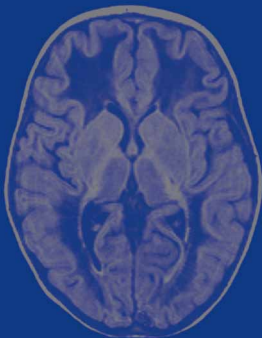


Marjo S. van der Knaap
Jaap Valk

Third Edition

Magnetic Resonance of Myelination and Myelin Disorders



 Springer

M.S. van der Knaap, J. Valk

Magnetic Resonance of Myelination and Myelin Disorders

Third Edition

Marjo S. van der Knaap
Jaap Valk

Magnetic Resonance of Myelination and Myelin Disorders

Third Edition

With 647 Figures in 3873 parts

With contributions by:

F. Barkhof
V. Gieselmann
G.J. Lycklama à Nijeholt
E. Morava
P.J.W. Pouwels
J.A.M. Smeitink

R. van den Berg
J.M.C. van Dijk
R.J. Vermeulen
R.J.A. Wanders
R.A. Wevers

Marjo S. van der Knaap, MD, PhD
Department of Child Neurology
VU University Medical Center
De Boelelaan 1117
1081 HV Amsterdam
The Netherlands

Jaap Valk, MD, PhD
Department of Radiology
VU University Medical Center
De Boelelaan 1117
1081 HV Amsterdam
The Netherlands

Third Edition

ISBN-10 3-540-22286-3 Springer Berlin Heidelberg New York
ISBN-13 978-3-540-22286-6 Springer Berlin Heidelberg New York

Second Edition
ISBN 3-540-59277-6 Springer Berlin Heidelberg New York

Library of Congress Control Number: 2004117334

This work is subject to copyright. All rights are reserved, whether the whole or part of the material is concerned, specifically the rights of translation, reprinting, reuse of illustrations, recitation, broadcasting, reproduction on microfilm or in any other way, and storage in data banks. Duplication of this publication or parts thereof is permitted only under the provision of the German Copyright Law of September 9, 1965, in its current version, and permission for use must always be obtained from Springer-Verlag. Violations are liable to prosecution under the German Copyright Law.

Springer is a part of Springer Science+Business Media
springeronline.com

© Springer-Verlag Berlin Heidelberg, 1989, 1995, 2005
Printed in Germany

The use of designations, trademarks, etc. in this publication does not imply, even in the absence of a specific statement, that such names are exempt from the relevant protective laws and regulations and therefore free for general use.

Product liability: The publisher can not guarantee the accuracy of any information about dosage and application contained in this book. In every individual case the user must check such information by consulting the relevant literature.

Editor: Dr. Ute Heilmann, Heidelberg, Germany
Desk editor: Dörthe Mennecke-Bühler, Heidelberg, Germany
Production: PRO EDIT GmbH, Heidelberg, Germany
Cover-Design: Frido Steinen-Broo, Pau, Spain
Typesetting and Reproduction: AM-productions GmbH, Wiesloch, Germany
Printing and Binding: Stürtz GmbH, Würzburg, Germany

Printed on acid-free paper 21/3151Di - 5 4 3 2 1 0

Preface

Preface to the Third Edition

Reading through the prefaces of the two previous editions, we can say that much of what was said there still holds. At the same time, however, much has changed. There has been immense progress in the technical possibilities of magnetic resonance and in the knowledge of genetic defects, biochemical abnormalities, and cellular processes underlying myelin disorders. This immense progress has prompted us to embark upon the enormous task of rewriting the previous edition and adding 40 chapters. In doing so we have tried to cover most white matter disorders, hereditary and acquired, and to present a collection of images to illustrate the field to the fullest possible extent. This edition will therefore be more complete than the previous ones. The number of illustrations has increased considerably. This was necessary to reflect not only the typical patterns of a disease, but to show also the variability that exists in some disorders. The best example of this is found in Alexander disease. Genetic verification now makes it possible to recognize very different patterns of imaging abnormalities, all related to a defect in the same gene. Today's increased insight into disease classification based on increased knowledge of related genes and proteins is best reflected in the chapter on congenital muscular dystrophies.

This is the first time that we have invited a number of experts in special fields to write or co-write a chapter, in order to assure the highest level of scientific accuracy. To assemble the knowledge presented in this work we have also harvested the literature, profiting from the work and discoveries of many others.

Our thanks go to our colleagues at the VU University Medical Center and to those in other hospitals who referred their patients to us. We are indebted to all colleagues who allowed us to use their MR images, published or unpublished, making it possible for us to present illustrations of nearly all known white matter disorders. Two colleagues were particularly helpful and provided us with essential and unpublished figures: our friends Susan Blaser, from the Hospital for Sick Children in Toronto, and Zoltán Patay, from the King Faisal Hospital in Riyadh.

Many people at the VU University Medical Center have been of great technical help to us in producing high quality images and in providing secretarial assistance. The contributions of these people are mentioned separately in the acknowledgements.

Our special thanks go to patients with white matter disorders and their families. They came to see us and were willing to work with us and to go through the procedure of diagnostic testing, including MR examinations. Many patients and families were also willing to participate in our research projects to advance the understanding of white matter disorders. Patients with white matter disorders are the focus of our work. They are our most important collaborators. Often they are children. To show our gratitude to them, we have decided that all profits of this book will go to the Foundation for Children with White Matter Disorders.

Amsterdam, May 2005

M.S. van der Knaap
J. Valk

Preface to the Second Edition

The first edition of this book was well received by readers and reviewers and we are very grateful for the positive reactions. We were convinced then, and even more now, that MRI and MRS have much to offer in diagnosis, therapy monitoring and research of hereditary and acquired myelin disorders.

In the last few years, a great deal of new information has become available concerning the genetic basis of inborn errors of metabolism and neurodegenerative disorders, the role of subcellular structures, the enzyme biochemistry, the pathophysiological mechanisms of posthypoxic-ischemic cerebral damage, and the inflammatory processes in infectious and inflammatory disorders. MR images of many rare disorders have become available, either in our own experience or published by other groups. MR spectroscopy could confirm its role in certain clinical applications. Because of these developments, it was necessary for us to rewrite the book almost completely. In some fields developments are so fast that we have not have caught all the latest developments. The pattern of the new approaches has, however, been established, making the assimilation of newly available information easy.

We are extremely grateful for the help of colleagues to make this book as complete as possible. The positive reactions of those from whom we requested MR pictures or other forms of support were of enormous encouragement to us during our efforts to complete this project.

We hope this work will be as warmly welcomed by our colleagues as the first edition.

Amsterdam, January 1995

M.S. van der Knaap
J. Valk

Preface to the First Edition

Magnetic resonance imaging (MRI) is now considered to be the imaging modality of choice for the majority of disorders affecting the central nervous system. This is particularly true for gray and white matter disorders, thanks to the superb soft tissue contrast in MRI which allows gray matter, unmyelinated, and myelinated white matter to be distinguished and their respective disorders identified. The present book is devoted to the disorders of myelin and myelination. A growing amount of detailed in vivo information about myelin, myelination, and myelin disorders has

been derived both from MRI and from MR spectroscopy (MRS). This prompted us to review the clinical, laboratory, biochemical, and pathological data on this subject in order to integrate all available information and to provide improved insights into normal and disordered myelin and myelination. We will show how the synthesis of all available information contributes to the interpretation of MR images.

Following a brief historical review of the increasing knowledge on myelin and myelin disorders, we propose a new classification of myelin disorders based on the subcellular localization of the enzymatic defects as far as the inborn errors of metabolism are concerned. This classification serves as a guide throughout the book. All items of the classification will be discussed and, whenever relevant and possible, illustrated by MR images.

We are aware of the fact that in a number of myelin disorders MRI is not a part of the usual diagnostic work up because a definite diagnosis is reached by other means, such as biochemical investigations of blood and urine, enzyme assessment or detection of specific antibodies. However, in many disorders MRI may facilitate a rapid diagnosis and early instigation of treatment, thus preventing structural cerebral damage. In other cases the role of MRI is to visualize the extent of brain damage and give an indication of the prognosis. In disorders which present in a non-specific way, for instance with behavioral problems or learning difficulties, MRI can be one of the first-line investigations. It is important to be acquainted with the various MRI patterns of the myelin disorders, as an early diagnosis may be of major importance in young families with a view to the provision of adequate genetic counseling.

MRS has been of limited clinical importance until now, and its application in patients only has a short history. We do, however, expect it to be a promising technique in the field of myelin and myelin disorders in clinical as well as in basic, experimental research and have, therefore, devoted a separate chapter to this subject.

This volume was written by a neuroradiologist and a neurologist/child neurologist. It is the product of close cooperation, animated discussions, strong arguments, restructuring, rewriting, and editing, in which they had an equal share. If the reader finds value in this monograph, it is because of this dual effort.

Amsterdam and Utrecht, March 1989

J. Valk
M.S. van der Knaap

Acknowledgements

The preparation of this book was a project of several years and could not have been concluded successfully without the support and collaboration of many people. Thanks to all.

Special thanks go to our colleagues: Jeroen Vermeulen and Leo Smit, pediatric neurologists, and Frederik Barkhof and Jonas Castelijns, neuroradiologists, at the VU University Medical Center (VUMC) in Amsterdam; Martin Heitbrink and Bart Wiarda, radiologists at the Medical Center Alkmaar; and Erik Veldhuizen, radiologist at the MRI center, Amsterdam, for their continuous support during this endeavor. We are grateful to the MRI technicians at the VUMC, who guaranteed the quality of the MR examinations and had the patience and empathy to deal with very sick children and their parents. We want to mention especially the help of Karin Barbiers and Erwin Kist, who headed this team and carried out the retrieval of older examinations to the Image Management System.

We received great support from the audiovisual center at the VUMC. We are especially indebted to Daan van Eijndhoven, Rene den Engelsman, and

Annuska Houtappels, who digitized older films and helped us improve the quality of the images.

Excellent secretarial help was provided by Sigrid Bruinsma, who single-handedly took care of the reference section. Staff members of the VUMC Library Els van Deventer, Linda Glas, Margreet Bosshardt, and Cisca Frederiks were very helpful in providing us with the necessary literature.

Technical support and guidance with computer programs and settings were provided by the Department of Informatics of the VUMC. We are grateful for their kind and prompt assistance. Special thanks go to Michiel Sprenger, Guido Zonneveld, and Peter Theijssmeijer.

We acknowledge the continuous friendly and encouraging support of the editorial staff of Springer-Verlag, Dr. Ute Heilmann and Mrs Dörthe Mennecke-Bühler.

Amsterdam, May 2005

M.S. van der Knaap
J. Valk

Contents

1	Myelin and White Matter	1	33	Trichothiodystrophy with Photosensitivity	268
2	Classification of Myelin Disorders	20	34	Pelizaeus–Merzbacher Disease and X-linked Spastic Paraplegia Type 2	272
3	Selective Vulnerability	25	35	18q- Syndrome	281
4	Myelination and Retarded Myelination . .	37	36	Phenylketonuria	284
5	Lysosomes and Lysosomal Disorders . . .	66	37	Glutaric Aciduria Type 1	294
6	Metachromatic Leukodystrophy	74	38	Propionic Acidemia	300
7	Multiple Sulfatase Deficiency	82	39	Nonketotic Hyperglycinemia	306
8	Globoid Cell Leukodystrophy (Krabbe Disease)	87	40	Maple Syrup Urine Disease	311
9	GM ₁ Gangliosidosis	96	41	3-Hydroxy 3-Methylglutaryl-CoA Lyase Deficiency	321
10	GM ₂ Gangliosidosis	103	42	Canavan Disease	326
11	Fabry Disease	112	43	L-2-Hydroxyglutaric Aciduria	334
12	Fucosidosis	119	44	D-2-Hydroxyglutaric Aciduria	338
13	Mucopolysaccharidoses	123	45	Hyperhomocysteinemias	342
14	Free Sialic Acid Storage Disorder	133	46	Urea Cycle Defects	360
15	Neuronal Ceroid Lipofuscinoses	137	47	Serine Synthesis Defect Caused by 3-Phosphoglycerate Dehydrogenase Deficiency	369
16	Adult Polyglucosan Body Disease	147	48	Molybdenum Cofactor Deficiency and Isolated Sulfite Oxidase Deficiency	372
17	Peroxisomes and Peroxisomal Disorders	151	49	Galactosemia	377
18	Peroxisome Biogenesis Defects	154	50	Sjögren–Larsson Syndrome	383
19	Peroxisomal D-Bifunctional Protein Deficiency	167	51	Lowe Syndrome	387
20	Peroxisomal Acyl-CoA Oxidase Deficiency	172	52	Wilson Disease	392
21	X-linked Adrenoleukodystrophy	176	53	Menkes Disease	400
22	Refsum Disease	191	54	Fragile X Premutation	406
23	Mitochondria and Mitochondrial Disorders	195	55	Hypomelanosis of Ito	409
24	Mitochondrial Encephalopathy with Lactic Acidosis and Stroke-like Episodes	204	56	Incontinentia Pigmenti	412
25	Leber Hereditary Optic Neuropathy . .	212	57	Alexander Disease	416
26	Kearns–Sayre Syndrome	215	58	Giant Axonal Neuropathy	436
27	Mitochondrial Neurogastrointestinal Encephalomyopathy	221	59	Megalencephalic Leukoencephalo- pathy with Subcortical Cysts	442
28	Leigh Syndrome and Mitochondrial Leukoencephalopathies	224	60	Congenital Muscular Dystrophies	451
29	Pyruvate Carboxylase Deficiency	245	61	Myotonic Dystrophy Type I	469
30	Multiple Carboxylase Deficiency	248	62	Myotonic Dystrophy Type 2	473
31	Cerebrotendinous Xanthomatosis . . .	252	63	X-linked Charcot–Marie–Tooth Disease	476
32	Cockayne Syndrome	259			

64	Oculodentodigital Dysplasia	479	86	Whipple Disease	658
65	Leukoencephalopathy with Vanishing White Matter	481	87	Toxic Encephalopathies	664
66	Aicardi–Goutières Syndrome	496	88	Iatrogenic Toxic Encephalopathies	679
67	Leukoencephalopathy with Calcifications and Cysts	505	89	Central Pontine and Extrapontine Myelinolysis	684
68	Leukoencephalopathy with Brain Stem and Spinal Cord Involvement and Elevated White Matter Lactate	510	90	Hypernatremia	690
69	Hypomyelination with Atrophy of the Basal Ganglia and Cerebellum	519	91	Marchiafava–Bignami Syndrome	695
70	Hereditary Diffuse Leukoencephalo- pathy with Neuroaxonal Spheroids	526	92	Posterior Reversible Encephalopathy Syndrome	699
71	Dentatorubropallidoluysian Atrophy	530	93	Langerhans Cell Histiocytosis	709
72	Cerebral Amyloid Angiopathy	535	94	Post-Hypoxic–Ischemic Damage	714
73	Cerebral Autosomal Dominant Arteriopathy with Subcortical Infarcts and Leukoencephalopathy	541	95	Post-Hypoxic–Ischemic Leukoencephalopathy of Neonates	718
74	Cerebral Autosomal Recessive Arteriopathy with Subcortical Infarcts and Leukoencephalopathy	549	96	Neonatal Hypoglycemia	749
75	Polycystic Lipomembranous Osteodysplasia with Sclerosing Leukoencephalopathy (Nasu–Hakola Disease).	552	97	Delayed Posthypoxic Leukoencephalopathy	755
76	Pigmentary Orthochromatic Leukodystrophy	557	98	White Matter Lesions of the Elderly	759
77	Adult-Onset Autosomal Dominant Leukoencephalopathies	559	99	Subcortical Arteriosclerotic Encephalopathy	767
78	Inflammatory and Infectious Disorders	561	100	Vasculitis	773
79	Multiple Sclerosis	566	101	Leukoencephalopathy and Dural Venous Fistula	801
80	Acute Disseminated Encephalomyelitis and Acute Hemorrhagic Encephalomyelitis	604	102	Leukoencephalopathy after Chemo- therapy and/or Radiotherapy	808
81	Acquired Immunodeficiency Syndrome	616	103	Gliomatosis Cerebri	818
82	Progressive Multifocal Leukoencephalopathy	628	104	Diffuse Axonal Injury	823
83	Brucellosis	635	105	Wallerian Degeneration and Myelin Loss Secondary to Neuronal and Axonal Degeneration	832
84	Subacute Sclerosing Panencephalitis	640	106	Diffusion-Weighted Imaging	839
85	Congenital and Perinatal Cytomegalovirus Infection	645	107	Magnetization Transfer Imaging	854
			108	Magnetic Resonance Spectroscopy: Basic Principles, and Application in White Matter Disorders.	859
			109	Pattern Recognition in White Matter Disorders.	881
				References	905
				Subject Index	1075

Contributors

F. Barkhof, MD PhD

Department of Radiology
and MR Center for MS Research
VU University Medical Center
Amsterdam, The Netherlands

V. Geiselmann, PhD

Institut für Physiologische Chemie
Rheinische Friedrich-Wilhelms-Universität
Bonn, Germany

G.J. Lycklama à Nijeholt, MD PhD

Department of Radiology
VU University Medical Center
Amsterdam, The Netherlands

E. Morava, MD

Nijmegen Center for Mitochondrial Disorders
and Department of Pediatrics
University Medical Center Nijmegen
Nijmegen, The Netherlands

P.J.W. Pouwels, PhD

Department of Clinical Physics and Informatics
VU University Medical Center
Amsterdam, The Netherlands

J.A.M. Smeitink, MD PhD

Nijmegen Center for Mitochondrial Disorders
and Department of Pediatrics
University Medical Center Nijmegen
Nijmegen, The Netherlands

J. Valk, MD PhD

Department of Radiology
VU University Medical Center
Amsterdam, The Netherlands

R. van den Berg, MD PhD

Department of Radiology
VU University Medical Center, Amsterdam
and Department of Radiology
Leiden University Medical Center
Leiden, The Netherlands

M.S. van der Knaap, MD PhD

Department of Child Neurology
VU University Medical Center
Amsterdam, The Netherlands

J.M.C. van Dijk, MD PhD

Department of Neurosurgery
Leiden University Medical Center
Leiden, The Netherlands

R.J. Vermeulen, MD PhD

Department of Child Neurology
VU University Medical Center
Amsterdam, The Netherlands

R.J.A. Wanders, PhD

Department of Clinical Chemistry
and Department of Pediatrics
Academic Medical Center
Amsterdam, The Netherlands

R.A. Wevers, PhD

Laboratory of Pediatrics and Neurology
University Medical Center Nijmegen St Radboud
Nijmegen, The Netherlands

List of Abbreviations

ACE	angiotensin converting enzyme	CAMFAK	cataracts–microcephaly–failure to thrive–kyphoscoliosis (syndrome)
ACTH	adrenocorticotrophic hormone	CD	Canavan disease; cluster determinant
AD	Alexander disease	Cho	choline
ADC	apparent diffusion coefficient	CIPO	chronic intestinal pseudo-obstruction
ADEM	acute disseminated encephalomyelitis	CIS	clinically isolated symptom
ADP	adenosine diphosphate	CK	creatine kinase
AD PEO	autosomal dominant progressive external ophthalmoplegia	CMD	congenital muscular dystrophy
AHEM	acute hemorrhagic encephalomyelitis	CMT	Charcot–Marie–Tooth disease
AIDS	acquired immunodeficiency syndrome	CMTX	X-linked form of CMT
ALD	adrenoleukodystrophy	CMV	cytomegalovirus
ALDP	ALD protein	CNP	2'3'-cyclic nucleotide 3'-phosphodiesterase
ALL	acute lymphocytic leukemia	CNS	central nervous system
AMN	adrenomyeloneuropathy	COFS	cerebro-oculofacioskeletal (syndrome)
ANCAs	anti-neutrophil cytoplasm antibodies	COX	cytochrome-c oxidase
ANCL	adult neuronal ceroid lipofuscinosis (or Kufs disease)	CPEO	chronic progressive external ophthalmoplegia
AP ₄	2-amino-4-phosphonobutyrate	CPM	central pontine myelinolysis
APLA	anti-phospholipid antibodies	CPSD	carbaryl phosphate synthetase deficiency
APBD	adult polyglucosan body disease	CPT	carnitine palmitoyl transferase
apoE	apolipoprotein E	Cr	creatine
APP	amyloid precursor protein	CREST	calcinosis, Raynaud syndrome, esophageal problems, sclerodactylia, and telangiectasia (syndrome)
aPTT	activated partial thromboplastin time	CS	Cockayne syndrome; concentric sclerosis (or Baló disease)
ASLD	argininosuccinate lyase deficiency	CSF	cerebrospinal fluid
ASSD	argininosuccinate synthetase deficiency	CSI	chemical shift imaging
ATP	adenosine triphosphate	CT	computed tomography/tomogram
BAEP	brain stem auditory evoked potential	CTX	cerebrotendinous xanthomatosis
BCNU	<i>bis</i> -chloroethyl-nitrosourea	DAB	diaminobenzidine
BDNF	brain-derived neurotrophic factor	DAGC	dystrophin-associated glycoprotein complex
bFGF	basic fibroblast growth factor	DAI	diffuse axonal injury
BIDS	brittle hair, impaired intelligence, decreased fertility, short stature (syndrome)	DAVF	cranial dural arteriovenous fistula
BMAA	β-N-methylamino-L-alanine	DHAPAT	dihydroxyacetonephosphate acyltransferase
BOMAA	β-N-oxalylmethylamino-L-alanine	DM 1	myotonic dystrophy type 1
BPD	D-bifunctional protein deficiency	DM 2	myotonic dystrophy type 2
CAA	cerebral amyloid angiopathy	DNA	deoxyribonucleic acid
CACH	childhood ataxia with central nervous system hypomyelination	DNC	deoxynucleotide carrier
CACT	mitochondrial carnitine/acylcarnitine transporter	dNTP	deoxyribonucleoside triphosphate
CADASIL	cerebral autosomal dominant arteriopathy with subcortical infarcts and leukoencephalopathy	DOA	dominant optic atrophy
cANCA	cytoplasmic form of ANCA	DOPA	dihydroxyphenylalanine
CARASIL	cerebral autosomal recessive arteriopathy with subcortical infarcts and leukoencephalopathy	DPHL	delayed posthypoxic leukoencephalopathy
		DRPLA	dentatorubropallidolusian atrophy

DS	diffuse sclerosis (or Schilder disease)	HCHWA-D	Dutch type of hereditary cerebral hemorrhage with amyloidosis
DSA	digital subtraction angiography	HDL	high-density lipoproteins
DTI	diffusion tensor imaging	HDLS	hereditary diffuse leukoencephalopathy with spheroids
DWI	diffusion-weighted imaging	5HIAA	5-hydroxyindoleacetic acid
EAA	excitatory amino acid	HIV-1	human immunodeficiency virus type 1
EAE	experimental allergic encephalomyelitis	HLA	human leukocyte antigen
ECD	ethyl cysteinat dimer	HMG-CoA	3-hydroxy-3-methylglutaryl-coenzyme A
ECG	electrocardiography/electrocardiogram	HMI	hypomelanosis of Ito
EDSS	Expanded Disability Status Scale	HMPAO	hexamethylpropyleneamine oxime
EEG	electroencephalogram	HSP	hereditary spastic paraplegia; heat shock protein
EGF	epidermal growth factor	HTLV	human T-cell lymphotropic virus
eIF	eukaryotic initiation factor	HUS	hemolytic-uremic syndrome
ELISA	enzyme-linked immunosorbent assay	HVA	homovanillic acid
EMG	electromyogram	IBIDS	ichthyosis, brittle hair, impaired intelligence, decreased fertility, short stature (syndrome)
EPI	echo planar imaging	IFN	interferon
EPM	extrapontine myelinolysis	Ig	immunoglobulin
EPMR	progressive epilepsy with mental retardation	IGF	insulin-like growth factor
ERG	electroretinography/electroretinogram	INCL	infantile neuronal ceroid lipofuscinosis (or Santavuori disease)
FA	fractional anisotropy	IP	incontinentia pigmenti
FAD	flavin adenine dinucleotide	IQ	intelligence quotient
FADH2	flavin adenine dinucleotide, reduced	IR	inversion recovery
FCMD	Fukuyama congenital muscular dystrophy	IRD	infantile Refsum disease
FD	Fabry disease	ISIS	image-selective in vivo spectroscopy
FISH	fluorescent in situ hybridization	ISSD	severe infantile sialic acid storage disease
FLAIR	fluid-attenuated inversion recovery	IVL	intravascular lymphomatosis
FSE	fast spin echo	JNCL	juvenile neuronal ceroid lipofuscinosis (or Spielmeyer-Vogt disease, or Batten disease)
FSH	follicle-stimulating hormone	KA	kainate
5-FU	5-fluorouracil	kDa	kiloDalton
FvLINCL	Finnish variant of late-infantile neuronal ceroid lipofuscinosis	KSS	Kearns-Sayre syndrome
GA	gestational age	LAMP	lysosome-associated membrane protein
GABA	γ -aminobutyric acid	LBSL	leukoencephalopathy with brain stem and spinal cord involvement and elevated white matter lactate
GAMT	guanidinoacetate methyltransferase	LCC	leukoencephalopathy with calcifications and cysts
GAN	giant axonal neuropathy	LCH	Langerhans cell histiocytosis
GDP	guanosine diphosphate	LDL	low-density lipoproteins
GE	gradient echo	LGMD	limb girdle muscular dystrophy
GEF	guanine-nucleotide exchange factor	LH	luteinizing hormone
GFAP	glial fibrillary acidic protein	LHON	Leber hereditary optic neuropathy
GIP	general insertion protein	LINCL	late-infantile neuronal ceroid lipofuscinosis (or Jansky-Bielschowsky disease)
GLD	globoid cell leukodystrophy	MAG	myelin-associated glycoprotein
Glx	glutamine, glutamate, GABA	MAP	microtubule-associated protein
GOM	granular osmiophilic material	MBS	Marchiafava-Bignami syndrome
GRACILE	growth retardation, aminoaciduria, cholestasis, iron overload, lactic acidosis, and early death (syndrome)	MBP	myelin basic protein
GROD	granular osmiophilic deposits		
GTE	glyceryl trierucate		
GTO	glyceryl trioleate		
GTP	guanosine triphosphate		
GVHD	graft-versus-host disease		
HAART	highly active/aggressive anti-retroviral treatment		
HABC	hypomyelination with atrophy of the basal ganglia and cerebellum		

MCE	multicystic encephalopathy	NCL	neuronal ceroid lipofuscinosis
MD	Menkes disease; myotonic dystrophy	nDNA	nuclear DNA
MDC1A	merosin-deficient congenital muscular dystrophy	NKH	nonketotic hyperglycinemia
MEB	muscle–eye–brain disease	NMDA	<i>N</i> -methyl- <i>D</i> -aspartate
MELAS	mitochondrial encephalomyopathy, lactic acidosis, and stroke-like episodes	NMO	neuromyelitis optica (or Devic disease)
MEPOP	mitochondrial encephalomyopathy with sensorimotor polyneuropathy, ophthalmoplegia, and pseudo-obstruction	NRTI	nucleoside analogue reverse transcriptase inhibitor
MERRF	myoclonic epilepsy with ragged red fibers	NT	neurotrophin
MHC	major histocompatibility complex	OCRL	oculocerebrorenal syndrome of Lowe
MHPG	3-methoxy-4-hydroxyphenylglycol	ODDD	oculodentodigital dysplasia
MICS	microcephaly–intracranial calcifications syndrome	OGIMD	oculogastrointestinal muscular dystrophy
MIL	multifocal inflammatory leukoencephalopathy	OHS	occipital horn syndrome
mIns	<i>myo</i> -inositol	OMgp	oligodendrocyte myelin glycoprotein
MLC	megalencephalic leukoencephalopathy with subcortical cysts	ONMR	onychotrichodysplasia, neutropenia, mental retardation (syndrome)
MLD	metachromatic leukodystrophy	OSP	oligodendrocyte-specific protein
MNGIE	mitochondrial neurogastrointestinal encephalomyopathy	OTCD	ornithine transcarbamylase deficiency
MOBP	myelin-associated oligodendrocytic basic protein	PACNS	primary angiitis of the CNS
MOG	myelin oligodendrocyte glycoprotein	PAF	platelet activating factor
MOM	mitochondrial outer membrane	PAN	polyarteritis nodosa
MOSP	myelin-/oligodendrocyte-specific protein	pANCA	perinuclear form of ANCA
MPP	mitochondrial processing peptidase	PAS	periodic acid–Schiff
MPS	mucopolysaccharidoses; mucopolysaccharidoses	PCD	pyruvate carboxylase deficiency
MPTP	methylphenyltetrahydropyridine	PCr	phosphocreatine
MR	magnetic resonance	PCR	polymerase chain reaction
MRA	magnetic resonance angiography	PDE	phosphodiesterases
MRI	magnetic resonance imaging	PDGF	platelet-derived growth factor
mRNA	messenger RNA	PDHc	pyruvate dehydrogenase complex
MRS	magnetic resonance spectroscopy	PEP	processing enhancing protein
MS	multiple sclerosis	PET	positron emission tomography
MSD	multiple sulfatase deficiency	Pi	inorganic phosphate
MSUD	maple syrup urine disease	PIBIDS	photosensitivity, ichthyosis, brittle hair, impaired intelligence, decreased fertility, short stature (syndrome)
MT	magnetization transfer		
mtDNA	mitochondrial DNA	PIP2	phosphatidylinositol 4,5-bisphosphate
MTI	magnetization transfer imaging	PKU	phenylketonuria
MTR	magnetization transfer ratio	PLOSL	polycystic lipomembranous osteodysplasia with sclerosing leukoencephalopathy
NAA	<i>N</i> -acetylaspartate		
NAAG	<i>N</i> -acetylasparyl glutamate	PLP	proteolipid protein
NAD	nicotinamide adenine dinucleotide	PMD	Pelizaeus–Merzbacher disease; proximal myotonic dystrophy
NADH	nicotinamide adenine dinucleotide, reduced	PME	phosphomonoesters
NALD	neonatal adrenoleukodystrophy	PML	progressive multifocal leukoencephalopathy
NARP	neurogenic muscle weakness, ataxia, and retinitis pigmentosa	PMP	peroxisomal membrane protein
NAWM	normal-appearing white matter	PNS	peripheral nervous system
NBCA	<i>n</i> -butyl cyanoacrylate	POLD	pigmentary orthochromatic leukodystrophy
		POLIP	polyneuropathy, ophthalmoplegia, leukoencephalopathy, and intestinal pseudo-obstruction
		PPAR	peroxisome proliferator activating receptor
		ppm	parts per million

PPRE	peroxisome proliferator response element	T	Tesla
PPT1	palmitoyl protein thioesterase 1	TE	toxic encephalopathy; echo time
PRES	posterior reversible encephalopathy syndrome	TI	inversion time
PRESS	point-resolved spectroscopy	TNF- α	tumor necrosis factor- α
PROMM	proximal myotonic myopathy	TORCH	toxoplasmosis, rubella, cytomegalovirus, herpes simplex
PTS	peroxisome targeting signals	TPP1	tripeptidyl peptidase 1
PVA	polyvinyl alcohol	TR	repetition time
PVL	periventricular leukomalacia	tRNA	transfer RNA
QA	quisqualate	TSD	Tay–Sachs disease
RCDP	rhizomelic chondrodysplasia punctata	TSE	turbo spin echo
RD	Refsum disease	TTD	trichothiodystrophy with photosensitivity
RF	radiofrequency	TTP	thrombotic thrombocytopenic purpura
RNA	ribonucleic acid	TvLINCL	Turkish variant of late-infantile neuronal ceroid lipofuscinosis
RPLS	reversible posterior leukoencephalopathy syndrome	TYROBP	TYRO protein tyrosine kinase binding protein
RPR	rapid plasma reagin (test)	UDP	uridine diphosphate
RR	relapsing remitting	US	ultrasound/ultrasonography
rRNA	ribosomal RNA	UV	ultraviolet
RXR	retinoic acid receptor	V-CAM	cellular adhesion molecules
SAE	subcortical arteriosclerotic encephalopathy	VDAC	voltage-dependent, anion-selective channel
SAP	sphingolipid activator protein	VDRL	Venereal Disease Research Laboratory (test)
SCA	spinocerebellar ataxia	VEGF	vascular endothelial growth factor
SCL	subcortical leukomalacia	VEP	visual evoked potential
SD	Salla disease	VLA-4	very late antigen 4
SE	spine echo	VLCFA	very-long-chain fatty acids
SIBIDS	osteosclerosis, ichthyosis, brittle hair, impaired intelligence, decreased fertility, short stature (syndrome)	vLINCL	variant late-infantile neuronal ceroid lipofuscinosis
SLE	systemic lupus erythematosus	VMA	vanillyl mandelic acid
SLS	Sjögren–Larsson syndrome	VWM	vanishing white matter
SP	secondary progressive	WD	Wilson disease
SPECT	single photon emission computed tomography	WM	white matter
SPG2	spastic paraparesis type 2	WWS	Walker–Warburg syndrome
SSEP	somatosensory evoked potential	XALD	X-linked adrenoleukodystrophy
SSPE	subacute sclerosing panencephalitis	XP	xeroderma pigmentosum
STEAM	stimulated-echo acquisition mode	ZS	Zellweger syndrome
STIR	short tau inversion recovery		

Myelin and White Matter

1.1 Introduction

Myelin makes up most of the substance of the white matter in the central nervous system (CNS). It is also present in large quantities in the peripheral nervous system (PNS). In both the CNS and the PNS, myelin is essential for normal functioning of the nerve fibers.

The white matter in the CNS is composed of a vast number of axons, which are ensheathed with myelin, which is responsible for the white color. Besides myelinated axons, white matter contains many cells of the neuroglia type, but no cell bodies of neurons. The axons it contains originate from neuronal cell bodies in gray matter structures.

There are two main types of macroglia in the white matter: astrocytes and oligodendrocytes. Among the many putative functions of glial cells, it is proposed that they contribute to the structural and nutritive support of neurons, regulate the extracellular environment of ions and transmitters, guide migrating neurons during development, and play an important part in repair and regeneration. The best known function of glial cells is the ensheathment of axons with myelin by oligodendrocytes.

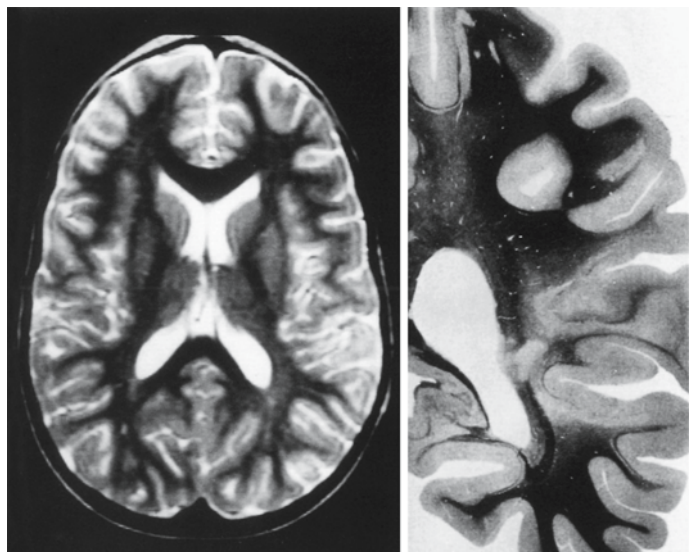
Gray matter contains the nerve cell bodies with their extensive dendritic arborization. The myelin content of gray matter structures is much lower, but

some myelin is present around intracortical and intranuclear fibers. The myelin content of the thalamus and the globus pallidus is relatively high.

1.2 Morphology of Myelin

Myelin is a spiral membranous structure that is tightly wrapped around axons. It has a very high lipid content and is soluble in fat solvents. Hence, when ordinary paraffin sections of the brain are prepared for light microscopic examination, most of the myelin dissolves away. After staining, the sites where myelin was present appear as round spaces that are empty except that each has a little round dot in the center, which represents a cross section of the axon. By means of fixatives that make myelin insoluble, it is possible to demonstrate it in paraffin sections. Osmic acid fixes myelin so that it does not dissolve in paraffin sections. Osmic acid itself stains myelin black. When examined under very low power, the white matter appears black (Fig. 1.1). If the white matter is examined under high power the myelin will be seen to be arranged in small rings around each nerve fiber. There are several myelin stains that can be used once the tissue has been fixed by some other means. Commonly used stains include hematoxylin, Luxol fast blue, and Oil-Red-O.

Fig. 1.1. T₂-weighted MR image compared with a postmortem section prepared with a myelin stain, illustrating the capability of MRI to reflect histology



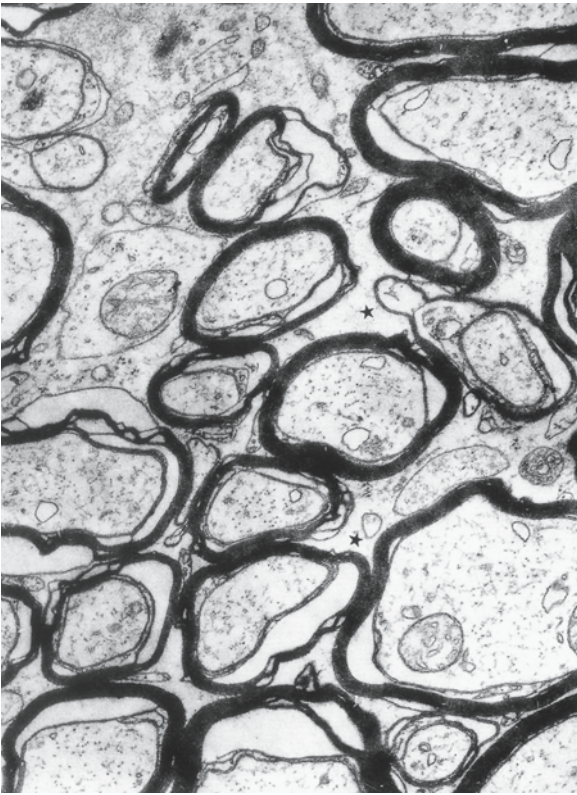


Fig. 1.2. Electron micrograph of white matter with myelin sheaths

The information derived from light microscopic investigations is limited and is inadequate when more detailed information about myelin structure is required. Analysis of the structure of myelin began in the 1930s, stimulated by polarization-microscope studies and X-ray diffraction work, which led to the suggestion that the myelin sheath was made up of layers or lamellae. The lamellar structure was confirmed by electron microscopic studies. In electron micrographs myelin is seen as a series of alternating dark and less dark lines separated by unstained zones. These lines are wrapped spirally around the axon (Fig. 1.2). The evidence available from studies using polarized light, X-ray diffraction and electron microscopy led to the current view of myelin as a system of condensed plasma membranes with alternating protein-lipid-protein-lipid-protein lamellae as the repeating subunit.

Plasma membranes are composed predominantly of lipids and proteins, and also contain carbohydrate components. The lipid elements of the membranes are phospholipids, glycolipids, and cholesterol. A common property of these lipids is that they are amphipathic. This means that the lipid molecules contain both hydrophobic and hydrophilic regions, corresponding to the nonpolar tails and the polar head groups, respectively. Hydrophobic substances are in-

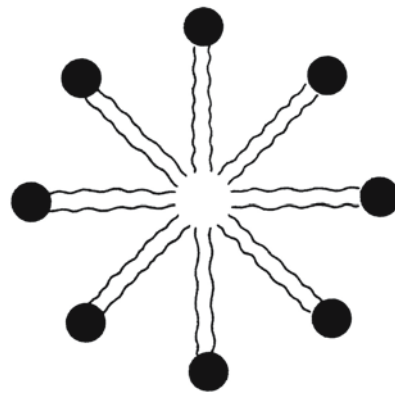


Fig. 1.3.
A micelle

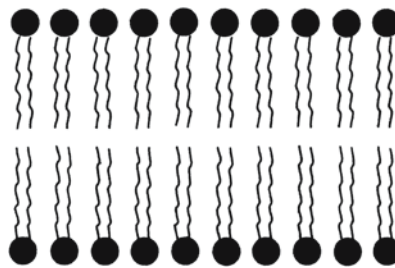
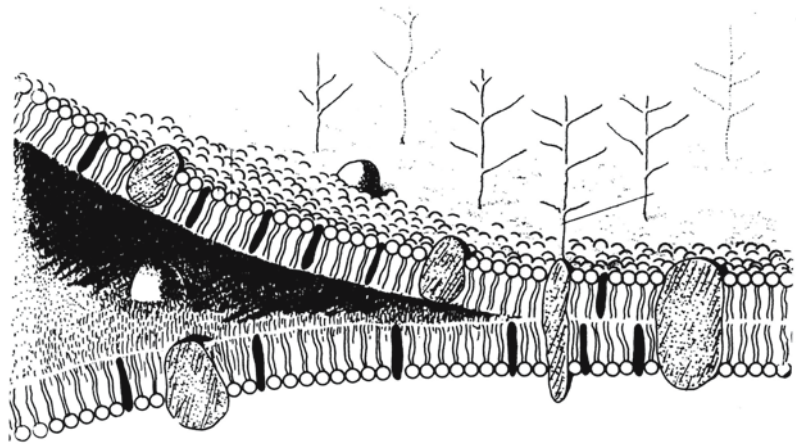


Fig. 1.4.
A lipid bilayer

soluble in water, but soluble in oil. Conversely, hydrophilic substances are insoluble in oil, but soluble in water. In an aqueous environment, the amphipathic character of the lipids favors aggregation into micelles or a molecular bilayer. In a micelle (Fig. 1.3), the hydrophobic regions of the amphipathic molecules are shielded from water, while the hydrophilic polar groups are in direct contact with water. The stability of this structure lies in the fact that significant free energy is required to transfer a nonpolar molecule from a nonpolar medium to water. Likewise, a great deal of energy is required to transfer a polar moiety from water to a nonpolar medium. Thus, the micelle provides a minimal energy configuration and is accordingly thermodynamically stable. The molecular bilayer, the basic structure of plasma cell membranes, also satisfies the thermodynamic requirements of amphipathic molecules in an aqueous environment. A bilayer exists as a sheet in which the hydrophobic regions of the lipids are protected from the water while the hydrophilic regions are immersed in water (Fig. 1.4). As the structure of the bilayer is an inherent part of the amphipathic character of the lipid molecules, the formation of lipid bilayers is essentially a self-assembly process.

In comparison with other molecular bilayers, the myelin bilayer is unique in having a very high lipid

Fig. 1.5. Membrane split open to demonstrate the layers. The lipid bilayer is interrupted by proteins embedded in this layer. Glycoprotein chains rise from the surface of the membrane



content and containing chiefly saturated fatty acids with an extraordinarily long chain length. This fatty acid composition leads to a closely packed, highly stable membrane structure. The presence of unsaturated fatty acids in a bimolecular leaflet leads to a more loosely packed, less stable structure, as unsaturated fatty acid chains have a kinked, hook-like configuration. Lipids containing such unsaturated fatty acids cannot approach neighboring molecules as closely as saturated lipids can, since the latter are rod-like structures. There will be much less total interaction between the tails of an unsaturated lipid and a neighboring molecule than between the tails of two saturated lipids, and the resulting binding forces will be much smaller. Lipids containing long-chain fatty acids are more tightly held in a membrane structure than those containing shorter chain fatty acids, since with increasing length of the hydrocarbon chain the binding interactions between the lipid molecules become stronger. It has also been suggested that very-long-chain fatty acids can form complexes by interdigitation of the hydrocarbon tail on one side with the hydrocarbon tail of a lipid on the opposite side of the bimolecular leaflet. Such complexes would contribute to the stability of the myelin membrane. If this lipid composition is changed, as is the case in a number of demyelinating disorders, it is clear that the stability of the myelin membrane may be diminished.

The bimolecular lipid structure allows for interaction of amphipathic proteins with the membrane. These proteins form an integral part of the membrane, with hydrophilic regions protruding from the inner and outer faces of the membrane and connected by a hydrophobic region traversing the hydrophobic core of the bilayer. In addition, there are peripheral proteins, which do not interact directly with the lipids in the bilayer, but are bound to the hydrophilic regions of specific integral proteins. Thus, the cell membrane is a bimolecular lipid leaflet coated with proteins on both sides (Fig. 1.5). There is inside-outside asymmetry of the lipids. In addition, integral and peripheral proteins

are asymmetrically distributed across the membrane bilayer and the protein composition on the inside is different from that on the outside of the bilayer.

On electron microscopic examination, a plasma membrane is shown as a three-layered structure and consists of two dark lines separated by a lighter interval. It is also revealed that the plasma membrane is not symmetrical in form: the dark line adjacent to the cytoplasm is denser than the leaflet on the outside.

From both X-ray diffraction and electron microscope data it can be seen that the smallest radial subunit that can be called myelin is a five-layered structure of protein-lipid-protein-lipid-protein (Fig. 1.6). The repeat distance is 160–180 Å. The dark lines seen in electron microscopic studies represent the protein layers and the unstained zones, the lipids. The uneven staining of the protein layers results from the way the myelin sheath is generated from the plasma membrane. The less dark lines (so-called intraperiod lines) represent the closely apposed outer protein coats of the original cell membrane. The dark lines (so-called major dense lines) are the fused inner protein coats of the cell membrane. High-magnification electron micrographs show that the intraperiod line is double in nature (Fig. 1.6).

The myelin sheath is not continuous along the entire length of axons, but axons are covered by segments of myelin, which are separated by small regions of uncovered axon, the nodes of Ranvier. The myelin lamellae terminate as they approach the node. The region where the lamellae terminate is known as the paranode. Electron micrographs of longitudinal sections of paranodal regions show that the major dense lines open up and loop back upon themselves, enclosing cytoplasm within the loop (Fig. 1.7). In that part of the paranode most distant from the node, the innermost lamellae of the myelin terminate first, and succeeding turns of the spiral of lamellae then overlap and project beyond the ones lying beneath. Thus, the outermost lamella overlaps all the others and terminates nearest the node, so that the myelin sheath

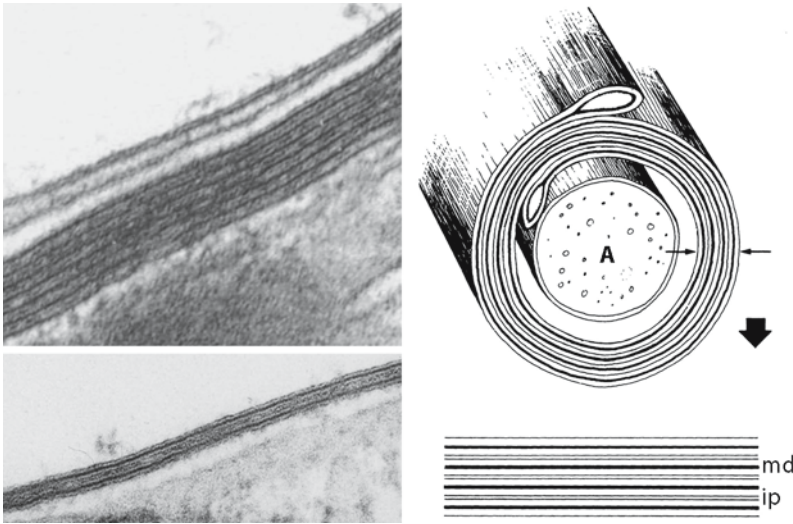


Fig. 1.6. The electron microscopic picture of a myelin sheath (*upper left*) reveals the five-layered structure of myelin with major dense lines and intraperiod lines. A higher magnification of two myelin lamellae (*lower left*) shows the periodicity of myelin even more clearly. On the *right*, a schematic representation of an electron microscopic picture of a myelin sheath surrounding an axon (A) demonstrates major dense lines (*md*) and intraperiod lines (*ip*)

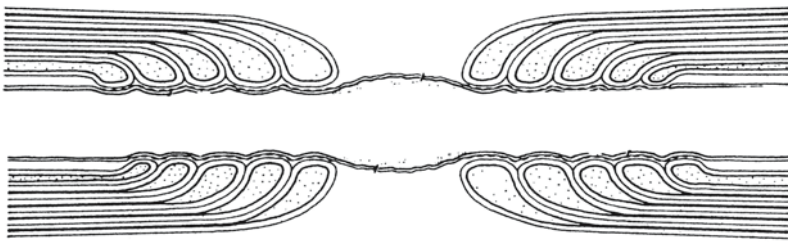


Fig. 1.7. Node of Ranvier, where the nerve fiber between two myelinated segments is bare. The outer myelin layers envelope the inner layer and cover these at the nodal junctions

gradually becomes thinner with increasing proximity to the node.

Schmidt-Lantermann clefts such as are described in the PNS are rare in the CNS. These are funnel-shaped clefts within myelin sheaths. They contain cytoplasm and extend from the soma of the myelin-forming cell to the inner end of the myelin sheath. In a transverse section of a myelin sheath they appear as islands of cytoplasm between openings of the major dense lines.

There is considerable variation in the number of myelin lamellae in the sheaths surrounding different axons. Generally, the larger the diameter of the axon the thicker its myelin sheath. In addition to this direct relationship between axon size and myelin thickness, the lengths of internodal segments also vary with the size of the axon: the larger the nerve fiber, the greater the internodal length.

1.3 Oligodendrocytes

Oligodendrocytes are the key cells in myelination of the CNS. They are cells of moderate size with a small number of short, branched processes. They are the predominant type of neuroglia in white matter and are frequently found interposed between myelinated axons. Actual connections between oligodendrocytes

and myelin sheaths can be observed. In the gray matter they aggregate closely around neuronal cell bodies, where they are called satellite oligodendrocytes. PNS myelin is formed by Schwann cells. The CNS myelin membranes originate from and are part of the oligodendroglial cell membrane. The oligodendrocytes form flat cell processes, which are wrapped around the nerve axon in a spiral fashion (Fig. 1.8).

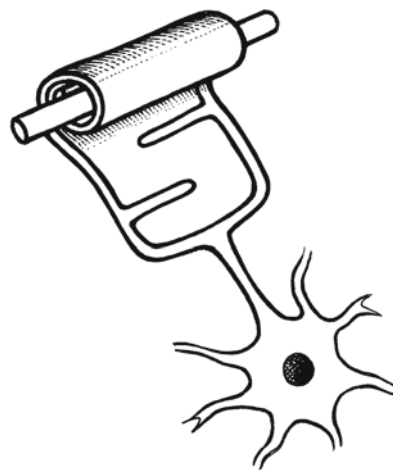
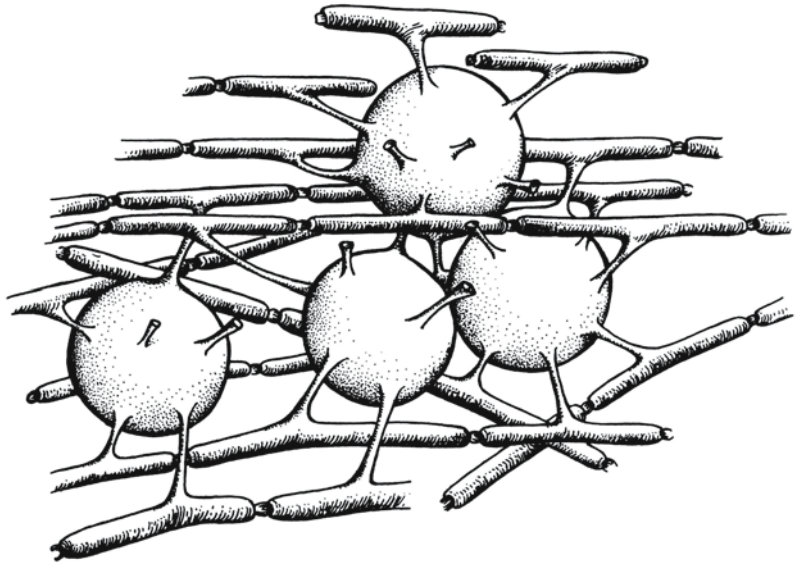


Fig. 1.8. Diagram showing the axon being rolled in the myelin sheath

Fig. 1.9. Impression of the three-dimensional structure of oligodendrocytes with their plasma membrane extensions as myelin sheaths covering the axons that cross their region



With the exception of the outer and lateral loops of the flat cell processes, the cellular cytoplasm disappears from these processes and the remaining cell membranes condense into a compact structure in which each membrane is closely apposed to the adjacent one. If myelin were unrolled from the axon it would be a flat, spade-shaped sheet surrounded by a tube containing cytoplasm.

Although the myelin sheath is an extension of the oligodendroglial cell membrane, the chemical composition of myelin is quite different from that of the oligodendroglial cell membrane. The oligodendroglial cell membrane is transformed into myelin in processes of modification and differentiation.

On the same axon, adjacent myelin segments belong to different oligodendrocytes. A single oligodendrocyte provides the myelin for many internodal segments of different axons simultaneously. One oligodendrocyte can be responsible for the production and maintenance of up to 40 nerve fibers (Fig. 1.9). This has implications for disease conditions and reparative processes, as the destruction of even only a few oligodendrocytes can have an extensive demyelinating effect.

Together with the Schwann cells of the PNS, oligodendrocytes are unique in their ability to produce vast amounts of a characteristic unit membrane. The ratio between cell body surface membrane and myelin membrane is estimated at 1:620 in the case of oligodendrocytes. The deposition and maintenance of such large expanses of membrane require optimal coordination of the synthesis of its various lipid and protein components and their interaction to ensure production of a stable membrane on the one hand and a well-regulated and controlled breakdown and replacement of spent components needed to support the myelin membrane on the other.

1.4 Astrocytes

Astrocyte functions have long been a subject of debate. Their major role has long been thought to be a sort of skeletal function, providing packing for other CNS components. It is becoming increasingly clear that astrocytes are of fundamental importance in maintaining the structural and functional integrity of neural tissue.

A well-known function of astrocytes is concerned with repair. When damage is sustained, astrocytes proliferate, become larger, and accumulate glycogen and filaments. This state of gliosis can be total, in which case all other elements are lost, leaving a glial scar, or occur against a background of regenerating or normal CNS parenchyma. Following demyelination, astrocytes synthesize growth factors thought to be involved in myelin repair. Astrocytes may also phagocytose debris in some conditions.

Astrocytes are involved in transport and in maintaining the blood-brain and CSF-brain barriers. End-feet of astrocytes form part of these barriers in perivascular and subpial regions. Endothelial tight junctions form the primary seal of the blood-brain barrier. The role of astrocytes in the blood-brain barrier is less well defined. They are physically separated from endothelial cells by the basal lamina and do not contribute directly to the physical barrier. Perivascular astroglial end-feet contain many transport proteins, including transporters of monocarboxylates, glucose, and glutamate, as well as water. Aquaporin-4 is the only known water channel in the brain and has a localization in the astroglial end-feet.

Astrocytes play a part in the process of myelin deposition. They promote the adhesion of oligodendrocyte processes to axons and stimulate myelin formation by local secretion of different growth factors. As-

trocytes and neurons are the sources of platelet-derived growth factor (PDGF), which promotes oligodendrocyte progenitors to proliferate, migrate, and differentiate. Astrocytes release basic fibroblast growth factor (bFGF), which promotes oligodendroglial differentiation. Extension of oligodendrocyte processes, a critical early step in myelin formation, is facilitated by astrocytic bFGF. Insulin-like growth factor I (IGF-I), which plays a crucial role in oligodendrocyte development and myelin formation, is produced by various cells, including astrocytes. It acts as an oligodendrocyte mitogen and a differentiation and survival factor and is one of the main regulators of the amount of myelin production. Astrocytes express neurotrophin-3 (NT-3), which promotes proliferation of oligodendroglial precursors and oligodendrocyte survival. There is evidence that NT-3 in combination with brain-derived neurotrophic factor (BDNF) can induce proliferation of endogenous oligodendrocyte progenitors and the subsequent myelination of regenerating axons. Astrocytes and oligodendrocytes communicate via gap junction-mediated contacts.

Astrocytes have a role in the conduction of nerve impulses. Astrocytes and axons have an intimate relationship at the node of Ranvier. Perinodal astrocytes and nodal parts of the axon have a high concentration of sodium channels, indicating specialization of astrocyte function at these sites.

Synthesis of the neurotransmitters glutamate and GABA (gamma aminobutyric acid) can originate either from glutamine or from α -ketoglutarate or another tricarboxylic acid cycle intermediate plus an amino acid as a donor of the amino group. Neurons lack the enzymes glutamine synthetase and pyruvate carboxylase, which are present exclusively in astrocytes. Astrocyte processes in perisynaptic regions take up the excitatory neurotransmitter glutamate from the synapse and recycle it to its precursor glutamine. Therefore, astrocytes are important in the synthesis and recycling of some neurotransmitters and protect neurons from excitotoxicity.

1.5 Biochemical Composition of Mature Myelin and White Matter

The most conspicuous feature of the composition of myelin as opposed to other membranes is the high ratio of lipid to protein. It is one of the most lipid-rich membranes, lipids making up 70–80% lipid by dry weight. In comparison with other membranes, the protein concentration of 20–30% is low. For example, the concentration of protein in liver cell membranes is 60%. Myelin is a relatively dehydrated structure, containing only 40% water.

CNS white matter is half myelin and half nonmyelin on a dry weight basis. Owing to the high myelin content, white matter has a relatively low water content and a high lipid content. The water content of white matter is 72% and that of gray matter 82%. The nonmyelin portion of white matter contains about 80% water.

Myelin is mainly responsible for the gross chemical differences between white and gray matter. Myelin is rich in all lipid classes, although nonpolar lipids and glycolipids (galactolipids) are particularly well represented. The lipids of CNS myelin are composed of 25–28% cholesterol, 27–30% galactolipid, and 40–45% phospholipid when expressed as percentages of total lipid weight. When lipid data are expressed as molar ratios, CNS myelin preparations contain cholesterol, phospholipid and galactolipid in a ratio varying between 4:3:2 and 4:4:2.

The biochemical composition of mature gray and white matter is shown in Table 1.1. With respect to white matter, separate figures are given for the myelin and nonmyelin portions, CNS white matter being half myelin and half nonmyelin on a dry weight basis. In Table 1.1 the lipid figures are expressed as percentages of total lipid weight. Since the water content and the dry weight lipid content of gray matter and white matter, myelin and nonmyelin, differ widely, the figures expressed in this way give no direct information about lipid concentration in either dry or wet tissue. However, from the data presented, these concentrations can be calculated.

When the lipid compositions of gray and white matter are compared, the most conspicuous difference to emerge is that white matter is relatively rich in galactolipids and relatively poor in phospholipids. Galactolipids (galactocerebroside and sulfatide) constitute 25–30% of the lipids in white matter, whereas they account for only 5–10% of those in gray matter. Phospholipids account for two-thirds of the total lipids in gray matter, but less than half those in white matter. There are, strictly speaking, no myelin-specific lipids that are not found elsewhere in the brain. However, the most specific distinguishing feature of myelin lipids is the high cerebroside content, and cerebroside can be considered the most typical myelin lipid. During development, the concentration of cerebroside in brain is directly proportional to the amount of myelin present.

Ethanolamine phosphoglyceride in plasmalogen form (plasmenylethanolamine) is the major myelin phospholipid. Approximately 80% of the ethanolamine phosphoglycerides of myelin and white matter are present in plasmalogen form, and only a small proportion are formed by phosphatidylethanolamine. Conversely, the plasmalogens, which comprise nearly one-third of the total phospholipids, are mainly of the ethanolamine type with lesser amounts of

Table 1.1. Composition of human CNS gray matter, white matter, myelin portion and nonmyelin portion of whole white matter. From Norton and Cammer (1984)

	Gray matter	White matter	Myelin	Nonmyelin ^d
Water ^a	82	72	44	82
Total protein ^b	55.3	39.0	30.0	62.2
Total lipid ^b	32.7	54.9	70.0	41.2
Cholesterol	22.0	27.5	27.7	14.6
Glycolipids	7.3	26.4	27.5	28.2
Cerebroside	5.4	19.8	22.7	19.9
Sulfatide	1.7	5.4	3.8	7.7
Phospholipids	69.5	45.9	43.1	51.9
Ethanolamine PG	22.7	14.9	15.6	6.8
Choline PG	26.7	12.8	11.2	16.5
Serine PG	8.7	7.9	4.8	20.4
Inositol PG	2.7	0.9	0.6	1.0
Sphingomyelin	6.9	7.7	7.9	5.6
Plasmalogens ^c	8.8	11.2	12.3	9.2

^a Percentage of total brain weight^b Figures for total protein and total lipid are percentages of dry weight; all others are percentages of total lipid weight^c Plasmalogens are primarily ethanolamine phosphoglycerides^d Figures for bovine brain, which are thought to be in close agreement with those for human brain (Norton and Autilio 1966)
PG phosphoglycerides

plasmalogen. Phosphatidylcholine is the major choline phosphoglyceride; only traces of choline phosphoglyceride have the plasmalogen form.

Gangliosides are minor myelin lipids and make up only 0.3–0.7% of total myelin lipids. They are localized mainly in neuronal membranes, and gray matter is 10 times as rich in gangliosides as in white matter. Gangliosides are complex sialic acids containing glycosphingolipids. GM₁, a monosialoganglioside, is the major myelin ganglioside accounting for about 70 mol % of the total myelin ganglioside content. Within the CNS, the ganglioside GM₄ (sialogalactosylceramide) is probably specific for myelin and oligodendroglia. It is a derivative of cerebroside.

Myelin lipids contain somewhat different fatty acid constituents than other membranes. Characteristic of myelin are α -hydroxy fatty acids in cerebroside and sulfatides and high amounts of long-chain fatty acids in the different lipid classes. There are monounsaturated fatty acids, but only low amounts of polyunsaturated fatty acids.

Table 1.2 shows the chemical structures of the main lipid constituents of myelin.

The protein composition of myelin is simpler than that of other membranes. Proteolipid protein and myelin basic protein encompass approximately 60–80% of the total protein. Most myelin proteins are unique to myelin.

Proteolipid protein (PLP) and its isoform DM 20 make up about 50% of the total protein in CNS myelin. Their concentration in white matter is about 5

times that in gray matter. The proteins are encoded by the same gene and are formed by alternative splicing of the primary gene transcript. The proteins differ by a hydrophilic peptide 35 amino acids in length, whose presence generates PLP. DM 20 is predominant in early development, whereas PLP is the major protein in mature myelin. The proteins are very hydrophobic.

There are multiple isoforms of myelin basic protein (MBP), arising from different patterns of splicing of the primary gene transcript. The heterogeneity is increased further by various posttranslational modifications. Myelin basic proteins account for 30–35% of the total myelin protein. MBP contains no extensive regions of hydrophobic residues and is hydrophilic. MBP is the antigen which, when injected into an animal, elicits a cellular immune response, producing the CNS autoimmune disease called experimental allergic encephalomyelitis.

There are several CNS myelin glycoproteins: myelin-associated glycoprotein (MAG), myelin/oligodendrocyte glycoprotein (MOG), and oligodendrocyte-myelin glycoprotein (OMgp). These are high-molecular-weight proteins. They are quantitatively minor myelin components: MAG accounts for about 1% of total protein and MOG, for 0.05%.

Other minor myelin proteins are oligodendrocyte-specific protein (OSP), which is a tight junction protein, myelin-associated oligodendrocytic basic protein (MOBP), a small basic protein distributed throughout compact myelin, and myelin/oligodendrocyte-specific protein (MOSP), which is located on

Table 1.2. Structure of the important myelin lipids

Cerebroside	sphingosine — galactose fatty acid
Sulfatide	sphingosine — galactose — sulfate fatty acid
Phosphatidylethanolamine	glycerol — fatty acid fatty acid phosphate — ethanolamine
Phosphatidylcholine = lecithin	glycerol — fatty acid fatty acid phosphate — choline
Phosphatidylserine	glycerol — fatty acid fatty acid phosphate — serine
Phosphatidylinositol	glycerol — fatty acid fatty acid phosphate — inositol
Ethanolamine plasmalogens	glycerol — *fatty acid fatty acid phosphate — ethanolamine
Sphingomyelin	sphingosine — fatty acid phosphate — choline
GM ₃ ganglioside	N-acylsphingosine glucose galactose — N-acetylneuraminic acid
GM ₂ ganglioside	N-acylsphingosine glucose galactose — N-acetylneuraminic acid N-acetylgalactosamine
GM ₁ ganglioside	N-acylsphingosine glucose galactose — N-acetylneuraminic acid N-acetylgalactosamine galactose

Sphingolipids of myelin are formed from sphingosine. N-acylsphingosine is termed ceramide. A phosphorylcholine group attached to ceramide forms sphingomyelin; glucose or galactose in glycosidic linkage forms cerebroside (most often: galactosylceramide). When the glucose or galactose is esterified with sulfate, sulfatide is formed. Phosphoglycerides contain two fatty acids in ester linkage at the α and β position of glycerol and at the α' position a phosphate group to which the moiety definitive of the class is linked. For example, a choline group defines phosphatidylcholine. The plasmalogens are similarly formed, except that at the α position of the glycerol there is a 1:2 unsaturated ether structure (*). Gangliosides are synthesized from N-acylsphingosine by stepwise addition of sugars and N-acetylneuraminic acid.

the extracellular surface of oligodendrocytes and myelin.

Highly purified myelin contains a number of enzymes. Two of these enzymes, 2',3'-cyclic nucleotide 3'-phosphodiesterase (CNP) and a cholesterol ester hydrolase, are found at much higher specific activities in myelin than in brain homogenates. It appears that these enzymes are fairly myelin specific, and are probably also present in oligodendroglial membranes. Many other enzymes are found that are not specific to myelin but also present in other brain fractions. The exact function of the two enzymes is not known. In particular, their contribution to the metabolism of myelin constituents is not known. CNP catalyzes the hydrolysis of several 2',3'-cyclic nucleotide monophosphates, all of which are converted to the corresponding 2'-isomer. The substrates of the enzyme are not present in nervous tissue. CNP is one of the proteins formerly called Wolfram proteins, a heterogeneous group of high-molecular-weight myelin proteins named after the investigator who first suggested that myelin contained proteins other than proteolipid protein and myelin basic protein.

1.6 Molecular Architecture of Myelin

The currently accepted view of the myelin structure is that of a double lipid bilayer, each coated on both sides with protein. The resulting repeating subunit consists of radial protein-lipid-protein-lipid-protein lamellae. Some proteins are fully or partially embedded in the bilayer, and others are attached to the surface by weaker linkages.

Both proteins and lipids have an asymmetrical distribution. Galactolipids, cholesterol, phosphatidylcholine, and sphingomyelin are preferentially located in the former extracellular half of the bilayer (intraperiod line). Ethanolamine plasmalogen and myelin basic protein are preferentially located in the former cytoplasmic half of the bilayer.

Membranes are fluid structures. Lipid molecules diffuse rapidly in the plane of the membrane, as do proteins, unless anchored by specific interactions. The spontaneous rotation of lipids from one side of the membrane to the other is a very slow process. The transition of a molecule from one membrane surface to the other is called transverse diffusion, or flip-flop. In view of the asymmetry of lipids in the bilayer, the transverse mobility must be limited. The diffusion within the plane of the membrane is referred to as lateral diffusion.

Proteolipid protein consists of alternating hydrophilic and hydrophobic sequences with four stretches of hydrophobic residues that are of sufficient length to span the lipid bilayer. It is an integral membrane protein that passes through the bilayer four times

(four transmembrane domains). The hydrophobic transmembrane segments are linked by hydrophilic portions on both sides of the membrane. This means that the protein has domains in both the intraperiod and the major dense lines. Probably both isoforms, PLP and DM 20, are involved in stabilizing the intraperiod line. Their role is described as that of 'adhesive struts' or 'spacers,' maintaining a set distance between apposed lamellae. DM 20 is the major proteolipid protein in early development, whereas PLP is the major product in mature myelin. It is believed that DM 20 has a still unidentified regulatory role in early oligodendrocyte progenitor development and differentiation, and that PLP plays a part later on in oligodendrocyte function, in the proper formation of the intraperiod line of myelin during its final elaboration and compaction.

Myelin basic protein is an extrinsic protein located on the cytoplasmic face of the myelin membranes at the major dense lines. It probably stabilizes the major dense lines by keeping the cytoplasmic faces of the myelin lamellae in close apposition. Myelin-associated oligodendrocytic basic protein is another small basic protein distributed throughout compact myelin at the major dense lines. There is evidence that MOBP reinforces the apposition of the cytoplasmic faces of the myelin sheath.

Gangliosides are located almost entirely on the external surface of membranes. They may have an important role in cell surface recognition and signal transduction processes such as those that occur during myelination.

Myelin glycoproteins are transmembrane proteins with the polypeptide extending through the lipid bilayer and the glycosylated portion of the molecule exposed on the outer surface of the bilayer. They are all implicated in recognition and cell-cell interactions.

MAG is one of these proteins. Its external region contains immunoglobulin-like domains. Thus, MAG is a member of the immunoglobulin superfamily. It is concentrated in the inner periaxonal membrane of the myelin sheath and absent from the compact multilamellar myelin sheath. The exposed, periaxonal position is compatible with its postulated involvement in oligodendrocyte-axon interaction, including maintenance of the structural integrity of the glia-axon adhesion in mature myelin. The observation that the protein can be detected at the very earliest stages of myelination has led to the hypothesis that the protein may also play a role in mediating the oligodendrocyte-axon recognition events that precede myelination and specify the initial path of myelin deposition.

MOG is another of the myelin glycoproteins. It also belongs to the immunoglobulin superfamily. The protein is located at the outermost layer of the myelin sheath and the oligodendrocyte plasma membrane.

The function of this glycoprotein is unknown. It may be involved in the adhesion between neighboring myelinated fibers and function as glue in the maintenance of axon bundles in the CNS. MOG may also be a cell surface receptor that transduces signals from the external milieu to the inside of the oligodendrocyte or myelin sheath.

The enzyme CNP is found in myelin and oligodendrocytes. Within the myelin sheath it is localized on the cytoplasmic side of noncompact regions, e.g., periaxonally and in the paranodal loops. CNP is essential for axonal survival but not for myelin assembly.

1.7 Myelinogenesis

The time-course of the appearance of newly synthesized lipids and proteins in myelin indicates that myelin is not laid down as a unit. Different components are synthesized and processed in different cellular compartments, are transported to the sites of myelin formation by different mechanisms, and show different rates of entry into the myelin sheath. For example, MBP enters the myelin sheath with almost no lag after synthesis, whereas proteolipid protein enters myelin with a lag-time of 30–40 min following synthesis. Once protein synthesis is stopped with cycloheximide, the entry of MBP is halted immediately, but proteolipid protein continues to be incorporated into myelin for 30 min. These data indicate that MBP and PLP are assembled by different mechanisms, with PLP taking a longer and more circuitous route through the cytoplasm. Lipids also continue to be incorporated into myelin for 4 h after protein synthesis has stopped.

MBP is synthesized on free polyribosomes near the plasma membrane or the adjacent myelin sheath. The myelin membrane is surrounded by and infiltrated with cytoplasmic channels, called the outer loops and longitudinal incisures of Schmidt-Lantermann, respectively. Myelin basic protein mRNA is translocated from the nucleus to the myelin membrane via these cytoplasmic channels. MBP synthesized here is rapidly sequestered into the myelin sheath and appears in the cytoplasmic leaflet of compact myelin (major dense lines). mRNAs for several other myelin proteins follow similar trafficking pathways.

Proteolipid protein and DM 20 are synthesized on polyribosomes bound to the endoplasmic reticulum. The nascent protein is inserted into the endoplasmic reticulum and passes through the Golgi apparatus to the plasma membrane and myelin sheath via vesicular transport. Inclusion in the plasma membrane occurs by fusion of the vesicles with the plasma membrane. The inside of the vesicle after fusion becomes the outside of the plasma membrane. As a conse-

quence, substances transported to the plasma membrane via vesicles end up in the extracellular leaflet of the myelin sheath. MAG resembles proteolipid protein as far as the site of synthesis and transport to the plasma membrane are concerned.

The same two mechanisms of synthesis and transport can be distinguished for myelin lipids, i.e., the routes of PLP and MBP, respectively. The endoplasmic reticulum is the site of synthesis of phosphatidylcholine and cholesterol. The Golgi apparatus is the site of synthesis of cerebroside, sulfatide, sphingomyelin, and gangliosides. The lipids are transported from the Golgi apparatus to the plasma membrane by a vesicle-mediated process. Expression on the cell surface occurs by fusion of the vesicles with the plasma membrane. The lipids are located predominantly in the extracellular leaflet of the myelin lamellae. In contrast, the myelin phospholipids that predominantly reside on the inner leaflet, including phosphatidylserine and ethanolamine plasmalogens, are synthesized in the superficial cytoplasmic channels of the myelin sheath and rapidly enter compact myelin, possibly with phospholipid transfer proteins as carriers. Several other phospholipids are also synthesized in the superficial cytoplasmic channels.

After reaching the outermost myelin layers, substances penetrate to the deepest layers over a period of a few days. This movement of substances from outer to inner layers occurs at rates consistent with lateral diffusion along the spirally wound bilayer.

1.8 Regulation of Myelinogenesis

Elaboration of the myelin sheath involves a precisely ordered sequence of events beginning with the initial ensheathment of the axon, proceeding to formation of multiple loose wrappings and eventually compaction to form the mature multilamellar myelin sheath. These processes imply a temporally regulated program of gene expression in the oligodendrocyte to ensure that the appropriate biochemical components are synthesized in the appropriate proportions at each stage of myelinogenesis. Just before the onset of rapid myelin membrane synthesis the expression of genes of myelin proteins is sharply up-regulated. There is evidence of a coordinated mechanism for synchronous activation of the myelin protein genes. This period of sharp up-regulation of expression of myelin genes is the most vulnerable part of the myelination process and is called the critical period.

Apparently, there are both tissue-specific and stage-specific mechanisms controlling myelin genes. Myelin genes are only expressed in oligodendrocytes and Schwann cells. The expression of the genes is de-

velopmentally regulated and is probably intimately associated with the stage of differentiation of these cells. Control mechanisms are active at the transcriptional level. Regulatory regions, including the promoter regions, have been identified for myelin protein genes. Key sites for tissue-specific expression of myelin proteins are clustered near the promoter regions, and within these clusters are several motifs that may be involved in coordinating the regulation of myelin-specific genes. The alternative splicing patterns produced from the primary myelin protein transcripts are also developmentally regulated. The splicing patterns for the different proteins have been shown to change in the course of development.

In both the CNS and the PNS, glial cells are influenced to produce myelin by both neuronal targets that they ensheath and by a range of hormones and growth factors produced by neurons and astrocytes. There is a continuous oligodendrocyte-neuron-astrocyte interaction in the process of myelination and myelin maintenance.

Proliferation of oligodendrocyte precursor cells depends on electrical activity of neurons. Oligodendrocyte number is also dependent on number of axons. Differentiation of oligodendroglia has been shown to depend heavily on the presence and the integrity of axons. Gene expression for myelin constituents is modulated by the presence of axons. Within oligodendrocytes, proteins are produced that are thought to be involved in the induction of myelination (e.g., glia-specific surface receptors for differentiation signals), in the initial deposition of the myelin sheath (e.g., axon-glial adhesion molecules), and in its wrapping and compaction around the nerve axon (e.g., structural proteins of compact myelin). A minimal axonal diameter is important for the initiation of myelination. Final myelin sheath thickness is also related to axonal size. This match is reached by local control mechanisms. Therefore, a single oligodendrocyte can be associated with several axons of different sizes, the myelin sheaths being thicker for larger axons. Larger axons also have longer internodes.

Astrocytes are essential in the process of myelination and myelin maintenance. They produce trophic factors, including PDGF, bFGF, IGF-I, and NT-3. These factors promote proliferation, migration and differentiation of oligodendrocyte progenitors, extension of oligodendrocyte processes, adhesion of oligodendrocyte processes to axons, myelin formation and myelin maintenance.

Hormones have a dramatic effect on myelinogenesis. A deficiency of growth hormone during the critical period leads to hypomyelination. Most of the effects of growth hormone are mediated by IGF-I. Administration of this substance in early development leads to an increase in all brain constituents, but par-

ticularly and disproportionately in the amount of myelin produced per oligodendrocyte. Thyroid hormone also has an effect on myelinogenesis. Hypothyroidism during early development leads to hypomyelination, whereas hyperthyroidism accelerates myelination. Steroids have a complex influence. None of the myelin protein genes is transcriptionally regulated by steroids, but steroids probably act at the post-translational level, stimulating the translation of MBP and PLP mRNAs and inhibiting the translation of CNP mRNA.

The importance of iron in myelination has been examined. Iron and the iron mobilization protein transferrin are localized in oligodendrocytes, and may participate in the formation and/or maintenance of myelin by complexing with enzymes involved in the synthesis of myelin components.

Myelination is vulnerable to undernourishment. If there is undernourishment during the critical period just prior to the onset of rapid myelin synthesis, myelination is more severely reduced than total brain weight, whereas the number of oligodendrocytes is unaltered. The hypomyelination is permanent. Severe undernutrition during the critical period leads to decreased levels of IGFs and a failure in up-regulation of myelin genes.

Successful myelination is also dependent on function. It is known that myelination is diminished by preventing the conduction of impulses in a nerve. Impulse conduction is a stimulus to myelination. Premature activity accelerates myelination. Hypermyelination has incidentally been noticed in cerebral anomalies, supposedly via the stimulus of epilepsy. It has been shown that oligodendrocyte progenitor cells express adenosine receptors, which are activated in response to action potential firing. Action potential firing leads to the nonsynaptic release of several substances from axons, including ATP and adenosine. Adenosine acts as a potent neuroglial transmitter to inhibit oligodendrocyte progenitor cell proliferation, stimulate differentiation, and promote the formation of myelin.

After formation the myelin sheath and the axon remain mutually dependent. The myelin sheath needs an intact axon, as demonstrated by the studies on Wallerian degeneration. On the other hand, for maintenance of the normal structure and function the axon requires an intact myelin sheath. Normal astrocytes are essential for an intact myelin-axon unit.

Since myelin, once deposited, is a relatively stable substance metabolically, it is relatively invulnerable to adverse external factors. Generalized vulnerability of myelin to noxious agents and adverse influences is likely to be confined to the period just before and during active myelination.

1.9 Myelination of the Nervous System

Myelination of each of the multiple connecting fiber systems of the CNS takes place at a different time in early development. Some fiber systems start to myelinate halfway through gestation or later and rapidly attain their maximal degree of myelination, whereas other systems attain their maximal degree of myelination only slowly. It is, therefore, not correct to refer to myelination as a singular process. There is a marked, temporal diversity in topographic patterns of myelination throughout the last half of gestation and during the first 2 postnatal years. Thus, at any time in the early development of the human brain there are multiple separate or intermixed regions of unmyelinated, partly myelinated, or completely myelinated tracts.

Myelination of the nervous system follows a fixed pattern consisting of ordered sequences of myelinating systems apparently governed by some rules:

1. The first rule, probably governing all other rules, is that tracts in the nervous system become myelinated at the time they become functional.
2. Most tracts become myelinated in the direction of the impulse conduction.
3. Myelination starts in the PNS before it starts in the CNS.
4. Myelination in central sensory areas tends to precede myelination in central motor areas.
5. Myelination in the brain occurs earlier in areas of primary function than in association areas.
6. Roughly speaking, myelination progresses from caudal (spinal cord) to rostral parts (brain) and spreads from central (diencephalon, pre- and postcentral gyri) to peripheral parts of the brain. However, there are many exceptions to this rule.

It is important to note that the times mentioned below for myelination of the different tracts and structures of the brain are only generalizations and approximations. In the first place, there is a considerable degree of normal variation. Secondly, the onset of myelination is difficult to define. It can be defined as the first myelin tube found on light microscopic examination, as the appearance of the first myelin lamella on ultrastructural examination, or as the first evidence of the presence of myelin constituents in immunological investigations.

In the 4th month of gestation myelin is first seen in the anterior motor roots and soon appears in the posterior roots.

In the 5th month of gestation myelination starts in the dorsal columns of the spinal cord and the anterior and lateral spinothalamic tracts for conduction of somesthetic stimuli.

In the 6th month of gestation myelination proceeds rapidly cephalad in the medial lemniscus and spinothalamic tracts in the brain stem tegmentum. Myelin begins to appear in the statoacoustic tectum and tegmentum and the lateral lemniscus for the conduction of acoustic stimuli. Myelin is seen in the inner, vestibulocerebellar part of the inferior cerebellar peduncle.

In the 7th month of gestation myelination is still largely confined to structures outside the diencephalon and cerebral hemispheres. Progress of myelination is seen in the optic nerve, optic chiasm and tracts, inferior cerebellar peduncle, the parasagittal part of the cerebellum, the descending trigeminal tract, superior cerebellar peduncle, capsule of the red nucleus, capsule of the inferior olivary nucleus, vestibulospinal, reticulospinal and tectospinal descending tracts to the spinal cord and posterior limb of the internal capsule.

In the eighth month of gestation, myelination starts in the corpus striatum (in particular globus pallidus), anterior limb of the internal capsule, subcortical white matter of the post- and precentral gyri, rostral part of the optic radiation as well as corticospinal tracts in midbrain and pons, transpontine fibers, middle cerebellar peduncles and cerebellar hemispheres.

In the ninth month of gestation, myelination continues in the thalamus (in particular ventrolateral nucleus), putamen, central part of the corona radiata, distal part of the optic radiation, acoustic radiation, anterior commissure, midportion of the corpus callosum and fornix.

However, in a child born at term, most of the structures and tracts mentioned are not fully myelinated and, in fact, in some myelination has just started. Apart from some myelin in the central tracts of the corona radiata connected with the pre- and postcentral gyri, and the primary optic and acoustic radiations, the cerebral hemispheres are still largely unmyelinated. During the first postnatal year, myelin spreads throughout the entire brain. By the postnatal age of 12 weeks myelination is well advanced in the corona radiata, the optic radiation and the corpus callosum, but the frontal and temporal white matter are still largely unmyelinated. By the age of about 8 months, the adult state is foreshadowed in that none of the fiber systems is still completely devoid of myelin sheaths. Myelin sheaths are still sparse in the temporal and frontal areas. It is not until the end of the second postnatal year that an advanced state of myelination is seen in all subcortical areas. Histologically, myelination reaches completion in early adulthood.

1.10 Compositional Changes in the Developing Brain

The DNA content of brain is considered to be a reliable indicator of cell number. The period of cellular proliferation can, therefore, be followed by measuring the amount of DNA per brain volume. In human brain two major periods of cell proliferation have been detected by measuring DNA levels. The first period begins at 15–20 weeks of gestation and corresponds to neuroblast proliferation. The second period begins at 25 weeks of gestation and continues into the 2nd year of postnatal life. This latter period corresponds to multiplication of glial cells and includes a second wave of neuronogenesis, producing mainly cerebellar neurons.

The ratio of protein to DNA indicates cell size. This ratio increases after neuronal division ends, reflecting in part the arborization of neuronal processes. The maximum ratio of protein to DNA is reached at 2 years of age.

The outgrowth of neuronal axons and dendrites results in a rapid increase in total ganglioside content in the brain. Increasing lipid content indicates membrane formation with, in particular, an increase in quantity of axonal, dendritic, and myelin membranes. The increasing lipid content is associated with a concomitant decrease in water content. The most rapid increase in lipid content of the brain begins after the period of greatest increase of DNA and protein and is closely related to the onset of myelination.

At birth, cerebral hemispheric white matter contains very little myelin and the white matter composition of neonates is very different from the composition of mature myelinated white matter. There is an important overall decrease in water content of the brain after birth and the change in water content is larger for white matter than for gray matter. The water content of neonatal gray matter is about 89% and of neonatal unmyelinated white matter about 87%, whereas the water content of adult gray matter is estimated to be 82% and of adult myelinated white matter 72%. The lipid composition of cerebral white mat-

ter at different ages is shown in Table 1.3. A major change is an increase in total lipid content, with a relative increase in glycolipids. One of these, cerebroside, is usually considered to be a marker for myelin as it is deposited at the same rate in the brain as myelin. However, cerebroside is not restricted to myelin and as much as 30% of it may be present in membranes other than myelin. There is a relative decrease (but absolute increase) in phospholipids in the white matter, which were relatively high in concentration in unmyelinated white matter and are relatively low in concentration in myelin. The relative contribution of cholesterol to total lipids remains constant, but the absolute cholesterol content of white matter increases with deposition of myelin. The changes in gray matter composition are much less important. Myelin deposition in gray matter is minor.

The changes in white matter composition are not caused only by glial cell proliferation, growth of axons and dendrites, and myelin deposition, but also by some changes in myelin composition. The composition of the myelin first deposited is somewhat different from that in adults. The most important changes are an increase in cholesterol and glycolipids as a proportion of total lipid and a decrease in phospholipids. In the immature brain significant amounts of glucose are present in the glycolipids, whereas in a mature brain glycolipids are present mainly as galactolipids. In contrast to the modest decrease in total phospholipids, more marked variations in the relative contribution of individual phospholipids are found. Sphingomyelin and ethanolamine phosphoglycerides increase, whereas choline phosphoglycerides decline. The molar ratio of galactolipids and choline phosphoglycerides appears to be a sensitive marker of myelin maturation.

In human unmyelinated white matter much of the cholesterol present is esterified. The same is true for cholesterol in newly formed myelin. During myelin maturation there is a decrease in the amount of cholesterol esters, and in adult white matter cholesterol is present almost entirely in the free form. The ratio of cholesterol to phospholipids in myelin increases after

Table 1.3. Lipid composition of human brain during development. From Svennerholm (1963)

	Lipid composition of (frontal) cerebral cortex			Lipid composition of (frontal) cerebral white matter		
	2 months	1 year	5 years	2 months	1 year	5 years
Age						
Total lipids ^a	28.4	31.3	29.5	29.5	49.6	58.2
Cholesterol ^b	21.5	19.8	19.3	26.4	25.0	24.4
Phospholipids ^b	76.8	7.6	75.6	66.1	53.4	49.8
Glycolipids ^b	1.8	2.6	4.1	7.5	21.6	25.8

^a Expressed as percentage of dry weight

^b Expressed as percentage of total lipid weight

birth and reaches the adult value at about 5 years of age. The ratio of galactolipids to phospholipids reaches the adult value at about the same time.

During development the ganglioside composition of myelin becomes simplified. The polysialogangliosides decline and the monosialoganglioside GM₁ content approaches about 90% of the total gangliosides with increasing age. The total ganglioside content remains constant.

Maturation of myelin is accompanied by an increase in hydroxy fatty acids and saturated and monounsaturated fatty acids.

Maturation of myelin is also accompanied by changes in the proteins. As the brain matures there is a change in occurrence of the major isoforms of the major myelin proteins. For example, initially, early in myelination, DM 20 is the principal isoform, whereas in adult brain DM 20 is present at much lower levels than the isoform PLP. With advancing development the contribution of PLP and MBP to myelin proteins shows a relative increase, whereas the high-molecular-weight proteins decrease.

On the whole, the differences in chemical composition of immature myelin and adult myelin are not striking, which suggests that only subtle remodeling of myelin occurs in humans once myelination has started. The major difference between white matter early in life and in adult life seems to be the quantity of myelin rather than its quality.

1.11 Myelin Turnover

The principal features of myelin metabolism are its high rate of synthesis during the active stages of myelination, when each oligodendroglial cell makes more than three times its own weight of myelin per day, and its relative metabolic stability after the completion of myelination. Individual components turn over at quite different rates. There are conflicting data about the precise half-lives of the various myelin lipids and proteins. This is understandable, since there are several variables in the experimental design that have considerable influence on the observed, real or apparent, half-lives. However, some general conclusions can be formulated. The concept of relative long-term metabolic stability of most myelin components has been confirmed. Some components do turn over much faster than others, and all components show both a slow- and a fast-turnover component. The data indicate that newly formed myelin is catabolized faster than old myelin. Hence, myelin that has been deposited early in life appears to have a higher metabolic stability than newly synthesized myelin.

1.12 Aging of Myelin

With increasing age, human brain weight decreases and water content increases. Levels of DNA and numbers of neurons in the cerebral cortex decrease significantly with aging. Little change is found in some regions, including the brain stem.

Multiple morphological changes take place with increasing age. The most prominent neuronal changes are the appearance of senile plaques (areas of degenerating neuronal processes, reactive nonneuronal cells, and amyloid), increasing deposits of lipofuscin, and areas of neurofibrillary tangles. Synapses and dendrites are lost with aging. Neurotransmitter systems are also affected by aging. Acetylcholinesterase, choline acyltransferase, tyrosine hydroxylase, DOPA decarboxylase, and glutamic acid decarboxylase, enzymes involved in cholinergic, and dopaminergic and GABA-ergic transmission, respectively, show appreciable decreases.

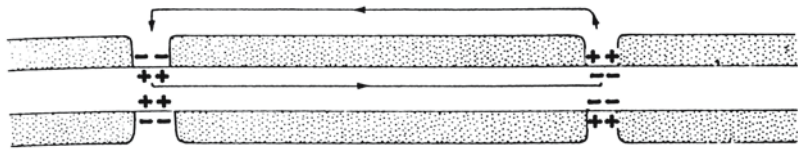
The total myelin content of white matter is reduced in old age. Low myelin concentrations of white matter most probably reflect the continuous loss of neurons with degeneration of axons and of the myelin sheaths. The lipid composition of myelin is quite constant during aging, with the possible exception of galactolipids, which tend to decline. Some differences are seen in the fatty acid composition of myelin phosphoglycerides and cerebrosides during aging. Myelin proteins do not undergo distinct quantitative changes in their relative proportions during old age.

1.13 Function of Myelin

Nerve fibers transmit information to other nerve fibers and to receptors of effector organs. The information is transmitted via an electric impulse called the action potential, which is conducted in an all-or-none way, i.e., the impulse is propagated or not. More detailed information is provided by temporal and spatial summation of many action potentials within one nerve. Myelin plays an important role in the impulse propagation. It is an insulator, but more important is its function to facilitate conduction in axons.

In a resting nerve fiber, polarization of the membrane exists: the inside is charged negatively compared with the outside. In an excited area the situation is reversed: the inside is charged positively compared with the outside. This is called membrane depolarization. There is a difference in potential between excited and adjacent resting fiber sections owing to the inversion of polarization in the excited area. In an effort to compensate this difference in potential, local circuits of currents flow into the active region of the axonal membrane through the axon and out through the adjacent, polarized sections of the

Fig. 1.10. Because of the myelin sheath, the conduction in a myelinated nerve fiber is saltatory, jumping from node to node



membrane. These local circuits depolarize the adjacent section of the membrane. As soon as this depolarization reaches the threshold of excitation, an action potential arises. These local circuits depolarize the adjacent section of membrane in continuous sequential fashion. Of course, the local circuits do not only flow in the direction of the impulse conduction. However, they cause no renewed excitation in the membrane that has just been excited because a temporary state of inexcitability, called the refractory period exists, which ensures that the fiber conducts the action potential in one direction and does not remain permanently excited. In unmyelinated fibers impulses are propagated in this way, and the entire membrane surface needs to be successively excited when an action potential travels along it.

In myelinated fibers, the excitable axonal membrane is only exposed to the extracellular space at the nodes of Ranvier. In the area of the node of Ranvier, the axon is rich in sodium channels. The remainder of the axolemma is covered by the myelin sheath, which has a much higher resistance and much lower capacitance than the axonal membrane. When the membrane at the node is excited, the local circuit generated cannot flow through the high-resistance sheath, and therefore flows out through the next node of Ranvier and depolarizes the membrane there (Fig. 1.10). In this so-called saltatory conduction, the impulse jumps from node to node, whereby the conduction velocity is considerably increased. Saltatory nerve conduction is not only faster, but it also saves energy because only parts of the membrane need to depolarize and repolarize for impulse conduction. For conduction velocities in unmyelinated fibers equivalent to those in the fastest conducting myelinating fibers, impossibly large unmyelinated fibers and energy expenditures several orders of magnitude greater would be required.

There are several factors that influence conduction velocity. Conduction velocity increases with increasing fiber diameter as a consequence of the smaller internal resistance, leading to an increased flow of current and thus shortening the time necessary for the excitation of the adjacent membrane section or the next node of Ranvier. Increase in myelin thickness, which accompanies increase in fiber diameter, also increases conduction velocity, mainly as the result of a change in myelin sheath capacitance. The internodal distance influences conduction velocity. With shorter internodal distances, the fibers behave more

and more like unmyelinated fibers while with longer internodal distances the current density at the next node of Ranvier becomes smaller. Consequently, there is an optimal ratio of internode distance to axon diameter. With increasing temperature conduction velocity increases, reaching a maximum at about 42 °C and decreasing thereafter.

1.14 Myelin Disorders: Definitions

‘Demyelination’ means, literally: loss of myelin and the literal interpretation of ‘demyelinating disorders’ is: disorders characterized by loss of myelin. The term demyelination is commonly used to indicate the process of losing myelin, which is caused by primary involvement of oligodendroglia or myelin membranes. Myelin loss that is secondary to axonal loss and simultaneous loss of axons and myelin sheaths is not usually included under the heading of demyelination.

However, there is considerable confusion about the meaning of the terms demyelination and demyelinating disorders. Sometimes demyelination is used to mean all conditions in which loss of myelin occurs, irrespective of whether the myelin membrane was primarily affected or was broken down secondary to or at the same time as axonal loss. This is probably partly because it is not always clear whether the loss of myelin is primary or secondary in nature. The mutual dependence of axons and myelin sheaths is an important factor in this respect. Demyelination will eventually lead to axonal loss, and in the end axonal degeneration will lead to loss of myelin. Hence, using histological examination it may be very difficult to differentiate between primary and secondary myelin loss. Another confusing factor is that some disorders show evidence of simultaneous primary neuronal degeneration and primary demyelination. The random use of related terms, such as dysmyelination, myelinoclastic disorders, white matter disorders, leukoencephalopathies and leukodystrophies add to the confusion.

Poser (1957) introduced the concept of ‘dysmyelination.’ He proposed dividing the disorders characterized by primary myelin loss into ‘myelinoclastic disorders’ and ‘dysmyelinating disorders’ (1961, 1978). He considered the myelinoclastic disorders to be the true demyelinating disorders, in which the myelin sheath is destroyed after having been normal-

ly constituted. Examples are multiple sclerosis and acute disseminated encephalomyelitis. The dysmyelinating disorders comprise those disorders in which “myelin is not formed properly, or in which myelin formation is delayed or arrested, or in which the maintenance of already formed myelin is disturbed.” Examples are metachromatic leukodystrophy and adrenoleukodystrophy. The idea behind the concept of dysmyelinating and myelinoclastic disorders is to distinguish between inherited disorders, especially inborn errors of metabolism, leading to disturbed myelination and myelin loss, and acquired disorders characterized by primary myelin loss. However, the definition of dysmyelinating disorders, as formulated by Poser, does not exclude all acquired disorders. There are many conditions characterized by a disturbance of myelination, and most of these are caused by external factors. Moreover, myelin may have been constituted normally in inherited disorders, only to be lost after many years.

There are several definitions of the term ‘leukodystrophy.’ Seitelberger (1984) defines leukodystrophies as degenerative demyelinating processes caused by metabolic disorders. Morell and Wiesmann (1984) state that leukodystrophies are disorders affecting primarily oligodendroglial cells or myelin. The disorders have to be of endogenous origin with a pattern compatible with genetic transfer of a metabolic defect. The clinical criterion is a steadily progressive deterioration of function. Menkes (1990) defines leukodystrophies as a group of genetically transmitted diseases in which abnormal metabolism of myelin constituents leads to progressive demyelination. Common concepts in these definitions are demyelination and inborn errors of metabolism. Heritability is implied. As such, the leukodystrophies are identical with inherited demyelinating disorders.

The terms ‘white matter disorders’ and ‘leukoencephalopathies’ comprise all disorders that selectively or predominantly involve the white matter of the CNS, irrespective of the underlying pathophysiologic mechanism and histopathologic basis. ‘White matter disorders’ is a literal translation of leukoencephalopathies. Sometimes these terms are used as if they are interchangeable with ‘demyelinating disorders,’ but usually they are used in the context of a wider range of disorders, characterized by either primary myelin loss or nonselective damage to myelin, axons and supportive tissue of the white matter. For instance, when the terms white matter disorder and leukoencephalopathy are applied in elderly people, ischemic white matter lesions are also implied, which do not involve or do not only involve a selective loss of myelin.

In this book the following definitions are used:

- ‘Demyelination’ is reserved for the process of myelin loss caused by primary and selective abnormality of either oligodendroglia or of the

myelin membrane itself. ‘Demyelinating disorders’ are conditions characterized by demyelination. Examples: metachromatic leukodystrophy, multiple sclerosis.

- ‘Hypomyelination’ is reserved for conditions with a significant permanent deficit in myelin deposition. The most extreme variant of hypomyelination is amyelination. Example: Pelizaeus-Merzbacher disease.
- ‘Dysmyelination’, as the literal translation of the name implies, is reserved for conditions in which the process of myelination is disturbed, leading to abnormal, patchy, irregular myelination, sometimes but not necessarily combined with myelin loss. Examples: some amino acidopathies, damaged structure of unmyelinated white matter after perinatal hypoxia or encephalitis.
- ‘Retarded myelination’ is reserved for disorders in which the deposition of myelin is delayed, but progressing. Examples: inborn errors of metabolism with early onset, malnutrition, hydrocephalus.
- ‘Myelin disorders’ comprise all the above-mentioned conditions.
- ‘White matter disorders’ and ‘leukoencephalopathies’ can be defined as all conditions in which predominantly or exclusively white matter is affected. Either myelin or a combination of myelin and other white matter components is involved. Hence, white matter disorders comprise all myelin disorders, but also, for instance, white matter infections and infarctions, which may affect various white matter components nonselectively.
- ‘Gray matter disorders’ comprise all disorders in which neurons and axons are predominantly or exclusively affected.

1.15 Levels of Myelin Involvement

Both inherited and acquired myelin disorders can arise at the level of the myelin membranes or the oligodendroglial cells. As a consequence, the processes of myelin build-up, maintenance, and turnover may be disturbed.

The processes of myelin build-up and deposition are highly complex and require the expression of many genes, the presence of many substances, the activity of many enzymes, optimal coordination of processes within the oligodendrocytes, and optimal cooperation with the environment. Complex and dynamic processes are particularly vulnerable, and the process of active myelination is easily disturbed. Some inborn errors of metabolism lead to a shortage of myelin components, and as a consequence to a disturbance of the process of myelination. An example is found in Pelizaeus-Merzbacher disease. Acquired dis-

orders, such as hormonal imbalances and severe malnutrition, can also lead to disturbed myelin build-up.

A disturbance of myelin maintenance and turnover can lead to demyelination. In some inborn errors of metabolism, the basic enzymatic defect involves the breakdown of one of the myelin components. This component is trapped in the myelin sheath, and its concentration increases gradually. Finally, the myelin composition is altered to such a degree that the stability is lost, leading to demyelination. Examples are metachromatic leukodystrophy and globoid cell leukodystrophy. Of the acquired demyelinating disorders, toxic disorders in particular can lead to a disturbance of myelin maintenance and turnover. Myelin is rich in lipids and has a long half-life. Consequently, lipophilic substances easily accumulate in myelin, disturbing the stability of the myelin membrane and leading to demyelination.

The myelin membrane may be intact and normal in appearance, biochemical composition, and function until it is attacked from the outside. This appears to be the case in several acquired demyelinating disorders, including inflammatory processes (e.g., multiple sclerosis, acute disseminated encephalomyelitis), metabolic disturbances (e.g., central pontine myelinolysis, Marchiafava-Bignami syndrome) and hypoxia (delayed posthypoxic demyelination).

Demyelinating disorders can also arise at the level of the oligodendrocytes. Damage to oligodendrocytes can lead to disturbances of myelin build-up, maintenance, and turnover. In some inborn errors of metabolism storage of unwanted material occurs, ultimately leading to dysfunction and death of oligodendrocytes. In globoid cell leukodystrophy the toxic substance psychosine is thought to lead to oligodendroglial cell death and myelin loss. In acquired demyelinating disorders, selective oligodendroglial cell death can also occur. This is the case, for instance, in progressive multifocal leukoencephalitis, in which viral infection of oligodendrocytes is present.

Of course, in many disorders more than one mechanism of myelin affection is involved. In disturbances of myelin build-up the myelin that is laid down may have an abnormal composition and configuration. Delayed myelination, dysmyelination, and early demyelination can occur at the same time. In other disorders, oligodendroglial cell death and myelin breakdown independent of oligodendroglial cell death occur simultaneously.

1.16 Biochemical Changes Related to Demyelination

Demyelinating disorders can be subdivided into two large categories: inherited disorders due to an inborn error of metabolism and acquired disorders sec-

ondary to adverse factors in the internal or external environment.

Biochemical analysis of myelin and white matter demonstrates an abnormal composition of the same type in many demyelinating disorders of diverse etiology. The concept of the nonspecific process of myelin breakdown suggests that when maintenance of normal myelin is no longer possible it follows a stereotyped route to complete destruction, largely irrespective of the initiating causes. The etiological factors can be wallerian degeneration, infections such as subacute sclerosing panencephalitis, or intoxications with such agents as triethyltin, but also inherited metabolic diseases, e.g., X-linked adrenoleukodystrophy, Canavan disease, and many other demyelinating diseases. In inherited diseases affecting myelin metabolism, biochemical analysis often reveals certain abnormalities superimposed on the nonspecific compositional abnormalities. These abnormalities are specific for a particular disorder or type of disorders. For instance, an elevation of the very long-chain fatty acids of the cholesterol esters is specific for a subgroup of peroxisomal disorders, including X-linked adrenoleukodystrophy. An elevation of sulfatide is found in the white matter of patients with metachromatic leukodystrophy. The specific biochemical abnormalities of myelin in the various disorders are discussed in separate chapters. Here we will limit our discussion to the nonspecific myelin abnormalities. It should, however, be kept in mind that the degree of abnormality varies considerably among different diseases and among different cases of the same disease depending on the stage of disease.

In degenerating myelin, the proportion of total protein to total lipid is not usually dramatically altered, but the proportions of individual lipids are abnormal. The amount of galactolipids is decreased, and cerebroside is usually much more severely affected than sulfatide. Moderate decreases of ethanolamine phosphoglycerides (mostly plasmalogen) are common. The amount of unesterified cholesterol is increased, often strikingly so, constituting almost half or even more than half the total lipid content, in contrast to approximately 27% in normal myelin. No esterified cholesterol is found in the degenerating myelin sheath. Such abnormal myelin is an intermediate form between normal myelin and completely catabolized myelin. The abnormalities are a result of partial degradation.

The compositional changes in white matter as a whole depend primarily on the extent of myelin loss and only secondarily on changes in myelin composition. Typical white matter changes are increased water content and reduced lipid-to-protein ratios, with specific decreases in such major myelin constituents as cholesterol, cerebroside, sulfatide, and ethanolamine phosphoglycerides. In addition, there

is an increase in cholesterol esters in whole white matter in a number of diseases, but not in all. The fatty acid composition of these esters is different from that of the small amount of esters normally present in white matter, but closely resembles the fatty acids linked to the 2-position in phosphatidylcholine. It is assumed that these esters come from myelin cholesterol and phosphoglyceride fatty acids. The presence of cholesterol esters is taken as evidence of an active phagocytosis of myelin and, as such, as an indicator of active demyelination, but the absence of cholesterol esters does not mean that there is no active demyelination. The presence of cholesterol esters is reflected in sudanophilia on histological examination. It is probable that the mechanism of breakdown is slightly different in sudanophilic myelin destruction and nonsudanophilic breakdown.

1.17 Demyelination: Loss of Function

In normal myelinated nerve fibers, conduction is saltatory and internodal conduction time is fairly regular. The conduction in demyelinated axons differs dramatically from that in normal fibers. The impulse conduction may be either saltatory or continuous. If the impulse conduction remains saltatory, the internodal conduction time varies widely from internode to internode. The internodal conduction time is prolonged by increased leakage of current between the nodes and by depression of excitability of the nodal membrane. There is, therefore, a decreased current generation capacity and an increased threshold for excitation. In demyelinated fibers, a very slow continuous conduction (about 5% of the conduction velocity of normal fibers) may be seen over short stretches. A so-called safety factor for impulse conduction can be calculated. If the required minimum is not reached, impulse propagation is blocked. Furthermore, the refractory period of demyelinated fibers is increased, which leads to failure to transmit high-frequency trains of impulses.

It is clear that demyelination, depending on its extent and severity, can lead to serious loss of function. However, damage to neurons, although not as prominent as destruction of myelin, may also play a part in the functional deficit. Especially in inborn errors of metabolism, substances may also accumulate in the membranes of axons, and in this way axonal dysfunction may arise, contributing to the functional loss.

1.18 Remyelination

Remyelination in the CNS is possible. Remyelinated fibers can be recognized because the internodes are too short and the myelin sheath is too thin for the size

of the axon. Even with time, there is no restitution of the normal axon-to-myelin ratio. The new myelin sheath in itself is normal with normal lamellar periodicity.

Remyelination also occurs when the demyelinated lesion was depleted of oligodendrocytes. The necessary supply of oligodendrocytes is provided by proliferation of remaining, mature oligodendrocytes and possibly also by proliferation of progenitor cells followed by differentiation into myelinating oligodendrocytes. It is often found that axons tend to be remyelinated in clusters, suggesting that a single oligodendrocyte myelinates many axons in the vicinity.

Remyelination among the demyelinating disorders is variable. The most successful examples of remyelination are found in those conditions in which demyelination has occurred rapidly, irrespective of whether the condition is acute and monophasic or relapsing and remitting. Remyelination is much more limited in demyelinating disorders with a protracted, chronic course. The presence of additional axonal damage has an adverse effect on potential remyelination. Some local factors, when present, may stimulate remyelination. There is evidence that epidermal growth factor, interleukin-2, immunoglobulins, platelet-derived growth factor and insulin growth factors may stimulate survival and proliferation of oligodendrocytes and remyelination. In contrast, the presence of T-CD4+ immune cells interferes with remyelination.

1.19 Retarded Myelination

The process of myelination is both complex and protracted. This means that the process is vulnerable to adverse factors over a long period of time, namely from the second half of gestation up to the end of the 1st or 2nd year of life. Many stress factors that act on the incompletely myelinated brain and interfere with the process of myelination do not have such a profoundly adverse effect on the mature brain. For instance, in the mature brain in which myelination is complete, stress factors such as malnutrition or hormonal imbalances will not appreciably reduce the amount of myelin.

Well-known factors potentially leading to retardation of myelination include malnutrition, hormonal imbalances (growth hormone deficiency, hypothyroidism, hypocortisolism, hypercortisolism), prenatal exposure to toxins (alcohol, anticonvulsants), chromosomal abnormalities, pre- and postnatal asphyxia, cerebral infections, hydrocephalus, and inborn errors of metabolism with early onset.

It is important to realize that myelination is dependent on normal function and interaction of oligodendrocytes, neurons, and astrocytes and that retarda-

tion of myelination can be related to dysfunction of oligodendroglia and myelin, dysfunction of astrocytes, or neuronal dysfunction. Cerebral infections and perinatal asphyxia may lead to disturbance of myelination through white matter damage or through neuronal damage. In addition, inborn errors of metabolism may disturb the process of myelination either directly, at the level of the oligodendrocyte or myelin sheath, or indirectly, at the level of the astrocyte or neuron. It is important to realize that a disturbance of myelination may also be seen in neuronal disorders with early onset. For instance, in Menkes

disease, Alpers disease, infantile neuronal ceroid lipofuscinosis, infantile GM₁ gangliosidosis, and infantile GM₂ gangliosidosis, all of which are neuronal disorders, myelination is severely retarded and the white matter looks severely abnormal on MRI, whereas in the later onset variants of neuronal ceroid lipofuscinosis, GM₁ gangliosidosis and GM₂ gangliosidosis these white matter abnormalities do not occur.

It has been demonstrated that myelination is an expression of the functional maturity of the brain. Retarded myelination is an expression of immaturity or dysfunction.

Classification of Myelin Disorders

The history of classifications of myelin disorders shows how each classification reflects the state of scientific development of its time. A revised classification based on the most recent scientific insights is proposed at the end of this chapter.

Interest in CNS myelin dates back to the nineteenth century. In 1854, Virchow was the first to suggest the name 'myelin' when he described the sheaths around axons in the CNS. It is not certain when Schwann (1810–1882) first described the cells since named after him, which supply the myelin sheaths around the peripheral nerve fibers. In 1878, Ranvier described the nodes that have since been given his name in his "*Leçons sur l'histologie du système nerveux*." He believed that the nodes prevented the essentially liquid myelin from flowing to the bottom of the nerve fiber (axon). But despite this conviction, he showed considerable insight into the functional role of the myelin sheath, both as an insulator and as a facilitatory agent in CNS functions. It was not until 1960–1961 that the role of the oligodendrocyte in the formation of myelin in the CNS became clear, and this was due to the work of Bunge.

During the nineteenth century and early twentieth century, important progress was made in the clinical and histological description of several demyelinating disorders. Multiple sclerosis was recognized as a clinical disease entity, and the characteristic histological abnormalities, in the form of multiple demyelinated, sclerotic plaques within otherwise normal white matter, were described. Prominent names in this development are Carswell (1838), Cruveilhier (1835–1842) and Charcot (1868).

In 1897, Heubner described a rare neurological disease in children, using the name diffuse sclerosis as opposed to multiple sclerosis. The disease was histologically characterized by diffuse demyelination of the cerebral white matter and eventual striking hardening of the white matter. Since that time, the term 'diffuse sclerosis' has commonly been used to describe cerebral diseases with diffuse demyelination and sclerotic hardening of the cerebral white matter. Pelizaeus in 1899 and Merzbacher in 1910 reported on a chronic progressive familial type of diffuse sclerosis.

In 1912, Schilder described a nonfamilial case of more acute diffuse cerebral demyelination in a child, and he suggested the name encephalitis periaxialis diffusa rather than diffuse sclerosis. In this case, more prominent signs of inflammation and a less symmet-

rical distribution were observed than in the familial cases described up to that time. Schilder considered that this disease was a nosological and histological entity related to multiple sclerosis and thought there were acute and chronic variants of diffuse sclerosis just as there were acute and chronic types of multiple sclerosis.

Since Schilder's time a number of familial neurological disorders have been recognized, which were histologically characterized by diffuse demyelination and again presented under the heading of diffuse sclerosis. In 1916, Krabbe described a familial infantile form of diffuse sclerosis. Another familial variant, with a later onset and a less rapid progression, was reported in 1925 by Scholz and in 1928 by Bielschowsky and Henneberg. Scholz noted that in this case the myelin breakdown products did not show the usual (orthochromatic) staining properties, but stained metachromatically.

In 1921, Neubürger drew attention to the fact that the term diffuse sclerosis was being applied to several very different disease entities, and he proposed a distinction between inflammatory and degenerative forms. In 1928, Bielschowsky and Henneberg suggested the name 'hereditary progressive leukodystrophies' for the degenerative forms of diffuse sclerosis and devised the following classification, based on the time of onset of the disease and its clinical course:

1. Infantile type of Krabbe
2. Subacute juvenile type of Scholz
3. Chronic type of Pelizaeus-Merzbacher

Hallervorden (1940) recognized that there were endogenous and exogenous factors causing diffuse demyelination and that a distinction was possible between disorders in which demyelination is invariably present and forms a specific part of the disease and disorders in which demyelination occurs occasionally and is nonspecific. He proposed a more extended classification based on these subdivisions:

- I. Endogenous central demyelination
 - A. Specific demyelinating diseases
 - a. Diffuse sclerosis of Krabbe and Scholz
 - b. Pelizaeus-Merzbacher disease
 - B. Nonspecific occasional demyelination
 - e.g. Tay-Sachs disease
- II. Exogenous central demyelination
 - A. Specific demyelinating diseases

- a. Inflammatory types:
 - Disseminated sclerosis (= multiple sclerosis)
 - Diffuse sclerosis (Schilder)
 - Concentric sclerosis (Balò)
 - Neuromyelitis optica (Devic)
 - Encephalomyelitis disseminata
 - Infectious encephalitis
- b. Toxic-metabolic types:
 - Funicular myelosis (= vitamin B₁₂ deficiency)
 - Marchiafava-Bignami disease
- B. Nonspecific occasional demyelination
 - a. Disturbances of blood flow, e.g. subcortical atherosclerosis (= Binswanger disease)
 - b. Edema
 - c. Toxic processes (carbon monoxide)
 - d. Tumors

Until that time, distinctions between different diseases had been based on neuropathological and clinical aspects of different demyelinating disorders. From about this time onwards, histochemical methods and chemical analyses became increasingly important. The classification proposed by Blackwood in 1957 is a reflection of this development. It is based not only on morphological but also on histochemical differences between various subgroups of diffuse sclerosis:

- I Disseminated sclerosis (= multiple sclerosis)
- II Diffuse demyelinating cerebral sclerosis
 - 1. With replacement of myelin by sudanophilic lipid
 - a. With large bilateral cerebral plaques
 - b. With concentric demyelination (Balò type)
 - 2. a. With replacement of myelin by metachromatic PAS-positive lipid (Norman type or Scholz type)
 - b. With associated degeneration of interfascicular oligodendroglia (Greenfield type)
 - 3. With replacement of myelin by nonmetachromatic PAS-positive lipid (globoid cell or Krabbe type)

Meanwhile, insight into normal biochemistry and into mechanisms of biochemical derangement was growing. The concept of hereditary inborn errors of metabolism caused by an enzyme defect leading to dysfunction and breakdown of myelin started to emerge. Fölling (1934) reported 10 patients in the same family with mental retardation and phenylpyruvic acid in their urine. Jervis discovered in 1947 that the underlying metabolic defect in phenylketonuria is a deficiency of phenylalanine hydroxylase. In 1955, Diezel found that the lipids stored in the globoid cells in Krabbe disease have very similar properties to those of cerebroside. In 1970, Suzuki

and Suzuki were the first to propose a deficiency of galactocerebrosidase as the underlying biochemical cause of this disease. Advances in histochemistry also made it possible to discover the basis of metachromatic leukodystrophy. Metachromasia had already been found by Alzheimer in 1910, by Scholz in 1925, and later by Von Hirsch and Peiffer (1955 and 1957). Edgar (1955) pointed out that this condition was characterized by a remarkable elevation of white matter hexosamine. In 1964, Austin et al. demonstrated a decrease in arylsulfatase A activity in metachromatic leukodystrophy.

The enzyme defects of an increasing number of hereditary diseases were detected, whereas in other cases the precise enzyme defect could not yet be discovered but typical biochemical abnormalities characteristic for the diseases could be demonstrated. The increased insight into hereditary metabolic disorders and the ongoing ability to distinguish different hereditary and acquired demyelinating disorders on the basis of a combination of clinical, histological and biochemical data, were reflected in the classification proposed by Raine (1984). Raine distinguished five main categories:

- I Acquired inflammatory and infectious diseases of myelin
 - 1. Multiple sclerosis
 - 2. Multiple sclerosis variants (Schilder, Balò, Devic)
 - 3. Acute disseminated encephalomyelitis
 - 4. Acute hemorrhagic leukoencephalopathy
 - 5. Progressive multifocal leukoencephalopathy
- II Hereditary metabolic disorders of myelin
 - 1. Metachromatic leukodystrophy
 - 2. Globoid cell leukodystrophy (Krabbe)
 - 3. Adrenoleukodystrophy
 - 4. Refsum disease
 - 5. Pelizaeus-Merzbacher disease
 - 6. Dysmyelinogenetic leukodystrophy (Alexander)
 - 7. Spongy degeneration (Canavan)
 - 8. Phenylketonuria
- III Acquired toxic-metabolic diseases of myelin
 - 1. Hexachlorophene neuropathy
 - 2. Hypoxic encephalopathy
- IV Nutritional diseases of myelin
 - 1. Vitamin B₁₂ deficiency
 - 2. Central pontine myelinolysis
 - 3. Marchiafava-Bignami disease
- V Traumatic diseases of myelin
 - 1. Edema
 - 2. Compression
 - 3. Barbotage
 - 4. Pressure release

In this classification, four of the five categories involve acquired demyelinating disorders, and only one

involves hereditary demyelinating disorders. The logical continuation of this development is a refinement of the classification of hereditary demyelinating disorders. For instance, in some diseases the inborn error affects the metabolism of amino acids, and in other diseases it affects the lipid metabolism. A further subdivision can be made among the disorders of lipid metabolism according to the type of lipids involved. In 1987, Poser proposed a classification of hereditary myelin disorders based on the biochemical group of compounds whose metabolism is disturbed. He distinguished six categories:

1. Disorders of glycosphingolipid metabolism
 - a. Ganglioside: GM₁ and GM₂ gangliosidoses, hematoside sphingolipodystrophy
 - b. Sulfatide: metachromatic leukodystrophy
 - c. Galactocerebroside: globoid cell leukodystrophy
2. Disorders of phosphosphingolipid metabolism
 - a. Sphingomyelin: Niemann-Pick disease
3. Disorders of fatty acid metabolism
 - a. Adrenoleukodystrophy
4. Disorders of amino acid metabolism
 - a. Phenylalanine: phenylketonuria
 - b. Branched-chain amino acids: maple syrup urine disease
 - c. Many other amino acidopathies
5. Multiple abnormalities
 - a. Mucosulfatidosis
6. Unknown abnormalities
 - a. Idiopathic spongy sclerosis (Canavan)
 - b. Fibrinoid leukodystrophy (Alexander)
 - c. Pelizaeus-Merzbacher disease
 - d. Idiopathic sudanophilic leukodystrophy

An important development during the last few decades concerns the knowledge of subcellular structures, their role in normal metabolism and the consequences of their dysfunction. Major subcellular structures are the nucleus, lysosomes, mitochondria, peroxisomes, cytoplasm matrix, smooth and rough endoplasmic reticulum, Golgi apparatus, ribosomes, and microtubules.

Demyelinating disorders have been described as resulting from nuclear, lysosomal, mitochondrial, peroxisomal, and cytoplasmic enzyme dysfunctions. Classification of hereditary demyelinating disorders according to the subcellular localization of the underlying metabolic defect stresses the clinical, biochemical, and neuropathological similarities within one category and the differences between the different categories. For the same reason, it is preferable to classify the acquired demyelinating disorders according to their underlying causes into noninfectious-inflammatory, infectious-inflammatory, toxic-metabolic, hypoxic-ischemic and traumatic. A number of

disorders remain for which the primary defect is largely or completely unknown.

An important point is that with increasing scientific insight the difference between 'primary demyelinating disorders' or 'myelin disorders' and 'primary neuronal or axonal degenerative disorders' is becoming less clear. It is evident now that in a classic 'primary demyelinating disorder' such as multiple sclerosis, early and important axonal damage and loss occurs. Some disorders, such as vanishing white matter, are characterized by serious loss of both axons and myelin sheaths, and it may be that neither of them is really 'primary.' Several 'primary neuronal disorders' with infantile onset are accompanied by prominent white matter abnormalities, which are not seen in the later onset forms of the same disorders. This is the case, for instance, in infantile GM₂ gangliosidosis, infantile GM₁ gangliosidosis, and infantile neuronal ceroid lipofuscinosis. We agree with Hallervorden and Poser that these disorders must have a place in a classification of myelin disorders, just as they also belong in a classification of neuronal disorders. Because of the difficulties in distinguishing 'primary neuronal/axonal disorders' from 'primary myelin disorders,' we use the neutral word 'leukoencephalopathies' to comprise all disorders that predominantly affect the white matter of the CNS, irrespective of whether or not the white matter abnormalities are the result of a primary abnormality of myelin.

We propose the following classification of leukoencephalopathies:

I Hereditary disorders

1. Lysosomal storage disorders
 - a. Metachromatic leukodystrophy
 - b. Multiple sulfatase deficiency
 - c. Globoid cell leukodystrophy (Krabbe disease)
 - d. GM₁ gangliosidosis
 - e. GM₂ gangliosidosis
 - f. Fabry disease
 - g. Fucosidosis
 - h. Mucopolysaccharidoses
 - i. Sialic acid storage disorders
 - j. Neuronal ceroid lipofuscinoses
 - k. Polyglucosan body disease
2. Peroxisomal disorders
 - a. Peroxisome biogenesis defects
 - b. Bifunctional protein deficiency
 - c. Acyl-CoA oxidase deficiency
 - d. X-linked adrenoleukodystrophy and adrenomyeloneuropathy
 - e. Refsum disease
3. Mitochondrial dysfunction with leukoencephalopathy
 - a. Mitochondrial myopathy encephalopathy, lactic acidosis, and stroke-like episodes (MELAS)

- b. Leber hereditary optic neuropathy
 - c. Kearns-Sayre syndrome
 - d. Mitochondrial neurogastrointestinal encephalomyopathy (MNGIE)
 - e. Leigh syndrome and mitochondrial leukoencephalopathies
 - f. Pyruvate carboxylase deficiency
 - g. Multiple carboxylase deficiency
 - h. Cerebrotendinous xanthomatosis
 - 4. Nuclear DNA repair defects
 - a. Cockayne syndrome
 - b. Trichothiodystrophy with photosensitivity
 - 5. Defects in genes encoding myelin proteins
 - a. Pelizaeus-Merzbacher disease
 - b. 18q⁻ syndrome
 - 6. Disorders of amino acid and organic acid metabolism
 - a. Phenylketonuria
 - b. Glutaric aciduria type 1
 - c. Propionic acidemia
 - d. Nonketotic hyperglycinemia
 - e. Maple syrup urine disease
 - f. 3-Hydroxy 3-methylglutaryl-CoA lyase deficiency
 - g. Canavan disease
 - h. L-2-Hydroxyglutaric aciduria
 - i. D-2-Hydroxyglutaric aciduria
 - j. Hyperhomocysteinemias
 - k. Urea cycle defects
 - l. Serine synthesis defects
 - 7. Miscellaneous
 - a. Sulfite oxidase deficiency and molybdenum cofactor deficiency
 - b. Galactosemia
 - c. Sjögren-Larsson syndrome
 - d. Lowe syndrome
 - e. Wilson disease
 - f. Menkes disease
 - g. Premutation fragile X
 - h. Hypomelanosis of Ito
 - i. Incontinentia pigmenti
 - j. Alexander disease
 - k. Giant axonal neuropathy
 - l. Megalencephalic leukoencephalopathy with subcortical cysts
 - m. Congenital muscular dystrophies
 - n. Myotonic dystrophy type I
 - o. Proximal myotonic dystrophy
 - p. X-linked Charcot-Marie-Tooth disease
 - q. Oculodigitodental dysplasia
 - r. Vanishing white matter
 - s. Aicardi-Goutières syndrome and variants
 - t. Leukoencephalopathy with calcifications and cysts
 - u. Leukoencephalopathy with involvement of brain stem and spinal cord and elevated white matter lactate
 - v. Hypomyelination with atrophy of the basal ganglia and cerebellum
 - w. Hereditary diffuse leukoencephalopathy with neuroaxonal spheroids
 - x. Dentatorubropallidoluysian atrophy
 - y. Amyloid angiopathy
 - z. Cerebral autosomal dominant arteriopathy with subcortical infarcts and leukoencephalopathy (CADASIL)
 - aa. Cerebral autosomal recessive arteriopathy with subcortical infarcts and leukoencephalopathy (CARASIL)
 - bb. Nasu-Hakola disease
 - cc. Pigmentary orthochromatic leukodystrophy
 - dd. Adult autosomal dominant leukoencephalopathies
 - II Acquired myelin disorders
 - 1. Noninfectious-inflammatory disorders
 - a. Multiple sclerosis and variants
 - b. Acute disseminated encephalomyelitis and acute hemorrhagic encephalomyelitis
 - 2. Infectious-inflammatory disorders
 - a. Subacute HIV encephalitis
 - b. Progressive multifocal leukoencephalitis
 - c. Brucellosis
 - d. Subacute sclerosing panencephalitis
 - e. Congenital cytomegalovirus infection
 - f. Whipple disease
 - g. Other infections
 - 3. Toxic-metabolic disorders
 - a. Toxic leukoencephalopathies (endogenous and exogenous toxins)
 - b. Central pontine and extrapontine myelinolysis
 - c. Salt intoxication
 - d. Marchiafava-Bignami syndrome
 - e. Vitamin B12 deficiency, folate deficiency
 - f. Malnutrition
 - g. Paraneoplastic syndromes
 - h. Posterior reversible encephalopathy syndrome
 - 4. Hypoxic-ischemic disorders
 - a. Posthypoxic-ischemic leukoencephalopathy of neonates
 - b. Delayed posthypoxic-ischemic leukoencephalopathy
 - c. Subcortical arteriosclerotic encephalopathy (Binswanger disease)
 - d. Vasculitis
 - e. Vasculopathy of other origin
 - 5. Traumatic disorders
 - a. Diffuse axonal injury
- The category of so-called cytoplasmic enzyme deficiencies is not listed in this classification. The rationale is that such a disease category would represent a

very heterogeneous group of disorders as the cytoplasm contains enzymes of many different biochemical pathways. This is why it is preferable in this case to make a subdivision according to the specific metabolic pathway involved. However, the group of amino acidopathies and organic acidopathies is heterogeneous, as some of the enzymes concerned are in fact mitochondrial or peroxisomal. In view of the relative homogeneity in clinical presentation, diagnostic tests, and treatment strategies, we prefer to place them in one category, which is also in keeping with general practice.

Over the years, this classification has been modified repeatedly. The basic defects of a steadily increasing number of hereditary myelin disorders have been elucidated, and the number of 'unknown' disorders is decreasing. Even the present classification of leukoencephalopathies is provisional and will have to be adapted in the future to take account of expanding scientific insights. The structure of the proposed classification allows easy integration of further information.

Selective Vulnerability

Within the context of this book, attention is paid to the concept of selective vulnerability, for two reasons. In the first place, the recognition of patterns of selective vulnerability contributes to the understanding of pathogenetic mechanisms of cerebral damage in the different disorders. In the second place, the recognition of patterns of selective vulnerability is of practical value and contributes to the diagnostic specificity of MRI interpretation. The concept of MRI pattern recognition is based on the concept of selective vulnerability.

Spielmeyer (1925), Meyer (1936), Vogt and Vogt (1937) and Scholz (1953) introduced the concept that, apart from the distribution of infarctions in vascular territories and border zones, specific brain regions may be more vulnerable to ischemic injury than others. Spielmeyer tried to find an explanation for this difference by suggesting that variations in the local vascular supply facilitated vascular insufficiency in such areas as the hippocampus. As we now know, structures of the CNS have different degrees of sensitivity to oxygen deprivation. Of the cellular elements of the CNS, the neurons are the most vulnerable, followed by oligodendroglia, astroglia and, finally, endothelial cells. Within the group of neurons, some neuronal cell types are more vulnerable to hypoxic–ischemic damage than others. Structures more liable to damage by hypoxia–ischemia are the hippocampus, the Purkinje cells of the cerebellum, the striatum, and the neocortex. Within these structures there is a further order of sensitivity among the different cell types, as indicated in Table 3.1. Vogt and

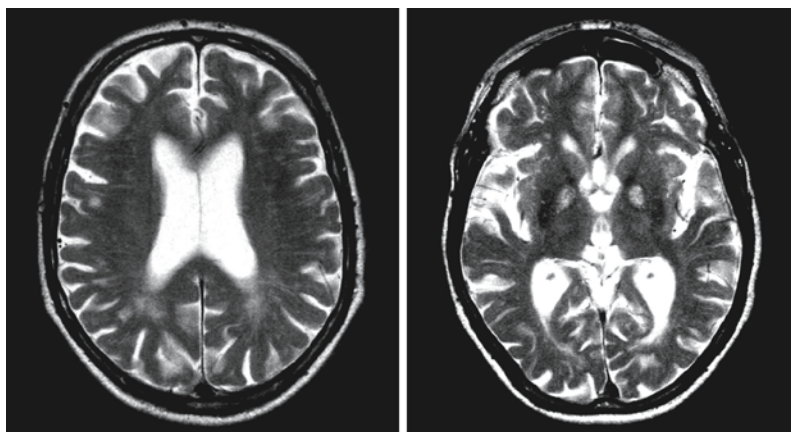
Table 3.1. Hierarchy of selective vulnerability to hypoxic–ischemic conditions for different CNS structures

Structure	Hierarchy of vulnerability
Hippocampus	CA ₁ > CA ₄ > CA ₃ > granule cells
Cerebellum	Purkinje cells > stellate or basket cells > granule cells > Golgi cells
Striatum	Small to medium-sized neurons > large neurons
Neocortex	Layers 3, 5, 6 > layers 2, 4

Vogt (1937) suggested the physicochemical properties of specific neurons as the reason for the unequal vulnerability to disease and introduced the term ‘topistic areas.’ The ‘pathocllisis’ of a region is determined by specific chemical and physical properties, which are also the essence of the specific function of that region. Meyer (1936) stated that it was too simple to assume that only the physicochemical or local vascular factors were involved, and that other factors should also be taken into consideration. Such factors, according to him, are the nature of the noxious agent, the ‘porte d’entrée,’ the path of distribution, and developmental factors.

Meyer initiated a discussion about the pathophysiology of the selective involvement of the basal ganglia in some disorders. He drew attention to the selective involvement of the globus pallidus in carbon monoxide intoxication (Fig. 3.1), which is more constant than the involvement of other structures, such as the pars compacta of the substantia nigra, cornu ammonis, Purkinje cell layer of the cerebellum, and

Fig. 3.1. Carbon monoxide intoxication in a 42-year-old male patient. The T₂-weighted images show the hyperintense lesion in the globus pallidus



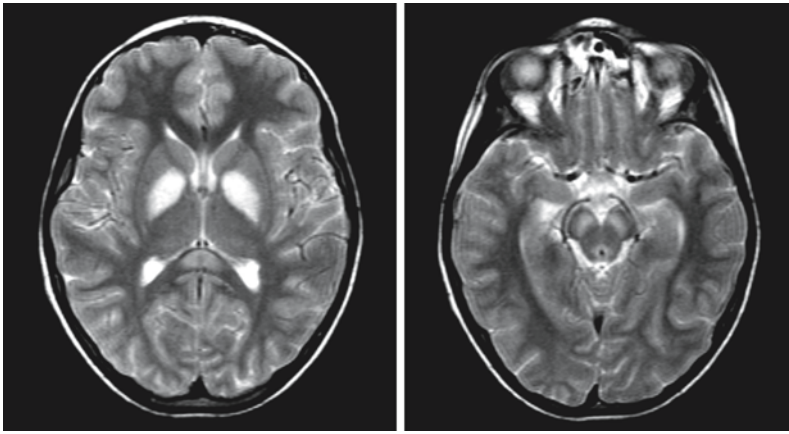


Fig. 3.2. Pyruvate dehydrogenase complex deficiency in an 8-year-old boy. The images depict selective involvement of the globus pallidus and the substantia nigra, the latter probably due to transsynaptic degeneration

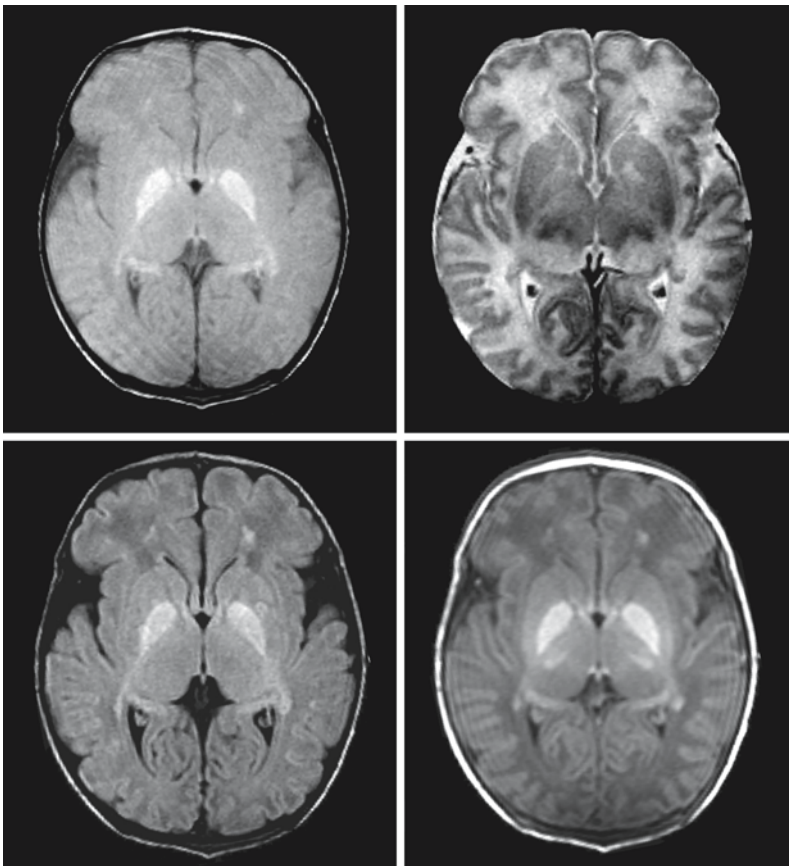


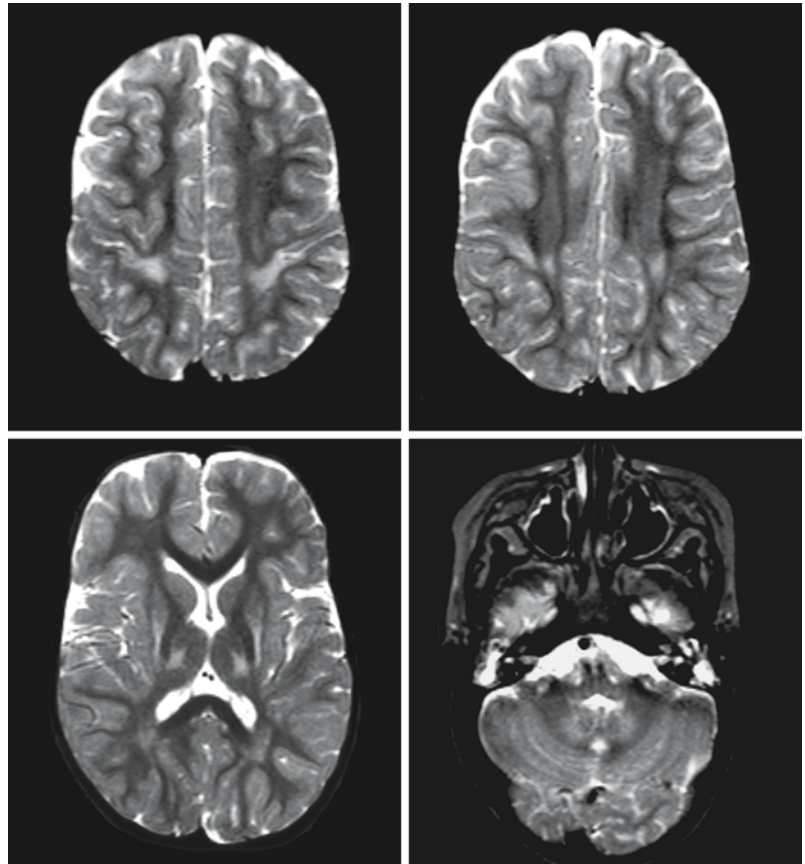
Fig. 3.3. Kernicterus in a 1-week-old neonate. The *upper row* shows a proton density and a T₂-weighted image at the level of the basal ganglia. The *lower row* shows a FLAIR and a T₁-weighted image at the same level. The images show the typical involvement of the globus pallidus and the pulvinar. The globus pallidus lesions are hardly seen on the T₂-weighted image, but the T₂-weighted image shows the abnormal signal of the pulvinar more clearly than the other images. It is not completely clear why the globus pallidus has a high signal on the T₁-weighted image

cerebral white matter. However, the globus pallidus may also be selectively involved in respiratory failure, mitochondrial defects (Fig. 3.2), kernicterus (Fig. 3.3), and intoxications with ether, potassium cyanide, and dinitrobenzol (leading to methemoglobinemia). Meyer, who was well aware of the differences of these conditions, suggested the common factor responsible for the involvement of the globus pallidus was interference with oxygen transport by either severe hypoxia or anemia or 'inhibition of the respiratory en-

zymes,' showing that awareness of something like the mitochondrial system already existed.

This discussion was renewed recently by Johnston and Hoon (1999), who compared three conditions in children: pyruvate dehydrogenase complex deficiency with a Leigh-like presentation and lesions in the basal ganglia (Fig. 3.2); kernicterus with abnormalities prominently involving the globus pallidus but also involving the nucleus subthalamicus (Fig. 3.3); and posthypoxic-ischemic encephalopathy caused by

Fig. 3.4. T₂-weighted series depicting the late pattern of acute profound ischemia in a term neonate. There is a triangular gliosis in the perirolandic white matter, with focal ulegria of the cortex. In addition, there are lesions in the dorsal part of the putamen, the ventrolateral part of the thalamus, and the dentate nucleus



acute profound asphyxia in a term neonate with basal ganglia abnormalities typically located in the dorsal part of the putamen and the ventrolateral part of the thalamus (Fig. 3.4). The authors try to explain the difference in location of the lesion by arguing that the neuronal circuit involved in asphyxia is different from that involved in mitochondrial disorders and kernicterus. They suggest that bilirubin toxicity is affecting mitochondria in the globus pallidus, in this way providing a link with mitochondrial respiratory chain disorders. They reason that, on the other hand, glutamate toxicity in particular affects the putamen, thalamus, and cerebral cortex in hypoxic-ischemic conditions.

In an earlier edition of this book (1995) we made the same observation as Johnston and Hoon in 1999: carbon monoxide intoxication affects the globus pallidus preferentially and most consistently, whereas hypoxia in cases of near-drowning or strangulation preferentially involves the putamen and caudate nucleus (Figs. 3.5, 3.6), layers 3, 5 and 6 of the cerebral cortex, and Purkinje cells in the cerebellar cortex. In carbon monoxide intoxication we assumed a mitochondrially mediated effect on the globus pallidus. However, our hypotheses are apparently too simple, and important details of the pathophysiology of the development of brain lesions elude our understand-

ing. It is a fact, for instance, that in inherited mitochondrial encephalopathies with cellular energy failure the putamen and caudate nucleus are usually preferentially affected and not the globus pallidus (Fig. 3.7). With this observation, it is questionable whether the preferential involvement of the globus pallidus in carbon monoxide intoxications can be blamed on mitochondrial dysfunction.

It is clear that hypoxia-ischemia, some toxic substances, some metabolites increased to toxic levels in inborn errors of metabolism, hypoglycemia, and some nutritional deficiencies (e.g. thiamine deficiency) all interfere with mitochondrial function. In more general terms, regardless of its cause, energy depletion will lead to failure of mitochondrial oxidative phosphorylation, ATP depletion, accumulation of glutamate and other excitatory amino acids, opening of ion channels, accumulation of Ca^{2+} in the cell, activation of polyunsaturated fatty acid cascades and, finally, cell death. It would be logical if all forms of cerebral energy failure, either caused by hypoxia-ischemia, hypoglycemia, primary mitochondrial dysfunction or deficiencies, intoxications and inborn errors of metabolism mediated through mitochondrial dysfunction, would lead to selective involvement of the same brain structures. This, however, is not true. It is correct that sometimes the pattern of abnormalities

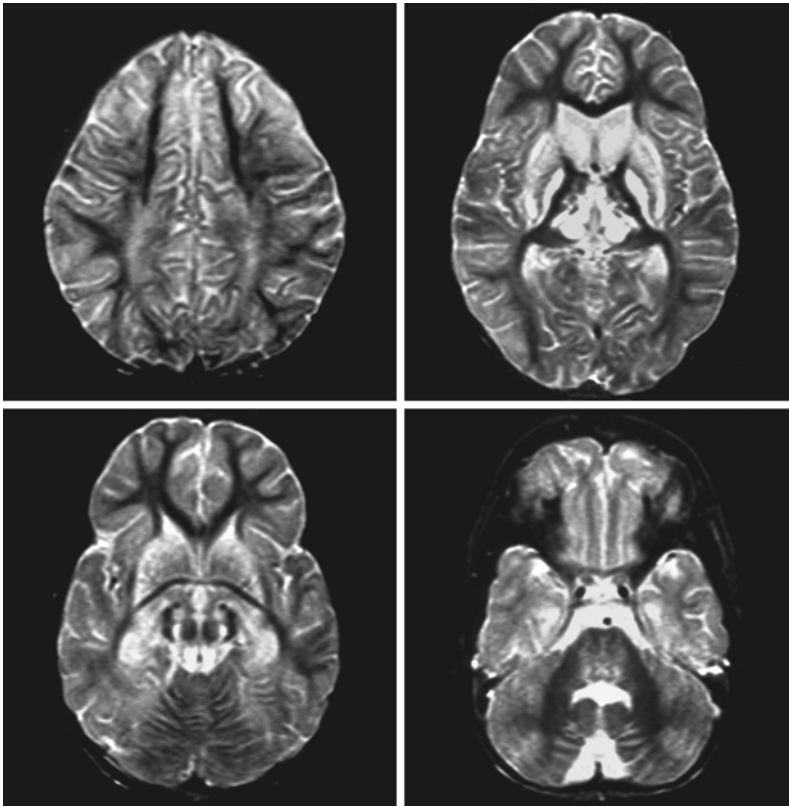


Fig. 3.5. A 3-year-old boy suffered near-drowning and prolonged attempts at resuscitation. Not only the striatum is involved, but also the globus pallidus, the thalamus, the hippocampus, and tracts in the brain stem. In addition, cortical laminar necrosis is seen in the higher slices

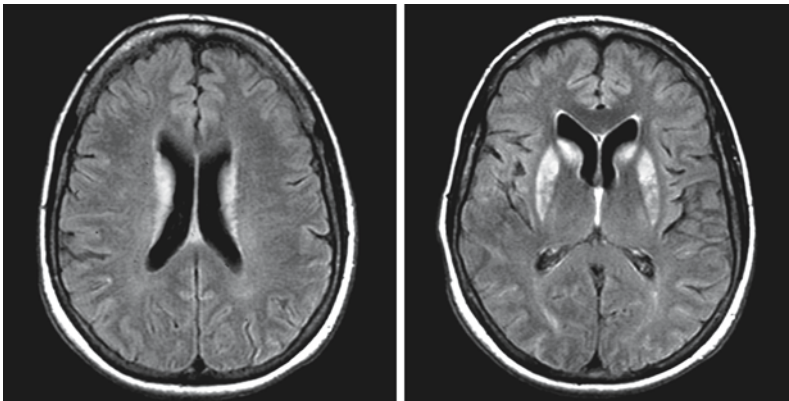


Fig. 3.6. A young woman has been anoxic for at least 3 min during resuscitation. The FLAIR images show that the lesions are confined to the striatum

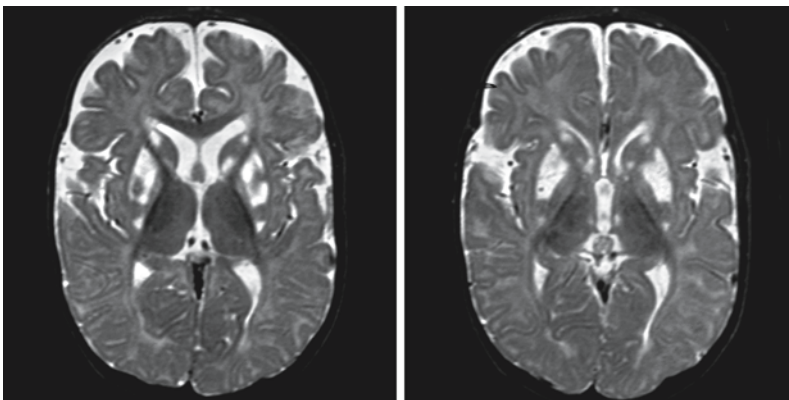


Fig. 3.7. Leigh syndrome in an 8-month-old boy, caused by the Leigh/NARP mutation with a high percentage of heteroplasmy. There are lesions in the putamen and caudate nucleus

Fig. 3.8. Leigh syndrome related to a complex I deficiency in a 3-year-old boy. The MR pattern shows symmetrical lesions in the wall of the third ventricle, the dorsal part of the midbrain, and the dentate nucleus. The mamillary bodies are not affected

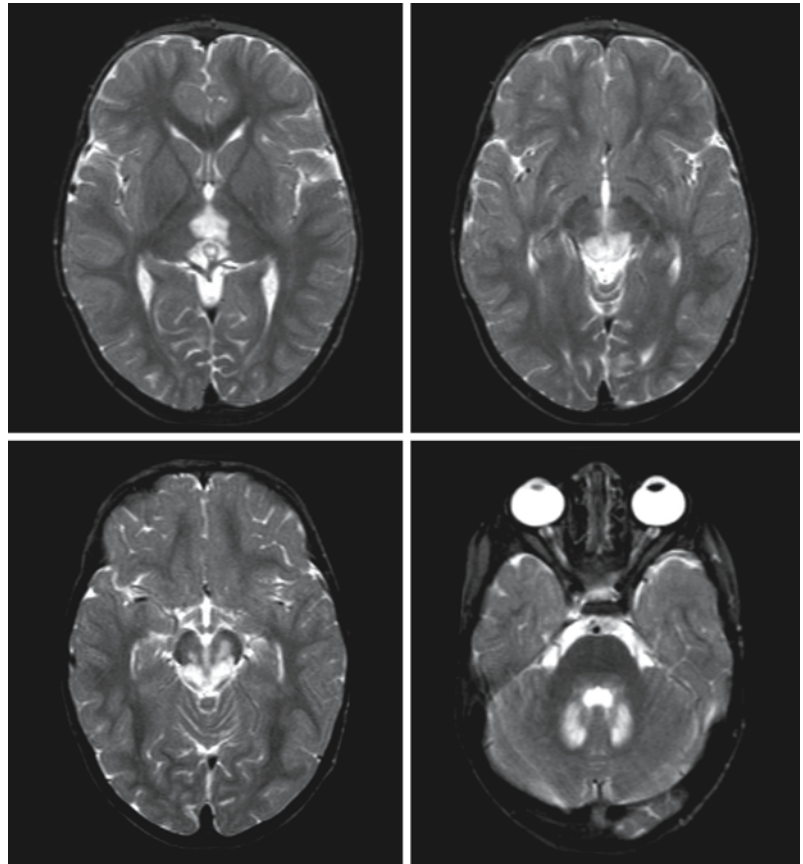
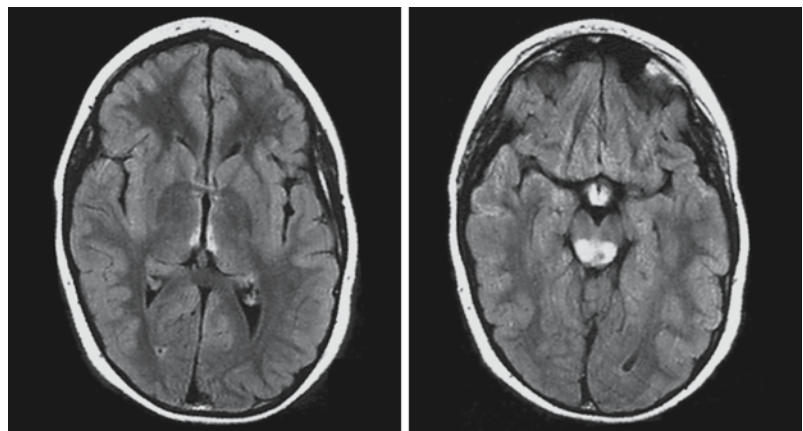


Fig. 3.9. Pattern of thiamine deficiency, which is very similar to that of Leigh syndrome (cf. Fig. 3.8). An important difference is that in thiamine deficiency the mamillary bodies are involved in most cases, whereas in Leigh syndrome they are not



in Leigh syndrome (Fig. 3.8) and the pattern of thiamine deficiency (Fig. 3.9) are very similar, although the lesions in the mamillary bodies, typical for thiamine deficiency, are consistently lacking in Leigh syndrome, but most different causes of energy failure lead to very different patterns of abnormalities (Figs. 3.1, 3.2, 3.4–3.13). The biochemical explanation for the differences in selectively involved structures is unclear, and apparently our present models are too simplistic.

Apart from mitochondrially mediated disorders, other conditions may involve the basal ganglia predominantly or selectively. This is the case in many inborn errors of metabolism other than mitochondriopathies, in hepatic failure (Fig. 3.14), and in classic Creutzfeldt-Jakob disease (Fig. 3.15). The explanations must be different from those so far proposed.

In glutaric aciduria type I there is typically involvement of the putamen and caudate nucleus, but not of the cortical layers and Purkinje cells. The neo-

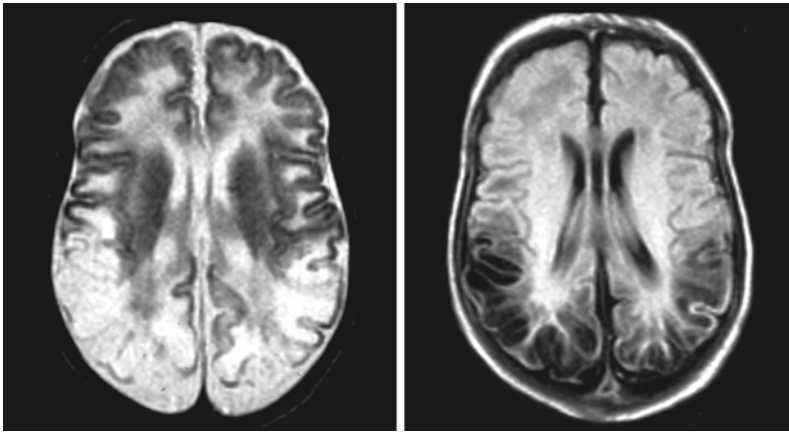


Fig. 3.10. Typical involvement of the parieto-occipital region in a neonate with hypoglycemia; in the worst cases this leads to multicystic encephalopathy restricted to this region. Selective vulnerability of this region for hypoglycemia disappears with age, indicating the influence of morphologic and biochemical maturation of the brain on the pattern of resulting damage

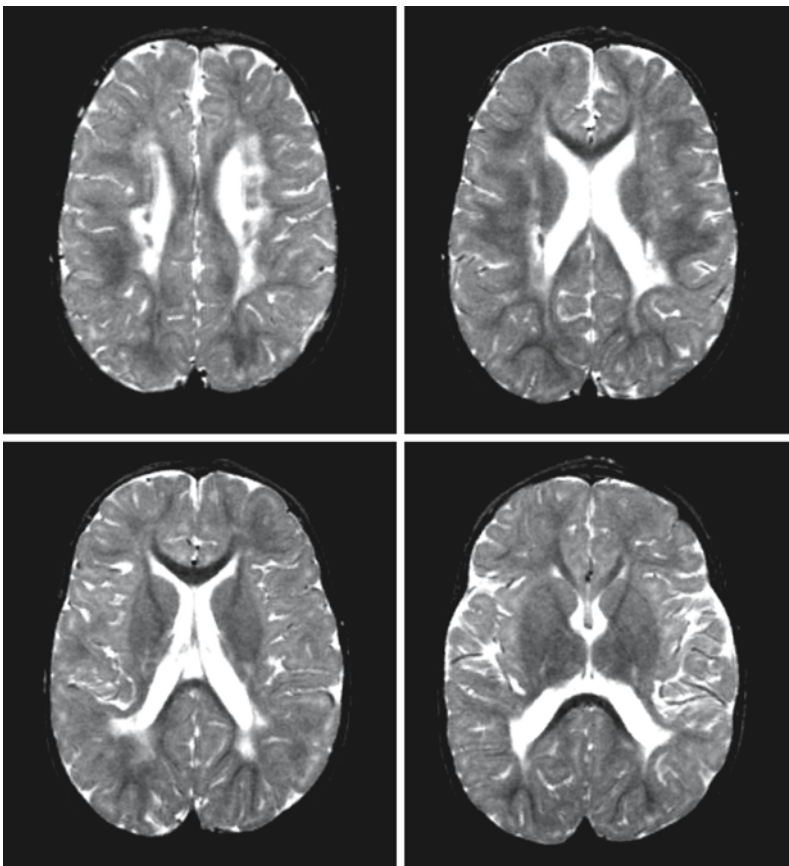


Fig. 3.11. Series of T₂-weighted images showing the classic triad of late sequelae of recurrent or prolonged partial hypoxia-ischemia in a preterm neonate: periventricular leukomalacia. There is a periventricular rim of signal abnormality; the ventricles have an irregular border, especially in the trigonum and occipital horns; and there is loss of white matter volume, the sulci in the parieto-occipital region abutting the ventricular walls

striatal dysfunction and degeneration in glutaric aciduria type I was demonstrated to be at least partly related to *N*-methyl-D-aspartate receptor-mediated neurotoxicity of the endogenously accumulating 3-hydroxyglutarate (Kolker et al. 2002).

In methylmalonic academia, as in carbon monoxide intoxication, there is preferential involvement of the globus pallidus. In this disease the selective lesion is due to accumulation of methylmalonate and alter-

native metabolites. Methylmalonate has been implicated in inhibition of respiratory chain complex II, and it also inhibits the tricarboxylic cycle (Okun et al, 2002).

Preference for the (neo)striatum in Creutzfeldt-Jakob disease is partly due to the local severe loss of parvalbumin-positive GABA-ergic inhibitory neurons. As in patients with liver failure and hepatocerebral syndromes, the striatum has a high signal

Fig. 3.12. In Kearns-Sayre syndrome, the subcortical white matter and the globus pallidus are preferentially affected

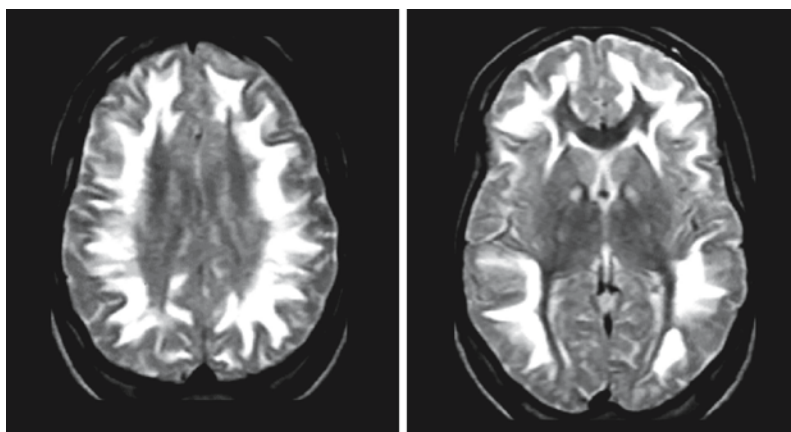


Fig. 3.13. In mitochondrial encephalopathy with lactic acidosis and stroke-like episodes (MELAS) the lesions have an infarct-like appearance on MR images, as shown on these transverse FLAIR images in a 9-year-old girl, but do not, as a rule, respect vascular territories. (Courtesy of Dr. M. Heitbrink and Dr. B. Wiarda, Department of Radiology, Medical Center Alkmaar, The Netherlands)

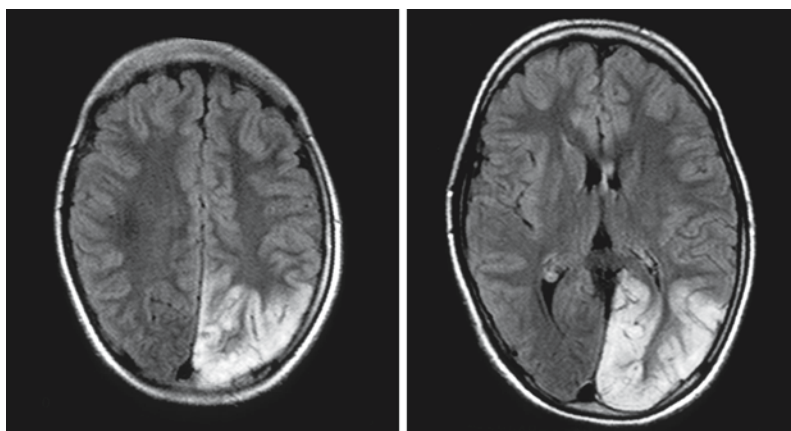
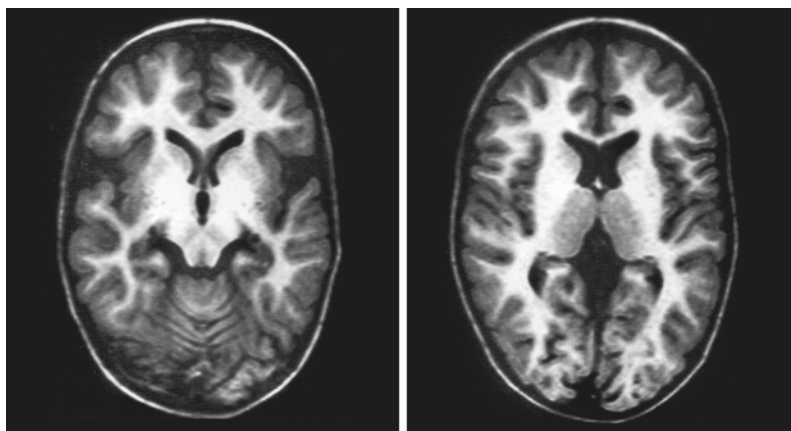


Fig. 3.14. IR images of a 3-year-old boy with hepatic failure, showing the effects of T_1 shortening of the basal ganglia. Because of the T_1 shortening, the basal ganglia can no longer be distinguished from the surrounding white matter



intensity on both T_1 - and T_2 -weighted images. In Creutzfeldt-Jakob disease this could be related to a higher concentration of manganese (Guentchev et al. 1999).

In intoxications with methylene dioxymethamphetamine (MDMA, or 'ecstasy') the lesions in the globus pallidus are due to severe brain dopaminergic neurotoxicity combined with less severe serotonergic neurotoxicity (Reneman 2001; Ricaurte et al. 2002).

Scholz (1953, 1963) stated that under specific pathophysiological conditions focal ischemic brain injury could be attributed to peculiarities of the vascular anatomy, while in other conditions the pattern of brain damage could only be explained by the unique properties of the cells themselves. One of the most important observations he made was the influence of the nature of the insult on the resulting damage to the CNS. In acute obstruction of cerebral ves-

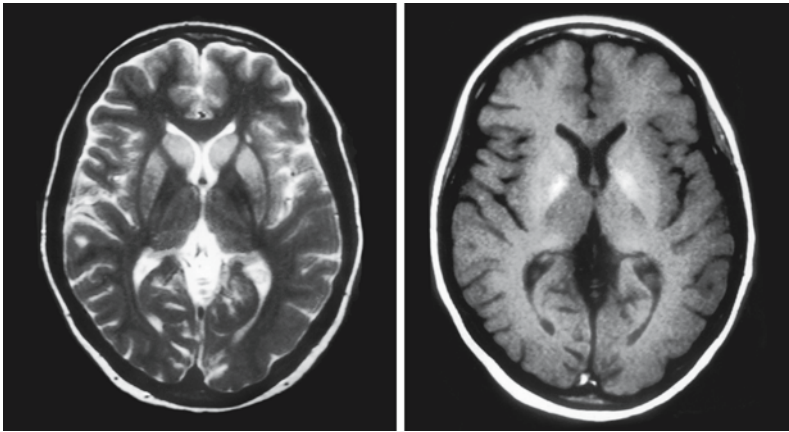


Fig. 3.15. Involvement of the basal ganglia is seen in sporadic 'classic' Creutzfeldt-Jakob disease. The putamen and caudate nucleus have a high signal on the T_2 -weighted image, whereas the globus pallidus has a high signal on the T_1 -weighted image

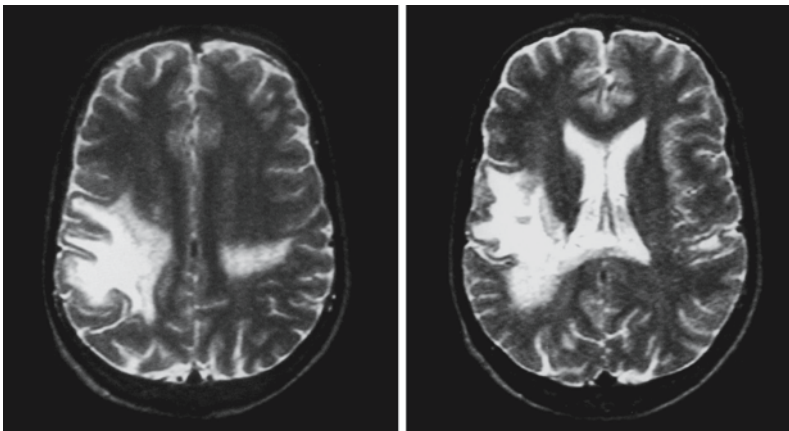


Fig. 3.16. In progressive multifocal leukoencephalopathy the white matter is predominantly involved, to a much greater extent than the gray matter. This results in a sharp demarcation of white from gray matter when the lesion abuts the cortex, as shown in these images

sels, he found experimentally that “the cerebral and cerebellar cortical layers, especially the Purkinje cells, were destroyed, whereas the shorter the duration of ischemia the greater the possibility for selection to take place and for the innate characteristics of the structures to be expressed in a special pattern of morphological alterations.” This, in fact, also seems to be true for other conditions, such as toxic encephalopathies and inherited metabolic disorders.

We could add that the “innate characteristics” mentioned by Scholz should not be seen as a static concept, but rather as a condition that is the product of genetic endowment, stage of development, interaction with other structures in neuronal functional circuits, and dependence on their functional activity and the local condition at the time of the insult.

There are several pathophysiological mechanisms that help to explain selective vulnerability of certain brain areas relative to others:

1. Level of activity is an important factor in selective vulnerability. Energy depletion by hypoxia-ischemia, toxic influences, and metabolic derangements will have the greatest effect on structures with the highest oxygen demand and chemical turnover. Gray matter in adults has a higher level

of activity than white matter and will as a rule be damaged first and most severely. In infants, actively myelinating zones have a high activity and are, therefore, liable to damage. In term neonates with acute profound asphyxia, lesions can be seen in primary myelinating zones in the cerebral cortex, subcortical tracts, and basal ganglia (Fig. 3.4).

2. Specific chemical affinity contributes to selective vulnerability. It has been known for a long time that certain areas in the brain are especially liable to damage by certain toxic agents. Hexachlorophene intoxication involves myelin sheaths exclusively. Hexachlorophene encephalopathy, induced in preterm neonates by washing them for antiseptic reasons with hexachlorophene-containing solutions, causes a myelinopathy with splitting of the myelin lamellae and intramyelinic vacuole formation. Vacuolating myelinopathy in the neonate always has a special distribution, irrespective of its cause, related to the distribution of myelinated versus unmyelinated areas. A clear example is found in maple syrup urine disease. Intoxication with triethyltin, cuprizone, toxic heroin, or poisoned cocaine also leads to myelin splitting and vacuolation. Furthermore, lipophilic substances

generally accumulate preferentially in myelin. Organic solvents such as are used by painters lead to irregular, patchy demyelination and can cause so-called house-painter's dementia or an organic psychiatric syndrome. Demyelination, loss of gray-white matter distinction, and signal changes in the basal ganglia have been described in toluene sniffers. Heavy metal poisoning also shows selective affinity for certain brain regions, as seen for example in Wilson disease (neostriatum, mesencephalon, dentatorubral tracts, nucleus dentatus), lead encephalopathy (cerebellar white matter in adults, cortical neurons in infants and children), and mercury poisoning in Minamata disease (occipital and parietal cortex).

3. Accumulation and/or deficiency of substances have different effects on different areas of the brain. In inborn errors of metabolism, the selection of primary targets and the pattern of spread of the lesions may be influenced by these factors. Differences in selective vulnerability may be explained by differences in residual activity of enzymes in the various cells, in importance of the enzyme function missing, in effects of the accumulation of abnormal breakdown compounds (psychosine in Krabbe disease), in sensitivity to lack of substances that are not formed, and presence of other factors within the cell with synergistic or antagonistic effects. It is often very difficult, if not impossible, to define the factors responsible for well-known patterns of selective involvement in inborn errors of metabolism. Shortage of dietary nutrients may also lead to selective damage. Malnutrition of infants in the 1st year of life leads to delayed myelination. Cobalamin deficiency in subacute combined tract degeneration leads to involvement of specific areas in the brain and spinal cord.
4. Patterns of selective vulnerability may be related to distribution of neurotransmitter systems. In some inborn errors of metabolism, some neurodegenerative disorders and some toxic-metabolic encephalopathies, selective vulnerability may result from interference with a neurotransmitter system. For instance, inborn errors of GABA metabolism have been described that lead to dysfunction of structures in which GABAergic neurotransmission is important. In Segawa syndrome, hereditary progressive dystonia with marked diurnal variation, disturbances of dopaminergic neurotransmission cause nigrostriatal dysfunction. In hyperammonemia, impairment of the neurotransmission by glutamate occurs.
5. The density of synapses for excitatory amino acids determines the sensitivity to adverse effects of these substances. Excitotoxicity due to overstimulation by excess excitatory amino acids (glutamate and aspartate) has recently been recognized as a final common pathway for inflicting injury upon the CNS. Many conditions can lead to an abnormal accumulation of excitatory amino acids. The preferential distribution of lesions by this mechanism will basically be in areas with the highest density of related receptors.
6. The density of mitochondria and varying percentages of mutated mitochondrial DNA have been suggested as explanations for the selective involvement of CNS structures in mitochondrial encephalopathies. Some reports have linked the percentage of mutated mitochondrial DNA in the basal ganglia in MELAS to local levels of lactate in MRS (Dubeau et al. 2000).
7. Antigen-antibody reactions may be at the root of selective CNS lesions. This is the case in a number of the paraneoplastic and parainfectious lesions of the brain. Antibodies against tumor antigens may, for example, cross-react with similar antibodies on Purkinje cells. Paraneoplastic CNS disorders such as limbic encephalitis and brain stem encephalitis may be caused by this mechanism. In parainfectious disorders, for example those related to *Mycoplasma pneumoniae* infections, the same mechanism may play a part and lead to myelin damage in patients with acute disseminated encephalomyelitis.
8. Bacterial, viral, or fungal infection may involve specific structures in the brain. For example, progressive multifocal leukoencephalitis is an infection of the oligodendrocyte, and thus predominantly involves white matter (Fig. 3.16). In other disorders the porte d'entrée may be responsible for the localization of the lesion, e.g., in herpes simplex encephalitis (Fig. 3.17).
9. Hyper- or hypo-osmolar conditions may cause white matter lesions in specific brain areas. In sodium intoxication in infants, unmyelinated areas appear to be most severely involved, probably because of the lower 'resistance' to the shifts of water. In central pontine myelinolysis the central part of the pons is mainly involved, for unknown reasons.
10. Another important factor is the nature (severity, duration, recurrence) of the noxious event. This can be seen in neonates with perinatal asphyxia. The pattern of brain damage in chronic or recurrent partial hypoxia-ischemia is very different from the pattern observed in acute profound hypoxia-ischemia. Whereas the first leads to periventricular leukomalacia (Fig. 3.11), the second leads mainly to lesions in the basal ganglia, thalamus, and perirolandic cortex (Fig. 3.4).
11. Trans-synaptic degeneration illustrates that the function of the brain depends on functional cir-

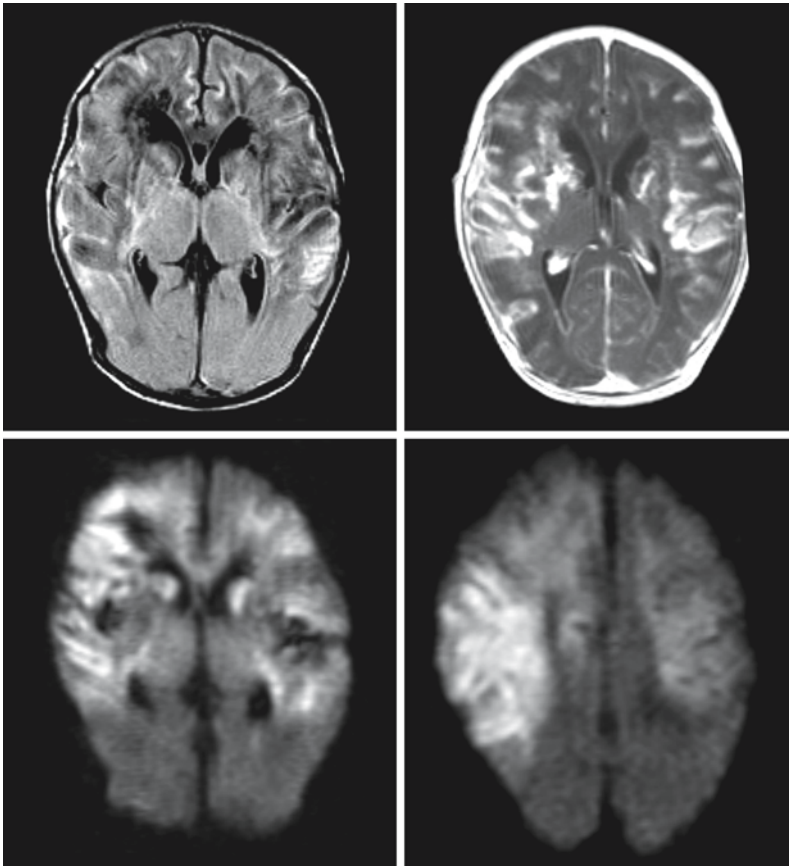


Fig. 3.17. Predominant but not exclusive involvement of temporal lobes is seen in herpes simplex infections, shown here in a FLAIR and a T₁-weighted image with contrast (*upper row*) and two trace diffusion-weighted images ($b=1000$) (*lower row*). The ADC values in the affected areas are low ($\sim 40\%$ relative to normal appearing tissue)

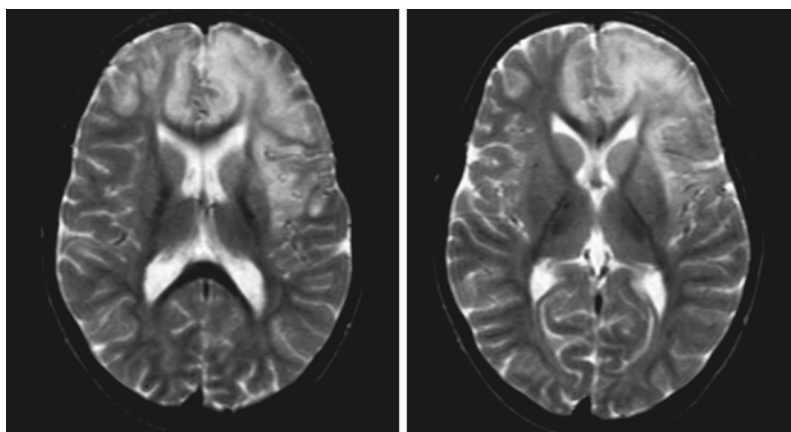
cuits, so that damage to one part of the circuit influences function, and possibly the structure of other parts of the circuit. This was established long time ago by Guillain and Mollaret for hypertrophic olivary degeneration. The Guillain-Mollaret triangle consists of the connections of three nuclei: nucleus ruber, nucleus dentatus, and nucleus olivary inferior. Disruption of this circuit by trauma, tumor, or surgery leads to lesions in the inferior olivary nucleus. It is important to recognize this as a product of trans-synaptic degeneration, and not, in tumor cases, as recurrent or multifocal tumor. Another example is substantia nigra degeneration secondary to lesions in the globus pallidus or secondary lesions in the limbic system when one part is affected (Fig. 3.2).

12. In neonates and infants the developmental stage is also of great importance in determination of which areas will be affected by a noxious agent. The patterns of hypoxic-ischemic lesions in preterm and term neonates are well described and show the changes in vulnerability, which depend on developmental factors. Another example is found in several neuronal storage disorders, such as GM₁ gangliosidosis, GM₂ gangliosidosis and neuronal ceroid lipofuscinosis. It is only in the early-infantile onset variants that the cerebral

white matter is involved, probably due to a combination of hypomyelination and white matter degeneration. These diseases primarily involve neurons and axons, and later onset variants lead to degeneration of gray matter structures only. However, if the disease has its onset before completion of myelination, the white matter of the CNS is also severely affected. It may be that the complex process of myelin deposition, which requires joint activity and cross-talk of oligodendrocytes, axons, and astrocytes, is disturbed because of axonal abnormalities. We found evidence for apoptosis of oligodendrocytes in infantile GM₁ gangliosidosis, and this may be the primary problem, but it may also be that this is the consequence of the failed collaboration and subsequently in itself a cause for further myelin loss.

Understanding mechanisms of selective vulnerability contributes to the understanding of patterns of cerebral involvement as shown by MRI. On the other hand, MRI gives us insight into patterns of selective vulnerability and into what we understand about them and what we do not. In disorders of quite different origins, some final common pathways may explain similarities in image abnormalities. On the

Fig. 3.18. Urea cycle disorder and encephalopathy related to a metabolic decompensation with hyperammonemia in a 6-year-old boy. Images show asymmetrical infarct-like lesions involving the frontal lobes, predominantly affecting the left hemisphere. The distribution of the lesions does not correspond to a vascular territory, and the lesions differ in some aspects from those seen in infarctions, especially with respect to the cortical involvement



other hand, even in disorders that have rather obvious similarities as far as pathogenesis is concerned, striking differences in image abnormalities are sometimes observed, indicating the inadequacy of our present understanding of pathogenetic and pathoplastic mechanisms.

An illustration of this inadequacy is provided by the involvement of cerebral structures in hyperammonemia. Impaired function of the urea cycle enzymes leads to hyperammonemia and raised concentrations of glutamine in the brain. Hyperammonemia can also be caused by hepatic failure of quite different origins (acquired, other inborn errors of metabolism) and still leads to an encephalopathy. MRS has revealed high concentrations of glutamine in the brain in hyperammonemia, irrespective of its origin. On the basis of similarities in the pathogenesis of encephalopathy in these disorders, a similar clinical picture and similar MR images might be expected. However, the expressions of these disorders, clinically and on MRI, are very different. In urea cycle disorders, large cerebral lesions involving cortex and white matter are seen, with asymmetrical distribution and asymmetrical neurological signs and symptoms (Fig. 3.18). In encephalopathy due to hepatic failure related to an acquired disease, brain involvement and neurological symptomatology are symmetrical. MRI shows a symmetrical T_1 shortening of the basal ganglia, including globus pallidus, putamen, caudate nucleus and other central gray matter structures (Fig. 3.14). This means that other factors in addition to hyperammonemia must be involved.

Selective vulnerability, and thus MRI pattern recognition, is not a static concept; it also refers to dynamic changes. It has become clearer with MRI than it ever was with neuropathology that among the white matter disorders there are great differences in early involvement of brain structures and spread in the course of time. In the lysosomal storage disorders involving the white matter, especially the sphingolipidoses, the temporal progression is remarkably con-

stant: the central white matter is involved first, including periventricular white matter and corpus callosum, and the demyelination proceeds centrifugally from there. The arcuate fibers are the last to be involved. An explanation proposed for this feature is that in these disorders abnormal substances accumulate in membranes, leading to a progressively altered myelin composition and progressively unstable myelin membrane that is liable to breakdown. As the arcuate fibers are the last to myelinate they contain the youngest myelin, which is altered least. However, some amino acidopathies and organic acidopathies primarily involve the arcuate fibers and the demyelination progresses in a centripetal way. It is obvious that the biochemical abnormalities and interactions are completely different in the latter disorders than in lysosomal disorders: interference with energy metabolism, lack of normal myelin components, and presence of toxic metabolites are important in amino acidopathies and organic acidopathies. However, it is still difficult to explain why the arcuate fibers are first affected. MRI shows an involvement of the periventricular white matter in the occipital lobe and the splenium of the corpus callosum in the early phases of most patients with the cerebral form of X-linked adrenoleukodystrophy. The disease spreads in a frontal direction. The reason for this occipital preference is unclear. It is noteworthy that in about 10% of patients with cerebral X-linked adrenoleukodystrophy the pattern is reversed, starting in the frontal lobes and the genu of the corpus callosum and progressing towards the dorsal parts of the brain. The reason for the frontal predominance in these patients is even less clear. The cerebral involvement in X-linked adrenoleukodystrophy tends to be symmetrical, as in the lysosomal disorders, but there are exceptions in which one side of the brain is far more severely involved than the other. It would be worth knowing whether the areas primarily involved are more vulnerable to the disease (and if so, why?) or whether the

areas that are primarily spared are more resistant to the process (and if so, why?).

Symmetry of cerebral involvement can be expected to be a general rule in inborn errors of metabolism, toxic encephalopathies, and neurodegenerative disorders, as toxic influences, genetic factors, and deficiencies of essential substances are thought to be similar for the left and right sides of the brain. In a number of disorders, however, asymmetrical involvement is the rule. An example is found once more in urea cycle disorders. In all urea cycle disorders, metabolic derangement is characterized by the accumulation of urea precursors, notably ammonium, and by increased glutamine in the brain. During episodes of metabolic derangement focal brain lesions occur, which are seen on MRI to be strikingly asymmetrical (Fig. 3.18). The large lesions can involve an entire hemisphere or a large part of it. Such an MRI pattern may be misinterpreted as an infarction, because the distribution of the lesion may suggest the involvement of one or more vascular territories. The MRI characteristics of the lesion, however, are different from those of infarctions, even though both show low signal intensities on T₁-weighted images and high signal intensities on T₂-weighted images. These differences can be described by the way in which gray and white matter are simultaneously involved, the way in which the whole affected area is swollen and demarcated from the rest of the brain, the slightly inhomogeneous change in signal intensity, and the often 'unusual' vascular territory that is occupied by the

lesion. The lesions in urea cycle disorders are not mediated by vascular changes, but are probably the result of a direct toxic effect in the involved area, mediated by the presence of elevated levels of glutamine. The asymmetrical and focal nature of the lesions is however unexplained, however. Another well-known example of asymmetry is found in MELAS, a mitochondrial disorder. The lesion usually has a cortical predominance and is restricted to one part of the brain, again simulating an infarction (Fig. 3.13). However, the lesion is not located in a vascular territory or a border zone area. Here too, there is no explanation for the asymmetry.

The basis of this book is the recognition of MR patterns that allow differentiation between disease categories and between disease entities. Knowledge of which structures are selectively damaged by a specific disease lies at the basis of this approach. MRI has an edge on histopathology, because it gives us the privilege of seeing patterns in an early stage of disease and allows us to follow their development. This has not only helped in pattern recognition of classified disorders, but also helped us to recognize unfamiliar patterns and to define new entities.

In all the chapters concerning specific disorders, one section is devoted to the description of MRI patterns of that specific disorder; another section is devoted to the description of pathogenetic mechanisms. As far as possible, these two will be linked. A separate chapter will deal with the principles of MRI pattern recognition.

Myelination and Retarded Myelination

4.1 Myelination

It was Flechsig (1920) who originally put forward the view that the degree of myelination of the CNS might be correlated with functional capacity. In his theory he stated that myelination started in projection pathways before association pathways, in peripheral nerves before central pathways, and in sensory areas before motor ones. Although he modified his theory slightly in response to his critics, he continued to maintain that fibers always myelinated in the same order: first the afferent (sensory), then the efferent (motor), then the association fibers.

The histological study of fetal development has confirmed that myelination proceeds systematically and, in nerve pathways with several neurons, in the order of conduction of the impulse. The first signs of myelination appear in the column of Burdach at the gestational age (GA) of 16 weeks, becoming stronger from the 24th week onward. The column of Goll starts to myelinate at 23 weeks of gestation. Cerebellar tracts start to myelinate at about 20 weeks of gestation, and the amount of myelin at birth is considerable. Pyramidal tracts start to myelinate at 36 weeks at the level of the pons, but at birth the amount of myelin is still small. In other tracts, for example, the rubrospinal tracts, the pattern of the pyramidal tract is followed. In a term neonate at a GA of 40 weeks myelin stains reveal myelin in the medulla oblongata, in the central parts of the cerebellar white matter, in the cerebellar peduncles and the vermis, in the medial lemniscus and fasciculus medialis longitudinalis in the pons and mesencephalon, in the posterior limb of the internal capsule, spreading into the globus pallidus and thalamus and, in the thalamocortical connections in the centrum semiovale, upwards to the parasagittal parts of the postcentral gyrus and backwards into the optic radiation. Paul Flechsig's lithographs (1920) demonstrate this myelination pattern beautifully (Fig. 4.1). Several authors, including Keene and Hower (1931) and Yakovlev and Lecours (1967), have published diagrams of the progress of myelination (Fig. 4.2).

MRI is unique in making it possible to visualize the progress of myelination *in vivo* in astonishing detail. It is now possible to describe the state of myelination in preterm and term neonates in detail and to follow this process through up to full maturation.

In the preterm child with a GA of less than 30 weeks the following structures show myelination:

cerebellar vermis, inferior cerebellar peduncles, vestibular nuclei, superior cerebellar peduncles and their decussation, dentate nucleus, medial longitudinal fasciculus, medial geniculate bodies, subthalamic nuclei, inferior olivary nuclei and ventrolateral nuclei of thalamus. Myelin can also be seen in the fasciculus gracilis and cuneatus and in their nuclei (Counsell et al. 2002; Sie et al. 1997).

In the period between 30 and 36 weeks of gestation the quantity of myelin in the aforementioned structures increases, but from weeks 30–36 of gestation no myelin is seen in any new sites on MRI. This is not in agreement with histological descriptions of the myelin process. Reasons for this are the lower sensitivity of MRI to small quantities of myelin, also the reason for a time-lag in myelination timetables between histology and MRI, and the higher spatial resolution of histological methods. At a GA of 36 weeks evidence of the presence of myelin appears on T_1 -weighted images in the posterior limb of the internal capsules (with higher intensity in the area of the corticospinal tracts) and in the tracts from and to the precentral and postcentral gyri in the corona radiata. In the period between 37 and 42 weeks of gestation myelination of these tracts also becomes visible on T_2 -weighted images. At this time myelination is visible in the tegmentum pontis but not in the basis pontis. Myelin now also appears in the lateral geniculate bodies and in the optic tracts, chiasm, and nerves. The myelin density in the basal ganglia and corticospinal tracts increases, and myelin shows up in the optic radiation.

During the 1st month after birth, myelination progresses rapidly. It becomes more prominent in the areas mentioned above. The pattern of myelin presence in the cerebellum changes (see below). On T_1 -weighted MR images myelin becomes visible in the rest of the striatum and caudate nucleus. Myelin in the optic pathways becomes more prominent, and myelin is also present in cortical layers of the primary motor and sensory cortex and in the hippocampus and parahippocampal gyrus. With increasing myelination in the occipital and parietal lobes, the splenium of the corpus callosum starts to myelinate. From the 3rd or 4th month onward myelination proceeds in the frontal direction, and from the 4th to 5th month onward, also in the temporal direction. The anterior limb of the internal capsule shows myelination from the 3rd to 4th month onward, proceeding in the 5th month to-

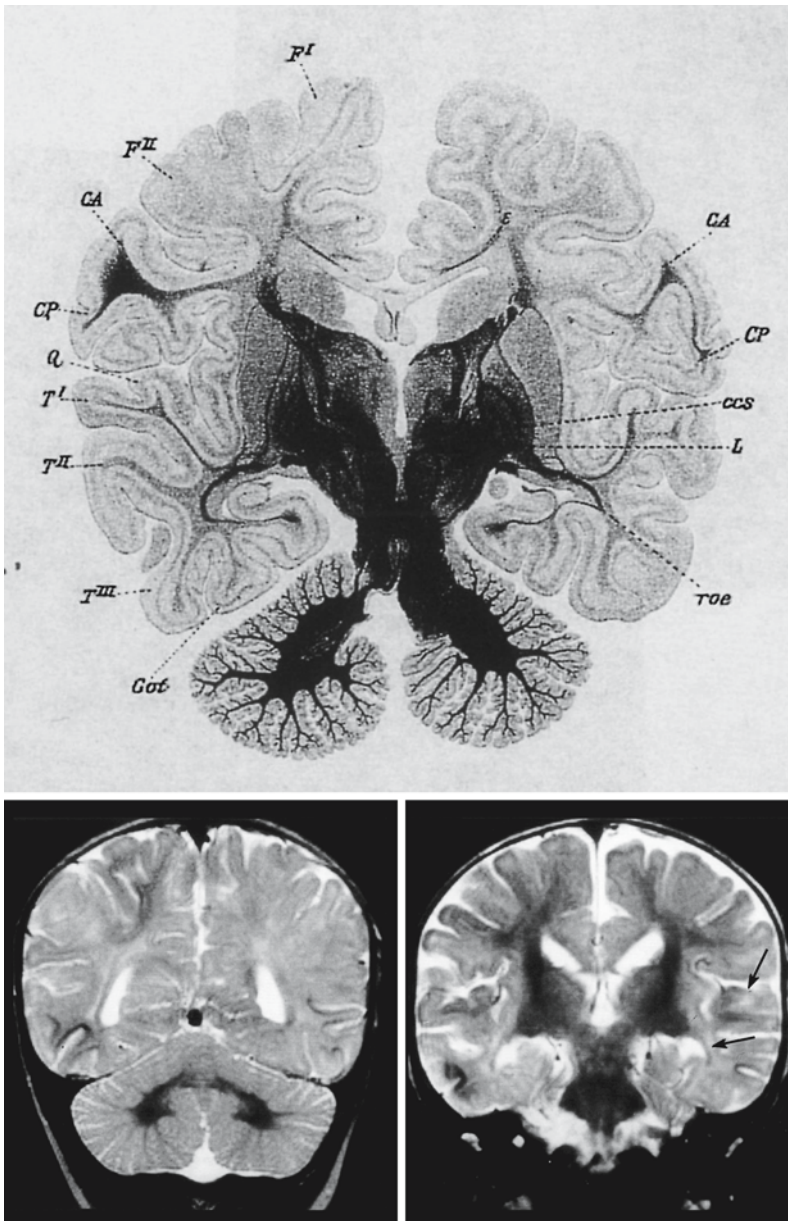


Fig. 4.1. Lithograph in left upper row is reproduced from work of Paul Flechsig (1920), who used refined histological techniques to depict ongoing myelination in the brain. Progress of myelination of a young infant is presented here. Note that myelin (dark in the image) is already circling around the temporal horn to reach the hippocampus and parahippocampal gyrus. Also note myelination of the auditory pathway in the superior temporal gyrus. The two T₂-weighted coronal MR images show the same features in vivo. Myelination in this case is somewhat further advanced than on the lithograph, already spreading towards the parietal U fibers

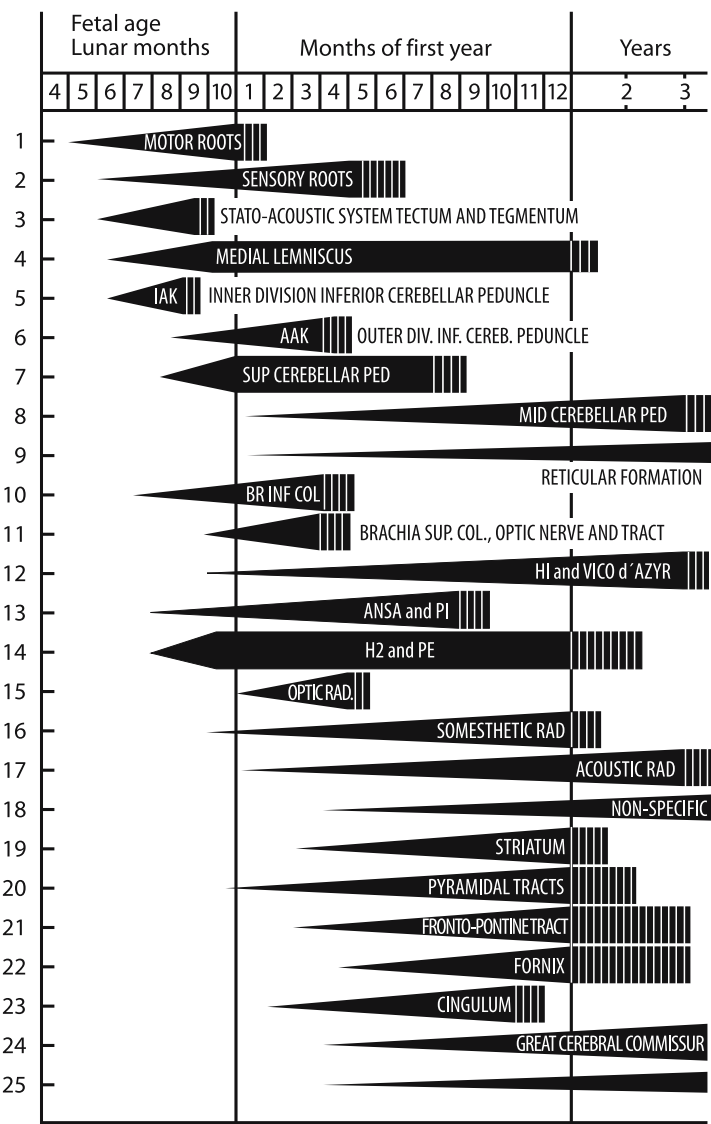
wards the genu of the corpus callosum. At 6 months myelination starts to spread in the frontal lobes, and on the T₁-weighted images the pattern of myelination is seen to be more or less complete at about 8 months. The corpus callosum reflects the myelination of the parts it connects. T₁-weighted images show myelin in the splenium at 3 months and in the genu at about 6 months of age; T₂-weighted images show this 4–6 weeks later.

It should be clear that we are describing 'apparent' myelination, i.e. myelination as it appears on T₁- or T₂-weighted images, which is dependent on pulse sequences and field strength. The apparent progress in myelination on T₂-weighted images lags behind that seen on T₁-weighted images. Because of this, myelina-

tion can be followed for much longer on T₂-weighted than on T₁-weighted images. On T₂-weighted images myelination does not reach the arcuate fibers in the frontal and temporal areas before the 12th–14th and 14th–18th months, respectively.

Myelination is not an all-or-none process. Myelinated white matter gradually replaces the unmyelinated white matter. In T₂-weighted series unmyelinated white matter has higher signal intensity than gray matter. With ongoing myelination, white matter becomes darker, and eventually it can no longer be differentiated from gray matter. This transition or 'cross-over' period is reached in the parietal and occipital areas between 8 and 10 months after birth. After this period myelinated white matter has lower

Fig. 4.2. Classic diagram of progression of myelination as conceived by Yakovlev and Lecours. Most of the structures mentioned can also be made visible on MRI. Appearance of myelination on MR images is 1 or 2 weeks behind this schedule with conventional MR techniques. From Yakovlev and Lecours (1967), with permission



signal intensity than gray matter on T₂-weighted images in this region. The frontal and temporal lobes show this cross-over at 12–14 and 14–18 months, respectively. T₁-weighted images show the same reversal in signal as the T₂-weighted images, but in the reverse direction. Unmyelinated white matter has a lower signal than gray matter, whereas myelinated white matter has a higher signal. Because of the preferential T₁-shortening effect of myelin, which exceeds the T₂-shortening effect, the signal reversal on T₁-weighted images occurs weeks to months before it occurs on the T₂-weighted images. This implies that there is a phase, for the cerebral hemispheric white matter mainly in the second half of the 1st year of life, in which white matter structures have a higher signal than gray matter on both T₁- and T₂-weighted images.

4.2 MRI Pulse Sequences

T₁-weighted spin echo (SE) or inversion recovery (IR) and T₂-weighted SE sequences are complementary. In the first 6 months of life, T₁-weighted images show to better advantage which areas contain myelin, while T₂-weighted SE images, with the proper pulse sequence, differentiate partially myelinated from non-myelinated and completely myelinated white matter more adequately. In MRI, pulse sequences should be chosen so that the contrast/noise ratio is as high as possible and the differences between tissues are maximal. It is, therefore, useful to consider the T₁ and T₂ values of gray matter and of unmyelinated and myelinated white matter in order to make an adequate choice. Holland et al. (1987) found that at a field strength of 0.35 T, T₁ of white matter is 1615±120 ms

(mean \pm standard deviation) at birth, 1150 \pm 60 ms at 6 months and 580 \pm 50 ms at 1 year; T_2 of white matter is 91 \pm 6 ms at birth, 64 \pm 6 ms at 6 months, 57 \pm 5 ms at 1 year and 53 \pm 3 ms at 3 years. For gray matter the corresponding T_1 measurements are 1590 \pm 60 ms at birth, 1300 \pm 70 ms at 6 months and 890 \pm 75 ms at 1 year, and the corresponding T_2 measurements 88 \pm 8 ms at birth, 67 \pm 7 ms at 6 months, 69 \pm 3 ms at 1 year and 62 \pm 3 ms at 3 years. The changes observed with increasing age can be explained by a decreasing water content and increasing myelin content. Protons in the myelin membrane are less mobile, water content is lower, and T_1 and T_2 are, therefore, shorter in myelinated areas.

A long TR, long TE sequence is advantageous to allow full benefit of the T_2 differences between gray matter, unmyelinated white matter and myelinated white matter and to minimize T_1 effects, which counteract the T_2 effects. We use a 3000/120 SE series, which shows unmyelinated white matter with high signal intensity, gray matter and partially myelinated white matter with intermediate signal intensity, and myelinated areas with low signal intensity. In our SE 3000/120 series, the transition or 'isointense' pattern between gray and white matter is reached in the parietal and occipital lobes in normal children by the age of 6–9 months. With a different pulse sequence, for instance SE 2000/80, this transition phase may be 7–12 months. Because of the heavier T_2 -weighting in our series, the T_2 -decay trajectories traverse each other at a somewhat steeper angle and the transition period is, therefore, more clearly marked and of shorter duration.

Fast or turbo spin echo (FSE or TSE) sequences are time-saving procedures and are frequently used in imaging of neonates and infants, but they have important disadvantages. Instead of one 'projection' or line in the k-space (the virtual spatial frequency space from where the image is reconstructed by Fourier transformation), FSE sequences generate multiple spin echoes from a single RF excitation, which are close enough together (echo spacing in the order of 15 ms) to provide multiple 'projections' or lines in the k-space. Imaging time is shortened by a factor of the number of echoes collected in the train. SEs are, therefore, acquired at slightly different TEs, which will affect the resulting image. The repetition of refocusing 180° pulses improves local magnetic homogeneity, thus diminishing magnetic susceptibility effects. On FSE and TSE images hemorrhages and calcifications will consequently be less conspicuous. Because of the short time interval between refocusing pulses, the apparent T_2 of adipose tissue becomes longer and the fat signal will be less suppressed than on conventional T_2 -weighted SE images. Fat will, therefore, appear bright on heavily T_2 -weighted FSE images. Other factors influence FSE images. The mag-

netization transfer component present in multislice conventional SE images is increased in FSE and influenced by the number of slices. From this it will be clear that MR images made with FSE sequences cannot be compared with conventional SE images. The influence of the FSE techniques on the estimation of the progress of myelination is probably negligible, but the influence on the depiction of disease conditions should be considered, especially when the abnormalities are subtle. In examination of neonates it is impossible to be sure in advance whether abnormalities will be found.

T_1 -weighted SE or IR series are of great importance for following the spurt of myelination during the first 6 months after birth. They demonstrate the progression of myelination beautifully, but they are less reliable than T_2 -weighted images for assessing the quantity of myelin deposited. The difference in T_1 between gray matter and unmyelinated white matter at birth gives the unmyelinated white matter a darker appearance than the cortex. With ongoing myelination the white matter will become brighter than the cortex. Between these structures, again, a cross-over or contrast inversion takes place. In T_1 -weighted images, however, this is a less striking event than in T_2 -weighted images. In premature neonates the unmyelinated white matter appears much darker than the rim of cortical gray matter. Even at 40 weeks of GA this difference is still present, although less marked. After that, the unmyelinated white matter rapidly changes its signal and becomes almost isointense with gray matter. The white matter structures in which myelin is advancing stand out as very bright and attract most attention in the assessment of myelination age. A comparison of T_1 - and T_2 -weighted images makes it clear that the T_1 -weighted images are more sensitive indicators of the presence of myelin, even when it is present only in small amounts. Partially myelinated structures, which are isointense or even still mildly hyperintense relative to gray matter on T_2 -weighted images, are already white on T_1 -weighted images. The reason for the higher myelin sensitivity of T_1 - than of T_2 -weighted images can be found in a number of factors at the molecular level. The special structure of the myelin membrane with a lipid:protein ratio of 70:30 (dry weight) and a cholesterol content of 30% is important. The construction of lipid layers separated by a 40-molecule thick layer of water, into which the hydrophilic phosphate polar groups of lipids and the cholesterol hydroxyls project, creates a unique lipid–water interfacial interaction seven times as intense as that at a typical protein–lipid interface. There is a field-dependent cross-relaxation between protons of myelin water and protons of myelin lipid, a phenomenon known as magnetization transfer. The apparent effect of these conditions is a shortening of T_1 induced by myelin, which is more pronounced than

would be expected to result from deposition of membranous structures alone.

Fluid-attenuated inversion recovery (FLAIR) images use a combination of an IR pulse with an inversion time chosen to suppress the water signal, followed by a heavily T_2 -weighted FSE. Because the water signal is suppressed, abnormalities will stand out clearly. FLAIR pulses are not very useful in the estimation of progress of myelination. The difference between gray, unmyelinated and myelinated white matter is much less on FLAIR images than on conventional T_1 - and T_2 -weighted images. It is probably the suppression of the water signal in the water-rich environment of the neonatal brain that is responsible for this diminished contrast, since the disappearance of 'free' water in the brain of neonates and its replacement by myelinated structures play a major part in the maturation process.

4.3 Diffusion-weighted Imaging and Diffusion Tensor Imaging

Diffusion-weighted imaging (DWI) and diffusion tensor imaging (DTI) use the microscopic movement of water molecules and the relative loss of phase of protons caused by this movement in different brain structures as a means of image contrast. Parameters that are frequently used are the apparent diffusion coefficient (ADC) of tissues and the relative anisotropy of brain structures, usually expressed as fractional anisotropy (FA).

The relative anisotropy is practically zero in gray matter in term-born neonates and in adults: diffusion in gray matter is isotropic. However, at a GA of 26 weeks cortical anisotropy is not zero, because at that time the cortical cyto-architecture is dominated by radial glial fibers and radially oriented apical dendrites of the pyramidal cells. This structure is disrupted in time by the addition of basal dendrites and thalamocortical efferents.

White matter ADC and FA depend on stage of maturation. During the early development of the brain ADC values are high, and they subsequently fall. This is because of the initial high water content and the subsequent overall decrease in water content together with the development of more densely packed structures with a high density of membranes that hinder free water movement. FA is initially low and increases rapidly. The increase in FA can be observed even in the premyelination state. The increase in FA during early development is not only the result of the progressing myelination; other contributing factors are the number of microtubule-associated proteins in axons, axon caliber changes, and a significant increase in the number of glia. More densely packed structures have higher FA. Both ADC and FA can be displayed in

Table 4.1. Apparent diffusion coefficient (ADC) ($\times 10^{-3} \text{ mm}^2/\text{s}$) and fractional anisotropy (FA) (10^3) in term neonates

Region	ADC	FA
Frontal white matter	1.62–1.73	190–210
Posterior limb internal capsule	1.06–1.01	410–500
Occipital cortex	1.15–1.20	150–180
Occipital white matter	1.58–1.69	330–370
Corpus callosum		
Genu	1.22–1.37	
Splenum	1.17–1.32	
Thalamus	1.23–1.08	
Mesencephalon (tegmentum)	0.99–1.09	420–480
Pons, anterior	1.13–1.27	
Pons, posterior	0.94–1.06	

images. In contrast with ADC maps, FA images show excellent gray–white matter contrast. In clinical practice, estimation of ADC and FA of different brain structures makes it possible to quantitate the progress of brain maturation, including myelination, and to visualize the formation of white matter tracts. In addition, DWI offers anisotropic diffusion maps that can be displayed separately for each diffusion gradient direction or as an averaged ADC map, the so-called trace map.

Measurements of ADC are available for different ages from the fetal period to adult age. ADC values decrease in between these points in time and development, from $1.50\text{--}1.95 \times 10^{-3} \text{ mm}^2/\text{s}$ for white matter in the fetal brain to about $0.87\text{--}0.95 \times 10^{-3} \text{ mm}^2/\text{s}$ in the mature brain. Maturity in this respect is reached at the age of approximately 2 years. For the basal ganglia the corresponding data are, respectively, $1.56 \times 10^{-3} \text{ mm}^2/\text{s}$ and $0.79 \times 10^{-3} \text{ mm}^2/\text{s}$. More detailed data are available for term neonates (see Table 4.1). ADC and FA values are different for different brain structures, depending on their structure and stage of development.

ADC values decrease with ongoing maturation and FA values rise. This process is exponential. The decrease in ADC and increase in FA are fast in the first 3–6 months, followed by a slower further decrease and increase, respectively. White matter anisotropy increases over the next 6 months, leveling in the 2nd year of life. The numbers in Table 4.1 are only guidelines. ADC and FA values reported from different centers can differ substantially. Data given here are in the same order of magnitude as those reported by Neill et al. (1998).

Detailed measurements of diffusion tensor characteristics related to brain maturation have been taken and have shown regional differences running parallel to the progress of myelination as seen on conventional MR images (Mukherjee et al. 2002). Unfortunately,

Table 4.2. Magnetization transfer ratio (%) during development

Projection fibers (pyramidal tracts)	At 1 month	23–25%
	At 3 months	25–27%
	At 6 months	31–33%
	At 20 months	34–37%
Association fibers	At 1 month	19–21%
	At 3 months	22–25%
	At 6 months	28–30%
	At 20 months	29–33%
Commissural fibers	At 1 month	23–24%
	At 3 months	24–25%
	At 6 months	29–33%
	At 20 months	34–37%

the reported values refer to 'eigenvalues' of the diffusion tensor and are not directly comparable to ADC and FA values.

4.4 Magnetization Transfer

With magnetization transfer (MT) quantitative information about the condition of brain tissue can be obtained by estimating MT ratios (MTRs), either voxel based and displayed as maps, or measured globally and displayed as MTR histograms. It has been shown that MTR changes in infants correlate with changes in the degree of myelination (Van Buchem et al. 2001). MTR can be used to quantitate the progress of myelination and monitor the regional development. MTR values (%) show an increase over time (Rademacher et al. 1999) (Table 4.2).

Gray matter structures also show an increase in MTR over time; these changes, however, are much less impressive (Rademacher et al. 1999).

It is possible to use MTR whole-brain histograms to monitor the progress of brain maturation. This will possibly develop into a method that will allow easy estimation of retarded maturation and be a good tool for individual follow-up studies (Van Buchem et al. 2001).

4.5 Myelination: Timetables

In daily practice it is useful to have a timetable of normal progress of myelination at hand. Even with a considerable variation, it is evidently possible to provide a time scale for normal development and to assess reliably significant delay in myelination. There are several approaches to making a timetable and each one has its own advantages and disadvantages. The methods can be subdivided in nonquantitative (visual inspection), semi-quantitative (ratios) and quantitative (absolute values).

Table 4.3. Signal intensity of central white matter relative to white matter on long TR SE images

Stage	Age	Short TE MWM	Long TE MWM
I	1st month	↑	=/↓
II	2nd months	=/↓	↓/↓↓
III	3rd–6th months	↓	↓↓
IV	7th–9th month	↓	↓↓
V	>9th month	↓	↓↓

↑↑ hyperintense, ↑ slightly hyperintense, = isointense, ↓ slightly hypointense, ↓↓ hypointense, SE spin echo, MWM myelinated white matter, TE echo time

Timetables can be based upon the *visual inspection* of changes on T₁- and T₂-weighted images. T₁-weighted images are very useful in the first 6 months of life, as discussed above, whereas T₂-weighted images provide more useful information after 6 months. Combination of T₁ and T₂ data has distinct advantages, especially in cases with delayed or distorted myelination.

At term birth, T₁-weighted images show evidence of myelination in the medulla spinalis, cerebellar white matter, dorsal part of the pons, mesencephalon, posterior limb of the internal capsule (in particular the area of the corticospinal tracts), and the postcentral parasagittal areas, as a continuation of the long ascending spinocortical tracts. The optic radiation becomes myelinated soon after birth. The splenium of the corpus callosum is myelinated in the 3rd month, the truncus in the 4th and 5th month, and the genu in the 5th and 6th months. In the 3rd and 4th months myelination spreads to the anterior limb of the internal capsule. From the parietal parasagittal area, myelination starts to spread in anterior and posterior directions. After this stage further distinction on T₁-weighted images becomes difficult.

Additional T₂-weighted images can be used to refine the assessment of myelination. Myelination of the central parts of the brain can be distinguished from the hemispheric white matter, making it possible to compose a timetable based on signal intensities with five steps of progression (see Tables 4.3, 4.4).

Some markers are useful in daily practice. On long TR, long TE SE images, the splenium of the corpus callosum has a low signal by 6 months of age, the genu at 8 months of age. The cross-over in the occipital lobe, when gray and white matter have a uniform and indistinguishable intermediate signal intensity (are isointense), occurs at about 7–9 months. At about 9 months the 'adult' contrast between gray and white matter starts to emerge in the occipital lobes. The anterior limb of the internal capsule is myelinated on the heavily T₂-weighted sequence at 8–11 months. At 12 months the frontal white matter starts to myeli-

Table 4.4. Signal intensities of peripheral white matter relative to white matter on long TR SE images

stage	age	Short TE		Long TE	
		UWM	MWM	UWM	MWM
I	1st month	↓	↑	↑	=
II	2nd month	=	=	↑↑	=
III	3rd-6th month	↑	=	↑↑	=
IV	7th-9th month		=		=
V	>9th month		↓		↓↓

↑↑ hyperintense; ↑ slightly hyperintense; = isointense; ↓ slightly hypointense; ↓↓ hypointense; MWM myelinated white matter; UWM unmyelinated white matter; TE echo time

nate; it should be nearly complete at 14 months of age. The temporal lobe is the last to myelinate; this occurs between 14 and 18 months of age. The U-fibers of the cerebral hemispheric white matter become fully myelinated between 18 and 24 months.

Use of marker sites can be helpful, especially for research purposes, to provide the necessary detail and quantitation. An approach defining specific targets for myelination, and scoring in a large population the time of onset and completion of myelination of such targets, leads to normal values with definition of normal variation.

In a *semi-quantitative* way the progress of myelination can be assessed by calculating a ratio between the averaged signal intensity of a chosen region of interest and dividing that by the averaged signal intensity of a fully myelinated structure. For this purpose the posterior limb of the internal capsule is often chosen, because myelination is complete at that structure at a GA of 44 weeks. A ratio so obtained is independent of type of equipment and field strength. In myelin disorders that also affect the posterior limb of the internal capsule, of course, this does not apply. The head of the caudate nucleus has also been used as a reference.

Some groups have used this more refined method of marker sites in combination with estimation of time of contrast cross-over between structures and used this approach to look at the detailed progress of myelination in the cerebellum and brain stem in the first months of life. Martin et al. (1990) took as target areas the cerebellar hemispheres, dentate nucleus, nucleus ruber, middle cerebellar peduncle, corpus medullare cerebelli, pontine tegmentum, basis pontis, medial lemniscus, and corticospinal tracts. They defined five stages of progress of cerebellar myelination, depending on the relative signal intensities of these regions. Landmarks of these studies used for time estimates were again the gradually darker appearance of myelinated areas on T₂-weighted images, the further extension of myelination towards the subcortical structures, and inversion of contrast between structures. An example of the first marker is the gradual

darkening of the rim around the dentate nucleus in the first weeks of life; of the second marker, the extension of myelin into the cerebellar folia; and of the third marker, the cross-over in signal intensities between the corticospinal tracts and the substantia nigra. When automatic scaling is used, which is usually the case on MR systems, it proves difficult to identify the five stages as described by these authors. Usually, however, three stages of maturation can be distinguished in the posterior fossa. The structures involved in the recognition of these three stages on T₂-weighted transverse images are: the basis pontis, the tegmentum pontis, the middle cerebellar peduncle, the dentate nucleus, the peridentate white matter, the corpus medullare cerebelli, and the white matter extending into the cerebellar folia (Fig. 4.3). In stage 1 (<1 month after term) the basis pontis is not myelinated, there is some myelin in the tegmentum of the pons and in the middle cerebellar peduncles, and the nucleus dentatus has a high signal intensity and is surrounded by a rim of lower signal intensity, followed by a high signal of the cerebellar white matter. In stage 2 (>1 months, <3–4 months) myelination starts to appear in the basis pontis; the tegmentum is still darker, however, and the dentate nucleus starts to appear darker. In stage 3 (>3–4 months), tegmentum and basis pontis are now approximately as dark as each other; the dentate nucleus and the cerebellar white matter appear completely dark and isointense with the middle cerebellar peduncle. After completion of these stages, myelination starts to extend towards the cerebellar folia, gradually shaping the 'arbor vitae' of the cerebellum.

We could make the assessment more detailed and add more structures: pyramidal tracts, medial lemniscus, and medial longitudinal fasciculus, structures that can be distinguished in good-quality images of the brain stem and cerebellum. A similar diagram could be produced for the mesencephalic structures, where the signal intensity, of the red nucleus, the substantia nigra, the corticospinal tracts, medial lemniscus, and inferior collicles changes with time, depending on the pulse sequence used.

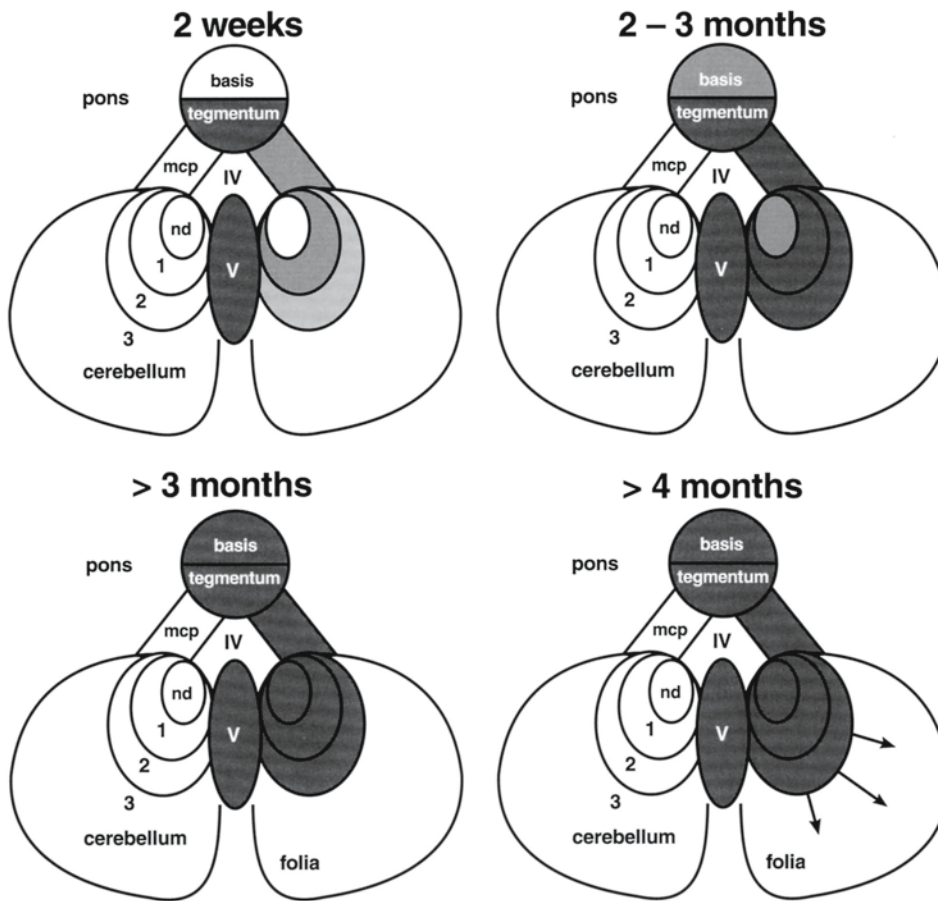


Fig. 4.3. Myelination of the posterior fossa (*nd* nucleus dentatus; *mcp* middle cerebellar peduncle; *V* vermis cerebelli; 1 peridentate white matter; 2 corpus medullare; 3 peripheral white matter; *IV* fourth ventricle)

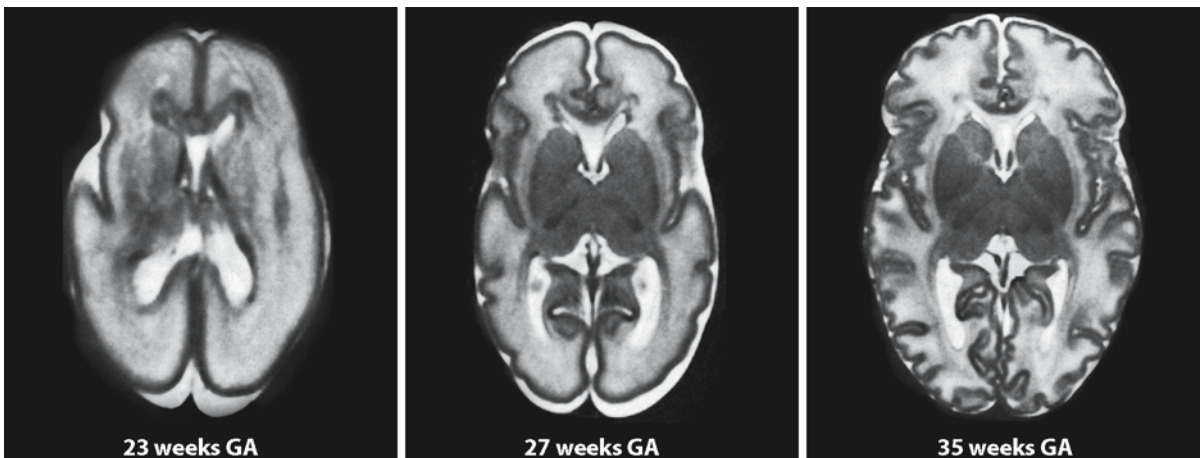


Fig. 4.4. Myelination and gyration are both part of the maturation process of the brain. These axial T_2 -weighted images obtained in infants with gestational ages (GAs) of 23, 27, and 35 weeks demonstrate brain maturation in that period. At 23 weeks of gestation the germinal matrix is visible at the trigonum, frontal horns and caudothalamic notch. The brain surface is still smooth. The sylvian fissure is hardly visible. At

27 weeks there are still remains of the germinal matrix, but it is less conspicuous. At 35 weeks of gestation myelination has started in the posterior limb of the internal capsule. (The *dark dot* represents the corticospinal motor tract.) The gyral development over this period is beautifully shown in these images. From Childs and Ramenghi et al. (2001), with permission

Quantitative measurements can be used to assess myelination of the brain in general, and in different structures in particular. Examples are measurements of T_1 , T_2 , ADC, FA, and MTR.

It is clear that myelination is not the only concern as far as development of the CNS is concerned. Progression of gyration should be included in an inventory of brain maturation. For premature children such a maturation index has been proposed (Childs et al. 2001), which provides a standardized method of assessing cerebral maturation. Four parameters are assessed in this scale: cortical folding, myelination, germinal matrix distribution, and glial cell migration (see also Fig. 4.4).

4.6 Gyration

The brain of premature children and neonates is immature, not only in myelination but also in development in gyri (gyration). Histopathological, intrauterine ultrasound and MR studies have yielded insight into the development of some major fissures, which provide landmarks of gyral development: the interhemispheric fissure (before 15 weeks of GA), the parieto-occipital fissure, the calcarine fissure, the central rolandic sulcus (visible at a GA of 23–25 weeks), and the development of the insula, visible at a GA of 18 weeks, with overriding frontal, temporal and parietal opercula at 28–29 weeks' gestation (Chi et al. 1977).

For MRI, insight into gyral development from the age of 26–28 weeks gestation is most important, as preterm infants often come for MRI. In premature infants the cerebral cortex is still entirely or relatively smooth and lacking in sulci, depending on the post-conceptual age of the infant. Over time, shallow sulci develop in an ordered sequence. The sulci increase in number and become deeper. The gyri become increasingly branched. Most of the process of a conversion of a smooth, lissencephalic brain into a nearly fully developed cortical gyral pattern occurs between 26 and 44 weeks of gestation. The mature pattern of gyri and sulci is normally reached at the age of 3 months after term. In our study of gyral development in preterm and term neonates (Van der Knaap et al. 1996) gyral development was graded for differ-

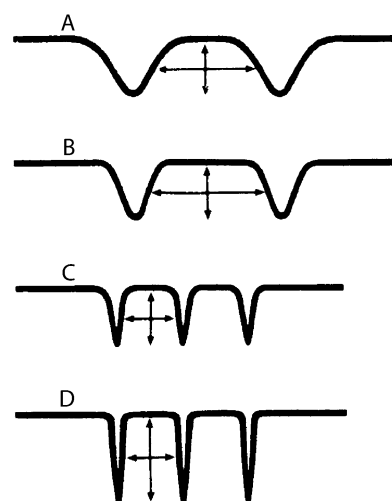


Fig. 4.5. A–D. Patterns of sulcus configuration for gyral development score 2 (A or B), score 3 (C), and score 4 (D). From Van der Knaap et al. (1996), with permission

ent brain areas using a five-point scoring system (Fig. 4.5): (1) The surface is smooth without gyri and sulci or there is, at most, some undulation of the cortical surface area. (2) Width of the gyri is greater than the depth of the sulci. (3) Width of the gyri is equal to the depth of the sulci. (4) Width of the gyri is less than the depth of the sulci. (5) Gyri and sulci are branched. Seven cortical areas were studied separately: (1) the frontal lobe minus the area of the central sulcus, (2) the area of the central sulcus, (3) the parietal lobe minus the area of the central sulcus, (4) the occipital lobe minus the medial area, (5) the medial occipital area, (6) the posterior part of the temporal lobe, and (7) the anterior part of the temporal lobe. The five stages of gyration distinguished are shown in Figs. 4.6–4.10. The ages of the children ranged from 30 to 42 weeks. At all ages the development of the rolandic area and the medial part of the occipital lobe (areas 2 and 5) was most advanced. In the parietal area, occipital area and posterior temporal area (areas 3, 4, and 6), an intermediate rate of gyral development was found. Gyral development was slowest and latest in the frontal and anterior temporal areas (areas 1 and 7).

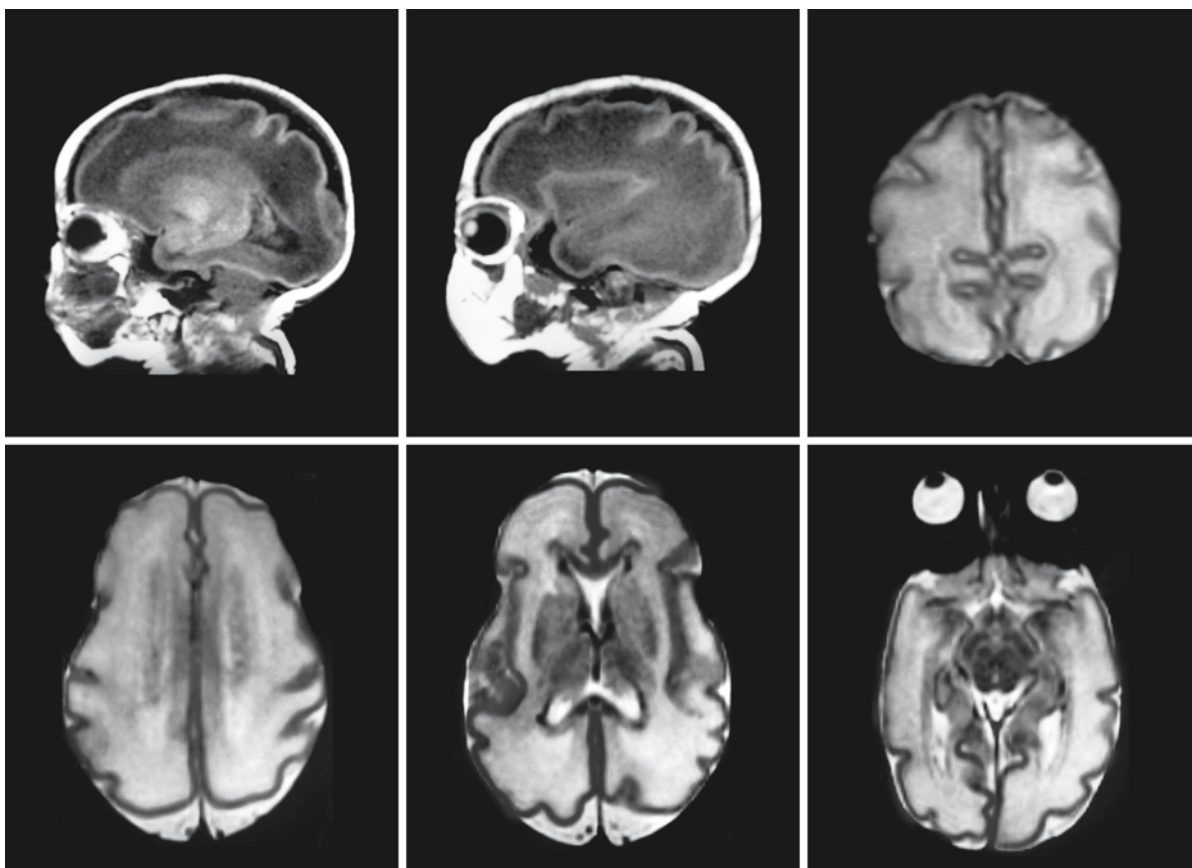


Fig. 4.6. Sagittal T_1 -weighted, and coronal and transverse T_2 -weighted images in a preterm infant at a GA of 30 weeks, showing stage 1 gyration. The depth of the central, parieto-occipital and calcarine sulci is about equal to the width of the

bordering gyrus. The frontal and temporal cortical surface is smooth; the cortex is slightly undulating in the posterior area. From Van der Knaap et al. (1996), with permission

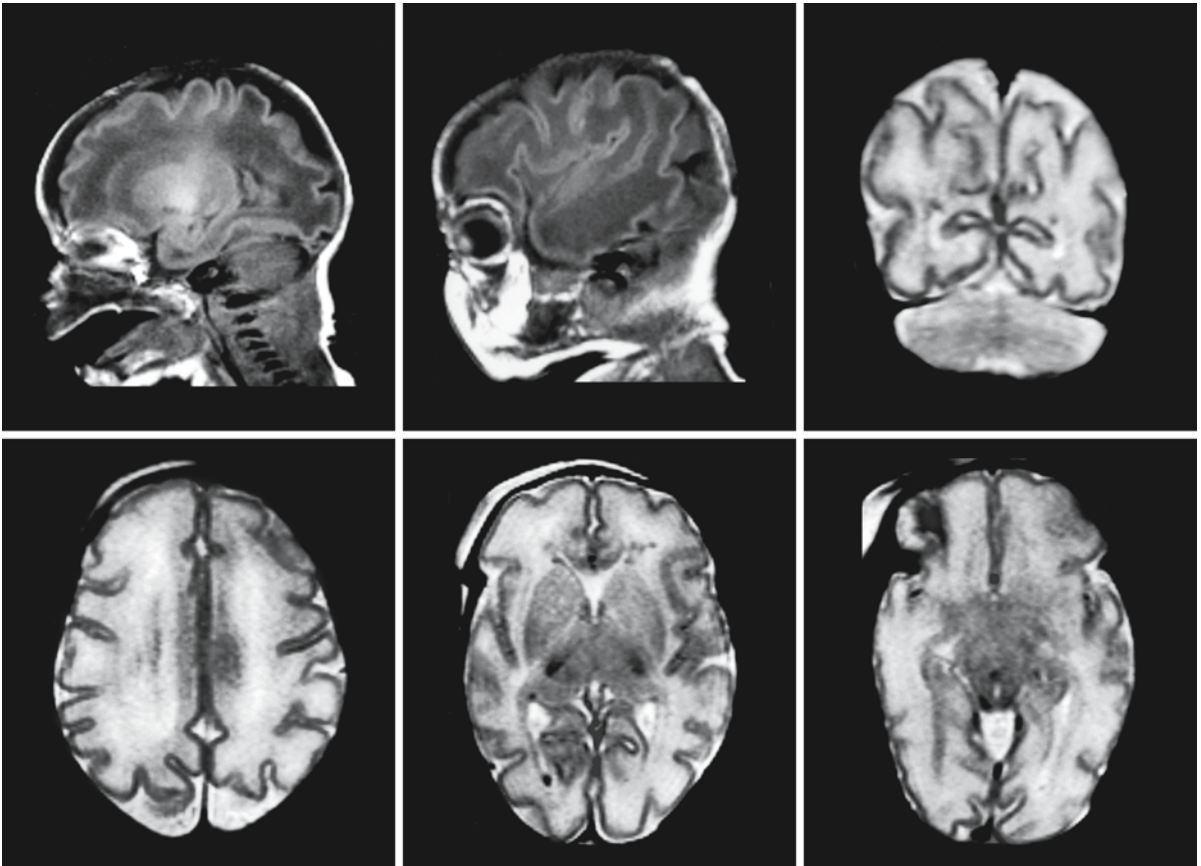


Fig. 4.7. Preterm infant at a GA of 32 weeks. Sagittal T₁- and coronal and transverse T₂-weighted images show gyration stage 2. The central and calcarine sulci are now deeper than

the bordering gyri. Compared with stage 1 sulci are better defined and increased in number in the remaining areas. From Van der Knaap et al. (1996), with permission

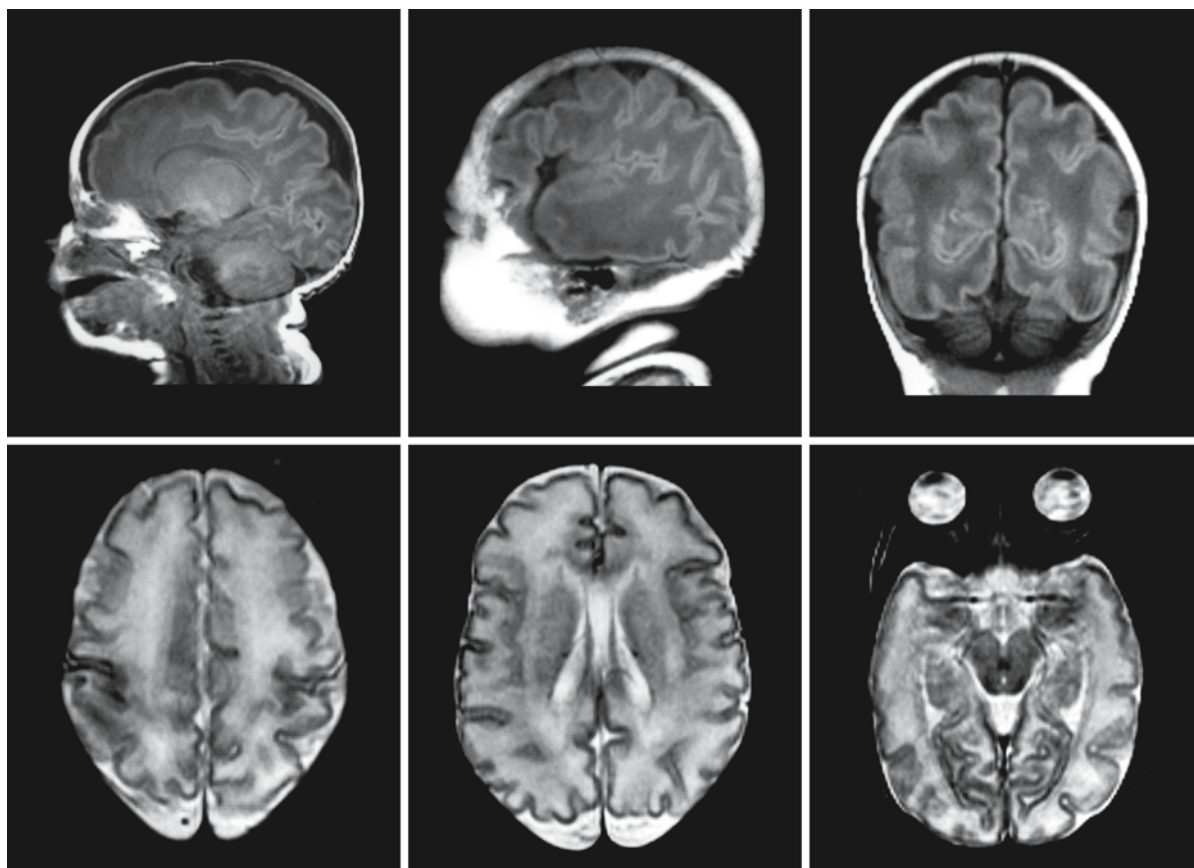


Fig. 4.8. Gyration at a GA of 36 weeks. Sagittal and coronal T_1 - and transverse T_2 -weighted images demonstrate stage 3 gyration. The central sulcus and sulci of the medial occipital area are now becoming branched. Sulci are becoming better

defined and more numerous. The depth of the sulci is equal or greater than the width of the gyri in most areas. From Van der Knaap et al. (1996), with permission

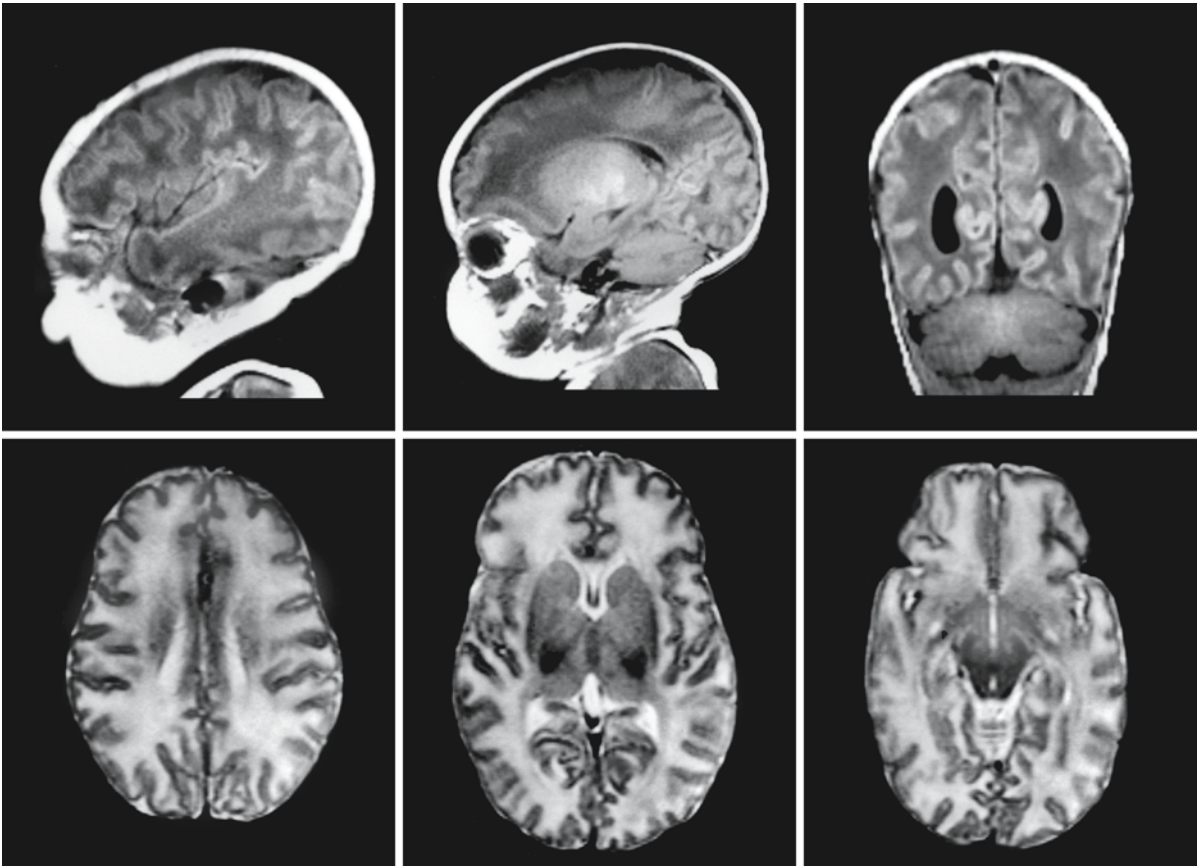


Fig. 4.9. Gyration at a GA of 39 weeks. Sagittal and coronal T_1 - and transverse T_2 -weighted images depict stage 4 gyration. The central and sulci of the medial occipital area are now branched. The number of sulci and gyri has increased again.

The sulci have a closed form in most areas. The depth of the majority of sulci is greater than that of the bordering gyri. From Van der Knaap et al. (1996), with permission

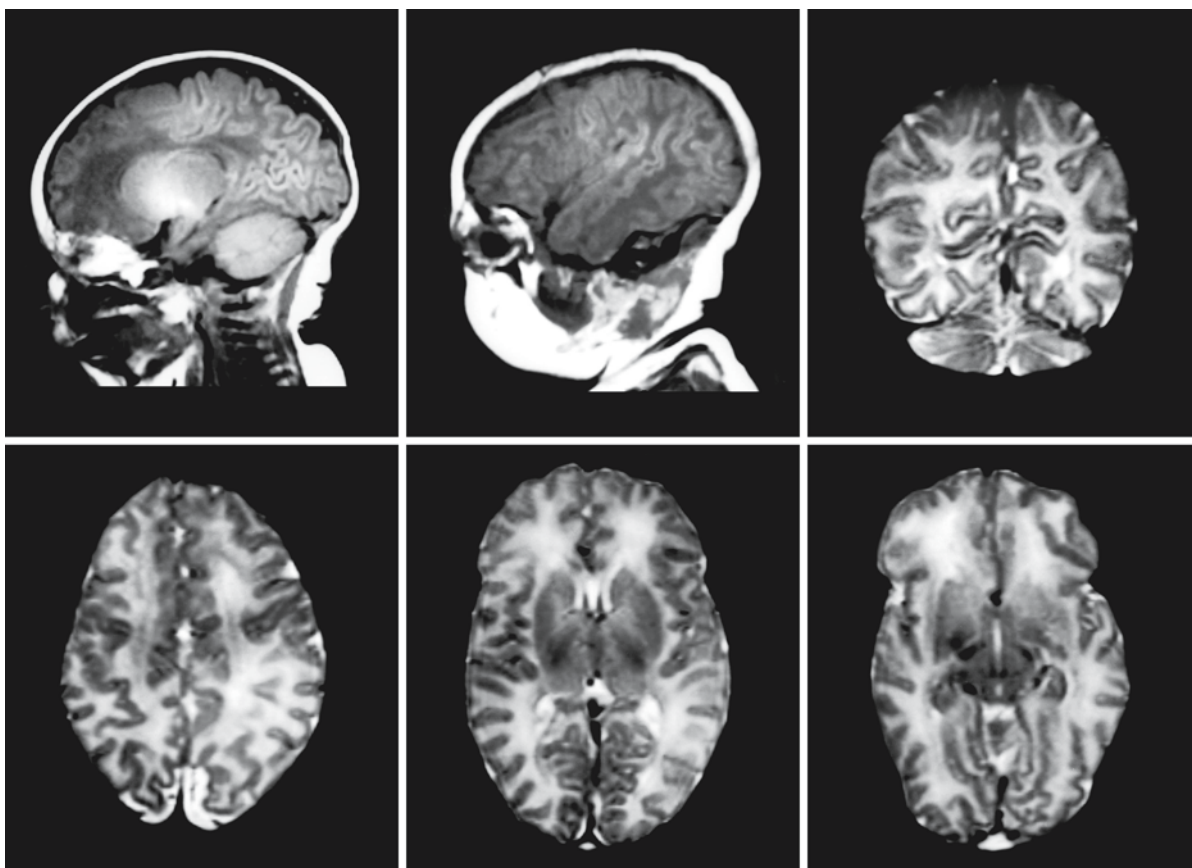


Fig. 4.10. Gyration at a GA of 42 weeks, depicted on sagittal T₁-weighted, and coronal and transverse T₂-weighted images, showing stage 5 gyration. Branching of sulci is now seen in all areas. From Van der Knaap et al. (1996), with permission

4.7 Delayed Myelination, Irregular Myelination, Hypomyelination, and Arrest of Myelination

Once MRI criteria for normal progress of myelination have been established, it is possible to diagnose delays in this process. If it is true that myelination expresses functional maturity a correlation between delay in myelination and delayed development of psychomotor functions can be expected. Roughly speaking, this appears to be the case. We have been able to confirm it in a group of children with hydrocephalus, in whom MRI and neuropsychological data were obtained before and twice after shunting. There was a strong correlation between (a) the progress of myelination as compared with the normal myelination standard and (b) the progress of mental development as compared with the normal developmental standard. It is important to follow up the progress of myelination in any child in whom a delay is suspected, to see whether, and if so when, the child catches up with normal myelination. It might be assumed that a longer delay in the restoration of the normal pattern would coincide with a poorer prognosis.

There are many possible causes for a delay in myelination: hypoxia-ischemia, congenital infections, congenital malformations, chromosomal abnormalities, congenital heart failure, postnatal infections, hydrocephalus, hypothyroidism, hypercortisolism, hypocortisolism, fetal intoxications, malnutrition, and inborn errors of metabolism. The delay is usually bilateral and symmetrical, but unilateral delay is seen in cases with hemimegalencephaly, unilateral porencephalic cysts, cerebral hemiatrophy, or unilateral periventricular leukomalacia.

The critical period in myelin development was initially thought to coincide with the proliferation of myelin-forming cells, rather than with the period of membrane accumulation. The mechanism of 'stunting' of oligodendroglial proliferation as a cause of hypomyelination has been under discussion, because in animal research no major deficits of oligodendrocytes could ever be established, except in severely starved animals. Therefore the induction of myelin membrane formation, rather than cell proliferation, seems to be the actual critical event. Damage in critical periods is often limited to areas in which myelination is beginning at that time. This knowledge is helpful in establishing the time of insult in infants and children.

Irregular myelination with local or generalized hypermyelination, or myelination not following the normal routes of progress, is rare, but is seen occasionally. Hypermyelination, or advanced myelination, has been observed in patients with Sturge-Weber syndrome. It has been suggested that epileptic seizures may stimulate myelination. However, advanced myelination or hypermyelination is not seen in most patients with infantile forms of epilepsy. Local hypermyelination in the basal ganglia is manifest histologically as the so-called status marmoratus, a late sequela of perinatal hypoxia. In this case the myelination does not involve the proper targets and does not occur around axons but around astrocytic extensions. Because of the low signal intensity of the basal ganglia on T₂-weighted images and the dark appearance of myelin in this sequence, MRI has so far not succeeded in identifying this condition.

Hypomyelination or arrest of myelination occurs in Pelizaeus-Merzbacher disease, a disorder of proteolipid protein synthesis, one of the major myelin proteins. In this disorder no myelin, or only very little, is produced. In Salla disease, a lysosomal storage disorder, and DNA repair disorders such as Cockayne syndrome and trichothiodystrophy with sun hypersensitivity hypomyelination is also present. To establish a secure diagnosis of retarded or arrested myelination, at least two observations sufficiently far apart are necessary.

4.8 Iconography of Myelination and Gyration

Illustrations in this chapter show the progress of gyration (Figs. 4.4–4.10) and myelination in normal neonates and infants (Figs. 4.11–4.23). Many examples of disturbances of myelination are found in the other chapters in this book. In Table 4.4 the myelination of some important structures on MRI is indicated. In some cases a more detailed look at structures in relation to their surroundings is useful, in order to see how contrast changes over time. The structures in the posterior fossa are a good example (Fig. 4.3). We also include an example of diffusion-weighted imaging in estimating the progress of myelination (Fig. 4.24).

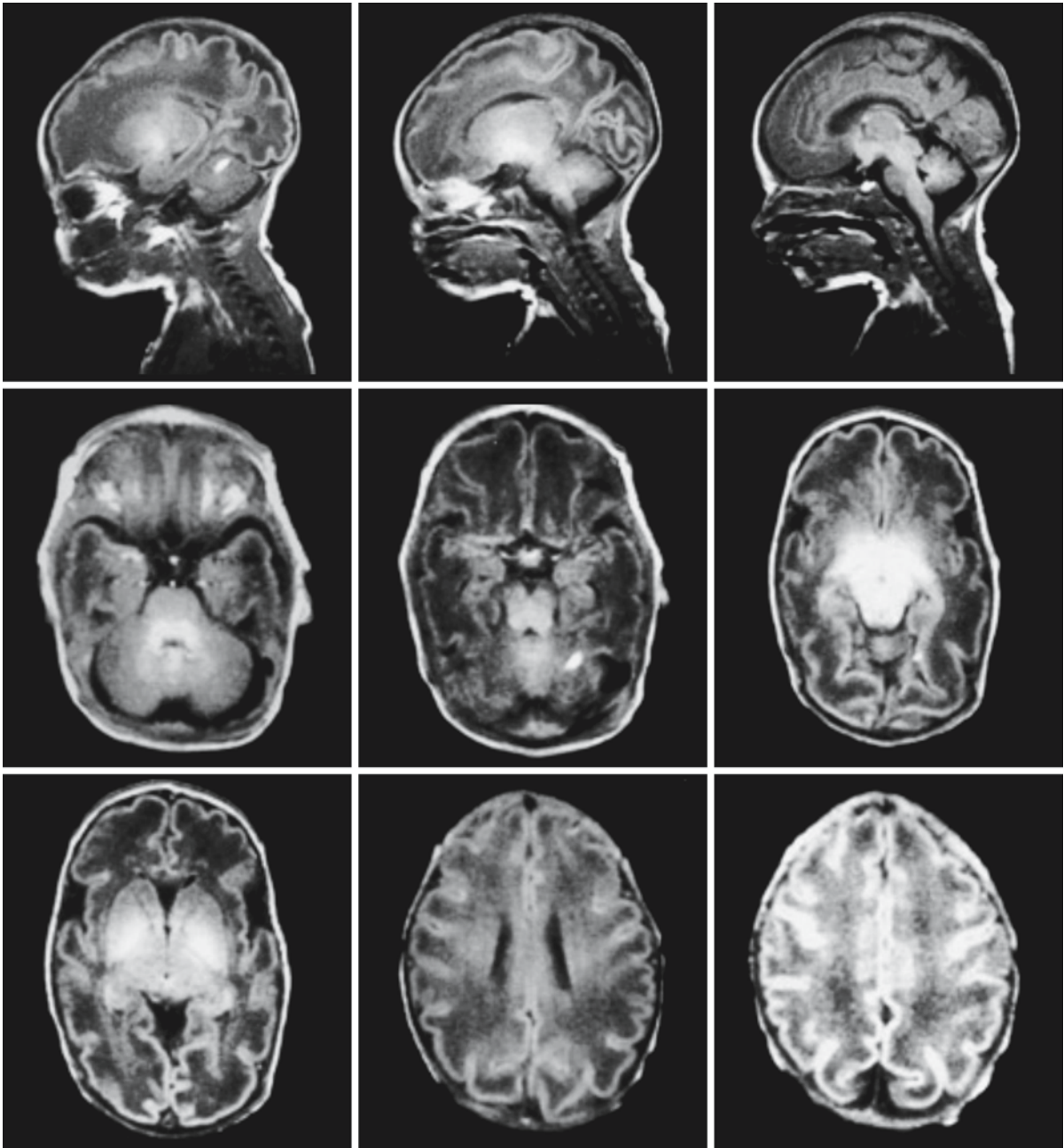


Fig. 4.11. Myelination at a GA of 32 weeks. The sagittal T_1 -weighted series (*upper row*) shows the features of the premature brain nicely: lack of gyration in the frontal areas, with some gyration in the parietal and occipital lobes. The midsagittal image shows myelin present in the medulla oblongata, the

dorsal part of the pons, the mesencephalon, and the corpus medullare of the cerebellum. The transverse T_1 -weighted series shows the same features and gives a good impression of the high water content of the unmyelinated white matter

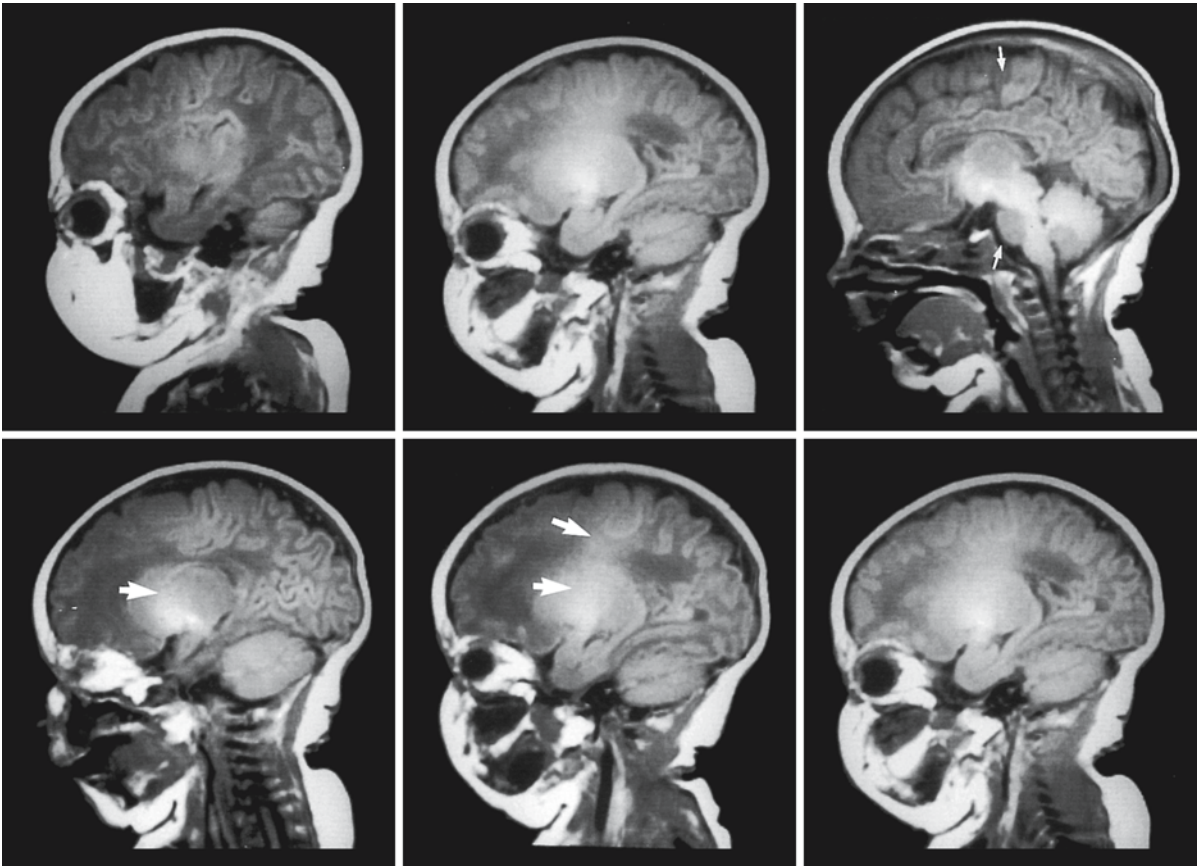


Fig. 4.12. Myelination at a GA of 39 weeks. A sagittal T₁-weighted SE series is shown from *right to left*. In the brain stem, the basis pontis is still not myelinated (*arrow*). The corpus cal-

losum is still thin and also unmyelinated. From the basal ganglia, myelinated white matter tracts can be followed towards the post-rolandic gyrus (*arrows*)

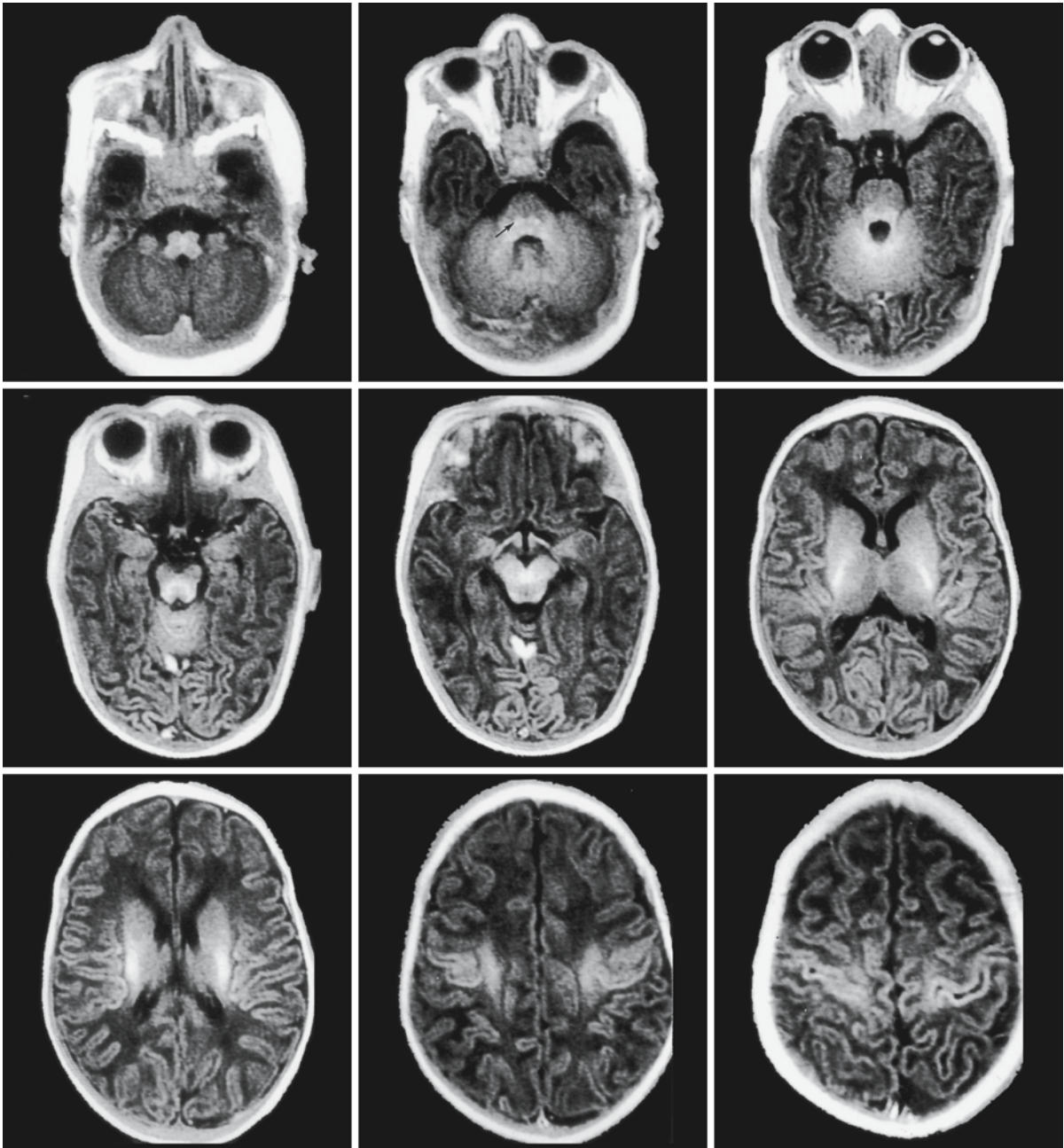


Fig. 4.13. Myelination 2 weeks after birth at term, as seen on a T₁-weighted transverse inversion recovery (IR) series. Myelination is seen in the medulla oblongata, middle cerebellar peduncle, tegmentum pontis (especially medial lemniscus, *arrows*), colliculus inferior, decussation of the superior cerebel-

lar peduncles, optic tracts, posterior limb of the internal capsule, white matter tracts in the basal ganglia and ascending tracts towards the post-rolandic gyrus. Note in the *upper images* that cortical gray matter is also myelinated

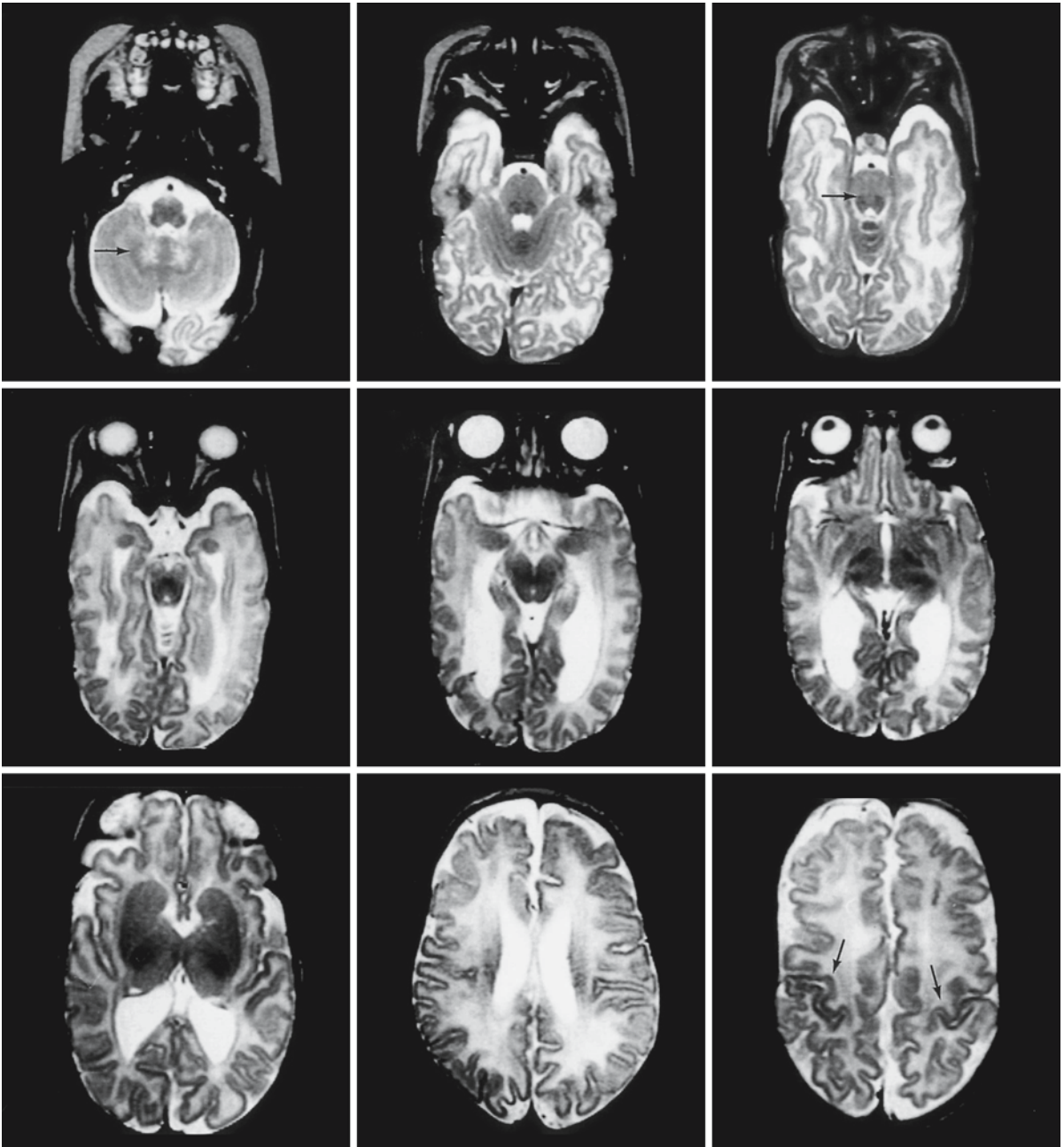


Fig. 4.14. T₂-weighted transverse series of myelination 2 weeks after birth at term for comparison. Cerebellar myelination is still in stage 1: the hilus of the dentate nucleus is bright; the dentate nucleus is surrounded by a dark band (*arrow*), again followed by bright cerebellar white matter. Contrast inversion of these structures during the progress of myelination

will give clues to the age of myelination. On T₂-weighted images the tegmentum pontis (*arrow*) and mesencephalon are darker than the ventral pons. Myelin can also be seen in the superior vermis, posterior limb of the internal capsule, basal ganglia and ascending tracts into the post-rolandic gyrus (*arrows*)

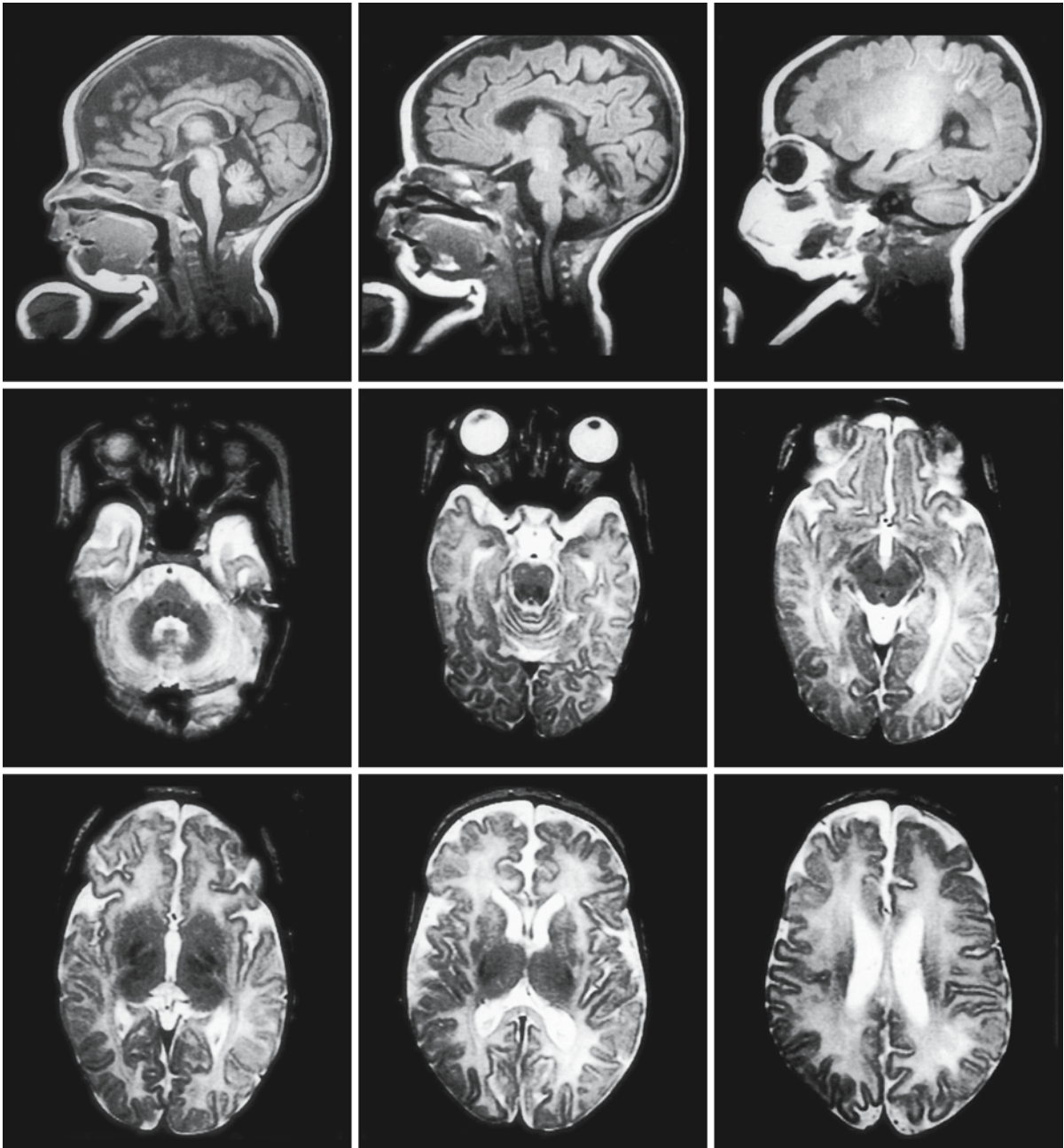


Fig. 4.15. In the posterior fossa T₂-weighted images show that cerebellar myelination has progressed to stage 2 in this 2-month-old infant. The bright ring around the dentate nucleus has disappeared, but the peripheral white matter of the cerebellum is still bright. There is still a difference between the

basis pontis and tegmentum pontis, although much less pronounced than before. In the mesencephalon, the pyramidal tracts and decussation of the superior cerebellar peduncles can be identified

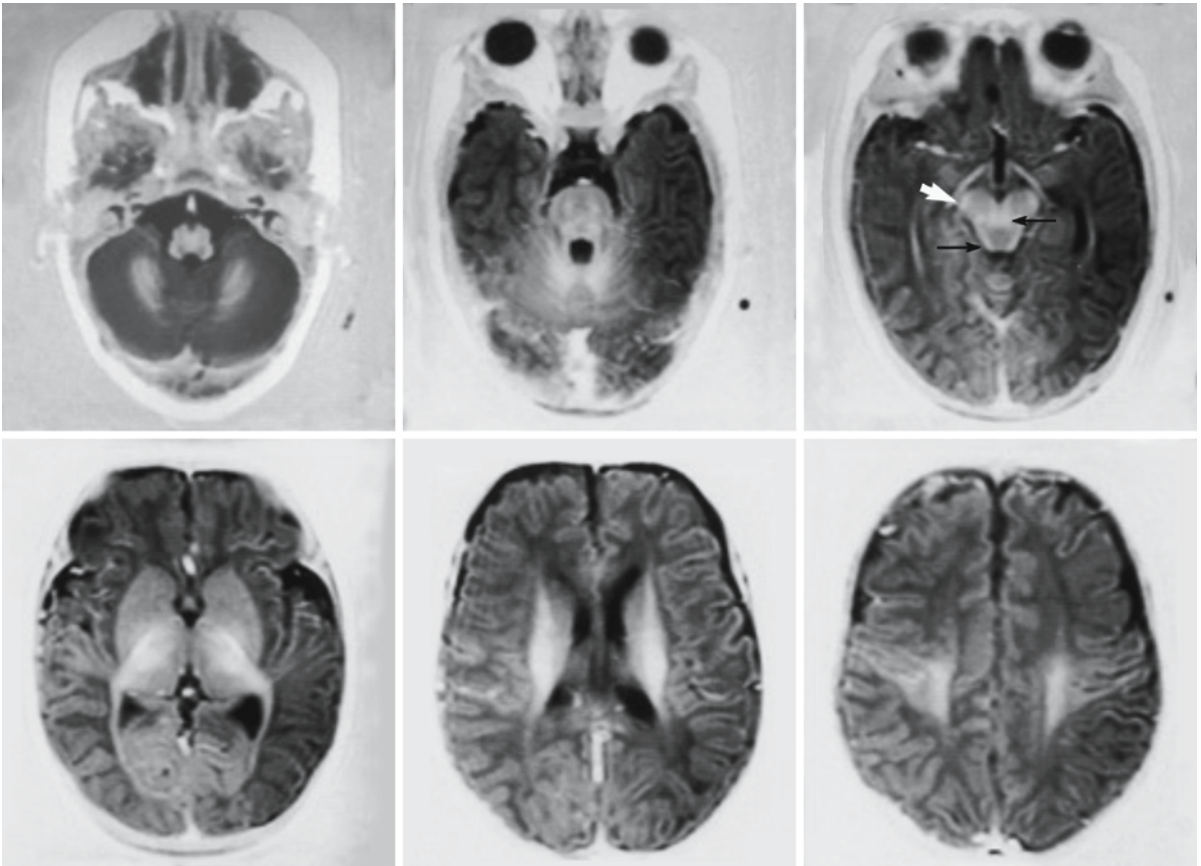


Fig. 4.16. IR images at 3 months. The myelinated structures can easily be identified. Note the beginning of myelination in the pyramidal tracts in the mesencephalon (*large white arrow*) and the strongly myelinated decussation of the superior cerebellar peduncles (*small black arrow*). The colliculus inferior (*black arrow*) and the auditory tracts are also clearly myelinat-

ed. The optic tract is myelinated, as is the optic radiation. The posterior limb of the internal capsule is fully myelinated at the postnatal age of 2 weeks. Myelin has now spread to the precentral gyrus and will advance dorsally and ventrally to myelinate the occipital, the frontal and, finally, the temporal lobes

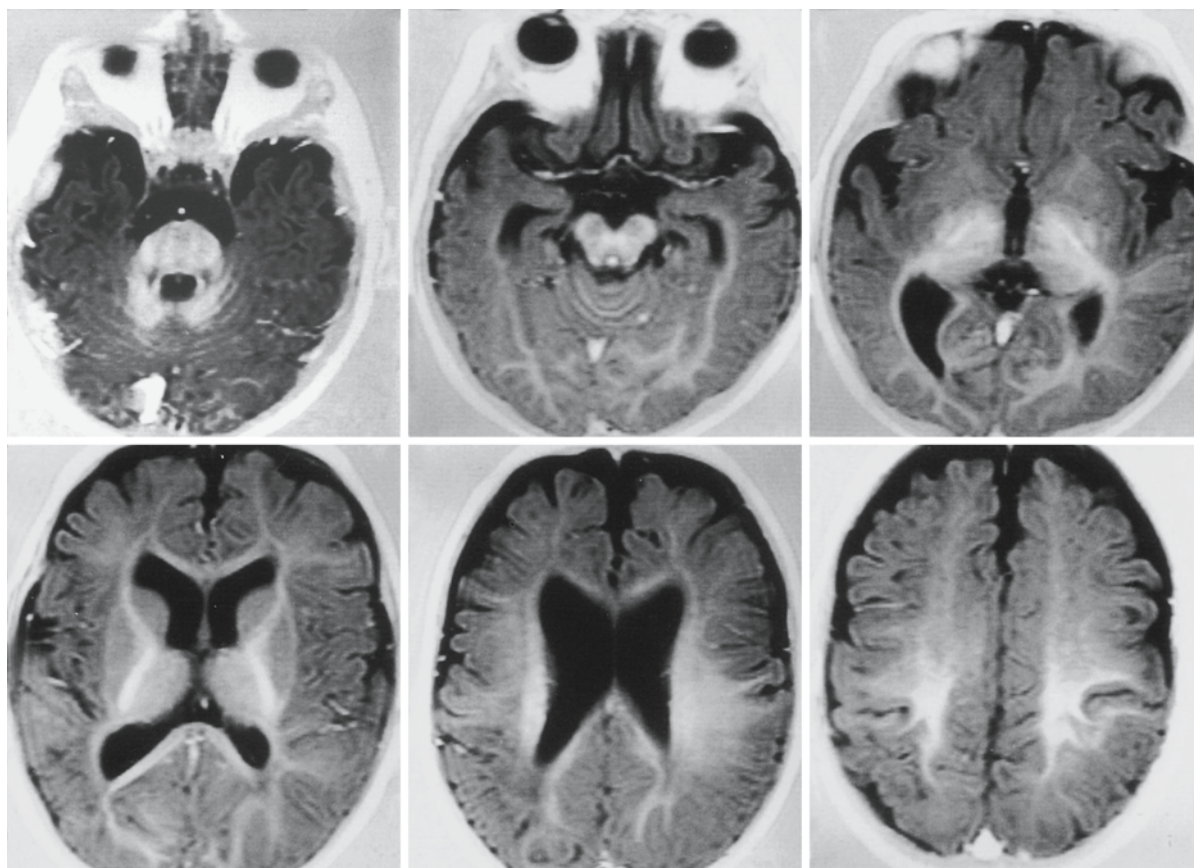


Fig. 4.17. At the age of 5 months the genu of the corpus callosum starts to myelinate. On IR images myelination will soon appear to be complete. T_2 -weighted images will then be more useful in providing information about maturation of the brain

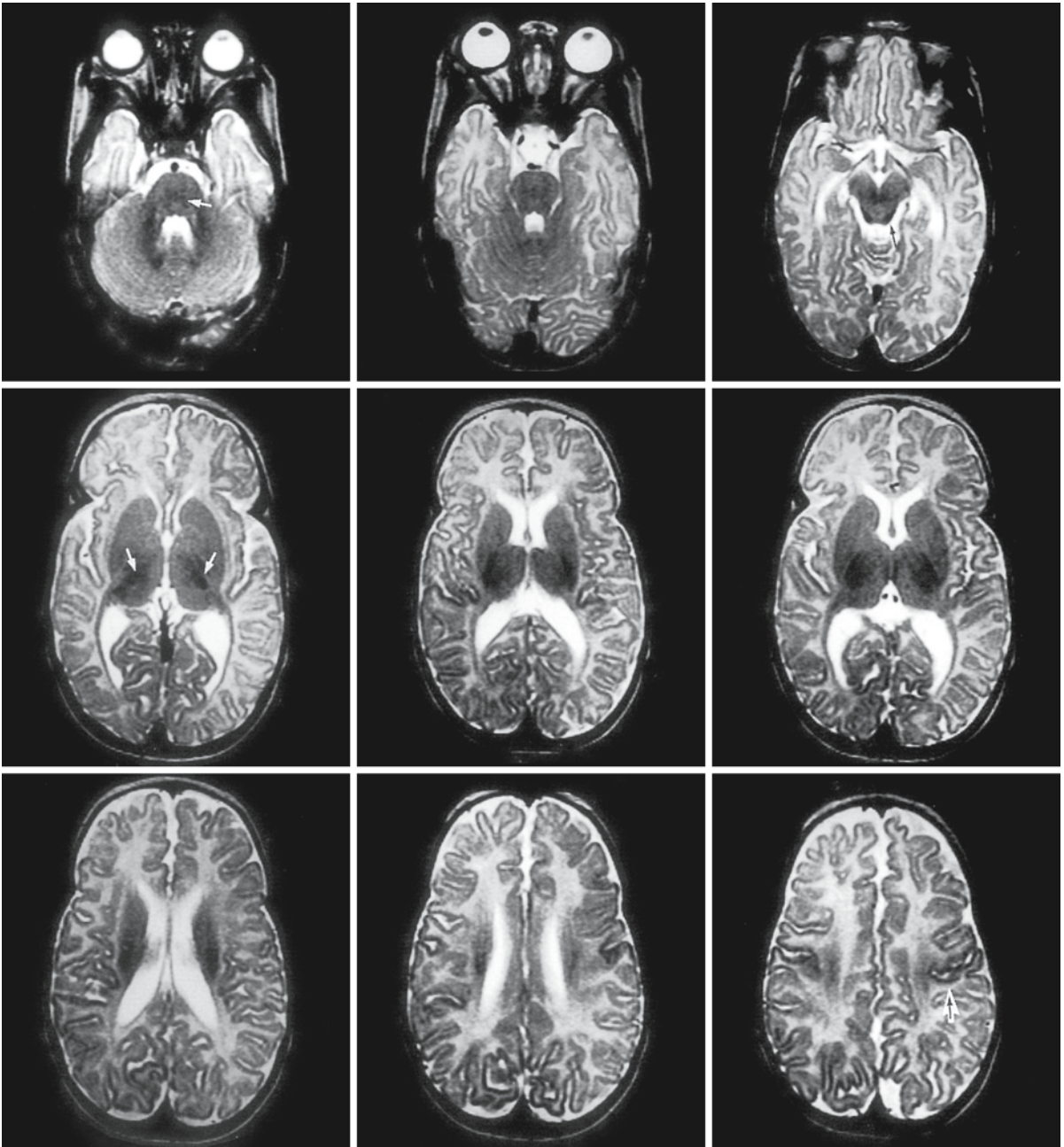


Fig. 4.18. T₂-weighted series at 4 months of age. In the pons, basis and tegmentum have a low signal; the medial lemniscus has an even lower signal (*arrow*), as do the middle cerebellar peduncles. The corpus medullare of the cerebellum is myelinated, but myelination is not yet extending towards the cortex. At the level of the mesencephalon, the decussation of the

superior cerebellar peduncles, the colliculus inferior (*arrow*), the pyramidal tracts, the corpus mamillare and the optic tract have a low signal. The posterior limb of the internal capsule is also dark (*arrows*). A difference is visible between the unmyelinated white matter in the frontal and temporal regions and the occipital and parietal region where myelination has started

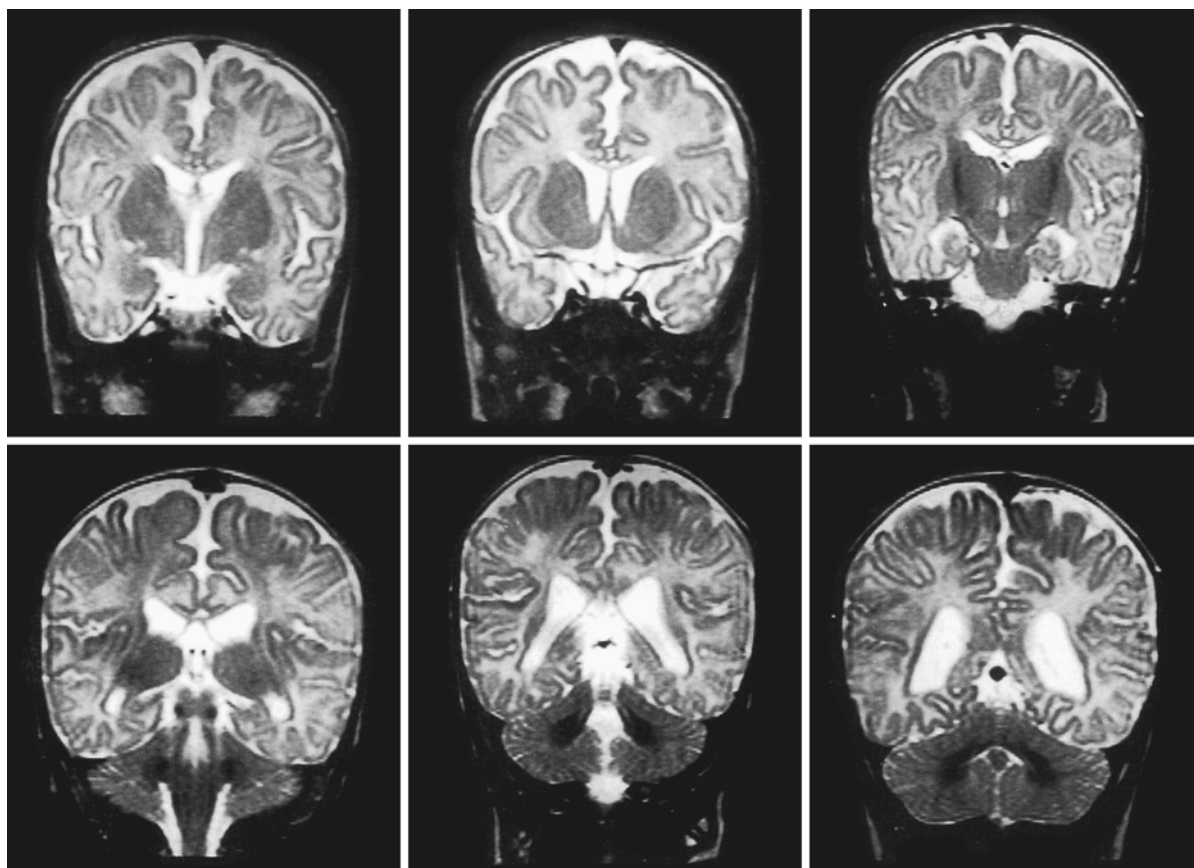


Fig. 4.19. T₂-weighted coronal images at the age of 4 months, showing the difference between still unmyelinated white matter in the frontal and temporal lobe and the more advanced myelination posteriorly

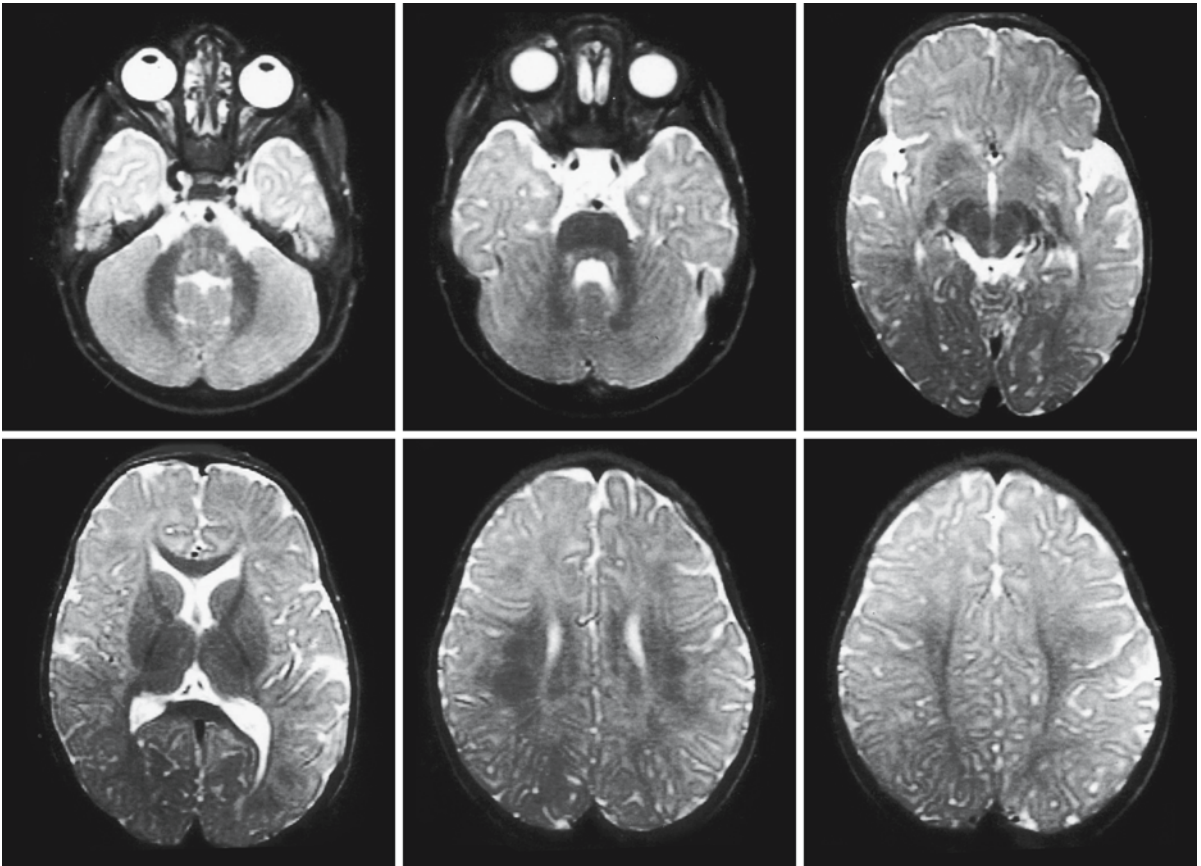


Fig. 4.20. Myelination at 7–8 months of age. On the T₂-weighted images the central parts are now myelinated, including the genu of the corpus callosum. The crossover between gray and white matter in the occipital and parietal areas has started; there is little contrast between gray and white matter. In the frontal and temporal regions this is not yet the case

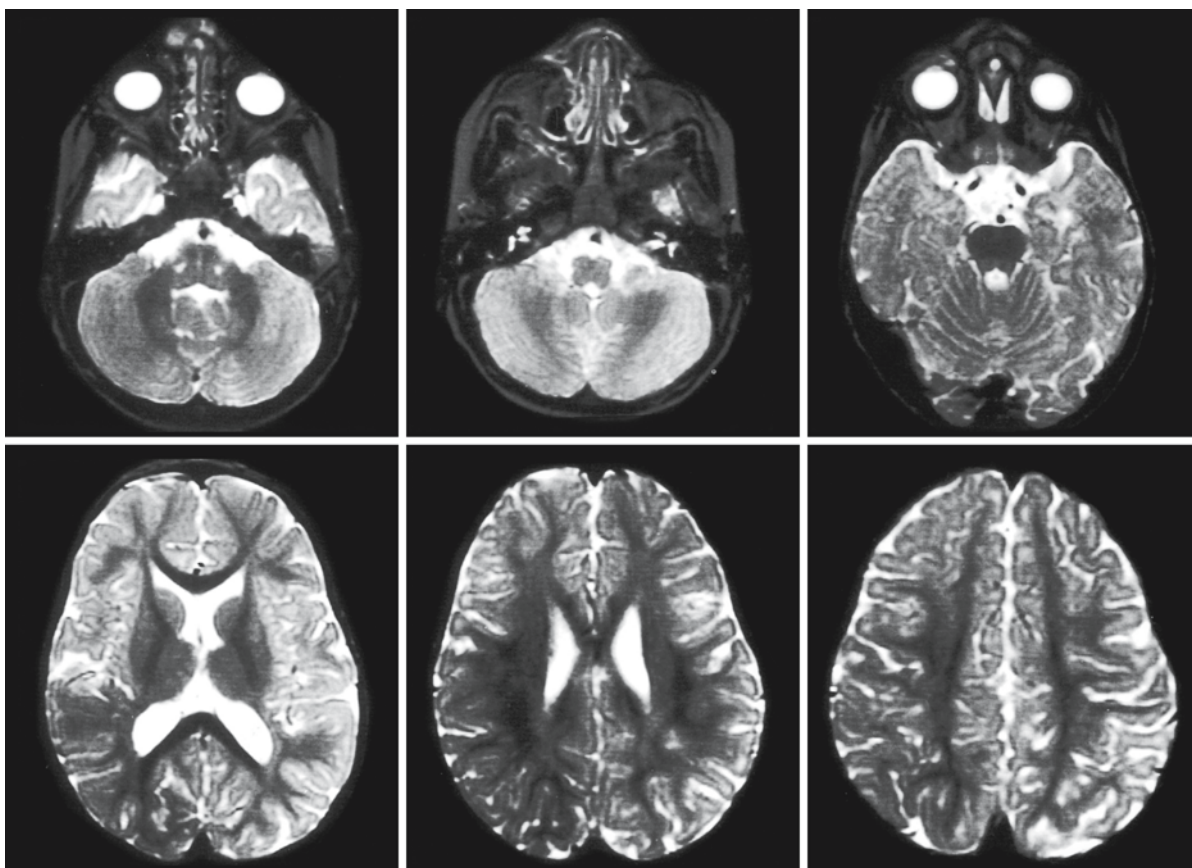


Fig. 4.21. Myelination at 12–13 months. The adult contrast is now emerging in all lobes except the temporal lobe, the latest to myelinate. The T_2 -weighted series shows that the spread of myelin into the arcuate fibers is still not complete

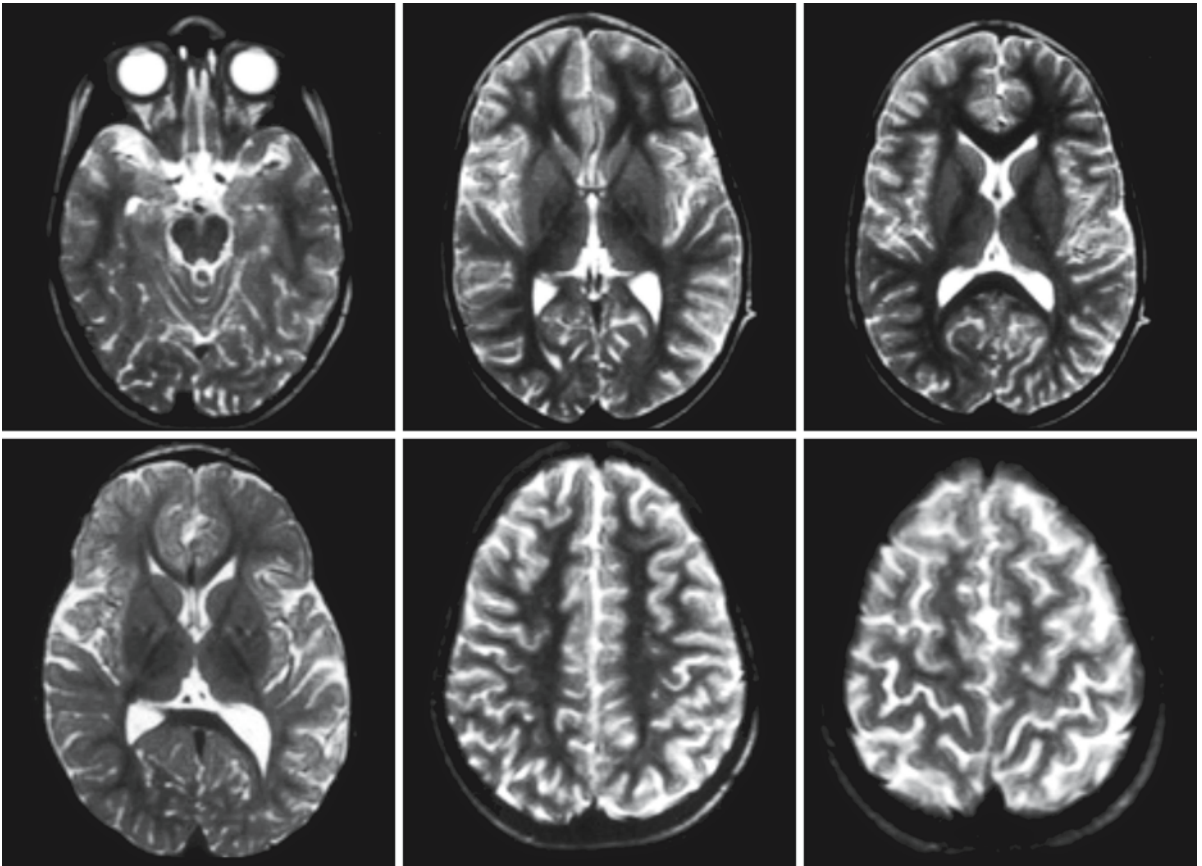


Fig. 4.22. Adult pattern of myelination on T_2 -weighted images in a 5-year-old child. The temporal lobes now also show the adult gray-white matter contrast

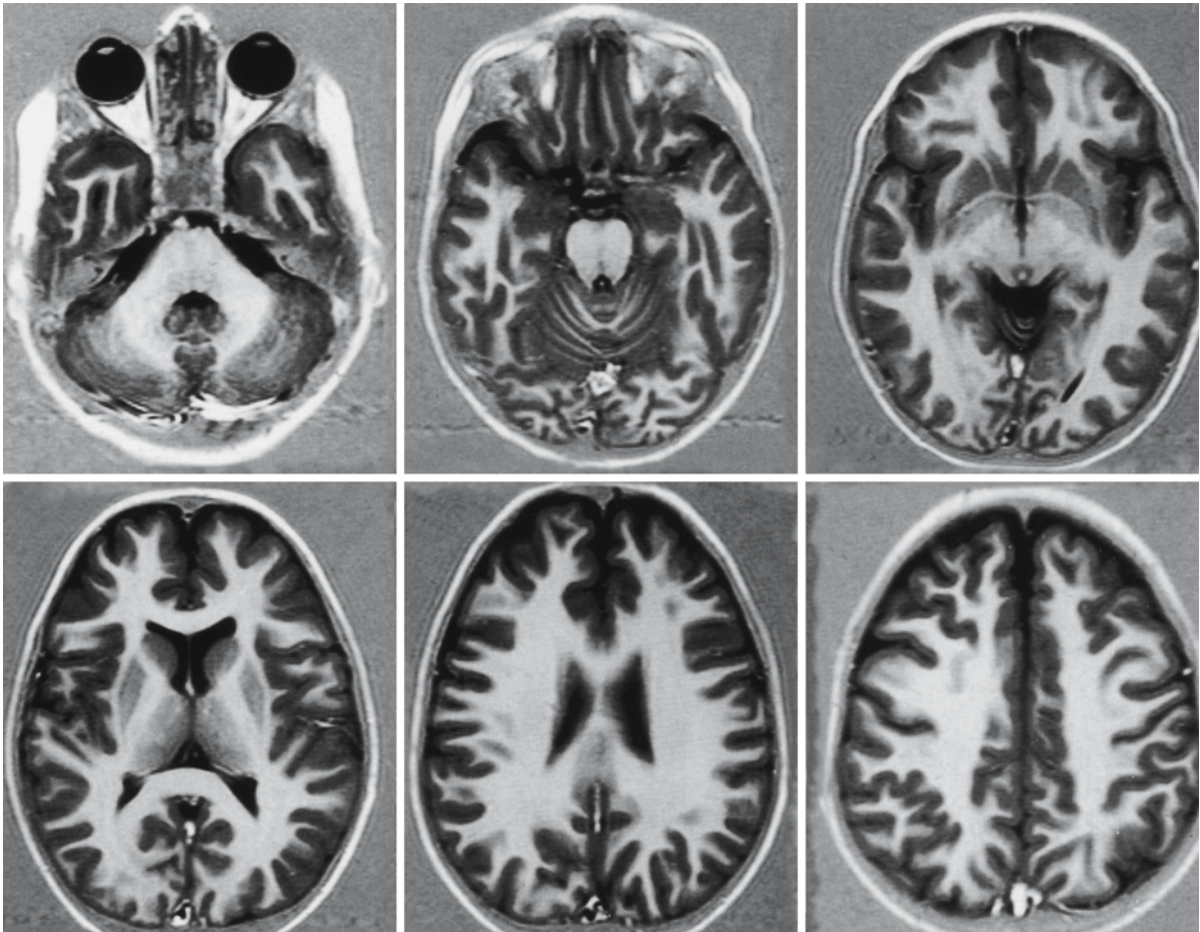


Fig. 4.23. Adult pattern of myelination on T₁-weighted (IR) images. These images were taken from a 5-year-old boy

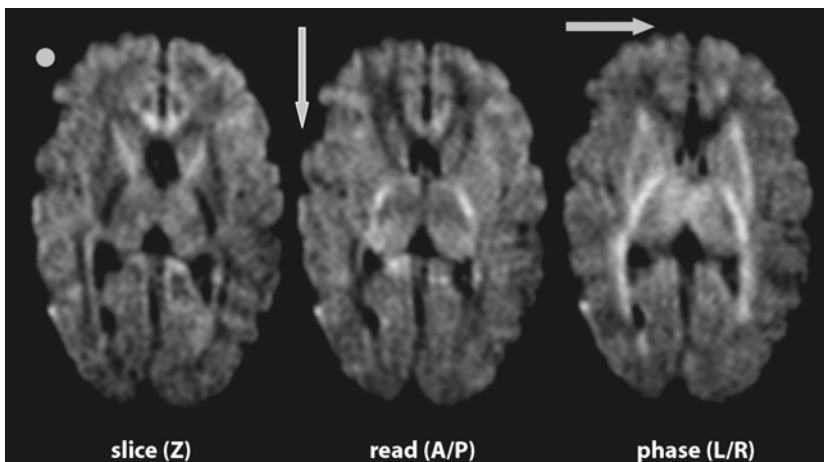


Fig. 4.24. Diffusion-weighted-imaging (DWI) and diffusion tensor imaging (DTI) allow further refinement and quantitation of the progress of myelination. These images depict single-shot EPI with single diffusion gradient in slice, read or phase direction at $b=1000$, showing anisotropy of myelinated fibers depending on the gradient direction in a baby boy 3 months of age

Lysosomes and Lysosomal Disorders

R.A. Wevers, V. Gieselmann

5.1 Lysosomal Biogenesis and Biochemical Functions

Lysosomes are hydrolase-rich organelles surrounded by membranes and with an acidic interior milieu. They are present in almost all types of body cells. Their number varies greatly, depending on cell type and function. They display considerable structural heterogeneity and appear in all shapes, sizes, and densities. They have been given their name because they are small bodies (soma = body) containing various enzymes that are hydrolytic (lysis = dissolution). These hydrolases catalyze reactions in which macromolecules and macromolecular structures are degraded into smaller components. Among the more than 50 different lysosomal enzymes so far identified are proteases, nucleases, glycosidases, lipases, phospholipases, sulfatases, and phosphatases. The variety of enzymes enables the lysosome to digest almost all types of biological macromolecules, such as proteins, polysaccharides, lipids, and nucleic acids. The low-molecular components released are transported to the cytoplasm to be reused. For this purpose the lysosomal membrane contains various transporters to translocate amino acids, sugars, and possibly nucleotides into the cytoplasm. The lysosomal membrane separates the hydrolytic enzymes from the cytoplasm to prevent uncontrolled lysis of cytoplasmic components. The acidic interior of lysosomes provides a favorable environment for the digestive activities of the enzymes: oligomeric proteins dissociate into monomers, proteins dissociate away from the protecting membrane, and stabilizing complexes become split. The low pH is generated by a complex multisubunit ATP-dependent proton pump. Several subunits of this proton pump are found on the cytosolic side of the lysosomal membrane, and others are integral lysosomal membrane proteins. Furthermore, the lysosomal membrane harbors various proteins, with highly glycosylated intralysosomal domains (e.g. LAMP1 and 2). The high carbohydrate content is thought to protect the lysosomal membrane from hydrolytic attack by the enzymes.

Lysosomal enzymes, along with secretory proteins and plasma membrane proteins, are synthesized on membrane-bound polyribosomes on the rough endoplasmic reticulum. An important question is how proteins, which are destined for specific intracellular compartments, are targeted at their destination from

their site of synthesis. The signal that specifies the destination of each nascent protein resides in its sequence or spatial structure. The cellular transport machinery recognizing these signals distributes the proteins to the diverse cellular compartments. Some signal peptides direct proteins specifically into the nucleus, mitochondria, or peroxisomes. Membrane, secretory, or lysosomal proteins are also sorted initially via signal peptides into the lumen of the endoplasmic reticulum. Here the lysosomal enzyme proteins undergo glycosylation, as do most of the secretory and plasma membrane proteins. The glycosylation step involves the transfer of a large oligosaccharide with high mannose content to selected asparagine residues of the nascent protein. Subsequently, the signal peptide is cleaved, the protein folds, and the processing of the asparagine-linked oligosaccharide begins. From the endoplasmic reticulum the proteins travel via vesicular transport to the Golgi apparatus. In the *cis* compartment of the Golgi complex, oligosaccharide side chains of lysosomal enzymes are phosphorylated and thus acquire mannose-6-phosphate moieties. In contrast, oligosaccharide side chains of secretory and membrane proteins are trimmed and remodeled further to yield complex-type side chains. The synthesis of the mannose-6-phosphate residues is initiated by a phosphotransferase, which specifically recognizes lysosomal enzymes. Recognition does not occur by way of a signal peptide but is mediated by a spatial signal depending on the three-dimensional structure of the enzymes. Given the structural diversity of lysosomal enzymes the precise nature of the signal shared by all enzymes is still a mystery. So far, only surface-located lysine residues seem to be an essential common component of this topogenic signal.

Phosphorylated lysosomal enzymes then proceed through the remainder of the Golgi complex (from *cis*- through *medial* to *trans*-Golgi). In the *trans*-Golgi network (TGN) they bind to mannose-6-phosphate receptors, which segregate the enzymes into distinct transport vesicles away from secretory and cell surface proteins. There are two mannose-6-phosphate receptors, which bind different but overlapping sets of enzymes. Once lysosomal enzymes are bound, the mannose-6-phosphate receptor-enzyme complexes are collected in clathrin-coated pits, which bud off to form coated vesicles. Most of these transport vesicles deliver the complexes to acidic early endosomes, but

complexes do also arrive at late endosomes. The low pH in the endosomes causes lysosomal hydrolases and receptors to dissociate. After dissociation, mannose-6-phosphate receptors are retrieved from this compartment and returned to the TGN, whereas lysosomal enzymes are delivered to mature lysosomes. Thus, receptors do not occur in lysosomes. Their absence is an important histochemical feature of lysosomes and differentiates them from late endosomes. Mannose-6-phosphate receptors also cycle between the endosomal compartment and the plasma membrane. One of the receptors can bind lysosomal enzymes at the plasma membrane and mediate their endocytosis and subsequent delivery to lysosomes. This is probably a recapture mechanism, since depending on cell type, 5–40% of newly synthesized lysosomal enzymes escape receptor binding in the TGN and are secreted. A proportion of these enzymes bind to the mannose-6-phosphate receptors on the plasma membrane and are recaptured, internalized, and delivered to lysosomes. Sorting signals within the cytoplasmic tails of the receptors are crucial for their correct intracellular trafficking.

Although the mannose-6-phosphate recognition pathway is a major route for targeting soluble lysosomal enzymes, there is evidence for an alternative mechanism, independent of mannose-6-phosphate, and localizing soluble acid hydrolases to lysosomes. Although it seems likely that this pathway is also receptor mediated, attempts to demonstrate this receptor have so far been unsuccessful. Only in cases of activator proteins – see below – has the multiligand receptor sortilin been shown to be involved in lysosomal trafficking independent of mannose-6-phosphate.

Lysosomal membrane glycoproteins travel the same route as soluble enzymes from the rough endoplasmic reticulum via the Golgi apparatus and endosomes to lysosomes. However, the transport of lysosomal membrane glycoproteins to lysosomes is independent of the mannose-6-phosphate receptor system, depending rather on signals in their cytoplasmic portion. An example is the classic lysosomal marker enzyme acid phosphatase. It is synthesized as a trans-membrane precursor protein with a large luminal domain and a short cytoplasmic tail. After reaching the TGN the enzyme precursor is repeatedly recycled between the cell surface and the endosomal compartment before reaching the lysosome. After its delivery to the lysosome, acid phosphatase undergoes proteolytic processing of the membrane-anchoring domain, resulting in conversion to a soluble form. Sorting signals for this mannose-6-phosphate receptor-independent pathway reside in the short cytoplasmic tail of the acid phosphatase precursor.

In addition to oligosaccharide processing, lysosomal hydrolases are synthesized as pre-proenzymes,

and almost all undergo proteolytic processing. The pre-piece is the signal sequence, which is cleaved immediately after transport into the endoplasmic reticulum. With the exception of aspartylglucosaminidase, which is already processed in the endoplasmic reticulum, the pro-piece is cleaved later in endosomal compartments. Cleavage is completed after arrival of the enzymes in the lysosomes. For lysosomal proteases, cleavage of proenzymes is accompanied by activation of the enzymes. Prior to arrival in the lysosomes the pro-piece keeps the proteases in an inactive state. In lysosomal enzymes other than proteases, however, the biological significance of this proteolytic processing is poorly understood.

Some enzymes involved in the degradation of sphingolipids need the assistance of enzymatically inactive activator proteins for hydrolysis of their substrates. So far, five different activator proteins encoded by two different genes have been identified. One gene codes for the GM₂ ganglioside activator protein only, whereas the other encodes a precursor protein that harbors four different but homologous sphingolipid activator proteins (SAPs). The mature SAPs A, B, C, and D – also called saposins – are generated from this precursor via proteolytic processing. They act on different enzymes and facilitate the degradation of various sphingolipids. They also differ in their mode of action. GM₂-activator protein and SAP-B bind the lipid substrates and present them to the respective enzymes, whereas SAP-C activates the enzyme directly.

Lysosomes are the final destination of endocytic, autophagic and phagocytic routes. The endosomal membranous network connects the lysosomes to the Golgi apparatus and the plasma membrane. Early endosomes start to accumulate internal membranes, and as this accumulation proceeds they mature into late endosomes. Since late endosomes are rich in luminal membranes they are also referred to as multivesicular bodies (MVBs) or multivesicular endosomes. Lipid and protein composition of these luminal membranes differs from that of early endosomes, suggesting a specific partitioning event during their generation. Thus, for some proteins it has been shown that tagging with ubiquitin directs them through this luminal compartment for lysosomal degradation, whereas other proteins seem to be quite stable in these membranes. This endocytotic lysosomal route can also be used to terminate growth factor receptor signaling, a process that is crucial for cellular regulation. Thus, ligand activation of epidermal growth factor receptor does not only activate downstream signaling pathways, but also induces endocytosis. Endocytosed receptors may be cycled back to the plasma membrane for continuous signaling or can be delivered to the lysosome for degradation, resulting in signal termination. Thus, the balance between recycling

and lysosomal delivery has a key role in regulation of the signal intensity of at least some tyrosine kinase receptors.

The MVBs/late endosomes can fuse homotypically, but they also fuse with lysosomes, forming a hybrid organelle. The dense lysosomes can be regarded as storage granules of hydrolytic enzymes, which fuse with late endosomes to perform their hydrolytic task on the late endosome contents. During this process continuous condensation occurs to recover lysosomes from this hybrid organelle.

Autophagy is the process by which the cell sequesters parts of its own cytoplasm, often containing entire organelles. In the first step, called autophagic sequestration, a cytoplasmic membrane, which is probably derived from the endoplasmic reticulum, envelops a region of cytoplasm in a closed vacuole called an autophagosome. Through fusion, the sequestered material is transferred to lysosomes. The lysosomal membrane protein LAMP2 seems to be essential for the maturation of autophagosomes. In normal cells this process is important because of its participation in cell renewal and turnover of worn-out cell constituents. In secretory cells there is a special kind of autophagy, called crinophagy. It occurs by way of direct fusion between secretory granules and lysosomes and results in the destruction of excess secretory material. Alternatively, in chaperone-mediated autophagy proteins can be unfolded in the cytoplasm and transported directly through the lysosomal membrane.

Finally, phagocytosis is the process by which cells internalize large particles, such as bacteria. Thus, phagocytosis is particularly active in neutrophils and macrophages. After internalization the interior of a phagosome initially resembles the extracellular milieu. However, phagosomes may fuse with endosomes and slowly acquire the characteristics of late endosomes and lysosomes. In this context it is important to note that lysosomes also generate peptides via hydrolysis of phagocytosed material to load MHCII molecules. Thus, lysosomes have an essential role in the immune system, maintaining the health of cells and the body's defense against foreign invaders.

Apart from the catabolic functions, lysosomes have also been shown to play an essential part in the repair of plasma membrane defects. In wounded cells lysosomes can fuse with the defective plasma membrane via a calcium-triggered exocytotic process. Lysosomes can thus serve as a reservoir allowing for rapid provision of membrane lipids in the case of extended defects that cannot be compensated by lipid biosynthesis within an appropriate time period. This clearly demonstrates that lysosomes also have anabolic functions.

5.2 The Pathobiochemistry of Lysosomal Disease in Humans

More than 45 different lysosomal diseases are currently known in man (Table 5.1). They can be caused by defects in the genes of individual lysosomal hydrolases, activator proteins, transporters, lysosomal membrane proteins, or enzymes modifying lysosomal hydrolases. In general a profound deficiency with residual activity of the respective protein <5% of normal is found in tissues of affected persons. Since undegraded substrates cannot leave the lysosomes, or only very slowly, these organelles are converted into storage granules, which steadily increase in size and number.

Over the years several classes of lysosomal diseases have been unraveled. In Table 5.1 and in the text below we have classified the lysosomal diseases primarily on the basis of functional characteristics, resulting in seven main groups. Furthermore, we have taken account of well-established clinical entities that are often based on the nature of the accumulating compound.

5.2.1 Defects in Individual Hydrolases

The molecular basis of most currently known lysosomal diseases is a deficiency of an individual hydrolase in the lysosome. These hydrolases have a role in the catabolism of different molecular species, such as lipids, mucopolysaccharides, and glycoproteins. This has led to a classification according to the biochemical nature of the substrate accumulating in a particular disease (see also Table 5.1).

In many lysosomal diseases lipid species accumulate. Examples of lipids that are involved are sphingomyelin (Niemann-Pick A and B), glucosylceramide (Gaucher), galactosylceramide and psychosine (Krabbe), globotriaosylceramide (Fabry), ceramide (Farber), sulfatides (metachromatic leukodystrophy), gangliosides (GM₁ and GM₂ gangliosidoses), cholesterol esters, and triglycerides (Wolman). This group of diseases can be referred to collectively as the lipidoses. Figure 5.1 illustrates the sequential action of the various enzymes involved in the pathway of lysosomal lipid metabolism.

In a second subgroup acid mucopolysaccharides, also called glycosaminoglycans, accumulate. These consist of long chains of repeating disaccharide units. Different subspecies exist, which are characterized by the composition of their repeating disaccharide units. Heparan sulfate, dermatan sulfate, chondroitin sulfate, keratan sulfate, and hyaluronan are representatives of the mucopolysaccharide family. The mucopolysaccharides are degraded in the lysosome. Defects in the enzymes involved in this catabolism cause

Table 5.1. A review of the lysosomal storage disorders, with the defective enzymes and proteins in each

A. Defects in individual lysosomal hydrolases	
1. Lipidoses	
a. Metachromatic leukodystrophy	Arylsulfatase A
b. Globoid cell leukodystrophy (Krabbe disease)	Galactocerebrosidase
c. GM ₁ gangliosidosis	β-Galactosidase
d. GM ₂ gangliosidosis:	
Tay Sachs disease	Hexosaminidase A
Sandhoff disease	Hexosaminidase A and B
e. Gaucher disease	β-Glucosidase
f. Fabry disease	α-Galactosidase A
g. Farber disease	Acid ceramidase
h. Niemann-Pick disease (types A and B)	Sphingomyelinase
i. Wolman disease and cholesterol ester storage disease	Acid lipase
2. Mucopolysaccharidoses	
a. Hurler disease and Scheie disease (I)	α-Iduronidase
b. Hunter disease (II)	Iduronate sulfatase
c. Sanfilippo disease (IIIA-D)	a. Heparin sulfamidase
	b. <i>N</i> -Acetyl α-glucosaminidase
	c. α-Glucosaminide <i>N</i> -acetyltransferase
	d. <i>N</i> -Acetylglucosamine 6-sulfatase
d. Morquio disease (IV)	Galactose 6-sulfate sulfatase
e. Maroteaux-Lamy disease (VI)	Arylsulfatase B
f. Sly disease (VII)	β-Glucuronidase
g. Hyaluronidase deficiency (IX)	Hyaluronidase
3. Disorders of glycoprotein degradation	
a. Sialidosis	Neuraminidase
b. Fucosidosis	α-Fucosidase
c. Mannosidosis (α and β)	α- and β-Mannosidase
d. Aspartylglycosaminuria	Aspartylglucosaminidase
4. Glycogen storage disorders	
a. Pompe disease	α-Glucosidase
5. Neuronal ceroid lipofuscinoses	
a. Infantile Finnish type NCL (Santavuori disease)	Palmitoyl thioesterase
b. Late-infantile NCL (Jansky-Bielschowsky disease)	Tripeptidyl peptidase I
6. Non classifiable	
a. Pyknodysostosis	Cathepsin K
b. Schindler disease	<i>N</i> -Acetyl α-galactosaminidase
B. Defects in activator proteins	
1. Lipidoses	
a. GM ₂ activator protein deficiency	GM ₂ Activator protein
b. Saposin B deficiency	Metachromatic leukodystrophy variant
c. Saposin C deficiency	Gaucher disease variant
d. Prosaposin deficiency	
C. Defects in the postsynthetic modification of lysosomal proteins	
1. Mucopolysaccharidoses	
a. I cell disease (mucopolipidosis II)	<i>N</i> -Acetylglucosaminylphosphotransferase
b. Pseudo-Hurler polydystrophy (mucopolipidosis III)	<i>N</i> -Acetylglucosaminylphosphotransferase
2. Non-classifiable	
a. Multiple sulfatase deficiency	F _{Gly} -Generating enzyme
D. Defects in structural lysosomal proteins	
1. Glycogen storage disorders	
a. Danon disease	LAMP2
E. Defect in a protective protein	
a. Galactosialidosis	Cathepsin A
F. Defects in transport and trafficking of substrates	
a. Cystinosis	Cystinosis
b. Salla disease	Sialin
c. Niemann-Pick disease type C	NPC1 or NPC2
G. Non-classifiable	
a. Mucopolipidosis IV	Mucolipin 1

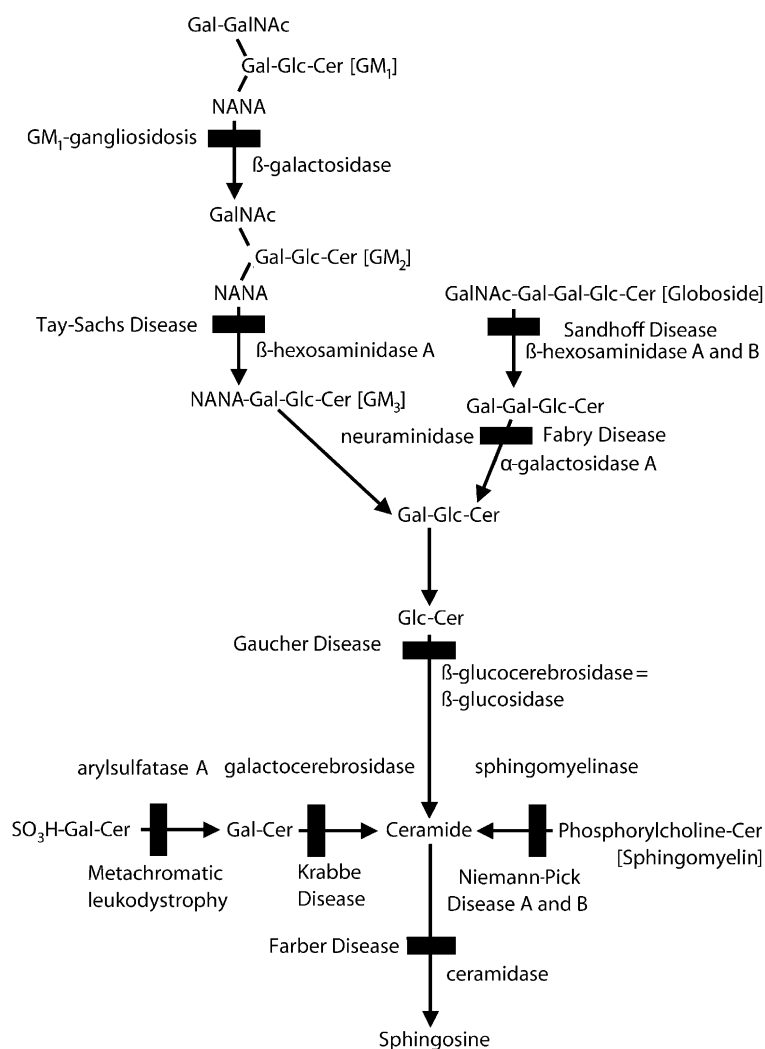


Fig. 5.1. Disorders in lysosomal lipid metabolism

a group of diseases collectively referred to as the mucopolysaccharidoses.

When glycoproteins are degraded in the lysosome, breakdown of the glycan part requires a set of glycosidases. Degradation of the glycans involves their sequential action. If one of these enzymes is deficient various oligosaccharides deriving from the glycan accumulate in tissues and body fluids. The material accumulating in the lysosomes is disease specific. As a group, these diseases can be referred to as glycoprotein degradation disorders.

The breakdown of glycogen, a glucose polymer, requires lysosomal α -glucosidase enzymatic activity. Defects in this enzyme lead to Pompe disease with massive glycogen storage in muscle and liver in the infantile-onset form of the disease. This disease is one of the family of glycogen storage disorders.

A last group in this category is formed by the neuronal ceroid lipofuscinoses (NCL). To date, eight main genetic forms are generally accepted to occur in man.

The NCLs collectively constitute the most common group of neurodegenerative diseases in childhood, with an estimated total incidence in the U.S. of 1:12 500. All NCL forms share unifying pathomorphologic features. In two subtypes the primary defect was found in a soluble lysosomal enzyme. The enzymes involved are protein thioesterase (PPT) and tripeptidyl-peptidase 1 (TPP1). The PPT enzyme removes fatty acids from several S-acetylated proteins. The function of TPP1, a serine protease, is the removal of N-terminal tripeptides from substrates with free amino termini. The *in vivo* substrates of PPT and TPP1 remain unknown. It may turn out that some of the remaining eight genetic NCL forms are also lysosomal diseases. Another lysosomal enzyme, cathepsin D, is for instance involved in an ovine neurodegenerative disease with ultrastructural features closely resembling human NCL. The human counterpart of this disease has not yet been identified.

Although the classification of lysosomal disorders according to storage compounds appears straightforward, it is important to realize that lysosomal enzymes are frequently specific not for a certain substrate, but for a component that may occur in different substrates. Thus, glycosidases are specific for particular sugar residues and the geometry of their linkage. The respective sugar and its linkage can occur both in lipids and in glycosaminoglycans. Degradation of both is affected in the case of enzyme deficiency, and both lipids and glycosaminoglycans accumulate. Thus, in some diseases the classification is somewhat artificial.

In Schindler disease the defective enzyme, α -*N*-acetylgalactosaminidase, is involved in various pathways, so that this disease cannot be assigned unambiguously to any one of the above groups. It exerts an action in the catabolism of various glycoconjugates with terminal α -*N*-acetylgalactosaminyl residues. Deficiency of the enzyme results in accumulation of glycopeptides, glycosphingolipids, and oligosaccharides in many tissues.

The defective enzyme in pyknodysostosis has been found in cathepsin K, a lysosomal protease. This enzyme is highly expressed in osteoclasts. The defect leads to a reduced capacity of this cell to remove organic bone matrix, thus causing defective bone growth and remodeling. This explains why the patients suffer predominantly from skeletal, orthopedic, craniofacial, and dental abnormalities.

5.2.2 Defects in Activator Proteins

Some enzymes require the presence of activator proteins or saposins for their catalytic function inside the lysosome. Examples are sphingomyelinase, aryl-sulfatase A, and α - and β -galactosidase. Since defects in activator proteins affect the degradation of sphingolipids only, all activator protein deficiencies are lipidoses. The clinical signs and symptoms frequently resemble those found in patients in whom the same glycolipid accumulates as the result of deficiency of hydrolase activated by the respective saposins (e.g., saposin B deficiency causes a variant form of metachromatic leukodystrophy).

5.2.3 Defects in the Postsynthetic Modification of Lysosomal Proteins

As outlined earlier, all soluble lysosomal enzymes are *N*-glycosylated and their oligosaccharide side chains receive mannose-6-phosphate residues, which are a lysosomal targeting signal, in the Golgi apparatus. Defects in a phosphotransferase initiating the synthesis of mannose-6-phosphate residues result in a de-

fect in the targeting of lysosomal enzymes towards the lysosome. This causes an intracellular deficiency of many lysosomal enzymes. The diagnosis can be confirmed by abnormally high enzymatic activity of many lysosomal enzymes in blood plasma. Because of the mistargeting, these enzymes are directed out of the cell and end up in the blood plasma. Defects in the phosphotransferase cause mucopolipidosis II (inclusion body or I cell disease) and III. Patients with mucopolipidoses II and III share clinical symptoms and biochemical characteristics with patients who have a mucopolysaccharidosis or a sphingolipidosis. Glycolipids as well as mucopolysaccharides accumulate in lysosomes in these diseases. Recently the primary defect in mucopolipidosis IV was found to be in the *MCOLN1* gene encoding for a protein, mucolipin 1. The function of the protein has not yet been fully characterized, and this disorder is therefore nonclassifiable (group G in Table 5.1).

Among the lysosomal storage disorders multiple sulfatase deficiency is particularly interesting. In this disorder the activity of all lysosomal and nonlysosomal sulfatases is reduced. Since sulfate groups occur in many different molecules a complex mixture of compounds accumulates. The enzymatic activity depends on a formylglycine residue (F_{Gly}) in the active center of all sulfatases. This amino acid residue is generated by a posttranslational modification from a cysteine residue. Patients with multiple sulfatase deficiency have defects in the *SUMF1* gene. The protein product of the *SUMF1* gene is the F_{Gly} -generating enzyme (=FGE) localized in the lumen of the endoplasmic reticulum. The function of this enzyme is to generate the formylglycine residue in the catalytic center of the sulfatases. When this modifying reaction is defective the sulfatases remain inactive. This causes accumulation of the various substrates. Therefore several compounds could be identified as storage material. The diagnosis can be established biochemically at the enzyme level by measuring various sulfatases in leukocytes, or preferably in fibroblasts.

5.2.4 Defects in Structural Lysosomal Proteins

Lysosomes have several structural proteins. Examples of such ubiquitous, highly glycosylated integral membrane proteins are LAMP1 and LAMP2 (LAMP = lysosome-associated membrane protein). They account for about 50% of the protein content of the lysosomal membrane. Recently the primary defect of Danon disease has been assigned to the *LAMP2* gene. This gene encodes LAMP2, which is thought to be a structural protein in the lysosome. This X-linked disease is characterized by lysosomal glycogen storage leading to cardiomyopathy and myopathy in patients

with normal α -glucosidase activity. It is not fully clear how a defect in this protein can lead to accumulation of glycogen. It can be anticipated that several new lysosomal diseases in this subgroup will be found in the future.

5.2.5 Defects in a Protective Protein

Galactosialidosis is caused by a defect in cathepsin A. This protein has a dual function: it is not only a protease, but also a protective protein. It combines with neuraminidase and β -galactosidase in an early biosynthetic compartment. By virtue of this association the complex is correctly delivered to the lysosomes. In the lysosome, cathepsin A protects the neuraminidase and β -galactosidase against rapid proteolysis and inactivation. In the case of cathepsin A deficiency both enzymes are rapidly degraded and thus deficient. Sialyloligosaccharides accumulate in the lysosomes of affected patients and are also excreted in the urine.

5.2.6 Defects in Transport and Trafficking of Substrates

Lysosomal degradation of macromolecules leads to the formation of smaller molecules, which generally are exported from the lysosome towards the cytoplasm. Some molecules require specific carriers to leave the lysosome. Defects in such carriers lead to accumulation of the molecule involved within the lysosome. Examples of such diseases are cystinosis and Salla disease. Cystinosis is characterized by intralysosomal storage of the amino acid cystine and is caused by defective carrier-mediated transport of cystine across the lysosomal membrane. The protein involved is cystinosin. In Salla disease intralysosomal storage of sialic acid occurs, caused by a defect in its transport across the lysosomal membrane by the transporter sialin.

Niemann-Pick disease type C is a lipid trafficking disorder. The majority of patients have mutations in the gene coding for the NPC1 protein. The postulated role for this protein involves modulation of the vesicular trafficking of cholesterol and glycolipids. Several lipids (sphingomyelin, phospholipids, glycolipids, and unesterified cholesterol) are stored in excess in the liver and spleen of these patients. Foam cells or sea blue histiocytes may be found in many tissues of affected patients. Primarily, the diagnosis requires the demonstration of excess cholesterol in fibroblasts with the so-called filipin staining test. In a small subgroup of patients with Niemann-Pick type C disease there are mutations in another gene coding for the NPC2 protein, a soluble lysosomal enzyme with un-

known function that is thought to work in a coordinate fashion with NPC1 protein.

5.3 Clinical Features and Diagnosis

A full survey of clinical symptomatology of lysosomal diseases is beyond the scope of this chapter. A few characteristics or general features can clearly be understood from the molecular basis of the diseases. Storage material often gives rise to organomegaly, for instance of liver or spleen. Another characteristic that may occur is the loss of acquired mental or motor skills in the course of time, which is due to an increase in storage material with time. Some clinical features, such as a cherry red spot in the retina or downward gaze paralysis, may be highly suggestive for lysosomal disease, and in some cases even pathognomonic for a specific disease. The same holds in the case of evidence for storage material in body fluids or tissues. Vacuolization may occur in peripheral white blood cells. The finding of sea blue histiocytes in bone marrow should also be followed up with a thorough work-up for lysosomal diseases. As most cell types in the human body contain lysosomes, many tissues or cell types can be involved in lysosomal diseases. Often these diseases affect the CNS, resulting in neurodegenerative disease. Others, such as Morquio and Pompe disease, leave the brain relatively unaffected. In general, the lysosomal diseases are multisystem diseases. Pyknodysostosis is an example of a disease in which the molecular defect, the deficiency of cathepsin K, seems to interfere predominantly with the function of only one cell type. Dysfunction of the osteoclast causes the clinical features of this disease.

Most lysosomal diseases show significant clinical heterogeneity. The onset of clinical signs and symptoms can occur in any decade of life, and even before birth. Hydrops fetalis has been observed as a presentation form in several lysosomal diseases. β -Glucuronidase deficiency is an example of a disease that can present as early as this. The time of presentation can vary rather widely within one disease. Pompe disease, for example, can have an early infantile onset: in such patients the course of the disease is invariably very severe and most of them die before the age of 6 months. Other patients with Pompe disease have adult-onset forms of the disease and have milder symptoms. The concept for our understanding of this variability in clinical presentation lies in the residual activity of the enzyme in a specific patient. However, with the methodology currently available it is not possible to predict the disease course from the residual activity in leukocytes or fibroblasts.

In recent years numerous mutations of genes for proteins that are deficient in lysosomal storage diseases have been described, leading to a better under-

standing of the biochemical consequences of mutations. Severe mutations that truncate the protein or shift the reading frame thereby alter the primary structure of the protein so that it has no residual biological activity. Such mutations almost always result in a severe clinical phenotype. In lysosomal storage diseases missense mutations are the most frequent. Often missense mutations lead to misfolded enzymes, which are not transported to the lysosomes but are retained and degraded in the endoplasmic reticulum. Alternatively, defective enzymes may still be sorted properly but become rapidly degraded on arrival in the lysosome. Mutations can be located in the active center of an enzyme or indirectly influence the catalytic activity of the enzyme. In some cases a combination of these effects is the cause of enzyme deficiency. Missense mutations can influence the catalytic activity of the enzyme as badly as truncating mutations. When they occur in less relevant parts of the coding region they may allow residual activity, resulting in a milder clinical phenotype. It is not always possible to show a clear genotype-phenotype relation. Most lysosomal diseases have an autosomal recessive mode of inheritance. Few diseases have an X-chromosomal inheritance. Fabry, Danon, and Hunter diseases are examples. Males have more severe clinical symptoms, as they only have one X chromosome. However, female carriers (=XX) can also have clinical symptoms of the disease because of uneven X inactivation (lyonization).

To confirm a clinical suspicion of a lysosomal disease at the biochemical level various approaches can be used as diagnostic strategy. In some lysosomal diseases undegraded substrates can be found in the urine. Investigations of urine samples are therefore often used as a first step towards establishing the

diagnosis. An increased concentration of urinary mucopolysaccharides can be found in the mucopolysaccharidoses. Subsequent electrophoresis of mucopolysaccharides will show which subtype of the mucopolysaccharides the patient cannot adequately degrade. Defects in mucopolysaccharide catabolism can affect the breakdown of heparan sulfate, dermatan sulfate, chondroitin sulfate, keratan sulfate, or hyaluronan. The result of electrophoresis will give a clue to the defective enzyme. Abnormal urinary oligosaccharides are present in the disorders of glycoprotein degradation shown in Table 5.1. Thin layer chromatography of oligosaccharides is also diagnostic in infantile Pompe disease, where a tetraglucoside deriving from glycogen accumulates in the urine. In late-onset Pompe disease this tetraglucoside is generally not found in the urine and other techniques are necessary to establish the diagnosis. In some diseases, then, accumulating material cannot be detected in the urine, and for some diseases the techniques that would be required to diagnose them at the metabolite level are too time consuming. This is the case for the lipidoses, defects in activator proteins, and the NCLs, for instance. In such cases direct enzyme analysis in leukocytes is often used as a first step in establishing the diagnosis. Cultured skin fibroblasts can generally also be used to confirm the diagnosis. A further test that may be relevant to the demonstration of lysosomal involvement is measurement of the activity of chitotriosidase. This enzyme is secreted by activated macrophages. In several lysosomal diseases increased chitotriosidase activity can be used as a nonspecific diagnostic marker.

The chapters below discuss only those lysosomal storage disorders that are accompanied by a white matter disorder.

Metachromatic Leukodystrophy

6.1 Clinical Features and Laboratory Investigations

Metachromatic leukodystrophy (MLD) is an autosomal recessive progressive disorder. Its incidence is estimated to be 1:40,000. The disease can be divided into three subtypes: the late infantile (40% of the patients with MLD), juvenile (40%), and adult (20%) variants. This subdivision is based on the age at onset, the duration, and the clinical picture of the disease. As a rule, only one variant of MLD occurs within one family, although exceptions have been reported.

The age of onset in the late infantile variant varies between 6 months and 3 years. Of the different subtypes, this variant is the one that shows the greatest uniformity with regard to clinical picture and course of disease. Most children learn to sit and walk with support normally, but show a delay in walking unaided. The first symptom is usually an unsteady gait due to muscle hypotonia. There are signs of a progressive polyneuropathy, ending in a generalized flaccid paresis of the arms and legs and a loss of tendon reflexes. The neuropathy may be painful. Cerebellar ataxia is also often an early sign. Nystagmus is usually present. Speech development is disturbed and dysarthria becomes manifest. Mental development stagnates and regression occurs. Gradually, involvement of the pyramidal system causes the flaccid paresis to be superseded by a spastic tetraplegia with abnormal reflexes, such as extensor plantar reflexes, but deep tendon reflexes are absent. Bulbar and pseudobulbar symptoms develop, leading to feeding difficulties. Speech is affected, and the child eventually becomes mute. Optic atrophy with impaired vision is present. Epileptic seizures occur in about 25% of the children. Eventually the child becomes blind and completely tetraplegic in a decerebrate state without purposeful movements. This final stage may last for several years. Death usually occurs about 5 years after the onset of clinical symptoms.

The age of onset in the juvenile variant ranges from 4 to 16 years. The disease occurs in apparently healthy, intellectually normal children. Early signs are a gradual deterioration in school performance, language regression, and clumsiness. There are usually also emotional and behavioral disturbances. These symptoms may be present for several months and up to a year before the onset of other neurological signs. A spastic paresis and cerebellar ataxia gradually de-

velop. On rare occasions the clinical picture is dominated by extrapyramidal features. Clinical symptoms of a peripheral neuropathy are often lacking, and deep tendon reflexes are usually brisk. Optic atrophy develops. Seizures occur in about 50% of the patients. Eventually complete tetraplegia with decerebration posture, brain stem dysfunction, and profound dementia evolves. Death usually occurs 5–10 years after onset.

Some authors prefer to divide the juvenile variant into two subgroups. An early juvenile variant has its onset between 4 and 6 years. The clinical symptomatology resembles that of the late infantile variant, showing gait disturbance and other motor dysfunction as early manifestations. The late juvenile variant has its onset between 6 and 16 years. In the clinical symptomatology, behavioral abnormalities, poor school performance, and language regression predominate as early abnormalities.

The adult form usually reveals itself between 16 and 30 years. Onset of the disease at 60 years or later has also been described. Most patients experience a gradual decline in intellectual abilities. At onset the clinical picture is often dominated by emotional lability, behavioral abnormalities, or psychiatric symptoms such as delusions and hallucinations. It is not uncommon for the patient to be treated initially for schizophrenia or a psychotic depression. After several months or years progressive spastic paresis of the arms and legs develops, with increased tendon reflexes and extensor plantar reflexes. Cerebellar ataxia and such extrapyramidal features as choreiform movements and dystonia may be present. Signs of peripheral neuropathy are often absent, although flaccid tetraparesis may occur in the terminal stage. Optic atrophy and signs of bulbar dysfunction may appear. Epileptic seizures are rare. A state of severe dementia gradually develops. The patient loses contact with the surroundings and lies in a decorticate or decerebrate posture; eventually a persistent vegetative state is reached. The duration of the disease varies from a few years to 15 years and longer. Although a rapid deterioration is seen in some patients, in most cases progression is slow over a period of years. Another, more rare presentation in adults is dominated by signs of a peripheral neuropathy.

CSF protein is elevated in the late infantile form and in most juvenile cases. In the adult form, CSF protein this is less often the case. The EEG is normal at

the beginning of the disease. At later stages it shows nonspecific abnormalities in the form of slowing of the background pattern, often together with paroxysmal or epileptiform activity. In the infantile and juvenile variants, the conduction velocity of peripheral nerves is markedly reduced. Particularly in adults, however, the nerve conduction velocity may be normal.

In all patients urinary sulfatide excretion is increased. The activity of arylsulfatase A in urine and in peripheral leukocytes is low, but may be normal in exceptional cases of activator deficiency (see below). In all cases of MLD a decreased catabolism of exogenous sulfatide by cultured fibroblasts can be demonstrated. In this test sulfatide is radiolabeled and added to cultured fibroblasts. The uptake of label by cells with subsequent metabolism is measured at frequent intervals. This procedure is not performed routinely, but only in specific situations. The definitive diagnosis of MLD is based on the determination of the activity of arylsulfatase A in peripheral leukocytes or fibroblasts. The diagnostic reliability of this test is hampered by the relatively frequent occurrence of so-called pseudodeficiency. In this condition low arylsulfatase A activity is found without associated clinical signs of MLD (see also section 6.4). For this reason, sulfatide excretion in urine should be used to confirm the diagnosis of MLD. It is increased in all cases of MLD, but normal in pseudodeficiency. DNA analysis is another option.

In cases in which symptoms are strongly suggestive of MLD and the enzyme activity in peripheral leukocytes is normal, deficiency of arylsulfatase A activator protein can be surmised. Additional tests then include the measurement of urinary sulfatides and the assessment of fibroblast sulfatide catabolism. A sural nerve biopsy can be performed to demonstrate the deposition of metachromatic material.

Determination of the enzyme activity in cultured chorionic villi or cultured amniotic fluid cells allows prenatal diagnosis. Assessment of sulfatide catabolism can be performed in amniotic fluid cells or fetal fibroblasts. DNA-based prenatal diagnosis is also an option. The detection of heterozygotes by determining enzyme activity in leukocytes and DNA techniques facilitates genetic counseling.

6.2 Pathology

Gross inspection of the brain reveals quite a firm consistency in most cases. The brain may be enlarged and heavier than normal, but in later stages reduced size is usually found. The cut surface shows discoloration of the white matter.

Initially, the involvement of the white matter in MLD is patchy, but after some time all the white matter is affected, often in a symmetrical fashion, so that the demyelinated lesions of the two hemispheres have a butterfly configuration. Sometimes, in cases of long duration, the white matter is reduced to a narrow strip 1–2 cm in diameter and shrinkage of the white matter has led to enlargement of the ventricles. Demyelination occurs predominantly in the cerebral hemispheres, especially in the centrum semiovale. Demyelination tends to be most intense in the periventricular area, diminishing towards the surface; the arcuate fibers are relatively spared. The internal capsule, cerebral peduncles in the midbrain, pyramidal tracts in the pons, and pyramids in the medulla are severely affected, but other brain stem tracts are usually only moderately or slightly demyelinated. The cerebellar white matter can also be demyelinated, but usually less so than the cerebral white matter.

Microscopic examination shows demyelination with paucity or complete loss of myelin from affected areas. Axons are relatively spared, but their density is reduced in severely affected areas. There is proliferation of astrocytes with fibrous gliosis. At the edge of affected areas and scattered throughout the lesions there are macrophages that contain the specific degradation products. Usually oligodendroglia are absent from lesions and are reduced in number even in areas where the myelin is still intact. No inflammatory cells are present in the lesions.

MLD is characterized by the deposition of metachromatically staining material in the white matter. The term 'metachromasia' designates the phenomenon of certain cationic dyes changing their color from blue to pink or brown when bound to certain anionic groups present in several organic compounds. In MLD, sulfatides are the organic compounds responsible for the metachromasia. The metachromatic material is mainly stored in the cytoplasm of the proliferated glial cells and macrophages, although some is also found in the oligodendroglia cells, in the neurons of cranial nerve nuclei, basal ganglia, and spinal cord, and seemingly extracellularly as free granules in the white matter. The greatest density of metachromatic deposits is seen in macrophages in perivascular spaces.

The cerebral cortex is relatively intact. Loss of neurons is slight or absent. The cortical neurons contain no metachromatic material. The cerebellar cortex is normal or may show a diffuse loss of granular cells. A decrease in the number of Purkinje cells may occur. In certain areas, metachromatic granular material is stored in the neuronal perikarya, although rarely in large amounts. Neuronal metachromatic deposits are preferentially found in the globus pallidus, thalamus,

subthalamic nucleus, hypothalamus, geniculate nucleus, amygdala, and dentate nucleus. The cerebral and cerebellar cortex, claustrum, and caudate nucleus, and also certain brain stem nuclei, tend to be spared.

Electron microscopy demonstrates inclusions bounded by a membrane of lysosomal origin. The morphological organization of the material varies in appearance, probably because of a difference in the lipid composition or in the physicochemical state of the lipids. Prismatic and tuffstone-like profiles are characteristic. In addition to the inclusions that stain metachromatically on light microscopic examination, lamellar inclusions are present in glial cells formed from fragments of degenerated myelin. The 'extracellular' deposits of metachromatic material described in light microscopic studies appear to be cytoplasmic processes containing inclusions in electron microscopy.

In MLD the peripheral nerves are affected by segmental demyelination. Signs of remyelination may be found. Metachromatic material is present in Schwann cells and macrophages.

Not only are there neuropathological changes in MLD, but also visceral abnormalities. Outside the CNS, metachromatic material is found in the liver, spleen and lymph nodes, gallbladder, pancreas, kidneys, adrenal glands, ovaries, ganglion cells of the retina, and leukocytes of peripheral blood and bone marrow. Storage in these organs is limited to certain cell types. Visceral accumulations are not accompanied by further morphological changes or obvious clinical dysfunction. Although MLD becomes manifest only with neurological abnormalities, it is clear that it is a generalized metabolic disorder.

6.3 Chemical Pathology

Biochemical analysis of the white matter shows a greatly increased amount of sulfatide with a concomitant decrease in cerebroside as the major chemical abnormality. Whereas in normal white matter the ratio of cerebroside to sulfatide is approximately 4:1, in MLD it can be below 1. There is not only evidence that the membrane-bound deposits seen in this disease contain sulfatide, but also that myelin, which still appears normal ultrastructurally, has an abnormally high sulfatide content. Other biochemical changes in the white matter are a consequence of loss of myelin with a decrease in cholesterol, phospholipid, and glycolipids other than sulfatides. There is no increase in cholesterol esters. There are relatively few chemical changes in gray matter.

6.4 Pathogenetic Considerations

MLD is a sphingolipidosis caused by deficient activity of the lysosomal enzyme arylsulfatase A (= cerebroside-3-sulfate sulfatase = cerebroside-3-sulfate-3-sulfohydrolase = sulfatide sulfatase). This enzyme catalyzes the hydrolysis of sulfatide, the sulfate ester of cerebroside. Desulfation is the first step in the metabolic degradation of sulfatides. Following this sulfate cleavage, cerebroside is then degraded by cerebroside galactosidase.

The three clinical forms of the disease (late infantile, juvenile, and adult onset) can be explained in part by different levels of residual enzyme activity. The arylsulfatase A gene, *ARSA*, is located on chromosome 22q13.3. Many different mutations have been found in the MLD gene. There is evidence of a genotype-phenotype correlation in MLD. Some mutations have been exclusively associated with either the infantile-onset or the later onset variants of the disease. Patients with two mutations that cause complete loss of enzyme activity always suffer from the early-onset form of the disease; patients with two mutations that lead to a low residual enzyme activity usually have the adult-onset form of the disease, whereas patients who are compound heterozygous for 'severe' and 'mild' mutations usually have intermediate phenotypes.

Individuals have been found with low (approximately 10–20%) arylsulfatase A activity but no clinical abnormalities. This is called arylsulfatase A pseudodeficiency. Individuals who are compound heterozygotes for the pseudodeficiency (PD) mutation and an MLD mutation have 6–10% residual arylsulfatase A activity but do not develop MLD. Thus, arylsulfatase A activities only slightly higher than those encountered in patients with two mild mutations (2–5%) are sufficient to sustain a normal phenotype.

Pseudodeficiency for arylsulfatase A causes diagnostic problems. Pseudodeficiency is related to two common polymorphisms, which are usually found together. These mutations can reduce arylsulfatase A activity to 10% of its control level, but do not lead to clinical symptoms. The allele frequency for pseudodeficiency is much higher (7–15%) than the MLD allele frequency (0.5%). Because homozygous pseudodeficiency is frequent (0.5–2% of the population), it is not uncommon for patients with pseudodeficiency and neurological symptoms of unknown origin to be misdiagnosed as having MLD. There are also serious problems with prenatal diagnosis of MLD in families in which the parents carry an MLD allele and a pseudodeficiency allele: MLD and pseudodeficiency cannot be distinguished on the basis of enzyme activity determinations using artificial substrates. Measurement of sulfatide excretion in urine and assays measuring the *in vivo* degradation of sulfatide in cultured fibro-

blasts allow the distinction between MLD and pseudodeficiency. Both are abnormal in MLD and normal in pseudodeficiency. Demonstration of metachromatic material in a sural nerve biopsy is also diagnostic for MLD. Alternatively, the pseudodeficiency allele can be determined directly by DNA techniques, on the basis of knowledge of the underlying sequence alterations. A problem encountered with this technique, however, is that given the high frequency of the pseudodeficiency allele, MLD mutations may also occur within the pseudodeficiency allele, rendering it nonfunctional. The frequency of MLD mutations in the normal and the pseudodeficiency allele is similar, so that 0.5% of the pseudodeficiency alleles harbors an MLD mutation. This finding calls for caution in the diagnosis of pseudodeficiency by DNA tests detecting the mutations of the pseudodeficiency allele. There is evidence that pseudodeficiency mutations may contribute to the phenotype when concurrent with disease causing mutations. Mutations that cause the later onset forms of MLD when they occur in the normal arylsulfatase A gene may lead to a more severe form when they occur in the pseudodeficiency gene.

A small subgroup of MLD patients are not deficient in arylsulfatase A, but in an activator protein that is essential for the enzymatic action of arylsulfatase A. The gene for the precursor of this protein, *PSAP*, is located on chromosome 10q22.1. This gene has been shown to code for a large precursor polypeptide, prosaposin, which is processed to yield four different activator proteins. Sphingolipid activator protein B, also called saposin B, SAP-B, or SAP-1, activates the hydrolysis of sulfatide by arylsulfatase A. In addition, it activates the hydrolysis of GM₁-ganglioside and globotriaosyl ceramide by β -galactosidase and α -galactosidase, respectively. The protein interacts with the substrate and solubilizes it for enzymatic hydrolysis. The deficiency of SAP-B causes a disease clinically resembling juvenile or late infantile MLD, but with histochemical and ultrastructural evidence of storage of gangliosides and other glycosphingolipids. The diagnosis is established in these cases by revealing metachromatic material in sural nerve biopsy, by finding an increased urinary sulfatide excretion, and by demonstrating deficient turnover of sulfatide in the loading test in cultured fibroblasts, all in the presence of normal arylsulfatase A activity. It can be shown in cultured fibroblasts that the defect in sulfatide catabolism can be corrected by adding activator protein. Deficient turnover of the other glycosphingolipids can also be shown in loading tests in fibroblasts.

Sulfatides are membrane lipids. They are important constituents of cell membranes, including myelin sheaths. Within the cell they are present in the mem-

branes of organelles. Sulfatide is predominantly present in membranes of myelin-producing cells and in myelin. The amount of this substance normally present in membranes of other organs is much lower. As a result of the block in catabolism, sulfatides accumulate in tissues that normally synthesize them. In the first place, they accumulate in membranes of myelin-producing cells and myelin sheaths, and within the lysosomes of these cells. The membrane build-up is basically normal in MLD. It is the membrane turnover that is abnormal. Sulfatide cannot be degraded and is trapped in the membrane. Simultaneously, the cerebroside content decreases as the conversion of sulfatide to cerebroside is impeded.

A number of pathogenetic mechanisms have been invoked to explain the demyelination in MLD. One of them is the fact that the myelin composition in MLD becomes increasingly abnormal and that therefore myelin possibly becomes increasingly unstable. As soon as the disturbance of the normal physicochemical stability reaches a critical point, demyelination starts. Another explanation proposed is that lysosomal storage of sulfatides in oligodendroglia and Schwann cells leads to cellular dysfunction and death, resulting in loss of all myelin sheaths maintained by these cells. Indeed, changes in the subcellular organelles, especially an increase in the numbers of lysosomes of these cells, have been observed before the detection of any morphological abnormalities in the myelin sheaths associated with them. A third mechanism that has been proposed is that sulfolactosylsphingosine, a compound closely related to the cytotoxic compound galactosylsphingosine or psychosine in globoid cell leukodystrophy, might accumulate and cause the death of oligodendrocytes and Schwann cells. However, there is no evidence for the enzymatic conversion of sulfatide to sulfolactosylsphingosine, and the concentration of this substance is not elevated in MLD.

The sulfatide accumulation in other organs (kidney, liver, pancreas, adrenal, gallbladder and intestinal tract) does not lead to impairment of functions. Only the gallbladder shows progressive functional impairment attributable to sulfatide accumulation, but gallbladder disease does not contribute to the fatal outcome of MLD. The tolerance of these tissues for sulfatides may be related to the fact that these organs have an excretory function and can discharge the accumulating lipid from the cell into urine, bile, or other fluids. Another important factor is that the sulfatide content of the cellular membranes in these organs is normally much lower than that of the myelin membrane, which has a remarkably high content of galactosphingolipids (cerebroside and sulfatide).

6.5 Therapy

Various forms of therapy have been attempted in an effort to alter the natural course of the disease, but with little success. Diets low in vitamin A or in sulfur (both substances are necessary for the synthesis of sulfatide) have failed to have any favorable effects. After intravenous and intrathecal infusion of arylsulfatase A the enzyme does not enter the brain, and no clinical benefit has been seen. Increasing numbers of patients have received hematopoietic stem cell transplants in attempts to correct their low cerebral arylsulfatase A levels and repair or retard their CNS deterioration. The results appear to depend largely on the stage of disease at transplantation and the rate of disease progression. The results of transplantation in the presymptomatic or early symptomatic stage are better than those of transplantation in the fully symptomatic stage of the disease with decreasing verbal and performance IQs. The chances are better in the late-onset cases, in which disease progression is slower. Stabilization and reversal of MRI abnormalities have been described, as has clinical improvement or arrested progression. However, slow progression despite successful engraftment has also been observed. The chances of stabilization or improvement have to be weighed against the possibility of major complications and death during or after the transplantation. The general experience is that hematopoietic stem cell transplantation has little or no beneficial effect on the polyneuropathy. Gene therapy still has to be tested in the clinical situation.

6.6 Magnetic Resonance Imaging

The CT scan findings in MLD are symmetrical, diffuse decreases in the density of cerebral white matter, with little evidence of cerebral atrophy until the later stages. Hypodensity of the cerebellar white matter has been observed less frequently. No contrast enhancement has been found.

Probably the first abnormalities to be noted on MRI are in the corpus callosum (Fig. 6.1). Subsequently, MRI discloses periventricular white matter abnormalities, with a more or less symmetrical distribution. The white matter lesions are highly confluent. In later onset cases involvement is often predominantly frontal, whereas in early-onset cases occipital predominance can be observed. However, in all variants the cerebral white matter tends to become diffusely affected. The arcuate fibers are relatively spared, but become involved in the later stages. Typically, a pattern of radiating stripes with a signal intensity closer to normal is seen within the abnormal cerebral white matter (Fig. 6.2). On microscopic examination, this radiating pattern is explained by the accumulation of products of myelin breakdown in perivascular macrophages and some sparing of myelin sheaths. This pattern is not evident in all cases (Figs. 6.3, 6.4), and it is lacking especially in far advanced cases with serious white matter atrophy (Fig. 6.5). The corpus callosum is invariably affected, connecting the lesions from both sides. Cerebral white matter atrophy occurs in advanced stages (Fig. 6.5). The posterior limb of the internal capsule becomes involved. Brain stem lesions are observed

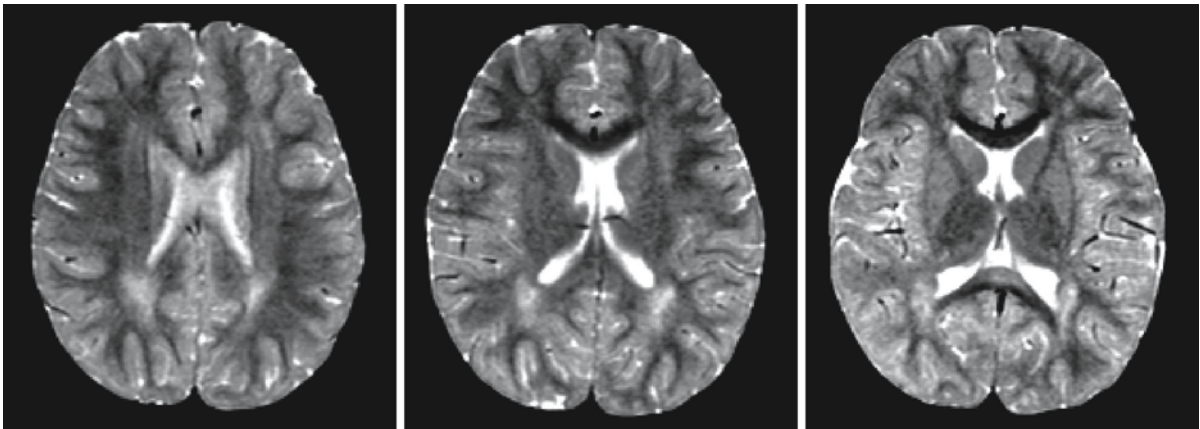


Fig. 6.1. MRI in a 5 1/2-year-old boy, who was diagnosed with metachromatic leukodystrophy (MLD) and extensive white matter abnormalities 3 years later. The areas of higher signal in the deep parietal white matter are often seen as a nonspecific finding, but the lesion in the splenium of the corpus callosum

should have been accepted as a warning against this interpretation. Courtesy of Dr. M.A.A.P Willemsen, Department of Pediatric Neurology, University Medical Center Nijmegen, The Netherlands

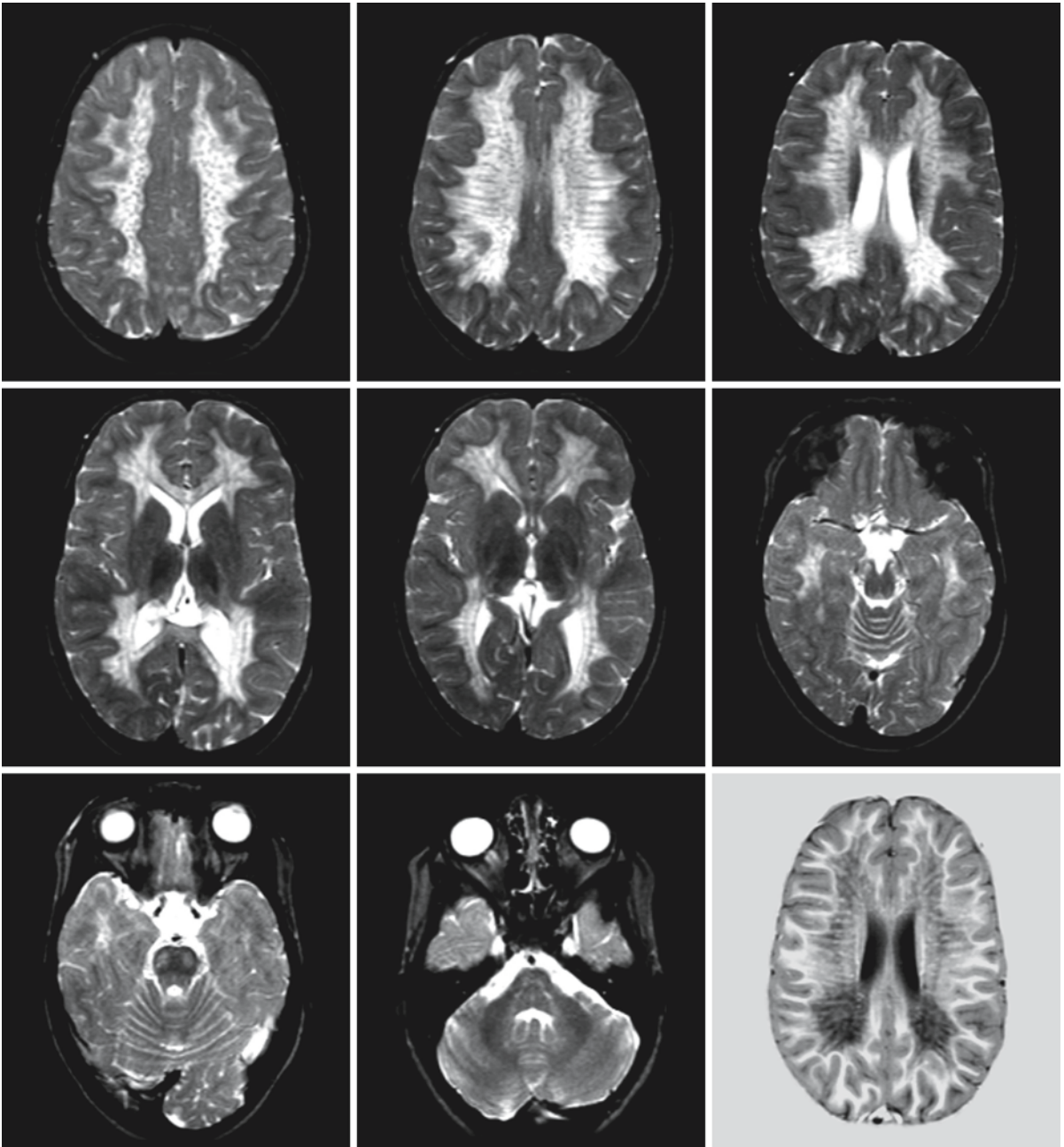


Fig. 6.2. A case of juvenile MLD in a 6-year-old girl. The cerebral white matter is diffusely involved, with sparing of the U fibers. Within the affected white matter a pattern of radiating stripes is seen of more normal signal intensity (low on T₂-

weighted images, high on T₁-weighted images). The corpus callosum, posterior limb of the internal capsule, and pyramidal tracts in the brain stem are involved

bilaterally in the pyramidal tracts, especially in the more advanced cases (Fig. 6.4). Some patients show involvement of the cerebellar white matter. No contrast enhancement is seen. Gray matter lesions are never conspicuous. Subtle abnormalities in signal intensity and atrophy of the basal nuclei have been observed.

The condition has to be differentiated from globoid cell leukodystrophy (Krabbe disease), the cerebral form of X-linked adrenoleukodystrophy, and inflammatory white matter disorders (acute demyelinating encephalomyelitis). The same pattern of radiating lines with a more normal signal intensity within extensive confluent white matter abnormalities can

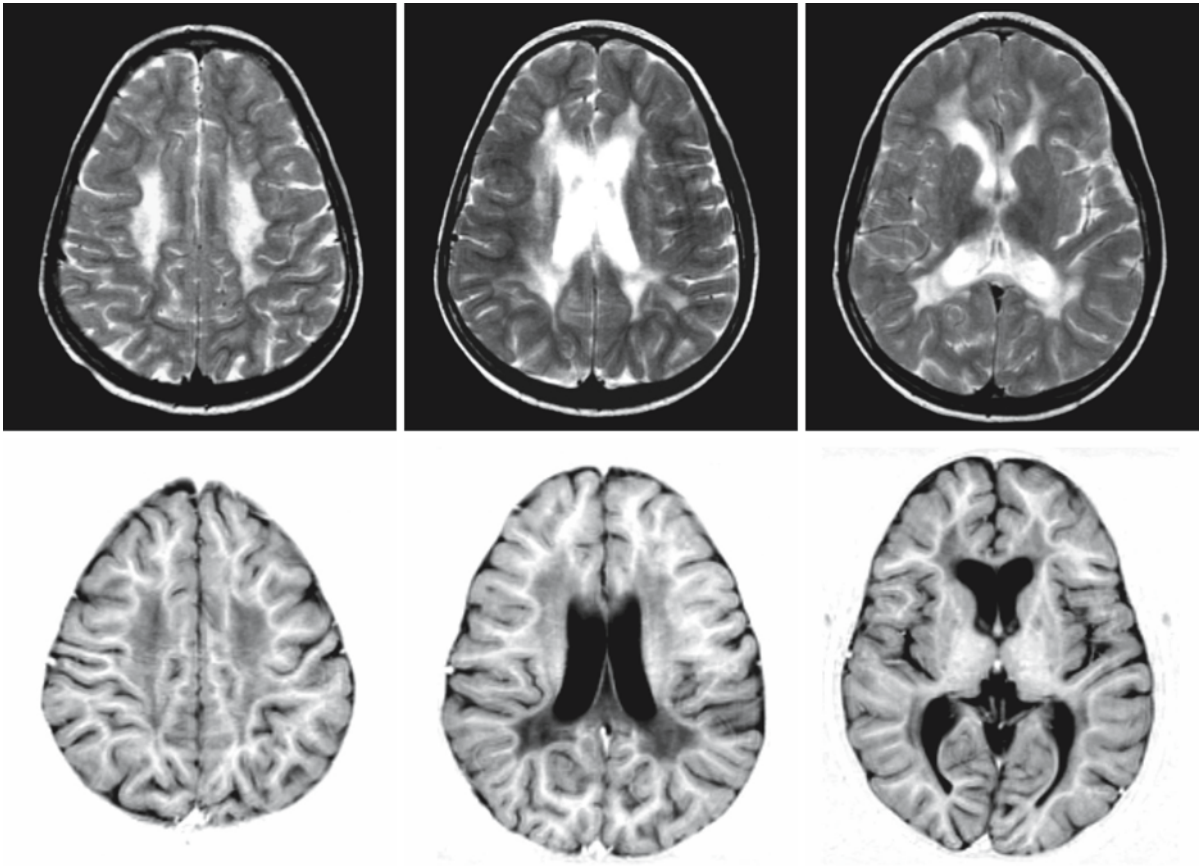


Fig. 6.3. A case of juvenile MLD in an 8-year-old girl. There is no evident stripe-like pattern

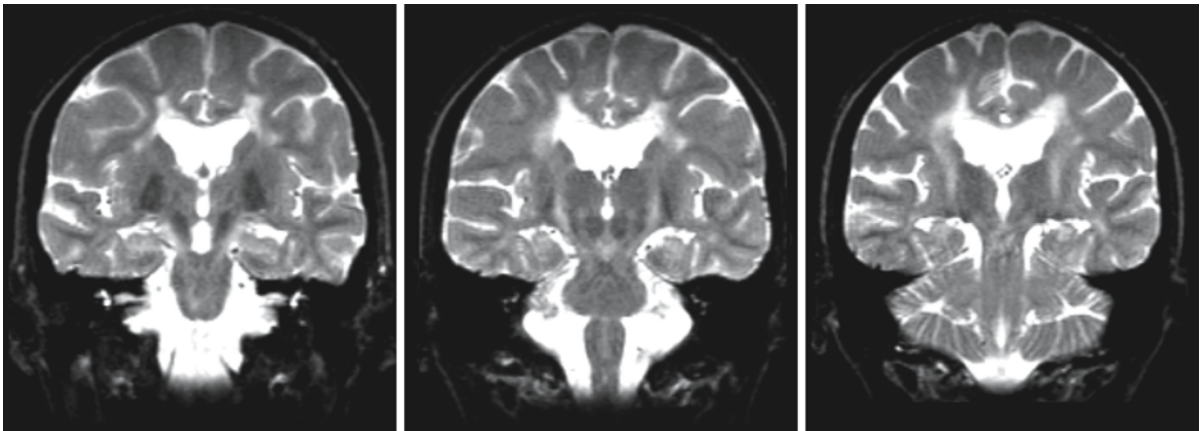


Fig. 6.4. An 18-year-old female patient with adolescent-onset MLD. Note the corticospinal tract involvement

be seen in globoid cell leukodystrophy, and in these cases the MRI abnormalities are indistinguishable from those in MLD. In early-onset globoid cell leukodystrophy, the cerebral atrophy is usually more pronounced and there are typically areas with increased density on CT in the cerebellum, thalamus, internal capsule, and corona radiata, which have nev-

er been observed in MLD. Contrast enhancement is generally present in the acute stage of inflammatory disorders. It is also present in most patients with patients with cerebral X-linked leukodystrophy. In cerebral X-linked adrenoleukodystrophy an occipital preponderance occurs most frequently, whereas MLD tends to have a frontal preponderance in juvenile and

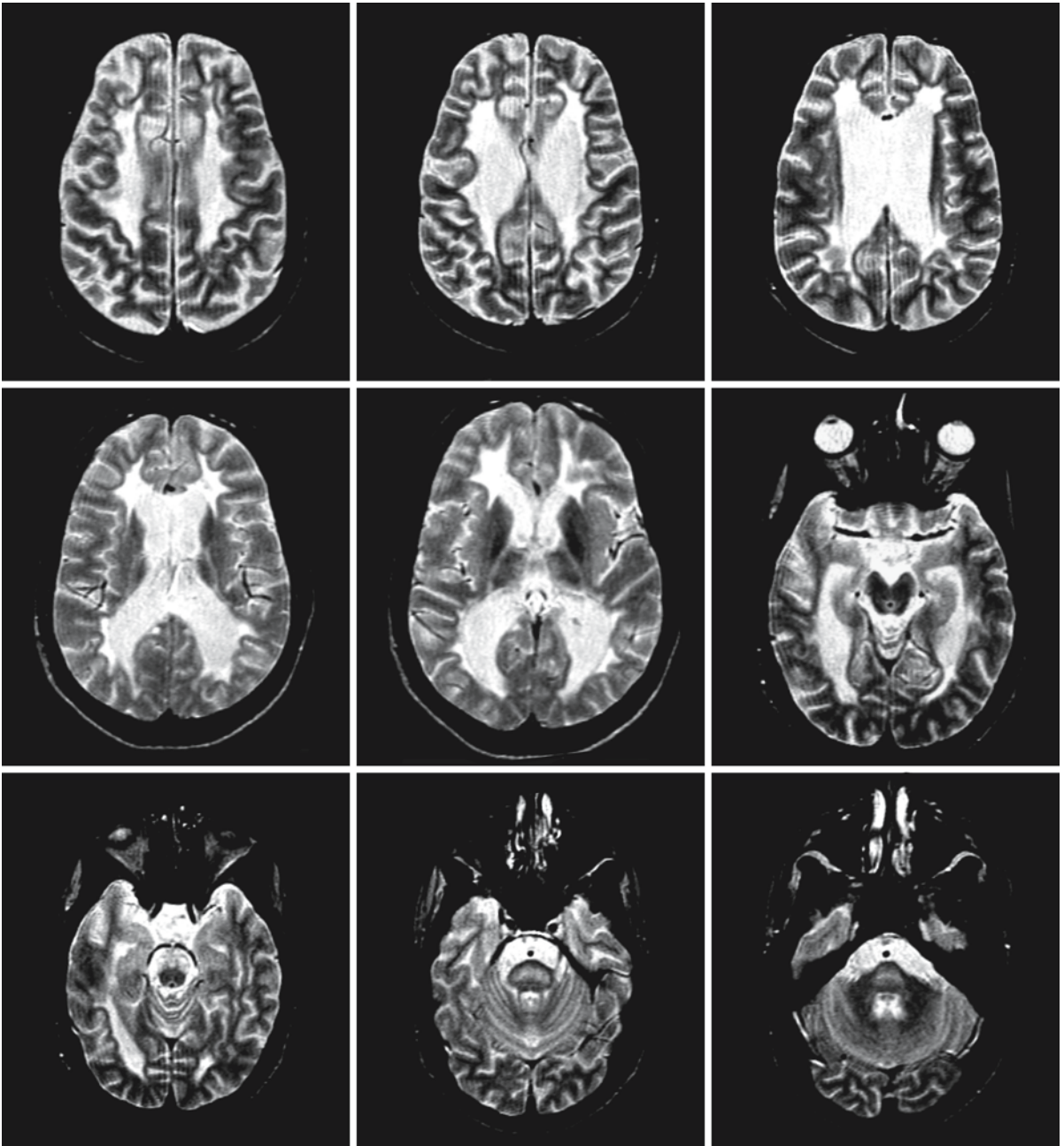


Fig. 6.5. In this MR series of a 29-year-old male with adult-onset MLD, extensive periventricular white matter abnormalities are seen, with serious atrophy. There is some frontal predomi-

nance of the abnormalities. The U fibers are still largely spared. Note the involvement of the corticospinal tracts in this case too

adult variants. The two zones typically present in cerebral X-linked adrenoleukodystrophy lesions are not present in MLD. In inflammatory disorders the demyelinating process is usually not perfectly symmetrical and the cortex is often not completely preserved.

Multiple Sulfatase Deficiency

7.1 Clinical Features and Laboratory Investigations

Multiple sulfatase deficiency (MSD) is a very rare disorder with an autosomal recessive mode of inheritance. It occurs with a prevalence of about 1 in 1.4 million births. The disease combines the features of metachromatic leukodystrophy and mucopolysaccharidosis. It is also called mucosulfatidosis, Austin variant or variant O. Three different types of MSD have been described: a neonatal form, an early-childhood form and a very rare juvenile form.

The early-childhood form is the usual, or classic, form of MSD. The clinical features are those of infantile metachromatic leukodystrophy with mild signs of mucopolysaccharidosis. Early development can be normal or delayed. Affected children usually acquire the ability to stand and to say a few words, but their development is less well advanced in the presymptomatic period than that of children with infantile metachromatic leukodystrophy. During the 2nd year of life the children develop signs of a progressive encephalopathy with loss of acquired abilities, progressive dementia, spasticity, microcephaly, blindness, hearing loss, and difficulties in swallowing. Tendon reflexes are variable. In the final stages there is often areflexia caused by the peripheral neuropathy. Features similar to those of mucopolysaccharidosis may occur early or later in the course of the disease. These include ichthyosis, mild coarsening of the facial features, hepatosplenomegaly, stiff joints, growth retardation, and skeletal anomalies. Hydrocephalus may occur. There is no corneal clouding. Optic atrophy, cherry-red macula, and retinal degeneration also occur in some cases. Death usually occurs when patients are between 10 and 18 years of age.

The neonatal form presents at birth with severe features suggestive of mucopolysaccharidosis, such as facial dysmorphism, short neck, corneal clouding, ichthyosis, cardiac valvular involvement, hepatosplenomegaly, and severe dysostosis multiplex. The children affected have macrocephaly caused by hydrocephalus. They have signs of a severe encephalopathy, with early death, usually before the end of the 1st year of life. A Saudi variant of the neonatal type of MSD has been described, with mild to moderate mental retardation, cranial synostosis and consequent deformities, and cervical cord compression or transection due to vertebral abnormalities. Severe

facial dysmorphism, corneal clouding, hepatosplenomegaly, dwarfism, severe dysostosis multiplex, and hirsutism are present, but no ichthyosis, no retinal degeneration, no deafness, and no progressive dementia. Some patients are macrocephalic, but they are rarely hydrocephalic. Some suffer from cardiac valvular involvement.

A rare juvenile type of MSD has been reported with onset in childhood. The disease is characterized by short stature, ichthyosis, hepatomegaly, moderate dysostosis multiplex and slowly progressive neurological abnormalities consisting of dementia, ataxia, quadriplegia, retinal degeneration, and blindness. Corneal clouding is not present.

Additional investigations show changes on bone X-ray, such as a J-shaped sella turcica, structural changes in vertebral bodies, scoliosis, gibbus, flared ribs, broad phalanges, abnormal metacarpals and, in the Saudi variant, synostosis of cranial sutures. Large basophilic to azurophilic granules are seen in lymphocytes of bone marrow and peripheral blood. There is an increased urinary content of sulfatide and mucopolysaccharides, including dermatan sulfate and heparan sulfate. CSF protein is increased. Nerve conduction velocity is slowed.

Diagnosis is established by demonstrating a deficiency of arylsulfatases A, B, and C and a number of sulfatases necessary in the degradation of mucopolysaccharides. Prenatal diagnosis can be made by demonstrating markedly reduced activities of sulfatases in cultured amniotic cells or chorionic villi. DNA-based diagnostic procedures are also possible.

7.2 Pathology

Pathological findings in MSD are those that might be expected in a combination of metachromatic leukodystrophy and mucopolysaccharidosis. There is widespread neuronal lipid storage in the cortex and subcortical gray matter structures. The storage is lysosomal. The neuronal deposits are finely granular and PAS positive, with slight reddish to purple metachromasia. On electron microscopy, neuronal inclusions range in configuration from zebra bodies, which are typically seen in mucopolysaccharidoses, to membranous cytoplasmic bodies such as are seen in neuronal gangliosidoses. There is loss of neurons in cerebral and cerebellar cortex and cortical atrophy.

The white matter shows demyelination with deposition of metachromatic material, oligodendroglial loss, relative axonal preservation, and marked gliosis. The U fibers are relatively spared. Mucopolysaccharides are stored in perivascular mesenchymal tissue, which may lead to the formation of macroscopically visible pseudocystic cavities. Meninges are thickened and cloudy. Obliteration of the subarachnoid spaces can lead to hydrocephalus. Abnormalities in peripheral nerves are typical of metachromatic leukodystrophy.

7.3 Chemical Pathology

Chemical analysis of the brain has shown increases in sulfatide, sulfated steroids (e.g. cholesterol sulfate), gangliosides, and mucopolysaccharides. The lipids stored in the white matter are predominantly sulfatides, while those stored in the gray matter are predominantly gangliosides and mucopolysaccharides.

7.4 Pathogenetic Considerations

In MSD activity of all known sulfatases is found to be reduced, including arylsulfatase A (metachromatic leukodystrophy), arylsulfatase B = *N*-acetylgalactosamine-4-sulfatase (Maroteaux-Lamy syndrome), arylsulfatase C = steroid sulfatase (X-linked ichthyosis), *N*-acetylgalactosamine-6-sulfate sulfatase (Morquio syndrome type A), heparan sulfate sulfatase (Sanfilippo A), iduronate-2-sulfate sulfatase (Hunter syndrome), *N*-acetylglucosamine-6-sulfate sulfatase (Sanfilippo D), and some other sulfatases. The residual activities of the sulfatases vary considerably in fibroblast lines from different patients. The lysosomal storage of sulfatides, mucopolysaccharides and sulfated steroids is a direct consequence of the enzyme deficiencies mentioned. The accumulation of gangliosides may be caused by inhibition of other lysosomal hydrolases due to the present lysosomal storage. It is probable that the different phenotypic expressions of MSD are due to differences in relative residual activity of the various enzymes.

The genes coding for the various deficient sulfatases are intact. The rate of synthesis of various sulfatases is normal in MSD, but they are degraded at an enhanced rate. The deficiency of the sulfatases results

from the lack of a posttranslational modification that is common to all sulfatases. The reduced activity of the enzymes is caused by a defect in the modification of a conserved cysteine residue to form formylglycine. The modification of the cysteine residue appears to be a prerequisite for the catalytic activity of sulfatases.

The gene mutated in MSD is *SUMF1*, which is located on chromosome 3p26. *SUMF1*, standing for sulfatase-modifying factor 1, encodes the protein formylglycine-generating enzyme (FGE).

7.5 Therapy

No effective form of treatment is known.

7.6 Magnetic Resonance Imaging

Imaging findings are scarce in MSD. In the classic early-childhood variant images are indistinguishable from those of infantile and juvenile metachromatic leukodystrophy with severe cerebral white matter abnormalities. The corpus callosum and long corticospinal tracts are also involved. The cerebellar white matter can be abnormal, but is not in all cases. In some patients a pattern of radiating stripes of more normal signal intensity is seen within the affected cerebral white matter (Fig. 7.1). In these patients the images are indistinguishable from those seen in metachromatic leukodystrophy. However, these stripes are not seen in all patients (Fig. 7.2). In the later stages of the disease severe white matter atrophy is seen (Fig. 7.2).

In the neonatal form of MSD more variable white matter involvement has been described. Myelination is delayed. In addition, scattered, small high-signal-intensity spots are sometimes seen in the white matter, which are more suggestive of mucopolysaccharidosis than of metachromatic leukodystrophy (Fig. 7.3). In some of the patients, white matter abnormalities are more extensive and confluent. Severe, highly confluent white matter disease can also be found. Dilatation of the ventricular system and prominence of the sulci are possible findings. Enlarged perivascular spaces within the white matter can be expected. At the cranio-cervical junction signs of cervical cord compression may be found, which is caused by atlantoaxial abnormalities.

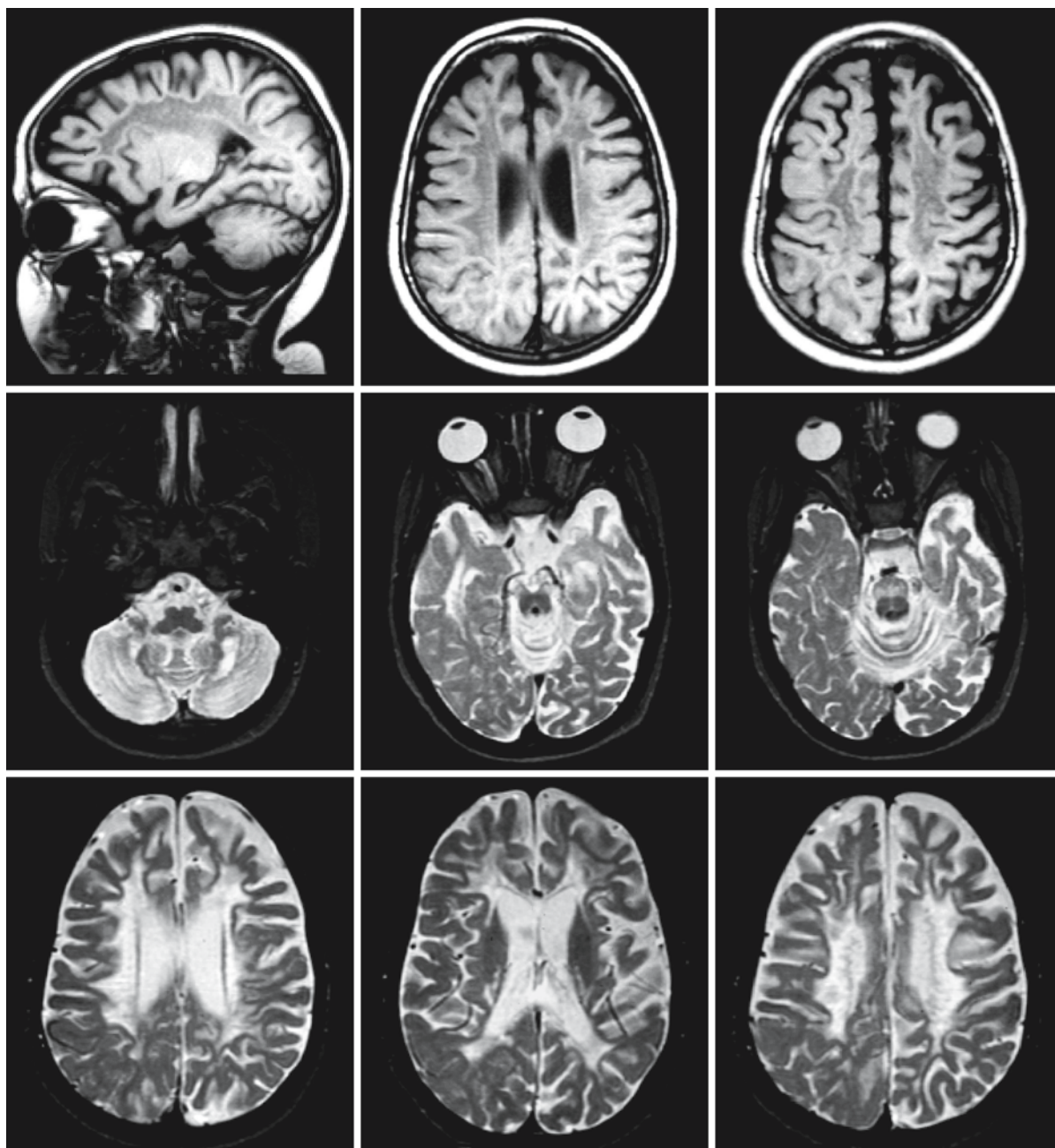


Fig. 7.1. A 5-year-old male patient with classic MSD. The images are indistinguishable from those seen in metachromatic leukodystrophy. The cerebral white matter is diffusely abnormal and contains countless radiating stripes of more normal

signal intensity. Within the brain stem the corticospinal tracts are involved. Courtesy of Dr. G. Mancini and Dr. H. Stroink, Sophia Children's Hospital, Erasmus Medical Center, Rotterdam, The Netherlands (see also Mancini et al. 2001)

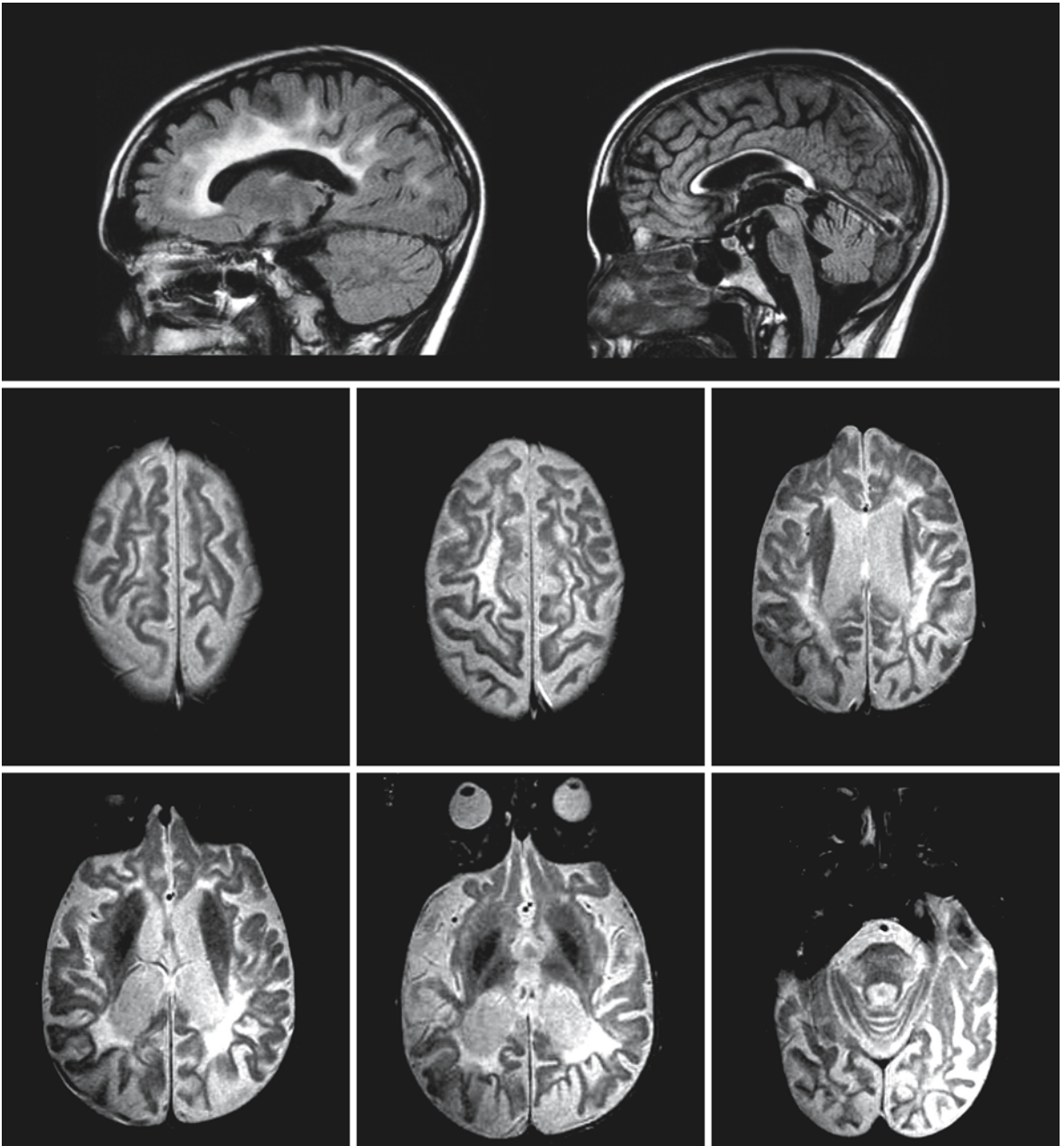


Fig. 7.2. A 7-year-old boy with MSD in an advanced stage. Note the serious white matter atrophy. Courtesy of Dr. S. Blaser, Department of Diagnostic Imaging, Hospital for Sick Children, Toronto

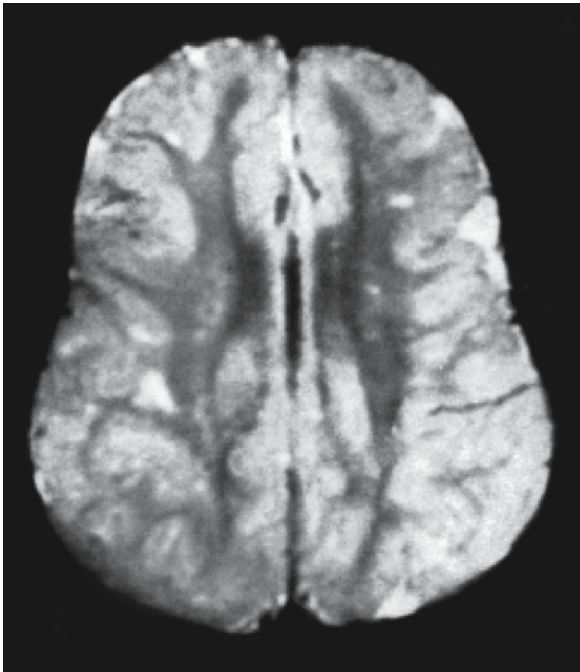


Fig. 7.3. A 4.5-year-old child with the Saudi variant of MSD. Note the multiple small high signal intensity spots bilaterally in the centrum semiovale. From Aqeel et al. (1992), with permission

Globoid Cell Leukodystrophy: Krabbe Disease

8.1 Clinical Features and Laboratory Investigations

Globoid cell leukodystrophy (GLD), also known as Krabbe disease, is a progressive white matter disorder with autosomal recessive inheritance. A number of clinical types can be distinguished, which differ in age of onset and in the rate of clinical deterioration. The early infantile or classic type is the most common. Its incidence is estimated at 1–2 in 100 000. The other types are: congenital, late-infantile, juvenile, and adolescent-adult. As a rule only one variant of GLD occurs within one family, although exceptions have been reported.

Clinical features and course of disease are fairly uniform in early-infantile GLD. During the first few months of life the infants are healthy and their psychomotor development is normal. The onset of clinical symptoms occurs between 1 and 6 months of age. Hagberg et al. (1969) distinguish three clinical stages. Stage I is characterized by hyperirritability and periods of crying, particularly when the infants are handled and nursed. They seem to be extremely sensitive to light and noise and often have excessive startle responses. Periods of fever often occur without signs of infection. The muscular tone increases. At the onset of the disease the deep tendon reflexes are normal. There is a stagnation of mental and motor development, soon followed by regression. In sporadic cases convulsions, hemiplegia, or predominant signs of peripheral neuropathy are the presenting abnormalities. Within 2–4 months of onset most patients reach stage II. This stage comprises the subsequent period of rapid and severe motor and mental deterioration. A constant opisthotonus and a hypertonic flexion of the arms and extension of the legs are present. The deep tendon reflexes can no longer be evoked. There are extensor plantar signs. Abilities previously achieved are lost. At the same time the general condition deteriorates, with more frequent hyperpyretic periods, often accompanied by intense sweating. Pulmonary infections are common. Myoclonic irregular jerks of the arms and legs, startle myoclonus, hypertonic fits, and other atypical seizures occur, as do typical, generalized tonic-clonic seizures and infantile spasms. The signs of visual failure and optic atrophy begin to appear. Stage III is the vegetative, burned-out stage. The children seem to have little or no mental activity and lie in a decerebrate posture. They are

blind and make no voluntary movements. Touching may elicit primitive generalized reflex movements. The children lack sucking abilities and have to be fed by nasogastric tube. The muscular tone often changes again. The opisthotonic posture disappears and is followed by a tendency to hypotonicity. The children become cachectic, and if they do not die of an intercurrent respiratory infection or of aspiration they succumb gradually. Death occurs between 5 months and 3 years of age.

In rare cases, GLD is already manifest during the neonatal period in the form of unspecific feeding difficulties, irritability, twitchiness, or respiratory problems. Both floppy and hypertonic neonatal variants have been described.

The later onset forms of GLD are clinically much more heterogeneous and progress more slowly. A subdivision into late-infantile onset (6 months to 3 years), juvenile onset (4–10 years) and adolescent-adult onset has been proposed, but the subdivision is arbitrary. In most children the onset of disease occurs before the age of 5 years; adolescent-adult onset is rare. There is no significant difference in symptomatology according to the age at onset. The initial signs in the late-onset forms of GLD are quite variable: spastic paraparesis, hemiparesis, cerebellar ataxia, isolated visual failure (as a result of either optic atrophy or bilateral involvement of the optic radiations), dystonia, epileptic seizures, psychosis, and mental deterioration. Of these signs, increasing difficulties in walking caused by spasticity or ataxia and isolated visual failure are the most frequent first manifestations. Irritability is not infrequently noted early in the disease. Peripheral neuropathy as an isolated presenting sign of the disease is a rare variant that can occur in late-onset types but has also been reported in infants. The rate of progression and duration of the disease are quite variable. Some patients, and especially those younger than 3 years, have a very rapid course of disease, becoming bedridden, tetraparetic, and demented in less than 3 months. Most patients, especially those with later onset, have a more chronic course. Death occurs after a highly variable period ranging from 18 months to more than 14 years. Bronchopulmonary infections are the most frequent cause of death.

In early-onset GLD an abnormally high protein level is always found in the CSF while the cell count is normal. Only occasionally are there more than

10 cells/ml, the majority of these being mononuclear leukocytes. The elevated CSF protein level is less constant in later onset forms of GLD, being found in about 50% of the patients. In early-onset GLD, the EEG is normal at the beginning of the disease, sometimes even after some months of manifest clinical symptoms. Abnormal findings tend to appear at the end of stage I. The pattern then becomes increasingly abnormal, characterized by markedly slow activity of high voltage. In the terminal stage the background activity is frequently interrupted by numerous fast, sharp-wave activities, episodic dysrhythmias, or epileptiform episodes. Sometimes a picture of hypsarrhythmia is found. Nerve conduction velocity is markedly reduced in all patients with early-onset GLD. In later onset forms the reduction in nerve conduction velocity is more variably present; conduction velocity can also be normal.

The diagnosis of GLD is established by showing a deficiency of galactocerebroside β -galactosidase (galactocerebrosidase) in white blood cells or cultured fibroblasts. It is not possible to distinguish between early-onset GLD and late-onset variants by comparing residual enzyme activities. There is a considerable overlap between the normal range and the carrier range of enzyme activity, so that carrier testing is often unreliable. In addition, very low levels of galactocerebrosidase activity (less than 10%) have been found in healthy people. The presence of polymorphic amino acid changes in the enzyme causes this wide range of activities. In some families additional studies, such as substrate loading tests in cultured skin fibroblasts, are necessary. DNA analysis may help in solving the problems with diagnosis. GLD can be diagnosed prenatally by assaying the enzyme activity in chorionic villi or amniotic fluid cells. DNA confirmation is an option.

8.2 Pathology

Gross examination of the brain reveals a moderate to marked reduction in size. On sectioning, the cortex appears to be relatively spared but there is a marked reduction in the amount of white matter, which shows a brownish discoloration.

Microscopic examination confirms that there is little or no involvement of cortical gray matter. The cerebral, cerebellar, and brain stem white matter shows diffuse demyelination throughout the brain, although there are regional variations in intensity. There is a distinct tendency for the U fibers to be preserved. The extent to which tracts in the brain stem and cord are affected varies. Long tracts, in particular the corticospinal and spinocerebellar tracts, and the dorsal columns are usually severely damaged. In the areas of demyelination axonal degeneration is ob-

served, but axons are relatively preserved in comparison with the degree of myelin loss. There is an early and marked loss of oligodendrocytes through apoptosis. There is diffuse fibrillary gliosis throughout the white matter with proliferation of astrocytes. In the central nuclei of the brain moderate neuronal loss can be observed, and sometimes intense gliosis.

The pathognomonic feature of GLD is the accumulation of globoid cells. These cells are multinucleated giant cells with ballooned cytoplasm containing finely fibrillary to granular material. Their cytoplasm stains eosinophilic in HE, moderately positive in PAS, and negative or faintly positive in Sudan Black preparations. There are also smaller rounded cells with single nuclei and accumulation of identical material in their cytoplasm. These are called epithelioid cells by some, and are included with the globoid cells by others. Globoid cells are present as single cells or, more often, as groups of cells in the affected white matter. They accumulate around blood vessels. They are not only present within the affected white matter, but can also accumulate in central gray matter structures. There is considerable variation in the distribution and number of globoid cells in individual cases, depending on the duration of the disease and the intensity of the histopathological process. They are lower in number in patients with long-standing disease who have burned-out pathology. At an ultrastructural level the globoid cells appear to contain specific straight and twisted tubular-type inclusions. The tubular inclusions are usually dispersed throughout the cytoplasm, and rarely membrane bound. The straight tubules are angular or crystalloid in cross section, while the twisted tubules are rectangular or oval. Sometimes myelin figures and lipid droplets are found in the cytoplasm of globoid cells. Globoid cells stem from phagocytic mesenchymal cells.

In GLD the peripheral nerves are also involved in the disease process. Light microscopic examination reveals segmental demyelination and variable axonal degeneration in early-onset forms. In adult patients, myelin sheaths have been reported to be abnormally thin for the fiber diameter, suggesting hypomyelination rather than demyelination. Usually no typical globoid cells are found. Electron microscopy shows that Schwann cells and endoneurial macrophages contain cytoplasmic inclusions similar to the inclusions in the globoid cells of the CNS.

8.3 Chemical Pathology

Chemical analysis of the brain shows that the gray matter is only moderately abnormal, while severe changes are present in the white matter. The white matter has an increased water content, and its lipid content is greatly diminished. Although both cerebro-

side and sulfatide are greatly decreased, as might be expected from the myelin loss, there is a significant change in the cerebroside-to-sulfatide ratio, from the normal value of 4:1 to as much as 10:1. Proportional to the total loss of myelin there is a decrease in the white matter content of total lipids, cholesterol, glycolipids, and ethanolamine phosphoglycerides. There is a relative increase (though an absolute decrease) of other phospholipids, such as choline phosphoglycerides, serine phosphoglycerides, and sphingomyelin. As a rule, no elevation of cholesterol esters is found. Galactosylsphingosine, also called psychosine, accumulates in considerable amounts in the white matter of GLD patients. Concentrations of up to 100 times the normal value have been found. Psychosine is not normally detectable in gray matter, but is elevated in GLD patients, though not nearly to the same extent as in white matter.

Analysis of isolated myelin in GLD reveals a relatively normal lipid composition. The cerebroside content of myelin is not elevated. A relatively high concentration of cerebroside is found in globoid cell-enriched fractions from the diseased white matter. There is cerebroside storage in globoid cells, while there is none in the white matter as a whole or in the myelin membrane.

8.4 Pathogenetic Considerations

The primary defect in GLD is a deficiency of galactosylceramidase, also called galactocerebroside β -galactosidase or galactocerebrosidase. This is a lysosomal enzyme that catalyzes the first step of cerebroside (= galactosyl ceramide) degradation and splits cerebroside into galactose and ceramide. Sulfatide is also normally degraded through cerebroside into ceramide and galactose. The gene coding for galactocerebrosidase, *GALC*, is localized on chromosome 14q31. Many different mutations in *GALC* have been identified in GLD. There is no clear genotype-phenotype correlation. One might anticipate that the difference in phenotypic expression in GLD would result from different levels of residual enzyme activity, but the currently available assay procedures reveal no consistent difference in residual enzyme activity between early- and late-onset forms.

Mammalian tissues contain two genetically distinct lysosomal β -galactosidases with different, though overlapping, substrate specificities: galactocerebroside β -galactosidase (galactocerebrosidase) and GM₁-ganglioside β -galactosidase. It has been demonstrated that under certain assay conditions GM₁-ganglioside β -galactosidase can also hydrolyze cerebroside. Psychosine (= galactosyl sphingosine) is hydrolyzed by galactocerebrosidase, but not by GM₁-ganglioside β -galactosidase. This difference in sub-

strate specificity explains why psychosine accumulates to give high levels in GLD brain, whereas cerebroside, while moderately increased in relative concentration, is decreased in absolute concentration.

Cerebroside is a constituent almost exclusively of oligodendrocytes, Schwann cells, and myelin sheaths. Metabolism of cerebroside is closely related to the metabolism of myelin. In immature brains, prior to myelination cerebroside is practically absent, and lack of galactocerebrosidase is therefore of little consequence. As soon as myelination begins the normal turnover of myelin starts. This coincides with a rapid rise of galactocerebrosidase activity in normal brain. In GLD brains cerebroside from catabolized myelin cannot be disposed of adequately because of the lack of the enzyme. GM₁-ganglioside β -galactosidase may be responsible for part of the cerebroside breakdown and prevent real accumulation of cerebroside. Excess of cerebroside in phagocytic cells leads to the transformation of these cells into globoid cells. In experimental studies the relationship between cerebroside and globoid cells has been confirmed. Intracerebral injection of cerebroside into rat brain elicits a globoid cell reaction, whereas the injection of many other substances does not lead to this response.

Psychosine is also a substrate for the deficient enzyme galactocerebrosidase. It is formed from UDP-galactose and sphingosine through the action of UDP-galactose : ceramide galactosyl transferase. It cannot be disposed of in GLD, because it is a very poor substrate for GM₁-ganglioside β -galactosidase. Psychosine is a highly cytotoxic substance. There is evidence that accumulated psychosine leads to production of cytokines and inducible nitric oxide synthase expression and contributes to apoptosis. It is probable that psychosine generated within oligodendrocytes during the period of active myelination accumulates until it reaches a toxic level. Apoptosis is selectively induced in oligodendrocytes because psychosine formation occurs primarily in these cells. This explains the early and marked loss of oligodendrocytes, resulting in loss of the myelin sheaths maintained by these cells. In GLD brains the concentration of psychosine correlates well with the severity of pathological changes. When the stage of massive death of oligodendroglial cells is reached, rapid myelin breakdown occurs, contributing more cerebroside, which may enhance the globoid cell reaction. The death of oligodendroglia prevents further myelination.

The sequence of events is well illustrated in the Twitcher mutant mouse, which has the same defect as is present in the human disease. Initial myelin development is normal, highlighting the point that myelin build-up is essentially normal in GLD. Subsequently, there is a declining rate of myelination, followed by demyelination and the appearance of globoid cells. It

is myelin turnover that brings the enzymatic defect to expression.

The difference in tissue reaction between CNS and PNS is difficult to explain. Phagocytic cells in the PNS contain abnormal inclusions similar to those in the brain, and it is not clear why they are not transformed to the typical multinucleated globoid cells. The almost obligatory involvement of the CNS and the variable involvement of the PNS, particularly in later onset forms of GLD, suggests that oligodendrocytes are more vulnerable to psychosine than are Schwann cells.

In the brain there is a regional variation in vulnerability to pathologic changes. In particular, the U fibers are typically spared. As the process of myelin build-up is normal in GLD and the defect involves myelin turnover and breakdown, the areas of the brain that myelinate last can be expected to be involved in later stages of the disease than are the early-myelinating areas. The U fibers are the last to myelinate, which may explain their relative preservation. In addition, in animal research the *in vivo* turnover rate of cerebroside appears to be higher in the areas of the white matter that are consistently more severely affected in GLD; this may furnish another part of the explanation for regional variation in white matter involvement.

GLD is a primary myelin disorder, and there are no morphological or functional abnormalities outside the nervous system. This is explained by the fact that cerebroside is present almost exclusively in nervous tissue, the amounts in organs outside the nervous system being quantitatively negligible.

Although GLD and metachromatic leukodystrophy are both caused by a genetic defect in the catabolism of myelin constituents and initial myelin build-up is normal in both disorders, there are interesting dissimilarities between GLD and metachromatic leukodystrophy. Metachromatic leukodystrophy is characterized by extreme storage of sulfatide, whereas GLD hardly deserves the name 'storage disorder.' In metachromatic leukodystrophy the composition of the myelin membrane is altered, with excessive sulfatide within the myelin sheath. In GLD, myelin is compositionally normal, and the relative rise in cerebroside relative to other lipids in the analysis of whole white matter appears to be related to an excess of cerebroside in globoid cells. It is likely that these differences can be explained by a difference in the rate of oligodendroglial cell death. In GLD these cells disappear rapidly, early on in the local disease process. This early cell death is probably caused by psychosine toxicity. With oligodendroglial cell death myelin membranes are lost simultaneously, before the defect in turnover can trap cerebroside or other abnormal constituents within the myelin sheath. In metachromatic leukodystrophy oligodendroglial cells disappear later,

more slowly, and to a lesser degree. Sulfatide is trapped in the myelin membrane and its content increases until the composition of the myelin sheath is so abnormal that the normal stability of the membrane is lost and demyelination ensues.

Sphingolipid activator proteins, i.e., saposins A, B, C, and D, are small glycoproteins derived from a common precursor protein, prosaposin. These activator proteins are required for degradation of sphingolipids. Total deficiency of all saposins and specific deficiencies of saposins B and C are associated with known human diseases. No specific saposin A or D deficiency is known in humans. It has recently been demonstrated that saposin A is indispensable for the degradation of cerebroside by galactocerebrosidase. A transgenic mouse with saposin A deficiency has been shown to develop a demyelinating disease similar to, but milder than, that seen in the Twitcher mouse. Saposin A deficiency can be anticipated among human patients with a late-onset slow-demyelination disease without galactocerebrosidase deficiency.

8.5 Therapy

To date, early-onset GLD has invariably proved fatal. The problem with early-onset forms of GLD is that neuropathological changes are already present in the second trimester of pregnancy and that any form of treatment is applied to an already damaged nervous system. Hematopoietic stem cell transplantation to infantile patients who are already clinically symptomatic has not resulted in beneficial effects. Reports on hematopoietic stem cell transplantation very soon after birth, before the onset of any clinical symptoms, are appearing, and the results are promising but must be confirmed in larger studies. Hematopoietic stem cell transplantation is now performed in increasing numbers of patients with later onset forms. Stabilization and improvement of clinical symptoms and MRI abnormalities have been reported. Early treatment, while the intellect is still intact and the motor disabilities are only mild, is essential.

Another therapeutic approach is one of substrate-reduction therapy. L-Cycloserine is an inhibitor of sphingosine synthesis by irreversible inhibition of 3-ketodihydrosphingosine synthase. Administration of L-cycloserine to animals leads to a reduction in the production of brain cerebroside, sulfatide, and gangliosides. Although the level of psychosine has not been measured, it is likely that it is also lowered, since psychosine is made up of sphingosine and galactose. Thus, L-cycloserine lowers the levels of substrates that are not digested in GLD. Twitcher mice treated with L-cycloserine have milder disease and live longer, but only if the treatment is started early. If combined with

bone marrow transplantation, L-cycloserine improves the outcome further. The problem with L-cycloserine is that cerebroside and sulfatide are essential for normal myelin structure and function. L-Cycloserine is toxic in higher doses. In addition, L-cycloserine has not yet been tested in humans. Gene therapy also has not yet progressed beyond the animal experimental stage.

8.6 Magnetic Resonance Imaging

In cases of early-onset GLD, the CT findings are quite characteristic. The abnormalities seen are related to the stage of the disease. In stage I there are either no changes at all, or symmetrically increased density in the thalami, corona radiata and, less often, posterior limb of the internal capsule, caudate nucleus, globus pallidus, and putamen. Sometimes more extensive hyperdense areas are noted, including the brain stem, cerebellum, dentate nucleus, optic radiation, central subcortical white matter, and cortical gray matter (Fig. 8.1). Pathologically, the hyperdensity on CT correlates with a higher concentration of globoid cells and proliferating glia. In stages II and III, symmetrical low-density areas in the periventricular white matter and corpus medullare of the cerebellum become obvious. The low density of the white matter is relatively less marked than in other leukodystrophies. The low density represents demyelination and increased water content. The severe fibrous astrogliosis that occurs in GLD may be responsible for the less intense hypodensity. In stage III diffuse brain atrophy, both central and peripheral, is observed. Sulci are widened, the head of the caudate nuclei is flattened, and the ventricles, including the third, are widened as a result of atrophy of the thalamus.

MRI confirms the presence of periventricular white matter abnormalities with relative sparing of the U fibers in early-onset GLD (Fig. 8.2). The corpus callosum is affected, connecting the lesions of both sides. A radiating pattern with stripes of more normal signal intensity is often observed within the cerebral white matter (Fig. 8.2), but this pattern is not obligatory. The stripes correlate with perivascular deposits of globoid cells in microscopic examination of the brain. The posterior limb of the internal capsule, cerebellar white matter, hilus of the dentate nucleus, and pyramidal tracts in the brain stem are involved (Fig. 8.2). In fact, involvement of the brain stem and cerebellum occurs early, before supratentorial white matter involvement. MRI can be deceptively normal in the initial stages of early-infantile GLD, which is probably largely related to the still immature myelination preventing recognition of the presence and

extent of white matter abnormalities. Signal abnormalities in the hilus of the dentate nucleus, cerebellar hemispheric white matter, and pyramidal tracts of the brain stem in infants only a few months of age should suggest the possibility of GLD. The areas of high density on CT may not be so clearly abnormal on MRI. These areas may have a relatively low or high signal intensity on T₂-weighted images and a normal, high, or low signal intensity on T₁-weighted images. With progression of the disease, the subcortical white matter also becomes involved and global atrophy ensues. An unusual finding reported in a few GLD infants is optic nerve enlargement. This is related to the presence of a very high number of globoid cells. In many patients MRI and CT provide complementary information, CT showing the characteristic hyperdensities and MRI showing the extent of the demyelination.

In cases of late-onset GLD, hyperdensities in the thalamus and basal ganglia have been found on CT. There are white matter abnormalities, and these may in part have a high density on CT. Both CT and MRI show a predominant involvement of the parieto-occipital periventricular white matter with extensions in the temporal direction and associated involvement of the splenium of the corpus callosum (Fig. 8.3). MRI may show a pattern of radiating stripes of more nearly normal signal intensity within the abnormal cerebral white matter. The U fibers are relatively spared (Fig. 8.3). The posterior limb of the internal capsule and pyramidal tracts in the brain stem are involved. The cerebellar white matter is spared. More extensive white matter lesions affecting the whole centrum semiovale probably represent a more advanced stage of disease. In the later stages atrophy becomes obvious.

Furthermore, adults may exhibit signal changes restricted to the corticospinal tracts, extending from the motor cortex through the posterior limb of the internal capsule into the pyramidal tracts of the brain stem, in either a symmetrical or an asymmetrical or unilateral distribution (Fig. 8.4). However, some adult patients have a normal brain MRI for a long time. Some adults present with signs of an isolated polyneuropathy. If they exhibit white matter abnormalities on cerebral MRI as described above, this should lead to inclusion of GLD in the differential diagnosis.

Variable, but at most subtle, enhancement has been described in GLD cases and may involve the normal-abnormal white matter junction at the border between the deep white matter and the U fibers, and also the corpus callosum, cranial nerves, and spinal nerve roots. However, in most cases no enhancement is seen.

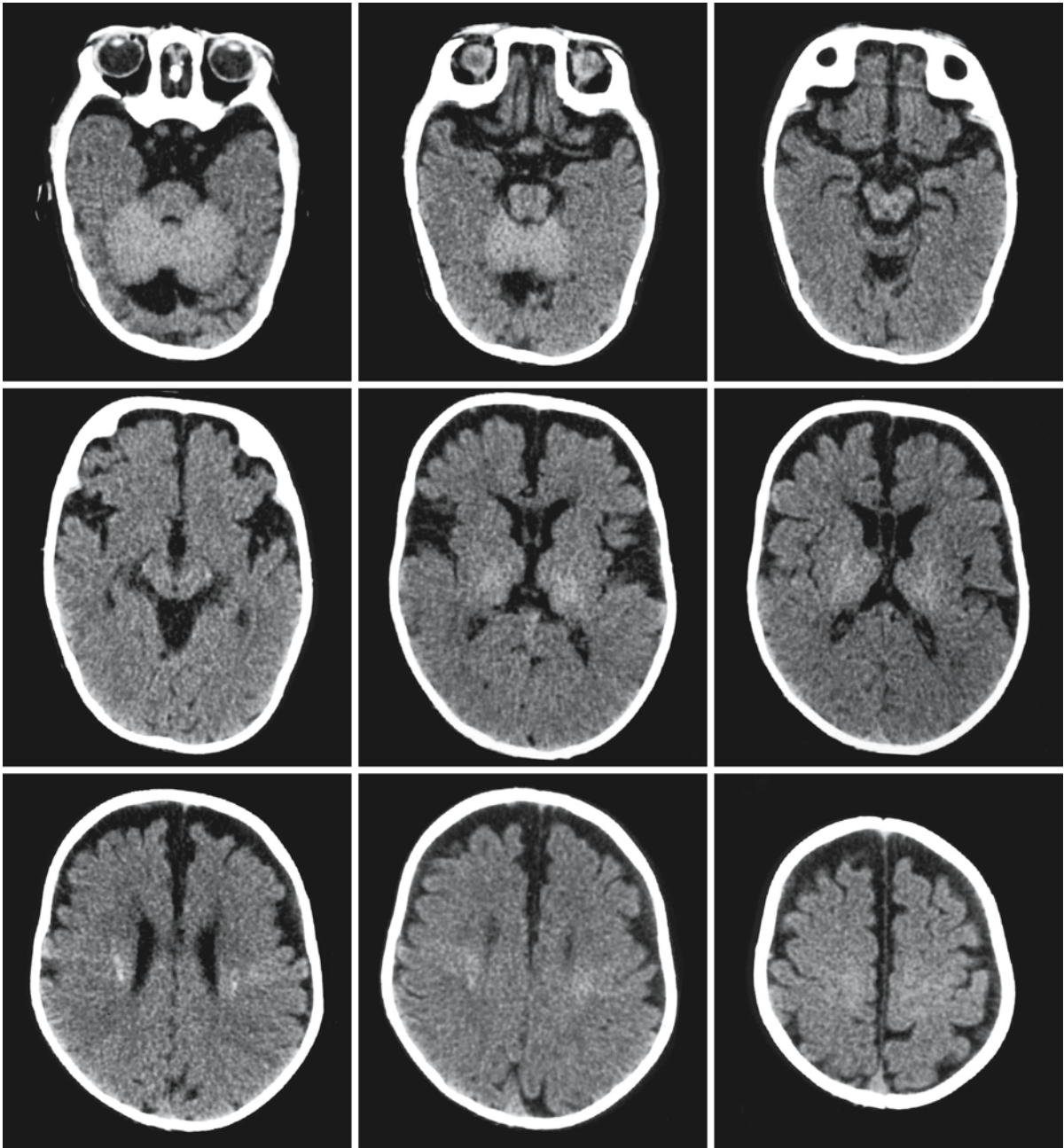


Fig. 8.1. CT findings in a 4-month-old boy with early-infantile GKD. The series demonstrates the hyperdensities in the primary myelination zones: brain stem, cerebellum, posterior limb of

the internal capsule, thalamus, and central part of the corona radiata. At this stage the CT appearance is almost diagnostic, and more characteristic than the MRI findings

Fig. 8.2. Early-infantile GKD in a 6-month-old girl. The *three upper rows* show transverse T_2 -weighted images. The periventricular white matter has a higher signal intensity than the directly subcortical white matter, although the latter is still unmyelinated. A stripe-like pattern is seen in the affected cerebral white matter. There is a significant atrophy of the cerebral

hemispheres. Cavitory lesions are visible in the posterior limb of the internal capsule. The cerebellar white matter and the hilus of the dentate nucleus are prominently involved. The T_1 -weighted transverse images (*lowest row*) confirm the stripe-like pattern in the abnormal white matter

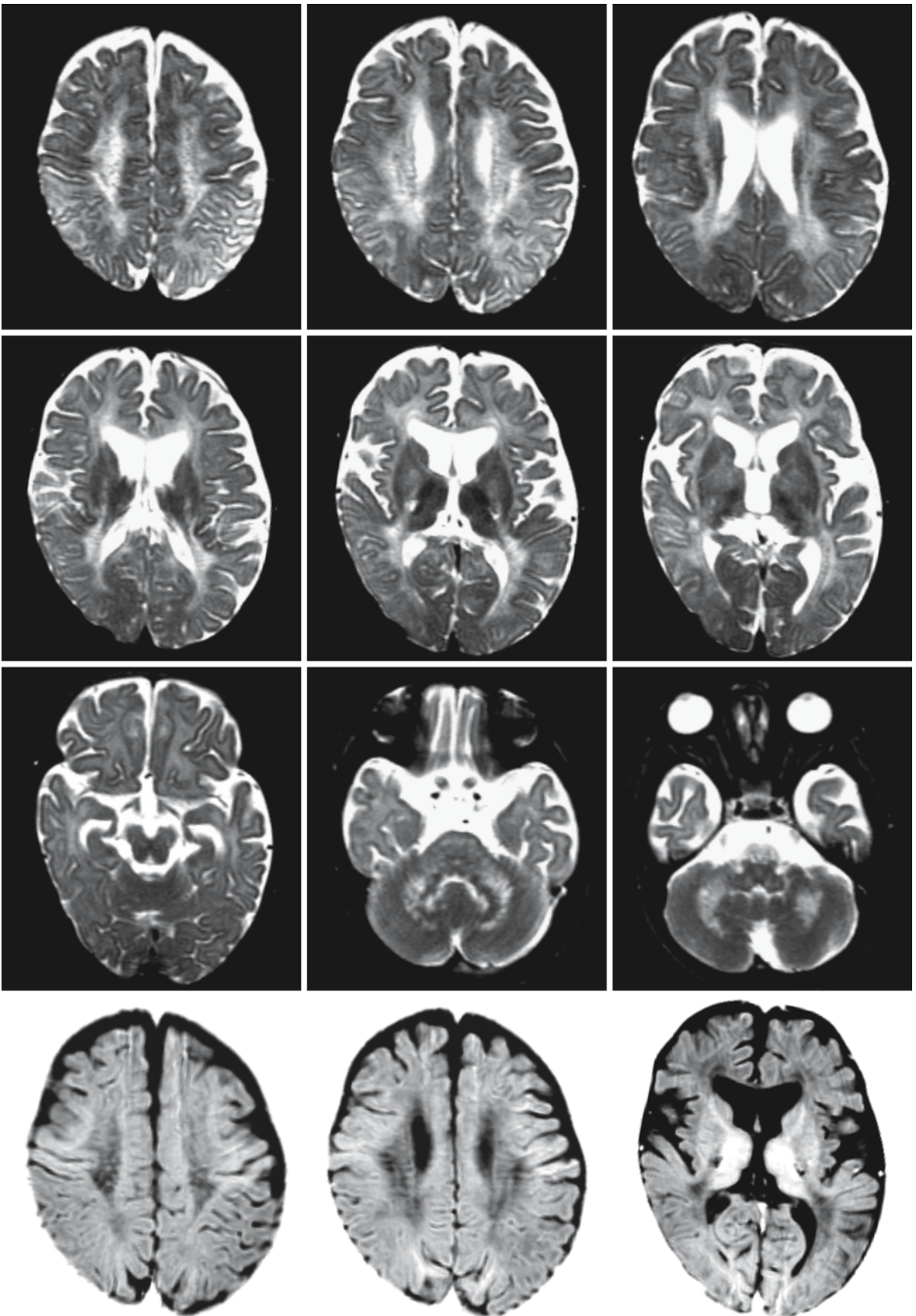


Fig. 8.2.

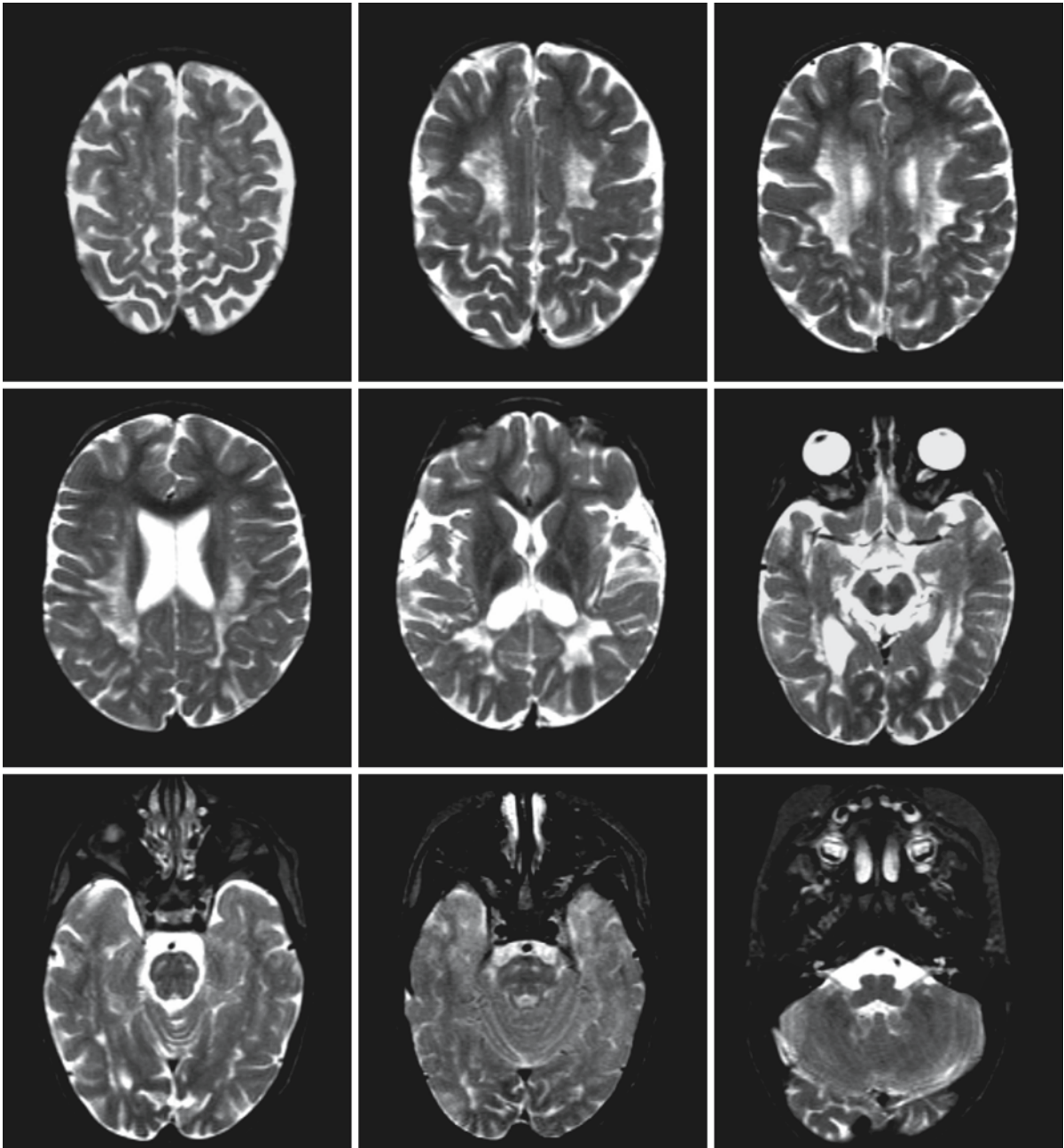


Fig. 8.3. Late-infantile GKD in a girl aged 4 years. There are extensive, symmetrical white matter abnormalities, predominantly involving the posterior part of the cerebral hemispheres. There is a subtle pattern of radiating stripes. The pos-

terior limb of the internal capsule and corticospinal tracts in the brain stem are affected. The cerebellar white matter is normal

The pattern of symmetrical and extensive involvement of the cerebral white matter, corpus callosum, internal capsule, and brain stem tracts is indistinguishable from the pattern observed in many metachromatic leukodystrophy patients, particularly when radiating stripes of more normal signal intensity are seen within the abnormal cerebral white mat-

ter. Patients with early-onset GKD usually have more pronounced cerebral atrophy than patients with early-onset metachromatic leukodystrophy. In patients with later onset metachromatic leukodystrophy, the white matter abnormalities often have a predominantly frontal location, whereas in patients with later onset GKD the parieto-occipital white matter is usual-

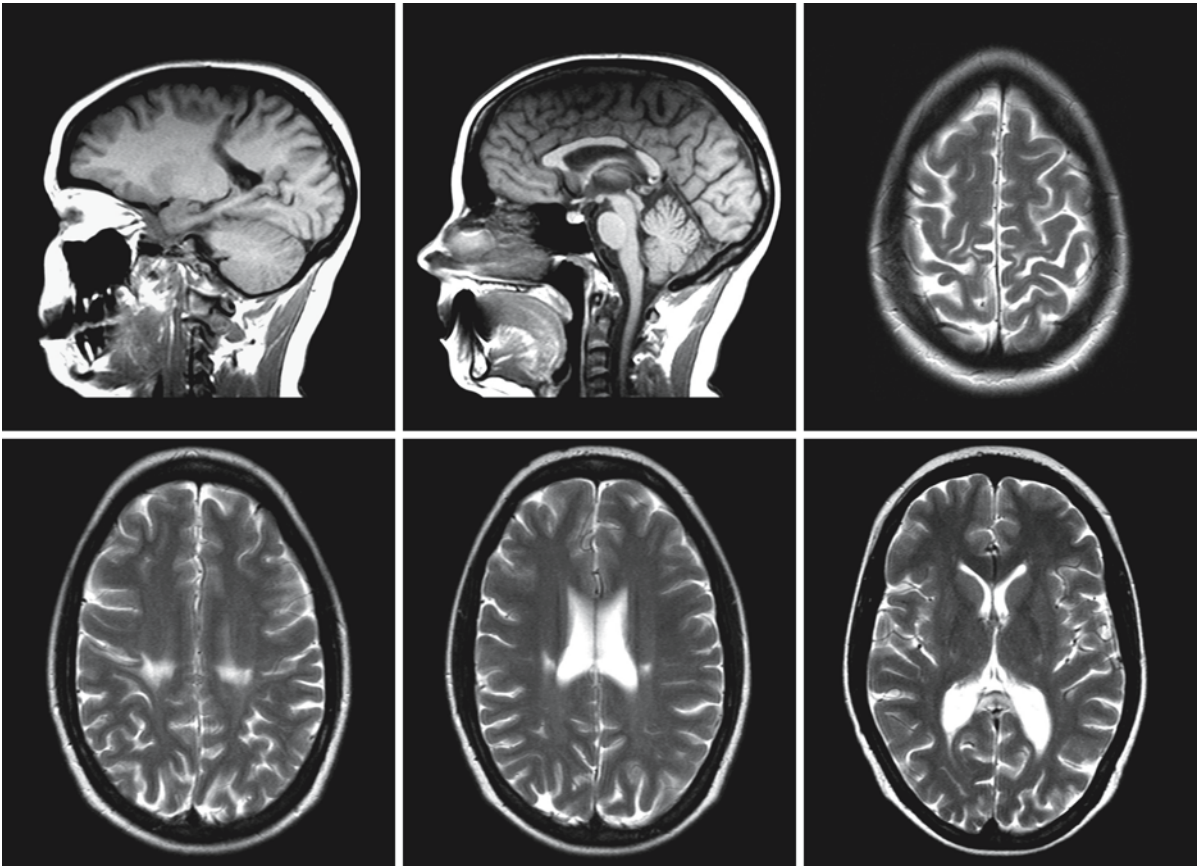


Fig. 8.4. Adult GLD in a female patient 25 years of age. Note the selective involvement of the corticospinal tracts. The connecting tracts through the corpus callosum are also affected,

as is the splenium. Courtesy of Dr. D. Loes and Dr. C. Peters, University of Minnesota, USA

ly predominantly involved. The hyperdense areas seen on CT in GLD are lacking in metachromatic leukodystrophy.

The CT scan findings with high density in the thalamus and basal ganglia are reminiscent of the CT findings in early-onset GM₁ and GM₂ gangliosidoses. The MRI findings are, however different (see related chapters).

The pattern with parieto-occipital predominance seen in later onset GLD patients resembles the pattern seen in cerebral X-linked adrenoleukodystrophy. However, the pattern consisting of two zones of different signal change within the abnormal white mat-

ter and a rim of contrast enhancement in between, which is so characteristic of X-linked adrenoleukodystrophy, has never been described in GLD, although contrast enhancement involving the splenium of the corpus callosum has been described in late-onset GLD patients.

The pattern with selective involvement of the corticospinal tracts may resemble the pattern seen in amyotrophic lateral sclerosis. However, the signal changes are less pronounced in the latter. In adrenomyeloneuropathy a similar pattern of MRI abnormalities can be observed, and this disease should be excluded by means of the appropriate laboratory tests.

GM₁ Gangliosidosis

9.1 Clinical Features and Laboratory Investigations

GM₁ gangliosidosis is an autosomal recessive disorder of GM₁ metabolism, resulting in variable neural and visceral accumulations. Three forms can be distinguished: infantile or type 1 GM₁ gangliosidosis, juvenile or type 2 GM₁ gangliosidosis, and adult, chronic or type 3 GM₁ gangliosidosis.

Type 1 infantile GM₁ gangliosidosis presents at or soon after birth, signs being poor sucking and feeding. The child is hypotonic and hypoactive and soon develops facial and peripheral edema. At times neonatal ascites and hydrocele are seen, and sometimes generalized edema. There are characteristic coarse facial features similar to those found in mucopolysaccharidoses. Facial abnormalities include frontal bossing, wide and depressed nasal bridge, long philtrum, and large low-set ears. The gums and tongue may appear hypertrophied. The cornea is clear. Hepatomegaly is present, and the spleen is often also enlarged. The dysmorphic features and hepatosplenomegaly gave this disease its other name: pseudo-Hurler disease. The skin is usually thick and rough. Exceptional cases of angiokeratoma corporis diffusum have been described. Failure to thrive and severe psychomotor retardation are early signs of the disease. Bilateral, cherry-red spots are found on the maculae in about half the patients. Early blindness occurs, which is cortical or retinal in origin. The child remains hypoactive and is weak. Noise frequently provokes an exaggerated startle response. Movements are poorly coordinated. Reflexes are hyperactive. Macrocephaly can develop, but is less marked than in Tay-Sachs disease. As the child gets older, broadness of the hands and shortness of the fingers become apparent. Joints become stiff. The wrist and ankle joints are often enlarged, but not tender. Flexion contractures frequently occur at elbows and knees. Kyphoscoliosis is frequently found. After a year, neurological deterioration is rapid, with epileptic seizures, progressive spasticity, and finally decerebrate rigidity, deafness, blindness, and loss of social contact. In rare cases cardiomyopathy with cardiac failure occurs. Flexion contractures of the arms and legs may become extremely severe. Respiratory problems are common, with frequent infections. Bronchopneumonia is a frequent cause of death, which usually occurs between 12 and 24 months.

In type 2 GM₁ gangliosidosis the clinical course is slower and the onset insidious. The children initially appear normal. The first clinical signs begin between 6 months (late-infantile form) and 2 years (juvenile form) of age. They usually consist of developmental arrest and gait disturbances. The subsequent course is characterized by progressive dementia, lethargy, epilepsy, an abnormally pronounced startle response to noise, spastic tetraplegia, cerebellar ataxia, loss of speech, and extrapyramidal features, such as choreoathetosis. Blindness is also a feature, but starts late in the course. No retinal degeneration or cherry-red spots are seen. The patients are not characterized by organomegaly or coarsening of facial features suggestive of mucopolysaccharidosis. Skeletal deformities are relatively mild. The average life span varies between 3 and 10 years. Death is usually caused by recurrent bronchopneumonia.

Type 3 GM₁ gangliosidosis is the adult or chronic variant. The clinical signs usually emerge in the second decade of life, but onset in the first decade has also been described. Gait disturbance and speech disturbance are early signs of the disease. Extrapyramidal features are usually most prominent and can take the form of slowly progressive dystonia, choreoathetotic movements, facial grimacing, blepharospasm, dysarthria, rigidity, parkinsonism with immobile face, bradykinesia, and typical gait abnormalities. In rare cases ataxia, pyramidal signs, mild intellectual impairment, and seizures occur. Bony abnormalities are minimal, if present. Cherry-red spots, visceromegaly, and facial dysmorphism do not occur.

In type 1 GM₁ gangliosidosis vacuolated lymphocytes are found in the peripheral blood smear, but these are not present in types 2 and 3. Large, foamy sea-blue histiocytes are present in the bone marrow in type 1; these cells are fewer in number in types 2 and 3. Rectal biopsy shows neuronal lipidosis in Meissner's plexus. Ultrastructurally, membranous cytoplasmic bodies similar to those seen in GM₂ gangliosidosis are seen within neurons. The membranous cytoplasmic bodies consist of spirally wound lamellae enclosed within a membrane of lysosomal origin. Other inclusions are more pleiomorphic in nature. Evidence of neuronal lipidosis on rectal biopsy can be found in all types of GM₁ gangliosidosis. Clear vacuoles can also be found in visceral histiocytes and parenchymal cells of visceral organs and

in epithelial cells in all types, but are less abundant in the later onset forms.

Radiological abnormalities in type 1 may be minimal at birth but become progressively more pronounced with time. By 6 months there is usually little difficulty in identifying them. The abnormalities include kyphoscoliosis and hypoplasia and beaking of one or more vertebrae. The long bones are wide in the center, tapering to both ends. There is generalized rarefaction of the cortex of most bones. With increasing age the externally thickened cortical wall is removed by expansion of the medullary cavity. The metacarpals are wedge-shaped, being expanded distally and constricted proximally. The sella turcica is shoe shaped, shallow, and elongated. In type 2, radiological changes are mild and involve mainly the vertebral bodies. In type 3 the radiological changes are minimal or absent. Flattening of vertebral bodies may be seen.

In types 1 and 2 the EEG shows progressive deterioration, but epileptic discharges are rare. The ERG remains normal.

Biochemical investigations disclose abnormal urinary oligosaccharide excretion. The concentration of the urinary oligosaccharides appears to correlate with the severity of the disease, the excretion being highest in type 1 and lowest in type 3 GM₁ gangliosidosis. The CSF protein is normal. In types 1 and 2 an increased concentration of GM₁ ganglioside may be found in plasma and CSF.

Demonstration of a deficiency of β -galactosidase activity in leukocytes or cultured fibroblasts is the most effective means of establishing the diagnosis. It is important also to analyze neuraminidase activity in order to exclude galactosialidosis. A decreased hydrolysis rate of GM₁ ganglioside can be demonstrated in cultured skin fibroblasts. DNA analysis for diagnostic purposes is possible. Prenatal diagnosis is possible by enzyme analysis in cultured amniotic fluid cells or chorionic villi or by DNA analysis.

9.2 Pathology

External examination of the brain in type 1 GM₁ gangliosidosis usually reveals no abnormalities, though sometimes some cortical atrophy is detected. The consistency of the white matter may be increased.

Light microscopy reveals neuronal storage throughout the nervous system, mainly in cerebral and cerebellar cortex, but also in basal ganglia, brain stem, spinal cord, and Meissner's plexus. The neurons have ballooning, foamy cytoplasm, and the nucleus is displaced to the periphery. Accumulation of storage material in proximal nerve cell processes results in the formation of meganeurites and megadendrites. There

is degeneration and loss of neurons. Storage bodies are also present in glia.

Electron microscopy demonstrates that the neuronal inclusion bodies are identical to the membranous cytoplasmic bodies seen in GM₂ gangliosidosis. They consist of spirally wound membranous lamellae enclosed within a limiting membrane of lysosomal origin.

The white matter in type 1 GM₁ gangliosidosis is gliotic, and there is a diffuse and profound paucity of myelin. Axons are relatively preserved. Where present, myelin is structurally normal, but the thickness of most myelin sheaths is reduced. The early myelinating structures have a myelin content that is normal for age, whereas the myelin content of later myelinating structures is much lower than expected. Oligodendrocytes are decreased in number, and apoptosis of these cells can be observed. The white matter abnormalities are probably the result of a combination of disturbed myelination and myelin loss.

In type 1 GM₁ gangliosidosis visceral storage is found. The liver is enlarged, and storage material is present in hepatocytes and in histiocytes in liver sinusoids. The renal glomerular epithelium shows marked vacuolization of the cytoplasm. The spleen, lymph nodes, thymus, and intestinal mucosa contain many foamy histiocytes. Large foamy histiocytes are present in bone marrow aspirates. Skin biopsies show foamy vacuolization of sweat gland epithelium, histiocytes, fibroblasts, and endothelium cells. The vacuoles appear empty. The stored oligosaccharides in visceral organs are extremely soluble in water and are lost on fixation.

In types 2 and 3 GM₁ gangliosidosis identical neuronal storage is seen. In type 3 the neuronal storage is present predominantly in the basal ganglia. White matter is either not affected at all, or only to a minimal extent. The visceral storage varies considerably. There may be no storage at all, or sparse histiocytes may be seen in spleen and liver. There may be foam cells in bone marrow and lymphatic tissue, and vacuolization of hepatic and renal cells similar in form to but less severe than in type 1.

9.3 Chemical Pathology

Gangliosides are glycosphingolipids that contain sialic acid in their oligosaccharide chain. In type 1 GM₁ gangliosidosis pronounced accumulation of the normal monosialoganglioside GM₁ occurs, accompanied by a minor accumulation of its asialo derivative GA₁ and of other minor glycolipids and glycopeptides. The total ganglioside content of the brain is increased, with an approximately 10-fold increase of GM₁ in gray matter and a 2-fold increase in white matter. In gray matter GM₁ ganglioside constitutes

70–90% of total ganglioside, instead of the normal about 25%. The level of total lipid in gray matter is slightly decreased, mainly due to a moderate decrease of phospholipids and glycolipids. In white matter a marked decrease of major myelin constituents is found, such as cholesterol, phospholipids, cerebroside, sulfatides, and proteolipid protein. Marked increases in free fatty acids and in cholesterol esters are found in most cases. The white matter chemical abnormalities are compatible with moderately severe myelin destruction. In the myelin membrane itself the concentration of GM₁ ganglioside is also several times the normal concentration. Other abnormalities in the composition of isolated myelin are a very high concentration of cholesterol, a low level of glycolipids, especially cerebroside, and a low concentration of phospholipids, especially ethanolamine phospholipids. These myelin abnormalities represent the transitional state of myelin undergoing nonspecific breakdown.

The neuronal inclusion bodies, the so-called membranous cytoplasmic bodies, have an extremely high ganglioside content. GM₁ accounts for approximately 95% of the total ganglioside content. Other components are proteolipid protein, phospholipids, and cerebroside. One of the glycolipids, cerebroside, consists mainly of glucocerebroside, which is an unusual cerebral constituent after the infantile period.

There is a 20- to 50-fold accumulation of GM₁ ganglioside in liver and spleen. Furthermore, there is visceral accumulation of galactose-containing oligosaccharides, which by far exceeds the accumulation of gangliosides. Some oligosaccharide fractions contain sialic acid. The oligosaccharide accumulation rather than the ganglioside storage is the chief cause of the visceral histiocytic vacuolation. Storage of galactose-containing, partially degraded, derivatives of keratan sulfate has been demonstrated in liver and brain.

In type 2 GM₁ gangliosidosis the concentration of GM₁ ganglioside and its asialo derivative are moderately elevated in the brain, to a considerably lesser degree than in type 1 GM₁ gangliosidosis. The myelin lipids, such as cholesterol, phospholipids, sulfatide, and cerebroside, are much closer to normal than in type 1 GM₁ gangliosidosis. Visceral accumulation of oligosaccharides is less marked.

In type 3 GM₁ gangliosidosis the accumulation of GM₁ ganglioside in the brain is more focal. Accumulation is most marked in the putamen and caudate nucleus, where GM₁ accounts for 50% or more of all gangliosides, whereas GM₁ accounts for about 30% of all gangliosides in the white matter and only a slight increase, if any, in the proportion of GM₁ ganglioside is noted in the cerebral cortex. Abnormal accumulation of asialo GM₁ is only noted in the basal ganglia. There are no abnormalities in the concentrations of other lipids, such as cholesterol, phospholipids, and

glycolipids. Visceral accumulation of oligosaccharides is minor.

9.4 Pathogenetic Considerations

GM₁ gangliosidosis is caused by a deficiency of the lysosomal degradative enzyme acid β -galactosidase. This enzyme is an acid hydrolase catalyzing cleavage of terminal β -linked galactose from a variety of substrates, including GM₁ ganglioside, its asialo derivative G_{A1}, lactosylceramide, galactose-containing oligosaccharides, and the mucopolysaccharide keratan sulfate. The gene coding for β -galactosidase, *GLB1*, is located on chromosome 3p21.33. Activity of β -galactosidase is also dependent on a functional protein, called protective protein/cathepsin A. This protein is encoded by *PPGB*, a gene located on chromosome 20q13.1. Protective protein associates with two enzymes, β -galactosidase and neuraminidase, in an early biosynthetic compartment, and by virtue of the association the two enzymes are correctly routed to the lysosome and protected against rapid breakdown by intralysosomal proteases. Some hydrolytic enzymes need nonenzymic factors (activator proteins) for degradation of sphingolipids in the lysosome. Substrates cleaved by β -galactosidase differ in their requirement of such activator proteins. Sphingolipid activator protein 1 (called SAP-B or saposin B) is required for the cleavage of GM₁ ganglioside by β -galactosidase. SAP-B acts on GM₁ as a kind of solubilizer. SAP-B shares a common larger precursor protein, called prosaposin, with some other SAPs. Prosaposin is encoded by a gene on chromosome 10q22.1, *PSAP*. SAP-B not only activates β -galactosidase to cleave GM₁ ganglioside, but also activates the cleavage of sulfatide by arylsulfatase A and globotriaosylceramide by α -galactosidase.

Two diseases have been recognized for deficiency of β -galactosidase: GM₁ gangliosidosis, a neurodegenerative disorder with visceral involvement, and mucopolysaccharidosis type IV B, also called Morquio B disease, a generalized bone disease. Molecular analysis has confirmed allelic mutations of the same gene in these two diseases with diverse phenotypic expressions. It has been suggested that this multiplicity of phenotypes can be explained by different alterations in the catalytic activity of the mutant enzyme, which differentially alters its activity on a variety of substrates. There is evidence that patients with Morquio disease type B retain a higher catalytic activity for GM₁ ganglioside than for oligosaccharides and mucopolysaccharides. The phenotypic variability in clinical symptomatology of GM₁ gangliosidosis may be explained in the same way. The early infantile form is characterized by neurological dysfunction in combination with bony abnormalities and

visceral storage. In later onset forms, progressive neurological symptoms are present but visceral and bony abnormalities are minimal or absent. Differences in residual enzyme activity, different types of mutations affecting different catalytic functions of the enzyme, different rates of turnover of the enzyme and substrates in brain, viscera, and bone may be responsible for these phenotypic variations. An attractive hypothesis is that in some cases the mutant enzyme possesses about the same low residual activity for each natural substrate (infantile type), whereas the mutant enzyme possesses significantly different residual activities for different natural substrates in other cases (juvenile and adult types).

Apart from GM₁ gangliosidosis and Morquio disease type B, β -galactosidase deficiency occurs in a number of disorders caused by different gene mutations: variant forms of metachromatic leukodystrophy, galactosialidosis, and I cell disease. Deficiency of the protective protein caused by a protective protein gene mutation leads to galactosialidosis. Deficiency of the protective protein gives rise to a secondary deficiency of both β -galactosidase and neuraminidase activity. SAP-B deficiency results in a form of metachromatic leukodystrophy, with a variable concomitant accumulation of gangliosides and other glycosphingolipids in addition to sulfatide storage. In I-cell disease, or mucopolipidosis III, deficiency of β -galactosidase is caused by a defect in posttranslational processing of the enzyme molecule.

In GM₁ gangliosidosis, GM₁ ganglioside and its asialo derivative accumulate in lysosomes owing to the impairment of normal degradation. GM₁ is a normal component of cellular membranes, and its content is especially high in neuronal plasma membranes, particularly in the regions of nerve endings and dendrites. GM₁ gangliosides act as binding molecules for toxins and hormones and are involved in cell differentiation and cell-cell interaction. They stimulate neurite outgrowth and enhance the action of nerve growth factor. In GM₁ gangliosidosis accumulation occurs predominantly in neurons, resulting in neuronal dysfunction and eventually neuronal cell death. There are several factors, which may contribute to neuronal dysfunction and death. The accumulated GM₁ ganglioside and its asialo derivative are relatively insoluble in water and aggregate within lamellated membranous bodies in lysosomes. Expanding lysosomes with increasing amounts of stored products may disturb intracellular transport, in this way disturbing cellular metabolism. Leakage of toxic intralysosomal products of enzymes into the cytoplasm during the process of intralysosomal storage may cause damage. Accumulation of GM₁ ganglioside in the neuronal membrane results in alterations of membrane structure. Gangliosides contain long, saturated fatty acids, which increase the packing density

of the membrane and reduce its fluidity. GM₁ ganglioside, specifically, has a pronounced effect on the reduction in membrane fluidity as the carbohydrate moieties of GM₁ reduce the rotational freedom within the hydrophobic regions of the membrane. The increased cholesterol content also contributes to the reduction of membrane fluidity. The altered membrane fluidity may influence the synaptic transmission and the activity of membrane-bound enzymes. GM₁ gangliosidosis is also characterized by inappropriate proliferation of secondary neurites and aberrant formation of synapses. This abnormal sprouting may lead to changes in neuronal connectivity, resulting in specific functional impairment. Evidence has been found for neurotransmitter dysfunction with disturbed neurotransmitter release and re-uptake and for specific dysfunction of cholinergic and GABAergic neurons.

The later onset forms of GM₁ gangliosidosis have more focal neuronal pathology, which is especially marked in basal ganglia and the spinal cord, whereas in the infantile form there is more generalized neuronal pathology, which is especially pronounced in cerebral and cerebellar cortex. We can only speculate on the explanation for this phenomenon. The regulation of substrate and enzyme synthesis and turnover may not be identical in different types of cells and may not be the same at all ages, which would change the distribution of cells in which saturation of the residual enzyme occurs earliest and is most prominent.

Significant white matter changes are only present in type 1 GM₁ gangliosidosis. There is a severe myelin deficiency, which is caused mainly by a disturbance of myelinogenesis with seriously delayed and arrested myelination. Myelin deposition occurs in close collaboration between axons, oligodendrocytes, and astrocytes. Altered neuronal/axonal membrane properties and disturbed oligodendroglial-axonal communication may be at the basis of the disturbed myelination process. Disturbances of oligodendroglial maturation and myelin production and early oligodendroglial cell death through apoptosis are contributing factors. However, there is also a component of myelin loss. The myelin loss may be secondary to degeneration of neurons as well as primary owing to oligodendroglial cell death, altered myelin composition, and myelin instability.

Galactose-containing oligosaccharides accumulate in the viscera, particularly in type 1 GM₁ gangliosidosis. These oligosaccharides are derived from the incomplete degradation of glycoproteins in lysosomes. The accumulation of these water-soluble compounds is responsible for the cytoplasmic vacuolation of visceral cells, the foamy histiocytosis in bone marrow, and the vacuoles in circulating lymphocytes. Storage of galactose-containing, partially degraded deriva-

tives of keratan sulfate occurs in liver, spleen, brain, and bone, especially in type 1. Storage of these compounds in bones is responsible for the bony deformities.

9.5 Therapy

At present there is no effective treatment for GM₁ gangliosidosis. Hematopoietic stem cell transplantation can be attempted, especially in the later onset forms, but insufficient data are as yet available to assess its potential. In addition, there is evidence in animal experiments that the low molecular compound 1-deoxygalactonojirimycin may increase β -galactosidase activity. The compound passes through the blood-brain barrier. Human studies are in progress. Gene therapy is still at the level of experimental research.

9.6 Magnetic Resonance Imaging

In type 1 GM₁ gangliosidosis CT of the brain typically shows a slightly increased density of the thalamus (Fig. 9.1). MRI shows diffuse white matter abnormalities, partly but not only explained by severely delayed and disturbed myelination. The signal abnormalities are more pronounced than would be expected if they were due merely to delayed myelination (Fig. 9.1). White matter gliosis and some myelin destruction add to the signal changes. We observed a very subtle pattern of radiating lines with a more normal signal

intensity within a patient's abnormal cerebral white matter, which we found to be related to a higher myelin content in perivascular regions. The brain stem, and sometimes the posterior part of the corpus callosum, are better myelinated, but the cerebellar white matter can be myelin deficient (Fig. 9.1). The basal ganglia and thalamus display subtle signal changes on MRI, with a slightly increased or decreased signal intensity of the thalamus and a slightly increased signal intensity of the basal ganglia on T₂-weighted images and a variably increased signal intensity of the thalamus on T₁-weighted images (Fig. 9.1, upper row). The pattern closely resembles the imaging findings in early-onset GM₂ gangliosidosis.

In type 2 GM₁ gangliosidosis, progressive atrophy of the cerebral hemispheres has been described with enlargement of the ventricular system and subarachnoid space and atrophy of the cerebellum and brain stem (Fig. 9.2). There are subtle white matter signal abnormalities, which are commonly seen in neuronal degenerative disorders and are secondary to loss of neurons and axons and their myelin sheaths (Fig. 9.2). The CT images that have been published suggest that the density of the thalamus and basal ganglia might possibly be mildly increased.

In type 3 GM₁ gangliosidosis, elevated T₂ signal and atrophy may be found bilaterally in the caudate nucleus and putamen. Hypointensity of the globus pallidus on T₂-weighted images has also been reported. In addition, cerebral atrophy and slight white matter signal changes secondary to neuronal degeneration can be found. The images are identical to those of adult GM₂ gangliosidosis.

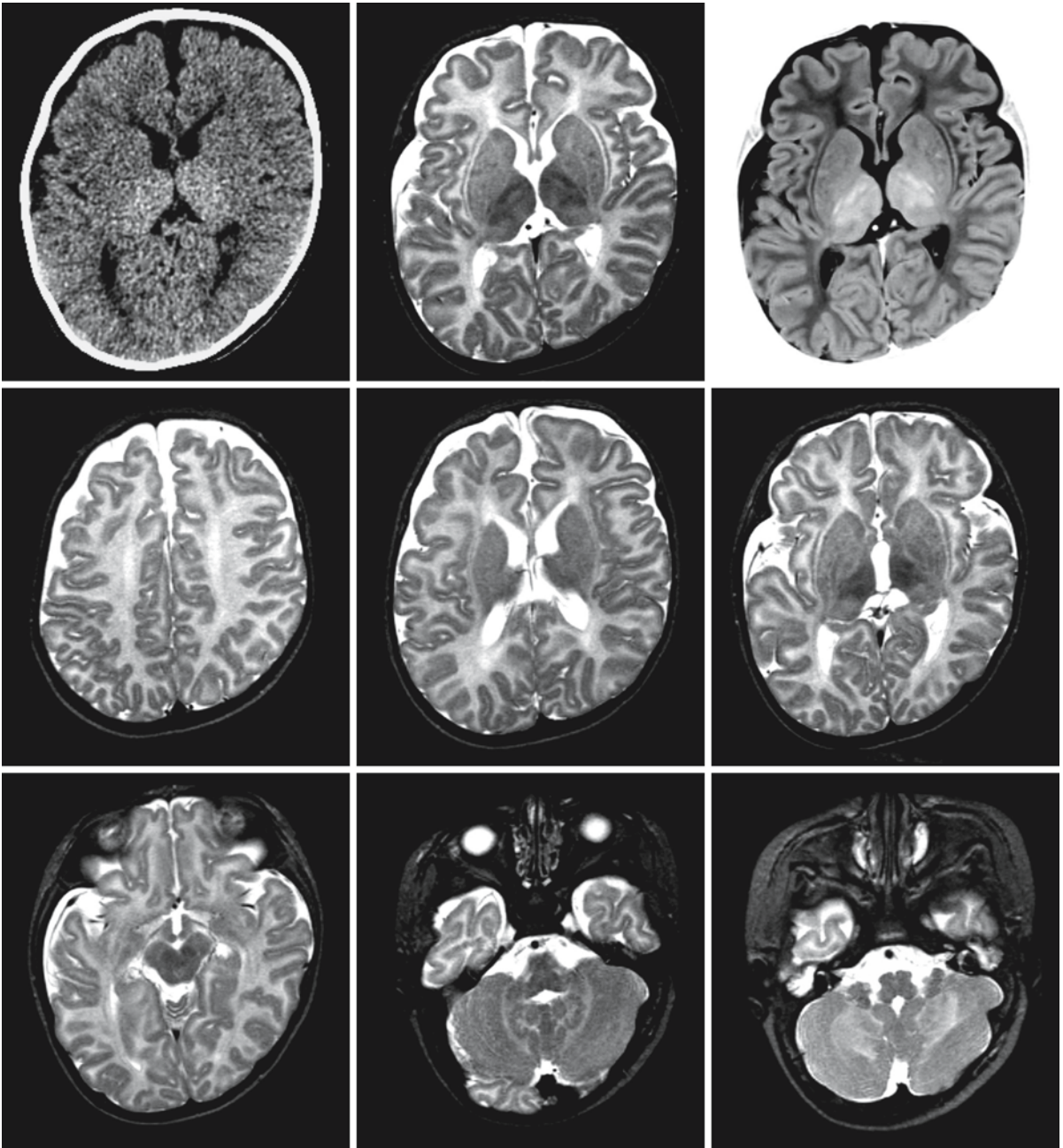


Fig. 9.1. CT scan and MR images in a 7-month-old boy with type 1 GM₁ gangliosidosis. Note the high density of the thalamus on CT. The thalamus and basal ganglia are diffusely slightly abnormal on both T₁- and T₂-weighted MR images (*first row*).

The cerebral and cerebellar white matter has a diffusely distributed high signal on T₂-weighted images, which is higher than is compatible with hypomyelination only

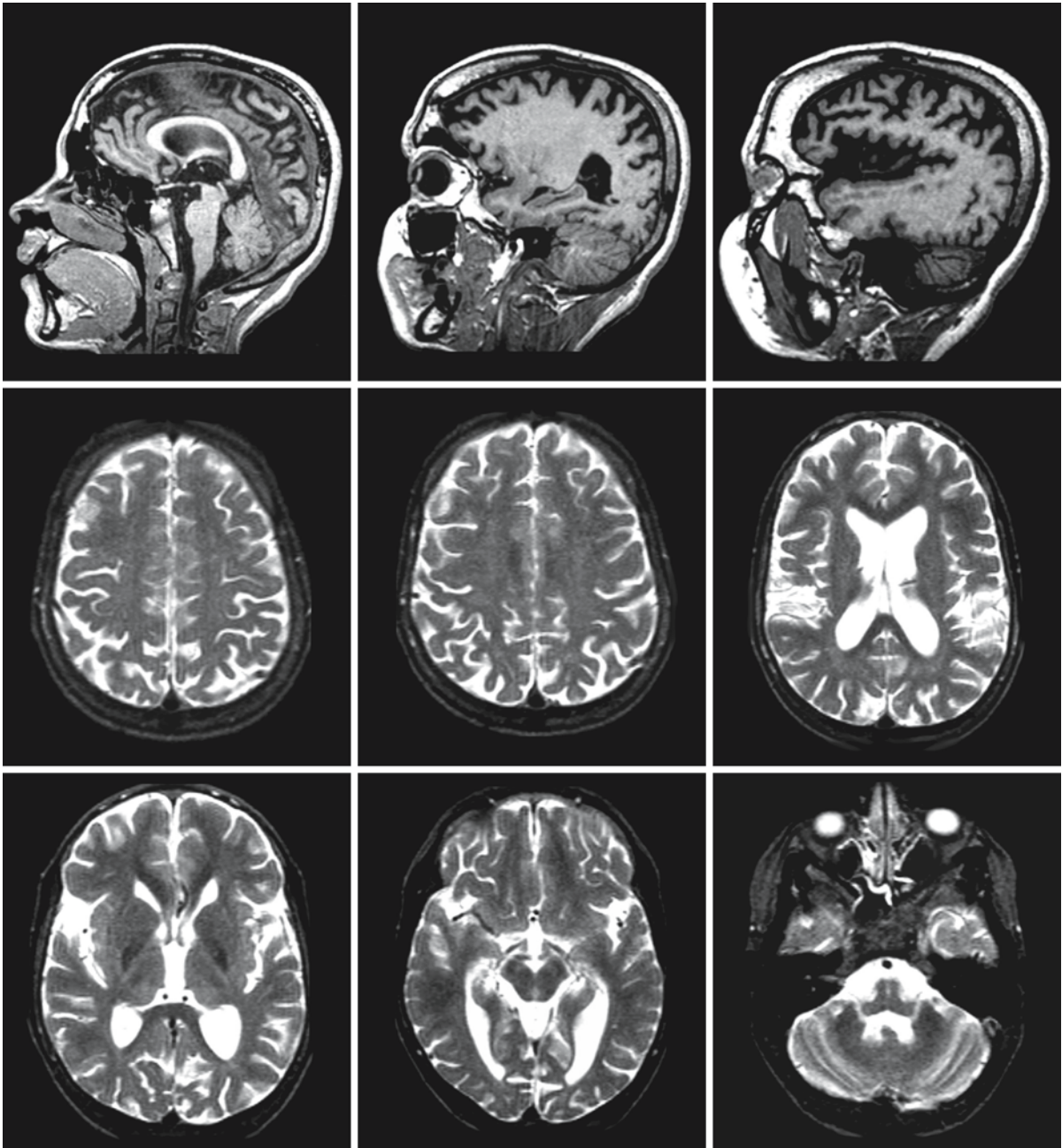


Fig. 9.2. Sagittal T₁-weighted and axial T₂-weighted images in a 9-year-old boy with type 2 GM₁ gangliosidosis. The thick skull indicates a long-standing disease process. The cerebral white matter has a slightly higher signal than normal on these

T₂-weighted images, and the cerebral hemispheres are mildly atrophic, suggestive of a primary neuronal degenerative process. The globus pallidus has a low signal

GM₂ Gangliosidosis

10.1 Clinical Features and Laboratory Investigations

GM₂ gangliosidoses are inherited disorders of GM₂ ganglioside metabolism. Its inheritance is autosomal recessive. There are three major, biochemically distinct types: B, O, and AB. Among the B and O types, infantile, juvenile, and adult forms can be distinguished; the AB variant is known only as an infantile form. Infantile type B is the classic Tay-Sachs disease (TSD), and infantile type O is the same as Sandhoff disease (SD).

TSD is common in Ashkenazi Jews of eastern European origin. In the United States carrier frequency is 1 in 30 among Ashkenazi Jews and only 1 in 380 among other groups. TSD infants seem normal at birth, and their early development apparently follows a normal pattern. The disease begins at the end of the first 6 months of life. An exaggerated startle response is often the earliest symptom, although it is frequently only recognized in retrospect. It is provoked by sudden noise and consists in extension, abduction, and elevation of the arms. Listlessness and irritability usually occur early in the course of disease. Gradually, psychomotor retardation and deterioration with loss of skills becomes evident. After 6 months of age the patient's vision noticeably deteriorates and hypotonic motor weakness becomes obvious. Affected infants may crawl, sit unaided, and pull themselves up to a standing position but do not usually manage to walk. By 1 year of age the deterioration of mental and motor capacities is obvious. The children no longer sit, hold, or transfer objects; they lose interest in their surroundings and usually lie placidly in bed. In the 2nd year hypotonic motor weakness progresses, and by the end of the 2nd year generalized flaccid paralysis has developed. The tendon reflexes are increased at all stages, and plantar responses may be extensor. In the later stages of the disease signs of spasticity, dystonia, rigidity, chorea and athetosis may be variably present. At the end of the 1st year of life most children are blind. Ophthalmoscopic examination reveals a cherry-red spot in one or both maculae in about 90% of the patients. Optic atrophy is also seen. Feeding becomes a problem in the 2nd year because of ineffective swallowing. Seizures are rare before the age of 1 year, but frequent thereafter. The epileptic manifestations may consist in tonic-clonic seizures, myoclonic epilepsy, and also gelastic epilepsy. A char-

acteristic sign in TSD is megalencephaly, which usually becomes prominent at about 2 years of age. By the age of 2 most patients are completely paralyzed, demented, blind, and deaf with frequent seizures. Decerebrate posturing may be present. Most patients die of bronchopneumonia and emaciation. Death usually occurs between 2 and 3 years of age, survival after the age of 4 being rare.

The clinical features of SD are similar to those of TSD, with the exception of hepatosplenomegaly, which does not occur in TSD. Occasionally there are bony deformities similar to those associated with infantile GM₁ gangliosidosis. Infantile GM₂ gangliosidosis type AB is also clinically similar to TSD. These disorders have no racial predilection.

In addition to the severe infantile forms of GM₂ gangliosidosis, later onset forms are known. The so-called juvenile form usually has its onset between 2 and 6 years of age. The adult, or rather chronic, form, has its onset between the end of the 1st decade and the 3rd decade of life. Even later onset has been described. However, the age of onset is difficult to determine because of the very slow progression of the disease. While the juvenile form has no ethnic predilection, the adult B form is more frequent among Ashkenazi Jews than in other ethnic groups. The main systems affected in the juvenile and adult variants are the cerebellum, the pyramidal cells, the lower motor neurons and, less frequently, the basal ganglia. Atypical spinocerebellar ataxia syndromes are common as modes of presentation of late-onset GM₂ gangliosidosis. They are characterized by slowly progressive ataxia, spasticity, dysarthria, and muscle atrophy. Such cases have been diagnosed as atypical variants of Friedreich ataxia, however, usually without sensory involvement. In some patients additional abnormalities in the form of supranuclear or internuclear ophthalmoplegia and sensory neuropathy have been described, but these are rare. Another relatively frequent presentation is as motor neuron disease. Clinical features include weakness, cramps, proximal muscle wasting, and fasciculations. This clinical picture closely resembles the Kugelberg-Welander phenotype of spinal muscular atrophy or bulbospinal neuronopathy. Amyotrophic lateral sclerosis-like syndromes present with involvement of both lower and upper motor neurons. Apart from paresis, atrophy and fasciculations, high reflexes, and extensor plantar reflexes are found. Upper limb postural tremor may

occur, as in other disorders of the lower motor neuron. Various extrapyramidal features have been described in late-onset GM₂ gangliosidosis, either in isolation or in combination with the more common motor neuron and cerebellar syndromes. Dystonia, rigidity, choreiform movements, and athetoid posturing have been noted. Another clinical characteristic of late-onset GM₂ gangliosidosis is the high incidence of recurrent psychosis. In addition, psychic changes include anxiety, depression, insomnia, aggressiveness, severe behavioral problems, and disintegration of the personality. The psychic changes may precede all other manifestations or may appear later. Neurovegetative disorders are common and take the form of sweating impairment, loss of libido, impaired esophagus motility, fixed cardiac frequency, and orthostatic hypotension. Intellectual deterioration is frequent. Epilepsy may occur, but is not obligatory. Blindness occurs late in the course of the disease. On ophthalmoscopic examination, optic atrophy and retinitis pigmentosa may be seen at that time, but a cherry-red spot is not a consistent finding and appears late if at all. In the juvenile variant death occurs between 5 and 15 years of age, often secondary to bronchopneumonia. Patients with the adult form usually live for some decades.

In the infantile variants, EEG is either normal or shows slight changes during the 1st year of life. In the 2nd year there are paroxysmal discharges of high-voltage, slow-wave activity with single and multiple spikes and sharp wave complexes. In the vegetative state of the disease there is a marked decrease in spike discharges. These findings are not specific for infantile GM₂ gangliosidosis. In later onset variants the EEG shows variable, nonspecific findings. Nerve conduction velocities are usually normal in the first stage of the disease and then decline. EMG shows fasciculations, especially in the proximal muscles, and signs of loss of motor units with collateral reinnervation. Muscle biopsy shows signs of neurogenic atrophy with type grouping and increased connective tissue. Sural nerve biopsy demonstrates decreased fiber density. A histogram of counted nerve fibers shows a decrease in the number of large myelinated fibers and an increase in small myelinated fibers, indicating active regeneration. Rectal biopsy reveals swollen ganglion cells with vacuolated cytoplasm. Ultrastructurally, the ganglion cells contain membranous cytoplasmic bodies, which are typically found in neurons in GM₂ gangliosidosis.

A definitive diagnosis is established by assaying hexosaminidase A and B in serum, leukocytes, or cultured skin fibroblasts. In the case of variant B, hexosaminidase A is deficient. In the case of variant O, both hexosaminidase A and hexosaminidase B are deficient. In the case of variant B₁, the activities of hexosaminidase A and B are found to be normal when

tested with the conventional, nonsulfated synthetic substrate, but a profound deficiency of hexosaminidase A activity is found on testing with the natural substrate GM₂ ganglioside or a sulfated synthetic substrate. Prenatal diagnosis of these variants of GM₂ gangliosidosis is possible in the first trimester of pregnancy by enzyme analysis in cultured amniotic fluid cells or chorionic villi.

In the case of type AB, the activities of hexosaminidase A and B are found to be normal, since in this type the defect is a deficiency of the GM₂ activator protein. In type AB the diagnosis requires either the demonstration of accumulating GM₂ ganglioside in the presence of normal hexosaminidase A and B activities or the demonstration of the GM₂ activator protein deficiency. GM₂ ganglioside accumulation can be demonstrated in brain biopsy tissue or alternative sources of nervous tissue (rectum, conjunctiva), and probably also in CSF, although the sensitivity and specificity of the latter test is not known. The deficiency of GM₂ activator protein can be demonstrated by feeding radiolabeled GM₂ ganglioside to cultured fibroblasts and correcting the disturbed degradation of this substance by the addition of purified GM₂ activator protein to the culture medium. The expression level of GM₂ activator protein can also be assessed in fibroblasts.

DNA analysis is possible for all variants of GM₂ gangliosidosis. If the mutations responsible are found in a family, carrier testing and prenatal diagnosis become more reliable. Pseudodeficiency may occur, and DNA analysis helps to ensure the presence of a benign pseudodeficiency allele. Accurate and inexpensive screening tests are available for detection of GM₂ gangliosidosis carriers. Enzymatic tests are used, which determine total serum hexosaminidase and hexosaminidase A activity; the leukocyte hexosaminidase assay is used for confirmation. Nowadays screening for common mutations is preferred in populations with a high carrier frequency for certain mutations.

10.2 Pathology

In infantile GM₂ gangliosidosis the gross changes in the brain vary with the length of the patient's life. The weight and volume of the brain increase massively during the 2nd year of life. The brain frequently weighs over 2000 g (normal weight 1000 g). Enlargement of the brain causes the gyri to become broadened. The cerebellum, however, is usually atrophic. On sectioning, the cut surface is abnormally firm. The hemispheric white matter may be gelatinous with local cavitation. The ventricles are variably enlarged.

Light microscopy shows ubiquitous involvement of the nerve cells throughout the brain, with a predilec-

tion for the neurons in the cerebral hemispheres over the ganglion cells of the motor cranial nerves or other brain stem nuclei. There is a diffuse disturbance of the cytoarchitecture of the gray matter with a reduction in the number of nerve cells, an unusual increase in size of the remaining neurons, and a concomitant augmentation in the number of glial elements. The neurons are large and distorted as a result of the deposition of lipid material. They have a distended, rounded outline; their nuclei are displaced to the circumference of the cell and are often shrunken and pyknotic. Cortical neuronal cells have swellings in the proximal axon segment or in the apical dendrite, resulting in so-called meganeurites. As the disease progresses, the neurons gradually disappear. There is a decrease in the number of axons seen within the white matter of the brain, which parallels the process of degeneration of the cerebral cortical nerve cells. With progression of the disease there are profound disturbances in myelination, with evidence of additional myelin loss. The myelin deficiency may be very extensive. In some patients the myelin deficiency is seen predominantly in the centrum semiovale with sparing of the subcortical U fibers, but in most patients it involves almost the entire white matter, including the U fibers. The internal capsule is usually well preserved. The preserved myelin sheaths frequently appear thinner than normal. Complete absence of myelin throughout the hemispheric white matter can occur if the patient survives for a long time. The white matter changes cannot be attributed to wallerian degeneration only. There is evidence for an additional role of both failure of myelination and active demyelination: the severity of myelin loss is often greater than the axonal loss, and the tendency to softening and cavitation in the most severely affected areas is consistent with active demyelination and not with wallerian degeneration only. As the disease progresses, the glial reaction increases and eventually large numbers of microglia can be observed as well as numerous proliferating astrocytes. The glial cells are swollen and filled with large globules. The contents of these glial cells show similar properties to those observed in neurons. The cerebellum shows extensive degenerative changes. Narrowing or reduction in size of the cerebellar folia is associated with decreased numbers of cells in the cerebellar cortex. The Purkinje cells show extensive damage and those remaining are filled with the same material that is present in the neurons of the cerebral cortex. The neurons of the cerebellar nuclei also show the typical ballooning due to deposition of lipids. The spinal cord neurons undergo changes similar to those seen elsewhere in the CNS. The neurons of the anterior horns are more intensely affected than those of the posterior and lateral horns. The spinal cord white matter frequently shows rarefaction of the nerve fibers, particularly in

the lateral columns and in the pyramidal tracts, but they are normally myelinated. Microscopic examination of the retina reveals extensive degeneration and loss of ganglion cells. The cytoplasm of the remaining cells is filled with lipid material similar to that seen in the neurons of the brain. These changes are particularly conspicuous in the area of the macula.

Electron-microscopic studies have shown that the cytoplasm of the distended neurons contains so-called membranous cytoplasmic bodies. These are membrane-bound structures, which contain closely packed lamellae, frequently arranged concentrically in a regular fashion. The lipid material, which is seen under light microscopy, is located in these membranous cytoplasmic bodies. They occupy a considerable proportion of the nerve cell cytoplasm. Their accretion within the neuronal cytoplasm causes the enormous ballooning of the cell and the displacement of the nucleus to the periphery. Accumulation of these storage bodies in proximal nerve processes leads to the formation of meganeurites and megadendrites. It has been shown that these storage bodies are lysosomal in origin. They are also found in axons and glial cells. In glial cells the deposits are more pleomorphic than in neurons.

Especially in SD, extraneuronal storage of lipids is found. Cells containing stored material are found in the spleen, in renal tubular cells, and in liver cells. The deposited material appears to be similar to that of the neurons.

In juvenile and adult GM₂ gangliosidosis pathological changes predominantly affect the anterior horn cells of the spinal cord, the cerebellar cortical neurons, brain stem nuclei, and basal ganglia. In these areas prominent neuronal storage and degeneration are present. The cerebral cortex is less severely or minimally involved. This is the reverse of what occurs in infantile gangliosidosis. The cerebellum is atrophic. Slight diffuse myelin loss within the cerebral and cerebellar white matter may be observed.

10.3 Chemical Pathology

GM₂ ganglioside is accumulated in abnormally large amounts in GM₂ gangliosidosis. In the brain, the concentration of gangliosides is 100–300 times that in normal brain. The storage patterns of the gangliosides exhibit some characteristic differences in the three variants of GM₂ gangliosidosis. In all cases the accumulation of the ganglioside GM₂ is most pronounced. It is accompanied by minor storage of its sialic acid-free derivative, GA₂. Variant 0 is characterized by the fact that the nervous tissue contains – in relative terms – the lowest amount of GM₂ and the highest amount of GA₂. Variant B and variant AB differ from each other in the extent to which GM₂ and

GA₂ are accumulated, the accumulation being higher in the AB variant. The gangliosides are mainly stored in the neuronal cells, but the ganglioside concentration of white matter is also increased. In late-onset forms of GM₂ gangliosidosis, cerebral levels of GM₂ and GA₂ are markedly increased above normal, but not to the extent seen in infantile forms. A regional variation in ganglioside accumulation in the brain can be seen, depending on the variation of neuronal storage in the different types of GM₂ gangliosidosis.

Some 30–40% of the lysosomal inclusion bodies consist of GM₂ ganglioside. Other components are proteolipid protein, cholesterol, phospholipids, and glycolipids.

Except for a high concentration of GM₂ ganglioside, the change in chemical composition of the white matter is nonspecific and reflects the extent of myelin deficit. The main findings are decreases in proteolipid protein, total lipids, glycolipids, and phospholipids and the presence of significant amounts of cholesterol esters as a sign of active myelin breakdown.

In the B variant and the AB variant, GM₂ ganglioside is not stored in large amounts outside the nervous system. In the O variant there is an extensive storage of globoside in the visceral organs, besides storage of GM₂ and GA₂ ganglioside. The level of globoside is approximately normal in the visceral organs in the B variant and the AB variant.

10.4 Pathogenetic Considerations

Gangliosides are glycosphingolipids, which contain sialic acid in their oligosaccharide chain. GM₂ gangliosidosis is caused by a deficient activity of the lysosomal enzyme β -hexosaminidase, also called GM₂ gangliosidase or β -N-acetylgalactosaminidase. This enzyme hydrolyzes the terminal N-acetylgalactosamine from the ganglioside GM₂. Hexosaminidase is composed of two subunits. The α - and the β -chain can associate in different combinations to produce isoenzymes of different structure and catalytic activity. Isoenzyme $\alpha\beta$ is called hexosaminidase A, isoenzyme $\beta\beta$ hexosaminidase B, isoenzyme $\alpha\alpha$ hexosaminidase S. Hexosaminidase A cleaves the substrates ganglioside GM₂, the asialo derivative GA₂, globoside, neutral oligosaccharides, and negatively charged substrates, such as terminal β -linked N-acetylglucosamine-6-sulfate contained in keratan sulfate, chondroitin sulfate, and dermatan sulfate. Hexosaminidase B has an overlapping substrate specificity and cleaves GA₂, globoside, and neutral oligosaccharides. Hexosaminidase B does not possess any significant ganglioside GM₂-cleaving activity. Hexosaminidase S has only negligible catalytic activity. Apart from the α - and β -chains of hexosaminidase, a third protein is necessary for in vivo catabolism of

GM₂ ganglioside: an activator protein. This activator protein is termed GM₂ activator protein (GM2AP) or sphingolipid activator protein 3 (SAP-3). The GM₂ activator protein has an isoenzyme specificity for hexosaminidase A, and not for hexosaminidase B or S. Interaction of the activator protein with GM₂ ganglioside or related compounds results in the formation of a water-soluble dimer. The activator-lipid complex binds to a specific recognition site of hexosaminidase A in such a way that the glycosidic bond is positioned at the active site in the α -subunit. Thus, the GM₂ activator functions as a transport protein rather than as an activator of the enzyme.

The different types of GM₂ gangliosidosis are characterized by the isoenzyme, which is missing. In type B, there is a deficiency of hexosaminidase A (isoenzyme $\alpha\beta$) resulting from mutations in the gene encoding the α -chain, *HEXA*, located on chromosome 15q23–24. In type O, both hexosaminidase A ($\alpha\beta$) and hexosaminidase B ($\beta\beta$) are deficient. This is the result of mutations in the gene encoding the β -chain on chromosome 5q13, *HEXB*. Type AB is caused by a deficiency of the GM₂ activator protein, encoded by a gene located on chromosome 5q31.3–33.1, *GM2A*. A special variant of GM₂ gangliosidosis has been described, the B₁ variant, which is allelic to the B variant. In the B₁ variant, a mutation affects a specific α -chain site to which the activator-substrate complex binds. The mutant enzyme has an almost normal activity towards substrates that are split at the active site located on the β -subunit (including non-sulfated synthetic substrates). It is virtually inactive towards the substrates that are exclusively or preferentially cleaved at the active site of the α -subunit (GM₂ ganglioside and also synthetic substrates containing a sulfate group). The B₁ mutation appears to be rare in the homozygous form, but may be more commonly encountered in the B/B₁ compound heterozygous form.

The time of onset and clinical severity of the disease are related to the rate of ganglioside accumulation, which is inversely related to the residual activity of hexosaminidase in the patient's tissues. The variable residual enzyme activities among infantile, juvenile, and adult-onset GM₂ gangliosidosis patients are related to different mutations present either in the homozygous or the compound heterozygous state. In its homozygous state the most common mutation in the α -subunit gene causes a total absence of hexosaminidase A and leads to the severe infantile form of the disease, TSD. In contrast, adult α -subunit mutations cause a severe, but not complete, deficiency of hexosaminidase A. Both the infantile and adult α -subunit mutations occur with enhanced frequency among Ashkenazi Jews. Compound heterozygotes carrying an infantile and an adult α -subunit mutation on homologous chromosomes have adult-onset GM₂

gangliosidosis. The patients who are homozygous for the B₁ mutation generally belong to the juvenile category. The clinical severity in compound heterozygotes depends on the other allele. When the other allele is totally inactive a late-infantile phenotype results. Compound heterozygosity in which the other allele carries an adult GM₂ gangliosidosis mutation is responsible for the patients with a chronic form of B₁ variant with survival into the third decade of life. For the β -subunit gene too, different mutations have been identified and variations in residual enzyme activity appear to explain the different clinical phenotypes.

Gangliosides are typical components of the outer leaflet of plasma membranes and are particularly abundant in the neuronal plasma membranes. An accumulation of these lipids will therefore occur predominantly in neurons. The accumulation of lipids occurs primarily inside the lysosomes, where they fail to be broken down in the absence of adequate hexosaminidase activity. The accumulating amphipathic lipids will precipitate and form lamellar structures. Although the stored compounds are normal, non-toxic, components of the cell, their excessive storage will interfere with normal cell function. In cells with extreme storage mechanical destruction of the neurons may occur. Undegraded storage material is not completely confined to the lysosomes, but can to some extent be recycled and reach other compartments, such as the Golgi apparatus and plasma membrane via normal membrane flow. This may lead to changes in the content and pattern of gangliosides in the neuronal plasma membrane. Gangliosides are implicated in cell-cell communication and recognition phenomena including dendritogenesis and synaptogenesis. Presence of abnormalities in gangliosides in neuronal plasma membranes interferes with the establishment of proper connections and leads to aberrant synaptogenesis. Inappropriate proliferation of secondary neurites, a tremendous increase in synaptic spines on neurons, and formation of meganeurites and megadendrites occurs. Increased ganglioside content in plasma membranes results in markedly reduced membrane fluidity. Evaluation of neurotransmitter metabolism has shown reduced high-affinity uptake of glutamate, GABA, and norepinephrine by synaptosomes. Other studies have suggested abnormal calcium homeostasis and interference with second messenger systems.

In the infantile form, mechanical storage is responsible for the megalencephaly and may be a major cause of neuronal dysfunction and death. In the late-onset forms the lipid accumulation is much less pronounced and the other mechanisms mentioned may be more important in explaining the neuronal dysfunction. It is difficult to explain why neurons from

different locations are preferentially involved in different variants of the disease. It may have something to do with the relative contribution of pathogenetic mechanisms mentioned in each particular variant. In addition, the regulation of substrate and enzyme synthesis and turnover may not be identical in different types of cells and may not be the same over the years, altering the distribution of cells in which saturation of the residual enzyme occurs most prominently. Impairment of cellular functions can occur at different threshold values of accumulated gangliosides in different types of cells at different times.

The white matter disease in infantile forms of GM₂ gangliosidosis can be explained by a combination of hypomyelination, myelin loss secondary to wallerian degeneration, and primary demyelination. The hypomyelination may be secondary to neuronal dysfunction, as a normal neuron-myelin interaction is necessary for normal myelin deposition. The demyelination might be explained by altered myelin composition, structure, and stability. The myelin membrane fluidity is decreased by the increased content of GM₂ ganglioside. GM₂ gangliosides contain long, saturated fatty acid moieties, which increase the packing density of the lipid matrix, resulting in reduced fluidity.

10.5 Therapy

Treatment in GM₂ gangliosidosis is largely restricted to supportive care and management of intercurrent problems. Attempts at enzyme replacement have been made by intravenous, intrathecal, and intraventricular injection of hexosaminidase preparations; these attempts have been unsuccessful. It has been suggested that hematopoietic stem cell transplantation might be successful in halting the disease, but the results so far have been disappointing. This form of treatment would have a better chance in the later onset and slower variants of the disease. Substrate deprivation is another option. This method uses a specific inhibitor of glycolipid biosynthesis to partially reduce the synthesis of the unwanted products. The feasibility of this approach is presently being tested with *N*-butyldeoxynojirimycin. Oral administration of the compound has been shown to result in the reduced storage of glycolipid in multiple organs, including the brain, and an improved clinical course in mice with GM₂ gangliosidosis. The combination of hematopoietic stem cell transplantation and substrate deprivation worked even better. The efficacy of the approach in humans has to be verified. Gene therapy is still in the experimental stage.

10.6 Magnetic Resonance Imaging

A characteristic abnormality in infantile GM₂ gangliosidosis is a homogeneously and symmetrically increased density within the thalami on CT scan (Fig. 10.1). Sometimes, the caudate nucleus, putamen, and globus pallidus are also hyperdense (Fig. 10.1). Thalami have a low or mixed low and high signal intensity on T₂-weighted MR images. They have a high signal on T₁-weighted images. In addition, MRI shows high signal intensity abnormalities on T₂-weighted images in the caudate nucleus, globus pallidus, and putamen on both sides (Fig. 10.2). These nuclei have a low or mixed low and high signal intensity on T₁-weighted images. The appearance of the cerebral white matter is at first suggestive of delayed myelination, but over time the signal intensity becomes more markedly abnormal, suggesting a combination of disturbed and abnormal myelination and myelin loss. The corpus callosum is well myelinated and intact. The cerebellar white matter may also be insufficiently myelinated and become more deeply abnormal in the course of the disease. In later stages cerebral and cerebellar atrophy ensues.

The finding of a high density of the thalamus on CT scans and low signal intensity of the thalamus on T₂-weighted MR images is also seen in globoid cell leukodystrophy (Krabbe disease). However, in the latter disease many more brain structures may show a

similarly high density on CT, the T₂ hyperintense signal abnormalities in the thalami and basal ganglia are lacking, and the white matter disease does not spare the corpus callosum. The images in GM₂ gangliosidosis are indistinguishable from those seen in GM₁ gangliosidosis.

In late-onset GM₂ gangliosidosis, CT and MRI show cerebral and cerebellar atrophy, generally in combination with slight white matter signal changes (Figs. 10.3, 10.4). These abnormalities are consistent with primary neuronal degeneration. Considering the histopathological findings, one might expect abnormalities in signal intensity on MR images of basal ganglia (Fig. 10.3.).

A highly unusual patient has been reported by Nassogne et al. (2003): this child presented with progressive cerebellar ataxia and Babinski signs at the age of 3 years. MRI revealed asymmetrical lesions in the brain stem and middle cerebellar peduncles with some mass effect. The lesions had a high signal on T₂-weighted images and a low signal on T₁-weighted images, and did not enhance after contrast. The slight mass effect suggested a tumoral or inflammatory process. A stereotactic biopsy was performed, and microscopy revealed evidence of lipid storage in neurons and glial cells. Enzymatic analysis revealed a deficiency of hexosaminidase A, indicative of variant B of GM₂ gangliosidosis.

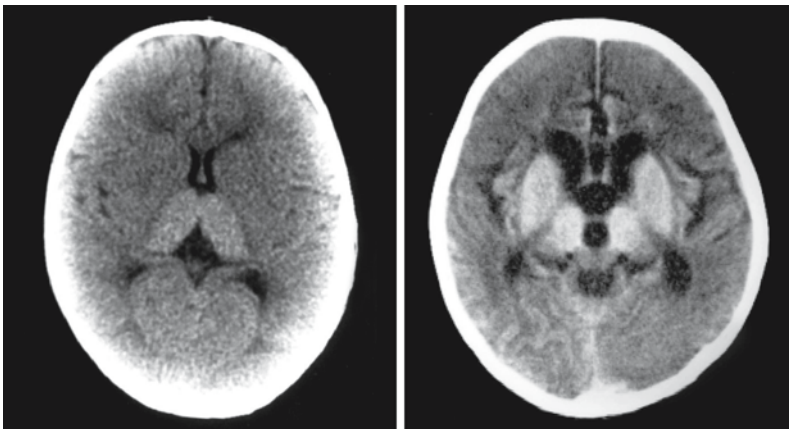


Fig. 10.1. The CT scan of a 12-month-old girl with SD (*left*) shows the hyperdensity of the thalamus on both sides. From Brismar et al. (1990), with permission. The CT scan of a 5-year-old child with TSD (*right*) shows hyperdensity of thalamus, globus pallidus, putamen, and caudate nucleus, together with some diffuse white matter hypodensity and cerebral atrophy. From Fukumizu et al. (1992), with permission

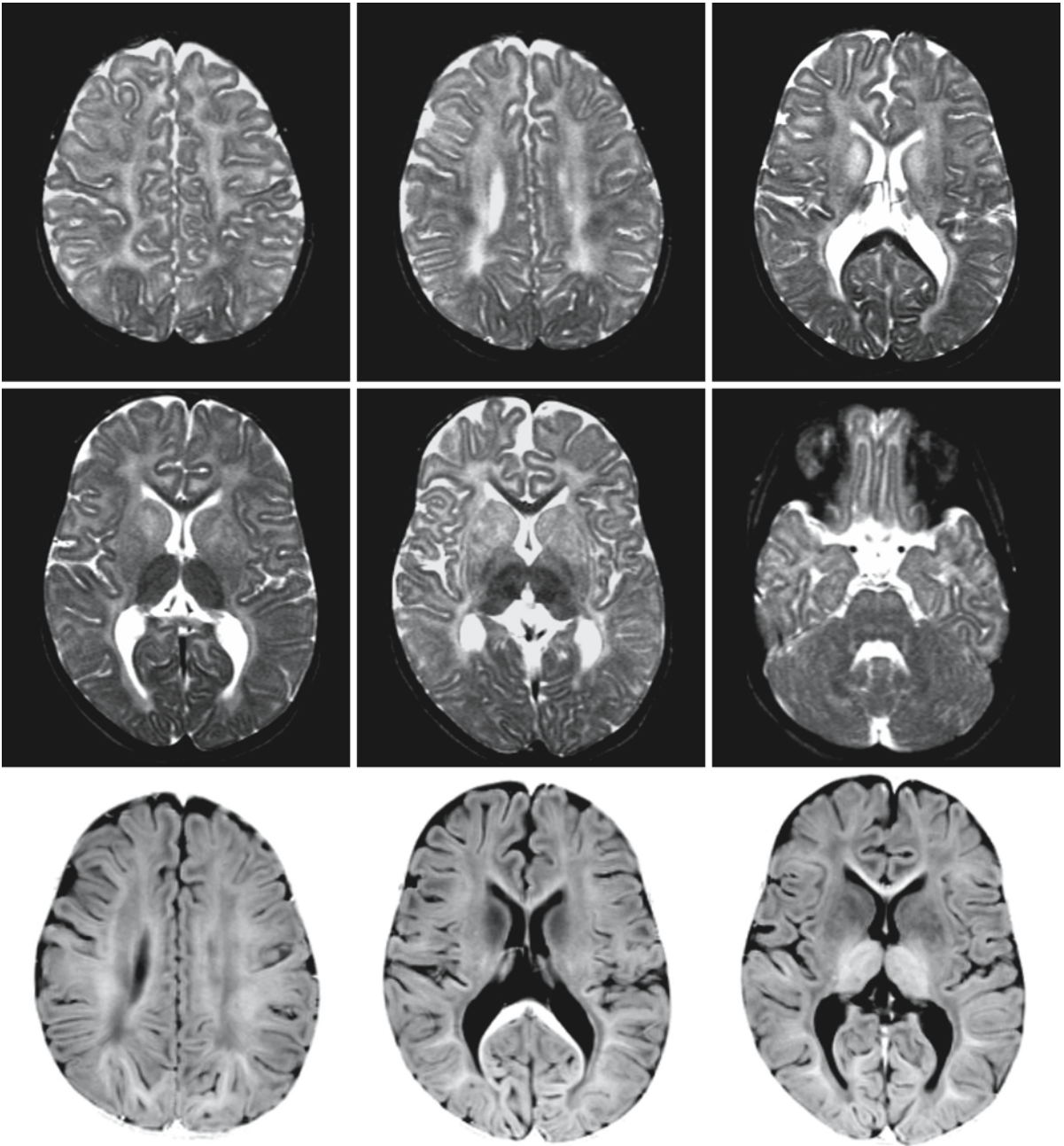


Fig. 10.2. The T_2 -weighted images of an 18-month-old girl with TSD show abnormal thalami, the signal intensity being too low. The caudate nucleus, globus pallidus, and putamen have a high signal intensity. The caudate nucleus has a slightly swollen aspect. The signal intensity of the cerebral white matter is diffusely abnormally high, except for the corpus callosum and internal capsule. The cerebellar white matter is also abnor-

mal. The T_1 -weighted images show that the basal ganglia have an abnormally low signal intensity, whereas the thalamus has an abnormally high signal. The signal intensity of the cerebral white matter is inhomogeneous on the T_1 -weighted images, high in some parts and low in others, suggestive of a combination of hypomyelination and myelin loss

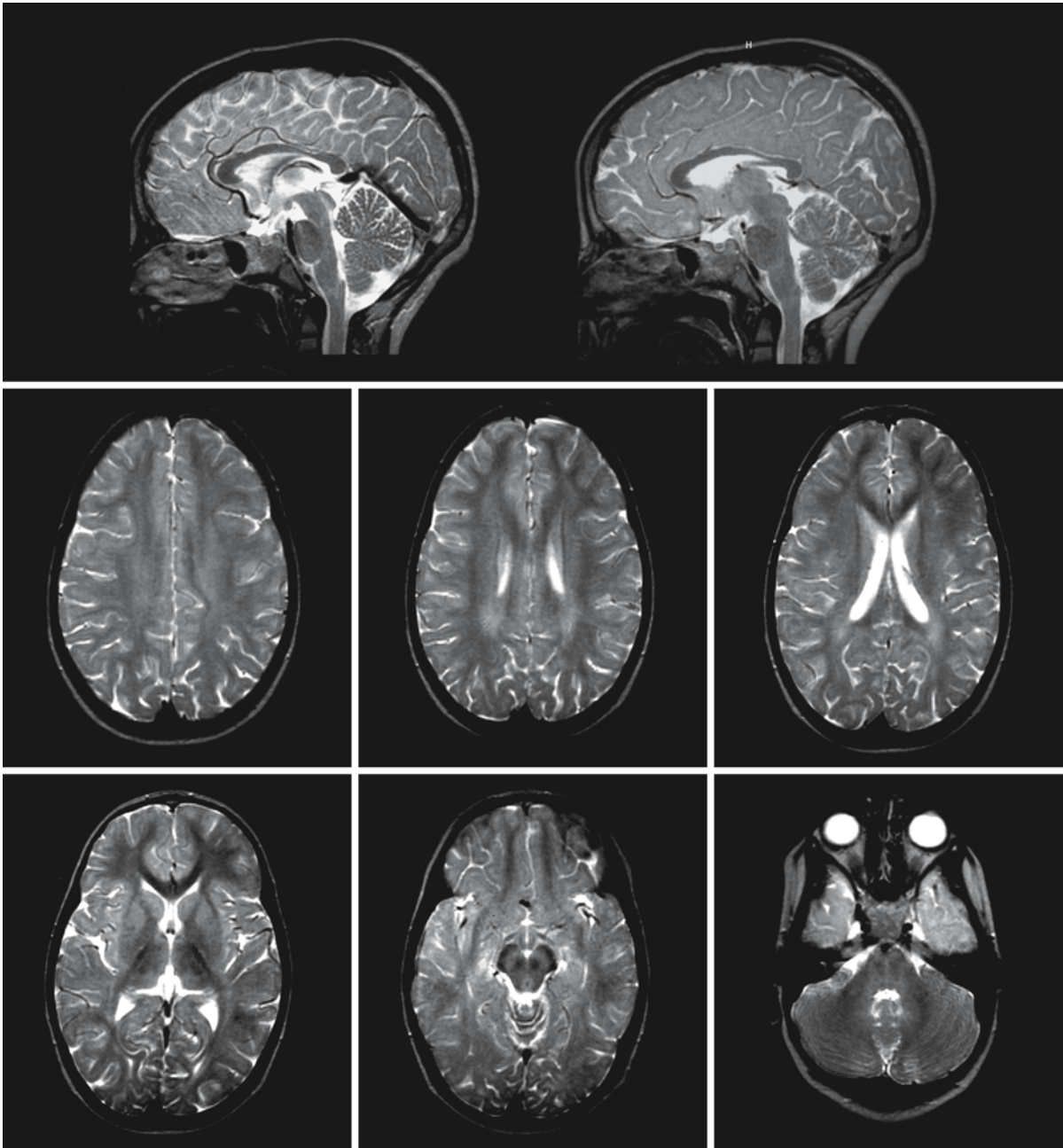


Fig. 10.3. T₂-weighted images in a 5-year-old boy with juvenile GM₂ gangliosidosis show that the cerebral white matter is slightly abnormal, suggestive of underlying axonal degeneration.

The basal ganglia also have a slightly abnormal signal. Courtesy of Dr. P.G. Barth, Department of Child Neurology, Academic Medical Center, Amsterdam, The Netherlands

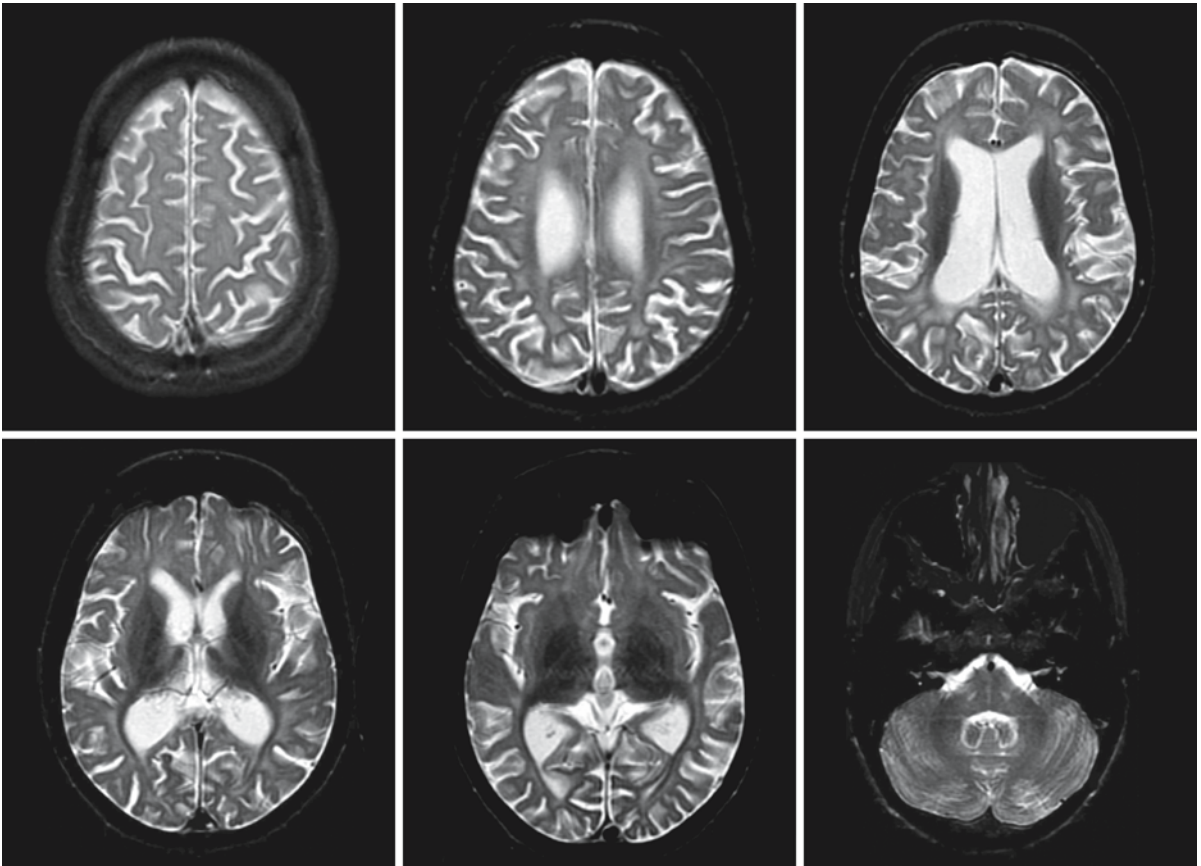


Fig. 10.4. T₂-weighted images in a 9-year-old girl with juvenile GM₂ gangliosidosis show a picture of advanced cerebral atrophy. There are mild signal abnormalities in the cerebral

white matter, as seen in neuronal degenerative disorders. Courtesy of Dr. S. Blaser, Department of Diagnostic Imaging, Hospital for Sick Children, Toronto

Fabry Disease

11.1 Clinical Features and Laboratory Investigations

Fabry disease (FD) is an X-linked recessive disorder. The onset of clinical symptoms usually occurs during childhood or adolescence, but may be as late as the third or fourth decade. Early manifestations consist of episodic pain in the extremities and a telangiectatic scaly maculopapular rash called angiokeratoma corporis diffusum. The angiokeratomas usually appear between the ages of 7 and 10 years and consist of dark red to black nonblanching macules and papules that range in size from punctate to 4 mm in diameter. They increase in number with time. They have a predilection for the genitals, the upper thighs, and the lower trunk, and spare the face, scalp, palms, and soles.

Pain is a predominant symptom of FD, both chronic acral paresthesias with burning discomfort in the hands and feet and episodes of excruciating pain, especially of the extremities. The pain crises, which last from minutes to several days, are often accompanied by fever and an elevated erythrocyte sedimentation rate. These episodes can easily be mistaken for rheumatic fever. The attacks are triggered by exercise, temperature change, fatigue, and emotional stress. The painful crises usually persist throughout life and are often the most debilitating aspect of the disorder.

Gastrointestinal symptoms consist of recurrent bouts of abdominal pain, described as colic with burning pain, located in the mid and lower abdomen. Nausea and vomiting are common. These symptoms tend to occur after meals and as a result patients are often afraid to eat. These complaints frequently lead to diagnosis as appendicitis or renal colic. Episodic diarrhea may occur, leading to diagnosis as colitis. Many patients are underweight.

Loss of autonomic nerve function leads to hypohidrosis, which begins at puberty and progresses to an absence of sweating by the third decade of life. Hypohidrosis results in temperature intolerance and overheating during the summer months. It contributes to the elevation in body temperature during a crisis. Saliva and tear formation is also decreased.

Ophthalmological abnormalities occur in more than 90% of the patients and often predate skin changes. Whorled corneal opacities (cornea verticillata), posterior linear lenticular cataracts with narrow wavy spokes, and dilatation and tortuosity of conjunctival and retinal vessels are frequent; anterior

lenticular deposits, periorbital edema, and retinal edema are less frequent. The corneal and lenticular opacities do not impair the visual acuity. Central retinal artery occlusion may cause acute blindness.

With increasing age, the major morbid symptoms result from the cardiovascular system. Cardiac disease is characterized by mitral insufficiency or aortic stenosis, left ventricular hypertrophy, hypertrophic obstructive cardiomyopathy, dysrhythmias, angina pectoris, myocardial ischemia and infarction, and congestive heart failure. Cardiac disease is worsened by systemic hypertension caused by renal vascular disease.

Cerebrovascular disease results mainly from small vessel involvement with transient ischemic attacks, ischemic infarctions, and cerebral hemorrhage. Clinical symptomatology includes hemiplegia, hemianesthesia, aphasia, and seizures. Dementia, personality changes, and psychosis may appear in older patients.

Less prominent clinical signs and symptoms include sensorineural hearing loss, tinnitus, delayed puberty, short stature, and dysmorphic facial features with thickening of the lips and nasolabial folds. Chronic airway obstruction may lead to decreased pulmonary function and, rarely, pulmonary insufficiency.

Over the years, the patients develop symptoms of chronic progressive renal failure with proteinuria, lymphedema, other signs of tubular dysfunction, renal hypertension, and uremia. The median survival of affected males is 50 years. The causes of death are predominantly cerebrovascular disease and renal failure, unless chronic dialysis or renal transplantation is performed.

Atypical variants have been described with mild single symptomatology at ages when patients with the classical disease are severely affected. Cardiac involvement can be the sole manifestation of the disease in some patients.

In heterozygous female patients, clinical expression is variable. Especially with increasing age, symptoms of the disease may become manifest. About 70% of carrier females experience some form of neuropathic pain. The typical whorled corneal opacities can be found in 70–80% of the female carriers. Angiokeratomas and hypohidrosis are found in some of the females. Gastrointestinal complaints are present in about 50%. Renal and cardiac disease, if present, is usually milder than in affected males. Transient is-

chemic attacks and cerebral infarction may occur, but much less frequently than in affected males. The median survival of carrier females is 70 years, which is an approximate reduction of 15 years from the general population.

Maximal motor and sensory nerve conduction velocities are usually normal. In contrast, quantitative assessment of thermal thresholds often reveals small-fiber neuropathy. The amplitudes of the motor and sensory nerve action potentials are also decreased.

The diagnosis of FD is established by demonstration of a deficiency of α -galactosidase A activity in plasma, leukocytes, urine, cultured skin fibroblasts, or single hair roots. Plasma, urine sediment, and cells can also be assayed for their content of accumulated globotriaosylceramide. The biochemical identification of female carriers is less reliable because of random X-chromosomal inactivation. In female heterozygotes 25–40% have levels of α -galactosidase A within the normal range. High-performance liquid chromatography of urinary sediment glycolipids is a more sensitive test for the detection of carriers. DNA analysis permits precise heterozygote detection and is preferred in families in which the molecular defect has been identified.

Prenatal diagnosis can be made by fetal sex determination and enzyme assay in cultured amniotic fluid cells or chorionic villi. In some pregnancies in which the fetus is a female carrier, enzyme activity may be very low or deficient in cultured amniotic fluid cells if they are derived from only a few cell clones which predominantly express the mutant X chromosome. Without knowledge of the sex of the fetus, this result can be misinterpreted as indicating an affected male fetus. In chorionic villi, an intermediate enzyme activity could either indicate an unaffected female carrier or could result from maternal tissue contamination of the sample from an affected male pregnancy. Hence, it is necessary to combine enzyme analysis with chromosome analysis. DNA analysis is the other option for prenatal diagnosis in families in which the molecular defect has been identified.

11.2 Pathology

The pathology of the nervous system is mostly related to vascular changes. Pathological lipid storage occurs in vascular endothelium throughout the brain and spinal cord, leading to thickening of vessel walls and obstruction of vessels resulting in infarcts. Small vessels are particularly involved. Lacunar infarcts are seen in the basal nuclei and central white matter. Larger infarcts may also be seen. The blood vessels of the peripheral nerves are involved as well.

Apart from vascular endothelium, lipid accumulation also occurs in the leptomeninges and the choroid stroma, in astrocytes, and in neurons in layers V and VI of the cerebral cortex, hypothalamus, amygdala, subiculum, entorhinal cortex, substantia nigra, periaqueductal gray, dorsal motor nucleus of the vagus, midline raphe nuclei in the medulla oblongata, intermediolateral cell column, dorsal root ganglia, anterior horn of the spinal cord, dorsal horn of the spinal cord, Meissner's and Auerbach's plexuses, and peripheral autonomic ganglia. Neurons in other areas of the CNS, including thalamus, subthalamic nucleus, caudate nucleus, putamen, red nucleus, and cerebellar cortex and nuclei do not show signs of lipid accumulation. Neurons of the more superficial layers of the cortex contain some lipid but are relatively spared. Quantitative studies of peripheral sensory neurons and spinal ganglia have shown preferential loss of small myelinated and unmyelinated fibers as well as small cell bodies of spinal ganglia.

Many organs other than the CNS are also affected. FD is characterized by widespread deposits of lipids, occurring predominantly in the lysosomes of endothelial, perithelial, and smooth muscle cells of blood vessels and, to a lesser degree, histiocytes and reticular cells of connective tissue. The deposits are also present in epithelial cells of the cornea, in renal glomeruli and tubuli, and in cardiac muscle fibers. The dermal lesions are dilated capillaries measuring 0.5–2 mm and underlying a hyperkeratotic skin.

Histochemical studies of the deposits show that they are PAS-positive, positive with Sudan black, show birefringence, and stain with Luxol fast blue. Electron microscopic examination reveals that the inclusions are intralysosomal and composed of tightly packed lipid lamellae, which may be concentric or parallel.

11.3 Chemical Pathology

FD is characterized by the accumulation of neutral glycosphingolipids, in particular globotriaosylceramide (= trihexosylceramide), galabiosylceramide (= digalactosylceramide), and, to a lesser extent, other galactolipids. In the CNS an increased content of globotriaosylceramide is found in FD patients, but no evidence has been found of an increase in galabiosylceramide. The most dramatic increases in globotriaosylceramide are found in the dorsal root ganglia, choroid plexus, and leptomeninges, where they can exceed 150-fold. Furthermore, globotriaosylceramide is present in CSF of FD patients, in contrast to normal CSF.

11.4 Pathogenetic Considerations

The basic defect in FD is deficient activity of α -galactosidase A, the lysosomal enzyme responsible for the hydrolysis of terminal α -galactosyl residues from glycolipids and glycoproteins. The gene encoding for the enzyme is *GALA* and is localized on the long arm of the X chromosome (Xq22.11). Different mutations have been identified. In male patients with classical FD (classical hemizygotes) there is no detectable enzyme activity and either no detectable enzyme protein or normal or decreased amounts of enzyme protein. In the latter case, presumably, the enzyme is altered and kinetically defective. In mild, atypical hemizygotes, some residual enzyme activity is found. Females have a variable clinical phenotype related to random X inactivation.

Glycosphingolipids are important constituents of plasma cell membranes and of some intracellular membranes including lysosomal membranes. Deficiency of α -galactosidase A leads to progressive accumulation of neutral glycosphingolipids with terminal α -galactosyl residues in lysosomes. The highest increase is found in globotriaosylceramide and digalactosylceramide. FD hemizygotes and heterozygotes who have blood group B or AB also accumulate B and B₁ glycosphingolipids, which are normal human erythrocyte antigens. Another neutral glycosphingolipid that can accumulate in FD is the P₁ blood group antigen.

There are several factors that may contribute to the phenotypic expression. First of all, there is the type of mutation. The blood group may also have an effect on the severity of the disease. It has often been reported that patients with blood group types B and BA are more severely affected than patients with blood group types O and A. This can be due to the fact that patients with blood groups B and BA accumulate the erythrocyte antigens B and B₁. In female heterozygotes, the phenotype is also influenced by the pattern of X chromosome inactivation.

The pattern of glycosphingolipid accumulation in FD differs from that in other glycosphingolipidoses. There is a very special cellular and tissue distribution of accumulated glycosphingolipids with particular involvement of vascular endothelium, smooth muscles, and neurons. Within the nervous system the pattern of involved neurons is also very special. A number of explanations have been given for this distribution of neuronal storage. Site-specific differences in globotriaosylceramide metabolism have been proposed. Absorption of high levels of globotriaosylceramide from blood has been suggested as the source of glycosphingolipids in cells, as concentrations of this substance are much elevated in the blood of patients with FD. Anatomical location in areas of reduced blood-brain barrier could potentially pro-

mote neuronal absorption from blood, but not all involved neuronal groups are in such areas. Absorption of globotriaosylceramide from the CSF into adjacent neurons could be a possible mechanism. Many of the involved neuronal groups are located adjacent to the CSF. There is, however, selective sparing of neighboring neuronal groups similarly exposed to CSF. Selective uptake and transfer of globotriaosylceramide by neurons could play a role.

Although structural compromise to the cerebral, renal, and cardiac arterial vasculature is believed to play a major role in the ischemic events in FD, there is also evidence for increased endothelium-mediated vascular reactivity and hyperdynamic cerebral circulation. Patients with FD have been found to have increased cerebral blood flow velocities. It is presently unclear how the disturbance in regulation of the vascular tone contributes to the ischemic incidents. The white matter involvement in FD is of hypoxic-ischemic origin, related to small vessel disease, and not demyelinating in nature.

The correlation of neurological complaints and lipid storage is hampered by the presence of a combination of neuronal storage, angiopathic infarcts in nervous tissue, and deposition of glycosphingolipids in end-organs such as the sweat glands in the skin. The episodic limb pain typical of FD has been ascribed to dorsal root ganglia neuropathy, peripheral small-fiber neuropathy, involvement of substantia gelatinosa neurons, and peripheral nerve ischemia due to involvement of the vasa nervorum. Autonomic dysfunction could arise from involvement of the autonomic nervous system at either central or peripheral level, but anhidrosis could also be explained by dysfunction of sweat glands. The episodic fever may be related to lesions of the hypothalamus and to the inability to sweat. The clinical correlate of the cerebral neuronal glycosphingolipid deposition is unclear. Psychosis, personality changes, and dementia have been described in FD but are not prominent phenomena. Seizures are rare. Apparently the accumulation of glycosphingolipids in neurons is a problem of lesser importance than their accumulation in endothelial cells, producing occlusive angiopathy and cerebral infarction.

11.5 Therapy

Recently, a breakthrough in the treatment of FD patients has been accomplished by the successful production of recombinant α -galactosidase A. The first results of trials of enzyme replacement therapy are very promising. Intravenous administration every other week was well tolerated and cleared the globotriaosylceramide deposits in the vascular endothelium of the kidney, heart, and skin and led to a decrease

in globotriaosylceramide concentration in urine sediment and plasma. The treatment led to significant improvement in renal function, cardiac function, cardiac conduction, and hearing. Clinically, the patients had less neuropathic complaints. Patients with FD have elevated cerebral blood flow velocities. These velocities improved significantly with enzyme replacement therapy. Similar positive results have been observed in affected carrier FD females.

Certain missense mutations produce catalytically active mutant α -galactosidase A that is unstable and rapidly degraded. Reversible competitive inhibitors of α -galactosidase A, such as 1-deoxygalactonojirimycin and galactose, have been shown to be able to increase or stabilize the activity of the residual mutant α -galactosidase A. Intravenous infusions of galactose every other day led to an increase in α -galactosidase A activity in circulating lymphocytes and endomyocardial cells and improved cardiac function in an FD patient with cardiomyopathy as the only clinical manifestation. These findings suggest that the administration of competitive inhibitors as chemical chaperones at subinhibitory intracellular concentrations may be efficacious in the treatment of particular variants of FD.

Substrate deprivation is a rational therapy for FD. This approach is based on the inhibition of an earlier step in the synthesis of the accumulating glycosphingolipids. Globotriaosylceramide contains glucosylceramide as its base cerebroside. D-threo-1-ethylenedioxyphenyl-2-palmitoylamino-3-pyrrolidinopropanol is a potent inhibitor of glucosylceramide synthase. Administration of the compound to FD knock-out mice led to a concentration-dependent decrease in globotriaosylceramide levels in kidney, liver, and spleen. The effects on brain levels were less profound. The results of human studies are still awaited.

Gene therapy for FD is in the experimental stage. Transplantation of genetically corrected bone marrow cells in α -galactosidase-A-deficient mice increased α -galactosidase A activity and decreased globotriaosylceramide storage in all organs except the brain.

Symptomatic care is important with regard to cardiac, pulmonary, and neurological manifestations. The pain in FD can in many cases be reduced by antiepileptic drugs, such as phenytoin, carbamazepine, gabapentin, and lamotrigine. Renal insufficiency requires chronic hemodialysis and/or renal transplantation. In addition to correcting the chronic renal failure, kidney transplantation provides a source of α -galactosidase A. Although a transient or sustained biochemical and/or clinical improvement has been

reported in several patients, in others no positive effect could be demonstrated. Significant lipid deposition and allograft dysfunction have been reported several years after transplantation. Several patients who underwent successful engraftment died 10–15 years later from complications of cardiac disease.

11.6 Magnetic Resonance Imaging

MRI in FD changes with the course of time. Increasing with age, 20–30% of the patients have a high signal in the pulvinar on T1-weighted images, whereas susceptibility-weighted T2* studies demonstrate low signal intensity in the more severe cases, suggesting mineralization of the pulvinar (Fig. 11.1). This has been confirmed by CT. CT may show more extensive calcium deposits, particularly in more severely affected patients, involving the cerebral cortical-subcortical junction, globus pallidus, pulvinar, and cerebellar corticomedullary junction. In cases of early and mild cerebral involvement, multiple bilateral lacunar infarcts are seen (Figs. 11.1 and 11.2). These may occur anywhere in the brain, in both gray and white matter structures. The number of small infarcts spread over the brain may become very high. In some patients an additional small rim of periventricular signal abnormality is seen (Fig. 11.3). In older patients extensive confluent periventricular white abnormalities are seen in combination with small lacunar infarcts elsewhere in the brain, especially the basal nuclei (Fig. 11.4). The pattern of extensive and confluent white matter involvement may resemble a demyelinating disease. However, the presence of additional small lesions in the basal ganglia and brain stem should suggest the possibility of an underlying vascular disorder. This pattern closely resembles the pattern of Binswanger disease. The anterior temporal abnormalities typically seen in CADASIL are lacking. Large infarcts in the territories of the major cerebral arteries and cerebral hemorrhages may also occur. Ectatic vessels are apparent in some patients. Dilatation of the ventricles and cortical sulci may occur in severe disease. If present, the hyperintensity of the pulvinar on T1-weighted images should suggest FD.

In female heterozygotes, MRI is often normal. However, multiple small lesions in the deep white matter, thalamus, and basal ganglia as well as more confluent periventricular white matter abnormalities in combination with lacunar infarctions elsewhere in the brain may occur, but usually at a later age than in affected males. Hyperintensity of the pulvinar on T1-weighted images may occur as well.

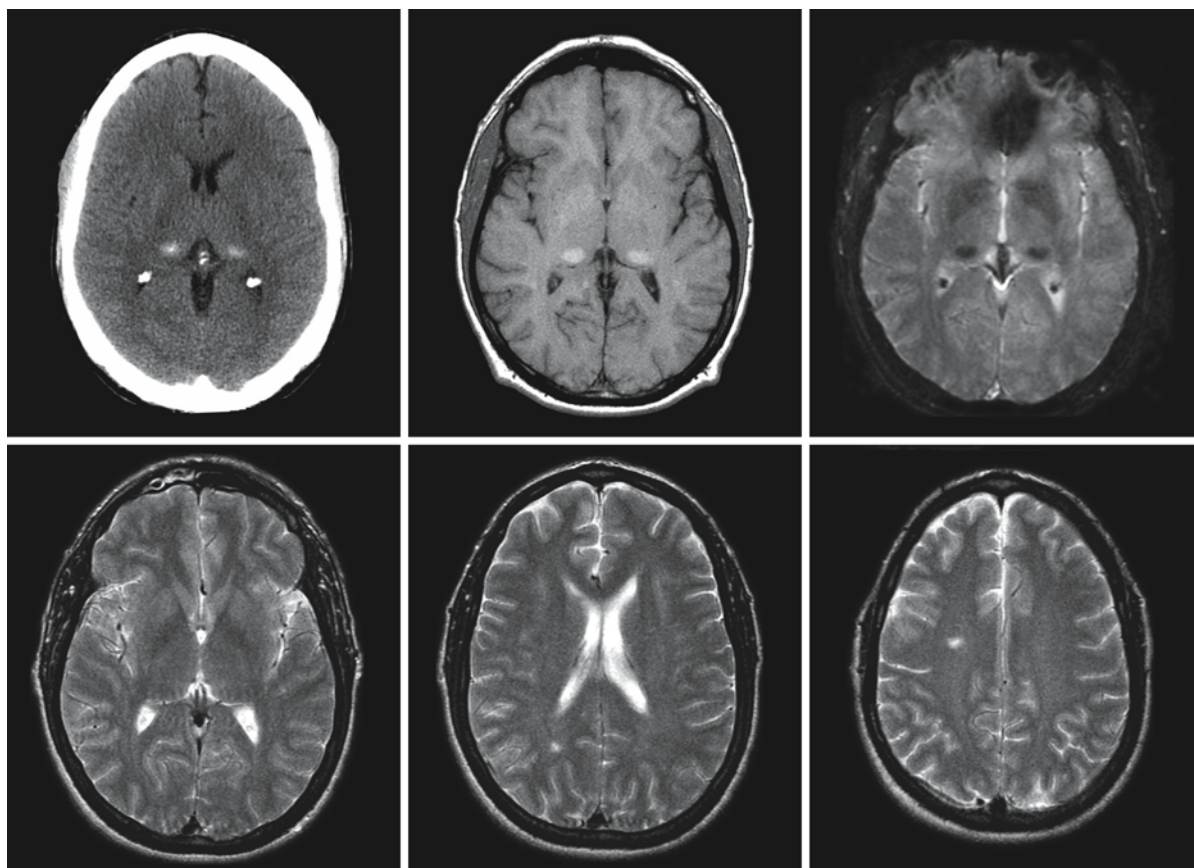


Fig. 11.1. A 42-year-old male patient with Fabry disease. The T_2 -weighted (FSE) images (*second row*) show two lacunar infarcts. The CT scan demonstrates calcium deposits in the pulvinar (*first row, left*). The pulvinar has a high signal on T_1 -

weighted images, a low signal on susceptibility-weighted T_2^* images (*first row, middle and right*). Courtesy of Dr. R. Schiffmann, Developmental and Metabolic Neurology Branch, National Institutes of Health, Bethesda, Maryland, USA

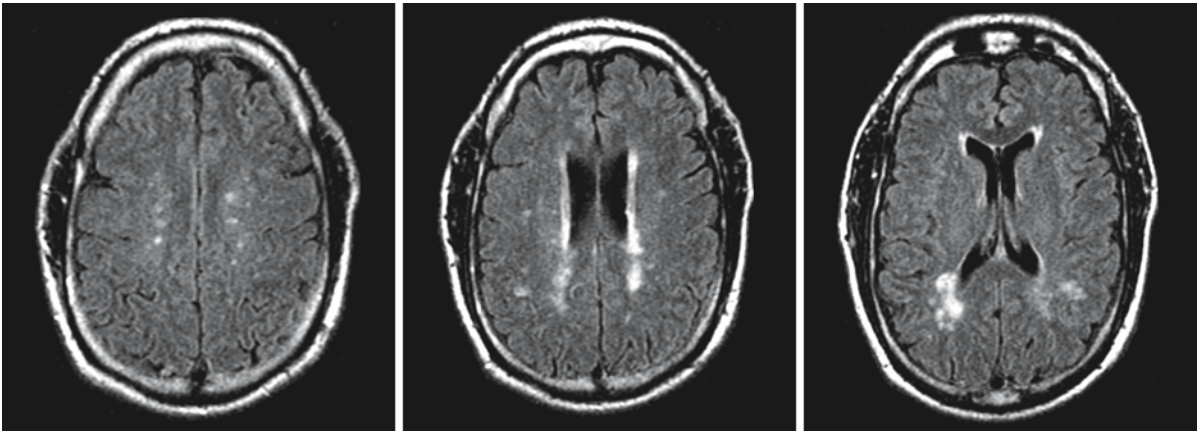


Fig. 11.2. FLAIR images in a 44-year-old male patient with Fabry disease show multiple small infarcts and a rim of high signal surrounding the ventricles. Courtesy of Dr. R. Schiff-

mann, Developmental and Metabolic Neurology Branch, National Institutes of Health, Bethesda, Maryland, USA

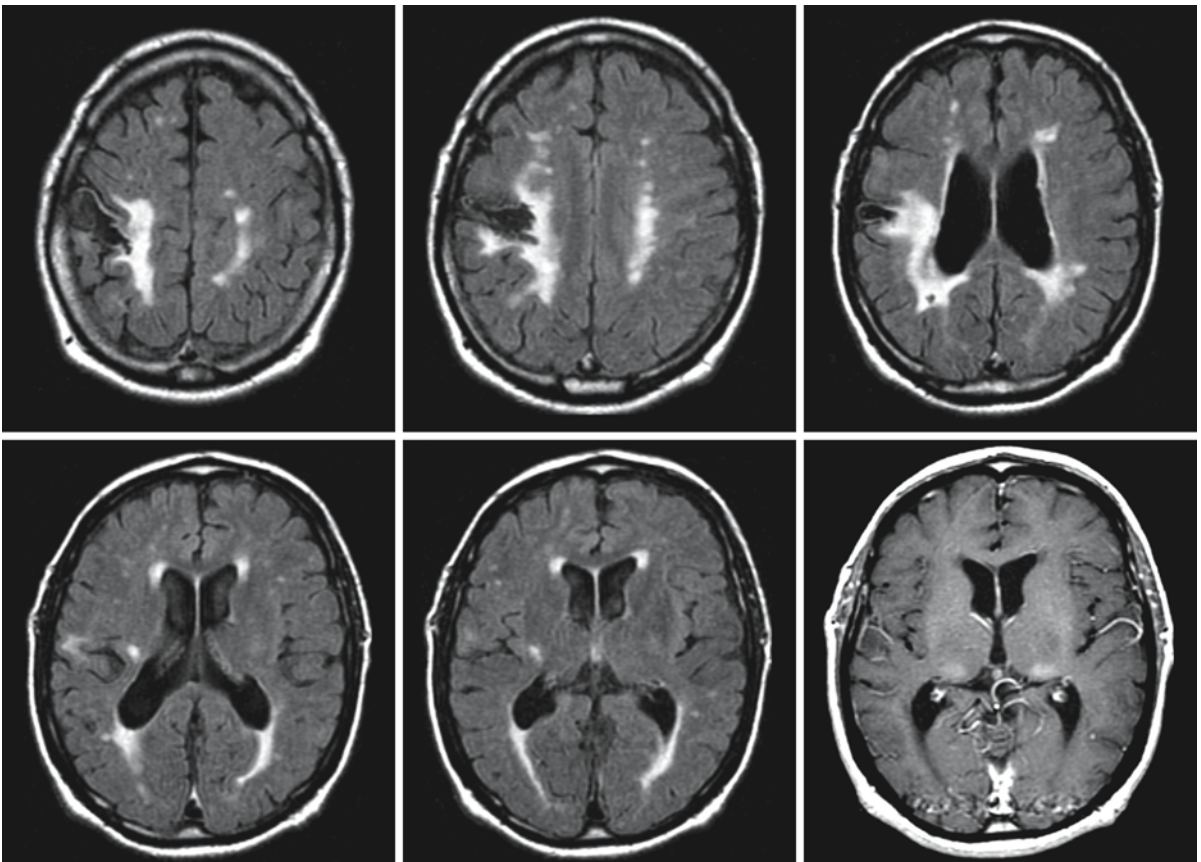


Fig. 11.3. FLAIR images and a T₁-weighted image (*second row, right*) of a 57-year-old male patient with Fabry disease, showing multiple infarctions which are partially confluent. There is a cystic lesion in the medial cerebral artery territory on the

right. The T₁-weighted image shows a high signal in the pulvinar. Courtesy of Dr. R. Schiffmann, Developmental and Metabolic Neurology Branch, National Institutes of Health, Bethesda, Maryland, USA

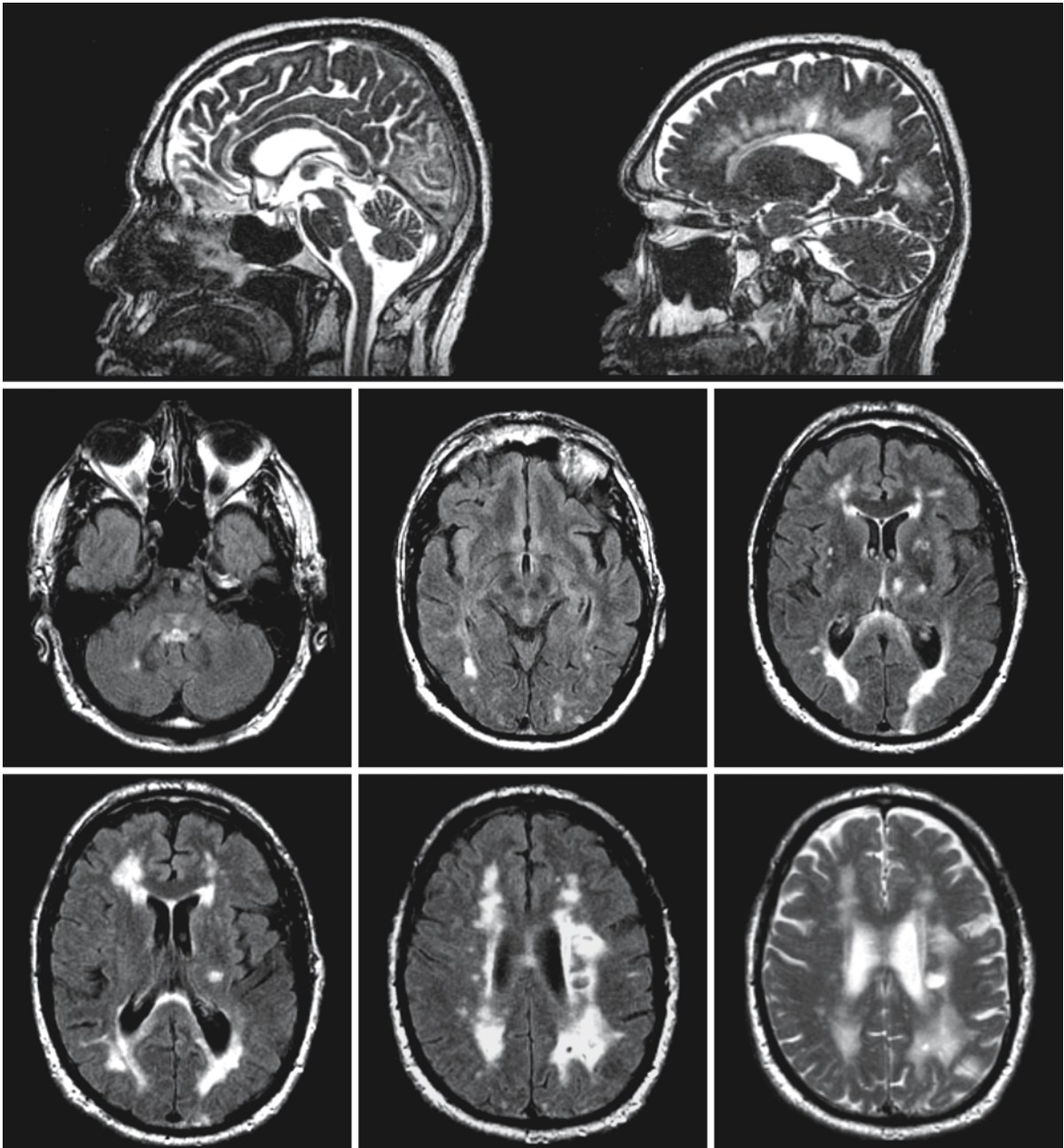


Fig. 11.4. Sagittal T₂-weighted images in a 58-year-old male patient with Fabry disease (*first row*) reveal lesions in the brain stem and corpus callosum. The axial FLAIR images demonstrate extensive, irregular lesions in the periventricular white matter. Comparing the FLAIR and T₂-weighted image at the

same level (*third row, right*) shows that part of the lesions are cystic. In addition, lesions are present in the brain stem, cerebellar white matter, and basal ganglia. Courtesy of Dr. R. Schiffmann, Developmental and Metabolic Neurology Branch, National Institutes of Health, Bethesda, Maryland, USA

Fucosidosis

12.1 Clinical Features and Laboratory Investigations

Fucosidosis is a very rare, autosomal recessive neurovisceral storage disorder. Two clinical variants have been described, but in fact the two types represent a continuous clinical spectrum. Mild and severe forms can occur within the same family.

Type I manifests before the end of the first year of life with frequent respiratory infections. From the age of about 1 year, mental and motor regression occurs. Initially, the children show signs of hypotonic weakness, but later hypertonia and spasticity develop. Seizures may occur. In the end stage decorticate and decerebrate postures are seen. The children's facial appearance resembles that seen in mucopolysaccharidosis type I, with coarse features and a protruding tongue. Other similarities between these disorders are growth retardation and a mild to moderate dysostosis multiplex. Hepatosplenomegaly, cardiomegaly, and anhidrosis with a marked increase in the sodium chloride content of sweat are present. Death occurs in the first decade of life.

Type II has a milder and more prolonged course. Mental retardation becomes evident between the ages of 1 and 2 years. The coarse facies, growth retardation, and skeletal deformities are very similar to those seen in mucopolysaccharidosis type I. Angiokeratoma corporis diffusum is a very special characteristic of this type and is identical to that occurring in Fabry disease. The content of sodium chloride in sweat is normal, although anhidrosis may be present. The patients suffer from similar but milder neurological signs than in type I. These patients survive much longer and often reach adulthood.

In the urine of patients with fucosidosis, an increased level of fucose-containing glycoconjugates is found, including fuco-oligosaccharides and fucoglycopeptides. There is evidence that fucosidosis types I and II can be distinguished by the pattern of urinary excretion. Cytoplasmic vacuolation in circulating lymphocytes is common in type I, less frequent in type II. Definite diagnosis is established by the demonstration of a deficiency of the lysosomal enzyme α -fucosidase in leukocytes, cultured fibroblasts, or other tissue cells. Prenatal detection is possible by assessing enzyme activity in amniotic fluid cells. DNA-based prenatal diagnosis is possible when

the mutations responsible in the family at risk have been identified.

12.2 Pathology

The brain may be enlarged or small, depending on the stage of the disease. The most striking feature is diffuse neuronal ballooning and neuronal loss. The cytoplasm of remaining neurons is packed with small vacuoles. These neuronal changes are seen everywhere in the gray matter. There are prominent white matter abnormalities, variably described as deficient myelination or demyelination. The white matter is deficient in myelin and gliotic.

Electron microscopy demonstrates that the vacuoles present in brain cells are membrane-bound. Many vacuoles contain two different components, moderately electron-dense reticular materials and parallel lamellae. The vacuoles are present in neurons, astrocytes, and oligodendroglia.

Enlargement of many internal organs is found, including liver, spleen, heart, pancreas, thymus, thyroid, and kidneys. Marked vacuolar storage is present in hepatocytes, Kupffer cells, and bile duct epithelium. The gall bladder may be "strawberry-like" and non-functioning and the adrenals may be small and atrophic. Granulovacuolar storage is seen in almost all organs, including kidney, spleen, lymph nodes, lungs, heart, endocrine glands, and sweat glands. In addition, vacuoles are present in vascular endothelial cells, fibroblasts, bone marrow cells, and circulating lymphocytes.

12.3 Pathogenetic Considerations

Fucosidosis is caused by a deficiency of the lysosomal enzyme acidic α -L-fucosidase. This enzyme hydrolyzes α -fucose from glycolipids and glycoproteins. Fucose is a normal sugar constituent of many tissue mucopolysaccharides, plasma glycoproteins, and tissue mucolipids. In fucosidosis, tissues store fucose-rich glycolipids, sphingolipids, glycoproteins, oligosaccharides, and mucopolysaccharides. The major part of the stored material consists of ceramide containing fucose and other hexoses. This material is derived from secretor antigens and blood group anti-

gens, which are fucose-rich glycolipids and glycoproteins. In the liver, there is a major accumulation of glycolipids. These are only present to a minor extent in the brain, where oligosaccharides predominate as storage material.

The gene encoding α -fucosidase, *FUCA1*, is located on chromosome 1 at position 1p34. The observed clinical variability among patients cannot be explained by the nature of the mutations in *FUCA1* and must be secondary to unknown factors. A region showing homology to the fucosidase gene was identified on chromosome 2 and designated *FUCA1P*. *FUCA1P* does not encode for fucosidase enzyme activity and is a so-called pseudogene. Because of the wide variation in clinical severity of fucosidosis, even within families, it is of interest to know whether the *FUCA1P* gene could encode for a protein product that might affect fucosidase enzyme activity. A third gene, *FUCA2* on chromosome 6, is thought to regulate the fucosidase activity, although it does not encode for the fucosidase enzyme.

12.4 Therapy

To date therapy has been entirely supportive. Hematopoietic stem cell transplantation has been performed in fucosidase-deficient animals. Following successful engraftment, increased levels of fucosidase activity were found in leukocytes, plasma, and neural and visceral tissue. The enzyme reaches viscera and peripheral nerves rapidly via phagocytes, but it takes months to achieve substantial levels of enzyme activity in the CNS. Long-term engraftment from an early age reduced the severity and slowed the progression of clinical neurological disease in these animals; transplantation after the onset of clinical signs was not effective. Hematopoietic stem cell transplantation has been performed in a few patients and the results are promising in those undergoing the transplantation early. At present, it is still uncertain whether early treatment will completely prevent the clinical signs of disease.

12.5 Magnetic Resonance Imaging

CT scan findings include hypodensity of the cerebral white matter and globus pallidus. Mildly increased density of the thalami has been reported.

The MR images obtained in a fucosidosis patient show symmetrical white matter abnormalities. In some patients, the white matter signal behavior on T_1 - and T_2 -weighted images is suggestive of moderate hypomyelination: the white matter is mildly hyperintense on both T_1 - and T_2 -weighted images (Fig. 12.1). In other patients, however, the white matter has in some parts a higher signal intensity on T_2 -weighted images than is usual for hypomyelination, and its signal on T_1 -weighted images is low in places, suggesting myelin loss (Fig. 12.2). The subcortical U fibers, internal, external, and extreme capsules, and cerebellar white matter also have an abnormal signal intensity. The corpus callosum is normal in signal, but may be thin. The cerebral white matter may have a decreased volume with enlarged CSF spaces. The internal medullary laminae of the thalamus and in some cases the lateral and medial medullary laminae of the globus pallidus and hypothalamus have a high signal on T_2 -weighted images. The globus pallidus, thalamus, and substantia nigra tend to have an abnormally low signal on T_2 -weighted images. Cerebral and cerebellar atrophy may be seen and may be marked, especially in older patients.

The involvement of a combination of cerebral hemispheric white matter, globus pallidus, and thalamus is reminiscent of Canavan disease and later-onset variants of maple syrup urine disease, but in the latter two conditions the white matter is swollen, whereas it is reduced in volume in fucosidosis. The images show resemblance with the pattern observed in infantile GM_1 and GM_2 gangliosidoses, although the hypointensity of central brain nuclei on T_2 -weighted images is not seen in the latter disorders.

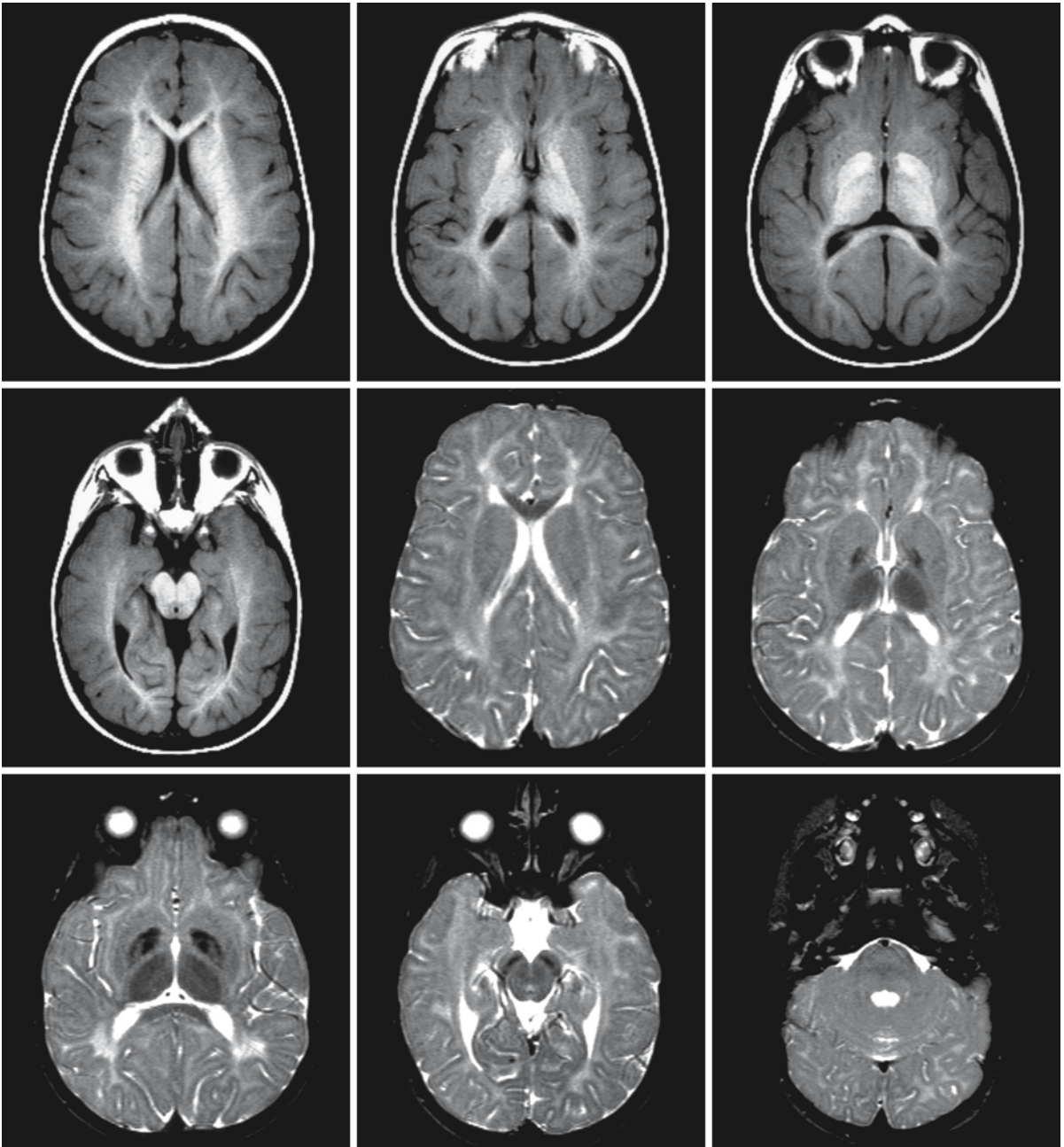


Fig. 12.1. The cerebral white matter in this 4-year-old patient with fucosidosis has a high signal on both T_1 - and T_2 -weighted images, suggestive of moderate hypomyelination. The globus pallidus, thalamus, and substantia nigra have a strikingly high

signal on T_1 -weighted images and low signal on T_2 -weighted images. Courtesy of Dr. S. Blaser, Department of Diagnostic Imaging, Hospital for Sick Children, Toronto

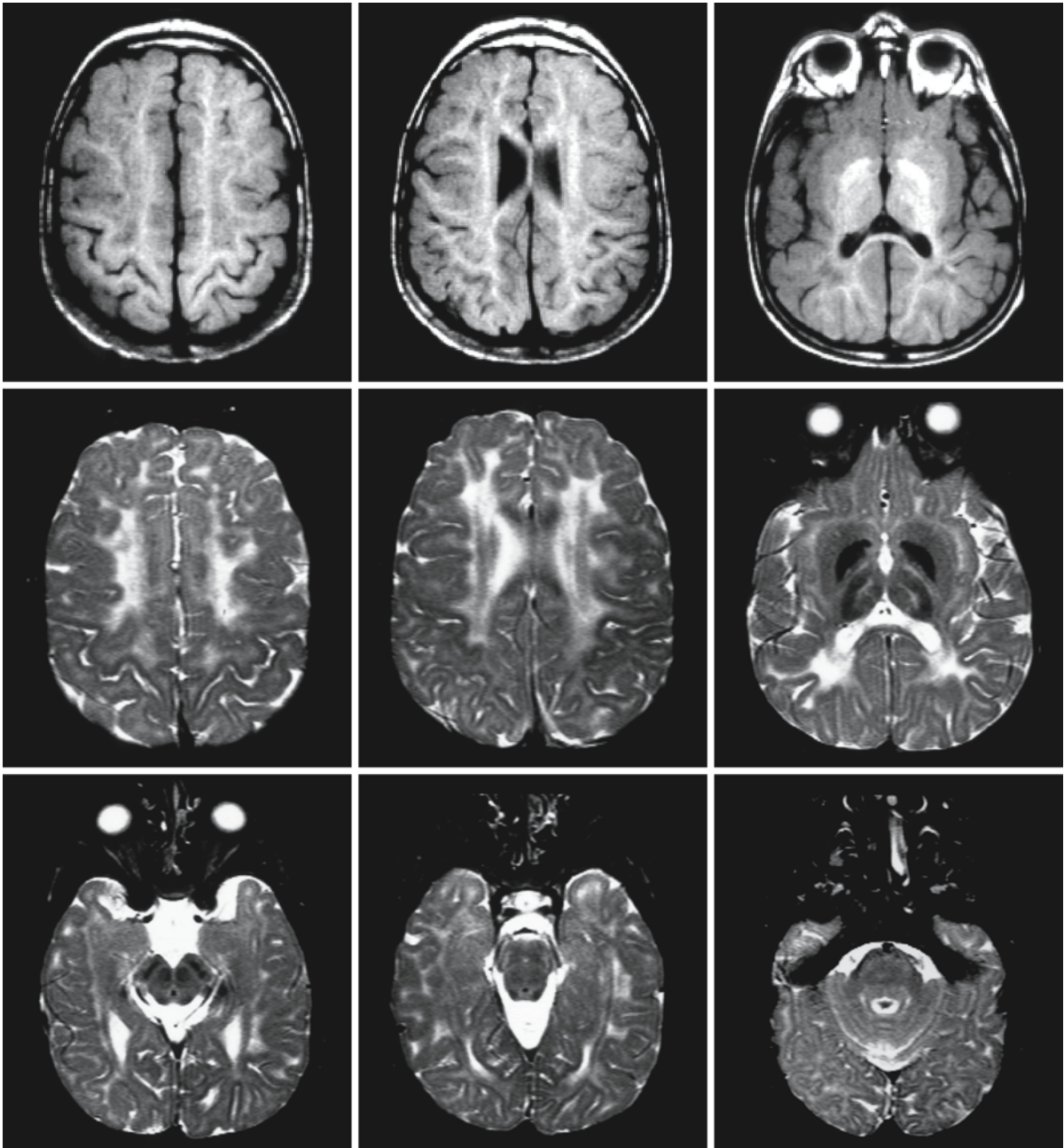


Fig. 12.2. Part of the cerebral white matter in this 7-year-old patient with fucosidosis has a high signal on both T₁- and T₂-weighted images, suggestive of moderate hypomyelination, but parts of the deep cerebral white matter have a higher signal on T₂-weighted images and a low signal on T₁-weighted images, suggestive of myelin loss. Note the signal

abnormalities in the internal laminae of the thalamus. Also note the very low signal of the globus pallidus, thalamus, and substantia nigra on T₂-weighted images. Courtesy of Dr. S. Blaser, Department of Diagnostic Imaging, Hospital for Sick Children, Toronto

Mucopolysaccharidoses

13.1 Clinical Features and Laboratory Investigations

The mucopolysaccharidoses (MPS) constitute a family of heritable disorders caused by the deficiency of specific lysosomal enzymes involved in the degradation of mucopolysaccharides (glycosaminoglycans). The mucopolysaccharidoses are classified into six groups, which are further subdivided on the basis of genetic, biochemical, and clinical findings (Table 13.1). These disorders share a number of characteristic clinical features, although there is considerable variability among the MPS types and within one type of MPS.

MPS type I, inherited as an autosomal recessive disease, can be divided into three subtypes: Hurler syndrome, Scheie syndrome, and Hurler–Scheie syndrome. The clinical phenotype in Hurler–Scheie syndrome is intermediate between the severe presentation of Hurler syndrome and the mild presentation of Scheie syndrome.

Children with Hurler syndrome (MPS I H) appear normal at birth. They may be unusually large in infancy, but subsequent growth is retarded, finally resulting in dwarfism. During the first year of life mental retardation becomes evident, and after several years this is followed by progressive deterioration.

Most children with Hurler syndrome manage to walk, but develop only limited language skills. They have a characteristic appearance. Prominent features are relative macrocephaly, a prominent forehead, coarse facial features, hypertelorism, flat nasal bridge, prominent bushy eyebrows, thick and dry hair, hirsutism, thick skin, enlarged tongue, hypertrophic gums, short and broad hands with stubby fingers, short and broad feet, exaggerated lumbar lordosis, thoracic kyphosis, and a protuberant abdomen, frequently with umbilical and inguinal hernias. On physical examination hepatosplenomegaly is found. Patients experience increasing joint stiffness and limitation of joint mobility, which may begin in early infancy. The preferentially affected joints are shoulders, fingers, and wrists. Deformities become apparent with claw hands and flexion contractures of elbows and knees. Vision becomes impaired due to progressive corneal clouding. Glaucoma, optic atrophy, and pigmentary retinal degeneration can contribute to the loss of vision. The majority of children have some degree of hearing loss, usually caused by a combination of conductive and sensorineural problems. Most patients have recurrent upper respiratory tract infections, copious nasal discharge, and ear infections. Valvular heart disease is common. Occasionally patients have progressive communicating hydro-

Table 13.1. Classification of the mucopolysaccharidoses

Number	Eponym	Enzyme deficiency	Urinary glycosaminoglycan
MPS I H	Hurler	α -L-Iduronidase	DS, HS
MPS I S	Scheie	α -L-Iduronidase	DS, HS
MPS I H/S	Hurler–Scheie	α -L-Iduronidase	DS, HS
MPS II	Hunter	Iduronate sulfatase	DS, HS
MPS III A	Sanfilippo A	Heparan N-sulfatase	HS
MPS III B	Sanfilippo B	α -N-Acetylglucosaminidase	HS
MPS III C	Sanfilippo C	acetyl-CoA: α -glucosaminide acyltransferase	HS
MPS III D	Sanfilippo D	N-Acetylglucosamine 6-sulfatase	HS
MPS IV A	Morquio A	Galactose 6-sulfatase	KS, C-6-S
MPS IV B	Morquio B	β -Galactosidase	KS
MPS V	No longer used	–	–
MPS VI	Maroteaux–Lamy	N-Acetylgalactosamine 4-sulfatase	DS
MPS VII	Sly	β -Glucuronidase	DS, HS, C-4-S, C-6-S
MPS VIII	No longer used	–	–

DS, dermatan sulfate; HS, heparan sulfate; KS, keratan sulfate; C-4-S, chondroitin-4-sulfate; C-6-S, chondroitin-6-sulfate.

cephalus caused by dysfunction of arachnoid villi, and some patients have overt signs of increased intracranial pressure. Signs of spinal cord compression may occur but are infrequent.

Not all mentioned signs and symptoms are obligatory and there is considerable clinical variability. However, progressive physical and neurological deterioration is the rule. Patients with Hurler syndrome rarely survive beyond the age of 16 years. Obstructive airway disease caused by deposition of mucopolysaccharides in soft tissue, respiratory infections, and cardiac disease are the usual causes of death.

Scheie syndrome (MPS I S) represents a mild variant of Hurler syndrome. Intelligence is normal. Common abnormalities are restricted mobility of joints, development of claw hands, hirsutism, variable deafness, corneal clouding, and aortic valve disease. Stature is normal. Glaucoma and pigmentary retinal degeneration may occur, which together with corneal opacities lead to impaired vision. Neurological problems may occur in the form of carpal tunnel syndrome and cervical cord compression by the thickened dura. Psychosis has been described in adults with Scheie syndrome. First abnormalities are usually noted in the second half of the first decade of life, and the disease is slowly progressive.

Hurler–Scheie syndrome (MPS I H/S) represents a variant of intermediate severity with onset of clinical signs and symptoms between 3 and 8 years. Most patients have normal or near-normal intelligence, but slowly progressive loss of mental capacities may occur. Coarsening of facial features, corneal clouding, joint stiffness, and valvular cardiac disease are frequent. Cervical spinal cord compression may occur. Development of communicating hydrocephalus is rare. Psychosis may occur in adulthood. Most patients survive well into adulthood. Cardiac complications and upper airway obstruction are the most common causes of death.

MPS type II or Hunter syndrome is an X-linked disorder with two clinical phenotypes, a severe type (MPS II A) and a mild type (MPS II B). The mild type is rarer than the severe type. The most important distinguishing feature is the presence or absence of mental deterioration. In the severe type progressive intellectual decline occurs, whereas intellectual performance remains normal or relatively normal in the mild type. The age at onset of the severe form is usually between 1 and 4 years of age. Early abnormalities are coarse facial features, enlargement of the tongue, growth retardation, mental retardation, severe behavioral problems, joint stiffness, gibbus formation, and skeletal deformities. Head growth is abnormally rapid initially, but slows down after several years. Retinal degeneration may occur, but there is no corneal clouding. Occasionally characteristic skin changes are found. They consist of pebbly, ivory-col-

ored patches over the lower angle of the scapulae and sometimes over the pectoralis area, in the neck and on the lateral sides of upper arms and thighs. Progressive neurological impairment dominates the course of the disease. By the age of 6 years, developmental skills begin to plateau and to regress. By the age of 10 years, 90% of the patients are bedridden. The neurological deterioration may be worsened by progressive communicating hydrocephalus. This problem usually arises between 7 and 10 years. Spinal cord compression may contribute to the neurological deterioration. Upper and lower respiratory tract disease is common. Tracheal stenosis may occur. Ear infections and progressive hearing impairment occur in most patients. There is a high incidence of hepatosplenomegaly and inguinal and umbilical hernias. Chronic and intractable diarrhea is a troublesome problem in many of the patients. Cardiac disease is present with valvular dysfunction, myocardial thickening, cardiac failure, pulmonary hypertension, coronary artery narrowing, and myocardial infarction. In end-stage disease convulsions may occur. Respiratory problems in the form of infection or obstruction or cardiac problems superimposed on a condition of emaciation are the usual causes of death. Death usually occurs between 8 and 15 years of age.

In the mild variant of Hunter syndrome, onset of disease is usually between 2 and 6 years. Coarse facial appearance is the commonest presenting feature. Intelligence is preserved and there are no behavioral problems. There are, however, obvious somatic problems: hepatosplenomegaly, cardiac symptoms (primarily valvular in origin), upper and lower respiratory tract disease, tracheal stenosis, and inguinal and umbilical herniae. Diarrhea is less frequent than in severe Hunter syndrome. Hearing impairment is common. Subtle corneal opacities have been found. Retinal degeneration is much less marked than in severe Hunter syndrome. The picture of chronic papilledema has been observed in about 60% of the patients, probably due to the deposition of glycosaminoglycans within the sclerae. The occurrence of hydrocephalus is exceptional. Head growth is, however, abnormally rapid with evident macrocephaly. Cervical myelopathy may occur secondary to atlantoaxial subluxation and dural thickening. Carpal tunnel syndrome is common. Death usually occurs in early adulthood, although survival into the fifth and sixth decade has been described. Death results primarily from cardiac problems, respiratory infections, and upper respiratory airway obstruction.

Female patients with MPS II are extremely rare and are explained by unbalanced expression of the mutant X chromosome.

Sanfilippo syndrome comprises four different diseases, MPS III A, B, C, and D, which are caused by different enzyme deficiencies. Clinically, however,

they are indistinguishable. Sanfilippo syndrome presents with great inter- and intrafamilial heterogeneity. The clinical characteristics of the disease are relatively mild somatic features and severe, progressive mental deficiency. Early psychomotor development is usually slightly or moderately delayed. Speech development, in particular, is often slow and poor. Intellectual deterioration is usually evident by school age. Dementia occurs early and progresses rapidly in some patients, but is more gradual in others. Behavioral disturbances are often dramatic with extreme restlessness and hyperkinesia. Some patients are withdrawn and lose contact with their environment. Aggression is often present in stressful situations. Most of the children are too mentally disabled to attend school, but some are able to attend primary school. Speech deteriorates, becomes slurred, the patient begins to stutter and eventually loses speech altogether. Motor functions are less frequently and less severely affected, but in some patients the gait becomes unstable with frequent falling. Facial changes are mild or absent in most of the patients. Skeletal involvement is minimal, with only mild dysostosis multiplex, kyphosis, scoliosis, and usually normal stature for age. Joint stiffness and contractures are mild and rarely cause loss of function. Some patients are macrocephalic, but most older patients have a normal head circumference and may even be microcephalic. Hepatomegaly is usual in younger patients, but is less frequent in older patients. Splenomegaly is rare. Other features that can be found are inguinal and umbilical herniae, coarse hair, hirsutism, and sensorineural hearing loss. Neurological findings are inconsistent; they may include hypotonia, hypertonia, hyporeflexia, hyperreflexia, tetraparesis, and muscular atrophy. Corneas are usually not clouded, but pigmentary degeneration of the retina may occur. Some patients develop epilepsy. Many patients develop swallowing difficulties with time, necessitating tube feeding at later stages. Infections and unexplained diarrhea are frequent problems. Cachexia and aspiration pneumonia are common causes of death. Death usually occurs in the second or third decade.

Morquio syndrome is characterized by marked skeletal involvement and preserved intellectual capacities. Two types can be distinguished, MPS IV A and MPS IV B, characterized by different enzyme deficiencies. Presenting features of Morquio syndrome are growth retardation with dwarfism, short neck and trunk, pigeon breast deformity, kyphosis, hyperlordosis, scoliosis, genua valga, valgus deformity of the elbow, and ulnar deviation and broadening of the wrist. The tone appears to be decreased due to ligamentous laxity. Decreased joint mobility may occur in the large joints. The teeth are usually widely spaced and there are numerous minute pits in the abnormally thin enamel, causing the surface of the teeth to be

rough and discolored. Facial features are usually coarse and the mouth wide. Corneal opacities may be present but are usually mild. Hepatomegaly, cardiac valvular abnormalities, and inguinal and umbilical hernias may occur. Intelligence is usually normal or just below normal. Neurological complaints are caused by compression of the medulla or spinal cord due to atlantoaxial subluxation and diffuse thickening of the cervical dura. The signs of cervical myelopathy are usually slowly progressive, but occasionally acute tetraplegia occurs. Cardiac valvular disease and cervical myelopathy contribute to death, which usually occurs in late childhood or early adulthood. Survival into the fourth and the fifth decade has been described. As a rule, MPS IV B has a later onset and slower course than MPS IV A, but severe forms of MPS IV B and mild forms of MPS IV A have been described. A variant of MPS IV B has been described with progressive mental handicap.

Maroteaux-Lamy syndrome or MPS VI clinically resembles Hurler disease, but intelligence is preserved. The disease usually presents in the third year of life and is characterized by growth retardation, coarse facial features similar to but milder than those seen in Hurler syndrome, corneal clouding, joint contractures, claw hand deformities, kyphosis, protrusion of the sternum, hepatosplenomegaly, umbilical and inguinal hernias, and mild hirsutism. Nerve entrapment syndromes may occur, in particular carpal tunnel syndrome. Myelopathy secondary to thickening of the cervical dura occurs frequently with the insidious development of spastic tetraparesis. Exceptional cases with mental retardation have been described. Cardiac valvular dysfunction resulting in cardiac failure is the most common cause of death. In the severe forms death usually occurs in the second or third decade, but patients with milder variants of the disease have a longer life expectancy.

Sly syndrome or MPS VII is also characterized by considerable clinical variation. In the severe neonatal form, hydrops fetalis and dysostosis multiplex are prominent early features; the course is rapidly fatal. The other end of the clinical spectrum is formed by patients with very mild clinical symptomatology, with normal intelligence, normal height, absence of coarse facial features, and minimal skeletal abnormalities. The classical form of the disease is characterized by coarse facial features, hepatosplenomegaly, diastasis recti, umbilical and inguinal herniae, thoracolumbar gibbus, short stature, metatarsus adductus, and variably present corneal clouding. Respiratory infections are frequent. Early psychomotor development is normal, but after 2 or 3 years of life retardation becomes evident. Retardation is usually moderate, but severe mental deficiency has also been reported. Epilepsy is rare.

Radiographs show skeletal changes in all MPS variants, but the dysostosis multiplex varies in severity. Typical findings are cortical sclerosis and thickening of the skull, which may involve the base and the vault. The pituitary fossa is often elongated and J-shaped. Teeth are widely spaced. The head is often scaphocephalic and there is early closure of cranial sutures, in particular the sagittal and lambdoid sutures. Orbits are shallow. Basilar impression may occur. In MPS IV odontoid dysplasia is a universal finding with a tendency to atlantoaxial subluxation. Various types of vertebral dysplasia are seen. Clavicles are short and stubby. There is anterior flaring of the ribs, hypoplasia of the inferior portion of the iliac bones, flared iliac wings, oblique acetabular margins, and a valgus deformity of the hips. Long bones are short and broad with metaphyseal and epiphyseal deformities. Cortical margins are wavy and scalloped. Metacarpals and phalanges are widened and shortened.

The MPS variants were originally classified according to the types of glycosaminoglycans excreted in the urine in addition to consideration of clinical features. In MPS I and II dermatan sulfate and heparan sulfate are excreted, but inheritance is autosomal recessive in MPS I and X-linked in MPS II. MPS III is associated with excretion of heparan sulfate. MPS IV is characterized by excretion of keratan sulfate, MPS VI by excretion of dermatan sulfate. MPS VII is associated with excretion of dermatan sulfate, heparan sulfate, and chondroitin sulfate. A problem in the diagnosis of MPS IV is that keratosulfaturia can be fairly easily missed. Special sensitive techniques are required for the detection of urinary keratan sulfate excretion. An additional problem of diagnosis in MPS IV is that keratan sulfate excretion may be diminished both early and late in the disease process.

Peripheral blood cells may also show changes related to the specific type of MPS. Alder-Reilly granulation, a coarse reddish-violet granulation present in neutrophils in blood films stained with May-Grünwald-Giemsa or Wright stain, is found in MPS VI and MPS VII. Vacuolated lymphocytes may be present in MPS IV B. Occasionally vacuolated lymphocytes with basophilic inclusions can be seen in any of the MPS variants. Metachromatic inclusions in lymphocytes are most prominent in MPS III. On the whole, however, vacuolation of lymphocytes is not usually prominent in MPS. Bone marrow aspirates will reveal the presence of storage cells.

Definitive diagnosis of the MPS is established by enzyme assays. It is important to realize that not all MPS patients have glycosaminoglycan elevations in urine. Therefore, enzyme assays should be performed in all cases with strong clinical suspicion. Prenatal diagnosis is possible for all MPS variants with enzyme assays on cultured amniotic fluid cells or chori-

onic villus cells. Prenatal diagnosis poses a problem in Hunter syndrome because of the X-linked mode of inheritance. When the cells obtained are derived from only a few cell clones which predominantly express the mutant X chromosome, very low enzyme activity may be detected in a carrier female fetus. Hence, sex determination is essential in prenatal diagnosis of Hunter syndrome. In families in which the molecular defect has been elucidated, DNA-based prenatal diagnosis is an option.

13.2 Pathology

Mental deficiency is an important clinical characteristic of MPS I H, MPS II, MPS III, and MPS VII. Neuropathological findings in the syndromes causing mental deficiency are similar. In particular, neuronal storage is confined to the MPS variants with intellectual problems.

The skull is sometimes grossly thickened. The leptomeninges are thickened and opalescent. There is a marked increase in connective tissue elements and there are numerous mononuclear cells containing large cytoplasmic vacuoles. These cells stain positive for glycosaminoglycans. The blood vessels running over the surface of the brain are prominent and enveloped by the thickened leptomeninges, which extend deep into the brain parenchyma.

The weight of the brain is usually at the upper limit of normal or slightly increased. The external surface is normal or the gyri are slightly atrophic. At the cut surfaces increased perivascular spaces with increased volumes of connective tissue are evident. Hydrocephalus is a common finding caused by impaired circulation of CSF through the subarachnoid spaces or dysfunction of the arachnoid granulations.

Within the brain there are two main pathological features which may occur in MPS: increase in perivascular connective tissue, and neuronal storage.

The neuronal changes are ubiquitous but their extent varies in different parts of the brain. Generally, the large nerve cells in the cerebral cortex and brain stem are the most severely affected. The cytoplasm of neurons is distended by an excessive amount of accumulated material, which stains positively with various Sudan dyes and PAS, corresponding to the presence of gangliosides. Variable numbers of neurons are in various stages of degeneration and shrinkage. Loss of nerve cells is usually mild. Electron microscopic examination of neurons shows several types of inclusions. The most characteristic are the zebra bodies. Zebra bodies are single membrane-bound vacuoles filled with stacked transverse lamellae, separated at intervals by larger clear spaces. In rare instances the lamellae have a concentric arrangement and look very similar to the membranous cytoplasmic bodies

seen in the gangliosidoses. Granular inclusions are less common than zebra bodies. Transitional forms between zebra bodies and bodies with granular material may occur. Inclusions resembling lipofuscin granules are infrequent. All inclusion bodies have acid phosphatase activity, indicating their lysosomal origin. In MPS the formation of meganeurites has been reported as well as the formation of ectopic secondary neurites. These are identical to those described in GM₁ and GM₂ gangliosidoses.

The cerebral white matter and basal ganglia are characterized by perivascular lacunation. Radially oriented, round to oval cystic white matter abnormalities are found at cut surfaces. On microscopic examination, the adventitia of vessels is abnormally thick and consists of a delicate fibrous network with numerous large cells containing large clear inclusions caused by storage of glycosaminoglycans. On electron microscopy they appear empty except for a variable amount of granular dispersed material. A few lamellar lipid inclusions resembling the zebra bodies are also observed. Loss of myelin may occur around the cysts but is not conspicuous. On occasion, focal areas of demyelination have been described. Some oligodendrocytes contain abnormal, clear inclusions.

In visceral organs a variable degree of cellular vacuolation is seen caused by glycosaminoglycan accumulation. Hepatocytes and Kupffer cells store glycosaminoglycans, in particular in MPS I, II, and III, in which hepatic fibrosis may occur. In addition to glycosaminoglycans, Kupffer cells may store gangliosides. Glycosaminoglycan storage is found in lymph nodes, spleen, kidney, and the heart. Cardiac valvular dysfunction is caused by the presence of large foamy cells and an increase of connective tissue. Fibroblasts in skin, cornea, and conjunctiva, endothelial cells of the vascular system, smooth muscle cells, skeletal muscle cells, macrophages, epithelial cells of distal and collecting tubules of the kidney, chondrocytes, osteoblasts, and periosteal cells of bone and cartilage show glycosaminoglycan storage. There are irregularities in enchondral ossification with variations in size and shape of the diaphyses of the long bones, periosteal fibrosis, and various degrees of fibrosis and lipid storage in marrow tissue.

13.3 Chemical Pathology

Chemical analysis of the brain and leptomeninges reveals a highly increased concentration of glycosaminoglycans. The level of glycosaminoglycans is much higher in the meninges than in brain tissue, where the largest amounts of glycosaminoglycans are found in vascular and perivascular tissue. In MPS I and MPS II, it is mainly dermatan sulfate that is stored, whereas in MPS III it is mainly heparan sulfate.

In MPS I, MPS II, and MPS III, chemical studies demonstrate that in neuronal perikarya glycosaminoglycans and gangliosides are increased. Ganglioside storage involves the gangliosides GM₂, GM₃, and GD₃. These substances together amount to 65 % of the gangliosides stored in neurons. The ganglioside storage is comparable in magnitude to the amounts stored in the gangliosidoses.

13.4 Pathogenetic Considerations

Proteoglycans are complex molecules consisting of long sulfated polysaccharide chains with up to 100 sugar residues covalently linked to a protein core. Glycosaminoglycans, formerly called mucopolysaccharides, are degradation products derived by proteolytic removal of the protein core of proteoglycans. Many enzymes are necessary in the intralysosomal stepwise degradation of each of the glycosaminoglycans dermatan sulfate, heparan sulfate, keratan sulfate, and chondroitin sulfate. In deficiencies of the related enzymes the undegraded or partially degraded glycosaminoglycans are stored in the lysosomes.

The respective enzyme deficiencies in the various forms of MPS are listed in Table 13.1. α -L-Iduronidase, the enzyme that is deficient in MPS I, is encoded by the gene *IDUA*, located on chromosome 4p16.3. It hydrolyzes terminal α -L-iduronate residues from dermatan sulfate and heparan sulfate. Iduronate sulfatase, the enzyme that is deficient in MPS II, is encoded by the gene *IDS*, located on chromosome Xq28. It removes a sulfate group from L-iduronate present in dermatan sulfate and heparan sulfate. In a concerted action, the four enzymes related to MPS III accomplish removal of the variably substituted α -linked glucosamine residues from heparan sulfate. Heparan N-sulfatase, the enzyme that is deficient in MPS III A, is encoded by the gene *MPS3A*, located on chromosome 17q25.3. It removes sulfate groups linked to the amino group of glucosamine. The enzyme is important in the breakdown of heparan sulfate. The enzyme is also called sulfamate sulfohydrolase or sulfamidase. α -N-Acetylglucosaminidase, the enzyme deficient in MPS III B, is encoded by the gene *NAGLU*, located on chromosome 17q21. It removes N-acetylglucosamine residues in heparan sulfate. Acetyl-CoA: α -glucosamide acetyltransferase, the enzyme that is deficient in MPS III C, is encoded by the gene *MPS3C*, located on chromosome 14. It catalyzes the acylation of glucosamine amino groups that have become exposed by the action of heparan N-sulfatase. After the acylation of glucosamine amino groups, α -N-acetylglucosaminidase removes the N-acetylglucosamine group. N-acetylglucosamine 6-sulfatase is deficient in MPS III D; the gene, *GNS* or *G6S*, is located on chromosome 12q14. This enzyme desulfates 6-sulfated N-

acetylglucosamine residues of heparan sulfate and keratan sulfate. Since hexosaminidase A can bypass the block in the degradation of keratan sulfate, only the block in the degradation of heparan sulfate is important. Galactose 6-sulfatase, the enzyme deficient in MPS IV A, is encoded by *GALNS*, located on chromosome 16q24.3. It cleaves sulfate from 6-sulfated galactose residues of keratan sulfate and 6-sulfated *N*-acetylgalactosamine residues of chondroitin 6-sulfate. β -Galactosidase, the enzyme deficient in MPS IV B, is encoded by a gene *GLB1* located on chromosome 3p21.33. It removes galactose residues of keratan sulfate. *N*-acetylgalactosamine 4-sulfatase, also called arylsulfatase B, is deficient in MPS VI. It is encoded by the gene *ARSB*, located on chromosome 5q13–14. It hydrolyzes the sulfate groups in the 4-position of *N*-acetylgalactosamine residues in dermatan sulfate and chondroitin 4-sulfate. Urinary chondroitin 4-sulfate is not elevated in MPS VI, probably because the enzymatic block is bypassed by the action of lysosomal hyaluronidase. β -Glucuronidase, the enzyme deficient in MPS VII, is encoded by the gene *GUSB*, located on chromosome 7q21.11. It removes β -glucuronate residues present in dermatan sulfate, heparan sulfate, and chondroitin sulfate.

The same enzyme deficiency underlies MPS IV B and GM₁ gangliosidosis. β -Galactosidase hydrolyzes terminal β -linked galactose residues found in GM₁ ganglioside, glycoproteins, and oligosaccharides, as well as keratan sulfate. Deficiency of enzyme activity toward all substrates causes GM₁ gangliosidosis. A mutation that predominantly impairs catalytic activity towards keratan sulfate results in MPS IV B.

In the absence of specific enzymes, nondegraded or partially degraded glycosaminoglycans accumulate in lysosomes and are partially excreted in urine. Glycosaminoglycans normally constitute the “ground substance” of connective tissue. They are attached to protein in proteoglycans, the macromolecular forms in which they exist in connective tissue. In MPS mainly bone and connective tissue are affected, causing the most characteristic clinical signs and symptoms: growth retardation, dysostosis multiplex, coarse facial features, joint stiffness, corneal opacities, valvular heart disease, and upper airway narrowing. In the CNS storage of glycosaminoglycans also occurs in connective tissue elements. Thickening of the leptomeninges may lead to hydrocephalus and to compression of the spinal cord in the cervical region, resulting in cervical myelopathy. Subluxation of the odontoid process can contribute to spinal cord compression. Storage in perineural tissue may lead to entrapment neuropathy. Within the brain, glycosaminoglycans are stored in the tissue around vessels.

In addition to glycosaminoglycans, there is evidence of accumulation of gangliosides (GM₂, GM₃, and GD₃) in the brain of MPS patients, especially in

MPS I, II, and III. Intralysosomal storage of gangliosides leads to the formation of zebra bodies and membranous cytoplasmic bodies, similar to those seen in GM₁ and GM₂ gangliosidoses. The question is what causes the storage of gangliosides. Apart from β -galactosidase, none of the enzymes involved in MPS plays a role in ganglioside breakdown. It has been demonstrated, however, that the activity of several additional lysosomal enzymes is reduced in the MPS, probably as a result of inhibition by the accumulating glycosaminoglycans, and this decreased enzyme activity may lead to ganglioside storage. The accumulation of gangliosides is probably responsible for the formation of meganeurites and ectopic secondary neurites, as these are also seen in GM₁ and GM₂ gangliosidoses. It is striking that the ganglioside storage is only found in MPS subtypes characterized by mental deficiency. These phenomena are most probably related.

There is a striking clinical variability within all MPS subtypes. An example is found in MPS I, in which Hurler syndrome is the most severe variant, Scheie syndrome the mild variant, and the Hurler-Scheie syndrome in between. The Scheie syndrome was previously classified as a separate disease entity, MPS V, until it became known that deficiency of the same enzyme underlies both Hurler syndrome and Scheie syndrome. It is probable that the clinical heterogeneity is caused by the presence of different mutant alleles, the Hurler patients having two severe mutations and the Scheie patients two mild mutations. It is likely that the type of mutation determines the residual activities of the mutant enzymes, which are associated with wide clinical variation within as well as between clinical subgroups. Environmental factors and modifying genes may also play a role in clinical severity, being in particular responsible for intrafamilial variability. A special phenomenon is the rare occurrence of clinical disease in female MPS II carriers, caused by unbalanced inactivation of the normal X chromosome.

13.5 Therapy

Hematopoietic stem cell transplantation presently represents the best therapeutic option in most MPS variants, if performed early in the course of the disease. In MPS I H, early transplantation with successful engraftment can preserve intellectual function and prevent or improve the systemic manifestations of the disease. Depending on the stage in which the transplantation is performed, mental decline is prevented or arrest or slowing of the mental regression is achieved. Progressive hydrocephalus requiring shunting does not occur after transplantation. Hepatosplenomegaly, joint stiffness, upper airway obstruction,

tion, and cardiac problems resolve or improve. However, hematopoietic stem cell transplantation does not reverse the progression of the skeletal abnormalities in MPS I H. Hematopoietic stem cell transplantation also leads to improvement in MPS I H/S and MPS I S, but these patients may be better candidates for enzyme replacement therapy. Hematopoietic stem cell transplantation in MPS II A and B may lead to improvements with respect to organomegaly, airway obstruction, and cardiac function. However, cognitive decline occurs despite early successful transplantation in MPS II A. In MPS II B cognitive function remains intact, as expected on the basis of the natural history of the disorder. As in MPS II, hematopoietic stem cell transplantation is able to effectively treat the somatic aspects of MPS III, but the progressive neurocognitive and behavioral deterioration that causes the dominant problems in the clinical picture of MPS III is not halted. For this reason, hematopoietic stem cell transplantation is generally not recommended for MPS III. Hematopoietic stem cell transplantation is unable to ameliorate the severe skeletal abnormalities which dominate the clinical phenotype in MPS IV, and this treatment is therefore not recommended for MPS IV. In MPS VI, hematopoietic stem cell transplantation leads to resolution of hepatosplenomegaly and airway obstruction, prevents further cardiopulmonary deterioration, and improves joint mobility. The skeletal abnormalities, however, do not benefit from the treatment. The experience in MPS VII is limited due to the rarity of the disease, but there is evidence for beneficial effects on neurocognitive, motor, and pulmonary outcome.

Enzyme replacement therapy has been applied so far only in MPS I. Administration of recombinant α -L-iduronidase leads to a decrease of the hepatosplenomegaly, increased growth rate in prepubertal patients, improved joint mobility, and decreased airway obstruction. This mode of treatment is considered for other MPS variants as well. Although systemic improvement is likely, no beneficial effects on the neurological manifestations is expected.

Various forms of *in vivo* and *ex vivo* gene therapy are being studied in animal models.

Symptomatic treatment is very important in MPS. Corneal transplantation can be performed in cases of corneal clouding; however, poor vision caused by retinal degeneration or optic atrophy cannot be reversed. Hearing aids may be helpful in cases of significant hearing loss. Exercise to optimize joint mobility should be started early. Airway obstruction may be alleviated by tonsillectomy, adenoidectomy, and, if necessary, tracheobronchial stent insertion. Sometimes a tracheostomy is required. Cardiac evaluation at regular intervals with echocardiography is important. Cardiac valve replacement is occasionally performed in cases of valvular disease. Bacterial endo-

carditis prophylaxis should be advised for MPS patients with valvular abnormalities. Progressive hydrocephalus may require ventriculoperitoneal shunting. Carpal tunnel syndrome is a common complication in MPS patients and surgical decompression should be performed early, before permanent nerve damage occurs. Cervical fusion to prevent atlantoaxial subluxation is performed to prevent or treat cervical spinal cord compression, especially in MPS IV. Anesthesia poses a particular problem in MPS. Atlantoaxial instability requires careful positioning and avoidance of hyperextension of the neck. Another problem may be difficulty in maintaining an adequate airway during anesthesia and postoperative airway obstruction. Sudden cardiovascular collapse may be caused by a combination of valvular disease, myocardial thickening, systemic and pulmonary hypertension, and narrowing of coronary arteries, all contributing to congestive heart failure.

13.6 Magnetic Resonance Imaging

The MRI abnormalities found in MPS vary greatly in severity from absent or negligible to severe, with a marked variation among sibs. However, in themselves, the abnormalities are fairly homogeneous.

Over the years many patients develop white matter abnormalities. These consist of multiple small spot-like lesions dispersed in the white matter, with a predilection for the parietal and occipital white matter. The signal intensity follows the signal intensity of CSF, indicative of the cystic nature of the lesions. The cystic areas often have a radial orientation from the subependymal region toward the cortex (Figs. 13.1 and 13.2). Punched-out cystic areas are often also present in the corpus callosum, best visualized on the sagittal images (Figs. 13.1 and 13.2). These cystic white matter lesions represent the perivascular lacunae seen on histopathological examination. In exceptional cases, the thalamus and basal ganglia have a honeycomb-like appearance, related to highly enlarged perivascular spaces in these areas. In addition, T₂-weighted and FLAIR images may show multifocal smaller and larger hyperintense areas, the signal intensity of which does not follow that of CSF. These areas may become extensive and confluent, and probably reflect gliosis, which is also seen on histopathological examination. The white matter abnormalities can be progressive on follow-up MRI. MRI and CT have demonstrated that white matter abnormalities may occur in all MPS variants. MRI may show a delay in myelination in young children.

Another frequent observation consists of ventricular enlargement, with or without accompanying enlargement of subarachnoid spaces. Enlargement of CSF spaces may occur in all MPS variants. The ven-

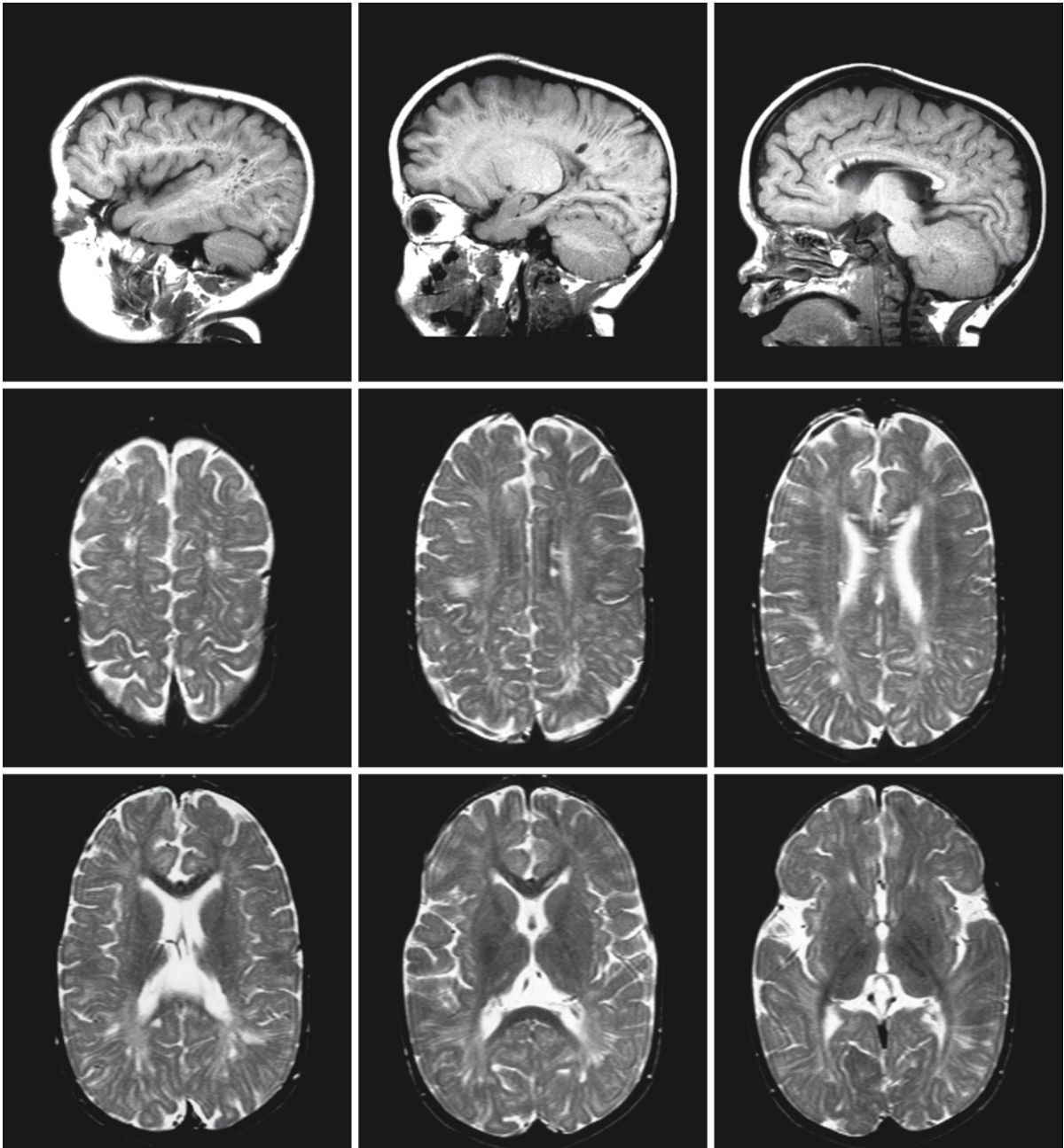


Fig. 13.1. A 3-year-old boy with Hurler syndrome (MPS I). The sagittal T₁-weighted images show the radial stripes of enlarged perivascular spaces, most prominent in the parietal region and also seen in the corpus callosum. The T₂-weighted

images confirm the enlarged perivascular spaces and show more extensive areas of signal abnormality in the region of the perivascular spaces. Courtesy of Dr. S. Blaser, Department of Diagnostic Imaging, Hospital for Sick Children, Toronto

tricular enlargement is of variable severity and is in some cases progressive. Some of the patients appear to have enlarged CSF spaces on the basis of diffuse atrophy of the brain parenchyma. In many cases, however, the enlargement of the CSF spaces is caused by hydrocephalus as a consequence of disturbed CSF reabsorption. Signs of hydrocephalus are upward bulging

Fig. 13.2. A 4-year-old boy with Hunter syndrome (MPS II). The sagittal and axial T₁-weighted images show the radial stripes of enlarged perivascular spaces, most prominent in the parietal region and the corpus callosum. The T₂-weighted images confirm the enlarged perivascular spaces and show more extensive signal abnormalities in the region of the perivascular spaces. Courtesy of Dr. S. Blaser, Department of Diagnostic Imaging, Hospital for Sick Children, Toronto

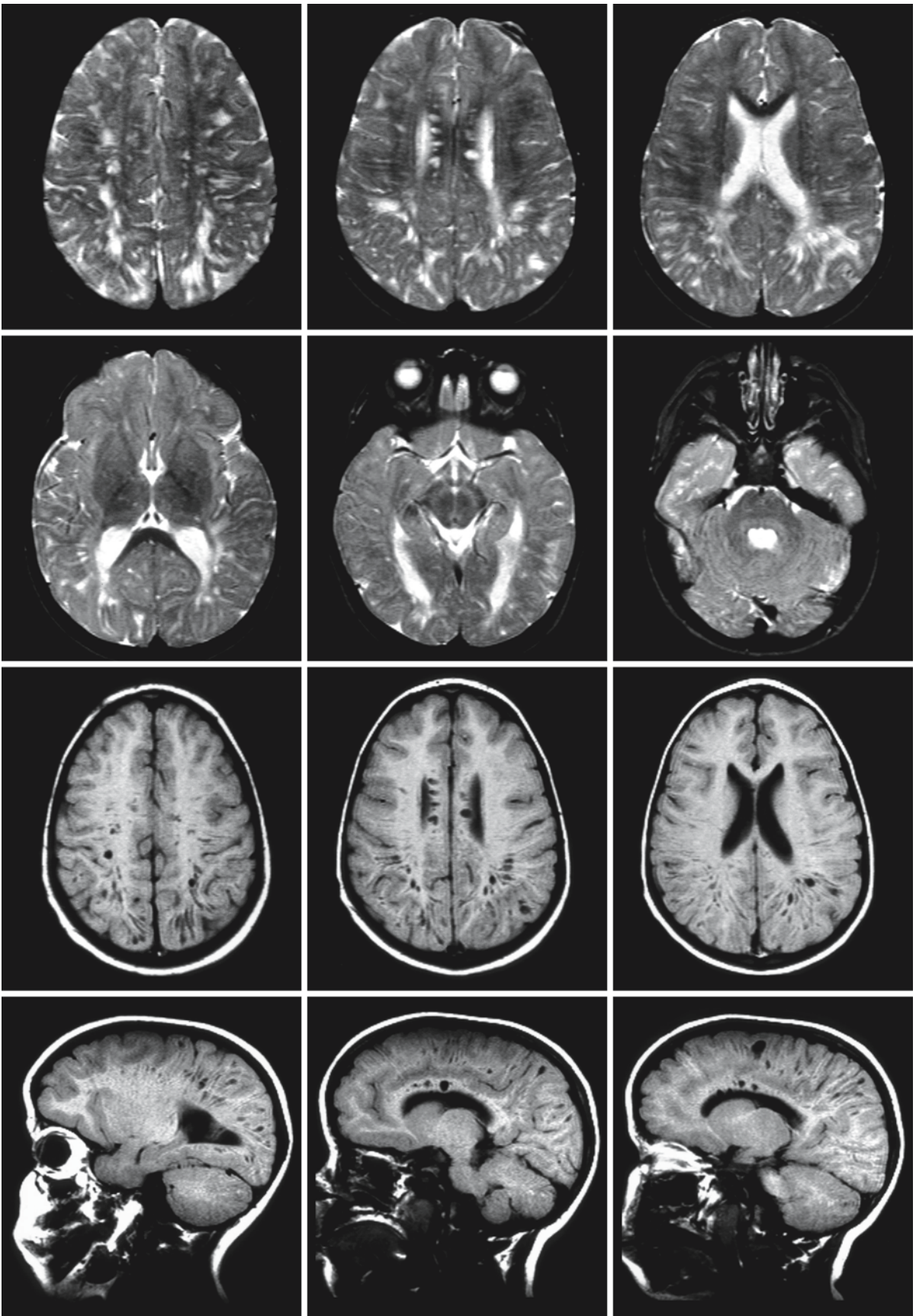


Fig. 13.2.

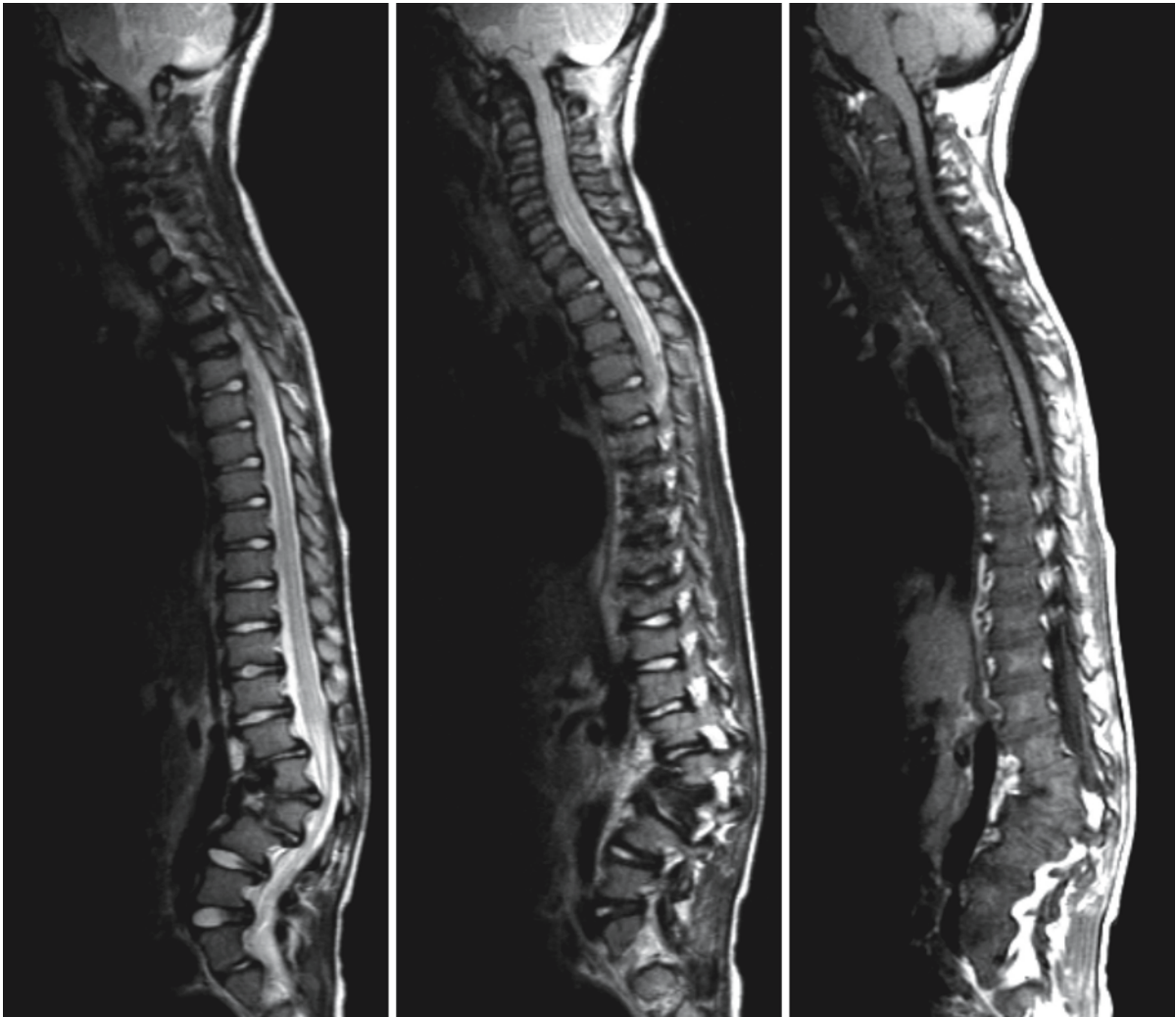


Fig. 13.3. Spinal MRI of a 5-year-old boy with Maroteaux–Lamy syndrome (MPS VI) shows abnormalities of the craniocervical junction, with deposits of mucopolysaccharide material around the dens, narrowing the spinal canal. The T₂-weighted images show no free CSF space around the cervical

spinal cord. The cervical vertebrae show platyspondyly. In the lower part of the vertebral column, T12, L1, L2, and L3 are dysmorphic with agenesis of the anterior parts of the vertebrae, resulting in local kyphosis

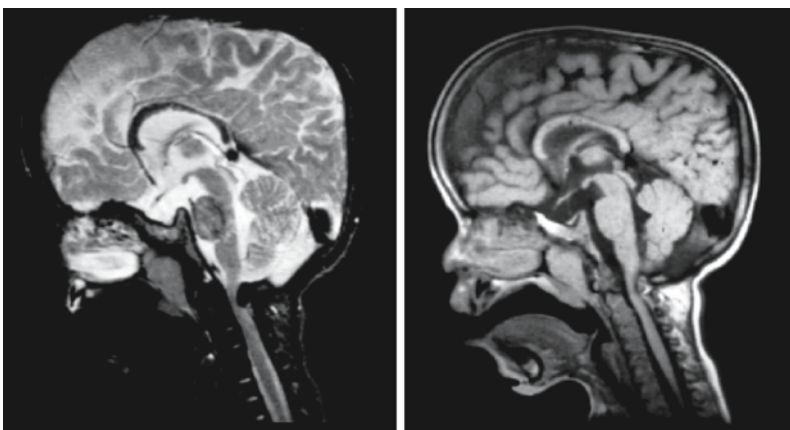


Fig. 13.4. A 5-year-old boy with Morquio syndrome (MPS IV). The mid-sagittal images show the intradural mucopolysaccharide deposits, leading to severe narrowing of the arachnoid space at the level of the craniocervical junction with compression of the spinal cord. Courtesy of Dr. P. Tortori Donati, Department of Pediatric Neuroradiology, G. Gaslini Children's Hospital, Genoa, Italy

Free Sialic Acid Storage Disorder

14.1 Clinical Features and Laboratory Investigations

The sialic acid storage disorders include severe infantile sialic acid storage disease (ISSD) and a milder variant, Salla disease (SD). Intermediate variants have also been reported.

ISSD is a rare disorder, presenting in the neonatal period with coarse facial features, hepatosplenomegaly, and often ascites or hydrops. Cardiomegaly and heart failure may also be present. The patients usually display generalized hypotonia. The subsequent clinical course is invariably characterized by failure to thrive and grossly delayed development. Most patients have hypopigmented skin and fair hair. Albinoid fundi and optic atrophy may be present. Mild hypertrophy of the tongue and gums may be seen. A nephrotic syndrome may complicate the course of the disease. Spastic tetraparesis develops with increased muscle tone and hyperactive tendon reflexes. Seizures may occur. There are recurrent respiratory tract infections. Hypothyroidism has been reported infrequently. The age at death varies from soon after birth to 5 years of age.

SD occurs with a relatively high frequency in Finland. Pregnancy and the perinatal period are uneventful. The first clinical signs usually appear at 6–9 months of age and include hypotonia, ataxia, and nystagmus. Gradually the patients develop spasticity. Many develop signs of athetosis. Motor development is delayed, and about 30% of the patients never walk without support. Speech development is also delayed, and the speech is dysarthric. The nystagmus disappears. Most patients acquire a divergent squint. Many patients are growth-retarded with a height below the second percentile. Mental development is delayed from early on, and most adults are severely mentally handicapped. Facial features may become coarse late in the course of the disease. Epileptic seizures may occur. Rarely, endocrine disturbances have been reported, including growth hormone deficiency and hypogonadotropic hypogonadism. The clinical course in SD patients is often static for many years, which delays evaluation for a metabolic disorder. The life span is relatively long. Most patients die in their thirties, but death in the seventies is also known to occur.

A few patients have been reported with a phenotype intermediate between SD and ISSD, and in fact

there is a phenotypic continuum between ISSD and SD.

Light microscopic examination of blood smears and bone marrow specimens reveal vacuolated lymphocytes in almost all ISSD patients and in most SD patients; young SD patients in particular may not have them. Electron microscopy of skin or conjunctival biopsy reveals vacuoles in many cell types including fibroblasts, smooth muscle cells, perineural cells, and Schwann cells. These vacuoles are bound by a single membrane and prove to be lysosomes. Most of them seem empty, but some contain small amounts of fibrillogranular material, membrane fragments, and occasional dark globules.

Dysostosis multiplex is found in about half of the patients with ISSD. Skeletal abnormalities are rare in SD and may include ovoid deformation of the vertebral bodies and a thickened calvarium of the skull. In SD EEG initially shows a slowing of background activity; in some patients epileptic activity is seen. With increasing age a gradual decrease in amplitude occurs; in adults a low-voltage EEG is a consistent finding. Motor and sensory nerve conduction velocities are reduced in about half of the SD patients. Somatosensory evoked potentials are abnormal in the majority of SD patients, but visual and brain stem auditory evoked potentials are usually normal. The most prominent changes in nerve conduction and evoked responses are seen in the patients with the most severe disease.

Demonstration of increased urinary excretion of free sialic acid and sialic acid accumulation in cultured fibroblasts is the mainstay of the laboratory diagnosis in both ISSD and SD. The levels of sialic acid excretion vary widely among patients. The level reflects more or less the severity of the clinical disease. Confirmation of the diagnosis by DNA analysis is possible.

Prenatal diagnosis is possible by assay of free sialic acid in a chorionic villus biopsy or by molecular studies. In all families in which the mutation is known, the latter option is the most reliable, in particular in SD, in which the increase in sialic acid in chorionic villi of an affected fetus is less pronounced than in ISSD. The use of cultured amniotic fluid cells is less appropriate because the elevation of the free sialic acid content in these cells may be only moderate.

14.2 Pathology

In ISSD, the brain has a firmer consistency at autopsy. There is some atrophy of the brain which a marked dilatation of the lateral ventricles. On sectioning, the white matter is firm and reduced in volume.

Histological examination shows clear vacuoles in neurons and astrocytes at all levels of the CNS. The stromal cells of the choroid plexus also contain these vacuoles. There may be neuronal loss in some areas. Axonal spheroids are present in all gray matter structures. The white matter is poorly myelinated and severely gliotic. The cerebellar white matter is also poorly myelinated and may show microcalcifications. Axonal spheroids are present in the cerebral and cerebellar white matter.

In SD, there is some external atrophy of the brain at autopsy. On sectioning, a marked reduction in white matter volume is found, whereas the cortex and basal ganglia are macroscopically normal. The corpus callosum is very thin. The cerebellum is atrophic with a markedly reduced white matter volume. Brain stem and spinal cord may appear thinner than normal.

Histological examination reveals storage of large amounts of lipofuscin in the perikarya of neurons in the cerebral cortex, thalamus, basal ganglia, brain stem nuclei, cerebellar cortex, and spinal cord. There may be extensive loss of Purkinje cells in the cerebellum. The cerebral and to a lesser extent the cerebellar white matter demonstrate severe myelin paucity with a marked loss of axons as well, accompanied by pronounced astrogliosis. The remaining axons frequently show spheroids.

On electron microscopy, a single membrane binds the cellular inclusions, indicative of lysosomes. They are filled with sparse fibrillogranular material and occasionally small neutral lipid droplets.

The sural nerve is normal on light microscopic examination, but electron microscopy shows vacuolar inclusions in the cytoplasm of Schwann cells.

In ISSD widespread storage of fibrillogranular material within large vacuoles is found in virtually all tissues of the body, including skin, conjunctiva, liver, kidney, myocardium, and bone marrow. Vacuolated lymphocytes can also be seen in blood. In SD the storage is less impressive.

14.3 Chemical Pathology

The material stored in ISSD and SD consists almost exclusively of *N*-acetylneuraminic acid. Studies of various tissues including the brain give identical results.

14.4 Pathogenetic Considerations

Free sialic acid storage disorders are autosomal recessive lysosomal storage disorders characterized by the accumulation of the acid monosaccharide sialic acid in lysosomes, caused by a defective efflux of sialic acid from the lysosomes. The basic defect in both ISSD and SD concerns the lysosomal free sialic acid transporter. The related gene *SLC17A5* is located on chromosome 6q14–15. The gene has also been designated *AST* (for anion and sugar transporter). This gene encodes the protein sialin, a predicted integral lysosomal membrane protein.

The anion and sugar transporter does not only transport sialic acid. The transporter carries acid monosaccharides, but also aliphatic nonsugar mono- and dicarboxylates. So, *N*-substituted acid monosaccharides (*N*-acetylneuraminic acid and *N*-glycolylneuraminic acid), glucuronic acids (the class of hexoses with a carboxyl on C-6), and glucoaldonic acids as well as lactic acid and α -ketoglutarate are all transported by the same carrier. Additionally, a large number of organic anions bind to the carrier, inhibiting transporter function.

Both ISSD and SD patients have mutations in the *AST* gene. Almost all Finnish SD patients have the same missense mutation in both alleles. The patients who are compound heterozygous for the Finnish mutation and another mutation usually have a more severe SD phenotype (intermediate phenotype). A variety of mutations, including deletions, insertions, missense, and nonsense mutations, are found in ISSD patients. These findings suggest that there is some genotypic–phenotypic correlation.

Sialic acids constitute a family of over 30 compounds derived from neuraminic acid. In humans, *N*-acetylneuraminic acid is the predominant sialic acid, referred to simply as “sialic acid.” Normally, a small portion of total sialic acid is free in tissues and body fluids. Most sialic acid is bound to glycoconjugates, providing these macromolecules with a negatively charged terminal sugar that serves many functions. No biological role is attributed to free sialic acid. Free sialic acid is produced in the lysosome by the degradation of sialylated oligosaccharides by neuraminidase. Sialic acid is removed from lysosomes for further metabolism by a specific membrane transporter system.

As a result of the defective transport of free sialic acid from lysosomes, patients store it excessively in many types of tissues and cultured fibroblasts and excrete large amounts in urine. Free sialic acid storage disorders must be discriminated from other forms of sialic acid storage, namely sialidosis, galactosialido-

sis, and sialuria. In sialidosis and galactosialidosis, bound sialic acid accumulates as the terminal sugar of complex oligosaccharides, which remain undegraded as a result of deficient lysosomal sialidase (neuraminidase) or as a result of a defect in protective protein. Sialuria results from the lack of feedback inhibition of the enzyme epimerase, which is involved in the biosynthesis of sialic acid from *N*-acetylmannosamine.

The pathophysiology of the myelin deficiency is unknown in ISSD and SD. Widespread storage of sialic acid in neurons and astrocytes may lead to dysfunction of these cells from early on. Myelin is deposited in a close collaboration and interdependence of neurons, oligodendrocytes, and astrocytes. This collaboration may be severely disturbed in the sialic acid storage disorders, leading to a profound deficiency of myelin.

14.5 Therapy

There is no causal treatment for sialic acid storage disorders. For both ISSD and SD, treatment is only supportive.

14.6 Magnetic Resonance Imaging

In ISSD MRI is characterized by a severe deficiency in myelin and a reduction in volume of the cerebral white matter, with enlargement of the lateral ventricles and in particular the subarachnoid spaces. The sylvian fissure may be wide open.

In SD MRI show a similarly serious myelin deficiency, but the reduction in cerebral white matter volume is less severe (Fig. 14.1). The lateral ventricles are

normal or moderately increased in size and the subarachnoid spaces are prominent. The corpus callosum is thin (Fig. 14.1). The brain stem and cerebellar white matter are usually better myelinated, although hypomyelination of the cerebellar white matter has also been observed (Fig. 14.1). The internal capsule is myelinated to a variable extent. In older patients variable atrophy of the cerebellum and brain stem is found. There is a correlation between the imaging findings and the clinical phenotype: better myelination is seen in patients with milder clinical symptoms.

The images in ISSD and SD are similar to those in Pelizaeus–Merzbacher disease. Proton MRS, however, distinguishes ISSD and SD from Pelizaeus–Merzbacher disease by showing elevations of sialic acid. Sialic acid (= *N*-acetylneuraminic acid) co-resonates with *N*-acetylaspartate. The result is a very high “NAA” peak at 2.02 ppm in a patient with a Pelizaeus–Merzbacher-like MRI. NAA is not equally high in Pelizaeus–Merzbacher disease.

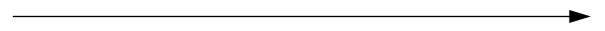


Fig. 14.1. The sagittal images in a 7-year-old girl with Salla disease demonstrate the thin corpus callosum and cerebellar atrophy. The axial T₂-weighted images show that the cerebral white matter has a high signal intensity throughout, consistent with myelin deficiency. The internal capsule is also hypomyelinated. The cerebellar white matter appears to contain more myelin, although still less than normal. The brain stem is myelinated best. Courtesy of Dr. J. Østergaard, Department of Pediatrics, and Dr. T. Christensen, MRI Research Center, University Hospital of Aarhus, Denmark. (Fig. 14.1 see next page)

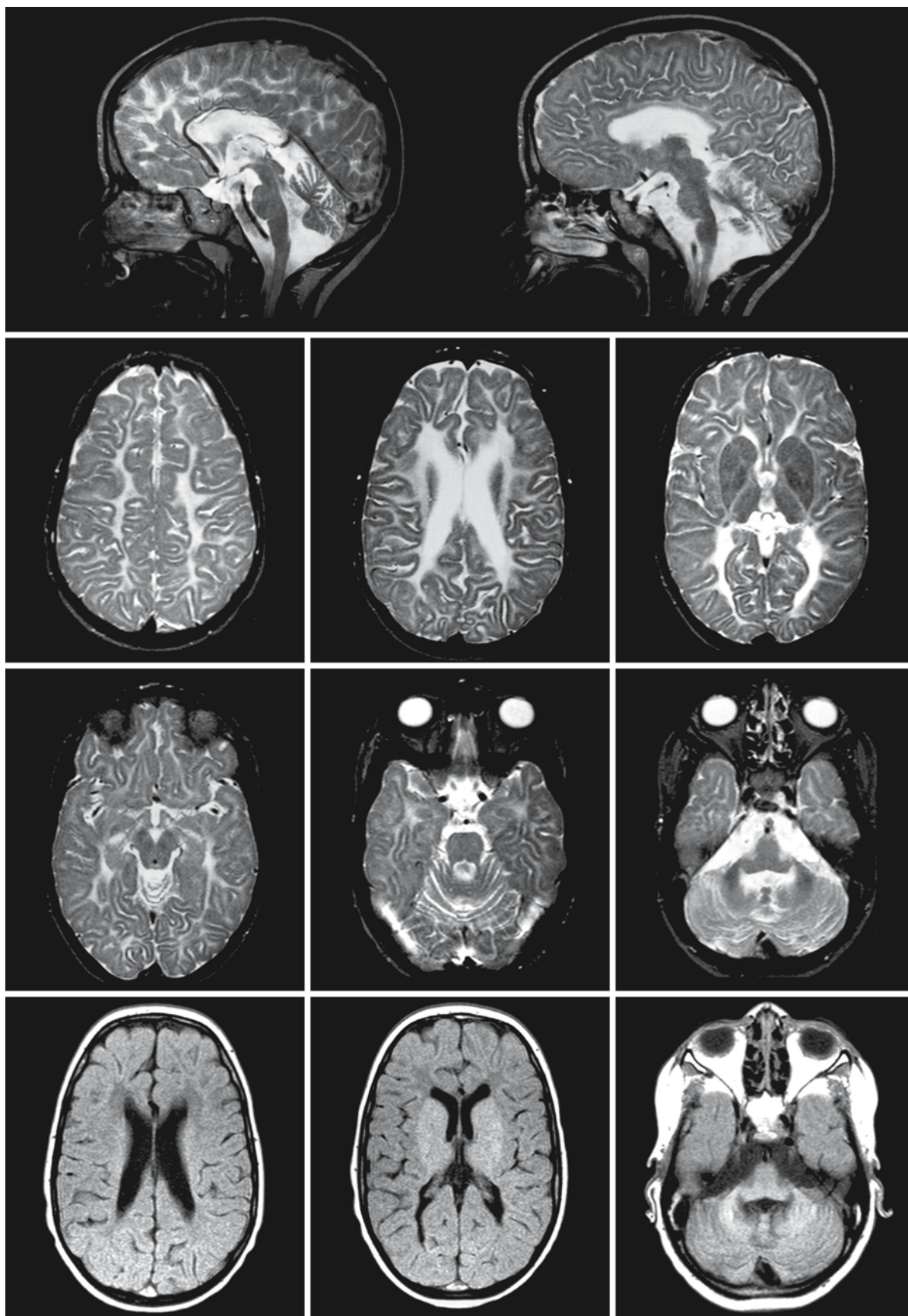


Fig. 14.1.

Neuronal Ceroid Lipofuscinoses

15.1 Clinical Features and Laboratory Investigations

The neuronal ceroid lipofuscinoses (NCL), often collectively called Batten disease, constitute a group of progressive neurodegenerative disorders characterized by accumulation of ceroid lipopigment in lysosomes in neurons and other cell types. They have an autosomal recessive mode of inheritance. Nine types are presently distinguished: infantile NCL (INCL or Santavuori disease), late-infantile NCL (LINCL or Jansky–Bielschowsky disease), the Finnish variant of late-infantile NCL (FvLINCL), variant late-infantile NCL (vLINCL), Turkish variant of late-infantile NCL (TvLINCL), juvenile NCL (JNCL, Spielmeyer–Vogt disease or Batten disease), adult NCL (ANCL or Kufs disease), Northern epilepsy or progressive epilepsy

with mental retardation (EPMR), and variant forms of late-infantile, juvenile, and adult NCL with granular osmiophilic deposits (see Table 15.1). The classification of NCL is based on the age at onset, clinical course of the disease, ultrastructural findings and, most of all, genetic defect.

INCL is the earliest and most severe form of NCL. The disease occurs most frequently in Finland, the incidence there being 7:100,000. Early psychomotor development is normal until the age of 6–18 months. Many children manage to stand up and to speak single words, but few learn to walk alone. Then rapid psychomotor deterioration sets in. Head growth slows down. The children develop muscular hypotonia, microcephaly, ataxia, choreoathetosis, stereotyped hand movements, myoclonic jerks, epilepsy, irritability, and visual failure. Most are restless and

Table 15.1. Classification of neuronal ceroid lipofuscinoses

Disease	Eponym	Deposits	Storage material	Gene location	Gene symbol	Gene product
Infantile form (INCL)	Santavuori	Granular osmiophilic deposits	SAPs A and D	1p32	<i>CLN1</i>	Palmitoyl protein thioesterase 1
Variant late-infantile, juvenile, and adult forms with GROD		Granular osmiophilic deposits	SAPs A and D	1p32	<i>CLN1</i>	Palmitoyl protein thioesterase 1
Late-infantile form (LINCL)	Jansky-Bielschowsky	Curvilinear bodies	Subunit c of ATP synthase	11p15	<i>CLN2</i>	Tripeptidyl peptidase 1
Juvenile form (JNCL)	Spielmeyer-Vogt/Batten	Fingerprint bodies and rectilinear profiles	Subunit c of ATP synthase dolichols, SAPs, amyloid- β peptide	16p12	<i>CLN3</i>	Membrane protein of unknown function
Adult form (ANCL)	Kufs	Curvilinear bodies, fingerprint bodies, rectilinear profiles	Subunit c of ATP synthase, SAPs, amyloid- β peptide	?	<i>CLN4</i>	?
Finnish variant late-infantile (FvLINCL)		Curvilinear bodies, fingerprint bodies, rectilinear profiles	Subunit c of ATP synthase, some SAPs A and D	13q22	<i>CLN5</i>	Soluble protein of unknown function
Variant late-infantile		Curvilinear bodies, fingerprint bodies, rectilinear profiles	Subunit c of ATP synthase	15q21–23	<i>CLN6</i>	Membrane protein of unknown function
Turkish variant late-infantile (TvLINCL)		Curvilinear bodies, fingerprint bodies, rectilinear profiles	?	?	<i>CLN7</i>	?
Northern epilepsy (EPMR)		Rectilinear profiles	Subunit c of ATP synthase SAPs, amyloid- β peptide	8p23	<i>CLN8</i>	Membrane protein of unknown function

sleep poorly. The stereotypical hand movements resemble those observed in Rett syndrome. Visual failure becomes apparent at between 12 and 20 months. Most patients are blind before the age of 2. Slow or absent pupillary responses, optic atrophy, and macular and retinal degeneration without pigment aggregations can be found on ophthalmological examination. Partial and generalized seizures and, occasionally, a Lennox–Gastaut-like epileptic syndrome are seen. Between 24 and 36 months most children have become bedridden. They are grossly mentally retarded and do not perform voluntary movements. Opisthotonus, decorticate posturing, and hyperexcitability to any kind of stimulation increasing the myoclonic jerks are characteristically present. Flexion contractures are common. After a number of years the hyperexcitability ceases. The final vegetative state is dominated by extensor posturing, unresponsiveness, blindness, gross microcephaly, stimulus-sensitive myoclonus, and seizures. Death ensues before the age of 15, usually between 8 and 11 years.

LINCL has its onset between 2 and 4 years of age. Usually epilepsy is the first symptom. Often several types of seizures occur, including generalized tonic–clonic seizures, myoclonic jerks, absences, and drop attacks. As disease progresses, myoclonia becomes the most predominant type. Onset of epilepsy is soon followed by mental and motor deterioration. Ataxia, especially truncal ataxia, hypotonia, and dysarthria, occur. Speech diminishes and disappears within a year. Typically, visual failure appears after the neurological symptoms and progression is slow. Blindness usually occurs at the age of 6 years. Funduscopic examination may initially be normal, but within 2 years after onset macular degeneration and retinal pigmentation are seen. Progression of disease is otherwise rapid with precipitous regression of mental and motor faculties. The initial hypotonia gives way to spasticity, painful flexor spasms, and severe flexion contractures. Excessive drooling and difficulty with swallowing occur. The final stage of the disease is one of unresponsiveness, myoclonic hyperexcitability, and blindness. Death occurs between 10 and 15 years.

The most important clinical difference between classic LINCL and FvLINCL is the later onset of clinical symptomatology in FvLINCL, usually between 4.5 and 7 years. The first symptoms are mental deterioration, clumsiness, and visual failure. Other symptoms, including epilepsy, ataxia and myoclonia, develop between the age of 7 and 10 years.

Incidence and prevalence figures for vLINCL, caused by *CLN6* mutations, are not known. Visual loss and seizures may occur initially, but in some children with the onset of the disease after 4 years, symptoms may start with epilepsy, ataxia, and myoclonus. Developmental regression occurs.

TvLINCL has its onset between 1 and 7 years of age. The disease is predominantly found within the Turkish population. Seizures and motor problems are early features. Visual impairment has a variable age of onset and is the leading symptom in some patients. Subsequently, motor and cognitive deterioration occurs.

JNCL is the most common type of NCL in the world, with the highest incidence in North European countries (0.5:100,000), in particular in Finland (5:100,000). The first clinical symptom is visual failure starting at the age of 4–8 years. Subsequently, mental slowing, epilepsy, and motor disturbances occur. The disease progresses at a slow pace. Long periods of ostensible arrest, sometimes even improvement, are common. Ophthalmological examination reveals macular degeneration and pigmentary retinal degeneration. Blindness is present by the age of 6–14 years. Seizures increase in frequency and severity and are usually of a generalized and complex partial nature. Mental deterioration with a widening gap between JNCL patients and classmates become obvious after the age of 12 years. Patients are unable to follow a regular school program and begin to lose acquired cognitive skills. A speech impediment becomes noticeable, in that the tone is monotonous. Patients also demonstrate echolalia and perseveration. Motor skills are lost. Rigidity, hypokinesia, and dystonia are frequently observed and movements are slow. Intention tremor, tremor at rest, and myoclonias are often noted. Spasticity does not set in until a late stage and is never severe. Many teenagers become depressed. Some manifest restlessness, rage, physical violence, insomnia, and visual and auditory hallucinations with paranoid delusions. Chewing and swallowing become more difficult, eventually necessitating nasal tube feeding. Myoclonia may become severe. Life expectancy is 18–25 years. Some patients have a so-called delayed-classic JNCL variant, which progresses less rapidly and leads to death after the age of 25. In addition, there are patients with so-called protracted JNCL. In these patients the first symptom, progressive visual loss, occurs at the same time as in classic JNCL, but mental and motor symptoms become manifest later, usually in the third or fourth decade of life. These patients have a different mutation in *CLN3*, with milder clinical phenotypes.

ANCL usually starts around the age of 25–30 years. Two main clinical subtypes are usually distinguished, although there is considerable overlap. Clinical phenotype A is characterized by behavioral changes, dementia, progressive myoclonus epilepsy, cerebellar ataxia, and dysarthria. Vision is normal and there are no signs of optic atrophy, macular degeneration, or pigmentary retinal degeneration. In the course of the disease seizures become intractable. Signs of involvement of the pyramidal, extrapyramidal and lower

motor neuron systems are absent or seen only terminally. Clinical phenotype B is characterized by behavioral changes, dementia, and motor abnormalities. Cerebellar or extrapyramidal features are prominent, the latter most frequently taking the form of a hyperkinetic movement disorder, rarely parkinsonism. Tic-like facial dyskinesias may be present. Pyramidal signs are rarely prominent. Visual failure and retinal abnormalities are not present. Seizures are rare and may only occur late in the course of the disease. In both phenotypes death usually occurs about 12 years after the onset of the disease, ranging from a few years to over four decades.

Northern epilepsy, also called progressive epilepsy with mental retardation (EPMR), is an autosomal recessive disease with onset between 5 and 10 years of age with generalized tonic-clonic seizures. In a minority of the patients complex partial seizures also occur during the first few years. The seizures increase in frequency, reaching a maximum at puberty. After puberty, the frequency of the seizures declines in a manner unrelated to changes in medication. After 35 years of age, many patients are almost seizure-free. Mental development is initially normal, but begins to deteriorate 2–5 years after the onset of the epilepsy. Deterioration continues during adulthood despite good epilepsy control.

Findings of repeated neurophysiological examinations are important in establishing the diagnosis. In INCL, EEG shows characteristic disappearance of sleep spindles from the age of 1.3 years onwards; sleep spindles are absent by 2.0 years at the latest. When the patient is 1.5–2 years old, the EEG slows and begins to attenuate, becoming isoelectric at the age of 3–4 years. There is no abnormal photic response. ERG abnormalities, especially a marked loss in amplitude, are early findings and may precede impairment of vision. ERG is usually negative at 12 months of age. VEP is markedly reduced in amplitude and becomes negative. It has been demonstrated that the SSEP becomes negative at an early stage, even before the ERG and VEP become negative. In LINCL, EEG already shows typical large polyspikes to a low rate of photic stimulation or single flashes at an early stage of the disease. ERG is negative by the age of 3–4 years. Other very typical findings are giant VEPs and SSEPs. In FvLINCL, the latency between onset of the first clinical symptoms of the disease and the appearance of the typical neurophysiological signs, including the negative ERG, the giant VEPs and SSEPs, and the EEG with spikes to a low rate of photic stimulation, is longer than in LINCL. These characteristic abnormalities appear several years after the onset of clinical symptoms, which is different from classic LINCL. In vLINCL the results of neurophysiological studies resemble those of classic LINCL. In JNCL, EEG findings are progressively abnormal, but not specific. There is

no abnormal photic response. ERG becomes absent by the age of 5–7 years. The amplitudes of the VEP and SSEP are reduced. In ANCL, the resting EEG is abnormal, but nonspecifically so. An intense photoparoxysmal response and an unusual sensitivity to low-frequency photic stimulation is of more diagnostic significance. ERG and VEP are normal. Giant short-latency SSEPs can be observed. They are common to many forms of progressive myoclonus epilepsy, and are of limited value in the differential diagnosis. In EPMR, EEG shows progressive slowing of the background activity, impaired reactivity to eye opening, and a disappearance of specific sleep patterns. In the fully developed disease, there is hardly any difference between waking and sleep recordings. The interictal epileptic activity is relatively scanty.

Ultrastructural findings are also important in the diagnosis of NCL. Skin, rectum, skeletal muscle, and conjunctiva biopsy are mostly used for this purpose. Peripheral lymphocytes can also be examined, in particular in JNCL. In this disorder peripheral lymphocytes can already be shown to contain vacuoles by means of light microscopy. Vacuolated lymphocytes on light microscopy are not a feature of the other NCL forms. Electron microscopic examination of lymphocytes can be very useful in the diagnosis and subclassification of NCL variants. A granular matrix indicates INCL; curvilinear profiles indicate LINCL; fingerprint profiles indicate JNCL. The biopsied tissues examined by electron microscopy show characteristic, membrane-bound deposits in vascular endothelium, sweat gland epithelium, smooth muscle cells, neurons, and in lymphocytes. In INCL, granular osmiophilic deposits are the predominant type of inclusions. In LINCL, FvLINCL, vLINCL, and TvLINCL curvilinear and fingerprint bodies and rectilinear profiles are seen. In JNCL, fingerprint bodies are most numerous. In EPMR rectilinear profiles are found. In ANCL either granular osmiophilic deposits or fingerprint and curvilinear structures are seen. In ANCL, a brain biopsy containing full-thickness cortex may be necessary to demonstrate the disease.

For INCL and LINCL and their variants, definite diagnosis is established by the demonstration of deficient activity of palmitoyl protein thioesterase 1 and tripeptidyl peptidase, respectively. Enzyme assays are relatively simple and rapid and should therefore be applied liberally in NCL patients to detect possible INCL and LINCL variants. DNA confirmation is an option in *CLN1*, *CLN2*, *CLN3*, *CLN5*, *CLN6*, and *CLN8*. Prenatal diagnosis is possible using enzyme or molecular studies, with the exception of ANCL and TvLINCL. Prenatal diagnosis using electron microscopy of chorionic villus specimens and amniotic fluid cells, searching for the characteristic inclusions in affected fetuses, is an option in these cases but requires special expertise.

15.2 Pathology

The hallmarks of neuropathological findings in NCL consist of neuronal lipofuscin storage and neuronal loss. The storage leads to displacement of the nuclei and distention of the proximal axon segment, but usually not to ballooning of the cells. On light microscopy the storage material is pale yellow with hematoxylin–eosin stains, slightly pigmented and granular. It is strongly PAS-positive, and stains with Sudan dyes and with many other stains for lipofuscin. Examination with ultraviolet light reveals bright yellow autofluorescence. The deposits are readily shown by an acid phosphatase reaction, indicative of their lysosomal location. The ultrastructural appearance of the storage material varies depending on the form of NCL.

In INCL atrophy of the brain is exceedingly severe, affecting cerebral hemispheres and cerebellum. The brain stem and spinal cord are relatively spared. Microscopic findings change with age. Up to the age of about 2.5 years, neuronal storage is observed with slight to moderate cortical neuronal loss, intense fibrillary astrocytosis, and presence of macrophages. The white matter shows mild changes. From about 2.5 to 4 years of age, neurons become grossly depleted. There is massive cortical macrophagocytosis and astrocytosis. The white matter shows moderate to severe loss of myelin and significant astrogliosis. The astrocytes are hypertrophic and contain storage material similar to that of nerve cells. Above the age of about 4 years, the atrophic cortex is entirely depleted of nerve cells and consists of a spongy network of fibrillary astrocytes and capillaries with some macrophages. The white matter shows complete loss of myelin and axons, also in the subcortical U fibers, and severe fibrillary astrogliosis. Only a very few myelinated nerve fibers are still present. At this stage the cerebellar cortex also shows complete atrophy. Most subcortical nuclei show florid neuronal storage, loss of neurons, macrophagocytosis, and astrocytosis, although the primary motor and sensory nuclei of brain stem and spinal cord are remarkably resistant. The stored material in INCL has a similar ultrastructural appearance wherever it is found. The substance is osmiophilic and consists of globules with a granular matrix, present either singly or as aggregates of globules. The single globules and the aggregates are stored in larger vesicles surrounded by a unit membrane of lysosomal origin. The deposits have been designated granular osmiophilic deposits (GROD) and can be found in neurons, ependymal cells, choroid plexus epithelium, astrocytes, macrophages, Schwann cells, smooth muscle cells, renal glomerular endothelium, renal distal tubular epithelium, Kupffer cells, vascular endothelium, germinal epithelium of the testis, sweat gland epithelium, thyroid follicle

cells, cells of the exocrine and endocrine pancreas, fibroblasts, and about 10% of lymphocytes.

In LINCL, neuropathological changes are less severe. The external atrophy is variable and sometimes more pronounced in the cerebellum than in the cerebral hemispheres. Neuronal storage, neuronal loss, and mild to moderate cortical astrocytosis are found, but neurons remain present, even in older patients. There is also neuronal storage and neuronal loss in the basal ganglia, thalamus, and substantia nigra, but neurons in the hypothalamus, brain stem nuclei other than the substantia nigra, and spinal cord are relatively preserved. There may be some loss of myelin in the white matter, but this is not marked. The white matter fibrillary gliosis may be more impressive than the myelin loss. In electron microscopy the stored material mostly has the appearance of curvilinear profiles, but may also take the form of fingerprint profiles. Curvilinear profiles consist of thin stacks of short, curved lamellae forming little arcs or semicircles. Accumulations of these are membrane-bound. These curvilinear bodies are also widespread outside the nervous system, similar to what is seen in INCL. Although no vacuoles containing lymphocytes are seen on light microscopy, curvilinear bodies may be shown in lymphocytes on electron microscopy.

The most important pathological difference between classic LINCL and FvLINCL is the presence of not only curvilinear bodies but also fingerprints and rectilinear profiles at electron microscopy in FvLINCL. Fingerprint profiles are formed by groups of parallel, paired lines, each pair of lines separated by a lucent space. The lines tend to be equidistant, straight or curved. Groups of lines form whorl-like patterns of fingerprints. Rectilinear profiles represent short, oligolamellar stacks with a prevailing straight course. They differ from curvilinear profiles in shape, width, and distinctness of the internal lines. In vLINCL, the neuronal and visceral storage is similar in distribution to that in classic LINCL and consists of a mixture of rectilinear, curvilinear, and fingerprint profiles.

Diffuse cerebral and cerebellar atrophy is also seen in JNCL, the degree being proportional to the duration of the disease. The cortical neurons show signs of storage and degeneration. Astrogliosis is usually mild. The white matter shows little evidence of myelin loss. In electron microscopy of stored material, the fingerprint pattern predominates, but may be admixed with curvilinear and rectilinear profiles. The deposits are membrane-bound. In JNCL, too, the storage bodies are widespread in other tissues than the nervous system. A small proportion of the lymphocytic vacuoles seen on light microscopy are shown on electron microscopy to contain fragments of fingerprint profiles.

In ANCL, variable cerebral atrophy is found. Neuronal storage and neuronal loss is found in the cerebral cortex (sometimes confined to layers III and V), the cerebellar cortex, and central nuclei. On electron microscopy fingerprint profiles, curvilinear bodies, or granular osmiophilic deposits are found. These storage bodies can also be found in several nonneuronal tissues.

In EPMR, most neurons have intracytoplasmic accumulations of autofluorescent storage material. In electron microscopy, the storage material is membrane-bound and consists of rectilinear profiles.

All infantile and childhood forms of NCL have a severe, progressive retinopathy. Ganglion cells show signs of lipofuscin pigment storage, similar to neurons in the brain. The same pigment is present in the cells of the bipolar layer. Most conspicuous is the degeneration and loss of photoreceptor cells, spreading from the macula outwards. Severe atrophy of all retinal layers develops, with narrowing of small retinal vessels and displacement of melanin-containing pigmented cells into the atrophic retina through the external limiting membrane. These displaced melanin-containing cells may also harbor NCL-type-specific lipopigments. On electron microscopy the storage material has the appearance specific for the form of NCL.

15.3 Chemical Pathology

Analysis of brain biopsy tissue from INCL cases shows lipid disturbance in the cerebral cortex, but a more severe reduction in myelin lipids in the cerebral white matter. At autopsy, when the end stage of the disease is reached, the cerebral and cerebellar tissues are extremely lipid-poor. The concentrations of cholesterol and phospholipids in cerebral gray matter are reduced to about 40% of those in age-matched controls. In cerebral white matter the lipid changes are even more pronounced. The concentration of cholesterol is reduced to about 10% of the control value, that of phospholipids to about 20%, and the concentrations of cerebrosides and sulfatides to values of often less than 1%. These results demonstrate an extreme reduction of myelin lipids, and in the terminal stage of INCL all attempts to isolate myelin from cerebral hemispheres and cerebellum fail. The ganglioside concentration and pattern of individual gangliosides are the same in gray and white cerebral matter, which means a more severe reduction in gangliosides for gray matter (to about 15% of control value) than for white matter (to about 40% of control value). Lipid changes are much less pronounced in brain stem and spinal cord. The other forms of NCL show only minor lipid alterations.

Protein is the major component of intralysosomal storage material, which accumulates in all forms of NCL. Over 40–60% of the dry weight of isolated storage material is protein. In INCL the saposins A and B constitute a major proportion of the accumulated protein. In LINCL, variants of LINCL, JNCL, and ANCL, subunit c of the mitochondrial ATP synthetase constitutes a considerable proportion (up to 85% in LINCL, about 20% in JNCL) of the accumulated protein. The protein molecules are intact and there is no evidence of any abnormality in amino acid sequences. Dolichols, which are unesterified alcohols, represent up to 2% of the dry weight of storage bodies. The dolichols are largely in the form of dolichyl pyrophosphoryl oligosaccharides.

15.4 Pathogenetic Considerations

NCL represents a group of unrelated disorders which share a number of clinical, biochemical, and histopathological characteristics. Although NCL variants are lysosomal storage disorders, they differ from the classic lysosomal storage diseases. The accumulated material consists mainly of proteins and not of lipids, making NCL a proteinosis rather than lipidosis.

The term “lipopigment” is a general one given to yellow-brown pigments that stain with lipid stains and fluoresce under ultraviolet light. The prototype pigment is lipofuscin (age pigment), ubiquitously present in cells of aged individuals. The term “ceroid” has been used to describe any abnormal lipopigment, including the lipopigment of NCL. The nature of the fluorophores in the NCL-specific ceroid has been studied but is still not clear.

At present there is evidence for at least eight genes that are related to NCL. Currently, six of them have been identified and characterized: *CLN1*, *CLN2*, *CLN3*, *CLN5*, *CLN6*, and *CLN8*. Two of these genes, *CLN1* and *CLN2*, encode lysosomal enzymes, palmitoyl protein thioesterase 1 and tripeptidyl peptidase 1, respectively. *CLN3*, *CLN6*, and *CLN8* encode proteins of predicted transmembrane topology, but their function is as yet unknown. *CLN5* is probably a soluble lysosomal protein. The genes associated with TvLINCL and ANCL are at present unknown. It is important to realize that one clinical type of NCL is not automatically equivalent to one genetic type. Some adult NCL patients have been shown to have a defect in *CLN1*. It cannot be assumed that all remaining ANCL patients have a defect in *CLN4*; there may be more than one related gene. Likewise, Turkish patients with a late-infantile onset of disease, who have the other NCL genes excluded, do not necessarily share a defect in the same gene (*CLN7*); again there may be more than one related gene.

Palmitoyl protein thioesterase 1 (PPT1) is a lysosomal enzyme that cleaves fatty acyl moieties (usually palmitate) from cysteine residues of proteins. Palmitoylation and depalmitoylation is a reversible and dynamic process, which may regulate the function of numerous proteins of the CNS that are implicated in important processes such as neuronal transmission, signaling pathways, and protein transport. Potential impairment of these processes by nonfunctional PPT1 could induce a deleterious effect on the functioning of neurons and neuronal death. PPT1 has been shown to depalmitate several neurospecific peptides *in vitro*, supporting a specific role of PPT1 in the CNS. PPT1 may also have a role in the protection of neurons against apoptosis. Recent evidence indicates that in neurons PPT1 is localized in synaptosomes and synaptic vesicles. The precise mechanisms leading to lysosomal storage of mainly saposins (sphingolipid activator proteins, SAPs) A and D remain elusive. SAPs A, B, C, and D are small glycoproteins derived from a precursor protein, prosaposin. SAPs are lysosomal proteins that facilitate the actions of several lysosomal hydrolases engaged in the degradation of sphingolipids. There is no evidence that SAPs are palmitoylated and could serve as substrates for PPT1. Accumulation of SAPs is not restricted to INCL. SAPs are also found in variable amounts among subunit c of ATP synthase in other NCL variants and they are found in GM₁ gangliosidosis, GM₂ gangliosidosis, type A Niemann–Pick disease, metachromatic leukodystrophy, and globoid cell leukodystrophy. The highest levels of SAPs are found in lysosomal storage disorders in which the stored lipids bind to SAPs. Although the lysosomal accumulation of SAPs may represent an epiphenomenon of no or minor significance, it is possible that the dysregulation of SAP metabolism plays a role in the pathogenesis of INCL. The severe paucity of myelin in INCL is striking and not shared by the other NCL variants. The myelin deficiency is more severe than can be explained by the neuronal loss. There is probably a component of hypomyelination. Early onset neuronal/axonal dysfunction may interfere with the complex interaction of oligodendrocytes, neurons/axons, and astrocytes that is necessary for myelin to be produced and deposited. A similarly severe myelin deficiency is seen in other neuronal storage disorders with infantile onset, including infantile-onset GM₁ and GM₂ gangliosidoses.

Tripeptidyl peptidase 1 (TPP1), also called pepstatin-insensitive proteinase, is a lysosomal enzyme with aminopeptidase activity, removing tripeptides from the N-terminus of proteins. Efficient protein degradation in lysosomes depends on concerted action of endopeptidases and exopeptidases, which provide dipeptides and free amino acids to be exported to the cytoplasm and further used according to the

metabolic needs of the cell. TPP1 could provide tripeptides for subsequent action of dipeptidyl peptidases and dipeptidases. The specificity and substrate range of TPP1 is still under investigation. TPP1 has been shown to degrade small peptides with an extended N-terminal domain. TPP1 appears to be involved in the initial lysosomal degradation of subunit c of ATP synthase, a very hydrophobic protein that accumulates in LINCL. The decreased TPP1 activity may be directly responsible for the accumulation of subunit c of mitochondrial ATP synthase and undigested small peptides. Whether and how subunit c accumulation is associated with progressive neuronal degeneration and death remains unknown. Storage of lesser amounts of subunit c is observed in other forms of NCL, mucopolysaccharidoses types I, II, and III, mucopolysaccharidosis type I, GM₁ and GM₂ gangliosidoses, and Niemann–Pick disease types A and C; the cause of this is unknown. So, the significance of the accumulation of subunit c in the pathophysiology of NCL is unclear.

CLN3, the gene for JNCL, encodes a putative integral membrane protein. The subcellular localization of the protein remains a subject of controversy. Available evidence indicates that CLN3 protein is trafficked through the endoplasmic reticulum and Golgi to the lysosome, where it is localized in the lysosomal membrane. It may also be present at the plasma membrane. Subunit c of mitochondrial ATP synthase constitutes part of the protein content of the storage material. Other identified constituents of the stored material include phosphorylated dolichols, small amounts of SAPs, amyloid- β peptide, and mannose-6-phosphate glycoproteins. Newly synthesized lysosomal enzymes are post-translationally modified by the carbohydrate residue mannose 6-phosphate. This residue serves as a recognition signal for mannose 6-phosphate receptors of proteins that are destined for lysosomes, where the recognition signal is removed. In JNCL the levels of mannose 6-phosphate glycoproteins are significantly elevated.

CLN5, the gene for FvLINCL, encodes a protein which was formerly predicted to be a membrane protein, but more recent evidence suggests it is a soluble lysosomal protein. There is evidence for interactions of the CLN5 protein with the CLN2 and CLN3 proteins. In contrast, there is no evidence for interaction between the CLN1 protein and the CLN2, CLN3, and CLN5 proteins. This is in line with the fact that the storage material in INCL is different from the material in other NCL variants. The lysosomal storage material consists mainly of subunit c of mitochondrial ATP synthase and small amounts of SAPs A and D.

CLN6, associated with vLINCL, codes for a transmembrane protein localized to the endoplasmic reticulum. Its function is unknown, but there is evi-

dence that defects in the protein lead to lysosomal dysfunction.

CLN8, associated with Northern epilepsy, also encodes a putative membrane protein. The *CLN8* protein is nonlysosomal. Most *CLN8* protein is localized in the endoplasmic reticulum with a proportion in the endoplasmic reticulum–Golgi intermediate compartment. It is involved in the early secretory pathway. It is proposed that the *CLN8* protein may play a role in the transport of proteins across the endoplasmic reticulum membrane. The storage material contains subunit c of mitochondrial ATP synthase, SAPs, and amyloid- β peptide.

Many different mutations have been identified in the NCL-associated genes. The age at onset of the disease is no longer the most important criterion for the subclassification of patients. Mutations in *CLN1* have been found to be associated with infantile, late-infantile, juvenile, and, rarely, also adult onset of the disease. Mutations in *CLN2* may give rise to late-infantile but also to juvenile disease onset. Late-infantile onset of the disease has been found in mutations of *CLN1*, *CLN2*, *CLN5*, and *CLN6*, and will be for *CLN7*. There is evidence for a genotype–phenotype correlation. Mutations that abolish all function of the encoded protein may lead to a more severe phenotype than mutations with some residual function of the protein. Mutations leading to intracellular misrouting of the encoded protein may be associated with a more severe phenotype.

15.5 Therapy

Treatment continues to be supportive only. Anticonvulsants are important and need to be tailored to the patient, seizure type, and side effects. Tegretol and lamotrigine may be helpful in the setting of behavioral disturbances. In the management of INCL, irritability, sleeping disorders, choreoathetosis, and late pains have responded best to baclofen, tizanidine, levomepromazine, and benzodiazepines. Only a few children with LINCL show significant irritability and sleeping disturbances. Behavioral problems, depression, and psychosis are often present in JNCL. Meaningful hobbies and individual, not too demanding teaching are of basic importance in the management of these problems. Medication is necessary periodically. Valproate and benzodiazepines can be of help in coping with the sleeping problems. Severe behavioral problems and psychotic symptoms can be treated with haloperidol, levomepromazine, and benzodiazepines. In the bedridden stage, motor restlessness or panic attacks can be alleviated with baclofen and tizanidine. Antiepileptics, neuroleptics, antidepressants, and anxiolytics have been used to try to suppress involuntary movements, but with no clear ef-

fect. Nasogastric tube or, preferably, gastrostomy tube feeding is important in the later stages of the disease and has prolonged and improved the quality of life.

Hematopoietic stem cell transplantation has been unsuccessful in halting the progression of the disease.

15.6 Magnetic Resonance Imaging

In INCL, CT scan of the brain shows severe atrophy, more severe in the cerebral hemispheres than in the cerebellum. Some atrophy of the brain stem can also be seen. The ventricles and subarachnoid spaces are enlarged. The entire white matter is hypodense and reduced in volume. The cortex is abnormally thin, whereas the volume of the basal ganglia is not reduced, except in the oldest patients. The calvarial bone is thickened in patients over 2 years of age. MRI is already abnormal in an early stage of disease in INCL, before the appearance of clinical symptoms. With increasing age there is increasing atrophy. The white matter has a high signal intensity on T_2 -weighted images in all stages of the disease (Fig. 15.1), but more seriously in the later stages (Fig. 15.2). The signal intensity is highest in the periventricular area. The corpus callosum and internal capsule are myelinated normally. With increasing age the loss in white matter volume becomes extreme (Fig. 15.2). The appearance of the white matter abnormalities suggests a combination of seriously delayed and disturbed myelination, increasingly severe gliosis, and some myelin loss. In the end only a thin cerebral mantle is left with highly abnormal signal intensity of the white matter throughout, compatible with complete absence of myelin and severe gliosis (Fig. 15.2). The cortex becomes increasingly thin. The basal ganglia and, in particular, the thalamus have a low signal intensity on T_2 -weighted images from early on (Figs. 15.1 and 15.2). The pattern of a strikingly low signal of the thalamus within cerebral white matter with a high signal intensity is quite characteristic of INCL. Initially, the volume of the thalamus and basal ganglia is relatively normal, but subsequently the central nuclei also become severely atrophic.

In the NCL variants of later onset, CT shows progressive atrophy involving cerebral hemispheres and cerebellum. The atrophy involves both gray and white matter (Figs. 15.3 and 15.4). In LINCL cerebellar atrophy is more severe than cerebral atrophy. MRI in LINCL, FvINCL, vLINCL, and TvLINCL shows a rim of mildly increased signal intensity around the lateral ventricles and in the posterior limb of the internal capsule (Fig. 15.3). Additionally, a decrease in signal intensity is seen in the thalami and, to a lesser degree, sometimes the basal ganglia on T_2 -weighted images. In JNCL abnormalities appear later and initial MRI may be normal. Apart from progressive atrophy, most

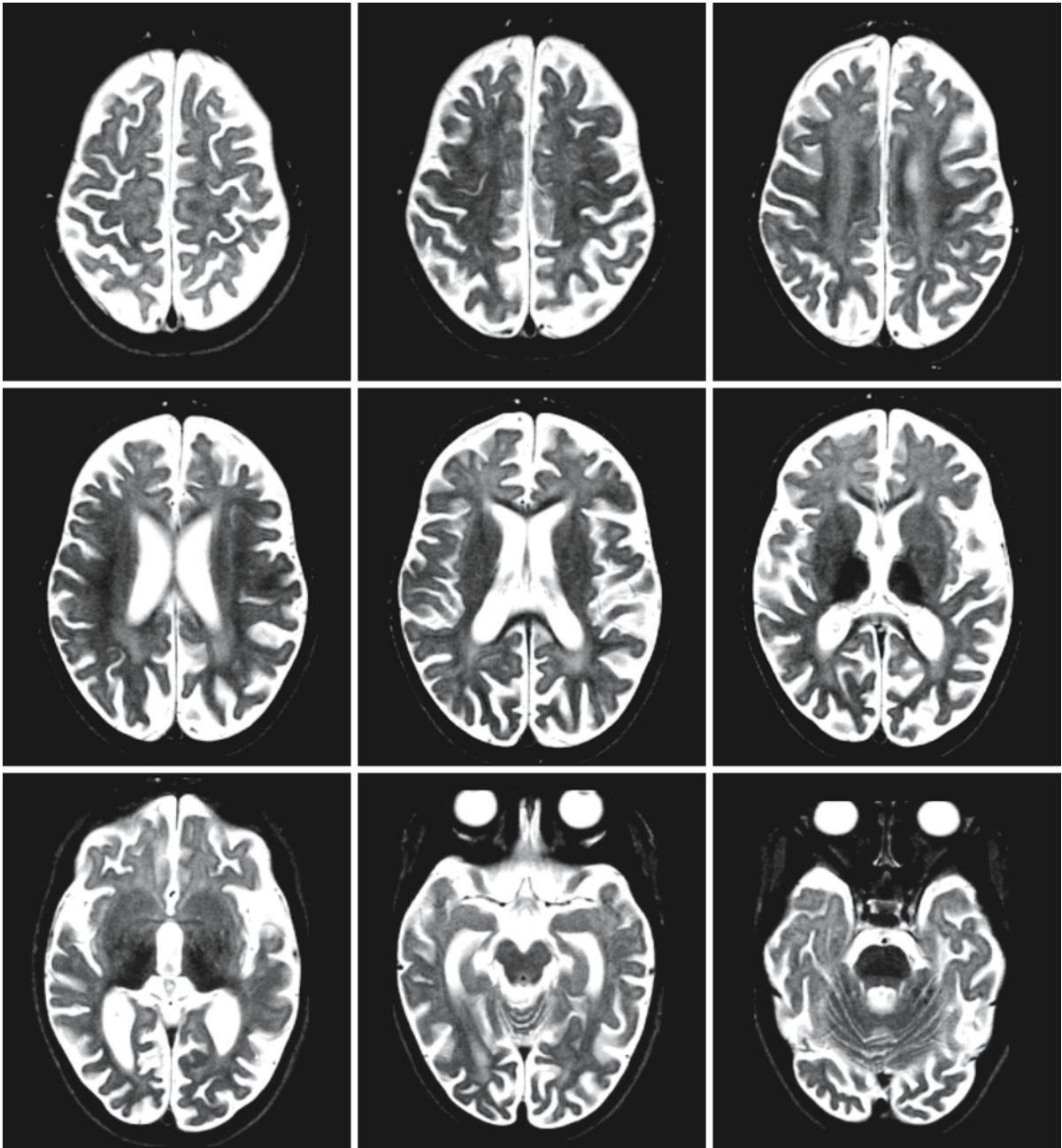


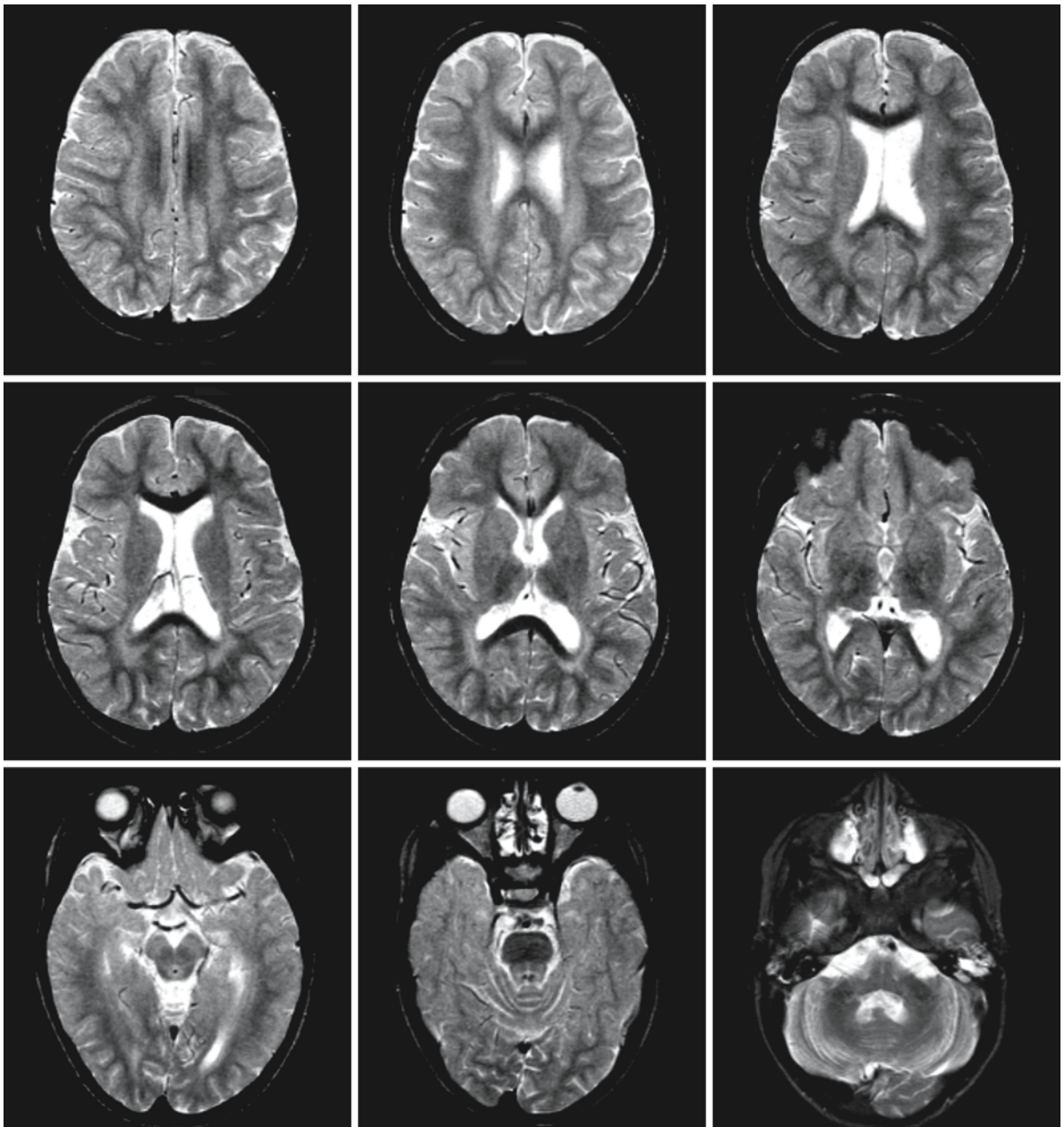
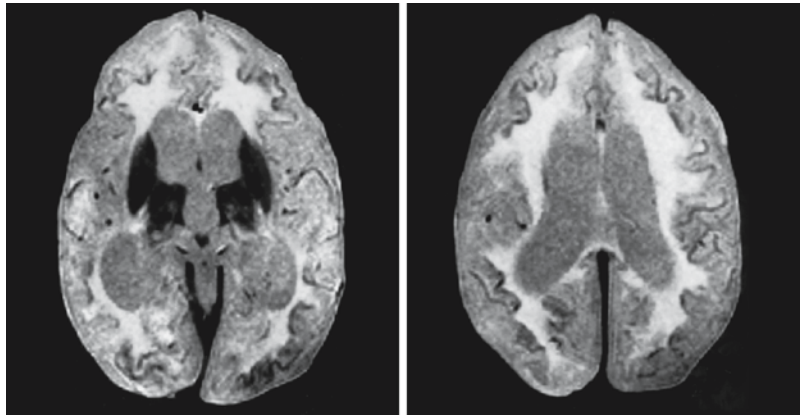
Fig. 15.1. MRI in a 21-month-old girl with INCL shows cerebral atrophy with enlarged ventricles and subarachnoid spaces. The white matter has a higher signal intensity than gray matter in most areas, consistent with disturbed and delayed

myelination. The corpus callosum has a low signal intensity, consistent with a higher myelin content. The thalami have a low signal intensity

severe in the cerebellum, the rim of mildly increased signal intensity in the periventricular white matter and posterior limb of the internal capsule may also be seen in JNCL. In ANCL, CT and MRI show atrophy. White matter abnormalities have not been reported. In early EPMR MRI is normal, but it shows atrophy in later stages of the disease.

Fig. 15.3. MRI in a 4-year-old Turkish boy with TvLINCL reveals a rim of slightly increased signal intensity around the lateral ventricles. The cerebellum is slightly atrophic

Fig. 15.2. A 6-year-old child with INCL. Note the severe generalized atrophy, and the low signal intensity of the thalami and basal ganglia on these mildly T₂-weighted images. The white matter has a high signal intensity throughout, consistent with absence of myelin and presence of gliosis. Courtesy of Drs. P. Santavuori and S.L. Vanhanen, Helsinki, Finland



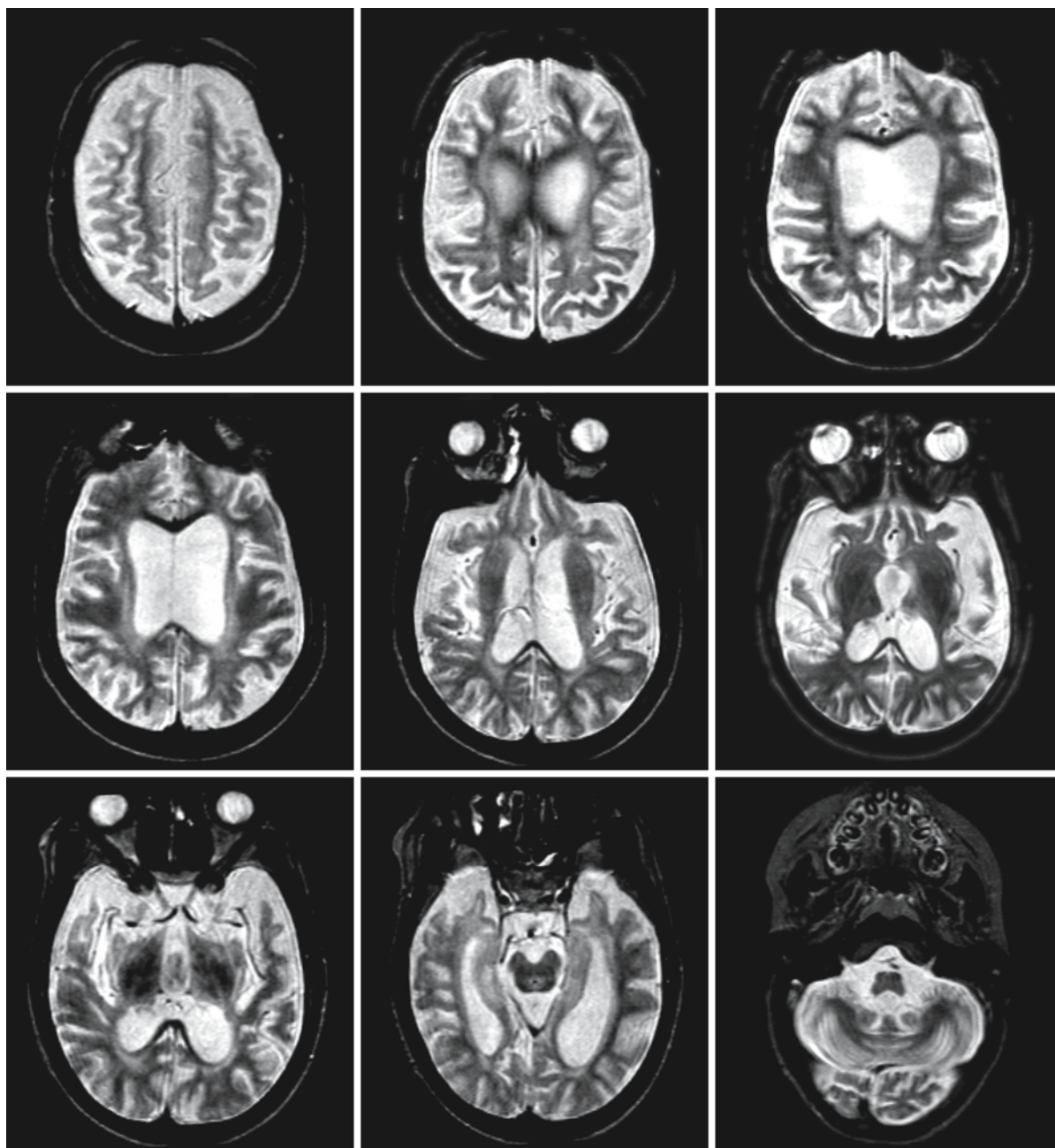


Fig. 15.4. MRI in the same boy with TvLINCL, now 8 years old. Note the serious generalized atrophy involving cerebral hemispheres, basal ganglia, and cerebellum. The cerebral white

matter has a slightly elevated signal intensity, as seen in neuronal degenerative disorders

Adult Polyglucosan Body Disease

16.1 Clinical Features and Laboratory Investigations

Adult polyglucosan body disease (APBD) is a rare autosomal recessive neurological disorder with an onset in the fifth to seventh decade of life. The clinical features consist of pyramidal tract signs, peripheral neuropathy with motor deficits, and usually pronounced distal sensory loss predominantly involving the lower limbs, hyper- or hypoactive reflexes, and urinary incontinence due to a neurogenic bladder. Most patients develop dementia, especially in the later stages of the disease. Cerebellar ataxia, extrapyramidal movement abnormalities, and seizures may occur. Some patients have predominantly signs of upper and lower motor dysfunction, prominent wasting of muscles, and fasciculations, suggesting a diagnosis of amyotrophic lateral sclerosis. The clinical course is progressive. The interval between onset of symptoms and death ranges from 3 to 21 years.

CSF protein levels are usually elevated. Neurophysiological studies show signs of an axonal sensorimotor peripheral neuropathy with normal to moderately slowed nerve conduction and signs of denervation in electromyography. SSEP studies show prolonged central conduction times. In the context of the above clinical symptoms, the demonstration of polyglucosan bodies in sural nerve biopsy or axillary skin biopsy confirms the diagnosis, especially if they are numerous. In some patients, especially patients of Ashkenazi Jewish ethnic background, deficiency of glycogen branching enzyme has been demonstrated in leukocytes and peripheral nerve biopsies. However, not all patients are deficient in this enzyme despite the otherwise indistinguishable clinical and histopathological findings. Prenatal diagnosis is possible in families in which deficiency of glycogen branching enzyme or the underlying genetic defect has been demonstrated.

16.2 Pathology

At autopsy mild external atrophy with prominence of sulci and widening of the lateral ventricles may be present. The spinal cord is atrophic. On sectioning, poorly demarcated areas of discoloration are seen within the white matter of the brain.

On microscopy, the most striking finding is the presence of many polyglucosan bodies throughout the nervous system. Most of them appear spherical, but there are also elongated thread-like forms, especially in the gray matter. They vary in size from 1 to 25 μm , even up to 50 μm ; the usual size is around 10 μm . The bodies are variably positive on staining with PAS, silver proteinate (Bodian, Bielschowsky), iodine stains, and alcian blue, but negative with Sudan black, luxol fast blue, and Congo red. With hematoxylin–eosin they show varying degrees of basophilia. Those in the white matter are usually more strongly basophilic than those in the cortex. Their location is intra-axonal and within astrocytic processes. Electron microscopy shows that polyglucosan bodies consist of non-membrane-bound, about 8-nm-wide branching filaments, associated to some extent with haphazardly distributed granular and amorphous, densely osmiophilic condensations. These are sometimes clumped together into much larger dense granular structures, which tend to aggregate in the center of the bodies to form round, target-like dense areas. Many of the polyglucosan bodies can be identified as being located within axons. The surrounding myelin sheaths are usually thinner than would be expected for the caliber of the axon. Polyglucosan bodies are not seen in neuronal cell bodies.

Within the cerebral hemispheric white matter there are extensive, ill-defined areas of myelin pallor, which involve the cerebral and cerebellar white matter bilaterally and symmetrically. Myelin loss is incomplete and more marked around the ventricles than in the subcortical white matter. In the affected areas, axons are relatively spared. In addition, small necrotic and even cystic lesions are frequently present in the subcortical white matter, globus pallidus, putamen, dentate nucleus, and the pons.

Examination of the sural nerve reveals the presence of numerous intra-axonal polyglucosan bodies in both unmyelinated and myelinated axons. The overlying myelin sheaths in myelinated axons are thin. The nerve may otherwise be normal or show moderate diffuse loss of both small and large myelinated axons. Onion bulbs may be found, suggesting demyelination and remyelination.

Polyglucosan bodies may also be found in other organs, such as the heart, liver, kidneys, lungs, skeletal, and smooth muscles. The presence of polyglu-

cosan bodies in myoepithelial cells of apocrine glands facilitates diagnosis by axillary skin biopsy.

16.3 Chemical Pathology

Polyglucosan bodies are composed principally of glucose polymers, with a small but variable component of phosphate and sulfate groups and less than 5% protein.

16.4 Pathogenetic Considerations

Type IV glycogen storage disease is a rare autosomal recessive disorder representing 0.3% of all cases of glycogenosis of any type. The disease is caused by a deficiency of the glycogen branching enzyme. Glycogen branching enzyme is encoded by the gene *GBE*, which is located on chromosome 3p14. There is evidence for the existence of different isoenzymes, probably generated by alternative splicing. The enzyme is involved in glycogen synthesis. Deficiency leads to accumulation of polysaccharides, which are resistant to amylase digestion and have longer outer chains and shorter branch points than normal glycogen.

Glycogen storage disease type IV is highly heterogeneous as to clinical symptoms and age of onset. The latter varies between the early neonatal period through childhood to late adulthood. The classical type is characterized by early onset and rapidly progressive hepatosplenomegaly, progressive cirrhosis with portal hypertension, ascites, esophageal varices, and death between 3 and 5 years due to liver failure, unless liver transplantation is performed. Nonprogressive hepatic variants have also been described. Patients with neuromuscular involvement have a myopathy with or without cardiomyopathy, neuropathy, and liver cirrhosis. The age at onset varies from neonatal to adulthood. Neonatal variants presenting with pronounced hypotonia are extremely rare. They resemble patients with the Werdnig–Hoffmann type of spinal muscular atrophy. They may have additional cardiomyopathy or hepatosplenomegaly. Presentation with hydrops fetalis is also very rare. APBD characterized by late onset and slowly progressive severe neurological symptoms can also be an expression of glycogen branching enzyme deficiency.

The phenotypic variability and tissue specificity described above may be due to particular mutations resulting in selective tissue-based expression or deficiency of isoenzymes. This hypothesis does not, however, explain the differences in phenotypic expression between patients with identical genotype.

Glycogen branching enzyme activity can be either deficient or normal in patients with APBD. Most patients of Ashkenazi Jewish ethnic background have a deficiency of this enzyme, but so do some patients of other ethnic background. It is likely that APBD is genetically heterogeneous and that the disease may have more than one biochemical etiology resulting in similar phenotypes.

Polyglucosan bodies are composed principally of glucose polymers and occur in various conditions. The polyglucosan bodies of APBD greatly resemble and may be identical to corpora amylacea, which accumulate in the CNS with normal aging, Lafora bodies present in Lafora body disease, and Bielschowsky bodies. Corpora amylacea are seen in a characteristic topography in the healthy nervous system with aging. They develop in astrocytic processes and are mainly distributed subpially, subependymally, and perivascularly, although intra-axonal corpora amylacea may also occur. Lafora bodies are found in association with Lafora body disease, a progressive myoclonus epilepsy. Lafora bodies appear in neuronal perikarya and processes, especially in the cerebral cortex, thalamus, globus pallidus, substantia nigra, and dentate nucleus. Bielschowsky bodies are found in the perikarya and processes of neurons. They differ from Lafora bodies in their much more limited distribution and pleomorphic appearance. They are usually only found in the external segment of the globus pallidus. They may represent a variant of Lafora body disease. Besides these specific conditions, polyglucosan bodies may be seen as a nonspecific phenomenon within the CNS in olivopontocerebellar atrophy and amyotrophic lateral sclerosis, and in peripheral nerves in exceptional cases of diabetes mellitus, motor neuropathy, familial spastic paraparesis, and spinocerebellar syndromes, as well as in normal aging.

It is unclear how the polyglucosan bodies arise in APBD. They may represent systemic glycogen storage due to deficiency of glycogen branching enzyme or another enzyme related to glycogen metabolism. The relationship with the CNS structural damage and dysfunction is unclear. It is conceivable that there is an underlying metabolic defect, which damages neurons by itself and as an independent side effect leads to the production of polyglucosan bodies. The growth of polyglucosan bodies within axons could also become deleterious for those axons, at the very least impeding or blocking axonal flow.

16.5 Therapy

There is at present no effective causal treatment for APBD.

16.6 Magnetic Resonance Imaging

MRI in patients with APBD shows extensive, often ill-defined abnormalities within the cerebral and cerebellar white matter (Figs. 16.1 and 16.2). The abnormalities are most prominent in the periventricular region and tend to spare the U fibers and the corpus

callosum (Fig. 16.1). The signal change is often most pronounced within the periventricular white matter, gradually becoming more normal in the deep white matter, and merging with normal white matter in the U fibers. In other patients, however, the white matter abnormalities are better demarcated (Figs. 16.1 and 16.2). In later stages, the corpus callosum and U fibers

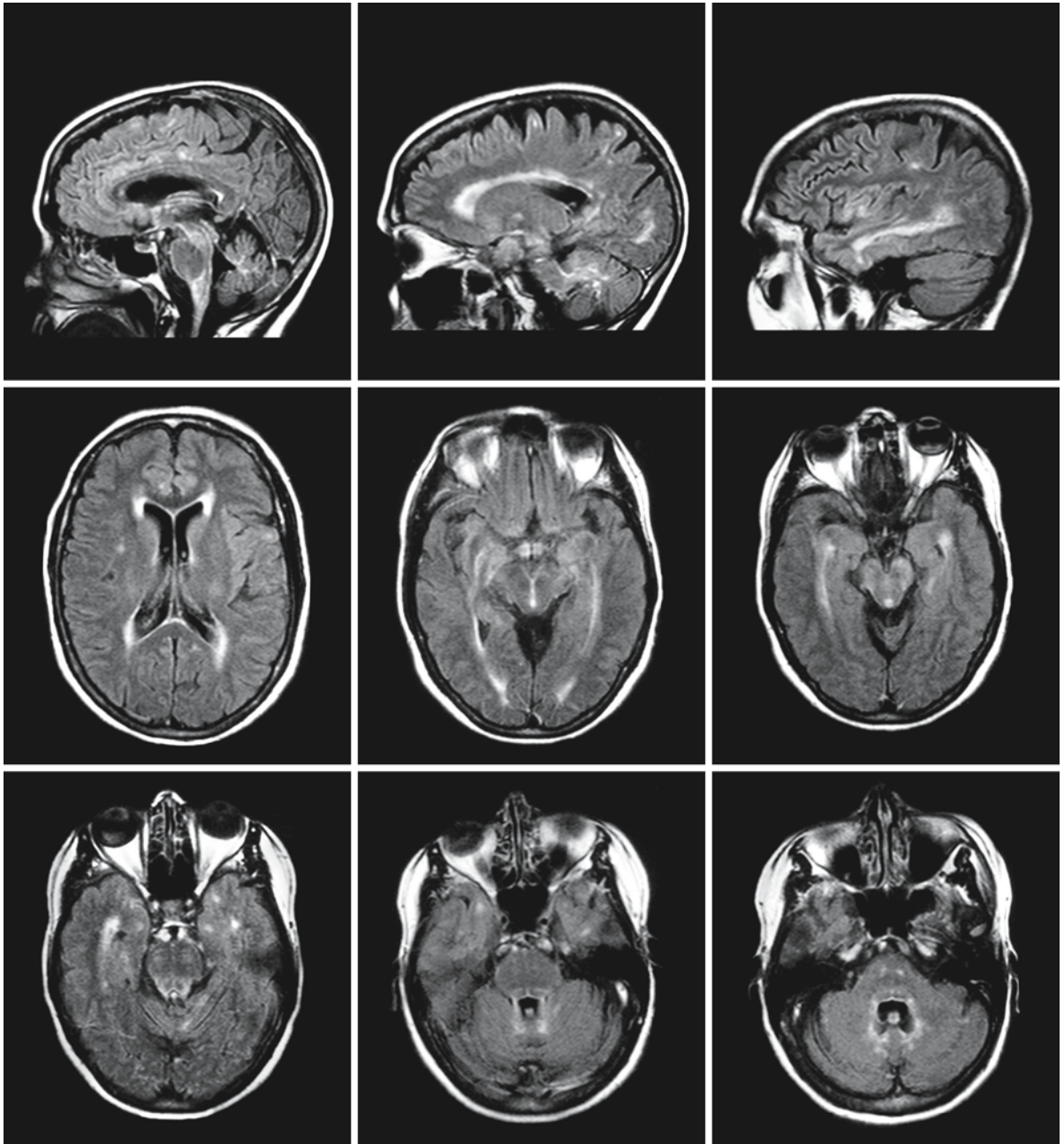


Fig. 16.1. FLAIR images in a 52-year-old female patient with APBD. Polyglucosan bodies were found in the sural nerve biopsy. There are confluent periventricular white matter abnormalities with relative sparing of the deep white matter and

U-fibers, where only small foci of abnormal signal are seen. Note the cerebellar and brain stem involvement. Courtesy of Dr.B.Barcelos da Nóbrega, Department of Radiology, School of Medicine, Federal University of Goias, Brazil

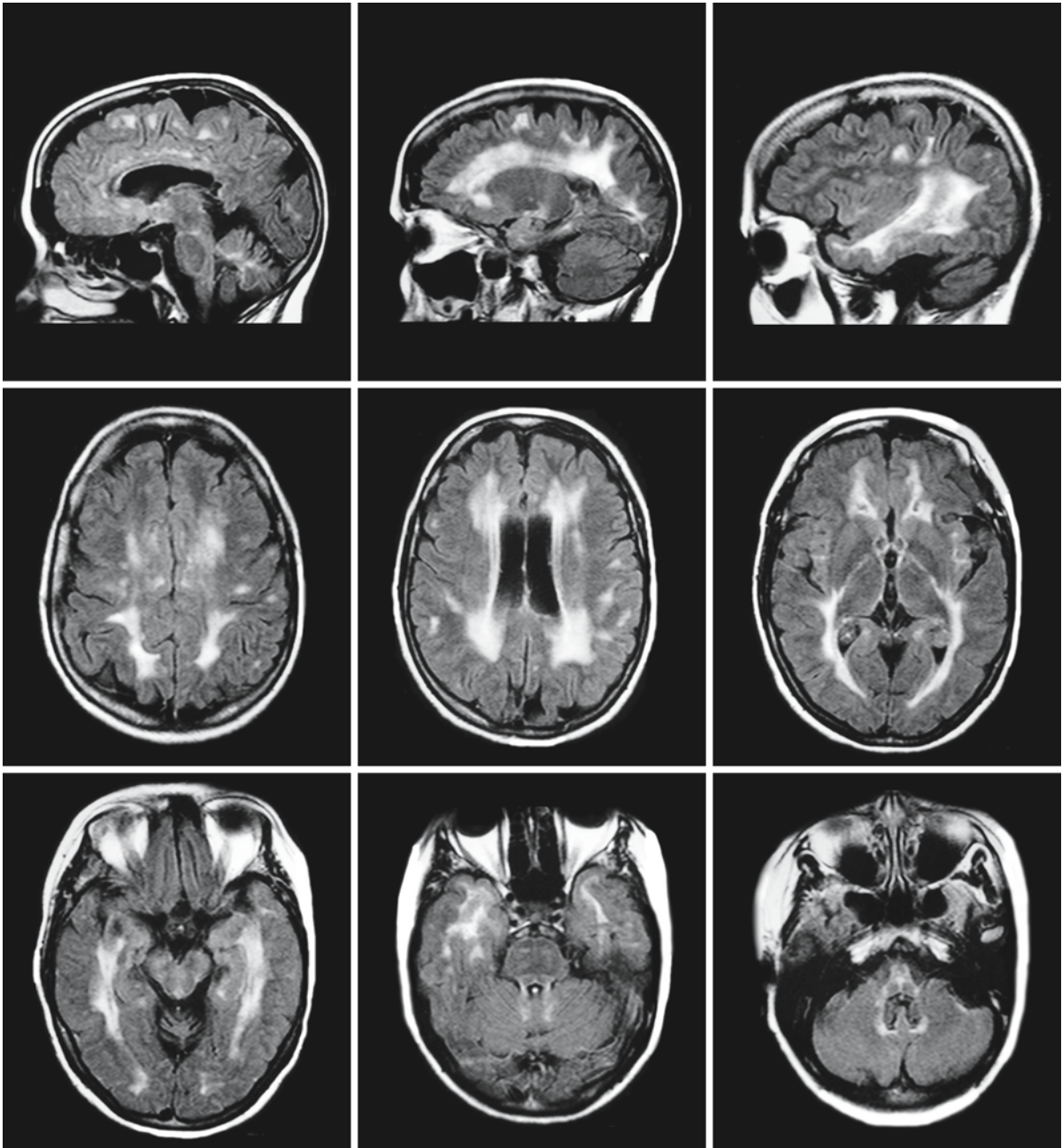


Fig. 16.2. FLAIR images in the 49-year-old sister of the patient in Fig. 16.1. Her disease is radiologically more advanced. There are confluent signal abnormalities in the periventricular white matter with some additional focal spots. The U fibers are relatively preserved. The corpus callosum has become thin. The

temporal white matter is prominently involved. Note the cerebellar and brain stem involvement. Courtesy of Dr. B. Barcelos da Nóbrega, Department of Radiology, School of Medicine, Federal University of Goias, Brazil

become involved as well (Fig. 16.2). The cerebral white matter may be decreased in volume with widening of the lateral ventricles and subarachnoid spaces and thinning of the corpus callosum. The frontal lobe tends to be involved more seriously, with

respect to both the white matter abnormalities and the atrophy. Within the brain stem signal abnormalities may be seen in the long tracts (Figs. 16.1 and 16.2). The cerebellum, brain stem, and spinal cord may be atrophic.

Peroxisomes and Peroxisomal Disorders

R. J. A. WANDERS

17.1 Peroxisomal Biogenesis and Biochemical Functions

Peroxisomes belong to the family of intracellular organelles, are present in virtually all eukaryotic cells with the sole exception of erythrocytes, and contain a fine granular matrix surrounded by a single membrane. Identification of peroxisomes in cells is greatly helped by the fact that peroxisomes stain dark when incubated in a medium containing diaminobenzidine (DAB) and hydrogen peroxide (H_2O_2) at alkaline pH thanks to the presence of catalase in peroxisomes. The availability of specific antibodies raised against peroxisomal matrix as well as membrane proteins, some of which are commercially available, has allowed unequivocal identification of peroxisomes using immunohistochemical, immunofluorescence, and immuno-electron microscopic methods. These methods have been used to study peroxisomes in different cells and have shown that the morphology of peroxisomes varies among different cell types, ranging from round to oval structures to elaborate tubular or reticular structures. Furthermore, the size and abundance of peroxisomes also vary widely, ranging from very small so-called microperoxisomes in fibroblasts ($<0.1\mu m$) to large peroxisomes in hepatocytes ($>1.0\mu m$). A striking feature of peroxisomes, at least in rodents, is their inducibility by a variety of dietary, hormonal, and other physiological effectors including fibrates such as clofibrate, bezafibrate, and phenofibrate. Fibrates exert their effect on peroxisomes via activation of one of the peroxisome proliferator activating receptors (PPARs), PPAR- α , which forms a heterodimer with the retinoic acid receptor (RXR) and activates the transcription of a range of different genes containing a peroxisome proliferator response element (PPRE) in their promoter regions. Several genes coding for different peroxisomal enzyme activities contain such a PPRE, which explains their inducibility by fibrates and other PPAR- α ligands. Although fibrates are effective hypolipidemic agents in humans as well, their effect on peroxisomes in humans in terms of peroxisome induction and upregulation of peroxisomal enzyme activities remains to be determined.

Although long regarded as relatively insignificant organelles with only a minor role in cellular metabolism, it is now clear that peroxisomes are essential subcellular organelles, as exemplified by the devastat-

ing consequences of a defect in peroxisome biogenesis as in Zellweger syndrome. In the last few years much has been learned about the biogenesis and metabolic functions of peroxisomes. With respect to peroxisome biogenesis, it is now clear that peroxisomal proteins are synthesized on free polyribosomes and are targeted to pre-existing peroxisomes by virtue of specific targeting signals contained within the amino acid sequences of the different peroxisomal proteins. Peroxisomal matrix proteins contain one of two different peroxisome targeting signals (PTS), the first of which, PTS1, is used by most of the peroxisomal matrix proteins. The PTS1 involves a C-terminal tripeptide of the sequence serine-leucine (SKL) or a variant thereof. The second peroxisomal targeting signal, PTS2, has been found in far fewer peroxisomal proteins and involves a stretch of nine amino acids, of which amino acids 1, 2, 8, and 9 are essential. The following consensus sequence has been found for the PTS2 motif (R/K)-(L/V/I)-XXXXX-(H/Q)-(L/A), in which X may be any amino acid. In human beings the PTS2 has only been identified in three peroxisomal proteins. Peroxisomal membrane proteins lack both a PTS1 and a PTS2 signal, implying the existence of additional signals, which remain ill defined. The identification of the PTS1 and PTS2 targeting signals was soon followed by the discovery of soluble receptors, called Pex5p and Pex7p, which recognize the PTS1 and PTS2 signals respectively. These two receptors pick up PTS1 or PTS2 proteins in the cytosol and direct these proteins to the peroxisomal membrane, where a complex network of proteins takes care of the transport of the PTS1 and PTS2 proteins across the peroxisomal membrane to end up in the peroxisome interior. On the basis of studies in yeasts, many of the proteins involved in correct transmembrane transport of PTS1 and PTS2 proteins have been identified. Proteins that are essential for peroxisome biogenesis have been termed peroxins and are written as "Pex" followed by a number and a small "p," e.g., Pex5p, Pex7p. The corresponding genes are called PEX genes, so that *PEX5* codes for Pex5p, *PEX7* for Pex7p, and so on. So far, 32 different peroxins have been identified in different species. Since peroxisome biogenesis is so markedly conserved among different species ranging from yeast to plants and humans, most of the peroxins have homologues in all the different species. So far 14 different PEX genes have been identified in humans.

As anticipated, mutations in any of these PEX genes will give rise to a defect in peroxisome biogenesis and underlie the disorders of peroxisome biogenesis.

Originally, peroxisomes were thought to play a role in hydrogen peroxide (H_2O_2) metabolism only. Peroxisomes contain a variety of H_2O_2 -generating oxidases and catalase, which cleaves H_2O_2 to H_2O and oxygen, thus constituting a simple respiratory pathway. In addition, peroxisomes carry out a series of other metabolic functions, the most important of which are fatty acid β -oxidation, ether phospholipid biosynthesis, fatty acid α -oxidation, glyoxylate detoxification, and L-pipecolic acid oxidation. There is much confusion about the role of peroxisomes in isoprenoid biosynthesis including cholesterol formation, for which reason we have decided to leave this potential function of peroxisomes out.

Fatty acid β -oxidation in peroxisomes involves a sequence of four reactions just as in mitochondria, in which an acyl-CoA ester undergoes dehydrogenation, hydration, dehydrogenation again, and thiolitic cleavage. Apart from this similarity, peroxisomal and mitochondrial β -oxidation differ in many respects, including the oxidation of different substrates in the two organelles. Mitochondria are able to oxidize short-, medium-, and long-chain fatty acids and are responsible for the oxidation of the bulk of dietary fatty acids. Peroxisomes, on the other hand, are not so important energetically, but are important for the degradation of a specific subset of fatty acids including very-long-chain fatty acids, pristanic acid, and di- and trihydroxycholestanic acid. The latter two acids are formed in the liver from cholesterol and are the direct precursors of the primary bile acid chenodeoxycholic acid and cholic acid, respectively. The difference between the functional roles of mitochondrial and peroxisomal β -oxidation is exemplified by the different clinical signs and symptoms of patients affected by a defect in mitochondrial versus peroxisomal β -oxidation. Another major function of the peroxisomal β -oxidation system concerns the "biosynthesis" of polyunsaturated fatty acids including docosahexaenoic acid ($C_{22:6\omega-3}$). Recent studies have clearly shown that the formation of $C_{22:6\omega-3}$ from linolenic acid ($C_{18:3\omega-3}$) involves active participation of the peroxisomal β -oxidation system at the level of the conversion of $C_{24:6\omega-3}$ to $C_{22:6\omega-3}$.

With respect to the enzymes involved in the β -oxidation of all these compounds, it was long thought that a single set of enzymes, including acyl-CoA oxidase, L-bifunctional protein with enoyl-CoA hydratase and 3-hydroxyacyl-CoA dehydrogenase activities, and peroxisomal thiolase would catalyze the β -oxidation of all these compounds. It now turns out, however, that peroxisomes harbor two acyl-CoA oxidases, one for straight-chain fatty acids like $C_{26:0}$, and one for branched-chain fatty acids like pristanic acid

and di- and trihydroxycoprostanic acid, two bifunctional proteins, and two peroxisomal thiolases. With respect to the bifunctional proteins, current knowledge holds that the second, more recently identified bifunctional protein, named D-bifunctional protein, is the single enzyme involved in the oxidation of $C_{26:0}$, pristanic acid, as well as the two cholestanic acids, whereas the two thiolases both play a part in the oxidation of these compounds. Apart from the differences in terms of enzymes involved in β -oxidation in mitochondria and peroxisomes, there are a number of other differences including the transport of fatty acids across the peroxisomal versus mitochondrial membrane. Mitochondrial entrance of long-chain fatty acids is mediated by a carnitine cycle involving carnitine palmitoyl transferase 1 (CPT1), mitochondrial carnitine/acylcarnitine transporter (CACT), and carnitine palmitoyl transferase 2 (CPT2), whereas transport of fatty acids across the peroxisomal membrane is probably mediated by membrane proteins belonging to the family of ABC transporters, of which four have been identified in peroxisomal membranes. One of these four is called adrenoleukodystrophy protein (ALDP), which is deficient in X-linked adrenoleukodystrophy and probably catalyzes the transport of very-long-chain fatty acids in their CoA-ester form. The end products of peroxisomal β -oxidation, including acetyl-CoA, propionyl-CoA, and medium-chain acyl-CoAs, are shuttled to mitochondria in the form of carnitine esters for final oxidation to CO_2 and water inside the mitochondria. The peroxisomal β -oxidation system does not only act on saturated fatty acids, but it is also capable of catalyzing chain shortening of monounsaturated and polyunsaturated fatty acids. To this end, peroxisomes are equipped with enzymes such as 2,4-dienoyl-CoA reductase and Δ^3, Δ^2 -enoyl-CoA isomerase.

The second important function of peroxisomes has to do with ether phospholipids. Ether phospholipids are a special class of phospholipids which differ from the regular, better-known diacylphospholipids in one major respect, which is the occurrence of an ether linkage rather than an ester linkage at the *sn*-1 position of the glycerol backbone. Two groups of ether phospholipids can be distinguished with either an 1-O-alkyl or an 1-O-alk-1-enyl-linkage. The latter phospholipids (1-O-alk-1-enyl-2-acyl phosphoglycerides) with an α -, β -unsaturated ether bond are also known by their trivial name *plasmalogens*. Platelet activating factor (PAF; 1-O-alkyl-2-acetyl-glycerophosphocholine) is the best-known ether phospholipid. Plasmalogens constitute 5–20% of the phospholipids of cell membranes and are present at high concentrations in the brain, especially in myelin. PAF induces both platelet and leukocyte aggregation and degranulation and is important in several disease processes including inflammation and

anaphylaxis. Peroxisomes are involved in the introduction of ether bonds in ether phospholipids, since the first two enzymes involved in ether phospholipid biosynthesis are localized in peroxisomes. These enzymes are dihydroxyacetonephosphate acyltransferase (DHAPAT) and alkyl-dihydroxyacetonephosphate synthase (alkyl-DHAP synthase), whereas all subsequent steps are catalyzed by enzymes in the endoplasmic reticulum.

The third important function of peroxisomes is fatty acid α -oxidation. Fatty acids such as phytanic acid (3,7,11,15-tetramethylhexadecanoic acid) with a methyl group at the 3-position cannot undergo direct β -oxidation. Instead, 3-methyl branched-chain fatty acids like phytanic acid first undergo α -oxidation in which the terminal carboxyl group is removed as CO_2 . The pathway of phytanic acid α -oxidation has long remained mysterious but has been resolved in recent years. It is now clear that phytanic acid is first converted into its CoA-ester followed by a series of enzymes including phytanoyl-CoA hydroxylase, 2-hydroxyphytanoyl-CoA lyase, and pristanal dehydrogenase, which are all peroxisomal enzymes, to produce CO_2 and pristanic acid (2,4,6,10-tetramethylpentadecanoic acid). Pristanic acid can then be activated via an intraperoxisomal acyl-CoA synthetase (VLCS) to produce pristanoyl-CoA followed by β -oxidation.

Detoxification of glyoxylate via the peroxisomal enzyme alanineglyoxylate aminotransferase (AGT) is another major function of peroxisomes. Deficiency of AGT as in hyperoxaluria type 1 leads to the accumulation of glyoxylate, which is subsequently converted into glycolate and oxalate, which precipitates as calcium oxalate in tissues.

A final important function of peroxisomes is the degradation of L-pipecolic acid via a peroxisomal oxidase called L-pipecolate oxidase. Pipecolic acid is a degradation product of L-lysine, which is normally degraded by the saccharopine pathway. However, L-lysine may also be degraded via the L-pipecolic acid pathway, which may be especially important in brain since the activity of the saccharopine pathway is low in brain. In the L-pipecolic acid pathway, L-pipecolic acid is produced from L-lysine via two enzymatic steps, and is then oxidized by L-pipecolate oxidase, a peroxisomal enzyme, at least in humans. The structure and function of the L-pipecolic acid pathway remain incompletely understood.

17.2 Peroxisomal Disorders

Disturbance of normal peroxisomal function is associated with far-reaching and devastating consequences. Zellweger syndrome is generally considered to be the prototype of the group of peroxisomal disorders.

Although different classifications have been proposed through the years, most authors now use a classification in two distinct categories: the disorders of peroxisome biogenesis, and the single peroxisomal enzyme deficiencies.

1. Peroxisome biogenesis disorders
 - (a) Cerebrohepato-renal syndrome (Zellweger syndrome)
 - (b) Neonatal adrenoleukodystrophy
 - (c) Infantile Refsum disease
 - (d) Rhizomelic chondrodysplasia punctata type 1
2. Single peroxisomal enzyme deficiencies
 - (a) X-linked adrenoleukodystrophy
 - (b) Acyl-CoA oxidase deficiency
 - (c) D-Bifunctional protein deficiency
 - (d) 2-Methylacyl-CoA racemase deficiency
 - (e) Adult Refsum disease
 - (f) Rhizomelic chondrodysplasia punctata type 2 (DHAPAT deficiency)
 - (g) Rhizomelic chondrodysplasia punctata type 3 (alkyl-DHAP synthase deficiency)
 - (h) Acatlasemia
 - (i) Mulibrey nanism

The first category contains peroxisomal disorders in which peroxisome biogenesis is deficient. In Zellweger syndrome (ZS), neonatal adrenoleukodystrophy (NALD), and infantile Refsum disease (IRD), together called Zellweger spectrum, both the PTS1 and PTS2 pathways are affected, which is associated with the generalized loss of peroxisomal functions, whereas in the other type of peroxisome biogenesis disorder, with rhizomelic chondrodysplasia punctata (RCDP) type 1 as sole representative, peroxisome biogenesis is only partially defective. In RCDP type 1 only the PTS2 pathway is blocked as a consequence of a nonfunctional PTS2-receptor (Pex7p) encoded by *PEX7*. In contrast to RCDP type 1, which is related to a single gene defect, the Zellweger spectrum disorders are genetically heterogeneous, with 11 different genes identified so far: *PEX1*, *PEX2*, *PEX3*, *PEX5*, *PEX6*, *PEX10*, *PEX12*, *PEX13*, *PEX16*, *PEX19*, and *PEX26*. In 65% of Zellweger spectrum patients, *PEX1* is the gene involved, which is explained, at least in part, by the occurrence of two frequent mutations in the *PEX1* gene. As a consequence, PTS2 proteins like peroxisomal thiolase, alkyl-dihydroxyacetonephosphate synthase, and phytanoyl-CoA hydroxylase are not properly targeted to peroxisomes, which explains a selective loss of peroxisomal functions (plasmalogen biosynthesis and phytanic acid α -oxidation).

In the second category, peroxisome biogenesis is intact, but the basic problem is at the level of one of the enzymes or transporters involved in each of the different metabolic pathways contained in peroxisomes.

Peroxisome Biogenesis Defects

18.1 Clinical Features and Laboratory Investigations

Peroxisome biogenesis disorders are genetically heterogeneous diseases with an autosomal recessive mode of inheritance. They include Zellweger syndrome (ZS, also called cerebrohepatorenal syndrome), neonatal adrenoleukodystrophy (NALD), and infantile Refsum disease (IRD). The clinical pictures of these disorders show similarities, but an important difference is a difference in severity, the clinical course being most severe in ZS and mildest in IRD. Exceptional patients present with a still milder phenotype.

After birth children with ZS show profound muscular hypotonia. Most patients lie motionless with weak or absent Moro reflex, tendon reflexes, and sucking and swallowing reflexes. Tube feeding is necessary. Typically, the children have craniofacial dysmorphism with a high and bulging forehead, flat occiput, upslanting palpebral fissures, puffy eyelids, hypoplastic supraorbital ridges, and a low and broad nasal bridge with hypertelorism and epicanthus folds, giving them a mongoloid appearance. In addition, Brushfield spots, peripheral pigmentary retinopathy, optic nerve dysplasia or hypoplasia, glaucoma, corneal clouding, cataracts, low-set malformed ears, high arched palate, micrognathia, and widely patent sutures and fontanels are present. Macrocephaly may be present. Some children have a cleft soft palate. The children have a severe visual and hearing deficit. Nystagmus is often present. Hepatomegaly, prolonged neonatal or later-onset icterus, and hemorrhages due to hypoprothrombinemia are common. Limb anomalies include cubitus valgus, camptodactyly, single transverse palmar creases, and talipes equinovarus. Failure to thrive and severe psychomotor retardation are conspicuous. Seizures are frequent. Cardiac defects are not frequent, but ventricular septum defect, patent ductus arteriosus, and patent foramen ovale may occur. Cryptorchidism is frequently observed in boys, clitoromegaly and labial hypoplasia in girls. About 90% of the patients die within the first year of life, death occurring in the majority within the first few months.

Most children with NALD have neurological abnormalities at birth, but some are initially near-normal. Hypotonia is moderate to severe, reflexes are hyporeactive. Craniofacial dysmorphism is milder than in

ZS. Widely patent fontanels are uncommon. The affected children show feeding problems, failure to thrive, hepatomegaly, and sometimes jaundice. Furthermore, the disease is characterized by seizures, sensorineural hearing loss, decreased vision with nystagmus, optic atrophy or dysplasia, and pigmentary retinal degeneration. The posterior eye segment abnormalities are identical to those of ZS, but anterior segment abnormalities are lacking. Macrocephaly may be present. Within the first year of life severe developmental retardation becomes apparent, although most infants reach some milestones before neurological deterioration occurs. The age at which regression begins varies from 12 months to more than 7 years. Progressive neurological dysfunction is characterized by cerebellar ataxia, spasticity of the arms and legs with truncal hypotonia, increased deep tendon reflexes, extensor plantar reflexes, and sensory defects. If not present from birth onwards, seizures usually occur in this period. Visual dysfunction progresses to blindness. Adrenal insufficiency is rarely clinically manifest. Exceptional patients are initially entirely normal or close to normal with onset of rapid neurological deterioration in the second year of life. The course of disease is more protracted in NALD than in ZS, death occurring between the ages of 1.5 and more than 10 years.

IRD is the mildest variant of the three mentioned disorders. The disease is usually not manifest at birth but presents itself within the first 6 months of life with psychomotor retardation, minor facial dysmorphism, mild hypotonia, sensorineural deafness, and visual impairment with retinal pigmentary degeneration, optic dysplasia, and nystagmus. Hepatomegaly and failure to thrive with growth retardation are common. Seizures occur but epilepsy is not as severe as in ZS. Many patients are able to sit and walk independently after several years, whereas others never acquire these abilities. The gait is usually ataxic and broad-based, and cognitive function in the severely retarded range. Life expectancy is considerably longer than in ZS and NALD, up to more than 2 decades.

Milder variants of peroxisome biogenesis defects with later onset and more protracted disease course have been described. One of the mildest variants reported concerns a family in whom adults with a normal or borderline intelligence only demonstrate sensorineural hearing loss and retinitis pigmentosa,

leading to a diagnosis of Usher syndrome (Raas-Rothschild et al. 2002).

In ZS, laboratory investigations may reveal many different, in themselves nonspecific biochemical abnormalities, such as hyperbilirubinemia, elevated liver enzymes, hypoprothrombinemia, reduced albumin level, hypocarnitinemia, hypocholesterolemia, generalized amino aciduria, and elevated CSF protein. These abnormalities are not necessarily all present. Elevated serum iron, iron saturation, and transferrin may be found, but these findings are inconsistent and transient. As a rule, an abnormally low cortisol response to ACTH stimulation is found despite normal basal cortisol level. More specific abnormalities are directly related to generalized deficiency of peroxisomal function. Plasma levels of very long-chain fatty acids are increased with an elevation of the $C_{26}:C_{22}$ and $C_{24}:C_{22}$ fatty acid ratio. Saturated as well as monounsaturated and polyunsaturated very-long-chain fatty acids are increased. Plasma pipelicolic acid and phytanic acid may be normal initially but increase with age. Plasma dicarboxylic acids are raised. Abnormal bile acids such as dihydroxycholestanoic acid and trihydroxycholestanoic acid are elevated. In urine elevated levels of dicarboxylic acids, dihydroxycholestanoic acid, and trihydroxycholestanoic acid are present. In platelets and red blood cells a deficiency of the peroxisomal enzyme dihydroxyacetone phosphate acyltransferase can be shown. The plasmalogen content of red blood cells is decreased in the first few months of life. The plasmalogen level of the red blood cells increases with age and may be normal in patients who are 4 months or older. The synthesis of platelet activating factor by leukocytes is deficient. The activity of dihydroxyacetone phosphate acyltransferase can be shown to be deficient in leukocytes and thrombocytes. In cultured fibroblasts a decreased content of plasmalogen and increased levels of very-long-chain fatty acids can be demonstrated. The β -oxidation of very-long-chain fatty acids, the de novo biosynthesis of plasmalogens, and the activity of dihydroxyacetone phosphate acyltransferase, alkyl dihydroxyacetone phosphate synthase, and phytanic acid oxidation can be shown to be deficient in fibroblasts. Finally, in fibroblasts catalase activity is not found in organelles, but in the cellular cytoplasm.

Laboratory abnormalities are essentially the same in NALD and IRD, but milder than in ZS. In ZS the accumulation of very-long-chain fatty acids includes the saturated and monounsaturated C_{26} fatty acid and is associated with a decrease in the C_{22} saturated fatty acid concentration. In NALD the rise in very-long-chain fatty acids is not associated with an increase in monounsaturated C_{26} fatty acid and the C_{22} fatty acid is on average higher than normal. In NALD, mild adrenal insufficiency and low cortisol response in ACTH stimulation is usually found, although appar-

ently normal adrenal function is not incompatible with the diagnosis. In IRD adrenal function is normal.

X-ray examinations in ZS often reveal calcific stippling of bony epiphyses. Stippled, irregular calcification of particularly the patellae, greater trochanters, triradiate cartilages, acetabulum, scapula, and sternum is seen in 50–70 % of the ZS patients. Ultrasound may detect multiple small renal cortical cysts, but they are often difficult to find. In NALD and IRD no calcific stippling of bony epiphyses is present. No renal cysts are found. ERG is extinguished at a very early age in ZS and the EEG is highly abnormal with epileptic discharges. BAEP shows reduced responses. In NALD and IRD the ERG becomes extinguished and BAEP is abnormal. Nerve conduction velocity may be decreased in NALD; it is normal in IRD.

Prenatal diagnosis can be performed with the help of various biochemical investigations in cultured chorionic villus cells and amniocytes. DNA techniques can be applied in families with known mutations.

18.2 Pathology

Brain weight in ZS is normal or may exceed normal. External examination reveals abnormalities in the cerebral convolutional pattern with areas of pachygyria and polymicrogyria. Polymicrogyria is typically present in the opercular regions of the frontal, parietal, and temporal lobes and within the insular region, with an increased number of gyri and decreased amplitude of the gyri. In the superior region, over the frontoparietal convexities, the polymicrogyric cortex merges with a pachygyric cortex, where convolutions are abnormally broad and reduced in number. There is a failure of full opercularization of the insula and the sylvian fissure is abnormally vertical in orientation. Otherwise the gyral pattern of the cerebral hemispheres is normal. Often the cerebellum is hypoplastic and the cerebellar cortex has areas of polymicrogyria. External appearance of the brain stem is normal.

On sectioning the gyral abnormalities are confirmed with moderate thickening of the cortical plate in the areas of abnormal gyration. The lateral ventricles are mildly enlarged and have a mildly colpocephalic configuration. There is a moderate symmetrical decrease in volume of the white matter. Olfactory bulbs and tracts and optic nerves are thin, as is the corpus callosum. Periventricular subependymal cysts, so-called germinolytic cysts, are often present over the heads of the caudate nucleus. In the brain stem, hypoplasia and dysplasia of the inferior olives is apparent.

Microscopic examination reveals that the cerebral cortex has a normal cytoarchitectonic pattern in the normally convoluted areas. The cytoarchitecture of polymicrogyric and pachygyric cortex is abnormal and there are heterotopias in the subcortical white matter under the regions of cortical abnormality. The migrational abnormality has principally affected neurons destined for the outer cortical layers. Many cells normally found in the outer cortical layers (layers II and III) are distributed in heterotopic positions within the deep cortical layers (layers V and VI) and in the white matter below the cortex. However, some of the neurons destined for the deep cortical layers are in their normal laminar positions. The difference between the pachygyric and polymicrogyric cortices is related to differences in intracortical cell patterns. The outer cortical layers are relatively more cellular in polymicrogyric cortex than in pachygyric cortex, whereas the reverse is true with regard to the deeper cortical layers. Within the cortex a marked astrocytic gliosis is present. Within the proliferated astrocytes, an excess of sudanophilic lipid material is seen. PAS-positive deposits are seen in the cortex of some of the patients related to glycogen deposition in the cytoplasm and nucleoplasm of neurons and astrocytes. Clusters of unusual histiocytes and multinucleated giant cells have been described with cytoplasm that is in part homogeneously PAS-positive and in part foamy and sudanophilic.

The white matter is characterized by a profound deficiency of myelin and presence of gliosis. Myelin deficiency is caused by delayed and disturbed myelination; active loss of myelin cannot be demonstrated. Throughout the white matter many astrocytes are present which are hypertrophic and contain sudanophilic lipid material in their cytoplasm. Lipid deposits are also seen in histiocytes and macrophages. No perivascular infiltration with inflammatory cells is present. The white matter abnormality is usually diffuse and generalized. In some cases the periventricular white matter is most severely involved with no myelin left in that area. Oligodendrocytes are reduced in number. There is a decrease of axons in the white matter corresponding to an area of pachygyria or polymicrogyria. The ventricles are partially denuded of ependyma and regionally the ependyma is a pseudostratified columnar epithelium resembling the epithelium seen in midfetal life. In many patients germinal cysts are present in subependymal areas.

The basal ganglia have a normal configuration, but at microscopic examination changes similar in nature to those in the cortex are seen, with an increase in astrocytes and the presence of lipid-laden cells. The optic nerves, chiasm, and optic tracts may show diffuse deficiency of myelin and presence of gliosis. The brain stem is normal in architecture, except for hypoplasia and dysplasia of the inferior olives, which

lack the usual delicately convoluted pattern. The brain stem is poorly myelinated. A diffuse increase in the number of astrocytes is found in gray and white matter and lipid-laden foamy cells are present. The cerebellum is often hypoplastic and its convoluted pattern abnormal. Areas of polymicrogyria are common and microscopic examination shows that cortical lamination is markedly abnormal at these points. Many heterotopic Purkinje cells are present in the subcortical white matter. A marked increase in astrocytes is present in the cerebellar cortex, and many glial cells and macrophages have vacuolated foamy cytoplasm filled with lipid droplets. The changes in the cerebellar white matter are similar to those in the white matter of the cerebral hemispheres. The dentate nuclei may be hypoplastic and dysplastic, showing the same lack of convolutions as observed in the inferior olivary nuclei.

Electron microscopy reveals that the lipid-laden cells contain typical trilamellar inclusions along with heterogeneous material. These inclusions are intralysosomal. The trilamellar structures are composed of two parallel electron-dense lines separated by an electron-lucent zone. They are identical to those encountered in other peroxisomopathies and may contain very-long-chain fatty acids. Structurally abnormal mitochondria have been reported in some cases.

Following birth hepatic cirrhosis may develop rapidly, although not invariably. The liver is enlarged in most ZS patients. Histological findings vary from near-normal to diffusely abnormal, dependent on the age of the patient. In the first 2 months of life, microscopic abnormalities are absent or mild and include fibrosis, cholestasis, and intrahepatic bile duct hypoplasia. In older patients fibrosis and distortion of liver architecture is more severe, ending in micronodular cirrhosis. Inconstant excess of hemosiderin in hepatocytes and in particular in Kupffer cells and macrophages may be related to age, with the greatest prominence between 5 and 18 weeks of age. In exceptional cases, accumulation of glycogen is found. On ultrastructural examination, no peroxisomes are seen in hepatocytes, where they are normally found in abundance. Invariably, abnormal mitochondrial morphology is seen. Intralysosomal trilamellar inclusions are present in Kupffer cells and macrophages. In the kidney multiple small cysts are present in the cortex, especially in the subcapsular region. The average diameter is 3 mm, with some reaching 8 mm. They are predominantly of tubular, occasionally of glomerular origin. Ultrastructural examination reveals no peroxisomes in renal tubular epithelium, where they are normally found in large numbers. Adrenal glands are either normal in size or small. The medulla is unremarkable. In the zona reticularis and inner fascicula large striated cells are seen with dense inclusions.

On ultrastructural examination, these cells contain trilaminar inclusions. Hyperplasia of pancreatic islets and pancreatic fibrosis have been observed in isolated patients. In muscle tissue myopathic changes and presence of abnormal mitochondria are occasionally observed.

In NALD brains, the gyrational abnormalities are much milder than in ZS. Areas of polymicrogyria and pachygyria, in particular in the area of the sylvian fissure, and a few islands of heterotopic neurons are seen within the white matter. The cerebral cortex is otherwise normal. Few cerebellar heterotopias are seen. Inferior olives may be dysplastic.

White matter degenerative changes are, however, much more severe in NALD than in ZS. Diffuse demyelination involves cerebellar white matter, brain stem, and cerebral hemispheres. Demyelination occurs in zoned lesions in X-linked adrenoleukodystrophy, but is more diffuse in NALD. The process is most severe in the cerebellar white matter, the pyramidal tracts in the internal capsule, brain stem and spinal cord, and in the parieto-occipital region. The cerebral arcuate fibers are relatively spared. In the areas of demyelination, the axons are relatively intact, but if demyelination is severe, axons may also be destroyed and cavitation may occur. In the affected areas gliosis is present and there is an accumulation of lipids, predominantly in histiocytes and macrophages, but little, if any, in astrocytes. Perivascular infiltration with mononuclear inflammatory cells may be present, but is then less severe than in X-linked adrenoleukodystrophy. On ultrastructural examination trilaminar inclusions have been found in vacuoles within histiocytes and macrophages in areas of demyelination. A polyneuropathy with thin myelin sheaths and trilaminar inclusions in Schwann cells and fibroblasts has been found in some of the patients.

Liver disease in NALD is less severe than in ZS. Hepatic fibrosis and micronodular cirrhosis may occur, but are not obligatory. Evidence of glycogen deposits may be present. Mitochondria have been described as either normal or abnormal in morphology. In most cases, absence or a marked reduction in number and size of peroxisomes has been reported, but enlarged hepatic peroxisomes have also been found. Histiocytes and macrophages that contain lipid storage material are present and may be abundant. On ultrastructural examination these cells are shown to contain the typical trilaminar inclusions. No renal cortical cysts are present. The adrenal cortex is atrophic and contains ballooned, lipid-laden cells. Electron microscopy reveals trilaminar inclusions in adrenocortical cells and in macrophages. Myopathic changes and mitochondrial abnormalities have been found in muscle tissue.

NALD is characterized by a generalized, systemic infiltration of many tissues by lipid-laden macro-

phages not seen in ZS. The storage cells harbor trilaminar inclusions and heterogeneous material. They are seen in multiple sites of the reticuloendothelial system and are not confined to sites of active degeneration such as the CNS. They occur in liver, spleen, lungs, lymph nodes, and gastrointestinal mucosa.

In IRD no malformations of the cerebral cortex are present and no neuronal heterotopias within the white matter. The white matter may be hypoplastic. White matter changes are mild. Myelin content is diminished, but there are no signs of active demyelination. In the areas of myelin deficiency and gliosis, one finds macrophages surrounding vessels and containing trilaminar lamellae. There may be cerebellar atrophy with reduced numbers of granular cells.

In the liver in IRD fibrotic changes may be present. Trilaminar lipid inclusions are seen in macrophages, Kupffer cells, and hepatocytes. Peroxisomes are absent or reduced in number and size. Mitochondria have abnormal morphology. No cortical renal cysts are seen. No adrenal degeneration is present. Foamy histiocytes may be seen in multiple organs.

18.3 Pathogenetic Considerations

The assembly of peroxisomes requires the interaction of a set of biogenesis proteins, peroxins, which are encoded by *PEX* genes. Peroxisomal matrix proteins are synthesized on free polyribosomes and are directed to the peroxisome by specific targeting signals, PTS1 and PTS2. Most peroxisomal proteins use PTS1; phytanoyl-CoA hydroxylase, alkylldihydroxyacetone phosphate synthase, and peroxisomal thiolase are the only three peroxisomal enzymes that use a PTS2 targeting sequence. PTS1 consists of a C-terminal tripeptide, SKL, that is recognized by the PTS1 receptor. There is a third mechanism for importation of peroxisomal membrane proteins (PMPs).

In peroxisome biogenesis disorders there is a defect in peroxisomal membrane synthesis or the matrix protein import. Complementation studies by somatic cell fusion studies have been extremely important in the elucidation of the basic defects in peroxisome biogenesis defects. In complementation studies cultured skin fibroblasts from different patients are fused and the resulting multinucleated cells are collected. Complementation is said to have occurred when the multinucleated cells show a restoration of function or structural features that were deficient in the unfused cell lines. Eleven different complementation groups have so far been identified for ZS, NALD, and IRD, and the underlying genes for the complementation groups are: *PEX1* (complementation group 1 or E), *PEX2* (group 10 or F), *PEX3* (group 12 or G), *PEX5* (group 2), *PEX6* (group 4 or C), *PEX10* (group 7 or B), *PEX12* (group 3), *PEX13* (group 13 or

H), *PEX16* (group 9 or D), *PEX19* (group 14 or J), and *PEX26* (group 8 or G). Almost all complementation groups are associated with more than one clinical phenotype and often with all three. Rhizomelic chondrodysplasia punctata patients belong to a separate complementation group (complementation group 11), related to the gene *PEX7*.

PEX1, located on chromosome 7q21–22, encodes Pex1p, a protein of the AAA ATPase family involved in peroxisome matrix protein import (AAA stands for ATPases associated with diverse cellular activities). *PEX2*, located on chromosome 8q21.1, encodes Pex2p, an integral peroxisomal membrane protein involved in matrix protein import. *PEX3*, located on chromosome 6q23–24, encodes Pex3p, a peroxisomal membrane protein factor for the proper localization of peroxisomal membrane proteins and involved in peroxisomal membrane biogenesis. *PEX5*, located on chromosome 12p13, encodes the PTS1 receptor, involved in peroxisome matrix protein import. *PEX6*, located on chromosome 6p21.1, encodes Pex6p, a protein of the AAA ATPase family involved in peroxisome matrix protein import. *PEX10*, located on chromosome 1p36, encodes Pex10p, an integral peroxisomal membrane protein involved in peroxisome matrix protein import. *PEX12*, located on chromosome 17q11–12, encodes Pex12p, an integral peroxisomal membrane protein involved in matrix protein import. *PEX13*, located on chromosome 2p14–16, encodes Pex13p, an integral peroxisomal membrane protein involved in matrix protein import. *PEX16*, located on chromosome 11p12–2, encodes Pex16p, an integral peroxisomal membrane protein involved in peroxisomal membrane biogenesis. *PEX19*, located on chromosome 1q22, encodes a peroxisomal membrane protein receptor involved in membrane biogenesis. *PEX26* encodes Pex26p, a peroxisomal membrane protein involved in peroxisome matrix protein import. It recruits Pex1p and Pex6p AAA ATPase complexes to peroxisomes.

Complementation group 1 is the largest and contains about 65% of the patients. The related clinical phenotype is highly variable and covers the entire clinical spectrum from ZS to NALD to IRD. There is some genotype–phenotype correlation. Patients with two null mutations have a more severe phenotype than patients with a residual function of Pex1p.

With defects in *PEX3*, *PEX16*, and *PEX19* no peroxisomal membrane structures are present at all. In the other complementation groups, the defect involves peroxisomal protein import but not the synthesis of peroxisomal membranes, and in cells belonging to these complementation groups remnant peroxisomal membrane structures are present, also called peroxisomal ghosts. These structures can be demonstrated in cultured fibroblasts by using antibodies to peroxisomal membrane proteins. These structures are

largely empty. They lack most of the peroxisomal matrix proteins; they contain the unprocessed precursor form of thiolase, unprocessed acyl-CoA oxidase, and residual dihydroxyacetone phosphate acyltransferase activity. Some catalase has also been found in the interior of peroxisomal remnant structures.

The absence of normal peroxisomes is associated with defective function of multiple peroxisomal enzymes. Several of the enzyme proteins, which are normally located in the peroxisomal matrix, are free in the cytosol and are stable and biologically active. This is the case with catalase, D-amino acid oxidase, alanine glyoxylate aminotransferase, polyamine oxidase and L- α -hydroxy acid oxidase. In contrast, other peroxisomal enzymes are synthesized normally, but are unstable in the cytosol, are rapidly degraded, and their enzyme activities are decreased. This is the case with the peroxisomal β -oxidation enzyme proteins, alkyl dihydroxyacetone phosphate synthase and dihydroxyacetone phosphate acyltransferase, and the plasmalogen synthesizing enzymes.

In the peroxisome biogenesis disorders, mitochondrial abnormalities are also found. Mitochondria are often morphologically abnormal. It is generally assumed that the mitochondrial abnormalities are secondary. There is a metabolic interdependence of mitochondria and peroxisomes. Participation in fatty acid metabolism is a property of both organelles. Peroxisomes shorten very-long-chain fatty acids prior to their oxidation by mitochondria. Defects in peroxisomal β -oxidation lead to accumulation of long-chain fatty acyl-CoAs, which have regulatory effects on a number of mitochondrial enzymes. The mitochondrial abnormality may contribute to the clinical disease. In some patients muscle pathology with abnormal mitochondria is observed, suggesting a mitochondrial myopathy. However, no changes in lactate, pyruvate, 3-hydroxy butyrate, and acetoacetate have ever been reported in patients, indicating that in vivo the proposed mitochondrial dysfunction is usually of no or only minor importance.

The peroxisome biogenesis defects are histopathologically characterized by a combination of malformative and degenerative abnormalities. The dysontogenetic or malformative changes include facial dysmorphism, renal cortical cysts, gray matter migrational disturbances, and abnormalities in myelin deposition. The degenerative, regressive changes include the pigmentary retinal degeneration, the liver fibrosis and cirrhosis, the adrenal cortical atrophy, and storage, demyelination, and neuronal degeneration. In ZS the dysontogenetic abnormalities predominate in the CNS. In NALD there are some dysontogenetic changes, but CNS pathology is dominated by degeneration and storage phenomena. In IRD both are mild or absent in the nervous system.

Mechanisms which interfere with migration in ZS and NALD do so to a partial degree only, as some neurons are in their normal position and only some of the neurons of a given class fail to complete their migrations. Neuronal migration is not disturbed in rhizomelic chondrodysplasia punctata. This observation makes a disturbance of plasmalogen synthesis or phytanic acid oxidation improbable as the cause of the migrational defect. The disturbance of neuronal migration in patients with D-bifunctional protein deficiency directs attention to the very-long-chain fatty acid and bile acid abnormalities. Neuronal migrational abnormalities may reflect the effect of accumulated very-long-chain fatty acids, since elevations consistently accompany the peroxisomal disorders with disturbed migration. The exception is X-linked adrenoleukodystrophy, in which very-long-chain fatty acids are elevated and no migrational disturbance is present. However, in X-linked adrenoleukodystrophy the increase in very-long-chain fatty acids is not as severe as in ZS or NALD, and is more restricted. In ZS, saturated, monounsaturated and polyunsaturated fatty acids are increased. In NALD and IRD, saturated and monounsaturated fatty acids are elevated, whereas in X-linked adrenoleukodystrophy, only saturated fatty acids are elevated. A possible role of accumulation of bile acid intermediates must also be considered. It is hypothesized that an accumulating substance interferes with the cell adhesion molecule interactions and linkages, which are necessary for normal migration of neurons along radial glial fibers. In ZS, ependymal abnormalities are found which are qualitatively similar but quantitatively less extensive than those found in classical lissencephaly. The abnormal ependyma may be a primary factor in the pathogenesis of migrational disturbances.

The white matter abnormalities vary among the disorders of peroxisomal biogenesis from predominantly deficient and disturbed myelination in ZS to predominant demyelination in NALD and variable white matter gliosis in IRD. In ZS myelin is severely deficient, but no signs of active demyelination are seen; in NALD the process of myelination is initially relatively normal, but demyelination follows. The difference between the two may be related to the degree of abnormality of membrane composition. Abnormal membrane composition is related to decreased availability of plasmalogens and accumulation of very-long-chain fatty acids and phytanic acid in the various membrane lipids. The more severe abnormality in ZS results in disturbed myelin formation, whereas in NALD myelin is laid down but subsequently broken down as a consequence of increasing instability. In IRD the biochemical abnormalities are mildest and white matter pathology only mild or minor. The inflammatory response in NALD may be related to the liberation of lipids containing very-long-chain fatty

acids in the process of myelin breakdown. These may be immunogenic and elicit an inflammatory response, as seen in X-linked adrenoleukodystrophy.

ZS, NALD, and IRD are all characterized by the presence of trilamellar inclusions in lysosomes, the amount of which increases with age. They consist of cholesterol-bound very-long-chain fatty acids. The storage is, as a rule, more abundant in macrophages than in parenchymal cells.

Hepatic fibrosis and cirrhosis are probably related to abnormal bile acid oxidation. Bile acid intermediates such as trihydroxycholestanoic acid with known hepatic toxicity may be important pathogenetically for both the development of bile duct paucity and hepatocellular injury.

The adrenal cortex is affected in all peroxisomal disorders with an elevation of very-long-chain fatty acids. The increase in these fatty acids causes an increase in membrane viscosity in adrenocortical cells, which in turn results in a decreased number of hormone receptor sites, subsequently leading to a decreased ability to respond to ACTH. Adrenal insufficiency followed by atrophy is due to the lack of response to ACTH.

18.4 Therapy

In treating patients with a disorder of peroxisome biogenesis, first of all supportive care is essential. In addition, it would seem rational to try to compensate as far as possible for the biochemical abnormalities that have been brought about by the peroxisomal dysfunction. Treatment would include oral supplementation of ether lipids and bile salts and dietary restriction of very-long-chain fatty acids and phytanic acid. The treatment has so far not resulted in definite clinical improvement or prolongation of life. Treatment with docosahexaenoic acid ethyl ester has been advocated on the basis of improvement of biochemical parameters and some neurological improvement in treated children. The rationale of the treatment is the observation of severe docosahexaenoic acid deficiency in tissues of children with disorders of peroxisomal biogenesis, while this substance is known to be an important constituent of brain membrane phospholipid and of photoreceptor cells. So far, the results of a controlled trial are lacking.

Administration of clofibrate fails to induce liver peroxisomes in ZS patients. Administration of 4-phenylbutyrate, a human peroxisome proliferator, increased the number of peroxisomes in fibroblasts of patients with a peroxisome biogenesis disorder (Wei et al. 2000). In NALD and IRD fibroblasts, but not in ZS fibroblasts, there was an increase in very-long-chain fatty acid β -oxidation and plasmalogen concentrations, and a decrease in very-long-chain fatty

acid concentrations. These data suggest that pharmacological agents that induce peroxisome proliferation may have a therapeutic potential in the treatment of patients with milder variants of peroxisome biogenesis defects.

The problem of any therapeutic trial in the disorders of peroxisomal biogenesis is that the dysontogenetic abnormalities cannot be changed by treatment and that only the degenerative changes acquired postnatally can, hopefully, be prevented.

18.5 Magnetic Resonance Imaging

In ZS the migrational derangement is well depicted by MRI. A very characteristic abnormality is the perisylvian polymicrogyria, which appears as a thickened cortical mantle consisting of many little dots (Figs. 18.1–18.3). The dots are cross-sections of the microgyri. The polymicrogyric cortex merges with

pachygyric cortex in the frontoparietal region (Figs. 18.1 and 18.2). The pachygyric cortex is visualized as broad convolutions of mildly thickened cortex. The cortex bordering the interhemispheric fissure and the occipital cortex are relatively normal. The gyral abnormalities are very extensive and serious in exceptional cases (Fig. 18.1). Small dots of ectopic gray matter may also be seen under the cortex and in the subependymal region (Figs. 18.2 and 18.3). The ventricular system is mildly enlarged and tends to have a primitive form with mildly enlarged occipital horns, which have a squared-off configuration. The ventricles are rarely markedly enlarged. Germinal cysts are often seen in the caudatothalamic groove in the early stages (Figs. 18.1 and 18.3). The corpus callosum is thin. The width of the white matter is reduced. Myelination is delayed and may be patchy, consistent with a disturbed myelination.

In NALD, CT has been shown to reveal progressive white matter hypodensities, particularly in the peri-

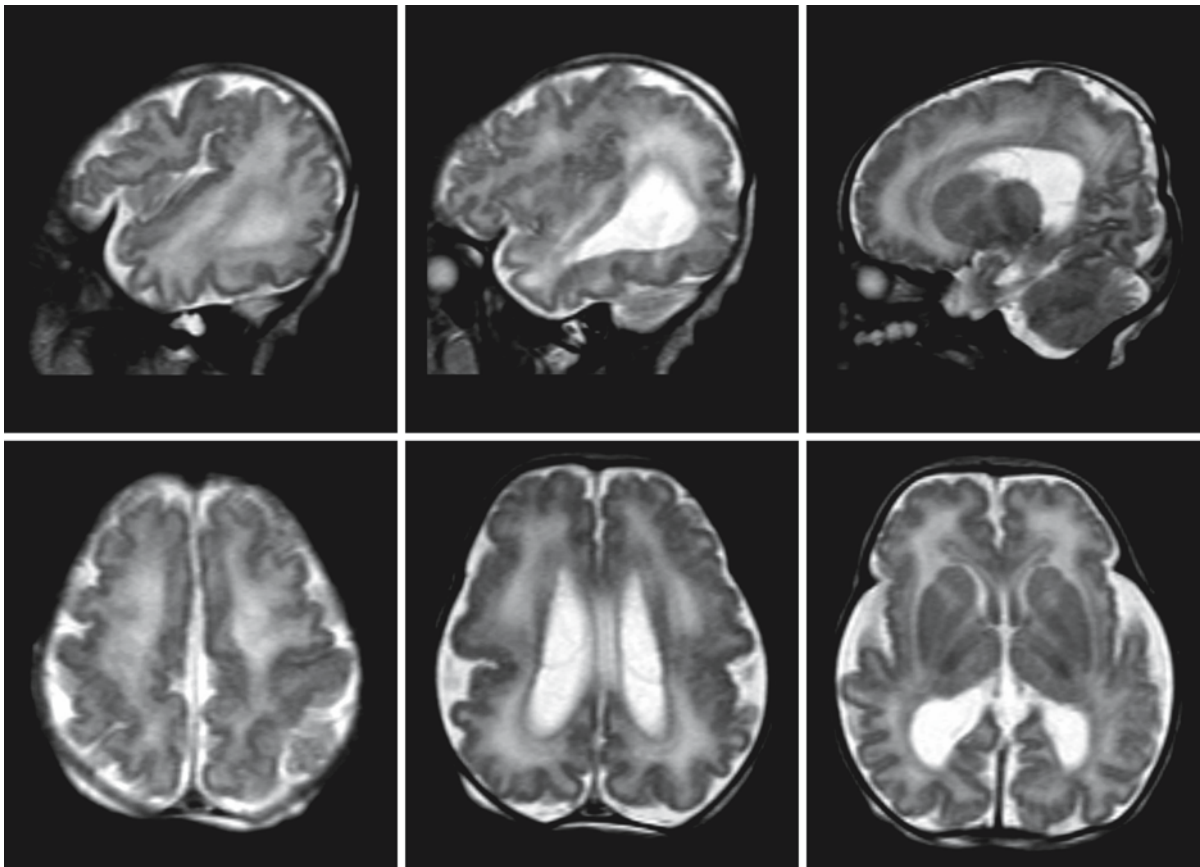


Fig. 18.1. Sagittal (*first row*) and axial (*second row*) T₂-weighted images in a neonate with ZS. The lateral aspects of the brain are diffusely pachygyric and polymicrogyric. The sylvian fissure is wide open. Note the huge subependymal cysts on both sides. (Courtesy of Dr. M.A. Breukels, Department of Pediatrics, and Drs. J.P. Westerhof and F. Kok, Department of Radiology, Elkerliek Hospital, Helmond, The Netherlands)

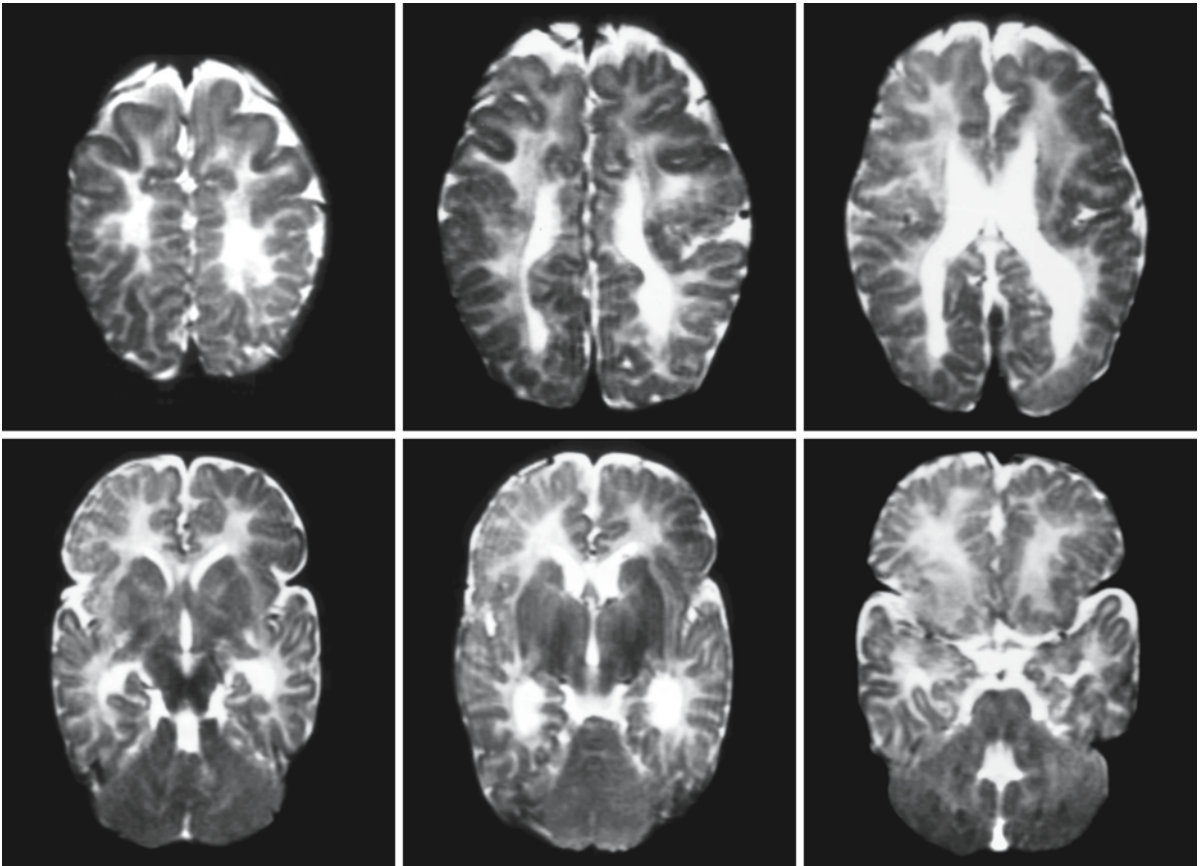


Fig. 18.2. Axial T₂-weighted images in a 3-month-old boy with a *PEX1* defect and the typical clinical course of ZS. The images show some ventricular enlargement. Myelination is sparse. In the frontal area the gyri are too coarse (pachygyria),

whereas polymicrogyria is present in the perisylvian region. There are several minor neuronal heterotopias in the periventricular region. The cerebellar vermis is hypoplastic

ventricular area, centrum semiovale, and cerebellum. The presence of extensive contrast enhancement in centrum semiovale, internal capsules, and cerebral peduncles has been reported. MRI may either show evidence of polymicrogyria in the area of the sylvian fissure (Fig. 18.4) or fail to show evidence of gyral abnormalities (Fig. 18.5). When demyelination starts, the earliest changes are seen in the cerebellum, involving both the hilus of the dentate nucleus and the peridentate white matter (Figs. 18.4 and 18.5). Other structures that become involved are brain stem tracts, in particular the pyramidal tracts, the posterior limb of the internal capsule, and the posterior cerebral white matter more than the anterior white matter (Figs. 18.4 and 18.5). On sequential MRI, the abnormalities are rapidly progressive.

In IRD MRI is normal in some patients, but is abnormal in others. MRI does not show migrational abnormalities. Symmetrical abnormalities in signal intensity may be seen in the hilus of the dentate nuclei and peridentate cerebellar white matter (Fig. 18.6). These seem to be the first and sometimes the only abnormalities present. Patchy, ill-defined abnormalities may be seen in the periventricular cerebral white matter (Fig. 18.6). The abnormal white matter merges into the normal white matter without sharp demarcation. The corpus callosum and posterior limb of the internal capsule may also be involved. There is no contrast enhancement. The white matter abnormalities may be slowly progressive over time, not necessarily associated with clinical decline. Profound cerebral and cerebellar atrophy may occur (Fig. 18.7).

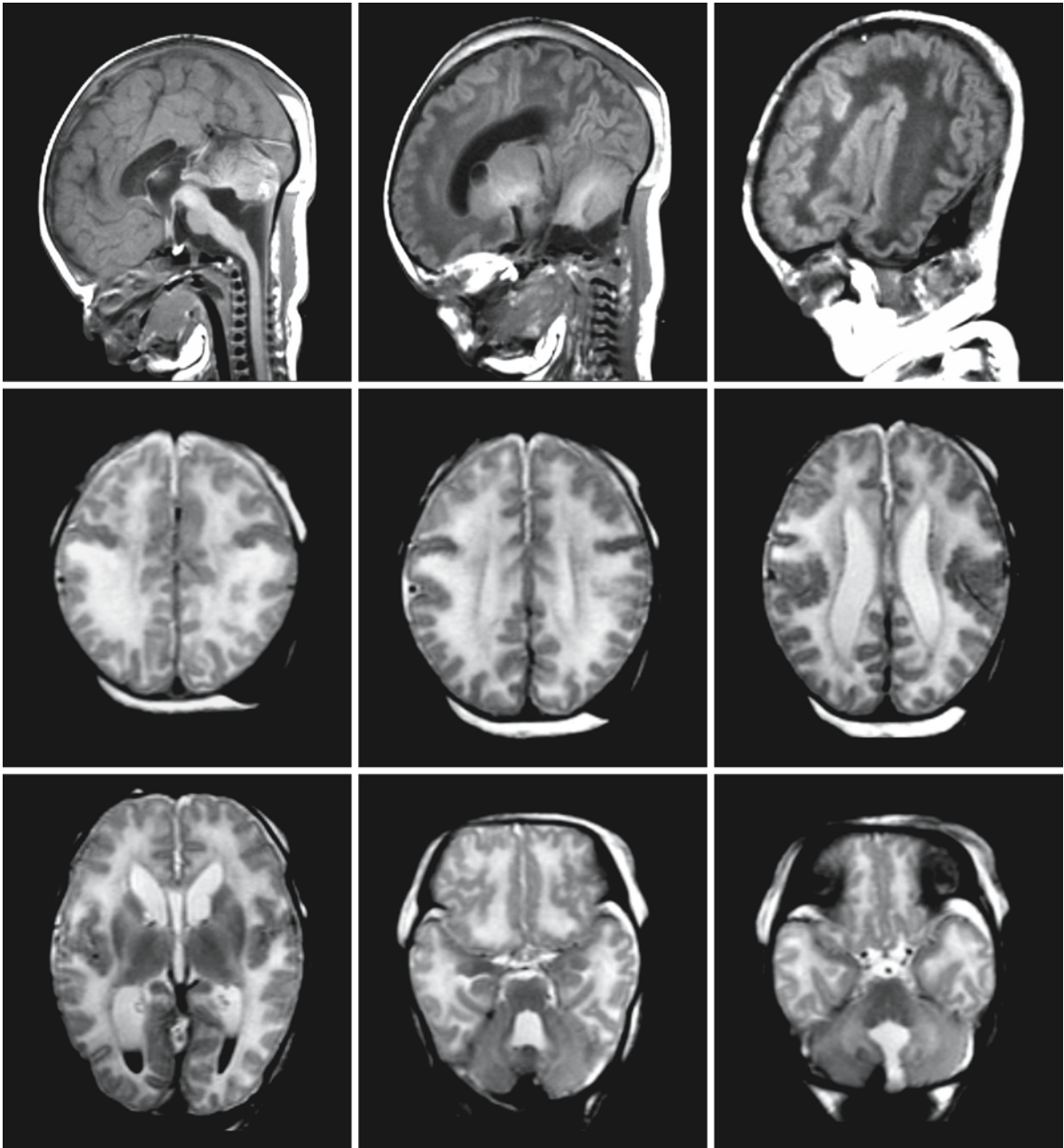


Fig. 18.3. A 1-week-old baby boy with ZS, related to a *PEX1* mutation. The *upper row* (T₁-weighted sagittal images) shows a thin corpus callosum, a hypoplastic vermis, and a subependymal cyst in the thalamocaudate notch. The sylvian fissure has a more vertical orientation than normal and is bordered by polymicrogyric cortex. The axial T₂-weighted images

show mildly enlarged lateral ventricles and absence of a large part of the vermis with an abnormally shaped fourth ventricle. The gyral deformity is most marked in the region of the sylvian fissure, with a combination of pachygyria and polymicrogyria. The *left image of the third row* shows a germinolytic cyst over the caudate nucleus and some blood in the occipital horns

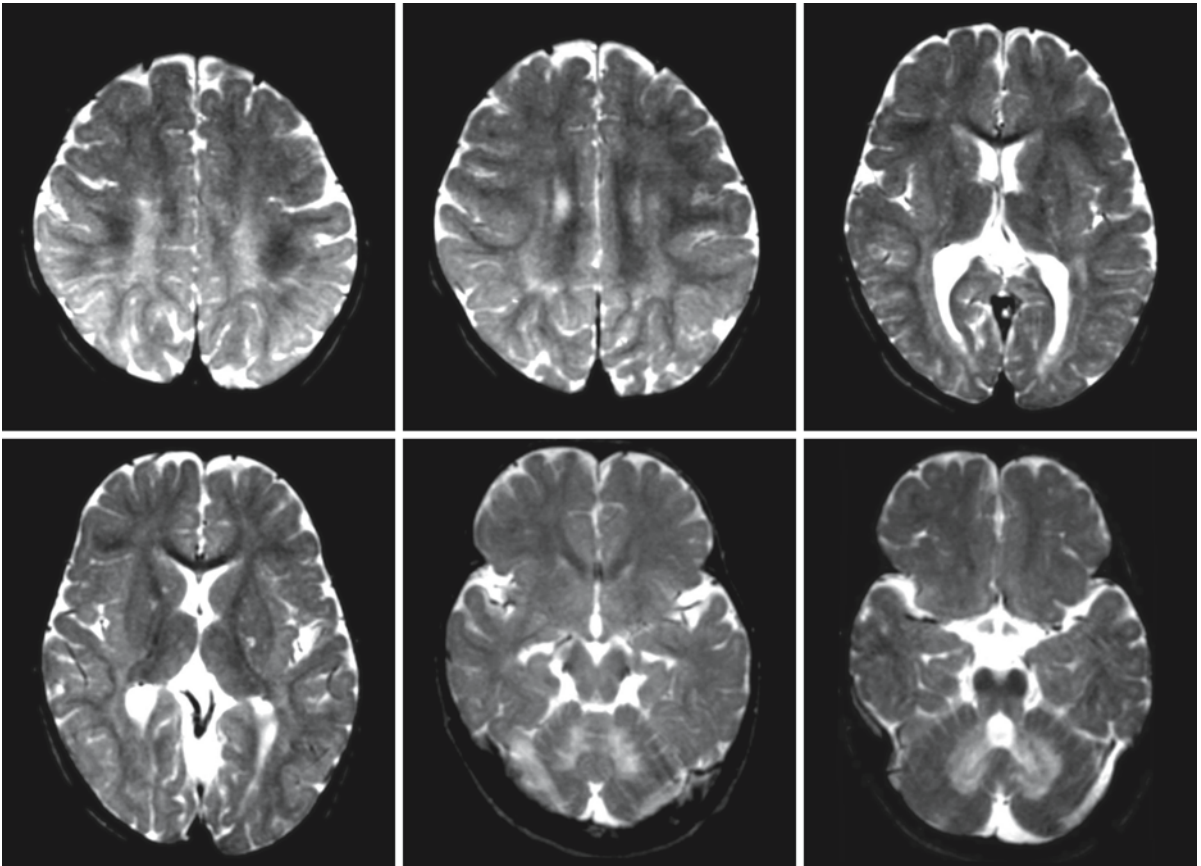


Fig. 18.4. A 2-year-old boy with a *PEX5* defect and progressive neurological deterioration with death at the age of 2.8 years. The images show white matter abnormalities in the hilus of the dentate nucleus, the cerebellar hemispheric white matter,

and the posterior cerebral white matter. The cortex in the area of the sylvian fissure appears mildly dysplastic with evidence of some polymicrogyria. Courtesy of Dr. P.G. Barth [Barth et al. 2001 (patient 3), 2004 (patient 4), with permission]

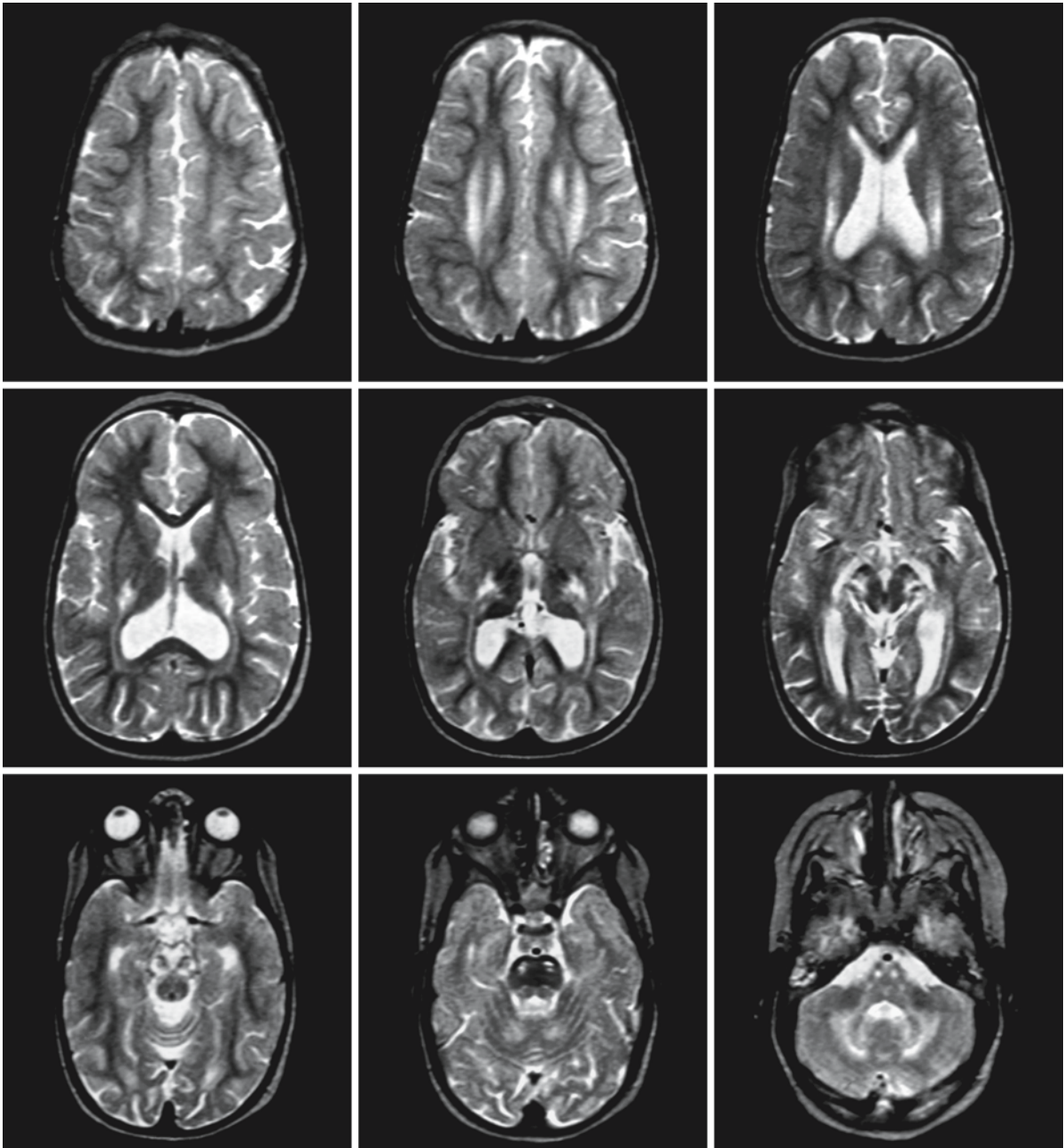


Fig. 18.5. A 2.5-year old girl with a *PEX5* defect and progressive neurological deterioration who died at the age of 3 years. The images show signal abnormalities in the hilus of the dentate nucleus, the cerebellar hemispheric white matter, pyrami-

dal tracts of the brain stem, and the posterior and central cerebral white matter. There is no evidence of cortical dysplasia. Courtesy of Dr. P.G. Barth [Barth et al. 1990, 2004 (patient 1), with permission]

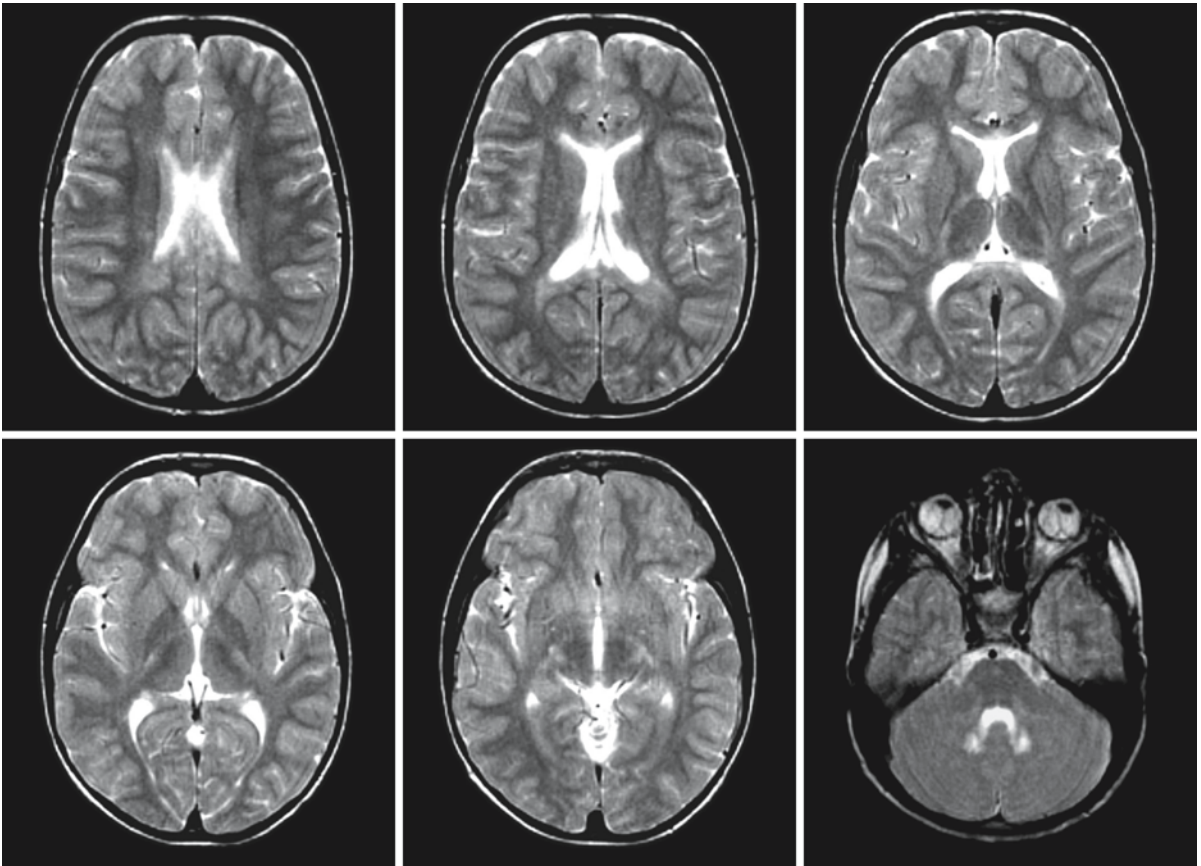


Fig. 18.6. A 10.5-year-old boy with a *PEX1* defect and a stable clinical course. Note the signal abnormalities in the hilus of the dentate nucleus, the corticospinal tracts at the level of the midbrain, the posterior limb of the internal capsule, the poste-

rior cerebral white matter, and splenium of the corpus callosum. Apart from the hilus of the dentate nucleus, the signal changes are mild and poorly demarcated. Courtesy of Dr. P.G. Barth [Barth et al. 2004 (patient 13), with permission]

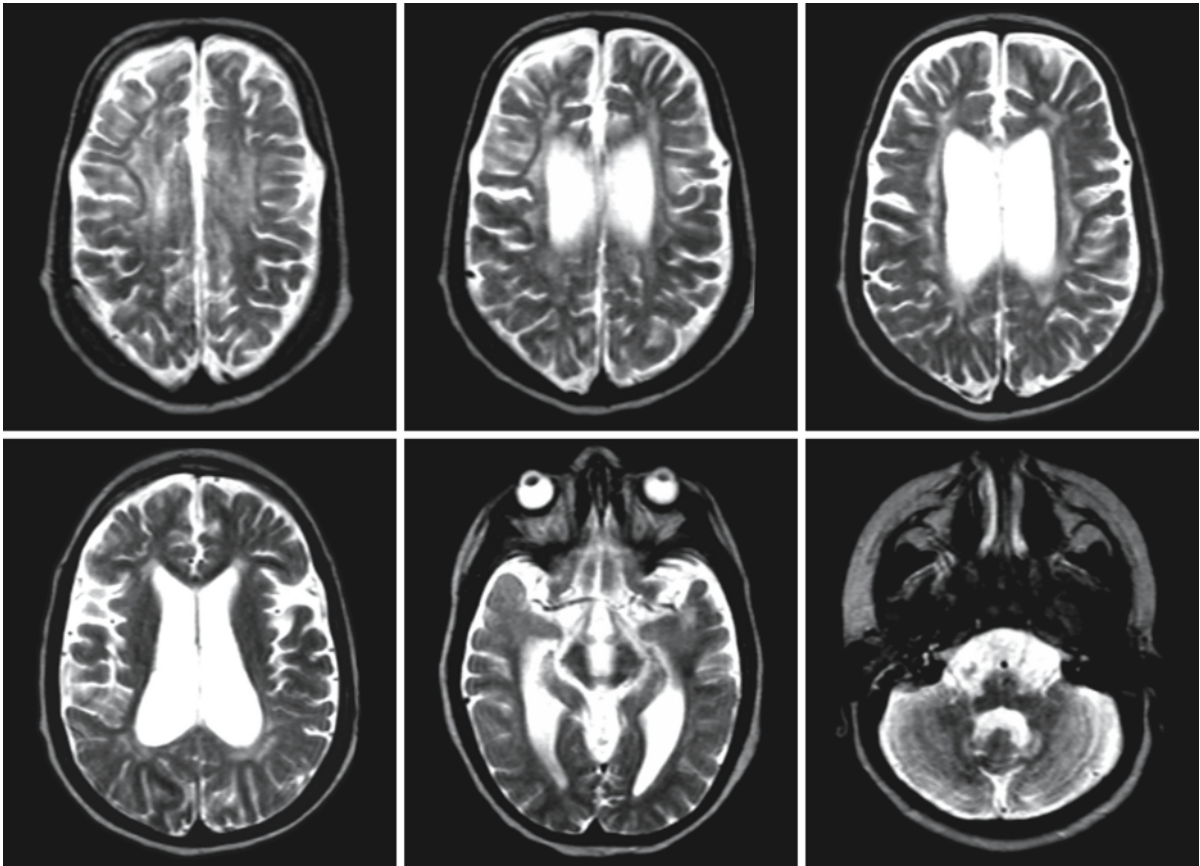


Fig. 18.7. T₂-weighted images of a 14-year-old boy with a *PEX1* defect and a very slow downhill course. The images show dilated ventricles and cerebral and cerebellar atrophy and widespread signal abnormalities in the atrophic cerebral

white matter, extending into the arcuate fibers. The hilus of the dentate nucleus is abnormal in signal. Courtesy of Dr. P.G. Barth [Barth et al. 2004 (patient 11), with permission]

Peroxisomal D-Bifunctional Protein Deficiency

19.1 Clinical Features and Laboratory Investigations

A limited number of patients have been described with isolated D-bifunctional protein deficiency (BPD), a disease with an autosomal recessive mode of inheritance. The children show severe CNS involvement with profound hypotonia from birth onwards. There are minimal spontaneous movements and the neonatal reflexes are depressed. Feeding problems are usually prominent. In most children dysmorphic features are present with high forehead, large open fontanel, flat nasal bridge, low-set ears, high-arched palate, and micrognathia, similar to the facial characteristics seen in patients with generalized peroxisomal dysfunction. Some infants have macrocephaly. Joint contractures may be present. Most patients suffer from severe epilepsy from the beginning and seizures are often uncontrollable. Psychomotor development is severely delayed and most patients fail to acquire any significant developmental milestones. Some patients have ocular abnormalities, including glaucoma, optic atrophy, pigmentary retinal degeneration, and cataract. Auditory dysfunction is present in some. Hepatomegaly is found in some of the patients. Adrenocortical insufficiency is manifest in few children. Death occurs most often between 4 and 12 months of age, but some patients survive a few years.

EEG is severely abnormal with epileptic discharges. BAEP findings are often abnormal. Nerve conduction velocities are normal. Skeletal X-ray survey is often normal, but calcific stippling of some joints may be seen. Renal ultrasound is normal.

Laboratory investigations reveal signs of adrenal insufficiency in some of the patients. In all patients very-long-chain fatty acids are elevated in plasma and fibroblasts. The plasma levels of bile acid intermediates (dihydroxycholestanoic acid and trihydroxycholestanoic acid) and pristanic acid may also be elevated, but not in all patients. When pristanic acid is elevated, phytanic acid is usually also elevated, although much less seriously and with an increase in pristanic to phytanic acid ratio. Plasma pipecolic acid and the de novo plasmalogen synthesis in fibroblasts are normal. A D-bifunctional protein deficiency is

demonstrated and mutations are found in the *D-BP* gene. Prenatal diagnosis is possible by measuring D-bifunctional protein activity in chorionic villus samples and, if the molecular defect has been resolved in the index patient, by DNA analysis.

19.2 Pathology

Postmortem examination of the brain reveals the brain to be relatively large. A combination of malformative and destructive abnormalities is usually found. Polymicrogyria is present in most but not all patients, in particular involving the lateral aspects of the brain in the area of the sylvian fissure. Scattered heterotopic neurons may be found in the centrum semiovale, the subcortical white matter, and cerebellar white matter. Mild dysplasia of the inferior olivary nucleus is noted. In addition, lack of stainable myelin is found in the cerebral and cerebellar white matter, probably partially related to a disturbance of myelination, but there is also evidence of active demyelination. The extent of both components also depends on the age at death. In infants of a few months the myelin content of the brain may be normal. In older infants, an evident deficiency of myelin is seen with relative sparing of the arcuate fibers. The active demyelination is most prominent in the cerebellar and occipital white matter. In the areas of active demyelination, axons are relatively spared. Lipid-filled, foamy macrophages, occasionally striated, and astrocytosis are seen in the areas of demyelination, cerebral cortex, and basal nuclei. The macrophages are located in the perivascular spaces. Cystic degeneration of the periventricular white matter has been observed. In the spinal cord the anterior and lateral corticospinal tracts and dorsal spinocerebellar tracts show loss of axons and myelin.

In liver, mild fibrosis is found. Electron microscopy of liver shows abundant peroxisomes. Additionally, adrenocortical atrophy is found with presence of lipid-containing, ballooned, striated cells. Electron microscopy reveals trilamellar lipid inclusions in these cells. Minute glomerular cysts may be seen in the kidney, but not in all cases.

19.3 Pathogenetic Considerations

D-bifunctional protein is involved in the β -oxidation process of both very-long-chain fatty acids, branched-chain fatty acids, like pristanic acid, and the oxidation of bile acid precursors. D-bifunctional protein has two catalytic activities: enoyl-CoA hydratase and 3-hydroxyacyl-CoA dehydrogenase activity. In some patients (group 2A), D-bifunctional protein is completely absent, which is associated with the loss of activity of both the enoyl-CoA hydratase and 3-hydroxyacyl-CoA dehydrogenase components. In group 2B patients, enoyl-CoA hydratase activity is deficient, whereas in group 2C 3-hydroxyacyl-CoA dehydrogenase activity is deficient. Group A and group C patients accumulate very-long-chain fatty acids, branched-chain fatty acids, and abnormal bile acid intermediates. Group B patients have elevated very-long-chain fatty acids and branched-chain fatty acids, but bile intermediates are normal, due to the normal 3-hydroxyacyl-CoA dehydrogenase activity.

In patients with BPD, mutations have been found in the gene *D-BP*, located on chromosome 5q23.1. The patient formerly classified as a thiolase-deficient patient (Goldfischer et al. 1986) also has a defect in the *D-BP* gene (Ferdinandusse et al. 2002).

It is striking that a disease caused by an isolated deficiency of one of the peroxisomal β -oxidation enzymes can have clinical symptomatology that is indistinguishable from that of peroxisome biogenesis defects. This observation indicates the pathophysiological significance of accumulation of very-long-chain fatty acids and abnormal bile acid intermediates. Evidently, the relationship between biochemical abnormalities and clinical symptomatology requires further elucidation.

19.4 Therapy

No specific treatment is possible. Supportive care is important.

19.5 Magnetic Resonance Imaging

A number of CT scans have been reported. Most were described as normal, some as showing white matter hypodensity and slight enlargement of the occipital horns of the ventricular system.

MRI shows a combination of polymicrogyria, especially over the lateral aspects of the brain in the area of the sylvian fissure, and white matter abnormalities (Fig. 19.1). The white matter abnormalities consist of delayed and disturbed myelination (Fig. 19.2), while in particular in the older infants with more advanced myelination active demyelination occurs (Figs. 19.3 and 19.4). The demyelination is most pronounced in brain stem tracts and occipital and cerebellar white matter (Fig. 19.4).

The combination of gyrational abnormalities and deficient myelination is also seen in Zellweger syndrome. The combination of gyrational abnormalities and demyelination with predilection for the cerebellar and occipital white matter is also seen in neonatal adrenoleukodystrophy. In BPD no inflammatory reaction is seen in the area of active demyelination. In conformity with this observation, no contrast enhancement was found on the CT of the child who had active demyelination at autopsy, unlike the situation in neonatal adrenoleukodystrophy, where extensive contrast enhancement is seen.

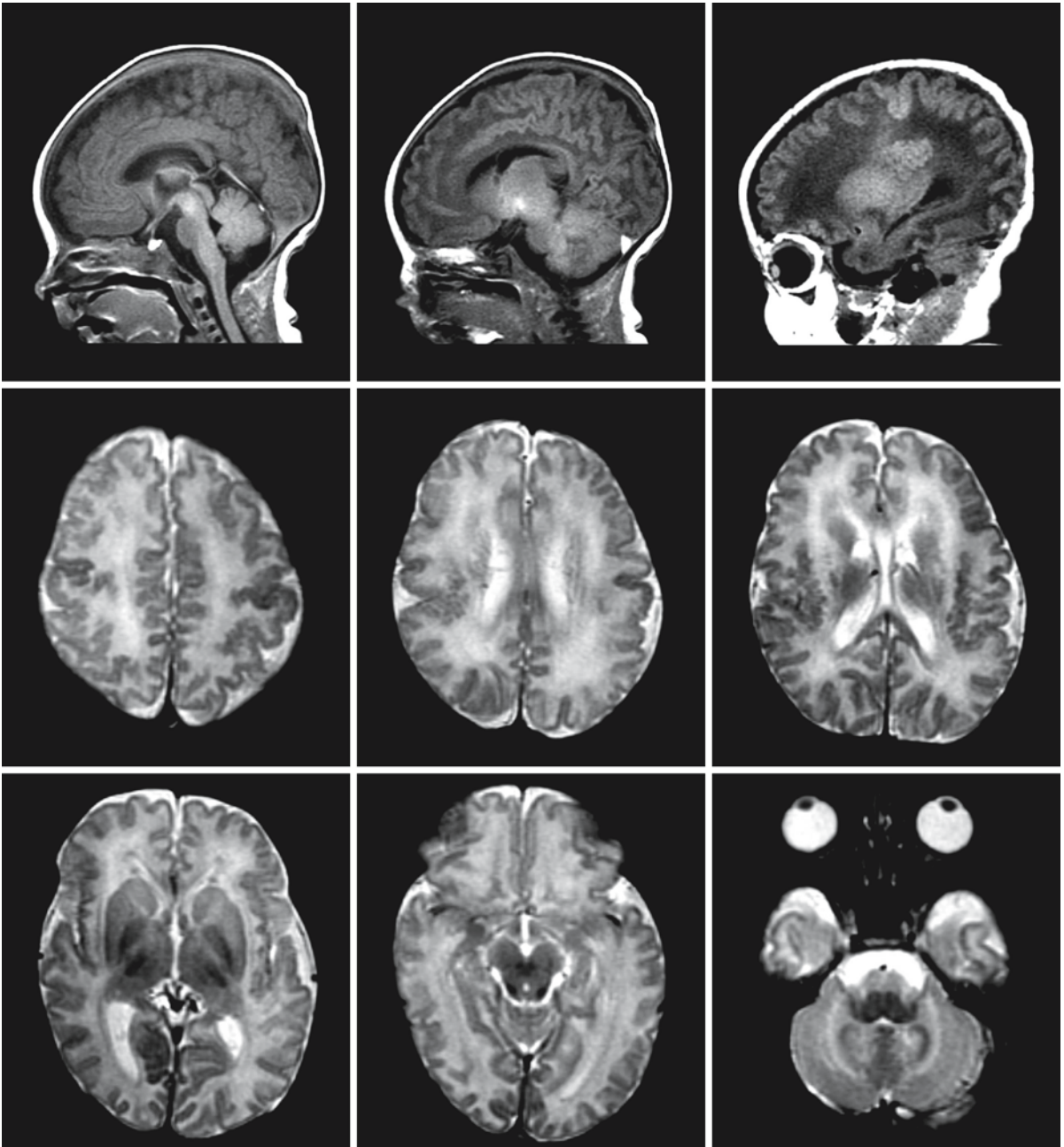


Fig. 19.1. Baby boy, 3 weeks old, with BPD. The sagittal T₁-weighted images show a germinolytic cyst in the thalamocaudate notch and polymicrogyria in the perisylvian region. The axial T₂-weighted images confirm the perisylvian polymicrogyria. There are possibly some small heterotopias around the

lateral ventricles. Myelination is compatible with a neonatal stage. These images are indistinguishable from those seen in Zellweger syndrome. Courtesy of Dr. D. Holder, Department of Pediatric Neurology, Cincinnati Children's Hospital, Cincinnati

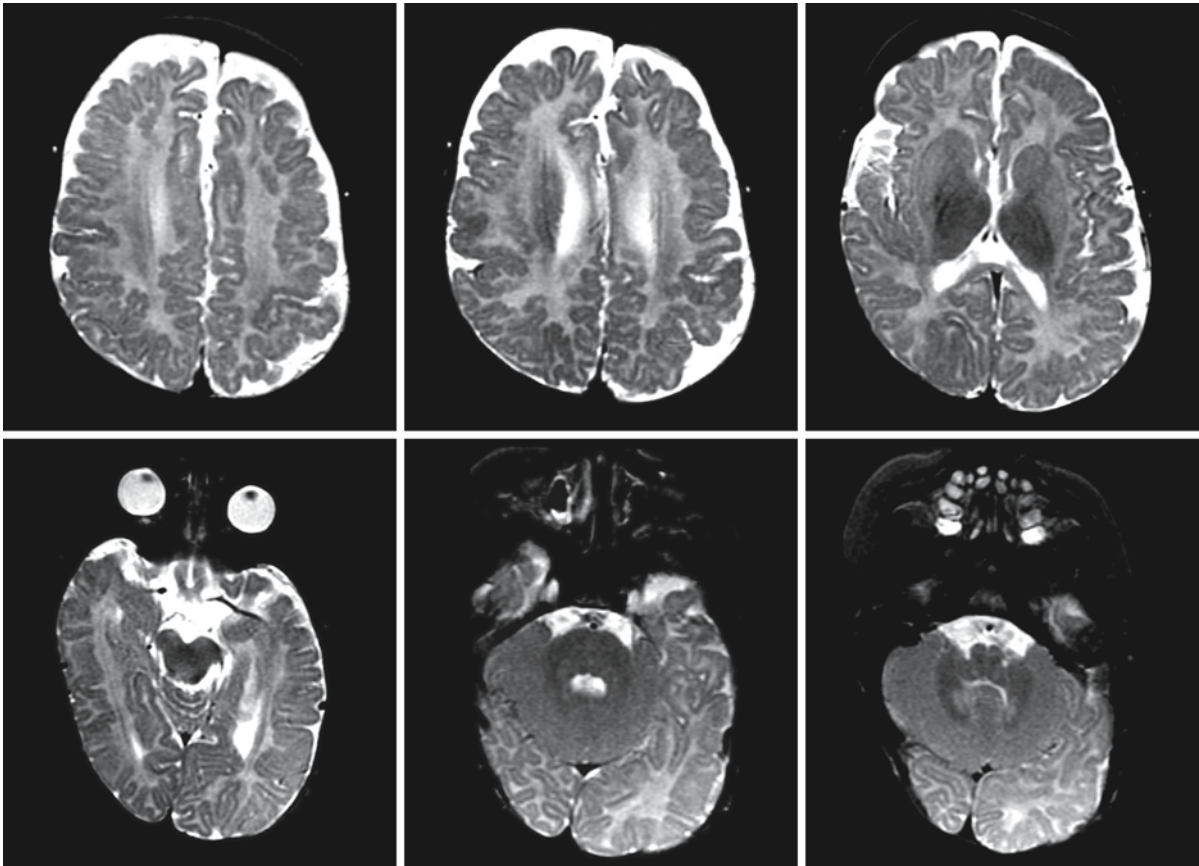


Fig. 19.2. Follow-up MRI of the same boy with BPD at the age of 6 months. The polymicrogyria in the perisylvian region is again visualized. The brain stem is now well myelinated, but there is little myelin in the supratentorial white matter. Note

the lesions in the hilus of the dentate nucleus. Courtesy of Dr. D. Holder, Department of Pediatric Neurology, Cincinnati Children's Hospital, Cincinnati

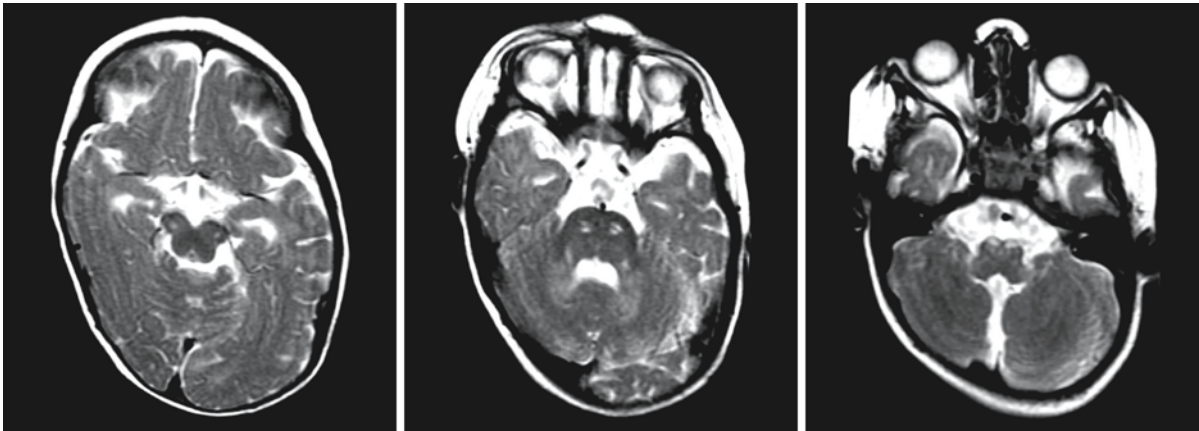


Fig. 19.3. Follow-up MRI of the same boy with BPD at the age of 22 months. Demyelination has started in the pyramidal tracts of the brain stem. The cerebellar white matter is also

affected. Courtesy of Dr. D. Holder, Department of Pediatric Neurology, Cincinnati Children's Hospital, Cincinnati

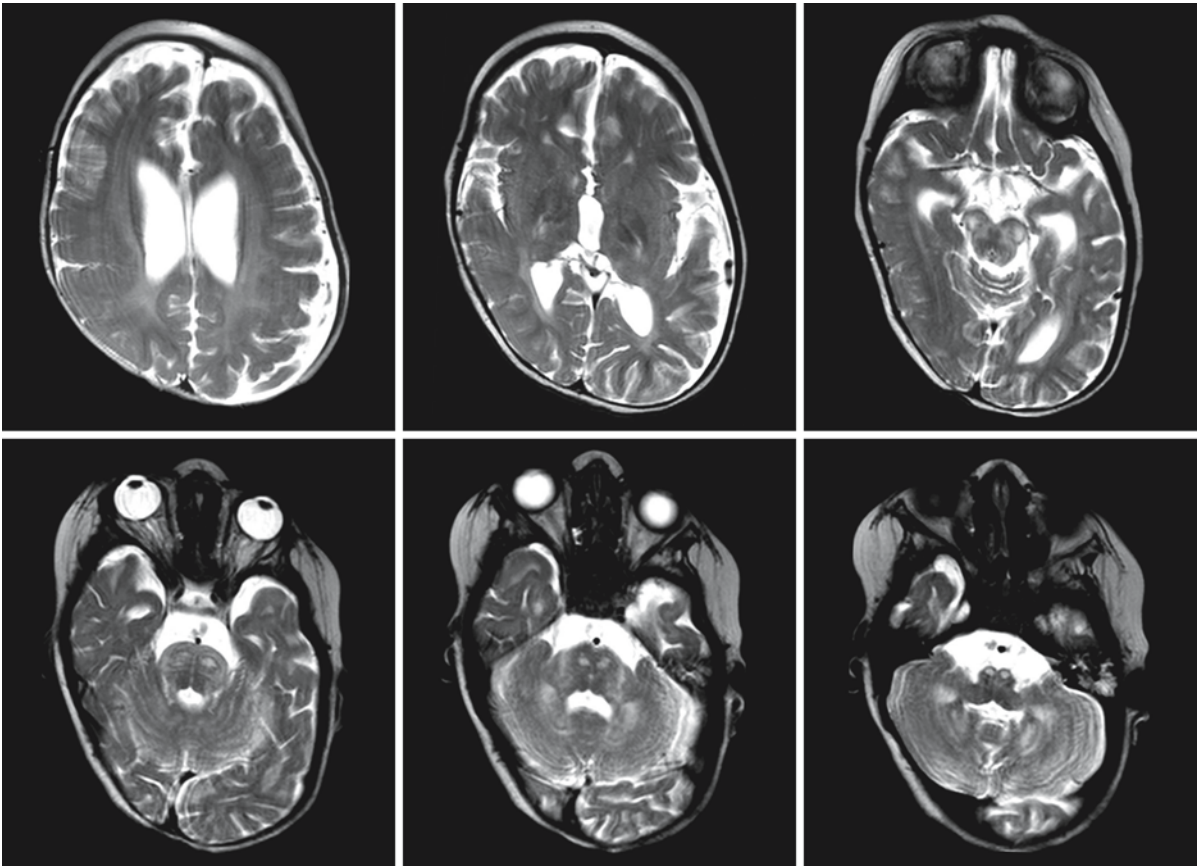


Fig. 19.4. Follow-up MRI of the same boy with BPD at the age of 26 months, shortly before he died. The process of demyelination now involves the brain stem more extensively. The posterior limb of the internal capsule and posterior cerebral

white matter are also involved. Courtesy of Dr. D. Holder, Department of Pediatric Neurology, Cincinnati Children's Hospital, Cincinnati

Peroxisomal Acyl-CoA Oxidase Deficiency

20.1 Clinical Features and Laboratory Investigations

A small number of patients has been described with isolated peroxisomal acyl-CoA oxidase deficiency. This autosomal recessive disease has also been referred to as pseudo-neonatal adrenoleukodystrophy (pseudo-NALD), because the clinical features are very similar to those of neonatal adrenoleukodystrophy. The disease had its onset in the neonatal period with hypotonia and seizures. Neonatal reflexes may be absent. Craniofacial dysmorphism may be present and include hypertelorism, epicanthus, low nasal bridge, low-set ears, and polydactyly, but some children have normal features. Hepatomegaly is present in some but not all patients. Psychomotor development is retarded, but several motor milestones can be reached and children may achieve walking although delayed. They may learn to speak a few words. Subsequently, neurological deterioration sets in, usually at the age of 1–3 years, with regression of motor abilities. The hypotonia gradually changes into hypertonia with hyperreflexia and positive Babinski signs. The epilepsy may become very severe with almost continuous epileptic seizures. Sensorineural hearing deficit becomes apparent. Whereas ophthalmological examination initially reveals normal pupillary light responses and normal fundi, increasing abnormalities are subsequently noted with nystagmus, strabismus, optic atrophy, tapetoretinal degeneration, and absent pupillary light responses. After a few years a vegetative state is reached, followed by death.

Neurophysiological investigations reveal increasing EEG abnormalities with epileptic discharges; the ERG may become flattened, and VEP may become almost entirely absent. Motor and sensory nerve conduction velocities are normal. Skeletal X-ray examination and ultrasound of the kidneys are normal.

Laboratory investigations show signs of mild liver dysfunction. Serum cortisol level is low, with an increased ACTH value. In serum and fibroblasts, very-long-chain fatty acids (VLCFA) are elevated, but no increase is found in plasma levels of phytanic acid, pristanic acid, pipecolic acid, and bile acids like dihydroxycholestanic acid and trihydroxycholestanic acid. In fibroblasts, VLCFA β -oxidation is seriously deficient, whereas de novo plasmalogen biosynthesis and other peroxisomal parameters are normal. The diagnosis is confirmed by measuring the activity of

acyl-CoA oxidase in fibroblasts. DNA confirmation by showing mutations in the acyl-CoA oxidase gene is possible. Prenatal diagnosis is possible using the same techniques.

20.2 Pathology

No postmortem examination of the brain has been performed in patients with pseudo-NALD. Liver tissue investigations show peroxisomes to be present in normal or increased numbers and to be increased in size.

20.3 Pathogenetic Considerations

The biochemical findings of an isolated accumulation of VLCFA in the absence of abnormal bile acid intermediates are consistent with an isolated deficiency of fatty acyl-CoA oxidase. Bile acid intermediates have their own CoA oxidase, whereas bifunctional protein and thiolase are active for all substances β -oxidized in peroxisomes. The gene encoding acyl-CoA oxidase or palmitoyl-CoA oxidase, *ACOX1*, is located on chromosome 17q25.

Two peroxisomal disorders, peroxisomal acyl-CoA oxidase deficiency (pseudo-NALD) and X-linked adrenoleukodystrophy, are characterized by an isolated accumulation of VLCFA. It is striking that both disorders may lead to demyelination with inflammation, as suggested by the contrast enhancement on neuroimaging. There are, however, also important differences. Patients with acyl-CoA oxidase deficiency display clinical abnormalities from birth on, while the clinical symptoms start much later in X-linked adrenoleukodystrophy. In acyl-CoA oxidase deficiency, the β -oxidation of C22 unsaturated fatty acids by chain-shortening and the β -oxidation of dicarboxylic acids are deficient in addition to the oxidation of VLCFA, such as C24:0 and C26:0 fatty acids. In X-linked adrenoleukodystrophy only the β -oxidation of the VLCFA is deficient. These differences may be important in explaining the clinical differences.

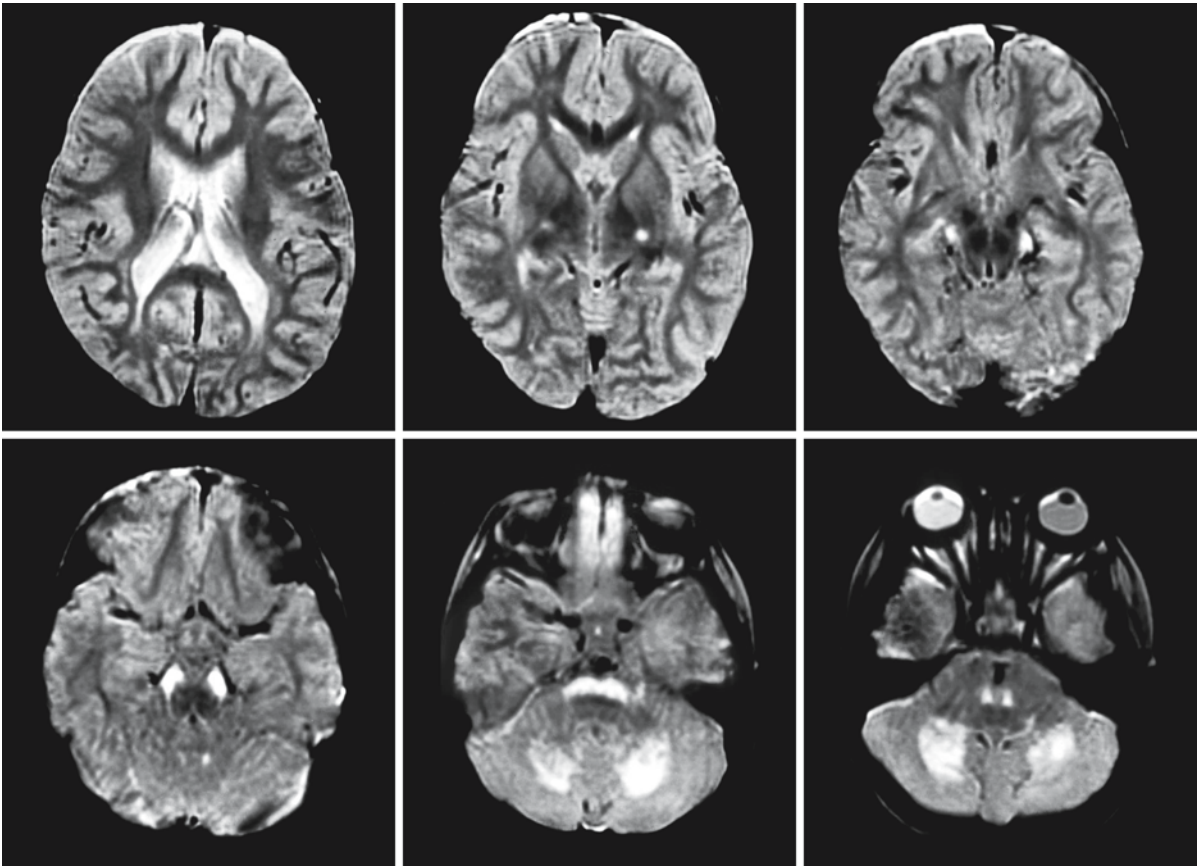


Fig. 20.1. A 3-year-old female patient with isolated peroxisomal acyl-CoA oxidase deficiency. Note the signal abnormalities in the corticospinal tracts in the brain stem and the cerebellar

white matter. The pyramidal tracts in the posterior limb of the internal capsule are affected. From Suzuki et al. (2002), with permission

20.4 Therapy

No specific treatment is available. Supportive care is important.

20.5 Magnetic Resonance Imaging

In several patients CT scan of the brain was performed at birth and found to be unremarkable. No evidence of cortical malformation was seen, although minor or mild abnormalities in gyration and heterotopias can easily be missed on CT. Repeat CT after the onset of neurological deterioration reveals symmetrical white matter hypodensities in the centrum semiovale and the occipital area with contrast enhancement of the border of the lesions. The CT findings are reminiscent of those reported in neonatal adrenoleukodystrophy.

MRI soon after the onset of neurological deterioration shows signal abnormalities in the cerebellar white matter, brain stem tracts, and middle cerebellar peduncles (Figs. 20.1 and 20.2). On follow-up, the pyramidal tracts at higher levels of the brain stem and the posterior limb of the internal capsule become abnormal in signal. Subsequently signal changes develop in the periventricular parieto-occipital white matter and the splenium of the corpus callosum (Figs. 20.2 and 20.3), spreading outward and forward, finally involving also the frontal white matter. If contrast is administered, enhancement is expected. No evidence of a migrational defect has been reported.

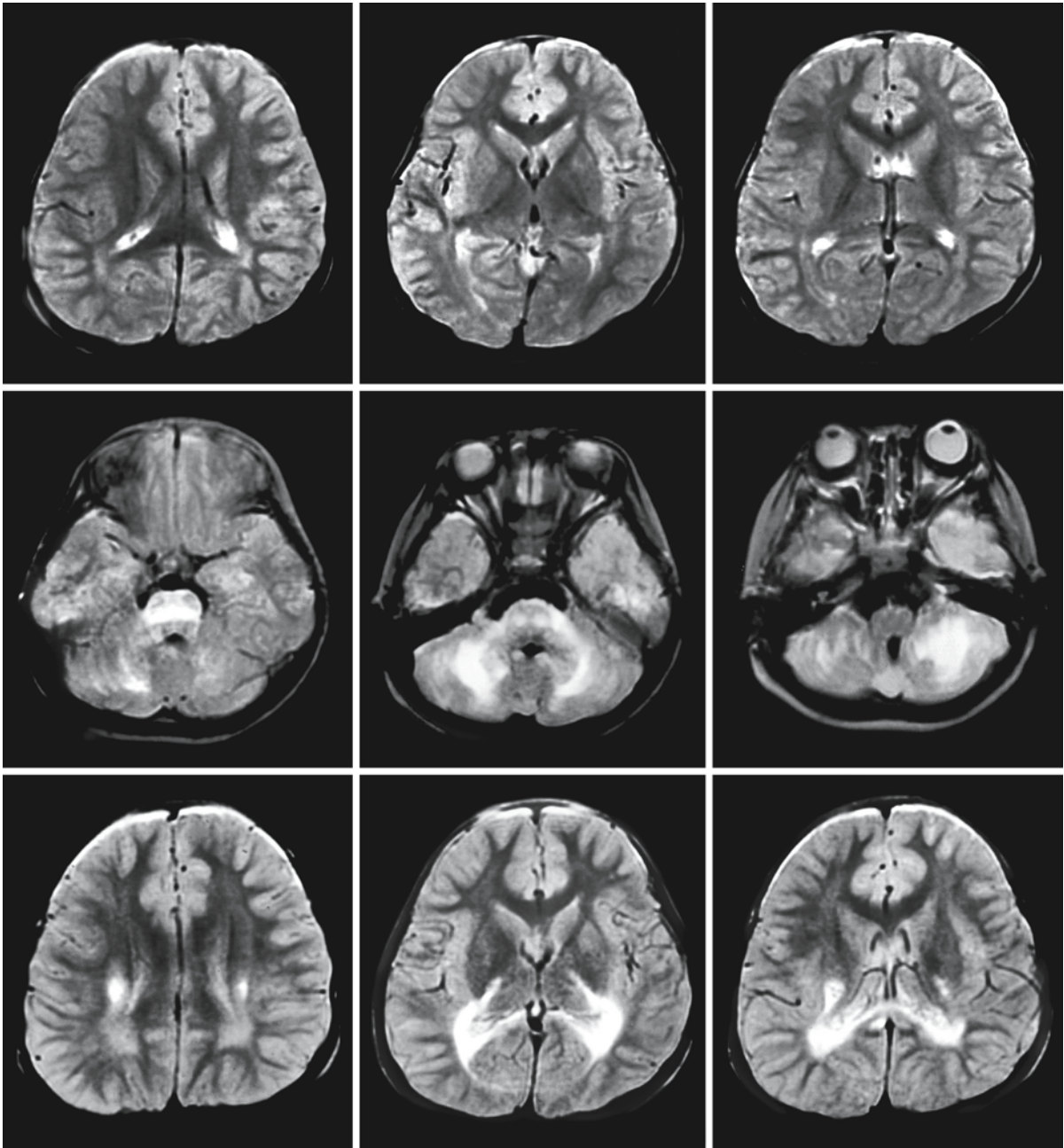


Fig. 20.2. The *first two rows* show the images of a male patient with peroxisomal acyl-CoA oxidase deficiency at the age of 3 years and 5 months. There are extensive signal abnormalities in brain stem tracts, middle cerebellar peduncles, and cerebellar white matter. There are incipient signal changes in the parieto-occipital white matter. The *third row* shows the images of

the same patient at the age of 7 years and 11 months. The posterior limb of the internal capsule, parieto-occipital white matter, and splenium of the corpus callosum now display prominent signal abnormalities. From Suzuki et al. (2002), with permission

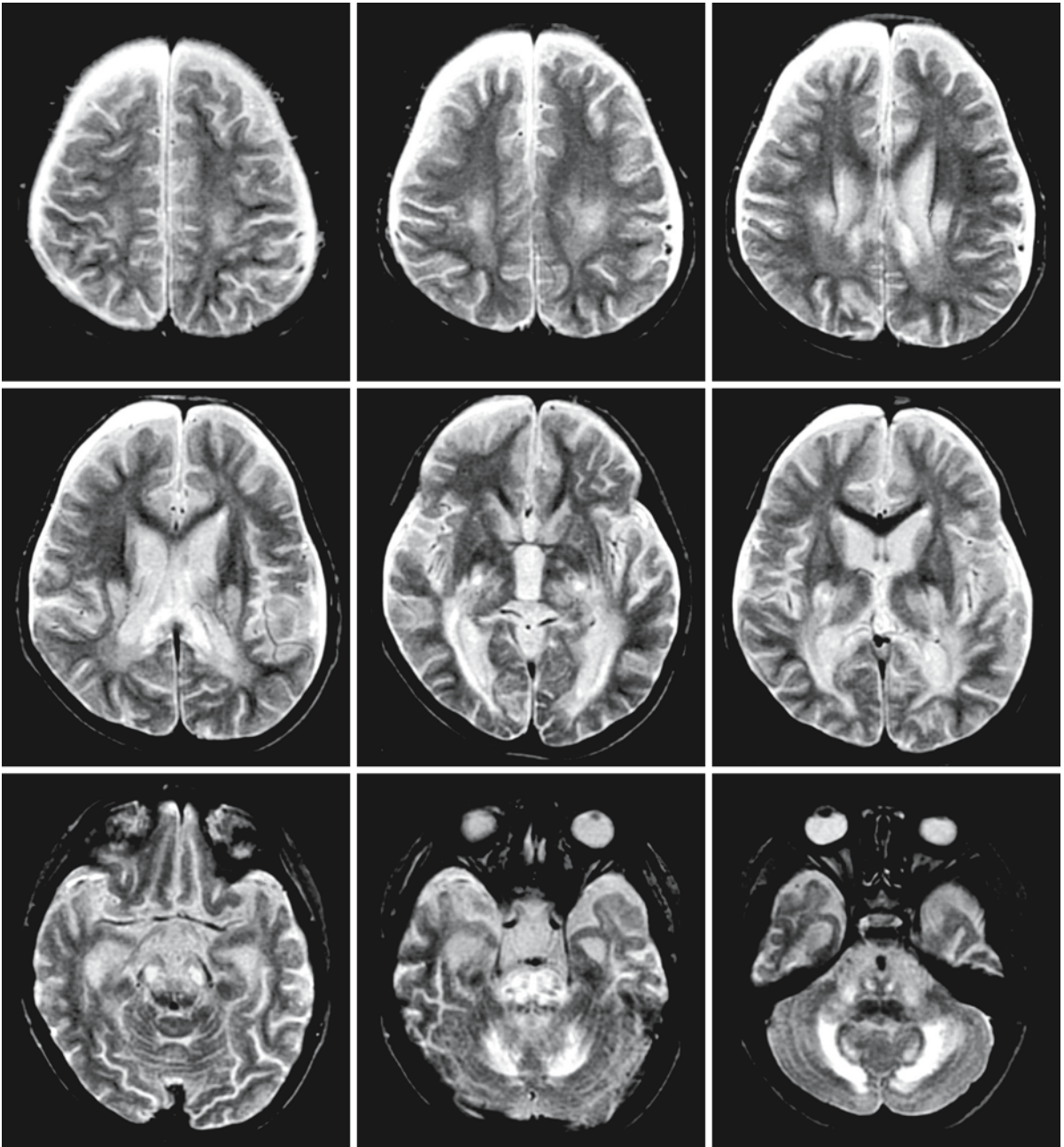


Fig. 20.3. Female patient with peroxisomal acyl-CoA oxidase deficiency at the age of 3 years and 3 months. Tracts in the brain stem (especially the corticospinal tracts), cerebellar white matter, hilus of the dentate nucleus, posterior limb of the internal capsule, thalamus, parieto-occipital white matter, and

splenium of the corpus callosum are affected. In addition, there is some generalized cerebral atrophy. The images resemble those of the cerebral form of X-linked adrenoleukodystrophy. From Suzuki et al. (2002), with permission

X-Linked Adrenoleukodystrophy

21.1 Clinical Features and Laboratory Investigations

X-linked adrenoleukodystrophy (XALD) is a genetically determined disorder that mainly involves the adrenal cortex and the CNS. Inheritance is X-linked recessive. The disease has a wide phenotypic variability. The rapidly progressive childhood cerebral form accounts for about one-third of the cases. Adrenomyeloneuropathy (AMN) has a later onset and slower progression and accounts for about 40–45% of the patients. The relative frequency of the Addison-only form varies with age and accounts for up to 50% of the cases in childhood. Less frequent variants include the adolescent and the adult cerebral forms. In addition, there are patients with unusual presentation and asymptomatic patients, a common observation below the age of 4 years and very rare above the age of 40. These different phenotypes may occur all within one affected family. Even identical twins may display different phenotypes. Females may also be affected, especially when they become older. The minimum frequency of males with the defect has been estimated to be 1:42,000 in the USA, whereas the minimum frequency of males with the defect and female carriers is estimated to be 1:16,800 (Bezman et al. 2001).

In the childhood cerebral form of XALD, the age at onset of neurological symptoms is usually between 5 and 9 years. Features of adrenal insufficiency may occur before overt neurological symptoms or may follow. In some cases a diagnosis of Addison disease is made 1–3 years before any neurological disorder is evident on the basis of increased pigmentation, fatigue, episodes of vomiting, or catastrophic reactions to intercurrent infections. In others, neurological deterioration may continue for some years without endocrine symptoms, and sophisticated investigations are needed to reveal evidence of adrenocortical dysfunction. Adrenocortical dysfunction is present in at least 80% of the patients.

The earliest neurological symptoms are often vague and frequently consist of behavioral changes. The changes vary from withdrawn to bizarre hyperactive and aggressive behavior and are often accompanied by poor school performance. Many boys receive psychiatric treatment until deteriorating learning capabilities and other neurological symptoms force recognition of the organic nature of the disease. Early neurological abnormalities are disturbances of

gait, loss of vision, and impaired auditory discrimination. The course of the disease is relentlessly progressive and spastic tetraplegia and dementia become manifest in months. Decreased vision is caused by optic atrophy or bilateral occipital white matter lesions or, more often, a combination of the two. Initially, neurological findings are often asymmetrical with hemiparesis or hemianopia. Frequently noted subsequent problems are dysarthria, dysphagia, and hearing loss. Cerebellar ataxia or sensory disturbances may be present, but are not usually prominent. There are no clinical signs of peripheral nerve dysfunction. Progressive dementia occurs. Epileptic seizures occur and are often multifocal in origin. The pace of deterioration is variable. In the final stage a spastic quadriplegia is present and a variable degree of decorticate posturing. The affected boys are blind, deaf, and mute. A vegetative state or death is reached in 1–5 years. Most patients die within 2 or 3 years after the onset of neurological symptoms, but some live for many years in a vegetative state. However, some patients stabilize for years in an earlier stage of the disease.

The adolescent (onset at 10–21 years) and adult (onset after 21 years) cerebral forms resemble the childhood cerebral form, except for the later onset. Just like the childhood form, the adolescent and adult cerebral forms have a rapidly progressive course. The disease is often misdiagnosed. It may present as a psychosis or dementing illness, or as a single focal brain lesion that can be mistaken for a tumor.

The usual age at onset of AMN is within the third or fourth decade, but ranges from 14 to 60 years. Most patients with an adult onset form of XALD have AMN. Neurological deficits are primarily due to a myelopathy and to a lesser extent a neuropathy. Affected males have a slowly progressive paraparesis, disturbed vibration sense of the legs, voiding disturbances, and a variable degree of sexual dysfunction. Signs of a distal polyneuropathy may also be found. Approximately two-thirds of the patients have overt or biochemical signs of adrenocortical insufficiency, which may precede or follow neurological dysfunction. Twenty percent of the patients have signs of hypogonadism with infertility. Many patients have scanty scalp hair. The disease is slowly progressive over decades. About half of the patients with AMN develop some cerebral involvement, with usually mild cognitive dysfunction. Visual memory, spatial cogni-

tion, and psychomotor speed are affected most. Psychological dysfunction may also occur, with emotional disturbances and depression. About 20% of the patients with AMN develop a rapidly progressive cerebral white matter involvement as seen in the cerebral forms of XALD.

In the Addison-only form no neurological dysfunction is found. However, all patients are at risk of developing overt neurological symptoms sooner or later. Some patients develop Addison disease in childhood and neurological abnormalities only arise in adulthood.

The asymptomatic group includes males in whom the typical biochemical abnormalities of XALD are found and who are completely healthy. Most of the males included in this group are small boys who were investigated because of clinically evident XALD in an older brother. The group also includes adolescents and a few older males. The oldest asymptomatic male ever mentioned was 62 years old.

There are a few patients with unusual forms of XALD. Patients have been reported with predominantly cerebellar ataxia or a spinocerebellar syndrome. One patient, aged 57 years, has been reported who showed rapid neuropsychiatric deterioration and signs of cerebral demyelination at the site of a severe cerebral contusion suffered several months previously. Cerebral XALD presents rarely as an acute encephalopathy with seizures, status epilepticus, headache, vomiting, lowering of consciousness, or even coma. Papilledema may be seen. The presence of fever may suggest encephalitis. After this acute episode, the patient recovers with temporary encephalopathic signs, which resolve in the course of days and weeks.

Female XALD carriers may also develop clinical problems. Most women below the age of 30 years are uninvolved. The percentage of females with neurological problems increases with age. Approximately 50% of the female carriers of 40 years and older display signs of a mild myelopathy with increased tendon reflexes and distal sensory changes in the legs, but no or mild disability. About 15% of the females of 40 years or older have an AMN-like clinical phenotype, but with later onset and milder symptomatology. Cerebral involvement and adrenocortical insufficiency are very rare among female carriers at all ages. Cerebral involvement is exceedingly rare in childhood and then probably related to skewed, highly unfortunate X inactivation or a partial deletion of one X chromosome and a mutated gene on the other chromosome. Some older female carriers have mild intellectual impairment, which is only detected by detailed psychological tests. An adult female has been described with a lethal cerebral leukodystrophy.

Laboratory testing usually reveals signs of adrenocortical dysfunction. Urinary excretion of 17-hydroxy-

corticosteroids and 17-oxysteroids may be reduced. Further evidence for primary adrenocortical insufficiency is found in impaired cortisol responsiveness to adrenocorticotrophic hormone (ACTH) in the presence of elevated baseline ACTH levels. Evidence of primary testicular insufficiency is provided by low testosterone levels and elevated luteinizing hormone (LH) or follicle stimulating hormone (FSH) levels. CSF protein is elevated in the majority of the symptomatic patients, sometimes combined with an elevation of γ -globulin level or moderate increase in lymphocytes.

Diagnosis of XALD depends upon the demonstration of abnormally high levels of saturated very-long-chain fatty acids (VLCFA) in plasma, cultured skin fibroblasts, or tissue. For routine purposes plasma is used. The concentration of C26:0 fatty acids is investigated as well as the ratios of C26:0/C22:0 and C24:0/C22:0 fatty acids. In over 90% of XALD patients all three parameters are abnormally elevated. In a minority of the patients only one or two of the three parameters are abnormal. VLCFA analysis and C26:0 fatty acid β -oxidation measurements in cultured skin fibroblasts are used for definite diagnosis. Patients with XALD already show the characteristic elevations in blood VLCFA during the first 2 weeks of life and even in cord blood.

Neurophysiological investigations are often used to establish the extent of disease in XALD. Nerve conduction studies usually show a normal conduction velocity in cerebral forms, but may also show a decreased velocity. In AMN the conduction velocity is decreased. In cerebral forms of ALD the EEG is as a rule abnormal, although nonspecifically, with diffuse slowing of the rhythm and a maximum usually in the posterior regions. Evoked potential studies may show abnormalities reflecting the central white matter involvement.

Investigation of the level of VLCFA is also a sensitive test in carrier detection: 85% of heterozygotes can be identified when the results of VLCFA assays in plasma and cultured fibroblasts are combined. Consequently, about 15% of the female carriers have false negative test results. Monoclonal antibodies have been raised against the XALD gene product (ALD protein, ALDP) and use of these antibodies in immunofluorescence studies of cultured skin fibroblasts or leukocytes may aid in the identification of heterozygous females, in particular when VLCFA concentrations in plasma and fibroblasts are normal. In 70–80% of the affected kindreds affected boys and men lack ALDP immunoreactivity; female carriers in these kindreds show a mixture of positive and negative immunoreactivity in their cells. Antenatal diagnosis can be established by measuring VLCFA in cultured amniocytes and chorionic villi, by measuring the activity of peroxisomal β -oxidation, and im-

munofluorescence analysis of ALPD. DNA techniques can also be used for carrier detection and prenatal diagnosis. A problem in genetic counseling and prenatal diagnosis is that the demonstration of the biochemical defect does not provide information about whether the patient will develop severe childhood XALD or the milder AMN.

21.2 Pathology

At autopsy the surface of the brain of a patient with cerebral XALD is either normal or shrunken, depending on the degree of tissue loss. The central white matter is grayish and indurated, sometimes cystic and cavitated. The thickness of the cortex is normal. The atrophic external appearance is, if present, secondary to loss of white matter. In cases of extensive loss of myelin the ventricular system is enlarged.

The pathological abnormalities are the same for childhood, adolescent, and adult cerebral XALD and consist of widespread demyelination of the white matter. The demyelinating lesion constitutes one large area extending across the corpus callosum and involving both hemispheres. In most cases of cerebral XALD the demyelinating process starts in the splenium of the corpus callosum and spreads bilaterally to the occipital region. Gradually the process spreads outwards and forwards as a confluent lesion until most of the cerebral white matter is involved. The frontal white matter is generally affected less severely and often asymmetrically. The subcortical U fibers are preserved until a far-advanced stage, and usually the U fibers in the occipital area are affected before those elsewhere. Other areas of the brain that are usually heavily involved are the fornix, the hippocampal commissure, the posterior limb of the internal capsule, the lateral two-thirds of the cerebral peduncles including the occipitoparietotemporopontine and pyramidal tracts, and the lateral lemniscus. In some patients the cerebellar white matter is involved, sometimes the cerebellar peduncles as well. In a smaller portion of the patients with cerebral XALD the demyelination starts bilaterally in the frontal area, also involving the anterior part of the corpus callosum. In these cases the anterior limb of the internal capsule and the medial third of the cerebral peduncles containing the frontopontine tracts are affected. In a few patients the demyelinating lesions are highly asymmetrical.

Within the white matter lesion three zones can be distinguished on histopathological examination. The outer zone shows evidence of active destruction of myelin with axonal sparing. Scattered PAS-positive and sudanophilic macrophages are present. The middle zone shows signs of active inflammation with

marked perivascular mononuclear cell infiltration. This zone contains many large ballooned macrophages laden with lipids. There are many preserved demyelinated axons and little myelin remains. The large central area is destroyed and burnt out. There is no evidence of an active process. Axons, myelin sheaths, and oligodendroglia are absent. There are few lymphocytes and only occasional macrophages surrounding blood vessels. This area is filled with a dense mesh of glial fibrils and scattered astrocytes. Sometimes cavitation or calcium depositions are seen in this area.

In the brain stem and spinal cord degeneration of the tracts appears to proceed at the same rate throughout, with no evidence of a dying-back phenomenon. Here too the demyelinating process occurs in a continuous fashion. No small independent foci of demyelination are seen. Perivascular accumulations of inflammatory cells may well be noted.

The cytoarchitecture of the cerebral cortex is normal. Only in more advanced cases may neuronal loss and gliosis be seen, especially in the deeper cortical layers. The cerebral cortical damage is mainly found in the occipital region where the demyelinating lesion may not spare the U fibers and may be contiguous with the deep layers of the cortex.

Electron microscopic examinations show that many macrophages and microglia contain distinctive cytoplasmic inclusions, consisting of linear lamellae. An individual lamella has a trilaminar structure, consisting of paired electron-dense leaflets separated by an electron-lucent space. These trilamellar structures are often closely associated with lipid droplets. They are not found in oligodendroglia or astrocytes. In addition, macrophages contain myelin debris.

Microscopic examination of peripheral nerves reveals either no abnormalities or demyelination. On ultrastructural examination abnormal cytoplasmic inclusions may be seen in Schwann cells and in endoneurial macrophages. These inclusions have the characteristic linear, trilamellar appearance.

Pathological studies in AMN demonstrate bilateral, usually symmetrical, long tract degeneration in the spinal cord with most prominent involvement of the corticospinal and dorsal tracts. The distribution of the degeneration of these tracts conforms to a dying-back pattern in that the greatest loss of myelinated fibers is found in the cervical dorsal tracts and the lumbar corticospinal tracts. Axonal loss is equal to or greater than myelin loss. The above findings provide strong evidence for primary axonal degeneration. There are no inflammatory cells. Microglia are increased in numbers and appear the dominant responding cells. Dorsal ganglion cells are not decreased in numbers but are decreased in size. Peripheral nerves display both axonopathic and myelinopathic features. In Schwann cells and macrophages

the typical trilamellar inclusions are present. There are no inflammatory cells.

The cerebral involvement in AMN is highly variable. In most AMN patients, patchy, poorly defined, small areas of demyelination are scattered throughout the cerebral hemispheres, with relative or total axonal sparing, activation of microglia, presence of striated macrophages with trilamellar inclusions, and absence of inflammatory cells. In some patients, moderate diffuse demyelination is observed in the cerebral white matter and to a lesser extent the cerebellar white matter, with sparing of the U fibers and without inflammation. Still others display inflammatory demyelinating lesions with axonal loss, qualitatively similar to cerebral XALD but much more localized. Some AMN patients develop the cerebral form of XALD with rapidly progressive inflammatory demyelination. In addition to these inflammatory demyelinating lesions, AMN patients also demonstrate noninflammatory, bilateral, fairly symmetrical lesions with comparable loss of axons and myelin sheaths, involving most often the brain stem corticospinal and spinocerebellar tracts, medial and lateral lemnisci, cerebellar peduncles, posterior limb of the internal capsule, and the optic radiations.

The adrenal glands in XALD show gross atrophy of the cortex, the medulla being normal. The zona reticularis and zona fasciculata are particularly affected with ballooned cortical cells, in which a striated appearance of the cytoplasm may be seen. These striated cells are specific for XALD. Ultrastructurally the striations are shown to consist of linear, trilamellar accumulations within the adrenal cortical cell cytoplasm. Lymphocytic infiltrates are found in a minority of the patients. Light microscopic examination of the testis often reveals no abnormalities, although fully developed Leydig cells may be lacking. Interstitial cells, presumptive Leydig cell precursors, may contain the characteristic trilamellar profiles. In all tissues, the morphology of peroxisomes is normal.

21.3 Chemical Pathology

XALD is a lipidosis, in which accumulation of saturated VLCFA occurs in all tissues, especially in CNS white matter, peripheral nerve, adrenal cortex, and testis. Substantial quantities of these VLCFA are deposited as cholesterol esters, which appear as the characteristic lamellated cytoplasmic inclusions. These VLCFA vary in chain length from C23 to C32 with a peak at C25–C26. Several other lipids also contain an increased percentage of saturated VLCFA. These increases in VLCFA are found in cerebral XALD, AMN, and female carriers.

The changes in lipid composition of myelin and whole white matter have been investigated separately

for regions with different stages of myelin breakdown in the cerebral form of XALD. In morphologically normal white matter, subtle changes in lipid composition are found. Phospholipids are increased, whereas galactolipids and cholesterol are slightly decreased. Only traces of cholesterol esters are found in histologically intact white matter. The fatty acid composition of cholesterol esters, cerebroside, and sulfatide in intact white matter is relatively normal, whereas phospholipids in the same area contain increased VLCFA, with the most striking increase in VLCFA in phosphatidylcholine. A moderate increase in VLCFA is seen in gangliosides. The area of active demyelination shows major changes in lipid composition. The water content is increased, the amount of total lipids is decreased, and there is a large increase in cholesterol esters, whereas unesterified cholesterol is severely decreased. Galactolipids are decreased, whereas phospholipids are stable as a proportion of total lipids. The fatty acid composition of cerebroside and sulfatide shows a slight elevation in VLCFA, whereas the VLCFA content of phospholipids, gangliosides, and cholesterol esters is greatly increased. The most striking rise in VLCFA among the phospholipids is seen in phosphatidylcholine and sphingomyelin. In the area of gliosis, the amount of remaining lipids is small, and the water content is high. The amount of galactolipids is relatively very low, whereas phospholipids and cholesterol are low in absolute content but constitute a relatively normal proportion of total lipids. Cholesterol esters are present in small but measurable amounts. Significant amounts of triglycerides and free fatty acids can also be measured. In gliotic tissue the VLCFA content of cerebroside, sulfatide, and phospholipids is barely elevated, whereas the VLCFA content of gangliosides and cholesterol esters is mildly to markedly elevated.

The adrenal and testicular content of cholesterol esters is abnormally high. The cholesterol esters contain an abnormally elevated amount of saturated VLCFA.

21.4 Pathogenetic Considerations

XALD is caused by mutations in the gene *ABCD1*, which is located on chromosome Xq28 and encodes ALDP, a peroxisomal ATP-binding cassette transmembrane transporter. A great number of different mutations have been identified. No consistent correlation between genotype and phenotype has been demonstrated.

The disease is biochemically characterized by elevated VLCFA due to reduced VLCFA β -oxidation. The first step in the β -oxidation of VLCFA is conversion of fatty acid to fatty acyl-CoA, catalyzed by the enzyme VLCFA-CoA synthase or ligase, present on the perox-

isomal membrane. The enzyme is more specifically called lignoceroyl- or hexacosanoyl-CoA synthase or ligase. The relation between ALDP and VLCFA-CoA ligase is still elusive. ALDP is not necessary for the import of this enzyme into peroxisomes or the import of VLCFA into peroxisomes. The reason for impaired VLCFA β -oxidation in XALD has yet to be found. A recent hypothesis assumes that ALDP facilitates the interaction between peroxisomes and mitochondria, and that ALDP deficiency leads to impaired β -oxidation in mitochondria. The repeated observation of structural mitochondrial abnormalities in XALD tissues, including lipid inclusions in mitochondria, is an argument in favor of this hypothesis.

The impaired degradation of VLCFA leads to enrichment of these fatty acids in various lipids at the expense of the normally degraded short-chain fatty acids. The accumulating fatty acids are saturated and have a chain length varying between C24 (lignoceroyl acid) and C32 with a peak at C26 (hexacosanoic acid). VLCFA are derived both from the diet and from endogenous synthesis by a microsomal system that elongates long-chain fatty acids. There is evidence that in XALD, not only β -oxidation of VLCFA is decreased, but fatty acid chain elongation activity is also elevated, contributing to the accumulation of VLCFA. It has been shown that the addition of monounsaturated fatty acids to culture medium has a dramatic effect in lowering the content of VLCFA in XALD fibroblasts. These monounsaturated fatty acids appear to inhibit the synthesis of VLCFA without having any effect on the degradation of VLCFA.

The exact mechanisms by which nervous tissue damage occurs are still unknown. There is a fundamental difference between the inflammatory demyelinating lesions seen in the white matter of patients with cerebral XALD and the axonopathic lesions seen in patients with AMN and AMN-like phenotypes. Both biochemical and immunological mechanisms may be important in the pathogenesis of the lesions. The greater length of the aliphatic chain causes VLCFA to be extremely insoluble. Abnormally high VLCFA levels alter membrane physiological properties and functions. Increasing levels of VLCFA in membranes may result in instability and breakdown of the membranes, leading to noninflammatory myelin loss and axonal degeneration, as seen in AMN. The destruction of adrenocortical cells, Leydig cells, and Schwann cells is also noninflammatory and may be related to the toxic effects of VLCFA. The rapidly progressive demyelination with a marked inflammatory reaction suggests additional immunological pathogenetic mechanisms in cerebral XALD. Further evidence for a role of immunological mechanisms is found in the occasional presence of signs of intrathecal immunoglobulin production, increased levels of IgA and IgG in XALD tissues, and high levels of

myelin antibodies in serum of XALD patients. Tumor necrosis factor- α (TNF- α), a proinflammatory cytokine thought to be responsible for tissue damage in inflammatory brain disorders including multiple sclerosis, is expressed in astrocytes and macrophages at the active edge of the lesion. Reactive astrocytes, macrophages, and T lymphocytes are the most prevalent cellular elements. Most lymphocytes are CD8-positive cytotoxic T cells. CD1 molecules, which play major roles in lipid antigen presentation, have been found to be present, most conspicuously in the acute inflammatory lesions. It is hypothesized that the primary biochemical abnormality in XALD, i.e. the abnormal accumulation of VLCFA, leads to membrane instability and breakdown, leading to liberation of VLCFA-containing moieties, which may be antigenic and elicit an immune response. Not only peptide antigens, but also lipid antigens may play a key role in the pathogenesis of inflammatory demyelination in cerebral XALD. Lipids containing an abnormally high proportion of VLCFA may stimulate nearby astrocytes, microglia, and macrophages to initiate a cytokine cascade resulting in further myelin destruction by T cells, B cells, and complement. This two-stage hypothesis explains why the zone of active inflammation in cerebral XALD is found behind the zone of active demyelination. This location of the inflammation contrasts with the situation in multiple sclerosis, in which the inflammation is most intense at the edges of the lesion, with little or no inflammatory response in the inner zones of the lesion. Others hypothesize that accumulation of VLCFA in membrane domains associated with signal transduction pathways may trigger inflammatory processes through activation of microglia and astrocytes, resulting in loss of myelin.

Adrenal cortical cells, Leydig cells, and Schwann cells are also involved in the disease process. They accumulate VLCFA incorporated in cholesterol esters in the form of lamellar cytoplasmic inclusions. A cytotoxic pathogenesis has been proposed for the adrenal, testicular, and Schwann cell lesions. Furthermore, it has been shown that accumulation of VLCFA in adrenal cortical cell membranes leads to increased membrane microviscosity and can interfere with ACTH responsiveness. Impaired ACTH receptor function has been found, probably contributing to the adrenocortical insufficiency. It is noteworthy that the destruction of these cells is accompanied by little or no inflammation.

All phenotypic variants of XALD have the same basic defect and all variants may occur within the same family. No differences in fatty acid abnormality could be established in fibroblasts, erythrocyte membranes, or blood in repeated investigations. There is evidence for an autosomal modifier gene, which would explain the phenotypic variability of XALD within pedigrees. This modifier gene probably modu-

lates the immune response, considering the marked difference in immune reaction between cerebral XALD and AMN. It is likely that environmental factors may also influence the phenotype, as disparate phenotypes can be seen in sets of identical twins.

Many female heterozygotes suffer from a late-onset, slowly progressive neurological disorder. Inactivation of one of the two X chromosomes in female somatic cells is considered to be a random process. However, there is some evidence that, in XALD carrier females, selection mechanisms favor cells expressing the mutant allele rather than cells expressing the normal allele. This observation may explain the relatively frequent occurrence of symptoms in female carriers. There is also evidence that skewing of X inactivation is an important factor in determining the severity of disease manifestations in female XALD carriers.

21.5 Therapy

First and foremost, family counseling, carrier detection, and prenatal diagnosis are important in preventing the occurrence of further cases in known families.

Symptomatic care is essential. Hormonal substitution is necessary to correct the adrenocortical insufficiency, if present. Testosterone administration can be of help in AMN patients who have testicular insufficiency. Psychiatric care may be necessary, in particular in adult patients with cerebral XALD.

An important difference between cerebral XALD and the more benign AMN is in the presence or absence of an inflammatory response. Various modes of immunosuppression and immunomodulation have been tried in order to influence the inflammatory reaction, including the use of steroids, β -interferon, cyclophosphamide, pentoxifylline, thalidomide, cyclosporine, plasmapheresis, and high-dose intravenous immune globulin, and unfortunately so far none of these has been effective. They do not influence the course of the neurological disease. Incidentally, improvement under steroids has been reported, but this effect may be temporary.

Therapeutic strategies aiming to lower VLCFA have been the cornerstone of therapeutic strategies for a long time. Dietary restriction of saturated VLCFA is insufficient to lower blood VLCFA. Monounsaturated fatty acids compete with saturated fatty acids for the microsomal fatty acid elongation system. Diets enriched in monounsaturated fatty acids lead to decreased synthesis of VLCFA and are more effective in lowering blood VLCFA. The best results are obtained by combining the two. Diets restricted in saturated VLCFA combined with the use of a 4:1 mixture of glyceryl trioleate (GTO; oleic acid is a C18 monounsaturated fatty acid) and glyceryl trierucate

(GTE; erucic acid is a C22 monounsaturated fatty acid), popularly referred to as Lorenzo's oil, can lead to complete normalization of blood levels of VLCFA. Moderate reduction in platelet count occurs as a side effect in 40% of the patients but does not lead to hemorrhages. This treatment does not alter the clinical disease course in patients in whom the neurological deterioration has already set in. However, there is increasing evidence that, depending on the degree of treatment compliance and decrease in VLCFA, the treatment has a protective effect when started in neurologically intact patients. Treated adequately, a smaller number of boys with the biochemical defect develop the aggressive cerebral form of the disease, and the onset of neurological symptoms is delayed. Unfortunately, dietary treatment is not an absolute preventive, and patients may still develop cerebral XALD despite perfect compliance and normalization of plasma VLCFA levels.

Another important cornerstone in the treatment of cerebral XALD is bone marrow transplantation. The outcome is highly dependent on the degree of cerebral involvement at the time of the transplantation. If applied early in the course of the disease, bone marrow transplants may prevent further deterioration and may even lead to improvement of cerebral lesions on MRI. In the brain, the donor-derived cells are microglia, and it is assumed that the beneficial effect of bone marrow transplantation is that donor microglia metabolize VLCFA, thus reducing their levels in the brain. The observation that improvement appears to commence only 6 months after transplantation is compatible with the slow turnover of microglia. The therapy is not recommended for patients with rapidly advancing or severe cerebral involvement, because these patients do not tolerate the temporary worsening associated with the procedure or the delay in onset of beneficial effect. Generally, an IQ of 80 (performance IQ appears to be especially important) is considered the limit because outcome in patients with a performance IQ below 80 is poor. In these patients transplantation may even lead to rapid worsening and sometimes an early death. Delayed stabilization in a poor neurological condition or vegetative state may also occur. Bone marrow transplantation is also not recommended for asymptomatic patients, because of the over 50% chance that they will not develop the serious cerebral form of the disease, and the high mortality associated with bone marrow transplantation. Transplantation is also not recommended in stable patients, because the duration of the stable period is unclear and may be many years. Unfortunately, the prognosis of XALD cannot be predicted by VLCFA measurement, mutation analysis, or the expression of the disease in relatives. It is presently not possible to predict whether a young asymptomatic boy is destined for a severe phenotype, for which

bone marrow transplantation should be performed, or a mild phenotype. For this reason, monitoring of the disease on MRI and using neuropsychological tests from the presymptomatic stage onwards is extremely important. As soon as lesions appear, and appear to be progressive, bone marrow transplantation should be attempted. Extensive screening of family members should be performed as soon as the diagnosis of XALD or AMN has been established in one patient and HLA typing should be initiated in all persons who are potential future candidates for bone marrow transplantation in order to search for a suitable donor and be prepared for transplantation. Bone marrow transplantation is presently not performed in adult patients with AMN. This is because the morbidity and mortality of bone marrow transplantation are higher in adults than in children, whereas AMN is a relatively slow disease that may take decades before death ensues. At present, it is not clear whether bone marrow transplantation at a young age for incipient cerebral XALD will prevent the development of AMN in adulthood.

Promising alternative therapies have been proposed, but no definitive data on their clinical effects are as yet available. 4-Phenylbutyrate up-regulates the expression of a protein referred to as ALDR, which is a protein with a high homology with ALDP and may be able to substitute at least in part for its function. The gene encoding this protein is called *ABCD2*. There is evidence that the drug may lead to lowering of plasma and tissue VLCFA. Lovastatin also induces the increased expression of ALDR. It improves the capacity of XALD fibroblasts to metabolize VLCFA and normalizes VLCFA in plasma of XALD patients. Lovastatin may also inhibit inducible nitric oxide synthase and proinflammatory cytokines. However, simvastatin, an analogue of lovastatin with similar pharmacokinetics and effects on plasma VLCFA, failed to decrease VLCFA tissue content.

Ultimately, gene therapy may hold the greatest hope for the treatment of XALD patients. One possible strategy would be bone marrow ablation followed by autologous transplantation with genetically corrected hematopoietic cells of the patient's own bone marrow. Transplantation and oligodendrocytes or pluripotent stem cells to repair damaged tissue are other options.

21.6 Magnetic Resonance Imaging

In imaging the brain of patients with XALD, different patterns can be detected. The most commonly occurring pattern in cerebral XALD consists of predominantly parieto-occipital white matter abnormalities (Fig. 21.1). The lesion starts in the splenium of the corpus callosum and spreads out into the parieto-oc-

cipital white matter. The arcuate fibers are relatively or completely spared, which is most easily seen on T₁-weighted images. In most patients two zones can be distinguished, the anterior zone where demyelination advances being less severely affected than the posterior zone. After administration of contrast, a rim of enhancement can be seen surrounding the most severely affected area, separating this area from the less severely affected and normal white matter (Fig. 21.1). These three zones are in accordance with the three zones recognized histologically. The outer and advancing zone is in the process of active demyelination without inflammation. The middle zone shows signs of prominent inflammation. The innermost and most posterior region is completely demyelinated and burnt out. In this latter area, cavitation and calcification may be present. The calcium deposits are best seen on CT (Fig. 21.2). The lesions are essentially symmetrical, but are often not so in detail. Demyelination advances in the frontal direction. Structures affected relatively early on are the lateral and medial geniculate bodies, in some cases the lateral-inferior part of the thalamus, the posterior limb of the internal capsule, and the external capsule. The frontal lobe is affected last and more variably. In the end, almost all cerebral white matter is affected. In the end-stage, serious white matter atrophy is seen. The cerebellum is not usually involved early in the course of disease, in contrast to the brain stem. Typically, the involved tracts are the occipitoparietotemporo-pontine and pyramidal tracts, the brachium of the inferior colliculus, the brachium of the superior colliculus, and the lateral lemniscus. The frontopontine tracts are preserved. This MRI pattern is present in about 80% of patients with childhood cerebral XALD and has a lower percentage in older patients. The overall fre-

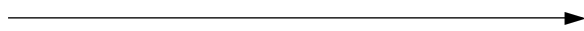


Fig. 21.1. An 8-year-old boy with cerebral XALD. The T₂-weighted axial images show the characteristic pattern of symmetrical lesions in the parieto-occipital white matter. The images show that the lesion contains three zones. The inner and more posterior zone has a slightly higher signal than the outer and more anterior zone; there is a rim of low signal in between. The contrast-enhanced T₁-weighted images confirm the two zones, the inner and more posterior zone having the lowest signal, whereas the outer and more anterior zone has a less low signal. The rim in between shows prominent contrast enhancement. The three zones of the disorder can be visualized this way: the outer and more anterior zone being inactive and completely demyelinated, zone 2 showing marked inflammation and advanced demyelination, and zone 3 representing the start of demyelination. Zones 1 and 3 can usually be distinguished on T₂-weighted images. The splenium of the corpus callosum is affected and the lateral part of the midbrain as well as the corticospinal tracts in the pons

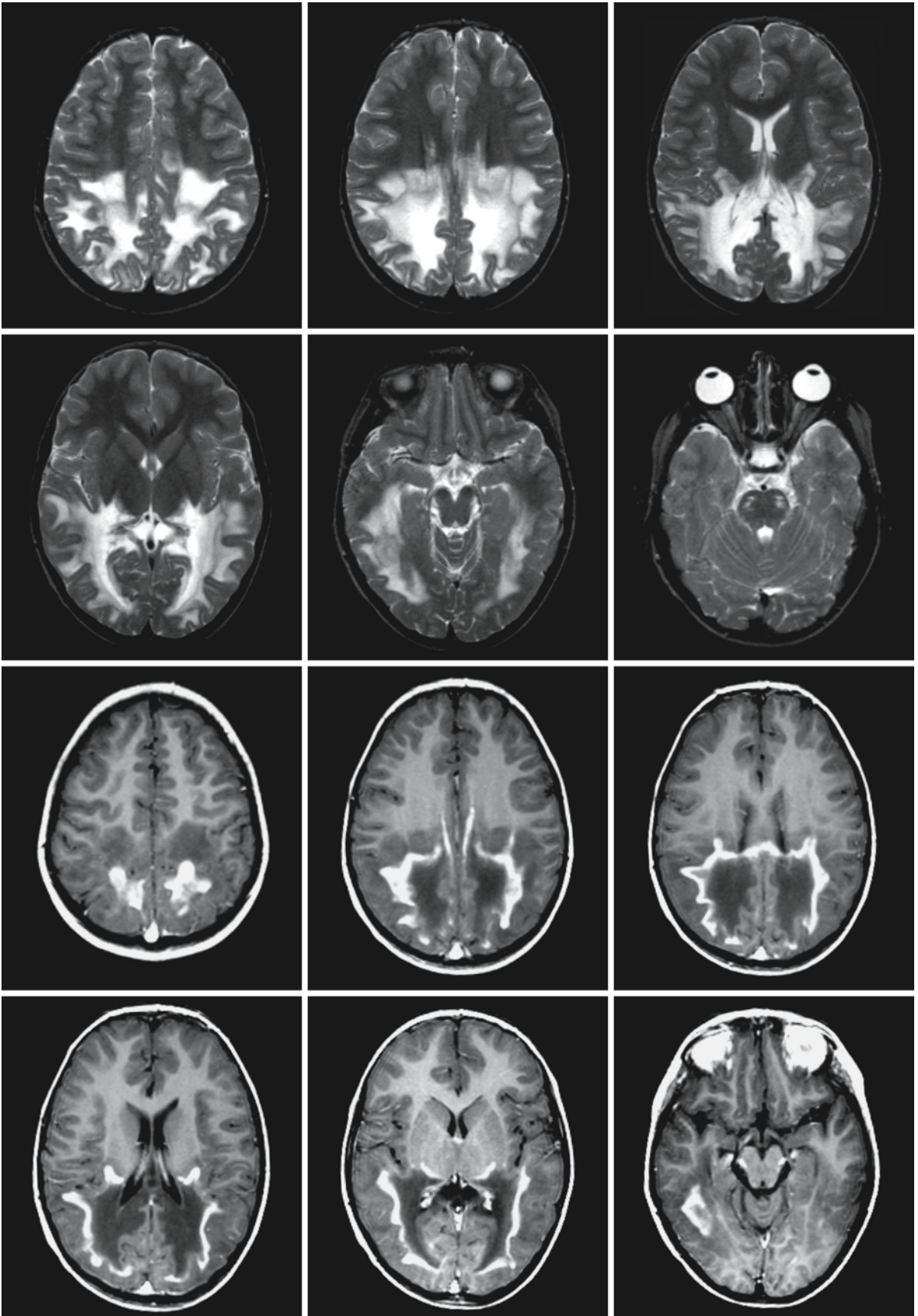


Fig. 21.1.

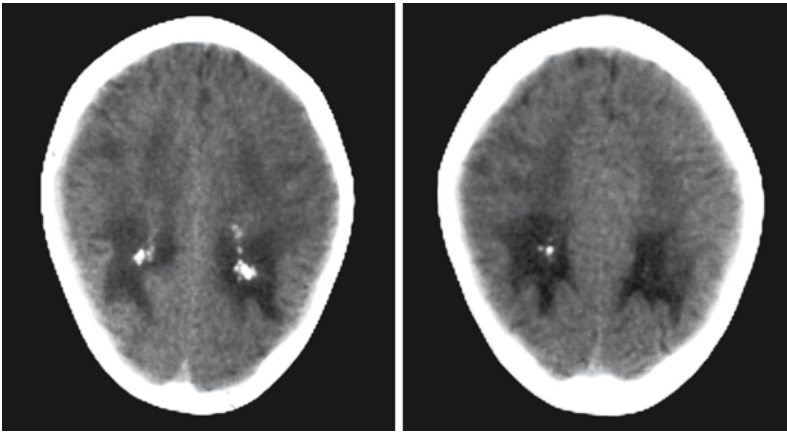


Fig. 21.2. CT scan of an 8-year-old boy with cerebral XALD shows calcium deposits in the lesion

quency of this pattern among patients with cerebral XALD is about 65–70%.

The pattern of cerebral XALD may be reversed, starting bilaterally in the frontal area with concomitant involvement of rostrum and genu of the corpus callosum (Fig. 21.3). In such cases the anterior limb of the internal capsule is involved instead of the posterior limb, and the frontopontine brain stem tracts instead of the occipitoparietotemporopontine tracts. Again, there are three distinguishable zones with contrast enhancement of the middle zone. This pattern is most commonly seen in teenagers and adolescents with cerebral XALD. The overall frequency among patients with cerebral XALD is about 15%.

In a few patients, there is concomitant but independent frontal and parieto-occipital white matter involvement. This pattern is rare and occurs mainly in children.

In some patients the frontopontine or corticospinal projection fibers are involved without involvement of the periventricular or deep white matter. In this pattern lesions are initially seen in the internal capsule and brain stem tracts. With progression of disease abnormalities most often develop in cerebellar peduncles, the splenium of the corpus callosum, and optic radiation. Contrast enhancement may be present. This pattern is seen in 10–15% of all cerebral XALD patients. It is mainly seen in adult XALD patients with clinical signs of AMN (Fig. 21.4), but has also been reported in children with mainly pyramidal signs.

Another pattern consists of symmetrical involvement of cerebellar white matter, middle cerebellar peduncles, and brain stem tracts. This pattern is rare and is mainly seen in adolescents.

In exceptional cases patients have unilateral disease initially and bilateral but markedly asymmetrical disease in later stages (Fig. 21.5). The presence of two zones in the lesion on unenhanced images and contrast enhancement of the rim in between these zones are helpful diagnostic clues. One asymptomatic

adult patient suffered a severe cerebral contusion in the left temporal area after which the course was downhill. Demyelination started in the area of the contusion, and proceeded to affect both hemispheres, but asymmetry remained. Marked contrast enhancement was seen and extensive inflammation on brain biopsy.

In general, patients with the parieto-occipital pattern and those with the frontal pattern have rapid disease progression if the abnormalities are present at an early age and if contrast enhancement is present. Patients with both frontal and parieto-occipital abnormalities have the most rapid disease progression. Patients with predominant involvement of frontopontine or corticospinal projection fibers or predominant involvement of the cerebellar white matter generally have much slower disease progression.

The primary finding in AMN consists of spinal cord atrophy. In half of the symptomatic AMN patients, abnormalities are noted on brain MRI. This percentage depends on age: it is lower among the younger AMN patients and higher among the older AMN patients. Involvement of corticopontine and corticospinal projection fibers, described above, is most commonly seen. However, AMN patients may also develop much more extensive white matter abnormalities, involving mainly the parieto-occipital white matter and splenium of the corpus callosum, the frontal white matter and anterior part of the corpus callosum, or the cerebellar white matter.

Only a few female heterozygotes show abnormalities on MRI of the brain and spinal cord, even when they display an AMN-like clinical phenotype. The pattern of full-blown cerebral demyelination is very rare.

Apart from its role in diagnostics, MRI has a major role in monitoring of the disease (Figs. 21.6 and 21.7). Monitoring is an essential part of treatment, first of all to determine which patients are eligible for a particular treatment and secondly to monitor treatment effects. At present, there are two cornerstones in the

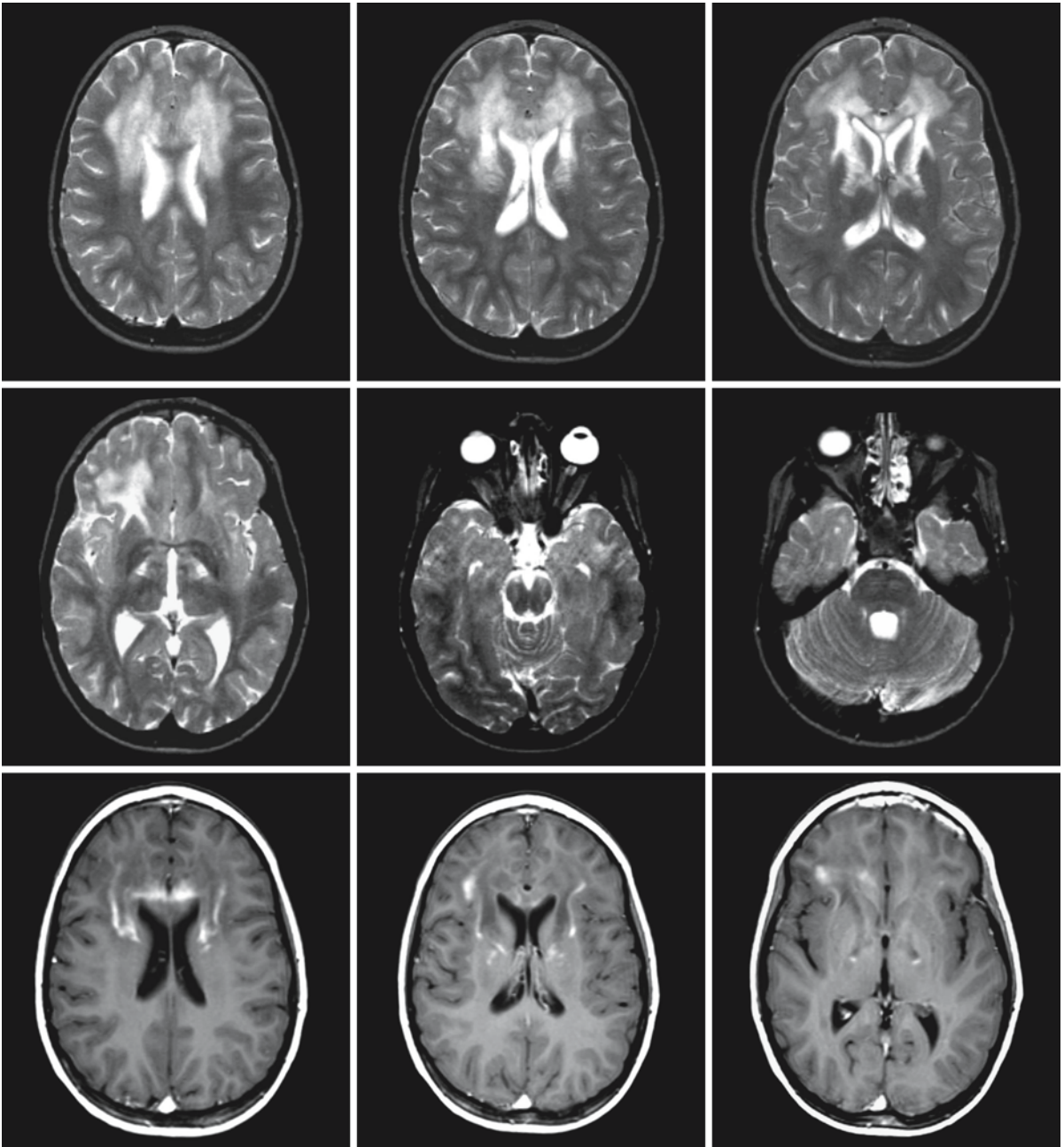


Fig. 21.3. A boy with cerebral XALD. The *first three rows* show images at the age of 9 years. Note the frontal predominance of the lesions with involvement of the genu of the corpus callosum and the anterior limb of the internal capsule. The U fibers are relatively spared. Also note the involvement of the fronto-

pontine tracts at the level of the midbrain. The three zones are visible, although less clearly than in Fig. 21.1, with enhancement of the middle zone on the T₁-weighted images. (Continue see next page)

treatment of XALD: dietary treatment and bone marrow transplantation. Dietary treatment should be applied in all asymptomatic patients in an attempt to delay and, hopefully, prevent the onset of clinical symptoms. Unfortunately, dietary treatment is not an absolute preventive. Bone marrow transplantation is

indicated for patients in whom cerebral demyelination is starting, especially young patients without AMN, but not for patients with a normal MRI or patients with entirely stable MRI abnormalities. Loes et al. (1994 and 2003) developed a 34-point scoring method for the grading of MRI abnormalities. It has

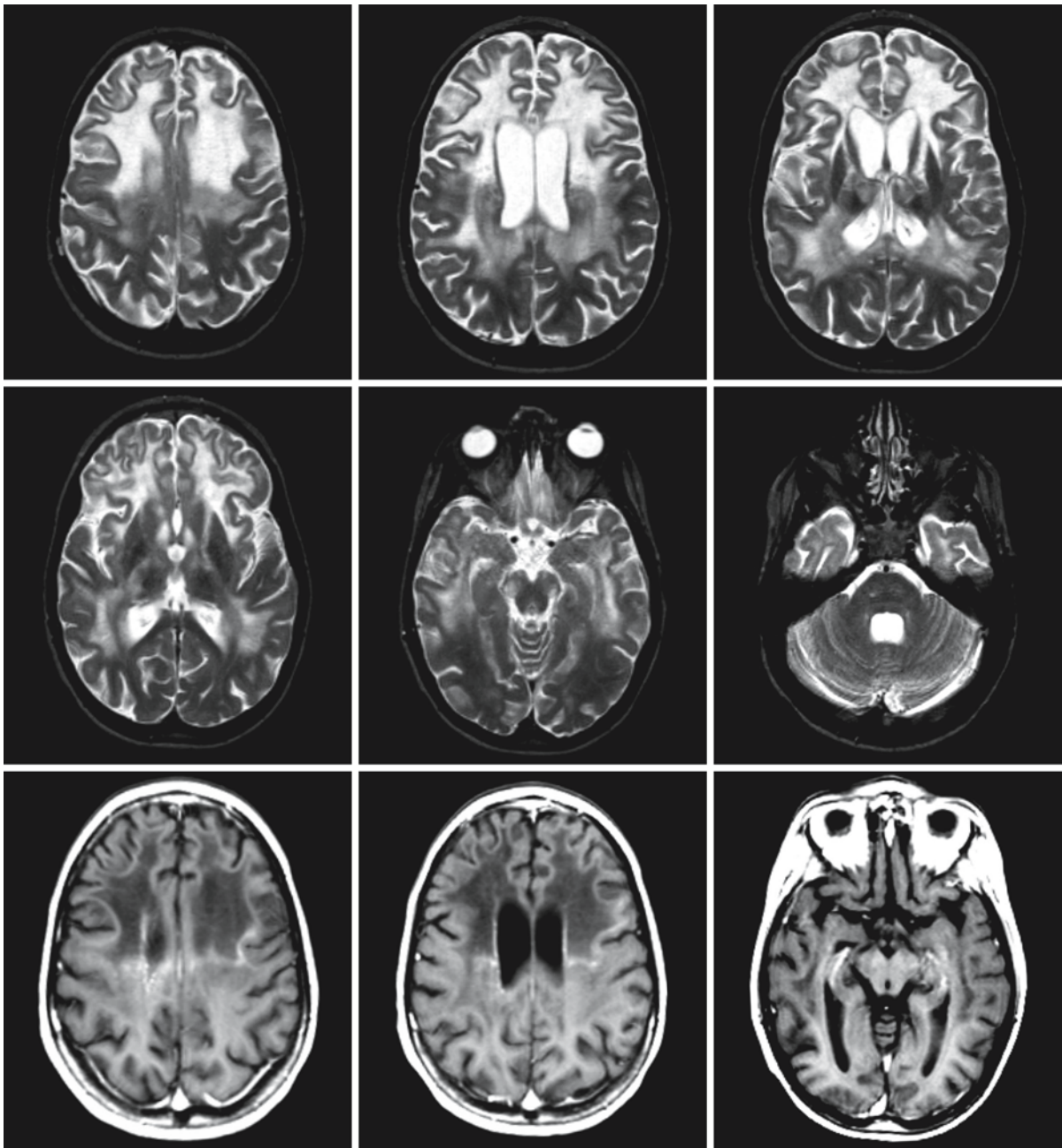


Fig. 21.3. (continued). A boy with cerebral XALD. The *second three rows* show the follow-up MRI, obtained 1.5 years later. The images demonstrate serious progression of the disease

with spread over almost the entire brain. Only the parieto-occipital region is partially spared. The cerebellar white matter remains intact

been found that the Loes score has predictive value. With a score higher than 3, almost all patients worsen, irrespective of age; only 10% remain neurologically stable. With a score of 1–3, 60% of patients worsen, irrespective of age, but survival is longer. If the Loes score is below 1, prognosis depends on the age of the patient: among patients aged between 3 and 7 years, 30% will develop rapidly progressive cerebral

demyelination; in the age group between 7 and 10 years, 10% will develop rapidly progressive cerebral demyelination; while in the age group above 10 years, rapidly progressive cerebral demyelination is rare and AMN is more likely. Contrast enhancement also has predictive value: absence of enhancement is associated with stable disease in 80–85% of the patients, whereas clear contrast enhancement is an indication

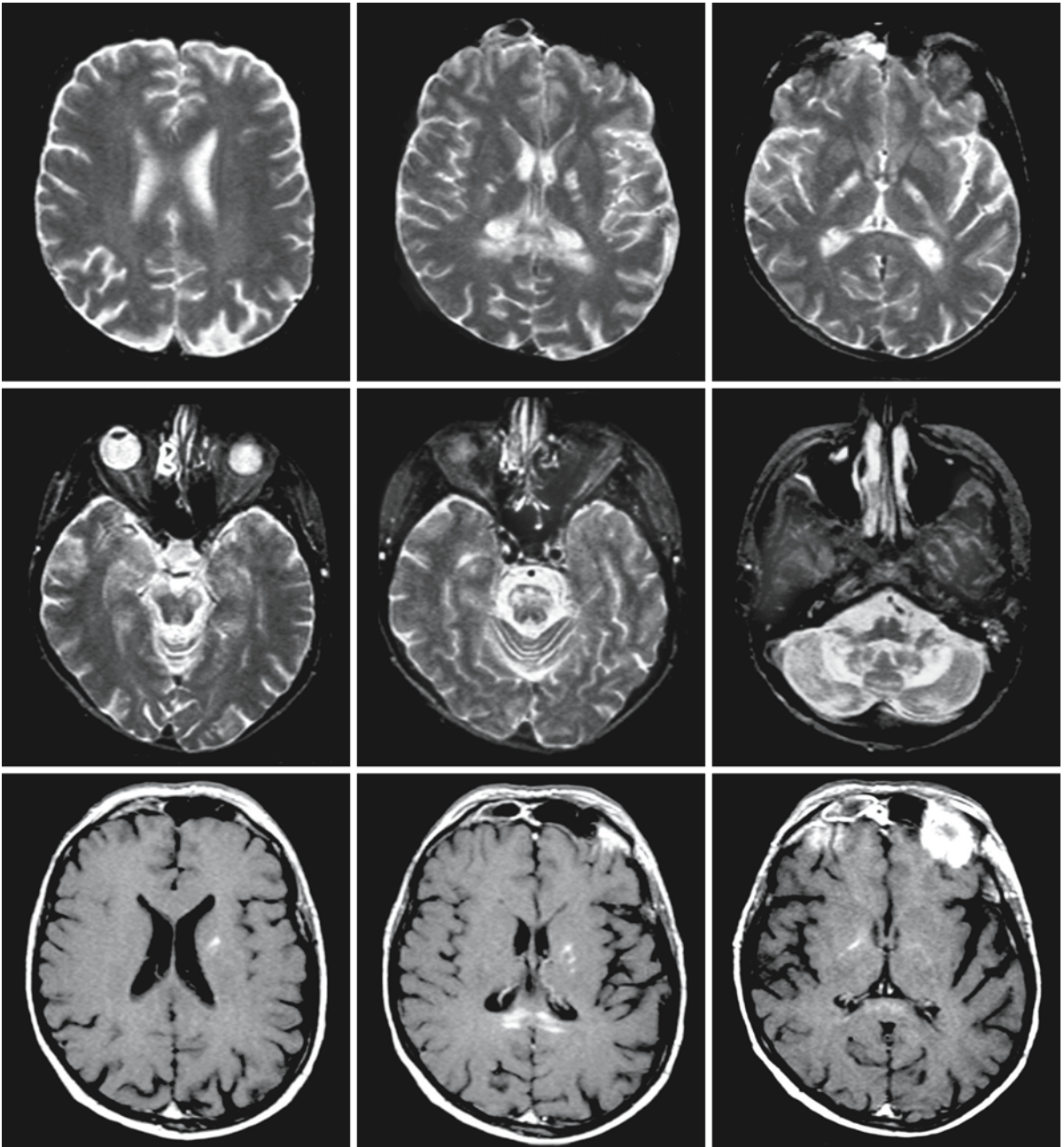


Fig. 21.4. A 45-year-old man with an AMN clinical phenotype. The T_2 -weighted images (*upper two rows*) show the involvement of the cerebellar white matter, the brain stem tracts, the

splenium of the corpus callosum, and the posterior limb of the internal capsule. Some enhancement occurs after injection of contrast (*third row*)

of active inflammatory demyelination and is associated with progression in 85–90% of the patients. Diffusion tensor imaging may be more sensitive than conventional MRI and show abnormalities in areas that are not (yet) abnormal on conventional images. The potential role of magnetization contrast imaging in the monitoring of XALD patients is presently not clear. The decrease in magnetization transfer ratios

reflects the three zones of white matter involvement, the lower ratios being present in the central burnt-out region. Normal-appearing white matter has a normal magnetization transfer ratio. The findings at MRS of the brain also have predictive value, in particular the findings just outside the visible lesion. If the *N*-acetylaspartate:choline ratio is decreased, this is evidence for impending demyelination in the area and disease

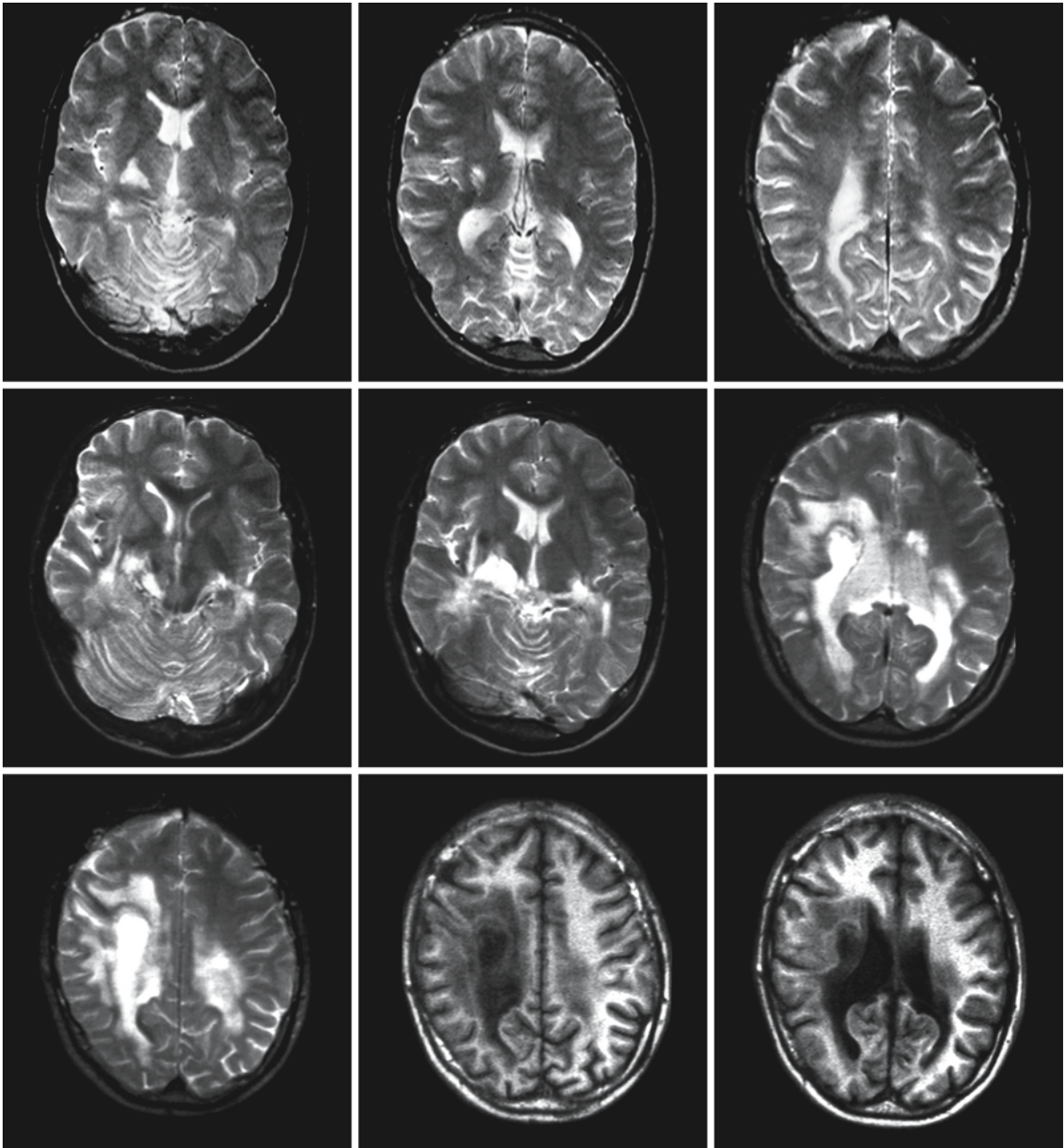


Fig. 21.5. Adult male patient with cerebral XALD. The MRI of the *first row* was obtained when he was 29 years old; the MRI of the *second and third rows* when he was 31 years old. The process started unilaterally and progressed to a bilateral but highly asymmetrical disease with predominant involvement

of the right side of the brain. Still the MR characteristics suggest cerebral XALD with a zoned lesion, the middle zone having a low signal on the T₂-weighted images. The zone are particularly prominent on the T₁-weighted images

progression. A normal *N*-acetylaspartate:choline ratio provides evidence for a stable situation. For these reasons, combined MRI and MRS studies every 6 months are recommended for asymptomatic XALD boys up to the age of 10 years. If abnormalities are seen on MRI, contrast-enhanced images are added to

the protocol. As soon as abnormalities are found, a repeat MRI is obtained after 2–3 months to document progression. If progression of abnormalities is demonstrated and the Loes score becomes 3 or higher, bone marrow transplantation is performed as soon as possible. Between the ages of 10 and 20 years, the

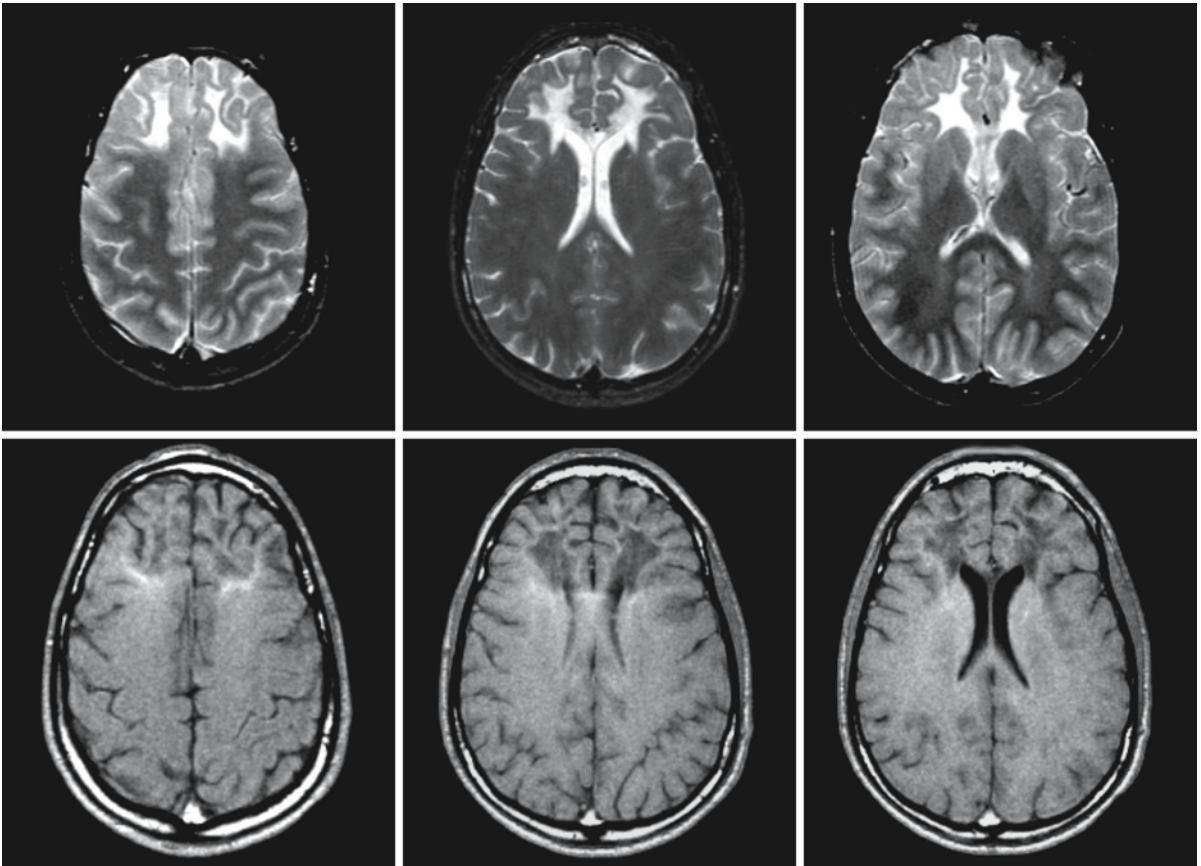


Fig. 21.6. This 18-year-old boy had learning and behavioral problems from early on. At the age of 15 years he experienced an encephalitis-like episode from which he fully recovered. Since then he has been clinically stable with a normal neurological examination. Between the ages of 15 and 18 years MRI findings have remained unchanged with frontal white matter abnormalities and white matter atrophy. The genu of the cor-

pus callosum is involved. The entire cerebral white matter appears slightly elevated in signal, with a loss of contrast between white and gray matter. There is some contrast enhancement at the rim of the lesion. In view of the static nature of the disease, hematopoietic stem transplantation has not been considered

frequency of MRI and MRS is decreased to once a year. After bone marrow transplantation, various outcomes are seen. In some patients MRI abnormalities regress or disappear; in others the abnormalities become stable. Unfortunately, bone marrow transplantation is not a great success in all patients and further deterioration may also occur.

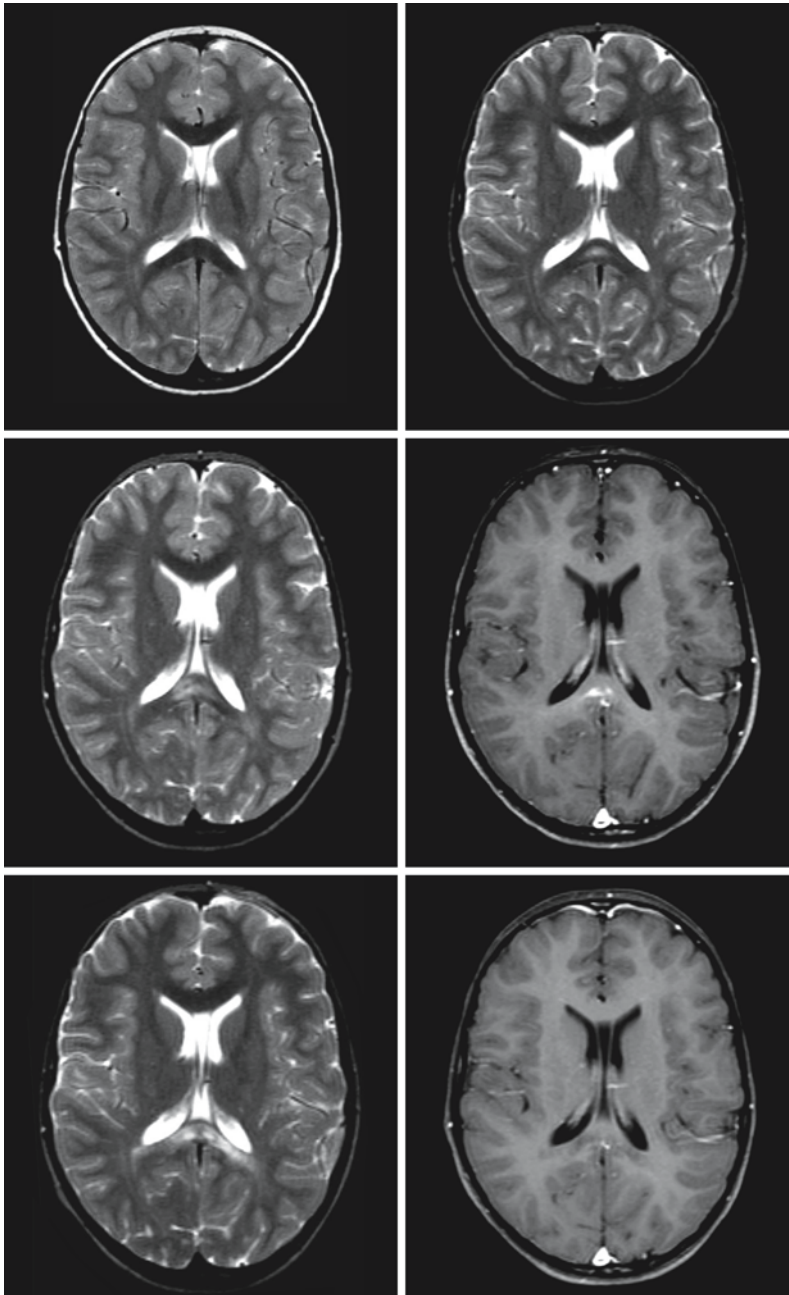


Fig. 21.7. This boy is the younger brother of the patient shown in Fig. 21.1. He was diagnosed with the biochemical defect of XALD after his brother was diagnosed with the disease. He was monitored by MRI and MRS every 6 months and normal results were found (*upper row, left*). When he was 6 years old a lesion was found in the splenium of the corpus callosum (*upper row, right*), which had increased in size after 3 months (*middle row, left*). At that time contrast enhancement of the lesion was found (*middle row, right*). Bone marrow transplantation was performed soon after without major complications. The first MRI after the procedure showed some further progression of the lesion, but the lesion has been stable since and he is now 9 years old (*third row, left*). There is at most minimal contrast enhancement remaining. He is clinically intact

Refsum Disease

22.1 Clinical Features and Laboratory Investigations

Refsum disease (RD), also called hereditary ataxia polyneuritis and hereditary sensory and motor neuropathy type IV, is a rare disorder with an autosomal recessive mode of inheritance, characterized by accumulation of phytanic acid. The age at onset of clinical signs and symptoms varies from early childhood to the fifth decade. The onset is insidious and may be difficult to determine precisely. Most patients have clear-cut manifestations before the age of 20 years. Symptoms may be precipitated by infections and low caloric intake. Dramatic exacerbations and remissions of symptoms may also occur spontaneously, without obvious antecedent cause. The main clinical features are visual disturbances, peripheral polyneuropathy, and cerebellar ataxia. Other frequently observed abnormalities are anosmia, cardiac problems, skin changes, sensorineural deafness, and skeletal abnormalities. Psychoses, particularly of a paranoid type, occur more frequently than one would expect on the basis of coincidence.

Initial visual disturbances include night blindness, which may be present for years before the diagnosis is established. Gradually, concentric constriction of the visual fields develops and finally only a tubular field of vision remains. Central vision may be intact or only minimally disturbed for years. In some cases optic atrophy, cataract, or vitreous opacities occur, contributing to visual failure and blindness. The funduscopic appearances are variable, also depending on the stage of disease. Typical pigmentary retinal degeneration is rare, and usually pigmentation looks like fine, small granules or has a salt-and-pepper appearance. In the majority of the patients pigmentation occurs in the peripheral retina; macular pigmentation is exceptional. In rare cases, no pigmentary degeneration is seen on funduscopy. The pupils are often small, and reaction to light, convergence, and accommodation is often minimal or absent.

Chronic progressive polyneuropathy is the second major manifestation of RD. The visual symptoms sometimes precede the polyneuropathy by several years. When the polyneuropathy develops gradually, it is usually symmetrical and initially distal, causing muscular weakness, atrophy, cutaneous hypesthesia, painful paresthesia, and disturbed position sense. Peripheral nerves are sometimes palpably enlarged.

There is a progressive lowering and loss of deep reflexes. The plantar responses are as a rule flexor or absent. Over a period of years the muscular weakness can become widespread and disabling, involving not only distal but also proximal musculature. Acute exacerbations are observed frequently in RD patients. When these happen, the weakness is not limited to distal muscles of the extremities, but proximal muscles are also paretic and cranial nerves may be involved. Periods of exacerbations may be followed by remissions in which the acutely developed weakness disappears.

Cerebellar ataxia forms the third major manifestation of RD. Its onset is later in the course of the disease. The ataxia is more marked than can be explained by the degree of weakness and sensory loss present. Nystagmus may be present as a sign of cerebellar dysfunction.

Cardiomyopathy is present in most patients, as demonstrated by cardiac enlargement, tachycardia, conduction disturbances, and ECG abnormalities. Sudden death is common during acute exacerbations and is probably caused by cardiac arrhythmias.

Skin changes vary from a dry, scaly skin to a condition of full-blown ichthyosis. The skin abnormalities change rapidly with the clinical state and are well correlated with plasma phytanic acid level. The skin problems tend to be more severe in children than in adults.

Bony deformities are frequently present. The skeletal manifestations include abnormalities of the metacarpal and metatarsal bones, which may be short or elongated; pes cavus; syndactyly; hammer toes; and epiphyseal dysplasia of the shoulders, elbows, and knees.

Renal dysfunction with amino aciduria and hypokalemia may occur.

The signs and symptoms of RD can be divided according to their liability to rapid change following changes in blood phytanic acid levels. Bony abnormalities are stationary. Visual disturbances, anosmia, and sensorineural deafness develop gradually, do not worsen rapidly on increasing phytanic acid levels, and do not improve on lowering of phytanic acid levels; only stabilization at the same level of impairment can be achieved by low blood phytanic acid levels. Peripheral neuropathy, cerebellar ataxia, and cardiomyopathy are slowly progressive but liable to deteriorate rapidly if phytanic acid levels rise. The component of

rapid deterioration responds well to lowering of phytanic acid levels, while the more chronic component responds slowly and often incompletely. Skin abnormalities are closely related to actual blood phytanic acid levels.

The clinical diagnosis of RD is not easy as no symptom is pathognomonic of the disease and the various signs and symptoms may develop in succession at different times. The demonstration of excessive amounts of phytanic acid in serum is the most valuable aid in the diagnosis of RD. Phytanic acid is not normally present in detectable amounts, and the absence of phytanic acid in the serum of an untreated patient suspected of suffering from RD makes the diagnosis highly improbable. In fact, so far no false negatives have been reported. However, elevated phytanic acid is not specific for the disease, since it may also accumulate in several other genetic diseases, including peroxisomal biogenesis defects and rhizomelic chondrodysplasia punctata type 1.

The protein in CSF is increased to levels between 1 and 7 g/l or even higher. The cell count is normal. Neurophysiological studies show a greatly reduced motor and sensory nerve conduction velocity and signs of denervation and reinnervation in the EMG. The nerve conduction velocity improves in conjunction with clinical improvement. The ERG shows absent or reduced reaction. ECG may reveal a prolonged QT segment and a widened QRS complex. When the urinary sediment of a patient with RD is stained for lipids, large amounts of fatty material can be detected.

A deficiency of phytanic acid α -oxidation can be shown in cultured fibroblasts. In RD patients the rate of α -oxidation of phytanic acid is less than 5% of normal, whereas in parents of RD patients the oxidation rate is about 50% of normal, indicating a heterozygous state. Phytanic α -oxidation activity can be determined in cultured amniotic cells, allowing prenatal diagnosis. DNA-based prenatal diagnosis is possible in families in which the mutations responsible have been identified.

22.2 Pathology

In RD the site of major involvement is the PNS, whereas the CNS shows more subtle abnormalities. On gross examination of the brain, the leptomeninges appear thickened and the cerebellum may appear moderately atrophic. On microscopic examination, deposition of fat is noted in the leptomeninges, ependymal cells, choroid plexus epithelium, and cells of the globus pallidus. The cerebral hemispheres are otherwise intact with normal cytoarchitecture of the cortex.

In the brain stem variable demyelination occurs mainly affecting the pontocerebellar tracts, medial lemniscus, olivocerebellar tracts, cerebellar peduncles, and corticospinal tracts. Axons are relatively spared. A variable number of fat-filled macrophages and hypertrophic astrocytes are present. Diffuse loss of neurons in the inferior olivary nuclei is commonly observed.

The cerebellar cortex is usually normal, although some neuronal loss may occur. The white matter within and surrounding the dentate nucleus is affected. Lipid-laden macrophages and hypertrophic astrocytes are present. Considerable loss of neurons is present within the dentate nucleus.

In the leptomeninges surrounding the spinal cord large amounts of fat are present. Sudanophilic granules of variable size are deposited in endothelial cells, histiocytes, and macrophages. Within the spinal cord there is marked demyelination of the posterior columns and demyelination of less severity in both spinocerebellar tracts. Retrograde changes and loss of motor neurons are observed in the anterior horns at all levels. In the spinal roots, especially at the level of the cauda equina, severe demyelination is observed together with complete destruction of some axons and axonal swellings. Onion-bulb formations are present.

The peripheral nerves, both somatic and autonomic, show macroscopic thickening. The changes in the peripheral nerves are constant, but their intensity varies greatly between cases. Nerve hypertrophy is usually most conspicuous in the lumbar and brachial plexuses. The hypertrophy is often irregular, forming localized swellings. Histological study of these swellings indicates that myelinated nerve fibers are reduced in number, and Schwann cell processes have given rise to typical onion-bulb formations. Many unmyelinated axons are present within the onion bulbs. The myelin sheaths are often abnormally thin and of unequal thickness, and segmental demyelination has been found. Axonal destruction is also present. In some onion bulbs the whorls are closely packed, but in others they are more loosely disposed and separated by large extracellular spaces of variable width. In the cytoplasm of the whorl-forming Schwann cells, several types of inclusion can be seen with help of electron microscopy: large crystalline inclusions and rounded osmiophilic bodies which are probably lipid in nature.

In the kidney, fat is accumulated in large amounts in the epithelial cells of the convoluted tubules. In the liver, fat is stored in mesenchymal and parenchymal cells. There are no or only slight signs of fibrosis. Peroxisomes are morphologically normal in RD.

22.3 Chemical Pathology

RD is a disorder of phytanic acid metabolism. Phytanic acid is a C20 multibranched fatty acid. It has been isolated in the brain and has been found to be present in much larger amounts in the white matter than in the gray matter. The presence of substantial portions of phytanic acid can be demonstrated without any appreciable alteration in total amounts of fat. Analysis of the lipid composition of the CNS reveals that the proportions of the remaining lipids are nearly normal. Phytanic acid is mainly present in phosphoglycerides, with higher proportions of phytanic acid in the choline phosphoglycerides than in the other phosphoglycerides. Lower concentrations are present in the galactolipids. Phytanic acid accumulates mainly in myelin and is found in higher concentrations in the choline phosphoglycerides from myelin than from gray matter or whole white matter. The proportions of phytanic acid in peripheral nerve myelin are even higher.

In several organs other than the nervous system there are accumulations of neutral lipids, especially in liver and spleen. A high proportion of the fatty acids consists of phytanic acid, incorporated in cholesterol esters and triglycerides. The heart muscle and blood also contain a large amount of phytanic acid.

22.4 Pathogenetic Considerations

Phytanic acid is a C20 multibranched fatty acid: 3,7,11,15-tetramethylhexadecanoic acid. The common pathway for fatty acid degradation is formed by the β -oxidation pathway in mitochondria and peroxisomes. The presence of a 3-methyl group in phytanic acid prevents it from undergoing β -oxidation. Instead, phytanic acid undergoes α -oxidation to pristanic acid in peroxisomes and pristanic acid is further degraded by β -oxidation. Phytanic acid is converted into phytanoyl-CoA by acyl-CoA synthase. Phytanoyl-CoA hydroxylase, a peroxisomal matrix protein, catalyzes the conversion of phytanoyl-CoA into 2-hydroxyphytanoyl-CoA, which is subsequently converted into pristanal, pristanic acid, and finally pristanoyl-CoA, a substrate for further β -oxidation.

The basic defect in RD is a defect in α -oxidation of phytanic acid in peroxisomes. In about 50% of the RD patients the defect involves the enzyme phytanoyl-CoA hydroxylase, resulting in an excessive accumulation of phytanic acid in blood and various tissues. The gene encoding this enzyme, *PHYH* or *PAHX*, is located on chromosome 10p13. Many different mutations have been identified in RD patients. A number of atypical RD cases have been related to a defect in the same gene. In one RD family, not only phytanic acid, but also pipecolic acidemia was elevated. This

family showed linkage to the *PAHX* locus on chromosome 10p13 (Tranchant et al. 1993; Nadal et al. 1995). In another patient with clinical findings of mental retardation and abnormally short metatarsals and metacarpals, but no other signs of classic RD, both phytanic acid and pipecolic acid were elevated (Baumgartner et al. 2000). Liver peroxisomes were reduced in number, had a larger average size, and lacked catalase. This patient was homozygous for a frameshift mutation in *PAHX* (Baumgartner et al. 2000).

RD is genetically heterogeneous and some patients have mutations in the gene *PEX7*, located on chromosome 6q21–22.2. Mutations in the latter gene are known to be associated with rhizomelic chondrodysplasia punctata (RCDP). This is another peroxisomal disorder characterized by proximal shortening of the extremities, contractures, growth failure, cataracts, mental retardation, and usually early death. RCDP is genetically heterogeneous with three distinct forms. A defect in the de novo plasmalogen biosynthesis is the central biochemical feature of RCDP. Only RCDP type 1, which is caused by mutations in *PEX7*, is also characterized by elevated phytanic acid. Mutations in *PEX7* lead to a defective PTS2 receptor, resulting in defective import of peroxisomal proteins with a PTS2 targeting signal. Phytanoyl-CoA hydroxylase, alkyl-dihydroxyacetonephosphate synthase, and peroxisomal thiolase are the three peroxisomal enzymes with a PTS2 targeting sequence. Alkyl-dihydroxyacetonephosphate synthase is involved in plasmalogen biosynthesis. In patients with a defect in *PEX7*, phytanoyl-CoA hydroxylase, alkyl-dihydroxyacetonephosphate synthase, and peroxisomal thiolase are deficient. Patients with RCDP types 2 and 3 have an isolated deficiency of either alkyl-dihydroxyacetonephosphate synthase or dihydroxyacetonephosphate acyltransferase, both resulting in a defect in plasmalogen biosynthesis. While patients with mutations in *PHYH* have an isolated phytanic acid α -oxidation deficiency, patients with mutations in *PEX7* have a deficiency of both phytanic acid α -oxidation and de novo plasmalogen biosynthesis. It is remarkable that mutations in *PEX7* can give rise to both RCDP and RD.

The genetic heterogeneity of RD is further emphasized by the finding of a 2-methylacyl-CoA racemase deficiency in some patients with retinitis pigmentosa and a late-onset sensory neuropathy (Ferdinandusse et al. 2000). In these patients both phytanic acid and pristanic acid are elevated, in contrast to true RD patients in whom only phytanic acid is elevated.

Phytanic acid is of exogenous, dietary origin. There is no evidence of any endogenous synthesis. It is consumed by humans in considerable quantities in dairy products, ruminant animal fats and meats, and certain fish. Phytol can be metabolized by humans to

phytanic acid, but most phytol in the diet, present in green vegetables, is bound to chlorophyll and little is absorbed. Hence, the contribution of phytol to the phytanic acid concentration in humans is low. In view of the large intake and the presence of only trace amounts in normal human tissue, the catabolic pathway that disposes of phytanic acid must be very efficient.

The accumulation of large amounts of this unusual fatty acid in various tissues and lipid classes in RD is probably the cause of a series of symptoms, both acute and chronic. Phytanic acid is readily incorporated into phospholipids. It is probable that the incorporation of phytanic acid into lipids of the myelin sheaths leads to a less stable myelin structure. The methyl branching of phytanic acid probably disrupts the packing of the hydrocarbon tails in the bimolecular lipid leaflet due to steric hindrance, and in this way destabilizes the myelin. Once phytanic acid levels reach a critical point, myelin dissolution occurs. The phytanic acid levels are higher in peripheral nerve myelin than in CNS myelin and demyelination starts earlier and is more severe in the PNS than in the CNS. A question is why the concentration of phytanic acid is higher in myelin of the PNS than in myelin of the CNS. The turnover rate of myelin is higher in peripheral nerves than in brain and spinal cord. Phytanic acid may, therefore, accumulate more easily in the peripheral nerves. Another possibility is that the blood–nerve barrier in the PNS is less restrictive than the blood–brain barrier in the CNS, allowing a more rapid increase in the phytanic acid content of peripheral nerves. The distribution of demyelination in the CNS, with preferential involvement of brain stem and cerebellum, remains to be explained.

Phytanic acid is an effective regulator of gene expression by virtue of its capacity to activate certain nuclear receptors affecting nuclear signal transduction pathways. It is likely that this effect is important in the pathophysiology of the disease in RD.

22.5 Therapy

As the origin of phytanic acid is exclusively exogenous, further accumulation of the substance can be prevented by a strict diet that is low in phytanic acid. There is no need to restrict phytol. Furthermore, the diet should contain enough energy to prevent considerable weight loss. An appreciable quantity of phytanic acid is present in hepatic lipid and body fat stores.

During conditions of increased mobilization of body fat, phytanic acid is liberated from body stores and the serum concentration increases even when intake of phytanic acid is low. During periods of significant weight loss and catabolic conditions related to febrile infections, serious worsening of neurological or myocardial pathology may occur, even resulting in death.

Strict diet and supply of sufficient energy to maintain a near-constant body weight lead to a gradual drop in serum phytanic acid levels to normal or slightly increased levels. Treated RD patients show clinical improvement. They no longer have apparently spontaneous relapses. The improvement in particular relates to the signs and symptoms that change rapidly: neuropathy, cerebellar ataxia, cardiomyopathy, and ichthyosis. Problems such as visual disturbances, anosmia, and deafness usually stabilize and do not deteriorate any further. Some clinical problems are due to irreversible damage and are not influenced favorably by lowering phytanic acid levels. Early diagnosis and treatment are important to prevent irreversible handicaps. The advice to ensure sufficient energy provision applies particularly at the start of treatment, when the serum phytanic acid levels are still very high. Later, when the phytanic acid content of the serum has been reduced to safer levels, a gradual weight reduction is acceptable. Dietary treatment is life-long.

Plasmapheresis provides the means to lower serum phytanic levels rapidly. Very high serum levels are toxic and may precipitate life-threatening symptoms. In these circumstances, plasmapheresis can be used as an emergency measure. Furthermore, plasmapheresis has been shown to be an excellent supplement to dietary treatment. When applied with a low frequency, it can compensate for a less strict dietary regimen. Dialysis is ineffective, as plasma phytanic acid is bound to lipoproteins.

22.6 Magnetic Resonance Imaging

There are no reports on MRI findings in RD, probably because of the rarity of the disease and the fact that the site of major involvement is the PNS rather than the CNS. In relation to histopathological findings, MRI signs of demyelination can be expected to occur mainly in brain stem tracts, cerebellar peduncles, and the cerebellar white matter.

Mitochondria and Mitochondrial Disorders

E. Morava, J.A.M. Smeitink

23.1 Mitochondrial Structure and Function

Mitochondria are membranous organelles that provide the energy necessary for the different cell functions. They are called mitochondria because of their threadlike appearance (Greek *mitos* = thread) on light microscopy. On electron microscopy they appear as vesicles bounded by two membranes. The inner membrane is thrown into folds that project like shelves into the mitochondria. These projections are called cristae. Mitochondria consist of four compartments: the outer membrane, the intermembrane space, the inner membrane, and the mitochondrial matrix. Mitochondria vary considerably in size in any one cell type, but most have a diameter of between 0.1 and 1.0 μm . In different cell types the size, shape, and number of cristae vary considerably. Most cells contain many mitochondria, the actual number differing in relation to the energy requirements of the type of cell. Mitochondria are dynamic organelles. They undergo frequent fission and fusion or branching, and they may alter their size and location in the cell under different conditions.

The main role of mitochondria is to synthesize adenosine triphosphate (ATP), the universal source of energy for the cell. Mitochondria convert the energy derived from oxidation of substrates into the high-energy bond of ATP, which is then transported into the cytosol in exchange for adenosine diphosphate (ADP). The process of production and storage of energy by mitochondria is called *oxidative phosphorylation*. In addition to this process, mitochondria also perform many other functions, including the first two reactions of the urea cycle, the synthesis of ketone bodies, and propionate metabolism.

Pyruvate and fatty acids are the most important substrates for energy production, although amino acids may also contribute in certain conditions, for instance during fasting.

Pyruvate represents the metabolic end point of glycolysis, which occurs in the cytoplasm and yields a small amount of ATP. Pyruvate is carried across the mitochondrial membrane into the mitochondrial matrix space by monocarboxylate translocase. Subsequently it is oxidatively decarboxylated by the pyruvate dehydrogenase complex (PDHc), which produces CO_2 and acetyl-CoA, while reducing one nicotinamide adenine dinucleotide (NAD^+) to $\text{NADH} + \text{H}^+$.

The pyruvate dehydrogenase complex is located at the inner border of the inner mitochondrial membrane.

Fatty acids with more than eight or ten carbon atoms require a specific carrier system to enter the mitochondrial matrix space (Fig. 23.1). They are activated to acyl-CoA by acyl-CoA ligase (= acyl-CoA synthetase) on the mitochondrial outer membrane. Fatty acyl-CoA is subsequently converted to fatty acyl carnitine in the intermembrane space by carnitine palmitoyl transferase 1 (CPT 1), which is located in the outer mitochondrial membrane. Fatty acyl carnitine is then translocated across the inner mitochondrial membrane in exchange for free carnitine, a reaction catalyzed by carnitine:acylcarnitine translocase, located in the inner mitochondrial membrane. On the inner surface of the inner membrane a second carnitine palmitoyl transferase, CPT 2, converts fatty acyl carnitine to acyl-CoA and free carnitine. Shorter-chain fatty acids (ten or fewer carbons) enter the mitochondria independently of the carnitine-requiring transport system, and are activated by short- and medium-chain acyl-CoA ligase to the respective acyl-CoA esters in the mitochondrial matrix. Acyl-CoA is the primary substrate for mitochondrial β -oxidation. This β -oxidation spiral involves four successive reactions, mediated by acyl-CoA dehydrogenase, 2-enoyl-CoA hydratase, 3-hydroxyacyl-CoA dehydrogenase, and 3-ketoacyl-CoA thiolase. The products of each turn of the spiral are acetyl-CoA and acyl-CoA, now two carbons shorter, with conversion of flavin adenine dinucleotide (FAD) to FADH_2 and NAD^+ to $\text{NADH} + \text{H}^+$. An acyl-CoA can recycle through β -oxidation spirals as many times as it can yield acetyl-CoA fragments. With each turn of the spiral, as the acyl-CoA becomes shorter, it encounters enzymes with different substrate specificities. An example of this is the series of chain-length-specific acyl-CoA dehydrogenases: long-chain acyl-CoA dehydrogenase mediates the reaction for acyl-CoA compounds from 8 carbons to 18 carbons; medium-chain acyl-CoA dehydrogenase from 4 to 12 carbons; and short-chain acyl-CoA dehydrogenase from 4 to 6 carbons. Fatty acids with double bonds require additional enzymes, δ^3 , δ^2 -enoyl-CoA isomerase and 2,4-dienoyl-CoA reductase. In the liver, the metabolic end product of each cycle of β -oxidation, acetyl-CoA, is primarily converted to ketone bodies, while in other tissues acetyl-CoA is completely oxidized via the citric acid

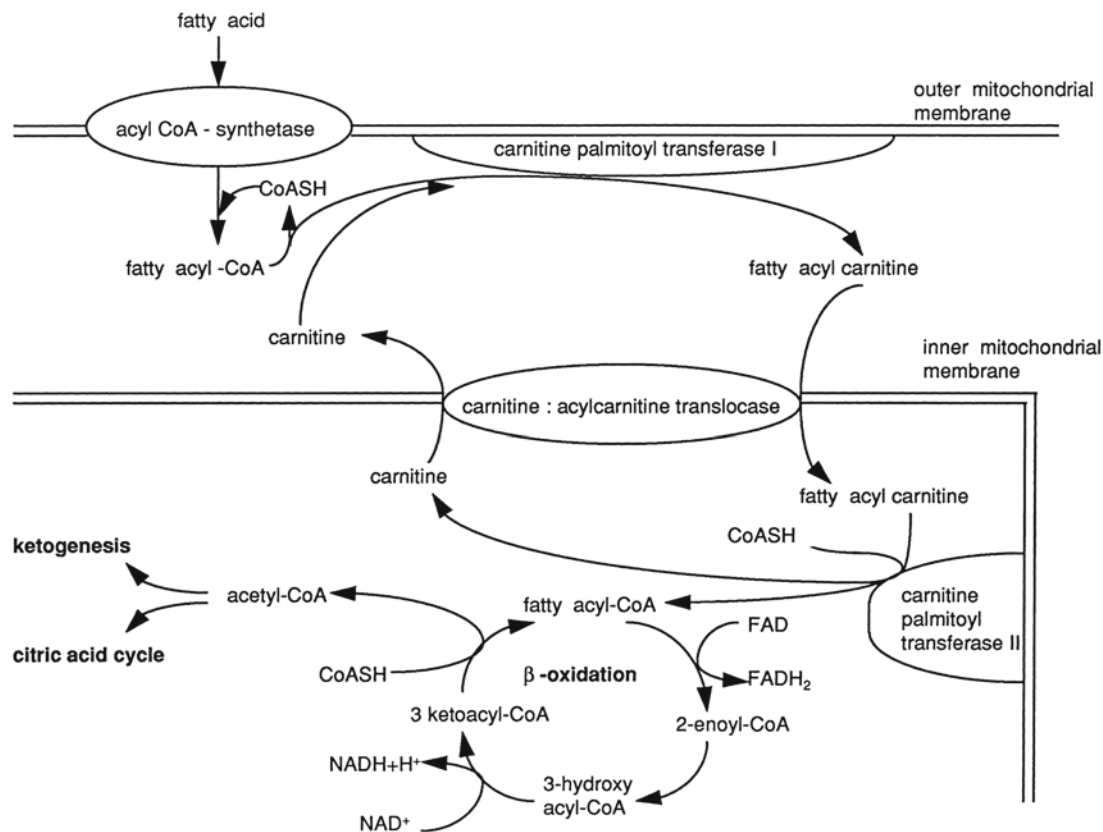


Fig. 23.1. Import and β -oxidation of fatty acids in mitochondria

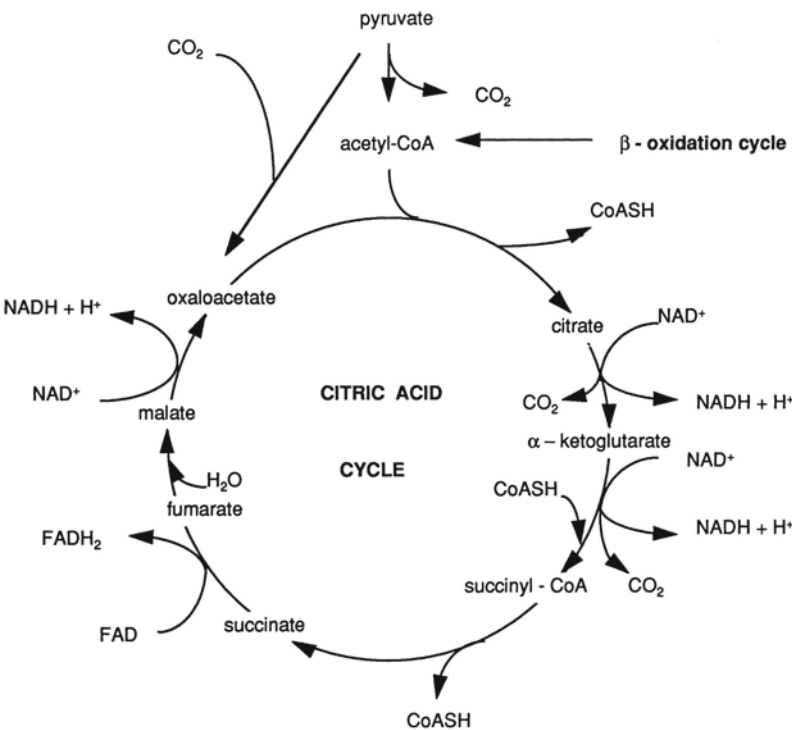


Fig. 23.2. Citric acid cycle in the mitochondrial matrix

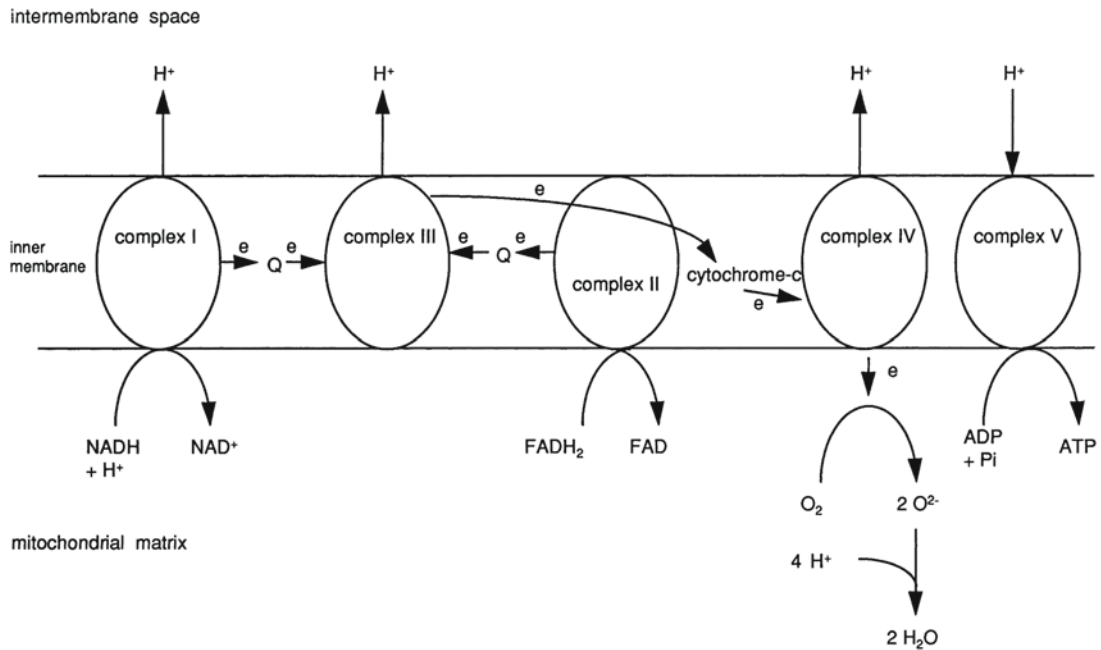


Fig. 23.3. Electron (e) transport chain in mitochondrial inner membrane

cycle. Electrons from the acyl-CoA dehydrogenase-mediated reactions are transferred to electron transfer flavoprotein to the electron transport chain.

Therefore, acetyl-CoA is produced from different sources. Carboxylation of pyruvate yields oxaloacetate and decarboxylation of pyruvate yields acetyl-CoA. Acetyl-CoA is produced in the β -oxidation of fatty acids. It can also be derived from breakdown of certain amino acids (for instance, leucine and isoleucine). Acetyl-CoA and oxaloacetate condense to form citrate. Citrate is decarboxylated in the *citric acid cycle* (also called *Krebs cycle*, *tricarboxylic acid cycle*, or *TCA cycle*, see Fig. 23.2), yielding CO_2 and reducing equivalents in the form of $\text{NADH} + \text{H}^+$ and FADH_2 . Certain amino acids can be converted to citric acid cycle intermediates, such as glutamate, aspartate, alanine, proline, and glutamine.

The reducing equivalents NADH and FADH_2 , produced by β -oxidation of fatty acids and the citric acid cycle, are reoxidized to NAD^+ and FAD by the respiratory chain. This oxidation sequence is tightly coupled to the phosphorylation of ADP to yield ATP. This process of so-called oxidative phosphorylation is responsible for the main production of ATP in most cells.

Oxidative phosphorylation (Fig. 23.3) is achieved by five multisubunit enzyme complexes (complexes I–V), all located within the mitochondrial inner membrane. Complexes I–IV constitute the *electron transport chain* (or *respiratory chain*). Complex I (NADH ubiquinone reductase = NADH-coenzyme Q

reductase) oxidizes NADH to NAD^+ and the electrons of the hydrogens are transferred to ubiquinone (CoQ) to yield ubiquinol (reduced CoQ). Complex II (succinate ubiquinone reductase) accepts reducing equivalents from succinate and also passes electrons down the chain to ubiquinone to yield ubiquinol. The electrons from ubiquinol are transferred to complex III (ubiquinol: cytochrome- c reductase), subsequently to cytochrome c , then to complex IV (cytochrome- c oxidase), and finally to oxygen, which combines with protons to form water. The energy released in the electron transport is used to pump hydrogen ions out of the mitochondrial inner membrane through complexes I, III, and IV. The resulting electrochemical gradient is exploited by complex V (ATP synthetase = ATPase). Complex V allows some of the protons to flow back into the mitochondria and uses the energy so generated for the synthesis of ATP from ADP and inorganic phosphate. ATP formed in the matrix space is then transported out of the mitochondria by adenine nucleotide translocase in exchange for ADP. The production and storage of energy by mitochondrial oxidative phosphorylation is a very efficient process with a high ATP yield. The rate of mitochondrial substrate oxidation is finely geared to the needs of the cell. The main control mechanism is the ratio of ATP to ADP. ADP is an activator of mitochondrial respiration.

Each complex of the respiratory chain is made up of a number of protein components. Complex I contains 46 polypeptides and has as prosthetic groups

flavin mononucleotide and several nonheme iron–sulfur clusters. Complex II consists of 4 subunits. Complex III is composed of 11 subunits including cytochrome *b*, cytochrome *c*₁, and a nonheme iron protein. Complex IV is composed of 13 different protein units, 2 cytochromes (*a* and *a*₃) and two copper atoms. Complex V is composed of 16 different polypeptides. Two small electron carriers, ubiquinone (coenzyme Q₁₀) and cytochrome *c* (a low molecular weight hemoprotein) act as shuttles between the complexes.

23.2 Mitochondrial Genetics

Human cells possess two different genomes: nuclear DNA (nDNA), a 3×10^9 -base-pair-long genome, present in two copies in each cell, and mitochondrial DNA (mtDNA), a 16,569-base pair-long genome, present in 2–10 copies per mitochondrion. Mitochondria are dependent upon the coordinated expression of these two parallel genetic systems.

Each mitochondrion contains on average five *mitochondrial genomes* and each cell contains hundreds to thousands of mitochondria. Consequently, there are hundreds or thousands of copies of mtDNA in each cell. In normal individuals all of these copies of mtDNA are identical (homoplasmy), but in disease there may be more than one distinct population of mtDNA (heteroplasmy), one being normal and the other being mutant. During cell division mitochondria (and mtDNA) are randomly distributed between daughter cells. As a consequence, the proportion of mutant genomes may shift in daughter cells.

mtDNA consists of two complementary strands: one filament is rich in guanine nucleotide residues, while the other is rich in cytosine residues. They are conventionally called heavy (H) and light (L) strands, respectively. mtDNA contains only 37 genes and codes for different proteins of the respiratory chain and the RNAs (transfer and ribosomal RNAs) necessary for expression of these genes (13 messenger RNAs [mRNAs], 22 transfer RNAs [tRNAs], and 2 ribosomal RNAs [rRNAs]). The 13 mRNAs specify as many polypeptides of the respiratory chain: 7 subunits of complex I, the cytochrome *b* subunit of complex III, 3 subunits of complex IV and 2 subunits of complex V.

In mtDNA, the gene organization is highly compact; all of the coding sequences are contiguous with each other and there are no introns. The only noncoding stretch of DNA is the displacement loop (D loop), a region of 1123 base pairs that contains the origin of replication of the H strand and the promoters for L- and H-strand transcription. The D loop is an important area of interaction of mtDNA with nuclear-encoded proteins regulating mtDNA housekeeping

functions. The genetic code used in the mitochondria differs from the universal code, making nDNA and mtDNA reciprocally untranslatable. The rate of spontaneous mutations of mtDNA genes is much higher than that of nDNA genes and repair mechanisms are limited and less efficient.

The entire mitochondrial genome of each individual, either male or female, is inherited from the mother, although the possibility is not excluded that a small contribution of the mitochondrial genotype may be of paternal origin. This is due to the fact that during egg fertilization the sperm cell contributes almost no cytoplasm to the zygote.

The replication and expression of mtDNA are controlled by nuclear genes. The *nuclear genome* furthermore encodes for most of the mitochondrial proteins and cooperates with the mitochondrial genome in the assembly of the multisubunit enzyme complexes of the oxidative phosphorylation apparatus. The D-loop region is an important area of interaction between nDNA and mtDNA.

The structural proteins of the oxidative phosphorylation (complexes I–V) are all dual-coded, except for complex II. Most mitochondrial membrane and matrix proteins are coded by nuclear genes and synthesized in the cellular cytoplasm on free polyribosomes and have to be imported from the cytoplasm into the mitochondria through a complicated translocation machine, which is under the control of the nuclear genome. In addition, nDNA encodes several factors controlling mtDNA replication, transcription and translation.

Most nuclear-encoded mitochondrial proteins destined for the inner three mitochondrial compartments (the intermembrane space, the inner membrane, and the mitochondrial matrix) are synthesized as larger precursors containing an amino-terminal extension (presequence). The presequences are the targeting signals of the precursor proteins and direct these proteins to mitochondria. The presequences consist of 20–80 amino acid residues. There is no apparent sequence identity among the different mitochondrial protein presequences, but a characteristic common to all of them is a relatively high content of positively charged and nonpolar residues and an almost complete absence of negatively charged residues. This finding suggests that the specificity of the presequences resides in a structural configuration rather than a particular biochemical motif. Most of the presequences probably adopt an α -helical structure. Most mitochondrial proteins, in particular matrix proteins, contain their targeting signal in a presequence, but there are a few exceptions. A few proteins do not have presequences and apparently contain a targeting signal in their mature form.

Presequences are recognized by specific receptors on the mitochondrial surface (a special class of mito-

chondrial outer membrane or MOM proteins). The receptors directly interact with another protein, the general insertion protein (GIP), and thereby donate the precursor proteins to this membrane insertion site. The further transport of precursor proteins occurs through contact sites, where the mitochondrial outer and inner membranes are closely apposed. The inner membrane has a translocation channel distinct from, but in dynamic interaction with, the translocation channel of the outer membrane. Import across the inner mitochondrial membrane requires ATP and the presence of a membrane potential across this membrane.

The configuration of proteins is important in the process of import across the mitochondrial membrane. Completely folded polypeptides are unable to traverse the membrane. Premature folding in the cellular cytoplasm of the precursor proteins is prevented by stabilization of the proteins in a translocation-competent, unfolded conformation with help of so-called molecular chaperones. Molecular chaperones do not form part of the final folded or assembled protein structure but prevent undesired folding and interactions of the substrate protein along its transport, folding, and assembly pathways. Appropriate peptide folding is attained after the chaperone has released the polypeptide substrate. The majority of the currently identified molecular chaperones belong to the class of so-called “heat shock proteins.” A different kind of molecular chaperones involved in mitochondrial precursor proteins consists of the so-called “presequence binding factors.” These proteins, through their interaction with the presequences of mitochondrial precursors, are also essential in the import pathway of proteins into mitochondria.

After import across the mitochondrial membrane, presequences are proteolytically removed in the mitochondrial matrix. This cleavage is necessary for further assembly of the newly imported polypeptides into functional proteins and complexes. Two different proteins are required for full protease activity: mitochondrial processing peptidase (MPP) and processing enhancing protein (PEP). The MPP component contains the catalytic activity, which is stimulated by PEP. After that, the proteins are sorted to their respective mitochondrial subcompartments.

The outer and inner mitochondrial membranes differ in permeability. The transport of metabolites and inorganic ions across the inner membrane is highly regulated. This relative impermeability is important in maintaining a membrane potential and pH gradient across the membrane necessary for oxidative phosphorylation. The permeability of the outer membrane is less restricted. The outer membrane contains pore-forming proteins called porins or voltage-dependent, anion-selective channels (VDAC). Whether the pore is open or partially closed is depen-

dent on the membrane potential. In addition to VDAC, other types of channels are present in the outer membrane. Probably the outer membrane has several permeability pathways differing in selectivity, regulation, and function.

23.3 Mitochondrial Disorders

Mitochondrial disorders are the most common in-born errors of metabolism, with an estimated incidence of 1 per 10,000 live births. They present as an extremely heterogeneous group of disorders with variable age of onset, progression, and severity. Considering the central role of mitochondria in cellular metabolism, it is not surprising that mitochondrial diseases are often multiorgan disorders with predominant involvement of brain and muscles. Mitochondrial disorders can follow either a maternal, autosomal, or X-linked mode of inheritance.

Many mitochondrial disorders follow maternal inheritance. A mother carrying a mtDNA mutation will transmit it to all her children, male and female, but only her daughters will pass it on to their children. At a clinical level maternal transmission may be difficult to detect. Due to heteroplasmy, unequal mitotic segregation, and threshold effect, different individuals in the matrilinear lineage may differ in symptomatology and in organ involvement; some may even be asymptomatic. In most cases of mitochondrial genomic defects, heteroplasmy is present, with occurrence of both wild type and mutant mtDNA. At cell division mitochondria and mtDNA are haphazardly distributed between the daughter cells and consequently the proportion of mutant genomes may differ between daughter cells. The percentage of mutant DNA versus normal DNA may, therefore, be very different in different children of the same mother, and in different tissues in the same person, and may alter in the course of time. Whether or not the mtDNA mutation is actually expressed is largely determined by the relative proportion of normal versus mutant genomes in a given tissue. A minimum critical number of mutant DNA is necessary to impair energy metabolism severely enough to cause dysfunction of that particular organ or tissue. This phenomenon is known as the threshold effect. The number of affected mitochondria and cells needed to cause organ dysfunction varies from tissue to tissue depending on the vulnerability of that particular tissue to impairments of oxidative phosphorylation. The relative reliance of tissues on oxidative phosphorylation energy decreases in the following order: CNS, skeletal muscle, heart, kidney, and liver. The presence of a mutation in a particular percentage of mitochondrial genomes may lead to signs of encephalopathy and/or myopathy, without any sign of dysfunction of other organs. The

metabolic vulnerability may also vary in the same tissue with time and according to functional demands. As the proportion of mutant mitochondrial genomes may shift in daughter cells, this may also be the cause of a change in phenotype. In general, there is a decline in oxidative phosphorylation capacity with age. The most likely mechanism for this phenomenon is the accumulation of damage to mtDNA in the face of insufficient ability to repair DNA alterations. This phenomenon may explain the late age of onset of clinical signs and symptoms in some patients, and the increase in severity of the disease with age.

The mitochondrial genome depends heavily on the nuclear genome, which encodes several factors involved in mtDNA replication, transcription, and translation. Faulty communications between nuclear and mitochondrial genomes may lead to either multiple mtDNA deletions or mtDNA depletion. These disorders are transmitted by mendelian inheritance, because the primary genetic defect resides in nDNA. The nuclear genome also contains the genes encoding structural mitochondrial proteins, most of the respiratory chain proteins, and the proteins necessary for the proper assembly of the oxidative phosphorylation complexes.

The classification of these pheno- and genotypically heterogeneous diseases is very difficult. Classification may be based on the clinical presentation, on the age of presentation and possible progression, or on the underlying biochemical or genetic defects. A previous classification by DeVivo (1993) is based on a genetic framework. The major subdivision is into nDNA defects, mtDNA defects, and intergenomic signaling defects.

This original classification developed further with time, e.g., with the description of defects in assembly factors, defects in mtDNA maintenance (replication control), and defects in oxidative phosphorylation system biogenesis. The classification of DiMauro and Schon (2003) has incorporated these recent insights:

1. Respiratory chain disorders due to defects in mtDNA
 - (a) Mutations in protein synthesis genes
 - (b) Mutations in protein coding genes
2. Respiratory chain disorders due to defects in nDNA
 - (a) Mutations in structural components of the respiratory chain
 - (b) Mutations in ancillary proteins of the respiratory chain
 - (c) Defects in intergenomic signaling affecting respiratory function
 - (d) Defects of the membrane lipid milieu
 - (e) Defects in mitochondrial motility, fusion, and fission

3. Disorders with indirect involvement of the respiratory chain
 - (a) Defects of mitochondrial protein importation
 - (b) Defects in mitochondrial motility
 - (c) Neurodegenerative disorders

For the clinician, the genetic origin of the mitochondrial defect is the most important item in the classification, recognizing two major groups: mtDNA defects (point mutations in structural proteins of the respiratory chain, point mutations in tRNAs and rRNAs, and major mtDNA rearrangements) and nDNA defects (defects in structural oxidative phosphorylation proteins, defects in genes encoding assembly factors, defects in genes involved in the biogenesis of the oxidative phosphorylation system, and defects in the maintenance of mtDNA).

In a simplified view, a positive family history suggestive of maternal inheritance may help in the early diagnosis in mtDNA defects, but the clinical presentation may be extremely variable in different family members. In many affected individuals the disease becomes evident only in early adulthood and may be organ-specific. Mitochondrial deletions, however, are most often sporadic, the symptoms may appear early, and the family history is negative.

In nDNA defects, the family history is noncontributory in most cases, the parents are healthy, the symptoms frequently arise soon after birth, and when progressive, the disease may be fatal in early childhood. Sibs may be affected to a variable degree (genetic and environmental factors), but the clinical variability is usually much less marked than in mtDNA defects.

23.3.1 Mitochondrial DNA Defects

A variety of defects in mtDNA can be distinguished: *point mutations*, *deletions*, and *duplications*. The DNA defects may involve genes coding for proteins of the respiratory chain (structural proteins) or genes coding for tRNA or rRNA. mtDNA depletion is related to a nDNA defect and is included under nuclear defects of mtDNA maintenance.

In cases of *mutations involving genes encoding structural proteins of the respiratory chain*, biochemical analysis reveals a defect restricted to one respiratory enzyme complex (complex I, II, III, IV, or V). In such patients the primary biochemical analysis, demonstrating a usually partial isolated complex deficiency, leads to targeted mutation analysis of particular mitochondrial structural genes. Different point mutations in genes coding for components of complex I have been observed in exercise intolerance, Leber hereditary optic neuropathy (LHON), Leigh

syndrome, Leigh-like syndrome, progressive epilepsy, adult-onset dystonia associated with neurological and ophthalmological symptoms, and in mitochondrial encephalomyopathy, lactic acidosis, and stroke-like episodes (MELAS) syndrome. mtDNA mutations involving components of complex III have been reported in patients with progressive exercise intolerance, proximal limb weakness with myoglobinuria, Parkinsonism, and LHON. In complex IV defects, structural mutations have been detected in patients presenting with isolated motor neuron disease, Leigh-like syndrome, MELAS, proximal myopathy with lactic acidosis, and LHON. In patients with neurogenic muscle weakness, ataxia, and retinitis pigmentosa (NARP) and Leigh syndrome, common mutations are known in a gene coding for an ATP synthetase (complex V) subunit.

A number of *point mutations in tRNA and rRNA genes* have been identified. Each tRNA mutation is generally associated with a distinctive phenotype, although some phenotypic overlap between the different tRNA defects is common. Well-known clinical phenotypes include myoclonic epilepsy with ragged red fibers (MERRF), MELAS, Leigh syndrome and variable combinations of myopathy, cardiomyopathy, chronic progressive external ophthalmoplegia (CPEO), diabetes mellitus, and hearing loss. Furthermore, a few rRNA mutations have been also described with a very similar phenotype of CNS involvement, deafness, neuropathy, and diabetes mellitus. Despite the overlap in the clinical symptoms mentioned, the association of different tRNA mutations with clinical syndromes is surprisingly specific considering that these mutations all act on the same mitochondrial function, i.e., the ability of mitochondria to translate their own genes. Since mutant tRNA is unavailable for translation, all mitochondrially encoded proteins are present in decreased amounts. Among the different clinical phenotypes the biochemical abnormalities are virtually indistinguishable, revealing multiple partial complex defects.

Large, single deletions of a substantial proportion of mtDNA have been described in CPEO, Pearson syndrome, and Kearns–Sayre syndrome (KSS). These syndromes are clinically overlapping. Muscle weakness and chronic progressive external ophthalmoplegia are also present in KSS. Many patients with Pearson syndrome die in early childhood from a combination of pancreatic, hepatic, renal, and bone marrow insufficiency with pancytopenia, but the few patients who improve and survive develop KSS and histological signs of a mitochondrial myopathy in later childhood. The deletions encompass many of the genes encoding for proteins of the respiratory chain, and also several tRNAs. This explains the decrease in presence of all mitochondrial translation products demonstrated by immunological analyses. Biochemical

analysis reveals decreased activity of complexes I, III, and IV, individually or in combination. The percentage of deleted mtDNA is similar in muscles of both CPEO and KSS patients, but deletions are restricted to skeletal muscle in CPEO and widely distributed in extramuscular tissue in KSS. In Pearson syndrome high amounts of mtDNA defects are present in bone marrow precursor cells. The proportion probably falls with age if the patient survives; however, repeated investigation has shown an increased proportion of deleted mtDNA in muscle tissue. Most (or all) of the cases associated with single DNA deletions are sporadic. The deletion probably occurs after egg fertilization and owing to unequal mitotic segregation is present in only some of the cells. The replication of deleted mtDNA occurs more rapidly and, in consequence, positive selection of respiratory-deficient cells may occur in tissues with rapid cell turnover.

Duplications of mtDNA are very rare in man. Sporadic cases of KSS with heteroplasmic mtDNA duplications have been described.

The relationship between mtDNA changes, biochemical defects of the respiratory chain, and clinical phenotype remains difficult to understand (genetic and phenotypic heterogeneity). One point mutation can be associated with different clinical phenotypes (for instance, the same mutation is present in both NARP and some cases of Leigh syndrome; the same mutation in a tRNA gene is found in MELAS, in maternally inherited myopathy and cardiomyopathy, and in maternally inherited diabetes mellitus). The phenotype related to the same abnormality in mtDNA may also vary within a single kindred. The same disease can be caused by different point mutations (see Chap. 25). Combined features of different syndromes have been observed in one patient (KSS combined with MELAS; MERRF with MELAS; Pearson syndrome progressing to KSS). Part of the relationship between genotype and phenotype can be explained by heteroplasmy with different percentages of mutant mtDNA in different tissues and changes of percentages over the course of time.

23.3.2 Nuclear DNA Defects

Nuclear genes responsible for oxidative phosphorylation defects can be categorized structurally and functionally into genes encoding structural components of the oxidative phosphorylation system, genes encoding assembly factors of the oxidative phosphorylation complexes, genes involved in the biogenesis of the oxidative phosphorylation system, and genes involved in the maintenance of the mtDNA.

Among the *defects in structural components of the oxidative phosphorylation system*, complex I deficiency is the most common. In general, isolated complex I

deficiency is one of the most frequent disturbances of the oxidative phosphorylation system and often follows an autosomal recessive inheritance. The clinical presentation in the majority of cases is of a Leigh or a Leigh-like syndrome, a leukodystrophy, or a cardiomyopathy. Mutations have been identified in seven of the 39 nuclear genes encoding structural subunits of complex I. Complex II comprises four nuclear encoded subunits. It has a dual function as an enzyme complex of the oxidative phosphorylation system and as an essential enzyme of the citric acid cycle. It consists of a flavoprotein (active site with covalently bound FAD) and an iron-sulfur protein, and is anchored to the membrane by two transmembrane proteins. A mutation in the flavoprotein coding gene of a patient with Leigh syndrome was the first mutation identified in a nuclear gene causing oxidative phosphorylation deficiency. Mutations in the genes encoding the iron-sulfur protein and the anchor proteins cause a different phenotype of hereditary paragangliomas and/or pheochromocytomas. Complex III transfers electrons from the ubiquinone pool to cytochrome *c*, and is composed of 11 subunits, of which ten are nuclear-encoded. Complex III deficiency is often associated with encephalomyopathy or cardiomyopathy. However, in the patient with the first mutation described in a nuclear-encoded subunit of complex III (an enzyme-binding protein), no psychomotor retardation or neurological impairment was detected, but hypoglycemia and lactic acidemia were. To date no mutations have been reported in the structural nuclear components of complex IV and complex V. Most syndromes with isolated complex IV deficiency are caused by mutations in genes encoding proteins involved in the proper assembly of the complex.

Assembly factors are proteins which mediate the process of assemblage of subunits and intermediate complexes into fully assembled oxidative phosphorylation complexes, and have chaperone-like functions. A few assembly factors have been identified for complex I and III, and many for complex IV. Mutations of the only known assembly factor gene responsible for isolated complex III deficiency (Rieske iron-sulfur subunit) are associated with neonatal proximal tubulopathy, hepatic involvement and encephalopathy, and with GRACILE syndrome (growth retardation, amino aciduria, cholestasis, iron overload, lactic acidosis, and early death), a fatal metabolic disorder with iron overload. Complex IV (COX) is composed of 13 structural subunits, ten of which are encoded by the nucleus. A large number of accessory factors are necessary for the assembly and maintenance of the active complex, and mutations in several of these factors have been described. The first gene encoding an assembly factor known to be responsible for COX deficiency is the *SURF1* gene. Leigh syndrome is the most common clinical manifestation observed in patients

with *SURF1* mutation, but milder neurological involvement with a malabsorption syndrome and cases with a leukoencephalopathy have been described in association with *SURF1* mutations as well. Mutations in two other COX assembly genes, *SCO1* and *SCO2*, frequently present with hypertrophic cardiomyopathy and encephalopathy, sometimes combined with hepatic failure. The *COX10* and *COX15* genes are involved in the synthesis of heme A, a prosthetic group of COX. Mutations in these genes result in a clinical manifestation comparable to that of *SCO2* mutations. A novel mutation has been recently described in the *ATP12* assembly gene of complex V with severe microcephaly, hepatomegaly, and early death.

As to *defects in the biogenesis of the oxidative phosphorylation system*, oxidative phosphorylation deficiencies can be caused by defects in the import of nuclear-encoded mitochondrial proteins into the mitochondrion. A mutation in the gene for subunit 8a of the translocase of the inner mitochondrial membrane, the *TIMM8A* or *DDP1* gene, causes human dystonia deafness syndrome, also known as Mohr-Trautenberg syndrome, a progressive neurodegenerative disorder. Friedreich ataxia, an autosomal recessive disorder, is caused by disturbances of the iron-sulfur cluster formation, related to an abnormal expansion of a GAA repeat in the first intron of the frataxin gene, which encodes a mitochondrial protein of unknown function. The defect in frataxin results in oxidative damage of the highly sensitive iron-sulfur protein complexes I, II, III, and the Krebs cycle enzyme aconitase. Hereditary spastic paraplegia (HSP) is a genetically heterogeneous neurodegenerative disorder characterized by progressive spasticity and weakness of the legs. A subtype of HSP is related to mutations in *SPG7*. Patients with this subtype show typical signs of mitochondrial disease (ragged red fibers and COX-negative fibers). The spastic paraplegia gene *SPG7* encodes a nuclear-encoded mitochondrial metalloprotease protein, which has both proteolytic and chaperone-like activities at the inner mitochondrial membrane. The oxidative phosphorylation system may be disturbed not only by defects in factors which are directly part of the system or involved in its biogenesis, but also by defects in factors that indirectly contribute to its function, such as alterations in the lipid composition of the inner membrane (Barth syndrome). Dominant optic atrophy (DOA) is caused by defects in the *OPA1* gene, which encodes a mitochondrial GTPase that is important for the formation and maintenance of the mitochondrial network.

Mutations in nuclear genes involved in mtDNA maintenance cause disorders that clinically resemble disorders caused by mtDNA mutations. This is understandable since the nuclear gene defect causes secondary mtDNA loss (mtDNA depletion) or formation of multiple mtDNA deletions. However, these disor-

ders follow a mendelian inheritance pattern. Multiple deletions of the mtDNA have been described in a number of clinical syndromes. The most frequently described is autosomal dominant progressive external ophthalmoplegia (AD PEO), for which three different disease genes have been identified: *ANT1*, encoding the adenine nucleotide translocator or ADP/ATP translocator; *POLG1*, encoding the catalytic subunit of the mtDNA-specific polymerase γ ; and *C10ORF2* encoding the Twinkle protein, a putative mtDNA helicase. For defects in *POLG1*, mutations with a recessive mode of inheritance have also been reported. The mtDNA depletion syndrome causes a rapidly fatal mitochondrial disorder in infancy. Quantitative analysis of the mtDNA reveals a severe depletion, varying from 50% up to 98% as compared to normal controls. Depletion of mtDNA correlates with the presence of multiple respiratory chain defects. Clinically three syndromes are distinguished: fatal infantile hepatopathy, congenital myopathy with or without nephropathy, and later-onset infantile

or childhood progressive encephalomyopathy. Two genes involved in mitochondrial deoxyribonucleoside metabolism, *TK2*, encoding thymidine kinase 2, and *DGUOK*, encoding deoxyguanosine kinase, have been associated with a myopathic form and a hepatoencephalopathic form of mtDNA depletion syndrome, respectively. Thymidine kinase 2 and deoxyguanosine kinase are both enzymes of the “salvage pathway,” which is the main supply of deoxyribonucleoside triphosphates (dNTPs) for mtDNA synthesis. The link between these salvage pathway enzymes and mtDNA depletion suggests their involvement in the maintenance of balanced mitochondrial dNTP pools. Deficiency of thymidine phosphorylase causes multiple mtDNA deletions and/or mtDNA depletion leading to mitochondrial neurogastrointestinal encephalomyopathy (MNGIE). Recently, mutations in a mitochondrial deoxynucleotide carrier (DNC) have been shown to cause failure of deoxynucleotide transport across the inner mitochondrial membrane in Amish congenital microcephaly.

Mitochondrial Encephalopathy with Lactic Acidosis and Stroke-like Episodes

24.1 Clinical Features and Laboratory Investigations

Mitochondrial myopathy, encephalopathy, lactic acidosis, and stroke-like episodes constitute the MELAS acronym. The disease shows maternal inheritance with considerable intrafamilial variation in expression of the disease. The age at onset varies between 3 months and 40 years, but in most cases first signs and symptoms occur before adulthood. Early development is normal in the majority of patients. The first manifestations of disease usually belong to the group of general features of encephalomyopathies. Growth disturbance and epileptic seizures are the most frequent first symptoms. The disease is progressive with increasing symptomatology. Learning disabilities, cognitive regression, exercise intolerance, and limb weakness are frequent manifestations of the disease. The myopathic features are rarely very prominent in MELAS. Stroke-like episodes are rarely early signs of the disease but have occurred before the age of 40 years in almost all patients. The stroke-like events give rise to both reversible and permanent neurological deficits. Hemiparesis and hemianopia or cortical blindness are seen most frequently. Seizures are common during the strokes. Episodic migrainous headaches with nausea and vomiting are common and often precede the stroke-like episodes. In some patients focal seizures progress to epilepsy partialis continua. All patients eventually develop cognitive impairment. In those with early-onset neurological impairment, development is generally delayed from early on in life, whereas in patients with later-onset impairment, the rapidity of disease progression and the number of cerebral infarcts have a direct impact on the presence and severity of cognitive impairment. Sensorineural hearing loss is frequent. Delayed puberty, infertility, and hypothalamic hypogonadism may be present. Diabetes mellitus, growth hormone deficiency, hypothyroidism, hypoparathyroidism, and hyperaldosteronism may occur. Less frequent findings, noted in less than half of the patients, include myoclonus, cerebellar ataxia, episodic coma, peripheral neuropathy, pigmentary retinopathy, ophthalmoplegia, ptosis, optic atrophy, hypertrophic cardiomyopathy, electrocardiographic evidence of pre-excitation, cardiac conduction block, and nephropathy. In relatives of typical MELAS patients a “partial” syndrome may be seen instead of the full-

blown MELAS picture. Short stature, sensorineural hearing loss, mild myopathy, cardiomyopathy, diabetes mellitus, and seizures without stroke or learning problems may be the only clinical manifestation of disease.

Some MELAS patients have manifestations which are typical of other mitochondrial syndromes. Patients with MELAS–MERFF overlap have myoclonic epilepsy and the associated EEG features in combination with clinical symptoms seen in MELAS, including stroke-like episodes. LHON–MELAS overlap leads to features typical of Leber hereditary optic neuropathy and stroke-like episodes.

On laboratory examination, most patients have lactic acidosis, although in some resting serum lactate is normal. CSF lactate is often also elevated. CSF protein is often found to be elevated. EMG may show a myopathic pattern. There may be neurophysiological evidence of a mixed axonal and demyelinating sensorimotor neuropathy. Some patients have ECG abnormalities with evidence of cardiomyopathy, Wolff–Parkinson–White abnormality, or conduction block. In most patients ragged red fibers are found on muscle biopsy.

Antenatal diagnosis is very difficult in defects of mitochondrial DNA. Because of heteroplasmy, a chorionic villus sample may not be representative of the level of mutant mitochondrial DNA in the embryo and it is therefore difficult to predict the future phenotype.

24.2 Pathology

On light microscopic examination of muscle biopsies, application of the modified Gomori trichrome stain often reveals the presence of ragged red fibers. With this stain the abnormal fibers demonstrate a mottled and irregular appearance with red-staining peripheral and intermyofibrillar zones. Histochemistry for oxidative enzymes, such as NADH dehydrogenase, succinate dehydrogenase, and cytochrome *c* oxidase, may yield abnormal staining patterns. On electron microscopy, the ragged red fibers display large aggregates of mitochondria, generally under the sarcolemma, but also between myofibrils. The mitochondria are frequently abnormal in size and structure. The mitochondrial cristae are often increased in number and irregularly oriented. The mitochondria may con-

tain different abnormal inclusions such as crystalline or paracrystalline structures or globular bodies.

Postmortem examination of the brain of deceased MELAS patients often reveals atrophy on external examination. The cerebellum, too, may have an atrophic aspect. Major blood vessels are normal. Microscopic examination reveals areas of extensive cortical laminar necrosis, usually in the occipital and posterior temporal areas. The cortical lesions usually have an asymmetrical distribution and are not related to vascular supply areas. The three deepest cortical layers are affected most severely. The gyral crests and sulcal depths are equally affected. The severity of the cortical damage varies from fractional neuronal loss to microcystic destruction. Gliosis is present. The cortical damage may have a spongiform aspect. In the area of cortical damage, there is a proliferation of capillaries. The lesions vary in age, the patient often having lesions of different ages. The adjacent subcortical white matter is involved with loss of myelin and presence of fibrous gliosis. The white matter damage may be spongiform. The periventricular white matter is usually not involved. However, diffuse white matter gliosis and atrophy may also be found. Calcium deposits are frequently present in the globus pallidus, less frequently in the caudate nucleus, lateral thalamus, dentate nucleus, subthalamic nucleus, substantia nigra, and red nucleus. The calcium granules are mostly deposited in and around capillary and small arterial walls. Otherwise the basal nuclei are intact and no neuronal loss is seen. Within the cerebellum pathological changes consist of some variable loss of Purkinje cells and granule cells. The dendrites of Purkinje cells may show remarkable segmented swelling, which is called cactus. On electron microscopy, accumulation of mitochondria, neurofilaments, and membrane complex is seen in the region of cactus formation. Brain stem and spinal cord may also contain spongiform lesions. Electron microscopy reveals abnormal accumulation of mitochondria in endothelial and smooth muscle cells of small arteries. The major cerebral arteries are normal.

24.3 Pathogenetic Considerations

Two heteroplasmic point mutations have been discovered in most cases of MELAS. In 80% of the patients a mutation is present in nucleotide 3243 of mitochondrial DNA, which affects a nucleotide position in the dihydrouridine loop of the tRNA specific to leucine (UUR codon) (tRNA^{leu(UUR)}). In addition, 7.5% of the patients have another mutation in the same tRNA^{leu(UUR)} gene at nucleotide 3271. The remainder of MELAS patients have other point mutations in the mitochondrial DNA; few have a deletion within the mitochondrial DNA. The 3243 mutation has also been

found in patients with chronic progressive external ophthalmoplegia and other neurological complaints, but without stroke-like episodes.

In MELAS, an isolated defect of complex I or combined defects in complexes I, III, and IV are found in muscle mitochondria. The presence of a mutant tRNA disturbs the mitochondrial gene translation machinery and leads to a decrease in all mitochondrially encoded proteins. The mechanism by which the tRNA^{leu(UUR)} gene mutation interferes with protein synthesis remains unclear, but defects in tRNA^{leu(UUR)} function, rRNA to mRNA ratio, impaired incorporation of leucine into mitochondrial translation products, and defects in rRNA processing are viable alternatives.

Among MELAS patients and their maternal relatives there is a clear relationship between percentage of mutant mitochondrial DNA and severity of disease. This is clearer for the level of mutant mitochondrial DNA in muscle than for that in blood. Asymptomatic relatives have the lowest percentage, oligosymptomatic relatives an intermediate percentage, and MELAS patients the highest. Among patients it has been found that the higher the percentage of mutant DNA is, the earlier the symptoms of stroke-like attacks appear.

The cause of the large cerebral lesions is a matter of debate. One hypothesis is that the relationship between mitochondrial dysfunction and cerebral pathology is explained by a mitochondrial vasculopathy of small arteries, observed in the "infarcted" areas. There is a marked increase in number of mitochondria in endothelial cells, smooth muscle cells, and pericytes of arterioles. The mitochondria are abnormal and enlarged. These vascular abnormalities may result in decreased blood supply. However, in SPECT and PET scan studies, evidence of patency of blood vessels is found in the acute stage of the infarct with the presence of a well-preserved blood flow. SPECT studies have repeatedly shown focal hyperperfusion before and during the stroke in MELAS and focal hypoperfusion in the chronic, atrophic stage. Hence, it is more probable that the metabolic demands exceed the potential of energy provision by the disturbed oxidative phosphorylation, leading to cell damage and edema.

24.4 Therapy

Various therapeutic strategies have been used in MELAS. In particular, administration of cofactors is often employed in an attempt to ameliorate the course of disease. Riboflavin is a precursor of both flavin monophosphate and flavin adenine dinucleotide (FAD), which are part of NADH-coenzyme Q reductase (complex I) and of complex II. Nicotinamide is a

precursor of NAD. Coenzyme Q₁₀ is given to substitute and supplement for endogenous coenzyme Q. Idebenone, a quinone compound similar to coenzyme Q₁₀, has the theoretical advantage of crossing the blood-brain barrier. Vitamin C and vitamin K₃ (menadione) are given to bridge a defect in the electron transport chain, as they accept and transport electrons. These drugs are given alone or in varying combinations. In patients with MELAS variable improvement has been reported, ranging from none to remarkable, but evidence for a consistent beneficial effect is lacking. Dichloroacetate inhibits the pyruvate dehydrogenase specific kinase, thereby activating the pyruvate dehydrogenase complex and reducing lactate levels. Oral creatine supplementation has been reported to lead to clinical improvement in incidental patients. Intravenous administration of L-arginine during acute stroke has also been reported to lead to improvement.

Symptomatic treatment of the neurological handicap, epilepsy, and endocrine dysfunction is important.

24.5 Magnetic Resonance Imaging

In MELAS CT often shows the presence of calcium deposits in the globus pallidus and caudate nucleus (Fig. 24.1). Sometimes the calcium deposits are more extensive and also affect the putamen and thalamus. During the acute phase of stroke-like episodes, one or more large hypodense areas are seen. The areas are swollen. They have, as a rule, an asymmetric distribution.

In MRI the calcium deposits in the basal nuclei are more difficult to see (Fig. 24.1). MRI shows the precise distribution of the lesions occurring during the stroke-like episodes. From MRI it is clear that the cortex is often more severely involved than the underlying white matter and that the periventricular white matter is most often preserved (Figs. 24.1 and 24.2). It is also the cortex that enhances after contrast injection (Fig. 24.1). The lesions are variable in size, sometimes small, often large, sometimes single, often multiple, and usually asymmetrical (Fig. 24.2). The distribution of the lesions does not follow vascular supply or vascular border zones. The occipital and posterior temporal areas are preferentially involved (Figs. 24.1 and 24.2). Other areas that may be involved are the thalamus, basal ganglia, and brain stem. Diffuse cerebellar involvement has also been described. In the acute stage the lesions are often swollen. The lesions may increase in size over days. In the course of a few weeks, the lesions may either resolve or leave behind an area of atrophy and altered signal intensity, in particular in the cortex (Fig. 24.2). Over the years MRI may show “migrating infarcts” that leave their traces

in progressive atrophy with enlargement of the ventricular system and subarachnoid spaces (Fig. 24.2). Cerebellar atrophy may be prominent.

Different MRI techniques can be of advantage in MELAS. Gradient-echo techniques are more sensitive to calcium than other techniques. FLAIR images are superior in showing small cortical lesions (Fig. 24.2). These lesions may arise without associated clinical symptoms of stroke. Diffusion-weighted imaging and mapping ADC values are of particular interest during the acute stages of a stroke-like episode (Figs. 24.3 and 24.4). The results reported so far are conflicting. A study with sequential imaging from day 3 up to day 25 shows that lesions in the acute phase may show normal or elevated ADC values in MELAS (Yoneda et al. 1999). Normal or elevated ADC values have also been reported in several other, less systematic studies. This, of course, is contrary to what is seen in ischemic infarctions. However, we and others (Wang et al. 2003) have found strongly reduced ADC values in acute lesions, suggesting cytotoxic edema. It remains unclear why ADC values are raised in the acute lesion in some patients with MELAS. It has been suggested that it is because of the presence of vasogenic edema, but this explanation seems too simple. There is evidence for hyperperfusion in acute MELAS lesions. Both this hyperperfusion with more prominent presence of blood in the voxels and the disruption of the blood-brain barrier may affect the ADC measurements. Perhaps the conflicting findings described are also reflected in the observation that some of the lesions in MELAS disappear after a couple of weeks, whereas others persist or result in focal atrophy. It seems a reasonable assumption that there are differences between subtypes of MELAS lesions, reflected in differences in MR measurements. A more systematic MR approach, follow-up, and analysis could probably better document these differences.

Cerebral angiography, xenon-enhanced computed tomography, and SPECT demonstrate patency of vessels in MELAS and, in fact, vasodilation. The regional cerebral blood flow is increased in the area of an acute lesion (hyperperfusion). This has been documented in SPECT studies with ^{99m}Tc-ethyl cysteinate




Fig. 24.1. A 21-year-old female patient with MELAS and the 3243 mitochondrial DNA mutation. Note the calcium deposits in the globus pallidus on CT (*second row, left*). The globus pallidus has a low signal on T₂-weighted SE images. There is a large lesion in the left temporo-occipital region, involving the cortex and to a lesser extent the subcortical white matter. A small lesion in the body of the caudate nucleus is seen on the right. After contrast administration (*third and fourth row*) it is mainly the affected cortex that enhances

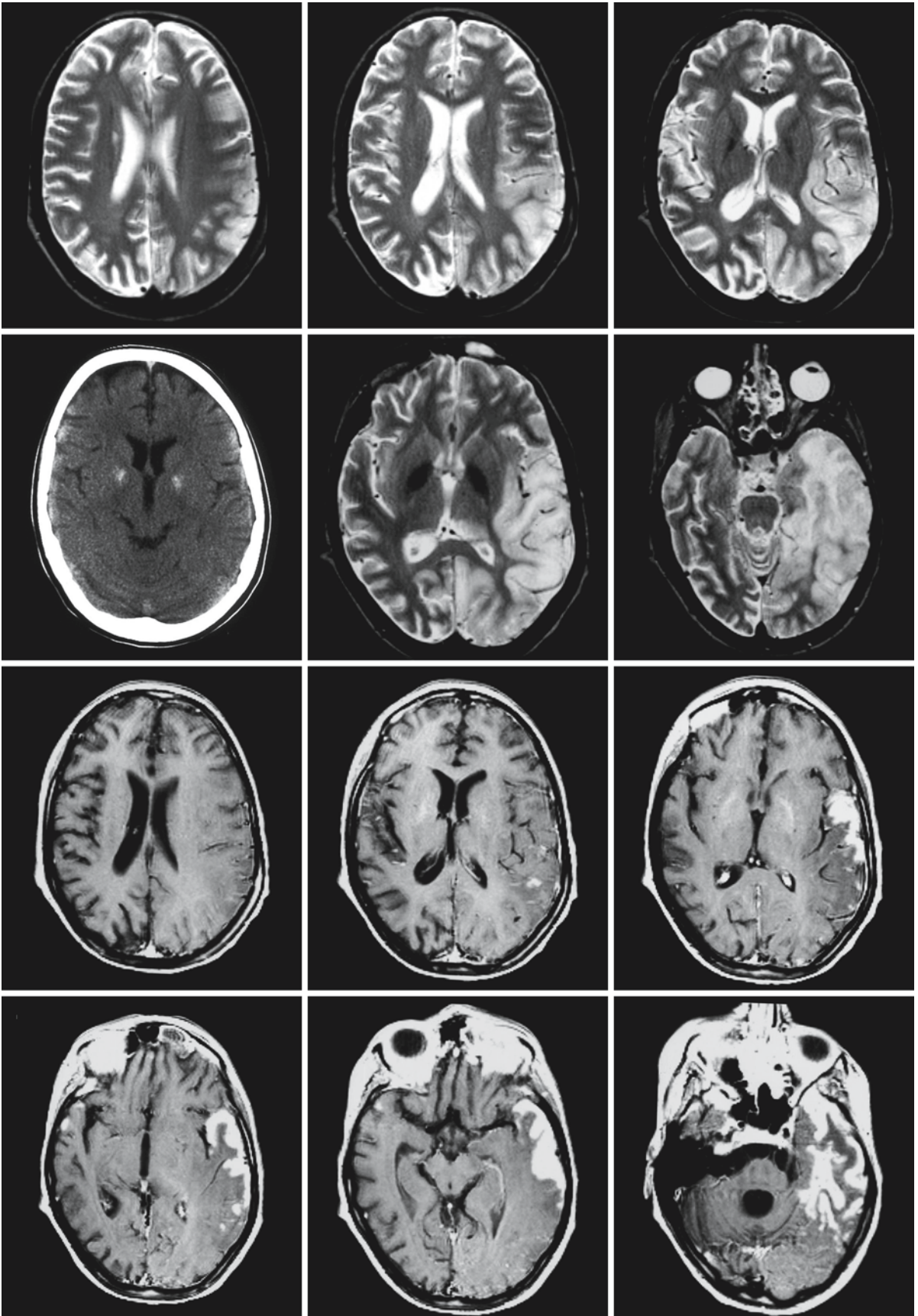


Fig. 24.1.

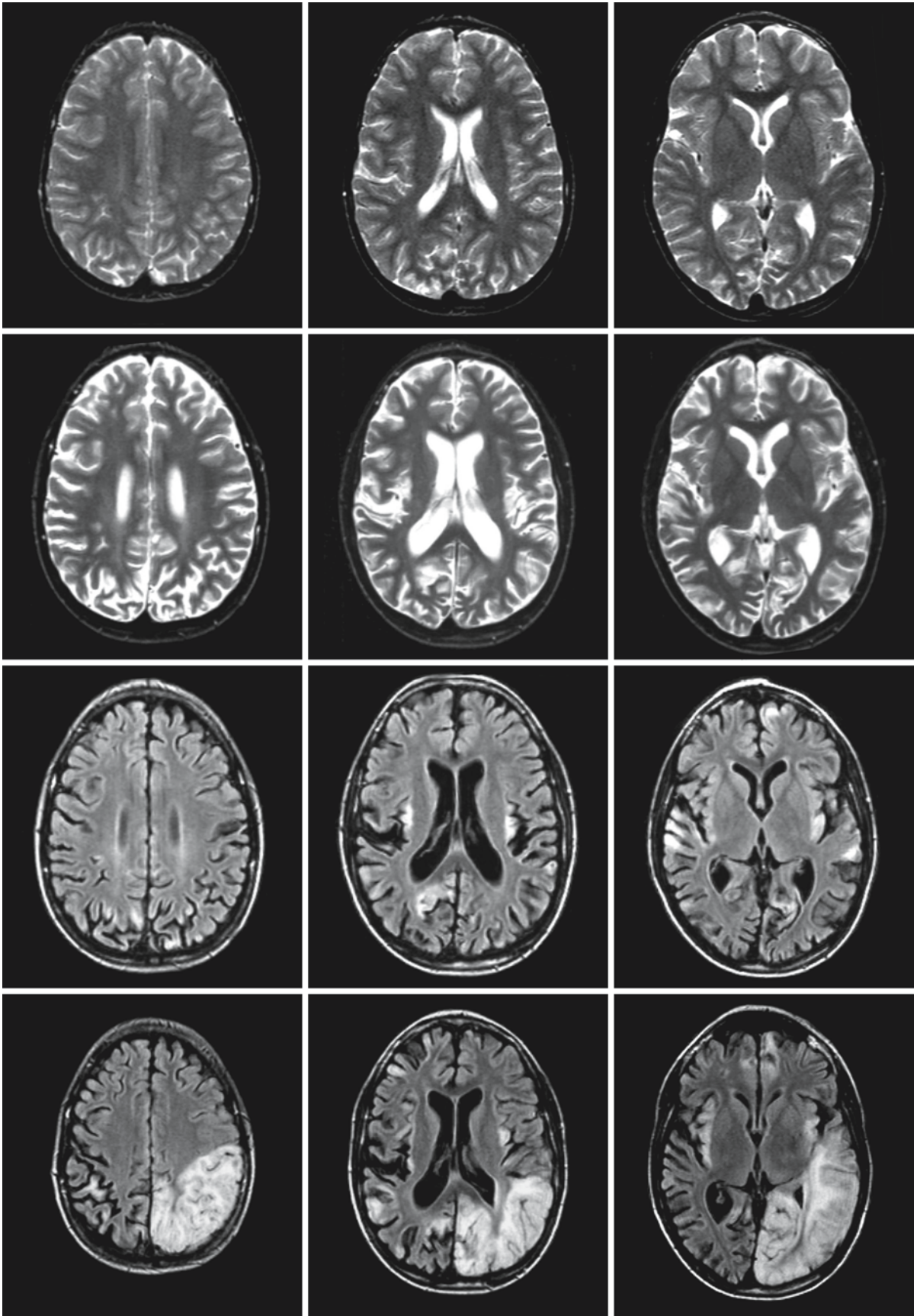


Fig. 24.2.

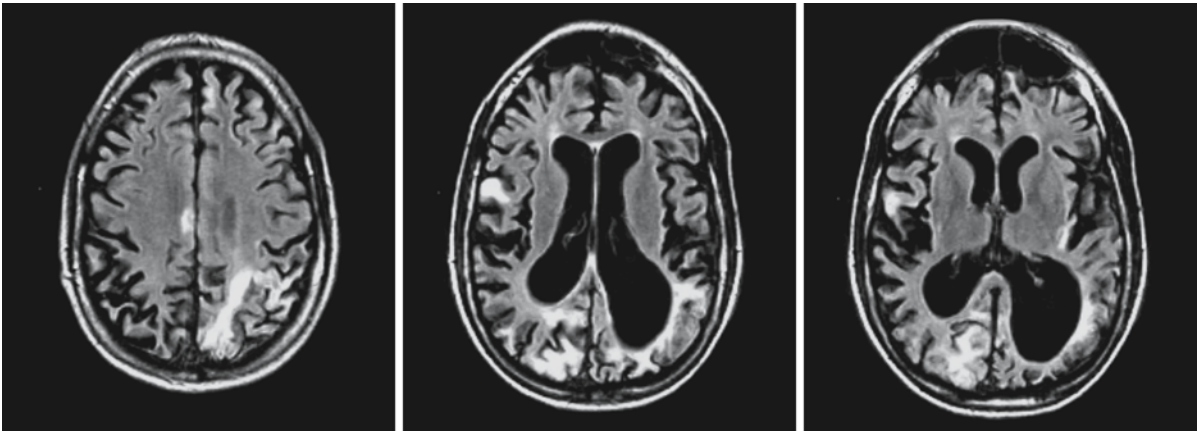


Fig. 24.2. A male patient with MELAS and the 3243 mitochondrial DNA mutation underwent MRI at the ages of 9 years (*first row*), 11 years (*second and third rows*), 12.5 years (*fourth row*), and 15.5 years (*fifth row*). At 9 years, he had seizures and some learning problems, but was otherwise normal. At 11 years, he had seizures and migrainous headaches and was evidently dementing. He had not had any stroke-like episodes. The MRI showed multiple small cortical lesions and generalized cerebral atrophy. The FLAIR images (*third row*) were much better at

showing the cortical lesions. At the age of 12.5 years he had an episode of dysphasia and right-sided hemiplegia and hemianopia. The MRI showed a large lesion in the left temporo-occipital region, involving both cortex and white matter. In addition, multiple old, small cortical lesions were seen. At 15.5 years the patient had serious dementia and dysphasia. MRI showed marked generalized cerebral atrophy as well as focal atrophy of the previously infarcted region

dimer (ECD) and ^{99m}Tc -D,L-hexamethylpropyleneamine oxime (HMPAO). The increased uptake of these substances in the lesion area also suggests a breakdown of the blood-brain barrier. Unfortunately, perfusion studies have not been performed systematically in a large group of MELAS patients, and no reports are available concerning MR perfusion studies of acute lesions. Especially, no data are available linking perfusion studies with ADC maps.

Proton MRS shows low *N*-acetylaspartate in acute lesions and highly elevated lactate. The decrease in *N*-acetylaspartate is at least partially reversible, and in the chronic stage lactate is usually normal or only mildly elevated. Elevated lactate may also be seen in areas that are not clearly abnormal on MR images, but the elevation is usually much more striking in acute and subacute lesions.

The obvious task for MR is to help distinguish between ischemic infarctions and the infarct-like lesions in MELAS. In the younger group it may be important to differentiate the infarct-like lesions of MELAS from the ischemic infarctions in the early

phases of moyamoya disease. The distribution of lesions in patients with moyamoya syndrome can be the same as in MELAS. The abnormal vessels in moyamoya syndrome, usually already seen on conventional MR images, but more clearly on MR angiography, will suggest the latter diagnosis. MELAS also has to be differentiated from vasculitic disorders presenting with multiple infarctions. In a case of predominantly temporal location of the acute lesion, herpes simplex encephalitis may be suspected. The raised serum lactate suggests mitochondrial dysfunction rather than herpes encephalitis, and the calcium deposits which are often present in the basal ganglia in MELAS patients may also help in differentiation. Other multifocal infectious and inflammatory lesions should be considered as well. Single and multiple large areas of abnormal signal intensity in the cortex and white matter are also seen in urea cycle defects. In MRS, however, findings are very different, with raised lactate in MELAS and raised glutamine in urea cycle defects. Assessment of blood lactate and ammonia levels shows a similar difference.

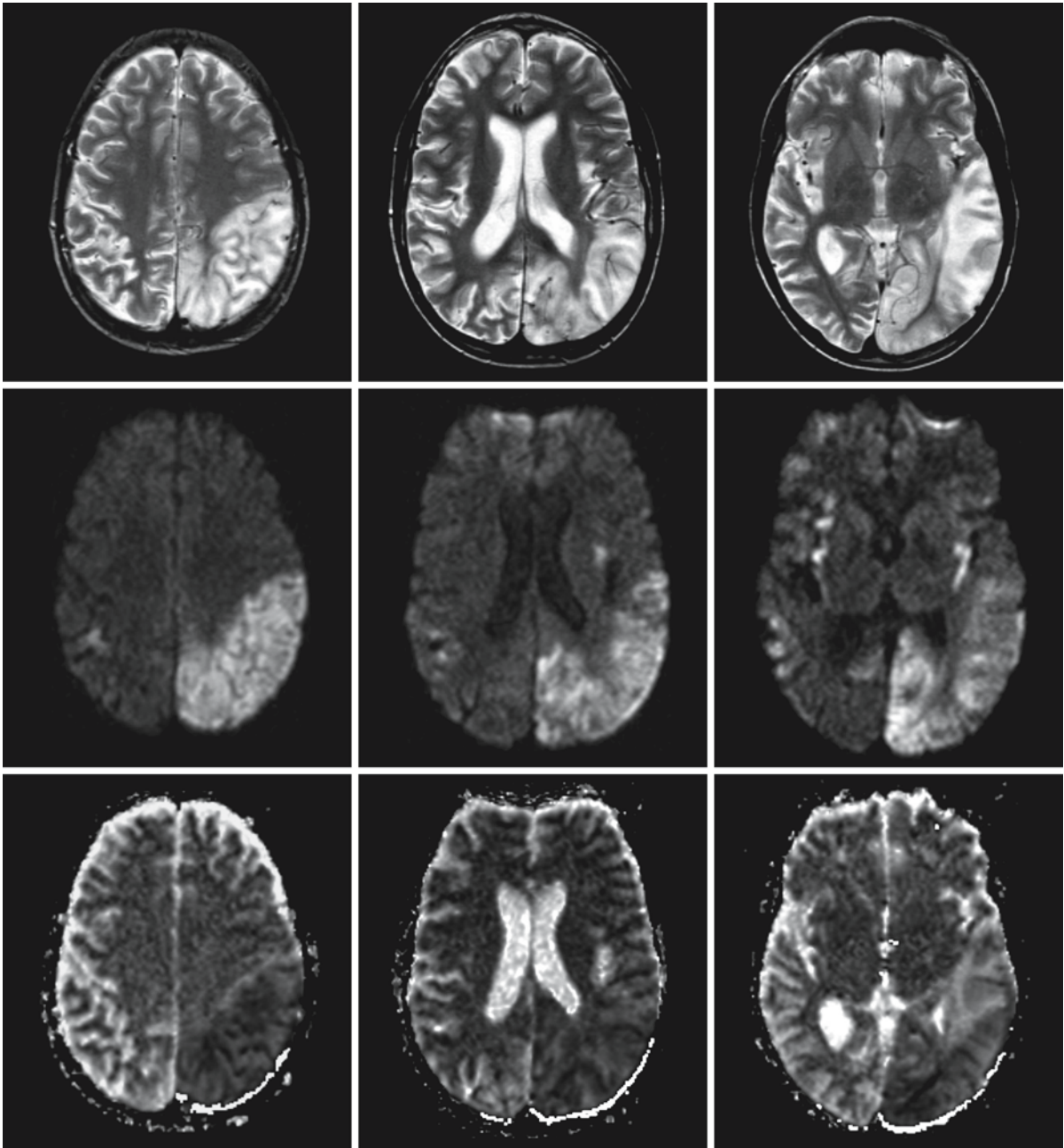


Fig. 24.3. Conventional and diffusion-weighted MRI of the patient in Fig. 24.2 at the age of 12.5 years. To be more precise, the stroke-like episode started with dysphasia, followed after 6 days by development of right-sided hemiplegia and hemianopia. The MRI was obtained 12 days after the onset of the episode. Displayed are T_2 -weighted SE images (*first row*), trace diffusion-weighted images with a b value of 1000 (*second row*), and ADC maps (*third row*). The T_2 -weighted images show the

extent of the lesion. The diffusion-weighted images show high signal in the lesion with an area of lower signal in the occipital white matter. The ADC maps show that the temporal lesion has a high ADC, whereas most of the occipital lesion has a low ADC. The difference in ADC may be related to the different age of the lesions. It could also be that the temporal lesion is more edematous, as suggested by the T_2 -weighted image

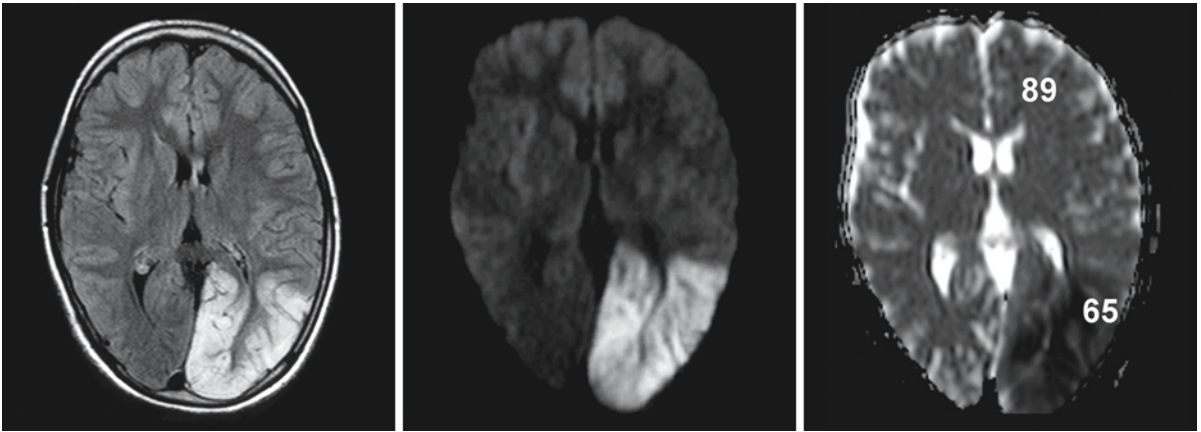


Fig. 24.4. Conventional and diffusion-weighted MRI of a 13-year-old MELAS patient with the 3243 mitochondrial DNA mutation. The MRI was obtained 3 days after the onset of right-sided hemianopia. The FLAIR image (*left*) shows a large

occipital lesion. On the trace diffusion-weighted image with a b value of 1000 (*middle*) the lesion has a high signal, whereas the lesion has a low signal on the ADC map (*right*). The measured ADC is very low

Leber Hereditary Optic Neuropathy

25.1 Clinical Features and Laboratory Investigations

Leber hereditary optic neuropathy (LHON) is a maternally inherited disorder that causes acute or subacute loss of bilateral central vision. The onset is usually asymmetrical, but the interval between involvement of the two eyes is usually less than a few months. Monocular involvement is extremely rare. Men are affected much more frequently than women and the age at onset is usually lower in males than in females. The male preponderance ranges from 80% to 90% in most white pedigrees to approximately 60% in Japanese families. The onset of visual loss typically occurs between the ages of 15 and 35 years, with an age range of 5–70 years. In most patients visual acuities deteriorate to worse than 2/20 in the course of several months, stabilizing thereafter. The loss of vision is usually permanent, but spontaneous improvement or recovery can occur. Transient worsening of vision with exercise or heat may occur (Uhthoff's symptom). Visual field defects are typically central or cecentral, but may also be bitemporal. Headache, eye discomfort, and flashes of light may occur at the time of vision loss. Color vision is affected severely, often early on in the course of vision loss.

The first sign of the disease, peripapillary telangiectatic microangiopathy, is ophthalmoscopically visible in the presymptomatic stage. At the onset of visual loss, the optic disc is swollen and there is marked dilatation and tortuosity of the peripapillary retinal vessels. However, vessels do not leak fluorescein on fluorescein angiography. The typical ophthalmoscopic findings may also be present in asymptomatic family members, but some patients with LHON never exhibit these characteristics, even if examined at the time of acute vision loss. After the development of visual loss, a capillary-poor retina with attenuated arterioles and a pale optic disc remain.

In the majority of patients with LHON, visual dysfunction is the only significant manifestation of the disease. In some pedigrees additional cardiac conduction abnormalities occur, in particular pre-excitation syndromes such as Wolff–Parkinson–White syndrome. Minor neurological abnormalities such as hyperreflexia, Babinski signs, mild ataxia, or peripheral neuropathy have been reported. Several pedigrees have been described in which some of the patients ex-

perience more severe neurological problems. An extrapyramidal movement disorder with bilateral lesions of the basal ganglia on MRI has been reported in several patients. Association with a Leigh-like encephalopathy with brain stem and basal ganglia involvement on MRI has also been observed. The most frequently observed association is with a multiple sclerosis-like disease, and multiple studies have shown that the association is more than coincidental. Episodic neurological abnormalities occur with partial or complete recovery. Apart from optic neuropathy, frequently observed signs include spasticity, cerebellar ataxia, sensory disturbances, vertigo, diplopia, internuclear ophthalmoplegia, and urgency of micturition. The clinical features are indistinguishable from those of multiple sclerosis, except for their occurrence in the context of a family history of LHON. Presence of severe and bilateral visual signs justifies considering the possibility of LHON in otherwise typical multiple sclerosis patients.

Laboratory tests are of limited use in LHON. Fluorescein angiography is helpful for the illustration and confirmation of the LHON fundusoscopic features. VEP studies confirm the absence of any response or presence of responses with prolonged latencies and decreased amplitudes. ERG is typically normal. In patients in whom the disease course resembles that of multiple sclerosis, CSF analysis may reveal an elevation of the IgG index and presence of oligoclonal bands. ECG may reveal conduction abnormalities. In the past, a definitive diagnosis depended on a positive family history, age at onset of the vision loss, and the characteristic circumpapillary microangiopathy of the optic disc in the acute stage. Demonstration of a point mutation in mitochondrial DNA in affected individuals confirms the diagnosis; DNA confirmation of the diagnosis can also be obtained in atypical or sporadic cases.

25.2 Pathology

In LHON severe axonal degeneration with myelin loss of the central part of the optic nerve and pregeniculate pathway is found. The nature of the cerebral multiple sclerosis-like white matter lesions has not yet been investigated.

25.3 Pathogenetic Considerations

A number of mitochondrial DNA mutations have been described in association with LHON. The mutations can be distinguished into high-risk mutations, called class I or primary mutations, and low-risk mutations, called class II or secondary mutations. The most frequent class I mutations include a mutation at nucleotide position 11778 in the mitochondrial gene encoding subunit 4 of complex I, present in 50% of European patients to 95% of Asian LHON patients; a mutation at nucleotide position 3460 in the gene encoding subunit 1 of complex I, present in about 15% of European patients; a mutation at position 14484 in the gene encoding for subunit 6 of complex I, present in about 15% of European patients; and a mutation at position 14459 in the gene encoding for subunit 6 of complex I. In addition, several class II mutations are known, the pathogenic role of which is much less clear. Generally, only one class I mutation occurs in a LHON pedigree and individuals harboring this mutation have a relatively high probability of vision loss. Class I mutations are not observed in the normal population. Class II mutations occur at a much higher frequency among LHON patients than among the normal population. When present in LHON patients, they occur in combination with other class I or II mutations. They may serve as additional predisposing or exacerbating genetic factors that increase the probability of expressing LHON. It is probably the synergistic effect of multiple mitochondrial DNA mutations that, by their accumulative effect on the oxidative phosphorylation, produces a pathogenic reduction in ATP-generating capacity.

For all class I mutations variable penetrance is observed among apparently homoplasmic LHON pedigrees. About 50% of males and 10% of females harboring a pathogenic mutation actually develop LHON. In spite of sharing the same mutations, males have a 4–5 times higher risk of being affected than females. About 15% of the patients are heteroplasmic for a class I mutation, and in about 35% of the families at least one heteroplasmic individual can be identified, but heteroplasmy is not sufficient to explain the observed phenotypic variation. Therefore, class I mutations appear to be necessary but not sufficient for the clinical manifestation of LHON. Additional genetic (nuclear or mitochondrial), environmental, or physiological factors may play a significant role in the expression of LHON. Both internal and external environmental factors may play a role. Systemic illnesses, nutritional deficiencies, and toxins that stress or inhibit the body's mitochondrial respiratory capacity could conceivably initiate or increase phenotypic expression of the disease. Adverse effects of tobacco smoke (cyanide present in tobacco smoke inhibits cytochrome-*c* oxidase activity) and alcohol have been

suggested but never proven. The male preponderance and earlier onset for males suggest a recessive susceptibility gene on the X chromosome acting in synergy with the mitochondrial DNA mutation. Affected females heterozygous for the X-chromosomal susceptibility gene may be involved because of unfortunate X chromosome inactivation.

Almost all class I mutations alter mitochondrial DNA-encoded subunits of complex I. The LHON mutations do not alter the amount, assembly, and stability of complex I. However, various mutations have been shown to affect complex I function, resulting in altered electron transport capacity, respiration rate, and ATP production. It is suggested that the decline in oxidative phosphorylation capacity caused by a combination of influences (class I and class II mutations, X-linked nuclear factor, other genetic factors, environmental factors, effects of aging) may result in optic atrophy, cardiac conduction abnormalities, and neurological disease. With regard to those pedigrees with LHON and neurological disease, it would appear that certain mitochondrial DNA mutations may be particularly responsible. The mutation at position 14459 is frequently associated with a combination of LHON and dystonia. Females with the 11778 mutation are especially likely to develop clinical and neuroimaging findings indistinguishable from multiple sclerosis.

25.4 Therapy

No effective treatment to prevent or halt LHON has as yet been found.

25.5 Magnetic Resonance Imaging

In patients with LHON, optic nerve abnormalities can be shown with STIR (short tau inversion recovery) sequences. Increased signal intensity of the mid and posterior intraorbital section of the optic nerve is seen, sparing the anterior portion. In most patients brain MRI is normal. In LHON associated with dystonia, bilateral putamen lesions have been found. In patients with a Leigh-like presentation, additional brain stem lesions are found. Cerebellar atrophy has also been reported. In patients with a multiple sclerosis-like disease, multiple small white matter lesions are seen as in multiple sclerosis (Fig. 25.1). The lesions are found in the periventricular and deep white matter of the cerebral hemispheres, in the brain stem, and in the cerebellum. The periventricular white matter is predominantly involved. On the basis of MRI only, differentiation between LHON and multiple sclerosis is not possible. In MRS we found no elevation of lactate in LHON.

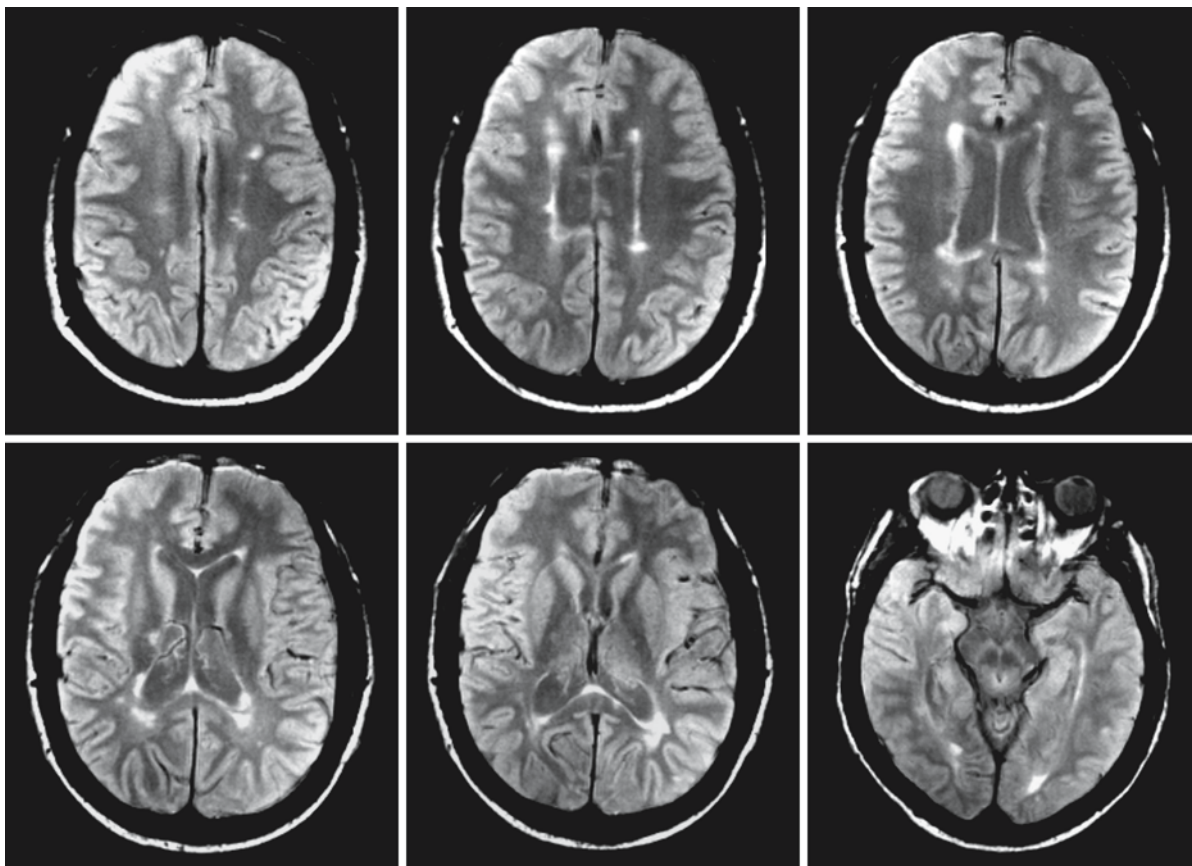


Fig. 25.1. Male patient, 43 years of age, with LHON. The transverse proton density series shows a white rim around the ventricles, involvement of the corpus callosum, and some isolated spots in the centrum semiovale. The ventricles are slightly enlarged

Kearns–Sayre Syndrome

26.1 Clinical Features and Laboratory Investigations

Kearns–Sayre syndrome (KSS) is a rare, sporadic disorder that affects males and females equally. Disease onset is before the age of 20 years. The sequence of manifestations is not constant, but the signs and symptoms in themselves are consistent. Early development is normal. Ptosis and chronic progressive external ophthalmoplegia are usually the initial signs. Apart from progressive external ophthalmoplegia the typical clinical triad includes pigmentary degeneration of the retina and cardiac conduction block. The fine salt-and-pepper type of atypical retinitis pigmentosa is usually associated with good visual function and follows a benign course. Incidentally, chorioideremia is present instead of pigmentary retinopathy. The most common cardiac conduction blocks are complete atrioventricular block, bundle branch blocks, and fascicular blocks. Other frequently noted signs are short stature due to progressive growth failure, delayed psychomotor development, sensorineural hearing loss, cerebellar ataxia, proximal myopathy, cardiomyopathy, and sensory neuropathy. Less frequent are pyramidal dysfunction and dementia. Seizures may occur. Endocrine disease is often present and may include primary gonadal failure, delayed puberty, diabetes mellitus, growth hormone deficiency, hyperaldosteronism, hypothyroidism, hypoparathyroidism, ACTH deficiency, and primary adrenal insufficiency. Hypomagnesemia may occur. Some patients have a mottled, hyperpigmented skin. Cardiac arrhythmias and congestive cardiomyopathy may be the cause of death. Cardiogenic embolism and stroke may also occur and contribute to the disability and the risk of death.

Incidental patients have been reported who suffered from Pearson syndrome in infancy, followed later by KSS. Pearson syndrome comprises refractory sideroblastic anemia requiring transfusions, thrombocytopenia, neutropenia, pancreatic insufficiency, and hepatic dysfunction. Onset is in infancy and most patients die in early childhood from a combination of pancreatic, hepatic, renal, and bone marrow insufficiency. Some children survive the infantile period and no longer need repeated blood transfusions. These patients subsequently developed KSS syndrome. Incidental KSS patients have also been reported who de-

velop aplastic anemia without other signs of Pearson syndrome.

Laboratory investigations in KSS almost invariably reveal an increased CSF protein level, usually above the level of 1 g/l. Blood and CSF lactate and pyruvate are usually elevated. Signs of variable endocrine dysfunction are frequently found. EMG may reveal signs of a myopathy. ECG shows evidence of a disturbance of cardiac conduction. Echocardiography and chest X-ray may show cardiomegaly.

Biochemical analysis of muscle tissue reveals decreased activity of respiratory complexes I, III, and IV, individually or in combination. The diagnosis is confirmed by demonstrating a heteroplasmic, single, large-scale deletion of mitochondrial DNA or, rarely, a mitochondrial DNA duplication.

26.2 Pathology

On light microscopic examination of muscle biopsies, application of the modified Gomori trichrome stain reveals the presence of ragged red fibers. With this stain the abnormal fibers demonstrate a mottled and irregular appearance with red-staining peripheral and intermyofibrillar zones. Histochemistry for oxidative enzymes such as NADH dehydrogenase, succinate dehydrogenase, and cytochrome-*c* oxidase may yield abnormal staining patterns. On electron microscopy, the ragged red fibers display large aggregates of mitochondria, generally under the sarcolemma, but also between myofibrils. The mitochondria are frequently abnormal in size and structure. The mitochondrial cristae are often increased in number and irregularly oriented. The mitochondria may contain different abnormal inclusions such as crystalline or paracrystalline structures or globular bodies.

In KSS the main finding on postmortem examination is a spongy state of the cerebral white matter due to splitting of myelin sheaths. The axons are generally preserved. The white matter changes are diffusely observed in the frontal, parietal, temporal, and occipital lobes of both hemispheres. It is the hemispheric white matter that is involved, whereas the corpus callosum and internal capsule tend to be preserved. The U fibers are preferentially affected. The cerebral cortex is intact. The basal ganglia are involved, in particular the globus pallidus and caudate nucleus, but the

putamen, thalamus, hypothalamus, subthalamic nuclei, and substantia nigra may also be affected. The basal ganglia lesions are characterized by loss of nerve cells, spongiosis, gliosis, and capillary proliferation. Within the globus pallidus perivascular depositions of calcium and intracellular depositions of iron may be seen. The same type of depositions may be seen within the caudate nucleus, dentate nucleus, and the putamen. Within the cerebellar cortex, loss of Purkinje cells may be seen. The cerebellar white matter displays spongiosis and gliosis. In the brain stem spongiosis and gliosis have been reported in white matter structures, in the pontine and midbrain tegmentum, red nucleus, substantia nigra, and other gray matter nuclei. Within the spinal cord vacuolation of tracts, in particular the dorsal columns, may be seen.

Cardiomyopathy with ragged red fibers may be found. The pancreas may display fatty infiltration. The adrenals may be atrophic and small. Glomerular and tubular abnormalities may be found in the kidneys. The lobules of the testes may be atrophic with marked overgrowth of fibrous tissue.

26.3 Pathogenetic Considerations

In most KSS patients large deletions of mitochondrial DNA are present. Large deletions of a substantial proportion of mitochondrial DNA have been described in chronic progressive external ophthalmoplegia (CPEO), Pearson syndrome, and KSS. These syndromes are clinically overlapping: muscle weakness and chronic progressive external ophthalmoplegia form part of the symptomatology in KSS. Although the size and the position of the large deletions ranges from 1.8 to 8 kilobases, the same 4.977-kilobase deletion is known to occur most often and is therefore known as “the common 5-kb deletion.” Most deletions are flanked by direct repeats, suggesting that homologous recombination or slip-replication may be responsible for the deletion. Despite the deletion, the mitochondrial genomes are usually competent for replication and transcriptionally active. Most frequently, the deleted segment encompasses some of the genes encoding the 13 proteins of the respiratory chain, but also several genes encoding tRNAs. This explains the decrease in all mitochondrial translation products demonstrated in immunological and biochemical analyses, leading to respiratory chain dysfunction. Biochemical analysis reveals decreased activity of complexes I, III, and IV, individually or in combination. Although large single deletions of mitochondrial DNA were initially thought to underlie KSS, the genetic abnormality is more complex. Mitochondrial DNA duplications appear frequently to be present as well, and there may be multiple deletions.

In all patients the deletions are heteroplasmic. Part of the relationship between genotype and phenotype can be explained by heteroplasmy with different percentages of mutant mitochondrial DNA in different tissues and changes of percentages with course of time. An increase with time of the mutated mitochondrial DNA fraction has been reported, paralleling the progression of the disease. In patients surviving Pearson syndrome it is likely that the patient initially had a high percentage of mitochondrial DNA with a deletion in blood cells. The spontaneous recovery indicates that selection favoring normal cells may occur *in vivo*. The percentage of deleted mitochondrial DNA is similar in muscles of both CPEO and KSS patients, but deletions are restricted to skeletal muscle in CPEO and widely distributed in extramuscular tissues in KSS. In Pearson syndrome mitochondrial DNA defects are present in high amounts in all tissue, in particular in blood and bone marrow. The proportion in blood and bone marrow probably falls with age if the patient survives, whereas conversely an increase in proportion of deleted mitochondrial DNA has been shown in repeated investigation of muscle tissue. In KSS patients the deletion is usually present in only a small proportion of peripheral blood cells.

The deletions are sporadic. The deletions are not present in mothers of patients or in children of affected mothers. Apparently, the deletions occur in the oocyte or zygote and affect somatic rather than germ cells. An alternative explanation for not finding the deletion in offspring of KSS mothers could be that oocytes containing mitochondrial DNA deletions may not be viable for gametogenesis and fertilization. By means of unequal mitotic segregation the deletion is spread among part of the cells of the body of the embryo and fetus. Replication of genomes containing the deletion occurs more rapidly, and as a consequence selection of respiratory-deficient cells may occur in the rapid-turnover tissues.

KSS is considered a clinical diagnosis and multiple KSS patients have been reported with other mitochondrial DNA abnormalities than those described above, including point mutations, multiple deletions, and mitochondrial DNA depletion. It is striking that as a rule these patients do not have the same abnormalities on MRI of the brain as are observed in patients with classical KSS. In most of these patients MRI of the brain is normal.

26.4 Therapy

Symptomatic treatment is important in KSS. Cardiac conduction defects often require medication or the implantation of a pacemaker. Endocrine dysfunction can be treated adequately.

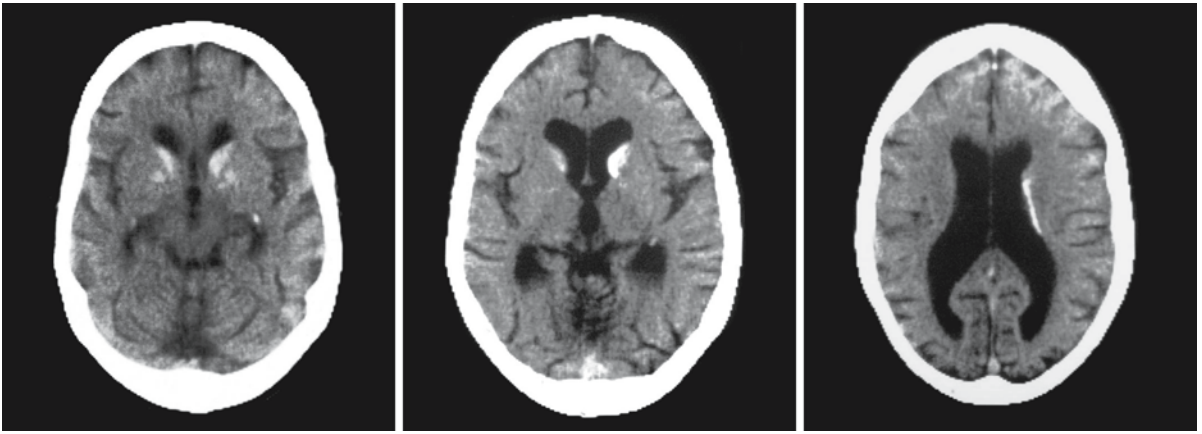


Fig. 26.1. Male patient, 29 years old, with KSS. The CT scan reveals calcium in the head and tail of the caudate nucleus and in the globus pallidus. There is some generalized atrophy

Administration of cofactors has often been employed in an attempt to ameliorate the course of disease. Coenzyme Q₁₀, cytochrome *c*, flavin adenine dinucleotide, riboflavin, thiamine, nicotinamide, vitamin C, and vitamin K₃ (menadione) have been given alone or in varying combinations and variable improvement has been reported. However, none of these has led to a consistent improvement of ocular movements, CNS symptoms, and cardiac function.

26.5 Magnetic Resonance Imaging

In KSS CT scan often reveals calcium deposits in the globus pallidus and caudate nucleus in addition to low density of the cerebral white matter and progressive atrophy (Fig. 26.1). In some patients the calcium deposits are more widespread and also occur in the cerebral white matter. In the absence of calcium deposition, low density of the globus pallidus may be apparent.

MRI often shows a characteristic pattern with symmetrical lesions of the globus pallidus and thalamus and subcortical white matter abnormalities (Figs. 26.2–26.4). Other central nuclei that are often involved include the caudate nucleus, substantia nigra, and red nuclei. The putamen is usually less prominently involved. The white matter abnormalities are symmetrical and tend to involve all subcortical white matter in a patchy or confluent way, sparing the periventricular white matter and corpus callosum, although in our experience the splenium of the corpus callosum is usually affected. The cerebellar white matter may also be involved. Often extensive brain stem abnormalities are seen, in particular involving the brain stem tegmentum. Cerebellar and to a lesser extent cerebral atrophy may occur.

The full-blown pattern in KSS is diagnostic. However, the pattern develops over time and in the earlier stages only limited abnormalities in some of the structures may be seen. In these patients, the differential diagnosis is longer. MRS shows elevated lactate in KSS, which may aid the diagnosis.

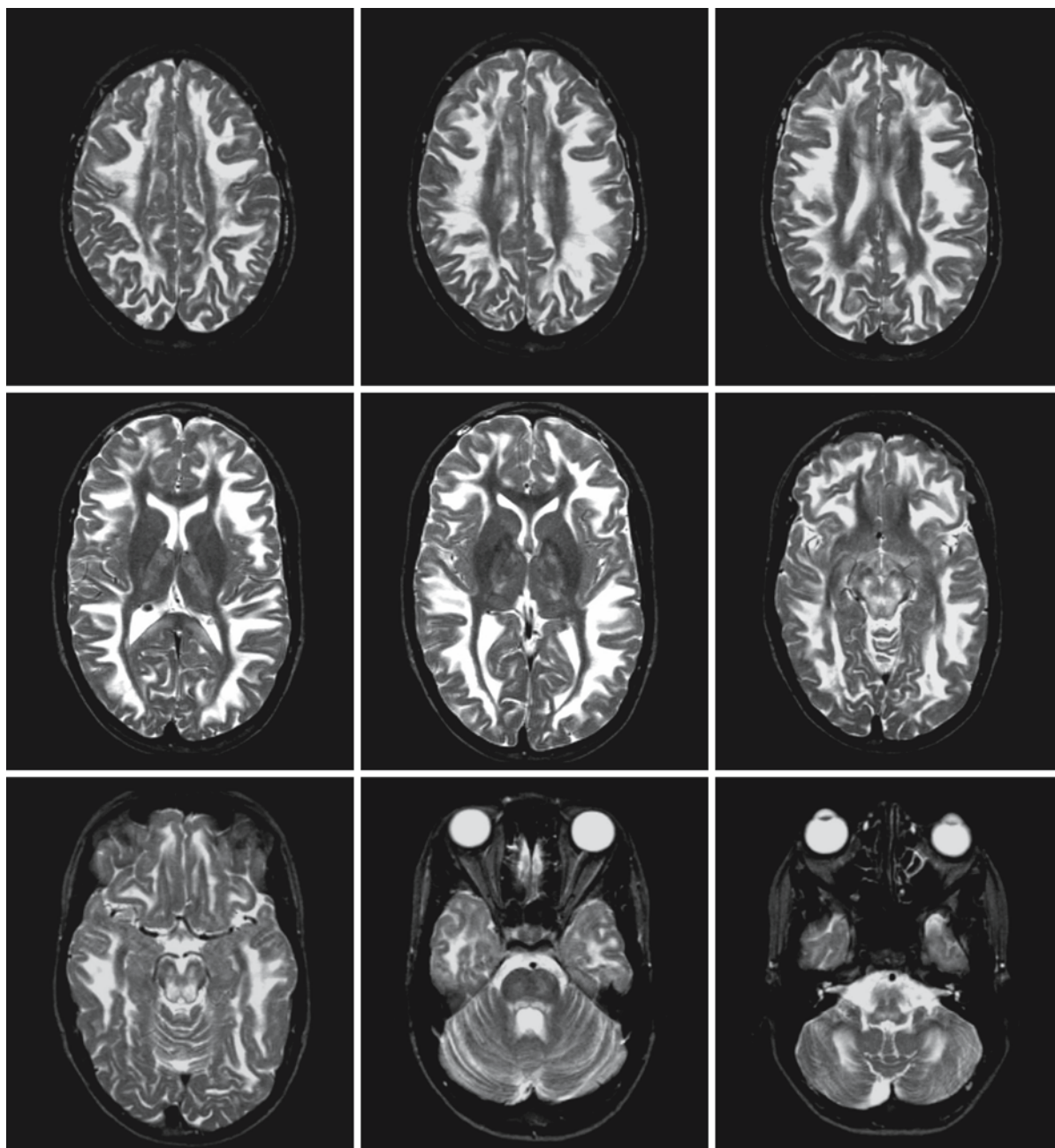


Fig. 26.2. A 15-year-old male patient with KSS. There are extensive cerebral white matter abnormalities with predominant involvement of the deep and subcortical white matter and sparing of the periventricular white matter and corpus callosum, except for the splenium. There are mild signal abnor-

malities in the thalamus and globus pallidus. It is not clear to what extent the posterior limb of the internal capsule is involved. Note the brain stem abnormalities, predominantly involving the midbrain, pontine tegmentum, and medulla. The cerebellar white matter is also involved

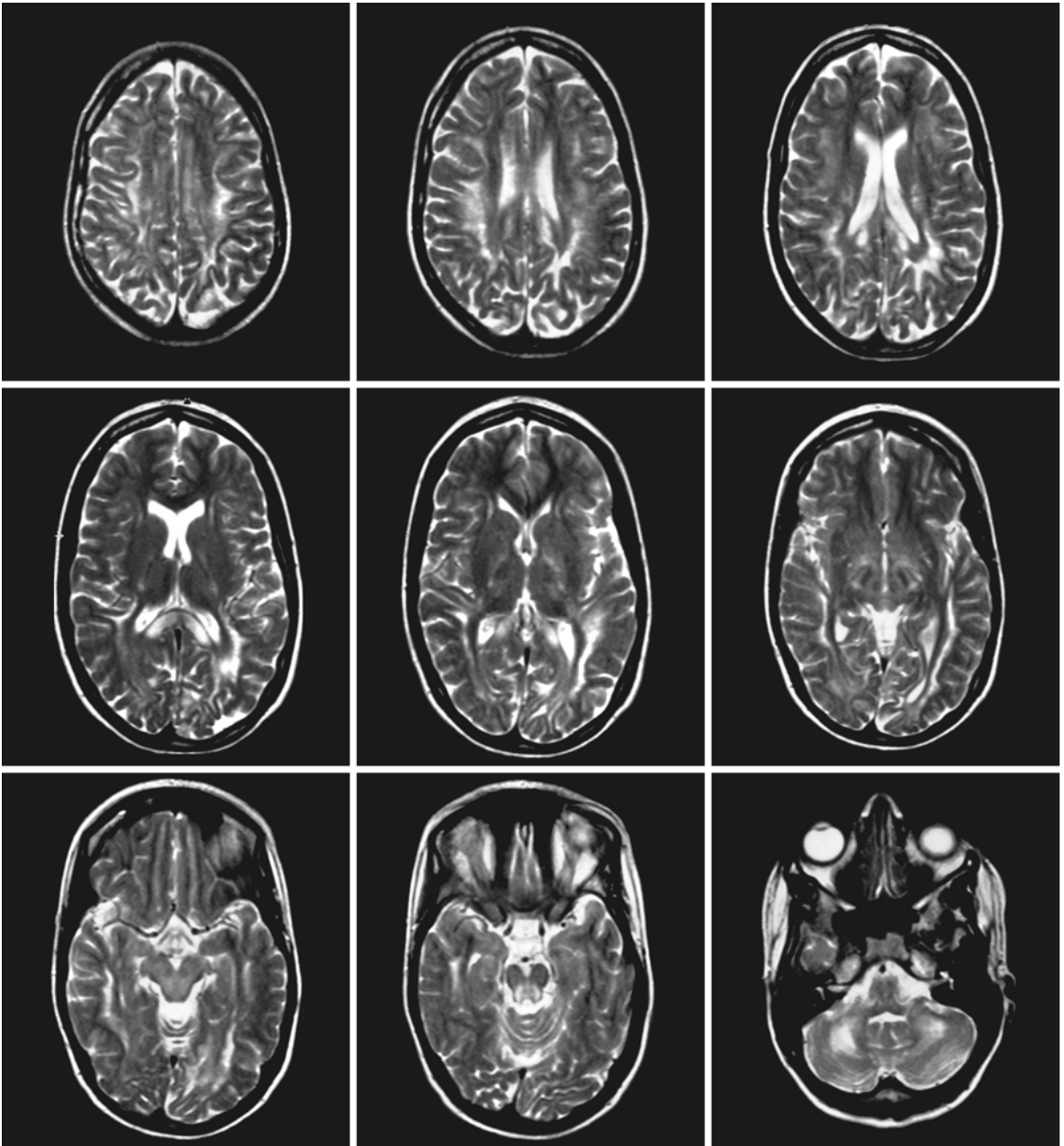


Fig. 26.3. A 21-year-old female patient with KSS. The white matter abnormalities are less impressive and appear to involve the deep white matter with relative sparing of the U fibers and complete sparing of a periventricular rim. The splenium of the corpus callosum is prominently involved. There are subtle sig-

nal changes in the globus pallidus, thalamus, and posterior limb of the internal capsule. Note the brain stem and cerebellar white matter abnormalities. Courtesy of Dr. T. van Laar and Dr. J.C.H van Oostrom, Department of Neurology, University Hospital Groningen, The Netherlands

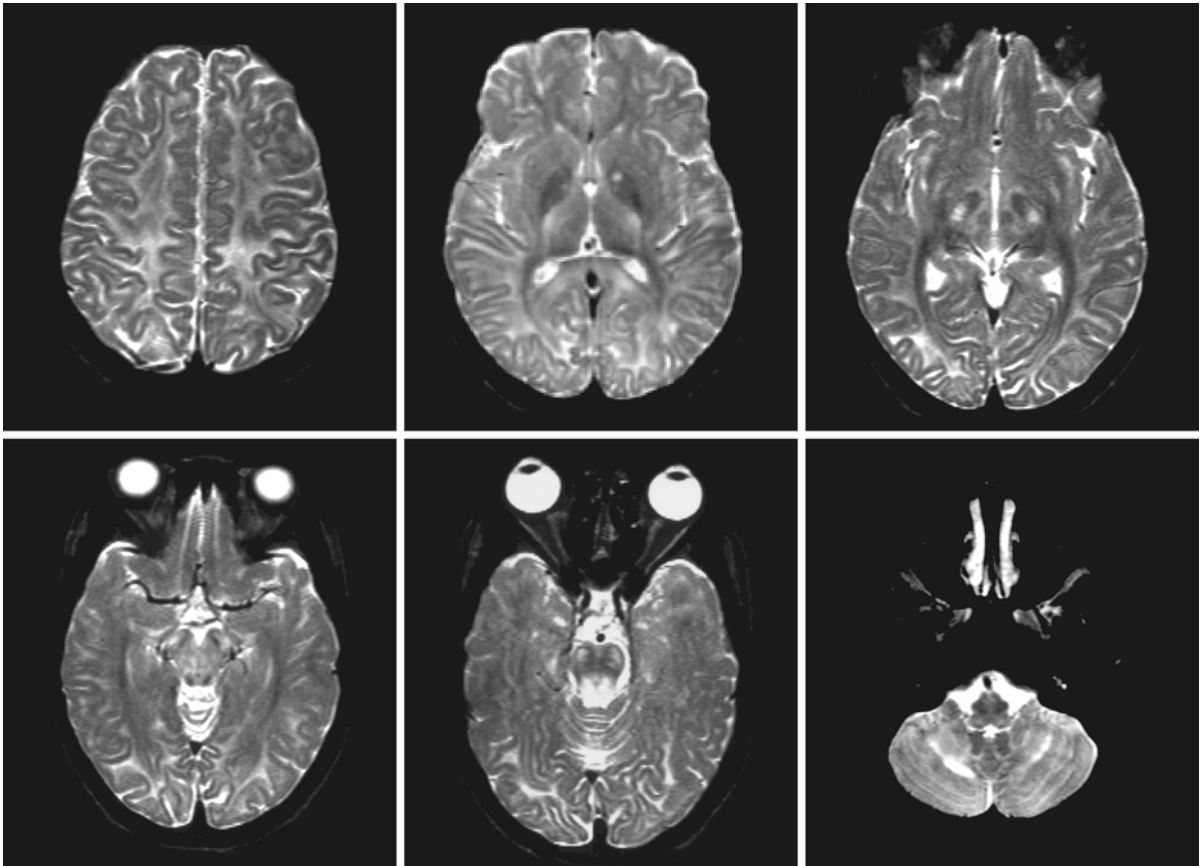


Fig. 26.4. The MRI of a 13-year-old female KSS patient displays more diffuse, mild signal changes in the cerebral white matter. The subcortical white matter in the parietal and occipital region has a more pronounced signal abnormality than the remainder of the cerebral white matter. The sparing of the periventricular white matter is less clear. Again, the splenium of the corpus callosum is involved. There are signal abnormal-

ities in the thalamus, globus pallidus, and corticospinal tracts in the posterior limb of the internal capsule, midbrain, and pons. The pontine tegmentum, cerebellar white matter, and medulla also contain signal abnormalities. Courtesy of Dr. S. Blaser, Department of Diagnostic Imaging, Hospital for Sick Children, Toronto, Canada

Mitochondrial Neurogastrointestinal Encephalomyopathy

27.1 Clinical Features and Laboratory Investigations

Mitochondrial neurogastrointestinal encephalomyopathy (MNGIE) is a multisystem mitochondrial disease which has also been described under a number of other acronyms: myoneurogastrointestinal encephalopathy (also MNGIE); polyneuropathy, ophthalmoplegia, leukoencephalopathy, and intestinal pseudo-obstruction (POLIP); oculogastrointestinal muscular dystrophy (OGIMD); mitochondrial encephalomyopathy with sensorimotor polyneuropathy, ophthalmoplegia, and pseudo-obstruction (MEPOP); and chronic intestinal pseudo-obstruction (CIPO) with myopathy and ophthalmoplegia.

The disease has an autosomal recessive mode of inheritance. In the majority of the patients symptoms have their onset between the first and fifth decade, with a mean of 19 years and extremes of 5 months and 45 years. Initial symptoms are most frequently gastrointestinal, ocular, or both. Gastrointestinal signs include dysphagia, borborygmi, abdominal pain, cramps, recurrent nausea, vomiting, diarrhea, malabsorption, diverticulosis, and pseudo-obstruction. In most patients, delayed gastric emptying and dysmotility of small intestine, esophagus, and/or pharynx are found. The gastrointestinal dysmotility is caused by visceral myopathy and visceral neuropathy. Some patients have liver problems, which may end in liver cirrhosis. Most often the liver problems are attributable to parenteral nutrition. Ocular signs include chronic progressive external ophthalmoplegia, ptosis, and pigmentary retinopathy. Other common clinical features include thin body habitus, short stature, tinnitus, sensorineural hearing loss, sensorimotor peripheral neuropathy, and myopathy. Limb weakness is either distal, proximal, or diffuse. Areflexia may be present. There is rarely evidence of CNS involvement. Mental retardation is rare. The average life expectancy in MNGIE is 38 years, with a range of 26–58 years.

Laboratory investigations may reveal elevated blood lactate and pyruvate. CSF protein level is often raised. Nerve conduction velocity is moderately to markedly decreased and EMG reveals signs of denervation. These findings are consistent with a combination of demyelination and axonal loss. In addition, some myopathic changes may be present in the EMG.

Some patients have an abnormal ECG with evidence of conduction disturbances. Laboratory studies show various mitochondrial abnormalities in skeletal muscle, including ragged red fibers with ultrastructurally abnormal mitochondria, muscle fibers with increased succinate dehydrogenase stain, cytochrome-*c* oxidase-negative fibers, and decreased activities of respiratory chain enzymes. In addition, multiple mitochondrial DNA deletions or mitochondrial DNA depletion or both are found.

The diagnosis is confirmed by demonstrating elevated thymidine levels in plasma and deficient thymidine phosphorylase activity in leukocytes. DNA-based confirmation of the diagnosis is also possible.

27.2 Pathology

In MNGIE cerebral gray matter structures are intact. Myelin pallor is found in the cerebral hemispheres, extending from the periventricular area into the arcuate fibers and into the internal capsule. The white matter is also pale in axonal preparations, but myelin pallor is relatively more marked. The corpus callosum is well myelinated. There are no signs of active myelin breakdown, no necrosis, and no significant astrogliosis. Electron microscopy provides some evidence of loosening and thinning of myelin sheaths. Similar changes are present in the cerebellar white matter. Myelin pallor is also seen in the central part of the pons. The optic nerves show myelin pallor, some vacuolation, and some axonal loss. In the cranial nerves myelin pallor and endoneurial fibrosis are seen. In the spinal cord, tracts are either normal or also show some myelin pallor and vacuolation, in particular involving the dorsal columns. Within the spinal roots marked endoneurial fibrosis and myelin pallor are present, the changes being more severe in the dorsal than in the anterior roots. Within peripheral nerves variable combinations of scanty presence of myelin sheaths, abnormal internodal length, (rarely) onion bulbs, axonal loss, excessive endoneurial fibrosis, and perineural thickening are seen. Thus, the neuropathy displays mixed features of segmental demyelination and axonal degeneration. Visceral nerves show axonal loss.

27.3 Pathogenetic Considerations

MNGIE is related to mutations in the thymidine phosphorylase gene, *TP*, located on chromosome 22q13.32-qter. Thymidine phosphorylase catalyzes the reversible phosphorolysis of the nucleoside thymidine to thymine and 2-deoxy D-ribose 1-phosphate. The enzyme is likely to have an important role in nucleoside homeostasis by regulating the availability of thymidine for DNA synthesis. The forward reaction, conversion of thymidine to thymine, is favored under physiological conditions, and a defect in thymidine phosphorylase leads to accumulation of thymidine. In normal cells, thymidine is either degraded to thymine by thymidine phosphorylase or salvaged to deoxythymidine monophosphate by thymidine kinase and reutilized for DNA synthesis through nucleotide pools. Because the thymidine salvage pathway is the only available metabolic pathway for thymidine in MNGIE patients, a large amount of thymidine should be salvaged to deoxythymidine monophosphate and subsequently converted to deoxythymidine triphosphate. The accumulation of thymidine is therefore likely to alter nucleoside and nucleotide pools. Mitochondria have separate and independently regulated nucleotide pools and distinct thymidine kinase. Mitochondria depend more on the thymidine salvage pathway than on the de novo synthetic pathway. Mitochondrial DNA constantly replicates, even in quiescent cells. Therefore a constant supply of nucleotides is essential for the maintenance of the mitochondrial genome. Because of these unique properties of mitochondria, the imbalance in nucleotide pools probably affects mitochondrial DNA more adversely than nuclear DNA, impairing mitochondrial DNA replication, repair, or both, and resulting in mitochondrial DNA depletion and multiple deletions.

Thymidine phosphorylase also has extracellular functions and is involved in angiogenesis and cell trophism. Thymidine phosphorylase is also called endothelial cell growth factor 1, because of its angiogenic properties, and gliostatin, to denote its inhibitory effects on glial cell proliferation. MNGIE patients do not have vascular problems, suggesting that decreased thymidine phosphorylase activity does not interfere with normal angiogenesis.

The nature of the nervous system pathology in MNGIE is enigmatic. In both the CNS and PNS, myelin and axons are involved, but myelin more so than axons. It is remarkable that in PNS histopathological abnormalities are associated with evident signs of dysfunction (peripheral polyneuropathy, visceral neuropathy), whereas patients rarely have overt signs of CNS dysfunction. This and the nature of the histopathological findings constitute arguments for abnormal myelination (dysmyelination) rather than demyelination.

27.4 Therapy

No successful treatment is available. The use of coenzyme Q, vitamin C, thiamin, riboflavin, and other vitamins does not halt progression of the disease. Treatment in MNGIE is largely supportive. Management of the gastrointestinal and nutritional problems is important. Parenteral nutrition may be necessary. Pharmacotherapy and celiac plexus neurolysis may achieve symptomatic pain relief in selected cases.

27.5 Magnetic Resonance Imaging

In MNGIE CT reveals diffuse hypodensity of cerebral and cerebellar white matter. MRI shows diffuse high signal intensity of cerebral and cerebellar white matter on T₂-weighted and FLAIR images, and usually but not invariably sparing of the U fibers and corpus callosum (Figs. 27.1 and 27.2). The thalami and basal ganglia may display patchy signal abnormalities (Fig. 27.1), but are spared in other patients (Fig. 27.2). The internal capsule, external capsule, brain stem, and middle cerebellar peduncles may be involved as well. In some patients the white matter abnormalities on MRI are more limited in extent and involve the periventricular white matter most prominently.

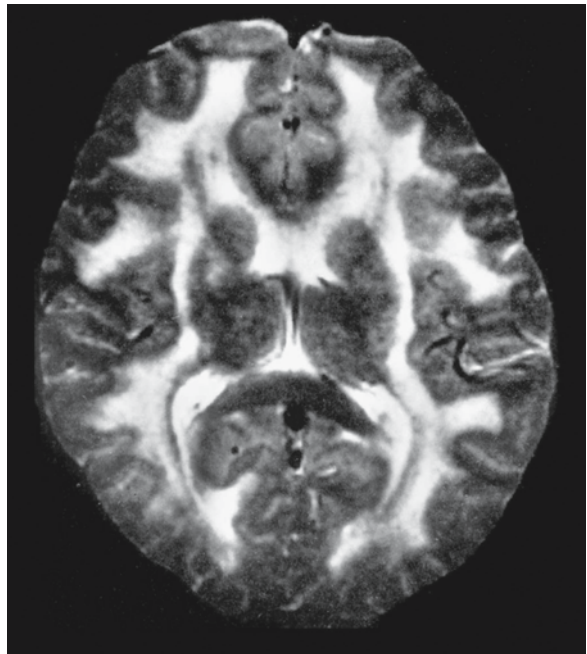


Fig. 27.2. A 17-year-old patient with MNGIE. Note the diffusely high signal intensity of the cerebral white matter on this T₂-weighted MR image. The corpus callosum, internal capsule, and optic radiation are spared. From Simon et al. (1990), with permission

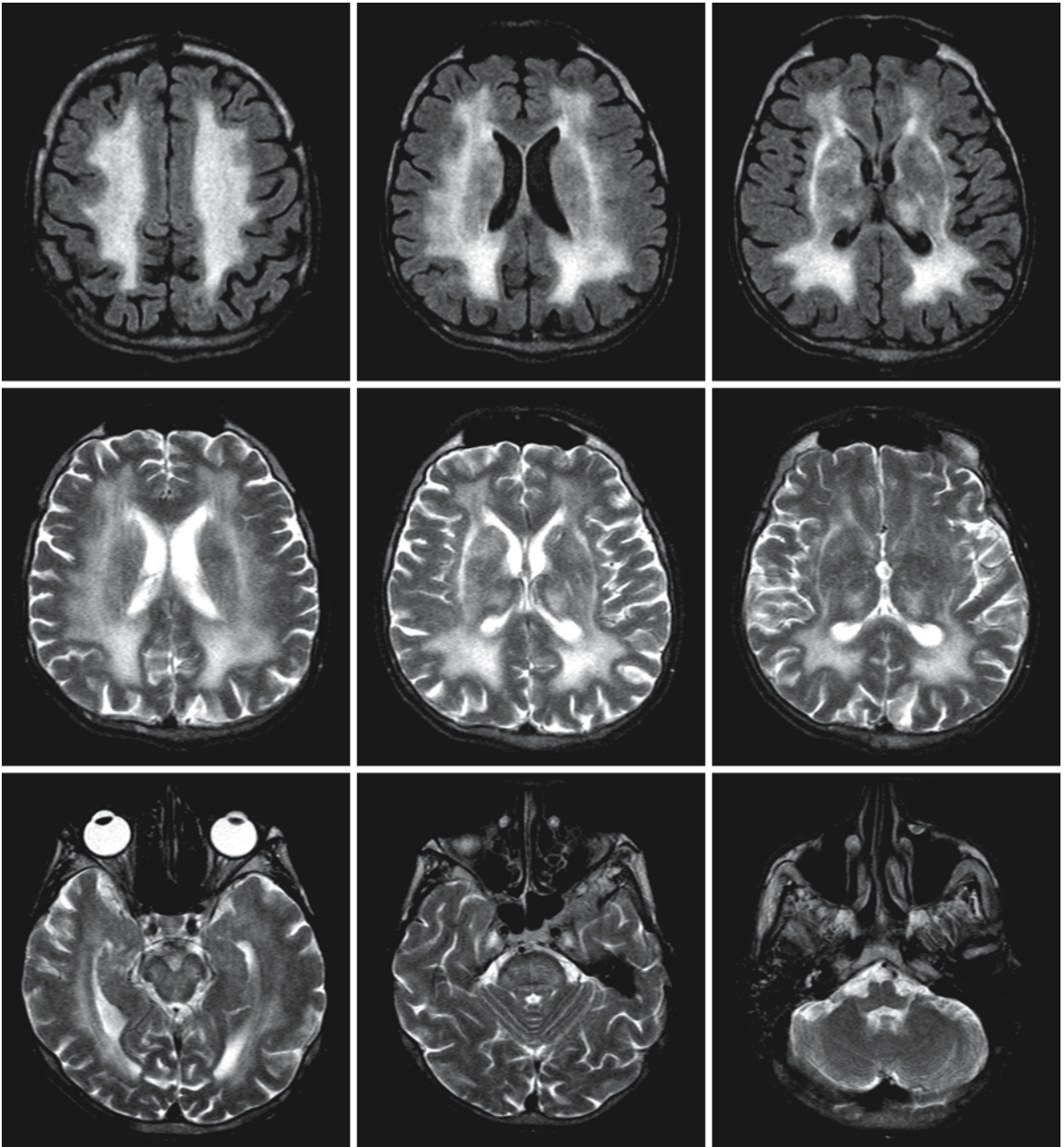


Fig. 27.1. The FLAIR images of a 47-year-old patient with MNGIE show diffuse signal abnormalities of the cerebral white matter with sparing of the corpus callosum. The basal ganglia,

thalami, and brain stem contain areas of abnormal signal. The cerebellar white matter is not affected. From Labauge et al. (2002), with permission

Leigh Syndrome and Mitochondrial Leukoencephalopathies

28.1 Clinical Features and Laboratory Investigations

Leigh syndrome, also called subacute necrotizing encephalomyelopathy, is a neurodegenerative disorder mainly occurring in infancy and childhood. The disease often starts before 1 year of age and leads to death in months or years. Juvenile and adult-onset forms have also been described. In most cases the disease has an autosomal recessive inheritance; in some cases inheritance is maternal or X-linked. Both sexes are affected, but among infants there is a 3:2 male predominance. The course can be acute, subacute, episodic, or chronically progressive. Generally, the later the onset, the slower the progression of the disease.

Although Leigh syndrome is a multisystem disorder, the clinical picture is dominated by signs of CNS dysfunction. In patients with neonatal and infantile onset, frequent signs are respiratory problems (irregular respiration, apnea, sighing, and hyperventilation), ocular abnormalities (strabismus, bizarre eye movements, external ophthalmoplegia, ptosis, optic atrophy, nystagmus, loss of vision, impaired pupillary reaction, retinal pigmentary degeneration), hypotonia, pyramidal signs (spastic paresis, hyperreflexia, extensor plantar reflexes), weakness, easy fatigability, and feeding problems (anorexia, difficulty in swallowing or sucking, vomiting, weight loss, and retarded growth). Episodes of lethargy, seizures, deafness, renal tubular dysfunction, and cardiac problems (cardiomyopathy and disturbances of cardiac rhythm with periods of tachycardia and bradycardia) may also be present. The same problems are frequent in later-onset forms of the disease, in addition to mental and motor retardation or deterioration, exercise intolerance, cerebellar signs (ataxia, dysarthria), and extrapyramidal signs (rigidity, hypokinesia, chorea, athetosis, myoclonus, tremor, ballismus). Sometimes there are signs of a peripheral polyneuropathy. In cases of acute onset, coma and convulsions, sometimes status epilepticus, may dominate the clinical picture. Causes of death are neurogenic disturbances of respiration, status epilepticus, sudden coma, pneumonia, hyperpyrexia, and cardiac problems.

Leigh syndrome is caused by a number of inborn errors of energy metabolism. Frequent causes are pyruvate dehydrogenase complex deficiency, complex I (NADH coenzyme Q reductase, NADH:ubi-

quinone oxidoreductase) deficiency, complex II (succinate dehydrogenase, succinate:ubiquinone oxidoreductase) deficiency, complex IV (cytochrome *c* oxidase) deficiency, and defects in subunit 6 of ATP synthase (complex V). Most of these defects may also lead to extensive leukoencephalopathy. A few patients with Leigh syndrome harbor a point mutation in the tRNA gene encoding lysine, usually associated with MERRF (myoclonus epilepsy and ragged red fibers), or have a mitochondrial DNA depletion.

Pyruvate dehydrogenase complex deficiency results in a wide spectrum of neurological disorders. Patients may have a neonatal or early-infantile-onset severe encephalopathy with profound lactic acidosis and early death. Some patients have a neurodegenerative course of the disease with an infantile or childhood onset and milder lactic acidosis (often typical of Leigh encephalopathy). At the mild end of the spectrum patients have mild, intermittent ataxia and normal intelligence. In patients with pyruvate dehydrogenase complex deficiency, worsening may be provoked by infections. Peripheral neuropathy has been reported in patients with a Leigh-like presentation and patients with intermittent ataxia. Patients with a neonatal presentation often have dysmorphic features, including a broad nasal bridge, upturned nose, micrognathia, low-set and posteriorly rotated ears, short fingers and arms, simian creases, hypospadias, and anteriorly placed anus. Most patients have a defect in the E_{1α} subunit of the pyruvate dehydrogenase complex, with an X-linked mode of inheritance. Females can also be symptomatic, depending on the pattern of X inactivation. In fact, the number of affected females is approximately equal to the number of affected males, consistent with a high rate of manifestations of the disease in heterozygous females. Male patients tend to have a more severe phenotype, but symptomatic females may also have a neonatal-onset devastating encephalopathy. Most defects in the E_{1α} gene seem to originate in the germline.

Isolated *complex I deficiency* most often leads to clinical symptoms in the neonatal or infantile period or early childhood, but onset may also be later. There are a great variety of clinical presentations. Often complex I deficiency is a multisystem disorder with fatal outcome. Up to 50% of patients with complex I deficiency present with Leigh syndrome or Leigh-like disease. Other commonly observed phenotypes are cardiomyopathy, fatal infantile lactic acidosis, macro-

cephaly with leukoencephalopathy, unspecified encephalopathy, and myopathy.

Complex II deficiency may lead to Leigh syndrome, diffuse leukoencephalopathy, late-onset ataxia and optic atrophy, myopathy with exercise intolerance, and isolated cardiomyopathy.

Cytochrome-c oxidase deficiency is associated with a wide range of clinical phenotypes including Leigh syndrome, leukoencephalopathy, unspecified encephalopathy, fatal infantile lactic acidosis, hypertrophic cardiomyopathy and myopathy, isolated myopathy, reversible cytochrome-c oxidase deficiency confined to skeletal muscle, motor neuron disease, spinocerebellar syndrome, myoglobinuria, hepatic failure, ketoacidotic coma, and renal tubulopathy.

Mutations in the mitochondrial gene encoding *subunit 6 of ATP synthase* are associated with two main phenotypes: the NARP syndrome (NARP standing for neurogenic weakness, ataxia, and retinitis pigmentosa, or neuropathy, ataxia, and retinitis pigmentosa) and maternally inherited Leigh syndrome. Other clinical features of NARP include mental retardation, dementia, seizures, behavioral problems, sensorineural deafness, and proximal muscle weakness. The severity of the phenotype is correlated with the load of the heteroplasmic mutation. Symptoms usually appear when mutant mitochondrial DNA exceeds 60%; retinal-dystrophy-related visual loss is the most prevalent symptom in the 60–75% range of mutant mitochondrial DNA; full-blown NARP syndrome usually occurs at between 75% and 90% heteroplasmy; whereas Leigh syndrome usually occurs at mutant mitochondrial DNA levels above 90%. In a few patients retinal dysfunction occurs at mutant loads even lower than 60% and manifests in an age-related fashion. Mutant loads tend to increase from mother to child, most frequently with a very rapid “leap” toward mutant homoplasmy. In some families, the mutation can only be demonstrated in the patient and not in the mother, other children, or maternal relatives, suggesting the possibility of a *de novo* mutation during oogenesis or after fertilization, or a germline mutation in the mother.

Laboratory investigations in Leigh syndrome reveal blood levels of lactate and pyruvate to be typically but not invariably elevated. In CSF, lactate and pyruvate are usually elevated. CSF protein is increased in about half of the patients. EEG shows normal findings or nonspecific abnormalities including diffuse or focal slowing and epileptic phenomena. EMG is either normal or shows signs of denervation or signs of a myopathy. Nerve conduction velocity is either normal or reduced. On biochemical analysis of intact mitochondria in muscle biopsy tissue, variable defects are encountered. Analysis of mitochondrial DNA may reveal mutations, whereas in some other cases defects in nuclear genes are encountered.

Since Leigh syndrome is a serious condition, prenatal diagnosis is important for families. In most cases of pyruvate dehydrogenase complex deficiency, the defect is in the $E_{1\alpha}$ subunit and the condition is X-linked. Mutation analysis is the preferred method for prenatal diagnosis. Affected male fetuses are likely to have a phenotype similar to that of previous affected male siblings. The problem is that the clinical presentation of an affected female cannot be predicted, since there is no way of assessing the X chromosome inactivation pattern in the fetal brain. In all mitochondrial defects with an autosomal recessive mode of inheritance, DNA-based prenatal diagnosis is possible as soon as the basic defect is known in the family. Prenatal diagnosis may also be considered if the complex I deficiency is expressed in both skeletal muscle and skin fibroblasts to rule out tissue specificity and if no mitochondrial DNA defects have been established or suspected. The situation is much more complicated for mitochondrial DNA mutations. The mother carrying a mitochondrial DNA mutation conveys the mutation to all her offspring. The clinical phenotype of these children is mainly determined by the load of mutated mitochondrial DNA in different tissues. As a consequence of the heteroplasmy, a chorionic villus sample may not be representative of the level of mutant mitochondrial DNA in the embryo. In addition, the level of mutant mitochondrial DNA may be different for different tissues within the embryo and change over time. A reliable prediction of the phenotype is therefore impossible. The mutations in the ATP synthase 6 gene are an exception. The distribution of mutant load among tissues is generally uniform in patients, lacking the skewed segregation seen in other mitochondrial DNA mutations, and there is a good genotype–phenotype correlation. These factors make it possible to provide reliable genetic counseling and prenatal diagnosis.

28.2 Pathology

The brunt of histopathological abnormalities in Leigh syndrome is borne by the central gray matter. The most consistent site of lesions is the brain stem gray matter. The lesions are usually bilateral, although not necessarily symmetrical. They are sharply delineated and not confined to the gray matter structures but often spread into the white matter. Preferential sites of affection are the periaqueductal region and brain stem tegmentum, posterior colliculi, substantia nigra, floor of the fourth ventricle, red nuclei, inferior olivary nuclei, dentate nuclei, putamen, caudate nucleus, and globus pallidus. Thalamus, hypothalamus, and subthalamic nuclei may also be involved, but less often. In the spinal cord, lesions are mainly located in the anterior horns, dorsal columns, and pyramidal

tracts. Lesions rarely occur in the cerebral or cerebellar cortex or mammillary bodies. Exceptional cases with predominant cerebral and cerebellar cortical damage have been described. Microscopic examination of the lesions shows a marked sponginess with loosening and rarefaction of the neuropil. There is a characteristic intense capillary proliferation. Astrocytosis and microglial proliferation are present and macrophages may occur. Nerve cells are remarkably well preserved, although there may be some nerve cell loss. The spongy lesions contain numerous vacuoles, enclosed by single or double membranes. Myelin splitting may contribute to the vacuolation. Cavitation and tissue collapse is the end result in most severe lesions.

In the majority of the cases the white matter is well preserved, but sometimes there is also extensive involvement of cerebral and cerebellar white matter, often with sparing of the corpus callosum and internal capsule. The white matter abnormalities are characterized by sponginess, deficient myelin formation, myelin loss, abundant presence of lipid-laden macrophages, marked capillary proliferation, prominent gliosis, and eventually also axonal loss. In all areas there is a gradient of damage, so that myelin sheaths and dendrites degenerate before axons and cell bodies do. In some patients the affected white matter is partially cystic, sometimes even extensively cavitated. The optic nerves and tracts are often affected by demyelination and gliosis.

In patients with a neonatal-onset encephalopathy related to pyruvate dehydrogenase complex deficiency, neuropathological findings are dominated by signs of dysgenesis of the CNS, with agenesis of the corpus callosum, dilatation of the ventricular system, dysplasia and ectopia of the inferior olivary nuclei, dysplasia of the dentate nuclei, absence or hypoplasia of the medullary pyramids, periventricular neuronal heterotopias, and delayed or deficient myelination. Degenerative findings, which may also be present, include gliosis and cystic degeneration of the white matter and vascular proliferation in the white matter and striatum. In patients with pyruvate dehydrogenase complex deficiency and intermittent ataxia, neuropathological findings consist of atrophy of cerebellar structures.

In the sural nerve, signs of demyelination and remyelination have been found as well as loss of myelinated and unmyelinated axons. Ragged red fibers are found in muscle tissue of some patients.

28.3 Pathogenetic Considerations

Leigh syndrome is caused by a number of inborn errors of energy metabolism. Frequent causes are pyruvate dehydrogenase complex deficiency, complex I

(NADH coenzyme Q reductase) deficiency, complex II (succinate dehydrogenase) deficiency, complex IV (cytochrome-*c* oxidase) deficiency, and subunit 6 of ATP synthase (complex V) deficiency. Rarely, patients with Leigh syndrome harbor a point mutation in the tRNA gene encoding lysine, usually associated with MERRF (myoclonus epilepsy and ragged red fibers), or mitochondrial DNA depletion.

The pyruvate dehydrogenase multienzyme complex catalyzes the thiamine-dependent oxidative decarboxylation of pyruvate to acetyl CoA in the mitochondrial matrix. The complex contains three catalytic components: pyruvate dehydrogenase (E_1), dihydrolipoyl transacetylase (E_2), and dihydrolipoyl dehydrogenase (E_3); two regulatory components, E_1 -kinase and E_1 -phosphatase; and protein X, a dihydrolipoamide dehydrogenase binding protein, necessary for proper interaction between the E_2 and E_3 components. The E_1 subunit is a heterotetramer composed of two α and two β subunits. The E_1 subunit contains a thiamin pyrophosphate binding site that is shared by the α and β subunits. The gene for the $E_{1\alpha}$ subunit, *PDHA1*, is located on the X chromosome. There is an autosomal counterpart located on chromosome 4. The $E_{1\beta}$ subunit gene, *PDHB*, is located on chromosome 3. The E_2 subunit is encoded by a gene on chromosome 3. The gene for the E_3 subunit, *PHE3*, is located on chromosome 7. The gene for protein X, *PDX1*, is located on chromosome 11. Pyruvate dehydrogenase deficiencies are most often associated with mutations in the gene that encodes the $E_{1\alpha}$ subunit of the complex. Primary defects in the other genes encoding other subunits of the complex are very rare. Consequently, transmission of pyruvate dehydrogenase deficiency occurs most often in an X-linked fashion, but sometimes in an autosomal recessive fashion.

Complex I (NADH coenzyme Q reductase, NADH: ubiquinone oxidoreductase) represents the largest complex of the mitochondrial electron transfer chain and consists of at least 35 nuclear-encoded subunits (NDUFV1–3, NDUF1–10, NDUFAB1, NDUFB1–10, NDUF51–8, NDUF1–2, and a 17.2-kDa subunit), and 7 mitochondrial-encoded subunits (ND1–6, ND4L). The overall function of the complex is to pass electrons from NADH to ubiquinone while pumping hydrogen ions out of the mitochondrial matrix into the inner membrane space. Complex I deficiency has an autosomal recessive or maternal mode of inheritance.

Complex II, or succinate:ubiquinone oxidoreductase, consists of a flavoprotein and an iron-sulfur protein, which together constitute the soluble enzyme succinate dehydrogenase. In addition, there are two membrane-anchored proteins. It catalyzes the oxidation of succinate to fumarate in the Krebs cycle and carries electrons to the ubiquinone pool of the respiratory chain. All four subunits of the complex are en-

coded by nuclear DNA. Complex II deficiencies have an autosomal recessive mode of inheritance.

Complex IV, or cytochrome-*c* oxidase, catalyzes the transfer of electrons from reduced cytochrome *c* to molecular oxygen. It is composed of 13 subunits, 10 of which are encoded by nuclear genes and 3 by mitochondrial genes. The catalytic core of the complex consists of the proteins COX I, COX II, and COX III, encoded by the mitochondrial genes *COI*, *COII*, and *COIII*, respectively. Heteroplasmic mutations in these three genes have been found in cytochrome *c* deficiency. Additionally, mutations in the mitochondrial tRNA gene for tryptophan and the tRNA gene for isoleucine may underlie a selective cytochrome-*c* oxidase deficiency. In these rare patients with a mutation in mitochondrial DNA, the disease has a maternal mode of inheritance. Autosomal recessive inheritance is much more common for cytochrome-*c* oxidase deficiency. Despite intensive studies, mutations have not been identified in any of the 10 nuclear-encoded genes in patients with an autosomal recessive cytochrome-*c* oxidase deficiency. In order to assemble a functional cytochrome-*c* oxidase complex, additional nuclear-encoded proteins, assembly factors, are necessary, including SURF1, SCO1, SCO2, COX10, COX11, COX15, and COX17. Mutations in *SURF1*, *SCO1*, *SCO2*, *COX10*, and *COX15* have been identified in patients with cytochrome-*c* oxidase deficiency. The genetic defect in the majority of the patients with cytochrome-*c* oxidase deficiency is still unknown. Mutations in *SURF1* most often lead to Leigh syndrome, but may also lead to a severe leukoencephalopathy. Mutations in *COX10* have been described in association with leukoencephalopathy and tubulopathy. However, mutations in *SURF1* and *COX10* may also be associated with other phenotypes. Recently, mutations in the gene *LRPPRC* have been found in patients with cytochrome-*c* oxidase deficiency and Leigh syndrome (the so-called French-Canadian subtype). The precise function of LRPPRC protein is presently not known.

Defects in subunit 6 of ATP synthase (complex V of the respiratory chain) are most frequently caused by the T8993G mutation in the mitochondrial DNA. The same mutation is associated with NARP. Defective catalytic properties of the enzyme complex may result from an impairment of the proton transport or from impaired coupling of proton translocation with ATP synthesis. There is a clear-cut reduction in the rate of ATP synthesis in patient cells with a high load of mutant mitochondrial DNA. The T8993C mutation is observed less frequently and seems to be associated with a somewhat less severe phenotype and a less severe reduction in the rate of ATP synthesis. The T9176C and T8851C mutation in the same gene have also been found in some patients with Leigh syn-

drome. These mutations have a maternal mode of inheritance.

A few patients with Leigh syndrome were found to harbor a point mutation in the mitochondrial tRNA gene for lysine, A8344G or G8363A, usually associated with MERRF (myoclonus epilepsy and ragged red fibers).

All defects underlying Leigh syndrome affect energy metabolism. There is a striking clinical and morphological similarity between Leigh syndrome and thiamine deficiency (beriberi). Thiamine is part of the pyruvate dehydrogenase, ketoglutarate dehydrogenase, and branched-chain keto acid dehydrogenase complexes, and deficiency leads to a disturbance in oxidation of pyruvate and consequently to energy failure. The only histopathological differences between thiamine deficiency and Leigh syndrome are that in thiamine deficiency the mammillary bodies are mostly involved and the substantia nigra is not, whereas in Leigh syndrome it is the substantia nigra that is often involved and the mammillary bodies rarely are. These differences, however, are not absolute.

28.4 Therapy

Therapeutic success is limited in Leigh syndrome. An important problem is that most of the brain damage is irreversible. Supportive care is important. Other possible therapeutic strategies include the removal of toxic metabolites, administration of artificial electron acceptors, administration of cofactors, administration of radical scavengers, and dietary interventions.

L-carnitine supplementation may have a nonspecific beneficial effect, in particular if toxic organic acid intermediates are present. Dichloroacetate has been used to lower blood and CSF lactate levels. Variable favorable results have been reported following the use of riboflavin (vitamin B₂), nicotinamide, coenzyme Q₁₀, vitamin C and menadione (vitamin K₃) in respiratory chain defects.

Thiamine treatment is effective in some patients with pyruvate dehydrogenase complex deficiency. The most rational therapeutic strategy in pyruvate dehydrogenase complex deficiency is the use of a ketogenic diet. Oxidation of fatty acids and ketone bodies provides alternative sources of acetyl-CoA not derived from pyruvate. This acetyl-CoA enters the citric acid cycle, thus bypassing the block at the level of pyruvate dehydrogenase. Dichloroacetate, a structural analogue of pyruvate, inhibits E₁ kinase, thereby keeping any residual E₁ in its active, dephosphorylated, form. Despite these therapeutic interventions, the outcome in patients with serious neurological disease is generally poor.

28.5 Magnetic Resonance Imaging

Irrespective of the underlying defect, the most commonly reported abnormalities on CT and MRI in Leigh syndrome involve the basal nuclei and brain stem (Figs. 28.1, 28.3, 28.9, 28.10, 28.14–28.16). The putamen and caudate nucleus are the most frequently affected, but the globus pallidus, subthalamic nucleus, dentate nucleus, substantia nigra, tegmentum of the pons, periaqueductal gray, red nucleus, the medulla, and other brain stem structures are also frequently involved. The colliculi, thalamus, hypothalamus, and cortex are less often involved. Although the lesions are often symmetrical, they may also be asymmetrical. These lesions may be swollen during the acute stage, may improve and become smaller, or may develop into focal atrophy or cystic lesions. During the acute stage, contrast enhancement may be present. Generalized cerebral and cerebellar atrophy has also been reported, and some of these patients develop secondary subdural effusions. Depending on the onset of the clinical symptomatology, myelination may be delayed or totally deficient.

Incidentally, focal or, more often, diffuse white matter abnormalities are seen on MRI, involving the cerebral white matter and often also the cerebellar white matter (Figs. 28.4–28.8 and 28.10–28.13). In some patients, the white matter disease is most prominent in the subcortical white matter; in some patients the white matter disease is mainly periventricular with sparing of the U fibers, whereas in other patients the cerebral white matter abnormalities are diffuse. Small cysts (or, in some patients, large cysts) may develop within the abnormal white matter (Figs. 28.4–28.6, 28.8, 28.10, 28.12, and 28.13) and their presence is particularly suggestive of a mitochondrial disease. The cysts are generally well delineated. This is in contrast with the diffuse melting away pattern of cystic degeneration usually seen in vanishing white matter disease. Foci of contrast enhancement within the abnormal white matter is another feature suggestive of a mitochondrial disorder and is, for instance, not seen in vanishing white matter disease (Figs. 28.5, 28.6, and 28.13). The concomitant presence of Leigh-like gray matter lesions is also suggestive of a mitochondrial disease.

The reported white matter abnormalities for each basic defect are specified below:

Pyruvate dehydrogenase complex deficiency is incidentally associated with diffuse leukoencephalopathy. Patients with neonatal presentation of pyruvate dehydrogenase complex deficiency usually have a distinct MRI pattern (Fig. 28.2) with signs of dysgenesis of the brain, including hypoplasia or agenesis of the corpus callosum and highly dilated lateral ventricles and third ventricle with a normal fourth ventricle. The cerebellum may be small with a cystic space

behind it. In other neonates, these dysgenetic changes are not seen, but the white matter has an abnormal and swollen appearance and there may be multiple subependymal cysts. In patients with episodic cerebellar ataxia, cerebellar atrophy may be seen.

Patients with isolated complex I deficiency may present with extensive cerebral leukoencephalopathy with initial swelling of the abnormal white matter and followed by macrocystic degeneration (Figs. 28.4 and 28.5). Focal areas of contrast uptake may be present (Figs. 28.5). A periventricular rim of white matter is sometimes spared. The corpus callosum is often involved, usually most seriously in its posterior part (Figs. 28.5). The cerebral or cerebellar cortex may be abnormal in signal with subsequent development of cortical atrophy (Fig. 28.5). There may also be lesions in the basal ganglia, thalamus, cerebellum, and brain stem. In other patients there are cerebral white matter abnormalities but they are less impressive and not cystic.

In complex II deficiency extensive cerebral white matter abnormalities may occur in the presence or absence of basal ganglia and thalamus lesions (Figs. 28.6–28.8). The U fibers tend to be spared. The corpus callosum may be involved in the process, often more seriously in its posterior part (Figs. 28.6 and 28.7). Focal areas of contrast enhancement may be present (Fig. 28.6). The abnormal white matter may be partially cystic (Figs. 28.6 and 28.8). Additional brain stem white and gray matter lesions may be present. The cerebellar white matter may also be involved.

In cytochrome-*c* oxidase deficiency, diffuse or less extensive leukoencephalopathy has been reported involving cerebral white matter (Figs. 28.10–28.13). The corpus callosum may also be involved (Figs. 28.10, 28.12, and 28.13). The internal capsule, cerebellar white matter, and U fibers are more variably affected. The abnormal white matter may contain small cysts (Figs. 28.10, 28.12, and 28.13), sometimes many cysts. The basal ganglia, thalamus, subthalamic nucleus, dentate nucleus, and brain stem may be normal or contain lesions (Figs. 28.10 and 28.11). After contrast, focal enhancement may be seen, probably occurring in necrotic lesions (Fig. 28.13).

In Leigh syndrome and NARP related to a mutation in the mitochondrial gene encoding the ATP synthase 6 subunit, leukoencephalopathy has not been reported.

Proton MRS of the brain usually reveals elevated lactate in the brain of patients with Leigh syndrome, most prominently in lesion areas. In diffuse cerebral white matter abnormalities with cystic degeneration, the presence of highly elevated lactate is an argument in favor of an underlying mitochondrial defect and against vanishing white matter disease. In pyruvate dehydrogenase complex deficiency, additionally ele-

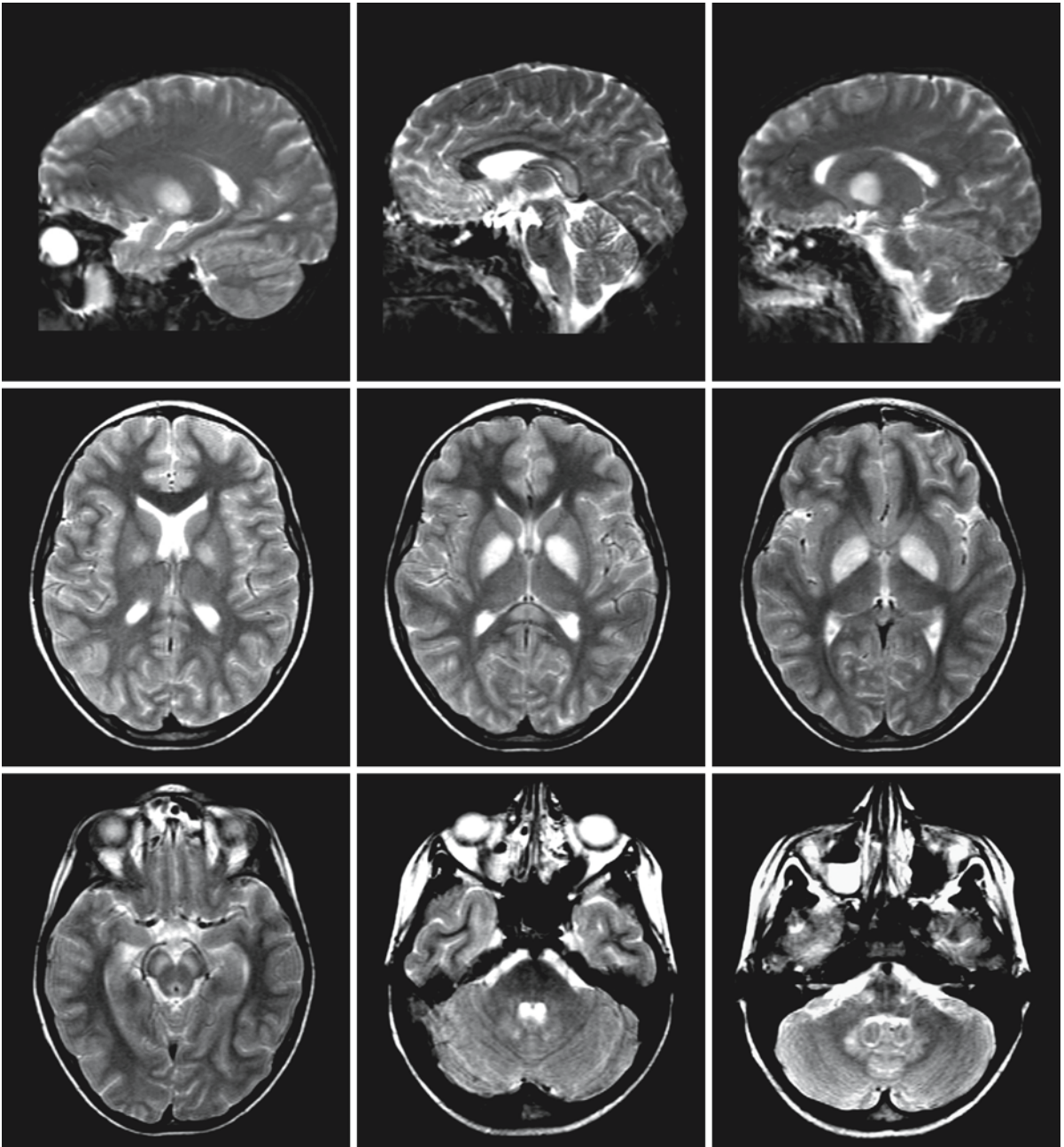


Fig. 28.1. An 8-year-old boy with pyruvate dehydrogenase complex deficiency and episodic neurological deterioration with Leigh-like features. There are lesions in the posterior part

of the corpus callosum, globus pallidus, substantia nigra, and dentate nucleus. The globus pallidus lesions are a typical feature of pyruvate dehydrogenase complex deficiency

vated pyruvate may be detectable at 2.37 ppm. In succinate dehydrogenase deficiency, highly elevated succinate is seen within the abnormal white matter in addition to the elevated lactate. Succinate is represented by a resonance at 2.40 ppm. More details and illustrations are found in Chap. 108.

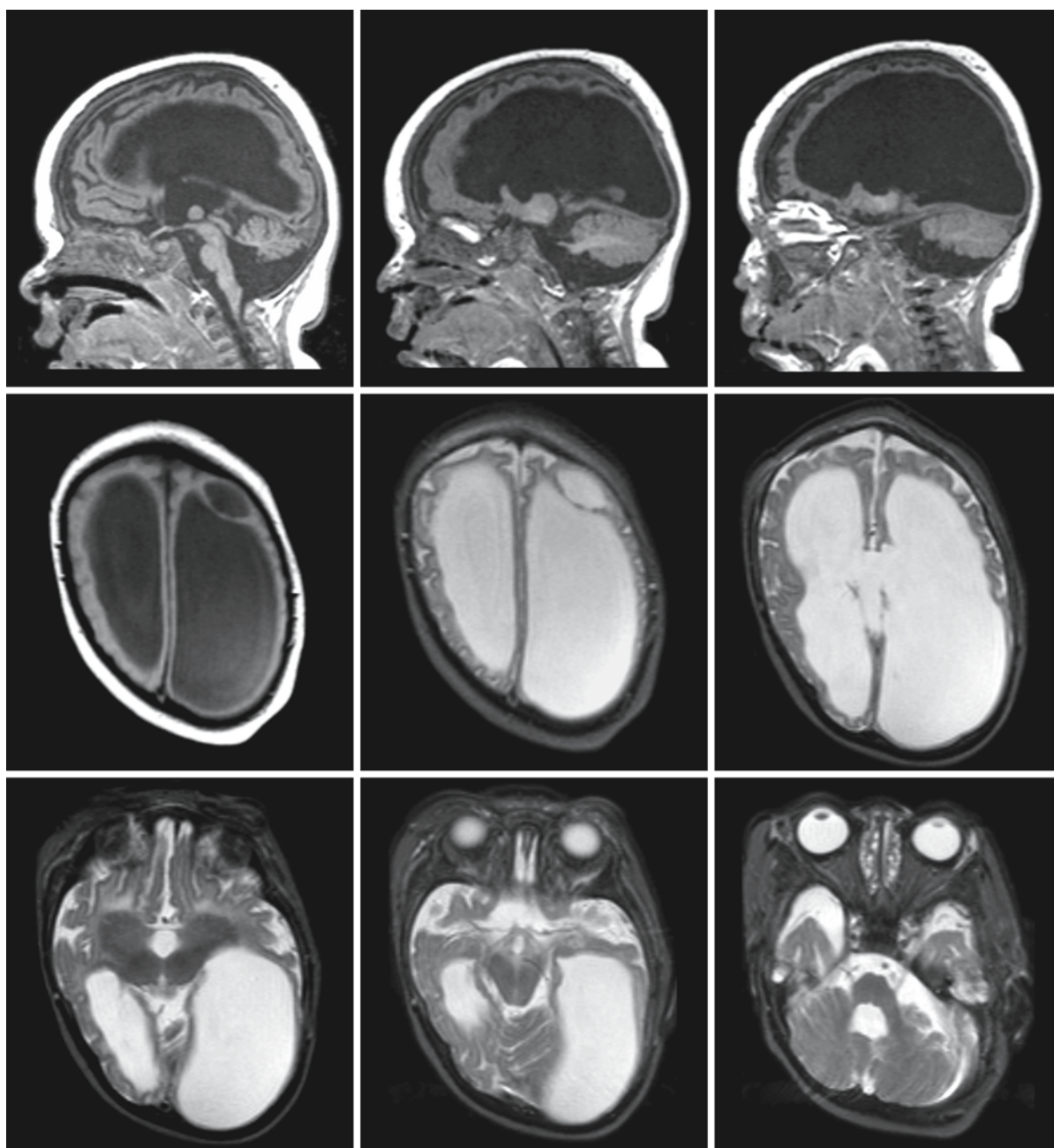


Fig. 28.2. An 8-month-old girl with pyruvate dehydrogenase complex deficiency and neonatal presentation. She has a severely dysgenetic brain with highly dilated lateral ventricles,

a very thin cerebral mantle, absence of the corpus callosum, a cyst in the left frontal area, and a small cerebellum

Fig. 28.3. A 3-year-old boy with isolated complex I deficiency, related to mutations in the NDUF57 subunit, and a Leigh-like presentation. The T₂-weighted (*first and second row*) and FLAIR images (*third row*) show lesions in the medial thalamus, mid-brain (including the periaqueductal gray), dentate nucleus, and medulla. Sagittal T₁-weighted images (*fourth row*) without (*left*) and with contrast (*middle and right*) show enhancement of small spots within the areas of abnormal signal

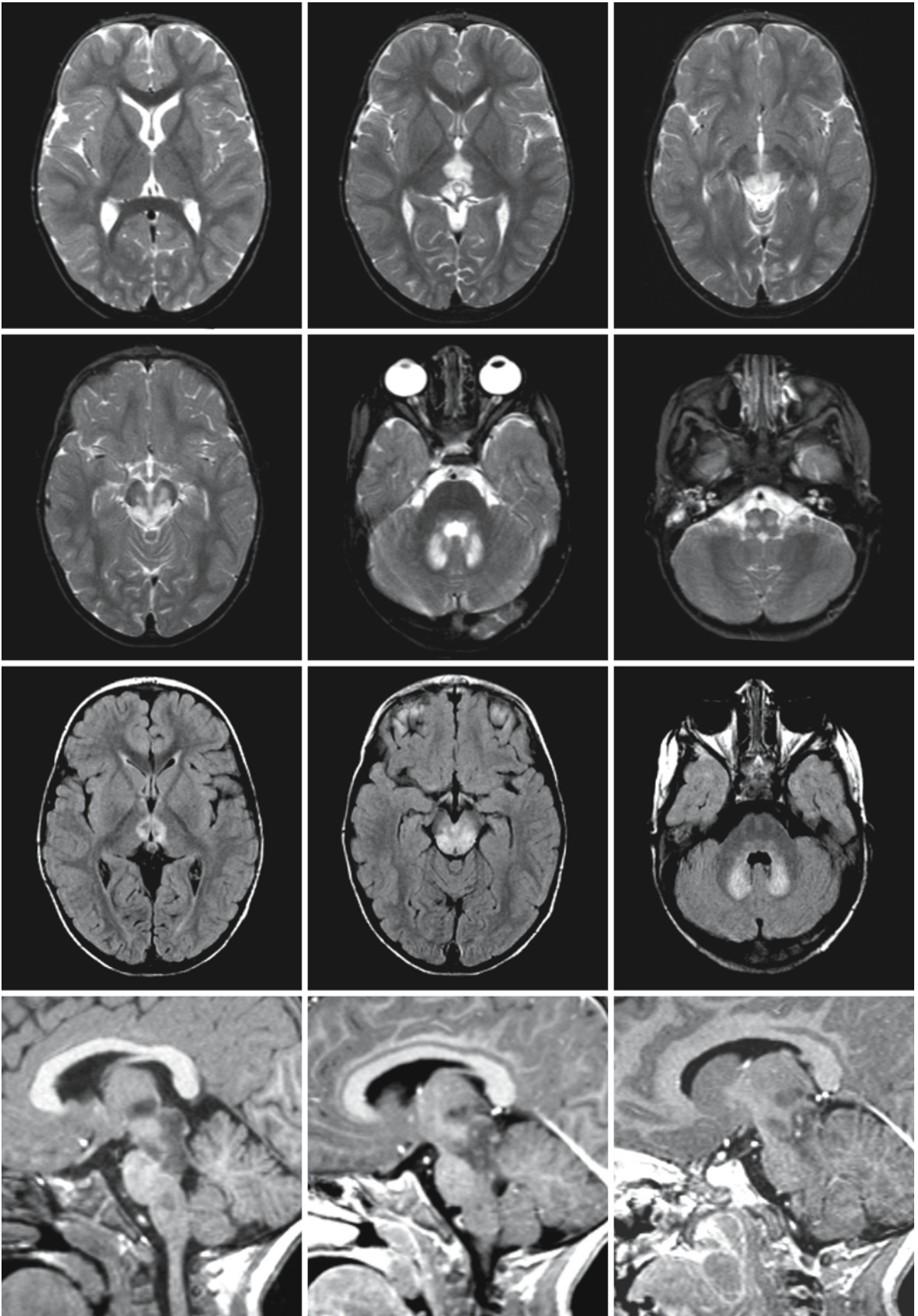


Fig. 28.3.

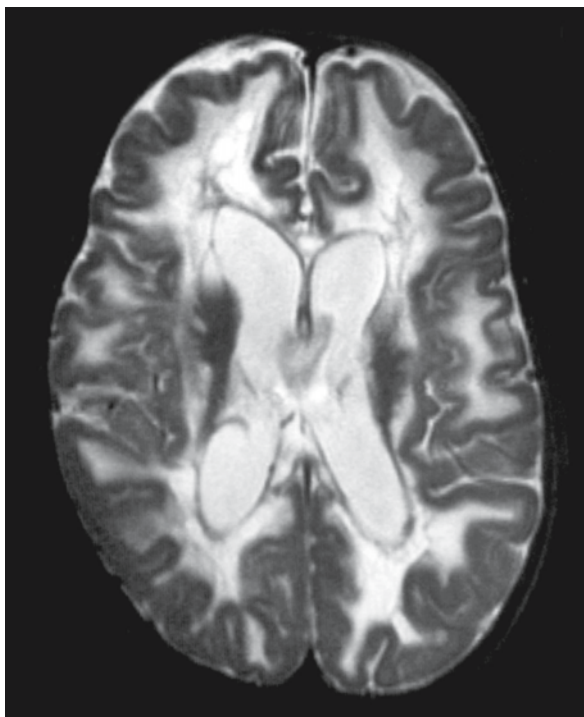


Fig. 28.4. A 1-year-old girl with complex I deficiency related to a mutant NDUFV1 subunit of mitochondrial complex I (Schuelke et al. 1999). Clinically she has a severe encephalopathy and macrocephaly. The MRI reveals a diffuse leukoencephalopathy with macrocystic degeneration. Courtesy of Dr. J.A.M. Smeitink, Department of Department of Pediatrics, Nijmegen Center for Mitochondrial Disorders, University Hospital Nijmegen, Nijmegen, The Netherlands

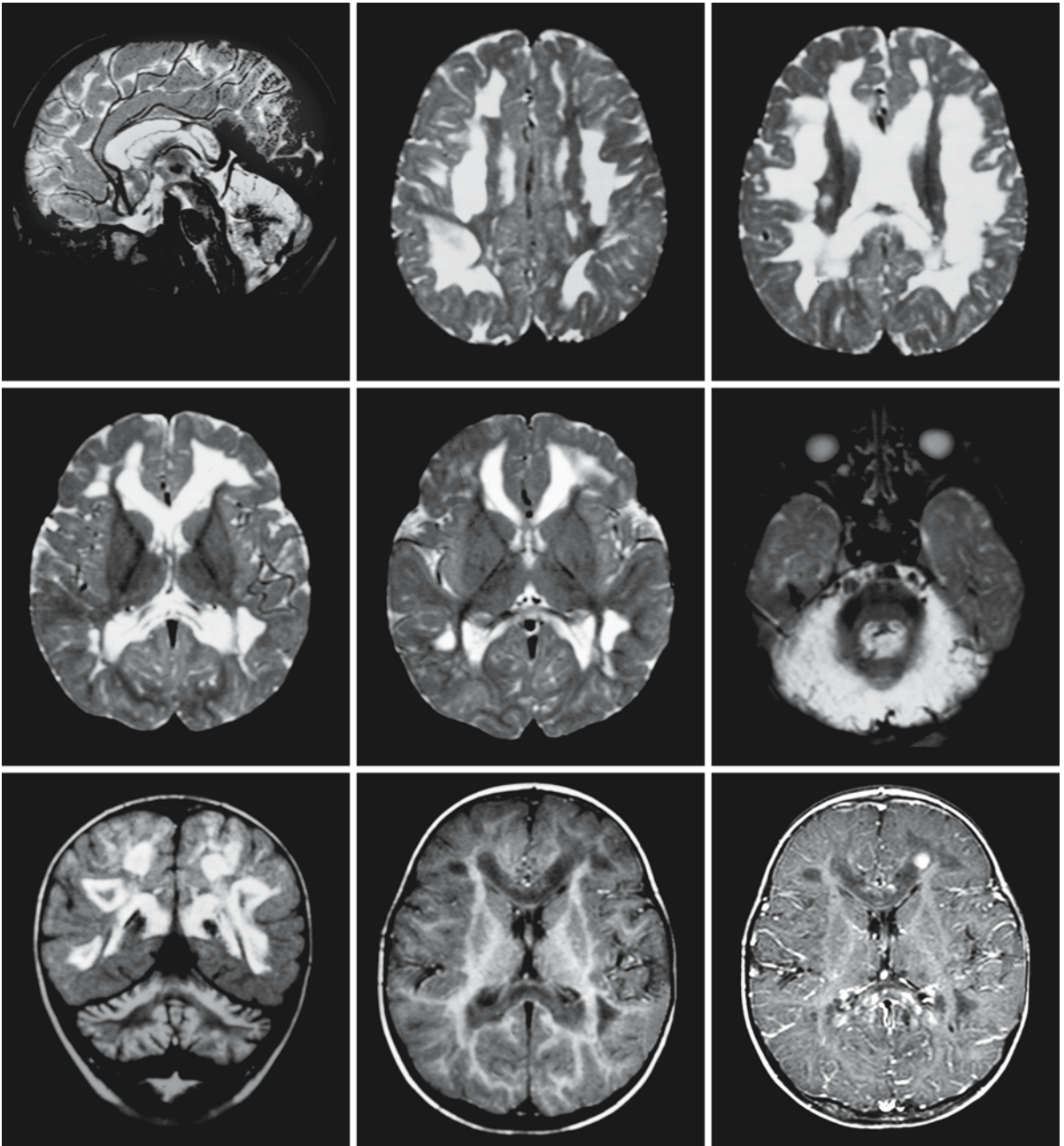


Fig. 28.5. A 19-month-old boy with isolated complex I deficiency. There are extensive, partially focal, but largely confluent cerebral white matter abnormalities. The internal capsule is spared, while the periventricular rim is partially spared. The corpus callosum is severely involved. The coronal FLAIR image (*third row, left*) shows that the abnormal white matter is partially cystic. The sagittal (*first row, left*) and transverse (*second row, right*) T₂-weighted images and the coronal FLAIR image (*third row, left*) demonstrate that the cerebellar cortex is dif-

fusely abnormal. The T₁-weighted images without (*third row, middle*) and with contrast (*third row, right*) demonstrate that there are foci of contrast enhancement within the abnormal white matter, most of all the posterior part of the corpus callosum. From Wolf et al. (2003), with permission; also courtesy of Dr. W. Evert, Children's Hospital Offenbach, and Dr. N. Rilling, Central Institute for Diagnostic and Interventional Radiology, Offenbach, Germany

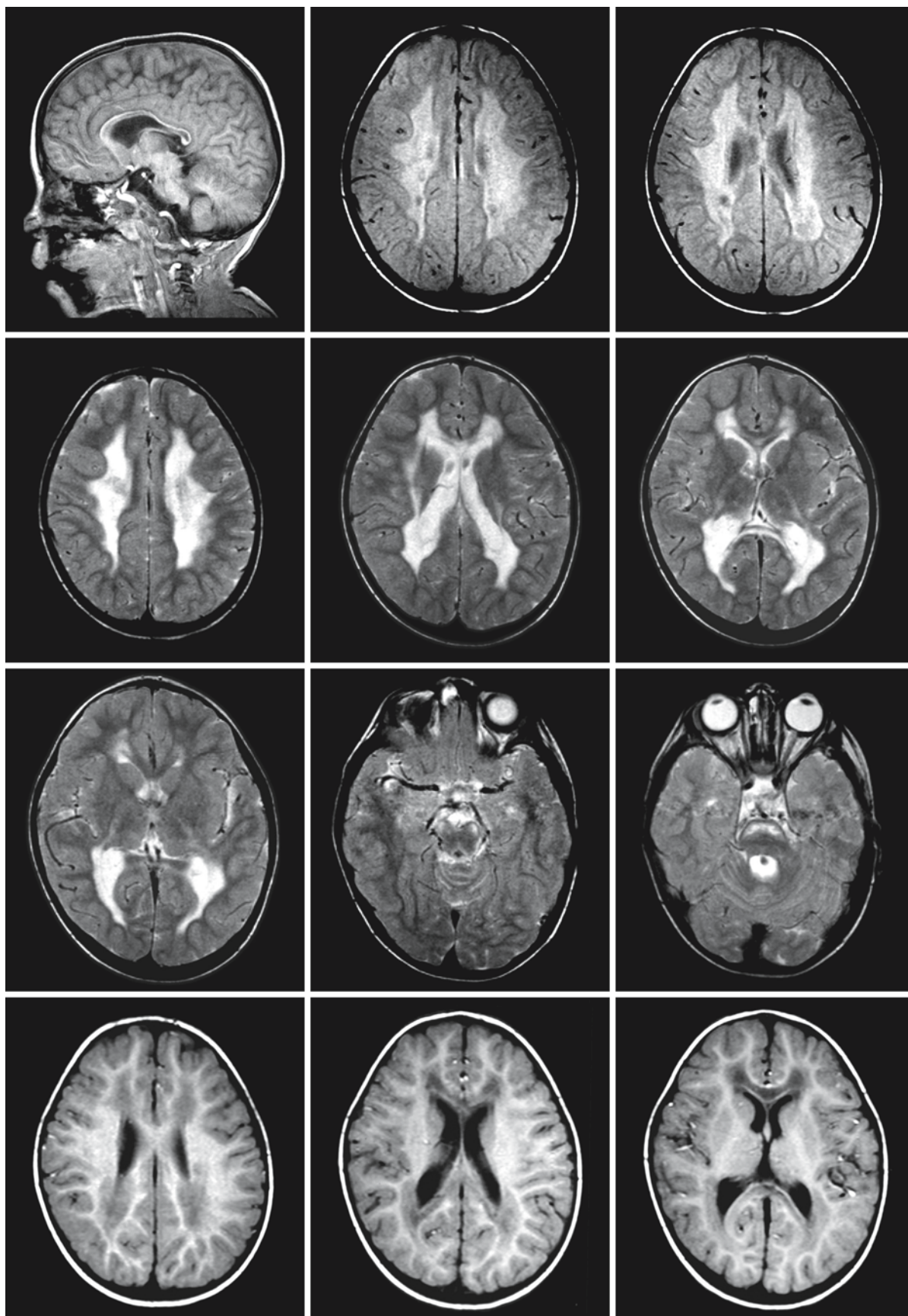


Fig. 28.6.

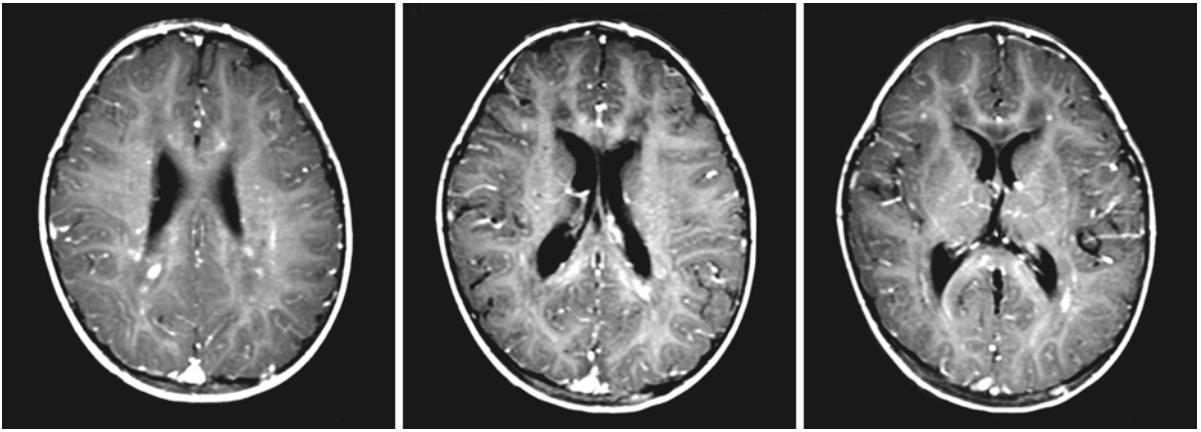


Fig. 28.6. (*continued*). A 2-year-old boy with complex II deficiency. There are extensive cerebral white matter abnormalities with sparing of the U fibers. The corpus callosum, posterior limb of the internal capsule, and corticospinal tracts in the brain stem are also involved. The sagittal T₁-weighted image and the transverse proton density images (*first row*) reveal that

the corpus callosum and cerebral white matter are partially cystic. There is a slit in the corpus callosum over its entire length. The T₁-weighted images without (*fourth row*) and with contrast (*fifth row*) demonstrate that there are foci of contrast uptake in the abnormal white matter. From Brockmann et al. (2002), with permission

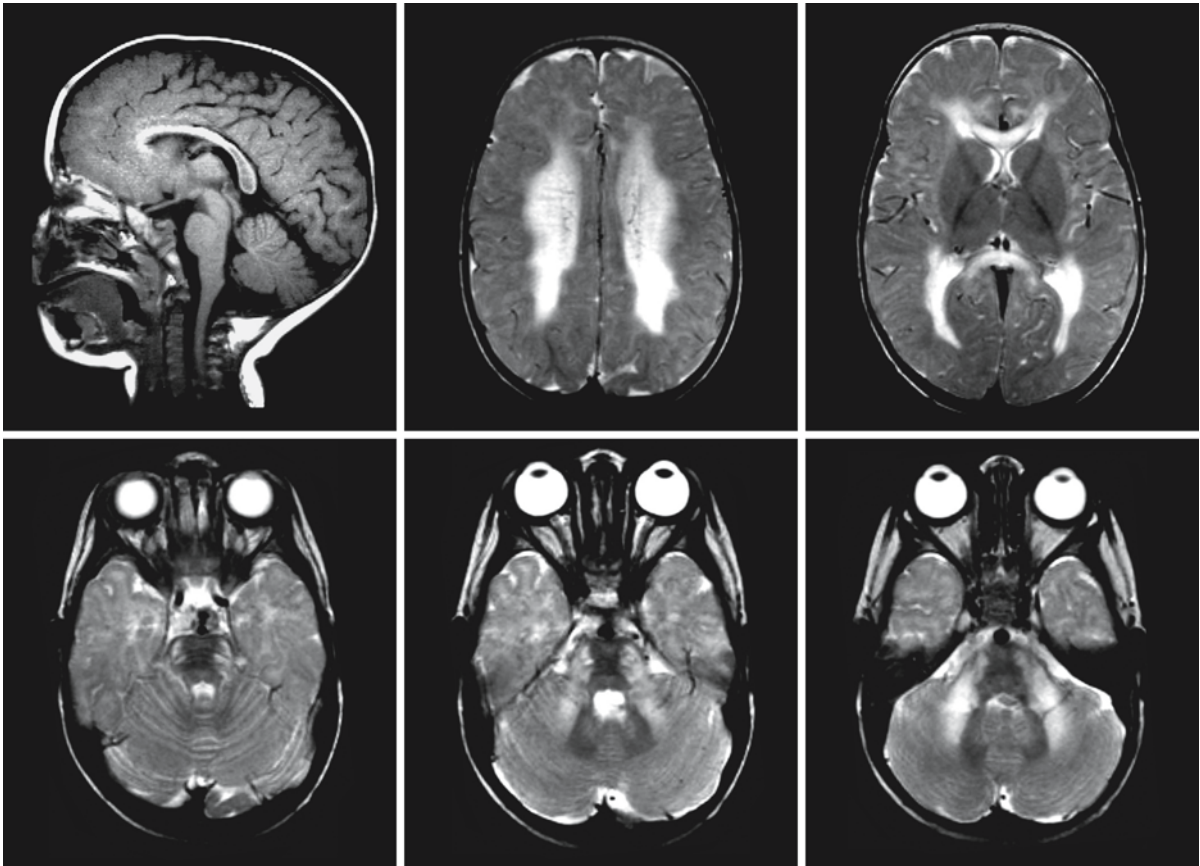


Fig. 28.7. An 11-month-old girl with complex II deficiency. There are extensive signal abnormalities in the periventricular and deep cerebral white matter and corpus callosum. There are signal abnormalities in the cerebellar white matter, middle

cerebellar peduncles, and lateral parts of the pons. Myelination is delayed for the age of the child. From Brockmann et al. (2002), with permission

Fig. 28.8. A 1-year-old girl with complex II deficiency. The cerebral white matter is diffusely abnormal. The corpus callosum, posterior limb of the corpus callosum, corticospinal tracts in the brain stem, middle cerebellar peduncles, and cerebellar white matter are also involved. There are small, well-delineat-

ed cysts within the abnormal cerebral white matter, best seen on the sagittal T₁-weighted images (*first row*) and axial FLAIR images (*fourth row*). Courtesy of Dr. A. Bizzi, Department of Neuroradiology, and Dr. G. Uziel, Department of Child Neurology, Istituto Nazionale Neurologico C. Besta, Milan, Italy

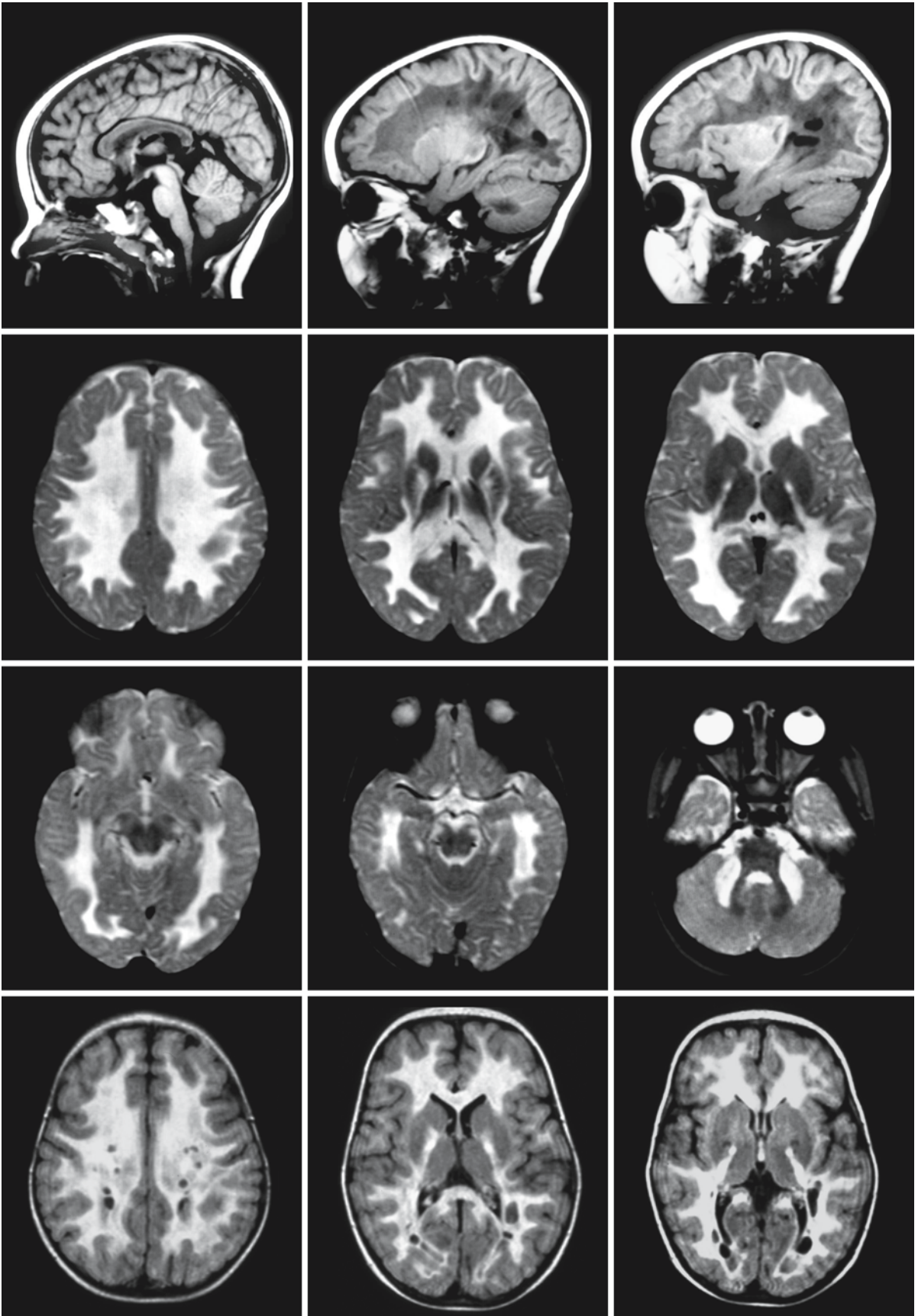


Fig. 28.8.

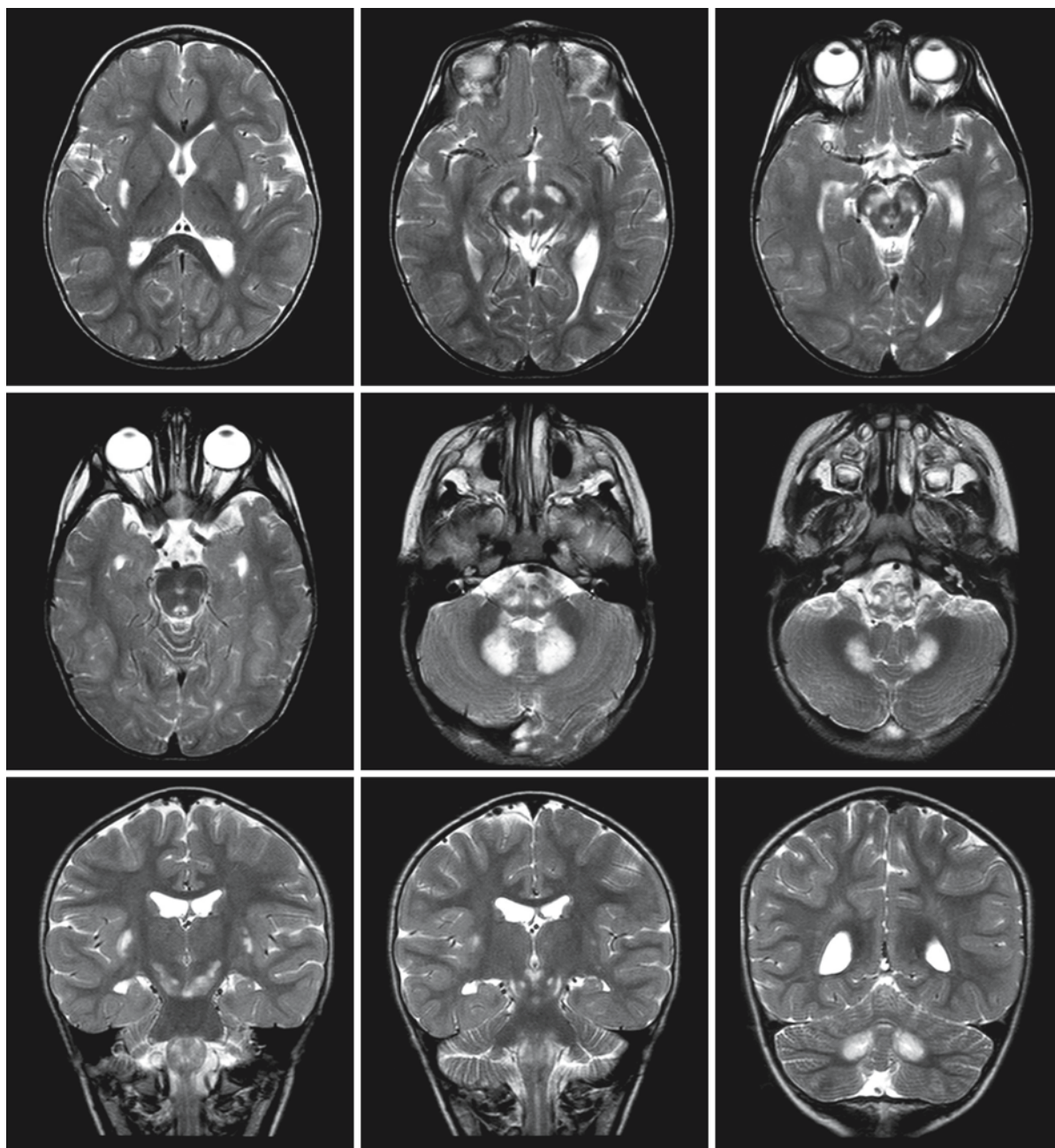


Fig. 28.9. A 3-year-old boy with cytochrome-*c* oxidase deficiency related to *SURF1* mutations. There are signal abnormalities in the posterior part of the putamen, the subthalamic nucleus, substantia nigra, dentate nucleus, periaqueductal gray,

and multiple nuclei in the medulla. From Rossi et al. (2003), with permission

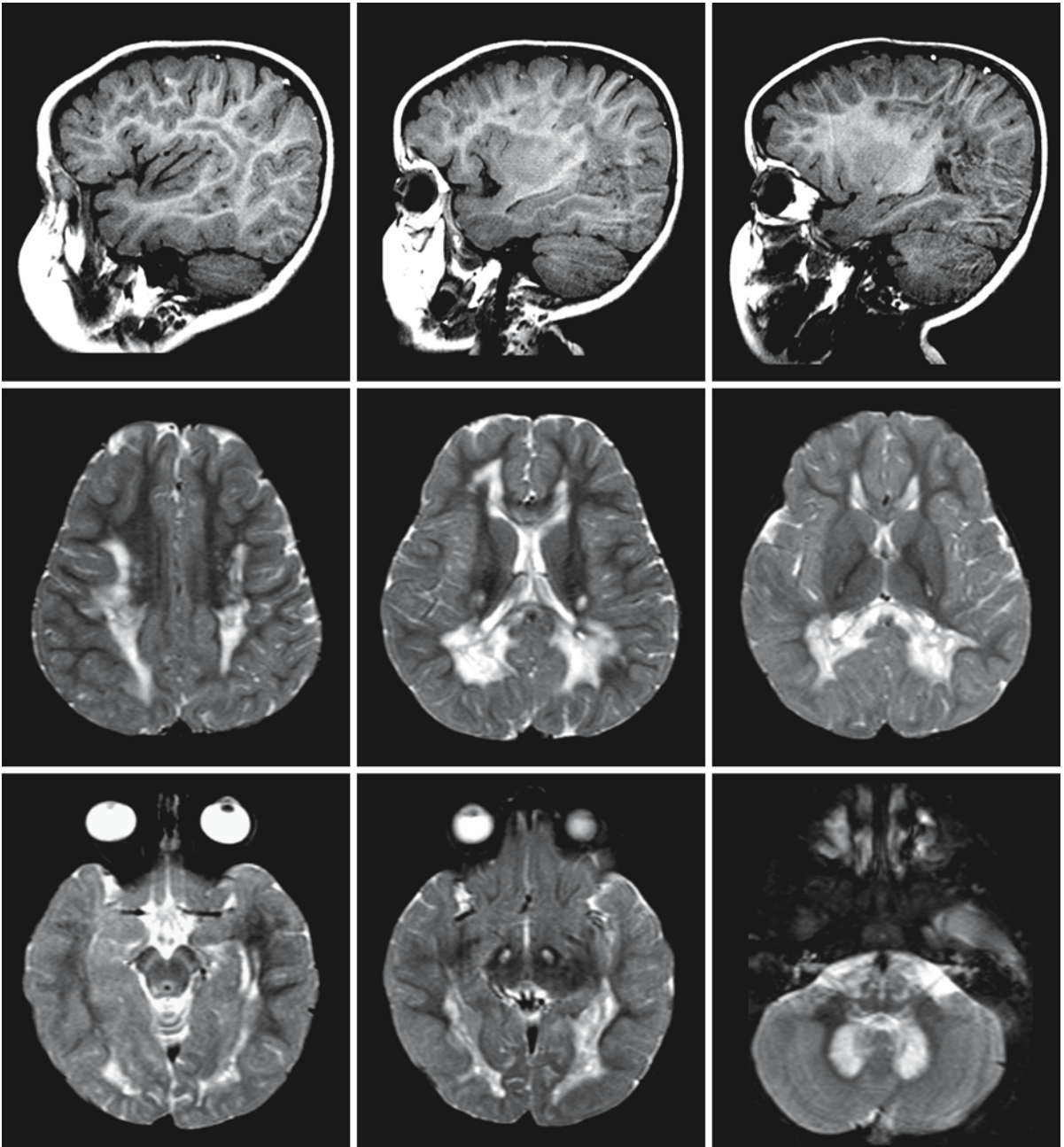


Fig. 28.10. A 2.5-year-old girl with cytochrome-c oxidase deficiency related to *SURF1* mutations. There are signal abnormalities in the subthalamic nucleus, substantia nigra, periaqueductal gray, dentate nucleus, posterior limb of the internal cap-

sule, corpus callosum, and the cerebral hemispheric white matter, posterior more than anterior. The abnormal white matter contains small cysts. From Rahman et al. (2001), with permission

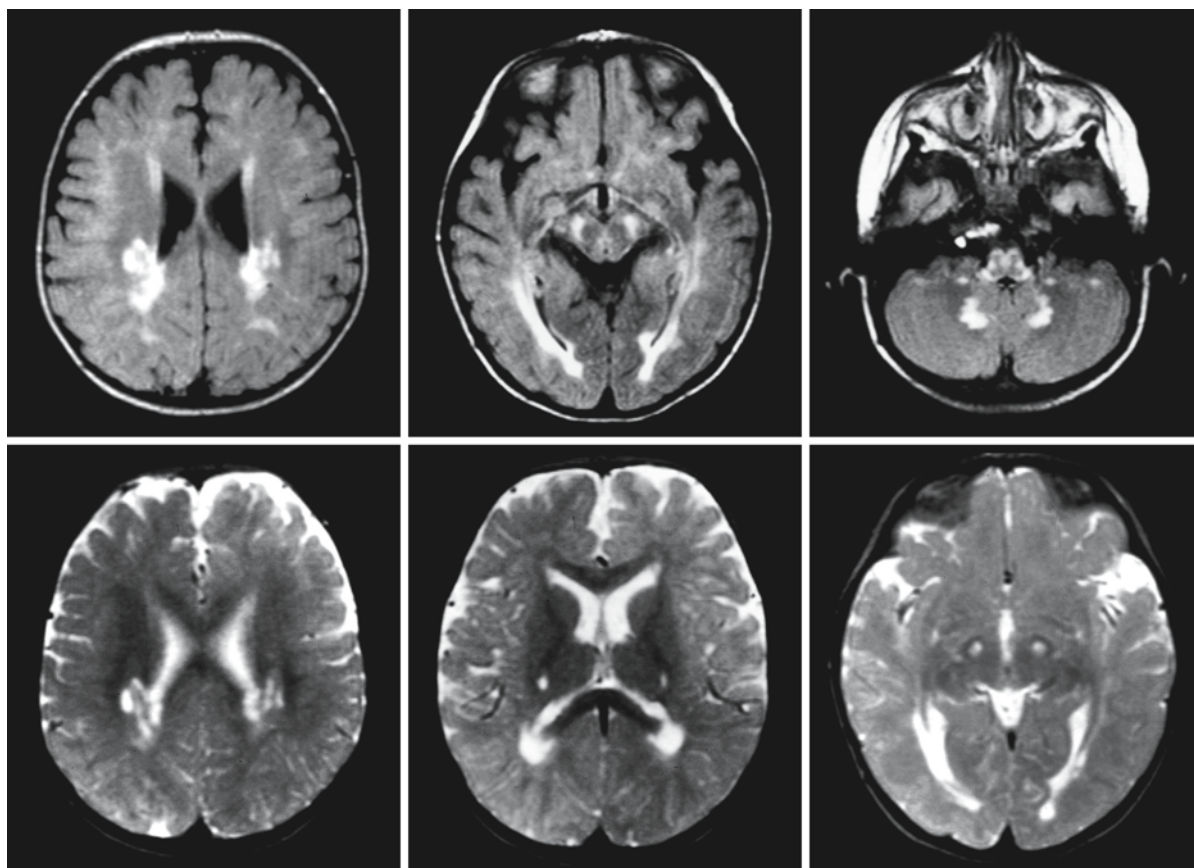


Fig. 28.11. A 1.5-year-old boy with cytochrome-c oxidase deficiency. There are signal abnormalities in the subthalamic nucleus, dentate nucleus, substantia nigra, and nuclei in the medulla. In addition, there are white matter abnormalities involving the periventricular parieto-occipital region and pos-

terior limb of the internal capsule. Courtesy of Dr. M. Savoirda, Department of Neuroradiology, and Dr. G. Uziel, Department of Child Neurology, Istituto Nazionale Neurologico C. Besta, Milan, Italy

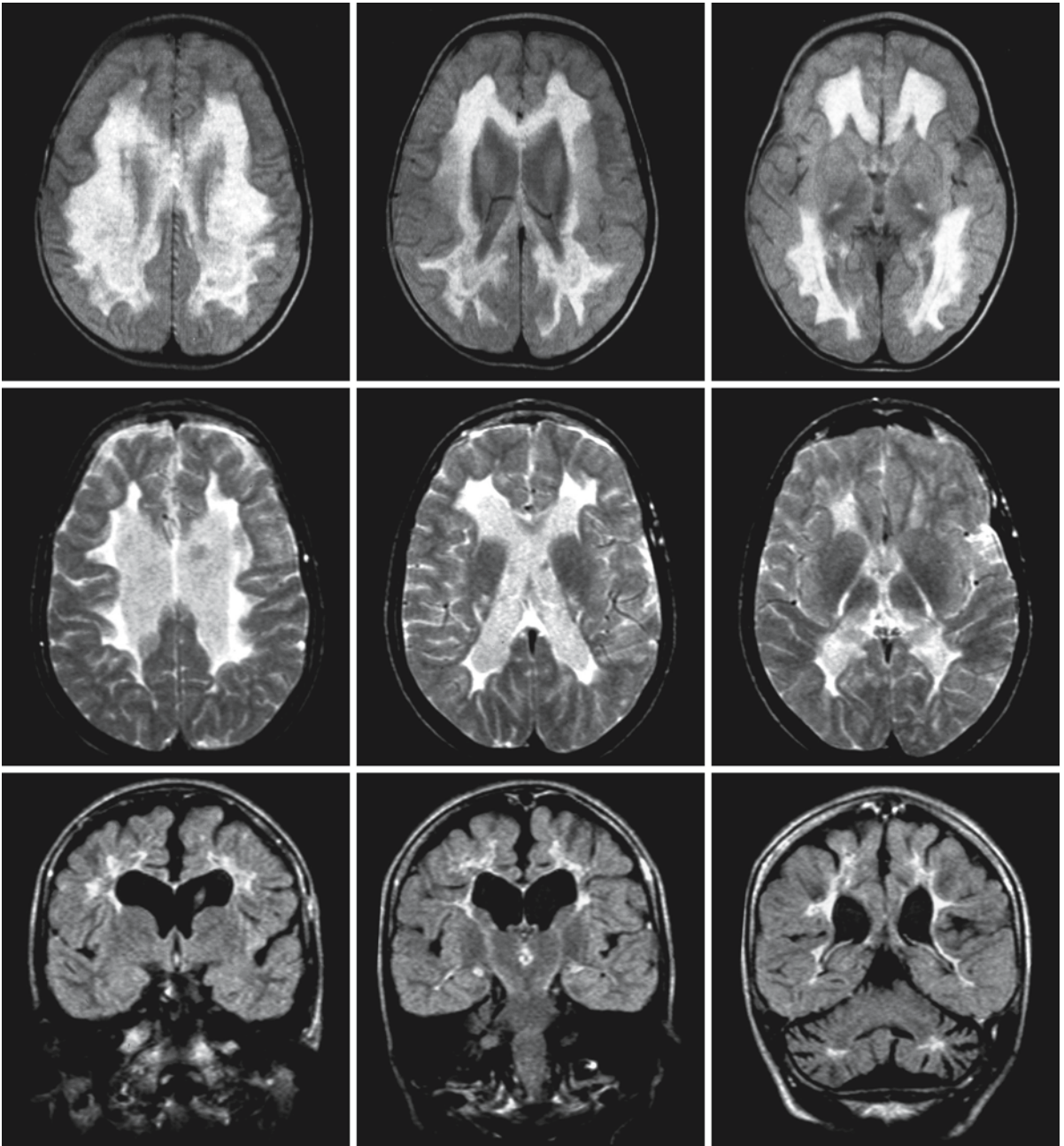


Fig. 28.12. Girl with cytochrome-c oxidase deficiency. The first MRI was obtained when she was aged 2.5 years (*first row*). These proton density images show extensive signal abnormalities involving all cerebral white matter including the corpus callosum, but sparing the U fibers. The images suggest some cystic degeneration, with a lower signal in some white matter areas. Follow-up MRI 10 years later (*second and third row*) re-

veals atrophy of the affected white matter. The coronal FLAIR images (*third row*) confirm the partial cystic degeneration. The deep cerebellar white matter is also affected. Courtesy of Dr. M. Savoiardo, Department of Neuroradiology, and Dr. G. Uziel, Department of Child Neurology, Istituto Nazionale Neurologico C. Besta, Milan, Italy

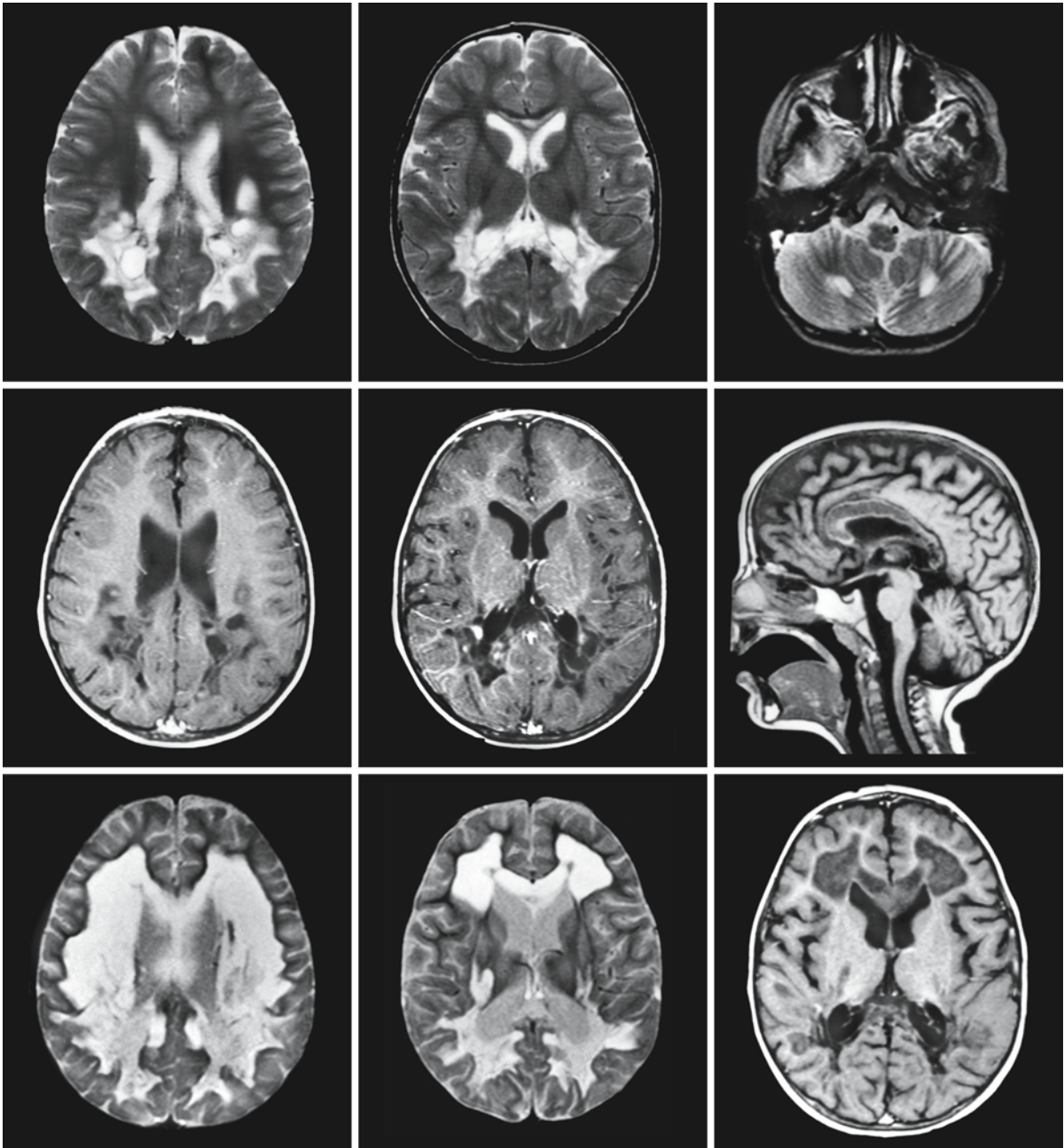


Fig. 28.13. Boy with isolated complex I deficiency. The first MRI (*first row; second row, left and middle*) was obtained at presentation at 3 years of age. Note the extensive signal abnormalities in the posterior cerebral white matter and posterior part of the corpus callosum. The abnormal white matter is partially cystic. There are foci of contrast enhancement within the abnormal white matter (*second row, middle*). The cerebellar

white matter is partially involved (*first row, right*). The second MRI (*second row, right, and third row*) was obtained after 3 months and shows progression of the white matter abnormalities. Only the U fibers are still spared, more so in the anterior than the posterior part of the brain. The corpus callosum is now involved throughout. From Topçu et al. (2000), with permission

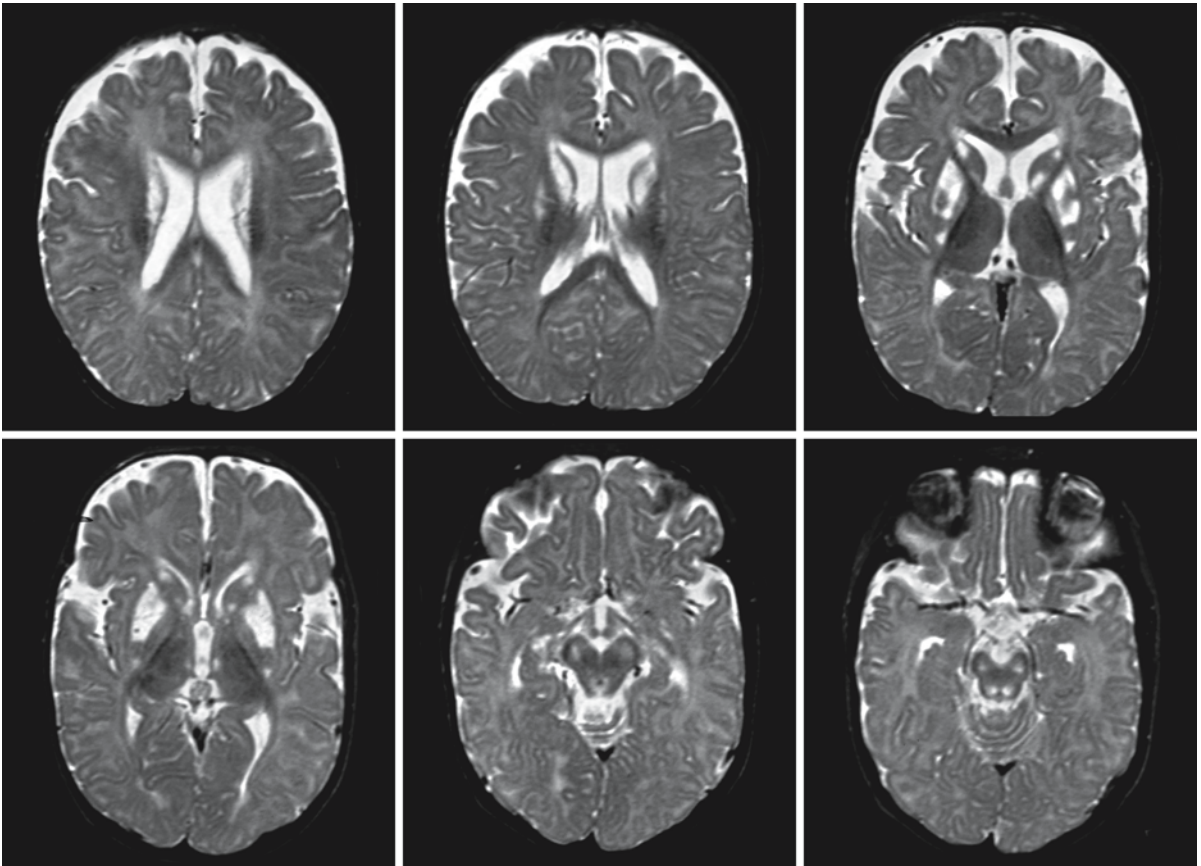


Fig. 28.14. An 8-month-old boy with Leigh syndrome related to a mutation in the mitochondrial gene encoding the ATP synthase 6 subunit. There are lesions in the caudate nucleus, putamen, globus pallidus, medial thalamus, substantia nigra, and periaqueductal gray. Myelination is delayed, but there are no white matter lesions

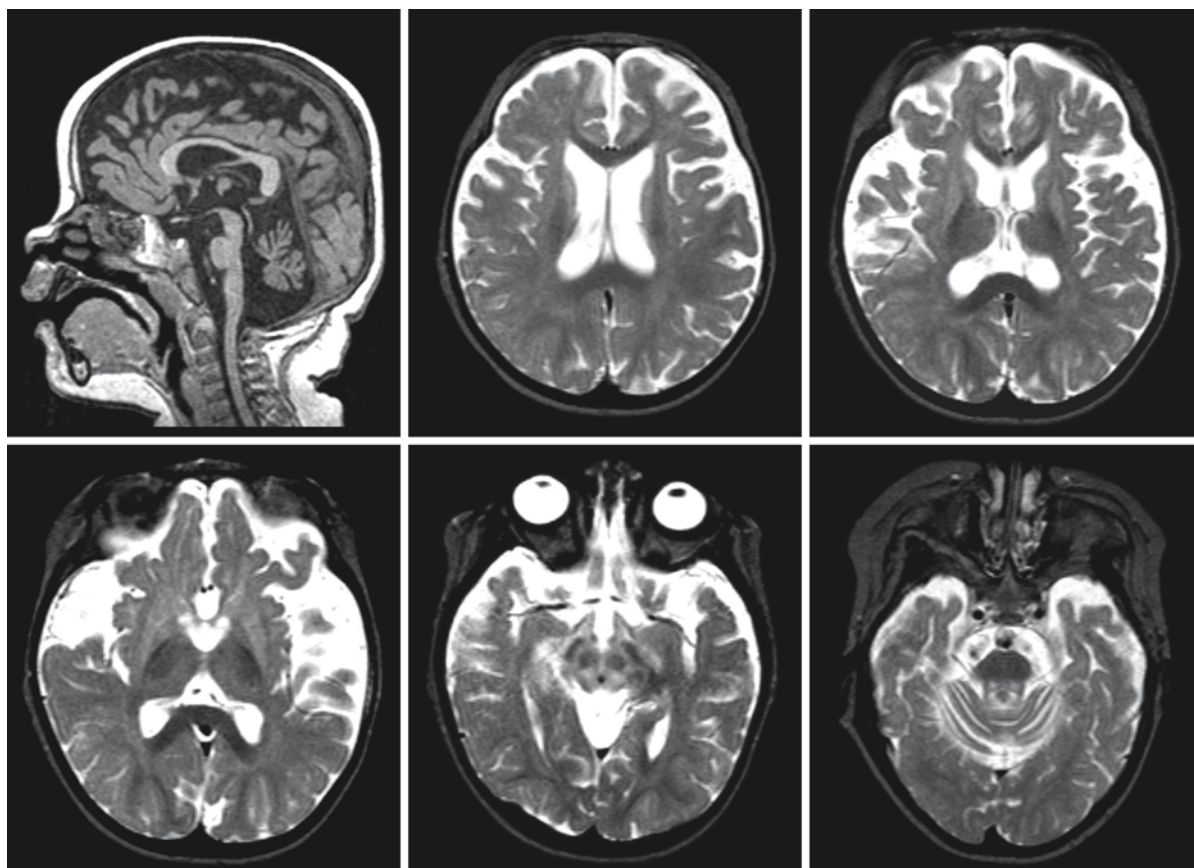


Fig. 28.15. A 2.5-year-old girl with Leigh syndrome related to an ATP synthase 6 subunit mutation. There is severe cerebral and cerebellar atrophy. Myelination is delayed. Faint lesions are visible in the basal ganglia, midbrain, and pontine tegmentum

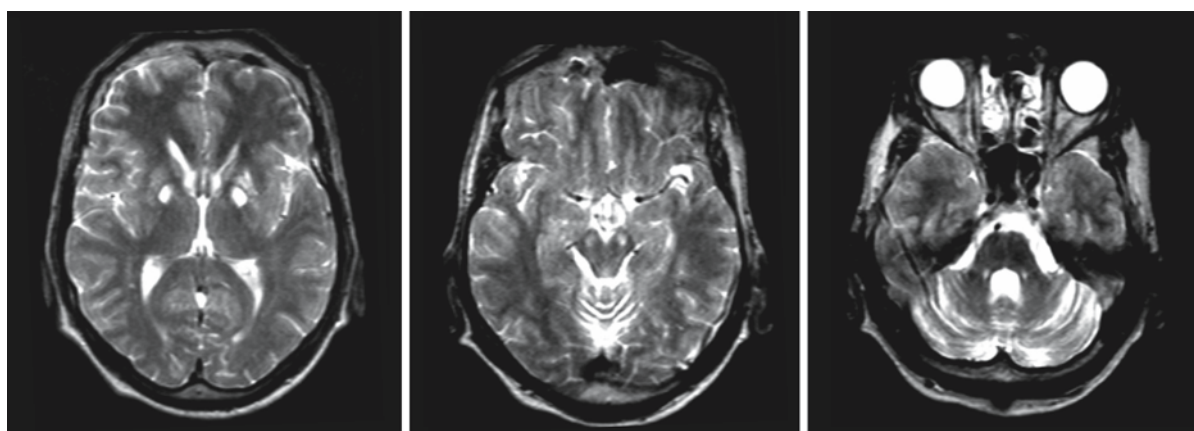


Fig. 28.16. A 38-year-old man with NARP and an ATP synthase 6 subunit mutation. There are lesions in the substantia nigra, caudate nucleus, putamen, and, most prominently, the globus pallidus. In addition, the cerebellum is atrophic. There are no white matter lesions

Pyruvate Carboxylase Deficiency

29.1 Clinical Features and Laboratory Investigations

Pyruvate carboxylase deficiency (PCD) is a rare disorder with autosomal recessive inheritance. Generally, three clinical and biochemical phenotypes of isolated pyruvate carboxylase deficiency can be distinguished. The group A or North American form or infantile form is less severe than the group B phenotype. Patients become symptomatic between 2 and 5 months of age with developmental delay, failure to thrive, apathy, hypotonia, spasticity, ataxia, nystagmus, and convulsions. Episodes of vomiting, tachypnea, tachycardia, ataxia, and lactic acidosis occur, precipitated by metabolic or infectious stress. Some patients die in the infantile period, while most of the survivors are grossly retarded. The group B or French form or neonatal form presents in the neonatal period with severe lactic acidemia and is clinically characterized by failure to thrive, anorexia, vomiting, hepatomegaly, weak cry, convulsions, stupor, hyporeactivity, irritability, hypotonia, tachypnea, dyspnea, respiratory failure, and subsequently hypertonia, extrapyramidal tract signs, and severely retarded development. Some infants have macrocephaly. Almost all children die within the first few months of life. The third variant is milder and has been described in a few exceptional patients who, despite episodic metabolic derangement with ketoacidosis from infancy onwards, have normal or near normal motor and mental development. These patients survive at least up to the third decade. Formerly, Leigh syndrome was thought to represent another clinical phenotype of pyruvate carboxylase deficiency, but this could not be confirmed.

In the North American phenotype lactic acidemia is associated with a normal lactate to pyruvate ratio. There is no hyperammonemia. Alanine and proline are elevated. In the French phenotype, laboratory investigations reveal lactic acidemia with a highly elevated lactate/pyruvate ratio and a lowered 3-hydroxybutyrate/acetoacetate ratio. Ketoacidosis and moderate hyperammonemia are present, and blood levels of alanine, citrulline, proline, and lysine are elevated. The level of aspartate is often decreased but may also be normal.

Diagnosis is established by demonstrating a deficiency in pyruvate carboxylase activity in fibroblasts, white blood cells, or liver cells. The activity of propi-

onyl-CoA carboxylase is normal, excluding multiple carboxylase deficiency. DNA confirmation is possible. Prenatal diagnosis can be performed by enzyme assessment in chorionic villi samples or cultured amniocytes. In families with known mutations in the pyruvate carboxylase gene, prenatal diagnosis using DNA techniques is also possible.

29.2 Pathology

In all reported cases, whether of the North American or the French phenotype, the brunt of abnormalities is borne by the white matter of the CNS. The brain may be swollen and the white matter may be friable and edematous. The hemispheric white matter is often grossly cystic, the cysts being located either in the periventricular or in the deep white matter. Subependymal cysts may also occur. Cystic degeneration tends to be symmetrical, but is not always symmetrical in detail. On microscopic examination diffuse myelin paucity, sponginess, and gliosis of the white matter are found, involving cerebral and cerebellar white matter and sometimes also the base of the pons. The myelin paucity is variably described as hypomyelination or demyelination. Probably, both are important. Perivascular accumulation of foamy macrophages is an argument in favor of a component of active myelin breakdown. The white matter is decreased in volume in cases of longer duration resulting in enlargement of the ventricular system. The corpus callosum is thin.

The condition of the gray matter is variable, but gray matter pathology does not dominate. In some cases all gray matter structures are completely normal. Some have noted depletion of neurons in the cerebral cortex. Some have noted that the globus pallidus, a nucleus rich in myelin, is involved in the process of myelin abnormality and loss. Some describe cystic degeneration of the deep gray nuclei.

29.3 Pathogenetic Considerations

Pyruvate carboxylase is a mitochondrial matrix enzyme, encoded by nuclear DNA. The gene, *PC*, is located on chromosome 11q13.4–13.5. Pyruvate carboxylase is a homotetramer consisting of four identical polypeptides, each with a covalently bound biotin

molecule. There are four major biotin-dependent carboxylases: pyruvate carboxylase, propionyl-CoA carboxylase, methylcrotonyl-CoA carboxylase, and acetyl-CoA carboxylase. There are no known tissue-specific isoenzymes of pyruvate carboxylase. The enzyme catalyzes the conversion of pyruvate, the end product of the glycolysis, into oxaloacetate, a citric acid cycle intermediate. It replenishes oxaloacetate for the citric acid cycle. Oxaloacetate is also in equilibrium with aspartate. Oxaloacetate is utilized in the synthesis of glucose, fat, some amino acids or their derivatives, and several neurotransmitters. The roles of pyruvate carboxylase in metabolism are tissue-specific. In gluconeogenic tissue (liver, kidneys), it catalyzes the first step in the synthesis of glucose from pyruvate. In lipogenic tissue (liver, adipose tissue, lactating mammary gland, adrenal gland), it participates in the export of acetyl groups, such as citrate, from the mitochondria to the cytosol. In the CNS, pyruvate carboxylase participates in the replenishment of neurotransmitter pools of glutamate, GABA, and aspartate.

Pyruvate carboxylase deficiency can occur as isolated pyruvate carboxylase deficiency, caused by a mutation in the pyruvate carboxylase gene, and as multiple carboxylase deficiency related to biotin deficiency. In isolated pyruvate carboxylase deficiency there is a defect in the conversion of pyruvate to oxaloacetate. Availability of the latter metabolite is essential for citric acid cycle activity. When oxaloacetate synthesis from pyruvate is limited, aspartate is converted to oxaloacetate and depletion of aspartate occurs. Aspartate is an important component of the shuttle mechanism transferring reducing equivalents across the mitochondrial membrane. Depletion of aspartate leads to accumulation of reducing equivalents (NADH) in the cytosol and mitochondrial NADH becomes more oxidized. This altered redox state results in an increase in the lactate to pyruvate ratio and a decrease in the β -hydroxybutyrate to acetoacetate ratio. Depletion of aspartate also interferes with urea cycle activity. Aspartate is a nitrogen donor for the urea cycle and depletion of aspartate leads to hyperammonemia, citrullinemia, and hyperlysinemia. Accumulation of acetyl-CoA may also occur under these circumstances and result in overproduction of ketone bodies. Despite the fact that pyruvate carboxylase is an important enzyme in gluconeogenesis, hypoglycemia is not a consistent finding in pyruvate carboxylase deficiency.

The different phenotypes of pyruvate carboxylase deficiency are related to the severity of enzyme deficiency. Many patients with the French phenotype have no immunologically detectable enzyme at all, but some have. In patients with the North American phenotype, the pyruvate carboxylase enzyme protein

can be shown to be present with immunological techniques, although deficient in activity. Presumably, the French phenotype is related to absent or almost absent residual enzyme activity, whereas in the North American phenotype the residual activity is enough to ameliorate the most severe symptoms of pyruvate carboxylase deficiency. However, environmental factors, including intercurrent illnesses and other stresses, such as fasting, may contribute to determining outcome.

29.4 Therapy

Treatment has proven to be quite difficult and disappointing in pyruvate carboxylase deficiency. Metabolic acidosis must be corrected by bicarbonate therapy. Aspartate supplementation has been recommended to increase oxaloacetate concentrations and overcome aspartate depletion, and some patients have actually shown improvement. Glutamine, also a precursor of oxaloacetate, may also have a beneficial effect. Citrate may result in reduction of the lactic acidosis. Thiamine has been advocated to stimulate the pyruvate dehydrogenase complex but is ineffective. Administration of biotin to stimulate pyruvate carboxylase has been beneficial in some patients, but in many patients it is disappointing. Avoidance of fasting with its attendant gluconeogenic stimulus is important, but high carbohydrate diets and high fat diets are not beneficial. Unfortunately, despite all therapeutic measures, the neurological outcome remains poor.

29.5 Magnetic Resonance Imaging

Reports on neuroimaging findings are scarce in pyruvate carboxylase deficiency. CT reveals diffuse hypodensity of the cerebral white matter. The white matter may be mildly swollen. MRI demonstrates signal abnormalities in the cerebral and cerebellar white matter and in brain stem structures, in particular the base of the pons (Fig. 29.1). In some patients the white matter degeneration is cystic. In the first few months of life, subependymal cysts may be seen (Fig. 29.1). Probably depending on the stage of the disease, the white matter has a swollen appearance (Fig. 29.1) or is atrophic. The corpus callosum is thin. In patients with severe atrophy, there may be subdural hygromas and hematomas. The signal abnormality of the cerebral white matter is partly related to delayed myelination; progress of myelination is seen over time. The white matter abnormalities tend to be diffuse in the early changes, but over time and with progress of myelination, they become more patchy and multifocal.

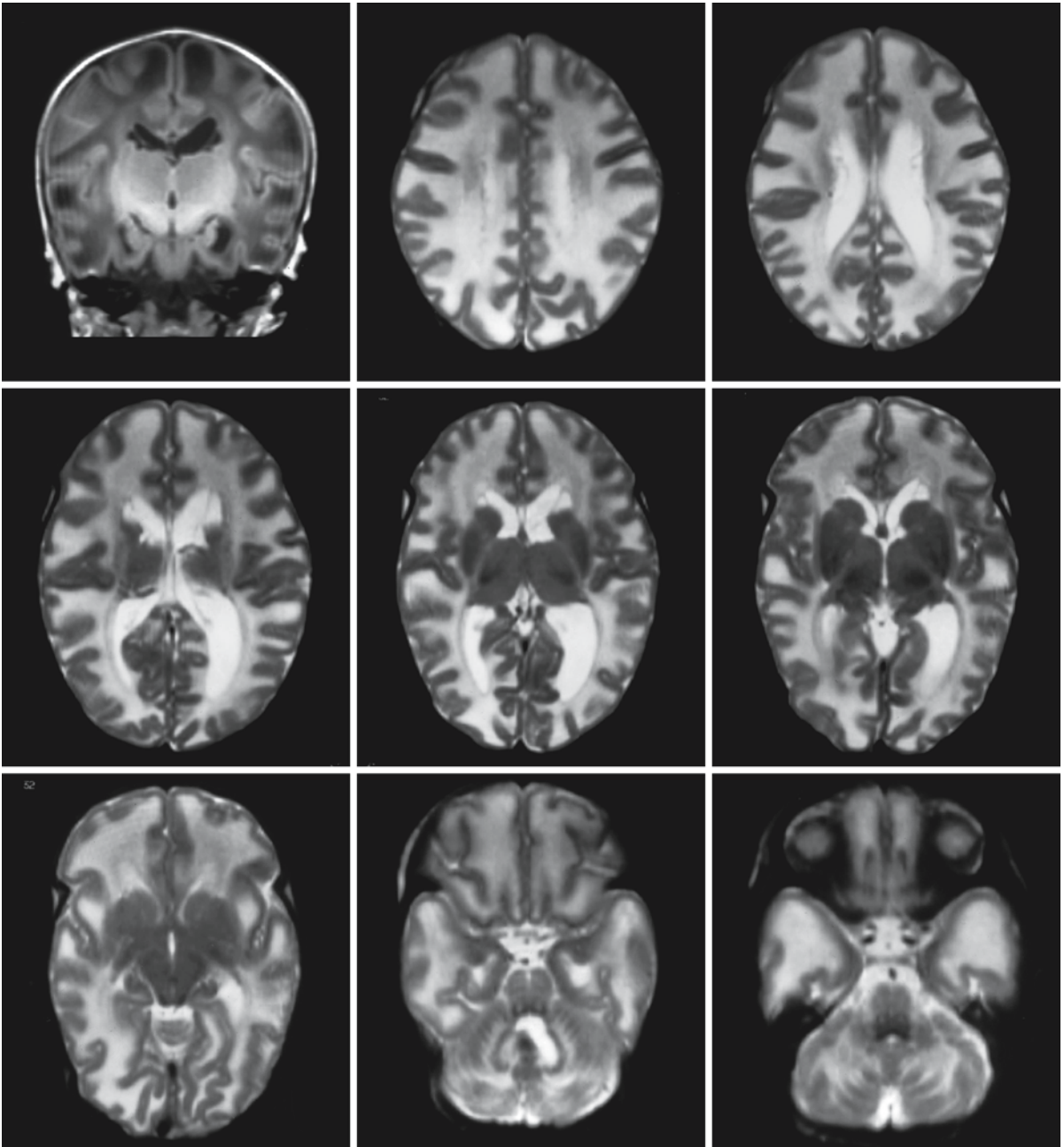


Fig. 29.1. The T_2 -weighted images of a female infant of 18 days with pyruvate carboxylase deficiency show that the cerebral and cerebellar white matter has a higher signal than normal for unmyelinated white matter, and is mildly swollen.

There are multiple subependymal cysts along the ventricles. Signal changes are seen in the base of the pons and the central tegmental tracts. Courtesy of Dr. U. Wendel, Department of Pediatrics, University Children's Hospital, Düsseldorf, Germany

Multiple Carboxylase Deficiency

30.1 Clinical Features and Laboratory Investigations

Two inherited defects in biotin metabolism are known: holocarboxylase synthase deficiency and biotinidase deficiency, both autosomal recessive disorders. A rare cause of biotin dependency is a genetic defect in the transport of biotin. Alimentary biotin deficiency is exceptional and may, for instance, be related to parenteral nutrition with a formula deficient in biotin, short bowel syndrome, or hemodialysis without biotin supplementation. Excessive intake of avidin, an egg-white glycoprotein that binds specifically and irreversibly to biotin, may also result in biotin deficiency. All lead to deficiency of multiple carboxylases: 3-methylcrotonyl-CoA carboxylase, propionyl-CoA carboxylase, pyruvate carboxylase, and the two isoenzymes of acetyl-CoA carboxylase.

The characteristic manifestations of multiple carboxylase deficiency consist of skin disease and neurological abnormalities. The skin abnormalities are described as seborrheic or atopic dermatitis. They consist of nonspecific, patchy, maculopapular, scaly and erythematous eruptions; they occur especially in moist and periorificial areas. In more severe cases lichenification, crusting, and open lesions may occur, that may become infected by *Candida*. The hair is often sparse and thin and partial or total alopecia may be present that can include the eyebrows and eyelashes.

Onset of clinical symptoms in patients with holocarboxylase synthase deficiency is between a few hours after birth and the age of 2 years. Most patients present in the first days or weeks after birth, but others present with acute metabolic derangement later, in the 2nd year of life. The symptoms may be precipitated by catabolism or increased dietary protein intake. The most common symptoms include tachypnea, stridor, skin rash, feeding difficulties, vomiting, hypotonia, developmental delay, tremor, ataxia, seizures, irritability, lethargy, and coma. Alopecia occurs in some of the patients. Disorders of immune function have been observed with a decreased T-cell count. The disease generally leads to severe neurological damage or death if untreated.

The age at onset in patients with a biotinidase deficiency is usually later and more variable. Most patients with a profound biotinidase deficiency have cutaneous and neurological symptoms in infancy or

early childhood, but patients with a partial biotinidase deficiency may not develop symptoms until adolescence. However, asymptomatic adults, both with a partial and a profound biotinidase deficiency, have been detected. When patients present, the symptoms are essentially the same, independent of age, although older patients tend to have fewer symptoms. Most patients present between the ages of 6 weeks and 18 months. Most have progressive encephalopathy, but some have episodes of acute deterioration. The most common symptoms are skin rash, partial or complete alopecia, hypotonia, spasticity, developmental delay, seizures including infantile spasms, and sensorineural hearing loss. In many patients the seizures are difficult to control with antiepileptic medication. Less common features are keratoconjunctivitis, ataxia, fatigue, lethargy, tachypnea, apnea, laryngeal stridor, scotomas, and loss of vision due to optic atrophy. Some patients develop feeding difficulties, vomiting, diarrhea, hepatomegaly, splenomegaly, or coma. Immunological dysfunction may occur in acutely ill patients. Older patients often present with optic atrophy, sensorineural hearing loss, and gait problems; some of them have a mental retardation, but others are intellectually intact. Biotinidase deficiency generally leads to progressive clinical symptoms ending in severe neurological damage or death if untreated.

Laboratory findings in affected children include metabolic acidosis, mild hyperammonemia, and organic aciduria. Increased urinary excretion is usually found of 3-methylcrotonylglycine and 3-hydroxyisovalerate reflecting methylcrotonyl-CoA carboxylase deficiency; 3-hydroxypropionate, propionylglycine, tiglylglycine, propionate, and methylcitrate reflecting propionyl-CoA carboxylase deficiency; and lactate, which likely reflects pyruvate carboxylase deficiency. In holocarboxylase synthase deficiency the biochemical abnormalities tend to be more severe and complete than in biotinidase deficiency. However, in some patients with holocarboxylase synthase deficiency the biochemical abnormalities are only mild, rather suggesting biotinidase deficiency. In some children with biotinidase deficiency, urinary organic acids are normal at presentation.

The diagnosis of holocarboxylase synthase deficiency is confirmed by showing deficiency of 3-methylcrotonyl-CoA carboxylase, propionyl-CoA carboxylase, pyruvate carboxylase, and acetyl-CoA

carboxylase in lymphocytes or fibroblasts in a medium with low biotin concentration. The enzyme activities remain severely deficient after in vitro preincubation with biotin. The diagnosis of biotinidase deficiency is confirmed by showing decreased or absent enzyme activity in serum, leukocytes, and fibroblasts. In biotinidase deficiency and acquired biotin deficiency, carboxylase activities in lymphocytes are usually decreased but may also be normal, depending on the degree of biotin deficiency; the carboxylase activities increase significantly or normalize after in vitro preincubation with biotin. Plasma biotin concentration is usually below normal in symptomatic patients with biotinidase deficiency and in acquired biotin deficiency, but normal in holocarboxylase synthase deficiency. Prenatal diagnosis can be performed by enzyme assays in cultured chorionic villi and amniotic fluid cells.

30.2 Pathology

Reports on neuropathological findings are scarce. The external appearance of the brain is usually normal. Ill-demarcated, partly necrotizing focal lesions are found in the white matter of the cerebral hemispheres, thalamus, hypothalamus, subthalamic nucleus, hippocampus, mammillary bodies, substantia nigra, red nucleus, oculomotor nuclei, periaqueductal gray matter in the midbrain, tegmentum of the pons, dorsomedial parts of the medulla oblongata, inferior olivary nucleus, deep cerebellar white matter, cerebellar nuclei, and the posterior, lateral, and anterior columns of the spinal cord. The lesions show rarefaction, microcavitation, sponginess, capillary proliferation, and gliosis. Reactive astrocytes and foamy macrophages are present. Myelin is lost and neurons are relatively preserved. The lesions are similar to those observed in Leigh syndrome and thiamine deficiency.

Another striking finding is vacuolation and edema of white matter tracts, including parts of the corpus callosum, fornix, the central tegmental tracts in the pons, the decussation of the medial lemniscus, the superior cerebellar peduncles, the pyramids, and anterior columns of the spinal cord. Abnormalities involving the lateral and posterior columns have also been reported. Myelin loss is seen with relatively less severe axonal loss. Defective myelination and gliosis of the cerebral and cerebellar white matter have also been reported. The optic nerves may display severe loss of myelinated fibers.

30.3 Pathogenetic Considerations

Biotin is an essential water-soluble vitamin and is the coenzyme for four carboxylases, propionyl-CoA carboxylase, 3-methylcrotonyl-CoA carboxylase, pyruvate carboxylase, and acetyl carboxylase, which are involved in the catabolism of several branched-chain amino acids, gluconeogenesis, and fatty acid synthesis. Each of the four carboxylases is synthesized in an inactive form called apocarboxylase and becomes enzymatically active only when it is linked covalently to biotin; it is then called holocarboxylase. Holocarboxylase synthase catalyzes the covalent binding of biotin to a lysine residue in the four biotin-dependent enzymes. Humans cannot synthesize biotin and therefore derive the vitamin from dietary sources or from recycling endogenous biotin. The carboxylases are degraded proteolytically to amino acids and biocytin (biotinyl-*N*- ϵ -lysine). Biocytin is then hydrolyzed by biotinidase to lysine and free biotin, thereby recycling the vitamin for reutilization. Biotinidase is also necessary for liberating biotin from dietary protein-bound sources to its free, bioavailable form. Additionally, biotinidase has biotinyl transferase activity, in which biotin from biocytin is transferred to other proteins. The gene encoding holocarboxylase synthase, *HLCS*, is located on chromosome 21q22.1. The gene encoding biotinidase, *BTD*, is located on chromosome 3p25.

The multiple carboxylase deficiencies are genetically determined or acquired disorders of biotin metabolism and result in impaired activity of all four biotin-dependent carboxylases. There are two forms of inherited multiple carboxylase deficiency: holocarboxylase synthase deficiency and biotinidase deficiency. In holocarboxylase synthase deficiency, the carboxylases remain in their inactive apo-form. In biotinidase deficiency, endogenous biotin cannot be recycled and dietary protein-bound biotin cannot be released. Biocytin is lost in urine, leading to progressive biotin depletion. The clinical symptoms of holocarboxylase synthase deficiency and biotinidase deficiency overlap, but ophthalmological abnormalities and hearing loss have not been observed in holocarboxylase synthase deficiency. The symptomatology in holocarboxylase synthase deficiency tends to be of earlier onset and more severe than in biotinidase deficiency, although there is a major overlap. In biotinidase deficiency, the level of the residual enzyme activity correlates with the development of clinical and biochemical abnormalities. Most patients with profound biotinidase deficiency develop early signs of the disease. Patients with partial biotinidase deficiency may be healthy and develop symptoms only under conditions of infection or starvation. A special variant of the disease is related to decreased affinity of biotinidase for biocytin, the so-called K_m variant

with a reduced maximum reaction velocity and an elevated K_m of biotinidase for biocytin.

30.4 Therapy

Holocarboxylase synthase deficiency can often be treated effectively with pharmacological doses of biotin. The required dose of biotin is dependent on the severity of the enzyme defect and has to be assessed individually. With treatment the symptoms usually either disappear or improve and further deterioration can usually be prevented. An important problem is that delayed diagnosis leads to permanent damage that cannot be undone with treatment. Unfortunately, some patients show only a partial response to biotin or no response at all. Persistence and even progression of the encephalopathy despite very high doses of biotin has been observed in some patients. It is likely that some defects in holocarboxylase synthase make it unresponsive to biotin supplementation.

The results of biotin treatment in biotinidase deficiency are even better. With treatment most or all symptoms disappear and further deterioration can be prevented. The only problem is that damage already acquired may not be entirely reversible. In particular auditory and visual deficits, but also intellectual impairment and motor deficits may persist in spite of treatment. For this reason, neonatal screening for biotinidase deficiency has been instituted in many countries. Early diagnosis and treatment prevent the onset of symptoms. Patients with a partial biotinidase deficiency and the biotinidase K_m variant should also be treated with biotin, especially as biotin has no known harmful effects.

Prenatal diagnosis is possible. If holocarboxylase synthase deficiency is detected, antenatal treatment can be started by treating the mother with biotin, preventing acute neonatal symptoms. Intrauterine treatment is not necessary for biotinidase deficiency, because of the later onset of symptoms.

30.5 Magnetic Resonance Imaging

CT of the brain may show basal ganglia calcification in untreated multiple carboxylase deficiency. Diffuse hypodensity of the cerebral white matter within the neonatal period with disappearance of the hypodensity after many months of treatment has been reported. The problem is that the cerebral white matter is always hypodense in neonates due to lack of myelin, and that disappearance of the hypodensity with ongoing myelination is a normal phenomenon. The white matter does, however, look more hypodense than normal and mildly swollen on the CT pictures

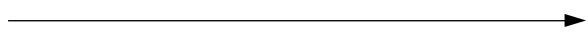


Fig. 30.1. A 1-year-old girl just diagnosed with biotinidase deficiency. The child presented with psychomotor retardation, spastic quadriplegia, and a severe seizure disorder. The MRI shows a severe delay in myelination. The white matter of the centrum semiovale looks spongy with many tiny cysts, which could also be enlarged perivascular spaces. The subarachnoid spaces are mildly enlarged, compatible with mild cerebral atrophy. Courtesy of Dr. Z. Patay, Department of Radiology, and Dr. P.T. Ozand, Department of Pediatrics, King Faisal Specialist Hospital and Research Center, Riyadh, Saudi Arabia

published, suggesting diffuse white matter vacuolation or edema.

MRI shows variable abnormalities in untreated multiple carboxylase deficiency, including delayed myelination, diffuse cerebral white matter signal abnormality and swelling, more patchy cerebral white matter abnormalities, and cerebral atrophy (Figs. 30.1 and 30.2). The white matter abnormalities and cerebral atrophy are at least partially reversible with treatment. These imaging abnormalities have a low diagnostic specificity. Signal abnormalities in central gray matter structures, brain stem, and spinal cord have also been reported, suggestive of a Leigh-like disease. These may be entirely or partially reversible with treatment. With Leigh-like abnormalities present on MRI, the possibility of multiple carboxylase deficiency should be considered.

One paper by Wiznitzer and Bangert (2003) reports signal changes in the spinal cord over its entire length in a patient with clinical ataxia and spastic paraparesis. The abnormalities disappeared with treatment.


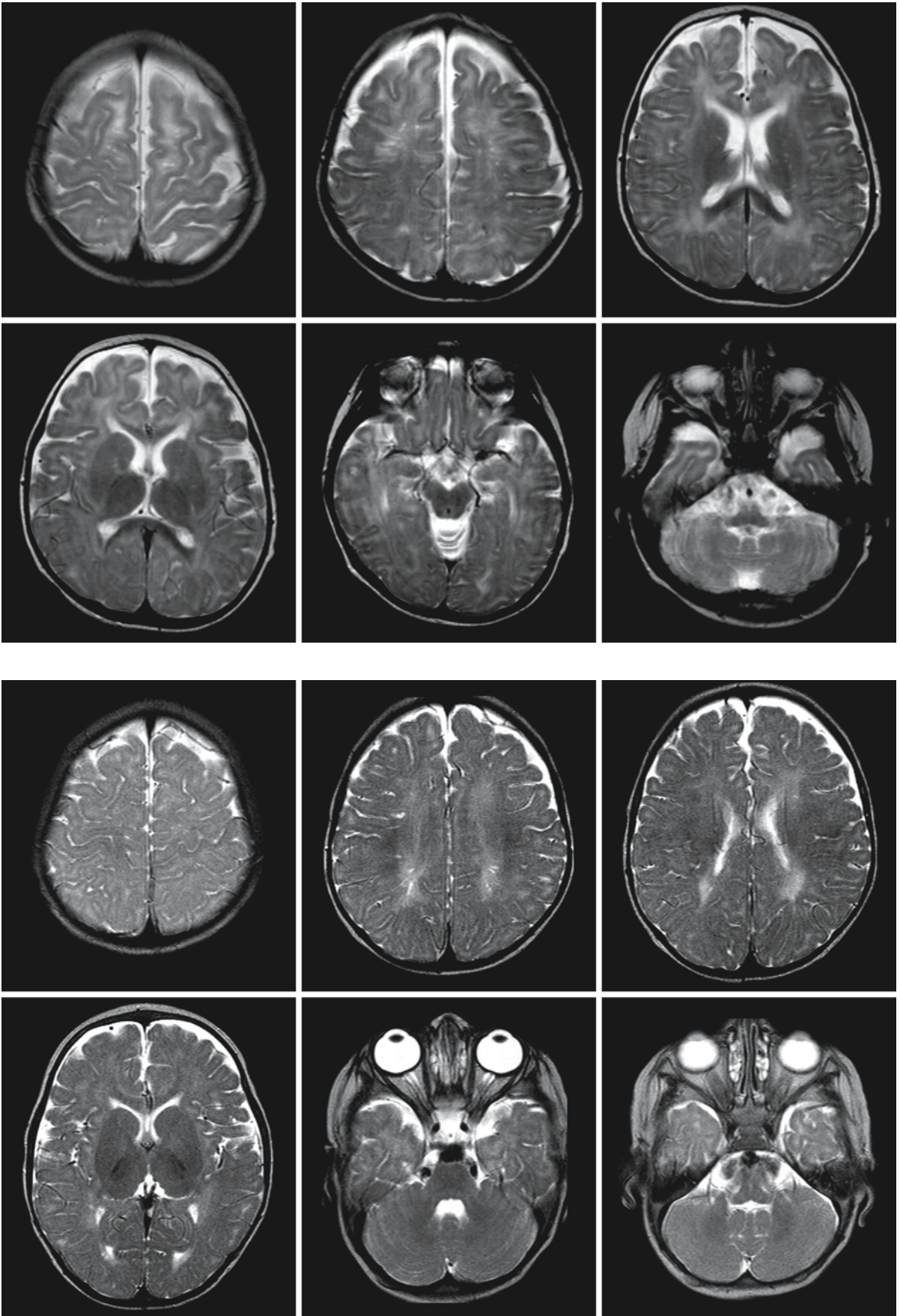


Fig. 30.2. A 1-year-old boy just diagnosed with biotinidase deficiency. He presented with an acute metabolic crisis. The MRI shows delayed myelination and mildly enlarged subarachnoid spaces. There are more prominent signal abnormalities in the deep parietal white matter, where the white matter also looks spongy with many tiny cysts, possibly enlarged perivascular spaces. Courtesy of Dr. Z. Patay, Department of Radiology, and Dr. P.T. Ozand, Department of Pediatrics, King Faisal Specialist Hospital and Research Center, Riyadh, Saudi Arabia



Cerebrotendinous Xanthomatosis

31.1 Clinical Features and Laboratory Investigations

Cerebrotendinous xanthomatosis (CTX) is a rare neurometabolic disorder with an autosomal recessive mode of inheritance. Prolonged neonatal cholestatic jaundice is common ("hepatitis of infancy"). Most patients are of borderline or low intelligence from the beginning and their school performance is poor. Chronic, intractable, and unexplained diarrhea is present in about 50% of the affected children. The more specific clinical manifestations usually appear in late childhood or early adolescence, or even later. The most commonly noted early manifestations of the disease include cataracts and xanthomas of tendons, especially the Achilles tendons, but also the tendons of the quadriceps muscle, the triceps muscle, and the finger extensors. During the second or third decade, neurological problems gradually become manifest with signs of cerebellar ataxia, spastic paraparesis and tetraparesis, signs of dysfunction of the posterior columns, and signs of peripheral polyneuropathy. Some patients have only signs of spinal cord dysfunction with pyramidal tract and dorsal column involvement. Tendon reflexes are generally hyperactive. Vibratory and position senses are diminished whereas the superficial sensory modalities remain relatively intact. Foot deformity, in particular pes cavus, is often noted. About 40% of the patients develop epilepsy with generalized tonic-clonic seizures. In most cases a decline of mental function occurs in the third decade, but there is wide diversity in the rapidity of the decline. Changes in personality and psychiatric problems may be present, varying from irritability, agitation, and aggressiveness to paranoid ideation, hallucinations, and catatonia. Premature atherosclerosis may lead to angina pectoris, myocardial infarction, and cardiac failure. Less frequent complaints are pharyngeal and palatal myoclonus, tachylalia, mask-like facies, parkinsonism, bulbar and pseudobulbar paresis with dysphagia and dysphonia, visual loss due to optic atrophy, palpebral xanthelasmas, corneal lipid arcus, generalized muscular wasting, bone fractures due to osteoporosis, impaired lung function due to pulmonary xanthomas, and signs of endocrine dysfunction. In untreated cases death usually occurs between the fourth and sixth decades.

The problem with the diagnosis of CTX is that there are no obligatory symptoms and that the devel-

opment of symptoms varies markedly in nature and degree of progression, even within one family. In particular in the absence of the typical tendon xanthomas, the diagnosis can be easily missed.

Laboratory investigations reveal normal or only moderately elevated serum cholesterol but a markedly increased level of serum cholestanol. CSF protein may be increased. CSF cholestanol levels are elevated. Low serum levels of 25-hydroxy vitamin D₃ and 24,25-dihydroxy vitamin D₃ may be found. The measurement of the serum cholestanol to cholesterol ratio has been advocated as a means of establishing the diagnosis, but elevated cholestanol and elevated cholestanol to cholesterol ratios are not very specific and can also be found in patients suffering from various liver diseases. A preferable method for establishing the diagnosis is to demonstrate the presence of abnormal bile alcohols in the urine. The diagnosis can be confirmed by demonstrating lack of 27-hydroxylase activity in cultured fibroblasts and by DNA techniques.

X-ray examination may reveal swelling of the Achilles tendons and, less frequently, of the tendons of the hamstrings, quadriceps, and finger extensors. Calcification of these soft tissue masses may be seen. Motor and sensory nerve conduction is often slowed. Evoked potentials, in particular SSEPs, are as a rule delayed. EEG shows diffuse slowing of background activity with poorly organized theta and delta waves.

Carriers of CTX can be identified by observing an abnormal increase in bile alcohols in their urine after administration of cholestyramine, a drug that leads to intestinal loss of bile acids and as a consequence to increased endogenous synthesis. Normal control persons fail to produce the unusual bile alcohols. Carrier detection can also be performed by analysis of 27-hydroxylase activity in cultured fibroblasts or by DNA techniques. Prenatal diagnosis is possible using the same techniques.

31.2 Pathology

On external examination of the brain, mild atrophy is found, especially of the cerebellum. Sometimes xanthomas are seen in the choroid plexus.

On microscopic examination, the cerebral cortex and hemispheric white matter usually appear normal. Sometimes gliosis and perivascular collections of

large mononuclear cells with foamy cytoplasm are found. Occasionally, prominent loss of myelin and axons may be found at the level of the corona radiata, periventricular white matter, and globus pallidus. Mononuclear cells with foamy cytoplasm may be present in the basal nuclei and thalamus. The globus pallidus especially may contain large mononuclear cells with foamy cytoplasm, accompanied by demyelination of the fibers of the ansa lenticularis as they pass through the internal capsule. The optic nerves and tracts may exhibit loss of myelin and axons associated with fibrillary gliosis and presence of perivascular lipid-laden mononuclear cells.

The most conspicuous abnormalities are found in the cerebellum. Xanthomatous tissue sometimes replaces most of the white matter. On microscopic examination extensive loss of myelin and axons is seen within the cerebellar white matter, with most severe involvement of the outflow tracts of the dentate nucleus and the superior cerebellar peduncles. In the affected areas many small and large cystic spaces and needle-like clefts are present. Large quantities of neutral fat accumulate within large mononuclear cells with foamy cytoplasm in the cysts and in perivascular spaces. The needle-shaped clefts contain crystalline deposits with staining properties of sterols. The crystalline deposits are surrounded by inflammatory cells and reactive multinucleated foreign-body giant cells. These cells represent the tissue reaction to deposition of sterols. There may be extensive loss of Purkinje cells and granule cells and destruction of the dentate and fastigial nuclei. Particularly in the dentate nucleus, severe neuronal loss may be found with presence of clefts containing crystalline lipid deposits, as well as reactive astrocytosis, focal calcification, and deposition of hemosiderin pigment.

In the brain stem the pyramidal tracts, medial lemniscus, transverse pontine fibers, and superior cerebellar peduncles are involved. At the higher levels of the brain stem, in particular in the red nucleus and substantia nigra, deposits of neutral lipids and crystalline sterols are present. Gray matter changes in the brain stem include loss of neurons, particularly in the inferior olives and other nuclei. In the spinal cord the pyramidal tracts and posterior columns demonstrate loss of myelin sheaths and axons.

In the peripheral nerves extensive axonal degeneration is found. There may be additional signs of segmental demyelination and remyelination with onion bulb formation. Histological examination of muscle tissue discloses signs of denervation and reinnervation with type grouping. On electron microscopy, large aggregates of mitochondria are seen, mainly in the subsarcolemmal region. The mitochondria show mild morphological abnormalities such as increased size and irregular cristae.

Microscopic examination of Achilles tendon xanthomas reveals islets of mononuclear cells with foamy cytoplasm and clefts filled with crystalloid material surrounded by multinucleated giant cells. The clefts are scattered in fan-shaped clusters without any relation to blood vessels. Under polarized light birefringence of the clefts is shown, suggesting presence of sterols. The cells filled with neutral fat are mainly present around blood vessels but also throughout the tissue.

Similar xanthomatous tissue can be found in the lungs and bones. In liver tissue fatty lipofuscin-like pigment granules have been reported in hepatocytes and Kupffer cells. Crystals are found in the cytoplasm of hepatocytes. Mitochondria are hypertrophied and peroxisomes are increased in size and number. Premature atherosclerosis of coronary arteries can be found.

31.3 Chemical Pathology

In CTX patients the lipids stored in the brain and in xanthomas consist of free and esterified cholestanol and cholesterol. Free cholestanol is found not only in the evidently affected areas of the brain, but also in areas which appear normal on histological examination. Cholestanol is found in myelin and also in all other membrane structures in the brain, including cell membranes and membranes of subcellular structures. The concentration of unesterified cholesterol is normal or only slightly increased. In demyelinated areas the concentrations of esterified cholestanol and cholesterol are elevated. Concentrations of cholesterol esters are nonspecifically elevated in many actively demyelinating disorders, but esterified cholestanol is not present in any of these disorders.

31.4 Pathogenetic Considerations

In CTX the basic defect is located in the mitochondrial enzyme 27-hydroxylase. This enzyme catalyzes the initial steps in the side-chain cleavage of sterols. The enzyme hydroxylates a spectrum of sterol substrates, including cholesterol and vitamin D₃. The sterol 27-hydroxylase gene, *CYP27*, is located on the distal portion of the long arm of chromosome 2 (2q35). Many different mutations have been identified. There is no clear correlation between genotype and phenotype.

The most important pathway for the metabolism and excretion of cholesterol in humans is the formation of bile acids. The two major bile acids, cholic acid and chenodeoxycholic acid, are formed in the liver and secreted in bile into the intestine. The enzymes involved in modifying the steroid nucleus of choles-

terol are mainly located in the endoplasmic reticulum and the cytosol. The enzymes involved in the side-chain degradation are mainly located in mitochondria and peroxisomes. The major pathway for side-chain cleavage is the 27-hydroxylase pathway.

Deficient activity of 27-hydroxylase results in a defect in bile acid biosynthesis. The formation of normal bile acids, in particular chenodeoxycholic acid, is reduced. Large amounts of unusual C27 bile alcohols are excreted in bile, feces, and urine. As bile acids are involved in a feedback regulation of the hepatic cholesterol production, the decrease in bile acids leads to enhanced cholesterol production and excessive production of bile alcohols.

Cholestanol is the 5 α -dihydro derivative of cholesterol. It normally represents about 0.1–0.3% of cholesterol in tissues and plasma. In CTX cholestanol is increased 10- to 100-fold, so that it accounts for 2% of plasma and tissue sterols with even greater enrichment in the brain (20–50%), tendon xanthomas (10%), and bile (10%). There is evidence that the increased synthesis of cholestanol is caused by the increased utilization of bile intermediates as precursors for cholestanol. The bile intermediates accumulating in CTX may be shunted into the cholestanol pathway.

Like cholesterol, cholestanol is transported by low-density lipoproteins (LDL) and high-density lipoproteins (HDL). Despite the enhanced production of both sterols, plasma LDL concentrations are low and HDL cholesterol levels are also diminished. The role of LDL is to transport cholesterol from the liver to peripheral tissues. LDL turnover is exceedingly rapid in CTX. The catabolism of LDL by the augmented expression of LDL receptors is sufficiently great to maintain low plasma concentrations, despite enhanced cholesterol production. The role of HDL is to transport cholesterol from peripheral tissues to the liver. HDL cholesterol levels are subnormal in many CTX patients. This may account for the accumulation of tissue sterols in atheromas and xanthomas by hindering reverse sterol transport.

Neurophysiology and histopathology suggest that axonal degeneration is primary in CTX, although there may also be a component of primary myelin loss. The precise pathophysiological mechanisms are unclear. Evidently, the deposition of cholestanol and cholesterol in the nervous system and the replacement of cholesterol by cholestanol must be important in the development of the nervous tissue damage. There is evidence that there is a subtle defect in the blood–brain barrier in CTX, probably caused by the accumulating toxic metabolites. The defect in the blood–brain barrier may be important in the accretion of cholestanol and cholesterol within the CNS. In CTX the fractional clearance of LDL is enhanced, most likely due to an increased activity of hepatic LDL receptors. LDL receptors within the blood–brain

barrier may be up-regulated as well, in this way contributing to the influx of sterols into the CNS.

31.5 Therapy

Treatment in CTX aims at breaking the vicious circle of defective endogenous bile acid synthesis leading to absence of negative feedback, which in turn leads to increased production of cholesterol, abnormal bile alcohols, and cholestanol. Treatment with oral bile acids, in particular chenodeoxycholic acid, repairs the negative feedback and leads to decreased production of cholesterol, cholestanol, and abnormal bile alcohols. Assessment of serum cholestanol and urinary bile alcohols can be used to monitor treatment. Once treatment starts, the diarrhea ceases. The progression of CNS damage is retarded or halted. Patients receiving therapy with chenodeoxycholic acid have been reported to show reversal of their neurological disability, with clearing of dementia and improved motor function. There is also evidence of improved results of paraclinical tests, such as nerve conduction velocity, evoked responses, EEG, and CT.

Combined treatment with chenodeoxycholic acid and 3-hydroxy-3-methylglutaryl coenzyme A reductase inhibitors such as simvastatin, lovastatin, or pravastatin – inhibitors of cholesterol synthesis, leads to a more pronounced reduction of cholesterol and cholestanol than treatment with chenodeoxycholic acid alone. Their long-term clinical efficacy of this combined treatment has still to be proven.

Some patients experience a more marked improvement than others. As the effects of therapy depend largely on the extent of irreversible structural damage to nervous tissue, early diagnosis and early treatment are important. If the disease is detected in early childhood, treatment of the patient not yet clinically affected can prevent occurrence of complaints. It is a treatment for life.

31.6 Magnetic Resonance Imaging

CT scan of the brain has been reported to show cerebellar hypodensity and in some cases also moderate hypodensity of cerebral hemispheric white matter. Increased density may be seen in the area of the dentate nucleus, corresponding to hemosiderin and calcium deposition in histopathology.

The most important and earliest MRI abnormalities are noted in the cerebellum. On T₂-weighted images the dentate nucleus and cerebellar hemispheric white matter have a high signal intensity (Figs. 31.1 and 31.2). The cerebellar foliae are prominent, indicative of atrophy (Fig. 31.2). In some patients, the dentate nucleus has a low signal intensity on T₂-weighted

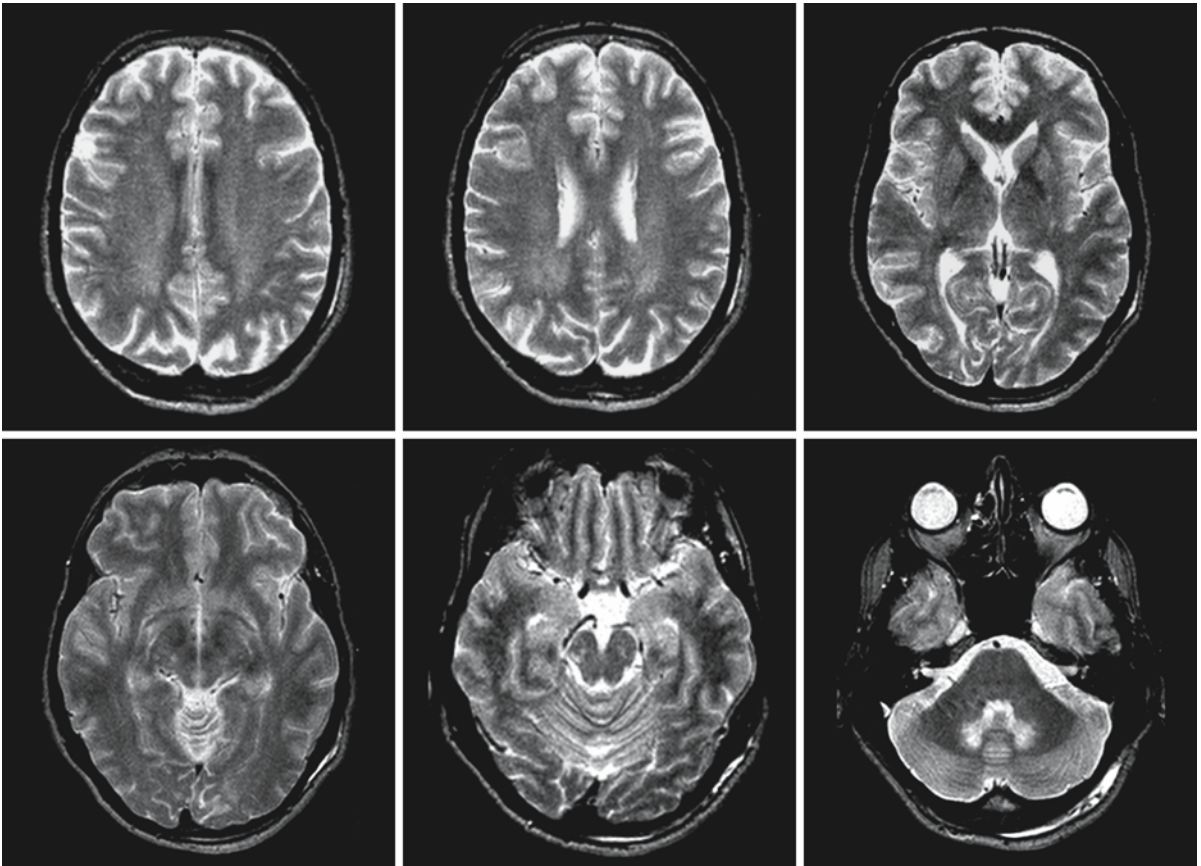


Fig. 31.1. The T_2 -weighted images in this 40-year-old male CTX patient reveal signal abnormalities in the dentate nucleus and medial lemniscus in the midbrain. In addition, there are diffuse, ill-defined slight signal abnormalities in the cerebral

white matter. Courtesy of Dr. F. Barkhof, Department of Radiology, VU University Medical Center, Amsterdam, and Dr. A. Verrips, Department of Pediatric Neurology, University Medical Center Nijmegen, The Netherlands

images (Fig. 31.2). In exceptional cases, the cerebellar white matter lesions are surrounded by a rim of markedly low signal intensity (Fig. 31.4). The low signal on T_2 -weighted images reflects the presence of macroscopic xanthomas or calcium and hemosiderin deposits. Symmetrical lesions are often present in the corticospinal tracts and medial lemniscus in the brain stem (Figs. 31.1 and 31.2). In some patients, the transverse pontine fibers contain signal abnormalities. Involvement of the inferior olives may occur.

In the supratentorial region, ill-defined slight signal changes are seen in the periventricular region in most patients, blending with the normal white matter without a sharp demarcation between the two (Figs. 31.1–31.3). They have a symmetrical distribution. These abnormalities may be confluent or patchy. U fibers and corpus callosum are spared. Slight enlargement of the ventricles and subarachnoid spaces may be seen. In a few patients, focal round or ovoid masses with low signal intensity on T_2 -weighted images are noted within the ventricles, probably reflect-

ing the presence of xanthomas within the choroid plexus (Fig. 31.4). T_2 -weighted images often reveal bilateral high-signal-intensity lesions in the globus pallidus and the adjacent part of the internal capsule, in the area of the ansa lenticularis (Fig. 31.3). The globus pallidus may have a low signal intensity, probably related to the high lipid content (Fig. 31.2).

Within the spinal cord, the lateral and dorsal columns may have a high signal intensity on T_2 -weighted images (Fig. 31.5). Lipid deposits in the Achilles tendon can be visualized (Fig. 31.6).

The full-blown MRI pattern of CTX, consisting of the typical cerebellar abnormalities with high-signal-intensity changes within the white matter and a low signal intensity of the dentate nucleus on T_2 -weighted images, has a high diagnostic value. When only high-signal-intensity lesions are present in the cerebellar (and also cerebral) white matter, other diagnoses should be considered, including adrenomyeloneuropathy and Refsum disease.

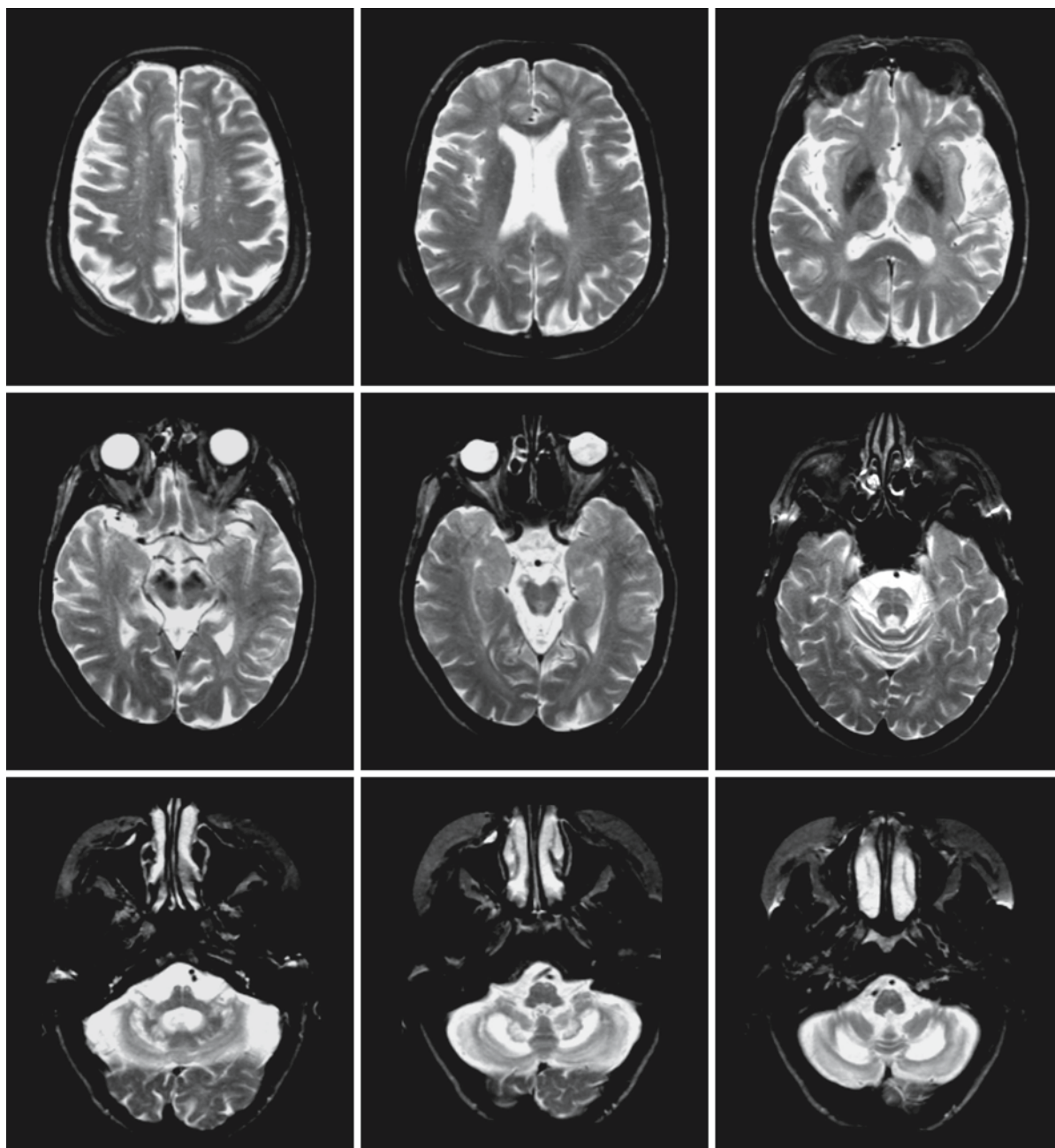


Fig. 31.2. The T₂-weighted images in this 48-year-old female CTX patient reveal diffuse, ill-defined slight signal abnormalities within the cerebral white matter, sparing the corpus callosum, and some cerebral atrophy. The globus pallidus has a low signal intensity. The pyramidal tracts in the brain stem, the medial lemniscus at the level of the pons, the cerebellar hemi-

spheric white matter, and the hilus of the dentate nucleus display an elevated signal intensity. The dentate nucleus stands out as dark. Courtesy of Dr. F. Barkhof, Department of Radiology, VU University Medical Center, Amsterdam, and Dr. A. Verrips, Department of Pediatric Neurology, University Medical Center Nijmegen, The Netherlands

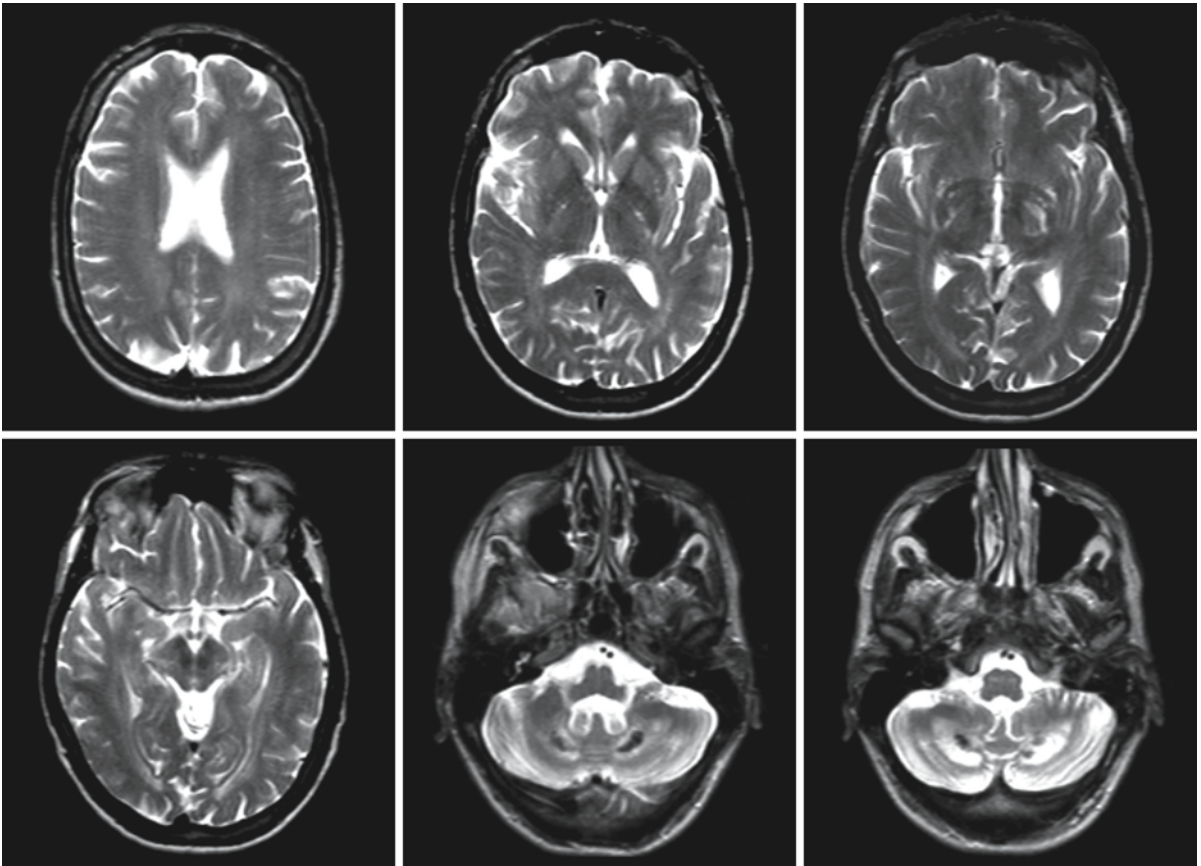


Fig. 31.3. Male, 38 years of age, with CTX. The T_2 -weighted images show a diffuse slight signal abnormality within the cerebral white matter. There are signal abnormalities in the medial globus pallidus and adjacent part of the posterior limb of the internal capsule, the pyramidal tracts, and medial lemniscus in the midbrain. The dentate nucleus has a low signal, whereas

the hilus of the dentate nucleus and cerebellar hemispheric white matter have a high signal. Note the cerebellar atrophy. Courtesy of Dr. F. Barkhof, Department of Radiology, VU University Medical Center, Amsterdam, and Dr. A. Verrips, Department of Pediatric Neurology, University Medical Center Nijmegen, The Netherlands

Fig. 31.4. Female, 43 years of age, with CTX. On the T_2 -weighted image on the *left*, the cerebellar white matter has a high signal intensity surrounded by a rim of very low signal intensity. The moderately T_2 -weighted image on the *right* shows the involvement of the corticospinal tracts in the midbrain. Note the round masses with low signal intensity in the choroid plexus of the lateral ventricles. From Fiorelli et al. (1990), with permission

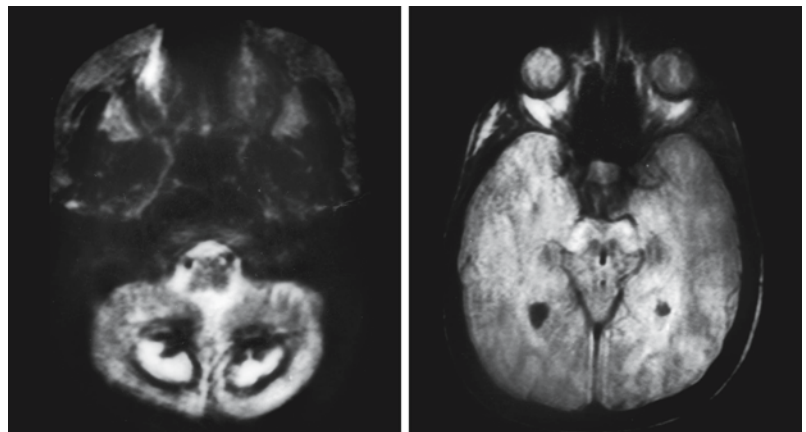




Fig. 31.5. Spinal images in a 41-year-old woman with CTX. The sagittal mildly T₂-weighted images reveal mild signal abnormalities in the spinal cord over its entire length. Courtesy of Dr. F. Barkhof, Department of Radiology, VU University Medical Center, Amsterdam, and Dr. A. Verrips, Department of Pediatric Neurology, University Medical Center Nijmegen, The Netherlands

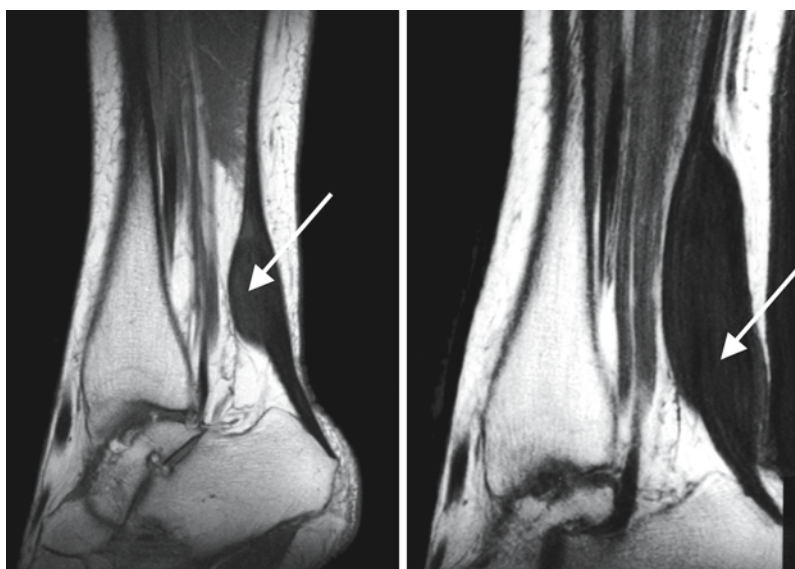


Fig. 31.6. The T1-weighted images show the typical swelling of the Achilles tendon in two CTX patients (arrows). Courtesy of Dr. F. Barkhof, Department of Radiology, VU University Medical Center, Amsterdam, and Dr. A. Verrips, Department of Pediatric Neurology, University Medical Center Nijmegen, The Netherlands

Cockayne Syndrome

32.1 Clinical Features and Laboratory Investigations

Cockayne syndrome (CS) is a rare, inherited disorder characterized by cachectic dwarfism, cutaneous photosensitivity, and progressive neurological dysfunction. The mode of inheritance is autosomal recessive. Two types of the disease are distinguished: classical CS or CS type I and severe CS or CS type II.

In CS type I, the children seem normal at birth. Their weight, length, and head circumference are normal. Growth failure generally begins within the first year of life and may be profound. Weight is affected to a greater extent than length, leading to cachectic dwarfism. Subcutaneous fat is lost diffusely and almost completely, giving the patients a starved appearance. A thin, prominent nose, narrow mouth and chin, sunken eyes, and loss of adipose tissue from the face result in the characteristic facies of an old man or woman. This appearance becomes more evident in older patients. However, percutaneous gastrostomy tube feeding allows better management of the feeding problems and the typical cachectic appearance may be lacking or delayed. Within the first 2 years almost all patients have become microcephalic. A thin and dry skin, fine hair, and large and sometimes malformed ears contribute to the characteristic facies of CS patients. Dermal photosensitivity appears as sun sensitivity resulting in desquamation, scarring, and atrophy of exposed areas. Pigmentary abnormalities with hypopigmentation and hyperpigmentation occur occasionally. Anhidrosis may be present. Dental problems are common with moderate to severe caries. The posture of CS patients is typical. Even at an early age there is abnormal flexion of hips and knees while standing. In older patients the posture is stooped due to kyphosis combined with progressive hip, knee, and ankle contractures. The trunk is small, the arms and legs are disproportionately long, and hands and feet are large.

The earliest commonly noticed neurological abnormality is delayed psychomotor development, which usually becomes apparent at the time when sitting, walking, and speech should develop. The delay in the acquisition of functions becomes progressively greater as the patient grows older. All patients with CS type I are mentally retarded, but mental capacities vary from mildly to profoundly deficient. Among the higher functioning patients, intellectual deterioration

usually becomes evident in the teenage years. Behavioral problems are rare and the patients are usually described as happy and social. In the course of the years progressive neurological abnormalities become apparent. Cerebellar signs are present with tremor, lack of coordination, dysarthric speech, and gait ataxia. Pyramidal signs are usually present with hypertonia and hyperreflexia. The gait disorder in patients who become ambulatory is striking and progressive, due to a combination of spasticity, ataxia, and contractures of the hips, knees and ankles. Sensorineural hearing loss occurs in over half the patients. Myoclonus and involuntary choreiform and athetoid movements are rare. Overt signs of peripheral neuropathy are rare until late stages of the disease, leading to a progressive, diffuse muscular atrophy, muscle weakness, and areflexia. Some patients have diminished lacrimation, decreased sweating, miotic pupils, and cool and acrocyanotic limbs. This could be due to autonomic dysfunction, but formal assessment of autonomic function has not been documented. Seizures occur late and in a minority of the patients.

Pigmentary degeneration of the retina of the salt and pepper type is found in the majority of the patients. The retinal changes are progressive, and during the first few years of life normal findings do not exclude the diagnosis of CS. Other common ophthalmological abnormalities are cataract and optic atrophy. Miotic pupils, which are poorly responsive to mydriatics, corneal dystrophy, and decreased or absent lacrimation may be found. Despite the extensive ocular abnormalities some visual acuity usually remains, although blindness may occur.

Renal problems develop in about 10% of the CS patients with decreased renal function, and very rarely renal failure. Hypertension may occur.

Undescended or small testes are seen in about 30% of male CS patients. In female patients breasts are often small and menstrual cycles irregular.

The neurological abnormalities in CS type I become gradually more severe and mental failure is progressive. Death by inanition and infection, most commonly respiratory infections, used to occur in the fourth decade of life. However, with improved nutrition and medical care, life expectancy may be longer.

Patients with CS type II have an earlier onset of symptoms and a more severe course than do CS type I patients. They often have a low birth weight and little postnatal increase in height, weight, and head

circumference, although some patients have a normal birth weight and normal weight gain during the first few months of life. The infants used to develop an emaciated appearance characteristic of CS with little subcutaneous fat, deep-set eyes, and a prominent, beaked nose, but with tube feeding weight for height can be normal or even high, and the typical lack of subcutaneous fat is not necessarily a feature of the disease. In the neonatal period the children are hypotonic, but they develop spastic quadriplegia. Few or no developmental milestones are reached; those that are reached are subsequently lost in the process of neurological deterioration. Congenital cataract is often present. Other reported ocular abnormalities include hypoplastic optic nerves, microphthalmia, iris hypoplasia, microcornea, and reduced lacrimal secretion. Kyphosis and progressive contractures of hips and knees occur and may already be present at birth. Photosensitivity is present but may be missed because of lack of exposure to sunlight in small infants. Generally, dental, auditory, and cutaneous complications are less commonly described in these patients, probably because of the severe neurological problems and early age at death. Death usually occurs by the age of 6 or 7 years, but may also occur during the first few months or years of life.

The clinical pictures of CS type II, cerebro-oculofacioskeletal syndrome (COFS syndrome) and cataracts-microcephaly-failure to thrive-kyphoscoliosis syndrome (CAMFAK syndrome) overlap. Some of the patients described with COFS or CAMFAK syndrome are in fact CS type II patients.

A few patients have the clinical features of classical or severe CS plus the skin abnormalities of xeroderma pigmentosum, including freckling and skin cancers.

Laboratory investigations of blood and CSF reveal no consistent and no diagnostic abnormalities. An elevated CSF protein content may be found. A few patients have biochemical evidence of decreased renal function with decreased creatinine clearance. In a few patients elevated serum cholesterol or lipoprotein levels have been noted. Nerve conduction velocities are markedly slowed, consistent with a demyelinating polyneuropathy, in the majority of the patients. In skeletal muscle, denervation changes can be found. EEG is normal in some patients, but may show slowing and sometimes epileptic discharges. Evoked potentials are often abnormally delayed. Radiological investigations of the skeleton in CS show microcephaly, with a thick cranial vault and sometimes intracranial calcifications. General skeletal maturation may be within normal limits or may be advanced or delayed. Less common findings include shortness and broadness of the metacarpals and phalanges, whose epiphyses sometimes have an ivory-dense appearance, and flattening of the vertebral bodies, lipping of

their upper and lower anterior margins, and osteoporosis.

The clinical suspicion of CS can be confirmed by UV irradiation of cultured skin fibroblasts of the patients. Cell lines from CS patients are hypersensitive to killing by UV, and show failure of DNA and RNA synthesis to recover to normal rates after irradiation. CS cells differ in some of their cardinal laboratory characteristics from xeroderma pigmentosum cells. CS cells and most xeroderma pigmentosum cells have defective DNA repair of actively transcribed genes, but only xeroderma pigmentosum cells have low DNA repair in the genome overall, as demonstrated by deficient unscheduled DNA synthesis after UV exposure. Patients with a combination of CS and xeroderma pigmentosum also have decreased unscheduled DNA synthesis after UV exposure. Prenatal diagnosis is possible using a test showing the defect in nucleotide excision repair or DNA analysis when the gene mutations responsible in a family have been demonstrated.

32.2 Pathology

The leptomeninges in classical CS appear thickened and fibrotic. The brain is usually small and has an atrophied appearance. Cerebellar atrophy is the most severe. On sectioning, the lateral ventricles appear to be enlarged and the corpus callosum is thin. The white matter is decreased in volume and has a mottled appearance. Calcium depositions are present bilaterally in the basal ganglia and dentate nuclei and may also be found in the white matter and cerebral and cerebellar cortices. The dura may be focally calcified.

Microscopic examination of the leptomeninges reveals increased collagenous connective tissue without any inflammatory changes. The principal finding in CS type I is lack of myelin. Numerous islands of preserved myelin are present within the white matter in a tigroid pattern. In the areas of myelin lack, axons are relatively preserved. There is no evident relationship between blood vessels and myelin loss or presence. All levels of the brain are involved, including cerebral hemispheric white matter, cerebellar white matter, and brain stem. The U fibers are not spared. In the spinal cord the descending tracts demonstrate a focal lack of myelin, whereas the ascending tracts have a relatively higher myelin content. The myelin-deficient areas contain fewer oligodendrocytes than the areas with more myelin. Sudanophilic lipids are scanty, but sometimes seen in the walls of vessels and in microglial cells in the brain parenchyma. No inflammatory infiltration is found. Astrogliosis is seen in the myelin-deficient areas. The cerebral cortex is generally intact, but sometimes there is a slight diffuse loss of

neurons. The cerebellar cortex is less well preserved and the number of Purkinje cells and granule cells is reduced. Calcium deposits are present perivascularly and within the neuropil. The typical locations of calcium deposits include the basal ganglia and dentate nucleus, and may also involve cerebral and cerebellar cortex and the white matter. The small deposits may coalesce into larger calculi. In some cases, nuclear abnormalities have been found in astrocytes and neurons. In these cases many of these cells have a single, large, hyperchromatic, atypical nucleus. Some cells are multinucleated. In a few cases neurofibrillary tangles have been found in the nucleus basalis, substantia nigra, locus caeruleus, and the cerebral cortex. Their presence may be considered to be a premature senile change of the brain or a nonspecific finding occurring in chronic neurological conditions.

Sural nerve biopsies demonstrate chronic segmental demyelination and remyelination with onion bulb formation. Onion bulbs are nonspecific signs of repeated demyelination and remyelination. They are more pronounced in older than in younger patients. In some cases of CS, electron-dense, membrane-bound, finely granular or lamellated inclusions have been reported in Schwann cells. The nature and role of these inclusions is unknown.

Renal pathology may include thickening of the glomerular basement membrane.

In CS type II, neuropathological findings are similar to those of CS type I. The leptomeninges are thickened. The brain is small and atrophic and the ventricles are enlarged. The white matter is reduced in volume. The cerebellum is small. In the CNS severe but discontinuous myelin deficiency is present with a tigroid pattern of islands with higher myelin content. There is concomitant white matter gliosis. The cerebrum, cerebellum, brain stem, and spinal cord are affected. Calcium depositions, present perivascularly and in the neuropil, may be found in basal ganglia, thalamus, dentate nucleus, and cerebral and cerebellar cortex and meninges. The cerebral cortex is intact; in the cerebellar cortex loss of Purkinje cells and granule cells is found. Bizarre astrocytes with large and multiple nuclei may occur.

32.3 Chemical Pathology

In CS the white matter shows a marked loss of myelin lipids and some increase in cholesterol esters. Besides these usual chemical changes related to demyelination, no specific abnormalities are found.

32.4 Pathogenetic Considerations

Three rare autosomal recessive disorders are associated with a defect in nucleotide excision DNA repair: xeroderma pigmentosum, CS, and trichothiodystrophy with photosensitivity. Xeroderma pigmentosum is characterized by photosensitivity, abnormal pigmentation, and a high incidence of sunlight-induced skin cancers; signs of neurological degeneration are rare. CS is characterized by photosensitivity, short stature, and a severe neurological degenerative disorder; there is no increased risk of skin cancer. Trichothiodystrophy, caused by a defect in nucleotide excision repair, is characterized by brittle hair and nails, photosensitivity, ichthyosis, and neurological problems, but no skin cancer. Rare patients have combined symptoms of xeroderma pigmentosum and CS. Complementation analysis by cell fusion has allowed a genetic classification of these disorders. Most CS patients belong to one of two complementation groups, CS-A and CS-B, which represent two different defective genes, the CSA gene located on chromosome 5 and the CSB gene on chromosome 10q11–21. The clinical phenotype of the patients (classical or severe CS) does not correlate with these complementation groups. Patients with combined xeroderma pigmentosum and CS belong to three of the xeroderma pigmentosum complementation groups: XP-B, XP-D, and XP-G. The patients in complementation group XP-G all have severe neurodegeneration and die in early childhood, but patients belonging to complementation group XP-D may also present with severe neurological problems.

Despite the high accuracy of the DNA replication process, some errors may arise spontaneously during DNA replication through intrinsic instability of chemical bonds in DNA. Furthermore, chemical compounds can cause alterations in the DNA. The chemical compounds that react with nucleic acids range from alkylating agents, polycyclic hydrocarbons, and aromatic amines to aflatoxin. DNA modifications can also arise endogenously through cellular metabolites, for instance through free radicals generated as by-products of oxidative metabolism. The most common physical agents causing DNA damage are UV and ionizing radiation. Unless repaired, DNA damage leads to defects in subsequent replication cycles and to abnormalities in transcription and translation of the information coded in DNA. The result may be cell death or genomic instability (mutagenesis).

There are different basic mechanisms by which lesions are eliminated from DNA: direct reversal, base excision repair, nucleotide excision repair, and DNA double-strand repair. Nucleotide excision repair is a complex process that detects, removes, and repairs many types of DNA lesions, in particular bulky lesions. The process involves at least 30 proteins, which

act in a stepwise fashion to recognize the damage, followed by enzymatic incisions in the damaged strand on both sides of the lesion, removal of the damaged single-stranded segment, repair synthesis to fill in the resultant gapped DNA duplex, and ligation of the repair patch to the existing DNA strand. Nucleotide excision repair has two subpathways: transcription-coupled repair and global genome repair. The transcription repair pathway repairs lesions in the strand of active, RNA-polymerase-II-transcribed genes. The global genome repair pathway removes lesions from genes that are transcriptionally inactive. Transcription-coupled repair is about three times faster than global genome repair.

In CS, the underlying defect affects not only the nucleotide excision repair, but also the basal transcription process and the sensitivity to apoptosis. Cultured fibroblasts from CS patients are more sensitive than normal to killing by UV irradiation and exhibit a marked, prolonged inhibition of synthesis of DNA and RNA after such irradiation. Damage produced by UV light in DNA in normal cells depresses rates of both DNA and RNA synthesis, but these rates soon become normal. In CS cells this rapid recovery does not occur. The rapid recovery of DNA and RNA synthesis in normal cells can be attributed to preferential rapid repair of DNA damage in regions that are actively transcribed, in contrast to much slower repair in the bulk of DNA. In CS cells, this preferential repair of transcriptionally active DNA does not take place, damage in these regions being repaired at the same (slow) rate as in the bulk of DNA. So, CS cells are defective in the transcription repair pathway, but proficient in the global genome repair of UV-induced DNA damage. CS cells also show evidence of a defect in basal transcription, not related to the defect in the transcription-coupled repair pathway. The initial inability to resume transcription may be attributed to a failure to remove DNA lesions from the transcribed strand of active genes, but defects in *CSB* result in failure of RNA polymerase II elongation complexes to resume transcription even after DNA damage is repaired. An arrest of transcription provides a strong signal for apoptosis. In addition, there is evidence that a defect in the ATPase domain of the *CSB* protein enhances the cellular liability to apoptosis.

The roles of the products of the genes *CSA* and *CSB* have been only partially elucidated. *CSA* is thought to associate with components of the DNA repair/basal transcription factor TFIIH and *CSB*. It could have a regulatory role in transcription-coupled repair. *CSB* is a DNA-dependent ATPase and stimulates the rate of elongation by RNA polymerase II. In addition, it has been shown that integrity of the ATPase domain of *CSB* is critical for prevention of DNA damage induced apoptosis.

With respect to the correlation between basic defect and the clinical features, it is interesting to consider the differences between CS patients and patients with xeroderma pigmentosum. The former lack the increased risk for skin cancer despite the presence of photosensitivity and the latter usually lack signs of neurodegeneration. Xeroderma pigmentosum patients are most often deficient in both transcription-coupled repair and global genome repair, although sometimes in global genome repair only. The photosensitivity of CS patients is due to the failure in rapid repair of crucial regions of DNA, which leads to hypersensitivity of the cells to the lethal effects of UV light. But considering the absence of neurodegeneration in most patients with xeroderma pigmentosum, the defect in excision repair cannot explain the neurological problems of CS patients in a straightforward fashion. It is generally accepted that a defect in basal transcription plays a role in the development of the non-xeroderma-pigmentosum problems. Cells with a high metabolic rate, such as cells of the nervous system, which generate high levels of reactive oxygen species, may be particularly vulnerable to the effects of a combination of endogenous (oxidative) DNA damage and transcription deficiency, induced by both DNA damage and dysfunction of CS genes. Furthermore, an arrest of transcription provides a strong signal for the apoptosis pathway. CS could be a disease characterized by excessive cell death by apoptosis. The apoptosis model could also explain the problem of stunted growth and provide the answer to the question why CS patients are not prone to skin cancer, even in the light of severe sunlight sensitivity: the damaged cells become apoptotic.

Xeroderma pigmentosum/CS patient belong to three complementation groups: XP-B, XP-D, and XP-G. XPB and XPD are DNA helicases and subunits of the DNA repair/basal transcription factor TFIIH. They are required for transcription initiation by RNA polymerase II under basal conditions and are involved in the early steps of the nucleotide excision repair pathway. XPG is involved in promoting efficient RNA polymerase II transcription, and a defect in XPG causes a deficiency in transcription. As in CS, the photosensitivity is attributed to the defect in nucleotide excision repair, whereas the non-xeroderma-pigmentosum manifestations are attributed mainly to crippled basal transcription.

32.5 Therapy

To date no effective mode of therapy has been found in CS and the management of the disease is purely symptomatic. Patients should be monitored for treatable complications, such as hypertension, hear-

ing loss, and dental caries. Physical therapy can be helpful to avoid contractures. Emollients for dry skin, avoidance of excessive sun exposure, and use of sun-screens are helpful in diminishing skin problems.

32.6 Magnetic Resonance Imaging

CT scan may demonstrate bilateral calcifications of the basal ganglia, dentate nucleus and areas of the cerebral and cerebellar white matter and cortex (Fig. 32.3), although in some patients the calcium deposits are very subtle (Figs. 32.1 and 32.2). Cerebral,

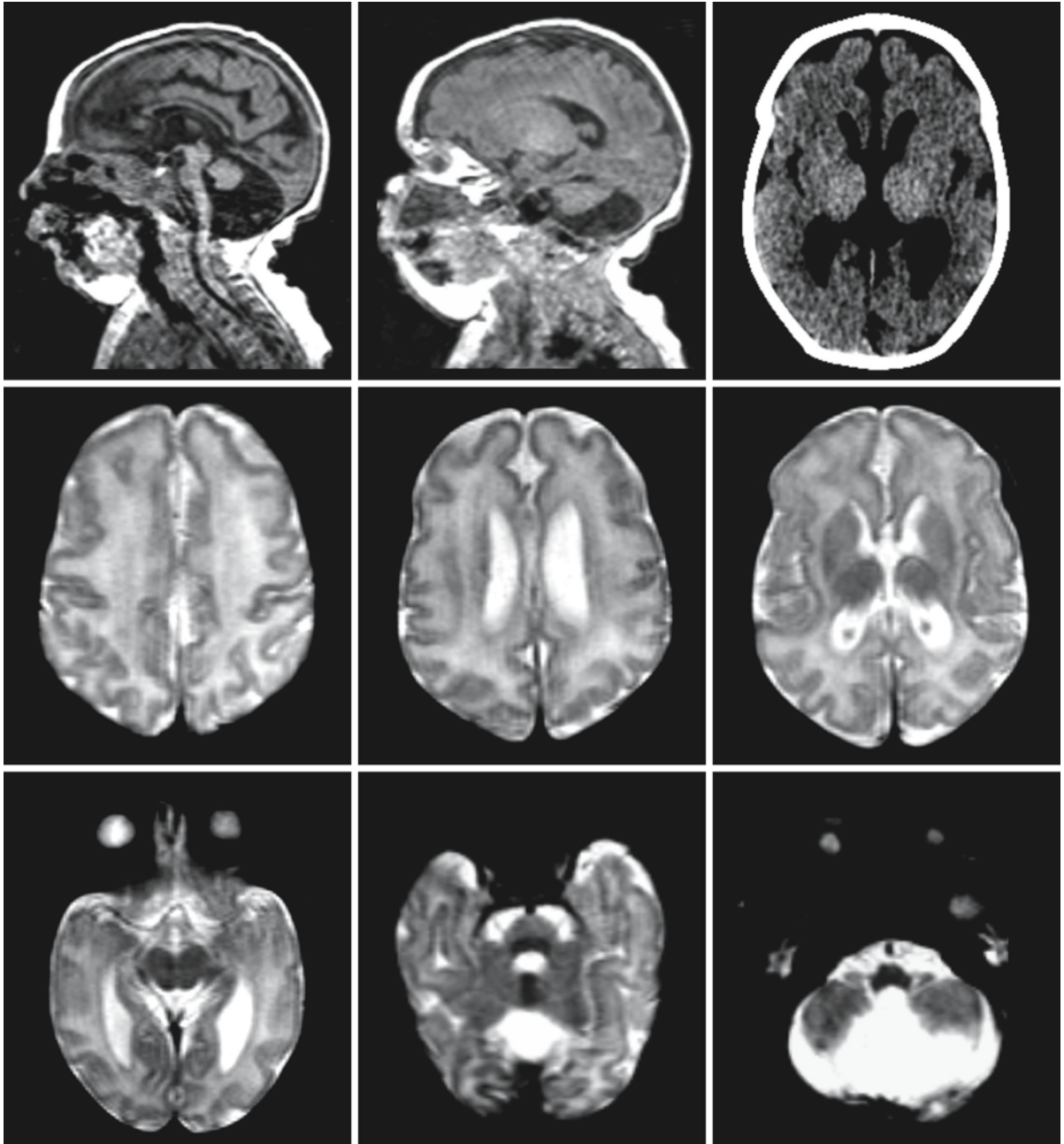


Fig. 32.1. Term born infant, now 5 weeks of age, with a clinical phenotype of CS type II and belonging to complementation group XP-G. Note the severe hypoplasia of the cerebellum and brain stem on the sagittal images. The CT scan shows evidence

of subtle mineralization of the basal ganglia and thalamus. The axial T₂-weighted images show that the brain has a somewhat immature gyral pattern for the age of the infant

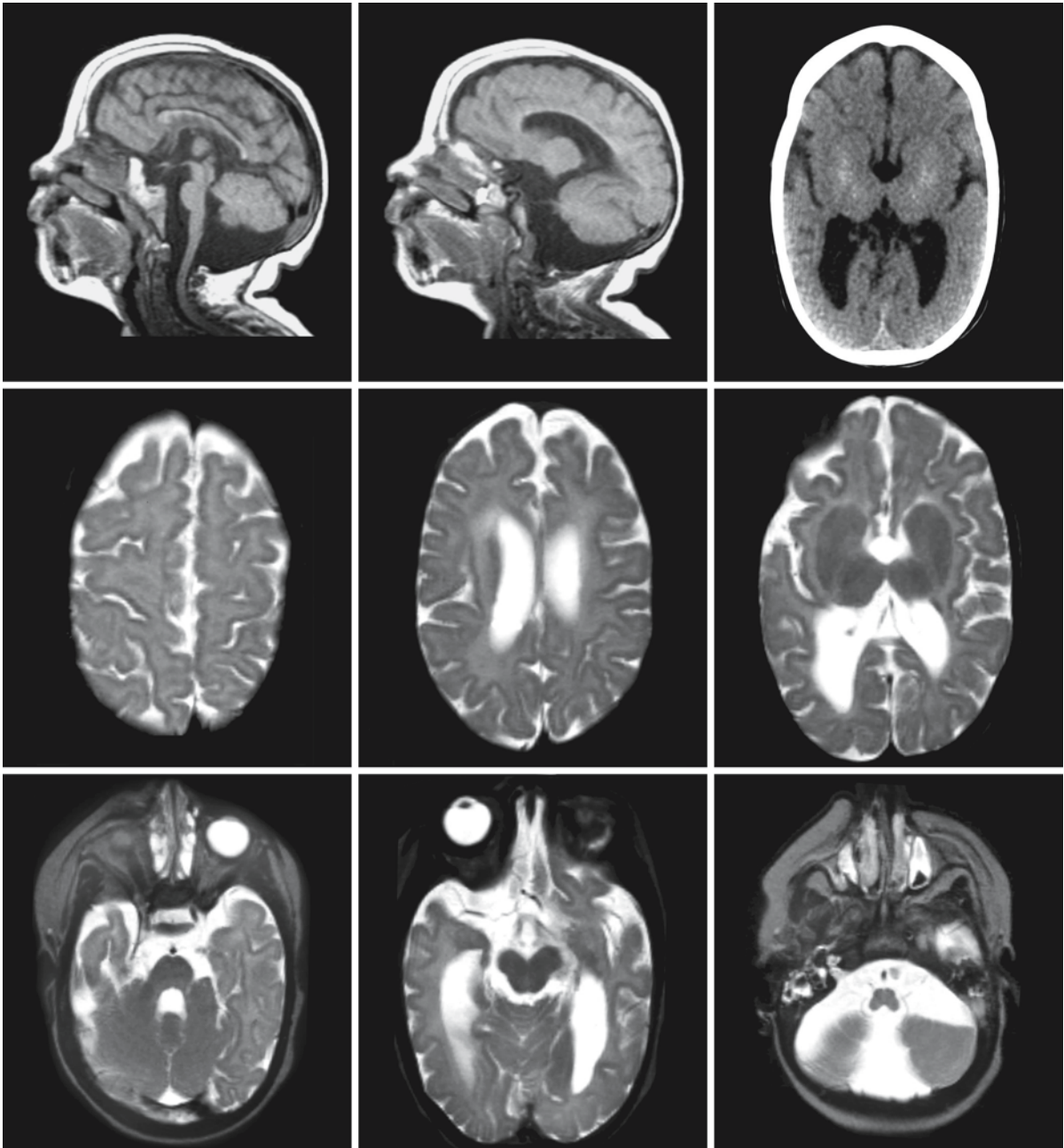


Fig. 32.2. An 18-month-old infant with a clinical phenotype of CS type II, belonging to complementation group CS-B. Note again the hypoplasia of the cerebellum and brain stem on the

sagittal images and the subtle mineralization of the basal ganglia and thalamus on the CT scan. The axial T₂-weighted images demonstrate seriously deficient myelination

cerebellar, and brain stem atrophy with prominence of sulci and ventricular enlargement is usually seen.

MRI confirms the presence of variable hypoplasia and atrophy, most pronounced in brain stem and cerebellum (Figs. 32.1–32.5). There is a loss of white matter volume and ventricles are mildly enlarged in most patients. MRI is less sensitive than CT in show-

ing the presence of calcium depositions, but may be more accurate in delineating the locations. The globus pallidus is most often involved, followed in frequency by the dentate nucleus. In addition, calcium depositions may be seen in the putamen and caudate nucleus, and as irregular, not necessarily symmetrical areas in the cortex and white matter of cere-

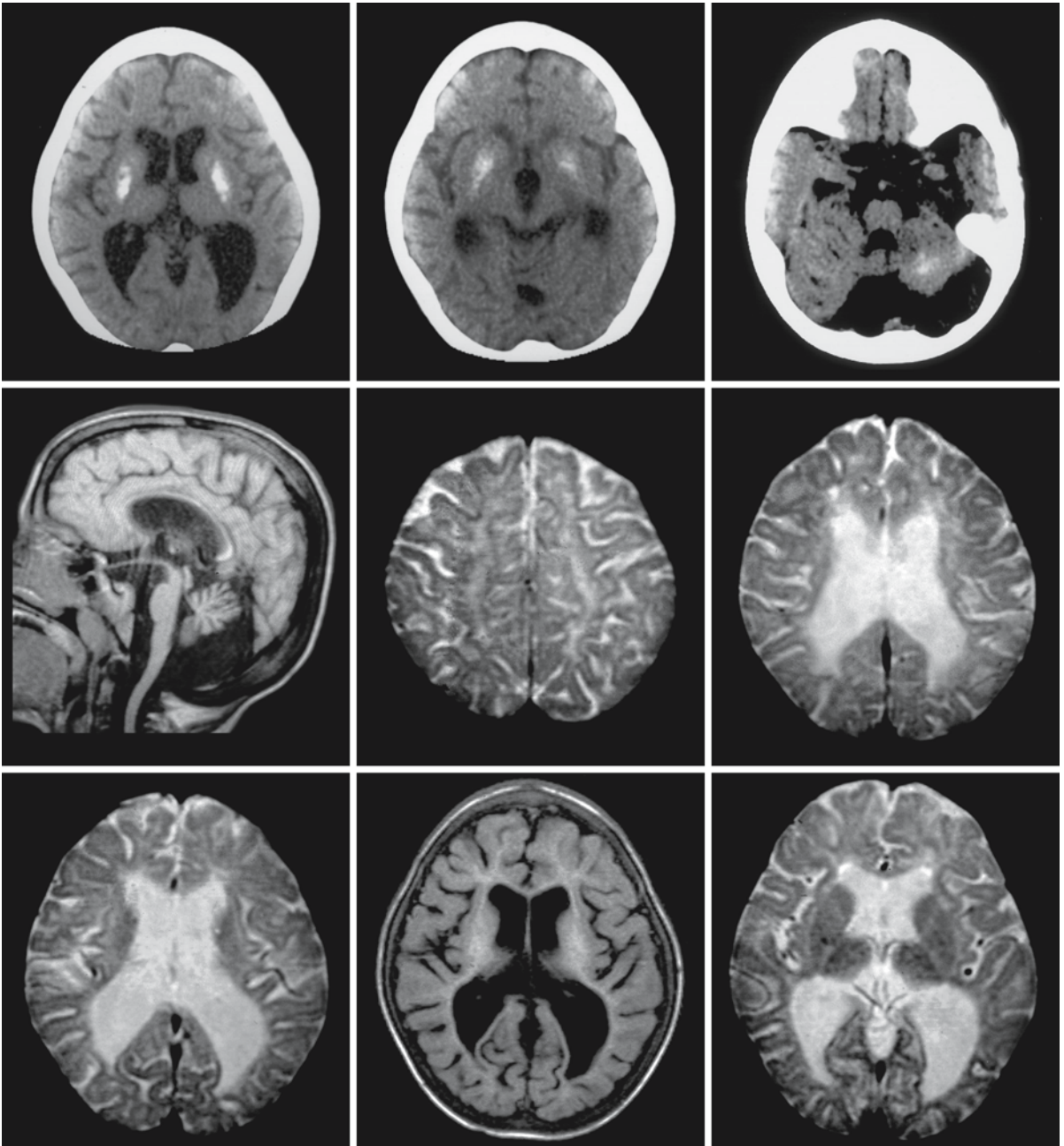


Fig. 32.3. A 6-year-old girl with CS type I. CT scans through the posterior fossa and the lateral ventricles show calcifications in the dentate nucleus and the basal ganglia. The T_2 -weighted MR images reveal white matter hypomyelination and atrophy.

The myelin deficiency is confirmed by the T_1 -weighted images (*middle image, third row*). The white matter has an irregular, tigroid appearance. Courtesy of Dr. I.N. Snoeck, Juliana Children's Hospital, The Hague, The Netherlands

brum and cerebellum. In addition, there are symmetrical white matter abnormalities. On T_2 -weighted images the signal intensity of the cerebral white matter is abnormally high, but usually not so high as in completely unmyelinated white matter in neonates. The white matter often seems to have a finely irregular, granular aspect, probably reflecting the tigroid pat-

tern of myelin presence (Figs. 32.3 and 32.4). In many of the patients the moderately high signal intensity is seen throughout the hemispheric white matter, including periventricular white matter and U fibers, sometimes also the internal capsule. The corpus callosum has a better state of myelination. In other patients the white matter is better myelinated in the sub-

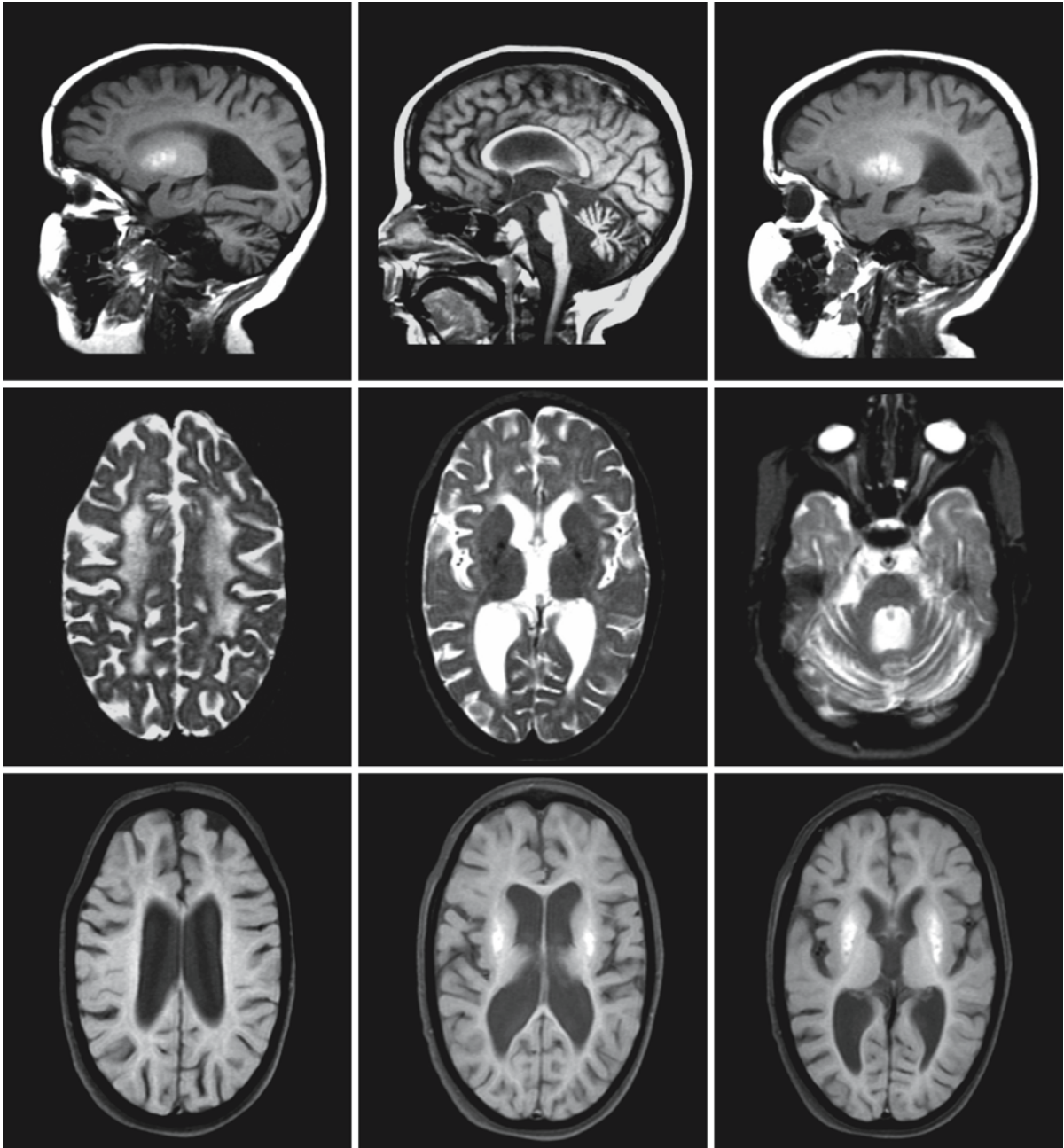


Fig. 32.4. A 7-year-old boy with CS type I. The sagittal images reveal serious cerebellar atrophy and some atrophy of the brain stem. The cerebral white matter has a high signal on the axial T_2 -weighted images with a finely irregular, granular as-

pect, probably reflecting the tigroid pattern of myelin presence. The T_1 -weighted gradient echo images (*third row*) reveal calcium in the putamen

cortical areas and the white matter hyperintensity is most marked in the periventricular area. Apparently delayed and disturbed myelination as well as demyelination play a role in CS. Images in type I and type II CS are essentially the same, but in type II CS the myelin deficiency is more profound and the cerebellum is as a rule very hypoplastic.

An MRI pattern combining hypomyelination and calcium deposition is highly suggestive of CS. The images are similar to those seen in Aicardi-Goutières syndrome, but the calcium depositions tend to be different. In Aicardi-Goutières syndrome the calcium depositions are typically punctate, with many small round deposits which may coalesce to larger irregular

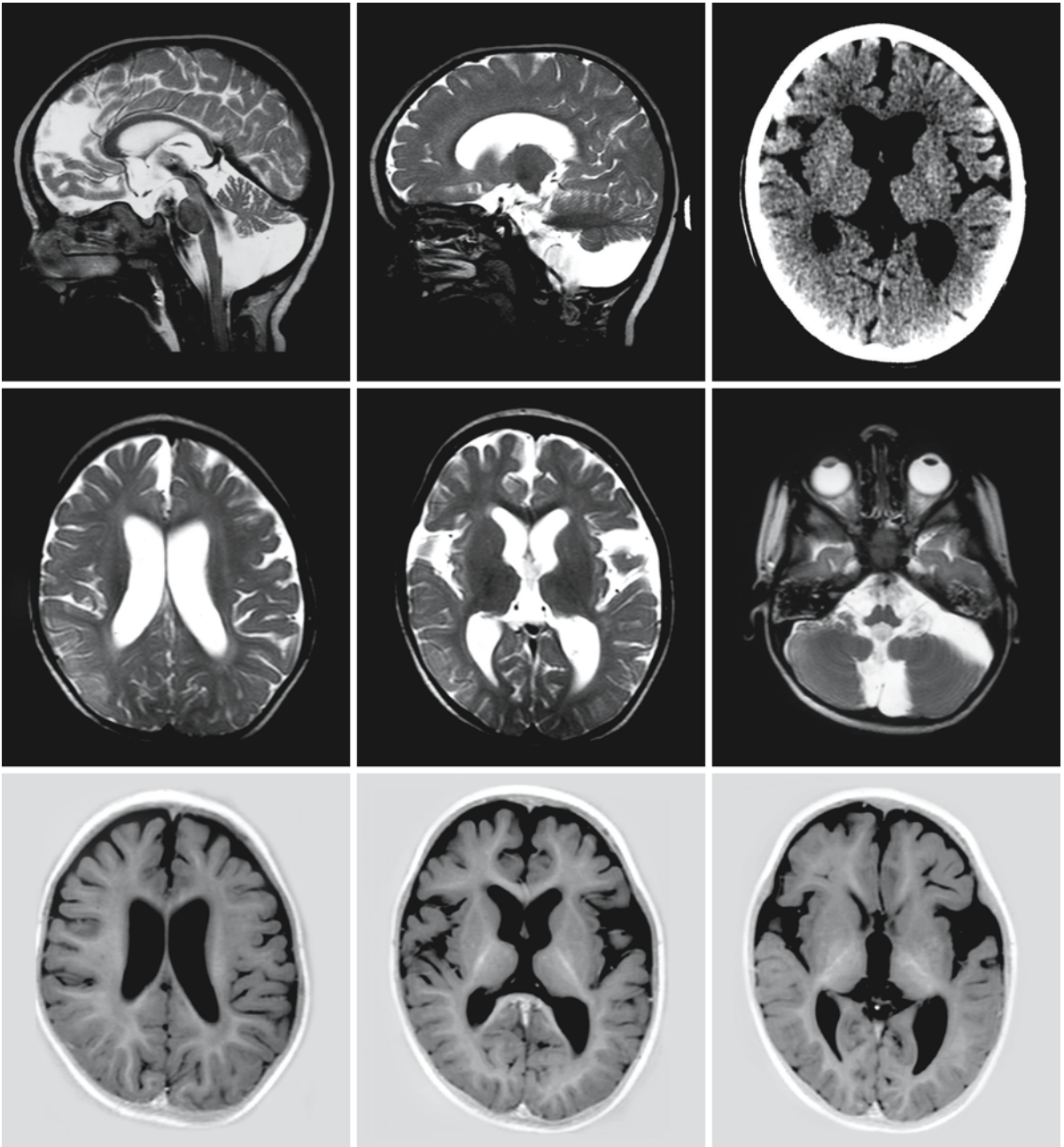


Fig. 32.5. This 3-year-old girl with CS type I has a relatively mild phenotype. The cerebellum is both hypoplastic and atrophic. The brain stem is relatively thin. The CT scan reveals

at most subtle mineralization of the basal ganglia. The cerebral white matter contains more myelin than in the other patients

areas. In CS the calcium depositions tend to have a more homogeneous aspect. Apart from the calcifications, the images showing severe hypomyelination resemble those of Pelizaeus–Merzbacher disease and Salla disease.

Trichothiodystrophy with Photosensitivity

33.1 Clinical Features and Laboratory Investigations

Trichothiodystrophy with photosensitivity (TTD) is a rare, inherited disorder with an autosomal recessive mode of inheritance. Multiple names and acronyms have been used for the same condition, including Tay syndrome, Pollitt syndrome, ONMR (*onychotrichodysplasia, neutropenia, mental retardation*), BIDS (*brittle hair, impaired intelligence, decreased fertility, short stature*), IBIDS (*ichthyosis, brittle hair, impaired intelligence, decreased fertility, short stature*), SIBIDS (*osteosclerosis, ichthyosis, brittle hair, impaired intelligence, decreased fertility, short stature*), and PIBIDS (*photosensitivity, ichthyosis, brittle hair, impaired intelligence, decreased fertility, short stature*). Presence of a defect in nucleotide repair has not been verified in all patients reported under these names. A few patients with features of both TTD and xeroderma pigmentosum have been reported.

One of the most striking clinical findings in TTD is the abnormal hair. The scalp hair is sparse, short, thin, brittle, and dry. The other clinical features of patients with TTD are highly variable in expression and severity. This partly explains the confusing nomenclature in the literature for what is probably the same disease. In many cases the brittle hair is associated with neuroectodermal abnormalities. Cutaneous signs include photosensitivity, ichthyosis, keratosis, and erythema. There is no abnormal pigmentation and no increased risk of skin cancer. Some children present at birth as collodion babies. Nails are dystrophic. Dental caries is common. Patients have short stature and may have microcephaly. Neurological and developmental impairments of patients with TTD are reminiscent of those found in Cockayne syndrome. The neurological signs may include spasticity with hyperreflexia, cerebellar ataxia, dysarthria, and neurosensory hearing impairment. The deep tendon reflexes may also be absent due to a concomitant polyneuropathy. Eye abnormalities may include nystagmus, retinal dystrophy, pale optic disc, cataract, and strabismus. Intelligence is impaired, but to a variable degree. Patients have a peculiar face with a beaked nose, receding chin, and protruding ears. They show genital abnormalities including cryptorchism, hypospadias, and hypoplasia of the genitalia. Delayed or absent puberty and laboratory evidence of hypergonadotropic hy-

pogonadism may be found. A few TTD patients have been reported who lose their hair and have more serious skin problems during episodes of fever. Within a period of a few months, the scalp hair returns. Some patients have increased susceptibility to infections due to chronic neutropenia, lymphopenia, or immunoglobulin deficiency. Life expectancy varies. Severely affected patients may die as early as at the age of 3 years, whereas other patients reach their thirties.

Polarization microscopy of the hair in TTD shows a typical appearance of alternating dark and light bands, giving the hair a tiger-tail pattern. Scanning electron microscopy usually reveals other abnormalities, including absent or damaged cuticle scales, irregular hair surface, trichoschisis, and trichorrhhexis nodosa (torsions of the flattened hair shaft). The hair and often the nails are characterized by a reduction in the cystine/cysteine and sulfur content, due to a decreased amount of sulfur-rich matrix proteins. These hair findings are not diagnostic of TTD as similar abnormalities may be found in other disorders, such as untreated argininosuccinic aciduria and acrodermatitis enteropathica.

The diagnosis can be confirmed by UV irradiation of cultured skin fibroblasts of the patients. Cell lines from TTD patients are hypersensitive to killing by UV, and show failure of DNA and RNA synthesis to recover to normal rates after irradiation. TTD cells have defective DNA repair of actively transcribed genes (transcription-coupled repair) as well as low DNA repair in the genome overall (global genome repair), the latter demonstrated by deficient unscheduled DNA synthesis after UV exposure. Prenatal diagnosis is possible using a test showing the defect in nucleotide excision repair or DNA analysis when the responsible gene mutations in a family have been demonstrated.

33.2 Pathology

At autopsy (unpublished data), micrencephaly is found. The most striking finding is a lack of myelin throughout the cerebrum and cerebellum, with a relatively higher myelin content in the brain stem. Loss of Purkinje cells is seen in the cerebellar cortex. Calcium deposits are less striking than in Cockayne syndrome, but may be present in the basal ganglia.

33.3 Pathogenetic Considerations

Three rare autosomal recessive disorders are associated with a defect in nucleotide excision DNA repair: xeroderma pigmentosum, Cockayne syndrome, and TTD. Xeroderma pigmentosum is characterized by photosensitivity, abnormal pigmentation, and a high incidence of sunlight-induced skin cancers, but rarely by signs of neurological degeneration. Cockayne syndrome is characterized by photosensitivity and a severe neurological degenerative disorder, but no increased risk of skin cancer. TTD is characterized by brittle hair and nails, photosensitivity, and neurological problems, but no skin cancer. Complementation analysis by cell fusion has allowed a genetic classification of these disorders. TTD patients belong to three complementation groups, XP-B, XP-D, and TTD-A. The *XPB* gene is located on chromosome 2q21 and the *XPD* gene on chromosome 19q13.2. The *TTDA* gene has not yet been characterized. The clinical phenotype of the TTD patients does not correlate with these complementation groups.

Despite the high accuracy of the DNA replication process, some errors may arise spontaneously during DNA replication through intrinsic instability of chemical bonds in DNA. Chemical compounds can also cause alterations in the DNA. DNA modifications can also arise endogenously through cellular metabolites, for instance through free radicals generated as by-product of oxidative metabolism. The most common physical agents causing DNA damage are UV and ionizing radiation. If not repaired, DNA damage leads to defects in subsequent replication cycles and to abnormalities in transcription and translation of the information coded in DNA. The result may be cell death or genomic instability (mutagenesis).

There are different basic mechanisms by which lesions are eliminated from DNA: direct reversal, base excision repair, nucleotide excision repair, and DNA double-strand repair. Nucleotide excision repair is a complex process that detects, removes, and repairs many types of DNA lesions, in particular bulky lesions. The process involves at least 30 proteins, which act in a stepwise fashion to recognize the damage, followed by enzymatic incisions in the damaged strand on both sides of the lesion, removal of the damaged single-stranded segment, repair synthesis to fill in the resultant gapped DNA duplex, and ligation of the repair patch to the existing DNA strand. Nucleotide excision repair has two sub-pathways: transcription-coupled repair and global genome repair. The transcription repair pathway repairs lesions in the strand of active, RNA-polymerase-II-transcribed genes. The global genome repair pathway removes lesions from genes that are transcriptionally inactive. Transcription-coupled repair is about three times faster than

global genome repair. Damage produced by UV light in DNA in normal cells depresses rates of both DNA and RNA synthesis, but these rates soon become normal. The rapid recovery of DNA and RNA synthesis in normal cells can be attributed to preferential rapid repair of DNA damage in regions that are actively transcribed, in contrast to much slower repair in the bulk of DNA.

The genes mutated in TTD are all related to the DNA repair/basal transcription factor II H (TFIIH). *XPB* and *XPD* are DNA helicases and subunits of TFIIH; *TTDA* is involved in the stabilization of TFIIH. The TFIIH complex regulates initiation of transcription by RNA polymerase II under basal conditions, and in the case of DNA damage it initiates nucleotide excision repair. TTD cells have a defect in both components of the nucleotide excision repair, the preferential repair of transcriptionally active DNA and in the global genome repair of UV-induced DNA damage. In addition, like Cockayne syndrome, TTD cells have a defect in basal transcription. The photosensitivity is attributed to the defect in nucleotide excision repair, whereas the other manifestations are attributed mainly to impairment of basal transcription.

Intriguingly, in view of the marked differences in clinical phenotypes, defects in two of the genes related to TTD (*XPB* and *XPD*) can also cause xeroderma pigmentosum and the combined symptoms of xeroderma pigmentosum and Cockayne syndrome. It has been suggested that clinical features of xeroderma pigmentosum result from mutations that affect only the nucleotide excision repair function of TFIIH, while features typical of TTD and Cockayne syndrome are due to impairment of its transcription role. This notion has been supported by the spectrum of mutations observed in the different patient groups, indicating that the site of mutation determines the clinical phenotype. It has been demonstrated that alterations in *XPB*, *XPD*, and *TTDA* associated with TTD specifically reduce the cellular content of TFIIH. However, the degree of reduction in the level of TFIIH does not correlate with the severity of the TTD phenotype, suggesting that the severity of the clinical symptoms in TTD cannot be related solely to the effects of mutations on the stability of TFIIH. Probably, the transcriptional activity of the residual TFIIH complexes also plays a role.

In all TTD patients known so far who show loss of hair during fever, the same missense mutation in the *XPD* gene has been demonstrated, either in the homozygous or the compound-heterozygous state. There is evidence that the *XPD* protein with this amino acid substitution is thermolabile, resulting in a further reduction of TFIIH-dependent basal transcription during fever.

33.4 Therapy

To date no effective mode of therapy has been found in TTD and the management of the disease is purely symptomatic. Patients should be monitored for treatable complications. Physical therapy can be helpful to avoid contractures. Emollients for dry skin, avoidance of excessive sun exposure, and use of sun-screens are helpful in diminishing skin problems.

33.5 Magnetic Resonance Imaging

CT scan may demonstrate bilateral calcifications of the basal ganglia, but in most TTD cases no calcium deposits are seen. Some cerebral atrophy may be seen with mildly enlarged lateral ventricles and subarachnoid spaces.

The most striking finding on MRI is diffuse hypomyelination involving the cerebral hemispheres and cerebellum (Fig. 33.1). Even the brain stem may be insufficiently myelinated. In addition, there may be some variable atrophy due to loss of white matter volume. However, atrophy is not present in all patients.

A neuroimaging pattern of hypomyelination and calcium depositions is highly suggestive of a DNA repair disorder, either TTD or Cockayne syndrome. The pattern is similar to that seen in Aicardi–Goutières syndrome, but the calcium depositions tend to be different. In Aicardi–Goutières syndrome the calcium depositions are typically punctate, with many small round deposits which may coalesce to larger irregular areas. In DNA repair disorders, the calcium depositions tend to have a more homogeneous aspect. In TTD patients without evidence of calcium deposits on neuroimaging, the pattern resembles that of Pelizaeus–Merzbacher disease and Salla disease.

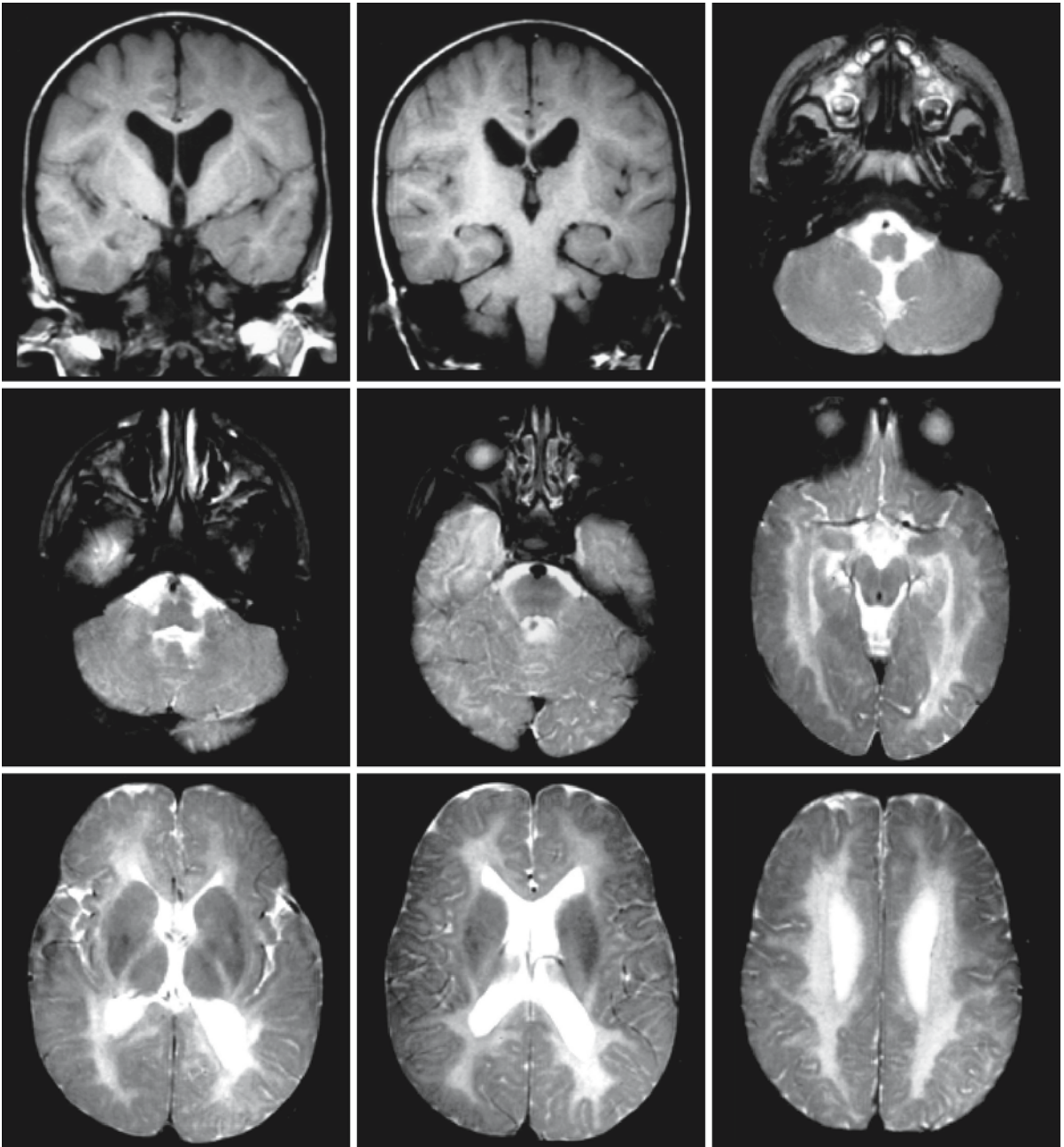


Fig. 33.1. The T_2 -weighted images in a 3-year-old boy with TTD show insufficient myelination of the cerebral white matter, which has a high signal. Even the corpus callosum and internal capsule are hypomyelinated. The cerebellar white matter seems to contain more myelin, but still less than normal.

The coronal T_1 -weighted images show that there must be some myelin, enough to give the white matter a moderately high signal. From Østergaard and Christensen (1996), with permission

Pelizaeus–Merzbacher Disease and X-linked Spastic Paraplegia Type 2

34.1 Clinical Features and Laboratory Investigations

Pelizaeus–Merzbacher disease (PMD) is a rare neurological disorder affecting the myelination of the CNS. The disease has an X-linked recessive mode of inheritance and is usually subdivided into three types: the classical type (type I), the connatal type (type II), and the transitional type (type III).

The classical type has its onset in the first year of life. Those affected are almost exclusively boys. The disease manifests initially by irregular nystagmoid eye movements referred to as “dancing,” “trembling,” or “roving.” In some children stridor occurs, caused by either laryngeal abductor paralysis or laryngomalacia. There is variable but always marked to severe developmental delay with only very slow developmental progress. Growth is retarded and the head size is small, in the low normal or microcephalic range. Seizures occur early in the course of the disease. Characteristically there is a tremor or bobbing, nodding, or shaking movement of the head. Signs of tetraspasticity, cerebellar ataxia, and extrapyramidal movement disturbances with hyperkinesia, dystonia, and choreoathetosis become manifest as the patient becomes older. Most patients never walk. The sensory system is usually well preserved. Optic atrophy with visual failure is common. The nystagmus disappears in the course of a few years. Social interactions are often relatively well preserved and the intellectual capacities are higher than the motor capacities. Skeletal abnormalities, such as osteoporosis and kyphoscoliosis, result from the chronic motor disease and occur after the disease has been manifest for many years. The course of the disease is chronic. Patients may improve in performance up to the age of 10–12 years. From that age onwards, a very slow progression of the neurological signs and a decline of mental level is usually noted. Death occurs in most patients in early or mid adulthood and is usually due to intercurrent illnesses.

Some patients have a milder variant. They may achieve aided or unaided walking and demonstrate slow neurological deterioration. They may have signs of polyneuropathy.

The connatal type, also called Seitelberger type, is a more rare and severe form of PMD. The disease is already manifest in the neonatal or early infantile period. The neonatal period may be characterized by

hypotonia, feeding problems, absent primitive reflexes, and sometimes stridor. Abnormal, nystagmoid eye movements and extrapyramidal hyperkinesia occur early, followed by the development of epilepsy, spasticity, cerebellar ataxia, and optic atrophy. Titubation is often present. From birth onwards there is a complete failure of psychomotor development or an early loss of attained milestones. Microcephaly and growth retardation develop in the subsequent years. Progression is rapid, with death occurring in the first decade, usually in early childhood.

The transitional form between the classical and connatal types has its onset in the neonatal or early infantile period, but its course is less rapid. The distinction between the classical, transitional, and connatal forms of PMD is ill-defined. The age of onset does not appear to be the most valuable discriminating factor between the types of PMD. The rate of progression is the most useful and earliest reliable means of differentiating the different types.

The nosology of PMD is a matter of debate. Some include all patients with evidence of severe hypomyelination on MRI and a Pelizaeus–Merzbacher-like clinical picture under the heading of PMD, even in sporadic cases, in female patients, or in the case of autosomal recessive inheritance. In particular with connatal onset, female patients can be found. An adult variant of PMD has been suggested: the Löwenberg–Hill type. We prefer to include under the heading of PMD only patients in whom a proteolipid protein (PLP) gene mutation has been found or in whom the family history indicates an X-linked recessive inheritance. Another basic defect should be sought for the remaining patients.

Mothers of boys suffering from classical PMD sometimes develop neurological problems including spasticity, bladder dysfunction, personality changes, dementia, and polyneuropathy. Incidentally female patients in sibships with classical PMD show identical clinical and postmortem neuropathological findings.

X-linked spastic paraplegia type 2 (SPG2) and PMD are allelic conditions. The pure form of SPG2 leads to spasticity only. The legs are more severely involved than the arms. An intention tremor may be present. There are no other neurological deficits and intelligence is normal. The disease is slowly progressive and the life span is nearly normal. The age of onset varies from a few years of life to the teenage period. The complicated form of SPG2 also leads to slow-

ly progressive spasticity, but there are additional signs in common with PMD, which may include nystagmus, optic atrophy, cerebellar ataxia, sensory disturbances, and dysarthria. Walking may be delayed but all patients achieve unaided walking. Mild mental retardation is present in some of the patients. Analysis of SPG2 and PMD families shows a great overlap of clinical findings, both within and between families. Therefore, mutations in the PLP gene lead to a spectrum of disorders ranging from connatal PMD through the various manifestations of the classical PMD disease to pure SPG2.

Routine and metabolic laboratory investigations are of no help in establishing the diagnosis. Nerve conduction velocities and electromyography are usually normal, but in some patients mild to moderate slowing of nerve conduction velocities and neurogenic changes in electromyography are found. Evoked potential studies are of some help in PMD. In BAEP studies usually only wave I or waves I and II are present and later components are absent, indicative of abnormalities at brain stem level. ERG is normal. VEP and SSEP are absent or abnormal with increased latency, abnormal shape, and decreased amplitude. Definite diagnosis in PMD and SPG2 is DNA-based. Prenatal diagnosis and carrier detection are possible using DNA techniques.

34.2 Pathology

In PMD, the brain is too light for the patient's age and shows signs of diffuse atrophy, involving cerebral hemispheres and in particular brain stem and cerebellum. On sectioning the white matter appears reduced in volume to a variable extent and the corpus callosum is markedly reduced in width. Microscopic examination shows lack of myelin in all parts of the CNS. The pathological picture is basically the same in all PMD patients irrespective of subtype, but with variable severity.

In connatal PMD, the pathological picture varies from a marked lack of myelin to a complete absence of myelin in all parts of the brain and spinal cord. The myelin present is usually found in the spinal cord and the deeper parts of the brain: the diencephalon (globus pallidus, posterior limb of the internal capsule, thalamus), the brain stem (tectum of pons and mesencephalon, mesencephalic pyramidal tracts), and the central part of the cerebellum. The myelin is usually present in perivascular islets. Also, residual myelin islets are sometimes present in the subcortical white matter, especially in the pre- and postcentral gyri. There are no signs of active demyelination. There are no or little sudanophilic breakdown products in the white matter. Oligodendrocytes are reduced in number or completely absent. The axons are

relatively well preserved. Some axonal loss may be seen in completely demyelinated areas. The severity of the concomitant fibrillary gliosis varies from slight to dense. The gray matter is also affected; the intracortical myelin is completely or almost completely absent, but the normal cytoarchitecture is preserved. The cerebellar cortex shows loss of Purkinje cells and granular cells. Myelin is also deficient in the optic nerves and chiasm.

The abnormalities in classical PMD are less pronounced and myelin deficiency is less severe. There is a patchy absence of myelin with preservation of numerous myelin islets giving the white matter a so-called tigroid pattern. Most of the myelin islets surround small blood vessels. The myelin sheaths in these islets are thin and composed of only a few myelin lamellae. Microscopically some remaining myelin sheaths are also seen in the areas, which are otherwise devoid of myelin. At most small amounts of sudanophilic lipid products are found. Oligodendrocytes are numerically reduced, especially in the areas lacking myelin. All parts of the CNS are affected in the same way, but the spinal cord, brain stem, cerebellum, diencephalic structures, and subcortical white matter show a relatively good state of myelin preservation. In all areas of the CNS axons are relatively well preserved. Where myelin is absent, the remaining white matter is mainly composed of naked axons. Fibrillary gliosis varies from slight to intense. The astrocytes are sometimes hypertrophied. The gray matter is also involved in the process; myelin sheaths are reduced in number or are absent, but the cortical cytoarchitecture as well as the individual nerve cells are normal, although a certain loss of and damage to nerve cells may be seen. In the cerebellar cortex, loss of Purkinje cells and granule cells may be evident.

Whereas most PMD patients do not show signs of primary axonal degeneration, evidence of length-dependent axonal degeneration is seen in patients with a PLP gene deletion or null mutation.

Myelin is present in normal amounts for age in the PNS, including spinal roots and cranial nerves with the exception of the optic nerve in most PMD patients. However, in some patients the peripheral nerves are affected and myelin loss is found.

The transitional type shows abnormalities intermediate in severity between the connatal and the classical types.

Electron microscopy demonstrates that the few oligodendrocytes present contain an excess of cytoplasmic dense bodies and a poorly developed endoplasmic reticulum. There is condensation of nuclear chromatin, strongly suggestive of apoptosis, as has been found in animal models.

Information on the neuropathology of SPG2 is limited. A severe myelin deficiency has been reported in the spinal cord, contrasting with a mild lack of myelin

in the cerebral hemispheric white matter with sparing of the U fibers.

34.3 Chemical Pathology

Chemical analysis of the remaining myelin in PMD reveals that its lipid content is greatly reduced and its protein content, conversely, relatively increased. Cerebrosides are reduced in quantity and sulfatides are greatly reduced in quantity. The remaining glycolipids contain an abnormally high proportion of glucose with a proportional reduction in galactose. The myelin ganglioside content and cholesterol content are near normal. Phospholipids are increased, particularly sphingomyelin, choline phosphoglycerides, and inositol phosphoglycerides, whereas ethanolamine phosphoglycerides and plasmalogens are reduced. Protein analysis shows that proteolipid protein is absent, myelin basic protein is decreased, whereas so-called Wolfram proteins are increased.

The chemical composition of whole white matter depends on the amount of myelin that is present. The water content is abnormally high. Those lipids that are generally recognized as myelin lipids are either absent or markedly reduced. No or very little sulfatide is present. A marked reduction is seen in cerebroside, cholesterol, and phospholipids. The cholesterol:phospholipid:cerebroside ratio is similar to the ratio in brain prior to myelination. Gangliosides are found in normal concentrations. No or only a very small amount of cholesterol esters are present. The protein composition of white matter is also altered with absence of proteolipid protein and reduction of other myelin proteins.

In contrast to white matter, the chemical composition of gray matter is much closer to normal. The concentration of sulfatides and cerebrosides is decreased, but the concentration of phospholipids, cholesterol, and gangliosides is normal or close to normal.

34.4 Pathogenetic Considerations

For many decades the pathogenesis of the lack of myelin in the CNS in PMD has been a matter of debate. The original contention of Merzbacher was that the lack of myelin sheaths was due to faulty or absent myelination. Subsequently, many authors have classified PMD among the leukodystrophies and described the histopathological findings as tigroid demyelination. However, several histological and chemical findings are not consistent with demyelination, but are consistent with a defect in myelin deposition. Histological examination fails to reveal signs of active demyelination. The small amounts of myelin degradation products are in conformity with at best a

very slow breakdown of myelin. Oligodendrocytes are found to be decreased in number, show morphological abnormalities, and appear inactive. The chemical findings of no or at most a low level of cholesterol esters in the white matter is not in agreement with active demyelination. The cholesterol:phospholipid:cerebroside ratio in PMD corresponds with the ratio in the brain prior to myelination. The low ratio of ethanolamine phosphoglycerides to choline phosphoglycerides in PMD is an indication of a poor state of maturation of the brain, as the ratio increases with maturation. The high glucose content of glycolipids is also an indication of the immature state of the brain; as maturation proceeds, glucolipids are replaced by galactolipids. The topography of the myelin present is in conformity with an arrest of myelination, which apparently occurs before birth (congenital form) or within the first year of life (classical and transitional form). So, the severity of the clinical phenotype seems to be related to the degree of myelin deficiency.

PMD caused by a defect in the gene coding for proteolipid protein (PLP). The *PLP* gene is localized on the long arm of the X chromosome (Xq21.33–Xq22). It codes for PLP as its major gene product and additionally for DM 20 due to alternate splicing of mRNA. DM 20 is identical to PLP but 35 amino acids shorter.

The oligodendrocyte is the predominant cell in which the *PLP* gene is expressed in the CNS. PLP and DM 20 are produced in the endoplasmic reticulum and routed through the Golgi to the plasma membrane. PLP is a major myelin membrane protein. Myelin basic protein and PLP normally constitute more than 80% of the total CNS myelin proteins. Myelin basic protein accounts for 30–40% of the total myelin protein, PLP for 40–50%. PLP and its less abundant isoform DM 20 are strongly hydrophobic transmembrane proteins. They are myelin-specific and almost entirely confined to the CNS. They are, however, minor constituents of the PNS and compose less than 1% of the mass of PNS myelin proteins. The compact lamellar structure of myelin is organized and stabilized by the two main myelin proteins, myelin basic protein as a peripheral membrane protein, and PLP as a strongly hydrophobic integral membrane protein. Myelin basic protein contributes to the compaction of the major dense lines and PLP to the tight apposition of the intraperiod lines in the myelin sheath. DM 20 is the predominant isoform in oligodendrocyte progenitors and is expressed before PLP in the developing brain. DM 20 has biological functions in the maturing CNS that are distinct from the role of PLP.

Although PLP and DM 20 have been studied extensively, their biological functions are still not known in detail. Mice in which PLP gene expression has been inactivated demonstrate only subtle defects in the ultrastructure of CNS myelin, demonstrating that

neither PLP nor DM 20 is necessary for normal myelin assembly. These mice develop widespread wallerian degeneration of CNS axons, demonstrating that PLP expression in oligodendrocytes is necessary for the maintenance of normal axonal integrity, probably through oligodendrocyte–axonal interactions.

Many different mutations in the *PLP* gene related to PMD have been identified. Gene duplications are the most common cause of PMD and account for over 60% of the mutations. Furthermore, missense mutations, insertions, deletions, and nonsense mutations have been found. Point mutations do not only occur in the coding regions of the gene, but may also affect splice sites and noncoding regions of the gene. The severity of the clinical phenotype is related to the nature of the mutations. The most benign course of PMD is seen in *PLP* gene deletions or null mutations, whereas most missense mutations lead to a serious disease with neonatal or prenatal onset. Gene duplications lead to a disease of intermediate severity (usually the classical phenotype). The disease severity in duplications is proportional to the degree of overexpression of the *PLP* gene. In some mutations only PLP is altered whereas DM 20 is produced correctly, resulting in the more benign phenotype of SPG2. SPG2 may also be seen in *PLP* null mutations or point mutations in some nonconserved regions of the *PLP* gene.

The mode of action of changes in or absence of PLP has not yet been fully elucidated. There is experimental support for the concept that missense mutations cause conformational changes of the protein, “misfoldings” that prevent proper processing of PLP and DM 20 after biosynthesis in the endoplasmic reticulum. The accumulation of the mutated proteins in the endoplasmic reticulum of oligodendrocytes leads to the so-called unfolded protein response, which sets into motion an apoptotic cascade. The greater the accumulation of mutated proteins, the more intense the unfolded protein response and the higher the likelihood of apoptosis of oligodendrocytes. Oligodendroglial cell death leads to hypomyelination. In mutations in which *PLP* is mutated but normal DM 20 is produced, the trafficking of mutated PLP to the cell surface is disrupted, but the trafficking of DM 20 is normal, a situation that leads to milder disease. Much more myelin is produced than in classical PMD, but the myelin is less stable. Myelin instability and loss may contribute to the clinical phenotype.

In gene duplications, the excessive biosynthesis of PLP and DM 20 has deleterious effects on oligodendroglia, leading to CNS hypomyelination and subsequent demyelination, but there is no evidence of activation of the unfolded protein response. Overexpression of the *PLP* gene leads to arrested maturation and death of oligodendrocytes. Overexpressed PLP is routed to late endosomes/lysosomes and causes sequestration of cholesterol in these compart-

ments. Oligodendroglia may be particularly sensitive to an imbalance in the synthesis and turnover of myelin components due to their high rate of myelin synthesis. Considering the premature death of oligodendrocytes in *PLP* gene duplications, it is likely that a death program is triggered early in the disease course.

Gene deletions and null mutations do not lead to accumulation of mutated protein in the endoplasmic reticulum, do not cause increased oligodendrocyte cell death and arrest of myelination, and lead to a mild phenotype. It is intriguing that in these conditions the formation of compact myelin can proceed, while PLP and DM 20 are absent. In null mutations axonal abnormalities with wallerian degeneration are found in the CNS. This suggests that PLP has a role in glial–axon communication and is somehow necessary for axonal maintenance. In patients with absent PLP expression, a demyelinating peripheral neuropathy has been reported. It has been demonstrated that PLP but not DM 20 is necessary for peripheral nerve function, suggesting that the PLP-specific domain plays an important role in this respect.

The cause of the secondary neurological deterioration in PMD is insufficiently clarified. It is possible that the small amount of myelin present is unstable, leading to a very slow breakdown. In some patients histopathology provides evidence for axonal loss. There seems to be an inverse relationship between initial clinical severity of the disease (and the severity of the myelin deficit) and axonal loss. Axonal loss is especially seen in patients with milder disease and more myelin, for instance in patients with a null mutation.

As a rule PMD affects hemizygous males. However, from the beginning the occurrence of PMD has also been noticed in girls and women. This phenomenon has been ascribed to highly unfortunate X inactivation. Some female patients may have transient neurological abnormalities of variable severity as children but gradually improve over a period of several years. This functional restoration is attributed to ongoing myelination by oligodendrocytes, in which the healthy X chromosome is not inactivated. However, in most patients the occurrence cannot be explained by mechanisms related to X inactivation. It has become apparent that female patients are more common in families with milder forms of PMD or SPG2. Women heterozygous for *PLP* mutations are mosaic: one population of oligodendrocytes expresses normal PLP and synthesizes normal myelin sheaths, whereas the other population expresses a mutant form of PLP. The lack of phenotype in most female PMD carriers can be attributed to the phenomenon that oligodendrocytes in which the mutant X chromosome is activated become apoptotic and are replaced by healthy oligodendrocytes. Most of the resulting population con-

sists of healthy oligodendrocytes at the peak of myelination. In contrast, in female carriers of a mild mutation the mutant oligodendrocytes survive and compete with normal oligodendrocytes. They produce structurally flawed myelin sheaths, which are susceptible to degradation. Because the affected females maintain a population of normal oligodendrocytes, they never display as marked a phenotype as male members of the same family.

34.5 Therapy

Apart from supportive care there is presently no effective therapy for PMD and SPG2. Transplantation of myelin forming cells is a promising strategy.

34.6 Magnetic Resonance Imaging

CT scanning is of little help in the diagnosis of PMD, showing only atrophy.

In contrast, the MRI pattern in PMD is usually highly suggestive of the disorder. In most cases, MRI shows an arrest of myelination in a stage that is in itself normal (Figs. 34.1 and 34.2). There is a correlation between the amount of myelin present and the clinical severity of the disease. In some cases of congenital PMD, no myelin at all is seen. The T_2 -weighted images show a high signal intensity of all unmyelinated white matter structures, whereas these structures have a low signal intensity on T_1 -weighted images. In fact, no high signal intensity areas are seen on T_1 -weighted images in these cases. In cases of classical PMD myelin is present in (parts of) the brain stem, (parts of) the cerebellar white matter, (parts of) the posterior limb of the internal capsule, the thalamus, and the globus pallidus. Often the pyramidal tracts in the brain stem lack myelin while the brain stem is otherwise better myelinated. In some cases additional myelin is present in the directly periventricular part of the corona radiata, in the subcortical white matter and cortex of the pre- and postcentral gyri, and in the directly periventricular part of the optic radiation. The myelinated structures have a low signal intensity on T_2 -weighted images and a high signal intensity on T_1 -weighted images. The pattern described is a normal stage of myelination for a neonate or an infant in the first few months of life, but not normal for the age of the patient. In addition, the cerebral white matter is variably but often markedly reduced in volume with a mild enlargement of the ventricular system, a thin corpus callosum, folding of the cortex in thin, deep gyri, and enlargement of the subarachnoid spaces (Fig. 34.1). The appearance of the white matter is often not completely identical to normal unmyelinated white matter, but may be somewhat

speckled, possibly reflecting the presence of some myelin in a tigroid pattern. Atrophy of brain stem and cerebellum may be striking. If MRI is performed during the first few months of life, the images are not diagnostic as they merely show some atrophy and delay of myelination or may even be near-normal in appearance, but repeated MRI confirms the absence of progress of myelination. The described pattern of myelin deficiency in a boy who is a few years old is highly suggestive of PMD. Proton MRS of the cerebral white matter may give normal results. In some patients an increased concentration of *N*-acetylaspartate is found, probably related to denser axonal packing in the absence of normal amounts of myelin.

Arrest of myelination may be seen in other conditions, such as severe asphyxia or late congenital infections, but as a rule in these conditions additional focal brain lesions are present which are lacking in PMD. Most conditions other than PMD, having an adverse effect on myelination, lead to delayed but slowly progressive myelination, with advancement of the degree of myelination on each repeat MRI if made after a sufficiently long interval. Hence, repeated MRI is of help in establishing the diagnosis of PMD. Serious and permanent hypomyelination is also present in some DNA repair disorders and sialic acid storage disorders. These can be ruled out on the basis of clinical findings and appropriate biochemical tests. In addition, patients with Cockayne syndrome typically have calcium deposits within the basal ganglia, a phenomenon lacking in PMD.

In cases of mild PMD, related to gene deletions or null mutations, more myelin is present in the cerebral hemispheres and corpus callosum (Figs. 34.3 and 34.4). The pattern of myelination may be patchy and myelination may involve the subcortical areas in particular. In a family with multiple males with mild PMD related to a null mutation (initiation codon mutation) we found considerable although incomplete initial myelination of the cerebral hemispheres (Fig. 34.3), with subsequent cerebral atrophy and diffuse loss of myelin in a way seen in primary neurodegenerative disorders, suggesting underlying axonal degeneration and secondary loss of myelin (Fig. 34.4). In MRS of one of these patients a strikingly decreased level of *N*-acetylaspartate was found within the cerebral white matter, in agreement with axonal degeneration. Decreases in *N*-acetylaspartate within the cerebral white matter have also been found in other patients lacking PLP.

Some female carriers of PMD have been shown to have multiple foci of increased signal intensity in the cerebral white matter, but others have not. MRI is not suitable as a tool for carrier identification. In some more seriously affected females, an MRI pattern of profound myelin deficit may be seen, similar to the pattern observed in male patients.

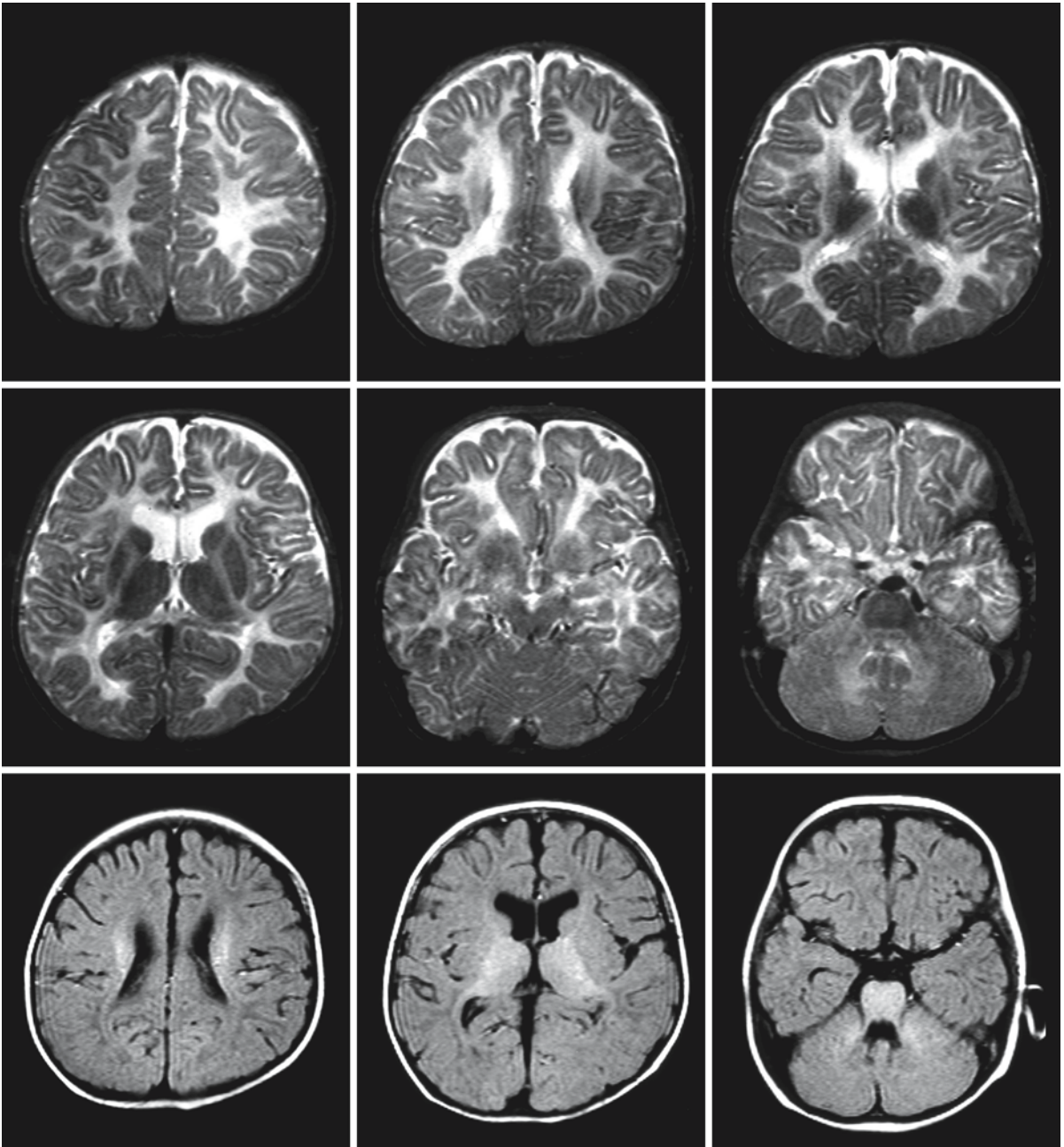


Fig. 34.1. Boy, 29 months old, with classical PMD. The T_1 -weighted images (*third row*) show presence of myelin in the central areas. On the T_2 -weighted images as well, some myelin is seen in the cerebellum and brain stem. The pattern of myelin

presence is consistent with arrest of myelination soon after birth. There is some cerebral atrophy. Courtesy of Dr. J.J.M. van Collenburg, Zwolle, The Netherlands

In SPG2 MRI abnormalities vary. Diffuse serious white matter changes may be seen as in males with classical PMD, with a high signal of the white matter on T_2 -weighted images and a low signal on T_1 -weighted images. In some cases the MRI is suggestive of diffuse or patchy mild hypomyelination with a mildly elevated signal on T_2 -weighted images, but also a high

signal on T_1 -weighted images. In other patients widespread or more limited focal lesions are seen within otherwise well myelinated white matter. Proton MRS of affected white matter in SPG2 patients has demonstrated decreased levels of *N*-acetylaspartate, indicative of axonal damage or loss.

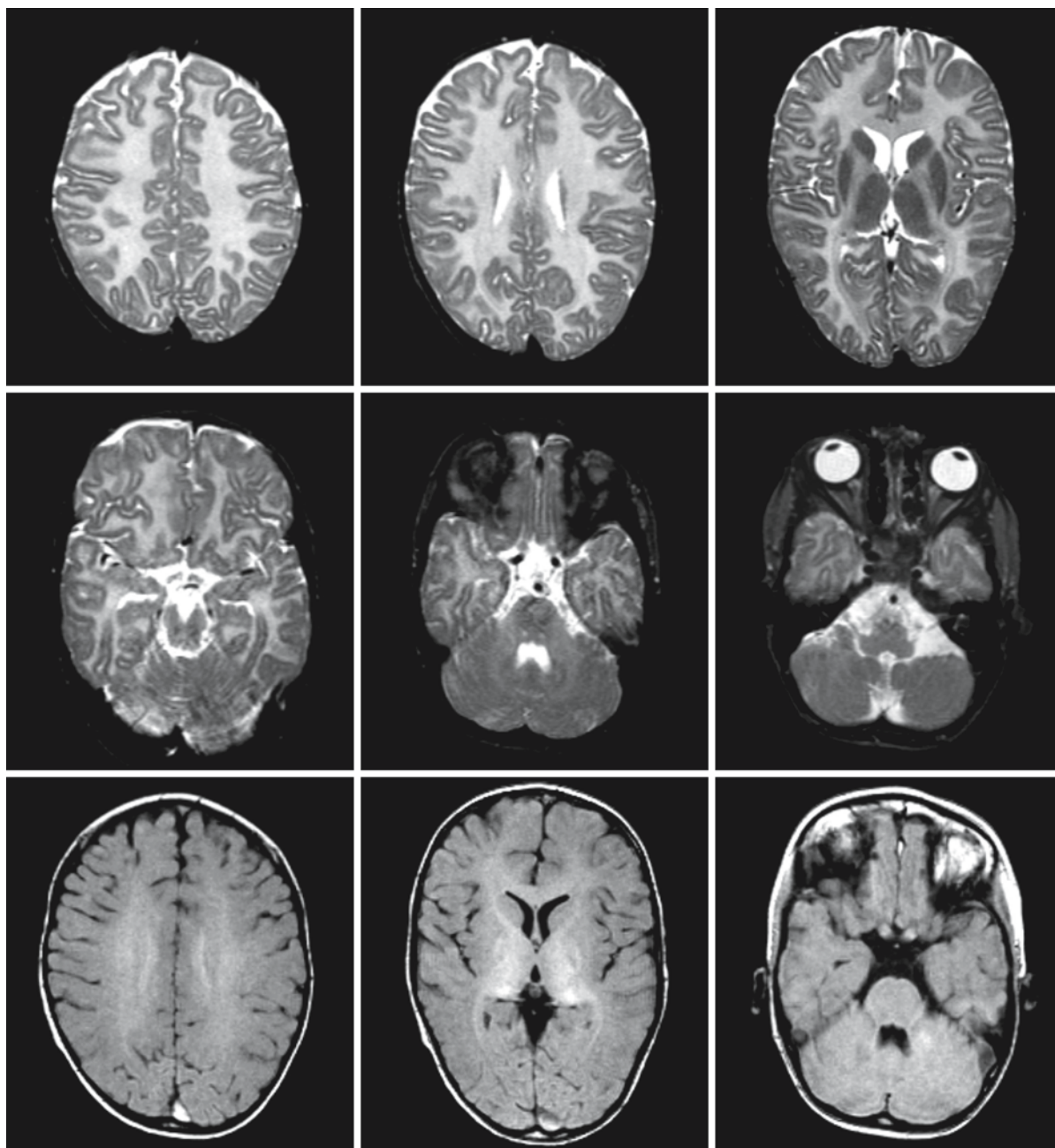


Fig. 34.2. A 6-year-old boy with classical PMD. The T_1 -weighted images reveal some myelin in the central white matter (*third row*), but the T_2 -weighted images show that the white

matter has a high signal intensity throughout. The brain stem and cerebellar white matter contain more myelin, but less than normal. It is striking that this patient has no atrophy

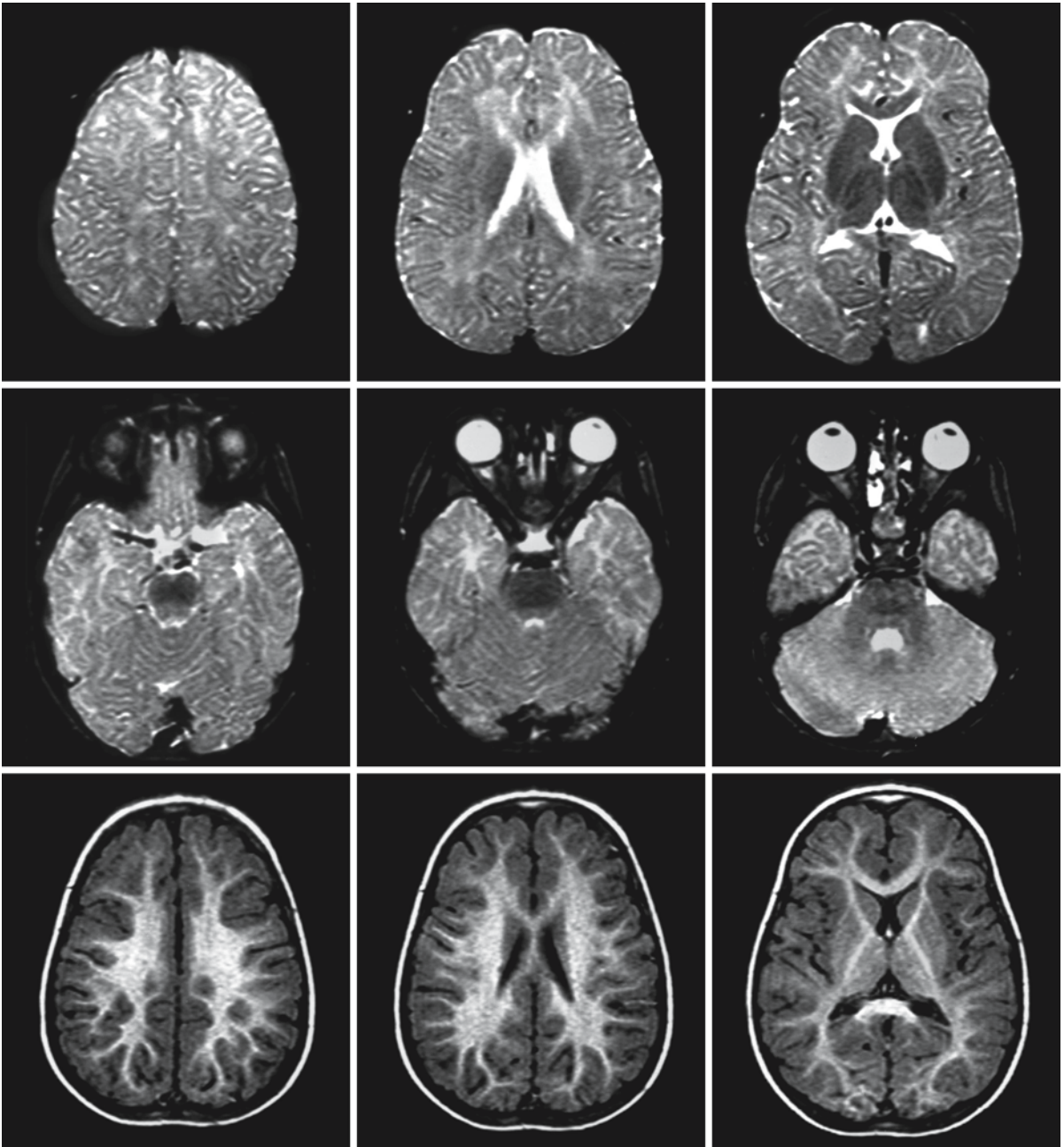


Fig. 34.3. This 2.5-year-old boy has a relatively mild form of PMD and an initiation codon mutation (Sisternans et al. 1996). The T₁-weighted images (*third row*) suggest an advanced stage of myelination, but the T₂-weighted images demonstrate that myelination is far from complete. Most cerebral

hemispheric white matter has a high signal; some deep white matter in the parieto-occipital region has a low signal. The corpus callosum and brain stem also have a low signal intensity on the T₂-weighted images

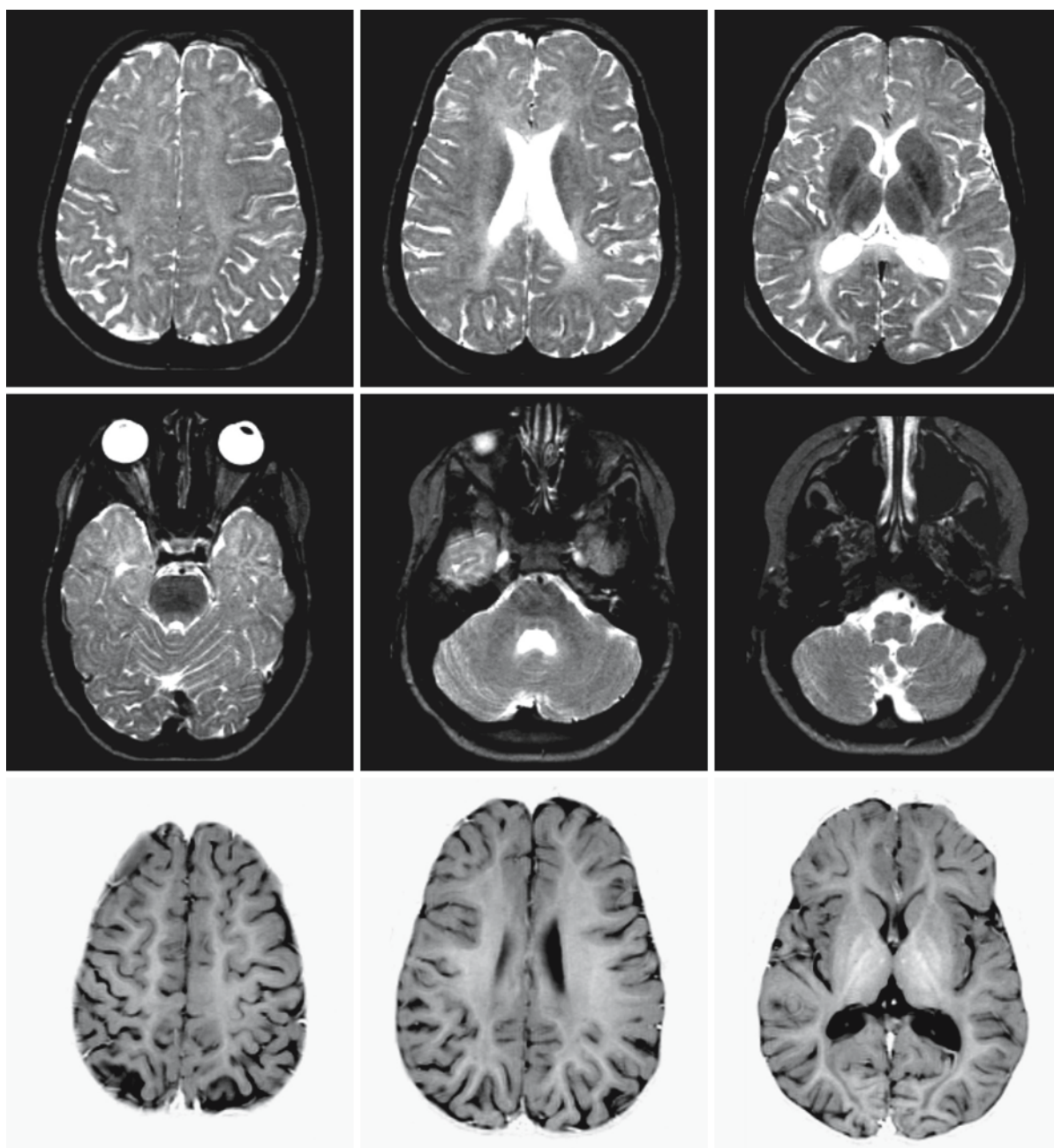


Fig. 34.4. The same boy as in Fig. 34.3, 8 years later. He has lost myelin. The corpus callosum and deep parieto-occipital white matter now have a high signal on the T₂-weighted images. The T₁-weighted images (*third row*) show a loss of contrast

between white and gray matter, indicative of diffuse myelin loss. Compared to 8 years ago, there is some diffuse cerebral atrophy

18q⁻ Syndrome

35.1 Clinical Features and Laboratory Investigations

The 18q⁻ syndrome is an autosomal deletion disorder with variable phenotype. Most patients have a *de novo* deletion, but in some patients it is inherited. The most frequent disease characteristics include mental retardation, short stature, microcephaly, midface hypoplasia, hypertelorism, epicanthus, carp-shaped mouth, high or cleft palate, preauricular skin tags, narrow or atretic ear canals, sensorineural or conductive hearing deficit, short neck, tapering fingers, clinodactyly, proximally placed thumbs, prominent finger whorls, widely spaced nipples, congenital heart disease, genital abnormalities, and foot deformities. Mental capacities vary from borderline to severely deficient. Apart from mental retardation, neurological abnormalities include hypotonia, seizures, nystagmus, poor coordination, tremor, and choreoathetosis.

Routine and metabolic laboratory investigations reveal no abnormalities. IgA deficiency and abnormalities in growth hormone production are relatively frequent. Peripheral nerve conduction is normal. Study of evoked potentials may reveal prolonged central conduction. Chromosomal analysis reveals a partial deletion of the long arm of chromosome 18, most often including the bands q22.3→qter. Inversion of the long arm of chromosome 18 with loss of the 18q23 region, translocations involving 18q, ring chromosome 18, and interstitial 18q23 deletions may also be seen.

35.2 Pathology

Reduction of cerebral white matter and delay of myelination are the main histopathological findings. Ventricles and subarachnoid spaces may be mildly enlarged.

35.3 Pathogenetic Considerations

18q⁻ Syndrome is a contiguous gene syndrome. It is likely that haplo-insufficiency of genes located in the deleted region explains the clinical phenotype and that the variability of the phenotype depends on the exact genes deleted. However, whether there is a correlation between the size of the deletion and the phe-

notype or not is still controversial. The deletion in the 18q⁻ syndrome includes the locus for the myelin basic protein gene (18q22–23). It is likely that the impairment in myelination of the CNS is at least partially related to haplo-insufficiency of the myelin basic protein gene. In patients with an interstitial deletion of chromosome 18, which retains the myelin basic protein region, myelination is normal (Linnankivi et al. 2003). The two most important proteins of CNS myelin are proteolipid protein and myelin basic protein. Myelin basic protein accounts for 30–40% of the total myelin protein, proteolipid protein for 40–50%. The 18q⁻ syndrome could be considered to be the autosomal counterpart of X-linked Pelizaeus–Merzbacher disease, which is caused by mutations of the proteolipid protein gene. However, an important difference is that one normal myelin basic protein gene is present in the 18q⁻ syndrome, whereas no normal proteolipid protein gene at all is present in males suffering from Pelizaeus–Merzbacher disease. Pelizaeus–Merzbacher disease is characterized by severe impairment of myelination of the CNS. The extent of impairment of myelin deposition is less severe and more variable in the 18q⁻ syndrome. The degree to which myelination is affected in the 18q⁻ syndrome has been found to correlate with the severity of the other features, whereas the myelin basic protein gene is included in the deletion in all patients. It is therefore unlikely that the presence of only one copy of the myelin basic protein gene is solely responsible for producing the abnormalities in myelination.

The so-called shiverer mouse has an autosomal recessive disease related to a mutation of the myelin basic protein gene. In this mouse a defect in CNS myelination is found. Clinical disease is characterized by generalized action tremor, increasingly frequent convulsions, and premature death. Histopathological examination reveals that CNS myelin is largely absent and, when present, appears as abnormal whorls of cytoplasm-filled membranes, tightly compacted at the intraperiod line, but uncompacted at the major dense line. The so-called myelin-deficient mouse has a duplication of the myelin basic protein gene and a low level of myelin basic protein mRNA. The phenotype of the myelin-deficient mouse is similar to that of the shiverer mouse, but less severe.

Myelin basic protein is also a component of PNS myelin. A curious feature is that absence or mutation of the gene has little effect on PNS myelin. PNS is on-

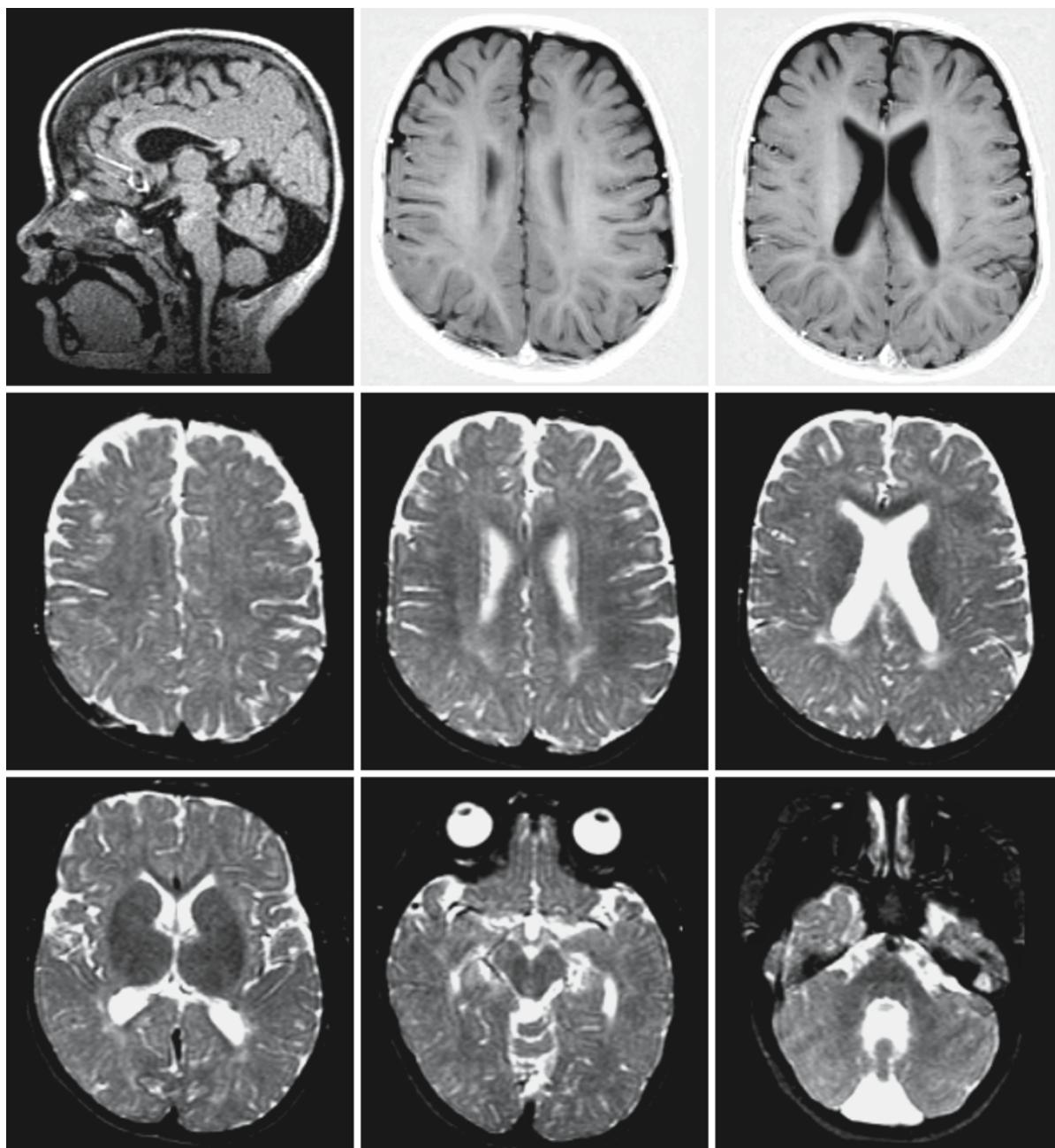


Fig. 35.1. A 2.5-year-old girl with 18q- syndrome. Note the delay in myelination, leading to poor contrast between gray and white matter. There are additional spots of abnormal sig-

nal intensity in the periventricular region. The corpus callosum is relatively well myelinated. The gyri have a relatively thin, atrophic appearance

ly subtly altered and is functionally normal. It is suggested that some component specific to peripheral myelin is functionally equivalent to myelin basic protein and capable of substituting for this protein in its absence.

35.4 Therapy

Supportive care is the only therapeutic option.

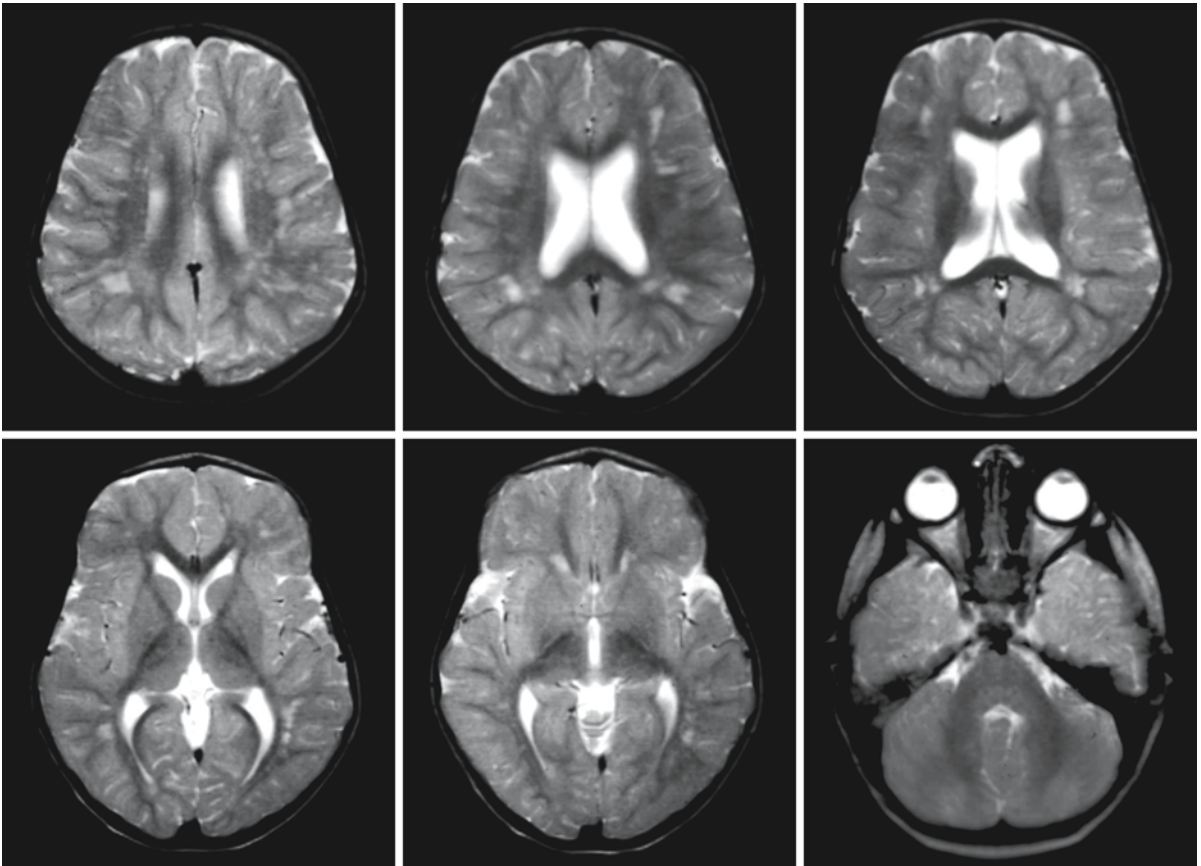


Fig. 35.2. The transverse T_2 -weighted MRI series of this 3-year-old boy shows widespread patches of hypomyelination. Myelination is delayed for the age of the child, most evidently

in the temporal lobes, where the white matter still has a higher signal intensity than the cortex. Courtesy of Prof. Dr. U. Stephani, Kiel and Prof. Dr. B. Terwey, Bremen, Germany

35.5 Magnetic Resonance Imaging

MR images show a variable myelin deficit. Initially, myelination is delayed (Fig. 35.1) but further advanced at every follow-up MRI. In older patients a stable picture of incomplete myelination is seen. The severity of the myelin deficit is variable. In some patients, a near-total absence of myelin in cerebral and cerebellar white matter, internal capsule, and corticospinal tracts is seen with relatively normal myelination of the corpus callosum. The cortical gyri are relatively thin and the sulci relatively deep due to reduction in white matter volume. Other patients have better myelination. The partial hypomyelination often leads to poor differentiation on MRI between white

and gray matter (Fig. 35.1). The myelin deficiency in the cerebral hemispheric white matter is often patchy with focal white matter signal abnormalities (Fig. 35.2). In some patients, hypomyelination of the corticospinal tracts in the brain stem and posterior limb of the internal capsule is present, but in most other patients these structures contain a considerable amount of myelin. The corpus callosum seems to have a relatively normal myelin content. Measurements of white matter T_1 and T_2 relaxation times show significant prolongation in patients with the 18q⁻ syndrome, even in structures that seem well myelinated such as the corpus callosum, compatible with incomplete myelination. In some patients the lateral ventricles are mildly enlarged.

Phenylketonuria

36.1 Clinical Features and Laboratory Investigations

Phenylketonuria (PKU) represents a heterogeneous group of disorders with autosomal recessive inheritance. PKU, or hyperphenylalaninemia, is caused by a deficiency of the phenylalanine hydroxylating system. The phenylalanine hydroxylating system consists of two essential components: phenylalanine hydroxylase and coenzyme tetrahydrobiopterin (Figs. 36.1 and 36.2). PKU is in most patients caused by deficiency of phenylalanine hydroxylase, and in a minority of patients by deficiency of tetrahydrobiopterin.

Classical PKU is due to severe phenylalanine hydroxylase deficiency. Infants with this disease are normal at birth. In the course of the first year of life psychomotor retardation becomes evident. Eczema is present in a considerable number of patients, usually from infancy to late childhood. The patients often, but not always, have blond hair, fair skin, and blue eyes.

They often have a mousy, musty odor. Seizures may occur, taking the form of tonic-clonic seizures, myoclonic seizures, and infantile spasms. Irritability, frequent vomiting, and insufficient growth are part of the clinical picture. The final mental level of PKU children is deficient, but the children are trainable. Verbal IQ is lower than performance IQ. The children are small and often microcephalic. Pyramidal signs are present with hypertonia, gait disturbances, hyperreflexia, and extensor plantar reflexes. Frequently a rapid, fine, and irregular tremor of the hands is present. Abnormal choreoathetoid movements may be present with twisting movements, continuous repetitious finger movements, and rhythmical swinging body movements. Psychiatric disturbances with severe hyperactivity, destructiveness, self-mutilation, and uncontrollable attacks of rage or excitement are common.

Worldwide neonatal screening programs have led to early detection of almost all PKU patients. Early dietary treatment prevents most of the described ab-

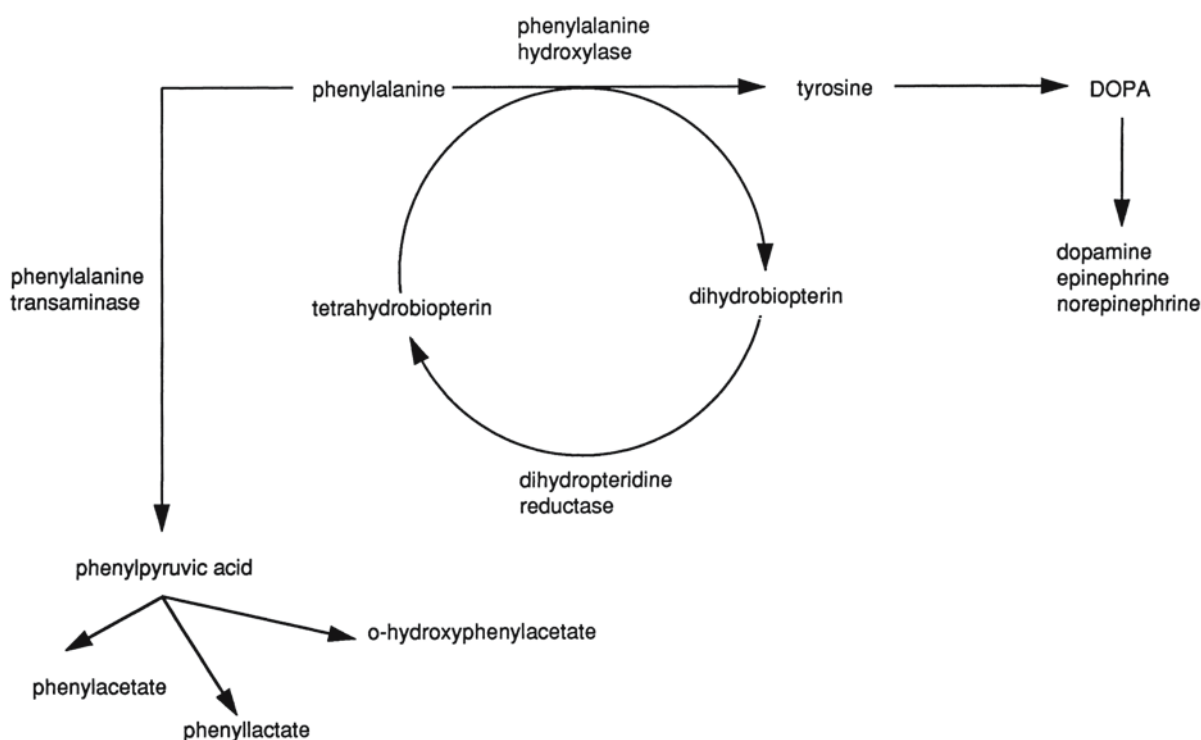


Fig. 36.1. Metabolism of phenylalanine

normalities, which are now rarely seen. Intelligence is usually within the normal range, although mean intelligence in patients with classical PKU who are treated early is roughly half a standard deviation lower than the IQ of unaffected siblings and population norms. Treated PKU patients are generally slower to acquire language and have a higher frequency of learning difficulties and behavioral disturbances, with hyperactivity, anxiety, and poor concentration. The better the dietary control in early and middle childhood, the better the outcome. Despite neonatal screening programs, there are still a number of patients with PKU who are not diagnosed in the neonatal period and start treatment late. In general, the later the onset, the lower the IQ scores. Strict dietary treatment was formerly thought to be important only during the period of major cerebral maturation and used to be moderated or stopped in mid to late childhood. However, there is now evidence that with discontinuation of strict diet and a rise in phenylalanine levels, some cognitive deterioration and emotional problems develop in many patients, together with an increase in motor problems consisting of tremor and signs of spasticity of the legs. Reinstitution of strict diet may result in disappearance of these problems.

Maternal PKU appears to have detrimental effects on embryogenesis and fetal development. The offspring of females with classical PKU, who are no longer being treated, show a high frequency of in-

trauterine and extrauterine growth retardation, microcephaly, and mental handicap, occasionally accompanied by malformations of the heart or other organs. The incidence of these aberrations appears to be correlated with the maternal concentration of serum phenylalanine. Reinstigation of dietary treatment prior to conception has a favorable effect on outcome.

Mild variants of classical PKU lead to less severe mental retardation if untreated. Patients tolerate a larger intake of phenylalanine and successful treatment requires a less rigid diet than in the case of severe classical PKU.

In so-called *persistent hyperphenylalaninemia* mildly elevated serum phenylalanine levels are found, but there are no clinical symptoms and treatment is not necessary.

Approximately 2% of newborns with PKU have a *tetrahydrobiopterin deficiency*. In the most severe patients microcephaly, developmental delay, and progressive neurological dysfunction occur, leading to death in childhood, although some patients stabilize or make some developmental progress. Early in life patients present with microcephaly, disturbed psychomotor development, and the other neurological problems associated with hyperphenylalaninemia. In addition, signs of extrapyramidal dysfunction are prominently present and consist of parkinsonism, chorea, dystonia, oculogyric spasms, or myoclonus.

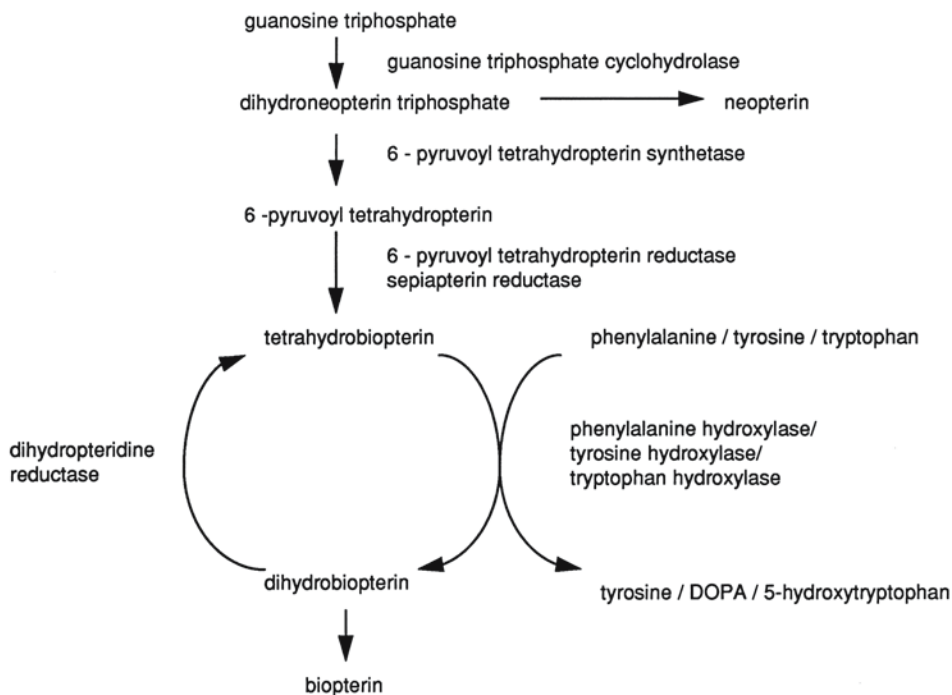


Fig. 36.2. Synthesis of tetrahydrobiopterin

Typical signs of parkinsonism are hypokinesia, bradykinesia, rigidity, and mask-like facies. In addition, sweating, hyperpyrexia without infection, drooling, swallowing difficulties, pinpoint pupils, truncal hypotonia, limb hypertonia and hyperreflexia, infantile spasms, and tonic-clonic seizures often form part of the clinical picture. In milder forms, symptoms are less marked and consist mainly of extrapyramidal dysfunction or slow development. In patients with pterin-4 α -carbolamine dehydratase as the cause of the tetrahydrobiopterin deficiency, there are generally no significant clinical abnormalities other than transient alterations in tone. In tetrahydrobiopterin deficiency caused by a defect in dihydropteridine reductase, rapidly progressive demyelination of the CNS may occur additionally, due to defective folate metabolism, and cause spasticity, pseudobulbar palsy, long tract sensory loss, and cognitive deterioration.

Neonatal screening is performed between 6 and 14 days after birth. Increased blood phenylalanine concentration indicates a positive test. In phenylalanine hydroxylase deficiency, phenylpyruvic acid and *o*-hydroxyphenylacetic acid are excreted in the urine (Fig. 36.1). The blood level of tyrosine is normal or lower than normal, which excludes hyperphenylalaninemia secondary to disorders of tyrosine metabolism. Apart from tyrosinemia, hyperphenylalaninemia secondary to prematurity, hepatic insufficiency, chronic renal insufficiency, and trimethoprim medication should be considered. An oral phenylalanine loading test is performed when the child is several months old and leads to elevated serum levels of phenylalanine without elevation of tyrosine. Severe and mild variants of phenylalanine hydroxylase deficiency are distinguished by the level of serum phenylalanine before treatment, the level of serum phenylalanine and the duration of the increase after phenylalanine loading, and the tolerance of phenylalanine in the diet. Residual phenylalanine hydroxylase activity can be determined in liver biopsy material. Prenatal diagnosis and carrier detection can be performed with the help of DNA techniques.

If elevated serum phenylalanine concentrations are found on neonatal screening, pterins in urine are analyzed and dihydropteridine reductase activity is measured to exclude dihydropteridine reductase deficiency and other disorders in the synthesis and recycling of tetrahydrobiopterin (Fig. 36.2). Assessment of the ratio between total biopterin and neopterin in urine is helpful in differentiating between the various enzyme defects. In dihydropteridine reductase deficiency, the total biopterin level is very high, whereas the neopterin level is normal or moderately increased; in 6-pyruvoyl tetrahydropterin synthetase deficiency, the neopterin level is elevated and the biopterin level is very low; and in guanosine triphosphate cyclohydrolase deficiency both neopterin and

biopterin levels are extremely low. Examination of urine pteridine profiles allows a tentative diagnosis of the basic defect. In cases of tetrahydrobiopterin deficiency, CSF and urine levels of homovanillic acid (HVA), 5-hydroxyindoleacetic acid (5HIAA), vanillyl mandelic acid (VMA), and 3-methoxy-4-hydroxyphenylglycol (MHPG), the major metabolites of dopamine, serotonin, and (nor)epinephrine in the human CNS, are reduced. The levels of these metabolites may also be reduced, although less markedly, in classical PKU. However, in classical PKU the levels normalize with a phenylalanine-restricted diet, which is not the case in disorders characterized by tetrahydrobiopterin deficiency. In dihydropteridine reductase deficiency, serum folate levels may be low. The diagnosis should be confirmed by enzyme studies in erythrocytes (dihydropteridine reductase, 6-pyruvoyl tetrahydropterin synthetase), lymphocytes (guanosine triphosphate cyclohydrolase), or liver biopsy (6-pyruvoyl tetrahydropterin synthetase, guanosine triphosphate cyclohydrolase). Prenatal diagnosis can be performed by assessing pterin levels in amniotic fluid or enzyme activity in fetal erythrocytes, amniocytes, or chorionic villi, depending on the different enzyme defects. A DNA-based prenatal diagnosis is possible in families with known mutations.

36.2 Pathology

In untreated classical PKU, the weight of the brain is below normal. The reduction in volume is greater in the white than in the gray matter. The ventricles are enlarged. The cortical pattern of gyri and sulci is normal.

Microscopic examination of the cortex reveals evidence of developmental arrest or delay of cortical neurons, with a reduction in number and size of cortical neurons, paucity of dendritic arborization, and reduced synaptic density.

In untreated PKU children variable white matter abnormalities are seen ranging from hypomyelination and spongy change to frank demyelination. Some PKU patients do not have white matter abnormalities, but the majority of the patients have white matter lesions. Hypomyelination is usually seen, affecting most severely the structures that myelinate late. In addition, a status spongiosus of the white matter is usually present. The status spongiosus is most marked in the optic tracts, periventricular white matter, centrum semiovale, and in the central part of the cerebellar white matter, although at times spongy lesions are also seen in the subcortical white matter. Apart from occasional sudanophilic fat droplets in perivascular spaces, there are no signs of active myelin loss. Gliosis is variable. In some patients, espe-

cially older untreated children and adults, areas of demyelination are seen in the periventricular and deep white matter, sparing the subcortical U fibers. In some cases the areas are sharply defined; in others the borders of the lesions are indistinct. In the areas of demyelination intense gliosis and deposition of sudanophilic material is seen. Oligodendrocytes are reduced in number. The axis cylinders are relatively better preserved than the myelin sheaths. The cerebellar white matter may also be involved. Spongy lesions may be noted adjacent to the demyelinated areas. With advancing age white matter changes tend to become more pronounced and diffuse, although not in all cases.

In patients with dihydropteridine reductase deficiency, additional neuronal loss, abnormal vascular proliferation, and calcium deposits in the walls of small, medium, and large arteries and veins, as well as diffusely scattered pericapillary and isolated calcium deposits have been reported in the basal ganglia, thalamus (Milandi et al. 1998), cerebral cortex, and white matter (Takashima et al. 1991). Diffuse myelin pallor of the cerebral and cerebellar white matter, spongy white matter changes, and multifocal perivascular demyelination occur as well.

36.3 Chemical Pathology

Analysis of cerebral lipids reveals a deficiency of myelin lipids, particularly cerebroside, sulfatide, and cholesterol. In the few studies performed, the deficiency of myelin lipids is more severe in older patients. Cholesterol esters are absent or present in only small amounts.

36.4 Pathogenetic Considerations

Phenylalanine is an essential amino acid, ubiquitous in dietary protein. It is normally transformed into tyrosine, which is in turn used for protein synthesis and is the immediate amino acid precursor for melanin, dopamine, norepinephrine, and epinephrine. The conversion of phenylalanine to tyrosine requires the presence of phenylalanine hydroxylase and tetrahydrobiopterin as a proton donor (Figs. 36.1 and 36.2). Tetrahydrobiopterin is reconverted from dihydrobiopterin by dihydropteridine reductase (Fig. 36.2). In the majority of cases, PKU is caused by a deficiency of the hepatic enzyme phenylalanine hydroxylase, and in a minority ($\pm 2\%$) by tetrahydrobiopterin deficiency, caused by a defect in its recycling or its synthesis (Fig. 36.2). Defects in dihydropteridine reductase and pterin-4 α -carbinolamine dehydratase affect the recycling. Defects in guanosine triphosphate cyclohydrolase I and 6-pyruvoyl tetra-

hydropterin synthetase affect tetrahydrobiopterin synthesis.

The phenylalanine hydroxylase gene, *PAH*, is located on chromosome 12q22–24.1. A large number of different mutations have been reported. There is evidence that the phenotypic heterogeneity of the disorder reflects underlying genetic heterogeneity. Some of the mutations lead to absence of residual hydroxylase activity, whereas others result in the presence of some variable residual activity. A good correlation has been found between the residual level of activity of mutant phenylalanine hydroxylase enzyme and the clinical severity of the disease. The residual enzyme activity also correlates with the pretreatment serum level of phenylalanine, serum phenylalanine levels measured in standardized loading tests, and phenylalanine tolerance. Severe classical PKU is caused by mutations with zero residual enzyme activity. Higher enzyme activity is associated with a milder phenotype. In persistent benign hyperphenylalaninemia without clinical manifestations the residual enzyme activity is relatively high. However, the genotype is not the only factor determining the phenotype. Different clinical outcomes despite comparable dietary control form evidence for additional factors. Phenylalanine is transported over the blood–brain barrier, and there is evidence that individual differences in this transport contribute to the severity of the neurological problems. The higher the affinity of the transporter for phenylalanine, the higher the cerebral phenylalanine levels despite similar blood phenylalanine levels, and the lower the IQ.

Deficiency of phenylalanine hydroxylase results in the accumulation of phenylalanine, which is transaminated to phenylpyruvate, phenyllactate, phenylacetate, and *o*-hydroxyphenylacetate (Fig. 36.1). The metabolites derived from phenylalanine contribute little to the cerebral damage in PKU. Probably the most important effects are related to direct toxic influences of phenylalanine itself. In theory, deficiency of phenylalanine hydroxylase activity could lead to systemic tyrosine deficiency. However, no consistent or significant reduction in plasma tyrosine has ever been demonstrated in untreated PKU patients, and postnatal tyrosine supplementation does not prevent occurrence of neurological abnormalities. Hyperphenylalaninemia has a number of adverse effects. Owing to the competitive nature of amino acid transport across the blood–brain barrier, the brain in patients with PKU is exposed to both high phenylalanine levels and low concentrations of other large neutral amino acids, including histidine, tyrosine, tryptophan, threonine, valine, methionine, isoleucine, and leucine, especially methionine and tyrosine. Hyperphenylalaninemia inhibits protein synthesis, which may be related to the inhibition of transport of amino acids across the blood–brain barrier. It may be that

the hypomyelination, almost invariably seen in untreated PKU patients, is related to the inhibition of protein synthesis. High levels of phenylalanine have a double effect on tyrosine and tryptophan metabolism. Not only is the transport across the blood-brain barrier inhibited, but high phenylalanine levels also lead to competitive inhibition of the enzymes tyrosine hydroxylase and tryptophan hydroxylase, enzymes involved in the synthesis of dopamine, (nor)epinephrine (from tyrosine), and serotonin (from tryptophan). As a result of both enzyme inhibition and deficiency of the amino acid substrates for these enzymes, the neurotransmitters dopamine, (nor)epinephrine, and serotonin are decreased in untreated patients with phenylalanine hydroxylase deficiency.

It is important to distinguish permanent from reversible effects of hyperphenylalaninemia. Reversible neuronal dysfunction, which disappears on treatment, is probably related to neurotransmitter dysfunction. If left untreated, reversible dysfunction may become irreparable damage consisting of a reduction in the number and growth of neuronal cells and synapses. The defect in protein synthesis may contribute to this damage. Reversible white matter damage consists of delay in myelination and white matter sponginess, probably related to a combination of phenylalanine toxicity on cells and disturbed protein synthesis. Longstanding, severely disturbed myelination and demyelination may only be partially repairable. The vulnerability of the brain for hyperphenylalaninemia is life-long. Discontinuation of diet may again lead to neuronal dysfunction with epilepsy, enhanced occurrence of EEG abnormalities and cognitive decline, and to white matter damage as evident from MRI.

The tetrahydrobiopterin deficiency states can be divided into defects in synthesis and defects in recycling (Fig. 36.2). Defects in synthesis are related to deficiency of guanosine triphosphate cyclohydrolase or 6-pyruvoyl tetrahydropterin synthetase. The genes encoding these enzymes, *GCH1* and *PTS*, are located on chromosomes 14q22.1–22.2 and 11q22.3–23.3, respectively. Dihydropteridine reductase deficiency and pterin-4 α -carbinolamine dehydratase deficiency are defects in recycling. The genes encoding these enzymes, *QDPR* and *PCBD*, are located on chromosome 4p15.3 and 10q22, respectively. Deficiency of guanosine triphosphate cyclohydrolase most often leads to dopa-responsive dystonia without hyperphenylalaninemia. Deficiency of each of the enzymes leads to tetrahydrobiopterin deficiency, which is a cofactor (proton donor) not only in the hydroxylation of phenylalanine to tyrosine, but also in the hydroxylation of tryptophan to 5-hydroxytryptophan and in the hydroxylation of tyrosine to L-dopa (Fig. 36.2). 5-Hydroxytryptophan is the precursor of serotonin and

melatonin; L-dopa is the precursor of dopamine, epinephrine, and norepinephrine. In addition, hyperphenylalaninemia has a competitive inhibitory effect on tyrosine hydroxylase and tryptophan hydroxylase. So, deficiency of these enzymes has a profound effect on multiple neurotransmitter systems, which explains many of the neurological features. This effect cannot be improved by lowering phenylalanine intake only. A special aspect of dihydropteridine reductase deficiency is related to folate metabolism. The enzyme also reduces dihydrofolate to tetrahydrofolate. Defective folate metabolism is important in dihydropteridine reductase deficiency. Megaloblastic changes of blood cells are unusual, even in very low folate concentration. However, progressive neurological damage is frequent. Histological changes in the brain are similar to those seen in congenital folate malabsorption and 5,10-methylene tetrahydrofolate reductase deficiency, and consist of multifocal perivascular demyelination.

36.5 Therapy

Classical PKU is treated with a low-phenylalanine diet. Some patients with phenylalanine hydroxylase deficiency are tetrahydrobiopterin-responsive. These patients benefit from use of tetrahydrobiopterin and may follow a less strict diet or avoid the diet altogether. The low-phenylalanine diet depends on the use of synthetic, phenylalanine-low substitutes for many natural foods (meat, fish, eggs, nuts, dairy products, bread), making the diet difficult to sustain over long periods. Treatment should be monitored regularly with assessment of serum phenylalanine levels. Both early start of dietary treatment and strict compliance with the diet contribute to a favorable intellectual outcome. IQ clearly correlates to the quality of dietary control. It is also important to be careful that patients do not develop nutritional deficiencies, in particular vitamin B₁₂ deficiency, from failure to consume appropriate supplements. Protein insufficiency, which leads to impaired growth, can be avoided by monitoring plasma prealbumin levels. Current treatment of PKU patients is not perfect, and cognitive level is, on average, lower than expected.

For many years it has been customary to stop dietary treatment in mid to late childhood or in adolescence on the assumption that hyperphenylalaninemia is only harmful in the immature brain. However, discontinuation of diet may lead to some cognitive deterioration and emotional problems in many of the PKU patients. They show a lack of concentration, and sometimes agitation and emotional instability. Hypertonia of the legs, hyperreflexia, and extensor plantar responses are frequently present and may lead to difficulty in walking. Epilepsy, slowness of speech,

dysarthria, and tremor, in particular intention tremor, may occur. With high levels of phenylalanine EEG shows background slowing. The sensitivity for phenylalanine fluctuations is greater among younger patients and decreases with age. The complaints may be reversible if phenylalanine restriction is resumed, but may become permanent if longstanding. Lifelong continuation of dietary treatment is advisable.

In particular, restriction of phenylalanine intake during pregnancy is important for the benefit of the offspring. The maternal PKU syndrome, occurring in children born to mothers with untreated PKU, consists of intrauterine growth retardation, congenital heart disease, dysmorphic signs, microcephaly, and mental deficiency. The syndrome can be prevented by adequate treatment during pregnancy.

In PKU related to tetrahydrobiopterin deficiency, the therapeutic goal is two-fold: not only to control the blood level of phenylalanine, but also to normalize monoamine neurotransmission. The administration of tetrahydrobiopterin is insufficient to achieve this latter purpose. The introduction of oral administration of a combination of tetrahydrobiopterin, L-dopa, carbidopa, and 5-hydroxytryptophan, given to bypass the impaired activity of tyrosine hydroxylase and tryptophan hydroxylases, is followed by some (and sometimes a dramatic) degree of clinical and biochemical improvement. Carbidopa is a peripheral decarboxylase inhibitor to prevent peripheral conversion of L-dopa to dopamine and so prevent systemic adverse effects and enhance central beneficial effects. The treatment should be monitored not only by evaluation of serum phenylalanine levels, but also by assessment of CSF neurotransmitter metabolites. In dihydropteridine reductase deficiency, the folate disturbance also requires treatment. Tetrahydrofolate should be administered in sufficient amounts to keep CSF concentrations in the high normal range. This level of tetrahydrofolate prevents the occurrence of demyelinating disease.

36.6 Magnetic Resonance Imaging

White matter abnormalities occur with high frequency in patients with classical PKU. These white matter changes have been reported in older children, adolescents, and adults. At present, there is no systematic MRI study involving infants and young children. From the studies performed it is apparent that white matter abnormalities are less likely to be present in children under strict dietary control and in patients with milder variants of PKU. The white matter changes are predominantly present in patients after they have stopped the phenylalanine-restricted diet. There is a positive correlation between the presence and severity of the white matter abnormalities and

both the degree of recent exposure to high phenylalanine levels and the number of years since the low-phenylalanine diet was stopped. The presence of white matter changes does not correlate with age at the start of dieting (early versus late treatment) or with the quality of dietary control during the first years of life or subsequent years. These data suggest that recently sustained exposure to high phenylalanine concentrations rather than the quality of long-term control is the major determinant of white matter signal abnormalities as detected by MRI. A few patients who developed neurological abnormalities several months or years after stopping or relaxing the phenylalanine-restricted diet underwent sequential MRI studies. Whereas initial MRI investigations showed white matter changes, follow-up scans after resumption of a strict diet showed resolution of the abnormalities within a few months in some but not all patients.

The earliest and most frequent abnormalities consist of high-signal-intensity lesions on T₂-weighted images in the parieto-occipital periventricular white matter (peritrial and peritrigonal region) (Fig. 36.3). In more severe cases, the frontal periventricular white matter is also involved and the white matter abnormalities may extend into the subcortical area, in particular in the posterior region (Fig. 36.4). The corpus callosum is relatively, but not always completely spared. The internal capsule, brain stem, and cerebellar white matter are most often preserved, although in some patients the cerebellar white matter and brain stem tracts are involved. The white matter lesions are symmetrical and either band-like or patchy and partly confluent in an irregular fashion. Additional isolated white matter spots may occasionally be present. Frequently the frontal, less often the occipital white matter changes have a peculiar configuration, extending like little "flames" from the ventricular border in line with the ventricles. In few patients some generalized cerebral atrophy is seen.

The nature of the white matter changes is still a matter of conjecture as there are no direct correlative studies comparing MRI and histopathological findings in the same patients. Considering the rapid reversal of MRI changes that may be produced by effective dietary intervention, white matter edema may be assumed. In view of the fact that reversibility of MRI changes was not confirmed in all cases, and considering the known histopathological sequence of events in untreated PKU patients (hypomyelination → white matter (myelin) vacuolation and edema → demyelination), an attractive hypothesis is that the early MRI changes observed represent white matter edema with intramyelinic vacuole formation, and that the late changes represent permanent myelin damage and loss. The initial stage is reversible, the later stage is not. Restricted diffusion has been found in the areas

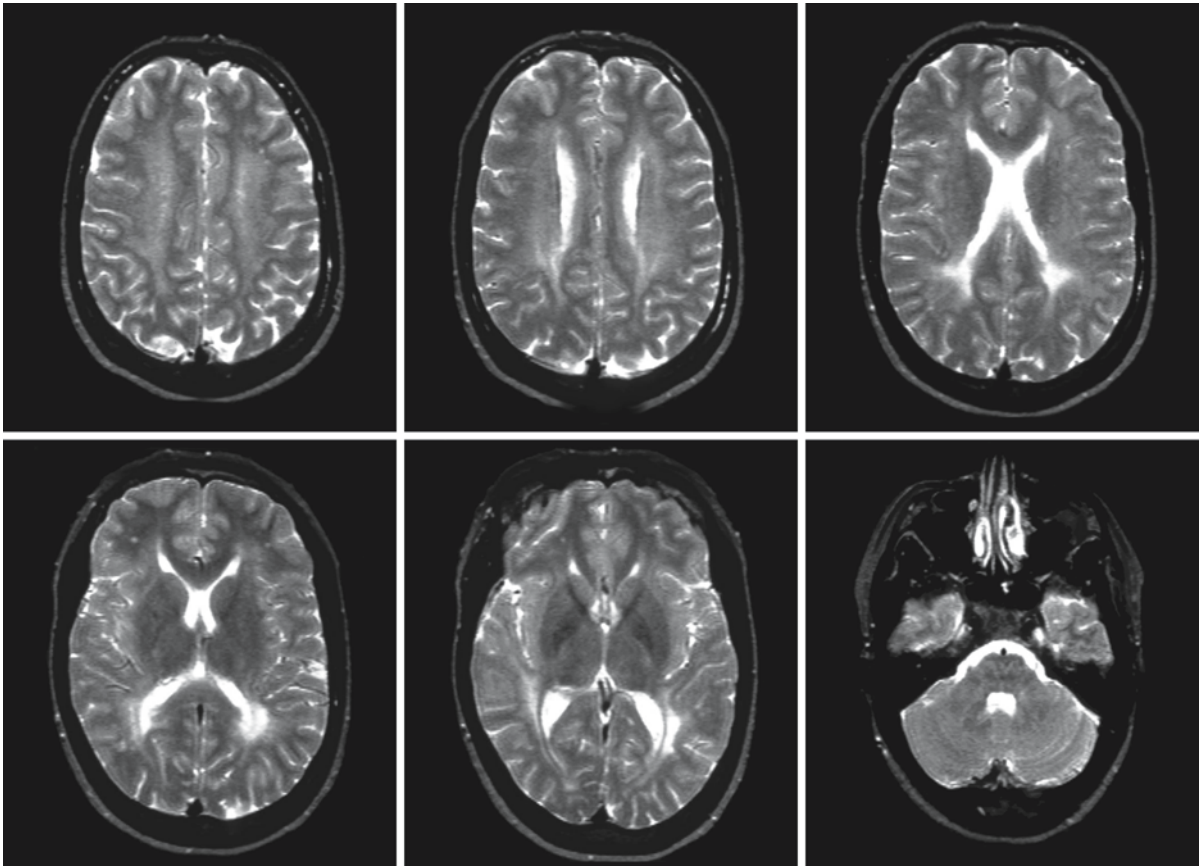


Fig. 36.3. A 24-year-old female patient with classical PKU. Note the periventricular zone of mild signal changes. There is a more prominently abnormal signal in the white matter bordering the frontal and, especially, the posterior horns of the lat-

eral ventricles. Courtesy of Dr. S. Blaser, Department of Diagnostic Imaging, and Dr. A. Feigenbaum, Department of Clinical Genetics, Hospital for Sick Children, Toronto, Canada

of white matter abnormalities (Philips et al. 2001; De-zortová et al. 2001), which would be compatible with myelin vacuolation as histopathological basis.

Clinically, the white matter changes correlate with motor problems, in particular spasticity of the legs, processing of visual information, sustained attention, and changes in mood and personality. No relationship between MRI changes and IQ has been found.

Proton MRS permits noninvasive measurement of brain phenylalanine levels. MRS has been helpful in studying the dynamics of phenylalanine transport across the blood-brain barrier after phenylalanine loading and in studying the relationship between phenylalanine levels in the brain and neurological functions.

The imaging changes observed in patients with PKU due to a deficiency of tetrahydrobiopterin are different from those in classical PKU. There are only a few reports on imaging findings, and so the incidence and extent of the abnormalities are not fully known. Several reports concern patients with pyruvoyl

tetrahydropterin synthetase deficiency (Brismar et al. 1990; Chien et al. 2002). CT is normal up to the age of about 1 year. In older children CT shows atrophy with enlargement of the ventricular system and subarachnoid spaces. In some of the patients, diffuse hemispheric white matter hypodensity is seen. MRI shows diffuse hemispheric white matter hyperintensity on T₂-weighted images in these patients, but in other patients the white matter is normal.

In dihydropteridine reductase deficiency a combination of gray and white matter changes is found (Figs. 36.5–36.7). CT scan shows cerebral atrophy with enlargement of the ventricular system and subarachnoid spaces. In addition, calcium deposits develop and are seen bilaterally in the basal nuclei (globus pallidus, putamen), thalamus, and cortico-subcortical junction. Variable white matter hypodensity is seen. MRI shows some evidence of calcium deposition in the areas mentioned, with mottled hyperintensity on T₁-weighted images and heterogeneous signal loss on T₂-weighted images, sometimes in

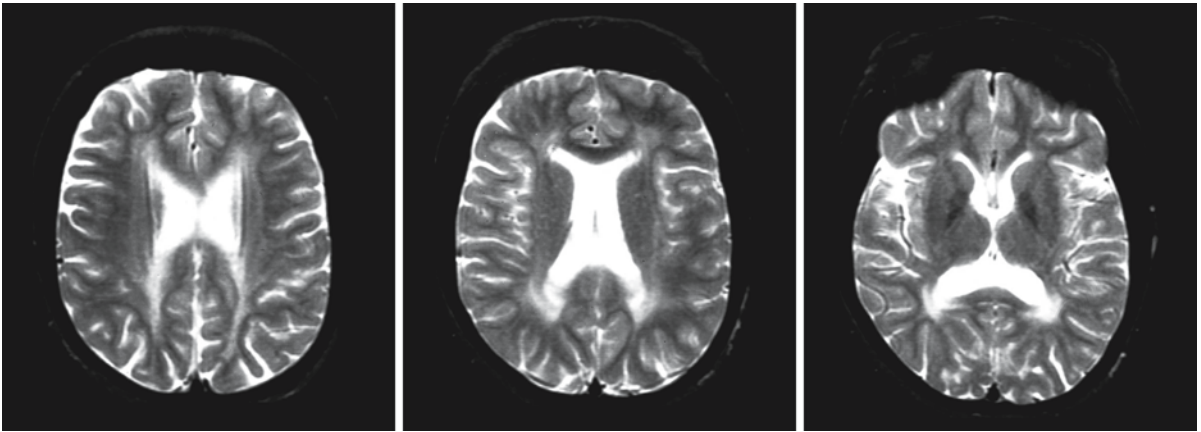


Fig. 36.4. A 17-year-old female patient with classical PKU. She has more prominent signal abnormalities in the periventricular white matter than the patient in Fig. 36.3. The corpus callo-

sum is spared. Courtesy of Dr. S. Blaser, Department of Diagnostic Imaging, and Dr. A. Feigenbaum, Department of Clinical Genetics, Hospital for Sick Children, Toronto, Canada

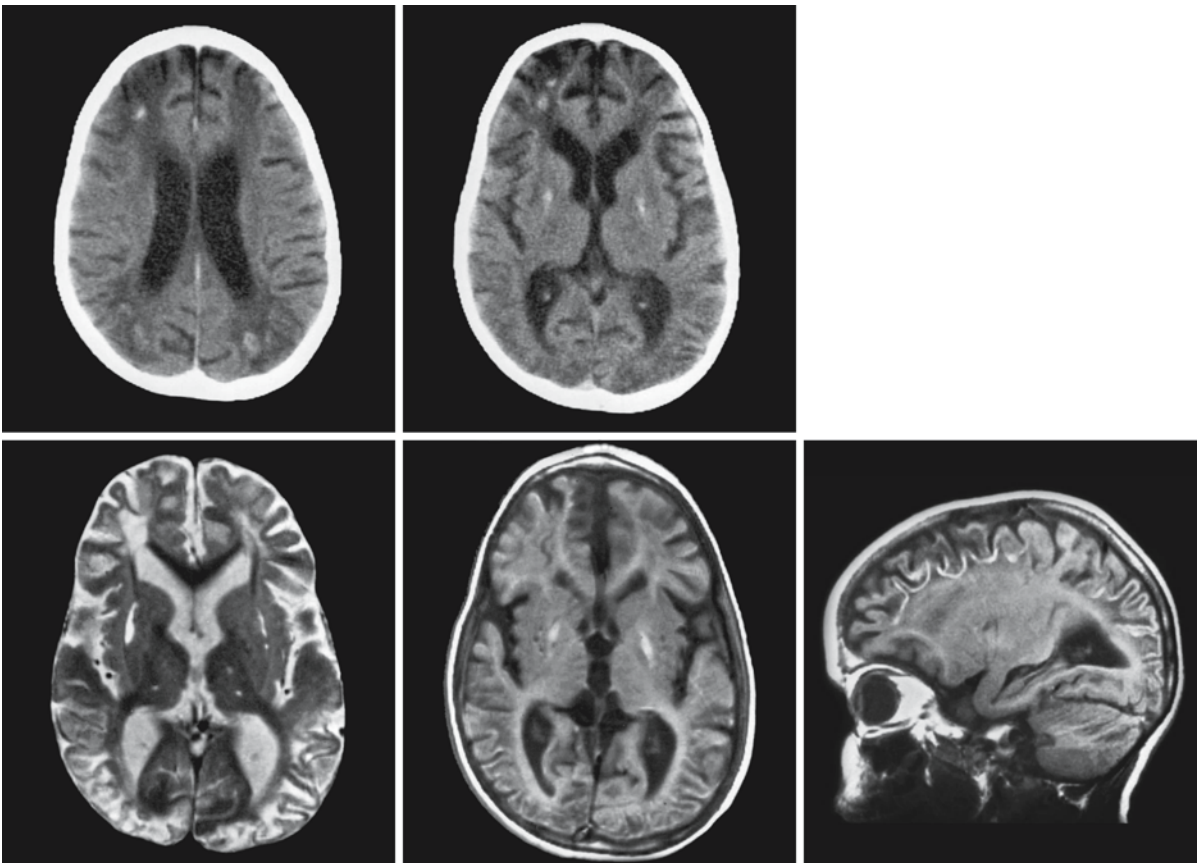


Fig. 36.5. A girl with PKU due to dihydropteridine reductase deficiency, age 2 years and 8 months. CT scan (*upper row*) shows some cerebral atrophy with dilated lateral ventricles. There are calcifications in the striatum and in the frontal and occipital gray and white matter junction. The white matter is hypodense in these areas. The transverse T₁- and T₂-weighted MR images at the age of 4.5 years (*second row*) show high signal intensity in the calcified spots in the basal ganglia on

T₁-weighted images. The subcortical white matter has too low a signal intensity on the T₁-weighted images, too high a signal intensity on the T₂-weighted images. The parasagittal T₁-weighted MR image shows a gyriform band of high signal intensity in the cortex and corticomedullary junction, probably due to calcification. From Gudinchet et al. (1992), with permission

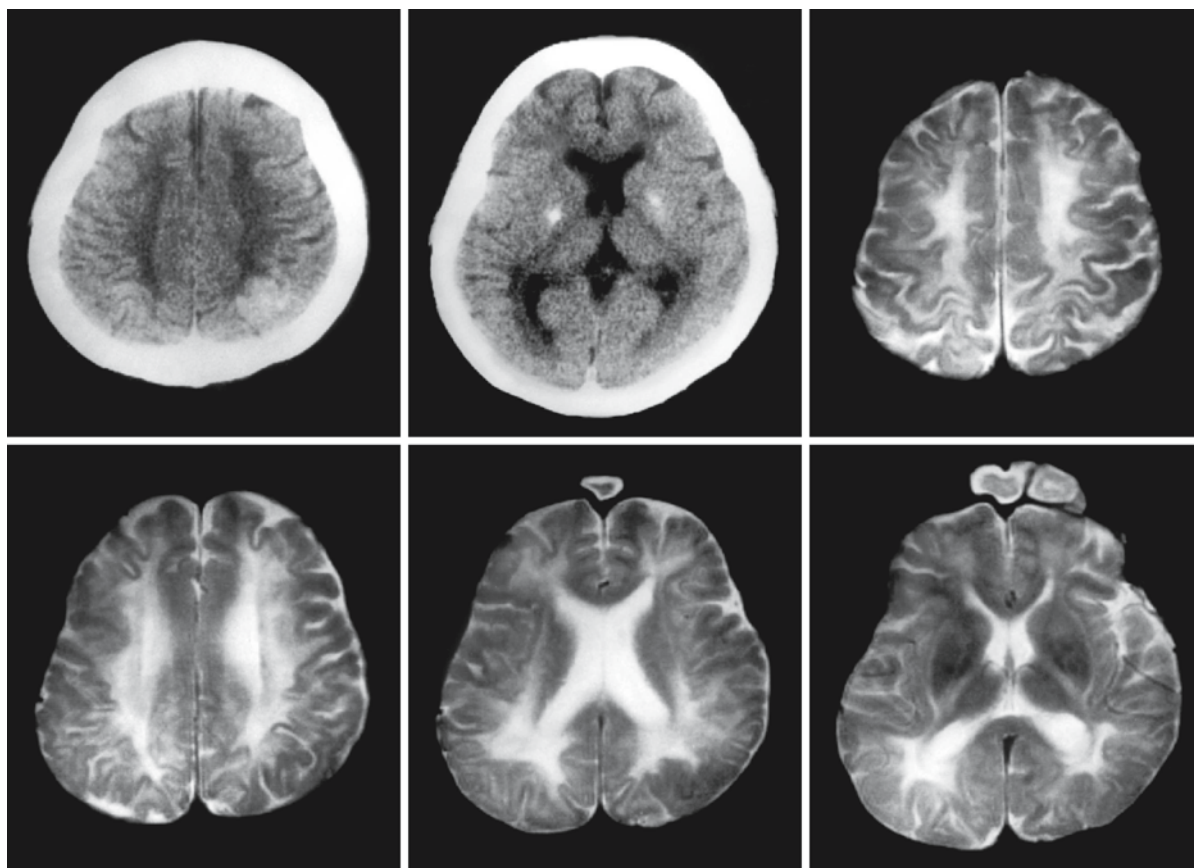


Fig. 36.6. A 20-year-old male with dihydropteridine reductase deficiency. CT (*upper row, left and middle*) shows some calcification of the basal ganglia and the parietal corticosubcortical junction. The MRI shows diffuse abnormality of the white

matter in the centrum semiovale, reaching the U fibers and involving the peritrigonal white matter and external and internal capsule. The frontal white matter is less severely affected. From Sugita et al. (1990), with permission

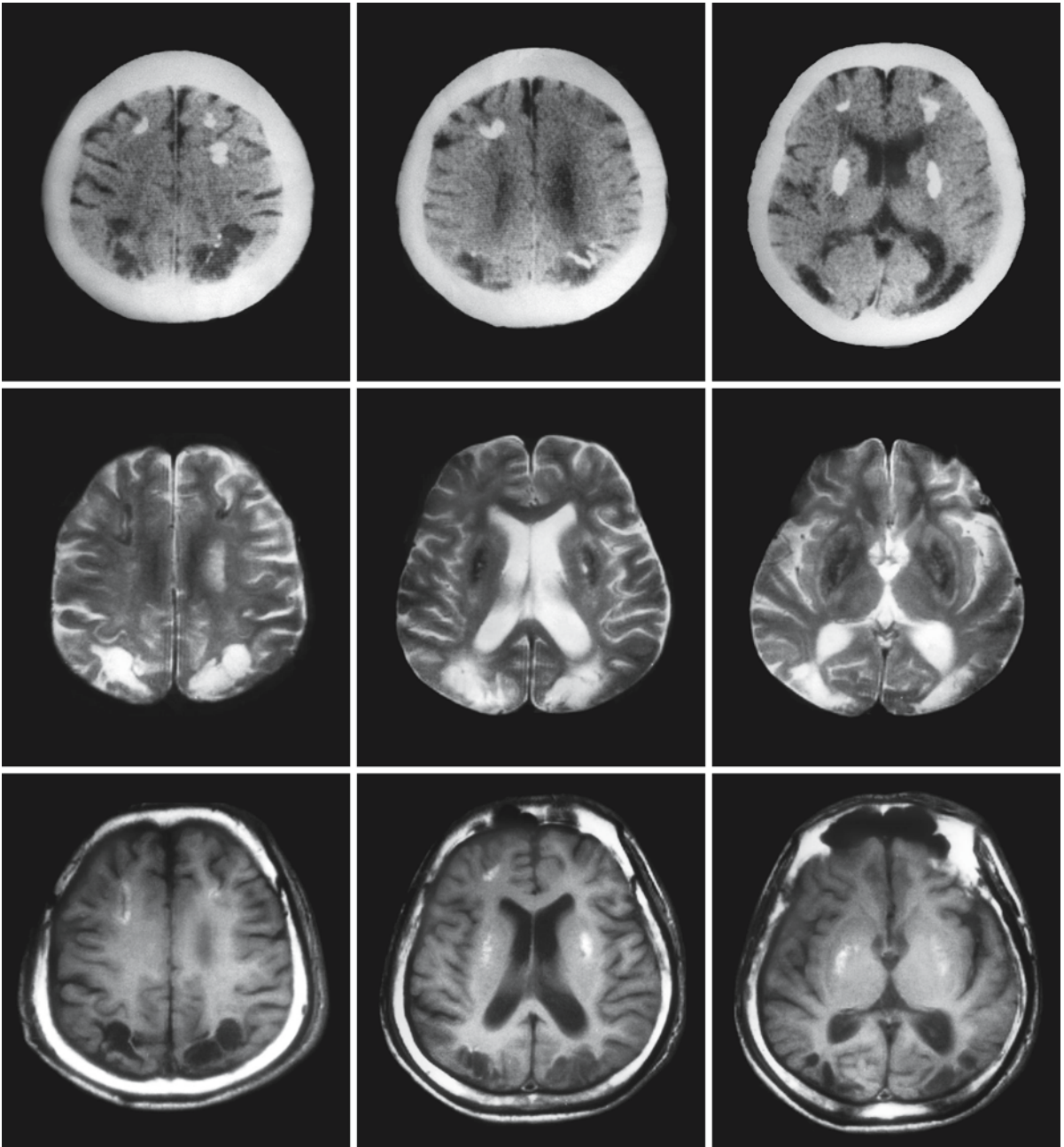


Fig. 36.7. A 26-year-old male with dihydropteridine reductase deficiency. CT (*first row*) shows extensive calcifications of the basal ganglia and in the frontal corticomedullary junction. The transverse T₂-weighted MR images (*second row*) show enlarged ventricles. The basal nuclei have a low signal intensity with a central area of high signal intensity, similar to the eye-

of-the-tiger phenomenon of Hallervorden-Spatz disease. The transverse T₁- (*third row*) and T₂-weighted images, like the CT scan, show cyst formation in the occipital lobes. Note the high signal intensity on the T₁-weighted image in a calcified areas. From Sugita et al. (1990), with permission

Glutaric Aciduria Type 1

37.1 Clinical Features and Laboratory Investigations

Glutaric aciduria type 1 is an autosomal recessive metabolic disorder with highly variable clinical symptomatology. The disease usually presents with an acute encephalitis-like encephalopathy in infancy or childhood after a normal initial development. In most cases the first episode occurs between the ages of 6 and 18 months. Frequently, the only abnormality preceding the first episode is a developing macrocephaly. The macrocephaly may already be present at birth. The encephalopathic episode is usually triggered by an infectious illness or vaccination. The episode is characterized by hypotonia, loss of head control, spasticity, dystonia, rigidity, orofacial dyskinesia, grimacing, seizures, opisthotonic posturing, lowering of consciousness, and coma. Recovery is slow and often incomplete. There is usually a preservation of intellect. After the first crisis, neurological signs may remain static for a long time, suggesting a diagnosis of postencephalitic damage. More often, the subsequent course of disease is slowly progressive with episodes of acute deterioration, often associated with an infection. Patients frequently have a tendency to sweat profusely. There may be episodes of unexplained fever. Ocular abnormalities are frequent, including intraretinal hemorrhages, cataract, gaze palsy, strabismus, ametropia, and pigmentary retinopathy. If untreated, death usually occurs in the first decade, in the course of an episode of acute deterioration during an infection or in the course of a Reye syndrome-like episode. In other patients the course of disease is more chronically progressive with retarded development during the first year of life. Subsequently, hypotonia, dystonia, athetoid involuntary movements, and spasticity develop gradually over the years with loss of motor skills. The progressive dystonia is disabling and leads to a loss of walking and writing abilities. Also, articulate speech may become progressively difficult and may be lost altogether. Mental capabilities are intact or relatively preserved. Some patients are stable for several years, suggesting a diagnosis of athetoid cerebral palsy. Occasional patients present as adults with signs of a progressive encephalopathy. Some patients remain asymptomatic, and asymptomatic adults have occasionally been found during screening of families known to be affected. Thus, there is a large phenotypic variation

within families. With early treatment the prognosis of the patients improves and most or all of the neurological damage can be prevented. Acute deterioration after instigation of treatment is rare.

In glutaric aciduria type 1, excessive urinary excretion of glutaric acid, glutaconic acid, and 3-hydroxyglutaric acid suggests the diagnosis. The defect in metabolism of glutaryl-CoA leads to accumulation of this substance in body fluids, partly esterified with carnitine and excreted as glutarylcarnitine. Carnitine deficiency can be the result of this excessive urinary carnitine excretion. Lysine, hydroxylysine, and tryptophan, precursors of glutaryl-CoA, are not elevated in urine or body fluids. During episodes of clinical decompensation, metabolic acidosis, ketosis, hyperammonemia, and elevation of serum transaminases may be found. Occasionally hypoglycemia occurs in an acute episode. The diagnosis of glutaric aciduria type 1 may be difficult to establish. Enhanced urinary excretion of the metabolites mentioned may be intermittent and only detectable during episodes of metabolic derangement. In some cases the urine concentration of glutaric acid, glutaconic acid, and 3-hydroxyglutaric acid may even remain normal during episodes of clinical decompensation. In most (but not all) of these patients a decrease in plasma carnitine levels and an increase in urinary glutarylcarnitine levels can be found, indicative of glutaric aciduria. In some patients only elevated levels of glutaric acid can be found in CSF. A definite diagnosis can be established by assay of glutaryl-CoA dehydrogenase in leukocytes and fibroblasts and by means of DNA analysis. Asymptomatic siblings of patients with glutaric aciduria type 1 should always be investigated and, if diagnosed with the same disease, treated. Prenatal diagnosis can be performed by enzyme assessment in chorionic villi or cultured amniotic cells and by DNA-based tests.

37.2 Pathology

External examination of the brain may reveal cerebral atrophy with an open operculum. Ventricular enlargement is often noted. Most commonly noted parenchymal abnormalities involve the putamen and head of the caudate nucleus, less often the globus pallidus. Changes tend to be more marked in patients who die after several years than in infants. The lesions

are characterized by loss of neurons associated with gliosis. The cortex is well preserved.

Marked spongiform changes are seen in the hemispheric white matter in some patients. It is the periventricular white matter that is particularly involved, whereas the subcortical U fibers are spared. In addition, optic nerves, corpus callosum, internal capsule, deep cerebellar white matter, and long tracts of the brain stem may be involved. Vacuolation is caused by myelin splitting and intramyelinic vacuole formation. In electron microscopy splitting is seen to occur along the intraperiod line. Mild spongiform changes due to myelin splitting may be seen in gray matter structures rich in myelin, such as the thalamus, globus pallidus, and brain stem reticular formation.

37.3 Pathogenetic Considerations

Glutaric aciduria type 1 is caused by deficiency of glutaryl-CoA dehydrogenase. Glutaryl-CoA, a catabolite of lysine, hydroxylysine, and tryptophan is dehydrogenated to glutaconyl-CoA and subsequently decarboxylated to crotonyl-CoA, both steps being catalyzed by a single enzyme, glutaryl-CoA dehydrogenase. The enzyme is active in mitochondria as a homotetramer. In glutaric aciduria type 1 this mitochondrial enzyme is lacking. A single case of peroxisomal glutaryl-CoA dehydrogenase deficiency has been described (Bennett et al. 1991). Mitochondrial glutaryl-CoA dehydrogenase is a flavin adenine dinucleotide (FAD)-requiring enzyme. Deficiency of this enzyme activity has been reported in glutaric aciduria type 1 and in multiple acyl-CoA dehydrogenase deficiency, also called glutaric aciduria type 2.

The gene encoding glutaryl-CoA dehydrogenase, *GCDH*, is located on chromosome 19p13.2. Many different mutations have been identified in glutaric aciduria type 1. There is no apparent correlation between genotype and phenotype. There is also a marked clinical variability among individuals who are homozygous for the same mutation. This suggests the existence of unrelated, genetically polymorphic protective mechanisms. Clinical variability may also be related to the flexibility of associated enzyme systems such as those involved in γ -aminobutyric acid (GABA) or glutamate metabolism. Additionally, environmental factors may be important in determining the severity of the phenotype.

The cause of striatal dysfunction and necrosis in glutaric aciduria has only been partially elucidated. A number of factors may contribute to the damage. Excitotoxicity of accumulating substances may be an important factor and involve activation of *N*-methyl-D-aspartate (NMDA) receptors, of which glutamate is the normal activator. Both glutaric acid and 3-hydroxyglutaric acid exhibit structural similarities to glutamate.

Both glutaric acid and 3-hydroxyglutaric acid are toxic to neurons in culture, and this neurotoxic effect can be prevented by preincubation with NMDA receptor blockers. In addition, glutaric acid, glutaconic acid, and 3-hydroxyglutaric acid are competitive inhibitors of glutamic acid decarboxylase, the enzyme involved in biosynthesis of GABA, an inhibitory neurotransmitter. Biochemical analysis of the brains of a few patients demonstrated elevated levels of glutaric acid in the frontal cortex and basal ganglia, very low glutamic acid decarboxylase activity, and very low concentrations of GABA in the caudate nucleus and putamen. Low CSF GABA levels have also been found. However, the low GABA is not necessarily related to inhibition of glutamic acid decarboxylase, but may also be the result of destruction or dysfunction of GABA-ergic neurons. Quinolinic acid, an intermediate in the metabolism of tryptophan and lysine, and a potent neurotoxin, may contribute to the neuronal damage in glutaric aciduria.

Even less is known about the pathogenesis of myelin splitting and vacuolation. Myelin splitting is probably caused by toxic effects of accumulating substances.

The cause of the macrocephaly has not been adequately explained. Contributing factors may be the presence of extracerebral fluid collections, hydrocephalus, and myelin splitting with intramyelinic accumulation of fluid. The pathogenesis of the extracerebral fluid collections is unexplained.

37.4 Therapy

During a metabolic crisis, it is essential to correct the metabolic decompensation as soon as possible to prevent and limit the irreversible brain damage. A high-calorie glucose infusion (if necessary together with insulin), intravenous lipids, intravascular volume expansion, and correction of acidemia and hypoglycemia are essential. Chronic treatment consists of a diet low in protein, in particular low in tryptophan and lysine, supplemented with carnitine. Carnitine is used to stimulate the formation and excretion of glutarylcarnitine. Riboflavin is a coenzyme for glutaryl-CoA dehydrogenase, but cofactor responsiveness is rare. A trial of riboflavin can be recommended, but the drug should be stopped if no beneficial biochemical effect is found. After the onset of neurological problems this treatment protocol leads to no or only modest improvement, but in most cases further deterioration is halted and subsequent episodes of acute encephalopathy are prevented. Early treatment has been shown to be effective in preventing the occurrence of most or all problems, and improvement or resolution of neuroimaging abnormalities can be observed. Some treated patients, however, still show

some deterioration, and unfortunately even a serious encephalopathic episode may occur.

There are some additional therapeutic options. In view of the decreased GABA levels, treatment with a GABA analogue, baclofen, is logical and has produced some symptomatic improvement with a decrease in dystonia. Gamma-vinyl GABA (vigabatrin) causes an irreversible inhibition of GABA transaminase, the first step of GABA catabolism, and in this way leads to increased GABA levels. Decreased dystonia has been noted with vigabatrin therapy. Valproate has been recommended because of its inhibitory action on GABA transaminase. However, valproate is partly excreted as valproylcarnitine and may cause further stress to the already compromised carnitine system.

Whether subdural fluid collections should be evacuated, and whether shunt implantation should be performed in cases of ventricular enlargement and progressive macrocephaly, is highly questionable. Resolution of these abnormalities, spontaneously or with metabolic treatment, has been documented. If metabolic treatment is not started, deterioration may continue despite neurosurgical intervention. A prompt diagnosis of glutaric aciduria type 1 is extremely important in this context. The stress of the subdural hygroma or hematoma itself and the stress of the surgery, combined with a catabolic state in a very ill child, may provoke serious neurological injury.

37.5 Magnetic Resonance Imaging

CT scan of the brain discloses enlarged CSF spaces in most untreated patients with glutaric aciduria type 1, even if asymptomatic. The most often noted are fluid collections over the convexities in the frontoparietal and frontotemporal areas. In some cases the frontoparietal fluid collections have the appearance of subdural hygromas, usually bilateral, occasionally unilateral. In most cases the fluid collections consist of enlarged subarachnoid spaces, frequently ascribed

to cerebral atrophy, sometimes to communicating hydrocephalus. Considering the presence of absolute or relative macrocephaly, mild enlargement of the ventricular system, and absence of significant cortical damage at autopsy, communicating hydrocephalus may be the most probable explanation. Both in the case of subdural hygroma and in the case of enlarged subarachnoid spaces, these spaces are crossed by bridging veins. As a consequence, patients with glutaric aciduria type 1 are prone to developing subdural hemorrhages after minor head trauma. Especially in the presence of retinal hemorrhages, a misdiagnosis of nonaccidental head injury and child abuse is readily made. In many patients with glutaric aciduria type 1, the sylvian fissure is wide open, forming a large CSF space anterior to the temporal lobes. Some authors ascribe these CSF collections to the presence of bitemporal arachnoid cysts, but this is rarely in conformity with the configuration of the CSF collections. Usually they are ascribed to either frontal and temporal atrophy or failure of opercularization. The aspect of the incompletely formed frontal and temporal operculum is most consistent with a failure of opercularization. However, in a few patients a normal sylvian fissure has been noted soon after birth,

Fig. 37.2. A 3-year-old girl with glutaric aciduria type 1, who presented with an acute encephalopathic episode at the age of 1 year. Note the mildly enlarged subarachnoid spaces, the open sylvian fissure, enlarged spaces anterior to the temporal lobe, and mildly dilated lateral ventricles. There are extensive mild signal changes in the periventricular white matter, sparing the corpus callosum and U fibers. Bilateral lesions are present in the putamen, caudate nucleus, globus pallidus, dentate nucleus, and pontine central tegmental tracts. The putamen and caudate nucleus are atrophic. Courtesy of Dr. Z. Patay, Department of Radiology, and Dr. P.T. Ozand, Department of Pediatrics, King Faisal Specialist Hospital and Research Center, Riyadh, Saudi Arabia

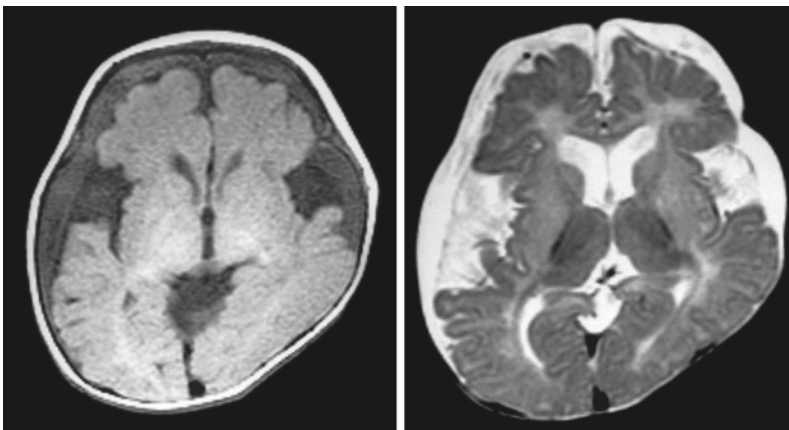


Fig. 37.1. Boy, 10 months old, with untreated glutaric aciduria type 1. The images show extensive bilateral subdural hygromas and frontotemporal hypoplasia with an open sylvian fissure. Note that the arachnoid and subdural spaces can be easily distinguished. Myelination is seriously delayed. The basal ganglia have a slightly abnormal signal intensity. From Osaka et al. (1993), with permission

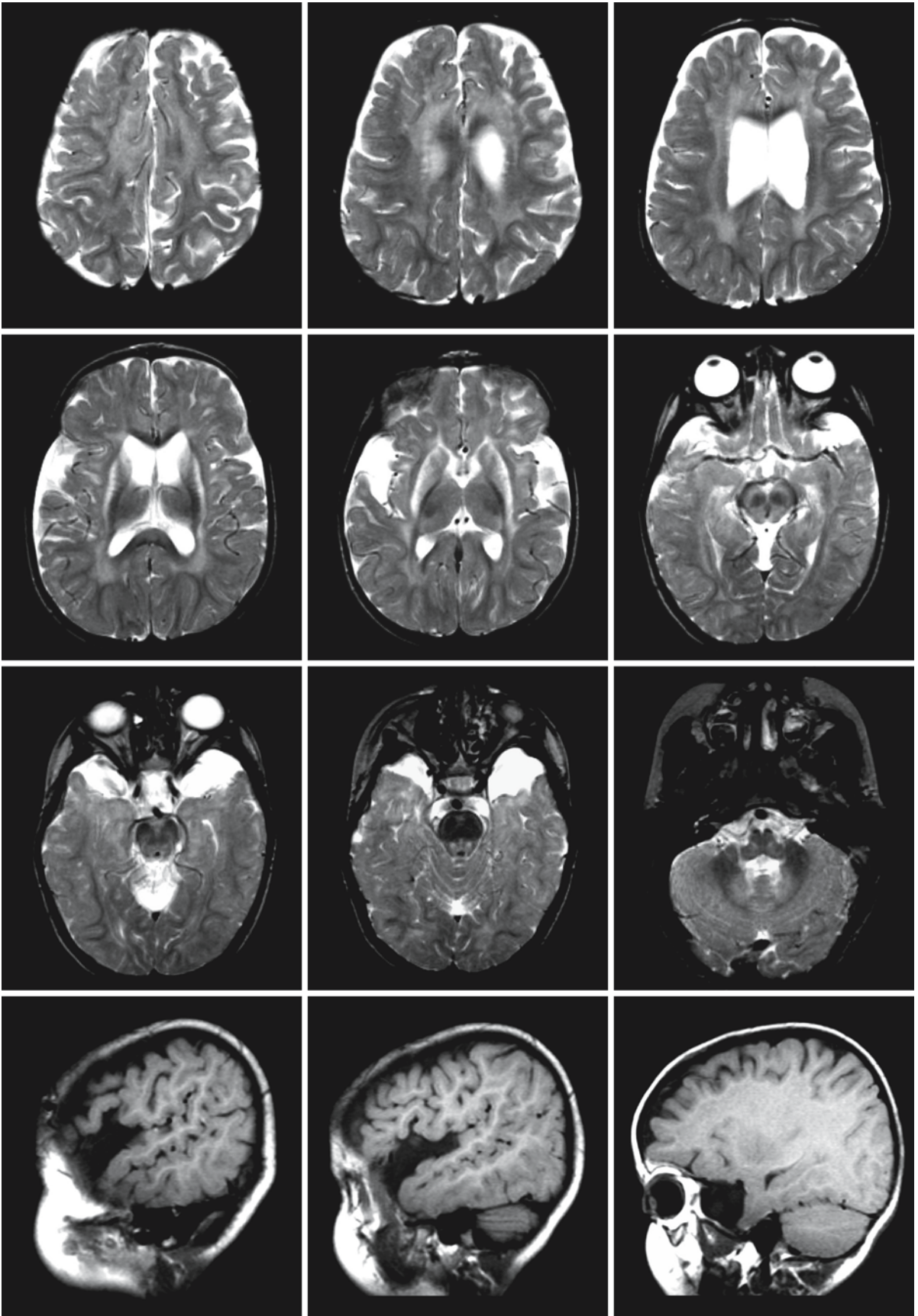


Fig. 37.2.

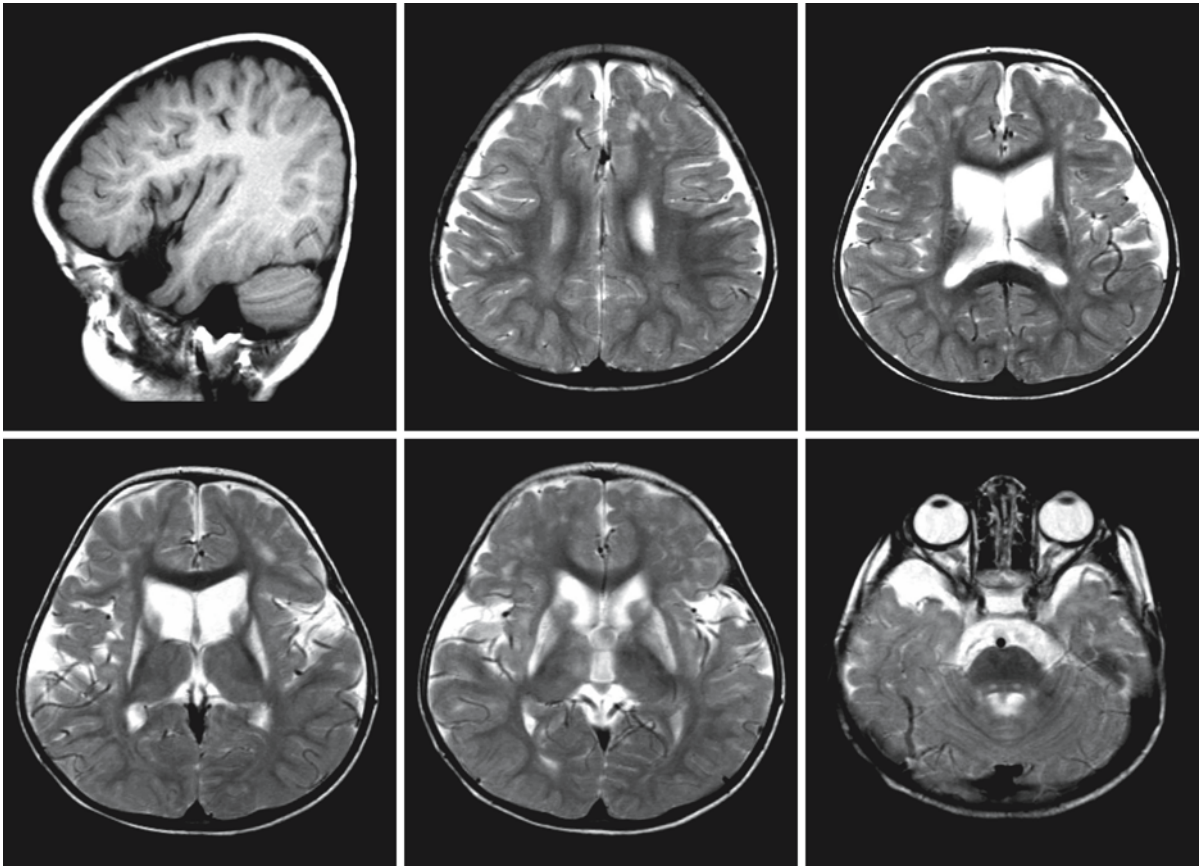


Fig. 37.3. A 3-year-old girl with glutaric aciduria type 1, who was diagnosed at the age of 15 months and has been non-compliant with treatment since. There is an open sylvian fissure and free space anterior to the temporal lobe. There are small spots of abnormal signal within the deep cerebral white matter. The putamen, globus pallidus, and caudate nucleus

have an abnormal signal and are atrophic. There are signal changes in the central tegmental tracts of the pons. Courtesy of Dr. Z. Patay, Department of Radiology, and Dr. P.T. Ozand, Department of Pediatrics, King Faisal Specialist Hospital and Research Center, Riyadh, Saudi Arabia

whereas wide open sylvian fissures are seen several months later, forming an argument for atrophy. Decrease of enlarged CSF spaces has been noted to occur spontaneously and with treatment. In some patients hemispheric white matter hypodensity has been found on CT.

MRI may depict transient subependymal cysts in young and often still presymptomatic infants. MRI also depicts the fluid collections (Figs. 37.1–37.3). In most cases, the aspect of the wide open sylvian fissures is not consistent with arachnoid cysts but more probably with hypoplasia of the frontal and temporal operculum (Figs. 37.1–37.3). The enlarged peripheral fluid spaces are the result of enlarged subarachnoid spaces, subdural spaces, or a combination of the two (Figs. 37.1–37.3). Subdural hematomas may also be seen. In some patients the brain has a highly atrophic appearance with greatly enlarged extracerebral fluid spaces (Fig. 37.1).

Bilateral lesions are often seen in central gray matter structures, variably including the putamen, globus pallidus, head of the caudate nucleus, dentate nucleus, and substantia nigra (Figs. 37.1–37.4). The lesions are swollen in the acute stage and subsequently become atrophic. Myelination may be delayed (Fig. 37.1). In some of the patients more prominent white matter abnormalities are seen, most often in combination with striatal lesions or enlarged fluid collections as described above (Figs. 37.2 and 37.4). The white matter abnormalities are extensive, symmetrical, and most marked in the frontal and occipital periventricular white matter and in the centrum semiovale. The arcuate fibers and corpus callosum are usually spared (Figs. 37.2 and 37.4). In other patients, more limited white matter abnormalities are seen (Fig. 37.3).

On the whole, the imaging findings are highly variable. In some patients no abnormalities are noted at all, whereas in others only or mainly enlarged CSF

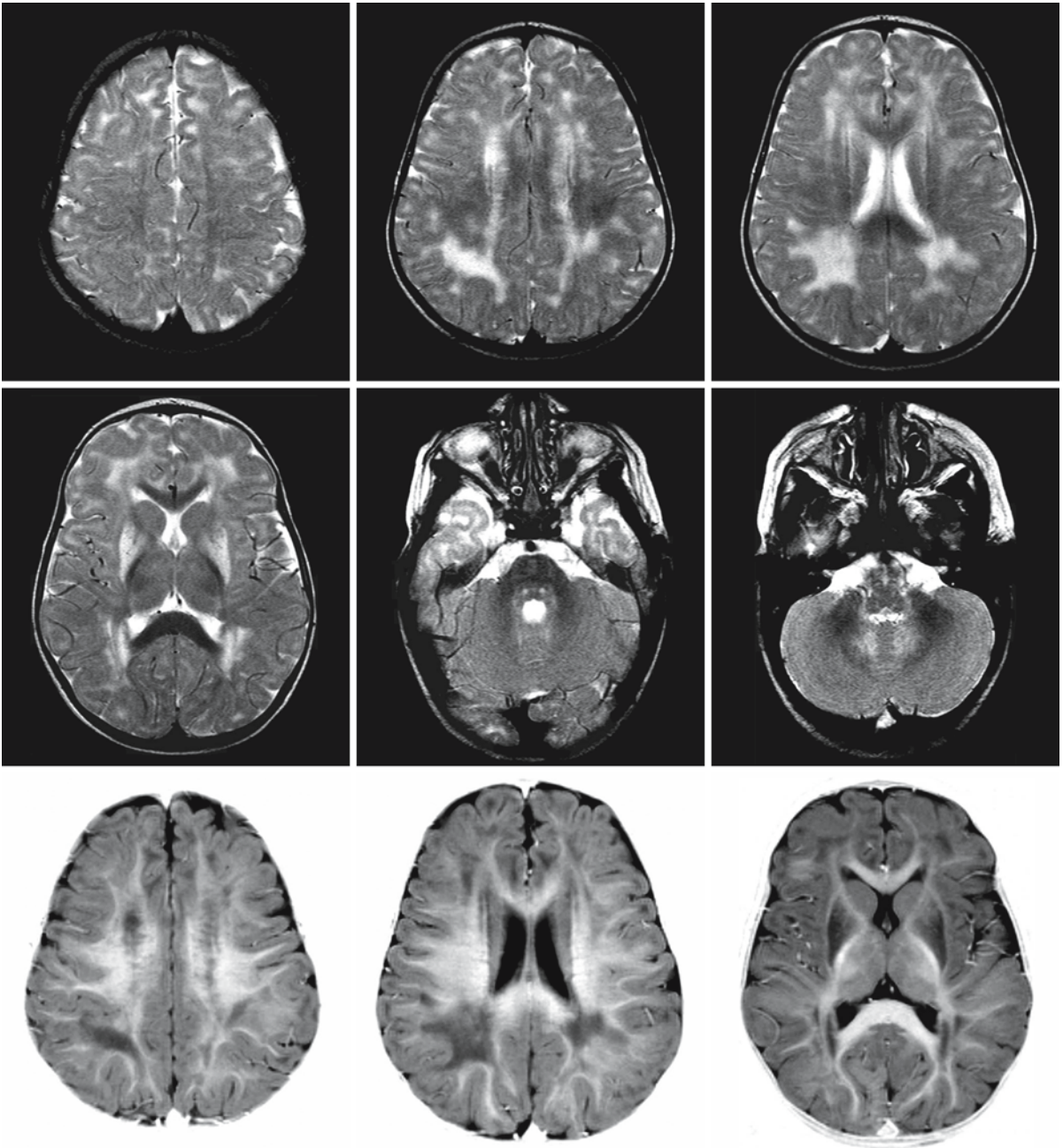


Fig. 37.4. A 14-month-old boy with glutaric aciduria type 1. He was diagnosed at 8 months and responded well to treatment. The cerebral white matter is abnormal, partly because of delayed myelination, partly because of white matter damage. It is easier to distinguish the two using T₁-weighted images

(third row). There are bilateral lesions in the putamen, globus pallidus, dentate nucleus, and pontine central tegmental tracts. Courtesy of Dr. Z. Patay, Department of Radiology, and Dr. P.T. Ozand, Department of Pediatrics, King Faisal Specialist Hospital and Research Center, Riyadh, Saudi Arabia

spaces are seen; other cases show a predominance of striatal lesions, while others have a combination of striatal and white matter abnormalities. Most cerebral abnormalities can be prevented by early treat-

ment. If already present, they tend to improve with treatment, depending partly on the reversibility of the abnormalities found.

Propionic Acidemia

38.1 Clinical Features and Laboratory Investigations

Propionic acidemia, formerly also called ketotic hyperglycinemia, is a disorder of organic acid metabolism with autosomal recessive inheritance. Two forms of the disease can be distinguished: the severe neonatal onset form and the late onset form.

Many patients with propionic acidemia present in the neonatal period with a progressive encephalopathy. They are normal at birth, but after a few hours or days deterioration sets in with lethargy, poor feeding, vomiting, tachypnea, and unexplained coma. Abnormalities in tone and movement occur. Limb hypertonia and opisthotonic posturing or axial hypotonia are often present. Abnormal pedaling movements, myoclonic jerks, tremors, and seizures may be present. Intracranial hemorrhage may occur as a result of serious thrombocytopenia. Hepatomegaly may be found on physical examination. In the more advanced stage, there are signs of respiratory distress and bradycardia. Mortality is high, and survivors frequently have severe lasting neurological impairment, in particular characterized by mental retardation and extrapyramidal movements. The disease course is most commonly characterized by repeated relapses.

In the late-onset form, the patients are older when they present with an acute encephalopathy. Most patients are older than 1 year at presentation, and some may even present in adulthood. The acute metabolic decompensations are precipitated by enhanced protein catabolism of exogenous origin (high protein intake) or endogenous origin (catabolic states, such as in fasting, infections, or other forms of stress), but sometimes no cause is found. The encephalopathic episodes are characterized by ataxia, lethargy, and coma, sometimes with focal neurological abnormalities like hemiplegia. Often the children already had chronic problems before the first episode, including chronic feeding problems, persistent vomiting, failure to thrive, hypotonia, osteoporosis, and developmental retardation. Some patients with the later-onset form of propionic acidemia are mildly retarded, but some patients have normal intelligence. Some patients have a lasting extrapyramidal movement disorder, usually chorea. These chronic problems can be present for a long time without acute metabolic decompensation and without correct diagnosis. The mortality rate of the encephalopathic episodes with delayed onset is

lower than that of the neonatal onset form, and the prognosis with respect to intelligence is better.

During episodes of acute metabolic decompensation, laboratory investigations reveal signs of dehydration, metabolic acidosis with ketonuria, elevated ammonia levels, and decreased carnitine levels. Lactate may be elevated and hypoglycemia may be present. Neutropenia and thrombopenia are consistent findings. Pancytopenia is rare. Specific laboratory findings suggesting the diagnosis are elevated plasma and urine levels of propionate, glycine, hydroxypropionate, propionylglycine, and methylcitrate. CSF glycine is not elevated, as is the case in nonketotic hyperglycinemia. The diagnosis is confirmed by assessment of the enzyme propionyl-CoA carboxylase in leukocytes or fibroblasts. Prenatal diagnosis can be performed by enzyme assessment in cultured amniocytes and chorionic villi or by DNA techniques.

38.2 Pathology

Few data exist relating to histopathological findings in propionic acidemia. In the neonatal form, myelin splitting and myelin vacuolation have been reported, affecting the structures that contain myelin in a term neonate: posterior limb of the internal capsule, globus pallidus, thalamus, myelinated brain stem tracts, cerebellar white matter, and spinal cord. The progress of myelination is normal for a neonate. The cortical cytoarchitecture is normal.

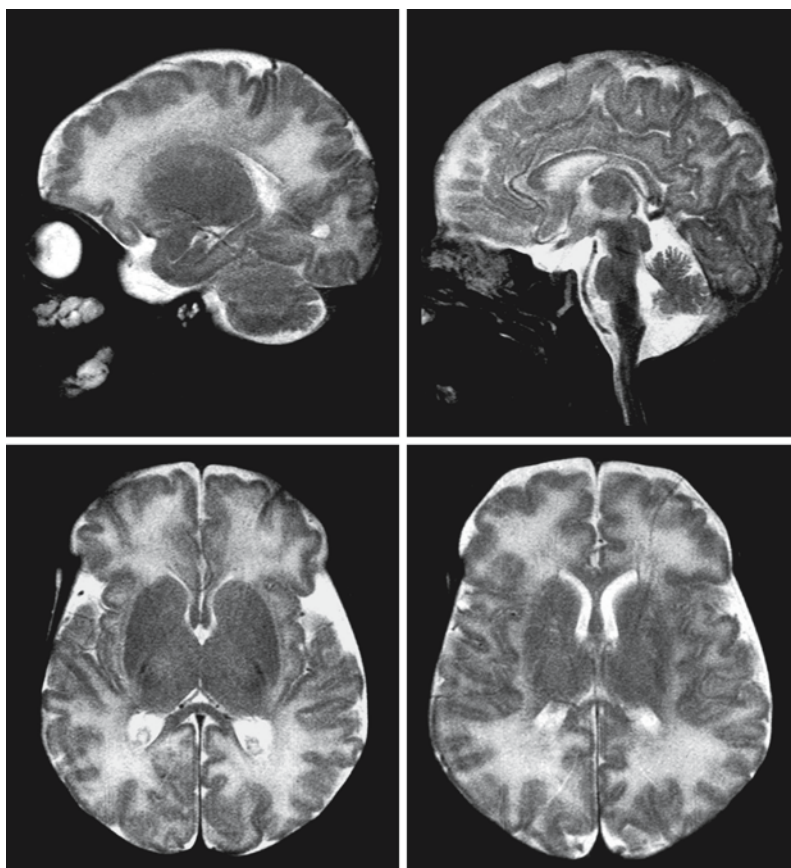
In older children, postmortem abnormalities mainly concern the basal ganglia. Atrophy, nerve cell loss, and gliosis are often found in the caudate nucleus and putamen, to a lesser extent in the globus pallidus and thalamus. Hypermyelination may occur in the affected basal ganglia. The white matter is often normal. However, atrophy and spongiosis of the cerebral white matter may also be found.

Examination of the liver may reveal fatty degeneration.

38.3 Pathogenetic Considerations

The basic defect in isolated propionic acidemia is a deficient activity of the mitochondrial enzyme propionyl-CoA carboxylase. This enzyme has biotin as its cofactor and consists of two nonidentical subunits (α

Fig. 38.1. A 2-month-old boy with early presentation of propionic academia. The cerebral white matter is slightly higher in signal intensity than normal for a neonate. Courtesy of Dr. Z. Patay, Department of Radiology, and Dr. P.T. Ozand, Department of Pediatrics, King Faisal Specialist Hospital and Research Center, Riyadh, Saudi Arabia



and β). Propionyl-CoA carboxylase deficiency can be caused by a defect in either the α -subunit or the β -subunit. The gene encoding the α -subunit is called *PCCA* and located on chromosome 13q32. The gene encoding the β -subunits is called *PCCB* and located on chromosome 3q13.3-q22. Multiple disease-causing mutations have been described in both genes.

Propionyl-CoA carboxylase converts propionyl-CoA into methylmalonyl-CoA, which is subsequently converted into succinyl-CoA, which enters the Krebs cycle. Isoleucine, valine, threonine, and methionine are precursors of propionic acid, explaining the observed protein and amino acid intolerance. Propionyl-CoA carboxylase is also involved in the degradation of fatty acids with odd-numbered chain lengths and cholesterol. It is presently not clear why some patients have a neonatal-onset devastating disease, whereas other patients have a later onset and milder disease course.

The myelinopathy with splitting and vacuole formation is seen in a number of inborn errors of metabolism, including Canavan disease, maple syrup urine disease, and nonketotic hyperglycinemia, and a number of intoxications, including hexachlorophene, cuprizone, and triethyltin intoxication. The myelinopathy is probably a toxic phenomenon.

38.4 Therapy

In episodes of acute metabolic decompensation, treatment consists of removal of toxic products by dialysis or exchange transfusions. At the same time further catabolism of proteins should be prevented and an anabolic situation should be achieved to prevent the production of more toxic products. This can be achieved by continuous parenteral nutrition with a protein-free product and continuous intravenous infusion of insulin. Insulin has the capacity to stimulate protein synthesis. Biotin can be added in an attempt to stimulate residual enzyme activity. Carnitine is administered to stimulate excretion of propionylcarnitine in urine.

Long-term treatment consists of dietary protein restriction while maintaining normal development and nutrition status and preventing catabolism. Chronic treatment with carnitine should be considered. Chronic use of metronidazole can be prescribed to reduce propionic acid production by bacteria in the gut. Despite adequate treatment, the outcome of patients with the severe variant of propionic academia is poor. Most of these patients have remaining morbidity and disability and recurrent metabolic decompensations may still occur. In these severe forms of propi-

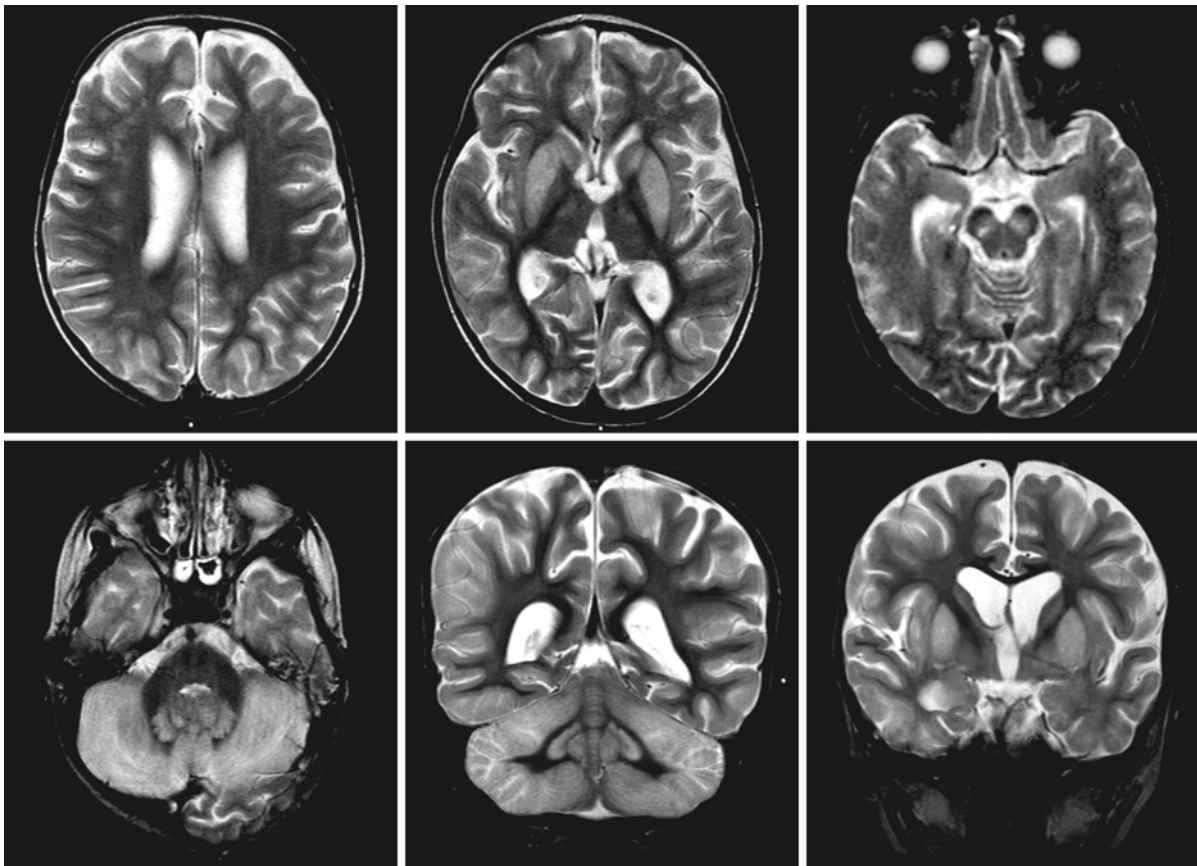


Fig. 38.2. This girl with propionic academia was diagnosed at the age of 3 weeks. She has had repeated crises and intensive care admissions since. The present MRI was obtained at the age of 2 years, when she was admitted in coma to the intensive care unit. The T_2 -weighted images show signal abnormality and swelling of the caudate nucleus, putamen, substantia ni-

gra, and dentate nucleus. The cerebral cortex has a slightly elevated signal intensity, while the cerebellar cortex and subcortical white matter have a more prominently elevated signal. Courtesy of Dr. Z. Patay, Department of Radiology, and Dr. P.T. Ozand, Department of Pediatrics, King Faisal Specialist Hospital and Research Center, Riyadh, Saudi Arabia

onic acidemia, liver transplantation can be considered. After the procedure, a diet with normal or only mildly restricted protein content can be resumed.

38.5 Magnetic Resonance Imaging

In patients with neonatal presentation of propionic academia and serious encephalopathy, an MRI picture similar to that of maple syrup urine disease, with signal abnormality and swelling of the myelin-containing structures (dorsal part of the pons, midbrain, cerebellum, posterior limb of the internal capsule, globus pallidus, thalamus, and central part of the corona radiata) would be expected. These have, however, not been reported. Diffuse slight cerebral white matter signal abnormality has been observed (Fig. 38.1).

In older patients with propionic academia and acute decompensation, MRI may reveal signal abnormalities and swelling of the basal ganglia, substantia nigra, and dentate nucleus (Fig. 38.2). The cerebral and cerebellar cortices and subcortical white matter may also display abnormal signal and mild swelling (Fig. 38.2 and 38.3). In the chronic phase, MRI findings include cerebral atrophy, variably delayed and disturbed myelination, and abnormalities in the caudate nuclei, globus pallidus, and putamen (Fig. 38.4). The basal ganglia may display signal changes and atrophy. However, none of these abnormalities is obligatory in patients with propionic academia. In one patient with hemiplegia during acute metabolic decompensation, MRI did not reveal a corresponding contralateral cerebral lesion, apart from slight local cortical atrophy.

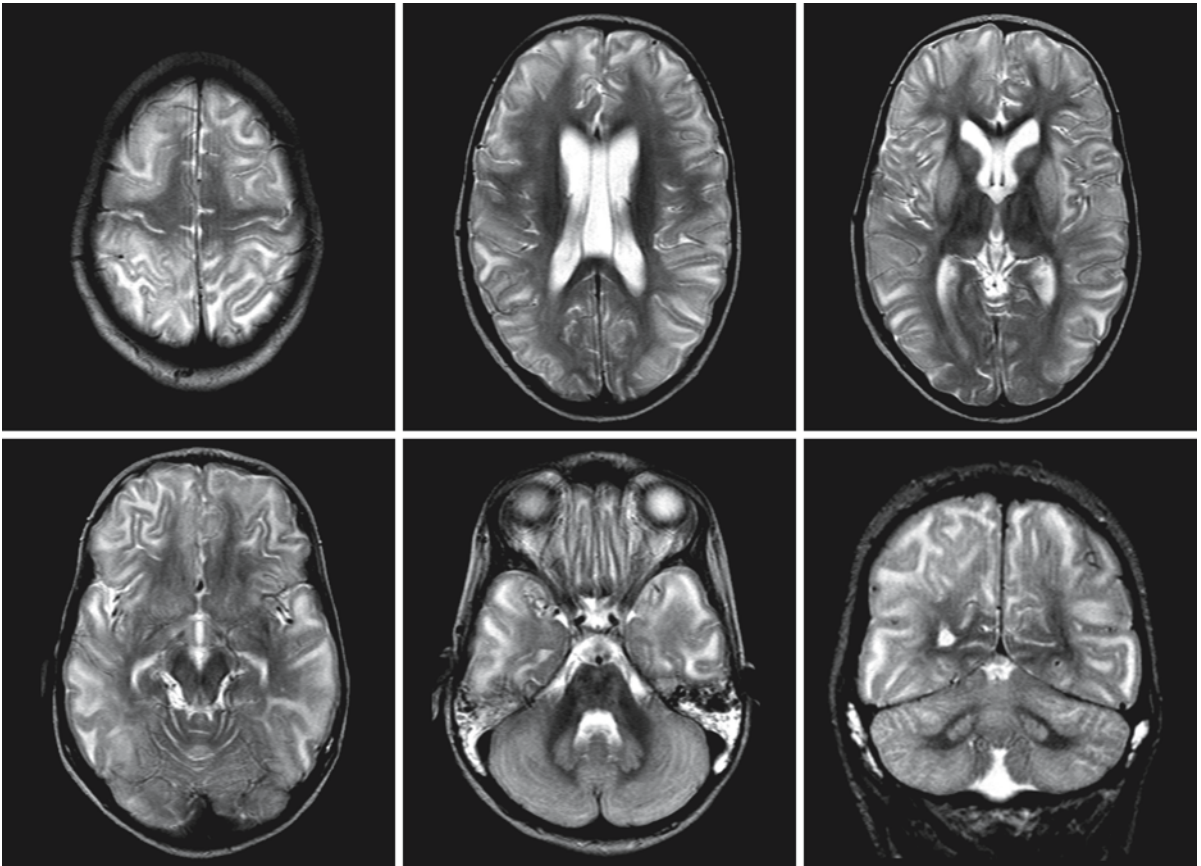


Fig. 38.3. A 6-year-old girl with propionic academia presented with an acute metabolic decompensation. Note the signal abnormalities in the cerebral and cerebellar cortex and the subcortical white matter on the T₂-weighted images. Signal

abnormalities are present in the caudate nucleus, putamen, and dentate nucleus. Courtesy of Dr. Z. Patay, Department of Radiology, King Faisal Specialist Hospital and Research Center, Riyadh, Saudi Arabia

With treatment, improvement may occur. It is striking that what looks like irreversible cerebral atrophy (Fig. 38.4) improves with treatment with an increase in volume of the cerebral mantle (Fig. 38.5).

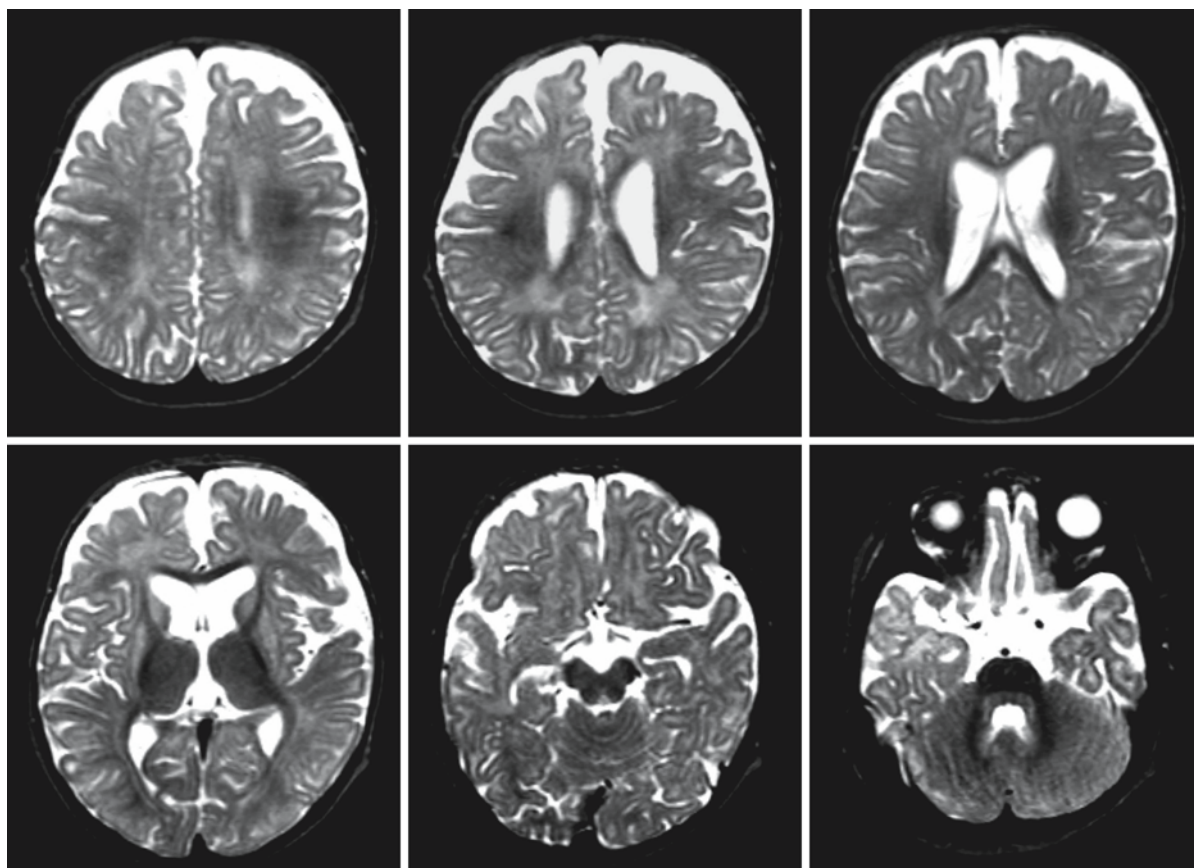


Fig. 38.4. A 10-month-old boy with untreated propionic acidemia, who had just been diagnosed at the time. The T₂-weighted images show delayed and irregular myelination. There is evidence of prominent cerebral atrophy with dilation

of the lateral ventricles and subarachnoid spaces. The caudate nucleus, putamen, and globus pallidus have an abnormal signal and are atrophic. The dentate nucleus also seems to have a slightly abnormal signal

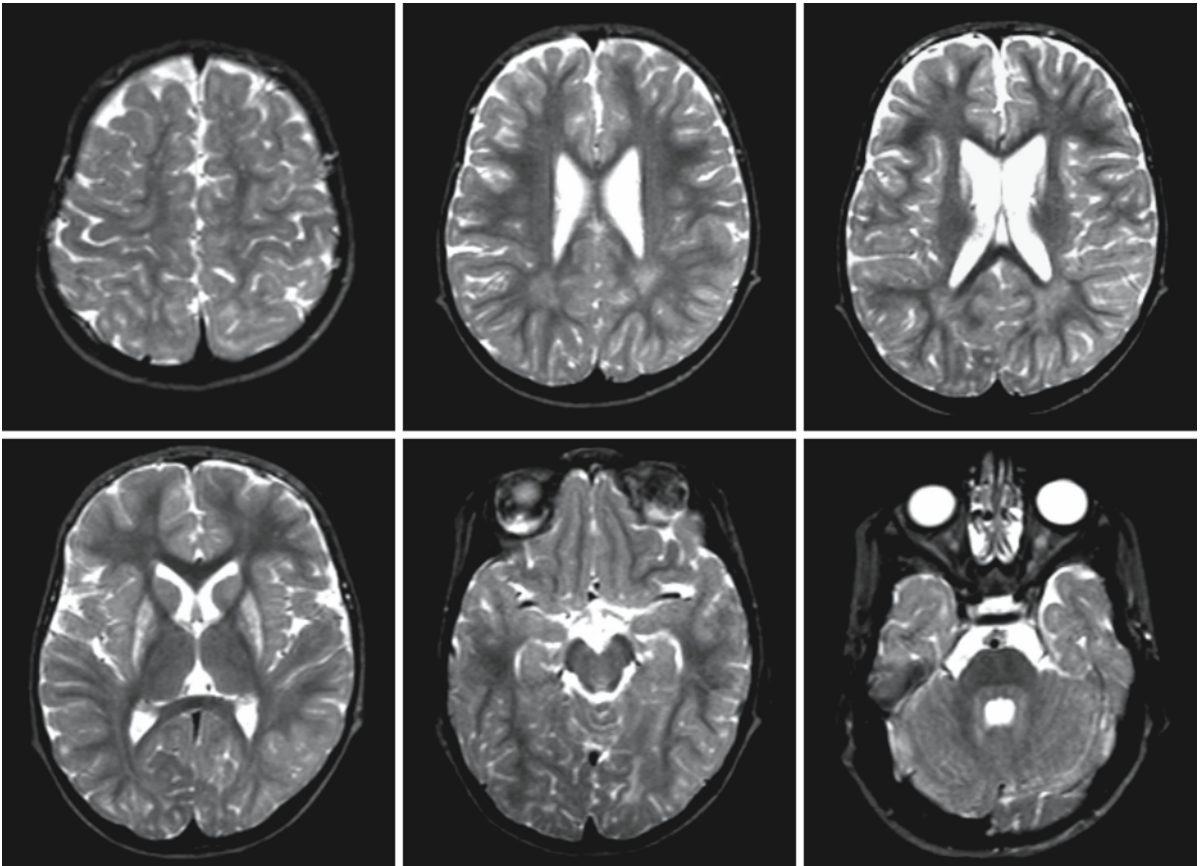


Fig. 38.5. Follow-up of the boy shown in Fig. 38.3. Dietary treatment and medication were started soon after the age of 10 months and this MRI was obtained at 3 years. Myelination is now much more advanced, but still incomplete in the periventricular occipital area, the temporal lobes, and the subcortical

area. There is a marked increase in cerebral volume as compared to the previous MRI. The basal ganglia lesions are still visible. The dentate nucleus also still has a slightly abnormal signal

Nonketotic Hyperglycinemia

39.1 Clinical Features and Laboratory Investigations

Nonketotic hyperglycinemia (NKH) is an autosomal recessive disorder of which different types are distinguished: neonatal, infantile, mild-episodic, late-onset, and transient.

Most NKH patients have the neonatal variant. They are normal at birth. Within a few days there are progressive neurological abnormalities, including lethargy, hypotonia, myoclonic jerks, seizures, coma, and apneic spells. Most infants require assisted ventilation. A few patients have been described with an increasing head circumference to above the 95th percentile and hydrocephalus on neuroimaging, requiring shunting. Many patients with neonatal NKH die within a few weeks. The patients who survive show signs of spasticity, opisthotonus, absence of any development, severe seizures, and microcephaly. Many children who survive the neonatal period die within the first year of life, but some survive into childhood or beyond in a severely disabled condition.

Patients with atypical NKH do not present in the neonatal period. In the infantile variant, seizures have a later onset, in the first year of life, and the patients tend to survive. Mental retardation is present but is not as severe as in the neonatal variant of NKH. Patients with mild-episodic NKH have mild mental retardation and episodes of agitation, ataxia, chorea, and vertical supranuclear ophthalmoplegia provoked by febrile illness. Patients with late-onset NKH have variable neurological features, including seizures, developmental delay, developmental regression, spasticity, ataxia, and optic atrophy. Patients with transient NKH are initially indistinguishable from patients with neonatal NKH. However, in the course of several weeks the patients recover, most often without neurological sequelae, although some patients have severe remaining neurological deficits.

In neonatal and transient NKH, a characteristic EEG pattern is seen during the first weeks of life with short bursts of high complex waves alternated with hypoactivity. In neonatal NKH, this burst-suppression pattern changes into hypsarrhythmia in the course of a few weeks.

Laboratory abnormalities include elevated levels of glycine in plasma and urine in the absence of ketoacidosis. The CSF level of glycine is elevated, as is the ratio of CSF to plasma glycine. Elevation of CSF

glycine is essential for the diagnosis. Patients with transient NKH initially have elevated CSF glycine and an elevated CSF:plasma glycine ratio, but in the course of 2–8 weeks plasma and CSF glycine levels return to normal.

NKH is caused by a defect in the glycine cleavage system. This system is specifically expressed in liver, kidney, brain, and lymphoblasts, but not in fibroblasts and leukocytes. Liver biopsy used to be necessary for enzymatic diagnosis of NKH. Since it was shown that the glycine cleavage system can be tested in lymphoblasts, enzymatic diagnosis of NKH has been performed using peripheral blood. However, the normal glycine cleavage activity in normal lymphoblasts is low, and the reliability of this method has been questioned. Patients with neonatal NKH have extremely low to undetectable glycine cleavage system activity, whereas in patients with atypical NKH some residual activity is found. Prenatal diagnosis using cultured amniotic cells is not possible, because the glycine cleavage system is not manifest in these cells. Prenatal diagnosis using chorionic villi tissue is feasible, although false negative and false positive prenatal diagnoses have been reported. DNA diagnosis is preferable when the mutation of the family is known.

39.2 Pathology

The external configuration of the brain in patients with neonatal NKH is usually normal with a normal gyral pattern. The quantity of myelin found by microscopic examination of the brain is normal, but all myelinated areas have a strikingly spongy appearance imparted by the presence of numerous vacuoles. In conformity with the neonatal state of myelination, the spinal cord, brain stem (in particular brain stem tegmentum), cerebellar white matter, posterior limb of the internal capsule, and optic nerves, tracts, and chiasm are prominently involved, whereas cerebral hemispheric white matter devoid of myelin is free of vacuoles. There is usually a correlation between myelin density and density of vacuoles. In electron microscopy, the vacuoles are found to be located within myelin sheaths and formed by splitting of myelin lamellae along the intraperiod lines. There are no sudanophilic deposits and there is a paucity of phagocytic and astroglial reactions. In children

beyond the neonatal period variable delay in myelination has been reported.

In some patients with neonatal NKH, pachygyria and agenesis of the corpus callosum have been reported at CT. These findings have, so far as we know, not been confirmed by more detailed MRI or autopsy findings.

Additional neuropathological changes can be found related to the serious condition of the child and occurrence of complications: neuronal incrustation with calcium in the cortex and thalamus, more acute anoxic neuronal changes in the cerebral cortex, and ischemic and/or hemorrhagic white matter changes in the periventricular area.

Neuropathological findings in patients with a neonatal presentation of NKH and survival beyond the first year of life include a variable diffuse decrease in white matter mass with some ventricular enlargement and a thin corpus callosum. The white matter of the CNS shows diffuse vacuolation, contrasting with the more restricted vacuolation in neonates, in whom unmyelinated white matter is not vacuolated. The amount of myelin may be normal or reduced without evidence of a progressive myelin disease or myelin loss. Cortical architecture is normal. The cerebellum may be of normal size or diffusely atrophic with a severe loss of Purkinje cells and granule cells.

39.3 Pathogenetic Considerations

The basic defect in NKH involves the glycine cleavage system. The glycine cleavage system is a mitochondrial multienzyme complex that is composed of four proteins: P protein (a pyridoxal phosphate-dependent glycine decarboxylase), T protein (a tetrahydrofolate requiring aminomethyltransferase), H protein (a lipoic acid containing hydrogen carrier protein), and L protein (dihydrolipoamide dehydrogenase). Three components, the P, T, and H proteins, are specific for the glycine cleavage system. L protein is a housekeeping enzyme, that is also used as the E₃ component of α -keto acid dehydrogenase complexes such as the pyruvate dehydrogenase complex. P, T, H, and L proteins are encoded by the genes *GLDC* on chromosome 9p23–24, *AMT* on chromosome 3q21.1–21.2, *GCSH* on chromosome 16q24, and *GCSL* on chromosome 7q31–32, respectively. The glycine cleavage system catalyzes the conversion of glycine and tetrahydrofolate to CO₂, NH₃, and methylenetetrahydrofolate.

The glycine cleavage activity is undetectable or extremely low in the neonatal type, whereas in the later-onset types there is still some residual activity. The majority of NKH patients have a defect in *GLDC* and the remainder have a defect in *AMT*. In transient neonatal NKH heterozygous *GLDC* and *GCSH* mutations have been found. However, the same mutation is

also found in family members who never have symptoms of NKH. Apparently carriership for NKH contributes to the development of transient NKH, but an additional unknown factor or factors contribute to the development of symptoms. Immaturity of the glycine cleavage system in the neonatal period may be a factor. Deficiency of the L protein presents with the symptoms of pyruvate dehydrogenase complex deficiency without hyperglycinemia.

In NKH, there is an elevated concentration of glycine in the brain and CSF. The glycine is held responsible for the neurological impairment. Glycine is a major inhibitory neurotransmitter in the brain stem and spinal cord, acting on strychnine-sensitive glycine receptors. The effects of high levels of glycine concentrations here are probably responsible for the hypotonia, lowered consciousness, and apnea present in neonates. Glycine is also active in the cerebral cortex and has excitatory properties here. It is a positive modulator of the *N*-methyl-D-aspartate (NMDA) receptor of glutamate, which plays an important role in glutamate-induced neurotoxicity. NMDA receptors are located throughout the brain. Glycine increases the frequency of NMDA receptor channel opening by accelerating recovery of the receptor following glutamate-induced desensitization. In this way, glycine potentiates the excitotoxic action of glutamate and may lead to intractable seizures. In animal experiments it has been shown that glycine administration enhances NMDA-induced seizures in mice whose classic glycine receptors located in spinal cord and brain stem had been blocked with strychnine. This experiment indicates that glycine is a harmful enhancer of the NMDA response. It has been shown that the developing brain has heightened susceptibility to NMDA-mediated injury, and high levels of glycine may be particularly devastating to the CNS of the neonate. This is in accordance with the clinical observation that most acute neurological problems are present in the neonatal period, and that stabilization is seen in patients who survive this period, albeit with a severe neurological handicap.

The relationships between high glycine levels and myelin vacuolation and between myelin vacuolation and clinical symptomatology are unclear. A myelin disorder does not, as a rule, lead to severe epilepsy, but rather to spasticity and other forms of loss of neurological function. The myelin disorder may explain at least part of the clinical impairment in the chronic stage of the disease. Myelin vacuolation is seen in inborn errors of metabolism (Canavan disease, maple syrup urine disease) and in intoxications (hexachlorophene, triethyltin, cuprizone). The pathogenetic mechanisms of myelin vacuolation are unclear in all these conditions, but are probably toxic in nature.

39.4 Therapy

Many therapeutic approaches have been used in the attempt to lower glycine concentrations in patients with the neonatal-onset form of NKH. Dietary restriction of glycine and serine or of all protein, administration of drugs to stimulate excretion of glycine in urine or bile, peritoneal dialysis, hemodialysis, and exchange transfusions have all failed to achieve much.

Another strategy is aimed at blocking the effects of glycine on NMDA receptors. Strychnine blocks glycinergic inhibitory effects, but strychnine is only effective on the classic glycine receptors present in the brain stem and spinal cord. Strychnine treatment is clinically ineffective. Diazepam is a competitor for glycine receptors. The drug has a favorable anticonvulsant effect. Treatment using NMDA receptor antagonists has also been attempted. Ketamine and tryptophan, both NMDA receptor antagonists, have been reported to lead to some reduction in irritability

and epilepsy and some improvement of sucking and gross motor movements.

So far a combination of the two strategies, using sodium benzoate and dextromethorphan, has had variable beneficial effect. Sodium benzoate is conjugated with glycine to form hippurate, which can be effectively excreted in the urine, in this way removing excess glycine. A lowering to normalization of plasma glycine level and a lowering of CSF level can be achieved with sodium benzoate, accompanied by increased alertness of the patient and a reduction of seizures. The effectiveness of sodium benzoate seems to be higher in patients with atypical variants of NKH with only moderately elevated glycine levels than in patients with neonatal NKH. Dextromethorphan, an NMDA receptor antagonist, has been used with variable success to reduce or stop seizures, improve alertness and social interest, and initiate some motor development. During temporary cessation of treatment and during febrile infections, temporary neurological deterioration can occur. Imipramine, another NMDA

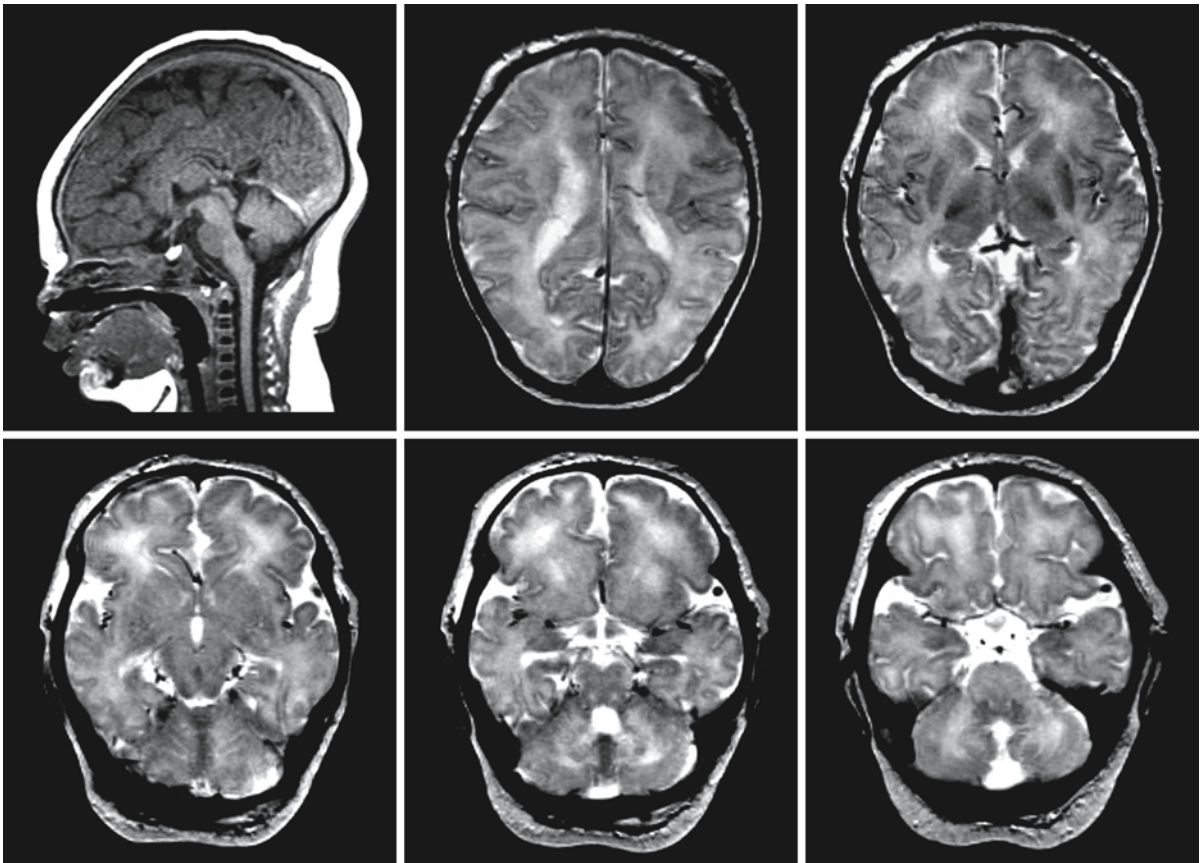


Fig. 39.1. Male neonate with NKH, born at term and now 4 days old. The brain looks diffusely abnormal and somewhat swollen. In large areas the contrast between cortex and white matter is decreased. The posterior limb of the internal capsule

has a high signal throughout on these T_2 -weighted images. The brain stem also has an abnormal signal. The corpus callosum is present

receptor antagonist, has also been reported to have beneficial effects. Despite treatment, the neurological handicap of the treated children remains serious and there is only minor psychomotor development.

39.5 Magnetic Resonance Imaging

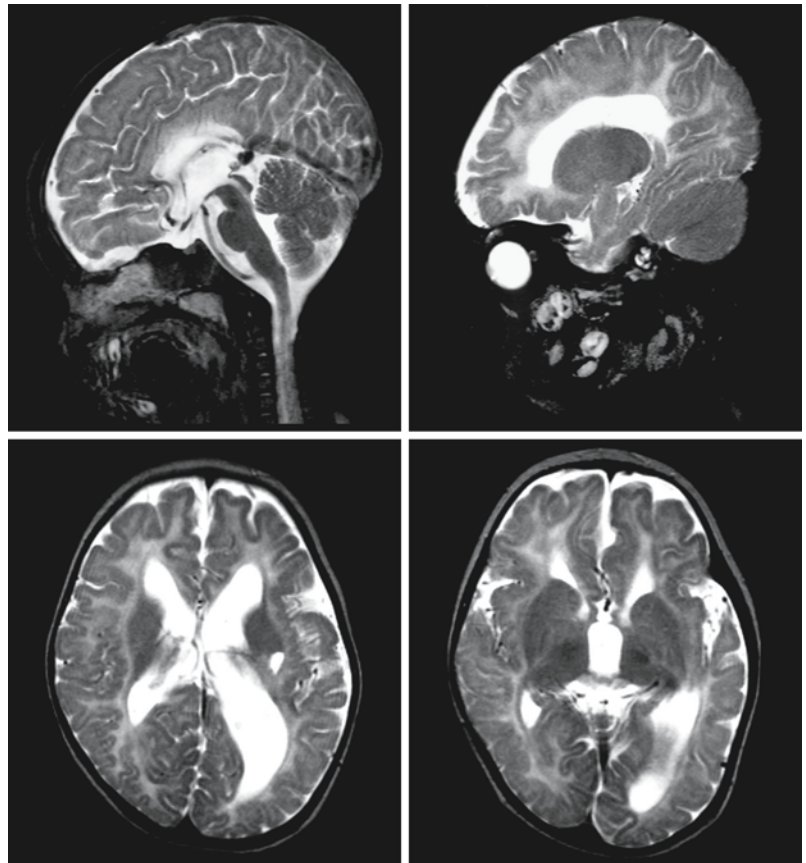
Limited imaging data are available in NKH. In the neonatal phase, MRI may show abnormalities in the signal intensity in the dorsal pons and midbrain and posterior limb of the internal capsule. These abnormalities are probably related to myelin vacuolation in myelinated areas. Diffusion-weighted MRI shows a high signal in these areas and the cerebral peduncles, whereas ADC values in these areas are low, indicative of restricted diffusion. The findings are reminiscent of those in maple syrup urine disease, but tend to be

less prominent (Fig. 39.1). We observed diffuse brain edema and swelling in a comatose neonate with NKH (Fig. 39.1).

On follow-up progressive cerebral and cerebellar atrophy is observed with ventricular enlargement, enlargement of the subarachnoid spaces, and thinning of the corpus callosum (Figs. 39.2 and 39.3). Myelination is seriously delayed (Figs. 39.2 and 39.3).

Long echo time proton MRS of the brain offers a noninvasive method for direct measurement of brain levels of glycine, if elevated, and can be used for diagnostic purposes and to monitor treatment. Glycine co-resonates with *myo*-inositol at 3.56 ppm. For this reason it is impossible to quantify glycine at short echo times. However, glycine has a much longer T_2 than *myo*-inositol and is also visible at long echo times (135–270 ms), when *myo*-inositol is no longer seen.

Fig. 39.2. Boy, 10 months old, with NKH. The corpus callosum is extremely thin and hardly visible on the sagittal images, but the presence of the cingulate gyrus indicates that it has developed normally. The transverse images confirm that there is a very thin corpus callosum. The white matter contains very little myelin. The volume of the cerebral white matter is reduced and the lateral ventricles are dilated. There is a lesion in the basal ganglia on the left. Courtesy of Dr. Z. Patay, Department of Radiology, and Dr. P.T. Ozand, Department of Pediatrics, King Faisal Specialist Hospital and Research Center, Riyadh, Saudi Arabia



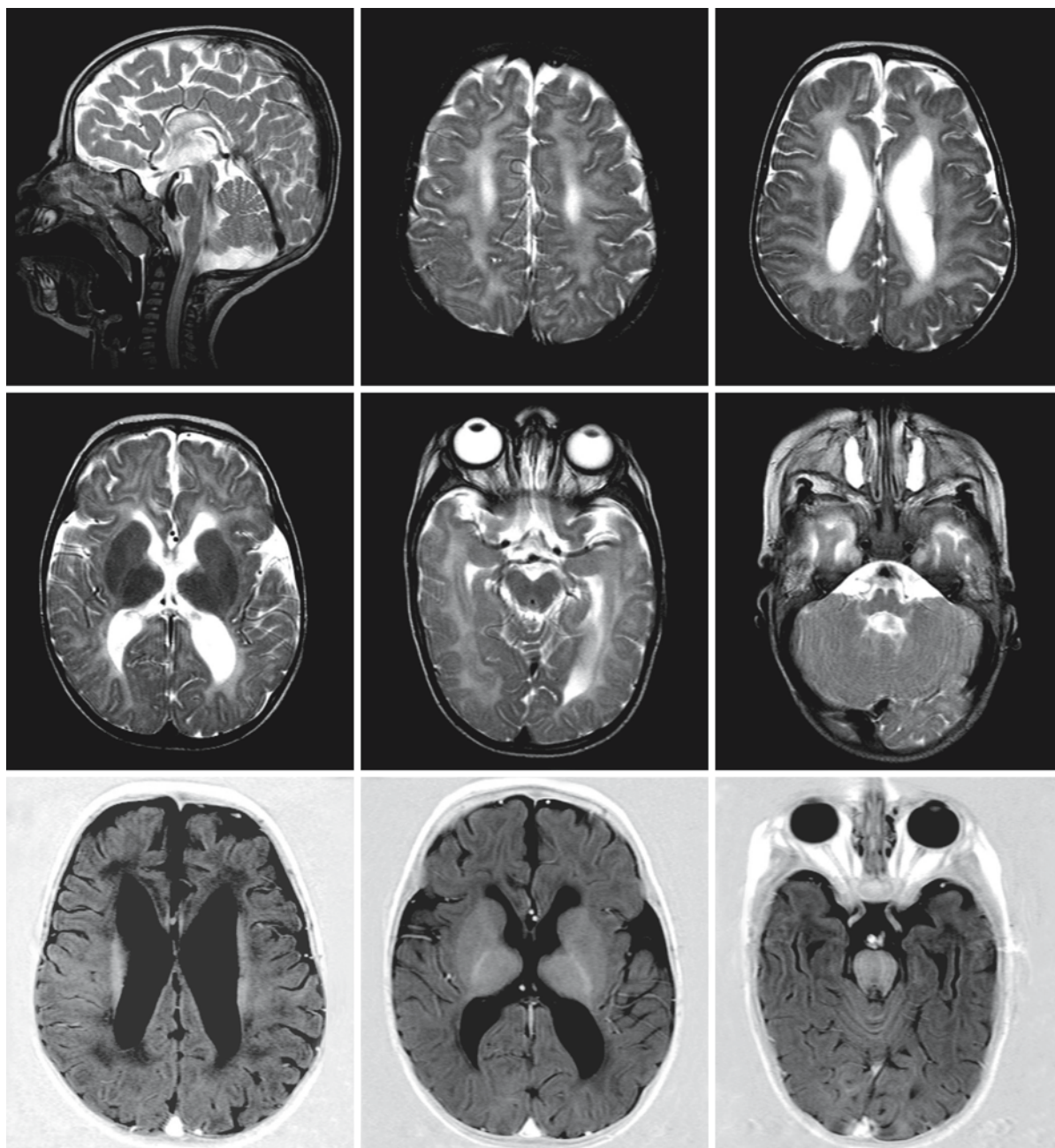


Fig. 39.3. Patient, 13 months old, with NKH. The sagittal image demonstrates that the corpus callosum is extremely thin but complete. The T_1 - and T_2 -weighted images show that the cerebral white matter contains very little myelin. The volume of the

cerebral white matter is mildly reduced and the lateral ventricles are dilated. Courtesy of Dr. Z. Patay, Department of Radiology, and Dr. P.T. Ozand, Department of Pediatrics, King Faisal Specialist Hospital and Research Center, Riyadh, Saudi Arabia

Maple Syrup Urine Disease

40.1 Clinical Features and Laboratory Investigations

Maple syrup urine disease (MSUD) is a heterogeneous disorder. Classification is based on clinical presentation and outcome. Five phenotypes can be distinguished: classical, intermediate, intermittent, thiamine-responsive, and dihydrolipoyl dehydrogenase (E_3)-deficient forms of MSUD. All forms have an autosomal recessive mode of inheritance.

Classical MSUD is the most severe and the most common form of the disease. Infants appear normal at birth. By the end of the first week symptoms emerge, with lethargy, poor feeding (but rarely vomiting), alternating periods of hypertonia and hypotonia, opisthotonus, convulsions, bulging fontanel, irregular respiration, and apnea. An odor of maple syrup is frequently noted, but may not initially be present. If the disease is not treated, rapidly progressive neurological deterioration occurs, with cerebral edema, coma, and death usually within the first month of life. If an untreated patient survives the first few weeks of life, signs of severe brain damage remain, with profound psychomotor retardation, spasticity, generalized dystonia, and cerebral blindness. Early diagnosis and treatment may avert or reverse the neurological abnormalities, but mental and neurological residua are common in treated patients. It has been shown that the length of time after birth for which the metabolic derangement is not adequately treated, and the quality of long-term metabolic control both have important influences on eventual intellectual capacities. If the disease is identified and treated within a few days after birth, IQ scores are higher and may be normal. A problem is that throughout life intercurrent illnesses, even minor illnesses, may lead to severe metabolic derangement, cerebral edema, and possibly death.

The intermediate variant of MSUD is milder and patients do not have catastrophic illness in the neonatal period. Many patients do not have episodes of acute metabolic decompensation. Progressive mental retardation is the major clinical feature, usually becoming apparent during the first year of life. Generalized hypotonia and an odor of maple syrup are present.

Patients with the intermittent form of MSUD show normal early development. They are at risk for acute metabolic decompensation during stressful situa-

tions. Clinical signs may be first seen between the ages of 2 months and 40 years, triggered by infection, vaccination, operation, or sudden increase in dietary protein. The episodic deterioration is characterized by maple syrup odor, cerebellar ataxia, irritability, and progressive lethargy. With supportive care the patient recovers, but will experience repeated similar episodes until the correct diagnosis is established and specific dietary treatment started.

Thiamine-responsive MSUD is not a well-defined subtype of MSUD. In the reported patients, the clinical course tends to be relatively mild, even if untreated, although thiamine responders may also have the classical, severe form of the disease. In general, these patients do not have acute neonatal illness and their early clinical course is similar to that of intermediate MSUD. The course of the disease is greatly ameliorated by simultaneous thiamine administration and dietary treatment. Outcome is favorable.

E_3 -deficient patients have a relatively uneventful first few months of life. Patients develop persistent lactic acidosis between 2 and 6 months of life and a progressive neurological deterioration sets in with hypotonia, developmental delay, and extrapyramidal movement abnormalities.

Laboratory investigations reveal ketoacidosis in episodes of metabolic decompensation. Concentrations of branched-chain amino acids (leucine, valine, and isoleucine) and related keto acids (α -ketoisocaproic acid, α -ketoisovaleric acid, and α -keto- β -methylvaleric acid) are elevated in blood, urine, and CSF. Smaller amounts of the respective 2-hydroxy acids are formed by reduction of the keto acids. An unusual isomer of isoleucine, alloisoleucine, is also found. Diagnosis is confirmed by demonstration of a deficiency of branched-chain keto acid dehydrogenase in leukocytes or cultured fibroblasts. DNA confirmation is an option.

In the early stages of untreated classical MSUD, EEG shows characteristic abnormalities, variously called a "comb-like" or "picket fence" rhythm or "central theta spindle." The pattern consists of bursts and runs of 5–7 Hz, primarily monophasic, negative, mu-like activity in the central and central-parasagittal regions during wakefulness and sleep with the most abundant bursts occurring during quiet, non-REM sleep. The background pattern shows diffuse slowing, loss of reactivity to auditory stimuli, burst-suppression patterns, and spike and sharp wave pat-

terns. The abnormalities disappear on treatment. Motor and sensory peripheral nerve conduction velocity is normal.

Prenatal diagnosis can be performed by assessing branched-chain keto acid dehydrogenase in cultured amniocytes or chorionic villus cells. In families with known mutations, DNA analysis can replace the enzyme assay.

40.2 Pathology

In young infants who die in the acute stage of the disease, the brain is enlarged due to generalized edema. Brain weight is increased. Gyri may be broadened and flattened. Microscopic examination reveals a status spongiosus of myelinated areas. Unmyelinated regions are not affected. Thus, in neonates the areas involved are the spinal cord, medulla oblongata, dorsal part of pons, midbrain, cerebellar white matter, cerebellar peduncles, posterior limb of the internal capsule, and central part of the corona radiata. Sponginess may also be present in the basal ganglia, in particular in the globus pallidus due to its density of myelinated fibers. The sponginess is caused by myelin splitting at the intraperiod line and intramyelinic vacuole formation. No signs of active myelin breakdown are seen and no sudanophilic breakdown products. In the spongy white matter marked astrocytic gliosis is present.

In older, untreated infants neuropathological findings may also be characterized by edema if the patient died during an acute metabolic decompensation. Further findings consist of a delay in myelination and a status spongiosus and astrogliosis of the myelinated white matter. Myelin stains reveal myelin paucity, but there is no evidence of active myelin breakdown. Oligodendrocytes are decreased in numbers. There are no phagocytic cells and no or little deposition of sudanophilic breakdown products. The myelin abnormalities occur in all regions; no areas are spared. Gray matter is essentially normal. In treated infants and children myelination is normal and white matter sponginess is minimal.

The neuropathology in E_3 deficiency resembles that of Leigh syndrome with lesions in the basal ganglia, thalami, and brain stem.

40.3 Chemical Pathology

In neonates the lipid composition of the brain is normal or near-normal. In older, untreated infants the findings of chemical analysis of the brain are in conformity with delayed myelination without active myelin breakdown. Major myelin components, including sulfatide, cerebroside, and proteolipid pro-

tein, are significantly reduced. Cholesterol esters are not elevated. Free amino acids in the brain are not altered with the exception of the branched-chain amino acids, which are markedly increased. Glutamine, glutamate, and GABA are significantly reduced. In older, treated patients, the lipid composition of the brain is normal.

40.4 Pathogenetic Considerations

MSUD is caused by a deficiency in activity of the branched-chain α -keto acid dehydrogenase complex. This is a mitochondrial multienzyme complex catalyzing the oxidative decarboxylation of branched-chain α -keto acids, which are derived branched-chain amino acids such as valine, leucine, and isoleucine by transamination. The multienzyme complex consists of three catalytic components: branched-chain α -keto acid decarboxylase (E_1), dihydrolipoyl acyltransferase (E_2), and dihydrolipoyl dehydrogenase (E_3). E_1 is a heterotetramer composed of two α and two β subunits. The complex also contains two specific regulatory enzymes, a kinase and a phosphatase, compounds that are responsible for regulating the catalytic activity through phosphorylation and dephosphorylation. E_1 is phosphorylated at two serine residues and hence responsible for regulation of the catalytic activity of the complex. Phosphorylation inactivates the complex and dephosphorylation activates it. E_1 binds thiamine diphosphate to create the active site for decarboxylation of the branched-chain α -keto acid substrate. E_2 catalyzes transfer of the acyl group from the lipoyl moiety to coenzyme A to give rise to a branched-chain acyl-CoA. It forms the structural core of the enzyme complex to which E_1 , E_3 , kinase and phosphatase are bound. E_3 is identical to the dehydrogenases associated with pyruvate dehydrogenase and α -ketoglutarate dehydrogenase complexes.

Mutation in any of the four genes encoding E_1 , E_2 , and E_3 may result in MSUD through dysfunction of the branched-chain α -keto acid dehydrogenase complex. The gene encoding $E_{1\alpha}$, *BCKDHA*, is located on chromosome 19 at position q13.1–13.2. The gene encoding $E_{1\beta}$, *BCKDHB*, is located on chromosome 6 at position p21–22. The gene encoding E_2 , *DBT*, is located on chromosome 1 at position p21–31. The gene encoding E_3 , *DLD*, is located on chromosome 7 at position q31–32. Patients with a deficiency of E_3 activity have combined deficiency of branched-chain α -keto acid dehydrogenase, pyruvate dehydrogenase, and α -ketoglutarate dehydrogenase complexes. So far, no clear relationship between genotype and phenotype has emerged. There is some relationship between clinical phenotype and residual enzyme activity.

Mechanisms for toxic effects of increased branched-chain amino acids and keto acids remain largely unelucidated. The toxic effects may be related to disturbance of neurotransmission, energy depletion, and direct myelin damage. Branched-chain keto acids and their hydroxy derivatives compete with glutamate for decarboxylation and so reduce GABA production. Excess leucine may reduce cerebral serotonin. α -Ketoisocaproic acid inhibits pyruvate dehydrogenase and α -ketoglutarate dehydrogenase, two important enzymes in mitochondrial energy production. The mechanism of myelin vacuolation and myelin damage is unknown. Hexachlorophene and triethyltin are toxins which also lead to myelin vacuolation. These substances are inhibitors of mitochondrial oxidative phosphorylation. From experimental studies it is known that lasting effects only follow chronic exposure and that early discontinuation of exposure is followed by repair. This course of events is similar to that observed in MSUD: early treatment leads to resolution of abnormalities. Only in untreated cases are lasting effects seen. The precise pathophysiological mechanisms of myelin splitting are unknown, either in exogenous intoxications or in MSUD. Evidence has been found that MSUD metabolites, in particular α -isocaproic acid, induce apoptosis in glial and neuronal cells, but the relationship with the *in vivo* pathology of MSUD is unclear.

40.5 Therapy

In cases of acute metabolic decompensation with very high blood and tissue levels of branched-chain amino acids and keto acids, emergency treatment is necessary. Exchange transfusions, peritoneal dialysis, hemodialysis, and hemofiltration are effective in acutely ill patients. These therapeutic measures must be supplemented by high-energy intake to reverse the catabolic condition caused by infection or fasting. For this purpose intravenous glucose, intravenous lipids, or a special formula containing a mixture of complete nutrients lacking only branched-chain amino acids can be used. Concomitant administration of insulin is very effective in achieving an anabolic situation. In acutely ill but not comatose patients, nutritional therapy may be sufficient. During the course of therapy, isoleucine and valine should be added to the regimen to prevent depletion of these essential amino acids and thus ensure effective protein synthesis.

Minor illnesses may lead to catabolic conditions with release of amino acids from body tissues. Toxic levels of branched-chain amino acids may be reached within a few hours with onset of as yet mild clinical symptoms. Immediate high-energy intake and temporary removal of all natural protein from the diet in such situations may prevent a full-blown metabolic

decompensation. Catabolic conditions after surgery can be prevented by administration of insulin and a branched-chain amino-acid-free parenteral nutrition regimen.

All patients with classical MSUD require life-long dietary treatment. The long-term treatment aims at maintaining the whole-body content of branched-chain amino acids close to the minimum requirement for normal body function. The amount of branched-chain amino acids necessary for adequate protein synthesis is given in the form of natural proteins in a protein-restricted diet. A branched-chain amino-acid-free mixture of amino acids is used to supplement the diet. The levels of branched-chain amino acids in blood are measured regularly to monitor treatment. Deficiency of branch-chain amino acids leads to growth failure, skin rash, exfoliative dermatitis, diarrhea, and de-epithelialization of the cornea. Patients with milder forms of MSUD tolerate a higher protein intake. In thiamine-responsive MSUD, use of thiamine increases protein tolerance. However, a protein-restricted diet should still be used and the plasma levels of branched-chain amino acids monitored. In order to test for thiamin-responsiveness, all patients should receive trial therapy with thiamin.

If onset of dietary treatment leads to lowering of blood levels of branched-chain amino acids within a few days after birth, and if adequate dietary control is maintained over the years, prognosis is excellent and intellectual capacities may be normal. Later onset of treatment or poor dietary control contribute to mental deficiency. With adequate dietary treatment and careful monitoring, female patients with MSUD may enjoy successful pregnancies.

Liver transplantation has been shown to increase whole-body branched-chain α -keto acid dehydrogenase activity to at least the level of very mild MSUD variants (Wendel et al. 1999). After liver transplantation, patients no longer need protein-restricted diets and the risk of metabolic decompensation during catabolic events is apparently abolished. However, liver transplantation comes with considerable risks and the benefits may not be significantly different from those of strict dietary treatment.

40.6 Magnetic Resonance Imaging

In MSUD with neonatal presentation, CT shows a very characteristic pattern with profound hypodensity and swelling of the cerebellar hemispheres, dorsal part of the pons, midbrain, posterior limb of the internal capsule, the globus pallidus, and often the thalamus. In addition, milder, generalized cerebral white matter hypodensity is seen.

MRI confirms the pattern. In MSUD with neonatal presentation, T_2 -weighted images show marked

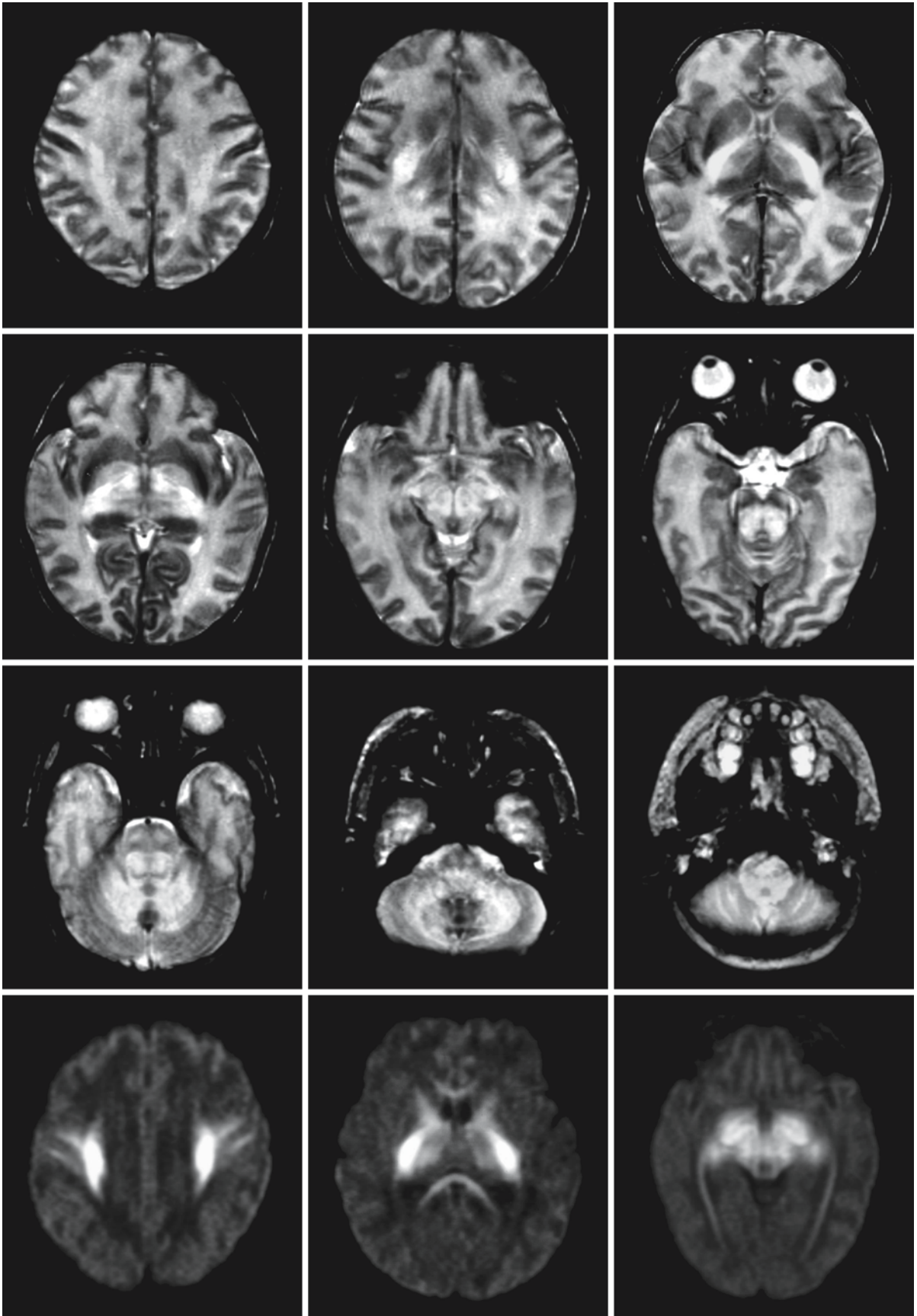


Fig. 40.1.

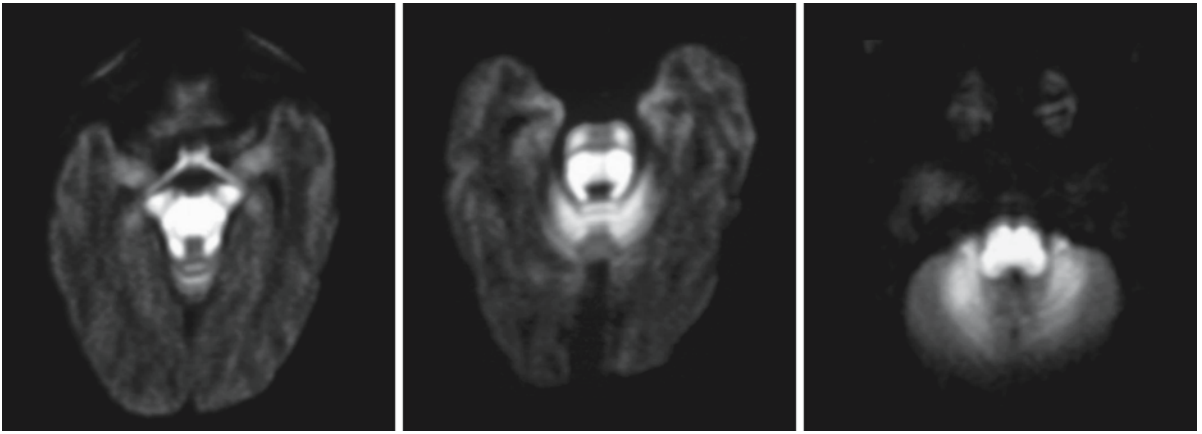


Fig. 40.1. (continued). Baby boy with MSUD. The T_2 -weighted images (first three rows) show an elevated signal intensity and swelling of the cerebellar white matter, the medulla, dorsal part of the pons, pyramidal tracts in the basis of the pons, midbrain, the posterior limb of the internal capsule, and central part of the corona radiata. The thalamus, too, has a slightly abnormal signal. The diffusion-weighted images (trace images, $b = 1000$, fourth and fifth rows) show restricted diffusion in the

cerebellar white matter, the medulla, dorsal part of the pons, pyramidal tracts in the basis of the pons, midbrain, posterior limb of the internal capsule, and central part of the corona radiata. The thalamus, anterior limb of the internal capsule, corpus callosum, and hippocampus display less severely restricted diffusion. Courtesy of Dr. Z. Patay, Department of Radiology, and Dr. P.T. Ozand, Department of Pediatrics, King Faisal Specialist Hospital and Research Center, Riyadh, Saudi Arabia

swelling and high signal intensity in the posterior part of the pons, in the midbrain, cerebellar white matter, posterior limb of the internal capsule, thalamus, globus pallidus, and central part of the corona radiata (Fig. 40.1). Besides, mild diffuse cerebral white matter edema may be present. Without treatment, the edema gradually decreases and atrophy ensues. Edema is most pronounced between the third week and the end of the second month. With treatment edema resolves more rapidly.

Remaining abnormalities in treated patients are variable, depending on the severity and duration of the initial episode of metabolic derangement and the subsequent metabolic control (Figs. 40.2–40.4). In some patients MRI becomes normal. In others some signs of atrophy, delay in myelination, and white matter abnormalities are found. Many patients have remaining signal abnormalities in the midbrain, thalamus, and globus pallidus.

If MRI is performed during a later episode of metabolic decompensation in otherwise adequately treated and normally developing children with classical MSUD, it shows brain swelling and abnormally increased signal intensity on T_2 -weighted images in the deep white matter and U fibers, internal capsule, basal ganglia, thalamus, hypothalamus, dentate nucleus, and brain stem. In deep coma, all white matter may be abnormal in signal and seriously swollen. If adequate treatment is initiated immediately, most or all abnormalities disappear.

Milder variants of MSUD usually come to medical attention in the second year of life because of retard-

ed development or signs of metabolic decompensation. MRI at that time (Figs. 40.5 and 40.6) shows more diffuse abnormality of the white matter of the cerebral hemispheres. The cerebellar white matter may have a striking stripe-like appearance, the stripes being partly related to enlarged perivascular spaces and partly to myelination in stripes, probably reflecting perivascular myelin deposition (Figs. 40.5 and 40.6). The brain stem is also involved. Both the thalamus and globus pallidus are affected, whereas the putamen and caudate nucleus are normal. The cortex is normal. Improvement after treatment has been reported. In adequately treated patients with milder variants of MSUD, CT and MRI may be normal.

Diffusion-weighted imaging shows restricted diffusion in the areas of acute myelin vacuolation with low ADC values (Fig. 40.1). In neonates, this results in a pattern of very high signal intensity in the medulla, dorsal part of the pons, the midbrain, cerebellar white matter, posterior limb of the internal capsule, thalamus, globus pallidus, and central part of the corona radiata. The restricted diffusion is probably related to decrease of the extracellular space because of the vacuoles within the myelin sheaths. Diffusion tensor imaging reveals decreased anisotropy in the same regions. In the unmyelinated white matter ADC values are increased, reflecting white matter edema.

Proton MRS is helpful in establishing a diagnosis in acute metabolic decompensation by revealing resonances related to branched chain amino acids and keto acids at 0.9 ppm. Lactate may also be elevated. These peaks disappear with treatment.

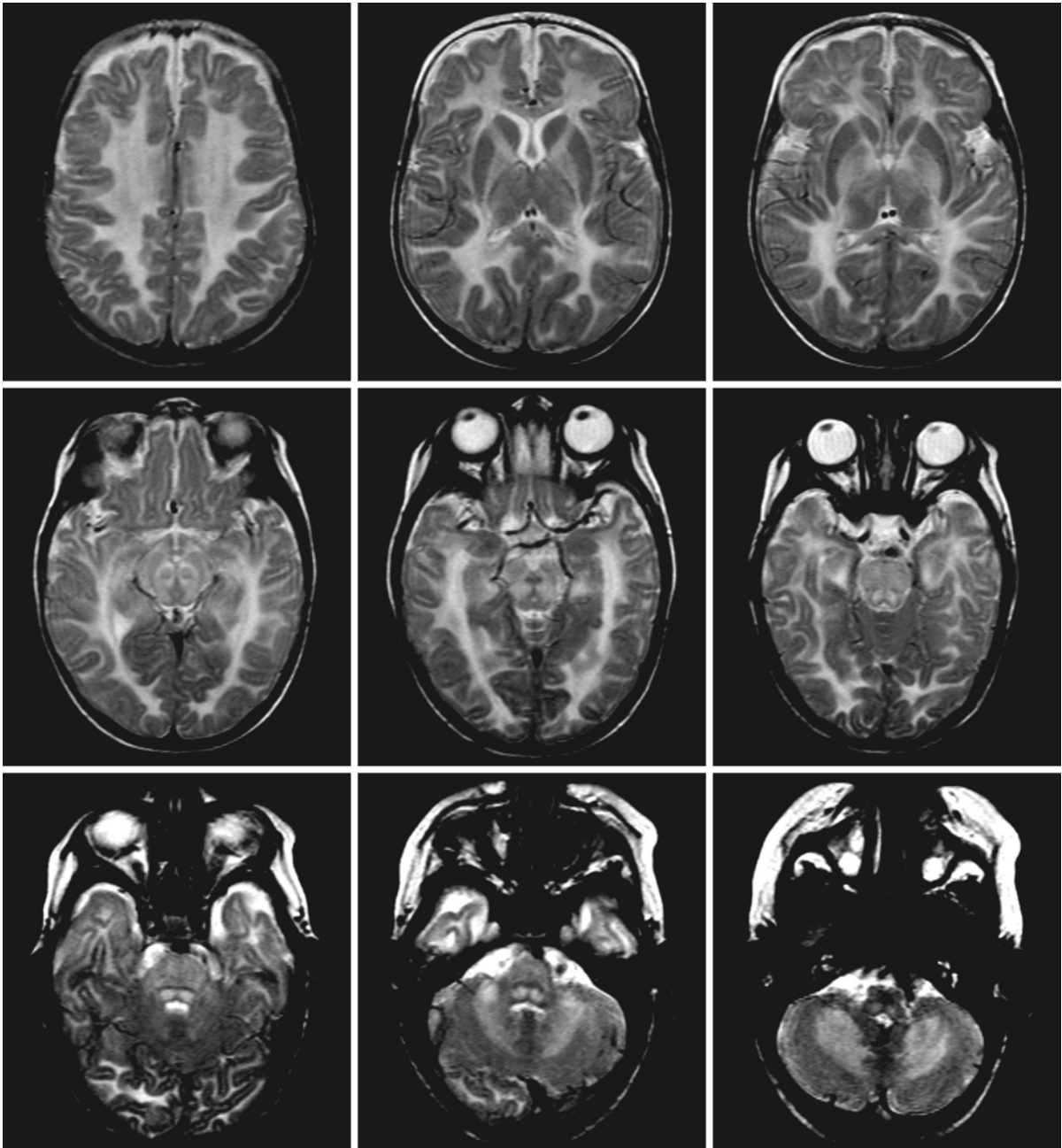


Fig. 40.2. A 4-month-old girl with neonatal-onset MSUD. She was diagnosed at 3 weeks and has been receiving treatment since that time. Diffuse signal abnormalities are still seen in the cerebral and cerebellar white matter, and brain stem at all levels. There is, however, much less swelling than in the neonatal stage. The thalamus and globus pallidus are abnormal, where-

as the putamen and caudate nucleus are spared. These abnormalities are very similar to those seen in Canavan disease. Courtesy of Dr. Z. Patay, Department of Radiology, and Dr. P.T. Ozand, Department of Pediatrics, King Faisal Specialist Hospital and Research Center, Riyadh, Saudi Arabia

The images of patients with classical MSUD during the neonatal period are diagnostic. All areas which are normally myelinated at that age have an abnormal signal intensity and are swollen. This pattern is exclusively seen in vacuolating myelinopathies of neonatal

onset. The images of patients with milder variants of MSUD during the second year of life are very similar to those of Canavan disease. However, clinical history and laboratory findings differentiate between the two.

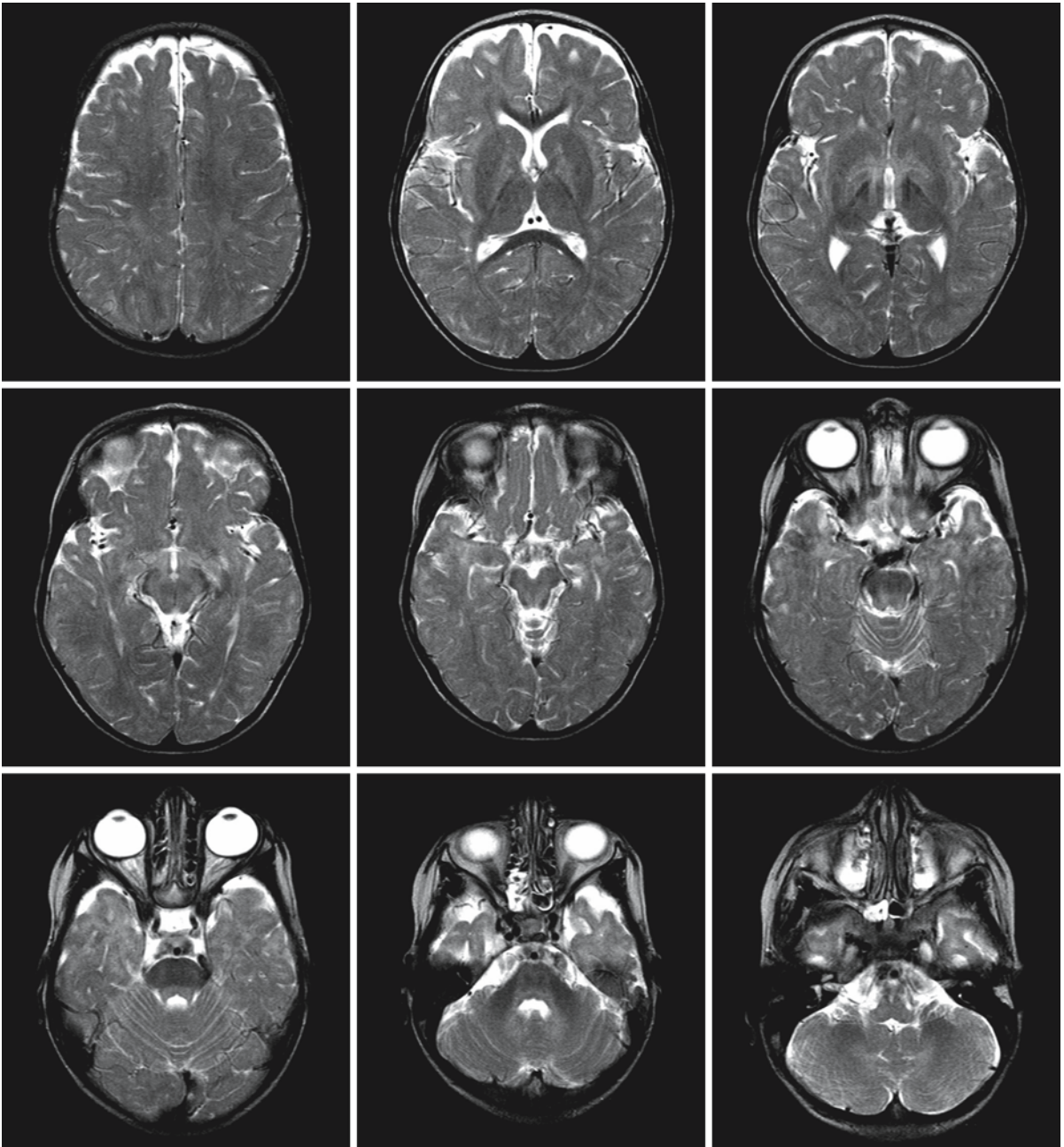


Fig. 40.3. The same girl as in Fig. 40.2, now at the age of 2 years. Under treatment most abnormalities disappeared. Myelination is mildly delayed. There are slight signal abnormalities in the globus pallidus. Courtesy of Dr. Z. Patay, Depart-

ment of Radiology, and Dr. P.T. Ozand, Department of Pediatrics, King Faisal Specialist Hospital and Research Center, Riyadh, Saudi Arabia

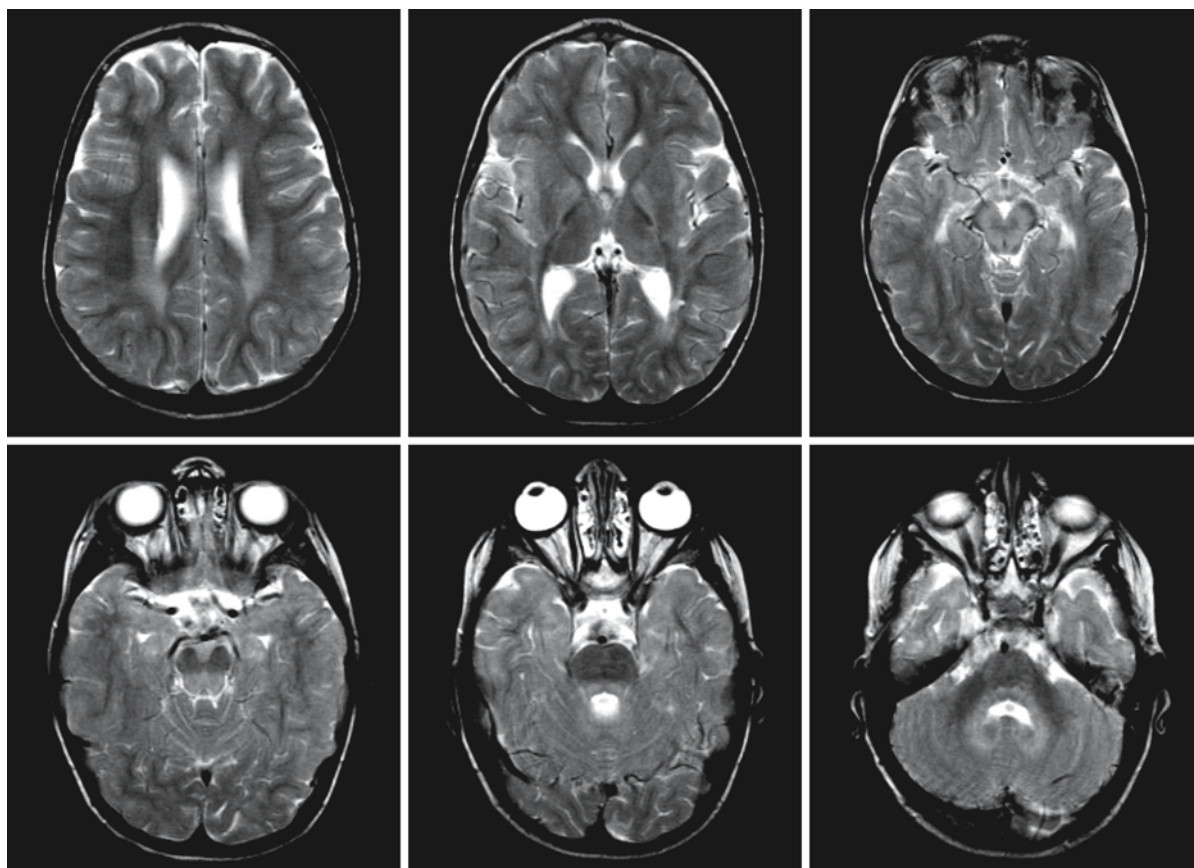


Fig. 40.4. Boy with neonatal presentation of MSUD. He has responded well to treatment and is now 6 years old. The MRI shows signal abnormalities in the periventricular white matter, globus pallidus, midbrain (especially the dorsal part), the dor-

sal pons, and the dentate nucleus. Courtesy of Dr. Z. Patay, Department of Radiology, King Faisal Specialist Hospital and Research Center, Riyadh, Saudi Arabia

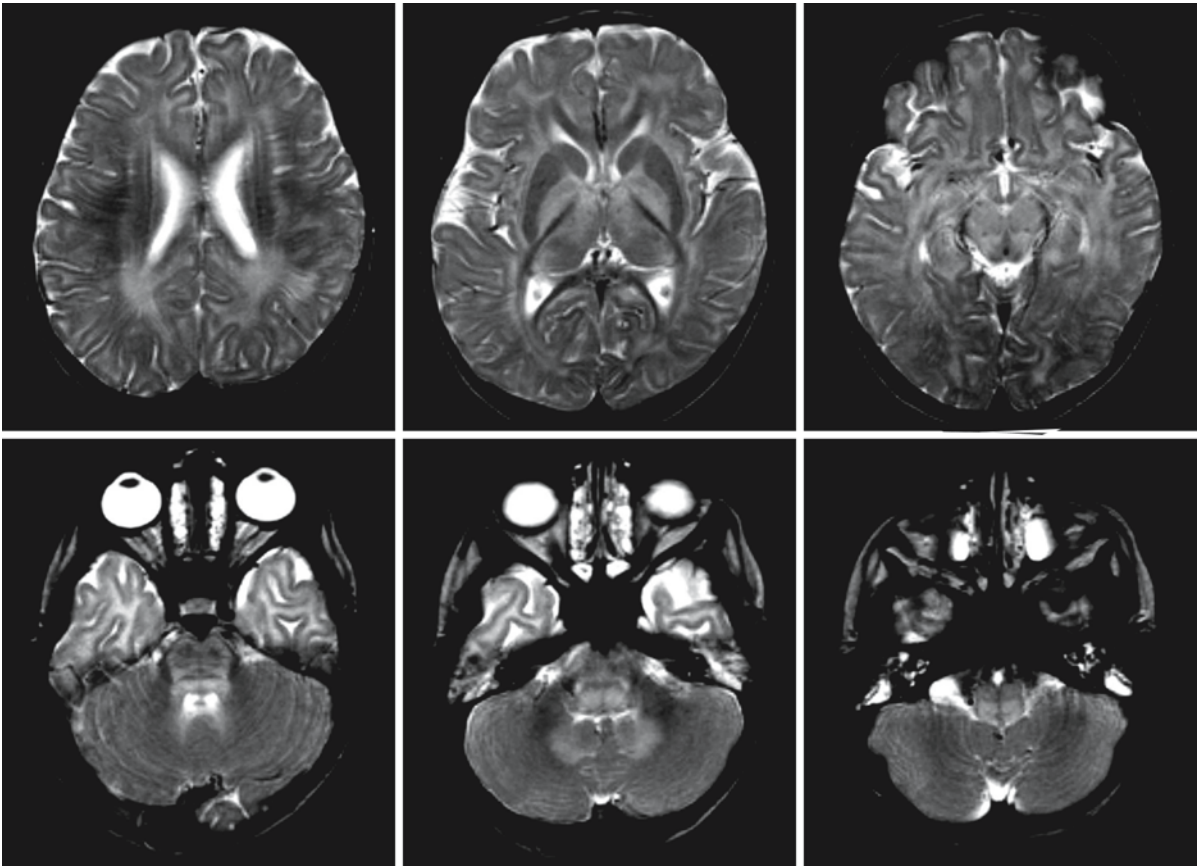


Fig. 40.5. An 18-month-old boy with intermittent MSUD. He experienced metabolic coma at 12 and 18 months. MRI shows extensive cerebral white matter abnormalities, in some areas with a stripe-like aspect. The thalamus and globus pallidus are abnormal, while the putamen and caudate nucleus are spared. The posterior limb of the internal capsule is spared. In addition,

there are signal abnormalities in the midbrain, pons, medulla, and dentate nucleus. He responded well to treatment and had a full clinical recovery. Courtesy of Dr. Z. Patay, Department of Radiology, King Faisal Specialist Hospital and Research Center, Riyadh, Saudi Arabia

Fig. 40.6. A 4-year-old boy recently diagnosed with MSUD. The T₂-weighted images (*first and second rows*) show extensive cerebral white matter abnormalities, which have a stripe-like aspect. The stripes are partly related to enlarged perivascular spaces and partly to myelin deposition in a stripe-like pattern, probably perivascular myelin deposition. The thalamus and globus pallidus are abnormal, while the putamen and caudate nucleus are spared. The posterior limb of the internal capsule is spared. There are signal abnormalities in the midbrain, pons, medulla, dentate nucleus, and cerebellar white matter. The

T₁-weighted images (*third row*) demonstrate mild diffuse hyperintensity of the white matter, consistent with diffuse hypomyelination. Within the white matter the enlarged perivascular spaces are beautifully seen. The sagittal (*fourth row, left and middle*) and coronal (*fourth row, right*) images confirm the presence of the enlarged perivascular spaces and the stripe-like pattern of myelin deposition. Courtesy of Dr. I. Verma, Department of Genetic Medicine, Sir Ganga Ram Hospital, New Delhi, India. (Fig. 40.6 see next page)

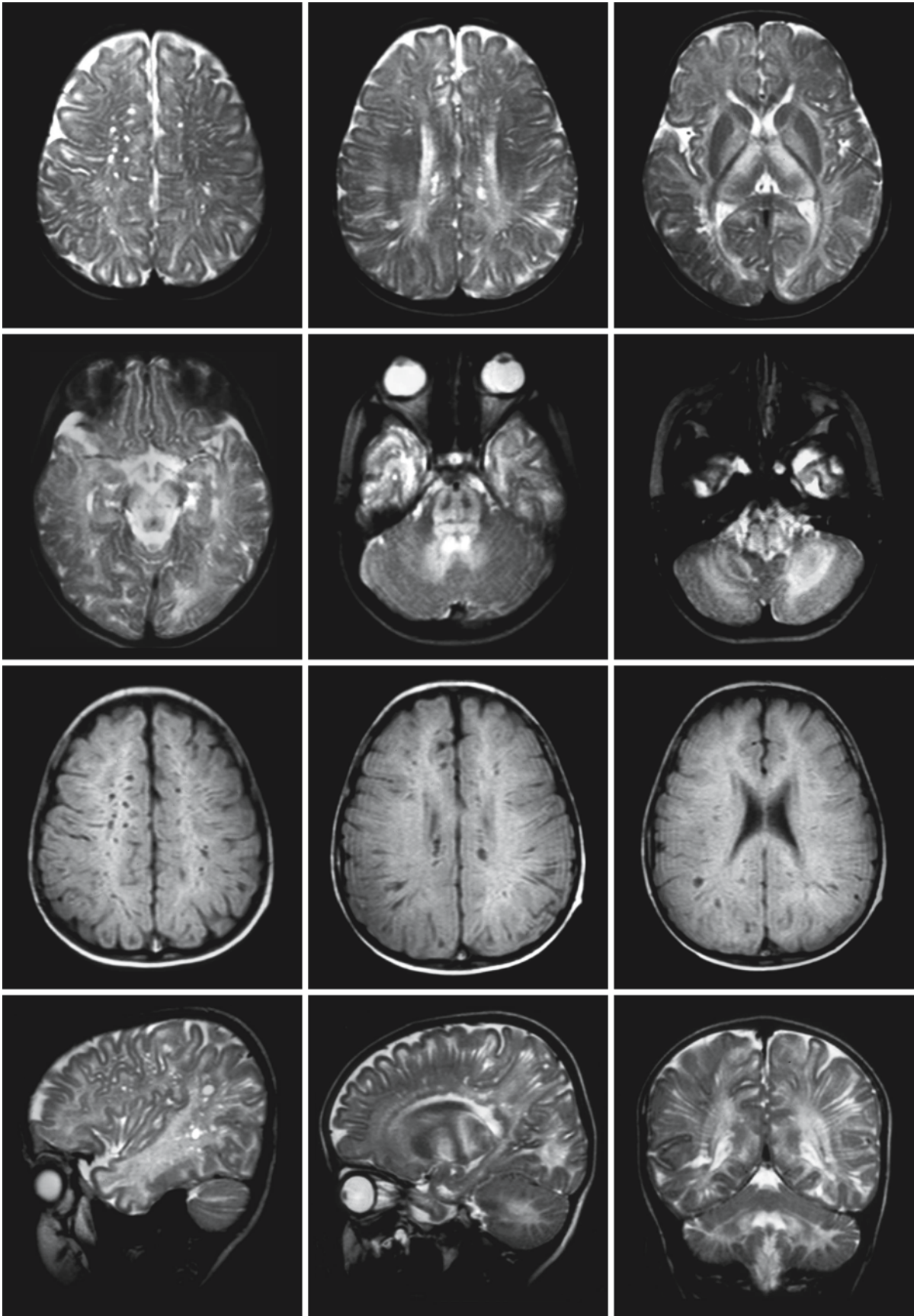


Fig. 40.6.

3-Hydroxy-3-Methylglutaryl-CoA Lyase Deficiency

41.1 Clinical Features and Laboratory Investigations

3-Hydroxy-3-methylglutaryl-coenzyme A lyase (HMG-CoA lyase) deficiency is a rare inborn error of metabolism with an autosomal recessive mode of inheritance. About 50% of the patients present in the neonatal period after a brief symptom-free period. Most of the rest become symptomatic before the age of 1 year. Presentation after the age of 2 years is rare. Episodes of deterioration are provoked by fasting, infections, and high protein intake. The episodes are characterized by lowering of consciousness, hypotonia, sometimes seizures, and apnea. Many patients have hepatomegaly. Some patients die from deep hypoglycemia. With appropriate treatment, most patients recover from their initial episode of metabolic decompensation, but there may be remaining neurological sequelae, including microcephaly, mental retardation, visual impairment, epilepsy, and central motor deficits.

Laboratory examinations during these episodes always reveal an acidosis and almost always hypoglycemia, which is often profound. Ketone bodies are inappropriately low. Lactate may be markedly elevated, especially in neonates. Many patients have abnormal liver function tests and hyperammonemia. Pancreatitis is another complication that may occur. Urinary organic acid analysis reveals increased excretion of 3-hydroxy-3-methylglutaric acid, 3-hydroxyisovaleric acid, 3-methylglutaconic acid, and 3-methylglutaric acid. 3-Methylcrotonylglycine may also be present. The diagnosis is confirmed by enzyme assessment in leukocytes or cultured fibroblasts. Fasting and leucine loading are usually unnecessary for diagnosis. They may be useful to determine fasting and protein tolerance, but they carry the risk of invoking metabolic decompensation and should be performed under close supervision. DNA confirmation is optional. Neonatal screening is possible using analysis of 3-methylglutaryl carnitine in blood. Prenatal diagnosis can be performed using metabolite measurements, enzyme assays, and molecular techniques.

41.2 Pathology

Zoghbi et al. (1986) reported the findings of a brain biopsy during an episode of metabolic decompensation. No abnormalities were found in the cerebral cortex. In the white matter spongiosis, reactive gliosis, and increased intracellular astrocytic glycogen were found. Gibson et al. (1994) reported spongiform degenerative changes and generalized edema in a child who died during a metabolic crisis. The histopathological basis of the focal and diffuse white matter signal abnormalities in well-treated and clinically normal patients is unknown.

41.3 Pathogenetic Considerations

HMG-CoA lyase is a key enzyme in leucine degradation and in ketogenesis. The gene encoding HMG-CoA lyase, *HMGCL*, is located on chromosome 1p35.1–36.1. The enzyme HMG-CoA lyase is located in mitochondria and peroxisomes of all tissues. Leucine is sequentially converted to 3-methylcrotonyl-CoA, 3-methylglutaconyl-CoA, and HMG-CoA. Fatty acid degradation leads to the formation of acetyl-CoA, which joins acetoacetyl-CoA to form HMG-CoA. HMG-CoA lyase catalyzes the conversion of HMG-CoA to acetoacetate. Acetoacetate and 3-hydroxybutyrate are the principal ketone bodies. 3-Hydroxybutyrate is derived directly from acetoacetate in a dehydrogenase reaction. A third ketone body, acetone, arises from decarboxylation of acetoacetate. Ketone bodies are formed predominantly from fatty acids and ketogenic amino acids, principally leucine. Ketone bodies are used as alternative source of energy for the brain when production of energy from glucose is insufficient to meet the demands. The main function of ketone bodies may be to provide the brain with a noncarbohydrate energy source during fasting. The brain cannot use fatty acids as an energy source. Under normal conditions, the main energy substrates of the brain are glucose and its derivatives, such as lactate, but during prolonged fasting ketone bodies supply almost two-thirds of the brain energy. Ketone bodies have a glucose sparing effect, turning down peripheral and central glucose utilization. They also reduce muscular proteolysis.

In HMG-CoA lyase deficiency multiple different mutations have been identified in *HMGCL* but so far no clear genotype–phenotype correlation has been found. HMG-CoA lyase deficiency causes a block in the production of ketone bodies, leading to exhaustion of glucose to very low levels under conditions when ketogenesis is required, that is, insufficient availability of glucose to meet energy demands. The metabolic decompensation is characterized by hypoketotic hypoglycemia. Infancy is the period of highest risk for decompensation.

In patients who survived a period of profound hypoglycemia in the neonatal period the remaining cerebral damage may mainly involve the posterior part of the brain, as typically happens in neonatal hypoglycemia. The cause of the remaining white matter abnormalities seen in patients with HMG-CoA lyase deficiency is unknown. These abnormalities must somehow be related to the specific metabolic derangement, because they are not seen in other disorders with hypoketotic hypoglycemia.

41.4 Therapy

The mainstay of treatment is suppression of ketogenesis. During a metabolic crisis, immediate attention should be focused on correction of the blood pH by sodium bicarbonate infusions and elevation of blood glucose by glucose infusions. In addition, patients may require measures of general support including assisted ventilation and repair of electrolyte and fluid deficits.

Long-term management of HMG-CoA-lyase-deficient patients should focus on avoidance of hypoglycemia and of long fasts. A high-carbohydrate diet is recommended with moderate protein and fat restriction. The leucine intake should be adjusted to insure normal growth. Patients should be under constant observation during periods of intercurrent illness. A high carbohydrate intake must be maintained during any metabolic stress. If high carbohydrate intake cannot be maintained, patients should be admitted for intravenous glucose administration.

Once the diagnosis has been established and this treatment strategy is applied, further neurological damage is usually prevented.

41.5 Magnetic Resonance Imaging

CT scan findings during a metabolic crisis in the neonatal period are characterized by white matter hypodensity and swelling. In the occipital region, contrast between the cortex and white matter may have disappeared and follow-up CT may show severe cystic degeneration of the occipital and parieto-occipital white matter. These findings are not specific for HMG-CoA lyase deficiency, but are characteristic sequelae of profound neonatal hypoglycemia. Follow-up MRI shows evidence of gliotic scarring and atrophy of the area involved (Fig. 41.1). In addition, lesions in the globus pallidus, thalamus, putamen, and caudate nucleus may occur following a neonatal hypoglycemic crisis (Fig. 41.1).

Hypoglycemia after the neonatal period usually leads to more diffuse cerebral cortical damage. In some children a stroke, e.g., a unilateral anterior and middle cerebral artery infarction arising during a metabolic crisis, has been reported. In an untreated infant with a moderately severe chronic metabolic derangement, macrocephaly and diffuse white matter hypodensity and swelling have been reported (Lisson et al. 1981; Leupold et al. 1982), suggesting diffuse white matter spongiosis. Cystic degeneration of the white matter was documented on follow-up.

MRI findings that are characteristic of HMG-CoA lyase deficiency include multiple abnormal white matter foci, varying in number from a few to, more often, a multitude and varying in size from very small – a few millimeters – to larger and more confluent lesions (Figs. 41.2 and 41.3). The abnormal white matter foci may be seen on a background of slight to mild signal abnormalities of almost the entire cerebral white matter, sparing the corpus callosum, variably sparing the U fibers (Fig. 41.2). The combination of diffuse mild and multifocal more serious cerebral white matter abnormalities is unique. In addition, signal abnormalities may be seen in the posterior limb of the internal capsule, hilus of the dentate nucleus, the dentate nucleus, and pontine tegmentum (Figs. 41.1–41.3). The cerebellar white matter is spared. These abnormalities are also seen in well-treated patients who have never experienced a metabolic crisis and who are clinically normal. The striking discrepancy between the serious white matter abnormalities on MRI and the lack of clinical findings in these patients is unexplained. This observation excludes demyelination as histopathological basis.

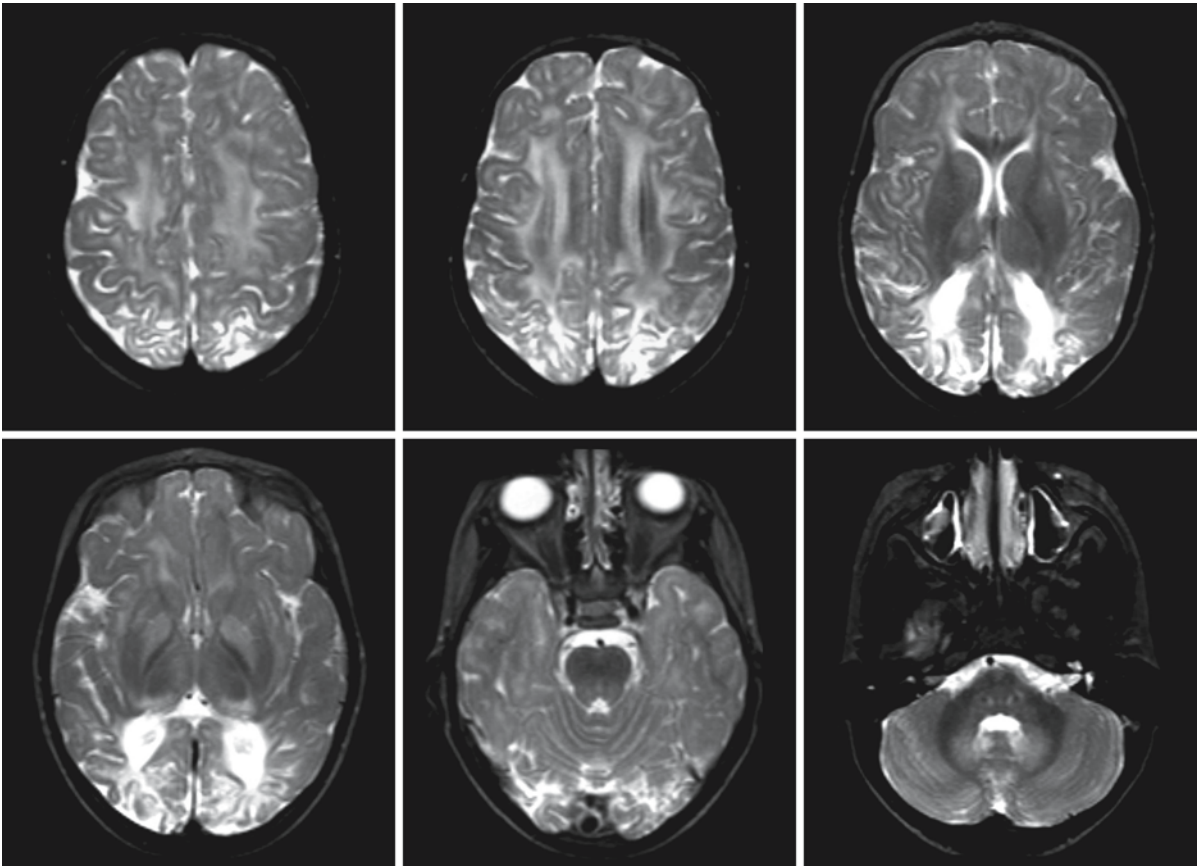


Fig. 41.1. This 4-year-old girl with HMG-CoA lyase deficiency experienced serious hypoglycemia in the neonatal period. She is severely retarded and has a visual impairment and microcephaly. MRI shows damage of the parieto-occipital white and gray matter, as may occur after neonatal hypoglycemia. In

addition, mild signal changes are present in the basal ganglia, thalami, and dentate nuclei. The cerebral white matter is diffusely abnormal. The corpus callosum is spared. From van der Knaap et al. (1998), with permission

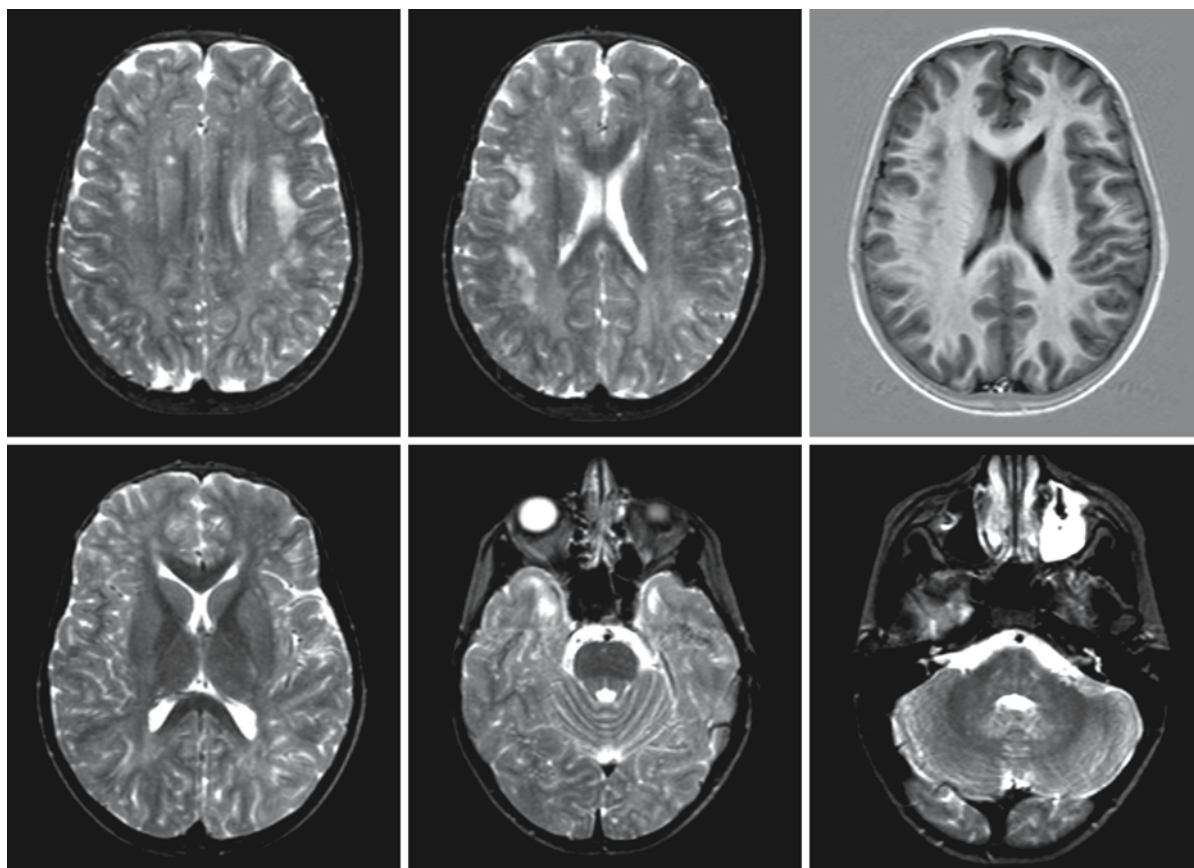


Fig. 41.2. The 10-year-old sister of the patient in Fig. 41.1 also has HMG-CoA lyase deficiency, but never developed symptoms of the disease. She was diagnosed after the diagnosis was established in her sister. The T₂-weighted images show diffuse mild signal changes in the cerebral white matter with additional spots of more prominent signal abnormality. The

T₁-weighted images only show the areas of more prominent signal abnormality; the diffuse signal changes are difficult to see. The corpus callosum is not involved. Signal abnormalities are also seen in the dentate nucleus and the hilus of the dentate nucleus. From van der Knaap et al. (1998), with permission

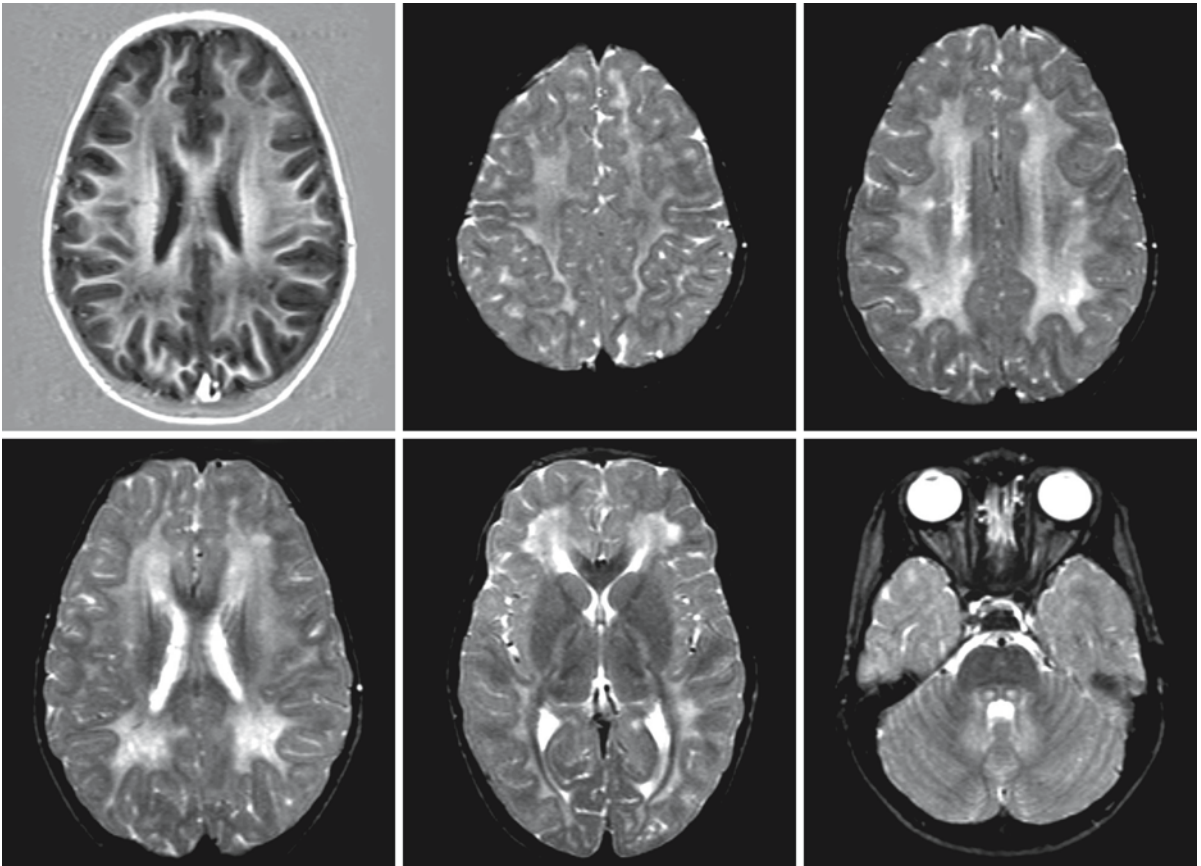


Fig. 41.3. A 6-year-old boy with HMG-CoA lyase deficiency. He had two episodes of hypoglycemia and lethargy in his third year of life, but his condition was never serious. His intelligence and neurological examination are normal. MRI reveals diffuse signal changes in the cerebral white matter, sparing the U fibers, with multiple foci of more prominent signal abnormali-

ty. These spots are also seen on the IR images (*upper row, left*). Slight signal changes are seen in the posterior limb of the internal capsule, thalami, pontine tegmentum, dentate nucleus, and outflow tract of the dentate nucleus. From van der Knaap et al. (1998), with permission

Canavan Disease

42.1 Clinical Features and Laboratory Investigations

Canavan disease (CD) is a rare hereditary neurological disorder affecting infants and children. The disease is also called spongy degeneration of the CNS of the Van Bogaert–Bertrand type. CD has an autosomal recessive mode of inheritance. It is most frequently found in children of Jewish Ashkenazi origin.

The infantile form of CD is the most common. The patients appear normal at birth and the initial stages of development are normal. The disease usually becomes apparent within the first 6 months of life. Early signs include hypotonia with poor head control, decreased motor activity, irritability, visual loss, poor sucking ability, and accelerated skull growth. An abnormal increase in skull growth results in macrocephaly in most of the patients. Failure of developmental progress and regression occur. Gradually, hypotonia of arms and legs is replaced by spasticity and tonic extensor spasms may occur. Axial hypotonia persists. Blindness with coarse nystagmoid eye movements and pale optic discs at funduscopy become evident. Occasionally sensorineural hearing loss is noted. Choreoathetosis, dystonia, and tonic or myoclonic seizures occur in some patients. Eventually a chronic vegetative state with decerebrate or decorticate rigidity appears. Autonomic crises may occur with episodically increased vasomotor responses, disturbed temperature regulation, and vomiting. The patients generally die before the age of 4 years. However, a considerable number of patients have a more protracted course with a life expectancy beyond 10 years, even into the third decade.

In the uncommon congenital variant, children may appear normal at birth or may be in a poor condition. During the first few days after birth, inactivity and lethargy become manifest. The children cry frequently and exhibit difficulties in sucking and swallowing. They are hypotonic. They die within a few days or weeks.

A separate juvenile variant of CD has been distinguished with normal development for several years. Occasionally, children with CD may achieve more developmental milestones than usual and may even achieve walking; they may have a highly protracted course of disease and live longer than expected; but an entirely normal development for several years has never been documented in patients in whom the

diagnosis of CD was proven with biochemical or DNA techniques, and the existence of a truly juvenile variant is doubtful.

Laboratory investigations in CD are diagnostic. An increased concentration of *N*-acetylaspartic acid is found in urine and plasma. CSF protein is sometimes raised. EEG is diffusely slow with paroxysmal features. Evoked potentials are delayed or absent. Nerve conduction velocity is normal. Decreased activity of the enzyme aspartoacylase is found in cultured fibroblasts. Carrier detection on the basis of enzyme assessment is a problem because of large overlap between activities found in carriers and controls. Prenatal diagnosis by assessment of enzyme activity in amniocytes and chorionic cells is unreliable owing to the low levels of aspartoacylase in these cells. Assessment of the level of *N*-acetylaspartate in amniotic fluid is more reliable. Prenatal diagnosis is also possible using DNA techniques.

42.2 Pathology

The brain is abnormally enlarged in CD. Otherwise the external appearance of the cerebral gyri, cerebellum, and brain stem are normal. On sectioning, an ill-defined demarcation between cortex and white matter is seen in all parts of the cerebral and cerebellar hemispheres. The deeper cortex and subcortical white matter are edematous and soft. Cavitation of the affected white matter is only seen in advanced stages of the disease. During the first few years, the ventricles are slightly narrowed. Thereafter, they gradually increase in size as a result of increasingly severe loss of white matter.

Histological examination shows vacuolation with the presence of innumerable minor vacuoles, most striking in the subcortical cerebral white matter and in the deep layers of the cortex, giving the affected areas a spongy appearance. The periventricular white matter is better preserved. No substances can be demonstrated within the vacuoles. Myelin degeneration is present in a distribution that closely follows the status spongiosus. Thus, moderate to severe loss of myelin is seen in the subcortical areas, whereas the periventricular white matter, corpus callosum, internal capsule, and fornix are less severely vacuolated and their myelin content is better preserved. In the areas of severe myelin loss axons and oligodendro-

cytes are largely intact. Myelin vacuolation and loss is accompanied by astrogliosis. Myelin breakdown products are scarce; some sudanophilic lipids may be present in macrophages. Cortical neurons are normal in number and appearance, while intracortical myelin is lost. Within the cortex, there is a marked proliferation of swollen astroglia with the morphologic features of Alzheimer type II cells. Their nuclei are abnormally large, variably shaped, with unevenly dispersed nuclear chromatin, which tends to accumulate near the nuclear membrane. The cytoplasm is swollen and watery. These cells are also seen in the subcortical white matter, but they do not prevail in other areas of vacuolated white matter.

On electron microscopy, the vacuoles observed in the white matter appear to be formed as a result of separation of myelin lamellae with intramyelinic vacuole formation. Splitting of the myelin lamellae occurs at the intraperiod lines, where external surfaces of the original oligodendroglial membrane were closely apposed in the formation of the myelin sheath. The swollen astrocytes with enlarged nuclei and watery cytoplasm contribute to the vacuolated aspect, in particular within the cortex. On electron microscopy these cells are shown to contain abnormal, enormously elongated mitochondria.

Sponginess is also present in the globus pallidus, thalamus, and hypothalamus, whereas caudate nucleus and in particular putamen tend to be better preserved. Alzheimer type II cells are present in the basal ganglia.

Within the cerebellum the most severe vacuolation is seen in the Purkinje cell layer, the deeper areas of the granule cell layer, and the subcortical white matter. Purkinje cells and granule cells are well preserved. Myelin loss is accompanied by astrogliosis, but axons are spared. The deep white matter of the cerebellum is better preserved. Vacuolation is present in the dentate nucleus, but nerve cells are intact.

Vacuolation, demyelination, and astrogliosis are present in the midbrain, pons, medulla, and spinal cord, both in descending and ascending tracts. However, the involvement of brain stem and spinal cord is variable in severity. Cranial nerve nuclei, other brain stem nuclei, and spinal cord gray matter also show a variable degree of vacuolation. The optic nerve, containing CNS myelin, is involved in the process. The other cranial nerves, the spinal roots, and the peripheral nerves are normal.

In protracted infantile patients, who survive for a relatively long time, the lateral ventricles are markedly dilated as a result of severe loss of white matter tissue. Myelin is now also lost in the deep white matter. In addition, neuronal loss is severe, and vacuolation is seen in all layers of the cortex.

In the congenital variant the sponginess is most severe in the cerebellum and brain stem, which are the parts with the highest myelin content at that time.

42.3 Chemical Pathology

In CD, chemical abnormalities in the brain are limited to the white matter; the chemical composition of the gray matter is near-normal. The most prominent white matter abnormalities are its increased content of water and *N*-acetylaspartate. Electrolyte analyses show that the composition of the excess fluid in the brain is similar to that of plasma ultrafiltrate. There is a drastic decrease in myelin lipids and protein as manifestations of the severe myelin loss. There is a marked decrease of galactolipids and a relatively smaller decrease in cholesterol and total phospholipids. No cholesterol esters are detected in the white matter.

The composition of myelin is altered. Cholesterol is increased, and phospholipids are decreased, especially ethanolamine phosphoglycerides. Galactolipids are severely diminished, cerebroside more so than sulfatide. The total ganglioside concentration is normal.

This abnormal pattern of white matter and myelin composition is also seen in several other diseases and is probably a result of nonspecific destruction of myelin.

42.4 Pathogenetic Considerations

CD is caused by a deficiency of aspartoacylase. The gene for aspartoacylase, *ASPA*, is located on the short arm of chromosome 17 (17p13-ter). Numerous different mutations have been described. Homozygosity for one particular mutation (Glu285Ala) is responsible for most Ashkenazi Jewish cases. In non-Jewish patients the mutations are different and more diverse. There is no evident correlation between genotype and phenotype. Siblings homozygous for the same mutation can have a very different course of disease and life span.

N-acetylaspartate is synthesized from acetyl-CoA and aspartate by *L*-aspartate-*N*-acetyl transferase. This reaction occurs exclusively in neurons of the CNS. *N*-acetylaspartate is metabolized to aspartate and acetate by aspartoacylase. Aspartoacylase is exclusively located in oligodendroglia. In deficiency of aspartoacylase *N*-acetylaspartate concentrations in the brain are elevated and the substance is excreted in large amounts in the urine.

The brain is the only organ in which the biosynthesis of *N*-acetylaspartate has been demonstrated. Its concentration in the brain is very high, and it is higher in gray than in white matter. *N*-acetylaspartate is second to glutamic acid in its abundance in the human brain. It has been shown that *N*-acetylaspartate is mainly or exclusively localized in neurons. To date, the functional role of this compound has not been elucidated. Some suggest it is involved in neurotransmission. The high concentration of *N*-acetylaspartate in neurons may be a form of chemical compartmentation serving neurotransmission. *N*-acetylaspartate is converted to aspartate and has been implicated in the formation of glutamate. It has been found that not only *N*-acetylaspartate but also *N*-acetylaspartylglutamate is elevated. Both aspartate and glutamate are excitatory neurotransmitters. *N*-acetylaspartylglutamate may be the storage form of glutamate. *N*-acetylaspartylglutamate may also by itself interfere with neurotransmitter receptors. Another suggestion is that *N*-acetylaspartate may act as an osmolyte and that its lack of hydrolysis leads to accumulation of water in brain cells. *N*-acetylaspartate may function as a molecular water pump in myelinated neurons. It has also been proposed that *N*-acetylaspartate is an acetyl group donor in the synthesis of brain lipids, including myelin lipids. In particular, the substance would be important in the formation of cerebronic acid, which is a precursor of ceramide, which in turn is a constituent of sulfatide and cerebroside. Some others suggest *N*-acetylaspartate is important in protein synthesis.

The relationship between accumulation of *N*-acetylaspartate and myelin vacuolation and formation of abnormal astrocytes has not been elucidated. Those who suggest that the substance is essential for the normal synthesis of myelin lipids explain the myelin abnormality by faulty formation of one of its constituents. However, the chemical composition of myelin in CD shows only nonspecific abnormalities related to the myelin breakdown process and no specific deficiencies of any of its components. Others suggest that accumulation of *N*-acetylaspartate may have toxic effects leading to myelin splitting. In this respect, the comparison to hexachlorophene intoxication and triethyltin intoxication is important, as both conditions are characterized by myelin splitting, vacuolation, and loss, and presence of Alzheimer type II cells with abnormal mitochondria, as is the case in CD. Hexachlorophene and triethyltin both interfere with mitochondrial oxidative phosphorylation. *N*-acetylaspartate is synthesized in mitochondria and if this substance accumulates, its toxic effects may well be mainly exerted in these organelles. However, the relationship between possible mitochondrial dysfunction and myelin vacuolation is unclear. De Coo et al. (1991) could not find evidence of mitochondrial

dysfunction, in contrast to earlier studies in which abnormalities in mitochondrial Na^+/K^+ -ATPase had been reported (Adachi et al. 1966, 1972). Those who believe that *N*-acetylaspartate is a molecular water pump and has an important role in osmoregulation hypothesize that the myelin vacuolation and other pathological changes are the consequence of continuous increased hydrostatic pressure.

42.5 Therapy

At present there is no specific therapy for CD patients. Seizures need to be controlled. Gene therapy has been attempted. Clinical results have so far not been impressive and at most some transient beneficial effects have occurred. Prolonged follow-up is not yet available.

42.6 Magnetic Resonance Imaging

CT shows diffuse hypodensity of the white matter of cerebral hemispheres and cerebellum. Involvement of the globus pallidus with sparing of caudate nucleus and putamen is usually seen.

In infants with CD, diffuse cerebral white matter changes are seen (Figs. 42.1 and 42.2). In older patients with CD, MRI shows that the most severe abnormalities are present in the subcortical white matter of the cerebrum and cerebellum (Fig. 42.3). Central white matter structures, such as the periventricular rim of white matter, internal capsule, and corpus callosum are better preserved (Fig. 42.3). As the disease progresses, the central white matter also becomes involved (Fig. 42.4). Thus, the spread of the white matter changes is centripetal. The white matter abnormalities are confluent and symmetrical in distribution. The subcortical white matter has a mildly swollen aspect, broadening the gyri. Over time, white

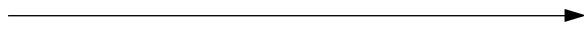


Fig. 42.1. A 4-month-old male infant with CD. Note the diffuse signal abnormality of the cerebral and cerebellar white matter on the T_2 -weighted images (*first three rows*). The globus pallidus and thalamus are involved, but the putamen and caudate nucleus are spared. The posterior limb of the internal capsule and brain stem are also abnormal. The FLAIR image (*fourth row, left*) demonstrates that the peripheral cerebral white matter has a high water content with a low signal intensity as compared to the central white matter. On the trace diffusion-weighted image ($b = 1000$; *fourth row, middle*) the central white matter (posterior limb of the internal capsule and the optic radiation) has a high signal, whereas the same structures have a low ADC in the range of 45–70 on the ADC map (*fourth row, right*), indicative of restricted diffusion in these regions

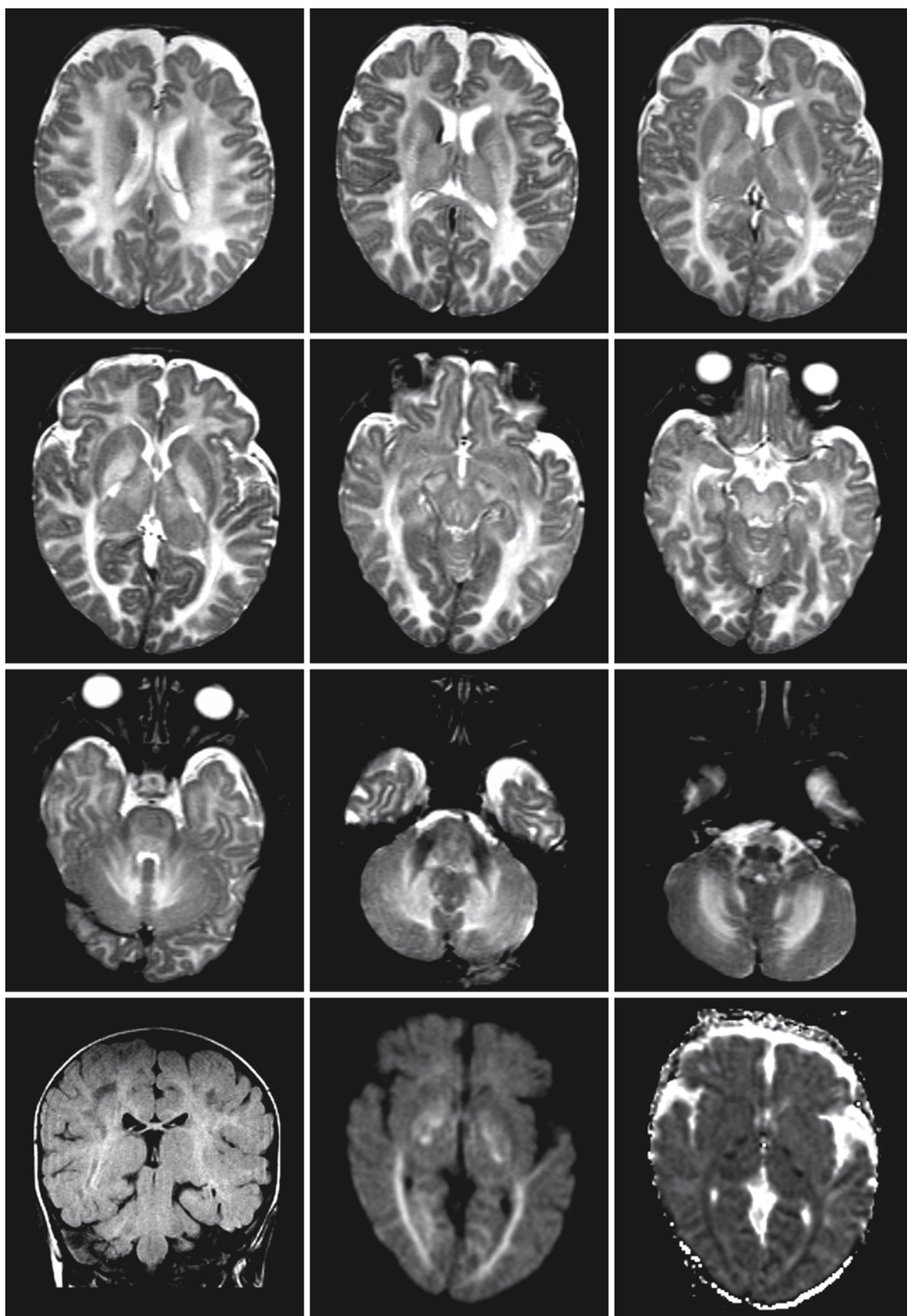


Fig. 42.1.

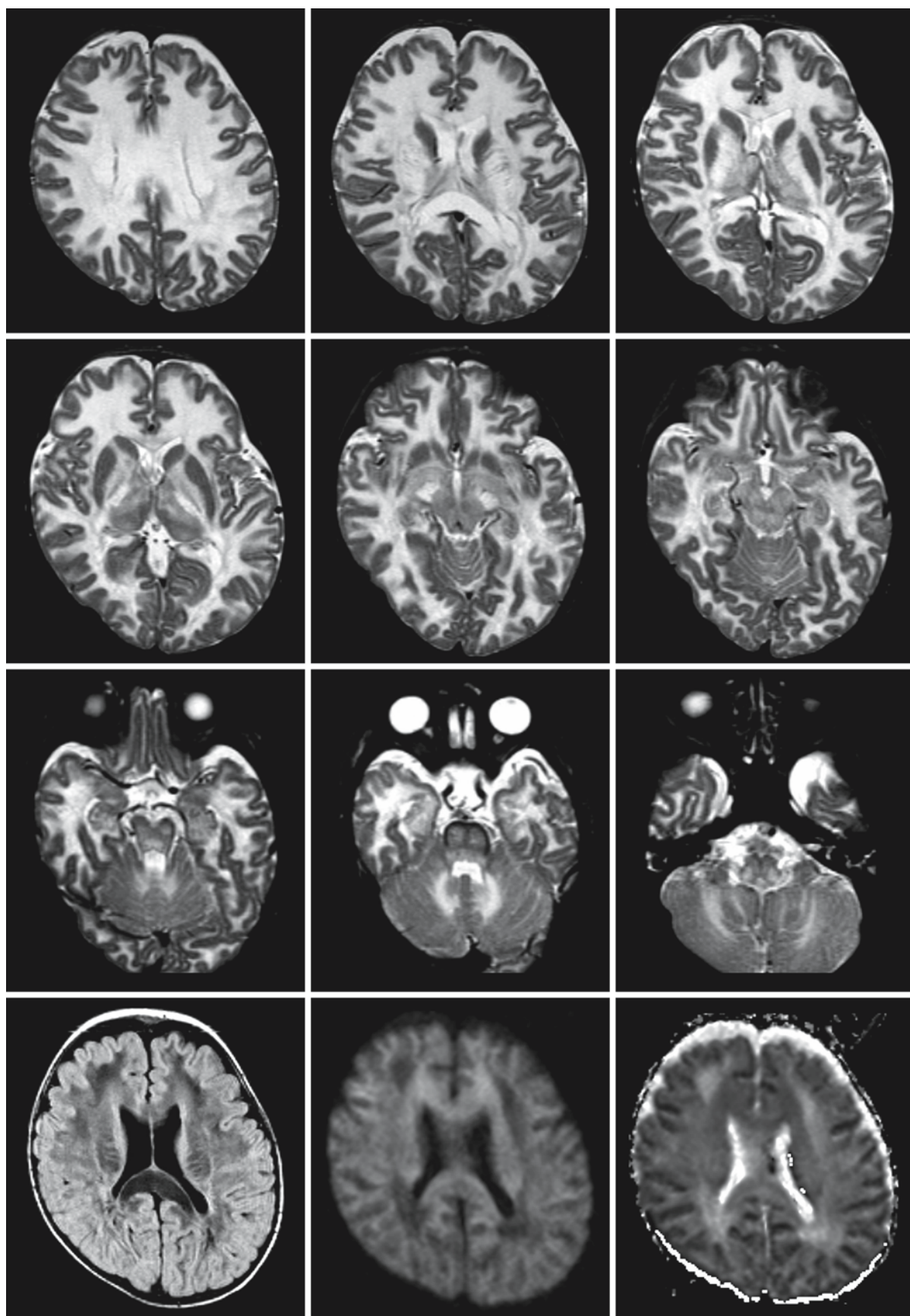


Fig. 42.2.

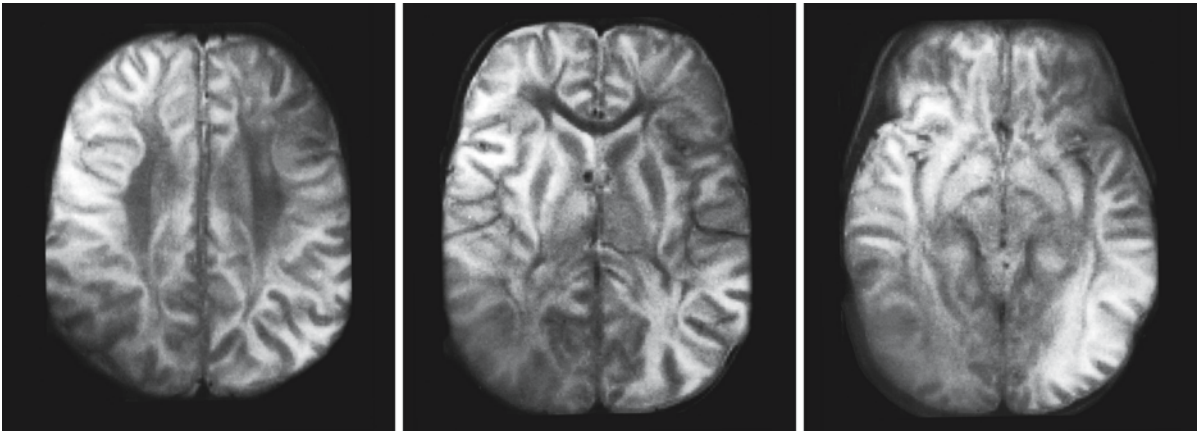


Fig. 42.3. A 21-month-old boy with CD. These T₂-weighted images show the involvement of the subcortical white matter, globus pallidus, and, to a lesser extent, the thalamus. The central white matter structures, including the corpus callosum,

periventricular white matter, and posterior limb of the internal capsule, are spared. The midbrain is diffusely abnormal. From Meyding-Lamadé and Sartor (1993), with permission

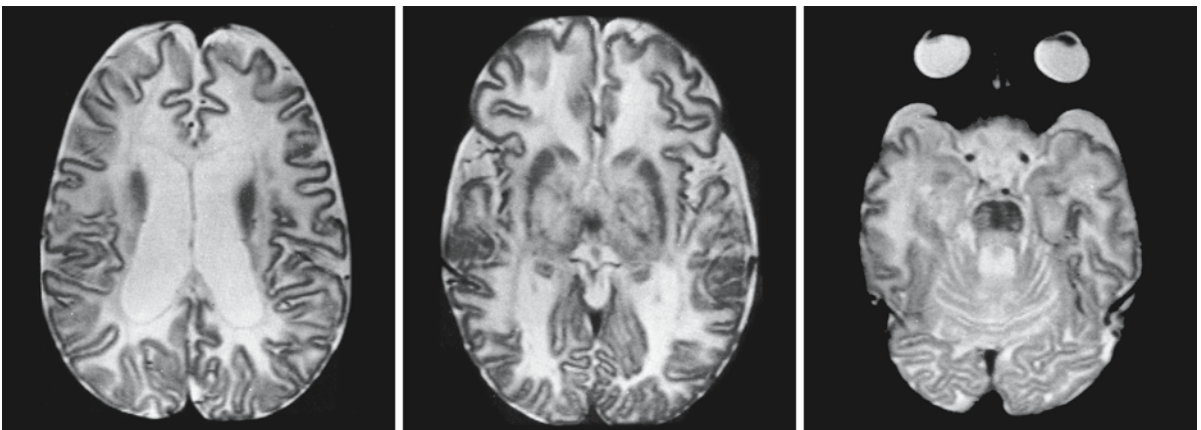


Fig. 42.4. A 32-month-old child with CD. These T₂-weighted images show there is now involvement of all white matter structures, including corpus callosum and periventricular white matter. The globus pallidus and thalamus are involved

bilaterally, whereas the putamen and caudate nucleus are spared. The brain stem contains signal abnormalities. There are signs of diffuse atrophy. From Kendall (1992), with permission

←
Fig. 42.2. The same boy with CD as in Fig. 42.1, now 12 months old. The pattern of abnormalities on the T₂-weighted images (*first three rows*) is essentially unchanged. The FLAIR image (*fourth row, left*) shows further white matter rarefaction with a lower signal of the cerebral white matter throughout. The trace diffusion-weighted image (*b = 1000; fourth row, middle*) shows that large parts of the cerebral white matter now have a low signal, whereas they have a high ADC in the range of 130–200 on the ADC map (*fourth row, right*), indicative of increased diffusion

matter atrophy occurs with marked dilatation of the lateral ventricles and to a lesser extent the subarachnoid spaces (Figs. 42.4 and 42.5). Bilateral involvement of the globus pallidus is seen and involvement of the thalamus often present (Figs. 42.1–42.4). The resulting image with sparing of putamen and caudate nucleus is very typical of CD. Brain stem tracts are involved as a rule (Figs. 42.1–42.5). The cerebellar white matter may also be affected. Over time, brain stem and cerebellar atrophy ensues (Fig. 42.5).

Diffusion-weighted imaging shows restricted diffusion with low ADC values early in the course of the disease (Fig. 42.1), whereas increased diffusion and high ADC values are found later in the course of the

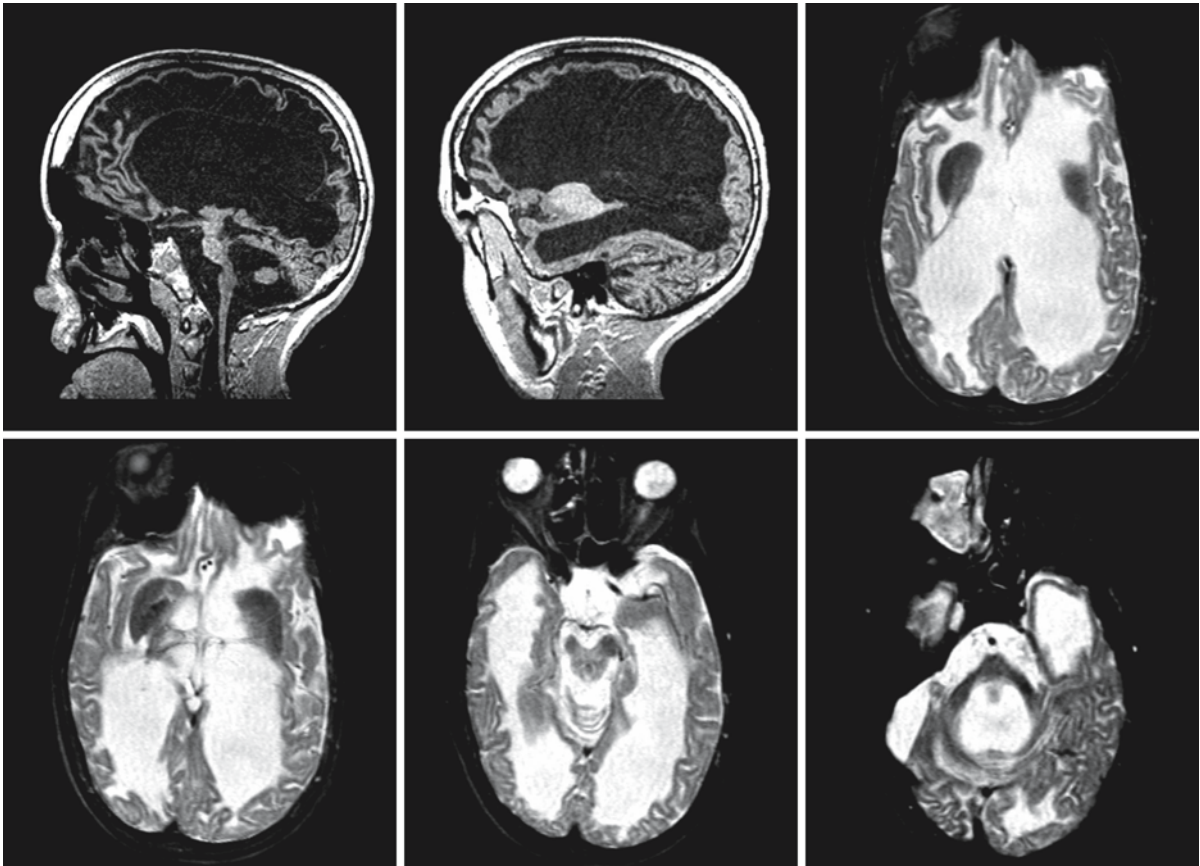


Fig. 42.5. A 19-year-old boy with CD. There is impressive cerebral and cerebellar atrophy. The images still show that the remaining cerebral white matter is abnormal, but they no longer display the features characteristic of CD

disease (Fig. 42.2). The explanation is probably to be found in the myelin vacuolation, which leads to restricting of the extracellular space in the early stages, whereas in the chronic stage destruction of the white matter matrix leads to increased size of the extracellular space. Similar observations have been done in maple syrup urine disease, a disease also characterized by myelin vacuolation.

Proton MRS of the brain in CD patients reveals a relatively high *N*-acetylaspartate resonance. The increase may only be relative in comparison with the concentration of the other metabolites, although increase in absolute values has also been reported. Lactate may be elevated. Choline is as a rule decreased. The decrease in choline suggests a component of hypomyelination rather than active myelin loss.

Zafeiriou et al. (1999) have reported MRI findings in two siblings with a mild and protracted course of disease. The diagnosis was confirmed by finding elevated *N*-acetylaspartate in urine and deficiency of aspartoacylase in cultured fibroblasts. MRI of the

brain (Fig. 42.6) revealed signal abnormalities limited to the U fibers, whereas the periventricular and deep white matter had a normal signal. In addition, signal abnormalities were seen in the caudate nucleus, thalamus, and capsule between globus pallidus and putamen. There were signal abnormalities in the external and extreme capsules. The rest of the putamen appeared to have a normal signal. The tegmentum of the pons, hilus of the dentate nucleus, and dentate nucleus were also involved. Thus, the pattern is very similar to the pattern described above for classical CD, the main difference being the fact that the cerebral white matter abnormalities were much more limited in extent and affected the U fibers only.

Two unusual patients with elevated urinary *N*-acetylaspartate and aspartoacylase deficiency in fibroblasts were reported by Toft et al. (1993). The clinical disease was much milder than in the usual form of CD, with normocephaly, epilepsy, and mild psychomotor retardation without regression at any time up to the age of 6 years. MR images showed sub-

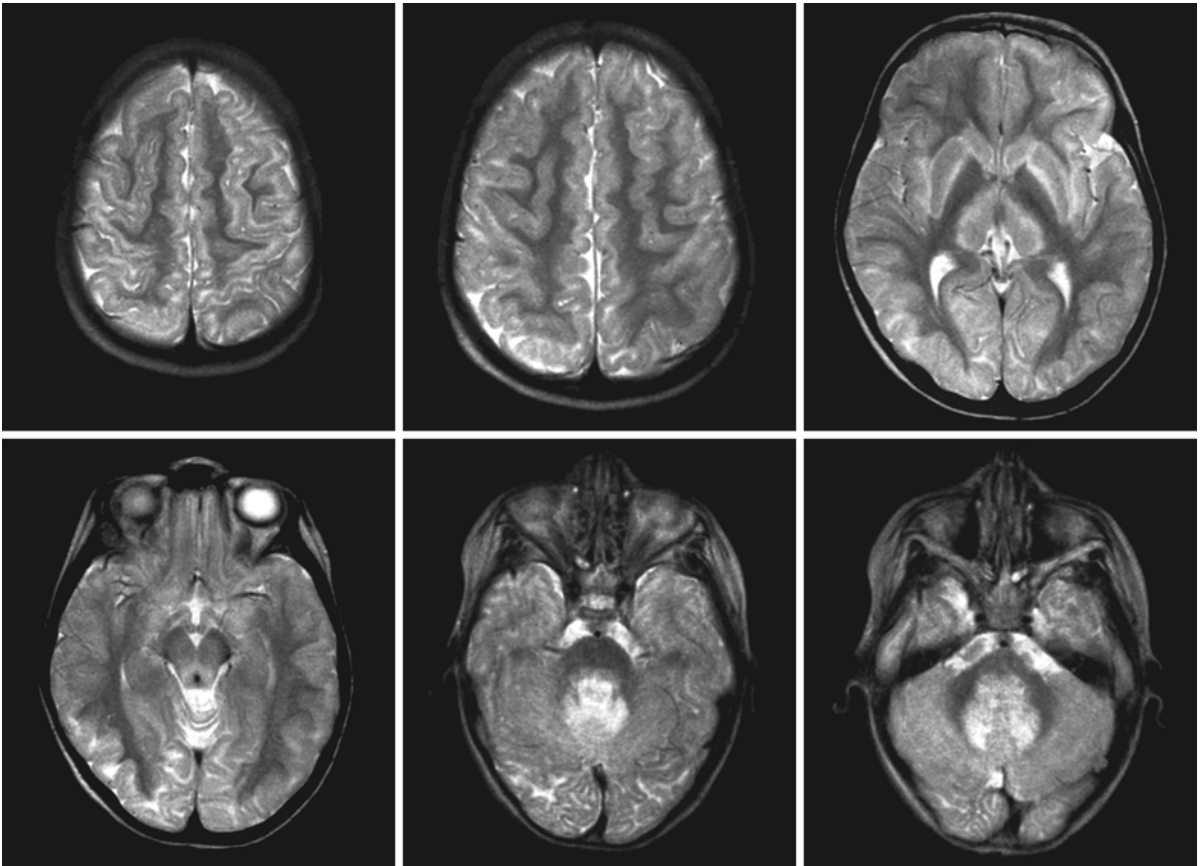


Fig. 42.6. A 4-year-old female patient with a mild variant of CD. The U fibers are diffusely abnormal, whereas the central cerebral white matter is normal. The thalamus, head of the caudate nucleus, external capsule, and capsule between globus

pallidus and putamen have an abnormal signal. In addition, signal abnormalities are present in the dentate nucleus and hilus of the dentate nucleus. Subtle signal changes are seen in the brain stem. From Zafeiriou et al. (1999), with permission

the subcortical white matter changes in one patient, whereas the white matter was normal in the other patient. Signal abnormalities were seen in globus pallidus, putamen, and caudate nucleus. Proton MRS did not reveal an elevation of *N*-acetylaspartate, which is highly unusual for CD. It is important to recognize that the assessment of aspartoacylase activity is difficult and not always reliable. Unfortunately, the diagnosis was not confirmed by demonstration of mutations in the *ASPA* gene.

The differential diagnosis of diffusely swollen white matter changes includes mainly late onset variants of maple syrup urine disease, Alexander disease, congenital muscular dystrophy, and megalencephalic leukoencephalopathy with subcortical cysts. In the presence of lesions of the globus pallidus with preservation of the caudate nucleus and putamen, the images are highly suggestive of CD, but maple syrup urine disease should be excluded by appropriate biochemical tests.

L-2-Hydroxyglutaric Aciduria

43.1 Clinical Features and Laboratory Investigations

L-2-Hydroxyglutaric aciduria is a rare neurometabolic disorder with autosomal recessive inheritance. The children are initially normal. In the second year of life a delay in unsupported walking, abnormal gait, speech delay, or febrile convulsions form the presenting symptoms in most cases. In other patients no abnormalities are noted until learning disabilities become apparent during early school years. Over the years slowly progressive neurological dysfunction is noted, characterized predominantly by cerebellar ataxia with nystagmus, dysarthria, head titubation, trunk ataxia, dysmetria, and intention tremor. Slow intellectual decline is noted in all patients. Frequently noted abnormalities are extrapyramidal signs such as dystonia and choreoathetosis, pyramidal signs, pseudobulbar signs, myoclonus, and macrocephaly. Seizures occur in the majority of the patients, especially in the context of fever. In some patients stable mental retardation is the only manifestation for years and the slowly progressive decline of motor and cognitive functions only starts in adolescence or adulthood. There is increasing evidence that patients with L-2-hydroxyglutaric aciduria have an increased risk of CNS malignancies of various types.

Laboratory investigations reveal elevated urinary excretion of L-2-hydroxyglutaric acid; plasma and CSF levels are also increased. Lysine levels in urine, plasma, and CSF may also be elevated. Prenatal diagnosis is possible by assessment of the L-2-hydroxyglutaric acid concentration in the amniotic fluid.

43.2 Pathology

Only a few descriptions of brain pathology are available. In 1994, Larnaout et al. described diffuse demyelination, spongiosis, and cystic cavitation of the cerebral white matter in a patient who died at the age of 30 years. The abnormalities were most pronounced in the subcortical region, in the axis of cerebral convolutions. In the cerebellum, loss of granule cells and Purkinje cells and moderate pallor of the white matter were noted. The dentate nucleus and globus pallidus showed marked cell loss and severe spongiosis. The putamen and caudate nucleus were less severely affected. Myelin was normal in the corpus callosum,

genu of the internal capsule, optic tracts, and optic radiations. Cerebral cortex, thalamus, brain stem, and spinal cord were normal.

43.3 Pathogenetic Considerations

L-2-hydroxyglutaric aciduria is caused by a deficiency of an FAD-linked, membrane-bound mitochondrial enzyme, L-2-hydroxyglutarate dehydrogenase, that catalyzes the oxidation of L-2-hydroxyglutarate to α -ketoglutarate. The gene encoding this enzyme, *C14orf160*, also called *DURANIN*, is located on chromosome 14q22.1. Elevated levels of L-2-hydroxyglutarate are probably toxic for the CNS. The elevations of lysine in blood and CSF may be secondary rather than primary, as lysine loading appears to have no effect on the level of L-2-hydroxyglutaric acid in blood.

Two patients have been reported with neonatal-onset encephalopathy, early death, and elevated L-2-hydroxyglutaric acid as well as lactate (Chen et al. 1996; Barth et al. 1998). It is likely that these patients had another, unrelated metabolic disease.

43.4 Therapy

Treatment is entirely symptomatic.

43.5 Magnetic Resonance Imaging

MRI in patients with L-2-hydroxyglutaric aciduria shows a highly characteristic and consistent pattern. The abnormalities begin within the subcortical white matter with multiple foci of high signal intensity on T₂-weighted images (Figs. 43.1 and 43.2). The lesions have a tendency to become confluent, first in the frontoparietal region (Fig. 43.1), later involving all subcortical white matter in a confluent manner (Figs. 43.2 and 43.3). In relatively mildly affected patients, the abnormalities remain multifocal and confined to the U fibers, whereas in patients with more serious neurological handicap, the cerebral white matter is more diffusely involved, although a rim of periventricular tissue remains spared. The white matter abnormalities are mildly swollen with some broadening of the gyri (Figs. 43.1–43.3). The aspect of swollen white matter changes is related to the spongi-

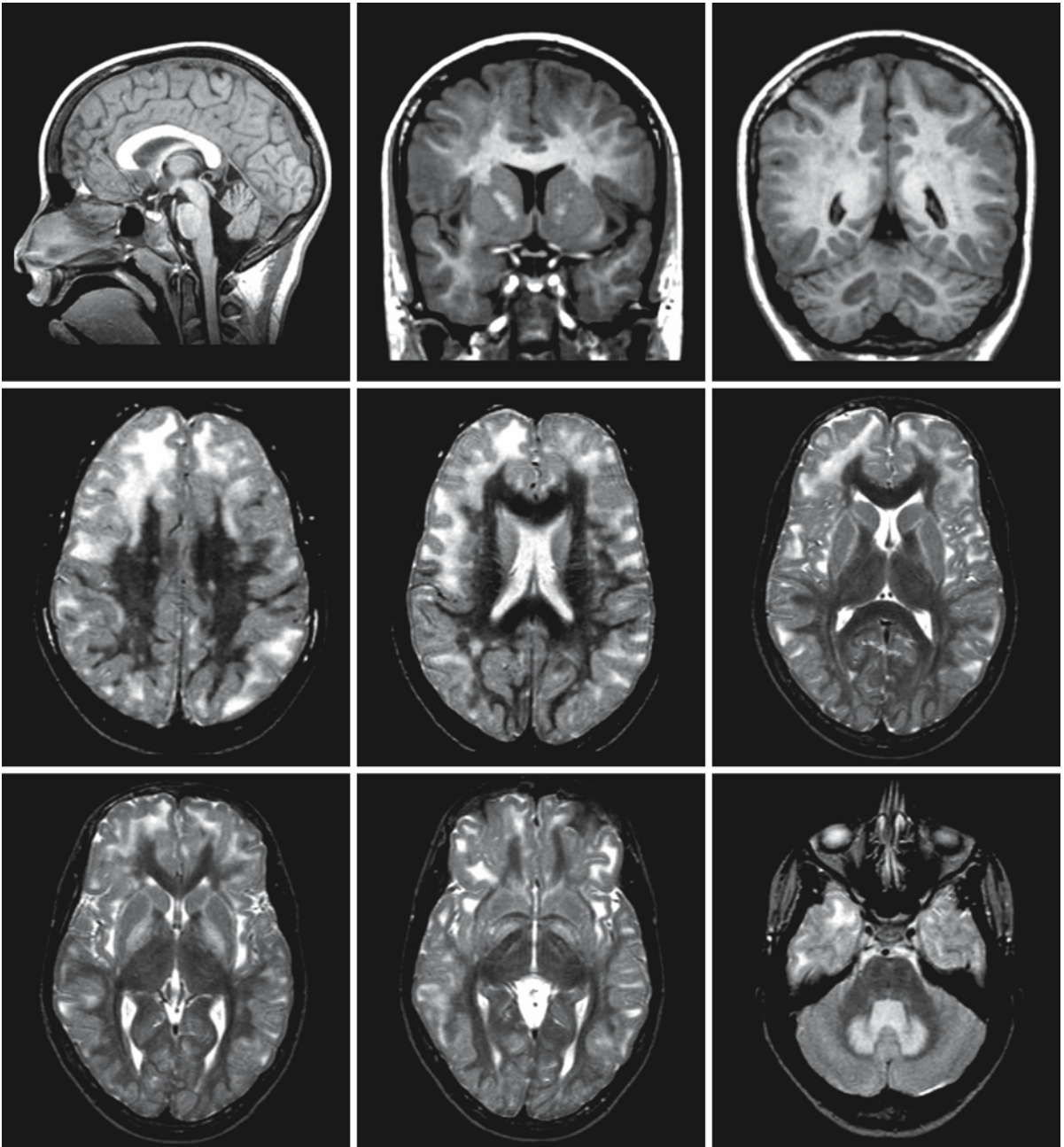


Fig. 43.1. A 12-year-old girl who has L-2-hydroxyglutaric aciduria, showing the involvement of subcortical white matter and the sparing of the central white matter including the corpus callosum. The subcortical lesions are partly multifocal,

partly confluent. Lesions are present in central gray matter structures, most prominently the globus pallidus and dentate nucleus. The sagittal image shows that part of the inferior vermis is absent

form nature of the leukoencephalopathy at histopathology. Diffusion-weighted MRI has revealed a high ADC and low signal on diffusion-weighted images in the abnormal white matter, consistent with increased freedom of water movements. Centrally located white matter structures, including periventricular white matter, corpus callosum, internal cap-

sule, and brain stem, are spared, although the internal capsule is involved in some cases. The lateral ventricles become slightly enlarged. In addition to the white matter abnormalities, changes in signal intensity are typically seen in the globus pallidus, caudate nucleus, and putamen (Fig. 43.1). The globus pallidus is usually most severely involved. The caudate nucleus may be

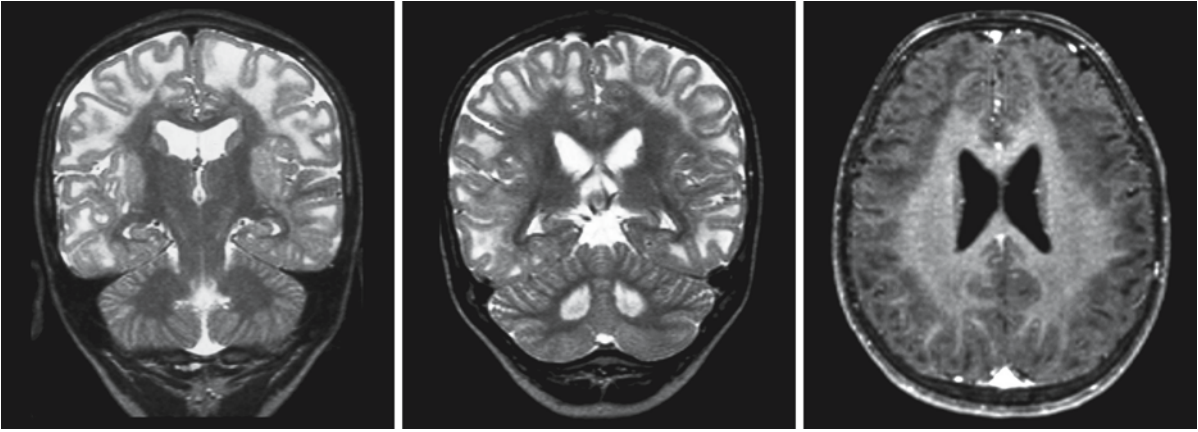


Fig. 43.2. MR images of a 10-year-old boy with L-2-hydroxyglutaric aciduria, showing confluent involvement of the subcortical white matter, which is also mildly swollen. The central

white matter structures are spared, which is nicely shown by the T₁-weighted image

atrophic. The cerebellar vermis becomes highly atrophic (Fig. 43.3). The cerebellar hemispheres are also atrophic, but less severely. In the dentate nucleus a change in signal intensity is present (Figs. 43.1–43.3). The cerebellar white matter is most often normal.

The pattern of symmetrical abnormalities with supratentorial subcortical white matter lesions, infratentorial atrophy of the cerebellum (vermis more than hemispheres), and lesions in both dentate nuclei is reminiscent of the patterns seen in Kearns–Sayre syndrome and Canavan disease. In both of the latter disorders brain stem involvement is as a rule present.

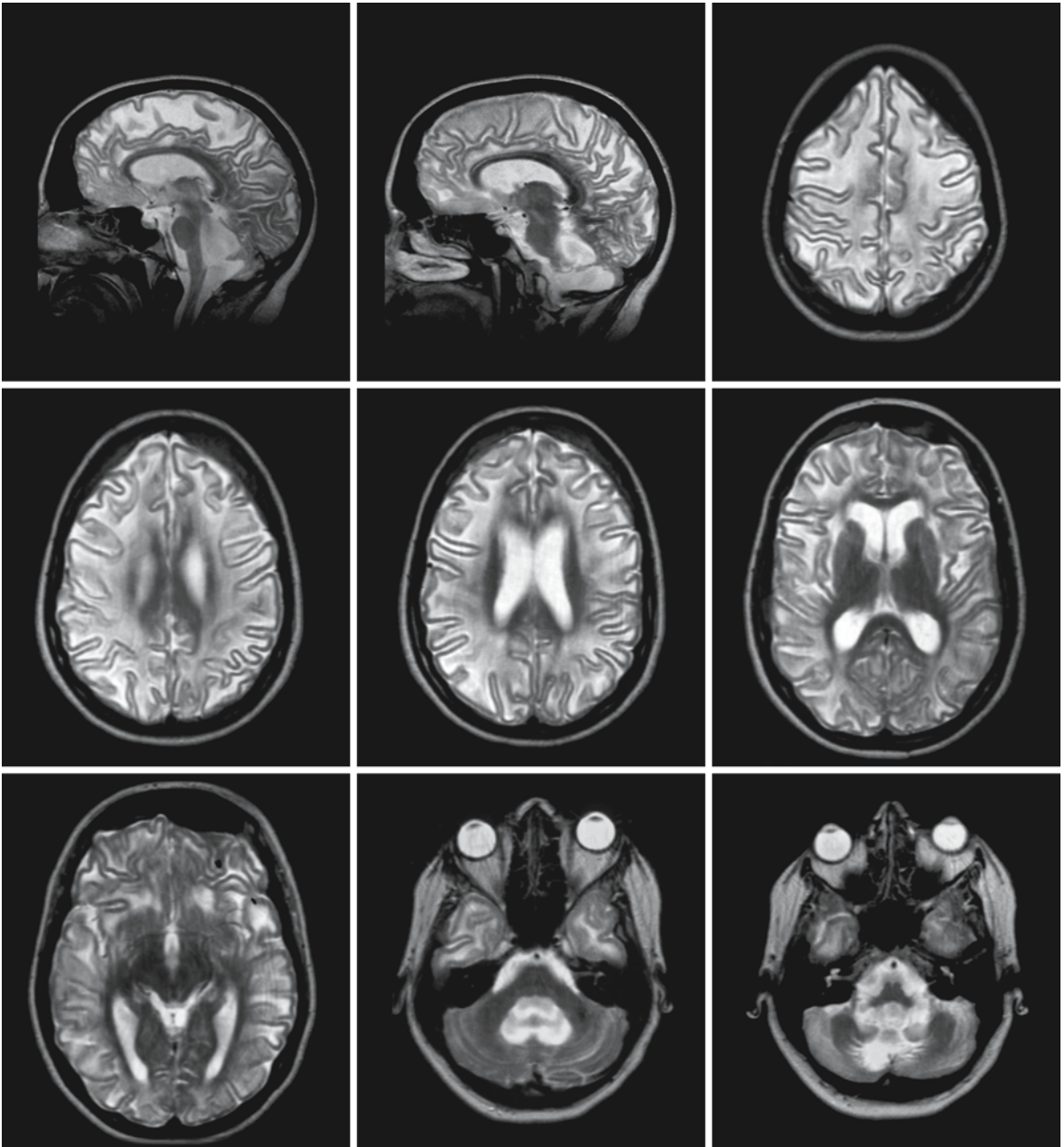


Fig. 43.3. The T_2 -weighted images of a 25-year-old female patient with L-2-hydroxyglutaric aciduria show involvement of all subcortical and deep cerebral white matter with sparing of a thin periventricular rim. The basal ganglia are atrophic and

the dentate nucleus has disappeared. What remains of the basal ganglia has a mildly abnormal signal. The cerebellum is highly atrophic. Courtesy of Dr. N. Giffin, Royal United Hospital Bath, Bath, United Kingdom

D-2-Hydroxyglutaric Aciduria

44.1 Clinical Features and Laboratory Investigations

D-2-Hydroxyglutaric aciduria is a rare neurometabolic disorder with autosomal recessive inheritance. Two different variants are distinguished: a severe variant and a mild variant. The two variants have never been observed within the same family.

Severe D-2-hydroxyglutaric aciduria results in neonatal- or early-infantile-onset encephalopathy with serious epilepsy, hypotonia, visual failure, and no or little development. The infants are often irritable and lethargic. Episodic vomiting may be present. Inspiratory stridor, dyspnea, and apnea may occur. Further signs may be spasticity, chorea, or dystonia. Both macrocephaly and microcephaly may occur. Many patients have signs of cardiomyopathy. Hepatomegaly is of rare occurrence. Signs of mild facial dysmorphism consisting of a flat face with a broad nasal bridge and external ear anomalies are frequent. Early death may occur, but the patients may also survive with severe developmental delay and epilepsy.

Mild D-2-hydroxyglutaric aciduria is clinically much more variable. Hypotonia, developmental delay of variable severity, and epilepsy are the most frequent signs of the disease. Macrocephaly may be present. Multiple cerebral infarctions associated with acute-onset neurological signs have been reported in one patient with D-2-hydroxyglutaric aciduria and no identifiable known vascular risk factors (van der Knaap et al. 1999b). Cardiomyopathy has been observed in few patients. However, some patients have no clinical problems that can be related to the D-2-hydroxyglutaric aciduria. These patients are detected in the course of screening for D-2-hydroxyglutaric aciduria in a family with a symptomatic child.

Laboratory investigations reveal elevated urinary excretion of D-2-hydroxyglutaric acid; plasma and CSF levels are also increased. The urinary organic acid profile often shows elevated excretion of 2-ketoglutarate, sometimes accompanied by elevated excretion of other citric acid cycle intermediates and lactate. Nonketotic dicarboxylic aciduria is observed in some patients. Prenatal diagnosis is possible by assessment of D-2-hydroxyglutaric acid concentration in amniotic fluid. A few patients with the severe phenotype have combined D- and L-2-hydroxyglutaric aciduria. It has been suggested that these patients rep-

resent a separate third variant. Prenatal diagnosis may not be reliable in this latter disorder.

44.2 Pathology

There is a detailed histopathological description of only one patient with a severe phenotype (Eeg-Olofsson et al. 2000). The boy had severe psychomotor retardation and epilepsy and died at the age of 14 years. The middle cerebral arteries showed multiple saccular aneurysms. There was diffuse atrophy of the cerebral white matter with marked dilation of the lateral ventricles. Microscopy showed loss of myelinated fibers and some astrogliosis within the cerebral white matter. The cerebral cortex was intact. The basal ganglia and cerebellum showed slight atrophy. Microscopically, there was some loss of Purkinje cells and a reduction of cerebellar white matter. The brain stem was intact.

44.3 Pathogenetic Considerations

D-2-hydroxyglutaric aciduria is caused by a deficiency of the mitochondrial enzyme D-2-hydroxyglutarate dehydrogenase, which converts D-2-hydroxyglutarate into 2-ketoglutarate. The enzyme is encoded by a gene with the code name *MGC25181*, located on chromosome 2p25.3. It is not yet known whether deficiency of this enzyme underlies the disease in all patients.

D-2-hydroxyglutaric acid is a metabolic intermediate in a variety of pathways. It is striking that the urinary organic acid profile often shows elevated excretion of 2-ketoglutarate. Sometimes the increased urinary excretion of 2-ketoglutarate is accompanied by elevated excretion of other citric acid cycle intermediates. The latter abnormalities probably reflect a secondary disturbance of the citric acid cycle and mitochondrial respiratory chain. It has been shown that elevated levels of D-2-hydroxyglutaric acid in brain tissue lead to strong inhibition of cytochrome-c oxidase activity (complex IV) in a dose-dependent manner in vitro (da Silva et al. 2002). Secondary respiratory chain dysfunction may be important in the pathophysiology of the clinical symptomatology in D-2-hydroxyglutaric aciduria. The nonketotic dicarboxylic aciduria observed in some patients may reflect a sec-

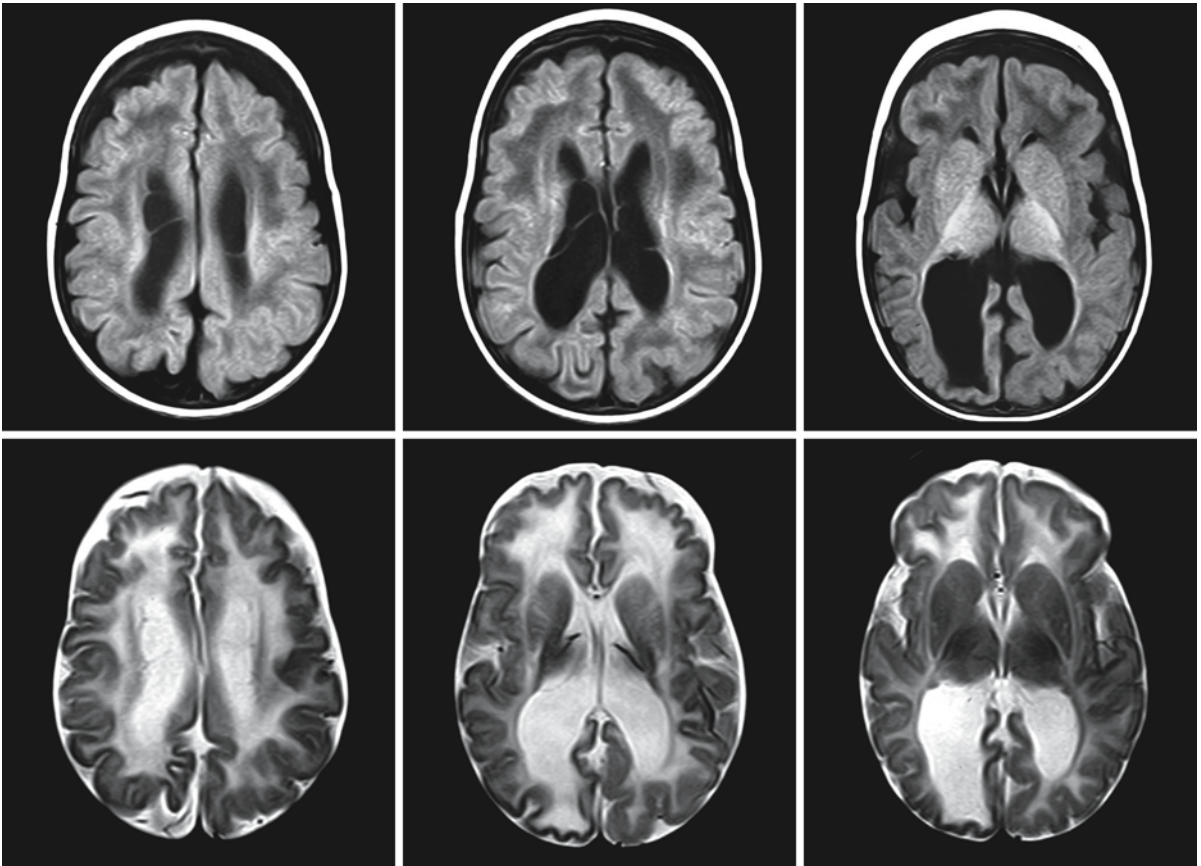


Fig. 44.1. T₁-weighted (*first row*) and T₂-weighted (*second row*) images in a 4-month-old patient with the severe variant of D-2-hydroxyglutaric aciduria. The lateral ventricles are enlarged, most pronouncedly in the posterior region. The subarachnoid spaces are also mildly enlarged. Myelination and

gyration are delayed. The opercula are insufficiently developed and the gyri are too coarse for the age of the infant. There are large subependymal cysts over the body of the caudate nucleus. From van der Knaap et al. (1999a), with permission

ondary disturbance of the mitochondrial fatty acid β -oxidation.

44.4 Therapy

Treatment is entirely symptomatic.

44.5 Magnetic Resonance Imaging

In the early-onset severe variant of D-2-hydroxyglutaric aciduria, MRI performed in the first few months of life shows signs of delayed cerebral maturation, including delayed myelination and gyration (Fig. 44.1). Gyri are insufficiently branched, and in some patients focal agyria is found, particularly in the occipital region. The sylvian fissure is wide open due to insufficient formation of the frontal and temporal opercula (Fig. 44.1). The lateral ventricles are usually mildly

enlarged, mainly in the posterior part. The ventricular enlargement is often combined with mildly enlarged frontal subarachnoid spaces and frontal subdural effusions (Figs. 44.1 and 44.2). Secondary subdural hematomas may occur. Within the first few months of life, subependymal germinolytic cysts are almost invariably present over the head and corpus of the caudate nucleus (Fig. 44.1). They disappear with time and are rarely seen after 6 months. Follow-up MRI in the second year of life shows more advanced gyration, but myelination remains delayed and in some patients patchy white matter abnormalities are seen (Fig. 44.2). The lateral ventricles may become highly enlarged due to white matter atrophy. In one patient, multiple aneurysms of the large cerebral arteries were found (Eeg-Olofsson et al. 2000; Fig. 44.3).

In the mild variant of D-2-hydroxyglutaric aciduria, subependymal cysts and delayed myelination may be seen on early MRI. The lateral ventricles and the subarachnoid spaces may be mildly dilated. Subdural

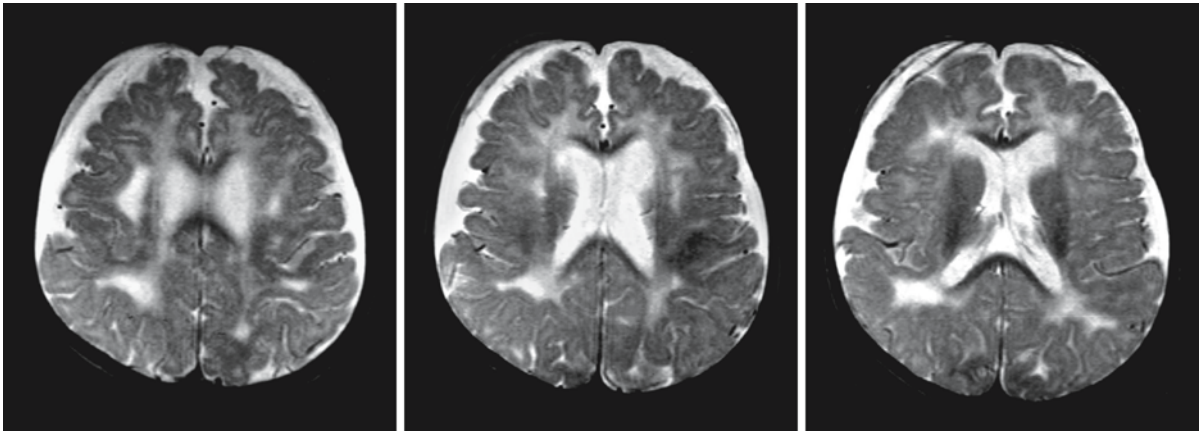


Fig. 44.2. T₂-weighted images in a patient with the severe variant of D-2-hydroxyglutaric aciduria at the age of 15 months. Myelination is seriously delayed. In addition, there are multifocal white matter abnormalities. The lateral ventricles

and subarachnoid spaces are mildly enlarged. There are small subdural effusions. From van der Knaap et al. (1999b), with permission

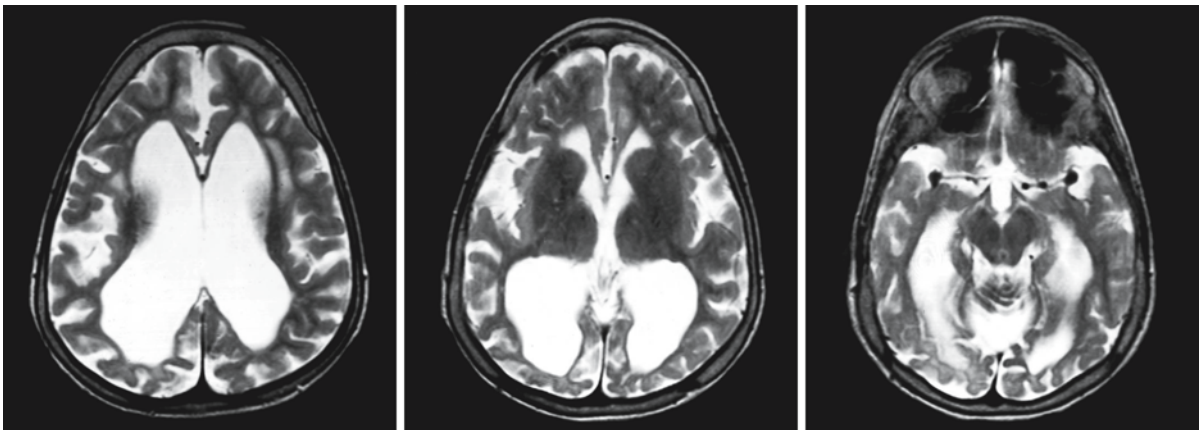


Fig. 44.3. T₂-weighted images in a patient with the severe variant of D-2-hydroxyglutaric aciduria at the age of 15 years. The lateral ventricles are seriously dilated. A focal area of abnormal signal is visible within the cerebral white matter on the

left. Note the aneurysms in the M2 segment of the middle cerebral arteries on both sides. From van der Knaap et al. (1999b), with permission

effusions may be seen. On follow-up, MRI may be normal, or it may show deficient myelination or bilateral multifocal, patchy abnormalities in the cerebral white matter or a combination of the two. The ventricles are often mildly dilated (Fig. 44.4). In one patient, multiple infarctions developed in the territories of

the major cerebral arteries (van der Knaap et al. 1999b).

The imaging findings in patients with combined D- and L-2-hydroxyglutaric aciduria are similar to those seen in the severe variant of D-2-hydroxyglutaric aciduria.

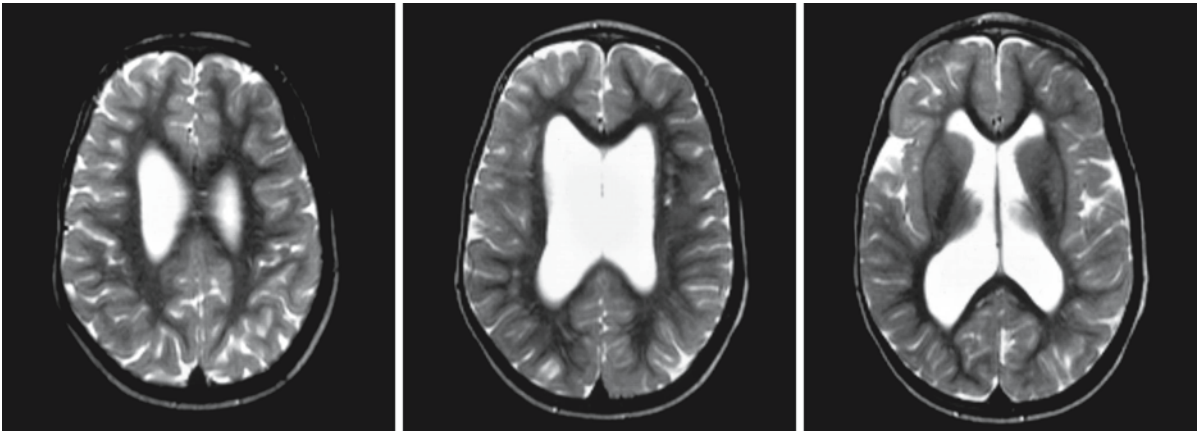


Fig. 44.4. T₂-weighted images in a patient with the mild variant of D-2-hydroxyglutaric aciduria at the age of 4 years. There are minor abnormal white matter spots. The lateral ventricles are mildly enlarged

Hyperhomocysteinemias

45.1 Introduction

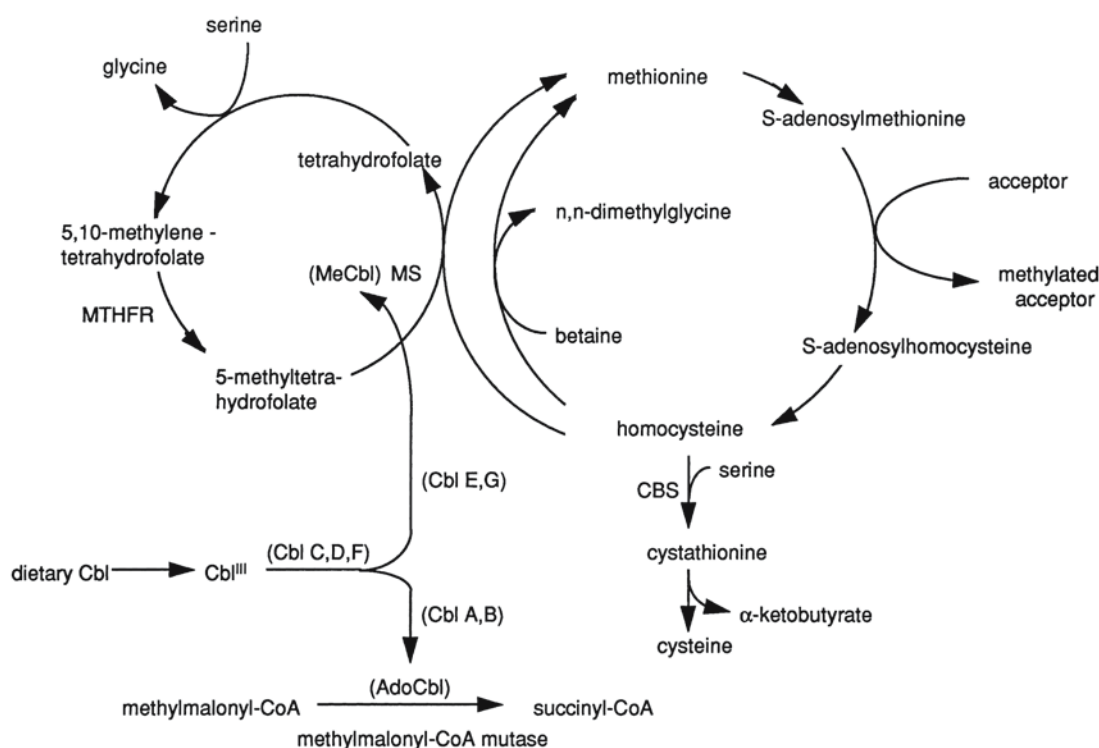
Hyperhomocysteinemias are associated with a diversity of neurological problems, ranging from mental retardation or deterioration to signs of subacute combined degeneration of cord and cerebral infarctions.

Homocysteine lies at an important branch point of sulfur amino acid metabolism. It is formed from methionine by demethylation. It may either be converted to cysteine through the transsulfuration reaction or remethylated to form methionine. Remethylation to methionine requires methyl donors such as betaine or 5-methyltetrahydrofolate. The metabolism of homocysteine requires folate and cobalamin (vitamin B₁₂) (Fig. 45.1). Consequently, a number of defects may underlie hyperhomocysteinemia: a defect in the transsulfuration pathway, a defect in cobalamin metabolism, and a defect in folate metabolism.

The most common defect of the transsulfuration pathway and the most frequent cause of severe hyperhomocysteinemia is a deficiency of cystathionine β -synthase. This enzyme normally catalyzes the conversion of homocysteine to cystathionine, which is converted to cysteine.

5,10-Methylenetetrahydrofolate reductase deficiency is the most common defect of folate metabolism. This enzyme deficiency leads to a lack of 5-methyltetrahydrofolate, a cosubstrate for the methionine synthase reaction, which in turn leads to an impairment of the remethylation of homocysteine to methionine.

So-called mild hyperhomocysteinemia, both in the fasting state and after methionine loading, can be the consequence of heterozygosity for cystathionine β -synthase deficiency. Heterozygosity for 5,10-methylenetetrahydrofolate reductase deficiency does not



CBS=cystathionine β -synthetase; MTHFR=5,10-methylenetetrahydrofolate reductase; MS=methionine synthetase; Cbl=cobalamin; MeCbl=methylcobalamin; AdoCbl=adenosylcobalamin

Fig. 45.1. Homocysteine metabolism

lead to hyperhomocysteinemia. However, homozygosity for a mutant form of 5,10-methylenetetrahydrofolate reductase, characterized by thermolability, can lead to mild hyperhomocysteinemia. Heterozygosity for this mutation does not lead to hyperhomocysteinemia. Compound heterozygosity for the classical and the thermolabile mutations of 5,10-methylenetetrahydrofolate reductase may also lead to mild hyperhomocysteinemia.

Folic acid deficiency leads to a disturbance of the folate cycle and, as a consequence, to hyperhomocysteinemia.

Inborn errors affecting intracellular cobalamin metabolism lead to a deficiency of methylcobalamin and/or adenosylcobalamin. Methylcobalamin is an essential cofactor for methionine synthase, the enzyme catalyzing the conversion of homocysteine to methionine. Adenosylcobalamin is a cofactor for methylmalonyl-CoA mutase. The inborn errors of cobalamin metabolism can be divided into three main groups: isolated defects in methylcobalamin synthesis, isolated defects in adenosylcobalamin synthesis, and defects in the synthesis of both methylcobalamin and adenosylcobalamin. The patients with isolated defects in methylcobalamin synthesis can be divided into two complementation groups (CblE and CblG), which are very similar clinically and biochemically with the presence of hyperhomocysteinemia. Both are characterized by a deficiency of methionine synthase, also known as methyltetrahydrofolate: homocysteine methyltransferase. Complementation group CblG deficiency of methionine synthase is caused by mutations in the gene encoding methionine synthase. In complementation group CblE the functional deficiency of methionine synthase is caused by a defect in the reductive activation of methionine synthase due to a defect in methionine synthase reductase. The patients with isolated defects in adenosylcobalamin synthesis can be divided into two complementation groups, designated CblA and CblB. Biochemically they are characterized by methylmalonic aciduria without hyperhomocysteinemia. As hyperhomocysteinemia is not present in these diseases, they are not discussed in this chapter. Among the patients with a defect in the synthesis of methylcobalamin and adenosylcobalamin, three complementation groups can be distinguished, CblC, CblD, and CblF. Biochemically they are characterized by presence of both hyperhomocysteinemia and methylmalonic aciduria. In CblC and CblD, there is a defect in cellular metabolism of cobalamin. In CblF there appears to be a defect in the process by which cobalamin exits from lysosomes after being taken up by receptor-mediated endocytosis.

Cobalamin cannot be synthesized by the body and is dietary in origin. Deficiency leads to a disturbance of function of both methionine synthase and methyl-

malonyl-CoA mutase and consequently to a combination of hyperhomocysteinemia and methylmalonic aciduria.

45.2 Clinical Features and Laboratory Investigations

Cystathionine β -synthase deficiency leads to the classical clinical picture commonly associated with the term "homocystinuria." The disease has an autosomal recessive inheritance. There is considerable clinical variability, even within the same family. Psychomotor retardation is often a feature of the disease and becomes evident during the first or second year of life. In the course of time, the optic lenses become dislocated in most patients. Other ophthalmological abnormalities include myopia and, less frequently, glaucoma, optic atrophy, retinal abnormalities, and cataract. There are often skeletal abnormalities including osteoporosis, scoliosis, arachnodactyly, thinning and lengthening of the long bones, and other abnormalities in the configuration and maturation of the skeleton. The combination of ectopic lenses and tall and thin habitus may give the patient a marfanoid appearance. Patients often present with signs of premature arteriosclerosis and thromboembolism. Vascular occlusion can occur in any vessel at any age. Fifty percent of the untreated patients suffer a cardiovascular incident before the age of 30 years, and cerebral infarction accounts for more than 60% of these incidents. Related neurological problems include hemiparesis and other focal neurological signs. In addition, generalized dystonia, other extrapyramidal movement disturbances, and epilepsy, usually with grand mal convulsions, may occur. Behavioral disturbances and personality problems occur in a considerable number of patients. There are no signs of bone marrow dysfunction.

The clinical severity of 5,10-methylenetetrahydrofolate reductase deficiency varies greatly from patient to patient, even within the same family. The disease has an autosomal recessive mode of inheritance. Onset of clinical manifestations varies from early infancy to adulthood. More than half of the patients become symptomatic during the first year of life. Among the most common early clinical manifestations are lethargy, epilepsy, hypotonia and severe developmental delay, often in combination with microcephaly. In early-onset disease, early death is not rare and can occur during an episode of apnea or may follow respiratory problems. In older children, a disturbance of gait is a common finding. Neurological examination reveals a combination of spasticity and sensory disturbances of the legs, consistent with combined dysfunction of the dorsal columns and pyramidal tracts of the spinal cord (combined degeneration

of the cord), variably mixed with signs of a peripheral polyneuropathy with weakness and sensory disturbances with a glove-and-stocking distribution. The disturbances of postural sense lead to loss of coordination. Seizures, psychiatric manifestations, athetosis, and parkinsonism may occur. There are no signs of megaloblastic anemia. Vascular complications are not common in patients with 5,10-methylenetetrahydrofolate reductase deficiency, but recurrent cerebral infarction and superior sagittal sinus thrombosis have been reported.

Longstanding mild hyperhomocysteinemia related to heterozygosity for cystathionine β -synthase deficiency and to thermolability of 5,10-methylenetetrahydrofolate reductase contributes to premature arteriosclerosis of small and large vessels, which may become manifest with transient ischemic attacks, lacunar infarctions, cerebral infarcts in large arterial territories, and spontaneous artery dissection. The clinical symptomatology of stroke in these patients does not differ from that in cerebrovascular disease of any other origin.

Folate deficiency is one of the most common vitamin deficiencies. The major causes are poor dietary intake; conditions leading to malabsorption, such as steatorrhea and sprue; and treatment with anticonvulsants such as phenytoin or with antifolate drugs including methotrexate, trimethoprim, and triamterene. In an advanced stage, the deficiency can cause macrocytic anemia, neutropenia, thrombopenia, or pancytopenia with macrocytosis. Neurological complications are exceptional. However, there is evidence that folate deficiency without cobalamin deficiency can also cause subacute combined degeneration of the cord and cerebral abnormalities. Hereditary congenital folate malabsorption has been described in a small number of patients. These patients present at the age of 2–5 months with severe megaloblastic anemia, diarrhea, mouth ulcers, and failure to thrive. Most patients show progressive neurological deterioration, with mild to severe mental retardation, seizures, peripheral neuropathy, ataxia, and athetosis. There is evidence that decreased serum folate is also an independent risk factor for ischemic stroke, probably related to the elevated homocysteine levels.

Inborn errors of cobalamin metabolism are autosomal recessive disorders with a variable clinical picture. Most cases become manifest in infancy, but delay in onset of clinical manifestations to adolescence or adulthood has been described. In infancy, the patients present with gastrointestinal signs and symptoms (feeding problems, vomiting, atrophic stomatitis, glossitis, alternating diarrhea and constipation, and failure to thrive), hematological signs (macrocytic anemia, less often thrombopenia, neutropenia, and leukopenia), and neurological problems compatible

with subacute combined degeneration of the cord, brain involvement (hypotonia, developmental delay, seizures, microcephaly, hydrocephaly), polyneuropathy, and pigmentary retinopathy. In young children neurological manifestations include psychomotor retardation or regression, lethargy, hypokinesia, hypotonia, brisk reflexes, ataxia, optic atrophy, and seizures. In older children the gastrointestinal problems are less prominent and hematological and neurological problems dominate, with signs of myelopathy, peripheral neuropathy, tremor, dementia and behavioral problems, and, rarely, optic atrophy or retinopathy.

Cobalamin deficiency can be observed in a number of conditions. Deficiency due to insufficient dietary intake is rare, but can be observed in strict vegetarians (vegans) and in breast-fed babies of mothers who are cobalamin-deficient. Cobalamin in the diet is released from protein in the acid environment of the stomach. Here it binds to R proteins of gastric and salivary origin. Pancreatic proteases digest the R proteins and liberate cobalamin in the upper small intestine, where it forms a complex with intrinsic factor, synthesized by gastric parietal cells. The newly formed complex binds with specific receptors in the terminal ileum and is transported into the enterocyte. The complex is dissociated and cobalamin is transported into the portal blood bound to transcobalamin II. Transcobalamin II is the transport protein for cobalamin and also facilitates cobalamin uptake by tissues. Disturbances of cobalamin uptake and transport can arise at all levels. R protein deficiency as an inherited defect has been described in a small number of patients. Intrinsic factor deficiency can be caused by deficient synthesis, synthesis of a mutant protein with decreased activity, autoimmune gastritis with antibodies against parietal cells and intrinsic factor, or gastrectomy. Cobalamin malabsorption may be due to defective receptor on the enterocyte, defective receptor internalization, surgical resection of the terminal ileum, inflammatory diseases of the ileum (sprue, ulcerative colitis, Crohn disease) and transcobalamin II deficiency. Nitrous oxide (N_2O) is a very special cause of deficient cobalamin activity. It oxidizes active cobalamin to an inert form. Long-term exposure to this anesthetic substance, formerly used in the artificial ventilation of patients with tetanus, leads to megaloblastic and aplastic bone marrow changes and combined degeneration of the spinal cord. Patients with latent cobalamin deficiency are exceedingly sensitive to neurological deterioration following nitrous oxide anesthesia.

The clinical signs and symptoms of cobalamin deficiency usually follow a chronic course and have a delayed onset because of the large cobalamin stores in the body. In infants fed on breast milk with a low cobalamin content, symptoms are delayed by several

Table 45.1. Laboratory findings in the hyperhomocysteinemias

	Homocysteine	Methionine	Methylmalonic acid	Macrocytosis
Cystathionine β -synthetase deficiency	↑	↑	–	–
5,10-Methylene-tetrahydrofolate reductase deficiency	↑	–	–	–
Cbl C, D, F	↑	–	↑	+
Cbl E, G	↑	–	–	+
Folate deficiency	↑	–	–	+
Cobalamin deficiency	↑	–	↑	+

months. The signs and symptoms are hematological (macrocytic anemia, usually mild thrombopenia, hypersegmentation of neutrophils, aplastic anemia), gastrointestinal (atrophic glossitis, stomatitis, constipation, diarrhea), and neurological. The neurological signs and symptoms usually follow a chronic course, but a more or less acute spinal cross-section syndrome does occur. Neurological abnormalities consist of a progressive spastic paraparesis with ataxia due to impairment of postural sense. The arms are usually affected later and to a lesser extent than the legs. Peripheral neuropathy occurs with progressive weakness, loss of reflexes (but plantar reflexes usually remain extensor) and distal sensory disturbances. Visual problems may occur caused by optic atrophy. Mental signs are frequent and range from disturbed development in infants to regression and dementia, lability, depression, irritability, confusion, psychosis, and lethargy in older patients. Affected infants are often microcephalic. Epileptic seizures may occur.

The most important laboratory investigations include assessment of the levels of homocysteine, methionine, and methylmalonic acid in plasma and urine and assessment of hematological abnormalities, in particular megaloblastic anemia (see Table 45.1). It is important to note that there may be no hematological abnormalities, even in the presence of overt neurological abnormalities. In cystathionine β -synthetase deficiency, low levels of cystathionine and cystine are additional findings. The homocysteine levels are highest in cystathionine β -synthetase deficiency, lowest in the so-called mild hyperhomocysteinemias. Mild hyperhomocysteinemia can be detected by performing a methionine loading test or by assessment of serum homocysteine levels during fasting. The assessment of the CSF level of S-adenosylmethionine is of value as a decrease is associated with present or imminent demyelination.

Direct enzyme assessment confirms the diagnosis in cystathionine β -synthetase deficiency and 5,10-methylenetetrahydrofolate reductase deficiency. The enzyme assessment can be performed in liver biopsy specimens, cultured fibroblasts, and lymphocytes. Serum folate is low in folate deficiency. In case of di-

etary cobalamin deficiency or deficiency due to gastrointestinal absorption problems, serum cobalamin levels may only be slightly or moderately low, despite other clinical evidence of important deficiency. Total serum cobalamin is normal in transcobalamin II deficiency, and in CblC, CblD, CblF, CblE, and CblG. Disturbances of cobalamin absorption can be investigated with the Schilling test. This test measures urinary excretion of radioactively labeled cobalamin after oral administration. If the urinary level is below normal, the test is combined with addition of intrinsic factor to distinguish between cobalamin deficiency caused by lack of intrinsic factor and other causes of disturbances of the vitamin absorption. Differentiation of CblC, CblD, CblF, CblE, and CblG is possible by biochemical and complementation studies on cultured fibroblasts.

Cystathionine β -synthetase activity and 5,10-methylenetetrahydrofolate reductase activity can be assessed in chorionic villi and cultured amniocytes, facilitating prenatal diagnosis. Prenatal diagnosis in disorders of intracellular cobalamin metabolism can be performed on amniocytes or chorionic villus samples. In many disorders, a DNA-based prenatal diagnosis is also possible.

In case of subacute combined degeneration of the spinal cord, CSF protein is usually slightly elevated. SSEPs show normal or moderately slowed peripheral conduction, normal conduction or mild slowing across the cervical portion of the median SSEP, and absence or severe slowing of impulse propagation along the spinal cord with the peroneal SSEP. The conduction velocity of peripheral nerves is normal or mildly to more markedly reduced. There may be signs of denervation.

45.3 Pathology

Two types of cerebral pathology are consistently seen in severe hyperhomocysteinemias: subacute combined degeneration of the spinal cord and brain and the cerebral consequences of premature vascular disease.

The vascular changes affect both arterial and venous systems. Histologically, the vascular disease is characterized by intima and media smooth muscle hyperplasia, with fibrosis and thickening of the elastic lamina.

Subacute combined degeneration of the spinal cord is a demyelinating disorder. The brain is often affected at the same time. The form the disorder takes, both clinically and histopathologically, is strongly influenced by the age of the patient, or rather, the progress of myelination at the time of onset of disease. In early infantile onset, the disease may take the form of delayed and disturbed myelination rather than demyelination, whereas after completion of myelination the classical picture of subacute combined degeneration of the cord and demyelinating brain disease arises.

Degeneration and demyelination of the spinal cord, in particular the dorsal and lateral columns, lent the disease its name: subacute combined degeneration of the cord. The midthoracic segments of the cord are mainly involved where a zone of white matter destruction may affect the whole cord and not only the long tracts. In the upper cervical segments the posterior columns are predominantly affected, and at the lower lumbar levels predominantly the pyramidal tracts. As pathological changes predominate in the midthoracic segments, subsequent wallerian degeneration may play a role in the involvement of the ascending tracts in the cervical segments and of the descending tracts in the lumbar segments. The first changes consist of swelling and splitting of myelin sheaths, followed by spongiform white matter degeneration and demyelination. Electron microscopy shows that the myelin splitting occurs at the intraperiod line. A variable astrocytic reaction is present; sometimes it is considerable.

In the cerebral white matter variable demyelination is present. In many cases the demyelinating lesions are small, ill defined, and located perivascularly. Their number is variable. They may be scanty or disseminated over wide areas. Sometimes the cerebral white matter changes become extensive and diffuse, but the internal capsule and brain stem remain relatively spared. In occasional cases a predominance of subcortical white matter involvement has been mentioned, with the brunt of abnormalities in the white matter at the junction of the cortex. The histology of the cerebral lesions is similar to that of the spinal cord. There is first a fusiform swelling of myelin sheaths, myelin splitting, and formation of intramyelinic vacuoles, followed by demyelination and finally also axonal degeneration. The optic nerves are often involved in the demyelinating process. The basal nuclei including the thalamus may also become involved in the process of myelin vacuolation. In more extensive white matter disease loss of white

matter volume occurs with enlargement of ventricles and subarachnoid spaces.

Peripheral nerves show signs of a combination of segmental demyelination and axonal degeneration.

In cystathionine β -synthase deficiency the main pathological findings are arteriosclerosis, arterial thromboembolism, and venous thrombosis in children and young adults. Resulting lesions consist of arterial and venous infarcts. Most often multiple small infarcts of different ages are seen, spread over the brain. In cystathionine β -synthase deficiency demyelination is rare. In one patient (Chou and Waisman 1965), a vacuolating white matter disease was documented, predominantly involving the subcortical white cerebral and cerebellar white matter, relatively sparing the corpus callosum, internal capsule, and brain stem. The spinal cord was also involved. In one patient a combination of demyelination and extensive vascular abnormalities with multiple small infarcts was found (Dunn et al. 1966).

In 5,10-methylenetetrahydrofolate reductase deficiency vascular pathology is present but less severe than in cystathionine β -synthase deficiency and cerebral infarcts are rare. Demyelination of brain and spinal cord as described above is the most common type of pathology. The findings in folate deficiency are similar.

In the inherited defects in cobalamin metabolism and in cobalamin deficiency, spongy demyelination in the patterns of subacute combined degeneration of cord and demyelinating brain disease is the predominant finding. Additional changes are present in arterioles and capillaries with thickening, fibrosis, and hyalination, but cerebral infarctions have not been reported.

To date, cerebral infarction is the only type of pathology that has been observed in mild hyperhomocysteinemia, in most cases related to heterozygosity for cystathionine β -synthase deficiency. This observation may be biased as children and young adults with cerebrovascular accidents are screened for the presence of mild hyperhomocysteinemia. Systematic data on neuropathological findings in unselected patients are not available.

45.4 Pathogenetic Considerations

Two types of pathology dominate in the hyperhomocysteinemias: vascular pathology and myelinopathy. The relative contribution to the clinical symptomatology varies by disease. In cystathionine β -synthase deficiency, and also in mild hyperhomocysteinemia, vascular pathology dominates, whereas in 5,10-methylenetetrahydrofolate reductase deficiency, disturbances of cobalamin metabolism (CblC, CblD, CblF, CblE, and CblG), exogenous folate deficiency,

and cobalamin deficiency, the myelinopathy dominates.

The pathogenesis of the vascular pathology is only partially understood. There is evidence from experimental animal work and from in vitro research that homocysteine damages the vascular endothelium. Injury of arterial and venous vessel walls predisposes to early platelet activation and thrombus formation. Homocysteine is rapidly auto-oxidized when added to plasma, and potent reactive oxygen species, including superoxide, hydrogen peroxide, and hydroxyl radicals, are produced during this process. These reactive oxygen species have been implicated in the vascular toxicity of hyperhomocysteinemia. Platelet abnormalities and abnormalities in soluble factors involved in blood coagulation may contribute to the thrombotic diathesis.

Plasma homocysteine levels are highest in cystathionine β -synthase deficiency, explaining the high incidence of vascular accidents in this disorder. It is remarkable, however, that vascular abnormalities and vascular accidents occur relatively frequently in the mild hyperhomocysteinemias, which have a lower level of homocysteine than for instance the inherited cobalamin disorders, whereas vascular pathology is rare in the latter conditions. The chronicity of elevated homocysteine levels before detection and treatment, in view of the absence of other clinical problems in heterozygosity for cystathionine β -synthase deficiency, may form part of the explanation.

Most current evidence points to deficiency of S-adenosylmethionine being critical to the development of demyelination. In the human brain S-adenosylmethionine is the universal methyl group donor, acting in a wide variety of biological methylations that modify proteins, nucleic acids, fatty acids, phospholipids, and polysaccharides. S-adenosylmethionine is necessary for the inactivation of catecholamines and other biogenic amines. The methyl transfer pathway provides precursors for polyamine synthesis. A relationship has been found between the presence of demyelination and deficiency of S-adenosylmethionine in the CSF, whereas remyelination under treatment is associated with a return of the S-adenosylmethionine level to normal. Additional evidence comes from animal experimental work, in which cycloleucine is used to elicit subacute combined degeneration of the spinal cord. Cycloleucine causes deficiency of S-adenosylmethionine by inhibition of methionine adenosyltransferase. The precise mechanism by which a deficiency of S-adenosylmethionine would lead to demyelination is not known. The failure of methylation of arginine₁₀₇-myelin basic protein may be important in this respect. In addition, methyl groups are necessary for synthesis of choline from ethanolamine, and these methyl groups are provided by S-adenosylmethionine. Defi-

cient synthesis of choline may contribute to the myelinopathy.

Administration of folic acid in patients with cobalamin deficiency may precipitate or exacerbate demyelination. Folic acid is not active and requires conversion to active tetrahydrofolate. This reaction is very slow. Folic acid competes with the transport of active tetrahydrofolate in the CNS. The resulting decreased availability of tetrahydrofolate for nervous tissue is probably the cause of enhanced demyelination.

The folate cycle is not only involved in the remethylation of homocysteine to methionine, a reaction that is crucial to the synthesis of S-adenosylmethionine, it is also involved in the transfer of methyl groups necessary for the synthesis of purines and pyrimidines, major constituents of DNA. There is general agreement that megaloblastic anemia or pancytopenia and the defective proliferation of rapidly dividing cells with sequelae such as glossitis, intestinal problems, and hypospermia, are related to impairment of DNA synthesis due to interference with folate metabolism. The main problem with folate metabolism in the cobalamin disorders (CblC, CblD, CblE, CblF, and CblG) and cobalamin deficiency is that 5-methyltetrahydrofolate is not converted to tetrahydrofolate, whereas the conversion of 5,10-methylenetetrahydrofolate to 5-methyltetrahydrofolate is irreversible. This is called the methyl-folate trap. The trap leads to deficiency of folate coenzymes derived from tetrahydrofolate, necessary in the production of purines and pyrimidines.

In cases of deficiency of folate or cobalamin, or in inborn errors of folate or cobalamin metabolism, CSF levels of 5-hydroxyindolacetic acid (5-HIAA) and homovanillic acid (HVA), metabolites of serotonin and dopamine, respectively, are decreased. The decrease is independent of the level of S-adenosylmethionine. Why these metabolites are reduced is not known. Neurotransmitter disturbances may be responsible for the frequently observed extrapyramidal movement abnormalities, epilepsy, and changes in mood and personality.

The gene encoding cystathionine β -synthase, *CBS*, is located on chromosome 21q22.3. Different mutations have been described. Cystathionine β -synthase requires pyridoxal phosphate (vitamin B₆) as a cofactor. In the case of a mutation, there is either no residual enzyme activity, reduced activity and normal affinity for the cofactor, or reduced activity and reduced affinity for pyridoxal phosphate. The vitamin-B₆-responsive patients do better in all aspects of the disease than nonresponsive patients, even if both groups are untreated. They have a higher IQ and all other manifestations of the disease occur later.

The gene for 5,10-methylenetetrahydrofolate reductase, *MTHFR*, is located on chromosome 1p36.3.

Many different mutations have been described. Thermolability of the enzyme is due to a C→T substitution at position 677 of the gene. Homozygosity for this mutation is associated with mild hyperhomocysteinemia. The 677T→C allele has a high prevalence (30–40%) in most populations, but varies greatly in different ethnic groups. About 10% of Caucasians are homozygous, but in populations of African descent the prevalence is 0–2%, whereas in Asians it is about 20%.

Functional deficiency of methionine synthase is caused either by mutations in the gene encoding methionine synthase, *MTR* (complementation group cblG), or in the gene encoding methionine synthase reductase, *MTRR*, leading to a defect in the reductive activation of methionine synthase (complementation group cblE).

Among the patients with a defect in the synthesis of both methylcobalamin and adenosylcobalamin three complementation groups are distinguished: CblC, CblD, and CblF. In cblC and cblD, there is a defect in cellular metabolism of cobalamin. In cblF there appears to be a defect in the process by which cobalamin exits from lysosomes after being taken up by receptor-mediated endocytosis.

45.5 Therapy

About half the patients with cystathionine β -synthase deficiency respond to large oral doses of vitamin B₆ (pyridoxine). After a variable period, up to a few weeks, homocysteine levels become normal, hypermethioninemia decreases, and hypocysteinemia increases to normal values. In some patients the response is only partial and very large doses of vitamin B₆ are needed. If this is not enough to correct the biochemical abnormalities, a diet low in methionine and high in cystine should be initiated. A mildly methionine-restricted diet may be advisable for vitamin-B₆-responsive patients too. Extra supplementation of betaine has been proposed to promote remethylation of homocysteine to methionine. Folate utilization may be increased in patients with cystathionine β -synthase deficiency, since it is required in methylation of homocysteine to methionine. Folate deficiency can mask vitamin B₆ responsiveness, and simultaneous administration of folate is necessary in some patients to achieve biochemical normalization. Aspirin has been used to reduce the tendency to develop thromboses, but has not proven to be beneficial. With early instigation of treatment, most of the clinical manifestations of the disease can be prevented or delayed.

Also, in mild hyperhomocysteinemia due to heterozygosity for cystathionine β -synthase deficiency, vitamin B₆ combined with folate can normalize plas-

ma homocysteine levels. The long-term effects of this treatment have not been fully assessed.

5,10-Methylenetetrahydrofolate reductase deficiency has proven very resistant to treatment and only limited success has been achieved. Therapeutic options include (1) use of folates such as folic acid or folinic acid in an attempt to maximize any residual enzyme activity; (2) use of methyltetrahydrofolate to replace the missing product; (3) use of methionine to correct the cellular methionine deficiency; (4) use of pyridoxine to lower homocysteine levels because of its role as a cofactor for cystathionine β -synthase; (5) use of cobalamin because of its role as a cofactor for methionine synthase; (6) use of carnitine; and (7) use of betaine in order to lower homocysteine levels and supplement methionine levels. In most patients several agents are used in combination.

Folate deficiency can be corrected by supplementation of the deficient substance.

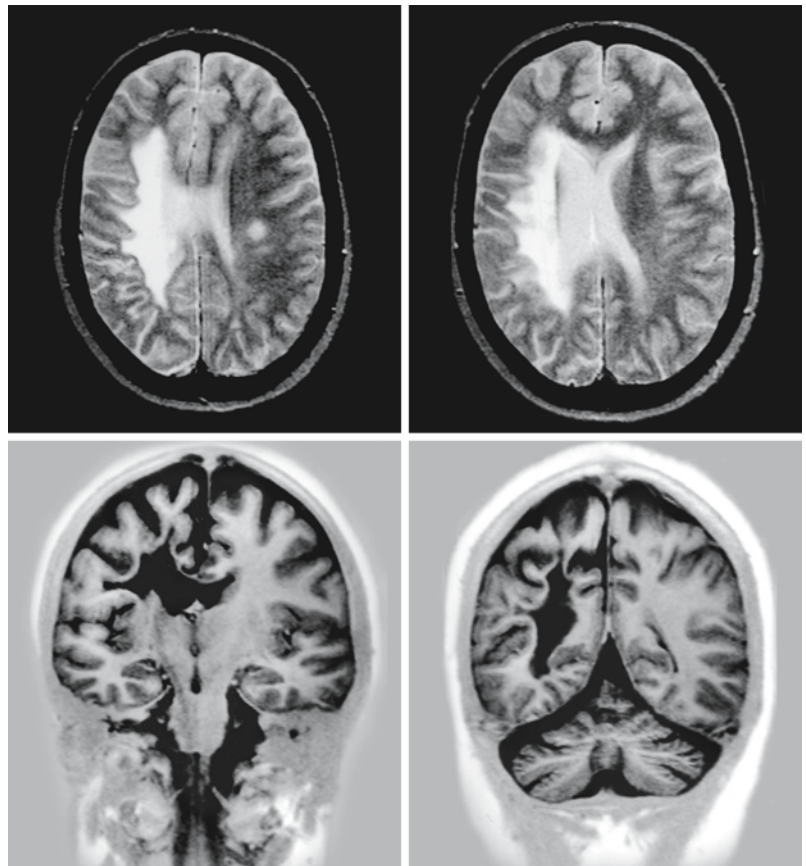
All inborn errors of intracellular cobalamin metabolism are treated with intramuscular hydroxycobalamin. After induction, the hydroxycobalamin can be given orally because cobalamin absorption and transport are normal. The biochemical and hematological response to the therapy is usually rapid. Plasma levels of methionine and homocysteine can be used to monitor treatment. In CblE and CblG the use of hydroxycobalamin is usually sufficient, although supplementation with methionine has been shown to have additional beneficial effects. In CblC of infantile onset, hydroxycobalamin cannot always fully reverse the clinical and biochemical abnormalities. Betaine can be used as additive. A synergistic action of betaine and hydroxycobalamin has been shown in CblC. The long-term outcome of treatment depends to a great extent on the swiftness with which treatment is started after onset of symptoms, or, in other words, on the extent of irreversible neurological damage.

In cobalamin deficiency of all causes, hydroxycobalamin can be administered. In transcobalamin II deficiency large doses of hydroxycobalamin are required to correct cellular cobalamin deficiency. The effect of treatment depends on the presence and extent of irreversible neurological damage.

45.6 Magnetic Resonance Imaging

The cerebral infarctions occurring in cystathionine β -synthase deficiency, both lacunar and large infarctions, can be visualized by MRI. The images as such are not specific, only the age category of the patient is unusual. Changes suggestive of single or multiple small infarcts are most commonly observed. When the lesions are scattered over the brain with a predilection for the periventricular area, the picture may resemble that of multiple sclerosis.

Fig. 45.2. A 43-year-old woman with mild hyperhomocysteinemia who had her first stroke with hemiparesis on the left at the age of 22 years. At that time a large medial cerebral artery infarction was found. Recently she developed signs of left hemisphere dysfunction. The MR images show an old, large middle cerebral artery infarction with wallerian degeneration of the connecting pyramidal tracts, through the internal capsule into the brain stem. There is a small lesion in the paraventricular white matter on the left. Courtesy of Dr. J.W. Snoek, Department of Neurology, Martini Hospital, Groningen, The Netherlands



Multiple systematic studies have documented an increased frequency of overt and silent infarcts of the brain in patients with mild hyperhomocysteinemia (Fig. 45.2). An increased incidence of spontaneous artery dissection has also been reported. One patient with mild hyperhomocysteinemia and severe cerebrovascular occlusive disease due to a moyamoya phenotype has been reported (Van Diemen-Steen-voorde et al. 1990).

In subacute combined degeneration MRI reveals spinal cord abnormalities with an increased signal intensity of the posterior part of the cervical spinal cord on T_2 -weighted sagittal and transverse images (Fig. 45.3). The abnormality in signal intensity is located in the dorsal and lateral columns. Contrast enhancement of the dorsal columns may be seen, but does not occur in all patients. With treatment, partial or complete resolution the lesion can follow.

MRI of cerebral white matter abnormalities has mainly been documented in patients with 5,10-methylenetetrahydrofolate reductase deficiency (Figs. 45.4 and 45.5) and disorders of intracellular cobalamin metabolism (Figs. 45.6–45.8). In untreated infants within the first year of life, MRI shows a delay in myelination with improvement after therapy (Figs. 45.4 and 45.6). In older untreated patients, an in-

creased signal intensity is seen in the cerebral white matter, sparing the brain stem and cerebellar white matter, consistent with demyelination or insufficient myelination (Figs. 45.5 and 45.7). The degree of signal abnormality varies from slight to prominent. There may be evidence of cerebral atrophy with increased size of the lateral ventricles and subarachnoid spaces. Improvement of the white matter signal and the cerebral atrophy is noted after therapy. Several patients with 5,10-methylenetetrahydrofolate reductase deficiency and disorders of intracellular cobalamin metabolism have been reported, who had internal hydrocephalus with marked enlargement of the lateral ventricles and macrocephaly, requiring shunt implantation (Fig. 45.8).

Delayed myelination and reversible cerebral atrophy has been documented in cobalamin-deficient infants (Fig. 45.9). In our cobalamin-deficient patient, aged 19 months, a severe cerebral hemispheric white matter abnormality was found, whereas the corpus callosum, internal capsule, and brain stem were spared (Fig. 45.9). The white matter abnormalities were most severe in the parietal area, extending through the corona radiata into the arcuate fibers. In addition, the hemispheric white matter had too high a signal intensity on T_2 -weighted images with a

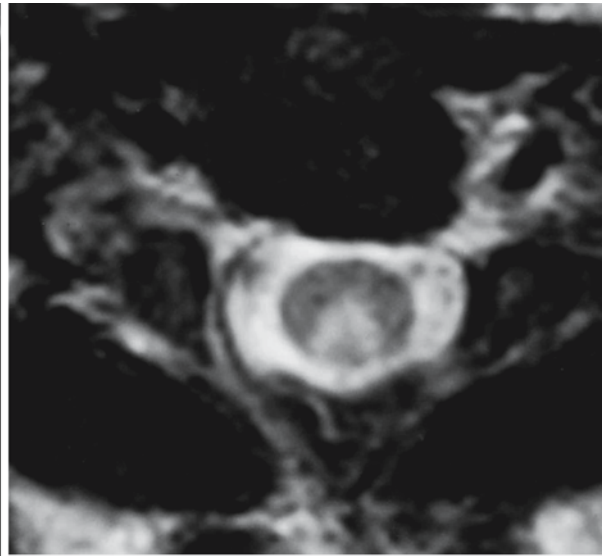


Fig. 45.3. Spinal images of a cobalamin-deficient patient with signs of subacute combined degeneration of the spinal cord. Note the selective involvement of the dorsal columns at the cervical level

patchy distribution, most pronounced in the subcortical white matter, probably related to delayed and disturbed myelination. The images also showed cerebral atrophy in the presence of clinical microcephaly. With cobalamin treatment, the white matter improved and the atrophy resolved with return of the head circumference to the normal centiles (Fig. 45.9). In older cobalamin-deficient patients, white matter abnormalities of variable extent have been described. These abnormalities are bilateral but not necessarily symmetrical. The white matter changes are most often located in the periventricular white matter as a confluent rim of signal change with additionally smaller lesions in the deep white matter (Fig. 45.10). In some patients, larger areas of white matter are abnormal, extending from the periventricular region

into the U fibers (Fig. 45.11), sometimes with some swelling leading to broadening of gyri. There may be signal abnormalities in the brain stem and middle cerebellar peduncles as well (Fig. 45.11). Small lesions in the basal ganglia have been reported. The abnormalities resolve partially with treatment (Figs. 45.10 and 45.11).

Finding evidence of combined degeneration of dorsal and lateral columns is highly suggestive of one of the hyperhomocysteinemic disorders and should direct the diagnostic work-up in the right direction. However, both the vascular abnormalities and the white matter abnormalities described above are non-specific. Metabolic screening of urine is most helpful in achieving the correct diagnosis.

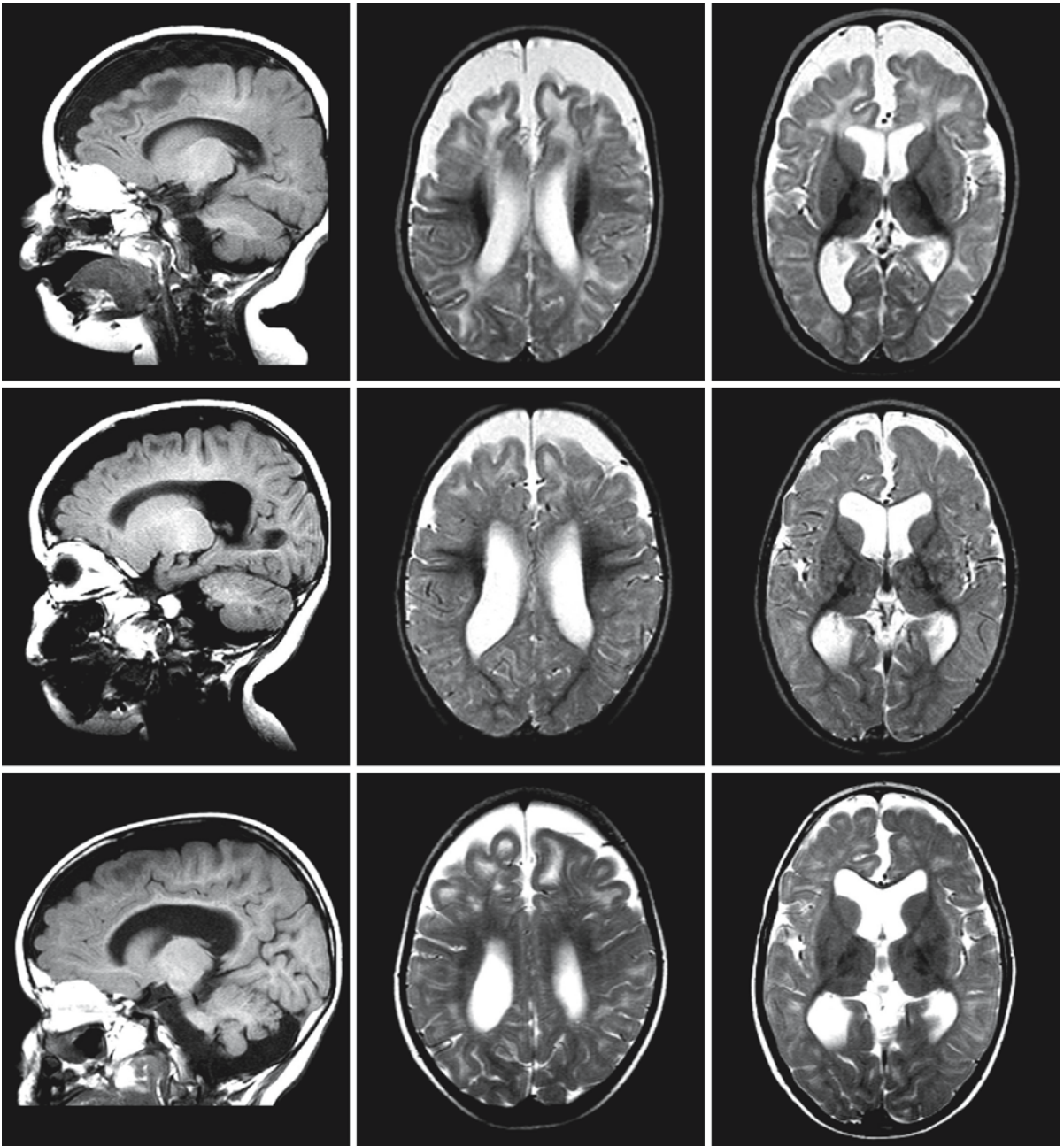


Fig. 45.4. Girl with methylenetetrahydrofolate reductase deficiency. The images in the *first row* were obtained at the age of 10 months. They show marked cerebral atrophy with widening of the lateral ventricles and subarachnoid spaces. In addition, myelination is delayed. The frontal and parietal white matter has a higher signal on T_2 -weighted images than expected for delayed myelination only. Treatment with betaine monohydrate led to marked clinical and biochemical improvement.

The second MRI series (*second row*) was obtained at 22 months and the third MRI was obtained at 4 years (*third row*). A decrease in cerebral atrophy and a progress of myelination are noted on follow-up, although the lateral ventricles and subarachnoid spaces remain dilated and myelination incomplete. There remain areas in the subcortical white matter with evidently elevated signal on the T_2 -weighted images. From Engelbrecht et al. (1997), with permission

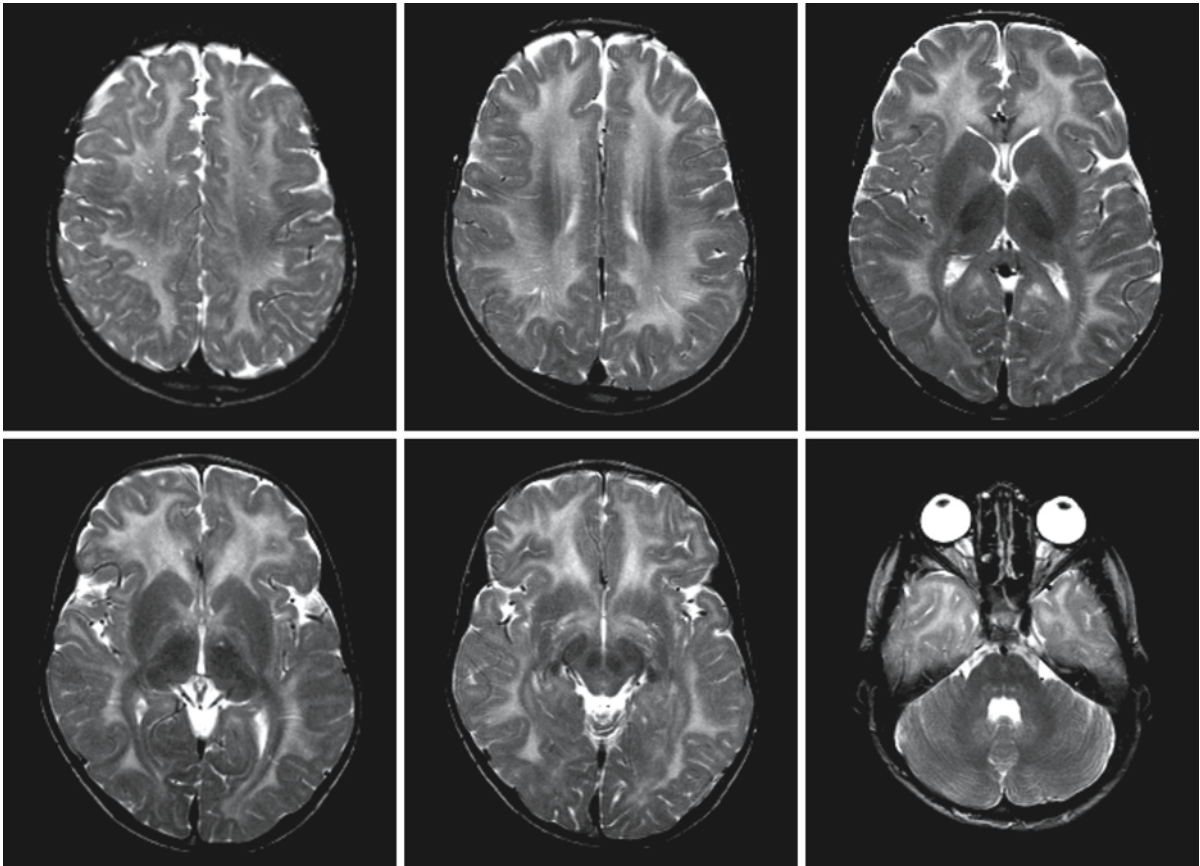


Fig. 45.5. Boy with methylenetetrahydrofolate reductase deficiency at the age of 5 years. The T_2 -weighted MR images show that the cerebral white matter has an elevated signal throughout. The corpus callosum also has a slightly abnormal signal.

The optic radiation and cerebellar white matter have a more normal signal. Courtesy of Dr. Z. Patay, Department of Radiology, King Faisal Specialist Hospital and Research Center, Riyadh, Saudi Arabia

Fig. 45.6. Girl with CblC. The first MRI was obtained at the age of 2.5 months (*first and second row*); the second MRI at the age of 24 months (*third and fourth row*). On the first MRI the cerebral white matter is abnormal and slightly swollen. Treatment with hydroxycobalamin led to clinical improvement. Follow-up MRI at 2 years reveals that myelination has progressed but

is still incomplete. There are more prominent white matter abnormalities in the periventricular region. Courtesy of Dr. C. Fonda, Division of Pediatric Radiology, A. Meyer Children's Hospital, Florence, Italy, and Dr. A. Rossi (Rossi et al. 2001b, with permission)

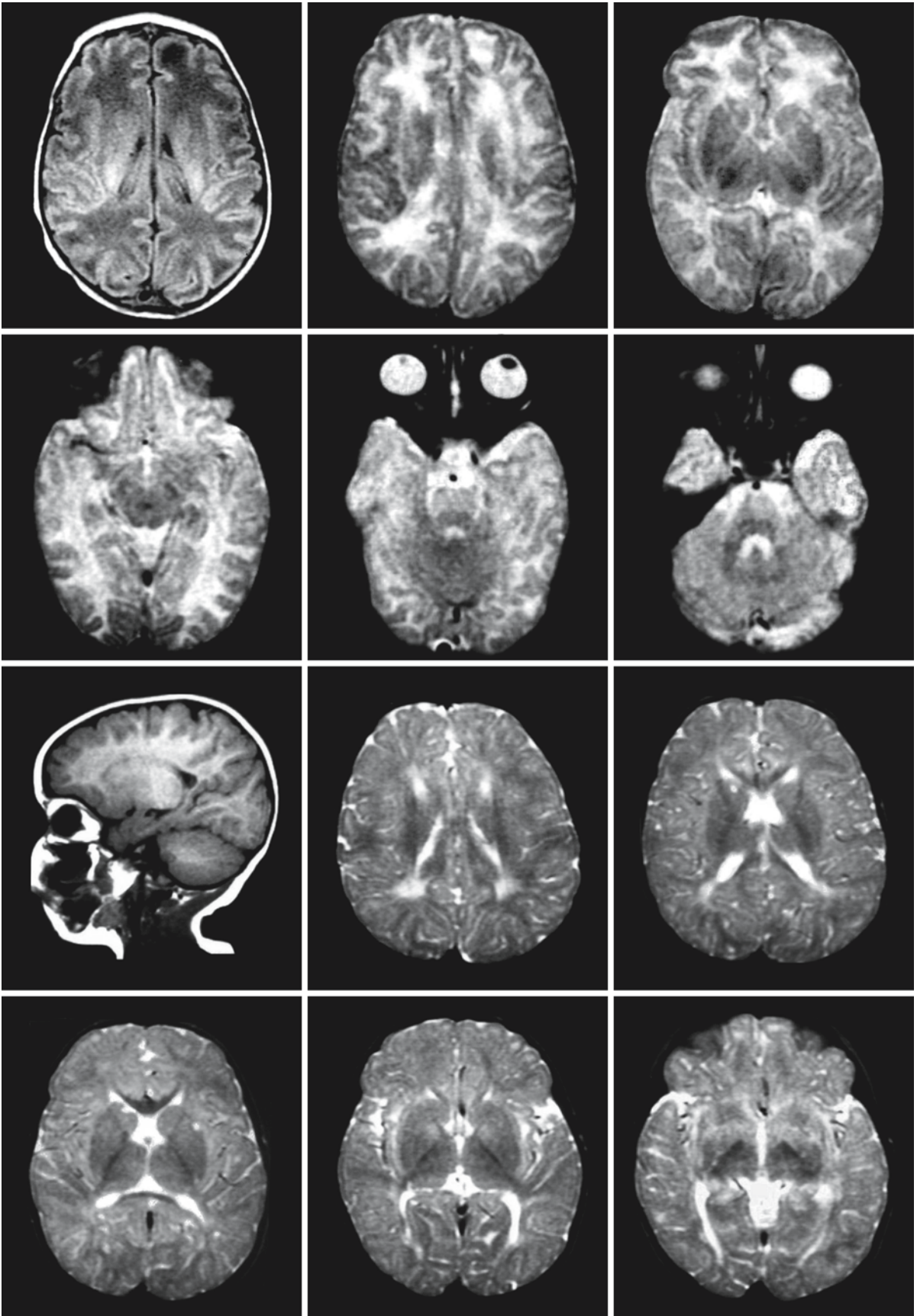


Fig. 45.6.

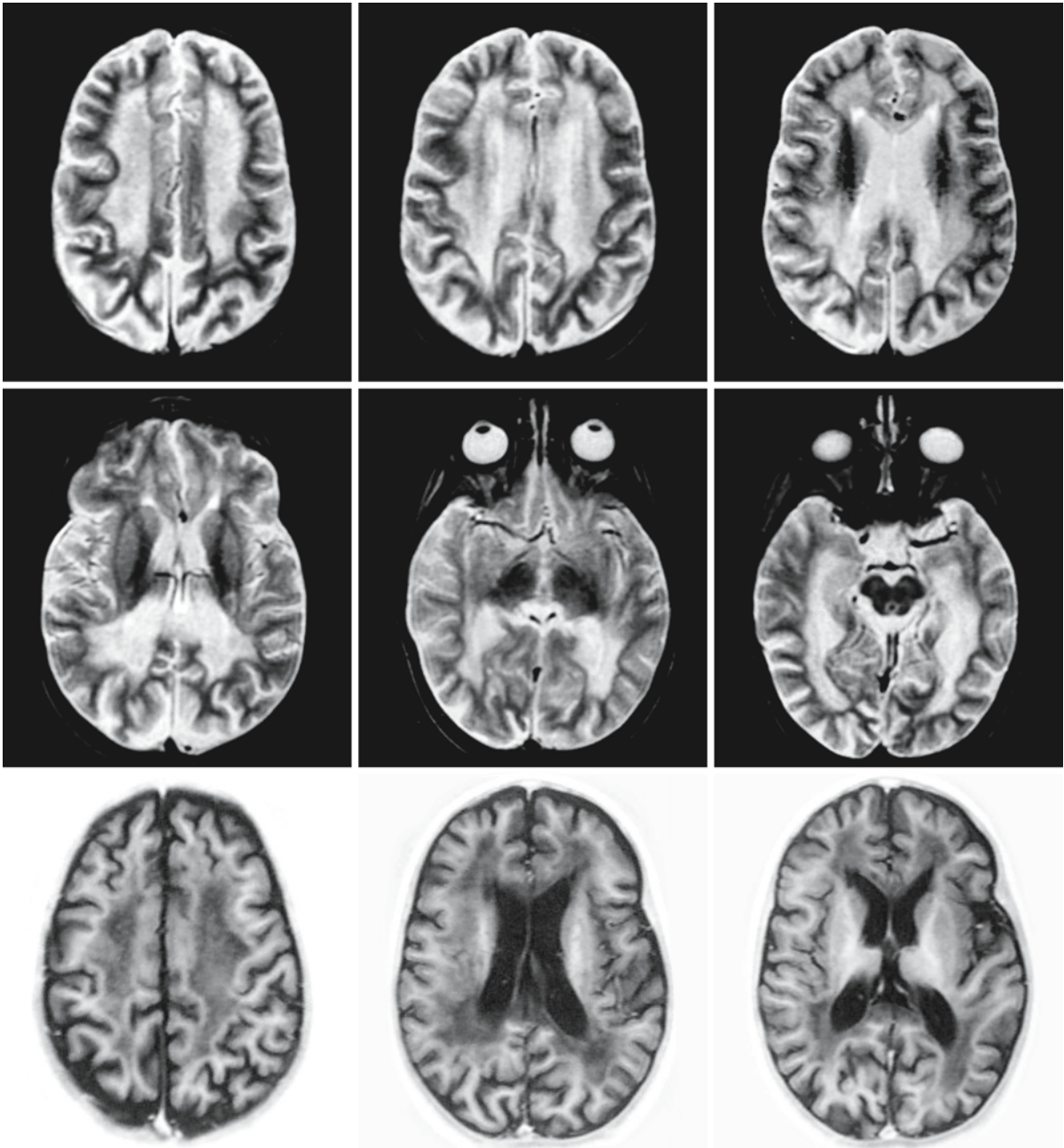


Fig. 45.7. A 6-year-old untreated male patient with CbIC. There are prominent abnormalities in the periventricular and deep white matter. The corpus callosum is also involved, but the internal capsule and brain stem are spared. There is some

cerebral atrophy with mild widening of the lateral ventricles and subarachnoid spaces. Courtesy of Dr. C. Fonda, Division of Pediatric Radiology, A. Meyer Children's Hospital, Florence, Italy

Fig. 45.8. Girl with CbIC. The first MRI was obtained at 3 months (*first and second row*), the second at 4 months (*third and fourth row*). Note the progressive hydrocephalus. The lateral ventricles have increased in size and the cerebral mantle has become thinner. The cerebral white matter has become increasingly abnormal in signal intensity. Courtesy of Dr. S. Blaser, Department of Diagnostic Imaging, and Dr. A. Feigenbaum, Department of Clinical Genetics, Hospital for Sick Children, Toronto, Canada

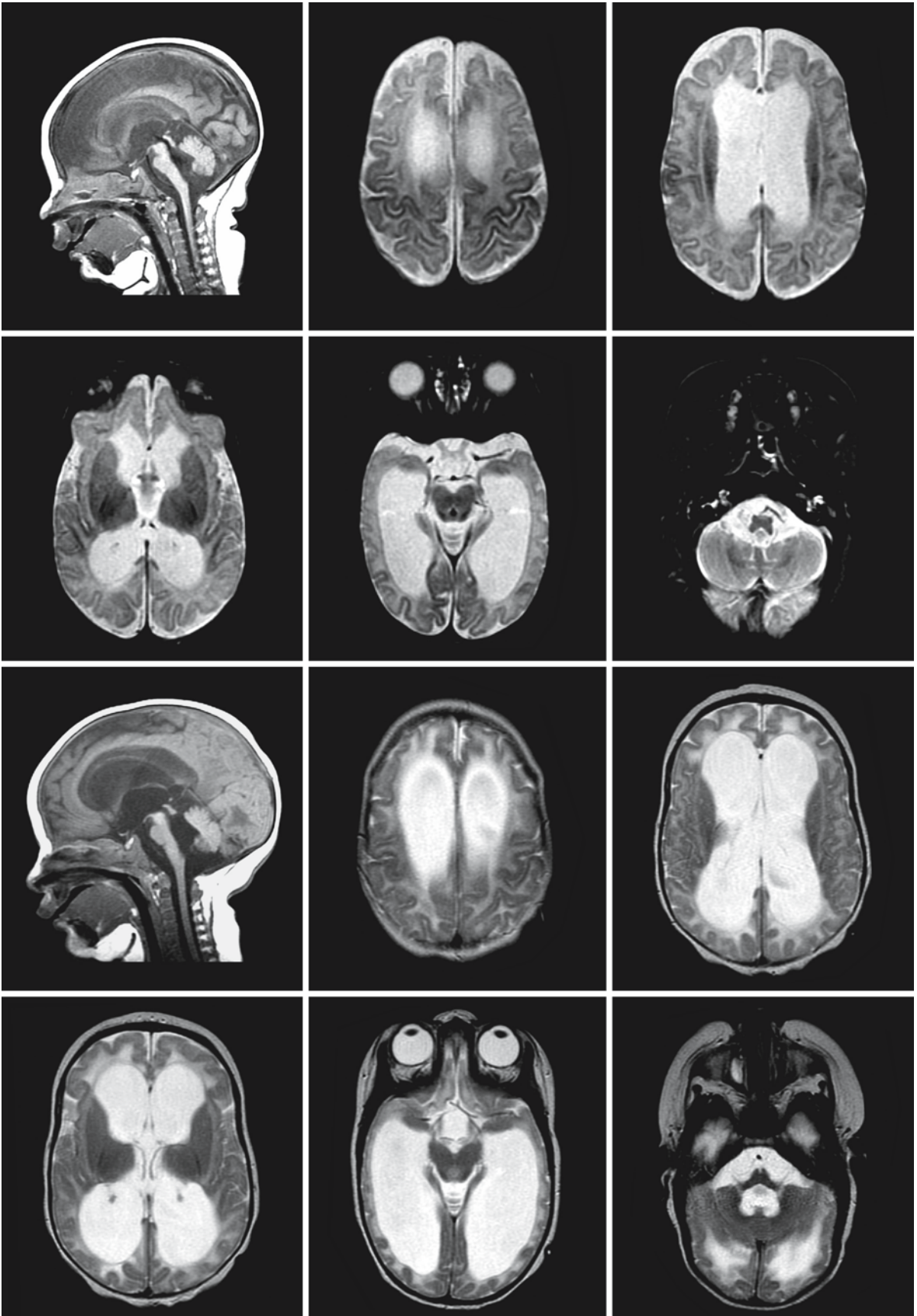


Fig. 45.8.

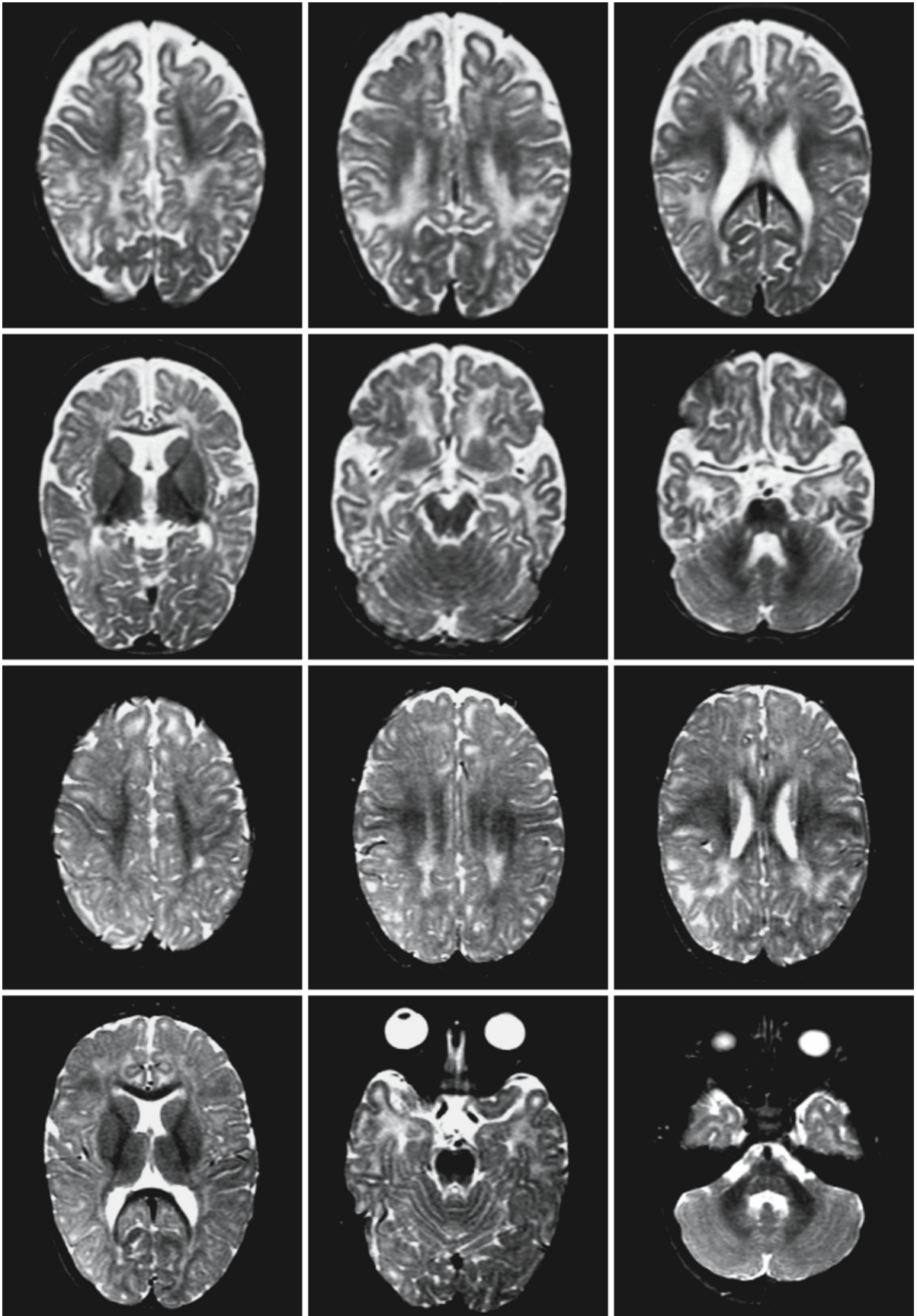


Fig. 45.9.

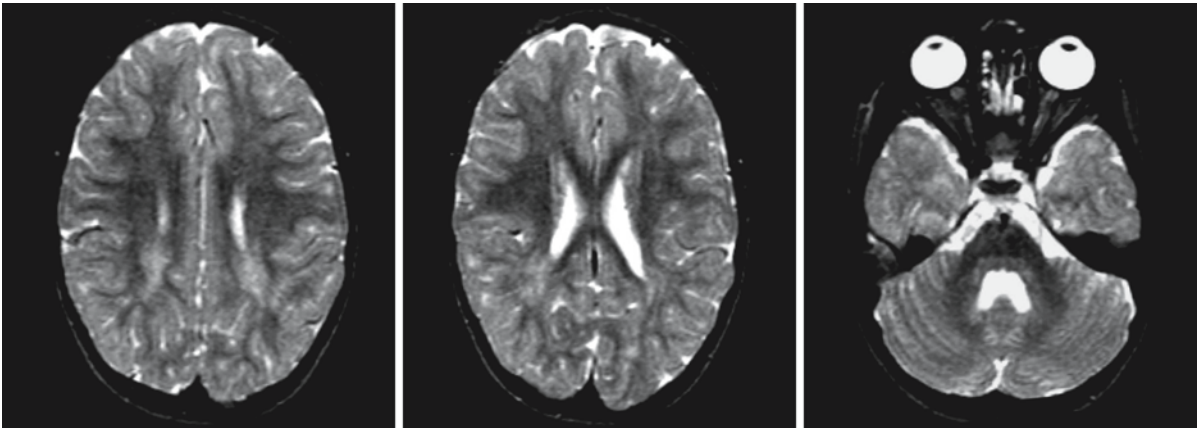


Fig. 45.9. Girl with cobalamin deficiency, 19 months old at the time of the first MRI (*first and second row*). She was breast-fed and her mother, being vegan, had a cobalamin deficiency. These T₂-weighted MR images suggest a combination of delayed and disturbed myelination of the cerebral hemispheres, and demyelination and gliosis in the tracts under the pericentral cortex. Corpus callosum, internal capsule, and brain stem are spared. In addition there is prominent cerebral atrophy

with enlargement of the ventricular system and subarachnoid spaces. The second MRI was obtained after 6 months of treatment (*third and fourth row*) and showed marked progress of myelination and improvement of the atrophy. The third MRI was obtained at the age of 4 years (*fifth row*). It shows that myelination is still incomplete in the U fibers and temporal lobe. There are some remaining areas of abnormal signal in the deep parietal white matter

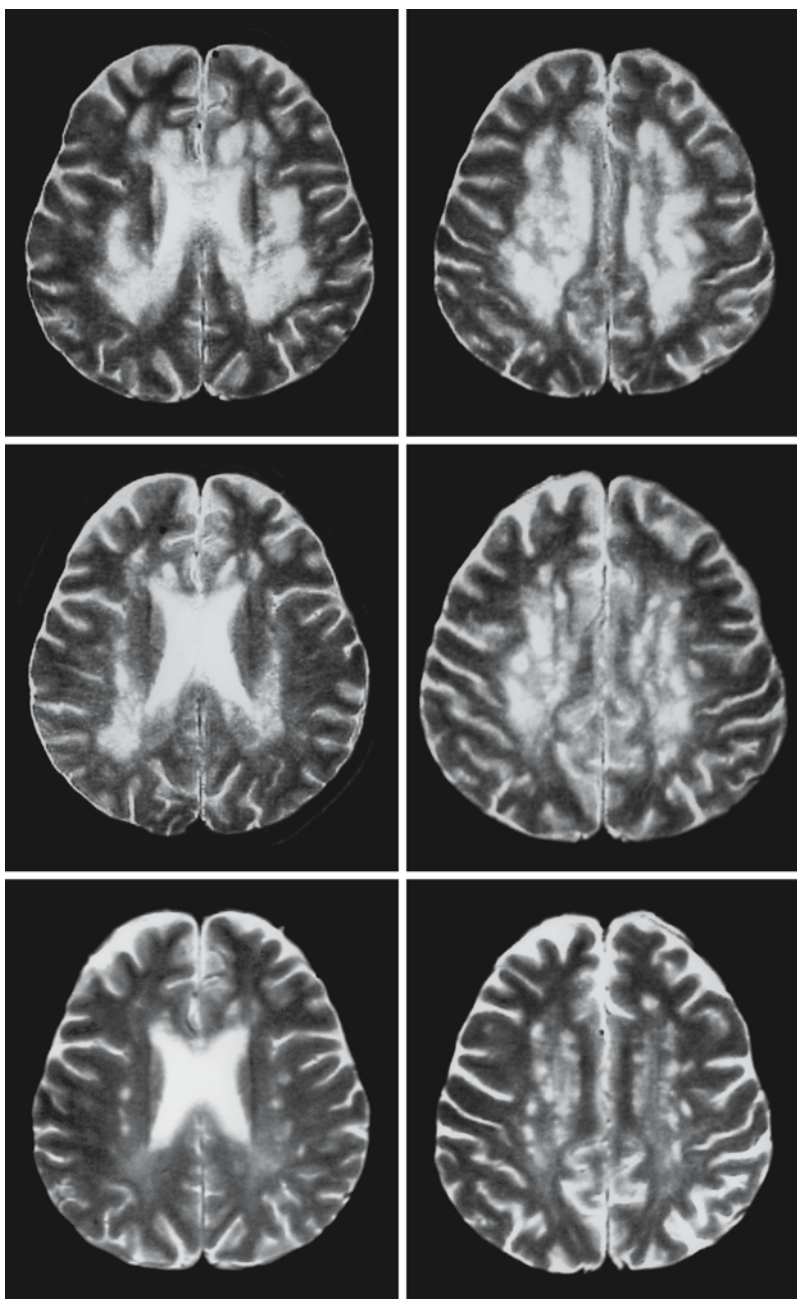


Fig. 45.10. A 51-year-old female patient with cobalamin deficiency. The first MRI (*first row*) was obtained before treatment and shows extensive, patchy cerebral white matter abnormalities with sparing of the U fibers. Follow-up MR images 2 months after installment of cobalamin supplementation (*second row*) and 44 months after initiation of treatment (*third row*) show a striking improvement, especially on the third MRI. From Stojavljević et al. (1997), with permission

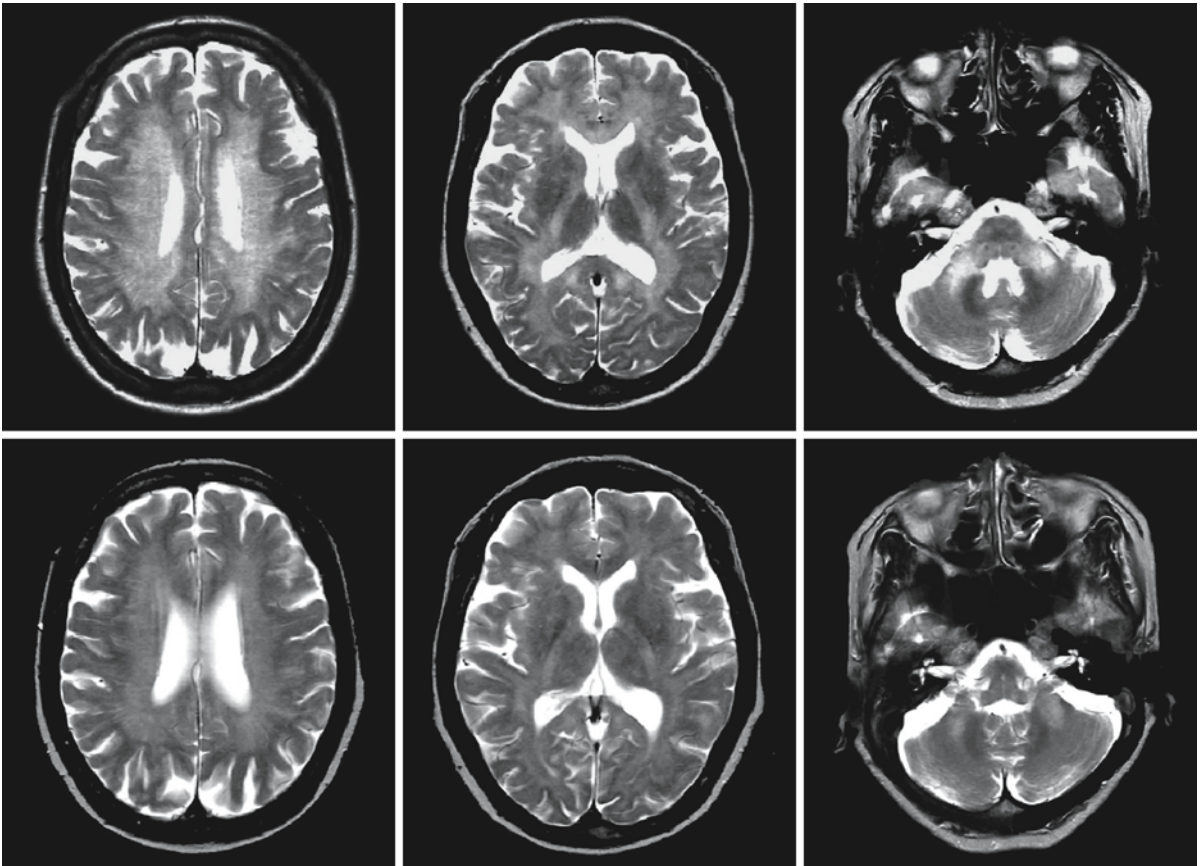


Fig. 45.11. A 48-year-old woman with cobalamin deficiency (*first row*) with follow-up 6 months after initiation of cobalamin supplementation (*second row*). Note the diffuse cerebral white matter abnormalities before treatment, also involving

the corpus callosum, posterior limb of the internal capsule, and middle cerebellar peduncles. With treatment improvement occurs. From Morita et al. (2003), with permission

Urea Cycle Defects

46.1 Clinical Features and Laboratory Investigations

There are five well-documented urea cycle defects (Fig. 46.1):

- Carbamyl phosphate synthetase deficiency (CPSD)
- Ornithine transcarbamylase deficiency (OTCD)
- Argininosuccinate synthetase deficiency (ASSD), also called citrullinemia
- Argininosuccinate lyase deficiency (ASLD), also called argininosuccinic aciduria
- Arginase deficiency, also called hyperargininemia

These disorders have an autosomal recessive mode of inheritance, with the exception of OTCD, which has an X-linked recessive inheritance. Clinical signs of metabolic derangement may appear at any time from early infancy to adulthood, but peak periods include the neonatal period, change to a diet with high protein content (replacement of milk feeding by a diet with higher protein content, parental nutrition), and episodes of infectious diseases. Valproate may also induce an episode of metabolic derangement.

In the case of neonatal presentation, a normal baby is born after normal pregnancy and delivery. After

one or two days the child becomes lethargic and hypotonic. Vomiting, seizures, hypothermia, and hyperventilation occur. Lethargy increases and coma follows. There are signs of elevated intracranial pressure with a bulging fontanel and increasing head size. In most cases the disease progresses rapidly to death within a few days. Survivors almost always have severe neurological sequelae.

In the case of later onset, the disease is chronic and episodic. Occurrence of symptoms may be related to protein intake, infections, trauma, surgery, or initiation of valproate treatment, but not infrequently an episode occurs without any obvious cause. The episodes are characterized by headache, lethargy, irritability, agitation, confusion, hallucinations, vomiting, hypotonia, ataxia, dysarthria, or coma. The presentation may also be stroke-like with signs of dysfunction of one cerebral hemisphere, in particular hemiplegia. In patients with later onset of clinical symptoms the mortality rate is still high, and highest during the initial presenting illness. In addition to the episodic worsenings, there are often chronic clinical signs, which may include learning problems or psychomotor retardation of variable severity, behavioral problems, ataxia, seizures, and hepatomegaly. Some patients voluntarily restrict their protein intake. Normal development and neurological function up to adulthood have been reported in rare cases. In ASLD, coarse and friable hair (trichorrhexis nodosa) is a special characteristic.

The clinical features and course of disease are indistinguishable in CPSD, OTCD, ASSD, and ASLD. It is only in hyperargininemia that the clinical manifestations differ. In the latter disease, the clinical symptoms are slowly progressive and include growth failure, psychomotor retardation, progressive spastic tetraplegia (the legs being more severely involved than the arms), tremor, ataxia, choreoathetosis, epilepsy, and hyperactivity. In addition, episodes of lethargy, vomiting, and coma may occur. There is some variability in onset and rate of progression of the disease. Life span is usually longer than in the other urea cycle defects.

Females heterozygous for OTCD are usually free of symptoms, but approximately 10% become symptomatic and have a milder and more variable course of disease than affected males. Symptoms are episodic and include headaches, vomiting, irritability, bizarre behavior, lethargy, ataxia, tremors, seizures, and co-

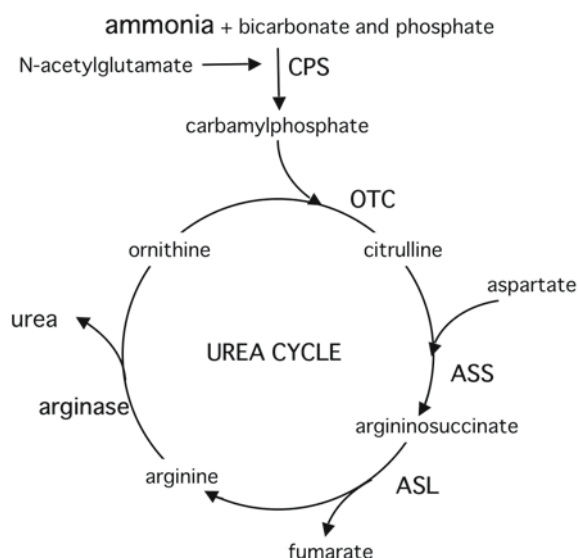


Fig. 46.1. The urea cycle. CPS, carbamyl phosphate synthetase; OTC, ornithine transcarbamylase; ASS, argininosuccinate synthetase; ASL, argininosuccinate lyase

ma. The presentation may also be stroke-like with recurrent episodes of hemiparesis. A high-protein diet, infection, surgery, and the postpartum state may precipitate attacks. Deterioration following use of valproate has been described repeatedly.

Laboratory investigations reveal hyperammonemia in all urea cycle disorders, with the exception of hyperargininemia, in which blood ammonium levels may be normal. Respiratory alkalosis is often present. Urinary orotic acid is increased because of the shunting of nitrogen waste from the urea cycle. In CPSD and OTCD citrulline is decreased in plasma. In ASSD plasma citrulline is elevated, whereas in ASLD argininosuccinate is elevated and citrulline is moderately increased. In these four disorders, plasma levels of glutamine and alanine are frequently raised, whereas arginine and ornithine are decreased. In hyperargininemia, arginine is elevated in plasma. In urine, elevation of arginine, lysine, cystine, ornithine, citrulline, glutamine, and orotic acid is found. A definite diagnosis can be established by enzyme assessment in liver cells. In hyperargininemia and ASLD, enzyme assessment is also possible in erythrocytes; in ASSD and ASLD, enzyme assessment is also possible in fibroblasts. DNA confirmation is possible for all urea cycle defects.

All five urea cycle defects can be diagnosed antenatally. The techniques available for prenatal diagnosis vary from measurement of abnormal metabolites in amniotic fluid, to DNA analysis in chorionic villi or amniocytes, to measurement of enzyme activity in cultured amniocytes or in utero liver biopsy samples. Protein loading, alanine loading, and allopurinol challenge to induce orotic aciduria can be used for carrier detection in OTCD. However, a negative test does not rule out the carrier status. DNA techniques can be used for carrier detection if the mutation in the affected patient is known.

46.2 Pathology

Neuropathological findings are variable and depend on the age of the patient and on the relative effects of present and past acute and chronic metabolic derangements. Neuropathological findings are similar in the different urea cycle disorders.

Actual high elevations of ammonium levels lead to brain swelling. On light and electron microscopy, astrocyte swelling is found. Hyperammonemia induces the so-called Alzheimer type II change in astrocytes. This change consists of an increase in the number and size of astrocytic nuclei, which may become nearly twice their normal size. These nuclei are vesicular with a prominent nuclear membrane and an optically empty nucleoplasm with sparse chromatin particles. The cytoplasm is not discernible with the light

microscope. Alzheimer type II astrocytes are mainly present in cerebral cortex, basal nuclei, cerebellar cortex and nuclei, and brain stem nuclei. The presence of Alzheimer type II cells depends on the presence of hyperammonemia. In adequately treated patients with normal ammonia levels Alzheimer type II cells are absent.

In neonates who die in the acute phase of metabolic decompensation, diffuse brain swelling is found. Alzheimer type II astrocytes are present in gray matter structures. There may be signs of acute neuronal injury. Myelination is normal for age. In some neonates a status spongiosus of cortex and white matter is observed.

In older infants, children, and adults, atrophy of the brain is often found with widening of the lateral ventricles and spaces between the sulci. The atrophy varies from mild to severe. Variable focal and multifocal corticosubcortical necrosis may be seen with a tendency to microcavitation. Acute lesions are swollen; old lesions are atrophic with presence of ulegria. On microscopic examination, cortical findings vary from normal to pseudolaminar neuronal necrosis to complete depopulation of the cortex and diffuse gliosis. The cortical damage may have a spongiform appearance. Neuronal loss, gliosis, and spongy changes may also be seen in basal nuclei, thalamus, and brain stem. White matter changes are variable. Myelination may be normal or mildly to severely delayed. Signs of active myelin breakdown may be present, but are not seen in all cases. The white matter may show diffuse gliosis. The white matter changes may be spongiform with presence of myelin splitting and vacuolation. In severe cases, there is diffuse loss of axons and myelin, and the white matter may be largely replaced by gliotic tissue.

In female carriers of OTCD, neuropathological findings are apparently mainly related to chronic hyperammonemia, which leads predominantly to neuronal damage. Variable, sometimes extreme cerebral atrophy is the predominant finding. The hemispheric walls are thin and the lateral ventricles are dilated. The cerebral cortex shows signs of neuronal loss and gliosis. There is also loss of neurons in the basal nuclei and thalamus. Alzheimer type II astrocytes are present in the cerebral cortex, basal nuclei, dentate nuclei, and brain stem nuclei. The white matter may be rarefied and gliotic with a reduced number of myelinated fibers.

46.3 Pathogenetic Considerations

The urea cycle (Fig. 46.1) serves two purposes: it contains, in part, the biochemical reactions required for the *de novo* biosynthesis and degradation of arginine, and it incorporates the surplus of nitrogen into urea,

which serves as a waste nitrogen product. The enzymes involved in urea synthesis are partly located within the mitochondria (carbamyl phosphate synthetase, ornithine transcarbamylase), whereas the other enzymes are located within the cytosol (argininosuccinate synthetase, argininosuccinate lyase, arginase). Carbamyl phosphate synthetase requires *N*-acetylglutamate for full activity. Most urea cycle metabolic capacity resides in the liver. The gene locations of the urea cycle enzymes have been identified and the genes have been characterized. The gene for carbamyl phosphate synthetase is located on chromosome 2q35; the gene for ornithine transcarbamylase is located on chromosome Xp21.1; the gene for argininosuccinate synthetase is located on chromosome 9q34; the gene for argininosuccinate lyase is located on chromosome 7cen-q11.2; and the gene for arginase is located on chromosome 6q23.

A urea cycle defect has two consequences: arginine becomes an essential amino acid (except in hyperargininemia), and nitrogen accumulates in a variety of molecules, in particular ammonia. Ammonia is highly toxic to the brain where it interferes with energy production and normal metabolism of neurotransmitters. Ammonia influences the glutamine-glutamate-GABA balance. Glutamate is the most important excitatory neurotransmitter, whereas GABA (γ -aminobutyric acid), formed by decarboxylation from glutamate, is the most important inhibitory neurotransmitter. In the presynaptic neuron, glutamate is formed from glutamine by glutaminase. After release by the presynaptic neuron, glutamate is taken up by the astrocyte, in which it is processed by glutamine synthetase into glutamine. Glutamine is transported to the presynaptic neuron, where glutaminase catalyzes the formation of glutamate available for neurotransmission. Hyperammonemia has a great impact on this cycle by stimulating synthesis of glutamine from ammonia and glutamate with consumption of ATP. The disturbance of the balance between excitatory and inhibitory neurotransmitters may contribute to the cerebral dysfunction. Glutamine synthetase is mainly located in astrocytes, and high plasma levels of ammonia lead to accumulation of glutamine within astrocytes. During hyperammonemia, the concentration of glutamine in the brain becomes highly elevated. It has been proposed that the consequent osmotic effect causes astrocytes to swell, with subsequent cerebral edema.

The excitotoxin quinolinic acid has been proposed to explain aspects of neuronal injury. Quinolinic acid accumulates under hyperammonemic conditions and derives from tryptophan metabolism. Under such conditions there is increased transport of tryptophan across the blood-brain barrier. Tryptophan oxidation leads to the formation of quinolinic acid, which acts as an excitotoxin at the *N*-methyl-D-aspartate

(NMDA) receptors. Moderate elevations of CSF levels of quinolinic acid have been found in patients with a urea cycle defect.

Unlike patients with liver failure, in whom ammonia is only one of several toxins, ammonia appears to be the only cause of the acute encephalopathy seen in patients with urea cycle defects, except for those with hyperargininemia, in whom an increase in arginine may also play a role. In hyperammonemia due to liver failure, MRI of the brain shows, as expected in generalized disorders, a symmetrical pattern. There are changes in signal intensity in the basal nuclei, in particular due to T_1 shortening. In contrast, brain pathology in urea cycle disorders is often characterized by focal, usually asymmetrical lesions. It remains to be explained why cerebral abnormalities related to hyperammonemia in urea cycle disorders are so different from those observed in liver failure, and why the lesions tend to be asymmetrical.

In all urea cycle disorders apart from hyperargininemia, arginine is deficient unless externally supplied. Chronic arginine deficiency is characterized by dermatological features with erythematous scaling. A dramatic improvement of this cutaneous eruption occurs with dietary arginine supplementation. High levels of citrulline or argininosuccinate are probably not toxic. The similarity in presentation among the different urea cycle defects is related to hyperammonemia. The variability in clinical severity is probably related to differences in mutations (and differences in levels of residual enzyme activity), differences in other genetic factors and environmental factors. In females carrying an OTC mutant allele on one chromosome, variability in expression is related to the proportion of hepatocytes in which the normal or mutant allele is active (lyonization).

Hyperargininemia has a clinical picture that is partially different from that of the other urea cycle defects. The progressive spasticity that dominates the clinical picture in hyperargininemia is not a feature of the other urea cycle defects. It has been proposed that arginine and its metabolites, the guanidine compounds, are responsible.

46.4 Therapy

Therapeutic strategies in urea cycle defects aim at reduction of protein intake, utilization of alternative pathways of nitrogen excretion, and replacement of deficient nutrients.

Emergency treatment consists of stopping all protein intake, starting high energy intake to prevent catabolic situations with breakdown of endogenous protein, and measures that lead to augmented nitrogen disposal. Sodium benzoate, sodium phenyl butyrate, or sodium phenyl acetate, supplied orally or

intravenously, can be used as substrates for an alternate route of nitrogen disposal. Lactulose binds ammonia in the intestinal tract and can increase ammonia disposal in feces. Arginine should be supplemented in all urea cycle defects except hyperargininemia. Hemodialysis can be used in life-threatening situations. Of course, the conditions initiating the deterioration (infections, insufficient intake) and complications (seizures) have to be treated too.

Chronic treatment of urea cycle defects consists of a protein-restricted diet, sufficient caloric intake to avoid catabolic situations, and supplementation of absent substances. Protein-restricted diets have to be supplemented with essential amino acid mixtures to avoid deficiencies. In all urea cycle disorders apart from hyperargininemia, arginine cannot be synthesized endogenously; it has become an essential amino acid and has to be supplied. If an essential amino acid is lacking, protein breakdown cannot be remedied. Long-term treatment that restricts intake of high-protein food, including milk and meat, leads to deficiency of minerals, trace elements, and vitamins, which also have to be supplemented. Infections and insufficient caloric intake due to anorexia carry the risk of triggering an episode of severe hyperammonemia. Therefore, such conditions have to be treated vigorously. The use of valproic acid as an antiepileptic drug should be avoided. Valproic acid may accelerate the appearance of hyperammonemia.

The overall long-term prognosis has improved with treatment, in particular in patients presenting after the neonatal period. However, a high percentage of treated patients are still mentally retarded. The mortality rate in the group with neonatal presentation is still very high, and most (or all) surviving patients are severely handicapped.

Enzyme replacement therapy through liver transplantation has been attempted, and it has been shown to be effective in correcting the metabolic defect. After liver transplantation no further brain damage is to be expected, but significant recovery of prior brain damage does not occur. Therefore, liver transplantation may be an excellent treatment for patients without major brain injury. However, in view of the potential morbidity and mortality associated with liver transplantation, the present experience is still too limited to allow a balanced opinion. Genetic correction of the patient's liver cells is a promising future option.

46.5 Magnetic Resonance Imaging

In urea cycle defects, cerebral abnormalities change depending on the stage of disease. In acute episodes of metabolic derangement, lesions appear, which may improve under treatment but leave traces. Chronic hyperammonemia also has deleterious effects. MRI has the advantage over neuropathological examinations of being able to depict the dynamics of cerebral lesions in urea cycle disorders.

In neonates, neuroimaging shows severe brain swelling. On CT diffuse cerebral hypodensity with loss of contrast between cortex and white matter may be seen. MRI shows diffuse cerebral edema (Fig. 46.2) and may demonstrate involvement of the basal ganglia with a high signal in the caudate nucleus, putamen, and/or globus pallidus on T₂-weighted images (Fig. 46.2) and a high signal in the globus pallidus and to a lesser extent the putamen on T₁-weighted images. The deep sulci of the insular and perirolandic region may also display T₁ shortening. MR spectroscopy may contribute by showing highly elevated glutamine levels. If the patient survives, diffuse brain atrophy follows. In some cases, focal or diffuse gross cystic degeneration of the cerebral hemispheres is seen on follow-up. The basal ganglia are often prominently involved as well, but the thalamus, brain stem, and cerebellum tend to be relatively spared.

In acute metabolic derangement in older infants and children, small and large areas of abnormal signal intensity are seen in the brain, most often involving both cortex and underlying white matter, giving them an infarct-like aspect (Figs. 46.4 and 46.5). Sometimes, the signal abnormalities involve only or mainly the cortex (Fig. 46.3). The acute lesions are moderately swollen. Often multiple lesions are present. The distribution of the lesions is as a rule asymmetrical or even unilateral (Figs. 46.4 and 46.5). In some cases one hemisphere is totally involved. However, in other patients almost the entire brain is affected (Fig. 46.3). A combination of high plasma ammonia levels and an MRI picture with one or more large, moderately swollen areas involving cortex and white matter is highly suggestive of a urea cycle defect. This pattern can be found in all urea cycle defects when an episode of acute metabolic derangement is present, including those in female carriers of OTCD (Fig. 46.4) and patients with arginase deficiency (Fig. 46.5). In the chronic stage, swelling resolves and focal areas of atrophy and patchy signal changes of cortex and white matter remain (Fig. 46.6). Sometimes, the lesions are restricted to the white matter.

In chronic hyperammonemia, defective myelination and progressive cerebral atrophy are seen. Some patients have some nonspecific focal white matter abnormalities.

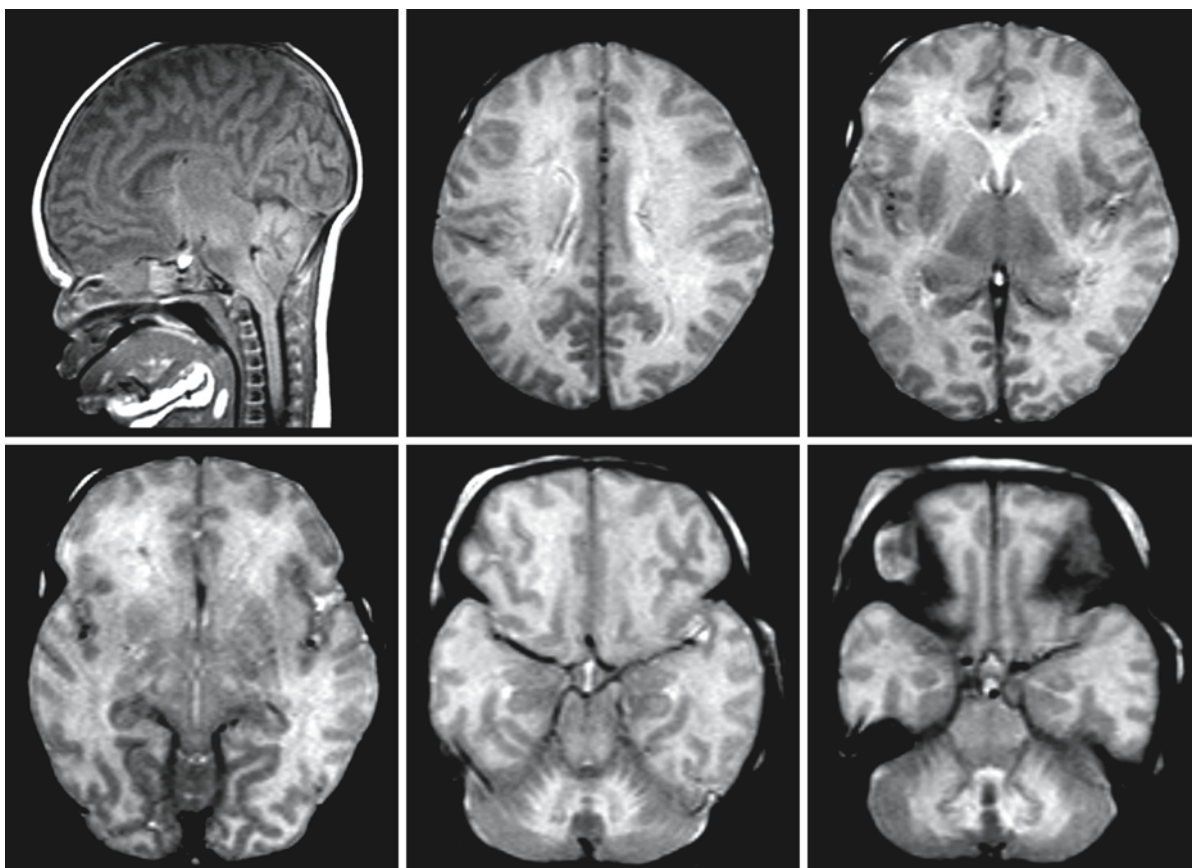


Fig. 46.2. MRI series of a baby boy, 6 days old, with ASD and extreme hyperammonemia. The T₁-weighted sagittal image shows generalized edema and tonsillar herniation. The T₂-weighted transverse images show generalized edema with, in

particular, severe swelling of the brain stem. Note the signal abnormalities in the putamen and caudate nucleus. MR spectra of this patient are shown in Chap. 108

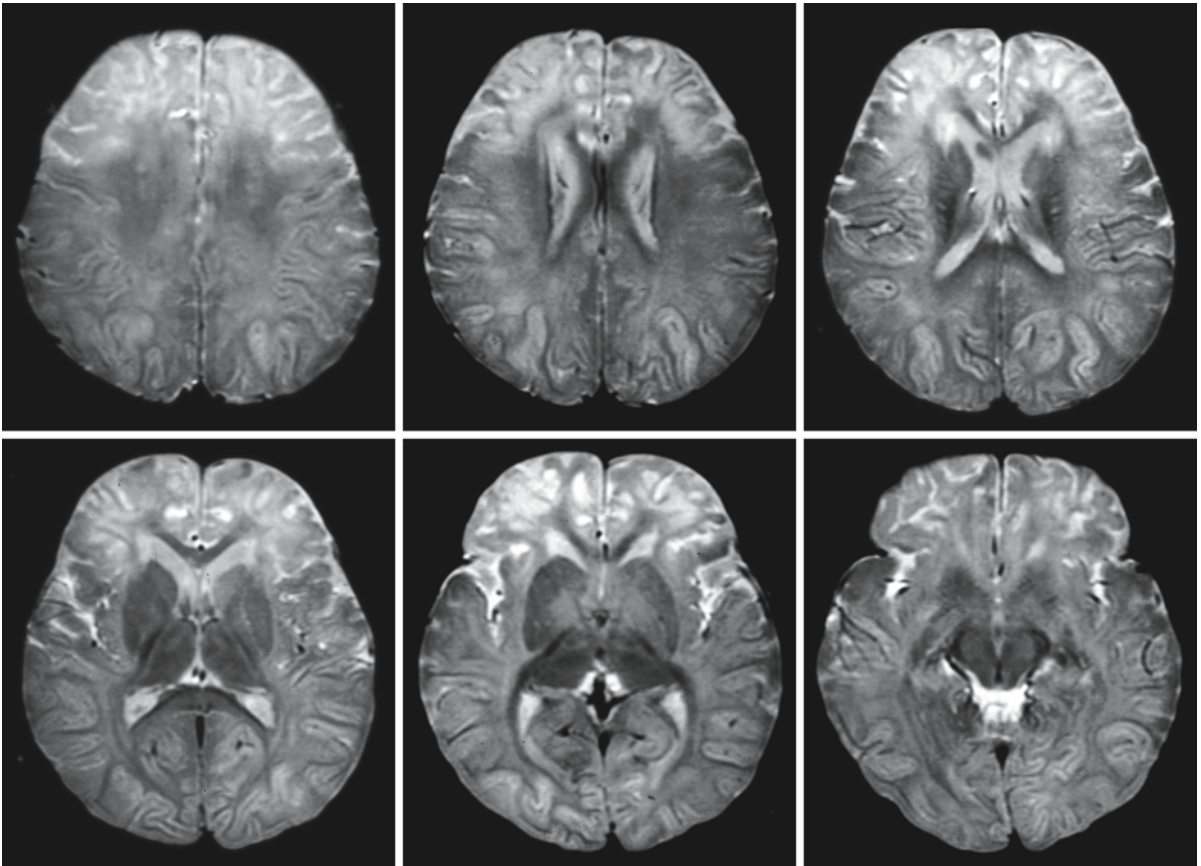


Fig. 46.3. A 2-year-old girl, a carrier of OTCD, with an acute episode of neurological deterioration and coma. The T₂-weighted transverse images show diffuse involvement of the cerebral cortex and subcortical white matter. Courtesy of Dr. S. Blaser, Department of Diagnostic Imaging, Hospital for Sick Children, Toronto, Canada

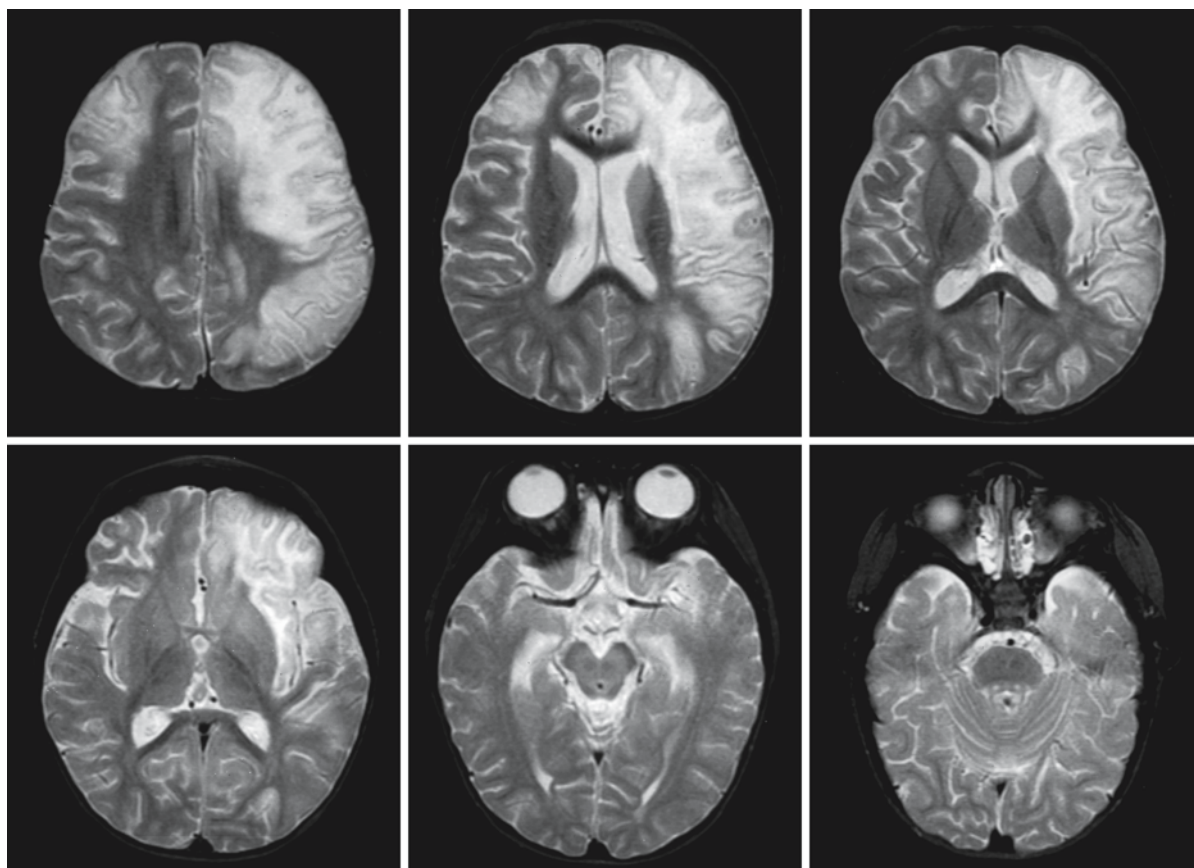


Fig. 46.4. A 2-year-old girl, a carrier of OTCD, with an acute episode of neurological deterioration and hemiplegia. The T₂-weighted images show an extensive area of high signal intensity and swelling in the left frontal and parietal white matter and cortex with blurring of the corticomedullary junction. A

smaller area of abnormal signal in the cortex and subcortical white matter is seen in the right frontal region. Courtesy of Dr. S. Blaser, Department of Diagnostic Imaging, Hospital for Sick Children, Toronto, Canada

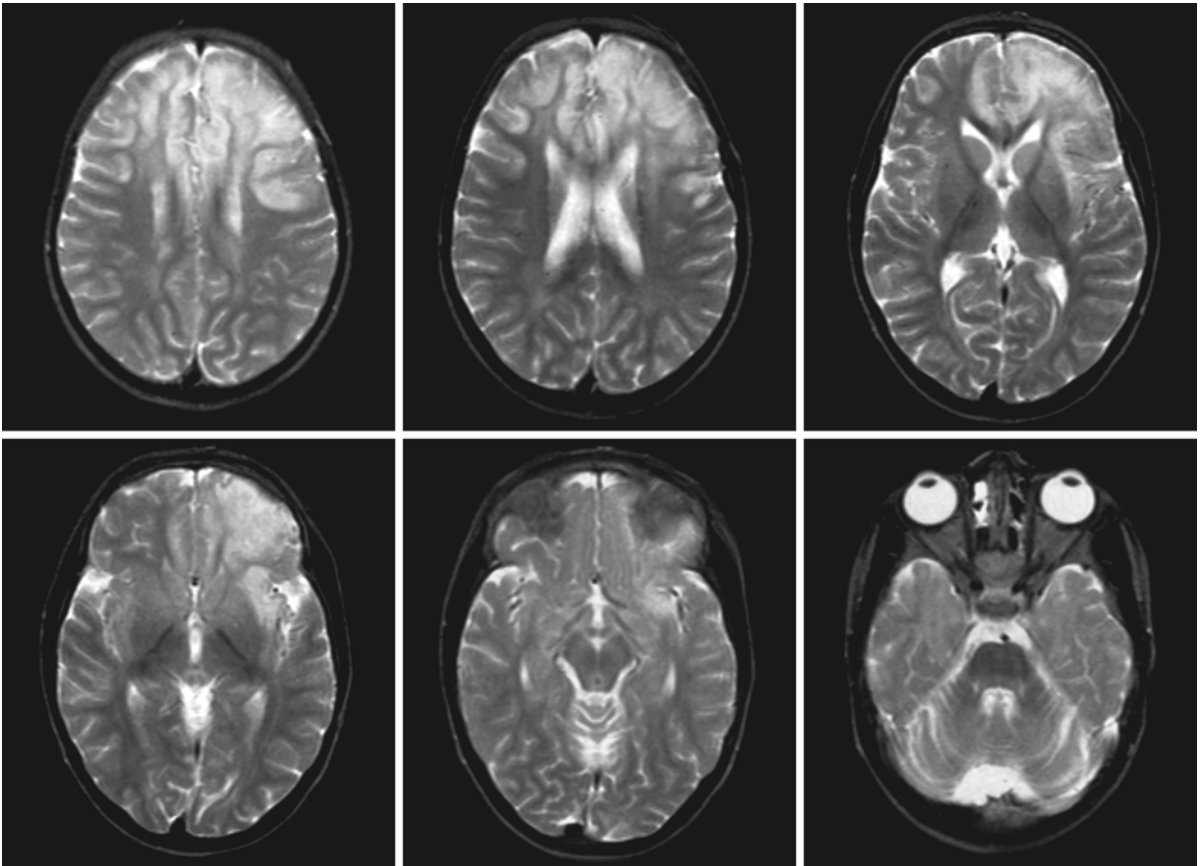


Fig. 46.5. A boy, 6 years of age, with hyperargininemia. The MR images were made during an episode of acute metabolic decompensation following protein-rich gavage feeding. The T₂-weighted transverse images show the signal changes bilaterally in the frontal lobes, accentuated on the left side, with involvement of both gray and white matter, blurring the gray-white matter junction. The corpus callosum is not involved, nor are the basal ganglia

ally in the frontal lobes, accentuated on the left side, with involvement of both gray and white matter, blurring the gray-white matter junction. The corpus callosum is not involved, nor are the basal ganglia

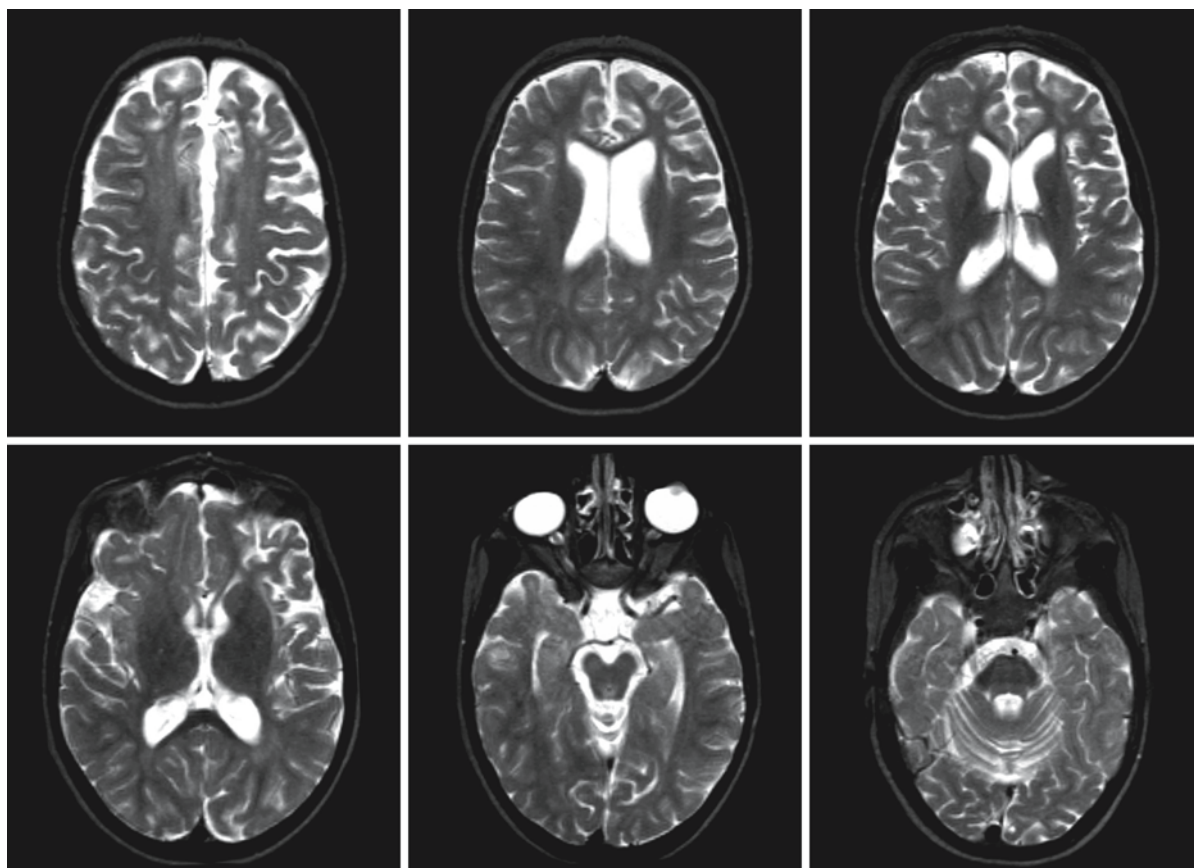


Fig. 46.6. The same boy as in Fig. 46.5, now 2 years later. The acute abnormalities have disappeared. Note the atrophy, most marked in the left frontal area

Serine Synthesis Defect Caused by 3-Phosphoglycerate Dehydrogenase Deficiency

47.1 Clinical Features and Laboratory Investigations

3-Phosphoglycerate dehydrogenase deficiency is a rare neurological disorder with a prenatal onset. All patients known so far have presented with congenital microcephaly. Some have contractures at birth. During the first months of life a severe psychomotor retardation becomes apparent. Between 2 and 14 months epilepsy starts, which is difficult to control with antiepileptic medication. Different types of seizures may be seen, including West syndrome and tonic, atonic, and myoclonic seizures. The patients develop spastic tetraparesis. Other features that may be seen are nystagmus, cataract, and hypogonadism.

Low levels of L-serine and glycine are found in the CSF and plasma in the fasting state. The levels are relatively lower in CSF than in plasma. Urinary amino acids are not informative. Another finding is a low level of 5-methyltetrahydrofolate in CSF without an elevated homocysteine concentration in plasma. Megaloblastic anemia and thrombocytopenia are variably present. The diagnosis is confirmed by demonstration of deficient 3-phosphoglycerate dehydrogenase activity in cultured fibroblasts. Prenatal diagnosis is possible by means of both enzyme assessment and DNA analysis.

47.2 Pathology

At present, no autopsy reports are available.

47.3 Pathogenetic Considerations

Deficiency of 3-phosphoglycerate dehydrogenase is a disease with an autosomal recessive mode of inheritance. The related gene, *PHGDH*, is located on chromosome 1q12. Different mutations have been described.

L-Serine is derived from four possible sources: dietary intake, biosynthesis from 3-phosphoglycerate, biosynthesis from glycine, and degradation of protein and phospholipids. It is likely that the predominant source of L-serine is different for different tissues and different stages of development. 3-Phosphoglycerate dehydrogenase catalyzes the first step in the synthesis of L-serine from the glycolytic intermediate 3-phosphoglycerate.

L-serine has a central role as a precursor for sulfur amino acids. It is a major source of one-carbon groups, providing formyl groups for purine synthesis and methyl groups for pyrimidine synthesis, the remethylation of homocysteine, and many other methylation reactions necessary in cellular metabolism. It is a precursor for the synthesis of phosphoglycerides and complex macromolecules such as sphingolipids and glycolipids. Serine can be converted to glycine, which has important neurotransmitter functions as an NMDA receptor agonist. The conversion of L-serine to glycine is accompanied by the conversion of tetrahydrofolate to 5,10-methylenetetrahydrofolate, which is subsequently reduced to 5-methyltetrahydrofolate. The latter is a methyl donor for the remethylation of homocysteine to methionine. L-serine can also be converted to D-serine, and D-serine is an even more potent NMDA receptor agonist than glycine. L-Serine is utilized in gluconeogenesis, but its role here is quantitatively of minor importance.

It is likely that, as soon as the blood-brain barrier is established, the CNS has to rely on its own synthesis of L-serine. 3-Phosphoglycerate dehydrogenase is highly expressed in fetal tissues including the CNS, especially in the ventricular and subventricular zone of the neural tube. This is the zone where the proliferation of neural cells takes place. It is likely that impairment of neuronal proliferation is responsible for the microcephaly observed in patients at birth. The role of L-serine in the CNS is not restricted to providing nucleotide precursors needed for cell proliferation. Serine has also a trophic effect on neurons and stimulates dendritogenesis and axon length.

The hypomyelination observed on MRI in patients with 3-phosphoglycerate dehydrogenase deficiency may be secondary to low concentrations of folate metabolites. Hypomyelination has been described in patients suffering from other inborn errors with a low CSF level of 5-methyltetrahydrofolate. Low levels of S-adenosylmethionine may be important in the white matter abnormalities observed in folate deficiency.

47.4 Therapy

Treatment with high doses of L-serine is usually very effective in controlling the seizures. Some patients need additional treatment with glycine to stop the seizures. There is some developmental progress after

onset of treatment, but the children remain seriously handicapped. The biochemical abnormalities normalize during treatment. The problem with treating children diagnosed some time after birth is that irreversible brain damage is already present, which cannot be reversed by treatment. There is preliminary evidence that treatment of mothers pregnant of an affected fetus with L-serine may prevent all or most of the clinical problems.

47.5 Magnetic Resonance Imaging

MRI in untreated patients shows a reduced volume of the cerebral white matter with enlarged subarachnoid spaces (Fig. 47.1). The sulci almost touch the walls of the lateral ventricles. The corpus callosum is thin and short (Fig. 47.2). The cerebral white matter is deficient in myelination, also in older children.

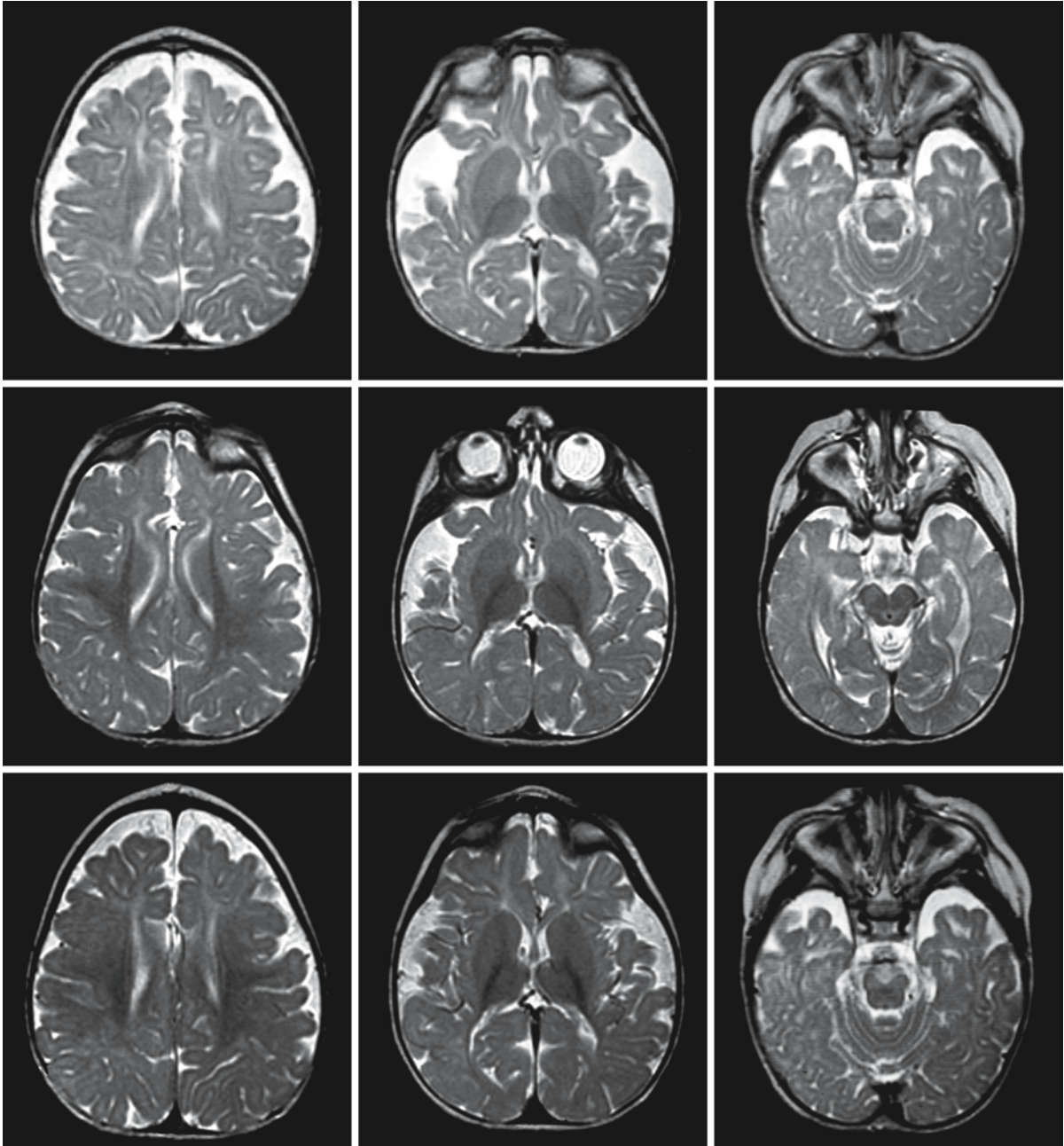
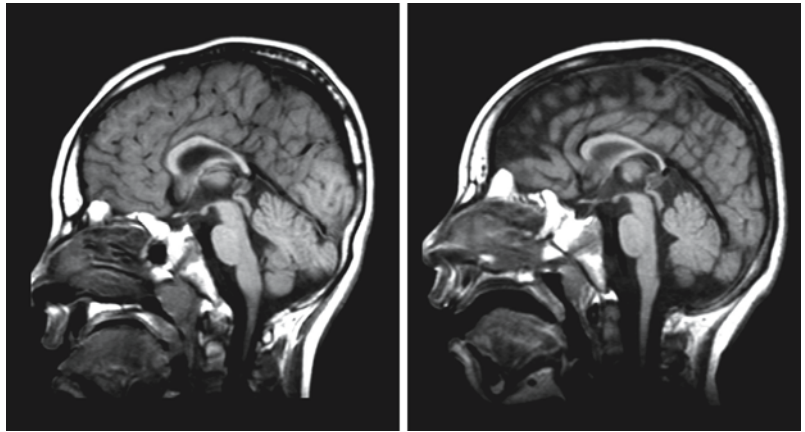


Fig. 47.1. Female patient with 3-phosphoglycerate dehydrogenase deficiency at the age of 12 months before the start of treatment (*first row*), and at the ages of 18 (*second row*) and 22 months (*third row*), both after treatment started. At 12 months there is serious myelin deficiency and atrophy of the cerebral

white matter. Under treatment the myelin content and the volume of the cerebral white matter increase, although they do not become normal. Courtesy of Dr. M. Pineda, Department of Neuropediatrics, Hospital Sant Joan de Déu, Barcelona, Spain

Fig. 47.2. Midsagittal image of two brothers with 3-phosphoglycerate dehydrogenase deficiency, showing the short and thin corpus callosum



Once treatment has been started, the white matter volume increases (Fig. 47.1). In some patients myelination progresses, but not in all. In the patients in whom myelination progresses, it still remains deficient and does not seem to reach completion. Longer follow-up is needed to document the long-term effects of treatment.

Molybdenum Cofactor Deficiency and Isolated Sulfite Oxidase Deficiency

48.1 Clinical Features and Laboratory Investigations

Molybdenum cofactor deficiency and sulfite oxidase deficiency are autosomal recessive inborn errors of metabolism with a similar clinical presentation. In molybdenum cofactor deficiency, not only sulfite oxidase but also xanthine dehydrogenase and aldehyde oxidase are deficient. Molybdenum cofactor deficiency occurs more frequently than isolated sulfite oxidase deficiency.

Patients with molybdenum cofactor deficiency usually present a few days after birth with feeding difficulties, seizures, axial hypotonia, and limb hypertonia. The seizures are usually tonic-clonic and difficult to control. In patients who survive the neonatal period, serious psychomotor retardation is seen. Many patients develop microcephaly. Lens dislocation develops in patients who survive the neonatal period. Other ocular abnormalities include spherophakia, iris coloboma, nystagmus, and enophthalmos. Cerebral blindness may occur. A few patients have a milder disease course, with onset after the neonatal period, usually precipitated by an infection. The clinical symptoms include hypotonia, extrapyramidal movement abnormalities, and sometimes lens dislocation. Most patients die at an early age. Exceptional patients have a still milder disease with a Marfan-like habitus, dislocated lenses, learning problems, occasional stroke-like episodes with unilateral motor deficits, and survival into the third decade.

In patients with sulfite oxidase deficiency, the clinical picture is on the whole more variable than in molybdenum cofactor deficiency. At the severe end of the spectrum, patients display signs of serious encephalopathy soon after birth, with seizures and spasticity and subsequently serious psychomotor retardation, lens dislocation, spherophakia, and early death, similar to the clinical picture of molybdenum cofactor deficiency. However, patients may also have a later onset, most often between the ages of 6 months and 1.5 years, and lack suggestive symptoms such as ectopic lenses and seizures. The onset of the disease is often precipitated by an infection, which is followed by developmental regression, hypotonia, and dystonia or choreoathetosis. Microcephaly may develop. An episodic course with stepwise deterioration has also been described.

Laboratory investigations in isolated sulfite oxidase deficiency reveal elevated urinary excretion of sulfite, thiosulfate, and taurine. Plasma and urinary amino acid profiles show the presence of S-sulfocysteine. Plasma cystine levels are decreased. Urinary excretion of xanthine and hypoxanthine are normal. Sulfite oxidase activity is deficient in cultured fibroblasts. In molybdenum cofactor deficiency, the same laboratory findings are present, with the exception of xanthine and hypoxanthine, which are elevated, and plasma and urinary uric acid, which are low to virtually absent. DNA-based diagnosis is possible for both disorders. Elevated urinary sulfite can be detected using dipsticks, but these are not very reliable and may show false negative results, because sulfite spontaneously oxidizes to sulfate on standing. Prenatal diagnosis is possible by enzyme assessment in chorionic villi or cultured amniotic cells. Prenatal diagnosis by DNA analysis is also an option.

48.2 Pathology

The neuropathology of both isolated sulfite oxidase deficiency and molybdenum cofactor deficiency is characterized by gross cerebral atrophy with deep sulci and dilated ventricles. The cerebral hemispheres are usually affected by multicystic degeneration, which involves the white matter and inner layer of the cortex. In some areas the cortex may show complete degeneration. The cavities are separated by thick glial scar tissue. The remaining white matter contains little myelin and is markedly gliotic. The basal ganglia, thalami, and cerebellum are atrophic and show neuronal loss and gliosis on microscopy. The basal ganglia may also be partly cystic. Remaining white and gray matter structures may show diffuse spongiosis and may contain areas of mineralization. The brain stem is atrophic and contains little myelin, but is better preserved.

48.3 Pathogenetic Considerations

Sulfite oxidase is encoded by the gene *SUOX*, located on chromosome 12q13.2–13.3. Molybdenum cofactor consists of a unique pterin, molybdopterin, and the metal molybdenum. The cofactor is synthesized in

humans by a complex pathway that requires the products of at least four different genes: *MOCS1*, *MOCS2*, *MOCS3*, and *GEPH*. Disease-causing mutations have been identified in three of these genes: *MOCS1*, *MOCS2*, and *GEPH*. *MOCS1* is located on chromosome 6p21.3, *MOCS2* on chromosome 5q11, and *GEPH* on chromosome 14q24. *MOCS1* and *MOCS2* have a bicistronic architecture, which means that each gene encodes two proteins in different open reading frames. The gene products, MOCS1A and B and MOCS2A and B, are expressed either from different mRNAs generated by alternative splicing or by independent translation of a bicistronic mRNA. The gephyrin protein is required during cofactor assembly for insertion of the molybdenum into molybdopterin. To date, no disease-causing mutations have been found in *MOCS3*.

Molybdenum cofactor deficiency results in simultaneous loss of all cofactor-dependent enzyme activities, including sulfite oxidase, xanthine dehydrogenase, and aldehyde oxidase. Sulfite oxidase catalyzes the oxidation of sulfite into sulfate. Xanthine oxidase catalyzes the decomposition of xanthine into uric acid. Aldehyde dehydrogenase catalyzes the formation of xanthine from hypoxanthine. In addition, this enzyme is thought to be part of a general detoxification system. Combined deficiency leads to a phenotype that is clinically quite similar to that of isolated sulfite oxidase deficiency. Therefore, it is likely that the neurological disease, characterized by a severe encephalopathy, results primarily from the sulfite oxidase deficiency. The pathological findings resemble those seen in severe perinatal asphyxia. The pathogenesis of the disease is not understood. It is not clear whether the damage arises from a toxic metabolite or from the deficit of a reaction product. The accumulating sulfite may be toxic. However, its mode of action is unclear, and it is also unknown why the brain is most seriously affected. The reaction of sulfite with disulfide bonds or with sulfhydryl groups is a general process that would be expected to occur in all organs. Ocular lens subluxation may be related to a disruption of cystine cross-linking by excess sulfite.

48.4 Therapy

No effective treatment is available for the severe variants of either isolated sulfite oxidase deficiency or molybdenum cofactor deficiency. The cofactor is exceedingly unstable and direct cofactor replacement is not feasible. Various therapeutic trials, including oral intake of molybdenum salts and low-sulfur amino acid diet, combined with oral sulfate supplementation, have failed. However, some measures may benefit individual patients. In particular in patients with a milder clinical picture, restriction of the intake of the

precursor sulfur amino acids may lead to some improvement. Cysteamine may be beneficial in absorbing excess sulfite.

Treatment of seizures is important. In particular vigabatrin has been successful in controlling the seizures.

48.5 Magnetic Resonance Imaging

Neuroimaging findings in patients with isolated sulfite oxidase deficiency and molybdenum cofactor deficiency are similar. CT scan of the brain has been reported to show diffuse edema in the neonatal period. Multicystic degeneration of the cerebral hemispheres and calcium deposits have been documented by follow-up CT.

In early postnatal presentation, MRI shows brain swelling and extensive areas of abnormal signal, consistent with edema and “hypoxic” changes within the cerebral cortex (Figs. 48.1 and 48.2). Follow-up MRI shows extensive cystic degeneration of the cerebral hemispheres, with large and smaller cysts within the white matter and enlargement of the ventricles and subarachnoid spaces (Fig. 48.2). The corpus callosum is thin. The cerebellum and brain stem are small, probably due to both hypoplasia and atrophy. The small cerebellum with enlarged pericerebellar spaces has been described as a Dandy–Walker variant, which is not correct, as the rest of the Dandy–Walker configuration is lacking. The basal ganglia and thalami are atrophic and may contain cysts. On more prolonged follow-up, the large cysts in the cerebral white matter may collapse and a seriously atrophic brain may remain. Not much myelin is deposited in the highly damaged, gliotic white matter. Because of the serious brain atrophy, subdural fluid collections develop easily.

The above pattern is indistinguishable from that seen in multicystic encephalopathy after perinatal asphyxia, neonatal presentations of a urea cycle defect, and some early-onset and severe mitochondrial disorders. It is essentially the pattern that is expected to develop in neonates after profound energy failure of any origin. It seems that serious edema preceding the multicystic degeneration is a common factor.

Some patients with milder forms of isolated sulfite oxidase deficiency or molybdenum cofactor deficiency have a much better preserved brain. Bilateral lesions in the globus pallidus with preservation of the rest of the brain have been found repeatedly (Fig. 48.3). In some patients more extensive abnormalities are seen, with signal abnormality and swelling of the caudate nucleus, putamen, globus pallidus, and cerebral peduncles in the acute stage (Fig. 48.4) and less prominent signal abnormalities and atrophy of these structures in the chronic stage.

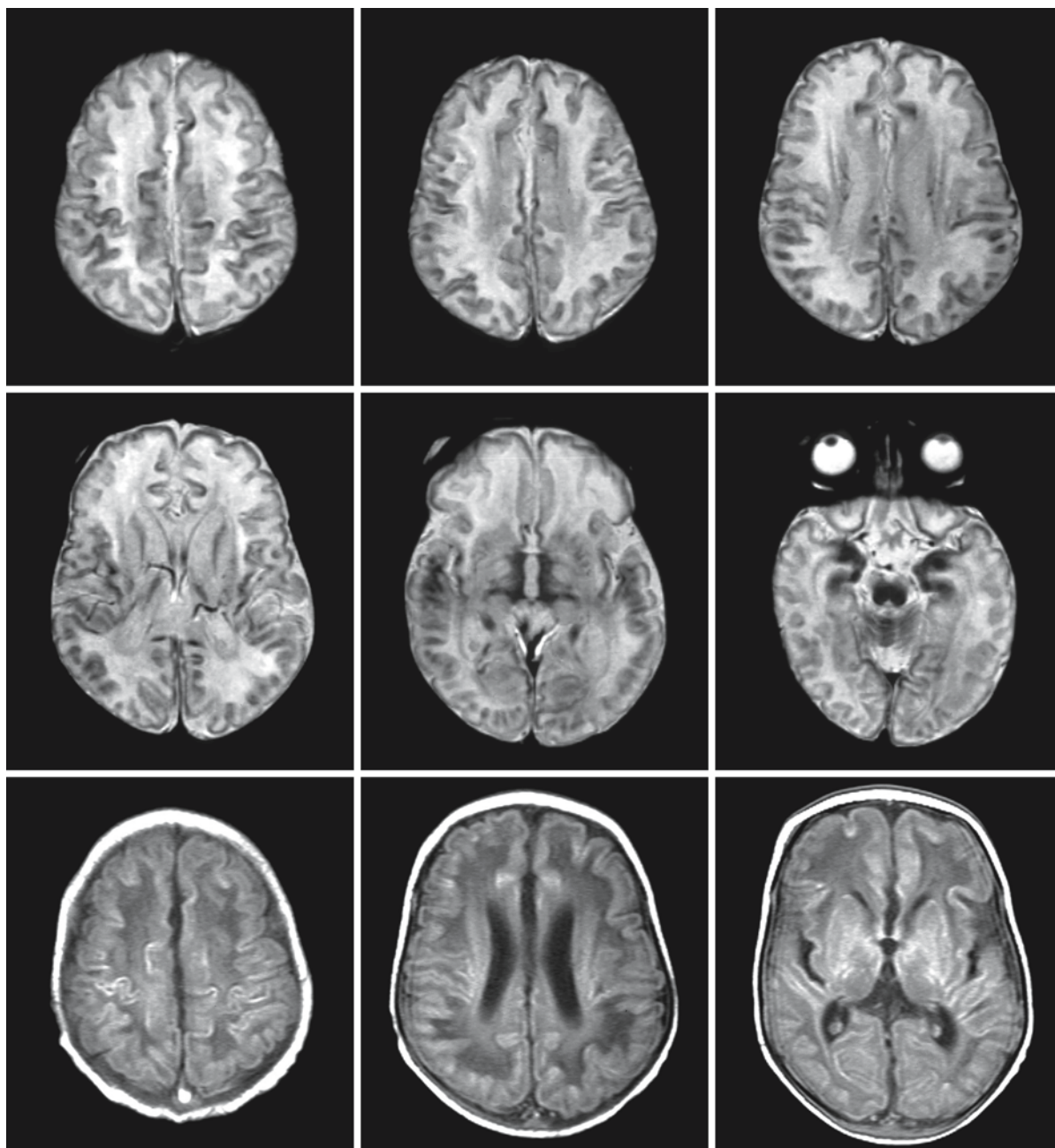


Fig. 48.1. Baby boy, 10 days old, with molybdenum cofactor deficiency. The T_2 -weighted images show serious involvement of the cortex and basal ganglia. These structures have a high

signal in parts on T_1 -weighted images, as seen in necrosis. Courtesy of Dr. S. Blaser, Department of Diagnostic Imaging, Hospital for Sick Children, Toronto, Canada

Selective involvement of the globus pallidus is rare and has been observed in creatine synthesis defects, succinic semialdehyde dehydrogenase deficiency, mitochondrial defects, hyperbilirubinemia, and carbon monoxide poisoning. Lesions in the globus pallidus are also relatively frequent in neurofibromatosis type I.

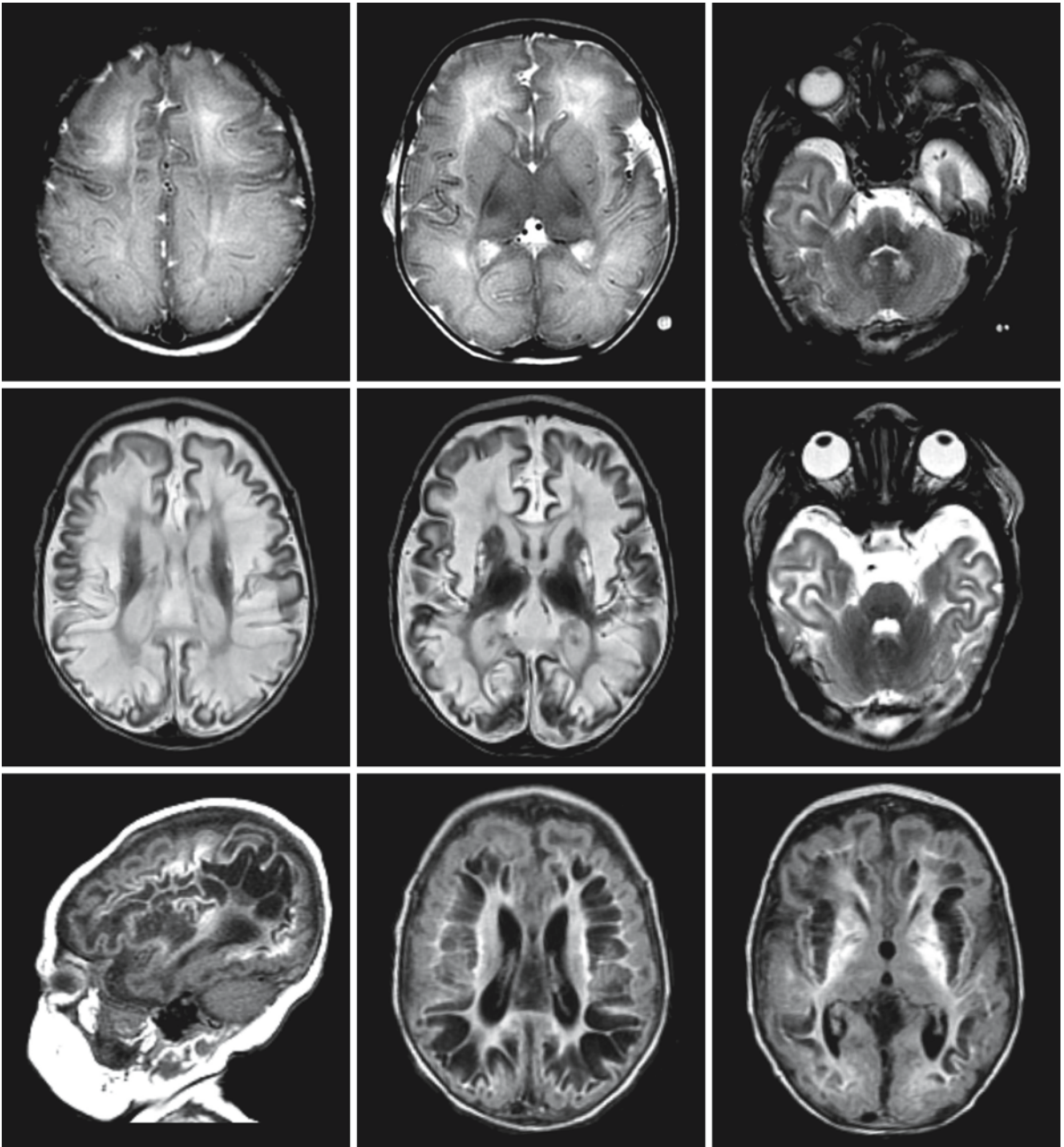


Fig. 48.2. Baby girl with isolated sulfite oxidase deficiency. The T₂-weighted images in the *first* row were obtained at the age of 5 days and show serious abnormalities of the cerebral cortex, white matter, and basal ganglia. The brain is diffusely swollen. The posterior fossa structures have a more normal appearance. The images in the *second* and *third* rows were

obtained at the age of 31 days and demonstrate cystic degeneration of the cerebral white matter. The basal ganglia and cerebral cortex also contain signal abnormalities. The brain stem and cerebellum are preserved. From Dublin et al. (2002), with permission

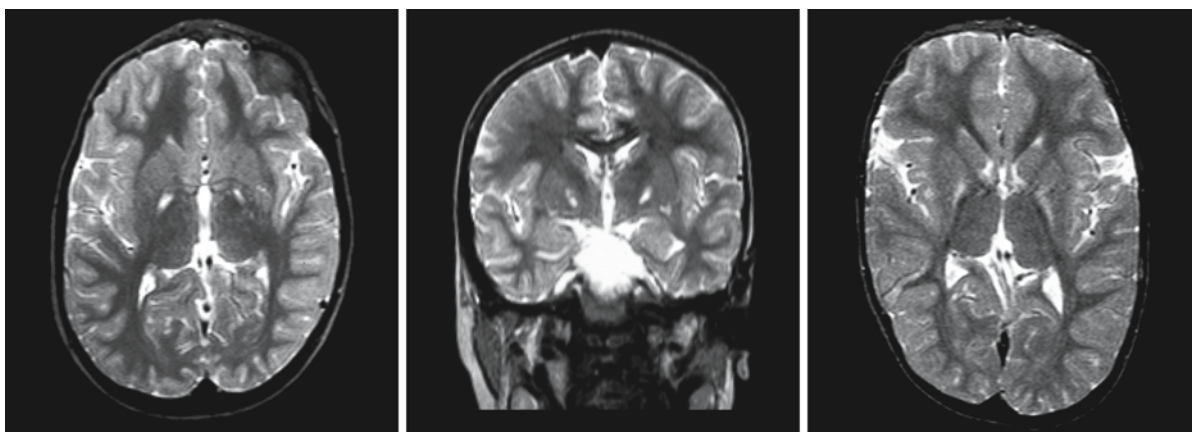


Fig. 48.3. Two brothers with isolated sulfite oxidase deficiency. Both are relatively mildly affected. The *left* and *middle* images represent the older brother at the age of 5 years. The

right image represents the younger brother, also at the age of 5 years. Both have isolated globus pallidus lesions

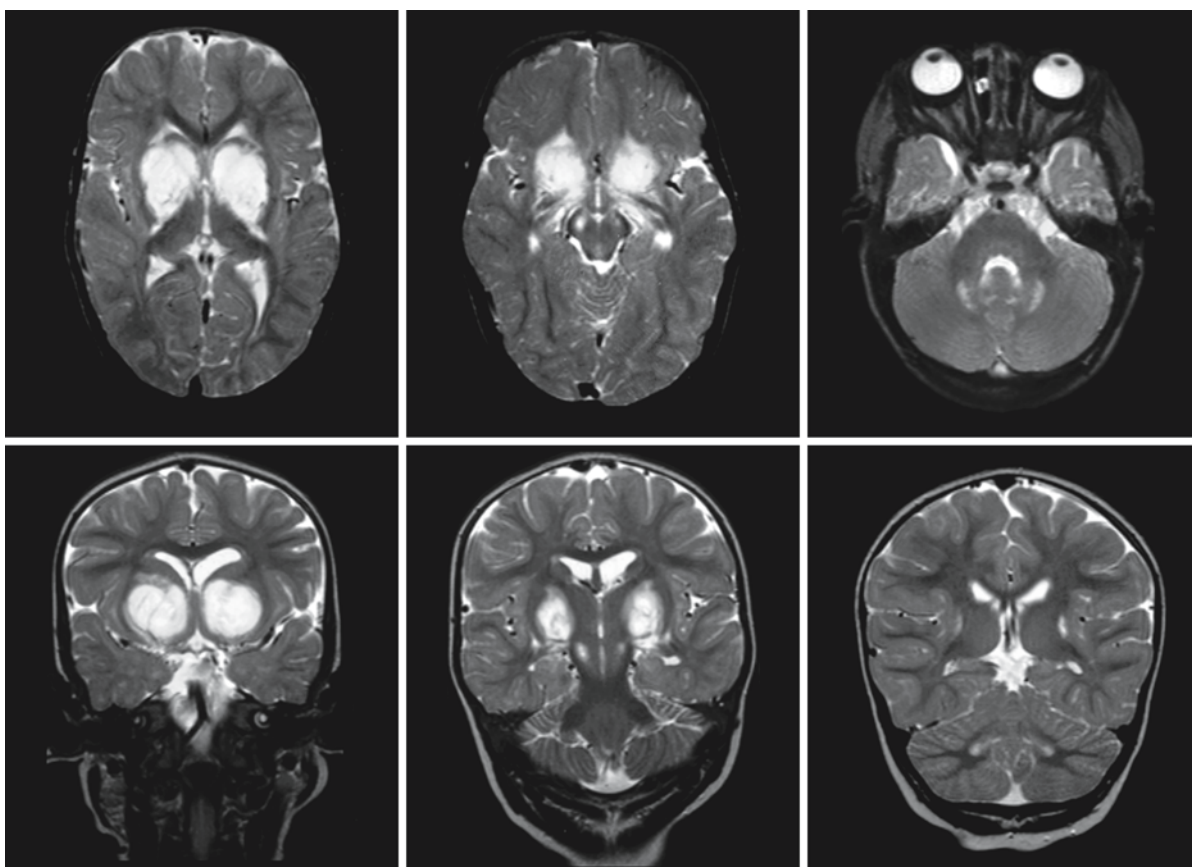


Fig. 48.4. Girl, 1 year and 9 months old, with molybdenum cofactor deficiency. Note the signal abnormality and swelling of the putamen, globus pallidus, caudate nucleus, substantia

nigra, and dentate nucleus. From Hughes et al. (1998), with permission

Galactosemia

49.1 Clinical Features and Laboratory Investigations

Three major types of galactosemia can be distinguished, based on three different enzyme deficiencies. The most commonly detected type, classical galactosemia or galactosemia type 1, is caused by a deficiency of galactose-1-phosphate uridylyltransferase. Galactosemia type 2 is caused by galactokinase deficiency. Galactosemia type 3 is the result of a deficiency of uridine diphosphate galactose-4-epimerase. All three types have an autosomal recessive mode of inheritance.

Galactosemia type 1 has an incidence of 1:30,000 to 1:60,000. Affected infants are normal at birth. Clinical manifestations develop a few days after the baby has started to have milk feeds. Symptoms include a failure to thrive, refusal to feed, vomiting, diarrhea, and hypotonia. Signs of deranged liver function with jaundice and hepatomegaly usually become apparent after the first week of life. Hemolysis occurs in some patients, contributing to the jaundice. There is an enhanced susceptibility to infections, in particular *Escherichia coli* infections. Sepsis often develops within the first 2 weeks of life. Ascites may occur and is a serious prognostic sign with an associated mortality of about 20%. Cataracts appear within days or weeks and become irreversible within a matter of weeks. There may be signs of elevated intracranial pressure with lethargy and diffuse cerebral edema on neuroimaging. If milk is not withdrawn, neonatal death may follow.

There are less severe variants of the disease. Clinical presentation may be later and less life-threatening. Some patients are seen later in the first year of life because of retarded psychomotor development, cataracts, and hepatomegaly. In rare cases, a child who is several years of age is presented with psychomotor retardation and cataracts. These children often have a history of reduced milk intake because of recurrent vomiting after drinking milk.

If galactose is not eliminated from the diet, cataracts, progressive liver failure, and mental deficiency develop in patients surviving the neonatal period. A galactose-free diet causes a striking regression of all signs and symptoms. Nausea and vomiting cease, lethargy disappears, weight gain ensues, liver problems clear, and cataracts regress. However, the long-term outcome is less optimistic. Over the years,

verbal and performance IQ slowly decline, and a substantial number of patients have subnormal intelligence. School achievements are often worse than those of healthy sibs. At the end of the first decade of life, many children develop tremor, resting and postural. Other neurological signs that may develop over the years include a cerebellar ataxia with clumsiness, intention tremor and dysidiadochokinesis, hyperreflexia, apraxia, seizures, and choreoathetosis. Some children have microcephaly. Many children have speech abnormalities, varying from dysarthria, verbal dyspraxia, and dysgrammatism to stuttering. Delayed growth is especially seen in girls, but final height is usually within normal limits. A high incidence of ovarian failure with hypergonadotropic hypogonadism has been documented in female patients. It may be manifest as delayed puberty, primary or secondary amenorrhea, or oligomenorrhea. Amenorrhea can also occur after pregnancy. Successful pregnancies in female patients are rare, but may occur. No correlation between onset and strictness of diet and development of late complications has ever been established. A relationship between development of cataract and dietary control is present. With introduction of tighter dietary control, lens opacities usually gradually resolve. The patients with milder variants of galactosemia type 1 have a better outlook with normal physical, motor and mental development when treated.

In patients with signs of CNS problems, EEG often shows nonspecific abnormalities. SSEPs show prolonged central conduction times.

Galactosemia type 2 is much rarer than type 1, and much milder. Cataracts are the only consistent manifestation of the untreated disorder. They develop insidiously within weeks of birth. In exceptional cases, mild hepatomegaly, mental retardation, or pseudotumor cerebri have been described.

Galactosemia type 3 exists in two forms. Infants with the mild form appear healthy and remain so. The severe form is similar to galactosemia type 1. Presentation is neonatal with jaundice, vomiting, weight loss, hypotonia, and hepatomegaly. Despite treatment, motor and intellectual development is retarded and neural deafness is present.

Whenever the diagnosis galactosemia is considered in neonates, it is essential to stop milk feeding immediately. In galactosemia type 1, a positive reduction test in urine may be the first diagnostic lead.

Apart from galactosuria, there may be evidence of a renal tubular defect with some proteinuria, glucosuria, amino aciduria, phosphaturia, and renal tubular acidosis. Galactitol in urine is elevated. The intermittent nature of the galactosuria makes its detection difficult, in particular when milk feeds are withheld from very ill infants. The diagnosis is confirmed by the finding of high levels of galactose-1-phosphate in red blood cells and the demonstration of a deficiency of galactose-1-phosphate uridylyltransferase in red or white blood cells. The assay on red blood cells may, of course, be falsely negative after exchange blood transfusion. When a child has received exchange transfusion, assays in blood must be postponed for 3–4 months. Enzyme activity can also be determined in cultured skin fibroblasts. Patients with some residual enzyme activity appear to follow milder clinical courses (mild variants) than patients with no demonstrable activity.

In galactosemia type 2, elevated galactose is found in blood and urine. Galactose-1-phosphate is not elevated. Final diagnosis is established by demonstrating a deficiency of galactokinase in red blood cells or fibroblasts.

In galactosemia type 3, elevated galactose is present in blood and urine. The diagnosis may be suspected when galactose-1-phosphate in erythrocytes is elevated and the activity of galactose-1-phosphate uridylyltransferase is normal. The diagnosis can be confirmed by demonstrating a deficiency of epimerase activity in red blood cells and leukocytes. In the mild form of galactosemia type 3, the enzyme deficiency is limited to blood cells and normal activity is found in fibroblasts and liver cells. In the severe form a generalized deficiency of epimerase is present.

In several countries, mass newborn screening is performed. Diagnostic difficulties arise in cases of partial galactose-1-phosphate uridylyltransferase deficiency. A mutation of the transferase gene, called the Duarte variant, causes diminished red cell transferase activity but usually no clinical disorder. The allelic frequency of the Duarte variant is high, and compound heterozygotes with one Duarte allele and one classical galactosemia allele constitute the most common biochemical phenotype detected by screening newborn infants. This condition is usually benign, but neonates may have symptoms of galactose toxicity. Several other benign mutations of the galactose-1-phosphate uridylyltransferase gene have been described.

Prenatal diagnosis can be performed by analysis of galactitol in amniotic fluid, by enzyme analysis in chorionic villus cells or amniotic fluid cells, and by DNA techniques. Prenatal diagnosis, however, is only rarely performed with a view to terminating the affected pregnancy.

49.2 Pathology

Few neuropathological descriptions are present and they only concern patients with classical galactosemia (type 1). External examination often reveals the brain to be mildly atrophic. The most prominent findings concern the cerebral white matter and cerebellar cortex. The cerebral white matter is diffusely gliotic. On myelin staining, patchy pallor is found, but no signs of active demyelination. The white matter changes are most pronounced in the periventricular area. The white matter may be reduced in volume with some enlargement of the lateral ventricles and subarachnoid spaces. The cerebral cortex may either be normal or exhibit some neuronal loss. Gliosis and pigmentary degeneration of the globus pallidus and reticular zone of the substantia nigra have been described. There is a loss of Purkinje cells within the cerebellar cortex.

49.3 Pathogenetic Considerations

Galactose is metabolized in three sequential enzymatic steps. The first step comprises the phosphorylation of galactose by galactokinase to form galactose-1-phosphate. The second step is mediated by galactose-1-phosphate uridylyltransferase and results in an exchange of galactose-1-phosphate for the glucose-1-phosphate moiety of uridine diphosphate glucose to form uridine diphosphate galactose and free glucose-1-phosphate. In the third step, uridine diphosphate galactose is transformed to uridine diphosphate glucose by the enzyme epimerase. In this step galactose is converted to glucose. This step can be reversed, leading to endogenous synthesis of galactose from glucose.

The most common type of galactosemia, type 1, is related to a deficiency of galactose-1-phosphate uridylyltransferase. The gene encoding this enzyme, *GALT*, is located on chromosome 9p13. A large number of mutations have been described. Furthermore, gene polymorphism has been found, leading to enzyme polymorphism. The most common variants are the Duarte variants (D_1 and D_2), but other benign variants have also been described. There is evidence that the molecular heterogeneity forms the explanation for the variable clinical outcome.

The human galactokinase gene, *GALK*, is located on chromosome 17p24. Patients with galactokinase deficiency have mutations in this gene. A second *GALK* cDNA has been found on chromosome 15. It is clear that only the first gene on chromosome 17p24 produces significant amounts of the enzyme; the role of the second gene is not known.

The epimerase gene, *GALE*, is located on chromosome 1p36. Different mutations have been detected in epimerase deficient patients.

The pathogenetic mechanisms of tissue damage in galactosemia are understood to only a limited extent. The mechanisms may be organ-specific.

Galactitol toxicity is probably responsible for the development of cataracts. In the presence of high galactose levels, the enzyme aldose reductase irreversibly reduces galactose to galactitol. Very little galactitol leaves the intracellular compartment and no further metabolism is possible beyond the galactitol step. The intracellular concentration of galactitol increases and alters the cell osmotic environment. Water is drawn into the cell and results in lens swelling, with denaturation and precipitation of proteins and disruption of lens architecture. Aldose reductase activity is also present in the brain, where galactitol may accumulate intracellularly and contribute to cellular swelling and death, especially in the early, untreated stage.

There is evidence that galactose-1-phosphate is responsible for many of the acute toxic effects in galactosemia, including liver, kidney, and brain damage. Galactose-1-phosphate may contribute to toxicity by reducing energy availability through inhibition of several enzymes involved in glucose metabolism.

The observations that a galactose-free diet is impossible and that galactose and galactose-1-phosphate can also be made from endogenous sources make it probable that galactose-1-phosphate and galactitol also contribute to the occurrence of late complications.

Galactose is part of many complex glycoproteins and glycolipids. Defects in galactosylation of proteins and lipids has been proposed as pathogenetic mechanisms for organ damage in galactosemia, by analogy to the congenital defects in glycosylation. In particular, the late complications of classical galactosemia have been ascribed to depletion of uridine diphosphate galactose (UDP-galactose), one of the products of galactose-1-phosphate uridylyltransferase activity. UDP-galactose is the donor of the galactosyl moiety in the biosynthesis of glycoproteins and glycolipids, including gangliosides, cerebroside, and sulfatide. A deficiency of UDP-galactose could limit the synthesis of these macromolecules, which include major myelin lipids. UDP-galactose is also needed for the synthesis of ovarian membrane glycoproteins and glycolipids. The theory is, however, difficult to reconcile with the metabolic pathways, which enable synthesis of UDP-galactose from glucose-1-phosphate by pyrophosphorylase and epimerase.

Depletion of *myo*-inositol and inositol phospholipids has been found in the brain of galactosemia patients. *Myo*-inositol is synthesized from glucose-6-

phosphate. Aldose reductase is activated by high levels of galactose, and activation of this pathway leads to *myo*-inositol depletion. *Myo*-inositol is an intracellular osmolyte. It is essential for the synthesis of inositol phospholipids, which are membrane components. An important surface signal transduction system relies on induction of hydrolysis of plasma membrane phosphoinositides to generate intracellular second messenger molecules, which induce the cell to respond to various extracellular agonists, such as neurotransmitters and peptide hormones. Insufficient levels of these membrane phosphoinositides may lead to impaired cell function.

49.4 Therapy

The predominant source of galactose is lactose, present in mammalian milk or artificial milk formulae and milk products. Lactose is a disaccharide. Prior to absorption from the intestine it is hydrolyzed to its constituent monosaccharides, glucose and galactose. Galactose is subsequently converted to glucose. Patients with galactosemia type 1 are treated with a galactose-free diet, causing all symptoms of acute galactose toxicity to disappear, including vomiting, diarrhea, jaundice, hepatomegaly, cerebral edema, and cataracts. Levels of galactose-1-phosphate in red blood cells and galactitol in urine drop. Treatment monitoring by assessment of galactose-1-phosphate in red blood cells or galactitol in urine is of limited value, since even with strict adherence to diet the values remain elevated. After increased galactose intake, it takes several weeks before galactitol in urine rises and even longer before galactose-1-phosphate rises. On the whole, changes in galactose intake have relatively little effect on metabolite levels. Perfect treatment is not attainable, probably because food products may still contain some galactose and, possibly more importantly, because of endogenous production of galactose from glucose. There is no evidence that the occurrence of late complications depends on strictness of compliance with the diet, which is also an argument in favor of endogenous galactose production. In addition, an abnormal prenatal intrauterine biochemical environment may be responsible for part of the cerebral and ovary dysfunction, which cannot be reversed by postnatal treatment.

There is no evidence that dietary treatment of heterozygous mothers pregnant with a galactosemic fetus has beneficial effects. Lactation in galactosemic mothers may cause a significant rise in galactose-1-phosphate in red blood cells and galactitol in urine. Considering these biochemical signs of self-intoxication, breast feeding is discouraged. Hormonal replacement therapy is given to female patients with ovary dysfunction.

Treatment of galactosemia type 2 may be limited to the elimination of milk from the diet. It is not necessary to apply a strict galactose-restricted diet.

Treatment of the mild form of galactosemia type 3 is not necessary. Treatment of the severe form is similar to treatment of galactosemia type 1, but more difficult. Patients with galactosemia type 3 are unable to synthesize galactose from glucose and are therefore dependent upon exogenous sources for galactose. When too small amounts of galactose are ingested, synthesis of galactosylated compounds, such as galactoproteins and galactolipids (present in myelin lipids), is impaired. Unfortunately, there is no easily available chemical parameter for monitoring how much galactose should be used.

49.5 Magnetic Resonance Imaging

Neuroimaging reports all relate to galactosemia type 1. CT scan of the brain has been reported to show signs of generalized atrophy in patients with neurological abnormalities. The ventricular system may be enlarged and the cerebellum atrophic.

The first abnormality noted by MRI is that after normal initial myelination the directly subcortical white matter does not become as hypointense on T₂-weighted images as in normal children older than 1 year, indicating hypomyelination (Figs. 49.1 and 49.2). This can still be seen in teenage and adult patients (Fig. 49.3). In addition, multiple foci of high signal intensity are seen in many patients, spread over the hemispheric white matter (Figs. 49.1 and 49.3). The foci are bilateral and more or less symmetrical in distribution, although not perfectly symmetrical. The white matter abnormalities are most pronounced in the periventricular area, round the frontal and occipital horns. In many patients the ventricular system is slightly enlarged. Cerebellar foliae are prominently visible in some patients. In patients with mild variants of galactosemia type 1 no abnormalities are noted on MRI.

In the early, untreated stages of the disease, proton MRS shows the presence of highly elevated peaks at 3.67 and 3.74 ppm, representing galactitol. In treated patients brain galactitol is below the level of detection for in vivo proton MRS. Under treatment, *myo*-inositol levels have been found to be normal.

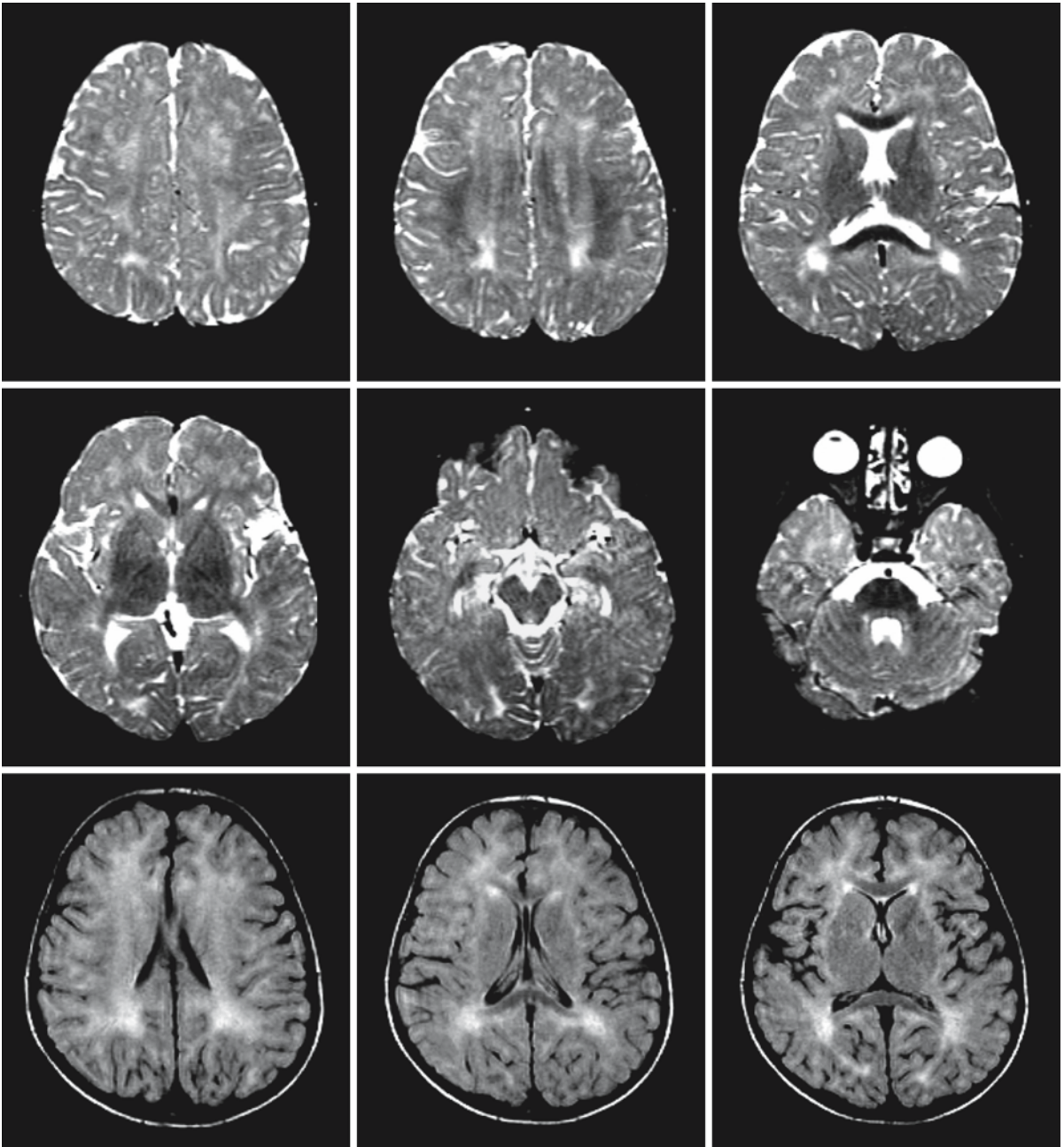


Fig. 49.1. A 4-year-old boy with galactosemia type 1. Note the seriously delayed myelination. In addition, the T_2 -weighted images show foci of elevated signal intensity in the periventricular region, most marked posteriorly. The FLAIR images (*third row*) confirm the white matter abnormalities

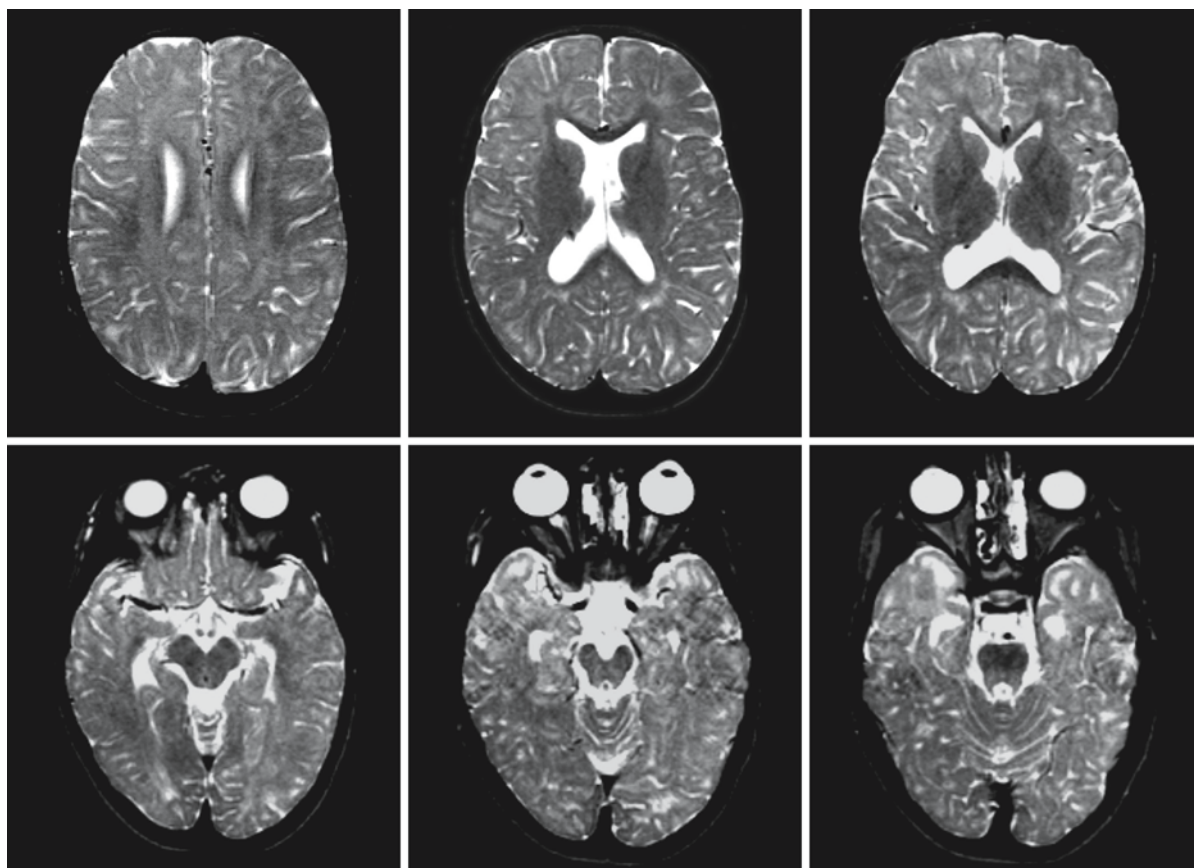


Fig. 49.2. A 6-year-old girl with galactosemia type 1. Again the process of myelination is seriously delayed. The anterior temporal white matter displays an abnormal signal

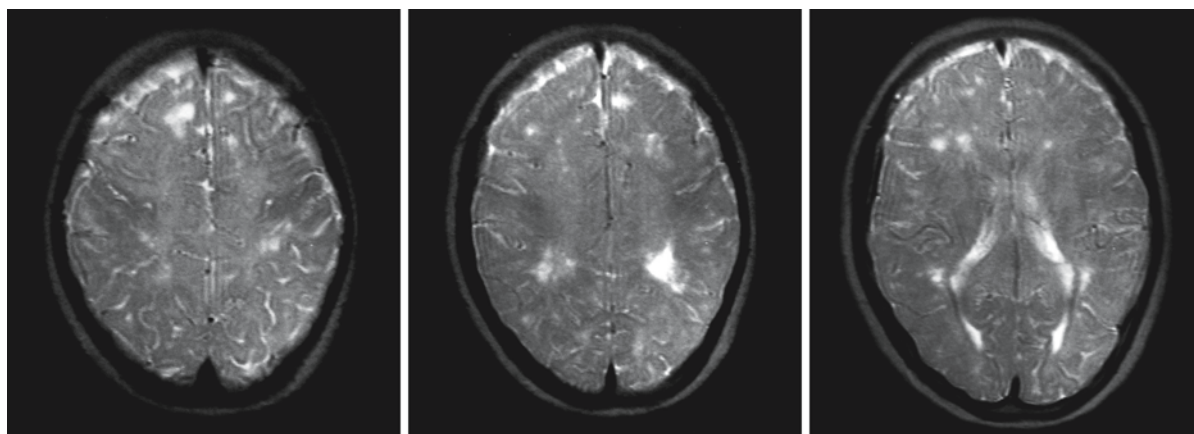


Fig. 49.3. Girl, 14 years of age, with galactosemia type 1. The T₂-weighted images show a combination of hypomyelination and patchy high signal intensity white matter abnormalities, consistent with gliosis

Sjögren–Larsson Syndrome

50.1 Clinical Features and Laboratory Investigations

Sjögren–Larsson syndrome (SLS) is a rare disorder with an autosomal recessive mode of inheritance. The three cardinal clinical signs are mental retardation, congenital ichthyosis, and spastic diplegia or tetraplegia. Most patients are born prematurely. The ichthyosis is usually present at birth and initial presentation may be as a collodion baby. The ichthyosis tends to worsen with time, and usually presents after infancy as a brownish verrucous, lichenified hyperkeratosis, more pronounced on the lateral aspects of the trunk, neck, lower abdomen, and the main flexures, with marked pruritus. The face is usually spared. Palms and soles may show hyperkeratosis and desquamation, but abnormalities are usually mild. Hair and nails are normal. The spasticity usually becomes manifest between 4 and 30 months of age. Many of the patients are never able to walk without assistance, and a considerable number are wheelchair-dependent. Those able to walk have a typical spastic gait. Tendon reflexes are high, and bilateral Babinski signs are often present. Mental deficiency varies from moderate to severe. Speech defect is usually present and can be attributed to a combination of mental deficiency and pseudobulbar palsy. Occasionally epilepsy is present. SLS patients have ocular abnormalities, consisting of bilateral glistening yellow-white dots in the macular region of the retina. They appear during the first 2 years of life and become more numerous over time. Photophobia and subnormal vision are frequently present. Short stature and thoracolumbar kyphoscoliosis may be present. The disease is not clearly progressive; the clinical signs are more or less stable over the years; most patients survive into adulthood. There is no correlation between the severity of the neurological symptoms and the ichthyosis.

The clinical diagnosis of SLS is confirmed by finding deficient fatty alcohol-NAD⁺ oxidoreductase activity in leukocytes and cultured fibroblasts and DNA analysis. Carrier detection can be performed by enzyme assessment in cultured fibroblasts or DNA analysis. Prenatal diagnosis is possible with the help of enzyme assessment or DNA techniques in families with known mutations.

50.2 Pathology

The external appearance of the brain is normal. A considerable deficit in myelin is seen in the periventricular and deep white matter, the area involved extending from frontal to occipital, sparing the U fibers. Ballooning of myelin sheaths is a notable feature within the areas of myelin deficit. Lipid-laden macrophages and histiocytes are present. Small lipid droplets are contained in the cytoplasm of microglia, scattered diffusely through the white matter. In the area of myelin paucity, degeneration and loss of axis cylinders and astrocytosis are found. The corpus callosum is well myelinated. Within the brain stem the pyramidal tracts show a deficit in myelin and loss of axis cylinders. Myelin paucity is also demonstrated in some of the descending tracts of the spinal cord, including the lateral corticospinal tracts, but the ascending tracts are normal. Cerebellar white matter is normal.

Microscopy of the cerebral cortex and central brain nuclei reveals in all areas an increase in astrocytes and accumulation of sudanophilic droplets of fat. Within the cerebellar cortex some loss of Purkinje cells is seen. Some neuronal cell loss may also be seen in the cerebral cortex, in particular Betz cells in the motor cortex, and in the basal ganglia, in particular in putamen and substantia nigra.

50.3 Pathogenetic Considerations

The basic defect of SLS is an impairment in fatty alcohol oxidation due to deficient activity of fatty alcohol-NAD⁺ oxidoreductase. This enzyme consists of two proteins that sequentially catalyze the oxidation of fatty alcohol to fatty aldehyde and fatty acid, reactions that are catalyzed by fatty alcohol dehydrogenase and fatty aldehyde dehydrogenase, respectively. SLS patients are specifically deficient in the fatty aldehyde dehydrogenase component. The gene coding for the enzyme is called *FALDH* or, more recently, *ALDH3A2* and is located on chromosome 17p11.2. The enzyme has a microsomal location. Fatty aldehyde dehydrogenase is necessary for the oxidation of fatty aldehydes derived from metabolism of fatty alcohols, phytanic acid, ether glycerophospholipids, and leukotriene B₄.

Fatty aldehydes and fatty alcohols are aliphatic lipids that exist as free molecules or as components of other lipids. As a consequence of the enzyme deficiency, fatty alcohols accumulate in SLS patients (octadecanol and hexadecanol). The levels of free fatty alcohols are increased in cultured fibroblasts and plasma. Although the primary enzyme deficiency is at the aldehyde step of the fatty alcohol oxidation, free fatty aldehydes are not increased in blood or cultured fibroblasts. This suggests that the defect in fatty aldehyde dehydrogenase results in a concomitant blockage of the fatty alcohol dehydrogenase within the enzyme complex, which limits the production of alcohol-derived fatty aldehyde. Another explanation would be that the aldehyde substrates are diverted into other metabolites.

The symptoms of SLS patients probably arise from membrane alterations resulting from accumulation of fatty-alcohol- or fatty-aldehyde-modified lipids and proteins. The biological consequences of either long-chain fatty alcohol or fatty aldehyde accumulation are unknown. Long-chain alcohols have been shown to partition into artificial lipid bilayers and synaptic vesicles. Accumulation of fatty alcohols in the skin of SLS patients probably alters the epidermal water barrier, which is critically dependent on the lipid composition of the stratum corneum, and leads to increased transepidermal water loss and ichthyosis. Furthermore, the catabolism of ether phospholipids (including plasmalogens) and sphingolipids, both of which are major components of myelin, generates fatty aldehydes that may be substrates for fatty aldehyde dehydrogenase. Accumulation of fatty alcohols or fatty aldehydes in myelin could alter myelin stability and lead to myelin loss.

It has been shown that fatty aldehyde dehydrogenase is also important in the α -oxidation of phytanic acid. The enzyme is involved in the conversion of pristanal into pristanic acid. Surprisingly, SLS patients do not accumulate phytanic acids in their plasma. It may be that another fatty aldehyde dehydrogenase takes over.

Fatty aldehyde dehydrogenase is involved in the ω -oxidation of leukotriene B_4 . Leukotriene B_4 is a potent proinflammatory mediator, synthesized from arachidonic acid. It is predominantly produced by polymorphonuclear leukocytes. The inactivation of leukotriene B_4 is regulated by microsomal ω -oxidation. The urinary levels of leukotriene B_4 and its metabolite ω -hydroxy leukotriene B_4 are elevated in SLS patients. ω -Hydroxy leukotriene B_4 is converted to ω -aldehyde leukotriene B_4 and subsequently ω -carboxy leukotriene B_4 . Urinary ω -carboxy leukotriene B_4 is not detectable, indicating a block in the degradation of leukotriene B_4 at the level of the conversion of ω -aldehyde leukotriene B_4 to ω -carboxy leukotriene B_4 . Elevated levels of leukotriene B_4 and ω -hydroxy

leukotriene B_4 are probably responsible for the pruritus. There is evidence that leukotriene B_4 probably plays a role during labor. Placental leukotriene B_4 production is low during the third trimester of pregnancy and increases in spontaneous labor. Elevated levels produced by the fetus may lead to preterm birth.

50.4 Therapy

Several studies have been performed in which dietetic therapy was aimed at the primary biochemical defect, trying to block the exogenous admission of toxic substances, the fatty alcohols. Unfortunately these studies had little if any success at all. Leukotriene B_4 is synthesized from arachidonic acid via the lipoxygenase pathway. The drug zileuton, used in asthma, inhibits 5-lipoxygenase and has a beneficial effect on the pruritus in patients. A favorable behavioral effect has also been observed. Some patients have been treated with acitretin, a retinoid, which leads to a marked improvement of the ichthyosis and pruritus. Symptomatic treatment includes care of the dermatological and neurological problems.

50.5 Magnetic Resonance Imaging

CT reveals diffuse or patchy cerebral white matter hypodensities, most marked in the frontal area. No enhancement is present after contrast administration.

MRI may show three types of white matter abnormalities. First of all, the process of myelination is mildly delayed and appears not to reach completion in SLS patients (Figs. 50.1 and 50.2). The directly subcortical U fibers and the white matter of the anterior part of the temporal lobes, which are normally among the last to reach complete myelination, retain a slightly higher signal intensity than the adjacent cortex on T_2 -weighted images. Secondly, some patients have a symmetrical periventricular rim of markedly increased signal intensity, most often predominantly involving the frontal and parietal lobes (Fig. 50.2). Thirdly, other patients have a symmetrical periventricular rim of slightly to mildly increased signal intensity, which often has a more posterior predominance (Fig. 50.3). The white matter changes become apparent during the process of myelination and seem to be stable. Follow-up MRI does not show an increase in the extent or severity of the white matter signal changes. In exceptional cases the white matter abnormalities are not confluent, but multifocal (Fig. 50.1). Typically, the corpus callosum and cerebellar white matter are spared. In exceptional cases the corpus callosum shows signal abnormalities. Brain stem pyramidal tract involvement may be seen. Mild cerebral atrophy is common leading to mild but sometimes

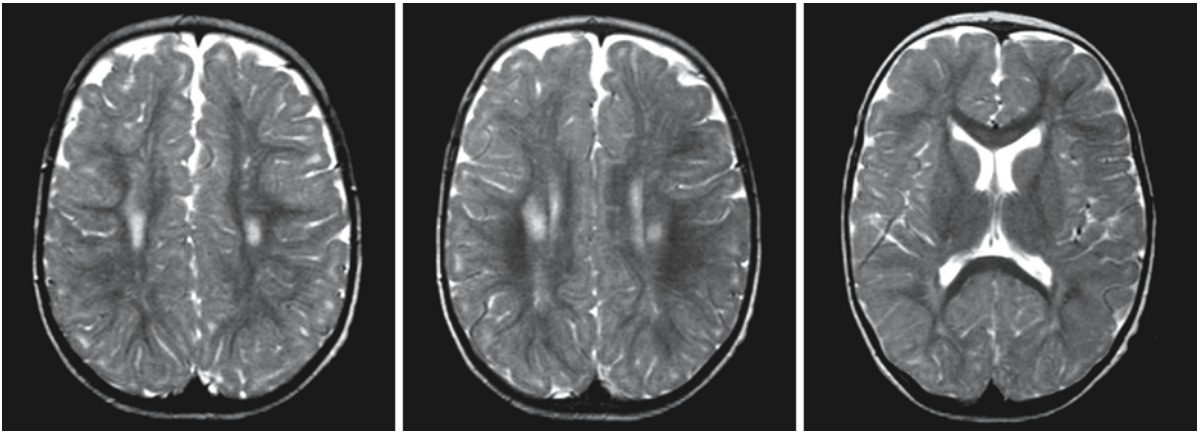


Fig. 50.1. A 2-year-old patient with SLS. Myelination is incomplete. The T₂-weighted images show a high signal in the directly subcortical white matter in all areas. There are focal

signal abnormalities in the periventricular white matter. Courtesy of Dr. M.A.A.P. Willemsen, Department of Pediatric Neurology, University Medical Center Nijmegen, The Netherlands

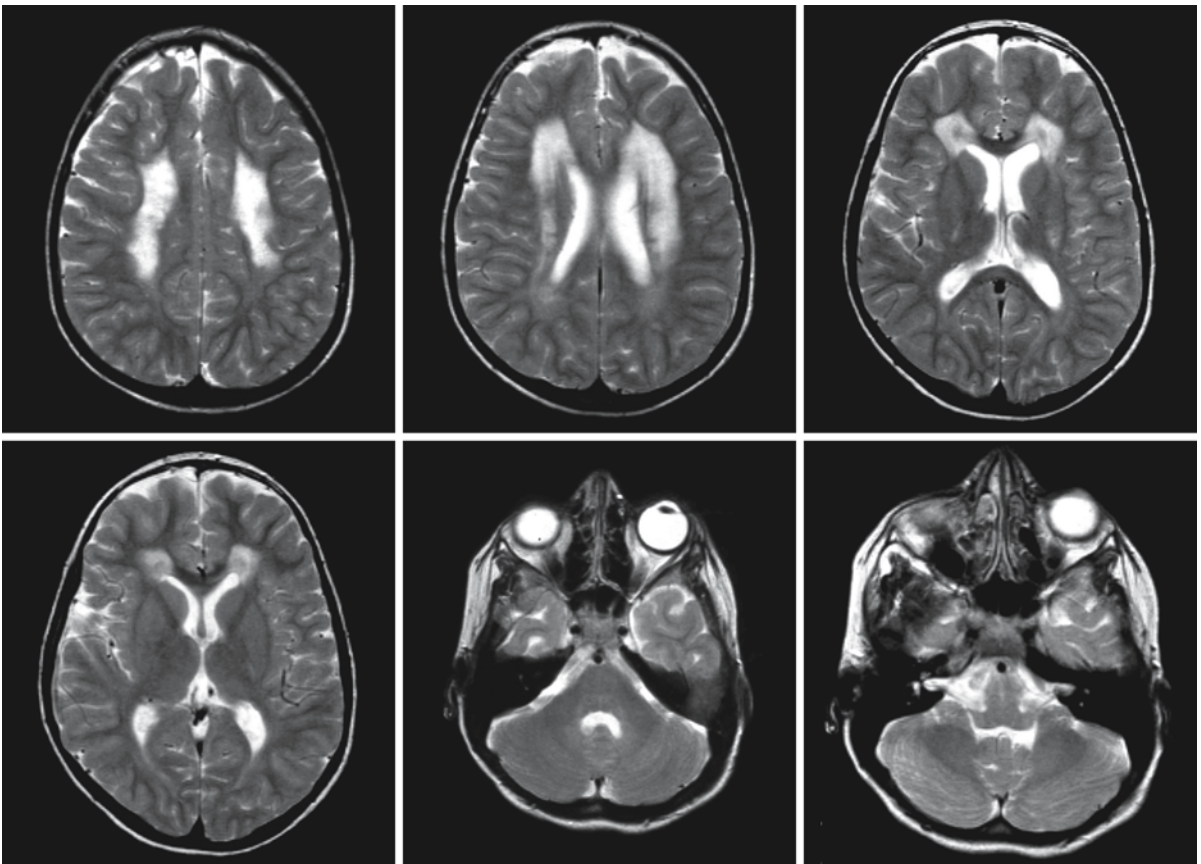


Fig. 50.2. A 10-year-old boy with SLS. Myelination is still incomplete, which is best seen in the basotemporal white matter (*second row, right*). There are prominent signal abnormalities in the periventricular and deep white matter, most pronounced in the frontoparietal region. The signal abnormalities

have a sharp demarcation. The corpus callosum is largely spared. Courtesy of Dr. M.A.A.P. Willemsen, Department of Pediatric Neurology, University Medical Center Nijmegen, The Netherlands

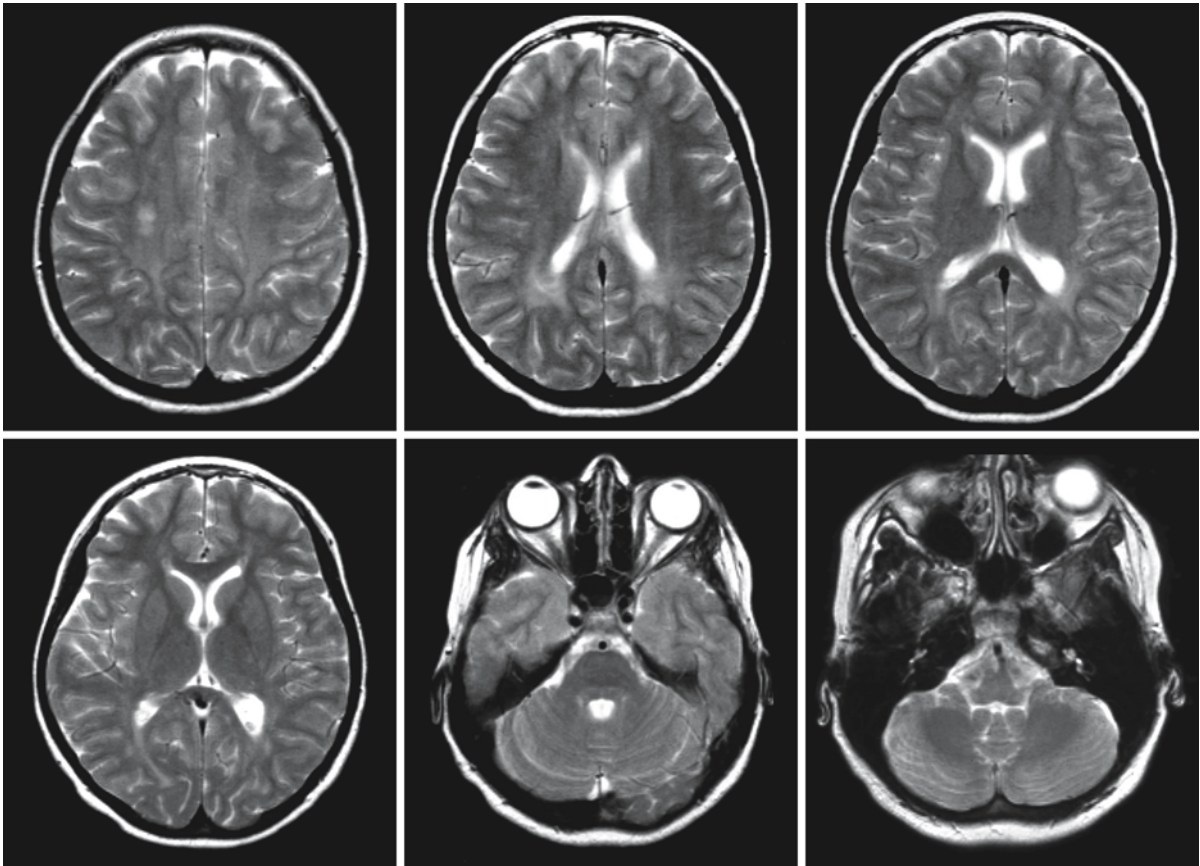


Fig. 50.3. An 8-year-old patient with SLS, brother of the patient shown in Fig. 50.2. In this patient there is a periventricular rim of mild signal abnormality, most pronounced in the poste-

rior region. The rim is poorly demarcated. Courtesy of Dr. M.A.A.P. Willemsen, Department of Pediatric Neurology, University Medical Center Nijmegen, The Netherlands

more marked dilatation of the lateral ventricles. There is no correlation between the severity of the white matter abnormalities and the severity of the neurological problems or the age of the patient.

MRS consistently shows a high and narrow peak at 1.3 ppm and a much smaller peak at 0.9 ppm in spectra of the cerebral white matter of SLS patients.

These resonances have been assigned to methylene and methyl groups of lipids, respectively. It is highly likely that the peaks represent accumulating fatty alcohols or fatty aldehydes. The peaks have their greatest height within the abnormal white matter. Neither of the peaks is seen in spectra from the cerebral cortex.

Lowe Syndrome

51.1 Clinical Features and Laboratory Investigations

Lowe syndrome, or oculocerebrorenal syndrome of Lowe (OCRL), is a rare, X-linked hereditary disease. It is present in all races, with a predominance in those of Caucasian and Asian ancestries. Rarely females are affected like males.

Males with OCRL present with congenital ocular manifestations including cataract, often associated with glaucoma and miotic pupils. Buphthalmos may be present. Sight is poor and eye movements are nystagmoid. Additional early features include muscle hypotonia, hyporeflexia, or areflexia and hypermobility of the joints. During the first year of life psychomotor developmental delay becomes evident. The infants have excessive crying with a high-pitched scream. Asymptomatic amino aciduria and proteinuria are usually found during this stage.

During early childhood the symptoms of renal tubular dysfunction develop with metabolic acidosis and losses of calcium and phosphate. Severe demineralization and rickets may develop and lead to frequent fractures, pain, and delay of normal physical development. Many patients develop scoliosis. Linear growth decreases after 1 year of age, and between 1 and 3 years of age height falls below the third percentile. Head circumference is either normal or borderline microcephalic. Noninflammatory arthropathy of unknown pathogenesis with pain, joint swelling, and contractures may occur, affecting both large and small joints. Mental retardation is usually moderate, but intelligence varies between normal and profoundly decreased. Some patients have epilepsy. Unusual stereotypic movements are often seen, especially repetitive shaking of limbs. Maladaptive behavior is frequently present and consists of temper tantrums, high-pitched scream, and stubbornness. A later occurring ocular complication is corneal keloid, consisting of scar-like opacifications of the cornea that can develop spontaneously or following trauma. The frequency of corneal keloid increases with age in OCRL patients.

Patients with OCRL continue to grow in early adulthood. Final height, however, remains below the third percentile of normal values. Severe bone disease leads to orthopedic disability. Renal dysfunction is slowly progressive with decreasing glomerular filtration rates. Terminal renal failure occurs in the mid-

thirties. Death may occur between the first and the fourth decade, secondary to inanition, pneumonia, or uremia.

Laboratory findings show renal tubular dysfunction similar to Fanconi syndrome. The tubular dysfunction leads to urinary loss of bicarbonate, glucose, calcium, phosphorus, protein, and amino acids. The results are metabolic acidosis, hypophosphatemia, secondary hyperparathyroidism, and rickets. Urinary excretion of carnitine is increased with decreased serum carnitine. The serum muscle enzymes creatine kinase, aspartate aminotransferase, and lactate dehydrogenase are sometimes elevated. Over the years progressive glomerular dysfunction develops with uremia. A linear relation between reciprocal serum creatine level and age reflects the progressive renal failure. Abnormalities of blood chemistry values are mitigated by replacement therapy for renal tubular losses.

Skeletal X-ray examinations reveal rachitic changes. EEG often shows nonspecific abnormalities, sometimes epileptic activity.

Progressive lenticular opacities are present in OCRL carriers, and even young carriers can be identified reliably in this way in known OCRL families. Lack of opacities in females cannot be considered as proof of not being a carrier, but is suggestive.

The biochemical assay for deficiency of phosphatidylinositol 4,5-bisphosphate 5-phosphatase in cultured fibroblasts is the definitive laboratory test for diagnosing patients and can be used for prenatal diagnosis. DNA techniques are available for diagnostic confirmation in patients, for carrier detection, and for prenatal diagnosis. De novo mutations or sporadic cases are frequent. Somatic and germline mosaicism has been described and must be taken into account for genetic counseling.

51.2 Pathology

In OCRL, data on neuropathological findings are limited. The brain weight is usually below normal. Moderate, diffuse atrophy may be seen with cerebral volume loss, some ventricular enlargement and thinning of the corpus callosum. The meninges are diffusely fibrotic without inflammatory changes.

Variable cortical changes have been described ranging from normal to neuronal loss in combination

with gliosis. Evidence of aberrant neuronal migration with pachygyria or polymicrogyria has also been reported.

The white matter changes described are variable. The most frequent finding is gliosis. More or less prominent myelin paucity has been described, either focal or diffuse. White matter abnormalities are most pronounced in the centrum semiovale and periventricular white matter. Spongy changes have been observed, frequently associated with perivascular lacunes. Active myelin breakdown has never been reported, and the myelin paucity is usually ascribed to deficient myelination. In rare cases, the white matter is normal.

The cerebellum may be atrophic or normal. Gliosis of the cortex and white matter have been observed.

Variable and inconsistent abnormalities of the peripheral nervous system have been reported. Nerve biopsy has been found to exhibit signs of axonal neuropathy in several, but not all patients. Muscle biopsy has indicated selective type 1 fiber atrophy with mild type 1 fiber predominance, considered to be consistent with congenital fiber type disproportion myopathy or, alternatively, to abnormal neuronal influence upon muscle. In other patients, muscle biopsy revealed no abnormalities.

Renal pathology demonstrates dilated tubules with atrophy of tubular epithelium. Many tubules contain eosinophilic, granular protein casts. Interstitial fibrosis is present. Glomerular changes have been observed, in particular on ultrastructural examination. Glomerular endothelial cells may be swollen with a reduction in the number of endothelial slit pores, fusion of endothelial foot processes, and thickening of the glomerular basement membrane.

51.3 Pathogenetic Considerations

OCRL is caused by defects in the *OCRL1* gene, located on chromosome Xq25–26. The gene product is phosphatidylinositol 4,5-bisphosphate (PIP₂) 5-phosphatase, an inositol polyphosphate 5-phosphatase belonging to the type II 5-phosphatase family. The type II phosphatases hydrolyze both water-soluble and lipid inositol polyphosphate substrates, whereas the type I phosphatases only hydrolyze water-soluble substrates. However, PIP₂ 5-phosphatase prefers the lipid substrate phosphatidylinositol 4,5-bisphosphate.

Many different mutations of the *OCRL1* gene have been described in patients, most of which are truncating mutations or missense mutations in conserved domains of the protein. In highly exceptional cases, the OCRL phenotype has been observed in female patients. In some of these female patients there is a mutation in the *OCRL1* gene on one chromosome, whereas there is a deletion of the region on the other

X chromosome. OCRL may also occur in XO patients. Unfortunate X inactivation is another possibility explaining exceptional female patients.

Inositol containing phospholipids are collectively referred to as phosphoinositides or phosphatidylinositols. They are minor but ubiquitous components of eukaryotic membranes. Phosphoinositides are important in signal transduction. The subcellular localization of PIP₂ 5-phosphatase is in the trans-Golgi network. The substrate of this enzyme, phosphatidylinositol 4,5-bisphosphate, serves as a substrate for the production of second messengers, promotes the polymerization of actin cytoskeleton, and plays a role in vesicular trafficking. In fibroblasts of Lowe patients a decrease in long actin stress fibers, enhanced sensitivity to actin depolymerizing agents, and an increase in actin staining in a distinctly anomalous distribution in the center of the cells have been demonstrated. Two actin-binding proteins, gelsolin and α -actinin, proteins regulated by both PIP₂ and Ca²⁺, have been found to have an abnormal distribution. Actin polymerization plays a key role in the formation, maintenance, and proper function of tight junctions and adherens junctions, which are critical in renal proximal tubule function and the differentiation of the lens. The relationship with the encephalopathy is less clear.

51.4 Therapy

The nephrologist should manage both the tubular and glomerular complications associated with the renal disease in OCRL. In renal tubular acidosis and rickets a combination of sodium-potassium citrate, phosphorus, and large doses of vitamin D has a beneficial effect. Ocular surgery is essential to prevent total blindness. The retina in patients with OCRL is usually well-formed and capable of receiving a light stimulus.

51.5 Magnetic Resonance Imaging

MRI in OCRL shows a more consistent pattern of abnormalities than would be suggested by the neuropathology. In patients with an advanced degree of myelination patchy, small and larger, isolated and partially confluent white matter changes are visible, suggestive of gliosis (Figs. 51.1 and 51.2). During the first months of life these white matter abnormalities may not be noticeable within the still unmyelinated white matter. The changes are most pronounced in the periventricular area and centrum semiovale, whereas the U fibers, corpus callosum, internal capsule, brain stem, and cerebellum are spared. The white matter abnormalities are highly variable in extent. In

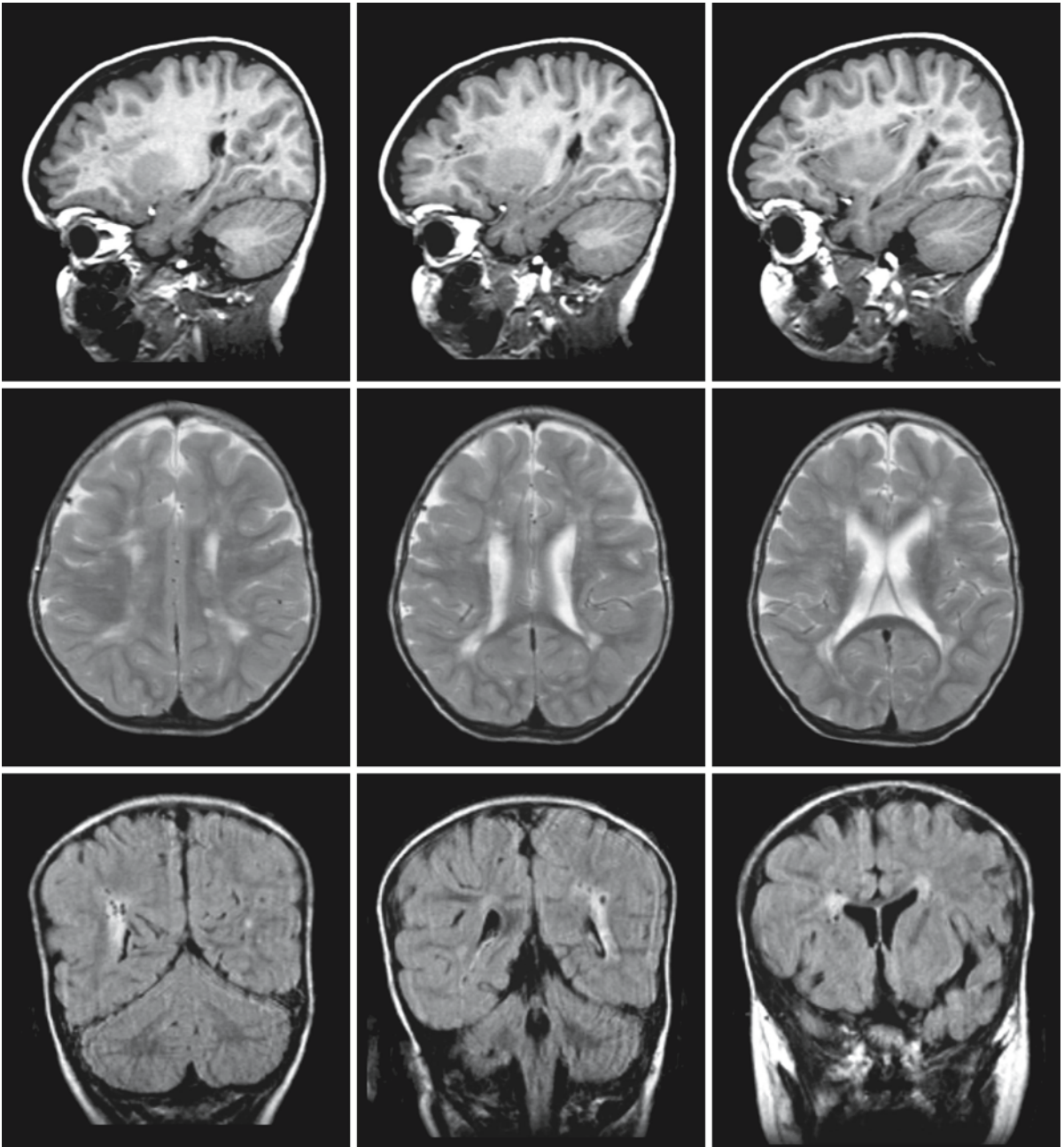


Fig. 51.1. MR study of a 17-month-old boy with OCRL. There are multifocal small lesions in the periventricular white matter and small cysts within the abnormal white matter

some patients only a few, small white matter lesions are present (Fig. 51.1), whereas in other patients the lesions are much more extensive (Fig. 51.2). The distribution of the white matter changes is symmetrical globally, but not in detail. Often multiple small cystic lesions are seen within the abnormal white matter. Mild ventriculomegaly may be present. No major cortical abnormalities have been reported.

The MRI pattern of multifocal, irregular, patchy white matter abnormalities with small cysts is reminiscent of the patterns seen in hypomelanosis of Ito and some mucopolysaccharidoses.

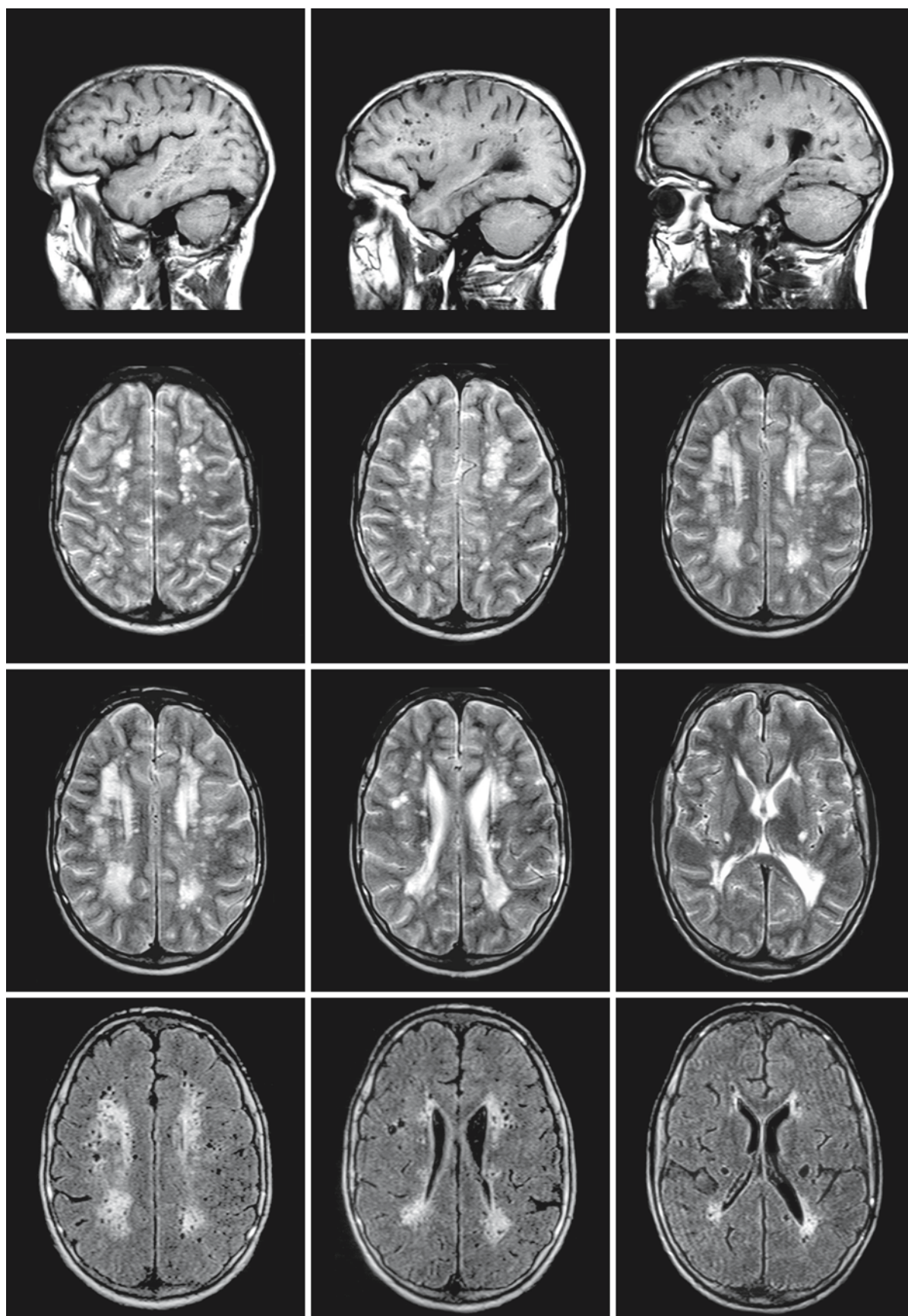


Fig. 51.2.

←

Fig. 51.2. An 8-year-old boy with OCRL. The T₂-weighted images (*second and third rows*) show multifocal small and larger, partially confluent lesions in the periventricular and deep white matter. The sagittal T₁-weighted (*first row*) and axial FLAIR images (*fourth row*) reveal a multitude of small cysts within and outside the abnormal white matter. Courtesy of Dr. L. Charnas, Department of Pediatric Neurology, and Dr. C Peter, Department of Pediatric Hemato-Oncology and Bone Marrow Transplantation, University of Minnesota, Minneapolis, USA

Wilson Disease

52.1 Clinical Features and Laboratory Investigations

So-called hepatolenticular degeneration was first described by the English neurologist S.A.K. Wilson in 1912 and has been named after him. Wilson disease (WD) is a genetically determined, autosomal recessive disease with a prevalence of 20 to 30 per million. The clinical picture is extremely variable, depending among other things on the age at presentation. Patients present with hepatic, neurological, or psychiatric symptomatology in roughly equal proportions, with some overlap. In children, hepatic manifestations predominate, whereas in adolescents and adults neuropsychiatric manifestations are more frequent. Symptoms rarely occur before the age of 6, and half of the patients are symptomatic by the age of 15. Onset after the age of 40 is rare, but patients presenting in the fifth and sixth decades of life have been described.

Hepatic manifestations in WD encompass a spectrum of acute and chronic liver diseases. Some patients, usually younger ones, present with fulminant hepatic failure, leading to jaundice, hypoalbuminemia, ascites, coagulation defects, hyperammonemia, and hepatic encephalopathy. Massive liver failure in WD is often accompanied by hemolytic anemia. However, if the liver failure is less massive, only some of the features of this syndrome may be present. In older patients liver failure tends to be chronic and is associated with portal hypertension, leading to gastric or esophageal varices and/or hypersplenism with thrombopenia or leukopenia. In addition, these patients often have hypoalbuminemia, edema, and ascites. Some patients present with a picture of acute hepatitis, which subsides spontaneously, and may be attributed mistakenly to a viral infection. In some patients cirrhosis is well compensated and the results of standard liver biochemical tests are normal. Most patients with WD, whatever their clinical presentation or presymptomatic status, have some degree of liver disease.

Patient with WD who present with neurological disease are typically in their late teens or twenties. The signs and symptoms are usually chronic, but occasionally acute in presentation. Frequent early symptoms include tremor, speech problems, clumsiness, dystonia, and personality changes. The tremor may be unilateral or asymmetrical. Kayser–Fleischer rings are almost invariably present in patients with

neurological manifestations of WD. The rings are typically 1–3 mm in diameter, green, yellow, or brown, and located at the periphery of the cornea. They begin as crescents in the superior quadrant and subsequently extend to the inferior, lateral, and medial regions until they become circumferential and broader, spreading centrally from the limbus. Kayser–Fleischer rings may sometimes be seen with the unaided eye, but a slit-lamp examination often is necessary to detect them. Adolescents may present with a deterioration of performance at school and in athletics, difficulties with handwriting, and loss of dexterity. Without treatment, neurological deterioration continues. The full-blown neurological picture of WD encompasses a variable combination of the following signs: dysarthria, drooling, dysphagia, grimacing, abnormal eye movements, dystonia, rigidity, bradykinesia, athetosis, wing beating, spasticity with increased tendon reflexes and Babinski signs, cerebellar ataxia, and tremor (resting, intention, or postural), but cognitive and sensory functions are typically preserved. Seizures may occur. Because of increasing difficulty in controlling movement, the patients become unable to feed themselves, and become bedridden. Flexion contractures develop. Ultimately, the patients become helpless, are usually alert, but unable to talk.

Psychiatric and behavioral symptoms are variable and include reduced performance at school or at work, inability to cope, depression, labile moods ranging from mania to depression, sexual exhibitionism, and psychosis. Personality changes, particularly irritability, emotionality, and increased anger are the most commonly noted problems.

Ophthalmological abnormalities include, first and foremost, the Kayser–Fleischer rings, and, less frequently, sunflower cataracts consisting of green, golden-brown, or gray granular deposits in the lens of the eye, appearing as discoid opacities in the anterior lens capsule with petal-like fronds that radiate toward the lens periphery like a sunflower. Neither Kayser–Fleischer rings nor sunflower cataracts affect vision significantly. Kayser–Fleischer rings are found in almost all patients with a neurological presentation and in about 30% of the patients with a hepatic presentation.

Hematological presentation is rare, but WD should be considered in young patients with nonspherocytic, Coombs-negative intravascular hemolysis of unclear etiology. Severe hemolysis frequently occurs in

the setting of fulminant hepatic failure and suggests a diagnosis of WD.

Patients may have abnormalities of renal tubular function with amino aciduria, proteinuria, uricosuria, hypercalciuria, hyperphosphaturia, or defective urine acidification. Occasionally, full-blown Fanconi syndrome is present. Renal stones are not uncommon.

Osteomalacia, rickets, osteoporosis, osteoarthritis, polyarthritis, localized bone demineralization, spontaneous fractures, peri- and intra-articular calcifications, and joint hypermobility may occur in WD. However, musculoskeletal symptoms are rarely the presenting complaints.

Hyperpigmentation of the skin may occur. Congestive heart failure and cardiac dysrhythmias have been reported. The most frequent endocrinological disturbances are gynecomastia and delayed puberty due to hepatic dysfunction. Primary or secondary oligo- or amenorrhea is common. Successful pregnancy is exceptional in untreated female WD patients, and spontaneous abortions occur frequently.

There is often an unacceptable delay in establishing a diagnosis of WD. Whenever the diagnosis is suspected, Kayser–Fleischer rings should be sought by an experienced ophthalmologist using a slit-lamp. Kayser–Fleischer rings are almost always present in WD patients with neurological problems, but their absence does not mean the diagnosis is wrong. Kayser–Fleischer rings are also not pathognomonic for WD, but may be seen in some other hepatobiliary diseases or as a result of topical ocular application of copper-containing solutions. In most patients suspected of WD, the diagnosis is confirmed by the presence of both Kayser–Fleischer rings and at least one, if not all three, of the biochemical markers: low serum level of ceruloplasmin, elevated free (nonceruloplasmin) serum copper concentration, and increased urinary copper excretion (24-h urine copper). However, the limited value of these tests should be recognized. Ceruloplasmin is low in about 80–90% of WD patients, but some WD patients have levels in the low-to-normal range due to hepatic inflammation, hepatic neoplasm, pregnancy, or use of estrogen. A low serum ceruloplasmin level is found in up to 20% of the heterozygotes for WD, even though they will never develop symptoms of WD. Low serum ceruloplasmin can also be found in other hepatic disorders, normal neonates and young infants, patients with malabsorption, malnutrition, or nephrosis, and in patients with hereditary hypoceruloplasminemia. Free serum copper and urinary copper concentrations can be elevated in other hepatobiliary diseases. In case of doubt, in particular if the ceruloplasmin level is normal and/or Kayser–Fleischer rings are absent, conditions most often seen in patients with hepatic presentation, liver biopsy for quantitative copper analysis, and micro-

scopic examination have a high diagnostic value. Hepatic copper concentrations are always elevated in untreated WD patients and also higher in patients than in heterozygotes. Histological abnormalities in WD range from steatosis to cirrhosis. Liver histology is normal in heterozygotes. However, in patients with chronic cholestatic liver disease, elevations of liver copper concentrations may be similar to those in WD patients, and incidental WD cases with normal copper levels in single biopsies have been reported, related to uneven copper distribution in the liver. In selected patients a test of incorporation of a copper isotope into serum ceruloplasmin is informative. Because the biochemical copper profile of a normal neonate mimics that seen in WD and clinical manifestations of WD are rarely seen before the age of 6 years, conventional screening of potentially affected children should not be performed before the age of 2–3 years. DNA techniques are available for definite diagnosis in patients suspected of WD and for distinction between presymptomatic patients and heterozygotes in families with WD and known mutations. Prenatal diagnosis is possible using DNA techniques.

52.2 Pathology

External examination of the brain usually reveals no abnormalities except for some shrinkage of the insular cortex.

Within the brain parenchyma of patients with manifestations of CNS disease, lesions are invariably present in the corpus striatum, which appears shrunken. Cavitation is often present in the putamen, sometimes also in the caudate nucleus, rarely in the globus pallidus, thalamus, and red nucleus. On microscopic examination, neuronal loss is found in the putamen and caudate nucleus. Astrocytic proliferation is present. Some astrocytes have the appearance of Alzheimer type II cells; few resemble Alzheimer type I cells. When cavities are present, variable numbers of lipophages and siderophages are seen in relation to the cavities; old and recent hemorrhages can be found. Depositions of copper have been described by some, in particular in the putamen. Less constantly and less severely involved nuclei are the globus pallidus, the subthalamic nucleus, the thalamus, dentate nucleus, substantia nigra, and other brain stem nuclei. Opalski cells are typically present in the thalamus, globus pallidus, and zona reticularis of the substantia nigra, less often in the caudate nucleus and putamen. Opalski cells are large cells with voluminous cytoplasm and small nuclei. Like Alzheimer type I and type II cells, they are of astroglial origin. Alzheimer type I cells and Opalski cells are characteristic of WD.

In some patients destructive lesions are present in the cerebral cortex and white matter. The distribution of the cortical involvement corresponds with that of the white matter involvement. These lesions may be very impressive and exceed the lesions in the basal nuclei. The lesions are typically located in the superior and middle frontal gyri; widespread involvement posterior to the frontal lobes is uncommon. The changes are usually symmetrical, but may be asymmetrical. Cavitation of the white matter lesions may occur. The outer layers of the cortex always retain sufficient structural integrity to form a continuous shell. In microscopic examination of the affected cortex, the deep cortical layers appear to be affected predominantly, whereas the more superficial cortical layers are relatively intact. The cortical abnormalities may have a spongiform appearance. Alzheimer types I and II cells and Opalski cells may be seen in the cerebral cortex. The white matter abnormalities vary from myelin paucity and spongy white matter degeneration to outright necrosis with presence of sudanophilic breakdown products. There may be proliferation of Alzheimer type I and type II astrocytes and Opalski cells.

The cerebellum is relatively spared. Some loss of cortical neurons may be seen. The dentate nucleus is more frequently involved. Cerebellar white matter pallor, gliosis, and degeneration have been described. Brain stem nuclei may be involved.

In patients with fulminant liver failure, the cirrhosis is predominantly micronodular, whereas in patients with longstanding liver disease large areas of macronodular cirrhosis are found. In the periphery of the nodules, copper pigments may be demonstrated histochemically. Electron microscopy demonstrates that hepatocytes contain giant mitochondria with paracrystalline inclusions. Multivesicular rounded granules in hepatocytes are thought to be characteristic of WD.

52.3 Pathogenetic Considerations

The gene responsible for WD is *ATP7B*, located on chromosome 13q14.3. The gene product is a cation transporting P-type ATPase protein, called ATP7B or Wilson disease protein (WNDP). Many different mutations have been identified in WD patients. It is reasonable to assume that the type of mutation might account, at least in part, for the clinical variability observed in WD patients. However, most patients are compound heterozygotes, which hampers the study of genotype-phenotype correlations. Considerable clinical variation is seen among patients within the same family, suggesting influence of other genetic and environmental factors.

Copper is an essential trace element, being an integral component of many important enzymes involved in cellular processes such as oxidative metabolism, free radical detoxification, neurotransmitter biosynthesis, and iron homeostasis. In excess, copper is also a very toxic ion, because it can oxidize proteins and lipids in membranes, bind to proteins and nucleic acids, and enhance the generation of free radicals. Dietary intake of copper generally far exceeds the trace amounts required. Consequently, efficient and appropriate mechanisms must exist to ensure copper homeostasis and to transport copper to the sites where it is required without allowing toxic accumulation of free ions. Clearance of excess copper is achieved via the hepatobiliary route. Various proteins have been recognized to be involved in copper homeostasis and transport: albumin for copper transport in the blood, ceruloplasmin as a copper donor to tissues and enzymes, and metallothionein for intracellular copper storage. The human copper chaperone Atox1 is a small cytosolic protein that plays a key role in the distribution of copper to the secretory pathway of the cell. Atox1 facilitates copper delivery to the protein ATP7B. ATP7B translocates copper in an ATP-dependent manner into the lumen of the trans-Golgi network for incorporation into copper-dependent enzymes, or exports excess copper out of the cell into the bile. Under steady state conditions ATP7B is localized primarily in the trans-Golgi network, where it pumps copper from the cytoplasm into the trans-Golgi network lumen. Under elevated copper concentrations ATP7B undergoes a reversible, copper-mediated translocation from the Golgi to the apical canalicular membrane, where it pumps copper into the bile. Deficiency of ATP7B leads to failure to excrete copper from the liver into bile and to incorporate copper into ceruloplasmin during ceruloplasmin biosynthesis in the liver. This results in toxic accumulation of copper in the liver, with subsequent overflow to the kidney, brain, and cornea. WNDP is present in hepatocytes, kidney, placenta, brain, heart, lung, muscle, and pancreas, but reversal of dysfunction of other organs after liver transplantation indicates that the primary genetic defect leading to copper accumulation resides in the liver.

Accumulation of copper leads to liver cirrhosis, progressive neurological damage and renal problems. Very high free serum copper levels, in particular caused by sudden massive release of copper from the liver, may result in hemolytic crises. The cause of pathology in WD is copper toxicity. Organs affected by the disease contain elevated copper levels, and lowering of copper leads to cessation of progression, some repair, and clinical improvement. Excess copper causes cell injury, inflammation, and cell death. Copper has damaging effects on mitochondria and per-

oxisomes. Effects on microtubules, on cross-linking of DNA, and on plasma membranes, as well as inhibition of a large number of enzymes, have also been shown. The state of copper is important. Copper bound to ceruloplasmin, metallothionein, or albumin is nontoxic. It is ionic copper or copper, which is easily dissociable, that is toxic. Copper toxicity probably occurs because of the generation of oxidant radicals. In this respect it is important to note that the pattern of preferential involvement of gray matter structures in WD shows some striking similarities to the patterns observed in respiratory chain defects and in hypoxia. Caudate nucleus and putamen are preferentially affected. Other frequently involved gray matter structures are thalamus, globus pallidus, subthalamic nucleus, and periaqueductal gray matter.

52.4 Therapy

Therapeutic strategies in WD can focus on inhibition of the intestinal uptake of copper, induction of metallothionein to detoxify copper, and chelation. When a diagnosis of WD is made, siblings of the affected patient should be screened. On average 25% of the siblings will be affected but still at the "presymptomatic" phase clinically, although they always have subclinical liver disease. WD is an almost completely penetrant disease, and individuals having two mutations in the WD disease gene have an almost 100% chance of acquiring neurological, psychiatric, or hepatic disease or a combination of these. It is therefore important to treat these presymptomatic patients prophylactically with anti-copper medication. Patients begin to have hepatic damage from about the age of 3 or 4 years. Patients should be treated as soon as a diagnosis has been made, but probably not during the first 1 or 2 years of their life. Treatment should be continued for life in WD patients, whether asymptomatic or symptomatic.

Nowadays, zinc is usually preferred as the first-choice drug in the treatment of WD patients, because it is almost completely nontoxic. Oral zinc in the form of zinc acetate or zinc sulfate inhibits intestinal copper absorption and promotes fecal copper excretion. There is also evidence that zinc may induce the synthesis of metallothionein in enterocytes and possibly hepatocytes. Although zinc appears to be a more potent stimulus to metallothionein synthesis than copper, copper is more avid in binding to metallothionein. Complexed copper may then either be transferred into the portal circulation or remain complexed within the cytosolic fraction of the enterocyte and be excreted in the feces with sloughed cells. Zinc therapy acts slowly, producing a modestly negative copper balance. Zinc therapy is usually well tolerated, gastric irritation being the most frequent side effect.

A few highly exceptional patients have been reported who show deterioration after the institution of oral zinc therapy.

Penicillamine has been considered the drug of first choice in WD for many years. It acts by reductive chelation, reducing the copper bound to protein, thereby decreasing the affinity of the protein for copper and allowing the penicillamine to bind copper. Reductive chelation is much more effective than chelators with a high affinity for copper, such as EDTA. The copper mobilized by penicillamine is excreted in urine. Penicillamine probably also induces hepatic metallothionein, thereby holding potentially toxic copper in a nontoxic form. Some patients improve clinically soon after therapy begins, whereas some may require several months of therapy before improvement occurs. In about 10–20% of WD patients with neurological complaints, temporary exacerbation of symptoms is seen with the institution of therapy. Unfortunately, some patients never recover to their pretreatment baseline. Inadvertent discontinuation of penicillamine therapy may lead to catastrophic clinical deterioration and death. Adverse effects of penicillamine are, unfortunately, common. A considerable number of the patients develop an early hypersensitivity reaction to penicillamine mandating its discontinuation. Treatment is restarted in conjunction with corticosteroids until tolerance develops. Long-term use of penicillamine can result in serious side effects forcing discontinuation of its use. These side effects include induction of a variety of autoimmune-like disorders and induction of skin problems due to alterations of dermal collagen and elastin.

Triethylene tetramine dihydrochloride (trientine or trien) is both a chelator, acting primarily by enhancing urinary excretion of copper, and an inhibitor of copper absorption in the intestine. Far less clinical experience has been gained with this drug than with penicillamine, but it can be used in WD patients who do not tolerate penicillamine. Tolerance of triethylene tetramine dihydrochloride is generally excellent. Toxicity during the first weeks of treatment may consist of bone marrow suppression or proteinuria. Later a variety of autoimmune disorders may occur.

Ammonium tetrathiomolybdate forms a tripartite complex with copper and protein that is very stable. Given with food, ammonium tetrathiomolybdate complexes food copper with food protein, rendering food copper, along with copper in saliva, gastric juice, and intestinal secretions, unabsorbable. This puts the patient in an immediate negative copper balance. In addition, tetrathiomolybdate is absorbed into the blood and complexes free copper with blood albumin. This complexed copper cannot be taken up by cells and is nontoxic. This drug has a faster effect than zinc and avoids the deteriorations that may be seen

with penicillamine. As such the drug is ideal for initial treatment. Possible side effects are related to copper deficiency and include mild bone marrow suppression. In addition, mild elevations of aminotransferases may be seen.

Because of the ubiquity of copper in our diet, a negative copper balance cannot be achieved by dietary modification alone. It seems prudent, however, to recommend that WD patients avoid food with a high copper content.

Despite the effectiveness of medication in most WD patients, occasional patients require liver transplantation because of hepatic failure. This procedure corrects the metabolic defect localized in the liver, and transplanted patients no longer need specific medication for WD.

The prognosis for WD patients has generally improved greatly with the advent of treatment. In particular, when treatment is started in a presymptomatic stage, patients never become symptomatic. Also, the vast majority of symptomatic patients improve considerably or recover completely. The patients with hepatic presentation have the least optimistic prognosis. Assuming they survive the initial episode, the greatest risks are bleeding from esophageal varices and hepatic insufficiency. The patients with neurological or psychiatric presentation have a better prognosis, although their quality of life can be problematic if the residual deficit is considerable. It is therefore important to start treatment as early as possible, before irreparable damage has occurred. Under adequate treatment, successful pregnancy is possible. Anti-copper therapy should be continued during pregnancy. Zinc is safest as both penicillamine and triethylene tetramine dihydrochloride are potentially teratogenic.

52.5 Magnetic Resonance Imaging

CT scan of the brain in WD may reveal a number of different abnormalities including mild ventricular dilatation, cortical atrophy, brain stem atrophy, hypodense areas in the region of the putamen, globus pallidus, and dentate nucleus, and white matter hypodensities, in particular in the frontal subcortical area.

MRI most often shows lesions in the thalamus, putamen, and caudate nucleus (Figs. 52.1–52.3). Within the putamen, the lateral rim is often most prominently affected (Fig. 52.1). Other gray matter structures which are also regularly affected are the globus pallidus, claustrum, and subthalamic nucleus. The lesions are usually bilateral and symmetrical; asymmetry is rare. The lesions most often have a high signal intensity on T₂-weighted images and a low signal intensity on T₁-weighted images (Figs. 52.1–52.3). These changes in signal intensity are thought to re-

flect edema, necrosis, and gliosis. In some patients, areas of low signal intensity are seen in the putamen, head of the caudate nucleus, globus pallidus, and thalamus on T₂-weighted images (Figs. 52.1 and 52.2). The nuclei either have a generalized low signal intensity or have small areas of low signal intensity within the bigger high signal intensity lesion. Some assume that the low signal intensity on T₂-weighted images is related to iron deposition, as phagocytes containing iron pigment after small hemorrhages are seen in histological specimens. Others assume that the low signal intensity is related to the paramagnetic effect of copper. It is well established that copper ions in vitro have a pronounced effect on both T₁ and T₂. An increased concentration of copper ions causes a decrease in T₁ and T₂. High signal intensity on T₁-weighted images has been found in the globus pallidus (Fig. 52.1) and, more rarely, in the putamen, caudate nucleus, and around the aqueduct. This may be explained by a paramagnetic effect of copper, but may also be related to hepatic dysfunction. Sometimes multiple small cavities are seen within the basal nuclei with a signal intensity similar to that of CSF on all sequences. No contrast enhancement is seen.

Atrophy is a frequent finding. It may be focal, most frequently involving the caudate nuclei and brain stem. The atrophy may also be generalized involving the cerebral hemispheres and the cerebellum, with enlargement of subarachnoid spaces and ventricular system.

Subcortical white matter lesions are not rare in WD, in contrast to what was formerly thought. The white matter lesions are most often found in the frontal lobes, sometimes with extensions into the parietal area (Fig. 52.3). White matter lesions in other areas are rare. Their location is largely subcortical and they may not reach the ventricular wall. The overlying cortex may also be involved (Fig. 52.3). The white matter lesions are usually large and confluent, but multiple, small, isolated lesions can also be found. In exceptional cases the white matter lesions are cystic. The white matter changes are often asymmetrical (Fig. 52.3), which contrasts with the symmetry of the gray matter lesions. The posterior limb of the internal capsule and the external capsule may be affected. Rare localizations are the splenium of the corpus callosum and the white matter of the parietal, temporal, and occipital lobes. No contrast enhancement is present.

Cerebellar lesions are less frequent. Bilateral lesions in the dentate nuclei are most often seen. The cerebellar white matter may be abnormal, especially in the area around the dentate nucleus (Fig. 52.1).

Brain stem lesions are frequent. The areas most frequently involved are the midbrain tectum and tegmentum, the red nucleus, substantia nigra, central part of the base of the pons, and pontine tegmen-

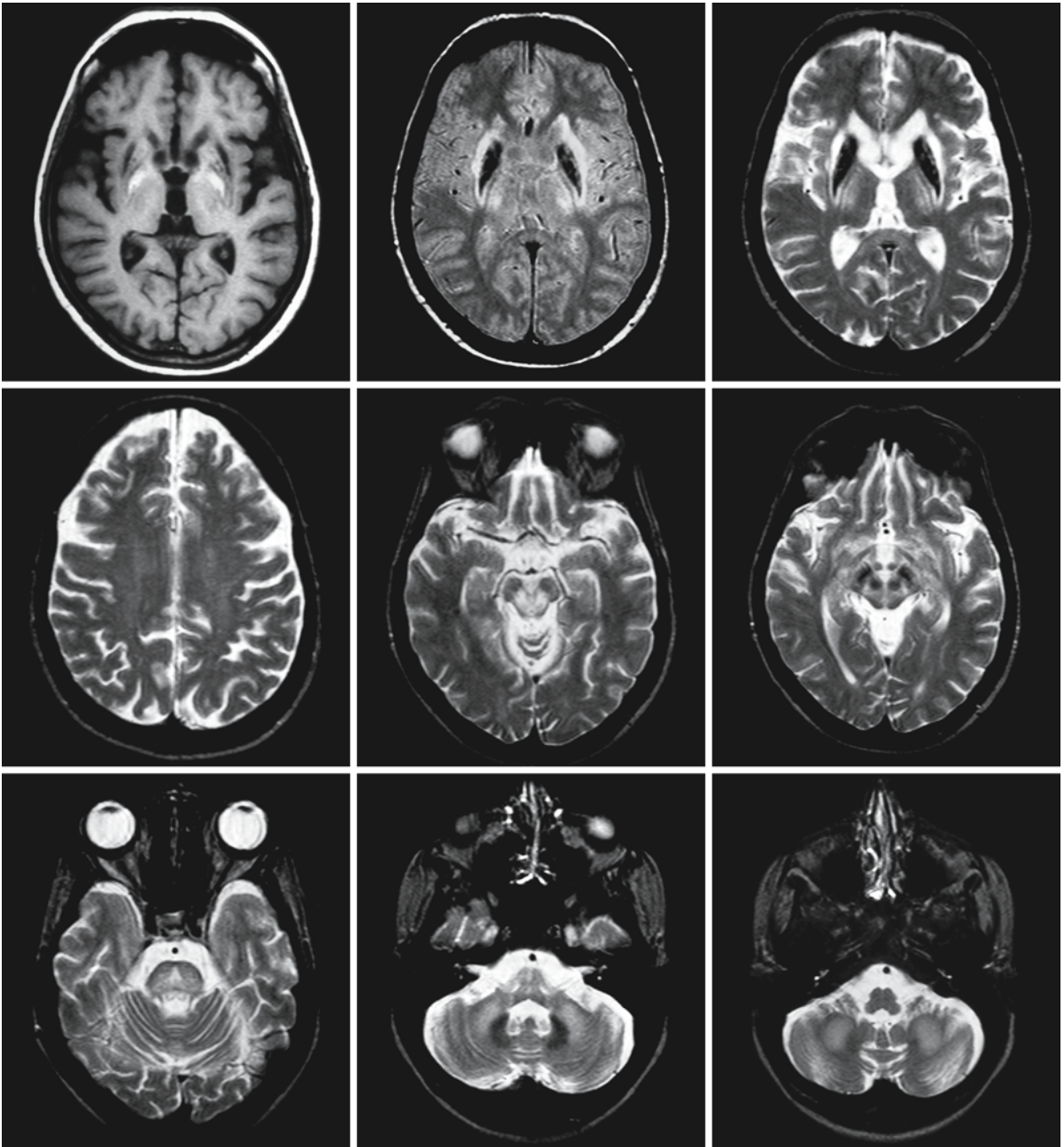


Fig. 52.1. A 37-year-old female with WD. Note the prominent abnormalities in the basal ganglia (*first row*). The caudate nucleus is markedly atrophic. The caudate nucleus, the peripheral rim of the putamen, and the claustrum have a high signal on proton density and T₂-weighted images, whereas the central part of the putamen has a low signal. The globus pallidus has a high signal on T₁-weighted images. The ventrolateral thalamus also contains signal abnormalities, the outer rim of the

thalamus standing out separately. Additionally, the T₂-weighted images (*second and third row*) show areas of high signal in the brain stem and cerebellar white matter, whereas the dentate nucleus has a low signal. The typical “panda face” is seen on the right in the second row. Courtesy of Dr. E. Gut, Department of Neuroradiology, Kliniken Schmieder, Allensbach, Germany

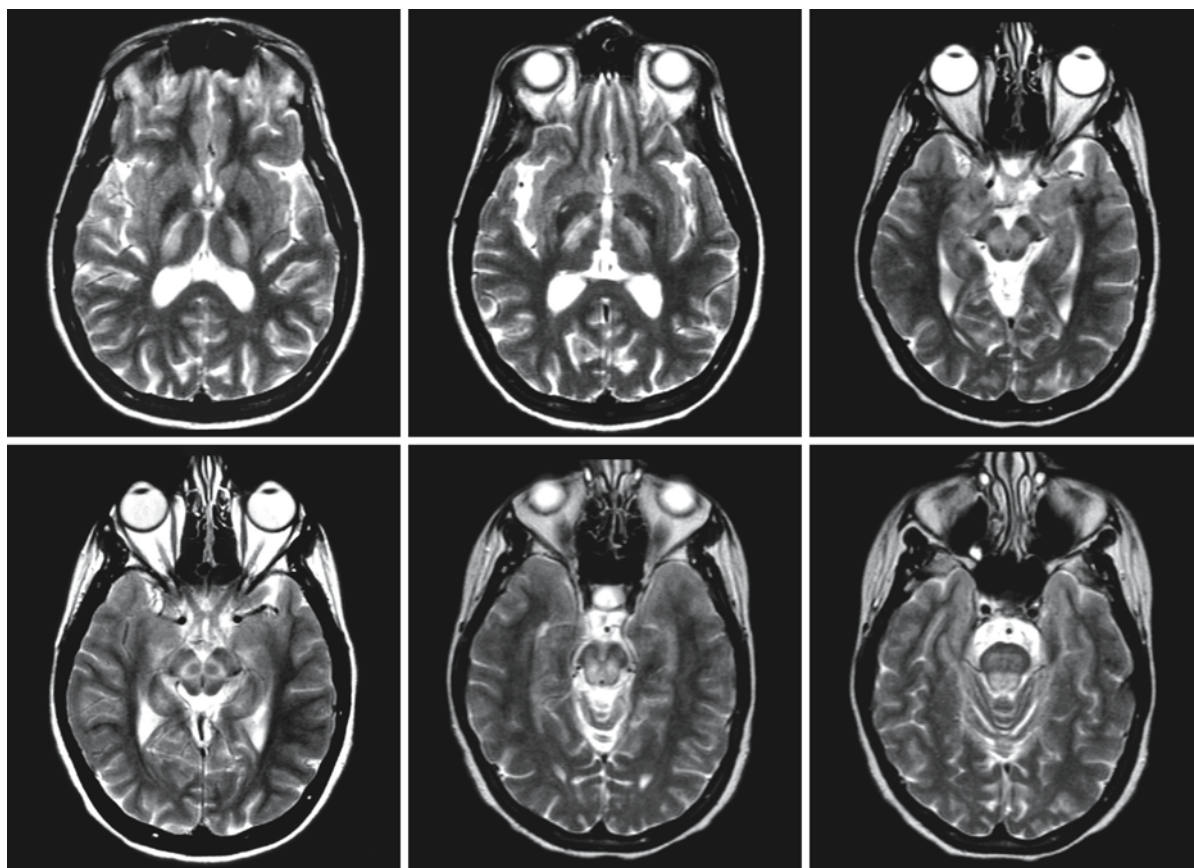


Fig. 52.2. A 31-year-old female with WD. The T_2 -weighted images show high signal intensity in the ventrolateral thalamus, its outer rim standing out separately. The putamen has an abnormally low signal with some tiny high-signal-intensity areas. The tectum and tegmentum of midbrain and pons have a high

signal. Within the midbrain, the typical panda face configuration is seen (*second row, left*). Courtesy of Dr. T. Naidich, Department of Radiology, The Mount Sinai School of Medicine, New York

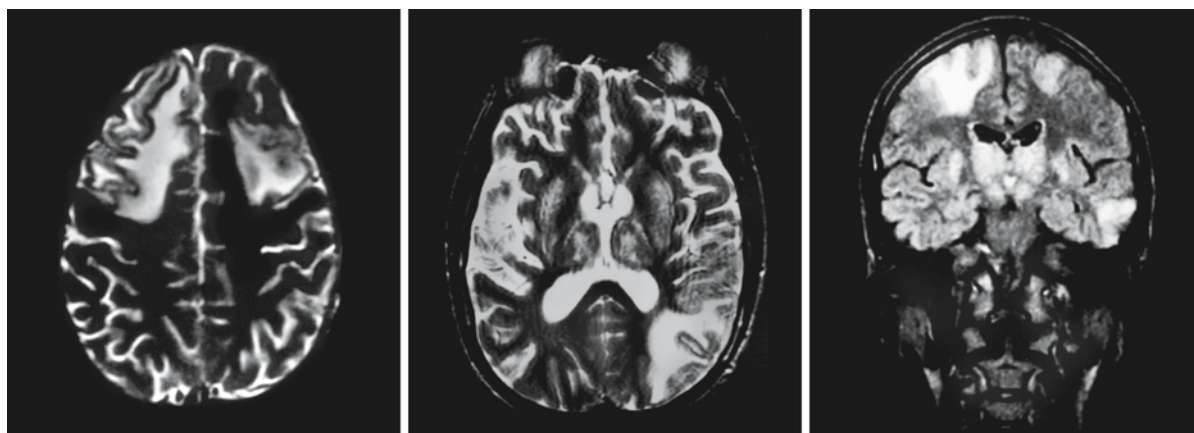


Fig. 52.3. A 13-year-old boy with WD. Note the involvement of the putamen and thalamus, the lateral rim of the thalamus standing out separately. Additionally, there are large focal

white matter lesions with an asymmetrical distribution. The overlying cortex is affected as well. From Hedera et al. (2002), with permission

tum. Atrophy of midbrain and pons may be seen. A T₂-weighted image through the midbrain may reveal the so-called “face of the giant panda” appearance, with a low signal intensity of the superior colliculus, loss of the normal, characteristic low signal intensity of the lateral portion of the substantia nigra, presence of the normal low signal intensity of the red nucleus, and high signal intensity of the tegmentum of the midbrain (Figs. 52.1 and 52.2).

MRI is of value in WD, both for diagnostic and monitoring purposes. The diagnosis of WD may be difficult, and MRI may suggest this possibility. The most important differential diagnostic options are respiratory chain defects and extrapontine myelinolysis, in particular if a central lesion is present in the basis of the pons. WD and Japanese encephalitis also show a very similar topography of the MRI abnormalities. However, brain stem lesions are more frequent in WD. WD patients more often have a mixed signal intensity of the basal ganglia and a typical linear rim of signal abnormality in the putamen. Thalamic hemorrhagic lesions and meningeal enhancement are more often seen in Japanese encephalitis. Clinical his-

tory and laboratory tests differentiate between these disorders.

MRI is abnormal in almost all patients with neurological complaints and in some neurologically normal patients. In exceptional cases normal MRI has been reported despite the presence of neurological abnormalities. With successful treatment, MRI abnormalities have been shown to improve or disappear.

Some correlations have been found between cerebral lesions and clinical symptomatology. Dystonia is related to putamen lesions; dysarthria correlates with lesions in both putamen and caudate nucleus. Both lesions in the substantia nigra and in the putamen and caudate nucleus are associated with parkinsonism. Abnormalities in efferent cerebellar pathways, including the superior cerebellar peduncle, red nucleus, and thalamus, are associated with clinical cerebellar signs. Lesions in the dentate nucleus are associated with a kinetic tremor and dysmetria. Lesions in the red nucleus are associated with proximal kinetic tremor. Generalized atrophy and subcortical white matter lesions are associated with cognitive decline.

Menkes Disease

53.1 Clinical Features and Laboratory Investigations

Menkes disease (MD), also called kinky hair disease or trichopoliodystrophy, is a rare, genetically determined disease with an X-linked recessive mode of inheritance. About 30% of cases are related to new mutations, and in these patients a positive family history is lacking. Rarely, females are affected, related to an accompanying chromosomal abnormality (for instance, XO or a translocation that disrupts the disease gene on the X chromosome) or carriership for a mutation and a highly unfavorable X inactivation pattern. The incidence has been estimated as 1 in 100,000–250,000 live births. However, the true incidence is unknown because patients may die in early infancy without a diagnosis. The clinical spectrum is broad.

In classical MD, premature birth and low birth weight are frequent. In the neonatal period, some patients display hypothermia, hypoglycemia, poor feeding, and hyperbilirubinemia. However, these features may also appear in otherwise healthy premature babies and rarely lead to a diagnosis in the neonatal period. The infants are normal up to the age of 2–4 months, when loss of developmental milestones, hypotonia, hypothermia, seizures, and failure to thrive occur. The hair abnormalities characteristic of MD usually become prominent at the age of 2–3 months. The hair is short, sparse, coarse, twisted, and often hypopigmented. It resembles steel wool. Eye lashes and eyebrows can also be affected. The infants have a cherubic face, with a decreased facial expression, prominent forehead, pudgy cheeks, sagging jowls, and scant eyebrows. The skin and joints are lax. The skin is lacking in pigment. Inguinal hernias may be present. Diverticula of the bladder and ureters predispose to urinary tract infections and sometimes rupture. Hydronephrosis may occur. Bone changes such as osteoporosis are always present, and fractures of the long bones and ribs may occur. Pectus excavatus is often seen. Diarrhea is common and intestinal hemorrhage may occur. The neurological deterioration in classical MD is severe. Most patients never achieve head control or independent sitting. The seizures are usually intractable. Subdural hematomas and effusions are often present. Infections are common, in particular respiratory and urinary tract infections.

Sepsis and meningitis are also fairly common. Death usually occurs before the age of 3 years.

Patients with unusually severe variants of MD have been reported who present soon after birth with extensive vascular disease with intracranial, gastrointestinal, intra-abdominal, pulmonary, and other hemorrhages, in the absence of a coagulopathy, finally resulting in hemorrhagic shock and early death. Additionally, brain infarcts may occur and multiple fractures may be present.

Milder variants of the disease occur, including mild MD and occipital horn syndrome (OHS). Patients with mild MD have a hypopigmented skin, laxity of the skin and joints, abnormal hair, and the characteristic facial appearance. The neurological symptoms are much milder than in classical MD. The predominant neurological manifestations of mild MD are prominent cerebellar ataxia and dysarthria, and moderate cognitive deficit.

OHS was previously known as type IX Ehlers-Danlos syndrome or X-linked cutis laxa. It is an X-linked recessive connective tissue disorder. The disease derives its name from distinctive cranial exostoses (occipital horns) resulting from calcification of the trapezius and sternocleidomastoid muscles at their attachment to the occipital bone. The predominant clinical manifestations of OHS are skeletal abnormalities including the occipital horns, short and broad clavicles, osteoporosis, laxity of the skin and joints, bruisable skin, and bladder diverticula. The urinary tract abnormalities lead to recurrent urinary tract infections. Most patients have inguinal hernias. The only apparent neurological abnormalities of patients with OHS are autonomic dysfunction and slight mental deficiency. The autonomic dysfunction may lead to diarrhea, orthostatic hypotension and syncope, and temperature instability with heat intolerance. Life expectancy is as a rule up to at least mid-adulthood.

Some patients have been reported with a mixture of manifestations of classical MD, mild MD, and OHS.

Most patients with classical MD show moderate to severe EEG abnormalities including hypsarrhythmia. Skeletal changes in classic MD are distinctive but not pathognomonic. They usually become apparent by the second month of life. They include wormian bones of the skull, generalized osteoporosis, metaphyseal spurring of long bones, and anterior flaring of the ribs. Rib and long bone fractures, including

metaphyseal fractures, are common. The clavicles are short with hammer-shaped distal ends. Radiographic abnormalities in OHS include osteoporosis, occipital and femoral exostoses, carpal coalescence, coxa valga, deformation of the radii, ulnae, tibiae, and fibulae, and short clavicles with hammer-shaped distal ends.

Microscopic examination of the hair in MD reveals pili torti (180° twisting of the hair shaft), often in combination with constrictions at regular intervals (trichorrhexis nodosa), varying diameters, transverse fractures of the hair shaft, and longitudinal splitting of the shaft.

Serum levels of copper and ceruloplasmin are very low in patients with classical MD. Interpretation is difficult in the first 2–3 weeks of life. Serum copper and ceruloplasmin levels are normally low at birth and rise over the first month. It may therefore be difficult to diagnose MD by these markers in the neonate. An abnormal plasma or CSF catecholamine pattern may be a more sensitive marker of copper deficiency, but a lumbar puncture is not feasible in neonates with a hemorrhagic disease. The defect in copper transport can be demonstrated by analysis of copper accumulation in cultured fibroblasts or lymphoblasts using radioactive copper (^{64}Cu). Copper levels and accumulation are elevated in MD. The activity of various copper-dependent enzymes, such as cytochrome-*c* oxidase, dopamine β -hydroxylase, and lysyl oxidase, are reduced. CSF lactate is elevated, as expected in cytochrome-*c* oxidase deficiency. Catecholamine levels are abnormal in serum and CSF, with elevated levels of the dopamine metabolite dihydroxyphenylacetic acid (DOPAC) and the catecholamine precursor dihydroxyphenylalanine (DOPA) and low levels of the deaminated norepinephrine metabolite dihydroxyphenylglycol (DHPG), indicating reduced activity of dopamine β -hydroxylase. As a result the ratios of DOPA to DHPG and DOPAC to DHPG are markedly elevated and valuable for a diagnosis. Generalized amino aciduria has been observed in a few patients with MD, but renal tubular damage is rarely a problem.

In patients with mild MD and OHS, serum levels of copper and ceruloplasmin are usually slightly to moderately decreased, but may also be normal or even lower than in patients with classical MD. The increased copper levels and ^{64}Cu uptake and retention in fibroblasts or lymphoblasts from patients with mild MD or OHS are indistinguishable from those in classical MD. The activity of lysyl oxidase is significantly decreased in skin and cultured fibroblasts from patients with OHS.

DNA-based diagnosis is possible. Female carriers are clinically almost always completely normal, with the exception that pili torti are seen in the hair of 50% of carriers. Heterozygous females can be diagnosed on the basis of these pili torti in their hair, patchy skin

depigmentation, and/or increased copper accumulation in cultured fibroblasts. However, some heterozygotes display no abnormalities, which can be explained by the individual X inactivation pattern. DNA-based diagnosis is very useful for carrier detection. Prenatal diagnosis can be performed on the basis of analysis of copper levels or ^{64}Cu uptake in cultured amniotic fluid cells or chorionic villi. DNA-based prenatal diagnosis is possible in families with a known mutation.

53.2 Pathology

In many infants with classic MD, chronic subdural hematomas are found. The brain shows as a rule severe and diffuse atrophy of the cerebral and cerebellar hemispheres. The cerebral arteries are thin-walled, tortuous, and ectatic. On sectioning, the white matter appears shrunken and the lateral ventricles are moderately dilated.

Microscopic examination of the cerebral cortex shows widespread neuronal loss and severe spongiosis. Areas of total devastation with microcystic rarefaction of the cortex may be present, and in some areas the cortex and subcortical white matter may be cavitated. Moderate nerve cell loss is also found in the basal ganglia. The thalamus and red nucleus may be particularly affected and show severe degeneration. The cerebral white matter is reduced in volume. Microscopic examination demonstrates severe myelin paucity and sometimes severe and diffuse gliosis. The myelin paucity is probably explained by a combination of poor myelination and myelin loss. A status spongiosus may be seen in the white matter but frank cavitation is rare.

The cerebellum is markedly atrophic. On microscopic examination, there is a striking loss of granule cells. The Purkinje cells are also diminished in number and show striking dendritic abnormalities, with presence of perisomatic dendrites radiating from the perikaryon. The apical dendrites may show deformities of the weeping willow or staghorn pattern. Dendritic swellings and axonal torpedoes may also be present. On electron microscopy, a marked increase in the number and size of mitochondria is found in the perikaryon of Purkinje cells and to a lesser extent of neurons within the cerebral cortex and basal ganglia. There are intramitochondrial electron-dense bodies.

In muscle biopsy of MD patients, mitochondrial abnormalities have been found, including enlarged mitochondria with disorderly and irregular cristae. Ragged red fibers have also been reported.

Ultrastructural studies of the skin reveal that dermal collagen fibrils have a heterogeneous size range, with a mean diameter smaller than normal. Dermal elastin fibers are scarce and considerably smaller

than normal. They consist of thin strands of amorphous elastin associated with numerous microfibrils.

Cerebral and systemic arteries and arterioles are tortuous with irregular lumina and frayed and split intimal linings. In the walls of arteries the amount of collagen is normal, but the fibrils display a broader range of diameters than normal, with a slightly smaller mean. Elastin fibers in the internal elastic lamina, tunica media, and intimal layers show considerable disruption, appearing fragmented and wider than normal and displaying irregular contours. Veins are less often affected.

53.3 Chemical Pathology

Lipid studies in MD show decreases in myelin lipids with increases in cholesterol and cholesterol esters. The presence of cholesterol esters points to active myelin loss. In the white matter galactolipids are decreased.

53.4 Pathogenetic Considerations

The gene for MD and its variants is *MNK*, also called *ATP7A*, located on chromosome Xq13.3. The gene codes for a transmembrane copper-transporting P-type ATPase. *ATP7A* is expressed in virtually all nonhepatic tissues. The protein is located in the trans-Golgi network, pumping copper into the Golgi apparatus to supply copper to the copper-dependent enzymes. In the presence of elevated extracellular copper concentrations, the protein relocates to the plasma membrane to pump excess copper out of the cells. When intracellular copper levels are reduced, the protein returns to the trans-Golgi network. This reversible relocation is very important for copper homeostasis.

Several key metabolic processes are copper-dependent, including oxidative respiration neurotransmitter synthesis, connective tissue formation, free radical detoxification, iron homeostasis, and pigmentation. Copper is required for the catalytic activity of a number of essential enzymes in these processes, the majority of which catalyze oxidation-reduction reactions. The ability of copper, like iron, to undergo reversible redox changes makes it a useful cofactor in redox reactions. However, both metals also catalyze the production of potentially damaging free radicals and are toxic in excess amounts. Organisms have several mechanisms to obtain and distribute copper safely and to excrete the excess.

Defects in *ATP7A* result in a defect in the copper excretion of cells and an accumulation of copper in their cytosol. Copper efflux requires *ATP7A* in most cells, hepatocytes being a notable exception. The

defect in the *ATP7A* protein leads first of all to reduced uptake of copper across the small intestine, because the copper accumulates in the intestinal epithelial cells and is not excreted into the blood. The reduced supply of dietary copper is further compounded by the defective distribution of copper within the body wherever *ATP7A* is required for copper transport. For example, *ATP7A* is involved in the transport of copper across the blood-brain barrier to the CNS, explaining the marked deficiency of copper in the brain of MD patients. In contrast with the overall copper deficiency in MD, copper accumulation occurs in certain tissues such as the intestinal epithelial cells, the kidney, and cultured cells, owing to the copper efflux defect. It is probable that copper is normally resorbed in the proximal tubules of the kidney, as under normal conditions very little copper is excreted in the urine. Patients with MD cannot deliver the resorbed copper from the epithelial cells of the proximal tubules into the blood.

Deficiency of copper-dependent enzymes causes the multiple abnormalities in MD patients. Hypopigmented hair is caused by the deficiency of tyrosinase, an enzyme required for melanin synthesis. The unusual hair, the pili torti, is caused by reduced keratin cross-linking, a process that is copper-dependent. Connective tissue abnormalities, including arterial vessel wall abnormalities, loose skin, and fragile bones, result from reduced lysyl oxidase activity and consequent weak cross-links in collagen and elastin. Deficiency of several enzymes, including cytochrome-*c* oxidase (oxidative respiration), superoxide dismutase (free radical detoxification), peptidylglycine α -amidating mono-oxygenase (modification of various peptide neurotransmitters), and dopamine β -hydroxylase (neurotransmitter biosynthesis), may contribute to the neurological damage.

Many different mutations have been found in *ATP7A*. In classical MD, most mutations are nonsense mutations, frameshifts, large deletions, and splice site mutations, which lead to absence of functional protein. In mild MD, missense mutations have been found that block copper-induced relocation of the mutated protein from the trans-Golgi network to the plasma membrane. The milder course of the disease suggests that the mutant protein retains some copper transport activity. Patients with OHS have splice site mutations that still permit the production of a small amount of normal *ATP7A* mRNA next to abnormally small transcripts. The milder clinical manifestations can be explained by the presence of small amounts of the normal protein. As most of the clinical symptoms in OHS are related to lysyl oxidase deficiency, it is assumed that this enzyme is more sensitive than the other cuproenzymes to copper deficiency.

53.5 Therapy

In the treatment of MD patients, the first important issue is early diagnosis. The second issue is to bypass the block in the intestinal absorption of copper. The third is to deliver circulating copper to the brain. The fourth is that copper must be available within cells to enzymes that require copper as a cofactor.

Oral administration of copper generally has no effect on circulating copper, but parenteral administration of copper in any form restores circulating copper and ceruloplasmin to normal levels. Among the different forms of copper, copper histidine has been reported to be taken up by the brain most efficiently. Copper uptake by hepatocytes and brain tissue is physiologically mediated by histidine. Therefore, copper histidine is generally used for parenteral administration. While low hepatic stores are quickly replenished by parenteral copper treatment, levels of copper in the brain only increase gradually, if at all, during treatment, consistent with trapping of copper within the cells forming the blood–brain barrier. The activities of copper-dependent enzymes remain subnormal under treatment in most patients. However, it is difficult to assess the activities of most enzymes serially, as repeated skin, muscle, and brain biopsies would be required to do that. The darkening of the hair under treatment indicates a higher activity of tyrosine hydroxylase. Ceruloplasmin is the only cuproenzyme whose activity always normalizes in response to copper treatment, because this enzyme is synthesized in the liver, where *ATP7A* is not expressed.

There are two major problems with this copper replacement therapy. First of all, there is usually a delay in diagnosis, and during this time brain damage continues which cannot be undone. Secondly, the block in intestinal copper absorption may be bypassed by parenteral administration, but the basic defect affecting transport of copper into the brain and intracellular copper metabolism in tissues throughout the body cannot be fully overcome by copper replacement.

Clinical outcomes of MD patients treated with copper replacement have generally been disappointing. Some patients who are treated from an early age, preferably <1 month, show outcomes better than expected, and some even attain normal developmental milestones. However, other patients do not fare well despite early treatment. When treatment is commenced at an older age, after onset of symptoms, significant neurological recovery is not possible, although decreased seizure frequency, reduced irritability, better sleeping, and slight advances in social development may be seen. Copper treatment may prolong life span, but not consistently in all patients.

Some striking exceptions have been observed. With early treatment neurological symptoms have

regressed or even disappeared in some MD patients, although an OHS-like clinical picture may persist in such patients. It has been suggested that mutations with preservation of some residual *ATP7A* activity may be requisite for significant clinical efficacy of copper replacement therapy (Kaler et al. 1996). One patient has been reported in whom mislocalization of the protein in the endoplasmic reticulum due to a certain mutation could be corrected by supplementation of copper (Kim et al. 2002). However, significant improvement has also been observed in some early-treated patients from classical MD families with severe mutations.

From a practical point of view, commencing parenteral copper histidine treatment as soon as the diagnosis of MD has been established may be advocated irrespective of the gene abnormality. Therapy should be continued until it becomes evident that cerebral degeneration cannot be arrested.

Symptomatic treatment including antiepileptic medication, maintenance of an adequate nutritional status, and physical therapy are important. Bisphosphonate therapy has been used to increase bone mineral density in MD patients. It is effective in the management of osteoporosis and contributes to the prevention of bone fractures.

53.6 Magnetic Resonance Imaging

One of the most striking findings on MRI in patients with classical MD is excessive tortuosity of the cerebral arteries. MRA confirms tortuosity, dilatation, and kinking of the arteries (Fig. 53.1). Tortuosity of the extracranial systemic arteries is also present.

Early MRI of the brain may be normal in classical MD. Soon, however, serious damage develops. Transient bilateral temporal lobe white matter abnormalities with prominent swelling and involvement of the overlying cortex have been observed (also seen in Fig. 53.1). In some MD patients, brain lesions arise that look like focal infarctions with a low ADC on diffusion-weighted images. The cerebral white matter may also be diffusely abnormal, mildly swollen, and have a highly abnormal signal. In that stage of the disease, there is no evident atrophy and there are no subdural fluid collections. The white matter swelling soon evolves into atrophy and the white matter remains poorly myelinated (Fig. 53.2). The atrophy is progressive over time. Some white matter areas may become cystic. Diffuse and serious cerebral and cerebellar atrophy leads to enlargement of the extracerebral spaces (Fig. 53.2). Subdural hygromas and hematomas easily develop and are almost invariably seen in MD (Fig. 53.2). As the atrophied brain recedes from the dura, the bridging cortical veins may tear, resulting in subdural effusions. The vulnerability of

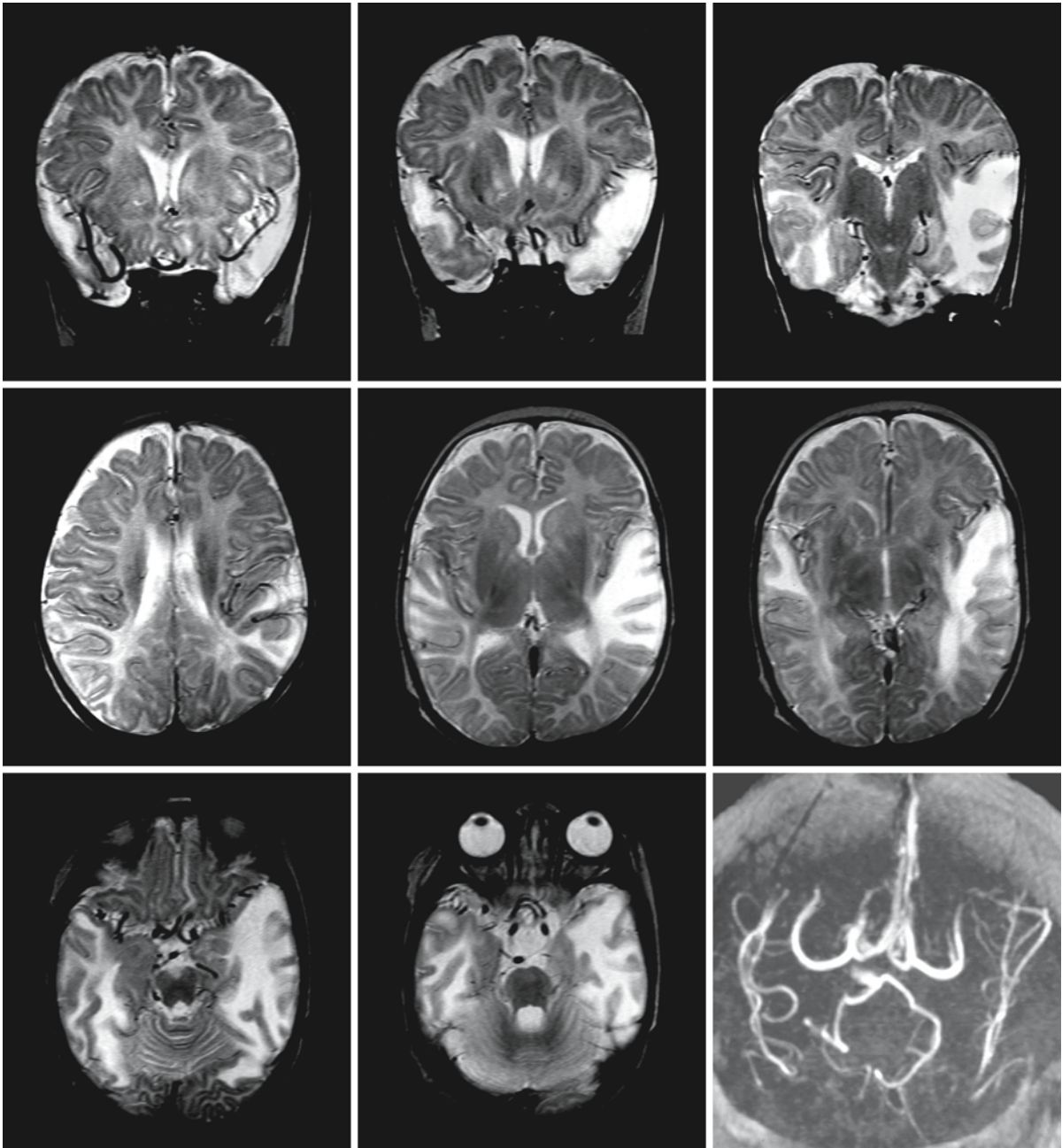


Fig. 53.1. A 5-month-old boy with MD. The large, swollen temporal lesions, which involve both white matter and overlying cortex, could be considered suggestive of herpes encephalitis. However, the arteries in the sylvian fissure and around the

brain stem show abnormal hypertortuosity, which is not a feature of herpes encephalitis. MRA confirms the tortuosity of the cerebral arteries. Courtesy of Dr. T. Aduc, Randburg, and Dr. M.M. Lippert, Pretoria, South Africa

the abnormal vessels in MD may contribute to the development of hematomas. In addition, there may be signal changes in the basal ganglia.

The most important item in the differential diagnosis is the shaken baby syndrome. The combination of subdural hygromas and hematomas of different ages and bone fractures is very suggestive of this di-

agnosis. However, the clinical picture with skin and hair abnormalities, tortuosity of the arteries on MRI, and the presence of other bone abnormalities should help in the differentiation. In patients presenting with predominantly white matter disease on MRI, tortuosity of the cerebral vessels is again an important diagnostic clue for MD.

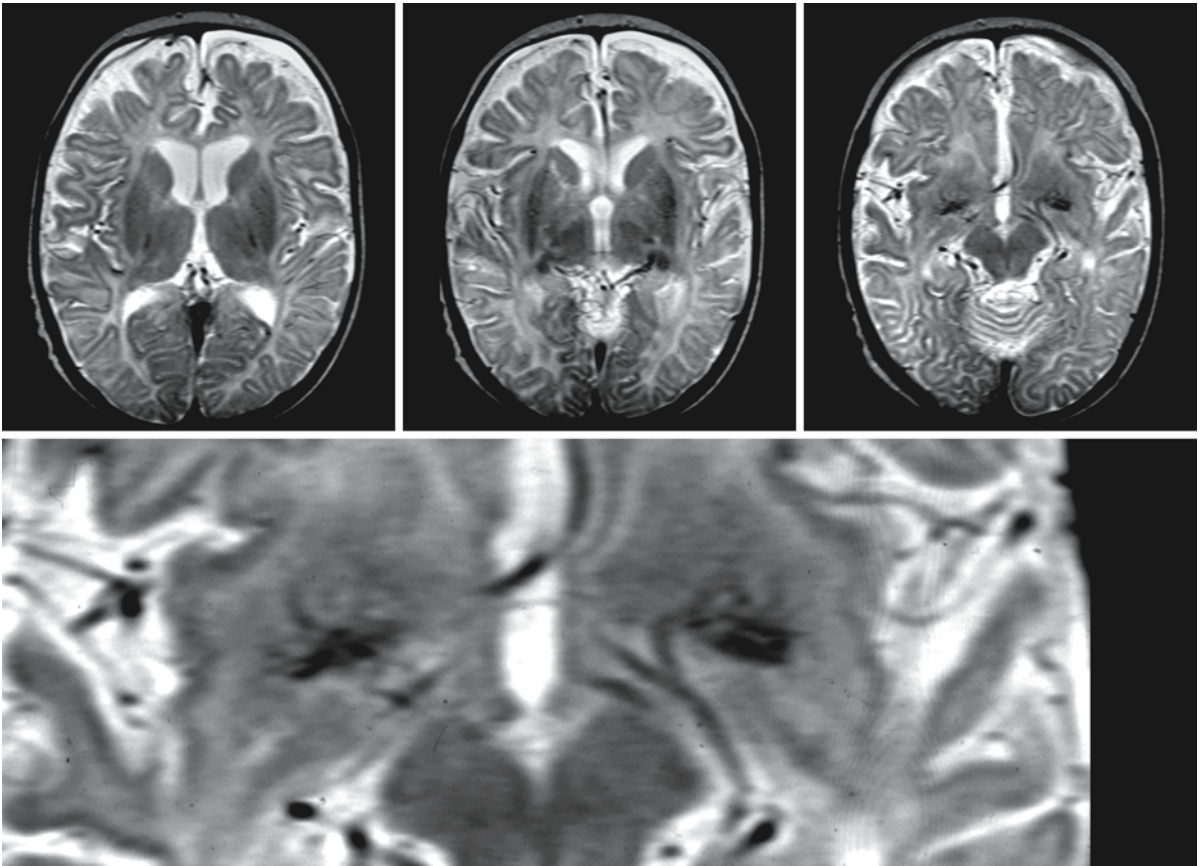


Fig. 53.2. The same boy as in Fig. 53.1, now 6.5 months old. Note the serious atrophy with enlargement of the subarachnoid spaces and small subdural effusions. The process of myelination is not showing any progress beyond the neonatal

stage. Bilaterally low in the basal ganglia a ball of tortuous and dilated vessels is seen, which is particularly clear in the enlarged view. Courtesy of Dr. T. Aduc, Randburg, and Dr. M. M. Lippert, Pretoria, South Africa

Fragile X Premutation

54.1 Clinical Features and Laboratory Investigations

Fragile X syndrome is one of the most common inherited forms of mental retardation. The disorder is caused by an expansion in excess of 200 repeats (full mutation expansion) of a trinucleotide element, (CGG)_n, located in the 5' untranslated region of the fragile X mental retardation 1 gene (*FMR1*). Trinucleotide expansions that are in the 55–200 repeats range are called premutations. Normal persons have a range of approximately 5–54 repeats.

Male carriers of premutations typically have normal intelligence, although emotional problems and subtle physical features occur in about 25%. Mental retardation and autism may occur. About 20% of female patients with a premutation experience premature ovarian failure and menopause. Some female premutation carriers have emotional problems, including anxiety, obsessional thinking, or depression.

Some male carriers of the fragile X premutation over the age of 50 years experience progressive neurological dysfunction with tremor and cerebellar ataxia, most frequently leading to gait difficulties and deterioration of fine motor skills. Additionally, progressive cognitive decline and behavioral difficulties arise, including memory loss, anxiety, mood lability, and reclusive behavior. In a few patients more serious dementia occurs. More variable features include parkinsonism, peripheral neuropathy with distal weakness and sensory loss, lower limb proximal muscle weakness, and autonomic dysfunction with urinary and bowel incontinence and impotence. Rarely, female premutation carriers develop tremor and ataxia, but they do not experience cognitive decline.

The diagnosis of fragile X premutation is established by demonstrating a CGG repeat with a length of 55–200 trinucleotide repeats in the *FMR1* gene.

54.2 Pathology

Neuropathologic findings include cerebral and cerebellar atrophy. There are eosinophilic intranuclear inclusions in neurons and astrocytes throughout the cortex, subcortical regions, and brain stem. The hippocampus and the frontal cortex are the most severely affected. There is evidence of cerebellar degeneration with Purkinje cell loss, torpedo formation, and

dystrophic axons. Spongiform changes are seen in the cerebellar white matter and middle cerebellar peduncles.

54.3 Pathogenetic Considerations

The fragile X syndrome is caused by an expansion in excess of 200 repeats of a trinucleotide element, (CGG)_n, located in the 5' untranslated region of the fragile X mental retardation 1 gene (*FMR1*) on chromosome Xq27.3. Trinucleotide expansions that are longer than 200 repeats are called full mutation expansions. Trinucleotide expansions that are in the 55–200 repeats range are called premutations. Normal persons have a range of approximately 5–54 repeats.

The pathophysiology of the neurological syndrome in older males with a premutation has not been fully understood. Repeat expansions are known to influence both transcription and translation. The full expansion of over 200 repeats generally leads to transcriptional silencing and deficiency or absence of the *FMR1* protein (FMRP). Lack of this protein leads to the fragile X syndrome. In patients with a fragile X premutation, FMRP levels are gradually reduced with increasing repeat number, despite elevated *FMR1* mRNA levels, suggesting that translation is impeded within the premutation range. The syndrome seen in older males with a premutation may be related to a gain of function with toxic effects related to elevated *FMR1* mRNA levels.

54.4 Therapy

No specific treatment is available.

54.5 Magnetic Resonance Imaging

In older male patients carrying the fragile X premutation and the clinical symptoms described above, MRI shows symmetrical signal abnormalities in the middle cerebellar peduncles and deep cerebellar white matter (Figs. 54.1 and 54.2). After contrast, no enhancement occurs. The dentate nucleus is spared. Mild to moderate atrophy of the cerebellum, midbrain, and pons is frequently present. Mild to moder-

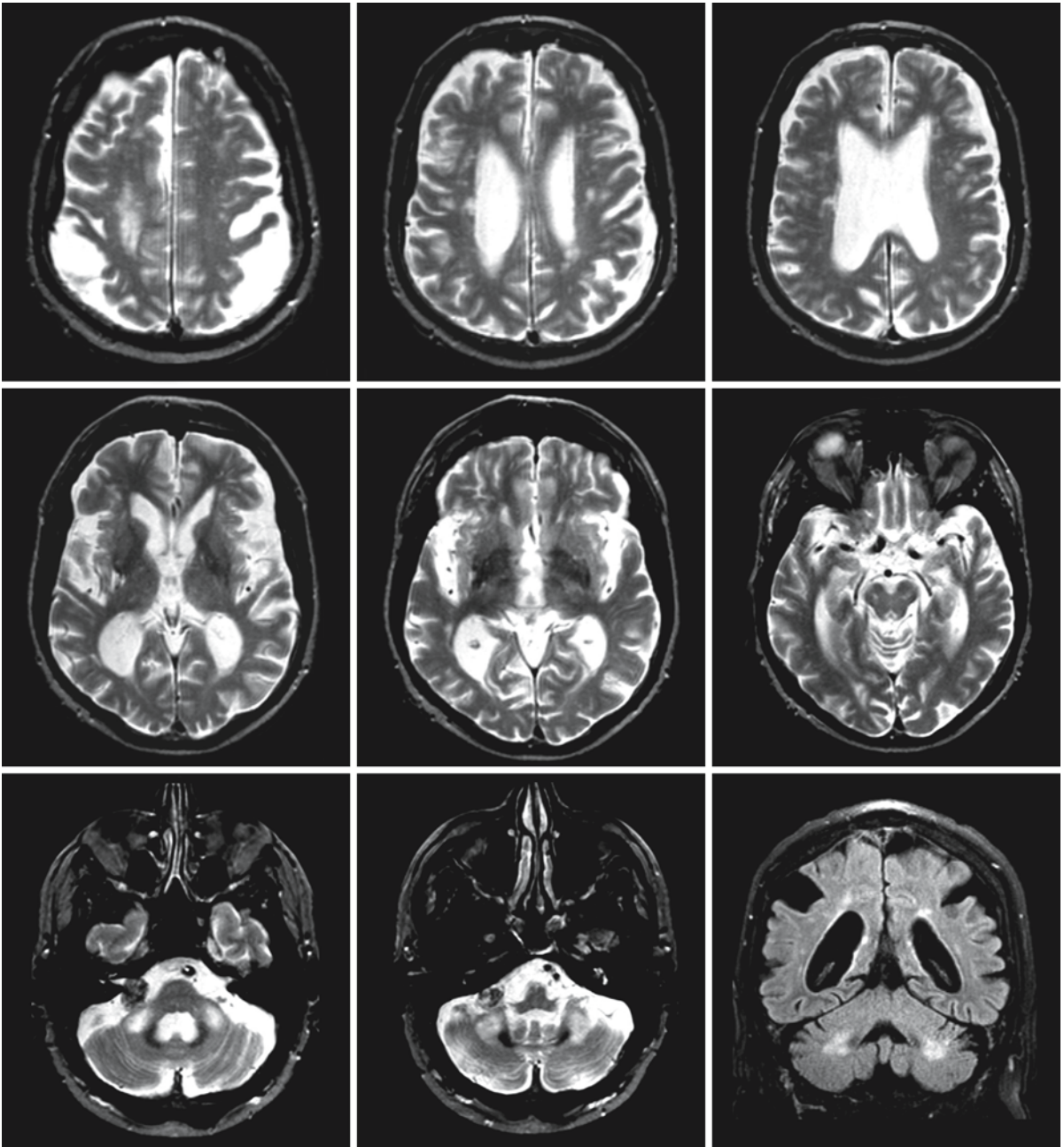


Fig. 54.1. A 61-year-old man with a fragile X premutation. A CGG repeat with a length of 80 trinucleotide repeats was demonstrated in the *FMR1* gene. Note the cerebral and cerebellar atrophy. There are signal abnormalities in the middle cerebellar peduncles and deep cerebellar white matter. There

are patchy signal abnormalities in the periventricular and deep cerebral white matter. Courtesy of Dr. J. Vandevenne, Department of Radiology, and Dr. A. Wibail, Department of Neurology, Hospitals Oost-Limburg, Genk, Belgium

ate cerebral atrophy with thinning of the corpus callosum is present in the majority of the patients (Figs. 54.1 and 54.2). In many patients additional white matter abnormalities are present in the frontal

and parietal periventricular and deep white matter (Figs. 54.1 and 54.2). MRI does not demonstrate the same abnormalities in asymptomatic older male patients carrying the fragile X premutation.

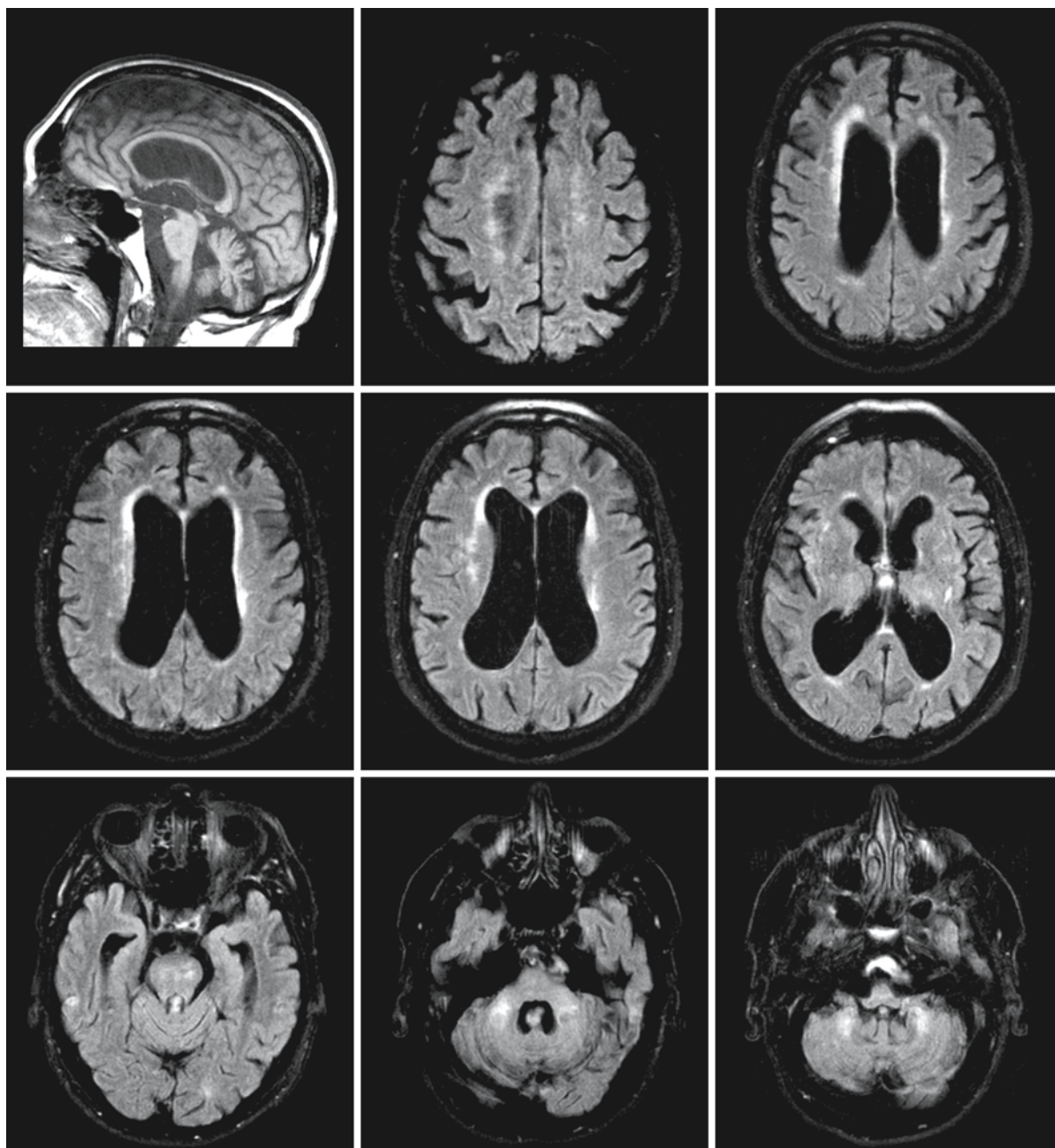


Fig. 54.2. A 63-year-old man with a fragile X premutation. A CGG repeat with a length of 90 trinucleotide repeats was demonstrated in the *FMR1* gen. These sagittal T₁-weighted image (first row, left) and axial FLAIR images show prominent cerebral and cerebellar atrophy. There is a periventricular rim

of elevated signal intensity. In addition, there are signal abnormalities in the base of the pons, middle cerebellar peduncles, and cerebellar white matter. Courtesy of Dr. J. Vandevenne, Department of Radiology, and Dr. I. Raets, Department of Neurology, Hospitals Oost-Limburg, Genk, Belgium

Hypomelanosis of Ito

55.1 Clinical Features and Laboratory Investigations

Hypomelanosis of Ito (HMI), formerly also called incontinentia pigmenti achromians, does not represent a distinct entity but is a symptom of many different states of mosaicism. HMI is characterized by unilateral or bilateral hypopigmented whorls, streaks, and patches. The abnormal pigmentation follows Blaschko lines. The Blaschko lines have a bizarre fountain-like pattern on the back, whorls on the abdomen and linear stripes on the limbs. Zones of hypomelanosis are easily seen in patients with a darker skin, but to see the zones in patients with a fair skin the use of Wood's light may be necessary. In most patients the zones are apparent at birth or within the first year of life. The mucous membranes are spared. The hypopigmented whorls represent the "negative pattern" of the hyperpigmented lesions seen in incontinentia pigmenti type II, an X-linked disorder that is lethal for males. Another difference with incontinentia pigment type II is that neonatal inflammatory skin abnormalities are lacking in HMI.

HMI is a nonspecific marker for genetic or chromosomal mosaicism in persons with a sufficiently dark skin to show lighter patches. Most cases are sporadic, but autosomal dominant inheritance is evident in some. Incontinentia pigmenti type I is a subtype of hypomelanosis of Ito, associated with an X chromosome/autosome translocation involving band Xp11.

Abnormalities of the eyes, hair, teeth, musculoskeletal system, heart, and CNS occur in some of the patients with HMI. Hypopigmented areas can be observed in the iris and the retina. Corneal opacities, macrophthalmia, microphthalmia, strabismus, epicanthal folds, choroidal atrophy, and optic nerve hypoplasia may occur. Abnormalities in hair color, alopecia, hypertrichosis, and trichorrhexia may be observed. Fingernails may be abnormal. Numerous types of dental dysplasia may be present. Macrocephaly is relatively common; microcephaly is less frequent. The face may be asymmetrical. Unilateral hypertrophy or hypotrophy of the body or part of the body may be present. Other abnormalities observed include hypertelorism, bifid uvula, cleft palate, small stature, scoliosis, clinodactyly, and syndactyly. Congenital cardiac abnormalities and unilateral kidney aplasia may be present. Occurrence of a tumor is a rare observation, and if present, it is most often be-

nign. CNS abnormalities are frequent and these are highly variable. Neurological impairment can be quite severe with hemimegalencephaly or migrational defects, leading to intractable seizures and serious mental and motor handicap. About 80% of the patients have mental retardation, which varies from mild to profound. Autism is seen in some patients. HMI has been associated rarely with vascular abnormalities such as moyamoya syndrome and intracranial arteriovenous malformations. If a parent is affected, he or she may only have cutaneous abnormalities and no neurological problems, whereas the offspring has evident neurological signs.

In patients with HMI chromosome mosaicism is often restricted to the skin, while blood karyotypes may be normal. For this reason skin fibroblast chromosome analysis is recommended. Mosaicism has also been found in keratinocytes obtained from the hypopigmented areas of the skin. The use of FISH facilitates the determination of the origin of the chromosomes involved and the extent of the mosaicism when one is detected.

55.2 Pathology

Some patients with HMI may have major brain abnormalities, including hemimegalencephaly and migrational abnormalities. The pathology of these abnormalities is not reviewed here. The pathological correlate of the white matter abnormalities observed relatively frequently in HMI is deficient myelination and gliosis.

55.3 Pathogenetic Considerations

HMI is a manifestation of etiologically heterogeneous conditions, the common factor being chromosomal or genetic mosaicism. A mosaic is defined as an organism composed of two (or more) genetically different populations of cells originating from a genetically homogeneous zygote. The mosaicism either involves a chromosomal abnormality or a gene mutation. The chromosomal mosaicism includes an array of different abnormalities: diploid/triploid mosaicism, diploid/tetraploid mosaicism, mosaicism for trisomies, unbalanced translocation between autosomes or an autosome and the X chromosome, chro-

mosomal deletions, and ring chromosomes. In the X-chromosome, band Xp11 is involved. HMI due to Xp11 alteration is caused by functional or genetic mosaicism. Functional mosaicism results from the Lyon effect of X inactivation.

Mosaicism can be recognized most easily in the skin, which exhibits patterns of differences in pigmentation following the Blaschko lines. The different degrees of pigmentation of the skin represent different cell populations. The abnormal cell line is confined to the skin with abnormal pigmentation; the normal skin contains almost only normal cells. It has been hypothesized that the genetic and chromosomal abnormalities result in abnormalities of pigmentation because of altered expression of genes in the pigmentary pathway. Such genes may be present in different regions of multiple chromosomes.

55.4 Therapy

No specific treatment is available.

55.5 Magnetic Resonance Imaging

In many patients with HMI, MRI of the brain is normal. Some patients with HMI have major CNS abnormalities, including migrational abnormalities and hemimegalencephaly. The migrational abnormalities may consist of cortical dysplasia or neuronal heterotopias. In hemimegalencephaly, the enlarged hemi-

sphere is dysplastic with a larger ventricle, a thickened, pachygyric or polymicrogyric cortex, and frequently heterotopic neurons in the white matter. Various other abnormalities have been found, including agenesis of the corpus callosum, asymmetrical or symmetrical ventricular dilatation, focal cerebral atrophy with porencephalic ventricular dilatation, hemiatrophy, diffuse cerebral atrophy, cerebellar hypoplasia or atrophy, vascular abnormalities, and, rarely, a tumor.

More subtle brain abnormalities in HMI consist of irregular, multifocal, and confluent abnormalities in the periventricular and deep white matter, usually with increased perivascular spaces within and, to a lesser extent, also outside these areas (Fig. 55.1). In some patients, enlarged perivascular spaces are seen without associated white matter signal abnormalities. The enlarged spaces may also involve the corpus callosum. The increased perivascular spaces are best seen on FLAIR images (Fig. 55.1). The white matter abnormalities are often bilateral but may be asymmetrical in distribution. They are static and probably reflect white matter gliosis and focal myelination defects.

Presence of brain abnormalities in HMI appears to be associated with an enhanced frequency of neurological problems. Major malformations are associated with a major handicap. White matter abnormalities with enlarged perivascular spaces are more commonly seen in patients with a mental handicap, although they have also been observed in HMI patients with a normal cognitive function.

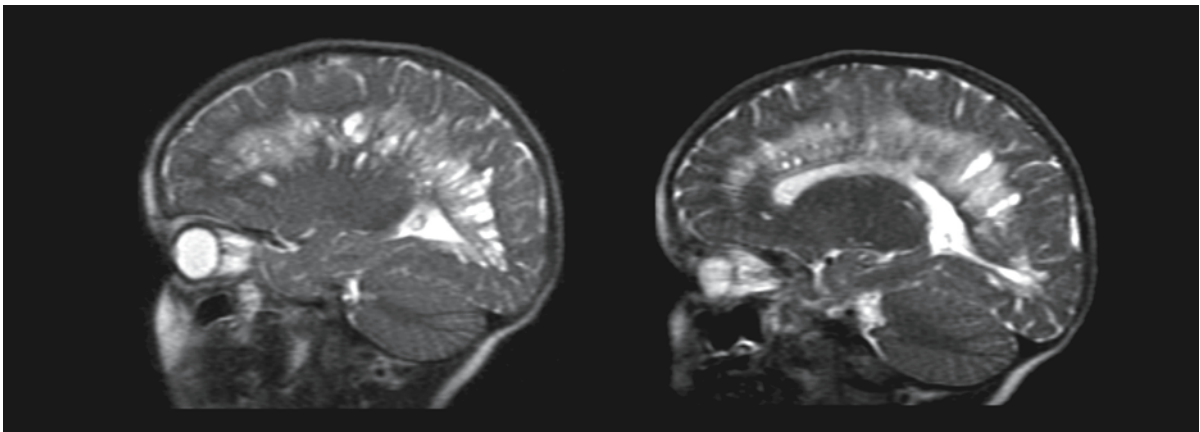


Fig. 55.1. A 5-year-old boy with HMI, mental retardation, and macrocephaly. The sagittal (*first row*) and axial (*second and third row*) T₂-weighted images show extensive, partly multifocal and partly confluent abnormalities in the cerebral white matter. The posterior fossa structures are spared. The FLAIR im-

ages (*fourth and fifth row*) allow distinction between enlarged perivascular spaces with a low signal intensity and gliotic white matter with a high signal intensity. Courtesy of Dr. S. Blaser, Department of Diagnostic Imaging, Hospital for Sick Children, Toronto, Canada

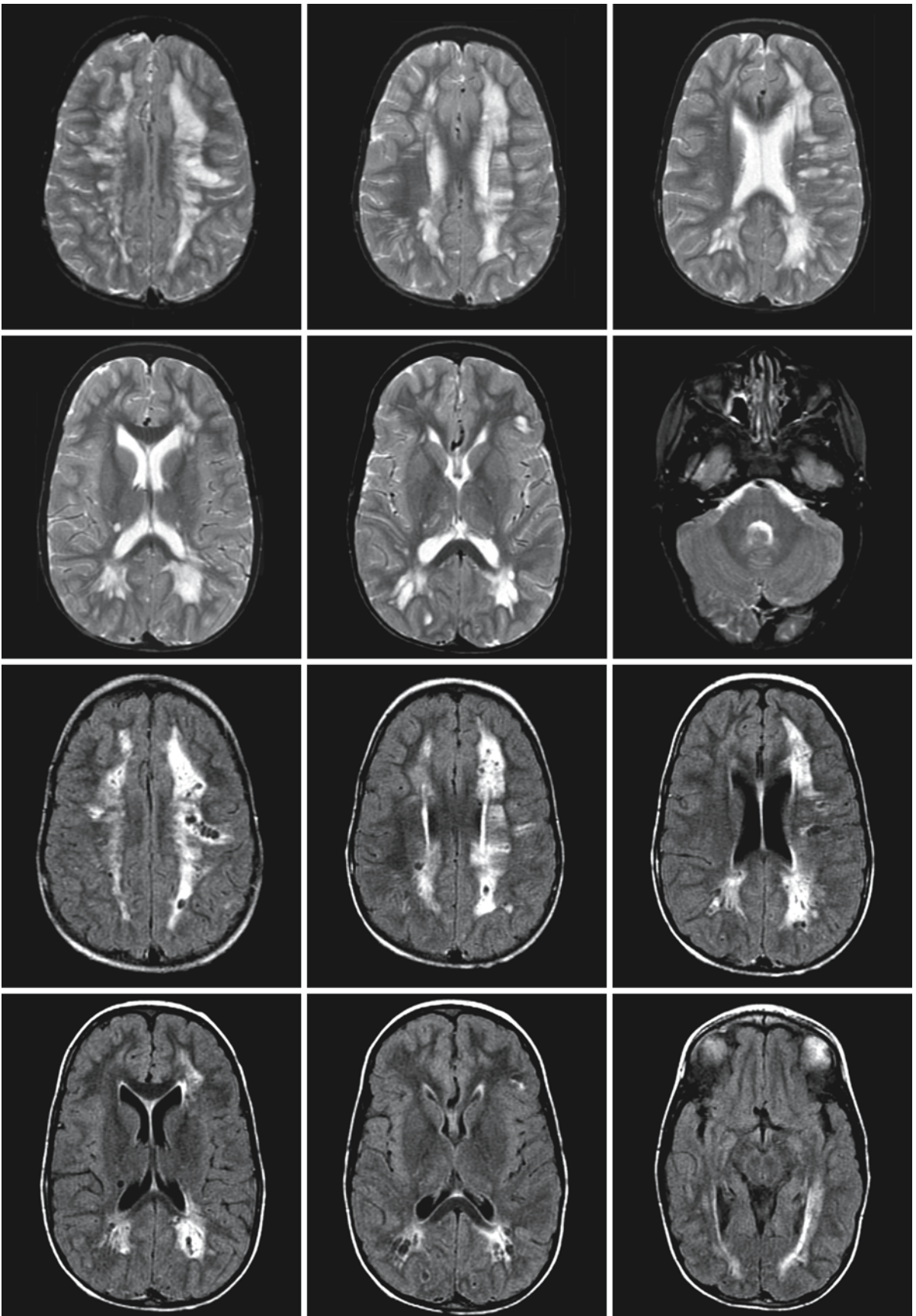


Fig. 55.1. (continued).

Incontinentia Pigmenti

56.1 Clinical Features and Laboratory Investigations

Incontinentia pigmenti (IP), formerly called incontinentia pigmenti type II or Bloch–Sulzberger syndrome, is an X-linked dominant disorder that is usually fatal prenatally in males. Fifty-five percent of the patients have a family history of the disease; the rest of the cases are caused by spontaneous mutations. So-called incontinentia pigmenti type I is unrelated to incontinentia pigmenti type II and is in fact a subtype of hypomelanosis of Ito, associated with an X chromosome/autosome translocation involving band Xp11. It has an X-linked dominant mode of inheritance. In contrast to incontinentia pigmenti type II, the typical neonatal inflammatory skin abnormalities are lacking. Incontinentia pigmenti type I is discussed in Chap. 55.

Affected females display skin abnormalities in four stages: (1) perinatal inflammatory vesicles, (2) verrucous patches, (3) hyperpigmentation, and (4) dermal scarring. In IP the pigmentary disturbance is a sort of self-tattooing. The lesions of the first phase are present at birth or appear within the first 2 weeks of life in 90% of the patients, although they may also appear later in infancy or childhood. They are erythematous, macular, papular, vesicular, and bullous, and suggest an inflammatory condition of the skin. Lesions of the second stage, appearing between 2 weeks and several months of life, are pustular, lichenoid, verrucous, keratotic, and dyskeratotic. The third stage is characterized by development of pigmentation, mainly at the sites of the earlier lesions. In the fully developed disease, the skin shows swirling patterns of melanin pigmentation, especially on the trunk, with a “marble cake” appearance. The pigmentary abnormalities usually disappear by the age of 20 years. The fourth stage is characterized by atrophic scarring. Hypomelanotic macules, most often located over the calves, may be the only dermatological indication of IP in adulthood. Late recurrences of the first-stage inflammatory lesions are uncommon and are usually preceded by an infectious episode.

IP may be associated with a variety of abnormalities of the eyes, teeth, and skeleton. Dystrophy of the nails is frequent but usually mild. Any of the cutaneous stages of IP may involve the scalp. Alopecia secondary to scarring is frequent. Malformed teeth, hypodontia, or adontia may occur. Ocular abnormalities

include cataract, strabismus, retinal pigmentary abnormalities, retinal detachments, infarction, vitreous hemorrhage, microphthalmia, and optic atrophy.

The brain is affected in 30–50% of the patients, causing mental retardation, spasticity (hemiplegia or quadriplegia), cerebellar ataxia, and seizures. The head circumference is usually normal at birth, but patients may develop microcephaly. Some of the patients have signs of serious encephalopathy in the neonatal period, with intractable seizures suggestive of viral encephalitis. Acute-onset stroke has been observed occasionally in infants and children with IP. Patients with structural brain abnormalities and neonatal seizures are at greater risk of motor and mental impairment.

In IP, laboratory studies usually reveal eosinophilia in the blood in the neonatal period. The disease is caused by mutations in the *NEMO* gene, located on chromosome Xq28. Cells expressing the mutated X chromosome are eliminated selectively around the time of birth, so females with IP display extremely skewed X inactivation, which can be demonstrated in peripheral blood leukocytes.

56.2 Pathology

Pathological findings in IP are highly variable and dependent on the stage of the disease. Fresh hemorrhagic necrosis within the cerebral white matter with perivenous and capillary hemorrhage, vascular congestion, edema, and inflammation surrounding the hemorrhage is seen in the early stages. The gray matter may also be affected, but usually to a lesser extent. In the more chronic stages, ulegyria, cystic changes in the cerebral white matter, neuronal loss, and gliosis are found.

56.3 Pathogenetic Considerations

Mutations in the gene *NEMO*, located on chromosome Xq28, cause IP. IP is allelic with ectodermal dysplasia, an- or hypohidrosis, and immunodeficiency, a disease caused by different mutations in the same gene. *NEMO* stands for nuclear factor (NF)- κ -B essential modulator. The gene is also called *IKBKG*, which stands for inhibitor of κ (kappa) light polypeptide gene enhancer in B cells, kinase of, gamma (γ). *NEMO*

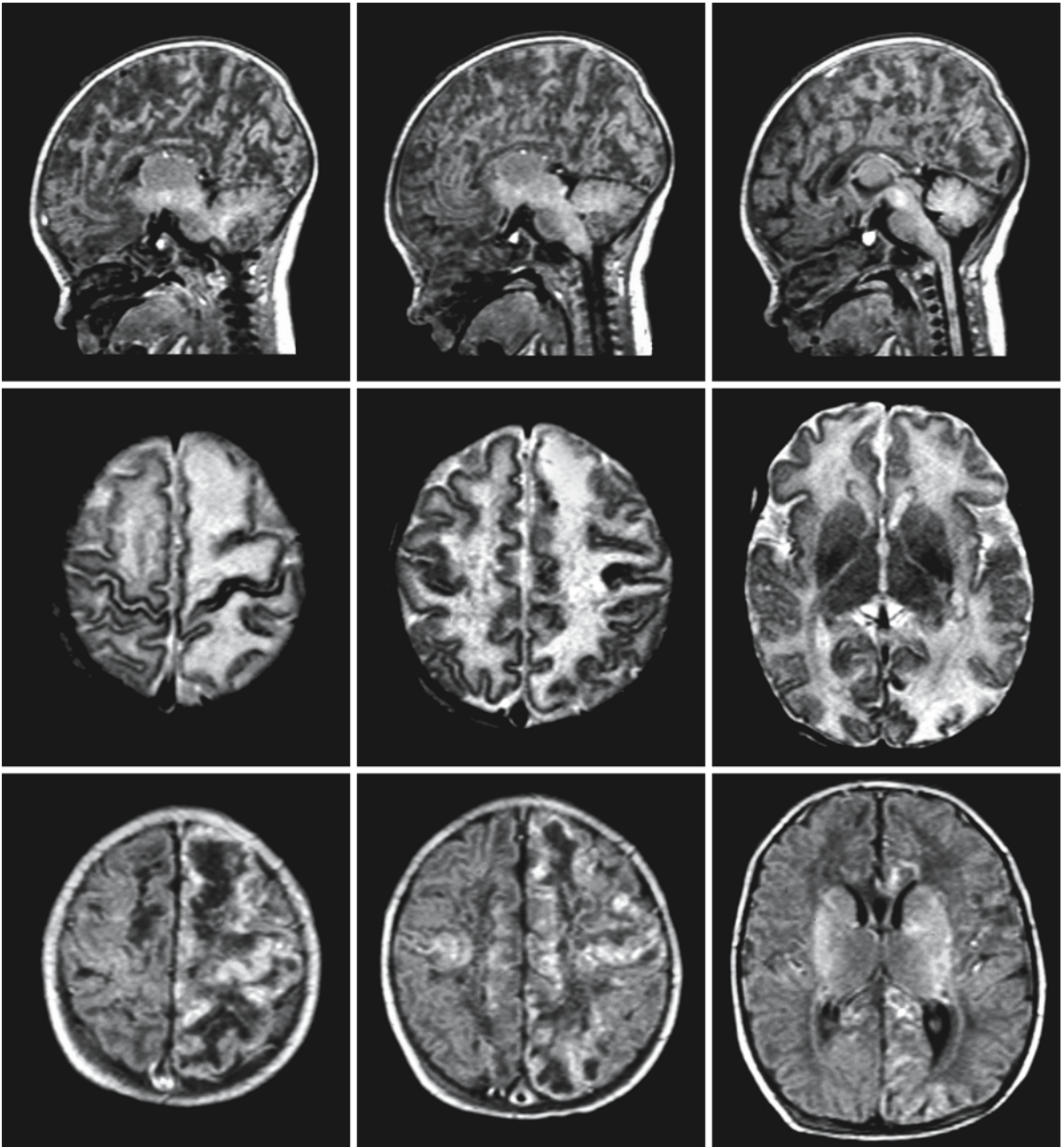


Fig. 56.1. Female neonate, 3 days old, with IP. She has signs of a devastating encephalopathy and vesicular skin lesions. Note the extensive damage to large parts of the cerebral white matter and cortex, more seriously on the left than on the right. The lesions have a swollen aspect. The high signal on the

T₁-weighted images (*third row*) indicates hemorrhagic necrosis. Courtesy of Dr. N. Wolf, Department of Pediatric Neurology, and Dr. A. Seitz, Department of Neuroradiology, University Hospital Heidelberg, Germany

is essential for NF- κ -B activation. Activated NF- κ -B normally protects against tumor necrosis factor alpha (TNF- α)-induced apoptosis.

The most common mutation in IP is a genomic rearrangement resulting in a large deletion within the *NEMO* gene. This rearrangement, which occurs dur-

ing paternal meiosis, is responsible for 80% of the new mutations. This mutation results in a lack of NF- κ -B activation, which leads to an extreme susceptibility to proapoptotic signals, leading to embryonic death in males and extremely skewed X inactivation in females with IP. The remaining mutations are small

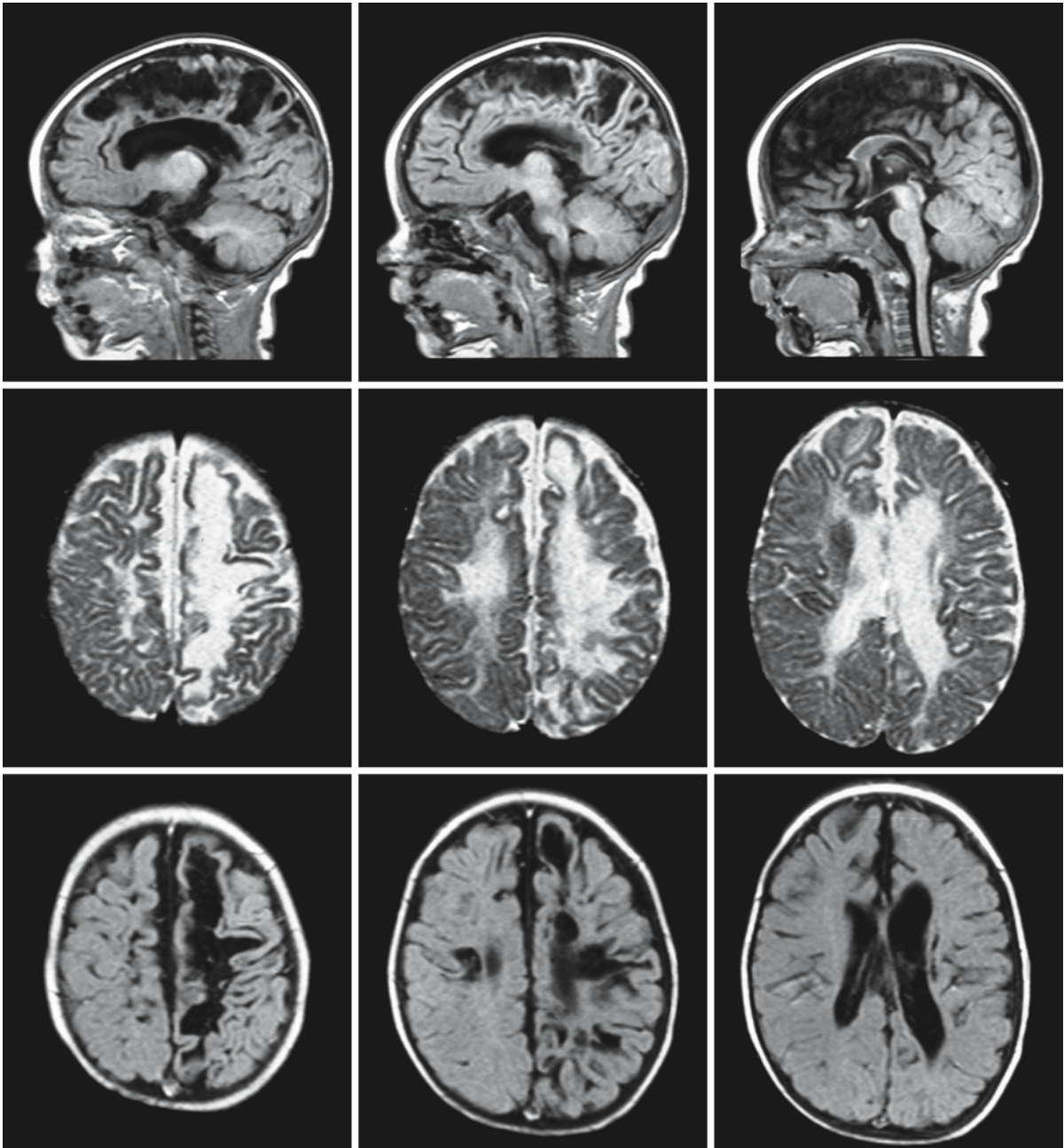


Fig. 56.2. Follow-up MRI of the girl shown in Fig. 56.1. She is now 5 months old. There is a serious cystic degeneration of the deep and subcortical cerebral white matter, more prominently on the left than on the right. The overlying cortex is also

involved. Courtesy of Dr. N. Wolf, Department of Pediatric Neurology, and Dr. A. Seitz, Department of Neuroradiology, University Hospital Heidelberg, Germany

duplications, substitutions, and deletions. In surviving males with IP, somatic mosaicism or a 47,XXY karyotype with skewed X inactivation has been found.

The evolution of the lesions in females can be interpreted as representing death of cells that have the mutant-bearing X chromosome as the active one and

their replacement by cells in which the normal X chromosome is active. This leads to extremely skewed X inactivation patterns in females, which save them from the lethal effect of the mutation. Other interpretations suggest a vasculopathy as the major pathogenetic mechanism for ophthalmological and brain damage.

56.4 Therapy

No specific treatment is available.

56.5 Magnetic Resonance Imaging

In IP, the MRI findings are highly variable. In neonates with signs of active encephalopathy, MRI shows variably extensive areas of hemorrhagic cortex and white matter necrosis and edema suggestive of encephalitis, in particular herpes encephalitis (Fig. 56.1). Cystic degeneration may follow (Fig. 56.2). In some patients the lesions are small, whereas in other patients the abnormalities involve most of one or both cerebral hemispheres. In the chronic stage, signs

of gliotic scar tissue, focal atrophy, and secondary cortical dysplasia in the form of ulegyria are common (Fig. 56.3). The scar tissue may be unilateral or bilateral, symmetrical or asymmetrical. The lesions usually involve both cortex and white matter of the cerebral hemispheres, but the most severe lesions are usually seen in the deep white matter. The lesions may also be similar to those seen in periventricular leukomalacia with mild, symmetrical or asymmetrical dilatation of the lateral ventricles due to loss of white matter volume, periventricular white matter signal abnormalities, and disfiguration of the lateral ventricles due to the gliotic scarring (Fig. 56.3). The corpus callosum is thin. Lesions may also be seen in the cerebellum. Developmental cerebral anomalies may also be present, including polymicrogyria and neuronal heterotopias.

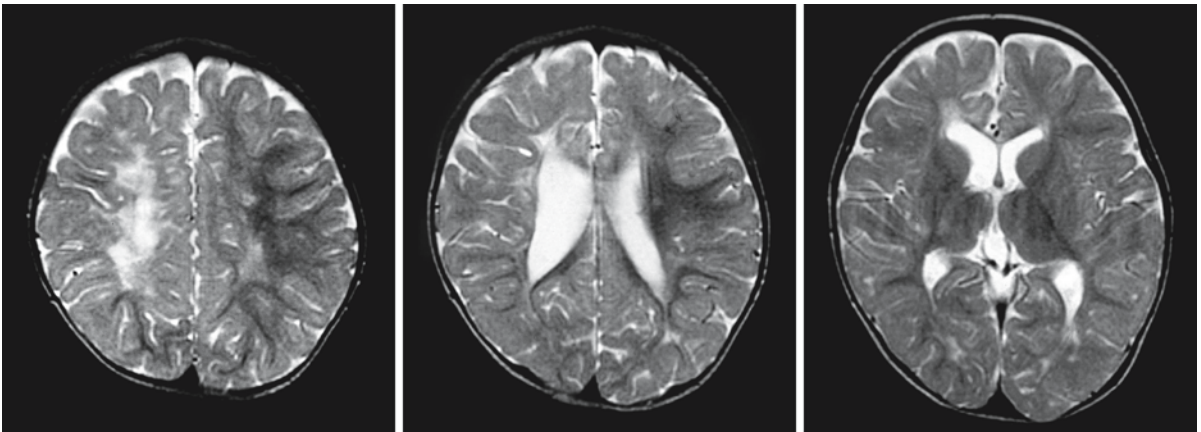


Fig. 56.3. A 13-month-old girl with IP. Note the extensive damage to the white matter of the right cerebral hemisphere. The white matter damage on the left is much milder. The lateral ventricles are dilated, more so on the right than on the left.

There is retraction of the cortex on the right, which is folded with deep narrow sulci (ulegyria). Courtesy of Dr. W.J. Feikema, Department of Neurology, Deventer Ziekenhuis, Deventer, The Netherlands

Alexander Disease

57.1 Clinical Features and Laboratory Investigations

Alexander disease (AD) is a rare disorder of the CNS. Almost all cases are sporadic, but there are occasional familial cases with an apparent autosomal dominant mode of inheritance. Three clinical subgroups of AD can be distinguished: infantile, juvenile, and adult.

In infantile AD, the onset of symptoms varies from birth to early childhood. The average age at onset is 6 months. There is increasing macrocephaly together with feeding problems, difficulty swallowing, choking, vomiting, failure to thrive, and signs of neurological deterioration. Slowing down of motor and mental development, loss of acquired developmental milestones, spastic quadriplegia, and seizures are usually present. Chorea-athetosis and other extrapyramidal signs may occur. In some patients there are clinical signs of elevated intracranial pressure with bulging fontanel, vomiting, and papilledema at funduscopy. Usually funduscopic findings are normal. Nystagmus and eye movement abnormalities may occur. The children may develop apneic attacks or chronic hypoventilation. The average duration of the illness is 2–3 years, ranging from a few months to 8 years.

In juvenile AD, the age at onset of clear symptoms varies from 4 to 14 years, with an average age of 9 years. However, in retrospect subtle signs of neurological problems have usually been observed since before the age of 2 years, mainly some developmental delay or seizures. Many of the patients have macrocephaly, but this is a less consistent finding than in infantile AD. The patients suffer from progressive bulbar and pseudobulbar symptoms, with delayed speech development, dysarthria, hoarseness, loss of speech, increasing swallowing problems, and apneic attacks. Many patients have bouts of vomiting, especially during morning hours. The swallowing problems and vomiting often lead to insufficient gain in weight, finally necessitating tube feeding. Spasticity, cerebellar ataxia, seizures, behavioral changes, and cognitive deterioration develop. The average duration of illness is 8 years.

In adult AD, the onset of symptoms is highly variable, occurring between the second and seventh decades. Some of the cases are familial, with an affected parent and one or more affected children. The clinical features reported are highly variable. In some pa-

tients the clinical course is episodic and progressive, as in multiple sclerosis. A chronic progressive course with bulbar and pseudobulbar symptoms, spasticity, cerebellar ataxia, and dementia has been reported. Nystagmus and other abnormalities in eye movements may occur. Some patients only have bulbar signs. Palatal myoclonus may present. Sometimes the disease remains asymptomatic and Rosenthal fibers are found at brain autopsy. Macrocephaly is not a sign of the disease in adults.

Laboratory investigations are not helpful in establishing the diagnosis of AD. CSF is normal or shows a nonspecific increase in protein level. The CSF α B-crystallin level may be elevated, as may be the CSF level of heat shock protein 27 (HSP27), but the sensitivity and specificity of these tests have not been assessed. High-voltage slow-wave activity and focal discharges are recorded on the EEG in most cases, with predominance of abnormalities over the frontal area. A brain biopsy or autopsy revealing the characteristic Rosenthal fibers used to be considered a prerequisite for a definite diagnosis. However, DNA-based diagnosis is now possible. Sporadic patients are heterozygous for a mutation in the *GFAP* gene which is de novo and not found in one of the parents. In familial cases, affected family members are heterozygous for a mutation in the gene, the disease being transmitted in an autosomal dominant fashion.

57.2 Pathology

In infantile and juvenile AD the brain is abnormally enlarged. External examination may reveal macrogyria. Olfactory bulbs and optic nerves are sometimes enlarged. In many patients the lateral ventricles are widened, either because of hydrocephalus or because of atrophy and tissue loss. Hydrocephalus, if present, is caused by narrowing of the aqueduct. Occasional cases have been reported with a greatly expanded cavum septi pellucidi, bulging into the lateral ventricles and compressing the foramina of Monro. Subependymal cysts may be seen beneath the inferior surfaces of both frontal horns. Thalami, basal ganglia, cerebellum, and brain stem may be atrophic on inspection.

On microscopic examination the most distinctive feature of AD is the presence of countless Rosenthal fibers throughout the CNS. Rosenthal fibers are irreg-

ularly shaped, elongated or round hyaline eosinophilic bodies up to 50 μm in length with a diameter of 1–25 μm . They are arranged radially around blood vessels and perpendicularly to the surface of the cerebral hemispheres, brain stem, cerebellum, and spinal cord in the subependymal and subpial regions. In addition, they are scattered throughout the white matter in all areas of the CNS. Rosenthal fibers are most prominent in the deep frontal white matter, the cerebral cortex, the periventricular region, the basal ganglia, thalami, and brain stem. Deposition of Rosenthal fibers in the cerebellum is variable, being sparse in some cases but prominent in others, involving the cerebellar white matter, dentate nucleus, or, rarely, the subpial layers of the cerebellar cortex. The fornix and optic nerves, chiasm, and tracts may contain many Rosenthal fibers. The peripheral or schwannian parts of the cranial nerves are always free of Rosenthal fibers, whereas the intraparenchymal root bundles may contain heavy deposits. The neurons of the cortex and basal ganglia are usually relatively well preserved regardless of the degree of Rosenthal fiber deposition, but there may also be a serious loss of neurons in the frontal cortex and deep gray matter structures. In the brain stem the subependymal accumulation of Rosenthal fibers may lead to narrowing of the lumen of the aqueduct, resulting in hydrocephalus.

Throughout the CNS there are accumulations of hypertrophic fibrillary astrocytes, most marked in the subpial, subependymal, and periventricular regions. Their distribution corresponds to the greatest concentration of Rosenthal fibers. The astrocytes are often large and may contain bizarre nuclei. They have large amounts of cytoplasm and, in their perikaryon, hyaline droplets which show the staining characteristics of Rosenthal fibers. On electron microscopy it is evident that the Rosenthal fibers are abundant in astrocytic processes and are present in smaller amounts in the astrocytic perikarya. On electron microscopy Rosenthal fibers appear as irregular, electron-dense, osmiophilic, granular deposits closely associated with intermediate glial filaments. The granular deposits are non-membrane-bound.

Another distinctive histological feature is paucity of myelin. The lack of myelin sheaths is generally most pronounced in the frontal white matter, temporal white matter, centrum semiovale, tegmentum of the brain stem, and ventral and lateral columns of the spinal cord. As a rule the frontal white matter is the most severely involved. There is little or no sparing of the arcuate fibers. The internal capsule, parieto-occipital white matter, and cerebellum are relatively better myelinated. However, in some cases the cerebellar white matter is also extensively involved. The brain stem involvement may be plaque-like with focal or multifocal areas of myelin paucity. In the areas of

myelin paucity most axons are intact. The affected white matter is markedly cellular due to abundance of abnormal, hypertrophied astrocytes. No inflammatory reaction is present. Oligodendroglia do not show any pathological changes, but may be reduced in number. Cavitation occurs relatively frequently in AD, is usually present in the deep white matter of the frontal lobes, and is sometimes seen in the parietal lobes adjacent to the lateral ventricles and the hilus of the dentate nucleus. In the end stage, the white matter may be severely reduced in volume.

In most cases there is a lack of myelin and at the same time a scarcity of sudanophilic material. Some authors suggest that the absence of typical features of active breakdown of myelin sheaths points to disturbed myelination rather than demyelination. However, in other cases the presence of sudanophilia and macrophages accumulating neutral fat have been reported. Possibly, myelin paucity can be explained by a variable combination of disturbed myelination and demyelination, disturbed myelination being most pronounced in the patients with early onset of disease.

In adult cases, more rarely in juvenile cases, and in exceptional infantile cases, the abnormalities may be much more limited. Usually, brain stem, cerebellar, and spinal cord abnormalities dominate, with Rosenthal fiber deposits and numerous hypertrophied astrocytes in subpial, subependymal, and perivascular regions. Myelin paucity may be present in the affected areas, but myelin density may also be normal. There may be focal, tumor-like lesions with mass effect. There may also be a striking atrophy of the lower brain stem and the upper part of the spinal cord. Microscopy of the lesions may demonstrate proliferated astrocytes with considerable pleomorphism of the nuclei and occasionally multiple nuclei, resembling an astrocytoma. The Rosenthal fiber deposition may also be more widespread throughout the CNS. Likewise, there may be more extensive white matter abnormalities, predominantly involving the frontal and parietal white matter. The white matter involvement may be patchy and multifocal or diffuse. Cavitations have been reported in the frontal white matter, but also in the brain stem, hilus of the dentate nucleus, and spinal cord.

57.3 Chemical Pathology

Chemical analysis of brain tissue in AD reveals signs of immature myelin with a relatively high content of glucolipids instead of galactolipids and with a relatively low cerebroside content. All myelin constituents are present in a lower than normal concentration as a consequence of the myelin paucity. Cholesterol esters are not elevated.

Rosenthal fibers consist of two components: bundles of intermediate filaments, and aggregates of dense material on the filaments. Biochemically, the major proteins of the aggregates are α B-crystallin and HSP27. A fraction of α B-crystallin is ubiquitinated. The filaments contain glial fibrillary acidic protein (GFAP) and vimentin. GFAP is also found in the granular aggregates.

57.4 Pathogenetic Considerations

AD is caused by mutations in the gene *GFAP*, which encodes GFAP and is located on chromosome 17q21. The disease has an autosomal dominant inheritance and almost all patients have a *de novo* mutation, i.e., which is not found in one of the parents. Familial cases are mainly seen in adult AD, where patients may have offspring. So far, only missense mutations have been found. It is most likely that the mutations observed in AD act in a gain-of-function fashion. *GFAP*-null mice have a subtle phenotype which does not resemble AD. On the other hand, transgenic mice with overexpression of human GFAP have a fatal encephalopathy that closely resembles AD. Astrocytes of these mice are hypertrophic and contain inclusion bodies that are histologically and antigenically identical to Rosenthal fibers. It is not yet known whether defects in other genes may be responsible for some cases of AD.

GFAP is an intermediate filament protein that is expressed almost exclusively in astrocytes of the CNS. Intermediate filaments are intermediate-sized fibrous cytoskeletal polymers, which together with smaller actin microfilaments and larger microtubules form the structural framework of the cytoplasm of all eukaryotic cells. GFAP is the major intermediate filament protein of astrocytes. It appears to play a role in the outgrowth of processes of astrocytes. A marked increase in GFAP is part of the complex changes seen in astrocytes after most types of CNS injury. Absence of GFAP leads to surprisingly few change in the unchallenged CNS, but if damage occurs, it is more severe in the absence of GFAP. For instance, experimental allergic encephalitis is more severe in *GFAP* knock-out mice. On the other hand, accumulation of GFAP in astrocytes apparently leads to a stress response that induces the small stress proteins α B-crystallin and HSP27 and leads to the generation of Rosenthal fibers.

Rosenthal fibers are inclusion bodies composed of intermediate filaments and the small stress proteins α B-crystallin and HSP27. α B-Crystallin and HSP27 are both members of the so-called small heat shock protein family. They are normally present in the brain in small amounts and are water-soluble. The expression of these proteins is enhanced by various stress

conditions. They accumulate in reactive and neoplastic astrocytes, and this accumulation is associated with translocation of the proteins from the soluble fraction to the insoluble or cytoskeleton-related fraction. In the Rosenthal fibers, α B-crystallin and HSP27 are present as insoluble aggregates bound to intermediate glial filaments. The association of α B-crystallin and HSP27 with intermediate filaments is probably critical in the formation of Rosenthal fibers. Ubiquitin is another component of the Rosenthal fibers. Rosenthal fibers contain mono- and polyubiquitinated conjugates of α B-crystallin. Conjugation with ubiquitin is the first step in a series of reactions that leads to intracellular nonlysosomal degradation of proteins. However, apparently stable ubiquitin conjugates can also be formed, suggesting that proteolysis is not the only function of ubiquitin conjugation. Ubiquitin is present in various abnormal filamentous neuronal inclusions, such as the neurofibrillary tangles of Alzheimer disease, Lewy bodies in Parkinson disease, and Pick bodies in Pick disease. The presence of ubiquitin in these inclusions may represent an abortive or only partially successful attempt to degrade proteins that accumulate in the abnormal states mentioned.

The formation of Rosenthal fibers is in itself a non-specific process. Rosenthal fibers accumulate in glial scar tissue and glial tumors, both of which are conditions characterized by genesis of intermediate filaments. They have been reported as a focal phenomenon in different types of glial tumors, multiple sclerosis, encephalomalacia, and syringomyelia. More widespread formation has been described in diffuse gliomatosis, central pontine and extrapontine myelinolysis, vincristine therapy, radiation therapy, and chronic inflammatory processes. Rosenthal fiber formation appears to reflect chronic pathological processes affecting astrocytes.

There is evidence that myelin paucity is explained at least in part by disturbed myelination. In truly demyelinating disorders, a macro- and microglial reaction of variable intensity is always found with evidence of phagocytic activity and presence of products of myelin breakdown. In AD, no phagocytic transformation of macroglia and microglia is seen, despite a conspicuous absence of myelin sheaths. There is a lack of histological and histochemical evidence for the presence of lipid products of myelin breakdown. There is chemical evidence of a disturbance of myelin maturation. To stress the differences between AD and the regular "myelinoclastic leukodystrophies," the disease has been called a "dysmyelinogenic leukodystrophy."

The nature of the relationship between astrocytic abnormalities and myelin paucity, whether due to disturbed myelination, demyelination, or both, is unknown. Astrocytes have multiple important func-

tions. They provide structural support within the nervous system, and they play a central role in regenerative repair. Astrocytic foot processes provide physical and electrical insulation for synapses. They have an important role in potassium distribution, preventing the accumulation of potassium in the extracellular space during neuronal activity. They are involved in the metabolism of various neurotransmitters, and probably have a reservoir function for nutrients. Astrocytes and their interaction with oligodendrocytes are a prerequisite for oligodendrocyte differentiation and survival and for the deposition and maintenance of myelin sheaths. There are gap junctions between astrocytes and oligodendrocytes, which provide a means of interaction. Astrocytes are the “third factor,” allowing oligodendrocytes to myelinate axons and to maintain the myelin sheaths already deposited around axons. These data indicate that astrocytic dysfunction in the immature brain of infants, in which myelin is still to be laid down, may have an adverse effect on the process of myelination and myelin maturation, resulting in disturbed myelination and hypomyelination. In older patients astrocytic dysfunction may lead to disturbance of myelin maintenance, resulting in demyelination. The reason why certain astrocyte populations are more involved than others is not clear.

The megalencephaly in AD is caused by a combination of astrocytic hyperplasia and massive deposition of Rosenthal fibers. The subsequent atrophy and cyst formation would be secondary to progressive astrocytic cell death in association with loss of other nervous tissue components. In neuroimaging the contrast enhancement is seen mainly in the frontal white matter, periventricular rim, basal ganglia, thalamus, hypothalamus, and brain stem, which are the areas with the highest Rosenthal fiber density. The contrast enhancement is probably caused by a defect in the blood–brain barrier related to impaired function to astrocytic foot plates. The Rosenthal fibers are particularly present in astrocytic cell processes and foot plates, and these foot plates form an integral part of the blood–brain barrier.

The topography of the pathological changes correlates with the clinical features. The frontal predominance of the white matter abnormalities correlates with the frequently observed behavioral problems. Most patients have epilepsy, which correlates with cortical involvement. Bulbar signs are prominent in AD patients, whereas brain stem involvement is almost invariably found in pathology and imaging. It is, however, important to note that in juvenile and adult AD the complete typical imaging picture is already present on early MRI studies obtained during the stage of minimal neurological dysfunction, and that the onset of neurological deterioration may be delayed for many years. Spasticity and ataxia occur usu-

ally relatively late, in the stage of cystic degeneration and atrophy of the white matter.

57.5 Therapy

Treatment is entirely supportive. No causal therapy is available.

57.6 Magnetic Resonance Imaging

In infantile AD, CT discloses bilateral, usually symmetrical, moderately well-demarcated areas of reduced density in the frontal lobes with extensions to the temporal and parietal lobes and the external and extreme capsules. The anterior limb of the internal capsule may be involved. The subcortical arcuate fibers are involved in the process. Temporarily, the white matter abnormalities may show mass effect with compression of the ventricles. A mild to moderate enlargement of the lateral and third ventricles ensues, caused either by atrophy or by hydrocephalus due to aqueduct stenosis. In all reported cases, the frontal white matter abnormalities are the most severe, and occipital white matter and cerebellum are completely or relatively spared. However, cerebellar white matter may also become extensively involved. In many cases a rim of normal or increased density is seen in the subependymal region, including frontal periventricular white matter, caudate nucleus, thalamus, hypothalamus, fornix, and the occipital periventricular white matter (Fig. 57.1). In some cases increased density has also been reported in the subpial cortical layers with a more patchy appearance. Contrast enhancement is seen in the areas of increased density (Fig. 57.1). Contrast enhancement has also been reported in the dorsal part of the brain stem. However, some patients show no contrast enhancement, probably depending on the time of examination, because the higher-density enhancing regions decrease as the disease progresses. The course of the disease is characterized by volume loss. Cysts arise in the white matter, especially the frontal white matter, and atrophy ensues. The extent of the white matter abnormalities may increase, but the increase is usually not very prominent. Contrast enhancement is usually absent in late stages of the disease.

In juvenile AD, CT findings include frontal white matter hypodensity. Areas of increased density and contrast enhancement are less prominent than in infantile AD. Over time, white matter atrophy occurs and cysts may form.

In adult AD CT abnormalities limited to the cerebellar white matter and brain stem have been reported. The lesions may be space-occupying.

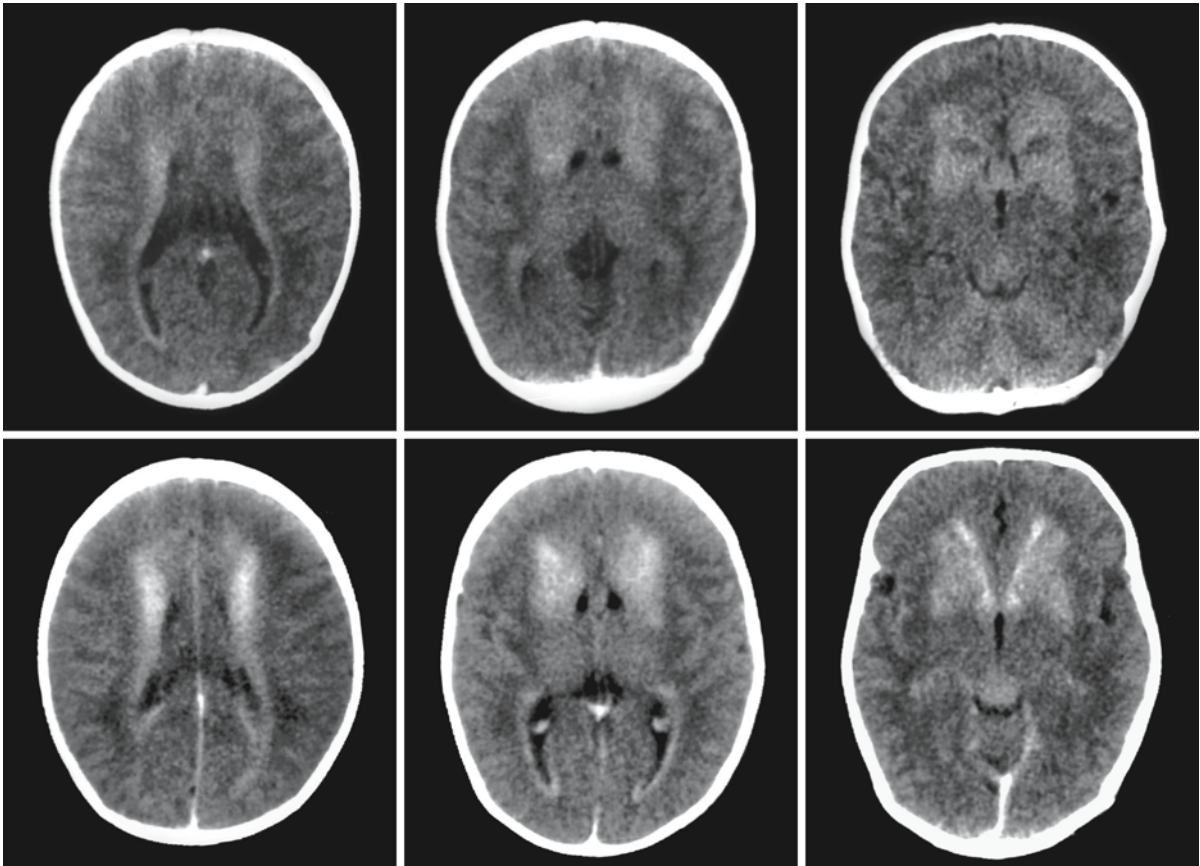


Fig. 57.1. A CT scan without (*first row*) and with contrast (*second row*) in a 4-week-old baby boy with infantile AD. Note the increased density in the frontal white matter, a periventricular rim, and part of the basal ganglia on the images without con-

trast. The same areas enhance with contrast. Courtesy of Dr. S. Blaser, Department of Diagnostic Imaging, Hospital for Sick Children, Toronto, Canada

In infantile AD, MRI shows abnormal signal intensity of the white matter in a symmetrical distribution with frontal predominance (Figs. 57.2–57.4). The abnormal white matter has usually a swollen aspect, with broadening of gyri and stretching of the overlying cortex (Fig. 57.4). However, in infantile cases it may be difficult or impossible to distinguish abnormal white matter from unmyelinated white matter and the frontal predominance may be evident only in the degree of hyperintensity on T_2 -weighted images or degree of hypointensity on T_1 -weighted images and the swelling (Figs. 57.2 and 57.3). In some infants there is no evident frontal predominance of white matter abnormalities. There is a characteristic periventricular rim of low signal intensity on T_2 -weighted images and high signal intensity on T_1 -weighted images (Figs. 57.2–57.4). There are usually prominent signal abnormalities and swelling of the caudate nucleus, other basal ganglia, and thalamus (Figs. 57.2 and 57.3). These structures may have a high signal on T_1 -weighted images (Figs. 57.3 and

57.4). In addition, there are usually lesions in the brain stem, most often involving the mid brain and the medulla (Figs. 57.2–57.4). The hilus of the dentate nucleus may have an abnormal signal. The fornix and optic nerves and chiasm may be thickened (Figs. 57.2 and 57.3). Contrast enhancement is often prominent and involves the frontal white matter, ependymal lining of the ventricles, the periventricular rim, the basal ganglia, thalamus, dentate nucleus, brain stem lesions, fornix, and optic chiasm in variable combinations (Figs. 57.2, 57.4, 57.5 and 57.7). The frontal cortex may also show contrast enhancement (Fig. 57.4). Special features may be hydrocephalus due to aqueduct stenosis and major enlargements of a cavum septi pellucidi and cavum Vergae (Fig. 57.6). Subependymal cysts may be seen at the level of the head of the caudate nucleus. Over time, cavitation of the frontal white matter may occur and may become prominent (Fig. 57.4). Atrophy of the affected white matter, basal ganglia, thalamus, brain stem, and cerebellum occur (Fig. 57.4).

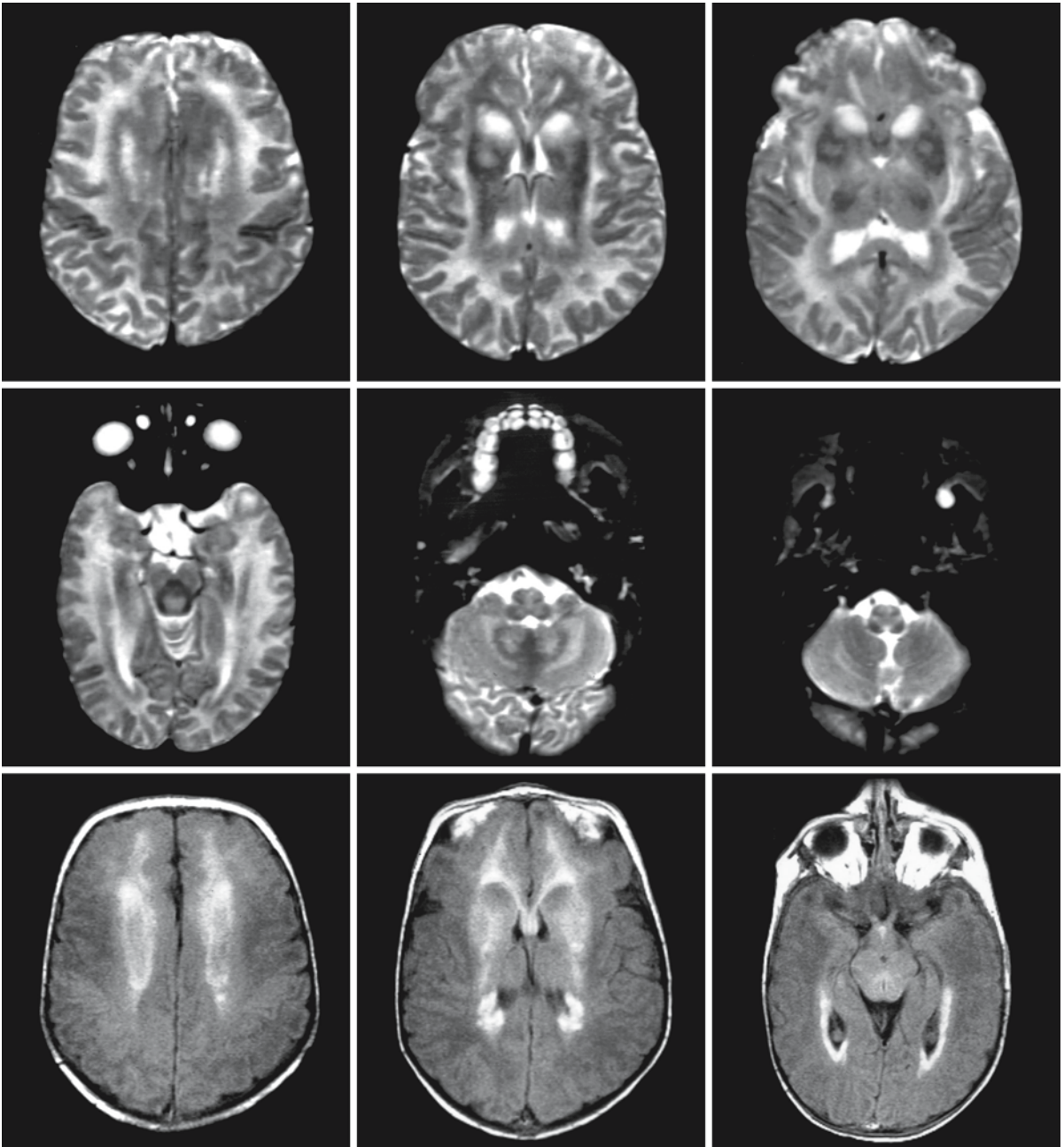


Fig. 57.2. MRI in the same boy as in Fig. 57.1, a few days later. The frontal white matter has at most a slightly abnormal signal intensity on the T_2 -weighted images; its signal intensity is close to normal for unmyelinated white matter. There is a periventricular rim of low signal intensity on the T_2 -weighted images, most prominent in the frontal region. The head of the caudate nucleus is highly swollen and abnormal in signal. The

fornix is thickened. The midbrain and medulla contain areas of abnormal signal. After contrast (*third row*), the T_1 -weighted images demonstrate enhancement of the periventricular rim, frontal white matter, fornix, basal ganglia, and a central area in the thickened optic chiasm. Courtesy of Dr. S. Blaser, Department of Diagnostic Imaging, Hospital for Sick Children, Toronto, Canada

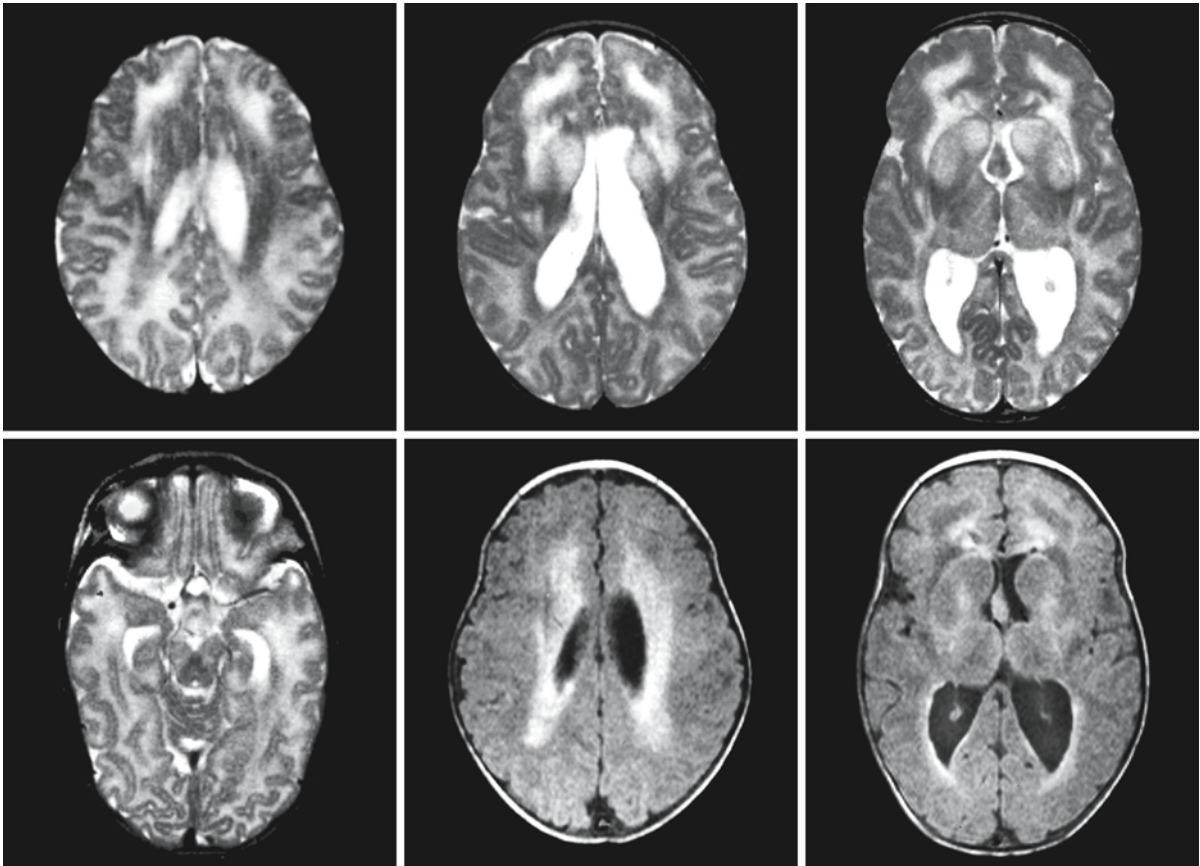


Fig. 57.3. MRI in a 7-week-old baby girl with infantile AD. The frontal white matter has a higher signal intensity than normal for unmyelinated white matter on the T₂-weighted images. There is a rim of low signal on the T₂-weighted images and high signal on the T₁-weighted images without contrast, extending into the frontal white matter. The caudate nucleus and

putamen have an abnormal signal intensity and are swollen. The thalamus and large parts of the midbrain have an abnormal signal. The fornix is thickened. From van der Knaap et al. (2001), with permission; additional images courtesy of Dr. S. Springer, Department of Pediatrics, Ludwig Maximilian University, Munich, Germany

In juvenile AD, there is a frontal predominance of the white matter abnormalities (Figs. 57.8–57.10). The occipital and temporal white matter may be largely spared, but in some patients only a thin rim of occipital arcuate fibers is spared. The abnormal frontal white matter is usually involved throughout and mildly swollen with some broadening of the gyri. However, in some patients the white matter changes are restricted to the frontal periventricular region and there is no evident swelling of the abnormal white matter. There is a rim of low signal intensity on T₂-weighted images and high signal intensity on T₁-weighted images (Figs. 57.8–57.11). The rim is often thin and discontinuous (Figs. 57.8–57.11). There are almost invariably some signal changes in the basal ganglia and thalamus, with some swelling (Figs. 57.8, 57.10 and 57.11). These structures may have a high signal on T₁-weighted images (Figs. 57.10 and 57.11). Very characteristic are the brain stem lesions, most

often seen in the midbrain (in the anterior part, the periaqueductal region, or the entire area except for the red nuclei and the colliculi) and the medulla (either in the central or the posterior part) (Fig. 57.9). The pontine tegmentum may be involved as well. Contrast enhancement may involve the frontal white matter, ependymal lining of the ventricles, the periventricular rim, the basal ganglia, thalamus, dentate nucleus, cerebellar cortex, brain stem lesions, and intraparenchymal trajectories of cranial nerves in variable combinations, but the enhancement is as a rule much more subtle than in infantile AD (Figs. 57.9 and 57.10). Over time cavitation of the frontal white matter may occur (Figs. 57.10 and 57.12). The cysts may become very large (Fig. 57.12), but in some patients cysts are never seen. Invariably atrophy occurs of the affected white matter, the basal ganglia, and the thalamus. The atrophic basal ganglia and thalamus have a high, normal, or low signal on T₂-weighted

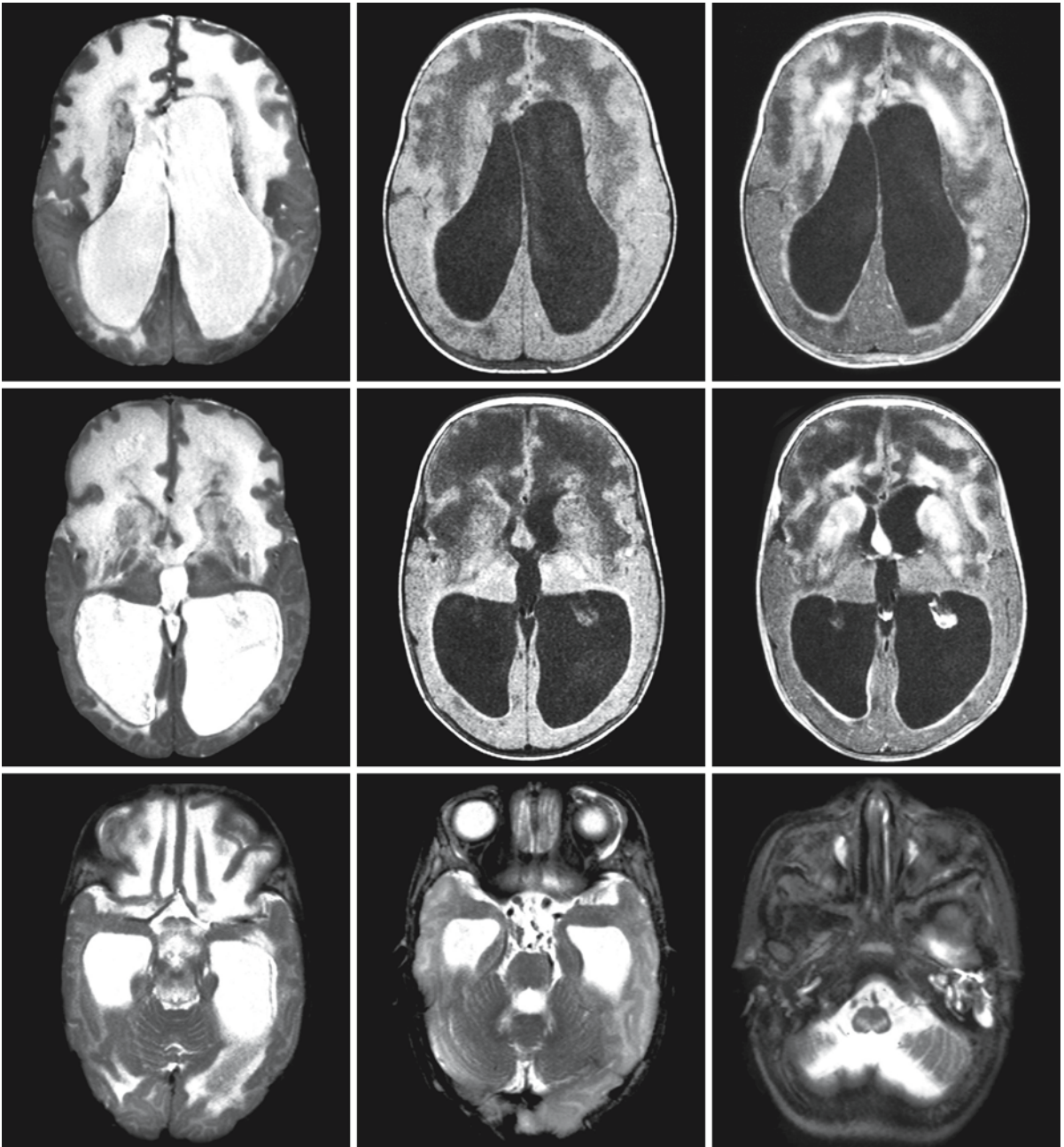


Fig. 57.4. The same girl as in Fig 57.3, now 3 months old. The *first and second rows* show the T_2 -weighted images (*left*), T_1 -weighted images without contrast (*middle*) and with contrast (*right*). The *third row* shows T_2 -weighted images at lower levels. The frontal white matter now displays much more prominent signal abnormalities and has a swollen appearance. There are small cysts in the frontal white matter. The lateral ventricles have become much wider, probably due to a combination of white matter volume loss and hydrocephalus caused by aqueduct stenosis. The basal ganglia are atrophic and have an ab-

normal signal. There is a thin periventricular rim of low signal on T_2 -weighted images and high signal on T_1 -weighted images, which enhances after contrast. Parts of the basal ganglia, frontal white matter and frontal cortex also enhance after contrast. The fornix is thickened and enhances after contrast. The midbrain, hilus of the dentate nucleus, and medulla contain areas of abnormal signal. From van der Knaap et al. (2001), with permission; additional images courtesy of Dr. S. Springer, Department of Pediatrics, Ludwig Maximilian University, Munich, Germany

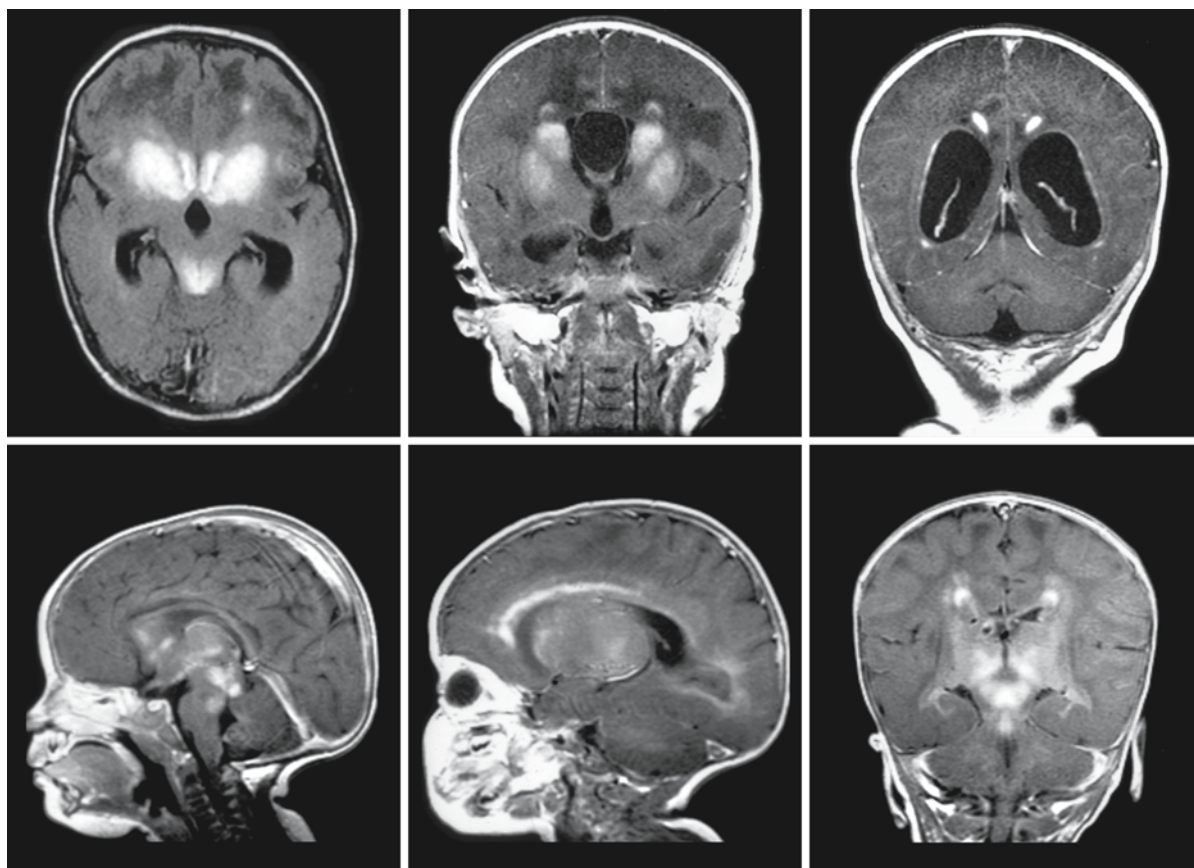


Fig. 57.5. T₁-weighted images with contrast in a 3-month-old girl (*first row*) and 6-month-old girl (*second row*) with infantile AD. The images of the *first row* show contrast enhancement of spots in the frontal white matter, the basal ganglia, thickened fornix, dorsal part of the midbrain, and ependymal lining.

There is cystic enlargement of the cavum septi pellucidi. The images of the *second row* demonstrate enhancement of a periventricular rim, basal ganglia, and spots in the brain stem and the colliculi

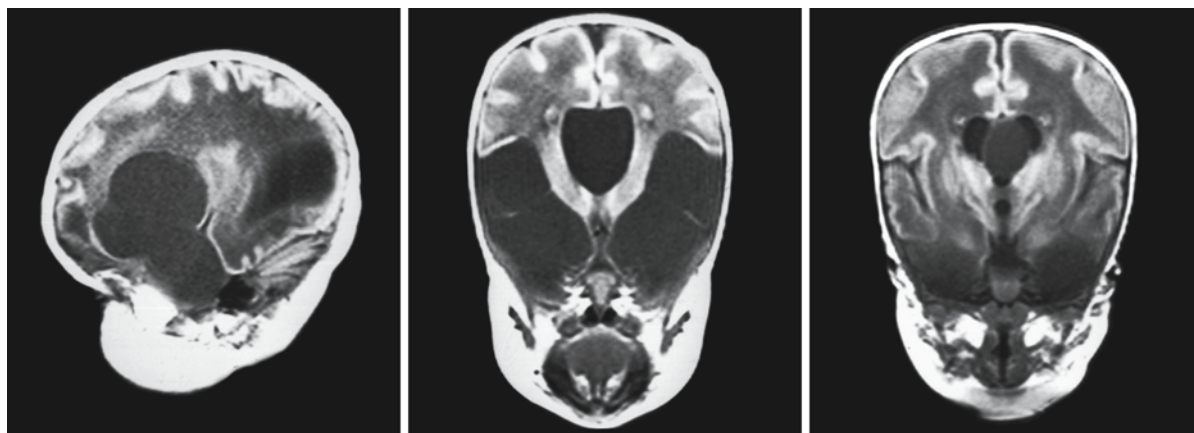


Fig. 57.6. The T₁-weighted sagittal (*left*) and coronal images (*middle and right*) of a 4-month-old girl with infantile AD show large frontotemporal cystic areas. The third ventricle is

wide; the cavum septi pellucidi is grossly dilated. Note the small areas of high signal at the frontal horns, frequently seen in AD

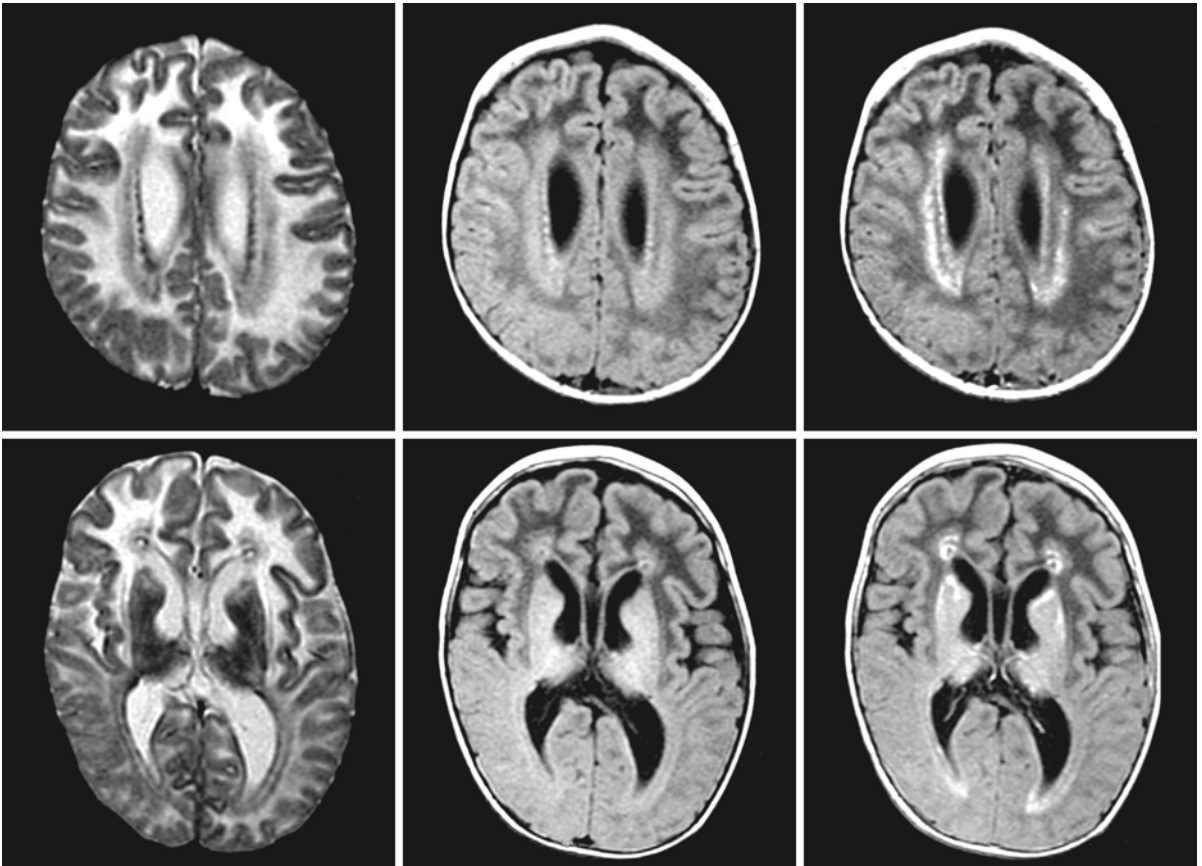


Fig. 57.7. T₂-weighted images (*left*), T₁-weighted images without contrast (*middle*), and T₁-weighted images with contrast (*right*) in an 18-month-old boy with late-infantile AD. The frontal white matter is abnormal in signal. The basal ganglia and thalami are of mixed signal and are atrophic. There is a periventricular rim with low signal on T₂-weighted images and

high signal on T₁-weighted images, which enhances after contrast. The rim is double, the inner rim being discontinuous. Note the small rings at the frontal horns, which enhance after contrast. These small rings are often seen in AD. Courtesy of Dr. N. Thomas, Department of Pediatric Neurology, Southampton General Hospital, Southampton, UK

images (Fig. 57.9). The brain stem and cerebellum may also become atrophic. The extent of the white matter abnormalities may increase over time, but the increase is usually not prominent.

MRI is capable of suggesting the diagnosis with a high probability of accuracy, as demonstrated by a high correlation with *de novo* *GFAP* gene mutations. MRI criteria have been defined and four of the five criteria have to be fulfilled for an MRI-based diagnosis.

1. Extensive, symmetrical cerebral white matter abnormalities with a frontal preponderance, either in the extent of the white matter abnormalities, the degree of swelling, the degree of signal change, or the degree of tissue loss (white matter atrophy or cystic degeneration)
2. Presence of a periventricular rim of decreased signal intensity on T₂-weighted images and elevated signal intensity on T₁-weighted images

3. Abnormalities of the basal ganglia and thalami, either in the form of elevated signal intensity and some swelling or atrophy and elevated or decreased signal intensity on T₂-weighted images
4. Brain stem abnormalities, in particular involving the mid brain and medulla
5. Contrast enhancement involving one or more of the following structures: ventricular lining, periventricular rim of tissue, white matter of the frontal lobes, optic chiasm, fornix, basal ganglia, thalamus, dentate nucleus, cerebellar cortex, and brain stem structures.

These criteria were designed to facilitate diagnosis in typical AD patients. However, unusual MRI patterns have been reported in DNA-confirmed AD patients, which do not fulfill the above criteria. In exceptional patients, the frontal white matter abnormalities are asymmetrical (Fig. 57.13). A patient with juvenile AD has been reported, in whom cerebellar white changes

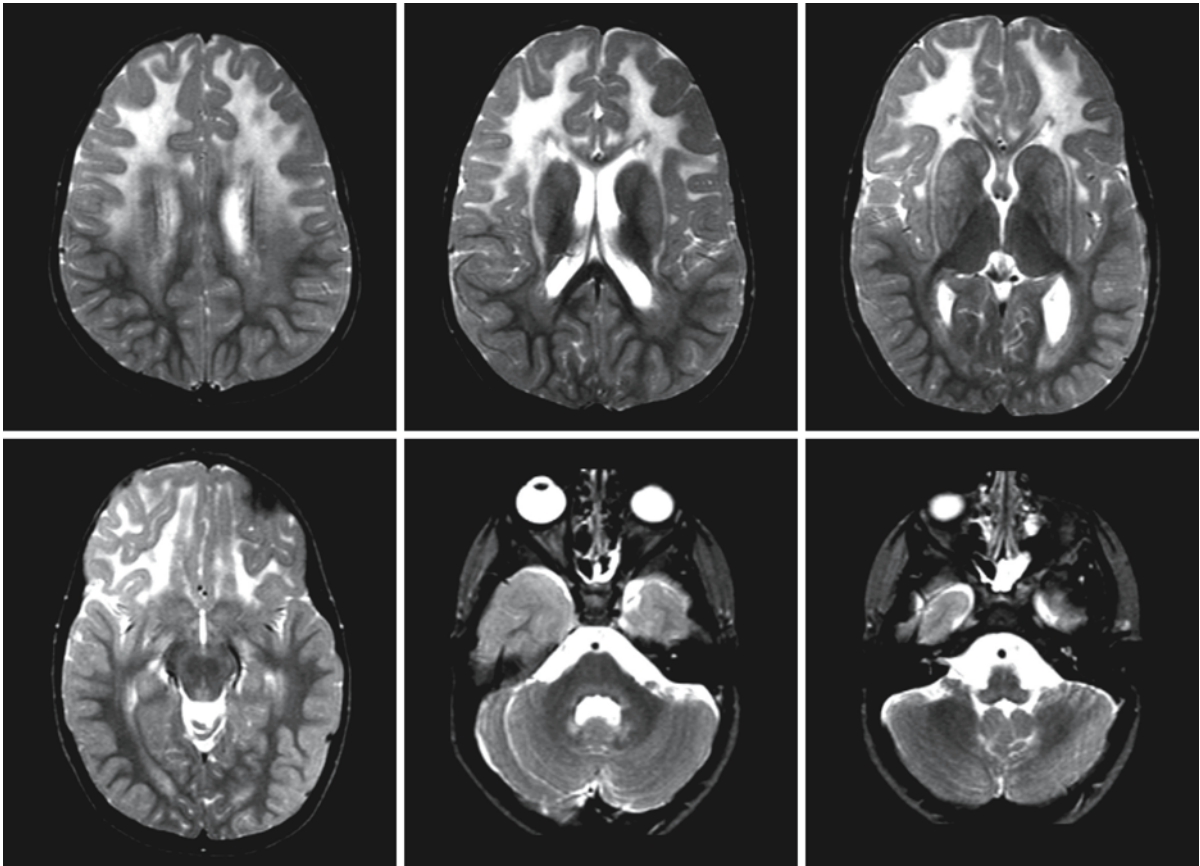


Fig. 57.8. Series of T₂-weighted images in a 5-year-old girl with juvenile AD. From these images the ventrodorsal gradient in white matter disease is evident. The basal ganglia have a slightly abnormal signal intensity and a somewhat swollen ap-

pearance. There is a thin periventricular rim of low signal. There are small dark round rings at the frontal horns. The hilus of the dentate nucleus is affected. There are no clear brain stem abnormalities.

and swelling were most prominent (Fig. 57.14). Over time he also developed frontal white matter changes (Fig. 57.15). Additionally, there are patients, as a rule with juvenile or adult AD, who exclusively or almost exclusively have brain stem, cerebellar, or spinal cord lesions in variable combinations (Figs. 57.16–57.19). These lesions may be space-occupying, suggesting a multifocal glioma (Figs. 57.18 and 57.19). They are often asymmetrical. These lesions may show contrast enhancement (Figs. 57.15 and 57.17–57.19). Few patients have been reported who only have atrophy of the lower part of the brain stem and upper spinal cord. None of these patients received contrast agent, so that the pattern of enhancement cannot be assessed.

The typical AD MRI pattern is quite specific, dissimilar from patterns observed in other white matter disorders. Several leukoencephalopathies share some of the MRI characteristics, but none shares all of them. Predominant involvement of the frontal white

matter together with involvement of diencephalic nuclei and brain stem tracts as well as contrast enhancement may be seen in X-linked adrenoleukodystrophy.

Fig. 57.9. Series of T₂-weighted (*first and second rows*) and contrast-enhanced T₁-weighted images (*third and fourth rows*) in a 10-year-old boy with juvenile AD. There are extensive cerebral white matter abnormalities with frontal predominance. There is a thin, discontinuous periventricular rim of low signal on the T₂-weighted images. The basal ganglia are atrophic. There is a lesion in the midbrain and the dorsal medulla. Both the cerebellar hemispheric white matter and the hilus of the dentate nucleus are abnormal, with the dentate nucleus prominently visible in between. After contrast administration there is some enhancement of parts of the ependymal lining of the lateral ventricles, the lesions in the midbrain and medulla, the dentate nucleus, and the cerebellar cortex. From van der Knaap et al. (2001), with permission

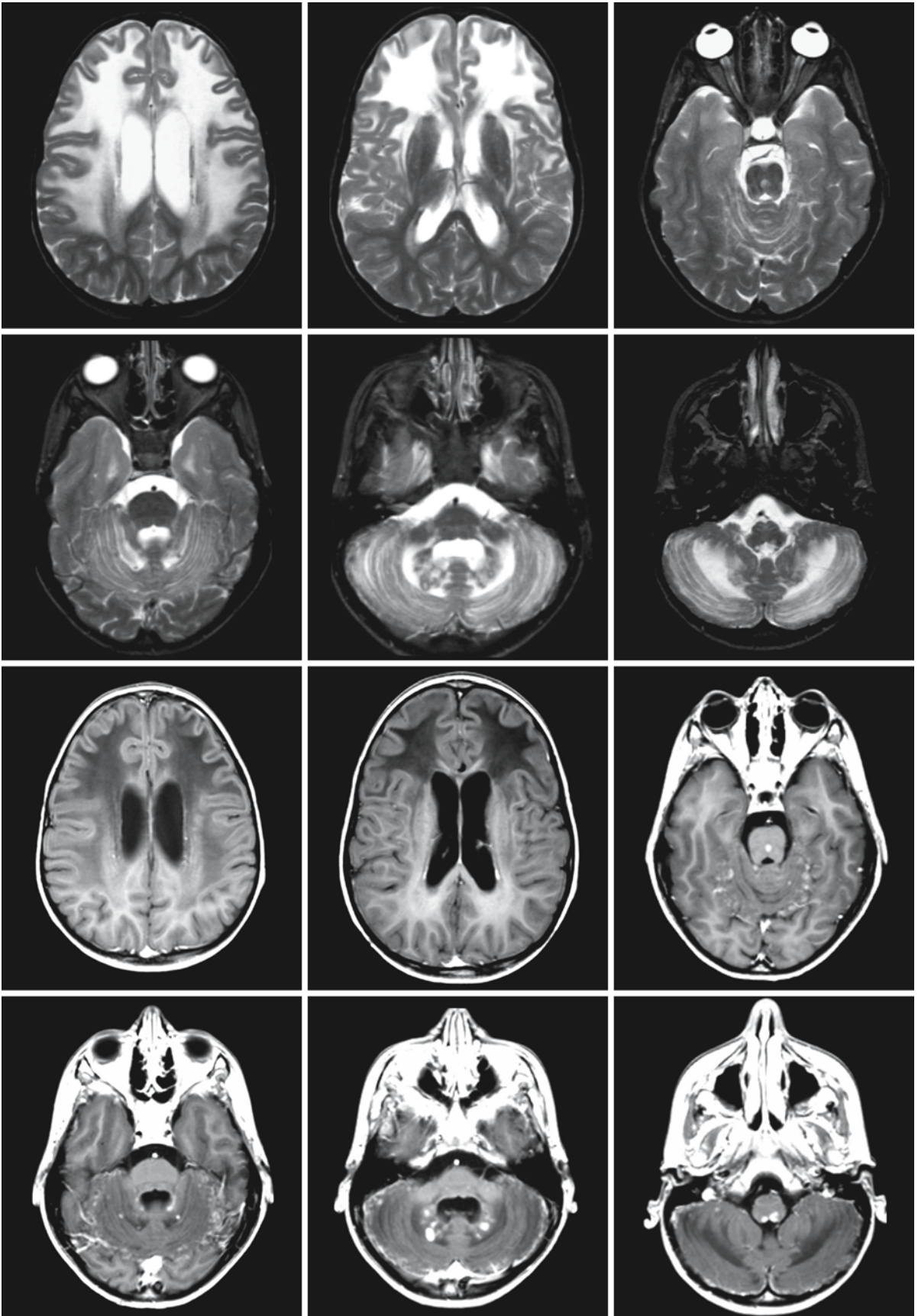


Fig. 57.9.

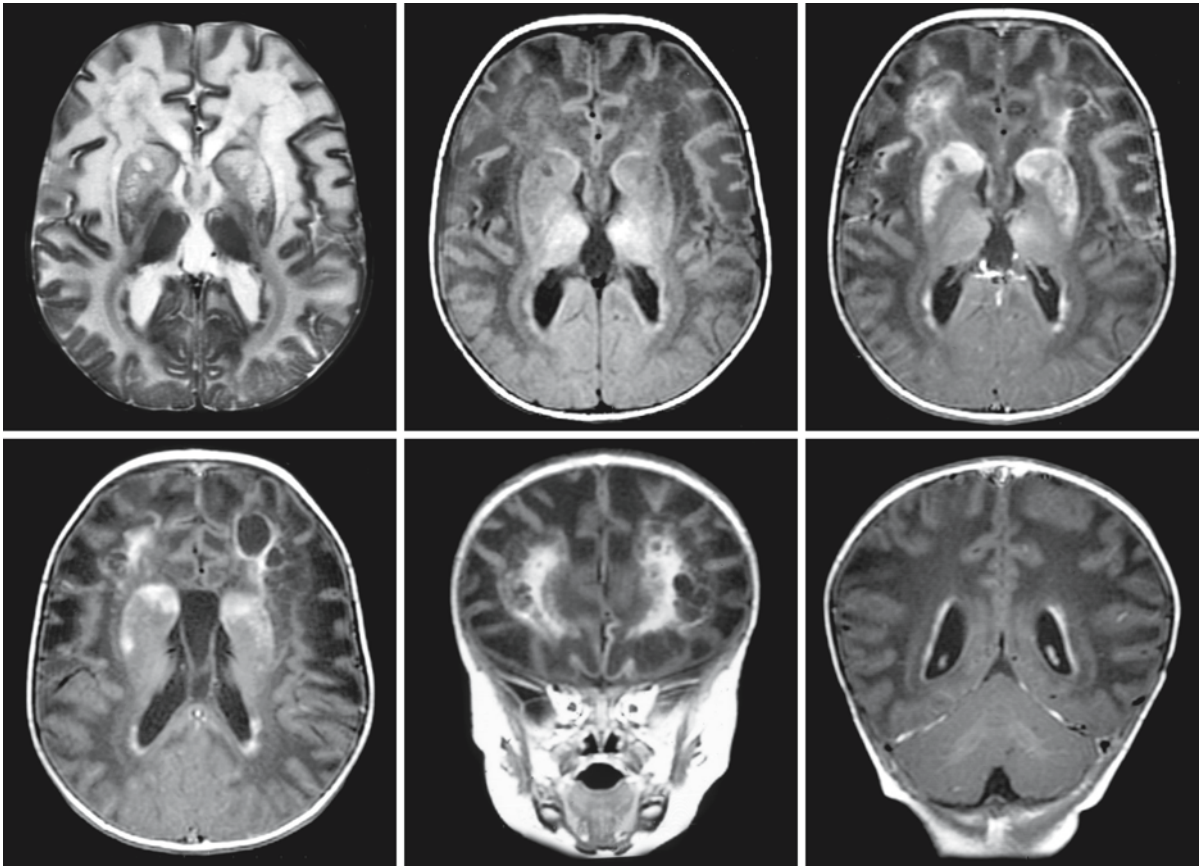


Fig. 57.10. An 8-year-old boy with juvenile AD. The *first row* contains a T₂-weighted image (*left*) and two T₁-weighted images, one without contrast (*middle*) and one with contrast (*right*), at the level of the basal ganglia. The *second row* contains T₁-weighted images with contrast. Note the extensive cerebral white matter abnormalities with frontal predominance, the periventricular rim with a low signal on the T₂-weighted image and high signal on the T₁-weighted image,

and the signal abnormalities in the basal ganglia. The fornix is thickened. After contrast administration, enhancement of the periventricular rim, basal ganglia, and frontal white matter is seen. There are cysts of variable size in the frontal white matter. There is a large cavum Vergae. Courtesy of Dr. C. Leite, neuroradiologist, and Dr. F. Kok, pediatric neurologist, University of São Paulo Medical School, São Paulo, Brazil

However, in this disorder only or mainly the geniculate bodies are involved among the diencephalic nuclei. The brain stem lesions primarily involve the corticospinal, corticobulbar, visual, and auditory tracts. Contrast enhancement occurs within the outer border of the white matter lesions. Similarly, some patients with metachromatic leukodystrophy have predominantly frontal white matter abnormalities together with involvement of the brain stem. The brain stem lesions involve the long tracts. Contrast enhancement is not a feature of this disease. Canavan disease is characterized by a combination of macrocephaly, extensive cerebral white matter changes (without frontal preponderance), and basal ganglia abnormalities. However, the thalamus and globus pal-

lidus are typically involved, with sparing of the caudate nucleus and putamen. Contrast enhancement does not occur. In merosin-deficient congenital muscular dystrophy, extensive cerebral white matter changes are present with relative sparing of the occipital white matter. However, the basal ganglia and brain stem are spared. In megalencephalic leukoencephalopathy with subcortical cysts, extensive cerebral white matter changes are observed with slight swelling. However, there are invariably anterior temporal cysts, and often subcortical cysts in the frontoparietal area, whereas the cysts in AD affect primarily the deep frontal white matter. Contrast enhancement is not a feature of megalencephalic leukoencephalopathy with subcortical cysts.

Fig. 57.11. One T₂- (left) and one T₁-weighted image (right) in a 6-year-old girl with juvenile AD, showing the typical characteristics. Note the high signal of the basal ganglia on the T₁-weighted image without contrast

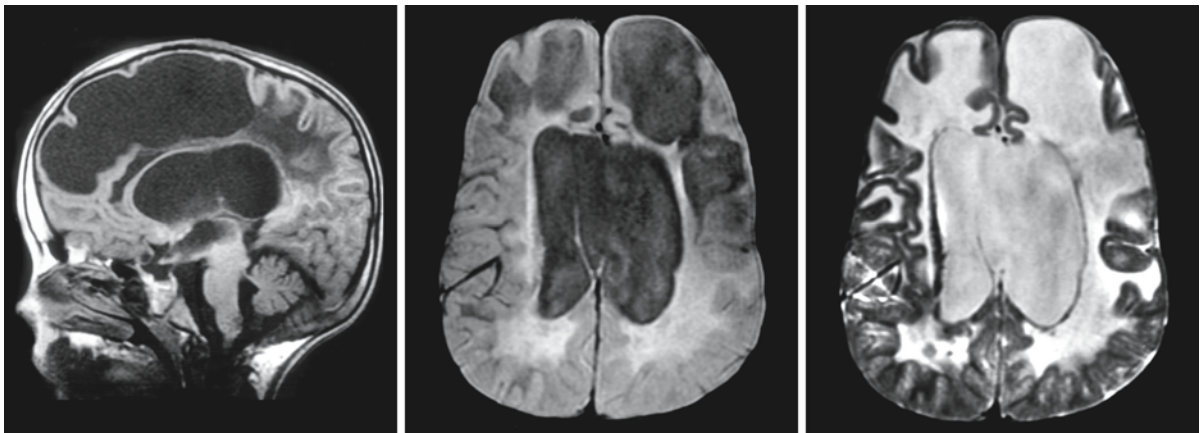
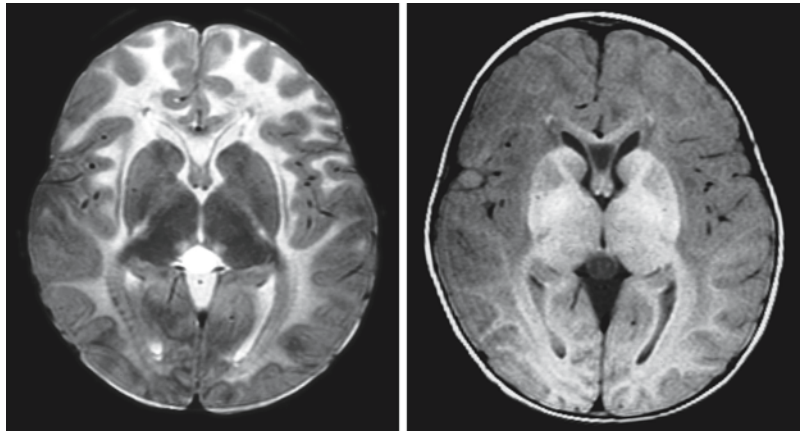


Fig. 57.12. A 7-year-old girl with juvenile AD. Note the huge cysts in the frontal white matter. Note also the periventricular rim of low signal on the T₂-weighted image. From van der

Knaap et al. (2001), with permission; additional images courtesy of Dr. S. Naidu, Department of Neurogenetics, Kennedy Krieger Institute, Baltimore, USA

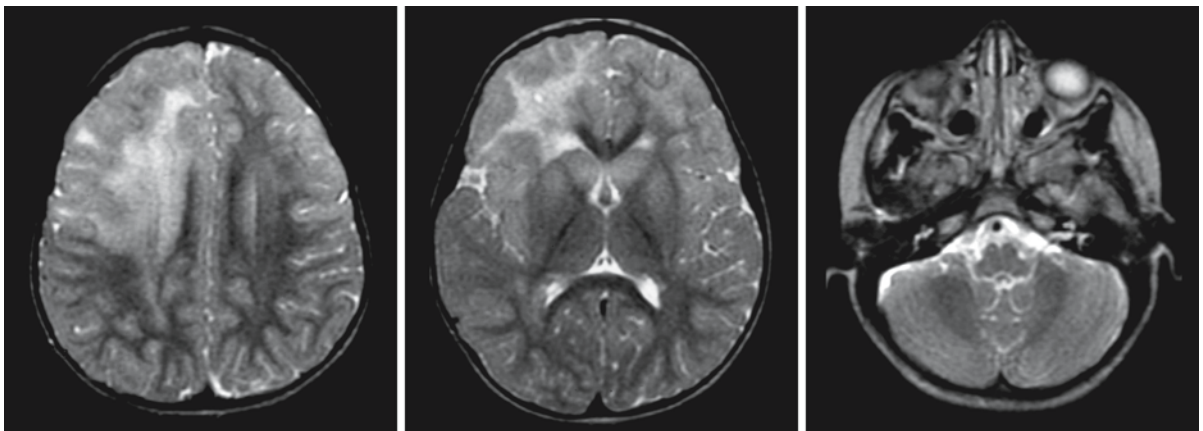


Fig. 57.13. This 5-year-old female with an unusual variant of AD has highly asymmetrical signal abnormalities in the frontal white matter. A brain biopsy was performed to rule out a low-grade glioma; Rosenthal fibers were found. Subsequently, a mutation in the *GFAP* gene was demonstrated, not present in

her mother (father not investigated). The basal ganglia are mildly abnormal in signal and are mildly swollen, suggestive of AD. There are no brain stem lesions. Courtesy of Dr. N. Thomas, Department of Pediatric Neurology, Southampton General Hospital, Southampton, UK

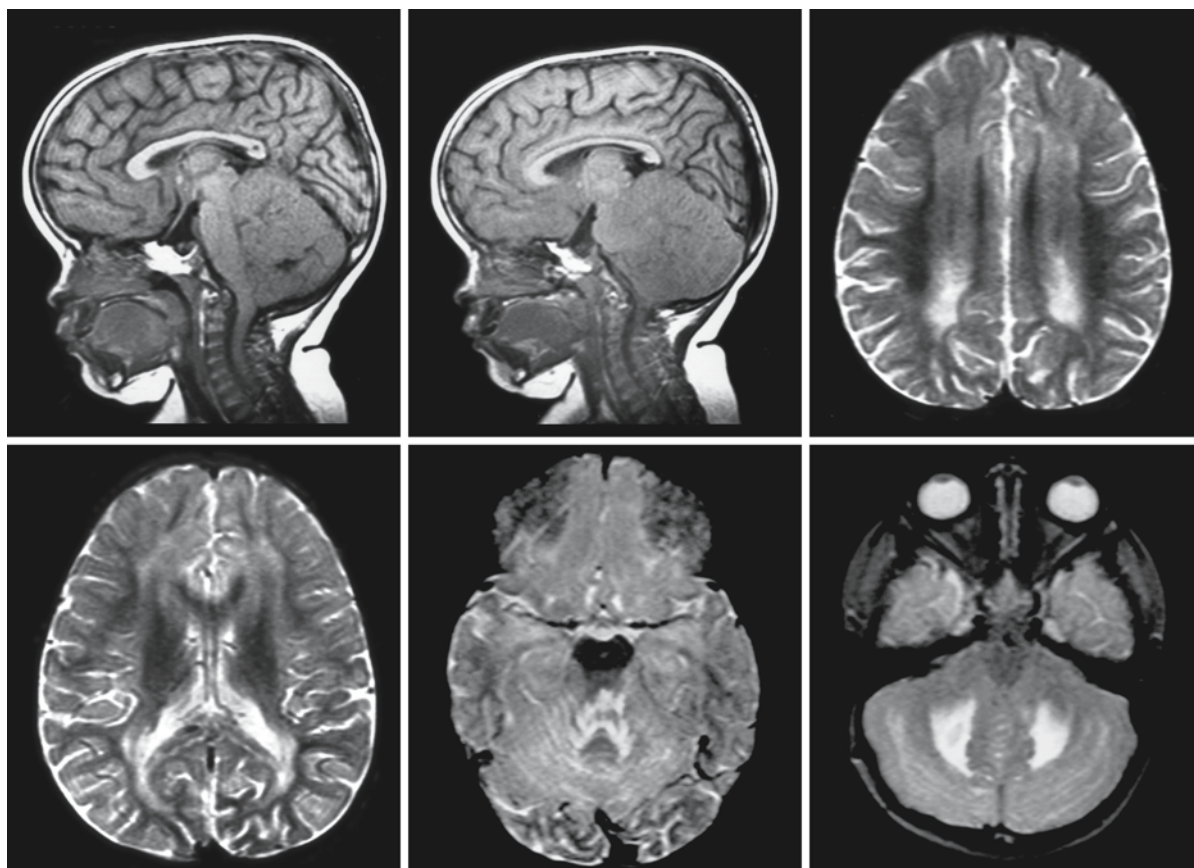


Fig. 57.14. A 3-year-old boy with an unusual variant of AD. His cerebellum is highly enlarged, leading to obstructive hydrocephalus for which a ventriculoperitoneal shunt was placed. The cerebellar white matter is abnormal in signal. He has mild

signal abnormalities in the periventricular white matter, most prominent in the posterior region. A cerebellar biopsy revealed Rosenthal fibers and a de novo mutation in the *GFAP* gene was found

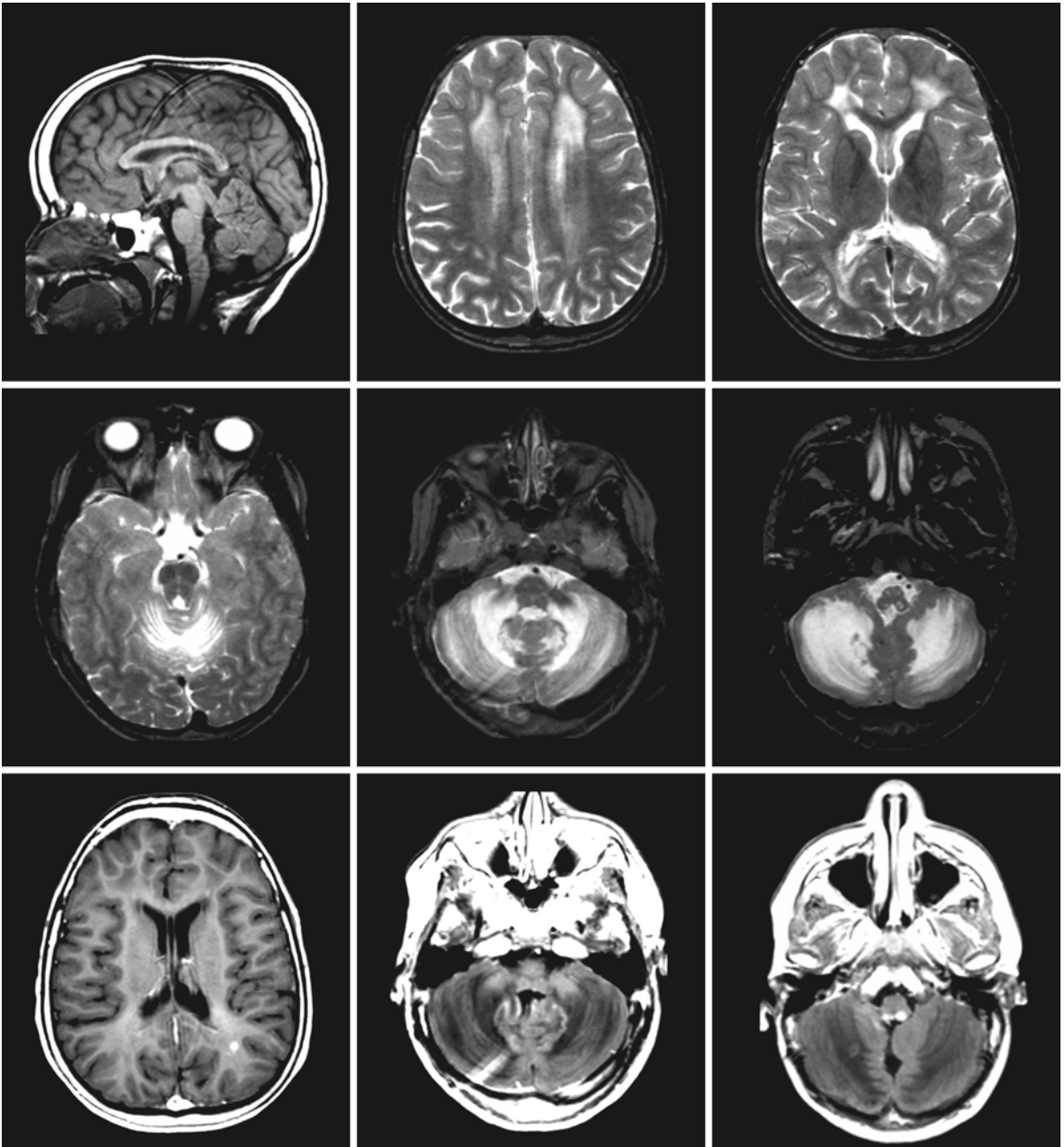


Fig. 57.15. The same boy as in Fig 57.14, now 12 years old. He is neurologically remarkably stable. His cerebellum is markedly reduced in size. There are periventricular white matter abnormalities with a frontal predominance. There are slight signal abnormalities in the basal ganglia. The cerebellar white

matter and hilus of the dentate nucleus display prominent signal abnormalities. The medulla contains lesions. After contrast administration, a lesion in the deep parietal white matter, spots in the dentate nucleus, and the dorsal part of the medulla show enhancement

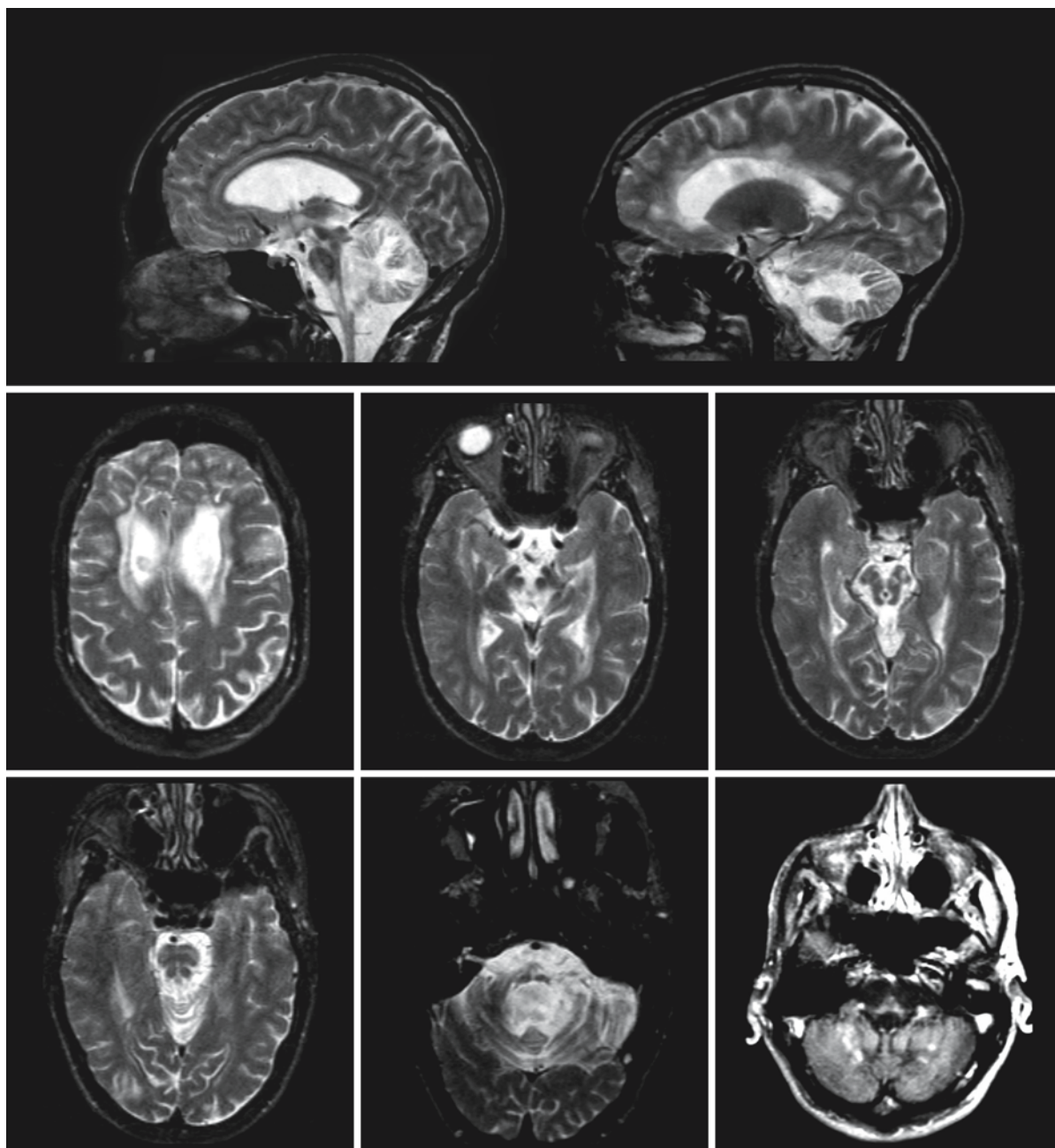


Fig. 57.16. A 32-year-old patient with adult AD. He had a slowly progressive neurological course and died soon after the MRI. Numerous Rosenthal fibers were found at autopsy and a mutation in the *GFAP* gene was found, not present in his mother (father not investigated). Most prominent features are

the cerebellar white matter abnormalities and the brain stem atrophy. The lower brain stem is extremely thin. There are also areas of abnormal signal within the brain stem. The contrast-enhanced T₁-weighted image (*third row, right*) shows foci of enhancement in the cerebellum

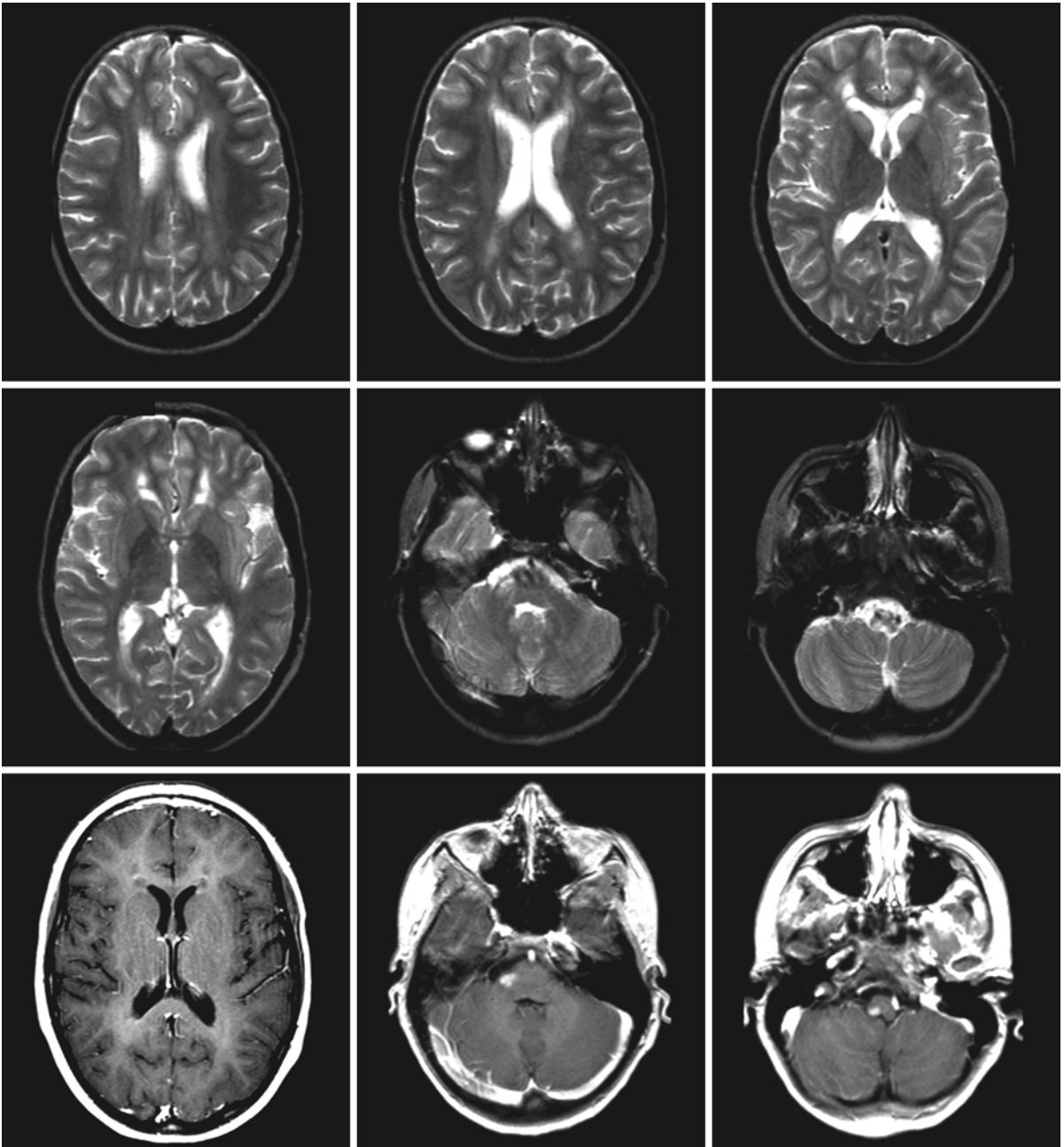


Fig. 57.17. An 11-year-old female patient with juvenile AD and a mutation in the *GFAP* gene. There are minimal supratentorial abnormalities. Some periventricular white matter abnormalities are seen, most pronounced at the frontal horns. The basal ganglia contain slight signal abnormalities. Several small lesions are present in the middle cerebellar peduncle on the

right and in the medulla. After contrast administration, enhancement of the latter lesions is seen. The small rings at the frontal horns also show some enhancement. Courtesy of Dr. R. Robinson, Department of Pediatric Neurology, Guy's Hospital, London, UK

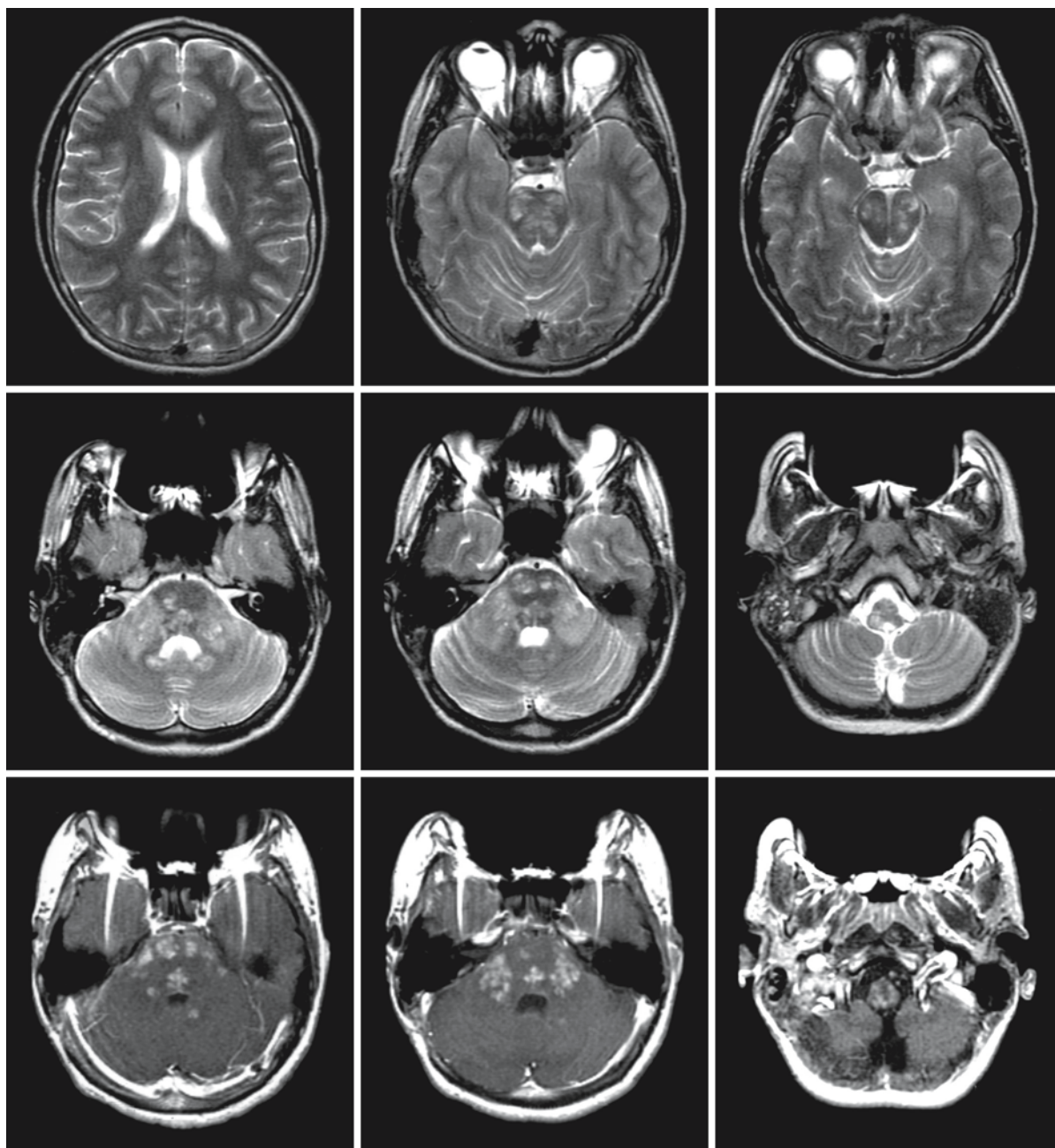


Fig. 57.18. A 14-year-old male patient with juvenile AD and a de novo *GFAP* mutation. There are no evident abnormalities in the supratentorial white matter. There are extensive multifocal and confluent abnormalities in the midbrain, pons, medulla, and middle cerebellar peduncles with some mass effect of the

middle cerebellar peduncles. The hilus of the dentate nucleus has an abnormal signal. After contrast administration, numerous foci of enhancement are seen. Courtesy of Dr. A. Reddy, Department of Hematology/Oncology, Children's Health System, Birmingham, Alabama, USA

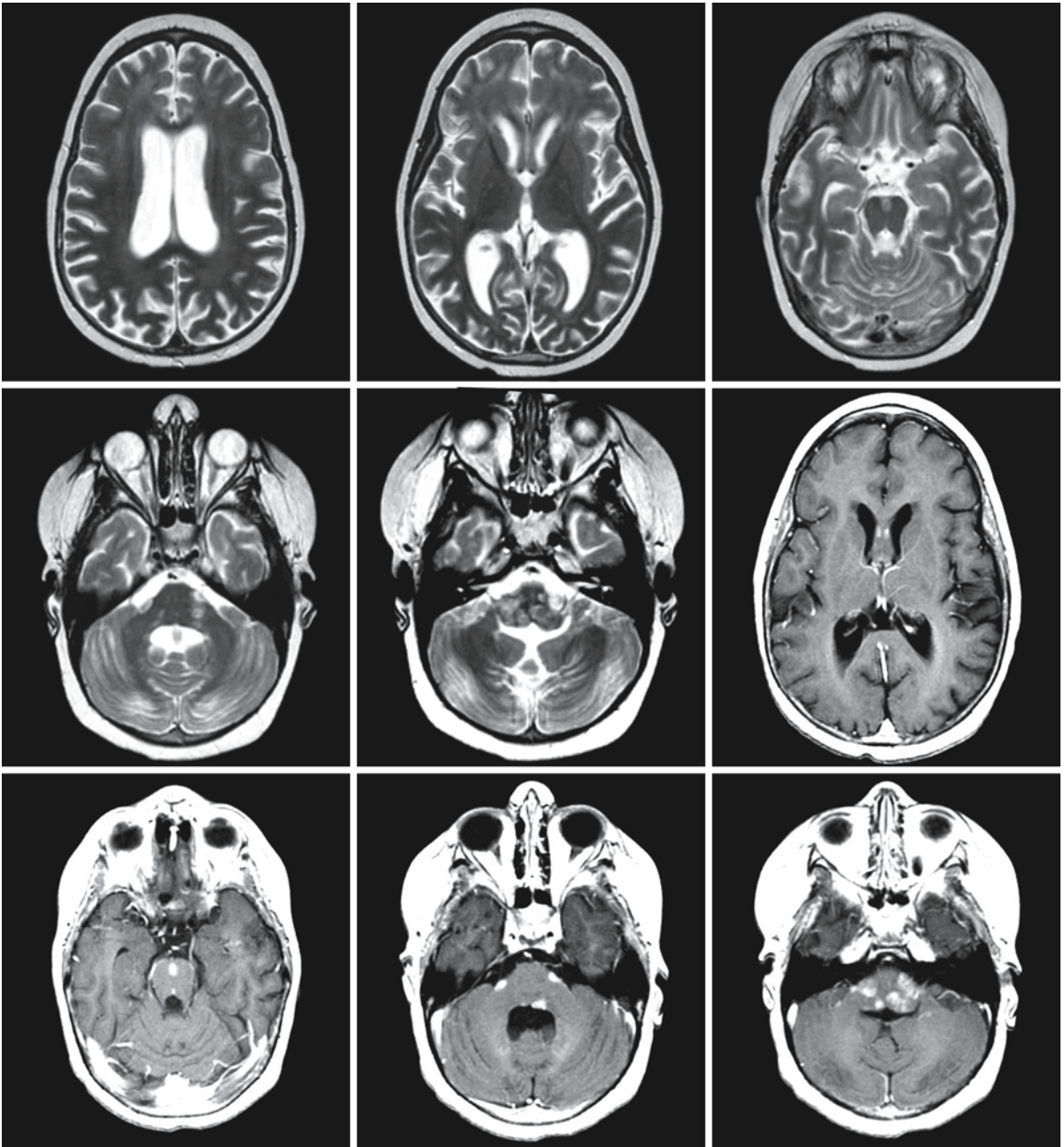


Fig. 57.19. A 7-year-old boy with juvenile AD. He had Rosenthal fibers at histological examination and a de novo mutation in the *GFAP* gene. Apart from a mild dilatation of the lateral ventricles and a thickened fornix, the T₂-weighted images do not show supratentorial abnormalities, neither in the white matter nor in the basal ganglia. There are multiple nodular lesions in the brain stem and middle cerebellar peduncles. The

pons is mildly atrophic. After contrast, enhancement of the fornix and the nodular lesions in the posterior fossa is seen. Courtesy of Dr. L. González Gutiérrez-Solana, Neuropediatrics Unit, Hospital Niño Jesús, Madrid, Spain, and Dr. A. Messing, Department of Pathobiological Sciences, Waisman Center and School of Veterinary Medicine, University of Wisconsin, Madison, Wisconsin, USA

Giant Axonal Neuropathy

58.1 Clinical Features and Laboratory Investigations

Giant axonal neuropathy (GAN) is an early-onset neurodegenerative disorder that affects both the PNS and CNS. The disease has an autosomal recessive mode of inheritance. Patients have characteristic tightly curled hair, often described as frizzy or kinky. Acquisition of motor milestones is delayed in most, but not all patients. The age at onset of progressive neurological problems is usually below 7 years. Patients develop a clumsy gait and progressive weakness of the legs. The weakness spreads to involve the arms as well. Neurological examination reveals signs of peripheral neuropathy with absent reflexes, muscular atrophy, weakness, and impaired sensation, most marked distally. There are usually also pyramidal signs, with extensor plantar reflexes. Subsequently, dysarthria, nystagmus, ataxia, scoliosis, and intellectual decline become apparent. Optic atrophy may occur. Patients may develop bulbar weakness, involving muscles of the face, tongue, and palate. Seizures may occur. Urinary retention and chronic constipation may be vexing problems and are related to involvement of peripheral autonomic nerves. Precocious puberty may occur. Most patients are of small stature. Patients usually become wheelchair-dependent in the first or second decade of life and die between the ages of 10 and 30 years.

Neurophysiological examination reveals signs of a severe axonal neuropathy. Somatosensory, visual, and brain stem auditory evoked potentials show prolonged conduction times or absence of reproducible responses. Sural nerve biopsy, showing axonal loss and large axonal swellings, which consist mainly of tightly packed neurofilaments, supports the diagnosis. DNA confirmation is possible.

58.2 Pathology

The brain is unremarkable on external examination. On sectioning, some dilatation of the lateral ventricles and thinning of the corpus callosum may be found. The cerebral and cerebellar white matter may be abnormal with sparing of the U fibers.

Histological examination of the cortex reveals increased numbers of astrocytes and scattered Rosenthal fibers. The Rosenthal fibers are positive in im-

munostaining for glial fibrillary acidic protein. In addition, occasional giant axons are found, measuring up to 100 μm or more in diameter. They are short, globular to fusiform or balloon-like enlargements or long cigar-like or corkscrew-shaped axonal thickenings. They stain positively with silver stains and anti-neurofilament antibodies. The cerebral white matter may be diffusely gliotic with a variable loss of myelin, the frontal and parietal lobes being most affected and the U fibers being relatively spared. In other patients, however, absence of myelin loss has been reported. Rosenthal fibers are aggregated around blood vessels. Low numbers of giant axons are seen within the cerebral white matter. The central gray matter structures also contain increased numbers of astrocytes, scattered Rosenthal fibers, and occasional giant axons. Optic nerves and tracts show fiber loss and gliosis. The cerebellar cortex displays loss of Purkinje and granule cells and hyperplasia of Bergmann astrocytes. In the cerebellar white matter, loss of nerve fibers and increase of astrocytic processes and Rosenthal fibers is found. Giant axons and Rosenthal fibers are scattered throughout the brain stem. In particular, the pyramidal tracts are shrunken and gliotic, display loss of nerve fibers, and contain many giant axons. The spinal white matter contains excessive numbers of astrocytes. There are subpial clusters of Rosenthal fibers. Giant axons are particularly numerous in the posterior columns, especially in the cervical region, and the lateral corticospinal tracts, especially in the lower thoracic and lumbar region. Electron microscopy of the axonal swellings reveals enormous accumulations of neurofilament, often arranged in a whorl-like, interlacing pattern. Nondescript electron-dense granules are interspersed among filamentous masses. The myelin sheaths of the enlarged axons are abnormally thin and disintegration of myelin lamellae may be seen.

Sural nerve biopsy reveals enlarged axons with spindle-shaped focal distensions of non-myelinated and thinly myelinated nerve fibers. Myelin sheaths around the swellings are abnormally thin and the largest swellings often lack a covering of myelin over a part of their length. Ultrastructurally, the distensions are composed of closely packed neurofilaments, which often form a whorl pattern. There are closely associated electron-dense granules. Microtubules, microtubule-mitochondrial complexes, and cisterns of smooth endoplasmic reticulum, instead of being

dispersed among the neurofilaments as in normal axoplasm, are frequently seen gathered together within the filament-free areas at the center or periphery of the axonal swelling. In muscles, the typical pattern of neurogenic atrophy is found.

In conclusion, the pathology is that of a distal axonopathy most severely affecting peripheral nerves, pyramidal tracts, posterior spinal columns, and the cerebellum. It is important to note that Rosenthal fibers have not been reported in all patients.

58.3 Pathogenetic Considerations

The gene related to giant axonal neuropathy, GAN, is located on chromosome 16q24.1 and encodes a ubiquitously expressed protein, gigaxonin.

Giant axonal neuropathy is characterized by cytoskeletal abnormality. The hallmark of the disease is the presence of giant axonal swellings, which are densely packed with aberrant neurofilaments, abnormal microtubule network, and accumulation of other membranous organelles. Neurofilaments belong to the intermediate filaments. In GAN, an abnormal accumulation of multiple tissue-specific intermediate filaments is found in a wider range of cells than only neurons, suggesting a generalized disorganization of intermediate filament networks. Aggregations of vimentin have been reported in endothelial cells, Schwann cells, and cultured skin fibroblasts, and aggregations of glial fibrillary acidic protein are found in astrocytes. Keratin intermediate filaments are altered, leading to the characteristic kinky hair.

The cytoskeletal network is responsible for cell architecture, intracellular transport, mitosis, cell mobility, and differentiation. It is composed of microtubules, actin microfilaments, and intermediate filaments, which interconnect through cross-linking proteins. The properties of the network formed are modulated by different associated proteins. Cytoskeletal organization and dynamics depend on protein self-associations and interactions with a variety of binding partners such as microtubule-associated proteins (MAPs).

Gigaxonin binds directly to microtubule-associated protein 1B light chain (MAP1B-LC), a protein involved in maintaining the integrity of cytoskeletal structures and promoting neuronal stability. The interaction of gigaxonin with MAP1B-LC enhances microtubule stability, required for axonal transport over long distance. In line with this, the neurofilament accumulations in GAN, leading to the segmental distension of axons, mainly affect distal portions of the long tracts. Some of the mutations found in GAN patients have been shown to lead to loss of gigaxonin–MAP1B-LC interaction. The devastating

axonal degeneration and neuronal death found in GAN patients point to the importance of gigaxonin for neuronal survival.

58.4 Therapy

No specific treatment is available. Therapy is supportive.

58.5 Magnetic Resonance Imaging

The MRI findings described in GAN are variable, probably at least partly depending on the stage of the disease. In some patients, no or minimal cerebral white matter abnormalities are present (Fig. 58.1). The white matter abnormalities may be diffuse and subtle (Fig. 58.3), sometimes with multifocal spots of more prominent signal change superimposed. In other patients, extensive and confluent white matter abnormalities are present, symmetrically involving the cerebral white matter in a diffuse fashion (Fig. 58.2) or with a predominance in the frontoparietal region. The corpus callosum and U fibers tend to be spared. The posterior limb of the internal capsule, pyramidal tracts, and medial lemniscus in the brain stem, middle cerebellar peduncles, hilus of the dentate nucleus, and cerebellar white matter may display signal changes (Figs. 58.2 and 58.3). The white matter abnormalities are progressive over time (Figs. 58.1 and 58.2). The lateral ventricles become mildly dilated due to white matter volume loss and the cerebellar vermis becomes atrophic over time.

In our experience the MR images in GAN have a certain resemblance to the images in Alexander disease, which is interesting since both are characterized by Rosenthal fiber deposition. The basal ganglia may have a slightly abnormal signal and a slightly swollen aspect (Figs. 58.1 and 58.3). The areas with high signal on T₁-weighted images include the ependymal lining (Fig. 58.1), a thin periventricular

Fig. 58.1. A 6-year-old female patient with GAN. The T₂-weighted images (*upper two rows*) show a diffuse slight signal abnormality of the cerebral white matter. The basal ganglia have a slightly abnormal signal and slightly swollen appearance. The T₁-weighted images (*third row*) show that the ependymal lining of the lateral ventricles and the globus pallidus have a slightly increased signal. After contrast administration (*fourth row*), subtle enhancement of the ependymal lining is seen. Courtesy of Dr. S. Blaser, Department of Diagnostic Imaging, Hospital for Sick Children, Toronto, Canada. (Fig. 58.1 see next page)

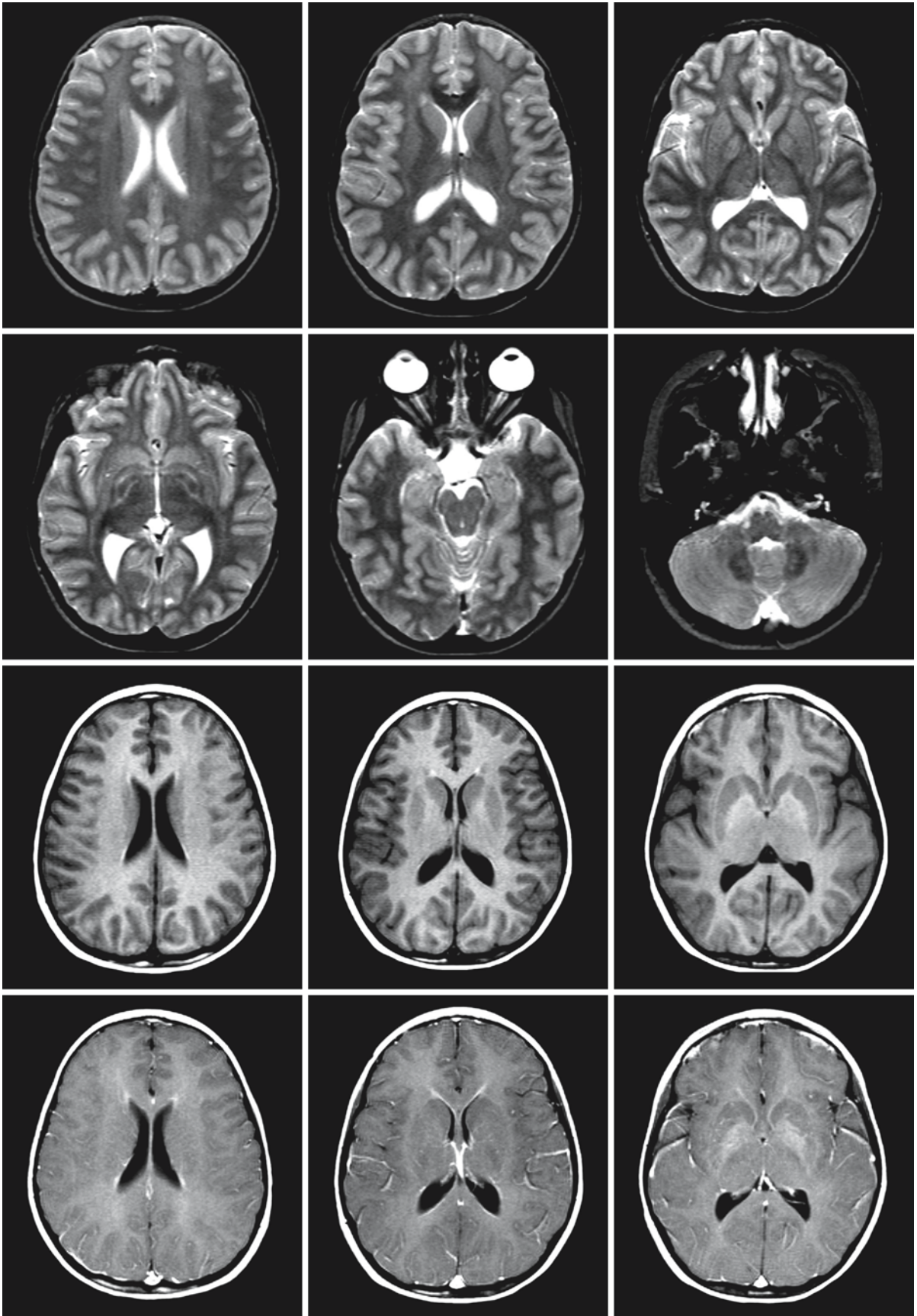


Fig. 58.1.

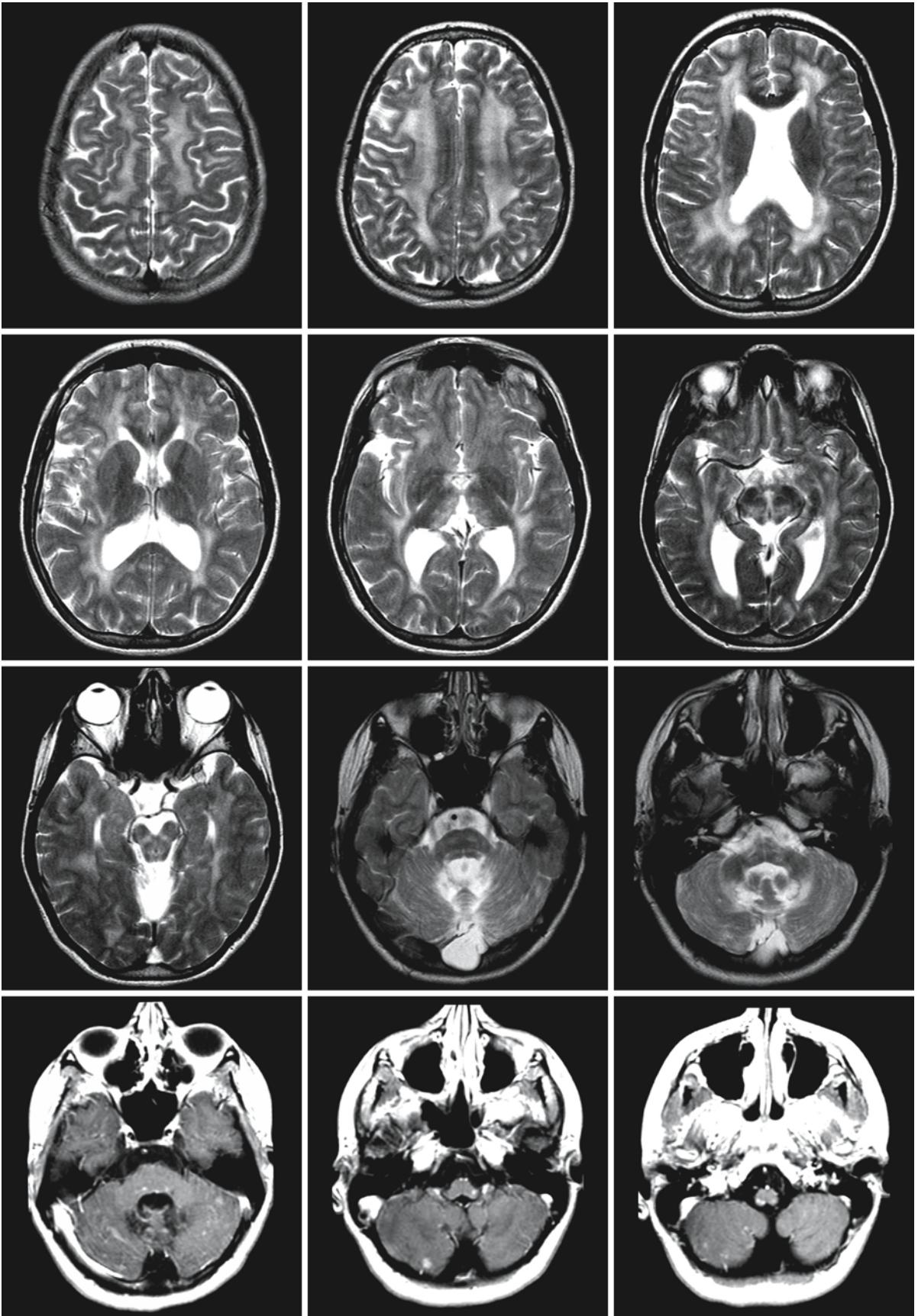


Fig. 58.2.

rim (Fig. 58.3), and the globus pallidus (Figs. 58.1 and 58.3). The thin periventricular rim may have a low signal on T₂-weighted images (Fig. 58.3). The ependymal lining shows subtle contrast enhancement (Figs. 58.1 and 58.3). Areas in the dorsal medulla may also show contrast enhancement (Fig. 58.2), which is often seen in Alexander disease.

Fig. 58.2. At the age of 14 years, diffuse cerebral signal abnormalities are seen in the same girl, sparing the corpus callosum and to some extent the U fibers. The posterior limb of the internal capsule, pyramidal tracts and medial lemniscus in the brain stem, hilus of the dentate nucleus, and cerebellar white matter are also involved. The contrast-enhanced T₁-weighted images reveal contrast uptake in multiple spots with the cerebellum, pons, and the dorsal part of the medulla. Courtesy of Dr. S. Blaser, Department of Diagnostic Imaging, Hospital for Sick Children, Toronto, Canada. (Fig. 58.2 see last page)

Fig. 58.3. The T₂-weighted images (*upper two rows*) of her brother, who also suffers from GAN, at the age of 3 years, show diffuse slight signal abnormalities in the cerebral white matter with sparing of the U fibers and corpus callosum. The posterior limb of the internal capsule, pyramidal tracts and medial lemniscus in the brain stem, hilus of the dentate nucleus, and cerebellar white matter are also involved. There is a thin rim of low signal around the lateral ventricles on the T₂-weighted images, most evident in the posterior region. This rim has an increased signal on T₁-weighted images (*third row*) and enhances after contrast (*fourth row*). The globus pallidus also has a slightly increased signal on T₁-weighted images (*third row*). Courtesy of Dr. S. Blaser, Department of Diagnostic Imaging, Hospital for Sick Children, Toronto, Canada.

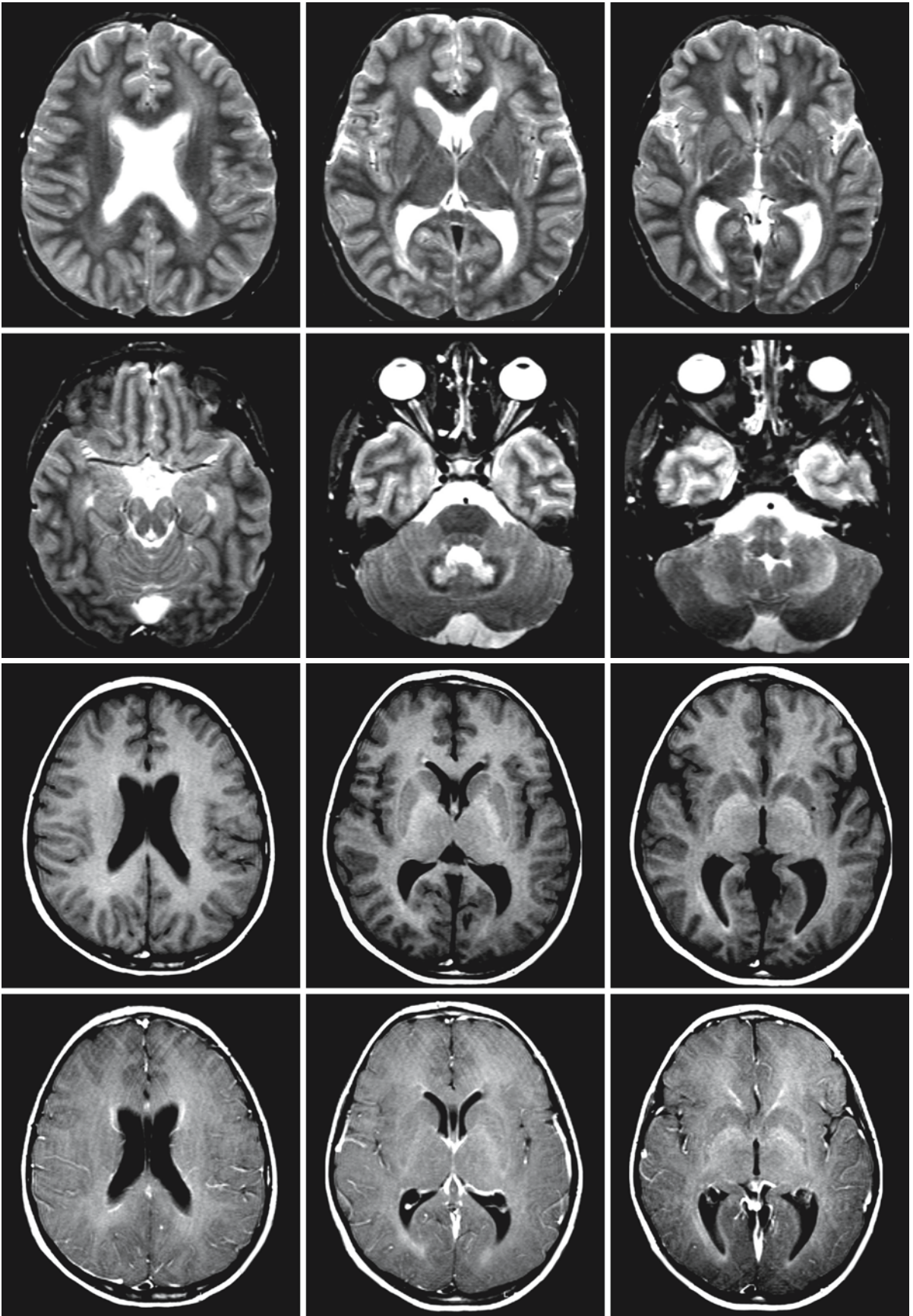


Fig. 58.3.

Megalencephalic Leukoencephalopathy with Subcortical Cysts

59.1 Clinical Features and Laboratory Investigations

Megalencephalic leukoencephalopathy with subcortical cysts (MLC) is a rare leukoencephalopathy with an autosomal recessive mode of inheritance. The disease is relatively prevalent among Turkish people and in a certain Asian-Indian community, the Agarwal ethnic group. Macrocephaly is present at birth or, more frequently, develops during the first year of life. The degree of macrocephaly is variable and is impressive in some of the patients. After the first year of life the head growth rate normalizes and growth follows a line parallel to the 98th percentile, usually several centimeters above it. Initial mental and motor development is normal in most cases, mildly delayed in some of the patients. Apart from progressive macrocephaly, the first clinical sign is usually a delay in walking. Walking is often unstable and the child falls frequently. After an interval of several years, a slow deterioration of motor function is noted with development of axial ataxia and ataxia of the extremities. Signs of pyramidal dysfunction are late and minor, and are as a rule dominated by the signs of cerebellar ataxia. Muscle tone tends to be low, apart from some ankle hypertonia. Reflexes become high and Babinski signs become apparent. Gradually the ability to walk independently is lost, and most children become completely wheelchair-dependent at the end of the first decade or in the second decade of life. Almost all patients have epilepsy from early on, usually easily controlled with medication. Mental deterioration is late and mild. Decreasing school performance becomes evident during the later years of primary school. In a minority of patients, intellectual capacities are mildly decreased from the beginning. A relatively late and slow decrease in intelligence is also noted in these patients. Speech becomes increasingly dysarthric and the patients may also develop dysphagia. Some patients display extrapyramidal movement abnormalities with dystonia and athetosis. Minor head trauma has been reported to induce temporary deterioration in some patients, most often with seizures or status epilepticus, prolonged unconsciousness, or acute motor deterioration with gradual improvement.

Some patients have a more severe clinical course and maintain the ability to walk independently only

for a few years or never achieve independent walking. Some patients have a more benign clinical course. As a teenager they may have normal mental and motor function and only have borderline macrocephaly. Some patients still walk independently in their forties. As the disease has been known for only a relatively short time, little information exists about average life span. Some patients have died in their teens or twenties, but others are alive in their forties.

In extensive laboratory investigations no abnormalities are found. CSF protein is normal. Peripheral motor and sensory nerve conduction velocities and electromyogram are normal. Evoked potentials are initially normal in most patients. BAEPs remain normal, but VEPs and SSEPs deteriorate over the years with prolongation of latencies and abnormal cortical responses. EEG is initially normal. Subsequently, background slowing occurs and abnormalities are seen such as sharp waves, spikes, and spike-wave complexes with variable location. Abnormal photoparoxysmal responses are seen in some of the patients but not in all.

Presently, the diagnosis is MRI-based. Analysis of the *MLC1* gene can be performed, and abnormalities are found in 60–70% of the patients with typical MRI findings. Some families without mutations in *MLC1* exclude linkage to the *MLC1* locus, implying that there must be another gene or genes related to MLC. Prenatal diagnosis is possible in families with known mutations in *MLC1*.

59.2 Pathology

Brain biopsy was performed in one patient (van der Knaap et al. 1996). The cortex was normal. A status spongiosus of the cerebral white matter was found with presence of innumerable vacuoles. Myelin sheaths had a normal thickness and density and there were only minor signs of myelin breakdown. The white matter showed intense fibrillary astrogliosis. Electron microscopy revealed splitting of myelin sheaths at the intraperiod line with intramyelinic vacuole formation. The splitting involved only the outer lamellae of the myelin sheaths; the vacuoles were covered by only one or two myelin layers. There was no evidence of axonal degeneration or loss. The cerebral cortex was normal.

59.3 Pathogenetic Considerations

There is one gene known to be related to MLC: *MLC1*, formerly called *KIAA0027*, located on chromosome 22qtel. Mutations in *MLC1* are found in approximately 70% of the MLC patients. Different mutations have been found. Within the Agarwal ethnic group, the patients are homozygous for the same founder mutation. Among Turkish patients, however, different mutations are found and there is no evidence for a founder mutation among them. There is no evident genotype–phenotype correlation. Some families without mutations in *MLC1* exclude linkage to the *MLC1* locus, implying that there must be another gene or other genes related to MLC.

MLC1 encodes a membrane protein of unknown function with eight transmembrane domains. The *MLC1* protein is highly conserved throughout evolution in a variety of different vertebrate species that produce myelin. Orthologues are not found in eukaryotes that do not produce myelin, suggesting an as yet undiscovered fundamental function of *MLC1* related to myelin. Sequence analysis of the *MLC1* protein does not reveal any similarity to known proteins or protein domains. Most proteins with eight transmembrane domains have a transport function. Both the C- and the N-terminus of *MLC1* are located within the cytoplasm. *MLC1* is expressed in the brain and all types of blood leukocytes. Within the brain, the *MLC1* protein is specifically expressed in astrocytic endfeet in perivascular, subependymal, and subpial regions. Astrocytic endfeet form part of the blood–brain barrier. This localization suggests a possible role for *MLC1* in a transport process across the blood–brain barrier. The blood–brain barrier is a diffusion barrier for the exchange of molecules and is formed by seamlessly joined endothelial cells of the capillary wall, the basal lamina, and astroglial endfeet. The role of astrocytes in the blood–brain barrier is not well defined. They are separated from the endothelial cells by the basal lamina and do not contribute directly to the physical barrier. Perivascular astroglial endfeet contain many transport proteins, including transporters of monocarboxylates, glucose, glutamate, and water.

Given the presence of vacuoles in the outer layer of the myelin sheaths in MLC, the role of astrocytic endfeet in water homeostasis in the brain is of special interest. Different water channel proteins or aquaporins are present in the brain. Aquaporin-4 shows a localization in the astroglial endfeet similar to *MLC1*. Aquaporin-4 is associated with the dystrophin-associated glycoprotein complex (DAGC). This complex links the actin cytoskeleton to the extracellular matrix. Interestingly, some congenital muscular dystrophies, which are caused by mutations in members of the dystrophin-associated glycoprotein complex, also

show white matter abnormalities on MRI. Especially the MRI pattern of merosin-deficient congenital muscular dystrophy is very similar to that of MLC. Myelin vacuolation is seen in both MLC and merosin-deficient congenital muscular dystrophy. Another possibility is that *MLC1* is involved in transporting molecules that are essential for oligodendrocytes or myelin. Mutations in *MLC1* may affect myelin sheath formation or compaction. An argument in favor of this possibility is the fact that the rapidly increasing macrocephaly of MLC develops during the period of most rapid myelin formation, the first year of life, whereas head growth rate slows down and becomes normal in the second year of life. It is probable that the myelin vacuoles arise during the myelin deposition. In agreement with this, Schmitt et al. (2003) show that *MLC1* mRNA expression in the murine brain peaks during a transitional period of astrocytic specialization that occurs in white matter during myelination, suggesting a role for *MLC1* in myelin formation.

The white matter has a very abnormal aspect on MRI at an early age (the youngest child was 1.5 years old when imaging was performed), when neurological examination is still normal or near-normal and evoked responses are normal. Thus, despite its highly abnormal appearance, the white matter is functionally intact or largely intact during these early years. Apparently the presence of the vacuoles in the outer part of the myelin sheaths permits normal function. Over the years, MRI shows some decrease in white matter swelling and some enlargement of lateral ventricles and subarachnoid spaces, a process accompanied by clinical deterioration. The basis of the deterioration is not known.

The gene *KIAA0027/MLC1* has also been implicated in catatonic schizophrenia. However, this has so far not been substantiated. Among patients and family members known to be carriers, the incidence of psychiatric illness is not increased.

59.4 Therapy

So far all attempts at treatment have failed. Patients have been treated with diuretics and acetazolamide, but neither the clinical symptoms nor the white matter swelling improved. Treatment with creatine monohydrate did not lead to objective improvement either.

59.5 Magnetic Resonance Imaging

In MLC the cerebral hemispheric white matter is diffusely abnormal and swollen (Figs. 59.1–59.6). The swelling is most marked during the first years of life, with obliteration of peripheral CSF spaces and nar-

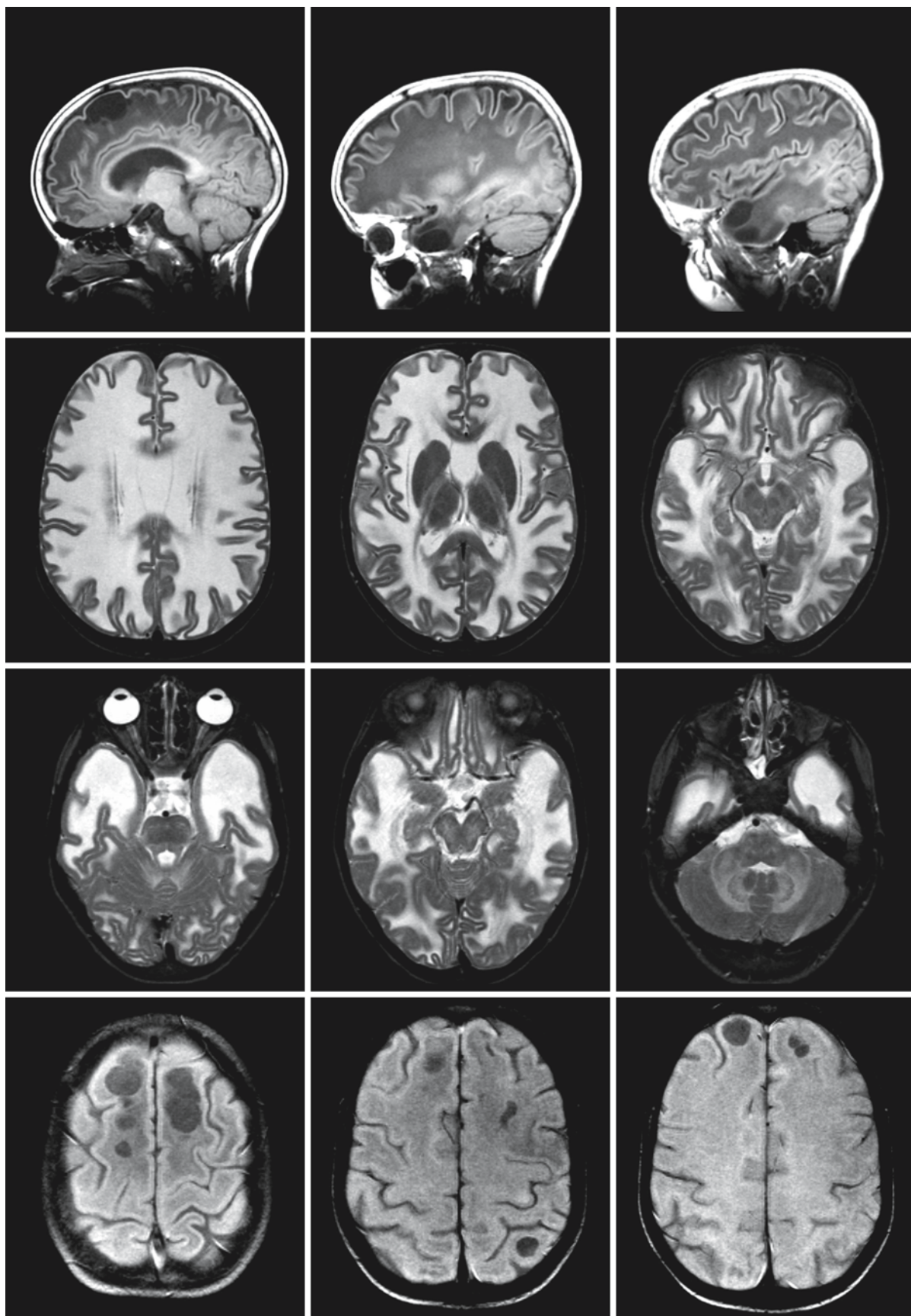


Fig. 59.1.

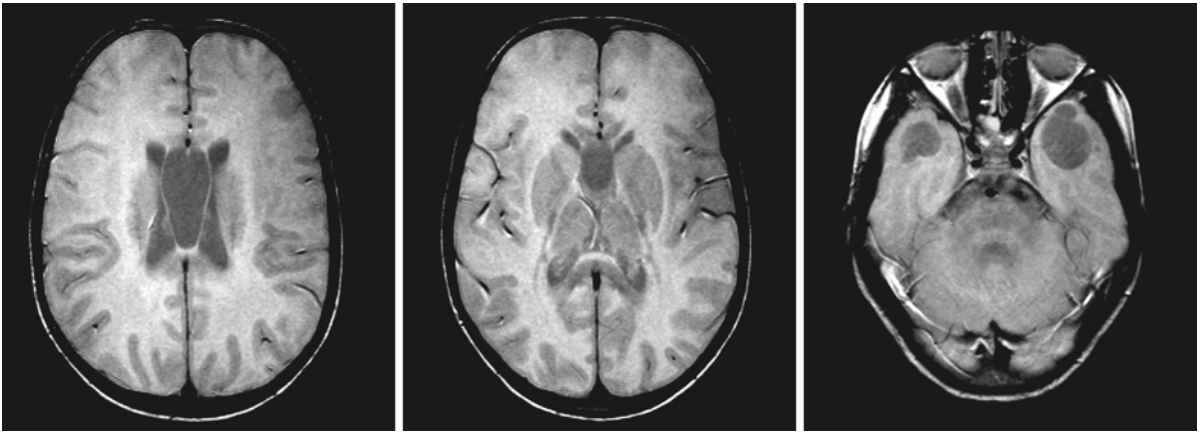


Fig. 59.1. (continued). MRI series of a 6-year-old girl with MLC. The *upper row* of T₁-weighted sagittal images show the swollen white matter and the cysts in the frontal and temporal region. The U fibers in the posterior region of the cerebral hemispheres, corpus callosum, brain stem, and cerebellum are relatively normal in signal intensity. The *second and third rows* shows these features on axial T₂-weighted images. A large cavum septi pellucidi and cavum Vergae are visible. The corpus

callosum is largely spared. The posterior limb of the internal capsule contains two lines of abnormal signal with a line of normal signal in between. The midbrain, pontine tegmentum, pyramidal tracts in the basis of the pons, and cerebellar white matter are mildly abnormal in signal but not swollen. The *fourth and fifth rows* contain the proton density images, which reveal the many subcortical cysts

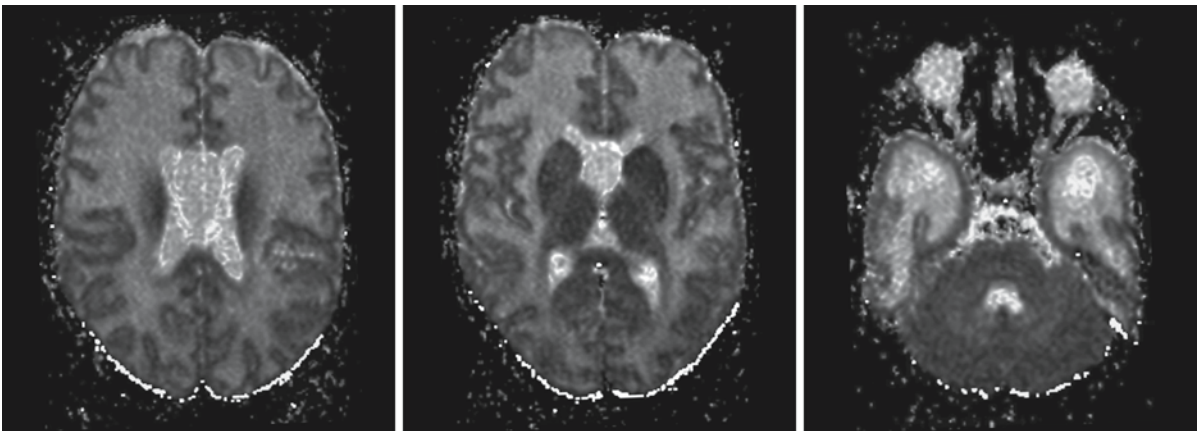


Fig. 59.2. Three ADC maps of the same patient as in Fig. 59.1. ADC values are highly elevated within the cerebral hemispheric white matter, for instance $2.06\text{--}2.47 \times 10^{-3} \text{ mm}^2/\text{s}$ in the frontal white matter (normal white matter ADC $0.85\text{--}0.95$).

ADC values are normal in the basal ganglia ($0.74\text{--}0.94 \times 10^{-3} \text{ mm}^2/\text{s}$) and mildly elevated within the cerebellar white matter ($1.10\text{--}1.32 \times 10^{-3} \text{ mm}^2/\text{s}$)

rowing of ventricles (Fig. 59.1). In older children and adults the hemispheric white matter swelling is less severe, peripheral CSF spaces are more prominently visible, and the ventricular system becomes enlarged (Fig. 59.3 and 59.4). On FLAIR images parts of the cerebral white matter may have a slightly lower signal intensity than the remainder of the abnormal white matter, related to the very high water content of the

white matter. The external and extreme capsules are prominently involved. The central white matter structures, including the corpus callosum, anterior limb of the internal capsule, posterior limb of the internal capsule (in part), and a periventricular rim of occipital white matter are relatively spared. The posterior limb of the internal capsule shows either a double line of abnormal signal intensity over its whole length

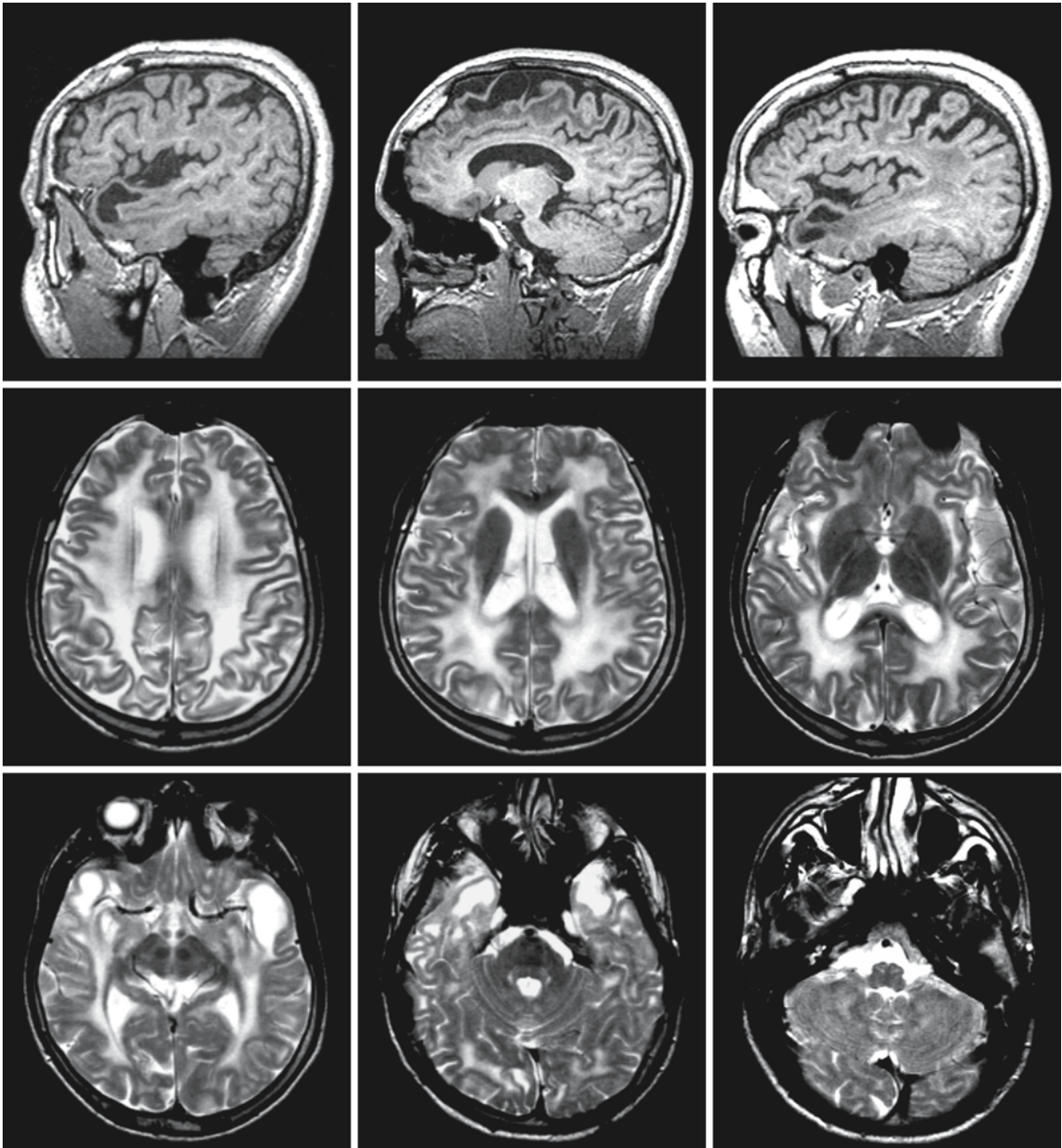


Fig. 59.3. An 18-year-old boy with MLC. The cerebral white matter is diffusely abnormal and mildly swollen, but less so than in the previous patient. Note again the sparing of the corpus callosum and the presence of a double line of high signal

from the posterior limb of the internal capsule. There are mild signal abnormalities in the cerebellar white matter. There are cystic lesions in the anterior temporal and frontal regions

(Figs. 59.1 and 59.3) or a signal abnormality mainly in its distal part (Fig. 59.4). Some sparing of arcuate fibers may be seen, most often in the occipital area (Figs. 59.3 and 59.4). In the majority of patients, the cerebellar white matter shows only a mild abnormality in signal intensity and no swelling (Figs. 59.1, 59.3 and 59.4). In some patients minor abnormalities are

seen in the brain stem, especially the pyramidal tracts (Fig. 59.1). There are almost invariably subcortical cysts in the anterior temporal region, often also in the frontal and parietal subcortical regions (Figs. 59.1 and 59.3–59.6). The cysts are bilateral. So far, the anterior temporal cysts have only been found to be lacking in some young infants and children with

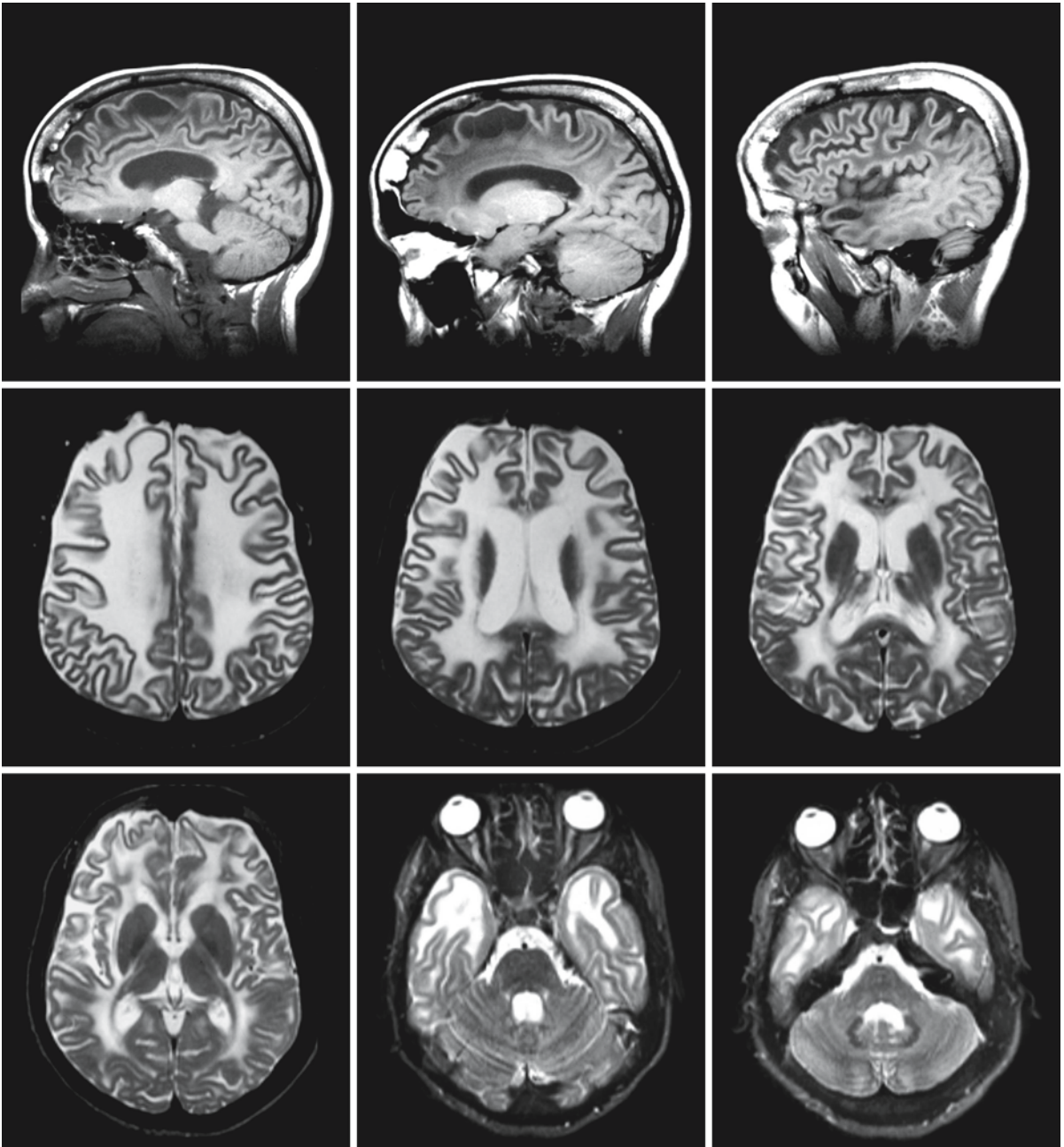


Fig. 59.4. A 20-year-old woman, showing that some atrophy has now developed

MLC. The cysts tend to become larger with age and may increase in number. In some patients they become very large (Fig. 59.5). The signal intensity of the contents of the cysts is always similar to that of CSF. In accordance with this, T_1 and T_2 of cyst contents and CSF are also similar. A patent and enlarged cavum septi pellucidi and cavum Vergae are often present (Figs. 59.1 and 59.3). Cortical gray matter structures and basal nuclei are always normal.

Since the gene for the disease has been found, less prominent white matter abnormalities have been documented in patients with clinically mild disease (Fig. 59.6). Early MRI may show the typical diffuse cerebral white matter abnormalities with swelling (Fig. 59.6a), whereas follow-up MRI may show that the cerebral white matter now has a normal signal intensity in large areas and is less swollen (Fig. 59.6b). It is mainly the subcortical white matter that remains

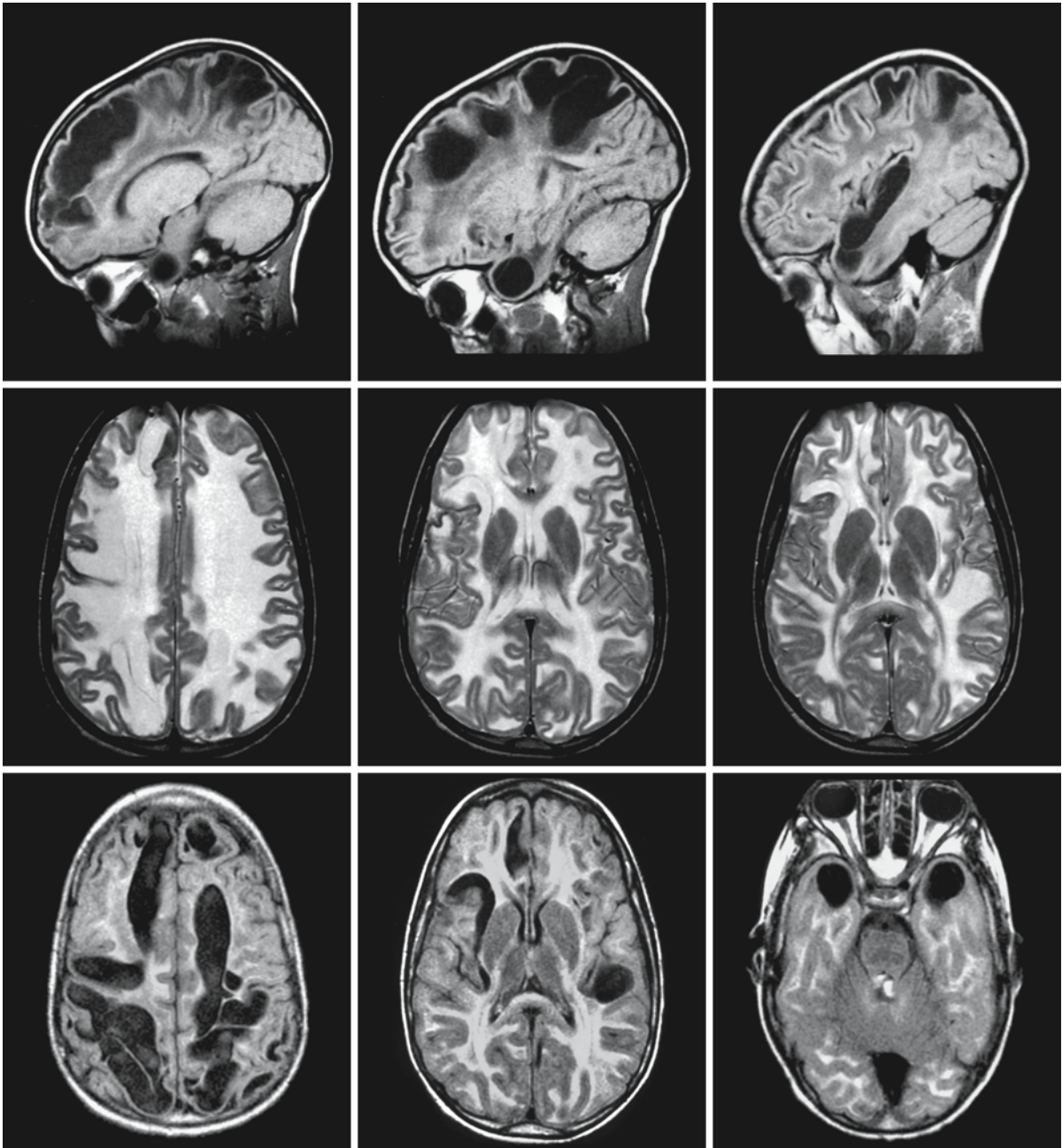


Fig. 59.5. A 5-year-old girl with MLC. The subcortical cysts are huge. Courtesy of Dr. J. Wolf, Biochemical Genetics Clinic, University of Wisconsin–Madison, Madison, Wisconsin, USA

abnormal. Still, the characteristic subcortical cysts are present.

MRS has revealed a reduction of all signals per volume, indicative of the high water content of the brain. Relative to creatine, *N*-acetylaspartate is decreased and *myo*-inositol is increased, suggesting axonal damage and gliosis. Diffusion tensor imaging shows increased ADC values in the cerebral white matter and reduced anisotropy (Fig. 59.2).

Similar white matter changes with swelling have been reported in Canavan disease, Alexander disease, L-2-hydroxyglutaric aciduria, and merosin-deficient congenital muscular dystrophy. However, in Canavan disease, as a rule, MRI demonstrates additional involvement of the thalamus and globus pallidus, not found in MLC patients. Special MRI findings in Alexander disease are a more prominent sparing of parieto-occipital white matter and often also sparing

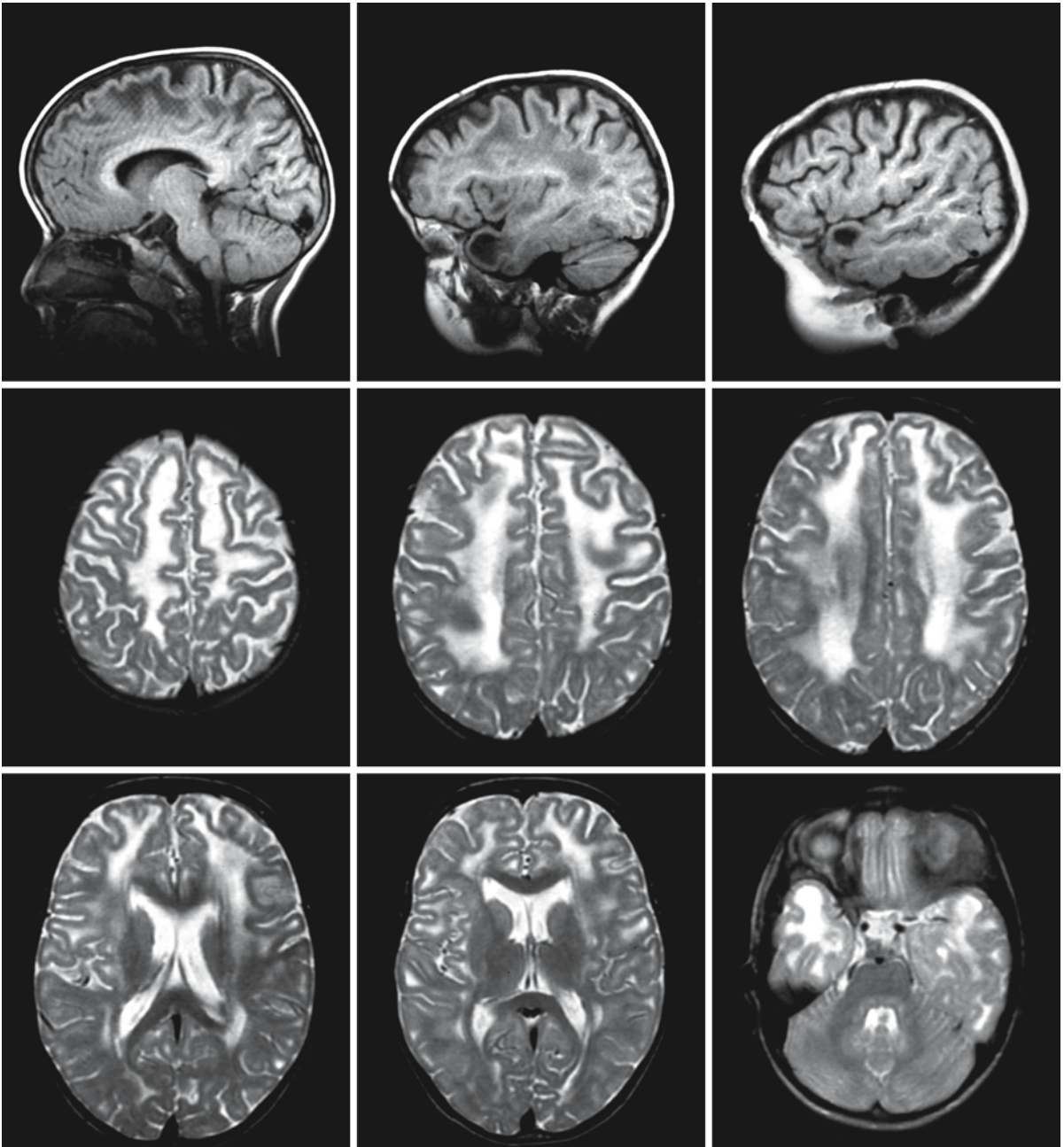


Fig. 59.6 a. Girl with DNA-confirmed MLC. The first MRI (a) was obtained at the age of 5 years; the second (b) at the age of 11 years. Whereas the first images show a classical pattern

of abnormalities (a), the white matter looks much more normal than usual for MLC on the follow-up MRI (b). The subcortical cysts, however, remain present

of the U fibers throughout. Basal ganglia and brain stem structures are typically involved. Contrast enhancement of certain brain structures is typically present. Cavitation starts in the deep frontal white matter. None of these features is present in MLC. In L-2-hydroxyglutaric aciduria MRI shows additional involvement of caudate nuclei, putamen, dentate

nuclei, and severe atrophy of the cerebellar vermis, not observed in MLC. The MRI abnormalities observed in merosin-deficient congenital muscular dystrophy are very similar to those observed in MLC. Subcortical cysts were observed in one patient with a later-onset variant of muscular dystrophy with leukoencephalopathy and swelling.

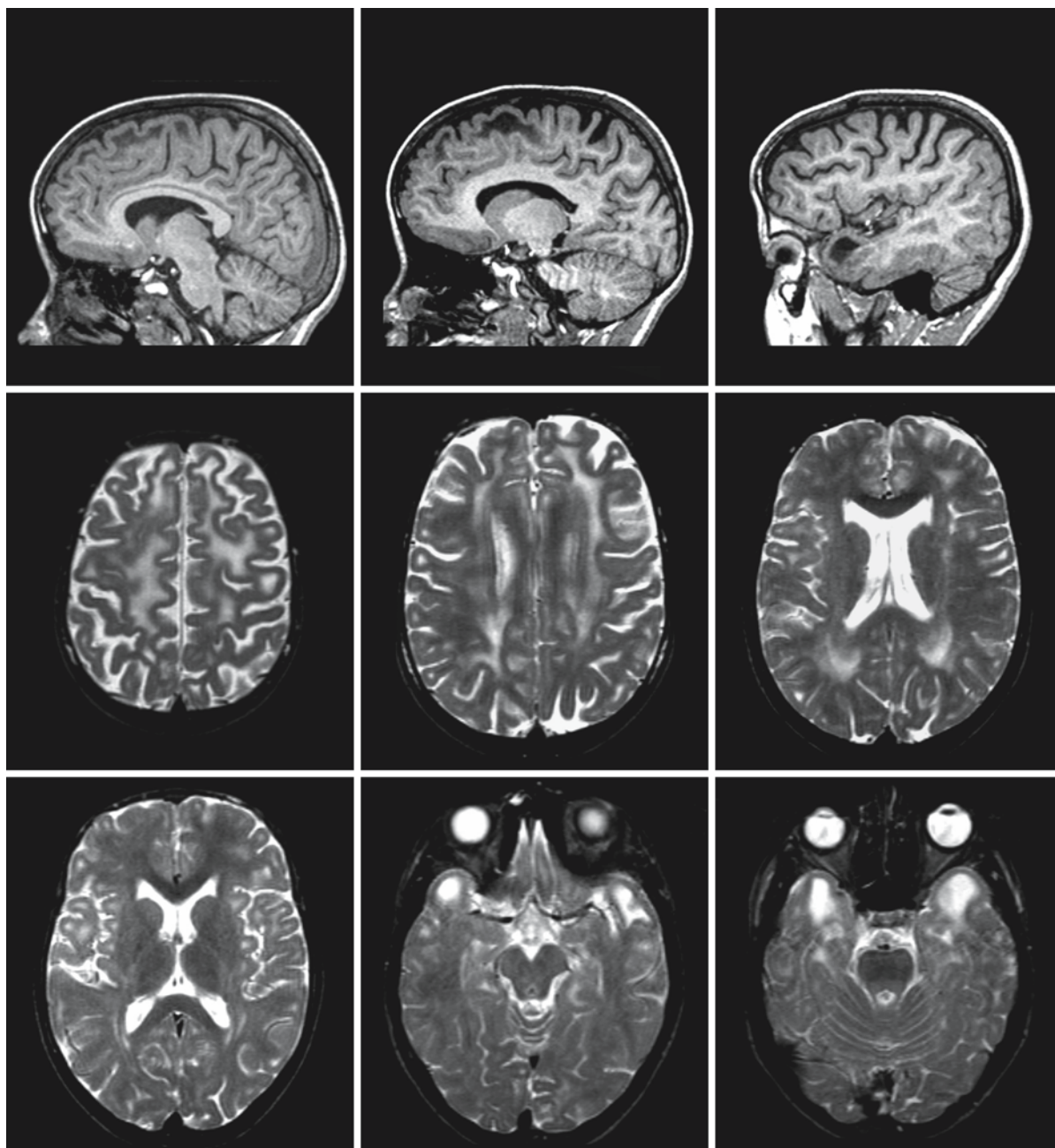


Fig. 59.6 b. (continued).

Congenital Muscular Dystrophies

60.1 Clinical Features and Laboratory Investigations

Congenital muscular dystrophies (CMD) are a heterogeneous group of congenital myopathies that are hereditary and often progressive. They are often associated with abnormalities of the brain and eyes. Only those types that are associated with significant white matter abnormalities are discussed in the present chapter.

1. Fukuyama congenital muscular dystrophy (FCMD)
2. Muscle-eye-brain disease (MEB)
3. Walker-Warburg syndrome (WWS)
4. Merosin-deficient congenital muscular dystrophy (MDC1A)
5. MDC1C
6. MDC1D

WWS has many alternative names, including Walker's lissencephaly, Warburg syndrome, cerebro-oculo-muscular syndrome, cerebro-ocular dysplasia-muscular dystrophy syndrome, and HARD±E syndrome (*hydrocephalus, agyria, and retinal dysplasia with or without encephalocele*). The disease has an autosomal recessive mode of inheritance. Severe neurological dysfunction is evident from birth onwards. Hypotonia is profound and neonatal reflexes are often poor or absent. In about 40% of the patients congenital contractures are present. The affected neonates are immobile and unresponsive. In many patients progressive hydrocephalus is evident from birth onwards with macrocephaly and bulging fontanel. Shunting may be required. In other patients hydrocephalus is not evident at birth but develops soon afterwards. A few patients have microcephaly. About 30% of the patients have an occipital meningocele or encephalocele. Epileptic seizures occur frequently. Ophthalmological abnormalities are multiple and diverse and include defects of the anterior and posterior chambers: corneal opacities, microcornea, megalocornea, iris atrophy, iris coloboma, iridolental synechiae, narrow iridocorneal angle with or without glaucoma and buphthalmos, cataract, persistent hyperplastic primary vitreous, chorioretinal coloboma, retinal dysplasia, retinal detachment, optic disc hypoplasia, optic disc coloboma, and unilateral or bilateral microphthalmia. Some patients have cleft palate and cleft lip. Genital abnormalities including small penis and undescended testes are common in males. In the

months following birth, the infants show profound mental and motor retardation with rarely any development beyond the newborn level. However, the clinical picture varies considerably, even within the same sibship. Survival varies from the neonatal period to over 5 years, but most children die within the first year of life.

In Japan, FCMD is the second most frequent of the muscular dystrophies, Duchenne muscular dystrophy being the most frequent. The disease is almost exclusively reported in Japan. Inheritance is autosomal recessive. Onset of clinical symptoms is in the neonatal or early infantile period with marked hypotonia and hypokinesia. Motor development is delayed to a variable degree. In most patients motor functions are acquired gradually and the maximum motor development has been reached by the age of 2–8 years. The majority of patients never manage to stand or walk; the highest developmental level is usually crawling on hands and knees. The distribution of affected muscles is generalized, but proximal muscles are slightly more severely affected than distal muscles. The facial muscles are also affected, resulting in a hypotonic facial expression. Muscular atrophy is prominent. Pseudohypertrophy of the calves is found in some patients. After the age of about 8 years, motor functions gradually deteriorate. Joint contractures are not usually found in the neonatal period, but flexion contractures of hips, knees, and elbow joints, limited ante flexion of the cervical spine, and contractures of the joints of the hands develop consecutively during the first few years of life. There is invariable involvement of the CNS, often with microcephaly, and always with severe mental retardation, which is not progressive. Seizures occur in more than half the patients, usually in the form of generalized tonic-clonic convulsions. In a minority, infantile spasms are found. Ophthalmological abnormalities are present in about half of the patients and include strabismus, nystagmus, optic nerve pallor, mild to severe myopia, cataract, and, less often, chorioretinal degeneration and retinal vascular abnormalities. The average life span in Fukuyama type CMD is estimated to be about 12 years; patients rarely live beyond the age of 20. However, with respiratory support patients may live beyond this age. In a few cases FCMD is more severe and resembles WWS in phenotype. In these cases patients have more severe muscular weakness, never achieving head control or the ability to sit without support, they may have pro-

gressive hydrocephalus requiring shunt implantation, and they have more severe ophthalmological abnormalities.

Most reports concerning MEB come from Finland. The disease has an autosomal recessive mode of inheritance. Clinical symptoms are similar to those of WWS, but tend to be milder. Muscle hypotonia and poor visual contact are noted in the neonatal or early infantile period. The typical facial appearance is characterized by a relatively large head with a high and prominent forehead, wide fontanel, flat midfacies, short nose, and short philtrum. In about half of the patients there are some signs of hydrocephalus during the first year of life, with a mildly increased head growth rate, but shunt implantation is required in only some of the patients. Motor development is variably but generally severely retarded. Some of the patients show hardly any developmental progress, whereas others achieve sitting without support at the age of 10 years and walking with support after more than 10 years of life. Muscle weakness is generalized, but in the extremities weakness is slightly more prominent in the proximal muscles. Facial muscles are usually not involved. Contractures develop gradually and not in every patient. There is always involvement of the CNS with marked mental retardation. However, some patients do acquire the ability to speak. Most patients develop seizures, and occasionally infantile spasms. Ophthalmological examination typically reveals severe visual failure with severe myopia. Additional ocular signs include glaucoma, retinal degeneration, choroidal hypoplasia, optic nerve pallor, and cataract. Between the ages of 5 and 25 years progress of psychomotor development ceases in many patients and deterioration sets in with loss of mental and motor abilities and development of signs of spasticity, particularly in the legs. The age at death is highly variable: some patients die at the age of 6 years, whereas others survive until their fifties.

In Europe, merosin-deficient CMD (MDC1A) is the commonest form of CMD. Inheritance is autosomal recessive. Generalized hypotonia is noted in infancy with a delay in motor development. Most children do not acquire independent ambulation. Muscle weakness and atrophy are severe and generalized and include facial weakness. Contractures are usually present, either at birth or later in life. Most children have a normal intelligence, some have a mild intellectual impairment, but severe mental deficiency is rare. Some of the patients have macrocephaly. Some children develop seizures. Eyes and visual function are normal. Additionally, there may be cardiac involvement that is usually subclinical, rarely clinically evident. There is neurophysiological evidence of peripheral nerve involvement with reduced motor and sensory nerve conduction velocities, but clinically the neuropathy is overshadowed by the myopathy. Pro-

gression of weakness may be noted at the end of the first decade, with death between 10 and 20 years. However, survival beyond 20 years has been described. Some patients have a milder presentation, related to partial merosin deficiency. Patients have later-onset slowly progressive muscle weakness, mainly limb-girdle type, and achieve ambulation. Rarely, they may display signs of CNS dysfunction. Some patients are adults and (still) asymptomatic.

A new CMD syndrome has been defined, designated MDC1C. The patients present soon after birth with hypotonia and severe weakness. They have weakness and wasting of the shoulder girdle muscles, and weakness and hypertrophy of the leg muscles. In some patients, cognitive development is normal, as is MRI of the brain, whereas other patients display mental retardation and, on MRI, cerebral white matter abnormalities and subcortical cerebellar cysts. MDC1C is allelic with limb-girdle muscular dystrophy 21 (LGMD21), a much milder muscular disease. MDC1C and LGMD21 may occur in the same family.

Another new CMD syndrome has been designated MDC1D. Apart from a congenital muscular dystrophy, mental retardation is present. The phenotypic variability still has to be defined.

In addition to the above, more or less well-delineated syndromes, there are many patients remaining who have an unclassified CMD. Some of these patients have merosin deficiency; most of them do not. Many of these patients do not have accompanying brain abnormalities, but some do. Some of the patients in this group of unclassified CMD cases have white matter abnormalities. Some patients have white matter abnormalities similar to MDC1A, whereas muscle merosin staining is normal. Other patients have more limited white matter abnormalities. Still others have cerebellar abnormalities, brain stem abnormalities, or gyral abnormalities. The classification and basic defects in these patients remain to be elucidated.

In laboratory examinations, a moderately increased CK level is consistently found in almost all patients. However, exceptional patients may have a normal CK level, and, therefore, a normal CK value does not rule out the presence of a CMD. Patients with a partial merosin deficiency have lower CK than classical MDC1A patients, who have markedly increased CK. Electromyography reveals signs of myopathy. In MDC1A, peripheral nerve conduction velocities are decreased. Muscle biopsy contributes to the diagnosis of CMD, revealing dystrophic changes. These include marked variation in fiber size with presence of atrophic and hypertrophic fibers, fiber necrosis with presence of phagocytes, increased number of fibers with internal nuclei, increased interstitial fibrosis, and replacement by adipose tissue. No inflammatory infiltration is found, with the exception of some pa-

tients with MDC1A, in whom the findings may be suggestive of myositis. There are no significant histological differences between the different CMD variants. However, the use of different antibodies contributes to establishing the correct diagnosis. In MDC1A there is isolated negative (usually completely negative) immunostaining for laminin- α 2 in muscle. In some patients with a milder phenotype a partial deficiency is found. Skin biopsy is also useful to assess the laminin- α 2 status of a patient. In FCMD, MEB, MDC1C, and MDC1D muscle, severely decreased immunostaining for α -dystroglycan and a variable but less severe reduction for laminin- α 2 are observed. In WWS immunostaining for α -dystroglycan is decreased, but immunostaining for laminin- α 2 tends to be normal, although decreased immunostaining has also been reported. It is important to realize that there are several antibodies against different epitopes of laminin- α 2. The results of immunostaining may be different with different antibodies. DNA-based prenatal diagnosis is possible in families with a known mutation in one of the genes related to the CMDs.

60.2 Pathology

In WWS the leptomeninges are thick and tend to obliterate the subarachnoid space with fibrous and heterotopic neuroglial tissue. The brain surface may be smooth on external examination, with only an interhemispheric fissure present and a markedly foreshortened sylvian fissure due to incomplete development of the opercula. The brain surface may also have areas of pachygyria and polymicrogyria with an irregular verrucous appearance. Bands of gliotic tissue cross the interhemispheric fissure, especially frontally, fusing the hemispheres. On sectioning, the lateral ventricles are markedly to severely enlarged; only in exceptional cases are the ventricles normal. The cerebral mantle is usually seriously reduced in width. The deep nuclei are present in their normal position but are usually small. The corpus callosum and septum pellucidum are often absent or hypoplastic. The aqueduct is small and stenotic. The quadrigeminal surface elevations are fused and the mammillary bodies do not protrude from the ventral surface. The brain stem is small and the pons markedly hypoplastic. Olfactory and optic nerves are attenuated or absent. The cerebellar vermis, especially the posterior vermis, and the cerebellar hemispheres are hypoplastic, often associated with an enlarged fourth ventricle and a retrocerebellar cyst, constituting a Dandy-Walker malformation. In about 25% of the patients a posterior encephalocele or meningocele is present, containing either an extension of a retrocerebellar cyst, cerebellar tissue, or, rarely, tissue of supratentorial origin.

Factors contributing to ventricular enlargement are aqueduct stenosis, disturbed fluid dynamics associated with the Dandy-Walker malformation, and blockage of the arachnoid granulations by fibroglial tissue. The cerebral cortex is abnormally thick with absent white matter interdigitations or with irregular, shallow indentations in the otherwise smooth cortical ribbon. On microscopic examination the cortex is severely disorganized, with no recognizable lamination and widespread disruption by gliofibrillary bundles accompanying vessels from the pial surface. Agyria or pachygyria with severe disorganization of the cortex and absence of lamination is called lissencephaly type II. Neuronal heterotopias are present scattered in the white matter and in the subependymal region. The white matter is reduced in volume, poorly myelinated, gliotic, spongy, and often strikingly edematous with occasionally cavitations. Myelination is virtually absent in some cases. In the brain stem corticospinal tracts are grossly absent. The pontine nuclei and middle cerebellar peduncles are usually absent. Within the smooth, afoliar cerebellar cortex microscopic changes are found similar to those in the cerebral cortex, but the abnormalities are less severe, as some organization into layers is usually present. Cerebellar white matter is better myelinated.

In FCMD superficial gliomesenchymal proliferation is present on the surface of the brain and spinal cord, leading to thickened leptomeninges adherent to the surface of the CNS. Microscopically, glioneuronal heterotopias are found in the leptomeninges. Extensive cortical dysplasia of cerebrum and cerebellum is present. The pattern of the cortical dysplasia is always symmetrical, but varies in severity from site to site and from case to case. As a rule, the cortical dysplasia is most prominent in the frontal and temporal lobes, whereas the occipital lobe is relatively spared. Occasionally the frontal cortex shows focal interhemispheric fusions. The primary sulci (central, calcarine, parieto-occipital, and cingulate) are present, secondary sulci are shallow, and the gyral surfaces have an irregular appearance. The cortical dysplasia may take the form of unlayered polymicrogyria (lissencephaly type II), or smooth, four-layered pachygyria, or verrucous dysplasia with superficial cellular nodules within a normally stratified six-layer cortex. The polymicrogyria is also called pachygyric polymicrogyria (or polymicrogyric pachygyria), because the microgyri are fused and the external appearance of the brain is pachygyric; polymicrogyria is only a microscopic finding. In most patients the three mentioned types of cortical dysplasia are present to a variable extent. Many breaches are present in the glia limitans-basal lamina complex overlying the cerebral cortex. In the CNS a basement membrane is observed in the boundary between nervous tissue and leptomeninges forming part of the pial-glial barrier. At

the site of the breaches, neural tissue protrudes. The exposed surfaces of the extruded neuroglial elements lack basal lamina, come into contact with adjoining elements, and fuse with each other, leading to development of polymicrogyria. During this process, vessels in the subarachnoid space, which were originally located over the cortical surface, become entrapped. The border between cerebral cortex and white matter is irregular. Ectopic nerve cells are found in the subcortical white matter, near the ventricles and disseminated within the white matter. The ventricles are often mildly dilated. Overt hydrocephalus is not present. The pyramidal tracts in the brain stem are hypoplastic and dysplastic and have an abnormal course. Within the cerebellar cortex, areas of polymicrogyria are present. In the cerebellum mesenchymal tissue proliferation appears to have occurred inside the cerebellar parenchyma to form numerous small cavities bordered by neuroglial elements. The cerebral white matter changes vary in severity. Myelin paucity and gliosis are seen, but without signs of breakdown, particularly in the younger children, whereas normal myelination may be seen in older children. In a patient in whom brain tissue was investigated at two different points of time, myelination was very poor and astrogliosis marked in brain biopsy material, whereas at autopsy 4 years later, myelination proved to be only slightly less than normal and astrocytosis was mild.

In MEB, the cerebral gyral pattern is coarse on inspection, with an abnormal nodular surface, suggestive of pachygyric polymicrogyria. Agyric areas have been found in the lateral convexity of the occipital lobes. On sectioning, the cortex is abnormally thick. Microscopic examination reveals that almost the entire cortex is severely disorganized apart from the basomedial occipital lobe and hippocampus. The abnormally thick cortex lacks horizontal laminae and vertical columns. The neurons are haphazardly oriented and form irregular clusters or islands separated by gliovascular strands extending from the pia. In places, irregular bundles of myelinated axons penetrate the cortex from the white matter. The pia-arachnoid is focally thickened and adherent to the cortex. The pial-cortical border is irregular. The white matter is reduced in volume and shows a moderate and variable degree of myelin pallor and gliosis. The ventricles are dilated to a variable extent. The septum pellucidum may be absent. The cerebellar cortex is also severely disorganized and lacks normal folia, especially on the upper surface. The vermis is severely hypoplastic. The interface between pia-arachnoid and cerebellar cortex is distorted. Gliovascular strands penetrate the cerebellar cortex. The brainstem is thin and the pons is flat.

In MDC1A only two histopathological reports have been published. Echenne et al. (1984) report on an 18-

year-old patient. The external appearance of the brain was normal. Furthermore, no abnormalities of cerebral and cerebellar cortex were found on microscopic examination and there were no neuronal heterotopias within the white matter. Extensive myelin pallor was found bilaterally with sparing of the arcuate fibers. Abnormalities were most severe in the frontoparietal white matter, whereas the occipital white matter was less severely affected. On microscopic examination there was a spongy appearance of myelin. Moderate astrocytic proliferation and vascular hyperplasia were found. No changes were found in basal ganglia, brain stem, or cerebellum, including cerebellar white matter. Taratuto et al. (1999) report on a 4-month-old patient. The patient had bilateral occipital cortical dysplasia with irregular lamination and fusion of adjacent gyri at microscopy. Multifocal glioneural leptomeningeal heterotopias were present. The white matter had a normal stage of myelination for a 4-month-old infant. The cerebellar vermis was hypoplastic. Sural nerve biopsy in MDC1A patients shows a reduction of large myelinated fibers, short internodes, enlarged nodes, excessive variability of myelin thickness, tomacula, and uncompacted myelin, but no evidence of demyelination.

60.3 Pathogenetic Considerations

The dystrophin-associated glycoprotein (DAG) complex is present in several tissues including muscle, heart, nerve, and brain. This complex has a crucial role in linking the cytoskeletal proteins with the extracellular basal lamina. In muscle this complex functions by linking the actin-associated cytoskeleton of the muscle fibers to the extracellular matrix via dystrophin and the laminin- α 2 chain of merosin. The dystrophin-associated glycoprotein complex is crucial for normal contraction of muscle. α -Dystroglycan is a peripheral membrane component of the dystrophin-associated glycoprotein complex. Structural defects in the dystrophin-associated glycoprotein complex, leading to defects in the linkage between merosin in the extracellular matrix and actin in the subsarcolemmal cytoskeleton, cause various muscular dystrophies. Duchenne and Becker muscular dystrophies are related to mutations in dystrophin. Mutations in various sarcoglycans result in limb-girdle muscular dystrophies. Mutations in the gene *LAMA*, which is located on chromosome 6q and encodes the laminin- α 2 chain of merosin, result in MDC1A. WWS, FCMD, MEB, MDC1C, and MDC1D are characterized by hypoglycosylation of α -dystroglycan. Glycosylation is the most common form of post-translational protein modification, necessary for proteins to achieve their proper structure, function, and stability. It is a complex process where sugars are added to pro-

teins as they pass through the endoplasmic reticulum and the Golgi apparatus. Attached glycans can be divided into two groups according to their linkage to the protein. *N*-Glycans are linked to asparagine; *O*-glycans are attached to serine or threonine. α -Dystroglycan is normally a heavily glycosylated protein, and hypoglycosylation abolishes the binding activity of the protein for laminin, neurexin, and agrin, all of which are components of the basement membrane. In 20% of WWS patients the disease is caused by mutations in the gene *POMT1*, which is located on chromosome 9q34.1 and encodes *O*-mannosyltransferase 1. FCMD is related to mutations in the gene *FCMD*, which is located on chromosome 9q31 and encodes the protein fukutin. The function of fukutin is unknown, but based on amino acid homology with several phosphoryl-ligand transferases, it is hypothesized to be a glycosyltransferase. MEB is caused by mutations in the gene *POMGNT1*, located on chromosome 1p33–34, which encodes the protein *O*-mannosyl- β 1,2-*N*-acetylglucosaminyltransferase-1 (POMGnT1). This enzyme uses an *O*-linked mannose as a substrate. Fukutin-related protein, encoded by the gene *FKRP*, located on chromosome 19q13.3, is highly homologous to fukutin and also a putative glycosyltransferase. Mutations in the gene *LARGE*, located on chromosome 22q12.3–q13.1, lead to MDC1D. Large is a putative glycosyltransferase.

In WWS, about 20% of the patients have a defect in *O*-mannosyltransferase 1, the enzyme that putatively catalyzes the first step in *O*-mannosyl glycan synthesis. The *O*-mannosyl glycans of α -dystroglycan are critical for binding laminin- α 2. WWS is genetically heterogeneous and several WWS families do not link to the *POMT1* locus. It is very likely that defects in the other proteins involved in *O*-mannosylglycosylation underlie the remaining, unexplained WWS patients.

FCMD occurs almost exclusively in Japan. About 95% of FCMD patients share a specific haplotype on one or both alleles in the critical region of chromosome 9, supporting the hypothesis of a founder of the disease in the Japanese population. In all patients sharing this haplotype, a 3-kb retrotransposal insertion into the 3'-untranslated region of the gene is found. Various other mutations have been found. The frequency of a severe phenotype with WWS-like manifestations such as hydrocephalus and microphthalmia is higher among patients who are compound heterozygous for the Japanese founder mutation than among the patients who are homozygous for the founder mutation. The observed lack of Japanese patients with two nonfounder mutations suggests that such cases might be fatal in utero. This may also explain why few FCMD patients have been reported in non-Japanese populations in which the Japanese founder mutation does not occur. The rare non-

Japanese patients with mutations in *FCMD* tend to have a very severe, WWS-like clinical phenotype.

MEB is caused by a defect in the *O*-mannosyl glycan synthesis. POMGnT1 normally adds an *N*-acetylglucosamine residue to an *O*-linked mannose. This is the second step in *O*-mannose glycosylation. It has been demonstrated that sialyl *O*-mannosyl glycan is the laminin-binding ligand of α -dystroglycan. The hypothesis that defects in *O*-mannosylation weaken the laminin-binding and consequently may be responsible for muscular dystrophy led to the detection of a defect in POMGnT1 as the cause of MEB. Some patients with severe *POMGNT1* mutations have a WWS-like phenotype. Patients with mutations near the 5'-terminus tend to have a more severe clinical phenotype than patients with mutations near the 3'-terminus.

Laminin is a heterotrimer composed of three different polypeptides, called α -, β -, and γ -chain, of which different subtypes are known. These chains assemble into a number of different laminin variants, but every laminin has one α -, one β -, and one γ -chain. Laminin-2, or merosin, is composed of α 2- β 1- γ 1. It is the α 2-chain that is mutated in MDC1A. Classical MDC1A is associated with mutations that drastically affect the expression or structure of laminin- α 2. A wide range of milder phenotypes is caused by partial laminin- α 2 deficiency, produced by mutations in *LAMA2* that permit production of a partially functional protein or a reduced amount of normal protein. Merosin is not only present in muscle tissue, but also in the brain. In the brain merosin is localized on the brain surface at the glia limitans and on the basement membrane of blood vessels. Furthermore, merosin is present in the endoneurial basement membrane that surrounds the myelin sheath of peripheral nerve fibers and individual Schwann cells. In laminin- α 2 deficiency, the basement membrane in skeletal muscle and peripheral nerves is disrupted or completely absent, indicating that laminin- α 2 is essential for formation of basement membrane in these tissues. There is evidence that the formation of a basement membrane is a prerequisite of myelination in peripheral nerves. Under conditions that prevent basement membrane formation, Schwann cells fail to ensheath and myelinate nerve fibers.

Defects in the gene *FKRP* lead to a severe form of CMD, designated MDC1C, and a milder limb-girdle muscular dystrophy, designated LGMD21. Most patients with MDC1C do not have structural brain abnormalities. However, it has been shown that severe mutations in *FKRP* may lead to an MEB or even WWS phenotype.

Large is a putative bifunctional glycosyltransferase. One putative catalytic region has a high homology to members of the bacterial WaaIJ family of putative α -glycosyltransferases involved in the syn-

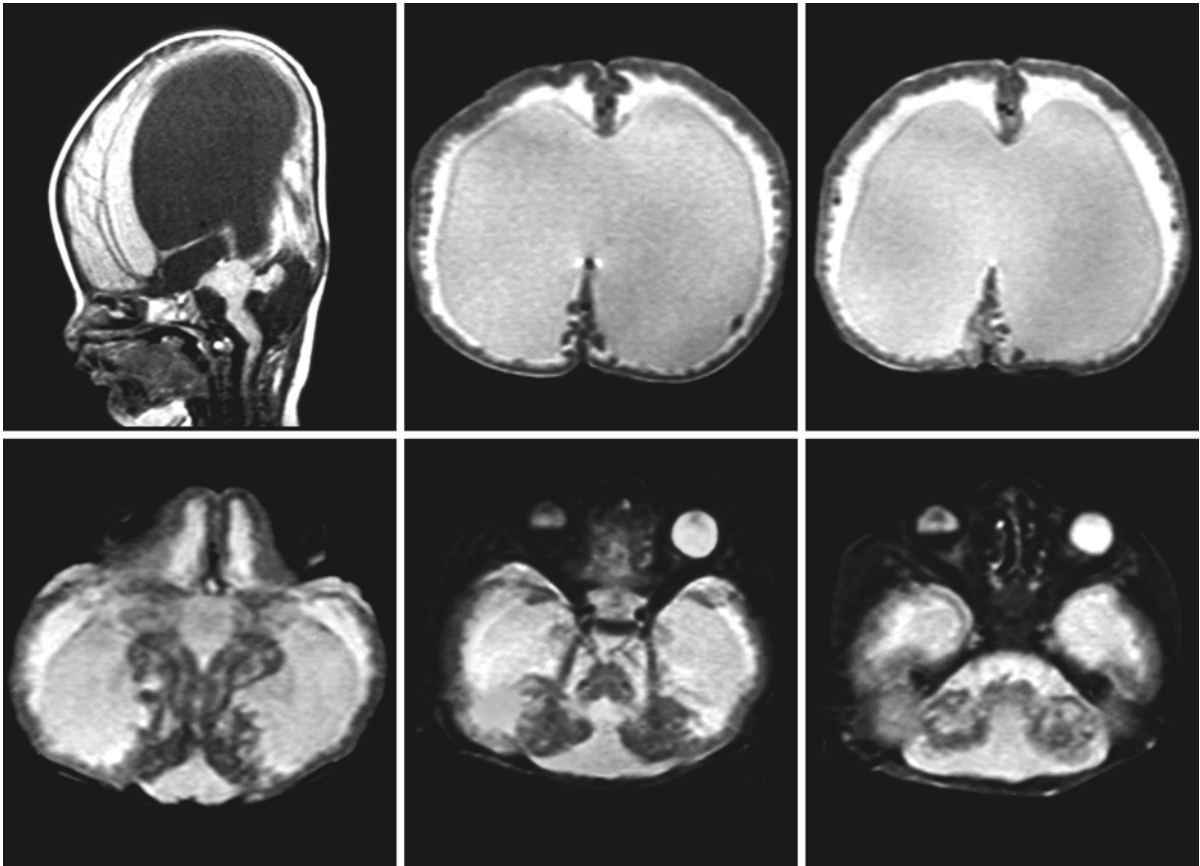


Fig. 60.1. A 4-month-old boy with WWS. The third and lateral ventricles are highly enlarged due to aqueduct stenosis. The corpus callosum is thin and high-arched. Note the presence of a cingulate gyrus, indicating that there is no agenesis of the corpus callosum. The septum pellucidum is absent. The colliculi are fused. The pons is extremely hypoplastic and there is a pontomesencephalic kink. The cerebellum is extremely hypoplastic with characteristics of a Dandy-Walker malforma-

tion. The cerebral cortex is agyric on the outside, whereas the irregular inner border indicates a disorganized, polymicrogyric cortex, compatible with lissencephaly type II. The cerebellar cortex is also disorganized. The cerebral hemispheric white matter has an abnormal signal throughout. Only the brain stem appears to contain some normal myelin. From Van de Knaap et al. (1997), with permission

thesis of lipopolysaccharides or lipo-oligosaccharides. The second catalytic domain is closely related to $I\beta$ -1,3-*N*-acetylglucosaminyl transferase, an enzyme required for the synthesis of the poly-*N*-acetyl-lactosamine backbone, which is attached to *N*-glycans, *O*-glycans, and glycolipids.

Whether the brain and eye symptoms in the WWS, FCMD, MEB, MDC1C, and MDC1D are related to the defect in glycosylation of α -dystroglycan or other proteins is less clear. Brain-specific disruption of α -dystroglycan during embryonic development causes neuronal overmigration and fusion of cerebral hemispheres in mice. This suggests that disrupted glycosylation of α -dystroglycan is also at least in part responsible for the brain abnormalities. The white matter abnormalities reported in the CMDs are variable and

their pathogenesis is unclear. Retarded but ongoing myelination may contribute in some cases, especially in FCMD and MEB. However, in FCMD and MEB, too, the cerebral white matter abnormalities have a higher signal on T_2 -weighted images and a lower signal on T_1 -weighted images than is compatible with straightforward hypomyelination, but reduction in the white matter abnormalities has been observed on follow-up. In WWS and MDC1A the white matter abnormalities are more impressive and mildly swollen, suggesting sponginess, which has been confirmed at autopsy. The role of the white matter abnormalities in determining the clinical picture seems to be minor in all CMD variants. The disease is mostly explained by the severity of the cortical dysplasia and the muscular dystrophy.

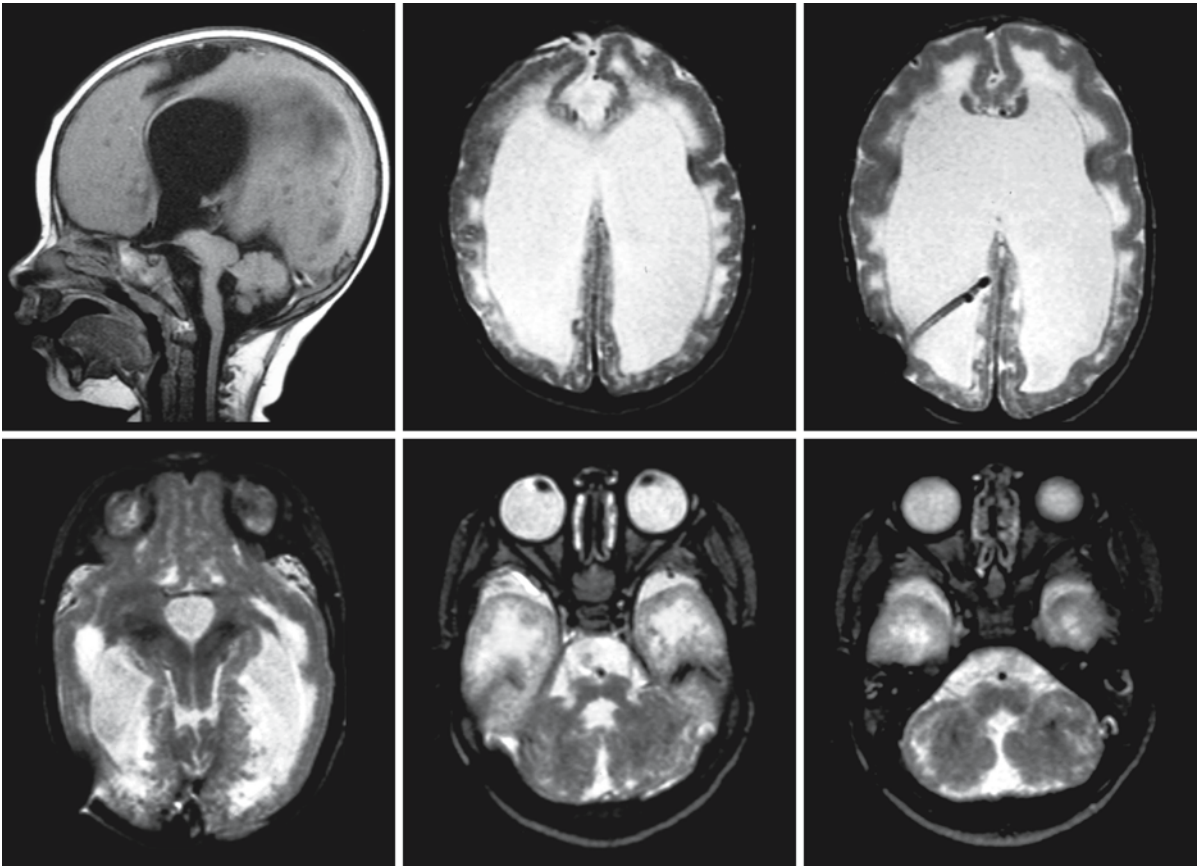


Fig. 60.2. A 10-month-old girl with WWS. The lateral and third ventricles are markedly dilated despite the shunting. Note the thin and high-arched corpus callosum, which is just visible. The septum pellucidum is absent. The colliculi are fused. The pons and cerebellar vermis are hypoplastic. The cerebral cortex is pachygyric. In the anterior region the cortex is abnormally thick, whereas it is thinner in the parietal areas. The irregular inner border indicates a disorganized, polymicrogyric cortex, compatible with lissencephaly type II. There is a rim of periven-

tricular heterotopias. The cerebellar cortex is also disorganized, with the presence of many small subcortical cysts. The cerebral hemispheric white matter has an abnormal signal throughout. Only the brain stem and cerebellar white matter appear to contain myelin. Courtesy of Dr. C.E. Catsman-Berrevoets, Department of Child Neurology, Sophia Children's Hospital and Erasmus University Medical Center, Rotterdam, The Netherlands

60.4 Therapy

No definitive treatment is possible, only supportive care. Physiotherapy is of major importance. In some patients a slight improvement in strength and a fall in CK activity have been noted on administration of corticosteroids. However, in other patients no improvement was found. Considering the major adverse effects of chronic use of corticosteroids, this mode of therapy remains controversial. Respiratory support may prolong life.

60.5 Magnetic Resonance Imaging

In WWS, MRI almost invariably shows severe hydrocephalus (Figs. 60.1–60.3). A normal ventricular size is highly unusual. Because of the severe hydrocephalus and very thin cerebral mantle, the quality of the white and gray matter may be difficult to assess. In patients in whom a cerebral mantle of some thickness is present, the abnormalities are easier to recognize. The cortex is either totally agyric (Fig. 60.1) or folded in broad, somewhat better formed gyri (Figs. 60.2 and 60.3). The cortex is smooth on the external side but the border with the white matter is irregular, reflecting the underlying polymicrogyria and disorganization of the cortex with frequent disruption by gliofibrillary bundles (Figs. 60.1–60.3). In some cases ex-

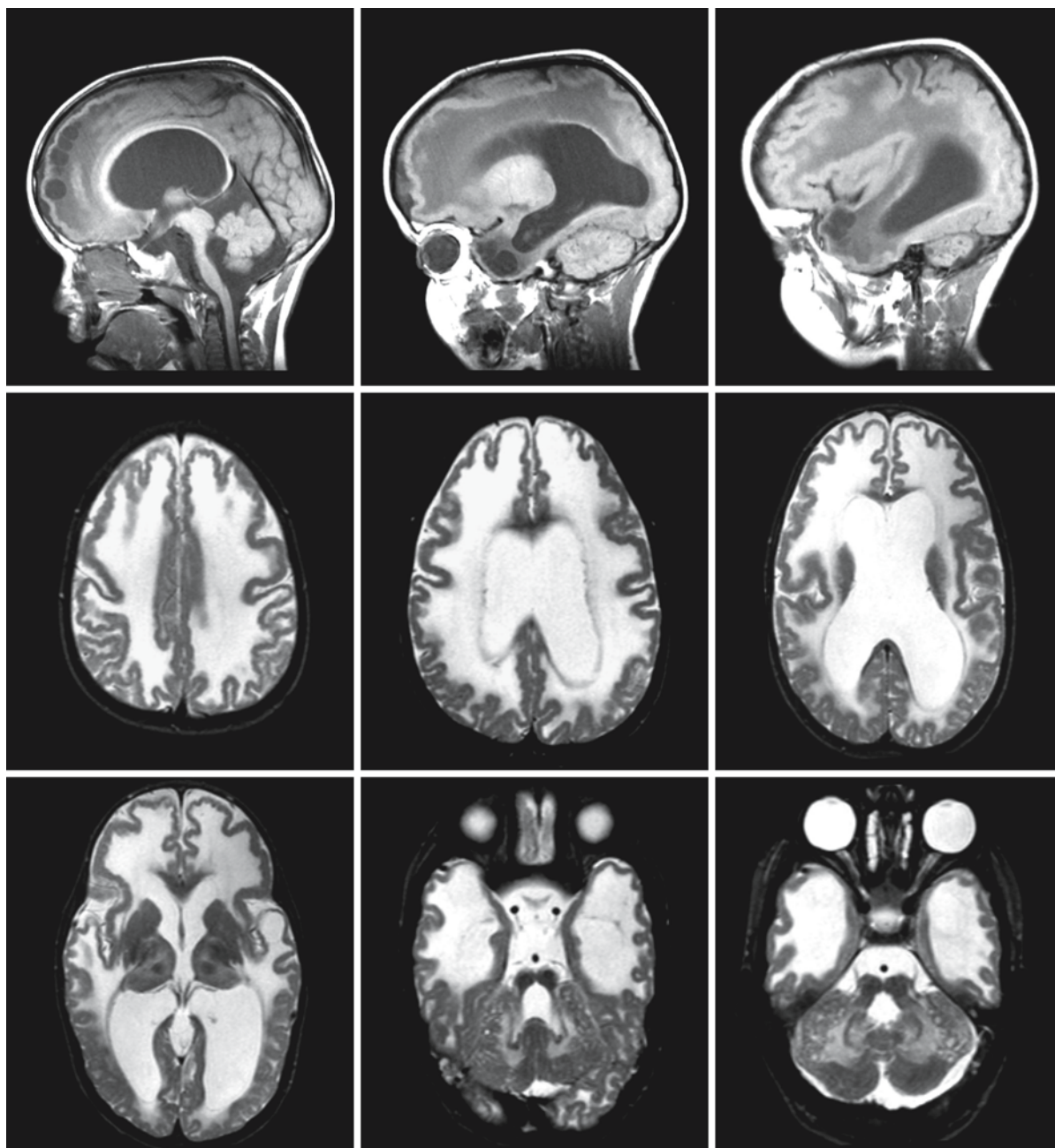


Fig. 60.3. A 6-year-old boy with WWS. The lateral and third ventricles are mildly dilated. The corpus callosum is high-arched. The septum pellucidum is partially absent. The colliculi are fused. The pons and cerebellar vermis are hypoplastic. The cerebral cortex is pachygyric and irregular, compatible with lissencephaly type II. There are many small periventricular heterotopias. The cerebellar cortex is disorganized, with the pres-

ence of many small subcortical cysts. The cerebral hemispheric white matter has an abnormal signal throughout and is swollen. There are multiple large subcortical cysts. The cerebellar white matter also has an abnormal signal intensity. Only the corpus callosum and the brain stem have a normal low signal. From Van der Knaap et al. (1997), with permission

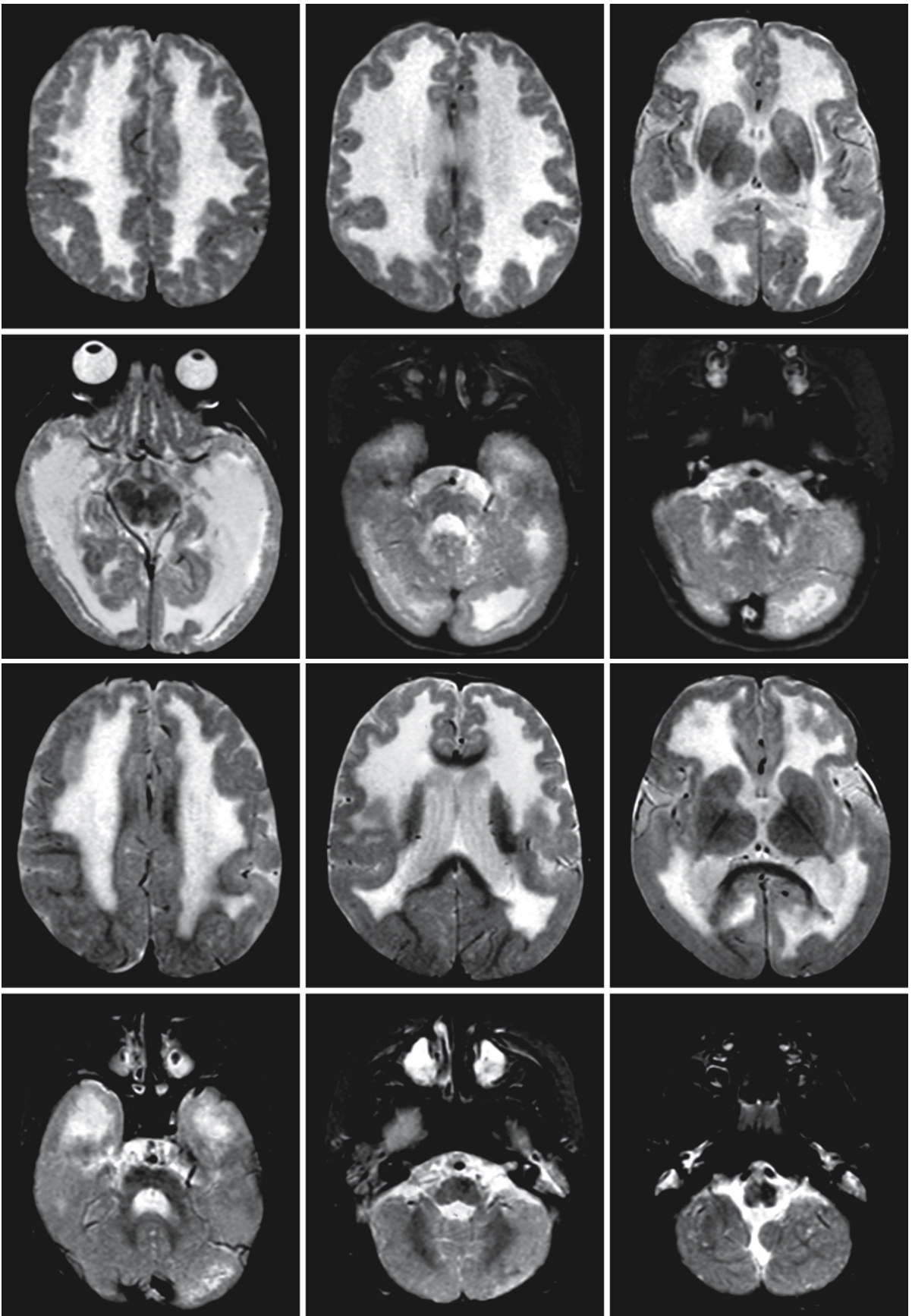


Fig. 60.4.

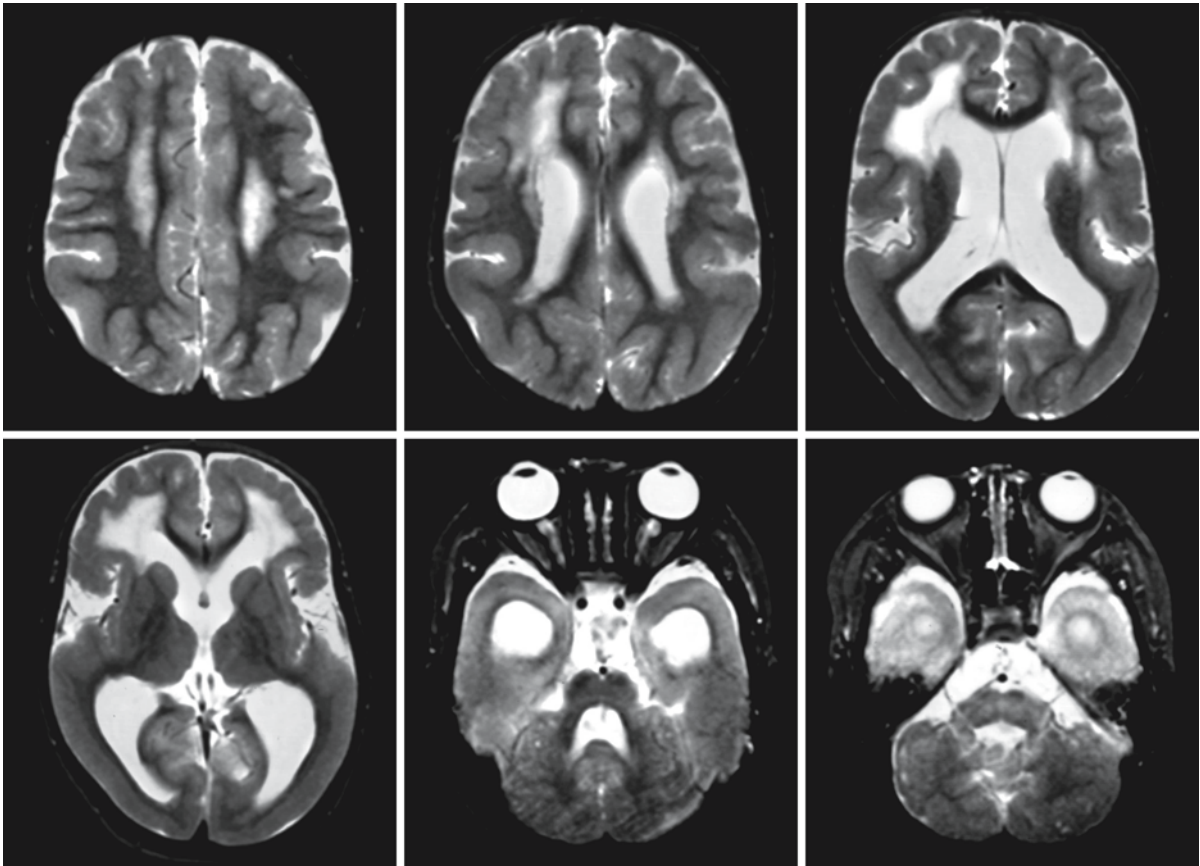


Fig. 60.4. (continued). A male patient with FCMD. The first and second rows show the MRI at 5 months, the third and fourth rows contain the MRI obtained at 21 months, the fifth and sixth rows show the MRI obtained at 7 years. The frontoparietal cortex displays the characteristics of a polymicrogyric pachygyria, whereas the occipital cortex is smooth and very thick. The cerebellar cortex is also dysplastic with distortion of the normal horizontal foliae and presence of subcortical cerebellar cysts. The pons is flat. The lateral ventricles are somewhat

dilated. The cerebral white matter is diffusely abnormal in signal at 5 months, but improvement is seen over time. At 7 years the posterior cerebral white matter is normally myelinated, whereas the frontal periventricular and deep white matter has an abnormal signal intensity. The corpus callosum and internal capsule have a normal signal intensity. Courtesy of Dr. N. Aida, Department of Radiology, Kanagawa Children's Medical Center, Yokohama, Japan

tensive subcortical and subependymal heterotopic neuronal nodules are seen (Figs. 60.2 and 60.3). The cerebral white matter has a high signal intensity on T₂-weighted images throughout and a low signal intensity on the T₁-weighted images (Figs. 60.1–60.3). The white matter may have a mildly swollen appearance and multiple cysts may be present within this highly abnormal looking white matter (Fig. 60.3). The corpus callosum is often very thin and high-arched, and may not be visible. However, the presence of a gyrus cinguli strongly suggests that it is not an agenesis of the corpus callosum, but rather an extreme thinning due to severe hydrocephalus (Figs. 60.1–60.3). The septum may be absent, probably also related to the long-standing hydrocephalus of antenatal origin (Figs. 60.1–60.3). The third ventricle

is also enlarged and the aqueduct is narrow. Fusion of the superior and inferior colliculi is typically seen (Figs. 60.1–60.3). There is often a pontomesencephalic kink and the pons is extremely hypoplastic (Figs. 60.1–60.3). The cerebellum is highly hypoplastic in all its elements, in particular in the vermis. The cerebellar surface is smooth, without foliae or with irregular, small foliae. Multiple small subcortical cerebellar cysts are seen (Figs. 60.2 and 60.3). In some patients the posterior fossa is extremely small, but in other patients the fourth ventricle is enlarged and in open communication with an enlarged retrocerebellar space, forming either the full-blown Dandy–Walker malformation or the less severe Dandy–Walker variant (Fig. 60.1). A posterior meningocele or encephalocele is often present.

In FCMD, MRI reveals cerebral cortical dysplasia, showing gyri that are too few and too broad, and incomplete opercularization (Fig. 60.4). In most areas the slightly thickened cortex has an irregular aspect with little dots and an irregular inner border, reflecting polymicrogyria and verrucose cortical dysplasia. This type of cortical dysplasia is seen in frontoparietotemporal areas (Fig. 60.4). In some areas the cortex is thicker and has a smooth inner and outer surface. This type of cortical dysplasia is mainly seen in the temporo-occipital region (Fig. 60.4). The ventricular system is mildly enlarged and often has a colpocephalic aspect. In neonates the cerebral white matter looks normal for unmyelinated white matter. In infants and young children the cerebral white matter looks diffusely abnormal, with a higher signal on T₂-weighted images and lower signal on T₁-weighted images than is compatible with straightforward hypomyelination (Fig. 60.4a). On repeated MRI progress of myelination is seen, the rate being variable (Fig. 60.4b,c). In some patients there is still hardly any myelin after several years. In some older children diffuse white matter lesions are seen. Most patients have multifocal lesions in the cerebral white matter (Fig. 60.4b, c). The lesions vary in size and distribution. In a few patients no white matter abnormalities are found. The corpus callosum, internal capsule, and brain stem display a normal myelin signal. MRI also shows cerebellar cortical dysplasia, with irregularly distorted folia. There are subcortical cerebellar cysts (Fig. 60.4b, c). The pons is flat (Fig. 60.4).

In MEB, MRI shows a variable ventricular enlargement, ranging from normal to markedly dilated. The cortical dysplasia is variable, both between different areas of the brain and between patients (Figs. 60.5 and 60.6). The frontal, temporal, and parietal areas are the most abnormal, whereas the configuration of the occipital cortex is close to normal. The cortex is slightly too thick and folded in broad gyri with an irregular inner border, compatible with pachygyric polymicrogyria (Figs. 60.5 and 60.6). Opercularization is incomplete. Neuronal heterotopias may be seen in the white matter. The cerebral white matter is either normal (Fig. 60.6) or contains multifocal white matter abnormalities (Fig. 60.5). The corpus callosum may be dysplastic and thin and the septum pellucidum may be incomplete. The superior and inferior colliculi are fused. The pons is hypoplastic. The cerebellum, in particular the vermis, may be small. The cerebellar cortex is dysplastic and there are multiple small subcortical cerebellar cysts (Figs. 60.5 and 60.6).

In classical MDC1A, MRI shows prominent white matter changes (Figs. 60.7 and 60.8). The white matter appears mildly swollen, leading to broadening of the gyri with stretching of the overlying cortex. On CT it is difficult to distinguish between primary cortical dysplasia and secondary broadening of the gyri as a

consequence of white matter swelling. MRI shows that the cortex is not thicker than normal and does not have the irregular inner border of pachygyric polymicrogyria (Figs. 60.7 and 60.8). However, some MDC1A patients have occipital cortical dysplasia with an agyric outer border but irregular inner border and evidence of subcortical ectopic neurons, similar to the lissencephaly type II seen in WWS (Figs. 60.9 and 60.10). In patients with occipital agyria the occipital horn of the lateral ventricles may be focally dilated (Fig. 60.9). The dysplasia is bilateral but may be larger on one side than the other, with also a more prominent enlargement of the occipital horn on the most seriously affected side. In MDC1A, the white matter is near-normal in the first few months of life (Fig. 60.9). From the second half of the first year onwards, MRI shows swollen white matter with a high signal on T₂-weighted images, low on T₁-weighted images. In most patients the white matter abnormalities are extensive and confluent, but in some patients they are a bit less extensive and sometimes they are multifocal. The abnormalities have a frontal predominance and the occipital white matter is better preserved. In some cases the subcortical areas are spared throughout. The corpus callosum, internal capsule, optic radiation, brain stem, and cerebellar white matter are consistently spared. The white matter changes appear to be nonprogressive over the years. In patients with occipital agyria, the occipital white matter may be markedly abnormal (Fig. 60.9). In some patients hypoplasia of the pons is seen (Fig. 60.7). The cerebellum may also be hypoplastic. In CMD patients with partial merosin deficiency, white matter abnormalities are more variable. Some patients have extensive white matter abnormalities similar to those seen in classical MDC1A. In others the white matter abnormalities are more limited in extent (Fig. 60.10). Occipital agyria may also occur in patients with partial merosin deficiency (Fig. 60.10).

In the two patients with adult-onset signs of muscular dystrophy and cerebral dysfunction reported by van Engelen et al. (1992), the white matter abnormalities are identical to those of MDC1A patients. A special finding is that the oldest patient, 29 years of age, has cysts in the subcortical area in the tips of the temporal lobes and the parietal area. With these cysts the MR pattern becomes indistinguishable from the pattern of megalencephalic leukoencephalopathy with subcortical cysts, described in Chap. 59.

In the MDC1C patients with mutations in the *FKRP* gene and cerebral abnormalities, variable cerebral white matter abnormalities and the presence of subcortical cerebellar cysts have been reported (Figs. 60.11 and 60.12). However, most patients with *FKRP* mutations have normal MRI.

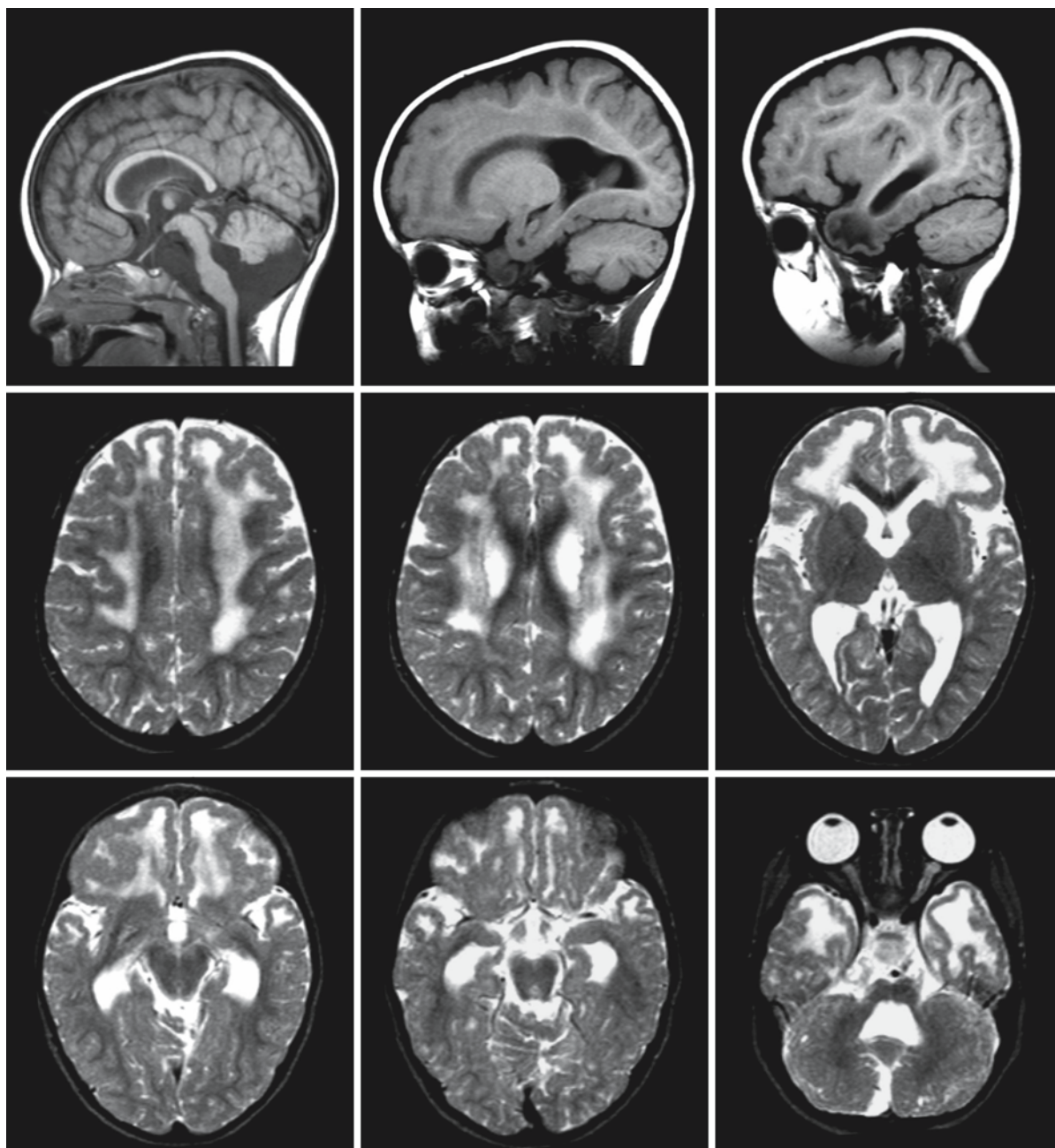
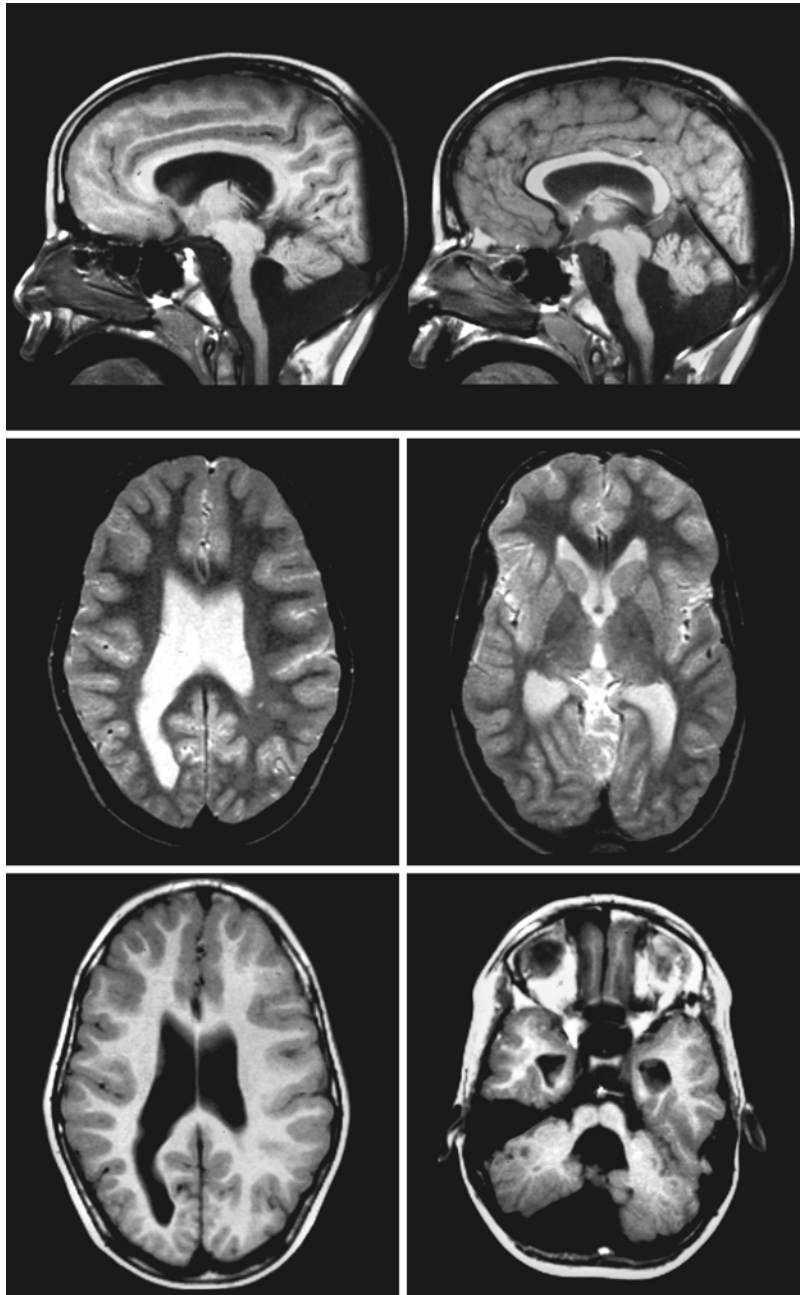


Fig. 60.5. A 2.5-year-old girl with MEB. The frontal, temporal, and parietal cortex is the most abnormal, whereas the configuration of the occipital cortex is close to normal. The abnormal cortex is slightly too thick and folded in broad gyri with an irregular inner border, indicative of pachygyric polymicrogyria. Neuronal heterotopias are seen in the white matter along the lateral ventricles. The frontal, parietal, and temporal

white matter contains extensive signal abnormalities, whereas the occipital white matter is normal. The corpus callosum, internal capsule, brain stem, and cerebellar white matter have a normal signal. The inferior vermis is hypoplastic. The superior and inferior colliculi are fused. The pons is hypoplastic. There are multiple small subcortical cerebellar cysts

Fig. 60.6. A 9-year-old boy with MEB. The frontal cortex is too thick and has an irregular inner border, indicative of underlying polymicrogyria. The inferior vermis is hypoplastic. The superior and inferior colliculi are fused. The pons is hypoplastic. There are multiple small subcortical cerebellar cysts. The lateral ventricles are mildly dilated, more so on the right than the left. The white matter is normal. Courtesy of Dr. P.G. Barth, Department of Child Neurology, Academic Medical Center, Amsterdam, The Netherlands



In the single MDC1D patient reported (Longman et al. 2003), MRI revealed diffuse cerebral white matter abnormalities with mild swelling of the abnormal white matter leading to broadening of gyri (Fig. 60.13). The cerebral cortex showed signs of diffuse polymicrogyria. The pons was hypoplastic.

It is clear that MRI plays an important role in the classification of CMD patients during life. The cortical dysplasia, pons hypoplasia, subcortical cerebellar cysts, and different types of white matter involvement are highly suggestive of the diagnosis CMD. MDC1A may be confused with megalencephalic leukoencephalopathy with subcortical cysts, but the subcortical cysts are as a rule lacking.

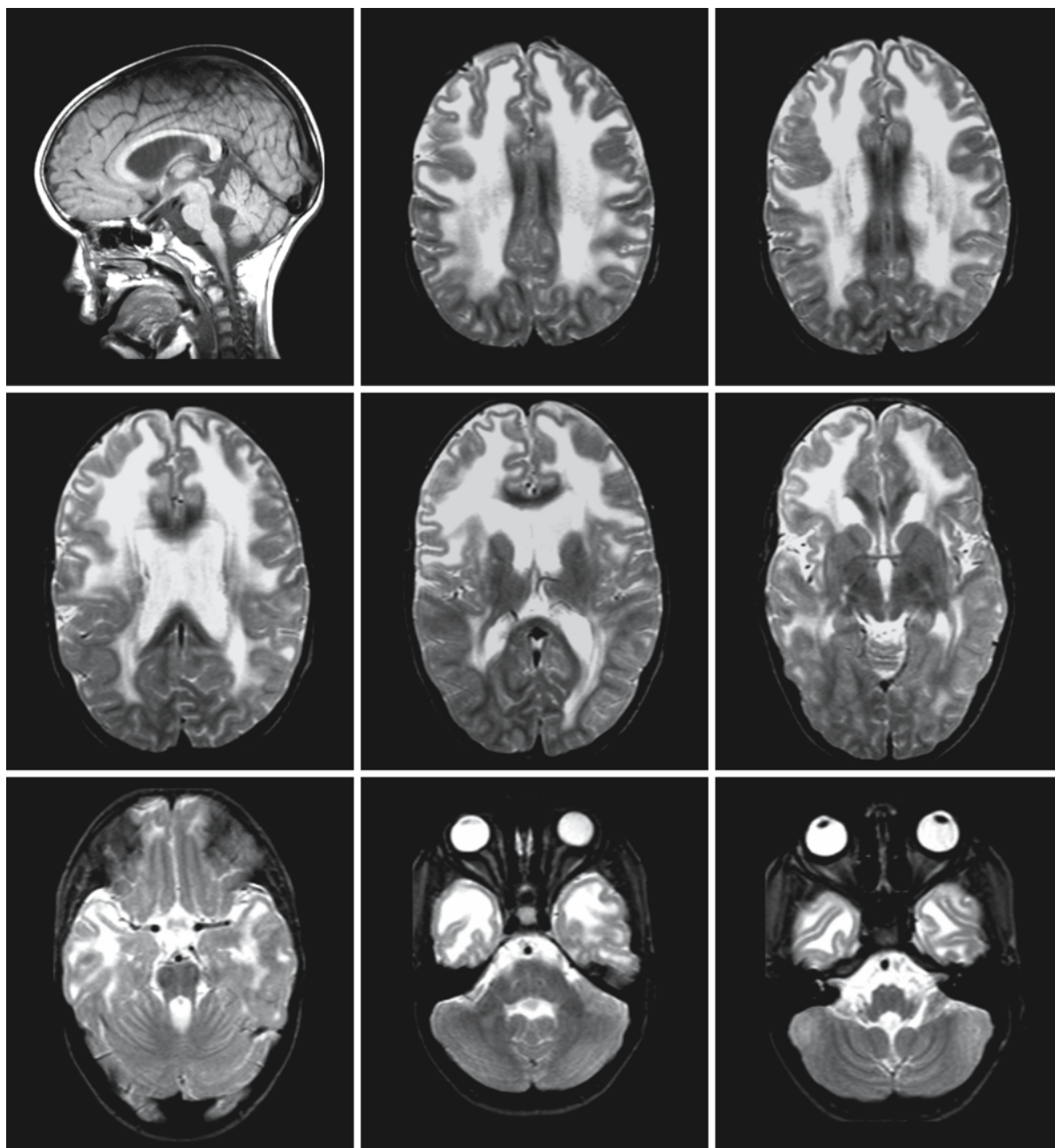


Fig. 60.7. A 6-year-old girl with classical MDC1A. The MRI shows prominent white matter changes. The abnormal white matter is mildly swollen with broadening of the gyri. MRI shows that the cortex is of normal thickness and does not have an irregular border. The frontal white matter is most abnormal

whereas the occipital white matter is better preserved. The corpus callosum, internal capsule, optic radiation, brain stem, and cerebellar white matter are spared. The pons is mildly hypoplastic

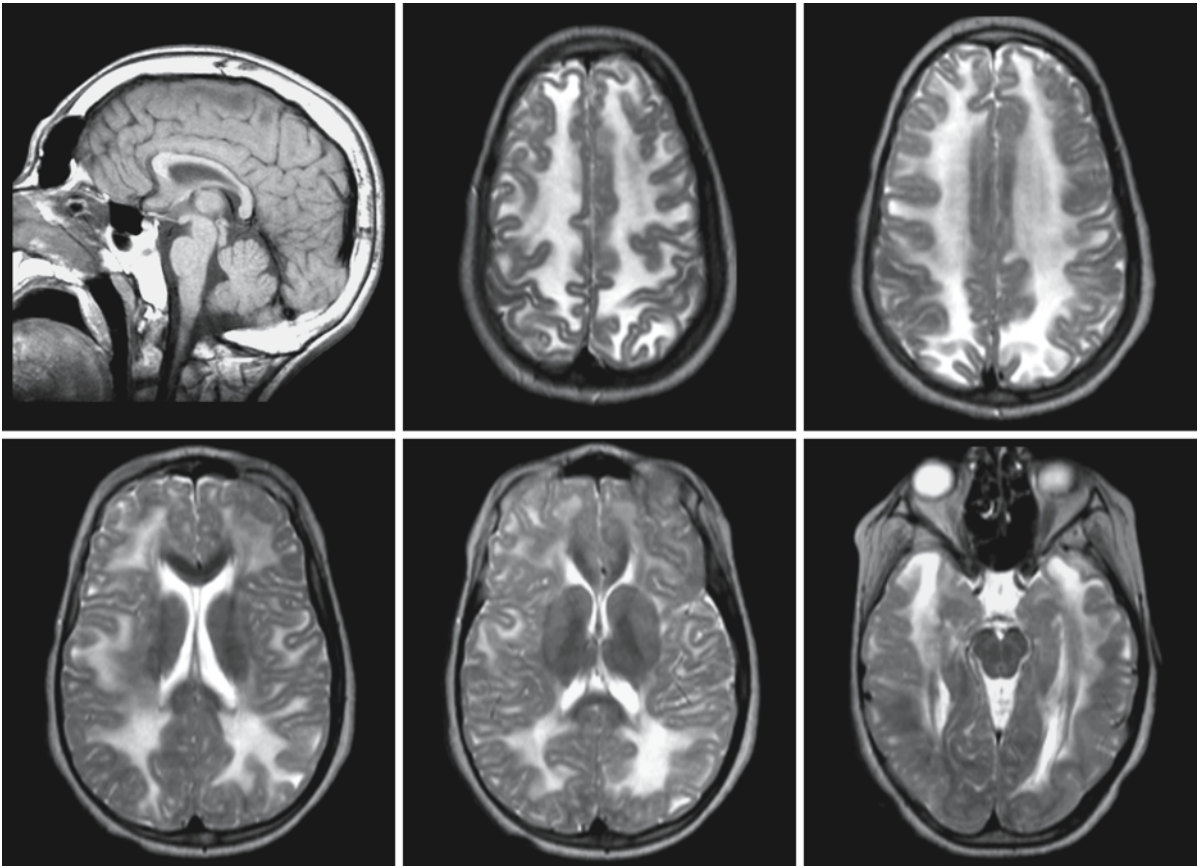


Fig. 60.8. A 9-year-old girl with MDC1A. The abnormalities are very similar to those seen in Fig. 60.7

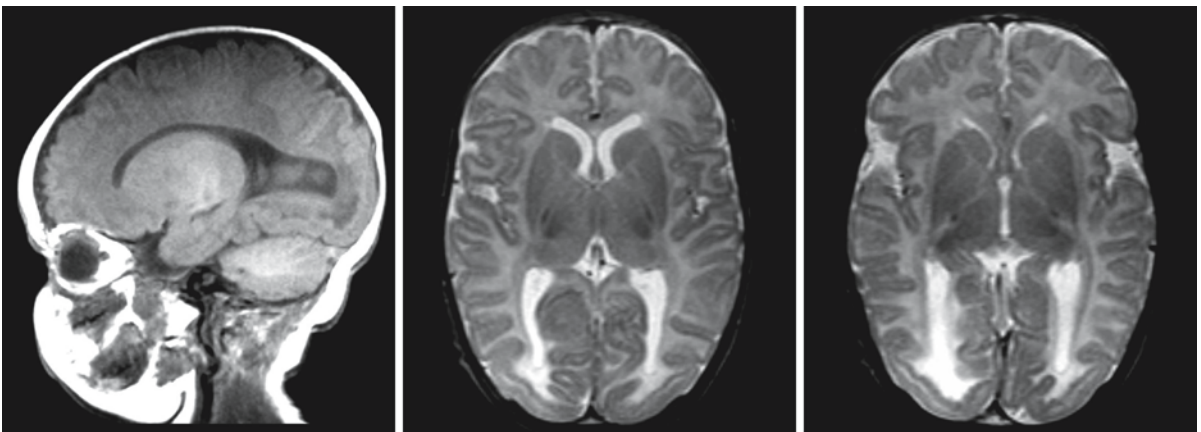


Fig. 60.9. A 2-month-old girl with MDC1A. Note the occipital agyria. The white matter under the area of agyria has an abnormally high signal. The remainder of the white matter looks normal for unmyelinated white matter

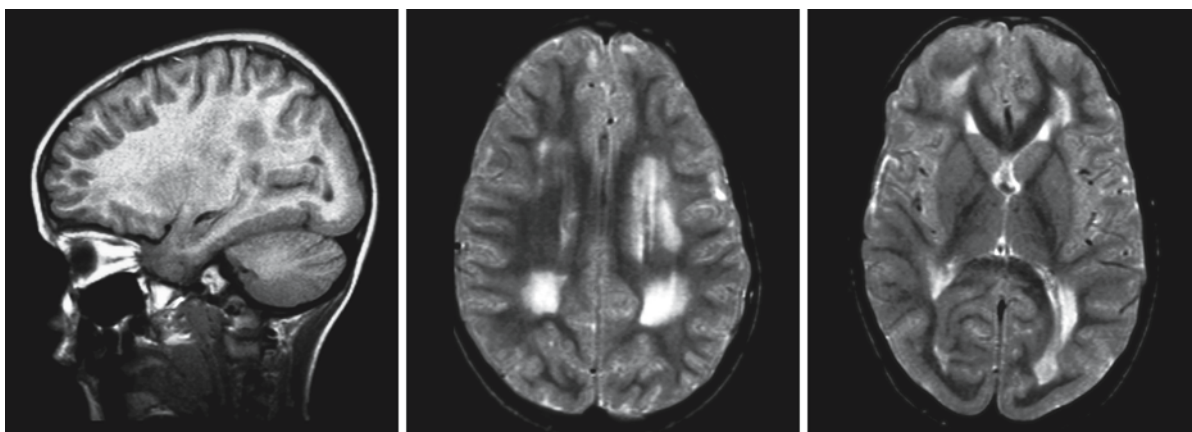


Fig. 60.10. A 7-year-old boy with CMD and partial merosin deficiency. Note the agyria in the occipital and basotemporal region. There are multifocal white matter abnormalities. Cour-

tesy of Dr. H. Stroink and Dr. C.E. Catsman-Berrevoets, Department of Child Neurology, Sophia Children's Hospital and Erasmus University Medical Center, Rotterdam, The Netherlands

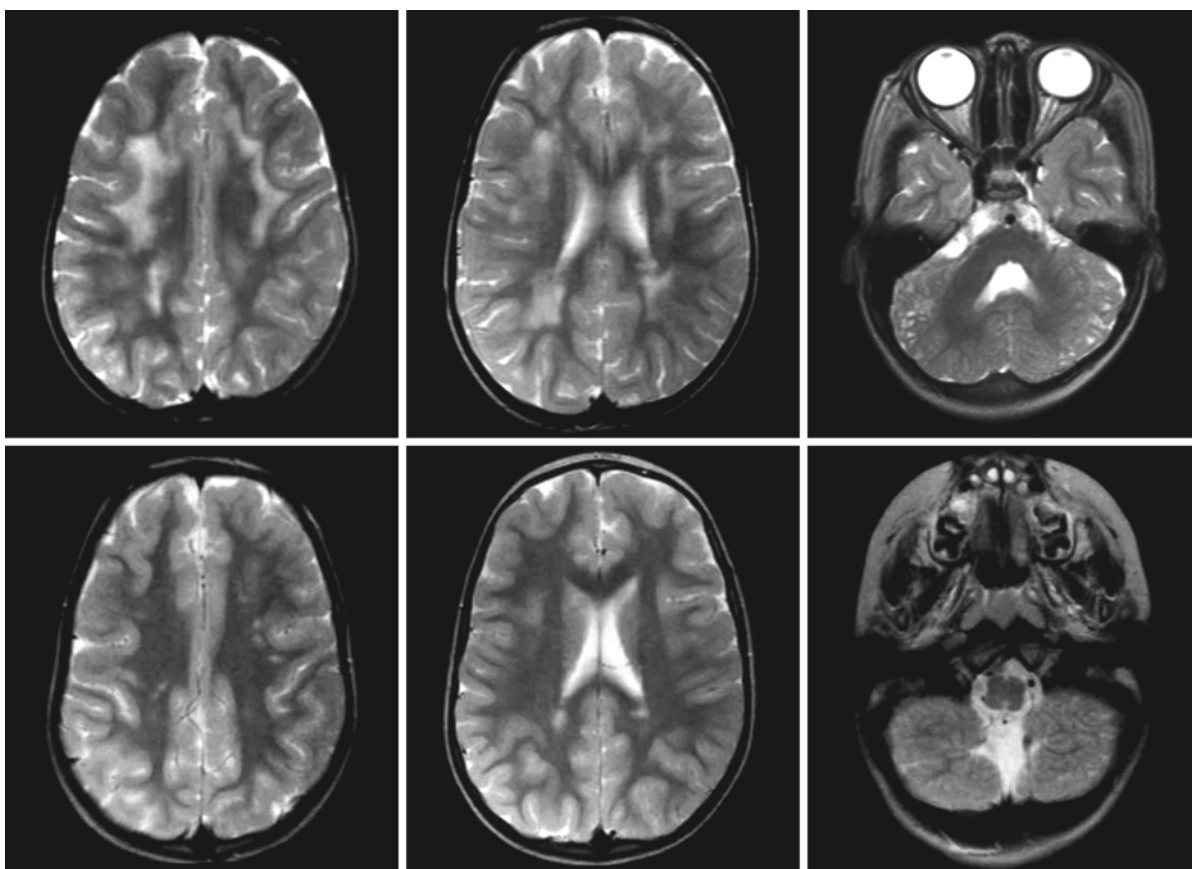


Fig. 60.11. A girl with MDC1C. The first MRI (*first row*) was obtained at the age of 3 years; the follow-up MRI (*second row*) at the age of 6 years. The initial MRI shows multifocal large white matter lesions, mainly involving the deep white matter. On follow-up, most white matter abnormalities have disappeared and only a few foci of abnormal signal remain. The cerebellar

cortex is dysplastic and there are subcortical cerebellar cysts. The pons is hypoplastic. From Louhichi et al. (2004), with permission, and courtesy of Dr. F. Fakhfakh, Laboratoire de Génétique Moléculaire Humaine, Faculté de Médecine de Sfax, and Dr. C. Triki, Service de Neurologie, CHU Habib Bourguiba, Sfax, Tunisia

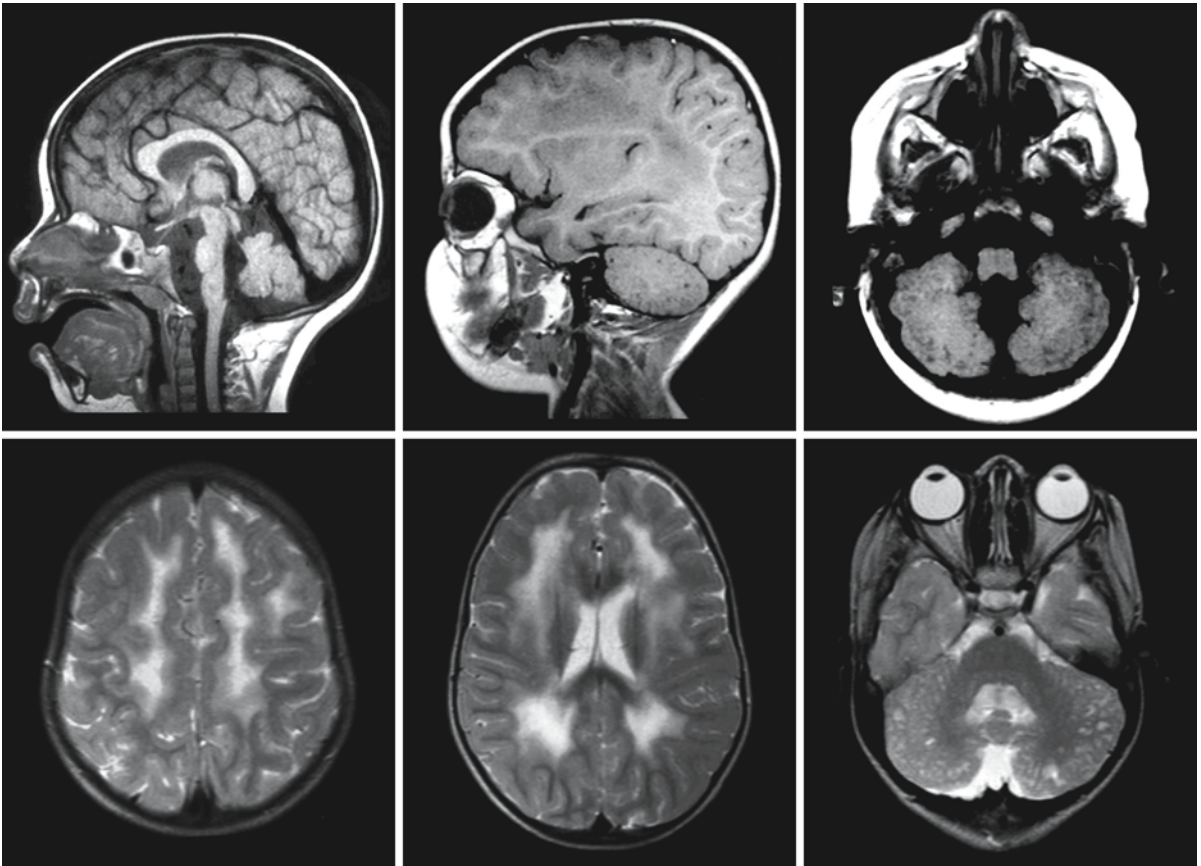


Fig. 60.12. A 7-year-old boy with MDC1C. The MRI shows extensive white matter abnormalities, which partially spare the U fibers. The pons and cerebellar vermis are hypoplastic. The cerebellar cortex is dysplastic and there are subcortical cere-

bellar cysts. From Louhichi et al. (2004), with permission, and courtesy of Dr. F. Fakhfakh, Laboratoire de Génétique Moléculaire Humaine, Faculté de Médecine de Sfax, and Dr. C. Triki, Service de Neurologie, CHU Habib Bourguiba, Sfax, Tunisia

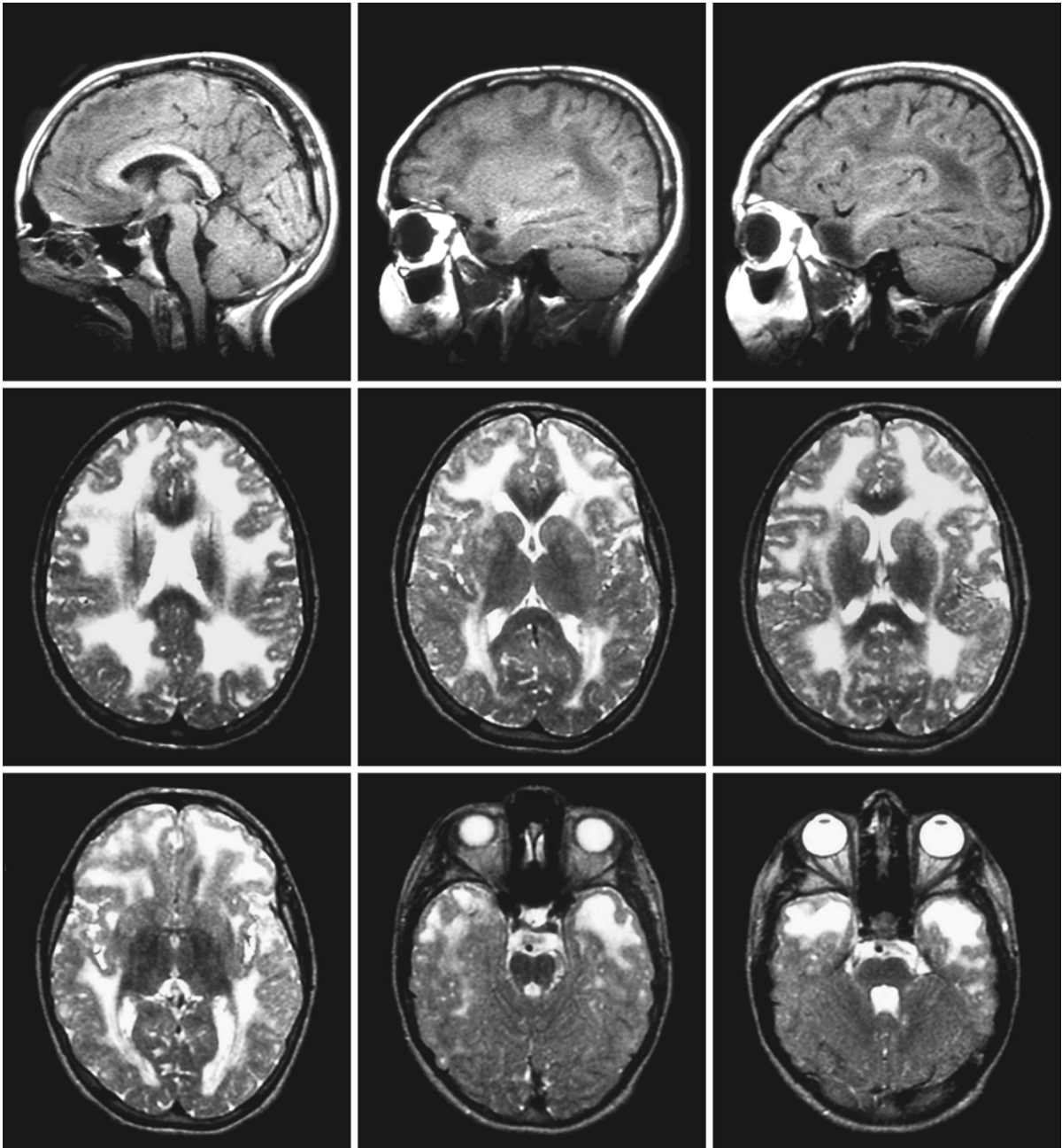


Fig. 60.13. A 14-year-old girl with MDC1D. The sagittal images show hypoplasia of the pons and fusion of the superior and inferior colliculi. There is no cerebellar hypoplasia and there are no evident subcortical cerebellar cysts. The cerebral white matter is diffusely highly abnormal in signal. In the frontal and particularly the anterior temporal region the abnormal white matter is swollen with broadening of gyri. The corpus callo-

sum, internal capsule, brain stem, and cerebellar white matter have a normal signal. The U fibers in the occipitotemporal region are spared. The cerebral cortex diffusely has an irregular border, suggesting underlying polymicrogyria. From Longman et al. (2003), with permission, and courtesy of Dr. F. Muntoni, Dubowitz Neuromuscular Centre, Hammersmith Campus, London, UK

Myotonic Dystrophy Type 1

61.1 Clinical Features and Laboratory Investigations

Myotonic dystrophy type 1 (DM 1) or Curschmann–Steinert disease is a dominantly inherited progressive myopathy. It is one of the most frequent muscle disorders, with a prevalence of approximately 1:8,000. Symptoms of the disease usually become apparent between the ages of 15 and 40 years, but may be found in childhood. Major symptoms include myotonia, progressive muscle weakness, and atrophy. In particular the face, jaw, neck, and distal muscles of the arms and legs are affected. Involvement of the bulbar muscles causes dysphagia and dysarthria. Myotonia leads to a prolonged after-contraction of the affected muscles, which persists after the voluntary muscle contraction has ceased. Myotonia is increased by fatigue, emotion, and cold. Other features of the disease include cataract, early frontal baldness (more conspicuous in males than in females), hearing impairment, and testicular atrophy leading to impotence and infertility. The heart is often affected. Cardiac conduction defects and dilated cardiomyopathy may occur and may contribute to a shortened life span. Smooth muscles, particularly those of the pharynx, esophagus, and gastrointestinal tract, are also involved. Hyperinsulinism occurs with enhanced frequency. Mildly impaired intelligence is frequently present. Hypersomnia may occur.

DM 1 has a congenital variant, with variable hypotonia and weakness present at birth. This variant is present in 10–15 % of the patients. In congenital DM 1 respiratory problems and feeding difficulties are common. Joint deformities may be present. Myotonia is not usually present in neonates and seldom develops until later in childhood. Cataracts and endocrine abnormalities usually develop even later. Mental retardation is present in nearly all patients with congenital DM 1 and is more severe than the cognitive problems seen in patients with adolescent and adult-onset disease. Some patients do not survive the neonatal period.

A characteristic feature of DM 1 is the tendency of the symptomatology to have an earlier onset and increasing severity with transmission to subsequent generations, a phenomenon called anticipation. In early generations, cataract is often the only abnormality; in a subsequent generation adult myotonia and weakness occur, while in the next generation con-

genital DM 1 is seen. The disease is transmitted as an autosomal dominant trait, but the mother is the affected parent in over 90 % of the cases of congenital DM 1.

Diagnosis is established by clinical examination and EMG. On EMG prolonged trains of high-frequency discharges arising from single fibers or groups of muscle fibers occur in response to electrode insertion or movement. EMG can be negative in young patients. Serum creatine kinase levels may be mildly elevated. DNA techniques are available to confirm the diagnosis and for prenatal diagnosis.

61.2 Pathology

Neuropathological data on DM 1 are scarce. Some external atrophy of the cerebral hemispheres may be present. Microscopic examination may reveal lesions within the cerebral white matter, especially in the subcortical areas. Microscopically, they are characterized by myelin paucity and preservation of myelin sheaths in perivascular regions in a tigroid pattern. Axons are relatively preserved. Macrophages containing fatty material and fibrillary astrocytes are scanty. It has been demonstrated that the areas of myelin paucity correspond with areas of signal abnormality on MRI.

Additional findings that have been reported are variable neuronal loss and astrocytosis in the frontoparietal and occipital cortices, neurofibrillary tangles in the limbic cortex, intracytoplasmic inclusion bodies within neurons of the thalamus and substantia nigra, disordered cortical architecture, and neuronal heterotopias. The neuronal heterotopias are frequently found adjacent to the areas of myelin paucity.

The absence of gliosis and lipid-laden macrophages within the areas of abnormal white matter as well as their association with neuronal heterotopias suggest that the white matter lesions are developmental abnormalities and not caused by demyelination.

61.3 Pathogenetic Considerations

DM 1 is caused by an expansion of an unstable cytosine-thymine-guanine (CTG) trinucleotide repeat in the 3' untranslated region of a protein kinase gene, *DMPK*, located on chromosome 19q13.3. In the normal population, the repeat length ranges between

4 and 37 copies, whereas alleles in DM 1 patients vary from 50 to several thousands of CTG repeats. The longer the CTG repeat sequence, the earlier the onset and more severe the clinical symptomatology. Alleles with 50–80 repeats are classified as protomutations, with which the DM 1 phenotype is mild and often does not cause subjective symptoms. Alleles with more than 80 repeats usually cause the classic DM 1 phenotype. The phenomenon of anticipation is associated with an increase in the length of the CTG repeat sequence with transmission to subsequent generations. Rare cases of reverse mutations have been reported, in which the prolonged CTG repeat sequence in the parent is decreased in size to a normal length in the offspring.

The expanded repeat is located in the 3' untranslated part of the gene. Three models have been proposed to explain how an expansion of this untranslated CTG repeat may cause the dominantly inherited DM 1 phenotype. Haploinsufficiency of the *DMPK* gene may produce cellular dysfunction. Alternatively, the expanded repeat may lead to a dominant gain of function. Finally, the CTG repeat expansion may change the chromatin structure, which interferes with the expression of adjacent genes.

The in vivo biological substrates of the enzyme DMPK are unknown. Since DMPK exhibits kinase activity, any perturbation of its expression or activity will potentially affect other molecules. Because DM 1 is characterized by muscle dysfunction and myotonia, ion channels could be substrates for DMPK. However, other proteins of as yet unknown function have also been found associated with DMPK. Dysfunction of such proteins may explain the extramuscular symptoms, including the mental deficit.

61.4 Therapy

First and most important is awareness of the potential problems associated with DM 1. Anesthesia and surgery come with particular hazards due to the combination of respiratory muscle weakness and increased sensitivity to anesthetics and muscle relaxants. Cardiac problems such as atrial fibrillation and flutter and heart block are important causes of death and require careful attention and treatment. Awareness of smooth muscle dysfunction and the associated potential gastrointestinal complaints including abdominal pains and pseudo-obstruction may prevent unnecessary surgery. Symptomatic relief of the myotonia can, if necessary, be obtained by drugs such as procainamide, diphenylhydantoin (phenytoin), and mexiletine. The effect of these drugs lies in the stabilization of the muscle membrane; they have no effect on muscle weakness. Physical therapy may be necessary. Cataract extraction can be important in order to preserve visual acuity.

61.5 Magnetic Resonance Imaging

It was already known from CT that mild ventricular enlargement and white matter hypodensity are not rare in DM 1.

MRI confirms the frequent presence of mild ventriculomegaly and enlargement of subarachnoid spaces (Figs. 61.1–61.4). In the majority of the DM 1 patients MRI also shows white matter abnormalities in the cerebral hemispheres (Figs. 61.1–61.4). The distribution of the white matter lesions is variable, ranging in location from predominantly in the periven-

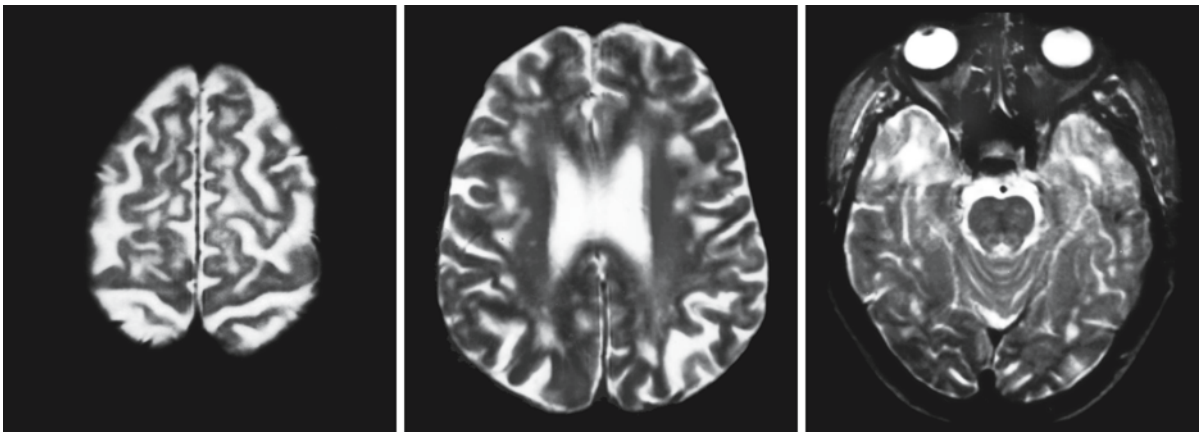


Fig. 61.1. These T₂-weighted MR images show the white matter changes in a 60-year-old female patient with DM 1. The white matter abnormalities are patchy and predominantly located in the subcortical areas. The temporal white matter is

involved as well. There is some atrophy with enlargement of the subarachnoid spaces. From Damain et al. (1992), with permission

tricular region to predominantly in the deep white matter or predominantly in the subcortical areas. In particular the anterior part of the temporal lobes is frequently involved (Figs. 61.1–61.4). The white matter changes are often patchy with in part isolated and in part irregularly confluent lesions of variable size. The lesions tend to be bilateral but are often not symmetrical in detail. The extent of the white matter changes varies from minor, with some small white matter lesions (Figs. 61.4 and 61.5), to more extensive and more confluent lesions (Figs. 61.1–61.3). In exceptional patients, the cerebral white matter abnormalities are diffuse. The white matter abnormalities may show an increase over time. The white matter changes occur both in congenital MD1 and later-onset forms and have the same imaging characteristics

in both conditions. Patients with congenital DM 1 tend more often to have enlargement of the lateral ventricles and a small corpus callosum.

Magnetization transfer ratios have found to be decreased not only in the MRI-visible white matter lesions, but also in the normal-appearing white matter, suggesting presence of more widespread structural abnormalities. T_2 relaxation measurements similarly revealed increased values within the white matter lesions, but again also in the normal-appearing white matter.

The pattern of MRI abnormalities with multifocal and often not entirely symmetrical lesions would rather suggest acquired disorders, especially inflammatory and infectious disorders. The pattern is particularly similar to that seen in congenital cyto-

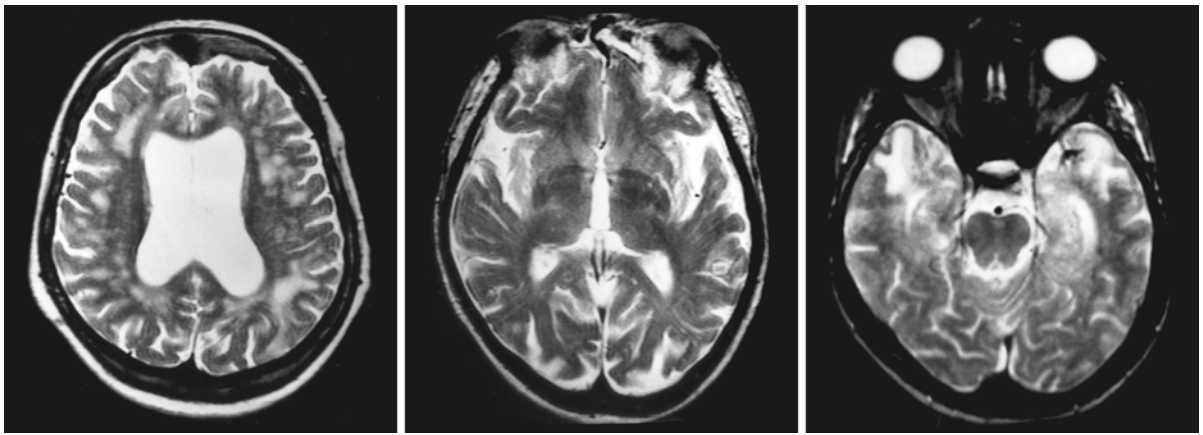


Fig. 61.2. A 63-year old female patient with DM 1. The patchy, multifocal white matter abnormalities mainly involve the deep cerebral white matter. The abnormalities are asymmetrical in distribution. The lateral ventricles and subarachnoid spaces

are mildly dilated. Note the temporal white matter abnormalities. Courtesy of Dr. G. Bachmann, Department of Diagnostic Radiology, Kerckhoff-Klinik, Bad Nauheim, Germany

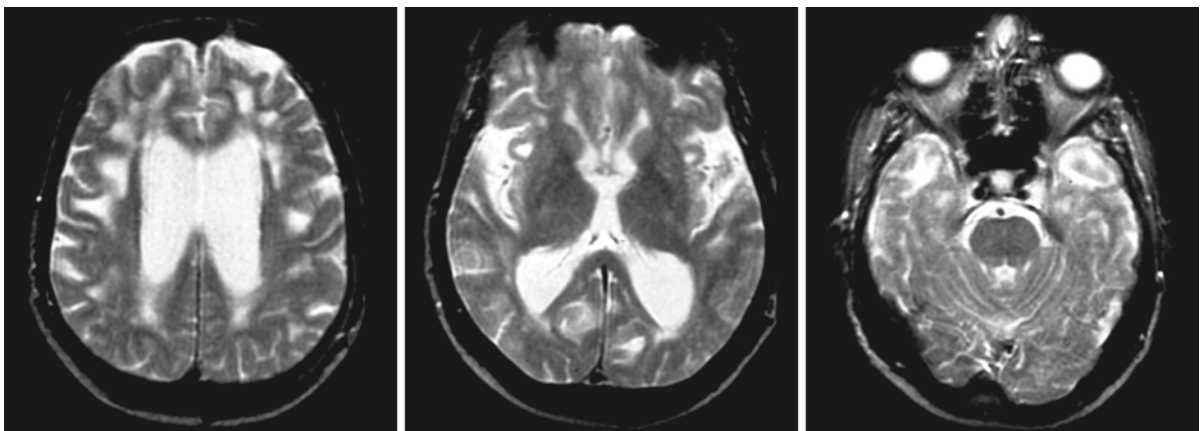


Fig. 61.3. The T_2 -weighted images in a 61-year-old male patient with DM 1 reveal similar abnormalities, again with a slightly asymmetrical distribution. Courtesy of Dr. A. Di Costan-

zo, Department of Neurological Sciences, Second University of Naples, Italy

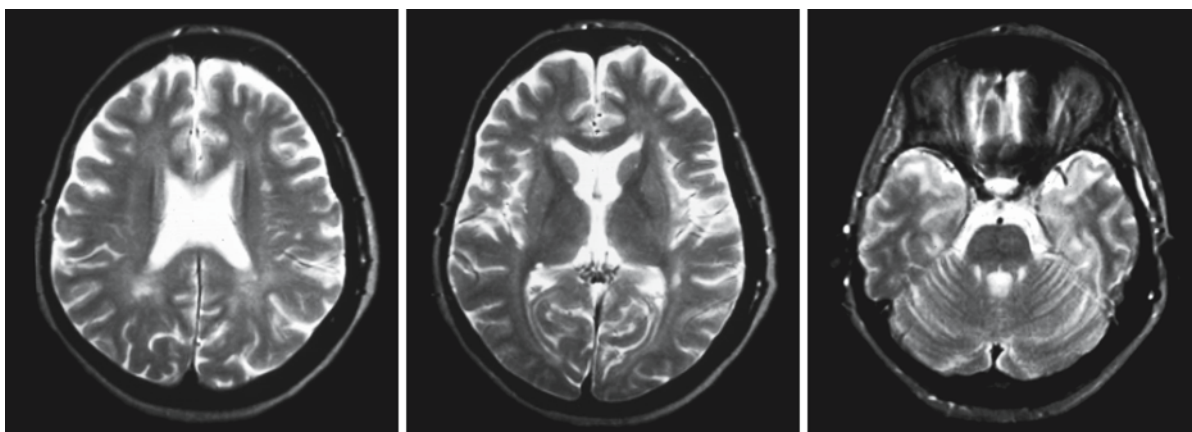


Fig. 61.4. This 54-year-old female patient with DM 1 has only mild white matter abnormalities. The temporal abnormalities are most pronounced. Courtesy of Dr. G. Bachmann, Depart-

ment of Diagnostic Radiology, Kerckhoff-Klinik, Bad Nauheim, Germany

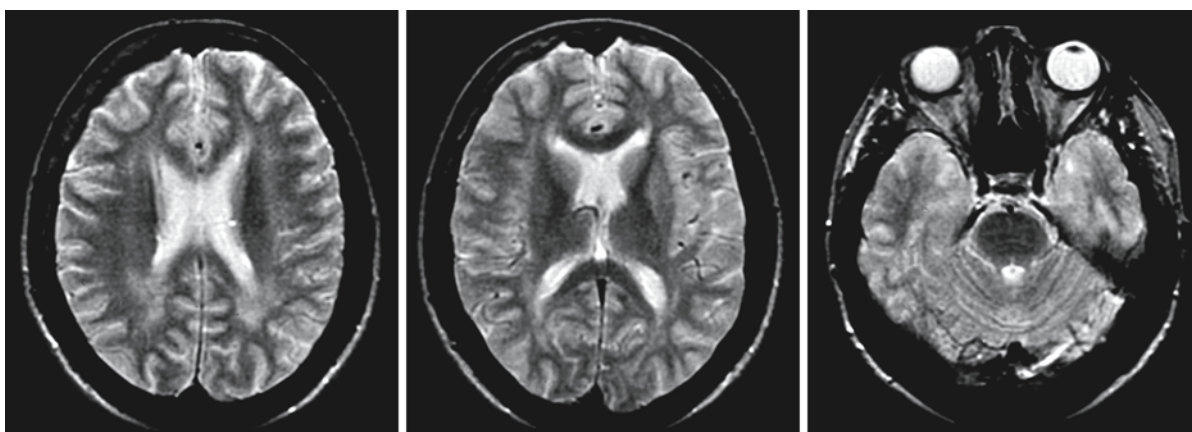


Fig. 61.5. This 34-year-old female patient with DM 1 has minimal white matter abnormalities. There is an indication of slight abnormalities in the anterior temporal white matter.

Courtesy of Dr. A. Di Costanzo, Department of Neurological Sciences, Second University of Naples, Italy

megalovirus infection. In the latter condition, multifocal lesions are seen, mainly in the deep cerebral white matter, and the anterior temporal lobes are frequently involved. However, in congenital cytomegalovirus infection, the largest lesions are as a rule present in the parietal region, which is not the case in DM 1. Of course, in the presence of myotonia, there is little reason for confusion.

Myotonic Dystrophy Type 2

62.1 Clinical Features and Laboratory Investigations

Myotonic dystrophy type 2 (DM 2) is a dominantly inherited progressive myopathy. DM 2 closely resembles adult-onset myotonic dystrophy type 1 (DM 1). Initially, three different disorders were delineated on the basis of clinical findings: proximal myotonic myopathy (PROMM), proximal myotonic dystrophy (PMD), and myotonic dystrophy type 2 ("DM 2"). Since all three have been shown to be part of one genetic spectrum, DM 2 is used for all three and has replaced the terms PROMM and PMD.

Patients with PROMM have been reported as being completely asymptomatic, mildly affected, or considerably disabled. Clinical onset is between 20 and 60 years of age. Most patients have cataract before the age of 50. The muscle weakness is predominantly proximal. Additional signs include muscle pain, fluctuating weakness and stiffness, muscle cramps, fasciculations, calf hypertrophy, tremor, seizures, sensorineural deafness, frontal baldness, male hypogonadism, insulin-resistant diabetes mellitus, hypothyroidism, hyperhidrosis, dysphagia, constipation, intermittent episodes of chest pain, and cardiac conduction defects. Cognitive impairment, hypersomnia, and apathy are rare and at most mild.

Patients with PMD have been reported to present with cataract, late-onset sensorineural hearing loss, late-onset prominent proximal weakness, wasting, myotonia and male hypogonadism.

"DM 2" as defined initially includes patients with myotonia, diffuse (proximal and distal) or exclusively distal weakness, frontal balding, cataracts, infertility, and cardiac conduction defects. Additional features include calf hypertrophy and hyperhidrosis.

So, like DM 1, DM 2 is a clinically heterogeneous multisystem disorder. Some affected DM 2 patients exhibit remarkable clinical similarity to those with classic DM 1, with myotonia, proximal and distal muscle weakness, frontal balding, cataracts, and cardiac conduction defects, whereas other patients can be more easily distinguished. One clear distinction is the absence of a congenital form of DM 2. Other differences include a lack of mental retardation in juvenile patients; less evident central hypersomnia; less distal, facial, and bulbar weakness; and less pronounced muscle atrophy.

In a large overview study on DM 2 (Day et al. 2003), 90% of the affected individuals had electrical myotonia, 82% had weakness, 61% cataracts, 23% diabetes mellitus, and 19% cardiac involvement. First symptoms of the disease occur between the ages of 13 and 67, with a median of 48 years. Muscle symptoms, including pain, stiffness, myotonia, and weakness, are the most common symptoms in DM 2 patients. Fluctuating or episodic burning muscle pain is frequently present, mainly during the night. Cataracts are a prominent and early feature, sometimes already seen before the age of 20. Cataract extraction may be necessary from as early as 30 years to as late as in the seventies. Cardiac complaints include palpitations, intermittent tachycardia, and episodic syncope. These symptoms increase in frequency with age. Cardiac conduction abnormalities and cardiomyopathy may underlie these complaints. DM 2 patients can develop fatal arrhythmias unexpectedly.

On EMG a broad spectrum of spontaneous activity, such as fibrillations, positive sharp waves, fasciculations, myotonic and pseudomyotonic discharges, neuromyotonia-like discharges, and high-frequency bizarre discharges, can be found. Motor unit action potentials may show reduced mean duration, increased polyphasia, and increased satellite potentials. Serum creatine kinase levels are usually elevated, typically less than five times the upper limit of normal, but may also be normal. γ -Glutamyl transferase is normal or mildly elevated. Primary male hypogonadism is found in the majority of the affected men, with elevated LH and FSH, low testosterone, and oligospermia. Hypogammaglobulinemia may be found. Thyroid function tests may indicate hypothyroidism. In the case of diabetes mellitus, insulin insensitivity is found with elevated basal insulin levels or prolonged insulin elevations. ECG shows impulse generation and conduction defects. Echocardiography may reveal a cardiomyopathy. DNA techniques are available to confirm the diagnosis and for prenatal diagnosis.

62.2 Pathology

Neuropathological data on DM 2 are lacking.

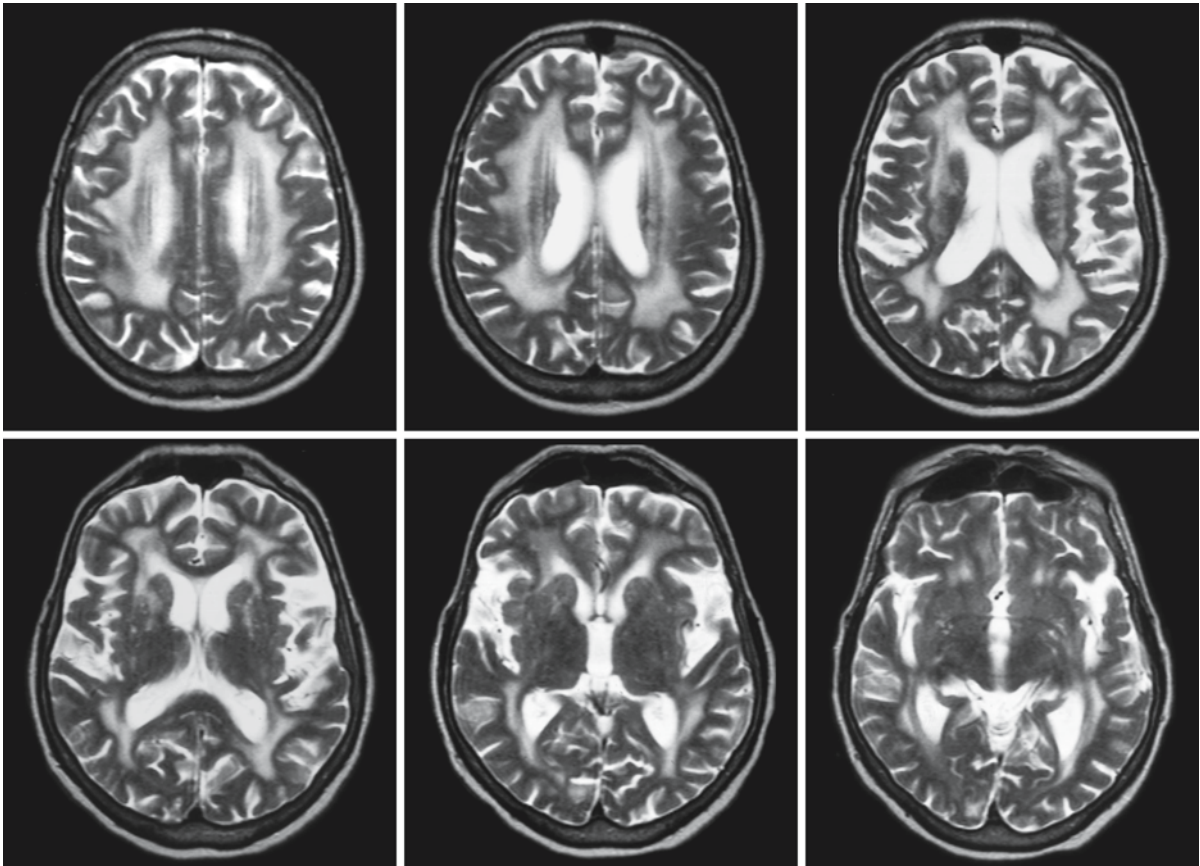


Fig. 62.1. The T₂-weighted images in this 66-year-old male patient with DM 2 show diffuse cerebral white matter abnormalities with sparing of the corpus callosum and relative sparing of the U fibers. Spots of abnormal signal are present in the basal ganglia. The anterior limb of the internal capsule and the

external capsule are also affected. The lateral ventricles and subarachnoid spaces are mildly dilated. Courtesy of Dr. E. Hund, Department of Neurology, and Dr. Sartor, Department of Neuroradiology, University of Heidelberg Medical School, Heidelberg, Germany

62.3 Pathogenetic Considerations

DM 2 is caused by an unstable expansion of a cytosine-cytosine-thymine-guanine (CCTG) repeat in intron 1 of the zinc finger protein 9 gene (*ZNF9*), a gene located on chromosome 3q21.3. The repeat length varies between 75–11,000, with a mean of approximately 5,000. Expansion sizes in the blood of affected children are usually shorter than in their parents. No significant correlation is found between the age of onset and expansion size.

The gene has two products, α -ZNF9 and β -ZNF9, produced by alternative splicing. ZNF9, also called cellular nucleic acid binding protein, contains seven zinc finger domains. It is thought to be an RNA-binding protein. It is widely expressed, with the highest expression in heart and skeletal muscle. The pathophysiology of the disease is presently unclear.

Not all families with a DM 2 phenotype display linkage with chromosome 3q21.3. So, there must be still other genes related to this phenotype.

62.4 Therapy

So far, there is no specific treatment for DM 2. Physical therapy may be of some benefit. In patients in whom myotonia is a prominent problem, mexiletine, phenytoin, or carbamazepine may be beneficial. When cardiac conduction defects are present, antiarrhythmic drugs should be avoided. Patients should undergo cardiological examination and follow-up as soon as the diagnosis is established. Cataracts may require surgical intervention at some point. Cardiac therapy, including pacemaker implantation, may be necessary. Patients should be checked for hypo-

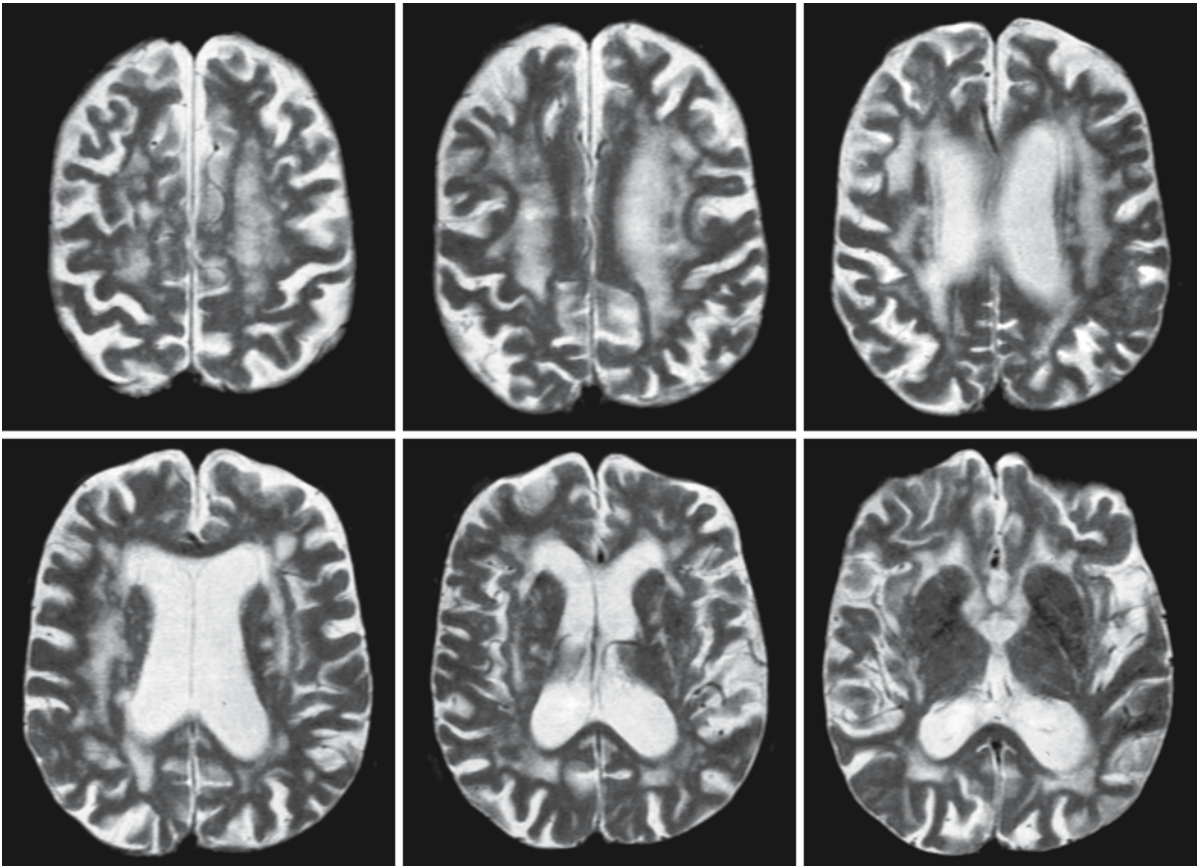


Fig. 62.2. The MRI of this 64-year-old female patient with DM 2 reveals extensive, patchy cerebral white matter abnormalities, sparing the corpus callosum and partially sparing the U fibers. The internal and external capsules are affected. There are spots of abnormal signal in the basal ganglia. The lateral

ventricles and subarachnoid spaces are dilated due to reduced volume of the cerebral white matter. Courtesy of Dr. E. Hund, Department of Neurology, and Dr. Sartor, Department of Neuroradiology, University of Heidelberg Medical School, Heidelberg, Germany

thyroidism regularly. Whether DM 2 patients experience respiratory depression in response to benzodiazepines, opiates, or barbiturates, whether myotonia is aggravated by depolarizing muscle relaxants, and whether DM 2 patients may develop malignant hyperthermia during or after anesthesia is unknown.

62.5 Magnetic Resonance Imaging

MRI of the brain is often normal, but may show rather extensive abnormalities in the cerebral white matter (Figs. 62.1 and 62.2). The U fibers tend to be spared. The white matter abnormalities may be diffuse (Fig. 62.1) or, more often, patchy (Fig. 62.2). These abnormalities may be accompanied by neurological problems including clinical episodes of stroke, parkinsonian features, seizures, and mental changes.

X-linked Charcot–Marie–Tooth Disease

63.1 Clinical Features and Laboratory Investigations

Charcot–Marie–Tooth disease (CMT) is a clinically and genetically heterogeneous group of peripheral nerve disorders characterized by distal weakness, atrophy, sensory loss, and decreased tendon reflexes. CMT has been classified according to the pattern of inheritance and whether the abnormalities primarily affect myelin (CMT1) or axons (CMT2). The X-linked dominant form of CMT (CMTX) shows both demyelinating and axonal aspects, causing problems in categorizing CMTX as a subtype of CMT1 or CMT2.

CMTX affects both males and females, but males are affected more severely than females, with onset of symptoms at an earlier age. Asymptomatic female carriers have been reported. The clinical manifestations of CMTX vary. Onset may be congenital or delayed until the third decade. Symptoms develop in a length-dependent distribution, meaning that the longest nerves are involved earliest. Thus, the weakness always starts in the lower leg muscles with stumbling and steppage gait. With progression of the disease, the weakness spreads to the hands. The weakness varies widely, from mild, causing no functional impairment, to severe, necessitating the use of a wheelchair. Foot deformities, including pes cavus and hammer toes, are common. Muscle atrophy and loss of tendon reflexes occur. Distal sensory loss with glove and stocking distribution occurs, involving touch, pin prick, temperature, vibration, and position sense. Many patients have balance difficulties with a positive Romberg sign. Scoliosis may occur. Breathing difficulties due to phrenic nerve involvement occur in some patients.

Most CMTX patients do not have overt clinical CNS manifestations, but subclinical evidence of CNS dysfunction is common. Hyperreflexia, extensor plantar reflexes, some spasticity, and cerebellar dysfunction have been observed in addition to the peripheral neuropathy. Some patients have sensorineural hearing loss. Patients may experience episodes of transient neurological problems of central origin, lasting hours to weeks. The problems may fluctuate in severity during that time. Signs reported include dysarthria, cerebellar ataxia, gait ataxia, pyramidal weakness of the extremities (hemiparesis, monoparesis, paraparesis, or tetraparesis), and cranial nerve palsies including third cranial nerve palsy, facial

weakness, bulbar dysarthria, dysphagia, and loss of the gag reflex. Nausea and vertigo may be present. The patients are usually alert during the episode, but somnolence, behavior abnormalities, and disorientation may also occur. They may complain of headache. After the episode, patients recover fully to their previous condition. The episodes seem to be provoked by minor infections, surgery, sports, or staying at high altitudes.

Nerve conduction velocities are reduced in CMTX, but the reductions are less severe than in the other forms of demyelinating CMT, consistent with moderate demyelination of the investigated nerves. The reductions in conduction velocities may be variable from one nerve segment to the other. Distal latencies are prolonged. Compound muscle action potentials and sensory nerve action potentials have reduced amplitudes. The electromyogram is usually normal, but sometimes fibrillation potentials are found, suggesting axonal involvement. Nerve conduction velocities are typically slower in affected males than in their affected female relatives. Abnormalities in brain stem auditory evoked responses have been reported repeatedly with slowed central conduction. Sensory evoked responses may also show a slowing of central conduction.

63.2 Pathology

Findings in sural nerve biopsy specimens are variably described as primary axonal degeneration and primary demyelinating. Findings include loss of myelinated fibers and the presence of groups of small, thinly myelinated and unmyelinated regenerating fibers. Axons with disproportionately thin myelin sheaths in relation to the axon caliber and small onion bulb formations, indicative of demyelination and consecutive remyelination, may be present.

No brain autopsy studies are available

63.3 Pathogenetic Considerations

CMTX is caused by mutations in the gene, called *CX32* or *GJB1*, coding for connexin 32, also called gap junction protein $\beta 1$. The gene is located on chromosome Xq13.1. Connexin 32 is a gap junction protein that is found in both the PNS and the CNS. It is incor-

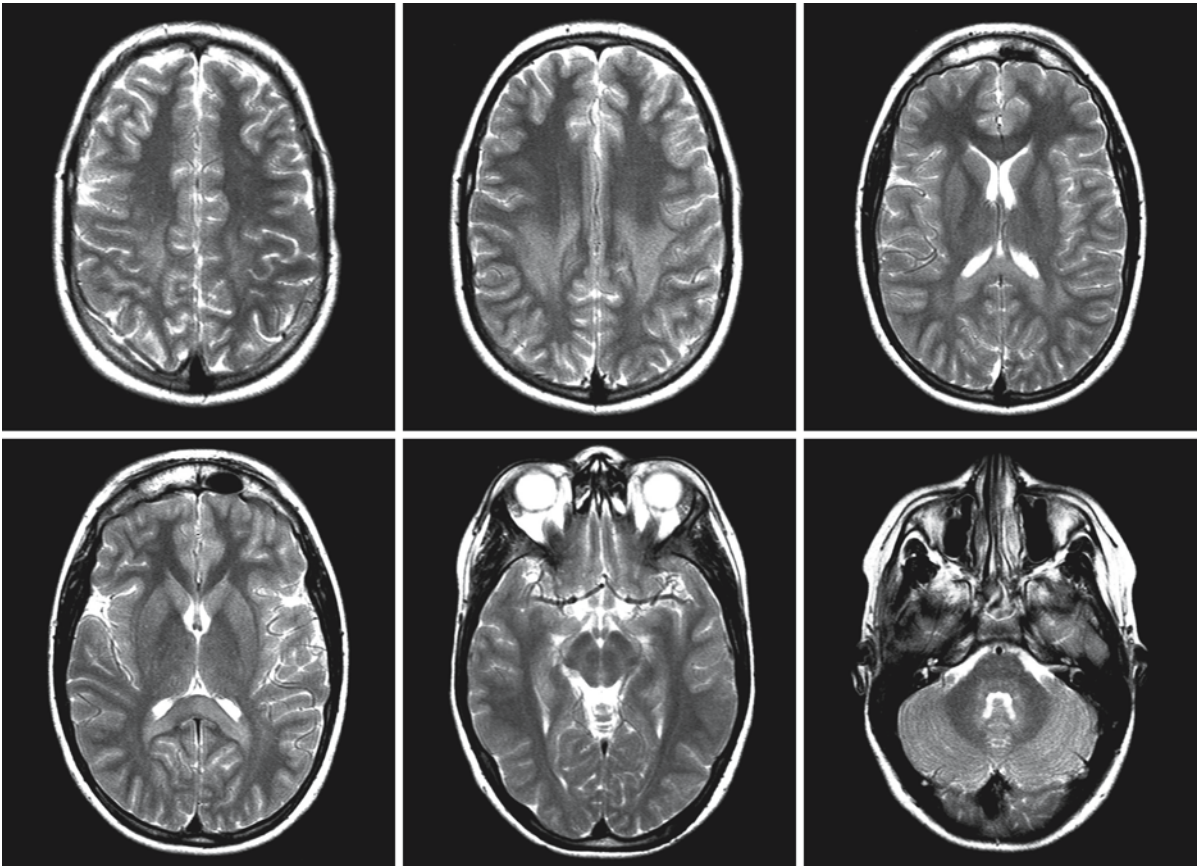


Fig. 63.1. MRI of a 14-year-old male patient with CMTX during an episode of CNS symptoms shows mild signal changes in the parieto-occipital white matter, sparing the U fibers. The spleni-

um of the corpus callosum is affected. There is no evident involvement of the brain stem and cerebellar peduncles. From Schelhaas et al. (2002), with permission

porated into cell membranes as a subunit of a hemichannel called the connexon. One connexon comprises six subunits and two connexons form a gap junction between two cells. Gap junctions are intercellular channels that span the space between two neighboring cells and result from the association of two half-channels, connexons, contributed separately by each of the participating cells. These gap junctions allow rapid exchange of ions, small metabolites, and second messengers between cells or parts of cells. In the PNS, connexin 32 is expressed in Schwann cells at the Schmidt–Lantermann incisures and the paranodal regions, the noncompacted parts of myelin. In the CNS it is expressed in oligodendrocytes and neurons. Connexin is also expressed in nonnervous tissues including liver, pancreas, and secretory epithelium.

Mutations either lead to loss of function or to altered gating properties of the gap junction channels. There is not yet a hot spot for connexin 32 mutations associated with CNS symptoms. The mutations associated with CNS disease have been found in the extra-

cellular, transmembrane, and intracellular domains of the protein. By analogy to channelopathies, altered gating properties of connexons due to mutated connexin 32 could give rise to transient CNS symptoms. Situations of metabolic stress may further alter the function of gap junctions and cause transient symptoms.

63.4 Therapy

At present, no specific therapy exists for patients with CMTX.

63.5 Magnetic Resonance Imaging

Outside the episodes of CNS dysfunction, MRI of the brain is most often described as normal. During the episodes of CNS symptoms, transient white matter abnormalities occur (Fig. 63.1). They are located in the central or posterior part of the centrum semio-

vale, the splenium of the corpus callosum, posterior limb of the internal capsule, and middle cerebellar peduncles. The U fibers are spared. The signal changes are milder than those seen in demyelination or white matter inflammatory disease. They are symmetrical and confluent. After contrast administration, no enhancement is seen. Diffusion-weighted imaging shows restricted diffusion. As the white mat-

ter abnormalities are reversible within a few months, the restricted diffusion cannot be caused by cytotoxic edema. Myelin splitting and intramyelinic edema, with compression of the extracellular space, is a more likely explanation.

No systematic study of CMTX patients has been performed to document the MRI findings of the brain outside the episodes of CNS dysfunction.

Oculodentodigital Dysplasia

64.1 Clinical Features and Laboratory Investigations

Oculodentodigital dysplasia (ODDD) is an inherited disorder that affects the development of the face, eyes, limbs, and teeth. The disorder has an autosomal dominant mode of inheritance. It displays a high penetrance but variable expression. There is also intrafamilial variation of the clinical characteristics. Isolated patients, related to de novo mutations, are frequently observed.

Affected patients have a narrow nose with thin, anteverted nostrils and a prominent columnella. Characteristic eye manifestations include short palpebral fissures, epicanthal folds, hyper- or hypotelorism, microphthalmia, and bilateral microcornea, often with abnormalities of the iris. Some patients develop glaucoma or optic atrophy. Bilateral complete syndactyly of the fourth and fifth fingers is the characteristic digital malformation (type III syndactyly). The third finger may also be involved. Syndactyly of the third and fourth toes may be present. Midphalangeal hypoplasia, distal phalangeal hypoplasia, or aplasia of one or more digits or toes may be present. Associated camptodactyly or clinodactyly of the fifth fingers is a common finding. The teeth are small and there is generalized hypoplasia of the enamel. Partial anodontia may be present. Caries and premature loss of teeth may occur. Less common features include dry, thin, slow-growing, and sparse hair (hypotrichosis), cleft lip and palate, conductive hearing loss, cranial and mandibular hyperostosis, and microcephaly.

Neurological symptoms are frequent in ODDD. Slowly progressive spastic paraparesis of the legs has been reported most often. Other reported problems include ataxia, dysarthria, ptosis, nystagmus, gaze palsy, strabismus, visual impairment, neurogenic bladder dysfunction, bowel disturbance, seizures, and mild mental retardation. However, the clinical expression of neurological features often varies widely among affected individuals within and between ODDD kindreds. The onset of the neurological problems is variable. It is usually evident by the second decade of life, but may be much later.

64.2 Pathology

No autopsy studies of ODDD are available.

64.3 Pathogenetic Considerations

ODDD is related to dominant mutations in the connexin 43 gene, *GJA1*, at chromosome 6q22–23. A high rate of de novo mutations is observed.

Connexin 43, like other connexin proteins, is a transmembrane protein with an intracellular N-terminus, four transmembrane domains, two extracellular loops, one cytoplasmic loop, and an intracellular C-terminus. Six connexins can form a hemichannel or connexon, a specialized intracellular structure surrounding a pore. Two connexons in apposing cell membranes can align to form an intercellular gap junction. These channels provide a direct low-resistance intracellular pathway for the passage of ions and small molecules. Gap junctions have been found in most tissues. Most tissues express more than one type of connexin. Multiple types of connexins can assemble to form gap junctions between cells, with the diversity of combinations influencing the nature of the cell-to-cell communication.

Almost all *GJA1* mutations in ODDD are missense mutations. The lack of mutations resulting in the introduction of a stop codon into the protein suggests that the mechanism underlying ODDD is not a loss of connexin 43 function. This hypothesis is reinforced by the finding that the mouse knock-out does not have an ODDD-like phenotype. There is a strong correlation between the sites of *GJA1* expression during mouse embryonic development and the ODDD phenotype, suggesting that connexin 43 plays a key role in normal facial and limb development. The pathophysiology of the disease in ODDD has still to be elucidated.

ODDD and Hallermann–Streiff syndrome share several clinical characteristics. Some patients with Hallermann–Streiff syndrome have two mutations in the *GJA1* gene, whereas their parents are carriers. However, in other typical Hallermann–Streiff syndrome patients no mutation in *GJA1* can be found.

64.4 Therapy

At present, only symptomatic therapy is available for patients with ODDD.

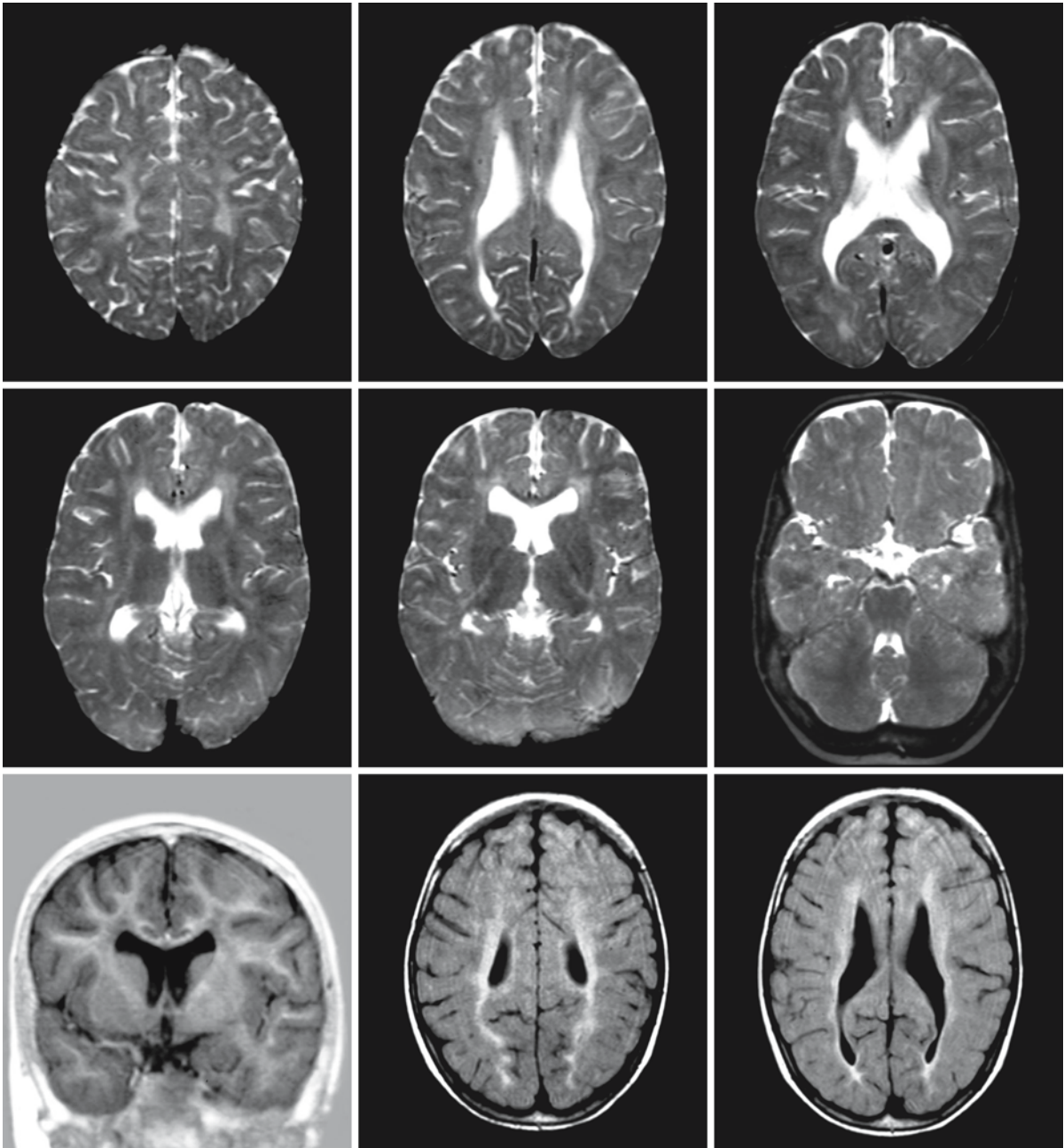


Fig. 64.1. A 5.5-year-old girl with ODDD. The T_2 -weighted images (first and second row) show ill-defined, mild periventricular signal abnormalities, extending downwards into the posterior limb of the internal capsule. The inversion recovery (third

row, left) and FLAIR images (third row, middle and right) show that the subcortical white matter is better preserved. Courtesy of Dr. B. Tinselsboer and Dr. F. Beemer, Department of Clinical Genetics, University Medical Center Utrecht, The Netherlands

64.5 Magnetic Resonance Imaging

In some patients with ODDD, MRI does not reveal abnormalities. Patients with ODDD and progressive neurological problems have white matter abnormalities on MRI (Fig. 64.1). The cerebral white matter is somewhat reduced in volume. A zone of mildly abnormal signal surrounds the lateral ventricles, rela-

tively sparing the U fibers. The signal abnormalities extend downwards into the posterior limb of the internal capsule and the corticospinal tracts in the brain stem. Low signal intensity on T_2 -weighted images has been reported in the pericentral cortex, globus pallidus, and substantia nigra. The imaging abnormalities in ODDD may not be very specific, but they are consistent among patients.

Leukoencephalopathy with Vanishing White Matter

65.1 Clinical Features and Laboratory Investigations

Leukoencephalopathy with vanishing white matter (VWM) has also been called childhood ataxia with central nervous system hypomyelination (CACH) and myelinopathia periaxialis diffusa. “Cree leukoencephalopathy” and “ovarioleukodystrophy” have both been found to be variants of VWM.

VWM is a disease with an autosomal recessive mode of inheritance. It has been shown to be one of the more prevalent leukoencephalopathies in children. Its incidence is similar to that of metachromatic leukodystrophy. The classical and most frequent variant has its onset in childhood, most often between the ages of 2 and 6 years. The disease is characterized by chronic progressive neurological deterioration with cerebellar ataxia, usually less prominent spasticity, and relatively mild mental decline. Optic atrophy with loss of vision may occur, but not in all patients. Epilepsy is present in most patients, but is rarely a prominent feature. Characteristically, there are additional episodes of major and rapid deterioration following minor head trauma and especially febrile infections. Occasionally, these episodes are provoked by fright. During these episodes, patients rapidly lose motor faculties and become very hypotonic. Irritability, vomiting, and seizures usually progress to somnolence and loss of consciousness. These episodes may end in coma. Death usually follows an episode of coma. If recovery occurs, it is usually incomplete.

Some patients have a more severe variant of the disease with onset within the first year of life and early demise. An example is found in so-called “Cree leukoencephalopathy,” a disease that was described among the Cree Indians. The onset of Cree leukoencephalopathy is between the ages of 3 and 9 months, and death occurs before the age of 2 years. Some (non-Cree) patients have an even more severe phenotype with antenatal onset. In the third trimester of pregnancy, decreased fetal movements, oligohydramnios, growth failure, and development of microcephaly occur. At birth, contractures may be seen. From birth onwards or from soon after birth, there are increasing problems, with a rapid downhill course characterized by feeding problems, vomiting, failure to thrive, irritability, apathy, axial hypotonia, limb hypertonia or hypotonia, seizures, apneic episodes, coma, respiratory failure, and death within a few

months. In these infants evidence may be found of involvement of other organs, including cataract (oil droplet cataract), hepatosplenomegaly, kidney hypoplasia, pancreas involvement, and ovarian dysgenesis.

At the other end of the clinical spectrum are patients who are completely normal until onset of the disease in adulthood. In some patients occasional seizures are the first sign of the disease. In other patients, the disease starts with psychiatric symptoms. Some patients slowly develop dementia. In other patients motor deterioration dominates the clinical picture. The episodes of major deterioration are usually less marked in patients with a later onset. Later onset most often implies a slower and more protracted disease course, although unexpected rapid progression and death within a few months may also occur. In adult females with the disease, primary or secondary ovarian failure may occur.

Laboratory tests are unrevealing in VWM. The only consistent abnormality ever demonstrated is moderately elevated CSF glycine. The CSF:serum glycine ratio is also elevated and may even be higher than 0.08. A ratio higher than 0.08 is thought to be indicative of nonketotic hyperglycinemia. It is not known whether CSF glycine is elevated in all patients with VWM and whether a normal level excludes the diagnosis. The glycine elevation is probably a non-specific finding related to ongoing excitatory brain damage. DNA testing is available for diagnostic confirmation, carrier testing, and prenatal diagnosis.

65.2 Pathology

In VWM, the brain is generally of normal size and weight, but in a few cases it is slightly heavier or lighter than normal. The gyri are usually normal or atrophic. When the brain is removed from the skull, the rarefied and cystic white matter usually collapses. On macroscopic examination, gray matter structures appear unaffected. The lesions are found primarily in cerebral white matter, with the cerebellum and brain stem much less severely involved. The cerebral white matter varies from gelatinous to cystic to frankly cavitary. The frontoparietal white matter, particularly deep and periventricular, appears to be more commonly involved, with relative sparing of the temporal lobe. White matter areas that are characteristically

relatively spared include the optic system, corpus callosum, anterior commissure, and internal capsule. The subcortical arcuate fibers also tend to be spared, but not consistently. In the brain stem the central tegmental tract at the level of the pons is often involved in a bilateral and symmetrical distribution.

Microscopically, the grossly affected white matter shows myelin pallor, thin myelin sheaths, vacuolation, myelin loss, cystic change, and rarely active demyelination. Lipophages containing myelin breakdown products are rare. There is no significant inflammatory response (lymphocytes, plasma cells, neutrophils, eosinophils). The gray matter is generally spared or greatly preserved in comparison to white matter. However, astrogliosis and microgliosis of the overlying cortex may be found. Subtle mineralization of the basal ganglia has been observed. While axonal loss is complete in areas of cavitation, the less involved areas demonstrate a more variable loss of axons. Sometimes the axonal loss is as severe as the myelin loss, but in other cases or areas axons are relatively spared. Myelin sheaths are abnormal and vary from pale to thin to vacuolated. Vacuolated myelin is noted in preserved areas, often near the cystic to cavitated lesions. The vacuoles are bordered by material staining positive with Luxol fast blue or with myelin basic protein, suggesting that these vacuoles reflect intramyelinic edema. Ultrastructural studies have revealed some myelin vacuoles suggestive of intramyelinic edema. However, a re-evaluation of the vacuolated white matter following the recognition of “foamy” oligodendrocytes has raised questions about how much vacuolation of white matter is related to intramyelinic edema and how much is due to the presence of these vacuolated oligodendrocytes. The radiating stripes within the rarefied white matter, seen on MRI, seem to correlate with blood vessels accompanied by reactive astrocytes.

Different types of glia are involved in the disease process. In and around the areas that are cavitated, oligodendrocytes demonstrate marked losses, although they are still relatively high in number as compared to other types of cells. In areas that are better preserved an increase in apparently mature oligodendrocytes is seen, most consistently in the arcuate fibers, other regions bordering the cystic to cavitated lesions, anterior commissure, the internal capsule, and the corpus callosum. Oligodendrocytes may have an abnormal appearance and look vacuolated or “foamy.” At the ultrastructural level the vacuoles are membranous structures associated with mitochondrial membranes, and, in places, contiguous with myelin lamellae. These oligodendrocytes also combine many mitochondria, proteolipid protein mRNA, and fingerprint structures – the latter two attributes also noted in nonvacuolated oligodendrocytes. Positive staining for both proliferative markers (Ki-67), antiapoptotic

markers (bcl2, survivin), and proapoptotic markers (bac, bax, TUNEL, and activated caspase-3) has been found in oligodendrocytes. There is a trend that in early-onset devastating encephalopathy, loss of oligodendrocytes dominates with enhanced staining for apoptosis markers, whereas in older patients with longstanding disease, proliferation of oligodendrocytes dominates with striking increases in their numbers. There is a meager to moderate response by astrocytes and microglial cells in this disease, even in areas near the cavitation. Only scant lipophages are seen, and the astrocytes appear to be dysmorphic with blunt, broad processes rather than their typical delicate arborizations.

65.3 Pathogenetic Considerations

VWM is related to defects in translation initiation factor eIF2B. eIF2B consists of five nonidentical subunits (eIF2B α , eIF2B β , eIF2B γ , eIF2B δ , and eIF2B ϵ), all of which are encoded by different genes (*EIF2B1*, *EIF2B2*, *EIF2B3*, *EIF2B4*, and *EIF2B5*, respectively) located on different chromosomes (12q24.3, 14q24, 1p34.1, 2p23.3, and 3q27, respectively). Mutations in any of these genes can independently cause the disease.

Translation of mRNA into polypeptides is one of the major energy-consuming processes in the cell and is therefore, not surprisingly, a tightly regulated process. The initiation phase, in which ribosomes are assembled on mRNA, is controlled via several different signaling pathways. Multiple so-called eukaryotic initiation factors (eIFs) are involved in translation initiation, and among them the guanine nucleotide exchange factor eIF2B plays a key regulatory role. A crucial step in translation initiation is the delivery by eIF2 of the initiator methionyl-transfer RNA (Met-tRNA_i) to the small ribosomal subunit. Upon recognition of the start codon and binding of methionine to it, the eIF2-bound guanosine triphosphate (GTP) is hydrolyzed and eIF2 is released in its inactive guanosine diphosphate (GDP)-bound form. In order to bind another Met-tRNA_i and initiate the production of another protein, active eIF2 must be regenerated by exchange of GDP for GTP. This step is catalyzed by eIF2B. The exchange of GDP for GTP by eIF2B is required for each round of translation initiation. Thus, eIF2B is necessary for the production of all proteins in the body. Regulation of this step can control global rates of protein synthesis under diverse conditions.

Protein synthesis is markedly inhibited under a variety of stress conditions and in the recovery phase that follows. This response is part of a protective mechanism of cells elicited by various stimuli, including thermal, chemical, oxidative, or physical trauma, called the cellular stress response or heat shock re-

sponse. Stress may lead to misfolding and denaturation of proteins, contributing to cell dysfunction and death. The inhibition of normal RNA translation during stress is thought to enhance cell survival by limiting the accumulation of denatured proteins and saving cellular energy.

Inhibition of mRNA translation can be achieved through the modification of several initiation factors. Most stress conditions, including heat stress, lead to activation of specific kinases that phosphorylate eIF2 on its α -subunit. In this phosphorylated form, eIF2 binds tightly with eIF2B and in this way is a competitive inhibitor of eIF2B, preventing the recycling of eIF2. The concentration of eIF2 usually exceeds that of eIF2B. Therefore, even modest levels of eIF2 α phosphorylation can potentially lead to complete inhibition of translation initiation and protein synthesis. In certain cell types, inactivation of eIF2B at 40–41 °C can be achieved without changes in eIF2 α phosphorylation. eIF2B activity can also be regulated through other pathways, such as phosphorylation at different sites, which can enhance or suppress eIF2B activity. Whether these latter pathways are involved in the regulation of eIF2B activity under stress conditions is unclear.

The essential role of eIF2B, both in normal protein production and in its regulation under different conditions, including elevated temperature, is reflected by the evolutionary conservation of the complex and the nonviability of yeast null mutants for each of the subunits except eIF2B α . In VWM patients, most mutations are missense mutations. So far, major mutations, which prevent the expression of full-length eIF2B subunits, have only been observed in the compound heterozygous state with a missense mutation as second mutation.

At a biochemical level, evidence has been provided that mutations reduce eIF2B activity. Certain mutations impair the ability to form the five-subunit eIF2B holocomplexes, leading to diminished eIF2B activity. Point mutations in the catalytic domain, located at eIF2B ϵ , impair its ability to bind eIF2. Some other mutations in eIF2B β actually enhance eIF2 binding, also impairing eIF2B function.

The pathophysiology of VWM is still difficult to explain. Serious deteriorations often follow febrile infections and other forms of cellular stress. Inhibition of eIF2B via the phosphorylation of eIF2 α is an important mechanism for slowing down protein synthesis in response to, for example, the accumulation of unfolded proteins in the endoplasmic reticulum. This regulation of eIF2B is likely to be of particular importance in preventing denatured proteins from accumulating during cellular stress and could provide a clue as to why VWM is exacerbated by episodes of infection and trauma. There is evidence of activation of the

unfolded protein response in VWM. However, many aspects of the disease are poorly understood. eIF2B is ubiquitously expressed in all cells of the body. It is unclear why the brain is preferentially or selectively affected, whereas other organs are only involved in the most serious variants of the disease.

It is becoming increasingly clear that there is some genotype–phenotype correlation. Some mutations are consistently, although not invariably, associated with a mild phenotype, whereas other mutations are consistently associated with a severe phenotype. One example is the Arg113His mutation in eIF2B ϵ , which in the homozygous state is almost always associated with a late onset and slow progress. It is remarkable that histidine is normal at position 113 in mouse and rat. However, childhood-onset patients homozygous for the Arg113His mutation have been observed too. The second example is the Arg195His in eIF2B ϵ , the Cree leukoencephalopathy mutation, which in the homozygous state is invariably associated with an early onset and early death. There is also evidence for a correlation between decrease in guanine-nucleotide exchange factor (GEF) activity of eIF2B and the age at onset of the disease. Mutations with a more serious impact on eIF2B function seem to be associated with a more serious disease course. However, there is also major variation between patients carrying the same mutations and between affected siblings in the same family. So, environmental and other genetic factors influence the phenotype as well.

65.4 Therapy

There is presently no causal treatment for VWM, but certain preventive measures seem advisable. Particular stress conditions should be avoided in patients with VWM: infections, high temperatures, and head trauma. Vaccinations to prevent infectious diseases are important. In the case of fever, it is essential to keep the temperature down with antipyretics, if necessary with cooling. It is important to be liberal with antibiotics. In children with frequent upper respiratory tract infections, daily low-dose antibiotics may be considered. Patients have reported deterioration after sun bathing. Playing for a long time in the full sun during hot weather may, therefore, be something to avoid. It is impossible to avoid the minor head traumas of daily life, but it is better to avoid certain types of physical contact sports. During episodes of major deterioration, corticosteroids have led to temporary improvements. However, this effect is not consistent and lasting beneficial effects have never been observed. Considering the potential adverse effects of steroids, in particular worsening of infections, their use during episodes of deterioration is not advocated.

65.5 Magnetic Resonance Imaging

MRI of the brain shows extensive cerebral white matter changes in VWM (Figs. 65.1–65.5). Over time, MRI shows evidence of disappearance of the affected white matter, which is replaced by fluid (Figs. 65.2 and 65.3). On T₂-weighted images, abnormal white matter and cystic white matter both have a high signal intensity and cannot be distinguished. Proton-density or FLAIR images are necessary to demonstrate the white matter rarefaction and cystic degeneration. Abnormal white matter has a high signal on proton-density and FLAIR images, whereas cystic white matter has a low signal intensity, similar to the signal of CSF. Rarefied white matter has an intermediate signal intensity, not as low as CSF. Within the rarefied and cystic white matter a stripe-like pattern is visible, suggesting remaining tissue strands (Fig. 65.6). Heavily T₂-weighted images are as a rule not suitable to show the stripes, because these images do not allow distinction between the stripes of abnormal white matter and rarefied or cystic white matter, both appearing bright. In exceptional cases, the stripes are dark on T₂-weighted images (Fig. 65.6). The U fibers are spared to a variable extent. In some patients a rim of subcortical white matter is spared, whereas in other patients the U fibers are abnormal (Fig. 65.7). The sparing of the U fibers is seen best on T₁-weighted images (Fig. 65.7). MRI has been performed in a few presymptomatic and oligosymptomatic individuals and in all persons diffuse cerebral white matter abnormalities have been found, although initially not necessarily with evidence of rarefaction or cystic degeneration (Figs. 65.8 and 65.9). In the end stage of VWM all cerebral hemispheric white matter may have vanished, leaving a ventricular wall and cortex with little or nothing in between (Figs. 65.2 and 65.3). It is striking that although the white matter may be highly cystic, the brain does not collapse and rarely shows evidence of external atrophy. On the contrary, the cerebral white matter may have a (mildly) swollen appearance with broadening of gyri (Fig. 65.3). Even when there seems to be hardly any cerebral white matter left, there is a distance between ependymal lining and the cortex, apparently filled with fluid. The lateral ventricles may be mildly to moderately dilated, but not seriously so. White matter swelling is predominantly seen in young children, whereas more serious atrophy is seen in teenagers and adults with VWM (Fig. 65.4).

Often a dilated cavum septi pellucidi and cavum Vergae are present. The inner rim of the corpus callosum is usually involved (Figs. 65.8 and 65.9), and in later stages the corpus callosum becomes thin (Fig. 65.10). The posterior limb of the internal capsule is often involved, whereas the anterior limb of the internal capsule is rarely involved. The anterior com-

missure is spared. The cerebellar white matter may have a normal (Fig. 65.4) or mildly abnormal signal (Figs. 65.1, 65.2 and 65.5). However, the process of rarefaction and cystic degeneration appears to be restricted to the cerebral hemispheric white matter. Over time, atrophy of the cerebellum and sometimes also the brain stem ensues. There are often signal abnormalities in the midbrain and pons, and sometimes in the medulla (Figs. 65.2 and 65.5). Especially, the central tegmental tracts in the pontine tegmentum are often involved. Unlike the cerebral and cerebellar white matter abnormalities, the brain stem signal abnormalities, when present, may improve again and even disappear. They seem to be particularly prominent during episodes of lowered consciousness (Figs. 65.2 and 65.5). MRI-visible spinal cord lesions are rare but may occur.

The cerebral and cerebellar cortex have a normal appearance. Most often, the basal ganglia and thalamus also have a normal signal intensity, but particularly thalamus and globus pallidus lesions may occur (Figs. 65.2 and 65.5). Thalamus lesions may also improve and disappear all together. The globus pallidus may have a low signal intensity on T₂-weighted images, suggesting mineralization (Figs. 65.4 and 65.5).

The above MRI description applies to the late-infantile, childhood, juvenile, and adult-onset disease (Figs. 65.1–65.10). The MRI picture may be much more difficult to diagnose in early-infantile VWM. In evidently affected neonates, the brain may only look immature with a gyral pattern that is too coarse for the gestational age of the child and with immature white matter having a high water content and little myelin, but little or no rarefaction (Figs. 65.11–65.13). Over time, the cerebral white matter may look increasingly abnormal, rarefied, and cystic, as seen in the later-onset variants of the disease, but the cerebral white matter may also become highly atrophic, the ependymal lining (almost) touching the depth of the gyri (Fig. 65.13), very much unlike what is seen in the later-onset variants of the disease. In these severely affected infants, the brain as a whole is highly atrophic, including also the corpus callosum, cerebellum, and brain stem. In early-onset VWM, the cerebellar white matter may also become cystic.

Proton MRS shows stage-dependent abnormalities. In the initial stages, when there is little white matter rarefaction, the white matter spectrum is relatively preserved. With ongoing rarefaction and cystic degeneration, the signals decrease, finally to disappear altogether. Finally, the spectrum is a CSF spectrum with some lactate and glucose and no or minor “normal” peaks. The cortex spectrum remains well preserved throughout.

A study using phosphorus MRS of the brain (Blüml et al. 2003) revealed evidence for an altered energy state of the residual cells in the cerebral white

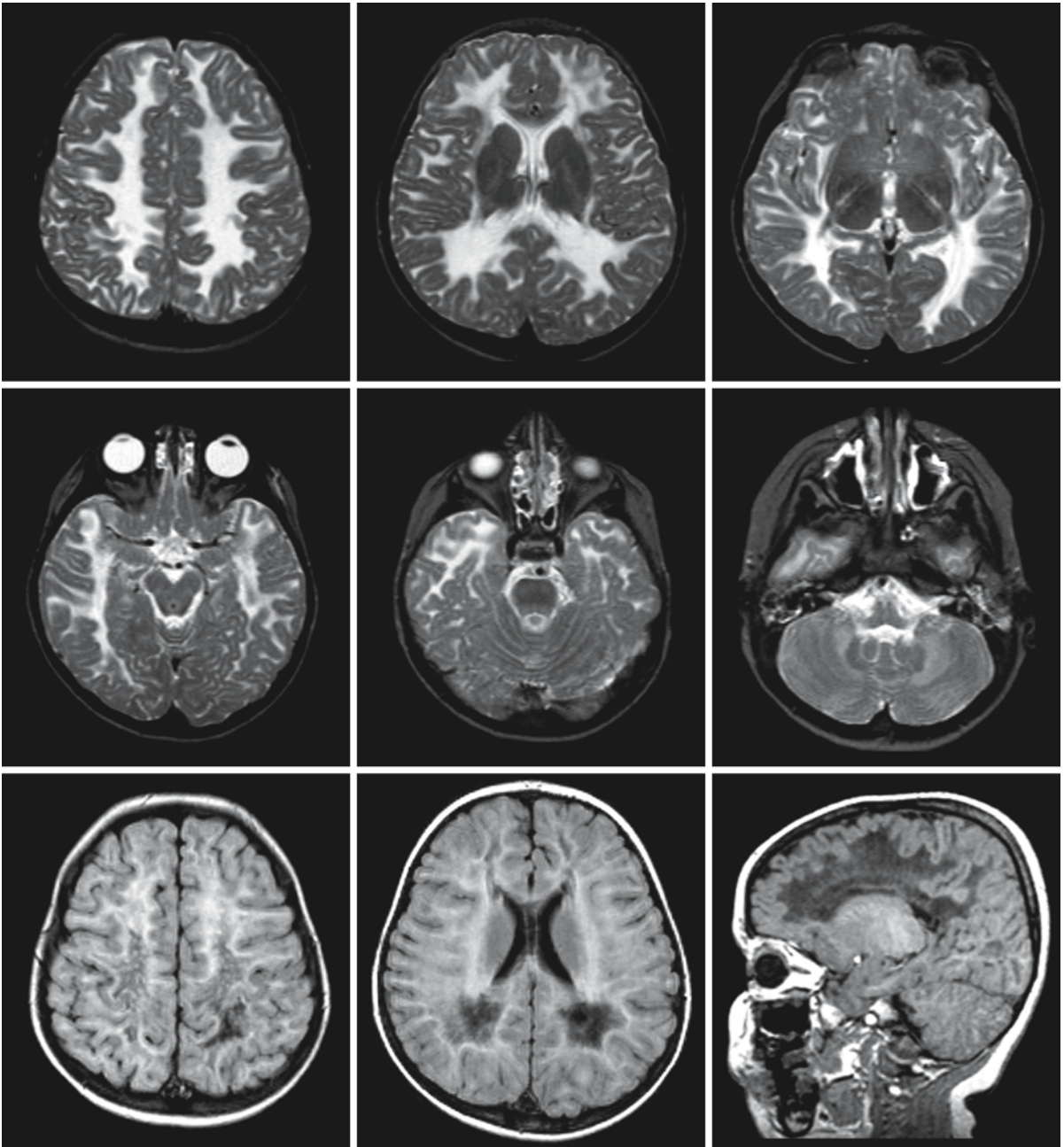


Fig. 65.1. The cerebral white matter is diffusely abnormal in this 3.5-year-old girl with VWM. The posterior limb of the internal capsule is affected. The brain stem is intact. The cerebellar white matter has a mildly abnormal signal intensity. The FLAIR images (*third row, left and middle*) demonstrate that within the white matter that is abnormal on the T₂-weighted images there are areas with a low signal intensity, close or equal to the

signal intensity of CSF, consistent with white matter rarefaction and cystic degeneration. Within these areas dots and stripes with a high signal intensity are seen, consistent with remaining strands of abnormal tissue. The sagittal T₁-weighted image (*third row, right*) shows a pattern of radiating stripes, compatible with better preserved tissue strands

matter. Nucleoside triphosphate and inorganic phosphate were reduced, whereas phosphocreatine was elevated. The relative preservation of gray matter over white matter may have contributed to this observa-

tion, the nucleoside triphosphate to inorganic phosphate ratio normally being lower in gray matter than in white matter. Of the metabolites involved in biosynthesis and catabolism of membrane phospho-

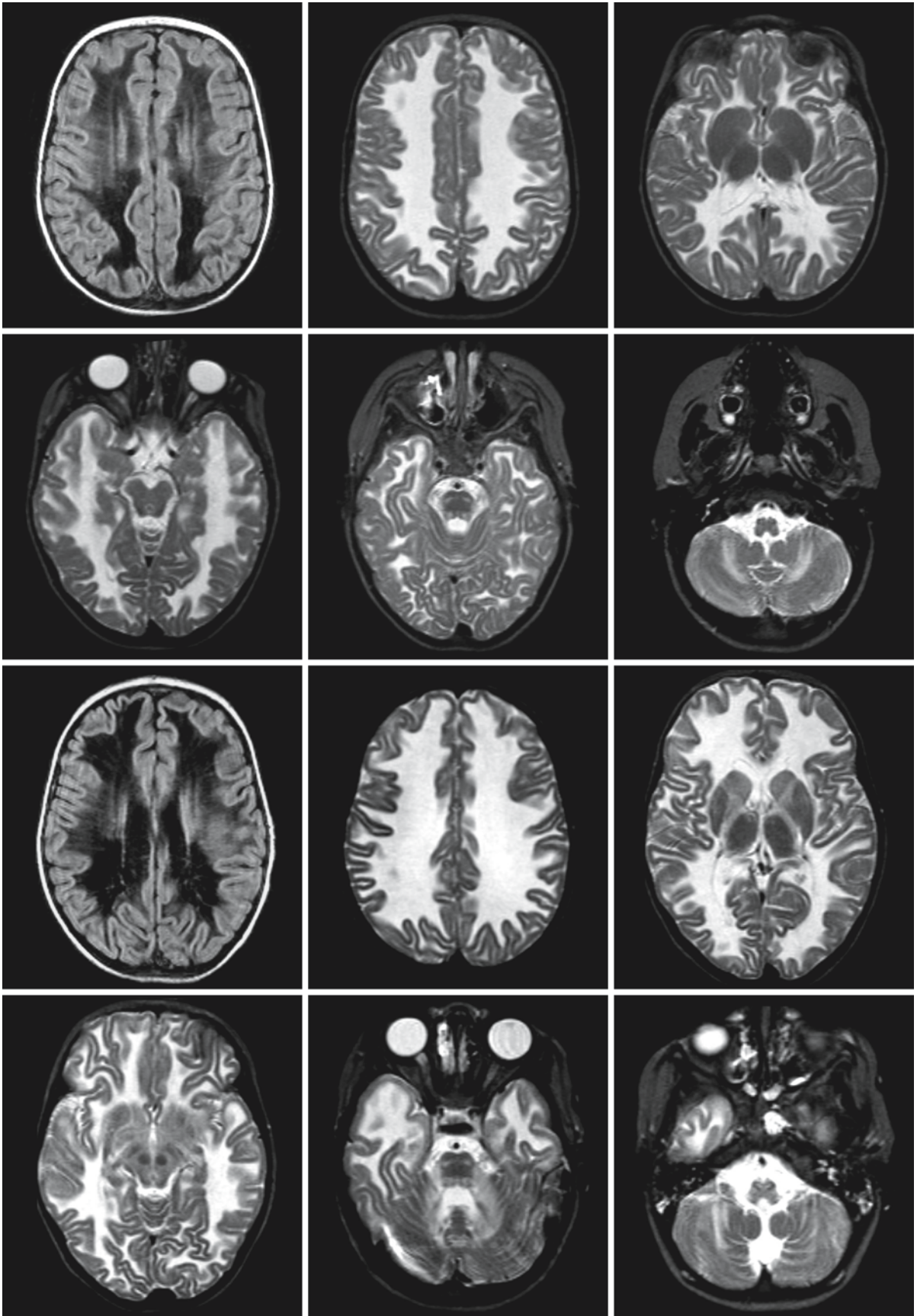


Fig. 65.2.

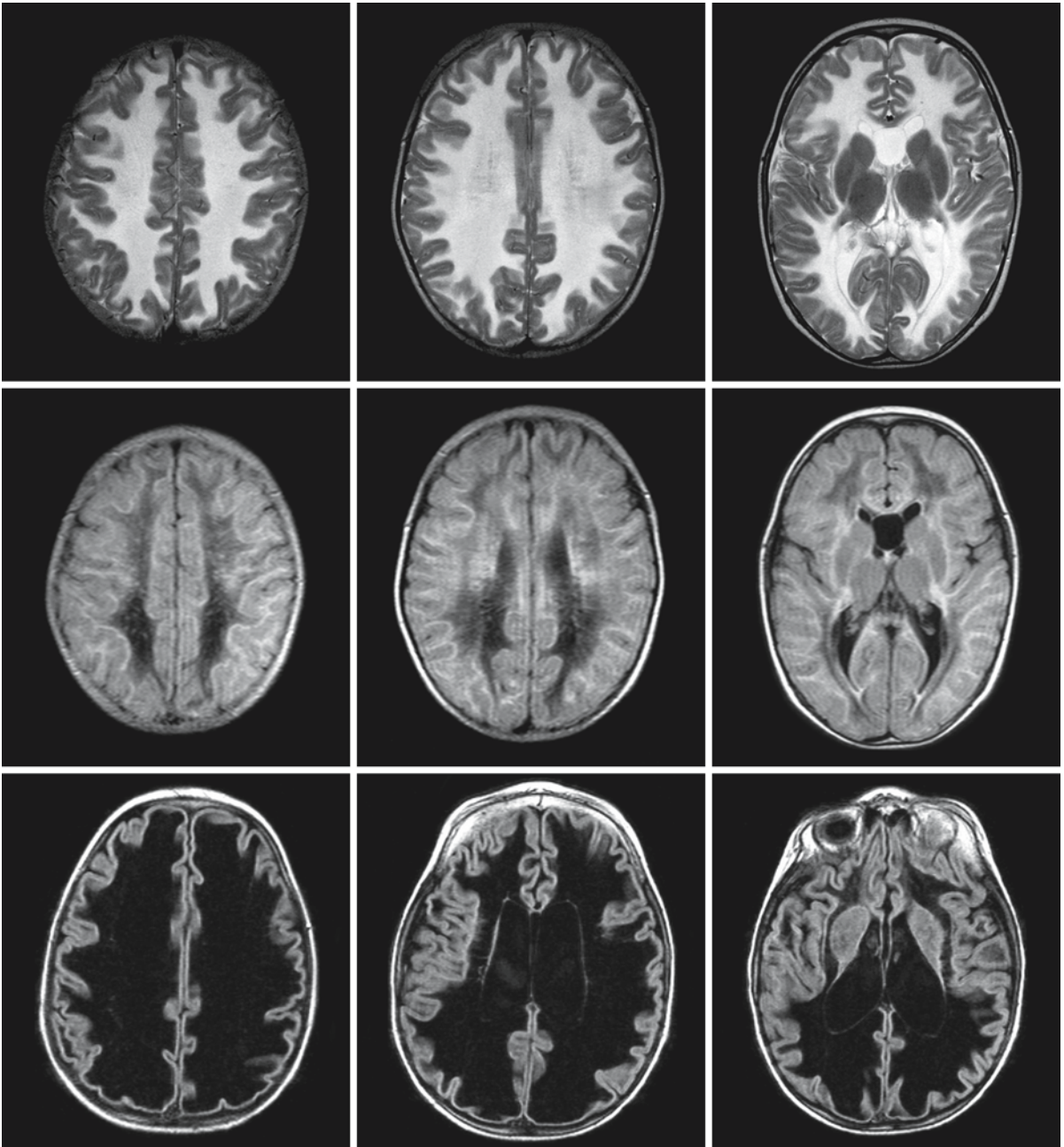


Fig. 65.3. The T₂-weighted (*first row*) and FLAIR images (*second row*) of a severely affected 2-year-old boy with VWM show the characteristic abnormalities. Note the large cavum septi pellucidi. Ten months later he has lost almost all functions. He is blind and has no intentional movements. The MRI was performed because he had papilledema at funduscopy. The FLAIR

images (*third row*) show that all cerebral white matter has vanished. The lateral ventricles are mildly dilated, but the cerebral cortex has not collapsed over the central structures. On the contrary, the vanished white matter look swollen with broadening of gyri

Fig. 65.2. The T₂-weighted images of this 3-year-old girl with VWM (*first two rows*) show diffuse involvement of the cerebral white matter, posterior limb of the internal capsule, and cerebellar white matter. Within the pons the central tegmental tracts and the pyramidal tracts are affected. The FLAIR image (*first row, left*) shows much more serious white matter rarefac-

tion and cystic degeneration than in the previous patient. Five months later (*third and fourth rows*), she is in coma. The FLAIR images (*third row, left*) show that the cerebral white matter is now largely cystic. The T₂-weighted images show that the globus pallidus, midbrain, and medulla now have an abnormal signal. The girl died soon after the MRI

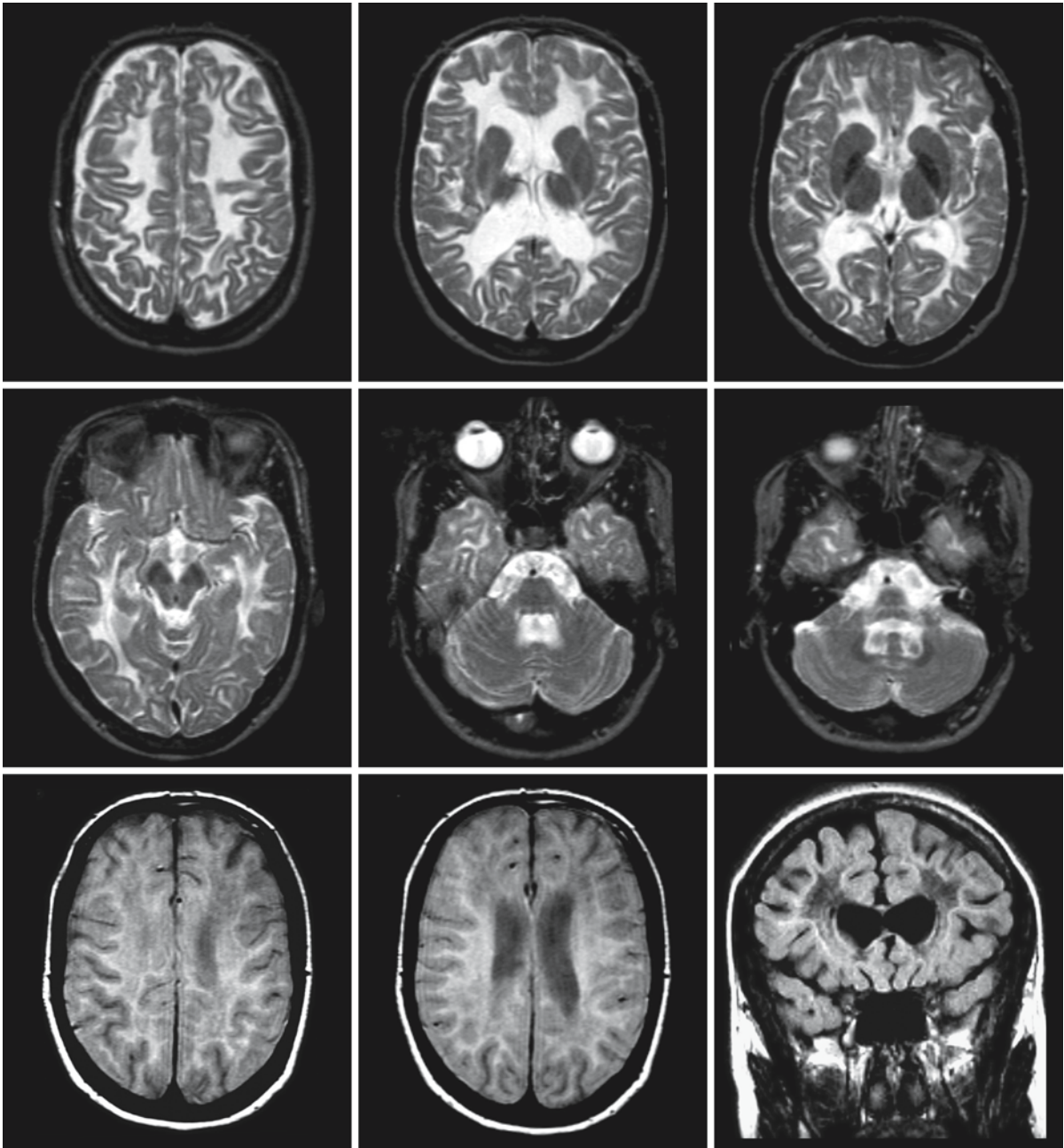


Fig. 65.4. This 18-year-old girl has a milder form of VWM. Although she has been symptomatic since the age of 4 years, she can still walk without support. The T₂-weighted images show diffuse white matter involvement with some atrophy, but the proton-density images (*third row, left and middle*) show that

the cerebral white matter is rarefied but not cystic. The FLAIR image (*third row, right*) shows the characteristic radiating stripes of better preserved tissue strands. The globus pallidus has a low signal intensity, probably related to mineralization. The brain stem and cerebellar white matter are intact

lipids, glycerophosphoethanolamine was reduced and phosphatidyl ethanolamine was increased, whereas choline-containing phosphorylated metabolites were unchanged. It is difficult to interpret these findings, most of all because the composition of the remaining brain tissue in VWM is dramatically

changed with serious rarefaction and altered ratios of composing cells. Why a defect in the regulation of protein synthesis would selectively affect ethanolamine phospholipid metabolism and leave choline phospholipid metabolism unaffected is presently unclear.

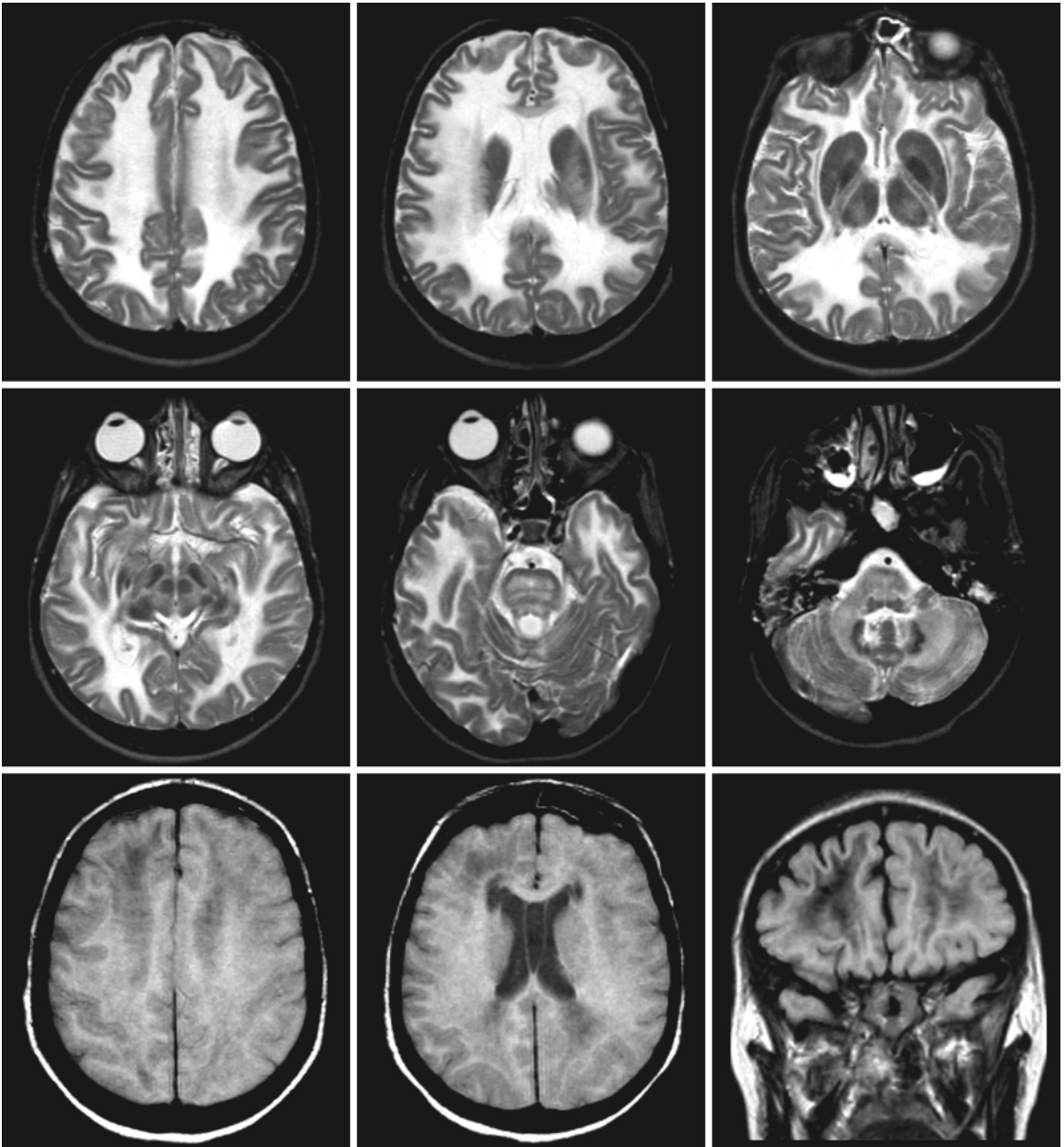


Fig. 65.5. The girl illustrated in this figure presented for the first time at the age of 16, lapsed into coma and died after 4 months. The T₂-weighted images show the diffuse white matter involvement, but the proton-density images (*third row, left and middle*) show that the white matter is rarefied but not cystic. This was confirmed at autopsy. Both the proton-density

and FLAIR (*third row, right*) images show evidence of some better preserved tissue strands. The T₂-weighted images show signal abnormalities in the internal capsule, thalamus, midbrain, basis of the pons, central tegmental tracts, middle cerebellar peduncles, cerebellar white matter, and medulla

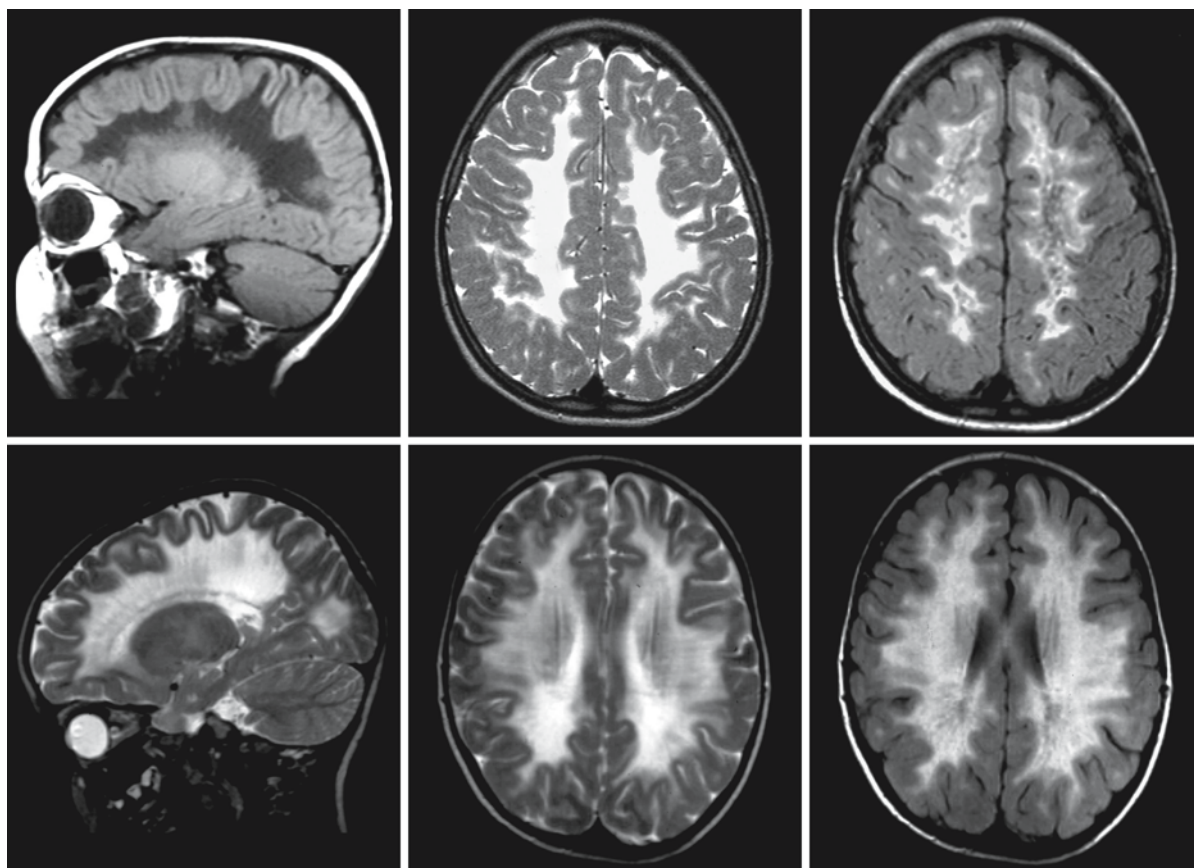


Fig. 65.6. The *first* row of images was obtained in a 5-year-old boy with VWM; the *second* row in a 6-year-old girl with VWM. In the boy the typical MRI features of VWM are seen with a pattern of radiating stripes on the sagittal T₁-weighted image (*left*), diffuse white matter abnormalities without evidence of stripes and dots on the axial T₂-weighted image (*middle*), whereas on the FLAIR image (*right*) the abnormal white matter has a high signal in some parts and a low signal in others, the latter compatible with rarefaction and cystic degeneration. Within the rarefied white matter of the centrum semiovale,

dots with a high signal intensity are seen, consistent with transections of strands of abnormal white matter. In the girl an unusual pattern is seen. The sagittal (*left*) and axial (*middle*) T₂-weighted images show the diffuse abnormality of the cerebral white matter. Within the abnormal white matter a pattern of dark radiating stripes is seen, apparently representing strands of normal tissue. The FLAIR image (*right*) shows some white matter rarefaction in the parietal area. Images of the second patient courtesy of Dr. T. Polster, Gilead Pediatric Center, Bielefeld, Germany

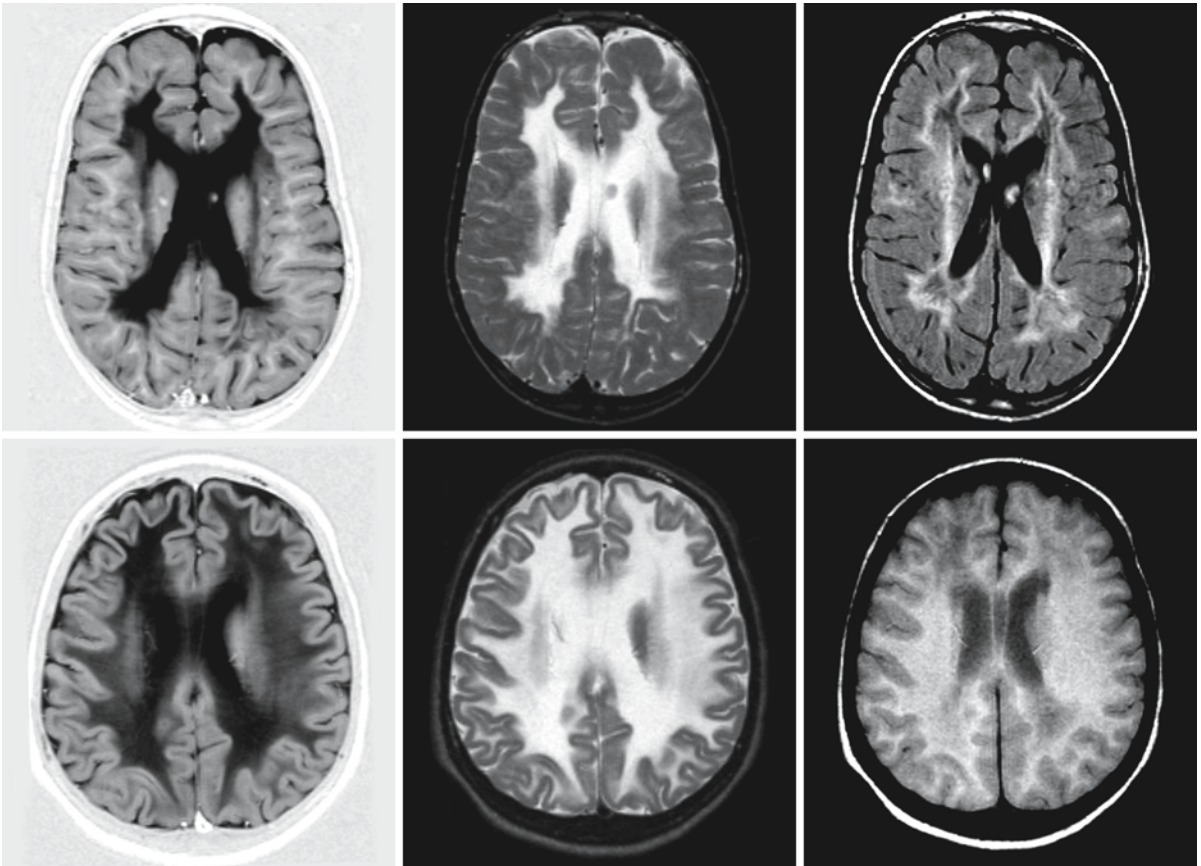


Fig. 65.7. The *first* row of images originates from a 9-year-old girl with VWM, the *second* row from a 16-year-old girl with VWM. The T_2 -weighted (*middle*) and FLAIR or proton-density (*right*) images reveal the characteristic features of VWM. The IR image (*left*) shows that the U fibers are spared in the first patient, whereas they are affected in the second patient

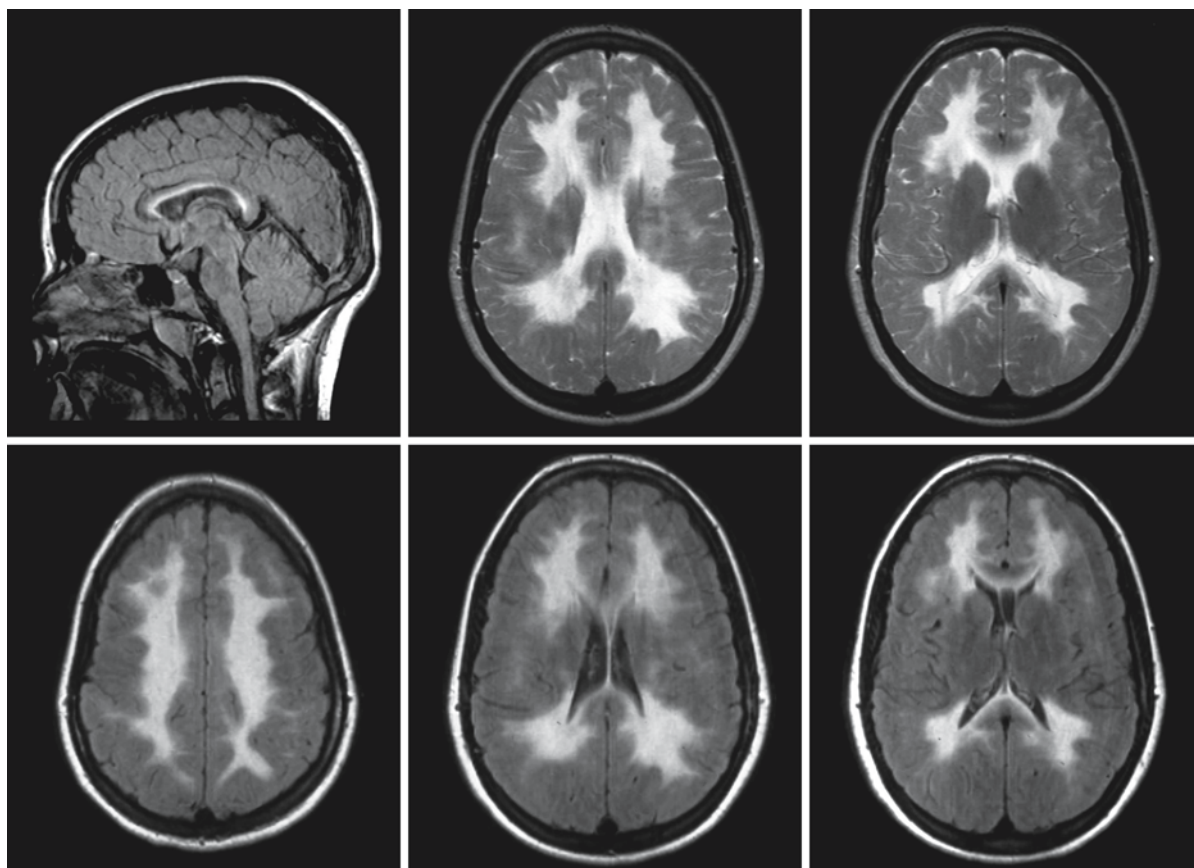


Fig. 65.8. This 18-year-old university student presented with a single seizure and had no abnormalities at neurological examination. She has a DNA-confirmed diagnosis of VWM. The T₂-weighted images (*first row*) show diffuse involvement of the

cerebral white matter and the inner rim of the corpus callosum. The FLAIR images (*second row*) do not show evidence of white matter rarefaction. Courtesy of Dr. E Storey, Neurogenetics Clinic, Royal Melbourne Hospital, Parkville, Australia

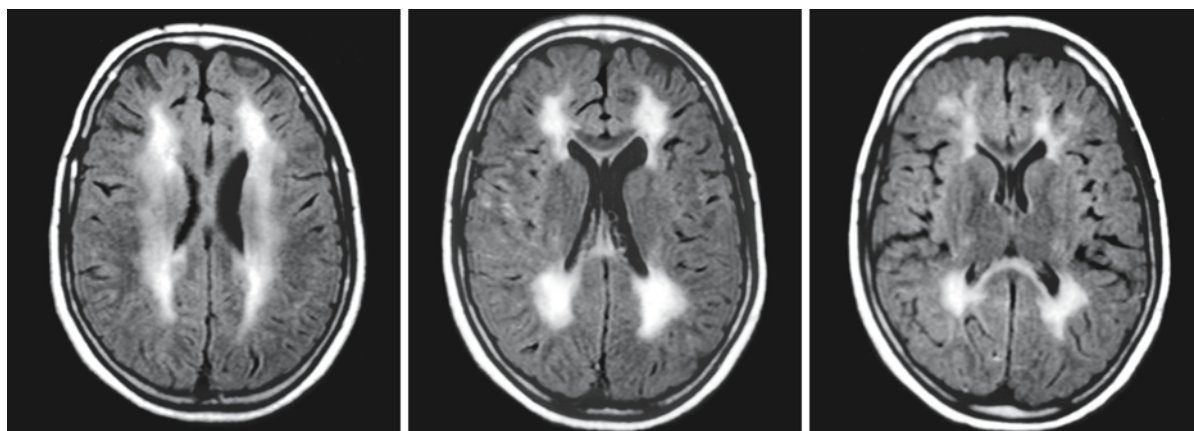


Fig. 65.9. A 13-year-old girl has a history of complicated migraines, but no abnormalities at neurological examination. She has a DNA-confirmed diagnosis of VWM. These FLAIR images show abnormalities in the periventricular and deep white

matter and inner rim of the corpus callosum with sparing of all subcortical white matter. There is no evidence of white matter rarefaction. Courtesy of Dr. M. D'Hooghe, Department of Neurology, Sint-Jan General Hospital, Brugge, Belgium

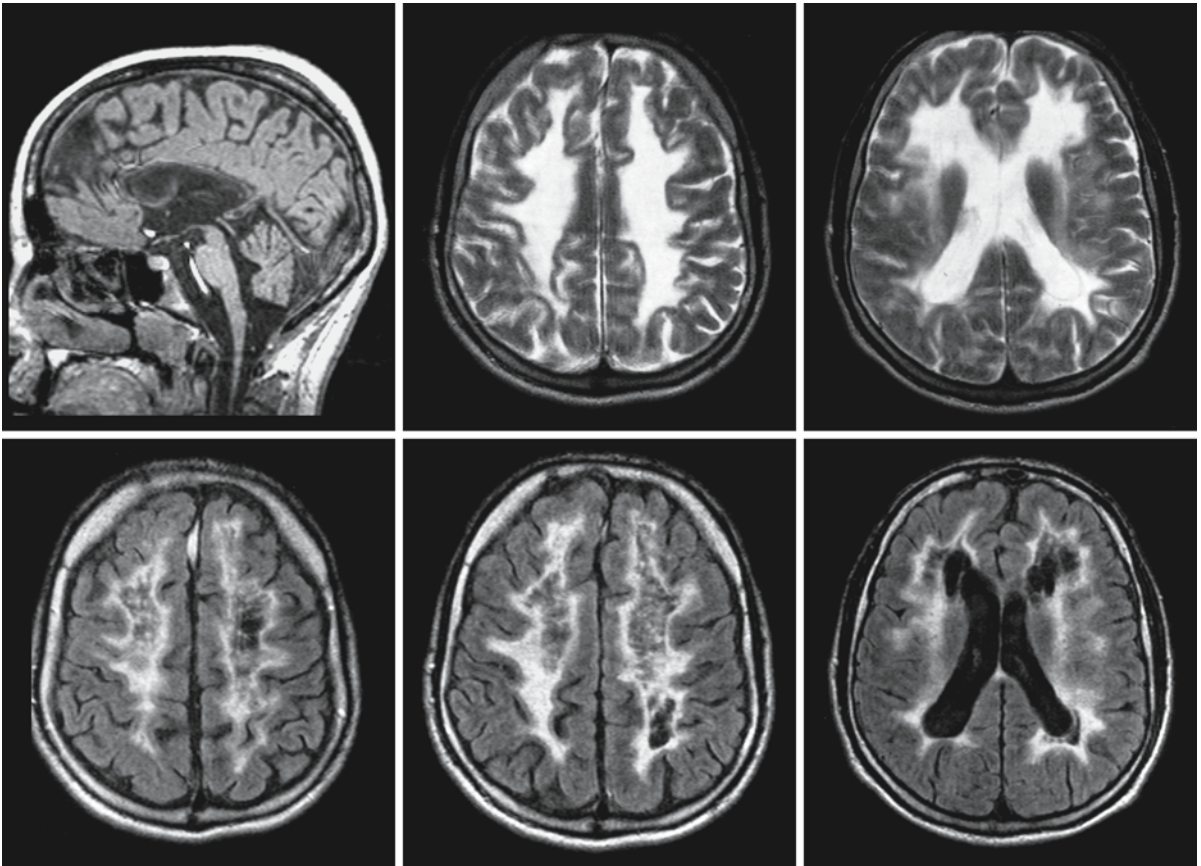


Fig. 65.10. A 49-year-old man with a history of presenile dementia and motor problems. His MRI is typical for VWM and the diagnosis was DNA-confirmed. Note the thin corpus callosum. From Prass et al. (2001), with permission

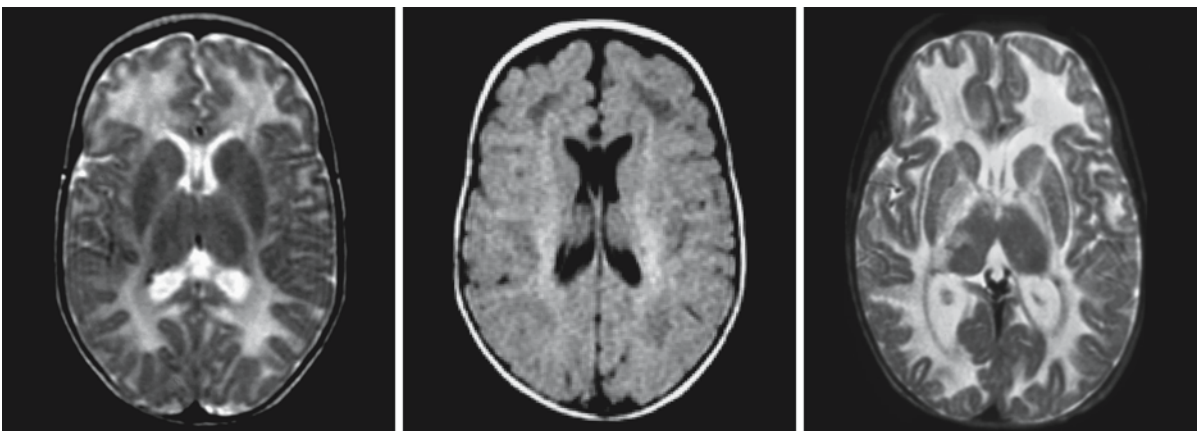


Fig. 65.11. The VWM patient in this figure had an antenatal onset of symptoms with decreased fetal movements and oligohydramnios. At birth she had dislocated hips and was hypotonic. She followed a rapidly downhill course with intractable seizures, feeding difficulties, hypotonia, apathy, and finally coma and respiratory failure. At physical examination oil droplet cataracts and hepatosplenomegaly were found. She died at 8 months. The *left* (T_2 -weighted) and *middle* (FLAIR) im-

ages were obtained at the age of 3 months and revealed most of all an immature brain with failure of myelination and insufficient gyral development. The FLAIR image shows some white matter rarefaction. The right image was obtained at 6 months and revealed more prominently abnormal cerebral white matter with additional involvement of the globus pallidus and the right thalamus. From van der Knaap et al. (2003), with permission

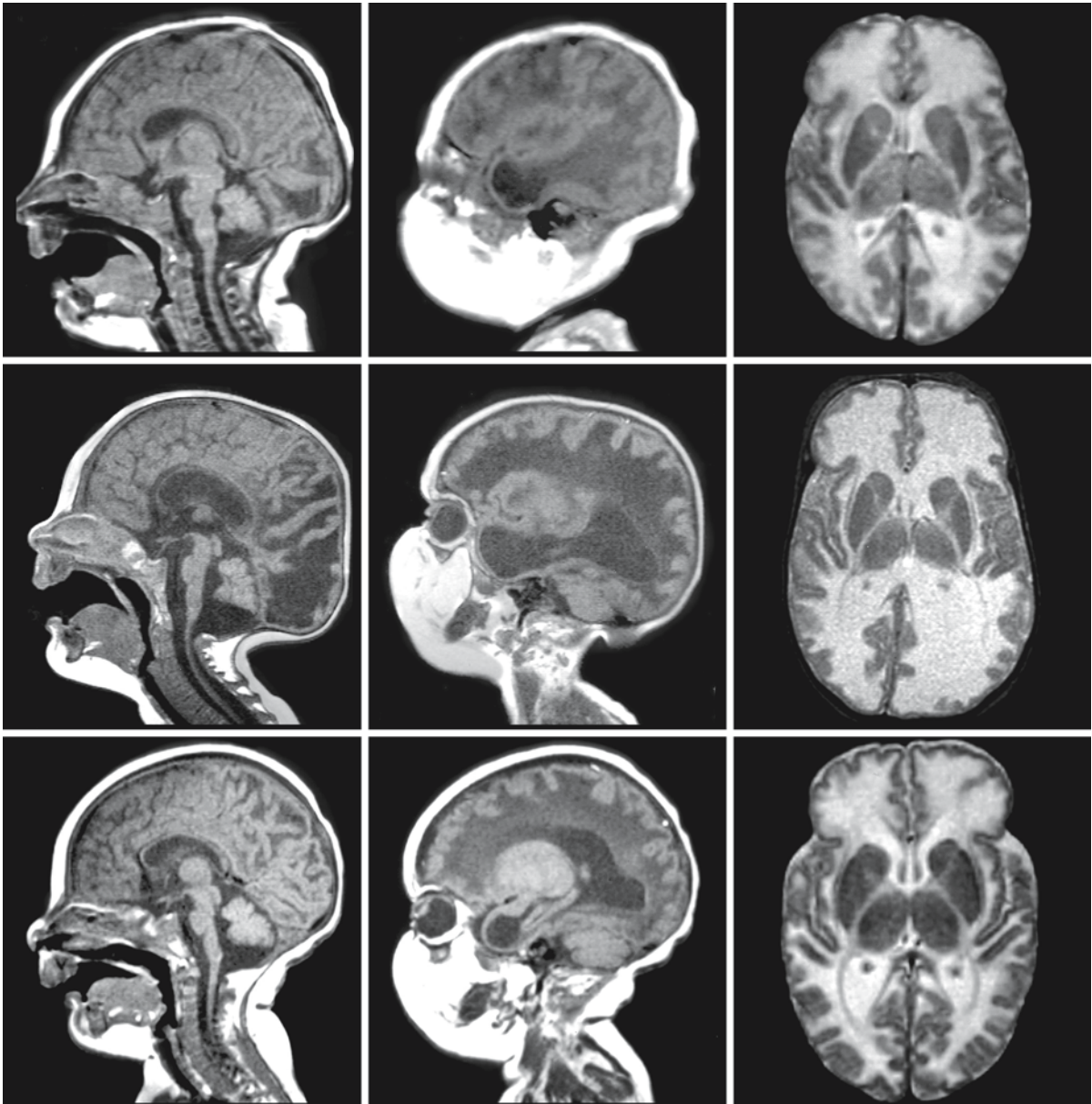


Fig. 65.12. This figure shows the images of two siblings with antenatal onset of VWM and death at the ages of 3.5 and 4 months, respectively. The *first* row of images was obtained at 1 month in a girl; the *second* row shows the follow-up images obtained at 4 months. The *third* row shows the images of her affected brother, obtained at 3 months. The images obtained at 1 month reveal an immature brain with failure of myelination and insufficient gyration. Note the swelling of the anterior temporal white matter, which contains a cyst. The images ob-

tained at 3 and 4 months revealed more prominent abnormalities of the cerebral white matter. Myelination and gyration have not progressed. There is white matter volume loss with enlargement of the lateral ventricles. Note the swollen and cystic anterior temporal white matter. The cerebellum is small and the brain stem looks atrophic. Courtesy of Dr. R. van Coster, Department of Pediatric Neurology, C. Hooft University Hospital, Gent, Belgium

Fig. 65.13. A patient with antenatal onset of VWM underwent MRI at the ages of 5 days (*first* and *second* rows) and 5 months (*third* and *fourth* rows). Initially, the brain has an immature appearance with coarse gyri and cerebral white matter with a high water content. The inferior horns of the lateral ventricles are dilated. On follow-up, most of the cerebral white matter has disappeared, but, unlike the typical appearance of vanish-

ing white matter, the ependyma touches the cortex. The lateral ventricles are now highly dilated. There is a cyst in the anterior temporal region. The remaining cerebral white matter looks highly abnormal and swollen. The cerebellum has become highly atrophic. The brain stem is also thin. From Boltshauser et al. (2002) and van der Knaap et al. (2003), with permission

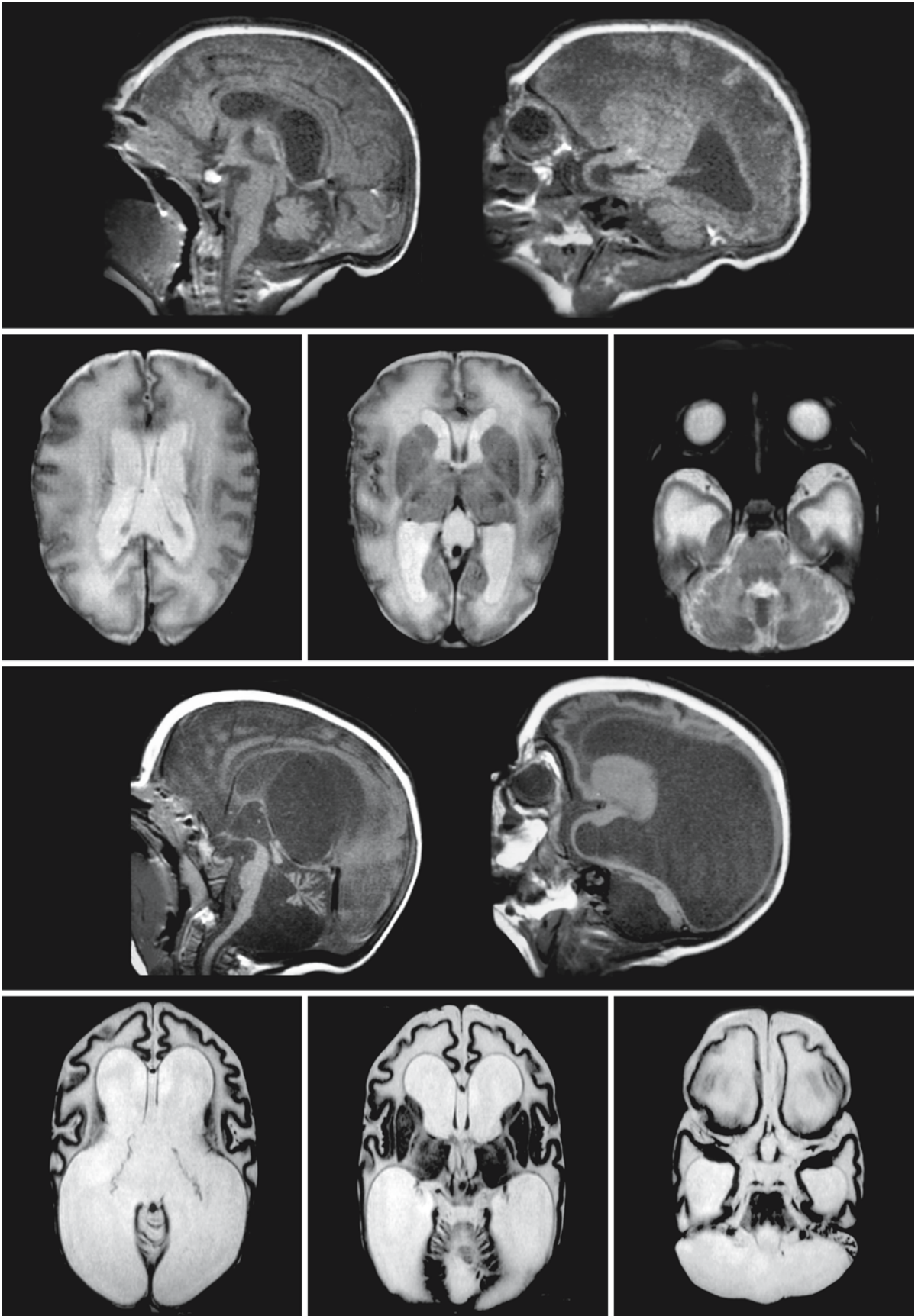


Fig. 65.13.

Aicardi–Goutières Syndrome

66.1 Clinical Features and Laboratory Investigations

Aicardi–Goutières syndrome is a rare leukoencephalopathy with an autosomal recessive mode of inheritance. The disease presents at birth or within the first few months of life. In some patients intrauterine growth retardation and a deceleration of head growth have been reported. Early postnatal signs are irritability, jitteriness, feeding problems, and failure to thrive. Often a high-pitched cry is noted. Recurrent febrile episodes of unknown cause may occur in the presence of normal laboratory investigations. Generalized hypertonia and spasticity are present from the beginning, or develop in the course of the first months. Dystonic posturing may occur. Truncal hypotonia, poor head control, and opisthotonic posturing are often noted. Head growth is usually poor with progressive microcephaly, but some patients have a normal head circumference. Gain in height and weight is usually normal or just below normal. Some but not all patients have seizures. Vision is often poor. Some patients have pale optic discs, whereas others have normal fundi. Pupillary reactions are normal. Nystagmus may be present. There is a variably severe developmental delay. In many patients no, or at most few, developmental milestones are reached. However, some patients achieve walking with or without support. Some patients learn to talk.

Some patients have extraneurological features. The most prominent of these are cutaneous lesions, which mainly affect the fingers and toes, and sometimes also the ear lobes, in the form of scaly erythematous lesions and an acrocyanotic appearance reminiscent of chilblains. Patients may have puffy edema and swelling of the proximal parts of fingers and toes tapering towards the end.

The disease is usually considered to be progressive, although in patients with severe and early-onset disease it may be difficult to determine whether this is the case. Patients with milder disease may show ongoing development for many years, although in others a clear regression is noted. Many patients die early, within either months or a few years of birth. Most children die in a vegetative state from pneumonia. However, survival beyond the teenage period has also been observed. When multiple affected patients are present within the same family, striking differences in the severity of the disease may be observed. Within

the same family, one affected child may achieve no developmental milestones at all and be severely spastic, whereas the affected sibling is walking with support.

Laboratory investigations have revealed no abnormalities apart from mild chronic lymphocytic pleocytosis in the CSF, with a cell count usually varying between 10 and 300 cells/mm³. The CSF lymphocytosis is more or less obligatory in the early stages of the disease, but may disappear afterwards. The duration of the persistence is probably quite variable. Protein level varies from normal to more than 1 g/l. There is no evidence of intrathecal immunoglobulin synthesis: IgG index is normal and there are no oligoclonal bands. Interferon- α is elevated in blood and CSF, but much higher in CSF than in blood, indicative of intrathecal synthesis. The elevation of interferon- α is probably consistently present, at least in the early stages of the disease and probably also for a long time thereafter. Electron microscopy of CSF lymphocytes may reveal tubuloreticular inclusions, indicative of interferon deposits. Similar deposits may also be present in endothelial cells on skin biopsy. There is no evidence of congenital infections; TORCH (*toxoplasmosis, rubella, cytomegalovirus, and herpes simplex*) screening is negative. Extensive screening for inborn errors of metabolism has never revealed abnormalities. In some patients increased CSF pterins and lowered CSF folate levels have been found.

Multiple patients have been reported with atypical findings. At present it is not clear whether these cases are variant forms of Aicardi–Goutières syndrome or should be considered separate, distinct disease entities. A few patients reported had atypical manifestations including microcytic anemia (Kumar et al. 1998) or growth hormone deficiency and retinal degeneration (Bönnemann et al. 1991). Another condition to be considered is the microcephaly–intracranial calcifications syndrome (MICS), also called pseudo-TORCH syndrome, which has a neonatal-onset encephalopathy and shares essential features with Aicardi–Goutières syndrome, especially calcium deposits within the cerebral white matter and basal ganglia, but also has features suggestive of a congenital infection, such as neonatal thrombocytopenia, hepatosplenomegaly, congenital microcephaly, and cataracts in the presence of negative TORCH antibodies (Burn et al. 1986; Reardon et al. 1994; Wiczorek et al. 1995; Monastiri et al. 1997; Slee et al. 1999; Vivarelli et al. 2001). Cree encephalitis, reported among the

Cree Indians, leads to microcephaly, intracerebral calcifications, hepatosplenomegaly, and thrombocytopenia, similar to the pseudo-TORCH syndrome (Black et al. 1988). Lupus erythematosus has been described in two siblings with a pseudo-TORCH syndrome born to consanguineous parents (Dale et al. 2000). The patients presented with early-onset encephalopathy and typical signs of pseudo-TORCH syndrome. Within a year they developed hypocomplementemia and a systemic lupus erythematosus-like rash. The diagnosis of systemic lupus erythematosus was made on the basis of a characteristic autoantibody profile. Finally, there are reports on patients who share similarities with Aicardi-Goutières syndrome patients, including the cerebral white matter abnormalities and punctate calcium deposits in the white matter and basal ganglia, but also have symptoms not reported in other patients, such as hypothyroidism and pericardial effusions, and lack CSF lymphocytosis and elevated CSF interferon- α levels (Schwarz et al. 2002).

66.2 Pathology

Postmortem investigations demonstrate gross atrophy of the cerebral hemispheres, corpus callosum, brain stem, and cerebellum. On sectioning, reduction in white matter volume and enlargement of the ventricles are noted. Calcium deposits are consistently present. Most dense calcium deposits are seen in the globus pallidus, putamen, caudate nucleus, thalamus, and dentate nucleus. Less dense calcium deposits are variably noted in the cerebral cortex, cerebral white matter, cerebellar white matter, and cerebellar cortex. The calcium deposits are usually punctate, but large concretions may also be seen. On microscopy the calcium deposits are shown to be vascular and perivascular. Many small vessels, both veins and arteries, exhibit thickened media and adventitial wall with circular and focal calcium deposits within the media, adventitia, and perivascular spaces. In addition, some lamellar calcium deposits not associated with blood vessels are seen in the cerebral and cerebellar white matter. The cerebral and cerebellar white matter and the brain stem display a diffuse inhomogeneous myelin deficiency associated with astrogliosis. Areas of complete myelin deficiency may show cavitation. Signs of active myelin breakdown are lacking; no sudanophilic material is present. Some ascribe the myelin deficiency to hypomyelination and others to myelin loss. In the cerebral and cerebellar cortex a multitude of wedge-shaped microinfarctions has been reported with abnormal small vessel proliferation. These infarctions are probably related to the widespread calcifying microangiopathy. Inflamma-

tion is minor and limited to the areas of necrosis and to the leptomeninges.

66.3 Pathogenetic Considerations

The disease has an autosomal recessive mode of inheritance. The basic defect is unknown. A genome-wide linkage study has revealed a locus for a disease gene on chromosome 3p21, but no gene associated with Aicardi-Goutières syndrome has yet been identified. Evidence for locus heterogeneity has been provided, suggesting the existence of at least one additional disease gene. The problem presently is the clinical definition of the disease. There is a striking clinical heterogeneity and it is not known whether Aicardi-Goutières syndrome, variant forms, MICS/pseudo-TORCH syndrome, and Cree encephalitis represent the same disorder or not. They may represent closely related but different disorders with defects in different single genes, probably all involved in similar or the same processes, or they may represent one disorder, associated with not a single but a small number of genes that are involved in the same process.

The chronic CSF lymphocytosis and elevated interferon- α levels are central and striking features in Aicardi-Goutières syndrome. Interferons constitute a family of signal proteins. Upon binding to specific receptors they induce activation of a signal transduction pathway that activates a broad range of genes, which are involved in antiviral, immunomodulatory, and antiproliferative activities. Interferon- α is increased to variable levels in viral infections, depending on the stage of the disease. Interferon- α does not cross the blood-brain barrier, so if levels are higher in the CSF than in the blood, it is a result of intrathecal synthesis. It is elevated in the CSF during viral meningitis and encephalitis, but elevation is not a sign of neurodegenerative disorders in general. It is probable that interferon- α is important in the pathophysiology of Aicardi-Goutières syndrome. Transgenic mice with astrocyte-targeted chronic overproduction of interferon- α develop progressive inflammatory encephalopathy with angiopathy and calcifications in the basal ganglia. These neuropathological features are very similar to those found in Aicardi-Goutières syndrome, suggesting a causal relationship between the elevated levels of interferon- α and the disease.

Histopathological findings suggest that a calcifying microangiopathy may underlie Aicardi-Goutières syndrome. Small vessels have a highly abnormal appearance with thickened walls and intramural and perivascular calcium deposits. The wedge-shaped microinfarctions in the cerebral and cerebellar cortices are highly suggestive of involvement of small arteri-

oles. The inhomogeneous, irregular aspect of the white matter abnormalities, with patches of preserved myelin and patches of myelin loss and cavitation alternating in an apparently haphazard way, is compatible with an underlying microangiopathy. A microangiopathy in the context of an inherited disease is not unique. The combination with microangiopathy and leukoencephalopathy is also seen in Labrune syndrome and CADASIL, although in the latter condition there are no calcium deposits. An open question is how an “interferonopathy” could be related to the calcifying microangiopathy seen in Aicardi–Goutières syndrome

66.4 Therapy

At present, there is no therapy apart from supportive care. Prenatal diagnosis is not possible as yet.

66.5 Magnetic Resonance Imaging

CT is very important in the diagnosis of this disease, readily demonstrating the presence of calcium deposits (Figs. 66.1, 66.3, 66.5, and 66.8). The calcium deposits are most often seen in the globus pallidus, putamen, caudate nucleus, thalamus, and dentate nuclei. Additionally, calcium deposits may be seen in the cerebral white matter, in particular in the periventricular area alongside the ventricle wall, and in the cerebellar white matter. The deposits are typically punctate, and may coalesce to form large concretions. However, in patients in whom the basal ganglia calcifications have become diffuse, there are usually still punctate calcifications elsewhere in the brain. In several affected sibs of typical cases of Aicardi–Goutières

syndrome, CT did not reveal any calcifications, or only in the cerebral white matter along the ventricles. Apparently the calcifications are a characteristic, but not obligatory part of the disease. Over time the calcium deposits tend to increase in extent and number. On CT, variable white matter hypodensity and atrophy has been reported.

Calcifications are less easily seen on MRI, but MRI more easily shows the abnormality of the white matter. With few exceptions, the cerebral and cerebellar white matter is diffusely abnormal (Figs. 66.2 and 66.6). In some patients the signal abnormality is mild and the white matter looks hypomyelinated rather than “diseased.” In these patients, MRI demonstrates the presence of myelin in some structures that normally myelinate early, suggesting arrest of myelination at an early stage. In other patients the white matter signal abnormalities are much more pronounced, suggesting that the white matter signal abnormality cannot simply be explained by insufficient and arrested myelination, but that there must be additional white matter damage. So, MRI suggests that the white matter abnormalities seen in Aicardi–Goutières syndrome are the result of a variable combination of hypomyelination, demyelination, gliosis, and white matter microinfarctions. In some patients, the cerebral white matter looks much better, with more myelin and only some focal white matter abnormalities (Fig. 66.4). Over time there is variable atrophy of the brain, in particular due to loss of cerebral white matter volume (compare Figs. 66.6 and 66.7). The atrophy becomes severe in some patients, whereas in other patients there is no evidence of progression of the atrophy. Some patients have subcortical cysts in the anterior temporal area (Figs. 66.2 and 66.7). These cysts may become large. Occasionally exceptional patients are seen who are the sibling of a more typically

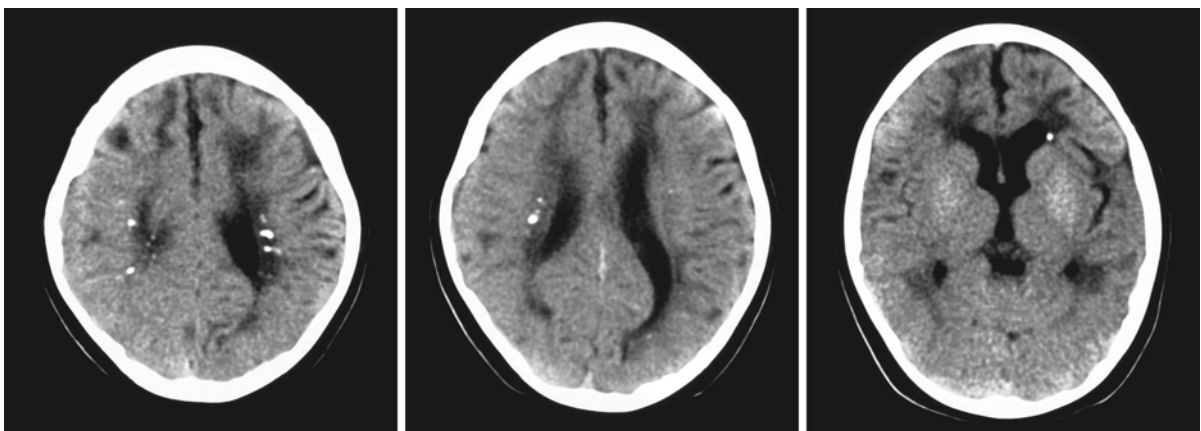


Fig. 66.1. CT of a 3-year-old severely affected patient with Aicardi–Goutières syndrome. There are calcium deposits in the basal ganglia and periventricular white matter. The calcium

deposits in the white matter have the typical punctate appearance, whereas the basal ganglia calcium deposits are more diffuse

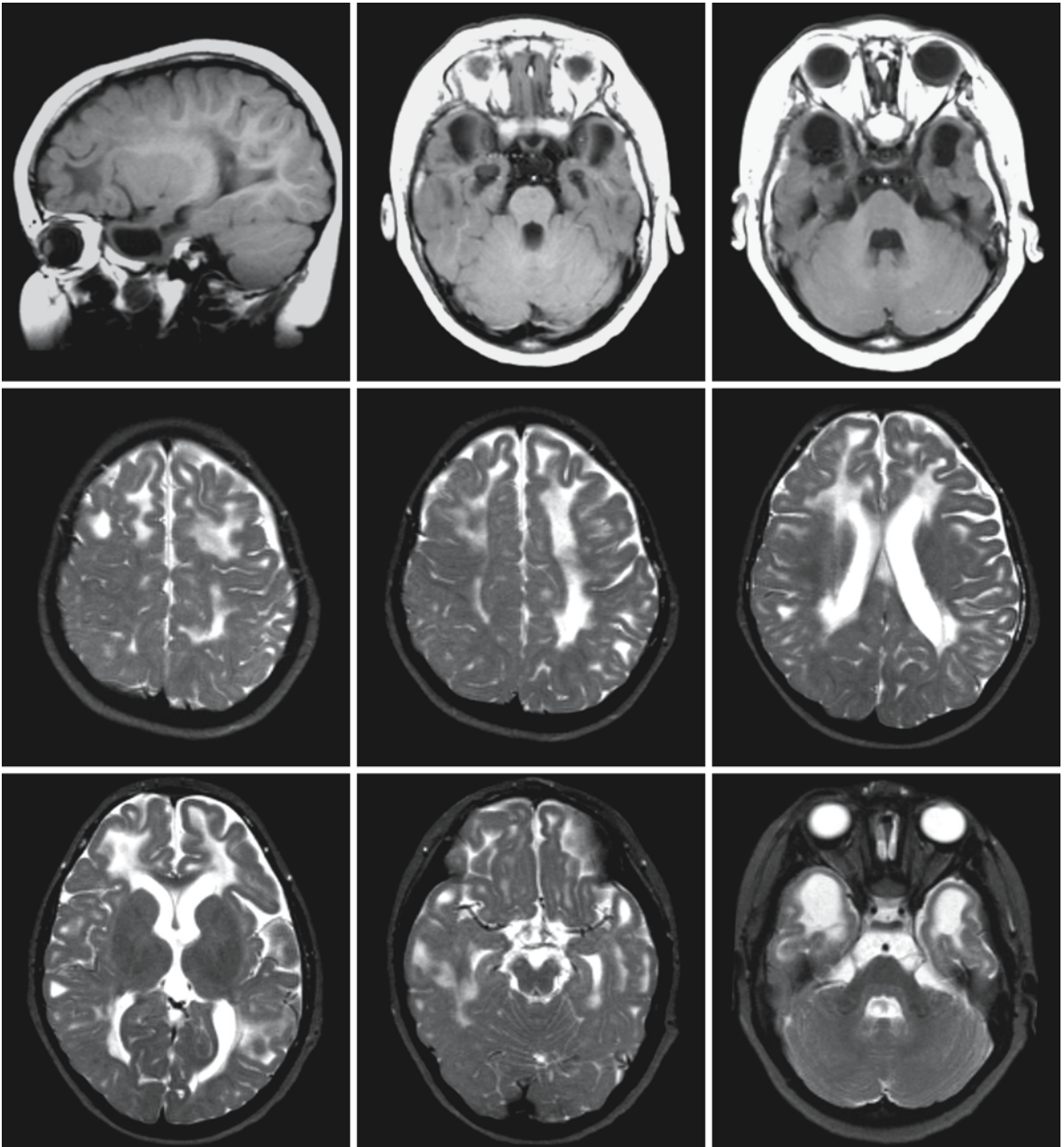


Fig. 66.2. MRI of the same patient as shown in Fig. 66.1 at the same age. The T₁-weighted images show cysts in the anterior temporal region. The T₂-weighted images show extensive

cerebral white matter abnormalities. The corpus callosum and internal capsule are spared

affected patient and in whom the cerebral white matter looks much closer to normal than is usual for Aicardi-Goutières syndrome.

The MRI pattern shows similarities to the leukoencephalopathy and calcium deposits seen in Cockayne syndrome. However, in the latter disease the calcium deposits tend to be larger and more confluent, while the punctate pattern is very typical of Aicardi-

Goutières syndrome. Congenital infections, in particular congenital cytomegalovirus infection and toxoplasmosis can lead to a similar pattern of calcium depositions and in particular congenital cytomegalovirus infection may be associated with extensive white matter abnormalities and anterior temporal subcortical cysts.

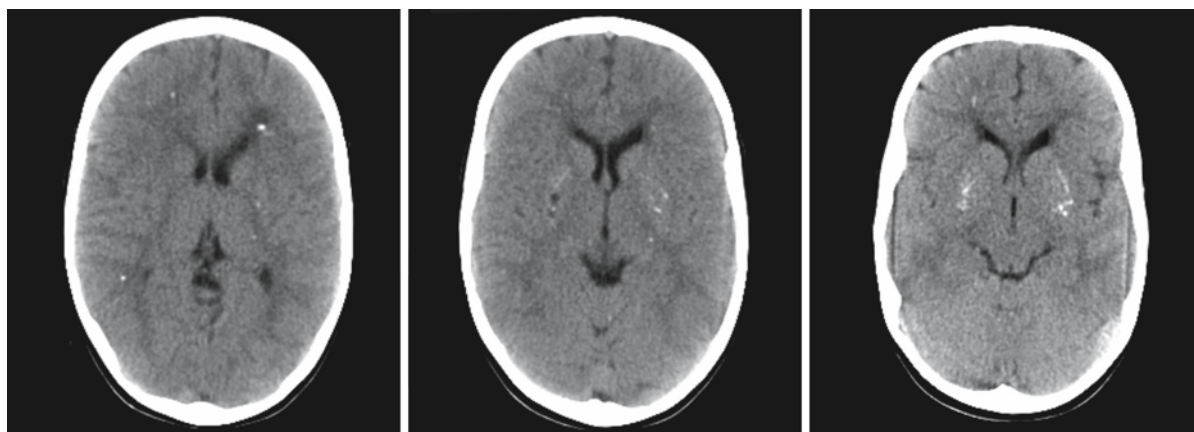


Fig. 66.3. CT scan of the affected brother of the patient shown in Figs. 66.1 and 66.2. He is 7 years old. He has a much milder phenotype and can walk with support. Note the subtle

punctate calcium deposits in the basal ganglia and cerebral white matter

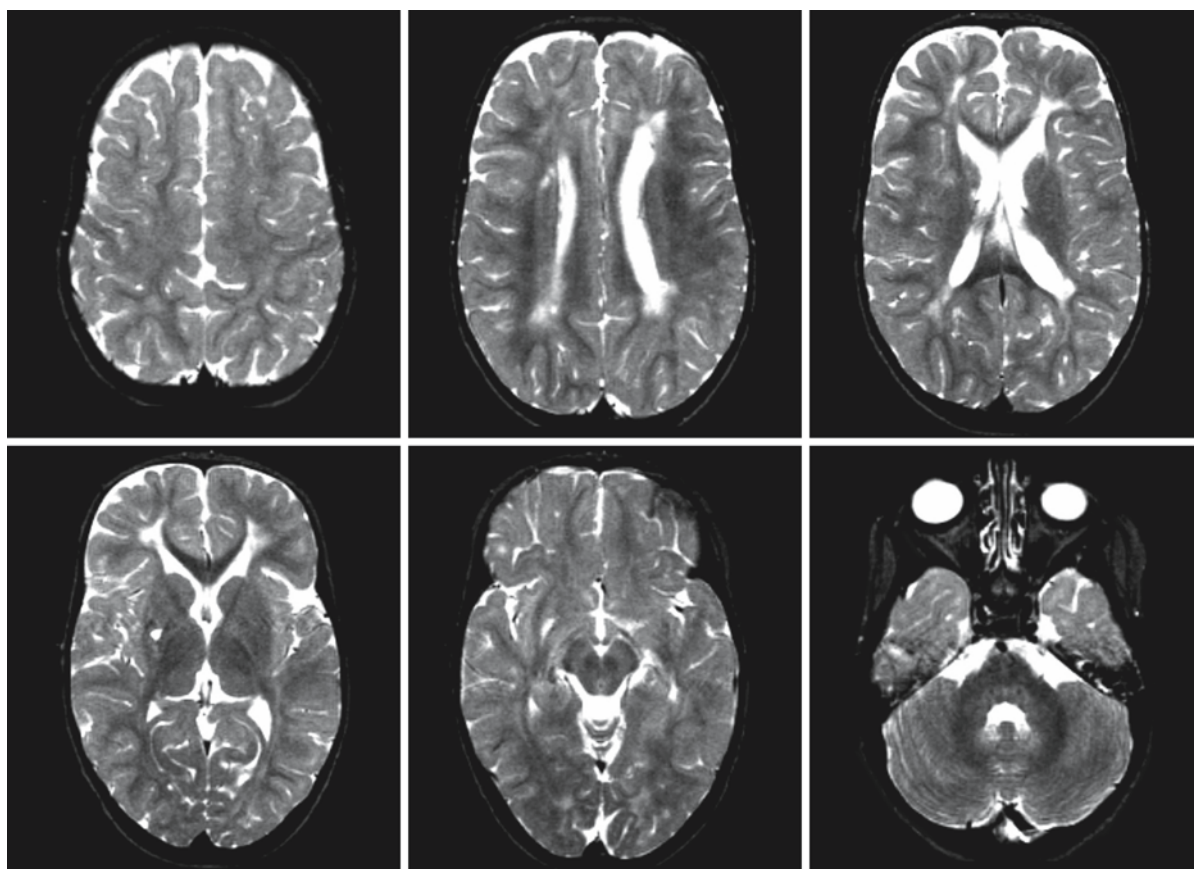


Fig. 66.4. MRI of the same patient as shown in Fig. 66.3 at the same age. The cerebral white matter looks much better. There are multifocal, partially confluent abnormalities in the periven-

tricular white matter. Myelination is delayed, as most evident in the temporal lobe

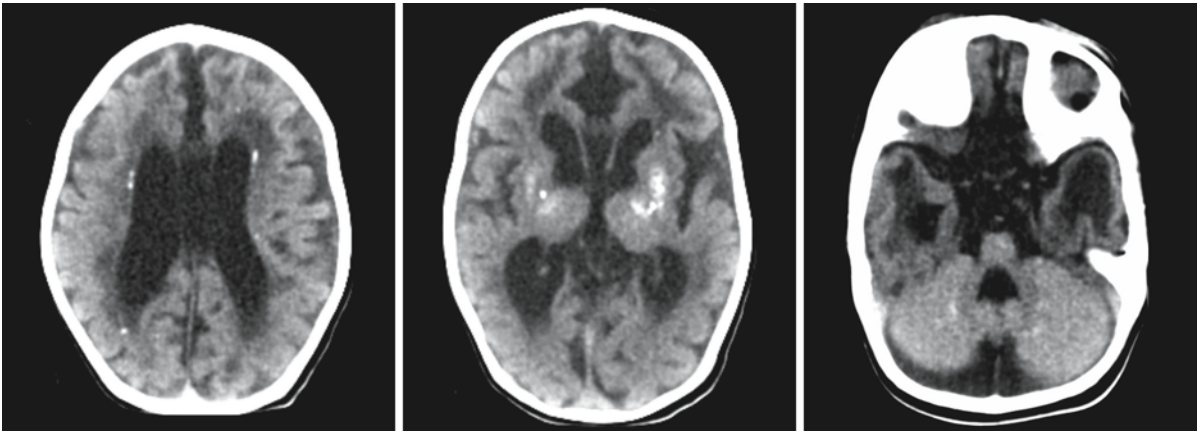


Fig. 66.5. CT scan of a 4-month-old patient with Aicardi–Goutières syndrome, who is extremely severely affected. He has a sister with the same diagnosis. There are punctate calci-

um deposits in the periventricular and deep white matter, basal ganglia, thalami, and dentate nucleus

Fig. 66.6. MRI of the same patient as shown in Fig. 66.5, also at the age of 4 months. Note the atrophy of pons and cerebellum. The anterior temporal white matter is swollen and highly rarefied. The cerebral white matter is reduced in volume and diffusely abnormal in signal intensity. There are small spots of low signal intensity in the periventricular white matter on the T₂-weighted image, reflecting calcium deposits. The coronal FLAIR images reveal subependymal cysts and highly rarefied or cystic anterior temporal white matter. (Fig. 66.6 see page 502)

Fig. 66.7. MRI of the same patient as shown in Figs. 66.5 and 66.6, now at the age of 16 months. Note the serious atrophy of the cerebral white matter. There are anterior temporal cysts. The subependymal cysts have disappeared (Fig. 66.7 see page 503)

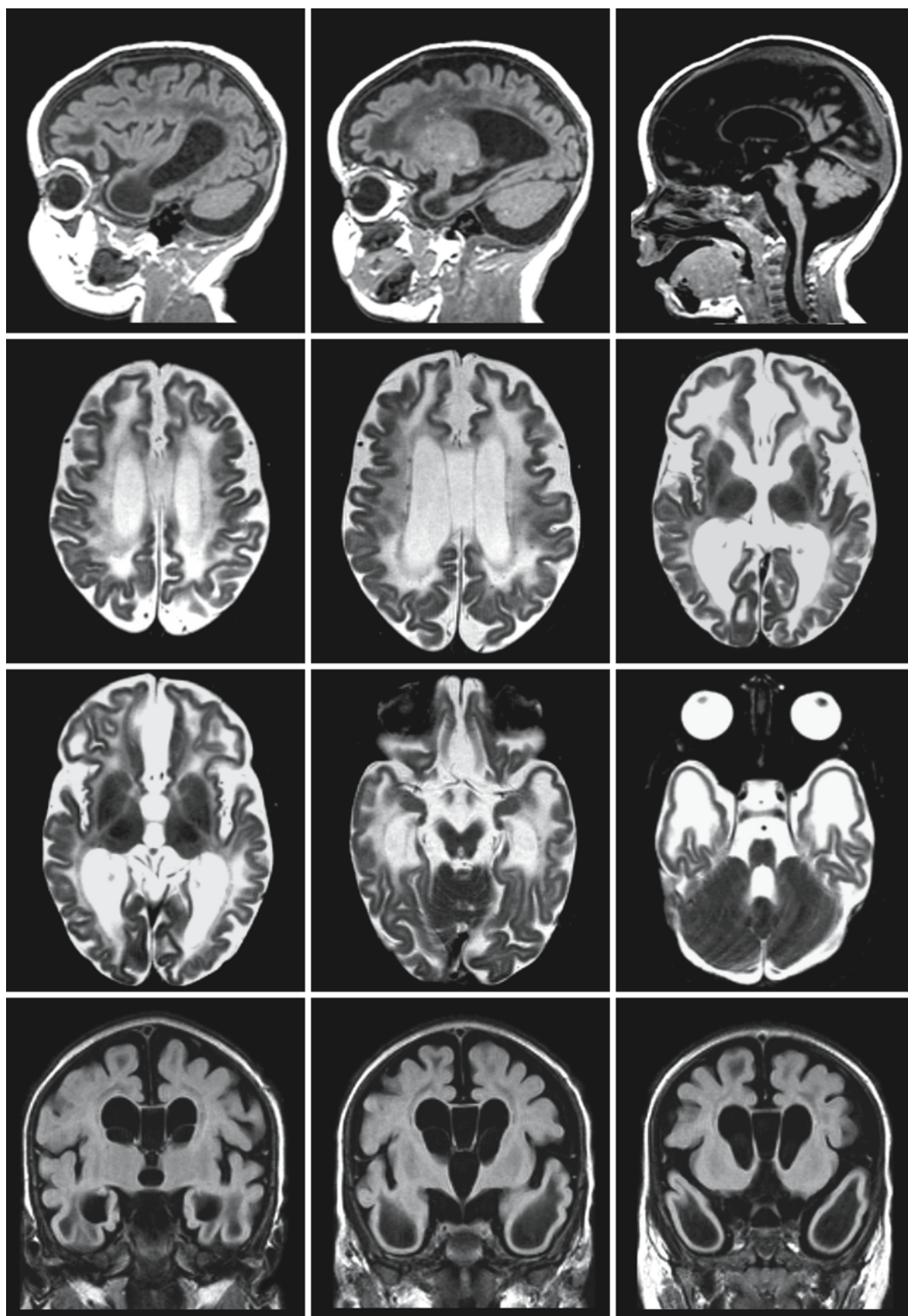


Fig. 66.6.

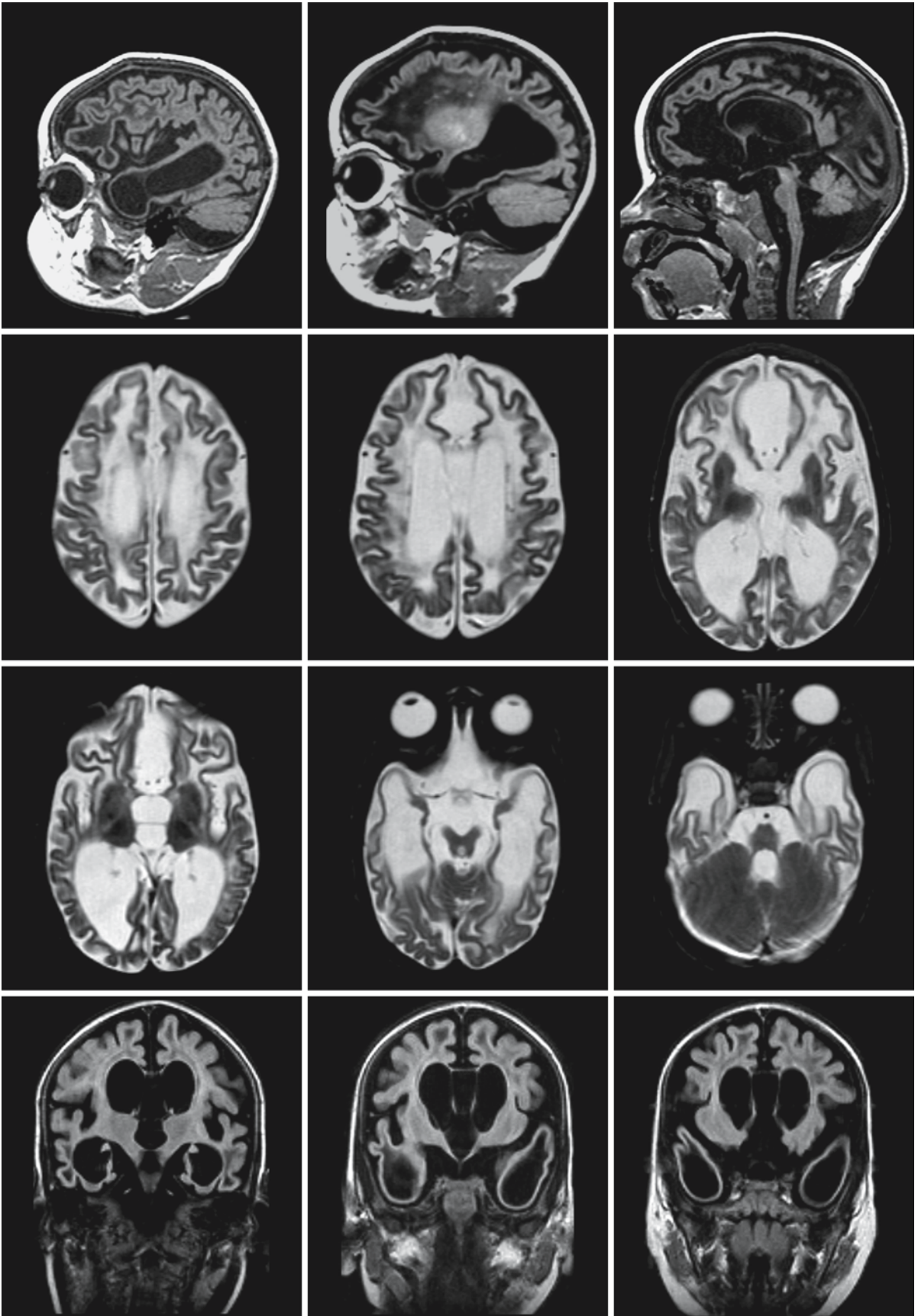


Fig. 66.7.

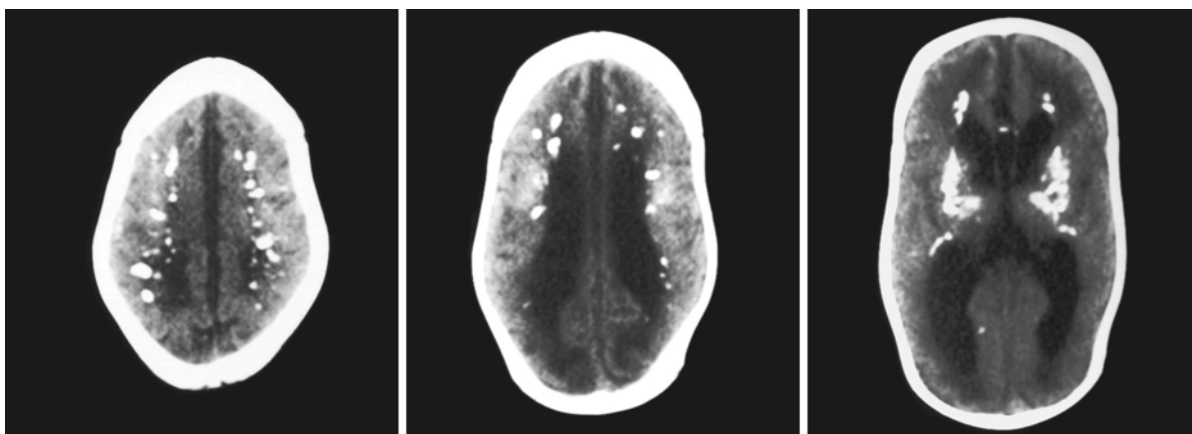


Fig. 66.8. CT of a 4-month-old patient with Aicardi–Goutières syndrome, demonstrating how extensive the calcium deposits may be. Courtesy of P.G. Barth, Department of Child Neurology, Academic Medical Center, Amsterdam, The Netherlands

Leukoencephalopathy with Calcifications and Cysts

67.1 Clinical Features and Laboratory Investigations

Leukoencephalopathy with calcifications and cysts (LCC) is a very rare leukoencephalopathy. Affected siblings have been reported, suggesting an autosomal recessive mode of inheritance. Onset varies between early infancy and adolescence. Some children display intrauterine growth retardation. The disease is slowly progressive with signs of spasticity, cerebellar ataxia, extrapyramidal movement abnormalities, epilepsy, and mental deterioration. In addition, the patients may develop focal neurological deficits and signs of increased intracranial pressure related to growing intracranial cysts which require neurosurgical treatment. Optic atrophy with deterioration of vision and blindness may occur. Some of the children have bilateral Coats retinopathy. Coats retinopathy is a congenital retinal telangiectatic disease, characterized by abnormal retinal vascular permeability and telangiectasia, leading to a progressive exudative retinal detachment and blindness.

As with all newly described syndromes for which the basic defect is not yet known, it is difficult to define the phenotype. Several patients have been reported who lack some of the features described above and have additional features not mentioned above. A few patients had additionally dyskeratosis congenita-like symptoms (sparse hair, dysplastic nails, pigmentation abnormalities of the skin) and Fanconi anemia-like features (thrombopenia and aplastic anemia). Other features reported include microcephaly, osteopenia, osteosclerosis with a tendency to fractures, and short stature.

Laboratory investigations are unrevealing. Blood calcium, phosphorus, and alkaline phosphatase are normal. Parathormone levels are normal. CSF is normal.

67.2 Pathology

The most prominent finding in tissue obtained in neurosurgical interventions consists of angiomatous changes. Numerous small, tortuous blood vessels are found with normal endothelial lamina but an irregular, often calcified wall. These vessels are surrounded by many whirled and irregular Rosenthal fibers, eosinophilic bodies, microcalcifications, and ferric

iron deposits. The white matter shows myelin loss, microcystic degeneration, and gliosis.

67.3 Pathogenetic Considerations

The disease probably has an autosomal recessive mode of inheritance. The basic defect is unknown. A genome-wide linkage study has been started.

The pathophysiology of the disease has not been elucidated, but it is clearly a proliferative angiopathy involving the vessels of the central nervous system and the retina. The genesis of the cysts is unclear.

67.4 Therapy

Growing cysts may require neurosurgical intervention to alleviate the elevated intracranial pressure. Other than that, only supportive care is available. Prenatal diagnosis is as yet not possible.

67.5 Magnetic Resonance Imaging

CT is very important in the diagnosis of LCC, readily demonstrating the presence of calcium depositions (Figs. 67.3 and 67.6). The calcium deposits are most often seen in the thalamus, basal ganglia, the deep white matter, the white matter–cortex border, cerebellar white matter, dentate nucleus, brain stem, and lining of the cysts. They are not necessarily symmetrical. They are progressive over time. The calcium deposits are different from those seen in Aicardi–Goutières syndrome. In the latter disease the calcium deposits are small and punctate, and even in patients with more confluent calcifications, smaller punctate calcifications can still be seen. In LCC the calcium deposits are larger and bulky.

Calcifications are less easily seen on MRI. Gradient-echo images can be used for that purpose (Fig. 67.1). MRI is, however, superior in depicting the abnormality of the white matter (Figs. 67.1, 67.2, 67.4, and 67.5). The cerebral white matter shows large areas of signal abnormality. The abnormal areas may have a mildly swollen aspect with broadening of gyri and stretching of the overlying cortex. The white matter abnormalities may be asymmetrical. They increase in extent over time.

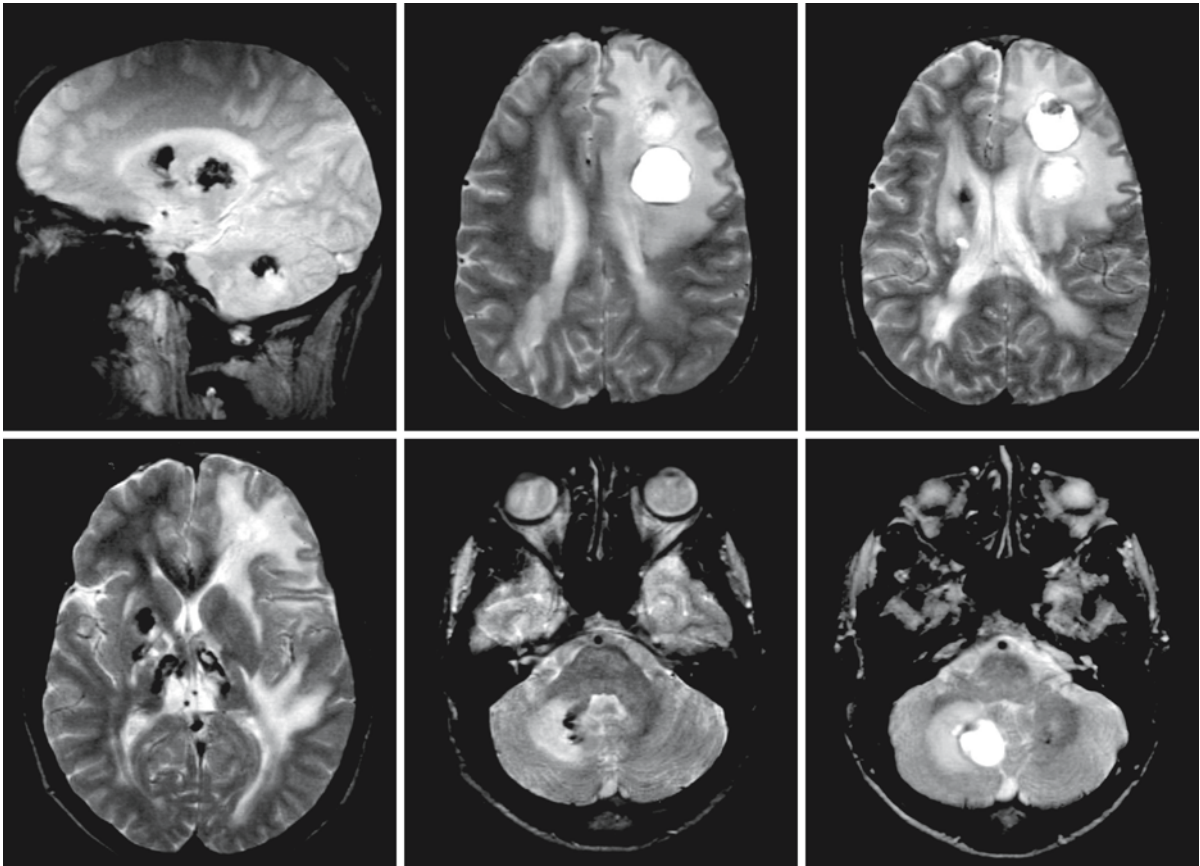


Fig. 67.1. A boy with LCC syndrome started to have increasing walking difficulties at the age of 9–10 years. The first MRI was obtained at the age of 10 years. Note the calcium deposits in the basal ganglia, thalami, dentate nuclei, and lining of the cysts in the deep frontal white matter on the left and the cerebellum on the right, indicated by a low signal intensity on the gradient-echo (first row, left) and T₂-weighted images.

The cerebral white matter abnormalities are more serious on the left; the cerebellar white matter abnormalities are more serious on the right. The abnormal white matter has a swollen aspect. We thank Dr. P.G. Barth, Department of Child Neurology, Academic Medical Center, Amsterdam, The Netherlands, for referral of the patient

In addition, growing cysts may be seen, most often located in the region of the basal ganglia and third and fourth ventricle (Figs. 67.1–67.6). They may become large and lead to compression of brain tissue or obstruct the normal CSF flow, leading to secondary hydrocephalus. Some of the cysts seem entirely intraventricular, whereas other cysts are evidently primarily intraparenchymal. It is important to stress that the cysts are not present in all patients, or not yet. Patients may be known for many years with calcium deposits and white matter abnormalities before they develop cysts.

The imaging pattern showing a combination of leukoencephalopathy and calcium deposits is reminiscent of that seen in other disorders leading to

white matter abnormalities and calcium depositions. However, the cysts are unique. In Aicardi–Goutières syndrome the calcium deposits are typically punctate. In Cockayne syndrome the calcium deposits tend to be larger and more confluent, but the white matter disease is symmetrical and there are no cysts. CNS infections, in particular congenital cytomegalovirus infection, may lead to calcium depositions and extensive white matter abnormalities, but the pattern of white matter abnormalities is typical and there are often anterior temporal subcortical cysts. In disorders involving parathormone, similar calcium deposits may be seen but the white matter abnormalities and cysts are lacking.

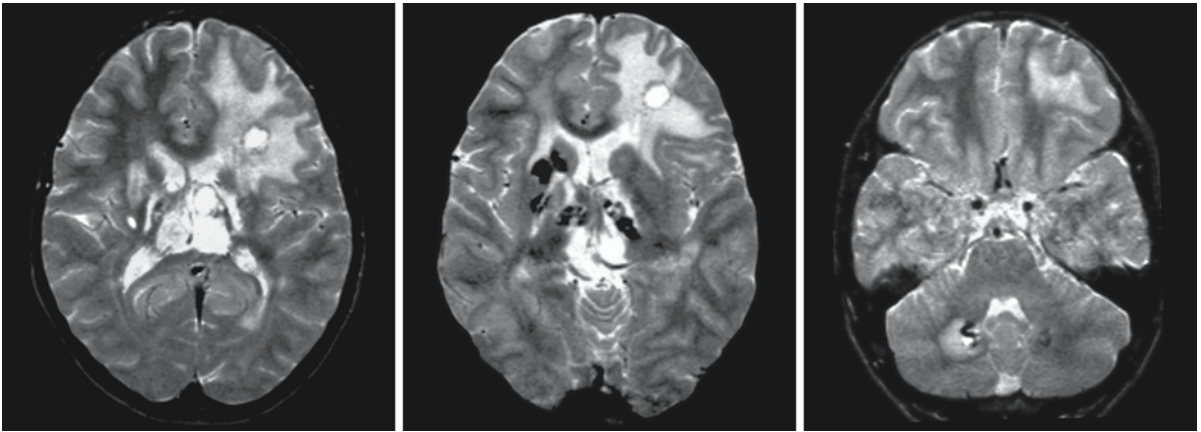


Fig. 67.2. The same patient 1 year later. With surgical intervention, the cysts have become smaller

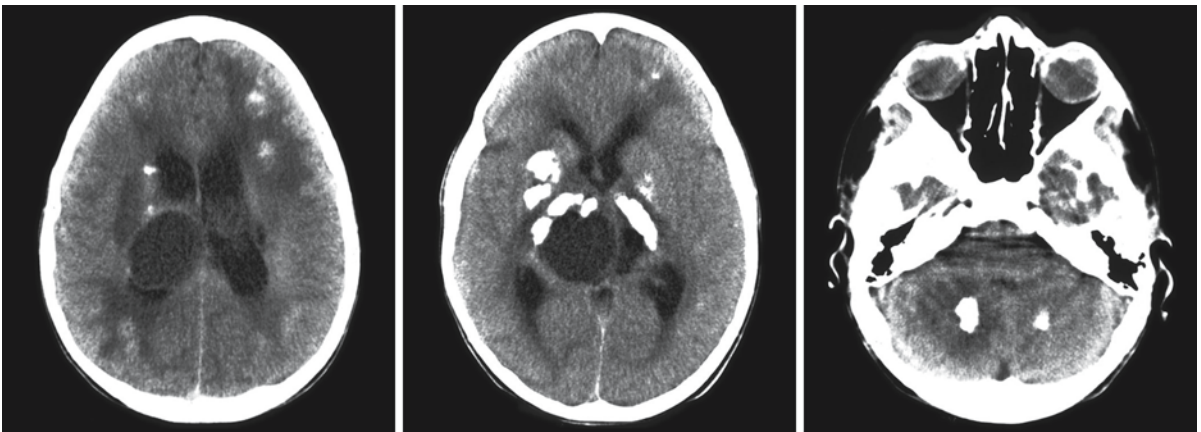


Fig. 67.3. The same patient, now 13 years old. There is a growing cyst in the region of the thalamus on the right. The CT scan shows the calcium in the basal ganglia, thalami, and dentate nuclei. There are multiple calcium deposits in the cortico-subcortical junction in the cerebral hemispheres

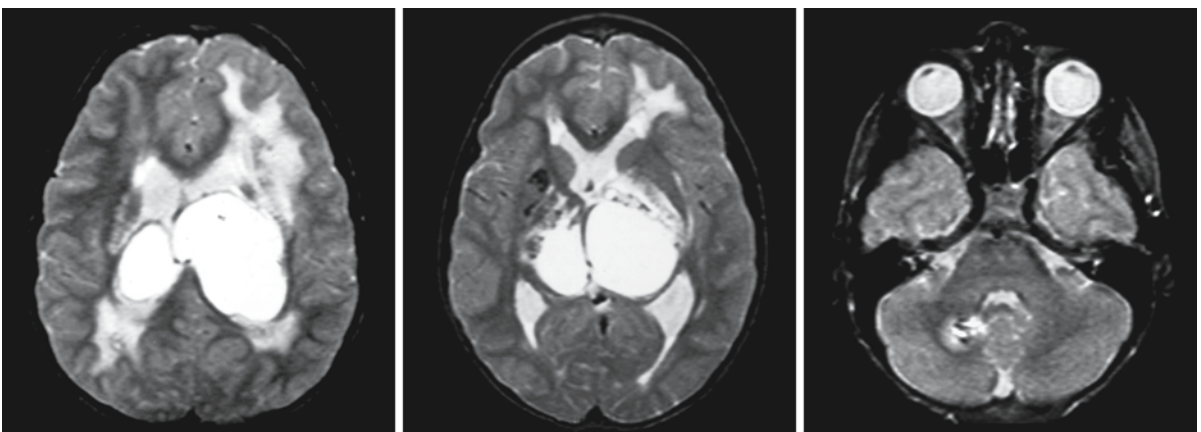


Fig. 67.4. The same boy, now 19 years old. There are large cysts in the region of the thalamus on both sides

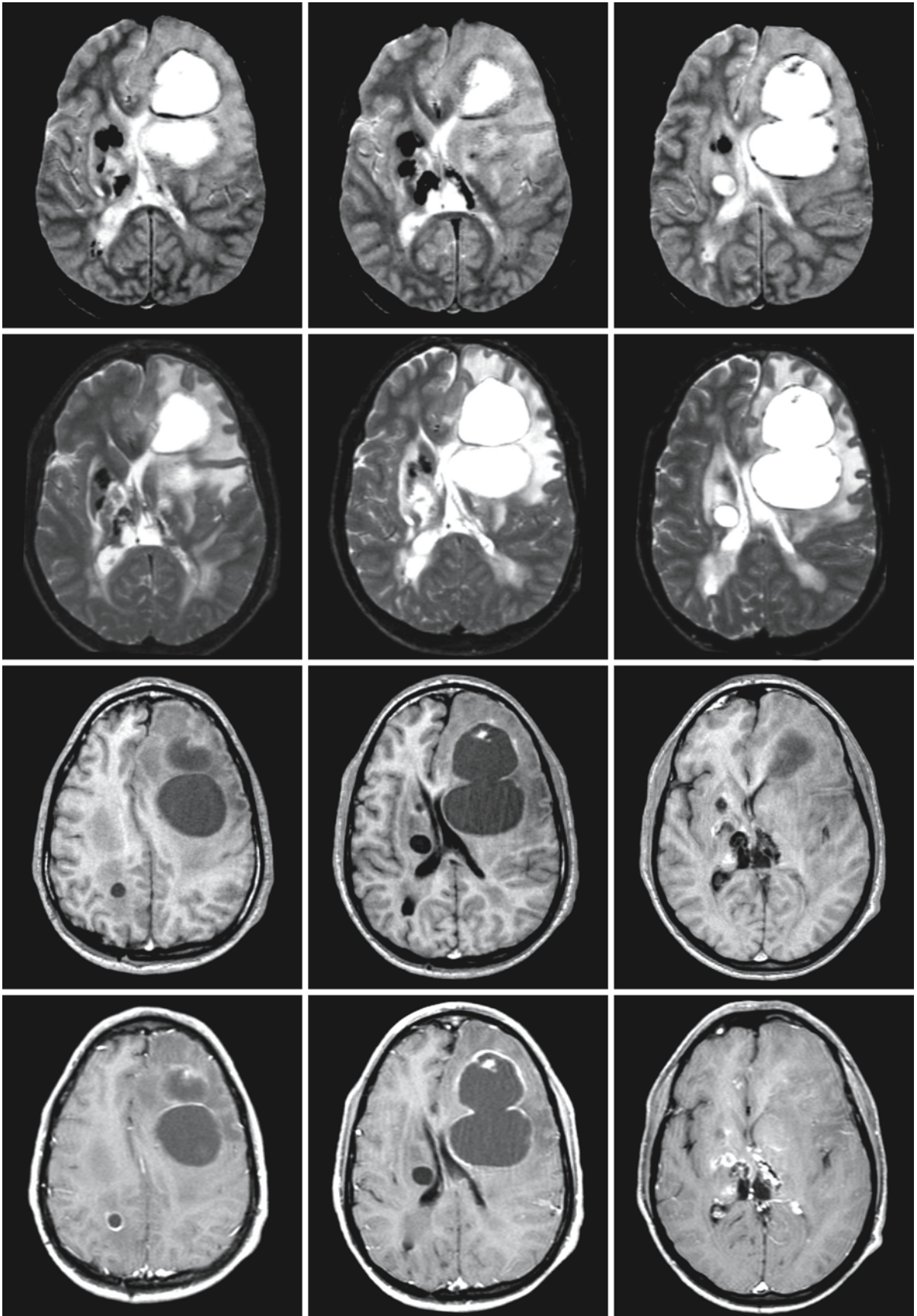


Fig. 67.5.

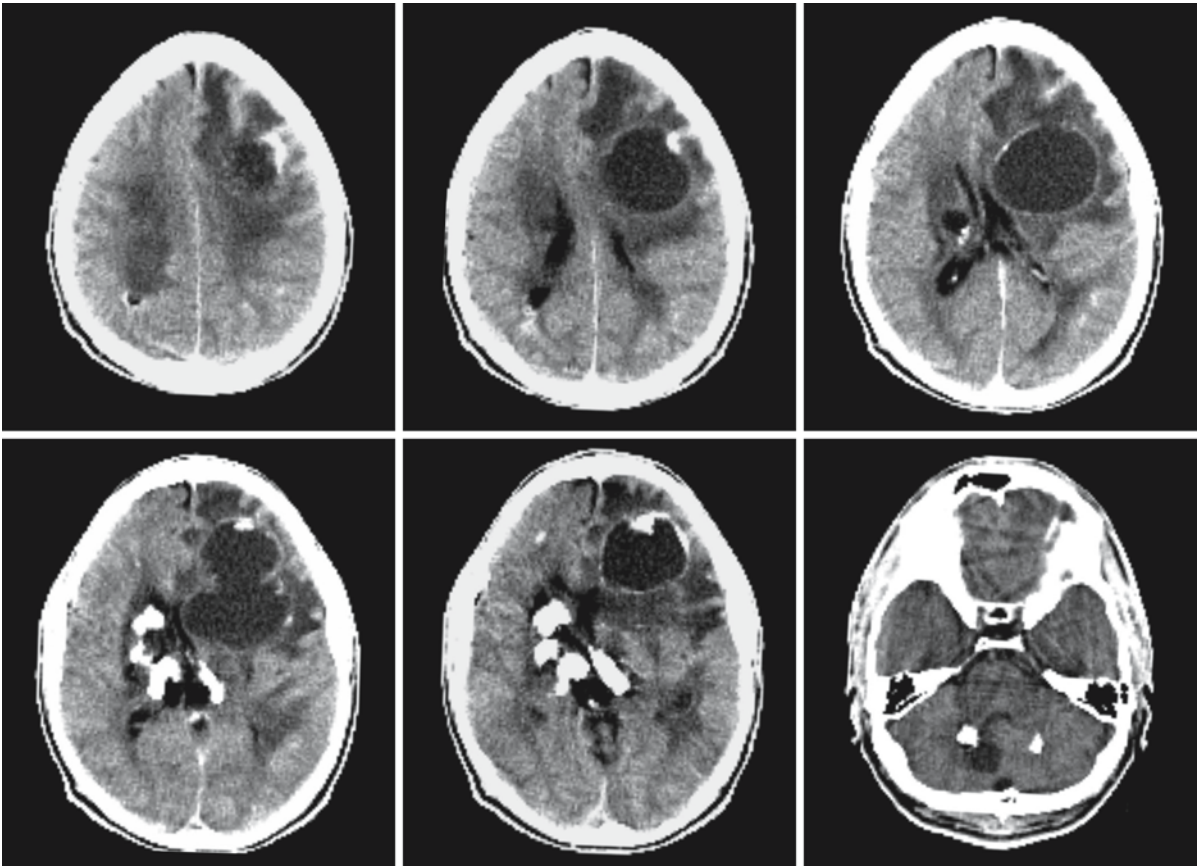


Fig. 67.6. CT scan at the age of 22 reveals the increase in calcium as compared to the first CT (Fig. 67.3)

←
Fig. 67.5. The same boy, now 22 years of age. The cysts in the region of the thalami have regressed without surgical intervention. The cysts in the left hemisphere have become very large and have led to a marked midline shift. The T₁-weighted images without (*third row*) and with contrast (*fourth row*) reveal enhancement in the areas of calcium deposits: the lining of cysts and the basal ganglia and thalami.

Leukoencephalopathy with Brain Stem and Spinal Cord Involvement and Elevated White Matter Lactate

68.1 Clinical Features and Laboratory Investigations

Leukoencephalopathy with brain stem and spinal cord involvement and elevated white matter lactate (LBSL) is a rare disorder with an autosomal recessive mode of inheritance. The initial development is normal. In some of the patients, independent walking is unstable from the beginning. Motor deterioration starts at a variable age in childhood or adolescence with signs of spasticity and ataxia involving the legs more than the arms. The disease is slowly progressive. Patients may become wheelchair-dependent in their teens or twenties, but some still walk in their forties. Manual dexterity also becomes decreased to a variable degree. At neurological examination, most patients have a distal decrease in position and vibration sense. Some patients develop epilepsy with infrequent seizures. Some of the patients have learning problems from early on, but cognitive decline is of late occurrence. Some patients have more serious disease than others. A striking feature is that some patients experience an episode of more rapid and partially reversible neurological deterioration accompanied by fever following minor head trauma.

Somatosensory evoked potentials with stimulation of the tibial and median nerves are delayed or negative. Sensory and motor nerve conduction velocities are normal.

Extensive laboratory investigations have been unrevealing. Only in some of the patients have mild elevations of serum or CSF lactate been found on several occasions. However, extensive mitochondrial work-up in fresh muscle tissue has not revealed abnormalities in any of the patients. No mitochondrial DNA mutations have been found.

Presently, the diagnosis is MRI-based. Prenatal diagnosis is unfortunately not possible.

68.2 Pathology

No pathology information is available.

68.3 Pathogenetic Considerations

The disease has an autosomal recessive mode of inheritance, but the genetic defect is unknown.

68.4 Therapy

No specific treatment is available. Supportive care is important.

68.5 Magnetic Resonance Imaging

LBSL has a distinct MRI pattern. The cerebral white matter is involved to a variable extent. In some patients the abnormalities are extensive (Figs. 68.1 and 68.2), in others they are more limited (Figs. 68.6 and 68.9). The white matter abnormalities are progressive over time, with new structures being involved and some white matter atrophy (Fig. 68.2). In all patients, even in the oldest, the U fibers are spared (Fig. 68.1). In some patients, the cerebral white matter abnormalities are homogeneous (Fig. 68.10), but in most patients the abnormal cerebral white matter has an inhomogeneous, spotty aspect (Figs. 68.1, 68.6, and 68.9). On FLAIR images the white matter abnormalities are also inhomogeneous with spots of lower signal intensity suggestive of focal rarefaction (Fig. 68.5). In the mildest form, there may be a few focal lesions in the cerebral white matter on a background of limited white matter abnormalities, both in extent and degree of signal change (Figs. 68.6 and 68.9). The corpus callosum is involved, almost always

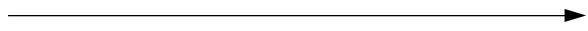


Fig. 68.1. A 34-year-old lady with LBSL, presently wheelchair-bound. The T₂-weighted images (*first, second, and third rows*) show extensive inhomogeneous signal abnormalities in the cerebral white matter with sparing of the U fibers. The posterior part of the corpus callosum is affected, whereas the anterior part is spared. Signal changes are also seen in the posterior limb of the internal capsule. Within the midbrain, signal abnormalities are seen in the pyramidal tracts. At the level of the pons, the entire basis, the medial lemniscus, mesencephalic trigeminal tracts, intraparenchymal parts of the trigeminal nerves, and superior cerebellar peduncles are affected bilaterally. At the level of the medulla, the inferior cerebellar peduncles, the anterior spinocerebellar tracts, the decussation of the medial lemniscus and the pyramids are involved. The cerebellar white matter is diffusely affected. The T₁-weighted images (*fourth row*) show the inhomogeneities in signal intensity of the abnormal white matter with foci of more prominent signal change.

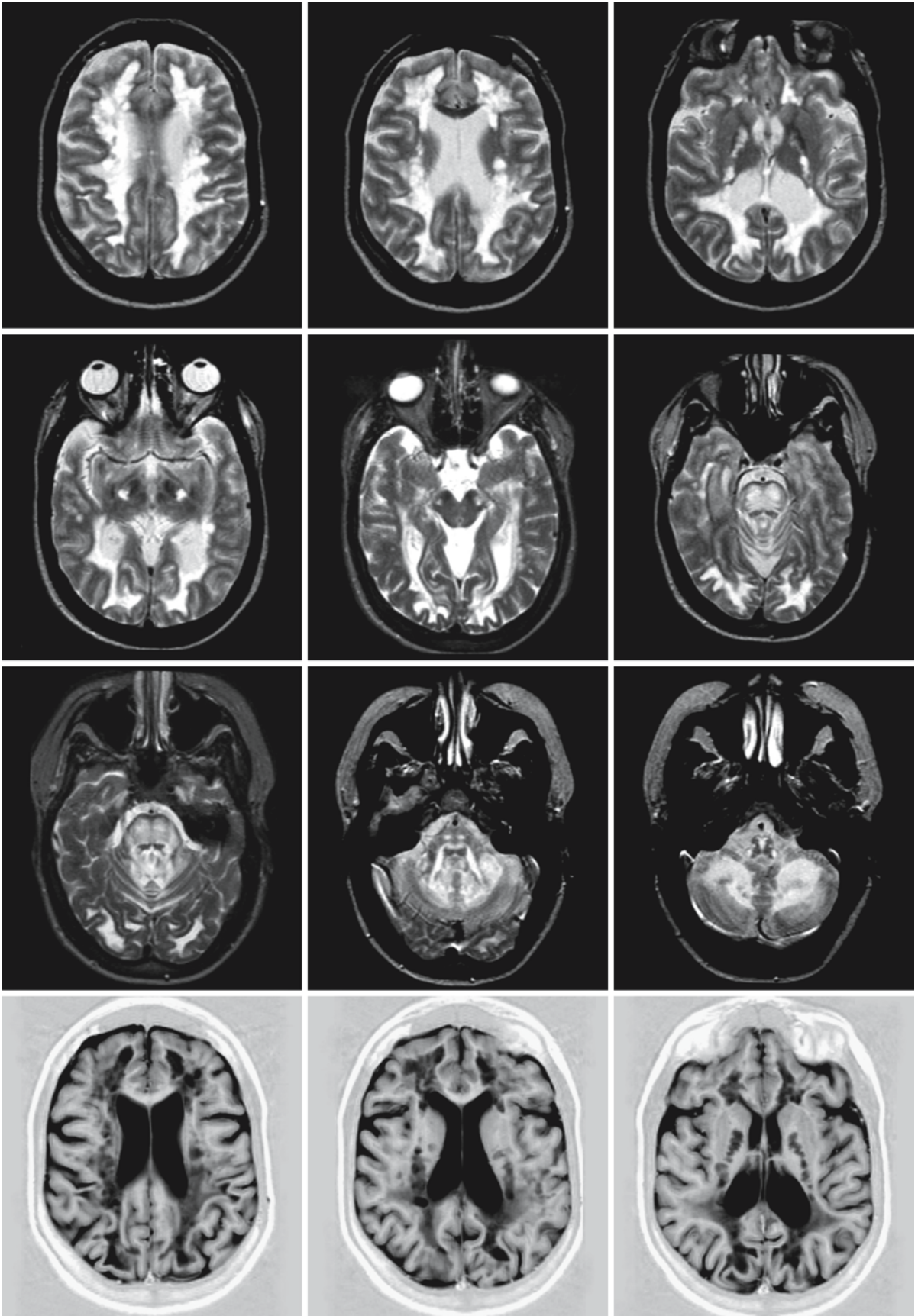


Fig. 68.1.

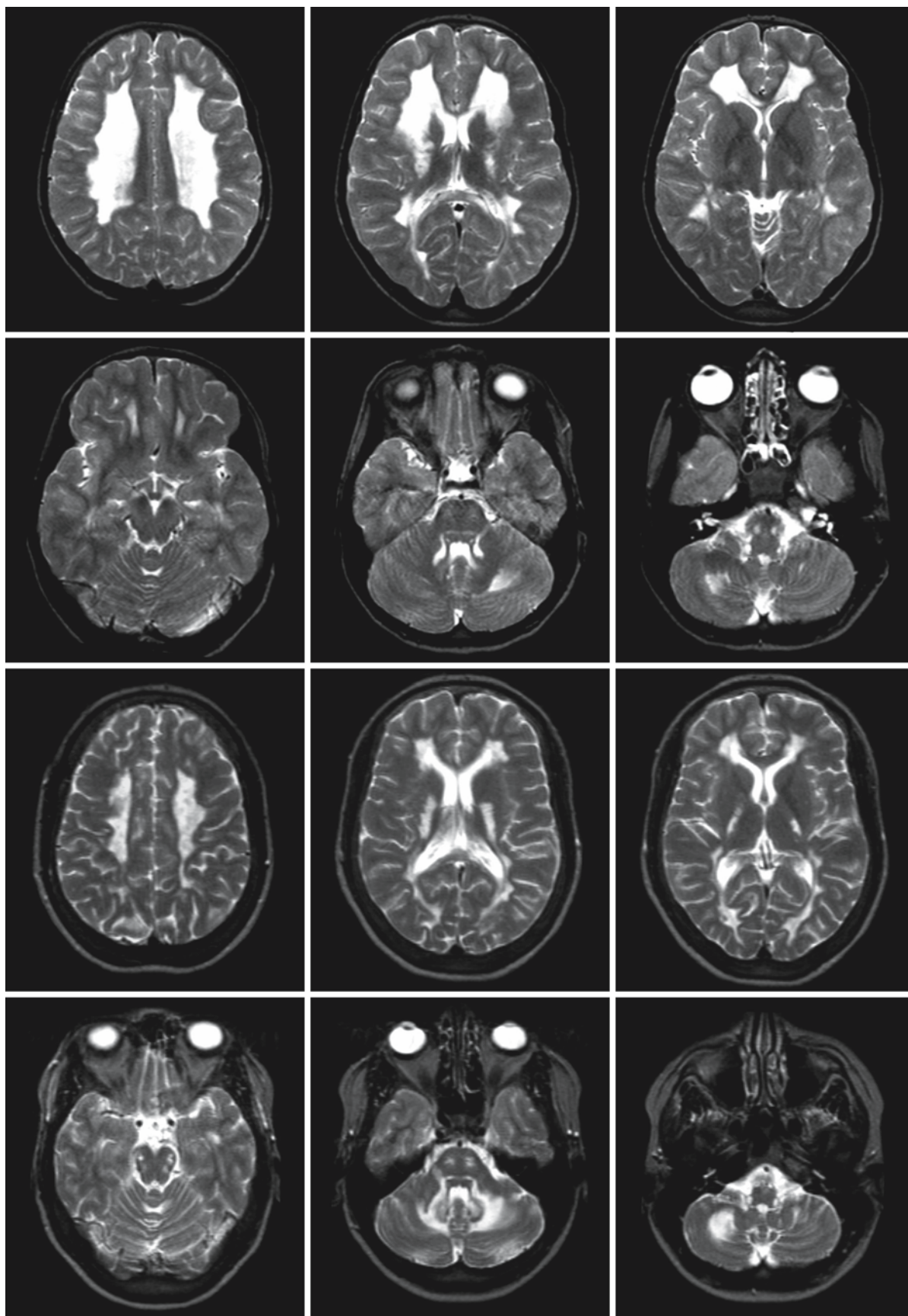


Fig. 68.2.

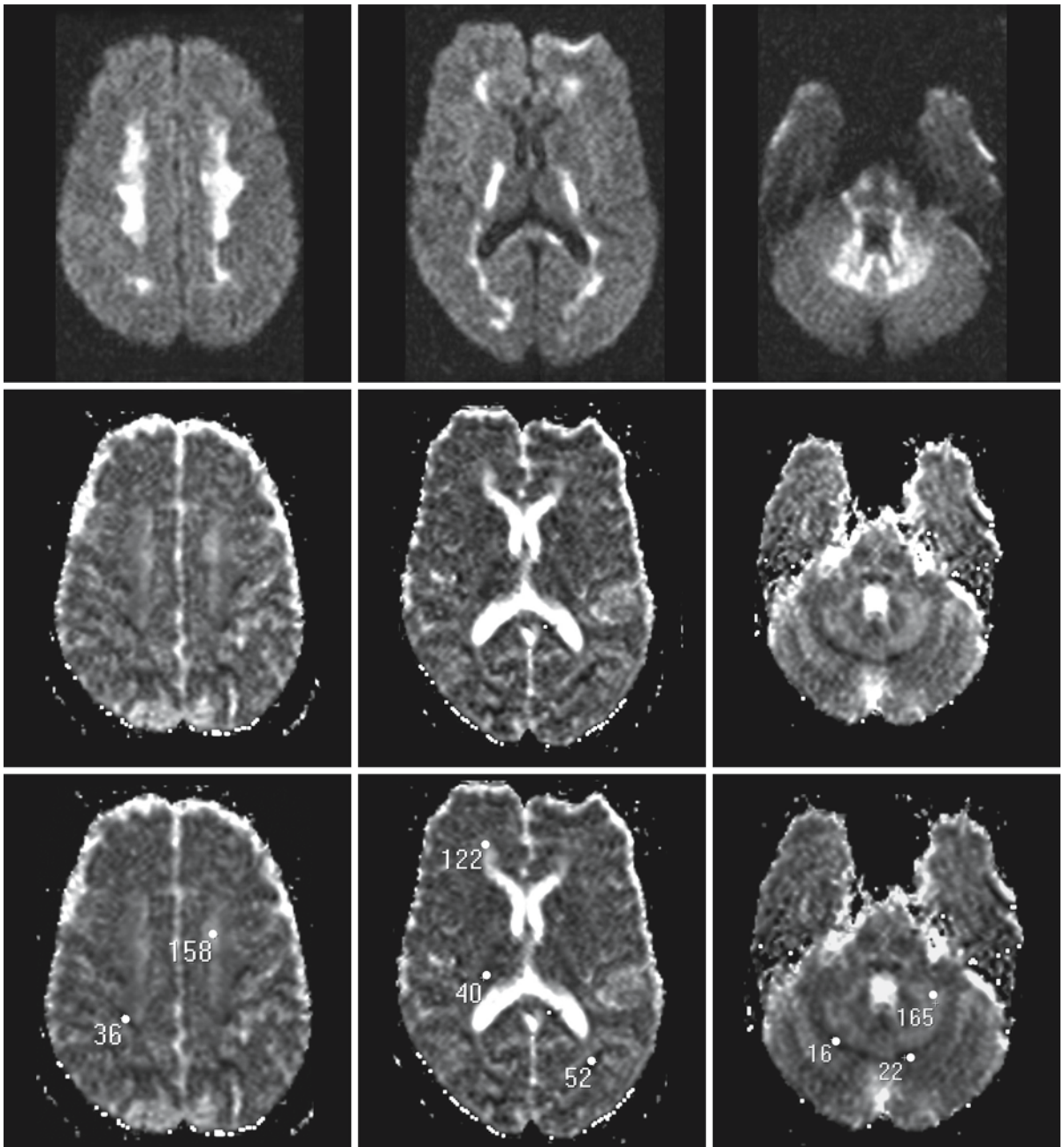


Fig. 68.3. Diffusion-weighted images of the same patient as shown in Fig. 68.2 at the age of 19 years. The Trace diffusion-weighted images (*first row*, b value = 1000) show a high signal intensity of the abnormal white matter. The ADC maps (*second*

and *third rows*) show that some areas, in particular rims of lesions, have a low ADC, whereas the remainder of the white matter has a high ADC

Fig. 68.2. These T₂-weighted images of a female patient with LBSL were obtained at the ages of 10 years (*first and second rows*) and almost 20 years (*third and fourth rows*). The typical abnormalities are present. Over time the supratentorial white matter becomes more atrophic and the abnormalities become less homogeneous. At the level of the midbrain signal abnormalities become visible in the pyramidal tracts and the medi-

al lemniscus. At the level of the pons, bilateral signal changes were seen in the medial lemniscus, mesencephalic trigeminal tract, intraparenchymal part of the trigeminal nerve, and the superior cerebellar peduncle, whereas on follow-up pyramidal tract abnormalities are seen as well. The cerebellar white matter abnormalities were initially subcortical and become diffuse



Fig. 68.4. Spinal images obtained in the patient shown in Figs. 68.2 and 68.3. The patient underwent multiple MRI studies in 10 years and the spinal imaging findings were always the same, with signal abnormalities in the dorsal columns and lateral corticospinal tracts over the entire length of the spinal cord

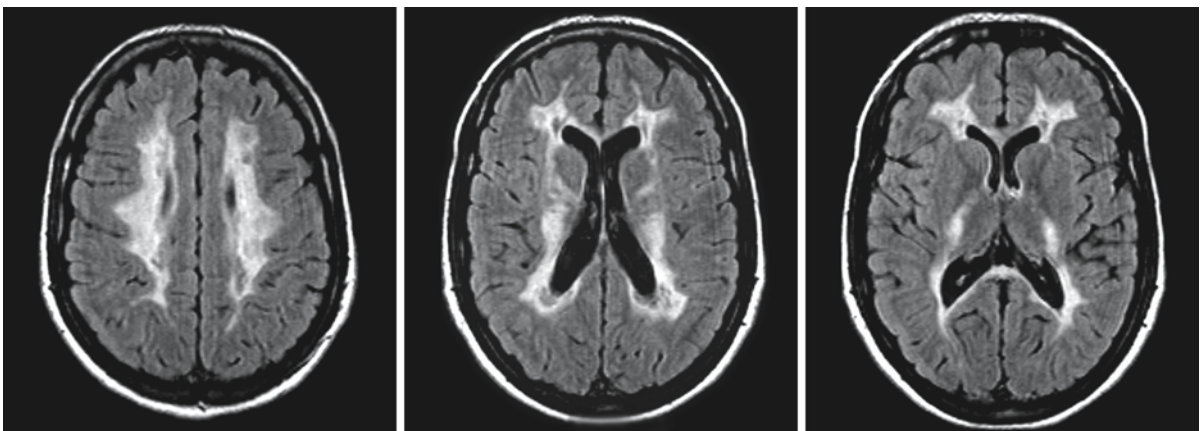


Fig. 68.5. FLAIR images of the patient shown in Figs. 68.2–68.4. These images show that the abnormal white matter is inhomogeneous with areas of lower signal, suggesting focal white matter rarefaction

more seriously in the posterior part than the anterior part (Figs. 68.1, 68.2, and 68.6), but sometimes the corpus callosum is homogeneously affected throughout. The posterior limb of the internal capsule is also affected (Figs. 68.1, 68.2, 68.5, 68.6, 68.9, and 68.10).

Within the brain stem and spinal cord, the disease involves certain tracts selectively. The pyramidal tracts are affected over their entire length extending downwards through the posterior limb of the internal capsule and the brain stem into the lateral corticospinal

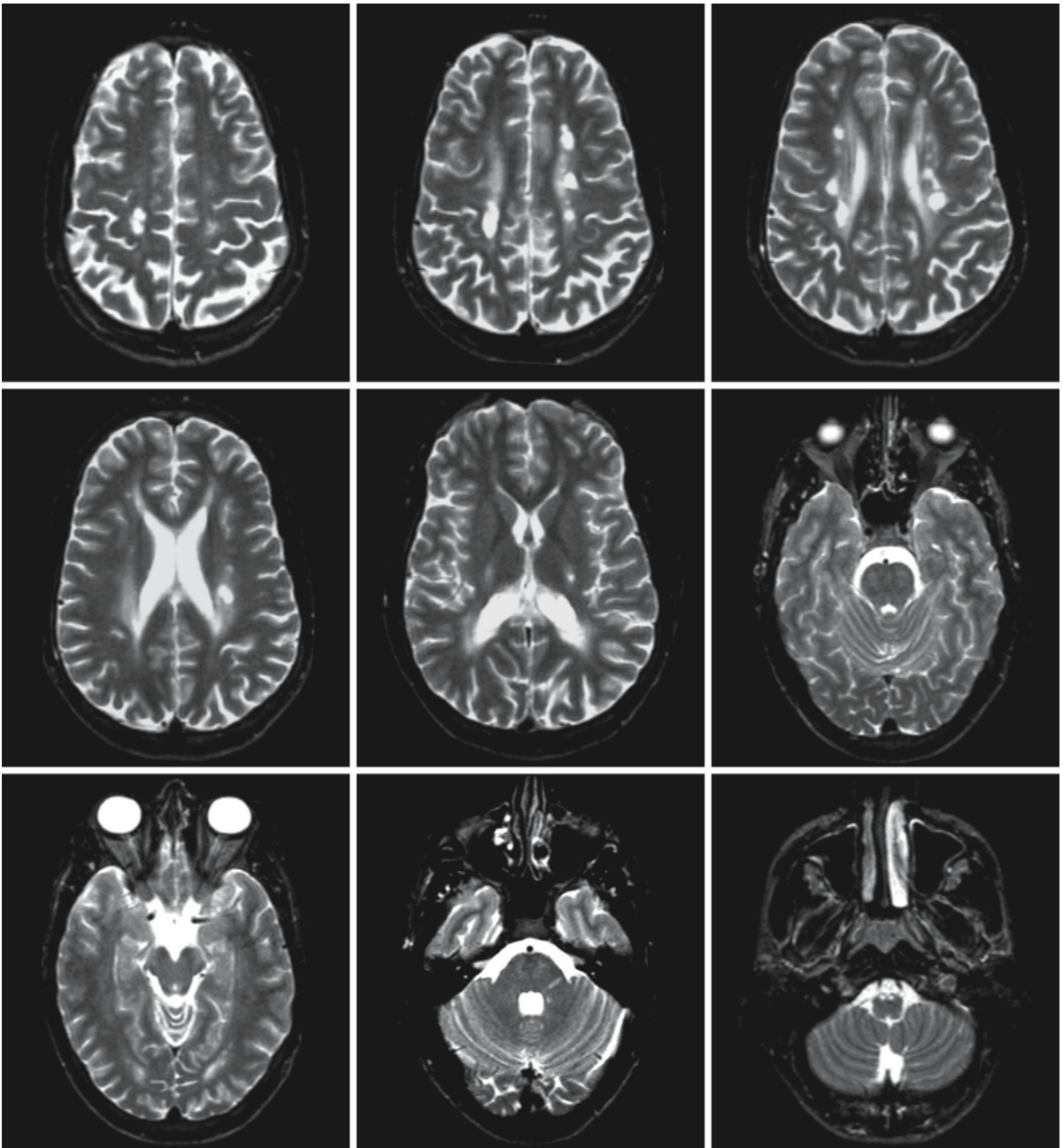


Fig. 68.6. Male LBSL patient at the age of 17 years. He has minimal neurological problems, mainly consisting of minor spasticity of the legs and some bladder dysfunction. The T_2 -weighted images show diffuse mild signal changes in the periventricular and deep cerebral white matter. There are superimposed focal lesions with more prominent signal change. The spleni-

um of the corpus callosum and posterior limb of the internal capsule are abnormal. At the level of the pons signal abnormalities are seen in the intraparenchymal part of the left trigeminal nerve. There is a small lesion in the superior cerebellar peduncle on the left. At the level of the medulla lesions are seen in the pyramids

tracts of the spinal cord (Figs. 68.1, 68.2, 68.4, 68.8–68.10). Sensory tracts are also affected over their entire length, involving the dorsal columns in the spinal cord, the medial lemniscus through the brain stem up to the level of the thalamus, and the corona

radiata above the level of the thalamus (Figs. 68.1, 68.2, 68.9, and 68.10). The transverse pontine fibers become involved in later stages of the disease (Fig. 68.1). Cerebellar connections are selectively involved, first the superior and inferior cerebellar pe-

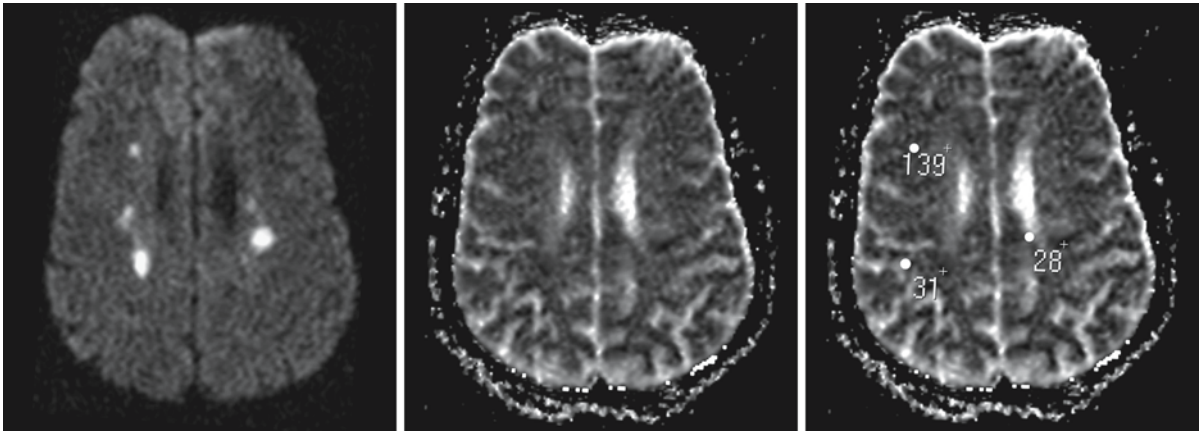


Fig. 68.7. Diffusion-weighted images in the same patient as in Fig. 68.6. The Trace diffusion-weighted image (*left*, b value = 1000) shows that the focal lesions have a high signal inten-

sity. On the ADC map (*middle and right*), the focal lesions have a low ADC, whereas the areas of subtle signal change on the conventional images have high ADC values

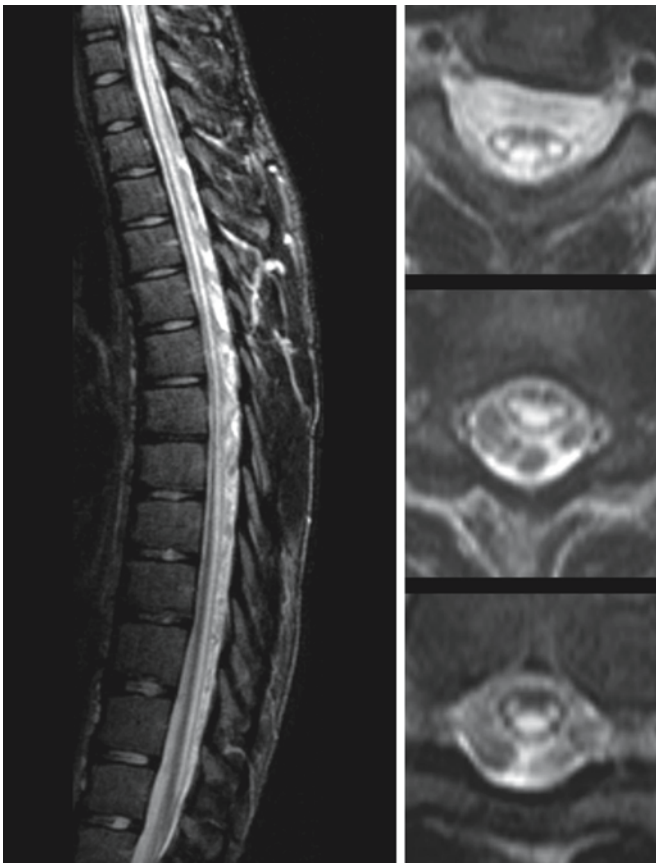


Fig. 68.8. Spinal images obtained in the patient shown in Figs. 68.6 and 68.7. There are signal abnormalities in the dorsal columns and lateral corticospinal tracts over the entire length of the spinal cord

duncles (Figs. 68.1, 68.2, 68.9, and 68.10), and only at a late stage the middle cerebellar peduncles (Fig. 68.1). The anterior spinocerebellar tracts at the level of the medulla also become abnormal (Fig. 68.1). A remarkable finding is the consistent involvement of the intra-

parenchymal trajectories of the trigeminal nerve and the mesencephalic trigeminal tracts (Figs. 68.1, 68.2, 68.9, and 68.10). The cerebellar white matter may also develop signal abnormalities, first in the subcortical regions (Fig. 68.2) and subsequently spreading in-

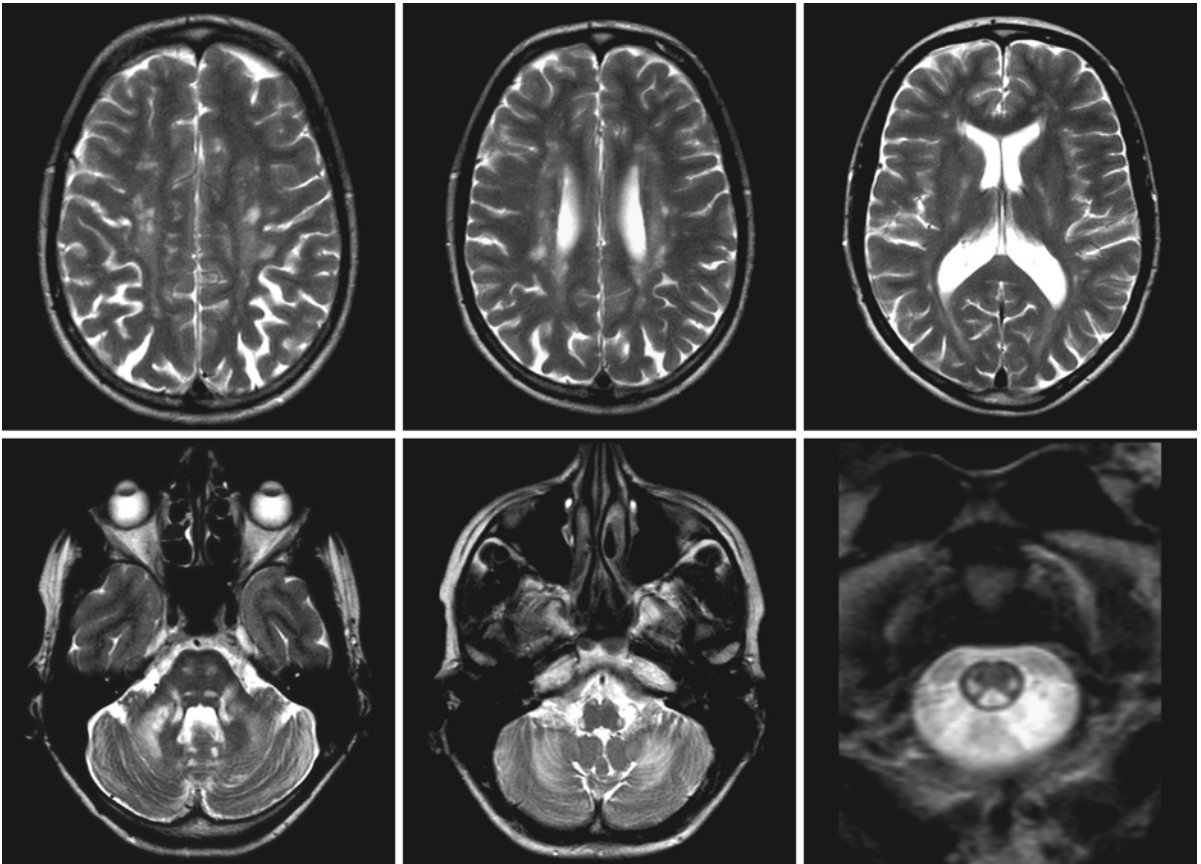


Fig. 68.9. A female 44-year-old LBSL patient with minimal neurological problems. In the periventricular and deep cerebral white matter subtle signal abnormalities are seen with small foci of more prominent signal change. The posterior limb of the internal capsule is affected. At the level of the pons, bilateral abnormalities are seen in the pyramidal tracts, medial lemniscus, superior cerebellar peduncles, and intrapar-

enchymal trajectory of the trigeminal nerve. At the level of the medulla, abnormalities are seen in the inferior cerebellar peduncles and pyramids. The lowest section is through the upper part of the cervical spinal cord and shows the involvement of the posterior columns and the lateral corticospinal tracts. Courtesy of Dr. M. Heitbrink and Dr. B. Wiarda, Department of Radiology, Medical Center Alkmaar, The Netherlands

wards to involve all cerebellar white matter throughout (Figs. 68.1 and 68.2). The cerebellum becomes atrophic over time.

The white matter abnormalities are progressive over time. Cerebral white matter abnormalities may be present without any abnormality in the brain stem or cerebellum, but at that time the spinal cord already contains signal abnormalities in the lateral and dorsal tracts. Without spinal imaging, an MRI-based diagnosis is not possible in the early or mildest stages of the disease. Over time, the brain stem abnormalities develop, and finally so do cerebellar white matter abnormalities.

A similar MRI pattern has not been described in any other condition; if present, it is diagnostic.

MRS shows a significant decrease in *N*-acetylaspartate and increase in *myo*-inositol in the abnormal white matter, suggesting axonal damage or loss

and gliosis, respectively. White matter choline is increased, too, but the increase is minor, suggesting mildly enhanced membrane turnover, possibly myelin loss. White matter lactate is elevated in almost all patients, but to a variable degree. Cortex spectra are normal. A minor increase in lactate in the cortex voxel is probably explained by admixture of both white matter and CSF in the voxel, lactate levels of up to 1.2 mmol/l being normal in the CSF.

Diffusion-weighted imaging in LBSL patients consistently shows high signal in the affected white matter on the Trace diffusion-weighted images (*b* value = 1000) (Figs. 68.3 and 68.7), most prominently in the focal lesions, with more severe signal change on the conventional images (Fig. 68.7). The ADC maps consistently show a complicated pattern with a mixture of high and low ADC values in areas with high signal on the Trace diffusion-weighted images. The

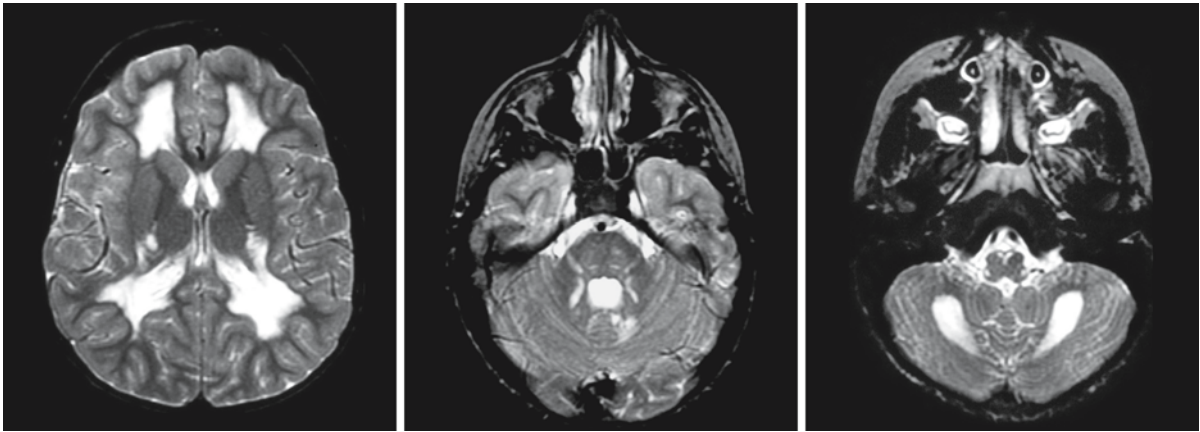


Fig. 68.10. A 10-year-old boy with LBSL. In this patient the cerebral white matter abnormalities are homogeneous. Courtesy of Dr. S. Blaser, Department of Diagnostic Imaging, Hospital for Sick Children, Toronto

low ADCs are mainly seen at the border of the white matter abnormalities (cerebral U fibers, peripheral rim of the cerebellar white matter abnormalities, the small focal lesions). The remainder of the abnormal white matter has elevated ADC values. The reason for

this is at present unknown, but it is clear that concepts such as vasogenic edema, cytotoxic edema, and T_2 shine-through effects are insufficient to explain these observations.

Hypomyelination with Atrophy of the Basal Ganglia and Cerebellum

69.1 Clinical Features and Laboratory Investigations

A distinct leukoencephalopathy has been described in a few patients, characterized by hypomyelination and atrophy of the basal ganglia and cerebellum (HABC), giving the disease its name. Both males and females are affected. It is highly likely that the disease is inherited. However, since all patients so far have been isolated cases, it is unclear whether the mode of inheritance is autosomal recessive, or whether it is autosomal dominant with all cases representing *de novo* mutations.

The disease has its onset in infancy or early childhood. The severity of the disease is highly variable. The most severely affected patients present soon after birth with poor eye contact and absence of any motor development. Ophthalmological examination reveals pale optic discs, consistent with hypomyelination of the optic nerves. Over the years there are signs of slowly progressive spasticity and extrapyramidal movement abnormalities including rigidity, dystonia, and choreoathetosis. The patients seem to have a better mental function than motor function and appear to have a social awareness. They may have some seizures. The severely affected patients tend to have a small stature and have a head circumference below the third percentile. Patients with intermediate severity of disease have delayed early development, but achieve grasping and unsupported sitting. In the mildest cases the patients may have normal initial development and they achieve unsupported walking. In these patients slow deterioration becomes evident in early childhood with increasing spasticity, ataxia, and often prominent extrapyramidal movement abnormalities consisting of dystonia, choreoathetosis, and rigidity. Some patients are predominantly spastic. The patients typically have learning problems, but further cognitive decline is at most minor. Occasional epileptic seizures may occur. Vision is normal and ophthalmological examination reveals no abnormalities. Height and head circumference are normal.

Laboratory examinations, including extensive metabolic studies, are unrevealing. CSF neurotransmitters and neurotransmitter metabolites have been studied in several patients and found to be within the normal range. Electroretinogram is normal. Visual evoked responses and somatosensory evoked responses are delayed. Brain stem auditory evoked re-

sponses show a normal latency for waves I and II, whereas the later waves are delayed or not recordable. Motor and sensory nerve conduction velocities are normal. Sural nerve biopsy is unrevealing.

69.2 Pathology

No autopsy studies are available.

69.3 Pathogenetic Considerations

The disease is most likely inherited, but the mode of inheritance is at present unclear. The disease is characterized by a disturbance of normal development and degeneration. From the beginning there is a picture of myelin deficiency. In some patients MRI suggests that there is some additional loss of myelin. There is progressive atrophy of the putamen, caudate nucleus, and cerebellum. The cerebral white matter also shows loss of volume over time. The putamen and caudate nucleus disappear without evidence of remaining scar tissue on MRI, suggesting atrophy by means of apoptosis rather than necrosis. The atrophy is more severe in the clinically more severely affected patients.

69.4 Therapy

At present, no specific therapy exists for patients with HABC. Seizures may require initiation of antiepileptic treatment. The severe extrapyramidal symptoms may require use of drugs also used for parkinsonism, including L-dopa. However, the extrapyramidal movement abnormalities tend to be drug-resistant. Some patients require intrathecal baclofen to reduce the serious hypertonia.

69.5 Magnetic Resonance Imaging

The diagnosis in HABC is MRI-based. Early MRI is characterized by the presence of very little myelin. In some patients, the putamen is already absent within the first year of life and the caudate nucleus is small, making the diagnosis of HABC possible (Fig. 69.1). However, in other patients the MRI within the first

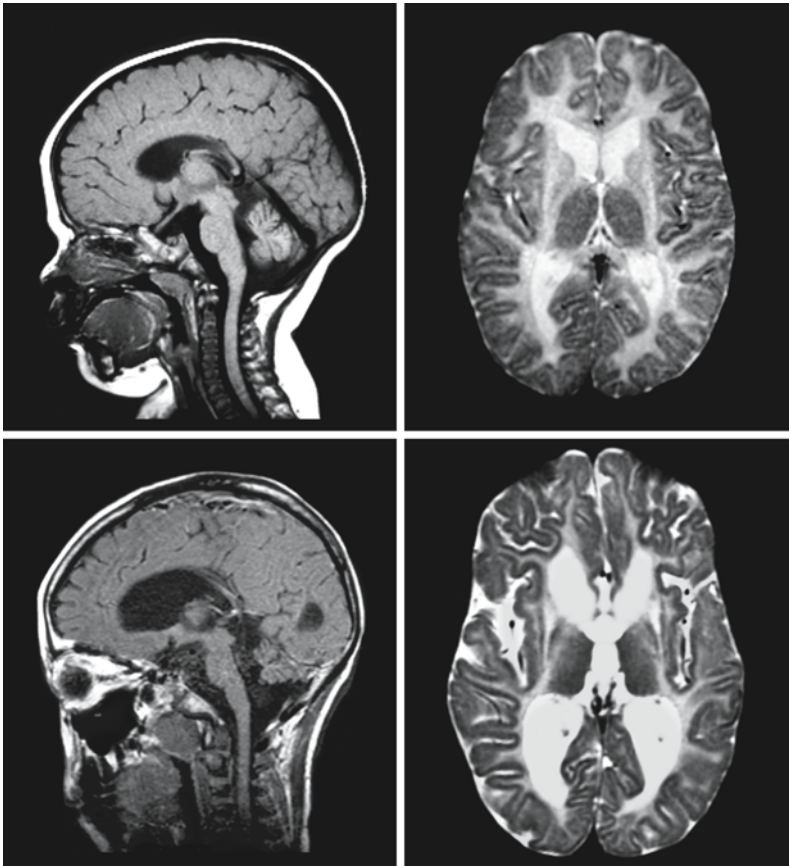


Fig. 69.1. Girl with HABC and a severe phenotype. At the age of 11 months (*first row*) the signal intensity of all cerebral white matter is high on the T₂-weighted image (*right*), consistent with hypomyelination. The same image shows that the thalamus is of normal size and the globus pallidus is visible, whereas there is no putamen. The caudate nucleus is very small and lacks the normal intermediate signal intensity. The follow-up images at the age of 10 years (*second row*) show the atrophy of the cerebellum. The T₂-weighted image (*right*) shows that the white matter still has a high signal and has become seriously atrophic. The thalamus and globus pallidus are of normal size but the putamen and caudate nucleus are not visible. From Van der Knaap et al. (2002), with permission

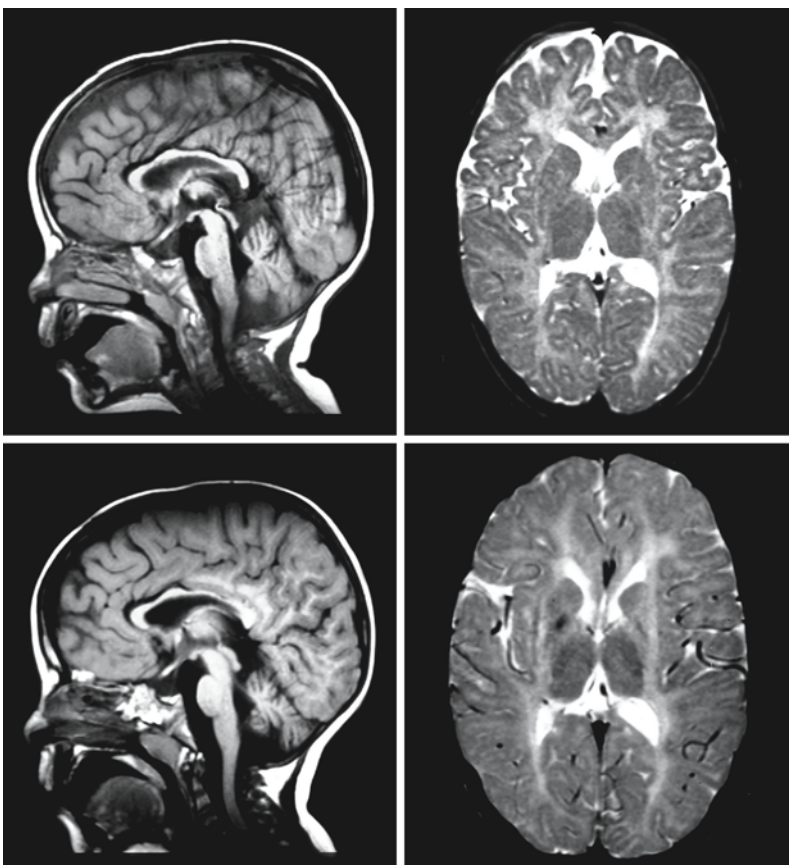


Fig. 69.2. Boy with HABC and a milder phenotype at the age of 18 months (*first row*) and 6 years (*second row*). The sagittal images (*left*) show progressive cerebellar atrophy over time. The axial T₂-weighted images (*right*) show persistent hypomyelination of the cerebral white matter. Initially, the basal ganglia have a normal appearance, but on follow-up the putamen has disappeared. Note the normal thalamus and globus pallidus. From Van der Knaap et al. (2002), with permission

year of life shows nothing other than myelin deficiency; the putamen and caudate nucleus are still present (Fig. 69.2). The severity of the myelin deficit is variable. In some patients the cerebral hemispheric white matter has a high signal intensity on T₂-weighted images and a low signal intensity on T₁-weighted images (Fig. 69.3), indicative of serious hypomyelination. In

other patients the white matter has a moderately high signal intensity on both T₂- and T₁-weighted images (Fig. 69.4), indicative of diffuse deposition of some myelin (moderate hypomyelination). It is striking that the pyramidal tracts in the brain stem are also hypomyelinated. Over time, the putamen disappears (Figs. 69.1–69.5). The caudate nucleus becomes

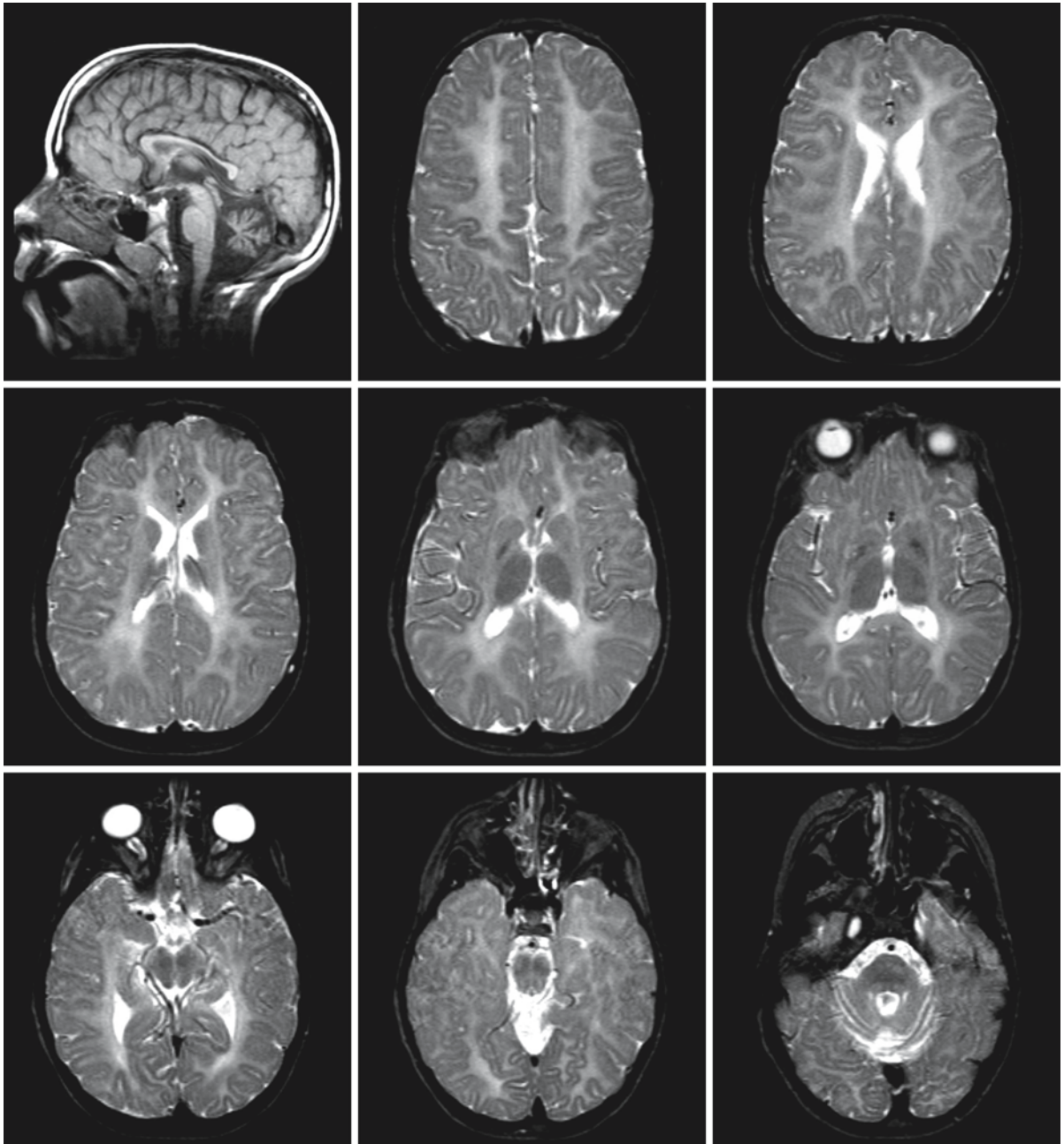


Fig. 69.3. A 9-year-old boy with HABC. The sagittal T₁-weighted image (*first row, left*) shows the prominent cerebellar atrophy. The cerebral white matter has a high signal intensity on the axial T₂-weighted images (*first, second, and third rows*) and a low signal intensity on T₁-weighted images (*fourth and*

fifth rows), consistent with a serious lack of myelin. On the T₂-weighted images the thalamus and globus pallidus are normal, whereas there is no putamen and the caudate nucleus is small

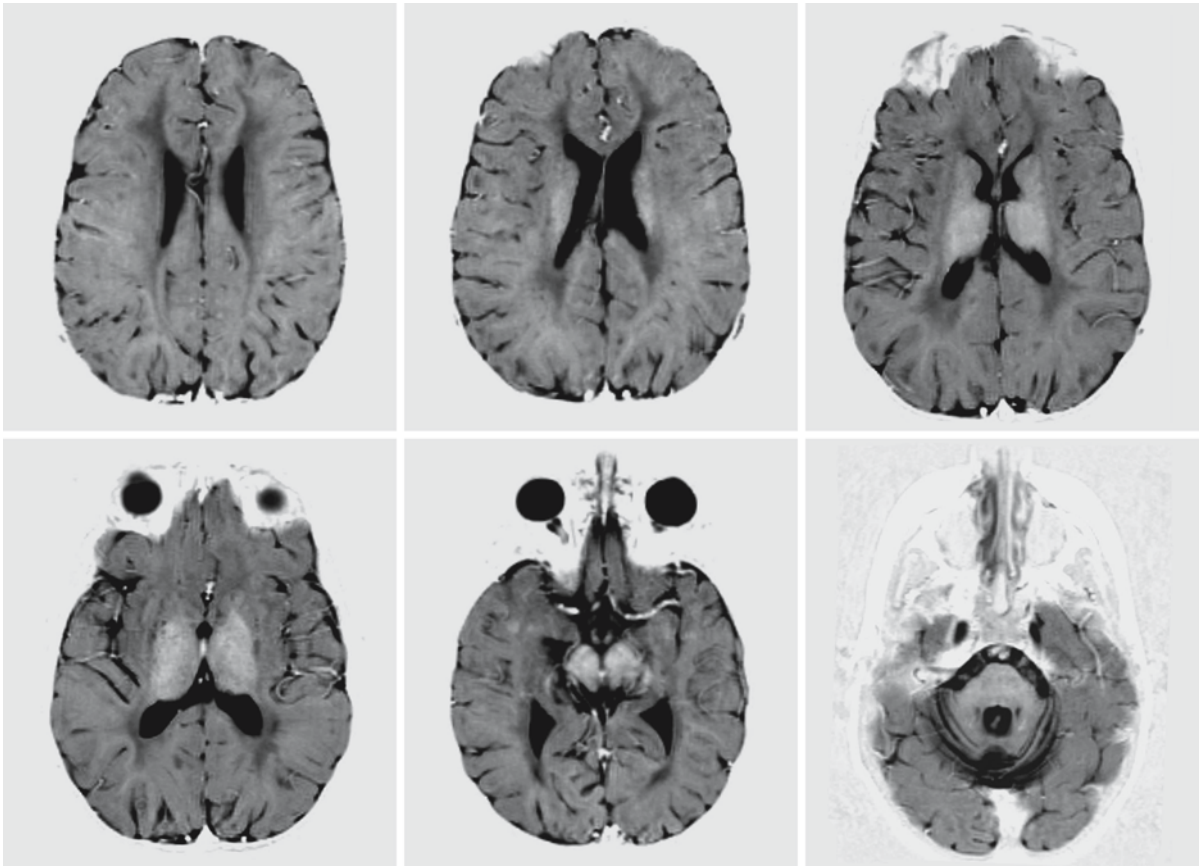


Fig. 69.3. (continued).

smaller, disappearing in some patients (Figs. 69.1 and 69.5). The thalamus and globus pallidus remain of normal size (Figs. 69.1–69.5). The cerebellum becomes progressively atrophic (Figs. 69.1 and 69.3). The atrophy affects the vermis more seriously than the hemispheres. Over the years, variable atrophy of the cerebral white matter occurs, associated with variable dilatation of the lateral ventricles. In some of the patients, there appears to be some additional loss of the little myelin present (Figs. 69.4 and 69.5). The atrophy of cerebral white matter and the basal ganglia is more serious in the clinically severely affected patients.

The full-blown picture of hypomyelination and missing putamen is diagnostic of HABC and does not suggest any other disorder. However, for as long as the putamen is still visible, other disorders leading to hypomyelination should be considered, including Pelizaeus–Merzbacher disease, Salla disease, and DNA repair disorders.

Proton MRS reveals that within the white matter total *N*-acetylaspartate and choline are normal, arguing against significant neuronal/axonal loss and active demyelination. *Myo*-inositol and total creatine are elevated, suggesting significant white matter gliosis.

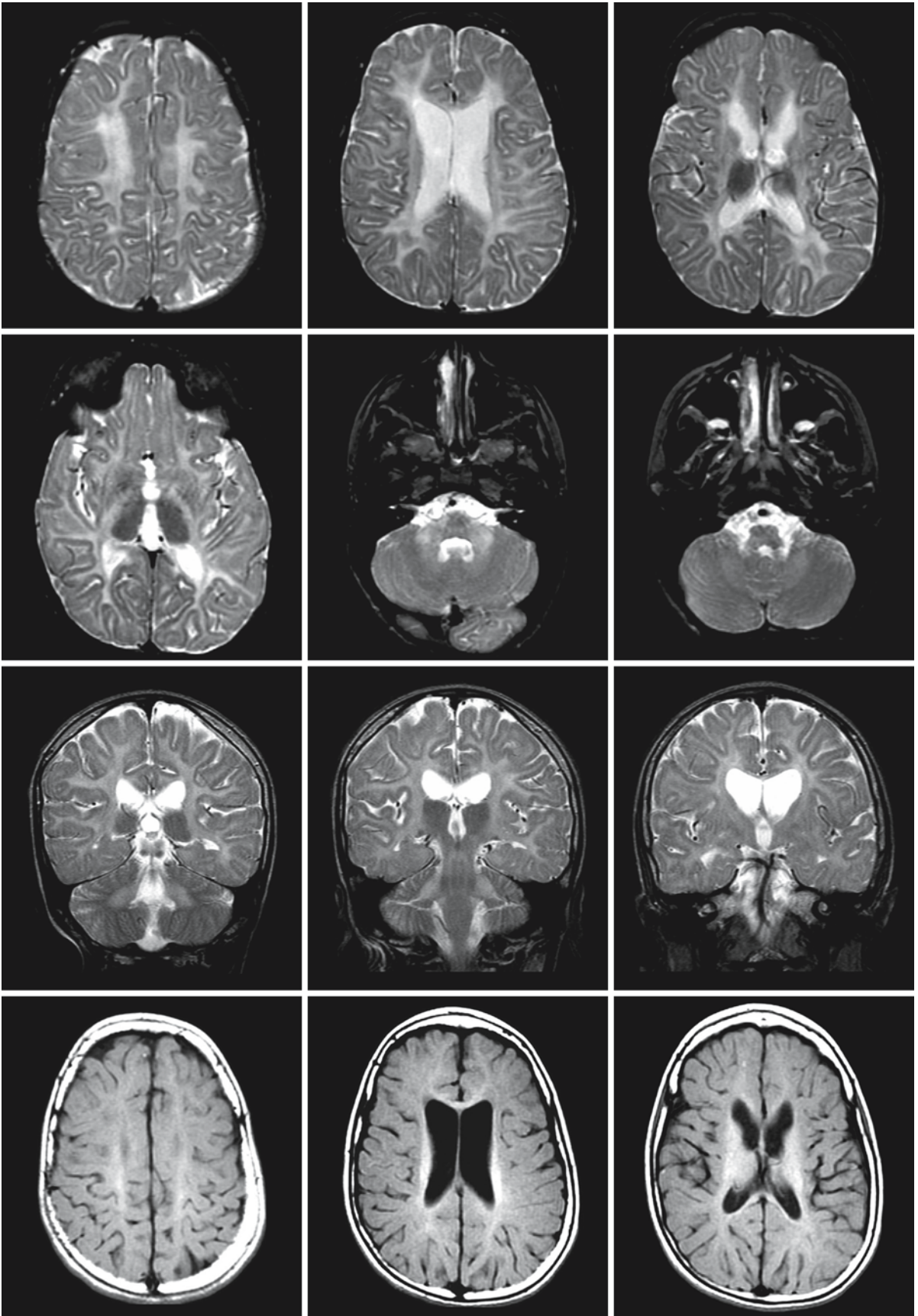


Fig. 69.4.

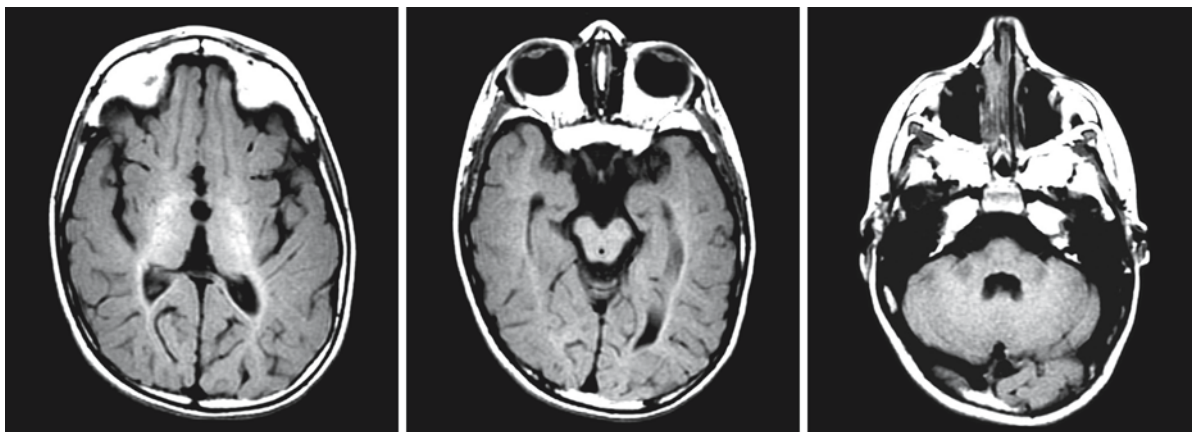


Fig. 69.4. (*continued*). A 6-year-old girl with HABC. The cerebral white matter has a high signal intensity on the axial (*first and second rows*) and coronal (*third row*) T₂-weighted images and an intermediate to high signal intensity on T₁-weighted images (*fourth and fifth rows*), consistent with moderate hypomyelination. The middle cerebellar peduncles and the cere-

bellar white matter are also insufficiently myelinated. The T₂-weighted images show a normal thalamus and globus pallidus, whereas there is no putamen and the caudate nucleus is very small. Courtesy of Dr. S. Blaser, Department of Diagnostic Imaging, Hospital for Sick Children, Toronto, Canada

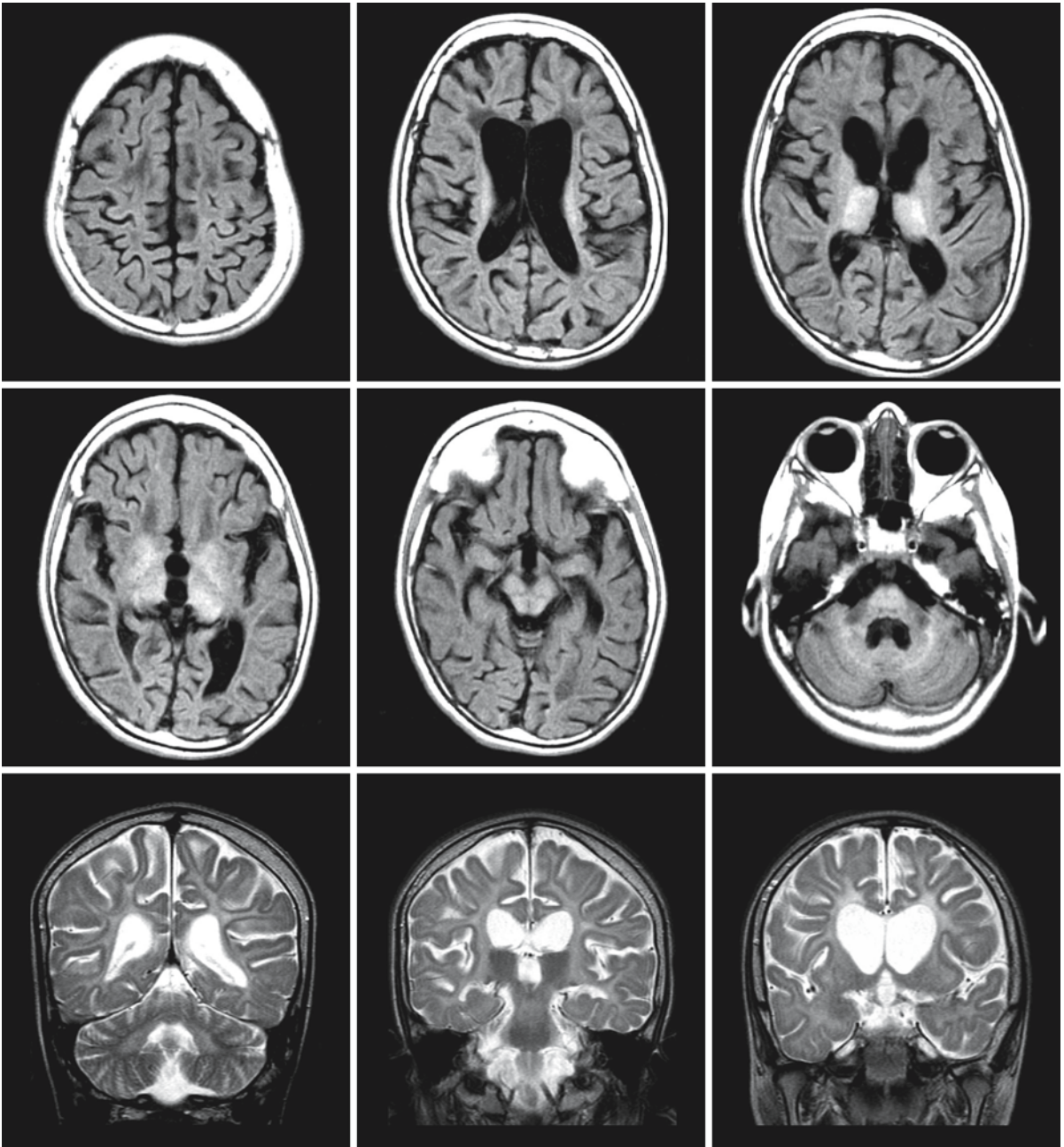


Fig. 69.5. The same girl as in Fig. 69.4, now 8 years old. She is clinically deteriorating. The T₁-weighted images (*first and second rows*) show white matter atrophy and loss of myelin. The coronal T₂-weighted images (*third row*) show that the caudate

nucleus is no longer visible. Courtesy of Dr. S. Blaser, Department of Diagnostic Imaging, Hospital for Sick Children, Toronto, Canada

Hereditary Diffuse Leukoencephalopathy with Neuroaxonal Spheroids

70.1 Clinical Features and Laboratory Investigations

Hereditary diffuse leukoencephalopathy with spheroids (HDLS) is an autosomal dominant progressive disease. The disease was described for the first time in multiple members of a large Swedish pedigree in 1984 (Axelsson et al. 1984). In this family, 17 of 71 subjects from 4 generations were affected. The age at onset varied from 8 to 60 years, with a mean of 36 years. The age at death was 39 to 89 years, with a mean of 57 years. The time between onset and death varied from 3 months to over 30 years. Some patients rapidly developed severe dementia and died within a few months of the onset of symptoms, whereas in others the course was prolonged with dementia developing over decades. Sporadic cases have also been reported.

The predominant clinical manifestations are psychiatric and include depression, anxiety, alcohol abuse, irritability, and aggressiveness. Psychotic symptoms may occur with confusion, delusions, and hallucinations. The most frequent neurological symptoms are dementia, seizures, impaired balance, retropulsion, gait apraxia, spasticity, ataxia, and urinary incontinence. Extrapyrarnidal symptoms may occur with hyperkinesia, chorea, tremor, and oral dyskinesia.

EEG usually shows nonspecific abnormalities with slowing of the background pattern and sometimes paroxysmal changes. The abnormalities often have a frontotemporal predominance. They may be asymmetrical. Routine and metabolic laboratory investigations reveal no abnormalities. The diagnosis is at present based on histopathological findings.

70.2 Pathology

External examination of the brain shows mild atrophy of the frontoparietal regions. The thalamus and the rostral part of the caudate nucleus may be mildly reduced in size. The lateral ventricles are moderately enlarged. The corticospinal tracts and the basis of the pons are atrophic. On microscopy, a widespread leukoencephalopathy is found, characterized by a commensurate loss of myelin sheaths and axons and the presence of numerous neuroaxonal spheroids in

the affected white matter. Neuroaxonal spheroids are round to sausage-shaped axonal swellings, which are easily identified with Bielschowsky, Bodian, and anti-neurofilament immunostains. The leukoencephalopathy is most severe in the frontal, frontoparietal, and temporal areas and may be mildly asymmetrical. The U fibers are relatively spared. The abnormalities tend to be most pronounced in the white matter below the pre- and postcentral gyri and extend through the posterior limb of the internal capsule into the pyramidal tracts of the brain stem. The corpus callosum is variably affected. The abnormal white matter may show vacuolization. Reactive astrocytes and macrophages are present, but no inflammatory cells. The cerebral cortex and basal ganglia are normal and contain no or only a few spheroids. Within the cerebellum, a marked loss of Purkinje cells is seen, but the cerebellar white matter is normal. Electron microscopy of the spheroids reveals neurofilaments scattered among electron-dense material and mitochondria.

70.3 Pathogenetic Considerations

The homogeneity of the clinical picture and histopathological findings strongly suggests that HDLS is a distinct disease entity. The disease has an autosomal dominant mode of inheritance. Isolated cases are probably the result of new mutations. The genetic defect and the pathophysiology of HDLS are as yet unresolved. Considering the more or less commensurate loss of axons and myelin sheaths, the preferential involvement of long tracts, and the presence of axonal swellings, it is likely that axons are the primary target of the disease.

Axonal spheroids are pathological findings characteristic of the neuroaxonal dystrophies. They occur most often in the context of neuronal degenerative disorders, such as infantile neuroaxonal dystrophy (Seitelberger disease) and Hallervorden–Spatz disease. The combination of leukoencephalopathy and neuroaxonal spheroids in the abnormal white matter is rare. Apart from HDLS, this combination is observed in dermatoleukodystrophy with neuroaxonal spheroids (Matsuyama et al. 1978) and polycystic lipomembranous osteodysplasia with sclerosing leukoencephalopathy (Nasu–Hakola disease). Both disorders are clinically different from HDLS.

70.4 Therapy

Supportive care is the only therapeutic option.

70.5 Magnetic Resonance Imaging

MR images demonstrate signal abnormalities bilaterally within the cerebral white matter, most pronounced either within the white matter under the pre- and postcentral gyri (Figs. 70.1–70.3) or within the frontal white matter. The signal abnormalities may be patchy or more confluent, and may be symmetrical or asymmetrical. They are ill-defined. The corpus callosum is thin and may contain areas of abnormal signal. The signal abnormalities extend downwards through the posterior limb of the internal capsule into the pyramidal tracts of the brain stem (Fig. 70.1). The affected cerebral white matter is atrophic with widening of the lateral ventricles and subarachnoid spaces (Figs. 70.1–70.3). The head of

the caudate nucleus may be flattened. There may be cerebellar atrophy.

The above MRI findings may confirm the diagnosis within a pedigree with known HDLS. However, the MRI findings in themselves are not specific and do not allow a definite diagnosis. The diagnosis needs to be confirmed by histopathology.

The differential diagnosis of HDLS includes disorders with frontal cortical degeneration, such as frontotemporal dementia and Pick disease. In these disorders MRI shows atrophy mainly of the frontotemporal areas. Sometimes there are additional white matter changes, which are ill-defined and usually mild. If present, they make differentiation from HDLS difficult.

The differential diagnosis also includes disorders with frontal lobe dysfunction caused by white matter degeneration, such as metachromatic leukodystrophy, X-linked adrenoleukodystrophy with frontal predominance, Nasu–Hakola disease, Binswanger disease, CADASIL, orthochromatic pigmentary leukody-

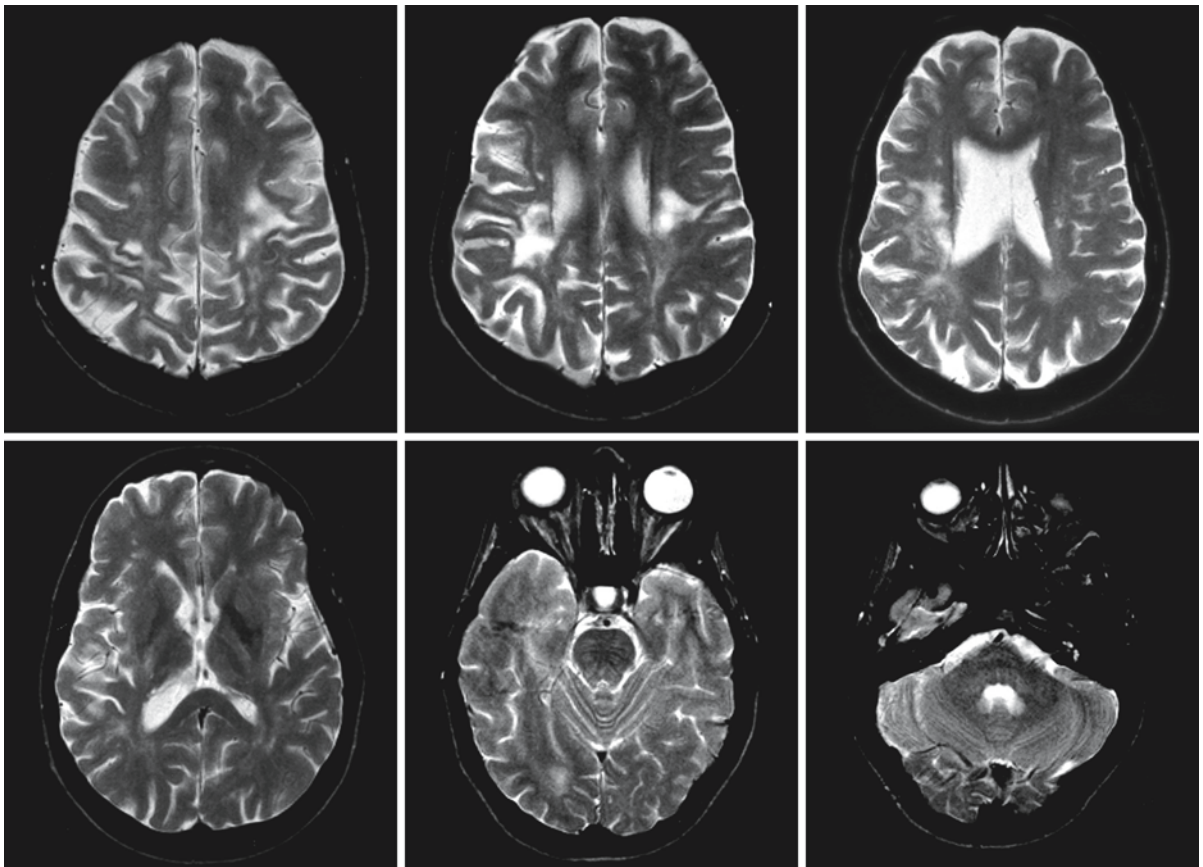


Fig. 70.1. A 26-year-old female patient with HDLS. This diagnosis was confirmed histopathologically in her father (Fig. 70.2). Note the patchy and asymmetrical abnormalities in the white matter under the central sulcus. The abnormalities

extend downwards into the posterior limb of the internal capsule and the pyramidal tracts in the midbrain. There is a mild cerebral atrophy. From van der Knaap et al. (2000), with permission

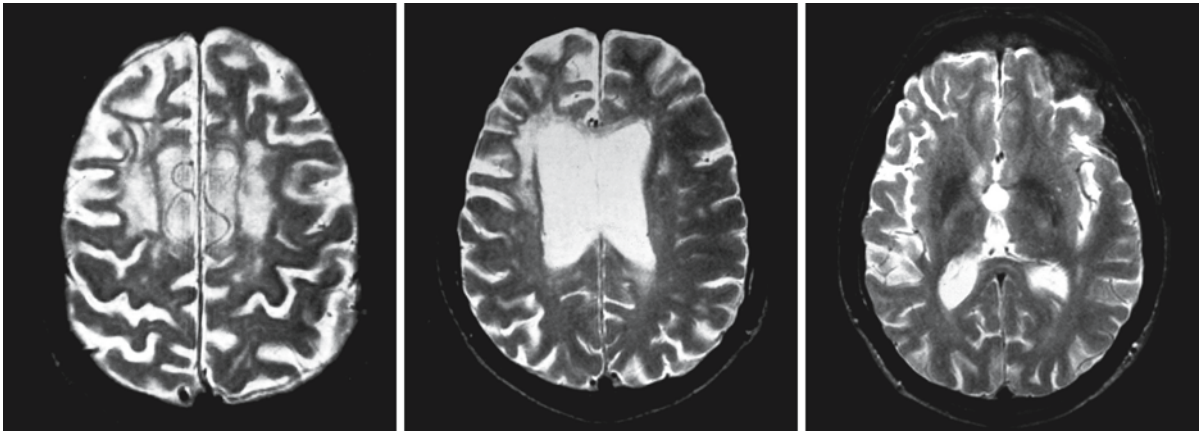


Fig. 70.2. A 55-year-old man with HDLS, father of the patient in Fig. 70.1. The diagnosis was confirmed at autopsy. There is serious cerebral atrophy. The white matter abnormalities are most prominent in the tracts under the pericentral cortex.

They are partially confluent, partially multifocal. The abnormalities extend downwards into the posterior limb of the internal capsule. From van der Knaap et al. (2000), with permission

atrophy, and adult-onset autosomal dominant leukodystrophies. Most disorders can be ruled out by typical clinical, physical, and laboratory findings and neuroimaging differences. Some disorders require histopathological confirmation.

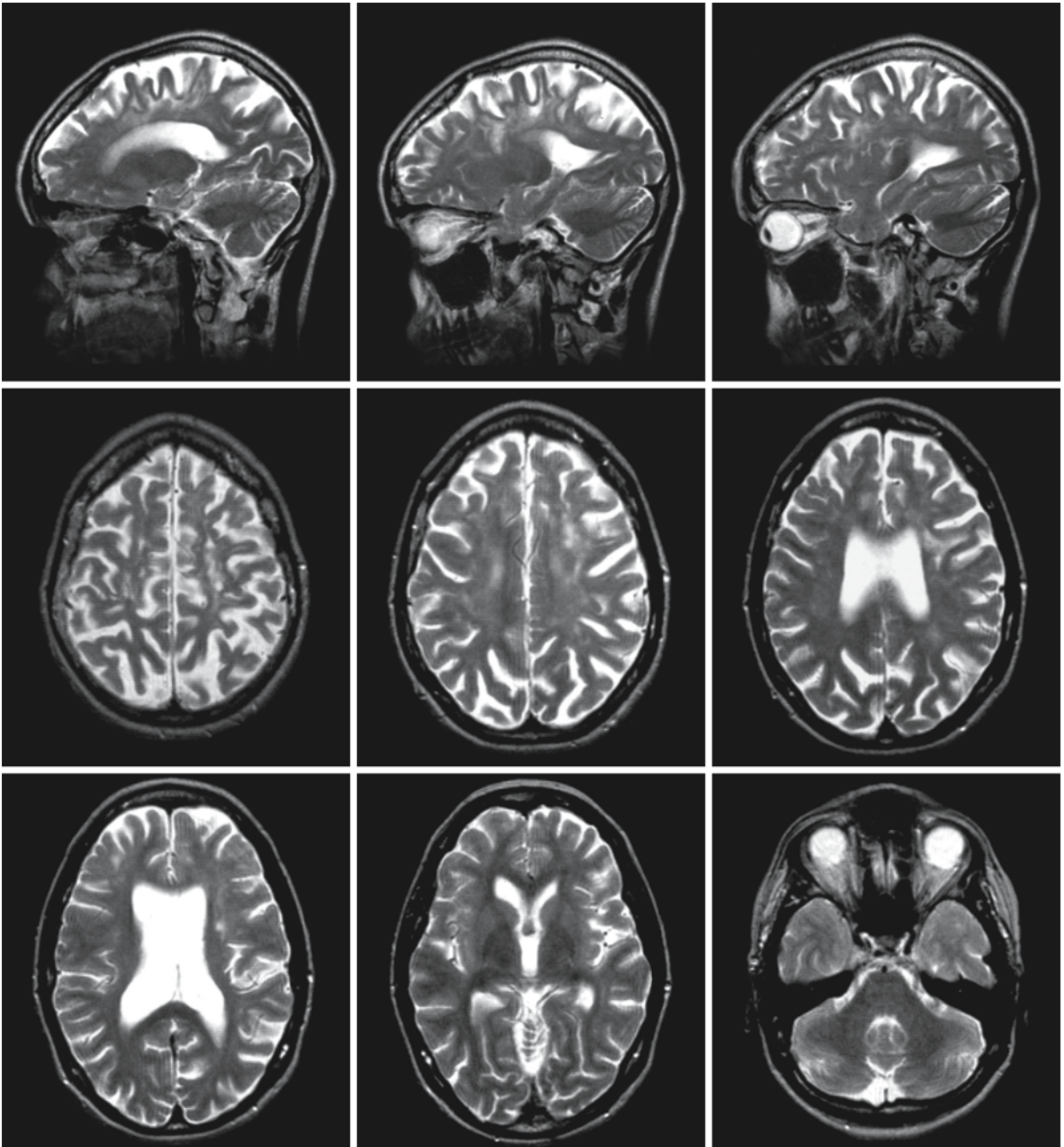


Fig. 70.3. A 38-year-old woman with HDLS. The diagnosis was confirmed at autopsy. There is prominent cerebral atrophy. There are patchy, multifocal abnormalities in the cerebral

white matter, most prominently in the central tracts. From van der Knaap et al. (2000), with permission

Dentatorubropallidoluysian Atrophy

71.1 Clinical Features and Laboratory Investigations

Dentatorubropallidoluysian atrophy (DRPLA) is a rare disease with an autosomal dominant mode of inheritance. The disease has a pronounced ethnic predilection and occurs most frequently in Japan. However, an increasing number of American and European patients have been described. Although sporadic cases have been reported, nearly all cases are familial with two or more successive generations affected. There is evidence of anticipation: in the next generation the disease tends to have an earlier onset and be more severe.

The presenting symptoms are a variable mixture of cerebellar ataxia, myoclonus, epilepsy, choreoathetosis, dementia, and psychiatric abnormalities. The age at onset ranges from the first to the sixth decade, with an average age of 32 years. In the early-onset forms progressive myoclonic epilepsy and dementia are the predominant symptoms, whereas in the patients with later onset progressive cerebellar ataxia and choreoathetosis are more prominent. Among the older patients two clinical presentations can be distinguished: a pseudo-Huntington form with prominent choreoathetosis, cognitive dysfunction, and psychiatric syndromes, and a form with progressive ataxia with less severe cognitive impairment.

In the younger group of patients, DRPLA has to be distinguished from other diseases with progressive myoclonic epilepsy, such as neuronal ceroid lipofuscinosis, sialidosis, myoclonus epilepsy with red ragged fibers (MERRF), and Unverricht disease. In the older patients DRPLA has to be distinguished from Huntington disease, which may have a very similar clinical presentation. Laboratory investigations are unrevealing in DRPLA, but DNA confirmation is possible.

71.2 Pathology

There are some variations in the histopathological findings between different families. Most data on histopathology in DRPLA come from Japanese patients, in whom histopathological findings are the most uniform. On gross inspection there may be some atrophy of the base of the pons and the cerebellar vermis. The principal histopathological alterations consist of severe neuronal cell loss and astrocy-

tosis in the globus pallidus, subthalamic nucleus, red nucleus, and dentate nucleus. Mild changes occur in the caudate nucleus, putamen, thalamus, and inferior olives. There is only subtle involvement of the substantia nigra. The superior cerebellar peduncles, containing the outflow tracts of the dentate nuclei, are atrophic. The base of the pons and the tegmentum of the midbrain and pons display variable atrophy. Unlike findings in other dementias, there is no significant cell loss in the nucleus basalis of Meynert. Immunohistochemistry demonstrates the presence of ubiquitin-positive intranuclear aggregates in neurons and also astroglia. In addition, filamentous ubiquitinated intracytoplasmic inclusions may be found in neurons of affected structures.

In younger patients patchy periventricular white matter abnormalities are found, whereas in older patients the white matter abnormalities are more confluent and symmetrical, and affect the deep white matter of the centrum semiovale. Microscopy reveals gliosis and demyelination in the affected areas. Occasionally the cerebellar white matter is involved. Intranuclear aggregates have been demonstrated in oligodendrocytes within the affected white matter.

Spinal cord involvement has been reported, with degeneration of the posterior columns, spinocerebellar tracts, corticospinal tracts, and anterior horn cells.

In the Haw River variant of the disease, marked neuronal loss of the dentate nuclei, microcalcification of the globus pallidus, neuroaxonal dystrophy of the nucleus gracilis, and demyelination of the centrum semiovale have been found.

71.3 Pathogenetic Considerations

DRPLA is caused by an unstable expansion of a cytosine-adenine-guanine (CAG) repeat in the gene *DRPLA*, located on chromosome 12p13.31. The product of *DRPLA* is atrophin-1, a protein that is widely expressed in many tissues including the brain. It shares no homology with other known proteins. Expansion of the CAG repeat in the *DRPLA* gene in normal subjects ranges from 10 to 21, in patients from 58 to 82. No overlap has been reported between normal alleles and mutant alleles.

In the brain atrophin-1 is located in the cytoplasm of neurons. In DRPLA subjects both expanded and normal alleles are detectable in the brain, with re-

gional variation. Atrophin-1 has been immunocytochemically localized to somatic and somatodendritic compartments of cortical and cerebellar neurons. In the cerebellum the protein is especially abundant in Purkinje cells and neurons of the dentate nucleus.

The unstable CAG repeat encodes for a polyglutamine repeat. Polyglutamine repeats also occur in myotonic dystrophy, fragile X syndromes, spinobulbar muscular atrophy (Kennedy disease), Huntington disease, spinocerebellar ataxia type 1 (SCA1), spinocerebellar ataxia type 2 (SCA2), Machado-Joseph disease (SCA3) and spinocerebellar ataxia type 7 (SCA7). The number of repeats clearly influences the phenotypic expression. As in other trinucleotide repeat syndromes, the number of repeats increases with successive generations. This leads to an earlier onset and worsening of the phenotype in every following generation, a phenomenon referred to as "anticipation." In the patients presenting with progressive myoclonic epilepsy end dementia (early presentation) the number of repeats is much higher than in the patients without the progressive myoclonic epilepsy (late presentation).

The molecular basis for the selective neuronal damage in dentatorubropallidoluysian atrophy is not yet fully understood. Misfolding and conformational alterations of the mutant protein due to polyglutamine expansion may lead to aberrant protein-protein interactions and targeting of the misfolded proteins for degradation. Ubiquitination of proteins in the aggregates indicates targeting for degradation. Protein aggregation is probably a critical molecular component of polyglutamine diseases. These aggregates are present as nuclear inclusions in the neurons selectively affected by the disease. Transglutaminases appear to play a role in the formation of the protein aggregates. Transglutaminases are a large family of proteins with the common capacity to catalyze cross-linking of protein substrates, resulting in the formation of large protein aggregates that are insoluble to all known protein detergents. These aggregates may contribute to neuronal dysfunction and degeneration. It may also be that mutant proteins are most toxic when roaming freely and that the aggregates represent the cell's effort to convert the toxic proteins into more innocuous clumps. The differences in clinical expression and cell specificity of the affected neurons in the different polyglutamine disorders could be related to different factors, including the cellular distribution of the polyglutamine protein, protein interactors, and cell specificity of certain modifying proteins. The latter group may include cell-specific transglutaminases and cysteine proteases.

Nuclear inclusions were previously considered to be a feature specific to neuronal degenerative dis-

eases, but recently histopathological studies have shown nuclear inclusions in oligodendrocytes of DRPLA patients as well. In transgenic DRPLA mice, too, oligodendrocytes demonstrated the same inclusions. Apparently not only neurons but also glial cells are affected in DRPLA. It is probable that oligodendroglial involvement is responsible for the white matter abnormalities that may be observed in DRPLA patients.

71.4 Therapy

No causal treatment is available, but symptomatic care is important. Anticonvulsants should be used when seizures are present. Psychiatric problems can be treated with appropriate psychotropic medications.

71.5 Magnetic Resonance Imaging

Standard sequences usually suffice to make an inventory of the abnormalities in DRPLA. Sophisticated techniques as diffusion tensor imaging may be useful to identify involved tracts, as may be fiber tracking. Gradient echo techniques may be useful in the detection of calcifications.

The characteristic findings on conventional MR include atrophy of the tegmentum of the midbrain, pons, dentate nucleus, superior cerebellar peduncles, and cerebellum (Figs. 71.1 and 71.2). The lateral ventricles show moderate to severe enlargement and commonly there is moderate but clear cortical atrophy. The globus pallidus and subthalamic nucleus are usually either normal or slightly atrophic on MRI. High signal intensity of the globus pallidus on proton-density and T₂-weighted images is often present from early on (Figs. 71.1–71.3). Bilateral symmetric signal changes in the thalamus and abnormal signal intensity in the midbrain and pons are characteristic (Figs. 71.1–71.3). The red nucleus characteristically has normal signal (Fig. 71.2). In older patients there is an increase of lesions in the midbrain and thalamus.

Although not invariable, white matter abnormalities are characteristically present in patients with DRPLA. In younger patients patchy periventricular areas with high signal intensity may be found on T₂-weighted, proton-density, and FLAIR images. Confluent white matter abnormalities are found in older patients with a diffuse increase in signal in the periventricular and deep white matter, only sparing most of the U fibers (Figs. 71.1–71.3). The pattern of cerebral white matter abnormalities in combination with signal changes in the globus pallidus, thalamus, and brain stem is typical of an advanced stage of DRPLA.

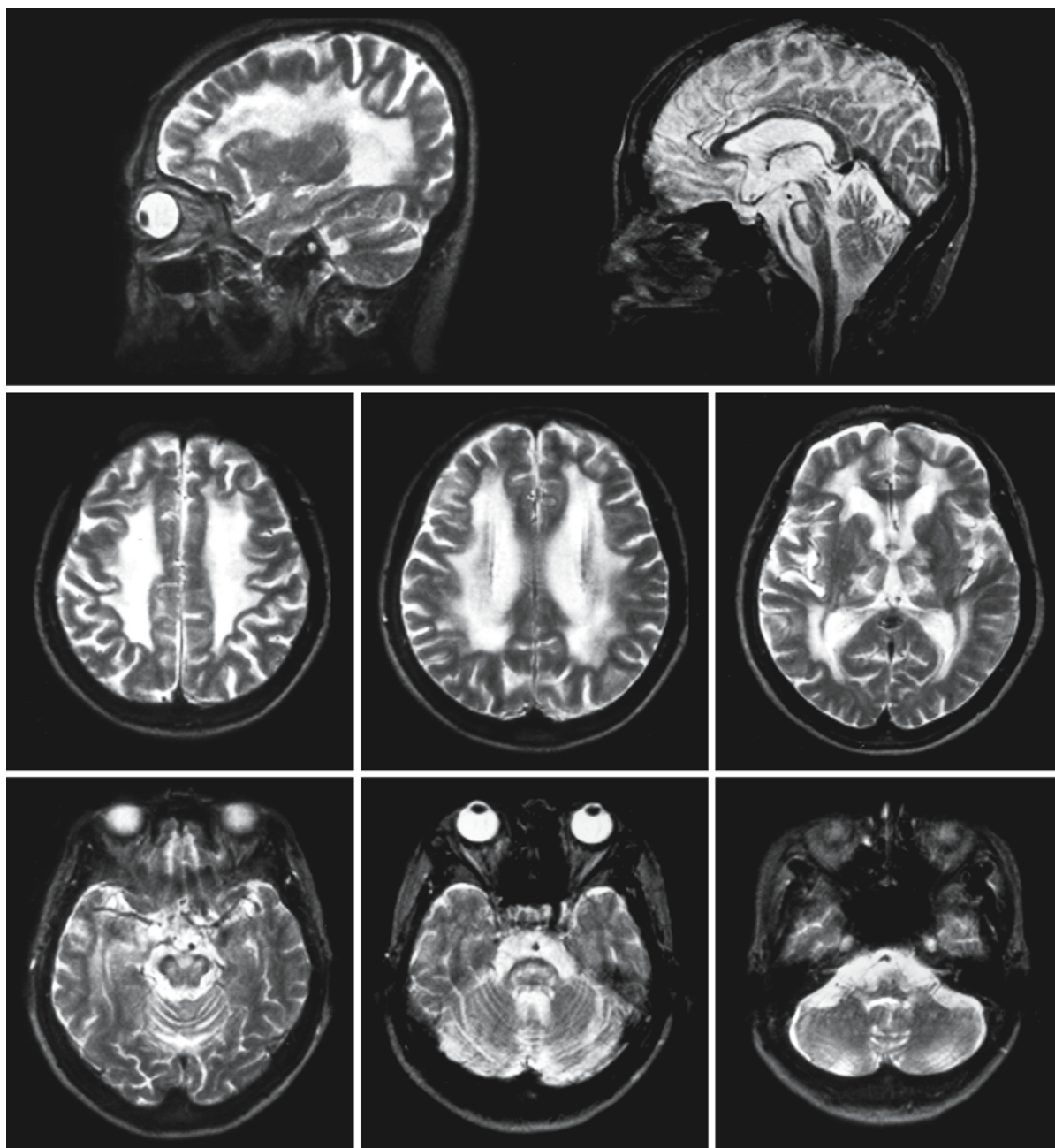


Fig. 71.1. A 73-year-old female patient with DRPLA. The mid-brain, pons, and cerebellum are atrophic. There is also some cerebral atrophy. There are diffuse signal abnormalities in the cerebral hemispheric white matter with partial sparing of the

U fibers and the corpus callosum. Note the signal abnormalities in the globus pallidus, thalamus, midbrain, and pons. From Uyama et al. (1995), with permission

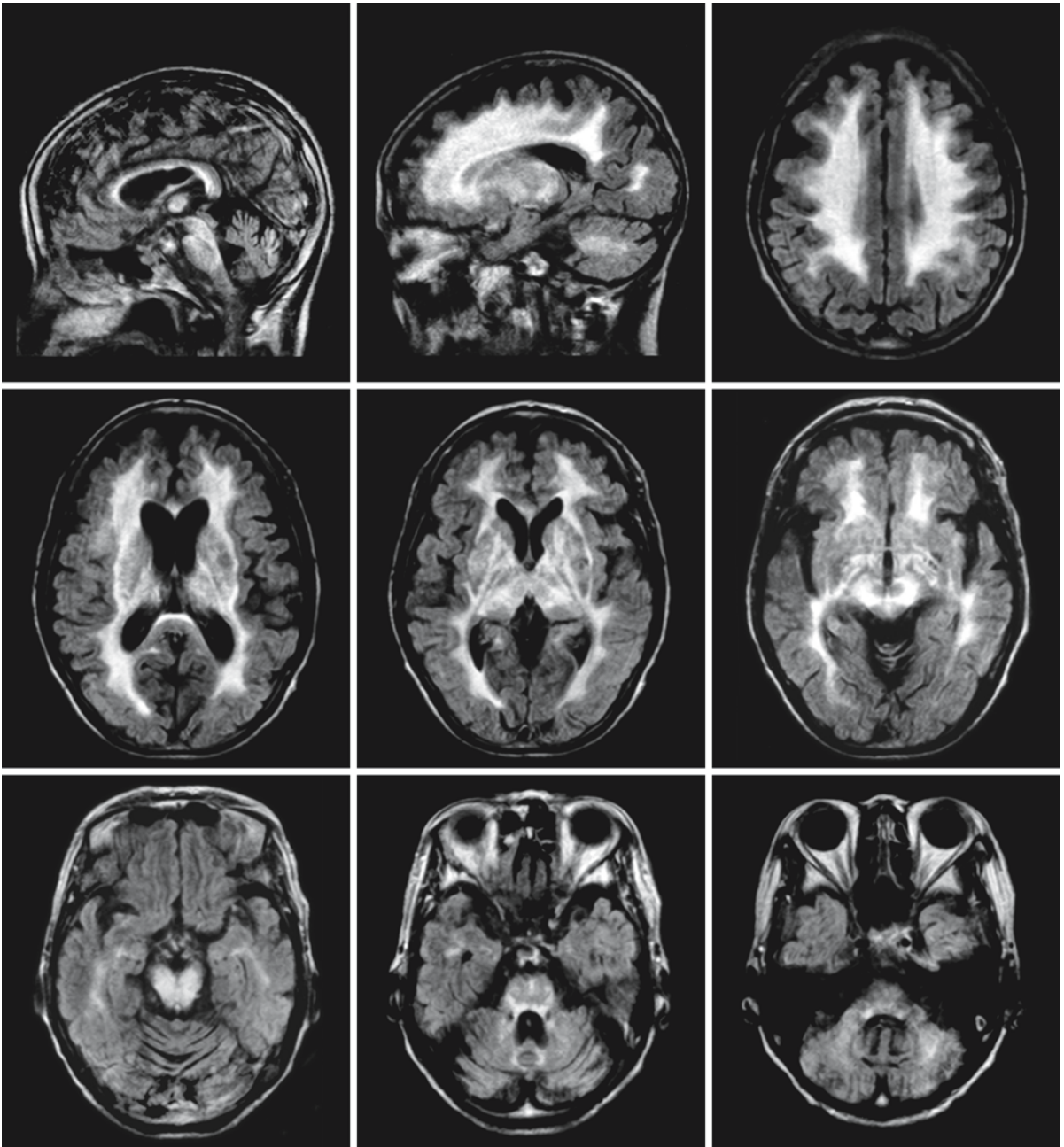


Fig. 71.2. A 60-year-old female patient with DRPLA. The sagittal and axial FLAIR images reveal extensive signal abnormalities in the cerebral white matter with partial sparing of the U fibers. The inner rim of the corpus callosum shows an abnormal signal. There are additional signal abnormalities in the

caudate nucleus, globus pallidus, putamen, thalamus, mid-brain, tegmentum of the pons, and dorsal part of the medulla. The red nuclei are spared. Note the atrophy of the cerebellum, pons and superior cerebellar peduncles. From Yoshii et al. (1998), with permission

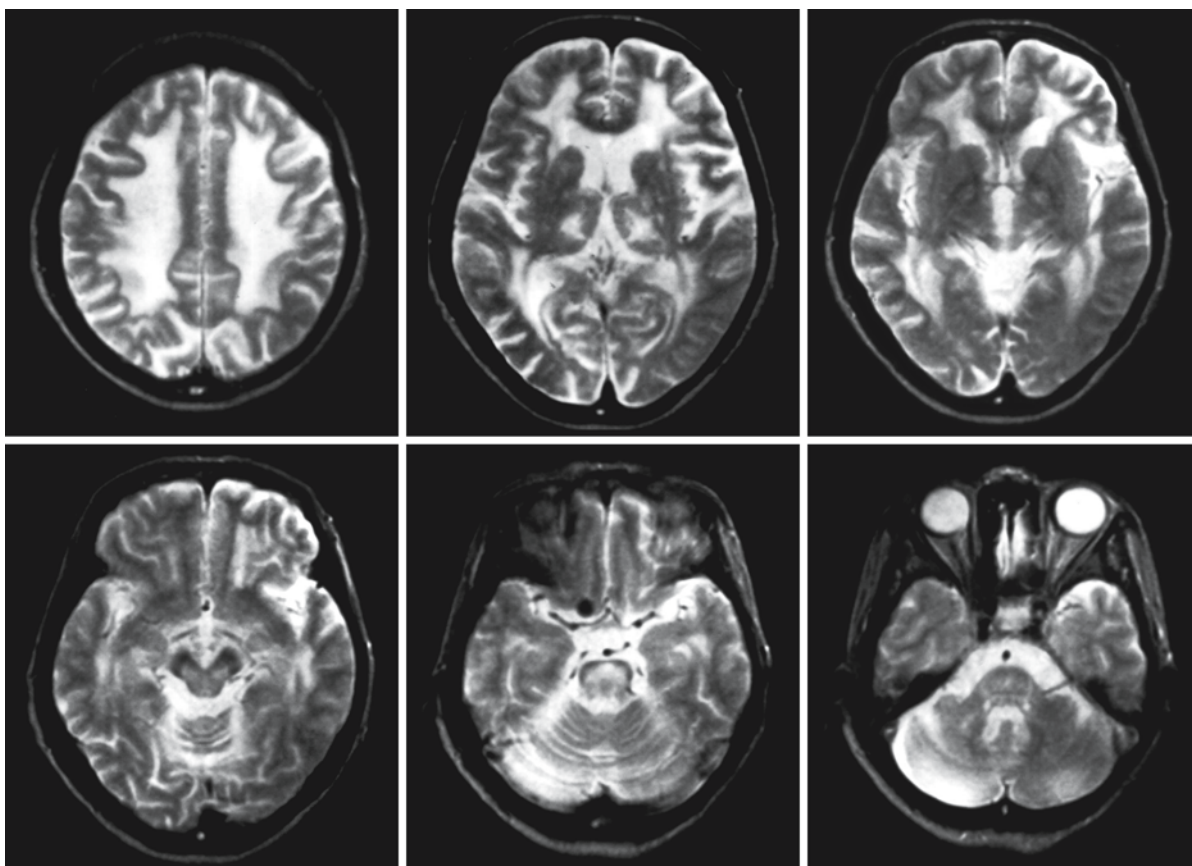


Fig. 71.3. A 68-year-old female patient with DRPLA. Note the evident pontine and cerebellar atrophy. There are extensive cerebral white matter abnormalities, sparing the corpus callo-

sum and some of the U fibers. There are also signal abnormalities in the globus pallidus, thalamus, midbrain, and pons. From Uyama et al. (1995), with permission

Cerebral Amyloid Angiopathy

72.1 Clinical and Laboratory Findings

Cerebral amyloid angiopathy (CAA) was recognized as a disease entity at the beginning of the twentieth century. The first reports appeared in the German literature in 1907 and 1909. In 1935 a familial form of this disease was reported from Iceland, later followed by the description of a Dutch family (1964), a Flemish variant (1992), and a British type (1996). In the latter variant hemorrhage is not a prominent feature, as it is in the Icelandic and Dutch type. Apart from the familial forms, there are also sporadic forms.

The classic presentation of CAA is lobar hemorrhage, often multiple, associated with an acute neurological presentation. CAA is responsible for 5–20% of nontraumatic cerebral hemorrhages and 30% of lobar hemorrhages. The most frequent locations are: frontal (35%), parietal (26%), temporal (14%), and occipital (19%). Cerebellar and basal ganglia hemorrhages are infrequent; brain stem hemorrhages are extremely rare. Sporadic CAA may present with a variety of symptoms other than lobar hemorrhage. There may be petechial hemorrhages in cortical and subcortical areas and these may produce either recurrent transient neurological symptoms or rapidly progressive dementia. Dementia is estimated to occur in about 40% of patients with CAA. The progression of dementia is as a rule much faster than in Alzheimer disease.

The familial forms of CAA have an autosomal dominant inheritance. There are differences in presentation between the affected families. The Icelandic form presents in the third decade with multiple intracerebral hemorrhages and infarctions. The disease progresses rapidly to dementia, paralysis, and early death. The Dutch form has a later onset, in the fourth to fifth decade of life. Chronic migrainous headache, as in CADASIL, may precede the onset by years. The presenting symptom is most often intracerebral hemorrhage, sometimes ischemic strokes. Neuropsychiatric symptoms and dementia are constant features. The Flemish variant presents with intracerebral hemorrhage and dementia. The British variant shows progressive dementia, spasticity, and ataxia (Worster-Drought syndrome). In this form the entire CNS is involved, including cerebral white matter, cerebellum, brain stem, and spinal cord. Hemorrhage is not prominent. Other families from Japan, Italy, and North America have been reported with oculo-

leptomeningeal amyloidosis. They vary in presentation but dementia, hemiplegic migraine, spasticity, blindness, and deafness are usually present. These patients have amyloid deposition in the vitreous and retinal vessels, leptomeningeal vessels, and other organs.

The incidence of sporadic CAA increases with age. The differentiation from other conditions with small vessel disease may be difficult. There is a relationship with sporadic Alzheimer disease. Amyloid deposition in vessel walls is also a factor of importance in sporadic and familial forms of Alzheimer disease. CAA is found in 92% of postmortem studies of brains of patients with Alzheimer disease. Amyloid deposition is accepted as one of the hallmarks of Alzheimer disease. CAA, however, can occur without any other sign of Alzheimer disease, and Alzheimer disease can occur without CAA. If CAA is present there is risk of lobar hemorrhage. There is no obvious relation with the occurrence, location, and severity of neuritic plaques or neurofibrillary tangles.

Apart from a relationship with Alzheimer disease, CAA is reported to occur in transmissible spongiform encephalopathies (prion diseases), especially in Gerstmann-Sträussler-Scheinker disease, and, less commonly, in Creutzfeldt-Jakob disease; in malignant neoplasms treated with irradiation, parkinsonism-dementia complex of Guam, and dementia pugilistica. A few cases of primary angiitis of the CNS have been reported in combination with CAA.

Routine laboratory tests are unrevealing. The diagnosis of CAA should be suspected on the basis of typical clinical and neuroimaging findings. The diagnosis may be confirmed by a leptomeningeal biopsy, but this is only done in exceptional cases. In familial CAA histological confirmation in one patient is necessary, whereas in other affected family members suggestive clinical and neuroimaging findings suffice for a diagnosis. The Boston group for research of CAA has come up with criteria for the diagnosis of CAA-related hemorrhage (see Knudsen et al. 2001). Patients fulfilling these criteria, however, have a hemorrhage, so that patients without hemorrhage are excluded. The MR criteria mentioned in this set of criteria also do not specify the mandatory inclusion of gradient echo techniques, which would help to identify patients with and without hemorrhages with CAA, in addition to being helpful to demonstrate other possible causes.

72.2 Pathology

Gross inspection of brain sections reveals a combination of larger and smaller hemorrhages, most often in the cortex and subcortical regions; small infarctions, mainly affecting the cerebral cortex; and extensive white matter abnormalities, mainly involving the deep and periventricular white matter, usually sparing the U fibers. Lacunae may also be present in the basal ganglia. Ventricular dilatation is usually also present.

On microscopic examination the lesions in the white matter consist of patchy gliosis and myelin loss, the latter in particular in the parieto-occipital areas. U fibers, corpus callosum, internal capsule, and optic radiation are usually spared. Perivascular spaces are enlarged and contain mononuclear cells and hemosiderin-laden macrophages. Around the ventricles Rosenthal fibers may be found.

The most striking finding in CAA is that smooth muscle in the vessel wall of small blood vessels is replaced by a hyaline, eosinophilic material. The deposits stain with Congo red, hence the name “congoophilic angiopathy.” The term “amyloid” is applied to a number of proteins sharing the property of Congo red staining, which then exhibits green birefringence under polarized light. This latter property is dependent upon the configuration of a twisted β -pleated sheet. This is a feature of amyloid laid down under different circumstances and in different organs of the body, which, despite identical staining properties, may have different amino acid sequences in the constituent polypeptide chains. Specific antibodies against amyloid β peptide ($A\beta$), cystatin C, and thyrostatin can be used for immunohistochemical characterization. It is of interest that in patients with a combination of CAA and Alzheimer disease the deposits in the vessel wall are immunoreactive with both anti- $A\beta$ and anti-cystatin C. Fibrinoid necrosis and hyaline changes in vessel walls are usually also present in sporadic cases of CAA and larger cortical vessels are often thrombosed. Ultrastructurally, amyloid fibrils in blood vessels appear as interwoven bundles of 10-nm filaments, short and disarranged. In early CAA only the outer part of the vessel wall is involved, but when the deposits become larger, they occupy the abluminal part of the basement membrane and adjacent smooth muscle cells show degenerative features. When severely affected, the walls of blood vessels may be replaced entirely by bundles of fibrils with loss of smooth muscle cells and with radiation of fibrils into the surrounding neuropil.

72.3 Pathogenetic Considerations

The central biochemical event in the pathophysiology of CAA is the polymerization of soluble subunit proteins into insoluble amyloid fibrils. Several different forms of amyloid subunit proteins are deposited in the vasculature leading to amyloid angiopathy, including $A\beta$ protein, cystatin C, transthyretin, and gelsolin.

$A\beta$ protein is a hydrophobic, nonglycosylated peptide of 39–43 amino acids. $A\beta$ protein is derived from the amyloid precursor protein (APP) encoded by the gene *APP* located on chromosome 21q22.1. *APP* is one of the genes for familial Alzheimer disease, AD1. In sporadic CAA, CAA with sporadic Alzheimer disease, familial Alzheimer disease, Down syndrome, and the Dutch type of CAA, the vascular amyloid is composed of $A\beta$ protein subunits. Subtle differences exist between the vascular amyloid in CAA and amyloid parenchymal deposits, such as in amyloid plaques in Alzheimer disease. Vascular amyloid is composed mainly of the 39-amino-acid $A\beta$ species, plaque amyloid predominantly of a 42-amino-acid $A\beta$ species. Different point mutations in *APP*, causing an amino acid substitution in the $A\beta$ protein, have been found in the Dutch type of hereditary cerebral hemorrhage with amyloidosis (HCHWA-D) and in Italian families with similar clinicopathological findings to those in HCHWA-D.

Additionally, the $\epsilon 4$ allele (apoE $\epsilon 4$) of apolipoprotein E (apoE) is a risk factor for CAA and Alzheimer disease and the $\epsilon 2$ allele has been linked to greater risk of CAA and cerebral hemorrhage. The mechanism underlying this increased risk is not completely clear, but there is increasing evidence that the ability of apoE to interact with $A\beta$ and influence its conformation and clearance plays a major role. ApoE appears critically involved in the conversion of $A\beta$ into forms which have a high β -sheet content with associated cellular toxicity.

In the Icelandic form of CAA, HCHWA-I, the vascular amyloid is composed of a mutated form of cystatin C, a cysteine proteinase inhibitor, playing a role in intracellular catabolism of peptides and proteins. Cystatin C is encoded by the gene *CST3*, located on chromosome 20p11.2.

In the familial oculo-leptomeningeal amyloidoses the vascular amyloid is transthyretin, a prealbumin that is also present in hereditary peripheral amyloidoses. Transthyretin is an amino acid residue carrier protein for thyroid hormone and retinol binding protein in plasma and CSF. The gene encoding transthyretin is *TTR*, located on chromosome 18q12.1. In CAA related to transthyretin most of the families (Japan, Portugal) have an association with the same point mutation in *TTR*, but other mutations have also been reported.

In the British form of CAA a novel 4-kDa protein fragment called amyloid-bri (ABri) was identified in isolated amyloid fibrils. ABri is a fragment of a precursor protein (BriPP), a putative type II single-spanning transmembrane precursor that is encoded by the gene *BRI*, located on chromosome 13. A mutation in the stop codon of this gene generates a longer open reading frame, resulting in a larger, 277-amino-acid protein, whereas the wild-type protein is 266 amino acids. Cleavage of 34 amino acids at the C-terminal end of the extended protein generates the amyloidogenic fragment, ABri.

The Finnish, gelsolin-related type of CAA is noted worldwide in relatives carrying the same mutation in the gelsolin gene on chromosome 9.

Amyloidosis is a phenomenon in which native globular proteins form long fibrils with a characteristic three-dimensional structure. Although emerging from different proteins, amyloid fibrils show a common X-ray diffraction pattern, indicative of a cross- β structure, where the β -sheets run parallel to the fibril axis and the β -strands forming the sheets are perpendicular to this axis. Well studied amyloidogenic proteins include the $A\beta$ protein. The tendency to self-aggregate into insoluble fibrils is stronger in $A\beta$ 42 fragments of APP than in $A\beta$ 39 or $A\beta$ 40 fragments. Factors promoting *in vivo* $A\beta$ -amyloid formation are:

- Overproduction, increased levels of APP (in gene overdose and trisomy 21)
- A highly amyloidogenic sequence (as in the codon 693 mutation of the Dutch variant of CAA)
- Altered proteolysis of APP (as in familial Alzheimer disease due to codon 692 mutation)
- A seeding nucleation event, analogous to seeding in crystal formation
- Time/patient age

Many theories describe the detailed process of amyloid deposition in the parenchyma or the vessel wall. In Alzheimer disease the amyloid cascade is a good example. It describes the stepwise progression in the deposition of amyloid in Alzheimer disease, starting with either the genetic influence of the *APP* or *presenilin 1* and *2* genes, or the failure of clearance of $A\beta$ because of the *apoE ϵ 4* allele, increasing the $A\beta$ 42 levels, followed by oligomerization of $A\beta$ 42 in limbic and association cortices, with gradual deposition of $A\beta$ 42 oligomers, activation of microglia, complement, astrocytes, altering neuronal ionic homeostasis, leading to oxidative injury, production of changes in tau proteins, and formation of tangles and plaques, leading to neuronal dysfunction, dementia, and death. Other theories try to explain why vascular amyloidosis in the absence of other risk factors leads to hemorrhage, an important feature in CAA. One of these theories suggests a cascade starting with amyloid deposition in the media and adventitia of cortical arteries, lead-

ing to loss of smooth muscle cells of the media, followed by vascular dilatation, spindle-shaped microaneurysms, intimal thickening with thinning and disruption of media and adventitia, changes in vascular permeability, invasion of plasma components into the vascular wall (fibrinoid necrosis), possible additional factors (e.g., hypertension, $A\beta$ -induced production of superoxide free radicals from endothelial cells), activation of fibrinolytic systems by $A\beta$, infiltration of inflammatory cells with production of cytokines, and the *ApoE ϵ 2* allele), ending in hemorrhage.

The frequency of sporadic congophilic angiopathy in the normal aging subject is variable. In patients over the age of 60 years presenting with lobar hemorrhage, the incidence is high. In stroke patients, too, with the proper techniques, MRI detects microhemorrhages in more than 20% of patients. In individuals without hemorrhage or other clinical symptoms, the percentages in population studies differ. There is little evidence of the disorder under the age of 60. In the population over 60 years of age there is evidence of congophilic angiopathy in about 30% of individuals. In normal aging the changes are usually mild and limited to the cerebral cortex, most often in the parieto-occipital region. The presence of microhemorrhages in a high percentage of normal aging people can induce false positives when brain biopsies are considered to obtain a histological diagnosis.

72.4 Therapy

There is no effective treatment for the underlying disease process of CAA. Once a patient is diagnosed with CAA, measures can be taken to prevent brain hemorrhage as much as possible. High blood pressure should be treated. Blood thinners such as Coumadin (warfarin), antiplatelet agents such as aspirin, or medications designed to dissolve blood clots may cause hemorrhage in patients with CAA, and should be avoided if possible. If these medications are required for other conditions, such as heart disease, the potential benefits must be carefully weighed against the increased risks. Seizures should be treated with antiepileptic drugs, although some drugs should be avoided because of their antiplatelet effect. Once a hemorrhage has occurred, supportive and symptomatic medical care is important. Sometimes neurosurgical intervention is necessary to reduce the pressure within the brain.

72.5 Magnetic Resonance Imaging

In patients presenting with an intracerebral hemorrhage, both CT and MRI will show the hemorrhage(s), together with its secondary effects, such as

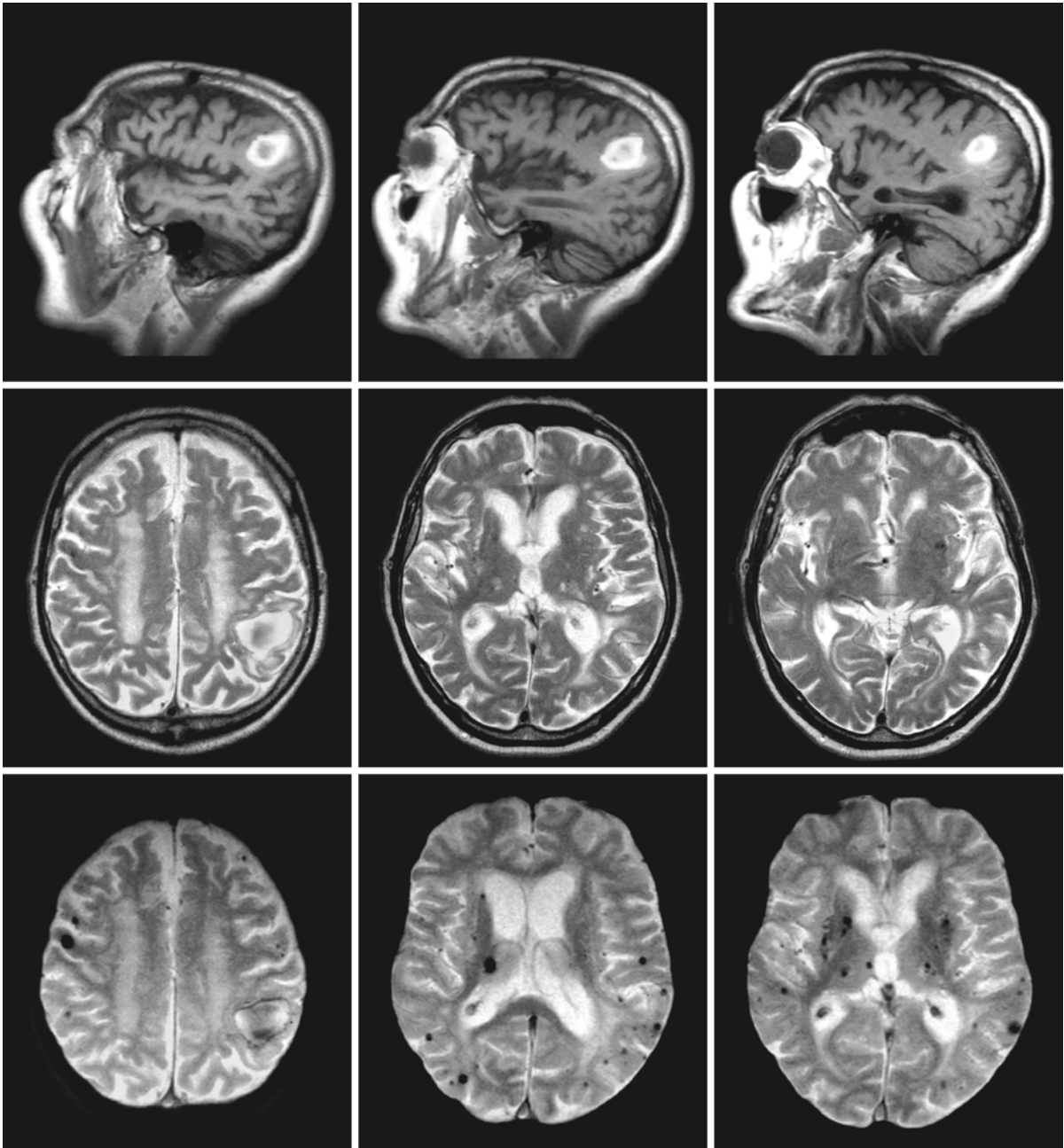


Fig. 72.1. A 54-year-old female with a familial history of amyloid angiopathy. The *first* row demonstrates T_1 -weighted parasagittal images of the left hemisphere with a parietal lobar hemorrhage. The *second* and *third* rows represent T_2^* - (GE)-weighted images revealing smaller and larger spots

of very low signal intensity, dispersed throughout the brain. The low signal intensity is caused by hemosiderin residues of microhemorrhages. The combination of lobar hemorrhage with multiple spot-like microhemorrhages is characteristic of CAA

Fig. 72.2. Transverse FLAIR images of a 72-year-old man with slowly progressive cognitive deterioration (*first* and *second* rows). The images show slightly asymmetrical confluent areas of hyperintensity in the deep and periventricular white matter, in some places extending into the U fibers. The underlying

cause of the white matter changes is not evident from these images. The images made with a T_2^* -weighted sequence (*third* and *fourth* rows) reveal multiple spots with very low signal intensity, representing microhemorrhages. These images suggest that the patient is suffering from a sporadic form of CAA

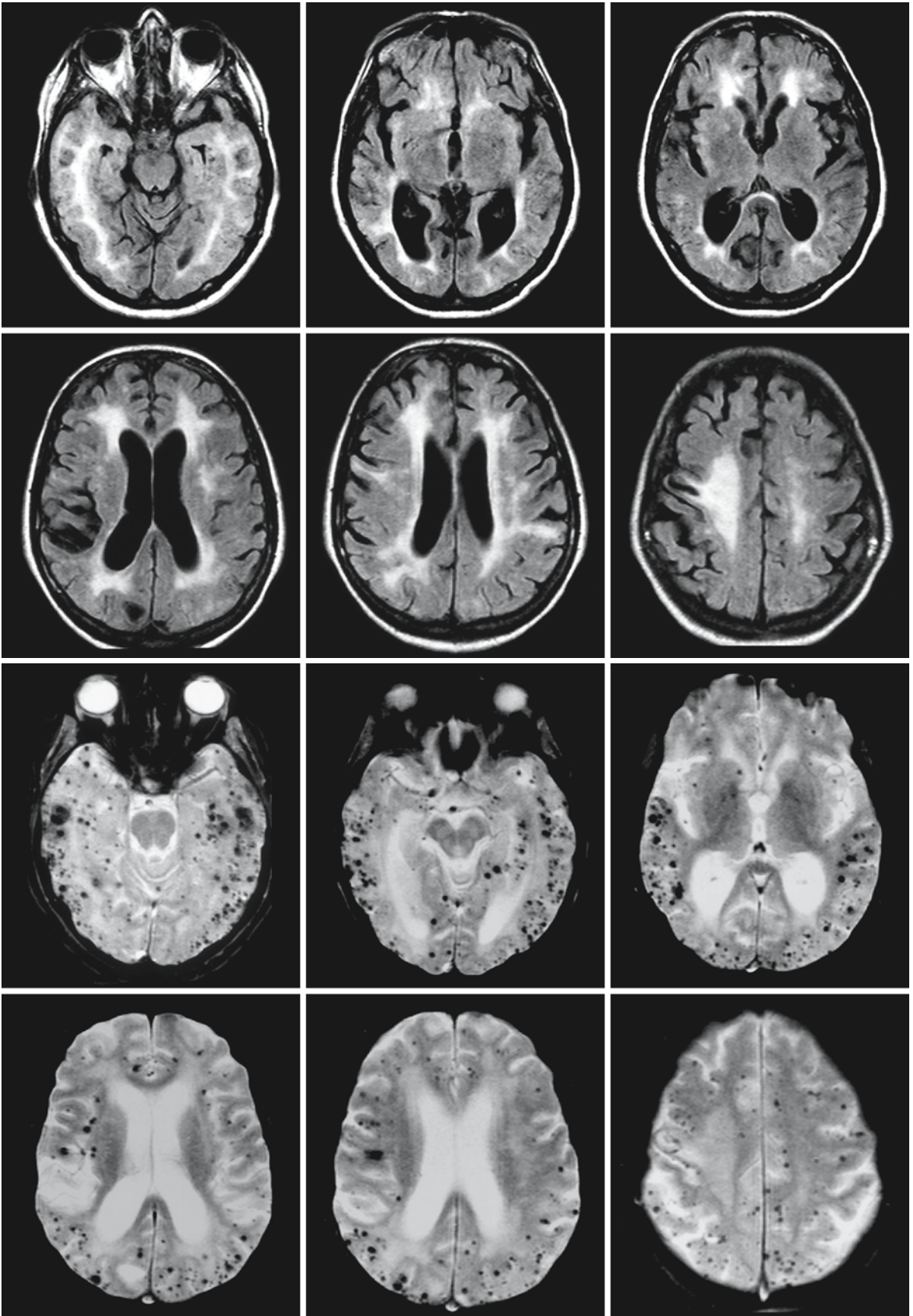


Fig. 72.2.

mass effect worsened by edema, imminent tentorial herniation, hydrocephalus, and breakthrough of blood into the ventricles and subarachnoid space. The location of the hemorrhage(s) is important: CAA hemorrhages are mainly lobar and predominantly in the parieto-occipital region (Fig. 72.1), in contrast to hypertension-related and aneurysm-related hemorrhages. In CAA hemorrhages in the brain stem and posterior fossa are rare. Especially cases with multiple hemorrhages are suspect for CAA, more so in the absence of vascular risk factors. In addition to hemorrhages MRI will show infarctions, when present, in more detail than CT. Lacunar infarctions will be seen best on FLAIR images, where they appear as black dots with a bright rim. In nearly all cases MRI will show extensive white matter abnormalities in the periventricular and deep white matter, but sparing the U fibers, with confluent and isolated lesions which are not necessarily symmetrical in distribution. There are often lesions in the basal ganglia; some-

times there is involvement of the midbrain and pons, and occasionally there is a lesion in the cerebellum.

The usual work-up for hemorrhages in the brain should be performed, including MR angiography, preferably phase contrast angiography when blood is present, and contrast administration to exclude metastases or arteriovenous malformations. The most important and mandatory MR sequence in cases of CAA is a gradient echo pulse sequence, because of its sensitivity to changes in magnetic susceptibility (Figs. 72.1 and 72.2). These T_2^* -weighted images may show multiple residues of petechial hemorrhages all through the brain (Figs. 72.1 and 72.2). This feature may be seen, however, in numerous disorders involving small vessels, such as hypertensive encephalopathy, vasculitides, atherosclerosis, CADASIL, or Rendu-Osler disease, and may be mimicked by multiple melanoma metastases. They are also present in a considerable percentage of normal aging individuals.

Cerebral Autosomal Dominant Arteriopathy with Subcortical Infarcts and Leukoencephalopathy

73.1 Clinical Features and Laboratory Findings

The acronym CADASIL stands for *cerebral autosomal dominant arteriopathy with subcortical infarcts and leukoencephalopathy*. This disease was formerly known as familial Binswanger disease or hereditary multi-infarct dementia. Although it was initially thought to be a rare disease, many families with CADASIL have now been reported worldwide. CADASIL is the most common hereditary form of stroke leading to progressive dementia.

The clinical picture is dominated by recurrent subcortical ischemic infarctions, beginning somewhere between 40 and 60 years, or occasionally at a younger age. There is usually a striking absence of vascular risk factors: there is no history of hypertension, no hypercholesterolemia, and no hyperhomocysteinemia. Migrainous headaches and psychiatric symptoms are frequent. They are often the initial symptoms and may precede other symptoms of the disease for many years. The neurological symptoms progress over months to years, most often in a step-like fashion, and may worsen in the second decade after onset. Hemiparesis, hemianopia, dysarthria, and cerebellar ataxia may characterize these events. Other symptoms include seizures, pseudobulbar palsy, urinary incontinence, and unexplained “CADASIL coma.” This latter event is a subacute encephalopathy, in some cases accompanied by fever, with focal neurological symptoms and seizures, eventually progressing to coma. The condition is reversible in most cases but may recur. In the history of nearly all the reported patients migraines with visual or sensory auras are present. In other patients the diagnosis “relapsing–remitting multiple sclerosis” was maintained for years. Psychiatric symptoms, including confusion, severe forms of depression, and signs of frontal dysfunction, are manifest in more than 30% of the patients. A subcortical dementia, similar to that seen in subcortical arteriosclerotic encephalopathy, evolves. There is considerable variability in clinical symptoms and course of disease among the patients, also within families. The median survival is 64 years for males and 69 years for females.

A definite diagnosis of CADASIL can be made on the basis of histopathological findings in skin, muscle, or brain biopsy or when the typical clinical findings can be linked to a mutation in the gene *NOTCH3*.

Table 73.1. Diagnostic criteria for probable CADASIL (Davous 1998)

1. Young age at onset (<50 years)
2. At least two of the following clinical findings:
 - Stroke-like episodes with permanent neurological signs
 - Migrainous headaches
 - Major mood disturbances
 - Subcortical dementia
3. No vascular risk factors related to deficit
4. Evidence of inheritance with autosomal dominant transmission
5. On MRI, white matter abnormalities without cortical infarcts

Diagnosis based on the electron microscopic demonstration of granular osmiophilic material (GOM) adjacent to the basement membrane of smooth muscle cells of arterioles has a specificity of 100%, but the sensitivity is rather low (~50%). Immunostaining with antibodies against the Notch3 protein may increase the sensitivity of skin biopsy techniques substantially; in patients with CADASIL, there is an abnormal accumulation of the Notch3 protein in the vessel walls. Diagnosis by mutation detection is also possible. In the absence of such evidence criteria for probable CADASIL have been proposed, which are summarized in Table 73.1.

Discovery of de novo mutations in isolated patients emphasizes that a possible diagnosis of CADASIL should not be rejected in the absence of a family history. Neuroimaging plays an important role in the initial diagnosis. The pattern of white matter abnormalities is highly suggestive (see below) and the MRI-based diagnosis of CADASIL can be substantiated with many more details than suggested under point 5 of the above criteria. Especially involvement of the anterior temporal pole has a high sensitivity and specificity (both 85–90%). CSF analysis shows oligoclonal bands in quite a number of cases, although these are considered to be nonspecific.

73.2 Pathology

The primary disease process is a vasculopathy, most prominently involving the small perforating arteries of the cerebral white matter. Within the media of the

small arterial vessels, deposits of GOM are seen on electron microscopy, which displace degenerating smooth muscle cells of the arterial media in small vessels, a feature now considered the pathological hallmark of CADASIL. GOM has an extracellular location and is not membrane-bound. The chemical nature of GOM is unknown. The material usually stains with PAS, consistent with acid polysaccharide. Other histochemical stains have shown that the material does not contain amyloid, elastin, chromatin, calcium, or iron. Immunoenzymatic and immunofluorescence studies have also shown absence of immunoglobulins or complement proteins, cystatin C, transthyretin, gelsolin, fibrinogen, cathepsin D and α_1 -antichymotrypsin. Although the disease manifests itself only through neurological and neuropsychiatric symptoms, it is a generalized disorder and the ultrastructural lesions of the arterial wall are also found in other organs, including the spinal cord, spleen, heart, muscle, skin, and peripheral nerves. Biopsy of these tissues can confirm the diagnosis. Skin biopsy is most often used for that purpose.

The concentric thickening of the wall leads to ischemia, infarctions, and myelin loss, which are shown by microscopic examination of the brain. Multiple small infarcts and lacunae are seen in the basal ganglia, thalamus, internal capsule, periventricular white matter, and brain stem. The cerebellum is less often affected. The periventricular white matter may be severely demyelinated. The U fibers and the cortex are usually spared. Cortical infarcts are rare and of small size. Fresh and old hemorrhages may also be found, most often in advanced stages of the disease.

73.3 Pathogenetic Considerations

CADASIL is related to dominant mutations in *NOTCH3* on chromosome 19q13.1. The gene codes for a large transmembrane receptor protein. The extracellular portion of the Notch3 protein contains 34 tandem repeats of an epidermal growth factor (EGF) motif, each of which contains six cysteine residues binding within the domains as three cysteine-cysteine disulfide bonds. Mutations that have been demonstrated in CADASIL occur within these EGF repeats and always involve either loss or gain of a cysteine residue. The mutations result in altered disulfide binding within the repeats by changing the number of cysteines from six to an odd number. There is evidence that mutations may lead to a gain of function. Other evidence demonstrates that some CADASIL mutations reduce the activity of the Notch3 receptor. There is considerable phenotypic variability, which is thus far unexplained.

In normal tissue, gene expression for *NOTCH3* is highly restricted to vascular smooth muscle cells. In

CADASIL, a dramatic and selective accumulation of the extracellular domain of the receptor protein occurs at the cytoplasmic membrane of vascular smooth muscle cells, in close vicinity to but not within GOM. This suggests that CADASIL mutations specifically impair the clearance of the notch3 ectodomain, but not the cytosolic domain, from the cell surface.

It is evident that the clinical manifestations, diverse as they may be, are the result of the vascular changes leading to hypoperfusion, demyelination, gliosis, and lacunar infarctions. How the genetic changes translate into the vascular changes and the phenotypic variability is still incompletely understood.

73.4 Therapy

As in other disorders with cerebrovascular disease, strategies are directed at improving cerebral perfusion. Anticoagulants and thrombolytic agents, such as warfarin and heparin, are not advocated because of the risk of hemorrhage. Aspirin, despite its low efficacy in some patients, is considered the best choice with the smallest chance of complications. Neuroprotective agents, antioxidants, *N*-methyl-D-aspartate (NMDA) antagonists, and voltage-sensitive calcium channel antagonists, for example nimodipine and flunarizine, also have been suggested. Other compounds, like propentofylline, a xanthine derivative with multiple actions, have been tested positively in Alzheimer disease, and might also be beneficial in vascular dementias.

73.5 Magnetic Resonance Imaging

Although there are many similarities between CADASIL, subcortical arteriosclerotic encephalopathy, and cerebral amyloid angiopathy, the MR pattern of fully developed CADASIL has several features that can make the MR diagnosis highly suggestive and, in combination with the clinical features and family history, even diagnostic.

MRI shows extensive white matter abnormalities in the absence of cortical infarcts (Figs. 73.1–73.3). There is a tendency to symmetry. The centrum semiovale is involved, with relative sparing of the U fibers. The abnormalities extend downwards into the external and extreme capsules. In the frontal lobes the white matter abnormalities extend into the U fibers. The white matter of the temporal lobes is involved in typical cases (Figs. 73.1–73.5). Moderate to severe involvement of the temporal lobes has a sensitivity of 89% and a specificity of 83%. Involvement of the extreme and external capsule has a sensitivity of 93%,

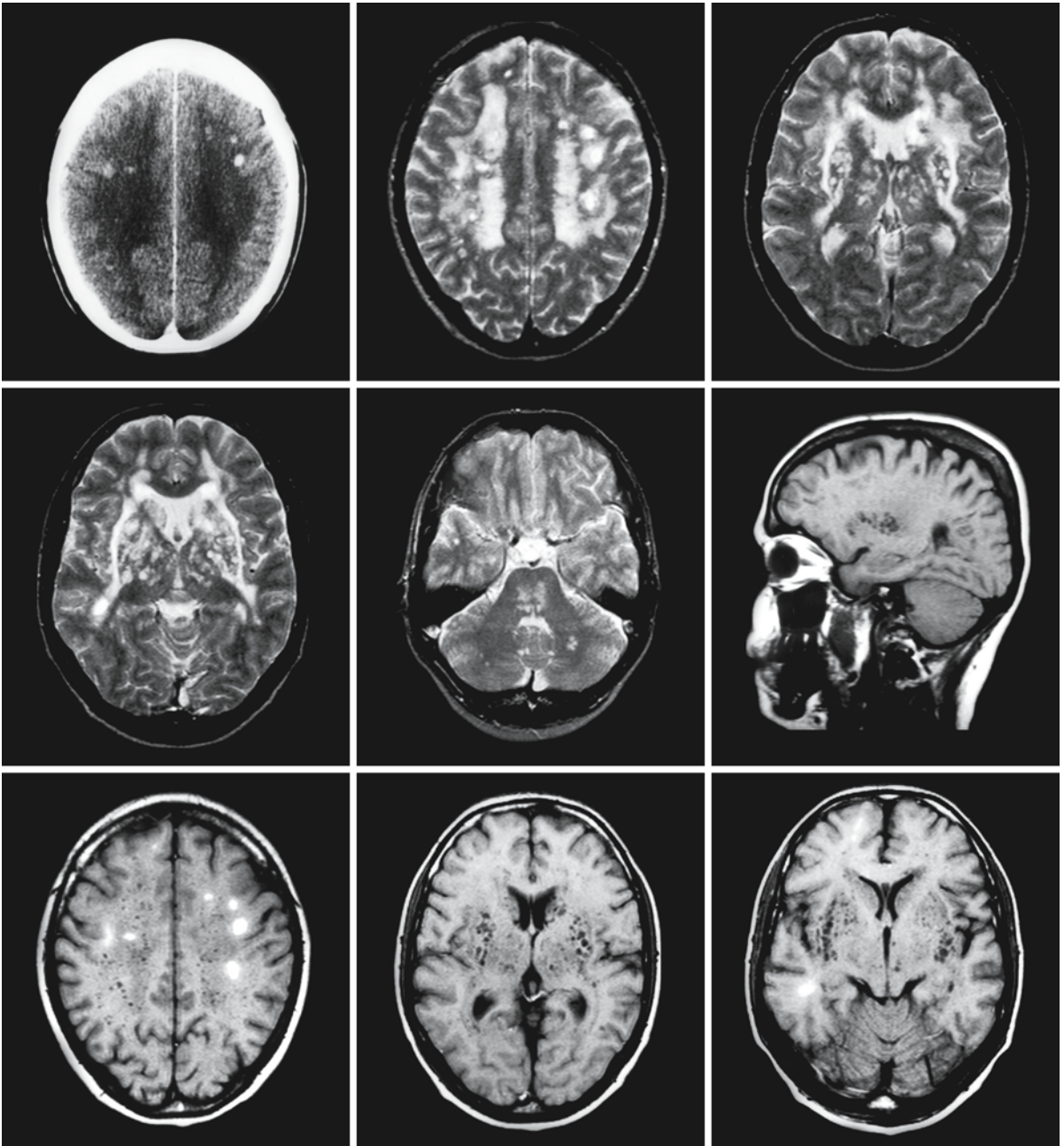


Fig. 73.1. Images of a 45-year-old woman with CADASIL, showing most of the typical MR features. The T_2 -weighted images (*first row, middle and right; second row, left and middle*) show nearly symmetrical involvement of the white matter in the centrum semiovale, with extensions into the arcuate fibers, the external capsules, and the temporal lobes. The corpus callosum is relatively spared. The involvement of the basal gan-

glia, thalamus, pons, and cerebellum is also more or less symmetrical. The CT scan (*first row, left*) and the T_1 -weighted images (*third row*) show multiple small hemorrhages in the centrum semiovale and the posterior temporal lobe on the right. The T_1 -weighted images, including the sagittal image (*second row, right*), show the widened perivascular spaces in the centrum semiovale and the basal ganglia.

but a low specificity of 45%. To differentiate between small lacunar infarctions and other white matter abnormalities, such as demyelination and gliosis, FLAIR images are very useful (Figs. 73.2–73.5). They show

the white matter changes with high signal intensity, whereas cystic infarctions have very low signal intensity. Diffusion-weighted imaging may demonstrate the relatively fresh infarctions.

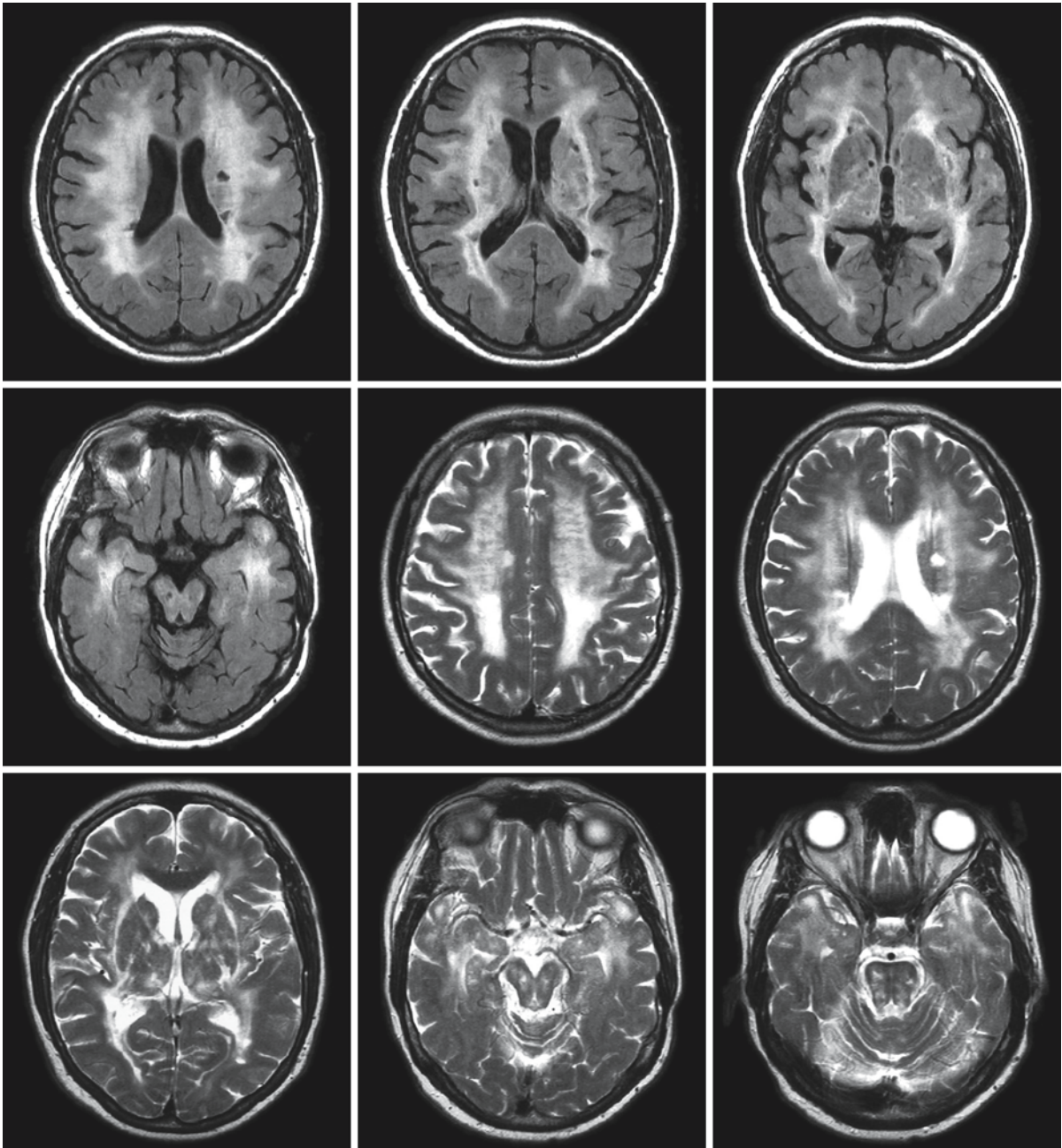


Fig. 73.2. The MR pattern in a 61-year-old woman with CADASIL is similar to the pattern seen in Fig. 73.1, although the white matter abnormalities are more confluent. There is cere-

bellar atrophy. Courtesy of Dr. K. Demuth, Department of Neurology, Marien Hospital, Stuttgart, Germany

Good quality images show that, apart from the signal changes in the white matter, the Virchow–Robin spaces are widened (Fig. 73.1). This leads to an *état criblé* of the basal ganglia. The widening of the perivascular spaces may also involve the centrum semiovale and the temporal lobes.

In longer-standing cases of CADASIL signal changes may occur in the basal ganglia. Apart from

the often multiple small or lacunar infarctions in the basal ganglia, one may see a more generalized low signal intensity on T₂-weighted images, in particular in the globus pallidus (Figs. 73.3 and 73.4). CT does not show calcification in the basal ganglia, so that the explanation must be deposition of other substances, for example iron.

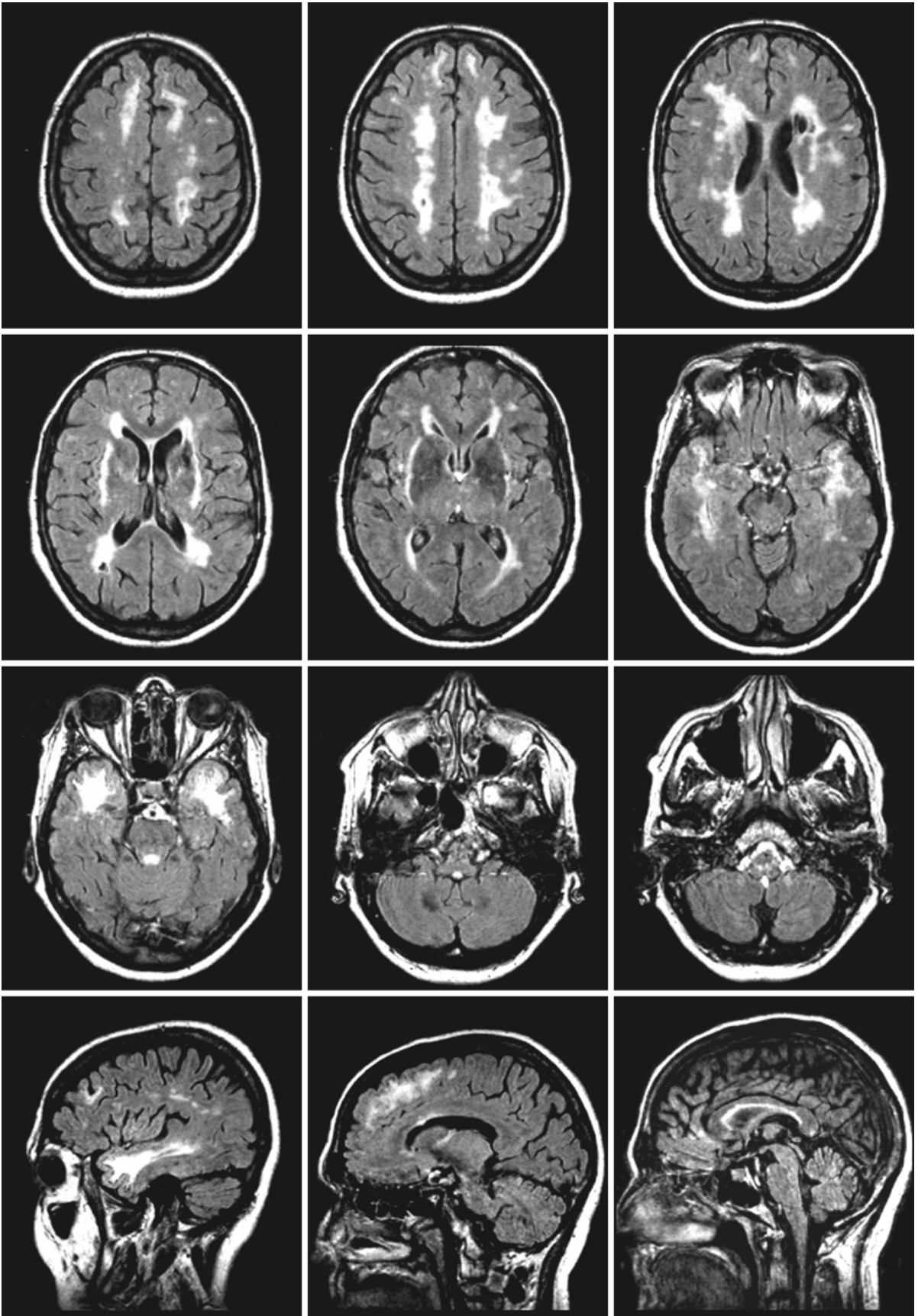


Fig. 73.3.

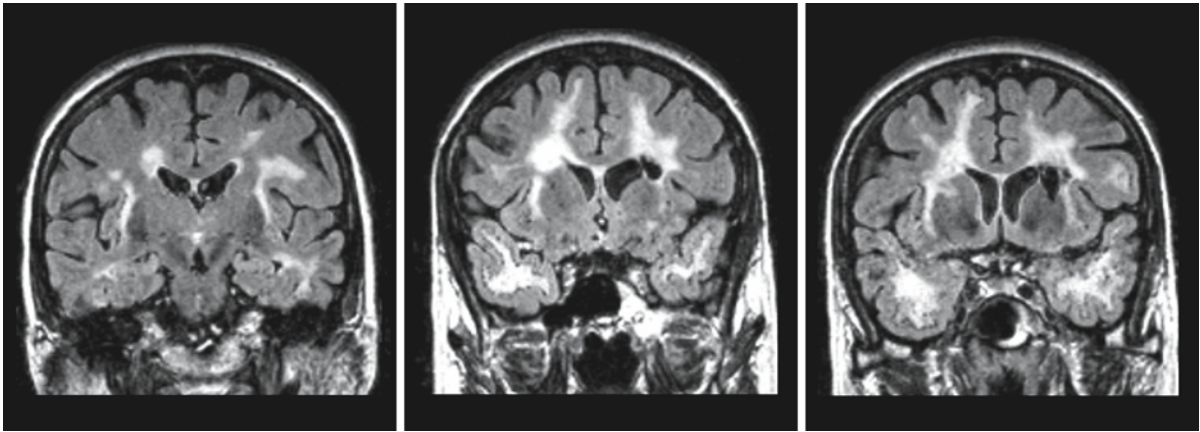


Fig. 73.3. (*continued*). Series of FLAIR images in a 59-year-old woman, a representative of a known CADASIL family. In this series many MR characteristics of CADASIL are present: more or less symmetrical involvement of the centrum semiovale, external capsules, temporal lobes, and basal ganglia; multiple lacunar infarctions; some involvement of the cerebellum. Even on the FLAIR images the basal ganglia have a relatively low

signal intensity. The sagittal (*fourth row*) and coronal (*fifth row*) FLAIR images further illustrate and complete this pattern. The frontal cortico-subcortical involvement is depicted, as are the multiple lacunar infarctions and the extension of the lesions into the external capsules and the temporal lobes. There is also involvement of the corpus callosum and the fornix (mid-sagittal image, *fourth row, right*)

Abnormalities in the mesencephalon, pons, and cerebellum are often less symmetrical than lesions in the cerebral hemispheres. One may find an occasional infarction in the mesencephalon, pons, and cerebellum, and a high signal in the transverse fibers of the pons (Figs. 73.1, 73.2, and 73.4).

MR angiography usually does not show the changes in the small vessels that cause the problems in CADASIL. At the same time intra-arterial DSA seems contraindicated because of the unexplained extremely high complication rate of up to 50% in intra-arterial DSA in CADASIL patients.

After contrast injection there is no enhancement seen in any of the lesions, unlike, for example, Binswanger disease, where new infarcts will display enhancement in the subacute phase, or multiple sclerosis, where acute plaques show enhancement.

Gradient refocused T_2^* -weighted images show in many cases spots of low signal intensity, representing microhemorrhages. This feature is also seen in other small vessel diseases. Small hemorrhages may also be seen on CT and T_1 -weighted images (Fig. 73.1).

MR diffusion-weighted imaging is capable of quantitative estimation of the structural damage of the brain, which in its turn may relate to the clinical severity of the disorder. Changes in diffusion-weighted imaging consist of an up to 60% increase in diffusivity in lesions with high signal intensity on FLAIR or T_2 -weighted images, with loss of diffusion anisotropy in those areas. In normal-appearing white matter, however, changes in diffusivity were also found. These findings do not explain one of the most intriguing MRI aspects of CADASIL, namely that many

of the above-mentioned findings may already be present in clinically unaffected members of patients' families.

In the early stages of the disease, the pattern of MRI abnormalities is less characteristic and more difficult to differentiate from other vascular disorders (Fig. 73.5). Abnormalities of the anterior temporal white matter and the external capsule are early findings and, in the presence of multiple small infarctions, suggestive of CADASIL.

The differential diagnosis of CADASIL includes other familial disorders presenting with multiple recurrent incidents and white matter lesions. Other familial disorders, in which recurrent incidents or step-like progression is a prominent symptom, include multiple sclerosis, the dyslipoproteinemias (e.g., familial hypercholesterolemia), disorders of connective tissue (Ehlers–Danlos syndrome, Marfan syndrome), hyperhomocysteinemia, amyloid angiopathy, and mitochondrial encephalopathies. Recurrent strokes in young adults may also be due to cerebral vasculitis, systemic lupus erythematosus, drug abuse (especially cocaine), cardiac diseases, sickle cell disease, etc. Most of these diseases can be ruled out by the mode of inheritance, the clinical appearance and course, biological tests, and laboratory findings. MRI of these diseases and disorders shows a pattern of irregular cortical and subcortical infarctions, lacking the tendency towards symmetry seen in CADASIL. In the disorders mentioned, the infarcts may involve both cortex and white matter, whereas CADASIL involves white matter and basal ganglia, without cortical infarctions. Temporal lobe involve-

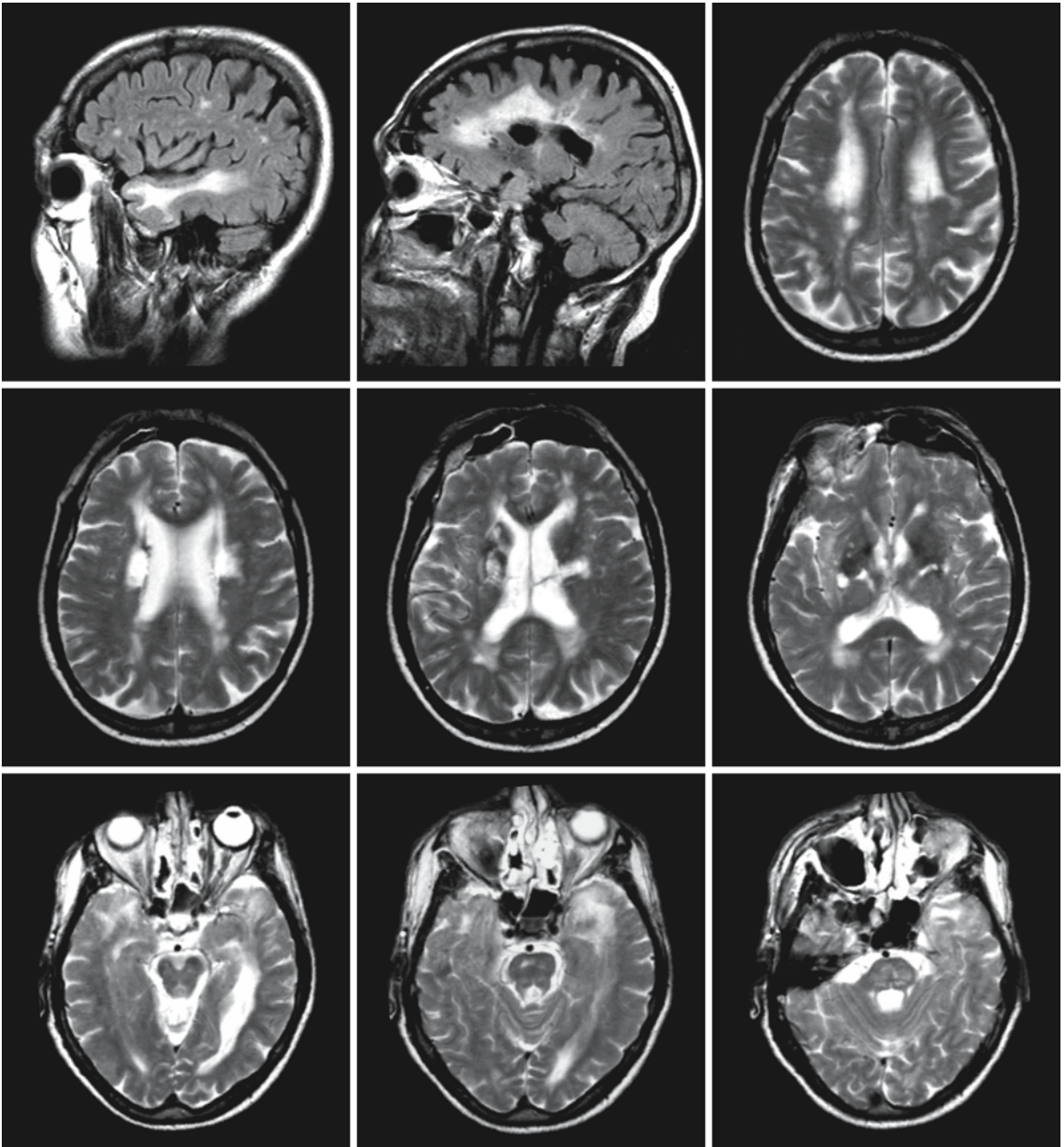


Fig. 73.4. In this 48-year-old man, a representative of another large family with CADASIL, the MR pattern is difficult to distinguish from that of other vascular disorders. The involvement of the centrum semiovale is patchy and less symmetrical than in more advanced CADASIL. There is incipient involvement of the

external capsules and evident involvement of the temporal lobes. There are many lacunar infarctions, which, together with the dark appearance of the globus pallidus, often seen in patients with CADASIL, indicate the correct diagnosis

ment also argues strongly for CADASIL. The differential diagnosis of white matter disorders with cognitive impairment and possible severe temporal lobe involvement is from myotonic dystrophy. Familial

hemiplegic migraine can be confused with the beginning of CADASIL, but does not show white matter abnormalities comparable to those of CADASIL.

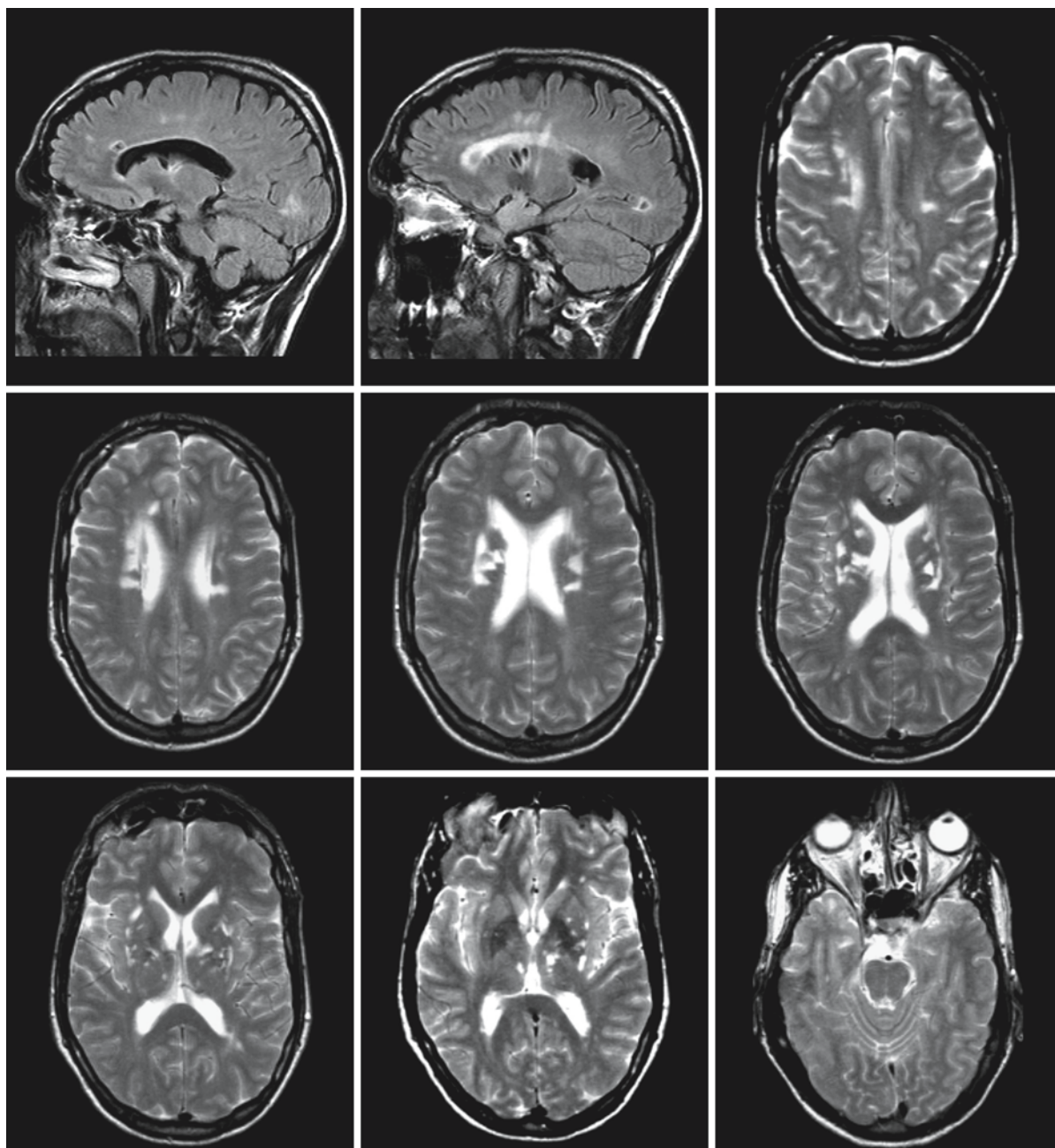


Fig. 73.5. A 31-year-old male member of the same family as the patient in Fig. 73.4. Without knowing the diagnosis in the family, it would be difficult to diagnose this patient with

CADASIL. The images show multiple lacunar infarctions. In addition, there is incipient involvement of the external capsules and the white matter of the anterior temporal lobes

Cerebral Autosomal Recessive Arteriopathy with Subcortical Infarcts and Leukoencephalopathy

74.1 Clinical and Laboratory Findings

This disease was first described in 1976 by Maeda et al. as a “familial unusual encephalopathy of Binswanger’s type without hypertension” in four patients, two of whom were brothers. In nearly all cases reported after this first publication, the parents were consanguineous, often first cousins, providing evidence for an autosomal recessive mode of inheritance. Over the years the syndrome has crystallized sufficiently to allow definition of the clinical picture. The disease occurs predominantly in males, with a male:female ratio of 7.5:1. So far, all patients described are Japanese. The disease has a relatively early age of onset, most often between 25 and 30 years. The course of the disease is relatively rapid and is characterized by step-like or chronic-progressive pyramidal and extrapyramidal symptoms, pseudobulbar palsy, and cognitive deterioration. The neurological symptoms are associated with alopecia from youth. There is diffuse hair-thinning with similarities to what is seen in radiation injury and systemic lupus erythematosus. Patients experience acute lumbago. The lumbago is caused by kyphotic and spondylotic changes of the vertebrae, often in an unusual location, the lower thoracic and higher lumbar region. Patients lack vascular risk factors, especially hypertension. Diffuse white matter disease is seen on MRI or at autopsy. The disease is often compared to Binswanger disease, but the MR images more closely mimic the MRI characteristics of CADASIL (see below). Life expectancy in these relatively young patients is shortened considerably. Most patients die within 10 years after onset of the disease in a vegetative state.

Laboratory examinations are unrevealing. There are no biochemical changes in blood or urine samples.

74.2 Pathology

The cortex is intact. There is diffuse demyelination of the cerebral white matter, with relatively well preserved U fibers. Within the affected white matter and within the basal ganglia, there are small softened and cystic foci. The corpus callosum is affected in about half of the patients. In the abnormal white matter arteriosclerosis is seen involving arteries of 100- to 400- μ m caliber, with fibrous intimal proliferation, severe hyalinosis, and splitting of the intima and the

elastic membrane. The thickened vessel walls do not stain with PAS stain or Congo red, there is no ultrastructural granular osmiophilic material in the vessel walls, and there is no β -amyloid immunoreactivity in vascular walls. The presence of PAS-positive material and the ultrastructural finding of granular osmiophilic material in the vessel walls are considered to be the hallmarks of CADASIL, making CARASIL distinct from CADASIL. There is also no increase of amyloid plaques or neurofibrillary tangles. Large arteries at the base of the brain display no or mild atheromatous changes; severe changes are rare. In visceral organs arterial changes are less severe. A muscle biopsy, however, may show the described vessel changes. The superficial temporal arteries are often involved, possibly explaining the alopecia.

74.3 Pathogenetic Considerations

In CARASIL the brain damage is caused by narrowing of the lumina of arterioles, especially of long perforating arteries supplying the periventricular and deep white matter. There is an obvious similarity to other diseases in which systemic narrowing of penetrating small medullary vessels is at the core of the pathophysiology. The resulting decrease in cerebral perfusion leads to white matter pallor, demyelination, gliosis, preinfarct status, and lacunar infarctions. The disease is hereditary, but not linked to the *NOTCH 3* gene, which is responsible for CADASIL. The genetic basis of CARASIL has not yet been elucidated.

74.4 Therapy

So far no therapy has been applied aimed at improvement of cerebral blood flow and counteracting ischemia, as described in the chapter on CADASIL. Treatment is mainly symptomatic. Disc herniation and lumbar stenosis may demand surgical intervention.

74.5 Magnetic Resonance Imaging

MRI shows a pattern of white matter involvement similar to that of CADASIL. The white matter lesions are confluent and more or less symmetrical (Figs. 74.1

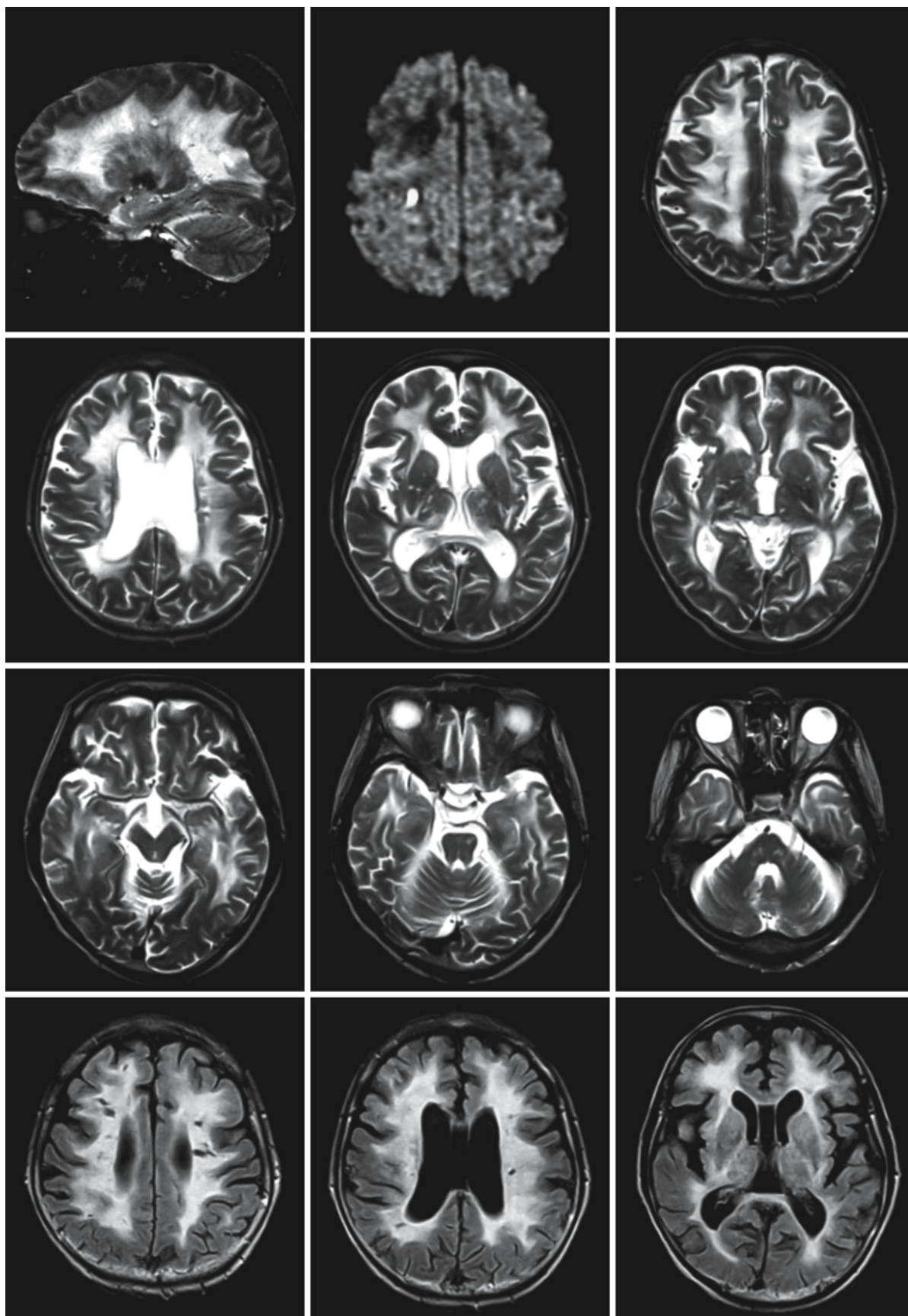


Fig. 74.1.

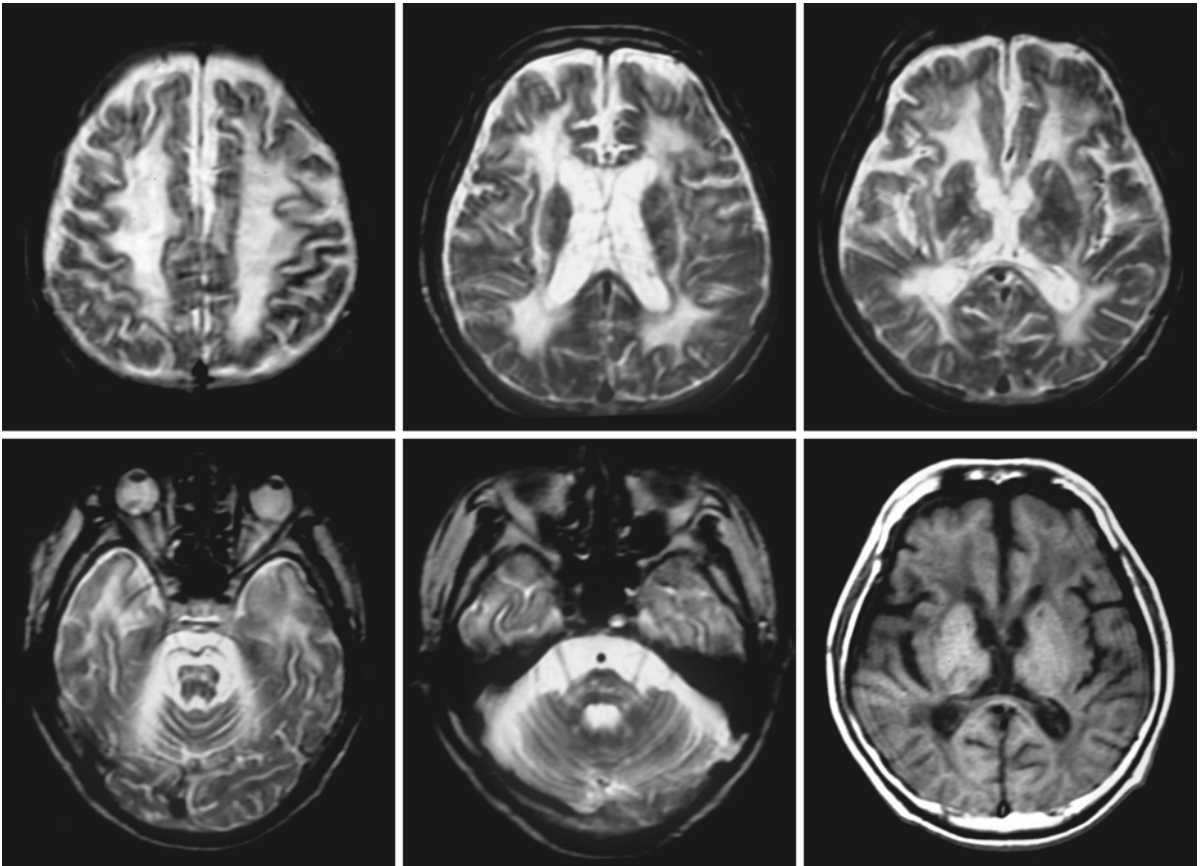


Fig. 74.2. A 42-year-old male patient with CARASIL. The MRI was obtained 16 years after the onset of the disease. Note the extensive cerebral white matter abnormalities, which do not spare the U fibers. The internal and external capsules are affected as well. The cerebral white matter is atrophic; the corpus

callosum is thin but seems to have a normal signal. There are many small lesions in the basal ganglia and brain stem. The T₁-weighted images do not show evidence of small hemorrhages. From Fukutake and Hirayama (1995), with permission

and 74.2). They involve the cerebral hemispheric white matter and both internal and external capsules. The temporal lobes are affected as well, including the temporal poles. The U fibers are relatively spared, but

certainly not completely spared (Fig. 74.1), and become extensively affected in later stages (Fig. 74.2). The corpus callosum tends to be spared. There are small focal lesions in the basal ganglia, thalami, and brain stem (Figs. 74.1 and 74.2). FLAIR images show small lacunae (Fig. 74.1), whereas diffusion-weighted images may reveal small fresh infarctions (Fig. 74.1). Over time, the white matter becomes increasingly atrophic (Fig. 74.2).

The pattern of confluent periventricular and deep white matter involvement in combination with multifocal small lesions of the basal ganglia, thalami, and brain stem is typically the pattern seen in vascular disorders. However, the white matter abnormalities are more homogeneously confluent than in Binswanger disease. Unlike in CADASIL, there are no petechial hemorrhages.

← **Fig. 74.1.** A 39-year-old woman with CARASIL. The MRI was obtained 17 months after the onset of neurological symptoms. There are symmetrical abnormalities in the cerebral hemispheric white matter and both internal and external capsules. The U fibers are partially spared. The corpus callosum is intact. There are small additional lesions in the basal ganglia and brain stem. The diffusion-weighted image (*first row, middle image*) shows a small fresh infarction. The FLAIR images (*fourth row*) reveal many small lacunae. From Yanagawa et al. (2002), with permission; additional images courtesy of Dr. S. Yanagawa, Department of Neurology, and Dr. S. Ikeda, Third Department of Medicine, Shinsu University School of Medicine, Matsumoto, Japan

Polycystic Lipomembranous Osteodysplasia with Sclerosing Leukoencephalopathy (Nasu–Hakola Disease)

75.1 Clinical Features and Laboratory Findings

Polycystic lipomembranous osteodysplasia with sclerosing leukoencephalopathy (PLOS), also called Nasu–Hakola disease, was described in the early 1970s by Nasu et al. (Japan) and Hakola (Finland). The disorder was recognized as a combination of abnormalities in the nervous system and adipose tissue in the skeleton. Initially most cases were reported from Japan and Finland, but over the years the disease has been reported on a more global scale, with papers from other Nordic countries, Italy, and Belgium to North America and South Africa. There is no doubt that other countries will follow. The disease has an autosomal recessive mode of inheritance. Patients are often born of consanguineous parents.

The initial development of patients is normal. The first symptoms develop in the second or third decade of life and are mainly related to the skeletal abnormalities. The disorder affects especially the distal parts of the long cancellous bones, metacarpals, metatarsals, and phalanges. The first symptoms are painful wrists and ankles, distortions and fractures, either occurring spontaneously or induced by minor trauma. In the third decade a slowly progressive dementia starts to develop, with the characteristics of a prefrontal psychological syndrome, including personality changes, euphoria, loss of social inhibitions, memory loss, and confabulations. Gradually other symptoms appear. Seizures enter the clinical picture, in addition to gait disturbances, paraplegia, choreiform movements, myoclonia, and urinary incontinence. In the last phase of the disorder, cortical involvement becomes manifest with manifestations such as aphasia, agraphia, acalculia, and alexia. Bulbar symptoms may develop as well. The prognosis is poor; the average life expectancy is 40 years. However, patients with a slower and more benign disease course have also been reported.

Laboratory findings may include an increased alkaline phosphatase level. Skeletal X-rays reveal multiple cystic lesions symmetrically located in the metatarsal areas of long bones, the phalanges, metacarpals, and metatarsals. Biopsy of the bone shows the characteristic histological membranocystic changes – lesions that can also be found in subcutaneous adipose layers. DNA confirmation of the diagnosis is possible.

75.2 Pathology

On gross inspection, the brain shows atrophy of variable severity, especially in the frontal and temporal regions. The large cerebral arteries at the base of the brain appear normal. On coronal sectioning, the ventricles are enlarged, again predominantly in the frontal and temporal lobes. There is a decrease in white matter volume. The white matter appears grayish and is of rubbery consistency. The basal ganglia and thalami are smaller than normal. The globus pallidus shows a brownish discoloration and contains deposits of sandy material.

Microscopy shows a diffuse, symmetrical myelin pallor and marked astrofibrillary gliosis of the cerebral white matter, predominantly in the frontal and temporal region, but also in the corpus callosum, internal capsule, and sometimes cerebellar white matter. The arcuate fibers are better spared in the temporal than in the frontal regions. There is little sudanophilic material in perivascular macrophages, although sometimes sudanophilic material is more prominent and diffusely scattered in the affected white matter. No metachromatic material is found. There are no signs of inflammation. Signs of axonal degeneration may be seen within the cerebral hemispheric white matter, basal ganglia, cerebellum, and brain stem, with axonal loss, fragmentation, and presence of spheroid bodies. Electron microscopy of these axonal spheroids reveals a compact collection of cell organelles, including degenerated mitochondria, neurofilaments, and vesicles with patchy dense material. The presence of these axonal spheroids may suggest a link to leukoencephalopathies with axonal spheroids. The cerebral cortex is usually intact. The thalamus is rarely seriously affected. In the globus pallidus and putamen, basophilic calcospherites and moderate neuronal loss are seen. There are changes in the blood vessels (small arterioles and capillaries), most prominently in the white matter. The vessels have plump endothelium. The basement membranes of these blood vessels are thickened and often multiplied, related to concentric deposition of collagen IV. Immunohistochemically extravasation of plasma constituents can be demonstrated.

Peripheral nerves may be affected and axonal degeneration has been reported.

In addition to the brain, adipose tissue and bone marrow are of interest. In adipose tissue and fatty

bone marrow, membranocystic lesions are found. Convoluted membranous structures lie scattered or conglomerated among mature fat cells. The membranes, which are mainly eosinophilic but partly basophilic, form irregular cystic cavities containing pale, homogeneous material. Ultrastructurally, the membranes consist of undulating bands composed of numerous minute tubular structures, arranged perpendicularly to the inner surface of the cavity. The cavity is filled with a lightly osmiophilic amorphous substance. The outer zone of the bands shows tubular crypts with microvesicles. The tubulovesicular structure of the membranocystic lesions arises at the lipid–cytoplasmic interface of degenerated fat cells and enters the interstitium to form the lesion, concurrent with the collapse of fat cells. There are also membranocystic structures with thinner membranes without tubular structures. Membranocystic structures are not specific for PLOSL. They can be induced by several forms of chronic circulatory insufficiency and trauma.

75.3 Chemical Pathology

Lipid analysis of brains of patients with PLOSL has revealed large amounts of free fatty acids, but no cholesterol esters. Within the white matter, total lipid, cholesterol, and cerebroside content are mildly to seriously decreased.

75.4 Pathogenetic Considerations

One gene for PLOSL is *TYROBP*, also called *DAP12*, located on chromosome 19q13.1. The gene encodes TYRO protein tyrosine kinase binding protein (TYROBP), also called DAP12. TYROBP is an adaptor molecule that couples a variety of cell surface receptors expressed by myeloid cells, including natural killer cells, and plays a major role in the transduction of cell activation signals. It is expressed by a wide variety of myeloid cells and also by microglia and osteoclasts. On the plasma membrane of these cells, TYROBP associates with activating receptors recognizing major histocompatibility complex class I molecules.

More recently, *TREM2* has been identified as the second PLOSL gene. The gene is located on chromosome 6p21.2. The protein TREM2 belongs to the immunoglobulin superfamily and forms a receptor signaling complex with TYROBP. Its pattern of expression closely follows the pattern of TYROBP. It triggers activation of immune responses in macrophages and monocyte-derived dendritic cells. PLOSL forms an example of a disease in which mutations in two different subunits of a multisubunit receptor complex result in an identical phenotypic appearance.

The TYROBP-mediated signaling pathway plays an important role in human brain and bone tissue. The pathogenesis of the disease has still to be clarified. The precise biochemical and structural steps leading to the histopathology of the disease are not yet understood. Patients with PLOSL have no defects in cell-mediated immunity, suggesting a remarkable capacity of the human immune system to compensate for the inactive TYROBP-mediated activation pathway. The characteristic bone cysts may reflect chronic dysfunction of osteoclasts.

75.5 Magnetic Resonance Imaging

The combined findings of X-rays of the skeleton and CT and MRI of the brain are diagnostic. X-rays of the long bones, phalanges, and metacarpal and metatarsal bones show the typical cystic changes, in many cases with evidence of earlier fractures. CT shows calcification of the basal ganglia, especially in the putamen and caudate nucleus (Figs. 75.1 and 75.2), sometimes also in the globus pallidus, rarely in the dentate nucleus (Fig. 75.2). The abnormalities in the white matter are better demonstrated on MRI. MRI shows bilateral, symmetric, cerebral white matter abnormalities with a high signal intensity on T₂-weighted and FLAIR images (Figs. 75.2–75.4). The

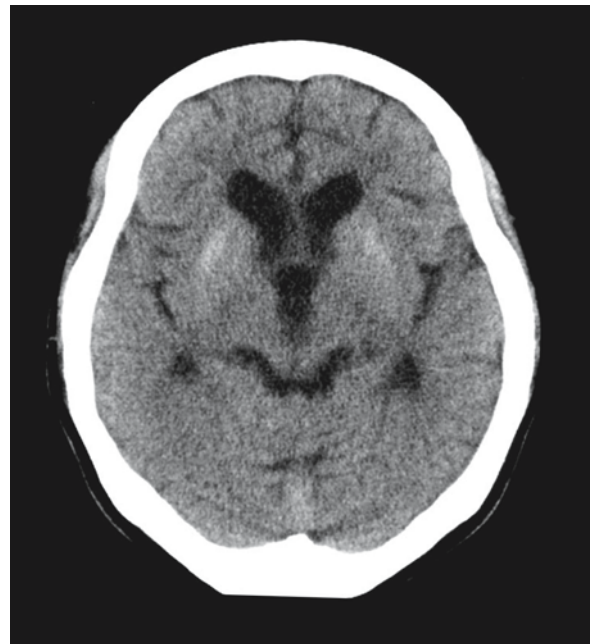


Fig. 75.1. Female PLOSL patient, 38 years old. The CT scan demonstrates the calcium deposits in the basal ganglia. Courtesy of Dr. Y. Ueki, Dr. N. Kohara, Dr. H. Fukuyama, and Dr. Y. Miki, Departments of Neurology and Brain Pathophysiology, Faculty of Medicine, Kyoto University, Kyoto, Japan

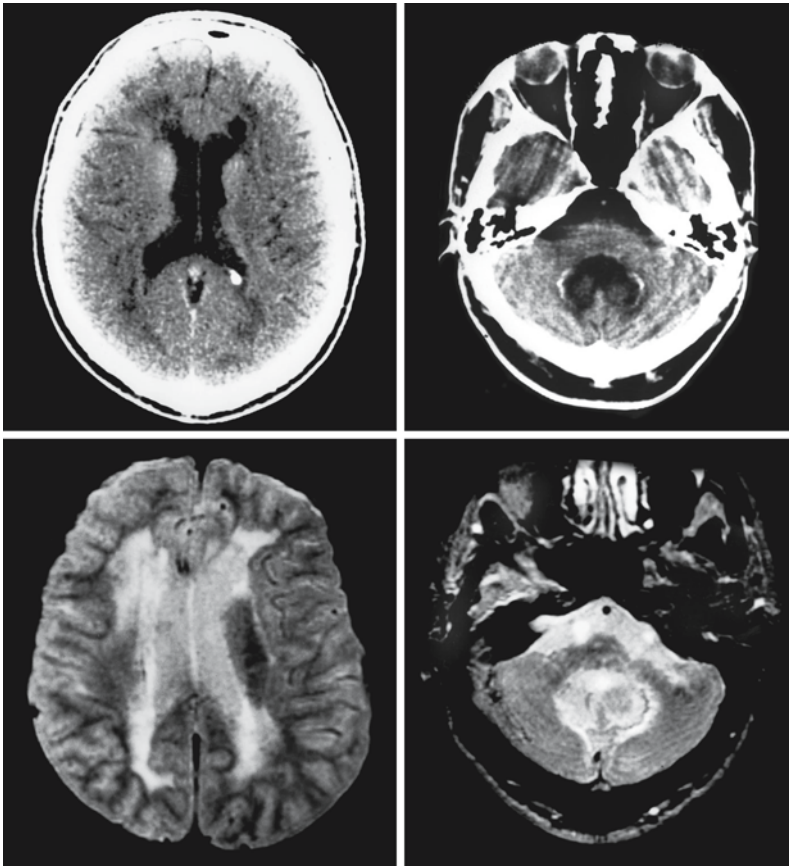


Fig. 75.2. Male PLOSL patient, 29 years old. The CT scan demonstrates the calcium deposits in the caudate nucleus and dentate nucleus. The MRI reveals abnormalities in the periventricular and deep white matter, sparing the U fibers. The hilus of the dentate nucleus and deep cerebellar white matter is affected as well. From Malandrini et al. (1996), with permission

signal change is often mild and ill demarcated. The temporal lobe tends to be better preserved (Figs. 75.3 and 75.4). The U fibers also tend to be spared (Figs. 75.2–75.4). On T_2 -weighted, but more conspicuously on gradient-recalled-echo images, the basal ganglia appear too dark in comparison with average normal findings in this age group (Figs. 75.3 and

75.4). There is progressive cerebral atrophy with widening of the ventricles and subarachnoid spaces (Figs. 75.3 and 75.4). The atrophy may dominate in the frontal area. Perfusion studies have been performed with SPECT and PET with evidence of hypoperfusion in the frontal and temporal lobes.

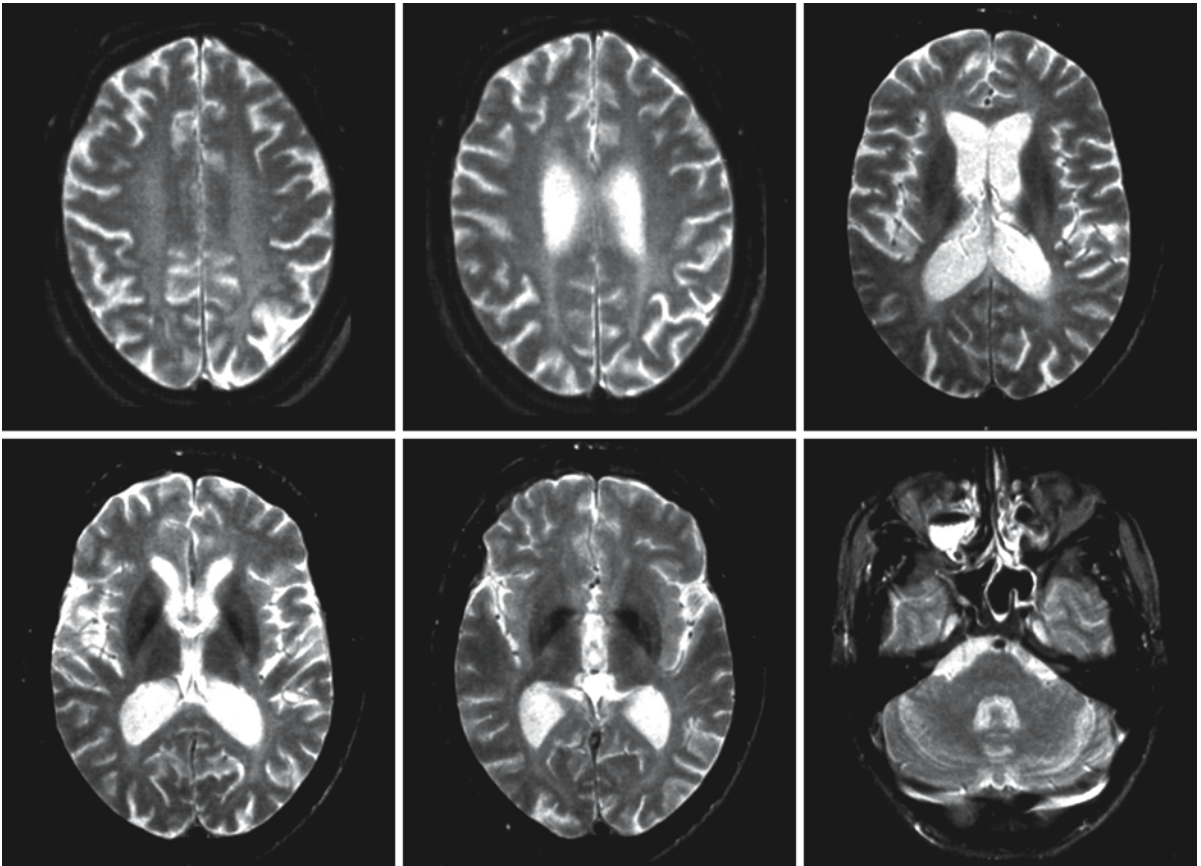


Fig. 75.3. A 32-year-old man with PLOSL. The T₂-weighted images reveal diffuse, ill-defined signal abnormalities in the cerebral white matter, relatively sparing the U fibers and temporal white matter. There is some cerebral and cerebellar atrophy with moderate widening of CSF spaces. Note the low signal

intensity of the putamen and globus pallidus, related to calcium deposits, as evident on the CT scan (not shown). Courtesy of Dr. T. Autti, Department of Radiology, Helsinki University Central Hospital, Helsinki, Finland

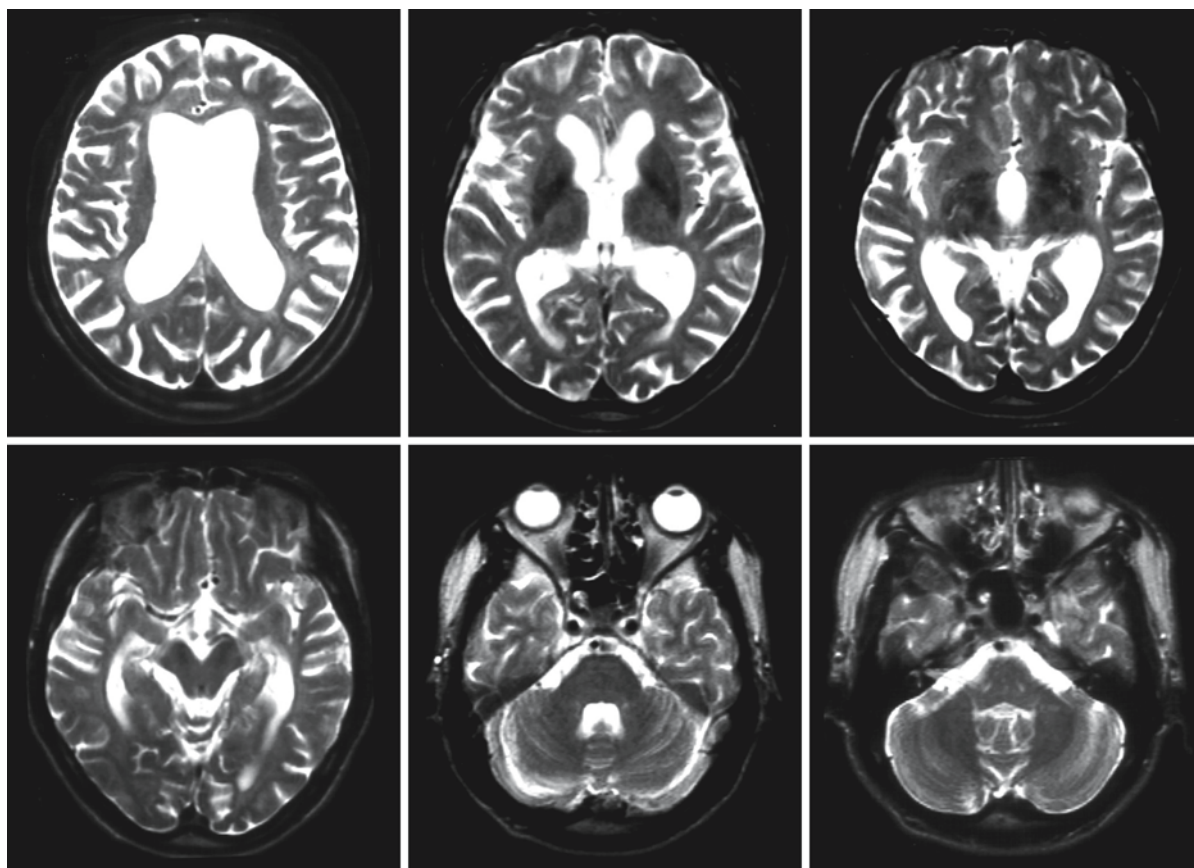


Fig. 75.4. Brother of the patient shown in Fig. 75.3, also suffering from PLOSL, 32 years old. Despite being the same age at MRI, this patient has much more severe cerebral atrophy and also some cerebellar atrophy. Note again the low signal inten-

sity of the basal ganglia on these T₂-weighted images. Courtesy of Dr. T. Autti, Department of Radiology, Helsinki University Central Hospital, Helsinki, Finland

Pigmentary Orthochromatic Leukodystrophy

76.1 Clinical Features and Laboratory Investigations

A limited number of families with pigmentary orthochromatic leukodystrophy (POLD) have been described. In several families affected siblings were observed, whereas the parents did not display signs of dementia, providing evidence for an autosomal recessive mode of inheritance. However, occurrence of patients in successive generations has also been reported, suggesting an autosomal dominant inheritance. Autosomal dominant inheritance with incomplete penetrance would explain the two observations. The mean age at onset of symptoms is 42 years \pm 11.5 (range 25–70 years). Women account for two-thirds of the patients. Childhood onset of POLD has been reported occasionally (Seiser et al. 1990; Harding et al. 1990).

Most patients present with dementia and behavioral disturbances. The disease is chronic-progressive and is characterized by progressive cognitive decline, spastic hemiplegia or tetraplegia, cerebellar ataxia, and pseudobulbar features with dysphagia, dysarthria, and finally loss of speech. Myoclonia and epilepsy are also relatively frequent findings. Optic atrophy and visual loss may occur. The duration of the illness is 7 \pm 5.5 years, with a range of 1–18 years, indicating that the rate of progression is highly variable. Two sisters with POLD had primary infertility with streak ovaries at autopsy.

The diagnosis is at present based on histopathological findings. When the diagnosis has been established by means of histopathology in one patient, MRI of the brain revealing a leukoencephalopathy is sufficient to confirm the diagnosis in family members who become clinically symptomatic.

76.2 Pathology

External examination reveals mild to marked atrophy of the cerebrum and cerebellum. On sectioning, dilatation of the lateral ventricles is found, in addition to gray-brown discoloration of the cerebral white matter, most marked in the frontal and periventricular regions.

Microscopic examination reveals prominent, symmetrical demyelination of the cerebral white matter

with relative sparing of the U fibers. The frontal white matter is most prominently affected. Axons are relatively spared, but axonal swellings may be seen in the affected white matter. The brain stem and cerebellar white matter are inconstantly and mildly affected. Wallerian degeneration may be seen in brain stem tracts. There are scanty macrophages containing sudanophilic material. Astrocytes, microglia, and macrophages contain a brown-yellow, autofluorescent pigment in the cytoplasm that stains positive with PAS. The inclusions have the staining properties of ceroid lipofuscin. Macrophages and astrocytes are inconstantly positive in iron stains. The demyelinated white matter is diffusely gliotic. Oligodendrocytes are markedly decreased in areas of demyelination, but preserved or relatively increased in numbers in the less severely affected areas. There are no inflammatory infiltrates.

Electron microscopy of the white matter shows that most macrophages and many astrocytes and oligodendrocytes are filled with membrane-bound intracytoplasmic inclusions containing electron-dense multilamellar material in a curved or straight parallel arrangement or with fingerprint profiles, accompanied by various amounts of lipofuscin and lipid droplets. Curvilinear profiles may also be observed.

76.3 Pathogenetic Considerations

At present, the basic genetic defect and the pathogenesis of the disease are unknown. One paper (Marotti et al. 2004) reports a father and two daughters with adult-onset leukoencephalopathy and at autopsy widespread destruction of cerebral white matter with presence of neuroaxonal spheroids as well as pigmented glial cells and macrophages. So in this family histology revealed characteristics of both POLD and hereditary diffuse leukoencephalopathy with spheroids (HDLS, Chap. 70), suggesting perhaps an etiological relationship between the two.

76.4 Therapy

Only symptomatic therapy is available for patients with POLD.

76.5 Magnetic Resonance Imaging

MRI has been reported in one patient (Dousset et al. 1998) and revealed extensive signal abnormalities in the cerebral white matter, accompanied by white

matter volume loss. The corpus callosum was also atrophic. The white matter abnormalities were bilateral but not entirely symmetrical. The MRI findings are not distinct and do not allow a specific diagnosis.

Adult-Onset Autosomal Dominant Leukoencephalopathies

Multiple families have been described with an adult onset leukoencephalopathy and an autosomal dominant mode of inheritance. When there is no specific disease marker, it is hard to tell whether families have the same disease or different disorders. In hereditary diffuse leukoencephalopathy with spheroids (see Chap. 70), the white matter disease is histopathologically accompanied by numerous neuroaxonal spheroids within the affected white matter, which is the basis for the diagnosis. In pigmentary orthochromatic leukodystrophy (see Chap. 76), histopathological examination reveals demyelination accompanied by astrocytes and phagocytic cells that contain in their cytoplasm membrane-bound inclusions of brown-yellow, autofluorescent pigment, which has the appearance of multilamellar material in a curved or straight parallel arrangement or with fingerprint profiles on electron microscopy. However, in other families with adult-onset autosomal dominant leukoencephalopathy such characteristic histopathological findings are lacking. In the present chapter we focus on those families in which MRI findings have been reported.

Adult-onset autosomal dominant leukoencephalopathy has been described in multiple members of an American-Irish family (Eldridge et al. 1984; Schwankhaus et al. 1988, 1994; Coffeen et al. 2000). In this family, the onset of clinical symptoms is in the fourth or fifth decade of life. The first symptoms consist of autonomic abnormalities, including bowel and bladder dysfunction, impotence, orthostatic hypotension, and decreased sweating. After several years, other neurological symptoms appear, such as loss of fine motor skills. Subsequently, overt cerebellar and pyramidal dysfunction develops, eventually leading to complete loss of voluntary movements. Signs of posterior column dysfunction are frequent. Behavioral problems, cognitive deficits, and abnormalities of the central visual pathways are mild and of later onset. Sensorineural hearing loss is common. The peripheral nervous system is spared. The disease is slowly progressive, and survival of 20 years is common. Laboratory tests are unrevealing. Evoked potentials show central conduction delays. Peripheral nerve conduction velocities are normal. A gene locus on chromosome 5q31 has been identified, but the gene itself has not yet been found.

Neuroimaging shows cerebral white matter changes with frontoparietal predominance in the ear-

ly stages. The abnormalities are patchy and inhomogeneous in signal intensity. The deep white matter is most prominently affected. The cerebral white matter abnormalities are progressive and extend posteriorly. They finally involve all cerebral white matter with relative preservation of the U fibers. Signal abnormalities in the middle cerebellar peduncles are early findings. In the later stages, the cerebellar white matter is also affected. Brain stem abnormalities are frequent, including involvement of the pyramidal tracts, medial lemniscus, and cerebellar peduncles.

Autopsy reveals widespread myelin loss in isolated and confluent patches in the cerebral white matter and relative preservation of axons within the affected areas. Irregular islands of relatively normal white matter are seen within and at the margins of the affected regions. In the areas of myelin loss, oligodendrocytes are abundant. The abnormal white matter is vacuolated. Despite the severity of the white matter abnormalities, macrophages, activated microglia, lipid accumulation, astrocytic proliferation, and fibrillary gliosis are scarce. Inflammatory infiltrates are absent. The U fibers are relatively spared. Gray matter structures are intact. The cerebellar white matter and cerebellar peduncles are severely affected, similar to the cerebral white matter. Brain stem tracts are also affected, but the changes are milder than in the cerebral and cerebellar white matter.

Calandriello et al. (1992) describe a family with an autosomal dominant leukoencephalopathy and a highly variable age at onset, ranging between 9 and 66 years, making evaluation of this family difficult. Details concerning MRI findings are lacking.

Abe et al. (1993) describe a family with adult-onset autosomal dominant leukoencephalopathy and clinically progressive tetraparesis, dysarthria, dysphagia, and urinary incontinence. Mental capacities seem to be relatively better preserved. MRI shows diffuse signal abnormalities of the cerebral white matter, brain stem tracts, and cerebellar white matter. A striking finding is the preservation of the optic radiation, considered to be a distinct finding.

Quattrocchio et al. (1997) and Bergui et al. (1997) describe a large Italian family with adult-onset autosomal dominant leukoencephalopathy and clinically progressive spasticity, pseudobulbar dysfunction, urinary incontinence, and sometimes action tremor. Apart from slight memory impairment, no cognitive decline is noted and there are no behavioral changes.

The peripheral nervous system is spared. The mean age at onset is 45 years and the duration of the disease 10 years. MRI of the brain shows diffuse signal abnormalities within the cerebral white matter, most prominently involving the deep cerebral white matter. The U fibers and corpus callosum are initially spared but become involved in the later stages of the disease. Some cerebral hemispheric atrophy develops over time. The posterior limb of the internal capsule and brain stem tracts become affected. The cerebellum and the optic radiation remain spared, even in the late stages of the disease. There are no data on histopathology.

Fukazawa et al. (1997) describe a family with an autosomal dominant leukoencephalopathy. The onset of clinical symptoms in this family is in childhood, but the progression is extremely slow, over decades. The first signs include cerebellar dysfunction and some mental deterioration. The subsequently developing spasticity leads to serious disability in the third or fourth decade of life. The MRI shows diffuse white matter signal abnormalities, involving all cerebral white matter from cortex to ventricular lining and also the internal capsule and corticospinal tracts in the brain stem. The cerebellum and remainder of the brain stem have a normal signal, although the cerebellum shows some atrophy. The findings may be compatible with hypomyelination, but data on histopathology are lacking.

In 2001 Tagawa et al. described another family with an adult-onset autosomal dominant leukoencephalo-

pathy. The disease is characterized by cerebellar ataxia as the initial symptom and later dementia and signs of pyramidal dysfunction. MRI shows a diffuse leukoencephalopathy involving all cerebral and cerebellar white matter and the brain stem. In addition, some cerebral atrophy develops. Histopathological examination reveals vacuolar degeneration of the white matter, sparing the U fibers.

In 2003, another family with adult-onset autosomal dominant leukoencephalopathy was reported by Letournel et al. The patients have a variable combination of dementia, motor signs, and epilepsy. MRI findings have not been reported in detail and histopathological finding are nonspecific, showing an orthochromatic leukoencephalopathy involving the cerebral hemispheres, but sparing the cerebellum and brain stem.

It is hard to tell whether consistent differences in clinical and MRI findings are sufficient to distinguish different disease entities. For instance, in some families signs of autonomic dysfunction are consistently present, whereas they are absent in other families. Likewise, the cerebellar white matter is consistently involved in some families, whereas in other families the cerebellum is consistently spared. It is presently important to document these families in every detail from clinical, MRI, MRS, and histopathological perspectives. It is to be expected that the underlying gene defect(s) will soon be found in the larger families, facilitating further analysis of the remaining families.

Inflammatory and Infectious Disorders

Although apparently different with respect to the underlying cause, inflammatory and infectious diseases have much in common. In both conditions the human defense system plays an active role, counteracting the cause of the disturbance, killing the intruder, and repairing the tissue damage.

Inflammation has principally a protective role. Paradoxically, in a large number of human diseases inflammatory reactions are part of the pathogenetic mechanisms causing tissue damage. Inflammatory reactions can be not only protective but also histotoxic. The inflammatory process is characterized by a complex interplay between blood cells, blood vessels, and tissue. Although the process is complex, it follows well-orchestrated patterns.

Many components of the defense system have to come into action to destroy the invading micro-organism or counteract adverse interactions. The defense system depends largely on the immune system, which can be subdivided into an *innate (nonadaptive)* and an *acquired (adaptive)* part. Repeated infections do not improve the innate system, whereas the adaptive immune system has a “memory bank” with improved resistance after repeated attacks. In both systems a *molecular* (soluble, humoral) component can be distinguished from a *cellular* component.

In the *innate system* the *soluble factors* are *lysozyme*, *complement*, *acute phase proteins*, and *interferon*.

The enzyme *lysozyme* is a soluble bactericidal substance, abundantly present in body fluids. It is capable of splitting the exposed peptidoglycan wall of susceptible bacteria.

Complement consists of a complex series of many proteins, and forms one of the enzyme systems in plasma triggered during inflammation. Once activated, the complement system produces a rapid, highly amplified response to a trigger stimulus, mediated by a cascade reaction, in which the product of one reaction is the enzyme catalyst of the next reaction. Components of complement are designated by the letter “C” followed by a number related to the chronology of its discovery. Unfortunately, the sequence in which the complement components come into action is not identical to the sequence of their discovery. The actions of activated complement range from increasing vascular permeability to mast cell degranulation, opsonization and phagocytosis of bacteria, neutrophil activation, chemotaxis, and lysis of bacteria and for-

eign cells. Two ways of activating complement are distinguished. One is the so-called alternative pathway, which is activated by a microbial polysaccharide. This pathway belongs to the innate, nonspecific immune system. The other, the classical pathway, is a specific response triggered by antibody–antigen complexes. Both systems work closely together.

Acute phase proteins are plasma proteins which undergo a dramatic increase in concentration in response to infection or injury. A number of factors belong to this group, including C-reactive protein (CRP) and fibrinogen. C-reactive protein has the ability to bind to a number of micro-organisms which contain phosphorylcholine on their membranes. The complex formed is able to activate complement by the classical pathway, resulting in opsonization of the microbe for adherence to phagocytes.

Interferons are broad-spectrum antiviral agents. Different molecular forms of interferon have been identified. There are at least 14 different interferons- α (IFN- α), produced by leukocytes, while fibroblasts and other cells produce interferon- β (IFN- β), interferon- γ (IFN- γ), and macrophage activating factors, which switch on the microbicidal mechanisms of the macrophage. A subpopulation of T lymphocytes, T helper cells, will produce lymphokines, amongst them IFN- γ , if bound to an antigen in association with a major histocompatibility complex (MHC) class II molecule on a macrophage surface. IFN- γ is also produced by cytotoxic T lymphocytes which recognize antigen in association with MHC class I molecules.

The *major histocompatibility complex* (MHC) is a complex of proteins which is of predominant importance in the transplant rejection process. In man the MHC is the *human leukocyte antigen* (HLA) cluster encoded for by chromosome 6. It has been recognized that proteins encoded in this particular region of chromosome 6 are involved in many aspects of immunological recognition, including both interaction between lymphoid cells and interaction between lymphocytes and antigen presenting cells. Three classes of MHC molecules are distinguished. Class I molecules associate with antigen on the surface of virally infected cells to signal cytotoxic T lymphocytes. Class II molecules signal T helper cells to activate B cells and macrophages. T helper cells are only activated when both antigen and MHC class II molecules are presented on the antigen-presenting cell. Class III genes encode components of the complement.

The *cellular part* of the *innate immune system* is formed by *phagocytes*, *natural killer cells*, and *mast cells*.

The *phagocytes* can be divided into monocytes and polymorphonuclear granulocytes. The latter can be further divided into neutrophils, eosinophils, and basophils, according to the histological staining of their granules. Granulocytes do not show any specificity for antigens, but together with antibodies and complement, they play an important role in protection against micro-organisms. Their predominant role is phagocytosis. In the process of phagocytosis both oxygen-dependent and oxygen-independent mechanisms play a role. The oxygen burst is the process in phagocytosis by which oxygen is converted to *free radicals*.

Oxygen radicals and their metabolites constitute an important class of inflammatory mediators. Free radicals are atoms or molecules containing an unpaired electron in the outer orbit. Phagocytic cells, when activated, exhibit a sharp increase in molecular oxygen consumption, the so-called respiratory burst, and produce a battery of biologically active oxygen radicals and derived metabolites. The stimuli for phagocyte-derived oxygen radical production are multiple, including endotoxins, γ -immunoglobulins, and cytokines. Reduction of molecular oxygen by addition of a single electron results in formation of the superoxide anion ($O_2^{\cdot-}$). In aqueous environments, $O_2^{\cdot-}$ exists in equilibrium with its protonated form, $H_2O^{\cdot-}$ (perhydroxyl radical). In the presence of superoxide dismutase $O_2^{\cdot-}$ can undergo dismutation, resulting in H_2O_2 formation. Hydrogen peroxide has the capacity to oxidize directly a wide spectrum of biological molecules. Phagocyte-derived oxygen radicals and their metabolites are important mediators of tissue damage in inflammatory disorders. The concurrent rise in pH due to free radical formation allows cationic proteins to function optimally, damaging the bacterial membrane. The process of phagocytosis is adequately supported by the complement system, which can prepare micro-organisms for phagocytosis by opsonization.

Natural killer cells are large granular lymphocytes with a characteristic morphology, capable of recognizing structures on high-molecular-weight glycoproteins which appear on the surface of virally infected cells and allow them to be differentiated from uninfected cells. At the binding site, pores are formed in the infected cell and the cell is then killed by nuclear fragmentation through calcium-dependent endonuclease. The various interferons produced by virally infected cells augment natural killer cytotoxicity and form an integrated feedback defense system.

Mast cells have a central role in the acute inflammation process. They are loaded with granules containing preformed mediators, which are released up-

on triggering. This triggering occurs by components of the complement system. Mast cell activation follows two major pathways. The first pathway involves the release of the preformed mediators from the granules, such as histamine, causing vasodilatation, increased capillary permeability, and chemokinesis; neutral proteases, which activate complement; eosinophil and neutrophil chemotactic factor; and platelet activating factor, which induces mediator release, including interleukins and tumor necrosis factor with multiple actions such as macrophage activation and triggering of acute phase proteins. The second pathway results in the release of newly synthesized mediators via the phospholipase A_2 pathway. This enzyme initiates arachidonic acid degradation. Breakdown of arachidonic acid is achieved by different enzymes. Lipoxygenase leads to the promotion of leukotrienes, which influence the microcirculation and enhance chemotaxis. Cyclo-oxygenase leads to the formation of prostaglandins and thromboxanes, which affect bronchial muscle, platelet aggregation, and vasodilatation.

Complex and efficient as the innate immune system appears, many micro-organisms find ways to circumvent these responses. Here the *adaptive immune system* is important, which also has humoral and cellular components. The *humoral adaptive immune system* leads to the formation of *antibodies*, which form specific responses to specific antigens. Antibodies form a highly specific answer to those micro-organisms which escape the innate immune system. Antibodies are capable of binding specifically to the attacking microbe, activating the complement system, and stimulating phagocytic cells. The antibody molecule therefore has three main regions, two regions concerned in communicating with complement and phagocytes, and one region for binding to an individual micro-organism. The latter region carries the external recognition function. The first two functions are constant. The recognition function, however, demands numerous adaptations of recognition sites. Antibodies, when bound to a microbe, will link to the first molecule in the classical complement sequence.

The *cells* involved in the *adaptive immune system* are mainly *lymphocytes*. All the cells of the immune system are derived from pluripotent stem cells through two main lines of differentiation: the lymphoid lineage, producing lymphocytes, and the myeloid lineage, producing phagocytes and mast cells. There are three kinds of lymphocytes with different functions: T cells and B cells and the so-called third population cells. T cells differentiate initially in the thymus; B cells in fetal liver, spleen, and in adult bone marrow. Morphologically, T and B cells are identical; functionally they can be distinguished. B cells are classically defined by the production of immunoglobulins (antibodies), which are presented on

the cell surface. The T cells can be subdivided into T helper cells, T suppressor cells, and T killer cells. Their function is to recognize foreign intruders, to activate B cells, and to kill invading micro-organisms. The third population cells do not consistently carry markers of either T or B cells. They possess specific receptors for γ -immunoglobulins and form the greater part of natural killer and antibody-dependent cellular cytotoxic effectors. In another classification system, dependent on the surface proteins reacting to clusters of antigens (CD = cluster determinants), lymphocytes can be subdivided in terms of different cell types. The T helper cells are classified as CD4+ cells (formerly T4 cells); the T suppressor/killer cells as CD8+ cells (formerly T8 cells).

To orchestrate the actions of all the cells involved in the inflammatory process, a great variety of solvable mediators are used for communication between the cells. On the effector side, too, many solvable factors play an important role in the inflammatory reaction. An important group of such mediators has been given the name *cytokines*. Cytokines can be divided into monokines, produced by monocytes and macrophages, and lymphokines, produced by lymphocytes. Cytokines are hormone-like substances and are the most important mediators of the action of T lymphocytes. The immune functions of T lymphocytes are reflected by a specific set of cytokines, the lymphokines, produced by these cells after activation. Subpopulations of T cells, such as T1 and T2 helper cells, can be distinguished by the specific lymphokines they produce. Important lymphokines, some of which have been mentioned before, are interleukins, interferons, lymphotoxin, growth factors, and tumor necrosis factor. CD4+ cell has the cytokine profile of the T1 helper cell. The T1 helper cell activates the B lymphocytes to produce antibodies and it causes eosinophilia and mast cell hyperplasia. The CD8+ lymphocyte has T2 cell characteristics and is responsible for cytotoxicity, complement fixation, and macrophage activation. The CD8+ lymphocyte profile, therefore, protects against viruses, tumors, and infections. It is also responsible for transplant rejection, inflammation, and autoimmune reaction. Cytokines form a functional network. The various factors, messengers, and effectors act in a subtle interaction. These interactions may be synergistic, additive, or antagonistic, and function in order to maintain a balance of optimal efficacy in the protection of the host.

The cooperative cellular and mediator activity in *inflammatory (either infectious or noninfectious) disorders* of the CNS can be briefly summarized as follows:

Circulating T cells recognize the antigen concerned in combination with the major histocompatibility complex class II on antigen-presenting cells and

start to proliferate. The antigen-presenting cells in the CNS may be perivascular macrophages, the gatekeepers of the CNS. Microglial cells may also act as antigen-presenting cells within the CNS. Sensitized or activated T cells start to release substances such as interferons (interferon- γ), which activate local cells such as microglia, astrocytes, and perivascular macrophages. This local activation results in upregulation of adhesion molecules on endothelial cells, enhanced expression of major histocompatibility complex, and release of chemoattractive substances, which attract and facilitate the entrance of more T cells, macrophages, and B lymphocytes. B cells are triggered to become plasma cells and produce antibodies. Macrophages, microcytes, astrocytes, and mast cells start to produce inflammatory mediators such as tumor necrosis factors, reactive oxygen species, interleukins, vasoactive amines, leukotrienes, complement, and hydrolytic enzymes. The result is, eventually, vascular dilatation, increased capillary permeability, exudation of fluid in tissue, and extravasation of numerous cells, leading subsequently to disruption of the blood-brain barrier, perivascular inflammation, formation of edema and demyelination. Phagocytosis of myelin by macrophages may be initiated by antimyelin antibodies, or by opsonization via their receptor for complement component.

Knowledge of the factors mediating inflammation has stimulated attempts to undo undesired reactions by counteracting or blocking the involved pathways. Interferon- γ , for example, proved to have a negative influence on the course of secondary progressive multiple sclerosis. Interferon- β , known to counteract the action of interferon- γ , seems to have a beneficial effect on the course of this disease.

In *infectious disorders* several pathogenetic factors play a role in evoking the host response. Exotoxins, for example, are produced by micro-organisms during their growth. They have a proteinaceous nature and therefore act as antigens. They evoke an antibody response and in this way give rise to neutralizing antitoxins. Endotoxins are membrane molecules, lipopolysaccharides, present in the outer cell membrane of gram-negative bacteria. The polysaccharide chain is variable and determines the antigenic structure of the bacteria. The lipid fraction anchors the lipopolysaccharide in the outer bacterial membrane, is less variable, and is responsible for the toxic effects. After liberation of the lipopolysaccharides from the bacterial membrane they adsorb on the lipid membrane of many cells, especially neutrophils. This triggers a whole cascade of immune reactions. Another way to evoke immune reactions is by presentation of antigens by specialized cells, also called antigen-presenting cells, such as the Langerhans and dendritic cells. These cells recognize the foreign intruders, probably by lack of identifying cell surface membrane

MHC class I compounds. Viruses use the replication system of host cells and bring their antigens to expression on the surface of the host cells, activating natural killer cells.

The presence and multiplication of the original micro-organism sustains the disease or expands it. The micro-organisms produce a gamut of products to assist in their spread, including streptokinase, hyaluronidase, and neuraminidase. In many cases it is difficult to distinguish the direct influence of the micro-organisms on the tissue from the immunological reaction the attack provokes. A demonstration of this is found in subacute sclerosing panencephalitis, caused by the measles virus. In subacute sclerosing panencephalitis, as in other persistent viral infections, deposits of immune complexes can be demonstrated in the wall of small cerebral blood vessels. The presence of immune complexes and the histological findings of perivascular edema, inflammation, and demyelination provide strong evidence that, in addition to the actual invasion by the virus, there is a contemporaneous immune-mediated response to this virus which is responsible for much of the tissue damage. The same could be true for subacute AIDS encephalitis and tropical spastic paraparesis due to HTLV-1 infection.

Selective neuronal and/or glial damage in infectious disorders and the predilection for particular areas (topistic areas) is in most cases difficult to understand. Experience has taught that herpes simplex virus has an affinity for the frontal and temporal lobes; fungal infections attack primarily gray matter structures; *Haemophilus influenzae* has a preference for cortico-subcortical areas; cytomegalovirus (CMV) encephalopathy and AIDS encephalopathy in adults are predominantly located in the cerebral white matter and spare the U fibers. There is often a considerable difference between the course of a disease and the predilection sites between congenital infections and infections acquired later, after birth. A good example is the difference between congenital, connatal, and adult CMV infection, and between congenital and postnatal toxoplasmosis.

In some infections the preferential location is simply related to the porte d'entrée. For example, infections that involve the leptomeninges will enter the brain via the Virchow–Robin spaces and are located predominantly in the cortex (*Haemophilus influenzae*) and in the basal ganglia (*Cryptococcus neoformans*) or both. In herpes simplex virus, a primary infection in the throat or mouth is followed by the persistent presence of latent virus in sensory ganglia and possibly also in the brain, after entry via the olfactory route. Following activation of the latent virus, direct spread may explain the frontotemporal predominance. Within the affected area, herpes simplex virus infects all types of cells.

For many viruses a necessary condition for the entry into cells is the availability of specific receptor molecules at the surface of such cells. The distribution of these receptor molecules will largely determine the specific regions of the brain preferentially attacked by the virus and the population of cells in the affected regions that are injured or destroyed. Some viruses like JC papovavirus, responsible for progressive multifocal leukoencephalopathy, infect oligodendrocytes with sparing of the neurons. This explains the affinity of this virus for white matter. Rabies virus has great affinity for the cerebellum and limbic system, whereas poliomyelitis affects the motor nuclei in the cortex, brain stem, and anterior horns of the spinal cord. Creutzfeldt–Jacob disease, caused by prions, has been shown by MRI to affect in particular the basal ganglia. These differences in topographical distribution are considered to be the result of specific receptor interactions.

Viruses enter the cells of the host either by fusing with the plasma membrane and discharging their contents directly in the cytosol, or by being internalized through the endocytotic pathway. The first way is used by herpes simplex and corona viruses. Internalization does not have special requirements in these cases. Other viruses do not have this option and have to follow the other path, involving binding to a receptor and collection of receptor–ligand complexes at the cell membrane. The viruses are then transported within endocytotic vesicles. After penetration of the cell membrane, the replicative machinery of the virus itself comes into play. Using the host cell system of nucleic acid (DNA/RNA) replication and transcription, viruses can replicate and transcribe their DNA or RNA and in so doing multiply themselves; the new virus particles leave the cell in search of new host cells. Ultimately the balance between the viral machinery and the host immune system will determine the outcome of the infection.

In the *noninfectious inflammatory disorders* other mechanisms play a role in invoking the host response, not all of which are well understood. The inflammatory reactions may be triggered by “primary” autoimmune reactions, in which autoantibodies are primarily directed against autoantigens, as is the case in vasculitis of the CNS, in systemic lupus erythematosus, Behçet disease, giant cell arteritis, and rheumatoid vasculitis. The hypothesis is that these primary autoimmune disorders are the result of a dysfunction of T cell regulation. The inflammatory response in the CNS may also be secondary to an infectious disease elsewhere in the body or a vaccination. Mycoplasma infections of the lung, for example, may lead to an acute disseminated encephalomyelitis, caused by the formation of antibodies that cross-react with CNS antigens on myelin membranes or surface molecules of CNS cells. This reaction resembles in many re-

spects the experimental allergic encephalomyelitis provoked by immunization with components of the myelin membrane (basic myelin protein, for example). Such a secondary autoimmune response probably also forms the basis of several paraneoplastic syndromes of the CNS, such as limbic encephalitis, and Purkinje cell degeneration. Here, too, the hypothesis is that antibodies formed against tumor antigens cross-react with structural components of the CNS.

As far as the involvement of myelin in inflammatory and infectious disorders is concerned, several bio-mechanisms can be distinguished:

- Immune reaction against one of the components of myelin. This occurs in acute disseminated encephalomyelitis. This condition can be simulated in an animal model, experimental allergic encephalomyelitis. In this experimental condition the animal has been sensitized against basic myelin protein.
- Specific infection of oligodendrocytes leading to cell death and subsequent loss of the myelin sheath extension of the oligodendrocytes. This is the case in progressive multifocal leukoencephalopathy.
- Myelin can also be an innocent bystander and become a victim in a process that hits all white matter components and possibly gray matter as well. This occurs in a multitude of infections, such as those caused by *Haemophilus influenzae* and herpes simplex virus, and in toxoplasmosis.
- Finally, dysmyelination may be the consequence of infectious or inflammatory changes to unmyelinated white matter, damaging the white matter matrix. Most of the congenital infections can have this effect, often in addition to other visible structural lesions.

Multiple Sclerosis

J. Valk, F. Barkhof

79.1 Clinical Features and Laboratory Investigations

Multiple sclerosis (MS) is the most common demyelinating disorder of the CNS. The peak incidence is at 30 years of age. MS rarely commences in childhood or after the age of 50 years. Females are affected twice as often as males. MS shows a characteristic geographical distribution. It is rare in tropical areas and increases in frequency at higher latitudes. It has been estimated, for example, that the prevalence in the United States varies from 6–14 per 100,000 inhabitants in the southern states to about 40–60 per 100,000 inhabitants in the northern states. No definite relationship has been established with the climatic characteristics of the latitude. Within this overall latitudinal distribution a rather large range of incidences of MS has been observed at the same latitudes. Occasionally clusters of MS have been reported. In these instances a remarkable number of patients acquire MS within a short period of time (a few months). Etiological factors for these MS pockets are as yet unknown. Sometimes such clusters of MS assume the proportions of an epidemic, the incidence of MS rising over a period of several years in a large area. In these cases the nature of the introduced environmental factor or factors still remains to be elucidated. The importance of environmental factors is stressed by the findings of migrational studies. A decrease in the risk of developing MS has been noted in young individuals migrating from high-risk to low-risk areas and an increase in risk after migration from low-risk to high-risk areas. Such changes in risk have not been found in older individuals, and the data suggest that the risk of acquiring MS is largely established around the age of 15. There is also strong evidence of a genetically influenced susceptibility to MS. In general, first-degree relatives of probands have a risk that is 30–50 times greater than the risk for the general population.

A number of variants of MS can be distinguished: classical MS (also called Charcot type), neuromyelitis optica (NMO, or Devic disease), concentric sclerosis (CS, or Baló disease), and diffuse sclerosis (DS, or Schilder disease).

The clinical presentation of *classical MS* is extremely variable. The extreme acute progressive form (Marburg type) is rare. For the more slowly developing forms it has become usual to distinguish four

main types. In most patients the disease starts with a *relapsing-remitting* course (RR), defined by the occurrence of relapses clearly separated in time, with stable intervals in between. Disability in RR patients develops because recovery between relapses is incomplete; in two-thirds of the patients the relapsing-remitting phase is followed by a *secondary progressive* course (SP) with increasing disability as measured on a disability scale over a period of 12 months. Finally there is a *primary progressive form* in 10–15% of the patients, with progressive disability from the onset. In this group the disease usually starts later and the female preponderance is less evident (Lublin and Reingold 1996). The term *benign form* (BF) is used when after initial relapses and remissions no further progression occurs and the patient is neurologically fully functional 15 years after the first symptoms. Special attention has been given in the last decade to patients with a *clinically isolated symptom* (CIS) because of the potential to delay or prevent the possible progression to MS with early treatment. Finally, *tumefactive forms* of MS present with symptoms of a space-occupying lesion. Medical history, the presence of other clinical symptoms or lesions on neuroimaging, and the therapeutic effect of corticosteroids may help in establishing the correct diagnosis.

In classical MS, clinical signs and symptoms are related to lesions present in various tracts of the CNS. Most last for days up to months or are permanent. Sometimes symptoms of extremely short duration occur, lasting for seconds to hours. Common features are fatigue, impairment of vision due to optic neuritis, motor disturbances caused by pyramidal tract involvement, sensory disturbances including Lhermitte's symptom, cerebellar ataxia and dysarthria, diplopia, micturition problems, sexual disturbances, hearing loss, vertigo, and balance abnormalities. Less common are epileptic seizures, signs of peripheral neuropathy, trigeminal neuralgia, hemifacial spasms, and dementia, although some degree of cognitive impairment is present in up to half of MS patients. There is almost always a tendency for the frequency of episodes to decrease as time passes, or for the progression in the progressive form to slow down.

The extent of the resulting disability is extremely variable. In general, it appears that the average life expectancy in young patients after the onset of MS is about 35 years. About 60–70% of patients remain ambulant. Long-term prognosis is not influenced by

pregnancy, illness, or anesthesia. Patients with many relapses in the early phase more rapidly acquire a severe state of disability than those with less frequent relapses (Confavreux et al. 2000). A large number of hyperintense lesions on T₂-weighted images is also indicative of more rapid deterioration. When more than 10 lesions are present, the EDSS score within 4 years will be higher than 6, which means inability to walk without support. Abnormal evoked responses in the early phase of the disorder are also indicative of a poor prognosis. It should, however, be noted that these predictors are rather weak.

NMO (*neuromyelitis optica* or *Devic disease*) is a clinical syndrome consisting of optic neuritis, often bilateral with total blindness, in combination with transverse myelitis, which usually has a thoracic localization. The optic neuritis and transverse myelitis either occur simultaneously or are separated by a brief interval of several days to several weeks. Men and women are affected more or less equally. The age of patients ranges from 5 to 65 years, but patients are rarely older than 50 years. The group most commonly affected is young adults. This disease occurs most frequently in the Asian population, where the overall incidence of MS is low. The prognosis is rather poor. Until recently, about 15–20% of patients died in the acute stage due to an ascending spinal disorder with respiratory paralysis; another 30% died with complications after many months. A poor neurological outcome with severe disability is reported in another 15% of patients. Complete or nearly complete recovery is found in about 35%. Improved supportive care has reduced mortality and residual disability. About half of the surviving patients experience no recurrence of neurological disease; about one-third of the remainder suffer a relapse of optic neuritis, one-third a relapse of optic neuritis and transverse myelitis, and one-third develop a multifocal white matter disease.

Wingerchuck et al. (1999) formulated absolute criteria and supportive criteria for the diagnosis NMO. The absolute criteria are: optic neuritis, acute myelitis, and no evidence of clinical disease outside the optic nerve and spinal cord. Supportive criteria are subdivided into major and minor support criteria. Major support criteria are: negative brain MRI at onset; MRI lesions in the spinal cord extending over more than three vertebral segments; and CSF pleocytosis >50 white blood cells/mm³. Minor supportive criteria are: bilateral optic neuritis; severe optic neuritis with fixed visual acuity of less than 20/200 in at least one eye; and severe, fixed, attack-related weakness in one or more limbs.

CS (*encephalitis periaxialis concentrica* or *Balo disease*) is a very rare MS variant, which usually affects young adults. For unknown demographic reasons there is a much higher incidence in the Philippines. Both sexes are affected more or less equally.

Compared to classical MS, CS runs a more rapidly progressive, usually monophasic course. The initial symptoms are often suggestive of a stroke; less frequently psychiatric symptoms predominate. The neurological symptoms are sometimes associated with fever and headache and then resemble the clinical picture of an infection or tumor. The disease is progressive and can be fatal, usually as a consequence of respiratory problems and infection. A more prolonged survival for several years has also been reported.

DS (*encephalitis periaxialis diffusa* or *Schilder disease*) is a demyelinating disease related to MS, which primarily affects children. Clinical features are intellectual impairment, epileptic seizures, signs of pyramidal tract involvement (occasionally unilaterally with hemiplegia), cerebellar ataxia, visual impairment (caused by retrobulbar neuritis or demyelination of the occipital lobes), pseudobulbar palsy (leading to problems with speech and swallowing), deafness, diplopia, extrapyramidal movement abnormalities, and incontinence. A predominantly psychiatric symptomatology is relatively frequent. In most cases there is rather rapid progression of neurological signs over the course of 1–2 years. In a minority, the demyelinating process is fulminant and accompanied by cerebral edema. Rarely, the course of disease is characterized by exacerbations. In exceptional cases significant and prolonged improvement occurs; an arrest of the disease is observed in exceptional cases.

Definite diagnosis has always been a problem in MS. The clinical features may mimic many other neurological disorders, including ischemic disorders, neoplastic diseases, vasculitides, granulomatous diseases, and infections. Definitive diagnostic tests are lacking. This diagnostic uncertainty has led to the definition of diagnostic criteria. In 1965, Schumacher was the first to draw up clinical criteria for the diagnosis of definite MS. The basic idea behind these criteria is that there must be symptoms and objective signs of multifocal white matter disease with dissemination in space and time, for which there is no better neurological explanation. These criteria have been repeatedly modified, and clinical criteria for possible and probable MS have been added (Rose et al. 1976). In 1983, Poser et al. were the first to draw up diagnostic criteria that were not completely clinical but incorporated supportive laboratory data (CSF abnormalities) and paraclinical evidence of multifocal white matter lesions (CT and evoked responses). Since that time, MRI has become more generally used and has acquired a prominent role as a paraclinical test. MR has the possibility to prove dissemination in time (by new enhancing lesions or new T₂ lesions) and dissemination in space (by multiple brain and spinal cord localizations). In the most recently proposed diagnostic criteria for multiple sclerosis by McDonald et al.

Table 79.1. Criteria for diagnosis of MS (McDonald et al. 2001)

Clinical presentation	Additional data needed for MS diagnosis
Two or more attacks; objective clinical evidence of 2 or more lesions	None
Two or more attacks; objective clinical evidence of 1 lesion	Dissemination in space, demonstrated by MRI or Two or more MRI-detected lesions consistent with MS plus positive CSF or Await further clinical attack implicating a different site
One attack; objective clinical evidence of 2 or more lesions	Dissemination in time, demonstrated by MRI or Second clinical attack
One attack; objective clinical evidence of 1 lesion (monosymptomatic presentation; clinically isolated syndrome)	Dissemination in space, demonstrated by MRI or Two or more MRI-detected lesions consistent with MS plus positive CSF and Dissemination in time, demonstrated by MRI or Second clinical attack
Insidious neurological progression suggestive of MS	Positive CSF and Dissemination in space, demonstrated by: (1) Nine or more T ₂ lesions in brain or (2) 2 or more lesions in spinal cord or (3) 4–8 brain lesions plus 1 spinal cord lesion or Abnormal VEP associated with 4–8 brain lesions, or with fewer than 4 brain lesions plus 1 spinal cord lesion demonstrated by MRI and Dissemination in time, demonstrated by MRI or (4) Continued progression for 1 year

If criteria indicated are fulfilled the diagnosis is “multiple sclerosis” (MS); if the criteria are not completely met, the diagnosis is “possible MS.” If the criteria are fully explored and not met, the diagnosis is “not MS.”

No additional tests are required; however, if tests (MRI, CSF) are undertaken and are *negative*, extreme caution should be taken before making a diagnosis of MS. Alternative diagnoses must be considered. There must be no better explanation for the clinical picture.

MRI demonstration of space dissemination must fulfill the criteria derived from Barkhof et al. (1997) and Tintoré et al. (2000).

“Positive CSF” is determined by oligoclonal bands detected by established methods (preferably isoelectric focusing) different from any such bands in serum, or by a raised IgG index.

(2001), these MRI criteria have been formalized. The MRI criteria for dissemination in space are based on the Barkhof criteria (Barkhof et al. 1997) with a modification as proposed by Tintoré et al. (2000). These new MRI criteria have been validated and make an earlier diagnosis of MS feasible without sacrificing accuracy (Barkhof et al. 2003; Dalton et al. 2003). Table 79.1 summarizes the diagnostic criteria as recommended by the International Panel on the Diagnosis of Multiple Sclerosis.

Valuable laboratory findings supporting the diagnosis of MS are oligoclonal bands in the CSF and an increased IgG index as a sign of increased synthesis of IgG within the blood–brain barrier. The sensitivity of assessment of the IgG index in MS is about 80% and

that of oligoclonal banding about 90%. The specificity and predictive value of these CSF investigations are highly dependent on the so-called pretest probability of MS. The problem is that a number of diseases mimicking MS, such as infections, acute disseminated encephalomyelitis, and vasculitis, are apt to lead to an increased production of IgG in the CSF with oligoclonal banding. It should also be noted that some patients with clinically definite MS have a normal IgG index and lack CSF oligoclonal bands. Levels of CSF IgM and IgA may also be elevated in MS. The CSF protein content may be slightly raised, but very rarely exceeds the level of 1 g/l. The white cell count may be increased, but only in exceptional cases is it higher than 20 cells/ml. Another CSF abnormality may be an

elevation of myelin basic protein in active MS. Its level is normal in stable MS. The finding of increased amounts of myelin basic protein is indicative of active demyelination and as such not specific for MS. Recently analysis of antibodies against myelin oligodendrocyte glycoprotein and myelin basic protein in patients with clinically isolated symptoms predict for early conversion to clinically definite MS (Berger et al. 2003). Free light chains of immunoglobulins and the $\kappa:\lambda$ light chain ratio may be increased in the CSF. Increased CSF free κ chains appear to be relatively specific for MS. Abnormally high levels have been found in 85% of patients with clinically definite MS, in 20% of patients with CNS infections, and only exceptionally in noninfectious controls. Concentrations of soluble adhesion molecules, sVCAM-1 and sICAM-1, in serum and CSF correlate with activity of MS, as indicated by gadolinium-enhancing lesions on MRI, and may possibly be used as a surrogate marker for disease activity.

A number of changes in the subset distribution of T lymphocytes has been reported in the peripheral blood of MS patients. CD (cluster of differentiation markers on hematopoietic cells) 4+ T cells (T helper-inducer cells) can be subdivided in two mutually exclusive subsets: “naïve” cells that have not yet been stimulated, and “memory” cells that have been stimulated before. These subsets can be recognized by differences in CD antigens. Memory cells can produce large amounts of cytokines after activation and show increased expression of a set of adhesion molecules, sVCAM-1 and sICAM-1. In the peripheral blood of patients with active MS, naïve cells are decreased in number; in inactive MS this fraction is normal. In the peripheral blood of patients with active MS, lymphocytes have been found with a higher expression of the activation marker CD26 than in patients with inactive MS and healthy controls. In CSF of active MS patients CD4+ T cells are relatively over-represented as compared to CD4+ T cells in peripheral blood. Among the CD4+ T cells in the CSF, memory cells are increased whereas naïve cells are almost absent. Subset changes, therefore, may reflect disease activity and can be used for monitoring purposes. Increased numbers of TNF-producing T cells are associated with an enhanced rate of lesion development on MRI (Killestein et al. 2001). More recently, the role of CD8+ T cells (suppressor-cytotoxic cells) has been reinforced, and again relationships with MRI lesion development have been found (Killestein et al. 2003). Further examinations are required to reveal the significance of these findings.

Other tests often used in the diagnostic assessment of MS are the visual, sensory and auditory evoked potentials (VEP, SSEP, and BAEP). These tests are helpful in detecting silent white matter lesions, thus providing evidence of multifocal white matter involvement

in cases of clinically indefinite MS. VEPs and SSEPs appear to have a higher diagnostic yield than BAEPs. However, abnormalities are nonspecific and must be interpreted with care in the context of the clinical picture.

In NMO, CSF abnormalities are similar to those in MS, with the exception of a more common occurrence of lymphocytic pleocytosis.

Laboratory examinations in CS rarely yield much information. CSF usually reveals no pleocytosis, sometimes an increased amount of red blood cells. Total protein is only occasionally elevated.

In DS the CSF is often normal, but slight lymphocytosis is occasionally found. The protein level is not infrequently elevated, as is the IgG index. Oligoclonal bands have been reported.

79.2 Pathology

Usually the external appearance of the brain is relatively normal in MS. In chronic cases slight atrophy may be present with widening of sulci and slight enlargement of the ventricular system. Occasionally firm, depressed lesions are seen on the surface of the brain stem, spinal cord, and in the optic nerves. On sectioning, numerous lesions of varying size become apparent in the white matter of CNS. Even more are revealed by microscopic examination, especially if MRI-guided. The distribution of plaques varies greatly among MS patients, but the following are recognized as preferential localizations: the periventricular white matter, in particular the lateral angles of the lateral ventricles, floor of the fourth ventricle, cerebellar peduncles, cervical part of the spinal cord, and the optic nerves. In severe, long-standing cases, numerous lesions are found in most parts of the CNS. Although the distribution of lesions is not precisely symmetrical, predominant involvement of one hemisphere is rare. A significant proportion of the plaques are found in the border zone between gray and white matter. The extent of cortical involvement has been underestimated for a long time. They are found with rigorous myelin stains (e.g., using antibodies against myelin basic protein or proteolipid protein), because the normal amount of myelin in the cortex is minimal and classical inflammatory changes are lacking (Peterson et al. 2001). In many cases a diffuse subpial demyelination can be found (Bö et al. 2003).

Microscopically, the earliest stage of the MS plaque consists of perivenular lymphocytic infiltration. Such lesions are now found more easily using postmortem MRI as a guide (De Groot et al. 2001). The subsequent stage is characterized by more diffuse tissue infiltration by inflammatory cells and macrophages associated with edema, demyelination, proliferation, and hyperplasia of astrocytes, and appearance of in-

creased numbers of lipid-laden macrophages and demyelinated axons. Axonal damage already occurs during the phase of acute demyelination. Loss of myelin and oligodendrocytes eventually becomes complete. As plaques enlarge and coalesce, the perivenular distribution becomes less apparent. Although variable between patients, axonal damage can be extensive from early on. In the course of time, axonal loss can become very substantial (Bjartmar et al. 2003). In the gray matter plaques, too, the myelin is predominantly affected and neuronal cell bodies are largely preserved. In lesions of several months' duration, inflammation is far less pronounced, fewer lipid-laden macrophages are seen, and fibrillary gliosis becomes increasingly prominent. Chronic-inactive MS plaques have a sharply demarcated border and are hypocellular, demyelinated, and gliotic with almost total oligodendrocyte loss. Inflammatory cells and lipid-laden macrophages are no longer present. The remaining elements are axons and astrocytic processes. Axonal damage has led to wallerian degeneration, which is most evident in the long tracts. Rarely is the damage sufficiently severe to produce a cyst. In the same patient lesions of different ages are present.

In MS, plaque-like areas are observed, in which myelin has not completely disappeared, and which do not have the appearance of the typical plaque. These lesions are called shadow plaques. The myelin sheaths in these plaques are abnormally thin and are of relatively uniform thickness. The internodes are short. The number of oligodendrocytes is increased in the lesion. These features are characteristic of remyelination, and so the shadow plaques probably represent areas of remyelination.

The description as given fits the relapsing-remitting form of MS. Histological examination is usually performed in patients who have suffered from the disease for a long time. An exception is the acute form of MS, in which the lesions are days to weeks old and show acute inflammatory and demyelinating changes. As a consequence of the lack of early histological information, there is no parallel description of histology in some clinical MS subtypes, such as benign MS. In primary progressive MS more diffuse demyelination with more diffuse and less intense inflammation is found. A mixture of the multiple lesions and the diffuse pattern is seen in patients in whom the disease was initially relapsing-remitting, but secondarily became progressive in its course.

Immunocytochemical studies have demonstrated that the inflammatory cells of acute MS plaques are mainly macrophages and lymphocytes, with few plasma cells. Macrophages stain positive for the major histocompatibility complex (MHC) class II, which implies a role for these cells in local antigen presentation to T cells. The T cells present are a mixture of CD4+ (helper-inducer) and CD8+ (suppressor-cyto-

toxic) T lymphocytes. Initially these T lymphocytes are predominantly present in the center of the plaque, but as the lesion enlarges, T cells move to the peripheral part of the lesion. The CD4+ cells invade the normal white matter. The majority of the inflammatory T cells in MS are memory cells. The margins of the plaque contain predominantly CD8+ cells and increased numbers of oligodendrocytes and astrocytes. With increasing age of the plaque, myelin and macrophages disappear from the central part; the plaque margins contain lymphocytes, oligodendrocytes, lipid-laden macrophages, and astrocytes, suggestive of low-grade activity at these margins. In chronic-active MS, small numbers of inflammatory cells are scattered throughout the normal-appearing white matter, suggestive of a diffuse, slow demyelinating process. Chronic-inactive MS lesions contain few inflammatory cells. In chronically affected tissue an interesting recent finding is the presence of T cells and their association with heat shock proteins expressed on oligodendrocytes. These cells have previously been implicated in the pathogenesis of rheumatoid arthritis, but the presence of these cells with still unclear function now seems to be a more general finding in autoimmunity. They may play a role either in tissue repair or in perpetuating the inflammatory process.

In the review of Lassman et al. (2001) four different types of histopathological reactions were distinguished, possibly reflecting four different types of MS lesions: (1) macrophage-mediated, with T-cell-mediated inflammation as a putative mechanism; (2) antibody-mediated, with T-cell-mediated inflammation with complement-mediated lysis of antibody-targeted myelin as a putative mechanism; (3) distal oligodendroglialopathy, with T-cell-mediated small vessel vasculitis with secondary ischemic damage of the white matter as a putative mechanism; and (4) primary oligodendrocyte damage and secondary demyelination, with T-cell-mediated inflammation and demyelination induced by macrophage toxins on the background of metabolically impaired oligodendrocytes as a putative mechanism. It is clear that such a postmortem classification does not easily translate into clinical practice, but it may help a better understanding of the differences between subtypes of MS.

In NMO the spinal cord, optic nerves, and chiasm appear swollen and congested externally if the patient has died relatively early in the course of disease. Demyelination and inflammation with perivascular lymphocytic infiltration and fat granules are seen at microscopy. In severe cases necrosis of gray and white matter occurs, leading to cavitation. However, at the periphery of such lesions the relative sparing of axons is evident. Acute lesions may be hemorrhagic. The spinal cord lesion is often large and extends over many segments, usually in the low cervical and high

thoracic areas. Lesions in the conus may also occur. In the optic nerves and chiasm extensive loss of myelin, gliosis, and some loss of axons occur. As a rule, additional areas of demyelination are found in the predilectional regions of classical MS, such as periventricular areas and brain stem.

The characteristic lesions in CS are areas of alternating zones of myelinated and demyelinated tissue, either with a concentric pattern or with a more irregular arrangement. The size of lesions varies from tiny to about 4–5 cm in diameter. The location and number of lesions vary widely. Sometimes large areas are almost completely involved. The lesions may occur anywhere in the CNS; only the spinal cord is rarely affected. The rings of the lesion terminate abruptly where they contact gray matter. The central core is the starting point of the lesion and consists of a venule with a cuff of inflammatory cells. In the course of time, the central core becomes intensely gliotic. The core is surrounded by zones of demyelination, in which axons are preserved and myelin is replaced by gliosis. With increasing distance from the core, the stage of myelin breakdown in the affected zones becomes less advanced, and the gliosis is less severe. Acute lesions are surrounded by edema. In chronic lesions the involved area becomes scarred and atrophic. The concentric lesion may become so disintegrated that it is difficult to recognize. Ultrastructural examination of the myelinated zones reveals that they are largely composed of thinly myelinated fibers. A few normally myelinated and some demyelinated axons are also present. These bands contain many cells, including oligodendrocytes, lymphocytes, and astrocytes. These changes are reminiscent of those seen at the edge of a chronic-active MS plaque and are interpreted by some as zones of remyelination. Throughout the white matter, numerous venules show cuffs of inflammatory cells. Very often there are also lesions characteristic of classical MS.

In DS widespread demyelination is found, with variable axonal damage in the centrum semiovale of both cerebral hemispheres, most often involving the occipital lobes. Usually the corpus callosum is also affected and interconnects the lesions of the two sides. The lesions are not completely symmetrical. They have a sharp edge. A rim of subcortical white matter is commonly preserved, but a lesion may also spread into the gray matter. In the acute stage demyelination is associated with dense perivascular infiltrates of lymphocytes, plasma cells, and lipid-filled macrophages. The myelin disintegration leads to the formation of sudanophilic material. Areas may become frankly necrotic, and cavitation may occur. Glial reaction is present, with giant multinucleated and hypertrophied astrocytes. In cases of long duration, inflammatory cells and macrophages containing sudanophilic material disappear. Evidence of wallerian de-

generation is common. There are not only naked axons but also axons partially covered with thin layers of myelin as signs of abortive remyelination.

79.3 Chemical Pathology

Chemical analysis of the composition of MS plaques reveals a number of alterations: increase in water, decrease in total lipid, in particular in cholesterol, cerebrosides, sulfatides, ethanolamine plasmalogens, and serine phosphoglycerides. Cholesterol esters are increased. In the lesion the major myelin proteins – myelin basic protein, proteolipid protein, and myelin-associated glycoprotein – are reduced. Myelin basic protein is in fact virtually absent from the center of most plaques, and the decrease in concentration of myelin-associated glycoprotein extends into the normal-appearing white matter around the plaque, suggesting that this protein disappears or is altered before myelin breakdown starts. The protein losses in the plaque are accompanied by an increase in proteins of a lower molecular weight, which may be proteolytic breakdown products. In and around the MS lesion proteinases and other hydrolytic enzymes are increased. The observed chemical changes in the MS plaques are variable and depend on the extent of demyelination. An early MS lesion contains more myelin and more sudanophilic material, which is biochemically defined as cholesterol esters. Old plaques have no or little myelin left and lack sudanophilic material.

Myelin isolated from the plaque has a composition typical of abnormal myelin during aspecific degradation. No myelin abnormalities specific for MS have been demonstrated.

Much effort has been devoted to the study of the chemical composition of normal-appearing white matter in MS. In the first place, the myelin yield of the normal-appearing white matter is strikingly low. There is a decrease in total lipid, in phospholipids (particularly ethanolamine plasmalogens), in both galactolipids (cerebroside, and sulfatide), and in myelin proteins. Frequently, cholesterol esters are found. Several investigators found an elevation of hydrolytic enzymes in normal-appearing white matter. These findings are qualitatively similar to those observed in MS plaques, but are considerably smaller in magnitude. All these data together provide strong evidence for the presence of minor microscopic abnormalities of the MS type in the white matter that appears macroscopically normal. This suggestion has been confirmed by microscopic examination of samples of normal-appearing white matter. It is clear that the disease process is widespread and not simply restricted to plaques. There is a general myelin deficit throughout the white matter.

79.4 Pathogenetic Considerations

The search for the cause of MS has engaged many investigators for many years. Three main lines can be distinguished in theories about the etiology of MS: one line stressing the importance of immunological reactions, the second line pointing to the evidence for genetic factors, the third one advocating environmental factors. These lines are complementary and not mutually exclusive.

A major theory proposes that MS results from alterations in the *immune system*. A suggestion in this direction came from the observation of some similarity between MS and experimental allergic encephalomyelitis (EAE) in animals. EAE is induced by immunizing animals with antigens normally present in the CNS myelin, such as myelin basic protein (MBP), proteolipid protein (PLP), and myelin oligodendrocyte glycoprotein (MOG), with an adjuvant containing heat-killed mycobacterium to stimulate the innate immune system. In about 1–2 weeks the animals develop encephalomyelitis with perivascular infiltrates composed of lymphocytes and macrophages in the white matter, followed by demyelination. In mice EAE is caused by activated CD4+ T cell lymphocytes specific for MBP, PLP or MOG, as proven in vitro and in cloning experiments. The lesions of EAE and of MS have the character of delayed hypersensitivity reactions. The sequence of events in EAE and possibly by analogy MS could be as follows: autoreactive T cells specific for myelin proteins may be present in the circulation of normal individuals. Immunization with a myelin antigen together with an adjuvant leads to T cell activation against epitopes of autologous myelin proteins. Activated T cells stick to the endothelial lining and cross into the cerebral parenchyma. In the CNS the activated T cells encounter myelin proteins and release cytokines that recruit and activate macrophages and other T cells that lead to myelin destruction. EAE has been used to analyze the specificity of myelin-reactive T cells and help to define immunodominant regions of myelin proteins that may be relevant to MS in humans.

Abnormalities of immunoregulation and of humoral and cellular immunity appear to be an important part of the disease process in MS. Inflammatory cells – lymphocytes, plasma cells, and macrophages – are present in perivascular areas in the CNS in active disease and take part in the disease process. In nearly all MS patients, there is evidence for an increased synthesis of immunoglobulins within the blood–brain barrier. A low CD8+ T suppressor cell activity and a high ratio of CD4+ T helper to CD8+ T suppressor cells is present in the blood during exacerbations of MS, and also chronically progressive MS patients have similar abnormalities of peripheral blood T lymphocyte subsets. The high levels of antiviral antibodies,

indicative of hyperactive B lymphocytes, and the deficiency of suppressor T lymphocyte function may be signs of a fundamental defect in immunoregulation. The role of CD8+ suppressor-cytotoxic cells versus CD4+ helper cells has been a point of discussion. These subsets interact with specific MHC molecules to regulate the immune response. MHC class II restricted CD4+ T cells are the major producers of cytokines and are associated with delayed-type hypersensitivity and antibody response. MHC class I restricted CD8+ T cells are associated with cytotoxicity. There is evidence that CD4+ cells are the key initiators of tissue destruction in MS. CD8+ T cells have received less attention, but there is growing evidence that MHC class I restricted CD8+ T cell responses may have a critical role in the pathogenesis of MS. In addition to CD4+ cells, CD8+ lymphocytes are present in active demyelinating lesions, and in fact predominate in many lesions. CD8+ T cells recognize peptides presented by MHC class I molecules. Adult oligodendrocytes express class I MHC molecules and do not express class II MHC molecules, even when stimulated by interferon- γ . This implies that when adult oligodendrocytes are targets for T cell reactivity, they will probably be recognized by MHC class I restricted CD8+ T cells and not by class II restricted CD4+ T cells.

The cause of the immunological alterations in MS and their role in the pathogenesis of MS have not yet been elucidated. The antibody response in the CSF may be an expression of an autoimmune process against normal or altered brain constituents. This autoimmune process may be idiopathic, or triggered by a viral infection or other exogenous or endogenous antigens that cross-react with brain constituents. Low concentrations of antibodies have been demonstrated in the CSF reacting with myelin proteins, oligodendroglia, glycolipids, and nuclear antigens, but no single MS-specific antigen that reacts with most of the IgG has ever been identified. It is not excluded that the observed antibodies are epiphenomena without pathogenetic importance. Another explanation may be that T helper-inducer lymphocytes in MS are activated and autoreactive. Many other changes in immune-related factors have been observed, such as circulating immune complexes, altered levels of cytokines and complement components, and increased prostaglandin synthesis, but the significance of these findings is not known. A convincing observation about the role of immune responses in MS has been the decrease in MS-activated lesions in pregnant women. There is a sharp decrease in lesions in all cases, with a return to the prepregnant status in the months after delivery. In another study, the beneficial effect of pregnancy was indicated by the finding that the mean disease duration before becoming wheelchair-dependent was 50% longer in pa-

tients who became pregnant after the first symptoms of MS.

Lymphocytes become activated by an unidentified cause and by a multistep process penetrate the blood–brain barrier. The capillary endothelial cells in the CNS are not fenestrated and are connected through tight junctions. The capillary endothelial cells express cellular adhesion molecules (V-CAM) and class II molecules of the MHC. Activated lymphocytes can pass the endothelial barrier assisted by adhesion molecules such as integrins, in particular α_4 integrin, which binds to V-CAM. Once the activated lymphocytes have extravasated, they still need help in passing through a barrier of extracellular matrix consisting of type IV collagen. T cells are then targeted to proteins of the myelin sheath, myelin basic protein, myelin oligodendroglial glycoprotein, and proteolipid protein, as well as stress proteins like α B crystallin, present in the myelin sheath after activation by the inflammatory response. T cells produce cytokines, notably TNF- β and TNF- α , and then influence macrophages, microglial cells and astrocytes to produce nitric oxide, a major mediator in inflammatory reactions, and osteopontin, a multifunctional protein abundantly expressed during inflammation. Macrophages and microglia are induced to phagocytose large pieces of the myelin sheath.

This short and incomplete summary of the initiation of the inflammatory process is intended to give an impression of the complexity of the process, in which the role of the many players only gradually becomes clear. Knowledge of this process in detail has already opened therapeutic windows and will open more in the future. It helps us to understand why many therapeutic interventions only yield partial results. Much still depends on the unraveling of the primary cause of the inflammatory reaction.

The evidence for *genetic factors* comes from reports of familial cases and unusually high-risk families, and from studies which consistently show higher concordance rates for MS in monozygotic twins than in dizygotic twins. The concordance rate in monozygotic twins reported in the literature varies from 10% to 70%, and that in dizygotic twins from 2.3% to 20%. Selection bias probably leads to overestimation of the rate of concordance among twins. On the other hand, however, a twin sample collected at one point in time probably underestimates the concordance rate, as more individuals will develop MS in the course of time, and the concordance rate will increase with increased duration of follow-up. The prevalence of MS among relatives of MS patients is increased, and the increase becomes more pronounced the closer the degree of kinship to the probandus. This observation is consistent with a genetic hypothesis, but common environmental experiences with relatives, and especially twins, may also play a role. The low overall twin

concordance rate (a concordance rate of 100% would be expected among monozygotic twins if MS were exclusively genetically determined), and the increased prevalence of MS in dizygotic twins as compared to siblings (1–6% of the siblings of MS patients are also affected) strongly suggests the involvement of environmental as well as genetic factors.

Further evidence for a genetic component in the etiology of MS comes from the observation of associations between MS and specific human leukocyte antigen (HLA) alleles. The HLA genes encoding for these antigens, which are expressed on cell surfaces of lymphocytes, are found on the short arm of chromosome 6. The HLA system consists of five loci – A, B, C, D, and DR – and each of the HLA loci has a large number of alleles. The HLA region can be used as an excellent genetic marker with known chromosomal location. There is a highly significant association between HLA-DR2 and MS and a less strong association between HLA-A3 and B7 and MS in Caucasians. However, there are great differences in observed HLA associations in populations of different racial background, and it is clear that the mentioned HLA alleles in themselves are neither necessary nor sufficient to lead to the development of MS. The meaning of the HLA associations is not entirely understood. A likely explanation is that the MS-related gene or genes lie on the same chromosome as the HLA genes and are in linkage disequilibrium with specific HLA alleles. This means that certain combinations of alleles occur significantly more frequently than would be expected by chance. It is also possible that specific HLA alleles are directly involved in the etiology of MS. The HLA system is part of the immune response system. Alleles of certain class II genes, HLA DR and HLA DQ, confer the strongest risk of MS. In addition to the well-established MHC association, genome-wide screens of families with multiple cases of MS also suggest a role for several additional unidentified genes, each with a modest effect. Transcriptional profiling using gene microarrays and large-scale sequencing of transcripts from MS lesion material reveal expression of genes involved in the pathogenesis of acute disease, like immunoglobulins, interleukin 6, and osteopontin.

It is clear that MS is not a genetically determined disease with a Mendelian mode of inheritance. It is more probable that multiple susceptibility genes for MS exist, and that the expression of subtle changes in these genes (polymorphisms) depends on environmental factors. The chromosomal localization of some of the genes determining susceptibility to MS is probably in or near the HLA region, or their expression depends on the action of certain HLA alleles. A method consisting of pooling DNA from MS individuals and typing these pools for around 60,000 microsatellite markers, suggested by Barcellos et al.

(1997), was realized in an extensive study known as Genetic Analysis of Multiple Sclerosis in EuropeanS (GAMES), described by Sawcer and Compston (2003). GAMES is essentially an indirect screen for association and is therefore dependent on the assumption that at least some of the markers tested will have alleles in linkage disequilibrium with gene variants that influence the susceptibility to MS. All previous genomic screens in MS families only suggested linkage with 6p21, the area containing the genes for the major histocompatibility complex. Although its approach has limits and flaws, GAMES may have the potential of identifying one or more novel associations outside the MHC region at 6p21.

Epidemiological studies of migrants suggest that *environmental factors*, particularly when present before the age of 15 years, are involved in the etiology of MS. One of the most important theories about the nature of the environmental factors speculates on a viral etiology. However, a causative virus has never been reproducibly isolated from the CNS of MS patients, nor has viral antigen been demonstrated in a consistent fashion. Ultrastructural examination of brain tissue has never unequivocally revealed virus particles. Antibodies to multiple viruses are elevated in the CSF of MS patients. It is probable that these antibodies result from a nonspecific immunostimulation. It is commonly accepted that relapses in MS are often triggered by infection with viruses. Viruses, such as herpes virus-6, influenza, measles, papilloma virus, and Epstein-Barr virus, have genes encoding peptides containing amino acid sequences similar to those found in the major structural proteins of myelin. Antibodies reacting with protein sequences from these microbes may cross-react with components of the myelin sheath. T cells also recognize peptide sequences in the myelin sheath that are shared with microbial sequences. Once an immune cell is activated, either by a foreign microbe or a self-protein, it may penetrate the blood-brain barrier and the inflammatory cascade as described above will follow (Buljevac et al. 2002).

The precise nature of the *relationship between MS, CS, NMO, and DS* is not known. The frequent occurrence of histopathological typical MS lesions in CS, NMO, and DS provides evidence for essential similarities in etiology and pathogenesis. In NMO, it is important to distinguish the MS-related disease from acute disseminated encephalomyelitis and a vasculitic process, especially lupus erythematosus, both of which may produce an identical clinical picture and a rather similar pathological picture. As NMO is relatively frequent in Asian populations, it has been suggested that racial-genetic factors lead to a modified appearance of MS.

In CS, some consider the concentric lesion to be a variant of an MS plaque in which the center of the lesion represents the initial small focus of acute demyelination, and in which the concentric rings are formed by a centrifugal progression of episodes of demyelination and remyelination. The zones of preserved myelin within the concentric lesions are supposed to be formed by episodic remyelination at the borders of demyelinating foci, which is followed by further centrifugal spread of the demyelination. A remarkable difference with MS is that the concentric lesion never invades gray matter structures, unlike MS plaques. There is, as yet, no explanation for the higher incidence of CS in the Philippines.

Loose and indiscriminate use of the term “diffuse sclerosis” (DS) has led to a great deal of confusion in nomenclature. Schilder was the first to describe the disease in three cases of what he called “encephalitis periaxialis diffusa.” However, on closer inspection of clinical data and neuropathological findings, it was concluded that one of these patients probably had X-linked adrenoleukodystrophy and another acute disseminated encephalomyelitis. Only one patient is now considered to be an example of DS. After Schilder many authors used the name “diffuse sclerosis” for a wide range of unrelated demyelinating disorders. It is true that a number of diseases, especially X-linked adrenoleukodystrophy, may be difficult to differentiate from DS on clinical and pathological grounds alone. In these cases, assessment of various enzyme activities and ultrastructural examination are indispensable in establishing the correct diagnosis. In the course of time, an increasing number of diseases could be distinguished from DS, and some investigators have suggested abandoning the term “Schilder DS.” However, we are of the opinion that the term “Schilder DS” should be reserved for myelinoclastic diffuse sclerosis as a variant of MS. The pathology of DS does not differ substantially in its light or electron microscopic appearances from the classical disseminated form of MS. The only difference involves the dimension of the demyelinating lesions and the rapid progression of the process. In 1985, Poser offered the following definition of DS: the disease is a subacute or chronic myelinoclastic disorder resulting in the formation of one or more, commonly two, roughly symmetrical plaques measuring at least 2×3 cm in two of the three dimensions, involving the centrum semiovale of the cerebral hemispheres. Other diseases that can lead to a similar picture should be excluded. According to this view, the pathogenesis of DS is largely identical with that of MS, and the question is which factor is responsible for the difference. It has been suggested that the large areas of demyelination may be due to the fact that the child’s nervous system, be-

ing still immature, is more susceptible to an injurious agent. It is improbable, however, that the immaturity of the brain alone accounts for the difference compared to classical MS, as classical MS can also occur during childhood.

The correlation between neuropathological lesions and clinical signs and symptoms is rather poor in MS. There are many silent lesions. Clinically silent lesions probably occur when demyelination affects some but not all fibers of a pathway, or when remyelination occurs. A conduction block occurs in demyelinated fibers, but conduction remains intact in unaffected fibers. The very transient symptoms in MS are probably related to a reduction of the functional reserve of a fiber tract for the conduction of nerve impulses because of demyelination. Slight alterations of conduction capacities, e.g., those due to a rise in body temperature, may result in the appearance of symptoms from a fiber tract in which a plaque has reduced the functional reserve but not to less than the minimum number of fibers necessary for normal function. Improvement occurs as soon as conduction of electrical impulses is restored. Recovery after a relapse is probably largely related to remyelination, which leads to abolition of the conduction block.

79.5 Therapy

The interest in an immunological basis for MS has led to the development of a variety of treatments designed to alter or suppress the immune response. One of the first of these studies advocated the use of adrenocorticotrophic hormone (ACTH) in acute exacerbations. It was demonstrated that ACTH shortens the recovery time but does not alter the eventual level of recovery. More recent studies indicate that high-dose intravenous methylprednisolone also hastens recovery, but that the effect on suppression of gadolinium-enhancing lesions, used as surrogate marker of MS activity, is short-lived. Intrathecal corticosteroids did not prove to be any more helpful than orally administered corticosteroids.

More aggressive immunosuppressive agents have also been used, such as azathioprine, cyclophosphamide, cyclosporin A, and total lymphoid irradiation. Plasma exchange has been used in limited studies. However, the limited beneficial effects of these treatment modalities usually do not outweigh the often serious side effects. Recently the intravenous administration of immunoglobulins has been the subject of interest.

Success has been reported with interferon beta-1b (IFNB) in relapsing-remitting MS, with significant favorable effects on exacerbation rates, times between first and second exacerbations, severity of exacerbations, MS activity, and lesion load as determined by

MRI. However, IFNB is only partially effective at the tested doses. Patients in the high-dose group continued to have exacerbations, although at a reduced rate and of milder clinical severity. The beneficial effect of IFNB is probably due to its ability to inhibit interferon- γ (IFNG) synthesis, to improve defective suppressor activity in MS patients, and to inhibit MHC class II antigen expression induced by IFNG on the surfaces of antigen-presenting cells. Patients in the chronic progressive phase still with relapses also benefit from continuous IFNB treatment. The indications for IFNB are relapsing-remitting forms of MS and clinically isolated syndromes. Interferons are less effective in primary progressive MS and secondary progressive MS.

Mitoxantrone (Novantrone in the US and Canada), which belongs to the group of tumor antibiotics, has been evaluated in a number of studies. Patients were treated with intravenous administration every 3 months for 24 months. Mitoxantrone was found to delay the time to first treated relapse and time to disability progression in patients with secondary progressive disease or progressive relapsing-remitting disease. Monitoring of white blood cells and liver function remained necessary because of an increased risk of infection.

Copolymer 1, known as glatimer acetate, is a mixture of polypeptides (L-alanine, L-lysine, L-glutamine, and L-tyrosine) that acts as an immunological agent and appears to simulate myelin basic protein. It has been reported to reduce the number of relapses with possible improvement of functional abilities. Its greatest advantage is its low toxicity. Glatimer acetate stimulates antigen-specific suppressor cells. T cells activated by glatimer acetate protect against inflammatory damage by the production of anti-inflammatory cytokines. It reduces the number of relapses. It is effective in MS patients under the age of 16 years. Long-term studies indicate that the EDSS score in patients treated with glatimer acetate hardly increases over the years and that outcome parameters such as brain atrophy and black holes show favorable results. In MRS studies the N-acetylaspartate (NAA) increases with treatment. Probably this effect is due to the increase of brain-derived neurotrophic factor under glatimer acetate treatment.

The glycoprotein $\alpha_4\beta_1$ integrin, also known as very late antigen 4 (VLA-4) is expressed on the surface of lymphocytes and monocytes and is an important mediator of cell adhesion and transendothelial migration. Treatment with an antibody against α_4 integrin reduced signs of disease activity and inflammation in mice and gave positive results in a small, placebo-controlled clinical trial with a humanized monoclonal antibody (natalizumab) (Miller et al. 2003).

New treatment modalities are based upon the understanding of T cell activation and cytokine produc-

tion in autoimmune diseases. From a therapeutic point of view there are several ways in which excessive effector functions of activated T cells can be counteracted, for instance by injection of monoclonal antibodies against T cell membrane molecules. The presence of excessive intrathecal immunoglobulins in MS may be related to the activation of CD4+ T lymphocytes, also inducing B lymphocyte production. A large multicenter anti-CD4+ antibody trial was started, but the lack of efficacy has ended this trial in an early phase. As monoclonal antibodies act more selectively, they may be more effective in suppressing disease activity.

Far fewer therapeutic trials have been performed in CD, NMO, and DS. In these groups no reports on the effects of INFB or glatimer acetate are available. In CD a beneficial effect of prednisone therapy has been described, but not consistently. In NMO remarkable improvement has been reported under treatment with corticosteroids, immunosuppressants, and lymphocyte plasmapheresis. However, due to the very low incidence of NMO, no controlled trial has provided proof of such favorable effects. In DS a good clinical reaction to corticosteroids, ACTH, and immunosuppressants is generally observed.

Many other attempts have been made to control the progress of MS. In this section we discuss some prominent endeavors – certainly not all of them – to demonstrate the many possible entries to the disease process.

Finally, and also importantly, there are many palliative measures to ease the problems of MS patients: physiotherapy is helpful in keeping the patient mobile as long as possible; spasmolytic drugs have a place in combating spasticity and bladder dysfunction; and antibiotics are necessary in intercurrent infections.

79.6 Magnetic Resonance Imaging

MR has obtained a prominent role in diagnosis, follow-up, therapy monitoring, and research in MS. MRI protocols for patients with or suspected of having MS depend on the clinical symptoms and the information required from the MRI. Different techniques yield different information (Table 79.2).

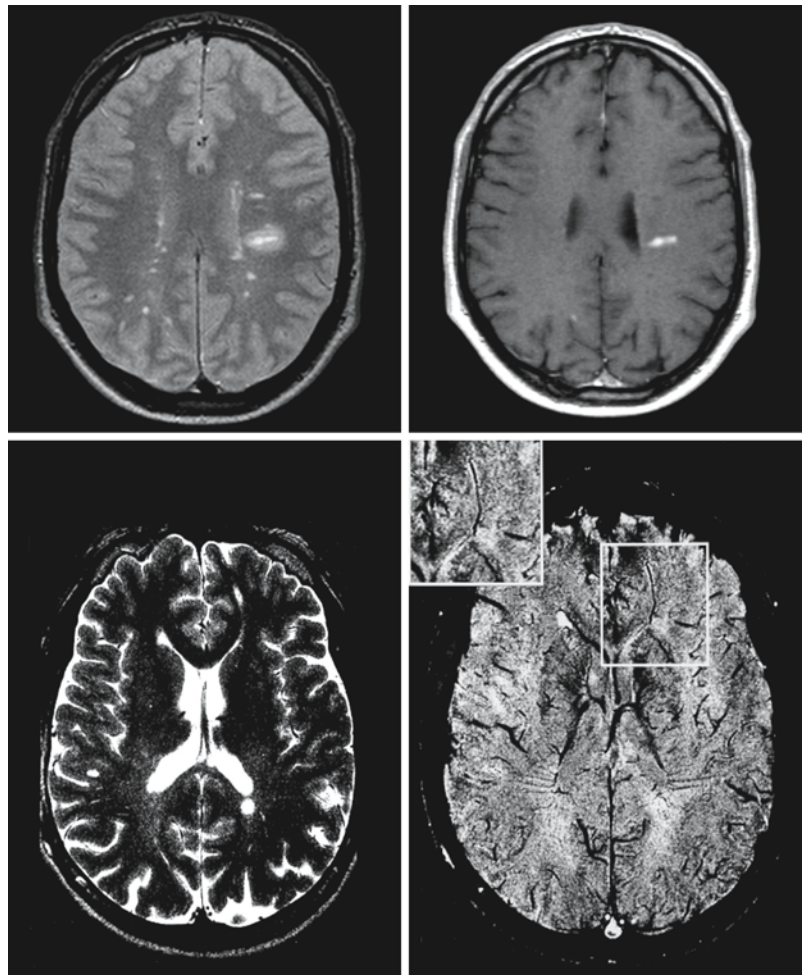
The most common MRI appearance of the relapsing-remitting and secondary progressive forms of MS consists of multiple lesions with intermediate or low signal intensity on T₁-weighted images, high signal intensity on T₂-weighted images, isolated or confluent or both, with a bilateral but usually not entirely symmetrical distribution, and preferentially located along the lateral angles of the ventricles in the efferent and afferent tracts of the corpus callosum (Figs. 79.1–79.5). Some of these lesions have a typical ovoid form, pointing towards the convexity of the brain, known as Dawson's fingers (Figs. 79.1, 79.5). This is the result of the perivenular distribution of MS lesions. This is known from histopathology, but can now also be illustrated by high-resolution MR venography (Fig. 79.1). The corpus callosum is thinner than usual and the inner rim has an irregular border related to the presence of lesions. Parasagittal and sagittal T₂-weighted and FLAIR images show this to best advantage (Fig. 79.5). Other lesions are spread over the frontal, parietal, and occipital white matter and, less frequently, the temporal lobes. There are no or few lesions in the basal ganglia. Lesions may occur in the midbrain (8%), pons (12%), cerebellar hemispheres (4%), and medulla oblongata (1–2%). Specific structures may be involved, such as the medial longitudinal fasciculus (clinically presenting as internuclear ophthalmoplegia), the trigeminal nucleus or emerg-

Table 79.2. MR sequences that may be included in a protocol with an indication of the MS features in which they are effective. This list serves as a general orientation and is not intended to be a protocol applicable to all MS patients.

<i>Conventional:</i>	
T ₁ -weighted, transverse	"Black holes," "gray" holes, prognosis
T ₂ -weighted and proton density, transverse	T ₂ lesions, distribution, lesion load
FLAIR (2D, 3D)	Most sensitive for T ₂ lesions
T ₁ -weighted with gadolinium	Active lesions, blood-brain barrier disruption
FLAIR sagittal	Corpus callosum lesions
STIR	Visual pathways, optic neuritis
Proton density, T ₁ -weighted, cardiac gated	Spinal cord lesions
<i>Special:</i>	
MTR or histograms	Structural integrity, follow-up, research, study of normal appearing white matter
DWI, DTI	Structural changes, ADC, FA, fiber tracking
MRS	Chemical composition

FLAIR, fluid-attenuated inversion recovery; STIR, short tau inversion recovery; DWI, diffusion-weighted imaging; DTI, diffusion tensor imaging

Fig. 79.1. The *upper row* of images shows *left* a proton density image with a typical ovoid lesion and *right* a T₁-weighted image with intravenous contrast, with enhancement of the lesion. The *lower row* of images shows a special high-resolution technique that allows submillimeter venography of the CNS. The image on the *right* shows the lesion extending from the frontal horn towards the convexity in its relation to the local perforating vein. From Tan et al. (2000), with permission



ing nerve (presenting as trigeminal neuralgia), and the vestibular nucleus (presenting with vertigo) (Figs. 79.6 and 79.7). Cortical lesions are often present but are difficult to appreciate on MRI. Cortical lesions extending into the white matter or lesions located in the U fibers are well detectable (Fig. 79.8). Such juxtacortical lesions form an important hallmark of MS on MRI and have been incorporated into new diagnostic criteria (McDonald et al. 2001, see Table 79.1).

Depending on the clinical request, contrast may be given. Active lesions may enhance. Enhancement indicates disruption of the blood–brain barrier, probably the first local change of a developing MS plaque. Inflammation and edema will follow. The enhancement lasts between 2 and 6 weeks. MRI provides the possibility to identify acute, new or reactivated, lesions (Fig. 79.9). Enhancing lesions are often used in clinical trials as surrogate markers for disease activity. Contrast-enhanced MRI can help, not only by demonstrating “dissemination in space” with the presence of more than one lesion in the CNS at different locations, but by also demonstrating “dissemination in time” in showing older nonenhancing or no

longer enhancing lesions together with new or reactivated lesions that enhance. The most important role of gadolinium-enhanced MRI has emerged as monitoring the efficacy of drug treatment (Figs. 79.10 and 79.11). Long-term follow-up studies have shown that newly appearing gadolinium-enhancing lesions are far more frequent than clinical exacerbations in relapsing-remitting and secondary progressive forms of MS. If one accepts gadolinium enhancement as a sign of new disease activity, this can serve as a means of monitoring the therapeutic response of the disease to new drugs. It has been shown that changes in the number of gadolinium-enhancing lesions during the course of the disease correspond better to changes in the EDSS than changes in lesion load on T₂-weighted images. The apparent advantage for therapeutic trials is the gain in time and the smaller study population one has to examine to obtain statistical significance of results. The eventual clinical trial based on clinical results can in this way be limited to the most promising therapeutic compounds.

Two manifestations of MS outside the brain deserve special mention: optic neuritis and spinal cord

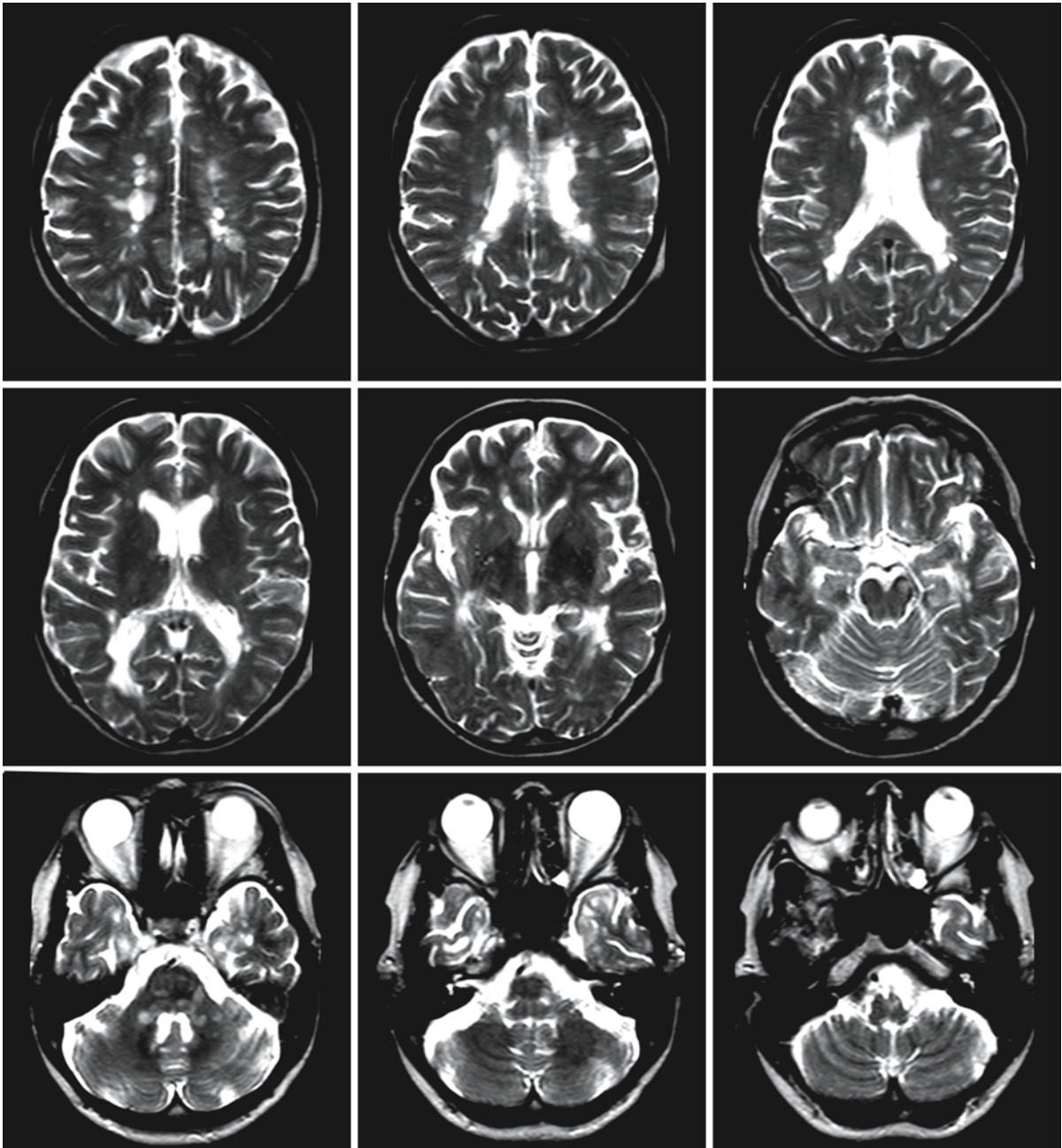


Fig. 79.2. The classical MR pattern of MS. The transverse T_2 -weighted series in this 42-year-old woman shows lesions in the centrum semiovale, around the lateral upper borders of

the ventricles, in the corpus callosum, in the mesencephalon, the pons, around the fourth ventricle, and in the medulla oblongata. There are no lesions in the basal ganglia

lesions, because they both require special MRI techniques.

The STIR sequence in particular has been effective in demonstrating optic neuritis. Other fat saturation techniques, using a saturation pulse to suppress the fat signal, can be combined with gadolinium enhancement (Fig. 79.12).

The majority of MS lesions of the spinal cord occur in the cervical spinal cord and the conus medullaris. In some patients lesions are solely present in the spinal cord. They appear most often as high-signal-intensity lesions on proton density and T_2 -weighted images and may enhance with contrast (Fig. 79.13). There is, as a rule, no or very little mass effect. Mass effect can, however, occasionally be considerable and

Fig. 79.3. Same patient as in Fig. 79.2. It is useful in patients suspected of having MS to include the spinal cord in the examination. The disability of the patient is often also or mainly related to the spinal cord lesions

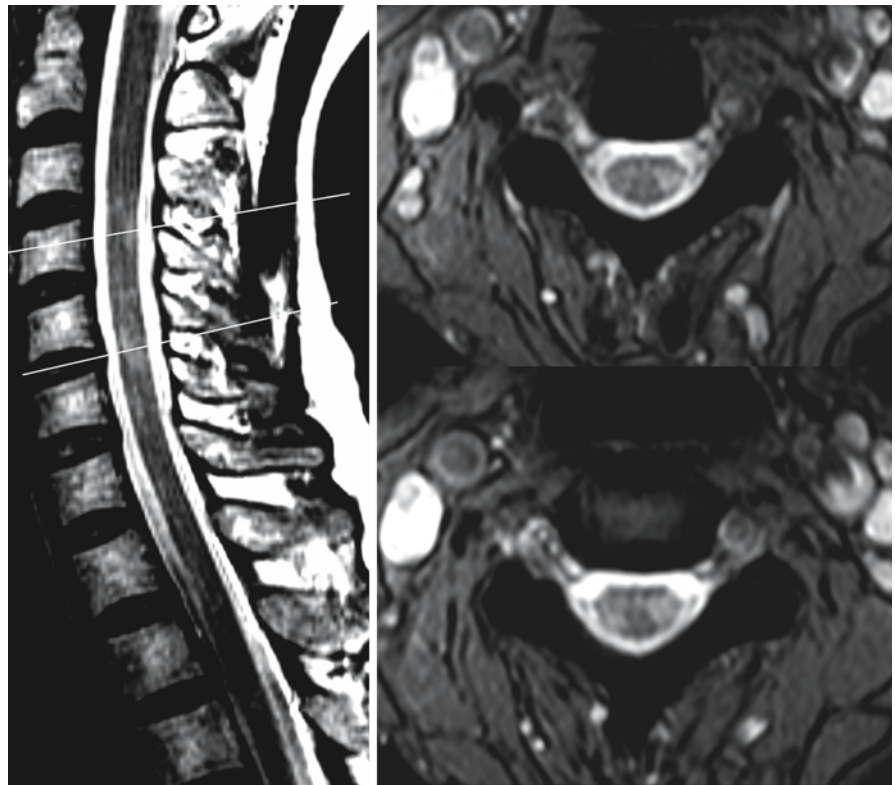


Table 79.3. Spinal lesions in patients with MS and patients with other neurological disorders. The difference is statistically significant (Bot et al. 2002)

Spinal cord	Normal	Abnormal
Other neurological disorders (n = 43)	39	4
MS (n = 25)	2	23

the lesion may then mimic an intramedullary tumor. When patients present with symptoms indicative of a spinal cord lesion, MRI of the spinal cord may be the first requested examination. If a lesion indicative of MS is found, an MRI of the brain should follow to look for corroborative evidence, in the form of lesions in the brain, to support the diagnosis of MS. The greatest technical problems in detecting spinal cord MS lesions are encountered in the thoracic region. Phased array coils have increased the signal-to-noise ratio and detail in studies of the spinal cord. Conventional dual-echo spin echo sequences with cardiac gating yield the best results (Fig. 79.14) (Lycklama á Nijeholt et al. 1996). In more than 90% of patients with MS, spinal lesions can thus be identified (Figs. 79.15–79.17). The detection of spinal lesions also helps in the differentiation of MS from vascular lesions (Table 79.3; Bot et al. 2002).

Indications, techniques, and the role of asymptomatic spinal cord lesions in the differential diagnosis from MS versus other diseases such as vascular disorders have recently been summarized (Lycklama á Nijeholt et al, 2003).

Many patients with definite MS do not fit the “typical” description given above. Nearly anything goes with MS. Lesions may show mass effect or become cystic. The distribution may not be typical. Criteria as suggested by Barkhof et al. (1997), incorporated in the McDonald criteria (see Table 79.1), are often helpful in establishing the diagnosis.

Sometimes MS presents with clinical signs of raised intracranial pressure and a tumefactive lesion on MRI, often enhancing. In quite a few patients this observation has prompted a brain biopsy. The presence of other white matter lesions and the “open ring” sign may lead to the correct diagnosis and management of the patient (Fig. 79.18). The open ring sign is often present in large, contrast-enhancing demyelinating lesions and consists of a partly enhancing ring around the lesion (Masden et al. 2000).

Much attention has also been given to clinical isolated symptoms (CIS) that may or may not progress to MS. This isolated symptom is often optic neuritis, but other signs are possible. MRI is a powerful predictor of the later diagnosis of definite MS, better than the presence of HLA-DR2 or CSF oligoclonal bands.

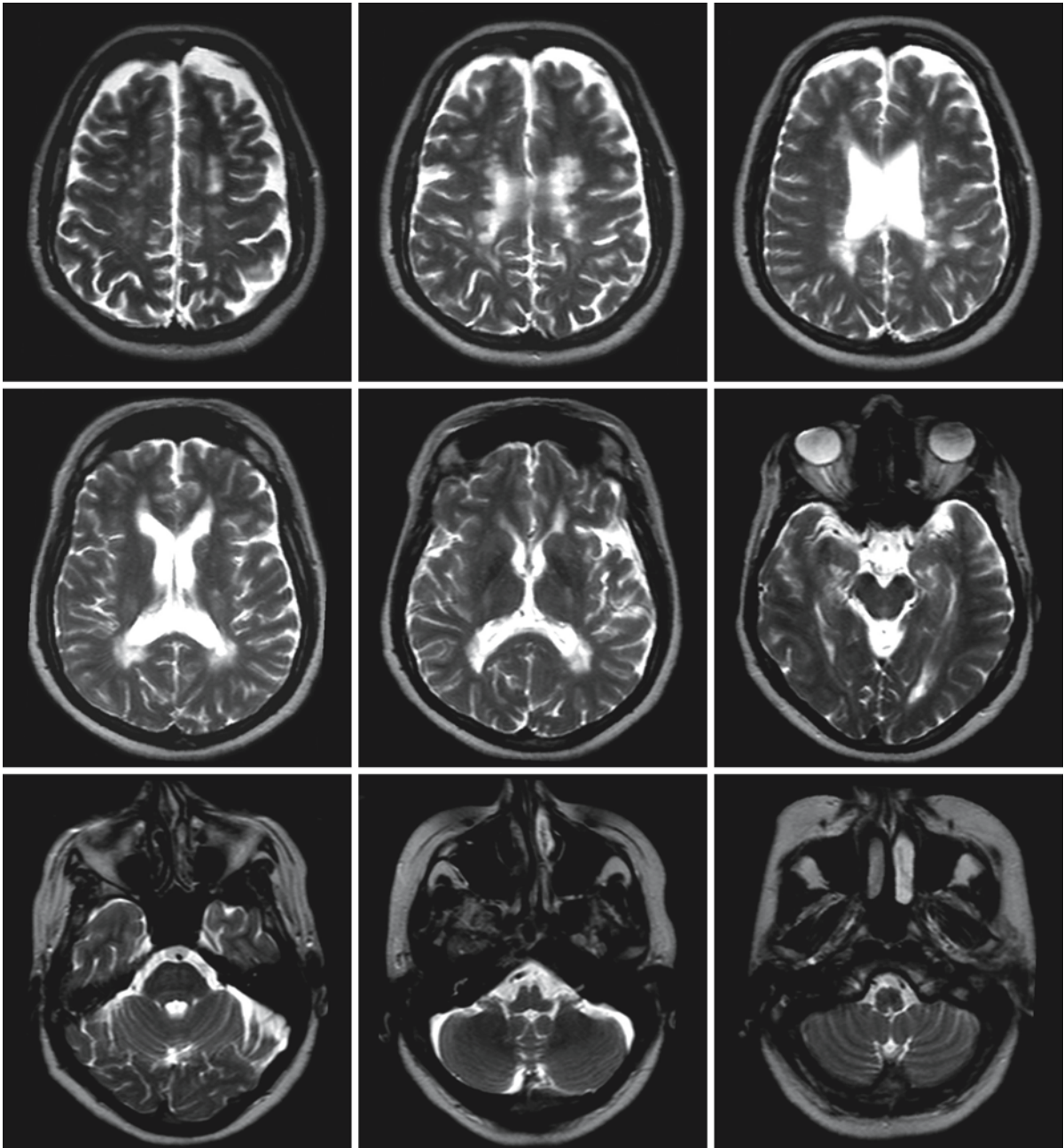


Fig. 79.4. A 38-year-old woman suspected of having MS. The MR picture is compatible with this diagnosis. The transverse T_2 -weighted images show lesions around the lateral borders

of the ventricles and the corpus callosum. There are no lesions elsewhere in the brain

Normal-appearing white matter (NAWM) has become an important issue in MRI of MS. MR techniques have confirmed the histopathological and chemical observations that white matter that appears normal on T_1 -weighted, T_2 -weighted, and FLAIR images show diminished structural integrity when magnetization transfer ratios (MTRs) are estimated (Fig. 79.19). With diffusion tensor imaging, ADC val-

ues of normal-appearing white matter are increased and FA values lower as compared to normal white matter in non-MS patients. Changes in metabolite concentrations on MR spectra lead to the same conclusion.

The relationship between the lesions demonstrated on MRI and clinical findings is generally speaking poor. In patients with advanced disease of the sec-

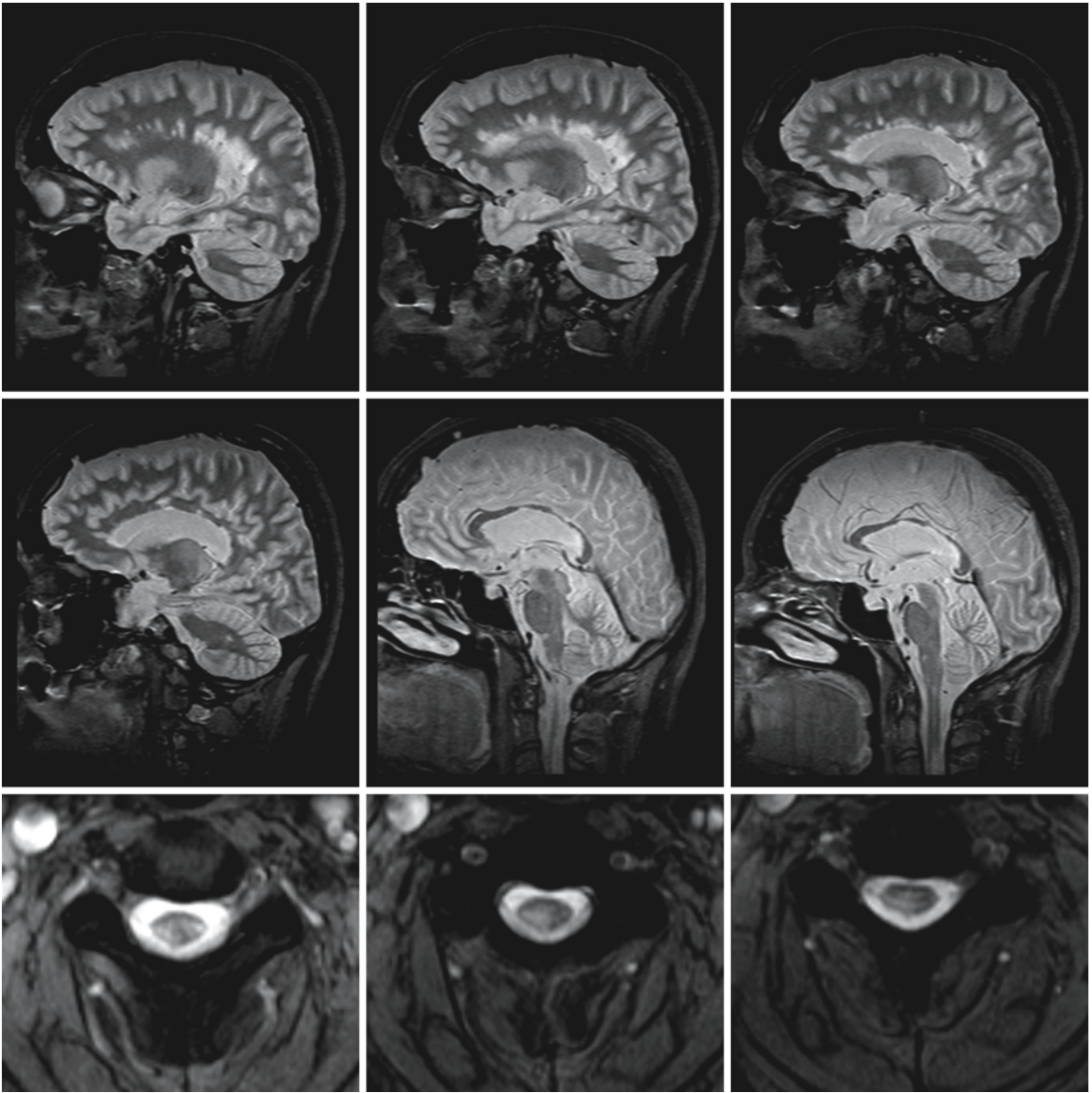


Fig. 79.5. Same patient as in Fig. 79.4. The *upper two rows* display sagittal and parasagittal proton density images, revealing the shape and extent of the lesions in the corpus callosum and

around the lateral ventricular borders. In this patient, too, multiple lesions in the spinal cord confirm the diagnosis

ondary progressive type, the correspondence between the developing atrophy and the number of white matter lesions and the EDSS disability score is better.

In estimating the prognosis of MS, so-called black holes have been proven to have a special place. “Black holes” are MS lesions that appear very dark on T₁-weighted images and bright on T₂-weighted images (Fig. 79.20). The presence of black holes correlates better with a poor prognosis than the presence of lesions on T₂-weighted images and gadolinium en-

hancement of lesions (Van Walderveen et al, 1995, 1998). Histopathologically, they correspond to areas with severe matrix destruction and axonal loss (Van Waesberghe et al. 1999).

There is a growing interest in remyelination, part of the healing process of MS. Some lesions disappear from MRI in MS patients with follow-up MRI, whereas others do not. The question is whether the disappearing lesions remyelinate and therefore become invisible, or shrink and turn into little gliotic scars. New MR methods may be helpful in answering this ques-

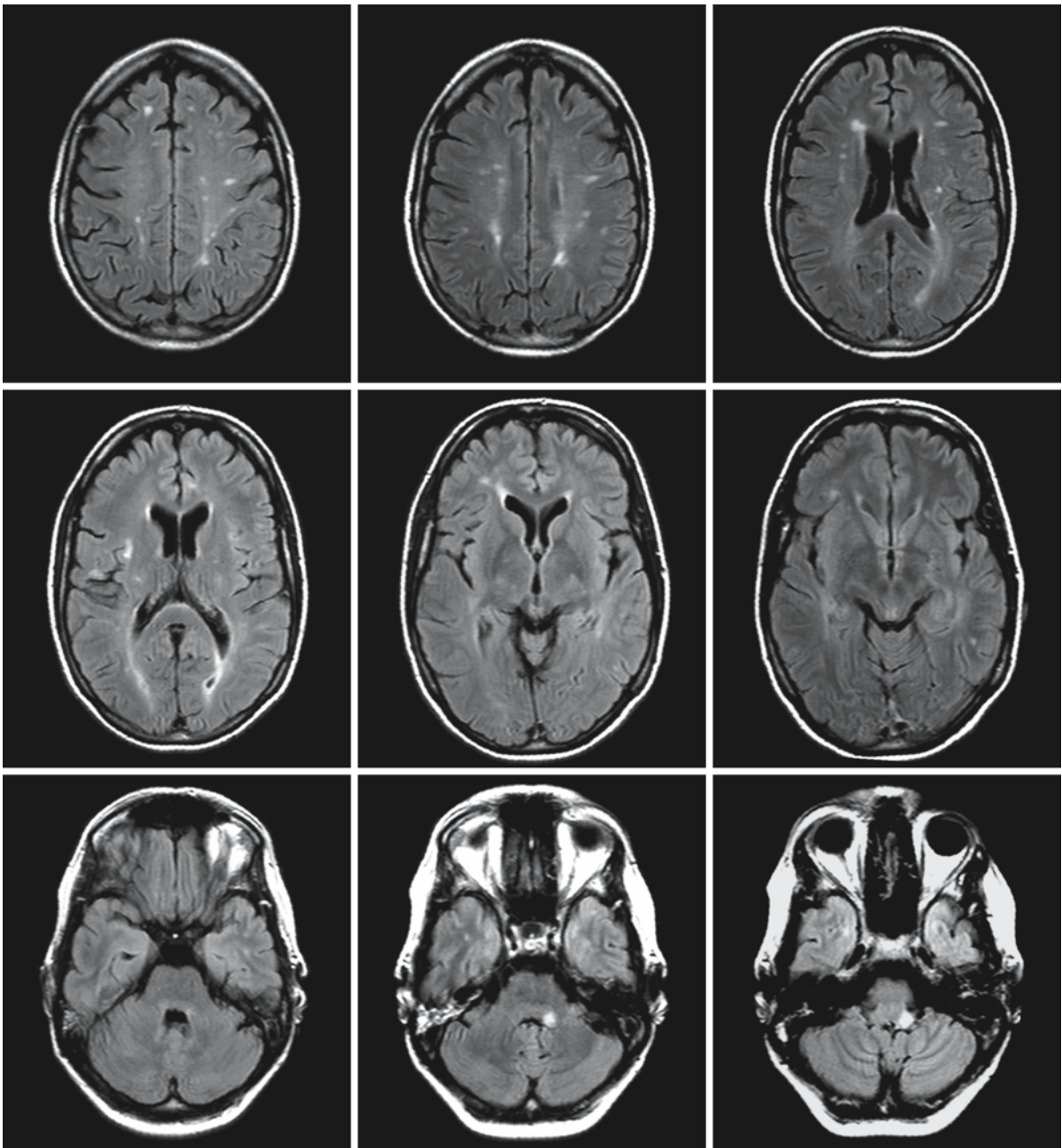


Fig. 79.6. Transverse FLAIR series of a 40-year-old woman presenting with a 6-week history of vertigo attacks. She had previously undergone operations on both ears for cholesteato-

mas. The surprise finding in this patient consisted of lesions supratentorially suggestive of MS and a distinct lesion on the left side in the vestibular nucleus and nerve

tion, for example by demonstrating changes in the MTR or ADC. Not all lesions that remyelinate necessarily disappear from the MR image; many maintain a high signal on T₂-weighted images. In a post-mortem study, MRI of the 1-cm-thick slices was used to detect lesions (Barkhof et al. 2003). In this study remyelination was found in 42% of the lesions, the remyelination being partial in 19% and full in 23%. The

conclusion of this study was that T₁-weighted images and MTRs have additional value in distinguishing lesions with and without remyelination (Barkhof et al. 2003). In addition, ADC values and contrast-enhanced T₁-weighted images may also hold information in patients with remitting MS (Fig. 79.21). MR data obtained in demyelinating lesions induced by lysophosphatidyl choline in animals showed high

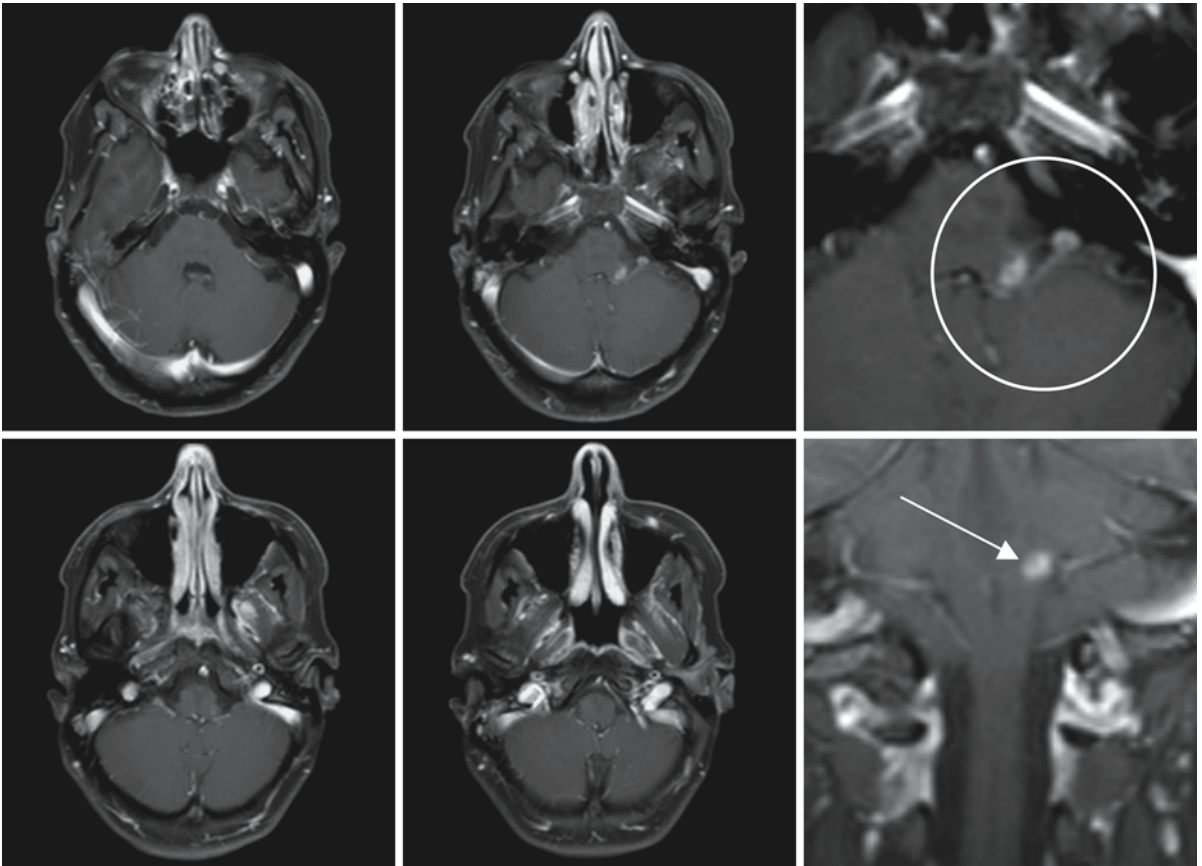


Fig. 79.7. T₁-weighted contrast enhanced images in the same patient as in Fig. 79.6. The two enlarged images on the *right* show the enhancement of the lesions in the vestibular nucleus and tract (*ring* and *arrow*)

ADC values in the peripheral edema and moderately low values in the center of the lesions in the early phase of the lesions. Substantial reduction of ADC values occurs in both parts of the lesions with remyelination (Degaonkar et al. 2002).

Several *special MR techniques* have been shown to be effective in extracting more information on the nature and degree of structural damage of brain tissue. They are mainly applied in research settings and in protocols of clinical trials.

Diffusion-weighted imaging usually reveals a high to very high signal in hyperacute lesions and sometimes low ADC values (Fig. 79.22). It is difficult to draw conclusions from that, because the underlying mechanism of the signal change in these cases is not completely understood. Low ADC values do not correspond entirely with enhancement, probably because enhancement depends on leakage through the blood-brain barrier, whereas low ADC values in MS lesions more likely reflect the initial inflammatory reaction. Low ADC values in MS are not indicative of cytotoxic edema. Diffusion tensor imaging and fiber tracking may be helpful in demonstrating the repair

in fiber tracts when remyelination occurs. Other techniques may also be considered, such as functional MRI in combination with fiber tracking.

Magnetization transfer ratios (MTRs) are often used in follow-up studies. Changes in MTR reflect changes in structural integrity and correlate with axonal damage. MTR histograms of the whole brain or segments (white matter, gray matter) are used as a tool to measure progression or regression of the disease.

Proton MR spectroscopy (¹H-MRS) has added considerably to the understanding of the pathophysiology of MS. ¹H-MRS has been performed as a single voxel technique or as chemical shift imaging (CSI) in acute, subacute, and chronic lesions, and also in normal-appearing white and gray matter, in particular in patients with relapsing-remitting MS and secondary progressive MS. MRS can analyze the biochemical changes and their time course. In acute lesions choline and lactate increase early in the demyelinating process, reflecting inflammation and demyelination, followed in most lesions by a decrease in NAA, reflecting axonal loss. The amount of NAA loss (be-

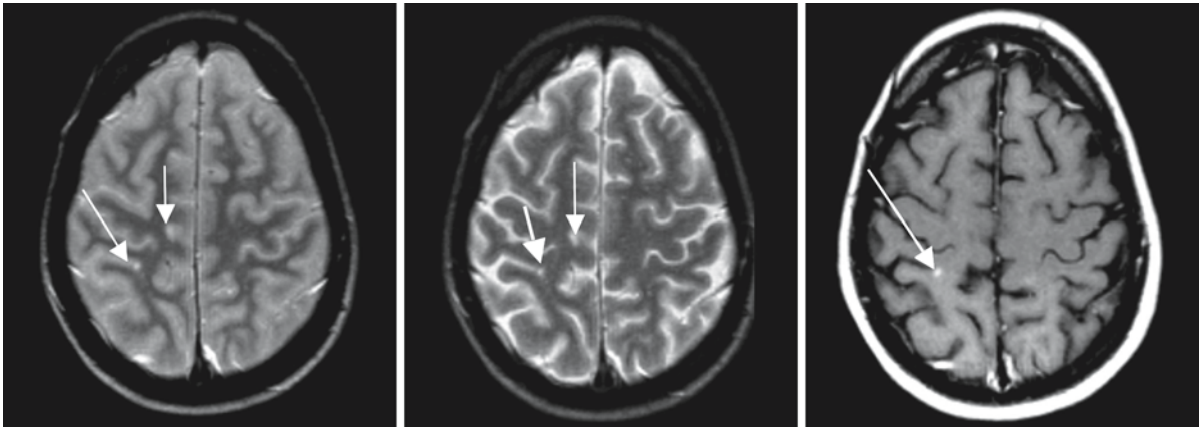


Fig. 79.8. Juxtacortical lesions are important in a definite diagnosis of MS, but can be difficult to identify on MR images. In this series of three transverse images tiny lesions are noted

on the proton density (*left*) and T₂-weighted images (*middle*). After contrast injection there is enhancement of one of the lesions (*arrows*)

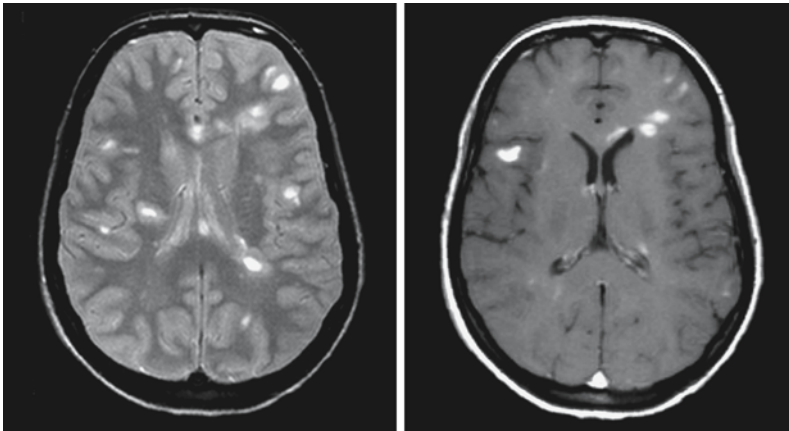


Fig. 79.9. On the *left* a proton density image shows multiple lesions, suggestive of MS. The T₁-weighted contrast enhanced image on the *right* shows enhancement of some, but not of all lesions, confirming dissemination in time and dissemination in space

tween 28% and 66%) reflects the severity of axonal damage, and correlates in a later phase with disability scores. Especially in patients with secondary progressive MS, the loss of NAA is more pronounced than in the more benign forms of MS. In ¹H-MRS with short echo times an increase in *myo*-inositol is seen, reflecting gliosis. The presence of “lipids” may also be noted. ¹H-MRS with metabolite nulling allows further identification of these “lipids” at 0.9 and 1.3 ppm and identifies them rather as proteins and polypeptides, probably products of myelin protein breakdown. When confirmed, these resonances can be used as markers of myelin fragments. Over time, partial or full recovery of NAA losses may occur. Full recovery may be seen in patients with mild disease and mild to moderate loss of NAA. Choline values decrease from high in the initial phase to normal in a period of 2 years. ¹H-MRS has shown gray matter involvement as

well as moderate NAA decrease and choline increase in normal-appearing white matter.

Special variants of MS may have a different MR appearance. MS can occur in very young children. As in adults, the diagnosis has to be considered when multifocal white matter abnormalities are seen, some of which may take up contrast after injection. The lesions in young children tend to be larger, more often involving the basal ganglia and less often involving the lateral borders of the ventricles. Although the numbers of childhood MS patients reported are small, it seems that the incidence of brain stem lesions is somewhat higher in children than in adults. As in adult MS, the contrast uptake disappears after several weeks and the lesions become less conspicuous on T₂-weighted images (Figs. 79.23–79.25).

In NMO, one does not necessarily expect lesions in the cerebral white matter as the clinical condition

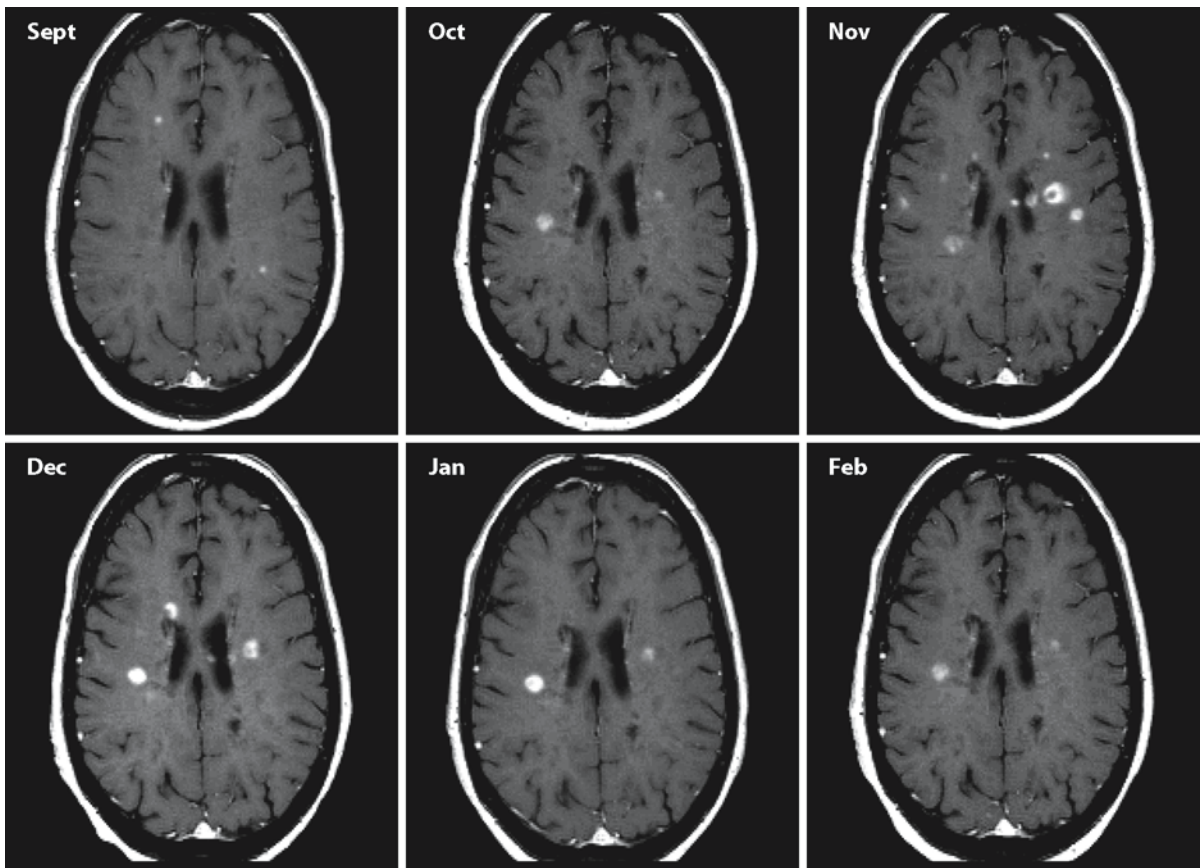


Fig. 79.10. Series of contrast-enhanced T₁-weighted images at the ventricular level, obtained in successive months. Enhancing lesions come and go. This type of serial study can be used as surrogate marker for disease activity in MS

mainly consists of problems of vision (optic neuritis) and paraplegia (transverse myelitis). In some cases, however, we have found multiple white matter lesions in the cerebral hemispheres. These MRI findings are in accordance with histology (Fig. 79.26).

In DS the lesions are large, at least 3×2 cm in size, mostly localized in the parietal region on both sides and, in accordance with the original drawings of Schilder, connected via the corpus callosum. From the drawings of Schilder's original publication (Fig. 79.27), one can also conclude that the lesions will appear symmetrical in some transverse sections but not in all. These lesions spare the arcuate fibers, unless the disease is very advanced. After injection of gadolinium there is enhancement of the peripheral active rim (Fig. 79.28). It may be difficult to distinguish DS from X-linked adrenoleukodystrophy on the basis of imaging findings. Bilateral, confluent white matter lesions connected via the corpus callosum and showing rim enhancement are also seen as a rule in X-linked adrenoleukodystrophy. However, in the latter disease the location of the lesions is preferentially occipital and the lesions are usually symmetrical. It is in the

atypical cases of X-linked adrenoleukodystrophy with frontal or parietal, asymmetrical lesions that confusion with DS may exist. However, with laboratory investigations it is easy to distinguish X-linked adrenoleukodystrophy from DS. DS is very rare, but it should be borne in mind when diagnosing cases of severe white matter affection occurring in the first two decades of life.

CS is easily recognizable on MRI and shows alternating layers of myelinated and unmyelinated fibers, leading to a striking appearance (Fig. 79.29). In CS the MR images show the ring-like lesions, often already visible on the proton density and T₂-weighted images, with an enhancing rim after contrast injection.

In the *differential diagnosis of MS*, it is important to realize that many other conditions can lead to multifocal lesions located chiefly in the white matter with prolonged T₁ and T₂. They are found in arteriosclerotic disorders, head trauma, migrainous headache, vasculitis (including systemic lupus erythematosus, other rheumatoid disorders, and Behçet disease), early metastatic lesions, leukemic deposits in the brain, Lyme disease, neurosarcoidosis, toxoplasmosis, and

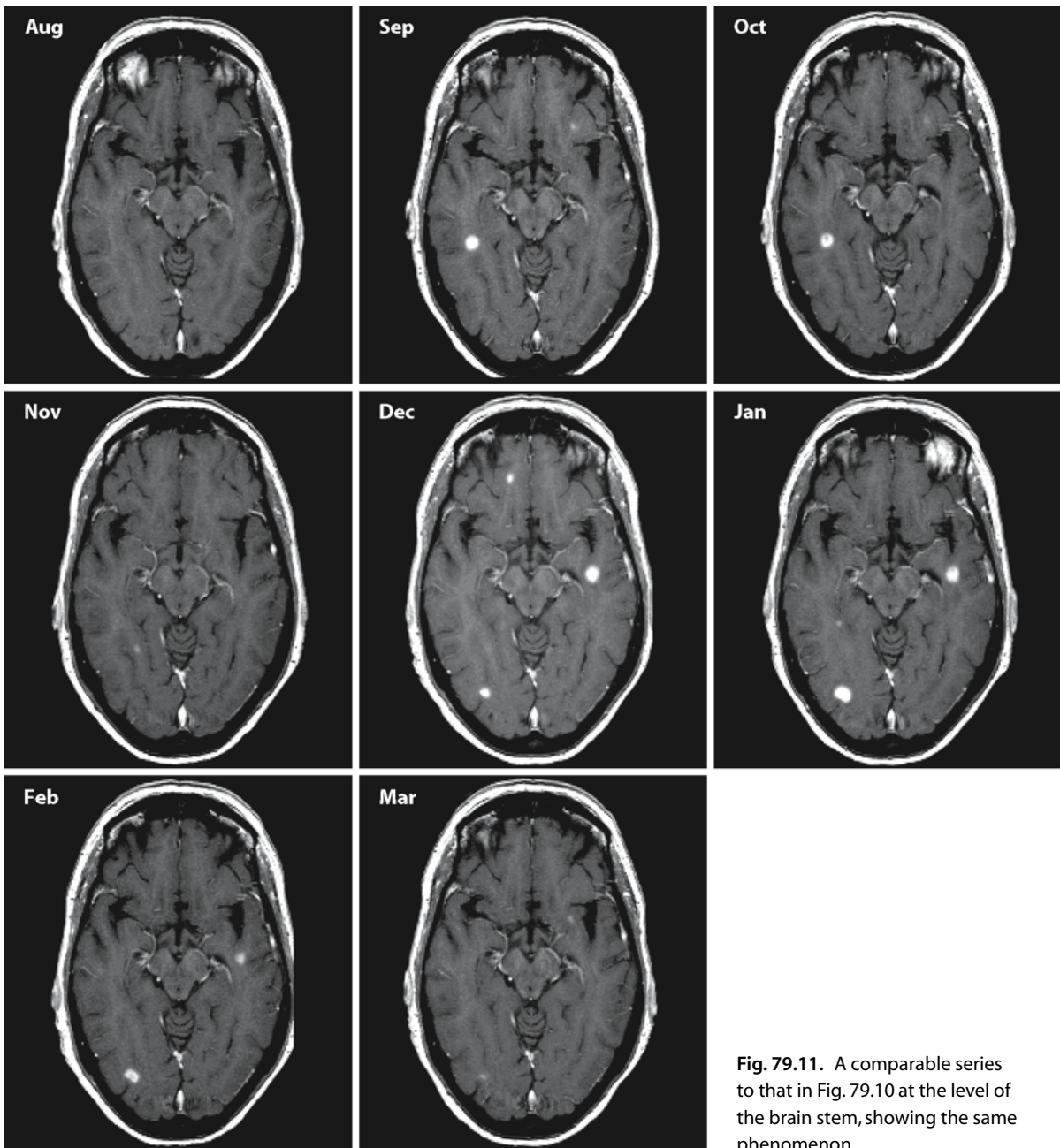


Fig. 79.11. A comparable series to that in Fig. 79.10 at the level of the brain stem, showing the same phenomenon

as age-related white matter changes in the elderly. Without further information, MRI cannot always reliably differentiate between conditions mimicking the MR pattern of MS. However, MRI is not the only tool which can be used to reach the diagnosis. Clinical evidence and the patient's history, age, and laboratory findings may suggest a diagnosis other than MS. The fact that some of the above-mentioned causes of

"MS-like" white matter lesions are often seen in the fifth and sixth decades of life, and that the incidence of MS is low in this age group, argues for the reservation of MRI as a tool in the classification of MS for research mainly in the under-50 age group. Spinal imaging may be of considerable help in the differential diagnosis of vascular disorders versus MS (Figs. 79.30, 79.31) (Lycklama á Nijeholt et al. 2003).

Fig. 79.12. Optic neuritis of the left eye. The coronal STIR image shows on the right side a normal optic nerve, with signal intensity identical to the white matter in the brain. On the left side the optic nerve has a bright signal, compatible with an active neuritis of the optic nerve

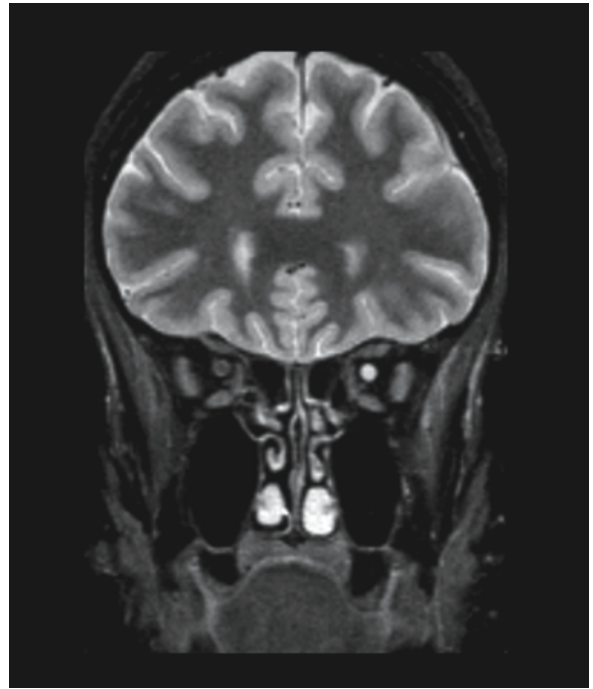


Fig. 79.13. Spinal imaging is extremely important in MS. On the T₂-weighted sagittal image on the *left* an intramedullary lesion is seen, enhancing on the T₁-weighted contrast enhanced image on the *right*



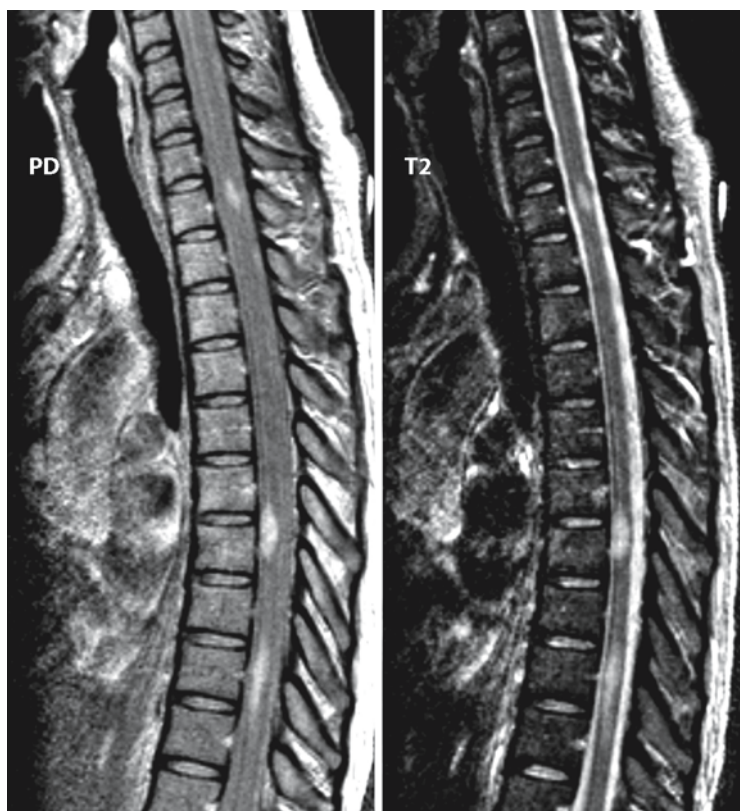


Fig. 79.14. To assure high-quality images of the spinal cord special techniques have to be employed. In these two images (proton density on the *left*, T₂-weighted on the *right*) cardiac gating was used to eliminate flow artifacts. On the proton density image the CSF is isointense with the spinal cord and the lesions stand out

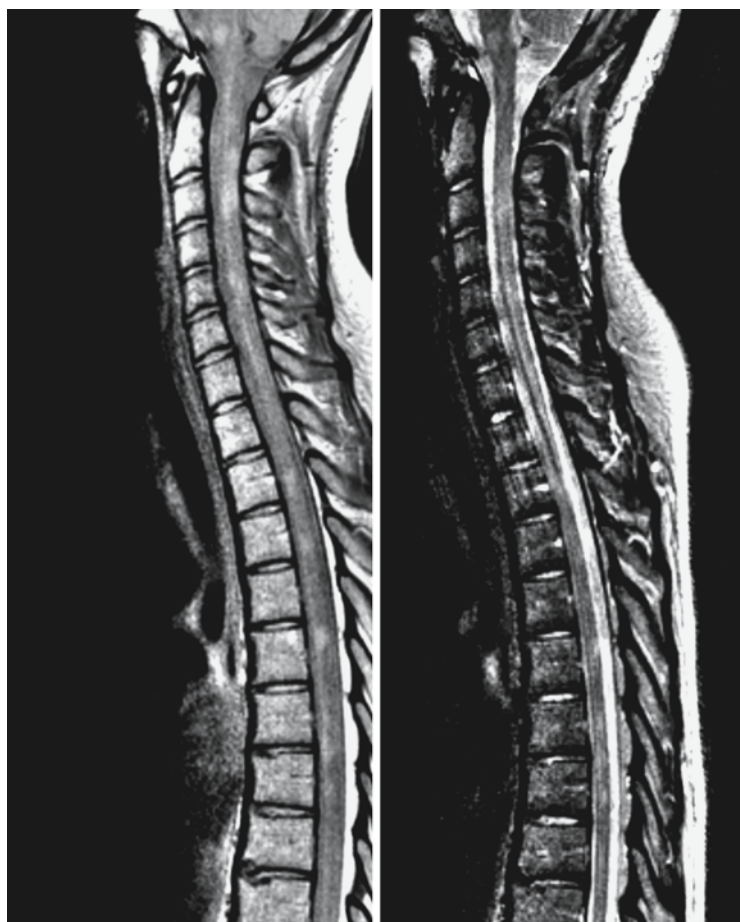


Fig. 79.15. The same technique is applied in this case, demonstrating that even in a case with severe atrophy and relatively wide CSF spaces, the influence of flow artifacts can be minimized. The lesions in the atrophic cord are well visible



Fig. 79.16. The technique employed in the previous images is also successful in the thoracic area. The lesions are well demonstrated. The transverse magnetization transfer gradient echo image (MT-FLASH) depicts the lesion in the axial direction

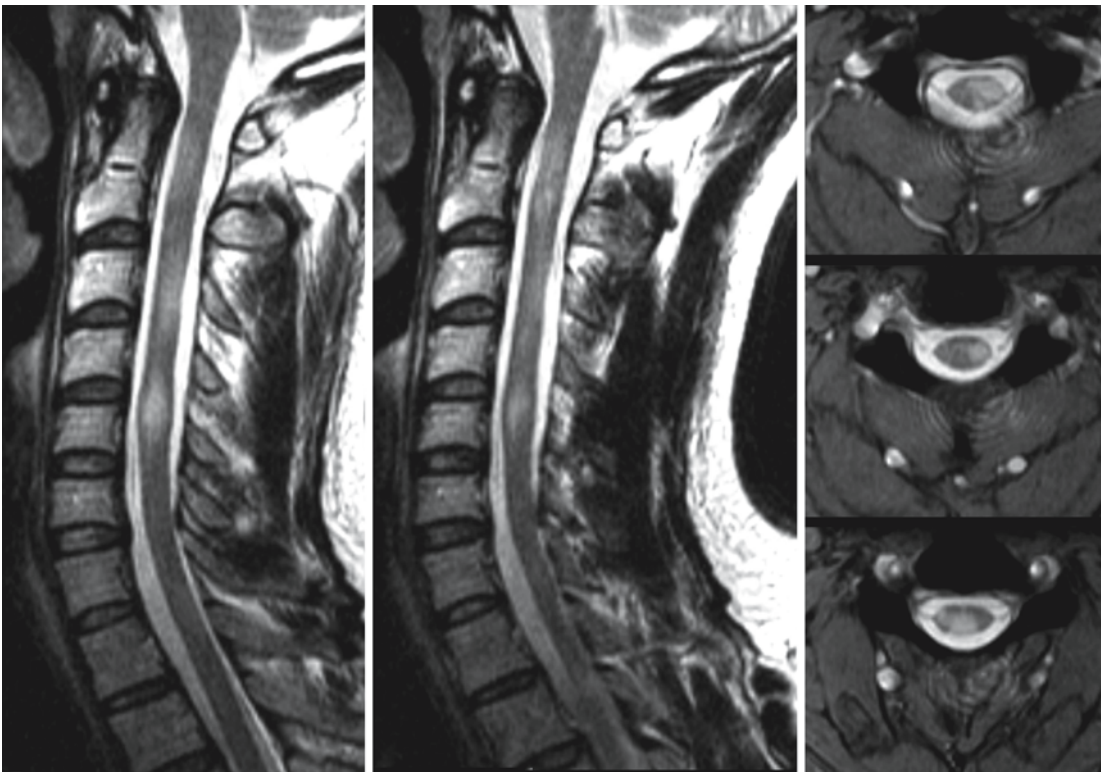


Fig. 79.17. Transverse images of the spinal cord lesions are important as well. There are several possible ways of obtaining good transverse images. This figure shows a series of sagittal

T₂-weighted images combined with a series of transverse T₂-weighted images, demonstrating the position of the lesions within the spinal cord structures

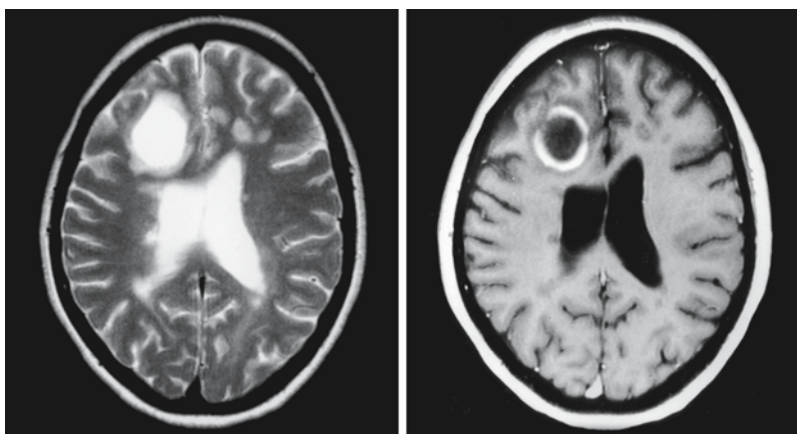


Fig. 79.18. Transverse T₂-weighted image and contrast-enhanced T₁-weighted image to demonstrate the “open ring” sign. The lesion shown on the T₂-weighted image is difficult to differentiate from a low-grade astrocytoma or abscess. After contrast the lesion shows ring enhancement, but the ring is not fully closed. This feature is rarely seen in tumors or abscesses, more often in tumefactive MS lesions

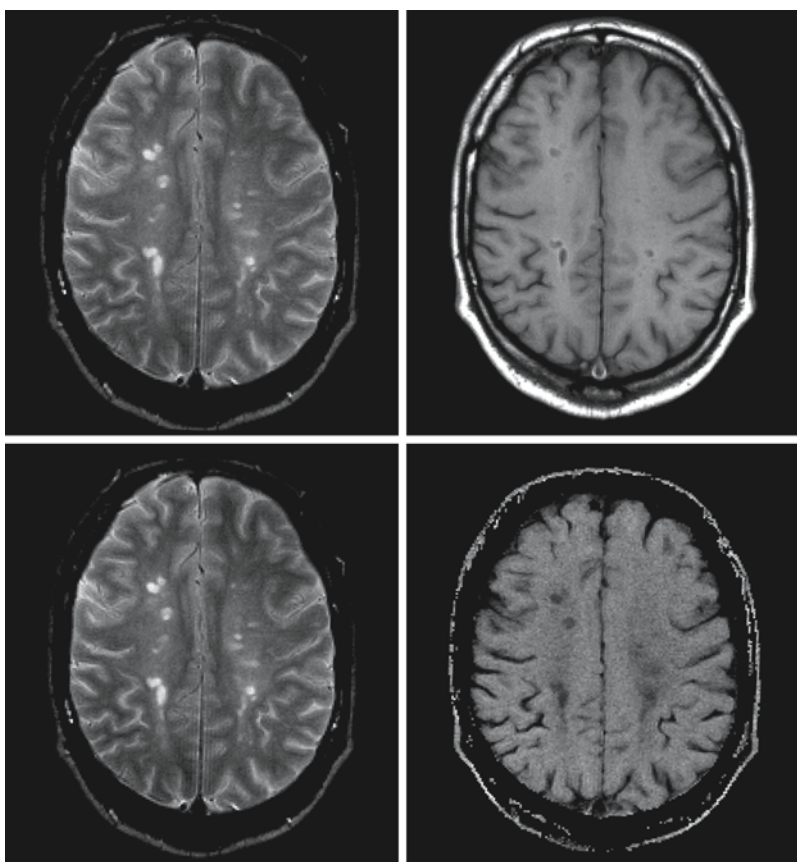
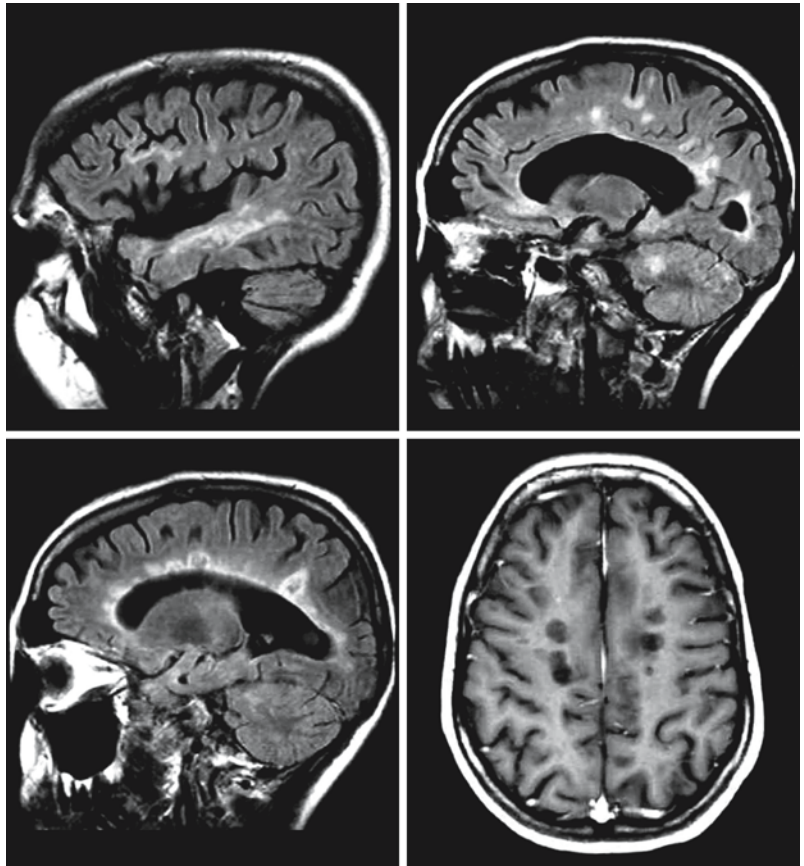


Fig. 79.19. These series of images represents magnetization transfer imaging. The *upper row* shows two transverse images, respectively T₂-weighted (*left*) and T₁-weighted (*right*). The *lower row* shows a T₂-weighted image after a magnetization transfer prepulse (*left*) and the resulting magnetization transfer map (*right*). This map allows direct measurements of the MTR, either pixel by pixel or by ROIs

Fig. 79.20. Three sagittal FLAIR images show typical MS lesions. The transverse T₁-weighted image shows "black holes." These images relate to a 43-year-old patient with a secondary progressive form of MS, now with severe disability and cognitive deterioration. The presence of black holes predicts a poor outcome



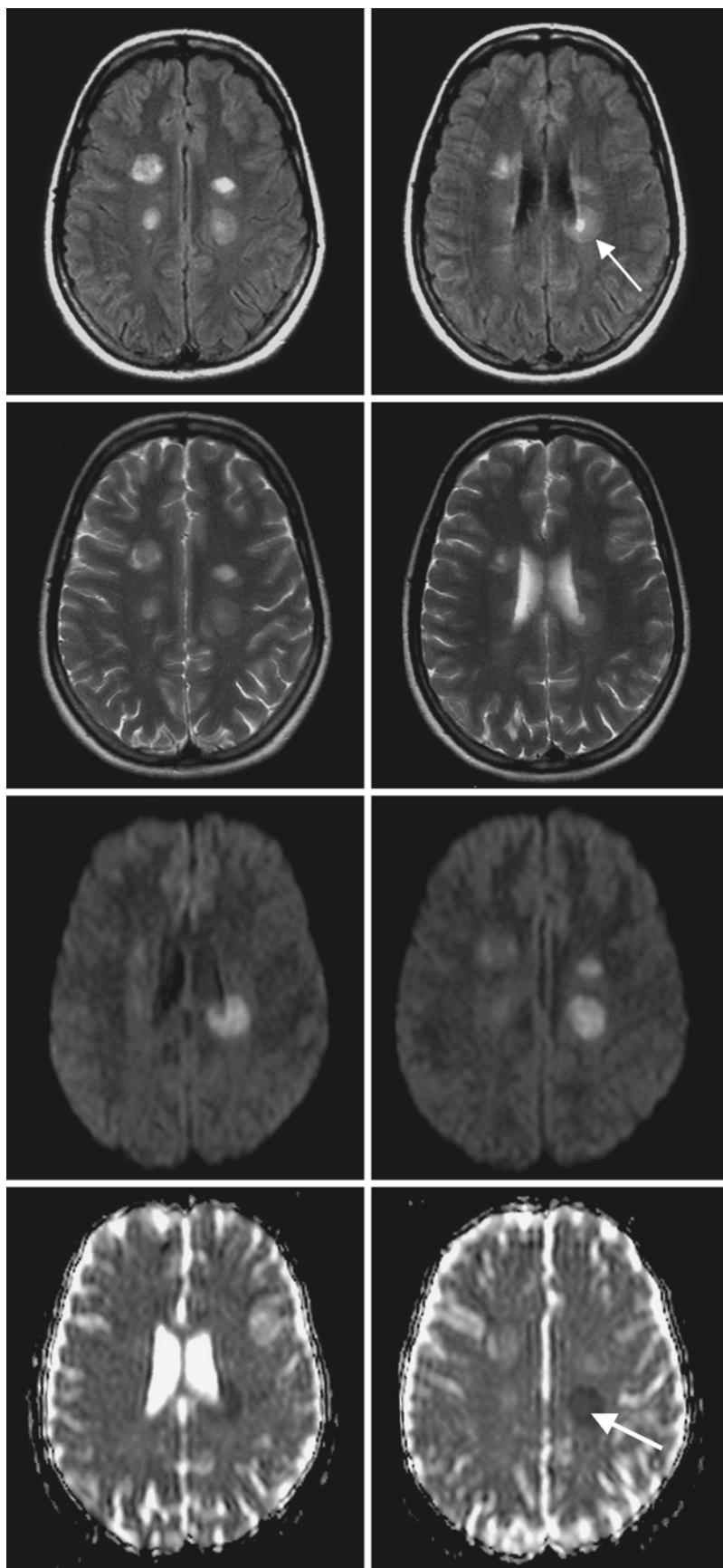


Fig. 79.21. This series of images probably illustrates one of the MR features of remyelination in a remitting patient. Presented are two FLAIR images (*first row*), two T₂-weighted images (*second row*), two Trace diffusion-weighted images with a b value of 1000 mm²/s (*third row*) and two ADC maps (*fourth row*). The FLAIR image shows a target lesion, with a higher signal centrally than the surrounding ring (*arrow*). This lesion has a high signal on the Trace diffusion-weighted image and low signal intensity on the ADC map ($0.52\text{--}0.64 \times 10^{-3}$ mm²/s), and no enhancement (not shown). The low ADC values in this area probably represent remyelination

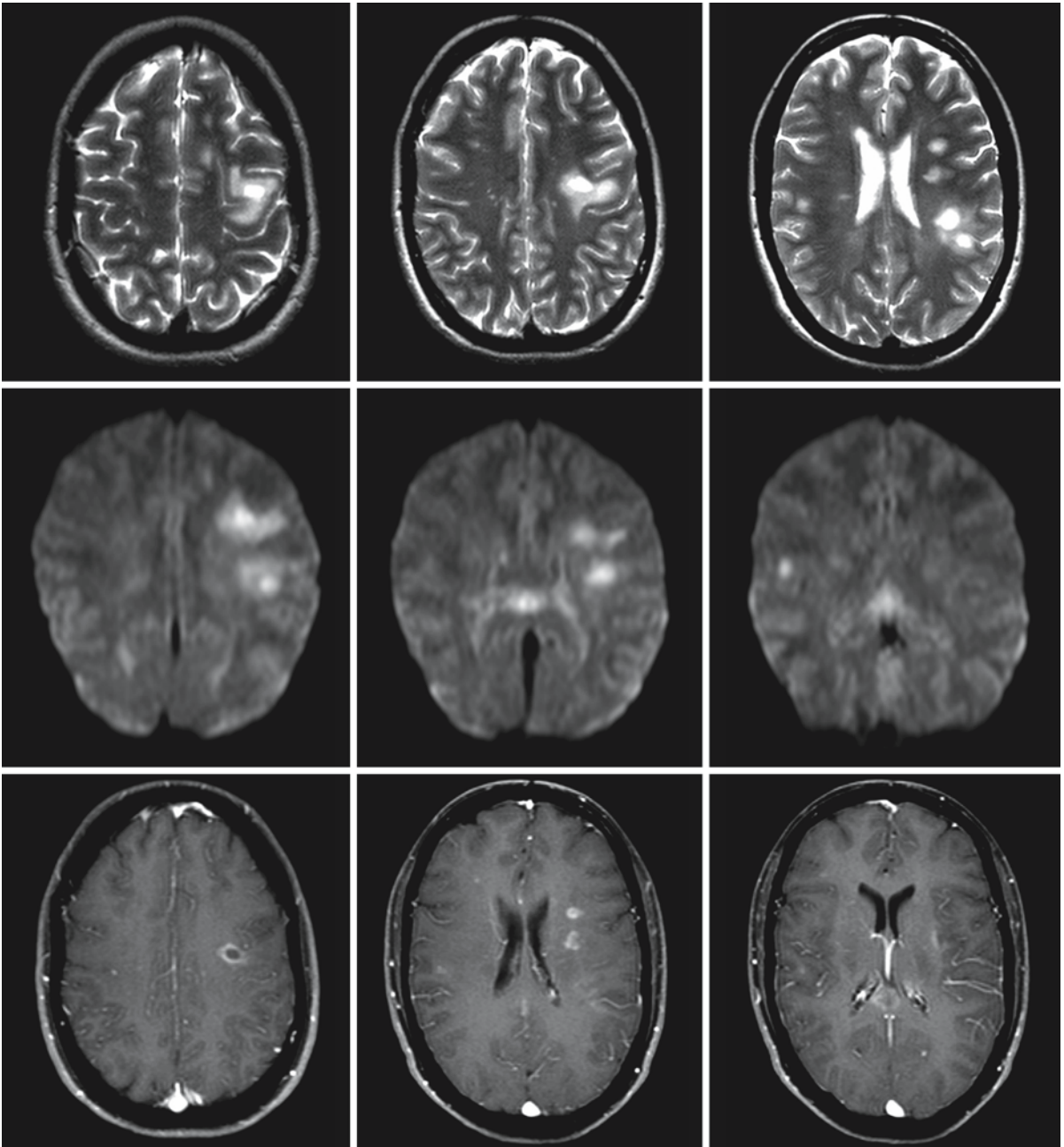


Fig. 79.22. The *upper* row of transverse T_2 -weighted images shows a number of lesions in a case of acute MS. The *second* row shows three Trace diffusion-weighted images ($b = 1000$), in which most of the lesions have a very high signal. The *third* row of T_1 -weighted contrast-enhanced images shows contrast uptake in some of the lesions. The ADC values in the lesions are just below normal

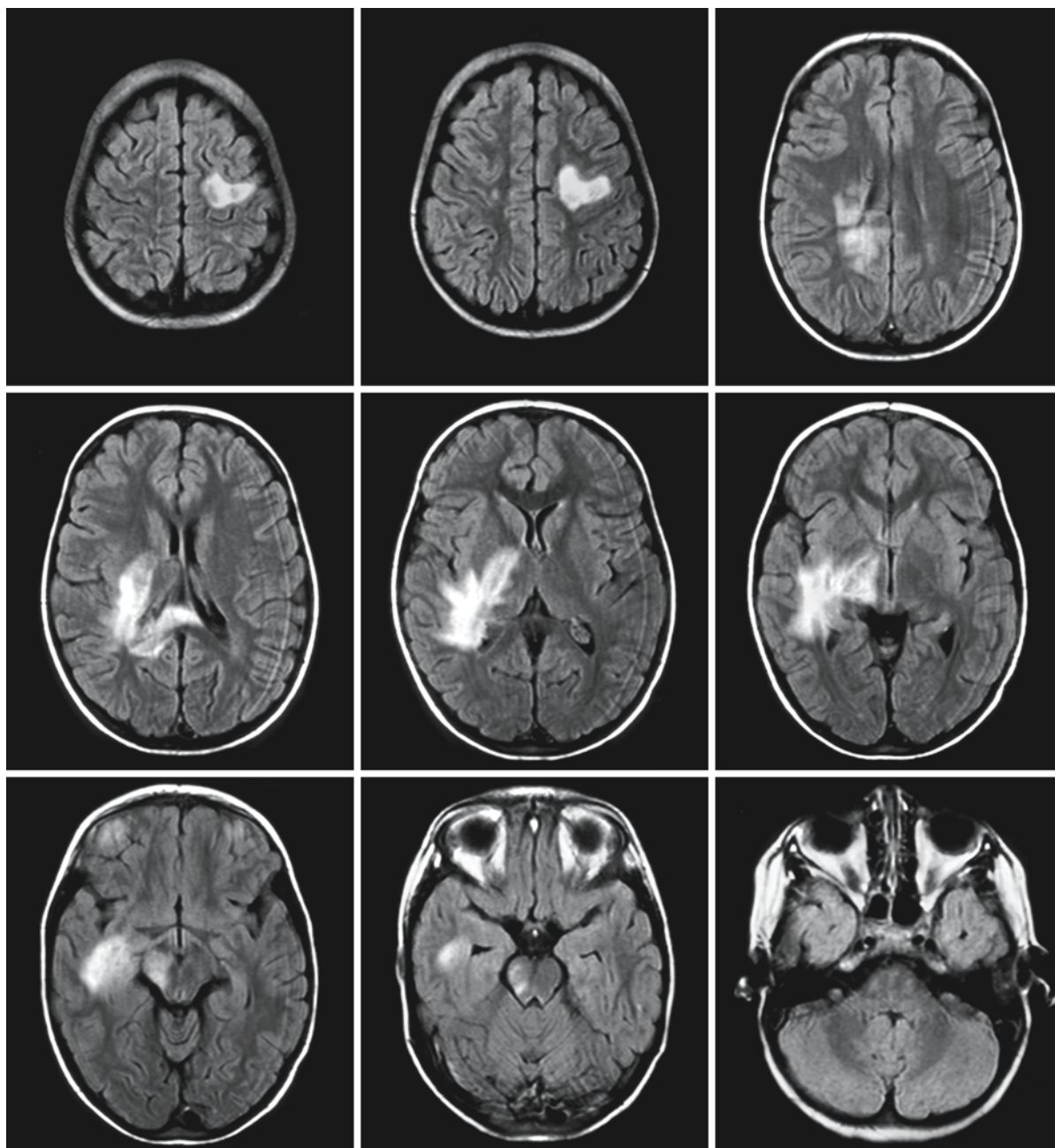


Fig. 79.23. MS in a girl of 6 years. The FLAIR images show a large lesion on the left side in the centrum semiovale, extending into the U fibers. A second lesion involves a large area at the right side near the trigonum, extending laterally into the basal ganglia, the internal capsule, the medial and lateral

geniculate bodies, and medially involving the splenium of the corpus callosum. There is also a lesion on the right side of the midbrain and pons. Courtesy of Dr. M.A.A.P Willemsen, Department of Pediatric Neurology, University Medical Center Nijmegen, The Netherlands

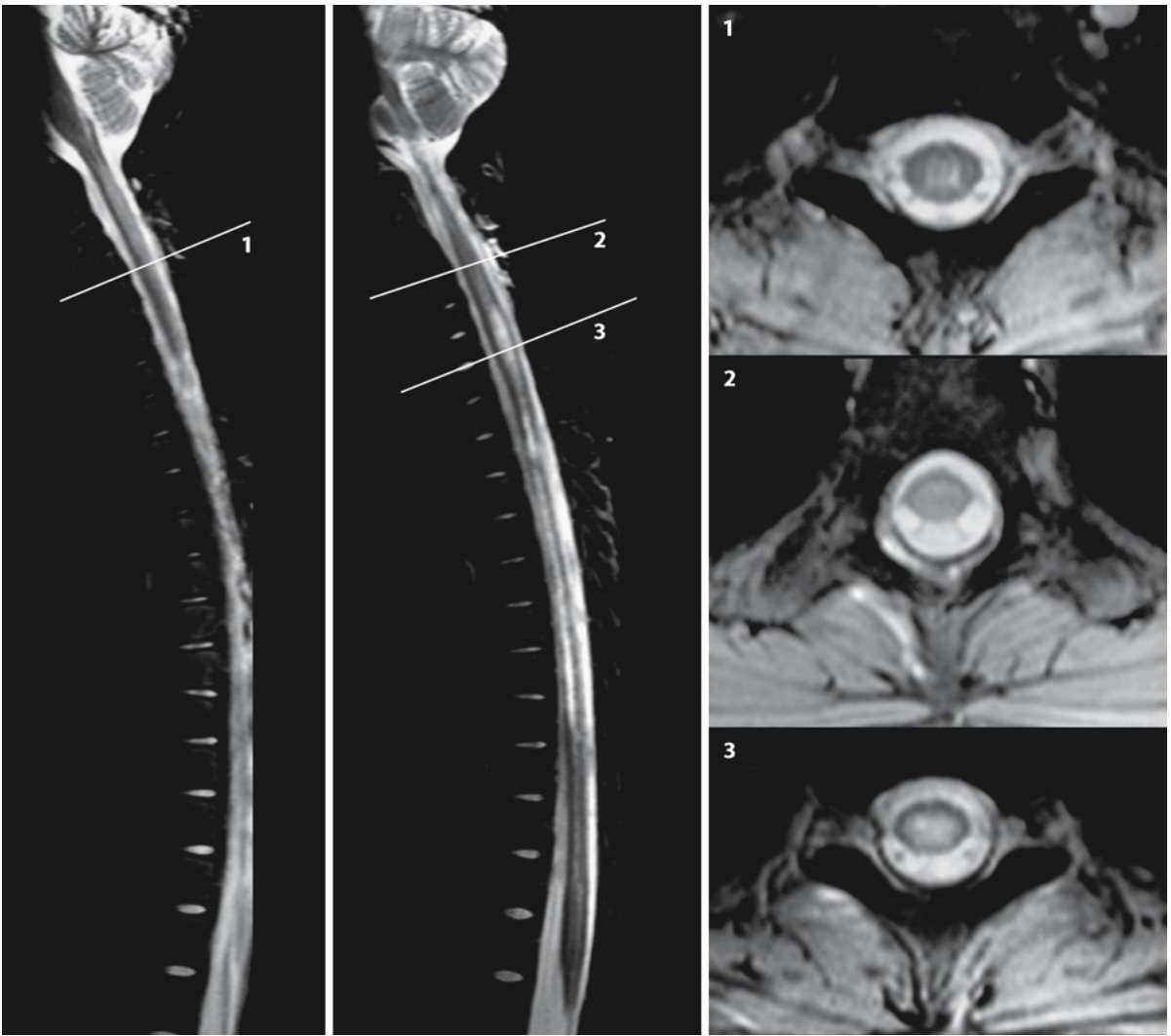


Fig. 79.24. Same patient as in Fig. 79.23. In children with MS, too, imaging of the spinal cord is important. The lesions in the spinal cord are well seen on the T_2 -weighted sagittal images;

the transverse images at the indicated levels give further information about the position of the lesions in the cord

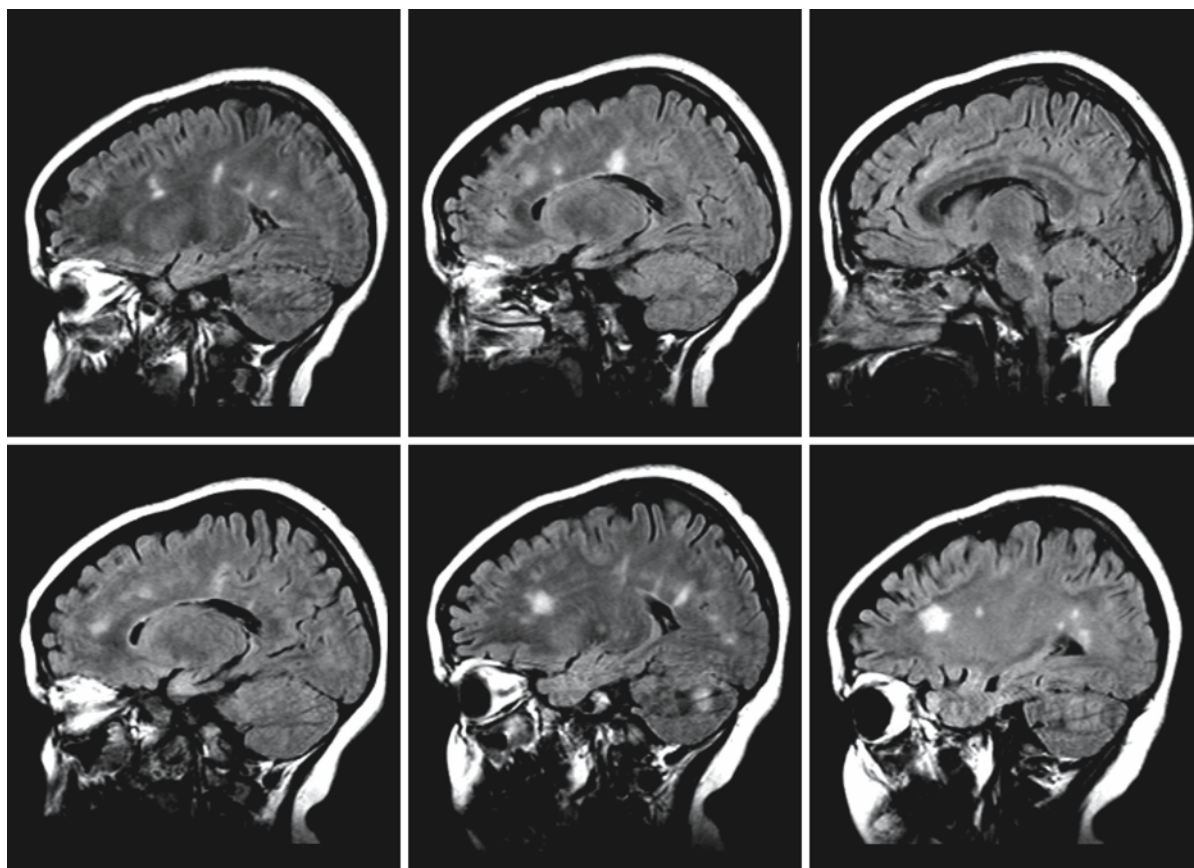


Fig. 79.25. Sagittal FLAIR images in a boy of 13 years shows the classic pattern of adult MS

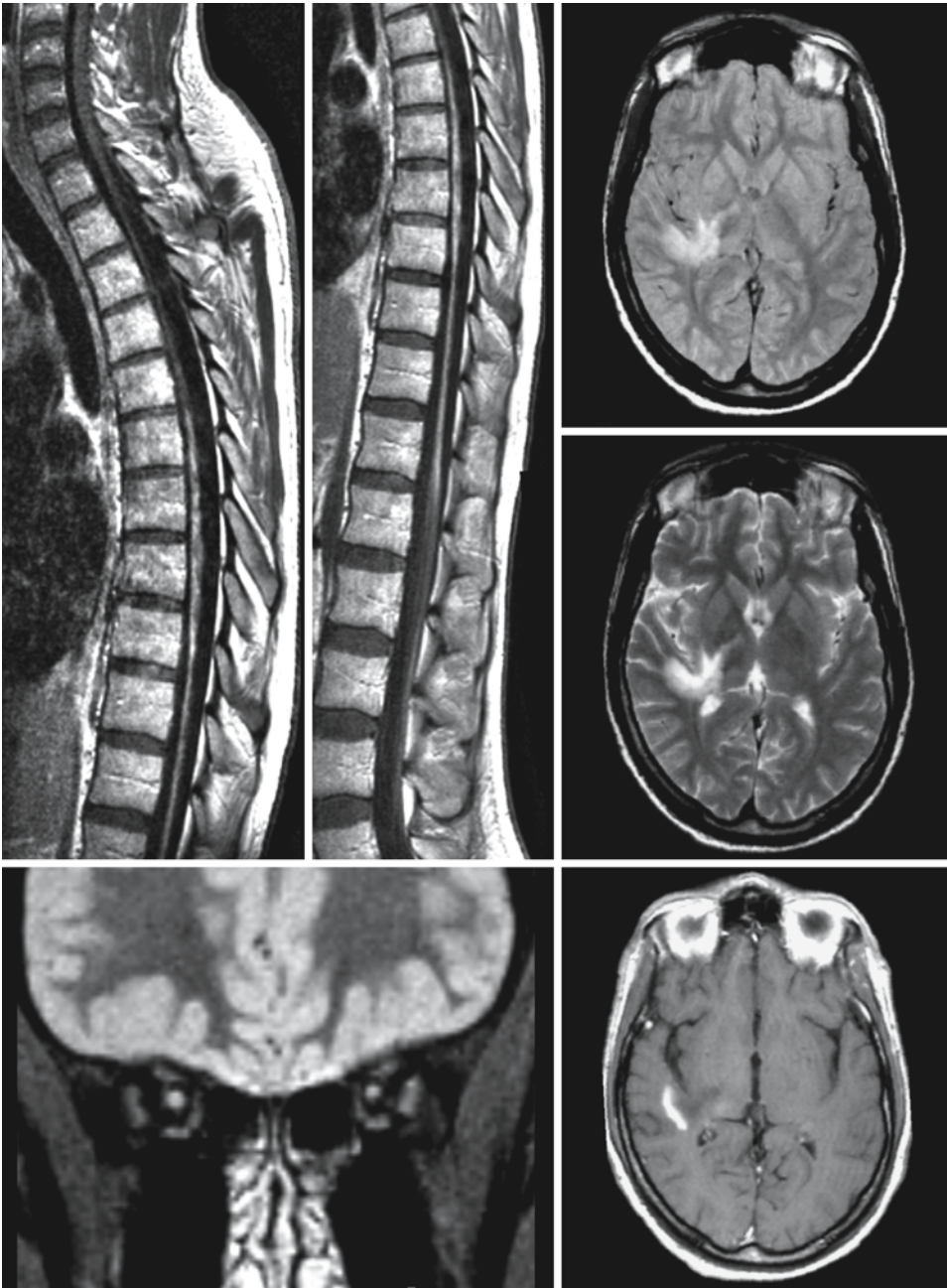


Fig. 79.26. A set of images illustrating neuromyelitis optica. The sagittal T₁-weighted contrast-enhanced images of the spinal cord show severe atrophy of the cord and multiple enhancing lesions. The coronal STIR image of the head shows an elevated signal of both optic nerves with atrophy on the left

side. In this case the images through the head (proton density, T₂-weighted, T₁-weighted with contrast) show a clinically silent lesion with enhancement. In other cases no abnormalities in the brain are found

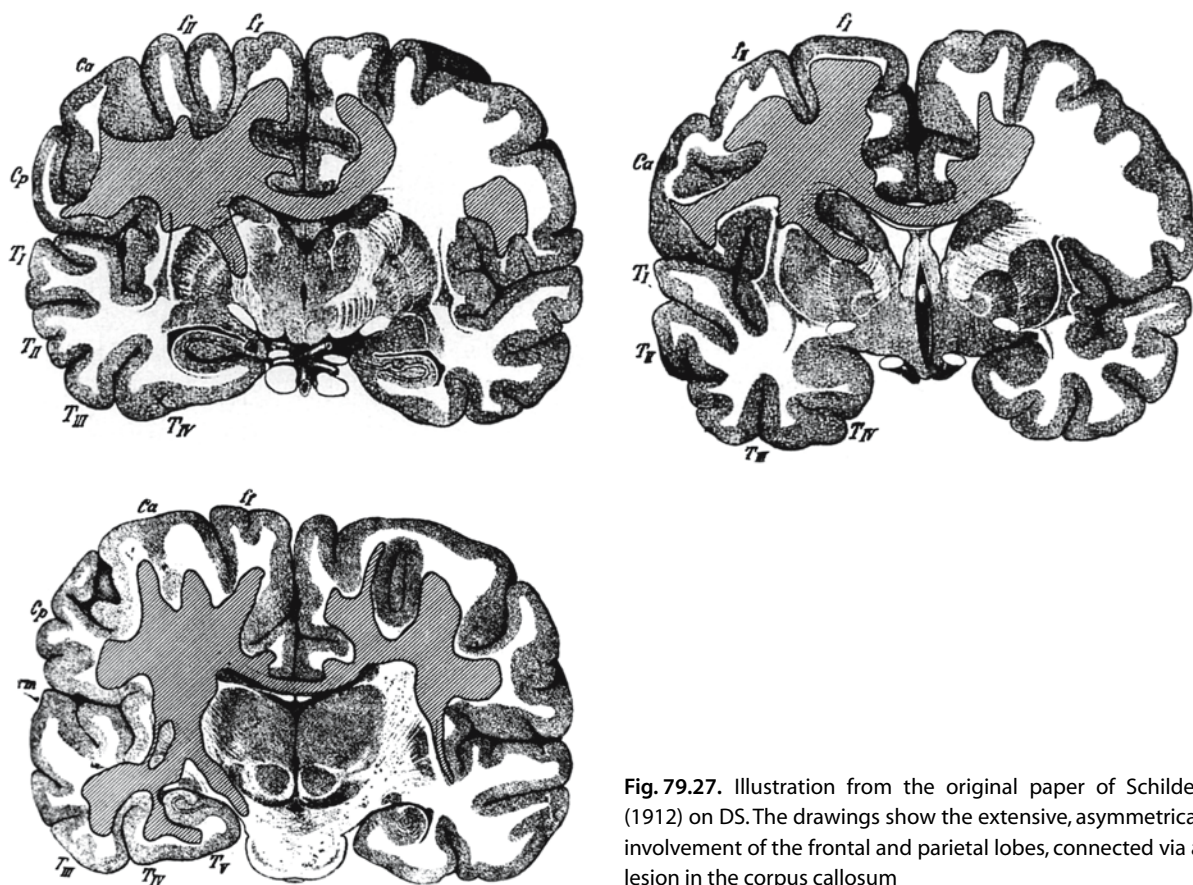


Fig. 79.27. Illustration from the original paper of Schilder (1912) on DS. The drawings show the extensive, asymmetrical involvement of the frontal and parietal lobes, connected via a lesion in the corpus callosum

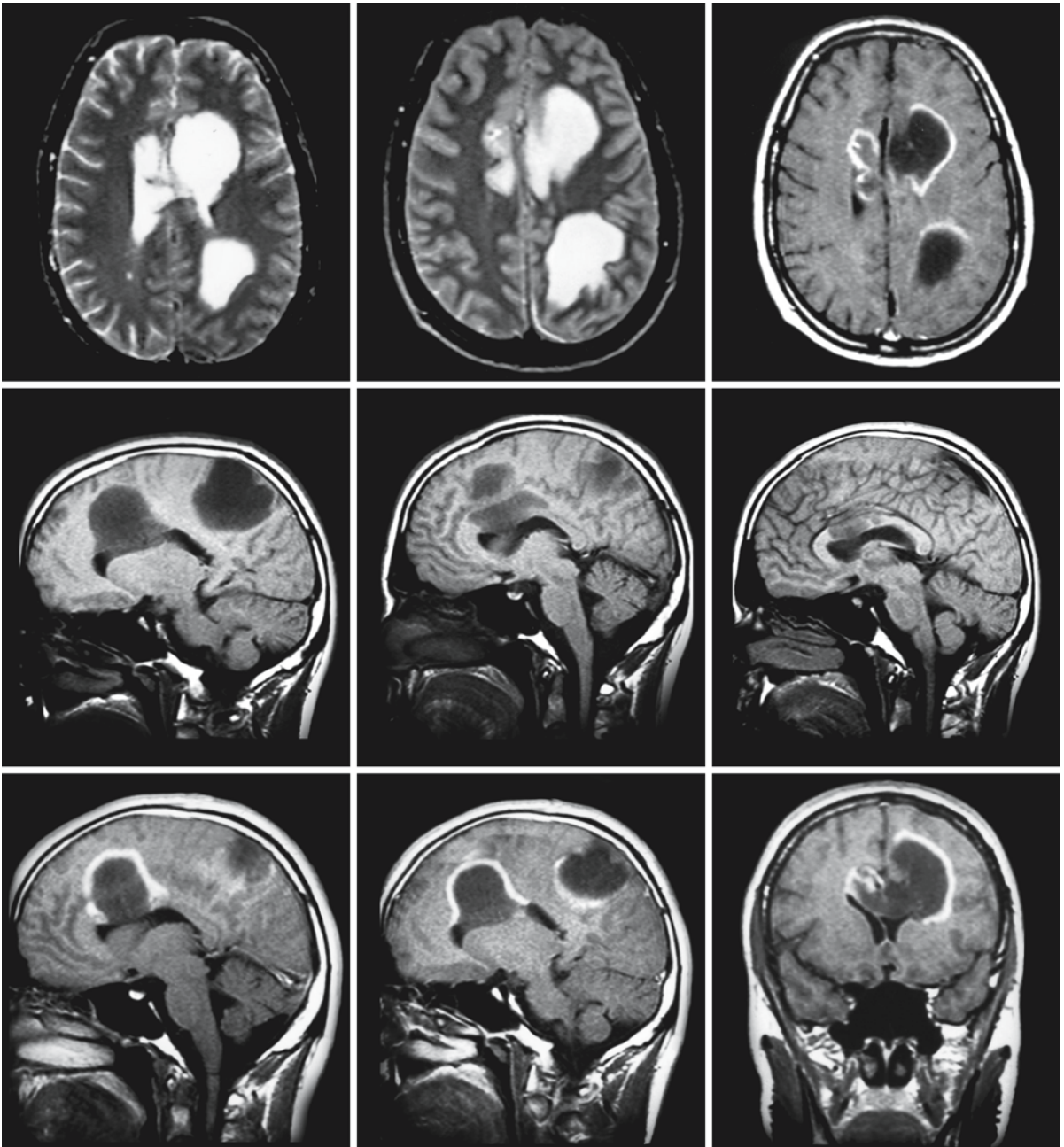


Fig. 79.28. A 27-year-old man with a recent acute exacerbation of neurological signs and symptoms, including hemiplegia, aphasia, headache, and drowsiness. The MR tableau is a collage of T_2 -weighted images (*upper left*) and T_1 -weighted images without and with contrast in three planes. Compare especially the coronal image with Schilder's diagram (Fig. 79.27).

Large lesions are seen on both sides in the frontal and parietal regions, with an asymmetrical distribution, preponderance on the left, and involvement of the corpus callosum connecting the lesions on both sides. There is ring-like enhancement in the zone of acute inflammation. There was considerable improvement after treatment with corticosteroids

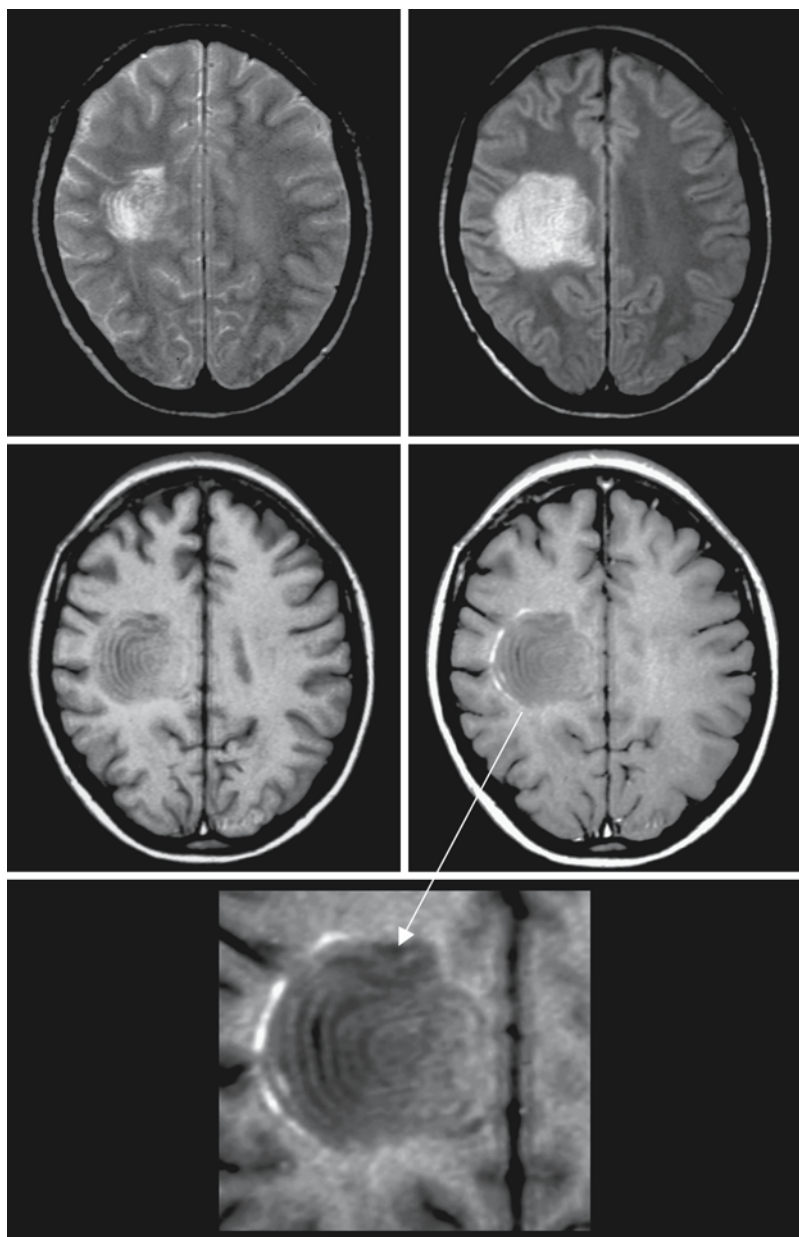


Fig. 79.29. A 25-year-old woman with CS. MRI shows a large lesion with a concentric pattern of rings in the white matter of the centrum semiovale on the right side. There is an abrupt termination of the concentric rings where the lesion abuts on the gray matter. After contrast injection only the outer rings enhance. From Korte et al. (1994), with permission

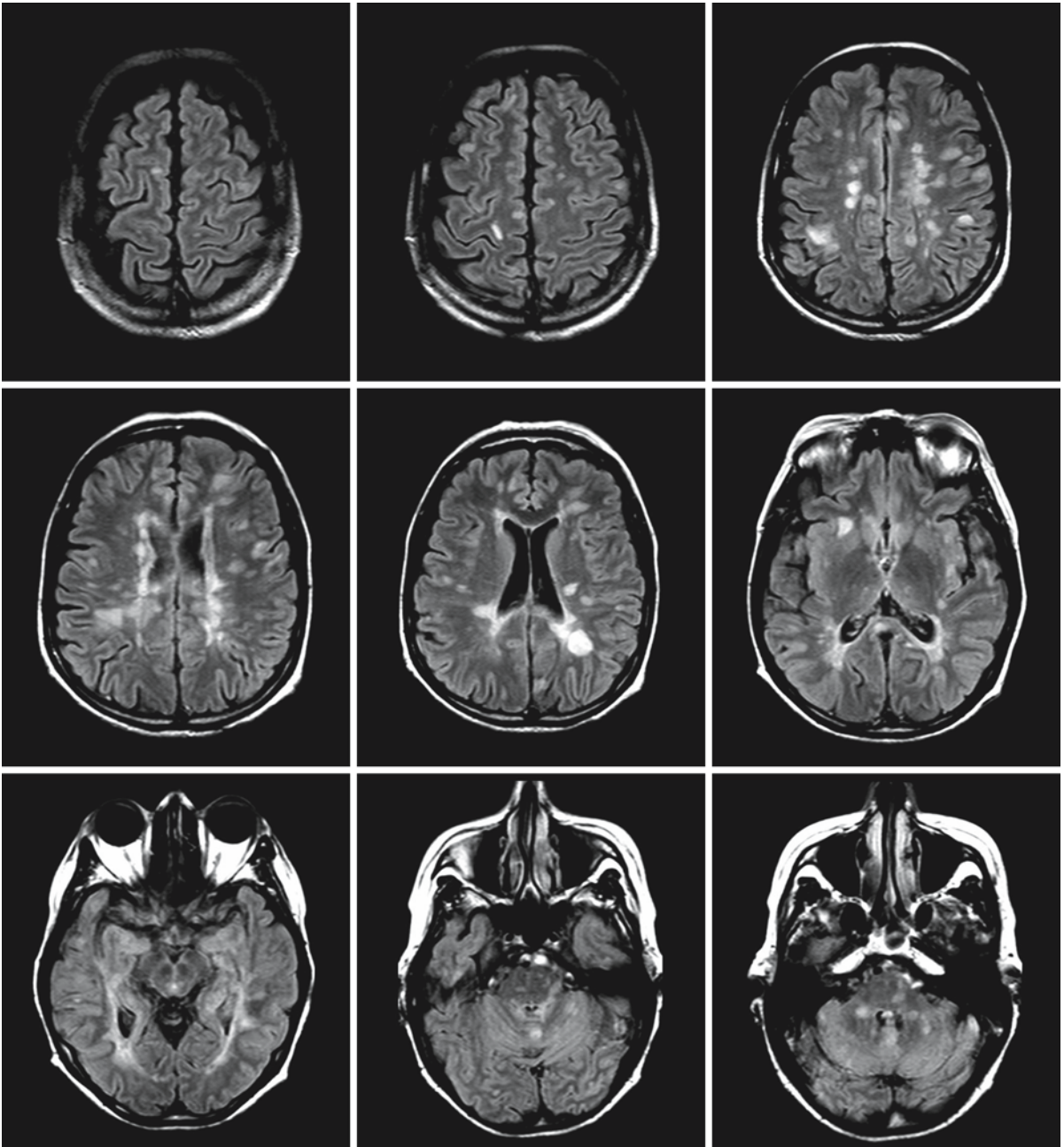


Fig. 79.30. In patients over 50 years of age, differentiation between MS and vascular lesions may be difficult. In this patient the FLAIR images of the brain are compatible with the diagno-

sis MS. The lesions in the spinal cord make this diagnosis more certain. (Fig. 79.30 continued see next page)

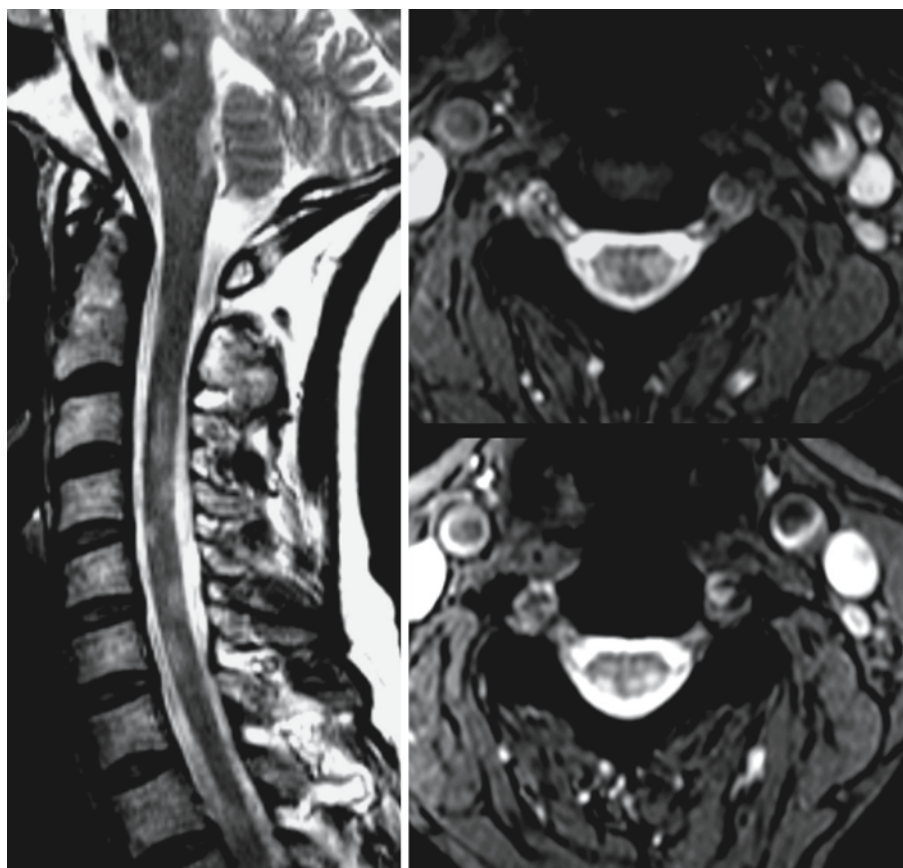


Fig. 79.30. (continued).

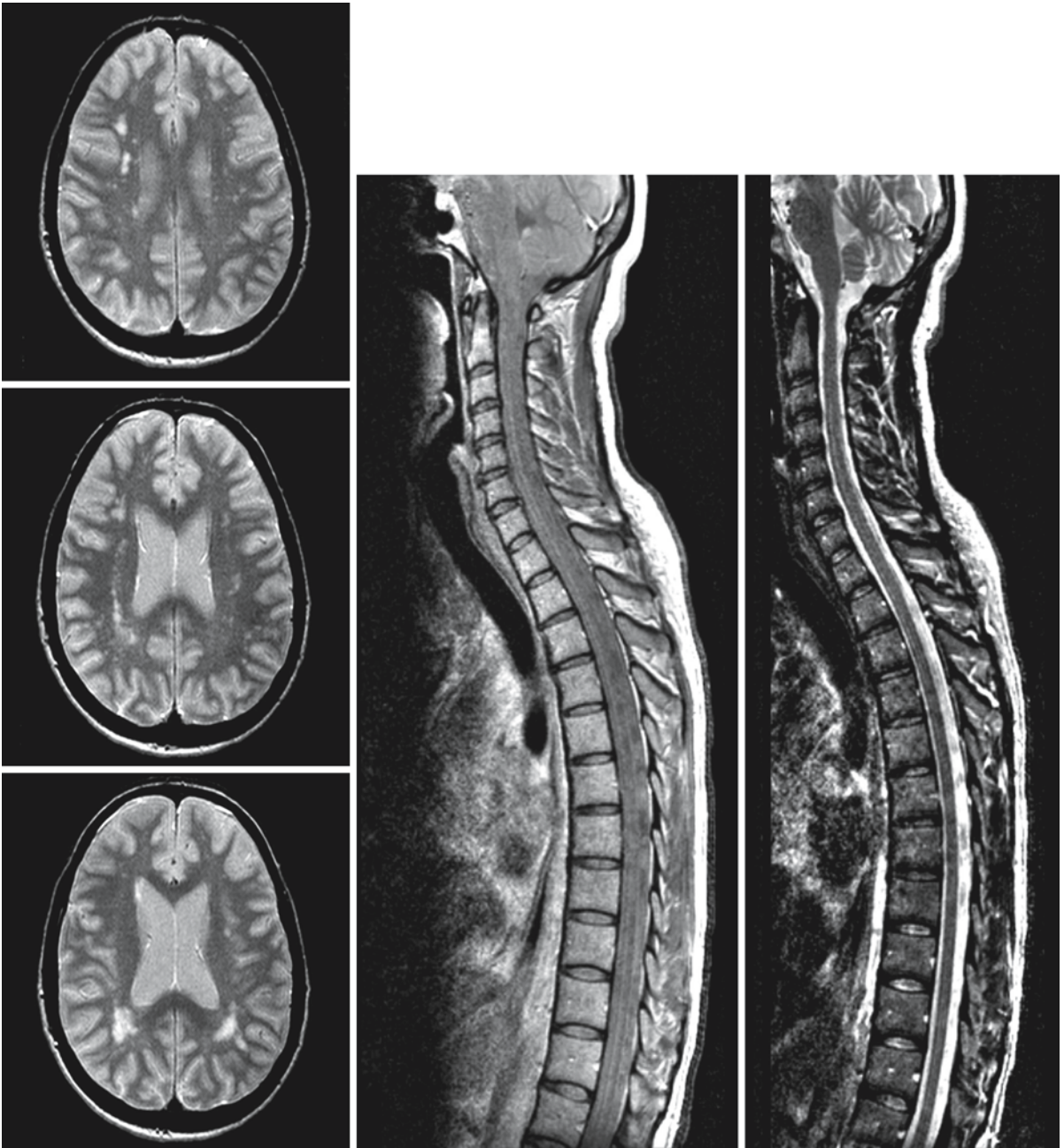


Fig. 79.31. This 50-year-old patient has a few scattered lesions in the brain. The spinal cord images do not reveal any abnormality. This argues strongly against MS (see Table 79.3)

Acute Disseminated Encephalomyelitis and Acute Hemorrhagic Encephalomyelitis

80.1 Clinical Symptoms and Laboratory Investigations

Acute disseminated encephalomyelitis (ADEM) is an uncommon inflammatory disorder within the CNS, predominantly within the white matter of the brain and spinal cord. "Postinfectious/postvaccination encephalopathy" is a synonym. Poser used the term "disseminated vasculomyelinopathy," indicating the probably causative small vessel vasculopathy (Poser 1969). Many other synonyms exist.

ADEM and acute hemorrhagic encephalomyelitis (AHEM) represent two clinical variants of a single pathological process. They follow a viral infection or vaccination or occur without recognized antecedent. Implicated viral infections are measles, chickenpox, rubella, smallpox, infectious mononucleosis, herpes simplex, herpes zoster, mumps, influenza, and *Mycoplasma pneumoniae* infection. They rarely occur following a bacterial infection. A nonspecific upper respiratory tract infection is the most common antecedent. The latent period varies from several days to several weeks, the mean being 4–6 days. Onset of the neurological symptoms is often abrupt, with convulsions and progression to somnolence and coma. Illness may also commence subacutely with symptoms of headache, fever, irritability, drowsiness, and vomiting. Nuchal rigidity may be present. The neurological signs are quite polymorphic and consist of hemiplegia, diplegia or tetraplegia, cerebellar ataxia, cranial nerve palsies, optic neuritis, nystagmus, sensory loss, and bladder dysfunction. Subcortical blindness is rare. Extrapyrarnidal movement abnormalities such as chorea, athetosis, and ballismus occur. The progression of the disease is variable. Patients with AHEM have a more severe clinical course and progress more rapidly into delirium and coma. The highest mortality is seen during the first week of the illness, and in fact most patients who survive the first week eventually recover, with varying degrees of disability. Prolonged disturbances in level of consciousness entail a poor prognosis both for morbidity and mortality. Possible neurological sequelae include epilepsy, spastic paresis, ataxia, decreased vision, and cognitive and psychiatric disturbances, but many patients have no remaining deficits. Most of the neurological syndromes have a monophasic course lasting several weeks. Recurrent attacks of ADEM/AHEM may occur. The occurrence of the neurological abnormalities is

apparently independent of the nature and severity of the antecedent infection or immunization.

There is a close relationship with the Guillain-Barré syndrome, and in fact a combination of ADEM and Guillain-Barré syndrome has been described. Clinically, ADEM can usually be distinguished from multiple sclerosis, because it presents with signs of severe multifocal involvement of the CNS at the same time. If initially monosymptomatic with optic neuritis, the optic neuritis tends to be bilateral. No clinical feature, however, is exclusive to one or the other disorder.

Laboratory investigations reveal a peripheral leukocytosis. The CSF shows pleocytosis. The cellular exudate is mainly lymphocytic and rarely exceeds 100 cells/ml in ADEM. In AHEM the initial cells are granulocytic, and erythrocytes are also often seen. Glucose concentration is normal. There is usually a mild elevation of the CSF proteins, with an oligoclonal banding pattern and a heightened IgG index as signs of intrathecal IgG synthesis. An elevated level of myelin basic protein is shown, indicating myelin destruction. CSF abnormalities may persist for a long time after clinical recovery. Rarely, the CSF is completely normal throughout the course of the illness. The EEG often shows bilateral slow activity. These abnormalities are nonspecific and add little to the diagnosis.

80.2 Pathology

Edema is often the most conspicuous gross finding in ADEM, but the external appearance of the brain may also be completely normal. Microscopic examination demonstrates a diffuse inflammatory process in the brain, brain stem, and spinal cord, with inflammatory cells around veins and venules. Sometimes the perivascular infiltrates are associated with signs of vasculitis, showing inflammatory cells in vessel walls with or without frank necrosis. The cerebral hemispheres are usually more or less symmetrically involved. Both the white matter and gray matter are affected, but the white matter shows more severe changes. The most distinctive histological change is perivascular demyelination. Within the lesions myelin sheaths are lost, but the axons are relatively unaffected. Occasionally the demyelinating lesions are confluent and form large demyelinated areas. At

later stages of the disease, the inflammatory exudate is replaced by fibrous gliosis.

In AHM, necropsy reveals the brain to be swollen and soft in consistency. On sectioning, numerous small hemorrhages are seen, mainly in the white matter. The cerebral cortex and basal ganglia are often spared. The hemorrhagic lesions are often but not always symmetrical. Confluence of many small lesions leads to large hemorrhagic lesions. On microscopic examination the abnormalities are seen to be related to blood vessels, predominantly small veins but also small arteries. There is necrosis of vessel walls, with fibrinous exudation, perivascular edema, hemorrhages, neutrophilic granulocytes in the vessel walls, perivascular spaces, and adjacent brain tissue, and perivascular demyelination. The demyelination is usually associated with necrosis and at least some loss of axons. In severely necrotic areas all axons may disappear. Perivascular demyelination is also seen surrounding apparently normal vessels.

Both in ADEM and in AHM the severity, type, and localization of the pathological changes are unrelated to the type of preceding disease. In both syndromes the parenchymal pathology is often associated with meningeal lymphocytic infiltrates.

80.3 Pathogenetic Considerations

The early theories on ADEM and AHM speculated that these syndromes might represent a delayed but direct invasion of the CNS by a virus or reactivation of a latent virus. There has, however, been a considerable amount of evidence against these theories. The pathological changes are fairly uniform and quite unlike those of the viral encephalitides, the demonstration of viral antigens or viral particles in the brain or the CSF being an exception.

Some observations led to the theory that ADEM and AHM represent an autoimmune response to myelin constituents. First of all, the same neurological syndrome was found in patients vaccinated with rabies vaccine grown in rabbit spinal cord. Secondly, a comparable neurological syndrome was reported in animals after the repeated injection of CNS homogenate in combination with Freund's adjuvant. This syndrome is known as experimental allergic encephalomyelitis. Pathologically, the lesions of ADEM and experimental allergic encephalomyelitis have marked similarities. The white matter shows perivascular cuffing by inflammatory cells and demyelination. The cerebral hemispheres, cerebellum, brain stem, and spinal cord are involved. A hyperacute form of allergic encephalomyelitis has been induced in animals with alteration of the immunization regimen. Pathologically, more hemorrhagic features are present, similar to AHM. Sensitization of lymphocytes

to nervous tissue antigen and especially to myelin basic protein has been shown in a variety of postinfectious neurological disorders, including ADEM and AHM. Experimental allergic encephalomyelitis results from T cell sensitization to myelin basic protein. The delayed hypersensitivity to myelin basic protein leads to an attack on myelin sheaths with subsequent demyelination. The demyelination is predominantly perivascular as the responsible T cells originate from the blood. ADEM and AHM may represent the human counterparts of experimental allergic encephalomyelitis with breakdown of tolerance to myelin antigens. It is possible that the viral proteins serve as an antigen that cross-reacts with myelin antigens. It is also possible that during the initial phase of viral invasion there is subclinical involvement of the CNS, with release or exposure of sequestered neural antigens and subsequent sensitization to them. These theories, however, do not explain the rarity of ADEM and AHM following a viral infection of the CNS, such as herpes virus or cytomegalovirus, nor its low incidence in general. How a wide variety of infections and vaccinations can induce similar sensitization to myelin antigens has also not been explained satisfactorily.

An alternative theory stresses the importance of the vascular changes, which are almost invariably present, and has coined the term "disseminated vasculo-myelinopathy." The detection of circulating antigen-antibody complexes in the serum of patients with a variety of postinfectious neurological disorders led to the assumption of a vascular lesion due to the entrapment of immune complexes in vessel walls and the subsequent inflammatory response. Because perivascular demyelination can result from vascular injury alone, the participation of delayed hypersensitivity would not be necessary. The presence or absence of immune complexes, the size and the number of the complexes, and not the antecedent illness would thus be the major factor in the development of ADEM and AHM, and the development of delayed hypersensitivity to myelin antigens would be merely an epiphenomenon resulting from nervous tissue damage. However, it is not clear why the nervous system should be preferentially involved in immune-complex-mediated vasculitis. Only some indirect evidence supports this theory: the detection of circulating complexes in some patients with various postinfectious neurological disorders, the presence of systemic features compatible with immune complex disease in occasional patients, and the occurrence of similar nervous system abnormalities in other human disorders caused by immune complexes. Immune complexes have, however, not been found at sites of vessel injury, and it is not impossible that the complexes themselves only represent an epiphenomenon.

The two hypotheses presented here are not mutually exclusive. Immune complex vasculitis results in increased vascular permeability. Changes in vascular permeability and perivascular inflammation can either alter the antigenicity of myelin or release an antigen previously sequestered by a competent blood-brain barrier. The cell-mediated immune response could then perpetuate the damage and lead to demyelination. In some patients perivascular demyelination is seen, whereas in others the pathological picture is dominated by perivascular necrosis. It is hypothesized that pure demyelination may be caused by delayed hypersensitivity to myelin antigens alone and that necrosis associated with inflammatory infiltration occurs when there is production of antibodies directed against several components of the brain parenchyma.

80.4 Therapy

Corticosteroids are central in the management of ADEM and AHM. Dramatic clinical improvement may be seen. Relapses may occur when steroids are withdrawn, and improvement may then recur when steroids are reinstituted. The fact that the improvement is sometimes absent or only slight may be explained by the presence of irreversible structural damage prior to institution of the steroid therapy. It is recommended that corticosteroid therapy be initiated as soon as possible in the treatment of these syndromes.

In desperate cases, alternative therapeutic strategies may include more drastic immunosuppression and plasmapheresis.

80.5 Magnetic Resonance Imaging

In ADEM, CT scan of the brain shows multifocal or diffuse white matter damage, but it may be normal in the acute stage, or may remain normal throughout. Not all lesions show enhancement after contrast injection. CT can seldom explain the full extent of clinical disability, and, conversely, several lesions may be seen for which no correlative clinical signs are observed. Clinical improvement is accompanied by disappearance of contrast enhancement and complete or partial resolution of low-density lesions.

In AHM the white matter lesions are characterized on CT by extensive edema with prominent mass effect and the presence of hemorrhages.

MRI in ADEM shows multiple, usually large white matter lesions with an asymmetrical distribution (Figs. 80.1–80.3). In very extensive cases, in which almost all white matter is involved, the asymmetrical distribution becomes less clear. Symmetry of lesions

is exceptional. Smaller, multiple sclerosis-like lesions occur in a small number of patients. The lesions have a preference for the occipital and parietal area. The white matter lesion may “spill into” the cortex with some focal cortical involvement (Fig. 80.3). Mass effect is rare but tumefactive lesions in the frontal and parietal lobes have been described. It should be noted that less frequently ADEM presents with involvement of the basal ganglia and brain stem (Fig. 80.4). Spinal MR is mandatory for a comprehensive inventory of lesions (Fig. 80.4). In nearly all cases spinal lesions can be demonstrated. Incidentally spinal lesions are the sole MR presentation of the disease. Some patients have optic neuritis (Fig. 80.4). After contrast injection the white and/or gray matter lesions may enhance (Fig. 80.3), but usually not all lesions enhance, and contrary to what is usually stated, our experience is that in many cases enhancement is at most subtle (Fig. 80.2), or is not present at all (Fig. 80.1). The enhancement is often patchy, while sometimes the whole lesion enhances. Ring enhancement may occur. The presence of both enhancing and nonenhancing lesions argues in favor of the lesions’ being in different stages of development, despite the supposed monophasic character of the disease. Repeated MRI during the course of the disease may show disappearance of some lesions and concurrent appearance of others. These observations modify the view that ADEM is always simply monophasic. Disappearance of white matter lesions is sometimes rapid (Fig. 80.5), but may also take a long time, as much as 18 months, and part of the white matter damage may be permanent (Fig. 80.6). New lesions may appear despite clinical improvement.

Diffusion-weighted imaging in ADEM reveals similar results as in multiple sclerosis. In the peracute phase of the lesion ADC values may be low; after 2–3 weeks, the ADC values are higher than average in the core of the lesion and mixed in the borders; in the late phase the abnormal findings tend to disappear.

Magnetization transfer ratios (MTRs) have been estimated in ADEM. Histogram MTR analysis of normal-appearing white matter in patients with multiple sclerosis and ADEM show significantly lower MTRs and peak positions and significantly higher diffusivity in multiple sclerosis than in ADEM, suggesting that




Fig. 80.1. A 2-year-old girl with ADEM. The T₂-weighted transverse images (*first and second rows*) show large, bulky lesions in the centrum semiovale, predominantly in the frontal lobe. There are also lesions in the midbrain and pons. This is the “common” pattern of ADEM. On the T₁-weighted contrast-enhanced images (*third and fourth rows*) no enhancement of lesions is seen, despite the acute clinical presentation

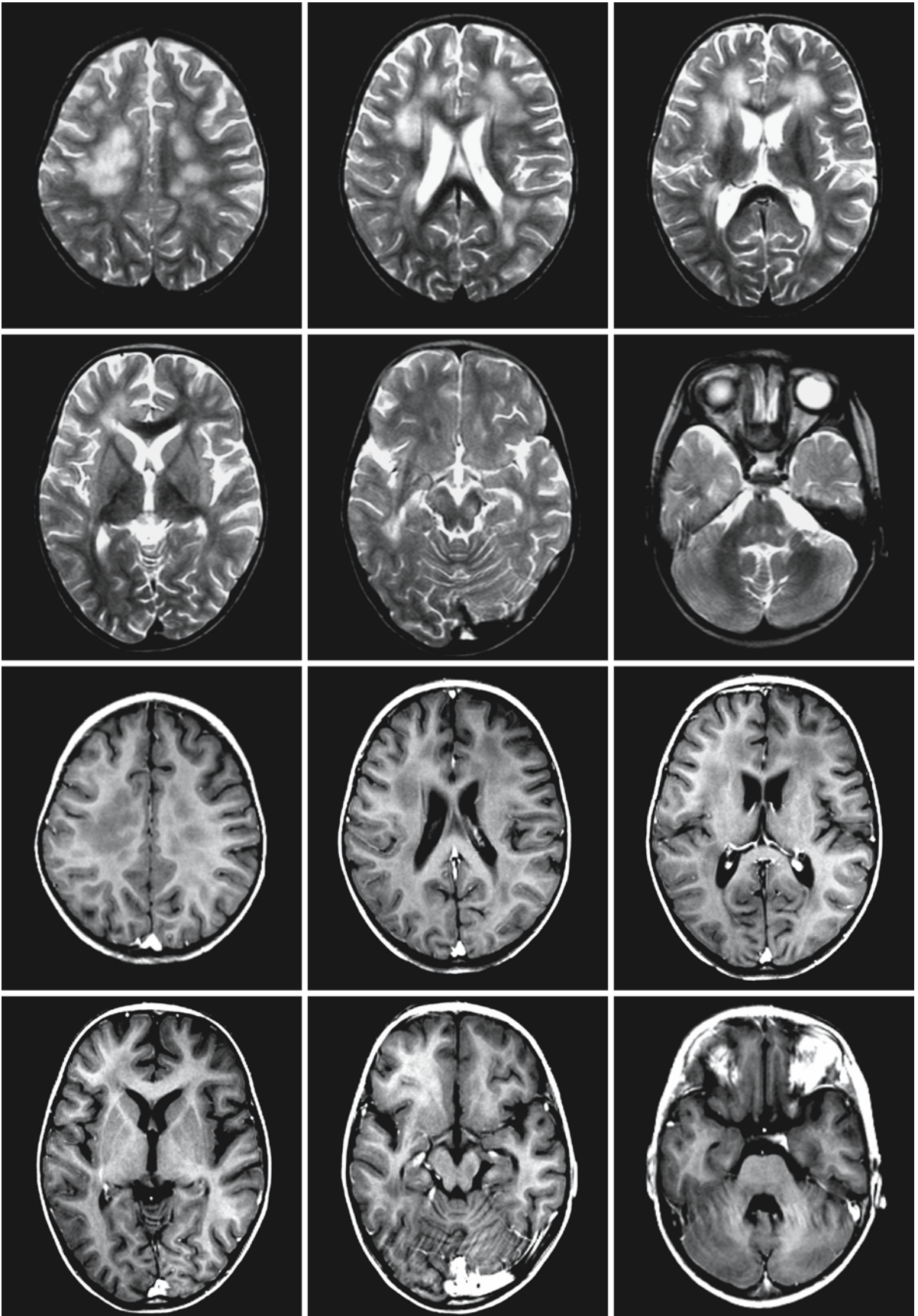


Fig. 80.1.

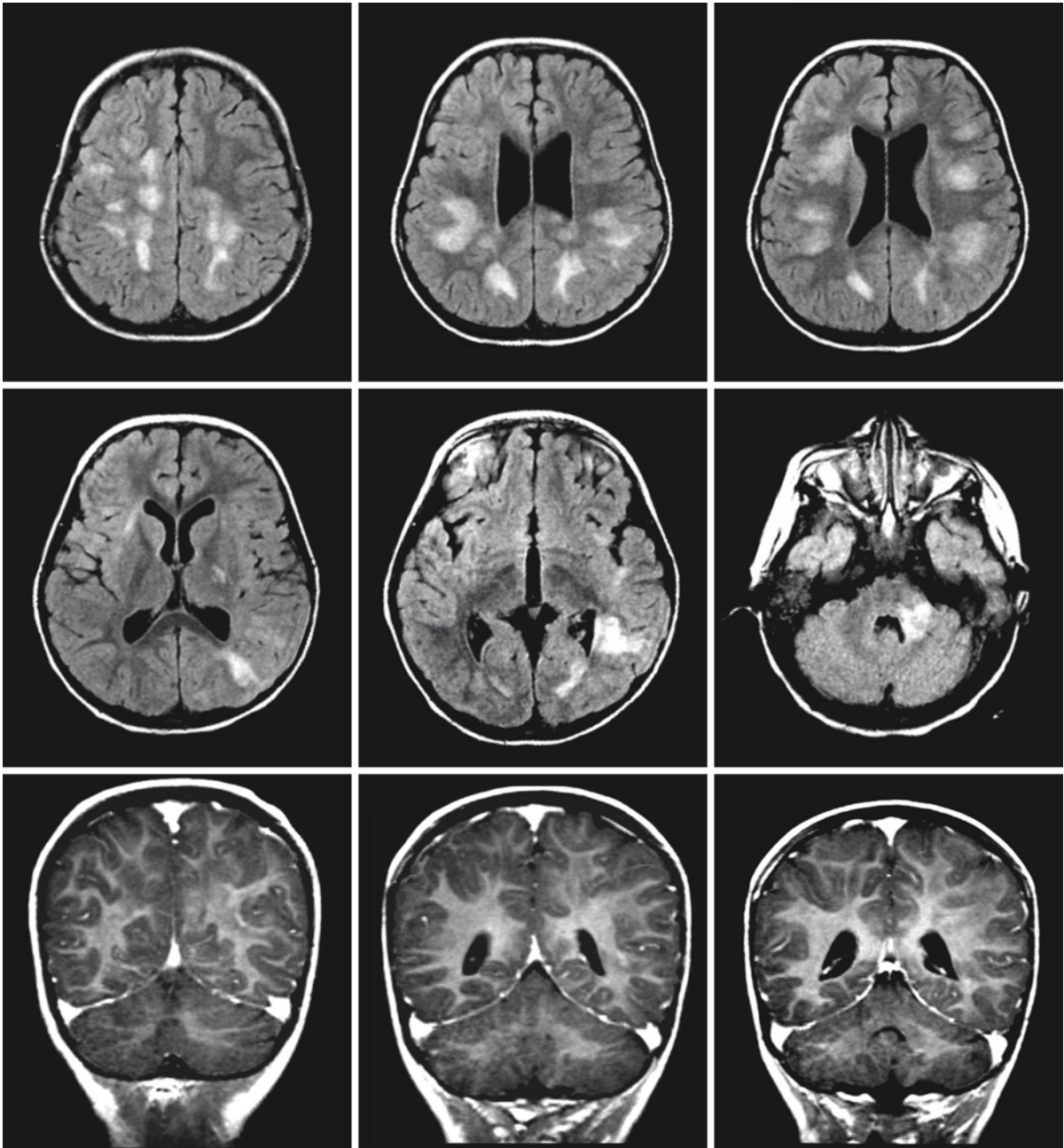


Fig. 80.2. A 5-year-old girl with a rapidly progressive presentation of ADEM. The transverse FLAIR images (*upper two rows*) show many lesions dispersed throughout the brain, with exception of the temporal lobes. There is also a large lesion in the

left middle cerebellar peduncle. T₁-weighted coronal contrast-enhanced images (*third row*) show only a few tiny spots of enhancement

in ADEM the normal-appearing white matter is less involved than in multiple sclerosis. These measurements have been made outside of the acute phase.

Apart from the difference in preferential involvement of brain structures, it may be difficult to distinguish ADEM from multiple sclerosis in the initial phase. Without a clinical history of a preceding infec-

tion or vaccination, or when the disease presents with a single symptom such as optic neuritis, it is impossible to differentiate between acute multiple sclerosis and ADEM on basis of MR images. In a later phase, comparison as described of MTRs and MRS in normal-appearing white matter can help in the decision. Repeated MRI examinations over a long period of

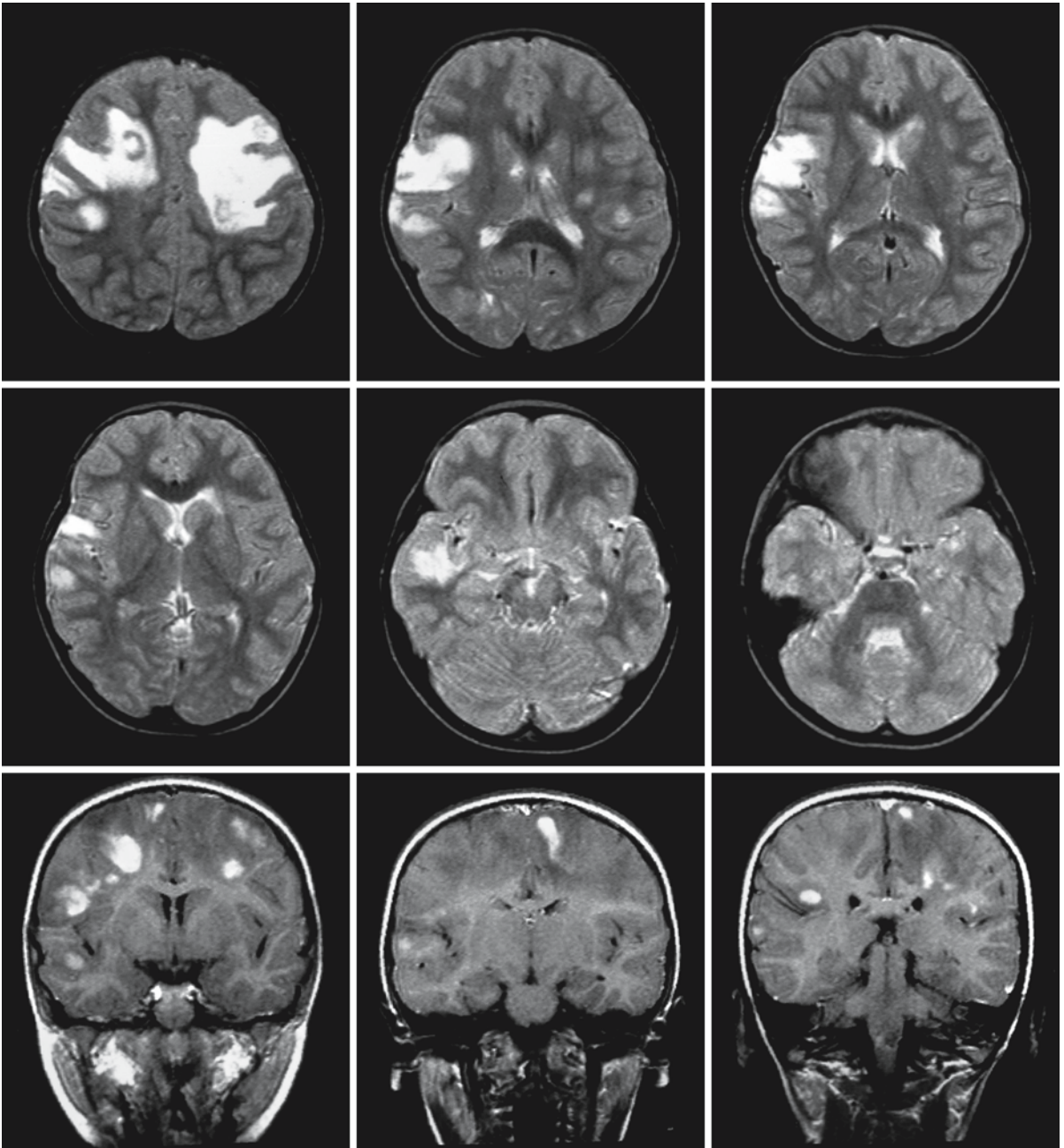


Fig. 80.3. In this 3-year-old girl with ADEM the T_2 -weighted transverse images (*upper two rows*) show large lesions that involve the subcortical white matter, with extension into the cor-

tex. After contrast injection the T_1 -weighted images (*third row*) show enhancement of many lesions

time may also be helpful, in particular in combination with follow-up of the clinical course. Stationary lasting lesions are indicative of ADEM, while newly appearing lesions argue against this diagnosis, but this is not an absolute rule. New lesions may appear in ADEM despite ongoing clinical improvement, but new lesions do, as a rule, not appear after the attack

when the patient is asymptomatic. New lesions on MRI repeated 3 months after the attack is considered to be predictive of multiple sclerosis. However, some ADEM patients have multiple episodes in the course of several years.

In exceptional cases, one may find a clinical picture suggestive of ADEM while MRI shows predominantly

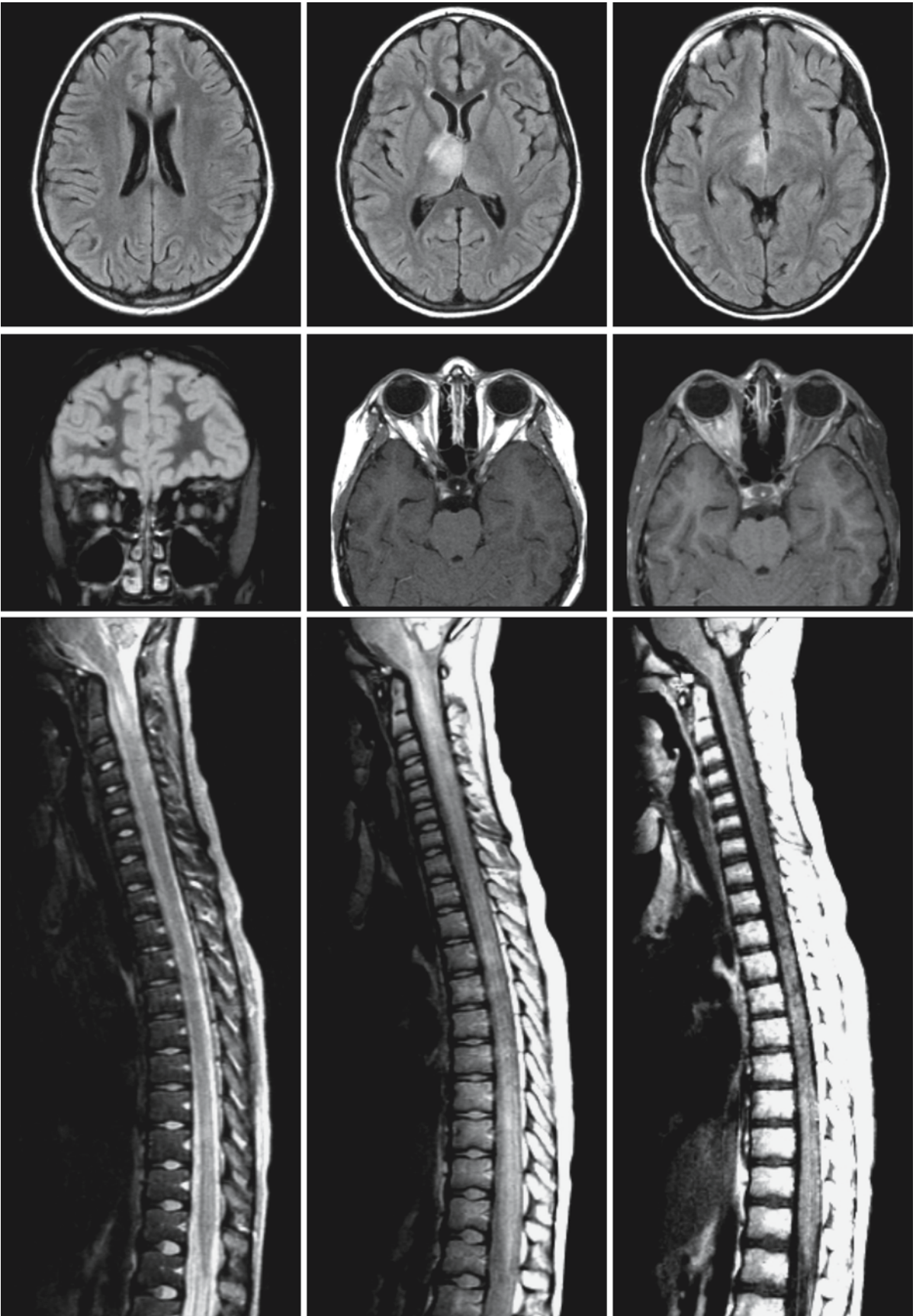


Fig. 80.4.

or exclusively gray matter lesions (Fig. 80.7). These gray matter lesions may disappear. Probably the “gray matter ADEM” is the counterpart of the “regular ADEM,” just as Guillain–Barré syndrome is usually a demyelinating polyneuropathy, but is sometimes axonal.

In AHEM, the hemorrhagic component can be identified on CT, but also with confidence by MRI, either by FLAIR or by gradient echo techniques. The hemorrhagic aspect, which is highly unusual in multiple sclerosis and its variants, may help to establish the correct diagnosis (Fig. 80.8).

Fig. 80.4. MRI in a 6-year-old girl presenting with lowered consciousness, spastic paraparesis, and diminished vision of the right eye. The FLAIR images (*first row*) show a gray matter lesion, a large lesion in the right thalamus with some mass effect. A coronal STIR image (*second row, left*) shows swelling and too high a signal in the right optic nerve, representing optic neuritis. The transverse T₁-weighted images after contrast injection (*second row, middle and right*) show enhancement of the right optic nerve. The *third row* shows the spinal images. A T₂-weighted sagittal image of the cervical and upper thoracic cord (*left*) shows a large intramedullary lesion in the upper cervical cord. The proton density image (*middle*) reveals multiple additional smaller lesions in the thoracic cord. A T₁-weighted contrast-enhanced sagittal image of the spinal cord (*right*) shows enhancement of multiple lesions

Fig. 80.5. An 11-year-old boy with ADEM. In the acute stage (*first two rows*), the T₂-weighted transverse images show extensive, patchy involvement of the white matter in the centrum semiovale, bilateral and symmetrical involvement of the internal capsule, involvement of the pulvinar, and also symmetrical involvement of structures in the pons. At follow-up, 2 weeks later (*third and fourth rows*), the lesions have disappeared completely, reflecting full clinical recovery. (Fig. 80.5 see next page)

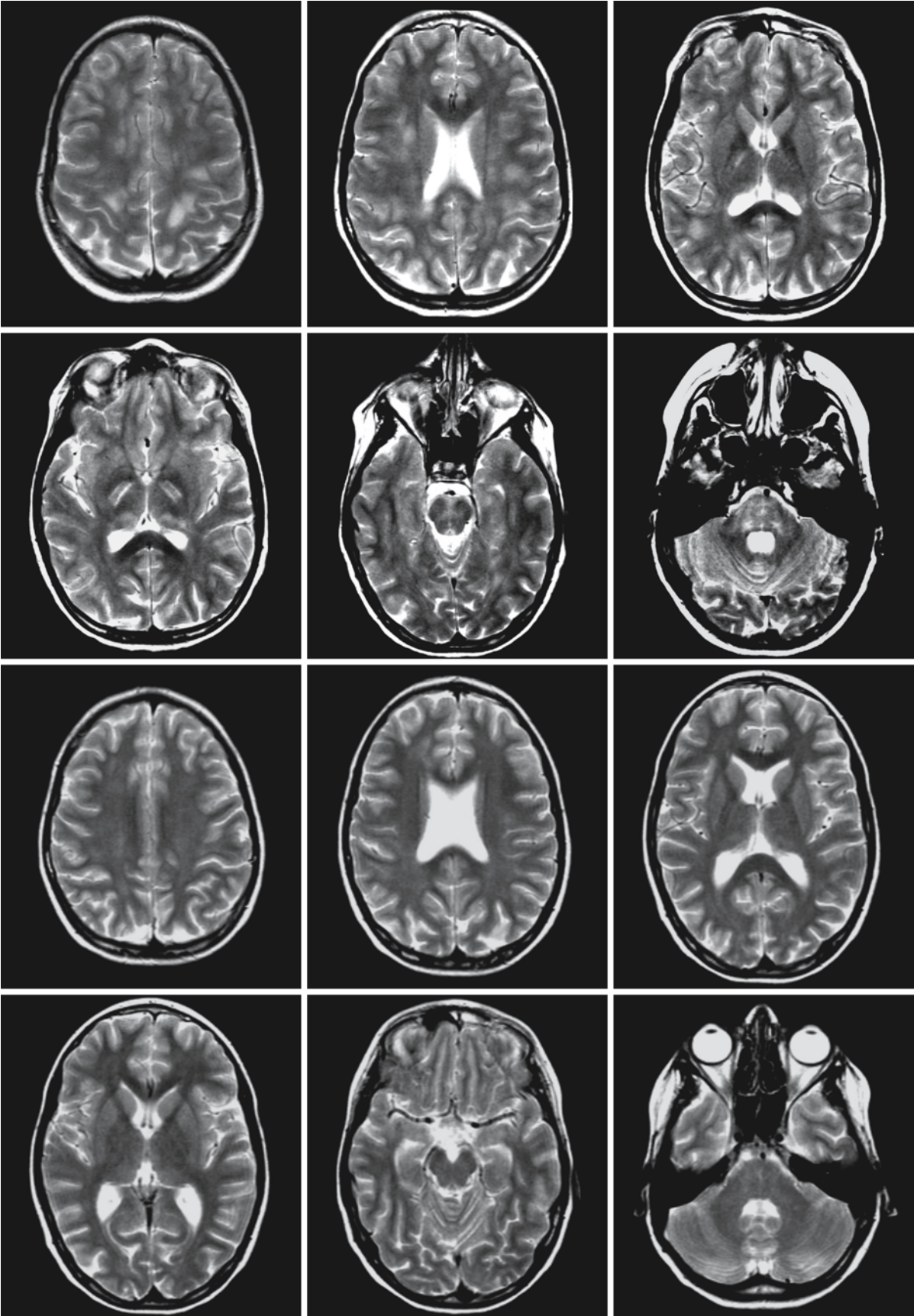


Fig. 80.5.

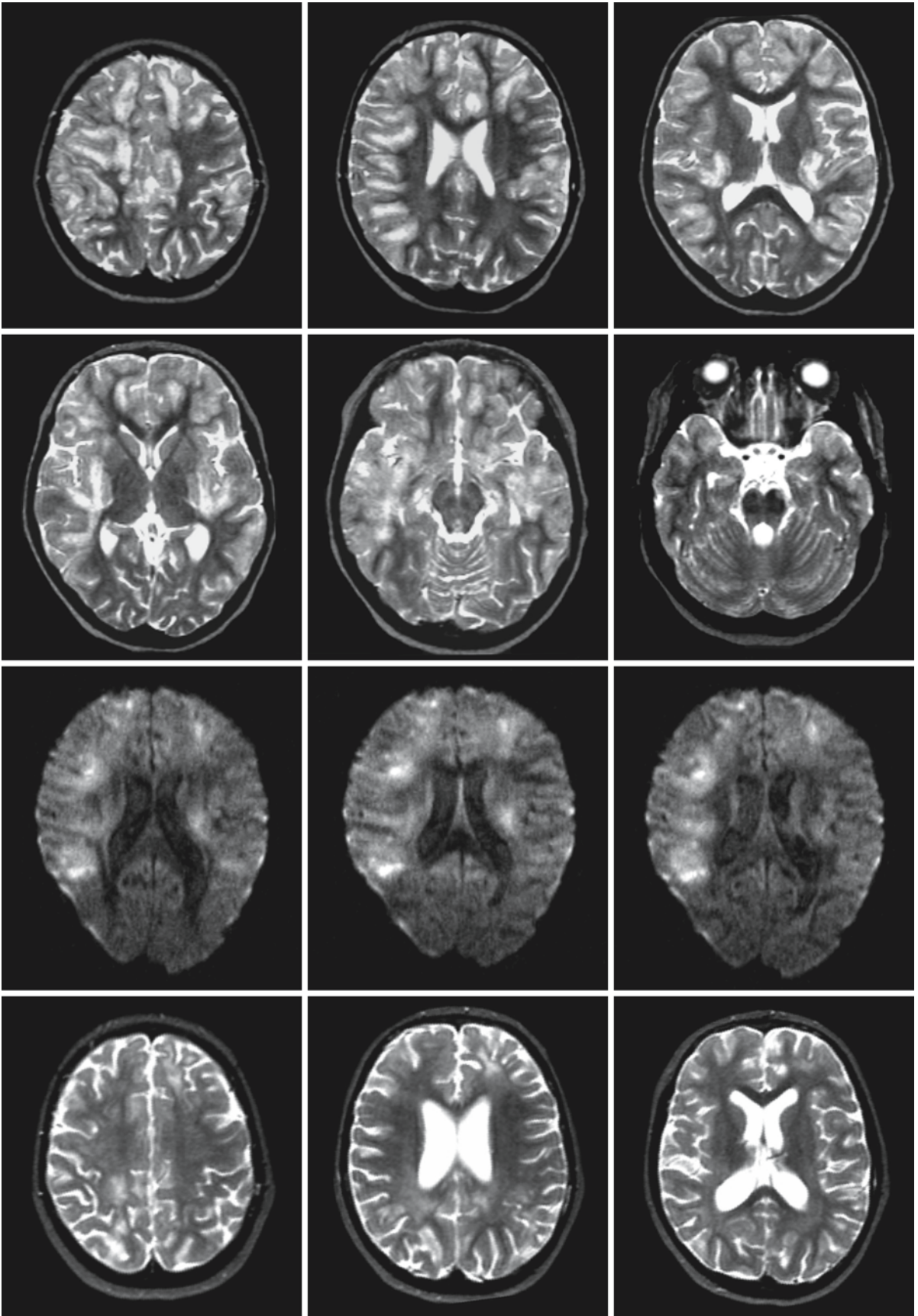


Fig. 80.6.



Fig. 80.6. (continued). In a 6-year-old girl with ADEM and a serious presentation, the T_2 -weighted images (*upper two rows*) show multifocal involvement of subcortical and deep white matter. Diffusion-weighted-Trace ($b = 1000$) images (*third row*) show high signal in the affected regions with greater con-

spicuity. The ADC values were low ($\sim 30\%$). Follow-up MRI after 6 months (*fourth and fifth row*) shows cortical and central atrophy and some ill-defined areas of signal abnormality in the cerebral white matter

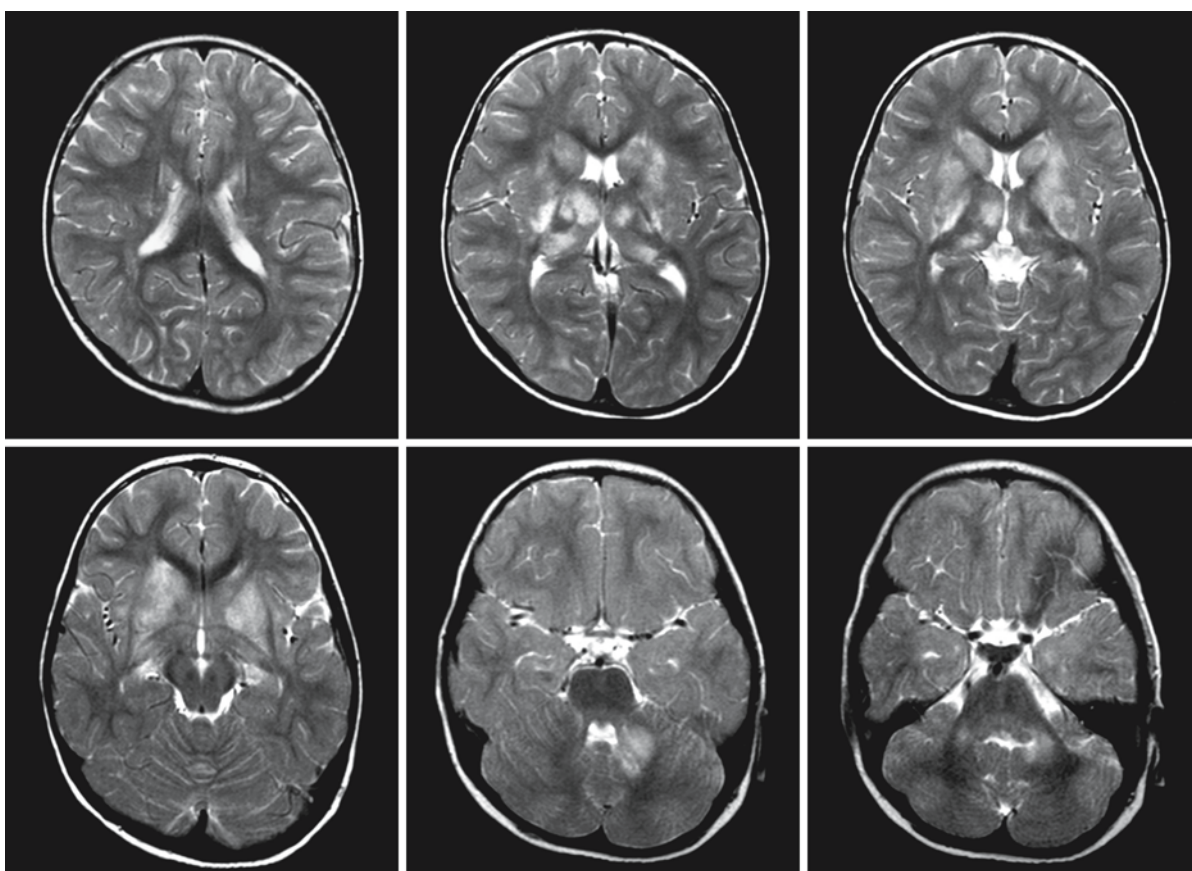


Fig. 80.7. In this 2.5-year-old boy with ADEM, the lesions are predominantly located in the gray matter. Exceptions are lesions in the middle cerebellar peduncle on the left side

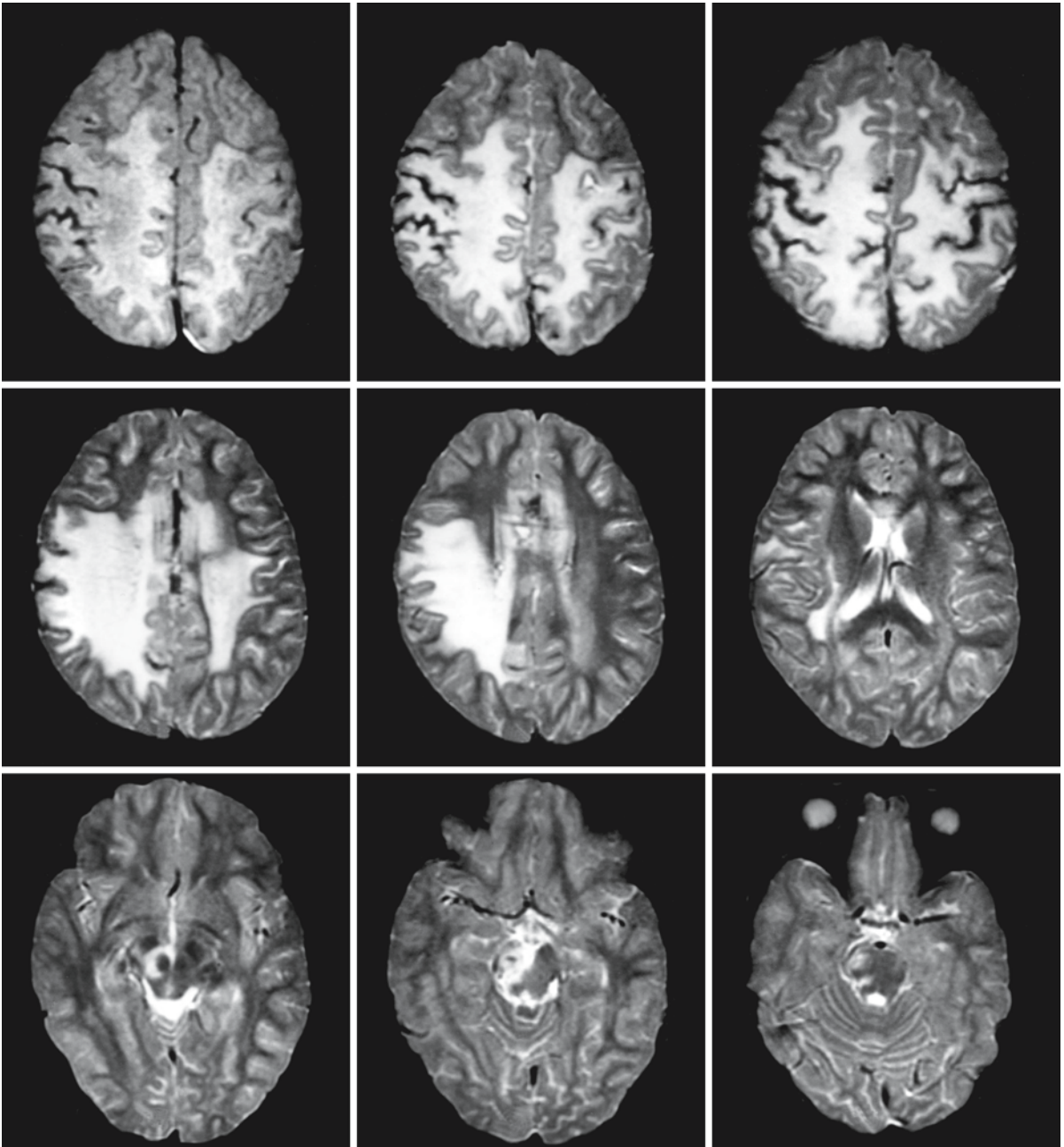


Fig. 80.8. An 8-year-old boy, acutely ill following a minor infection a few weeks before admission. The T_2 -weighted images show involvement of the pons and mesencephalon, especially on the right side, and large, confluent areas of abnormal white matter in the cerebral hemispheres. The gyral pattern in the

rolandic area shows too low a signal intensity, caused by the presence of breakdown products of blood, including hemosiderin. The presence of considerable hemorrhage classifies this patient as a case of AHM. Courtesy of Dr. A. Goulao, Lisbon, Portugal

Acquired Immunodeficiency Syndrome

81.1 Clinical Features and Laboratory Investigations

The acquired immunodeficiency syndrome (AIDS), as defined according to the criteria of the Centers of Disease Control, is a state characterized by one or more opportunistic diseases indicative of underlying cellular immunodeficiency, in the absence of underlying causes of cellular immunodeficiency other than human immunodeficiency virus type 1 infection and in the absence of all other causes of reduced resistance reported to be associated with opportunistic diseases. The opportunistic diseases in AIDS include opportunistic infections and neoplasms that can result from immunodeficiency. AIDS is caused by a retrovirus named human immunodeficiency virus type 1 (HIV-1). This virus has previously been designated human T cell lymphotropic virus type III (HTLV-III), lymphadenopathy-associated virus (LAV), and AIDS-related virus (ARV). High-risk groups in non-Third-World countries have been defined as homosexual or bisexual males, intravenous drug abusers, immigrants from Haiti and Central Africa, blood transfusion recipients, heterosexual partners of HIV-infected individuals, children of mothers infected with HIV, and hemophiliacs who have received factor VIII concentrate. About 72% of AIDS patients originate from the first of these risk groups and 17% from the second group. The other risk groups constitute only minor percentages of the total AIDS patient population.

AIDS can manifest itself in many different ways. Most patients present with malignant tumors and/or infections that are infrequently seen in immunocompetent individuals. The most common tumors in AIDS are Kaposi sarcoma, primary CNS lymphoma, systemic non-Hodgkin lymphoma, and plasmocytoma. The opportunistic infections most frequently include *Pneumocystis carinii* pneumonia, toxoplasmosis, cryptococcal meningitis, candidiasis of the upper gastrointestinal tract, and many infections with other viruses, fungi, mycobacteria, and parasites. Nonspecific signs and symptoms of the disease are weight loss, fatigue, malaise, night sweats, fever, cysts in the parotid glands and generalized lymphadenopathy. Neurological signs and symptoms are frequent and are reported in 30–75% of patients. Malignant lymphoma and metastatic Kaposi sarcoma may affect the CNS. Opportunistic infections of the CNS include

herpes simplex encephalitis, herpes zoster encephalitis and radiculitis, cytomegalovirus encephalitis, papovavirus infection with progressive multifocal leukoencephalopathy, infection with *Aspergillus fumigatus*, *Candida albicans*, and *Cryptococcus neoformans*, nocardiosis, coccidioidomycosis, *Mycobacterium tuberculosis* infection, atypical mycobacterial infections, toxoplasmosis, and neurosyphilis. However, only a minority (about 30%) of the CNS affections can be attributed to opportunistic infections. A primary HIV-1 infection is the most common cause of neurological dysfunction. Acute diffuse leukoencephalitis, subacute encephalitis, aseptic meningitis, vacuolar myelopathy, and inflammatory demyelinating peripheral neuropathy are generally assumed to be caused by direct HIV-1 infection. It should be noted that the following clinical descriptions refer to untreated patients. With treatment the disease course will be halted or modified.

Acute diffuse leukoencephalitis has been described in a limited number of cases. Clinically this disease is characterized by rapid mental deterioration, progressive tetraparesis, and in some cases death within a few days. A relapsing-remitting course of disease has also been described, indistinguishable from multiple sclerosis.

Subacute HIV-1 encephalitis, also called AIDS encephalopathy or AIDS dementia complex, is the most frequent neurological manifestation of AIDS and eventually afflicts many AIDS patients. Subacute HIV-1 encephalitis usually develops after other complications of AIDS have appeared, but it may also be the first major or even the sole clinical manifestation of HIV-1 infection. In subacute HIV encephalitis cognitive, motor, and behavioral abnormalities are usually early features. Early cognitive abnormalities are impaired memory, loss of concentration, confusion, and slowing of mentation and movement. The onset of dementia is usually insidious, but a rapid onset over a period of a few days and accelerations are not rare. Behavioral abnormalities include apathy, social withdrawal, dysphoric mood, organic psychosis, and regressive behavior. Early motor symptoms are lack of balance, weakness of the legs, tremor, and loss of coordination. Neurological examination often reveals ataxia and pyramidal tract signs. The majority of patients develop a severe and global dementia within 2 months after the onset of symptoms, but sometimes the initial course is more protracted, and a mild or

moderate impairment of intellectual functions is present for several months prior to the subsequent onset of a more severe global dementia. The dementia of subacute HIV-1 encephalitis has been described as subcortical because of the relative absence in many patients of seizures and other signs of focal cortical involvement. The affected patients usually remain alert. Neurological symptoms in the end stages are variable and include aphasia, ataxia, hypertonia, motor weakness with paraparesis, quadriparesis or hemiparesis, pseudobulbar palsy with dysphagia and dysarthria, tremor, blindness, extrapyramidal signs with rigidity, incontinence, myoclonus, epileptic seizures, and sometimes organic psychosis. Retinopathy is found in about one-third of the patients with subacute HIV-1 encephalitis. Cotton wool spots are the most frequently observed retinal abnormalities; less frequently a hemorrhagic retinitis is seen. Optic neuritis is a rare finding. Death usually occurs within 1 year after the first signs of encephalopathy are noted.

Other neurological complications include cerebral hemorrhage and cerebral infarction. Thrombocytopenia predisposes AIDS patients to cerebral hemorrhage, while nonbacterial thrombotic endocarditis may lead to cerebral infarction.

The majority of children with AIDS are born to women who have AIDS or pre-AIDS themselves and who are intravenous drug abusers, sexual partners of male members of high-risk groups, or of Haitian origin. In a smaller percentage of the affected children, transfusion-associated AIDS has been implicated. Clinical characteristics of AIDS in children include failure to thrive, generalized lymphadenopathy, hepatosplenomegaly, recurrent bacterial infections, and infections with opportunistic agents. Neurological abnormalities are variable. The most consistent findings are acquired microcephaly and moderate to severe mental retardation. Motor deficits ranging in severity include pyramidal tract signs with spastic paraparesis or tetraparesis and pseudobulbar palsy. Hypotonia with hyperreflexia is frequent in affected children, especially early in the course of disease. In some children, psychomotor retardation is stationary. In others progressive mental and motor deterioration occurs with a remitting course. Subacute HIV-1 encephalitis can be found in this latter group of patients.

Vacuolar myelopathy is a common neurological complication in AIDS. It is frequently difficult to correlate spinal cord abnormalities with clinical symptoms and signs in individual patients since many patients have coexistent encephalopathy or peripheral neuropathy. Clinical features may be a spastic monoparesis, paraparesis, or tetraparesis with hyperreflexia and extensor plantar reflexes, but sometimes reflexes are absent. Incontinence and sexual disturbances are frequent, as are sensory abnormalities with sensory ataxia. Neuropathologically, myelopathy

of grades I, II, and III can be distinguished. A steadily progressive spastic-ataxic paraparesis, which usually evolves over several weeks to months, is most characteristic of patients with grade III, severe myelopathy. Signs and symptoms are similar but less severe in patients with grade II myelopathy. Clear myelopathic signs are infrequent in patients with grade I myelopathy.

Patients with AIDS are susceptible to a number of PNS complications. Peripheral nerve affections occur in about half of the patients with subacute encephalitis. Cranial nerve signs are less prominent. Apart from herpes zoster radiculitis, a distal symmetrical peripheral polyneuropathy, chronic inflammatory demyelinating polyradiculoneuropathy, and mononeuritis multiplex have been described. Distal symmetrical peripheral neuropathy manifests itself by distal sensory disturbances and a mild degree of weakness in the distal muscles of the lower extremities. The symptoms are predominantly sensory with burning, painful paresthesias and numbness. In more advanced stages the muscular weakness may become more marked and spread to the arms. Chronic inflammatory demyelinating polyradiculoneuropathy resembles the Guillain-Barré syndrome but the course is subacute or, more often, chronic. Weakness is most severe in distal muscles but also affects proximal muscles. Sensory abnormalities are usually less marked. In severe cases weakness becomes generalized, and facial diplegia, bulbar weakness, and respiratory difficulties result. In mononeuritis multiplex, nerve dysfunction is relatively abrupt in onset. In the course of time, multiple nerves become involved, resulting in patchy weakness and sensory loss.

Diagnosis of HIV-1 infection cannot be made with standard serological tests in the early phase of the disease. Recombinant enzyme-linked immunosorbent assays (ELISAs) are commonly negative in the early phase, as are tests for antibodies. Serological tests become positive after 3–4 weeks. Early diagnosis is possible with the serum or plasma viral p24 antigen test, also used in blood donors to detect viral infection. Estimation of plasma viral RNA levels is even more sensitive than the p24 antigen test. Counts of CD4+ lymphocytes give important information of the immune status of the patient. Studies of T lymphocyte subpopulations in AIDS reveal a depletion of CD4+ T helper cells with an inversion of the CD4+ helper to CD8+ suppressor cell ratio. In active HIV-1 infections the count is low. The most specific diagnosis of HIV infection is by direct identification of the virus in tissue or blood of suspected patients or indirectly by demonstrating the presence of antibodies to the virus. Longitudinal studies have shown that in serum, HIV-1 antigens appear early and transiently after primary HIV-1 infection. Antibody production follows, after which HIV antigens may disappear.

Immunological investigations may include tests demonstrating cutaneous anergy to recall antigens, depressed response in lymphocyte transformation assays, and usually a decreased natural killer cell activity. Lymphopenia may be present. These immunological abnormalities may be absent early in the disease. Abnormalities in B cell function and humoral immunity have been reported. Immunoglobulin levels may be high due to nonspecific polyclonal B cell activation. Circulating immune complexes may be present. Serological studies for a number of infections are frequently positive, such as hepatitis A and B, herpes group viruses, and toxoplasmosis. If indicated, cultures of body fluids for bacteria, mycobacteria, viruses, and fungi may be performed.

The CSF of patients with HIV infection of the CNS usually has slightly raised protein content and less often a mononuclear pleocytosis with cell counts of up to 50 cells/mm³. The CSF of children with AIDS encephalopathy shows these abnormalities less often. The CSF of patients with AIDS encephalopathy often contains oligoclonal immunoglobulin bands, which have anti-HIV activity. CSF anti-HIV antibodies are present in most AIDS patients, irrespective of the presence of neurological complications. These antibodies occur early in the course of the disease, indicative of an early seeding of HIV to the CNS. A longitudinal study showed that HIV-1 antigen is present transiently in CSF before the occurrence of antibodies. HIV-1 antigen continues to be present in children and adults with progressive AIDS encephalopathy. As a rule, it is not found in the CSF of asymptomatic seropositive controls, some of whom have anti-HIV antibodies in the CSF. Persistence of HIV-1 antigens in the CSF most probably reflects ongoing CNS involvement. HIV-1 antigens in the CSF are not a result of leakage of viral proteins through the blood-brain barrier, as in some patients the quantity of HIV-1 antigens is larger in CSF than in serum, whereas other patients have extremely high serum levels and no HIV-1 antigens in the CSF. The same arguments apply to anti-HIV antibodies, proving that the synthesis of these CSF antibodies occurs within the blood-brain barrier.

EEG often shows moderate, generalized slowing of the background pattern in subacute HIV-1 encephalitis, occasionally with non-periodic high-voltage spiking. Even in patients with seizures or myoclonic jerks, paroxysmal discharges are not usually seen. In patients with distal symmetrical peripheral neuropathy the nerve conduction velocity is normal or slightly reduced. EMG shows some signs of denervation in distal muscles. In chronic inflammatory demyelinating polyneuropathy a marked slowing of nerve conduction is the rule. The abnormalities are frequently patchy. F responses are prolonged or absent, which is in conformity with a component of radiculopathy.

Conduction block is a common finding. EMG is either normal or shows signs of denervation and reinnervation.

81.2 Pathology

It has been estimated that approximately 40% of patients with AIDS have clinically apparent CNS dysfunction. At autopsy, neuropathological abnormalities are found in about 80% of patients, and 20% of patients have multiple coexisting CNS disease processes. Neuropathological signs of subacute HIV-1 encephalitis are found in about 50% of patients with AIDS, and it is accordingly the most common CNS illness associated with AIDS.

The brains of patients with *subacute HIV-1 encephalitis*, also called giant cell encephalitis or microglial nodule encephalitis, usually show some degree of atrophy at postmortem examination. Mild to moderate ventricular dilatation is associated with an apparent reduction of cerebral white matter volume and shrunken cortical gyri. The most prominent microscopic abnormalities in the brain involve the white matter and deep gray matter. Subacute HIV-1 encephalitis is characterized by intraparenchymal and perivascular infiltrations of lymphocytes and macrophages, located in both gray and white matter. The perivascular infiltrations occur typically around capillaries and venules and are most frequently detected in the centrum semiovale, basal ganglia, and pons. In mild cases the infiltrates are lymphocytic and scanty. In more severe cases, inflammatory infiltrates are composed mainly of foamy macrophages, in some instances intermixed with multinucleated giant cells. These multinucleated cells are thought to be derived from macrophages as they display macrophage markers, and are considered to be a histopathological hallmark of HIV-1 encephalitis.

The most common white matter abnormality is diffuse pallor, demonstrated by myelin staining. The borders of these large areas of pallor are ill defined. The subcortical white matter is relatively spared. There is some variability in the regional intensity of the pallor, which is most prominent in the centrum semiovale. The myelin loss is accompanied by a loss of axons, but the axons are relatively better preserved. Diffuse reactive astrocytosis occurs and generally parallels the inflammatory and parenchymal changes. In addition, most patients have small, poorly defined foci of more complete demyelination. These usually have a perivascular distribution. The lesions are associated with inflammatory infiltrates, which are composed of lymphocytes, lipid-laden foamy macrophages, reactive astrocytes, microglia, and sometimes multinucleated cells. Another common finding is vacuolation of the white matter, most frequently ob-

served in the centrum semiovale and less commonly in the internal capsule, brain stem, and cerebellum. Electron microscopic examination shows intramyelinic vacuoles.

The cerebral cortex is relatively normal. Astrocytosis is usually found only in the deep cortical layers. Considerable neuronal damage and loss is seen only in cases of severe white matter changes. Inflammatory infiltrations with presence of macrophages, lymphocytes, multinucleated cells, and reactive astrocytes are present in the basal ganglia and brain stem. Sometimes focal areas of coagulation necrosis with cavitation are seen, principally in the basal ganglia.

Microglial nodules with multinucleated giant cells are found in both gray and white matter, in the latter case often accompanied by demyelinating lesions. HIV-1 virus has been identified in these nodules. In a number of cases, however, the microglial nodules contain cells with the intranuclear and intracytoplasmic inclusion material typical of cytomegalovirus infection. Microglial nodules may be the consequence of either HIV-1 infection or cytomegalovirus infection. Cytomegalovirus-associated nodules are usually distinguished by their predominant localization within the cortical gray matter and by the presence of characteristic intranuclear inclusion bodies within or near the nodules.

Ultrastructural studies of the brain in subacute HIV-1 encephalitis reveal many virus-like particles in the cytoplasm of most macrophages and multinucleated giant cells and, less often, in astrocytes, but not in neurons and oligodendrocytes. These particles are double-membraned structures, which contain cylindrical nucleoids, characteristic of the Lentivirus subfamily of the retrovirus group. These structures have been identified as HIV-1. In addition to complete infectious HIV-1 virions, HIV-1 RNA, HIV-1 DNA, and HIV-1 core proteins have been identified in the brains and also in the CSF of patients with subacute HIV-1 encephalitis. Macrophages and multinucleated cells of macrophage origin appear to be infected, but there is evidence that some other cells are also infected to a lesser extent.

Histological examination of *acute diffuse leukoencephalitis* reveals demyelination, most pronounced in the centrum semiovale. There is also axonal loss, but axons are relatively better preserved than myelin. Microglial nodules and multinucleated giant cells may be present but have also been reported as absent. Inflammatory reaction is variable. The demyelinating lesion may extend into the frontal, occipital, and temporal area. The basal ganglia, thalamus, and brain stem may also be involved in the process. The lesions may be large and multifocal or highly confluent, symmetrical or asymmetrical. Presence of HIV-1 genome in the brain has been shown. Tests for all other infections, in particular cytomegalovirus, are negative.

In *multiple sclerosis-like leukoencephalopathy*, multiple, large, well-defined areas of demyelination can be shown, which may involve hemispheric white matter, internal capsule, basal ganglia, optic tracts, corpus callosum, brain stem, and cerebellum. These lesions are characterized by myelin loss with presence of lipid-laden macrophages and preservation of axons and nerve cell bodies, associated with marked gliosis and presence of perivascular inflammatory infiltrates. Multinucleated giant cells and microglial nodules are reported as absent. Direct evidence of HIV-1 infection has not (yet) been provided, although increase in CSF HIV-1 antigen during exacerbations has been demonstrated in some cases.

In *children with progressive HIV-1 encephalopathy*, brain weight is below normal for age, and sometimes there is obvious atrophy. Most of the brains show evidence of white matter disease, including pallor, diffuse lack of myelin, and astrocytosis. Probably both hypomyelination and demyelination are responsible for the diffuse lack of myelin. The axons are relatively better preserved than in adults. Calcification often occurs within or adjacent to the walls of small vessels in the basal ganglia and central white matter of the cerebral hemispheres, especially in the frontal lobes. Inflammatory cell infiltrates which resemble classic microglial nodules but which are larger are commonly observed. They consist of microglia, astrocytes, lymphocytes, a few plasma cells, and often multinucleated cells, some of which have the proportions of multinucleated giant cells. The inflammatory infiltrates are most often located in basal ganglia and pons, but are also found in other gray and white matter structures of brain and spinal cord. In addition, vascular or perivascular inflammation may be present, involving small or medium-sized arteries or veins. The inflammation of intraparenchymal vessels is accompanied by intimal fibrosis of medium-sized vessels and endarteritis obliterans with focal thrombosis of small vessels.

Spinal cord disease afflicts approximately 25% of AIDS patients. Pathological changes are most prominent in the lateral and posterior columns at the thoracic level, less severe in the anterolateral and anterior columns. White matter changes are often asymmetrical and are not confined to specific anatomic tracts. Microscopically, the disease is characterized by intramyelinic vacuoles, similar to those seen in cerebral and cerebellar white matter. Axons are intact except in the most severely affected areas. The white matter vacuolation is associated with few lipid-laden macrophages, usually located within the vacuoles. Reactive astrocytes are rare, and inflammation is not present as a rule.

81.3 Pathogenetic Considerations

Human immunodeficiency virus type 1 (HIV-1) has been identified as the primary cause of AIDS. HIV-1 is the prototypical member of the Lentivirinae subfamily of retroviruses affecting humans. Lentiviruses characteristically cause indolent infections in their host. These infections are notable for involvement of the nervous system, long periods of clinical latency, and weak humoral immune responses complicated by persistent virus presence. One feature that distinguishes the lentiviruses from other retroviruses is the remarkable complexity of their viral genomes. Most retroviruses capable of replication contain only three genes. HIV-1, however, contains in its RNA genome at least six additional genes. It is probable that the distinct but concerted actions of these additional genes underlie the profound pathogenicity of HIV-1. From a therapeutic standpoint, this same genomic complexity may also be the Achilles heel of the virus.

A broad-based search for antagonists specific for these HIV-1 gene products has started. High-resolution electron microscopy has revealed the HIV-1 virion as an icosahedral structure containing 72 external spikes. These spikes are formed by the two major viral envelope proteins, gp120 and gp41. The HIV-1 lipid bilayer is also studded with various host proteins, including class I and class II major histocompatibility (MHC) antigens, acquired during virion budding. HIV-1 has a selective tropism of CD4+ T helper-inducer lymphocytes. The human CD4+ T lymphocyte and monocyte are the major cellular targets for HIV-1 infection, because the CD4+ membrane antigen represents the principal, if not sole, high-affinity receptor for this retrovirus. After entry of the CD4+ T lymphocyte, the viral RNA is transcribed into DNA and subsequently integrated into the CD4+ T lymphocyte DNA during cell division. In inactive CD4+ T cells much of the viral DNA remains unintegrated in the cytoplasm. The HIV replication cycle is restricted until the CD4+ T cell is activated by other pathogens (for instance, hepatitis B virus, herpes simplex virus, cytomegalovirus) or by allogeneic stimulation (for instance, exposure to allogeneic semen, blood, or allografts). After activation, transcription occurs in RNA, followed by protein synthesis. Viral proteins and viral RNA assemble. Mature viruses are formed by budding from the cytoplasmic membrane. In the process of HIV replication the CD4+ T cell is killed. The mechanism of cell death is unclear. The killing of CD4+ T lymphocytes leads to depletion of this type of cells. Faster depletion of CD4+ T cells may result from enhanced susceptibility to superinfection by other pathogens, for example, by cytomegalovirus. CD4+ T lymphocytes play a central role in the immune response, and their depletion leads to many immunological abnormalities. The cellular (T

cell) immune system essentially ceases to function, but there are also marked abnormalities in B cell activation (humoral immune system) and immunoregulation. There is a state of polyclonal B cell activation with high immunoglobulin levels and a poor antibody response to new antigens. The deficiency of cellular immunity leads to an extreme susceptibility to viruses, fungi, mycobacteria, and parasites – agents that require cell-mediated immunity for containment. Neoplasms arising in a cellular immunodeficiency state include primarily lymphomas and Kaposi sarcoma. The B cell dysregulation may explain the frequent occurrence of severe pyogenic infections, in particular with *Streptococcus pneumoniae* and *Haemophilus influenzae*. The elevated production of nonspecific immunoglobulins may lead to autoimmune processes such as immune thrombocytopenia. In addition, CD4+ T antigens are also present on the cell surface of certain types of macrophages and monocytes, which may therefore also be infected by HIV-1. The infection of these cells results in additional immunological deficits, especially in chemotaxis.

HIV-1 leads to a persisting infection. The viral genetic information is integrated in the DNA of the host cell and the virus can only be destroyed by killing the infected cells. It has been demonstrated that a small percentage of infected cells may survive and contribute to virus persistence. Infected monocytes and macrophages may contribute to the persistence of HIV-1 as they appear to be relatively resistant to the cytolytic effect of HIV-1.

HIV-1 appears to be transmitted predominantly by contact with infected blood or semen. However, the virus has also been isolated from cervicovaginal secretions, tears, urine, saliva, breast milk, and CSF. These fluids could possibly also be involved in the transmission of AIDS. HIV may be transmitted to a child in utero, during birth, or postnatally through infected breast milk.

The clinical picture of patients with HIV-1 infections can range from asymptomatic (carrier with viremia or antibody or both) through chronic generalized lymphadenopathy to a variable degree of clinically manifest immunodeficiency. Estimation of viral load and CD4+ lymphocytes may help to predict which patients are likely to have the full-blown disease. The latency period between infection and full-blown AIDS ranges from several months to several years.

Substantial evidence supports a direct etiological role for HIV-1 in subacute encephalitis, aseptic meningitis, vacuolar myelopathy, and peripheral neuropathy. The intra-blood-brain-barrier synthesis of HIV-1-specific antibodies has been demonstrated in the majority of AIDS patients with neurological symptoms but also in patients without these. The

oligoclonal IgG bands in the CSF of AIDS patients have been demonstrated to contain anti-HIV activity. The presence of HIV-1 antigens in CSF appears to be strongly associated with CNS involvement. HIV-1 has been isolated from CSF in patients with subacute encephalitis and aseptic meningitis. The fact that virus has been isolated from CSF cannot be attributed solely to the presence of infected lymphocytes since many samples are free of cells. HIV DNA and RNA sequences have been demonstrated in CNS tissue of patients with subacute encephalitis. HIV-1 has been isolated from brain in subacute encephalitis, from the spinal cord in vacuolar myelopathy, and from the sural nerve in a patient with peripheral neuropathy. The multinucleated giant cells seen in subacute encephalitis show a striking similarity to the multinucleated cells that develop from the fusion of T lymphocytes infected by HIV-1 *in vitro*. Ultrastructural examination has identified intact retroviral particles within the multinucleated giant cells in some cases. The multinucleated cells are probably of macrophage origin, as they share morphological features and macrophage markers. Very similar multinucleated giant cells have been reported in lymph nodes in AIDS patients. There is evidence that the multinucleated giant cells are of hematogenous origin. It is possible that the virus penetrates the CNS by migration of infected mononuclear cells from the blood, but a direct viral invasion of the CNS is not excluded. Immunohistochemical identification of HIV antigen has shown that the most frequently infected cells include macrophages, microglia, and multinucleated giant cells; less frequently capillary endothelial cells, astrocytes, and oligodendroglia are infected, and also neurons, but only rarely. The virus is concentrated in, although not limited to, the white matter.

The precise mechanisms underlying the structural cerebral damage remain to be determined. The low-level infection, sometimes seen in a few neurons, astrocytes, and oligodendrocytes, cannot be held responsible for the severe CNS damage that is often present. The functional and structural damage of the CNS is therefore probably related indirectly to the HIV-1 infection, which primarily affects monocytes and macrophages and to a lesser degree endothelial cells. Data indicate that the extent of endothelial and macrophage infection is more commensurate with the clinical findings than the extent of neuronal and glial infection. This observation led to the suggestion that the CNS dysfunction reflects an infection of the endothelial cells that impairs the blood-brain barrier and leads to fluctuations in fluid and electrolyte levels and to structural damage. Another possibility is that activated macrophages secrete a variety of materials, such as tumor necrosis factor, interleukin, and proteolytic enzymes, that cause brain tissue damage and impairment of neurological function. An alterna-

tive is that the release of HIV-1 envelope glycoproteins from infected macrophages may interfere directly with neuronal function as these HIV-1 proteins may directly suppress neuronal responses to neurotropic factors and cause shortened neuronal survival.

The frequent involvement of the CNS in AIDS is probably related to a number of factors. The brain is an immunologically privileged organ. HIV-1 within brain tissue may be hidden and protected from immune surveillance. In addition, the damage to the immune system caused by HIV infection promotes the persistence of viral infection. In infants the known susceptibility of the immature CNS to viral invasion plays a role and may explain the high incidence of AIDS encephalopathy in young children infected with HIV.

81.4 Therapy

Therapy for HIV-1 infection has been increasingly successful in considerably reducing morbidity and mortality. This has been achieved by a logical attack on targets provided by the life cycle of the HIV-1 virus and by using a combination of therapies in the so-called highly active anti-retroviral treatment (HAART). To understand the different approaches it is most illustrative to follow this life cycle of HIV-1 and indicate where interference with the cycle is possible.

The HIV-1 virus consists of an outer envelope of protein, fat, and sugars wrapped around an inner core, the capsid, which contains genetic information in the form of two strands of RNA, and a number of special enzymes. Proteins of HIV-1 are strongly attracted to CD4+ surface receptors presented on dendritic cells, macrophages, monocytes, and, most abundantly, on T4 lymphocytes (helper cells). After binding to the CD4+ surface receptor, other proteins, such as glycoproteins gp120 and gp41, are activated, allowing the HIV cell to fuse with the outside of the cell. The therapeutic intervention at this point is administration of entry blockers. Attempts have been made to use CD4+ protein decoys, which have so far not been very successful. More promising as an entry inhibitor seems enfuvirtide (T20). Enfuvirtide is a complex peptide consisting of 36 amino acids. The compound binds to a subunit, gp41, of the glycoprotein gp120, located on the viral envelope, blocking the entry of the virus in the cell. Data about side effects and long-term results are still scarce.

Once the viral capsid is inside the cell, the two strands of RNA are transcribed into DNA, the "proviral" DNA, by the enzyme reverse transcriptase. Interventions at this step have been successful and several types of reverse transcriptase inhibitors have been

developed and play an important role in combination therapies. The main groups are nucleoside reverse transcriptase inhibitors, nonnucleoside reverse transcriptase inhibitors, and nucleotide reverse transcriptase inhibitors.

Approved reverse transcriptase inhibitors include:

- Nucleoside analogues: zidovudine, didanosine, zalcitabine, stavudine, lamuvidine, abacavir
- Nucleotide analogues: tenofovir disoproxil fumarate
- Non-nucleoside reverse transcriptase inhibitors: delavirdine, efavirenz, nevirapine

The next step in the development of new virions is the entry of the proviral DNA into the cell's nucleus, where the enzyme integrase connects the viral DNA with the host cell's DNA. Integrase inhibitors are still under research, but may eventually open a therapeutic window at this level.

When the T lymphocyte is activated, special enzymes transcribe DNA into messenger RNA. In this phase, transcription inhibitors could be expected to have therapeutic action, but so far they do not play an important role in HIV therapy.

Messenger RNA is now translated into new viral proteins, which are kept inside the cell. In the final part of the process these strings of proteins are cut up by the enzyme protease to form proteins that will handle the different functions of the new HIV virus. The logical answer to this phase was the development of protease inhibitors, which has been successful. Protease inhibitors now play a prominent role in HIV therapy. Approved protease inhibitors are: saquinavir, ritonavir, indinavir, nelfinavir, amprenavir.

This is not the place to give recommendations on combination therapy, which would be very soon outdated. Federal guidelines and recommendations are available on the Internet and updated regularly (<http://www.projinf.org/fs/antiVirSrat.html>). On this site generic names and brand names of the antiviral drugs are given, together with the names of the pharmaceutical companies. Federal guidelines are given for the circumstances in which therapy should start, how best to combine preparations, changes of therapy, when indicated, and advice for treatment of pregnant women. It is common policy now to prescribe a combination of a protease inhibitor with two nucleoside analogues. Initially the combination therapy had the disadvantage that many pills had to be taken every day, some before meals, some after meals, three or four times a day. This hardly promoted therapy compliance, seriously contributing to the risk of drug resistance. There are attempts to replace these regimens by a once-a-day intake of drugs, and several drugs have already been approved for once-a-day use. The newer therapeutic regimens have been successful in restoring at least some immunocompetence in the

patients. Patients with progressive multifocal encephalopathy have shown temporary improvement. The improved CD4+ cell count is another sign of improvement.

Side effects of these multidrug regimens are common, myopathy, neuropathy, gastrointestinal problems, pancreatitis, bone marrow and hepatic toxicity, and fat redistribution being the most common. Both lipodystrophy and lipohypertrophy are possible, lipohypertrophy probably caused by the protease inhibitors and lipodystrophy caused by the reverse transcriptase inhibitors. Lipohypertrophy causes a protease paunch and buffalo hump. Lipodystrophy can disfigure the face and often requires cosmetic surgery. Bone marrow suppression is another possible side effect, leading to anemia and thrombopenia. Children born from mothers using antiretroviral drugs during pregnancy may present with severe mitochondrial disorders related to depletion of mitochondrial DNA. The effects of HIV nucleoside analogue reverse transcriptase inhibitors (NRTIs) on mitochondrial function have been known for some time. NRTIs are phosphorylated intracellularly to dideoxynucleoside triphosphates. These compounds compete with the natural substrates (deoxythymidine triphosphates) for HIV reverse transcriptase, but, since they lack a 3' hydroxyl group, the effect is termination rather than lengthening of the DNA chain. They are also substrates for DNA polymerase γ , the enzyme required for replication of mitochondrial DNA. Mitochondrial DNA encodes crucial mitochondrial proteins and is present in multiple copies per cell. Decreased concentrations of mitochondrial DNA have been shown in muscles of patients with zidovudine-induced myopathy. NRTIs are widely used to diminish the rate of transmission of HIV across the placenta from infected mothers to children. In a series of 1784 children (Blanche et al. 1999), 8 children with probable mitochondrial dysfunction were observed, without HIV infection, a much higher frequency than could be expected in the normal population (1 in 5,000–20,000). Quite a few uncertainties remain (Morris and Carr 1999). At this moment continuation of the policy of the treatment of HIV positive pregnant women with antiretroviral therapy is still recommended.

A more definite approach is the development of an HIV-1 vaccine. The development of such a vaccine has been complicated by the remarkable sequence heterogeneity of the HIV-1 envelope proteins. Hyperimmunization of chimpanzees with HIV-1 envelope protein did not protect them against HIV-1 infection after injection of small quantities of the same strain of bHIV-1. More recent vaccination studies in Asian monkeys with a simian virus (SIV-1) infection, which causes an AIDS-like disease, have generated more positive results and suggest that an effective HIV-1 vaccine may be an achievable goal.

Preventive measures still prevail in the battle against AIDS, the universally propagated “safe sex” being the major public prevention factor. Other preventive measures are directed towards the avoidance of contact with infected blood, screening of blood donors for AIDS, and inactivation of virus in blood products such as factor VIII concentrate. Specific measures have also been advocated in the management of HIV-1-positive pregnant women, in order to reduce the risk of neonates acquiring the disease in the peri- or postnatal period.

In opportunistic infections and CNS tumors appropriate therapeutic measures have to be taken. Identifying the causative agent in infections or the nature of the tumor is, therefore, important and the major role of MRI.

81.5 Magnetic Resonance Imaging

Neuroimaging studies are essential in the evaluation of AIDS patients with neurological symptoms. A high percentage of the patients infected with HIV-1 have CNS complications, including the AIDS dementia complex, opportunistic infections, and brain tumors. The primary purpose of brain imaging is to detect potentially treatable opportunistic lesions.

Most patients with advanced subacute HIV-1 encephalitis have CT evidence of cerebral atrophy with enlargement of subarachnoid spaces and ventricles. CT evidence of atrophy may precede clinical signs of encephalitis, whereas in other cases initial CT scans may be normal and the atrophy becomes evident on later scans. Marked hypodensities in the white matter of both cerebral hemispheres are sometimes noted. An additional abnormality shown by CT scan in some children with HIV-1 infection of the CNS, and less frequently in adults, is calcification of basal ganglia and, less often, of the periventricular white matter and the frontal subcortical white matter. CT scans may also reveal abnormalities which are a conse-

quence of opportunistic infections, tumors, and vascular lesions of the brain. The presence of more than one type of lesion within one patient frequently complicates the interpretation of CT findings.

MRI has greater sensitivity than CT in identifying CNS lesions in this patient population, with the exception of calcifications. HIV-1 infection of the brain leads to a number of patterns identifiable on MRI.

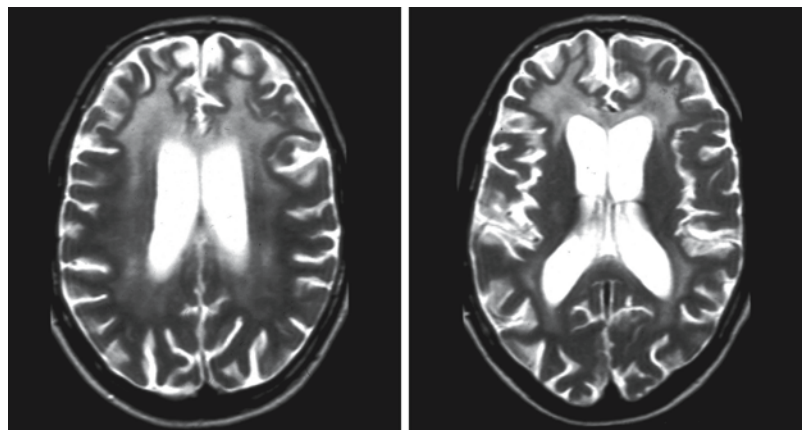
The most common pattern seen in AIDS dementia complex is generalized atrophy with widened ventricles and enlarged cortical sulci. Probably, however, atrophy is a relatively late finding. MRS is more sensitive, already showing a decrease in the *N*-acetylaspartate (considered to be a neuronal marker) while images are still normal.

The second pattern represents the subacute HIV-1 encephalitis and reflects the histological findings of diffuse, mild myelin pallor or demyelination with preference for the frontal and parietal lobes. MRI shows symmetrical periventricular areas of mildly increased signal intensity of the white matter, not involving the U fibers, with preferential involvement of the frontal and parietal lobes (Figs. 81.1 and 81.2). There is no enhancement after contrast injection. The brain stem and cerebellum are not involved. In the course of the disease the white matter abnormalities progress, resulting in severe hemispheric involvement (Fig. 81.2).

In acute diffuse leukoencephalitis, large multifocal or more diffuse and extensive white matter abnormalities are present. In the case of multifocal lesions, these are not necessarily symmetrical (Fig. 81.3). Hemispheric white matter, internal capsule, thalamus, and brain stem may be involved. In cases in which the disease course resembles multiple sclerosis, multifocal white matter involvement is seen (Fig. 81.3). Contrast enhancement of the lesions has not been reported.

The frequency of superimposed infections is relatively low, but double and multiple infections may occur. Of the opportunistic infections, cerebral toxo-

Fig. 81.1. T₂-weighted transverse images of 40-year-old male AIDS patient with an advanced stage of subacute HIV encephalitis. The MR images show widening of the ventricles and cortical atrophy. There are symmetrical signal abnormalities in the cerebral white matter, most prominently involving the frontal lobes. In the posterior regions, the signal abnormalities are more subtle and the U fibers are spared



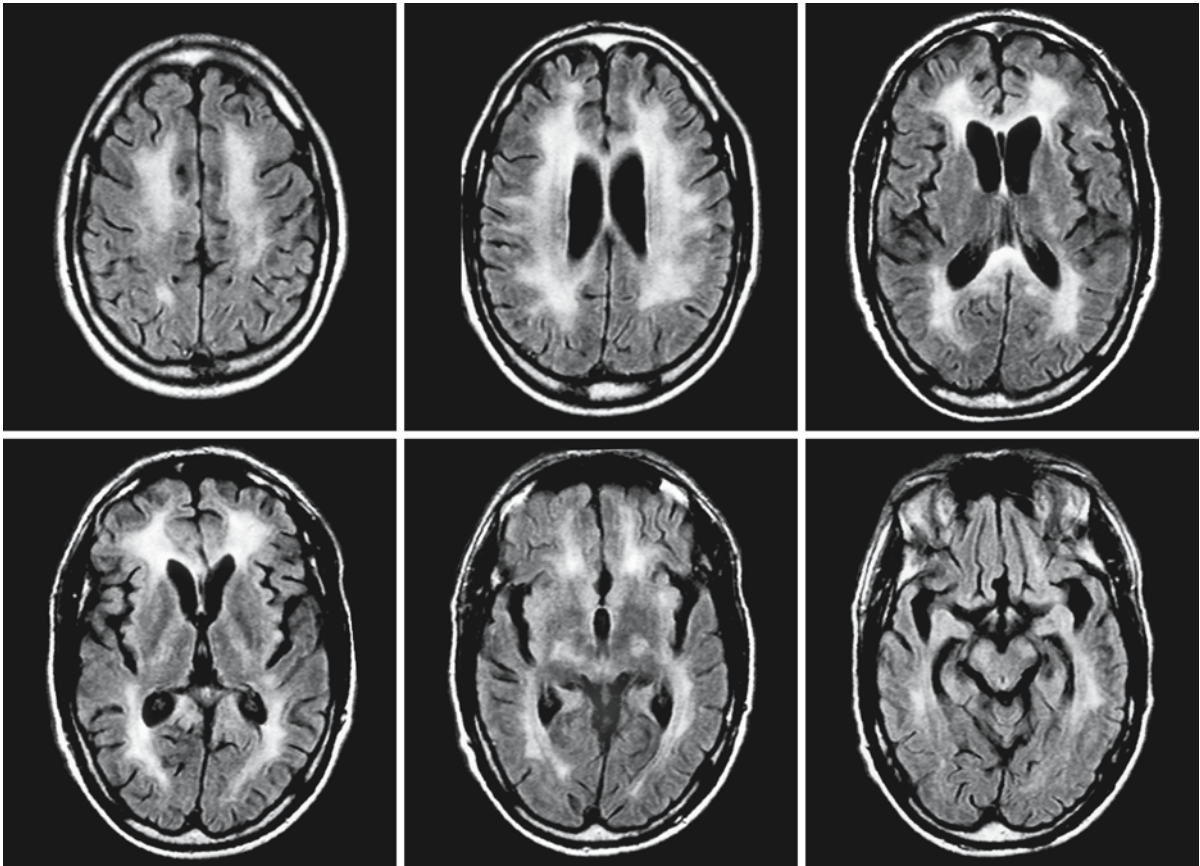


Fig. 81.2. A 48-year-old man presenting with AIDS presented with headaches, loss of concentration, mild cognitive impairment, and changes in behavior. The transverse FLAIR images show symmetrical involvement of the periventricular and deep cerebral white matter, sparing the U fibers. The posterior limbs of the internal capsules are involved, continued in the

corticospinal tracts of the midbrain and the white matter of the temporal lobes. There is slight cerebral atrophy. This pattern is characteristic of subacute HIV infection. Courtesy of Dr. M. Heitbrink and Dr. B. Wiarda, Department of Radiology, Medical Center Alkmaar, The Netherlands

plasmosis is the most common. It is the presenting opportunistic infection in at least 5% of the AIDS patient population. The lesions of toxoplasmosis are multifocal and unequal in size (Fig. 81.4). Sometimes the lesions show the so-called “target” sign, with a rim of high signal intensity on T_2 -weighted images and a core that is isointense with normal white matter. Lesions occur in all areas including the subcortical region, basal ganglia, brain stem, and, less frequently, the cerebellar hemispheres (Fig. 81.4). The lesions can be very large, have contact with the ventricles, and mimic a lymphoma. After contrast injection the lesions usually enhance. In about 5% of the cases, however, no or only slight enhancement is seen. This may be due to the absence of inflammation as a consequence of the defective immune system of the patient, resulting in little or no capsule formation around the toxoplasmosis abscess. Possibly, this finding predicts a poor prognosis. Pragmatically one could consider

anti-toxoplasmosis treatment when multiple focal lesions with ring enhancement are seen. If toxoplasmosis is present, the lesions will improve within a few weeks of therapy. Differentiation of larger single lesions is from lymphoma. Progressive multifocal leukoencephalitis is discussed in Chap. 82. In this disease, the lesions are confined to the white matter and extend into the arcuate fibers. There is a typically sharp border between gray matter and demyelinated white matter, leading to a characteristic pattern. Usually the lesions do not enhance, but there are exceptions. *Cryptococcus neoformans* infection is the most frequent intracranial fungal infection (2–7.5% of AIDS patients). The infection is preferentially located in the basal ganglia spreading along the Virchow–Robin spaces. This pattern of spread may produce a typical appearance, suggestive of this type of infection. Cytomegalovirus encephalitis resembles in many aspects the subacute AIDS encephalitis and

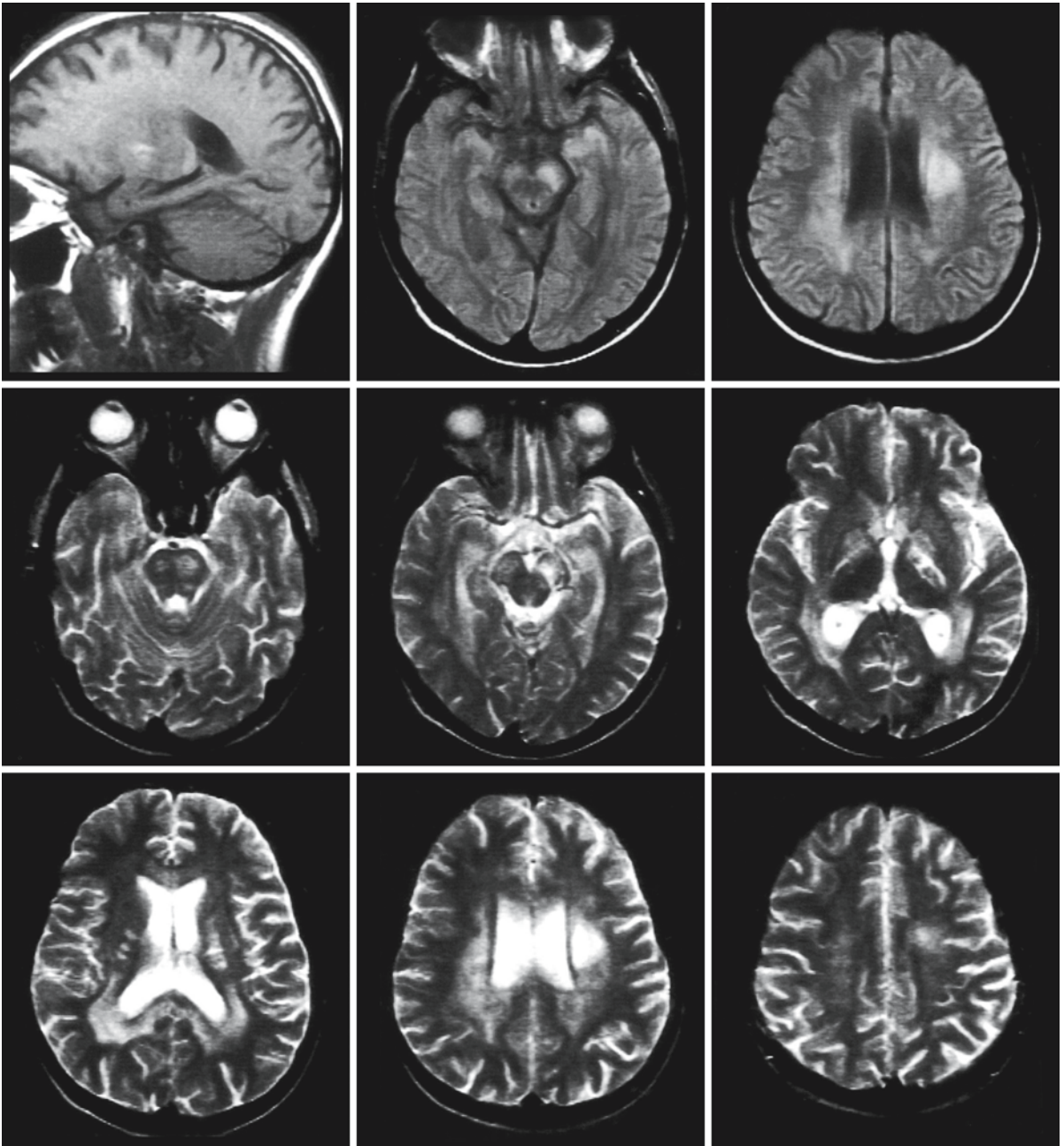


Fig. 81.3. A 24-year-old man, suffering from AIDS, presented with a rapidly progressive neurological syndrome and mental and emotional deterioration. The T₁-weighted sagittal image (*first row, left*) shows a high-signal-intensity lesion in the basal ganglia on the left side, probably a hemorrhage. The transverse proton density (*first row*) and T₂-weighted images (*sec-*

ond and third rows) show lesions consistent with acute diffuse leukoencephalitis. There is mildly increased signal intensity in the centrum semiovale and around the ventricles, also involving the posterior limb of the internal capsule and the white matter tracts in the pons. The lesions are asymmetrical at the level of pons, midbrain, and periventricular area

may present with the same clinical symptoms. Patients may also be asymptomatic. On MRI, diffuse, symmetrical, periventricular high-signal-intensity changes are seen on T₂-weighted images, indistinguishable from subacute HIV encephalitis. In some

cases a ventriculitis will develop. After contrast injection this appears as an enhanced subependymal rim around the ventricles.

Of the CNS tumors complicating AIDS, primary lymphoma is the most frequently observed (about

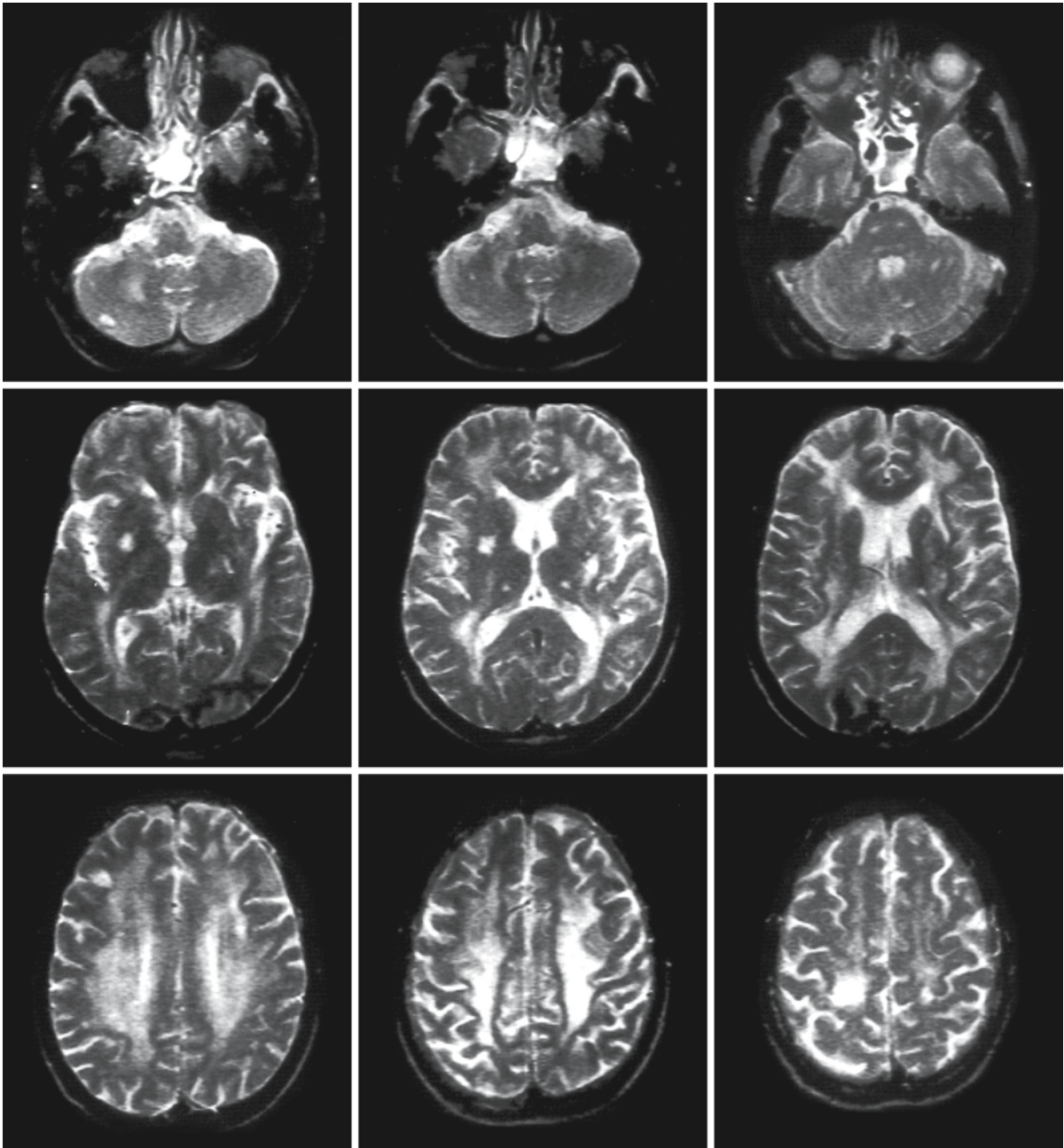


Fig. 81.4. A 48-year-old male AIDS patient was admitted to the hospital with general malaise and left-sided hemiparesis, cerebellar ataxia, and diplopia. He also showed intellectual deterioration. The MR images show two types of lesions. The first type consists of multiple smaller, isolated lesions in the

cerebellum, pons, and basal ganglia. The second type of lesion consists of a more symmetrical involvement of the periventricular and deep cerebral white matter. The latter type of lesion represents subacute HIV encephalitis; the dispersed, smaller lesions were demonstrated to be toxoplasmosis

5% of AIDS patients). In AIDS, lymphomas may be multifocal, which is rare in other patients. Also, the enhancement of lymphoma in AIDS patients may be less homogeneous. Differentiation from toxoplasmosis on MRI may be difficult. Both can present as single or multifocal lesions with mass effect; both can be

connected with the ventricular wall and enhance after contrast administration. Thallium-201 SPECT may offer a solution in distinguishing between infection and lymphoma. Leptomenigeal lymphoma can be diagnosed by the presence of pericerebral tissue that enhances with contrast. Metastases of Kaposi sarco-

ma have been observed in the CNS and in the skull base, but are extremely rare.

In HIV-1 encephalitis in children, apart from the ventriculomegaly and atrophy also found in adults, there is often symmetrical bilateral calcification of the basal ganglia and the white matter adjacent to the frontal horns. Contrast enhancement of the basal ganglia may also occur, sometimes starting unilaterally, becoming bilateral later on. Calcifications may also be related to a concurrent cytomegalovirus infection. White matter disease is not a prominent feature

of HIV-1 encephalitis in children, although white matter changes may be present. Opportunistic infections are less frequent in children than in adults. Central mass lesions are usually caused by primary lymphoma.

In the spinal cord lesions have been described in AIDS patients. On MRI these lesions are not distinguishable from lesions as seen in transverse myelitis in multiple sclerosis. Swelling of the cord is seen initially with moderate enhancement, eventually followed by atrophy.

Progressive Multifocal Leukoencephalopathy

82.1 Clinical Features and Laboratory Investigations

Progressive multifocal leukoencephalopathy (PML) is a rare demyelinating infection of the CNS caused by a polyomavirus, the JC virus. It usually occurs in immunodeficient patients. Its association with such underlying diseases as lymphoma, multiple myeloma, leukemia, sarcoidosis, tuberculosis, Whipple disease, systemic lupus erythematosus, systemic carcinomas, renal transplantation, bone marrow transplantation, AIDS, and immunosuppressed states is well documented, although the disease has also been reported in patients without evidence of an immunological deficit. During the last few years, PML has most often occurred in the context of AIDS. The prevalence of PML in AIDS patients is estimated to be in the range of 4–7%, which is probably an underestimation. In most cases, PML is a late complication of a pre-existing chronic systemic disease, which has typically been present for a long time before the neurological abnormalities appear. This underlying disease does not differ appreciably either in its clinical or pathological aspects from the same disease in other patients in whom PML does not occur. There is no way of predicting the occurrence of PML. PML occurs predominantly in adults. There is a male preponderance in the proportion of about 5:3.

The clinical signs and symptoms of PML are those expected from the presence of multiple CNS lesions of varying size, mainly affecting the white matter of the cerebral hemispheres but indiscriminate in their localization. In the early stages the most frequently observed signs are monoparesis, hemiparesis, personality change, cognitive impairment, ataxia, dysarthria, dysphasia, and cerebral visual impairment. Quadriparesis, severe dementia, and coma characterize the more advanced stages. Headaches and seizures are unusual, and there is no evidence of increased intracranial pressure. Rarely, involuntary movements indicative of an extrapyramidal disorder are observed, such as choreiform movements, dystonia, athetosis, or parkinsonism. Once the disease appears, it generally progresses until the patient dies. Usually, as with many incapacitating cerebral diseases, death results from terminal bronchopneumonia. In most patients a period of about 2–6 months elapses between the first appearance of neurological symptoms and death. In a few patients the illness is extremely

brief, lasting only a few days. At the other end of the scale, the disease can last for a year or more. In AIDS patients with secondary PML some survival time can be gained by treatment with highly aggressive antiretroviral therapy (HAART). Patients showing spontaneous improvement have also been described.

It is clear that a wide range of clinical neurological abnormalities may be encountered in PML and no syndrome is especially distinctive of the disease. The combination of a coexisting chronic systemic disease with fairly rapidly progressive multifocal or diffuse cerebral disease should suggest the presence of PML.

As a great proportion of the general population, probably 80–90%, has been exposed to JC virus in the form of a banal childhood upper respiratory tract infection and thus has developed IgG antibodies against the JC virus, serological tests are not helpful in establishing the diagnosis. Routine cytochemical CSF examinations, such as cell count and protein concentration, are also of little value, because abnormalities may be due to the underlying pre-existent disease. The JC virus has never been cultured from blood or CSF, nor have viral antigens been identified in the CSF. In patients who are not suffering from HIV infection, detection of intrathecal antibodies against the JC virus has a sensitivity of about 70% and a specificity of 99%. As in other microbial diseases, the PCR technique of amplifying DNA has had a major impact on the diagnosis of PML. Detection of JC viral DNA by PCR in the CSF has a sensitivity of about 75% and specificity between 90% and 99%. The high specificity obviates in many cases the need for a brain biopsy. However, the problem of false negative results in 25% of the cases remains, which may prompt a second CSF examination or still make a brain biopsy necessary. Semiquantitative measurements of JC viral DNA load in CSF shows correlation with survival and could be used as a method of monitoring therapeutic efficacy, in addition to clinical and neuroimaging findings.

82.2 Pathology

The brain displays no external abnormalities in PML. On sectioning, multiple grayish granular-appearing lesions are seen in the white matter, often associated with a loss of the distinct border between the cortex and subcortical white matter. Asymmetrical involvement is the rule. Although the lesions are often found

bilaterally, they are usually more extensive in one cerebral hemisphere than in the other.

Microscopically the lesions vary from small foci of demyelination to extensive areas of myelin loss, occupying a major portion of a cerebral lobe or hemisphere. The small foci tend to be round or oval, but the larger areas of demyelination are irregularly outlined, probably resulting from coalescence of smaller lesions. The lesions may occur anywhere in the white matter of the CNS, no part of the CNS being entirely spared. However, the lesions tend to be less frequent in the brain stem and the cerebellum, and involvement of the spinal cord and peripheral nerves is uncommon. Localization of lesions in the corticomedullary junction and subcortical white matter is very typical. The deep cortical layers often also show loss of myelin sheaths, but the cortical cytoarchitecture remains intact.

The lesions are characterized by loss of myelin with relative sparing of the axons. Sometimes the axons are destroyed along with the myelin, leaving nothing but a meshwork of astrocytic processes and glial fibrils or actual cavities. In the center of the lesion, where myelin sheaths have been destroyed, oligodendrocytes are absent. At the periphery of the lesions the oligodendrocytes are markedly altered, with enlargement of their nuclei and effacement of the normal chromatin pattern. These abnormal nuclei often contain basophilic or eosinophilic inclusion bodies. Another cellular change is a conspicuous alteration of astrocytes. Some of the astrocytes in and around the lesion are enlarged into gigantic forms, and their nuclear structure is profoundly altered. Hyperchromatism, occasionally bizarre lobulation of the nucleus, multinucleation, and mitotic figures are characteristic abnormalities. The change in individual cells is at times so severe that the cells become indistinguishable from the neoplastic cells that characterize malignant astrocytomas. The relative absence of a cellular inflammatory reaction is striking. In many cases inflammatory cells are absent altogether, and in other cases they are few. Numerous lipid-laden macrophages can be identified within the area of demyelination.

PML does little damage to nerve cell bodies. Lesions may be situated in gray matter structures, especially the deep cortical layers. Within these lesions the myelin sheaths are destroyed, and the astrocytes and oligodendrocytes show the characteristic changes, whereas most of the nerve cells appear to be intact.

Electron microscopic studies show virus-like particles within the abnormal oligodendrocytic nuclei and, to some extent, also in altered astrocytes. These particles are seen in isolation, in irregular groups, in a crystal-like pattern, or in the form of filaments. The size, shape, surface details, and arrangement of these particles are characteristic of the polyomavirus sub-

group of papovaviruses. This observation is confirmed by immunofluorescent studies with the use of specific antibodies against polyomavirus. Using the in situ hybridization techniques with a polyomavirus DNA probe, the infection of oligodendrocytes and astrocytes with this virus can also be shown.

82.3 Pathogenetic Considerations

PML is a demyelinating disease associated with a polyomavirus, which belongs to the Papovaviridae. The family Papovaviridae consists of two genera, *Papillomavirus* and *Polyomavirus*. These are small DNA-containing viruses. A human polyomavirus, designated JC virus after the individual from whom it was first isolated, has been implicated as the etiological agent in nearly all cases of PML. In a minority of the cases a related polyomavirus, simian virus 40 (SV40), has been held responsible for the disease. Although the disease PML is rare, infection with the JC virus is quite common. Antibodies to JC virus have been found in up to 90% of the population, and the prevalence of antibodies rises with increasing age. Infection is usually acquired early in life: by the age of 15, 65% of children have anti-JC virus antibodies. In any given PML patient there is no information about whether these antibodies were present before the onset of the disease. The virus is distributed throughout the world.

The question of how JC virus can be ubiquitous yet not cause more widespread clinical illness is not simple to answer. Recent research has provided information about the pathways the JC virus utilizes to enter the human host and ultimately the brain. Traffic of JC virus through the body is complex, involving cellular receptors, DNA-binding proteins, and a variety of viral regulatory regions in multiple target cells. JC virus DNA has been detected in human tonsil tissue, including stromal cells and lymphocytes. Therefore, tonsils may be the initial site of infection. For this infection to occur virions have to bind to special receptors, enter cells, and have their DNA integrated into host cell DNA. Viral DNA is replicated and translated into proteins, and via a number of steps JC virions are assembled and passed to circulating tonsillar lymphocytes. As with other human viral pathogens, susceptibility to infection is determined at least partly by viral attachment to cellular receptors. This specificity of receptors plays a role in the types of cells that are most vulnerable to infection. Different JC virus genotypes with different regulatory regions have consistently been found in different tissues, probably contributing to differential vulnerability of different tissues to infection. Viral reactivation occurs by immunosuppression of the host. Reactivated JC virus will infect B lymphocytes. These cells can cross the blood-brain barrier and infect oligodendrocytes.

Oligodendrocytes have a receptor profile that makes them extremely vulnerable to JC virus infection. Viremia would be another explanation of the transport of JC virus from infected organs to the brain, but this has never been observed. T cells cannot be carriers either, because JC virus cannot infect T lymphocytes or bind to T cell membranes. Infected B lymphocytes have been found in multiple PML brain tissue samples.

Various papovaviruses are known to induce cell transformation *in vitro* and are oncogenic in hamsters. Papovaviruses, as mentioned before, are subdivided into two subgroups: the papillomaviruses, known to cause warts and cervical carcinoma, and polyomaviruses, such as the JC virus, causing PML and of which the oncogenicity is a suspicion of more recent date. Papovaviruses, their antigens, or viral DNA sequences have been detected in some human tumor cells. Pathologically, two cell types in the brain are infected by the polyomavirus in PML. First, oligodendrocytes are lytically infected, and virus particles fill the nucleus to give it a characteristic appearance. Oligodendroglial cell death causes demyelination. It is postulated that there is also an infection of the astrocytes, in which the viral genome is integrated into the cellular DNA, leading to cell transformation. The fact that astrocytic cell transformation in PML is virally induced is indirectly supported by the known oncogenic potential of papovaviruses in hamsters, the reported simultaneous occurrence of PML and gliomas, and the demonstration of shared internal capsid antigens of a polyomavirus in the nucleus of giant astrocytes in PML.

A defect in cell-mediated immune defenses appears to be a central factor in the reactivation process of JC virus and the development of PML. The lack of cellular inflammatory reaction in white matter lesions also supports the notion of a deficit in cellular immunity. Yet this deficit alone does not provide an adequate explanation for the occurrence of PML since diseases associated with such immunological deficiency and treatment with immunosuppressive drugs are relatively frequent, while PML is rare. The problem is made even more difficult by the fact that PML may even occur in the presence of apparently intact immune responses.

Simian virus 40 is of minor importance in PML. In general, infection with this virus is rare in humans, only 5% showing antibodies. The source of the virus is unknown.

82.4 Therapy

At present the prognosis in PML is generally poor. Treatment with idoxuridine and vidarabine, both antiviral agents, has been shown to be nonbeneficial.

Cytarabine (arabinosylcytosine) administered intravenously and intrathecally has been demonstrated to be more promising in PML. The rationale for the use of this agent is that polyomaviruses are DNA viruses, and that cytarabine impairs DNA synthesis. Long-term survival of PML patients treated with cytarabine has been reported. The improvement of the neurological condition varies from moderate to marked in these patients. In some patients there is very rapid improvement, occurring within 48 h of initiation of therapy. In others there is a delay of several weeks. Sometimes cytarabine is only transiently beneficial, and sometimes it has no beneficial effect at all. Neither type and duration of underlying disease nor duration and course of neurological symptoms prior to treatment appear to yield a clue as to the different responses to therapy. Some studies, however, have been unable to find the same positive results using cytarabine. Treatment of PML with a combination of cytarabine and interferon has occasionally been reported as successful. Treatment of patients with HIV-1 infection and PML with highly aggressive antiretroviral therapy has led to a better immune status in patients, and sometimes also to a positive effect on the coexisting PML.

Therapy should be directed at eradication of the viral infection not only by specific antiviral agents but also by enhancing host immune defenses. Lowering of the immunosuppressive medication may be appropriate. Early diagnosis before actual destruction of nervous tissue has occurred may be necessary for treatment to be successful.

82.5 Magnetic Resonance Imaging

CT scan shows low-density white matter lesions with characteristically scalloped lateral borders following the contours of the gray-white matter junction, whereas the medial border is smoother in outline. Enhancement of some of the lesions may be seen. Small and early lesions are not detected, and CT often shows no abnormalities in the early stages of the disease.

MRI shows that PML lesions can be found anywhere in the white matter of the cerebral hemispheres, the brain stem, and the cerebellum, but most often involve the cerebral subcortical area (Figs. 82.1–82.3). The lesions have an intermediate to low signal intensity on T₁-weighted images, and a high or very high signal intensity on T₂-weighted images. The affected white matter appears somewhat swollen, which becomes more evident in those areas where the U fibers are involved. The subcortical white matter lesions then have a scalloped appearance, outlining the overlying cortex and stretching it (Figs. 82.1, 82.2 and 82.4). The sharp edge between affected white matter

Fig. 82.1. The characteristic image of PML: a large lesion in the right parietal lobe, involvement of the corpus callosum, and a smaller lesion in the left hemisphere. These T₂-weighted images show a sharp border between the hyperintense white matter lesion and the normal cortex. The cortex is stretched out over the lesion. In this case there was no enhancement

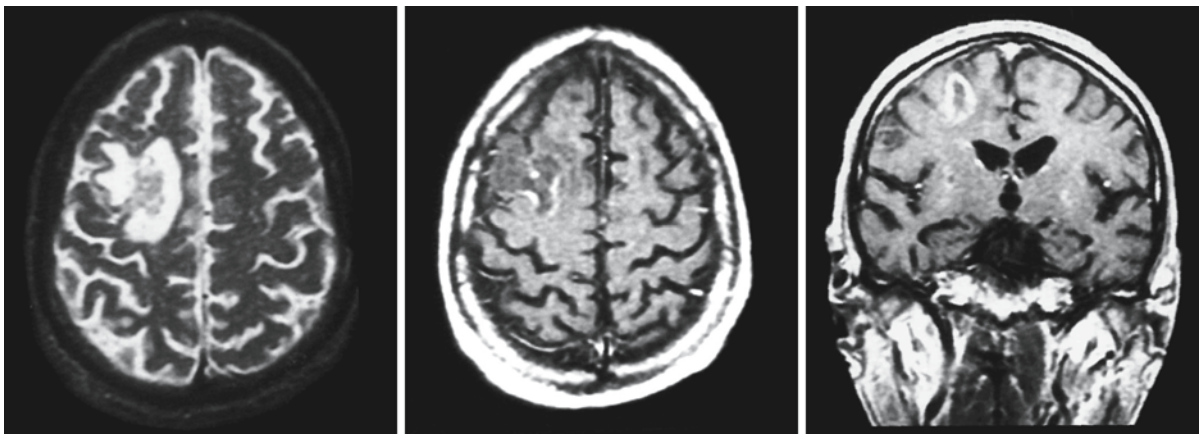
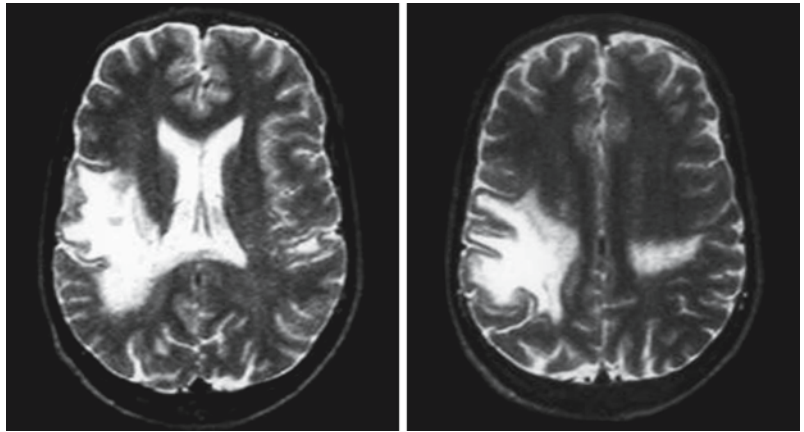


Fig. 82.2. A 63-year-old male with AIDS and PML. These images show a large frontal lesion on the right side with partial enhancement after contrast injection, as is seen on the transverse and coronal T₁-weighted contrast-enhanced images

and cortical gray matter is due to the anatomical barrier formed by the noninfected neuronal layer with its relative myelin paucity as opposed to the myelin-rich white matter and infected oligodendrocytes. In exceptional cases MRI shows some extension of a white matter lesion into the cortex, probably where intracortical myelin has been attacked (Fig. 82.3). Lesions of the external capsule have been found in 38% of PML patients, and posterior fossa lesions in 32% (Fig. 82.4). Isolated posterior fossa lesions have been reported occasionally. Basal ganglia may be involved, particularly in the myelin-containing laminae separating the various nuclei and subnuclei (Figs. 82.3 and 82.4). The myelin content of the thalamus and globus pallidus is higher than of the putamen and caudate nucleus, and lesions would be expected to occur more often in these areas. Involvement of the corpus callosum is often seen (Figs. 82.1 and 82.4). Although the epithet “multifocal” suggests more than one lesion in all cases, this is not necessarily true. Single lesions may occur. Confluence of several lesions may give rise

to the appearance of a widespread white matter disorder (Fig. 82.4). Enhancement after the injection of gadolinium is seen in a minority of patients, but is not exceptional (Figs. 82.2 and 82.4). If enhancement is seen, it is usually only present in some of the lesions; it is faint and peripheral. More solid enhancement is seen in rare cases. There is evidence that mass effect and (temporary) enhancement on MR images, as expressing the presence of an immune reaction of the patient, represent positive predictive factors for more prolonged survival. PML lesions have different appearances on diffusion-weighted images depending on the stage of the disease. Newer lesions and the advancing edge of large lesions have a high signal on Trace diffusion-weighted images and a normal to low ADC. Older lesions and the center of large lesions have a low signal on Trace diffusion-weighted images and increased ADC values. High signal on Trace diffusion-weighted images and low ADC mark the regions of active infection with cell swelling, distinguishing them from burnt-out areas of gliosis.

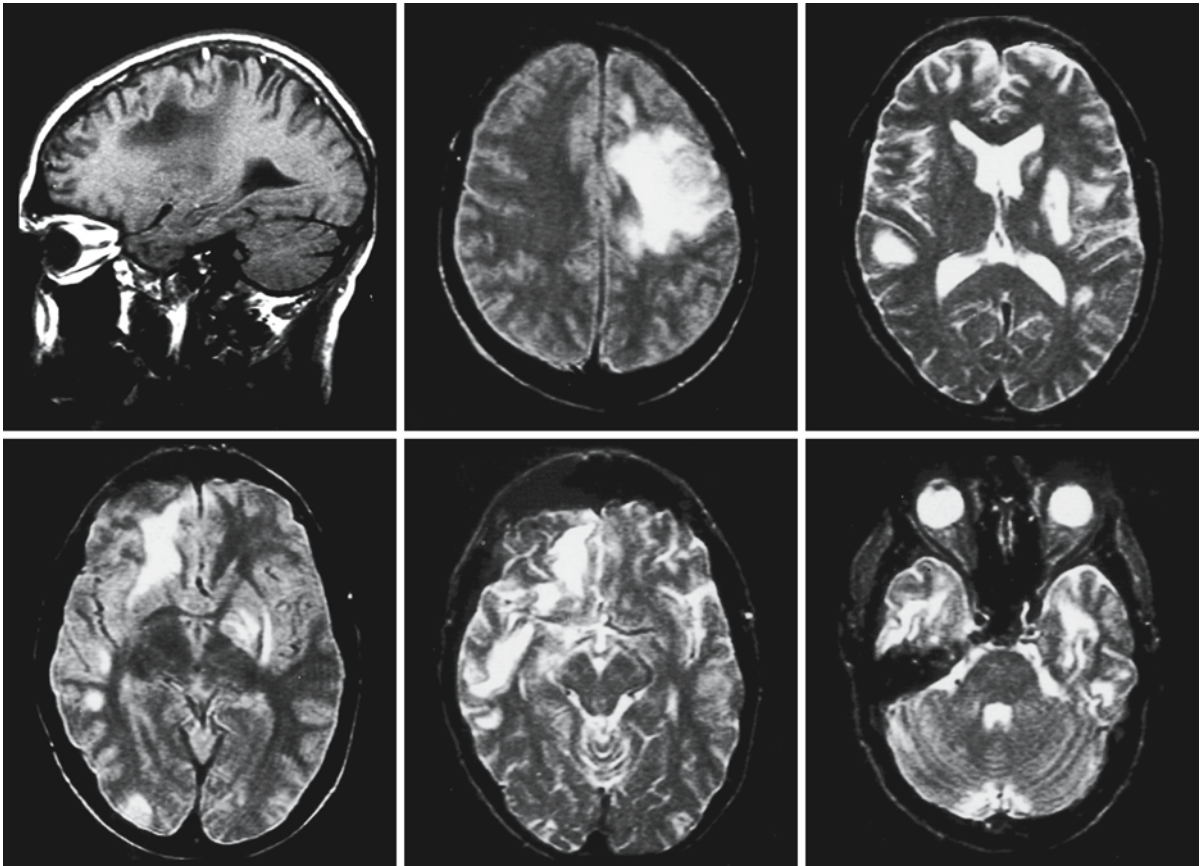


Fig. 82.3. One parasagittal T_1 -weighted and a series of T_2 -weighted MR images obtained in a 48-year-old man with AIDS and PML are shown. The images show multiple lesions in the white matter. Note that gray matter structures are also in-

involved; putamen, globus pallidus, and caudate nucleus on the left are affected, and some lesions extend into the cortical gray matter

PML has to be differentiated from other multifocal white matter disorders, especially from those occurring in AIDS patients, such as cytomegalovirus infections, and from acute and subacute HIV encephalitis itself. These latter infections, however, do not usually involve the U fibers, do have different signal intensity characteristics on T_1 - and T_2 -weighted images, and tend to be symmetrical. Lesions in systemic lupus erythematosus may sometimes mimic PML, while PML may also occur in the context of systemic lupus erythematosus. Multifocal white matter involvement with some swelling of the subcortical lesions and stretching of the overlying cortex may also be seen in noninfectious inflammatory disorders, in particular multiple sclerosis and acute disseminated encephalomyelitis. Similar lesions have been reported in the context of the reversible posterior encephalopathy syndrome. In vasculitis, posterior reversible

encephalopathy syndrome, and noninfectious inflammatory disorders, white matter lesions are as a rule also asymmetrical, and differentiation from PML may be impossible on the basis of MRI features alone. Clinical and laboratory information is necessary. In several inborn errors of metabolism and in several toxic encephalopathies, spongiform white matter changes occur, resulting in some white matter swelling and stretching of the overlying cortex, which is otherwise intact. The appearance of the white matter changes shows similarities to those observed in PML, but the white matter abnormalities are usually symmetrical and usually generalized rather than multifocal. Some cases of PML resemble gliomatosis cerebri on MRI. However, in gliomatosis cerebri the border between white and gray matter is as a rule blurred, contrasting with the sharp border seen in PML.

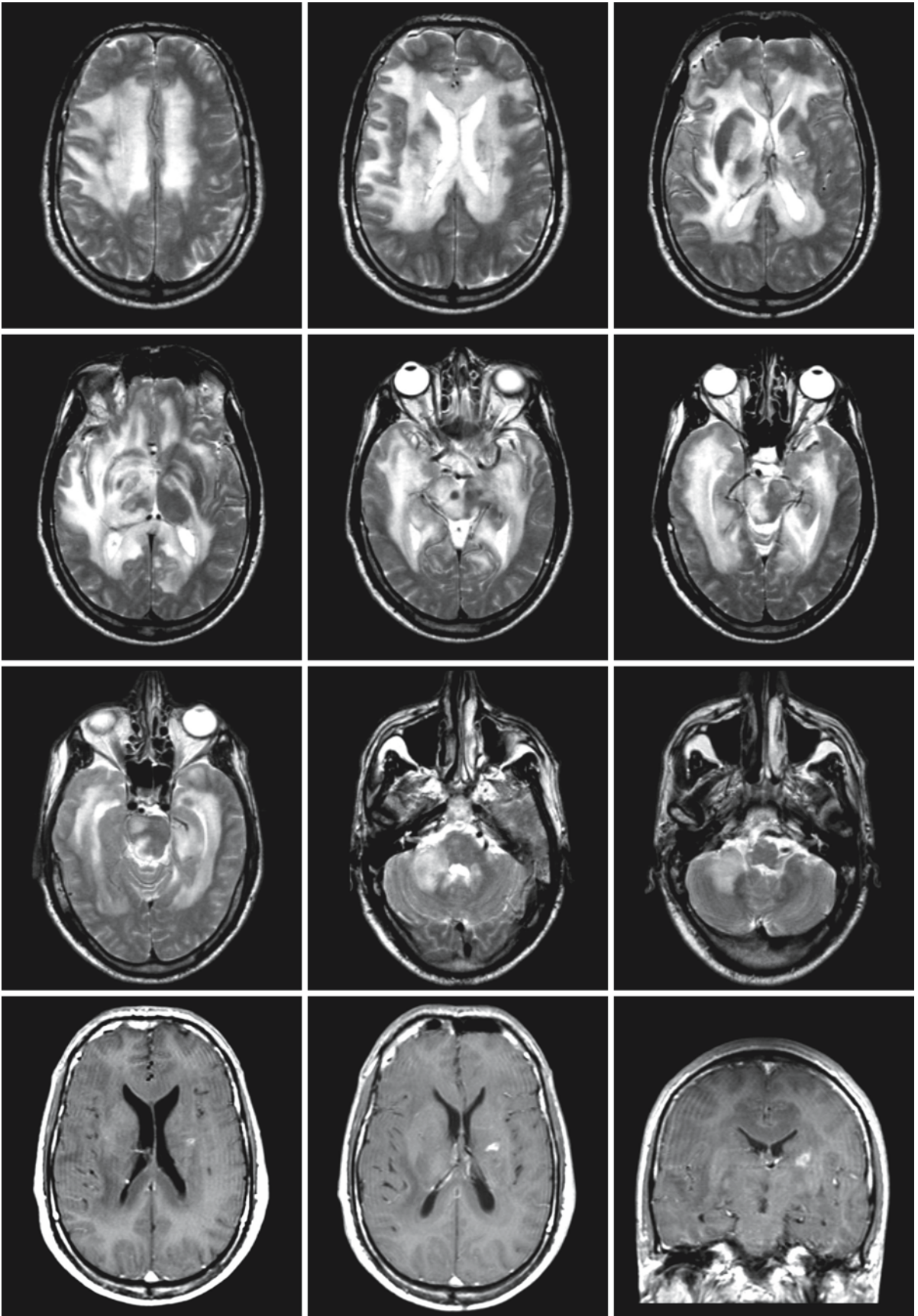


Fig. 82.4.

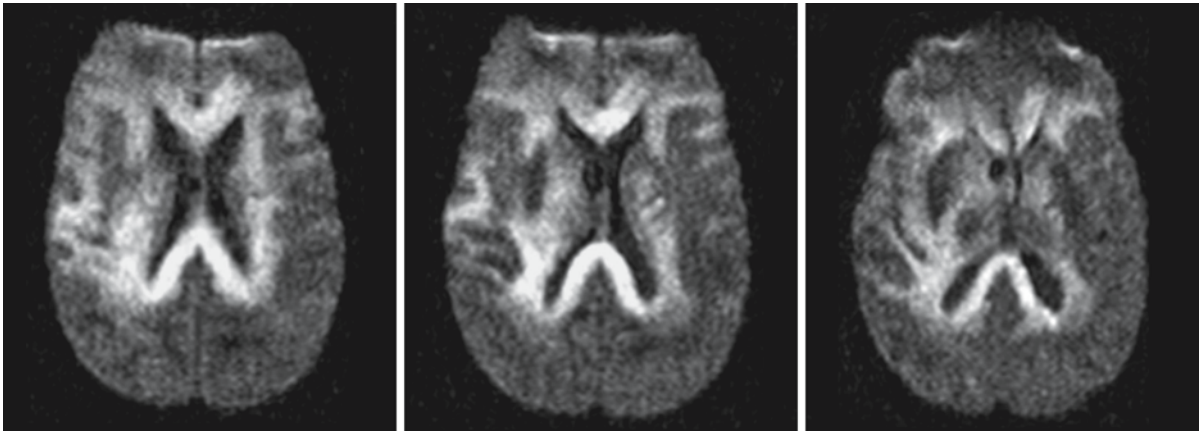


Fig. 82.4. (*continued*). A 43-year-old man with rapidly progressive neurological deterioration caused by PML. This series of T₂-weighted images (*first, second, and third rows*) show extensive involvement of white matter structures. The cerebral white matter is affected, more seriously on the right side, with involvement of the corpus callosum. The abnormal white matter is mildly swollen with thickening of the corpus callosum. The images could be considered suggestive of gliomatosis cerebri, but there is a sharp demarcation between the affected cerebral white matter and the unaffected overlying cortex. The basal ganglia are involved, but the structures mainly affected

are the internal capsule and the laminae separating the different nuclei, resulting in a pattern of concentric partial circles. The brain stem and middle cerebellar peduncle on the right are affected. The affected white matter is mildly hypointense on T₁-weighted images (*fourth row*). There is one small focus of contrast enhancement. Diffusion-weighted Trace images ($b = 1000$, *fifth row*) show large areas of hyperintensity, which correspond to low ADC values and restricted diffusion. These findings indicate active infection of large areas, consistent with the dramatic clinical picture in the patient

Brucellosis

83.1 Clinical Features and Laboratory Findings

Brucellosis is a zoonosis endemic in the eastern part of the Mediterranean, the Arabian peninsulas, and the Indian subcontinent. Infection of humans occurs by ingestion of raw meat, milk products, or direct contact with infected animals. Four species of *Brucella* can infect humans: *Brucella melitensis*, *Brucella abortus*, *Brucella suis*, and *Brucella canis*. After infection, bacteremia follows and the disease spreads to many organs and organ systems. *Brucella* species diffusely colonize the lymphoreticular system, with proliferation of lymphocytes and macrophages. Formation of granulomas follows.

The clinical symptoms are protean. The disease usually starts with an episode of malaise, fever, and arthralgia, and progresses slowly to more severe constitutional symptoms, including headache, nausea, vomiting, otalgia, hearing loss, ophthalmoplegia, and cardiac and neurological symptoms. Involvement of the CNS occurs in three major forms: *leptomeningeal involvement* in the bacteremic phase of the disease, *peripheral nervous system* involvement with polyradiculoneuropathy, and slowly progressive *central nervous system* involvement with mild confusion, focal neurological symptoms such as dysarthria, and cognitive impairment, but occasionally also with multifocal serious symptoms due to multiple brain abscesses. In children and occasionally in adults the clinical and MRI features may resemble those of acute disseminated encephalomyelitis (ADEM). In some cases diabetes insipidus is present as the result of granulomatous involvement of the sellar contents. Spinal symptoms may result either from direct involvement of the spinal cord or from compression due to involvement of the vertebral column with formation of granulomas.

Laboratory confirmation of brucellosis may be difficult. The CSF shows usually only mild pleocytosis and normal protein and glucose concentrations. IgG antibodies against *Brucella* may be found in the CSF, even with negative serum titers. Enzyme-linked immunosorbent assay (ELISA) of the CSF may further assist in the diagnosis. In rare cases brain biopsy may lead to a correct diagnosis.

83.2 Pathology

There are few reports on the neuropathology of neurobrucellosis. They describe various degrees of vascular inflammation, ranging from chronic infiltration with lymphocytes, plasma cells, and macrophages to acute polymorphic infiltration that may cause abscesses, necrosis, and aneurysm formation. Diffuse meningeal inflammation may occur as well as inflammatory cell infiltration of the perineurium of nerve roots. Little has been published about the nature of the involvement of the cranial nerves and the inner ear. Inflammation of the inner ear seems a more probable cause of the progressive hearing loss than affection of the eighth cranial nerve.

Although demyelination is presumed by several authors to be present in patients with white matter abnormalities, especially those presenting with the clinical picture of ADEM, no histopathological evidence of demyelination has been provided. Occasionally data have been obtained because a brain biopsy was performed. In a patient with diffuse white matter involvement and progressive encephalopathy, biopsy revealed abundant inflammatory cells in the white matter, with lymphocytic infiltrates in the leptomeninges surrounding the cortical vessels (Seidel et al. 2003). No significant demyelination was found in the affected area. Reactive astrogliosis was found in the cortex. Marked activation of microglia was demonstrated by immune staining of MHC complex class II antigens. The infiltrates in the white matter consisted mainly of CD8+ T-cell lymphocytes.

83.3 Pathogenetic Considerations

Brucellae are intracellular, nonmobile, gram-negative coccobacilli capable of replication within mononuclear phagocytes. Ingestion of infectious products, most often unpasteurized milk, is followed by hematogenous dissemination, residence of the brucellae in the reticuloendothelial system, and subsequent involvement of multiple organs or organ systems, resulting in a variety of clinical symptoms. In 4–15% of patients the CNS is involved. The presence of the brucellae leads to an inflammatory-granulomatous response and, in the CNS, sometimes to multiple brain abscesses. Involvement of venous structures may lead to sinus thrombosis. The abundance of

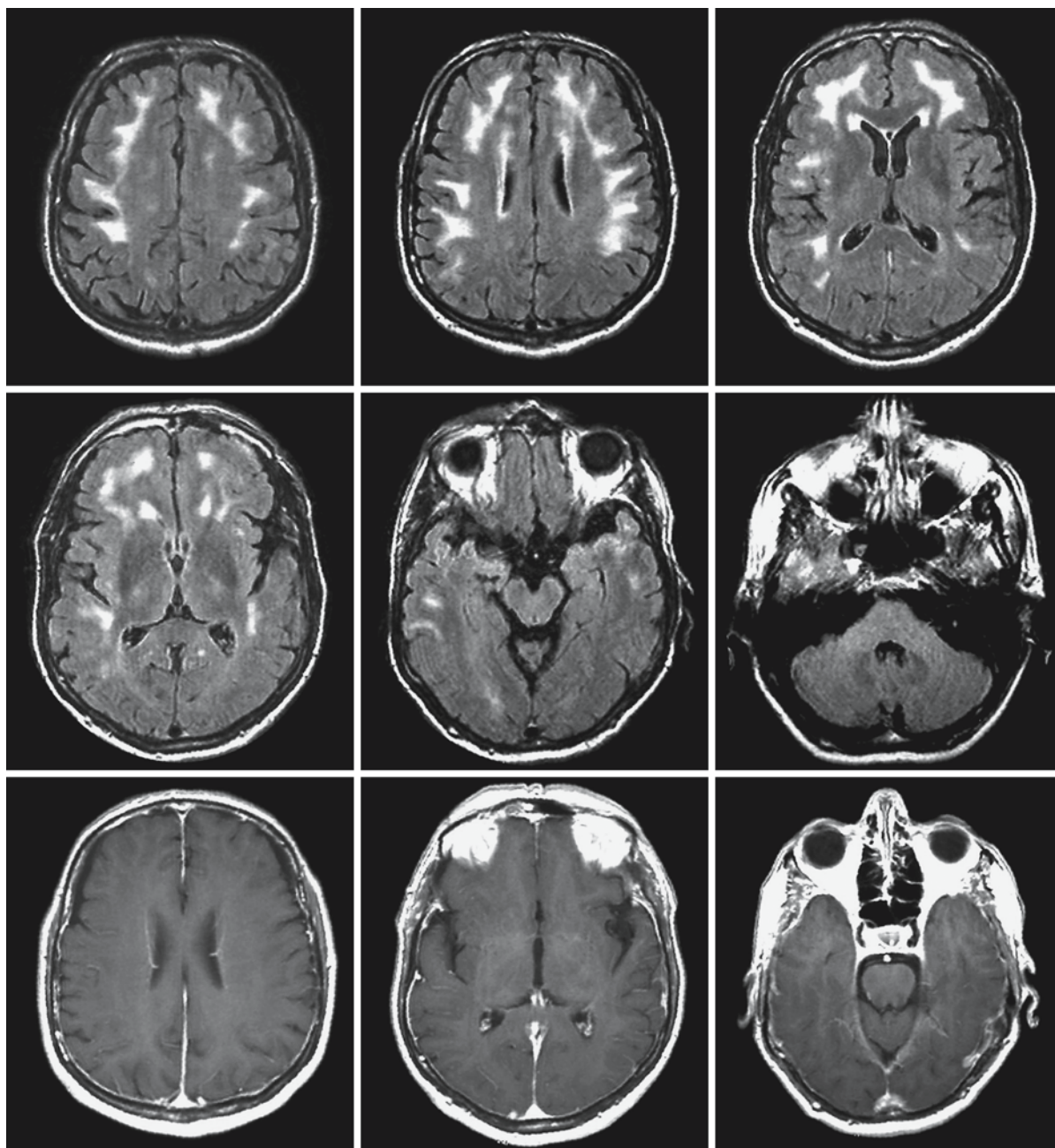


Fig. 83.1. Brucellosis in a 70-year-old man. The FLAIR images (*first and second rows*) show frontoparietal involvement of the arcuate fibers and a hyperintense rim around the ventricles.

The T₁-weighted images after contrast (*third row*) show enhancement of the leptomeninges. From Al-Sous et al. (2004), with permission

CD8+ T-cell lymphocytes in white matter lesions suggests that the white matter lesions are induced by T-cell-mediated toxic injury. This would imply that the pathogenesis of the lesions is different from lesions seen in autoimmune-related disorders such as acute disseminated encephalomyelitis. It is unclear why in some cases the sellar region is involved or the spinal cord in others.

83.4 Therapy

The correct diagnosis is essential because brucellosis is a treatable condition. Once diagnosed, neurobrucellosis can be treated with a combination of antibiotics. Most often this is done by an intravenous course for several weeks, followed by an oral course for many months.

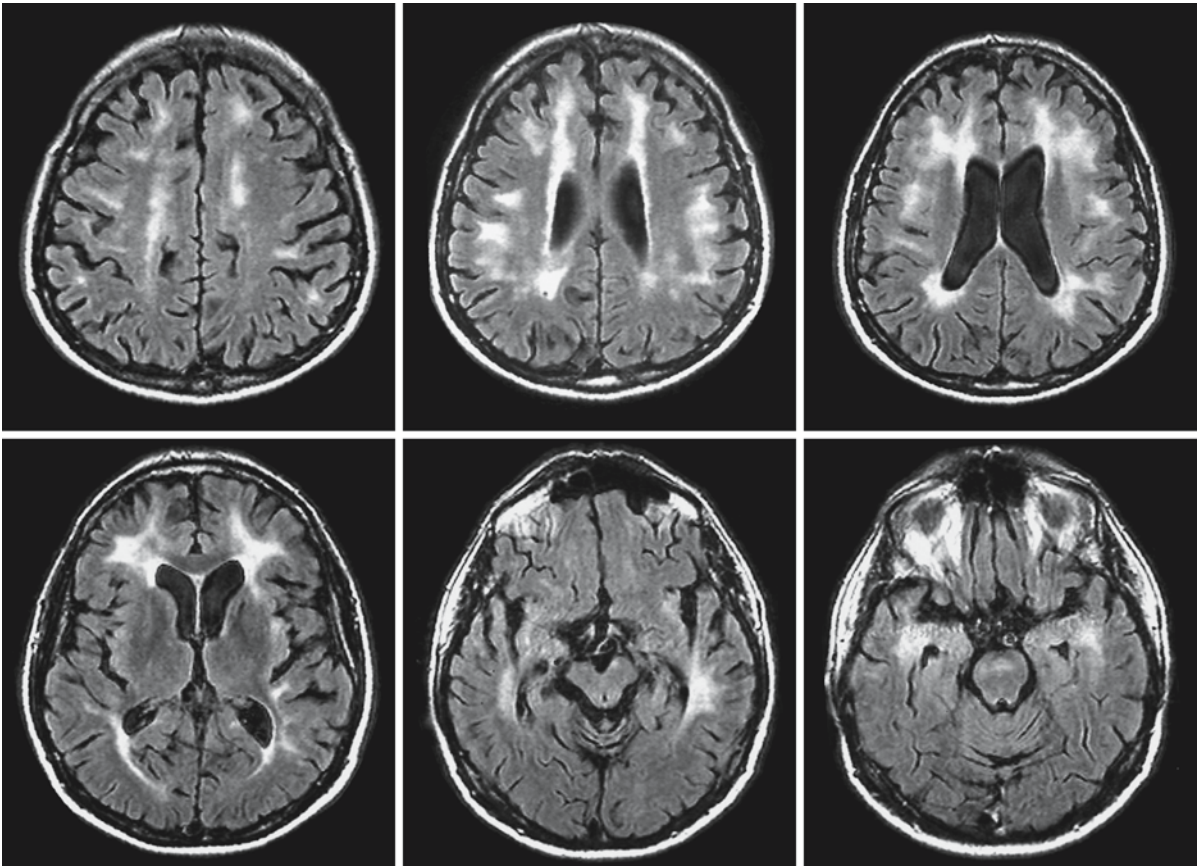


Fig. 83.2. Brucellosis in a 50-year-old man. The FLAIR images show a more irregular pattern of involvement of the arcuate fibers and a more prominent rim around the ventricles, with

extension into the deep frontal white matter, than seen in Fig. 83.1. In this case there are also lesions in the midbrain and pons. From Al-Sous et al. (2004), with permission

83.5 Magnetic Resonance Imaging

An MR inventory of suspected inflammatory-granulomatous disorders should aim at the depiction of the various disease manifestations of these disorders, guided by the clinical symptoms. The structures that should obtain special attention are:

- The leptomeninges, especially in the early phase of the disease (T_2 -weighted images, T_1 -weighted images without and with contrast, in transverse and coronal planes) (Fig. 83.1)
- The white matter (proton density, T_2 -weighted, and FLAIR images, contrast-enhanced T_1 -weighted images) (Figs. 83.1–83.3)
- The sellar region (sagittal and coronal T_1 -weighted images with fat-suppression, without and with contrast enhancement (Fig. 83.4))
- The spinal cord (sagittal T_1 - and T_2 -weighted images of the entire spinal canal, transverse images when lesions are present (Figs. 83.3 and 83.5))

Leptomeningeal involvement occurs usually in the early phase of the disease.

White matter involvement may occur in a number of different patterns. First of all, a multiple sclerosis or ADEM-like type of involvement may occur with asymmetrical large patchy hyperintense lesions on T_2 -weighted and FLAIR images (Figs. 83.1 and 83.2). Secondly, a symmetrical pattern of diffuse involvement of subcortical white matter is sometimes seen without involvement of the corpus callosum. Sometimes the abnormalities are more extensive and diffusely involve the subcortical and periventricular regions, again without participation of the corpus callosum (Fig. 83.3). Occasionally there are (asymmetrical) lesions in the basal ganglia (Fig. 83.3). Some of these basal ganglia lesions may be hemorrhagic and some may enhance after contrast administration. In later phases lacunar infarctions may be seen, mainly in the basal ganglia. In all cases and especially in the early phase of the disease, leptomeningeal enhancement may occur (Fig. 83.1).

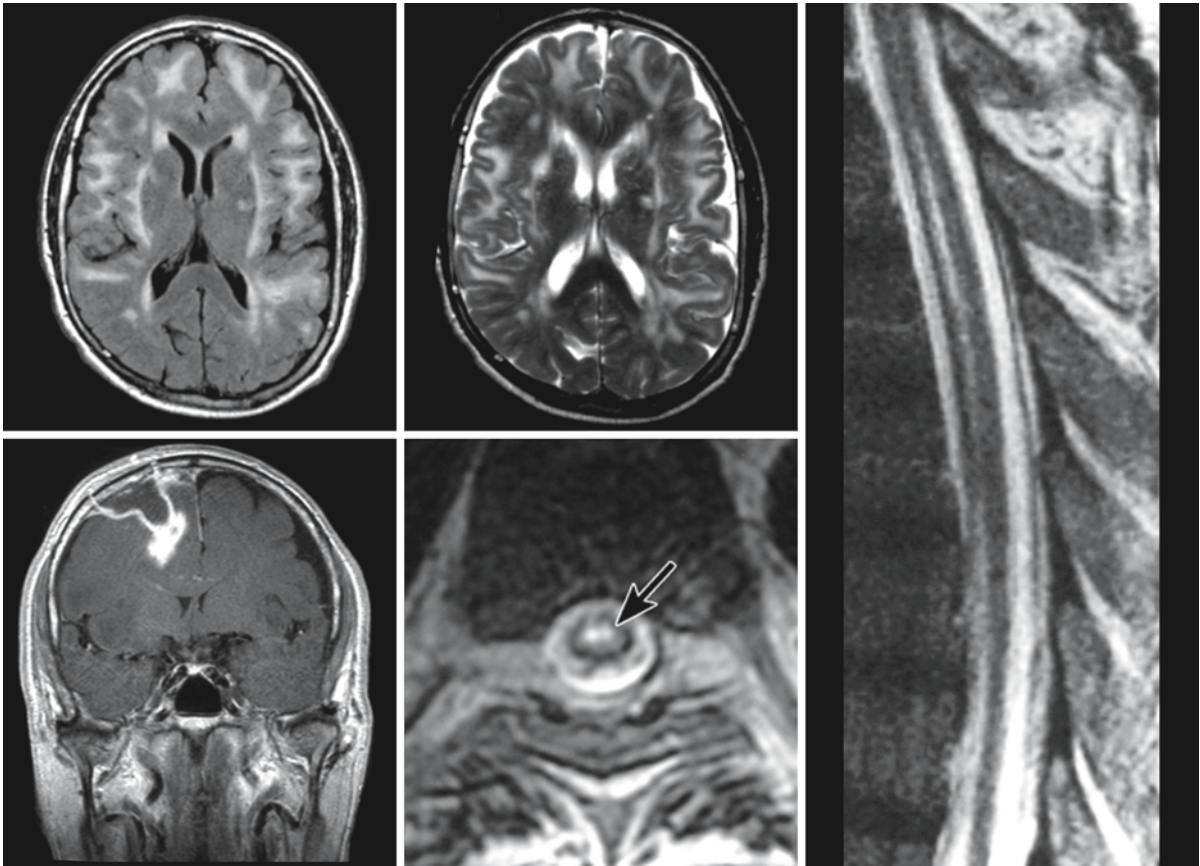


Fig. 83.3. Brucellosis in a 65-year-old patient with both cerebral and spinal abnormalities. The two upper images on the left, FLAIR and T₂-weighted respectively, show symmetrical involvement of most of the cerebral white matter, most prominently of the arcuate fibers and the external capsule. The lower left image, T₁-weighted with contrast, shows meningeal involvement and abscess formation with a cyst-like component

and a more solid component in the deep frontal white matter. The abscess is surrounded by an enhancing rim; the solid part of the lesions enhances in toto. The sagittal and transverse T₂-weighted images of the thoracic spinal cord show a lesion in the center of the thoracic cord (arrow). From Seidel et al. (2003), with permission

Lesions in the perisellar, suprasellar, and intrasellar region may be the only intracranial manifestation of brucellosis (Fig. 83.4). They may also occur in combination with white matter lesions.

Spinal cord abnormalities may show enhancement in the acute phase. Nerve roots may also show enhancement (Fig. 83.5). In the later phases spinal cord atrophy is usually found.

Unusual manifestations are superior sagittal sinus thrombosis and single or multiple brain abscesses (Fig. 83.3).

When multiple sclerosis-like white matter abnormalities are present, the differential diagnosis in-

cludes inflammatory conditions like multiple sclerosis, acute demyelinating encephalomyelitis, neuroborreliosis, and systemic lupus erythematosus. When more diffuse and symmetrical white matter abnormalities are present, the differential diagnosis may be more difficult and may include many inherited conditions, depending on the exact pattern of abnormalities present. Leptomeningeal enhancement after contrast injection may support the diagnosis of neurobrucellosis. The peri-, intra-, and parasellar manifestations have to be differentiated from neurosarcoidosis, pituitary tumors, Langerhans cell histiocytosis, and Whipple disease.

Fig. 83.4. Brucellosis in a 30-year-old woman. Coronal T₁-weighted images with contrast show a suprasellar granuloma as the sole manifestation of the disease. The differential diagnosis of this phenomenon includes Langerhans cell histiocytosis, Whipple disease, neurosarcoidosis, and Tolosa-Hunt syndrome. From Al-Sous et al. (2004), with permission

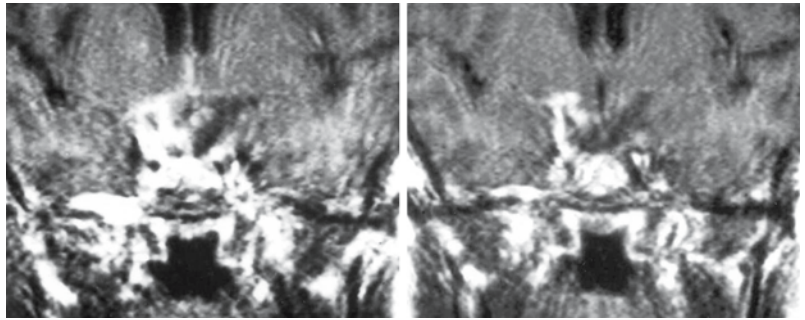
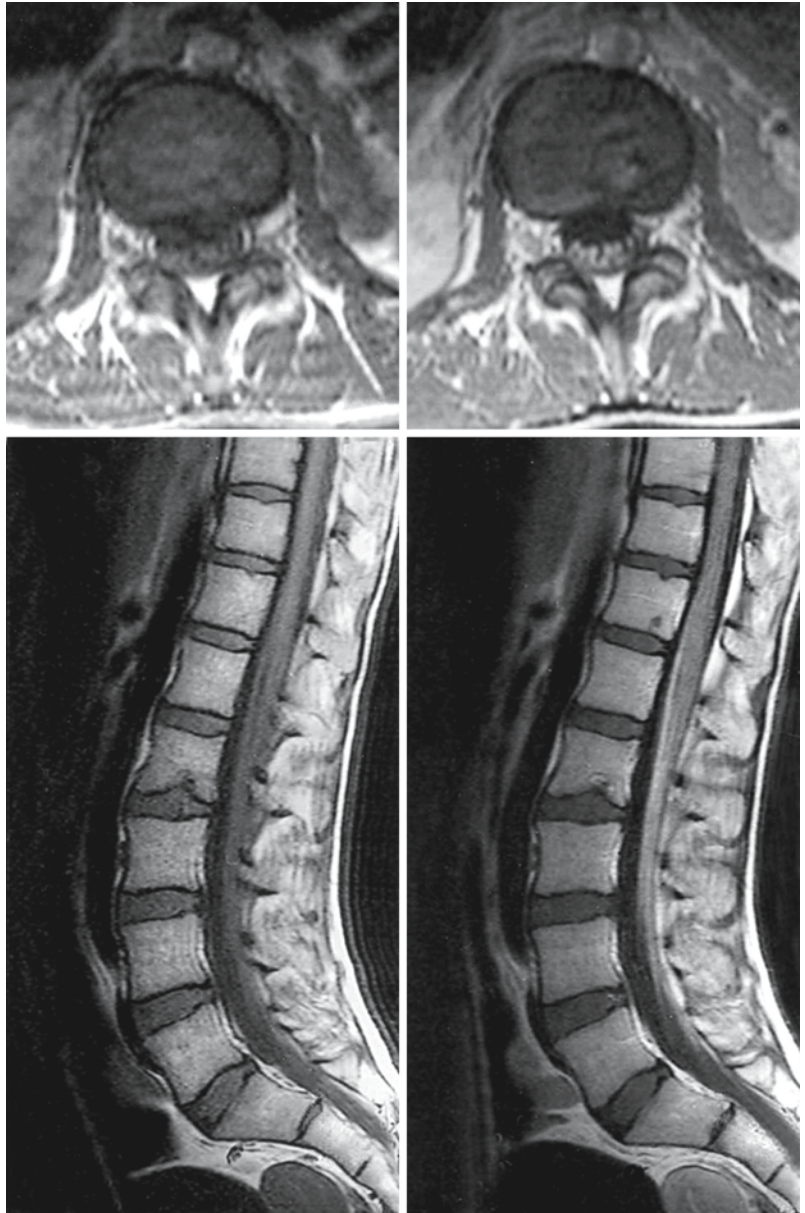


Fig. 83.5. T₁-weighted images in the transverse and sagittal plane in a 32-year-old man with brucellosis. The images on the *left* are T₁-weighted images without contrast, those on the *right* with contrast. After contrast administration, caudal roots show enhancement. From Al-Sous et al. (2004), with permission



Subacute Sclerosing Panencephalitis

84.1 Clinical Features and Laboratory Investigations

Subacute sclerosing panencephalitis (SSPE) is one of the slow virus infections of the CNS. It is a rare disorder, but it is the commonest of the chronic virus infections to affect children. It is caused by measles virus and occurs in approximately 4:100,000 cases of measles. SSPE is a disease of childhood and adolescence, with an age of onset range of 4–25 years and a peak incidence at 9–17 years. SSPE is rare in adults. The disease occurs on average 9 years after the initial infection. There is a racial difference in incidence of SSPE: in the United States the incidence is four times higher in whites than in blacks. Boys outnumber girls by 3 or 2 to 1. Children who acquire measles infection under the age of 1 year are more likely to develop SSPE. The mean age at infection is 12–14 months. In exceptional cases SSPE can also occur after live measles immunization, but the incidence is highly reduced after immunization. Since the introduction of measles vaccination, the incidence of SSPE has become very low in countries where a high immunization coverage (~95%) is achieved.

The clinical syndrome of SSPE is rather variable. The duration of the disease ranges from 3 months to more than 7 years. Although there is a marked variation in presenting signs and in the sequence of events, four clinical phases can usually be discerned. Stage I is characterized by an insidious deterioration of behavior and intellectual performance. The duration of this stage is usually several months, but the exact time of onset of the disease is often difficult to determine. Personality changes occur with withdrawn, timid, or aggressive behavior. These changes are followed by lethargy, drooling, slurred speech, and paucity of speech. Soon after the onset of intellectual deterioration, visual disturbances can often be detected. These are either related to progressive chorioretinitis or to lesions of the central visual pathways. In stage II, massive, repetitive, and frequent myoclonic jerking occurs. The myoclonia develops slowly and irregularly, but gradually affects all somatic muscle groups, especially the axial muscles, in a reasonably symmetric fashion and at a regularly repetitive rate. The myoclonus may be sufficiently severe to throw the child to the floor. The jerking interferes with intentional movements, giving the impression of clumsiness. The jerking is absent during sleep. Seizures of a more conventional type may also occur, such as focal motor,

generalized, and psychomotor convulsions. They may even precede the myoclonic jerking. Mental deterioration becomes progressively more obvious. At this stage, choreoathetosis, ataxia, tremor, and spasticity are common. The duration of stage II varies from 1 month to 1 year or more. In some patients the disease is arrested in stage II and remains in this stage for years. In stage III there is severe dementia. The spasticity increases, and the child becomes bedridden. Extrapyrarnidal dysfunction of the parkinsonian type is frequent. Nasogastric tube feeding is often required at this time because of progressive bulbar palsy. Hyperthermia may be found without evidence of infection. It is the rule that the myoclonia diminishes in stage III. Stage IV is the final stage in which the child is in a vegetative state, characterized by mutism and decorticate or decerebrate postures. There is no bladder or bowel control. Ophthalmological abnormalities occur in 50% of patients and include optic atrophy and chorioretinitis. The chorioretinitis may be most marked at the maculae, where scars are seen with characteristic pigmentation. There are signs of autonomic dysfunction, such as hyperthermia, severe perspiration, and changes in heart rate and blood pressure. The duration of stage IV varies from 1 to 6 years. Most patients die during stage III or IV from cardiorespiratory complications related to impaired central mechanisms controlling temperature, cardiac, and respiratory functions. Another common cause of death is infection. Spontaneous long-term remissions are exceedingly rare, but may occur.

The clinical diagnosis of SSPE is confirmed by the finding of increased levels of anti-measles virus antibody in serum and CSF with an elevated CSF-to-serum ratio in antibody level. The CSF is clear, and the pressure and glucose concentration are normal. Moderate pleocytosis (5–20 mononuclear cells per milliliter) is often present. The protein level is usually normal or mildly elevated; a level that exceeds 0.90 g/l is uncommon. The level of IgG as a percentage of total protein is highly increased, and oligoclonal bands are present. Measles-specific IgG antibodies represent nearly 10–20% of total serum IgG and about 75% of the total CSF IgG. There is always an elevated CSF-to-serum ratio of IgG, especially of measles virus antibodies, indicating local production of measles virus antibodies within the CNS.

Another confirmatory finding is a characteristic EEG pattern of periodic complexes consisting of bilateral synchronous, symmetric, 2- to 4-Hz high-am-

plitude sharp and slow wave bursts, which may occur every 5–7 s. These periodic complexes occur simultaneously with the involuntary myoclonic movements. In stage I the EEG may be normal or show only mild to moderate, nonspecific slowing. Stage II is characterized by the occurrence of the periodic complexes; the background pattern is still relatively normal. In stage III, the background rhythm slows, and fewer bursts of periodic complexes occur. Stage IV has slow delta activity and rare SSPE complexes. These complexes in association with myoclonic seizures provide strong corroborative evidence of SSPE. However, periodic complexes are also seen in other diffuse cerebral disorders, such as some lysosomal storage disorders, mitochondrial encephalopathy (MERRF), cerebral anoxia, and widespread infections of the brain.

84.2 Pathology

The pathology of SSPE is restricted to the CNS. The leptomeninges are thickened. The brain may show atrophy during the terminal stages of disease but is otherwise normal on external examination. On slicing the brain, discolored areas are seen. Microscopically, the disease appears to be multifocal in character and may involve all portions of the CNS, with the exception of the cerebellum, which is rarely affected. The frontal lobes are involved first, followed by the parietal, temporal, and occipital lobes, basal ganglia, brain stem, and spinal cord. The typical pathological findings include perivascular infiltration by mononuclear cells in gray and white matter and proliferation of both macroglia and microglia. Astrocyte proliferation can be particularly pronounced in white matter. Neuronal degeneration and neuronal loss may be severe. Neurofibrillary tangles are seen. Demyelination is focal and not always conspicuous. The subcortical white matter is mainly affected, first with inflammation and then with destruction. In the later stages of the disease both cortical atrophy and demyelination are more pronounced. Intranuclear and intracytoplasmic inclusions are present in neurons, astrocytes, and oligodendrocytes. Immunohistochemistry has revealed measles virus antigen in neurons, oligodendrocytes, and inflammatory cells. CD4+ T lymphocytes have been demonstrated in the perivascular areas and CD8+ T lymphocytes in the parenchyma.

Ultrastructural examination shows the presence of paramyxovirus particles. A spectrum of viral inclusions and particles has been reported. Some inclusions fill nuclei, whereas smaller particles, nucleocapsids, and virions of different configurations are found in either the nucleus or the cytoplasm of oligodendroglial cells and neurons. Nuclear bodies and granulo-filamentous inclusions occur in astrocytes.

84.3 Pathogenetic Considerations

Measles virus is a member of the *Morbillivirus* genus in the Paramyxoviridae family. SSPE is a rare complication of measles infection and differs from the acute measles encephalitis that may occur during or immediately after acute measles infection. The main risk factor is acquiring the infection at or before the age of 1 year. The elevated serum and CSF anti-measles virus antibody levels in patients suspected of having SSPE are indicative of an active measles virus infection of the brain. Inclusions with paramyxovirus particles have been demonstrated in neuronal and glial cells in SSPE. The cellular inclusions react with anti-measles virus antibodies. For a long time, however, the virus could not be recovered from brain tissue by conventional methods. Successful isolation of the measles virus was finally accomplished by cocultivating brain cells of SSPE patients with cells known to support measles virus replication. After the isolation of the virus, the agent was studied extensively to determine its structural and biological characteristics. Its ultrastructural features are similar to those of measles virus. Further studies of the immune response in patients demonstrated the absence of serum antibody to the matrix (M) protein of measles virus. The M protein is associated with the inner surface of the viral membrane. It is important in the assembly of the virus particle, which occurs by a budding process from the surface membrane of the infected cell. Subsequent studies demonstrated the absence of measles virus M protein in the brain tissue of patients with SSPE. More recent studies have demonstrated that the measles viruses isolated from the CNS of SSPE patients have major mutations in the M protein gene. As a consequence, the budding process is defective. Without budding, the replicating intracellular virus may go into a dormant phase. However, M protein gene mutations thought to be characteristic of SSPE viruses have also been found in measles virus isolated in the acute stage of measles infection and it is therefore unclear whether these mutations are critical for the development of SSPE. Regardless of the precise explanation, the absence of M protein explains many of the virological features of SSPE. Lack of M protein results in a persistent, abortive infection, in which no mature infectious virus is produced in the extracellular space. The internal components of the virus accumulate in the cells. It is thought that in the time between primary measles virus infection and the onset of SSPE symptoms, viral nucleocapsids, RNA, and probably other gene products accumulate in cells of the nervous system and spread from cell to cell through the nervous system. The onset of SSPE symptoms is usually ascribed to altered cell function and cell death, resulting from excessive accumulation of viral products. The intracellular virus is never in

contact with the extracellular space, as a consequence of the absence of M protein and the resulting inability of the virus to assemble and bud. Only when cells begin to deteriorate and die does the virus make contact with the immune system, causing a rise in anti-measles antibodies, except antibodies to M protein. The antibodies produced are ineffective in eradicating the intracellular virus.

Other mutations in the measles virus genome may contribute to the risk of SSPE. Fusion protein (F protein) and hemagglutinin (H protein) are two surface glycoproteins. Truncations in the cytoplasmic domain of the F protein impede efficient virus assembly and budding. Loss of glycosylation in the H protein leads to inefficient membrane transport. These features lead to reduced amounts of envelope protein on the cell surface and may prevent association with the M protein, which leads to hampered assembly and budding of mature measles virus particles. Mutations in H and F proteins may also lead to enhanced cell-cell fusion and spread of the virus from cell to cell, making it possible for the defective virus to accumulate readily and spread without the need at any stage for viral maturation and budding.

Host factors seem also to be important in predisposing individuals to SSPE. In human beings the primary infection seems to occur during a critical period in early life when passive maternal immunity has faded, in particular before the age of 1 year. Immaturity of the host immune system and CNS has been suggested to contribute to the increased risk for SSPE development among infants. Other genetic factors (male versus female; racial differences) seem to contribute and may determine components of the immune system.

84.4 Therapy

There is no effective treatment for SSPE. The disease leads to death in most cases, but there may be spontaneous temporary improvement or an arrest of further progression for a number of years. Attempts to alter the disease course with antiviral agents, such as amantadine (Symmetrel), 5-bromodeoxyuridine, or inosiplex (Isoprinosine, Viruxan) have failed, which is not surprising in view of the marked cell-associated nature of the virus. Intraventricular interferon- α -2b, usually applied in combination with oral inosiplex, seems to have a higher remission and survival rate. Some patients have been treated with a combination of intraventricular interferon- α -2b and ribavirin. Subcutaneous interferon- β has been applied in patients who could not receive interferon- α and has also demonstrated beneficial effects. Both medications are broad-spectrum antiviral agents with activity against both DNA and RNA viruses. In the case reports of a few patients, the addition of rib-

avirin stopped the progression of brain atrophy and improved the clinical condition.

The problem in trials concerning SSPE is the very small number of patients that can be included in the Western hemisphere, so that multicenter, international collaboration is necessary.

84.5 Magnetic Resonance Imaging

CT is normal during the initial stage of the disease, shows multiple low-density areas in the white matter and basal nuclei in subsequent stages, and shows severe atrophy in the end stage. Low-density areas may show contrast enhancement.

In the earliest stage, MRI may be normal, but it shows abnormalities before CT does. Early changes may involve the basal ganglia (Fig. 84.1), lateral geniculate bodies, or the disease may present with multifocal white matter lesions, which have a preference for hemispheric subcortical white matter (Fig. 84.2). In more extensive lesions, the deep and periventricular white matter are involved additionally (Fig. 84.3). The abnormalities are often asymmetrical (Fig. 84.2), but in many cases they are extensive and symmetrical (Fig. 84.3). The overlying cortex is often also affected (Fig. 84.2). Large focal lesions involving white and gray matter, resembling infarctions, may occur. These lesions may enhance initially and subsequently become nonenhancing. The white matter changes may decrease or resolve, even in the presence of clinical deterioration. Bilateral striatal lesions (Fig. 84.1), bilateral lesions in the middle cerebellar peduncles, brain stem lesions, and cerebellar abnormalities may occur. In end-stage disease, severe atrophy of cerebrum, basal ganglia, brain stem, and cerebellum is found, often with global and generalized white matter signal abnormality.

MR spectroscopy, either as chemical shift imaging or as single voxel measurements, may help to estimate the stage of the disease. In stage I, MRS findings do not differ significantly from those in normal age-matched volunteers. In stage II, there is still a normal *N*-acetyl-aspartate/creatine ratio, but an increased choline/creatine ratio. The *myo*-inositol/creatine ratio is increased in this and the subsequent stages. This would correspond with an early inflammatory reaction. In stage III, MRS shows decreased *N*-acetyl-aspartate/creatine, increased choline/creatine, increased *myo*-inositol/creatine, and elevated lactate and lipid peaks, suggesting demyelination, gliosis, neuronal loss, and macrophage activation, macrophages being highly dependent on anaerobic glycolysis.

The differential diagnosis includes other causes of multifocal abnormalities of gray and white matter, including acute disseminated encephalomyelitis, progressive multifocal leukoencephalopathy, multiple sclerosis, and vasculitides. In some cases of SSPE,

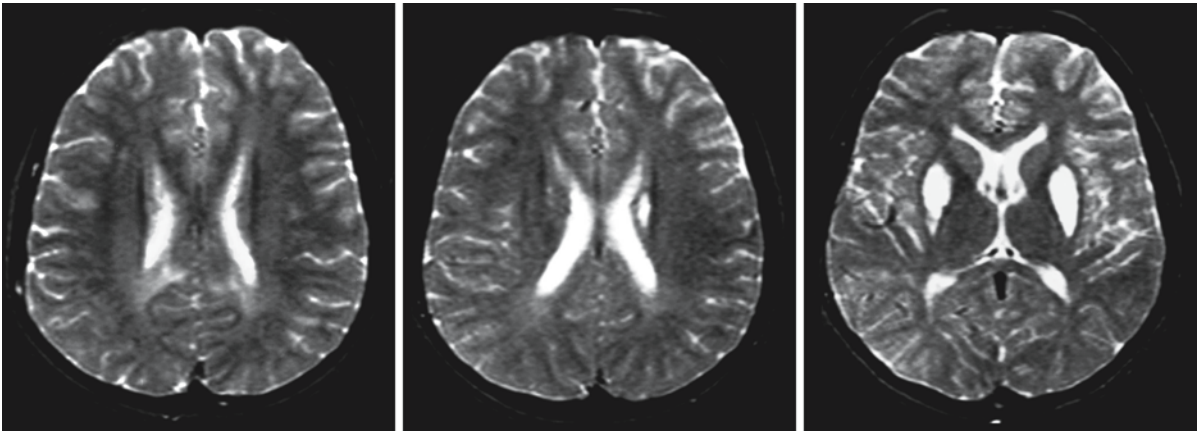


Fig. 84.1. In this 9-year-old boy with SSPE, MRI initially showed only a few moderately abnormal white matter lesions in the centrum semiovale. The MRI in this figure was performed 7 months later, when signs of neurological dysfunction were

much more severe, and shows lesions of the body of the caudate nucleus on the left and in the putamen on both sides. There is still a somewhat higher signal intensity of the parietal deep white matter

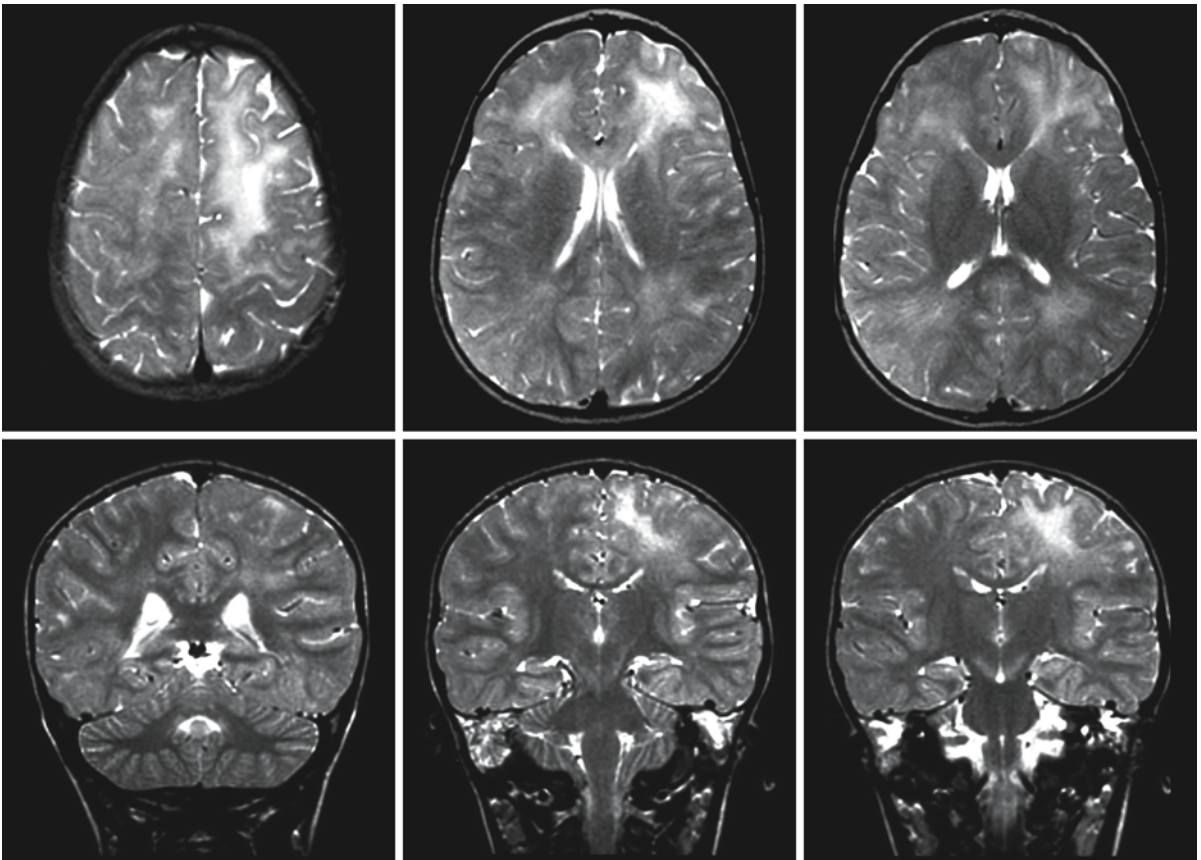


Fig. 84.2. In this 3-year-old boy with SSPE, T₂-weighted transverse and coronal images show asymmetrical involvement of the subcortical and deep white matter, most severe on the left.

The overlying cortex is also abnormal. Courtesy of Dr. M. Pineda, Department of Neuropediatrics, Clinic-Hospital Sant Joan de Déu, Barcelona, Spain

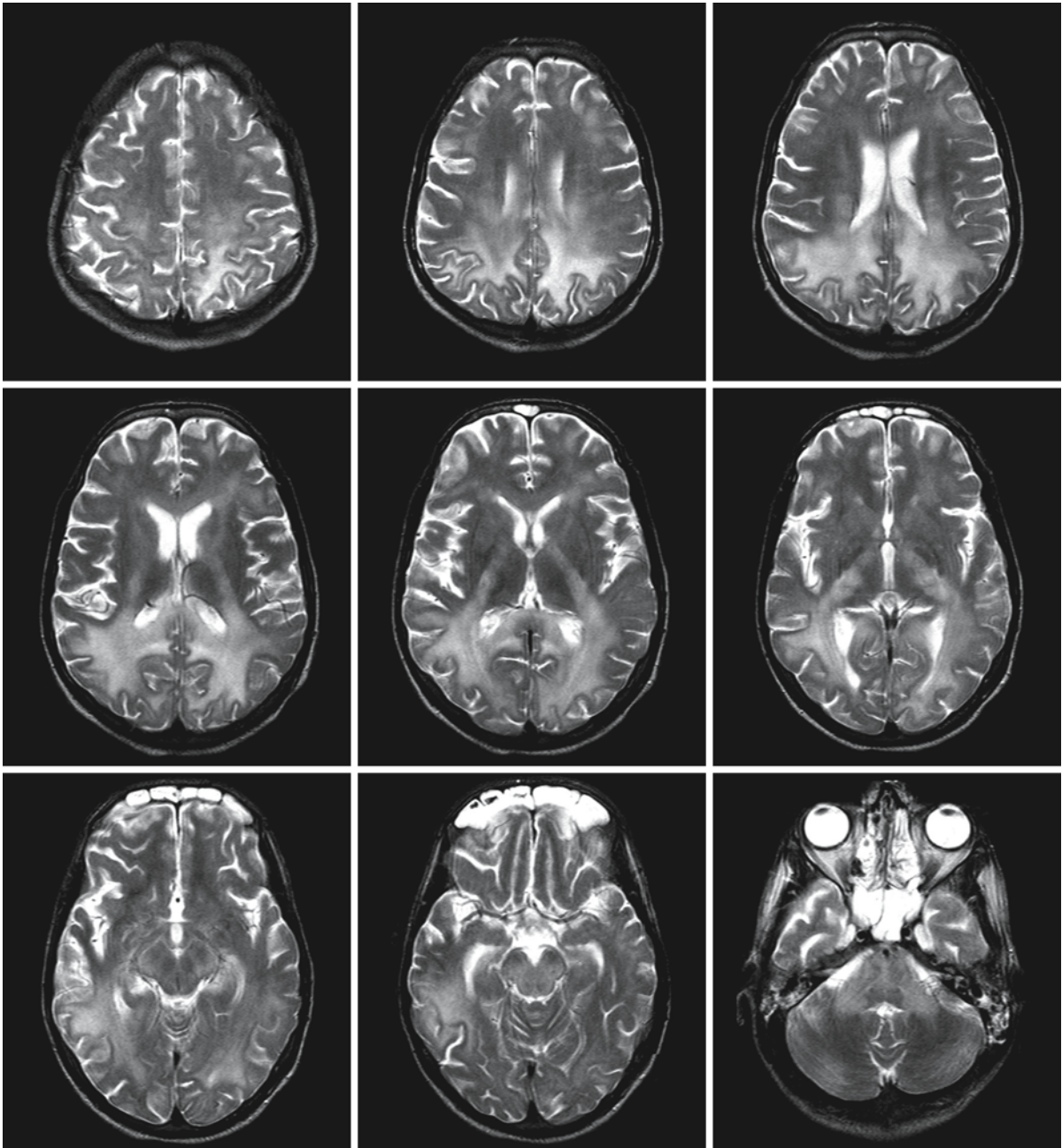


Fig. 84.3. This 20-year-old man with SSPE is in a far advanced stage of the disease. There are extensive abnormalities in the cerebral white matter, most severe in the posterior region, also involving the splenium of the corpus callosum, reminiscent of the cerebral form of X-linked adrenoleukodystrophy. However, there is no enhancement after contrast (not shown). There are

also extensive signal abnormalities in the brain stem, middle cerebellar peduncles, internal capsule. The basal ganglia display subtle signal abnormalities. There is some atrophy. Courtesy of Dr. Z. Patay, Department of Radiology, King Faisal Specialist Hospital and Research Center, Riyadh, Saudi Arabia

MRI shows symmetrical white matter lesions in the occipital area and splenium of the corpus callosum, simulating X-linked adrenoleukodystrophy. In cases with involvement of the basal nuclei, the differential diagnosis includes Creutzfeldt–Jakob disease, mito-

chondrial disorders, in particular Leigh syndrome, and other neurodegenerative disorders. EEG and laboratory findings help to establish the correct diagnosis.

Congenital and Perinatal Cytomegalovirus Infection

85.1 Clinical Features and Laboratory Investigations

Cytomegalovirus (CMV) is a member of the Herpesviridae family of large DNA viruses, along with herpes simplex virus types 1 and 2, Epstein-Barr virus, varicella-zoster virus, and human herpes viruses 6 and 7. These viruses share the biological properties of latency and potential reactivation. Infection with one member of the family does not confer immunity against infection or disease with the other members of the herpes family. Naturally acquired CMV infection induces cross-reactive immunity to infection with new strains of CMV, but this protection is not complete, because reinfection with a second strain of CMV has been documented.

Infection with CMV occurs in several ways: first, by close or intimate contact of either a sexual or nonsexual nature with another person who is shedding the virus in bodily secretions; secondly, vertically from mother to infant by transplacental infection; thirdly, by blood product transmission from a CMV-seropositive donor. In congenital and neonatal CMV infection, the mother plays a dominant role. Infection of the mother with CMV can be either a primary infection or a reactivation of an earlier infection. The risk of congenital CMV infection in the infant is much higher in the case of a primary infection in the mother than in the case of reactivation of an old infection. The transmission rate in a primary infection is 40–50%, whereas it is approximately 1–2% in recurrent infection. Infants may also be infected during delivery from CMV-infected maternal vaginal secretions or, postnatally, by infected breast milk. Children not congenitally or perinatally infected may acquire the disease during the toddler or preschool years by contact with family members or other children. Blood transfusions can also be a source of CMV infection; donor-to-recipient transmission of CMV has been documented. CMV may also be transmitted and produce a congenital infection if a pregnant woman or her fetus receives a blood product transfusion from a CMV-seropositive donor.

Approximately 1% of all newborns are congenitally infected with CMV, making CMV the most common congenital infection. Of the neonates infected with CMV, approximately 10% will have symptoms at birth that are commonly associated with congenital CMV disease, including intrauterine growth retarda-

tion, jaundice, hepatosplenomegaly, petechiae or purpura, and pneumonia. Hepatomegaly, splenomegaly, and petechiae are the most common. The liver is usually smooth and nontender and commonly measures 5 cm or more below the right costal margin. Ascites may be present prenatally and persist postnatally for 1–2 weeks. The hepatomegaly usually resolves by 3 months of age, and persistence beyond 1 year is highly unusual. Mild hepatitis is usually present. Hyperbilirubinemia, on the other hand, may be quite striking, with very high conjugated (direct) bilirubin levels. The abnormal results of liver function tests gradually resolve during the first few weeks of life. Chronic hepatitis due to congenital infection with CMV is unusual but may occur. Enlargement of the spleen is very common in congenital CMV infection, and in some cases it may be the only abnormality detectable at birth. Petechiae in congenital CMV disease are usually pinpoint and generalized over the infant's trunk and extremities. If present at birth, they can be transient and resolve within 48–72 h. They can be the only apparent manifestation of CMV infection. However, more commonly, the triad of hepatomegaly, splenomegaly, and petechiae is seen. Petechiae are usually, but not always, accompanied by thrombocytopenia, and platelet counts in the first few weeks of life range from 2,000/mm³ to 125,000/mm³. Hemolytic anemia may also be present. Pneumonitis is unusual but, if present, it is usually a severe, interstitial pneumonitis occurring in the context of a diffuse, multisystem infection. Post-transfusion CMV infection in neonates, especially premature infants, may cause a syndrome of shock, lymphocytosis, and pneumonitis. The mortality rate of neonatally symptomatic CMV infection is 10–30%.

CNS manifestations are common in neonates with a symptomatic CMV infection and include lethargy, poor feeding, seizures, hypertonia or hypotonia, microcephaly, chorioretinitis, and sensorineural deafness. Ocular involvement with CMV occurs in 10–20% of symptomatic infants. Most commonly it produces a chorioretinitis that is usually old and inactive at birth. The retinitis is usually unilateral but can produce blindness if the macula is involved, as well as strabismus and optic atrophy. Congenital CMV and congenital toxoplasmosis produce similar lesions; however, congenital CMV characteristically does not produce microphthalmia or cataracts, and alternative diagnoses, such as congenital rubella or toxoplasmo-

sis or metabolic disorders, should be considered if these eye findings are present. Microcephaly may be present at birth. It may be part of the overall small size of a growth-retarded infant or may be disproportionate and accompanied by normal weight, length, and chest circumference. Infants may also have septal defects, biliary atresia, inguinal hernias, hip dislocation, and other musculoskeletal abnormalities. In addition, infants with toxoplasmosis, herpes simplex, syphilis, and HIV infections may be coinfecting with CMV, and infants with metabolic disorders may have congenital CMV infection as well.

About 90% of the infants with an intrauterine CMV infection are asymptomatic at birth. Ten to fifteen percent of the infants with a congenital CMV infection that is clinically silent in the neonatal period, and almost all neonates with a neonatally symptomatic infection, develop persistent problems, most commonly neurological impairment, sensorineural hearing deficits, and decreased vision related to chorioretinitis or optic atrophy. Approximately half of the infants with symptomatic and 15% of infants with asymptomatic congenital CMV infection will have or develop an associated hearing loss. The hearing loss may still develop many years after the initial infection and may fluctuate in severity. The vision loss, too, may be progressive or of late onset. The severity of the neurological impairment is highly variable. At the severe end of the spectrum are profound mental deficiency and motor handicap, often with serious spasticity; at the mild end are learning, behavioral, and motor coordination problems. Epilepsy may occur, in particular in patients with more severe handicap. The encephalopathy has never been observed to be progressive.

These numbers indicate that congenital CMV is one of the leading causes of mental deficiency. The numbers also indicate that most infants with a congenital CMV infection have no sequelae at all.

The diagnostic time frame for congenital or perinatal CMV infection is only the first 3 weeks after birth. CMV infection is very common and a postnatal infection may readily occur. It is therefore important that the test is performed soon after birth. Positive tests after the age of 3 weeks can indicate either a congenital, perinatal, or postnatal infection.

An important test for the diagnosis of congenital CMV infection in neonates is the isolation of the virus from urine, saliva, or tissue obtained during the first 3 weeks of life. All infants in whom the diagnosis is suspected should have a viral culture performed. The virus is usually present in a very high titer, and cultures are commonly positive within 2–3 days of incubation. Excretion of the virus in the urine may persist for years.

Standard serological tests, such as detection of CMV IgG and IgM antibodies, alone or as part of a TORCH titer panel, are commonly used to diagnose

congenital CMV infection, but this approach has several drawbacks. Although the absence of IgG antibodies to CMV in cord or infant blood probably rules out congenital CMV infection in an immune-competent mother–infant pair, the presence of IgG antibodies has limited value, because 50–80% of women of childbearing age will have anti-CMV IgG antibodies that will be transplacentally transferred to their infant. A significantly higher titer of IgG antibodies to CMV in the infant than in the mother may imply an active congenital infection, but in practice this difference is usually difficult to ascertain. Serological samples obtained serially at 1, 3, and 6 months may rule out congenital infection if the level of CMV antibodies gradually declines, but if the levels persist, serological test results alone cannot determine whether the infection was of congenital or postnatal origin. The presence of IgM antibodies at birth, however, is highly suggestive of a congenital CMV infection, provided the test was performed properly, but confirmatory urine culture for CMV is recommended for a definitive diagnosis. It is important to realize that a negative CMV IgM antibody test does not exclude the diagnosis of congenital infection. Anti-CMV IgM antibodies are found in only 70–80% of the congenitally infected infants. More recently, the PCR technique has been introduced to demonstrate the presence of the virus in tissue or body fluids. CMV DNA has been detected by PCR in urine, saliva, and CSF.

The biggest problem with establishing the diagnosis of congenital CMV has been that it cannot be confirmed after the neonatal period. In the absence of overt neonatal signs, infants with congenital or perinatal CMV infection are not tested for the presence of the virus, viral DNA, or antibodies within the appropriate time frame of 3 weeks. The infants with a neonatally asymptomatic congenital CMV infection who develop neurological sequelae usually come to medical attention after the age of 6–9 months because of developmental delay or hearing loss, and at that time it is no longer possible to confirm the diagnosis with conventional techniques. However, the PCR technique allows a delayed diagnosis if neonatal body fluids are still available. The Guthrie card is usually the only source of neonatal blood kept beyond the neonatal period. The Guthrie card is the filter paper used to collect blood spots in the neonatal period for neonatal screening tests. These cards are stored for a variable number of months to years. The introduction of PCR on Guthrie cards for the diagnosis of congenital CMV creates the opportunity for correct diagnosis beyond the neonatal period. The sensitivity of the PCR for CMV DNA on Guthrie cards is 100% and the specificity is 99%. The only disadvantage of the test is that the PCR is negative if the neonate no longer had viremia. The chance that a neonate with a congenital CMV infection no longer has viremia is very small but

may exist, especially if the CMV infection occurred long before birth.

In the neonate with congenital infection, the differential diagnosis includes any of the TORCH (*toxoplasmosis, rubella, CMV, herpes simplex*) agents. Congenital toxoplasmosis may mimic congenital CMV infection. In parts of Europe, particularly France and Belgium, congenital toxoplasmosis is a common and significant problem. It is less common in the USA. Other congenital infections to be considered include lymphocytic choriomeningitis virus (LCMV) infection, syphilis, enteroviral disease, and human immunodeficiency virus (HIV) infection.

85.2 Pathology

Pathological data in congenital and neonatal CMV infections stem from lethal infections and are therefore highly biased towards the severe end of the clinical spectrum. Some of these infants were stillborn; others survived for several days or weeks. Microcephaly was present in most of the patients. Other findings included meningoencephalitis, periventricular necrosis with associated calcifications, more diffuse calcifications, extensive cortical necrosis with calcifications frequently involving the convexity of the gyri, disturbance of neuronal migration (ranging from lissencephaly to polymicrogyria), ventriculomegaly, cerebellar hypoplasia, and marked disruption of the cerebellar architecture. In about half of the cases intranuclear inclusion bodies are found, while systemic inclusion bodies are found in nearly all cases, in particular in the kidney, lungs and liver.

In clinical specimens, one of the classic hallmarks of CMV infection is the cytomegalic inclusion cell. These massively enlarged cells (the property of cytomegaly gave CMV its name) contain intranuclear inclusions, which histopathologically have the appearance of owl's eyes. The presence of these cells indicates productive infection, although they may be lacking even in actively infected tissues. In most cell lines, CMV is difficult to culture in the laboratory, but *in vivo* infection seems to involve chiefly epithelial cells, and, with severe disseminated CMV disease, involvement can be observed in nearly all organ systems.

There are no pathology data on the nature of the white matter abnormalities observed in children with a mild neurological handicap.

85.3 Pathogenetic Considerations

CMV is a member of the family of eight human herpes viruses, and is designated human herpes virus 5 (HHV-5). It is the largest member of the herpes virus

family, with a double-stranded DNA genome of more than 240 kilobase pairs, capable of encoding more than 200 proteins. The function of most of these proteins remains unclear. As with the other herpes viruses, the structure of the viral particle is that of an icosahedral capsid, surrounded by a lipid bilayer outer envelope.

Better understanding of the process of viral replication provides insights into molecular mechanisms of immunity and opens therapeutic windows. CMV replicates very slowly in cell culture, reflecting its very slow pattern of growth *in vivo* (in contrast to herpes simplex virus infection, which progresses very rapidly). The replication cycle of CMV is divided temporally into three regulated classes: immediate early, early, and late.

Immediate early gene transcription occurs in the first 4 h following viral infection, and key regulatory proteins are made which allow the virus to take control of cellular machinery. The major immediate early promoter of the CMV genome involved in this part of the process is one of the most powerful eukaryotic promoters described in nature, and has been exploited in modern biotechnology as a useful promoter for driving gene expression in gene therapy and vaccination studies.

Following synthesis of immediate early genes, the early gene products are transcribed. Early gene products include DNA replication proteins and some structural proteins.

Finally, the late gene products are made approximately 24 h after infection, and these proteins are chiefly structural proteins that are involved in virion assembly and egress. Synthesis of late proteins is highly dependent on viral DNA replication and can be blocked by inhibitors of viral DNA polymerase, such as ganciclovir. The lipid bilayer outer envelope contains the virally encoded glycoproteins, which are the major targets of host neutralizing antibody responses. These glycoproteins are candidates for human vaccine design. The proteinaceous layer between the envelope and the inner capsid, the viral tegument, contains proteins that are major targets of host cell-mediated immune responses. Of these tegument proteins, the most important is the so-called major tegument protein, UL83 (phosphoprotein 65 [pp65]). Another clinically important protein, the UL97 gene product, is a phosphotransferase. Although the function of this protein in the viral life cycle is unknown, this protein is clinically important because a substrate of the kinase is the antiviral drug, ganciclovir, which, once phosphorylated, becomes an effective anti-CMV drug.

Immunity to CMV is complex and involves humoral and cell-mediated responses. Several CMV gene products are of particular importance in CMV immunity. The outer envelope of the virus, which is derived from the host cell nuclear membrane, con-

tains multiple virally encoded glycoproteins. Glycoprotein B (gB) and glycoprotein H (gH) appear to be the major determinants of protective humoral immunity. Antibodies to these proteins are capable of neutralizing the virus, and gB and gH are targets of investigational CMV subunit vaccines. However, although humoral responses are important in control of severe disease, they clearly are inadequate in preventing transplacental infection, which can occur even in women who have anti-CMV antibodies.

The generation of cytotoxic T cell responses against CMV may be a more important host immune response in the control of infection. In general, these cytotoxic T cells involve major histocompatibility complex (MHC) class I restricted CD8+ responses. Although many viral gene products are important in generating these responses, most CMV-specific cytotoxic T cells target pp65, an abundant phosphoprotein in the viral tegument, the product of the CMV *UL83* gene.

Recent investigations into the molecular biology of CMV have revealed the presence of many viral gene products which appear to modulate host inflammatory and immune responses. Several CMV genes interfere with normal antigen processing and generation of cell-mediated immune responses. To date, three viral gene products have been identified that inhibit MHC class I antigen presentation. One is the *US11* gene product, which exports the class I heavy chain from the endoplasmic reticulum to the cytosol, thus rendering it nonfunctional. Another is the *US3* gene product, which retains MHC molecules in the endoplasmic reticulum, preventing them from traveling to the plasma membrane. Finally, the *US6* protein inhibits peptide translocation by transporters associated with antigen processing. Other viral gene products, encoded by the *UL33*, *US27*, and *US28* genes, are functional homologues of cellular G-protein-coupled receptors. They may, via molecular mimicry, subvert normal inflammatory responses, and in the process promote tissue dissemination of virus and interfere with host immune response. The CMV genome also encodes a homologue of the cellular MHC class I gene, which appears to contribute to the ability of CMV to evade host defense. The *UL144* gene encodes a structural homologue of the tumor necrosis factor receptor superfamily, which may contribute to the ability of CMV to escape immune clearance.

Little is known about the molecular mechanisms responsible for the pathogenesis of tissue damage caused by CMV, particularly for congenital CMV infection. Although the CNS is the major target organ for tissue damage in the developing fetus, culturing CMV from the CSF of symptomatic congenitally infected infants is difficult. Because CMV can infect endothelial cells, it has been postulated that a viral angiitis may be responsible for perfusion failure of

developing brain. Others have postulated a direct teratogenic effect of CMV on the developing fetus. Observation of CMV-induced alternations in the cell cycle and CMV-induced damage to chromosomes supports this speculation; however, this hypothesis has been difficult to verify experimentally.

It has been hypothesized that the nature and extent of the cerebral abnormalities is related to the gestational age at the time of the infection. Infection of the fetus early in pregnancy would lead to abnormalities in migration with cortical dysplasia, whereas infections late in pregnancy would lead to white matter abnormalities only. This hypothesis is probably generally correct. However, we have seen patients in whom a primary CMV infection was documented in the mother shortly before conception, and in whom only a mild encephalopathy with multifocal white matter lesions without gyral abnormalities was found. It is, of course, possible that the transplacental transfer of the virus occurred late in pregnancy.

85.4 Therapy

Four antiviral chemotherapeutic agents – ganciclovir, foscarnet, cidofovir, and formivirsen – are licensed specifically for treatment of serious, life-threatening or sight-threatening CMV in immunocompromised patients. Currently a randomized, controlled multicenter clinical trial evaluating the use of ganciclovir for the treatment of infants with symptomatic congenital CMV infection and evidence of CNS involve-




Fig. 85.1. Boy with congenital CMV infection (diagnosis confirmed by a positive PCR for CMV DNA on the Guthrie card), who presented in the course of the first year of life because of serious developmental delay, spasticity, and microcephaly. A CT scan was performed at 9 months of age (*first row*) and showed many small calcifications, especially at the cortico-subcortical junction. Some small calcium deposits are seen in the basal ganglia and deep white matter. In addition, the CT suggests a diffuse cortical dysplasia. MRI was performed at the age of 16 months. The T₂-weighted images (*second and third rows*) reveal extensive cortical dysplasia, most seriously affecting the lateral sides of the brain. The cortex is too thick, the outside folding is too coarse, whereas the inner border of the cortex is irregular, compatible with polymicrogyric pachygyria. In addition, the images show ventriculomegaly, dilated inferior horns, and multifocal white matter abnormalities, the largest lesions being present in the deep parietal white matter. The T₁-weighted images (*fourth row*) confirm the cortical dysplasia (*left*), the dilated inferior horn (*middle*), and tiny high-signal-intensity spots in the white matter (*right*), probably related to calcium deposits

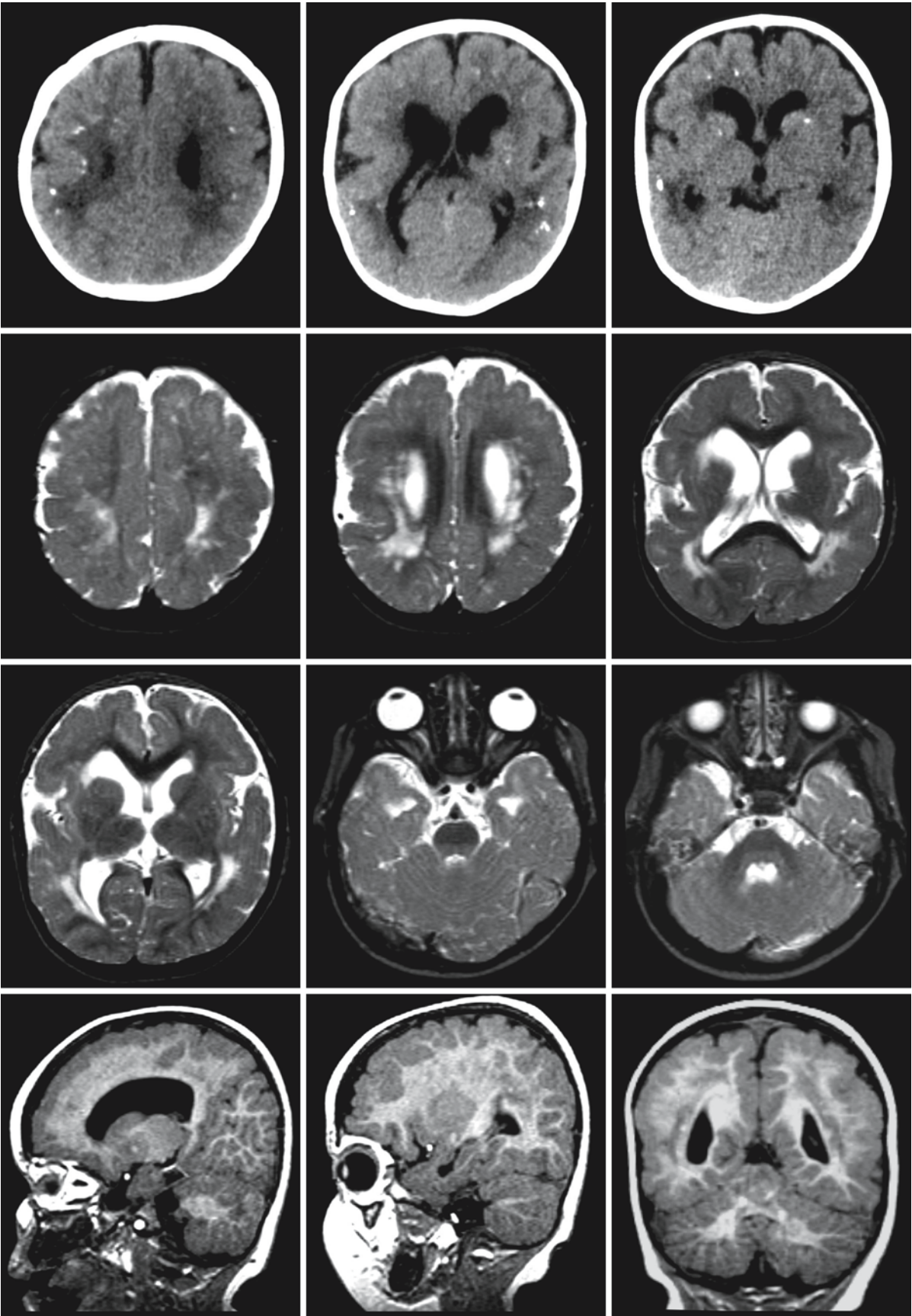


Fig. 85.1.

ment is in progress. It is unknown whether this early and intensive administration of ganciclovir will hasten resolution of acute disease, beneficially influence growth and development, decrease auditory and visual impairments, or improve intellectual outcome in these infants. There is evidence that with ganciclovir treatment the incidence of delayed hearing loss is lower. However, because of the potential bone marrow suppression, the possibility of as yet unforeseen long-term effects, and the as yet unproven benefit on long-term neurodevelopmental outcome, it is recommended that ganciclovir should not be routinely used to treat infants with congenital CMV disease until the results of ongoing clinical trials establish its safety and efficacy. Anecdotal evidence suggests that critically ill newborns, especially those who are premature and have CMV pneumonia, may benefit from ganciclovir treatment. Because of the side effects of therapy with currently available antiviral agents, treatment of newborns with an asymptomatic congenital CMV infection is presently not advocated, even though these infants are particularly at some risk for developing hearing loss.

The antiviral drugs that are now in use for the treatment of CMV either directly or indirectly inhibit viral polymerase or are able to reduce viral proliferation in patients with signs of CMV disease. These drugs, however, do not clear the virus completely and have serious side effects. Strains of CMV with reduced susceptibility to these antiviral drugs have been reported. There are, fortunately, newer therapies on their way, based upon better knowledge of the physiology and life cycle of the virus. Attempts are being made to improve the efficacy of orally taken drugs. Research is also going on in purine and pyrimidine nucleoside analogues, as well as in nonnucleoside CMV inhibitors and CMV protease inhibitors. The ultimate goal is the development of a vaccine that prevents congenital CMV disease.

85.5 Magnetic Resonance Imaging

Most published neuroimaging reports concern CT scans obtained during the follow-up of patients with a neonatal *symptomatic* congenital CMV infection. Frequent findings are intracranial calcifications (33–54%), unilateral or bilateral ventriculomegaly (10–37%), white matter abnormalities (0–22%), neuronal migration abnormalities with cortical dysplasia (0–10%), and an extensive, destructive encephalopathy (5–13%). Occasionally, subdural effusions or hemorrhage are seen. In 20–30% of the children no abnormalities are found.

In patients with a neonatal confirmed but *asymptomatic* congenital CMV infection, CT scans show milder abnormalities, and shows them less frequent-

ly. White matter abnormalities are reported in 14% of the children, whereas no abnormalities were demonstrated in 86% of the children. Few children have calcifications or mild ventriculomegaly (Fig. 85.1).

Characteristically the calcifications in congenital CMV are distributed in a linear, periventricular pattern ranging from tiny, punctate lesions to large deposits of calcium that appear to line the entire ventricular system. Calcifications also may involve the cortical and subcortical regions or involve the basal ganglia (Fig. 85.1). Infants with intracranial calcifications are more likely to display cognitive and audiological deficits later in life than those infants who do not have detectable abnormalities.

With respect to MRI, conventional MR sequences, including T₁- and T₂-weighted images, are useful to show morphological and structural details. Gradient echo sequences should be added to better show calcifications. Either an inversion recovery technique or a T₁-weighted 3D gradient echo sequence can help to assess the presence and extent of the cortical gyral abnormalities.

Studies reporting MRI findings in patients with neonatal *symptomatic* congenital CMV infection are restricted to small numbers. The findings include dilated ventricles, enlarged subarachnoid spaces, cerebral gyral abnormalities, cerebellar hypoplasia, cerebellar cortical dysplasia, delayed myelination, and white matter lesions. The ventricular dilatation may be extreme with serious thinning of the cerebral mantle. In the early stages, subependymal germinal cysts and intraparenchymal, intraventricular, and subdural hemorrhages may be present.

In patients with proven but neonatally *asymptomatic* congenital CMV, white matter abnormalities are frequently observed. The occurrence of anterior temporal cysts, often in combination with dilated inferior horns has been described repeatedly.

The gyral abnormalities in congenital CMV mainly involve the lateral aspects of the cerebrum (Figs. 85.1 and 85.2), although they may also be diffuse (Fig. 85.3). In patients with diffuse gyral abnormalities, the cortex may be thin and almost agyric. In addition, the lateral ventricles are often dilated in these patients. If the abnormalities are more limited, they most often consist of polymicrogyria (polymicrogyric pachygyria). The cortex is slightly thickened and folded in abnormally broad and shallow gyri (Figs. 85.1 and 85.2). The inner border of the cortex is irregular, indicative of underlying polymicrogyria. The gyral abnormalities may be unilateral or asymmetrical (Figs. 85.4 and 85.5). They may also present in the form of schizencephaly.

The pattern of white matter abnormalities observed in congenital CMV infection is distinct. Most often, the white matter abnormalities consist of multifocal lesions with the largest lesions in the parietal

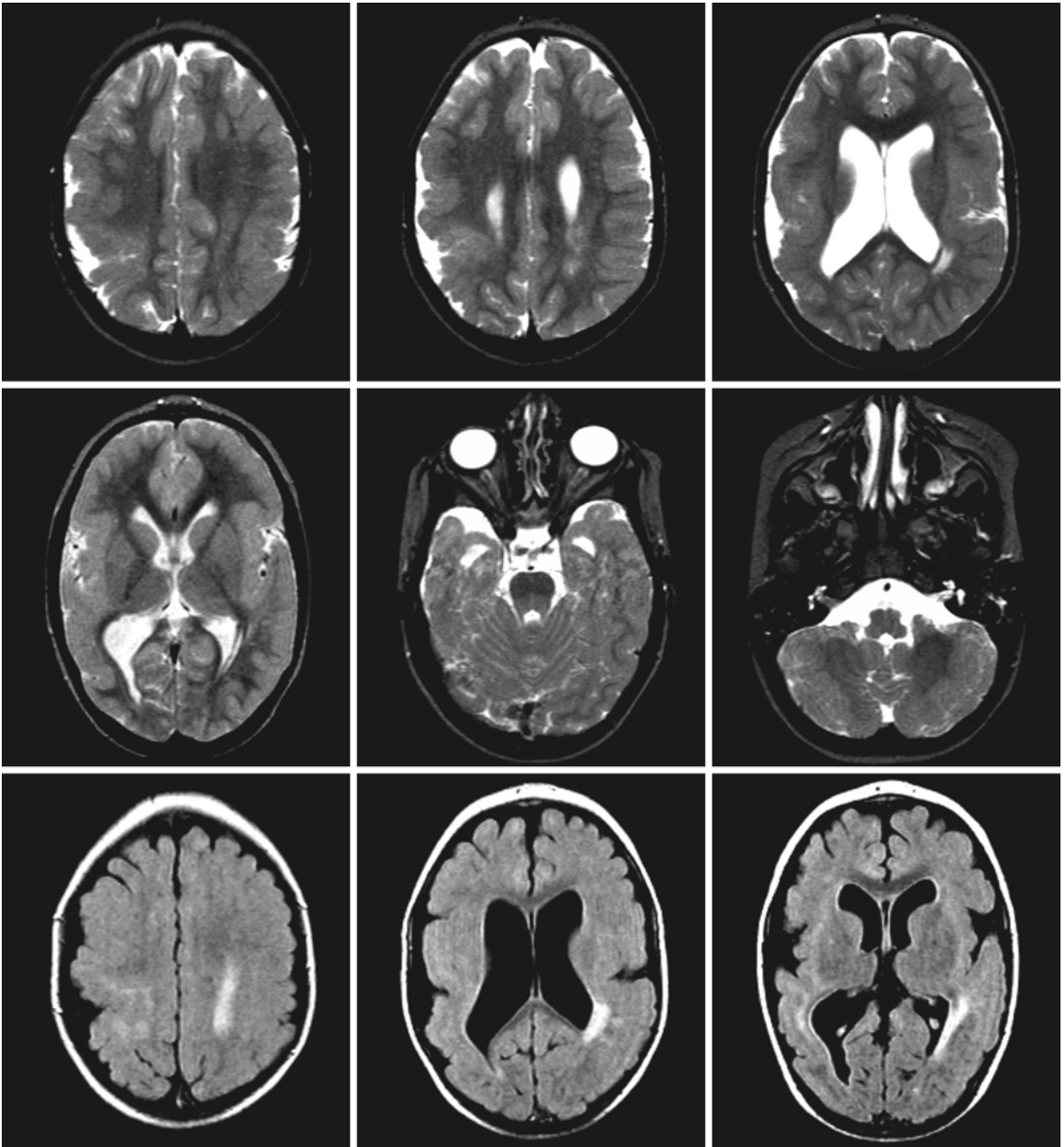


Fig. 85.2. Images of a 3-year-old girl with congenital CMV (diagnosis confirmed by a positive PCR for CMV DNA on the Guthrie card). The T₂-weighted images (*first and second rows*) show polymicrogyric pachygyria, more severe on the right than on the left, and dilated ventricles, larger on the right side.

The inferior horns of the lateral ventricles are dilated. Along the border of the left ventricle, in the parietal region, white matter lesions are seen. The FLAIR images (*third row*) show the white matter lesions more clearly

area and with predominant involvement of deep white matter, relatively sparing the immediately periventricular and subcortical white matter (Figs. 85.6–85.8). Numerous small additional lesions are usually seen in the frontal white matter (Figs. 85.6 and 85.8). The white matter abnormalities are as a rule bi-

lateral but not always symmetrical. In patients with gyral abnormalities, both diffuse (Fig. 85.3) and multifocal (Figs. 85.1, 85.2, 85.4 and 85.5) white matter abnormalities may occur. The white matter abnormalities may be limited in extent (Figs. 85.2 and 85.4), but may also be extensive (Figs. 85.3 and 85.5). In partic-

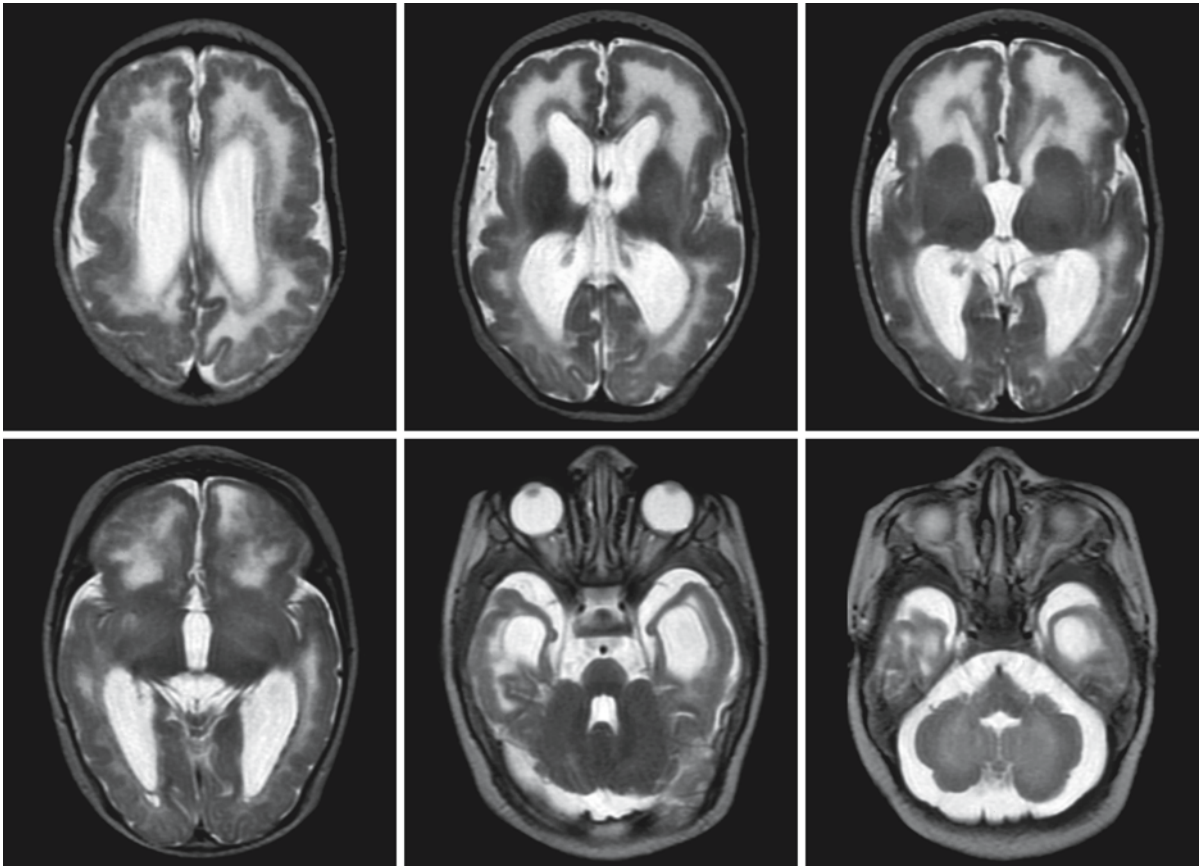


Fig. 85.3. A 11-month-old boy with CMV (diagnosis confirmed by a positive PCR for CMV DNA on the Guthrie card). The T₂-weighted images show polymicrogyria of both hemispheres, but also of the cerebellar cortex. Only the posterior part of the brain has better gyral development. There is a rim

of low signal intensity around the ventricles, probably a rim of ectopic neurons. The lateral ventricles are dilated. The inferior horns are markedly dilated and the hippocampus has an abnormal shape. Note the diffusely abnormal cerebral white matter

ular when the abnormalities are extensive, they are often mistaken for a genetic leukoencephalopathy and extensive laboratory tests are performed in that direction.

In addition, anterior temporal abnormalities, including abnormal and swollen white matter, subcortical cysts, and focal enlargement of the anterior part of the inferior horn, either alone or more often in combination, have been demonstrated to be particularly suggestive of congenital CMV (Figs. 85.1–85.8). The enlarged inferior horns are related to an abnormal configuration of the hippocampi, which have a vertical orientation instead of the normal horizontal orientation, and are abnormally small (Fig. 85.7).

The MRI pattern suggestive of congenital CMV does not resemble the pattern of any of the known leukoencephalopathies with the exception of some of the congenital muscular dystrophies. A combination of cortical dysgyria and diffuse or multifocal white matter abnormalities is also seen in Walker–Warburg

syndrome, muscle–eye–brain disease, and the Fukuyama type of congenital muscular dystrophy. However, in addition to muscle weakness, patients with these latter conditions have other MRI abnormalities, such as pontine hypoplasia and subcortical cerebellar cysts. None of these are seen in congenital CMV. A combination of multifocal white matter abnormalities and anterior temporal cysts has been reported previously in a few children with a clinically static encephalopathy (Olivier et al. 1998). It has been suggested that this might be a novel, genetically determined leukoencephalopathy. Considering our findings, congenital CMV should also be considered.

A CT scan showing calcification could raise the suspicion of congenital toxoplasmosis. In contrast to congenital CMV, the intracranial calcifications observed in congenital toxoplasmosis are usually scattered diffusely throughout the brain and not in the classic periventricular distribution of CMV, which may be an important clue.

Fig. 85.4. A 6-year-old boy with congenital CMV infection, diagnosed at birth. Note the unilateral left-sided gyral abnormalities. The abnormalities in the deep parietal white matter are most pronounced on the right. The inferior horn is dilated on the left

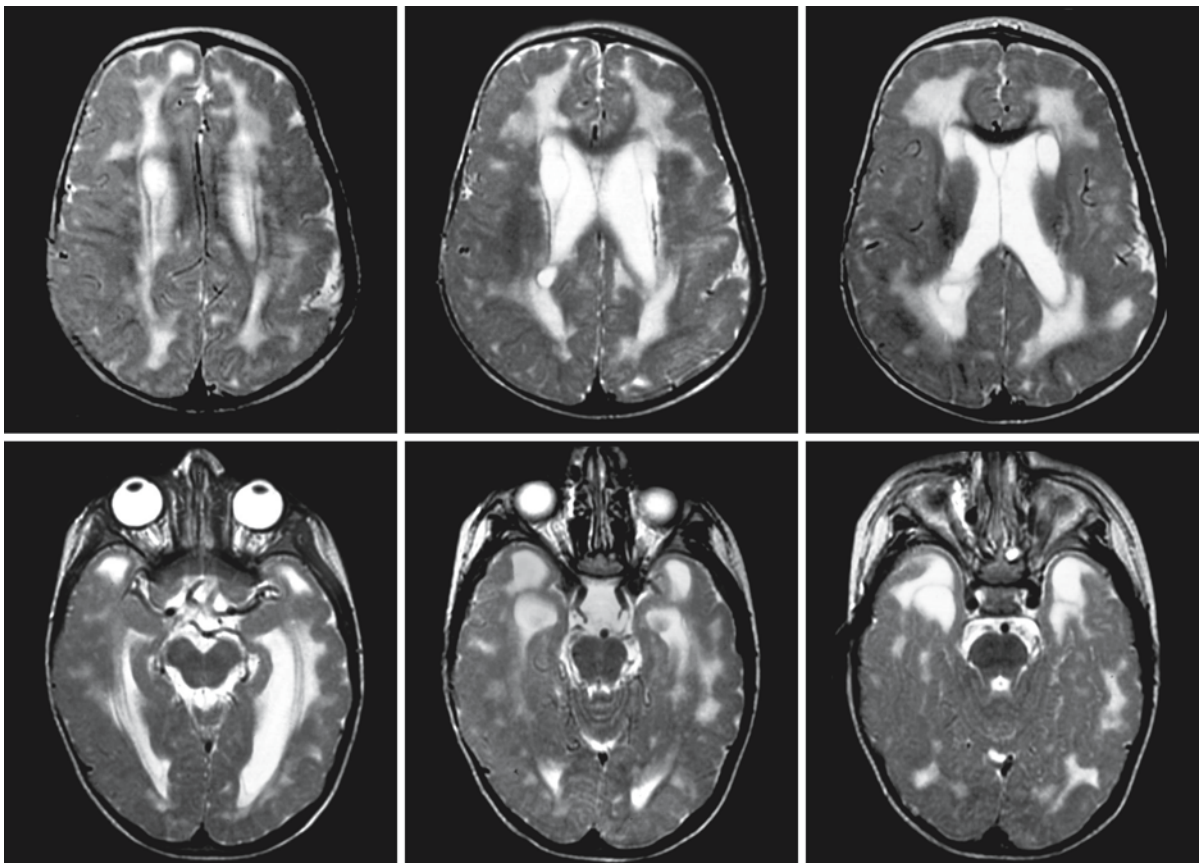
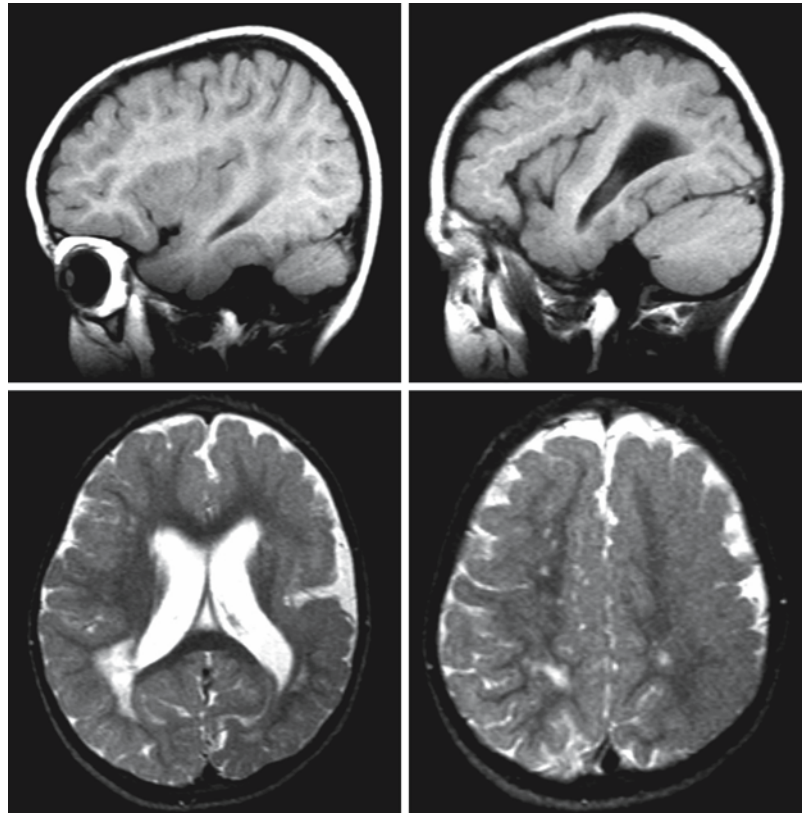


Fig. 85.5.

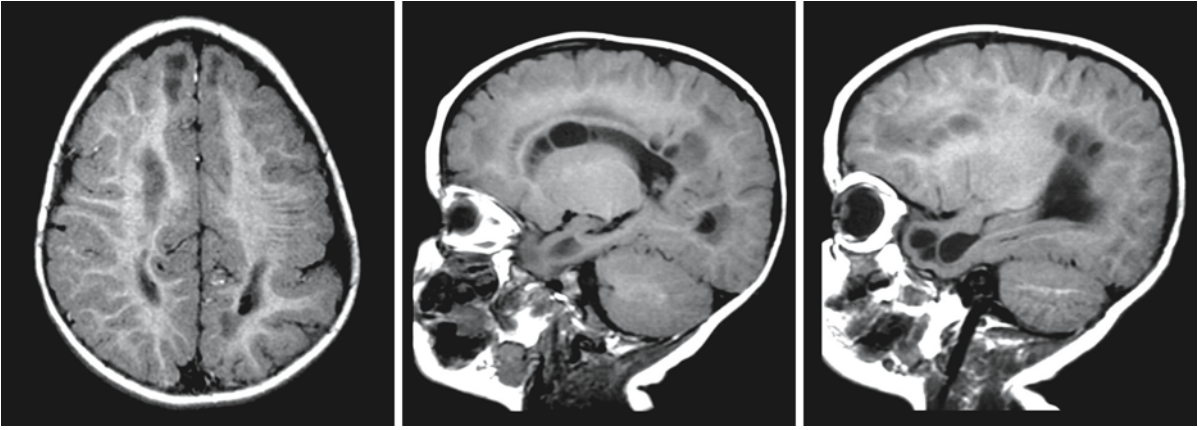


Fig. 85.5. (continued). A 17-month-old boy with congenital CMV (diagnosis confirmed by a positive PCR for CMV DNA on the Guthrie card). The T₂-weighted images (*first and second rows*) depict extensive, partly confluent, partly multifocal white matter abnormalities. On the left side of the brain, cortical dysplasia is present, best visible on the higher sections. The inferior horns of the lateral ventricles are dilated and the anterior temporal white matter is abnormal and swollen. The

T₁-weighted axial image (*third row, left*) shows the left-sided gyral abnormalities. The sagittal T₁-weighted images (*third row, middle and right*) demonstrate the presence of multiple intraparenchymal and intraventricular cysts. Note the cysts in the anterior temporal white matter and the enlarged inferior horn. Courtesy of Dr. A. Clarke, Department of Pediatric Neurology, St. George's Hospital, London, UK

Fig. 85.6. The boy presented with neonatal signs of a congenital CMV infection and was diagnosed in the neonatal period. The first MRI was obtained at the age of 1 month (*first and second rows*). The T₂-weighted images show that the cerebral white matter has an abnormally high signal intensity and is slightly swollen. The abnormalities are most pronounced in the posterior region. It is difficult to identify lesions within the high signal intensity of unmyelinated white matter. The sagittal T₁-weighted images (*first row, left and middle*) show swelling of the anterior temporal white matter, a small cyst in the inferior horn, and a subependymal cyst in the thalamocaudate notch. The follow-up MRI was obtained at the age of 1.5 years (*third and fourth rows*). The T₂-weighted images show the typical multifocal white matter abnormalities with the largest lesions in the deep parietal white matter. Note the signal abnormality in the anterior temporal white matter.

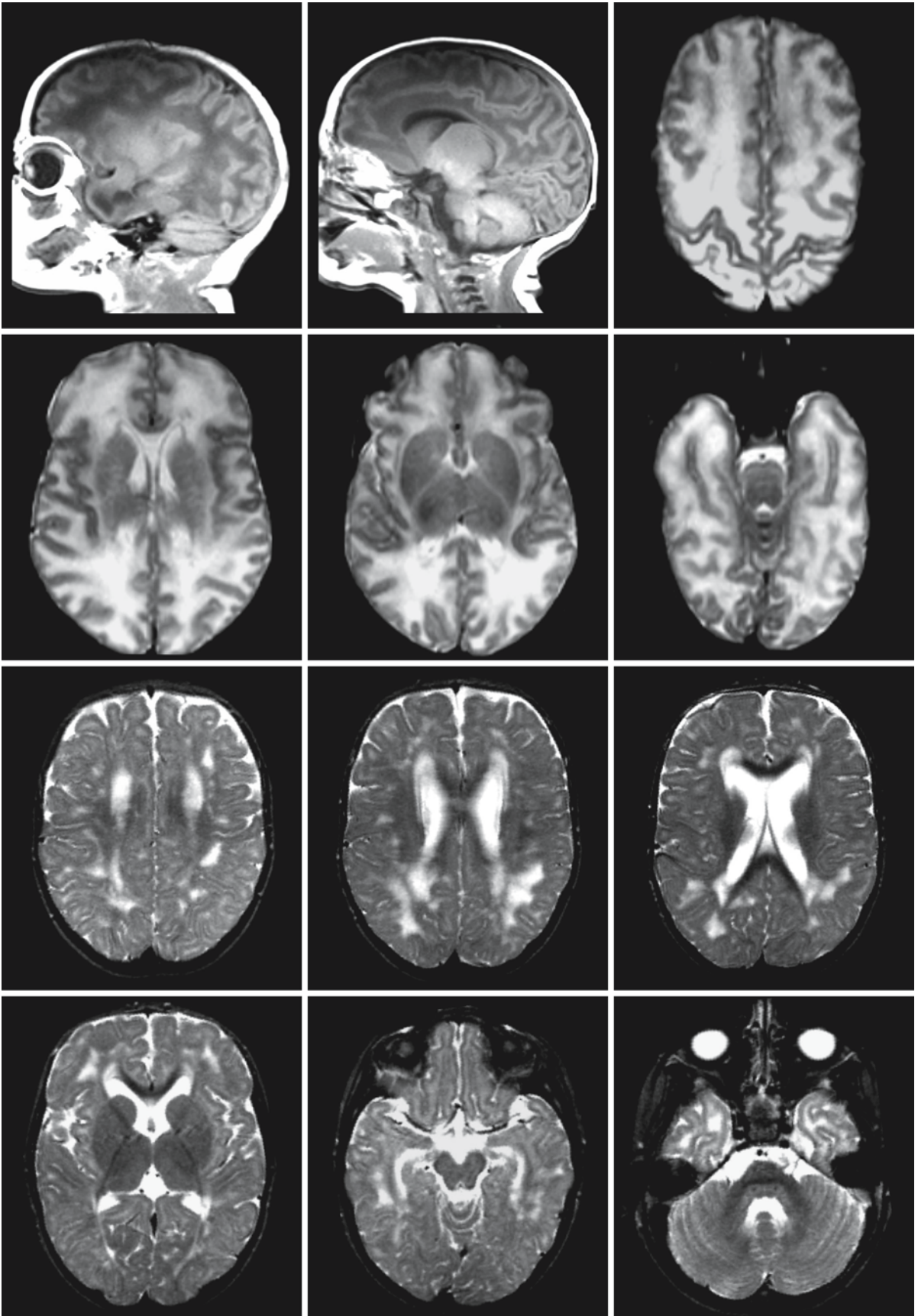


Fig. 85.6.

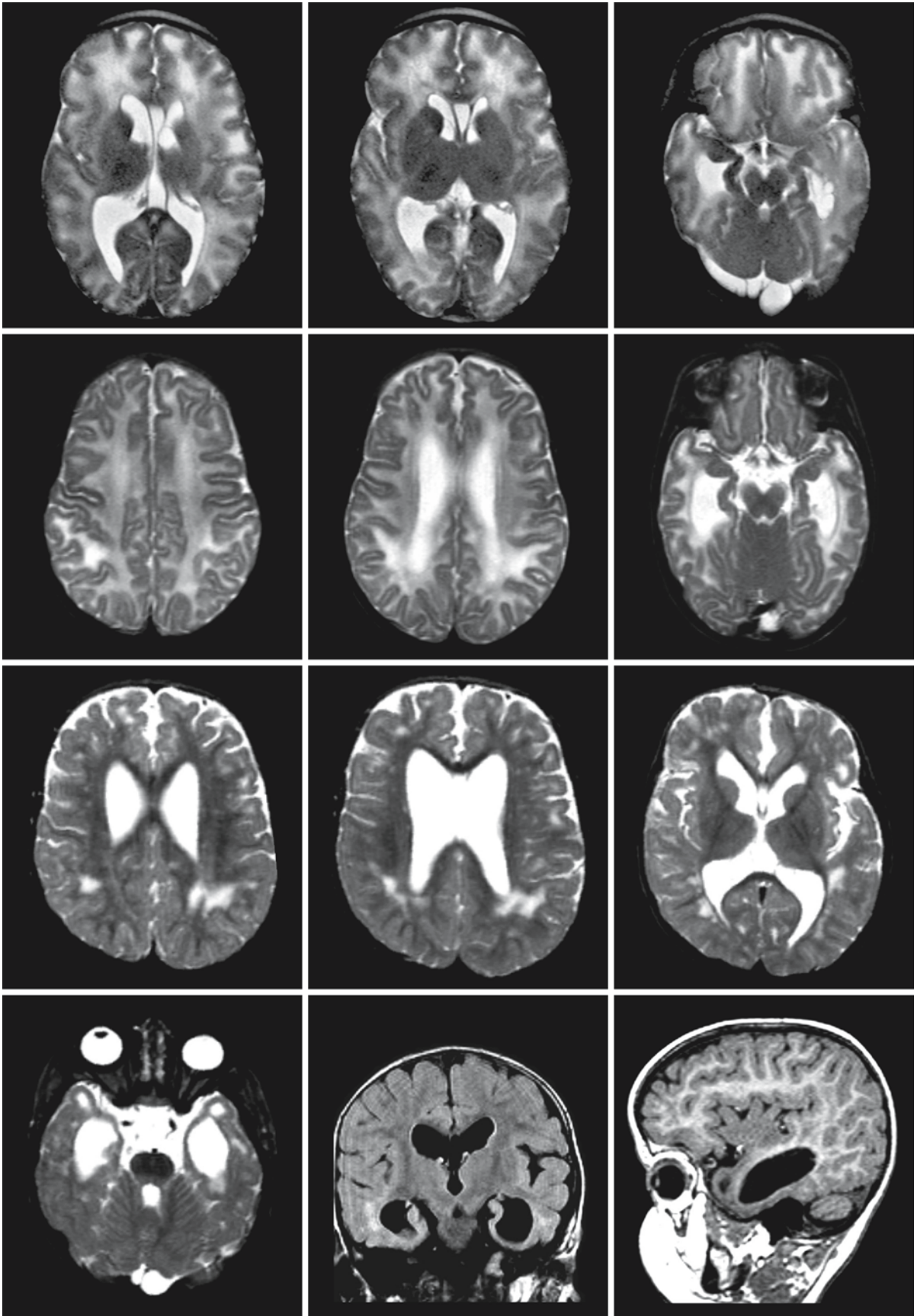


Fig. 85.7.

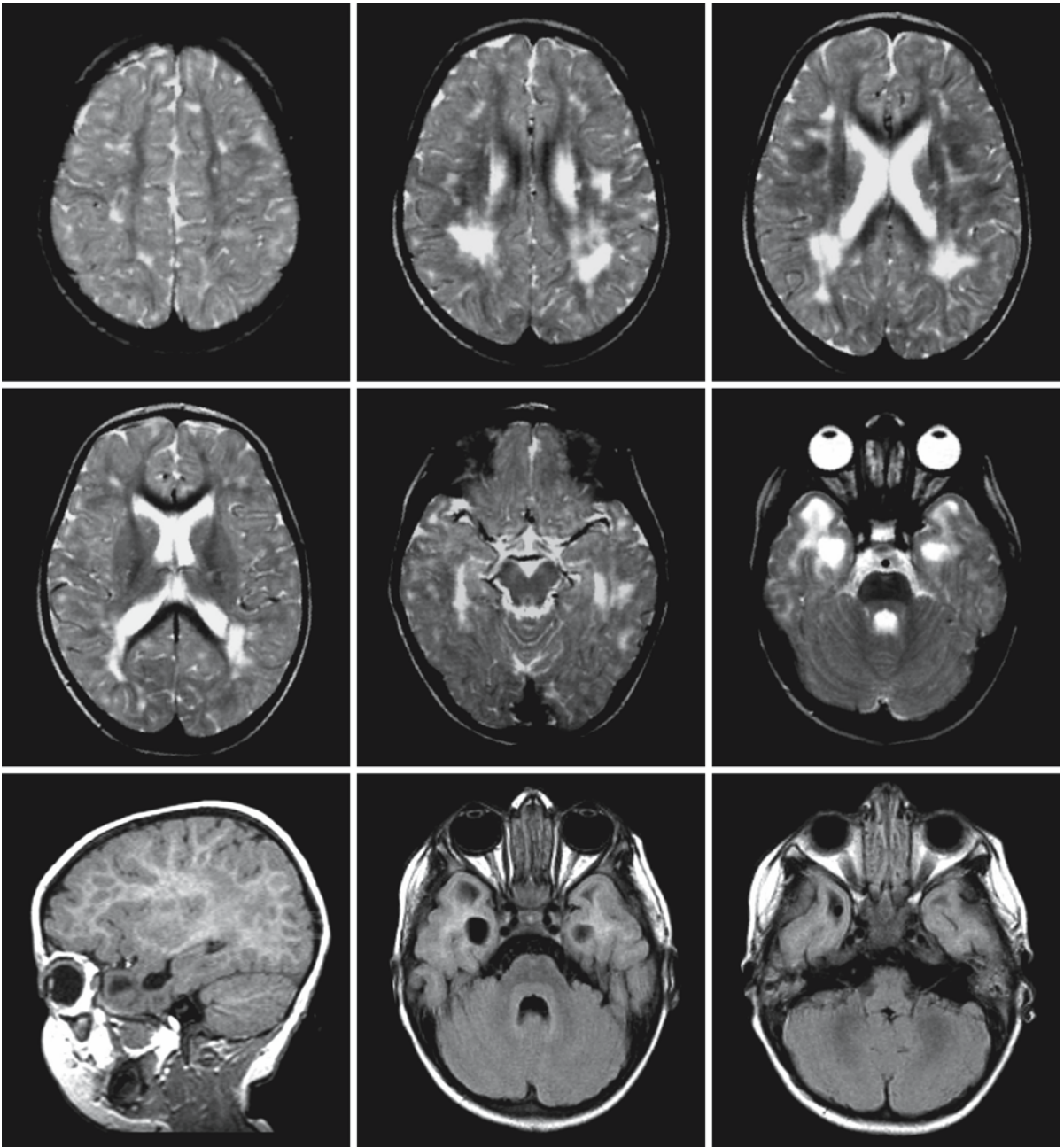


Fig. 85.8. A 1.5-year-old boy, diagnosed with congenital CMV in the neonatal period. Note the multifocal white matter abnormalities with the largest lesions in the deep parietal white matter. The inferior horn is dilated and the anterior temporal

white matter is highly abnormal in signal and has a somewhat swollen appearance. The FLAIR images (*third row, middle and right*) suggest that the anterior temporal white matter is almost cystic

Fig. 85.7. A baby girl presented soon after birth with an encephalopathy. She was diagnosed with a congenital CMV infection on the basis of a positive PCR for CMV DNA on the Guthrie card. The first MRI was obtained at 6 weeks (*first row*), which showed diffusely mildly abnormal cerebral white matter but no well-delineated lesions. There are subependymal cysts in the left thalamocaudate notch and in the left inferior horn. The hippocampus has an abnormal shape. Follow-up MRI at the age of 4 months (*second row*) shows that the parietal white matter is now evidently more abnormal than the re-

mainder of the cerebral white matter. The subependymal cysts have disappeared. MRI obtained at the age of 2.5 years (*third and fourth rows*) shows that the cerebral white matter looks much better myelinated. There are some remaining multifocal white matter abnormalities, most prominent in the deep parietal region. The inferior horns are highly dilated. The coronal FLAIR image (*fourth row, middle*) shows the abnormal shape of the hippocampus. The sagittal T₁-weighted image (*fourth row, right*) shows a cystic lesion anterior to the highly dilated inferior horn.

Whipple Disease

86.1 Clinical Features and Laboratory Investigations

Whipple disease is a multisystem granulomatous disorder. There is a male:female ratio of 6:1. The peak age of occurrence is between 50 and 55 years, but Whipple disease may also occur in childhood and in senescence. Many organs may be involved, but predominantly the gastrointestinal tract is affected. Migratory, nonerosive arthritis of the large joints may precede the intestinal symptoms by 2–10 years. The chief complaints of patients with systemic Whipple disease are diarrhea, weight loss, fever, arthritis, and abdominal swelling. Hypothalamic–pituitary involvement is common in patients with systemic Whipple disease and may lead to symptoms such as asomnia or hypersomnia, hyperphagia, polydipsia and weight gain. Physical findings in the multiorgan form of the disease may include lymphadenopathy, hypotension, hyperpigmentation, hepatomegaly, splenomegaly, ascites, edema, cardiac murmur, pericarditis, pneumonia, and occasionally ophthalmoplegia.

The CNS is involved in conjunction with other organs in 10–40% of patients. CNS complaints may include headache, diplopia, depression, personality changes, and cognitive decline. In a few patients the CNS is the sole site of infection, without any sign of involvement of other organs. The neurological symptoms in these cases are protean and include slowly progressive dementia, headache, hypothalamic dysfunction, meningitis, seizures, supranuclear ophthalmoplegia, myoclonus, ataxia, nystagmus, uveitis, papilledema, hemiparesis, peripheral neuropathy, and myopathy. A movement disorder referred to as oculomasticatory myorhythmia, characterized by rhythmic opening and closure of the mouth by action of the masticatory muscles, in combination with a slow (1-Hz) convergent–divergent pendular nystagmus, is considered virtually pathognomonic of Whipple disease of the CNS. The triad of progressive dementia, myoclonus, and external ophthalmoplegia is also highly suggestive of the disease.

Laboratory findings in systemic Whipple disease include elevated erythrocyte sedimentation rate, elevated liver enzymes, low serum potassium and calcium, low serum protein and albumen, anemia, low

serum iron, low serum carotene, proteinuria, hematuria, and steatorrhea. In Whipple disease with CNS involvement, CSF oligoclonal banding and an increased IgG level have been reported. In the initial phase an inflammatory reaction with CSF pleocytosis and elevated protein are usually seen. Increased IgA intrathecal synthesis, continuing even under therapy, has also been reported, probably indicating a still active infection.

The diagnosis is confirmed by either PCR of the CSF or light and electron microscopy of a biopsy of the jejunum, a retroperitoneal lymph node, or of affected brain tissue, demonstrating the presence of the bacillus *Tropheryma whippelii*.

86.2 Pathology

The gross pathological features of Whipple disease include generalized cerebral atrophy and small chalky nodules or granulomas up to 2 mm in diameter, scattered diffusely over the cerebral and cerebellar cortex and the subcortical white matter. The changes are focal, so that one area of the brain may be normal whereas an adjacent area may show florid abnormalities. Microscopically the granulomas contain strongly PAS-positive-staining macrophages, surrounded by large reactive astrocytes. With more widespread disease, PAS-positive cells infiltrate the white matter and may also extend into the subarachnoid spaces and be associated with death of neurons, formation of vacuoles, and demyelination. Bacilli and debris of bacilli may be found in the PAS-positive material. Microinfarctions have been reported and are probably caused by microthrombi related to vegetations on the heart valves, as found in a substantial number of patients at necropsy.

Epon-embedded toluidine-blue-stained semithin sections prepared for electron microscopy demonstrate gliotic gray matter with perivascular accumulation of macrophages containing multiple intracytoplasmic osmiophilic dark granules. Ultrastructurally these dark granules consist of lipofuscin and unique membrane-bound inclusions containing numerous membranous profiles. Transitional forms from these unique inclusions to lipofuscin are also observed.

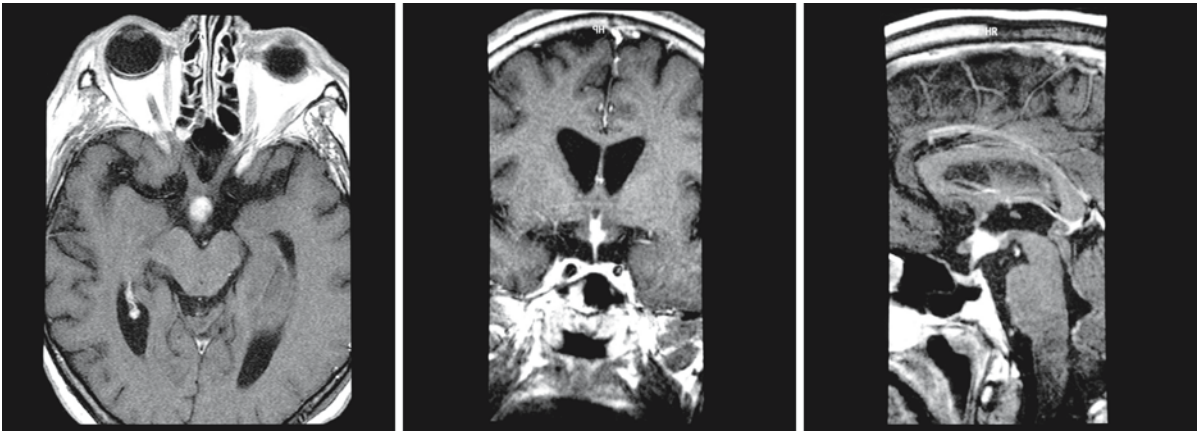


Fig. 86.1. Lesions in the hypothalamus often occur in Whipple disease and are demonstrated here in T₁-weighted, contrast-enhanced images in three planes in a 44-year-old man

with hypopituitarism. Similar lesions may be seen in Langerhans cell histiocytosis, neurosarcoidosis, brucellosis, and hypothalamic tumors. From Brändle et al. (1999), with permission

86.3 Pathogenetic Considerations

Whipple disease is caused by a bacillus with unique characteristics. With electron microscopy it has been consistently recognized in affected tissue, either free or degraded to varying degrees within macrophages. It is a weakly gram-positive rod-shaped bacillus which is not acid-fast. It is 1–2 μm in length and has a thick wall, the inner layer of which stains with PAS dyes. Its presence accounts for the brightly staining PAS-positive macrophages which are seen in biopsy material and contain bacillary debris. Culturing of the bacillus has proven to be difficult.

Molecular genetic techniques led to the identification of a 1321-base 16S rRNA gene sequence in tissue derived from small bowel biopsy of patients assumed to have Whipple disease. Using PCR, positive reactions have been obtained from other tissues, including heart, vitreous fluid, peripheral blood cells, and pleural effusions. It has been difficult to identify sequences from brain tissue; recently, however, a high yield has been obtained with PCR of the CSF. The bacillus was eventually characterized by 16S rRNA gene analysis to be a member of the actinomycetes. The bacillus has been given the name *Tropheryma whippelii*. It is still unclear whether all forms of Whipple disease are caused by this bacillus.

The occurrence in nature of this bacillus is still unclear. This is also the case with the transmission of the disease to humans and the pathophysiology once the infection is established. Humans are the only host for the disease. There is no evidence for human-to-human transmission and the disease does not occur in clusters. Because the main site of the disease is in the gastrointestinal tract, it has been assumed that infection follows ingestion, subsequently spreading hematogenously or via lymphatic channels. It is also

unclear how the infection breaches the blood–brain barrier. During active disease bacilli are found in macrophages and free in the affected area.

86.4 Therapy

Therapy consists of a combination of antibiotics, including penicillin, streptomycin, tetracycline, and trimethoprim–sulfamethoxazole. Treatment is continued for 1–2 years and relapses may occur even after many years.

86.5 Magnetic Resonance Imaging

As variable as the protean neurological manifestations of Whipple disease are the findings with MRI. Lesions may involve gray and white matter without a distinct pattern. To illustrate this we cite a number of findings in patients with confirmed Whipple disease:

- Lesions in the mammillary bodies and hypothalamus (Figs. 86.1 and 86.2)
- Lesions in the hippocampal gyrus, uncus, and medial or mediobasal temporal lobes (Fig. 86.2)
- Lesions in the hypothalamus, thalamus, and basal ganglia
- Lesions in the optic chiasm and tracts (Fig. 86.2)
- Diffuse cerebral atrophy and ventriculomegaly
- Lesions in the brain stem (Fig. 86.3)
- Spinal involvement (Fig. 86.3)
- Multiple lesions throughout white and gray matter, varying in size (Fig. 86.4)

A constant feature is enhancement after contrast. The enhancing lesions are very similar to those seen in other inflammatory and infectious disorders. From

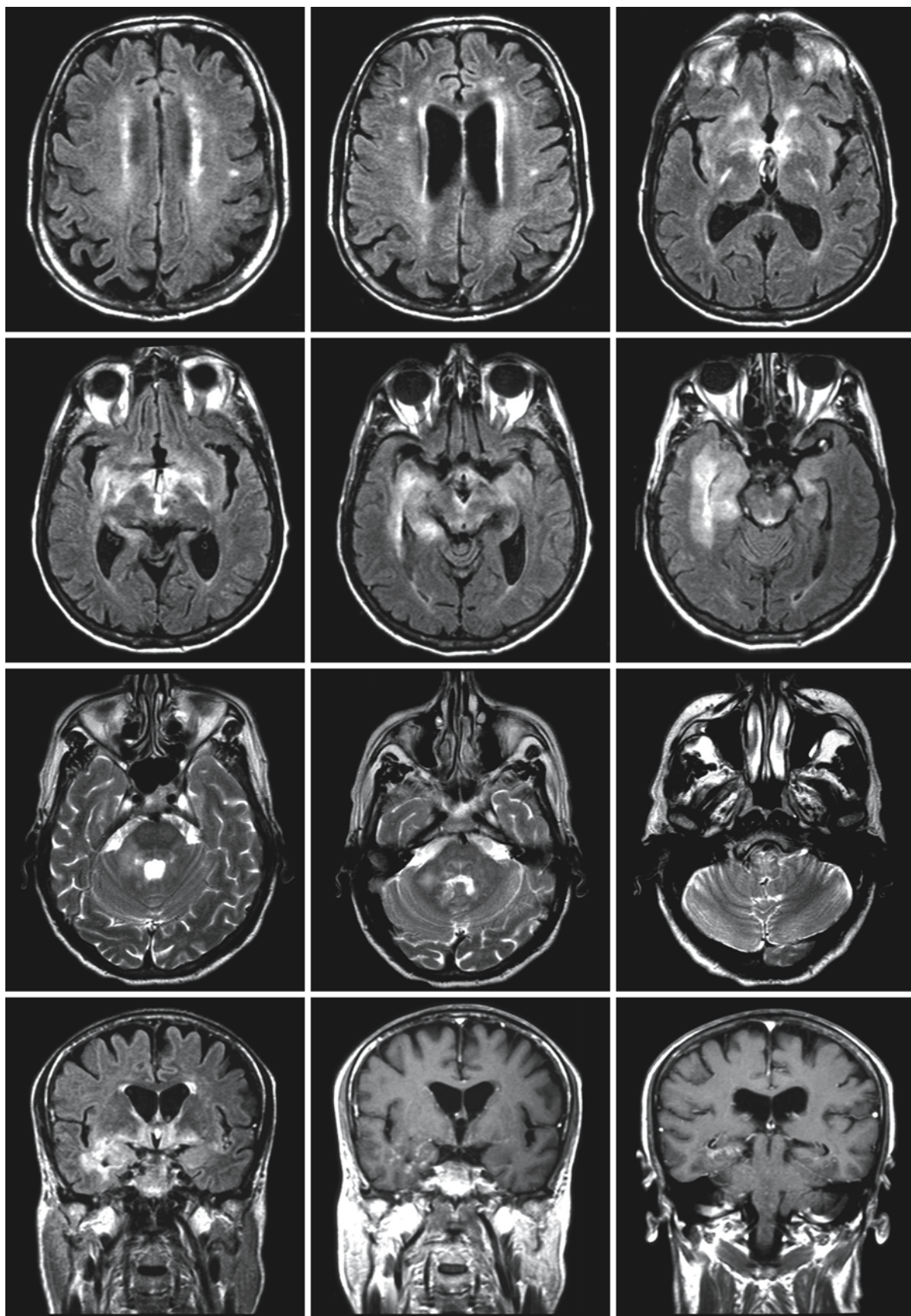


Fig. 86.2.



Fig. 86.3. The patient shown in Fig. 86.2 also has a lesion in the spinal cord (*arrows*). From Kremer et al. (2001), with permission and courtesy of Dr. S. Grand, Magnetic Resonance Imaging

Unit, Centre Hospitalier et Universitaire de Grenoble, Grenoble, France

←
Fig. 86.2. A 68-year-old man with Whipple disease. The axial FLAIR (*first and second rows*) and T₂-weighted images (*third row*) show a periventricular hyperintense rim and small focal lesions in the deep white matter. The lower slices show lesions in the posterior limb of the internal capsule, hypothalamus, thalamus, the mediobasal parts of the temporal lobes, the anterior commissure, mammillary bodies, optic chiasm, mesencephalon, pons, middle cerebellar peduncles, and medulla. The coronal images (*fourth row*), FLAIR (*left*) and T₁-weighted after contrast injection (*middle and right*), show enhancement of the involved structures in the hypothalamus and mediobasal temporal area, with an asymmetrical distribution. From Kremer et al. (2001), with permission and courtesy of Dr. S. Grand, Magnetic Resonance Imaging Unit, Centre Hospitalier et Universitaire de Grenoble, Grenoble, France

the description of these lesions there seems to be some preference for the hypothalamus and medial temporal lobe. A clear message from these findings is that contrast must be given in patients with an unusual pattern of lesions and an unexplained neurological disorder.

The differential diagnosis of multiple enhancing lesions of variable size involving both gray and white matter is from multiple metastases, infectious and inflammatory disorders, including multiple sclerosis, acute disseminated encephalomyelitis, systemic lupus erythematosus, and Behçet disease. In patients with predominant lesions in the hypothalamus and suprasellar region, the differentiation is from Langerhans cell histiocytosis, sarcoidosis, brucellosis, lymphoma, and other tumorous processes.

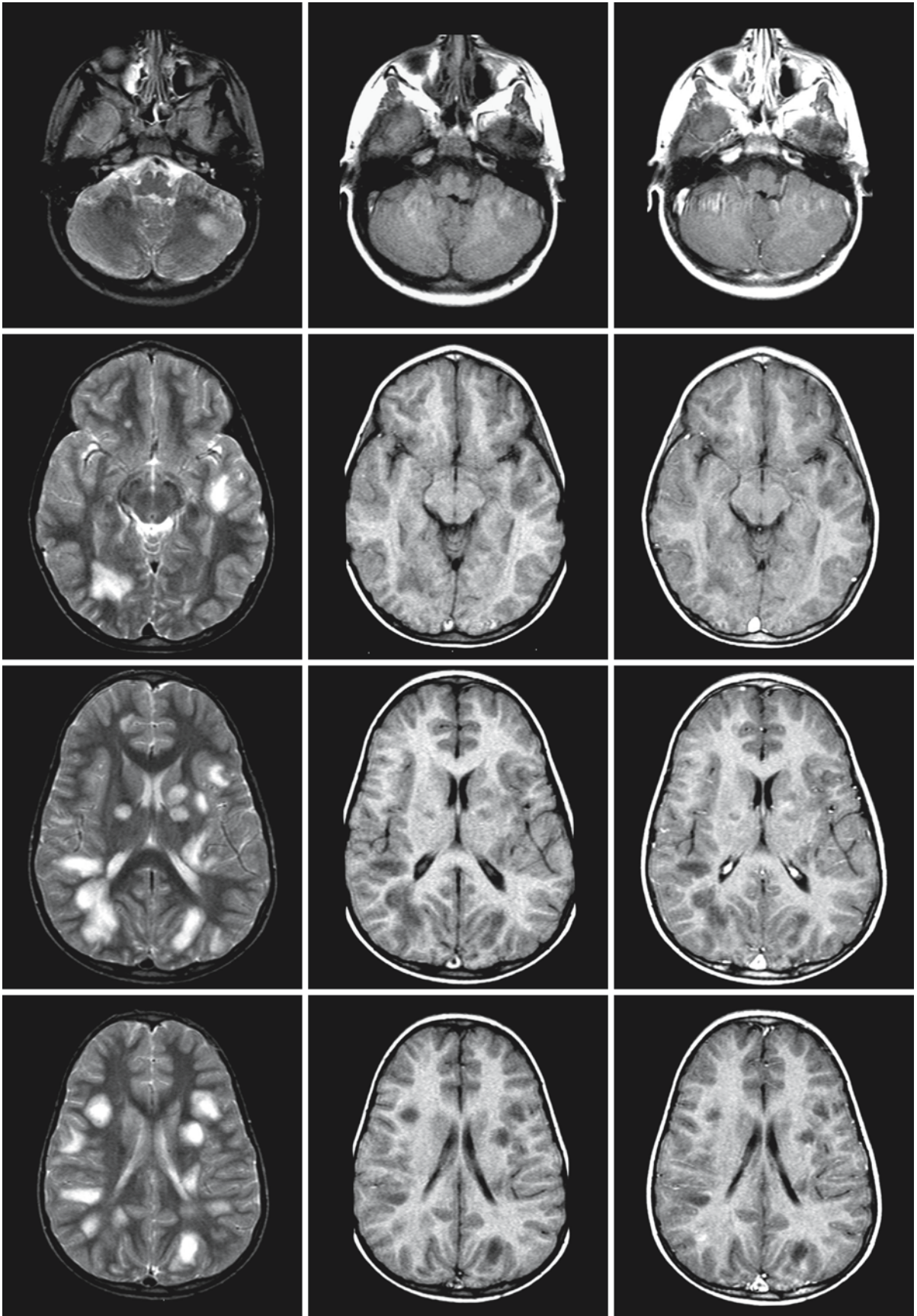


Fig. 86.4.

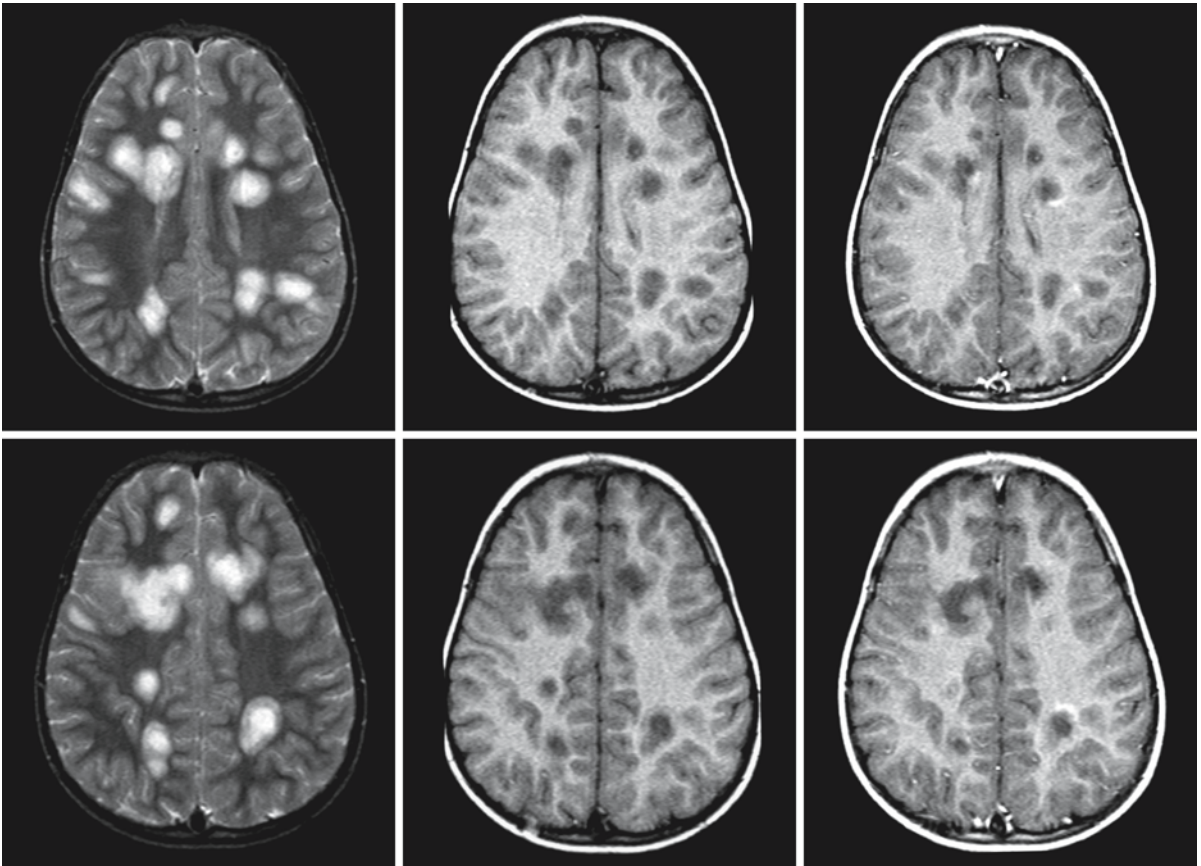


Fig. 86.4. (*continued*). A 4-year-old boy with Whipple disease. T₂-weighted images are in the *left column*, T₁-weighted images are at the same level in the *middle column*, and T₁-weighted images with contrast in the *right column*. The images give an overview of the lesions. The multifocal lesions are rounded,

isolated, of different sizes, involving both white and gray matter, randomly spread over the brain in an asymmetrical fashion. Note that only few lesions enhance and that the enhancement is partial. Some show a vague ring-like enhancement. From Duprez et al. (1996), with permission

Toxic Encephalopathies

There is growing awareness that chronic intoxications by industrial, agricultural, iatrogenic, and environmental pollution may have teratogenic or oncogenic effects or may cause neurological or psychiatric syndromes. A toxic encephalopathy (TE) is the result of the interaction between a chemical compound and the brain. Disturbance of normal brain function may be caused by multiple factors, such as depletion of oxidative energy, mitochondrial dysfunction, interference with biochemical pathways, alteration of membrane function and stability, enzymatic dysfunction, derangement of neurotransmission, and altered ion balance. It has often taken some time before the true cause of the encephalopathy was recognized, reflecting the difficulty in recognizing that slow deterioration of neurological functions may indicate poisoning by a toxin. In many cases, religious, superstitious, or racial “explanations” have been believed for a long time. The list of examples of TEs is long. Well-known examples include:

- 1941 Spastic paraparesis, caused by *Lathyrus sativus* peas; the toxic agent was identified as β -N-methylamino-L-alanine (BMAA)
- 1953 Guamanian type of parkinsonism, caused by the seeds of *Cycas circinalis*; the toxic agent was originally identified as β -N-oxalylmethylamino-L-alanine (BOMAA); later this theory was withdrawn, because blood concentrations were too low to explain the disease
- 1948 Hexachlorophene encephalopathy, especially in neonates
- 1950 Encephalopathy caused by monosodium glutamate in baby food
- 1953 Minamata disease (mercury encephalopathy)
- 1960 House painter’s dementia, caused by organic solvents and carbon disulfide
- 1983 Methylphenyltetrahydropyridine (MPTP), “synthetic heroin”, causing striatal dopamine deficiency and parkinsonism

In the past few decades drug-related encephalopathies due to heroin, cocaine, or ecstasy, and iatrogenic intoxications due to more aggressive therapies against cancer and graft-versus-host disease, have become more prominent and widespread.

TE presents with one or more of the following neurological or psychiatric symptoms (Bonhoeffer types): decreased concentration and consciousness; excitability and convulsions; motor and sensory

disturbances; extrapyramidal movement abnormalities; disturbance of specific senses; disturbance of coordination; and behavioral and psychological changes.

In many forms of TE, clinical manifestations are acute and severe, requiring immediate treatment. Imaging of the brain is then only of secondary interest, although in unsuspected cases MRI may play a leading role in diagnosis. The role of imaging is as a rule more important in cases of subacute or chronic TE with slowly progressive neurological damage. In such cases, MRI may demonstrate striking abnormalities and can be of importance for further diagnosis and therapy monitoring. However, even in cases with histologically proven cerebral damage, MRI is not always positive. For example, tardive dyskinesia is a severe movement disorder due to the chronic use of neuroleptic drugs. Histology shows a decrease in the number of ganglion cells in the substantia nigra. MRI shows no abnormalities. In other cases, too, when the encephalopathy is the result of interference with neurotransmitters, for example in the malignant neuroleptic syndrome, MRI fails to show abnormalities.

Knowledge of the biomechanisms whereby toxins of endogenous or exogenous origin cause encephalopathy helps us to understand the patterns of lesions seen in imaging studies. MRI abnormalities are, as a rule, symmetrical as toxins have no left/right preference. Characteristic MRI patterns showing involvement of particular brain structures are the result of differences in regional vulnerability of brain tissue to environmental perturbations and to biochemical changes. Here the concept of *selective vulnerability* comes in (see also Chap. 3).

As a general rule, specific groups of toxins tend to affect specific brain structures more than others. That is, certain regions and systems within the brain have greater affinity for and greater sensitivity to specific types of toxins. These regions of identical affinity and vulnerability were recognized by German neuropathologists in the first part of the twentieth century, who designated them the *topistische Bezirke* or topistic areas. Topistic areas often involve more than one structure; they often encompass a whole functional chain of neurons and tracts.

The principle of *functionally related systems* is well established in neurology. Topistic areas related to functional systems can be readily identified during normal physiological development of the brain and

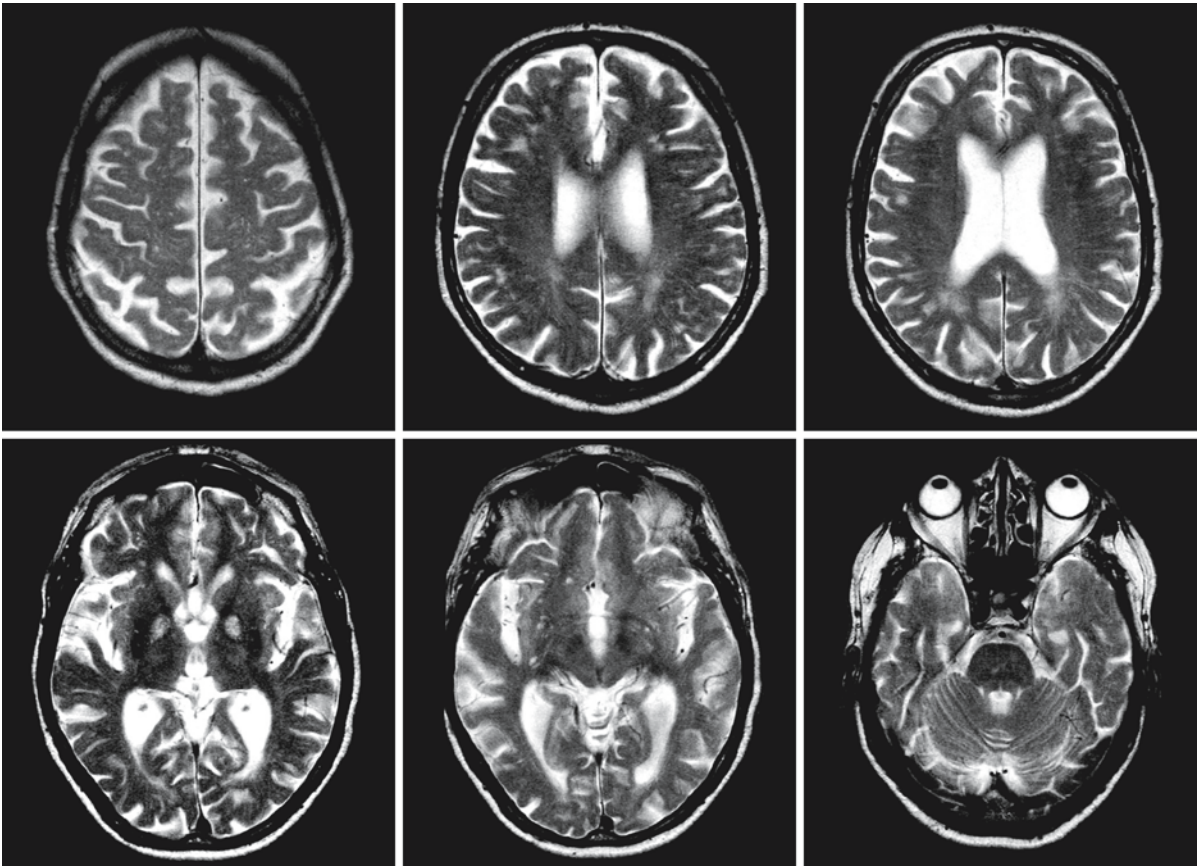


Fig. 87.1. T₂-weighted series of transverse images in a 63-year-old man with carbon monoxide intoxication. The globus pallidus shows high signal intensity, whereas the other brain

structures are initially spared. In the subsequent days a delayed leukoencephalopathy may follow

in systemic degenerative disorders. As early as 1920, Flechsig recognized that functionally related systems myelinate at the same time. Similarly, functionally related and interdependent nuclei appear to degenerate at the same time in multiple system atrophy and progressive supranuclear palsy.

Other mechanisms of selective vulnerability in TE are related to the *similarity in particular physico-chemical characteristics* that make different geographic areas equally vulnerable to a particular noxious agent. Apparently diverse areas may prove to have similar oxygen requirements, chemical composition, and/or neurotransmitter dependency and density.

Gray matter structures have higher cellular activity and a higher oxygen requirement than white matter structures and, therefore, are more vulnerable to oxygen deprivation. The damage that results from oxygen deprivation is actually mediated by toxic products, such as excitatory amino acids and free radicals inducing irreversible neuronal damage and death. The selective vulnerability of gray matter

structures to energy depletion is also reflected in the preferential affliction of gray matter structures in carbon monoxide intoxication, affecting especially the globus pallidus (Fig. 87.1), and Leigh disease, where the putamen, caudate nucleus, globus pallidus, periaqueductal gray matter, tectum and tegmentum of the midbrain, and dentate nuclei may be involved. Wernicke encephalopathy, a toxic encephalopathy caused by thiamine deficiency in alcoholics, shows a similarity in pattern of involvement to Leigh disease, presumably because thiamine deficiency also influences energy metabolism. A difference is that in Wernicke encephalopathy the mammillary bodies are nearly always involved and putamen and caudate nucleus are nearly always preserved (Fig. 87.2). The reason for this difference is unknown.

An example of selective vulnerability resulting from specific chemical composition is found in myelin. Myelin has high lipid content and a slow turnover. As a result, all the myelinated tracts are particularly vulnerable to the accumulation of lipophilic substances and to lipid peroxidation. Lipophilic sub-

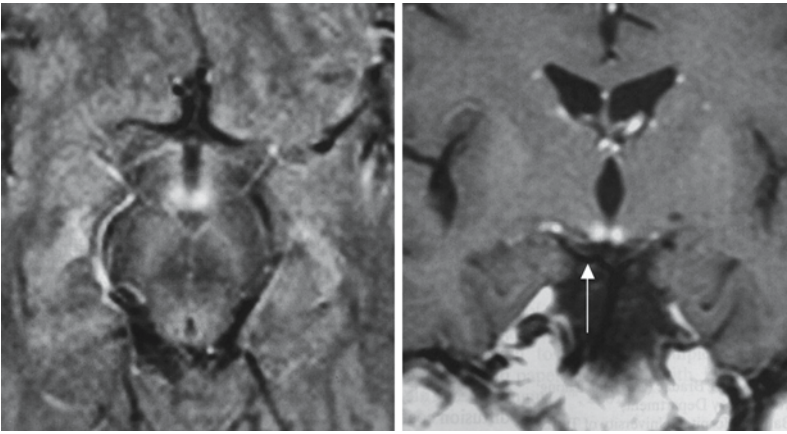


Fig. 87.2. In the acute phase of Wernicke encephalopathy the mammillary bodies are nearly always involved. The axial proton density image shows the lesions. On the coronal T₁-weighted contrast-enhanced image the mammillary bodies show uptake of contrast

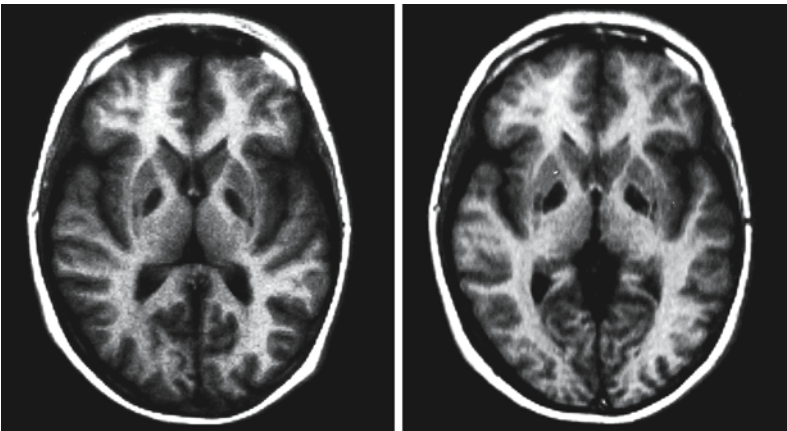


Fig. 87.3. T₁-weighted images of a 18-year-old girl with severe behavioral disturbances after having taken a love potion containing ecstasy. Cyst-like lesions are seen in the globus pallidus and the posterior parts of the putamen on both sides

stances easily cross the blood–brain barrier. One instance of such intoxication has become notorious in medical literature: hexachlorophene encephalopathy, a vacuolating myelinopathy, which was found in infants who were washed with antiseptic hexachlorophene solutions for dermal problems. The skin of preterm neonates proved to be more permeable to these agents than the more mature skin, resulting in increased absorption and toxicity. In adults, vacuolating myelinopathy has been described after the use of hexachlorophene solutions in vaginal tampons and as an antiseptic agent on burned areas. Intoxication with triethyltin has identical effects.

Topistic areas related to the *distribution of a particular neurotransmitter* are best visualized by positron emission tomography (PET). PET, for example, shows the distribution of ¹⁸fluorodopa in the basal ganglia. Methylphenyltetrahydropyridine (MPTP) interferes selectively with the dopamine neurotransmitters and leads to severe parkinsonism. Tardive dyskinesia and malignant neuroleptic syndrome are other examples of TEs with involvement of topistic areas related to specific neurotransmitters. In this kind of involvement of a neurotransmitter system, imaging modalities

do not usually show abnormalities. However, in some cases MRI successfully depicts the topistic areas, as shown in a case of ecstasy intoxication (Fig. 87.3).

Selective vulnerability is also related to *the level of activity during development*. This concept was particularly stressed by Dobbing (1968) and has broadened the insight into the origin of congenital malformations of the CNS. The greatest impact of noxious agents is on those structures that grow and develop at the highest rate at the time of insult. Thus, migrational disorders result when toxic insults occur in the third to fifth month of gestation, the period in which neuronal migration occurs. Similarly, disorders of myelination are observed when toxic insults occur during the last trimester of pregnancy and the first year of life, because myelination of the CNS occurs at a high rate in these periods. Since normal myelination depends upon complex interactions between axons, myelin-forming oligodendrocytes, and the provision of substrates by the environment, the delicate interactive process is easily disturbed by adverse factors such as nutritional deficiencies, inborn errors of metabolism, and intoxications.

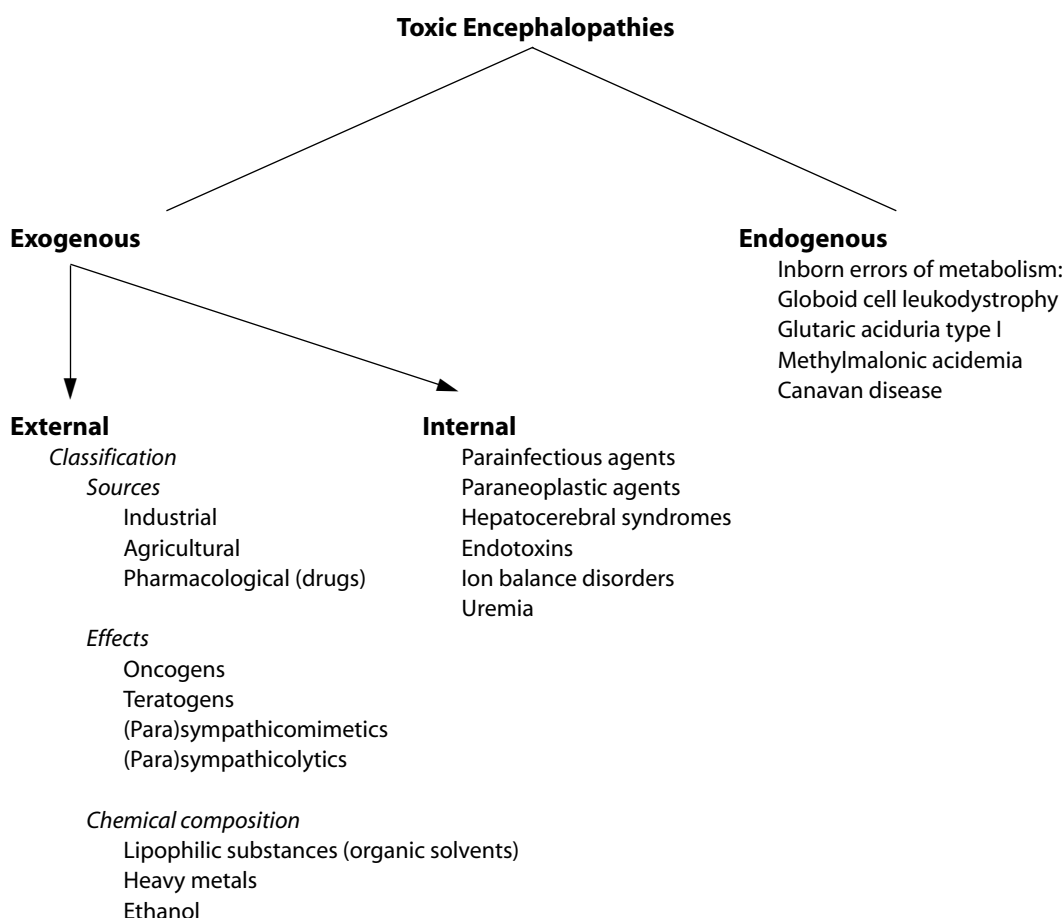


Fig. 87.4. Classification of toxic encephalopathies

In this respect, it should be mentioned that age can be a prominent pathoplastic factor in TE. Many fetal intoxications, such as those caused by maternal use of antiepileptic or antidepressive drugs, maternal alcohol abuse, and maternal drug abuse, lead to serious syndromes of which the fetal alcohol syndrome and fetal hydantoin syndrome are well-known examples. Fetal intoxications may result in cerebral maldevelopment, cerebral disruptions, and arrest or delay of cerebral maturation. The effects of intoxications may also be different in different age groups. Lead intoxication in adults differs in presentation from that in childhood. This is also true of salt intoxication, where the progress of myelination is an important factor in the distribution of the toxic damage.

To facilitate the analysis of TEs, we have classified them according to origin of the toxins within or outside the blood–brain barrier (endogenous versus exogenous). Exogenous TEs are then further subdivided depending on whether the toxic substance originates inside or outside the body (exogenous-internal versus exogenous-external) (Fig. 87.4). This classifi-

cation is imperfect because it depends, in part, on the point of view of the observer. A bacterial endotoxin can be classified either as exogenous-external, because the infection by gram-negative bacteria stems from outside the body, or as exogenous-internal because the endotoxin causing the related encephalopathy is produced by the bacteria within the body. We prefer exogenous-internal, because the toxin itself is produced within – and in interaction with – the body. The largest group of toxins is exogenous-external. Toxins within this group are usually categorized by chemical composition, source, or effect. Dietary and metabolic deficiencies may lead to abnormal biochemical processes that produce effects comparable to intoxications.

The group of *exogenous-external* TEs includes all intoxications from iatrogenic, agricultural, industrial, environmental, and social (drugs, alcohol, nicotine) sources that affect the CNS. Belonging to this group are intoxications with the *Lathyrus sativus* peas, organic mercury poisoning, organic lead poisoning, and toluene exposure, as well as other well-known en-

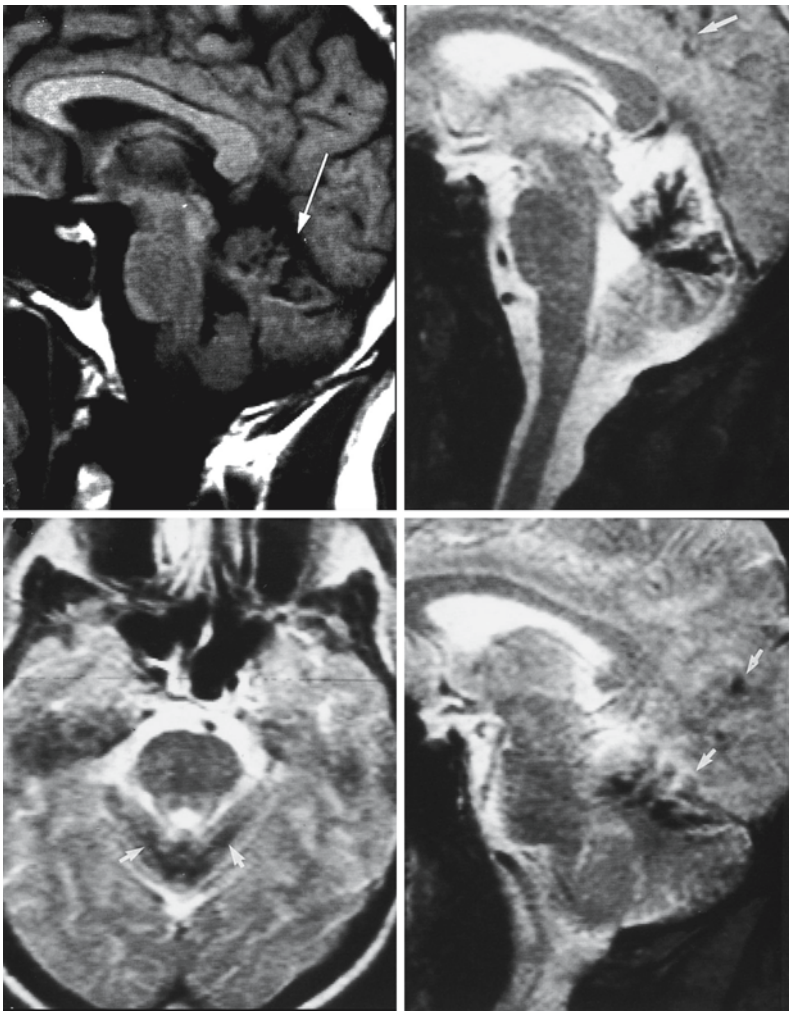


Fig. 87.5. Mercury encephalopathy in a 50-year-old man with a 2-year course of progressive cerebellar and focal cerebral signs following use of a mercury-containing compound to prevent tulip bulbs from cropping. In particular on the gradient echo images, which are more sensitive to magnetic susceptibility changes, the abnormal mineral depositions are clearly shown in cerebellar tissue and, to a less severe extent, in the occipital area

cephalopathies associated with ethanol abuse, such as the Marchiafava–Bignami syndrome, Wernicke encephalopathy, and Korsakoff syndrome. Iatrogenic exogenous-external TEs include all TEs caused by the ingestion of prescribed drugs, such as chemotherapeutic agents, anticonvulsants, tranquilizers, and anesthetic gases, or caused by medical treatment, such as progressive aluminum encephalopathy in patients undergoing renal dialysis. Some fetal intoxication syndromes can also be considered in this category. A few examples are mentioned here.

Organic Mercury Poisoning. Ingestion of fish caught in the poisoned bay of Minamata led to a neurological disorder that was eventually identified as being caused by organic mercury. Mercury intoxication has also been reported following accidental ingestion of wheat that had been treated with organic mercury compounds to prevent cropping. Neuropathology shows degeneration of the granular layer of the cerebellum and patchy loss of cells in the cerebral cortex,

in particular the calcarine cortex. MR images show the deposition of mercury in cerebellar structures and under the occipital cortex (Fig. 87.5).

Lead Encephalopathy. Children may have a lower tolerance to lead than adults. Acute lead intoxication is associated with convulsions, delirium, meningism, and papilledema. Chronic intoxication is associated with dementia, peripheral neuropathy, anemia, and a variety of visceral features. Neuropathologically the mildest chronic form of lead intoxication is the selective, segmental demyelination of peripheral nerves. In acute cases there may be demyelination and necrosis of central and cerebellar white matter. Neuronal damage is pronounced.

Aluminum Dementia. Aluminum has been indicated as a toxic factor in dialysis dementia. The excessive aluminum was probably derived from the high aluminum concentration in the dialysate and from the phosphate binding gels, which contain aluminum.

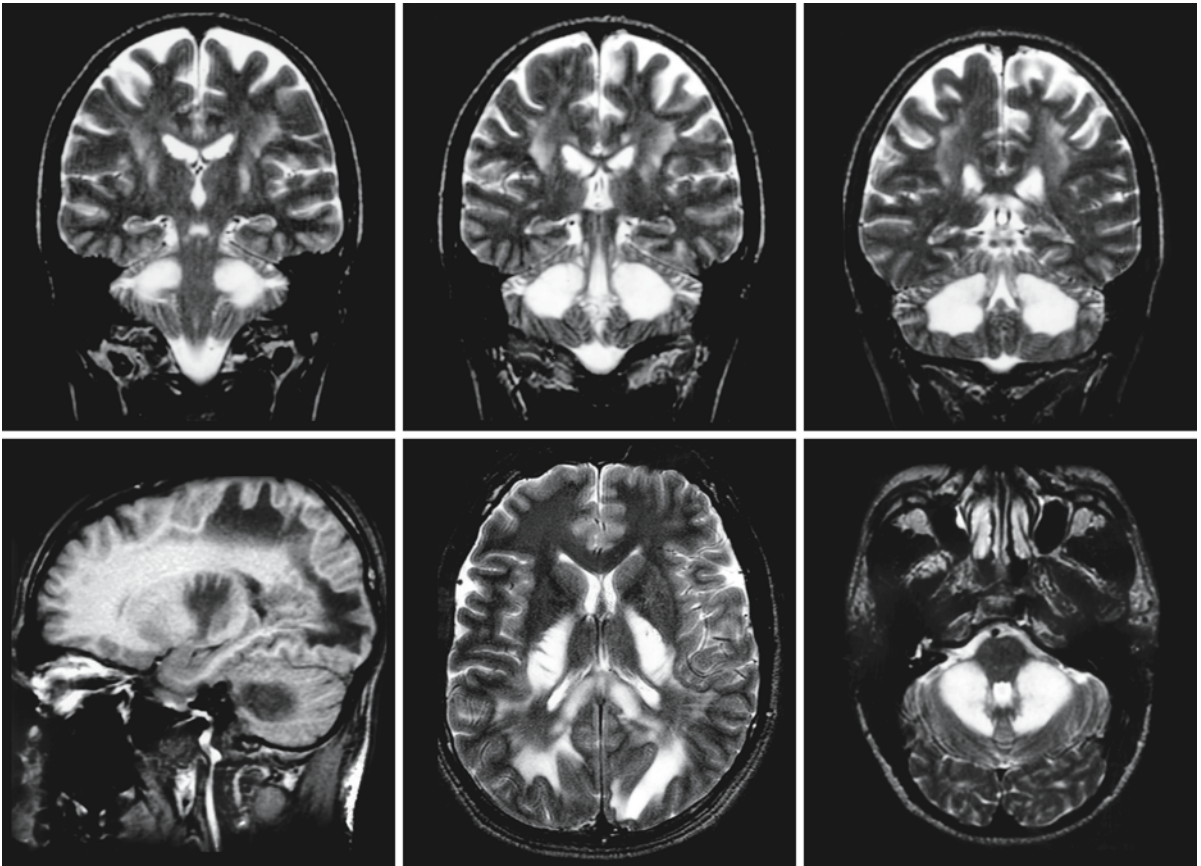


Fig. 87.6. Two men, aged 34 (*first row*) and 26 years (*second row*), with severe neurological disability after sniffing toxic heroin. There are lesions in the parieto-occipital white matter, splenium of the corpus callosum, the posterior limb of the in-

ternal capsule (note the swelling), and the cerebellar white matter. In all patients investigated in Amsterdam, an identical MRI pattern has been observed

Wernicke Encephalopathy. Wernicke encephalopathy results from a deficiency of vitamin B₁ (thiamine), and, as such, is not confined to chronic alcoholics. Because vitamin B₁ is a cofactor of transketolase, thiamine deficiency causes decreased activity of this enzyme. The precise relationship of reduced enzyme activity to damage in the characteristic “topistic area” represented by Wernicke encephalopathy is conjectural. Korsakoff disease is now generally seen as a chronic stage of Wernicke encephalopathy, with consistent atrophy of the mammillary bodies and variable involvement of the dorsomedial nucleus of the thalamus.

Cytostatic Agents. Cytostatics, such as methotrexate and 5-fluorouracil, especially in combination with levamisole, can lead to severe changes in the white matter when they are used to treat extracranial malignancies or intracranial tumors (often in combination with radiotherapy). These reactions will be dealt with in Chap. 88.

Immunosuppressive Agents. In graft-versus-host disease, immunosuppressive agents such as cyclosporine and tacrolimus are used to prevent the repelling of transplanted organs. They may cause what is usually referred to as posterior reversible encephalopathy syndrome. This reaction will be discussed separately in Chap. 92.

Heroin Pyrololite. During the 1980s, it was discovered that a group of chronic heroin addicts in Amsterdam manifested progressive neurological symptoms after sniffing heroin (“chasing the dragon”). On neuropathological examination, a vacuolating myelinopathy was discovered in these cases. MR studies revealed extensive involvement of the white matter of the cerebral hemispheres and the cerebellum and clearly depicted the affected tracts from the parietal cortex to the brain stem (Fig. 87.6). The toxic substance in the heroin has not been identified. One assumes that it must be a lipophilic substance. Identical neurological findings and MRI abnormalities have

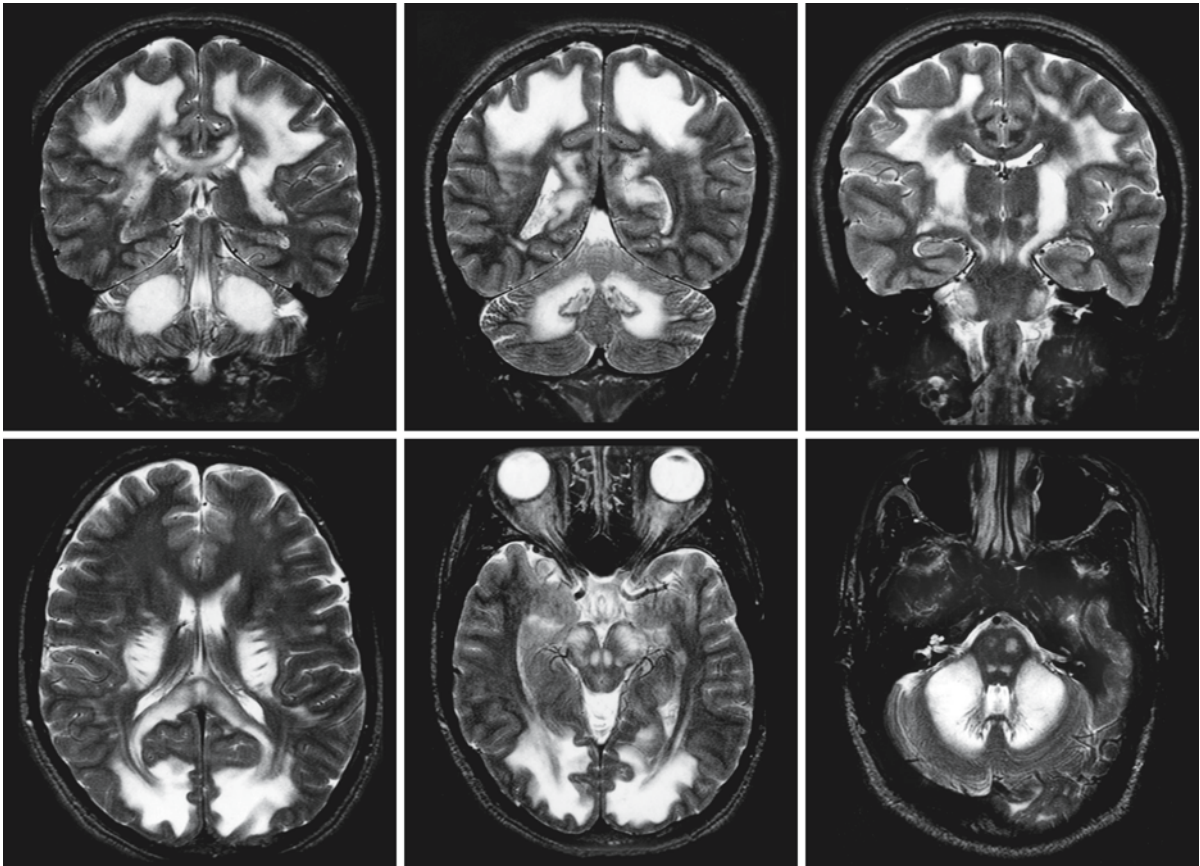


Fig. 87.7. Series of T₂-weighted MR images in transverse and coronal planes of a 22-year-old male cocaine sniffer. The abnormalities are similar to those found in patients sniffing heroin. The swelling of the white matter suggests that a vacuol-

ating myelinopathy also exists in this case. The images beautifully demonstrate all involved structures. Courtesy of Dr. J. Tamraz, Department of Magnetic Resonance and Neuroimaging, Hôtel-Dieu de France, Université Saint-Joseph, Beirut, Lebanon

been found among cocaine addicts (Fig. 87.7). Abuse of cocaine more often leads to vascular complications.

Organic Solvents. Individuals who have been professionally exposed over a long time to the inhalation of organic solvents may develop an organic psychological syndrome with loss of concentration, irritability, emotional instability, and memory disorders. Although in most cases no structural abnormality can be proven by MRI, in a number of cases changes in the white matter, sometimes also the gray matter, varying in degree from mild to severe, may be found in individuals who have been exposed many years to organic solvents or pesticides. In the United States of America a National Exposure Registry has published data on a longitudinal surveillance of populations exposed to low concentrations of specific substances in the environment. The trichloroethylene subregistry contained 4041 individuals, who were divided into four subgroups by types of exposure (chemicals), dura-

tion, and level of exposure. The authors (Burg and Gist 1999) compared the reporting rates for 25 health outcomes across subgroups. Statistically significant increases in reporting rates were seen with, increased maximum trichloroethylene exposure for the outcome stroke, increased cumulative chemical exposure for respiratory allergies, and duration of exposure for hearing impairment. Another registry study among a population of demented individuals concluded that there was no support for the hypothesis that occupational exposure to organic solvents is a cause of dementia (Palmer et al. 1998). More recently, 74 patients were examined who had a long history of exposure to carbon disulfide. They were assessed with respect to neuropsychological performance and MRI abnormalities (Cho et al. 2002). MRI findings revealed a significantly higher number of lacunae in the high exposure group than in a group with lower exposure. Periventricular hyperintensities were most often located in frontal and occipital areas (Fig. 87.8). Neuropsychological differences between those groups

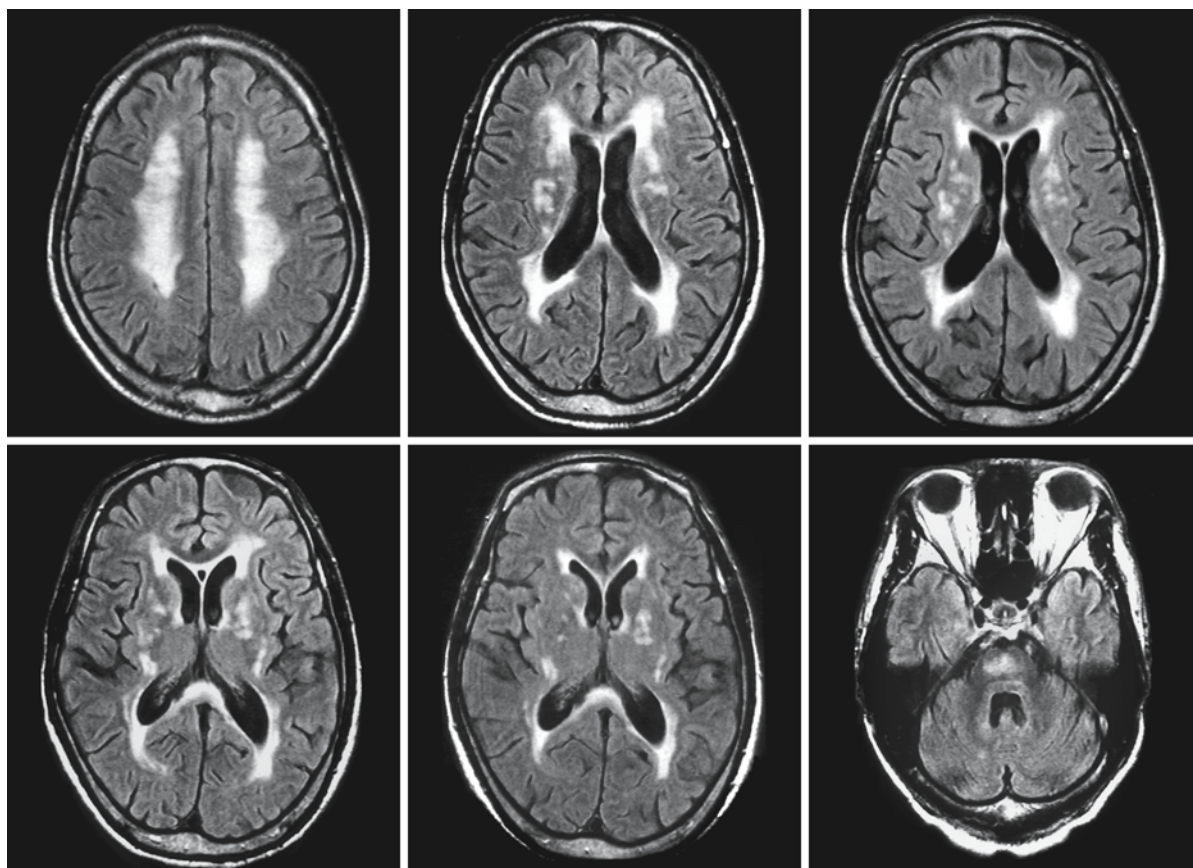


Fig. 87.8. FLAIR series in a patient with carbon disulfide intoxication. The images show a nearly symmetrical hyperintensity of the deep and periventricular white matter and the corpus callosum. There are multiple small basal ganglia lesions, some-

what less symmetrical. The central part of the pons is affected. Courtesy of Dr C.C. Huang, Department of Neurology, Chang Gung Memorial Hospital and University, Taipei, Taiwan

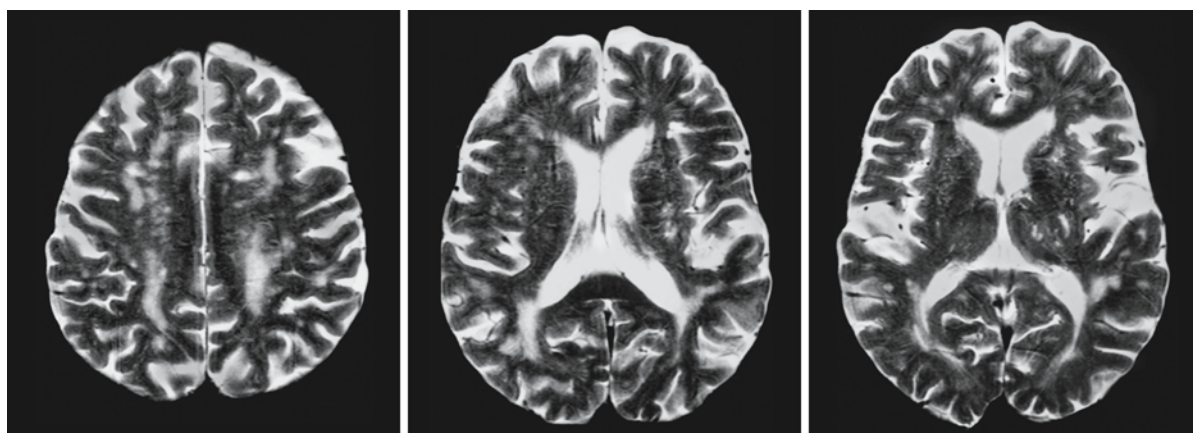


Fig. 87.9. A 68-year-old man with progressive memory loss, who worked in the paint industry for many years and was professionally exposed to organic solvents. The T₂-weighted MR images show lesions scattered through the centrum semio-

vale, both isolated and more confluent. The ventricles and subarachnoid spaces are moderately enlarged, related to cerebral atrophy. There are some isolated lesions in the basal ganglia

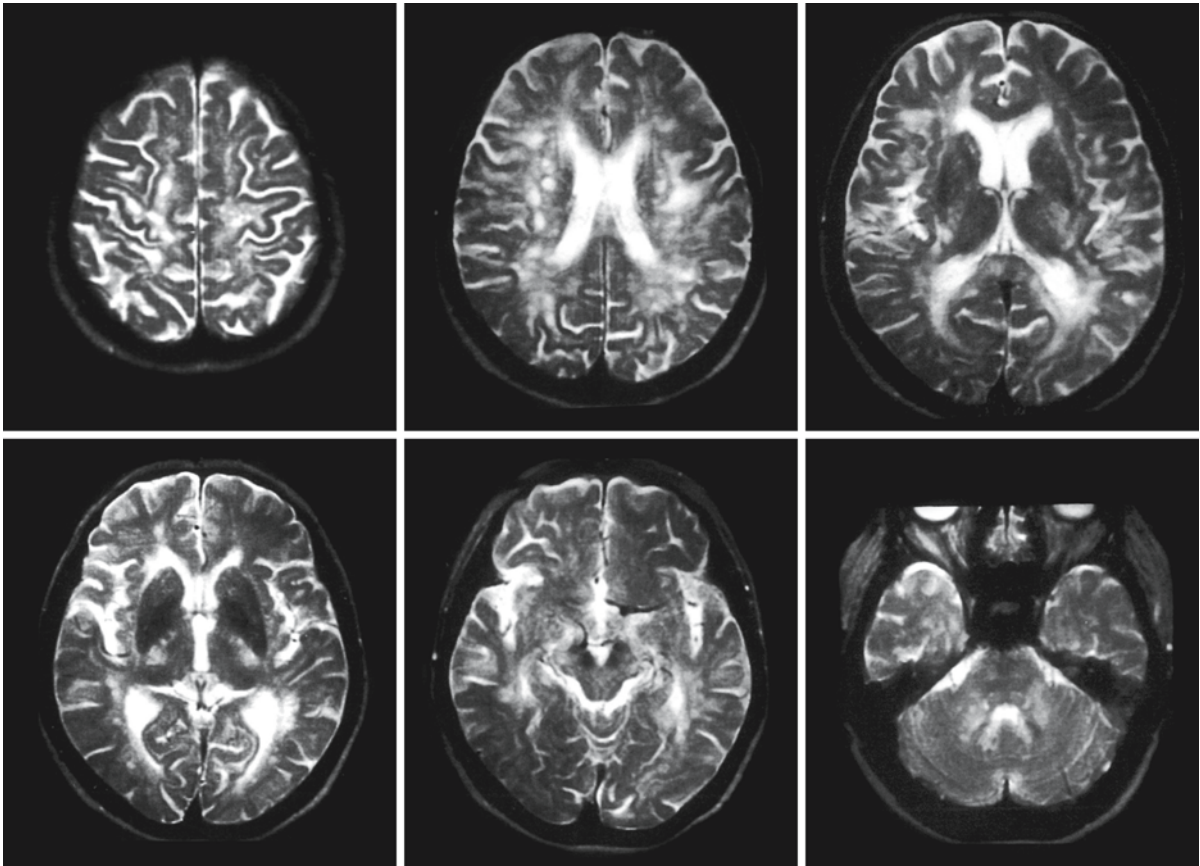


Fig. 87.10. T₂-weighted series of a 64-year-old female patient with progressive subcortical dementia and gait disturbances. This patient had been handling insecticides and pesticides for

over 30 years. There are widespread, focal, in some areas confluent, signal abnormalities in the white matter of the hemispheres and middle cerebellar peduncles

were not significant. In our own experience with MR and EEG studies of 50 persons with long-lasting exposure to organic solvents MR showed only minor white matter abnormalities in two persons. Whether this was related to the exposure to organic solvents remained unclear. On the other hand, we have seen two patients with severe exposure to organic waste products and pesticides for more than 30 years who had severe white matter abnormalities dispersed over the entire brain (Figs. 87.9 and 87.10).

Toluene is one example of a typical lipophilic substance that persists in the myelin for a long time, leading to myelin and gray matter damage. Toluene is a volatile liquid that is used as an industrial solvent. It is inhaled by some individuals as a form of substance abuse. Long-term abuse leads to cognitive deterioration, cerebellar ataxia, tremor, and anosmia. Chronic use of toluene leads to white matter lesions in 46% of the patients, cortical and central atrophy in 26%, and thalamic hypointensity in 20% (Aydin et al. 2002). The white matter changes in 41 patients were focal in 53% and diffuse in 47% (Aydin et al. 2002). White

matter changes started in the deep white matter and progressed to the periphery. Other reports state diminished distinction between gray and white matter.

Another highly lipophilic substance, is fentanyl, a synthetic opioid many times stronger than morphine. It is used in anesthesia and in intensive care units. We observed a patient who had attempted suicide by transdermal application of fentanyl. MRI in this comatose patient showed extensive white matter abnormalities, with ADC characteristics of increased diffusivity (Fig. 87.11). The leukoencephalopathy was most prominent in the parieto-occipital region. In this respect the pattern resembles the pattern seen in posterior reversible encephalopathy syndrome. In this case the abnormalities were not transient; the patient did not survive.

Common to disorders caused by *exogenous-internal toxins* is a focal or generalized process in the body outside the blood-brain barrier that produces a toxin that crosses the blood-brain barrier, enters the brain, and gives rise to encephalopathy. Encephalopathies related to toxins released by bacteria elsewhere in

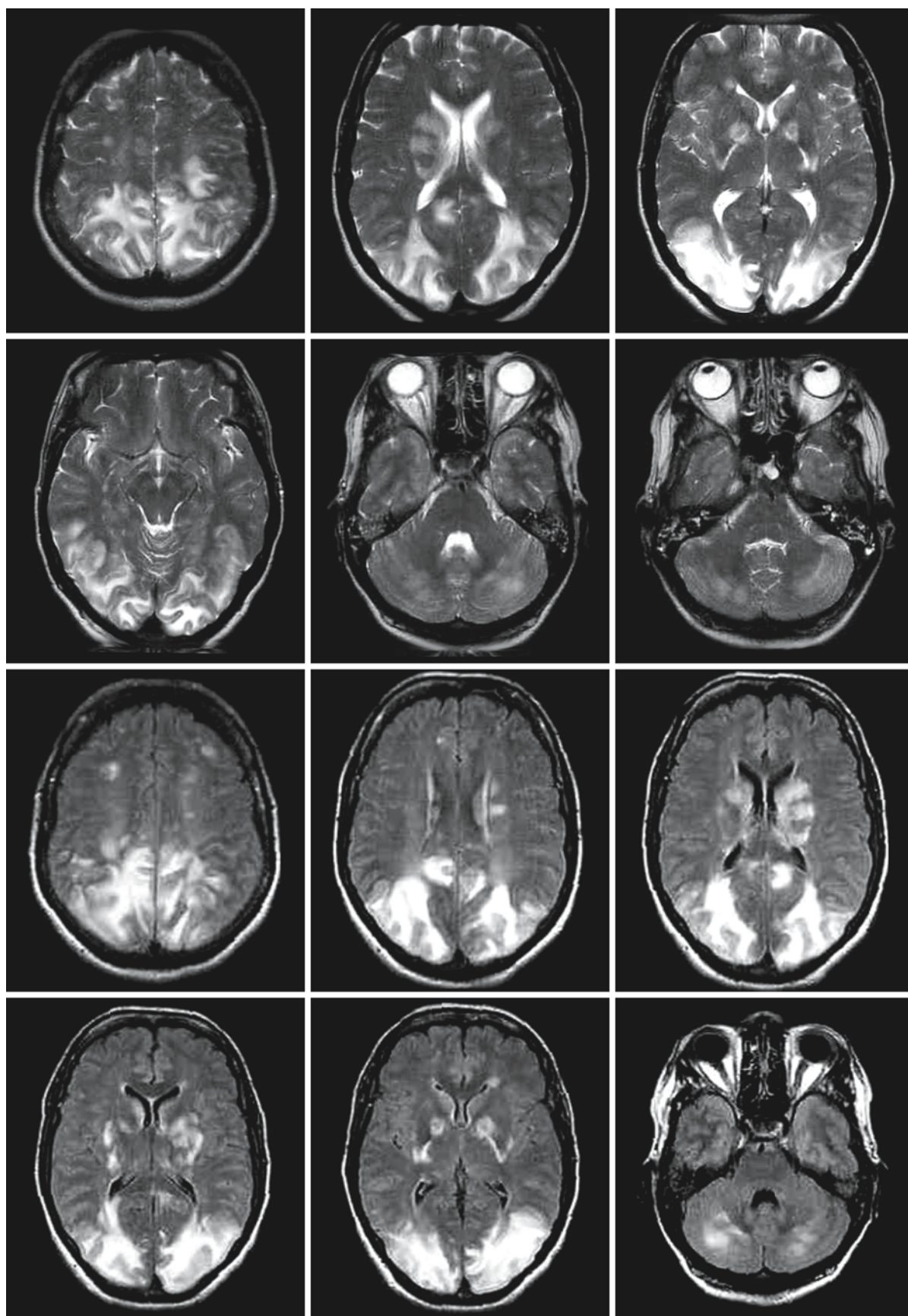


Fig. 87.11.

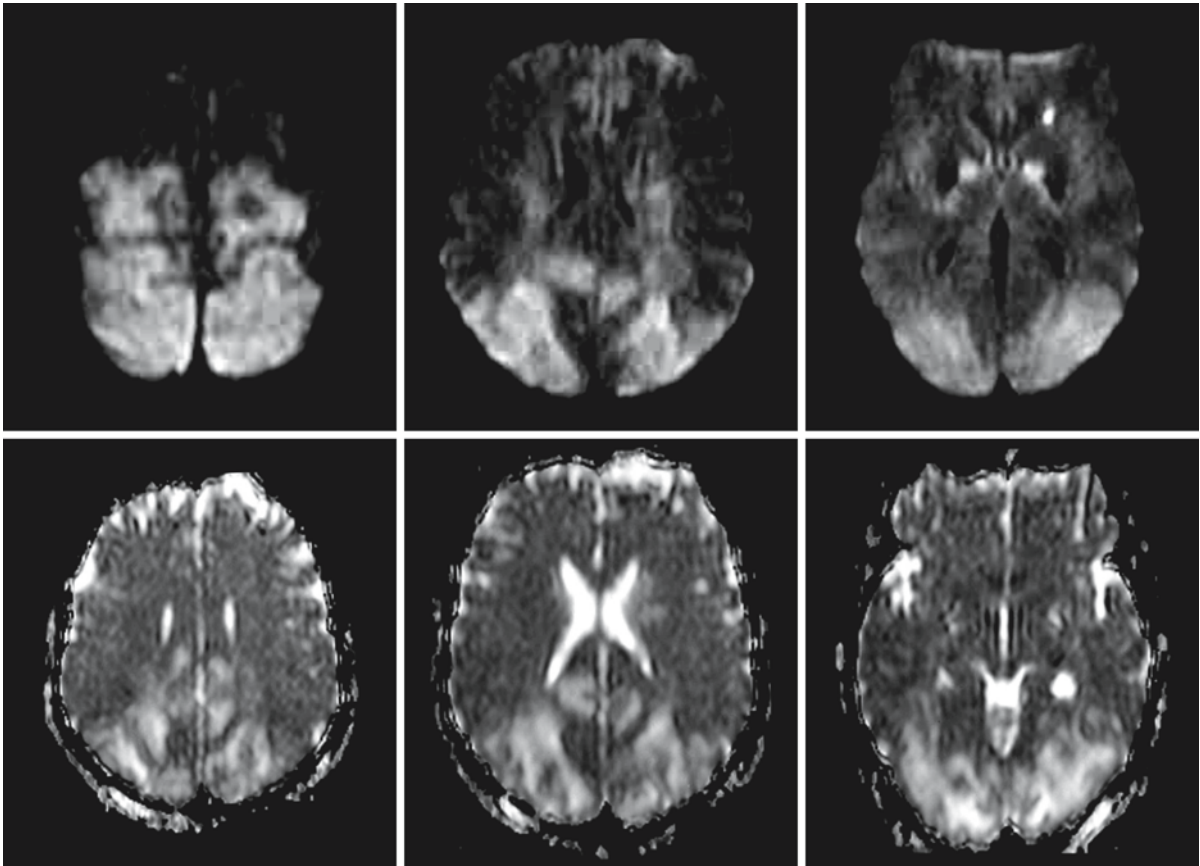


Fig. 87.11. (continued). A 39-year-old nurse committed suicide using fentanyl dermal patches. The T_2 -weighted images (first and second rows) show predominant involvement of the parieto-occipital areas, but also involvement of the basal ganglia (especially the globus pallidus) and the posterior limb of the internal capsule. The FLAIR images (third and fourth rows) more clearly show that there is also cerebellar involvement.

The lesions have a high signal on the Trace diffusion-weighted images (fifth row, $b = 1000$); the ADC values are, however, high (sixth row). This MR pattern is comparable to what is seen in posterior reversible encephalopathy syndrome. Courtesy of Dr. M. Heitbrink and Dr. B. Wiarda, Department of Radiology, Medical Center Alkmaar, The Netherlands

the body, and also paraneoplastic syndromes and parainfectious degeneration can be included in this category. Tumors may contain antigens that lead to the formation of antibodies which cannot distinguish between tumor cells and own-body cells, for example Purkinje cells. Malignant disease anywhere in the body may have a remote effect on the peripheral nerves, the spinal cord, and on the brain, causing peripheral neuropathy, subacute necrotizing myelopathy, and encephalomyeloradiculitis. The encephalomyeloradiculitis group includes two special forms: brain stem encephalitis, and so-called limbic encephalitis in which the changes are restricted to the limbic system (Fig. 87.12). The different manifestations presumably reflect the different antigenic content of these brain structures. It is possible that a more general toxic effect plays an additional role.

Parainfectious encephalopathy has been reported with *Escherichia coli*, *Mycoplasma pneumoniae*, and diphtheria infections. The reaction may be toxic, allergic, or both.

Changes in the ion balance are held responsible for central pontine and extrapontine myelinolysis. Hyponatremia is considered to be an important initial factor in these disorders, subsequently precipitated by (too) fast restoration of the blood sodium concentration. These conditions are discussed in more detail in Chap. 89.

Inborn errors of metabolism may lead to accumulation of toxic substances produced outside the blood-brain barrier and their then crossing the blood-brain barrier, leading to toxic brain damage. Many of the disorders described in the first part of this book may be considered an exogenous-internal TE. Examples are many of the amino acidopathies

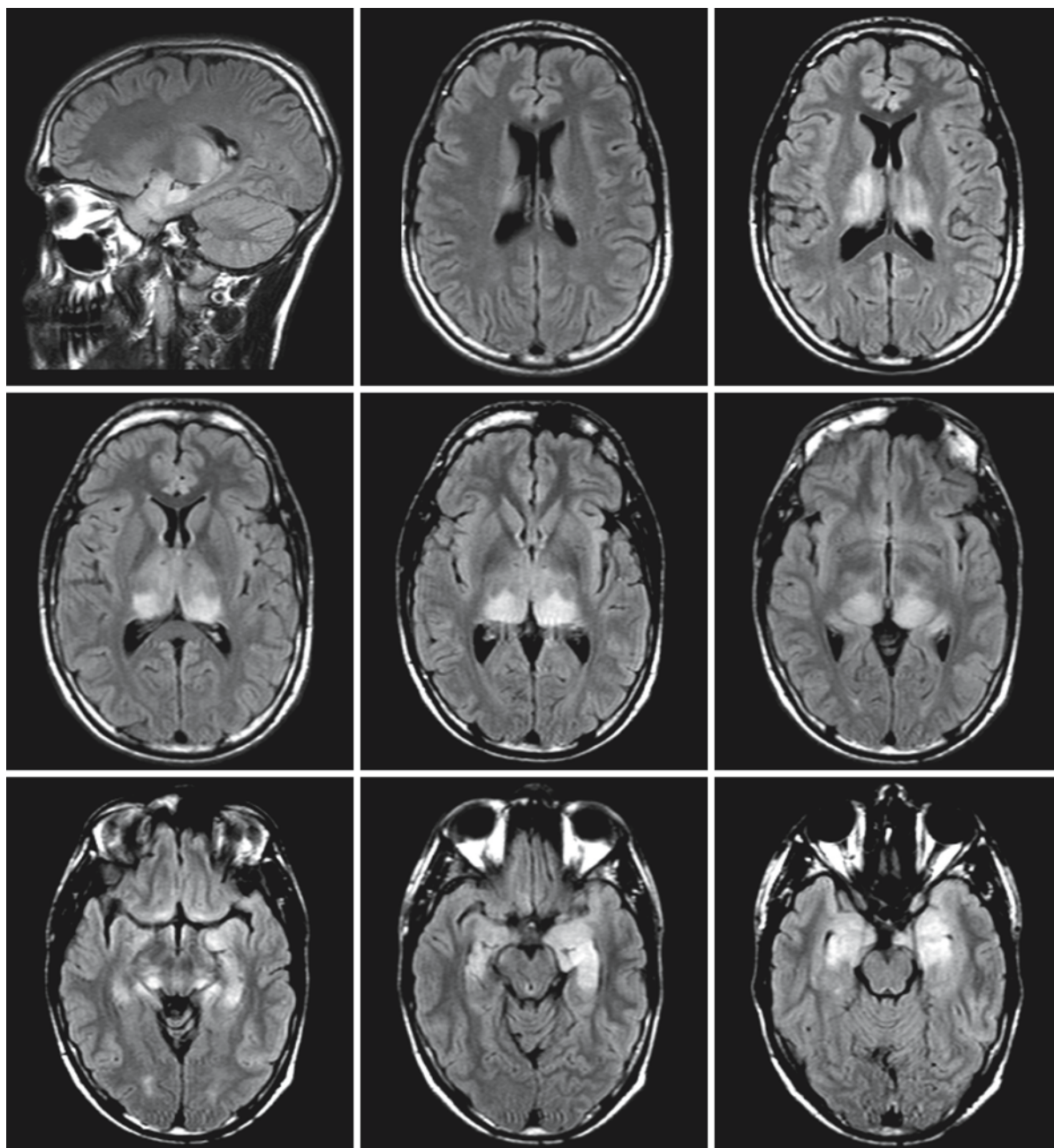


Fig. 87.12. Patient with limbic encephalitis. The images show the typical symmetrical involvement of the medial parts of both temporal lobes, including the hippocampus, involve-

ment of the thalamus, in particular the pulvinar. In this case there are also symmetrical lesions in the posterolateral parts of the midbrain

and organic acidopathies, including the urea cycle disorders. In Wilson disease, the encephalopathy is related to excessive deposition of copper in the brain, especially in the globus pallidus.

Hormonal abnormalities in infants may disturb the normal process of myelination. Thyroid deficiency in the neonatal period causes disturbed development of the CNS with a decreased formation of

myelin. Hypocortisolism, hypercortisolism, and a deficiency of growth hormone also result in hypomyelination in infants.

Failure of internal organs may lead to exogenous-internal TEs. Well-known examples are renal failure and hepatic failure. Hepatocerebral syndromes manifest by cerebral atrophy, by changes in signal intensity in the basal ganglia, and by T₁-shortening of the

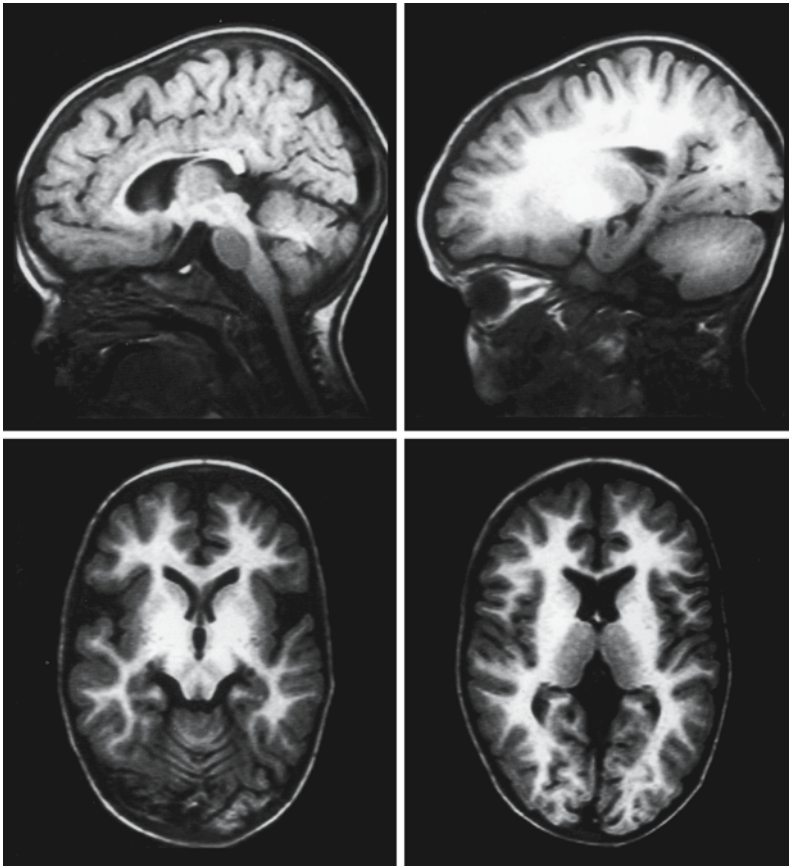


Fig. 87.13. T₁-weighted (SE) sagittal and transverse (IR) images in 3-year-old boy with hepatic failure and hepatic encephalopathy. The images show the typical T₁ shortening in the basal ganglia but also of the white matter. Due to T₁ shortening the basal ganglia can hardly be distinguished from the surrounding white matter. The pons shows T₁ shortening in the posterior part, leading to a pattern on the T₁-weighted sagittal image as seen in neonates

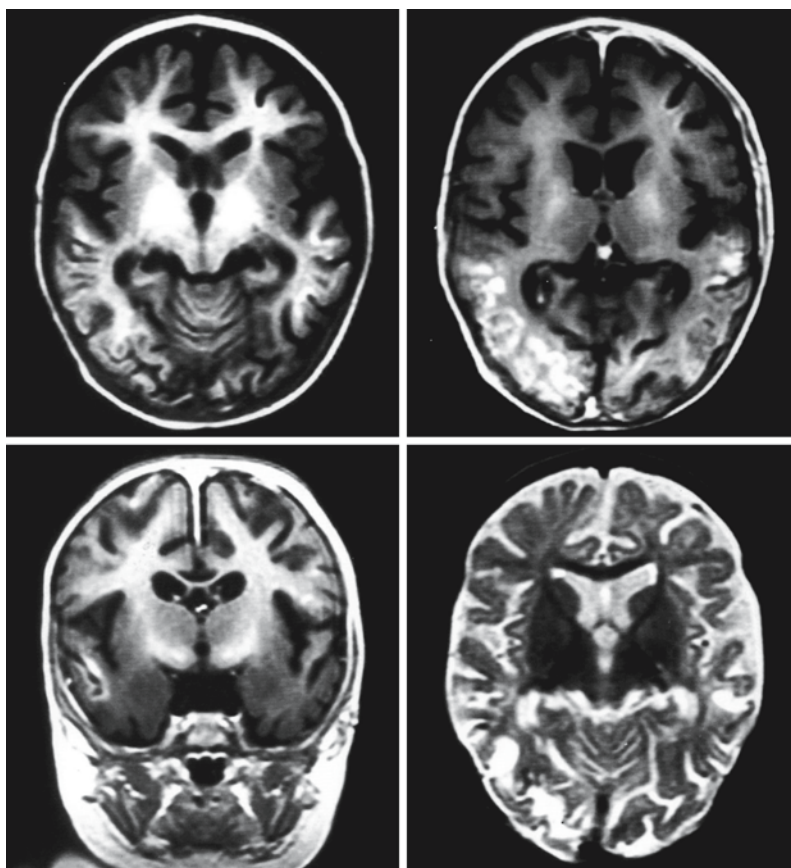
white matter (particularly in infants and children). ¹H-MR spectroscopy shows an increase in glutamine and a depletion of *myo*-inositol. Ammonia plays a key role in hepatic encephalopathy. It appears to cause neurotoxicity by interacting with the glutamate/glutamine/GABA balance. Apart from its other roles in metabolism, glutamate is the most important excitatory neurotransmitter. γ -Aminobutyric acid (GABA), formed by decarboxylation from glutamate, is the most important inhibitory neurotransmitter. In the presynaptic neuron glutamate is formed from glutamine by glutaminase. After neurotransmission glutamate is taken up by astrocytes where it is processed by glutamine synthetase into glutamine. Glutamine is transported to the presynaptic neuron where glutaminase catalyzes the formation of glutamate available for neurotransmission. Hyperammonemia has a great impact on this cycle by stimulating glutamine synthesis via glutamine synthetase, by possible inhibition of glutaminase, and by inhibition of glutamate reuptake by the astrocyte. However, the relation between the neurotransmitters' changes and the T₁ shortening as seen on MR is not clear. Other explanations for the T₁ shortening of the basal ganglia have been suggested, such as accumulation of manganese or of lipid particles. In MR images, T₁ shortening in the basal

ganglia can make the basal ganglia indistinguishable from white matter on T₁-weighted images (Fig. 87.13). At the same time, there is T₁ shortening in the white matter, typically sparing the pons. In older patients, this spread of T₁ shortening over the white matter is less clear. The T₁ shortening of gray and white matter may be observed with a number of toxic-metabolic conditions, not just hepatic encephalopathy. For instance, we have seen this phenomenon in a child with hemorrhagic shock and encephalopathy syndrome (Fig. 87.14). It has also been reported in patients who received parenteral nutrition over a long period.

GABA is considered to be an inhibitory neurotransmitter and the counterpart of glutamate. It has been used in anesthesia for good reasons, but has obtained a bad reputation as a "rape" drug. We have observed cortical infarctions and neurological deficits after the use of this drug, probably at excessive dosage (Fig. 87.15).

The *endogenous forms of TE* are the smallest group. A number of inborn errors of metabolism should be included here, because their effects are mediated by a toxic substance produced locally. In particular, this is the case in lysosomal storage disorders, such as Krabbe disease or globoid cell leukodystro-

Fig. 87.14. A 7-month-old girl with hemorrhagic shock and encephalopathy syndrome. Hemorrhagic laminar cortical lesions are seen in the occipital lobe. There is also a striking T_1 shortening in the globus pallidus on the T_1 -weighted images. The T_2 -weighted transverse image (*second row, right*) shows generalized atrophy, presence of lesions in the occipital area, but no clear signal changes in the basal ganglia



phy. The primary defect is galactocerebroside β -galactosidase deficiency. This enzyme has two functions: it degrades cerebroside into galactose and ceramide and it hydrolyzes psychosine (galactosyl sphingosine). Psychosine is a toxic metabolite that is essentially nonexistent in normal brain. Presence of elevated psychosine in Krabbe disease causes early, very rapid, almost complete death of the oligodendroglia with extensive loss of myelin sheaths maintained by these cells. In addition, inability to degrade cerebroside leads to an abnormally high concentration of this substance within the myelin membrane, eventually resulting in myelin instability and breakdown. In Krabbe disease, the disturbance of both functions of galactocerebroside β -galactosidase contributes to the myelin loss. In metachromatic leukodystrophy it is the local storage of sulfatide that causes myelin damage and loss. Other inborn errors of metabolism, glutaric aciduria type 1 and methylmalonic acidemia, produce compounds with a direct toxic effect on the basal ganglia (see also Chap. 3).

The toxic interactions interfering with fetal development can be considered as exogenous-external intoxication, reaching the unborn child via the mother. The fetal syndromes are unique, because the effect of the toxin depends upon the stage of development the

child has reached, as well as upon the nature of the toxin, its concentration, and the duration of the exposure. Toxic or teratogenic substances have a great impact on the developing fetus. The effects are often widespread and involve multiple parts of the body or the whole body in addition to the brain. The gamut of possible dysgenesis is extensive and ranges from fatal malformation with early spontaneous abortion to mild alteration in morphology and function. The sources of the toxins include:

1. Medical treatment. Syndromes can result from the use of established drugs prescribed to the mother, but taken during pregnancy. Most such cases are accidental. A few arise when drugs are given knowingly in desperate cases. Antiepileptic drugs are known to cause developmental damage, resulting, for example, in the fetal hydantoin syndrome and the fetal valproate syndrome.
2. Alcohol and drug abuse. An important cause of fetal dysgenesis is the use of drugs or alcohol during pregnancy. The fetal alcohol syndrome has been reported extensively in the literature. These children are growth retarded, have short palpebral fissures, a low nasal bridge, epicanthus, a long convex upper lip, and mental retardation. The numerous CNS anomalies of the fetal alcohol syndrome in-

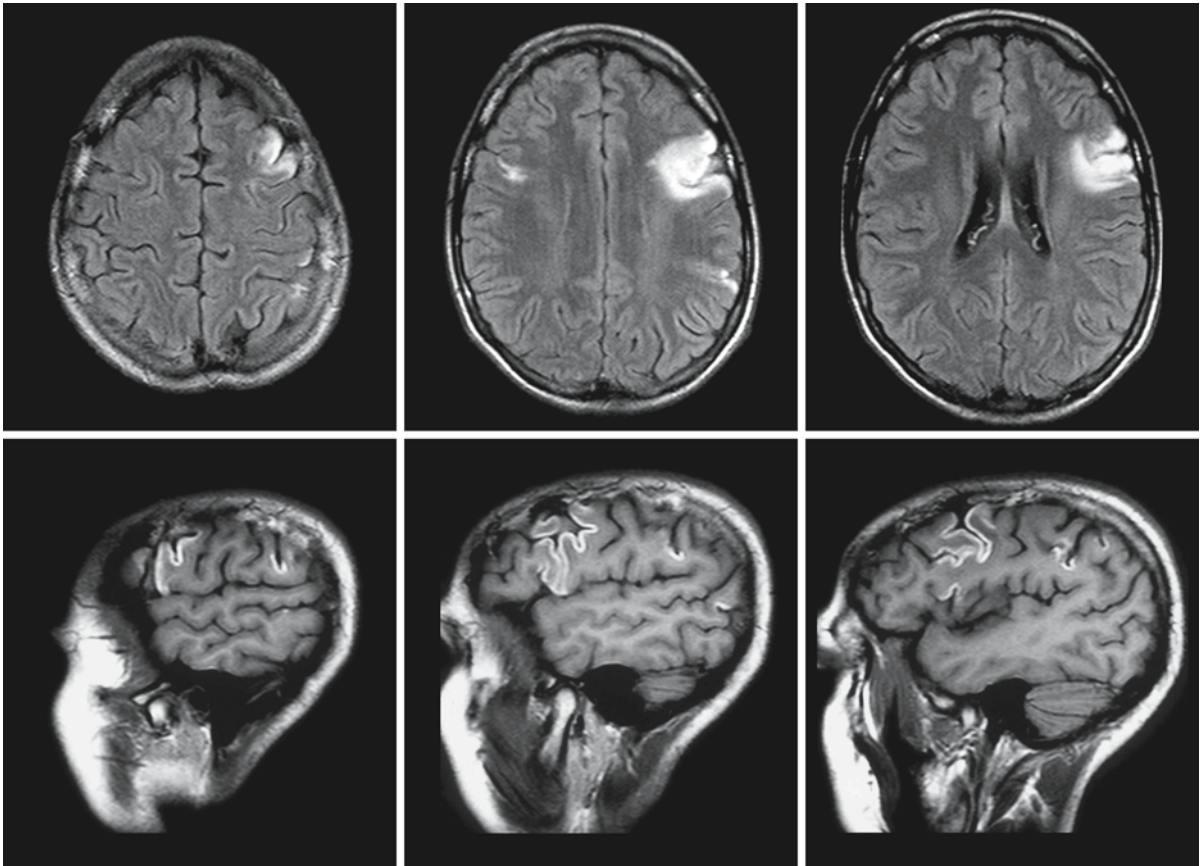


Fig. 87.15. Transverse FLAIR (*first row*) and sagittal contrast enhanced T₁-weighted images (*second row*) of a 17-year-old girl who had been administered GABA and subsequently

raped. GABA was used to subdue the victim. The images show multiple cortical infarctions

clude: derangement of neuronal and glial migration, microcephaly, hydrocephaly, porencephaly, agenesis of the corpus callosum, meningocele, and Dandy–Walker malformation.

3. Metabolic disorders of the mother. Fetal development may suffer if the mother has a metabolic disorder. Diabetes mellitus may be one causative factor in the caudal regression syndrome, a complex abnormality of the caudal end of the embryo with

anal atresia, sacral dysgenesis or agenesis, high position of the conus medullaris, and diverse urological, neurological, and orthopedic disorders. Microcephaly can be caused by maternal phenylketonuria.

4. Teratogenic chemical substances. Compounds with teratogenic action may be encountered in the direct environment (pollution, professional contact with chemicals).

Iatrogenic Toxic Encephalopathies

In the last decades more aggressive treatment methods have been used to control otherwise fatal diseases. This kind of treatment has a considerable impact on the temporary improvement, cure, and survival rate of patients with life-threatening conditions. It has been known for a long time that radiation therapy of the brain, either for prophylaxis as in acute lymphoblastic leukemia (ALL) of childhood, or for therapeutic reasons as in tumors of the brain, can lead to radiation damage of the brain, either as radiation necrosis or leukoencephalopathy, focal or diffuse (see Chap. 102). When radiation therapy is used in combination with intravenous or intrathecal methotrexate, the lesions can be even more pronounced. The introduction of bone marrow and organ transplantation in the treatment of a number of disorders has increased the numbers both of reversible and of permanent lesions in the central and/or peripheral nervous system related to the medical treatment before and after the intervention. This means that radiologists are increasingly being confronted with lesions of the brain that are therapy-related, either during the period of intervention, during the months following it, or even after an intervention that took place many years previously

The list of compounds that can be responsible for brain lesions is long, and for many of them the nature of the damage they may cause is known. Table 88.1 shows where the pharmaceutical compound has its place in present treatment plans. Notice that for some interventions an aggressive pretreatment is necessary. This pretreatment may cause lesions of the brain, but it has also been shown that the choice of pretreatment medication can influence the later outcome of drugs used after the intervention.

In this chapter we will discuss the side effects of drugs used in modern therapeutic strategies. Fortunately most of these side effects are reversible or, despite their visibility on MRI, do not lead to permanent major neurological dysfunction. An early clinical and radiological diagnosis is important. The therapeutic regimen should be modified or aborted and, if necessary and possible, replaced by a therapy with similar effect. This will in most cases lead to disappearance of the clinical symptoms and MR manifestations, but not in all.

The reported reactions to the drugs cited in the Table 88.1 may be divided in two groups of abnormalities:

88.1 Multifocal Inflammatory Leukoencephalopathy

In the patients with multifocal inflammatory leukoencephalopathy (MIL) the lesions may appear multiple sclerosis-like (Fig. 88.1). There are multiple lesions in the centrum semiovale, some with the appearance of Dawson's fingers. Many lesions may enhance after contrast injection. The enhancement may be ring-like. In other cases the lesions have the appearance of progressive multifocal leukoencephalopathy, with larger confluent lesions extending into the arcuate fibers. Sometimes the multiple enhancing lesions are taken for cerebral metastases and brain biopsy may be performed. The latter is also prompted by the clinical presentation of a multifocal neurological syndrome with subacute confusion, ataxia, dysarthria, diplopia, seizures, and other neurological signs. Neuropathology of MIL shows marked

Table 88.1. Schematic overview of the most common drugs used before and after the central intervention. The list of drugs is incomplete

Pretreatment	Treatment	Post-treatment
Immunosuppression	Radiotherapy	Anti-GVHD
Chemotherapy	Bone marrow transplant	Cyclosporine
Cyclophosphamide	Organ transplant	Tacrolimus (FK506)
Doxorubicin	Cytostatics	Corticosteroids
Vincristine	Chemotherapy	
Prednisone	5-Fluorouracil	
L-Asparaginase	Levamisole	
Cytosine arabinoside	Pegaspargase	
Cisplatin	Progenitor stem cell support	
BCNU		

GVHD, graft-versus-host disease; BCNU, 1,3-bis-(2-chloroethyl)-1-nitrosurea

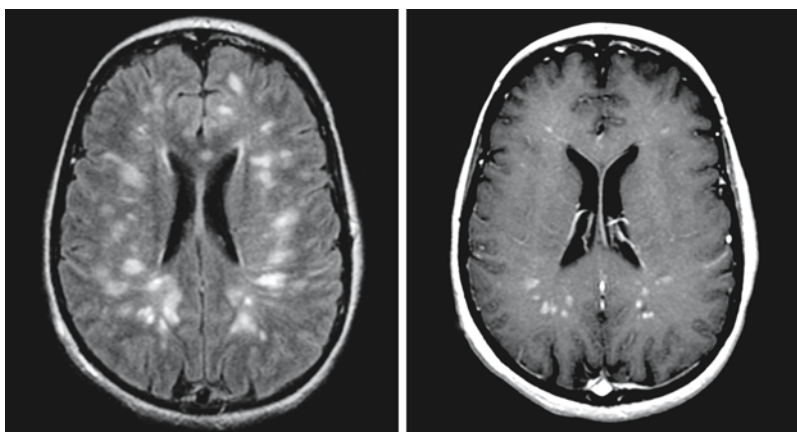


Fig. 88.1. Multifocal inflammatory leukoencephalopathy in a 57-year-old woman during adjuvant therapy with levamisole for malignant melanoma. Over a period of 3 weeks the patient became progressively confused and ataxic. The proton density image (*left*) shows multifocal white matter lesions, which enhance after contrast (contrast-enhanced T₁-weighted im-

age on the *right*). After discontinuation of levamisole and under treatment with steroids, the clinical picture improved dramatically. The MRI improved too. From Kimmel et al. (1995), with permission, and courtesy of Dr. E.F.M. Wijdicks, Department of Neurology, Mayo Clinic, Rochester Minnesota, USA

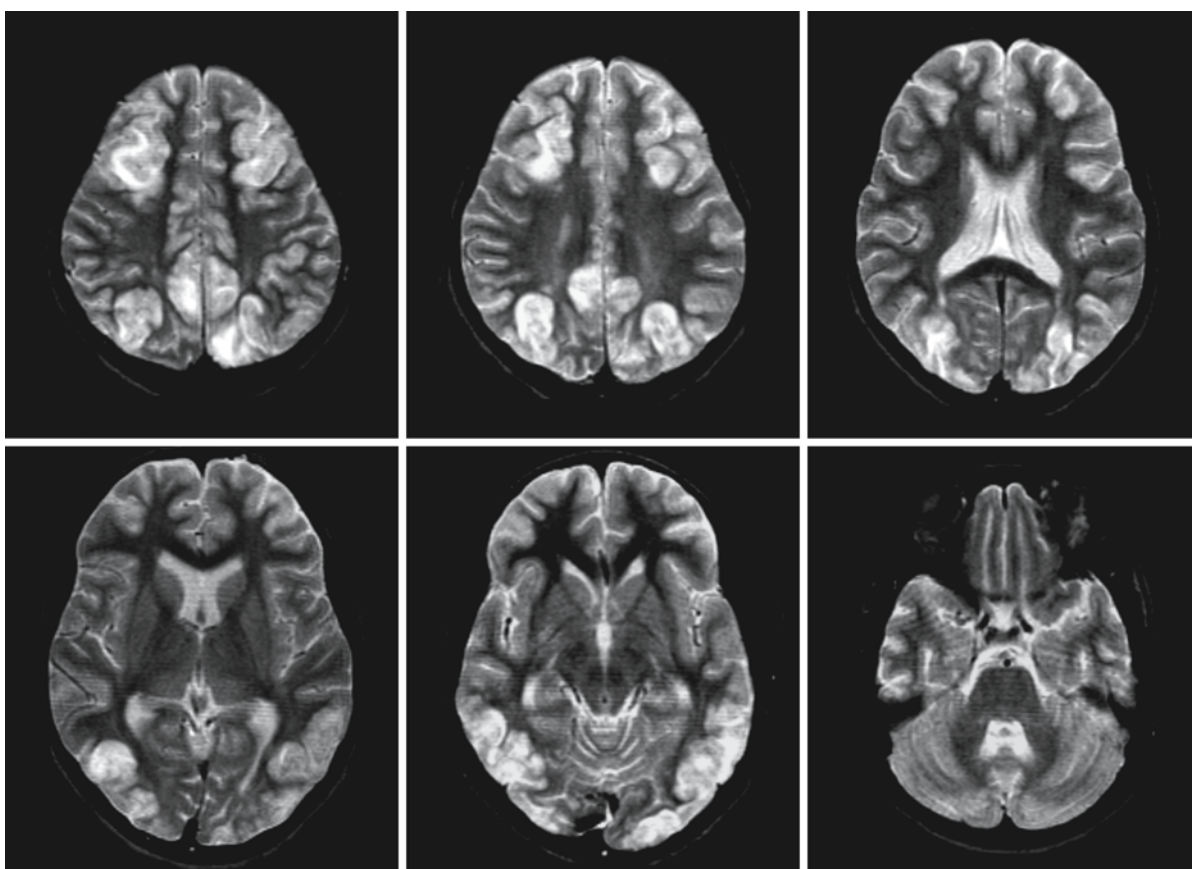


Fig. 88.2. The T₂-weighted images show the classical pattern of the posterior reversible encephalopathy syndrome with involvement of the border zones between the middle and pos-

terior cerebral artery and the middle and anterior cerebral artery

focal cellularity of the white matter, with mononuclear cells scattered throughout the white matter and around the blood vessels. The mononuclear cells are mainly macrophages. Knowledge of the drugs the patient is taking will, of course, lead to the correct diagnosis and treatment. MIL is mostly seen in patients with colon cancer treated with a combination of 5-fluorouracil (5-FU) and levamisole, the latter probably playing the dominant role and 5-fluorouracil acting as potentiator of the immunostimulatory actions of levamisole (Fig. 88.1). A patient has been reported who developed MIL after treatment with 5-fluorouracil alone. This patient, however, had a deficiency of dihydropyrimidine dehydrogenase, an enzyme necessary for 5-fluorouracil catabolism. MIL has also been described in patients treated with 5-fluorouracil derivatives, such as tegafur [1-(2-tetrahydrofuryl)-5-fluoro-uracil] and carmofur (1-hexylcarbamoyl-5-fluoro-uracil). After discontinuing the therapy the encephalopathy usually still progresses for 1 or 2 months, and then gradually clinical and radiological improvement occurs, although often incomplete.

88.2 Posterior Reversible Encephalopathy Syndrome

Drugs used in the prevention of graft-versus-host disease (GVHD) may lead to a reversible encephalopathy syndrome, posterior reversible encephalopathy syndrome (PRES), that bears resemblance to what is seen in acute hypertensive encephalopathy (Figs. 88.2–88.4; see also Chap. 92). In fact, the reaction may be mediated by hypertension, but there are exceptions. Clinically the presentation of the syndrome consists of altered mental status, headaches, seizures, and cerebral blindness. Drugs most often used in GVHD are cyclosporine and tacrolimus. Cyclosporine is of great importance in organ and bone marrow transplantation. The activity of cyclosporine is T-cell-mediated and inhibits calcineurin, which plays a role in calcium-mediated cell death. Cyclosporine is also used in autoimmune disorders, insulin-dependent diabetes mellitus, inflammatory bowel disease, chronic asthma, rheumatoid arthritis, aplastic anemia, and psoriasis. Tacrolimus (FK 506) suppresses both the cell-mediated and humoral immune responses by selectively inhibiting the expression of T lymphocytes of a subset of early-phase activation genes, including interleukin (IL)-2, IL-3, IL-4, interferon- γ , tumor necrosis factor, and granulocyte colony-stimulating factor. Tacrolimus binds, as cyclosporine, to specific intracellular protein ligands, which play a role in maintaining the stability of intracellular structures. Tacrolimus and cyclosporine inhibit the activity of calcineurin, but it is unclear how this relates to the development of leukoencephalopathy. The PRES reac-

tion is only one of the possible neurological side effects of these drugs, and effects on other organs are also known. In PRES there is, as in hypertensive encephalopathy, preferential involvement of the occipital lobes, but other locations – the frontal lobes, border zones, mesencephalon, and pons and cerebellum – have also been reported. The preference for areas in the vertebrobasilar arterial territory is considered to be due to the lack of sympathetic–parasympathetic fibers around these vessels, with poorer autoregulation as a result. There are many other suggestions for how to explain the selective damage: for example, local endothelial damage with the release of vasoactive peptides leading to labile blood pressure and vasospasm, and thrombotic microangiopathy leading to microvascular damage. None of these theories is completely satisfactory. In some cases only the subcortical white matter is involved, the gray matter being spared. In other cases the cortex is also involved. There is evidence for a relation between the conditioning regimens used before allogeneic bone marrow transplant and the type of lesions observed under post-treatment medication. Patients under post-treatment medication who were pretreated with cyclophosphamide and a chemotherapeutic agent, such as busulfan or thiotepe, develop cortical abnormalities with various degrees of subcortical white matter involvement. Nontransplant and transplant patients treated with cyclophosphamide and total body irradiation have lesions in the subcortical and deep white matter, without cortical involvement. This exemplifies how the final result is the last stage of a complex process. Cyclosporine-related toxicity is more often seen in liver transplantation than in cardiac or renal transplantation. The elimination of cyclosporine is through hepatic metabolism via the P-450 cytochrome oxidase system, and the concentration of biologically active cyclosporine depends on the blood cholesterol level. For this reason, cyclosporine toxicity occurs especially in the period shortly after liver transplantation, when the new liver has not regained its full functional capability. It is also clear that the pre-existing condition of the patient, which necessitated the liver transplant and may have included a hepatocerebral syndrome, alcoholic liver cirrhosis, and a severe degree of alcohol-related neurological disease, may obscure the symptoms of cyclosporine or tacrolimus toxicity. In these potentially reversible toxic disorders diffusion-weighted images and ADC maps are important. They help to differentiate between cytotoxic edema and vasculolating myelinopathy on one hand, and vasogenic edema on the other. As a rule, increased diffusivity is seen in reversible conditions and is helpful in the initial diagnosis, whereas decreased diffusivity usually predicts a poorer prognosis.

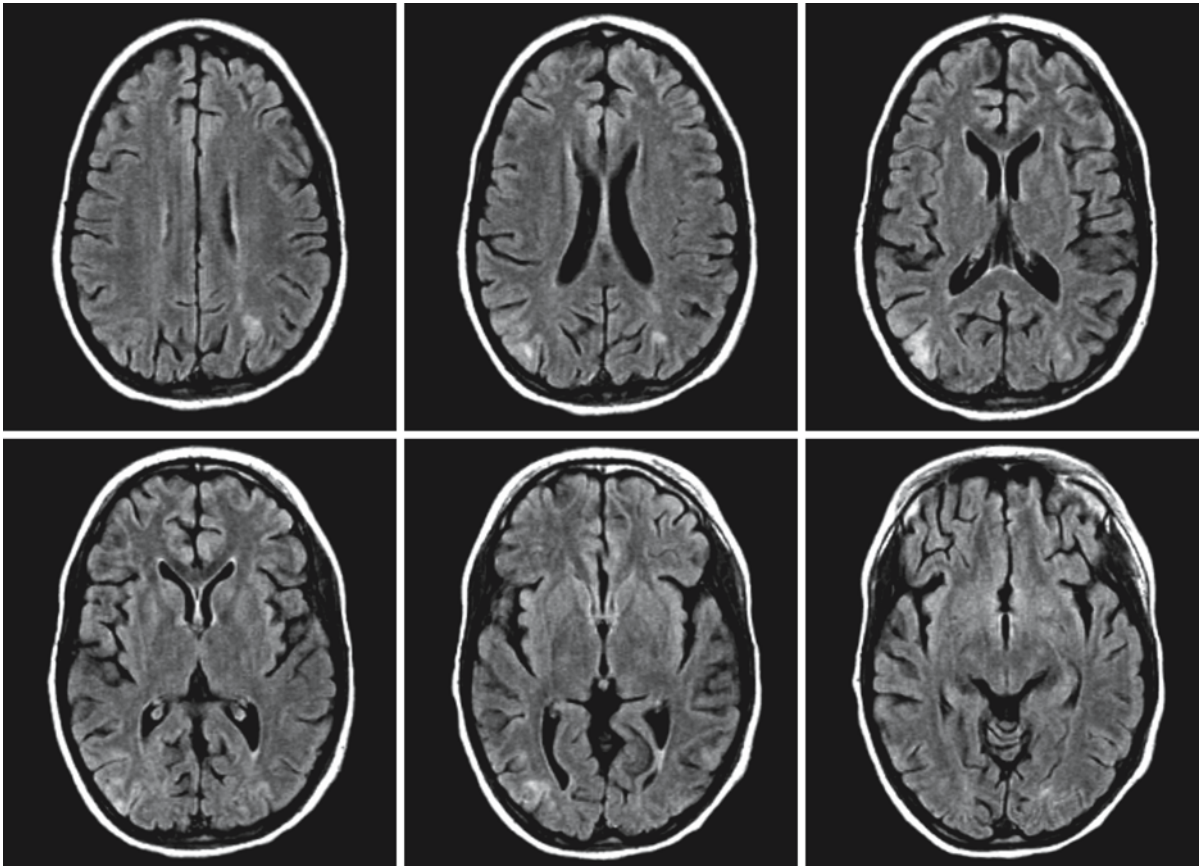


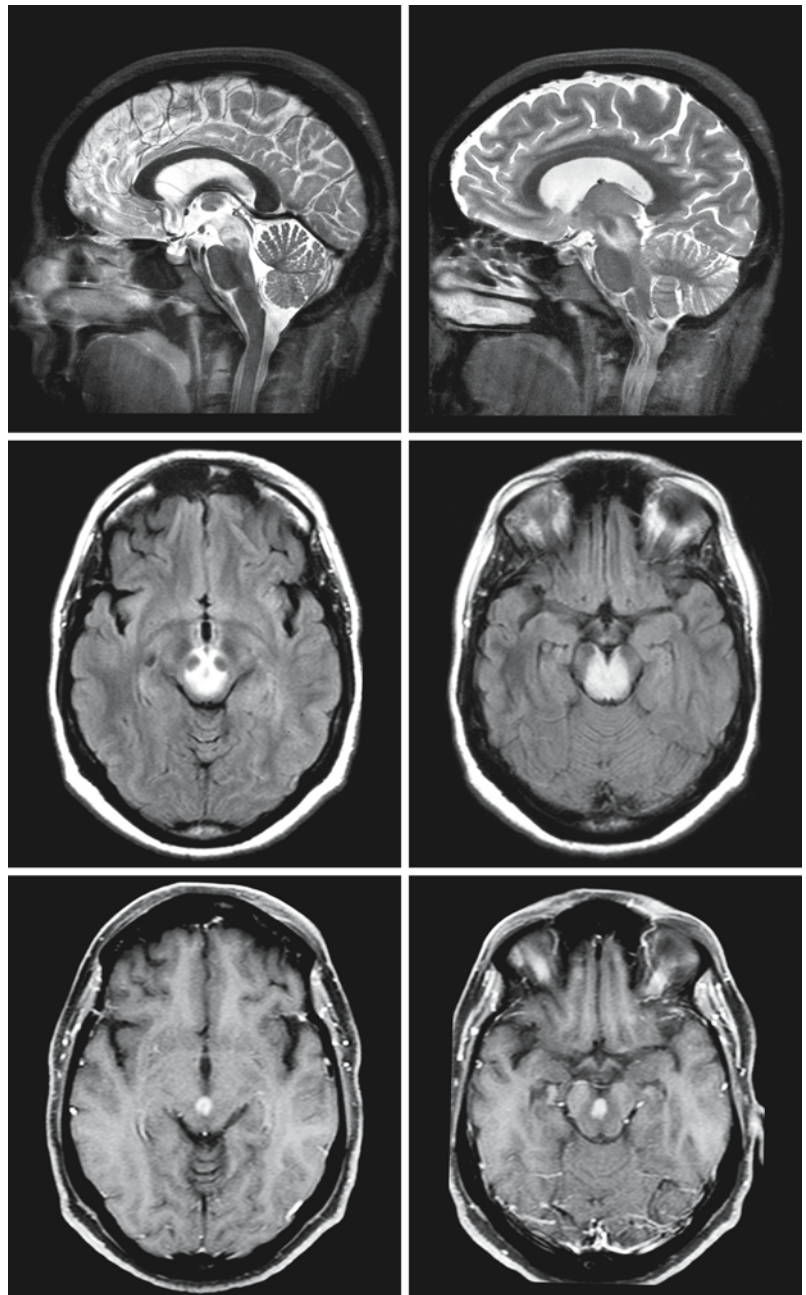
Fig. 88.3. Images of a 14-year-old girl with Henoch-Schönlein purpura treated with cyclosporine. T₂-weighted images did not show abnormalities, despite neurological symptoms.

FLAIR images show some minor lesions in the typical spots in the posterior parts of the hemispheres

In the last years it has become clear that toxic effects may appear a long time, even many years, after the intervention, and the link between the intervention and the brain abnormalities may not be obvious. We have just started to learn that even many years

after bone marrow transplant, which involves the use of total body irradiation and immunosuppressive and chemotherapy, severe, fatal leukoencephalopathy may occur.

Fig. 88.4. A 45-year-old woman underwent lung transplantation and treatment with cyclosporine to prevent graft-versus-host disease. The sagittal T₂-weighted images (*first row*) show a lesion selectively located in the mesencephalon and upper pons. The FLAIR images (*second row*) show this lesion even more clearly. The contrast-enhanced T₁-weighted images (*third row*) demonstrate that the core of the lesion enhances. After the medication was changed, the lesion disappeared within 2 weeks



Central Pontine and Extrapontine Myelinolysis

89.1 Clinical Features and Laboratory Findings

Central pontine myelinolysis (CPM) is a demyelinating disorder affecting mainly the central part of the pons. In some cases, CPM is accompanied by extrapontine myelinolysis (EPM, together CPM/EPM). CPM/EPM is not a primary disease but develops against a background of other, usually severe conditions, apparently as a complication of the main disease. It occurs most often in alcoholics but has also been reported in association with diabetic ketoacidosis, psychogenic excessive water drinking, inappropriate antidiuretic hormone secretion, malnutrition, and chronic debilitating diseases. It is probable that the underlying cause of myelinolysis in all these disorders is a derangement of serum sodium concentration, particularly a rapid correction of hyponatremia and rapid changes in osmotic conditions.

Most of the patients are severely ill as a result of the primary disorder. It takes a period of a few days for patients to develop the clinical symptoms caused by CPM/EPM. Mental confusion is present in many but not all cases. Sometimes patients suddenly lapse into coma for no apparent reason. No particular type of mental change is specific for CPM and EPM, as there are a variety of associated clinical conditions, some of which have their own mental counterparts, such as Wernicke encephalopathy, delirium tremens and various metabolic encephalopathies. Frequently a bulbar or pseudobulbar syndrome is present, manifesting itself in dysarthria or anarthria, dysphagia, and sometimes weakness of the neck muscles. Involvement of the facial nerve is uncommon; when present, it is usually of the central type and part of a hemispheric syndrome. Occasionally a limitation of conjugate movement of the eyes is found. Oculomotor or abducens nerve dysfunction is rarely observed. Pupillary disturbances may be present. The weakness of the limbs is often severe, resulting in tetraparesis or tetraplegia. The usual type of motor weakness is flaccid with hyporeflexia. Extensor plantar reflexes and abnormal bulbar reflexes are often present. Because of the weakness the testing of cerebellar function is often impossible. Extrapontine features may occur. Sensory findings are rare.

The clinical manifestations of CPM/EPM vary, according to the extent of the lesions, from minimal to a complete locked-in syndrome or coma. The constella-

tion of neurological findings is not specific for CPM/EPM and may also be seen in other types of brain dysfunction, particularly in pontine infarction or hemorrhage. Clinically, CPM/EPM can only be suspected, especially if the neurological condition of a patient deteriorates after correction of hyponatremia (serum sodium less than 120 mEq/l). Symptoms of the disease appear within hours or up to a week after correction of hyponatremia. Many patients with neurological manifestations of CPM/EPM die of complications or underlying disease. However, other patients survive with partial or complete recovery.

In CPM the EEG is rarely abnormal, because even large lesions of the base of the pons are compatible with a normal EEG. The most frequently observed EEG abnormality is a generalized slowing, correlating with the level of consciousness. In EPM, the EEG may show focal abnormalities. BAEPs and SSEPs often show abnormalities consistent with a pontine lesion, but may also be completely normal. The abnormalities are nonspecific.

89.2 Pathology

In CPM there is usually a single symmetrical lesion, often with a typical "ω" form, located in the central part of the base of the pons. It can be large, occupying almost the entire base of the pons, or very small. Generally the lesion is continuous and sharply defined, although an island of tissue is occasionally preserved. In exceptional cases the lesion develops unilaterally or appears to be multifocal. Rarely, the lesion spreads into the tegmentum pontis or into the middle cerebellar peduncles. It does not usually extend to the surface of the pons.

Histologically, there is severe and sometimes complete loss of myelin in the lesion, with a concomitant loss of oligodendrocytes. Demyelination affects both the long tracts (pontocerebellar transverse fibers and the long descending tracts) and the pontine nuclei. The axons are usually well preserved, although a considerable loss of axons may occur. The most severely affected area may be cystic in nature due to almost total disappearance of myelin and axons. Axonal loss is associated with degenerative changes in nerve cells. However, on the whole, neurons of the pontine nuclei are relatively spared even in areas of severe demyelination. Reactive astrocytosis and macrophage re-

sponse are usually present. Macrophages contain remnants of disintegrated myelin and lipid material. Neither vascular disease nor inflammation is seen.

In EPM, which accompanies CPM in 10% of patients, similar demyelinating lesions occur outside the pons, with a predilection for the white matter of the cerebellum, especially the folia. Also affected are the mammillary bodies, the tegmentum of the mid-brain, the lateral geniculate bodies, the thalamus, striatum, the internal, external, and extreme capsules, the anterior commissure, the fornix, the deep layers of the cerebral cortex and subjacent white matter of the crowns and sides of the cerebral gyri. Not all these structures are necessarily affected in any one patient; the precise localization of demyelinated lesions varies from patient to patient. In exceptional cases, histological abnormalities consistent with the diagnosis EPM occur without any pontine lesion.

89.3 Pathogenetic Considerations

CPM and EPM have been reported in quite a number of conditions: alcoholism, psychogenic water drinking, diabetic ketoacidosis, subdural abscess, brain tumor, cerebral trauma, meningitis, encephalitis, renal dialysis, malnutrition, lung infections, adrenocortical insufficiency, postoperative hyponatremia, inappropriate antidiuretic hormone secretion, extracerebral malignancy, and other chronic debilitating diseases. The etiology is not completely understood. Abnormalities in serum sodium levels have been the subject of considerable interest in this respect. There is evidence that rapid correction of hyponatremia may cause CPM/EPM. Clinical observations strongly suggest this causal relationship as the clinical symptomatology in CPM/EPM is usually preceded by a rapid rise in serum sodium after a period of sustained hyponatremia. Usually, no neurological injury is seen when the chronic hyponatremia is corrected slowly. In all diseases inferred to be able to induce CPM/EPM, hyponatremia is a common complication, for which rigorous treatment is often instituted after hospitalization.

There are strong indications that CPM/EPM is indeed an iatrogenic disease. The first description of this syndrome dates from the 1950s. It is inconceivable that it could have been missed by neurologists and pathologists of the nineteenth and early twentieth centuries with their strong reliance on post-mortem examination. In the 1950s more liberal use was made of intravenous tubing, and there was interest in treating alcoholic withdrawal states by massive administration of intravenous fluid. Thiazide diuretics were introduced for clinical use at this time. These factors probably contributed to the genesis of hyponatremia. Alcohol has an antidiuretic-hormone-

blocking effect. Alcohol withdrawal leads to rapid return of antidiuretic hormone function, thus causing hyponatremia. With intravenous tubing, aggressive treatment of hyponatremia by infusion of hypertonic solutions became possible in any of the implicated diseases. The clinical syndrome and the characteristic histological lesions of CPM/EPM can be reproduced in experimental work with dogs and rats by rapid correction of hyponatremia. In these experiments, hyponatremia in itself does not appear sufficient to induce CPM/EPM, and neither self-correction of the serum sodium nor a rapid rise from normonatremia to hypernatremia results in CPM/EPM.

However, there are other, conflicting data. Some investigators found that the rate of increase in serum sodium in patients with CPM/EPM had been more rapid than in patients with hyponatremia but without CPM/EPM. Others found no difference in the rate of increase of serum sodium in the two groups. Sometimes patients with a slow rise in serum sodium still develop CPM/EPM. Some authors stress that most of the patients developing CPM/EPM became hypernatremic after correction and state that it is the elevation of serum sodium to hypernatremic levels rather than the rapid correction that predisposes to CPM/EPM. Others have found that CPM/EPM can develop without overcorrection, while a mild hyponatremia still exists. In a recent discussion, attention was paid to the combined role of hyponatremia and hypoxia. The new point of view was that independent of the rate of correction of the hyponatremia, brain stem lesions develop when hypoxia is present.

The exact pathogenesis of demyelination in CPM/EPM is not clear. It is known that generalized cellular edema is the hallmark of acute hyponatremia. In cases of chronic hyponatremia, brain cells have adapted to this condition by extruding sodium, potassium, chloride, and water. The loss of more solute than water renders cellular and extracellular fluid equally hypotonic, but reduces cell swelling. Restoration of normal serum osmolality removes water from the hypotonic tissue and causes the adapted, normovolemic brain cells to shrink to volumes less than normal. As brain cells replenish lost electrolytes, the normal cellular volume is re-established. Complications may result if normonatremia is achieved too rapidly before cellular restoration of lost solute. The rapid rise in sodium level results in an osmotic endothelial injury and in opening of the blood-brain barrier. The proposed mechanisms for opening the blood-brain barrier are endothelial cell shrinkage allowing fluid into the intercapillary and pericapillary spaces. Others suggest that the barrier opening is in fact due to enhanced vesicular transport. In any case, the penetration of the blood-brain barrier is proven by the presence of biliary pigment in the myelinolytic lesion of some highly jaundiced patients. It is hypothesized

that the endothelial injury leads to a release of myelinotoxic factors from the damaged cells, in turn leading to demyelination. Alternatively, and not necessarily mutually exclusively, the osmotic opening of the blood–brain barrier results in vasogenic edema. Indeed, edema has been observed in CPM lesions. It is known that edema may itself be myelinotoxic. If the presumption of this mechanism is correct, it may explain the localization of lesions, which preferentially develop at sites characterized by an extensive admixture of gray and white matter. Of all regions in the brain, the pons has the greatest degree of gray–white apposition. Areas such as the basal ganglia, thalamus, geniculate bodies, and cortex–white matter junctions also have extensive apposition of gray and white matter. Edema or related myelinotoxic factors are principally derived from the highly vascular gray matter and are thus able to affect the adjacent heavily myelinated white matter. However, the mechanism whereby edema may cause demyelination remains to be determined. An alternative hypothesis states that edema of the pons would result in strangulation of tracts and nuclear masses. In the base of the pons, longitudinal and transverse fibers interlace. Because of this grid-like anatomy, the pons is particularly susceptible to damage when edema occurs, as the edema literally strangles the myelin sheaths and small blood vessels. If mild, this would result in a reversible physiological block of neurotransmission. If edema persisted and became more severe, irreversible demyelination would occur.

Although the summarized views seem reasonable, there are some objections. This grid pattern is not present in extrapontine localizations of myelinolysis. There are regions in the brain in which myelinated fibers are interspersed with layers of gray matter that do not show myelinolysis. And, finally, the factor of edema, invoked in several theories of myelinolysis, is little documented.

Another variable to be considered is the role of the underlying condition. The over-representation of alcoholics in the myelinolysis population requires explanation. It may simply be related to the fact that alcoholics admitted to hospital are in withdrawal and at the same time vigorously treated with intravenous fluids. Another possibility is that the alcoholic state or the withdrawal of alcohol somehow makes the brain more sensitive to the rapid rise of serum sodium from hyponatremia. This is conceivable, since alcohol reportedly affects brain hydration. Thiamine deficiency may be another factor. Thiamine deficiency may cause depletion of ATP, which may affect the transport of electrolytes in the cell membranes, producing endothelial damage and making cells more vulnerable to osmotic change. The fact that CPM/EPM has been observed in the setting of a variety of medical disorders other than alcoholism suggests that seri-

ously ill patients are in general vulnerable to the disease. Again, this fact may simply indicate that very sick patients face an increased risk of hyponatremia or a greater likelihood of undergoing vigorous correction of hyponatremia. The other possibility is that the brains of debilitated patients are less resistant to a rapid rise in serum sodium. Here, too, thiamine deficiency may play a role.

89.4 Therapy

No therapy is available for CPM/EPM. As soon as the neurological symptomatology has developed, only symptomatic measures can be taken. Prevention must therefore be the focus of clinical efforts. The prevention of CPM/EPM relates to the medical approach to hyponatremia, especially chronic hyponatremia. As there are different opinions about the role of hyponatremia and the rise of serum sodium level in the genesis of CPM/EPM, there are likewise many guidelines for the correction of hyponatremia. In severe hyponatremia with a serum sodium concentration below 120 mmol/l, correction is necessary. The recommended rate of correction varies between 0.5 to 2 mmol/l per hour, or 12 to 48 mmol/l per day. The fact that hyponatremia itself may lead to brain damage forms an argument against very slow correction. After reaching a concentration of 120–130 mmol/l, water restriction in combination with a diet with normal salt content is recommended. In chronic asymptomatic hyponatremia, simple water restriction and a diet with normal salt content may suffice from the beginning. Others prefer a combination of normal saline with fluid restriction. Of course, diuretics, which cause salt loss, are discontinued. It is advisable to avoid hypernatremia. In the light of recent discussion, one should also be aware of the influence of hypoxic–ischemic conditions and avoid or correct those as soon as possible.

In addition to the rate of sodium correction, the total osmotic load from contrast material in neuroimaging must be considered. Intravenous contrast material should not be used in the immediate post-correctional period of hyponatremia.

89.5 Magnetic Resonance Imaging

CT scanning may show fairly characteristic abnormalities in CPM, consisting of a roundish or “ω-” or “batwing-shaped” hypodense area in the midline of the pons, approximately equidistant from the floor of the fourth ventricle and the ventral surface of the pons, with, in the acute phase, peripheral enhancement after contrast injection. The fourth ventricle shows no displacement, and the brain stem is of nor-

Fig. 89.1. A 56-year-old man with an episode of general malaise, vomiting, and desiccation. Hyponatremia of 111.5 mmol/l was corrected in 2 days to 134 mmol/l, followed by severe neurological symptoms. Midsagittal T₁ and transverse T₂-weighted MR images demonstrate the characteristic features of CPM in the subacute phase, typically sparing the outer rim of the pons

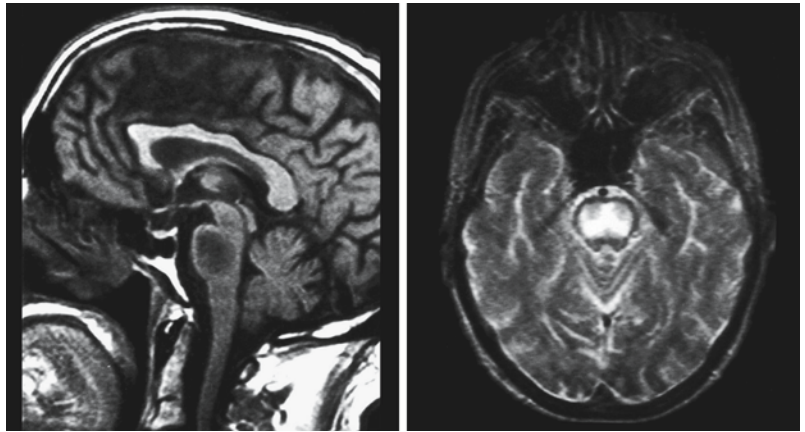
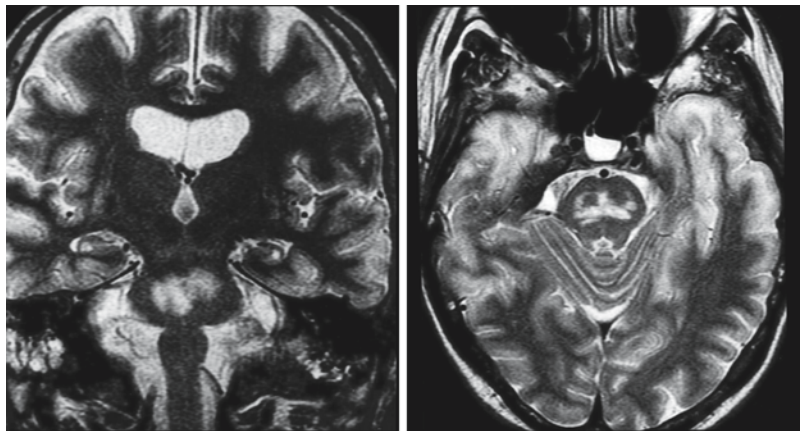


Fig. 89.2. A 44-year-old man with chronic alcohol abuse and hyponatremia. The MRI was obtained in the acute phase of CPM. The characteristic ω -shaped lesion central in the pons in the acute phase is especially well seen on the transverse T₂-weighted image. Courtesy of Dr. B.G. Ziedses des Plantes Jr., Deventer Hospital, Deventer, The Netherlands



mal size. The CT scan can also detect abnormalities consistent with EPM. Sometimes the CT scan is found to be normal in CPM/EPM. In some patients the hypodensities of the CT scan disappear as the patient improves, but persistence of hypodensities has also been observed despite clinical cure. CT findings appear to correlate rather poorly with the clinical syndrome. Furthermore, the specificity of CT findings in CPM is not high, as differentiation between CPM and other pontine lesions, especially pontine infarction, is often difficult or impossible. It is not an infrequent occurrence that posterior fossa artifacts, characteristic on CT, prevent optimal assessment of the pontine area.

MRI is capable of showing the characteristics of CPM and EPM in more detail. MRI is normal or may even show low signal intensity in the pons on T₂-weighted images at onset of clinical symptoms. In classic cases of CPM, repeat MRI after a few days shows symmetric high signal intensity on T₂-weighted images, representing myelinolysis of the base of the pons, spreading centrifugally from the median raphe, characteristically leaving the outer rim of the pons unaffected (Figs. 89.1 and 89.2). Hence, the ven-

trolateral longitudinal fibers are spared. In severe cases, necrosis and cavitation may develop. The lesions may spread into the pontine tegmentum and mesencephalon. Most reports reject a correlation between the severity of the MRI findings and the clinical condition. On the other hand, in the follow-up of patients a good correlation between clinical improvement and the fading of lesions on MRI is observed. Even with complete clinical restoration, however, abnormalities on MRI remain visible for a long time. Ring enhancement of the lesions in the pons after injection of intravenous contrast has been observed in the acute phase. Although in MRI the quantities of injected contrast material are far less than in CT, administration of contrast should be avoided, if possible, in order not to aggravate the patient's ionic imbalance. Moreover, enhancement of the lesions in the pons does not contribute to the diagnosis. Diffusion-weighted imaging may add helpful information. In the acute phase Trace diffusion-weighted images show a high signal in the central pontine lesion with corresponding low ADC values, in conformity with initial cellular edema. In a few days ADC values pseudonormalize.

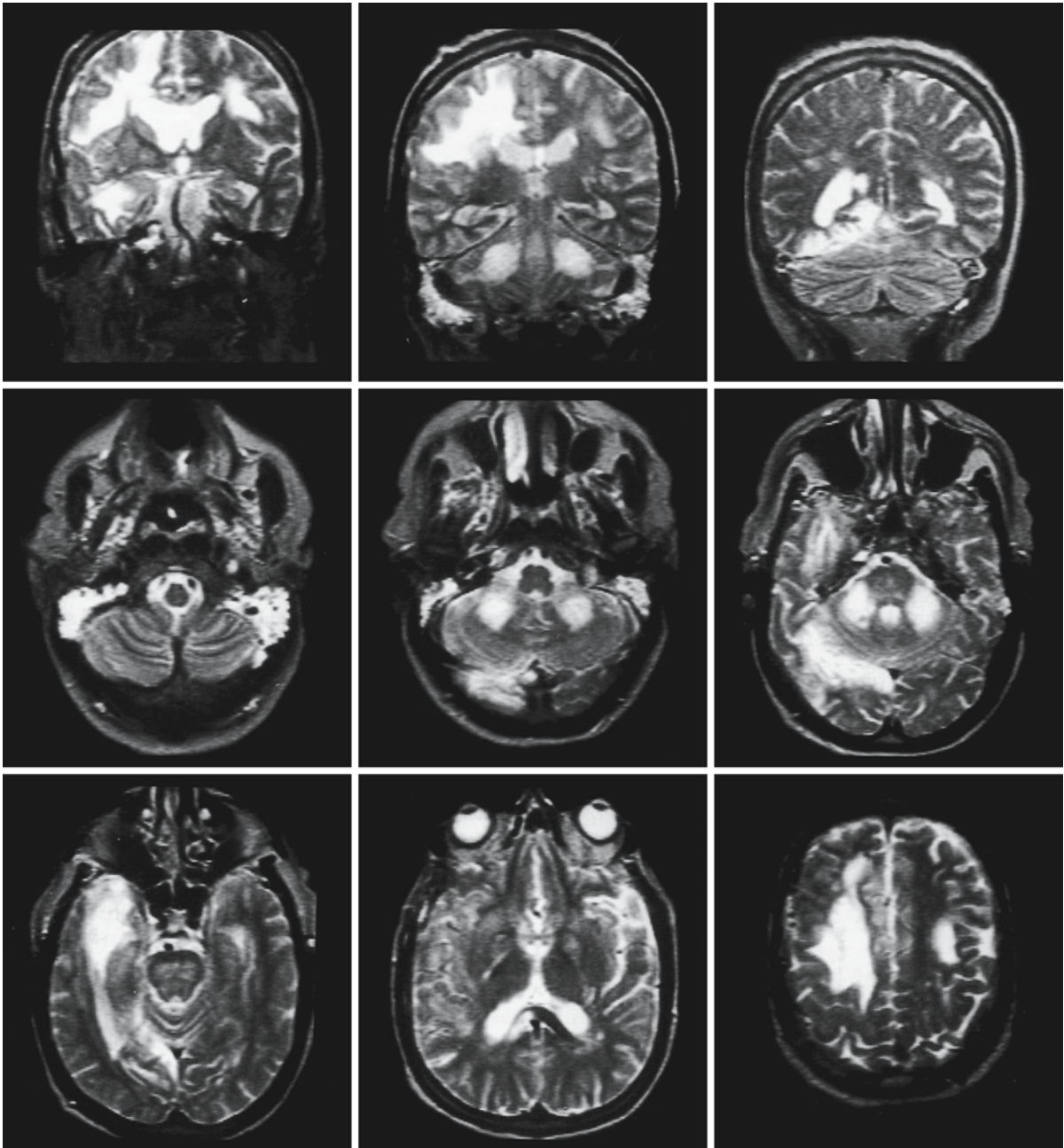


Fig. 89.3. A 64-year-old man became critically ill after surgery for removal of a meningioma. Surgery and postoperative course were complicated by severe blood loss and hyponatremia, both of which were corrected. After initial good recovery, deterioration of the clinical condition occurred. The T_2 -weighted coronal and transverse images show the postopera-

tive edema in the right temporal lobe. Furthermore, there is extensive myelinolysis in the cerebellar white matter, the middle cerebellar peduncles, the internal capsule, and the subcortical white matter, with preponderance on the right side. The pontine white matter is slightly affected. Gradual return to normal occurred in the weeks that followed

The findings as described are highly characteristic of CPM. With the typical antecedents there is no great difficulty in establishing a diagnosis. Differentiation in less clear cases is mainly from pontine glioma and pontine infarctions.

Sometimes lesions in the basal ganglia are seen together with the typical lesions in the pons. These cases can be considered transitional between CPM and CPM/EPM. In EPM, lesions are most often seen in the putamen and caudate nucleus. In addition, lesions

may occur in the globus pallidus, thalamus, geniculate bodies, mammillary bodies, hippocampus, internal and external capsule, corpus callosum, anterior commissure, and cerebellar and cerebral gyral convolutions (Fig. 89.3). Lesions may also be confined to the middle cerebellar peduncles (Fig. 89.3). EPM may occur in isolation or be combined with CPM. Estab-

lishing the diagnosis EPM is not difficult in the presence of the characteristic pons lesion. The differential diagnosis in EPM without a pontine lesion is more difficult and includes acute disseminated encephalomyelitis, encephalitis, and toxic-metabolic encephalopathies.

Hypernatremia

90.1 Clinical Features and Laboratory Findings

It has been known for a long time that hypernatremia is a highly toxic condition which, if not adequately and immediately treated, may end with severe neurological deficits, coma, and death. In most patients hypernatremia is a result in most patients of dehydration due to either insufficient intake or excessive loss of water, as in diarrhea, vomiting, adrenal dysfunction, or hypothalamic dysfunction caused by head trauma, brain surgery, pituitary tumors, craniopharyngiomas, other brain tumors, abscesses, or hemorrhages. Hypernatremia may also follow the discontinuation of intake of lithium after long-lasting treatment. This results in a defect in concentrating urine, leading to hypernatremia.

Another, less frequent, cause of hypernatremia is a too high intake of salt, either accidentally or nonaccidentally, in the latter case often as form of abuse or punishment. Attempts at abortion by intra-amniotic injection of hypertonic salt solution may lead to serious hypernatremia. Accidental disasters of intake of high doses of salt have been reported, when in the nursery sugar is inadvertently replaced by salt in preparing one of the formulas for neonates or when a 10% salt solution is used for infusion in neonates instead of a 10% glucose solution. Use of the wrong fluid for emetics, gastric lavage, and other medical interventions has been reported as an iatrogenic cause of hypernatremia in other cases. A separate chapter in salt poisoning is the nonaccidental, forced intake of too large quantities of salt as form of punishment, purification for religious motives, or child abuse. In many cases in children nonaccidental salt poisoning is part of the “Munchausen by proxy” syndrome.

The initial clinical presentation of hypernatremia may vary from drowsiness, inactivity, and irritability to altered consciousness, confusion, seizures, and evidence of dehydration, including sunken eyes, dry mouth, dry mucosa, doughy skin turgor, raised blood pressure, and irregular pulse. Coma may ensue. Further deterioration may occur after the initial diagnosis and installation of treatment, and severe neurological deficits may develop and remain even after successful regulation of the osmotic balance. The death rate among patients with serious hypernatremia is high.

Laboratory findings include a serum sodium level higher than 150 mEq/l by definition. Sodium excretion is usually found at maximum physiological rates of 270–290 mEq/l in urine, but is sometimes in excess of that, as high as 400 mEq/l, the latter at the expense of fluid homeostasis and thus leading to volume depletion.

90.2 Pathology

In the fatal incidents in neonates and infants pathological findings are uniform. Most of the abnormalities are found in the lungs and brain. In the lungs hemorrhages are found, sometimes very extensive. In the brain, subdural and focal subarachnoid hemorrhages are seen. On sectioning, petechial and larger, more confluent hemorrhages are seen, in particular in the basal ganglia and the white matter. The cerebral and cerebellar cortex is relatively spared. In the basal ganglia discolored spots are seen. The substance of the white matter in the centrum semiovale is macroscopically changed, with areas of gray-brownish discoloration.

Microscopic examination confirms the multiple petechial hemorrhages, together with thrombosis in many small vessels. Around these thrombotic vessels ring-like hemorrhages are present, with perivascular edema. The discoloration seen in the white matter appears to be related to the thrombotic vessels and focal hemorrhages. Hemosiderin is present in these lesions, making it possible to date these hemorrhages to the onset of the clinical symptoms. In some patients thrombosis of venous sinuses is seen. The overall picture is that of a hemorrhagic encephalopathy, with thrombosis, derangement of microcirculation, and necrosis.

90.3 Pathogenetic Considerations

The fluid balance of the body is maintained by multiple hormonal and neurogenic mechanisms. These keep the total quantity of fluid, the concentration of solutes, and thus the osmolality of body fluids within narrow limits. Disruption of these homeostatic mechanisms may lead to either overhydration with hypo-osmolality, or dehydration with hyperosmolality. Ex-

cessive intake of fluid on the one hand, or excessive intake of salt on the other, may cause the regulatory capacity of the homeostatic system to be exceeded. Damage of the regulatory systems in the hypothalamus, by trauma, brain surgery, tumor, or other expanding lesions, may also lead to deregulation of the osmotic sensors or deficiency of antidiuretic hormone.

The effects of hypernatremia on the brain appear with some delay. It takes time before the blood-brain barrier is disrupted. In experiments, animals with hypernatremia show similar clinical signs as humans: lethargy, irritability, tremor, ataxia, seizures, and eventually coma and death. On autopsy shrinkage of the brain is obvious with hemorrhagic fluid present around the brain. In some instances there are massive subdural hematomas. These are probably caused by tearing of veins which bridge the space between the brain and the calvarium. Smaller hemorrhages at the brain surface and in the parenchyma are the result of direct damage to the endothelium of the smaller vessels and capillaries. Increased osmolality of the blood causes water to move from the brain toward the blood. The brain reacts to the osmotic insult with the generation of intracellular osmolytes, so-called idiogenic osmolytes. These osmolytes serve to regulate volume and can reach high concentrations within cells. The intracellular osmolality is thereby increased and the loss of cellular fluid counteracted. Several substances have been identified as putative organic osmolytes, among them *myo*-inositol, *N*-acetylaspartate, glycerophosphoryl choline, and taurine. However, rapid correction and normalization of blood osmolality may subsequently lead to relative hyperosmolality of the brain, resulting in shift of fluid from the intravascular compartment to the brain parenchyma, brain edema, and possibly pontine and extrapontine myelinolysis.

90.4 Therapy

Therapy consists mainly of restoring the osmotic balance and bringing the sodium levels back to normal values. Too rapid correction of the sodium levels may be followed by pontine and extrapontine myelinolysis, a complication more often seen in too rapid correction of hyponatremic states. For this reason it has been advised that the decrease in plasma sodium should not exceed 0.5 mEq/l per hour and that

normalization of serum sodium levels should be achieved in 48–72 h. Dialysis has also been advocated. The damage done to brain, lungs, and kidney develops rapidly, and hypernatremia, especially in children, is fatal in over 50% of cases. Treatment should therefore start as soon as possible. Special attention is, of course, also necessary for renal, pulmonary, and cardiac function. Even when the patient survives, severe neurological deficit may remain.

90.5 Magnetic Resonance Imaging

Very few reports are available on neuroimaging findings in patients with hypernatremia. On CT, extensive cerebral and cerebellar hemorrhages have been described. CT may also show bilateral transient thalamic hypodensity. One report describes the MR findings in a neonate with hypernatremic dehydration. This was a 15-day-old girl who received insufficient quantities of breast milk for several days. MR showed a superior sagittal sinus thrombosis with a venous hemorrhagic infarction, and some smaller hemorrhages with surrounding edema.

We have seen a 2.5-month-old child, a victim of child abuse, who was given a small amount of sodium. On admission the blood sodium level was 200 mEq/l. The first MRI showed extensive abnormalities confined to the nonmyelinated frontotemporal areas, whereas the myelinated areas seemed to be preserved (Fig. 90.1). The lesions showed irregular enhancement, indicating a defective blood-brain barrier (Fig. 90.1). After the initial phase of swelling, shrinkage of the affected parts followed with evidence of hemorrhagic necrosis (Fig. 90.2). Finally, serious atrophy of the frontal and temporal lobes and gliosis developed (Fig. 90.3). The child remained severely neurologically damaged.

When MRI is required in patients suspected of having hypernatremia, the protocol should include gradient echo images to identify hemorrhage, pathologically a constant finding. Proton MRS could be of interest because it will be able to monitor osmolytes such as *myo*-inositol. The presence of hemorrhages, however, would probably disturb magnetic field homogeneity.

When nonaccidental salt poisoning is suspected, one should be alert for other possible signs of child abuse.

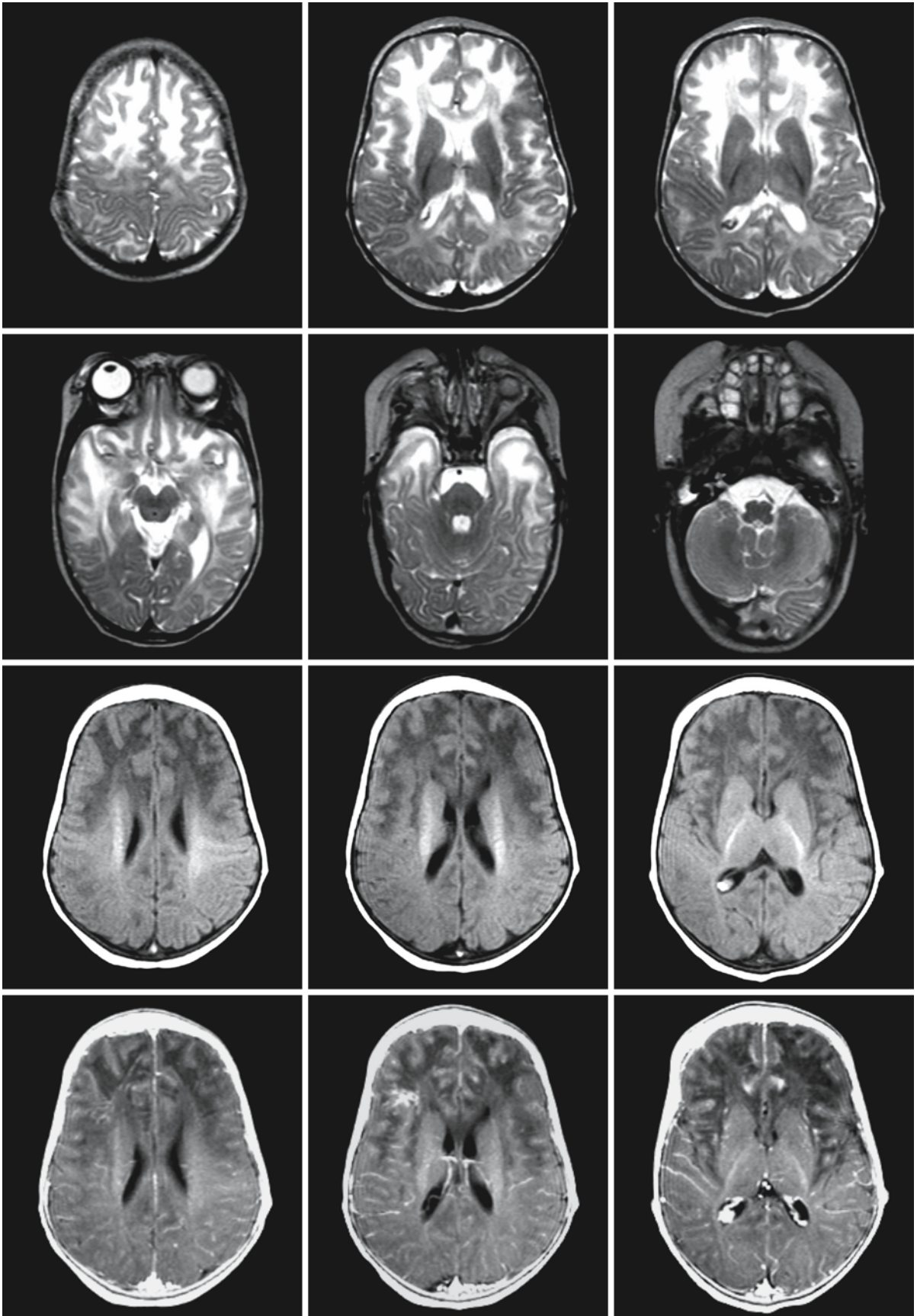


Fig. 90.1.

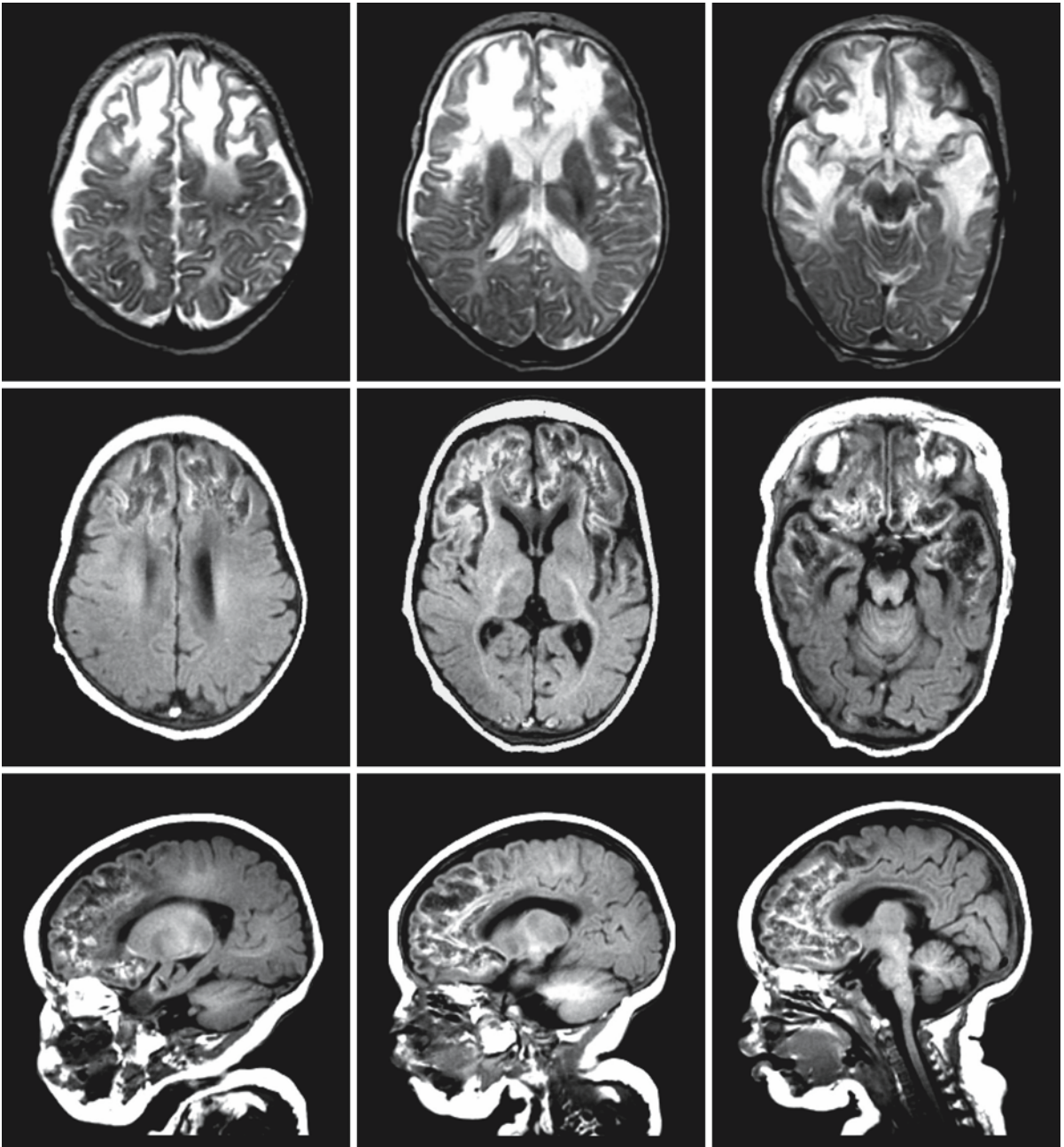


Fig. 90.2. After 1.5 weeks atrophy of the affected areas evolves. The T₁-weighted axial (*second row*) and sagittal images (*third row*) demonstrate the hemorrhagic component of the necrosis



Fig. 90.1. A 2.5-month-old girl was the victim of nonaccidental salt intoxication. The T₂-weighted images (*first and second row*) show involvement of the, at this stage of development, unmyelinated parts of the brain: the frontal and temporal lobes. The involved parts are partly swollen. The myelinated internal capsule, brain stem, and cerebellar white matter are intact. The T₁-weighted images (*third row*) show that myelination is normal and that the unmyelinated cerebral white matter has a low signal intensity. After contrast injection (*fourth row*), there are some areas of contrast enhancement as evidence of disruption of the blood–brain barrier

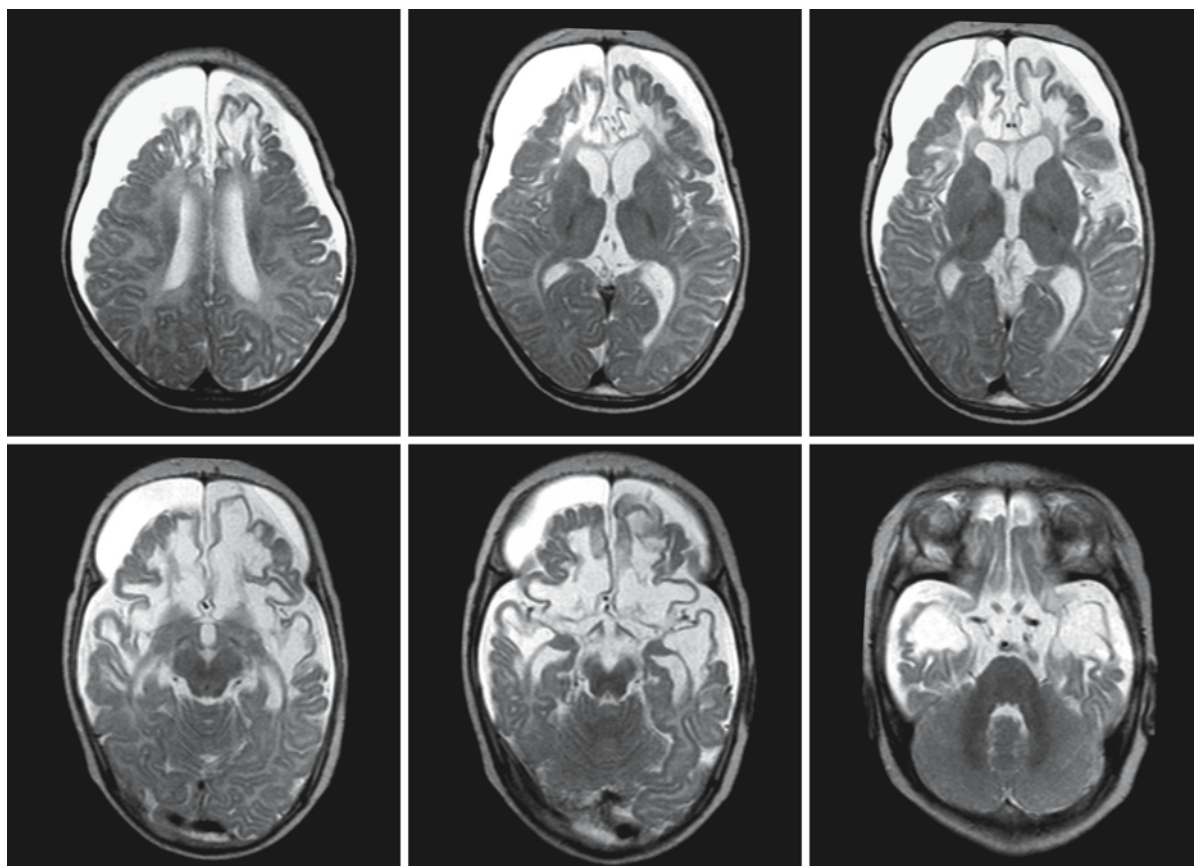


Fig. 90.3. Another month later, severe atrophy of frontal and temporal lobes and ventriculomegaly are seen. Bilateral frontal subdural effusions are present

Marchiafava–Bignami Syndrome

91.1 Clinical Features and Laboratory Investigations

Marchiafava–Bignami syndrome (MBS) is a disorder characterized by primary degeneration of the corpus callosum in chronic alcoholics. Although a high proportion of reported cases have been Italians, drinking Italian wine, the condition has also been described in many non-Italians drinking non-Italian wine. Most affected cases were middle-aged men whose daily wine consumption had been 21 or more for many years.

The disease has three major clinical forms: acute, subacute, and chronic. The acute form is characterized by sudden onset with severe disturbances of consciousness, sometimes heralded by convulsions. The initial phase is followed by the development of persistent coma or stupor with pyramidal signs and hypertonia. Patients are generally mute, but if they say a few words, they appear to be severely dysarthric. They may die within a few days. The subacute condition is characterized by rapidly progressive dementia, sometimes following an initial acute state with temporary coma or convulsions. The dementia has characteristics of a split-brain syndrome. The patients are usually dysarthric. Hypertonia of the limbs is quite common and marked by strong opposition to any movement, either flexion or extension. There is spastic flexion of the arms and extension of the legs with hyperreflexia and extensor plantar reflexes. A facial grimace and trismus may be present, as well as opisthotonus. In the end stage the patients are unable to walk or stand. Severe dementia usually progresses to a vegetative state and death within a few months. In the chronic form, which is much less common, dementia progresses slowly over a number of years. Neurological examination reveals diffuse rigidity, dysarthria, and inability to stand or walk, as in the subacute form. This condition progresses steadily towards death several years later. It should be noted, however, that in a few cases improvement of the patient's condition and disappearance of image abnormalities have been reported.

Laboratory investigations may reveal vitamin deficiencies due to malnutrition but they are probably not directly related to MBS. Combinations of Wernicke encephalopathy with MBS have been described. There is no laboratory test for MBS.

91.2 Pathology

The principal pathological change is necrosis of the corpus callosum. The necrosis may involve the entire length of the corpus callosum or only a part of it. The middle layers of the splenium and genu are mainly affected, an upper and lower rim of the callosal fibers usually being preserved. The lesion extends laterally to the edges of the corpus callosum. When necrosis is incomplete, demyelination is found, with relative preservation of axons and a moderate glial reaction. In cases of total necrosis, both myelin and axons have disappeared and are replaced by an accumulation of macrophages and perivascular cells together with a variable glial reaction. The lesion is sharply delineated. In acute cases the lesion appears in the form of a band of edematous necrosis with fresh coagulation. An upper and a lower band of normal callosal tissue remains. In cases of long duration, the corpus callosum is thinned and atrophic with a slit or band of demyelination in the middle, most conspicuous in genu and splenium. Macrophages accumulate in perivascular areas.

Other regions of white matter are sometimes involved, including the centrum semiovale in the frontal, parietal, and occipital region as an extension of the lesion of the corpus callosum. Sometimes the lesion includes all the white matter up to the U fibers. Furthermore, the cerebellar peduncles and the anterior commissure may be affected. The fornix is thought never to be affected. Also, these lesions are primarily characterized by demyelination with accumulation of macrophages. In complete necrosis axons are also lost. The ventricles are moderately enlarged, and in most cases there is some cortical atrophy. There is occasionally cortical laminar necrosis and, exceptionally, necrosis of the basal ganglia.

91.3 Pathogenetic Considerations

The pathogenesis of MBS is still unknown. A toxic factor present in cheap red wine seems to be the closest constant association, but the factor responsible has never been identified. It has been shown that vitamin deficiencies are not important in the pathogenesis, as a supply of vitamins does not prevent MBS in animals. There are, however, a few descriptions of the

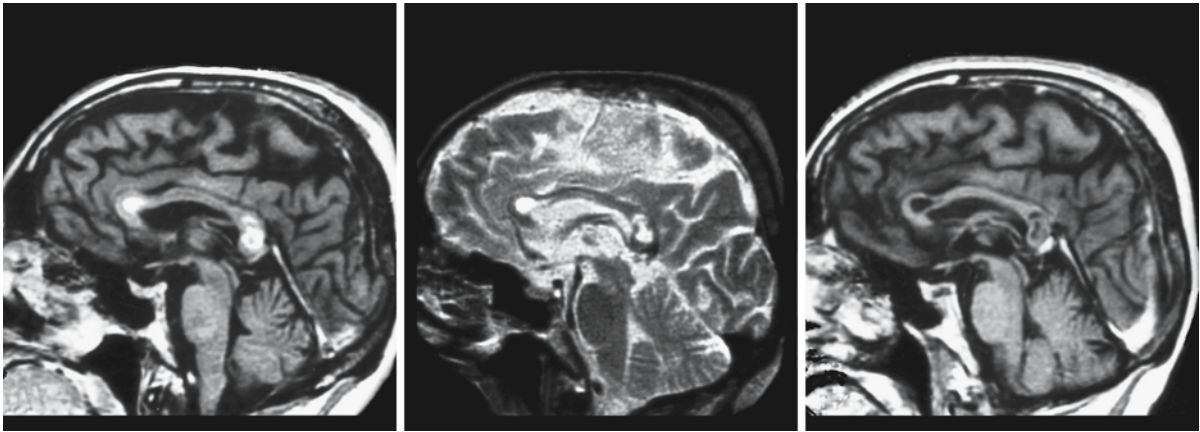


Fig. 91.1. A 53-year-old man with MBS with acute onset. MRI on the ninth day (*left image*) shows contrast-enhancing lesions in the genu and the splenium of the corpus callosum. At 3 weeks the images (*middle and right images*) show involvement

of the middle layer of the corpus callosum, in particular in splenium and genu, but no contrast enhancement. The splenium and genu show cystic degeneration. From Caparros-Lefebvre et al. (1994), with permission

combination of MBS with Wernicke encephalopathy. Lesions of the white matter affecting the corpus callosum and anterior commissure have been described following chronic cyanide intoxication and chronic methyl alcohol intoxication. However, the pathogenetic similarities on the molecular level between MBS and these intoxications are unclear. Why the central layers of genu and splenium of the corpus callosum are preferentially affected in MBS remains obscure. The cause of the additional gray matter lesions, usually in the form of laminar necrosis of the cerebral cortex, has not been explained satisfactorily. The most attractive hypothesis would seem to be that the cortical necrosis is secondary to the callosal lesion, which leads to loss of neurons due to secondary degeneration.

91.4 Therapy

There is no effective treatment for MBS; only symptomatic treatment is possible. However, it is important not to overlook other complications of long-standing alcoholism, particularly vitamin deficiencies and disturbances of electrolytes.

91.5 Magnetic Resonance Imaging

CT scan may show abnormality of the corpus callosum with some swelling and edema in the acute form. The corpus callosum lesions in the subacute or chronic forms of the disease, which are not associated with swelling, may be more difficult to detect on CT. Extensive hypodense areas may be found in the cerebral hemispheric white matter. Contrast enhancement

has been described in the early stages of the disease. In the later stages there is atrophy of the corpus callosum, progressive and marked widening of the cerebral sulci, and dilatation of the lateral ventricles.

The corpus callosum lesions are much more easily visualized by MRI (Figs. 91.1 and 91.2). The sagittal MR images are diagnostic: they show the typical pattern of the corpus callosum splitting into three layers, with relative sparing of the upper and lower layers. In the initial stages of the disease the corpus callosum appears swollen and contrast enhancement may be present, in particular in the genu and splenium. Callosal hemorrhage may occur in the subacute stage. The middle layer may become cystic in the later stages of the disease and the corpus callosum becomes atrophic. Cerebral hemispheric white matter may be involved, with a less characteristic appear-

Fig. 91.2. A 56-year-old man with MBS. The *first and second rows* of images were obtained in the acute phase. The sagittal T₂-weighted images (*first row*) show that especially the middle layer of the corpus callosum is involved. The axial FLAIR images (*second row*) show the predominant involvement of the corpus callosum with some additional lesions in the deep periventricular white matter. A follow-up MRI was obtained 50 days later (*third and fourth rows*). The sagittal T₁-weighted images (*third row*) show cavitation of the middle layer of the genu and splenium of the corpus callosum. The hyperintense lesions on the axial T₂-weighted images (*fourth row*) are less conspicuous. From Yamamoto et al. (2000), with permission

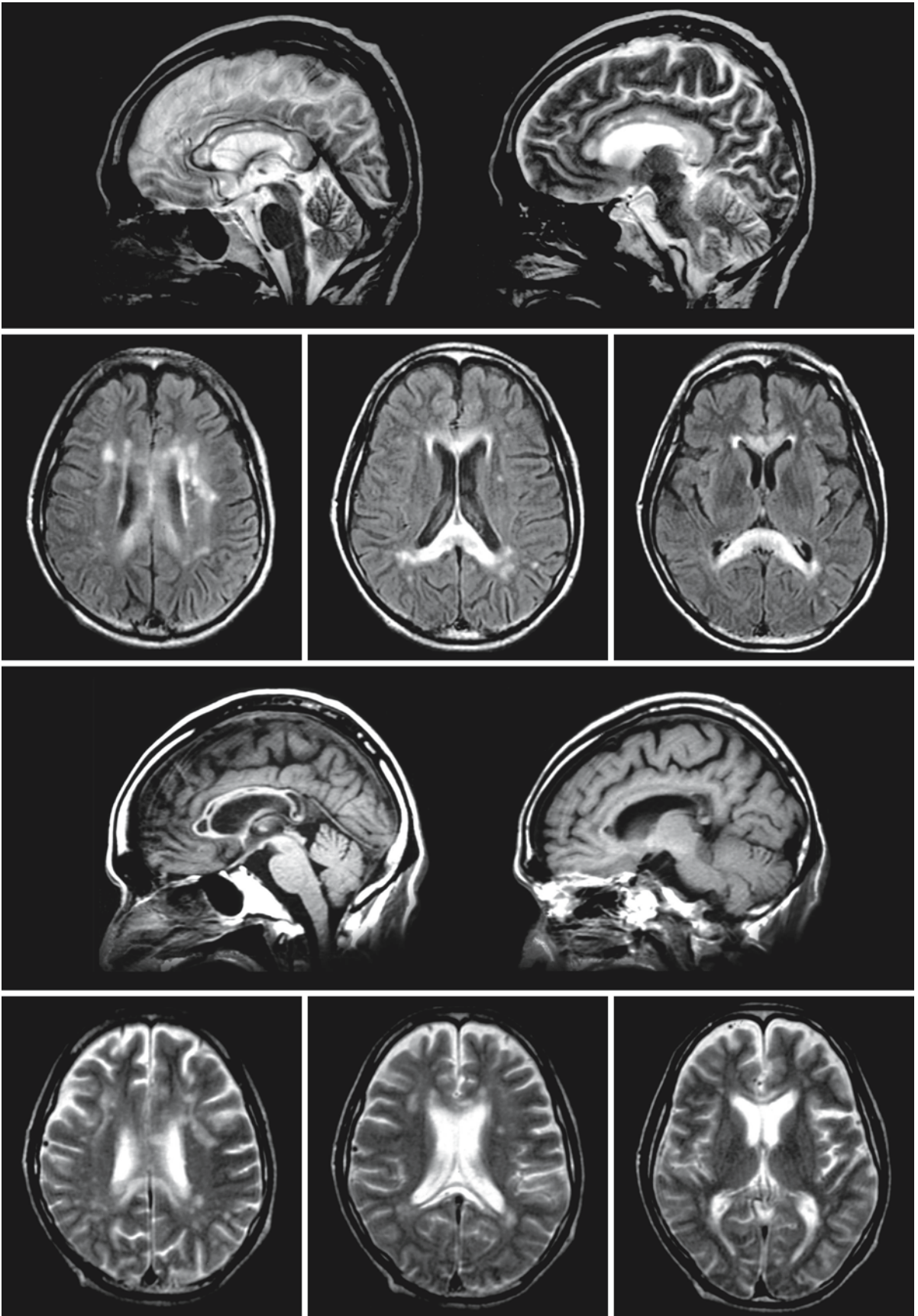


Fig. 91.2.

ance. Apart from the corpus callosum, other inter-hemispheric commissural fibers may be involved, such as the anterior commissure. Cortical laminar necrosis and basal nuclei involvement, when present, can be visualized by MRI. Involvement especially of the putamen, in some cases even reversible, has been described.

Because in nearly all patients excessive alcohol abuse plays a dominant role, the MRI study should also look for signs of other alcohol and thiamine deficiency-related abnormalities, such as changes in mammillary bodies, walls of the third ventricle and basal ganglia, tectum and tegmentum of the midbrain and pons, dentate nucleus and cerebellar cortex.

There are many diseases that produce lesions in the corpus callosum, the most prominent being multiple sclerosis. Others are acute disseminated encephalomyelitis, progressive multifocal leukoencephalopathy, adrenoleukodystrophy, and mitochondrial disorders. These disorders rarely produce the split corpus callosum pattern seen in MBS. Cyanide intoxication is said to present occasionally with splitting of the corpus callosum. The context is then obviously different. In most patients with MBS, the mid-sagittal MR image, showing the splitting of the splenium and genu of the corpus callosum into three layers, together with the medical history and clinical findings of MBS, lead to the correct diagnosis.

Posterior Reversible Encephalopathy Syndrome

92.1 Clinical Features and Laboratory Investigations

Hypertensive encephalopathy may lead to reversible clinical symptoms including headache, nausea, vomiting, altered mental functioning, cerebral blindness, and epileptic seizures.

The syndrome can be present in a number of conditions characterized by hypertension: eclampsia, renal insufficiency, hemolytic-uremic syndrome, thrombotic thrombocytopenic purpura, and acute intermittent porphyria. In most cases the symptoms and MR abnormalities will disappear with antihypertensive treatment. With or without hypertension, the clinical and MR pattern may also be seen in patients undergoing anticancer therapy, bone marrow, or organ transplantation, using either anticancer medication or immunosuppressive therapy (see also Chap. 88).

Because of the first reported findings on MRI and the transient nature of the clinical symptoms, the name reversible posterior leukoencephalopathy syndrome (RPLS) was suggested. When it became clear that often gray matter was also involved, the name was changed into posterior reversible encephalopathy syndrome (PRES). This name has stuck so far, but does not cover the entire spectrum of manifestations of transient clinical symptoms and MRI abnormalities seen in relation to hypertensive and drug-related encephalopathies.

92.2 Pathology

Pathological descriptions are rare, as expected in a usually reversible disorder. Occasionally the results of a brain biopsy are mentioned, usually with vasogenic edema as the only finding. The best data have been obtained in eclampsia, because in the first half of the twentieth century the condition could be lethal. The descriptions give a varied picture of cerebral pathology, with white matter edema, most pronounced in the watershed areas, sometimes with pronounced mass effect, potentially resulting in tentorial herniation. In addition, there may be microinfarctions, cortical petechiae, and pericapillary hemorrhages. Larger hemorrhages may occur in subcortical regions, deep white matter, and basal ganglia.

92.3 Pathogenetic Considerations

There are many theories trying to explain the nature and location of the lesions seen in PRES. The underlying problems are complex, and it is likely that multiple factors play a role in the pathogenesis. This point can be illustrated by a discussion of a few different underlying disorders.

Transient symptoms of hypertensive encephalopathy were recognized clinically even in the first half of the twentieth century in pre-eclampsia and eclampsia. The clinical picture of pre-eclampsia consists of hypertension, confusion, proteinuria, and edema occurring in the second half of pregnancy. Symptoms vary in severity and multiorgan involvement is common. Neurological symptoms include headache, confusion, hyperreflexia, visual hallucinations, and cerebral blindness. Eclampsia is characterized by the occurrence of an epileptic seizure or coma in a patient with a pre-eclampsia syndrome. This syndrome and the neurological implications have been studied extensively. Many factors have been identified that predispose to eclampsia, including an immunological maternal reaction (probably triggered by placental debris), dietary factors (such as deficiency of magnesium, calcium, and zinc, and excess of sodium) and genetic factors (such as abnormal alleles for the genes of tumor necrosis factor- α , angiotensinogen, factor V, and nitric oxide synthase). The maternal response leads to widespread cellular dysfunction with increased capillary permeability, raised fibronectin levels, and damaged endothelium. Subsequently, coagulation abnormalities develop with increased activation and consumption of platelets, low antithrombin III levels, abnormal prostaglandin levels, and in some cases diffuse intravascular coagulation. Endocrine abnormalities include activation of the renin-angiotensin-aldosterone axis, abnormal catecholamine levels, and abnormalities of progesterone metabolism. This constellation leads to hypertension, edema, proteinuria, bleeding tendencies, renal dysfunction, liver damage, and neurological abnormalities. The hypertension exceeds the regulatory capacity of the vessel walls (muscular regulation), so that the local autoregulation (regulating size of the vessels and the admitted blood flow) depends solely on the sympathetic innervation of the vessels, which is relatively poor in the vertebrobasilar system. Hypertension and

immune-mediated endothelial dysfunction lead to extravasation of red cells and plasma proteins, resulting in cerebral edema. Vasospasm, prostaglandin deficiency, defects in the e-NOS gene coding for nitric oxide synthase, and endothelial damage play a role in the eventual progression of the lesion to ischemia and infarction. Thus, in eclampsia a varied picture of cerebral pathology, with cerebral edema, micro-infarctions, cortical petechiae, and pericapillary hemorrhages, results in the clinical manifestations of headache, confusion, visual disturbances, and seizures.

Reversible leukoencephalopathies predominantly in the posterior cerebral areas also have been described in the hemolytic-uremic syndrome (HUS) and thrombotic thrombocytopenic purpura (TTP). In these disorders PRES is only one of many possible manifestations. Both disorders are microangiopathic hemolytic anemias characterized by hemolytic anemia, thrombocytopenia, CNS dysfunction, fever, and/or renal dysfunction. HUS is usually seen in infants and children, whereas TTP more often presents in adults. Clinical findings include acute renal insufficiency and encephalopathy, often with seizures, hemorrhagic colitis, and upper respiratory infection. MRI and CT abnormalities develop over days, showing patchy white matter areas in the frontal, parietal, and occipital gray and white matter. In patients who died, occlusive platelet thrombi were found, primarily confined to the cortical gray matter. There was mild endothelial proliferation in the larger vessels. Capillaries showed proliferation, or “wickerwork” formation. Many causes have been described for HUS and TTP. In children hemorrhagic colitis is the most frequent cause; in adults, immune-mediated diseases, for example, systemic lupus erythematosus. HUS and TTP are classified as “uremic encephalopathies.” The imaging findings may be similar to those described in hypertensive encephalopathies of other origins. Most probably the encephalopathy is the result of more than one factor. In patients with severe hypertension it is assumed that acute increase of blood pressure exceeds the limits of local autoregulation. Distal vessels and capillaries are exposed to too high a pressure and to hyperperfusion. This causes damage to the endothelium so that blood plasma and, in some cases, erythrocytes can pass the blood-brain barrier.

Reversible encephalopathic clinical symptoms and lesions on MRI resembling those of PRES may also be seen in acute intermittent porphyria. Acute intermittent porphyria is a disorder with an autosomal dominant mode of inheritance, caused by a deficiency of porphobilinogen deaminase. More than 80% of carriers never develop symptoms. Symptoms are often precipitated by the influence of drugs, hormones, and nutritional factors that change the rate of heme synthesis in the liver. Patients with acute intermittent

porphyria present with subacute episodes of abdominal pain, vomiting, nausea, bowel distension or ileus, and neurovisceral and circulatory disturbances. The neurological problems are extremely variable and include autonomic neuropathy, peripheral axonal neuropathy, and CNS dysfunction. In subacute attacks, central and peripheral neurological symptoms may become prominent. Patients may have seizures, visual hallucinations, and cerebral blindness. Bilateral lesions in the parieto-occipital and posterior frontal lobes have been found in these patients. The lesions disappear after treatment. The similarity of the clinical and imaging pattern to other cases of PRES is evident. Some of the patients have hypertension during these subacute episodes, but not all. It is likely that other factors play a role in the development of CNS dysfunction.

Hypertension has not been found in all patients with PRES. Nocturnal registration of blood pressure in patients with PRES without hypertension has shown transient rises in blood pressure, a “riser” pattern, in some patients. It remains to be proven whether that is the case in a significant number of patients with PRES.

In eclampsia, HUS, and TTP, as well as in acute intermittent porphyria and other disorders in which PRES develops, hypertension is only one of the factors that play a role in the development of the encephalopathy. This explains why not all patients develop the syndrome under the same conditions. Autoregulation of blood flow (velocity) and flux (volume) is dependent on local vascular wall (muscular) response and neuronal, sympathetic regulation. The predominant involvement of the parieto-occipital lobes, but also the involvement of brain stem and cerebellum, may be explained by the relative poverty of the sympathetic innervation of the vertebrobasilar vascular system. Other factors mentioned as contributing to PRES are direct toxic influences on the endothelium, vasoconstriction due to the liberation of endothelin, and the formation of microthrombi. What is not explained in any of these theories is the location of lesions in border zones, both parieto-occipital and frontal, suggesting temporary hypoperfusion as responsible factor.

92.4 Therapy

When hypertension is present, treatment of the hypertension and any underlying disease may lead to disappearance of clinical symptoms and MR abnormalities, usually within 14 days. This, of course, also depends on the underlying cause. In patients with eclampsia, delivery of the child when possible and, where necessary, treatment of hematological abnormalities, renal disorders, and hypertension should be

instituted. The positive influence of magnesium sulfate on the eclamptic condition has been recognized for many years, as has the role of pyridoxine in the past few decades. In patients in whom PRES is caused by immunosuppressive and/or chemotherapeutic drugs, the drug regimen has to be abandoned or changed. Once the treatment is stopped, further deterioration may occur for 1 or 2 weeks before improvement sets in. Complete disappearance of clinical and imaging symptoms and signs may occur, but residual damage is not rare.

92.5 Magnetic Resonance Imaging

In many cases of PRES and its variants CT shows hypodensity in the affected areas, predominantly the parieto-occipital regions. In some cases hemorrhages are seen, related to extravasation of erythrocytes.

MRI is more sensitive than CT and allows better delineation of the abnormalities, such as an inventory of all involved areas, their location in border zones, and the involvement of gray as well as white matter. Standard MR techniques, such as T₁-weighted, proton density, T₂-weighted, and FLAIR images demonstrate the lesions. FLAIR usually depicts hemorrhages fairly well. Gradient refocused images should be added to pick up microhemorrhages. Contrast enhancement may be seen in some of the lesions.

The lesions are predominantly located in the parieto-occipital region. In that location they tend towards symmetry, but asymmetrical presentations are not rare. The splenium of the corpus callosum may be involved. Usually the deep white matter is involved, but the overlying cortex is usually affected as well. In other cases the lesions are located in the parieto-occipital and frontal border zones (Fig. 92.1), suggesting that an episode of hypoperfusion has occurred. One must be aware of other presentations: PRES may affect solely the thalamic nuclei, the frontal border zones, the midbrain, the pons, or the cerebellum (Figs. 92.2 and 92.3). In the initial period some mass effect may be present, with secondary effects such as hydrocephalus. In some patients the lesions are extensive (Fig. 92.1); in others they are much more limited (Fig. 92.4). With treatment MRI abnormalities disappear completely or nearly completely in most patients (Figs. 92.2 and 92.5).

Differentiation from other disorders depends on the location. When the border zones alone are affected, other disorders leading to hypoperfusion must also be considered. Isolated involvement of the pons has to be differentiated from central pontine myel-

olysis. Isolated thalamic involvement also occurs in deep venous thrombosis. With a protracted state of the lesions low-grade gliomas have to be ruled out. When only the midbrain, pons, or cerebellum is affected, a correct diagnosis may be extremely difficult and depends on careful interpretation of all MR data in relationship to all the available clinical data.

Most important are the addition of diffusion-weighted imaging and the use of ADC maps (Fig. 92.6). These techniques allow differentiation of areas with low diffusivity, which may progress to infarction, and areas with high diffusivity, probably representing vasogenic edema, which may revert to normal. Unfortunately, results reported in the literature are contradictory. Some authors report decreased diffusivity; others show increased ADC values, or "pseudo"-normalized ADC values, the latter, according to the authors, the result of intravoxel presence of both vasogenic and cytotoxic edema. However, most evidence so far suggests that lesions with a high ADC, probably representing vasogenic edema, are reversible, whereas lesions with a low ADC, representing cytotoxic edema, are irreversible.

Perfusion studies with SPECT and MRI have also shown conflicting results. Both hypo- and hyperperfusion have been reported in the involved areas, as has diffuse hypoperfusion over the entire brain. Because in many cases border zones are involved, one might expect hypoperfusion to occur at some point during the development of the disorder. Perhaps the differences in results of perfusion studies may be explained by differences in the time elapsed between onset of the disorder and the time of the MR examination. The severity and rate of development of the process and underlying factors may be also of importance.

MRS has revealed diffuse metabolic abnormalities in PRES, even in areas that have a normal signal on imaging. Reduced ratios of *N*-acetylaspartate over choline and *N*-acetylaspartate over creatine, with high choline concentrations in the normal-appearing white matter have been reported. Quantification of the metabolites confirmed these findings: low concentration of *N*-acetylaspartate and high concentration of choline. After treatment MRS findings return to normal. Unfortunately there are also MRS studies reporting either no biochemical abnormalities in the affected areas during the acute stages of the disease, or no improvement of the MR spectra despite disappearance of clinical symptoms. Because most studies comprise a single observation or data on a small number of patients, it remains difficult to draw general conclusions.

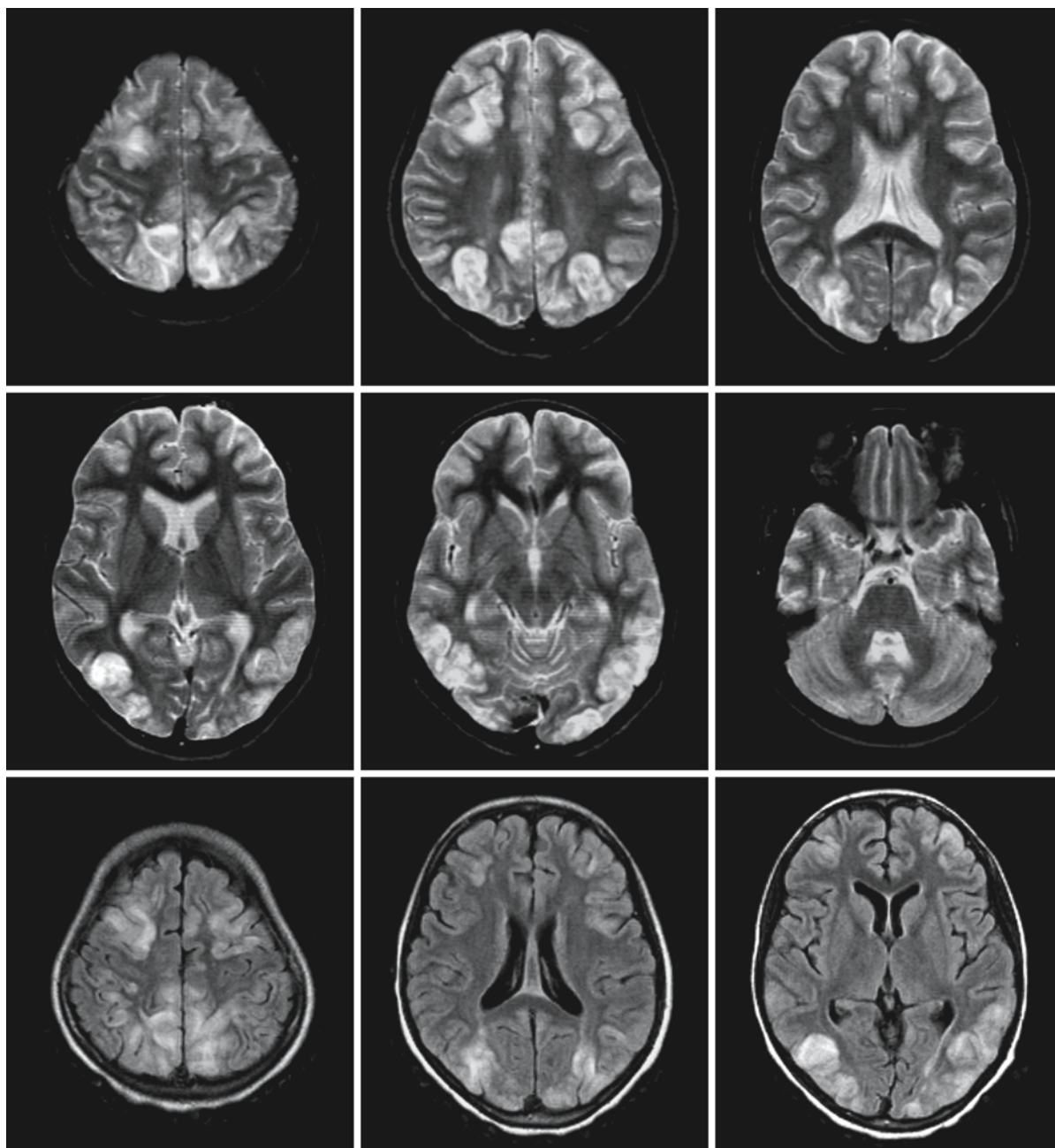


Fig. 92.1. An 11-year-old girl with hypertensive encephalopathy. T₂-weighted images (*first and second row*) show the typical pattern of the posterior reversible encephalopathy syndrome (PRES): nearly symmetrical lesions in the parieto-occipital lobes and the frontal border zones. The lesions involve both

gray and white matter. No abnormalities are seen in midbrain, pons, or cerebellum. On FLAIR images (*third row*) the lesions are more conspicuous, but FLAIR may be less good in depicting lesions in the posterior fossa

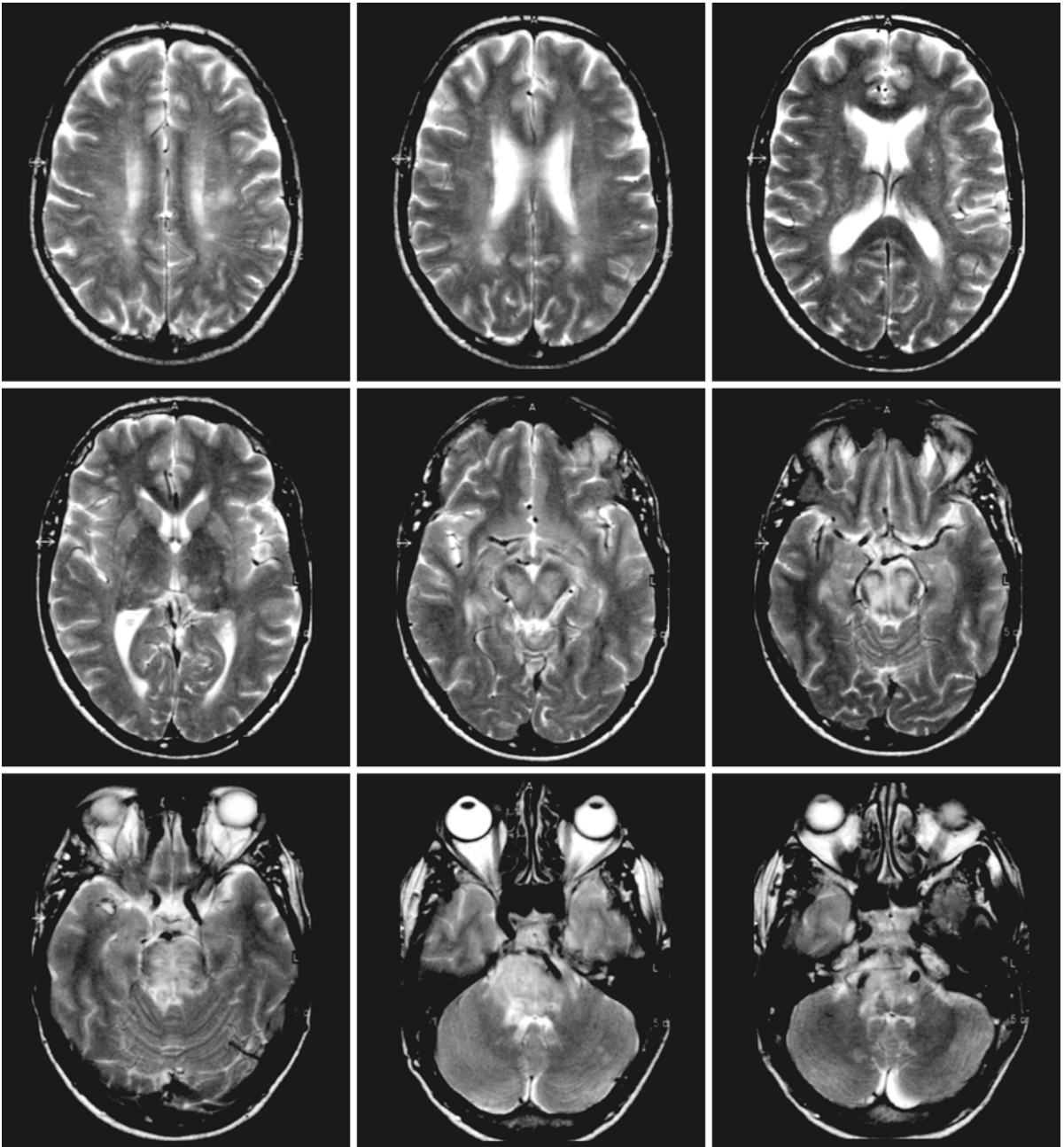


Fig. 92.2. T₂-weighted transverse images in a 58-year-old man with hypertensive encephalopathy (*first three rows*). There are diffuse mild white matter abnormalities in the cerebral hemispheres, but the more important abnormalities are seen

in the midbrain and pons. These latter lesions show some swelling. A repeat MRI was obtained a few weeks later (*fourth and fifth rows*) and show that with treatment all lesions have disappeared

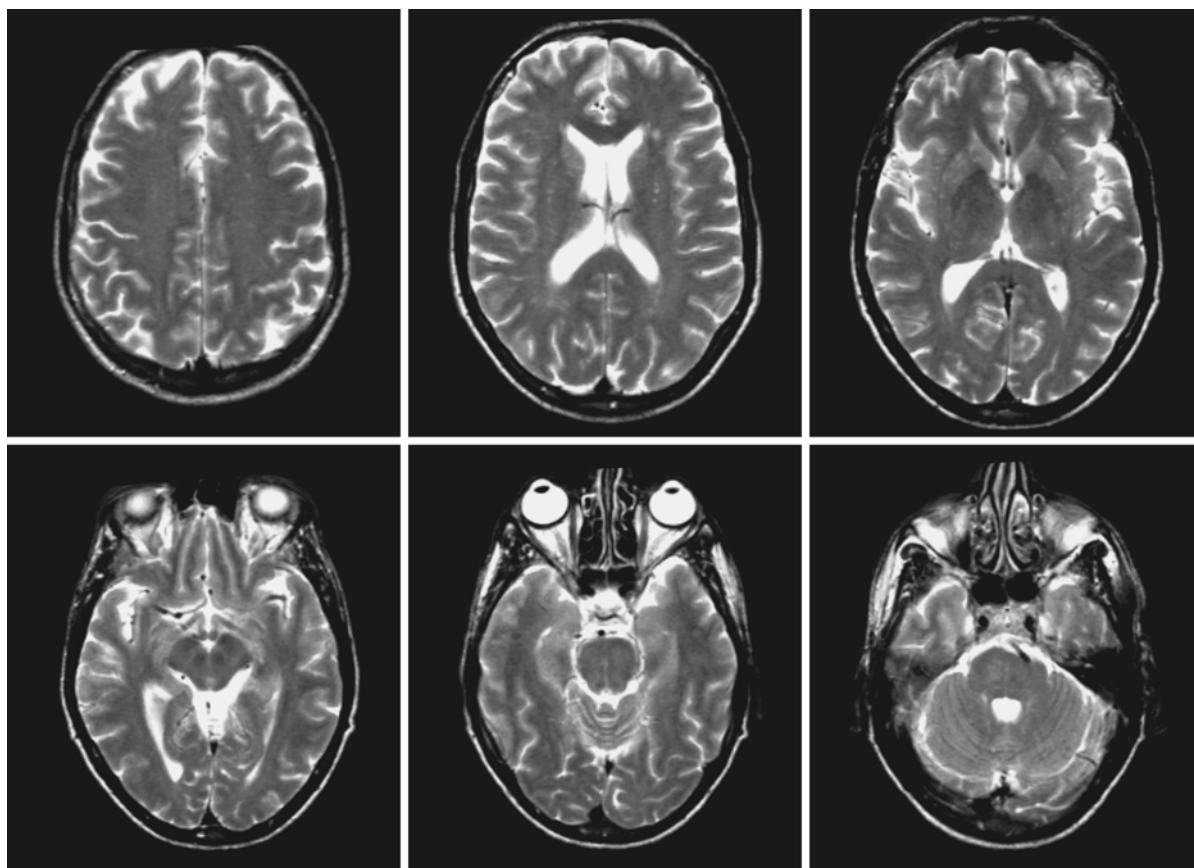


Fig. 92.2. (continued).

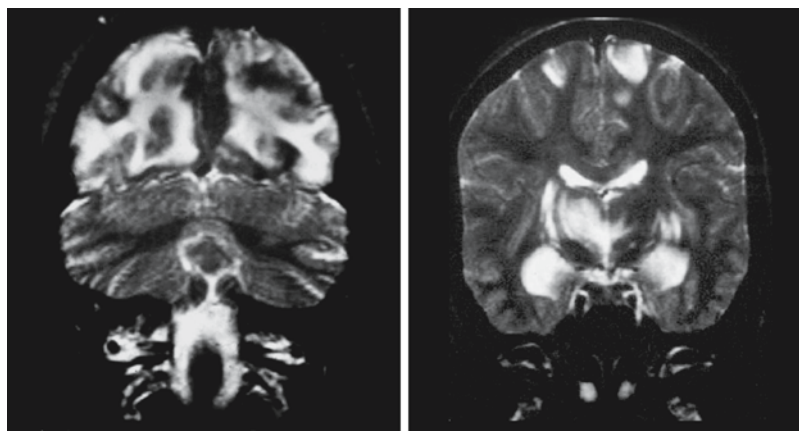


Fig. 92.3. Two coronal T₂-weighted images of a 32-year-old pregnant woman with eclampsia. The *left* image shows extensive involvement of the parieto-occipital lobe; the *right* image shows involvement of the basal ganglia, predominantly on the right side, and of the mesial temporal structures. After delivery and therapy an almost complete recovery followed

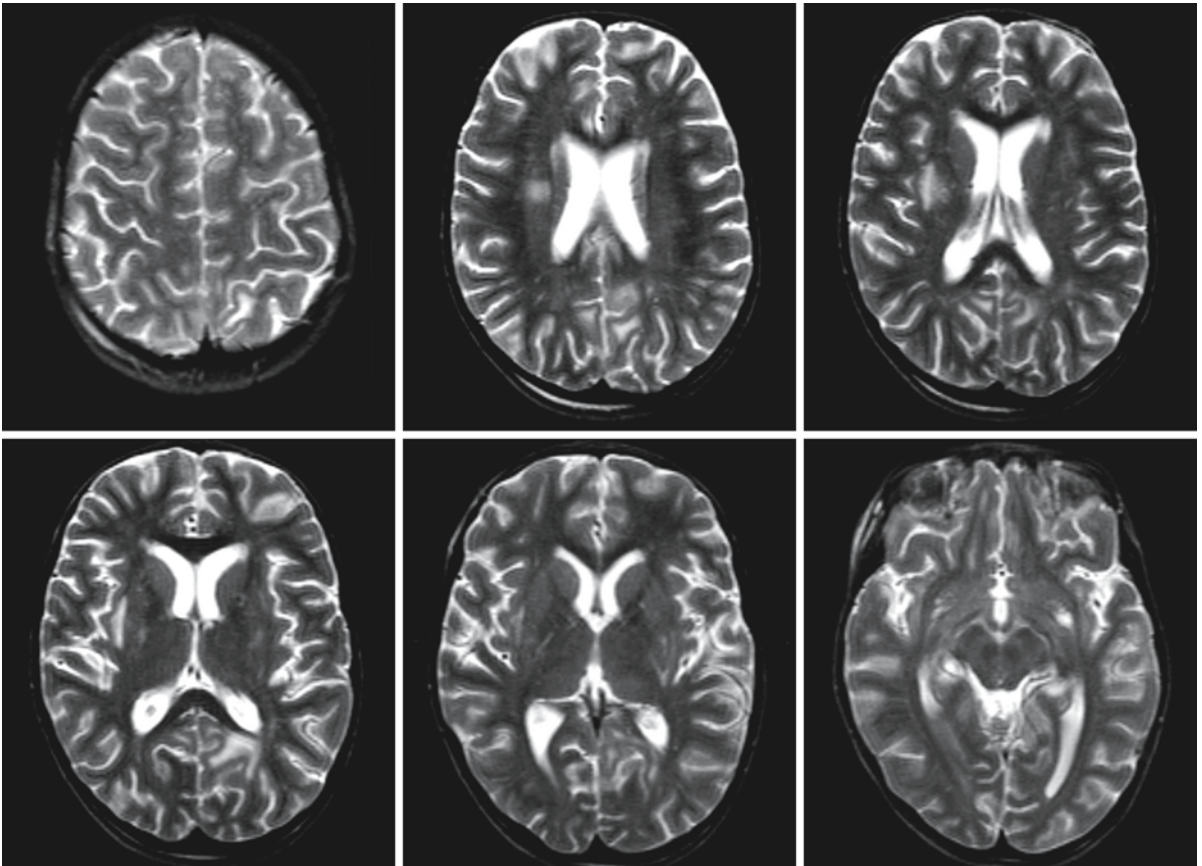


Fig. 92.4. In this 7-year-old girl with reflux nephropathy and hypertensive encephalopathy the T₂-weighted images show only a few lesions with an asymmetrical distribution

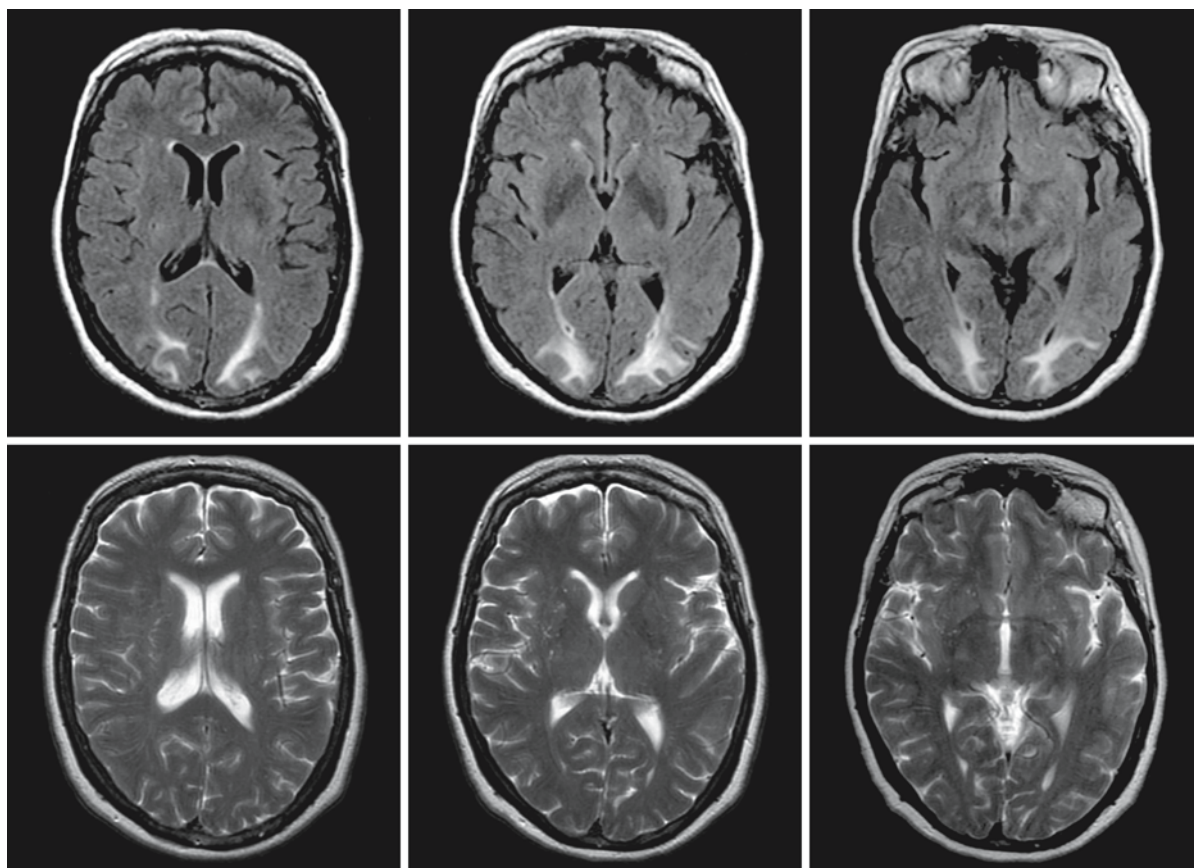


Fig. 92.5. A 63-year-old woman was admitted to the intensive care unit with septic shock, respiratory infection, and diarrhea. After recovery she complained of memory problems. The *upper row* of FLAIR images shows lesions in this phase. The *lower row* of T₂-weighted images shows complete disappearance of

the lesions on follow-up. The MRI findings are highly suggestive of PRES, although the causative factors in this patient are not known. Courtesy of Dr. E.P.J. Arnoldus, Department of Neurology, TweeSteden Hospital, Tilburg, The Netherlands

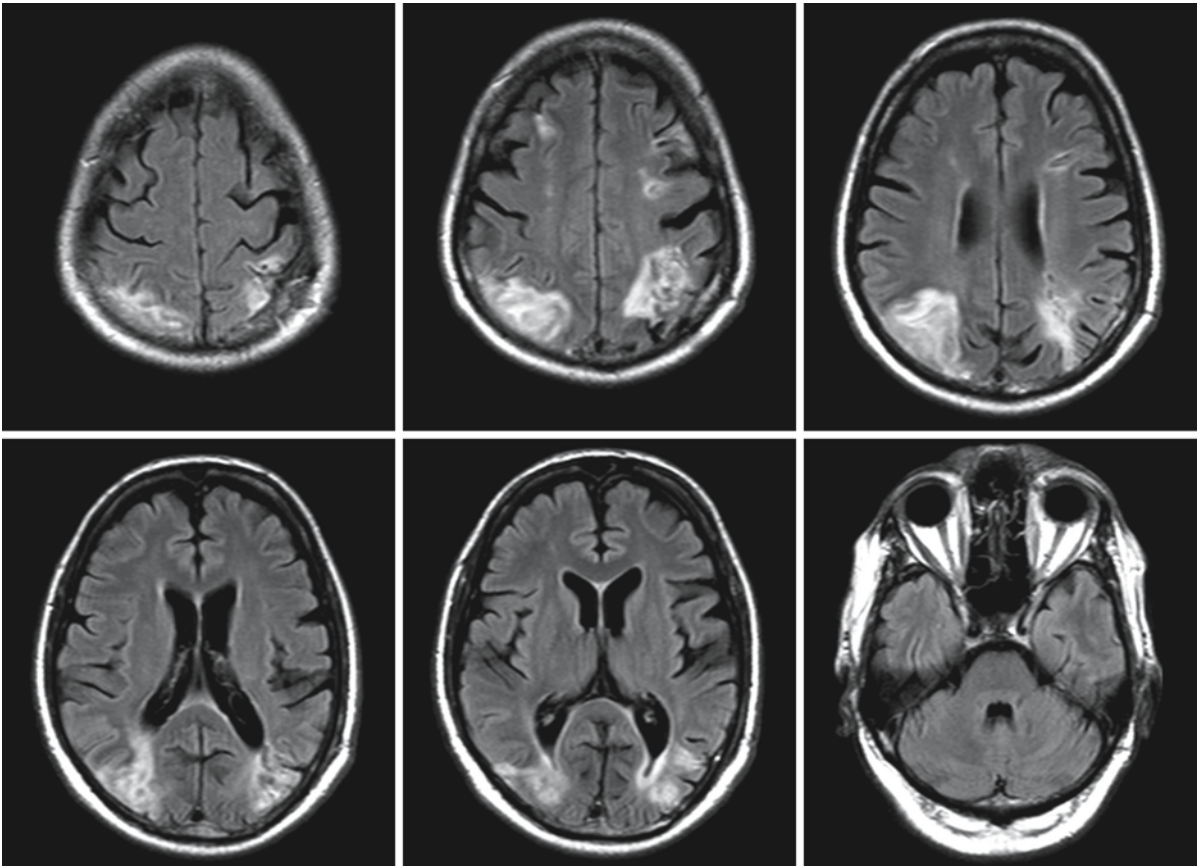


Fig. 92.6. The *first two rows* contain the FLAIR images of a 52-year-old man with hypertensive encephalopathy, showing the common MR pattern of PRES lesions. The *third and fourth rows* show Trace diffusion-weighted images ($b = 1000$), with bright spots in the parieto-occipital area, more extensive on

the right side, and some tiny hyperintense spots in the frontal border zones. The *fifth and sixth rows* show ADC maps with a mixture of higher and lower than average values in the involved areas

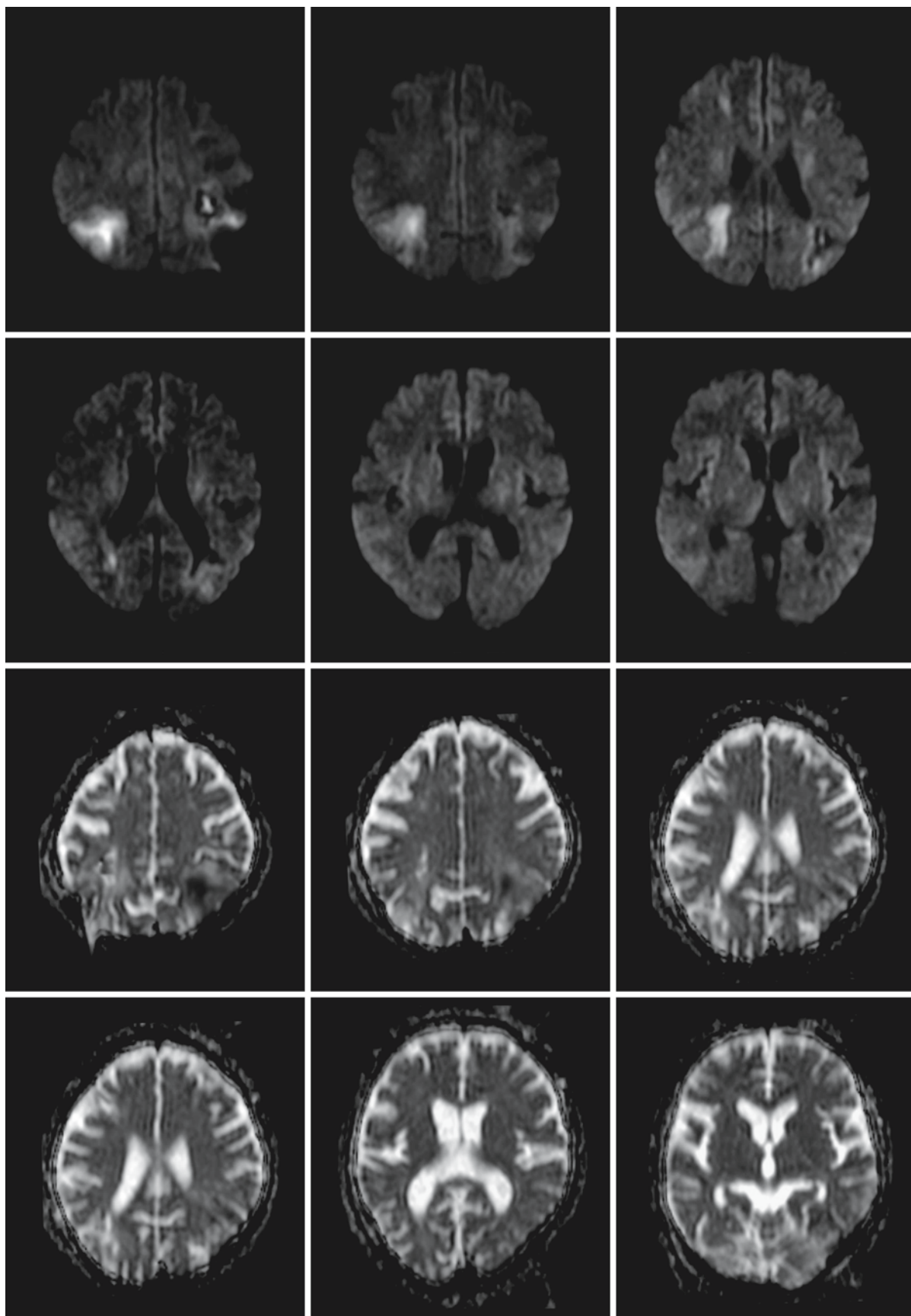


Fig. 92.6. (continued)

Langerhans Cell Histiocytosis

93.1 Clinical and Laboratory Findings

Histiocytosis-X was the name initially given to a group of disorders with seemingly unrelated clinical features, but characterized by the same pathological finding: infiltration of the involved tissue by large numbers of histiocytes, often organized as granulomas. The disease was later renamed Langerhans cell histiocytosis (LCH), after the cell (X) was identified as the Langerhans cell. LCH includes eosinophilic granuloma, Letterer–Siwe disease and Hand–Schüller–Christian disease. The eosinophilic granuloma involves the bone. Letterer–Siwe disease is a multiorgan disease in children under the age of 2 years. Hand–Schüller–Christian disease includes the triad of exophthalmos, diabetes insipidus, and bone lesions.

The second type of histiocytic disorders comprises non-Langerhans histiocytosis, which includes Erdheim–Chester disease, isohemophagocytic lymphohistiocytosis, and histiocytosis with massive lymphadenopathy. Erdheim–Chester disease is mentioned explicitly here, because it can mimic many of the features of brain involvement in LCH.

The third type of histiocytic disorders comprises malignant histiocytosis.

LCH can now be defined as abnormal proliferation of clonal, dendritic Langerhans cells, which can be found in lungs, bone, skin, liver, spleen, lymph nodes, thymus, bone marrow, brain, pituitary, and other endocrine organs. In adults usually only two organs are involved, whereas in younger children LCH is most commonly a multiorgan disease.

Primary involvement of the brain is rare in LCH. Patients who develop CNS disease are likely to have multiorgan disease, with lesions in the calvaria and the temporal and orbital bones. Involvement of the brain and related structures can be subdivided into four different forms: (1) involvement of the pituitary–hypothalamic structures; (2) intra- or extra-axial granulomatous lesions; (3) abnormalities in the posterior fossa, in particular the cerebellopontine pathways; and (4) combinations of these three manifestations, with overlapping symptoms.

Involvement of the pituitary–hypothalamic structures leads to the most common symptom of cerebral involvement, diabetes insipidus. Diabetes insipidus can precede other CNS lesions by more than 3 years. When diabetes insipidus occurs as isolated symptom, it is often referred to as Ayala disease or Gagel granu-

loma. The symptoms and signs of pituitary–hypothalamic involvement vary widely and may include changes in social behavior, appetite, changes of sleep pattern, polyuria and polydipsia, indicating posterior pituitary dysfunction, and growth failure, precocious or delayed puberty, amenorrhea, hypothyroidism, or hypocortisolism, indicating anterior pituitary dysfunction.

Intra- and extra-axial granulomas cause symptoms dependent on their location. The intra-axial lesions can occur in many places, supra- and infratentorial, and behave as space-occupying lesions. Extra-axial lesions may exist as a continuous extension from bone lesions, or they may develop as lesions from the leptomeninges. They may exert pressure on the brain. LCH may also occur in the choroid plexus.

Involvement of structures in the posterior fossa, in particular the cerebellum, are, after diabetes insipidus, the second most common manifestation of CNS involvement in LCH, and may occur many years after the initial diagnosis of LCH. Lesions in the posterior fossa may consist of local granulomas, or of symmetrical abnormalities in the white matter of the hilus of the dentate nucleus and corpus medullare of the cerebellum. Related clinical features are ataxia, reflex abnormalities, tremor, dysarthria, and dysphagia. Combinations of the symptoms and progression of the disease are not rare and may lead to severe CNS deterioration.

Combinations of diabetes insipidus and cerebellar symptoms also occur in Erdheim–Chester disease. Other manifestations of this disease can also be similar to LCH.

Diagnosis of LCH in nearly all cases demands a biopsy and histological confirmation of the pathological Langerhans cell.

93.2 Pathology

Histologically, the granulomatous lesions consist of a proliferation of clonal Langerhans cells, combined with an inflammatory reaction. Four stages are usually distinguished: a hyperplastic–proliferative stage, a granulomatous stage, a xanthomatous stage, and a stage of fibrosis. Lesions in the first stage are most likely to show the characteristics of LCH. Electron microscopy reveals Birbeck granules, characteristic of LCH. Immunostaining can be performed for the

S-100 protein and for CD1a (OKT6) antigenic reactivity, but these tests have a lower level of confidence. Histochemistry demonstrates that LCH and adjuvant T cell lymphocytes in lymph nodes produce high levels of several cytokines, including tumor necrosis factor- α (TNF- α), granulocyte-macrophage colony-stimulating factor (GM-CSF), interferon- γ , and interleukins (IL)-1, -2, -3, -4, -7, and -10. In pulmonary lesions LCH expresses the costimulatory molecules B7-1 and B7-2.

In the lesions in the cerebellar hemispheres no Langerhans cells can be demonstrated. The lesions are characterized by demyelination, gliosis, and loss of Purkinje and granular cells.

93.3 Pathogenetic Considerations

LCH is a proliferative disorder of mesenchymal cells, and can therefore only develop where mesenchymal tissue is present: within the CNS in the meninges, the adventitia of blood vessels, and among free microglial cells. It is unknown what triggers the transformation of normal antigen-presenting dendritic Langerhans cells into the clonal Langerhans cells that are defective in this ability. Clonal proliferation leads to functional deficiency. One theory assumes that LCH cells arise from the adventitia of blood vessels, causing perivascular histiocytic aggregates that develop into larger granulomatous masses with variable portions of foamy histiocytes, eosinophils, microglia, lymphocytes, and plasma cells. In later stages fibrosis and astrocytic gliosis become dominant. Why granulomas have a special affinity to the pituitary and hypothalamic structures remains so far an unanswered question.

The symmetrical lesions located in the cerebellar white matter, also involving Purkinje and granular cells, but without Langerhans cells on histological examination, require a separate explanation. One of the theories compares the cerebellar and pontine lesions in LCH to the cerebellar degeneration seen in paraneoplastic syndromes. In this paraneoplastic syndrome antineuronal (anti-Yu) antibodies can be demonstrated. The search for antibodies against cerebellar tissue has, however, been negative in LCH patients. Another theory proposes a toxic role for the high concentrations of cytokines produced by LCH cells, but again definitive proof is lacking.

93.4 Therapy

Therapy in LCH with CNS involvement is dependent on the nature and extent of the lesion and the secondary implications. It is important to realize that in some patients the lesions tend to regress sponta-

neously with transformation to a fibroxanthomatous state. Such lesions lose the characteristics of LCH. The involvement of other organs, which is usually present, also needs consideration in the treatment planning.

Surgical removal may be an option for intracerebral granulomas. When the resection is incomplete radiotherapy is usually added. Extra-axial locations at the convexity, subdural or arachnoidal, are resected when possible. Lesions of the skull base are less suited to radical surgical removal. Radiotherapy and chemotherapy are then the remaining options. In patients with multiple lesions radiotherapy combined with chemotherapy may control the disease for many years. In patients with diabetes insipidus primary treatment depends on the neuroimaging findings. In patients with a nearly empty sella and lack of high signal on T₁-weighted MRI of the posterior part of the pituitary, substitution therapy is indicated. In patients with granulomatous involvement of the pituitary-hypothalamic system, surgery, irradiation and chemotherapy in addition to hormonal substitution therapy have to be considered. Substances with favorable effects on LCH are steroids, vinblastine, and etoposide (VP16). Etoposide is a semisynthetic epipodophyllotoxin used in the treatment of malignancies of the macrophage and monocyte lineage, but also effective in LCH. It is noteworthy that etoposide may cause a high signal intensity of the basal ganglia on T₁-weighted MR images.

Lesions in the cerebellar white matter not containing Langerhans cells cause a treatment dilemma. If an autoimmune cause is supposed, one could expect benefits from corticosteroids or immunosuppressive therapy. If another explanation is supposed, for instance cytokine toxicity, therapy is unclear. So far no definite guidelines have been suggested for the treatment of the cerebellar white matter abnormalities.

93.5 Magnetic Resonance Imaging

MR is aimed at depicting the different possible manifestations and the different stages of LCH of both the skull and the intracranial contents. To visualize lesions of the skull, the cranial vault as well as the skull base, one can effectively use T₁-weighted images, with and without fat suppression, with and without contrast. This can be combined with using the same T₁-weighted sequences for visualizing the intracranial contents, both the extra- and intra-axial structures, as these sequences are also effective in depicting subdural and leptomeningeal disease manifestations. Granulomatous LCH lesions in the skull base and brain will enhance after contrast injection. In addition T₂-weighted and FLAIR images are indicated to survey the intracranial contents for other manifestations.

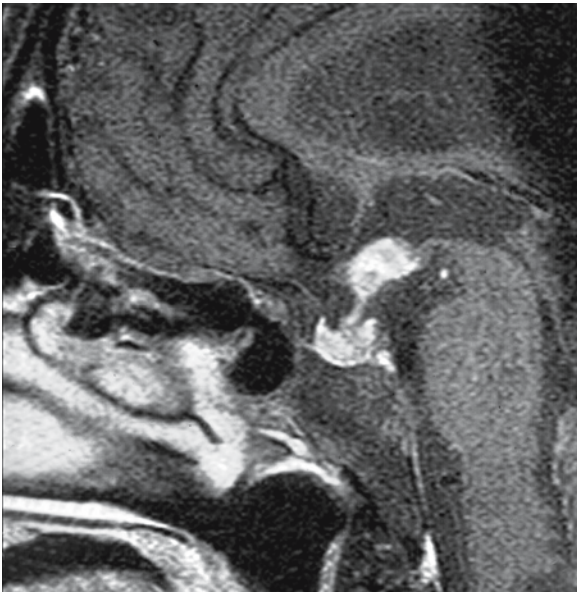


Fig. 93.1. A 65-year-old female patient with histologically confirmed LCH. The midsagittal, T₁-weighted, contrast-enhanced, fat-saturated image depicts a lesion mainly involving the hypothalamus

In patients with involvement of the pituitary–hypothalamus axis, sagittal and coronal T₁-weighted images with fat suppression, without and with contrast injection, will show in some patients a partially empty sella and lack of the bright signal of the posterior pituitary, and in other patients a granulomatous lesion in the suprasellar region, around the pituitary stalk, with or without extension into the skull base and meninges (Fig. 93.1). Infundibular thickening and infundibular atrophy are frequent findings. Other isolated or multifocal intracerebral lesions, for example LCH of the choroid plexus, or space-occupying lesions in the frontal, temporal, parietal, or occipital

lobes, show up on the sequences indicated above. In all cases one can expect enhancement of the granulomatous lesions.

There are also two possible types of lesions in the posterior fossa. First of all, granulomatous manifestations of LCH can be observed, space-occupying, enhancing after contrast, and usually asymmetrical. Secondly, bilateral, symmetrical, confluent signal abnormalities can be seen in the white matter of the hilus of the dentate nucleus, the corpus medullare of the cerebellum, and the pons (Figs. 93.3 and 93.4). The bilateral cerebellar lesions do not represent LCH lesions, do not show mass effect, and do not enhance (Figs. 93.3 and 93.4). In these patients, the dentate nucleus often has a high signal on T₁-weighted images. The globus pallidus and, less often, the caudate nucleus may also have a high signal intensity on T₁-weighted images (Figs. 93.3 and 93.4). Within the supratentorial white matter, enlarged perivascular spaces are frequently present. Contrast enhancement following a vascular pattern may be present. More prominent, patchy white matter abnormalities not following a vascular pattern may also be present.

In Erdheim–Chester disease, a non-Langerhans histiocytosis, similar lesions as described for LCH may be seen (Figs. 93.2 and 93.5). Granulomatous lesions may be found in the sellar and suprasellar region as well as in other areas (Fig. 93.2). Progressive intra-axial lesions have been reported involving the pons, superior part of the medulla oblongata, the cerebellar peduncles, and areas around the fourth ventricles, as well as an extra-axial mass with encasement of the vertebral artery. Autopsy in one of these cases revealed histiocytic infiltration of the cerebellar pathways, in particular the base of the pons and the middle cerebellar peduncles. The nonenhancing symmetrical bilateral lesions in the cerebellar hemispheres with clinically a progressive spastic–ataxic syndrome may also occur in Erdheim–Chester disease (Fig. 93.5).

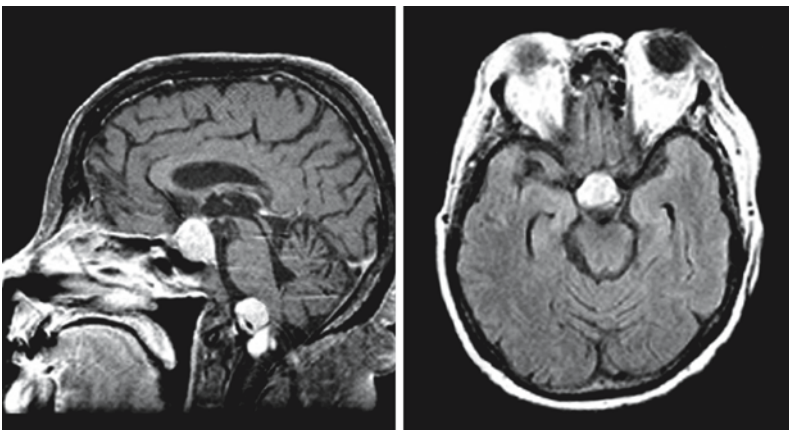


Fig. 93.2. A 55-year-old woman with Erdheim–Chester disease, as confirmed at autopsy. The sagittal T₁-weighted image with contrast shows an intra- and suprasellar process, enlarging the sella turcica and reaching upward unto the optic chiasm. A second, extra-axial lesion is located anteriorly in the craniovertebral junction. Both lesions enhance homogeneously. The axial FLAIR image reveals the lesion with high signal intensity. From Thorns et al. (2003), with permission

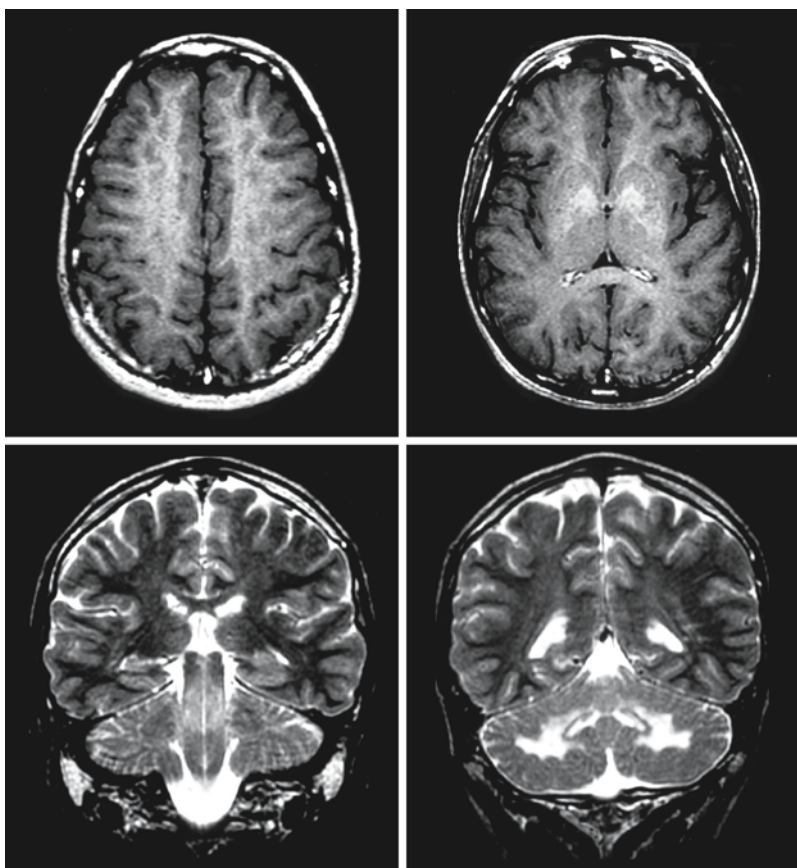


Fig. 93.3. A 16-year-old male patient with LCH. The T₁-weighted images (*upper row*) reveal high signal intensity in the globus pallidus. The coronal T₂-weighted images (*second row*) of the posterior fossa show hyperintensity of the cerebellar white matter and the brain stem

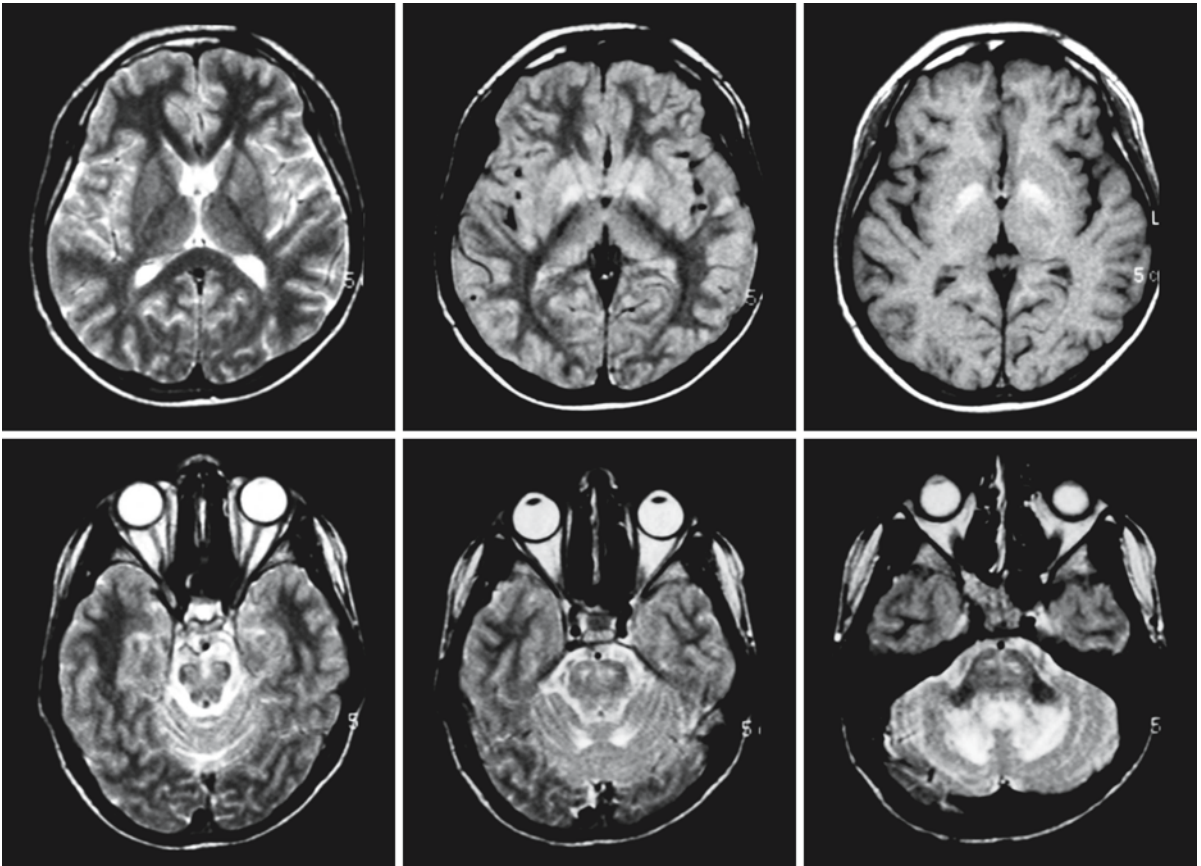
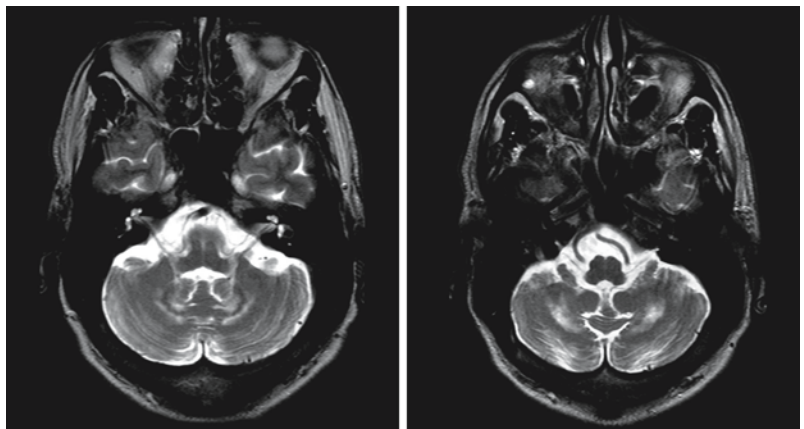


Fig. 93.4. A 17-year-old boy with LCH. The *upper row* shows T₂-weighted (*left*), proton density (*middle*), and T₁-weighted (*right*) images at the level of the basal ganglia. The globus pallidus has an increased signal on all these images. The *second*

row shows the T₂-weighted images at the level of the brain stem and cerebellum. The tracts in the midbrain and base of the pons as well as the cerebellar white matter display a high signal. From Saatci et al. (1999), with permission

Fig. 93.5. A 44-year-old man with Erdheim–Chester disease. The T₂-weighted images show hyperintensity of the cerebellar white matter. From Weidauer et al. (2003), with permission



Post-Hypoxic–Ischemic Damage

94.1 Pathogenetic Factors

In hypoxic and ischemic conditions the supply of oxygen and nutrients to brain tissue is compromised. If this condition lasts for some time, changes occur in cells and tissues, eventually leading to cell death.

The first change to occur at a molecular level is the replacement of the highly efficient aerobic glycolysis, which delivers 38 molecules of adenosine triphosphate (ATP) for one molecule of glucose, by inefficient anaerobic glycolysis with only 2 molecules of ATP for one molecule of glucose. Under aerobic conditions the major product of glycolysis is pyruvate, which is metabolized to acetyl-CoA (activated acetate), which enters the citric acid cycle. Under anaerobic conditions, pyruvate is not converted into acetyl-CoA, but into lactate, a potentially harmful compound.

Energy depletion leads to membrane depolarization and disturbed transport of ions across membranes of organelles and cells. Concentration and voltage gradients are no longer maintained; water is osmotically drawn into the organelles and cells, causing them to swell. These changes may be reversible, but if the hypoxic condition lasts too long, irreparable damage with cell death will occur. Morphologically this point of no return is indicated by the appearance of cloudy precipitations within the mitochondria. Apparent changes in the inner membrane of the mitochondrion, where oxidative phosphorylation takes place, occur much later.

94.2 Reperfusion Damage

Repair of the condition that has caused the hypoxic–ischemic changes, with restoration of blood circulation and oxygen supply, can introduce additional damage in ischemic cells. This means that cells that are reversibly damaged are again threatened, now by the harmful effects of reperfusion. Two factors are assumed to play a critical role as causative agent in this additional damage: the calcium factor and the oxygen paradox.

The concentration of Ca^{2+} in blood is much higher than in the cell. A Ca^{2+} gradient is maintained across the cell membrane with ATP as energy donor. Lowering of the ATP concentration leads to influx of Ca^{2+} and Na^+ into the cell. Ca^{2+} is first stored in organelles,

such as the endoplasmic reticulum and mitochondria, and it is not until these are flooded that the cytosol concentration of Ca^{2+} will increase. Ca^{2+} is a cofactor for certain enzymes, including proteases and phospholipases, which will attack functional components of the cell such as lipids and proteins. High Ca^{2+} levels in the cytosol are at the core of many detrimental biochemical cascades.

The oxygen paradox is based on the observation that oxygen supplied after a hypoxic episode causes additional damage. This is explained by the action of oxygen radicals. Free radicals are compounds with a lone electron in an outer orbital, which are, therefore, highly reactive. They are normally present in the mitochondrial electron transport chain of all cells and are kept under control by physical and chemical coupling. The defense mechanisms against the toxic effect of oxygen radicals include a low oxygen pressure at the cellular level, and enzymatic decomposition of oxygen radicals by enzymes and scavengers, such as superoxide dismutase and catalase, as well as antioxidants, such as α -tocopherol (vitamin E) and ascorbic acid (vitamin C). The latter compounds are fat-soluble and water-soluble, respectively. Superoxide dismutase snatches away the superoxide ion; catalase counteracts the effects of hydrogen peroxide. However, under conditions of hypoxia–ischemia, and in particular after restoration of oxygen supply, these defense mechanisms may be overwhelmed. One of the cascades that then become active is the xanthine oxidase reaction. Under anaerobic conditions, ATP is broken down in larger than usual quantities via ADP to AMP, to inosine and hypoxanthine, and finally to uric acid under the enzymatic influence of xanthine dehydrogenase. The raised Ca^{2+} concentration in the cytosol activates proteases, which convert xanthine dehydrogenase into xanthine oxidase, thereby producing a superoxide anion (O^\cdot). Superoxide anions, once formed from this xanthine oxidase system, react with iron salts to form perhydroxyl radicals (OH^\cdot). This chemical process is described as the superoxide-driven, iron-promoted Haber–Weiss reaction. This reaction occurs when free Fe^{2+} is present: under hemorrhagic conditions or in structures whose natural iron content is high. Targets for the perhydroxyl radicals are polyunsaturated fatty acids, compounds that are highly vulnerable to peroxidation. Polyunsaturated fatty acids reside in the midzone of biomembranes, spatially separated from the site of generation

of active oxygen. Under hypoxic-ischemic conditions, with activation of Ca^{2+} -dependent enzymes in the cells, in particular proteases and phospholipases, this is no longer the case. The polyunsaturated fatty acids in the cell membrane come under attack and become new sources of oxygen radicals. The superoxide anion withdraws a proton from a polyunsaturated fatty acid, creating a lipid with an unpaired electron. This newly created lipid radical (L^{\cdot}) reacts with O_2 (reperfusion) and forms a lipid peroxy radical (LOO^{\cdot}). This compound will withdraw a proton from a nearby polyunsaturated fatty acid, creating a new radical and initiating a chain reaction. Iron plays a very important catalytic role in lipid peroxidation. In a normal adult about 4 g iron is present in hemoglobin. Myoglobin contains 10% of total body iron and a small part is present in enzymes and in the transport protein transferrin. The remaining iron is found in storage proteins such as ferritin. Free iron is not usually present in peripheral blood. Iron from ferritin is liberated at pH values lower than 6, which may occur under conditions of severe hypoxia. Superoxide anions are also capable of dissociating the iron-ferritin complex. Lipid peroxy radicals can even dissociate iron from hemoglobin molecules. Hemorrhagic conditions, such as hemorrhagic infarctions, infections, contusions, and subarachnoid hemorrhages, create the optimal environment for these deleterious reactions.

In the formation of free radicals the polyunsaturated fatty acid arachidonic acid, abundant in cell membranes, has a special place. Arachidonic acid is metabolized by at least three enzymes: cyclooxygenase, lipoxygenase, and cytochrome P-450 oxygenase. All three pathways are capable of producing superoxide radicals. The cyclooxygenase pathway leads to the formation of prostaglandins and thromboxanes, which influence, amongst others, the microcirculation. The lipoxygenase pathway leads to the formation of leukotrienes, which may induce edema and necrosis and further inhibit microcirculation. Cytochrome P-450 oxygenase leads directly to the formation of oxygen radicals. There is interaction at each level of the components of this cascade, leading to either stimulation or inhibition of effects of the other components.

Free radicals are formed by many other mechanisms. They can be formed by membrane-bound enzymes on the surface of neutrophils and phagocytes, which are activated by endotoxins from bacteria, or by cytokines, inducing the so-called oxygen burst of phagocyte membrane compounds in the acute phase of infections.

Nitric oxide (NO^{\cdot}) is a reactive free radical, which can inhibit mitochondrial respiration. It is one of the major defense molecules against microbes and malignant cells. It has recently been reported to act as a highly unorthodox messenger molecule within the

CNS and there is evidence that it may contribute to excitotoxicity. It is a simple molecule which is synthesized from L-arginine by the enzyme nitric oxide synthase. Nitric oxide synthase is present in endothelial cells. There are several isoforms and the neuronal isoform is activated by high cytosol Ca^{2+} . Once formed, nitric oxide diffuses to neighboring cells and reacts with guanylate cyclase, inducing the formation of cyclic guanosine monophosphate from guanosine triphosphate. Cyclic guanosine monophosphate influences the relaxation of smooth muscles, including blood vessels. Nitric oxide preferentially combines with superoxide anions when present, leading to the formation of highly reactive peroxynitrite, which causes cell damage. The resulting drop in cyclic guanosine monophosphate leads to vasoconstriction. On the other hand, nitric oxide can be changed to a chemical state that has the opposite effect, i.e., a protective effect. In the presence of electron donors such as ascorbate or cysteine, nitric oxide becomes nitrosonium ion (NO^+), which binds to a regulatory site on the most prominent receptor of excitatory amino acids, resulting in decreased activity of this receptor. The deleterious action of free radicals, as mentioned before, is dependent on the presence of oxygen. Therefore, most of the damage occurs during reperfusion after ischemia. The capacity of tissue to neutralize free radicals is called the antioxidance capacity. During ischemia and reperfusion, this capacity decreases rapidly. The decrease is greater in experiments in which some blood is still perfusing the ischemic area than when the oxygen supply is totally arrested. This is understandable because the presence of oxygen is needed for free radical damage to occur.

The recognition of the harmful effects of free radicals has induced a worldwide search for counteracting compounds. Several pharmaceuticals are under consideration as cerebroprotective agents. Free radical scavengers are used to diminish negative effects of cranial trauma or cerebral hypoxia. Substances such as vitamin E, N-acetylcysteine, and dimethylsulfoxide are used for this purpose. Vitamin E works by offering a competitive binding site to superoxide anions. Allopurinol counteracts the effects of xanthine oxidase, and is effective in diminishing the influence of one of the cascades. The 21-amino steroids (lazaroids) have been proven to be potent inhibitors of lipid peroxidation. Calcium entry blockers are considered to prevent high Ca^{2+} concentrations in the cytosol and inhibit the formation of Ca^{2+} -dependent enzymes. Not all newly conceived drugs have met the theoretical expectations. Often, of course, in clinical situations the therapy starts when most of the damage has already been done. Moreover, the processes behind post-hypoxic-ischemic encephalopathy are complicated. And also: free radicals are not the only factors that have to be taken into account.

94.3 Excitatory Amino Acids

Overstimulation of neurons by excitatory amino acids (EAAs), in particular glutamate and aspartate, can lead to cell dysfunction and, eventually, neuronal death. EAAs serve as excitatory neurotransmitters, as opposed to inhibitory neurotransmitters, of which γ -aminobutyric acid (GABA) is the most prominent. These amino acids play a role in the normal messenger system of the CNS. Under normal circumstances the potentially harmful accumulation of EAAs is prevented from happening. After conversion from glutamine, glutamate is released in the synapse, making contact with glutamate-responding receptors. On the distal side of the synapse, glutamate is broken down to glutamine, which re-enters the presynaptic side, or is taken up by a glutamate transporter into a nearby astrocyte for further transformation. The ensuing neuronal depolarization is very short-lived. This glutamate reuptake chain is energy-dependent. In energy-deprived conditions glutamate accumulates in the extracellular space and causes neuronal overstimulation. There are several mechanisms leading to abnormal glutamate accumulation. For example, the role of the glutamate transporter in the astrocyte may be compromised, because of the collapse of the gradients for Na^+ and K^+ across the cell membrane. Its function may even be reversed and the transporter may become a source of extracellular glutamate. Or, in case of cell injury, glutamate may leak out of damaged cells. Every cell contains enough glutamate to cause damage to many neighboring cells.

Further analysis of the excitatory synapses reveals that at least three types of glutamate receptor can be distinguished. The EAA receptors are classified according to their typical agonists: *N*-methyl-D-aspartate (NMDA), quisqualate (QA), kainate (KA), and 2-amino-4-phosphonobutyrate (AP_4). Each class of receptor has distinct pharmacological properties and anatomical distribution. The NMDA receptor is the best understood. It contains an NMDA recognition site and a cationic ionophore, allowing Na^+ and Ca^{2+} to enter the cytosol. Other sites are an Mg^{2+} binding site and a Zn^{2+} binding site, probably for noncompetitive inhibition of the ionophore. A glycine site has also been recognized for positive allosteric modulation at the receptor site. Agonists and antagonists of each of these sites are known. For example, agonists for the NMDA site are L-glutamate and L-aspartate; an antagonist is carboxypiperazine propyl 1-phosphonate. At the ionophore site antagonists are phencyclidine, imine maleate (MK 801), ketamine, and dextromethorphan. At the glycine site, glycine and D-serine are agonists; kynurenate is an antagonist.

Agonists and antagonists for the quisqualate and kainate receptors have also been identified. They are directly involved in the regulation of Ca^{2+} and Na^+

concentration in the cell. These non-NMDA receptors open channels to allow Na^+ and Cl^- into the cell under anoxic conditions, passively causing the entrance of H_2O and cell edema.

The action of these EAA receptors is fundamental in the concept of excitotoxicity. Effects of overstimulation by EAAs have been considered to play a role in many different neurological disorders, for example, in epilepsy, hypoglycemia, trauma, AIDS dementia complex, Huntington chorea, amyotrophic lateral sclerosis, toxic encephalopathies, and perhaps Alzheimer disease, making the described mechanism a “final common pathway” of neuronal injury.

Evidence has been provided to support the concept that in vivo high levels of endogenous EAAs, such as glutamate and aspartate, also play a critical role in brain damage caused by hypoxic–ischemic insults. As has already been stressed, glutamate reclaim after the synaptic release is highly energy-dependent. In low-energy states glutamate accumulates in the extracellular spaces, leading to neuronal overstimulation with excessive anionic and cationic fluxes and, in the acute phase, to intracellular edema and osmotic lysis, which may be the cause of instant cell death. Resulting high concentrations of Ca^{2+} in the cytosol contribute to delayed cell death. In vitro tests have shown that these two processes, the osmotic instant lysis and the delayed Ca^{2+} -dependent neuronal death, can be separated by manipulating the conditions. The possibility of preventing each type of damage by different biochemical environments also confirms this difference. This knowledge is potentially of use in therapeutic interventions.

Antagonists of EAAs have been tested in cell cultures, animal experiments, and clinical trials of their “cerebroprotective” properties. In the clinical tests, especially, the results so far have been disappointing. This may be because the whole process is extremely complicated and an antagonist interferes somewhere in this complex process with unexpected reactions and effects, or because there is insufficient passage through the blood–brain barrier, or because the administration of drugs in humans usually occurs when the damage has already been done.

94.4 Patterns of Morphological Changes of White Matter in Hypoxic–Ischemic Encephalopathy

Hypoxemia, a reduced oxygen content of the arterial blood, occurs clinically in many conditions, including asphyxia, severe pulmonary failure, respiratory insufficiency, arrest, and incorrect anesthesia. Ischemia or oligemia is a reduction in blood flow. This condition exists where arteries are occluded, in exsanguination, and in cardiac arrest. Hypoxia, ischemia, and hypo-

glycemia have the same effect on the brain. Neurons are usually most susceptible, but there is also a hierarchy of vulnerability within the group of neurons, as is discussed in the chapter on selective vulnerability (Chap. 3). Under certain conditions, however, for example an early stage of development, white matter may be more vulnerable than gray matter. This is particularly the case in preterm infants.

Several patterns of morphological post-hypoxic–ischemic damage can be distinguished:

1. Focal lesions, the distribution of which depends at least in part on vascular patterns:

- (a) *Arterial territorial pattern*. If the perfusion through one major artery fails, the territory supplied by this artery is compromised. The initial cytotoxic edema affects all structures, gray and white.
- (b) *The arterial border zone pattern*, due to diminished perfusion, mostly leads to changes in the parietal region, or along the frontal parasagittal border between middle and anterior cerebral arteries. Other border zones may, however, also be involved.
- (c) *Focal symmetrical abnormalities* occur preferentially in the basal ganglia in patients with chronic hypertension and concurrent vascular changes. *Etat lacunaire* is the ancient denotation of a condition in which multiple small, old, cystic infarcts are seeded throughout the basal ganglia, leading to a highly characteristic appearance. This condition is difficult to separate from the *état criblé* (cribriform atrophy) caused by the widening of the Virchow–Robin spaces around tortuous vessels.
- (d) *Periventricular leukomalacia* occurs in older patients in subcortical arteriosclerotic encephalopathy, also referred to as Binswanger disease. Periventricular leukomalacia also occurs in prematurely born infants.

2. Lesions due to generalized hypoxia–ischemia:

- (a) *Cortical and subcortical gray matter damage*. Typical involvement of the “topistic” areas as described by Vogt and Vogt (1937) is the result of generalized hypoxia–ischemia. Morphologically changes occur in the most vulnerable areas, resulting in cortical laminar necrosis, Sommer’s sector necrosis (hippocampus necro-

sis), striatum necrosis, and Purkinje cell necrosis. At least two factors are involved in this selective involvement of particular brain structures. First the *distribution of excitatory amino acid receptors* is important. The differences in concentration of EAA receptors can lead to focal damage in areas with higher receptor density. These areas are to a large extent the areas involved as mentioned above. Secondly, a role is also played by *reperfusion damage and free radical action*. As has been explained, the Haber–Weiss reaction occurs especially in areas with a high iron concentration, including the thalamus, globus pallidus, substantia nigra, and several cortical layers.

- (b) *Specific involvement of zones of active myelination*. Following asphyxia in term-born neonates, lesions are frequently seen in the dorsal part of the putamen, the ventrolateral nucleus of the thalamus, and in the hippocampus. They are often combined with damage in the white and gray matter bordering the central sulcus, leading to local atrophy and sclerotic ulegyria. The explanation for the vulnerability of these affected areas at this time is the active myelination taking place at term in these areas, with high chemical turnover and high regional blood flow.

- (c) *Diffuse white matter injury*. In delayed post-hypoxic–ischemic demyelination there is usually diffuse involvement of all the white matter. This is seen in rare cases after cardiac arrest, errors in anesthesia, and in toxic encephalopathies, in particular after carbon monoxide and cyanide poisoning. The same pattern is seen in diffuse white matter injury after irradiation and chemotherapy, in which diffuse vascular changes play an intermediary role.

3. Miscellaneous lesions affecting both gray and white matter:

A number of congenital conditions such as encephaloclastic schizencephaly, hydranencephaly, and porencephaly are probably the result of hypoxic–ischemic conditions during pregnancy. The conditions that primarily lead to white matter changes will be discussed in separate chapters.

Post-Hypoxic–Ischemic Encephalopathy of Neonates

J. Valk, R.J. Vermeulen, M.S. van der Knaap

95.1 Clinical Features and Laboratory Investigations

Periventricular leukomalacia (PVL) is a post-hypoxic–ischemic leukoencephalopathy resulting from pre- or perinatal hypoxic–ischemic insults. Little (1861) was the first to describe the clinical picture of the condition. It occurs in particular in preterm neonates with a gestational age of 32–36 weeks. Major risk factors are prematurity and intrauterine infection. Before that time, at a gestational age of 28–32 weeks, germinal layer, intraventricular, and intraparenchymal hemorrhages predominate. PVL is rarely seen in term neonates; if present, it is often in combination with cardiac disorders, intrauterine growth retardation, or any other sign of intrauterine incidents. There is a distinct relationship between PVL and the clinical concept of “cerebral palsy,” although it should be realized that the concept of cerebral palsy comprises all infants with a stable handicap which occurred before the age of one year. The increasing technology in neonatal medicine has made it possible to keep more premature infants alive. As a consequence, PVL as a cause of cerebral palsy has increased in relative frequency.

The typical location of PVL in the periventricular region, interfering with the corticospinal tracts of the legs more than of the arms, is responsible for the resulting spastic diplegia, tetraplegia (legs more severely affected than arms), or hemiplegia (leg more severely affected than arm). Patients with motor disability and PVL have a relatively high incidence of seizures. Epilepsy in patients with PVL is associated with multiple seizure types. Mental development is relatively better preserved than motor development, although there is increasing evidence that there are also cognitive deficits in PVL. Extension of the leukomalacia into the optic radiation may lead to cortical blindness or, more often, delayed visual maturation. The CNS manifestations of PVL take 1 or 2 years to show the full clinical impact.

In older preterm infants the white matter damage tends to have a more peripheral, subcortical location. This condition is known as subcortical leukomalacia (SCL). In fact, PVL and SCL form a continuum, and SCL as a rule includes periventricular white matter damage. Clinically, so-called SCL leads to a more severe handicap than PVL. The children have spastic tetraplegia, are mentally more severely retarded, and

often have epilepsy. Delayed visual maturation and cerebral visual failure are usually present.

A third group of neonates develop a multicystic encephalopathy (MCE). Patients with MCE are more often born at term than preterm. In the majority of the children the clinical signs of a devastating encephalopathy are unexpected. The typical clinical course usually includes initially not very alarming signs of fetal distress, such as prolonged bradycardia or meconium-stained amniotic fluid, followed by moderate starting problems after delivery and rapid partial recovery. Several hours later a devastating encephalopathy develops, characterized by lowered consciousness, seizures and, on ultrasound, generalized cerebral edema. These patients have a very poor outcome, with microcephaly, severe developmental retardation, spastic tetraplegia, visual handicap, and seizures.

A special clinical picture is seen as the result of acute profound hypoxia–ischemia in term or post-term babies. In the course of the first year of life an extrapyramidal movement disorder becomes apparent with choreoathetosis, dystonia, and orobuccolingual dyskinesia in combination with variable spasticity and variable mental retardation, although mental capacities are often better preserved. The motor handicap is usually very severe, the combination of extrapyramidal and pyramidal abnormalities leading to serious impairment of intentional movements. This clinical picture is associated with lesions of the basal nuclei and the central, perirolandic cortical and subcortical area. A similar clinical condition may occur in preterm neonates, when they undergo a similar episode of acute profound hypoxia–ischemia, but the central cortical and subcortical areas are not similarly involved, probably due to the state of myelination in the preterm born infants.

It is estimated that post-hypoxic–ischemic encephalopathy is the cause of 90% of cases of cerebral palsy. For decisions on how to proceed with the treatment of a very sick patient in the neonatal intensive care unit, it is extremely useful to be able to predict the outcome of damage at an early stage. For the prediction of the outcome of pre- and perinatal injury one has to rely in the early phase on clinical symptomatology and paraclinical test results available at the time. A classification of the severity of post-hypoxic–ischemic encephalopathy was proposed by Sarnat and Sarnat (1976) for neonates with a gesta-

tional age of over 36 weeks. This classification, based on clinical and EEG findings, has been shown to have prognostic significance and is the standard of clinical scoring in neonatal intensive care unit in infants with post-hypoxic-ischemic encephalopathy. Stage I usually occurs during the first 24 h of life and is characterized by jitteriness, a state of irritability, hyperalertness, sympathetic nervous system preponderance, uninhibited reflexes, and a normal EEG. Stage II consists clinically of hypotonia, lethargy, or obtundation for at least 12 h after birth, strong distal flexion, parasympathetic predominance, and multifocal seizures. EEG displays periodicity, sometimes preceded by continuous delta wave activity. The period between 48 and 72 h is critical, during which the encephalopathy either worsens or improves. Stage III is characterized by suppression of brain stem and autonomic functions, stupor or coma, and generalized flaccidity. Mechanical ventilation is necessary. The EEG is isoelectric or shows a burst-suppression pattern. Persistence of stage II for less than 5 days and absence of entry in stage III are associated with favorable outcome. Entry into stage III, failure of the EEG to return to normal, or persistence of stage II for longer than 7 days predicts a poor neurological outcome.

In a large cohort, including 1807 preterm (32–36 weeks gestational age) and very preterm (25–32 weeks gestational age) infants it was shown that there was a significant inverse relationship between umbilical cord pH and base excess values and subsequent adverse outcome for infants delivered preterm (Victory et al. 2003). Determination of CSF lactate levels in 150 nonasphyxiated and 46 asphyxiated neonates showed a significant relationship between elevated lactate levels, fetal distress, and APGAR scores and seems to be an objective way of assessing the severity of cerebral hypoxia (Mathew et al. 1980).

Abnormal VEP and SSEP results carry some negative prognostic value.

Ultrasound (US), being versatile and a bedside examination, is the imaging modality of first choice in the neonatal intensive care unit. It can help to identify areas of hyperechogenicity located around the trigonum or the frontal horns with onset 3–7 days after the hypoxic-ischemic incident. This hyperechogenicity is either transient or progresses to cysts in about 7–14 days. This time delay is also reported in histological studies. US can be helpful in demonstrating SCL, depending on the type of equipment. US is also helpful in demonstrating germinal layer hemorrhage, intraventricular hemorrhage, ventricular dilatation, intraparenchymal hemorrhage, focal infarctions, porencephalic cysts, and lesions in the basal ganglia. An important acquisition is the ability to measure flow velocity and pulsatility index in major cerebral vessels with the Doppler ultrasound tech-

nique. A lowered pulsatility index is associated with more severe post-hypoxic-ischemic encephalopathy, although the overlap with normal is rather large.

Near-infrared spectroscopy is a method with potential to measure changes in the oxy-deoxyhemoglobin ratio in the brain and to estimate cerebral blood flow. The method has the advantage of being bedside and providing continuous information. There is, however, only a limited window available, because of interference with the skull. The method is in clinical use in some intensive care units and in research settings.

PET studies have occasionally been used to determine the metabolic rate and the cerebral blood flow of the various brain regions. This is rather a research than a clinical tool for post-hypoxic-ischemic encephalopathy in neonates.

Clinical signs, EEG, US, and evoked potentials are of the highest importance as predictors of the outcome of perinatal asphyxia in the acute stage, especially in those newborns that require intensive treatment to survive. In early stages of post-hypoxic-ischemic damage special MR techniques, including diffusion-weighted imaging and MRS, have proved to be of great importance in the prediction of outcome. In a later phase the extent of lesions on MRI, in particular the presence of subcortical damage, glial retraction, and ulegyria, the presence of secondary phenomena, such as atrophy and hydrocephalus, and the disturbance of myelination are helpful in predicting the degree of future disability.

95.2 Pathology

PVL was described histologically for the first time in 1867 by Virchow and in 1868 and 1873 by Parrot. They described “pale” infarcts in the periventricular white matter as yellowish or chalky plaques, 1–6 mm in diameter, 1–15 mm from the ependymal surface of the lateral ventricles. Softening of the plaques forms cavities filled with a milky fluid. The most common localizations are the area anterior to the frontal horn, the superolateral angles of the lateral ventricles, the peritrigonal area, and the area around the occipital horns.

Microscopically the lesions initially show coagulation necrosis, with nuclear pyknosis and sponginess of the tissue. Astrocytic proliferation at the borders sets in after a few days and varicose axon swellings develop. Microglia proliferate and lipid-laden macrophages accumulate. The organizing lesions are delineated by active gliosis. Cavitation forms within a few weeks. The cavities are lined by fibrillary glial scar tissue. Swollen axons mineralize quickly and persist for many months. Most of the infarcts are ischemic and lack hemorrhage. Vascular-occlusive changes are usu-

ally absent. Occasionally hemorrhages are found with a distribution similar to that of the leukomalacia. They are due to secondary hemorrhages into periventricular infarcts. Under certain circumstances these hemorrhages can become massive.

The severity of the gliotic reaction and its extent depend on age. Before 24–28 weeks gestational age, the immature brain cannot fully respond to insults with astrogliosis. In premature neonates of 28–32 weeks gestational age, gliosis is usually limited to the periventricular area (PVL). In older premature neonates gliosis extends more often into the subcortical area (SCL). This subcortical extension of the gliotic lesion is probably related to both gestational age and the severity of the hypoxic–ischemic insult. If subcortical cysts develop and the child dies during this stage, multicystic subcortical degeneration is found at autopsy. If the child survives, the cysts usually disappear and gliotic scarring occurs with retraction of white matter deforming ventricular system and cortex. The distribution of these lesions follows a pattern parallel to the periventricular area, closer to the cortical lining, extending from the frontal to the occipital region. The scars of PVL and SCL remain visible throughout life. The residual lesions of PVL are characterized by irregular borders of the ventricles, where periventricular cysts have made contact with the lumen of the ventricles, with glial retraction often at the level of the trigonum, focal loss of white matter, and deep sulci abutting the walls of the ventricles. In the case of SCL, glial retraction disfigures the centrum semiovale and causes crowding of gyri, eventually leading to parietal and occipital ulegyria (= sclerotic polymicrogyria).

In term neonates the pattern of damage is different. The post-hypoxic–ischemic lesions occur preferentially in a triangular area in the parasagittal, cortical, and subcortical region bordering the sulcus centralis. The resulting gliotic scar has a typical triangular shape with retraction of the parietal cortex, leading to local ulegyria. This is often combined with lesions in the dorsal part of the putamen and the ventrolateral part of the thalamus. The hippocampus may also be involved. The nuclei of the brain stem and the dentate nucleus may also be affected in this condition, and pontosubicular necrosis, a histological entity, could also fit into this gamut of post-hypoxic–ischemic damage of the term neonate.

Histopathology in MCE reveals multiple cystic cavities in the white matter, extending from the ventricular wall to the inner cortex, affecting frontal, parietal, and occipital lobes. Septa bridge the cyst walls. The medial and lateral parts of the temporal lobes are usually spared. Some convolutions are shrunk, and ulegyric regions are present. The lateral ventricles are dilated, but do not communicate with the cysts. The corpus callosum and fornix may be re-

markably thinned. Softening of the putamen, globus pallidus, and lateral thalamus may be present. There are foci of necrosis involving different levels of the brain stem down to the lower medulla. The spinal cord is not involved. Microscopically intensive gliosis and the presence of fat-laden macrophages are seen in the walls of the cysts. In the basal ganglia symmetrical necrotic changes are apparent: the neuropil is destroyed and few neurons remain. Scattered calcifications and encrusted neurons are seen in the cerebral cortex and basal ganglia. In the cerebellum there is loss of Purkinje cells, many of which are swollen, with cactus-like dendrites in the molecular layer.

95.3 Pathogenetic Considerations

PVL and germinal-layer-related hemorrhages are considered to be due to hypoxic–ischemic insults of the preterm neonate, occurring in the pre-, peri-, or postnatal period. Age seems to be the pathoplastic factor. The incidence of germinal-layer-related hemorrhage is highest before the 32nd week of gestational age; the highest incidence of PVL lies between the 32nd and 36th week of gestational age, but there certainly is an overlap, and both conditions may be present at the same time. Both conditions are rare in neonates born at term. The high incidence of germinal-layer hemorrhage before the age of 32 weeks' gestation can be explained by the presence of the germinal layer up until that time. After the 32nd week of gestation the germinal layer rapidly disappears. This germinal layer or matrix layer is considered to be the nurturing bed for the neuronal and glial cells of the developing brain. It is extremely well vascularized, whereas the vascular channels have thin endothelial walls without supportive tissue. The germinal layer therefore bleeds easily. A hemodynamic contribution comes from the pressure-passive cerebral blood flow in stressed premature children, causing a direct dependency of the cerebral blood flow on the systemic blood pressure and blood flow. The existence of a patent ductus arteriosus (ductus Botalli) and its drug-induced (indomethacin) closure can have a profound influence on the cerebral circulation, as it lacks the regulatory mechanism to buffer these changes. Another important factor is the immaturity of the lung, which requires mechanical ventilation with high pressures leading to indirect changes in the blood pressure. All these factors explain the relative high frequency of development of germinal-layer hemorrhage in early preterm babies. The hemorrhages potentially break through into the ventricles, which may or may not expand. Under certain conditions there is also a breakthrough of hemorrhage into the parenchyma. The intraparenchymal hemorrhages have a poor prognosis. There is growing evidence that

intraparenchymal extension of the hemorrhage occurs in tissue that has already suffered from hypoxia. In other words, the hemorrhage occurs in infarcted tissue, usually a venous infarction.

In explaining the selective vulnerability of white matter in PVL and SCL, multiple risk factors probably play a role. There are three major factors in the selective vulnerability of the periventricular white matter in premature infants: the incomplete state of development of the vascular supply to the cerebral white matter; the maturation-dependent impairment in regulation of cerebral blood flow; and the maturation-dependent vulnerability of the oligodendroglial precursor cells. The first two factors are the underlying cause of susceptibility to ischemic factors. Arterial end zones and border zones around the ventricles are defined by branches of arteries penetrating the cerebral wall from the pial surface and arteries from the choroid plexus penetrating the ventricular wall. Pressure-passive cerebral blood flow in stressed premature children causes a direct dependency of the cerebral blood flow on the systemic blood pressure and blood flow, hypotension leading to decreased cerebral perfusion. It has been shown that oligodendroglial precursor cells are highly vulnerable to attacks by free radicals, which are generated by the cascade of events in ischemia-reperfusion events. Mature oligodendroglia are more resistant to this type of insult. The presence of intraventricular and intraparenchymal blood is a risk factor. In free radical attacks the presence of oxygen and free iron is an important catalyst for the Haber-Weiss reaction and the formation of the perhydroxyl radicals, and the subsequent process of lipid peroxidation. Iron is present in hemorrhagic tissue. Fe^{2+} can be liberated from ferritin when the pH value is lower than 6. Iron is also actively acquired during the differentiation of oligodendroglia. In the ischemia-reperfusion cascade elevation of extracellular glutamate, contributing to excitotoxicity, is a factor contributing to tissue damage. Cytokines released in the presence of maternal (antenatal) and fetal or neonatal infection contribute to the tissue damage. Hypocarbica leading to vasoconstriction has been shown to be a contributing factor to the white matter damage in premature neonates. This finding is of clinical importance, since premature children with respiratory distress supported by artificial ventilation are at risk of developing hypocarbica. Detailed knowledge of all the pathogenic factors active in this field is essential to pave the way for interventions and treatment regimes.

The pathophysiology of encephalopathy in prematurely born neonates differs in many aspects from that of term-born neonates. In the postnatal period, the preterm neonate with a low birth weight and immature organs is going through an extremely stressful period, in which the baby depends on a special en-

vironment, monitoring, and life support measures. These include artificial ventilation, administration of surfactant, gastric tube feeding, and drug-induced closure of the ductus arteriosus, to mention but a few. Often there were already prenatal problems, which after preterm birth continue into postnatal problems. It is often not possible to pinpoint one precise hypoxic-ischemic incident as the cause of brain damage. In term-born neonates, on the other hand, most cases of hypoxia-ischemia are due to a single, severe, perinatal incident. The cerebral damage resulting from an acute episode of severe asphyxia is completely different from the cerebral damage in premature neonates. Selective vulnerability of the brain in this type of incident is apparently dictated by the biochemically most active parts of the brain, which demand the most glucose and oxygen: the zones of active myelination. The resulting damage in the term-born neonate has the form of the so-called central cortico-subcortical pattern, with leukomalacia in the myelination zone, extending band-shaped from the basal ganglia into the pre- and postcentral gyri. There are also lesions in the dorsal part of the putamen, the ventrolateral part of the thalamus, and the hippocampus, also actively myelinating at that time. In the premature neonate with a single episode of acute profound asphyxia, there are as a rule only lesions in the basal ganglia and thalami. This can be explained by the fact that the central cortico-subcortical area is not yet myelinating in premature infants. As far as lesions in the basal ganglia and hippocampus are concerned, excitotoxicity and high local density of glutamate receptors also play a role.

The pathophysiology of MCE is less clear. MCE is usually considered a rare condition in neonates, but still accounts for about 10% of the patients with post-hypoxic-ischemic injury (Sie et al. 2000a). The risk factors for this group show a striking difference as compared to patients developing PVL and those developing the cortico-subcortical pattern. PVL is mainly found in preterm infants who suffer from prolonged and repeated partial hypoxia-ischemia; the cortico-subcortical pattern mainly in term-born infants, following a single episode of acute profound hypoxia-ischemia; MCE is mainly seen in term-born infants, initially with signs of mild hypoxia-ischemia, not requiring vigorous resuscitation at delivery, followed by a delayed-onset devastating encephalopathy with generalized brain edema. This sequence of delayed-onset neuronal death resembles the sequence of ischemia-reperfusion damage and secondary energy failure as substantiated in animal experiments.

Without being linked directly to the concept of MCE, it has been noted that neonates, after an initial period of suboptimal responses, improve to a better functional level within the first day, only to present with a catastrophic reaction about 24 h after the first

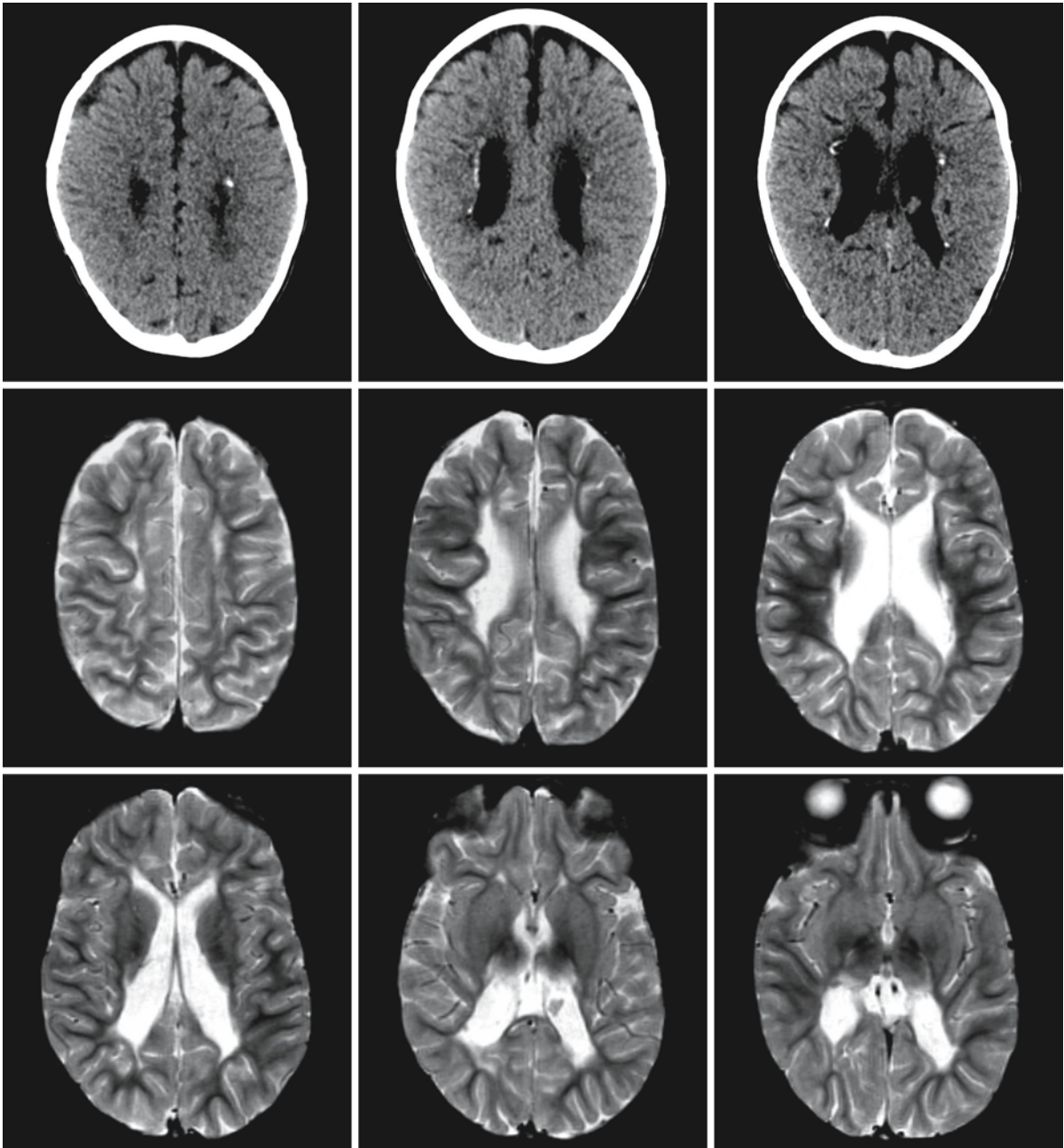


Fig. 95.1. A CT scan of a girl with PVL at the age of 2 years (*first row*) shows asymmetrical ventriculomegaly and calcifications around the ventricles. The T₂-weighted MR images obtained at the age of 3 years (*second and third rows*) show severe PVL

with dilatation of the lateral ventricles, deformation of the ventricular walls (due to scarring), white matter volume loss, and periventricular gliosis. In addition, pulvinar lesions are present

episode. The explanation for the first episode of sub-optimal function is sought in the acute reaction of neurons to energy depletion and cell membrane paralysis with edema, swelling, and impaired function. When the cell survives, a second, calcium-dependent mechanism is triggered, leading via activation of enzymes, formation of free radicals, lipid per-

oxidation, and accumulation of excitatory amino acids to delayed cell death. This sequence of events does not differ in essence from the general cascades triggered whenever energy failure occurs and can be seen as a final common path of secondary neuronal death.

95.4 Therapy

Because of the serious consequences of post-hypoxic-ischemic damage, many attempts have been directed at preventing PVL and other forms of post-hypoxic-ischemic damage from happening. Intensive check-ups during pregnancy, early in utero diagnosis of congenital abnormalities, electronic fetal monitoring during delivery, and technically advanced neonatal intensive care units have not, however, led to a reduction in the incidence of cerebral palsy, which stands at 1–2 per 10,000 newborns. This is at least partially due to a population shift. Neonates of very low birth weight can now be kept alive and carry high risk factors for the development of post-hypoxic-ischemic damage. Preventive measures applied in the past to reduce brain metabolism and thus to increase the resistance against hypoxia, such as the use of phenobarbital and low body temperature, have failed to improve the outcome. Better understanding of the pathophysiological mechanisms underlying post-hypoxic-ischemic encephalopathy has triggered new efforts to develop cerebroprotective drugs. It has become clear that disrupted calcium homeostasis within ischemic cells is an essential factor in delayed cell death. Energy depletion leads to high calcium concentration within the cytosol, triggering many other cascades that can damage the cell. Calcium entry blockers would seem to be a logical answer to this problem. Results of trials, however, have not been satisfactory. One of the cascades triggered by high cytosol calcium is the transformation of xanthine dehydrogenase into xanthine oxidase, both of them enzymes of the adenosine-nucleotide biochemical pathway. The formation of xanthine oxidase leads to formation of free radicals and to cell damage by lipid peroxidation after reperfusion. It was hoped that blocking of this cascade would improve the outcome. Free radical scavengers have also been tested for their ability to prevent reperfusion damage. Substantial

beneficial results have not yet been reported. Energy depletion leads to the accumulation of excitatory amino acids, glutamate in particular. Glutamate exerts its stimulating action via at least three different receptors, which have unequal topographical distribution. Of the glutamate receptors, the pharmacological properties of the NMDA receptor are best understood. An attempt has been made to counteract excitotoxicity by the administration of antagonists for specific sites of the NMDA receptor. Although neuroprotective effects have been obtained in vitro, clinical trials in preterm neonates have been disappointing. This is probably because glutamate is extremely important for many reactions, and nonselective inhibition may lead to tampering with the other functions of this neurotransmitter. For instance, maturing neuroreceptors in developing neurosynapses also play a role in the maturation of brain parts and brain functions; in the fetal period they are intermediates of cell plasticity and essential in processes of memory and learning.

Once a static encephalopathy has developed, the child should be given physical therapy, special education if necessary, and neurological treatment to limit secondary consequences such as spasticity and epilepsy.

95.5 Magnetic Resonance Imaging

Because of its versatility and ability to be used at the bedside, neurosonography (ultrasound, US) will remain the first-line imaging modality in intensive care units for neonates. Detection and staging of germinal-layer-related hemorrhage can be done satisfactorily with US. This is also true for the evolution of PVL, which can be followed day by day. Many other brain conditions can be correctly diagnosed by US: for example, cerebral infarctions, hydrocephalus, porencephaly, hydranencephaly, and congenital anomalies,

Table 95.1. MRI sequences for the evaluation of neonates

Sequence	Purpose/contribution
Sagittal T ₁ -weighted spin echo	Small hemorrhages, cysts, congenital anomalies
Proton density and T ₂ -weighted spin echo	Signal changes of white matter and cortical rim, ventricular size
FLAIR	Differential diagnosis: asphyxia versus infection
Gradient echo	Macro- and microhemorrhages, calcifications
IR	Progress of myelination, gray/white matter differentiation
T ₁ -weighted + contrast	Cortical laminar necrosis, infections
DWI–anisotropy–Trace	Infarcted and preinfarcted tissue, pattern of abnormalities
DTI-FA; fiber tracking	Quantitative estimation of brain maturation
MRS	Biochemical developmental age; presence of lactate
MRA	Vascular anomalies, abnormal vein of Galen

FLAIR, fluid-attenuated inversion recovery; IR, inversion recovery; DWI, diffusion-weighted imaging; DTI-FA, diffusion tensor imaging–fractional anisotropy; MRS, MR spectroscopy; MRA, MR angiography

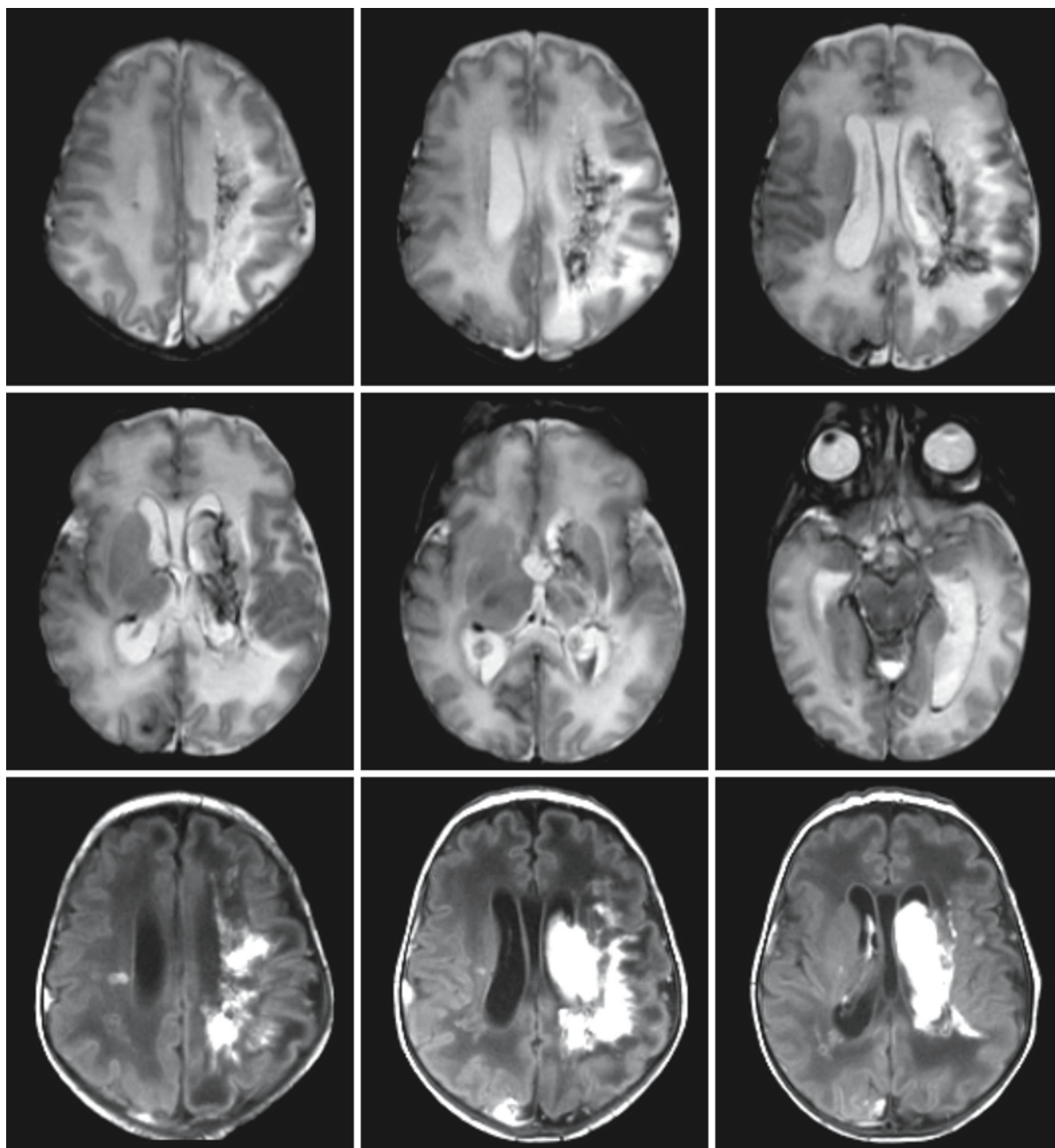


Fig. 95.2. a Boy born at 38 weeks of gestation. The pregnancy was complicated by hypertension and perinatal asphyxia occurred. MRI at the age of 1 week showed mildly dilated lateral ventricles. T₂-weighted (*first and second rows*) and T₁-weighted

(*third row*) images show an intraparenchymal hemorrhage on the left. This type of hemorrhage usually has its origin in a venous infarction and suggests a previous condition of venous congestion

such as schizencephaly, corpus callosum agenesis, vein of Galen malformations, and Dandy–Walker malformations.

The role of CT is limited to the diagnosis of hemorrhages and of calcifications, an important feature of some disorders, for example bilateral thalamic necrosis. In later cases of PVL, CT may be helpful to show

calcifications in the damaged periventricular region (Fig. 95.1).

When uncertainty remains after US, or discrepancy exists between US findings and clinical condition, MRI is indicated. The role of MRI in the diagnosis of post-hypoxic–ischemic conditions in neonates has become increasingly prominent. This is the result of

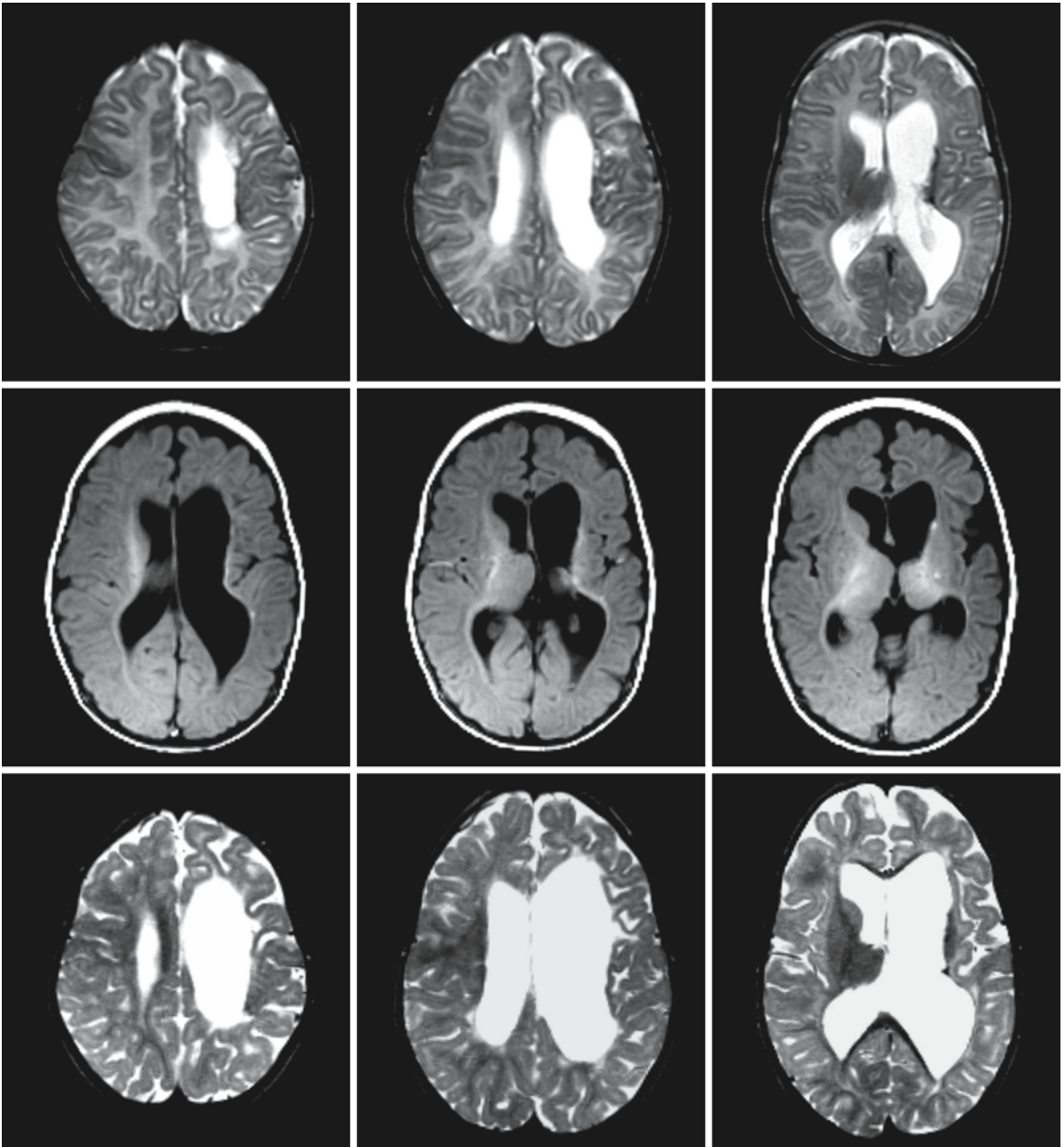


Fig. 95.2. b Follow-up studies after 3 months (*first row*, T₂-weighted; *second row* T₁-weighted) and 18 months (T₂-weighted, *third row*) show that the left lateral ventricle is enlarged and

there is loss of white matter in the left hemisphere. Myelination is delayed in the left hemisphere

improvement of MR techniques and, not least, to better adaptation of the MR procedure to the needs of preterm or term neonates. These improvements consist of improvement of monitoring vital signs with MR-compatible equipment, the development of MR-compatible incubators containing the usual life support systems, adapted head coil for neonates, and the

development of faster and new MR sequences. When the requirements for MRI of neonates are fulfilled, a protocol for MRI of neonates could include quite a gamut of sequences (Table 95.1). With the sequences listed in Table 95.1 it is possible to survey the condition of the neonatal brain tissue and in many cases to predict outcome, which is often of major importance

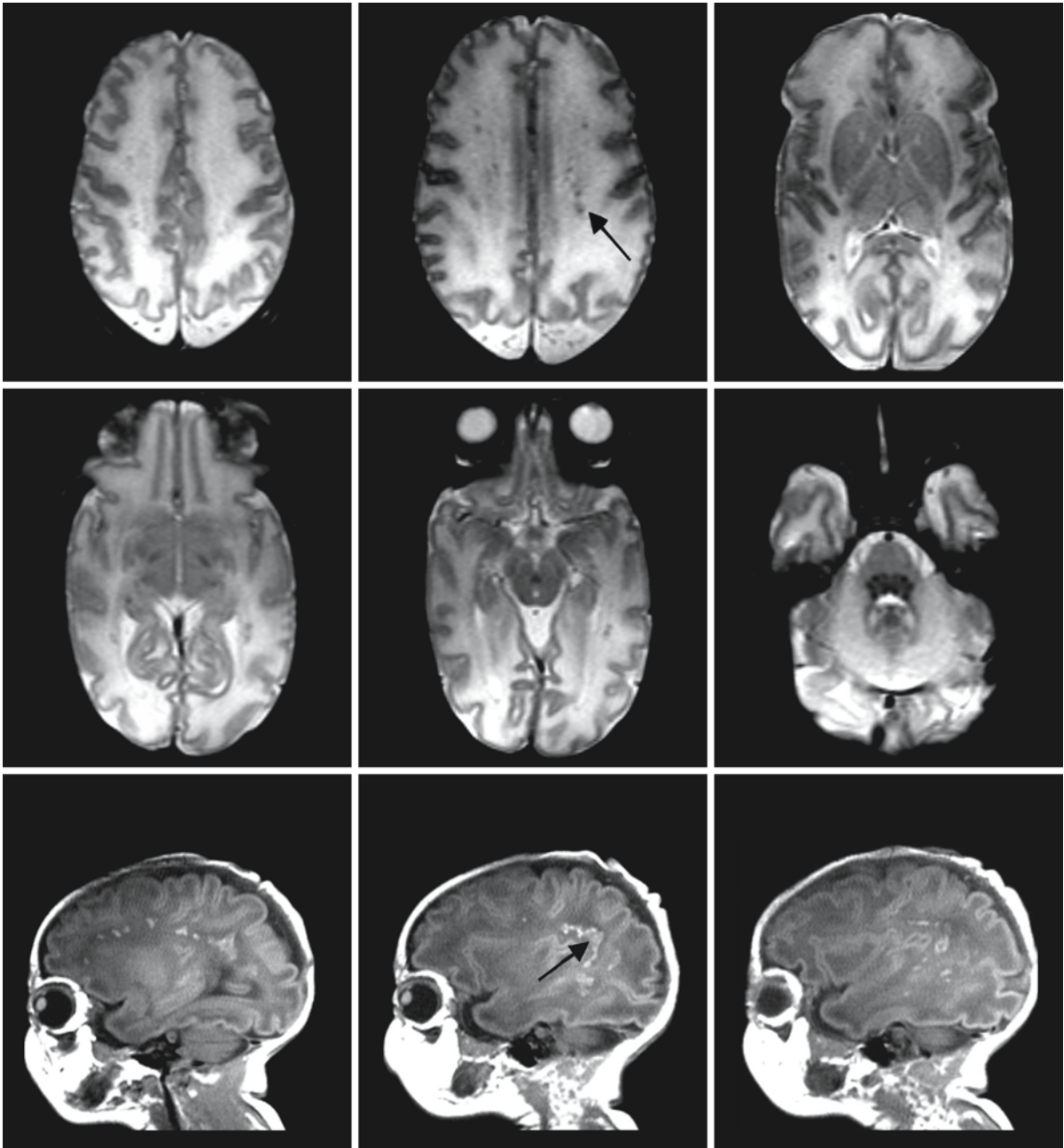


Fig. 95.3. a A boy born at 34 weeks' gestation with respiratory insufficiency. The T_2 -weighted images (*first and second rows*) show a row of dark dots along the lateral upper borders of the ventricles (*arrow*) and narrow ventricles. Sagittal T_1 -weighted

images (*third row*) show the row as bright dots along the ventricular borders, representing small hemorrhagic lesions (*arrow*)

in patient management. In daily routine not all these sequences will be applied; the first six, however, can considerably help in the initial diagnosis. Fast (turbo) spin echo sequences decrease acquisition time but have the disadvantage of canceling inhomogeneities in the local magnetic field and thus masking the pres-

ence of hemorrhages or calcifications. MRS may contribute to the prediction of outcome of post-hypoxic–ischemic damage in the neonatal period. An elevated level of lactate, particularly when present in the basal nuclei of a term neonate, predicts a poor outcome.

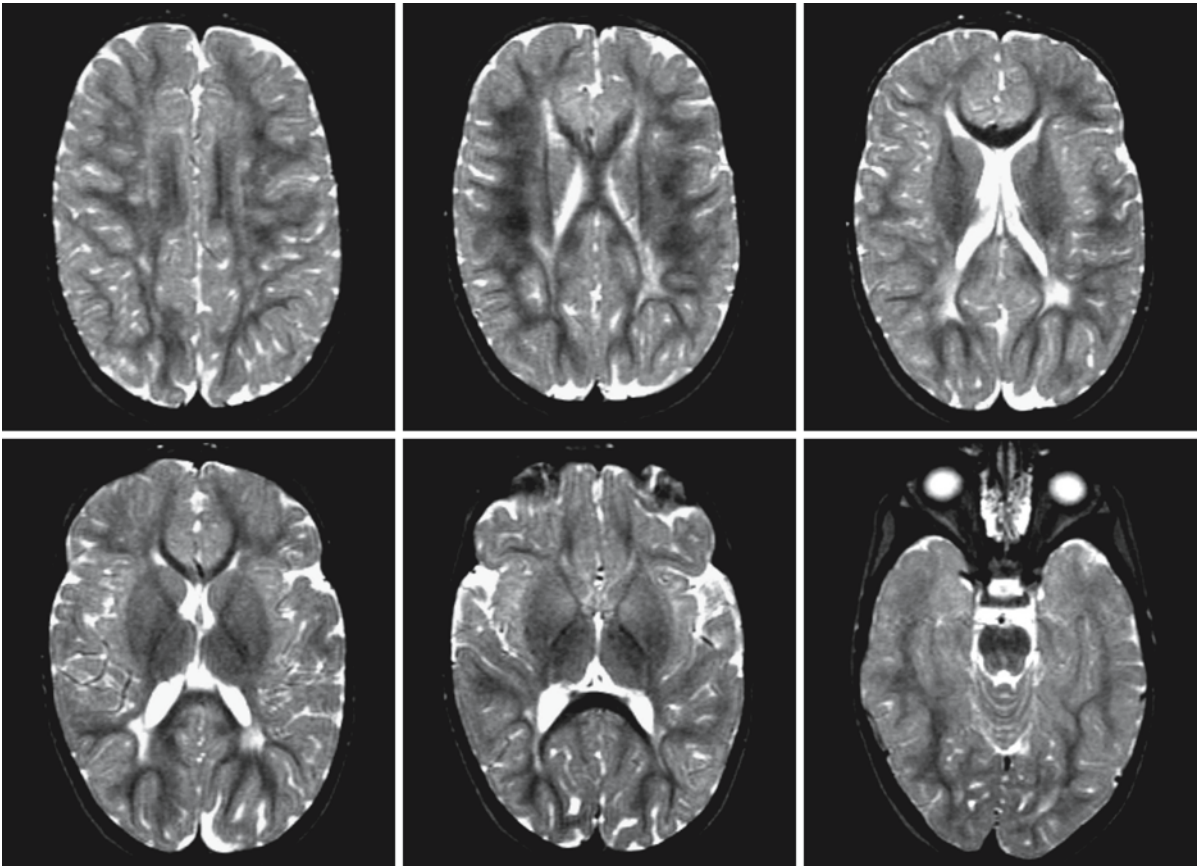


Fig. 95.3. b Follow-up at the age of 18 months. The T_2 -weighted images show the typical triad of PVL: irregular borders of the lateral ventricles, especially the trigonum; white matter

volume loss, also predominantly in the peritrigonal area with cortical sulci abutting the ventricles; and periventricular gliosis

MR patterns in post-hypoxic–ischemic encephalopathy can be subdivided into early and late, residual, patterns.

Post-hypoxic–ischemic encephalopathy in preterm neonates encompasses several conditions.

Venous infarctions, often in the wake of germinal-layer- (or matrix-) related hemorrhage, are often still referred to as grade 4 hemorrhages. Venous infarctions, frequently located along the border of the lateral ventricles, may occur isolated or together with more extensive PVL (Fig. 95.2).

The most important post-hypoxic–ischemic encephalopathy in preterm neonates is PVL. In the first postnatal week the diagnosis may be difficult. Small bright foci around the ventricles on T_1 -weighted sagittal or hypointense foci on T_2^* -weighted transverse images (Figs. 95.3a and 95.4a) are not always followed by cystic changes. More extensive lesions usually do (Figs. 95.3b and 95.4b). It is difficult in the first week to differentiate periventricular white matter changes, with high signal on proton density and T_2 -weighted images, from normal white matter, which

also has high signal intensity due to the high water content of the premature brain. In this early phase diffusion-weighted images (Trace images, ADC maps) are helpful. In acute PVL, the affected area has lower signal intensity on ADC maps and decreased ADC values. However, it should be noted that the hemorrhagic components also influence the ADC due to susceptibility effects. Diffusion tensor imaging and quantification of fractional anisotropy values may assist in the diagnosis. In the second week of life the changes become more obvious, also on conventional images. ADC values become higher; subependymal cystic changes appear around the ventricles and will often make contact with the ventricles. The most common late pattern of PVL consists of slightly widened lateral ventricles with irregular borders; loss of white matter volume, with cortical sulci nearly touching the ventricular walls; gliosis in the periventricular area; and focal or diffuse thinning of the corpus callosum (Figs. 95.1, 95.3b, 95.4b, 95.5, and 95.6). The presence of gliosis depends on the gestational age at the time of the insult; immaturity of astrocytes be-

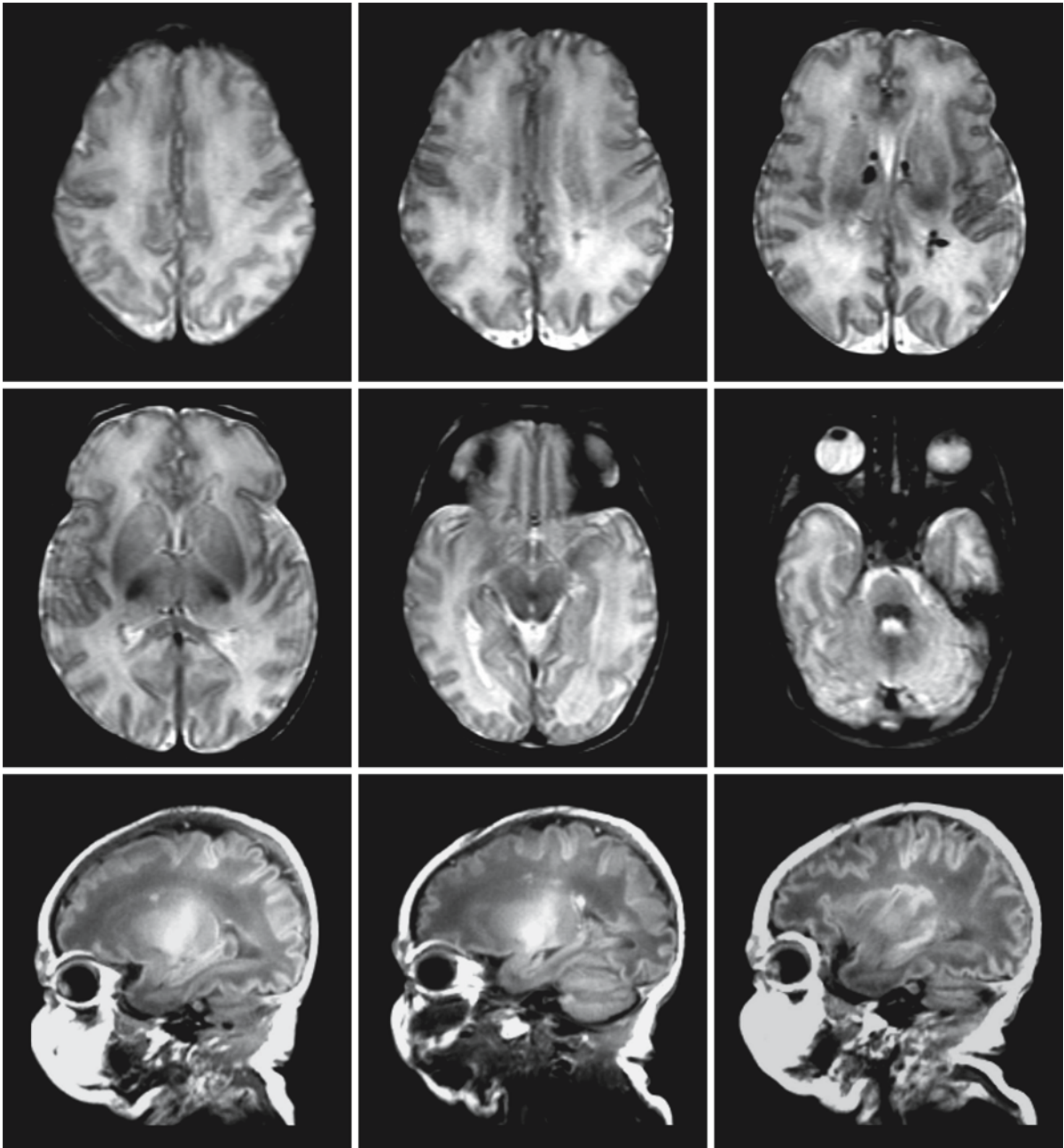


Fig. 95.4. a Boy born at 36 weeks' gestation. In the last trimester there were diminished fetal movements. During delivery worsening of the condition occurred with cardiac decelerations, necessitating emergency cesarean section. He had low APGAR scores. The T₂-weighted images (*first and second*

rows) show small hemorrhages in the germinal matrix along the ventricular border. The sagittal T₁-weighted images (*third row*) show a number of bright spots along the border of the lateral ventricles, consistent with hemorrhages

fore 28 weeks' gestation may lead to less prominent or absent gliosis. DTI fiber tracking may show the defects in the ascending and descending cortical tracts. Severe cases of PVL are often associated with lesions in the thalamus, especially in the pulvinar (Fig. 95.1).

PVL is not the only manifestation of post-hypoxic–ischemic encephalopathy in preterm neonates. Findings at autopsy are enlightening. In 97 autopsies of preterm neonates (Skullerud and Westre 1986), 48 had germinal-layer-related hemorrhage, 23 had PVL,

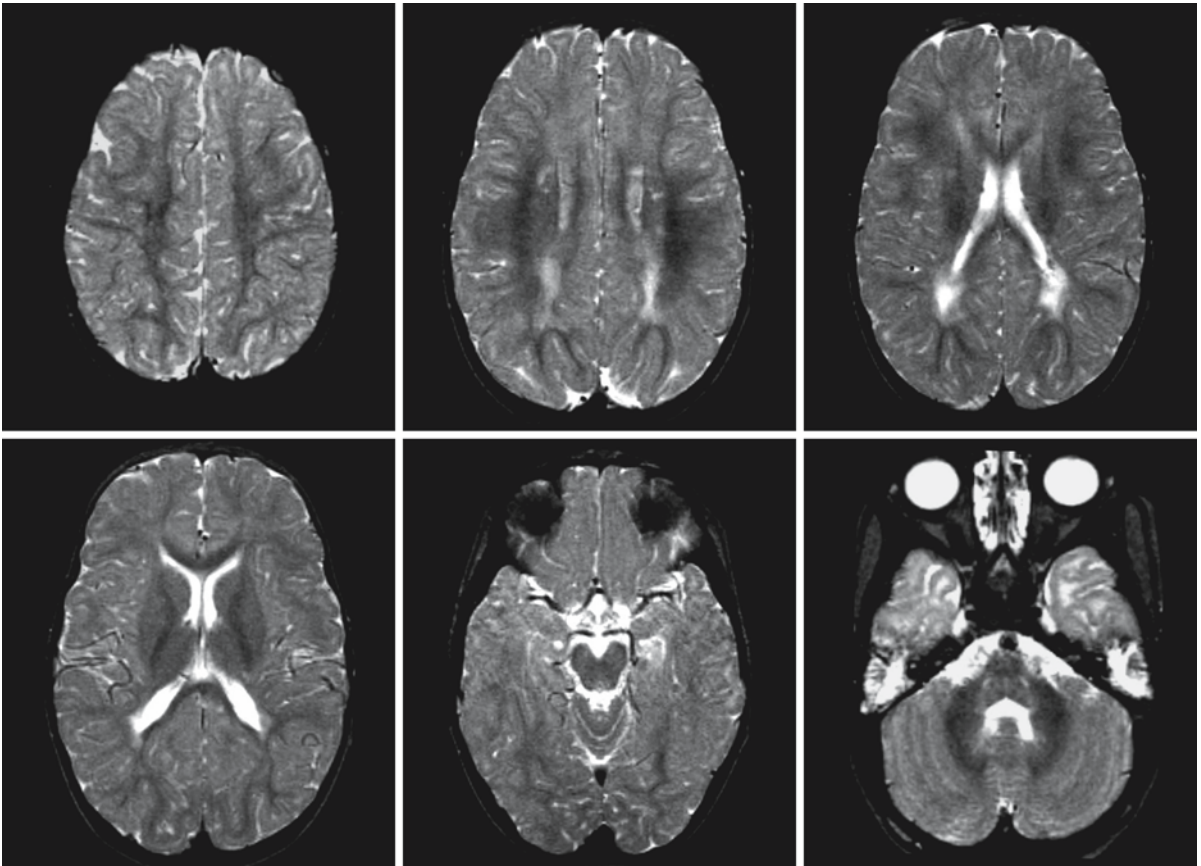


Fig. 95.4. b T₂-weighted images at 18 months show the triad of PVL. Myelination is delayed

and 57 had pontosubicular necrosis. Of course these findings are not representative of the surviving group. The diagnosis pontosubicular necrosis is rarely considered in MR reports of preterm neonates and may demand more attention. Sagittal proton density and T₂-weighted images may help to demonstrate abnormalities in the subiculum.

PVL may occur in term-born neonates, but less frequently than in preterm neonates. Acute profound hypoxia-ischemia occurs more frequently in term neonates. Conventional MR images, including contrast-enhanced images, may show diffuse cerebral edema. Because the cerebellum is less susceptible to hypoxia, it often is not involved. This results in what may be called a “white cerebrum” on ADC maps or “black cerebellum” sign on Trace diffusion-weighted images, the reverse of what was already known on CT as the “white cerebellum” sign (Figs. 95.7 and 95.8). This appearance is even more obvious on coronal diffusion-weighted Trace images. When the insult is less severe, another typical pattern develops with lesions in the basal ganglia and the central cortico-subcortical area (Figs. 95.9 and 95.10). On conventional images this pattern of damage may be difficult to ap-

praise in the acute phase; the images suggest most often diffuse edema. Diffusion-weighted Trace images bring out the pattern with high signal intensity, with low ADC values in the affected areas. This pattern typically involves the perirolandic cortex, the corticospinal tracts, the dorsal part of the putamen, the ventrolateral part of the thalamus, the hippocampus, and, in the most severe cases, dentate nucleus and brain stem nuclei. The typical late manifestation of severe post-hypoxic-ischemic damage in the term-born neonate consists of gliosis and or atrophy in the above-mentioned brain areas (Figs. 95.9 and 95.10).

In MCE the initial pattern seen on MR is generalized brain edema of the hemispheres, with sparing of the cerebellum. This is followed by the development of large subcortical cysts that may be spread through all cerebral lobes or confined to the frontal and parieto-occipital lobes. The cerebellum is least affected (Figs. 95.11 and 95.12).

Aside from the described patterns, other presentations of post-hypoxic-ischemic encephalopathy are possible. Cortical laminar necrosis (Fig. 95.13) usually shows on T₁-weighted and FLAIR images as a thin rim of higher signal intensity within the cortical

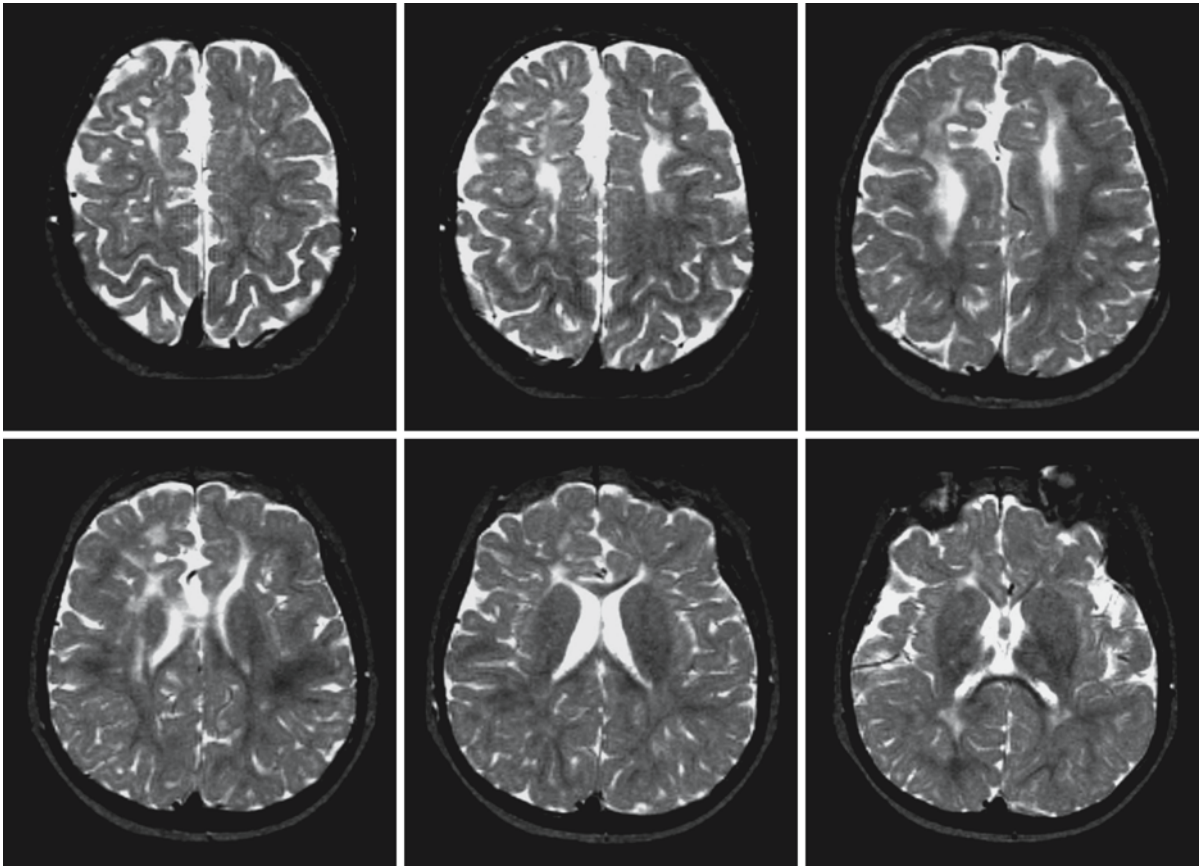


Fig. 95.5. A girl was born at a gestational age of 31 weeks with perinatal asphyxia and respiratory distress at birth demanding prolonged artificial ventilation. At 2 years T_2 -weighted images

show white matter loss and gliosis restricted to the frontal lobes. Frontal localization of PVL is unusual

layer. On proton density and T_2 -weighted images the cortical ribbon in the affected areas is usually less clearly seen. After contrast injection there may be enhancement of this rim. On follow-up this will result in gliosis and atrophy of the affected areas.

In neonates territorial infarctions are relatively rare, but will be seen occasionally. Often they involve the territory of the middle cerebral artery (Fig. 95.14).

The infarction most often involves the entire middle cerebral territory. A polycystic degeneration of the affected area follows.

In our experience border zone infarctions are relatively rare, but do occur (Fig. 95.15).

Other lesions caused by intrauterine hypoxic conditions of the neonate include hydranencephaly, porencephaly, and acquired schizencephaly.

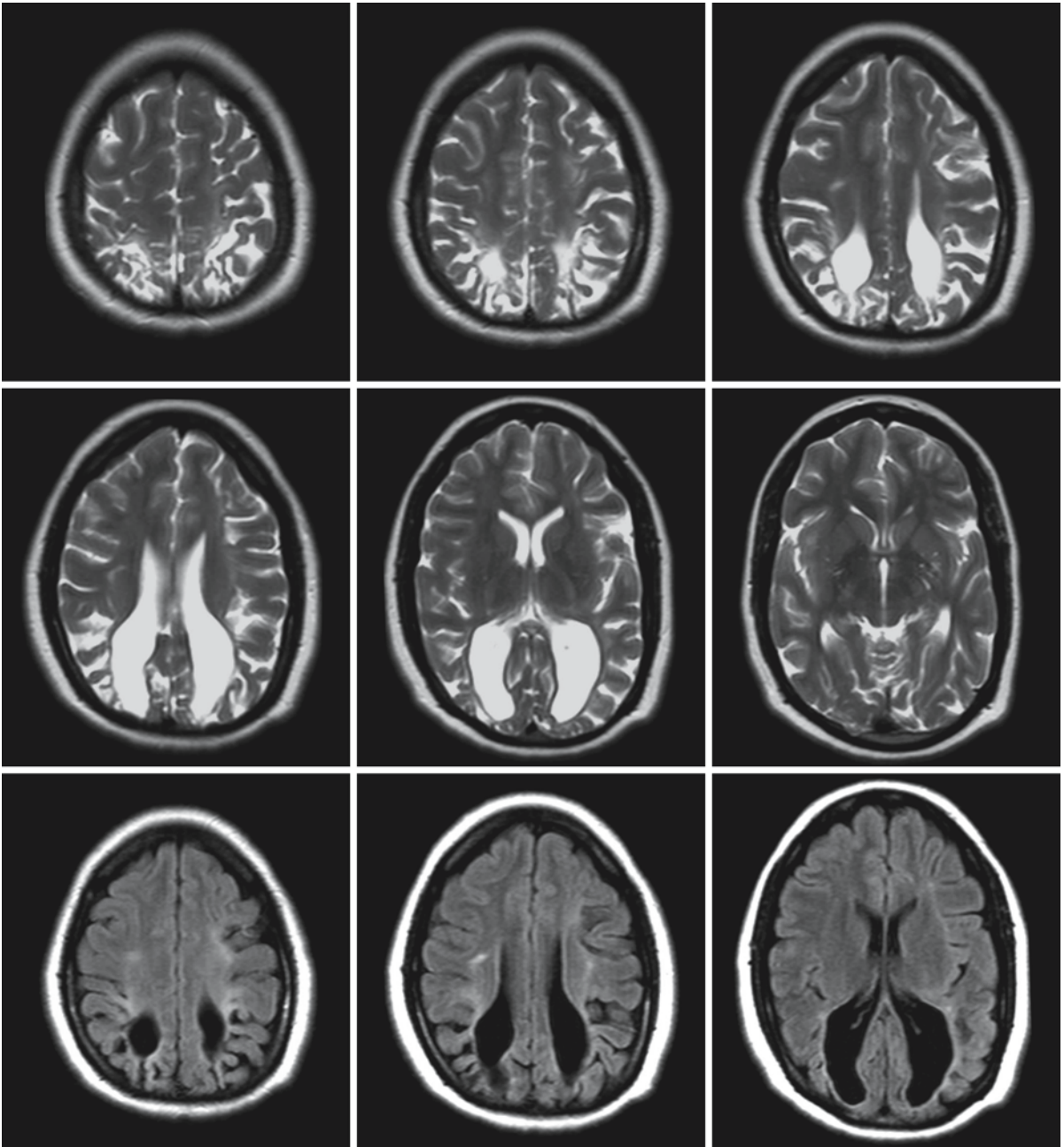


Fig. 95.6. Images of a 32-year-old mentally retarded and visually handicapped man with a history of perinatal asphyxia. It is unclear whether he also suffered from hypoglycemia. The T₂-weighted (*first and second rows*) and FLAIR (*third row*) images show severe white matter loss and gliosis in the parieto-occipital area and crowding of the occipital gyri (ulegyria)

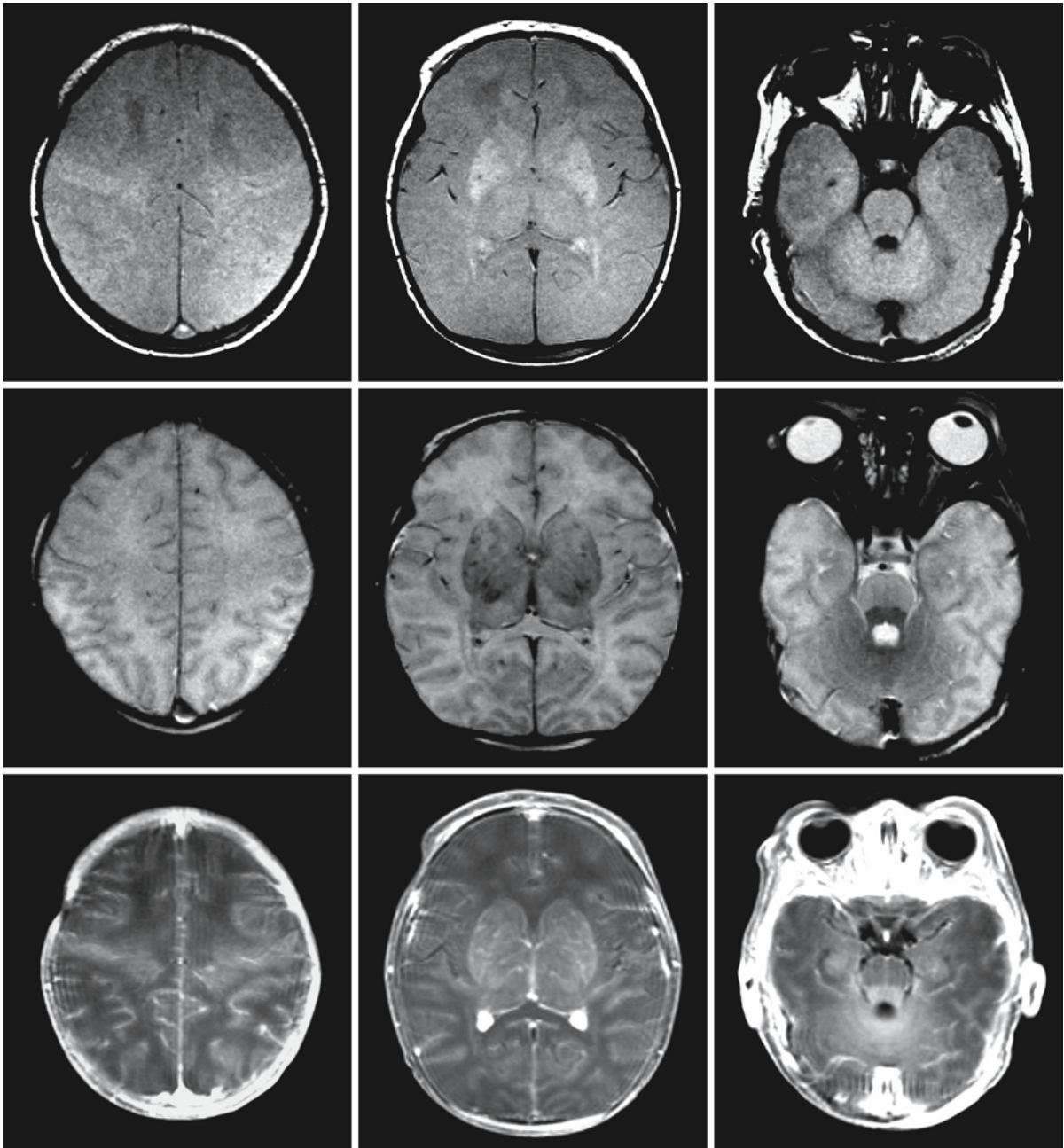


Fig. 95.7. **a** Images of a female neonate, born at a gestational age of 41.5 weeks, who suffered from extremely severe perinatal asphyxia. The MRI was obtained at 4 days. The proton density images (*first row*) show an almost complete loss of white–gray matter demarcation. The basal ganglia stand out as white. The T₂-weighted images (*second row*) confirm the loss of the cortical ribbon with decreased demarca-

tion between white and gray matter. There is generalized edema. The brain stem and cerebellum are the only structures that seem to have preserved their normal gray–white differentiation. The contrast-enhanced T₁-weighted images (*third row*) show diffuse faint enhancement of the basal ganglia and perhaps the cortex

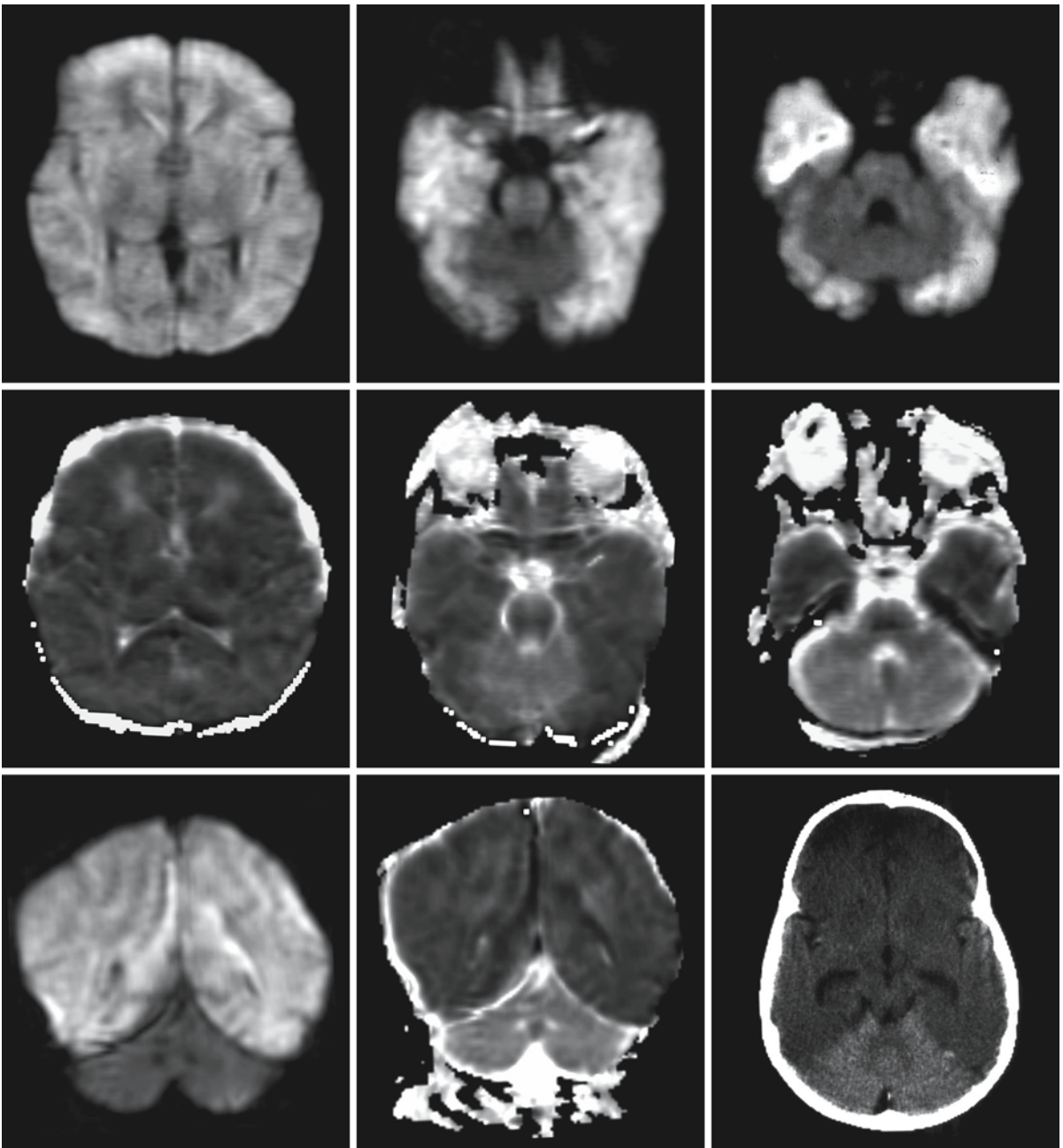


Fig. 95.7. **b** Transverse diffusion-weighted Trace images (*first row*, $b = 1000$) and ADC maps (*second row*) show diffuse abnormalities in the supratentorial regions, which makes them difficult to read: because all structures are abnormal, they do not stand out as abnormal as compared to normal structures. The *lower slices* show the normal brain stem and cerebellum. The

coronal images (*third row*, Trace diffusion-weighted image *left*, and ADC map in the *middle*) are much easier to interpret. Only the cerebellum has a normal aspect. This "dark" cerebellum on Trace images is the counterpart of the "white" cerebellum as seen on CT in severe hypoxia (*third row, right*)

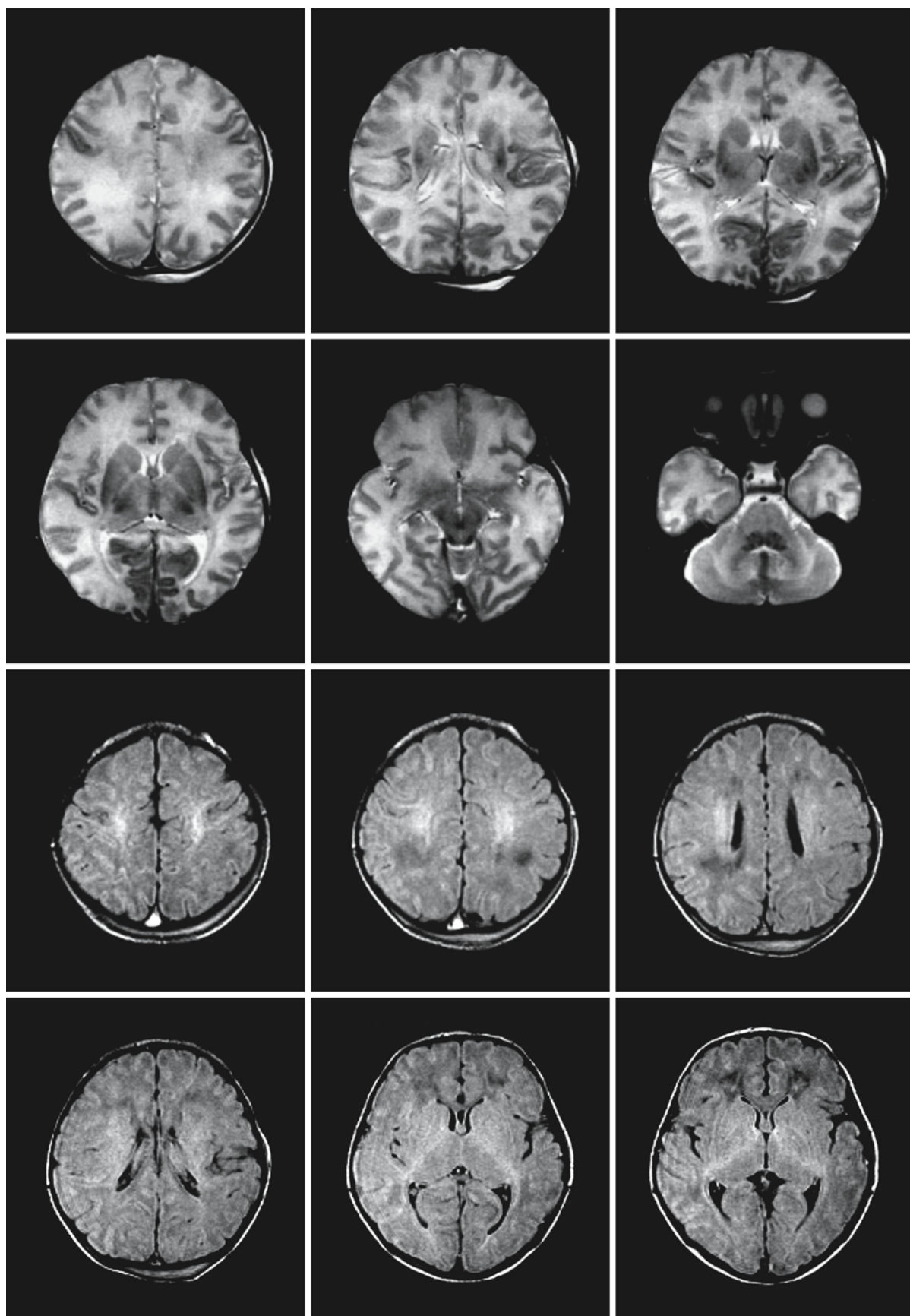


Fig. 95.8. a

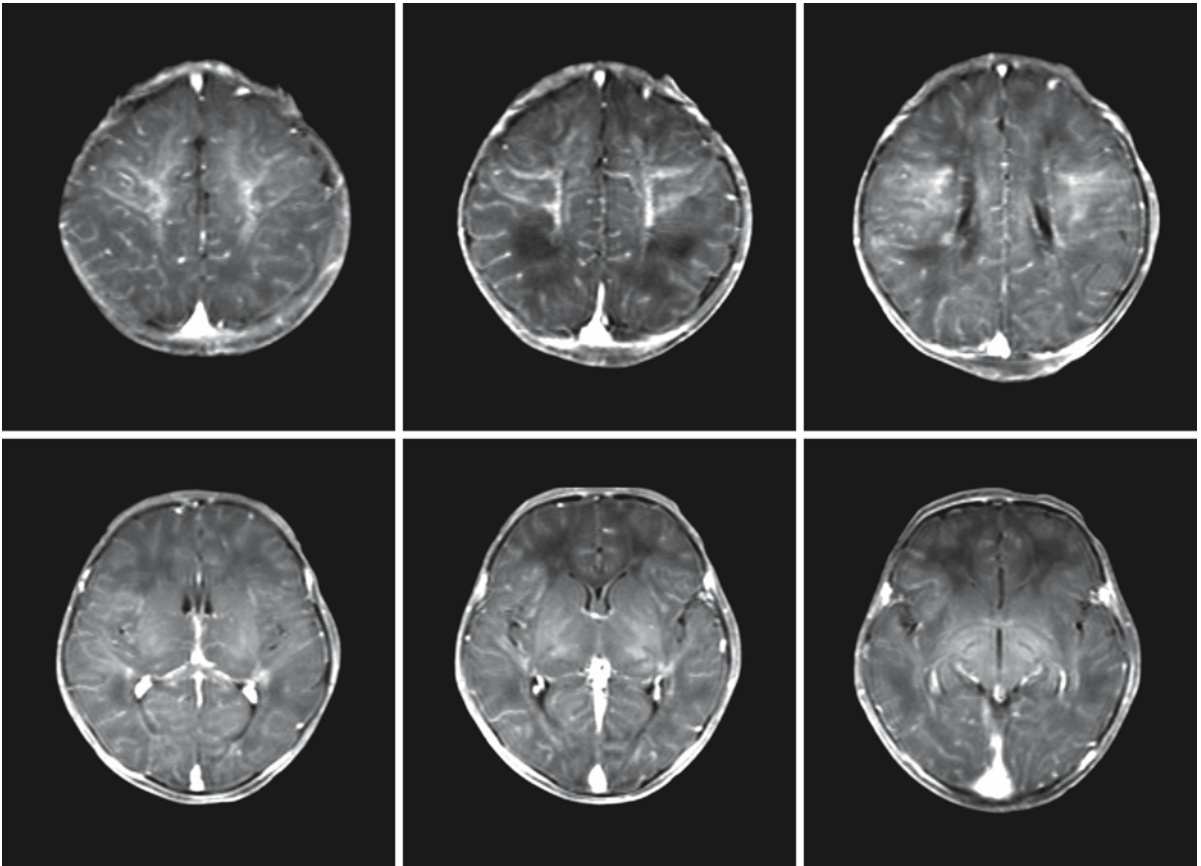


Fig. 95.8. (continued). a Images of a term-born male neonate, victim of a very difficult delivery and repeated attempts at vacuum extraction. The MRI was obtained at the age of 4 days. The T₂-weighted images (*first and second rows*) show loss of the cortical ribbon with decreased demarcation between white and gray matter over the large parts of the brain and

generalized edema. The FLAIR images (*third and fourth row*) show fuzziness of brain structures. The contrast-enhanced T₁-weighted images (*fifth and sixth rows*) show a remarkable pattern of enhancement in the rolandic area. It remains difficult to assess the condition of the neonate's brain

Fig. 95.8. b Diffusion-weighted Trace images (*first and second rows, b = 1000*) and ADC maps (*third and fourth rows*) show involvement of the cortical and subcortical structures of both hemispheres. Only the cerebellum has a normal aspect. (Fig. 95.8. b see next page)

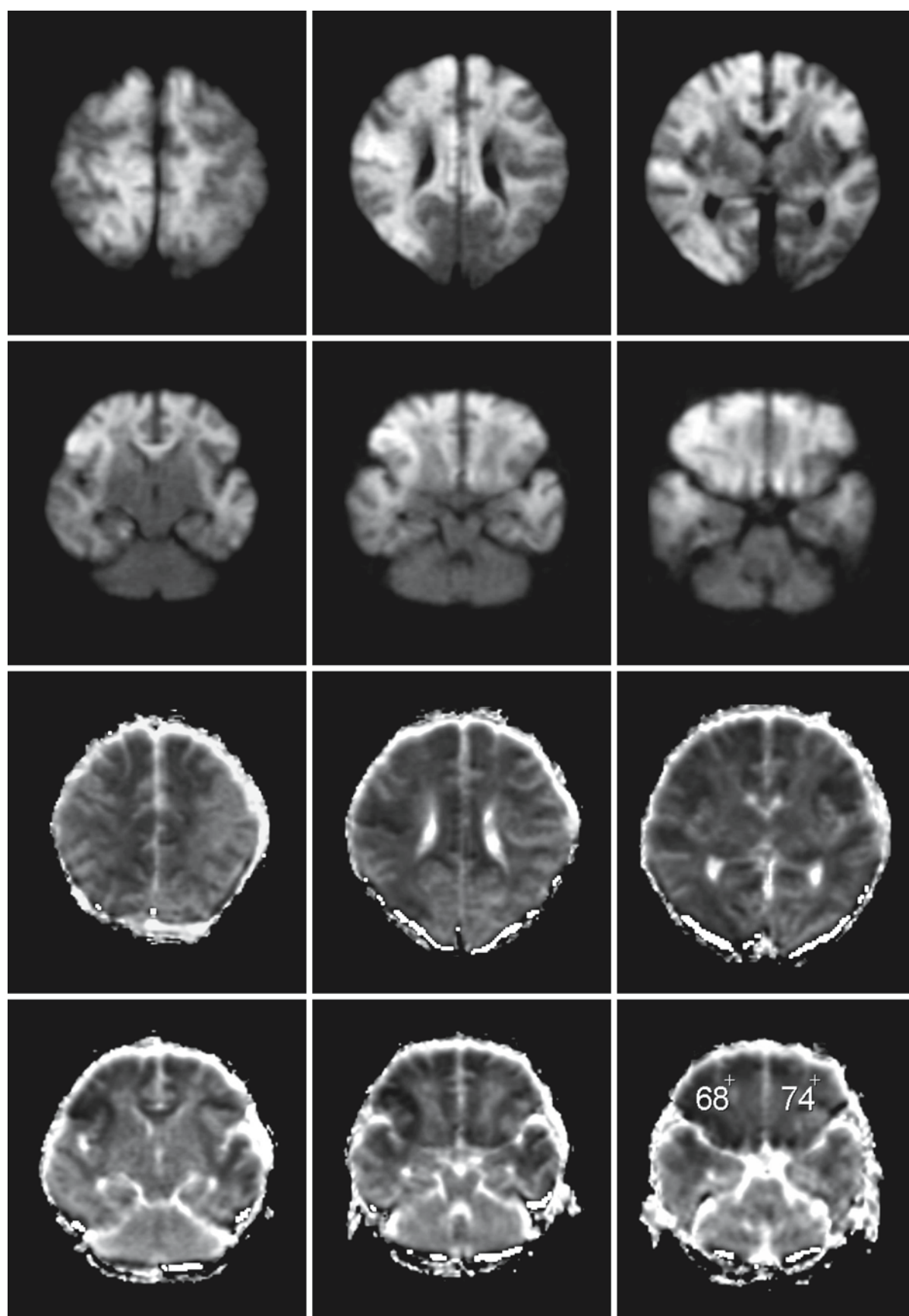


Fig. 95.8. b

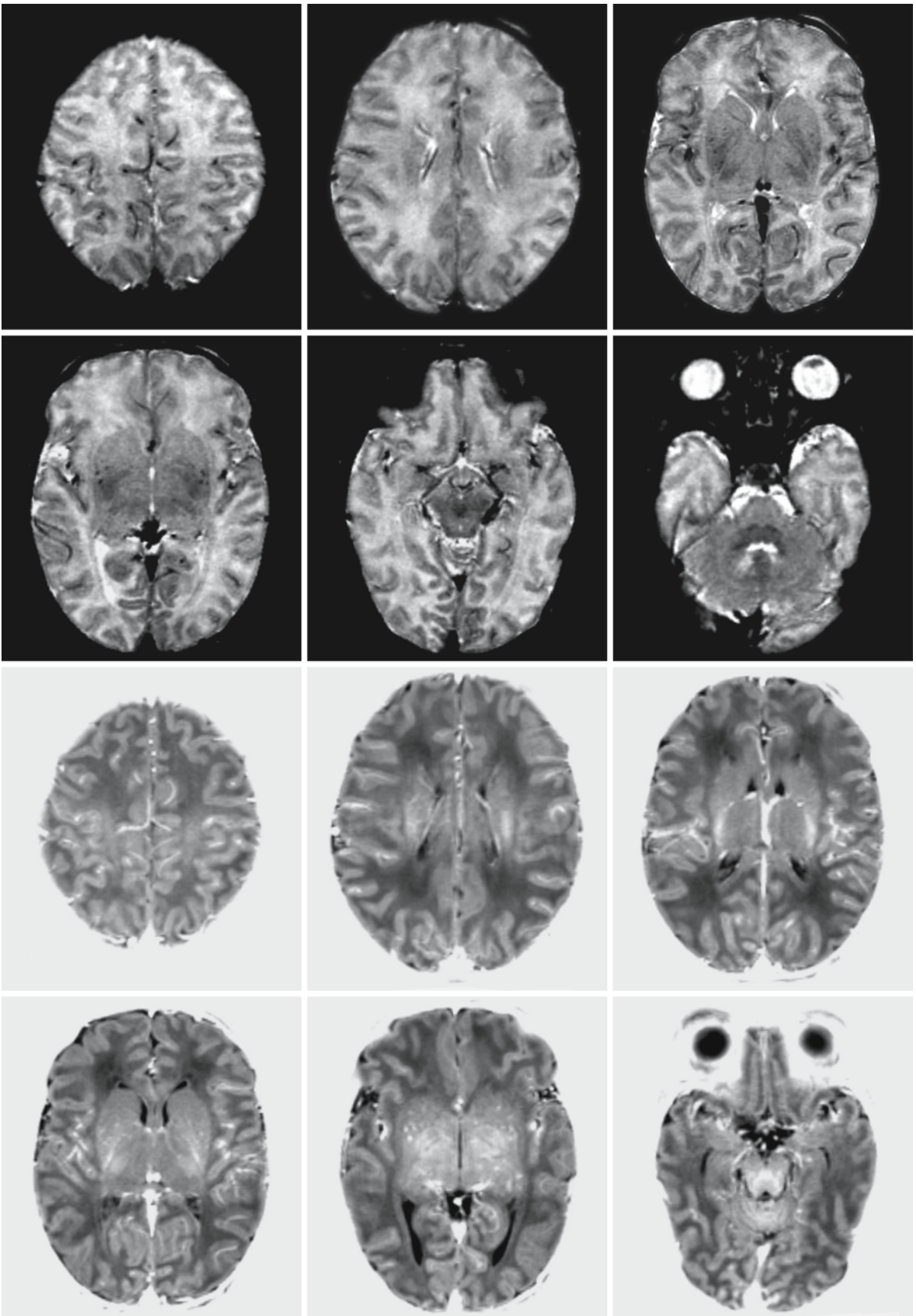


Fig. 95.9. a

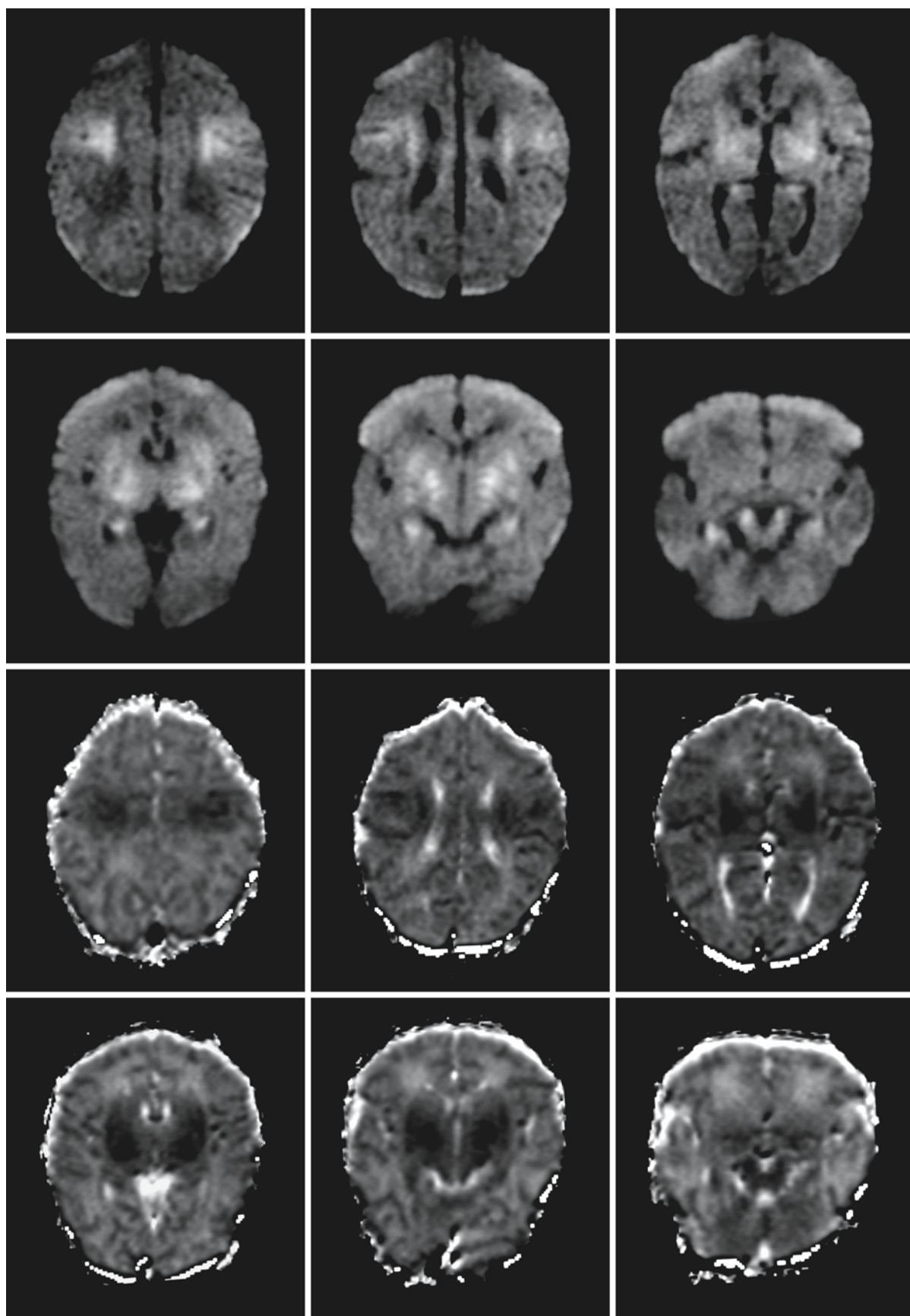


Fig. 95.9. b

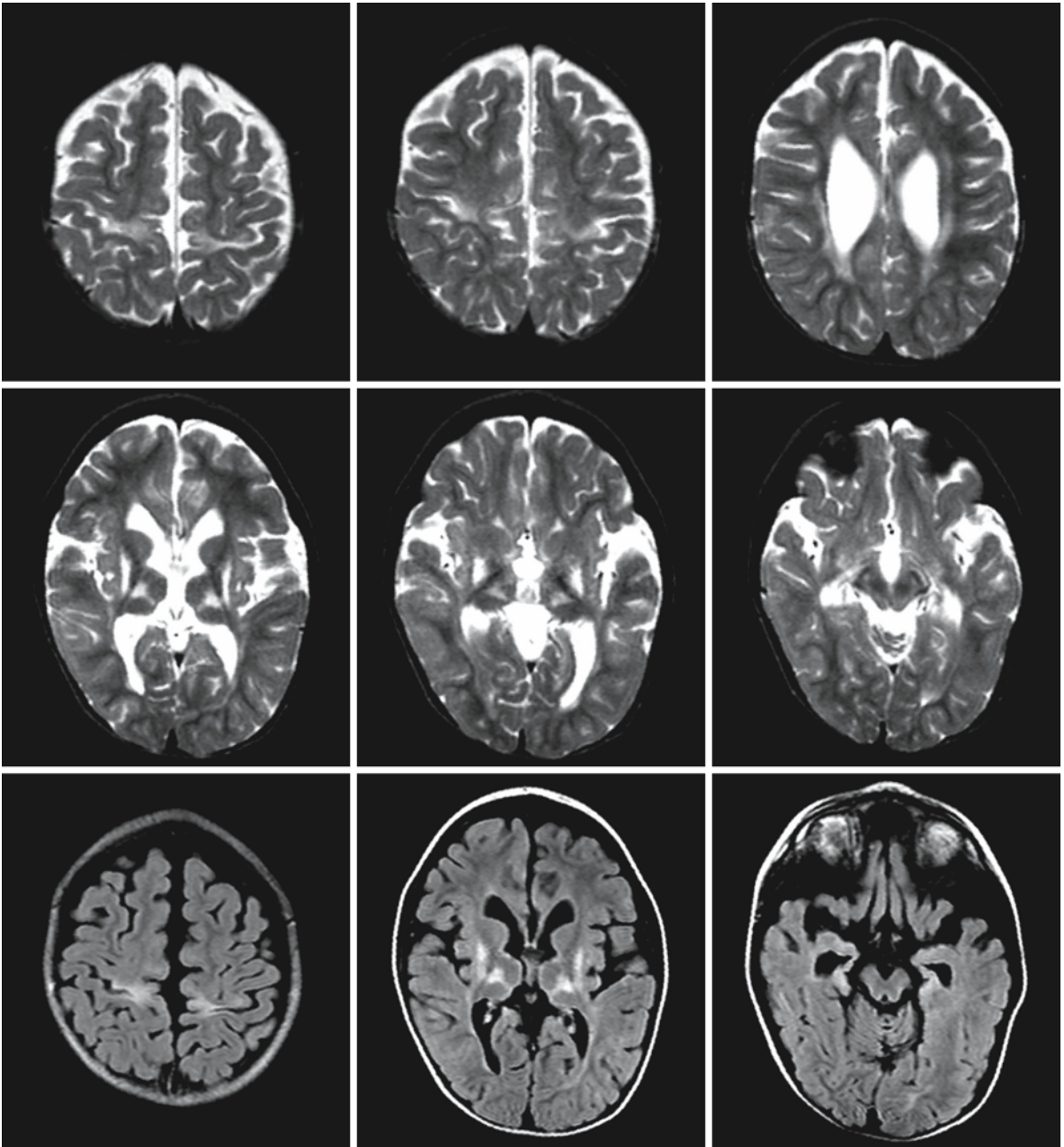


Fig. 95.9. c

Fig. 95.9. **a** A boy was born at 42 weeks gestational age by emergency cesarean section. There was a severe hypoxic–ischemic insult. The T_2 -weighted images (*first and second rows*) show perhaps a less clear cortical ribbon in the parietal region and ill-defined basal ganglia, but the abnormalities are not prominent and the images are difficult to interpret. The contrast-enhanced T_1 -weighted images (*third and fourth rows*) confirm the fuzziness together with some enhancement of the basal ganglia. **b** Diffusion-weighted Trace images (*first and second rows*, $b = 1000$) reveal the cortico-subcortical pattern

and help to establish the prognosis of the child. The ADC maps (*third and fourth rows*) confirm the low ADC values in the bright areas of the Trace images. **c** Follow-up MRI at 2 years shows the pattern also on conventional images. The T_2 -weighted images (*first and second rows*) show a gliotic lesion involving the cortex and subcortical white matter in the perirolandic area, and lesions in the dorsal part of the putamen, the ventrolateral part of the thalamus, the substantia nigra, and the hippocampus on both sides. The pattern is even more conspicuous on FLAIR images (*third row*)

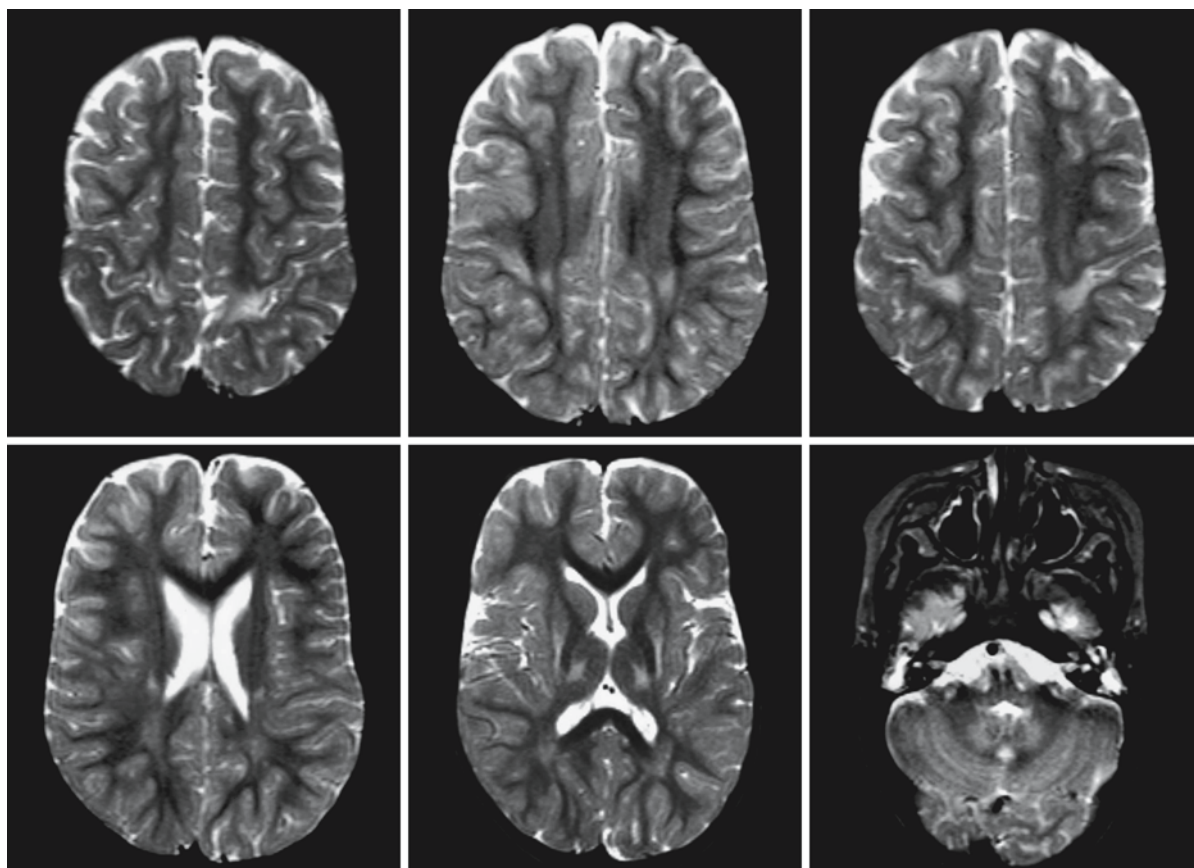


Fig. 95.10. The same pattern of periolandic cortico-subcortical gliosis and lesions in thalamus, putamen, and dentate nucleus in a 3-year-old girl who had a history of severe perinatal asphyxia at term birth

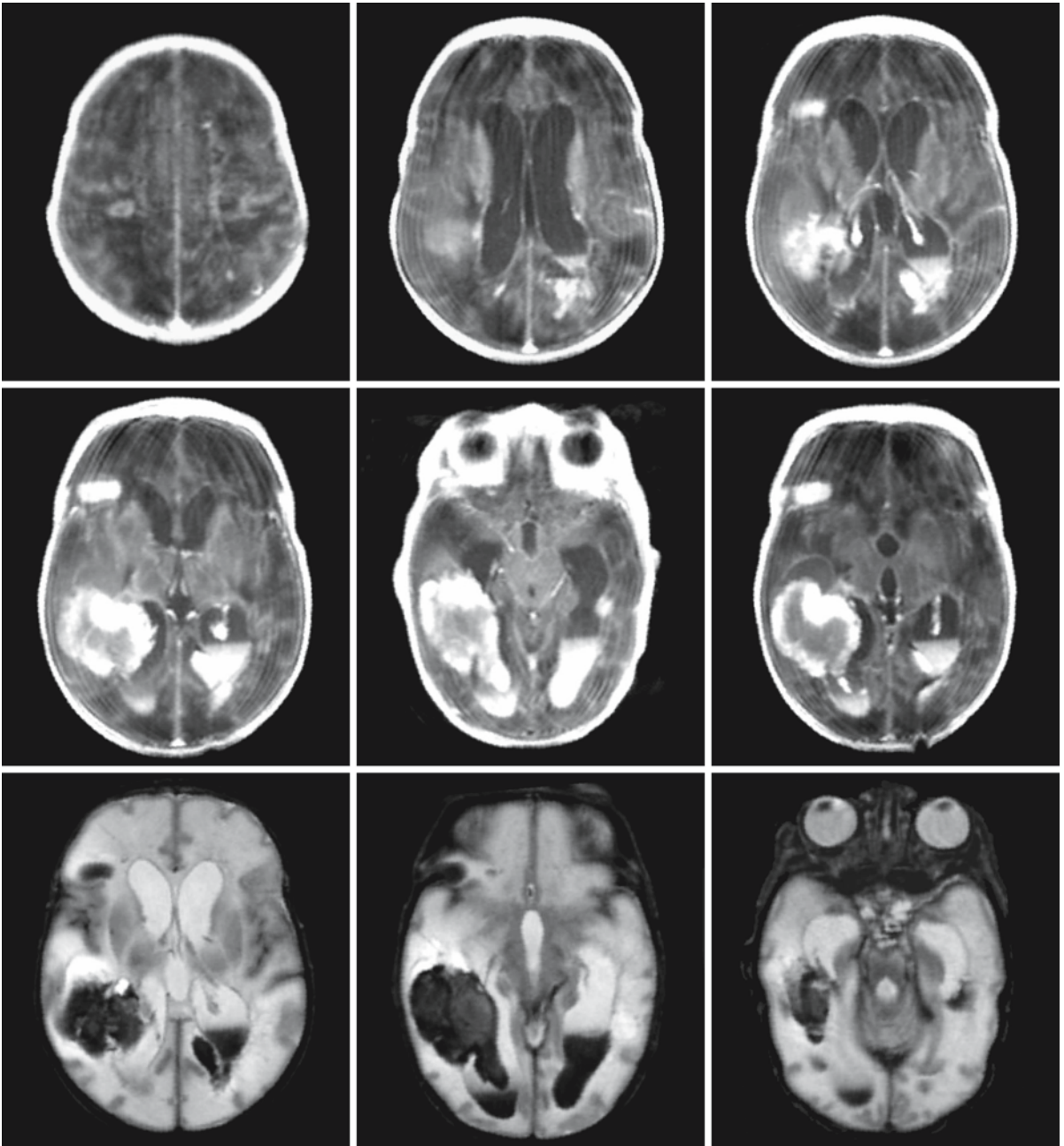


Fig. 95.11. a A boy was born at 32 weeks gestational age after fetal distress. He had a severe anemia and rhesus antagonism. T₁-weighted (*first and second rows*) and T₂-weighted (*third row*) images 1 month after birth show extensive intraparenchymal

hemorrhages and ventriculomegaly. There is also blood in the ventricles. The cerebral white matter is swollen and has an abnormal signal intensity. (Fig. 95.11. b see next page)

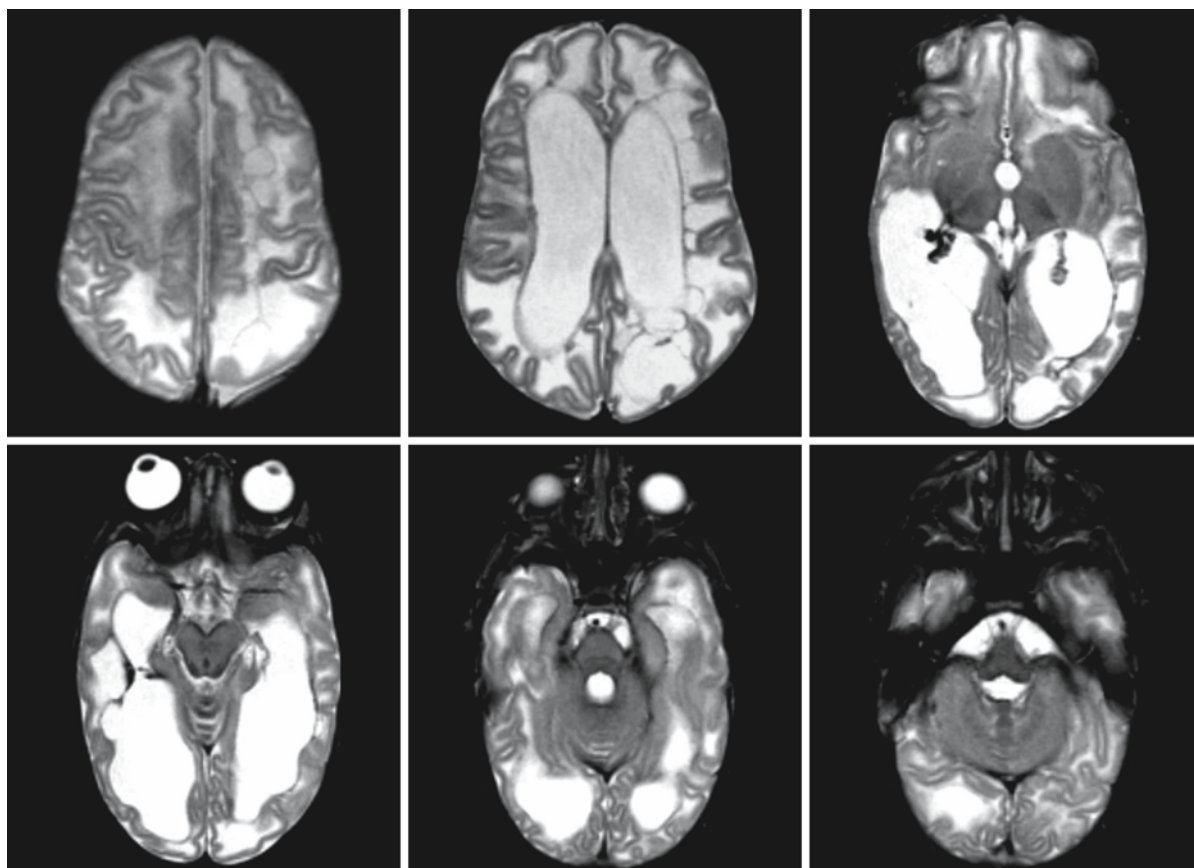


Fig. 95.11. b T₂-weighted series at the age of 2 months show a multicystic encephalopathy

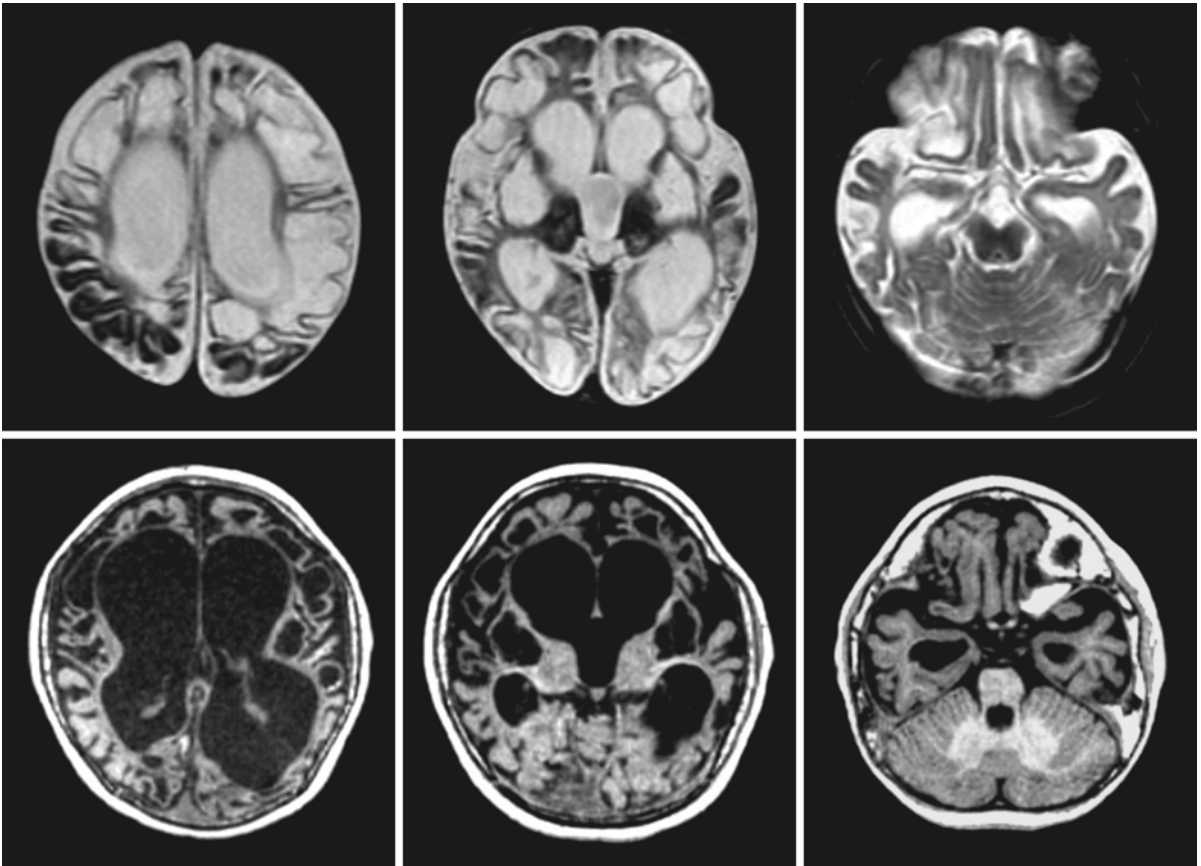


Fig. 95.12. A boy was born at 42 weeks' gestation. An initially mild hypoxic–ischemic encephalopathy was soon followed by a catastrophic encephalopathy. This MRI at the age of 2 years shows a multicystic encephalopathy and ventriculomegaly. The basal ganglia are also cystic. The brain stem and cerebellum are spared

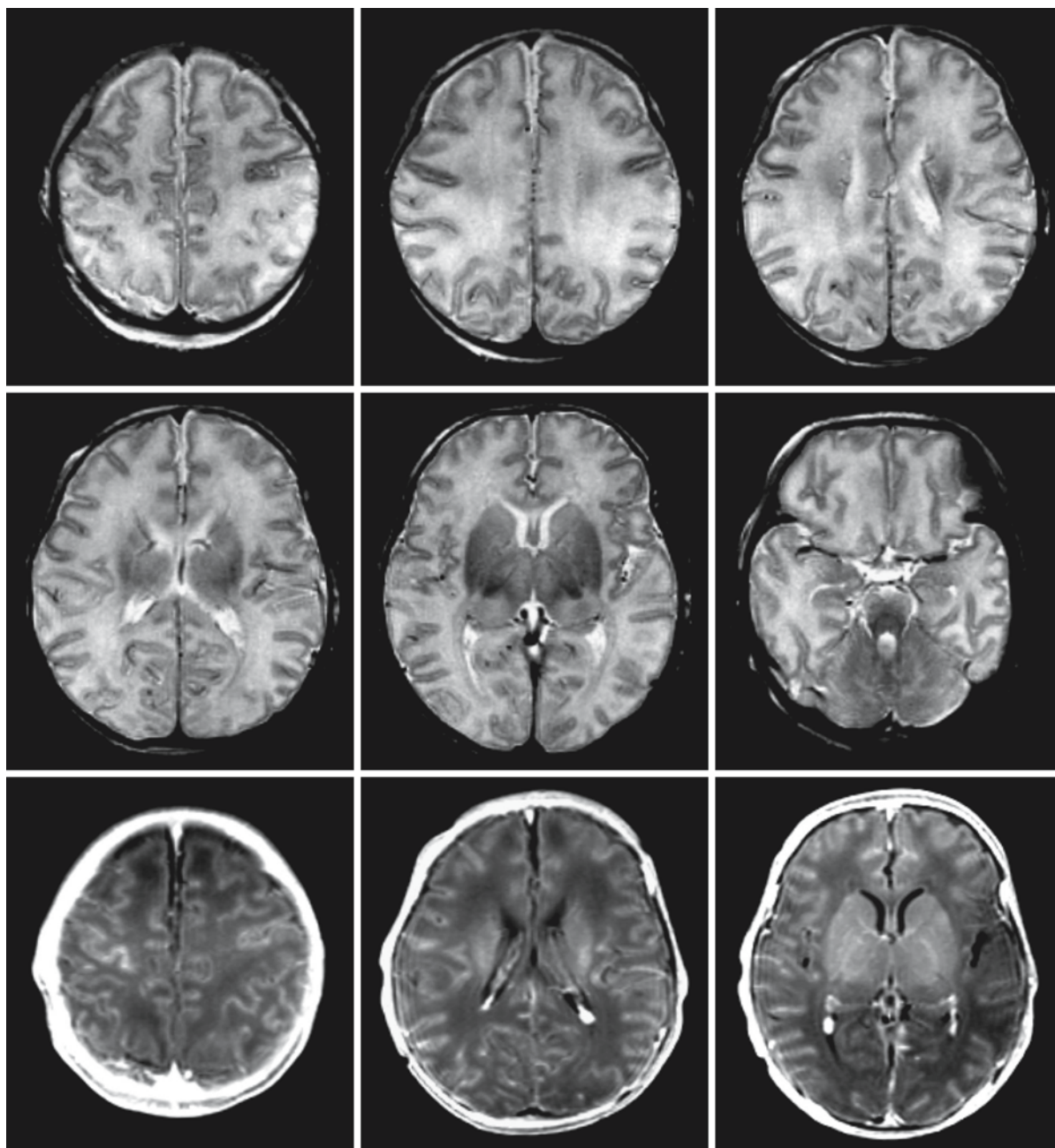


Fig. 95.13. a A boy was born at 39 weeks' gestation with serious perinatal asphyxia and a poor start. MRI was obtained at 3 days. The T₂-weighted images (*first* and *second* rows) show a poorly defined cortical ribbon in the parieto-occipital re-

gions and fuzziness of the basal ganglia. Contrast-enhanced T₁-weighted images (*third* row) show enhancement of the perirolandic cortex on the right, but no clear other abnormalities

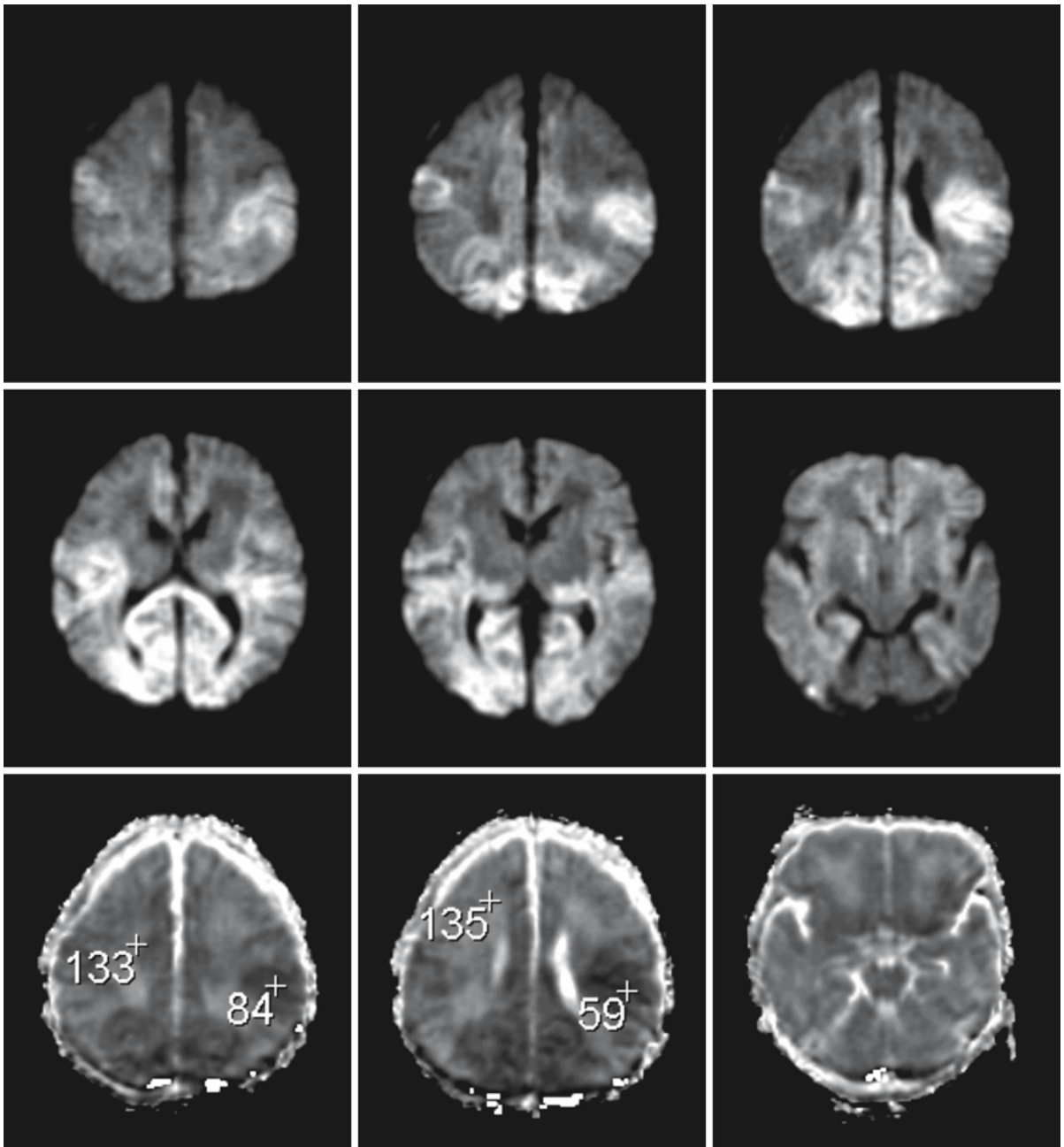


Fig. 95.13. b Diffusion-weighted Trace images (*first and second rows*, $b = 1000$) and ADC maps (*third row*) show a different pattern than in previous patients. The basal ganglia are not

involved, whereas the parieto-occipital and perirolandic cortex is severely involved. The ADC values in the affected areas are low, as is indicated for some spots

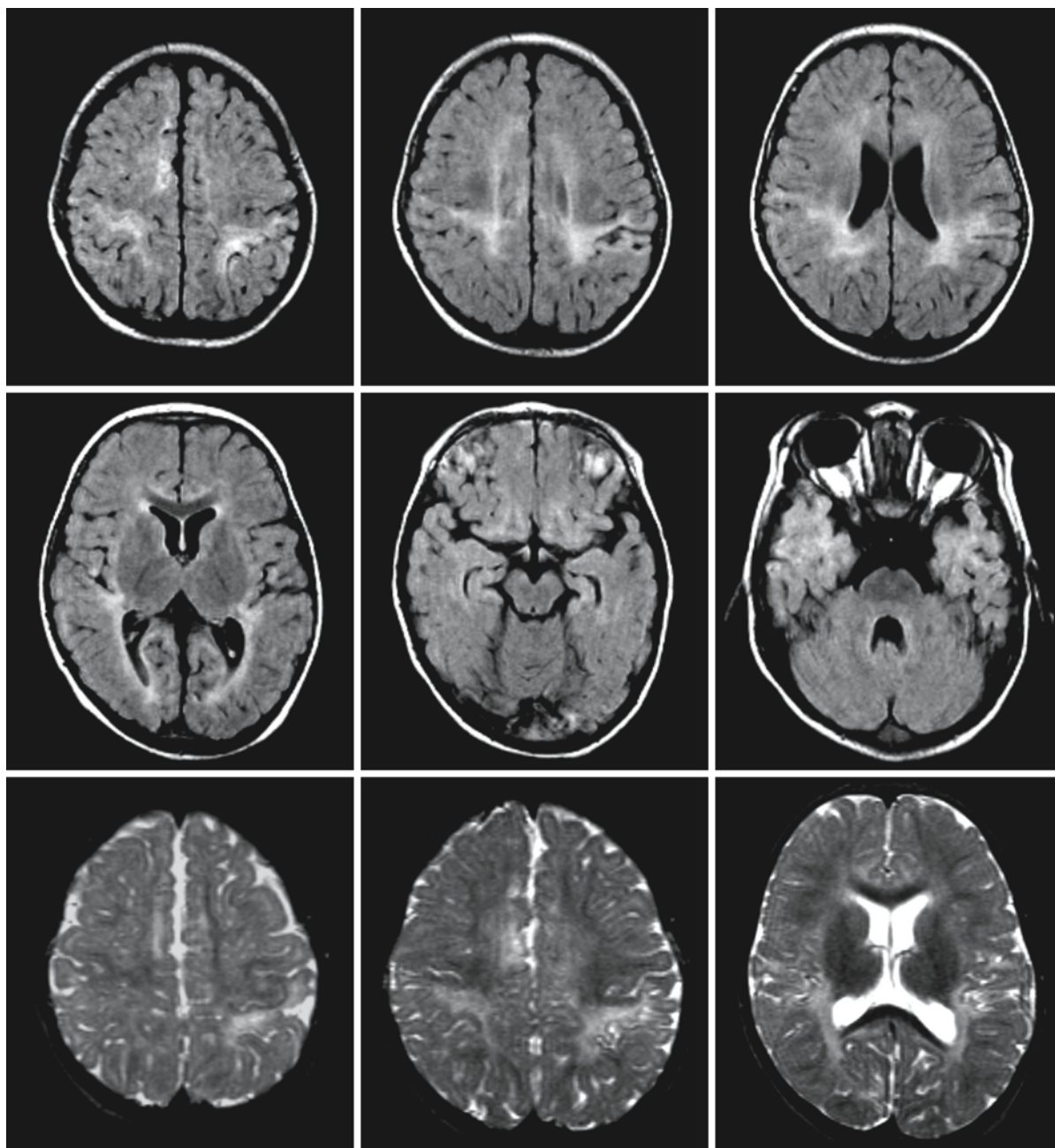


Fig. 95.13. *c* Follow-up MRI was obtained at the age of 14 months. The FLAIR (*first and second rows*) and T₂-weighted images (*third row*) show gliosis in the cortex and subcortical

tracts in the perirolandic area, as is seen in the cortico-subcortical pattern. There are no abnormalities in the basal ganglia. Additional gliosis is present in the parieto-occipital region

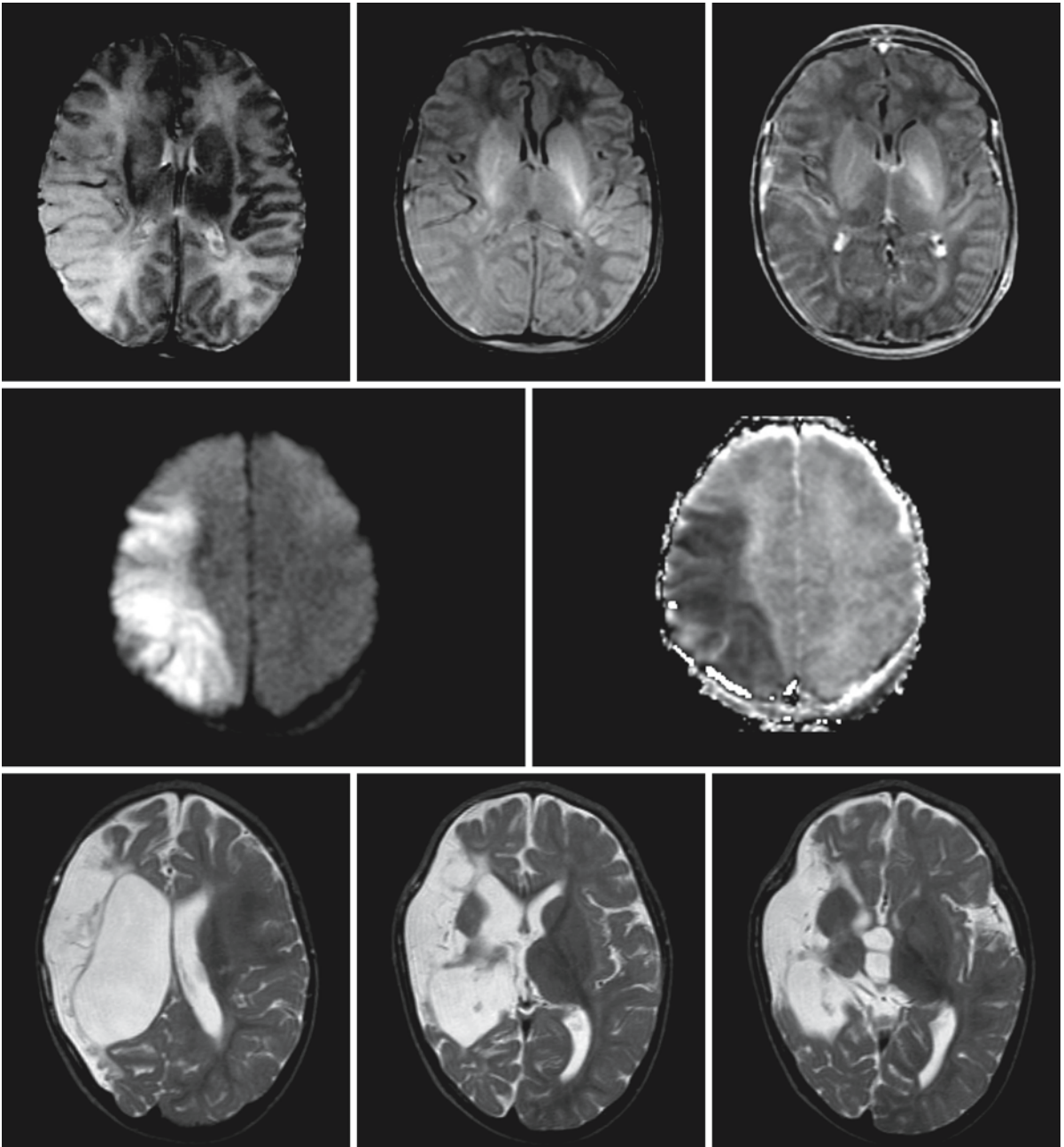


Fig. 95.14. A term-born neonate was born by vacuum extraction. The *upper row* of conventional T_2 -weighted and T_1 -weighted images without and with contrast show an infarction in left middle cerebral artery territory, most clear on the T_2 -weighted images. The *second row* shows a diffusion-weighted Trace image (*left*, $b = 1000$) and ADC map (*right*) at the same level, both indicating restricted diffusion in the infarcted area.

Follow-up images after a few years (*third row*) show the typical pattern of remains of a perinatal middle cerebral artery infarction. The entire right hemisphere is smaller than the left. The middle cerebral artery territory has undergone polycystic degeneration, with now only some membranous remains in the area

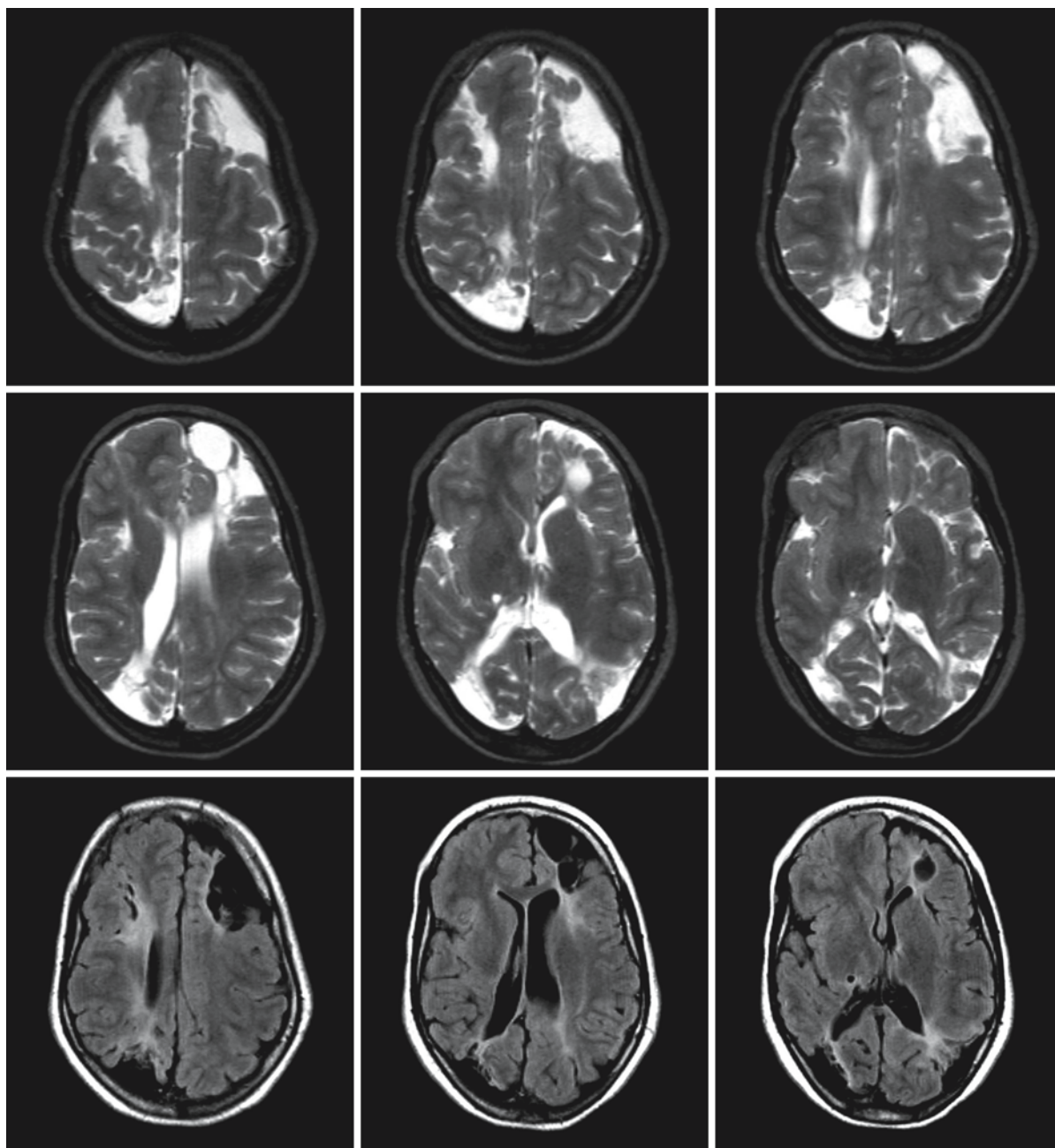


Fig. 95.15. A female infant was born at a gestational age of 35 weeks. Soon after birth she started to have epileptic seizures and developed microcephaly, developmental delay, and spas-

tic tetraparesis, left more than right. The MRI at 7 years shows the pattern of extensive border zone infarctions. The gliosis is best seen on the FLAIR images (*third row*)

Neonatal Hypoglycemia

R.J. Vermeulen, J. Valk

96.1 Clinical and Laboratory Findings

Neonatal hypoglycemia is a condition that frequently occurs in sick newborns. The symptomatology in the acute stage can range from agitation, somnolence, and epileptic seizures to status epilepticus and coma. Several groups of neonates are at risk of hypoglycemia because of a lack of glucose reserves (dysmaturity and prematurity) or an increased need for glucose related to high weight and maternal diabetes. The causes of severe neonatal hypoglycemia are diverse and can be separated in three large groups: hyperinsulinism (Beckwith–Wiedemann syndrome, nesidioblastosis–adenoma spectrum, hyperplasia of the pancreas, leucine sensitivity), endocrine deficiencies (cortisol deficiency, growth hormone deficiency, glucagon deficiency, hypothyroidism, panhypopituitarism), and hereditary metabolic defects (defects in carbohydrate, amino acid, organic acid, and fatty acid metabolism).

Long-term outcome of infants with severe neonatal hypoglycemia varies from fatal, through poor with severe mental retardation, epilepsy, and visual impairment, to absence of evident neurological consequences. Visual impairment is an important clinical manifestation of neonatal hypoglycemia and results from the preferential damage of the parieto-occipital white and gray matter. In addition, optic atrophy has been described, most probably secondary to the lesions in the parieto-occipital region through the mechanism of transsynaptic degeneration.

It should be noted that there is no consensus about the exact definition of hypoglycemia. It has been shown that even moderate hypoglycemia is a potential hazard for the neonatal brain. For instance, glucose levels below 2.6 mmol/l can be associated with motor and cognitive impairment. Deterioration of motor and cognitive skills is not only related to the depth of the hypoglycemia, but also to the number of days with hypoglycemic episodes.

96.2 Pathology

Most data on hypoglycemic brain damage have been obtained in adults. In human adults it is often difficult to distinguish hypoglycemic from hypoxic–ischemic brain damage on morphological grounds. There are, however, differences in distribution of the neu-

ronal damage and histochemical differences. Hypoglycemia leads to reduced concentrations of pyruvate and lactate and diminishes the production of protons by the Krebs cycle, resulting in tissue alkalosis, while hypoxia–ischemia is characterized by elevated lactate and acidosis. In contrast to hypoxia–ischemia, hypoglycemia does not lead to pannecrosis, but to selective neuronal necrosis. This neuronal necrosis involves the cerebral cortex, the hippocampus, the caudate nucleus, and sometimes the spinal cord. In contrast to hypoxia–ischemia, the brain stem and the cerebellum are spared in hypoglycemia. In addition, the cortical neuronal necrosis is more superficial in hypoglycemia, whereas the middle cortical layers are preferentially targeted by hypoxia–ischemia. Axon-sparing parenchymal lesions with selective dendritic swellings are often considered a hallmark of hypoglycemic damage. These swollen dendrites contain swollen mitochondria. In the next phase swollen mitochondria are seen in the cell body and cell membrane irregularities appear. Finally, the neurons become necrotic, as indicated by mitochondrial flocculent densities and frank membrane rupture. There is a free admixture of amorphous cytoplasm within the extracellular space, indicating cellular dissolution. The cytoplasm of the affected cells stains acidophilic in light microscopy. The dendritic death of neurons is characteristic of excitotoxicity.

Neuropathological observations of damage to the neonatal brain in pure hypoglycemia are limited. In the few studies of untreated or inadequately treated hypoglycemic neonates, involvement of all parts of the brain and the anterior horns of the spinal cord has been observed, with particularly severe lesions in the posterior parts of the cerebrum, the parieto-occipital lobes. Involvement of arterial border zones, as may be seen in hypoxic–ischemic encephalopathy, is not seen. As in adults, cortical involvement includes the superficial cortical layers and not the deeper layers as in hypoxia–ischemia. Microscopically the findings include acute degeneration of nerve cells and glial cells. In most infants the nerve cells in the cortex are small with abnormal nuclei. There is a regional distribution of neuronal damage, with the most severe signs of acute degeneration in the occipital cortex and the least signs of involvement in the temporal cortex. Fragmented cells may be demonstrated in the caudate nucleus and putamen, the claustrum, and the granular layer of the cerebellum. Another type of damage is

found in large neurons (thalamus, hypothalamus, globus pallidus, and Purkinje cells) showing chromatolysis with swelling and granularity of the cytoplasm. Large vacuoles may be observed in the motor nuclei of the brain stem.

96.3 Pathogenetic Considerations

Hypoxia–ischemia and hypoglycemia both lead to energy failure, and one would expect similar patterns of brain damage. There are, however, major differences, especially well known from the patterns of brain damage following perinatal asphyxia and neonatal hypoglycemia. Only in neonatal hypoglycemia is preferential damage of the parieto-occipital region seen. The differences require an explanation.

The immature brains of neonates have the facility to use alternative energy donors (for instance lactate and ketone bodies), an ability that gradually disappears with age. This and the lesser energy demand of the neonatal brain explain why the immature brain is more resistant to hypoglycemia than more mature brains. This is probably the reason why hypoglycemic brain damage rarely occurs in neonates without a predisposing factor. Glucose utilization in newborns as measured with 2-deoxy-2- ^{18}F fluoro-D-glucose PET does not demonstrate a higher glucose turnover in the occipital cortical area than in other cortical areas.

Neuronal death by hypoxic–ischemic energy depletion includes instant cell death and delayed cell damage and death, the latter mediated by a cascade of events including membrane depolarization, calcium influx into the cytosol, release of proteases and lipases, formation of free radicals, lipid fragmentation and formation of arachidonic acid, and lipid peroxidation. Brain damage in hypoglycemia is not the direct and immediate result of the lack of glucose, but follows the steps of delayed cell death.

It has been suggested that one of the important differences between hypoxic–ischemic and hypoglycemic conditions concerns the cerebral blood flow. The two- to threefold increase in cerebral blood flow that occurs in patients with hypoglycemia is then assumed not to occur in hypoxia–ischemia. This, however, is not true in all cases of hypoxia–ischemia, where an initial rise in cerebral blood flow of the same order may occur, followed by a decrease when generalized hypoxia–ischemia also affects the cardiac muscle. The cardiac muscle seems more resistant to low glucose levels than to hypoxia–ischemia. This difference could be important. Correction of the hypoglycemia leads to a decrease in cerebral blood flow to values about 30% below normal. PET studies reveal that under hypoglycemic conditions the metabolic

rate of the brain does not change, in contrast to under conditions of hypoxia–ischemia, where the metabolic rate decreases. A difference between the posterior part and the rest of the brain has, however, not been demonstrated.

Low glucose levels lead to a reduction of energy supply and to protein and lipid catabolism. Because of the lower glucose levels, levels of lactate and pyruvate are also reduced. Consequently proton production by the Krebs cycle is reduced, leading to tissue alkalosis, in contrast to ischemia, which is characterized by elevated levels of pyruvate and lactate and acidosis. In hypoglycemia decarboxylation of pyruvate is decreased, leading to a shortage of CoA, a major intermediate in the pathway to oxaloacetate. Oxaloacetate is the α -keto acid in a transamination reaction with glutamate, yielding aspartate and α -ketoglutarate. Shortage of oxaloacetate subsequently leads to a reduction of tissue glutamate and an increase in aspartate. This increase in the aspartate/glutamate ratio is the reverse of what is seen in hypoxic–ischemic conditions. Aspartate is more selectively active on NMDA receptors than glutamate. NMDA antagonists are, at least in experimental situations, more effective in hypoglycemia than in hypoxia–ischemia. However, no pattern of distribution of NMDA receptors is known that would explain the vulnerability of the posterior part of the cerebral hemispheres in neonates.

Delivery of glucose to the brain requires so-called glucose transporter proteins. Endothelial cells play a crucial role in the transport of glucose over the blood–brain barrier since they are equipped with GLUT1 glucose transporters. In addition, GLUT3, a neuronal glucose transporter, shows a developmental regulation of expression, at least in the newborn rat. However, it has not been reported that this transporter has a regional distribution that would explain the selective vulnerability of the parieto-occipital region. The GLUT5 transporter is selectively expressed in microglia, whereas the other types of glucose trans-




Fig. 96.1. A male neonate suffered from severe and repeated hypoglycemia. This first MRI was obtained at the age of 16 days. The T_2 -weighted images (*first and second rows*) show blurring of the cortical ribbon in the parieto-occipital and temporal areas and swelling of these areas. The signal intensity of the white matter is too high for normal unmyelinated white matter in these regions, suggesting edema. There is also a high signal intensity in the peripheral parts of the cerebellar hemispheres, which is extremely unusual in post-hypoxic–ischemic encephalopathy. The T_1 -weighted images (*third and fourth rows*) show areas of cortical laminar hyperintensity in the frontal and parietal areas and loss of gray–white matter distinction in the posterior parieto-occipital and temporal area.

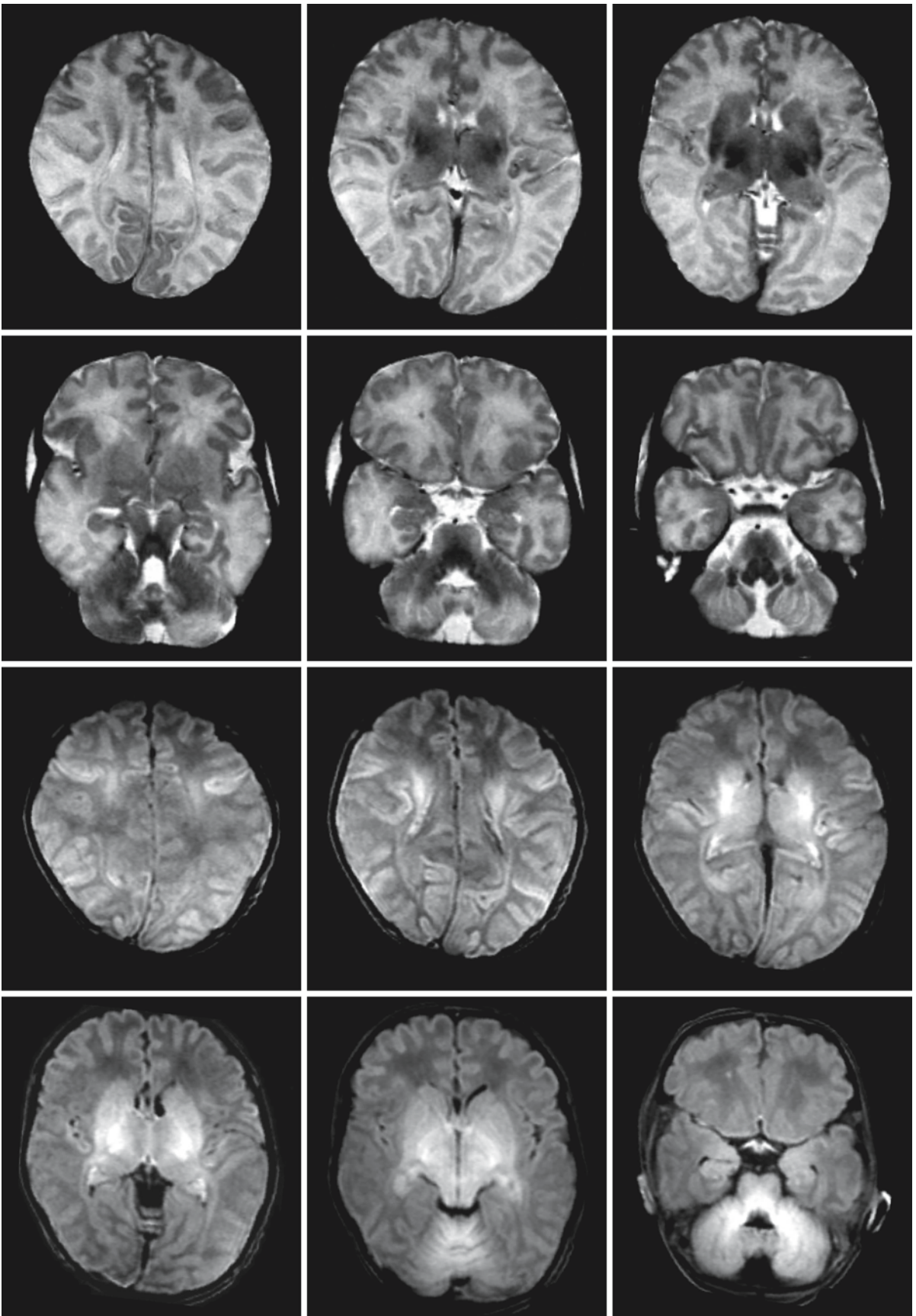


Fig. 96.1.

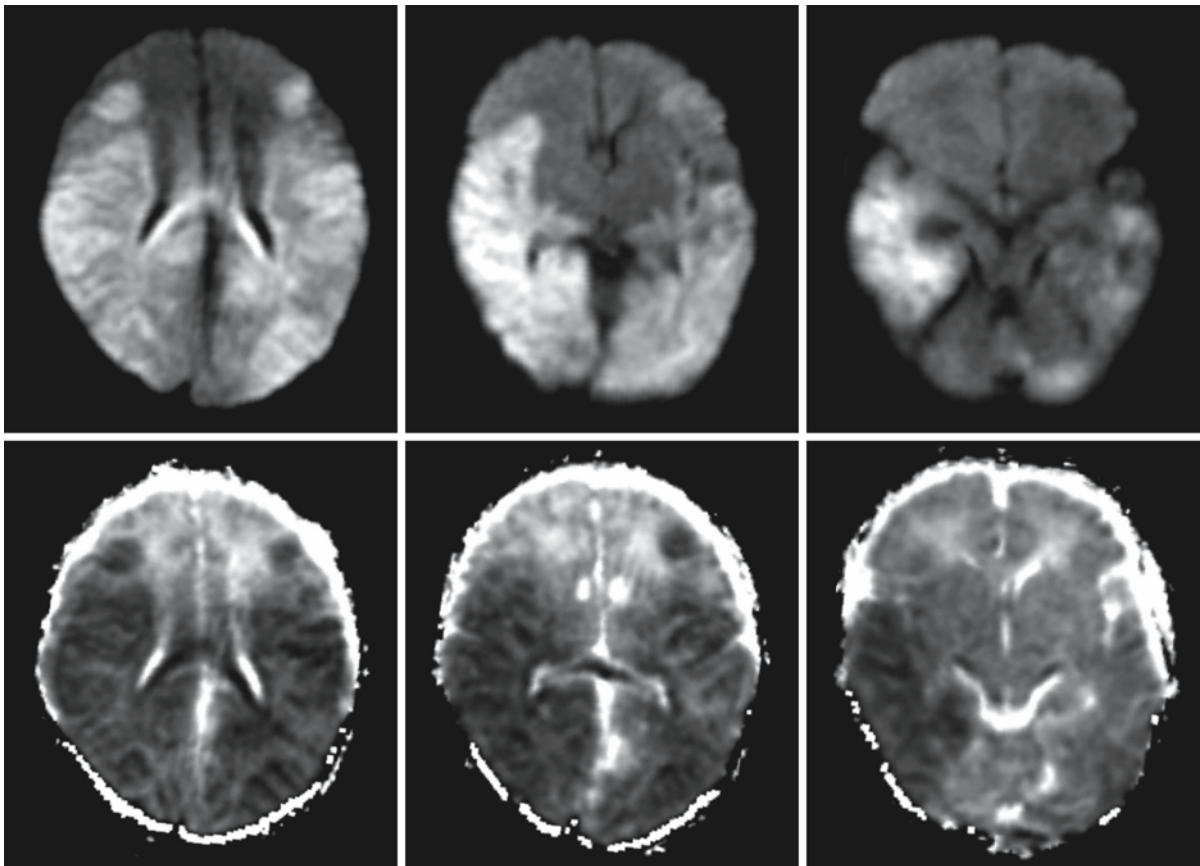


Fig. 96.2. Diffusion-weighted imaging was performed in the same boy at 16 days. The Trace diffusion-weighted ($b = 1000$) images (*first row*) show extensive hyperintensities, most pro-

minent in the parieto-occipital area, but also in both frontal and temporal lobes. The ADC maps (*second row*) confirm the severe restriction in water diffusion in the affected areas

porters (2, 4, and 7) are only expressed at very low levels in the brain.

So none of the factors mentioned above would explain either the selective involvement of the parieto-occipital gray and white matter in neonates or the sparing of the cerebellum and brain stem.

96.4 Therapy

Prevention is the most important form of treatment. It is essential to identify infants at risk of hypoglycemia and to detect the first signs of its occurrence. Special risk factors have been discussed above. In the postnatal period maintenance of body temperature, oral feeding within 3–4 h after birth and monitoring the clinical signs of hypoglycemia (jitteriness and seizures) are important in the prevention and early detection of hypoglycemia. Even in neonates with only mildly low glucose levels, treatment should be initiated, starting with a bolus infusion followed by a continuous glucose infusion. Importantly, hyper-

glycemia should be avoided because of the risk of neurological complications. After correction of the hypoglycemia, tapering of intravenous glucose infusion should be slow in order to avoid secondary hypoglycemia. In addition, treatment of any specific causes underlying the hypoglycemia, including endocrine dysfunction and inborn errors of metabolism, should be instituted as appropriate.

96.5 Magnetic Resonance Imaging

The standard protocol used for preterm and term neonates, described in Chap. 95, is also appropriate for imaging hypoglycemic brain lesions. This protocol includes T_1 -weighted, proton density, and T_2 -weighted images for morphological and pathomorphological information. Gradient echo refocused images are used to detect hemorrhagic components and calcifications. In addition diffusion-weighted Trace images and ADC maps should be obtained, to reveal the extent of damage and to discover abnormal

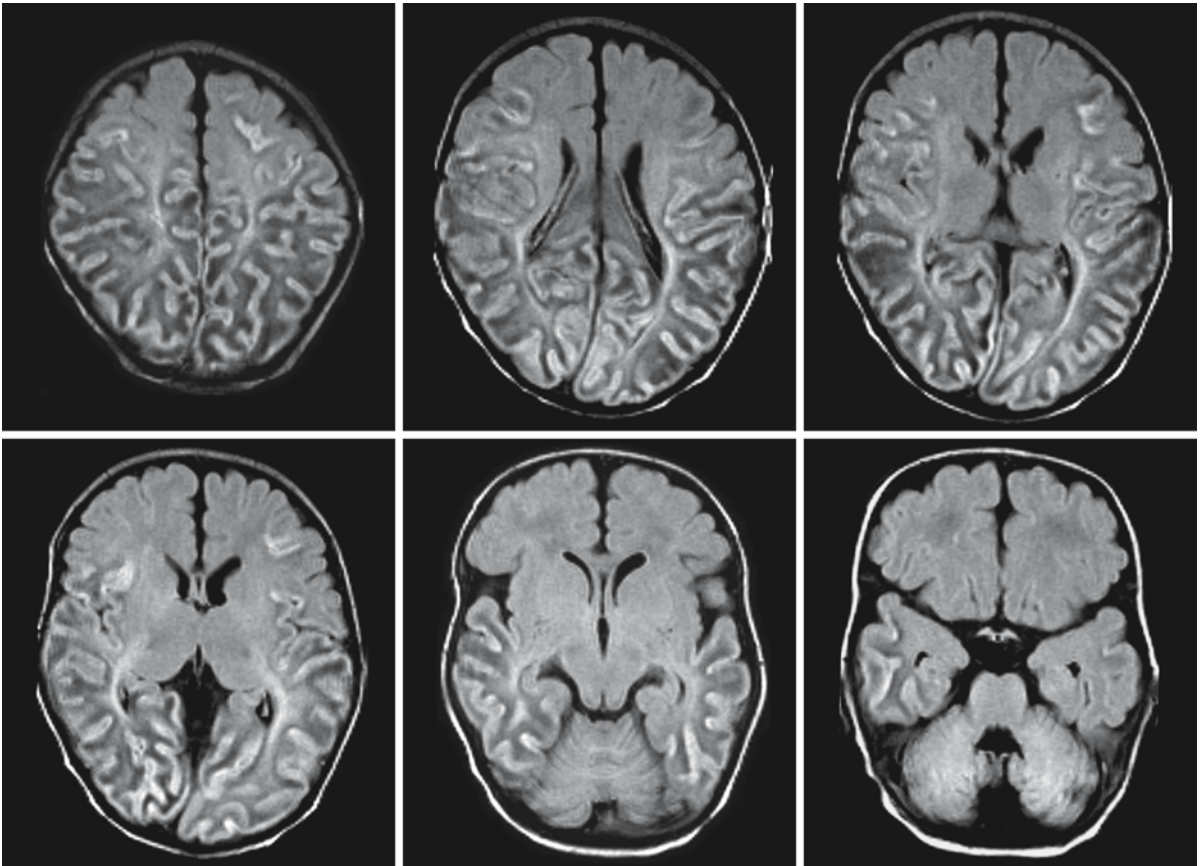


Fig. 96.3. This series of FLAIR images, obtained at 21 days in the same boy, confirm the extensive cortical involvement. Only the most anterior part of the frontal cortex seems spared.

The underlying white matter has become dark, suggesting white matter degeneration and rarefaction

areas with a normal appearance on conventional sequences. Where available, MRS should be part of the examination.

The most constant finding on MRI in early hypoglycemic encephalopathy consists of hyperintense and swollen areas on proton density, T_2 -weighted, and FLAIR images, predominantly located in the parieto-occipital lobes (Fig. 96.1). The lesions tend to be more or less symmetrical and may involve the splenium of the corpus callosum. T_1 -weighted images may show linear high-signal changes in the depth of the cortical sulci, in particular in the parieto-occipital areas (Fig. 96.1). After intravenous gadolinium the latter abnormalities may become more conspicuous. In the initial phase the affected areas show high signal intensity on diffusion-weighted Trace images and ADC values are decreased by about 25–40% compared to normal (Fig. 96.2). Very low ADC values (0.50–0.70) of the affected parieto-occipital lobes suggest irreversible cytotoxic edema leading to permanent loss of brain tissue. Follow-up FLAIR images show cortical hyperintensity, whereas the white matter becomes

dark (Fig. 96.3), compatible with ongoing cortical necrosis and white matter degeneration and rarefaction. Soon macrocysts develop, the cysts extending from cortex to ventricular wall (Fig. 96.4). The cortex covering these cysts is extremely thin. However, the initial hypoglycemic brain lesions are reversible in some cases or are reversible in part of the brain (compare Figs. 96.2 and 96.4). In the final stages MRI shows tissue loss, especially of the white matter, with crowding of the overlying gyri (ulegyria) in the parieto-occipital region. Usually the trigonum and occipital horns of the lateral ventricles are dilated.

MRS should show low concentrations of lactate in the initial lesions, in contrast to what is seen in perinatal asphyxia. MR phosphorus spectroscopy is able to confirm the alkalosis in hypoglycemia versus the acidosis in hypoxia–ischemia.

The differential diagnosis in the early phase of hypoglycemia includes only a few other disease states. The most prominent is bilateral occlusion of both posterior cerebral arteries, as may occur in patients with preceding severe brain edema. The P3 segment

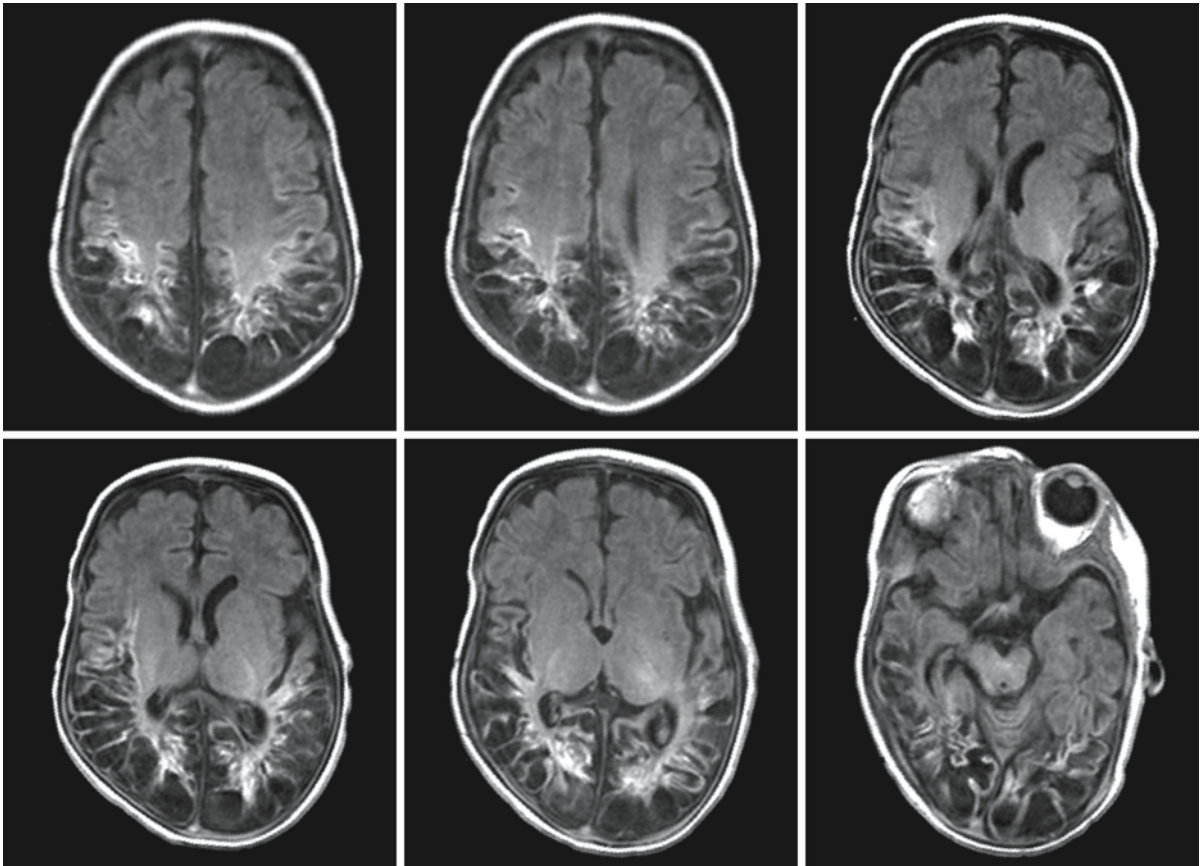


Fig. 96.4. This series of T₁-weighted images was obtained in the same boy at 6 weeks. There is multicystic degeneration of both parieto-occipital lobes. The lesions are partly hemor-

rhagic. Note that not all areas with severe diffusion restriction underwent the same degeneration

of the posterior cerebral artery may be compressed against the tentorial ridge and bilateral posterior territorial infarctions may result. Concurrent hypoxic-

ischemic damage is often present in hypoglycemia, which may make the hypoglycemic damage pattern less clear.

Delayed Posthypoxic Leukoencephalopathy

97.1 Clinical Features and Laboratory Investigations

The usual pathological sequels of hypoxia in the CNS consist of damage to the neurons of the cortex and the subcortical gray matter structures. Selective injury to the cerebral white matter as a consequence of hypoxia–ischemia occurring in the neonatal period is far less common after hypoxia–ischemia occurring later in life. However, as early as 1925 the German pathologist Grinker noticed a diffuse symmetrical leukoencephalopathy occurring days after carbon monoxide intoxication. The condition was named after him: Grinker myelinopathy. As in the original description, posthypoxic leukoencephalopathy may occur immediately subsequent to a hypoxic–ischemic insult, but usually there is an early phase of improvement after the initial stage of cerebral injury, followed, several days or weeks later, by recurrence of impaired consciousness and other neurological signs. In these cases CT and MR show more or less severe leukoencephalopathy, and therefore this condition is referred to as delayed posthypoxic leukoencephalopathy (DPHL). The neurological abnormalities in DPHL vary from patient to patient and include spastic paresis of the extremities, a parkinsonian syndrome, choreiform movements, visual failure, myoclonus, seizures, psychosis, and mental deterioration. The condition results in a chronic state of global dementia, a vegetative state, or death, but recovery may also occur.

The most common cause of DPHL is intoxication with carbon monoxide or cyanide. This may happen accidentally, but also occurs in homicidal or suicidal cases. In the USA not less than 6.4% of suicide attempts involve carbon monoxide. This figure is probable not far from that in other countries in the western hemisphere.

Laboratory tests in the acute phase include, first of all, determination of blood gases to assess oxygenation and acid–base status, since acidosis frequently accompanies the hypoxia. In cases of suspected carbon monoxide poisoning, the level of carboxyhemoglobin is determined. In carbon monoxide poisoning, the ECG often shows signs of ischemia with inverted T waves and ST wave depression. If other intoxications are suspected, specific laboratory estimations of the level of toxic agents are necessary. The diagnosis of DPHL is established at a later stage with the help of

clinical history, physical findings, and imaging techniques. The EEG contains diffuse bilateral slow wave activity with low voltage.

97.2 Pathology

The neuropathological findings are highly variable, depending on the severity and nature of the insult and the time between the event and the pathological examination of the brain. Here only the neuropathological findings of DPHL in the more chronic stage of the disease are described.

The external appearance of the brain is normal or mildly atrophic. On sectioning, confluent white matter lesions are found bilaterally, with a fairly symmetrical distribution. Microscopically, the central white matter of both hemispheres contains areas of diffuse demyelination with loss of oligodendroglial cells and proliferation of astrocytes. The axons are relatively spared, but areas of extensive necrosis may occur with loss of both myelin and axons. Such necrosis is seen predominantly in arterial end and border zones of the deep white matter, while in the less distant arterial end fields of the white matter only demyelination is observed. The arcuate fibers and white matter underneath the ependyma are better preserved. Patches of myelin persist around numerous vessels.

The cortex is usually spared, but concomitant areas of necrosis may be present in the cerebral cortex, especially in an arterial border zone distribution. Necrotic areas are often present in the basal ganglia. The brain stem and cerebellum are usually, but not always, unaffected.

97.3 Pathogenetic Considerations

The susceptibility of tissues to anoxic–ischemic damage depends on the extent of vascular supply, the presence and quality of collateral circulation, the metabolic activity, and thus the energy demands of the particular tissues. In intoxications the specific chemical affinity and vulnerability of certain brain structures also play a prominent role, as in the initial phase of carbon monoxide poisoning. In the brain anoxic–ischemic processes most commonly affect the cerebral cortex, while the white matter is completely

or relatively spared. This observation can be explained by the fact that the white matter is metabolically less active than the cortex. Other explanations are found in the distribution of excitatory amino acid synapses and local physicochemical factors at the cellular level.

However, a diffuse injury of the white matter is seen in DPHL. DPHL occurs under circumstances of prolonged hypoxia, hypotension, and metabolic imbalance. The underlying causes comprise respiratory failure, cardiac arrest, and systematic hypotension. Precipitating events are carbon monoxide poisoning, cyanide poisoning, carbon disulfide poisoning, heroin overdose, morphine intoxication, anesthetic accident, postoperative shock, and many other events.

The white matter lesions of DPHL are located in arterial end and border zones. For their arterial blood supply, the cerebral cortex and arcuate fibers depend on cortical branches of the major cerebral arteries and their leptomeningeal anastomoses. For their supply the periventricular and deep white matter are dependent on penetrating arteries which traverse the brain from the cortex towards the ventricular ependyma. These arteries have few collateral branches; one artery nourishes one white matter unit. The basal ganglia receive their supply from end arteries. The deep white matter lesions of DPHL are frequently accompanied by lesions in the basal ganglia, as well as in border zones of the cerebral cortex. However, there is no clear correlation between gray and white matter damage, and white matter damage does not appear to depend directly on the degree of anoxia. Although some consider the white matter lesions to be merely a border zone effect, it is probable that something other than hypoxia alone is required for lesions of this kind to be produced. There are several reasons for this assumption. Cerebral DPHL occurs only rarely, in contrast to the much more frequent anoxic-ischemic gray matter damage. In addition, gray matter structures are relatively spared in DPHL, which suggests that the hypoxic-ischemic process in itself is not profound as these structures are rather sensitive to lack of oxygen. This leads to the impression that white matter damage is particularly likely to occur under conditions of prolonged depression of both oxygenation and circulation. Acidosis may be another adverse factor in this context. Drug overdose, for instance morphine intoxication, leading both to a depression of respiration and to hypotension, is particularly apt to lead to DPHL, much more often than, for instance, a cardiac arrest without antecedent impairment of respiration.

Carbon monoxide intoxication relatively frequently leads to DPHL. It causes tissue hypoxia by reversibly binding to hemoglobin in red blood cells, thereby reducing the oxygen-carrying capacity of the blood. The presence of carboxyhemoglobin shifts the

oxyhemoglobin dissociation curve to the left, and tissue oxygen tension must therefore fall to much lower levels before the remaining oxyhemoglobin can give up its oxygen, a factor aggravating the tissue hypoxia. Moreover, carbon monoxide inhibits cellular respiration by binding to cytochrome oxidase. In addition to hypoxia, carbon monoxide often causes general hypotension by the formation of carboxymyoglobin in the myocardium, which in turn leads to myocardial dysfunction. This combination of hypoxia and general circulatory collapse probably explains why DPHL is so often seen in carbon monoxide poisoning.

Cyanide may also lead to DPHL. Cyanides have specific inhibitory effects on the cytochrome oxidase respiratory enzyme system of cells due to a strong affinity of cyanides for the iron core of the cytochromes. In this way cyanides lead to tissue hypoxia despite the presence of sufficient amounts of oxygen.

97.4 Therapy

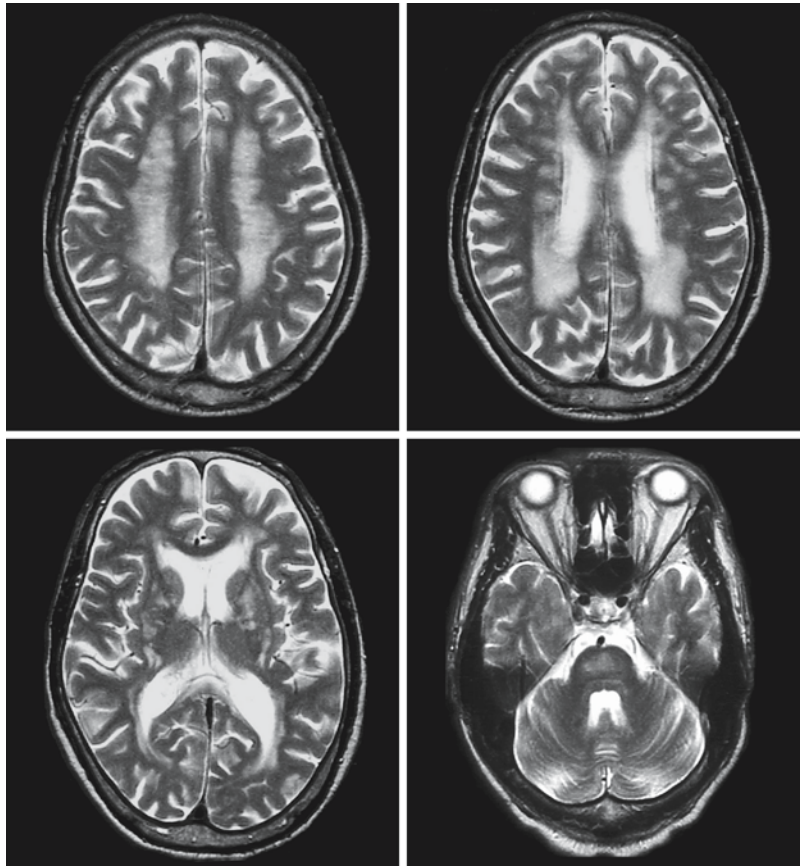
Prevention of cerebral hypoxia and ischemia and the prompt restitution of normal oxygenation, blood pressure, and acid-base balance after any hypoxic-ischemic insult are the only possible measures in the prevention and treatment of DPHL. The treatment of choice for patients with carbon monoxide poisoning is exposure to hyperbaric oxygen in order to wash out the carbon monoxide as soon as possible. Cyanide poisoning can be treated with hydroxycobalamin and sodium thiosulfate in the acute stage. Adequate treatment of the acute poisoning may prevent the occurrence of DPHL. Once DPHL has developed, the only option is to provide supportive care.

97.5 Magnetic Resonance Imaging

In DPHL, the involvement of the white matter is generally symmetrical and confluent and located in arterial border and end zones, due to the underlying systemic cause. In carbon monoxide poisoning, extensive, confluent deep white matter involvement with late occurrences has been reported, but more focal and asymmetrical white matter involvement has also been observed.

White matter lesions may be accompanied by lesions in gray matter structures in arterial terminal and border zones of the cortex and in the basal ganglia as the remains of the initial event. In carbon monoxide intoxication, the globus pallidus is preferentially affected. In cases where the original hypoxic-ischemic encephalopathy had another origin, other gray and white matter structures may also be involved. There are remarkably few reports on imaging findings in DPHL. The contribution of MRS is

Fig. 97.1. A 56-year-old man with chronic exposure to carbon disulfide. The T₂-weighted images show nearly symmetrical involvement of the deep white matter. There is also a moderate cerebral atrophy. The basal ganglia and the pons show lesions. From Ku et al. (2003), with permission and courtesy of Dr C.C. Huang, Department of Neurology, Chang Gung Memorial Hospital and University, Taipei, Taiwan



described in few articles. Diffusion-weighted Trace images and ADC maps have the possible contribution of distinguishing more recent from older lesions.

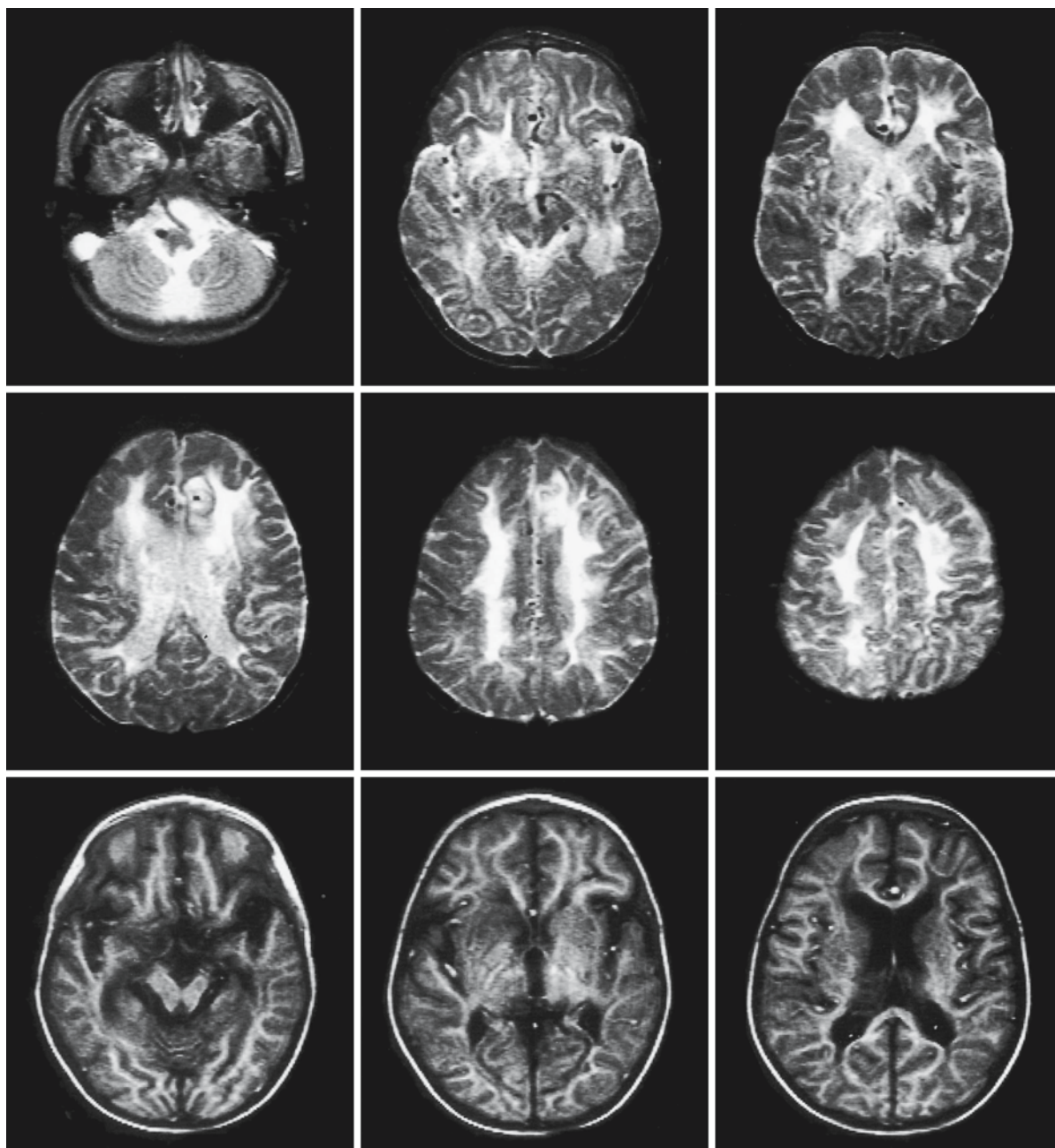


Fig. 97.2. A 6-year-old boy underwent surgery for a congenital cardiac defect. Postoperatively he did well. Four weeks later he showed behavioral changes. He suffered two cardiac arrests, necessitating resuscitation, after which he remained subcomatose. Neurological recovery was slow and only partial. He

showed signs of spastic tetraplegia. MRI shows extensive changes in the white matter, largely sparing the arcuate fibers. There are also lesions in the internal capsule, basal ganglia, and mesencephalon. The cerebellum is not affected

White Matter Lesions of the Elderly

98.1 Clinical Features and Laboratory Findings

Age-related changes of the brain have been documented in numerous MRI and histopathological studies. Changes that are found at histopathological examination in elderly individuals without neurological or neuropsychological deficits – in other words, in normal aging – include enlargement of the ventricles and the cerebral sulci reflecting gray and white matter loss, decrease in neurons and synapses, and increase in lipofuscin and mineral deposits in brain structures. On MRI white matter hyperintensities may appear on T_2 -weighted and FLAIR images, increasing with age, varying from multifocal spots in the deep white matter or a pencil-stripe-like rim around the ventricles to a confluent, bilateral, more or less symmetrical, periventricular leukoencephalopathy. The more or less extensive signal changes of the periventricular and deep white matter have been given the descriptive name “leukoaraiosis” (white matter rarefaction) by Hachinski et al. (1987), and have been the subject of many studies since then. Attempts have been made to document these changes more precisely with a variety of MR techniques, to search for neuropathological correlates, and to find out which white matter signal alterations represent apparently innocent changes by clinical standards, and which signal alterations indicate future clinical progress towards cognitive impairment and eventually vascular dementia. Similar attempts have been made from the neuropsychological point of view, where the search is still going on to define “age-related memory disorder,” “age-associated mental impairment,” “benign senescent forgetfulness,” and “mild cognitive impairment” (with decliners and nondecliners) in such a way that homogeneous subgroups can be identified for further studies. Again an important aim is prediction of outcome. The combined efforts of all disciplines involved so far have not come up with a final answer.

Much was expected of quantitative MR techniques. These techniques can more precisely indicate that with age more white matter than gray matter is lost; that increases in relaxation times are more pronounced in white matter than gray matter; that there is an increase of apparent diffusion coefficients in both white and gray matter, but more so in white than in gray matter, indicating more free water movement

and change of water content, with consequently loss of fractional anisotropy; and that there are decreasing magnetization transfer ratios, indicating loss of structural integrity of the brain tissue. MRS reveals a decrease of *N*-acetylaspartate, reflecting loss of neurons and axons. Reduced cerebral perfusion is reported as measured with MR techniques and PET, with unchanged oxygen extraction on PET. Impressive as these findings may seem, they have not enabled definition of clear cut-off points between successful aging, mild cognitive impairment, and progression towards multi-infarct dementia in the individual case.

98.2 Pathology

Reports on the pathological substrate of leukoaraiosis on MRI, either in normal aging or in patients with different degrees of cognitive decline, show a wide variety of findings. This is not surprising, given the bias in the examined populations, which most often involve only a small number of patients. In nearly all cases gross anatomy shows that the cerebral cortex appears normal or shows only minor changes. The white matter is either macroscopically normal or shows a grayish discoloration, with a rubbery consistency. White matter volume may be reduced. White matter abnormalities may be focal, isolated, or more confluent. The basal ganglia do not, as a rule, show changes. At microscopy, there are variable degrees of ependymal denudation and frontal and peritrigonal white matter changes, consisting of loosely structured tissue with widened Virchow–Robin spaces. The periventricular changes vary from white matter pallor (meaning less intensive myelin staining, the earliest change in the periventricular white matter, without overt demyelination, axonal loss, presence of foamy macrophages, or gliosis) to periventricular demyelination (describing overt myelin loss with astrocytic proliferation and in some cases some inflammatory reaction). The lesions may be patchy or more confluent. In more severe cases the periventricular and deep white matter changes are continuous. The cause of these changes is to be found in vessel wall abnormalities. These abnormalities range from non-specific intima thickening without narrowing of the lumen, to changes in the smooth muscle walls of the small vessels leading to gradual narrowing or occlusion of the small vessels.

There is no sharp transition between these relatively mild changes and the pattern seen in vascular dementia patients. In patients with vascular dementia, there are also lacunar infarctions, involvement of the corpus callosum, involvement of the basal ganglia (the latter often showing an *état criblé* or *état lacunaire* or both), abnormalities of the transverse fibers of the pons, and coagulation necrosis and cavitation of the deep white matter.

98.3 Pathogenetic Considerations

There are large differences in the estimation of the presumed clinical significance of white matter abnormalities in the elderly, and there is a great variability in reported histopathological correlates. The most prevalent morphological substrate is perivascular tissue change. Reasons for the perivascular tissue changes are supposed to be the thickening of vessel walls (by a number of different causes), damage to the surrounding tissue by a waterhammer effect of pulsating arterioles with diminished elasticity, and perivascular edema resulting from leakage of the blood–brain barrier. In a high percentage of cases hypertension plays a prominent role, and it is certainly a major factor in changing the vessel walls by lipohyalinosis and consequently narrowing of the lumina of small brain vessels. Several other disorders lead to the same result, despite the different material deposited in the vessel walls, with amyloid angiopathy, arteriosclerosis, and CADASIL as examples. Some factors must be responsible for the selective involvement of the periventricular and deep white matter as a common finding. Several factors have been suggested.

Chronic hypoperfusion may have a selective influence on oligodendrocytes and myelinated axons, as was supported by animal experimentation. Experimental studies of brain ischemia on rat and gerbil brains show that both oligodendrocytes and myelinated axons are highly vulnerable to ischemia and that chronic cerebral hypoperfusion leads to progressive rarefaction and glial activation in the white matter. Three hours after carotid occlusion in rats, oligodendrocytes display characteristics of irreversible injury, such as pyknosis and plasma membrane rupture. Three factors, in these experiments, led to vacuolation of the white matter: intramyelinic fluid accumulation, enlarged extracellular spaces, and swelling of astrocytic processes. These changes precede irreversible neuronal injury, indicating a time-independency of these processes and partly explaining the selective vulnerability of white matter in chronic hypoperfusion. Animal models, however, cannot easily be designed to mimic the age-related changes in the human brain and explain the various kinds of pathol-

ogy and the influence of lesions on neuropsychological functioning.

The distribution of the lesions may also be explained by the unique blood supply to the periventricular and deep white matter. Arteries originating in the arachnoid spaces perforate the brain tissue, running from the cortical surface towards the periventricular white matter. Although De Reuck's hypothesis (1971) of subependymal border zones has been challenged, it remains true that there is a scarcity of anastomoses of the large perforating arteries in these areas, so that in fact one vessel irrigates only one metabolic unit. Recurrent transient drops in cerebral blood flow can lead to ischemia in these units, often referred to as incomplete infarction. These changes may progress in some patients, explaining the whole range of abnormalities found in histopathology, from white matter sponginess, pallor, patchy demyelination, astrocytic proliferation, to more serious changes such as coagulative necrosis and cavitation. In this view leukoaraiosis is the expression of a diffuse cerebral hypoperfusion of variable severity, in its mildest form showing changes in the white matter on MRI without pertinent pathological findings other than possibly death of oligodendrocytes, and without neurological and/or neuropsychological deficits, and in its most severe form bearing the characteristics of subcortical arteriosclerotic encephalopathy.

Focusing on white matter abnormalities in the elderly, population-based studies have tried to identify risk factors for both the occurrence of white matter hyperintensities on T₂-weighted images, and factors predicting the long-term outcome of members of these populations. Not surprisingly, these factors include higher age, higher ischemic score on the Hachinski scale (0–18), history of stroke, lacunar infarction on MRI, hypertension (systolic >140 mmHg; diastolic >95 mmHg), male gender, atrial fibrillation, coronary artery infarcts, diabetes mellitus, smoking, alcohol abuse, drug abuse, hyperhomocysteinemia, antiphospholipid antibodies, several coagulation disorders, the presence of the apolipoprotein E ε4 allele, and probably other genetic factors. A study involving psychiatric patients showed periventricular and deep white matter abnormalities in a high percentage of patients with major depression. Important as these

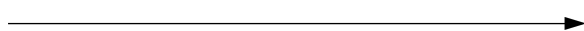


Fig. 98.1. a FLAIR (upper two rows) and T₂-weighted (lower two rows) images of a 64-year-old woman with "benign senescent memory impairment." The images show hyperintense changes in the deep and periventricular white matter and basal ganglia. The FLAIR images show the abnormalities with greater conspicuity. Clinical and MRI follow-up over the course of 4 years did not show any progression (nondecliner)

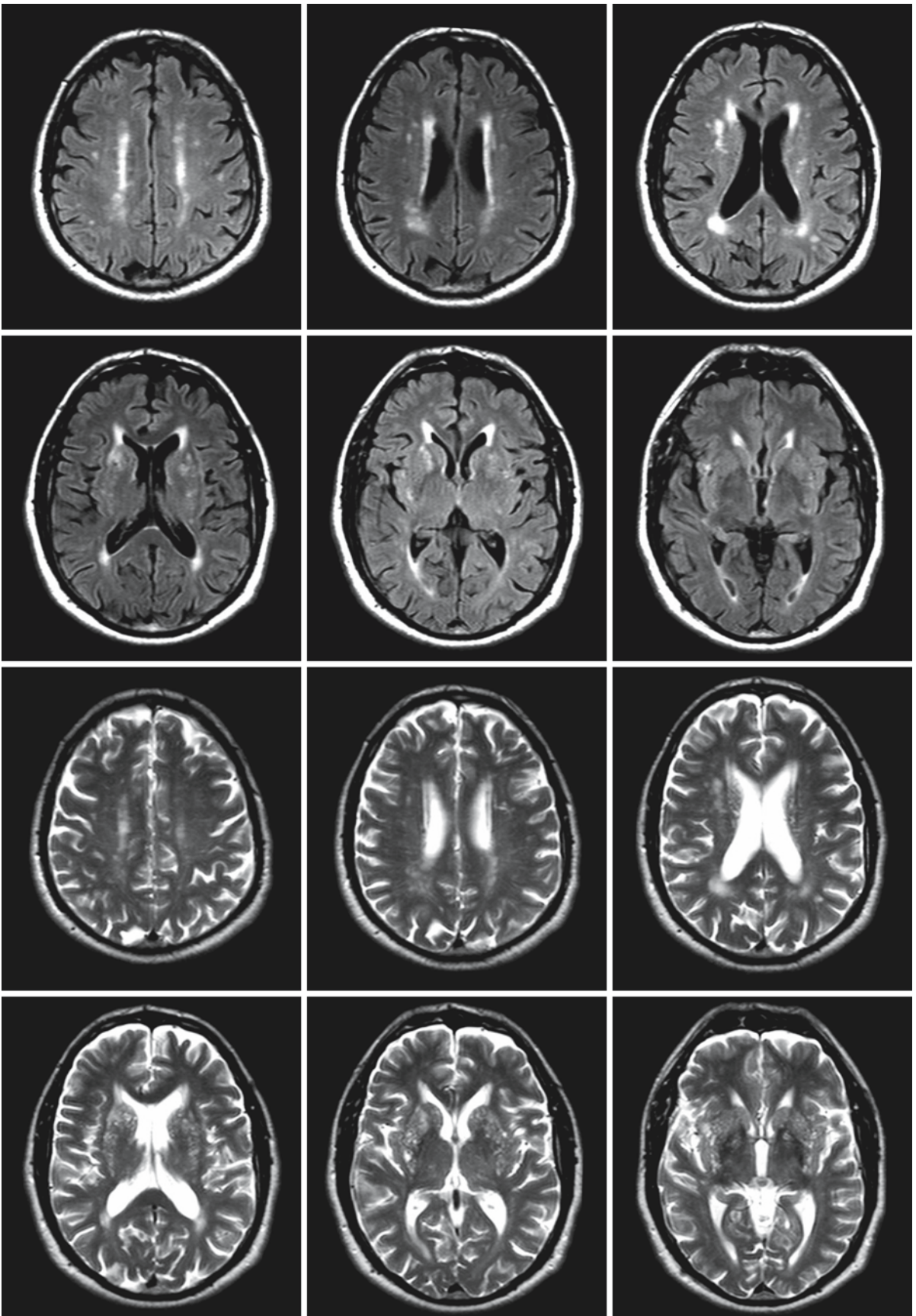


Fig. 98.1. a

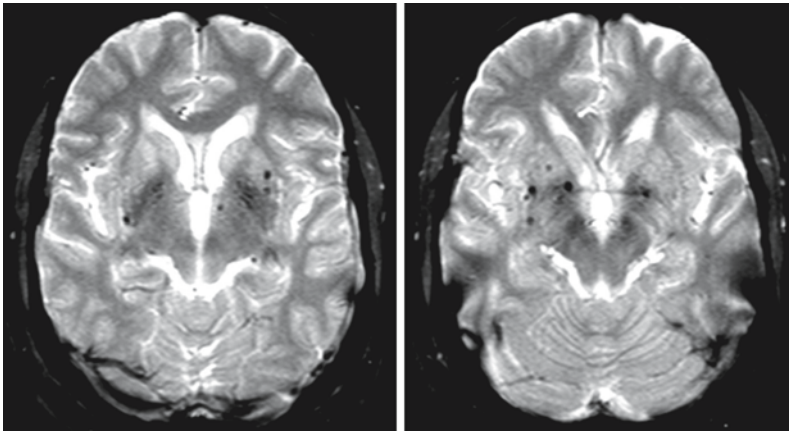


Fig. 98.1. b The gradient echo images of the same 64-year-old woman show hemosiderin deposits, residues of microhemorrhages, in the basal ganglia, more prominent on the left side, and around the anterior commissure. CT scan showed no calcifications

studies are to establish rules for population-based prevention, in individual cases they offer only guidelines.

The overall impression one may develop is that leukoaraiosis is too general a concept, so that examined populations and selected cases do not form a homogeneous entity. Certainly some general rules for prevention have been drawn from the research results obtained so far, but future research should aim at the definition of more homogeneous subgroups to obtain better insight in the pathophysiological mechanisms underlying the final common visual product leukoaraiosis.

98.4 Therapy

The development of leukoaraiosis is strongly related to age, and secondarily to risk factors. As they get older, nearly 100% of people will have white matter lesions. At the moment of detection of white matter lesions, whether related to neurological or neuropsychological complaints or as an incidental finding, risk factors should be searched for, where possible treated, and habits such as smoking, excessive drinking, and lack of exercise should be changed. The most important way to take action is by promoting preventive measures that would improve the lifestyle and health of the general population.

98.5 Magnetic Resonance Imaging

With the introduction of CT it became clear that there were age-related changes of the brain, amongst them more or less extensive periventricular areas of hypodensity. MRI showed these changes to better advantage as hyperintense changes on T_2 -weighted images, and later even better on FLAIR images. Many scales were developed to grade these signal abnormalities and to relate them to neurofunctional deficits, when

present. The lesions seen on MRI in older individuals can be graded as follows:

- Frontal and occipital caps: white matter hyperintensity around the frontal horns and the triangular area of the ventricles
- A periventricular 1- to 3-mm-thick rim of high signal intensity, best seen on proton density or FLAIR images (These two findings are considered to be without clinical significance and represent areas of looser tissue and widened Virchow–Robin spaces)
- Patchy deep white matter lesions, partly isolated, partly confluent
- Confluent deep white matter hyperintensity, continuous with periventricular white matter changes
- One or a few lacunar infarctions within the affected deep white matter

MR has been used extensively to study the process of aging of brain structures in vivo. Pathological studies of the brain depict the terminal phases of disease only and are limited by the relatively small number of samples that can be examined per patient, as a rule in the order of 350–450 at most. In contrast, MR data about normal aging are abundant and can be used as reference data for MR studies in older patients, for example to provide normal values per age group of ventricular and sulcal width, hippocampal and temporal lobe volume, magnetization transfer ratios and histograms, fractional anisotropy, apparent diffusion coefficients, T_1 and T_2 relaxation times, regional cerebral blood volume, and metabolite concentrations.

General experience is that over the age of 50 years one may expect to see white matter abnormalities in patients and controls, increasing exponentially with age (Figs. 98.1 and 98.2). Population-based studies have linked these white matter abnormalities to various risk factors, and also tried to find predictive factors that would indicate risks for future strokes and cognitive decline. The problem with these studies,

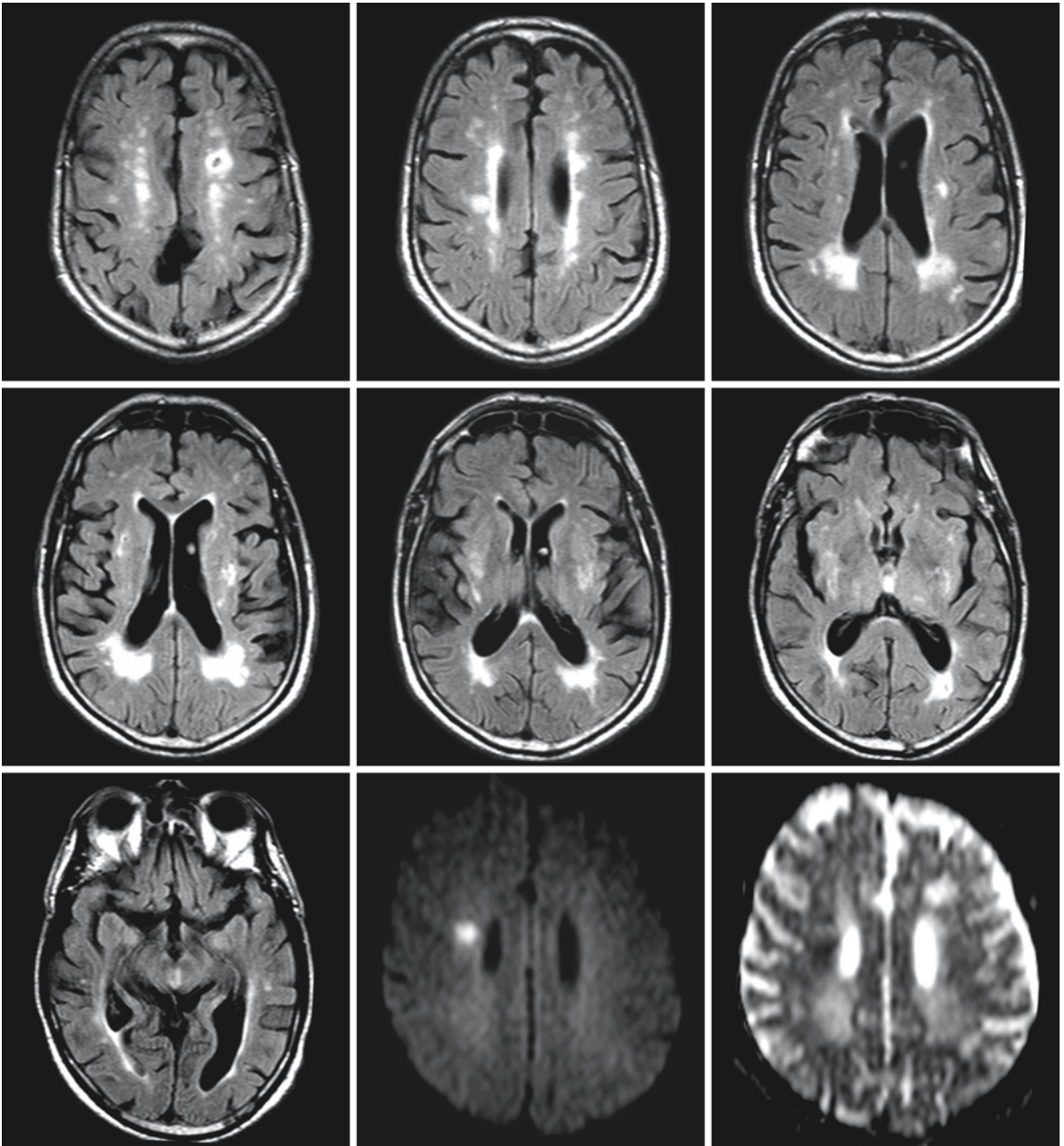


Fig. 98.2. FLAIR images of a 71-year-old man presenting with mild apraxia of the left arm and no cognitive impairment. In the periventricular white matter hyperintensities a few lacunar

infarctions are noted. The Trace diffusion-weighted image and ADC map (*third row, middle and right*) show a small recent infarction with low ADC values in the right periventricular area

especially those that include large populations, is that only basic MR techniques have been used – T_1 - and T_2 -weighted images – without employment of techniques that allow a better definition of tissue characteristics. The inclusion, for example, of gradient echo refocusing pulse sequences would have shown the members of these populations with micro-

hemorrhages (Fig. 98.1) and thus have identified a group with possibly a different pathogenesis, other risk factors, and different prognosis. Other MR sequences would possibly have led to further differentiation, for example, on the basis of the estimation of tissue integrity with magnetization transfer ratios, or on the basis of the change of brain metabolites in

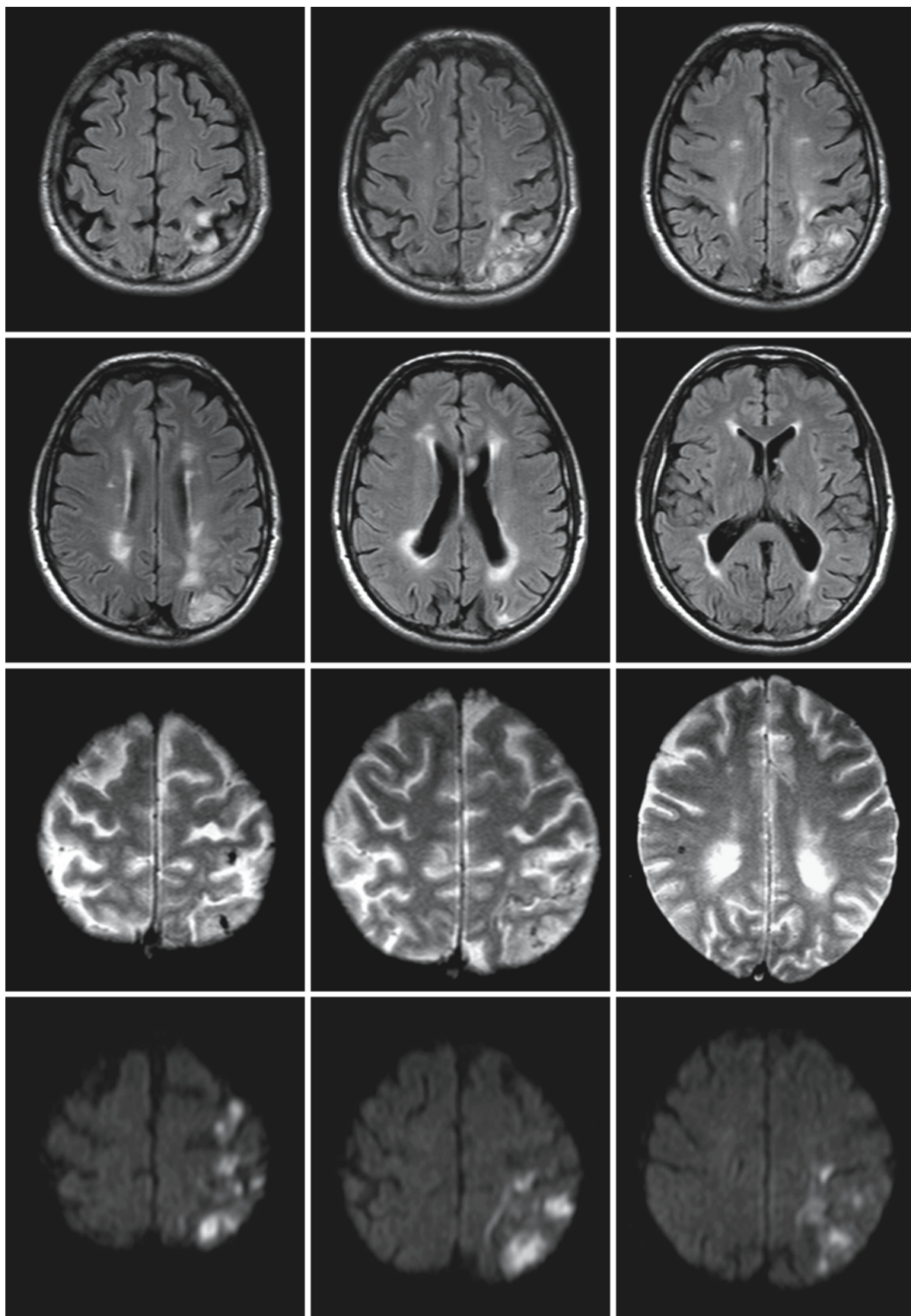


Fig. 98.3.

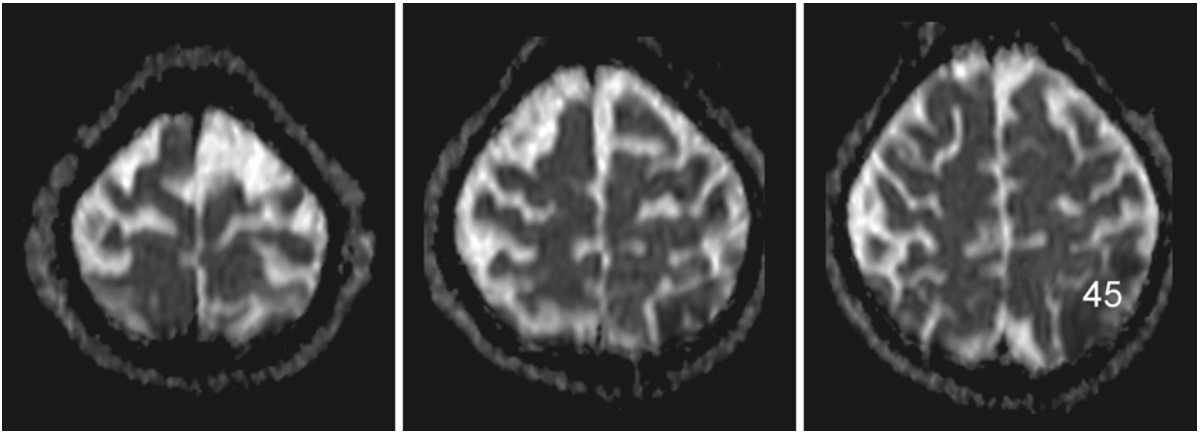


Fig. 98.3. (continued). A 62-year-old man without cognitive complaints, presenting with left-sided hemianopia. The FLAIR images (*upper two rows*) show hyperintensities consistent with normal aging, except for the left parietal lesion, involving cortex and subcortical white matter. The gradient echo images (*third row*) show a few low-intensity spots in the left parietal

area, and a single spot in the right parietal area. The *fourth row* shows Trace diffusion-weighted images with $b = 1000$; the *fifth row* shows ADC maps. The left parietal lesion is bright on the Trace images and has ADC values as low as $0.52 \times 10^{-3} \text{ mm}^2/\text{s}$, confirming the presence of a fresh infarction

MRS, including the presence of lactate in the lesions. Probably the most important MR technique to relate the white matter abnormalities to clinical findings is perfusion imaging. This allows not only the estimation of the degree of hypoperfusion in the involved areas, but also the reserve capacity of the tissue, giving a quantitative measure of the severity of the white matter damage.

In daily routine one will be confronted mainly with patients referred for memory disorders and cognitive decline. Apart from ruling out rare causes such as brain tumors, chronic subdural hematomas, and so on, a protocol should be used that will enable assessment of most of the factors responsible for cognitive decline according to present knowledge. This means an inventory of cerebral and cerebellar cortical and deep gray matter structures, including the hippocampus and temporal lobe structures, of white matter abnormalities, and of the presence of microhemorrhages (Fig. 98.1). In patients with rapidly progressive cognitive decline diffusion-weighted imaging with ADC maps should be added to the program (Figs. 98.2 and 98.3). In centers dedicated to the research of mild cognitive impairment, or where vascular factors seem to be important, MR angiography should be included. MRS and chemical shift imaging may give additional

information about neuronal and axonal loss, and about the presence of lactate, indicating anaerobic glycolysis.

In many patients follow-up studies will be required. Postprocessing of data is then also very important, to obtain adequate comparable information. This will give a clue with respect to the rate of progression, and information about the efficacy of therapeutic measures and changes in lifestyle (Fig. 98.4).

Differential diagnosis is important, because many other disorders may present with deep white matter abnormalities. Disorders with multifocal and partially confluent white matter abnormalities, often accompanied by cognitive impairment, are amyloid angiopathy, CADASIL, multiple sclerosis, cerebral vasculitis, systemic lupus erythematosus, chronic exposure to organic solvents (housepainter's dementia), and several infections including HIV encephalopathy and progressive multifocal leukoencephalopathy. In Alzheimer disease, in particular in the late-onset forms, white matter abnormalities are common. Disproportional hippocampal atrophy suggests Alzheimer disease. It is important to realize that more and more "mixed" dementias are being recognized, caused by a combination of vascular and neurodegenerative factors.

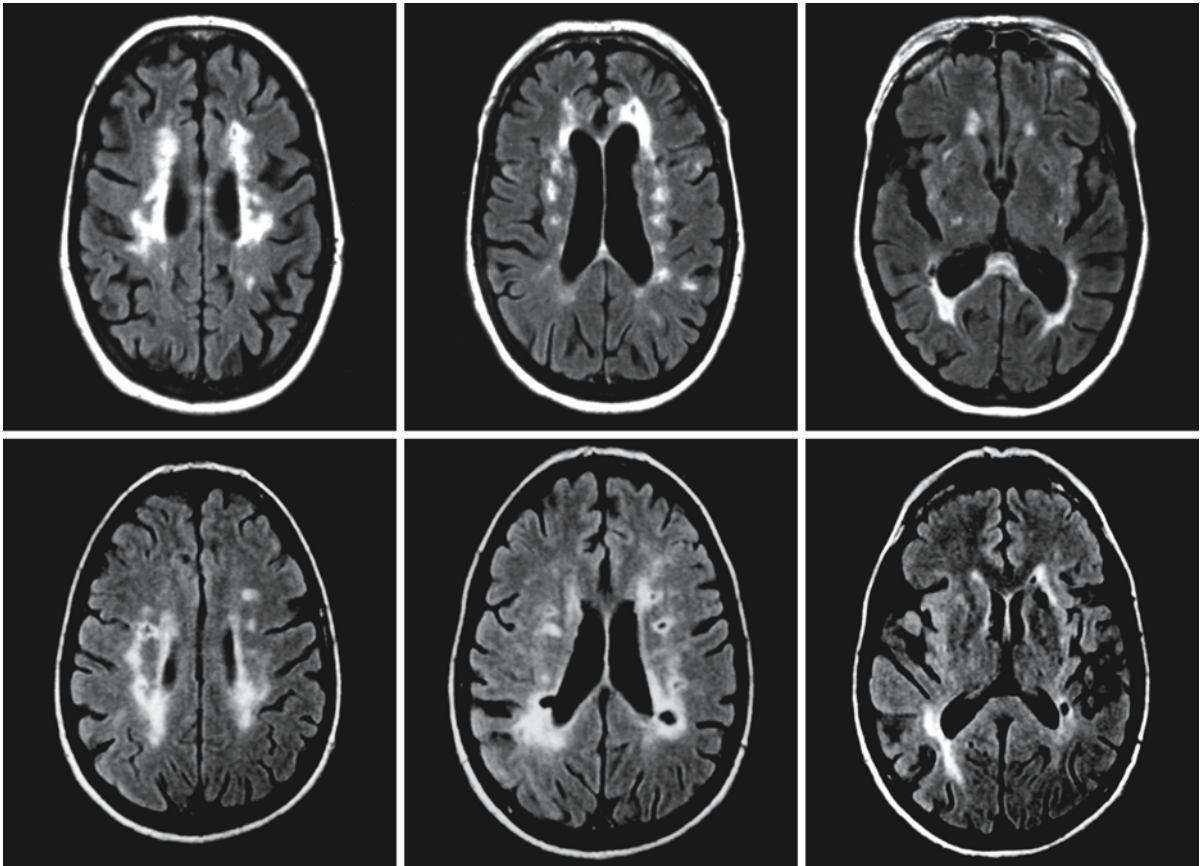


Fig. 98.4. FLAIR images of a 67-year-old woman with mild cognitive impairment (*first row*). There are white matter hyperintensities in the deep and periventricular white matter and corpus callosum, and scattered small lesions in the basal ganglia. Images of the same patient 4 years later (*second row*) show progression of the abnormalities, with lacunar infarctions in both hemispheres and the brain stem (not shown).

Also clinically there was clear progression of the cognitive disorder. ADC values in this patient in the centrum semiovale had gone up from $0.85\text{--}0.95 \times 10^{-3} \text{ mm}^2/\text{s}$ to $1.20\text{--}1.25 \times 10^{-3} \text{ mm}^2/\text{s}$; fractional anisotropy values changed from 0.450 to 0.224, indicating loss of structural integrity. MRS showed lactate in the lesions in the last examination. All evidence is that this patient is a decliner.

Subcortical Arteriosclerotic Encephalopathy

99.1 Clinical Features and Laboratory Investigations

This disease was first described by Binswanger in 1894 as *encephalitis subcorticalis chronica progressiva*, later renamed by Olzewski (1962) as subcortical arteriosclerotic encephalopathy (SAE). It was believed for a long time that the disease was very rare. Only a few documented cases appeared in the literature before the advent of CT and MRI. CT and, even more, MRI have made it clear that white matter abnormalities are frequent in the brains of older patients. This has opened a discussion that is still going on about the diagnostic criteria for the disease. These criteria comprise:

- A vascular risk factor or evidence of systemic vascular disease
- Evidence of focal cerebral disease
- Evidence of subcortical dysfunction
- Bilateral deep white matter abnormalities on CT or MRI
- Absence of multiple or bilateral cortical lesions on CT or MRI
- Absence of severe dementia (mini mental scale >10)

The age of onset is between 40 and 60 years and most patients have a history of chronic hypertension, often poorly controlled, and often one or more vascular incidents. The patients usually present with a slowly developing subcortical frontal dysfunction with loss of interest, lack of drive, alternations in mood and personality, loss of appropriate social conduct and lack of judgment, parkinsonian gait disturbances, urinary incontinence, and pseudobulbar palsy. Minor strokes may occur with a variable degree of improvement of the neurological deficits. Gradually the dementia progresses and more neurological symptoms become manifest, including dysarthria, clumsiness, disturbances of gait, ataxia and apraxia, and finally profound global dementia. It may be difficult to distinguish SAE on clinical grounds from Alzheimer disease and other vascular dementias.

There are no specific laboratory markers for the disease. Discussion has been going on for a long time whether or not SAE is a disease entity, but after the reviews of Fisher (1989) and Caplan (1995) there seem to be sufficient arguments to do so.

99.2 Pathology

Externally the brain in patients with SAE appears normal. The brain weight is average. In most cases the arteries at the base of the brain show moderate to severe arteriosclerosis. The lateral ventricles are moderately to highly enlarged. In advanced cases the cerebral hemispheric white matter appears wrinkled, firm, rubbery, and discolored gray or yellow, especially in the periventricular, frontal, and parietal regions. Histopathologically, the white matter lesions consist of partial loss of myelin sheaths, oligodendroglial cells, and axons, producing a decrease of the meshwork density of white matter tissue, along with mild reactive fibrillary gliosis and sparse macrophages. Arteriosclerosis is invariably present in these areas of incomplete infarction, and there is severe stenosis of the smallest vessels by fibrohyaline material. The U fibers are usually spared. The temporal lobes, too, in contrast to the findings in CADASIL, are uninvolved. *État criblé*, widening of the Virchow–Robin spaces, is an almost constant feature. *État criblé* results from spiraled elongation of penetrating arteries and arterioles in white matter and central gray matter nuclei. Blood vessels in areas of *état criblé* are thickened, ectatic, and have sclerotic walls. The perivascular tissue shows reactive astrocytosis and isomorphic gliosis with glial fibers extending along degenerated axons. There is perivascular leakage of serum proteins. Multiple lacunar infarctions, *état lacunaire*, are also a frequent finding. Lacunes are small cavitory lesions that result from ischemic strokes due to occlusion of penetrating cerebral arterioles. Lacunes predominate in the basal ganglia, internal capsule, pons, and centrum semiovale. Fresh lacunes show necrosis and liquefaction, followed by absorption of necrotic material by fatty macrophages. In the chronic stage an irregular cavity remains, whose walls show dense fibrillary connective tissue and gliosis. Reabsorption of minute hemorrhages may also result in lacunes leaving hemosiderin-filled macrophages in the walls and in the vicinity of the lesions.

99.3 Pathogenetic Considerations

The main characteristic of SAE is arteriosclerosis with narrowing and occlusion of the deep perforating cerebral arteries and their branches. These arteries

and arterioles are end vessels without collateral circulation. They form an arterial end and border zone in the periventricular region. The cortex and subcortical white matter are within the territory of supply of the cortical vessels and their leptomeningeal anastomoses.

SAE is characterized by microinfarctions, focal or diffuse demyelination, and gliosis of the periventricular and deep white matter, in combination with lacunar infarctions in the basal ganglia and brain stem. It is commonly accepted that SAE type encephalopathy is caused by ischemia in the distal watershed territories described above. The ischemia is the combined effect of arteriosclerosis and decreased brain perfusion from hypotension or low cardiac output. Elongation of the medullary arteries with dilatation of the perivascular spaces leads to an *état criblé*.

There are numerous risk factors underlying these changes, such as age, hypertension, hypotension, smoking, inadequate diet, and diabetes mellitus. A number of genetic factors may also play a role. Hyperhomocysteinemia and hyperlipidemia have been identified as important risk factors. Effects of sustained daytime hypertension, hypertensive crises, and the absence of a normal nocturnal dip in blood pressure are considered to be particularly damaging. Another factor that may play a role in the development and progression of SAE is coagulation activation, leading to a hypercoagulable state. In a selected group of SAE patients, fibrinogen, thrombin-antithrombin complex, prothrombin fragment₁₊₂, and cross-linked D-dimer were found to be significantly increased. Obstructive sleep apnea, which produces increased platelet activation, higher epinephrine levels with vasoconstrictive effect, and higher blood pressure, also plays a role.

There is little doubt that the changes caused by these factors are responsible for the abnormalities seen on MRI. That these MRI changes do not necessarily have the same histopathological background is illustrated by the observation that some patients with severe periventricular abnormalities on MRI have a mild clinical presentation, whereas other patients with much less severe MRI abnormalities have advanced clinical symptoms.

99.4 Therapy

There is no cure for SAE. Whenever hypertension is present, treating it may slow down the progress of disease. Other risk factors such as hyperlipidemia and hyperhomocysteinemia should be treated, and bad habits such as smoking and excessive drinking should be given up. There is some evidence that in an early stage the disease can still be influenced by these measures. Some success has been booked with med-

ication. The robust evidence for the effectiveness of cholinergic treatments in Alzheimer disease, and the frequent occurrence of mixed dementias, has led to the testing of galantamine (Reminyl) in a group of patients with SAE. Galantamine has a dual cholinergic mode of action, and reduces behavioral symptoms in Alzheimer disease. This is the result of its potential to modulate systems involving other neurotransmitters such as serotonin and dopamine, which affect mood and emotional balance. Application of galantamine in SAE patients led to significant cognitive improvement over 6 months, long-term maintenance of cognition for at least 12 months, and improvement of both behavioral and functional symptoms. These data suggest a result that is, so far, unsurpassed by other drugs or treatment regimens.

99.5 Magnetic Resonance Imaging

In patients with presenile dementia and a history of hypertension the diagnosis SAE depends on two parameters: the clinical establishment of a subcortical type of dementia and the establishment of diffuse damage to periventricular and deep white matter by means of an imaging modality, CT or MRI. In uncomplicated cases of SAE, CT and MRI identify a relatively well preserved cortex, moderately to more seriously enlarged ventricles, and a broad area of reduced density around the ventricles on CT or, on MRI, a zone of high signal intensity on T₂-weighted and FLAIR images, involving the periventricular and deep white matter (Figs. 99.1–99.3). The more central lesions, closest to the ventricles, are usually confluent; farther away from the center there are often many isolated lesions of different size (Figs. 99.1 and 99.3). Within the confluent areas there may be spots with still higher signal intensity on T₂-weighted images, possibly representing infarctions. In some cases small cavities are present with low signal intensity on FLAIR images, often with a bright rim, as residues of lacunar infarctions (Fig. 99.3). In the early phases of the disease the U fibers are usually spared (Fig. 99.1). In cases of longer standing white matter disorder the subcortical fibers may also be partially involved (Figs. 99.2 and 99.3). In some cases cortical infarctions are also seen. Apart from the periventricular and deep white matter lesions there are often isolated hyperintense lesions scattered throughout the basal ganglia, the pons, and midbrain, representing small infarctions (Figs. 99.1 and 99.2). Widened Virchow–Robin spaces and lacunar infarctions are best seen on FLAIR images (Fig. 99.3). The corpus callosum is usually less affected than in multiple sclerosis, but this is a rule with many exceptions. Sagittal FLAIR images will often show involvement of the under layer and thinning of the corpus callosum (Fig. 99.3).

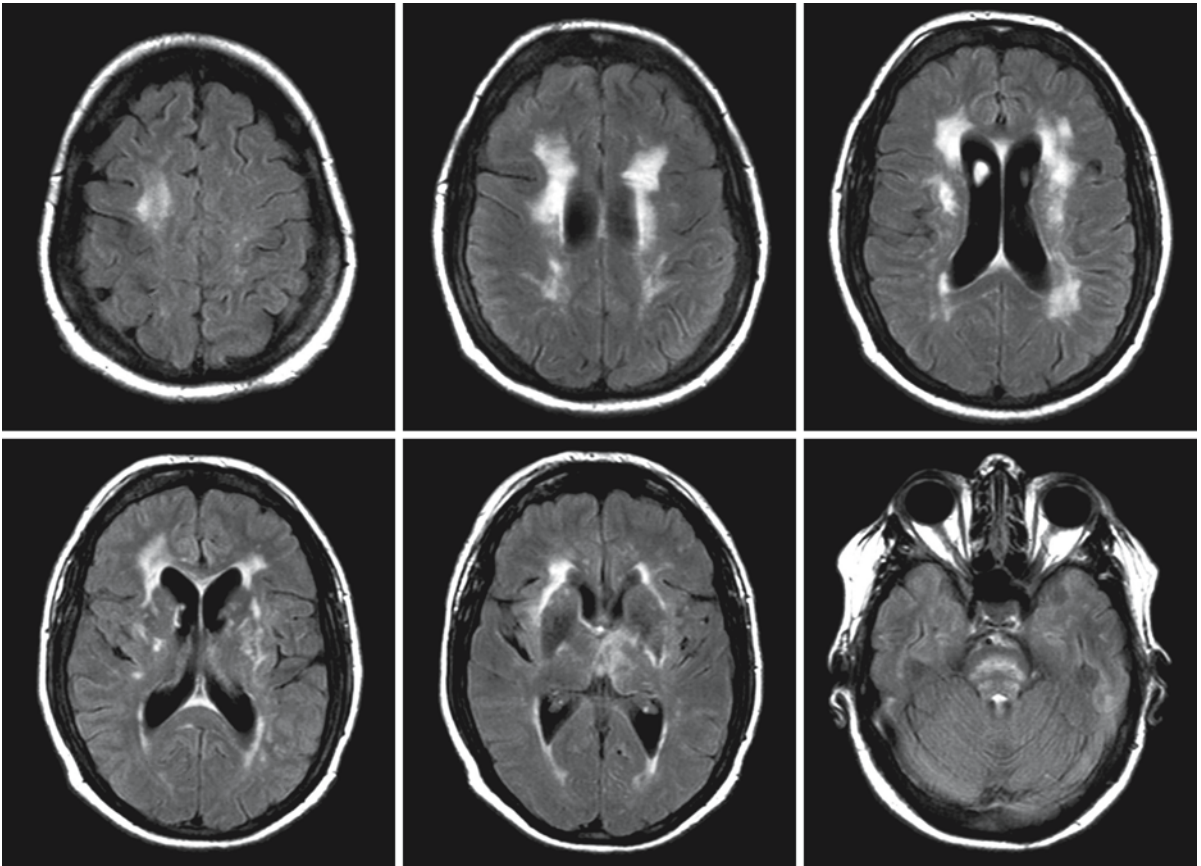


Fig. 99.1. FLAIR images of a 56-year-old woman. The patient had the antecedents of SAE with longstanding hypertension and multiple transient ischemic attacks. Her images show some of the characteristics seen in CADASIL, with the involve-

ment of the external capsule and the dark appearance of the globus pallidus, but the temporal lobes are not affected. Family history and tests for CADASIL were negative

Standard MRI series are fully capable of displaying most of the cerebral abnormalities. Fast imaging sequences can often be used to advantage. FLAIR is very useful to show older lacunar infarctions and enlarged perivascular spaces within the affected white matter and the basal ganglia as spots with low signal intensity, and to show the demarcation of the ventricles from the periventricular abnormalities. FLAIR is also useful when estimation of lesion load is required in research programs. Gradient refocused images should be standard in a MR protocol for dementing illnesses in the older age group, because they will show spots with high magnetic susceptibility, representing hemosiderin deposits in microhemorrhages. They are found in a high percentage of patients with SAE and in many other vascular disorders. Diffusion-weighted imaging may be helpful in identifying fresh infarctions, which will otherwise be lost in the brightness of the lesions that probably represent old infarctions, myelin loss, and gliosis. MRS usually shows decrease

in *N*-acetylaspartate and, in some cases, presence of some lactate.

The differential diagnosis includes in the first place periventricular and deep white matter changes which occur in normal elderly people with varying severity. The differentiation from normal pressure hydrocephalus may be difficult when the ventricles are greatly enlarged. Additionally, the combination of SAE and normal pressure hydrocephalus seems very possible. Stiffening of the walls of the ventricles in SAE may even play a role in the pathogenesis of normal pressure hydrocephalus. Other vascular diseases such as amyloid angiopathy and CADASIL have to be considered. Unlike CADASIL, patients with SAE do not have prominent abnormalities in the external and extreme capsules and the anterior temporal lobes, although the images may show some similarities (Fig. 99.1). Rarer are vasculitides, Fabry disease, Lyme disease, HIV infection, leukoencephalopathy after chemotherapy or radiotherapy, and toxic encephalo-

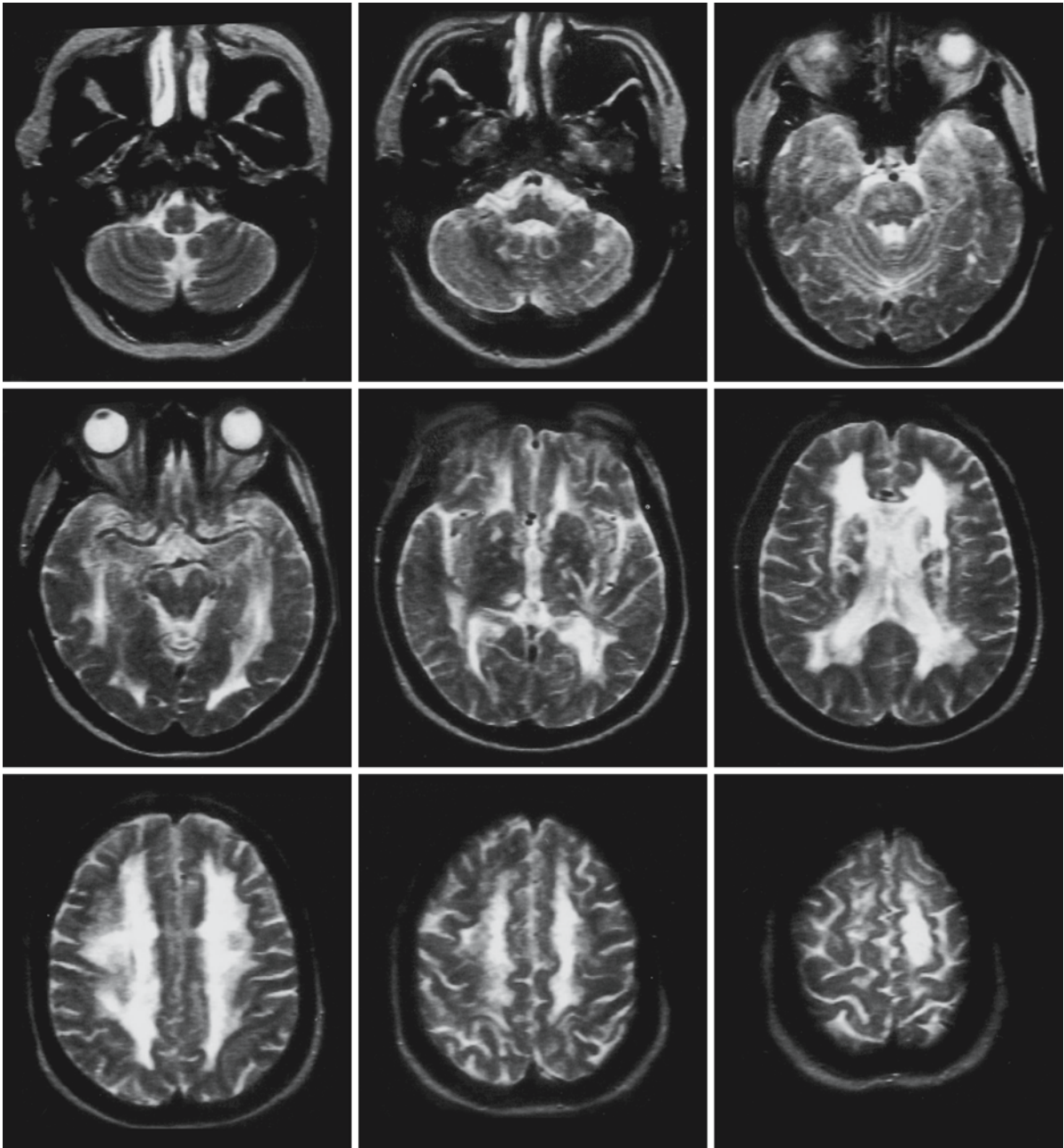


Fig. 99.2. A 58-year-old man with progressive subcortical dementia and transient ischemic attacks. The T₂-weighted series shows a periventricular leukoencephalopathy extending into the centrum semiovale, in some areas also involving the U

fibers. Small lesions are seen in the left cerebellar hemisphere. Diffuse hyperintensities are present in the pons. There are small, punctate lesions in the basal ganglia and in the corpus callosum

Fig. 99.3. A 64-year-old man with more advanced dementia and a history of hypertension and transient ischemic attacks. The axial FLAIR images (*first and second rows*) show ventriculomegaly, periventricular leukoencephalopathy, and prominent white matter atrophy. État criblé of the basal ganglia is

visualized. The sagittal FLAIR images (*third and fourth rows*) show more clearly the involvement of the corpus callosum and the fornix, both thinned and partly hyperintense. The état criblé of the basal ganglia is beautifully seen

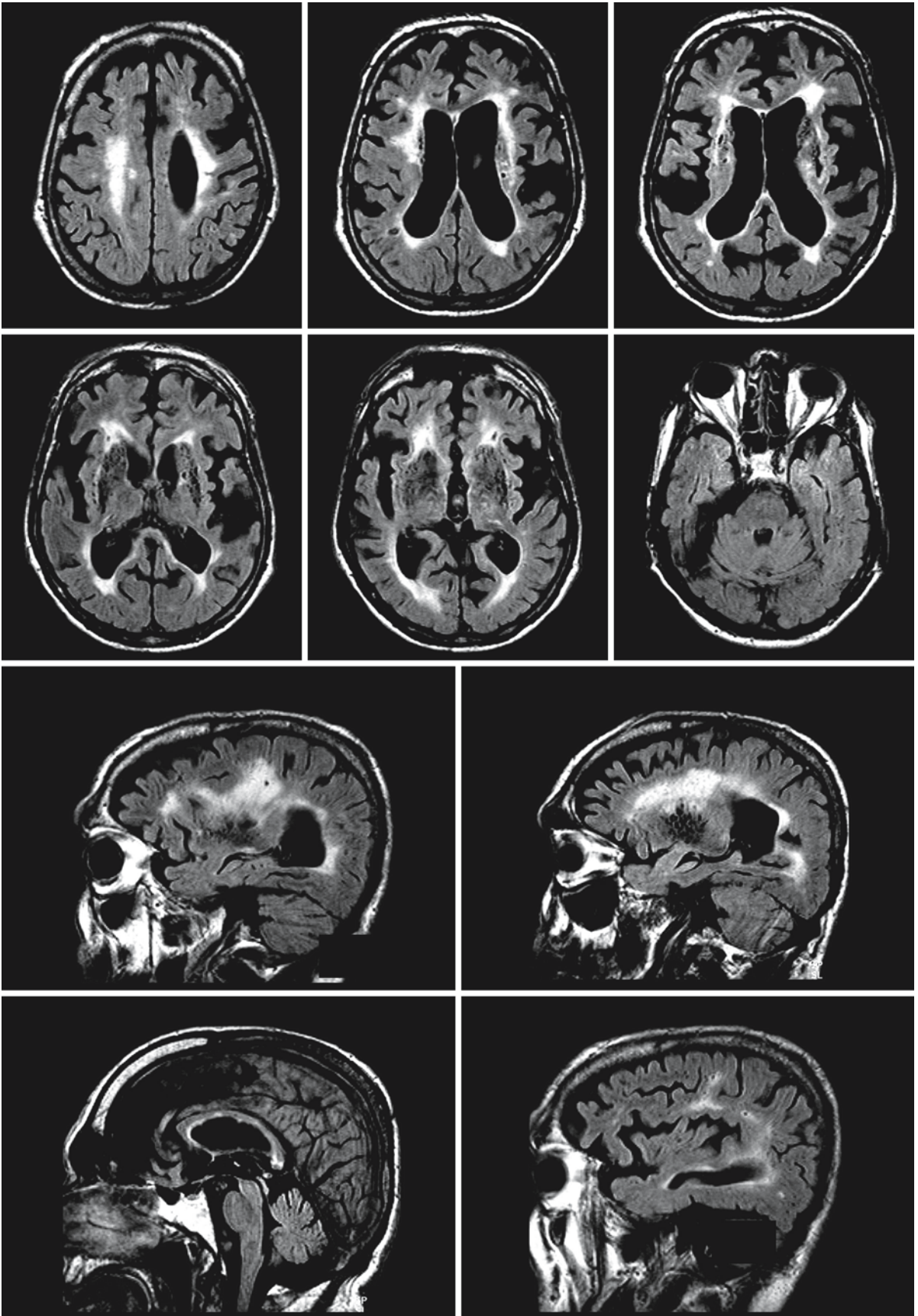


Fig. 99.3.

pathies. In general, vascular diseases share a pattern of irregularly confluent periventricular white matter abnormalities with often multiple isolated lesions at the periphery, multifocal lesions in the basal ganglia,

and often also brain stem lesions. The presence of small lacunes adds to the suspicion of a vascular disorder.

Vasculitis

100.1 Introduction

The term “vasculitis” refers to inflammation of the vessel walls. There are many causes of vasculitis, but they result in only a few histological patterns of vascular inflammation, of which necrotizing vasculitis and granulomatous reaction are the most prominent. Because vessels of any type in any organ can be affected, there are a wide variety of clinical manifestations. This, combined with etiological nonspecificity of the histological lesions, complicates the diagnosis of vasculitis. The past few decades have seen important progress in this field, enabling a laboratory diagnosis in some cases. A good example is the discovery in 1982 of the anti-neutrophil cytoplasm antibodies (ANCA), subdivided into a perinuclear form (pANCA), related to Churg–Strauss syndrome and microscopic polyarteritis, and a cytoplasmic form (cANCA), related to Wegener disease. The blood tests for these antibodies are now widely available, but they need careful application and interpretation. Other findings, such as the detection of anti-neuronal antibodies, anti-centromere antibodies, and anti-phospholipid antibodies (APLA), have shed some light on the pathophysiology of a number of disorders and have demonstrated a link between systemic lupus erythematosus (SLE) and Sneddon disease. Many more autoantibodies have been identified and they may help in better understanding the complex pathology underlying these disorders. Despite these discoveries the diagnosis of vasculitis remains often difficult, in particular in the primary vasculitides of the CNS.

To organize the discussion we suggest the following classification:

A subclassification that may be helpful in reaching a diagnosis is division according to the size of vessels affected by the disorder, even though there is a considerable overlap. Takayasu disease and giant cell arteritis affect large vessels; primary angiitis of the CNS and polyarteritis nodosa affect medium-sized vessels; Wegener granulomatosis, Churg–Strauss syndrome, rheumatoid disorders, SLE, microscopic polyarteritis, scleroderma, and many other vasculitic disorders involve small vessels: arterioles, capillaries, and venules. Behçet disease involves all types and sizes of vessels, arterial or venous (Fig. 100.1).

100.2 Clinical Presentation and Laboratory Findings

As in all relapsing multifocal disorders that may affect both gray and white matter, the clinical manifestations of the disease depend on the localization of the abnormalities, progression over time, and the nature of the disease. Symptoms may be neurological or psychiatric or both, and cognitive deterioration may be the leading feature. When the cerebral manifestations are part of a systemic disorder the diagnosis may be easier, unless the cerebral symptoms are the first or only manifestation.

Clinically there are many factors to consider: age, gender, presence of skin lesions, involvement of other organs (in particular kidneys, lungs, and paranasal sinuses), medication, drug abuse, and neurological

Fig. 100.1. Different vasculitic disorders may preferentially attack blood vessels of a particular size. AS, arteriosclerosis; cAA, cerebral amyloid angiopathy; CADASIL, cerebral autosomal dominant arteriopathy with subcortical infarcts and leukoencephalopathy; PACNS, primary angiitis of the CNS; PAN, polyarteritis nodosa; MPAN, micropolyarteritis nodosa; SLE, systemic lupus erythematosus

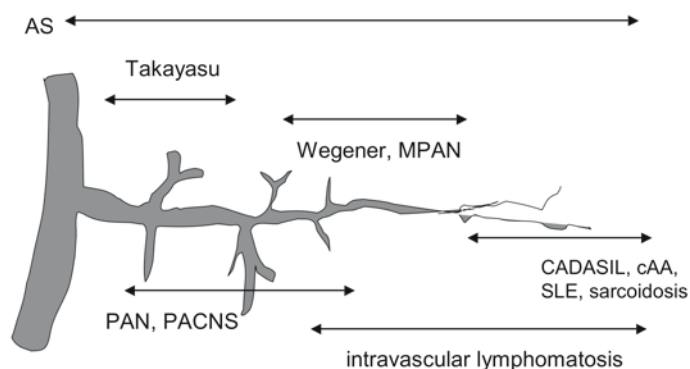


Table 100.1. Classification of CNS vasculitis (including nonvasculitic disorders that may present with similar pathology to some of the vasculitides)**Primary vasculitis of the CNS**

Granulomatous angiitis of the CNS
(primary angiitis of the CNS)
Giant cell arteritis (arteritis temporalis)
(Benign primary angiitis of the CNS)

Secondary vasculitis of the CNS

Systemic vessel wall disease

Takayasu arteritis
Polyarteritis nodosa
Moyamoya syndrome

Autoimmune-mediated disorders

Rheumatoid arteritis
Systemic lupus erythematosus^a (SLE)
Sneddon disease^a
Anti-phospholipid antibody (APLA) syndrome
Sjögren disease
Scleroderma
Neurosarcoidosis
Wegener granulomatosis^b
Churg–Strauss syndrome^b
Microscopic polyarteritis^b
Behçet disease

Infectious vasculitis

Borreliosis (Lyme disease)
Lues
Tuberculosis
Varicella-zoster
Herpes zoster ophthalmicus (delayed hemiplegia)

Drug-related vasculitis

Aminopenicillins	Ergot alkaloids
Allopurinol	Interleukin-2
Retinoids	Methylphenidate
Quinolones	Penicillin
Cocaine, heroin, amphetamines, ecstasy	

Disorders primarily obstructing the vascular lumen^c

Disorders of coagulation
Intravascular lymphomatosis
Sickle cell disease

^a APLA-related disorder.

^b ANCA-related disorder.

^c Disorders that may present with similar pathology to some of the vasculitides, but have an endoluminal cause and often require different treatment.

signs, including cognitive deterioration, focal cortical symptoms, stroke-like episodes, etc.

Relevant laboratory tests include erythrocyte sedimentation rate, complement activation, immune status and antibodies in blood and CSF, protein and cell content of the CSF, and assessment of coagulation factors. All these items may be unrevealing, even in histologically confirmed cases of vasculitis.

MRI may play an important role, even though the abnormalities found on MRI are usually not diagnostic. It is rare, however, that cerebral vasculitis exists with a negative MRI. A normal MRI should even lead to reconsideration of the diagnosis. MRA may be helpful in showing the vascular abnormalities, but special contrast-enhanced techniques should be used. Intra-arterial DSA may be helpful in some cas-

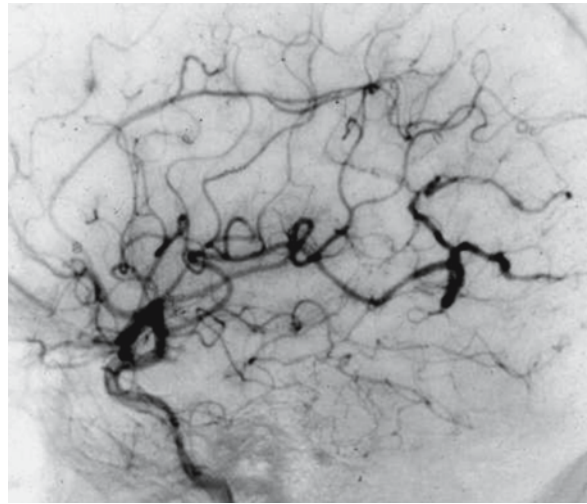


Fig. 100.2. Intra-arterial DSA of the right internal carotid artery in a 37-year-old woman with biopsy-proven granulomatous angiitis of the CNS, showing the irregular size of the lumen of the posterior temporal artery. Other vessels also show irregular borders

es, for example, in moyamoya syndrome, Takayasu disease, and infectious vasculitis. In quite a number of cases a leptomeningeal or brain biopsy will still be required, especially in primary angiitis of the CNS, to ascertain the diagnosis. However, this is not full proof either.

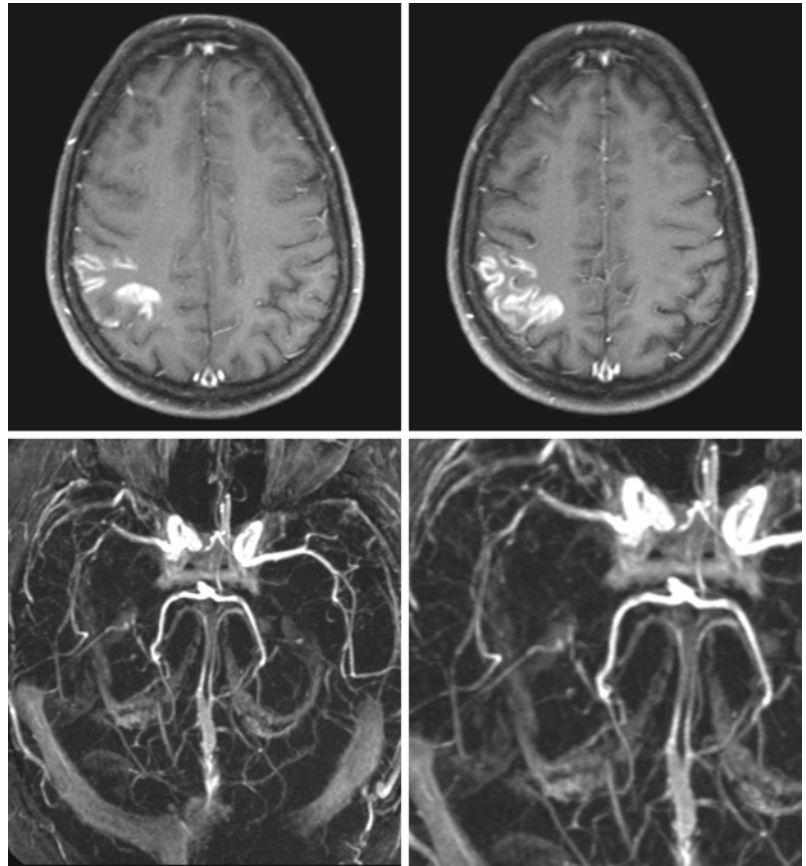
The most important features and data of the different forms of vasculitis will be briefly reviewed.

100.2.1 Primary Vasculitis of the CNS

Granulomatous angiitis (also primary angiitis of the CNS, PACNS) is the most important representative of primary vasculitides of the CNS. The presenting clinical signs of granulomatous angiitis are nonspecific, often suggesting global dysfunction of the CNS. Acute or subacute onset confusion, headache, change of personality, paresis, cranial neuropathy, or loss of consciousness are often presenting signs but as such nonspecific. The most frequent presenting symptoms of granulomatous angiitis are headache (68%), paresis (56%), and confusion (55%). In almost 25% of the patients fever and elevated blood pressure are noted. Dermatological abnormalities are rare. Funduscopy reveals vascular changes in 25% of patients.

The erythrocyte sedimentation rate is in most cases elevated. CSF pressure is usually increased, and CSF is nearly always abnormal with increased total protein, lymphocytic pleocytosis, and in 30% of the patients decreased glucose levels.

Fig. 100.3. T₁-weighted images with contrast (*first row*) of a 46-year-old woman with granulomatous angiitis of the CNS, showing an enhancing infarction in the right parietal lobe. MRA (*second row*) shows rapid and irregular tapering of the more distal branches of the middle and posterior cerebral arteries



Postmortem examination of brain tissue and examination of brain biopsy material show an inflammatory process of small arteries and arterioles, preferentially involving deep white matter and leptomeningeal vessels. Intima proliferation and fibrosis are frequent, with multinuclear giant cells of the Langhans type and foreign body type. In comparison with the other vessel layers, the media is relatively spared. Granulomata with macrophages and lymphocytes are present. The cause of the disease is unknown.

MRI and angiography are helpful in revealing the CNS lesions, consisting of multiple white and gray matter lesions and changes of caliber in the cerebral vessels (Figs. 100.2 and 100.3). MRA is usually not informative, but may show vascular irregularities (Fig. 100.3). The MRI pattern is not specific, but may suggest a vasculitis by a combination of multiple white and gray matter lesions and infarctions of different sizes (Fig. 100.4). Diffusion-weighted imaging may show lesions with high signal intensity and low ADC values, representative of infarctions.

Without treatment the disease is usually fatal. However, granulomatous angiitis responds to high-dose steroids and cytotoxic agents such as cyclophosphamide and azathioprine.

Giant cell arteritis or *arteritis temporalis* usually occurs in patients, male and female, who are over the age of 55 years. It often involves the superficial temporal arteries, which become swollen, tortuous, tender, and nodular. Pulsations are usually diminished. Eventually the vessels become hardened and shrink. Clinical problems most often consist of acute visual failure of one eye. Signs of CNS dysfunction are relatively rare. However, all larger and medium-sized vessels of the head and neck may become involved. Of particular interest are the carotid, vertebral, and ophthalmic arteries, including the ciliary arteries and the central artery of the retina. The cervical portions of the carotid and vertebral arteries are usually involved, the intracranial arteries to a lesser extent, and the spinal arteries least of all.

The erythrocyte sedimentation rate is in most cases elevated. Histologically segmental, multifocal panarteritis is found. The intima of the vessels is thickened by subendothelial fibrosis, narrowing or occluding the lumen. The internal elastic lamina is severely but irregularly fragmented. The media is infiltrated by small and large mononuclear cells, some of the epithelioid type. Giant cells of either Langhans or foreign body type are almost invariably present, either in the media close to the damaged internal elastic lami-

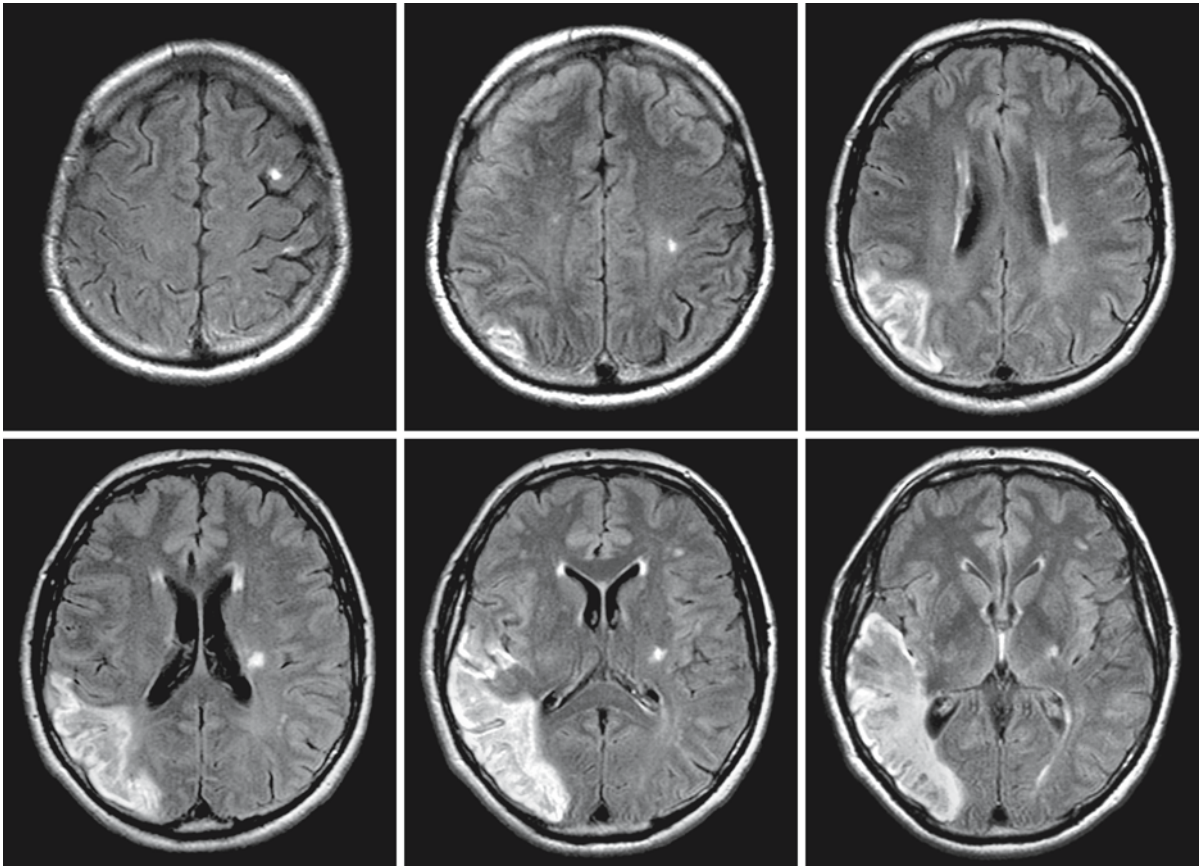


Fig. 100.4. A 57-year-old woman with multiple stroke-like episodes over the years. FLAIR images show a large temporo-parieto-occipital infarct on the right side and several lesions in the left hemisphere, with some focal cortical atrophy. Note that the distribution of the infarction does not reflect a single

vascular territory, similar to what is seen in MELAS. A mitochondrial disorder was ruled out and the diagnosis granulomatous angiitis of the CNS was established. Courtesy of Dr. M. Heitbrink and Dr. B. Wiarda, Department of Radiology, Medical Center Alkmaar, The Netherlands

na or in the adjacent intima. With healing there is scarring and occasionally aneurysm formation. In some cases the vessels are occluded by organizing thrombus.

MRI will show intracerebral lesions, but there is no specific pattern. MRA usually lacks resolution to visualize the abnormal vessels. Intra-arterial DSA may be more helpful in showing the diseased vessels. Diagnosis, however, is usually established by biopsy of the temporal vessels. A negative biopsy does not exclude the diagnosis.

Therapy includes the use of corticosteroids and immunosuppressives.

Benign primary angiitis of the CNS is best characterized as a self-limiting form of granulomatous angiitis of the CNS. This, of course, is a diagnosis a posteriori, because there are no criteria by which to distinguish progressive forms from nonprogressive.

100.2.2 Secondary Vasculitis of the CNS

100.2.2.1 Systemic Vessel Wall Disease

Takayasu arteritis affects the aortic arch and its branches, in particular in young women of Asiatic origin. The smaller intracranial vessels are usually not involved. The neurological symptoms are variable because they depend on the extent of the blood vessel abnormalities, in particular the involvement of the carotid and vertebral arteries. Visual problems are relatively frequent, most often as one-sided amaurosis fugax. Many other neurological symptoms are possible, including hemiparesis, aphasia, cranial nerve palsies, coordination problems, and vertigo.

Laboratory investigations are unrevealing. Histologically there are lesions in the media and adventitia of the vessels, but they are predominant in the adventitia. The lesions demonstrate collagenous proliferation and perivascular lymphocyte infiltration. The media shows an inflammatory granulomatous re-

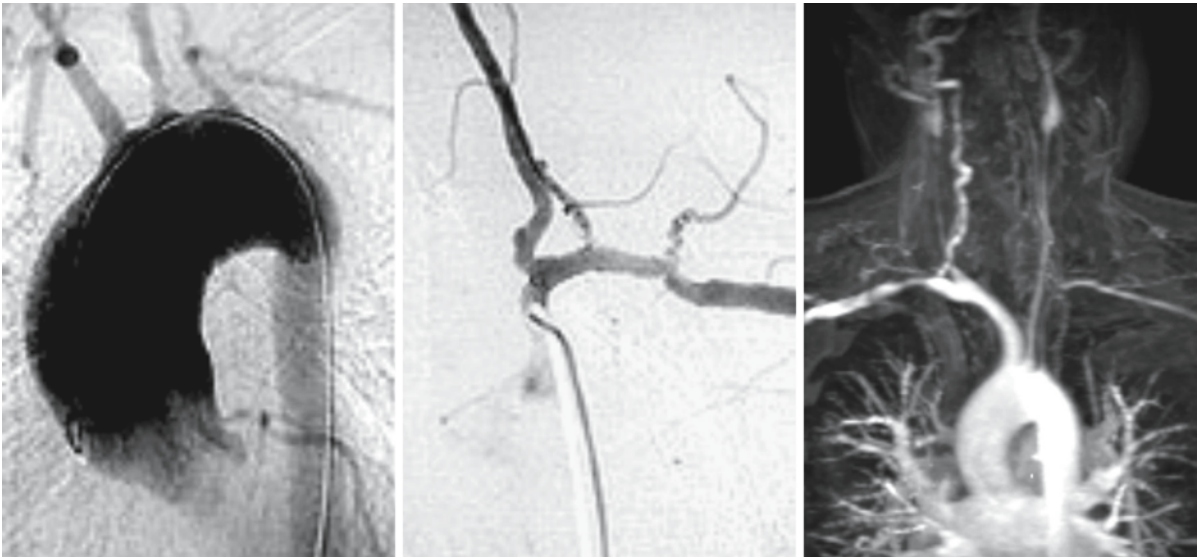


Fig. 100.5. Two intra-arterial DSA images (*left*) of Takayasu disease. On the *left-hand* image the narrowing of the neck vessels is clearly visible. The selective injection of the subclavian

artery (*middle*) shows irregular narrowing of the arteries. The MRA image on the *right* shows narrowing and wall irregularities of the subclavian arteries and the neck arteries

action, narrowing the lumen. The cerebral lesions are secondary to either diminished perfusion or emboli.

MRA, especially contrast-enhanced MRA of the aortic arch and branches, is now fully capable of making an inventory of all involved vessels (Fig. 100.5).

Treatment consists of corticosteroids, immunosuppressives, and, where necessary, interventional radiology or vascular surgery for bypasses, stent placement, and transposition of vessels.

In *polyarteritis nodosa* CNS manifestations usually develop in patients who have had systemic disease for several years, in particular with involvement of the kidneys and the lungs. Clinically two main groups of CNS involvement can be distinguished: one with general signs of CNS involvement, including changes of consciousness and epileptic seizures; the other with focal or multifocal signs, including ataxia, aphasia, hemiparesis, sensory disorders, ophthalmoplegia, and visual disorders. The most common neurological presentation is polyneuropathy.

The erythrocyte sedimentation rate is often but not always increased. CSF is usually normal. Histologically the small arteries and arterioles are most often affected, especially in the leptomeninges, the deep white and gray matter, and the choroid plexus. The affected vessels show fibrinoid or hyaline necrosis of the media and destruction of the internal elastic lamina. Inflammatory granuloma affects the entire thickness of the vessel wall, with secondary intima lesions, eventually obstructing the vessel lumen. Segmental vessel wall necrosis may lead to the formation of

small aneurysms. The parenchymal lesions are small infarctions, multiple and disseminated, sometimes hemorrhagic. Part of the *periarteritis nodosa* group is abuse-associated vasculitis, best described in intravenous methamphetamine users, and hepatitis B virus-associated vasculitis. In these cases, too, the disorder is systemic.

MRI shows the cerebral involvement as multiple white and gray matter lesions, both lacunar and territorial infarctions. High-resolution MRA may also show vascular abnormalities.

Moyamoya syndrome, (*moyamoya* meaning “puff of smoke,”) was long considered an ethnic disease limited to patients of Japanese ancestry. Today, however, it is clear that the disease occurs in Europe and America as well. The disease is a progressive arteritis of the supraclinoid portion of the carotid arteries, eventually leading to complete occlusion. The disease usually starts at a young age, rarely under the age of 10 years. The fact that the disease is limited to the carotid arteries has led to the suggestion that the disease is related to a defect in embryogenesis, which is different for the carotid arteries from what it is for the vertebrobasilar system. In the later phases an extensive collateral circulation characteristically develops, partly via external carotid arteries, partly via the posterior cerebral artery circulation.

Laboratory investigations are unrevealing in *moyamoya syndrome*. Histopathological examination in *moyamoya syndrome* reveals that the principal alterations are stenosis and occlusion of the distal portions of the internal carotid arteries and the proximal

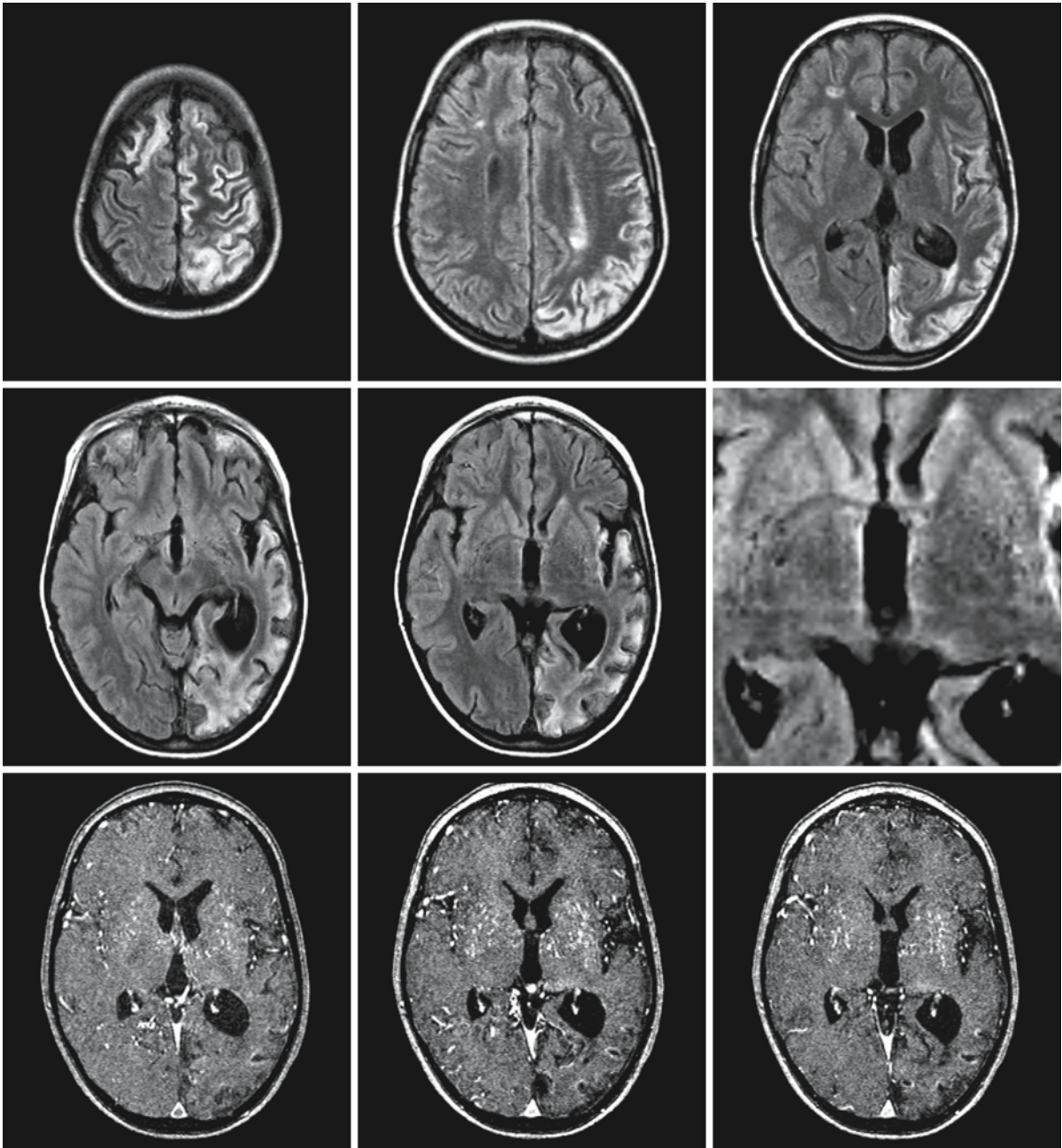
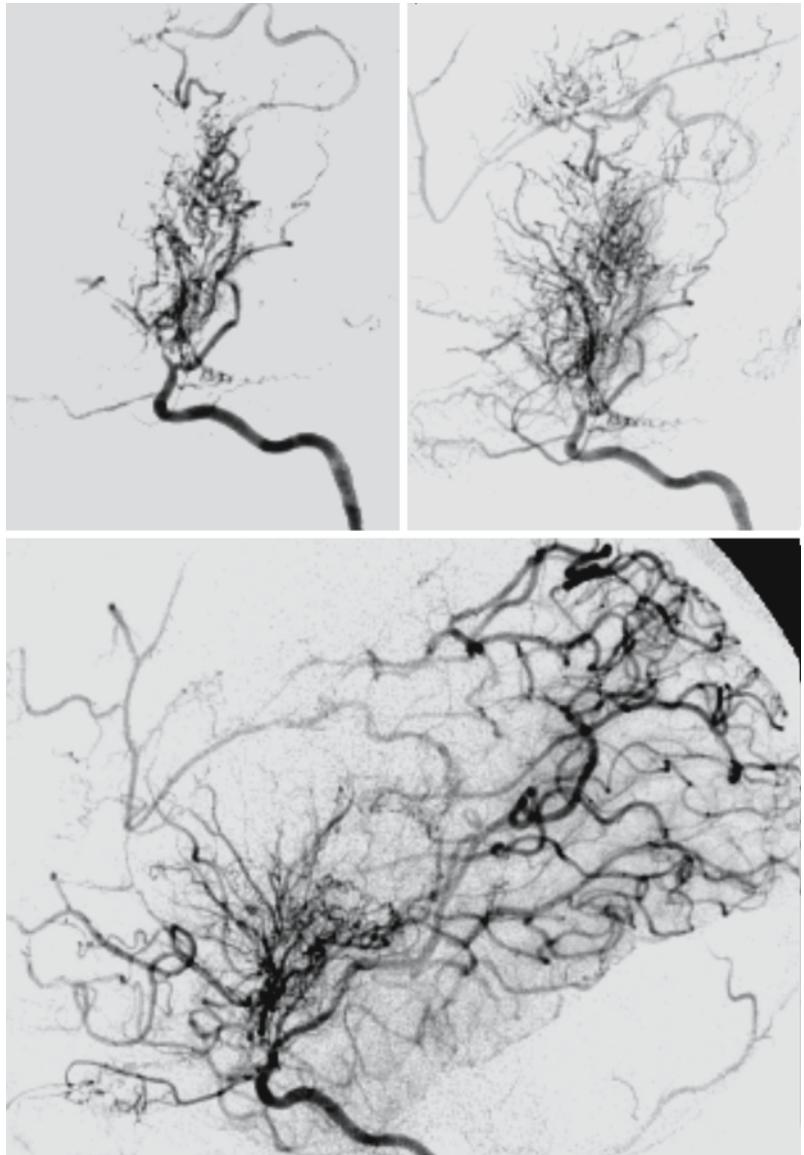


Fig. 100.6. FLAIR images of a 9-year-old boy with moyamoya syndrome and multiple cortical infarctions (*first two rows*). The image pattern is similar to what is seen in MELAS, but the images through the basal ganglia suggest the presence of many abnormal vessels. The *third row* shows the source images of the MRA, revealing the abundance of small and very small vessels all through the brain, reflecting the collateral circulation,

most intensive in the basal ganglia. The intra-arterial DSA of the left internal carotid artery (*fourth row*, next page) shows the typical changes of moyamoya syndrome with a “puff” of abnormal vessels in the center. The later phase (*fifth row*) shows the remaining circulation via the posterior cerebral artery, with the collateral “puff of smoke” in the basal ganglia, and the leptomeningeal collaterals in the parietal lobe

parts of the anterior and middle cerebral arteries. This is combined with numerous dilated, thin-walled collateral arteries branching from the posterior parts of the circle of Willis. In the stenotic arteries the

intima shows massive fibrous thickening, without atheromatous features. The internal elastic lamina is usually preserved but extremely wavy and often duplicated or triplicated. The media is atrophic. There is

Fig. 100.6. (continued).

no inflammatory infiltration, but thrombosis, recanalization, and aneurysm formation may occur.

The diagnosis can be established with radiological techniques. The anastomoses via lenticulostriate arteries in the basal ganglia give rise to the typical appearance of a cloud (“puff of smoke”) on intra-arterial DSA (Fig. 100.6), whereas on MRI the usual appearance is of multiple infarctions, both territorial and hypoperfusion-related border zone infarctions. Either the cortex or the cerebral white matter is principally affected (Figs. 100.6 and 100.7). On high-resolution images multiple dilated small vessels may be visible in the basal ganglia (Figs. 100.6 and 100.7). In advanced cases there may be dilated small vessels scattered throughout the brain.

There is no real cure for the disease, but microvascular surgery may help to restore some of the perfusion by vascular anastomoses

100.2.2.2 Autoimmune-Related Disorders

The *rheumatological syndromes* associated with CNS disease due to vasculitis include a broad spectrum of autoimmune diseases. At one end of this spectrum one finds organ-specific diseases with organ-specific antibodies, for example Hashimoto disease of the thyroid. In the middle of the spectrum the lesions tend to be localized in one organ but the antibodies are not organ-specific. A typical example is primary biliary cirrhosis, where the small bile ductules are the main target of inflammatory cell infiltration but the serum

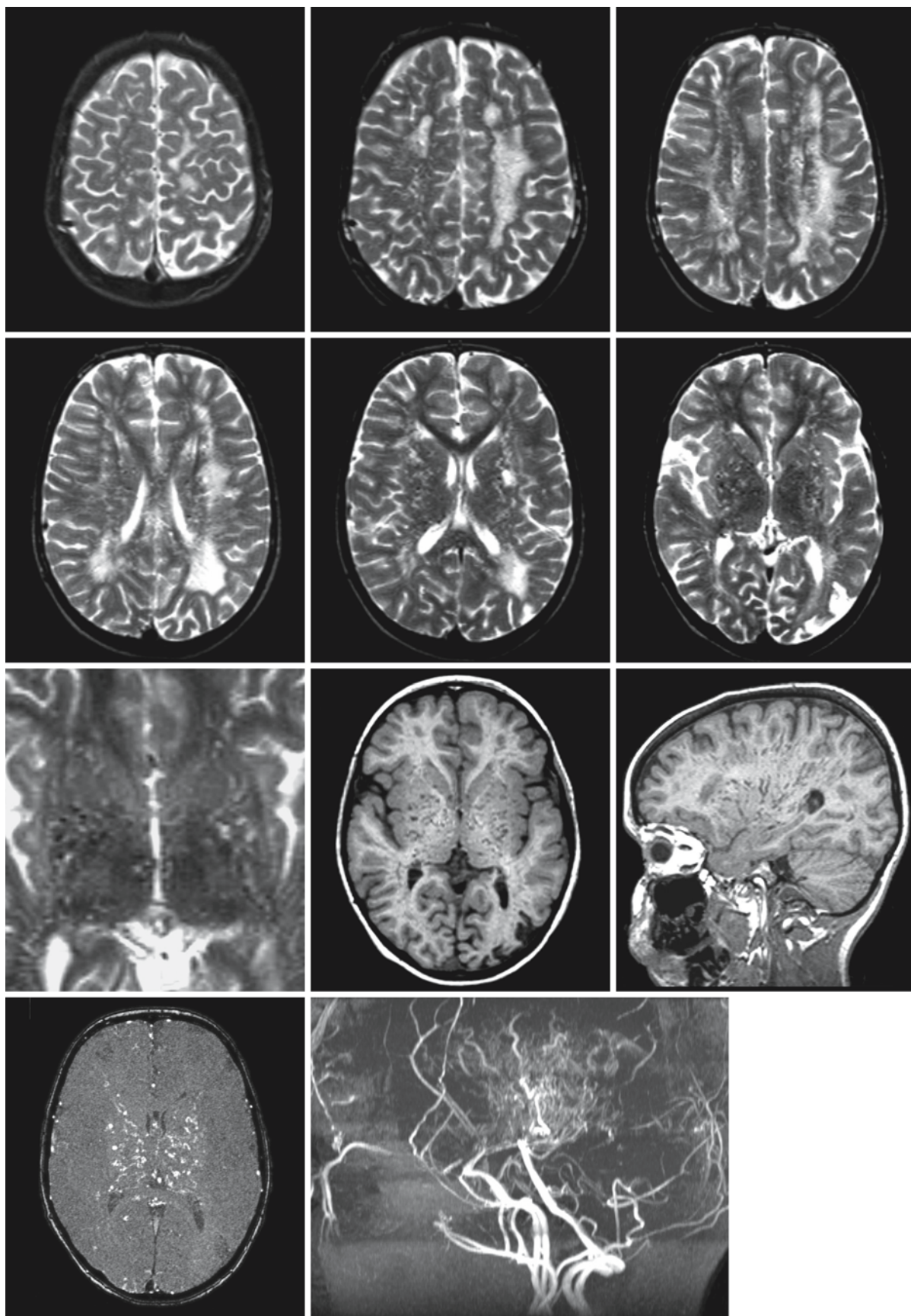


Fig. 100.7.

Fig. 100.7. A series of T₂-weighted images (*first and second rows*) of a 9-year-old boy with moyamoya syndrome. There are extensive white matter abnormalities in the deep white matter of the cerebral hemispheres suggesting a leukodystrophy. Note that within the abnormal white matter many punctate lesions are present, with high signal intensity in parts and low signal intensity in others. The blown-up image of the basal ganglia shows this to better advantage (*third row, left*). The axial and sagittal T₁-weighted images (*third row, middle and right*) show that there is an abundance of small abnormal vessels in the brain parenchyma. The source images of the MRA and the MRA itself (*fourth row*) confirm this. The MRA demonstrates that the large cerebral arteries are occluded. Note the contribution of external vessels to perfusion of the cerebral parenchyma on the left side of the image. The intra-arterial DSA confirmed the diagnosis of moyamoya syndrome

antibodies, mainly antimitochondrial, are not organ-specific. At the other end of the spectrum the disorder is not organ-specific; lesions and antibodies are not confined to a single organ. In SLE, and many other autoimmune disorders, lesions are seen in the skin, renal glomeruli, joints, serous membranes, and blood vessels.

Rheumatoid disease with CNS vasculitis is a relatively rare occurrence. In all patients joint disease is apparent. Patients may have had demonstrable rheumatoid arthritis for between 1 and 30 years prior to the onset of their neurological problems. CNS disease manifests itself nonspecifically by a multitude of possible neurological signs and symptoms, including seizures, dementia, hemiparesis, cranial nerve palsies, blindness, cerebellar ataxia, and dysphasia.

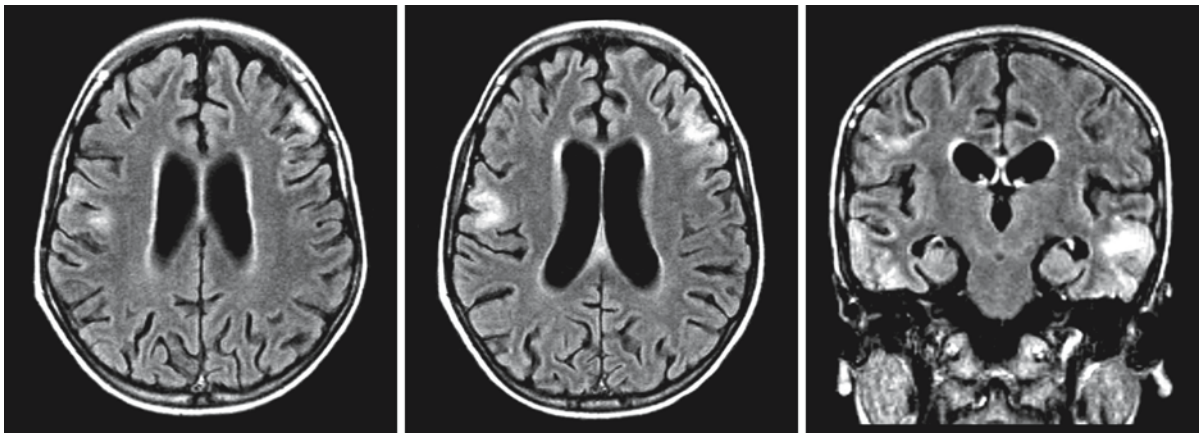


Fig. 100.8. The transverse and coronal FLAIR images of a 9-year-old boy presenting with progressive dementia show multiple, mainly cortical infarctions. The MRI would be com-

patible with a diagnosis of MELAS. In this case the clinical and laboratory diagnosis was SLE

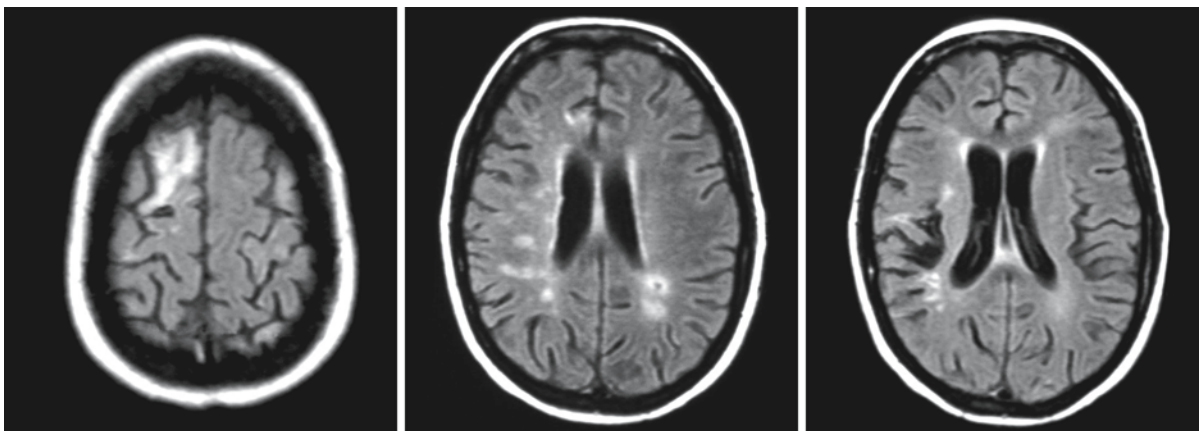


Fig. 100.9. The FLAIR images of a 25-year-old woman with a multiple sclerosis-like presentation show an MRI pattern compatible with this diagnosis. Shortly after the MRI she was diag-

nosed with SLE. Courtesy of Dr. M. Driessen-Kletter, Department of Neurology, Twenteborg Hospital, Almelo, The Netherlands

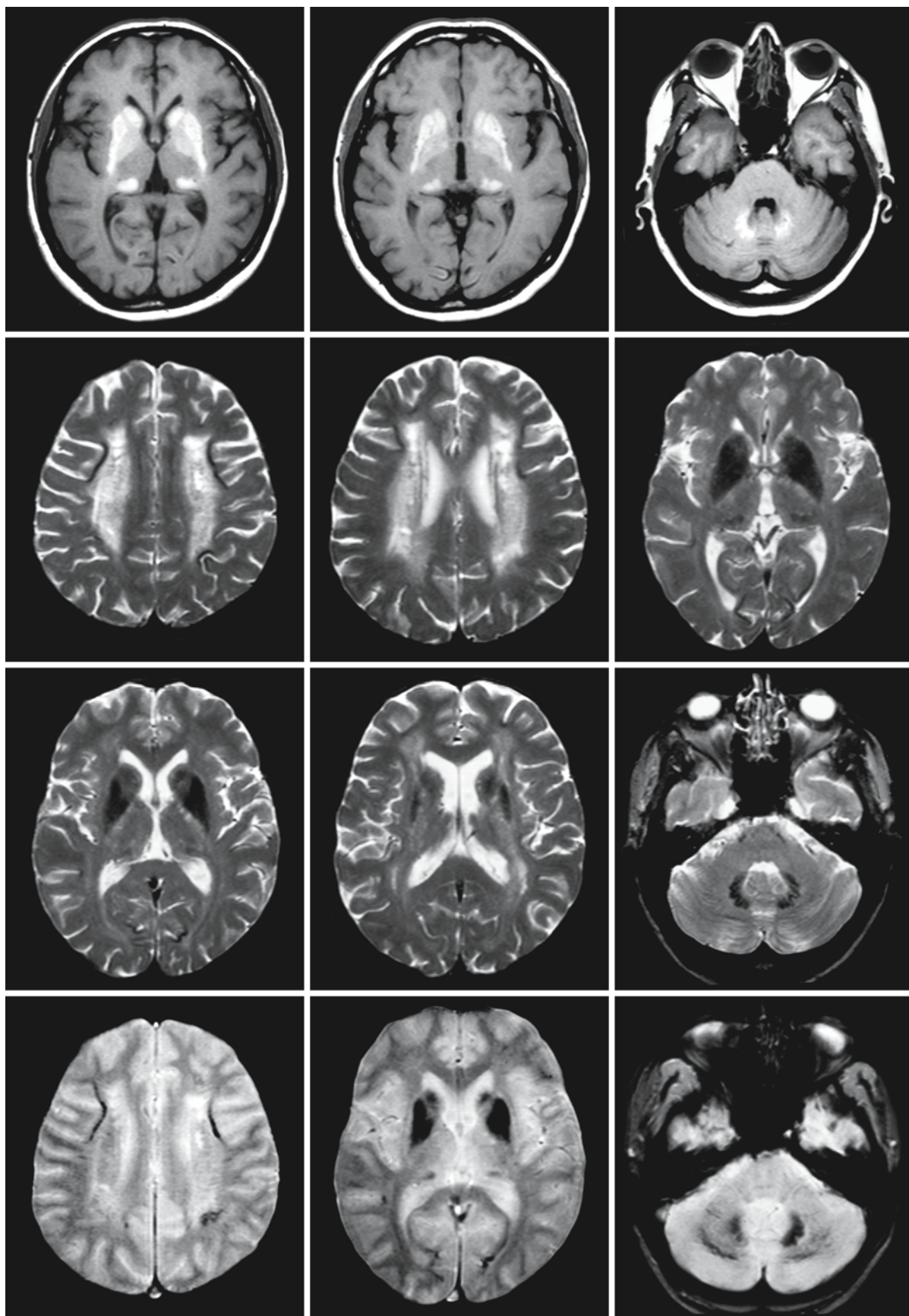


Fig. 100.10.

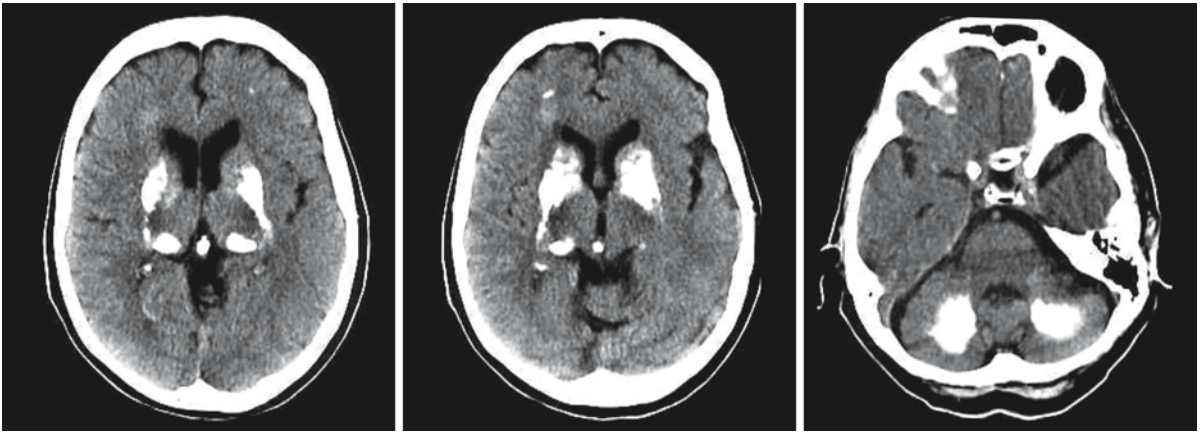


Fig. 100.10. (continued). Images of a 50-year-old female patient with SLE. The *upper row* of T₁-weighted images show high signal intensity in the basal ganglia, the pulvinar, and the dentate nucleus. The T₂-weighted images (*second and third rows*) demonstrate a broad rim of hyperintensity around the lateral ventricles. The basal ganglia, pulvinar, dentate nucleus, and multiple areas of the cortico-subcortical junction appear

very dark, suggesting calcium deposits. Gradient echo images (*fourth row*) show hypointensity in the same areas. The CT images (*fifth row*) confirm that there are massive calcifications in these areas. Note that the corpus medullare of the cerebellum is also calcified. Courtesy of Dr. E. Gut, Department of Neuro-radiology, Kliniken Schmieder, Allensbach, Germany

Serum rheumatoid factors are present and the erythrocyte sedimentation rate is elevated. Histological examination reveals in a number of cases amyloid deposits together with signs of vasculitis.

MRI is nonspecific and in most cases shows scattered white matter lesions, sometimes mimicking multiple sclerosis. The presence of systemic abnormalities will in most cases suggest the diagnosis.

Therapy of rheumatoid disorders is often complex and may include antiphlogistic medication, corticosteroids, immunosuppressives, cytokines and many supportive measures.

Systemic lupus erythematosus (SLE) is a chronic, relapsing-remitting disease, with variable involvement of different organ systems. The disease occurs preferentially in adolescent and young adult women. Frequent findings include malar rash (butterfly rash), nonerosive arthritis involving multiple joints leading to tenderness, swelling, and effusion, serositis of pleura or pericardium, renal abnormalities, Raynaud phenomenon, lymphadenopathy, and gastrointestinal complaints. Cerebral involvement often presents with neuropsychiatric symptoms. Neurological disease is the second or third leading cause of death after renal disease. Neurological manifestations usually follow systemic manifestations by more than a year. The symptomatology is related to the site of CNS involvement. Also, there may be spinal cord involvement with transverse myelitis.

There are criteria for the diagnosis of SLE (American College of Rheumatology), which contain both clinical symptoms and more or less specific laboratory findings, such as hemolytic anemia with reticulo-

sis, lymphopenia, elevated anti-DNA antibodies, false positive test to syphilis (VDRL), complement activation, and an abnormal titer of autoantibodies, such as lupus anticoagulant, anti-cardiolipin and other APLA. Immune complexes and diminished levels or altered metabolism of the fourth component of the complement cascade have been found in the CSF of patients with CNS disease. Antibodies to neuronal antigens, often cross-reacting with lymphocytic antigens, are preferentially seen in the serum and CSF of patients with neurological manifestations. The principal diagnostic test for the disease is the presence of antinuclear antibodies; antibodies against double-stranded native DNA are specific for SLE.

Histological true vasculitis of the CNS is rare, but vasculopathic changes are common. Microscopic changes are most marked in small vessels and consist of acute fibrinoid necrosis and marked thickening of the vessel wall with minimal inflammatory cell infiltration. Some vessels are occluded by thrombi with corresponding microinfarcts. Autoimmune factors that play a role in the cerebral vascular changes in SLE have been identified as lupus anticoagulant, APLA, and anti-cardiolipin antibodies. They link SLE with the pure anti-phospholipid syndrome and with Sneddon disease, which is probably a variation of the anti-phospholipid syndrome.

Many different MRI patterns can be encountered in SLE. Sometimes the MRI pattern mimics MELAS, showing mainly cortical infarctions (Fig. 100.8). Sometimes it mimics multiple sclerosis (Fig. 100.9). In other cases there are more widespread white matter lesions (Figs. 100.10 and 100.11). In some patients se-

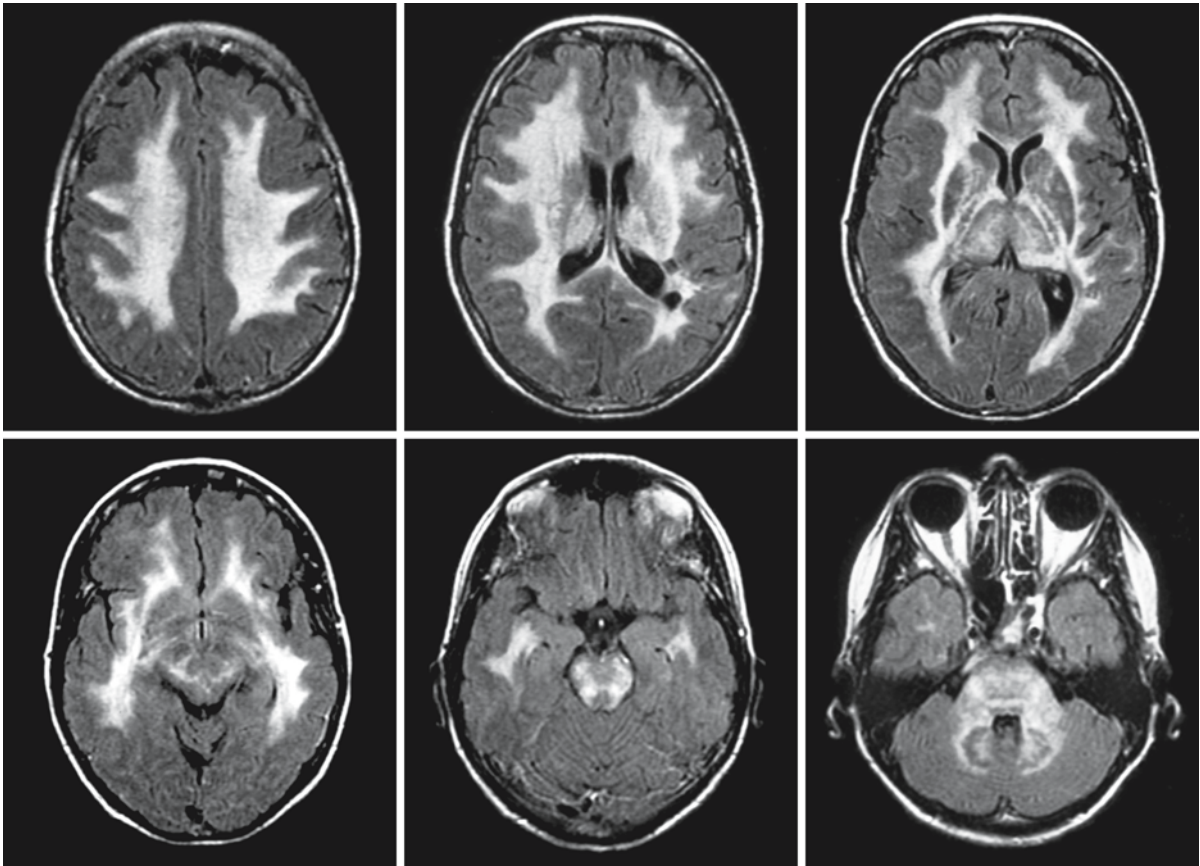


Fig. 100.11. A 56-year-old woman with a long history of complicated SLE. There is symmetrical involvement of the cerebral hemispheric white matter, the anterior and posterior limbs of the internal capsule, the external capsule, the thalamus (especially the pulvinar), the midbrain, pons, middle cerebellar pe-

duncles, the hilus of the dentate nucleus, and the peridentate white matter. Courtesy of Dr. R. Schiffmann, Developmental and Metabolic Neurology Branch, National Institutes of Health, Bethesda, Maryland, USA

vere involvement of the basal ganglia is seen, a pattern that has to be differentiated from central venous thrombosis. In still other patients there is extensive calcification of the basal ganglia, dentate nucleus, centrum semiovale, and cortico-subcortical junction (Fig. 100.10). Enhancement may occur in active lesions. In some cases, despite neuropsychiatric symptoms, conventional MRI is normal. In those cases estimation of magnetization transfer histograms may detect abnormalities, without otherwise visible lesions.

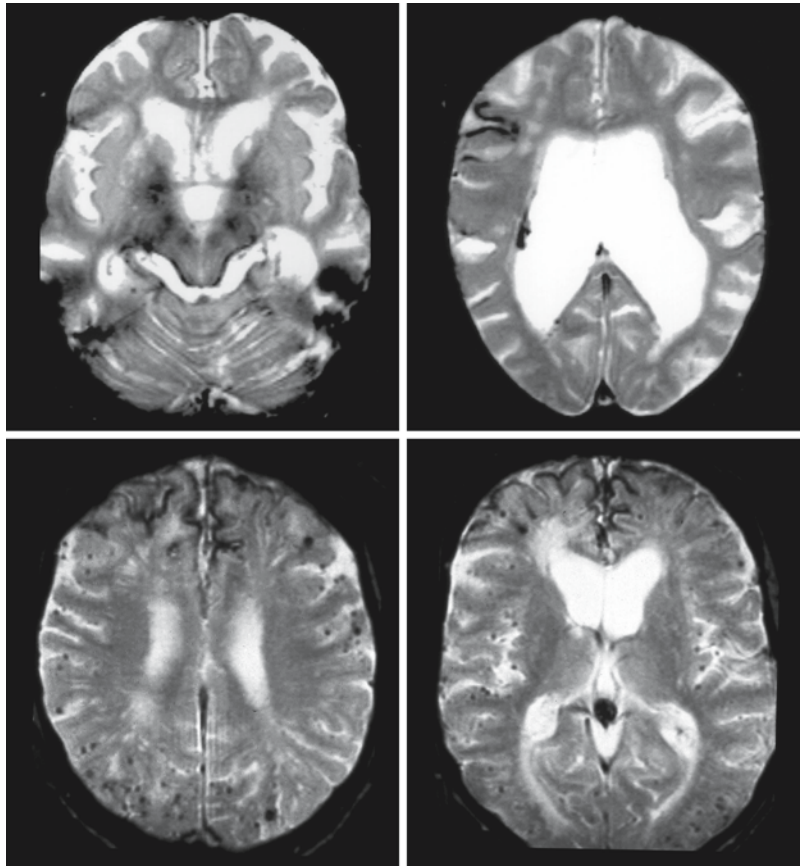
Therapy is usually with corticosteroids and immunosuppressives.

Sneddon syndrome is characterized by a combination of generalized livedo racemosa (or reticularis), a cutaneous condition featured by a reddish-purple reticulated pattern predominantly present on trunk and extremities, and diffuse intravascular coagulation leading to cerebrovascular manifestations. The skin abnormality is not specific, but may be also be associated with polyarteritis nodosa, SLE, rheuma-

toid arthritis, thrombocytopenic purpura, and polycythemia. At an early age the patients develop cerebrovascular manifestations, including larger and smaller arterial territorial infarctions, with severe neurological consequences and often cognitive deterioration.

Sneddon syndrome is linked with the presence of anti-cardiolipin antibodies (one of the APLA), and therefore Sneddon syndrome may be regarded as belonging to the APLA-related disorders. However, the presence of APLA is highly variable in Sneddon disease (41% positive). In APLA-positive patients, audible mitral regurgitation is observed more frequently. There is a close relationship between Sneddon syndrome, SLE, and “pure” APLA syndrome. It has been suggested that Sneddon syndrome might cover a continuum of various clinical and biological entities, ranging from APLA-related SLE patients, to primary APLA-positive patients, and Sneddon syndrome in the middle.

Fig. 100.12. Gradient echo images of two patients with Sneddon syndrome. The upper two images are of a 53-year-old woman who has suffered multiple infarctions in the past. She is now wheelchair-bound and suffering from progressive cognitive impairment. The lower two images are of a 42-year-old woman who has also suffered multiple transient ischemic attacks and permanent infarctions. She also has impairment of cognitive functions. In both women there is ventriculomegaly. The gradient echo images show the preferential occurrence of the hemorrhages at the surface of the brain and the ependymal lining. This is not often seen in other vasculitides. The superficial hemorrhages result in focal superficial hemosiderosis. The black rim around the brain stem in the upper images is also caused by hemosiderin. In the lower images punctate black dots are seen nearly everywhere in the brain, reflecting microhemorrhages



Nonspecific laboratory findings include an elevated erythrocyte sedimentation rate. The finding of APLA in addition to typical skin abnormalities confirms the diagnosis.

Histopathologically Sneddon syndrome particularly attacks small cortical arteries. Infarctions are, therefore, most often located in cortical areas. They are often hemorrhagic, and hemosiderin deposits are also found in the leptomeninges.

MRI shows a variable number of smaller and larger infarctions, in which cortical involvement is most prominent. With gradient echo techniques multiple hemosiderin deposits with extensive superficial hemosiderosis is the most common finding. In our experience this finding is more constant in Sneddon syndrome than in other vasculitides (Fig. 100.12).

Treatment according to the guidelines for SLE and APLA syndrome is the rule.

Anti-phospholipid antibody syndrome. Anti-phospholipid antibodies (APLA) are antibodies against phospholipids and are found in a variety of clinical disorders. The discovery of APLA followed the observation that in a patient with SLE the activated partial thromboplastin time (aPTT) was prolonged (lupus anticoagulant). Despite this, patients with high levels of APLA do not develop hemorrhagic complications

unless they also have thrombocytopenia. On the contrary, patients present with a hypercoagulable state which leads to thrombotic complications, stroke, myocardial infarctions, dementia, and fetal loss.

APLA syndrome is found in up to 30–50% of patients with SLE. Patients without SLE or other systemic disease can also develop APLA syndrome, referred to either secondary or primary or pure APLA syndrome. Children may develop secondary APLA syndrome during viral infections. Up to 30% of patients with HIV-infection develop secondary APLA syndrome. “Pure” APLA syndrome occurs in patients without any of these antecedents.

Venous thrombosis is a relatively frequent occurrence in APLA syndrome. About 30% of patients with APLA syndrome acquire deep venous thrombosis. In patients with APLA syndrome and SLE the figure is even 40%. In drug-induced or parainfectious APLA syndrome it is less than 5%. Patients with APLA syndrome may prove difficult to treat for venous thrombosis and they have a high rate of recurrence. In young adults with APLA syndrome there is an increased risk of arterial disease, leading to myocardial infarctions, stroke, and a higher incidence of peripheral vascular occlusions. In addition to brain damage by territorial infarctions, patients often present with

early-onset dementia, the average age at onset being 52 years. In these patients there is usually no history of major strokes. Associated findings include livedo racemosa, Raynaud phenomenon, superficial thrombophlebitis, cardiac valve vegetations, and mitral regurgitation.

Laboratory testing for APLA syndrome is complex and several subtests are involved. There is no simple screening test for the condition. Testing should be done when one or more of the major clinical manifestations occur: arterial or venous thrombosis, thrombocytopenia, or frequent miscarriages. Primary APLA syndrome patients are more often male, and have a low titer of anti-nuclear antibodies.

MRI can, with the appropriate techniques, demonstrate the involvement of the CNS. MRI shows white matter abnormalities, suggestive of small vessel disease. Apart from the white matter involvement, lesions usually extend into the cortical layers. In fresh infarctions diffusion-weighted imaging is helpful. Gradient echo sequences will show microhemorrhages when present.

Therapeutically one has to be aware that, although APLA syndrome is considered to be an autoimmune disease, immunosuppressive therapy does not prevent recurrent thrombosis, fetal loss, or neurological syndromes and should therefore not be considered. A possible exception to this rule is the treatment of catastrophic cases, in which also plasmapheresis may be attempted. In thrombotic forms anticoagulant therapy is usually the treatment of choice.

In *Sjögren syndrome*, an autoimmune disorder, neurological complications are not uncommon, most often affecting the PNS. CNS involvement is reported in 25–30% of the patients, presenting as trigeminal neuropathy, recurrent aseptic meningoencephalitis, or unifocal or multifocal cerebral parenchymatous lesions. Also lesions of the spinal cord may occur resulting from a necrotizing vasculitis and leading to transverse myelitis, chronic progressive myelitis, a Brown-Séquard syndrome, or a neurogenic bladder. Patients may also present with neuropsychiatric symptoms. The involvement of the salivary and lacrimal glands (the “sicca” manifestations) is usually manifest before CNS or PNS symptoms, but may also appear later. More general constitutional symptoms may also be present, such as fatigue, malaise, low-grade fever, Raynaud syndrome, lymphadenopathy, arthralgia, myalgia, as well as involvement of lungs, kidneys, muscles, and joints. Lymphoproliferative disorders are potential complications. This disease has much in common with rheumatoid arthritis and SLE.

Pathological studies of peripheral nerves and muscle show acute or chronic vasculitis or perivascular inflammation. In a few cases in which biopsy of the CNS was performed, either an unambiguous vasculitis was found or, more typically, a mononuclear vas-

culopathy with a perivascular mononuclear reaction infiltrating in the cerebral parenchyma, usually involving the white matter.

On MRI more or less extensive white and gray matter lesions have been reported, including partial territorial infarctions. Microbleeds, present in histopathological studies, can be seen on gradient echo sequences. Lesions in the posterior fossa are rare. The MRI pattern is not specific and the differential diagnosis includes multiple sclerosis, SLE, Behçet disease, and microscopic polyarteritis nodosa.

Scleroderma (*scleros*=hard, *derma*=skin) is a progressive disease that leads to hardening of the skin and connective tissue and is part of the group of arthritic conditions called connective tissue diseases. There are two main forms of scleroderma, a localized and a systemic form. The localized form is subdivided into two forms, morphea and linear scleroderma. Morphea is a cutaneous lesion with indurated, slightly depressed plaques of thickened dermal fibrous tissue, white or yellowish, with pinkish-purplish halo. The linear form of scleroderma is a line of thickened tissue, which affects the skin, but can also affect the muscles and bone underneath, limiting movements of limbs when affected. The underlying cortex can also be affected when the abnormality occurs on the forehead. Linear scleroderma is usually present on arms, legs, or on the forehead. It may appear as a long streak resembling a deep saber wound, often referred to as “en coup de sabre.” The systemic form of scleroderma can affect any part of the body, skin, blood vessels, and internal organs. The systemic form is also referred to as diffuse scleroderma or CREST (calcinosis, Raynaud syndrome, esophageal problems, sclerodactylia, and telangiectasia) syndrome. The presence of two of the five symptoms mentioned is enough to make the diagnosis CREST. When CREST is present together with other symptoms of scleroderma, it is referred to as “limited scleroderma plus CREST.”

In scleroderma many organs and organ systems may be involved, including skin; blood vessels; respiratory system; musculoskeletal system; cardiovascular system; genitourinary system; ears, nose, and throat (sicca syndrome); renal system; endocrine system; PNS; and CNS. Focusing on neurological involvement: peripheral nerve manifestations may lead to pain and paresthesias from nerve entrapment, for instance trigeminal neuralgia and carpal tunnel syndrome. Involvement of the CNS may lead to (partial) territorial strokes, epileptic seizures, with as pathological substrate focal narrowing of middle-sized arteries, and more or less extensive intracerebral calcifications, probably related to an underlying cerebrovascular pathology. Some patients present with recurrent loss of consciousness and multiple spontaneous intracerebral hemorrhages.

Anti-centromere antibodies have been found in patients with scleroderma and Raynaud syndrome and in CREST patients and may facilitate the diagnosis. Extractable nuclear antibodies and other autoantibodies may also be found. When peripheral skin lesions are present, the diagnosis can be confirmed by skin biopsy. The skin is thickened as a result of overproduction of collagenous tissue, overgrowing hair follicles and sweat glands.

Histologically there are two major findings: fibrotic changes, resulting from endothelial damage of small vessels and subsequent collagen deposition, and vasculopathy, consisting of fibrinoid necrosis of arterioles, lymphoid hyperplasia, and thickening of the basement membrane.

The cause of scleroderma is unknown. Recently it has been suggested that cellular microchimerism with a lifelong status could form an immunological basis for amplification of autoimmune reactions leading to clinical manifestations of systemic sclerosis. Microchimerism has been defined by the presence of a small number of circulating cells transferred from another individual. This transfer may occur during pregnancy between mother and fetus or, in multigestational pregnancies, between fetuses. Other causes are blood transfusion, bone marrow transplantation, and organ transplants. Microchimerism has been implicated not only in systemic sclerosis, but in the pathogenesis of autoimmune diseases more generally. An increased number of microchimeric cells has been found in peripheral blood and tissues of patients with systemic sclerosis, and they have been proven to be specifically activated and capable of recognizing human leukocyte antigens (HLA) from patients.

At this moment there is no specific treatment for scleroderma. Attempts are under way to build upon the remarkably successful use of TNF- α neutralizing treatments for rheumatoid arthritis, which may have paved the way for similar approaches in rheumatoid-like disorders.

MRI is nonspecific and presentations vary widely. Infarctions may occur in middle-sized artery territories. In addition, macro- and microhemorrhages and extensive calcifications may be present. In other cases lesions mimic patterns found in multiple sclerosis. Where frontal linear scleroderma is present one may expect underlying cortical abnormalities, calcifications, and atrophy.

Neurosarcoidosis occurs in approximately 5% of patients with systemic sarcoidosis, also called Besnier-Boeck-Schaumann disease. Sarcoidosis is a systemic granulomatosis of unknown cause, especially affecting the lungs with lung fibrosis, but also found in hilar lymph nodes, skin, liver, spleen, eyes, phalangeal bones, parotid glands, and the CNS. In the CNS facial nerve paralysis is the most common manifestation,

but findings may also mimic tuberculosis, multiple sclerosis, lymphomas, and fungal infections of the brain. Extra-axial manifestations may show features comparable to convexity meningiomas. Spread along the perivascular spaces, leptomeningeal involvement, involvement of the optic nerve, the pituitary gland, the floor of the third ventricle, and the hypothalamus have all been reported. Spinal manifestations are not rare.

Although the cause of sarcoidosis still is unknown, it is generally accepted that sarcoidosis results from exposure of genetically predisposed individuals to specific environmental agents. The finding of associations between the human leukocyte antigens of the major histocompatibility complex and sarcoidosis supports this hypothesis. So does the difference in prevalence rates between ethnic groups. Another possible association is between sarcoidosis and bacterial DNA, especially DNA of *Propionibacterium acnes* or *granulosum*. Further studies will have to confirm the value of these findings.

Laboratory tests are not very helpful in establishing the diagnosis. A positive angiotensin converting enzyme (ACE) test in the CSF may support the diagnosis, but the test may also be negative or neutral. The results of this test should therefore be interpreted with care. The cell count in the CSF is usually slightly elevated, as is the protein content.

Histologically the manifestations can be divided into those with proliferation of granulomatous tissue, leading to more solid lesions in the suprasellar region, the brain, and spinal cord, and those with leptomeningeal and perivascular involvement with features of an inflammatory vasculitis.

MRI can portray the major manifestations: the suprasellar-leptomeningeal involvement (Fig. 100.13) and the spread along the perivascular spaces (Fig. 100.14), in both cases with enhancement after contrast injection. In other cases the lesions mimic multiple sclerosis patterns. In several patients an extra-axial process very similar to a meningioma has been described. Intramedullary lesions are also easily demonstrated on spinal MR.

Therapeutically corticosteroids may be beneficial. In more chronic cases cyclophosphamide and methotrexate are treatment options.

Wegener granulomatosis (Wegener disease) may lead to cerebral lesions, either as lesions primarily located in the nasal cavities and sinuses and extending intracranially, or as necrotizing cerebral vasculitis, nearly always in the presence of active sinusitis, otitis, or lung disease. A limited form of Wegener disease, without upper and lower respiratory tract disease, has been repeatedly described and has a better prognosis. The clinical features are protean, but ocular manifestations are common.

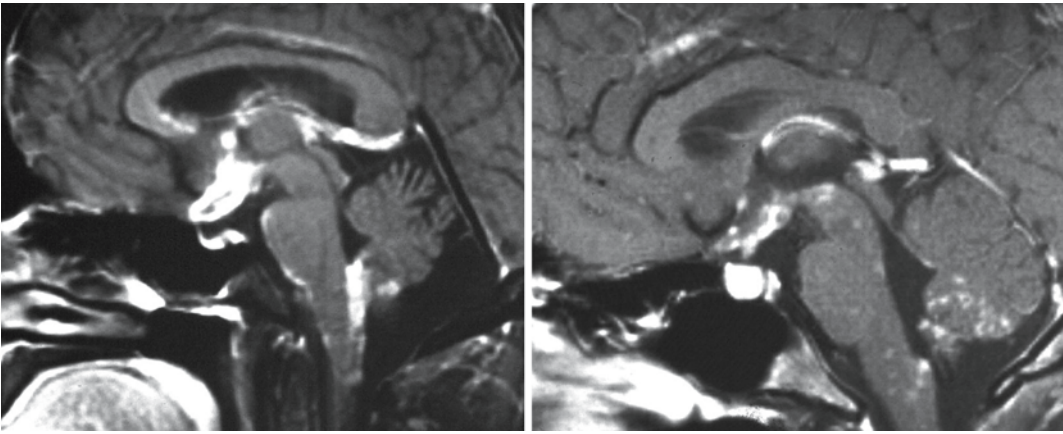


Fig. 100.13. Sagittal T₁-weighted, contrast-enhanced, fat-suppressed images of a patient with neurosarcoidosis, showing the characteristic images of involvement of the hypothalamus, pituitary stalk, the leptomeninges around the brain stem and cerebellum, in the sulcus cinguli, and in the foramen of Magendie

mus, pituitary stalk, the leptomeninges around the brain stem and cerebellum, in the sulcus cinguli, and in the foramen of Magendie

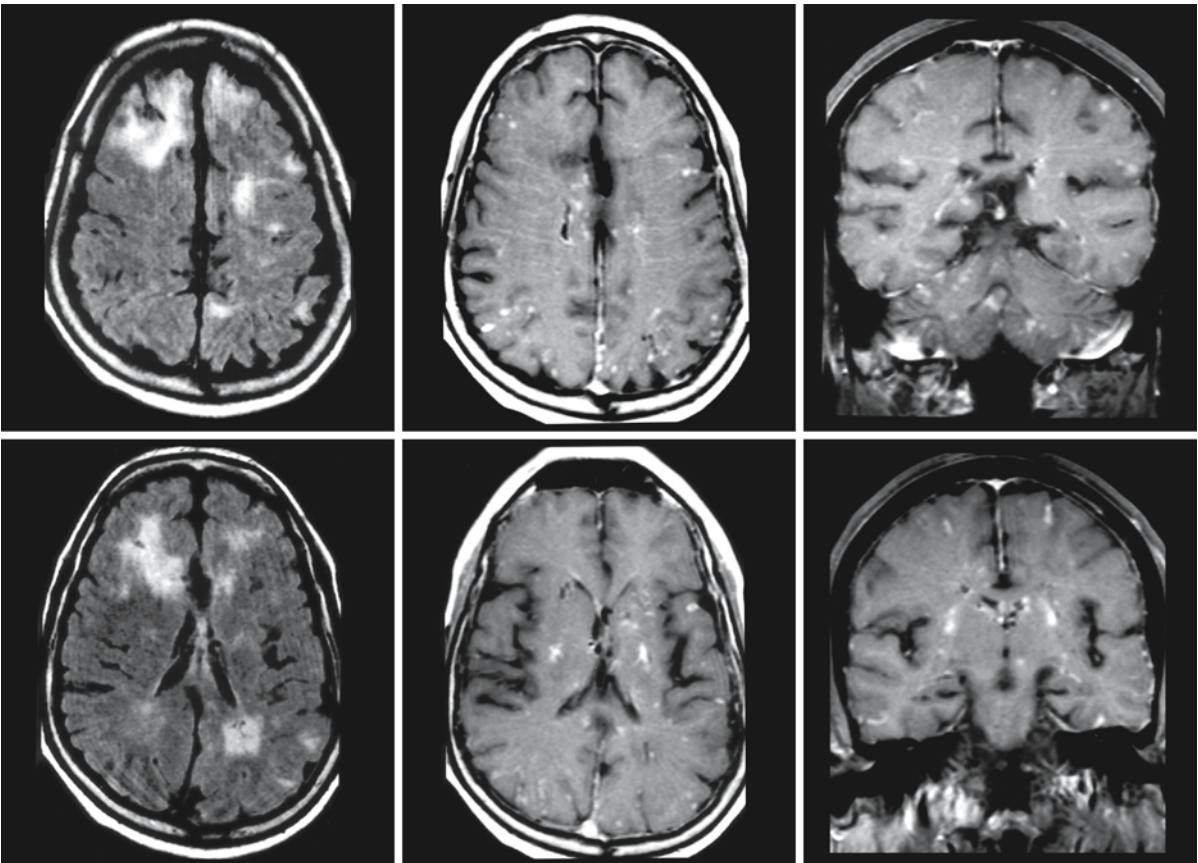


Fig. 100.14. In this patient with neurosarcoidosis, the involvement concerns the perivascular spaces. The two FLAIR images (*left column*) show multiple infarct-like lesions involving in

both cortex and white matter. After contrast injection (*middle and right columns*) enhancement occurs, in part with a stripe-like pattern following the course of the perivascular spaces

The diagnosis may be sustained by the presence of cytoplasmic anti-neutrophil antibodies (ANCA). The optimal evaluation of serum ANCA levels requires assessment of the presence of two principal ANCA targets: myeloperoxidase and proteinase 3. The cytoplasmic (c-ANCA) staining pattern of neutrophils stems largely from antibodies to proteinase 3; the perinuclear (p-ANCA) staining pattern is derived from antibodies to myeloperoxidase and several other antigens, including lactoferrin, cathepsin G, and elastase. ANCAs are detected in patients with different disorders, such as infections, inflammatory bowel disease, autoimmune hepatitis, and malignancies. With the presence of c-ANCAs, high titers of proteinase 3, and the absence of antinuclear antibodies, the diagnosis of Wegener disease becomes more definitive.

Histologically Wegener disease is characterized by necrotizing panarteritis of the middle great vessels. Multiple foci of arteritis develop in the nasal sinuses, the respiratory tract, the eye, and the kidneys. There is much similarity between Wegener disease and involvement of the CNS by other granulomatous and arteritic diseases, including Churg–Strauss syndrome and microscopic polyarteritis nodosa.

There is a close relationship between Wegener disease, Churg–Strauss syndrome, and microscopic polyarteritis (as distinct from polyarteritis nodosa). The latter involves predominantly if not exclusively arteries, whereas the other disorders virtually always affect vessels smaller than arteries.

In limited Wegener disease the histopathological characteristics are similar to those of the typical disease, but without the upper and lower respiratory tract and kidney involvement. The ANCA test is less likely to be positive. In limited Wegener disease 50–60% of the patients have sinusitis, and 6% have hearing loss due to formation of granulomatous tissue between eustachian tube and tympanum. Destruction of the petrous part of the temporal bone and inflammatory masses at the base of the skull may also be present. Erosion of the lamina papyracea of the orbital walls may occur. Involvement of single or multiple cranial nerves may occur, especially of the eighth, ninth, tenth, and twelfth cranial nerves. The cranial neuropathies are caused either by necrotizing small vessel vasculitis or by a granulomatous process in the meninges.

Leptomeningeal enhancement on contrast-enhanced MRI has been described in Wegener granulomatosis. Isolated intracranial or spinal lesions may also be seen (Fig. 100.15). The lesions will enhance after contrast injection (Fig. 100.15). MR and CT examinations of the nasal sinuses and mastoids are important in the evaluation of cerebral involvement by continuous extension.

Churg–Strauss syndrome belongs to the group of necrotizing vasculitides. It is characterized by an eosinophil-rich and granulomatous inflammation and necrotizing vasculitis involving the small- to medium-sized vessels, affecting particularly the respiratory tract. The disease is associated with asthma and peripheral eosinophilia, often combined with necrotizing glomerulonephritis. Cerebral manifestations occur in about 10% of the patients. About 60% of patients are p-ANCA-positive. MRI findings are variable and the cerebral lesions are similar to those seen in many other vasculitides. They consist of macro- or microinfarctions and micro- or macrohemorrhages.

Microscopic polyarteritis (polyangiopathy) is also characterized by necrotizing vasculitis of the small vessels, arteriolae, capillaries, or veins, without granulomas. The disease is nearly always associated with necrotizing glomerulonephritis and often with pulmonary capillaritis and hemorrhage. Peripheral neuropathy occurs less frequently than in polyarteritis nodosa. Sinusitis, which is rare in polyarteritis nodosa, occurs in 9% of patients with microscopic polyarteritis. CNS involvement is rare, but when present will be caused by necrotizing vasculitis.

The p-ANCA reaction is found in 50–80% of the patients with microscopic polyarteritis and in less than 20% of patients with polyarteritis nodosa. Histologically there is necrotizing vasculitis of small vessels, with microinfarctions and microhemorrhages.

MRI may show any degree of small vessel disease, with involvement of both white and gray matter. Additionally, MRI may show small and larger infarctions. MRA is usually negative.

Behçet disease is a multisystem recurrent vasculitis of supposedly autoimmune origin, involving many organs. The original clinical triad of symptoms includes oral ulcers, genital ulcers, and anterior or posterior uveitis. The disease is frequently encountered in a specific geographic distribution extending from Japan to the eastern Mediterranean countries, passing through China and Iran: the area that was supposedly the ancient silk route. The disease mainly affects young adults. The female:male ratio is 11:1 in Turkey, less pronounced in other countries. In Turkey the prevalence is 80–300 per million inhabitants, whereas the prevalence is 1 per 100,000 in the USA.

Behçet disease is known to cause a variety of other manifestations, such as arthritis, arterial and venous thrombosis, pulmonary angiitis, cardiac disorders, cutaneous lesions, rectocolitis, and lesions of the CNS. CNS involvement is estimated to occur in 5–50% of the cases. Neurological manifestations occur in a wide variety of forms, due to the involvement of either the leptomeninges, the brain parenchyma, or the blood vessels. All sizes of blood vessels are involved, and arteries as well as veins. Clinically the CNS involvement becomes apparent as meningo-

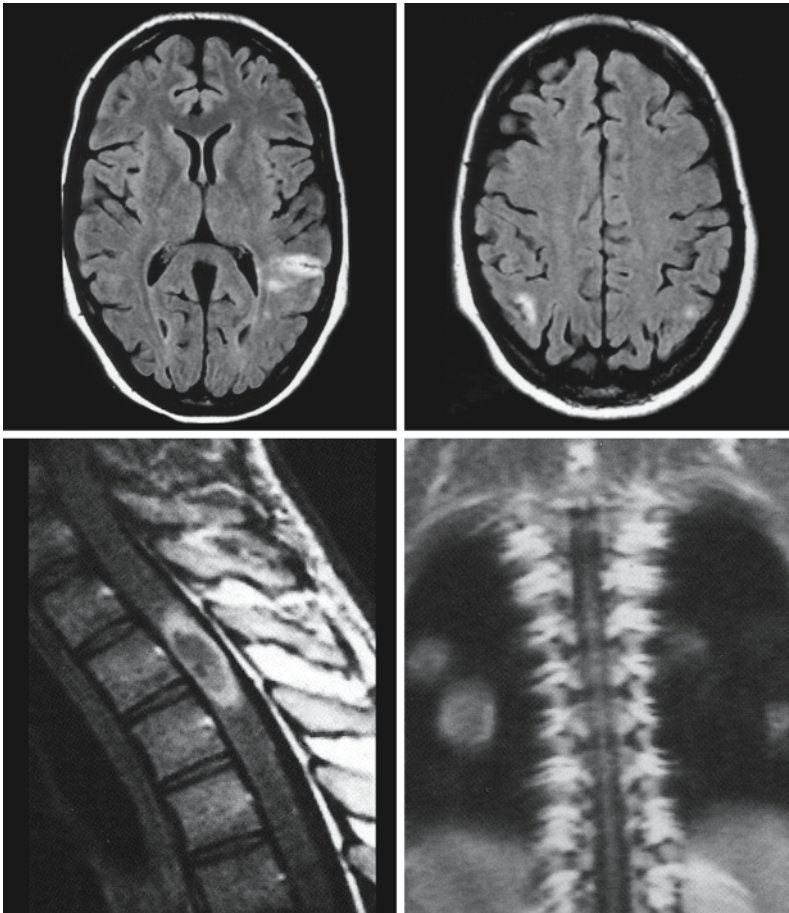


Fig. 100.15. A 9-year-old boy with Wegener disease. The FLAIR images through the brain show subcortical and cortical spots with hyperintensity. In the thoracic spinal cord there is an intramedullary lesion with ring enhancement and lower signal intensity in the core of the lesion. In the lungs there are multiple granulomas

cephalitis, cranial nerve palsies, cerebellar ataxia, spastic para- or tetraparesis, raised intracranial pressure, and dementia. Parenchymal CNS involvement occurs in the majority of the patients, predominantly in the basal ganglia and brain stem and spinal cord. CSF showed pleocytosis and elevated protein or an elevated CSF pressure.

The cause of Behçet disease is unknown. Viral and bacterial infections have been suggested, until now without sufficient evidence. It is widely assumed that Behçet disease is an autoimmune disorder, even though not all the facts agree with that view. Arguments against the autoimmune hypothesis are the male predominance, the lack of any specific antigen or antibody, and the lack of a relationship with HLA class II antigens. Genetic susceptibility, however, exists in some populations. In Turkey 84% of patients with Behçet disease are positive for HLA B51, which is not found in other populations.

Histologically the vasculitis in the CNS is characterized by perivascular cell infiltration, infarctions with small necrotic areas surrounding the blood vessels, microhemorrhages, loss of myelin, and gliosis. Behçet disease is unparalleled among the vasculitides

in its ability to attack blood vessels of any kind and any size, veins as well as arteries, with preference for certain organs. In the brain Behçet disease involves predominantly the white matter of the cerebral hemispheres, the basal ganglia, and the brain stem. Obstruction of arteries may lead to territorial infarcts; involvement of smaller vessels leads to small vessel disease and lacunar infarctions; thrombosis of venous structures may lead to venous infarctions or raised intracranial pressure.

MRI plays an important role in the diagnosis and follow-up of neuro-Behçet, and should aim at depicting the various forms of CNS involvement:

- White matter abnormalities often involve the cerebral hemispheres, with isolated and confluent lesions in the centrum semiovale and somewhat less prominent involvement of periventricular areas than in multiple sclerosis. However, they are often difficult to distinguish from multiple sclerosis.
- Lesions are often present in the basal ganglia, mid-brain, and pons; the brain stem lesions are more frequent, larger, and more extensive than in multiple sclerosis (Figs. 100.16 and 100.17).

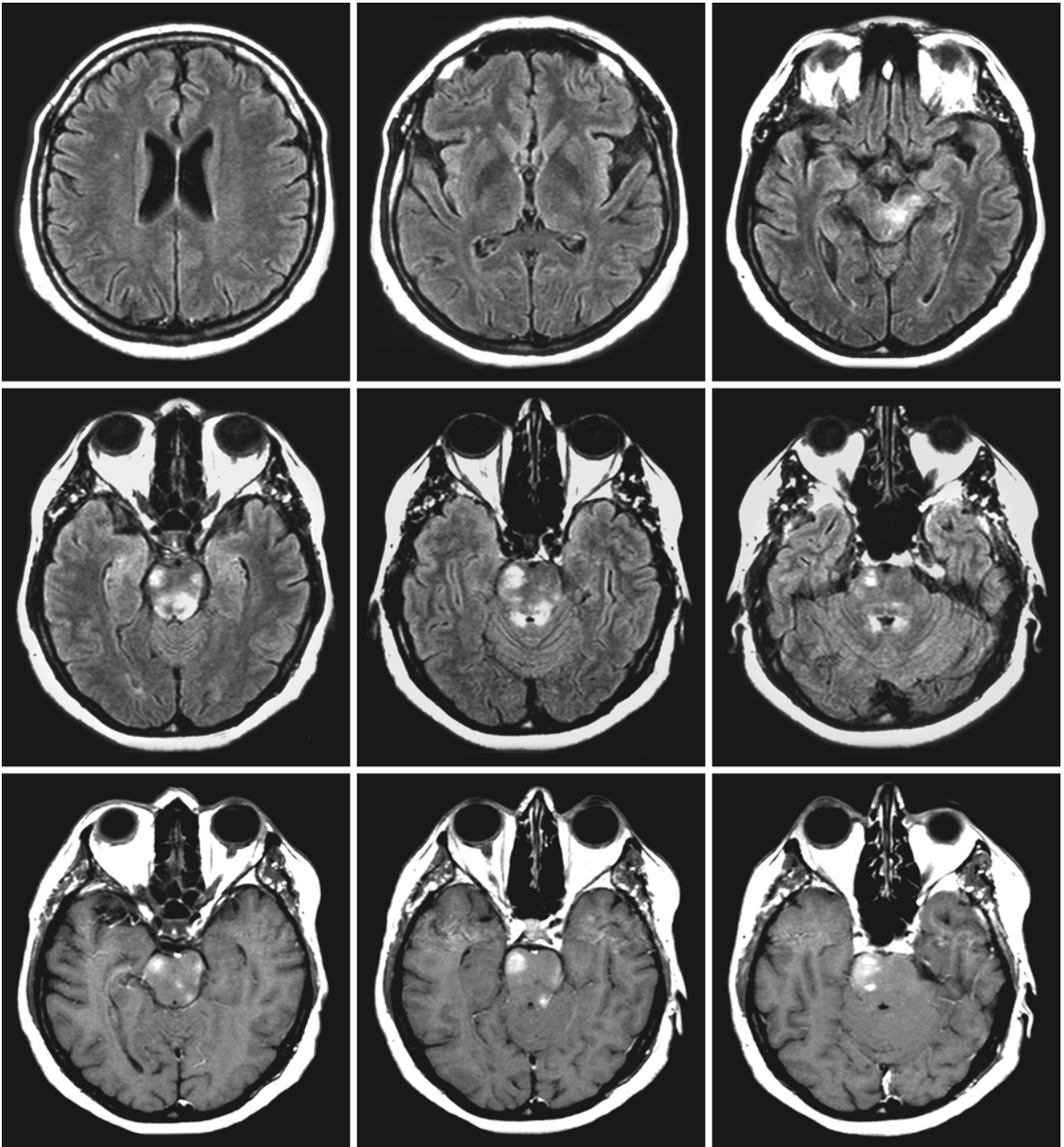


Fig. 100.16. Behçet disease may cause lesions anywhere in the brain, but most often involves the brain stem and basal ganglia in an asymmetrical fashion. The FLAIR images (*first and second rows*) of a 53-year-old woman depict the lesions in the midbrain, pons and around the fourth ventricle. Note the

enhancement of the lesions on the T₁-weighted images after contrast (*third row*). Courtesy of Dr. G. Akman-Demir, Department of Neurology, Medical Faculty, Istanbul University, Istanbul, Turkey

- Small, and occasionally large, infarctions may be present; diffusion-weighted images may be added to the usual protocol, which includes proton density, T₂-weighted, and FLAIR images, in order to catch fresh infarctions.
- Leptomeningeal involvement is especially to be expected in patients presenting with cranial nerve palsies and in those with meningoencephalitis; contrast administration and T₁-weighted images with fat suppression are required for adequate depiction.

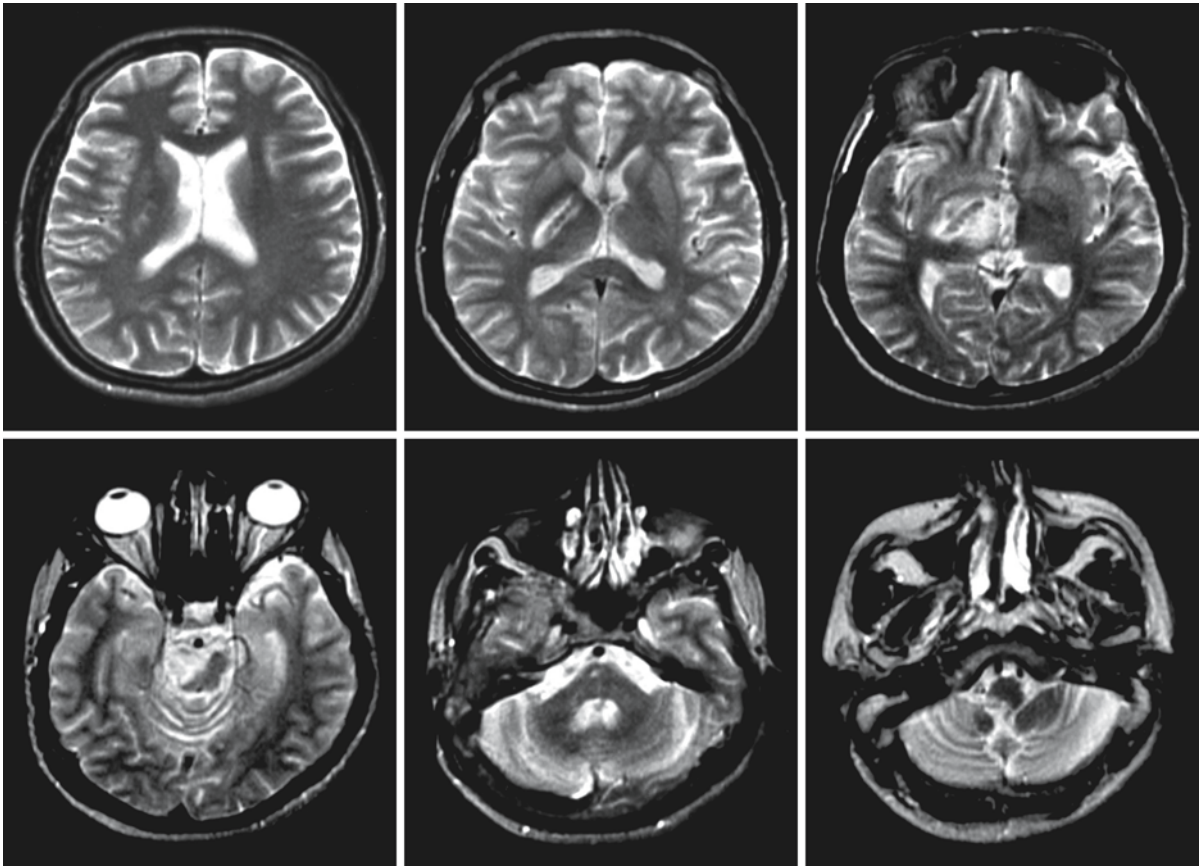


Fig. 100.17. A 28-year-old man with Behçet disease. Note the involvement of the internal capsule on the right, the midbrain and the medulla. Courtesy of Dr. G. Akman-Demir, Department

of Neurology, Medical Faculty, Istanbul University, Istanbul, Turkey

- Visualization of microhemorrhages, as often seen in pathological specimens, demands a gradient echo technique on MRI.
- In patients with raised intracranial pressure, thrombosis of the large venous sinuses has to be ruled out; on a T₁-weighted sagittal image this may already be obvious when the superior sagittal sinus is involved. Thrombosis of other intracranial veins can be made visible with MR phlebography.
- In patients presenting with large territorial infarctions MRA may show the occluded vessels.
- Spinal cord lesions will be visible on proton density and T₂-weighted images, and the spinal lesions will usually enhance after contrast injection, as will many of the intracranial lesions in Behçet disease (Fig. 100.16).

Therapy in Behçet disease may be topical when oral aphthae and genital ulcers are concerned. More extensive systemic involvement usually requires corticosteroid and immunosuppressive therapy.

100.2.2.3 Infectious Vasculitis

A number of infectious disorders may give rise to vasculitis and related cerebral lesions. *Lyme disease* (neuroborreliosis) is an infectious disease caused by *Borrelia burgdorferi*, which may affect many organs, such as skin (90% of all patients), joints, heart, CNS, and PNS. The first manifestation is often a skin lesion, known as erythema (chronicum) migrans. This may be followed by bacterial dissemination, presenting initially as a flu-like disorder, with fever, malaise, and diffuse pain. About 15% of patients subsequently develop one or more features of CNS involvement: lymphocytic meningitis (in the USA) or meningoencephalitis (in Europe), uni- or bilateral facial paresis (to be differentiated from neurosarcoidosis and Guillain-Barré syndrome), and polyradiculitis (which may mimic Guillain-Barré syndrome). In a minority of patients focal encephalomyelitis will develop with prominent white matter involvement on MRI.

In untreated or unsuccessfully treated patients, late neurological symptoms may develop, which include chronic encephalomyelitis, with focal neurological

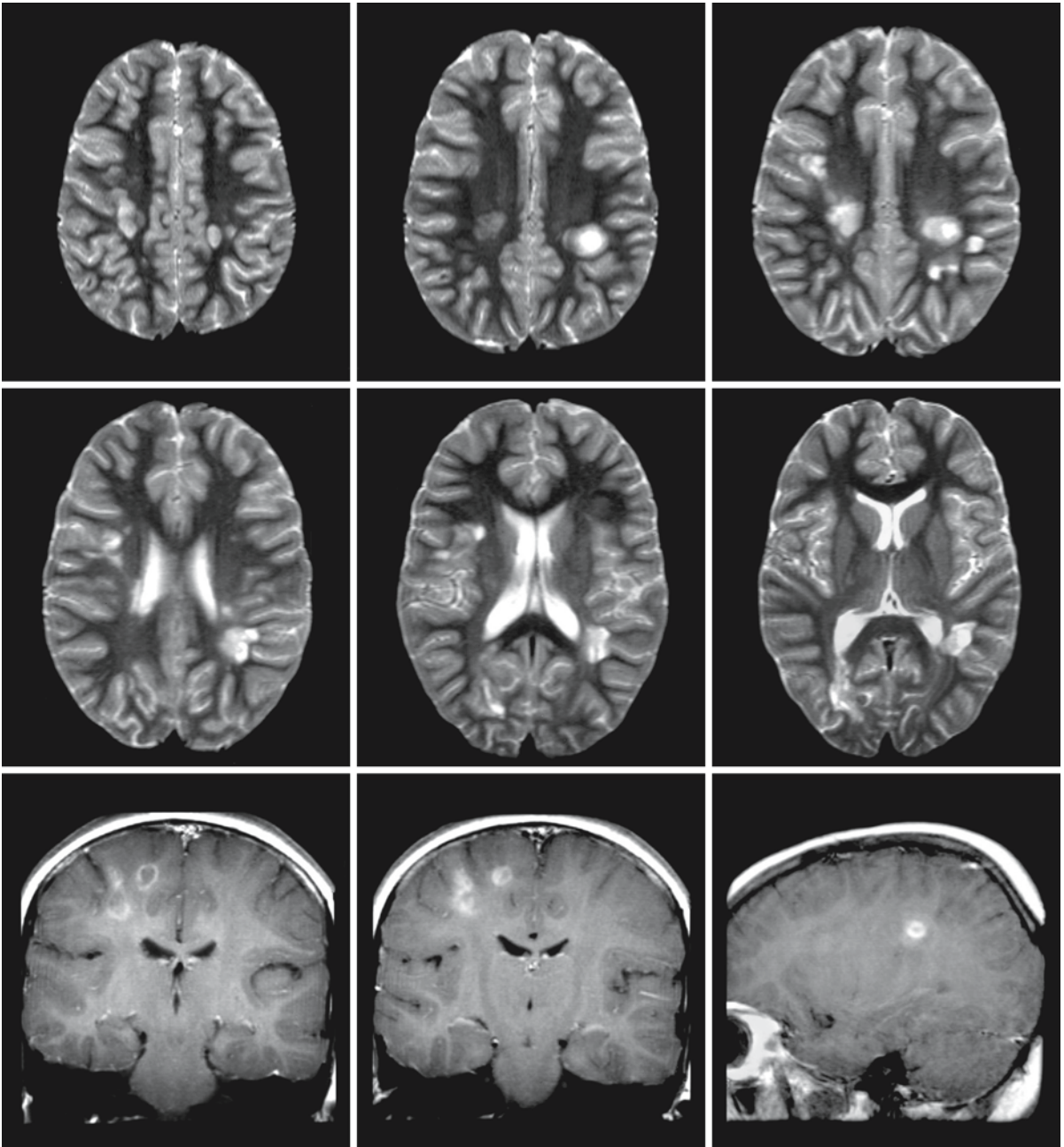


Fig. 100.18. Images of a 10-year-old girl with neuroborreliosis. The T_2 -weighted images show multiple lesions of different sizes, asymmetrically spread through the centra semiovalia of both hemispheres. The T_1 -weighted, contrast-enhanced images in the coronal and sagittal planes show that several

lesions enhance. These images do not allow differentiation from acute disseminated encephalomyelitis (ADEM) or multiple sclerosis. From Demaerel et al. (1995), with permission and by courtesy of Dr. P. Demaerel, Department of Radiology, University Hospitals Gasthuisberg, Leuven, Belgium

abnormalities and also focal abnormalities on MRI. A chronic infection may lead to confusional states, with memory loss and cognitive impairment. Due to limitations in diagnostic technology, Lyme disease is still primarily a clinical diagnosis, usually accepted only when the antecedents of the patient include a tick-

bite, erythema migrans, and one or more of the manifestations within the scope of Lyme disease.

The cause of Lyme disease is an infection by a member of a group of spirochetes, originally named *Borrelia burgdorferi*, now referred to as *Borrelia burgdorferi sensu lato*, subdivided into at least three

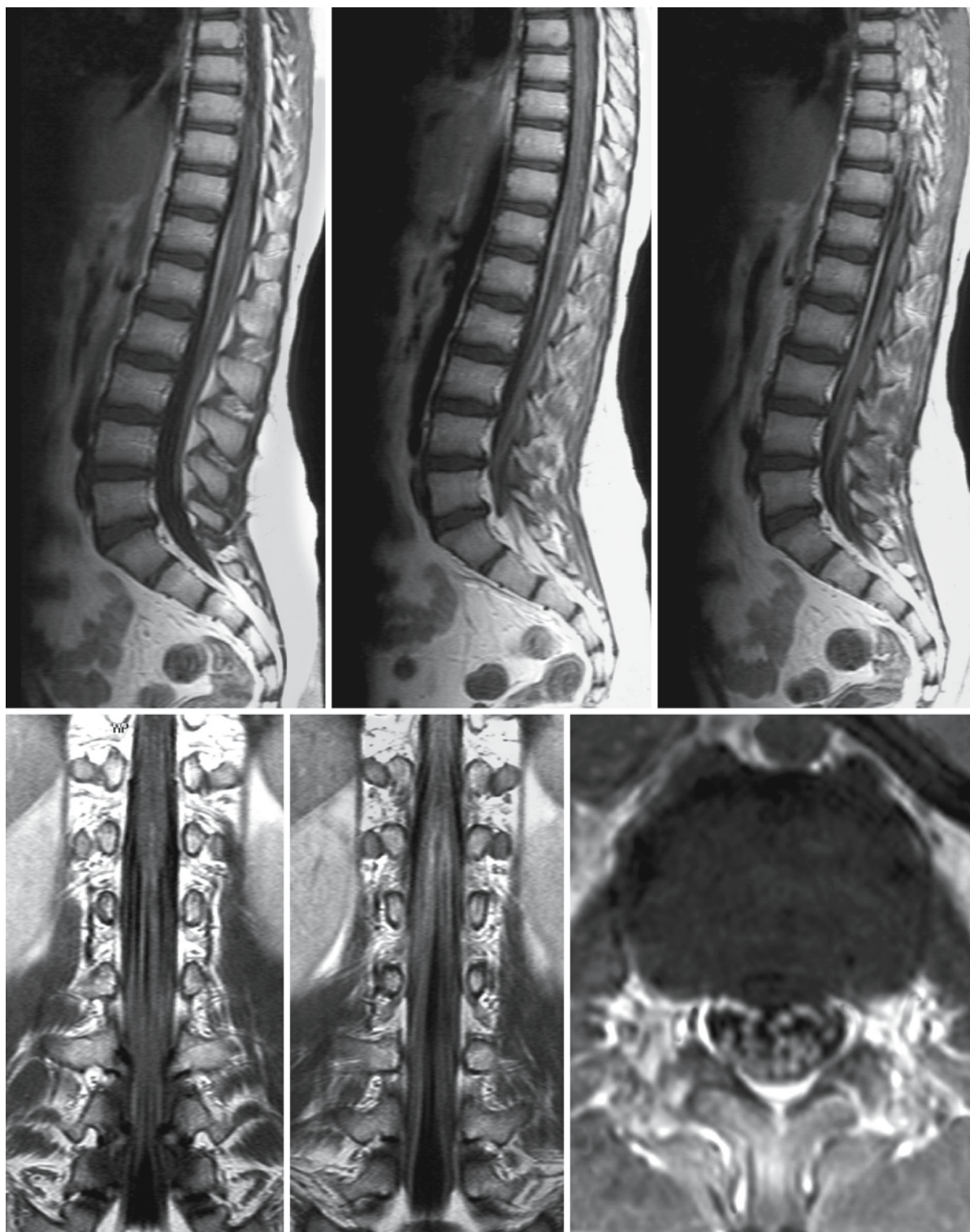


Fig. 100.19. A 10-year-old boy with Lyme disease presented with low back pain radiating to his legs. The T₁-weighted, contrast-enhanced sagittal images (*first row*) of the lower thoracic and lumbar spine show the enhancing and thickened caudal roots. In the coronal plane (*second row, left and middle*) and

transverse plane (*second row, right*) the enhancement and thickening of nerve roots is confirmed. From Demaerel et al. (1998), with permission and by courtesy of Dr. P. Demaerel, Department of Radiology, University Hospitals Gasthuisberg, Leuven, Belgium

species: *Borrelia burgdorferi* sensu stricto, *Borrelia burgdorferi garinii*, and *Borrelia burgdorferi afzelii*. The first group is responsible for the North American Lyme infections, the latter two for the European forms, which have some differences in clinical features. The disease is a zoonosis, with humans as inadvertent host. The disease is transmitted to humans by a bite from the hard-shelled ixodid ticks. These ticks are especially abundant in areas where the ecological circumstances, climate, food, and the different vectors for their procreation are present. The life cycle of the ticks runs a three-phase course over a 2-year cycle. Even in areas with a high proportion of infected ticks only 1–2% of humans with a tick bite will become infected.

Diagnosis of Lyme disease is not straightforward. Serological tests take a long time and may be unreliable because of crossover reactions, which can lead to false positives. CSF examination may be positive for inflammatory markers, pleocytosis, slight rise in protein, and usually normal glucose. A test can be performed to show anti-*Borrelia* antibodies with a Lyme-specific ELISA. PCR may be applied to detect bacterial DNA.

There is no specific MR pattern of Lyme disease. There may be many small lesions dispersed through the hemispheres, sometimes very similar to the pattern of multiple sclerosis (Fig. 100.18). Lesions in the corpus callosum are less common. After injection of contrast, active lesions may enhance (Fig. 100.18). Special techniques should be used to image the cranial nerves when involved; in the active phase these will also enhance. Leptomeningeal enhancement may occur in patients with meningoencephalitis, but in our experience this is rare in the chronic form. Lesions in the spinal cord and involvement of nerve roots may also occur (Fig. 100.19).

Antibiotic therapy is effective when given appropriately and cures up to 90–95% of patients. In patients with chronic disease the percentage is lower, 80–85%.

Tuberculosis is caused by *Mycobacterium tuberculosis*. Involvement of the brain is usually due to hematogenous spread from a primary focus, in most cases the lungs. Intracranial manifestations include extension of a subpial or subependymal focus, resulting in involvement of the basal leptomeninges, which causes basal leptomeningitis. Occlusion of the CSF pathways leads to hydrocephalus. The infection may also induce vasculitis of the smaller and middle-sized cerebral arteries, often the lenticulostriate arteries or the posterior cerebral artery branches, the thalamoperforate arteries, leading to small infarctions in the basal ganglia and deep white matter. Multiple miliary abscesses may also occur, as well as tuberculous intraparenchymal granulomas (tuberculomas), cerebritis, larger abscesses, and pachymeningitis. Spinal cord

infection is less common, but arachnoiditis and focal intramedullary tuberculomas may occur. Tuberculous spondylitis may lead to secondary involvement of spinal cord and roots. Because of migration of individuals from regions in the world where tuberculosis is still endemic and the higher incidence of cases in immunocompromised individuals, one should be aware of the possibility of a tuberculous infection.

The demonstration of *Mycobacterium tuberculosis* or bacterial DNA in the body fluids or biopsy material makes a certain diagnosis. Brain involvement is often secondary to a pulmonary infection. Indirect markers are pleocytosis in the CSF, high protein and low glucose levels and presence of indicators of inflammation in the plasma. Often CSF has transformed into a thick, yellowish fluid, which may be the cause of a communicating hydrocephalus.

Histologically, the different forms of tuberculosis of the brain and meninges have different aspects. Tuberculomas occur in the brain parenchyma and in the leptomeninges and choroid plexus. The larger tuberculomas have a granulomatous border, often with Langhans giant cells, encompassing a central caseating necrosis. They are usually small and multiple, but incidentally may become larger and have mass effect. Leptomeningeal tuberculosis can consist of isolated tuberculomas of varying size, often associated with tuberculomas in the brain tissue. A second form appears as generalized meningitis, presenting as a grayish, gelatinous, thick exudate, predominantly at the base of the brain. The exudate consists of polymorphonuclear cell infiltrations, fibrin exudation, endarteritis, hemorrhages and caseous necrosis. Perivascular intraparenchymal inflammatory extensions are frequent and hemorrhagic infarctions may ensue.

MR images, standard morphological and T₁-weighted images with and without contrast, where available with fat suppression, depict the described manifestations and secondary effects (Fig. 110.20). MRA demonstrates the affected vessels. Diffusion-weighted imaging will show infarction or abscesses.

Therapy consists of tuberculostatic medication and necessary supplements.

Syphilitic angiitis is caused by a spirochete, *Treponema pallidum*, and presents clinically as a multi-system infection. Neurosyphilis is one of its manifestations. Neurosyphilis can be classified into distinct syndromes that span all stages of dissemination of the disease.

In the first phase the local genital infection and skin abnormalities prevail, but a meningeal syphilitic infection at the onset may lead to cranial nerve palsies and ocular changes. Four to 7 years after the primary infection, a meningovascular syphilis may develop, with focal nervous system ischemia, secondary to thrombosis. Parenchymatous manifestations of neurosyphilis occur 10–30 years after the primary infec-

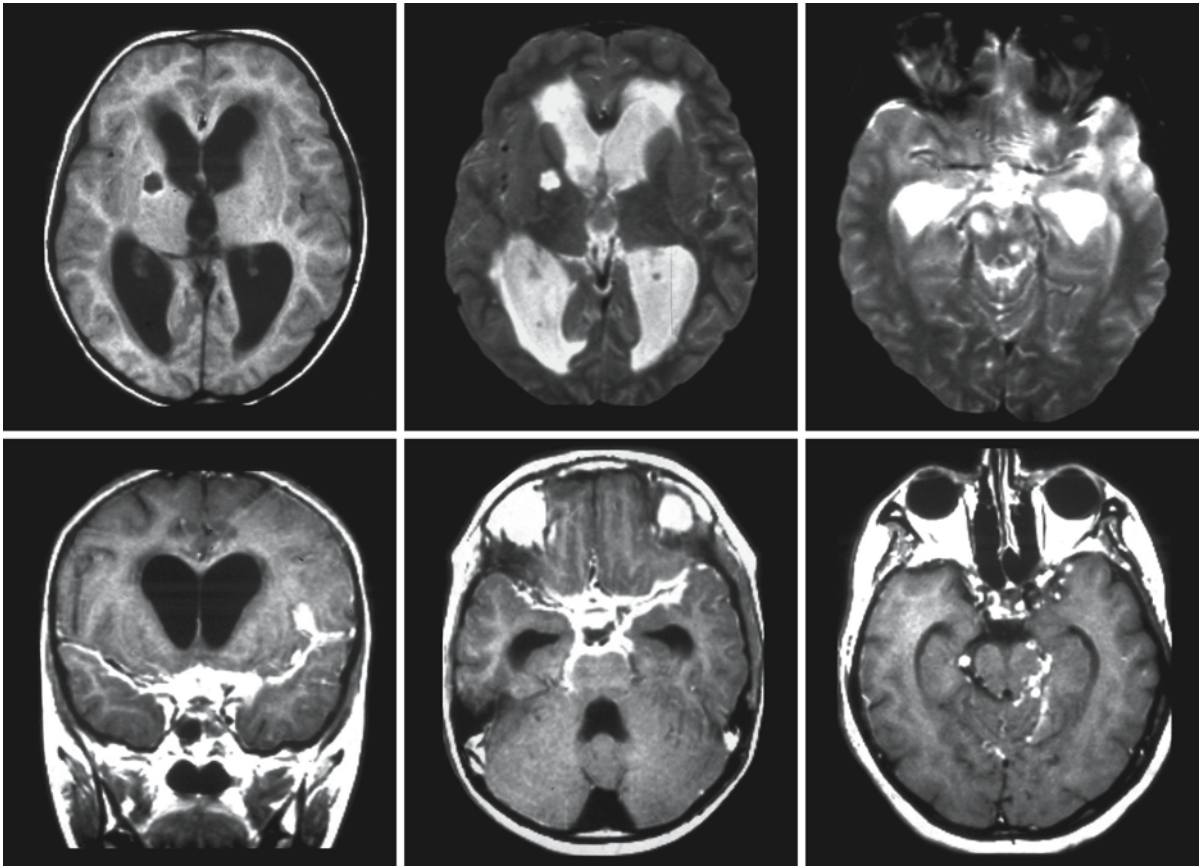


Fig. 100.20. Tuberculous meningoencephalitis. The *first row* shows one T₁-weighted and two T₂-weighted images; the *second row* shows T₁-weighted images with contrast. The images in the *first row* show ventriculomegaly and periventricular

leukomalacia. Focal lesions are seen in the basal ganglia and mesencephalon. The contrast-enhanced images show the typical basal leptomeningitis

tion with general paresis or tabes dorsalis. In this late phase other parenchymatous lesions, gummata, or cranial nerve involvement, hearing loss, or optic neuritis may occur. In this late phase cognitive decline, delusions, and paresis are part of the clinical picture, although nowadays, because of proper treatment, rarely observed. In combination with HIV infection, the neurological manifestations of neurosyphilis occur at an earlier date, accelerate faster, and are more severe.

The gold standard for the diagnosis is the demonstration of spirochetes by dark-field examination, which is easy when skin or genital lesions are present. In neurosyphilis this is more difficult and the diagnosis is suggested by clinical findings, medical history, and CSF analysis. Serological studies can confirm the diagnosis. *Treponema* tests include the fluorescent treponemal antibody absorption double staining hemagglutination test, and the *Treponema* immobilization test. Nontreponemal tests, such as the Venereal Disease Research Laboratory (VDRL) test and the

rapid plasma reagin (RPR) test, are more sensitive than specific. False positive results can be obtained in SLE, herpes simplex infections, pregnancy, and Lyme disease.

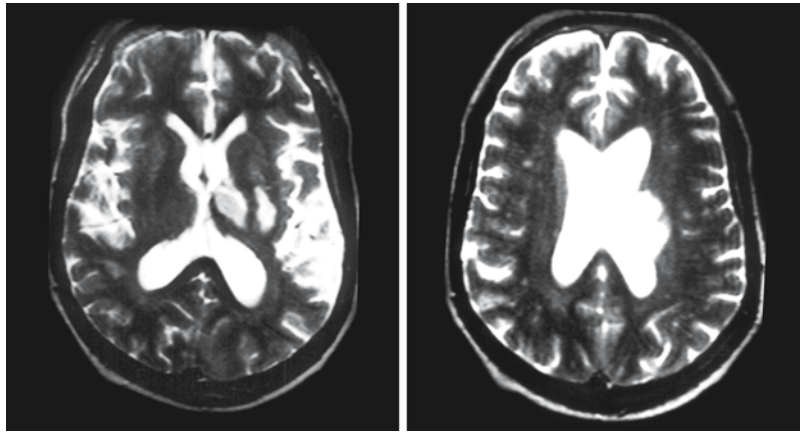
Pathophysiologically the infection leads to an obliterative endarteritis of terminal arterioles, resulting in inflammatory and necrotic lesions.

MRI is not specific in cases of neurosyphilis. Contrast-enhanced T₁-weighted images show the leptomeningitis, infarctions, and gummata when present. In HIV-positive patients the diagnosis may be even more difficult.

When treated in time the infection can be cured. Various regimes of antibiotics are now available. In patients with HIV, however, treatment failure is frequent.

Varicella-zoster complications stem from infection with the varicella-zoster virus, a virus that occurs exclusively in humans and causes chickenpox (varicella). It then becomes latent in cranial nerve and dorsal root ganglia, and frequently reactivates decades later

Fig. 100.21. Left-sided infarction of the brain following left-sided herpes zoster ophthalmicus



to produce shingles (herpes zoster) and postherpetic neuralgia. Latency depends on age of the virus and immune status of the patient. The reactivated virus may cause symptoms in elderly immunocompetent individuals or in immunocompromised patients and may produce disease of the brain and spinal cord. Recently varicella-zoster virus has been detected in blood vessels and other tissues by PCR, and this has widened the clinical spectrum of acute and chronic disorders ascribed to varicella-zoster virus, including large vessel granulomatous arteritis, myelitis, and small vessel encephalitis, all of which may occur without the rash typical of varicella-zoster.

Varicella-zoster becomes latent in ganglia along the entire neuraxis. Unlike herpes virus, it cannot be cultivated from human ganglia. With special techniques, such as in situ hybridization, Southern blot, and PCR analysis, viral DNA has been found in trigeminal and thoracic ganglia. Early reactivation of the virus after chickenpox with an interval of only several months, associated with granulomatous arteritis of the medium-sized vessels, may be seen in children presenting with an infarction. These infarctions may be located in the posterior fossa, with basilar artery arteritis, or, more often, in the carotid artery territories, causing either larger territorial infarctions or infarctions in the territories of the lenticulostriate arteries. Myelitis in immunocompetent individuals is usually less severe than in immunocompromised patients. In the latter group small vessel encephalitis may develop, with poor prognosis.

MRI is not specific in varicella-zoster vasculitis, but may show resulting infarctions. MRA may indicate the affected middle-sized vessels.

There is no curative therapy for the vasculitis, which is in most cases self-limiting. Supportive measures depending on the neurological symptoms are indicated.

Delayed contralateral hemiplegia following *herpes zoster ophthalmicus* tends to occur in middle age

(mean age 55 years, range 7–96 years). The hemiplegia occurs one week to 2 years after the onset of the herpes zoster ophthalmicus. Delayed hemiplegia following herpes zoster ophthalmicus has often been considered to be the equivalent of granulomatous angiitis. Sufficient clinical differences, however, exist to justify the assumption of two distinct entities. Symptoms tend to be milder in this disorder than in primary granulomatous angiitis of the nervous system. Most patients with this disorder survive, even without steroids.

Microscopic tissue examination reveals the same histological abnormalities in both disorders.

MRA is nonspecific, but will show the unilateral involvement of the brain (Fig. 100.21).

100.2.2.4 Drug-Related Vasculitis

There is a long list of drugs that may cause drug-induced vasculitis, including therapeutic and diagnostic pharmaceuticals and substances used in drug abuse. To the first category belong, among many others, allopurinol, amphetamine, ergot alkaloids, ephedrine, ginseng, interleukin-2, methylphenidate, oxymethazoline, penicillin, and hepatitis B vaccine. To the second category belong cocaine, heroin, methylphenidate, and methamphetamines. In many cases of the first group the vasculitis is restricted to the skin, but extension to other organs is very well possible. Extension to the brain is rare.

Cocaine may lead to vasculitis, vasospasm, and increased platelet aggregation resulting in infarctions (strokes), leukoencephalopathy, and hemorrhages. Chronic cocaine dependency has also been linked to a moyamoya-like vasculopathy, with obstructed vessels and extensive collateral circulation, in particular the basal ganglia. The risk of myocardial infarction is increased in young individuals using cocaine.

In heroin abuse strokes and hemorrhages are less frequent than in cocaine abuse. A spongiform leukoencephalopathy is far more frequent in heroin

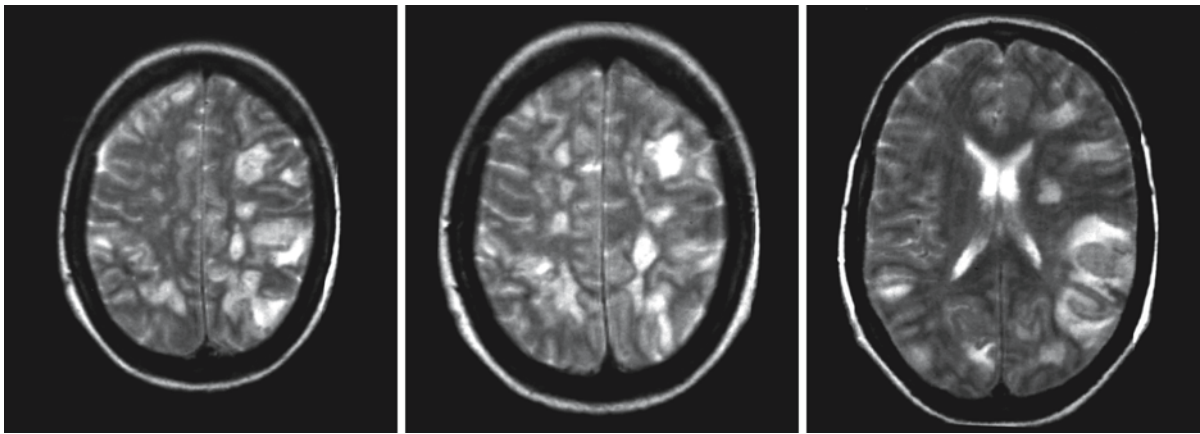


Fig. 100.22. A 43-year-old woman presenting with a series of transient ischemic attacks, all related to different brain localizations. T₂-weighted images of the brain show multiple lesions of different sizes involving cortex and subcortical white

matter and deep white matter. This pattern can be seen in intravascular coagulation, for example in sepsis, but also in intravascular metastases. In this case the cause was intravascular lymphomatosis

abuse (see Chap. 87), but has occasionally been described in cocaine abuse.

MRI patterns in drug-related vasculitides are inconsistent and depend on the vessels involved. Lesions will usually have the features of infarctions. Diffusion-weighted imaging, therefore, should be part of the MR protocol.

100.2.3 Disorders Primarily Obstructing the Vessel Lumen

Hypercoagulable states. There are a number of inherited and acquired disorders that lead to a change in the complex process of coagulation, which may invoke hemorrhages when hemostasis is insufficiently controlled or thrombosis with obliteration of vessel lumina when coagulation surpasses its necessary biological function and causes unsolicited thrombosis. Such inherited factors are: elevated von Willebrand factor, factor V Leiden, fibrinogen polymorphisms, protein C and protein S deficiencies, and many others. In various conditions hypercoagulation may be induced by changes in the blood composition, as may happen in cancer patients, and in postoperative and post-traumatic conditions with extended immobilization. The resulting lesions will occur in unpredictable places and therefore neurological signs and MR findings are not specific.

Intravascular lymphomatosis (IVL) is a very rare non-Hodgkin lymphoma characterized by proliferation of lymphoma cells in the vascular lumina, both arterial and venous, without involvement of adjacent parenchymal tissue. IVL with cerebral involvement is predominantly of B cell lineage. Patients with cerebral

IVL have been described in the age range of 30–80 years. The clinical signs and symptoms of IVL may mimic those of vasculitis, and the cerebral form has a variable presentation. Often there are stroke-like episodes or repetitive transient ischemic attacks. Focal cortical symptoms, confusion, disorientation, dementia, and seizures may follow. Meningoencephalitis-like presentation has also been described.

Proper diagnosis is important, because IVL is a treatable condition and early diagnosis may prevent irreparable damage. Manifestations in other organs – skin or lungs, for example – anemia, and high erythrocyte sedimentation rate may help to arrive at the correct diagnosis. Usually the diagnosis can be made by examination of blood or bone marrow samples, biopsies of skin lesions, or bronchial lavage in pulmonary manifestations.

Cerebral manifestations as seen on MRI include infarct-like lesions dispersed throughout the brain (Fig. 100.22), venous occlusion of the large sinus or cortical veins with venous infarctions, and enhancement of leptomeninges after contrast injection. Diffusion-weighted imaging may help to indicate the nature of the cerebral lesions and identify them as infarctions. MRA may show abnormalities of arteries but is not diagnostic. In cases where there is venous involvement, MR phlebography is useful to show the obstructed veins.

Treatment consists of polychemotherapy.

The name of *sickle cell disease* stems from the abnormal form of the red blood cells, which look like crescents. It is an autosomal recessive disease which has its highest incidence in Africa. It is caused by a defect in the β -hemoglobin gene. Sickle cell anemia will develop in homozygously affected individuals. Het-

erozygous carriers will have some abnormal erythrocytes, but symptoms will be only precipitated under conditions with low oxygen tension, such as in high-lying geographical regions. Sickle cells are less prone to parasitic (malarial) infection than normal blood cells. It is hypothesized that in former centuries carriers of sickle cell disease were more likely to survive malaria and were responsible for the recurrence of sickle cell carriership in subsequent generations. Today the disease affects 1 in 500 newborns with Afro-American parents and 1 in 1000 newborns with Hispano-American parents in the USA. The disease is found everywhere in Africa, throughout Middle and South America and Cuba, and in Mediterranean countries such as Italy, Greece, and Turkey.

The clinical picture is highly variable, as many different organs may suffer ischemic insults. The nature of the disease, however, is such that it often causes cerebrovascular accidents. Sickle cell disease is one of the many sources of watershed and arterial territorial infarctions in children and relatively young adults. Neurological symptoms depend on the location of the infarctions.

At the molecular level sickle cell anemia is caused by a single base mutation leading to the substitution of valine for glutamic acid at position 6 of the β -hemoglobin molecule. Homozygously affected individuals have abnormal hemoglobin, hemoglobin S. Under circumstances with low oxygen tension and acidosis the abnormal hemoglobin molecules polymerize, resulting in increased cell rigidity and the characteristic sickle shape. This leads to sludging in smaller vessels and to hemolysis. The majority of strokes occur in younger patients. Many factors can precipitate stroke, such as dehydration, pregnancy, low hematocrit value, cardiomegaly, and abnormal liver functions.

Sickled cells are less flexible, which slows their passage through the vessels. The red blood cells containing the abnormal hemoglobin S seem also to be abnormally adherent to the endothelium. Because of the stasis, platelets will also become more adherent, and fibrin deposition follows, with subsequent occlusion of the lumen. Ischemic infarctions account for 70% of cerebrovascular episodes, and these infarctions are most often caused by occlusion of large arteries at the base of the brain. Occlusion of smaller vessels most often involves smaller cortical branches.

On MRI lesions may include small, disseminated infarctions, border zone or territorial infarctions, and in rare cases thrombosis of the large venous sinuses. MRA may show obstructed vessels.

The anticancer drug hydroxyurea has given patients with sickle cell disease some hope. It was found that taking this drug caused an increase in the production of fetal hemoglobin, which is normally present only in newborns. The presence of sufficient fetal

hemoglobin causes the red blood cells to stop sickling. It has been proven effective in preventing crisis. The long-term side effects of this medication are, however, still unknown. Animal experiments with gene replacement of the defective gene have given new hope.

100.3 Magnetic Resonance Imaging

Vasculitis can lead to a wide variety of MRI patterns. The lesions can be focal, asymmetrically distributed throughout the brain parenchyma, sometimes mimicking multiple sclerosis, or lesions can be more confluent. Infarctions may occur in vascular territories or border zones, or they may present as small lacunar infarctions. Involvement of the basal ganglia, thalamus, midbrain, pons, medulla oblongata, and leptomeninges is often seen. Lesions may become hemorrhagic and macro- and microhemorrhages may occur. With cortical and leptomeningeal localizations superficial hemosiderosis may follow. In later phases of the disease atrophy may become apparent.

It is evident that the MRI pattern of vasculitis is not specific. Disorders which may share this gamut of MRI patterns include multiple sclerosis, acute disseminated encephalomyelitis, extrapontine myelinolysis, progressive multifocal leukoencephalopathy, radiation vasculopathy, subcortical arteriosclerotic encephalopathy (Binswanger disease), eclampsia, neoplasms and emboli. Clinical and laboratory data are helpful in further differentiation of these disorders.

Some of the vasculitic disorders may present with a more characteristic MRI pattern. Vasculitis in SLE can lead to extensive calcifications, which may be prominent in the basal ganglia, the geniculate bodies, and the dentate nucleus. On T_1 -weighted images this may lead to high signal intensity in the involved areas, sometimes blotting out the basal ganglia. This phenomenon may also be seen in such disorders as hypoparathyroidism, pseudo-hypoparathyroidism, liver failure, and parenteral nutrition. The signal intensity on T_2 -weighted images is decreased. These calcifications are largely symmetrical, but there seem to be exceptions to this rule.

An MRI protocol covering the features of vasculitis should include T_1 - and T_2 -weighted, FLAIR images, and diffusion-weighted imaging (Trace images and ADC maps). In addition gradient echo images are mandatory to note the hemosiderin deposits, which are ubiquitous in most cases of vasculitis. MRA can be helpful, but a contrast-enhanced high-resolution (512×512) sequence should preferably be used. We prefer slow machine injection of 15–20 ml contrast, about 1 ml per second, followed by 20 ml of saline, during the MRA acquisition, with a presaturation slab

blocking the larger venous sinuses. With this protocol, MR images will show the central cerebral vessels as well as their second and third ramifications. After this procedure a contrast-enhanced, fat-suppressed, T₁-weighted image is obtained in at least one direction to identify enhancement of lesions, a frequent observation in vasculitis.

When unusual MR patterns are present, vasculitis should be always be considered a possible cause, especially with clinical suspicion. The combination of MRI findings with the clinical and laboratory data

may lead to the correct diagnosis. It should be noted that in most of the vasculitic disorders, but in particular in SLE and Behçet disease, mild to extensive white matter disease can be found in absence of clinical neurological abnormalities. The reverse is also true: in SLE, despite evident neurological manifestation, the findings at MRI and autopsy may be disappointing. Quantitative estimation of CNS involvement may be reached by magnetization transfer ratio histogram analysis, diffusion tensor imaging, ADC mapping, and MRS.

Leukoencephalopathy and Dural Arteriovenous Fistulas

R. van den Berg, G.J. Lycklama à Nijeholt, and J.M.C. van Dijk

101.1 Clinical Features and Laboratory Investigations

Cranial dural arteriovenous fistulas (DAVFs) represent 10–15 % of all intracranial arteriovenous lesions. The exact etiology of cranial DAVFs is still unknown. Development of DAVFs has been described after surgery, head trauma, and in relation to dural sinus thrombosis. In adults, it is generally accepted that DAVFs are acquired conditions. Pediatric cases are rare; DAVFs have infrequently been demonstrated in utero and may be present in neonates, associated with a dural sinus malformation.

Clinical symptoms of DAVFs are related to the fistula itself, e.g., pulsatile tinnitus, or to the venous hypertension in the involved venous territory. The clinical symptomatology and the risk of aggressive complications, such as intracranial hemorrhage, correlate directly with the venous drainage pattern of DAVFs. Depending on the venous drainage and the flow characteristics, DAVFs may cause orbital symptoms including exophthalmia and cranial nerve deficits. A focal area of cortical venous reflux – retrograde drainage in a cortical leptomeningeal vein – may cause focal neurological deficits, such as aphasia or motor weakness. DAVFs can also cause remote symptoms. Lesions located in the cavernous sinus, tentorium, and foramen magnum can cause venous congestion of the brain stem or spinal cord with related symptomatology. The retrograde transmission of the arterial pressure in a more extensive venous network, in combination with impaired venous outflow through the sinuses, may lead to venous hypertension, resulting in CSF absorption abnormalities and papilledema. These venous pressure disturbances may lead to symptoms of parkinsonism, such as rigidity, bradykinesia, and gait disturbances, and global cognitive dysfunction with dementia as the most severe presentation.

The presence of cortical venous reflux in cranial DAVFs carries an annual mortality rate of 10.4 %. The annual risk of hemorrhage is estimated to be 8.1 % per year. The risk of nonhemorrhagic neurological deficit is 6.9 % per year. The annual event rate for patients with aggressive DAVFs is therefore 15 %.

101.2 Pathology

Histopathologically, DAVFs are located within the wall of the sinus. The fistula itself has no intervening capillary bed or nidus and consists of small venules. Intimal hyperplasia of both dural arteries and veins is noticed. The arterioles show hypertrophied walls, mainly characterized by media hyperplasia. Organized thrombi have been demonstrated in the dural sinuses in up to 100 % of cases.

Immunohistochemically, DAVFs show strong staining for basic fibroblast growth factor (bFGF) in the subendothelial layer and hypertrophied media of the arteries in the sinus wall and in the fibrous connective tissues around the sinuses, sparing the endothelium. Vascular endothelial growth factor (VEGF) stains positively in the endothelium of the dural sinus, small arteries, and veins in the sinus walls. In addition, VEGF stains positively in the endothelium of many capillaries in the sinuses that are obstructed by an organized thrombus. No such findings are encountered in dural sinuses of control specimens. The factors stimulating bFGF and VEGF are not known, but it is postulated that tissue hypoxia and or intraluminal shear stress resulting from venous hypertension stimulates the expression of these angiogenic growth factors.

The acute and chronic parenchymal abnormalities in the case of cortical venous reflux (aggressive type of fistulas) are related to venous hypertension. Acute changes include diffuse cerebral edema and petechial hemorrhages within the gray and white matter. Chronic changes include markedly dilated and thickened, hyalinized walls of the parenchymal veins. Gliosis may occur within the white matter.

101.3 Pathogenetic Considerations

The association of DAVFs with venous thrombosis has been described frequently. Another important factor contributing to the development of DAVFs is venous or sinus hypertension. Sinus thrombosis does not always lead to the development of DAVFs, and it has been stated that venous hypertension is a prerequisite for formation of a DAVF, even in the absence of sinus thrombosis. DAVFs have also been reported to develop following intracranial surgery, trauma, surgery in remote areas of the body, and in the post-

Table 101.1. Classification of cranial dural arteriovenous fistulas

Borden classification	
1.	Venous drainage directly into dural venous sinus or meningeal vein
2.	Venous drainage into dural venous sinus with cortical venous reflux
3.	Venous drainage directly into subarachnoid veins (only cortical venous reflux)
Cognard classification	
I.	Venous drainage into dural venous sinus with antegrade flow
IIa.	Venous drainage into dural venous sinus with retrograde flow
IIa-b.	Venous drainage into dural venous sinus with retrograde flow and cortical venous reflux
IIb.	Venous drainage into dural venous sinus with antegrade flow and cortical venous reflux
III.	Venous drainage directly into subarachnoid veins (only cortical venous reflux)
IV.	Type III with venous ectasias of the draining subarachnoid veins

partum period. The wide variety of etiological factors should not be regarded as direct causes of DAVFs; rather, they represent environments that may be conducive to the development of a DAVF in particular patients.

Two principal theories on the pathogenesis of DAVFs have been proposed. The first claims that DAVFs are caused by enlargement of preexisting microfistulas in the dura. These microfistulas enlarge because of increased venous pressure, associated either with sinus thrombosis or with sinus outflow obstruction. The second theory points to the development of angiogenic factors, such as the above mentioned bFGF and VEGF, either directly from the organization of a sinus thrombosis or indirectly from local tissue hypoxia due to an increased venous pressure.

Many classifications have been proposed for DAVFs, of which the Borden classification and the Cognard classification are most commonly used. The common concept of both classifications is to differentiate between DAVFs with antegrade drainage in the dural sinus (benign type: Borden 1, Cognard types I and IIa), and DAVFs with cortical venous reflux (aggressive type: Borden 2 and 3, Cognard type IIb and higher) (Table 101.1). The importance of the venous drainage pattern lies in the correlation with clinical symptomatology and the risks of hemorrhage. The retrograde transmission of the arterial pressure in the venous network leads to venous hypertension and congestion and impairs parenchymal venous

drainage. This causes chronic (venous) ischemia. In those cases where extensive reflux is seen in combination with impaired venous outflow through the sinuses, venous pressures can rise to very high levels.

101.4 Therapy

The natural history of the disease is related to the venous drainage pattern of the DAVF. DAVFs with antegrade drainage only present with focal symptoms due to the fistula itself, and morbidity and mortality are limited. In these cases treatment should aim only at diminution of the focal symptomatology. DAVFs with cortical venous reflux, however, may lead to severe complications and require aggressive treatment. Disconnection of the cortical venous reflux is obligatory to protect the patient from sequelae such as intracranial hemorrhage and nonhemorrhagic neurological deficits. Partial treatment will not reduce the risk of occurrence of these complications.

Both endovascular embolization and surgery are available to treat DAVFs. Surgical disconnection of the fistulous vein(s) used to be the gold standard for treatment, but with the introduction of liquid adhesive embolics, which have been shown to produce a durable result without recanalization, these techniques should be regarded as equal. The choice of treatment mode should be decided by the interventional neuroradiologist and the neurosurgeon.

If endovascular treatment is chosen, the arterial route is used preferentially. The goal of arterial embolization, in which a liquid embolic agent such as *n*-butyl cyanoacrylate (NBCA) should be regarded as superior to polyvinyl alcohol (PVA) particles, is to penetrate the fistulous point and to occlude the proximal part of the refluxing vein. If this cannot be accomplished, occlusion of the fistulous vein through an alternative route is indicated. The least aggressive is selective disconnection of the refluxing vein(s). This will leave the DAVF itself untreated. If the fistulous zone is more extensive and the cortical venous reflux is found on multiple sites of the dural sinus, or if venous hypertension is the main problem, obliteration of the sinus may be the only treatment option left. However, first a thorough angiographic examination of the venous drainage of the normally draining veins, including the veins of the posterior fossa, is necessary. Sacrifice of the dural sinus can only be performed if adequate venous drainage of the brain is guaranteed. Only if the sinus is no longer used for the drainage of the brain parenchyma, and the veins of the posterior fossa do not enter the involved segment, the sinus can be sacrificed.

Selective disconnection of the cortical venous reflux or sacrifice of (a part of) a dural sinus can also be performed by an open surgical approach or by a com-

bination of endovascular and surgical approaches. In patients with occlusion of the affected sinus at both proximal and distal sites (isolated sinus), a direct approach to the diseased sinus can be obtained through a small burr hole that allows direct puncture of the dural sinus. Subsequently the fistulous zone of the DAVF can be closed using coils or other thrombotogenic material.

101.5 Magnetic Resonance Imaging

In the presence of a DAVF with cortical venous reflux, unenhanced CT images may show hypodensities, representing areas of gliosis, edema, or venous ischemia. Abnormally enlarged pial veins can be depicted due to their increased density compared to the brain parenchyma (Fig. 101.1). Contrast-enhanced CT will show extensive enhancement of the enlarged pial venous network.

In the absence of cortical venous reflux, a DAVF might be occult on MRI. In such cases, the location of the DAVF within the dura and the lack of a mass effect on the brain parenchyma make it very difficult to see the nidus of the fistula on MRI. MRA is more sensitive in depicting the nidus, although the lack of flow information in time is one of the drawbacks. MRA after injection of a bolus of intravenous contrast may solve this limitation.

In DAVFs with cortical venous reflux MRI shows prominent flow voids on the surface of the brain corresponding to dilated cortical vessels, or more subtle serpiginous or dot-like vascular structures (Fig. 101.2). These are highly suggestive of the correct diagnosis. Hydrocephalus secondary to the venous hypertension in the superior sagittal sinus can be present. The brain parenchyma, particularly the white matter, may show T_2 hyperintensity (Fig. 101.2). This is related to venous hypertension and congestion of the brain in the earlier stages and gliosis in later stages. The cerebral involvement may be extensive (Fig. 101.2) or focal (Fig. 101.4). Dependent on the localization of the shunt, the cerebellum, deep gray nuclei, or brain stem may be affected. DAVFs have been described as the cause of bilateral thalamic hyperintensities on T_2 -weighted images.

The differential diagnosis in bilateral thalamic T_2 hyperintensities should include basilar artery infarction, tumor infiltration, and deep venous occlusion. The differential diagnosis of more diffuse T_2 hyperintensities would include superior sagittal sinus thrombosis with venous congestion, diffuse glioma, and other leukoencephalopathies. However, the combination of an abundance of dilated pial vessels, contrast enhancement of these vessels, and deep white matter T_2 hyperintensity is highly suggestive of a DAVF and mandates further angiographic analysis.

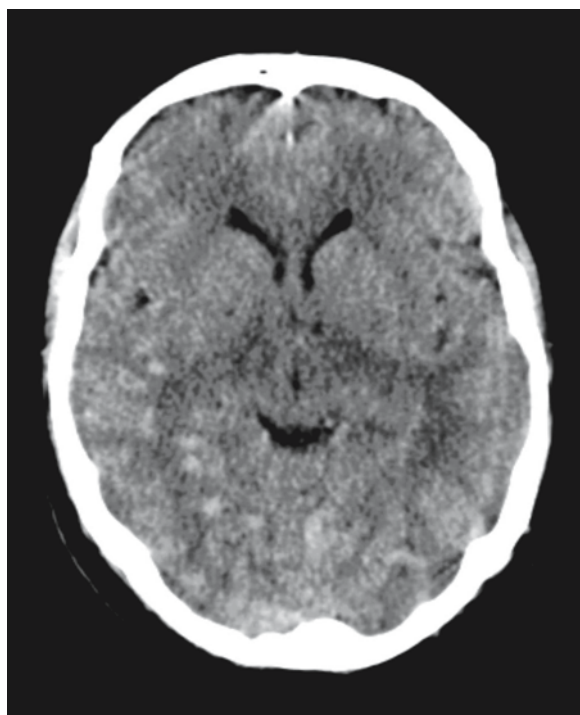


Fig. 101.1. A 57-year-old man presented with rapid cognitive decline related to a DAVF located in the torcular region. On the plain CT scan dilated pial veins are demonstrated in the right temporal region

Angiography is obligatory to confirm the diagnosis DAVF and for treatment planning. Selective contrast injections into the different branch arteries of the external carotid artery will reveal rapid arteriovenous shunting through the fistula into the cerebral venous system, thereby arterializing the venous system. Important concomitant findings are outflow obstruction due to venous sinus occlusion, which can result in extracranial drainage via collateral routes, including the orbital system, and which augments the risk of retrograde flow into the cortical and cerebellar veins. The transit time of contrast when injected selectively into the internal carotid artery is delayed, compatible with venous congestion. In the normal situation venous drainage is seen 4–6 s after the beginning of the arterial phase. In addition to the analysis of the venous reflux, the venous drainage of the brain should be examined with the same diligence, not only to detect focal areas of delayed venous drainage, but also to determine whether sacrifice of a dural sinus or a refluxing vein is a potential treatment option.

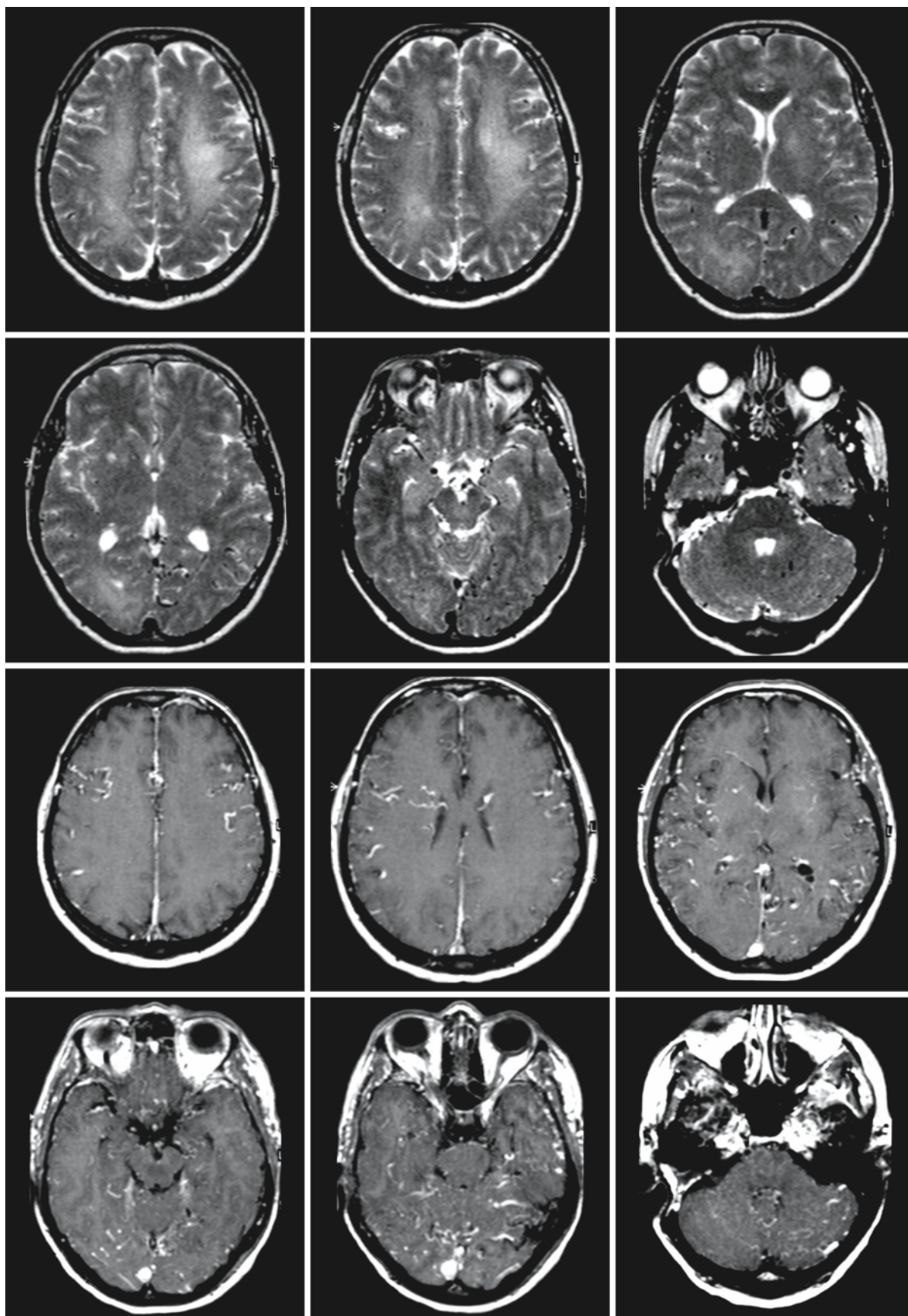


Fig. 101.2.

Fig. 101.3. Angiography of the patient presented in Fig. 101.2. Selective injection of the external carotid artery (*first row, left*) shows hypertrophy of the superficial temporal artery and middle meningeal artery. Immediate enhancement of the superior sagittal sinus is seen, suggesting the presence of a DAVF. Selective internal carotid artery injection (*first row, right; middle row, left*) shows filling of the artery of the falx cerebri through a (hypertrophied) ophthalmic artery (*first row, right*). There is early enhancement of the superior sagittal sinus, consistent with a DAVF. There is slow passage of contrast through the brain parenchyma because of venous congestion, resulting in a late parenchymal and venous phase. This is also illustrated by the poor visibility of peripheral arteries in the early phase (*middle row, left*) and by the “pseudo-phlebitic” aspect of the brain parenchyma in a later phase of the angiogram (*middle row, right*). After treatment by both an endovascular approach (selective glue injections in external carotid branches feeding the arteriovenous fistula) and by direct placement of coils in the superior sagittal sinus (*third row, left; middle row, right*), there is a marked reduction in the size of external carotid artery branches. The internal carotid artery injection after treatment shows abnormal drainage of the brain due to occlusion of the superior sagittal sinus (*third row, right*). The brain is no longer using the superior sagittal sinus for its drainage. However the transit time of contrast is much shorter. The cognitive symptoms of the patient have disappeared almost completely

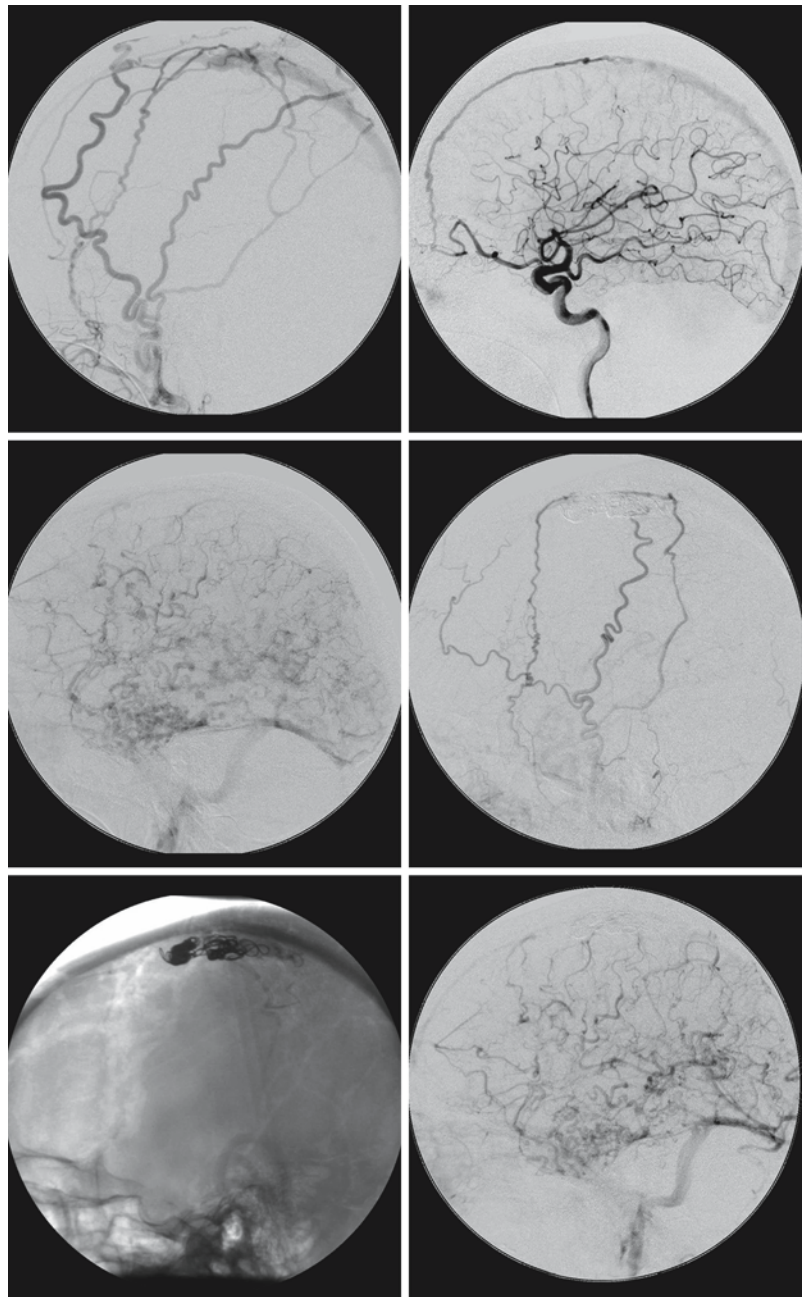


Fig. 101.2. A 67-year-old woman had in her medical history an operation for an acoustic neurinoma on the right. She presented with a rapid cognitive decline. The T₂-weighted images (*first two rows*) show a diffuse signal increase in the deep white matter of both cerebral hemispheres. Abnormal flow voids are visible on the cerebral surface and in the brain parenchyma, especially in the temporal lobes and in the posterior fossa. The T₁-weighted images after contrast (*third and fourth rows*) show extensive enhancement of cortical and parenchymal veins

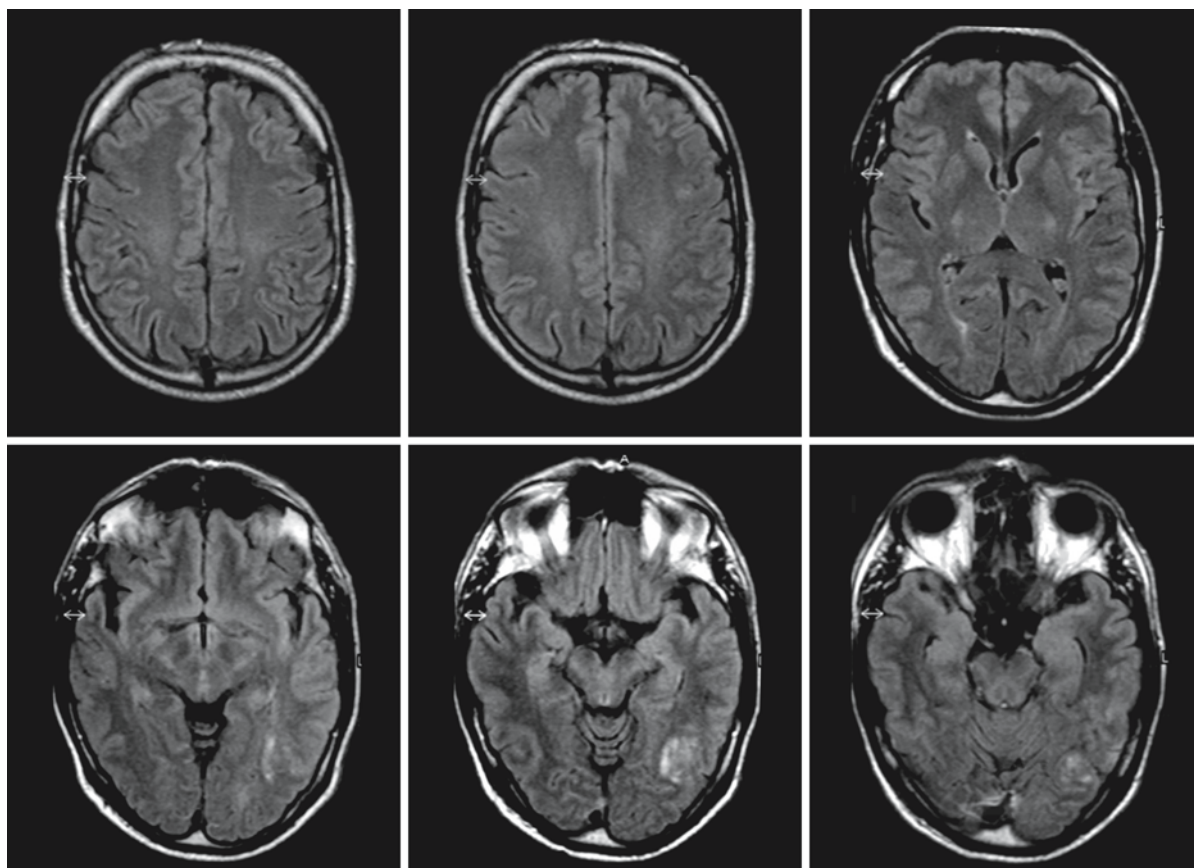
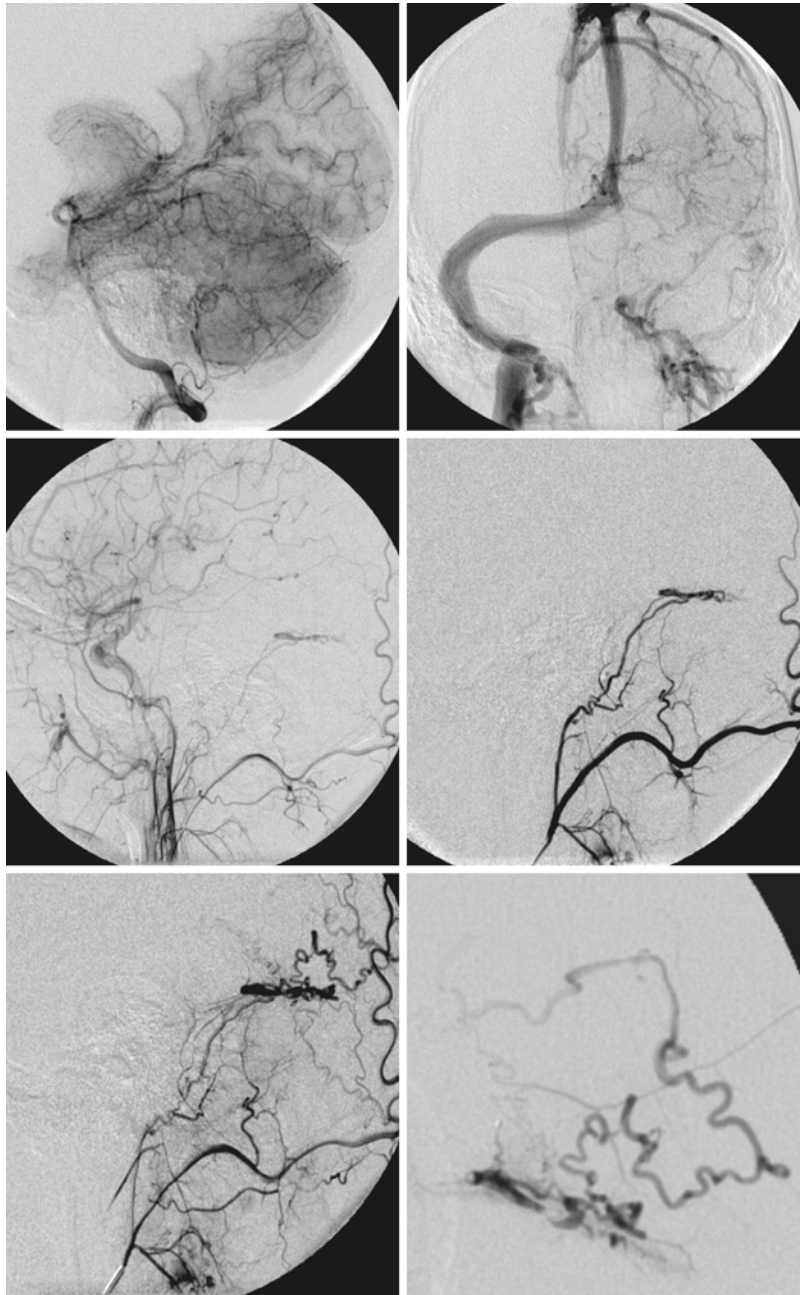


Fig. 101.4. FLAIR images of a 51-year-old patient who had a single epileptic attack with visual signs. The images show an area of increased signal in the left occipital lobe (*second row*)

Fig. 101.5. Angiography of the patient presented in Fig. 101.4. Selective injection of the left vertebral artery shows no definite abnormalities (*first row*), except for nonenhancement of the left transverse and sigmoid sinus. Selective external carotid artery injection shows early filling of a dural tentorial sinus, located in the tentorium cerebelli, due to a DAVF located there. The fistula is fed by a transmastoid branch of the occipital artery (*second row, right*). There is reflux from the dural sinus into cortical veins in the area (*third row*), leading to local venous congestion



Leukoencephalopathy After Radiotherapy and Chemotherapy

102.1 Clinical Features and Laboratory Investigations

In the treatment of malignancies three modalities play a major role: surgery, radiotherapy, and chemotherapy. Other treatment modalities such as hyperthermia and laser coagulation, often image-guided, are of some, but lesser importance. Radiotherapy and chemotherapy are not only applied in the treatment of primary brain tumors and metastases, but intrathecal and intravenous administration of chemotherapeutic drugs, together with cranial or total neuraxis irradiation, are also widely used in the prophylaxis of cerebral involvement in extracerebral malignancies.

For many years the brain was considered to be relatively resistant to therapeutic doses of irradiation and chemotherapy, because neurons do not multiply and the turnover of glial cells is relatively slow. Also, the blood-brain barrier may prevent the penetration of chemotherapeutics into the brain. These concepts have to be modified, because it has become clear that adverse effects are not exceptional.

In the classical description of the effects of radiotherapy three types of damage are distinguished according to their time of occurrence: acute reactions, which occur during the time of treatment and may change the treatment schedule; early delayed reactions, which are usually transient and appear from a few weeks to a few months after treatment; and late delayed reactions, with onset from several months to several years after treatment.

Acute reactions are usually mild and of little consequence, but severe reactions may occur. Clinically they may present as mild signs of increased intracranial pressure. The patient may become confused, incoherent, and disoriented. In more severe cases the patient suffers from headaches, nausea, vomiting, and sometimes elevation of body temperature. Seizures occasionally occur, and the patient may lapse into coma. Discontinuation of the treatment and corticosteroid administration may be necessary and life-saving.

Early delayed reactions are usually transient and disappear without treatment. Various clinical symptoms have been reported: somnolence, nausea, vomiting, dysarthria, dysphagia, cerebellar ataxia, and nystagmus.

Late delayed reactions are generally irreversible. The process begins insidiously with personality changes, gradually progressing over several months. Initially there is excessive drowsiness and loss of initiative and interest. In the course of time there is a decrease of cognitive functioning, confusion, irritability, and memory loss, eventually leading to global dementia.

This classical description is used to describe time-linked reactions after radio- and chemotherapy. In addition, the “focal radiation injury” and “focal white matter injury” resulting from stereotactic radiosurgery, gamma knife surgery, or intensity-modulated radiotherapy may be seen as fitting within the classical concept. Clinically some of these injuries have important consequences. Focal radiation injury caused by irradiation of extracranial structures, e.g. of nasopharyngeal squamous cell tumors or pituitary tumors, may lead to damage of the brain – in these cases, damage to both temporal lobes, resulting in a complex behavioral change, the Klüver-Bucy syndrome.

There are a number of irradiation- and chemotherapy-related patterns that need special consideration because of their consequences for the prognosis and sometimes the need for therapeutic management. This holds especially for multifocal inflammatory leukoencephalopathy (MIL), and the posterior reversible encephalopathy syndrome (PRES). MIL and PRES are addressed separately in Chaps. 88 and 92.

102.2 Pathology

Neuropathological changes in acute reactions after radiotherapy are primarily characterized by cerebral edema, with flattening of gyri, obliteration of sulci, and signs of tentorial herniation. The lateral ventricles are narrowed. Vascular changes are present and consist of fibrinoid necrosis and thickening of the endothelium with extravasation of fibrinous material and perivascular lymphocytic infiltration.

Because the early delayed reaction is usually transient and nonlethal in nature, the amount of information available on the histopathological features is limited. Foci of demyelination with central necrosis and petechial hemorrhages have been described. Lymphocytes and plasma cells are found in the perivascu-

lar spaces, and there is pronounced microglial and astrocytic proliferation in the affected areas. Vascular changes are not prominent in the affected areas, but occasionally the lesions are more marked and show fibrinoid necrosis, fibroproliferative vessel thickening, enlargement of endothelial cells, and capillary proliferation. The cytoarchitecture of the gray matter is usually intact.

The neuropathological findings of the late delayed leukoencephalopathy are rather specific. The changes consist of demyelination, astrogliosis, multifocal coagulative necrosis, and cavitation. The periventricular white matter and the centrum semiovale are involved bilaterally, whereas the subcortical arcuate fibers, the cerebral cortex, and deep gray matter structures are usually spared. Within and around the necrotizing lesions conspicuous swelling of axons occurs. An inflammatory response is usually absent. There are marked vascular lesions, characterized by hyalinization, fibrosis, and necrosis of vessel walls and vascular thrombosis. Areas of endothelial proliferation and various degrees of adventitial fibroblast proliferation are found. Obliteration of the lumen may result. Deposition of iron salts and calcium in the vessel walls may occur. Calcifications may be extensive and be present in the subcortical areas, the basal ganglia, and, less commonly, in the pons. It is noteworthy that mineralizing angiopathy is more often seen in children than in adults.

The installment of prophylactic irradiation and radiotherapy for acute lymphatic leukemia and the treatment of genetic disorders with bone marrow transplantation have focused attention on the side effects of these therapies. In most patients these reactions are transient and have the nature of temporary white matter edema, as has been confirmed by an occasional biopsy, and more recently by quantitative MR data. Multifocal white matter necrosis has the same neuropathological features as the radiation necrosis described above for late delayed post-irradiation reactions.

102.3 Pathogenetic Considerations

Cranial irradiation and systemic, intracarotid, intravenous, and intrathecal chemotherapy, alone or in combination, may result in lesions of the CNS, of either the white matter, the gray matter, or both. In cases of combined therapy it is impossible to delineate the relative contributions of radiation and chemotherapy to the development of cerebral lesions. The total radiation dose and possible overdosage on specific targets, as well as the dose of systemic intravenously or intrathecally administered chemotherapeutic agents all influence the outcome. Some chemotherapeutic agents are radiosensitizers, for example *bis-*

chloroethyl-nitrosourea (BCNU), methotrexate, and cisplatin. They enhance the effect of radiation-induced changes. On the other hand, radiation may induce changes in the permeability of the blood-brain barrier and thus affect the delivery of potentially toxic agents. Other factors in the patient, such as nutritional status, type of primary malignancy, or pretransplant status, and the presence of a paraneoplastic syndrome, may well contribute to the development and severity of cerebral lesions.

The acute post-therapy syndrome is thought to be due to vasogenic edema resulting from damage to the capillary endothelium.

Early delayed reactions are believed to be due to demyelination and may be reversible to some degree. There are suggestions that they may be the result of an autoimmune reaction following sensitization for some myelin antigen that has become exposed by therapy-induced tissue necrosis. Antigens are released in the intracellular spaces by damaged myelin and glial cells, and may evoke hypersensitivity reactions. This hypothesis has never been proven, but the perivascular inflammatory reaction may be an argument. Another mechanism which may account for the marked demyelination in the absence of vascular changes in early delayed post-treatment leukoencephalopathy is primary damage to glial cells, in particular oligodendrocytes. Sometimes striking glial proliferations are noticed, associated with bizarre cells and giant multinuclear astrocytes, supporting this hypothesis.

In the late delayed reactions vascular changes with secondary ischemic changes form the most likely explanation for the tissue damage. The endothelium of blood vessels is one of the most sensitive tissues of the brain. Damage to the endothelium leads to endothelial proliferation and changes in the vessel wall, with subsequent obliteration of the lumen and ischemia. Small vessels are usually most affected, but larger arteries may also suffer, and may be partially or totally occluded, possibly with formation of moyamoya-like collaterals.

It is important to realize that the adverse consequences of irradiation of the brain, in particular in combination with chemotherapy, may be more severe in infants and children than in adults. The consequences for the immature brain may differ from those for the more mature brain. From the management of medulloblastomas in young children it has become clear that aggressive treatment approaches, especially craniospinal irradiation, can harm the developing brain. It is hard to predict what dose of radiotherapy will be harmful in each individual child. It is well known that very young children will have significant learning problems after full-dose radiotherapy, and that even older children may develop difficulties in school. However, a reduction in dosage may also re-

duce efficacy on the tumor. Hence, approaches using reduced-dose craniospinal irradiation and chemotherapy, in order to reduce cognitive, endocrine, and psychological deficits, may decrease late effects, but carry with them the risk of having more treatment failures.

The combination of radiotherapy and chemotherapy leads to synergistic inhibition of the synthesis of macromolecules and DNA repair, possibly further contributing to the damage. In a postmortem study of children with childhood leukemia treated with different modes of application of this combined therapy, comparing those who showed leukoencephalopathy and those who did not show leukoencephalopathy, it became clear that the development of white matter damage did not correlate with age, despite the different stages of myelination and neuronal differentiation in the pediatric age group. Nor was there a relationship with intercurrent infections, nutrition, or the presence of CNS leukemia. There was a clear relationship with the radiation dose the child had received in combination with intrathecal methotrexate. The total amount of intrathecally administered methotrexate seemed less important. The dose of methotrexate was important when given intravenously: the incidence of leukoencephalopathy increased with the total dose of intravenously administered methotrexate.

To add substance to this discussion, the multicenter study of the German Late Effects (of acute lymphatic leukemia treatment) Working Group, summarizes findings in a large population treated with standard protocols (Hertzberg et al. 1997). In this study 118 former patients with acute lymphatic leukemia in first continuous remission underwent CT and/or MRI. The group was subdivided into: group A (39 patients), receiving intrathecal methotrexate and systemic medium-high dose methotrexate; group B (41 patients), receiving cranial irradiation (16.8 Gy) and intrathecal methotrexate or systemic methotrexate; and group C (38 patients), receiving irradiation (17.1 Gy) and intrathecal methotrexate. Abnormal MRI and CT scans were found in 61 of the 118 patients, consisting of white matter changes (diffuse or focal), brain atrophy, and calcifications. Of these 61 patients, 15 were from group A (38.5%), 23 from group B (56.1%), and 23 from group C (60.5%). Patients with definite CNS changes showed impaired neuropsychological function. It is clear from this report that methotrexate without irradiation can also lead to serious CNS changes, both of gray and white matter. This has been reported in more detail by Löwblad et al. (1998). They describe the cases of four children treated with high-dose intravenous and intrathecal methotrexate without irradiation. In all these cases the cure was prolonged, lasting for more than 1 year. These children developed serious CNS abnormalities with diffuse hyperintense white matter

changes on T₂-weighted images and subcortical hyperdensities on CT, consistent with calcifications. The authors attribute these changes to a mineralizing angiopathy, commonly thought to be the result of cranial irradiation in combination with chemotherapy. From this and other reports it has become clear that chemotherapy without irradiation may also lead to leukoencephalopathy and mineralizing angiopathy.

102.4 Therapy

In acute reactions corticosteroids are useful in alleviating cerebral vasogenic edema and may be life-saving in patients with imminent tentorial herniation. The importance of recognizing early delayed reactions is the fact that they are usually transient and do not necessarily require intervention or indicate a failure of therapy. In the late delayed reaction corticosteroids play a minor role. In cases with focal radiation necrosis, surgery is an option. In patients with neurological syndromes caused by toxic effects of cytostatic or immunosuppressive drugs that may be reversible, abortion of the therapy or a switch to other drugs may have a beneficial effect. Psychiatric syndromes, especially when caused by more permanent damage of both temporal lobes, as happens in the irradiation of nasopharyngeal and pituitary tumors, are difficult to treat and may require special measures.

102.5 Magnetic Resonance Imaging

MRI is generally the first choice of imaging modalities in the follow-up of patients treated with cranial irradiation and/or chemotherapy, because its sensitivity is much better than that of CT. Only in the detection of microcalcifications, such as occur in mineralizing angiopathy, does CT have an advantage. All stages of radiation and chemotherapy injuries

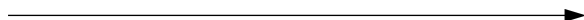


Fig. 102.1. A 62-year-old woman treated with chemotherapy and irradiation for a right frontal glioma. The initial tumor is barely visible on the FLAIR images (*first three rows*) within a now much larger area of high signal involving the periventricular and deep frontal white matter, right more than left, and the corpus callosum. T₁-weighted images after contrast (*fourth row*) show a rim of a few millimeters' thickness along the wall of the left lateral ventricle as well as an enhancing dot in the right frontal area. The white matter changes can be attributed to the irradiation and chemotherapy. The enhancement, which did not change during further follow-up, probably represents either inactivated tumor tissue, or, more probably, radiation-induced changes

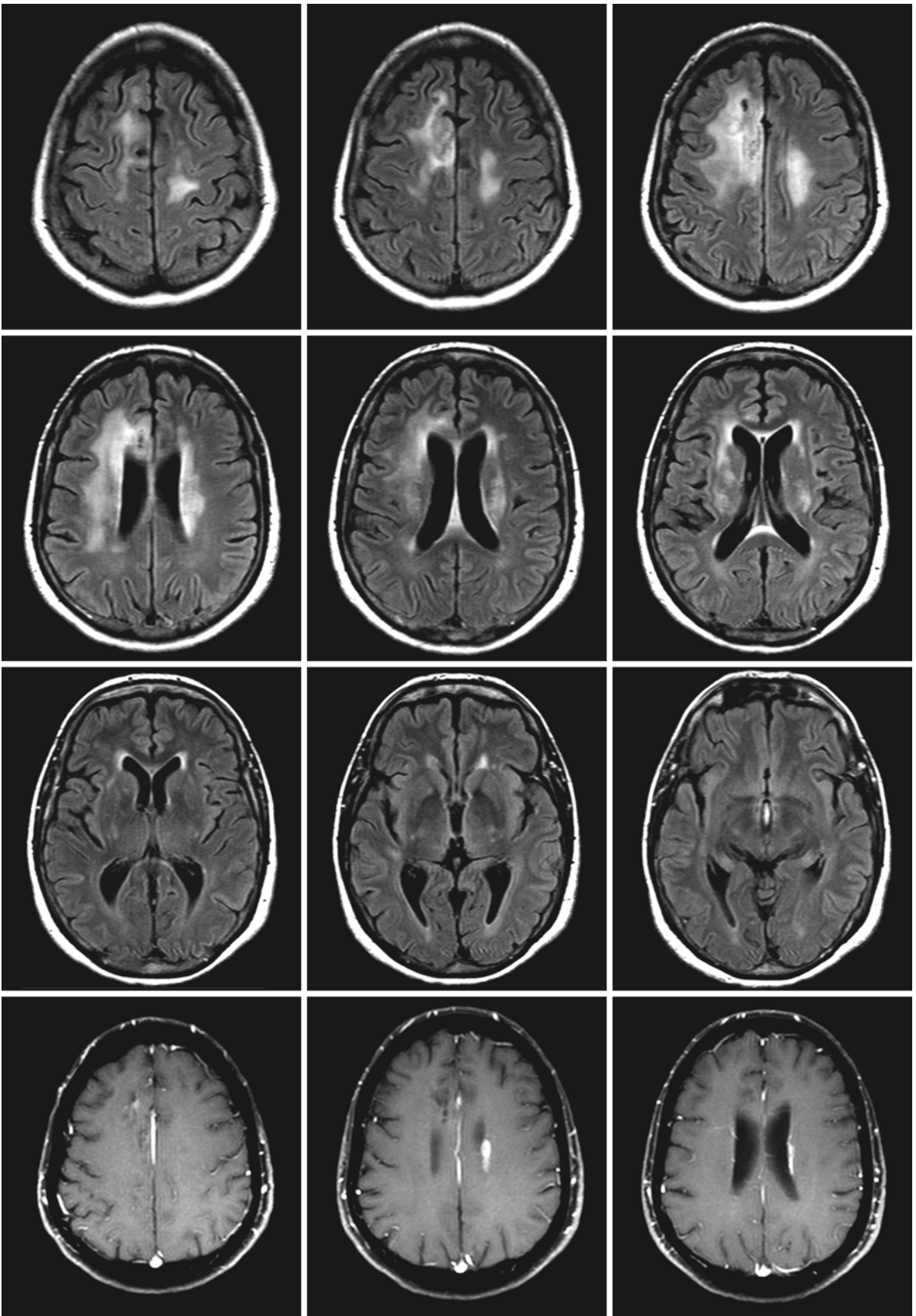


Fig. 102.1.

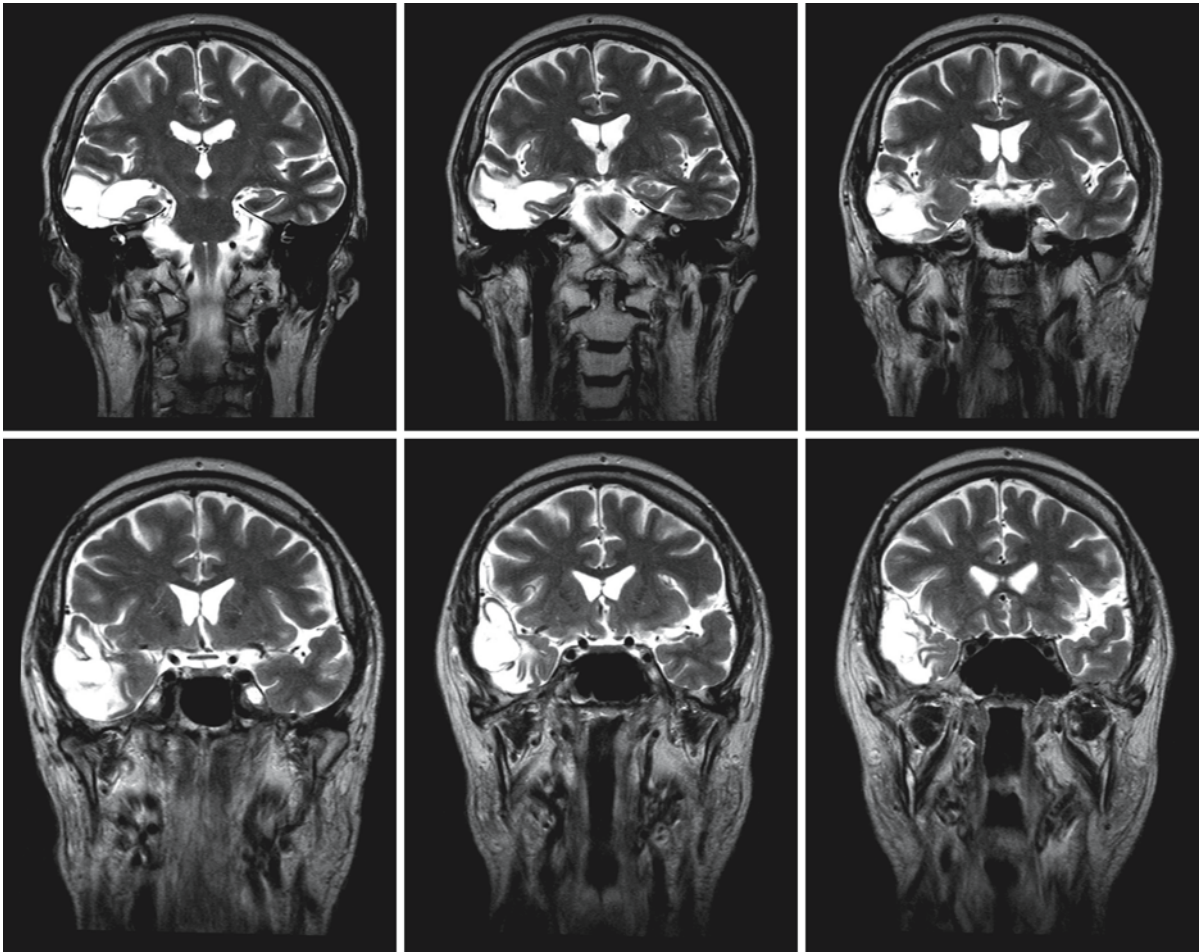


Fig. 102.2. A 52-year-old male patient presented with a partial seizure. He had been treated previously for a right-sided nasopharyngeal squamous cell carcinoma with partial excision and radiotherapy. The right temporal lobe was included in

the irradiation field. Coronal T₂-weighted images show the impact of the radiation on the right temporal lobe, involving both white and gray matter

have in common an increase in free tissue and, sometimes, intracellular water. The consequence of this is a higher signal intensity on T₂-weighted and lower signal intensity on T₁-weighted images. This signal behavior may, however, reflect many forms of underlying pathology, such as impairment of the blood–brain barrier due to endothelial damage and vasogenic edema, demyelination, gliosis, ischemia, and tissue necrosis. Newer techniques, such as diffusion-weighted imaging, perfusion imaging, and proton MRS, have been of considerable help in the determination of the structural tissue changes. Diffusion-weighted imaging, in combination with calculated ADC maps, or diffusion tensor imaging with the calculation of fractional anisotropy, have made it possible to differentiate between vasogenic edema and cytotoxic edema, and permits a better estimation of the prognosis of the abnormalities found. Contrast administration plays an important role, even though it does not dif-

ferentiate radiation necrosis from tumor recurrence. Perfusion imaging and MRS have a prominent role in distinguishing tumor recurrence from radiation necrosis. In necrotizing tissue perfusion is low, whereas in tumor recurrence it is usually high. MRS – if possible, chemical shift imaging to cover the whole area – shows in tumor recurrence high choline, lactate, and often the presence of some residual brain metabolites, for instance *N*-acetylaspartate in reduced concentration. In necrotic tissue *N*-acetylaspartate is usually absent, as is choline, whereas lactate is present. It is, however, not rare that both tissue necrosis and tumor recurrence are present at the same time. Microbleeds can be made visible on MR images with gradient echo or hybrid spin-echo–gradient-echo techniques.

In the acute reaction MR findings are nonspecific. The images may be completely normal or subtly abnormal with poorly defined multifocal areas of hy-

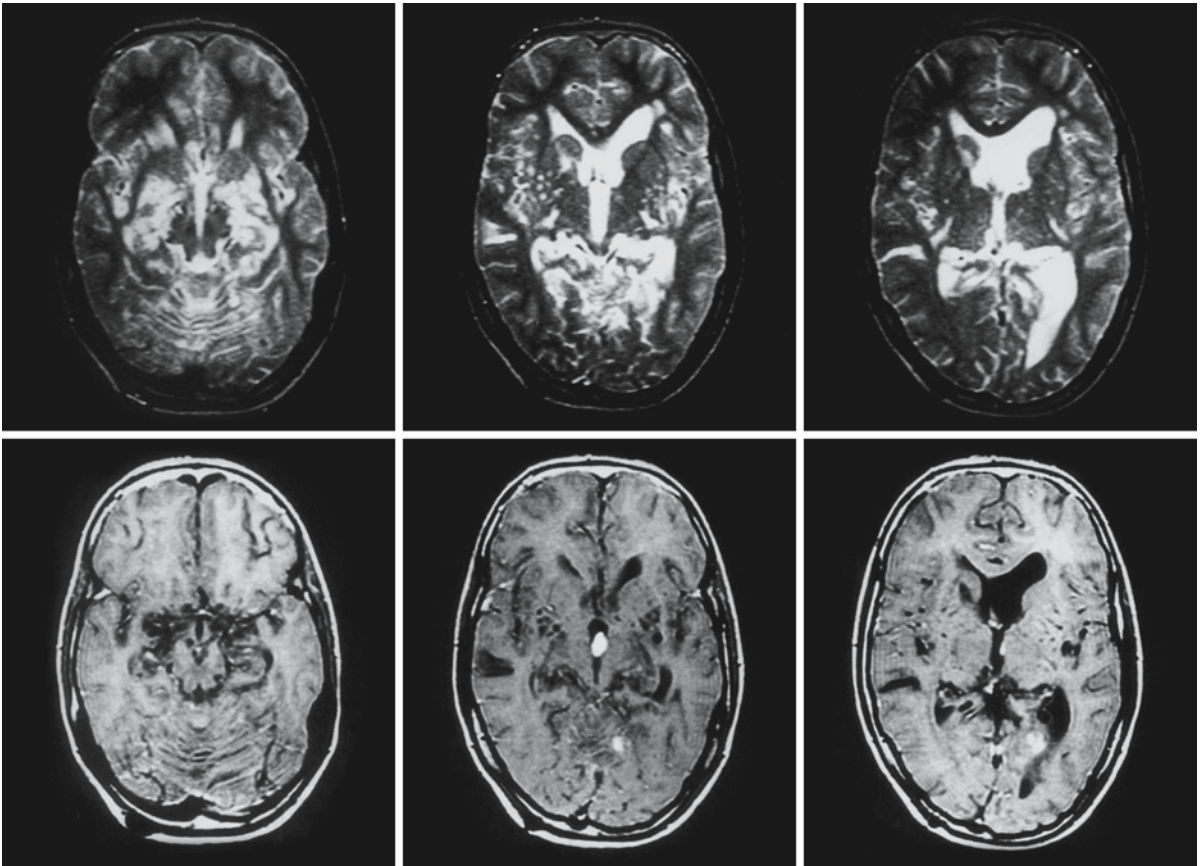


Fig. 102.3. A 4-year-old boy was treated prophylactically with irradiation and intrathecal methotrexate because of acute lymphocytic leukemia. The T₂-weighted images (*upper row*) show involvement of the basal ganglia, internal capsule, and

cerebral peduncles in the midbrain. The T₁-weighted images (*second row*) reveal cysts in the basal ganglia, indicating that cystic necrosis has developed. With contrast, an enhancing recurrent tumor is seen in the third ventricle

perintensity on T₂-weighted images, most often in both hemispheres. The abnormalities usually disappear spontaneously, given an uneventful clinical course.

In early delayed reactions, occurring a few weeks to months after treatment, the white matter changes are also usually transient. Changes on MRI include high signal intensity on T₂-weighted or FLAIR images in the basal ganglia, the cerebral peduncles, and the deep white matter. Diffusion-weighted imaging also shows high signal intensity in these areas, with also a high ADC value. The term “T₂ shine-through” is sometimes used for this phenomenon, but seems not quite correct, because the combination of high signal on diffusion-weighted imaging and high diffusivity may reflect an underlying condition, most probably, but not only, vasogenic edema. It is in general an indication of a benign nature of the lesion. In some patients who develop a diffuse leukoencephalopathy a few weeks to a few months after treatment, the course is not benign and the white matter abnormalities are

not reversible. Enhancing lesions within the white matter correlate with tissue necrosis at autopsy.

Transient white matter abnormalities are often found in patients treated for acute lymphocytic leukemia with prophylactic cranial irradiation, chemotherapy, and bone marrow transplantation. The lesions are located in the periventricular area and may be more or less extensive. There is no clear relationship between the severity of the lesions on MRI and the clinical condition and outcome. Diffusion-weighted imaging and ADC maps may be helpful by showing the nature of the lesions. The lesions may remain visible for a long time after the clinical disappearance of symptoms.

Late delayed reactions occur months to years after the initial treatment. Depending on the field of irradiation the lesions are more focal (Figs. 102.1–102.3) or more generalized (Figs. 102.4 and 102.5). So-called “diffuse radiation injury” can be caused by irradiation, by combined irradiation and chemotherapy, and by chemotherapy alone. The white matter lesions,

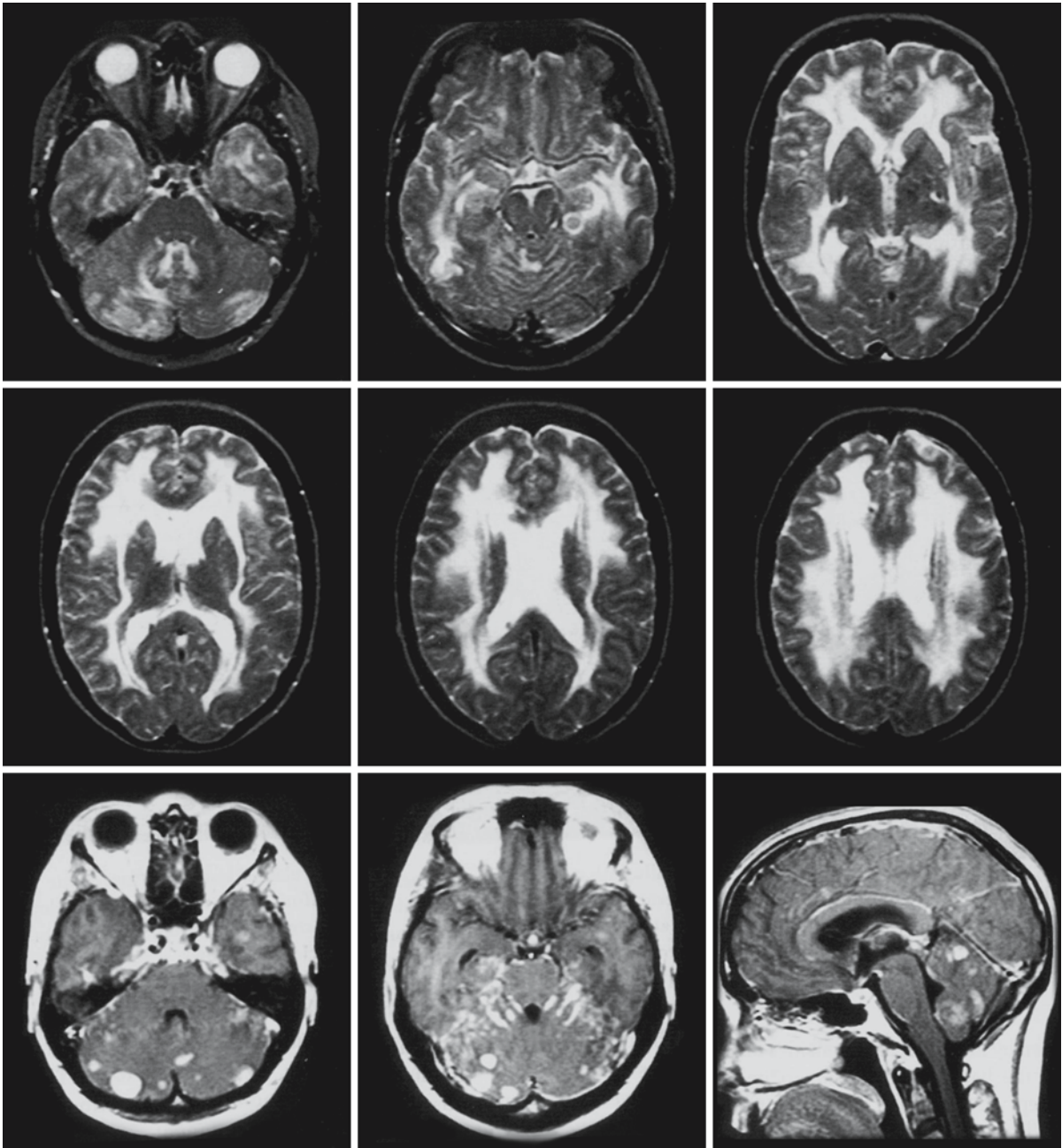


Fig. 102.4. A 29-year-old woman with disseminated breast carcinoma. Metastases in the brain were treated with radiotherapy and systemic cytostatic treatment. The T₂-weighted transverse series 6 months after radiotherapy (*upper two rows*) shows diffuse symmetrical deep white matter hyperintensity,

also involving the external capsule and the temporal lobes. In the cerebellum there are multiple, asymmetrical lesions and linear high-signal bands in the cerebellar foliae. T₁-weighted images after contrast (*third row*) show multiple metastases and leptomeningeal carcinomatosis

when irradiation has covered the whole brain, are located in the white matter of both hemispheres and are symmetrical and confluent. Combinations of diffuse radiation injury and recurrent tumor may occur (Fig. 102.3). The lesions of late delayed reactions have a high signal intensity on proton density, T₂-weight-

ed, and FLAIR images. ADC values are usually only slightly above those of normal cerebral tissue. Despite the sometimes extensive white matter lesions, patients may be asymptomatic. In more severe cases there may be slowing down of mental activity and cognitive impairment. The most severe form of late

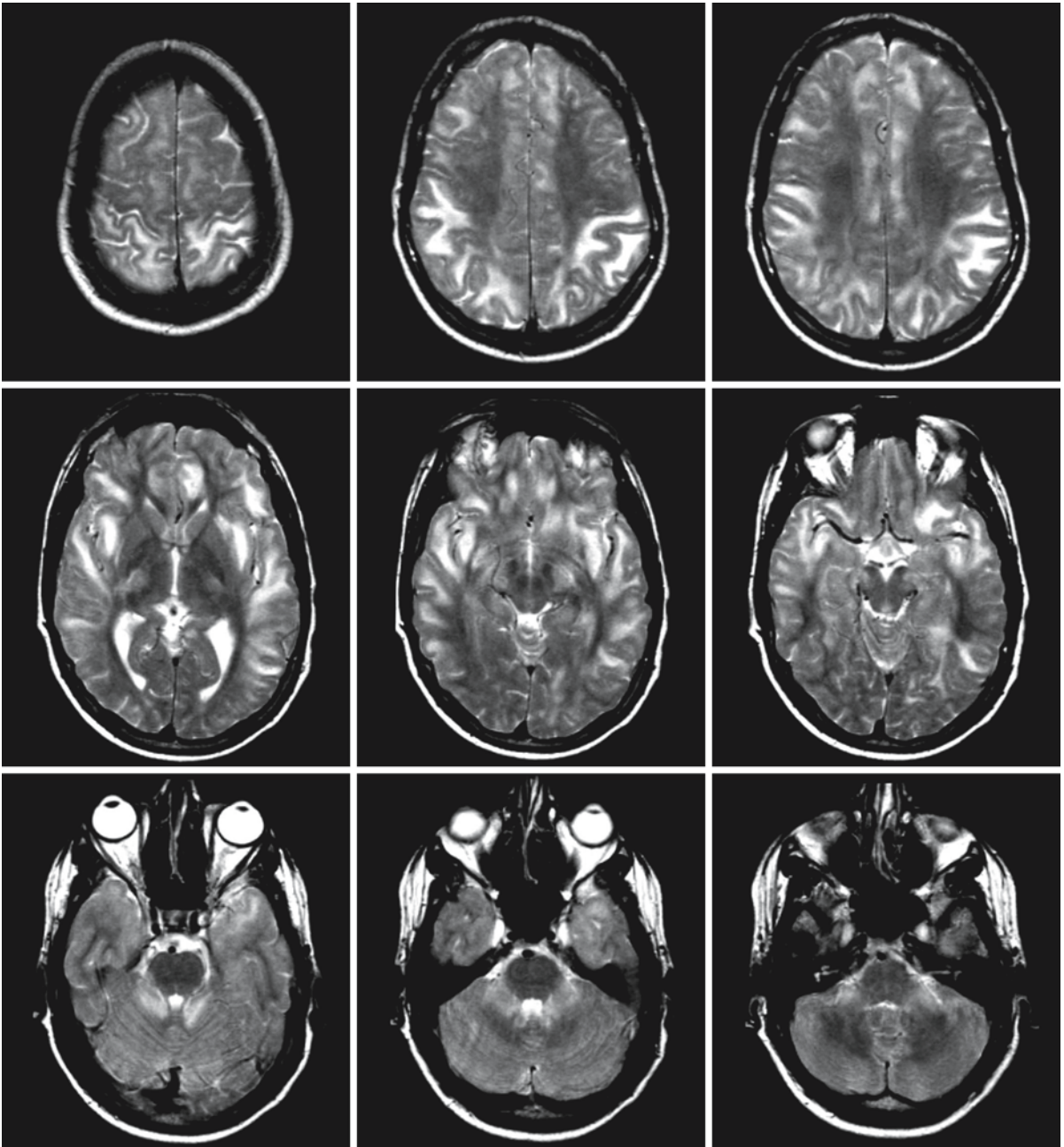


Fig. 102.5. A 24-year-old man was treated for acute lymphocytic leukemia with chemotherapy and intrathecal methotrexate. Two months later he developed progressive encephalopathy. The T_2 -weighted images show extensive involvement of

arcuate fibers in parietal, frontal, and temporal lobes, as well as bilateral involvement of the posterior limb of the internal capsule, thalamus, corticospinal tracts in the midbrain, and both middle cerebellar peduncles

delayed reaction is necrotizing encephalopathy with areas of focal necrosis (Fig. 102.3). The borders of these lesions may enhance. To verify this diagnosis, perfusion studies may be performed, showing reduced perfusion, or MRS, showing loss of metabolites without a rise in choline concentration and with various amounts of lactate.

A disseminated necrotizing leukoencephalopathy with characteristic contrast enhancement of the white matter has been reported in patients with acute lymphoblastic leukemia after intense chemotherapy with methotrexate and prophylactic cranial irradiation, with either a fulminant or a less fulminant course. In these cases methotrexate was delivered both intra-

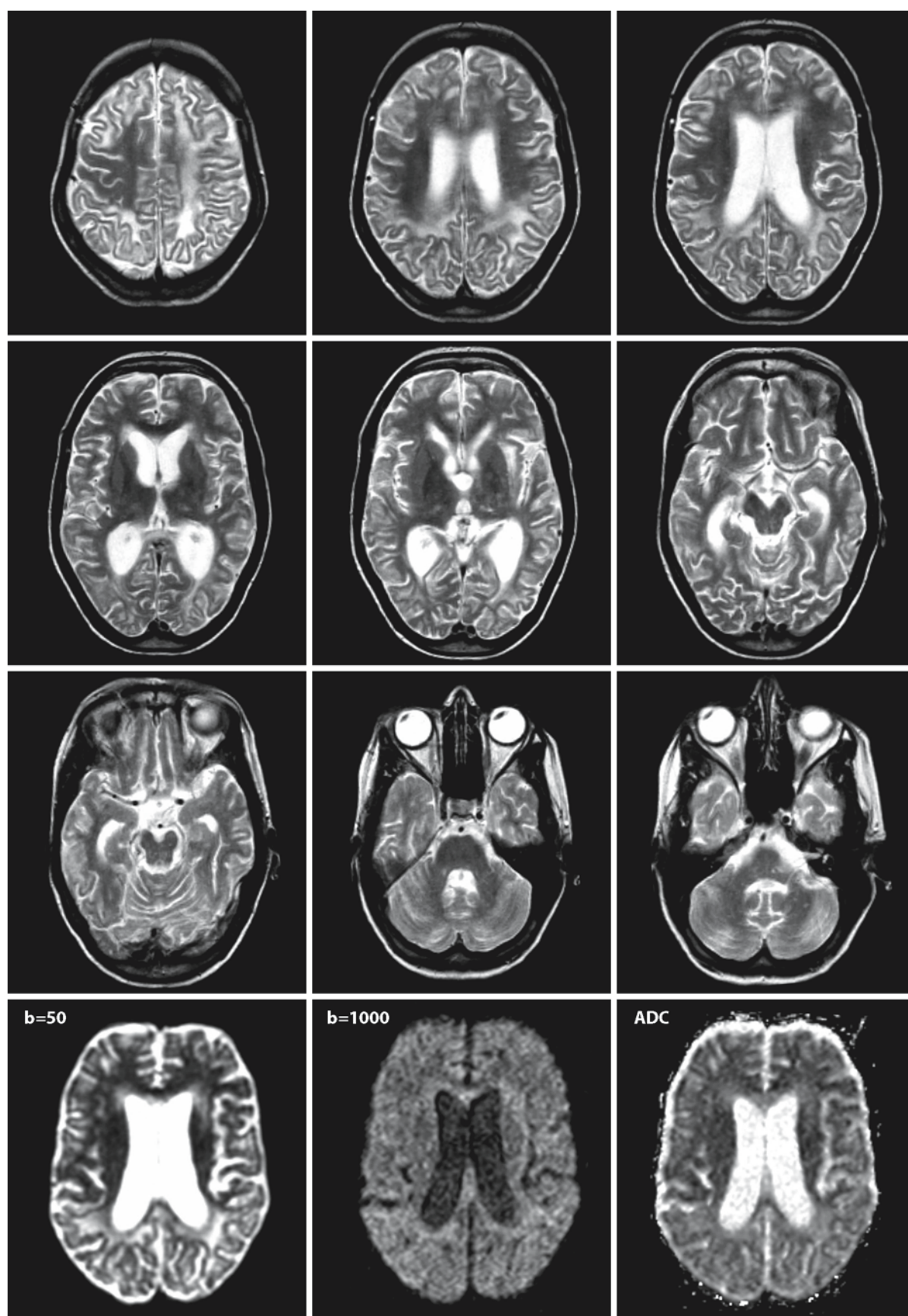
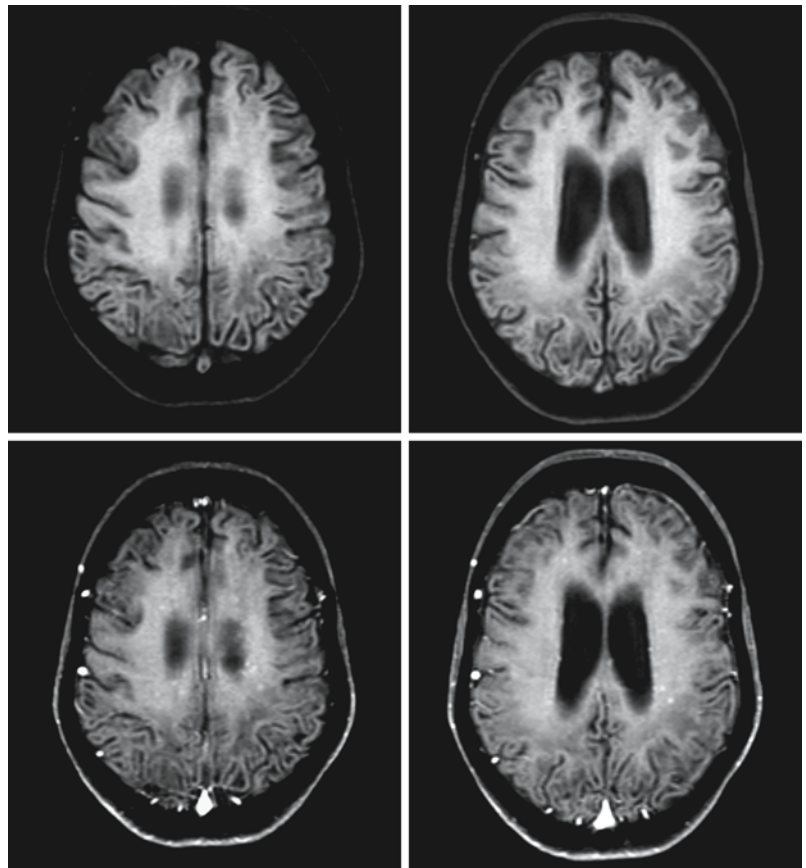


Fig. 102.6.

Fig. 102.7. The T₁-weighted images of the same patient as illustrated in Fig. 102.6, without (*first row*) and with contrast (*second row*), reveal multiple small punctate areas of contrast uptake, suggesting perivascular enhancement. These findings suggest an underlying angiitis or vasculopathy



venously and intrathecally. MRI initially shows extensive white matter abnormalities, with focal but symmetrical enhancement. On follow-up studies the



Fig. 102.6. An 18-year-old girl was treated 7 years ago with chemotherapy, irradiation, and autologous bone marrow transplantation for a non-Hodgkin lymphoma. She has been tumor-free since the treatment. However, since 1.5 years after the treatment she has developed slowly progressive encephalopathy with recently more rapid decline. The encephalopathy was characterized by concentration and memory problems, personality changes, subsequent global cognitive impairment, and finally increasing ataxia and spasticity. The T₂-weighted images (*first three rows*) show extensive white matter changes, especially involving the arcuate fibers. There is some cerebral atrophy with ventriculomegaly, including the temporal horns, and widening of the subarachnoid spaces. There are bilateral lesions in the thalamus. Diffusion-weighted images (*fourth row*) at different b values and an ADC map show increased ADC values in the abnormal white matter areas (ADC values in the affected region 1.24–1.55). These values, unfortunately, only reflect the final phase of the process. Because of the insidious start and progress of the encephalopathy, initial ADC values are not available

enhancement disappears but atrophy sets in, leading to death within a few years. The MR pattern differs from that seen in autoimmune suppressive therapy-related MIL.

Severe late delayed reactions may also develop after treatment with a combination of irradiation, chemotherapy, and bone marrow transplantation. Years after treatment, and following an initially good response, a progressive encephalopathy may develop with loss of mental faculties and an array of neurological symptoms and ending in death. MRI shows white matter abnormalities predominantly involving the arcuate fibers and progressive atrophy (Figs. 102.6 and 102.7).

Mineralizing angiopathy is more often seen in children than in adults. In children it is the most common abnormality seen on MRI and/or CT. Calcifications are found in the subcortical white matter and sometimes in the basal ganglia, in particular in the putamen.

Lesions after gamma-knife therapy, stereotactic radiosurgery, and localized overdosage are not fundamentally different from the classic description. Here, too, the whole gamut of reactions is possible: from vasogenic transient edema, to severe white and/or gray matter lesions, to a cavitating (leuko)encephalopathy.

Gliomatosis Cerebri

103.1 Clinical Features and Laboratory Investigations

Several synonyms are used for this condition: diffuse glioma of the brain, gliomatosis diffusa, gliomatous hypertrophy, blastomatous type of diffuse sclerosis, and central diffuse schwannosis.

The clinical presentation is variable. Headache is present in most cases, and may be accompanied by focal seizures, changes in mental state, psychiatric syndromes, ataxia, dysphagia, dysphasia, and memory loss. The clinical picture suggests in most cases a multifocal progressive disorder. Initially, however, symptoms may be difficult to interpret, with only loss of concentration, behavioral problems, or psychiatric symptoms. Some patients present with diminished vision only, and papilledema is found at fundoscopy. The clinical symptoms are often discrepantly mild in view of the extensive abnormalities found on MRI, but they are progressive and lead to death. The median survival time is 14 months.

Over the last 5–10 years there seems to have been an increase in the number of cases of gliomatosis cerebri, and younger patients are affected than in former years. The reason for this is unclear.

103.2 Pathology

Macroscopically, there is swelling of the involved structures. Although all parts of the brain may be involved, including the brain stem and cerebellum, there is a preference for the central, periventricular areas and mesolimbic parts of the temporal lobe. The microscopic hallmark of gliomatosis cerebri is the presence of many moderately pleomorphic glial cells, infiltrating pre-existing structures, without significant destruction. Natural borders between structures are not respected. Usually, these cells are astrocytic in type and react positively with glial fibrillary acidic protein (GFAP). In other cases, the infiltrating cells have oligodendroglia-like elements and only a few cells are GFAP-positive astrocytes. Locally further dedifferentiation may take place, and some parts of the lesion may progress to anaplastic astrocytoma or glioblastoma multiforme. Finally, the entire neuraxis may be involved.

103.3 Pathogenetic Considerations

No familial cases of gliomatosis cerebri have been reported. One study looking at the chromosomes of cells of gliomatosis cerebri revealed that the majority of the abnormal cells had the karyotype 44 XY, (del(6)(q25), del(14)(q21), del(15;21)(q10;q10), add(18)(q22), del(19)(p12), add(20)(p13), -21. A smaller proportion of cells had 88 chromosomes with a doubling of the normal karyotype. With the exception of the chromosome 6 deletion, these chromosomal changes do not resemble those found in astrocytomas, suggesting that gliomatosis cerebri is a separate entity (Hecht et al. 1995). Herrlinger et al. (2002) summarize the molecular genetic findings and find that genetic alterations in diffuse gliomatosis are not different from those found in infiltrating astrocytomas. They conclude on these grounds that gliomatosis cerebri should be considered a particularly invasive subform of glioma, rather than a distinct tumor entity that is entirely different from other cerebral gliomas. An extra argument for this is found in the dedifferentiation of gliomatosis cerebri into anaplastic astrocytomas and glioblastoma multiforme.

In one report, gliomatosis cerebri was seen following radiation and chemotherapy for a extraneural metastasis of primary nongerminomatous germ cell tumor in the pineal region, providing evidence for exogenous induction of the tumor.




Fig. 103.1. Series of transverse T₂-weighted images in a 56-year-old woman (*first two rows*). She has a history of changes in personality over the past 2 years, leading to suspicion of frontotemporal dementia. The images show bilateral, nearly symmetrical signal abnormalities of the frontal lobes, connected via the genu of the corpus callosum and spreading toward the deep insular structures on both sides. The affected corpus callosum is markedly swollen. There is diminished gray–white matter distinction in the involved areas. The *third and fourth rows* contain diffusion-weighted images (Trace diffusion-weighted images with $b = 1000$ in the *third row*; ADC maps in the *fourth row*). The Trace diffusion-weighted images show a moderate increase in signal intensity in the involved area, whereas the ADC values are too high, indicating increased mobility of water. Note that this combination of moderately high signal increase on Trace diffusion-weighted images together with high ADC values in the affected area does not reflect vasogenic edema

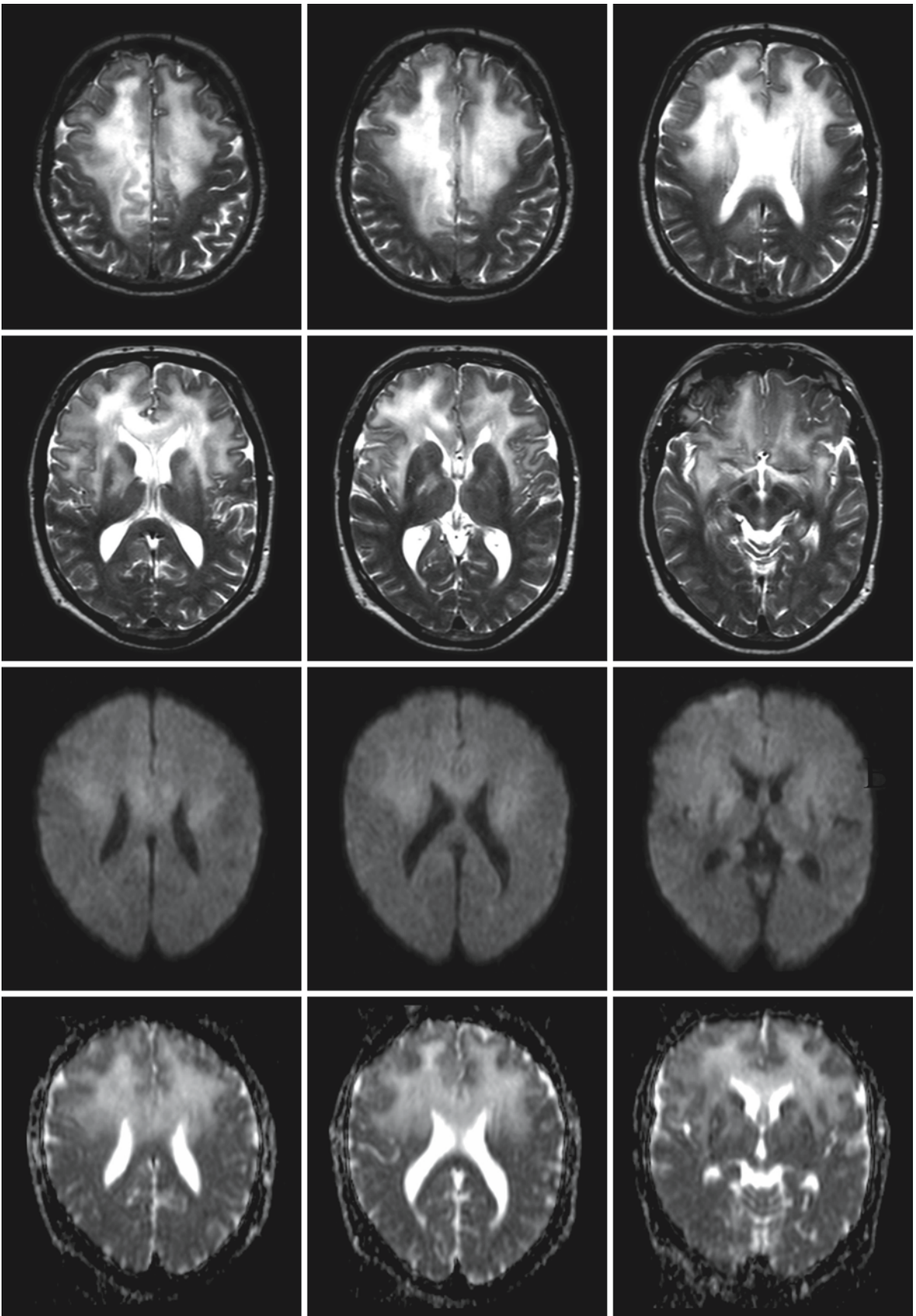


Fig. 103.1.

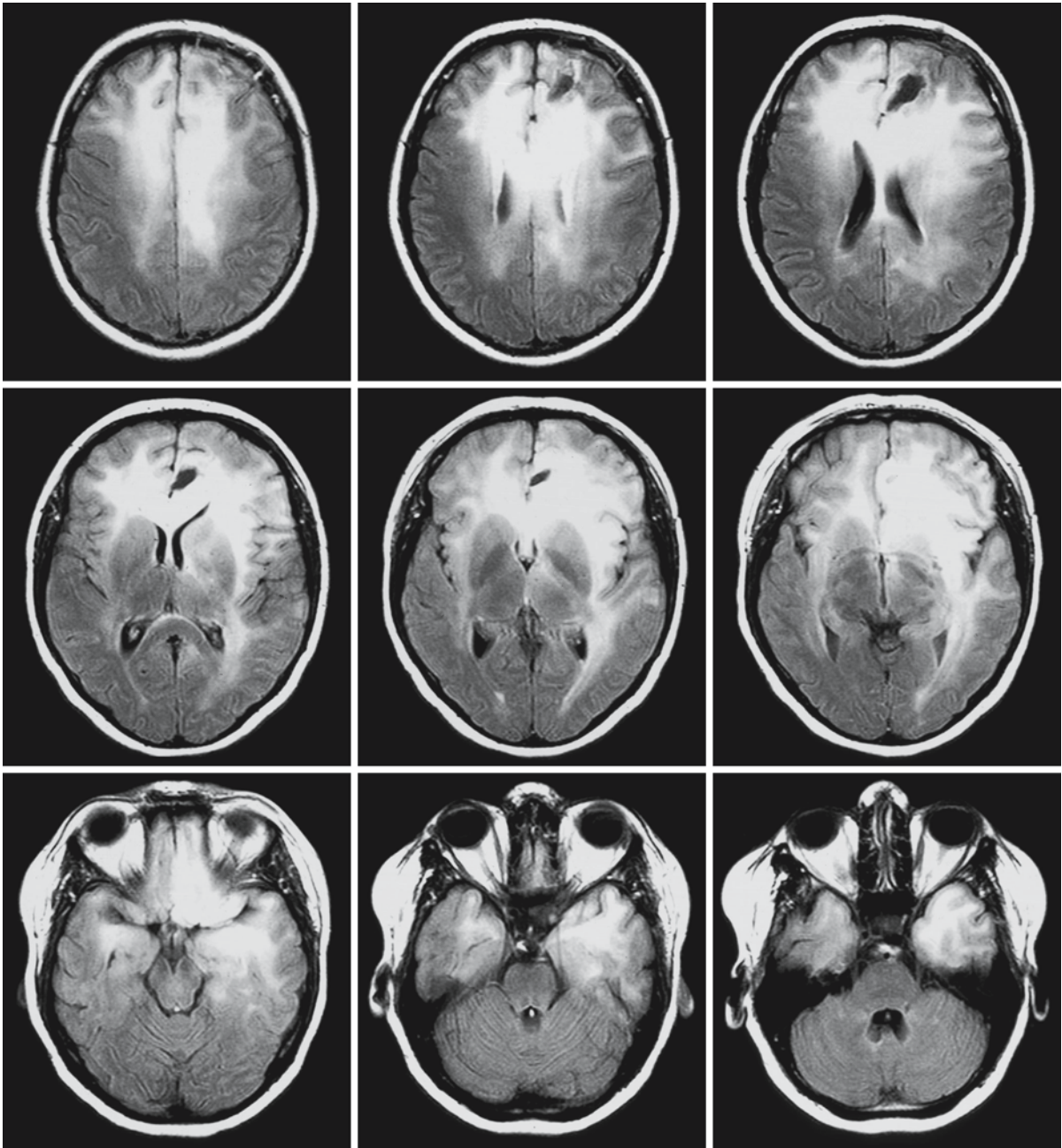


Fig. 103.2. Series of FLAIR images in a 25-year-old man with biopsy-proven gliomatosis cerebri. The biopsy was taken from the left frontal lobe. In this case the abnormalities are mildly asymmetrical and have a prominent mass effect. There is clear

involvement of the temporal lobes. In many places where the tumor touches upon the cortico-subcortical junction, the gray–white matter differentiation has disappeared

103.4 Therapy

Because neurosurgery is not an option in most cases, radiotherapy and chemotherapy are the only remaining therapies available. The results have been disappointing for many years, but with the drug temozolomide longer survival has been achieved.

103.5 Magnetic Resonance Imaging

Most useful for the diagnosis of gliomatosis cerebri are proton density, T_2 -weighted, and FLAIR sequences. They show increased signal intensity of the involved areas, with poor demarcation from noninvolved tissue, and with mass effect. When the cortico-subcorti-

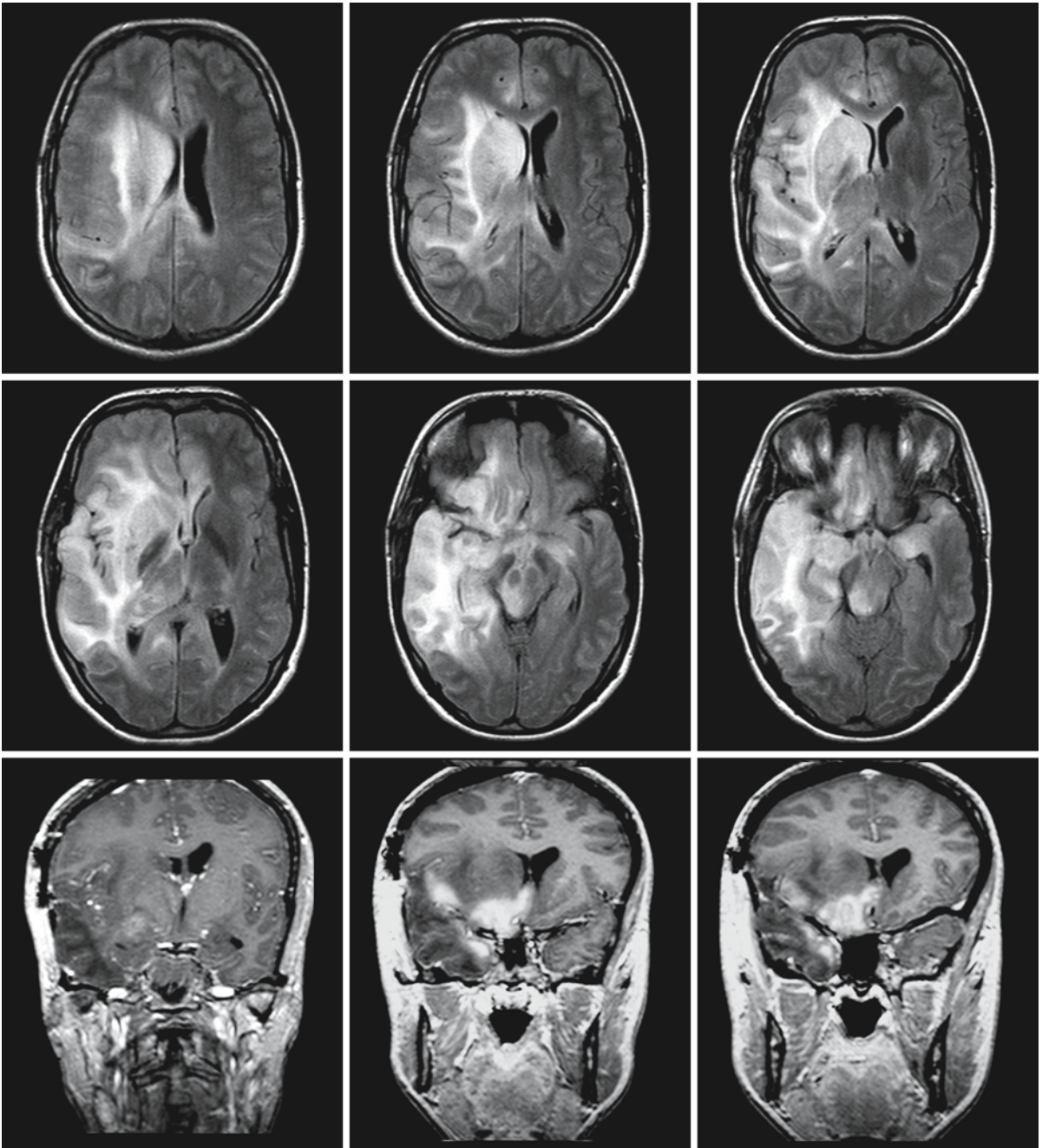


Fig. 103.3. This 17-year-old girl presented with bilateral papilledema and no other neurological signs. The FLAIR images (*upper two rows*) reveal an asymmetrical presentation of gliomatosis cerebri with most prominent abnormalities on the right. The *third row* shows coronal T₁-weighted images with contrast. The *left-hand* image was obtained directly after con-

trast administration, showing some contrast enhancement in the right frontal lobe. The two images on the *right* were obtained 1 h after the injection and show much more prominent contrast enhancement. The latter images make clear that the damage to the blood–brain barrier is far more extensive than the first postcontrast image would suggest

cal junction is involved, there may be a striking loss of demarcation of gray and white matter and the suggestion of some swelling (Figs. 103.1–103.3). When the periventricular structures are involved, the ventricle

will be locally narrowed, with distortion of its normal border (Figs. 103.2 and 103.3). In these centrally located cases, the corpus callosum is nearly always involved and may be severely swollen (Fig. 103.2).

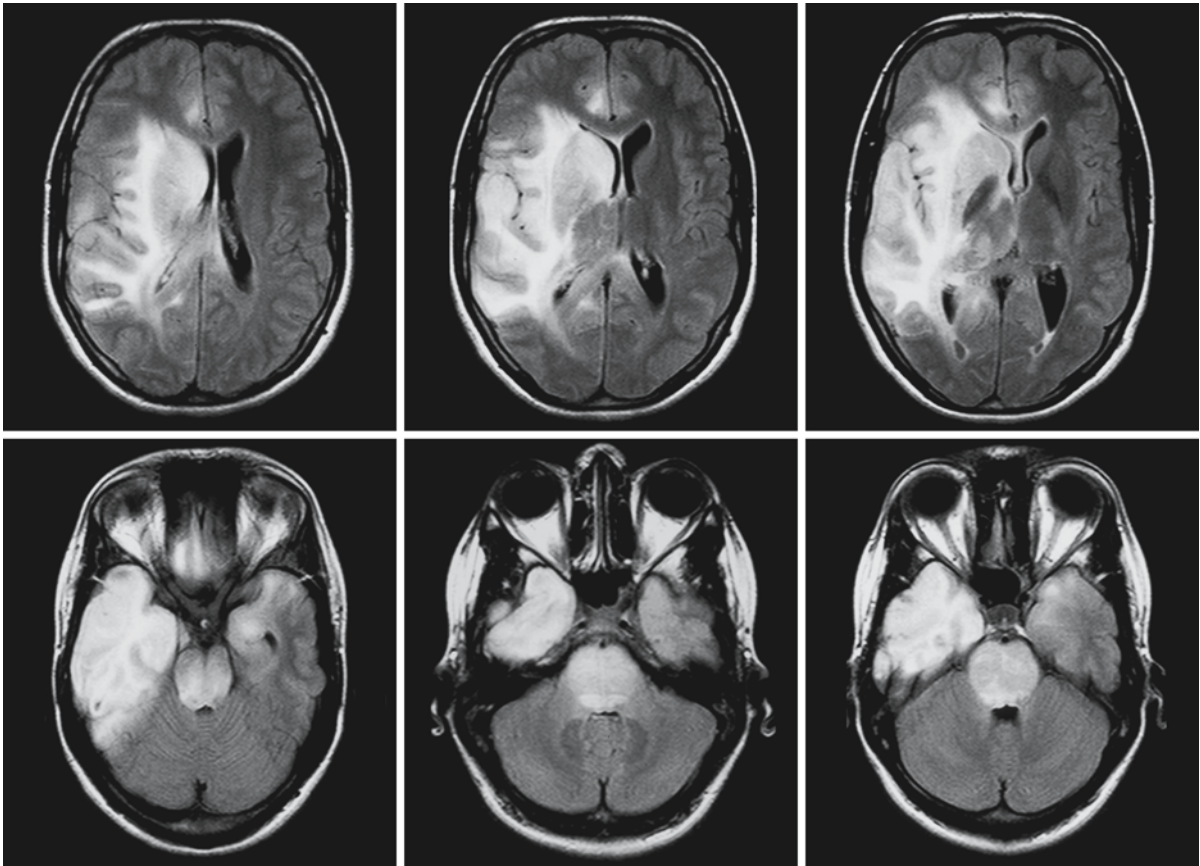


Fig. 103.4. Follow-up study of the same girl shown in Fig. 103.3, 6 months after radiotherapy and chemotherapy. It is clear that the process has advanced and the brain stem is seriously involved

There may be a striking symmetry of the abnormalities (Fig. 103.1), although this may disappear when the disease progresses. The disease may also be highly asymmetrical in the initial stage (Fig. 103.4). In some patients the spread of the disease clearly follows white matter tracts, with less severe involvement of gray matter structures. Focal calcification has been reported.

In most cases, there is no or only partial enhancement of the involved structures after contrast injection. This, however, depends on the technique used. With triple-dose gadolinium one may see some enhancement; a delayed scan (e.g., 1 h delay) may show enhancement in an unexpectedly large area (Fig. 103.3). Leptomeningeal dissemination may be observed, the disseminated lesions showing contrast enhancement.

Diffusion-weighted imaging with ADC maps is useful, in combination with chemical shift imaging and perfusion imaging, to find the places with the highest malignancy to direct a brain biopsy, when considered necessary, or to direct a local boost or intensity-modulated radiotherapy. In the affected areas MRS shows decreased *N*-acetylaspartate, normal or increased choline, and, in some patients, strikingly increased *myo*-inositol. *Myo*-inositol is exclusively present in glial cells.

The MR pattern of the disease is nearly always diagnostic. In cases with central location and symmetrical involvement of the thalamus, central venous thrombosis has to be excluded, for which purpose MRA can be used. Postictal changes may mimic the MR appearance of gliomatosis cerebri. In these cases the abnormalities disappear within 14 days.

Diffuse Axonal Injury

104.1 Clinical Features and Laboratory Findings

Head trauma, especially in motor vehicle accidents, can lead to a wide spectrum of cerebral and intracranial lesions, with usually different clinical presentations (epidural and subdural hematomas, subarachnoid and intracerebral hemorrhages, cerebral contusions, generalized cerebral edema, and secondary phenomena, such as hydrocephalus, raised intracranial pressure, and tentorial herniation), and different findings on CT and MRI.

About 50% of patients with traumatic acceleration–deceleration injuries are diagnosed with diffuse axonal injury (DAI), also called shearing injury. Clinically, DAI is characterized by loss of consciousness following the accident, usually without a lucid interval, a very low score on the Glasgow Coma Scale, and discrepantly subtle abnormalities on CT scans. When lesions are seen on CT, they consist mainly of petechial hemorrhages at the cortico-subcortical junction, in the body or splenium of the corpus callosum, and/or in the basal ganglia and brain stem.

Intracranial pressure measurements in patients with DAI are, at least in the beginning, normal, in contrast to the case with most of the other brain injuries.

DAI may result in death. It is unclear how often death occurs in DAI, but one may assume that it occurs in a high percentage of the patients. When it comes to a correct estimation of the frequency of death, the problem is that numbers provided by different specialists – neurologists, traumatologists, and neuropathologists – are not consistent. In some reports (by neurologists) it is stated that DAI rarely results in death, whereas others (neuropathologists) claim that DAI is an important cause of death in acceleration–deceleration trauma. This difference is at least partly due to the different populations they encounter. About 90% of patients with a clinical diagnosis of DAI, however, will remain in a vegetative condition.

In the first episode patients with DAI stay in the intensive care unit, in many cases artificially ventilated. During this period it would be important for the management of these patients to have a reliable prediction of outcome, most importantly to maintain the option to discontinue treatment that will not further improve the condition of the patient. Clinical and neurophysiological data are important in that re-

spect. EEG will reflect the seriousness of the functional disturbance of the brain, and will provide important information. MRI, in particular with more recent MR techniques, such as diffusion-weighted imaging, perfusion imaging, and MRS, may be helpful in predicting outcome.

104.2 Pathology

Pathological findings depend heavily on the time between the initial accident and the postmortem analysis. Because of the many secondary reactions that occur after the initial trauma, histological findings may be different in different stages. Unfortunately, very often the time between the accident and death is not reported.

In general, macroscopic findings may be normal or reveal focal atrophy, either cortical or in the rostral part of the brain stem. In early cases brain edema may be severe and tentorial herniation may be present.

Microscopic examination may demonstrate that axons are torn completely, but more often the damage is incomplete. Focal alterations in the axoplasmic membrane may result in impairment of the axoplasmic transport. Swelling ensues and the axon is dissected. Early damage to the axons is shown by the presence of large numbers of eosinophilic and argyrophilic bulbs on nerve fibers, forming the so-called retraction balls, the pathological hallmark of shearing injury. Macroscopically, lesions in DAI are usually ovoid or elliptical, following the long axis of the injured axons. Their distribution is not uniform or symmetrical, but they occur particularly at the junction of gray and white matter, in the corpus callosum, septum, fornix, internal capsule, deep gray matter, tegmentum, and cerebellar foliae dorsal to the dentate nuclei. The lesions are often hemorrhagic; the hemorrhages occur in a linear pattern, following the distortion of layers. In later stages, atrophy dominates the picture. Of the basal ganglia, the lateral and ventral nuclei of the thalamus are most atrophic, usually with sparing of the anterior and dorsomedial nuclei, the pulvinar, the centromedian nuclei, and lateral geniculate bodies. Cholinergic neurons have been found to be more susceptible than neurons belonging to other categories of neurotransmitters. Immunocytochemical staining for β -amyloid precursor protein (β -APP) detects with great sensitivity axons that have im-

paired fast axonal transport. In normally functioning axons β -APP is transported with fast axonal transport and never builds up to a concentration that allows its detection in tissue samples. When this fast axonal transport system is damaged, β -APP rapidly accumulates in the disrupted segment. This accumulation occurs before morphological methods detect the axonal damage. It is not known whether axonal damage thus detected is potentially reversible. The β -APP staining technique has demonstrated that even in apparently minor head trauma damage may occur to axons. In animal experiments there is a good correlation between the amount of axonal damage and the clinical outcome.

104.3 Pathogenetic Considerations

DAI is a shearing injury. It has been found experimentally that shearing injury is not induced by linear or translational forces but rather by rotational forces. A sudden acceleration–deceleration impact can produce rotational forces. Where the lesions occur depends on the distance to the rotational center, the arc of rotation, and the duration and intensity of the force. Because of the relative fixation of certain parts of the brain to the rigid skull, the deep and superficial portions may not move at the same rate and can even move in different directions. This will result in shear strain that manifests across the axons and results in axonal injury and rupture. Different brain parts have different consistencies depending on cell composition and cell density. Injuries to the brain will be most prominent at their junction, where differences in tissue densities are greatest. One such vulnerable site is the gray–white matter junction, involved in 60–70% of patients with DAI. Other vulnerable sites are the corpus callosum, corticospinal tracts, basal ganglia, and the brain stem. The initial damage to the brain is followed by secondary reactions related to hemorrhage, edema, changes in local perfusion, and triggering of biochemical cascades. Swelling of the brain may lead to tentorial herniation; swelling of the brain stem may lead to hydrocephalus. Disruption of neuronal and axonal connections leads to wallerian degeneration and atrophy.

It is probably the extent of the lesions and the involvement of the rostral brain stem that leads to the vegetative state in many of the patients. It is thought that damage to the rostral part of the brain is the cause of a reduction in dopamine turnover. In the first few hours after the traumatic brain injury, catecholamines in the CSF are raised. Soon the catecholamine production is chronically decreased and the levels in the CSF drop. Plasma norepinephrine levels have been shown to correlate with the Glasgow Coma Score and may correlate with the outcome of

brain injury. Homovanillic acid, a breakdown product of the adrenergic neurotransmitter systems, is significantly decreased soon after brain injury, and the level correlates with the depth of coma.

104.4 Therapy

Dopamine, one of the catecholamines, is an important neurotransmitter in the CNS. In DAI a reduction of dopamine turnover has been found. This observation has prompted the introduction of amantadine (Symmetrel) therapy in DAI. Amantadine is a drug known from treatment of Parkinson disease. Amantadine causes release of dopamine from central neurons, facilitates dopamine release by nerve impulses, and delays the uptake of dopamine by neural cells. It may also have a profound *N*-methyl-D-aspartate receptor antagonist effect, which may contribute to the neuroprotective effects after injury, by decreasing glutamate concentrations and thus excitotoxicity. In a randomized crossover design study in DAI patients, there was a consistent trend toward more rapid functional improvement with amantadine treatment, regardless of when during the first three months after injury the amantadine treatment was started (Meythaler et al. 2002). From these findings it is also clear that medication that results in dopaminergic blockade is contraindicated in the early stage of recovery from DAI.

104.5 Magnetic Resonance Imaging

In emergency departments CT is usually the first imaging modality used in cases of head trauma. In most presentations of head trauma CT is capable of producing a correct diagnosis. CT has the advantage over MRI of more clearly showing skull fractures. In DAI there is usually a discrepancy between the depth of the coma as expressed in the Glasgow Coma Score and the lack of or subtle findings on CT (Fig. 104.1). White matter abnormalities develop over time (Fig. 104.1).

MRI is the best imaging modality by which to confirm the diagnosis and to classify the lesions, usually employing the grading scale of Gennarelli. This scale divides the findings into three groups: lesions with and without hemorrhage at the gray–white matter junction, especially in the temporal and frontal areas (type 1), combined with lesions in and around the corpus callosum (type 2), and with lesions in the basal ganglia and the rostral brain stem (type 3). The scale roughly correlates with outcome.

Conventional MRI with T_1 -weighted, T_2 -weighted, T_2^* -weighted, and FLAIR images is more sensitive in depicting tissue changes than is CT (Figs. 104.2–

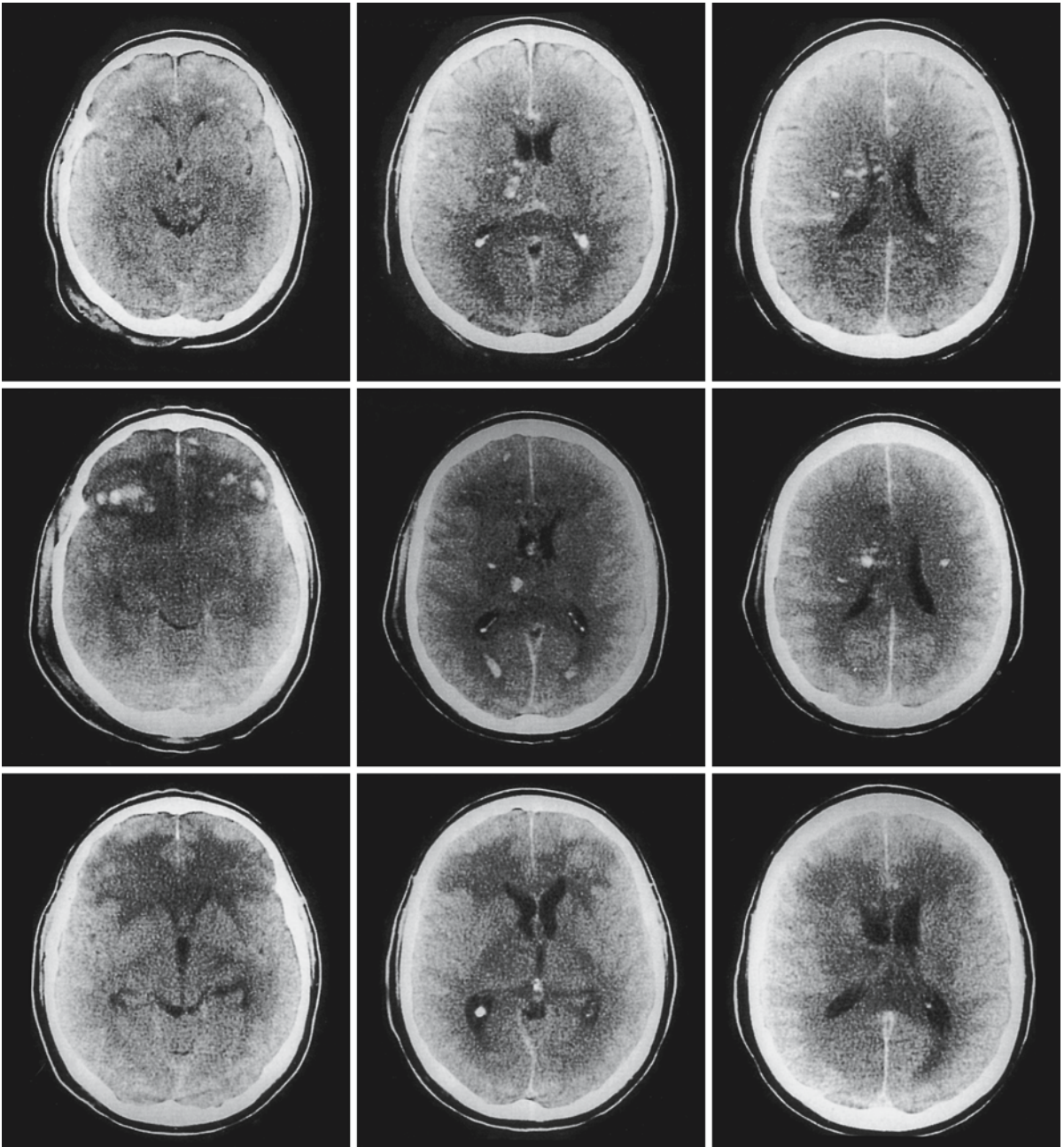


Fig. 104.1. A 36-year-old man with severe head trauma. The *first row* of images, obtained on admission, shows evidence of white matter shearing in the frontal subcortical region, corpus callosum, basal ganglia, and thalami with presence of small hemorrhages. The *second row* of images, obtained 1 week later, shows the hemorrhages to be more pronounced. There is

a developing leukoencephalopathy in the frontal region. The *third row* shows the images obtained 6 weeks after the accident. The hemorrhages have now disappeared. The frontal cortex seems intact, whereas the frontal white matter is hypodense, related to wallerian degeneration

104.5). The role of T_2^* -weighted images in establishing the diagnosis is considerable. Even early on hemosiderin deposits depict the linear nature and multiplicity of lesions (Figs. 104.2 and 104.5). The role of MR is even more pronounced when newer tech-

niques, such as diffusion-weighted images with Trace and ADC maps, tensor diffusion imaging with fractional anisotropy and fiber tracking, perfusion imaging, and magnetization transfer ratio maps are added to the protocol. These techniques allow assessment of

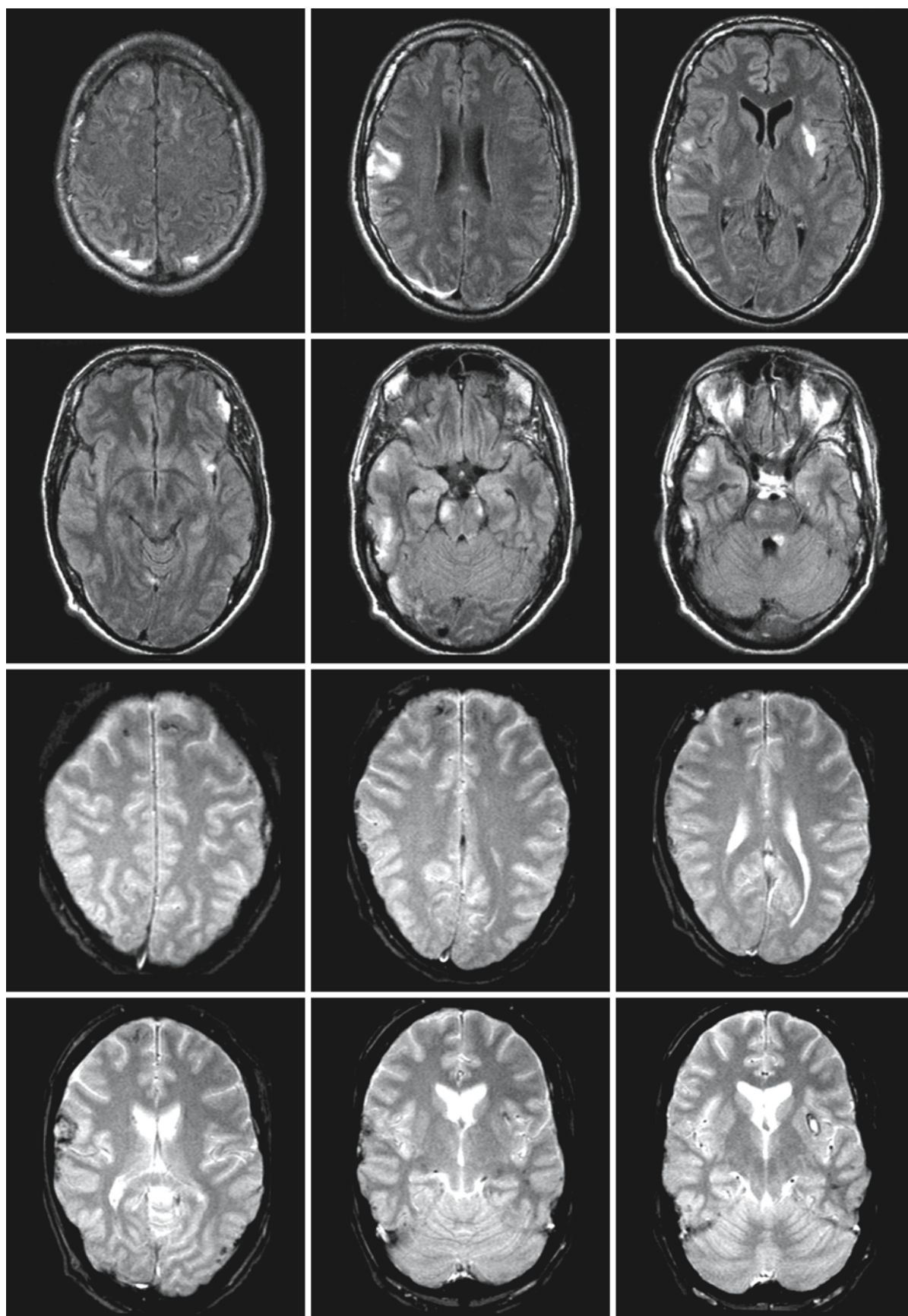


Fig. 104.2.

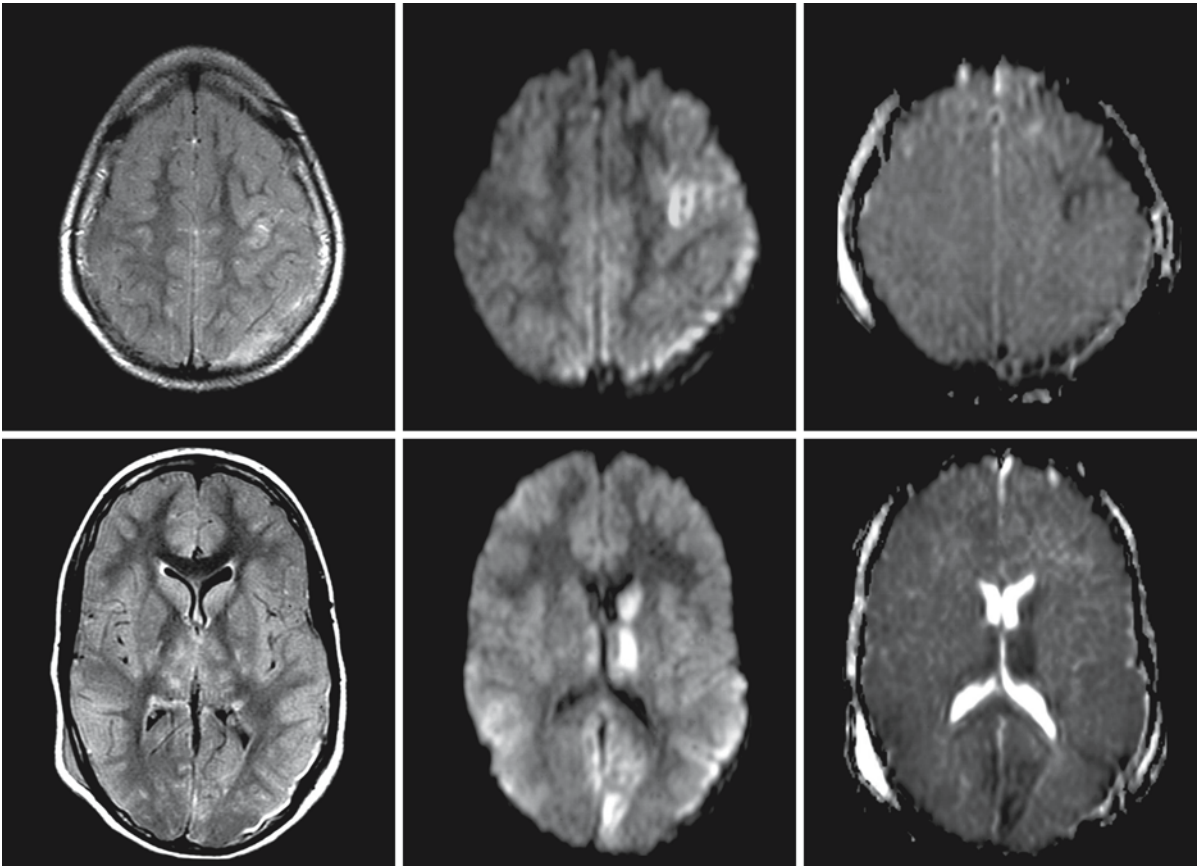


Fig. 104.3. A 14-year-old girl was the victim of a traffic accident. The FLAIR images on the *left (first column)* show some subdural blood in the left occipital region and a lesion in the left frontal lobe. There are lesions in the basal ganglia and thalami. Diffusion-weighted Trace images (*second column*) show

the lesions with greater conspicuity, especially those in the basal ganglia, thalami, and the medial parts of the occipital lobes. ADC values (*third column*) are low (<40–50% of normal values) in the affected areas

the presence and extent of lesions at an early stage, of the loss of structural integrity, and of changes in brain perfusion.

Diffusion-weighted imaging, commonly using a combination of Trace diffusion-weighted images and

ADC maps, is extremely sensitive in depicting post-traumatic changes at a very early stage. Most of the lesions show a high signal on the Trace diffusion-weighted images. Many of these lesions show a lower than normal ADC value (Figs. 104.3 and 104.6). It remains to be seen whether, as suggested, lower ADC values correspond with poorer outcome.

It is too early to describe the potential role of diffusion tensor imaging in combination with fiber tracking. One can imagine that fiber tracking may illustrate the disrupted connections in the brain and predict the loss of local functionality.

MRS has been repeatedly mentioned as capable of better predicting the functional outcome of brain injuries. The MR parameter used in these studies is the *N*-acetylaspartate concentration. The *N*-acetylaspartate concentration is thought to reflect the quantity and integrity of axons and neurons in the voxel. Since axonal damage is a good predictor of outcome, there is obviously a role for MRS. The drawback here is that

Fig. 104.2. A 43-year-old female, hit by a car, remained comatose with low Glasgow Coma Scale values. The FLAIR images (*first and second rows*) show small lesions at the cortico-subcortical junction in both frontal lobes, a small hemorrhagic lesion in the posterior corpus callosum, contusions in the right frontal operculum and the left putamen, blood around the parieto-occipital lobes on the right, a contusion in the right temporal lobe, and bilateral lesions in the midbrain, pons, and left superior cerebellar peduncle. Gradient echo images (*third and fourth rows*) show hemosiderin deposits in some of the lesions, especially in the cortico-subcortical lesions in the frontal lobes

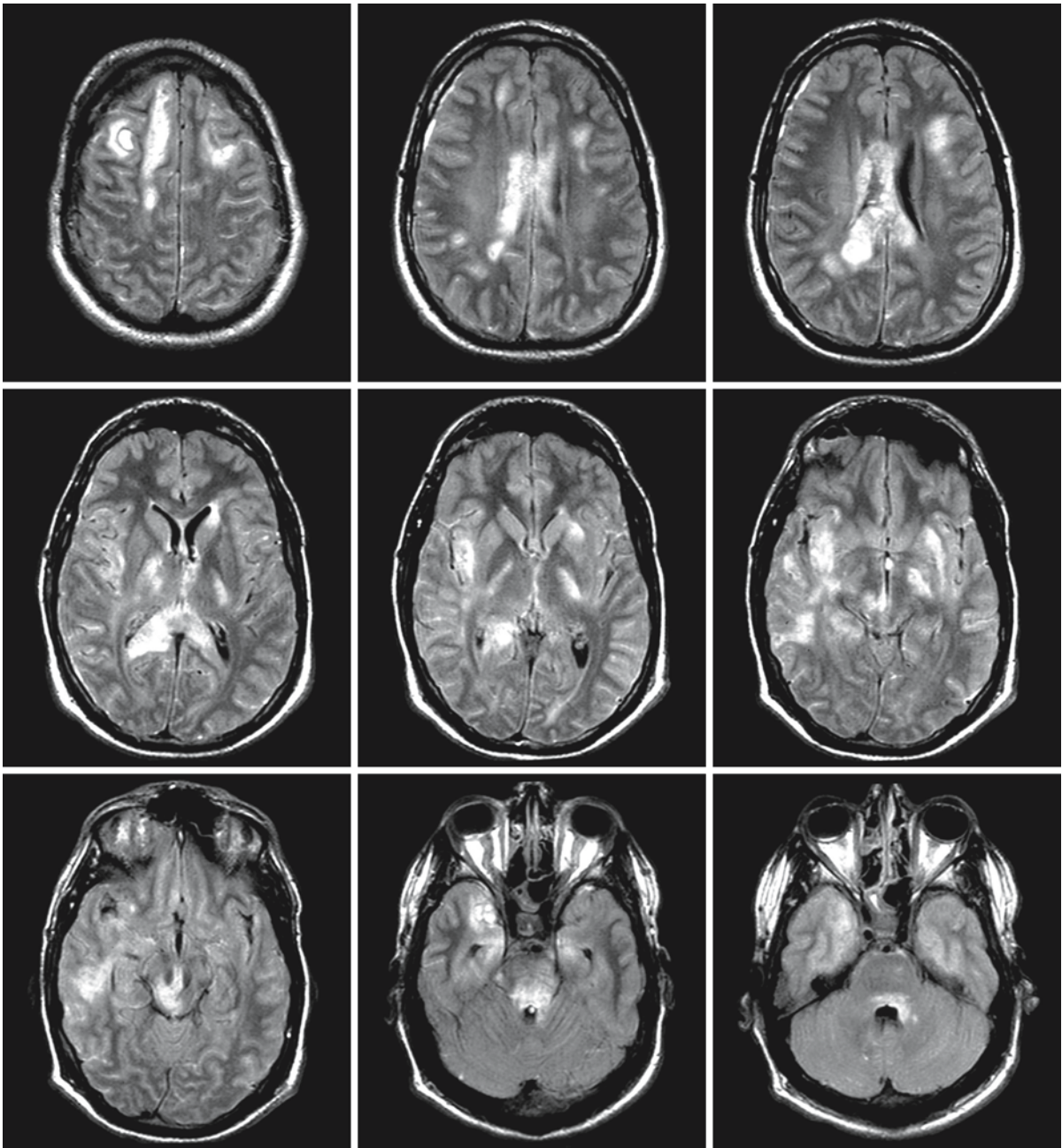


Fig. 104.4. Series of transverse proton density images of a 32-year-old man who was involved in a frontal collision show lesions at the cortico-subcortical junction, in the truncus and splenium of the corpus callosum, basal ganglia, thalamus, pos-

terior limb of the internal capsule, and in the rostral brain stem. All three types of the Gennarelli scale are present in this patient (see also Fig. 104.7)

in most studies MRS is postponed until the patient is in a stable condition, which means a considerable time interval between the accident and the performance of MRS, varying between 3 and 35 days.

The most important patient management decisions should ideally be made in the first 2 weeks, when patients are still in the intensive care unit and ventilator-dependent.

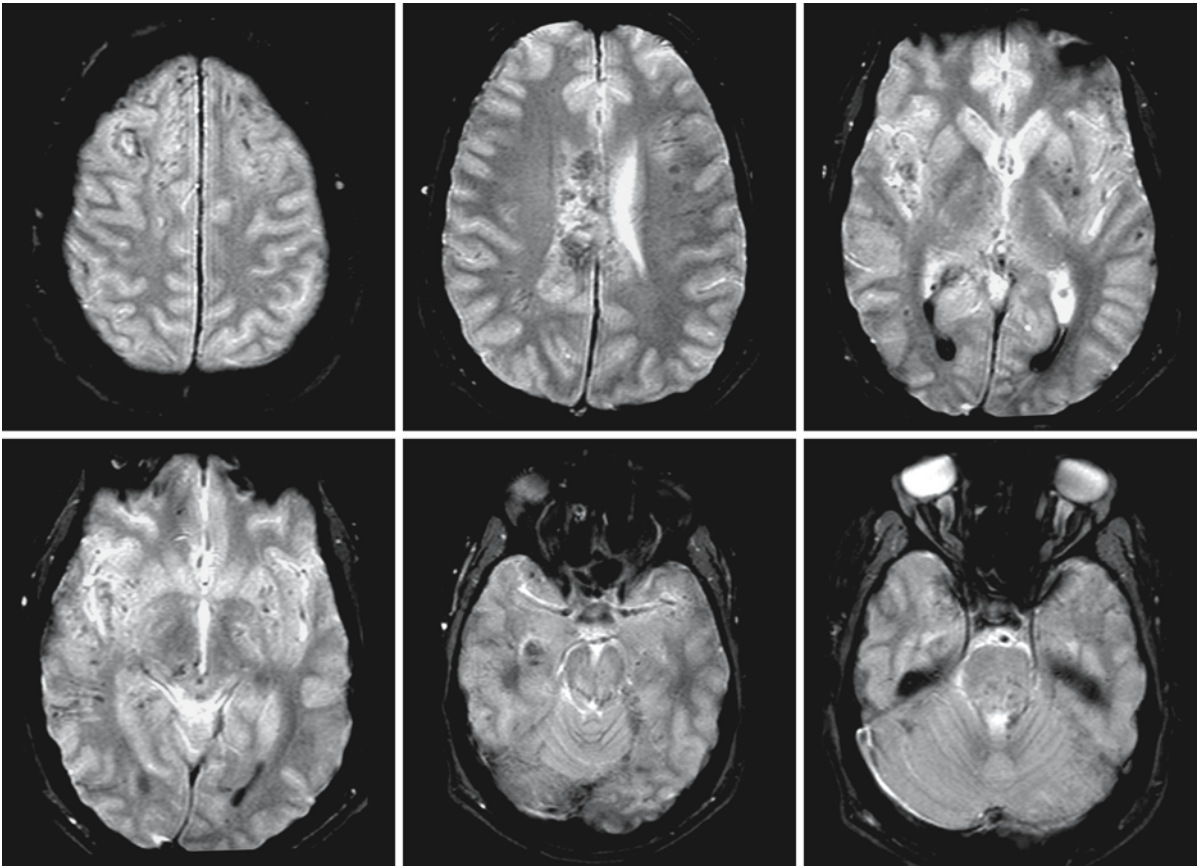


Fig. 104.5. Gradient-echo (FLASH) images of the same patient as in Fig. 104.4 show the hemorrhagic component in each of the lesions. Blood has also leaked into the ventricles

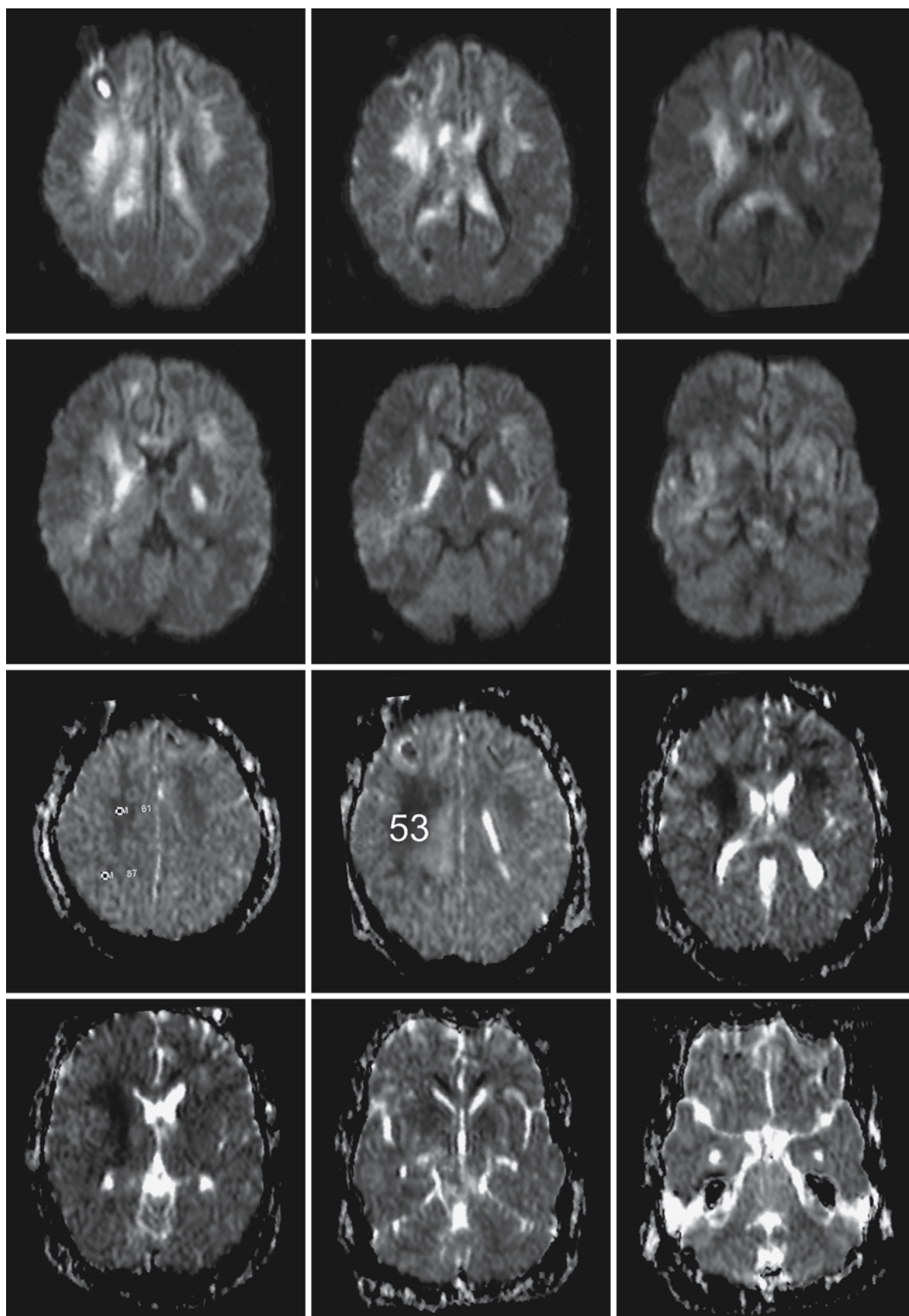


Fig. 104.6.

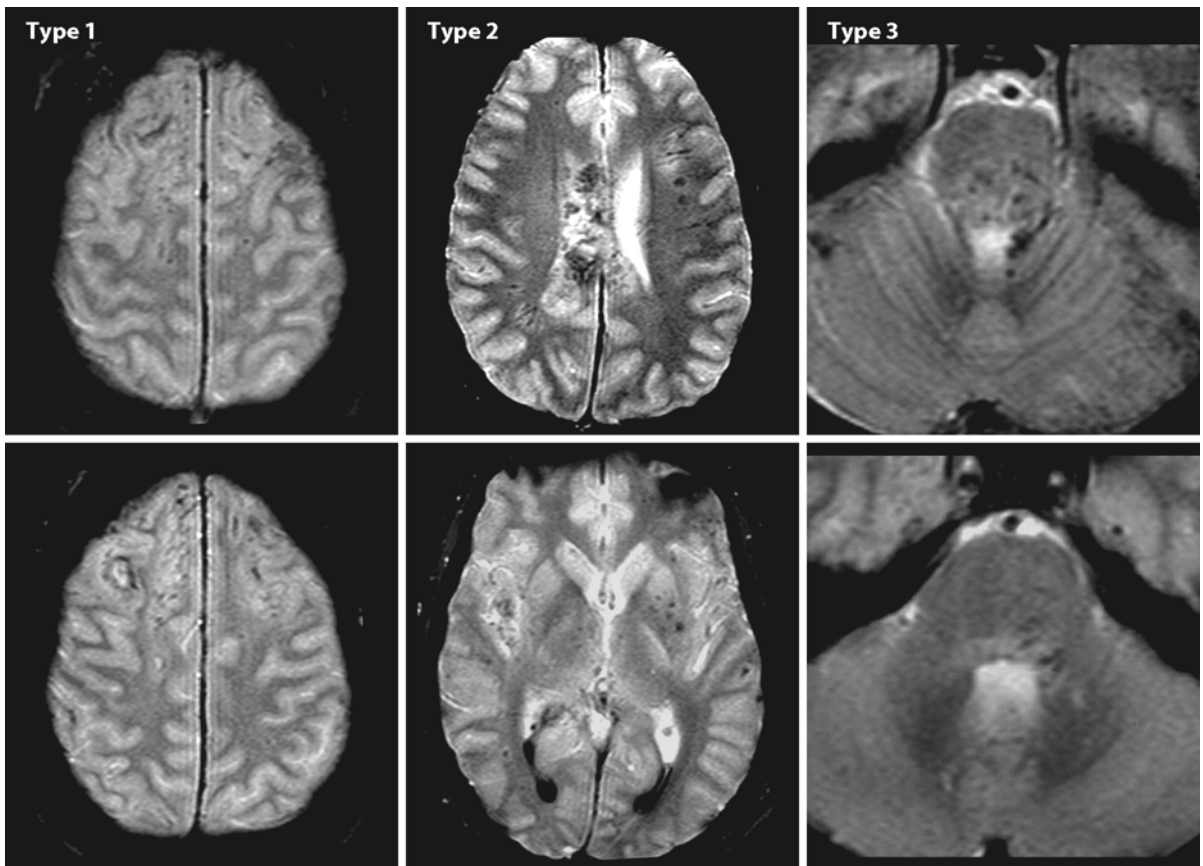


Fig. 104.7. The three types according to Gennarelli are all present in this patient and shown in this figure. The images on the left (*first column*) show the cortical lesions. The middle images (*second column*) reveal the corpus callosum lesions. The images on the right (*third column*) demonstrate the brain stem lesions

Fig. 104.6. Diffusion-weighted Trace images of the same patient as in Figs. 104.4 and 104.5 (*first and second rows*, $b = 1000$) show high signal intensity in nearly all lesions. ADC maps (*third and fourth rows*) show very low values (as low as $0.53 \times 10^{-3} \text{ mm}^2/\text{s}$, normal $0.85\text{--}0.95 \times 10^{-3} \text{ mm}^2/\text{s}$) in some of the lesions

Wallerian Degeneration and Myelin Loss Secondary to Neuronal and Axonal Degeneration

105.1 Introduction

There are basically two causes of wallerian degeneration in our definition: neuronal cell death and axonal lesions. It should be noted that our definition is wider than usual and includes not only acute axonal lesions, but neuronal and axonal lesions of any kind. Degeneration of the entire arborization of a neuron with its axon and axonal branches inevitably follows necrosis of the neuronal cell body. Examples are degenerative diseases affecting neuronal cell bodies and axons, such as amyotrophic lateral sclerosis, Friedreich ataxia, olivopontocerebellar atrophy, and neuronal ceroid lipofuscinosis. A lesion of the axon that leads to an interruption of its continuity gives rise to degeneration of the distal part, whereas the proximal portion as a rule survives. The myelin in the distal portion undergoes dissolution as a consequence of the axonal degeneration, as the integrity of the myelin sheaths depends on continued contact with a viable axon. The changes in the distal part of the interrupted nerve are called wallerian degeneration in a narrower sense, following Waller's original description of the changes that he observed after cutting the glossopharyngeal and hypoglossal nerves in the frog in 1850.

Any lesion of axons that leads to an interruption and any lesion of nerve cell bodies that leads to cell death are followed by wallerian degeneration. In all white matter disorders, wallerian degeneration eventually plays a role, as myelin loss is followed by secondary axonal degeneration, which in turn is followed by wallerian degeneration of the distal parts of the axons and their myelin sheaths. Wallerian degeneration as such cannot be considered a condition that primarily affects myelin. Nevertheless, wallerian degeneration with myelin loss secondary to neuronal and axonal degeneration are discussed here as a component of all disorders and because the MRI appearance may be mistaken for primary white matter affection. This is especially the case when the cortex and the neuronal cell bodies are unaffected. An example is the traumatic shearing of nerve fibers, which may lead to bilateral extensive white matter degeneration, whereas the cortex is remarkably normal.

105.2 Pathology

Characteristic of wallerian degeneration is the fact that the sequence and timing of its changes are highly stereotyped. The cascade of events is similar in the PNS and CNS, but much slower in the CNS. Most experimental studies of wallerian degeneration in the CNS have been carried out in the optic nerve, degenerating as a result of enucleation of the eye. Tract degeneration in the dorsal column of animals has also been studied after myelotomy. Human studies mainly concern wallerian degeneration after hemorrhage, stroke, tumors, and traumatic lesions.

Abnormalities in axons severed from their neuronal perikarya precede changes in the myelin sheath. There is no spatiotemporal gradient of degradation: abnormalities appear over the whole length of the axons simultaneously. About 8–15 days after the event, the axons have disintegrated, whereas the myelin still appears normal. Most axonal debris disappears from degenerating tracts within about 1 month. In the process of wallerian degeneration, degradation of myelin sheaths becomes apparent after 30–90 days and the myelin sheaths disintegrate. The breakdown of myelin into simpler lipids does not start until after about 100 days and takes place in the cytoplasm of phagocytic cells.

The pivotal process of wallerian degeneration is granular disintegration of the cytoskeleton, in which the normal cytoskeletal elements of the axon, the neurofilaments and microtubules, are abruptly depredated to granular and amorphous debris. This change occurs throughout the distal stump in the first 48 h after dissection. Granular disintegration of the cytoskeleton is the result of the activation of ion-sensitive proteases within the distal stump. A rise in intra-axonal calcium to critical levels initiates the proteolysis of the axoplasm. The reason for the rise in calcium is still unclear. Some evidence suggests that macrophages may also participate in the granular disintegration of the cytoskeleton: anti-macrophagic antibodies appear to delay axonal breakdown. The proteases, however, appear to be intrinsic to the axon. Granular disintegration of the cytoskeleton is associated with loss of the axolemma as well as the axoplasm, so that the myelin sheath surrounds an apparently empty cylinder formerly occupied by the axon. The granular debris still contains some axonal residua, as shown by the ability to stain the degenerating

fibers by silver impregnation for long periods after axotomy, and by the staining with some anti-neurofilament antibodies, even in the absence of surviving filamentous organelles. Following granular disintegration of the cytoskeleton, the myelin sheaths lose their regular smooth outline and undergo segmentation into short portions with closed ends, termed “ovoids,” which break down into smaller globules. The myelin collapses radially upon itself, the lamellae become loose, and the periodicity of myelin is gradually lost. Clearing of the debris is performed by macrophages. Without macrophages there is no efficient clearing. In the PNS this is achieved by circulating macrophages; in the CNS the process is much slower and not completely understood.

Electron microscopy reveals the degenerating axons and axonal debris to be surrounded by myelin sheaths, occasionally irregularly folded. The myelin sheaths initially show a regular structure with major and minor dense lines and a periodicity of 105 Å. Splitting of myelin lamellae is noted. The structure of myelin lamellae continues to change with time, developing into uniformly layered structures with a periodicity of 40–50 Å. At this stage, the myelin degradation products become smaller and are phagocytosed. Unstructured lipid droplets as well as complex lamellar inclusions are typically found in phagocytic cells during the later stages of degeneration. Inclusions of unstructured lipid crystals are sometimes seen. In the final stages, numerous different inclusions are seen.

The role of oligodendrocytes in wallerian degeneration in the CNS is not clear. It is probable but not certain that oligodendrocytes do not participate, or participate only to a minor extent. Macrophages, astrocytes, and multipotent glial cells have been observed to contain myelin debris.

Histological evidence indicates that wallerian degeneration takes place at different rates depending on a number of variables. The most important factor in determining the course of the wallerian degeneration is whether the axonal or neuronal lesion is acute and monophasic or chronically progressive.

105.3 Chemical Pathology

Biochemical analysis of CNS myelin undergoing wallerian degeneration shows a gradual decrease in all myelin constituents but otherwise a remarkable normality in the composition of the remaining myelin. Only an increase in cholesterol esters and a slight decrease of ethanolamine phosphoglycerides have been demonstrated. Neither are any major abnormalities found in the protein constituents. Basic protein is lost from the myelin sheath relatively early in the process of myelin degradation, due to an increase in proteinase activity. This occurs before phagocytosis of

myelin by macrophages and astrocytes and results in transformation of myelin sheaths into uniformly layered lipid structures. Cholesterol esters are the major constituents of the lipid droplets and the crystal inclusions of phagocytic cells. The change in biochemical composition of whole white matter depends on the extent of myelin loss. Cholesterol esters are relatively elevated.

105.4 Pathogenetic Considerations

Wallerian degeneration entails both breakdown of the axon and clearance of myelin from the distal stump of the transected nerve fibers as described in the previous paragraph. Wallerian degeneration is one of the most prevalent types of cellular pathology in nervous system disease.

The pathogenesis of wallerian degeneration depends largely upon the type of initial injury. The time schedule differs according to whether the lesion occurs acutely (as in stroke, intracerebral hemorrhage, and traumatic diffuse axonal injury), more slowly (as in progressive neurodegenerative disorders such as amyotrophic lateral sclerosis, Friedreich ataxia, neuronal ceroid lipofuscinosis, and Alzheimer disease), or is accompanied by an inflammatory reaction (in infectious or inflammatory disease, such as multiple sclerosis and HIV encephalopathy).

The isolation of myelin retaining an almost normal protein and lipid composition despite wallerian degeneration as late as 90 days after the injury is consistent with the morphological evidence that in wallerian degeneration in the CNS the breakdown of myelin occurs mainly within the cytoplasm of phagocytic cells. It would seem that the myelin sheath is degraded as a unit, with nonselective digestion of myelin constituents, cholesterol esters being the only residual constituents.

A model of four stages of myelin degradation in wallerian degeneration has been proposed (Lassman et al. 1978a, b):

1. The stage of mechanical deterioration of myelin sheaths, showing normal myelin periodicity under the electron microscope.
2. The stage of degradation of digestible proteins, resulting in the transformation of myelin sheaths into uniformly layered structures.
3. The stage of lipid degradation, accompanied by the occurrence of unstructured lipid droplets and crystals in phagocytic cells.
4. The stage of deposition of poorly digestible lipids or lipoproteins, resulting in numerous different electron microscopic inclusion types in phagocytic cells. Resolution of tissue debris and atrophy are the final stage in the process.

These four stages are reflected in MRI.

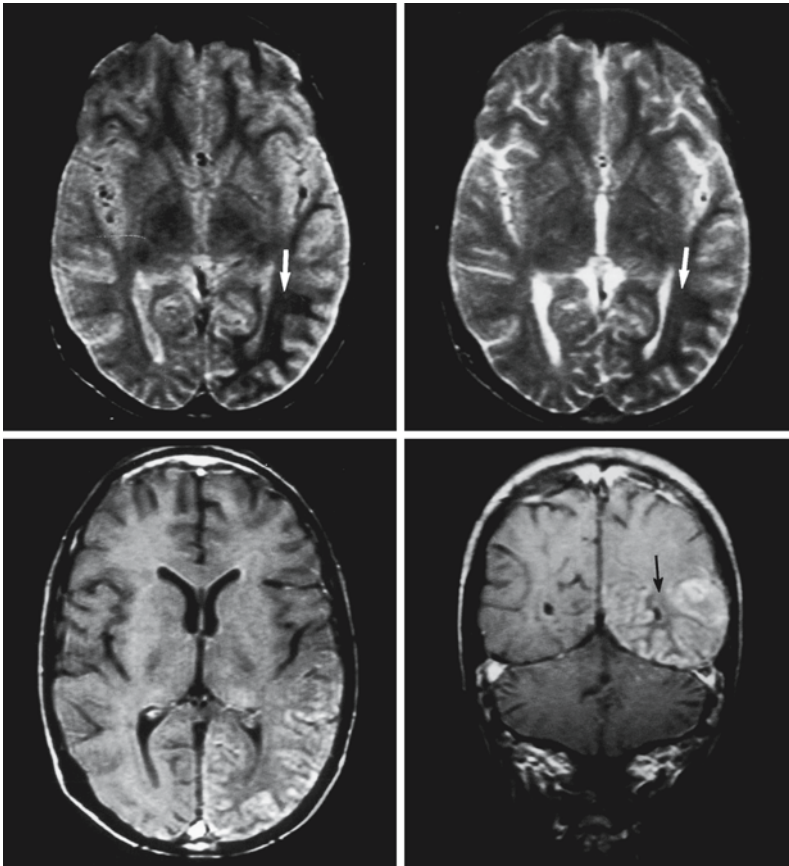


Fig. 105.1. A patient with subacute meningoencephalitis involving the leptomeninges over the left hemisphere and the cortex in the occipital region. On the T₂-weighted images (first row) the white matter underneath the affected cortex has a lower signal intensity than the white matter elsewhere. This represents the second stage of wallerian degeneration. The second row shows T₁-weighted images after contrast with occipital cortical enhancement

105.5 Magnetic Resonance Imaging

In the CNS, wallerian degeneration of long tracts can usually be well depicted. As a multiplanar modality, the MR plane can be chosen to depict the signal changes over their full length. Depending on the location of the primary lesion or lesions, wallerian tract degeneration can be unilateral or bilateral, and, if bilateral, symmetrical or asymmetrical. Normally the long tracts of densely packed white matter have somewhat lower signal intensity on proton density and T₂-weighted images than the remainder of the white matter. In wallerian degeneration the signal in the tract is lower or higher than usual compared to the normal white matter tracts, depending on the stage of degeneration. In fact MRI can help to distinguish the four stages of wallerian degeneration, each resulting from a rather well-defined phase in the process of degeneration:

1. Physical degeneration of the axon occurs first, with only mild biochemical changes. This happens in the first 2–4 weeks after the incident. This stage is not visible on conventional MR images.
2. The first stage is followed by myelin protein breakdown without myelin lipid breakdown. The resulting material with high lipid content is considered

to be hydrophobic, causing low signal intensity on proton density and T₂-weighted images. This occurs between 4 and 14 weeks after the incident (Fig. 105.1).

3. Next, myelin lipid breakdown starts to take place, with gliosis and increased water content, leading to a higher signal intensity of the involved tracts on proton density and T₂-weighted images (Figs. 105.2 and 105.3).
4. Finally, after a number of months to years, the abnormal tissue constituents are removed and atrophy results (Fig. 105.4).

Conventional MRI is able to depict stages 2–4. Although there is considerable overlap in time, each phase has been recognized. There is a crossover of contrast between the degenerating tract and the surrounding tissue between stages 2 and 3, “fogging” the MR depiction of wallerian degeneration.

Most attention has been paid to local wallerian degeneration following *acute focal* lesions and involving single tracts, most often sensorimotor tracts. *Acute diffuse* wallerian degeneration occurs in cases of diffuse axonal injury, with disruption of corticomedullary connections. The wallerian degeneration leads to diffuse white matter degeneration in the

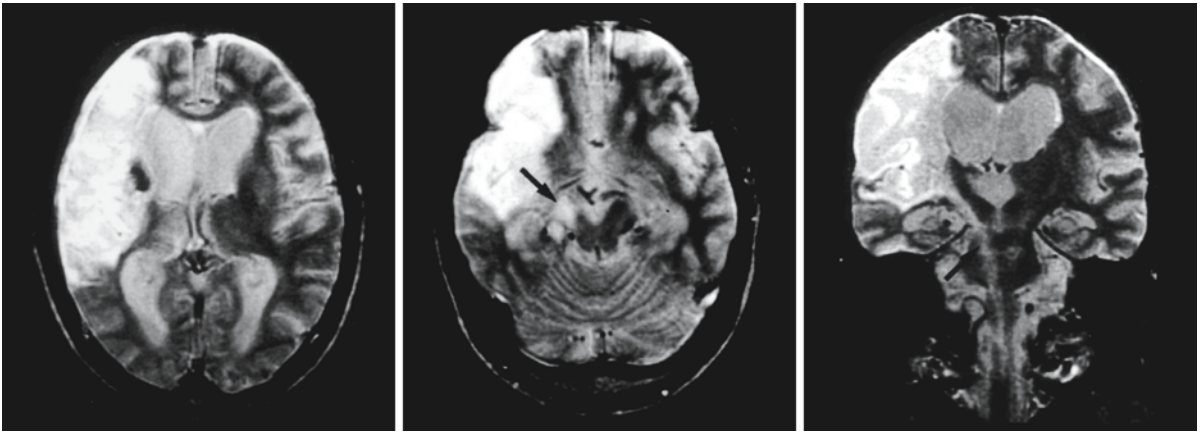


Fig. 105.2. The third phase of wallerian degeneration is clearly displayed on these T_2 -weighted images, showing the initial lesion and the corticospinal tracts undergoing wallerian de-

generation all the way down into the brain stem. From Waragai et al. (1994), with permission

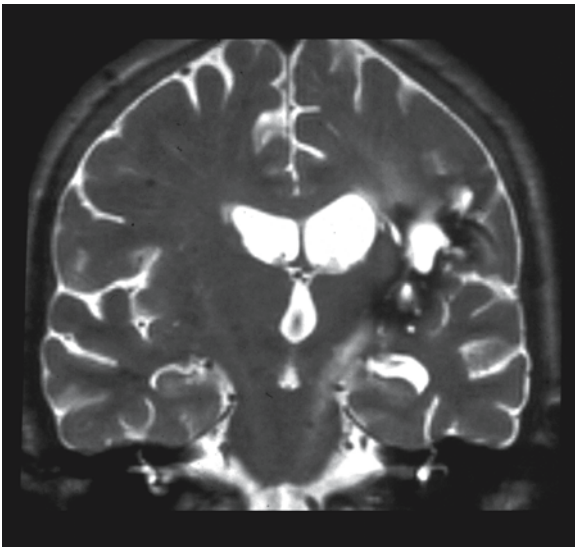


Fig. 105.3. Prototype of wallerian degeneration late in the third phase. The T_2 -weighted image shows a hemorrhagic lesion in the corona radiata on the left. Wallerian degeneration is seen in the corticospinal tract with high signal intensity. Atrophy is setting in

course of weeks (see Chap. 104). The subcortical and deep white matter have a low density on CT images and remarkably low signal intensity on proton density and T_2 -weighted MR images. This occurs in a phase where protein degradation is most prominent and lipid degradation still absent. In the next phase the involved area shows higher signal intensity on T_2 -weighted and FLAIR images. Finally, atrophy with focal gliosis results.

In addition, *focal or diffuse, low-grade* wallerian degeneration occurs in neurodegenerative disorders

with loss of neurons, such as in amyotrophic lateral sclerosis, neuronal ceroid lipofuscinosis, Niemann-Pick disease type C, Friedreich ataxia, Alzheimer disease, and in slowly developing inflammatory disorders. Neurons and axons disappear gradually and not all at the same time. That means that stages of wallerian degeneration overlap and that there are no stages to be visualized separately. In these disorders, MRI shows cortical atrophy and often, in addition, a slight to moderate increase of signal intensity in the cerebral hemispheric white matter (Fig. 105.5). The changes in normal-appearing white matter in relapsing-remitting and secondary progressive forms of multiple sclerosis are probably also, at least in part, the result of wallerian degeneration.

Wallerian degeneration has also been reported in the spinal cord, in particular in the posterior columns. This occurs after trauma of the spinal cord or in the course of a myelopathy, either caused by degenerative changes of the vertebral column, or by infectious or inflammatory lesions. From the lesion in the spinal cord wallerian degeneration occurs in two directions: downwards in the motor tracts, and upwards in the sensory tracts. In some degenerative cases there is a gap between the location of the original myelopathic lesions and the wallerian degeneration, the latter becoming visible several segments higher in the afferent tracts. Given time, the parts in between also show signal intensity changes in the affected tracts.

To improve the detection of wallerian degeneration on MR, special techniques, such as diffusion-weighted imaging and magnetization transfer ratio (MTR) measurements can be used. The most important advantage is that with these techniques changes can be detected in an earlier phase than with conventional MRI. In the first stage of wallerian degeneration

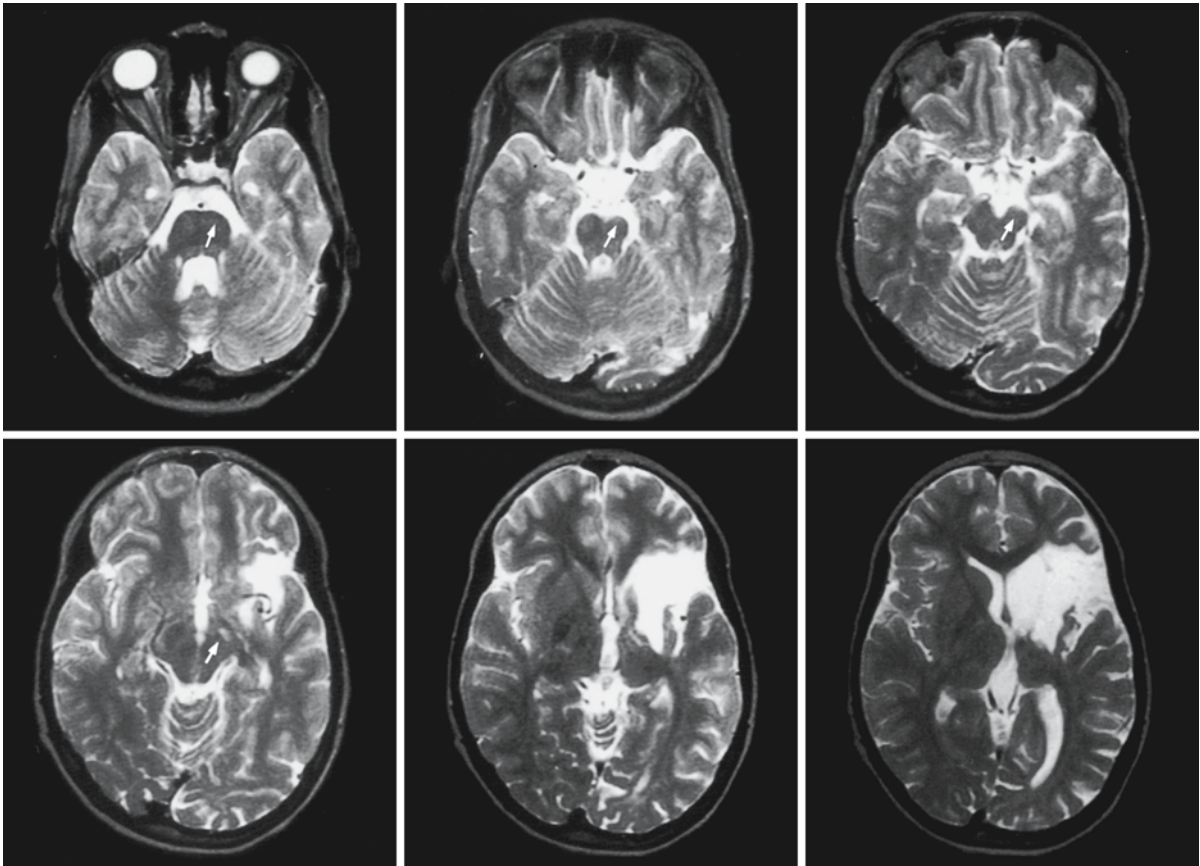


Fig. 105.4. T₂-weighted transverse series show a left opercular infarction. In the fourth stage of wallerian degeneration, atrophy results, as is shown in the brain stem (arrows)

tion following an acute lesion, diffusion-weighted imaging reveals a decreased apparent diffusion coefficient in the tracts involved in the degenerative process (Figs. 105.6 and 105.7), whereas the MTR in these tracts is increased, and anisotropic diffusion-weighted imaging or diffusion tensor imaging reveals loss of anisotropy in the affected tracts. The subsequent changes are more gradual and are progressive over time. From the second stage of wallerian degeneration onwards and continuing in the subsequent stages, the ADC is increased, MTR is decreased, and further loss of anisotropy occurs.

Long-term follow-up studies with diffusion tensor imaging in patients with more slowly progressive tract degeneration, such as in amyotrophic lateral sclerosis, show loss of anisotropy, decreased ADC val-

ues, and a decreased MTR in the tracts involved. The MTR shows changes in the affected tracts before there are abnormalities in T₂ that lead to signal changes on conventional images (including FLAIR). Follow-up studies show increasingly abnormal values over time. In contrast with wallerian degeneration following an acute incident, there is no transition from one phase of degeneration to the other.

MRS allows detection of changes in concentration of *N*-acetylaspartate in regions with loss of neurons or axons. Follow-up studies with MRS in patients with amyotrophic lateral sclerosis demonstrate that a marked decrease in the *N*-acetylaspartate/choline ratio is associated with the development of signs of upper motor neuron disease, and may even precede the appearance of pyramidal signs.

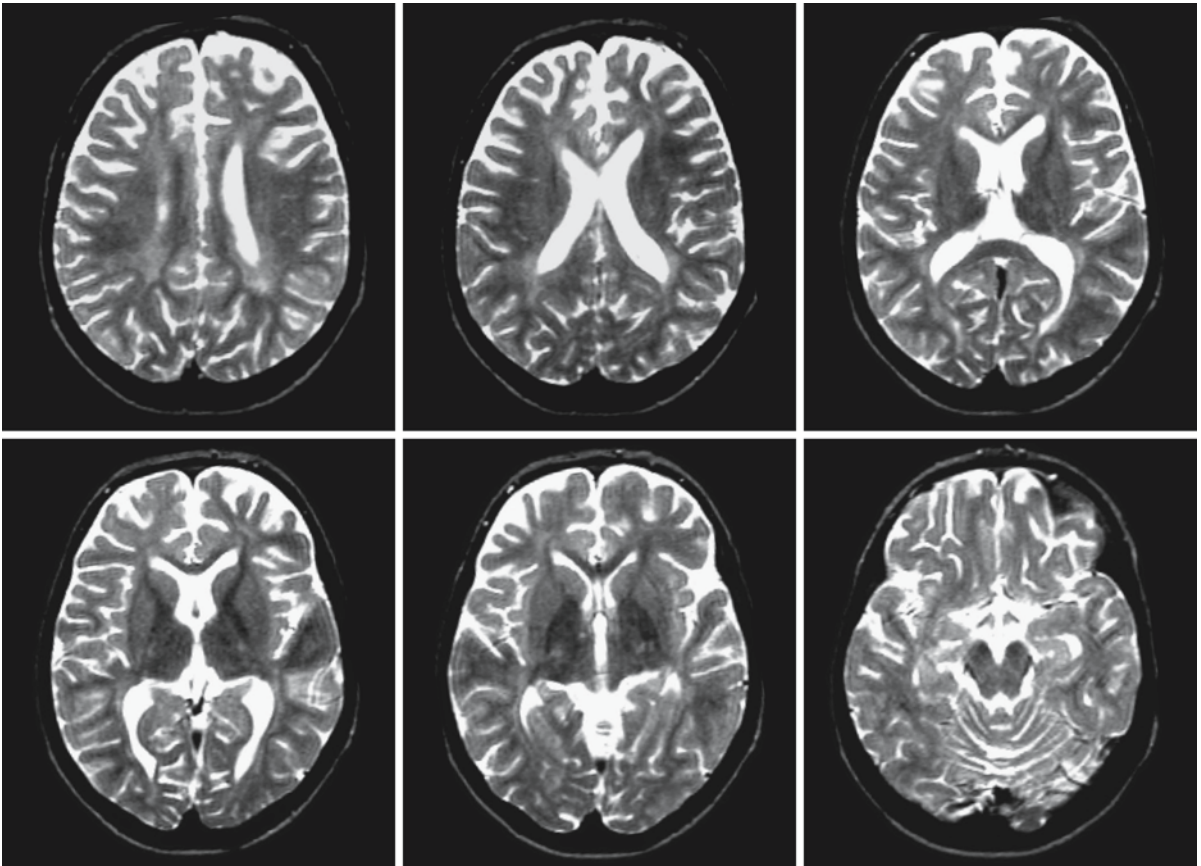


Fig. 105.5. In this 10-year-old boy with Niemann–Pick disease type C, wallerian degeneration is seen in the white matter, secondary to cortical neuronal loss. There is a diffuse increase in signal intensity of the cerebral white matter on T₂-weighted images and loss of distinction between gray and white matter.

Note the cerebral atrophy. A combination of atrophy and subtle white matter signal abnormalities is suggestive of primary neuronal or axonal degeneration rather than a primary myelinopathy

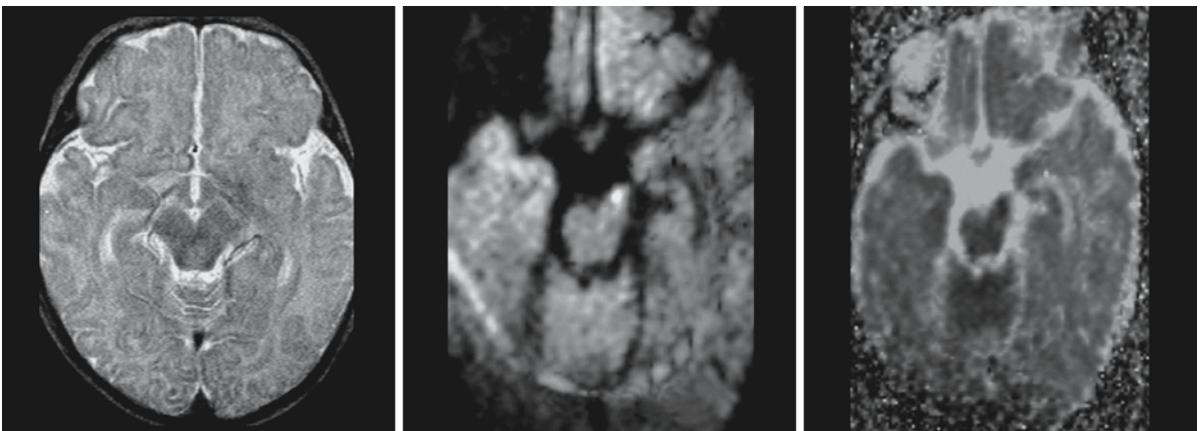


Fig. 105.6. A 5-week-old female infant with onset of seizures 3 days before the MRI. Neurological examination revealed right arm impairment. MRI reveals a left middle cerebral artery infarction. The images at the level of the midbrain are shown. The T₂-weighted image (*left*) reveals no abnormalities. The

Trace diffusion-weighted image (*middle*) reveals a high signal in the left cerebral peduncle, whereas the ADC map (*right*) reveals a decreased ADC in that area. From Mazumdar et al. (2003), with permission

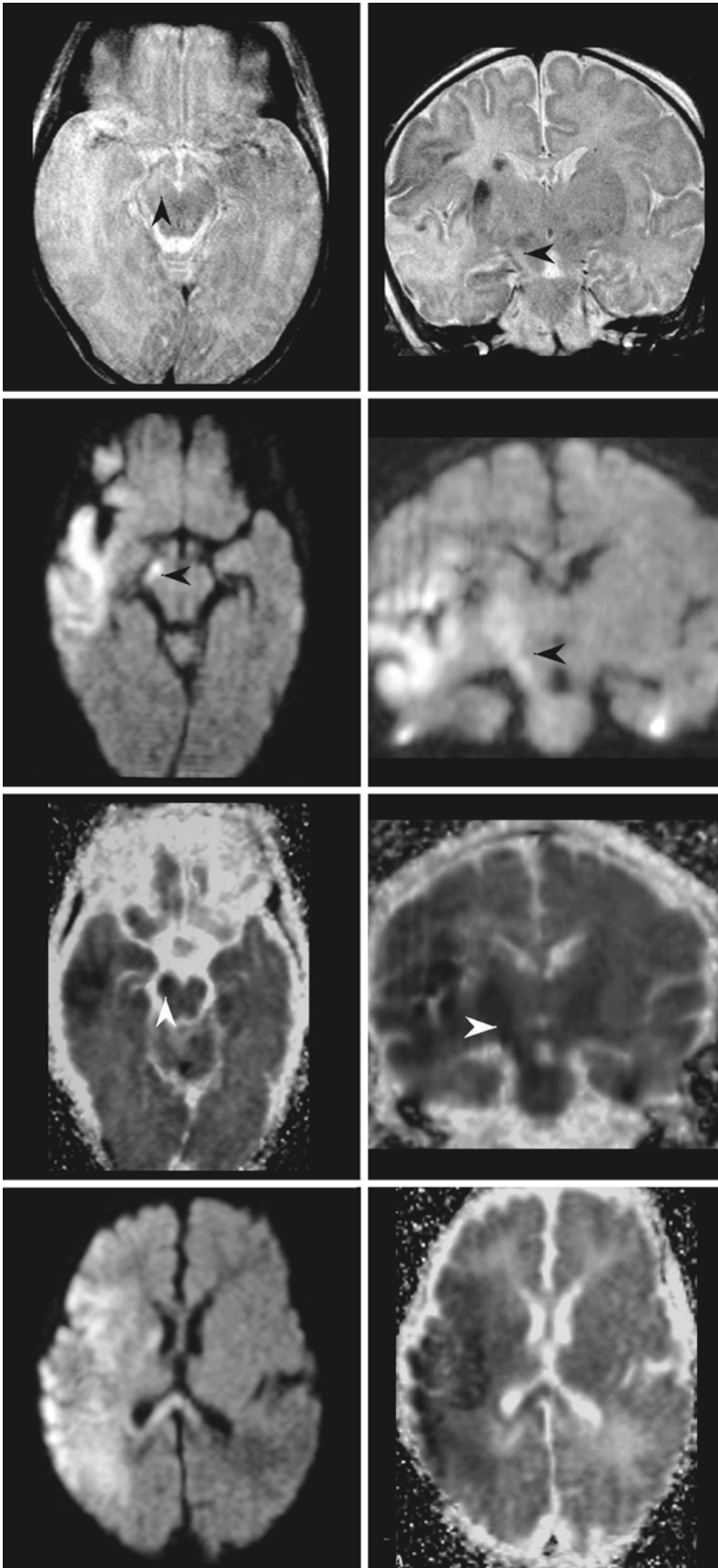


Fig. 105.7. A 4-day-old neonate with right middle cerebral artery infarction. The two images in the *first row* are T₂-weighted fast spin echo images (*left* transverse, *right* coronal). Increased signal intensity is present in the white matter of the right temporal lobe and insular region; the overlying cortex has a high signal in some parts, a low signal in others. A focus of hemorrhage is seen in the corona radiata and putamen. The images show abnormally high signal in the right corticospinal tract (*arrowheads*). Diffusion-weighted images (*second row left* transverse, *right* coronal) show increased signal intensity in the territorial infarct and the right cerebral peduncle (*arrowheads*). The corresponding ADC maps (*third row left* transverse, *right* coronal) show reduced ADC values in the infarcted region and the right cerebral peduncle (*arrowheads*). Images of the *fourth row* containing the transverse diffusion-weighted image (*left*) and corresponding ADC map (*right*) show involvement of the splenium of the corpus callosum with decreased diffusion. From Mazumdar et al. (2003), with permission

Diffusion-Weighted Imaging

106.1 Introduction

A drop of ink in a glass of water will spread throughout the water by a process known as diffusion. This phenomenon was first observed by Brown in 1827 and bears his name, brownian movement. His experiments, executed with *Clarkia* pollen spread on a water surface, led to wide speculations about the nature of the movements observed. "He suspended some of the pollen grains in water and examined them closely, only to see them 'filled with particles' that were 'very evidently in motion'. He was soon satisfied that the movement 'arose neither from currents in the fluid, nor from its gradual evaporation, but belonged to the particle itself'. In due course he was to carry out careful experiments to disprove these alternative explanations, and it has been shown that Brown was able to anticipate the later objections of those who would doubt his capacity to have observed what he claimed. It must have been tempting for Robert Brown to assume, as had other workers before him, that here was the very essence of life." (Ford, 1992)

Much later it became clear that the movement of particles was the result of random movement of water molecules. Temperature proved to be an important factor in determining the rate of the movement of molecules, and therefore the process is also referred to as thermodynamic movement. The human body consists to 60–80% of water. Molecular movements in the body are modified by complex tissue compartments. The brain, for example, consists of many different structures, restricting to a greater or lesser extent the free movements of water molecules. This leads to differences in diffusion of water molecules between different brain structures, which makes diffusion a potential source of image contrast. When water movement is relatively unrestricted in all directions, diffusion is *isotropic*; when restrictions are present in one or more directions, water movement is *anisotropic*. Diffusion in gray matter in adults is nearly isotropic; on the other hand, diffusion in white matter, with its compact and organized structure of myelinated axons and fiber tracts, is anisotropic. Disease states may also lead to changes in the freedom of water diffusion.

It has become possible, by using MR techniques with a spatial resolution in the order of square millimeters, to measure changes in the freedom of water

movement at the molecular level. MRI is based upon the resonance condition of protons brought about by a strong static magnetic field. Protons in this condition can absorb and subsequently release energy of a special frequency (resonance frequency). The response or released energy of the protons can be collected by coils placed around the body or a body part as the MR signal. The MR signal is used to reconstruct images and depends on many factors, such as pulse sequence, slice thickness, matrix, and number of acquisitions. The strength of the signal is ultimately the sum of protons in and out of phase in a pixel (picture element) or, more correctly, in a voxel (volume element). With all other parameters identical, the signal is at its maximum when all protons in a voxel are in phase. The signal decreases when a number of protons are out of phase (or dephased). Diffusion of water molecules leads to dephasing of protons and therefore loss of signal. This means that in MR images unrestricted diffusion leads to loss of signal and restricted diffusion leads to a smaller loss of signal. On a relative scale this means that tissue with restricted diffusion will appear brighter in the image, while tissues with less restricted diffusion will appear darker.

The contribution to dephasing of protons caused by diffusion of water molecules in the order of cell dimensions, 5–25 $\mu\text{m}^2/\text{s}$, is not detectable on images made with standard MR pulse sequences. Two developments were necessary to realize the visualization of diffusion effects with MR equipment. The first was the improvement of the temporal resolution by ultra-fast imaging techniques (now usually single shot echo planar pulse sequences). These techniques have the advantage of "freezing" motion. Motion in the order of cell dimensions is rapidly overshadowed by movements of the patient, voluntary and involuntary, by respiration, and pulsation of vessels and cerebrospinal fluid. The second requirement was the introduction of a set of strong, opposed "diffusion" gradients enhancing the diffusion process. Application of these techniques has made it possible to introduce diffusion-weighted imaging (DWI) into clinical practice. The MR application of DWI is practiced on two levels: a relatively simple level with rapid acquisition of clinically useful information, and a more complex level allowing more precise estimation and quantization of anisotropy and 3D analysis of the data.

106.2 DWI Techniques

For DWI it is necessary to use ultrafast sequences to “freeze” motion, as mentioned above. Even then, however, the small contribution of diffusion to the dephasing of protons is not visible on single shot echo planar images and is easily overshadowed by T_2 effects. It is necessary to enhance the diffusion effects by applying strong, opposed diffusion gradients (Stejskal–Tanner sequence) (Stejskal and Tanner 1965; Fig. 106.1) that cancel all “coherent” motion within the voxel and enhance the effect of diffusion of protons.

The *diffusion sensitivity* is expressed as the *b value of the sequence* and usually varies between 500 and 4000 s/mm^2 . On commercial scanners the maximum value often does not exceed 2000; usually $b = 1000 \text{ s/mm}^2$. Quantitative information about diffusion can be obtained in several ways. The simplest way is to measure the *apparent diffusion coefficient (ADC)* of the tissue. There is an exponential decrease in signal intensity with increasing *b* values. The ADC is measured by estimating the slope of the exponential curve describing the signal intensities at different *b* values. Measurements at two or more different *b* values (usually 500 and 1000) are used to calculate the ADC. The word “apparent” refers to the fact that in vivo it is not possible to measure the “pure” *diffusion coefficient D*. The diffusion coefficient measured – the apparent diffusion coefficient – averages different tissues with different diffusion coefficients present in one voxel; it is also influenced by other parameters, such as the presence of microparticles of iron. ADCs

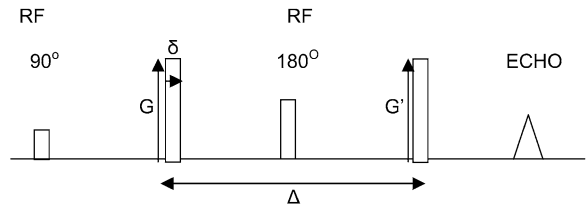


Fig. 106.1. Stejskal–Tanner pulse sequence, in which *G* is the diffusion gradient strength, Δ the distance between diffusion gradients, and δ the duration of the diffusion gradient. The diffusion sensitivity (gradient moment or *b* value) of this sequence increases when (1) the gradient strength (*G*) increases, (2) the duration of the gradient (δ) is longer, and (3) the time between the opposed gradients (Δ) is longer. These relations are brought together in the following equation: $b = \gamma^2 G^2 \delta^2 (\Delta - \delta/3)$, in which γ is the gyromagnetic ratio

describe the effective averaged diffusion per voxel. The diffusion coefficient in free water at 25 °C is about $25 \times 10^{-3} \text{ mm}^2/\text{s}$. In brain tissue ADC values are in the order of $0.70\text{--}0.90 \times 10^{-3} \text{ mm}^2/\text{s}$. In acute lesions, such as in acute ischemia, the ADC values decrease by about 50% to reach values of $0.40\text{--}0.60 \times 10^{-3} \text{ mm}^2/\text{s}$. In chronic ischemic lesions, with liquefaction and necrosis, these values may go up to $1.80\text{--}2.40 \times 10^{-3} \text{ mm}^2/\text{s}$.

In routine DWI, diffusion gradients are applied in three orthogonal directions. Images can be obtained on the basis of the results of each gradient separately, in respectively the slice (*s*), read (*r*), and phase (*p*) direction (Fig. 106.2). Where fiber tracts are parallel

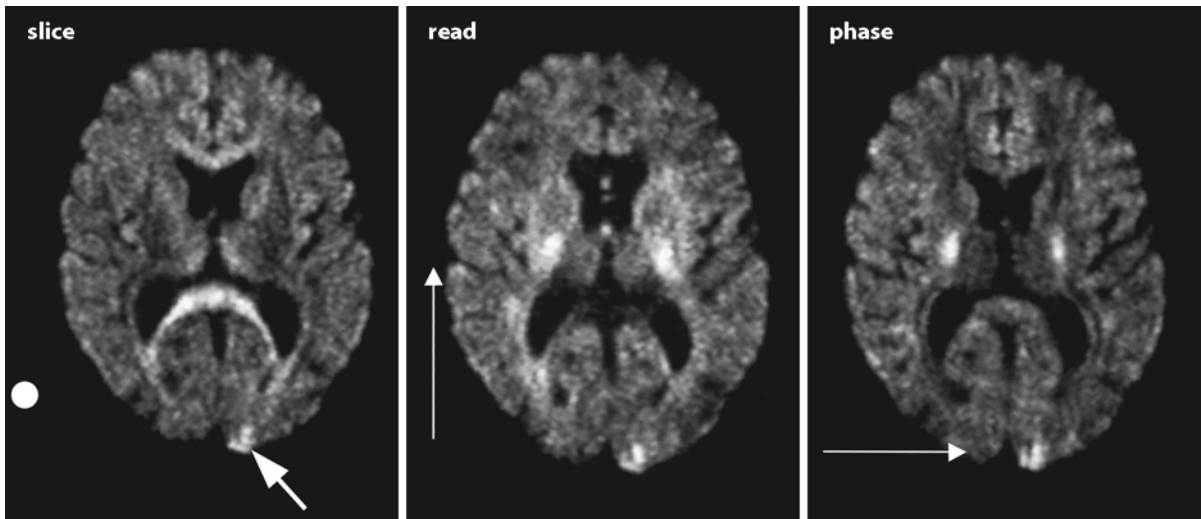
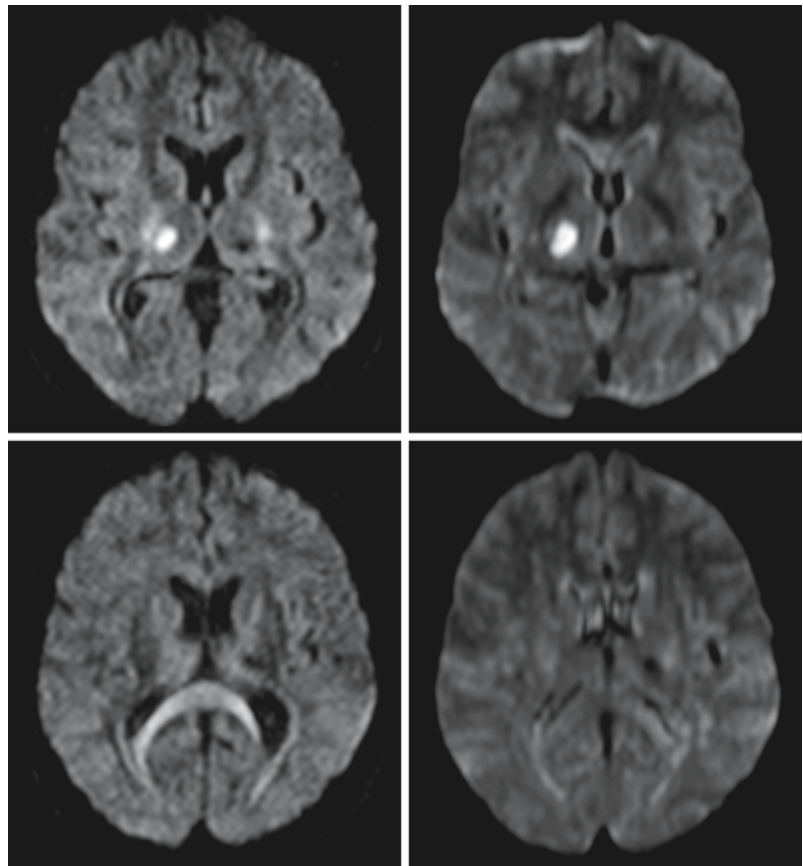


Fig. 106.2. Diffusion-weighted images in a patient with a right-sided homonymous hemianopia, made with three different diffusion gradients in *x* (read), *y* (phase), and *z* (slice) directions, showing anisotropy dependent on the direction of the

diffusion gradient. Tracts perpendicular to the gradient show high signal intensity, tracts parallel to the gradient show lower signal intensity. Note that the small lesion in the left occipital pole demonstrates restricted diffusion in all three directions

Fig. 106.3. The images on the left are made with a single diffusion gradient. In the *left upper image* one sees, in addition to the bright spot in the thalamus, high signal intensity in fiber tracts perpendicular to the gradient direction. The *lower left image* shows anisotropy of the splenium of the corpus callosum with a gradient in the slice direction. The images on the *right* are Trace diffusion-weighted images, which average diffusivity of three (or more) gradient settings to minimize the influence of anisotropy in the image. The *upper right image* now shows only the lesion in the right thalamus. The *lower right image* does not show any areas of restricted diffusion



with the direction of the applied gradient, signal loss due to diffusion will be at its maximum; where fiber tracts are perpendicular to the gradient direction, signal loss due to diffusion will be at its minimum and the signal will remain relatively high. The opposite is true for ADC maps: the greater the restriction in diffusion, the lower the ADC value, and the lower the signal intensity of that area. There is an important disadvantage to using images with the application of only one diffusion gradient in one direction. Fiber tracts perpendicular to the gradient direction have a relatively high signal, which may obscure hyperintense lesions with restricted diffusion in or in the neighborhood of these structures or simulate a hyperintense lesion. This pitfall can be omitted by averaging the ADC values of the measurements with (at least) three diffusion gradient directions (Fig. 106.3).

Diffusion is a process in time. That means that the MR sequence has to cover a minimum time slot to observe the diffusion process. Therefore, a relatively long echo time has to be applied, resulting in a T₂-weighted EPI sequence. This leads to a high signal intensity of structures with a long T₂. This high signal area may retain its brightness on diffusion-weighted images, simulating restricted diffusion. This phenomenon is referred to as “T₂ shine-through” effect. ADC maps do not share this problem. It is therefore

extremely important for the demonstration of restricted diffusion to look at the ADC values and verify the presence of a decreased ADC (Fig. 106.4).

Diffusion can be viewed as the product of the degrees of freedom of movement of water in three dimensions (*x*, *y*, and *z*). With equal movement opportunity in all directions (isotropy), the product is a rounded sphere and the diffusion vectors are equally long. Where diffusion is anisotropic, the product is an ellipsoid, the vectors unequal in different directions. The main vector, its size and direction can be estimated. With gradients applied in three directions, the *D* value can be estimated voxel by voxel by averaging the *D* values obtained in three (or more) different gradient directions: $D = (D_{xx} + D_{yy} + D_{zz}) / 3$. This averaging procedure will also cancel anisotropy in the image. The resulting image is called a *Trace image* (Figs. 106.3 and 106.5).

Diffusion Tensor Imaging In isotropic substances, diffusion can be described by a single parameter, the diffusion coefficient, or rather, the apparent diffusion coefficient, ADC. The attenuation of the MR signal depends on *D* and the *b* value, characterizing the gradient pulse:

$$A = \exp(-bD)$$

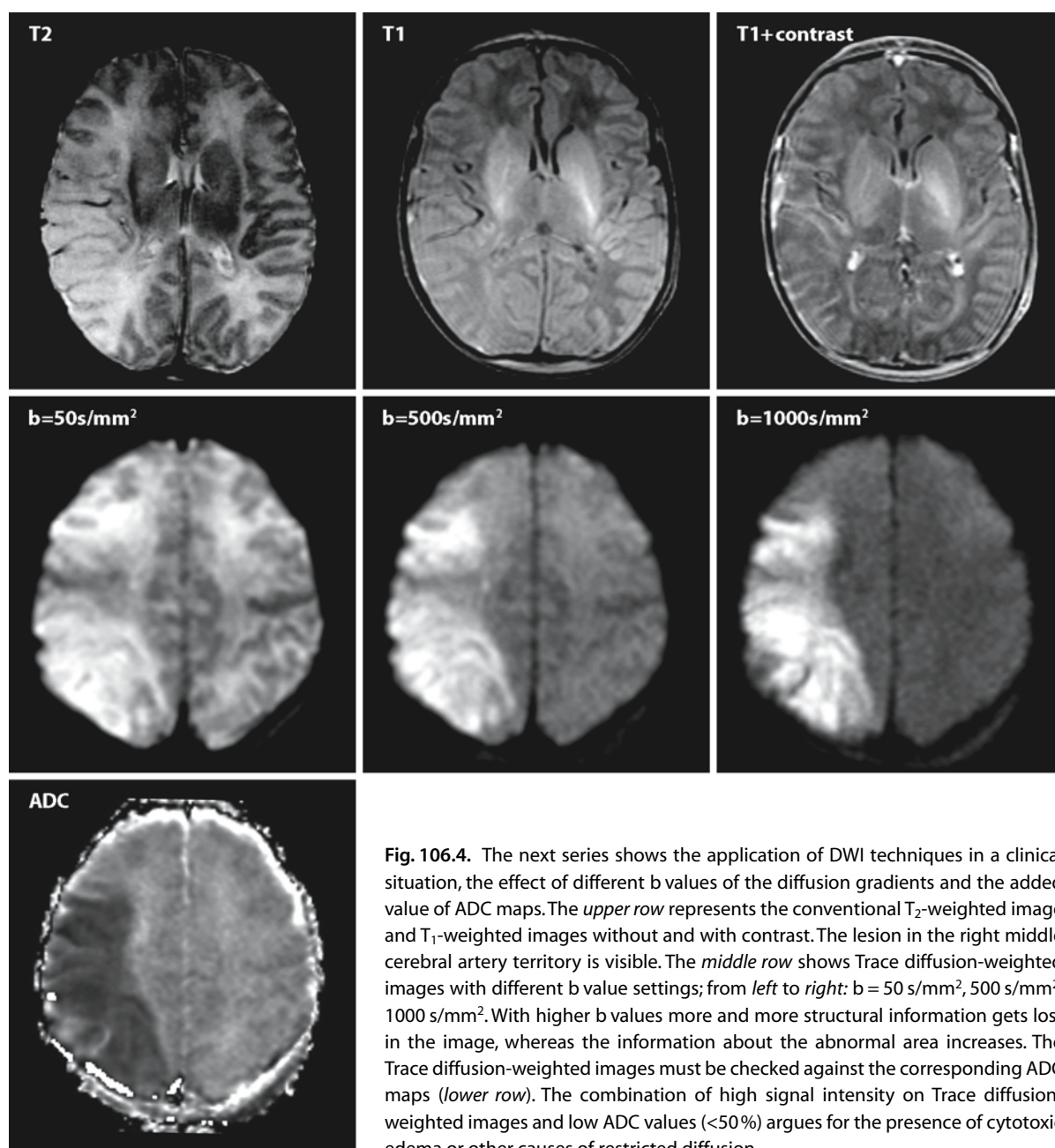


Fig. 106.4. The next series shows the application of DWI techniques in a clinical situation, the effect of different b values of the diffusion gradients and the added value of ADC maps. The *upper row* represents the conventional T₂-weighted image and T₁-weighted images without and with contrast. The lesion in the right middle cerebral artery territory is visible. The *middle row* shows Trace diffusion-weighted images with different b value settings; from *left to right*: b = 50 s/mm², 500 s/mm², 1000 s/mm². With higher b values more and more structural information gets lost in the image, whereas the information about the abnormal area increases. The Trace diffusion-weighted images must be checked against the corresponding ADC maps (*lower row*). The combination of high signal intensity on Trace diffusion-weighted images and low ADC values (<50%) argues for the presence of cytotoxic edema or other causes of restricted diffusion

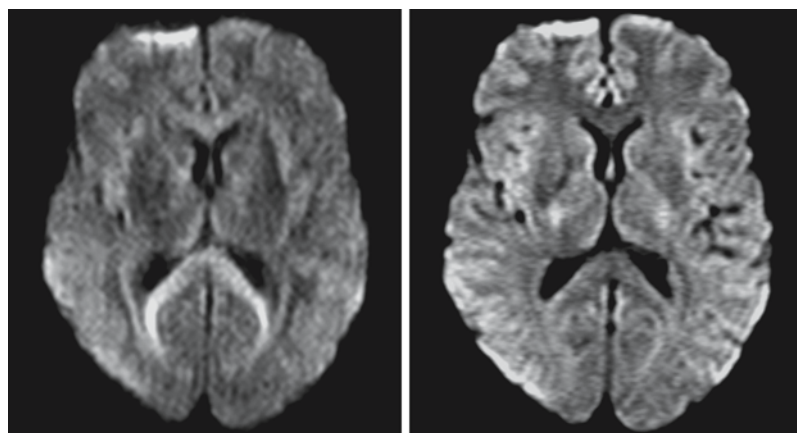


Fig. 106.5. The image on the *left* was obtained with a single gradient in the slice direction. In the Trace diffusion-weighted image on the *right* the effect of anisotropy in the splenium of the corpus callosum, as seen on the *left*, has disappeared

$$\underline{D}^{\text{eff}} = \begin{matrix} & \begin{matrix} D_{xx} & D_{xy} & D_{xz} \end{matrix} \\ \begin{matrix} D_{yx} \\ D_{yy} \\ D_{yz} \end{matrix} & \\ & \begin{matrix} D_{zx} & D_{zy} & D_{zz} \end{matrix} \end{matrix}$$

Fig. 106.6. Diffusion tensor (matrix). In isotropic conditions D_{xx} , D_{yy} , and D_{zz} suffice to determine the diffusion vectors. In anisotropic conditions D_{xy} , D_{xz} , and D_{yz} are also important to define the strength and directions of vectors in a voxel

in which A is attenuation, b is diffusion sensitivity, and D is the diffusion coefficient. With anisotropy present, a single parameter is no longer sufficient. With the mathematical description of the *diffusion tensor*, effects can be fully extracted, characterized, and exploited. The tensor D^{eff} is necessary to describe the molecular movements in each possible direction. In this model isotropic diffusion can be depicted as a rounded sphere, anisotropic diffusion as an ellipsoid tilted in the direction of the main orientation of the diffusion (Fig. 106.6).

The anisotropic diffusion process in each voxel can be characterized by D^{eff} , consisting of a 3×3 tensor matrix consisting of nine combinations, of which three are similar and six are independent. By sampling signal attenuation after applying diffusion-sensitizing gradients in at least six different noncollinear directions, these six (or more) elements can be determined. They represent diffusion along the three main coordinate axes of the ellipsoid, thus defining the shape of the ellipsoid (Fig. 106.7).

The data so obtained are rotationally independent: the head can be placed in an arbitrary position in the main magnet and this will not influence the results. The data can be used to calculate either the “*diffusivity*”, $\langle D \rangle$ (the directionally averaged ADC), or the degree of anisotropy, most often expressed as *relative anisotropy (RA)*, or as *fractional anisotropy (FA)*. In 2D representations of diffusion tensor imaging (DTI), FA is the most frequently used of many possible parameters describing anisotropy. RA is the ratio of variance of the eigenvalues to their mean. FA is the ratio of the anisotropic component of the diffusion tensor over the whole diffusion tensor. FA indicates how elongated the ellipsoid is (0 = isotropy, 1 = maximum anisotropy, often multiplied by 1000). FA is usually displayed as a map in gray shades (higher FA values reflecting more pronounced anisotropy show a higher signal intensity on gray scale images, low values appear darker) (Fig. 106.8) or in color codes. FA images show more contrast between gray and white matter than do T_1 - and T_2 -weighted images. The reason for this difference is still not fully clear, but may have to do with the major difference in density of axon fibers. In the literature ratios are used to quantify FA values, because values are not the same on all systems. The ratio is calculated as:

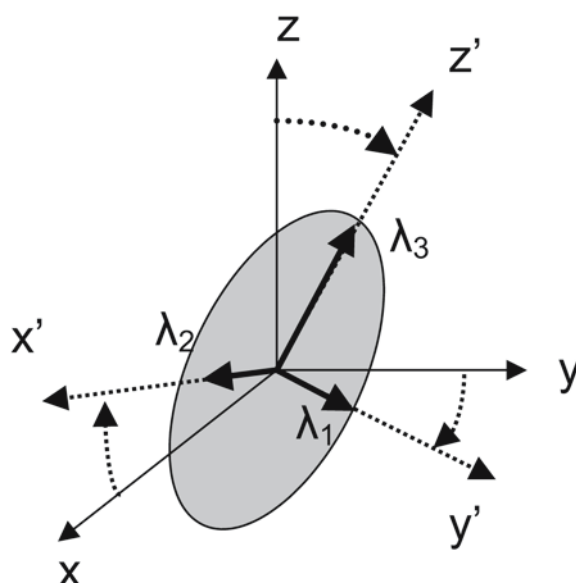


Fig. 106.7. Ellipsoid representing the diffusion tensor. The ellipsoid is characterized by the maximum diffusion in each direction and represents the relationship between the principal coordinate axes (x' , y' , and z') and the laboratory reference frame (x , y , z). The radii (bold black arrows) represent the magnitude and direction of the diffusion after unit time. The λ_1 , λ_2 , and λ_3 represent the so-called eigenvalues of diffusivity in all directions, shaping the ellipsoid

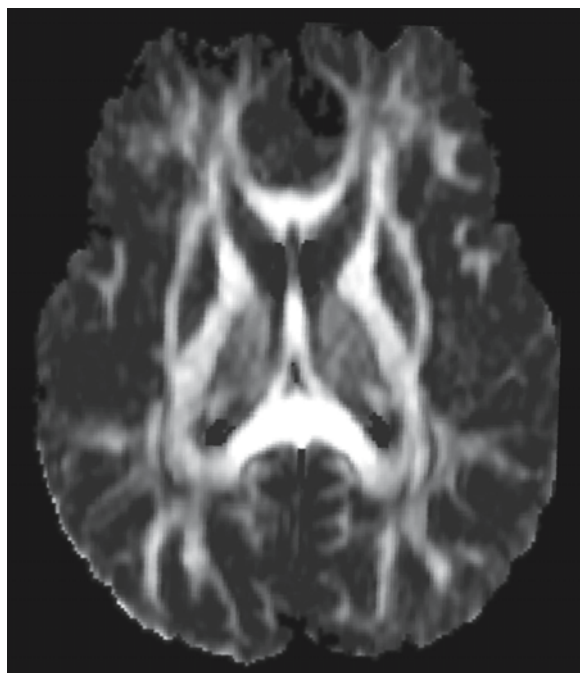


Fig. 106.8. A fractional anisotropy (FA) map provides a measure of anisotropy of different structures. Differences in FA between gray and white matter structures are greater than differences in T_1 , T_2 , or ADC values. In a FA map the distinction between gray and white matter structures is superb

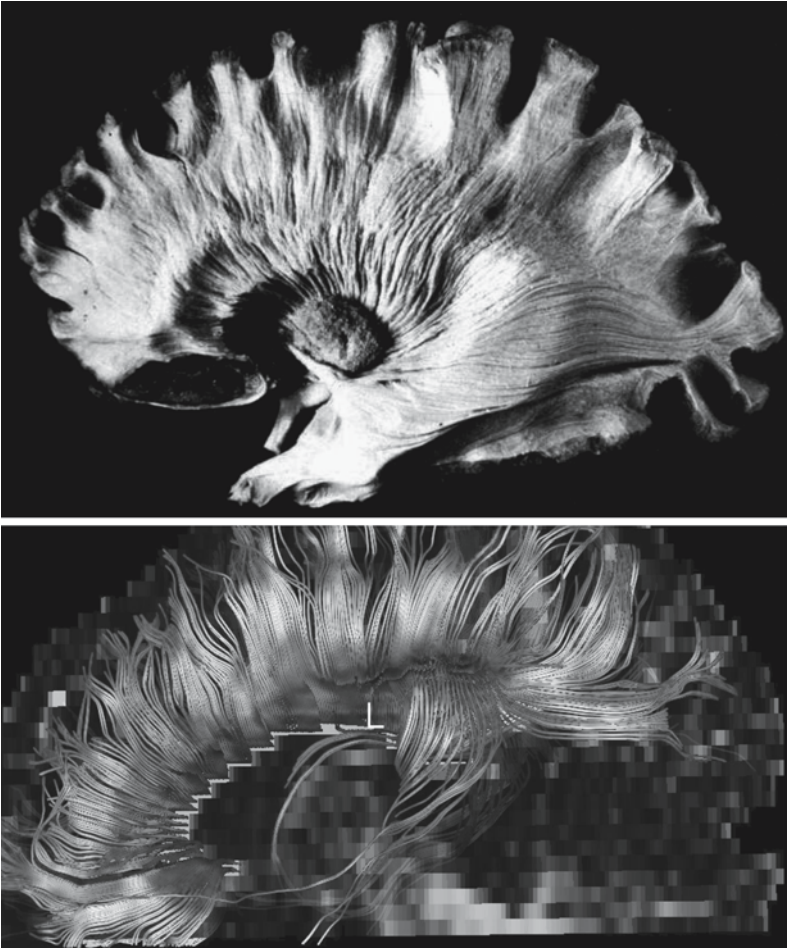


Fig. 106.9. Diffusion tensor imaging allows fiber tracking as is demonstrated in this image. DTI was done with 12 diffusion gradient directions. Fibers were tracked connecting left and right hemisphere via the corpus callosum, showing the potential of the method. The upper image shows a comparable anatomical specimen

$$rFa = \frac{\text{FA lesion}}{\text{FA reference point}} \times 100\%$$

or, somewhat more complex:

$$\Delta FA = \frac{\text{FA patients} - (\text{FA controls})}{(\text{FA controls})} \times 100\%$$

in which equation “(FA controls)” stands for the mean value from the regions of interest in volunteers. In particular in multicenter studies and trials ratios will have to be used to overcome inequalities in equipment performance.

A map can also be produced displaying the principal vector orientation per voxel. This is most often displayed as a color map in which the vectors (small arrows) are presented in color codes per direction.

DTI may be used to create a 3D map by connecting adjacent vectors with nearly the same orientation. Software programs usually allow the setting of a threshold that indicates the degree of accepted anisotropy (FA value), and also the setting of an arbitrary angle to decide whether a fiber connection will be accepted. The result is fiber tracking; white matter tracts can be visualized (Fig. 106.9). DTI cannot dis-

tinguish afferent from efferent tracts; the spatial resolution within acceptable acquisition times is still crude; and crossing fibers may lead to confusing results. Nevertheless, the potential of the method is, especially in combination with other techniques such as functional MRI, impressive.

106.3 DWI and Pathophysiological Backgrounds

DWI, usually in its simplest form with three diffusion gradients, anisotropy images, Trace images, and ADC maps, is now widely used in clinical practice. It has become a valuable tool in the detection and diagnosis of a growing number of neurological disorders. The pathophysiological background of the changes in the acute phase of diseases and the changes over time into subacute and chronic conditions are only partly understood. Diffusion is a parameter that is independent of the relaxation properties (T_1 and T_2) of tissue. Brain tissue consists of cell structures, with membranes dividing tissue fluid into extracellular and intracellular compartments, organelle compartments,

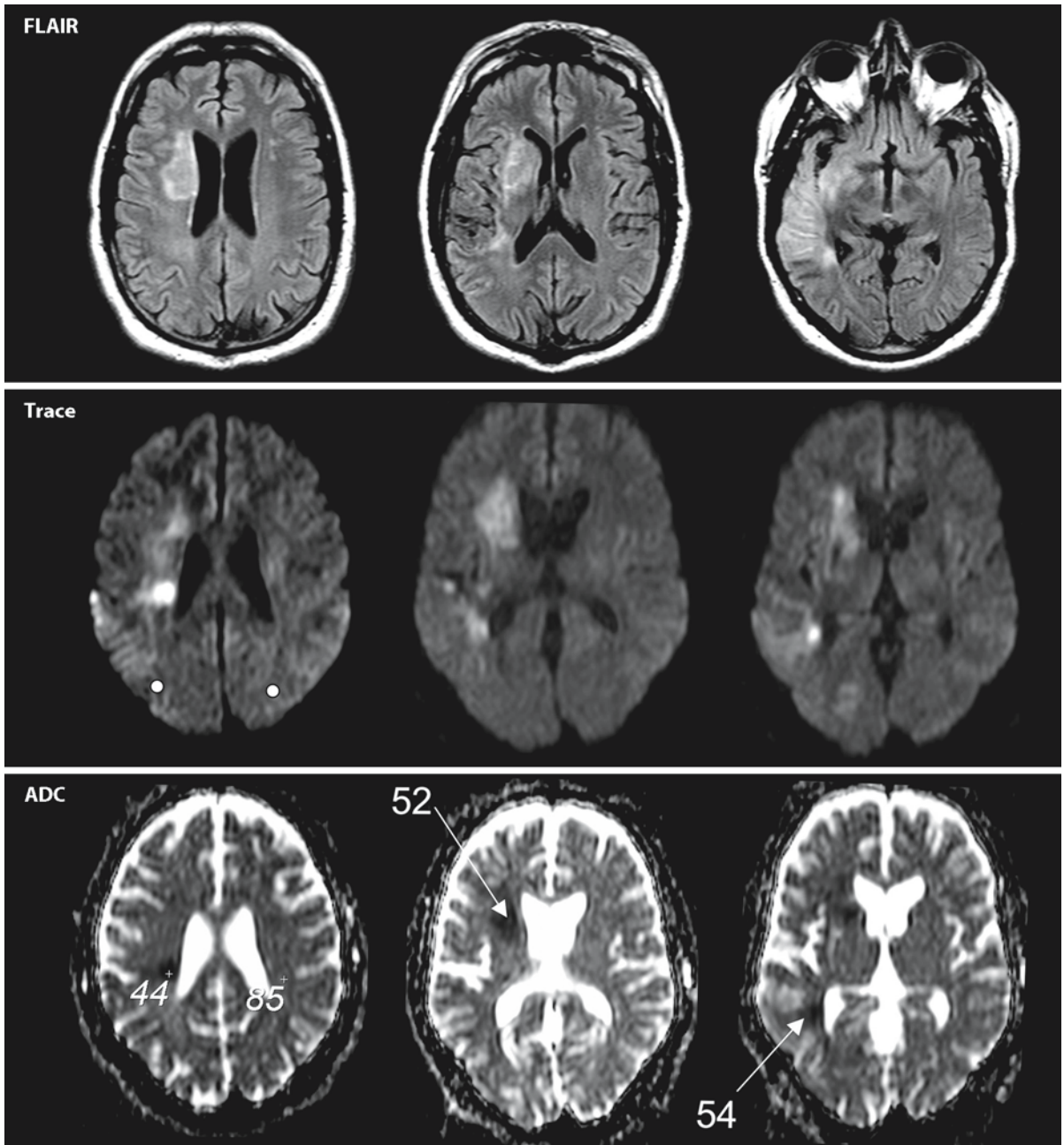


Fig. 106.10. DWI and ADC maps, often in combination with perfusion imaging, play an important role in stroke units, to identify salvageable tissue. This set of images shows such a practical application in a 66-year-old stroke patient. The *upper row* of FLAIR images shows lesions in the right middle cerebral artery territory. The *second row* of DWI–Trace images shows

bright signal in these lesions. The *lower row* of ADC images shows very low ADC values in the lesions, confirming the presence of cytotoxic edema. The added value to the FLAIR images is the time dependency of the DWI–ADC techniques, allowing an estimate of the age of the infarction

blood compartments consisting of arterioles, venules, and capillaries sustaining the microcirculation, and fiber tract compartments with myelin and axons, all having their impact on the complex process of diffusion.

The best understood changes are those in acute ischemic lesions (Fig. 106.10). Hypoxemia and ischemia lead to membrane depolarization, changes in membrane permeability, changes in ion exchange, and influx of water into the cell. Swelling of cells, both

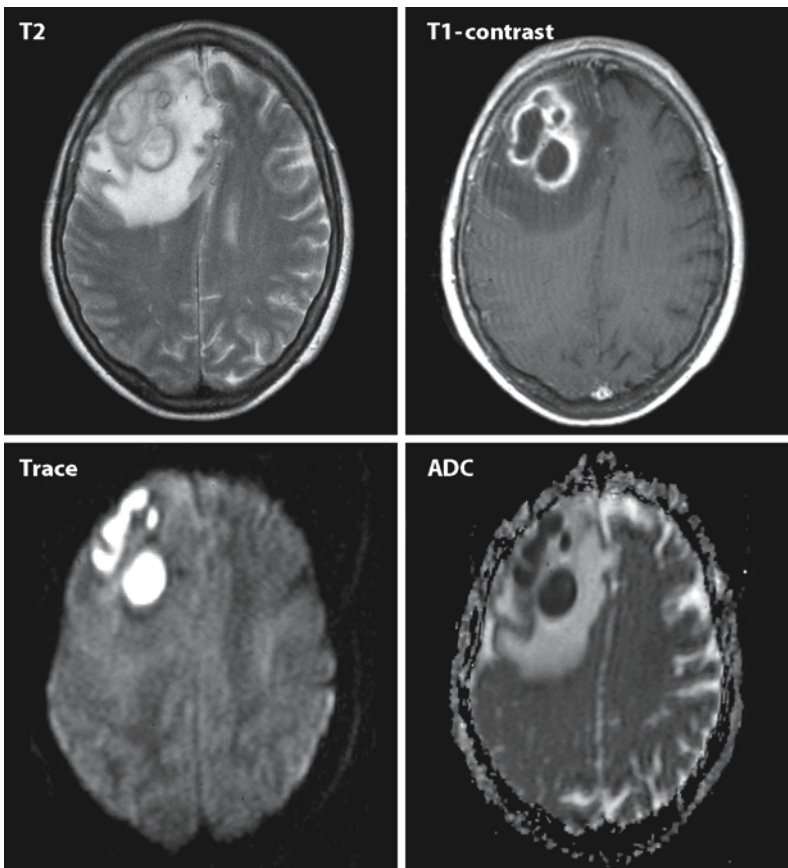


Fig. 106.11. The practical use of DWI and ADC maps is also demonstrated in this 38-year-old female, in whom the conventional images suggested the diagnosis glioblastoma multiforme. The patient showed no sign of infectious disease either clinically or biochemically. The *upper two images*, T₂-weighted and T₁-weighted with contrast, show a multicystic lesion in the right frontal lobe, with edema and ring enhancement. The Trace images and ADC map on the lower row show that within the cysts water diffusion is severely restricted, indicating a possible abscess, which was confirmed at surgery

glia and neurons, lead to compression of the extracellular space and restriction of movement of extracellular water, and probably also to restriction of intracellular water movements due to changes in organelles. This results in a high signal on DWI-Trace images and low ADC values. Subsequent lysis and shrinking of cells and rarefaction of tissue leads to increase of extracellular space and water content, with consequently a decrease of signal intensity on Trace images and increase of ADC values. The time frame for these changes in arterial territorial infarctions is in the order of 2–4 weeks. It should be noted that this time frame is different in border zone infarctions, where high signal on Trace images and low ADC values persist for much longer, even months. This is the result of a more chronic and persistent perfusion deficit.

In acute encephalitis and cerebritis, for example, in herpes simplex encephalitis, ADC values can be as low as in ischemic lesions. In viral infections there is swelling of cells and decrease of extracellular space in the initial phase, comparable to what happens in ischemia. It remains to be seen whether ADC and FA provide a means of estimating prognosis or of estimating disease activity in subacute lesions or recurrent infection.

Many other factors may influence the degree of freedom of movement of water molecules in brain tissue. High cellular density and high nucleus/cytoplasm ratio of packed cells in tumors may cause low ADC values. In brain abscesses, the restriction of water movement is based upon cellular density, formation of septa, and gelatinous or caseous contents of the abscess cyst (Fig. 106.11). Epidermoids also show restricted diffusion, caused by the gelatinous condition of the fluid and the presence of septa.

In focal epilepsy there is a reduction of 20% of ADC values of the tissue involved in the ictal phase, while MRA, MR perfusion studies, and SPECT show evidence of hyperperfusion in that area. In the interictal phase, the ADC values return to normal in days to weeks. In addition to swelling of involved neurons, the increase in regional blood volume may influence the measurements by an increase of magnetically active blood products, for example deoxyhemoglobin. Blood present in post-traumatic or postoperative cysts may lead to a pseudo-low ADC and in that way suggest an abscess. T₁-weighted images usually will solve this problem, when it arises.

In white matter disorders, inherited or acquired, multiple factors resulting in changes in diffusivity

have to be considered, such as cellular density and swelling in acute inflammation or infection (multiple sclerosis, acute disseminating encephalomyelitis, viral encephalitis), restriction of water movement in acute intramyelinic edema (posterior reversible encephalopathy syndrome) and vacuolating myelinopathy in toxic and metabolic conditions (maple syrup urine disease, Canavan disease, megalencephalic leukoencephalopathy with subcortical cysts, heroin intoxication, hexachlorophene intoxication, CO intoxication), and axonal swelling in neurodegenerative and traumatic disorders (amyotrophic lateral sclerosis, wallerian degeneration, diffuse axonal injury).

106.4 Brain Maturation and DWI–DTI Changes

DWI and DTI have the unique capability to show changes in anisotropy. Anisotropy is largely due to the presence of myelinated fiber tracts. It has been shown, however, that changes in anisotropy (FA) occur before myelination becomes visible, confirming that anisotropy is partly the result of precursors of myelin and, probably more importantly, axonal or fiber density. The changes in FA in different brain areas have been extensively documented. FA shows an increase over time, while ADC values drop. Unfortunately the methods used to establish timetables are

not quite comparable. Measures such as “apparent” anisotropy are less well defined than FA and RA and less reproducible. ADC values may also differ according to the machine and pulse sequences used, for example due to the b value setting and the number of applied diffusion gradients. Roughly, the ADC values are high in neonates, different in different anatomic regions, varying from 1.05 to $1.64 \times 10^{-3} \text{ mm}^2/\text{s}$. At the age of about 10 months this range is in the order of 0.75 to $0.92 \times 10^{-3} \text{ mm}^2/\text{s}$, close to values seen in young adults (Table 106.1).

A difficulty with reporting on quantitative diffusion data in neonates and children is that few of the data are obtained by methods that fully account for the effects of diffusion anisotropy. ADC values are often obtained by measurements in one direction only. When anisotropy is present, these estimations are not accurate. Even when measurements are made in three orthogonal directions, it is not possible to accurately and quantitatively determine anisotropy. The full diffusion tensor must be sampled in at least six different directions. Another concern is partial volume averaging in structures close to CSF spaces, because this will artificially increase the measured ADC values. Numerical data available at this moment should be applied with great care in clinical situations.

The development of anisotropy is reflected in the FA values in Table 106.2.

Table 106.1. ADC values in full-term neonates (adapted from Neil et al. 1998)

Region	ADC values ($\times 10^{-3} \text{ mm}^2/\text{s}$)
White matter centrum semiovale	1.30–1.60
Head of caudate nucleus	1.18–1.31
Insular gray matter	1.12–1.24
Lentiform nucleus	1.15–1.22
Thalamus	1.01–1.15
Anterior limb internal capsule	1.14–1.24
Posterior limb internal capsule	1.03–1.09
Cerebellar hemisphere	1.07–1.14

106.5 Hypoxic–Ischemic Conditions in Neonates

DWI and DTI have a great impact on the diagnosis of post-hypoxic–ischemic changes in neonates. On conventional MR sequences patterns of hypoxic–ischemic encephalopathy in preterm and term neonates are often difficult to visualize in the immediate postnatal period. This is due to the only partly myelinated state of the neonate’s brain, with a high signal on T_2 -weighted images of the unmyelinated parts, obscuring the lesion. DWI often reveals the abnormal areas with high sensitivity. In particular the extent of lesions in early periventricular leukomalacia, in the cortico-subcortical pattern, and in basal ganglia

Table 106.2. Regional FA values at different ages (adapted from Schneider et al. 2004)

	2 Months	12 Months	24 Months	144 Months
Genu corpus callosum	0.41	0.52	0.63	0.72
Splenium corpus callosum	0.45	0.61	0.68	0.76
Frontal white matter	0.16	0.29	0.34	0.39
Centrum semiovale	0.28	0.38	0.42	0.53
Posterior internal capsule	0.52	0.63	0.68	0.76

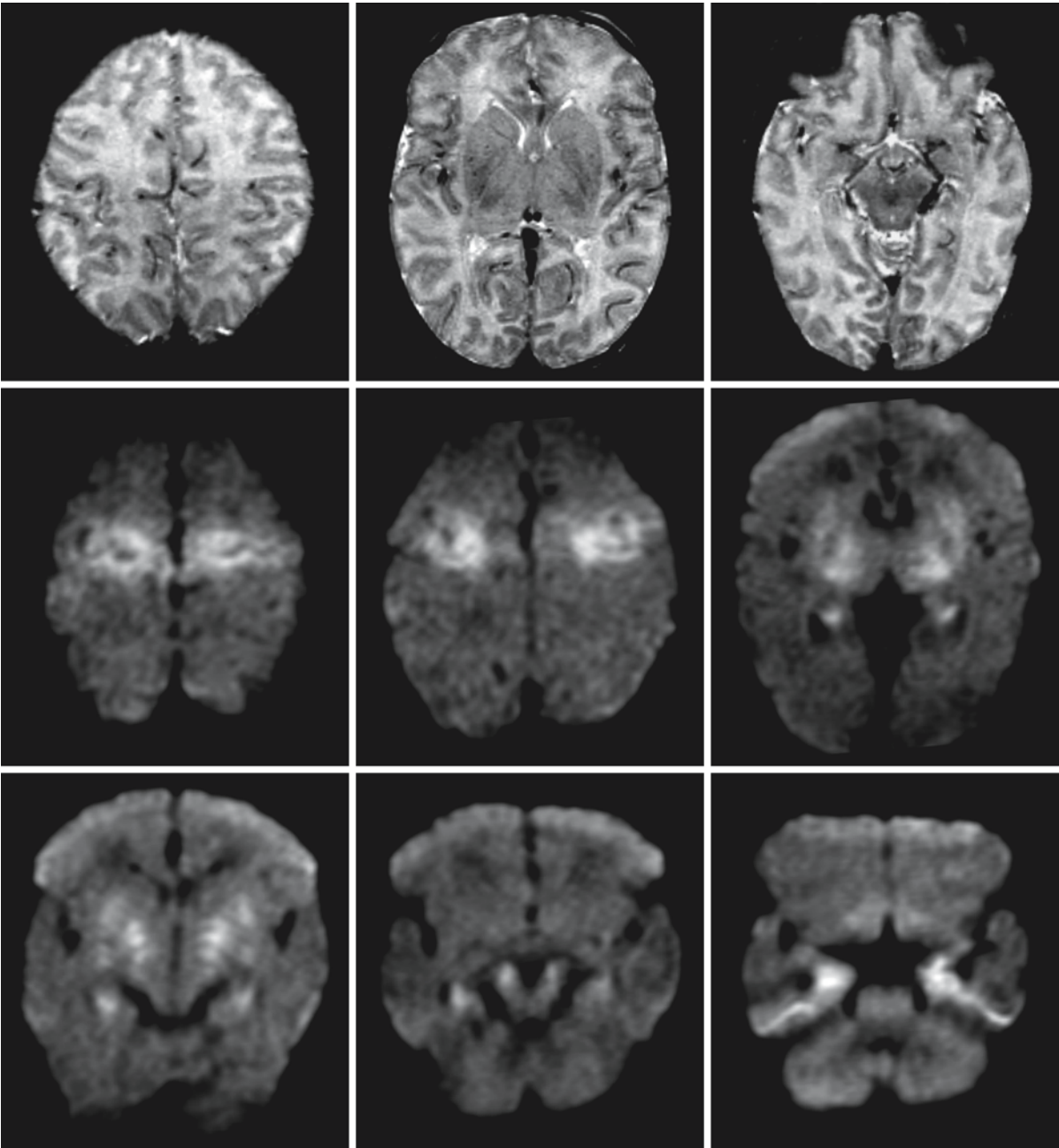


Fig. 106.12. Images of a term-born neonate with acute profound hypoxia-ischemia. The *upper row* of conventional T₂-weighted images show generalized edema, including swollen and abnormal basal ganglia. The *lower two rows* of DWI-Trace

images demonstrate the typical cortico-subcortical pattern, allowing an early diagnosis with a poor prognosis. It may take much longer before this pattern emerges on conventional images

lesions can be visualized within hours after the insult (Fig. 106.12). When interpreted with care, DWI and DTI data are extremely helpful.

As an example, the values in periventricular leukomalacia are instructive, because they seem to allow early confirmation of the presence of the lesions (Table 106.3).

Table 106.3. ADC values in early periventricular leukomalacia ($\times 10^{-3} \text{ mm}^2/\text{s}$) (adapted from Bozzao et al. 2003)

Region	Non-PVL	PVL
Posterior limb internal capsule	1.06	0.96
Corona radiata	1.23	0.97
Frontal white matter	1.35	1.19
Parietal white matter	1.52	1.15

PVL, periventricular leukomalacia

106.6 Leukoencephalopathies

DWI and DTI have been applied extensively in multiple sclerosis. In most studies estimation of FA and ADC has been used to compare different forms of multiple sclerosis and different tissue components, such as plaques, white matter around plaques, normal-appearing white matter, and enhancing versus nonenhancing lesions. Some of the results are summarized in Table 106.4.

From Table 106.4 it is clear that the discriminating power of FA is considerably greater than that of ADC. As expected, an increase in ADC is linked to a decrease of FA.

The findings in normal-appearing white matter of a high ADC and low FA correspond with findings in MTR and MRS studies. DWI and MTR findings correlate better with the disability scores of multiple sclerosis patients than do conventional MR estimates and even lesion load estimations. In primary progressive multiple sclerosis conventional MR abnormalities are minimal. DTI reveals abnormal values of FA and ADC in the corpus callosum and internal capsule of these patients. Hypointense lesions on T₁-weighted images, known as black holes and indicating a poor prognosis, have the lowest diffusivity of all multiple sclerosis lesions. T₁ isointense lesions have the highest FA of all lesions studied and apparently have maintained tissue integrity.

Normal-appearing gray matter in multiple sclerosis has also been the subject of a number of studies. In histogram analysis of diffusivity of gray matter in patients with primary progressive multiple sclerosis, patients with secondary progressive multiple sclerosis, and controls, statistically significant differences were found. The ADC and FA values in normal-appearing gray matter are respectively higher and lower than in controls, although the differences are less pronounced than in white matter. The differences between patients with primary progressive multiple sclerosis and controls were clearly less than between secondary progressive multiple sclerosis patients and controls, but still significant.

DWI and DTI have a place in research on patients with inherited leukoencephalopathies, but have also obtained a place in the clinical work-up of this cate-

gory of patients. Some findings of DWI and DTI have direct implications for the management of patients. An important example is found in X-linked adrenoleukodystrophy. DTI can play a role in the detection of early abnormalities in patients, not yet seen on conventional images. Early changes are important in estimating when to offer the patient hematopoietic stem cell transplantation. DWI and DTI should be compared in this respect with MRS and magnetization transfer imaging.

In progressive inherited disorders the time factor plays an important role. In early metachromatic leukodystrophy ADC values are low and DWI shows a high signal. This effect is not completely understood, but is thought to be related to the accumulation of abnormal metabolites (sulfatides). In later phases of the disease, ADC increases and FA decreases as sign of disintegration of affected structures. Similar findings are reported in globoid cell leukodystrophy.

The type of underlying pathology is important. In maple syrup urine disease with neonatal onset, myelin vacuolation occurs in all myelinated parts of the brain in the newborn. These parts show low ADC values with about 80% decrease, and very high signal intensity on DWI (Fig. 106.13). In other disorders, such as nonketotic hyperglycinemia, Kearns–Sayre syndrome, Canavan disease, L-2-hydroxyglutaric aciduria, and heroin encephalopathy, intramyelinic edema is also present and supposed to be the cause of restricted water movement and low ADC values in the early phase of the disease. In chronic myelin vacuolation, as seen in megalencephalic leukoencephalopathy with subcortical cysts and the end stages of Canavan disease, no evidence of restriction of water diffusion is found, but increased diffusion is found (Fig. 106.14).

Among the white matter disorders in children, hypomyelination is a frequent finding. It is striking that whereas the signal intensity of cerebral white matter is high on T₂-weighted images in both hypomyelination and demyelination, diffusion anisotropy can distinguish the two. Whereas diffusion anisotropy decreases in diseases characterized by myelin loss, marked diffusion anisotropy remains present in hypomyelinating conditions. This is an argument suggesting that it is not just myelination of fiber tracts that is responsible for the anisotropy, but rather that the tracts themselves are responsible (Fig. 106.15).

The combination of the nature of white matter changes and the changes over time in the lesion dictates the findings on DWI and DTI, usually expressed as ADC and FA values. This largely explains the controversies in reports on ADC and FA findings in several disorders, in particular posterior reversible encephalopathy syndrome and some inborn errors of metabolism. An example is found in the reports in the literature on ADC values in mitochondrial encephalopathy with lactate acidosis and stroke-like

Table 106.4. FA and ADC in different multiple sclerosis lesions (from Guo et al. 2002)

Lesions	FA	ADC ($\times 10^{-3} \text{ mm}^2/\text{s}$)
Plaque	0.280	1.03
Periplaque white matter	0.383	0.79
Normal-appearing white matter	0.493	0.74
Control white matter	0.537	0.73

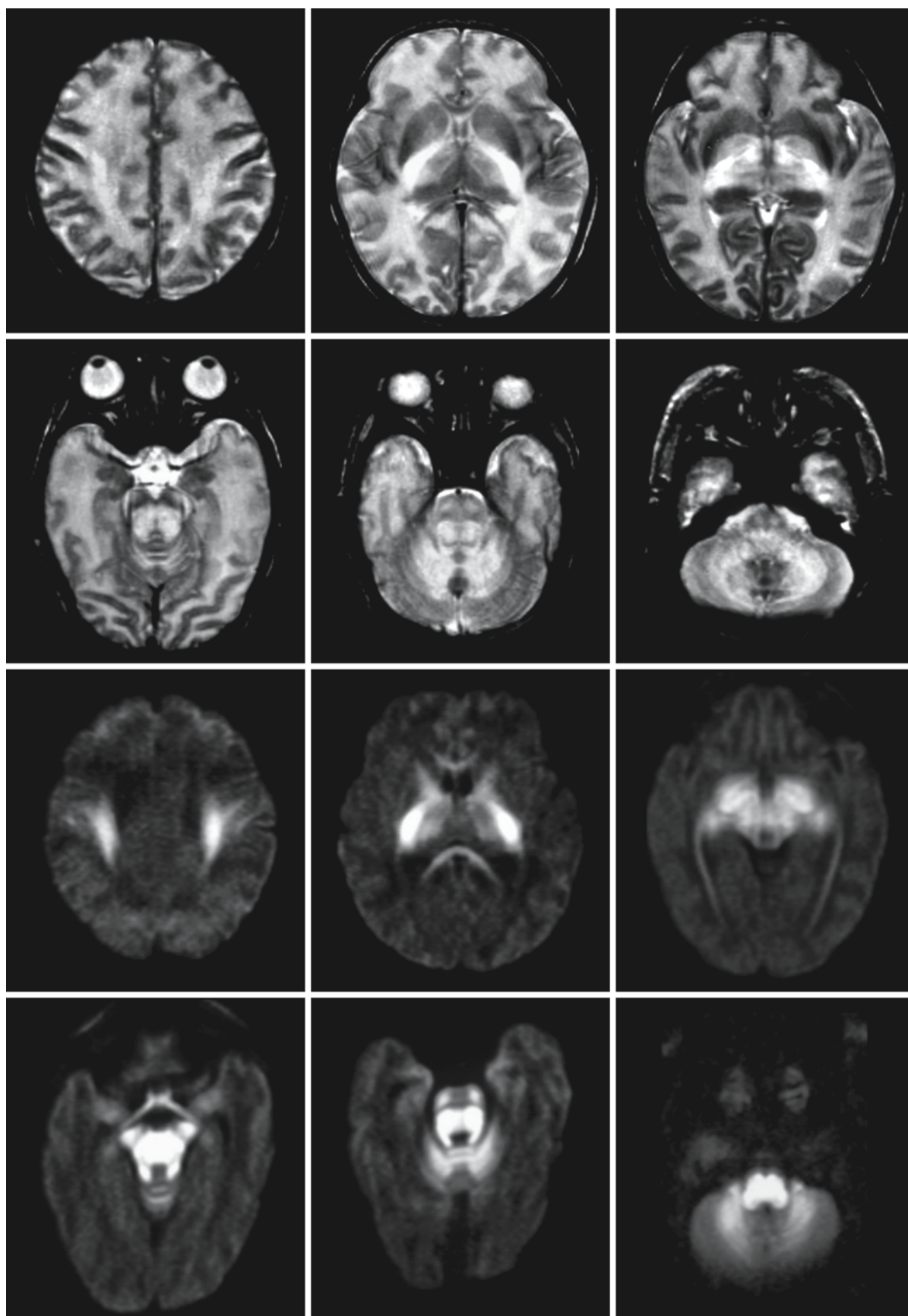


Fig. 106.13.

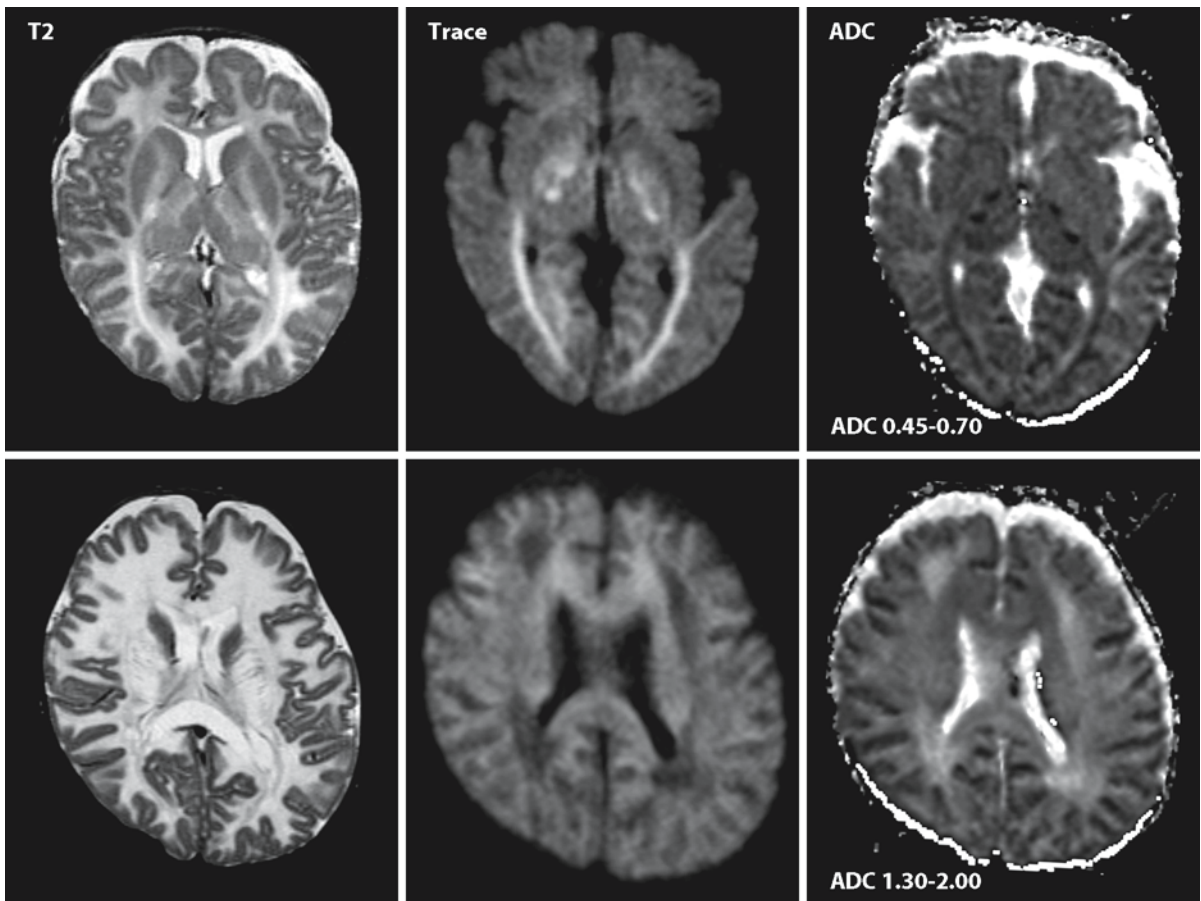


Fig. 106.14. Images of an infant with Canavan disease at the ages of 4 months (*upper row*) and 12 months (*lower row*). Initially the ADC values in the affected white matter areas are low. In the following months they become much higher than the values of normal tissue. Canavan disease is characterized by a

vacuolating myelinopathy, as is maple syrup urine disease, initially with compression of the extracellular space and restricted diffusion. The increase in ADC values probably indicates that the tissue disintegrates and becomes rarefied over time

episodes (MELAS). Both low and high ADC values have been found in fresh lesions (Fig. 106.16). This could depend on the delay between the insult and the measurement. It could also mean that MELAS produces two different types of lesions, of which the

infarctions have low ADC values and follow the time course and structural changes seen in common infarctions of vascular origin, whereas the “other” lesions with high ADC values shortly after the insult represent another type of pathology, yet to be elucidated.

In ischemic white matter lesions, for example subcortical arteriosclerotic encephalopathy, loss of structural integrity is expressed by a relatively high ADC ($1.12 \pm 15 \times 10^{-3} \text{ mm}^2/\text{s}$) and moderately low FA values (0.480–0.530). Figures in the same order have been obtained in patients with CADASIL. In these vascular disorders there is a strong correlation between the measure of loss of integrity and results of cognitive tests.



Fig. 106.13. A neonate with maple syrup urine disease. The pathological substrate is a vacuolating myelinopathy, which only affects myelinated areas. On the T_2 -weighted images (*first and second rows*) the myelinated parts of the brain show swelling and higher signal intensity than the surrounding unmyelinated structures. The differentiation of abnormal from normal tissue can be optimized by Trace diffusion-weighted imaging (*third and fourth rows*). Note that the optic tract and chiasm are also myelinated at this stage

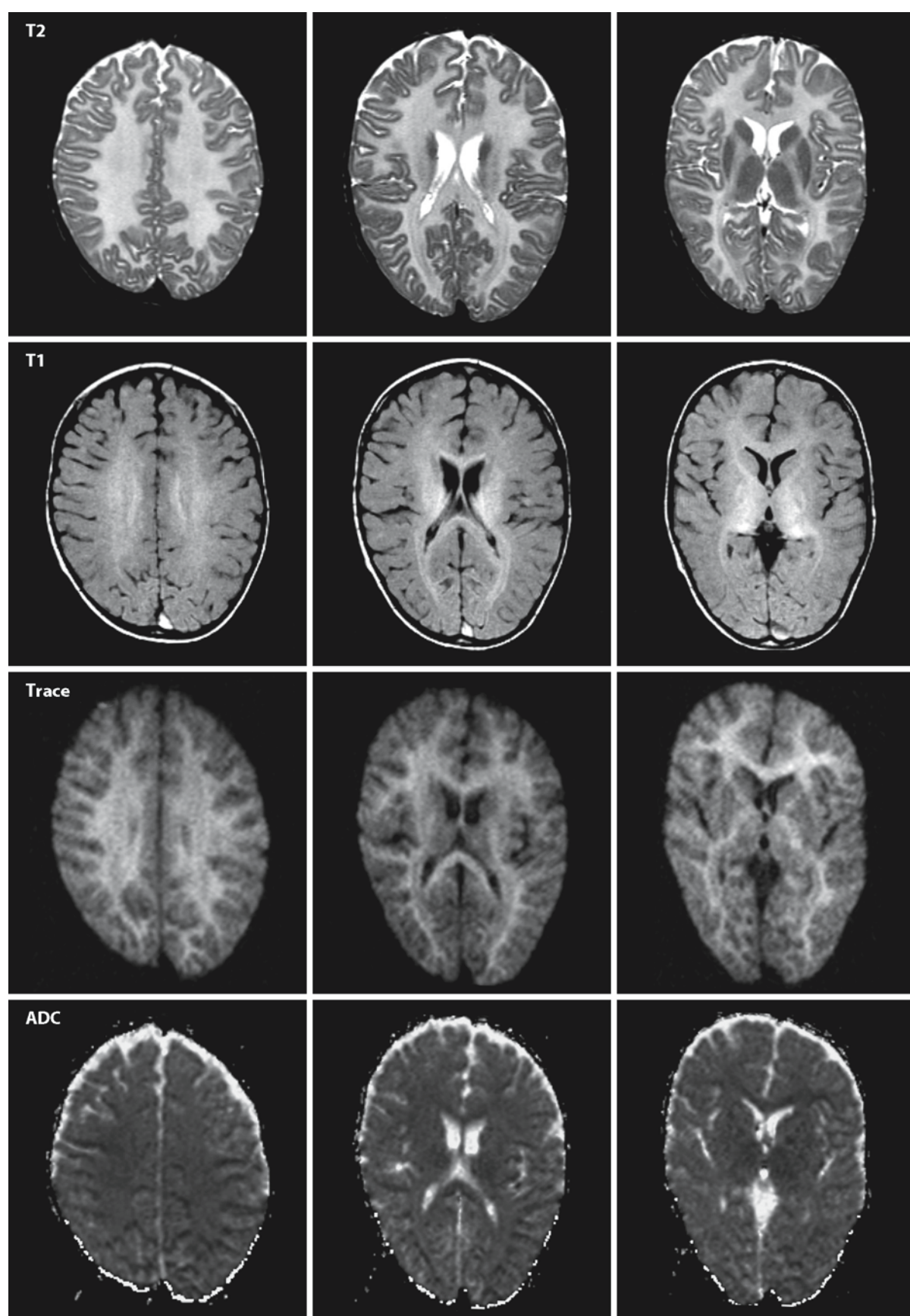


Fig. 106.15.

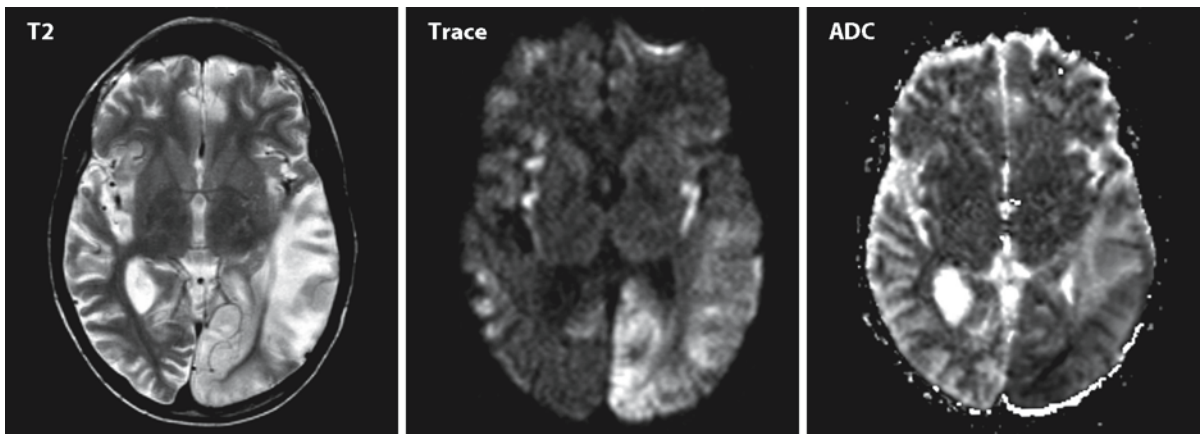


Fig. 106.16. A 12-year-old boy with MELAS develops a stroke-like episode, initially with dysphasia, followed by hemianopia. The ADC map is most informative, showing a high ADC in the

temporal infarction and a low ADC in the occipital infarction, suggesting the influence of time on the ADC

←
Fig. 106.15. A series of T₂- (first row) and T₁-weighted (second row) images of a 6-year-old boy with Pelizaeus–Merzbacher disease, showing severe hypomyelination. Unlike what one would expect, Trace diffusion-weighted images (b value 1000, third row) do not add much information and the ADC values (fourth row) are close to normal: ADC of frontal white matter is 0.76–0.84, that of the basal ganglia 0.54–0.84, and that of the cortex 0.84–0.89 × 10³ mm²/s

Magnetization Transfer Imaging

107.1 Techniques

Conventional MRI depends on the contribution to the MR signal of the freely mobile protons of water molecules because of their great abundance and slow relaxation, leading to a high and sharp resonance with a bandwidth of approximately 20 Hz. Protons bound to macromolecules form a second pool and do not directly contribute to the MR signal because of their relatively low concentration and rapid relaxation, resulting in a low resonance with much broader bandwidth of several thousand hertz. The broad peak of these frequencies is symmetrically arranged around the resonance of mobile protons. Indirectly these bound water molecules can influence the MR signal because there is a physicochemical exchange and cross-relaxation between the two pools of protons. Dipole-dipole coupling results in an exchange of magnetization, called *magnetization transfer*, where each pool has influence on the relaxation rate of the other. Wolff and Balaban (1989) demonstrated *in vitro* and *in vivo* that it is possible to selectively excite the bound pool of protons by using a radiofrequency (RF) pulse that is off-resonance for the free water protons. The excitation of the macromolecular bound protons leads to transfer of magnetization to the mobile water protons in the magnetization transfer (MT) process. This results in decrease of the MR signal after on-resonance excitation.

The rates of MT between macromolecular bound protons and mobile water protons differ between tissues, resulting in different degrees of signal decrease for different tissues, generating a new form of MR contrast. The rate of MT is dependent on a number of factors: the relative proportion of the two pools of protons; the magnetic field strength; the power of the preirradiation with an off-resonance RF prepulse; and the imaging parameters. The contrast on T_1 -weighted images is normally already partially determined by magnetization transfer, so the more T_1 -weighted the image, the smaller the extra MT effect. The highest MT effect is obtained when an MT prepulse is applied to a proton density spin echo or gradient echo sequence. The initially used continuous irradiation with an off-resonance frequency, administered with a separate RF unit, is currently replaced by a sinc-shaped pulse wave of short duration, applied between each on-resonance excitation using the main RF transmitter. In conventional multislice MRI a

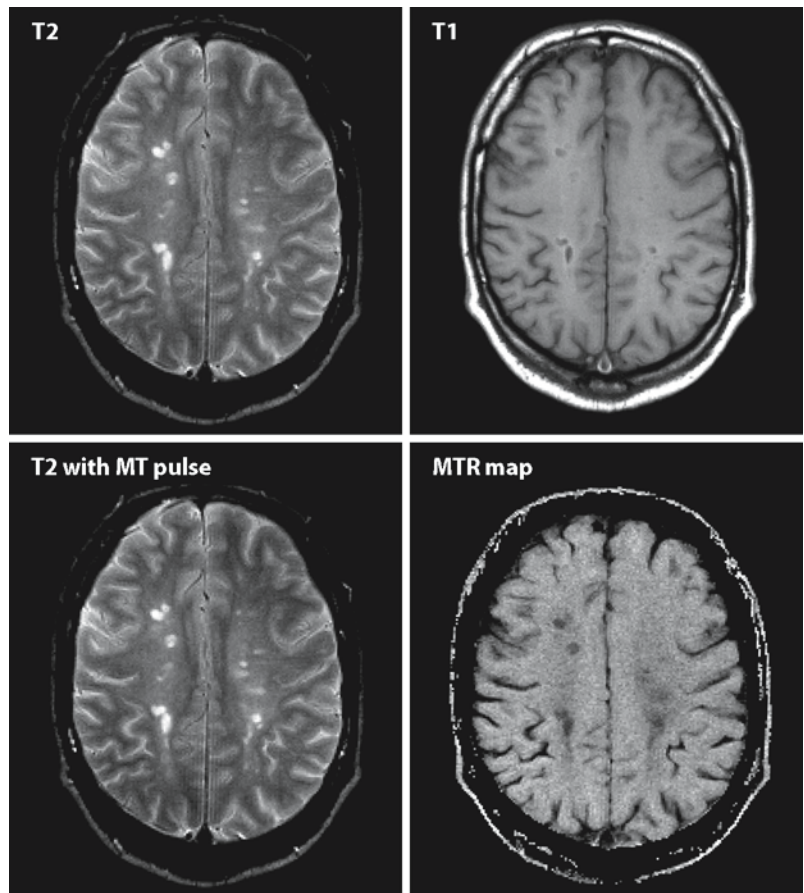
weak MT effect is always present, because each slice-selective pulse will serve as an off-resonance pulse for the adjacent slices. This effect is stronger when fast MR sequences are used with a high number of refocusing pulses.

Myelin forms a major part of the white matter. It is a lipid bilayer, in which proteins are embedded. The major lipids in myelin are cholesterol and glycerophospholipids. The lipid bilayer is wrapped in the form of large lamellae around the axons, with a small quantity of extracellular fluid between the layers. This creates a huge surface for interaction between the bound and free water molecules, which facilitates MT. Compartmentalization of the extracellular fluid further contributes to the MT effect. The MT effect of the myelin bilipid-water interface is responsible for the bright appearance of myelin on T_1 -weighted images. Both cholesterol and cerebrosides are particularly important in determining the myelin bilipid-water interface interactions, which facilitate T_1 relaxation due to MT. The signal loss of normal white matter due to MT effects ranges from 30% to 50%. It depends on the RF power applied and scan parameters. Gray matter shows a somewhat smaller MT effect than white matter. CSF, containing practically no macromolecules, shows a 0–2% signal reduction due to MT.

Magnetization transfer imaging (MTI) is used for two reasons. First, MT effects lead to a general signal reduction of the MR image, often referred to as background suppression. The diminution of signal intensity of brain tissue can be applied to increase the contrast between nonenhancing and enhancing tissue in studies with contrast injection. Background suppression with MT is also used in MR angiography. Secondly, MTI can be used as a separate imaging technique to characterize lesions. In tissue characterization, the magnetization transfer ratio (MTR) is commonly used. The formula is simple: $MTR = [(M_0 - M_s) / M_0] \times 100\%$, in which M_0 is the signal intensity obtained without the MT prepulse, M_s or M_{sat} the signal intensity with the prepulse applied. The stronger the MT effect, the higher the MTR. MTR is lower when there is less effect of the macromolecular proton pool. Thus, MTR is a measure of the degree of the structural integrity of brain tissue.

MT can be applied in different ways. MTR measurements can be displayed as a MTR map in which each voxel value represents the percentage of signal loss caused by MT (Fig. 107.1). The MTR map allows

Fig. 107.1. The *upper row* shows a T₂-weighted image without MT pulse and a T₁-weighted image in a patient with multiple sclerosis. The *second row* shows on the *left side* the T₂-weighted image with MT pulse. From the images without and with MT pulse, the MTR map can be calculated, which is displayed on the *right*. From this map MTR values (percentage) can be obtained per voxel or per ROI



voxel-by-voxel measurement or estimation of the average MTR for a specific region of interest. Another approach of MTR data that has attracted much attention is the creation of MTR histograms, either of the whole brain parenchyma or of segmented areas, such as the basal ganglia or the frontal lobe. White and gray matter can also be separated. In a number of postprocessing steps the intracranial contents are separated from the skull and orbital contents by a semiautomated software program. In the next step MTRs for every intracranial voxel are calculated. Implementation of a threshold value of 10–20% separates the CSF from the brain parenchyma. Voxels with a value higher than the 10–20% threshold are defined as brain parenchyma. The frequency distribution of MTR values can now be displayed as an MTR histogram of the whole brain (Fig. 107.2). The peak height is defined by the highest number of voxels with a certain MTR value. This measure is influenced by changes in brain tissue related to demyelination, gliosis, and axonal loss, but also by atrophy. The peak value, therefore, has to be normalized by dividing the peak height by the total number of segmented voxels. The relative peak height thus obtained is a measure of the amount of remaining brain tissue, independent of brain size and atro-

phy. A measure of atrophy can be obtained by dividing the number of voxels representing CSF by the total number of segmented voxels.

A drawback of both 2D and 3D MT is that MT values vary considerably between scanners, even with similar implementations. This is especially important in multicenter trials, and in follow-up studies when a different scanner is used for the same patient.

107.2 Normal Age-Dependent Changes

Important changes in MT have been reported related to brain maturation. With increasing density and complexity of brain tissue, MT changes, mainly expressed as an increase in MTRs. The changes in the MT of white matter run parallel with the progress of myelination. Fiber density or axonal density, however, plays an important role as well. Generally speaking, with increasing age of the infant, there is an increase in MT effect and a higher MTR. This effect is greater in white matter than in gray matter structures. In the neonatal brain MTR values are fairly homogeneously distributed, related to the fact that at that time there is little structural difference between gray and white

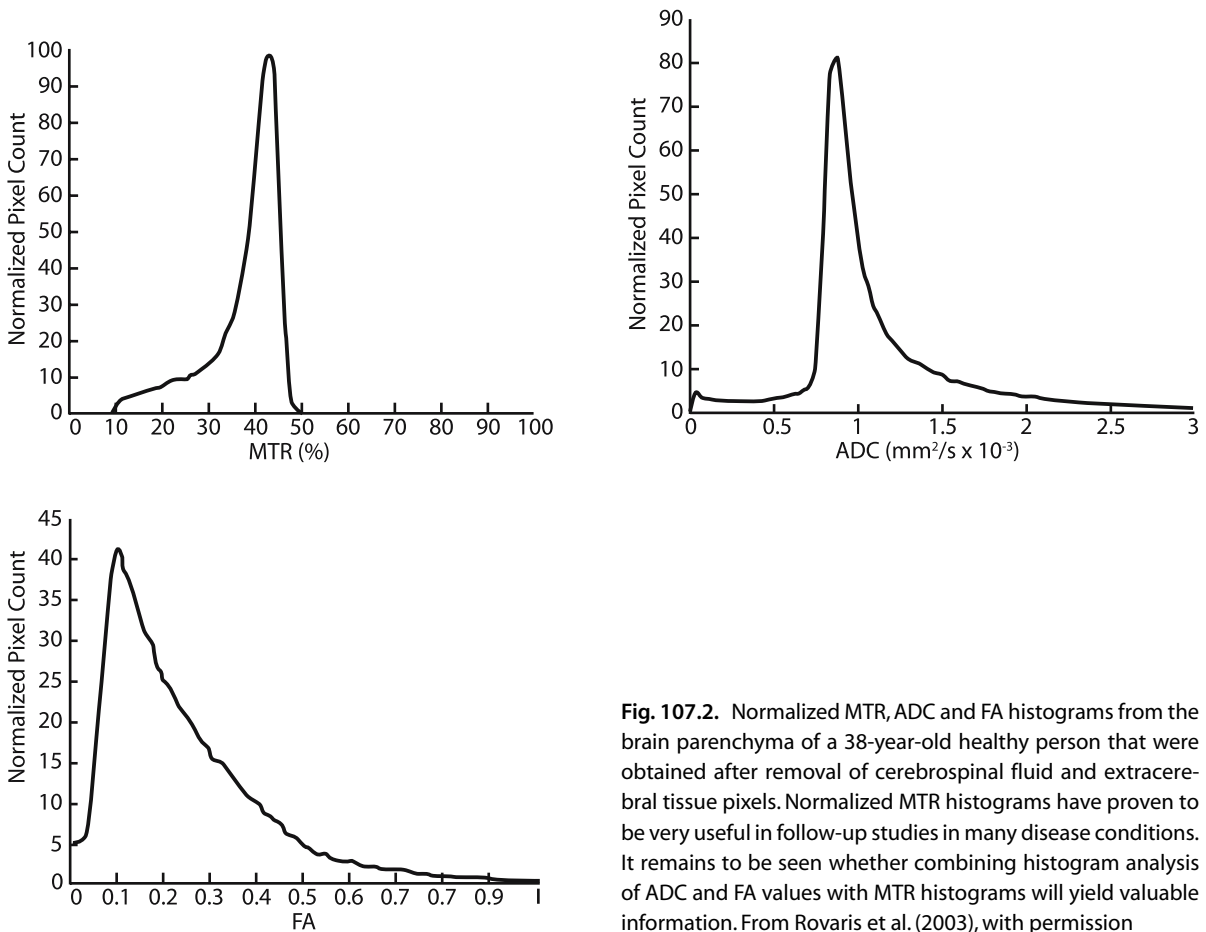


Fig. 107.2. Normalized MTR, ADC and FA histograms from the brain parenchyma of a 38-year-old healthy person that were obtained after removal of cerebrospinal fluid and extracerebral tissue pixels. Normalized MTR histograms have proven to be very useful in follow-up studies in many disease conditions. It remains to be seen whether combining histogram analysis of ADC and FA values with MTR histograms will yield valuable information. From Rovaris et al. (2003), with permission

matter. MTR values in the unmyelinated neonatal white matter are in the order of 13–19%, followed by a two- to threefold rise to 34–38% with myelination. Local differences in fiber density and myelin density lead to increasing regional variation in MTR. The highest MTR values after myelination are found in the corpus callosum and posterior limb of the internal capsule, the lowest values in the frontal and occipital white matter; this is probably related to fiber density. Overall the most rapid changes in MTR in white matter occur during the first year of life. The changes in MTR of gray matter are less conspicuous and level off at the age of 10 months. The peak height of the MTR histogram, however, continues to change over a longer period of time, up to the age of approximately 4 years.

107.3 Magnetization Transfer in Disease States

MT prepulses, MTI, and MTR can be used for a number of clinical applications. First of all, background reduction, as produced by MT prepulses, can be used

to improve the results of MR angiography, where the interest lies in the depiction of arteries and veins and less in the visualization of background structures. For this reason, MT prepulses are a standard part of many MR angiography pulse sequences. Background reduction can also be applied to improve the effect of contrast enhancement. This can be used to reduce the contrast dose or to have more contrast effect with the same dose, for instance in the search for the number of enhancing multiple sclerosis (MS) lesions or multiplicity of metastases.

The second application is based upon the possibility offered by MT to give a quantitative impression of the structural integrity of brain tissue. In order to assess the local structural integrity two types of MT postprocessing are currently in use: a 2D estimation of the MT effect, preferably as a MTR map, or measurement of the MT effect in regions of interest. By using whole brain histograms, the lesion load of the entire brain can be assessed. These techniques are applied to disorders characterized by focal or diffuse disintegration of cerebral tissue. They can be used to quantitatively assess the degree of tissue damage in areas that are also abnormal on conventional MR

Table 107.1. MTR and axonal density in normal appearing white matter and multiple sclerosis lesions versus degree of T₁-hypointensity

Degree of T ₁ -hypointensity	MTR (range)	% axonal density (range)
normal appearing white matter (n=24)	0.32 (0.26–0.36)	90 (60–100)
isointense (n=18)	0.24 (0.21–0.33)	80 (20–100)
mildly hypointense (n=38)	0.24 (0.16–0.31)	50 (10–100)
severely hypointense (n=53)	0.15 (0.10–0.28)	30 (0–70)

images, but they are also used to assess structures that are normal-appearing on conventional images. Changes in MT effect may occur in regions where conventional MR techniques do not show abnormalities, for instance in normal-appearing white and gray matter in MS, wallerian degeneration, amyotrophic lateral sclerosis, systemic lupus erythematosus, AIDS-related dementia, Alzheimer disease, X-linked adrenoleukodystrophy, and in many other disorders. In all these disorders, lower MTR values in normal-appearing structures signify a diminution of structural integrity and the presence of a disease state.

MT has been applied most extensively in MS, adding to our understanding of the disease. First of all, lesions visible on conventional images can be studied. MTR values for lesions visible on T₂-weighted MR images are significantly lower than for normal-appearing white matter, although with a wide range of MTR values. Average MTR for MS lesions was found to be 26.3%, with a lower mean value in chronic progressive (23.3%) than in relapsing-remitting MS (27.6%) (Filippi 1999). Follow-up studies show a further reduction of MTR values over time, more pronounced in patients with secondary progressive MS than in those with relapsing-remitting MS. Decreased MTR values were also found in normal-appearing white matter in the neighborhood of focal T₂ lesions. Using threshold techniques, lesion segmentation can be obtained and the MTR lesion load can be estimated. MTR histogram analysis reveals that there is a loss of high MTR values and a gain of voxels with low MTR values in MS patients as compared to normal persons. The increase in voxels with a low MTR value, however, makes up for only a low percentage (in the order of 15%) of the total decrease in voxels with a high MTR value, suggesting that a higher percentage of “lost” voxels can be attributed to white matter atrophy.

MT has been one of the techniques confirming that normal-appearing white matter in MS is not normal. With MT, subtle but consistent abnormalities have been found, more pronounced with increasing disability and in progressive MS. MT has also been used to study gray matter involvement. MTR of gray matter is significantly lower in patients with relapsing-remitting MS than in controls, confirming that MS is a diffuse disease affecting the whole brain.

Table 107.2. MTR in different zones of cerebral X-linked adrenoleukodystrophy

Tissue	MTR (%)
Unaffected white matter	46
Zone of inflammation and partial myelin loss	35
Zone of severe myelin loss and gliosis	20

(Melhem et al. 1996)

A correlative MTR–histopathology study in multiple sclerosis has shown that myelin is not the only factor involved in the MT effect. A significant correlation could be demonstrated between MTR and axonal loss (Van Waesberghe et al. 1999), indicating that the MTR reflects not only myelin density but also axonal density.

Table 107.1 shows the relationship between axonal density and MTR. It also demonstrates the relationship between hypointensity of MS lesions on T₁-weighted images, MTR, and axonal density (Van Waesberghe et al. 1999).

MTR has been applied to compare MS clinical subtypes (relapsing-remitting MS, secondary progressive MS, and primary progressive MS) and to correlate the data with disability scores. While the MTR of white matter is not significantly different for the different MS subtypes, MTR histogram analysis reveals a significant distinction between relapsing-remitting and progressive MS and between primary and secondary progressive MS. Findings in primary progressive MS are interesting. Primary progressive MS shows few lesions on conventional MR. MTR histograms show a lower peak height in primary progressive MS than in all the other MS subgroups, with an about normal average brain MTR and normal peak position, suggesting that there is a markedly reduced amount of normal brain tissue (Filippi 1999). The correlation between MTR results and disability is better than the correlation between estimations of lesion load and disability. Cognition tests showed correlations with MT parameters of brain atrophy and remaining normal brain tissue (Kalkers et al. 2001). Correlation between gray matter involvement and EDSS is seen as an indication that estimation of gray matter abnormality may be useful in assessing clinical disability.

MTR can be used in monitoring of the disease in MS. In view of all the therapeutic trials going on in this disease, objective and quantitative parameters are essential to monitoring the disease course and the efficacy of the treatments applied. For instance, MTR has been used to estimate the effect of interferon beta-1a (Kita et al. 2000) and interferon beta-1b (Richert et al. 1998) in MS patients. In these studies MTR was found to be comparable with the more common estimation of the number of new enhancing lesions over time.

Another important application of MT is in X-linked adrenoleukodystrophy. Monitoring of the onset of cerebral demyelination is extremely important in young boys. As soon as the first significant signs of progressive cerebral demyelination are found, hematopoietic stem cell transplantation is performed in an attempt to halt the disease. Because of the significant

morbidity and mortality of the procedure, and the fact that one cannot predict which boy carrying the biochemical and genetic defect will develop the devastating cerebral demyelinating disease and which boy will develop adrenomyeloneuropathy, the later-onset and milder form of the disease, hematopoietic stem cell transplantation cannot be performed at an early age as a preventive measure. Careful monitoring at regular intervals is presently the best solution. Conventional MRI is important but it has been shown repeatedly that proton MRS, diffusion tensor imaging, and MT are more sensitive and are able to demonstrate the onset of the disease and quantify disease progression where conventional MRI does not (yet) show changes. It has been shown in X-linked adrenoleukodystrophy that MTRs correlate closely with the degree of loss of tissue integrity (Melhem et al. 1996).

Magnetic Resonance Spectroscopy: Basic Principles and Application in White Matter Disorders

M.S. van der Knaap, P.J.W. Pouwels

108.1 Basic Principles

Pauli was the first, in 1924, to suggest that electrons spin at high speed. Because the spinning electrons have mass, they have a certain angular moment and, thus, as spinning electric charges, a magnetic moment. Later, it was observed that certain nuclei also have magnetic moments. What these nuclei have in common is the fact that they are isotopes with an odd atomic mass and/or odd atomic number, whereas nuclei with both an even atomic number and an even atomic mass do not have a magnetic moment. Subsequently it was noted that when these nuclei are placed in a powerful magnetic field, they show a precessional motion about the axis of the field. In 1946 Bloch and Purcell simultaneously discovered the possibility of resonant energy absorption and emission of precessing nuclei, the basis of magnetic resonance imaging (MRI) and spectroscopy (MRS). For this work they were awarded the Nobel Prize in 1952. MRS has developed into a very important tool in molecular chemistry and physics to reveal molecular structure, chemical reaction rates, and diffusion processes. The first spectroscopy experiments on living systems were performed on small-bore systems with tiny objects, such as red blood cells and excised tissue. Wider bores have since been developed, allowing the study of muscle disorders and experimental work with small animals. Subsequently, *in vivo* MRS of human brain and other organs has also become possible.

Atomic nuclei are composed of protons and neutrons. These nuclear particles exhibit spin. A proton is positively charged, and this spinning charge generates a small magnetic field. Although a neutron is electrically neutral, its component electrical charges are not uniformly distributed within its volume, and thus the neutron also generates a magnetic field when spinning, but smaller than that produced by a spinning proton. The magnetic moments of these particles are directed randomly, and they cancel each other out in nuclei with an even number of protons and neutrons. When the nucleus has an odd number of neutrons and/or protons, the nucleus has a net spin, and this spinning charge has a magnetic moment. These nuclei exhibit the magnetic resonance phenomenon. Nuclei of interest for *in vivo* spectroscopy are ^1H , ^{31}P , ^{23}Na , and also ^{13}C , ^{15}N , ^{17}O , and ^{19}F as markers of biochemically interesting compounds. If there is no external magnetic field, the nuclear magnetic

moments have a random direction and there is no net magnetic vector. The intrinsic magnetic phenomena can be detected by applying an external magnetic field. The nuclear magnetic moments tend to align themselves parallel or antiparallel to the external magnetic field. On the other hand, however, nuclei tend to be in constant random motion due to thermal effects. The percentage of nuclei that align with the external magnetic field depends on the strength of the magnetic field relative to the random thermal effects. Slightly more nuclei align with the external magnetic field than against it, because the first position is more stable than the second. Stability is related to the amount of energy that a nucleus possesses. Stability is greater at low energy levels. In fact, there is a continuous transition of nuclei between high- and low-energy positions, but there is a slight net surplus in the low energy position ($1:10^5$ at 1.5 T).

A spinning nucleus precesses about the axis of the magnetic field. This motion is called Larmor precession, and its frequency the Larmor frequency. The Larmor frequency (ω) depends on the magnetic field strength H_0 and characteristics of the particular nucleus, as expressed in the gyromagnetic ratio γ . This dependency is represented in the Larmor equation $\omega = \gamma H_0$. Resonance is a property of physical systems to oscillate at a preferred frequency which is characteristic of the system. The characteristic frequency is referred to as the resonance frequency. The most efficient energy transfer to atomic particles precessing in magnetic fields occurs in their resonance frequency, the Larmor frequency. For magnetic field strengths used in MRS these resonance frequencies are within the radiofrequency (RF) band of the electromagnetic spectrum. A short burst of RF energy is known as an RF pulse. When an RF pulse is administered, this energy is absorbed, and more nuclei move into the high-energy position. When the RF pulse is terminated, the nuclei return to equilibrium and energy is released at the same frequency. The RF signal emitted can be detected.

The basis of MRS is the chemical shift phenomenon. The atomic nucleus is surrounded by an electron cloud and other atomic nuclei. If an external magnetic field is applied, precession is also induced in this electron cloud, resulting in a small magnetic field. This small magnetic field has an influence on the atomic nucleus and modifies the effect of the external magnetic field at the site of the nucleus. Because of

this slight change in the local magnetic field, the nucleus resonates at a slightly different frequency. This shift in frequency is called chemical shift. The chemical shift is determined by the electrochemical environment of the resonating nucleus, and therefore the precise shift is characteristic of a particular atomic nucleus in a particular compound. The bandwidth of the RF pulse, of course, must contain all the frequencies that are necessary to excite the particular atomic nucleus in compounds of interest. The RF signal obtained in an MRS experiment contains many slightly different frequencies. Fourier transformation of the signal transforms a complex time-domain signal into a complex frequency-domain signal. The resulting spectrum depicts all the nuclear resonances as a function of their frequency. Each peak in the spectrum represents the atomic nucleus in a particular compound. The area under each peak is proportional to the number of nuclei producing that peak. MR spectra can be calibrated to yield absolute concentrations of the metabolites represented. The chemical shift depends on the magnetic field strength. However, in MRS the resonance frequencies are not expressed in absolute units (hertz) but in relative units (parts per million, ppm) related to the resonance frequency of a given reference compound. The relative units, ppm, are independent of magnetic field strength. In this way the results obtained in experiments performed at different magnetic field strengths become directly comparable with respect to chemical shift. Another phenomenon that determines the appearance of a spectrum is the influence of other nuclei in the same molecule on the nucleus of interest, which is called J-coupling. If there is no coupling, the resonance remains a single peak (a so-called singlet). If a certain nucleus in particular compound – in the case of ^1H -MRS a proton – is influenced by other protons only a few chemical bonds apart, coupling will induce a splitting of the resonance. Depending on the number of neighboring protons, the resonance may be split into a doublet, a triplet, or more complex patterns. Due to J-coupling spectra will look different at different field strengths.

The nuclei that one would like to observe can be selected by using the appropriate RF pulse. MRI most commonly makes use of the magnetic properties of protons and is in fact ^1H MRI. The protons that contribute to the signal intensity on the images are mainly present in water and fat. MRS, however, focuses not only on protons (^1H -MRS), but also on phosphorus (^{31}P -MRS) and, less frequently, on other nuclei such as ^{13}C , ^{15}N , ^{19}F , and ^{23}Na . In human tissues, these nuclei are present in much lower concentrations than are protons, and the overall sensitivity of the nuclei is much lower than that of protons. Table 108.1 lists the resonant frequencies and relative MR sensitivities of various nuclei at a magnetic field strength of 1.5 T.

Table 108.1. Resonance frequencies and relative MR sensitivities at 1.5 T

Nucleus	Larmor frequency in MHz	Relative MR sensitivity
^1H	63.86	1
^{31}P	25.85	0.066
^{19}F	60.08	0.83
^{23}Na	16.89	0.093
^{13}C	16.06	0.016
^{15}N	6.47	0.001

MRS methods are relatively insensitive. Weak MR signals are measured from relatively low-concentration compounds. For this reason spectra are obtained from relatively large volumes of interest (so-called voxels). The voxel size necessary to produce a spectrum with a reasonable signal-to-noise ratio is larger for nuclei with low abundance and low inherent sensitivity. For ^1H -MRS voxels typically have a size of 4–12 ml, whereas for ^{31}P typical voxel sizes are in the range of 24–63 ml. A further improvement of the spectral signal-to-noise ratio is obtained by signal averaging. For ^1H -MRS 64–128 acquisitions are common, whereas 128–256 acquisitions are generally used for ^{31}P -MRS. It is also essential to use MR instruments with optimal technical equipment to ascertain optimal primary sensitivity. The magnetic field should be extremely homogeneous over the volume analyzed. Any significant inhomogeneity in the magnetic field spreads out and blurs chemical shift spectral lines due to the spread of Larmor frequencies across the volume. The resulting spectral line broadening is undesirable because it reduces the signal-to-noise ratio and hampers the ability to distinguish two closely neighboring resonance lines. The frequencies and frequency separations increase linearly with field strength. High magnetic field strengths are therefore necessary to optimize spectral resolution. High spectral resolution is particularly important for proton spectroscopy, where most interest is focused on metabolites within a narrow chemical shift range, and where the peaks of the metabolites often overlap. For MRS in human beings, a magnetic field strength of 1.5–4 T is used. In experimental work with animals, magnetic field strengths of 4–8 T or even higher are preferred.

For the purpose of cleaning the final spectrum or obviating unwanted resonances, the spectroscopist has access to many suppression and editing techniques. The largest peak in the ^1H spectrum represents water. The concentration of water is about 10^4 – 10^5 times higher than the concentration of the other metabolites. Consequently, the water peak dom-

inates the spectrum, while the other resonances are barely visible. For this reason, water suppression techniques are invariably applied to remove the water peak from the spectrum and make the other peaks better visible and quantifiable. Lipids present in the skull and subcutaneous tissue are another potential problem, as their concentration is also high and their resonances overlap with those of interesting brain metabolites. Several techniques are available to overcome the contamination of a spectrum by fat: location of the volume of interest far from the skull, fat suppression techniques, and outer volume suppression when an entire brain slice is investigated.

Even with all these precautions, MRS remains a relatively insensitive technique requiring concentrations at least in the millimolar range for metabolites to be visualized. Many important but too diluted compounds have so far remained undetectable by *in vivo* MRS. In addition, only molecules sufficiently small and mobile to tumble freely render MR signals useful for *in vivo* work. No useful signals can be obtained from large molecules such as proteins, even soluble ones, nor from most membrane compounds or small molecules bound to large ones. The broadening of spectral lines makes differentiation of these molecules impossible. However, under certain conditions they will contribute to the spectrum as a "macromolecular baseline."

For *in vivo* MRS it is important that a volume of interest can be selected from which the spectrum is derived. A simple technique is the placement of a surface coil over the volume of interest. The spatial definition of such coils is rather poor since the intensity of signal reception decreases with distance. Several techniques have been devised to improve the spatial response of surface coils and to make positioning of the volume of interest more accurate. One major disadvantage remains, which is that surface coils are only suitable for volumes of interest near the surface. Image-localized single voxel spectroscopy by gradient control allows direct and precise definition of a volume of interest on a proton image. Major advantages are the ability to select volumes located in the deeper parts of the brain and the ability to define a volume of interest guided by the abnormalities seen on the image, avoiding contamination of the spectrum by signals from undesired regions. In chemical shift imaging (CSI), also called spectroscopic imaging, spectra are obtained from many contiguous voxels at the same time, covering more or less an entire brain slice. ^1H CSI is usually applied to investigate one of multiple brain slices of 1–2 cm thickness with an in-plane resolution of $1 \times 1 \text{ cm}^2$. The information thus obtained can be used to construct maps for separate metabolites, which display the distribution of a particular metabolite over the brain slice.

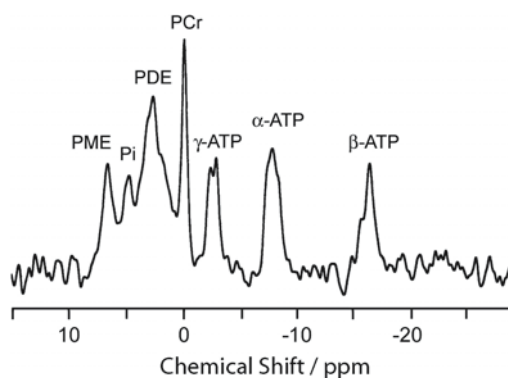


Fig. 108.1. Localized ^{31}P spectrum of the human brain. The spectrum is obtained at 1.5 T with the ISIS technique, TR 3750 ms, 256 measurements, voxel size 63 ml

108.2 Metabolites

In a spectrum from the human brain, ^{31}P -MRS reveals seven major peaks (Fig. 108.1): phosphomonoesters (PME), inorganic phosphate (P_i , including H_3PO_4 , H_2PO_4^- , HPO_4^{2-} , and PO_4^{3-}), phosphodiester (PDE), phosphocreatine (PCr), and the γ -, α -, and β -phosphate groups of adenosine triphosphate (ATP), resonating at 6.5, 4.9, 2.6, 0, -2.6, -8.0, and -16.5 ppm respectively. ADP contributes to the γ - and α -ATP peaks. NAD and NADH contribute to the α -ATP peak.

The main component of the PME peak is phosphoethanolamine. Other components are phosphocholine, glycerol 3-phosphate and sugar phosphates. Minor components are phosphoserine and phosphoinositol. Phosphoethanolamine is a precursor in the anabolism of phosphatidylethanolamine and a product in the catabolism of sphingomyelin. Phosphocholine is a precursor of phosphatidylcholine and sphingomyelin and a product in the catabolism of sphingomyelin. Glycerol 3-phosphate is a precursor of phosphatidylethanolamine, phosphatidylcholine, and plasmalogens and a product in the catabolism of the same compounds. The PME peak is elevated in all rapidly growing tissues with rapid membrane synthesis, such as tumors and the growing brain. It is probable that the elevation is caused by the enhanced presence of compounds meant for the production of membrane phospholipids. Generally, the PME peak is considered to reflect phospholipid anabolic activity. This notion has been confirmed by the finding that the level of PME correlates linearly with the rate of phospholipid synthesis.

The ^{31}P spectrum of the brain contains a large, broad peak centered in the PDE region, underlying the remainder of the spectrum (Fig. 108.2). This large, broad peak originates from large, relatively immobile membrane phospholipids. This broad component is commonly removed from the spectrum by filtering

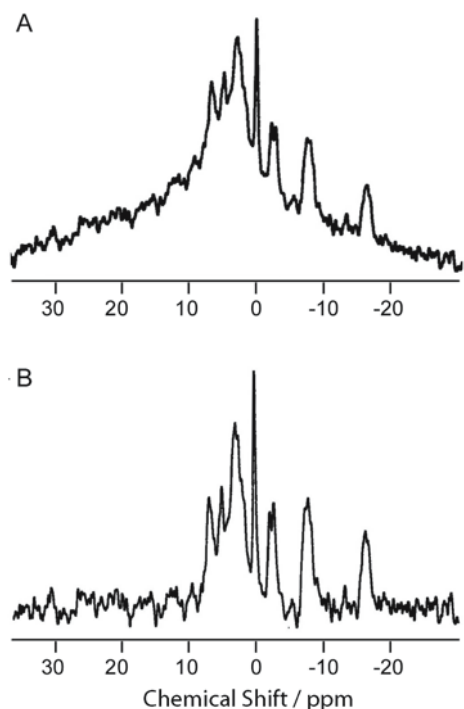


Fig. 108.2. A An unfiltered ^{31}P spectrum of the brain. B The same spectrum after filtering. The spectra are obtained at 1.5 T with the ISIS technique, TR 3750 ms, 256 measurements, voxel size 63 ml

techniques as a standard processing procedure. The remaining PDE peak contains mainly contributions from more mobile phospholipids and relatively minor contributions from phospholipid breakdown products, including glycerophosphocholine and glycerophosphoethanolamine, freely soluble cytosolic molecules. These latter compounds are catabolic products of phosphatidylcholine, phosphatidylethanolamine, and plasmalogens.

The ^{31}P spectrum contains multiple peaks representing high-energy phosphorus compounds (ATP and PCr) and P_i . Intracellular PCr acts via the creatine kinase reaction as a buffer to maintain a constant ATP level in the face of variable energy demands. In conditions of decreasing ATP, PCr reacts with ADP to produce ATP and creatine with creatine kinase as catalyzing enzyme. The reaction is reversible and PCr can be re-synthesized from creatine and ATP. This so-called creatine phosphate shuttle facilitates energy distribution and responds to energy demands. The PCr/ P_i ratio is often used as a measure of the energy status of the brain. The ATP level only drops when PCr is exhausted. In view of the metabolic stability of ATP, it has often been used as an internal reference for quantitation. In particular the β -ATP peak, which does not contain any contributions of other compounds

known to be present in brain tissue in significant amounts, is used as a reference.

The chemical shift of P_i relative to PCr is a function of pH. The pH determines the relative amounts of H_2PO_4^- and HPO_4^{2-} in the equilibrium $\text{H}_2\text{PO}_4^- \rightleftharpoons \text{HPO}_4^{2-} + \text{H}^+$, and the precise resonance frequency of P_i as a whole. Using the equation of Petroff et al. (1985), the pH can be deduced from the chemical shift of P_i relative to PCr. This pH holds for the compartment in which these phosphates are present, which in the brain is the intracellular compartment.

Peak assignment in the ^1H spectrum is problematic because of overlapping resonances. Straightforward assignment is possible for the singlet representing the *N*-acetyl methyl resonance of *N*-acetylaspartate (NAA) at 2.02 ppm, the methyl and the methylene resonance of total creatine (Cr), including free creatine and phosphocreatine, at 3.02 ppm and 3.93 ppm, respectively, and the methyl resonances of choline-containing compounds (Cho) at 3.22 ppm (Fig. 108.3). The methyl resonance of *N*-acetylaspartyl glutamate (NAAG) is a shoulder on the methyl resonance of NAA with only a slight difference in chemical shift (2.05 as opposed to 2.02 ppm). It is responsible for about 10–25% of the NAA peak. Since the singlet resonances of NAA, Cr, and Cho exhibit relatively long T_2 relaxation times, they may be specified in spectra at long echo times (135 or 270 ms) (Fig. 108.3a). When shorter echo times (15–30 ms) are used, a considerably increased number of resonances with short T_2 relaxation times can be visualized (Fig. 108.3b). Most obvious are the appearance of a strong signal from multiple collapsed resonances of *myo*-inositol (mIns) at 3.56 ppm. A complex pattern of coupled resonances between 2.1 and 2.5 ppm together with a further group of resonances around 3.8 ppm are assigned to glutamine and glutamate. Resonances of γ -aminobutyric acid (GABA) are overlapped by the larger resonances of Cr, glutamate, and NAA (GABA resonances at 1.90, 2.30, and 3.03 ppm). Additional resonances are seen originating from the aspartyl group of NAA (2.48, 2.60, and 2.66 ppm), glucose (3.43 and 3.80 ppm) and *scyllo*-inositol (3.35 ppm). The singlet of glycine (3.55 ppm) overlaps with the mIns peak. The quartet of taurine (centered at 3.35 ppm) partly overlaps with *scyllo*-inositol. Lactate is not usually visible under normal conditions, but can be visualized as a doublet centered at 1.33 ppm if elevated. Alanine can only be seen when increased in concentration, then giving rise to a doublet at 1.47 ppm. Pyruvate is below the level of detection under normal circumstances, but when elevated it gives rise to a single peak at 2.36 ppm. In case of elevated tissue levels of free lipids, for instance as a result of myelin breakdown or spectral contamination by fat from the skull, broad resonances are seen at 0.9 and 1.3 ppm originating from the methyl and methylene groups of the

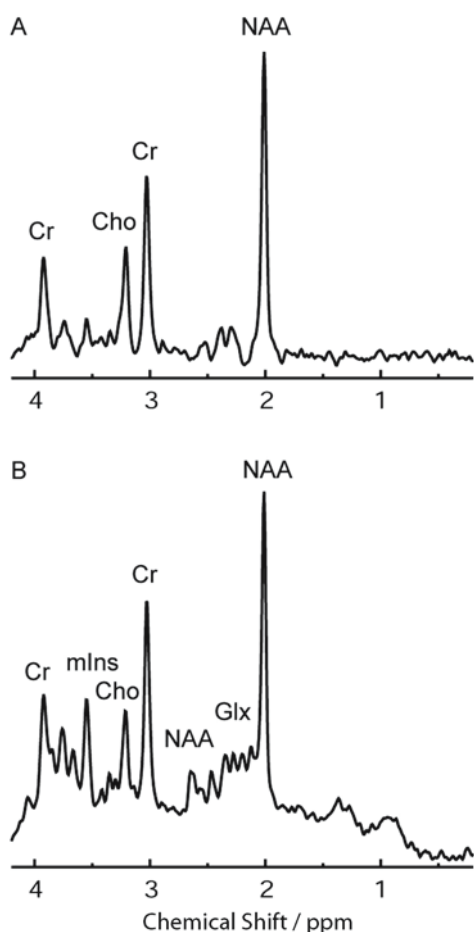


Fig. 108.3. Localized ^1H spectra of parietal cortex (12 ml) of a 4-year-old healthy girl, obtained at 1.5T. **A** At a long echo time of 135 ms (PRESS, TR/TE = 3000/135 ms) only singlet resonances of NAA, Cr, and Cho are visible. **B** At a short echo time of 20 ms (STEAM, TR/TE = 6000/20 ms) additional resonances of mIns, Glx (glutamate and glutamine), and other metabolites are present in the spectrum

lipids. Because of severe overlap of resonances in spectra recorded with short echo times, it is difficult to quantify metabolite concentrations. Special techniques such as spectral editing have been developed to quantify glutamine, glutamate, and GABA separately. Alternatively, a spectrum can be quantified by describing it as a linear combination of model spectra of all individual metabolites included in a database using prior knowledge.

NAA is a compound found at high concentration in the CNS, whereas only traces are found in other tissues. In the mature brain NAA is almost entirely confined to neurons and their axons: 40% of the NAA is in the nerve-ending mitochondrial fraction and 60% is in the cytosol. In cell cultures NAA has also been demonstrated in oligodendroglial precursor cells.

NAA and its derivative NAAG are synthesized in neuronal mitochondria. However, the catabolic enzyme for NAA hydrolysis, aspartoacylase, is expressed only in oligodendrocytes, and the catabolic enzyme for NAAG is expressed only in astrocytes. Little is known about the role of NAA in normal function or disease states. Possible functions include a role as precursor of the putative neurotransmitter NAAG, as storage form of the neurotransmitter aspartate, as acetyl donor in lipid synthesis (important in myelin synthesis), as stabilizer of the concentration of acetyl-CoA, as molecular water pump, and as having a role in osmotic regulation, protein synthesis, and cell signaling. NAA is considered to be a neuron- and axon-specific marker. In disease conditions NAA is often low, related to neuronal or axonal dysfunction or loss. Partial recovery of NAA level has been described in improving cerebral disorders. It is, therefore, not correct to interpret a decrease in NAA as a straightforward indication of irreversible neuronal loss. However, it is difficult to separate the effects of recovery of NAA concentrations in recovering neurons from the effects of tissue contraction after removal of damaged tissue elements. Temporary reductions in NAA have been ascribed to temporary metabolic depression and decreased mitochondrial energy production.

The Cr peak represents the total amount of creatine and phosphocreatine present in the creatine kinase shuttle. The total creatine pool remains fairly constant under a variety of conditions. For this reason Cr has often been used as internal reference for quantitation. However, since Cr is not constant under all conditions, other means of referencing are preferable. The Cr concentration of glia is relatively high and consequently increased Cr is seen in conditions of gliosis. Cr is only present intracellularly, and Cr has also been considered a marker for cellular density.

The Cho peak contains contributions from various compounds. Water-soluble choline-containing compounds in the brain, including choline, glycerophosphocholine, and phosphocholine, are responsible for the largest part of the peak. A smaller contribution to the peak comes from choline-containing phospholipids, including sphingomyelin and phosphatidylcholine. Acetylcholine is also a water-soluble compound, but has a low concentration. Elevated Cho is seen in conditions of high cell density and enhanced membrane turnover, such as brain growth, myelination, demyelination, inflammation, and tumor growth. Cho is also an osmolyte and its level may reflect compensation for osmotic changes.

Lactate occupies a special position in energy metabolism. Being the end product of glycolysis, it rises in concentration whenever the glycolytic rate in a volume of tissue exceeds the tissue's capacity to catabolize lactate or export it to the blood stream. Lactate levels are increased under conditions of anaerobic

glycolysis, for example in failure of energy supply or in respiratory chain defects. Macrophages are highly dependent on anaerobic glycolysis for their energy production. Elevated lactate is also seen in conditions characterized by the presence of increased numbers of macrophages, such as active demyelination and tissue necrosis. Increased lactate secondarily leads to increased alanine, which may become visible in the spectrum.

The mIns peak is also a composite peak, containing contributions from *myo*-inositol as main component, and, additionally, inositol monophosphate, phosphatidyl inositol (a membrane phospholipid), and inositol diphosphate as minor components. Inositol diphosphate is, however, a very important component, functioning as a second or third messenger for various hormone actions. Inositol diphosphate is active in releasing calcium from the endoplasmic reticulum and mitochondria. Many enzymes are dependent upon the inositol-induced calcium release. The function of *myo*-inositol itself is still largely unknown, but it may be the storage form of the inositol-dependent messenger system. Another important function of *myo*-inositol is that of osmoregulator. In diabetes mellitus, inositol phosphate has been considered as a mediator of some of the secondary complications, in particular polyneuropathy. In galactosemia some of the late complications have been attributed to depletion of *myo*-inositol. Also in hepatic encephalopathy a depletion of *myo*-inositol is seen. *myo*-Inositol is only present in glia and mIns can therefore be used as a glial marker. In conditions of gliosis, the mIns level is increased. *scyllo*-Inositol is a stereoisomer of *myo*-inositol and usually the variation in *myo*-inositol level and *scyllo*-inositol level change simultaneously. However, in some individuals high *scyllo*-inositol levels are found in the presence of normal *myo*-inositol levels.

Glutamate is the most important excitatory neurotransmitter, whereas GABA, formed by decarboxylation from glutamate, is the most important inhibitory neurotransmitter. In the presynaptic neuron glutamine is converted to glutamate and ammonia by glutaminase. Glutamate can either be converted to GABA by glutamic acid decarboxylase or be released in the synaptic cleft. After release by the presynaptic neuron, glutamate is taken up by the astrocyte in which it is processed by glutamine synthetase into glutamine, which is transported back to the presynaptic neuron. This cycle operates between the presynaptic neuron, the neuronal cleft, and the astrocyte. Hyperammonemia has a great impact on this cycle by stimulating glutamine synthesis via glutamine synthetase, by possible inhibition of glutaminase, and by inhibition of glutamate reuptake by the astrocyte. In hyperammonemia glutamate decreases and glutamine increases. Glutamate may be elevated in conditions of

active tissue damage, such as hypoxia-ischemia, as one of the so-called excitatory amino acids. Apart from its role as neurotransmitter and precursor of GABA, glutamate is important as a Krebs cycle component via α -ketoglutarate. Considering its predominantly glial localization, glutamine may be considered a glial marker.

Taurine is a key component of the cytosol buffer and serves to optimize cytosol buffering capacity at physiological pH. It is involved in neurotransmission, osmoregulation, and brain growth. It controls magnesium homeostasis and calcium homeostasis.

108.3 Normal Values: Age Dependency and Regional Variability

The major biochemical changes related to processes of brain maturation are reflected in spectroscopic changes (Figs. 108.4 and 108.5).

The most striking finding in ^3P -MRS (Fig. 108.4) of neonatal brain is a very high PME peak, in particular in fetuses and preterm babies, in whom the PME peak is higher than all other peaks in the spectrum. Relative to β -ATP, PME decreases with ongoing brain maturation, to reach final values at about 2 years of age. In terms of absolute metabolite concentrations also, PME decreases with increasing age. The elevation of the PME peak in early development is mainly related to elevated phosphoethanolamine. The high PME peak can be attributed to active membrane phospholipid synthesis, in particular active myelination. Myelination is almost complete at the age of 2 years.

PDE is very low in fetal brain. PDE increases with ongoing brain maturation, but is still relatively low in term neonates. The PDE/ β -ATP ratio and absolute concentrations of PDE increase with age. Final values are reached at the age of about 2 years. PDE originates to a large extent from phospholipids and to a smaller extent from low-molecular-weight soluble metabolites in phospholipid breakdown. The increase in PDE with increasing brain maturation is primarily related to the increasing membrane density of the brain, which is largely caused by progressing myelination. With increasing membrane content of the brain, membrane turnover also increases, and, accordingly, so does the concentration of intermediary products of phospholipid breakdown, contributing to the height of the PDE peak.

The PME/PDE ratio can be used as a maturation index for brain development.

There are major changes in energy metabolism related to brain maturation. On the basis of findings in animal experimental research it was assumed that the cerebral concentration of ATP, reflected in β -ATP, does not change with age and is constant irrespective

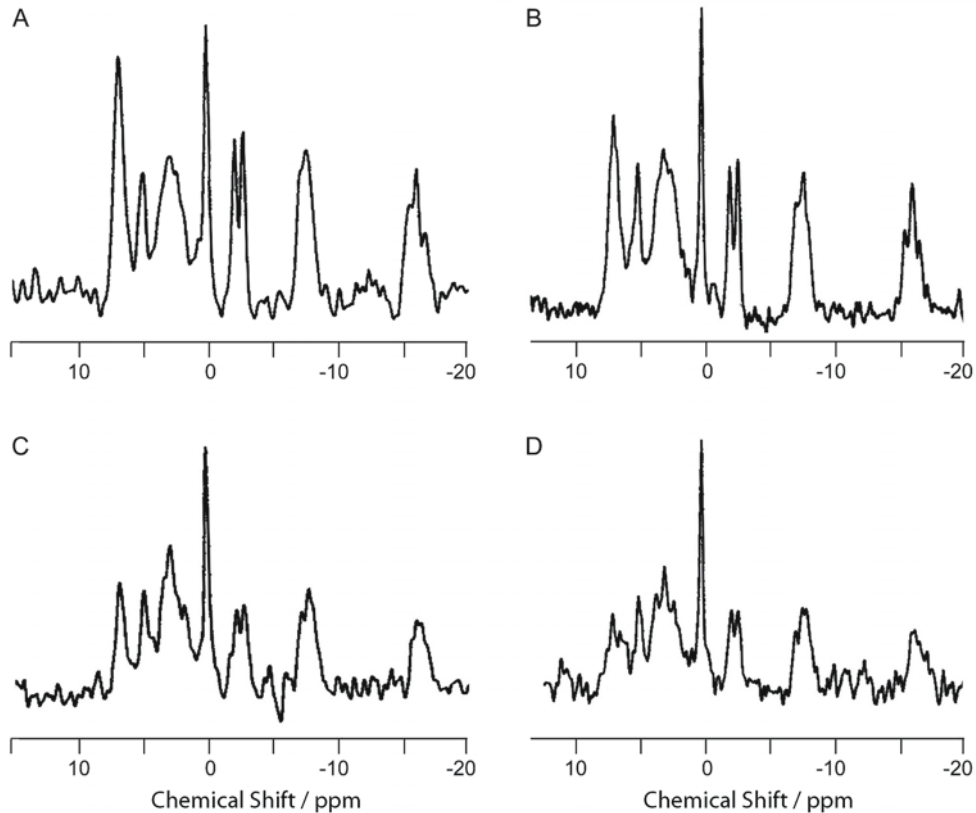


Fig. 108.4. Four ^{31}P spectra of the brain obtained at different ages after birth at term: 1 month (A), 4 months (B), 2 years (C), and 15 years (D). Note the decrease in PME and increase in PDE

and PCr relative to β -ATP with increasing age. The spectra are obtained at 1.5 T with the ISIS technique, TR 3750 ms and 256 measurements, voxel size 54–63 ml

of maturational stage. However, evidence has been provided by Buchli et al. (1994) that the ATP concentration of the brain increases significantly with age during early development. Relative to β -ATP, PCr increases rapidly after birth and reaches final values after a few months. P_i/β -ATP does not undergo significant changes. Buchli et al. (1994), using absolute quantitative data, found some postnatal increase in P_i and a more marked increase in PCr and ATP. So, there is a maturational increase in the creatine kinase reaction rate with age. PCr/P_i is considered a measure of the phosphorylation potential and energy status of the examined tissue; the increase may, therefore, imply an increase in energy reserve in infant brain tissue. This increase would be compatible with the increase in rate of energy metabolism observed in post-natal cerebral maturation.

Human cerebral pH shows some decrease with ongoing cerebral maturation.

^1H spectra also undergo major developmental changes. In neonates, in particular in preterms, the spectrum is dominated by Cho and mIns peaks, whereas in the adult the NAA peak is largest (Fig. 108.5).

NAA is low at birth. NAA/Cr ratio and absolute NAA values have been shown to increase after birth. The steepest increase occurs during the first year of life, with very gradual increases during childhood, and final values are reached around the age of 10 years. The increase in NAA can be attributed to processes of neuronal maturation, including increase in number of axons, dendrites, and synaptic connections.

There is a rapid increase in the cerebral Cr concentration before and around term, and final values are reached after a few months. The difference from adult values is small but significant. Therefore, Cr is an internal reference of limited value, especially in early development.

Cho is high in neonates and decreases thereafter. Cho/Cr ratio and absolute Cho values decrease with increasing cerebral maturation, and final values are reached after 3–5 years. The high Cho in early development can be attributed to a high rate of membrane synthesis and turnover, in particular related to the process of myelination.

The mIns concentration is high at birth and decreases rapidly. Final values are reached within the

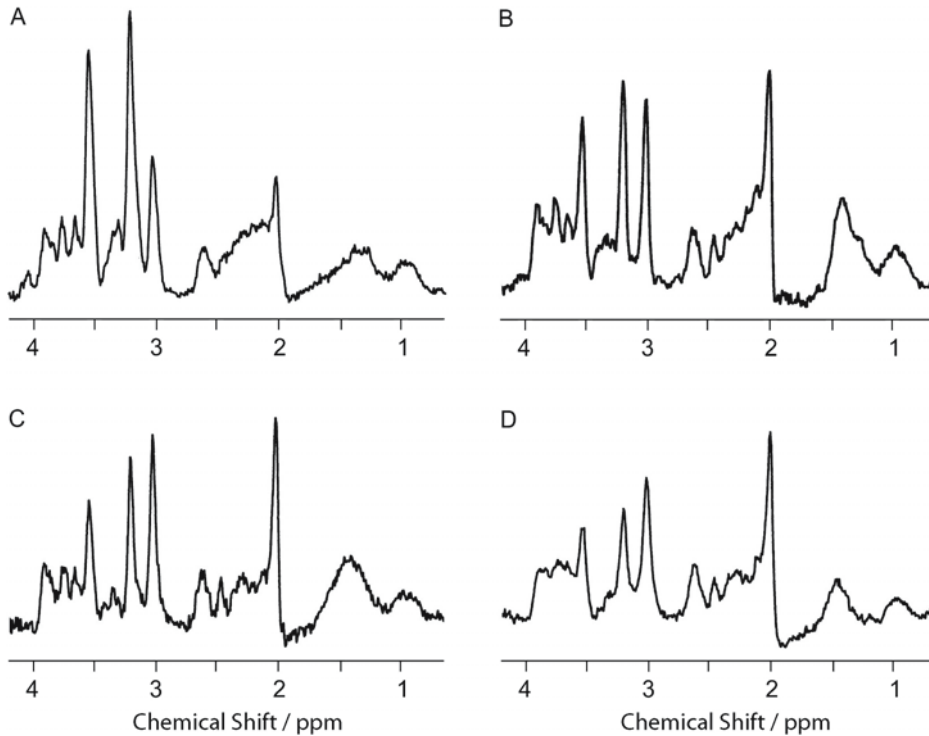


Fig. 108.5. Four ^1H spectra of parietal white matter obtained at 1.5 T (STEAM, TR/TE = 2500/20 ms) and at different ages: 32 weeks postconceptional age (A), 3 months after term birth

(B), at 4 years (C), and at 9 years (D). Note the increase in NAA and decrease in Cho and mIns relative to Cr with increasing age

first year of life. The significance of the high mIns concentration in early development is not known.

The resonances originating from taurine are high at birth, and gradually decrease.

The peaks originating from glutamine and glutamate do not change significantly.

Metabolite concentrations show regional variability, determined by the structures included in the study (Fig. 108.6). Depending on the size of the individual voxels, partial volume effects are important. Due to the cortical foldings it is not possible to obtain spectroscopic data from a voxel containing cortex only, and it is difficult to choose a voxel containing white matter only. The impact of the problem is more severe on ^{31}P -MRS than on ^1H -MRS, because larger voxels are used. In ^{31}P -MRS, PME, PDE, and P_i are higher in white matter than in gray matter, whereas PCr is higher in gray matter. In ^1H -MRS it is possible to obtain spectra from voxels containing mainly cortex or white matter or central nuclei. It has been shown that NAA, Cr, mIns, glutamate, and glutamine are higher in gray matter spectra than in white matter spectra, whereas Cho is higher in white matter spectra (Fig. 108.6). The normal spectroscopic findings in the intact brain stem, cerebellum, and basal ganglia are again different. The maturational changes as de-

scribed above are valid for brain structures in general, but they may differ in detail for different brain structures. These regional and age-dependent spectral changes make it necessary to obtain region-specific normal values for different ages.

108.4 MRS in Cerebral Disorders: Process-Specific Abnormalities

Two types of spectroscopic abnormalities are seen in white matter disorders:

1. Process-specific spectroscopic abnormalities, related to delayed maturation and tissue damage.
2. Disease-specific spectroscopic changes, directly related to the particular disorder under investigation.

In this section, the process-specific abnormalities are discussed.

In retarded brain maturation, MRI only shows delayed myelination, because, apart from gyration, processes of neuronal maturation cannot be visualized. In MRS one expects metabolite levels appropriate for a younger age than the age of the patient. The use of MRS to provide quantitative measures for

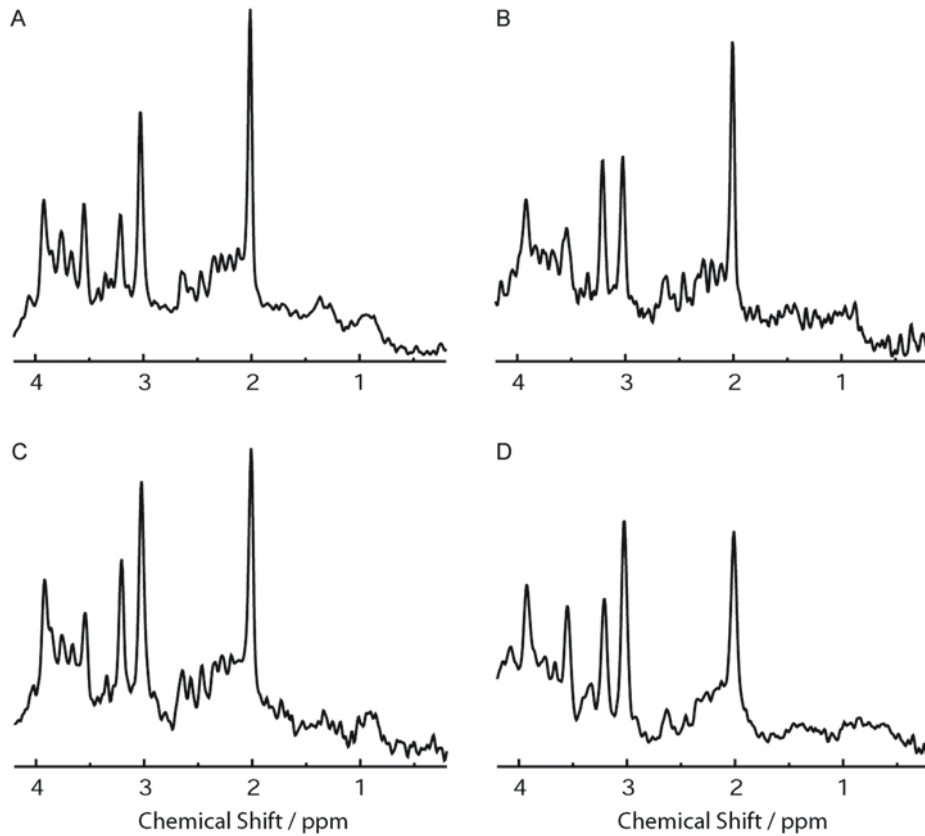


Fig. 108.6. ^1H spectra of a 4-year-old healthy girl, obtained with STEAM (TR/TE = 6000/20 ms) at 1.5 T. Spectra are from (A) parietal cortex (10 ml), (B) parietal white matter (4 ml),

(C) basal ganglia (5 ml), and (D) cerebellar vermis (8 ml). The spectra are plotted on the same vertical scale to allow a qualitative comparison

processes of cerebral maturation is limited by the rather wide normal variation.

In demyelinating disorders, it is primarily the myelin sheath that is lost; secondarily, axonal damage and loss occurs. Histologically, demyelinating disorders are characterized by rarefaction of the white matter with respect to its normal constituents. Gliotic scar tissue fills in the free spaces that arise as a consequence of the loss of myelin and axons. Consequently, demyelinating disorders do not lead to significant cerebral atrophy in the early stages. Only when the demyelination is severe and long-standing does atrophy ensue. The rarefaction of white matter implies that the total amount of membrane phospholipids per volume of brain tissue decreases, resulting in a decrease in PDE in the ^{31}P spectrum (Fig. 108.7). The decrease in the ratio of PDE to β -ATP has been shown to be proportional to the extent of the demyelination. The PME peak, which is proportional to the rate of membrane phospholipid synthesis, remains normal until demyelination is very severe. In severe demyelination a variable decrease in PME/ β -ATP ratio is observed. The neuronal damage and loss accom-

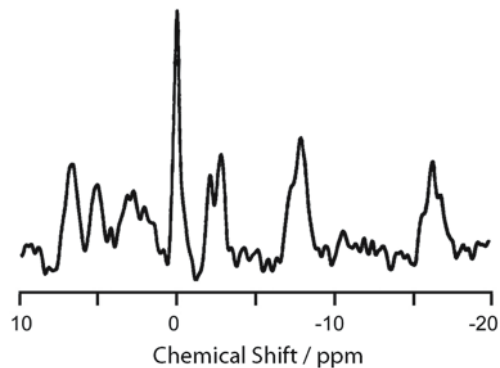


Fig. 108.7. ^{31}P spectrum of a patient with severe demyelination. Note the very low PDE. Compare this spectrum to that of Fig. 108.1, which was obtained from a normal child of the same age

panying demyelination are reflected in a decrease in NAA in the ^1H spectrum. The decrease in NAA occurs early in the process. The extent of NAA loss can vary considerably, depending on the stage of the disease

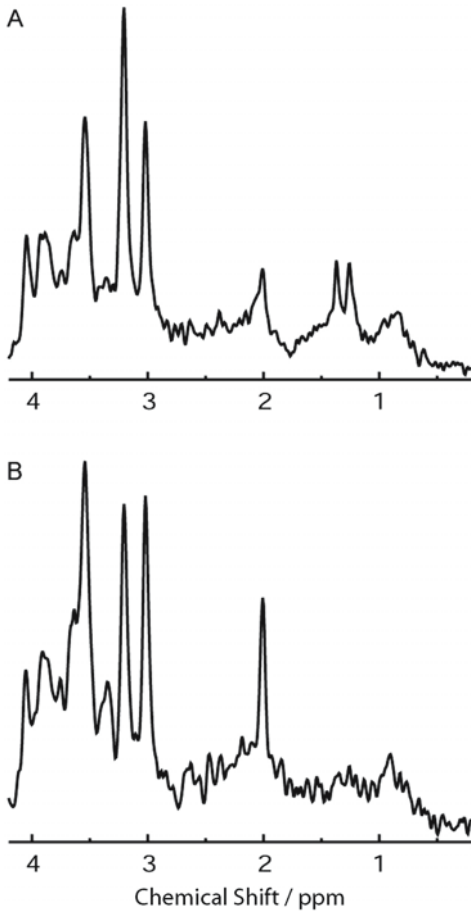


Fig. 108.8. ^1H spectra obtained with STEAM (TR/TE = 6000/20 ms) at 1.5 T. **A** The white matter spectrum (5 ml) of a 9-month-old girl with advanced-stage infantile Krabbe disease shows almost complete absence of NAA, increased Cho and mIns, as well as a clear elevation of lactate, represented by the doublet at 1.33 ppm. **B** The white matter spectrum (5 ml) of a 4-year-old girl with the much slower disease course of late-infantile/early-juvenile Krabbe disease is characterized by a strong elevation of mIns and a less severe decrease of NAA

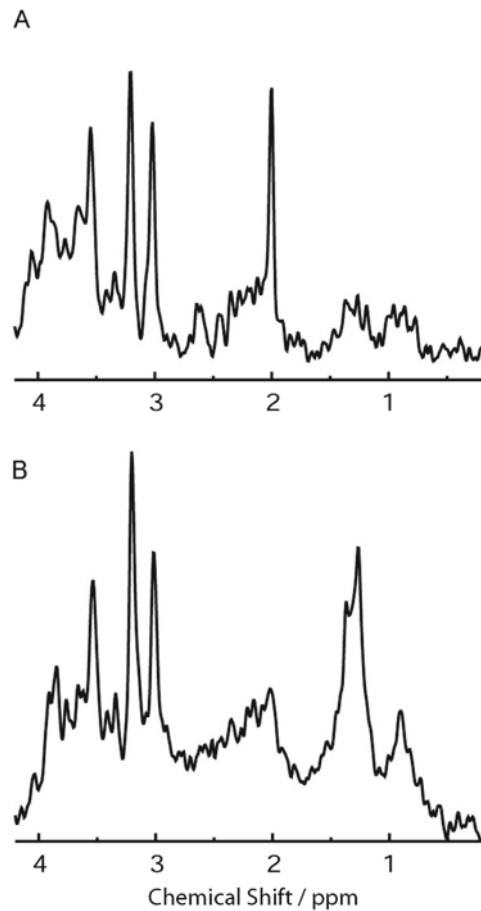


Fig. 108.9. ^1H spectra of white matter affected by demyelination (4–5 ml, STEAM, TR/TE = 6000/20 ms, 1.5 T) show variable extents of metabolic abnormalities. **A** In a 4-year-old X-linked adrenoleukodystrophy patient with nonprogressive lesions, metabolic abnormalities in the affected white matter are limited to a small decrease of NAA and increases of Cho and mIns. **B** In a 10-year-old X-linked adrenoleukodystrophy patient with highly active demyelination, a complete absence of NAA, a strong increase of Cho, and lipid resonances at 0.9 and 1.3 ppm, overlapping with a doublet of lactate, are found

and destructiveness of the process, as illustrated in Fig. 108.8 for patients with infantile and juvenile Krabbe disease. In active demyelination Cho is elevated, related to enhanced membrane lipid turnover (Fig. 108.9). In addition, elevated protein and lipid peaks at 0.9 and 1.3 ppm are occasionally seen, related to the enhanced presence of myelin breakdown products (Fig. 108.9b). A variable increase in lactate occurs in active demyelination, presumably related to the infiltration of the tissue by macrophages (Fig. 108.9b). Increased levels of glutamate/glutamine have been observed, which may be related to processes of active tissue degeneration. The concentration of mIns increases as a consequence of gliosis (Fig.

108.10a). In the end-stage phase of demyelination, Cho decreases again, lactate and lipids disappear, and the spectrum becomes “empty,” dominated by a high mIns peak. The cortex spectrum remains relatively intact (Fig. 108.10b).

In primary neuronal degenerative disorders, neurons undergo degenerative changes, die, and disappear, together with their axons and myelin sheaths. White matter rarefaction does not occur and gliosis is usually inconspicuous. Tissue loss is primarily evident as atrophy. As expected, the PDE/ β -ATP ratio has been found to remain within the normal range, even in far advanced disease. The neuronal damage is reflected in a decrease in NAA, but the decrease in

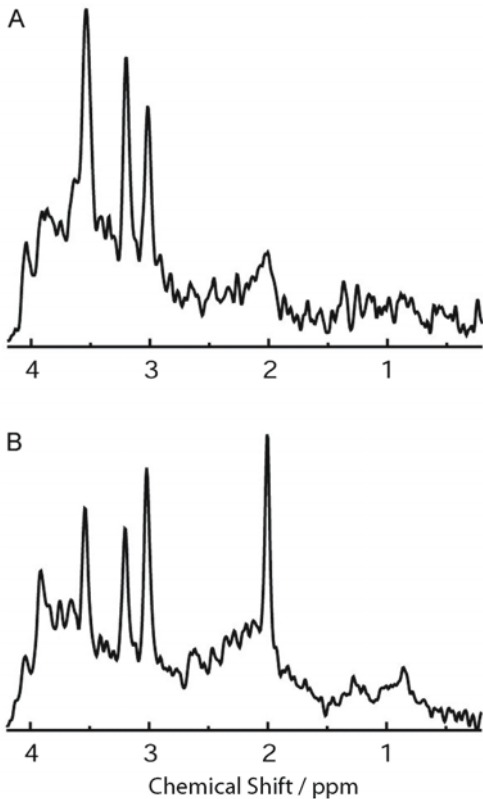


Fig. 108.10. The ¹H spectrum of affected white matter (A; 5 ml, STEAM, TR/TE = 6000/20 ms, 1.5 T) of a 10-year-old girl with an advanced stage of metachromatic leukodystrophy only contains signals of mIn, Cho, and Cr, indicating the pure gliotic contents of the tissue. **B** In contrast, the spectrum of the cortex (8 ml) still contains a relatively high signal of NAA

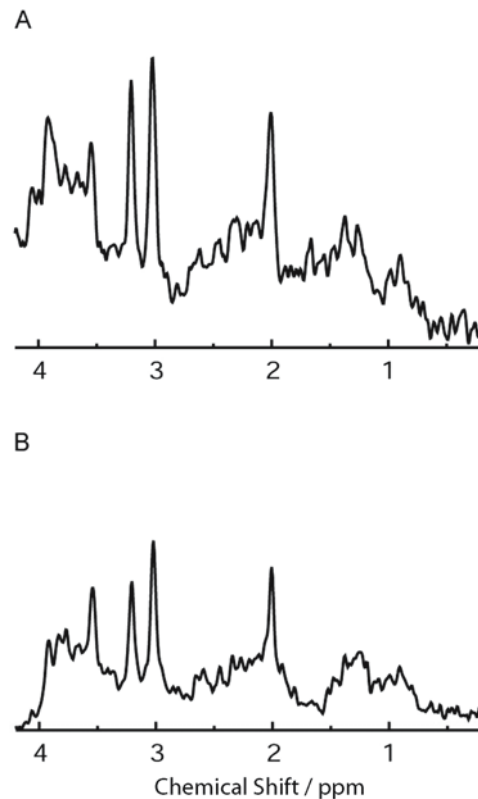


Fig. 108.11. The ¹H spectrum of white matter (A; 5 ml, STEAM, TR/TE = 6000/20 ms, 1.5 T) of an 8-year-old boy with the Turkish variant of late-infantile neuronal ceroid lipofuscinosis shows a marked decrease of NAA and an increase of lactate. **B** The loss of NAA is also pronounced in the cortex spectrum (8 ml). In the cortex spectrum all signals are relatively low due to atrophy and admixture of more CSF than usual

NAA underestimates the neuronal/axonal loss as compared to primary demyelinating disorders because of tissue contraction (Fig. 108.11a). However, in neuronal degenerative disorders the decrease in NAA in the cortex spectrum is more marked (Fig. 108.11b) than in demyelinating disorders (Fig. 108.10b). In neuronal degenerative disorders the NAA decrease occurs before evident atrophy on MRI. So, in this respect, MRS is more sensitive than MRI. In neuronal degenerative disorders, Cho may be elevated related to enhanced membrane turnover. Some elevation of mIn is sometimes seen, related to some gliosis.

In hypomyelination, the level of Cho tends to be low, indicative of decreased (myelin) membrane synthesis and turnover (Fig. 108.12). In the case of concomitant white matter gliosis, mIn and Cr are elevated, as is seen in H-ABC (*hypomyelination with atrophy of the basal ganglia and cerebellum*) (Fig. 108.13). In the case of concomitant axonal damage and loss,

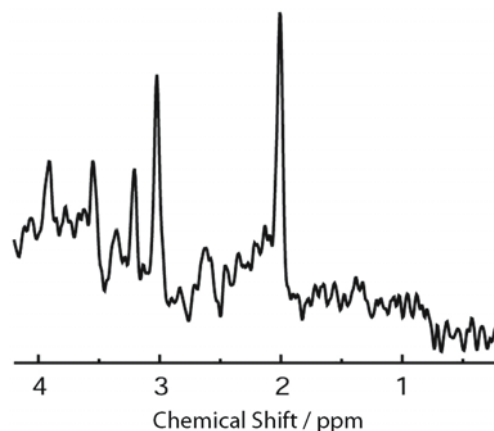


Fig. 108.12. The ¹H spectrum of white matter (5 ml, STEAM, TR/TE = 6000/20 ms, 1.5 T) of a 25-year-old male with hypomyelination shows a decrease of Cho whereas all other metabolite concentrations are within normal ranges

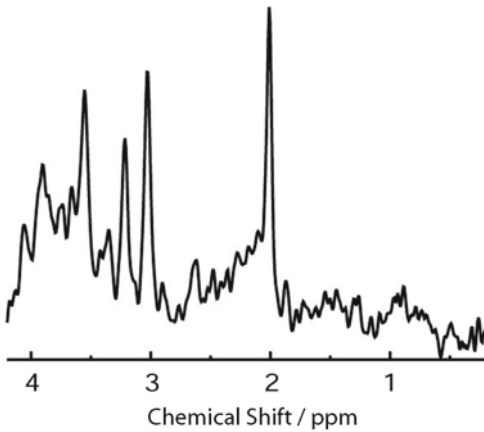


Fig. 108.13. The ^1H spectrum (5 ml, STEAM, TR/TE = 6000/20 ms, 1.5 T) of an 8-year-old boy with H-ABC at 1.5 T, shows a slight decrease of Cho, as well as an increase of Cr and especially of mIns

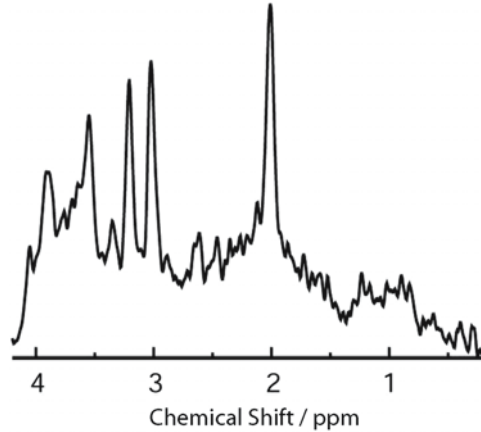


Fig. 108.15. The ^1H spectrum (6 ml, STEAM, TR/TE = 6000/20 ms, 1.5 T) of a white matter lesion of a 44-year-old female with relapsing-remitting multiple sclerosis shows a decrease of NAA and an increase of mIns

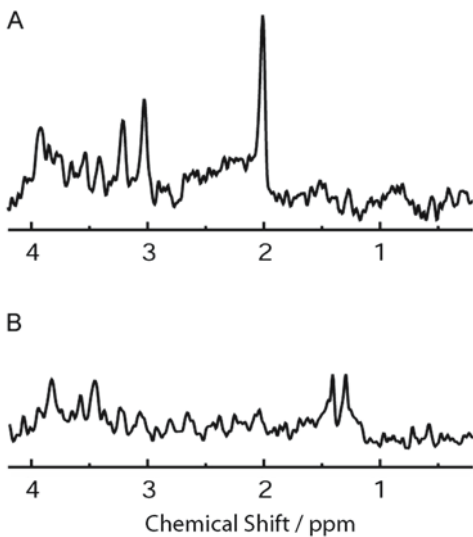


Fig. 108.14. ^1H spectra of white matter (6 ml, STEAM, TR/TE = 6000/20 ms, 1.5 T) of patients with vanishing white matter. **A** In the spectrum of a 10-year-old girl with mild disease all metabolites are only slightly decreased, indicating a rarefaction of the white matter. **B** The spectrum of a 3-year-old girl with totally cystic white matter on MRI only contains lactate (doublet at 1.33 ppm) and glucose (signals at 3.4 and 3.8 ppm), indicating the replacement of white matter by CSF

white matter NAA is decreased. Some have found an increased NAA in the white matter of patients with Pelizaeus–Merzbacher disease, which can be explained by the higher axonal density per tissue volume in the absence of myelin sheaths.

In several disorders, white matter pathology is dominated by white matter rarefaction and cystic degeneration. Examples are vanishing white matter disease and severe variants of sulfite oxidase deficiency/molybdenum cofactor deficiency. In particular in vanishing white matter, the process of progressive white matter rarefaction can be followed with ^1H -MRS. The peaks representing metabolites normally present in the spectrum gradually become lower and disappear (Fig. 108.14). The peaks representing lactate and glucose become visible (Fig. 108.14). Lactate and glucose are normally below the level of detection in brain tissue, but they have a higher concentration in the CSF, which makes them detectable in highly rarefied and cystic white matter, where most of the white matter has been replaced by tissue water or CSF.

Acute inflammatory white matter lesions, related to encephalitis, acute disseminated encephalomyelitis, and multiple sclerosis, are characterized by a decrease in NAA and variable increases in Cho, lactate, lipids, and mIns (Fig. 108.15). The findings are indistinguishable from those seen in active demyelinating metabolic disorders and related to the same basic pathological processes, including axonal damage and loss, enhanced membrane turnover, macrophage infiltration, enhanced presence of membrane breakdown products, and gliosis.

As MRS allows in vivo assessment of cerebral energy metabolism, it can be applied to evaluate cerebral consequences of cellular energy failure in mitochondrial defects. Inborn errors involving mitochondrial oxidative phosphorylation and electron transport may lead to failure to synthesize sufficient ATP, accumulation of ADP, and failure of PCr synthesis from Cr. In addition, mitochondrial dysfunction may lead to

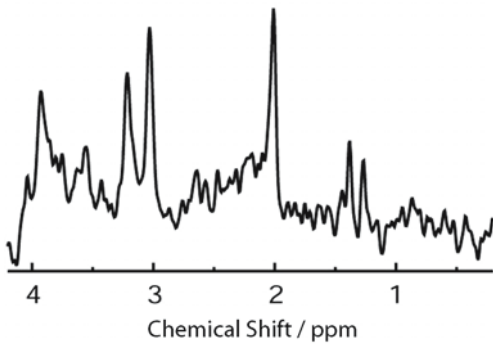


Fig. 108.16. The ^1H spectrum of white matter (5 ml, STEAM, TR/TE = 6000/20 ms, 1.5 T) of a 15-year-old boy with Kearns-Sayre syndrome shows a decrease of NAA and mIns, as well as an increase of lactate (doublet at 1.33 ppm) and glucose (resonances at 3.43 and 3.8 ppm)

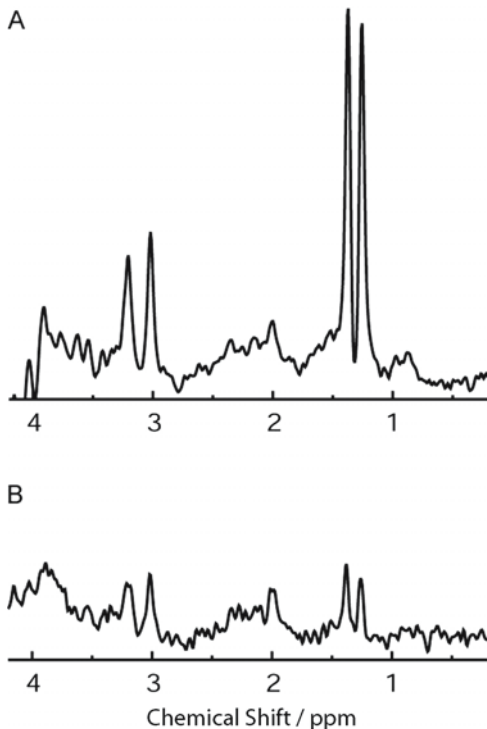


Fig. 108.17. **A** The ^1H spectrum of an acute lesion in the occipital cortex (8 ml, STEAM, TR/TE = 6000/20 ms, 1.5 T) of a 12-year-old boy with MELAS shows a prominent doublet of lactate and complete loss of NAA. **B** The spectrum of an adjoining older lesion in the parietal cortex (6 ml) contains only some small signals from remaining lactate, Cho, and Cr

accumulation of unoxidized reducing equivalents in the form of NADH, NADPH, and lactate. Alanine may be elevated secondary to the lactate elevation. The pattern of metabolic disturbances in mitochondrial

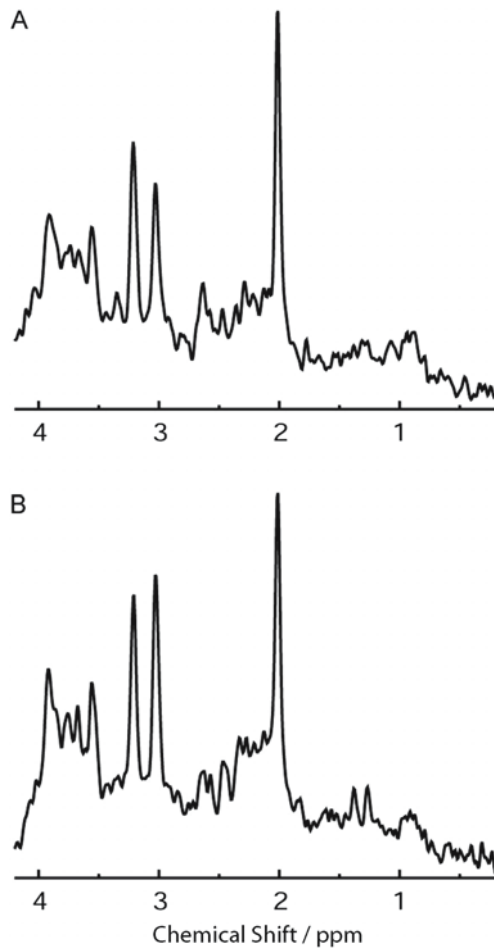


Fig. 108.18. **A** The ^1H spectrum of white matter (5 ml, STEAM, TR/TE = 6000/20 ms, 1.5 T) of a 2-year-old boy with Leigh syndrome (Leigh/NARP mutation) is completely inconspicuous. **B** A spectrum of the lesion in the basal ganglia (4 ml) in the same patient contains a small lactate doublet. It should, however, be noted that lactate is not necessarily detected in patients with mitochondrial disorders, not even in areas which are abnormal on MRI

disorders is, in most respects, indistinguishable from that of hypoxia. In ^1H -MRS in a variety of mitochondrial encephalopathies, including Leigh syndrome, NARP syndrome, Kearns-Sayre syndrome (Fig. 108.16), MELAS (Fig. 108.17), MERFF, and Leber hereditary optic atrophy, variable elevations of cerebral lactate are found, but lactate is not unequivocally elevated in all patients and/or in all brain structures (Fig. 108.18). Cross et al. (1993) found a good correlation between CSF levels of lactate: when the CSF lactate was below 2.5 mmol/l, no lactate was seen in ^1H spectra of the brain, whereas in all cases with a CSF lactate above 4.0 mmol/l, elevated lactate was found in MRS. However, patients have been described repeat-

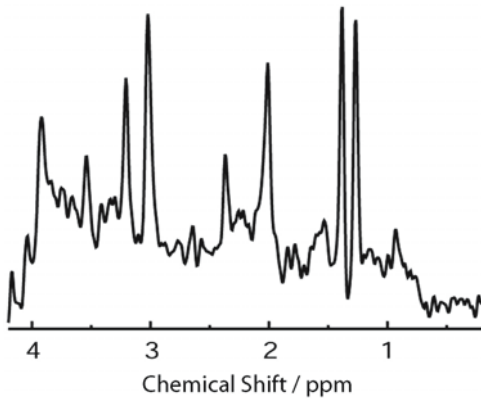


Fig. 108.19. The ^1H spectrum of frontal cortex (5 ml, STEAM, TR/TE = 6000/20 ms, 1.5 T) of a 7-month-old girl with pyruvate dehydrogenase complex deficiency shows not only a prominent lactate doublet (1.33 ppm), but also a clear singlet at 2.36 ppm, which can be assigned to pyruvate. The spectrum is further characterized by decreased signals of NAA and mIns

edly with absence of lactate in ^1H spectra of the brain, while CSF lactate was high, as well as patients with elevated lactate in ^1H spectra of the brain while CSF lactate was normal. There is a regional variability in elevations of cerebral lactate, lactate being most pronounced in regions where MRI shows fresh structural abnormalities, as illustrated in Fig. 108.17. The lactate decreases again when the lesion turns into inactive scar tissue. In some patients the elevated alanine can be visualized. Elevated cerebral glucose levels may be seen (Fig. 108.16), ascribed to a high degree of nonoxidative glycolysis. In pyruvate dehydrogenase complex deficiency, elevated cerebral pyruvate may be demonstrable in addition to the elevated lactate (Fig. 108.19). ^{31}P -MRS in mitochondrial disorders may reveal a decrease in PCr and increase in P_i in the presence of a normal pH, while calculations yield an increase in ADP, a decrease in phosphorylation potential, and an increased percentage of the maximal rate at which ATP is being synthesized, the latter reflecting the increased demand on the mitochondria able to participate in oxidative phosphorylation. These abnormalities are, however, again not invariably present. The above ^1H and ^{31}P spectroscopic features are a measure of the derangement of cerebral energy metabolism and can be used to monitor the course of disease in mitochondrial disorders, in particular to evaluate the effects of treatment. In addition, nonspecific spectroscopic changes can be present in mitochondrial disorders, in particular a decrease in NAA, glutamate, and Cr in lesions, related to neuronal dysfunction and loss.

Similar spectroscopic changes related to cellular energy failure are present in hypoxic-ischemic encephalopathy of neonates. In the acute phase of cere-

bral hypoxia-ischemia, acute reciprocal changes occur in the concentrations of PCr and P_i , so that the PCr/ P_i ratio falls. Only when PCr/ P_i reaches a low value does the concentration of ATP also decline. Intracellular pH is reduced. These changes are rapidly reversed when cerebral perfusion and oxygenation are restored. Over the subsequent few days, spectral abnormalities develop again in spite of the absence of any ongoing hypoxia-ischemia. Again there are roughly reciprocal changes in PCr and P_i and, in severely affected infants, a fall in ATP. However, intracellular pH tends to rise rather than to fall. Later P_i increases, well out of proportion to the fall in PCr, and in severely damaged brains PCr and ATP are absent, leaving only a large residual P_i peak in the spectrum. In less severely affected infants who recover, the ^{31}P metabolite ratios return to normal over the course of about 2 weeks, but sometimes the total phosphorus signal is reduced, indicating permanent loss of cells. The explanation of the presence of two stages is that the initial acute hypoxic-ischemic episode initiates a series of reactions, which later cause progressive disruption of oxidative phosphorylation in brain tissue. This disruption is termed "secondary energy failure." This course of events explains why ^{31}P -MRS findings are often normal on the first day of life, to become abnormal over the subsequent few days. The ^{31}P -MRS findings appear to have prognostic value. Of the children whose PCr/ P_i falls below the 95% confidence limits for normal infants, two-thirds die and almost all survivors have a serious neurological handicap. Nearly all infants with a decrease in ATP die. With respect to ^1H spectroscopic findings, it has been shown that lactate is elevated during the hypoxia-ischemia, to recover partially soon after restoration of normal oxygenation of the brain and rise again during the first 2 days, mirroring the phenomenon of secondary energy failure seen in ^{31}P -MRS. NAA begins to decrease several hours after the hypoxic-ischemic episode. mIns may also increase within the first few days. Glutamate may be relatively elevated for a while after the acute hypoxic-ischemic incident, suggesting excitotoxic effects. In contrast to the normalization of the ^{31}P spectra, ^1H spectra remain abnormal. NAA may recover partially, but does not return to normal. The increased lactate may persist for weeks. ^1H spectroscopic findings also have prognostic value. The lowest NAA levels are found in the children with the poorest outcome. The presence of elevated lactate and also of mIns carries a poor prognosis with respect to survival and neurological handicap.

In conditions of chronic hypoxia-ischemia, such as subacute arteriosclerotic encephalopathy and CADASIL, damage-specific spectroscopic abnormalities are found, including decreased NAA and increased Cho and mIns, whereas lactate may be normal or mildly elevated.

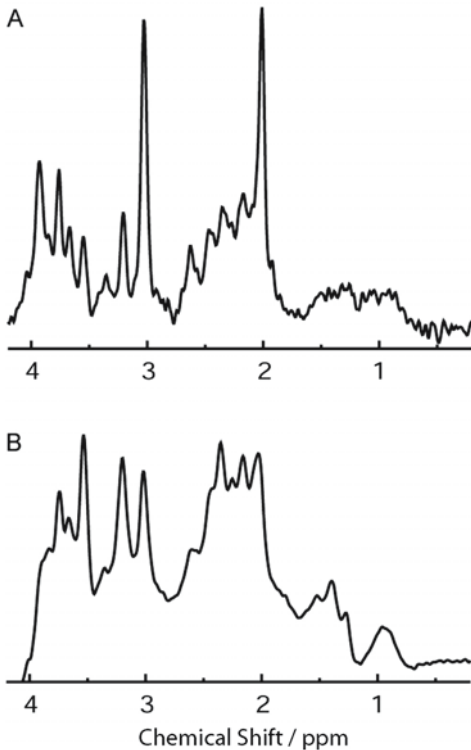


Fig. 108.20. **A** The ^1H spectrum of basal ganglia (8 ml, STEAM, TR/TE = 6000/20 ms, 1.5 T) of a 6-year-old boy with a portocaval shunt and serum ammonia levels of 150–200 $\mu\text{mol/l}$ shows the effects of hyperammonemia in the brain: apart from an increase in glutamine, the spectrum is characterized by low signals from mIns and Cho, compensating the osmotic pressure. **B** The resonances from glutamine dominate the spectrum obtained from basal ganglia and white matter (27 ml, STEAM, TR/TE = 2500/20 ms, 1.5 T) in a 1-week-old neonate suffering from argininosuccinate lyase deficiency (urea cycle defect) and serum ammonia levels of more than 1000 $\mu\text{mol/l}$. The signals of the osmolytes mIns and Cho are small in comparison to the usually much higher levels in neonates

The ^1H spectrum contains resonances of several metabolites that have a function as idiogenic osmolytes. mIns is probably the most important among them, but Cho, Cr, NAA, glutamine and glutamate also have a role in maintaining iso-osmosis. It has been shown that in hypernatremia mIns, *scyllo*-inositol, Cho, Cr, and glutamine/glutamate are elevated, returning to normal when the serum sodium level returns to normal. In hyponatremia, mIns, Cho, Cr, and NAA are decreased and return to normal with normalization of the serum sodium level. In our patient with extremely elevated levels of D-arabitol and ribitol in the brain (see below), NAA, mIns, Cr, and Cho are decreased, probably a compensatory reaction to the osmotic effects of the accumulating polyols.

In cases of hyperammonemia of any origin, including urea cycle defects, propionic acidemia, Reye syndrome, Wilson disease, and other causes of hepatic failure, ^1H spectra show changes directly related to the high levels of ammonium. Hyperammonemia has a great impact on the equilibrium between glutamate, glutamine, and GABA by stimulating glutamine synthesis from glutamate, resulting in an accumulation of glutamine and a depletion of glutamate. Elevated levels of glutamine can be visualized easily by ^1H -MRS (Fig. 108.20). Other consistent and striking spectroscopic changes in hyperammonemia concern a decrease in mIns and Cho (Fig. 108.20). As mIns is an osmolyte, depletion of mIns is probably an osmotic response to glutamine accumulation. In addition, mIns is a precursor of glucuronic acid, which helps to detoxify xenobiotics by conjugation. Depletion of mIns could partially be the result of excessive detoxification. The decrease in Cho is probably also an osmotic response. In cases of neuronal damage, NAA is decreased, but in many patients with hyperammonemia, NAA is normal. The spectroscopic changes directly related to hyperammonemia are reversible after normalization of ammonia levels, implying that ^1H -MRS is a very useful tool for monitoring cerebral abnormalities in hyperammonemias.

108.5 MRS in Cerebral Disorders: Disease-Specific Abnormalities

Specific changes, related to the specific disorder, can be found in particular in some of the inborn and acquired errors of metabolism.

The relative increase in NAA in Canavan disease is well known (Fig. 108.21). It is specifically the metabolism of NAA that is disturbed in this disorder. When absolute quantitation is used and metabolites are expressed in millimoles per liter of brain tissue, Cho and Cr appear to be low and NAA can vary between the normal range and up to a two-fold elevation. In direct biochemical measurements the increase in the level of cerebral NAA expressed in micromoles per milligram protein is much more pronounced. The apparent discrepancy between MRS and biochemical findings can be explained by the different way of expressing the concentration: per volume (MRS) or per dry weight (biochemical analyses). In Canavan disease, the white matter has a reduced myelin content and cellularity, and the white matter is converted into a loose, vacuolated meshwork, with glia and bare axons left as tissue elements. This serious white matter rarefaction implies that a large part of the selected volume of interest for MRS consists of water. The low Cho with low Cho/Cr ratio in Canavan disease is probably related to the very low membrane content of the white matter. In itself the elevation of NAA is

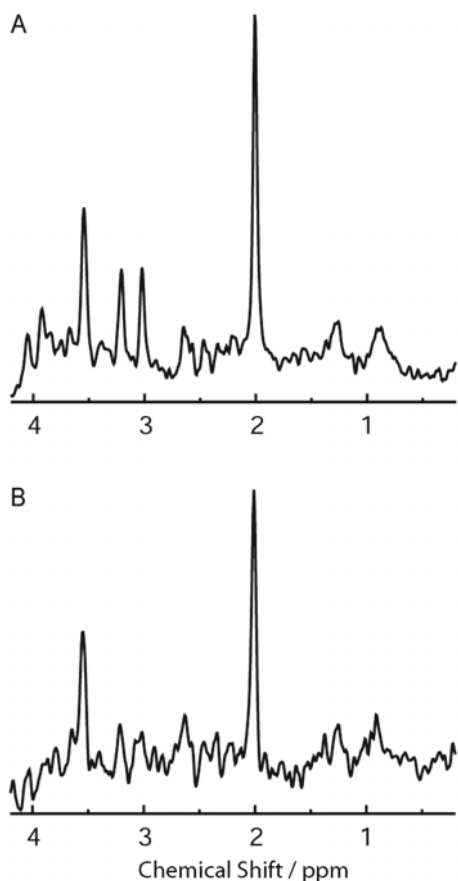


Fig. 108.21. **A** The ^1H spectrum of white matter (4 ml, STEAM, TR/TE = 6000/20 ms, 1.5 T) of a 4-month-old boy with Canavan disease shows elevated signals of NAA and mIns, whereas Cr and Cho are decreased. **B** Only NAA and mIns are visible in the white matter spectrum (3.5 ml, STEAM, TR/TE = 6000/20 ms, 1.5 T) of the same patient at the age of 1 year.

specific for Canavan disease, as in all other conditions NAA is normal or decreased, but not increased. In addition, mIns is increased and in some of the Canavan patients lactate is elevated.

One patient has been described who had no detectable NAA in the brain (Martin et al. 2001), probably related to an as yet unidentified defect in NAA synthesis (Fig. 108.22). Surprisingly, the clinical picture was characterized by psychomotor retardation only, whereas MRI revealed delayed myelination at the age of 3 years.

Salla disease and severe infantile sialic acid storage disease are characterized by accumulation of *N*-acetylneuraminic acid (sialic acid). *N*-acetylneuraminic acid resonates close to the methyl resonance of NAA, leading to a pseudo-elevated NAA peak in the ^1H white matter spectrum. In addition, the Cho peak is abnormally low, related to hypomyelination, and the Cr peak is elevated, probably related to white matter gliosis.

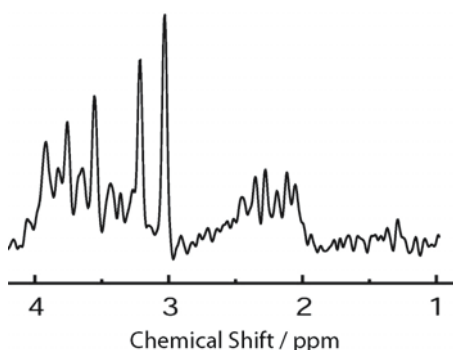


Fig. 108.22. The ^1H spectrum of white matter (6 ml, PRESS, TR/TE = 6000/30 ms, 2 T) of a 3-year-old with an NAA deficiency does not contain signals from NAA or NAAG. From Martin et al. (2001), with permission

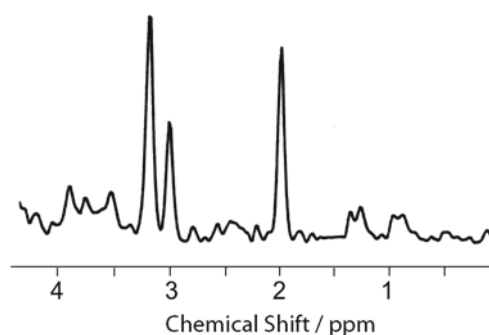


Fig. 108.23. The ^1H spectrum of predominantly white matter (27 ml, STEAM, TR/TE = 1500/270 ms, 1.5 T) of a 3-year-old boy with maple syrup urine disease in the acute state shows next to the doublet of lactate a doublet around 0.9 ppm, assigned to the methyl group of branched-chain amino acids (probably leucine) or keto acids. From Felber et al. (1993), with permission

In maple syrup urine disease, ^1H -MRS during acute metabolic decompensation shows elevated lactate and resonances around 0.9 ppm corresponding to cerebral accumulation of branched-chain amino acids and keto acids (Fig. 108.23). NAA is decreased. With treatment and clinical recovery the ^1H spectra normalize.

In nonketotic hyperglycinemia, ^1H spectra show an elevated glycine signal at 3.55 ppm at both short and long echo times. Using a short echo time, the glycine peak co-resonates with the mIns peak, but using echo times of 135 or 270 ms, the peak at 3.55 ppm represents glycine only, glycine having a much longer T_2 than mIns (Fig. 108.24). There is evidence that the time course of glycine content in brain tissue, as shown by MRS, correlates more closely with the clinical course than do plasma and CSF glycine values.

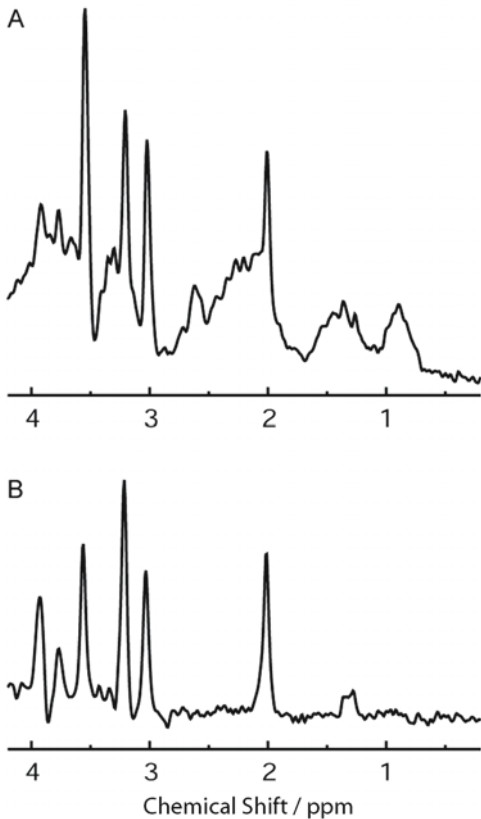


Fig. 108.24. **A** The ^1H spectrum of cortex and white matter (12 ml, STEAM, TR/TE = 2500/20 ms, 1.5 T) of a 1-week-old neonate with nonketotic hyperglycemia shows a very high signal at 3.55 ppm. **B** A spectrum obtained with a long echo time (PRESS, TR/TE = 2500/270 ms) shows that this signal is largely due to glycine, since mlNs does not contribute to the spectrum at such long echo times

Succinate dehydrogenase deficiency is a mitochondrial disorder with a defect in complex II. Elevated succinate, represented by a resonance at 2.40 ppm, can be found in some patients (Fig. 108.25), providing evidence for the diagnosis (Brockmann et al. 2002).

A severe reduction of the Cr peak in ^1H MR spectra of the brain is a central feature of the so-called creatine deficiency syndromes (Fig. 108.26). The lack of creatine in the brain can be caused by a defect in the synthesis of creatine due to either guanidinoacetate

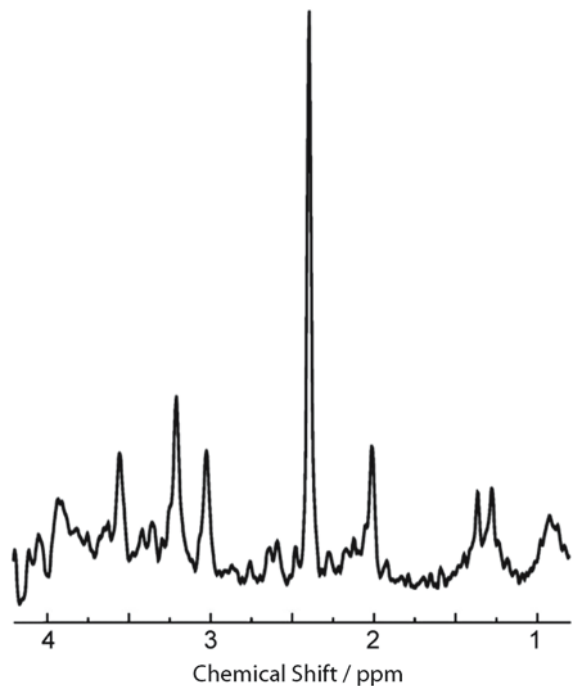


Fig. 108.25. The ^1H spectrum of white matter (4 ml, STEAM, TR/TE = 6000/20 ms, 2 T) of a 17-month-old girl with succinate dehydrogenase deficiency is dominated by the singlet from succinate at 2.40 ppm. In addition, NAA is severely reduced, and lactate is elevated. From Brockmann et al. (2002), with permission

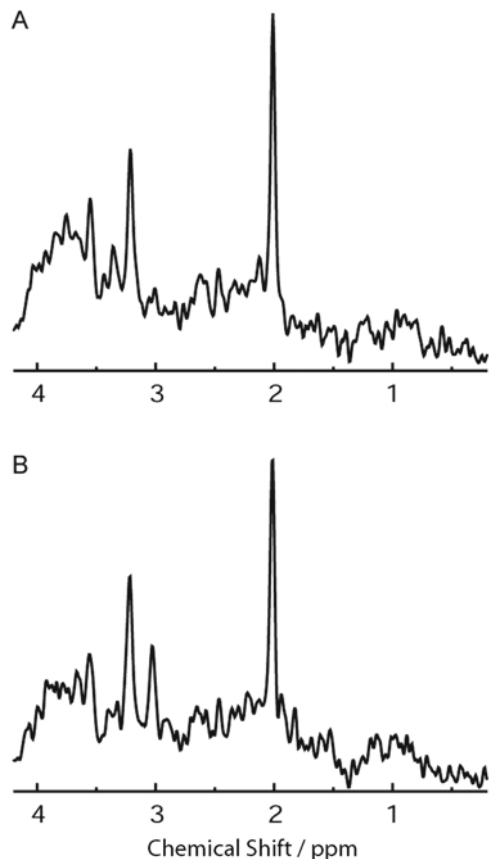


Fig. 108.26. **A** The ^1H spectrum of white matter (4 ml, STEAM, TR/TE = 6000/20 ms, 1.5 T) of a 2-year-old boy with guanidinoacetate methyltransferase deficiency does not contain signals from Cr. **B** The presence of Cr 3 months later shows the positive effect of treatment with oral creatine supplementation in patients with a creatine synthesis defect

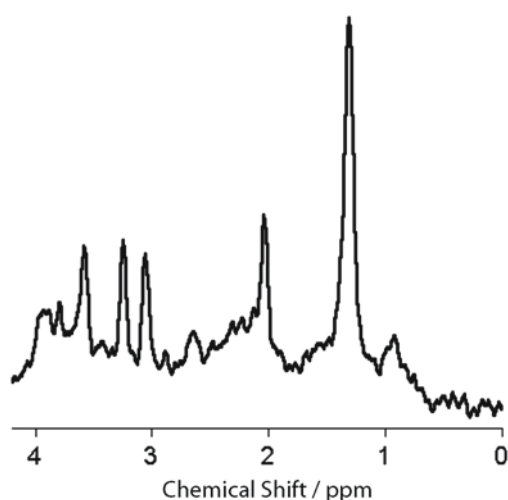


Fig. 108.27. The ^1H spectrum of white matter (8 ml, STEAM, TR/TE = 3000/20 ms, 1.5 T) of a 16-year-old boy with Sjögren–Larsson syndrome shows a prominent signal at 1.3 ppm, probably representing long-chain fatty alcohols. Courtesy of Dr. M.A.A.P. Willemsen, Department of Pediatric Neurology, University Medical Center St Radboud, Nijmegen, The Netherlands

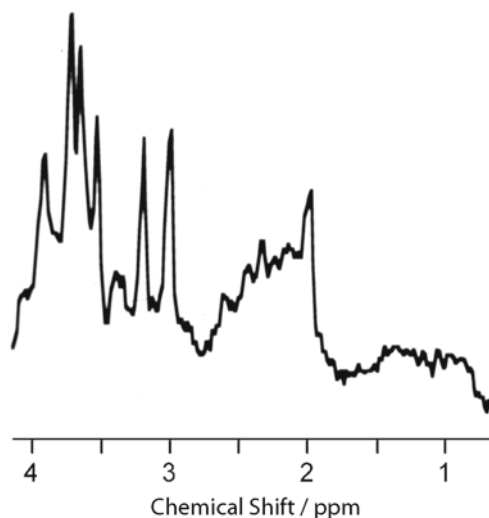


Fig. 108.28. The ^1H spectrum of basal ganglia (3.5 ml, STEAM, TR/TE = 1600/10 ms, 1.5 T) of a 9-day-old patient with galactosemia due to a deficiency of galactose-1-phosphate uridyl-transferase. Resonances at 3.67 and 3.74 ppm correspond to galactitol. From Wang et al. (2001), with permission.

methyltransferase (GAMT) deficiency or glycine amidinotransferase (AGAT) deficiency, or by a defect in the transport of creatine across the blood–brain barrier (X-linked creatine transporter defect). In GAMT deficiency, the spectrum may also reveal a resonance at 3.78 ppm, representing guanidinoacetate, which is not seen in the other creatine deficiency syndromes. In the defects in creatine synthesis, oral creatine substitution leads to striking improvement of the symptoms of the patients and a return of the Cr peak into the spectrum, although the Cr concentration remains below normal. Oral creatine substitution does not influence the cerebral creatine level in patients with a transporter defect.

In Sjögren–Larsson syndrome a prominent singlet is found at 1.3 ppm, the lipid region of the spectrum (Fig. 108.27). The peak is seen at both short and long echo times. In addition, in most patients increased resonances at 0.8–0.9 ppm are seen. These findings are compatible with the presence of an abnormal amount of lipids, the methylene protons resonating at 1.3 ppm and the methyl protons resonating at 0.8–0.9 ppm. The peaks are only found in the cerebral white matter with the highest levels in the periventricular region, where T_2 -weighted images show signal abnormalities, and not in the cerebral gray matter or cerebellum (Willemsen et al. 2004). The identity of the lipids responsible for the peaks has not yet been elucidated, but most likely the resonances represent long-chain fatty alcohols.

^1H -MRS allows monitoring of the cerebral phenylalanine levels in phenylketonuria (PKU). The α and β protons of phenylalanine give rise to complex multiplets of low intensity at the region between 3 and 4 ppm, which cannot be distinguished from overlying strong signals of abundant metabolites under in vivo conditions. In contrast, all signals of the phenyl protons collapse into a single peak at 7.36 ppm of sufficient intensity for quantitation. However, this region of the spectrum, too, normally contains several overlapping peaks between 6.5 and 8.5 ppm. The most efficient way of removing these background signals is to use the spectra of normal controls for subtraction. As the cerebral phenylalanine level in classical phenylketonuria patients under free nutrition is typically below 1 mmol/l, selection of a large volume of interest for MRS, of the order of 25 ml or larger, is required to obtain a sufficient signal-to-noise ratio for reliable quantitation. PRESS is preferable to STEAM for better signal to noise. In addition, short echo times of 20 ms or less are necessary to minimize signal loss due to T_2 -weighting of the spectrum. Blood–brain barrier kinetics for phenylalanine entry into the brain can be studied using ^1H -MRS. Brain phenylalanine levels do not correlate closely with blood phenylalanine levels. The individual variation in brain-to-blood phenylalanine ratio is large, even among patients with similar blood levels. This individual variability may contribute to the different neurological outcomes in PKU patients.

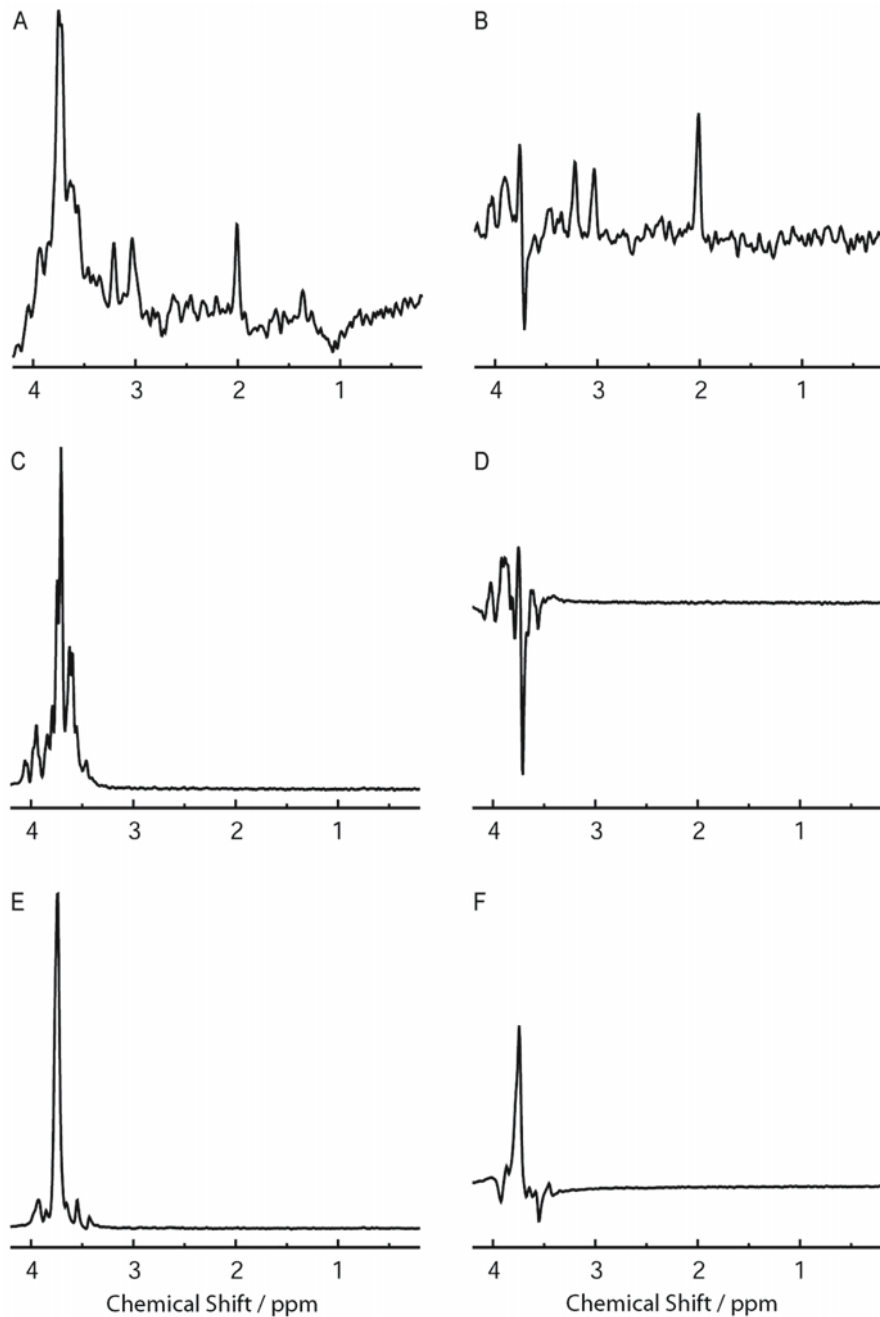


Fig. 108.29. ^1H spectra of white matter (5 ml) of a 14-year-old boy with deficiency of ribose-5-phosphate isomerase leading to polyol accumulation, obtained with (A) STEAM (TR/TE = 6000/20 ms) and (B) PRESS (TR/TE = 3000/135 ms) at 1.5 T. The large signals between 3.6 and 3.8 ppm are partly inverted due

to J-coupling in the long echo time spectrum. Comparison with model spectra of D-arabitol (C, D) and ribitol (E, F), acquired with corresponding short echo times (C, E) and long echo times (D, F) illustrates the contribution of the two polyols to the spectra in A and B

Untreated galactosemia is characterized by elevated galactitol concentrations in the brain, which disappear with treatment. Galactitol gives rise to resonances at 3.67 and 3.74 ppm (Fig. 108.28).

One patient has been described with highly elevated levels of the polyols ribitol and D-arabitol in the brain (van der Knaap et al. 1999). The patient suffered from a slowly progressive encephalopathy and peripheral neuropathy. MRI of the brain revealed exten-

sive white matter abnormalities, most pronounced in the subcortical area, with some swelling of the abnormal white matter. ^1H -MRS of the brain revealed highly elevated peaks between 3.6 and 3.8 ppm, which could be identified as representing D-arabitol and ribitol (white matter concentrations 8.9 mmol/l and 2.9 mmol/l, respectively) (Fig. 108.29). The presence of these polyols could be confirmed in all body fluids with a brain:CSF:plasma gradient of 70:40:1 for D-arabitol and 125:55:1 for ribitol, suggesting a neurometabolic defect. The basic defect has been demonstrated to be a deficiency of ribose 5-phosphate isomerase, a defect in the pentose phosphate pathway (Huck et al. 2004).

In diabetes mellitus, ^1H -MRS is able to detect the brain levels of glucose (resonances at 3.43 and 3.80 ppm) and the ketone bodies acetone (resonance at 2.22 ppm), acetoacetate (resonance at 2.26 ppm) and β -hydroxybutyrate (doublet at 1.2 ppm), allowing monitoring of glucose metabolism at a brain level. In cystic leukoencephalopathies, ^1H -MRS of cystic areas reveals the resonances of glucose and lactate, present in the CSF. An important example is vanishing white matter disease, in which the white matter is typically rarefied and cystic. ^1H MR spectra of the white matter reveal that the peaks representing metabolites normally present in the spectrum are very low or absent and that peaks of lactate and glucose are visible.

108.6 Monitoring

Both the process-specific and disease-specific spectroscopic abnormalities provide excellent possibilities for disease monitoring. With respect to monitoring of disease-specific abnormalities, a good example is found in the creatine synthesis defects. Oral creatine supplementation leads to clinical improvement. Unfortunately, assessment of metabolites in body fluids is of little help in monitoring the treatment of the disease. ^1H -MRS gives the most direct measure of the efficacy of the treatment in the cerebral creatine level.

Process-specific spectroscopic findings can also be very useful in monitoring disease. Among the inherited white matter disorders, an example of the important role of MRS in monitoring disease is found in X-linked adrenoleukodystrophy (XALD). Central issues in the treatment of males carrying the biochemical defect of XALD are the questions of in which patient and when to perform hematopoietic stem cell transplantation. This form of treatment is only applied for the rapidly progressive cerebral disease, which usually has its onset in childhood, and not for the later-onset variant adrenomyeloneuropathy (AMN). The outcome of hematopoietic stem cell transplantation in cerebral XALD is highly dependent on the degree of

cerebral involvement at the time of the transplantation. If applied early in the course of the disease, hematopoietic stem cell transplants may prevent further deterioration and may even lead to improvement or disappearance of cerebral lesions on MRI. The therapy is not recommended for patients with rapidly advancing or severe cerebral involvement, because in these patients the procedure may lead to acceleration of the disease or survival in a very poor neurological condition or vegetative state. Hematopoietic stem cell transplantation is not recommended for asymptomatic patients, because of the more than 50% chance that these patients will not develop the serious cerebral form of the disease, the absence of a way of predicting whether they will, and the high mortality associated with hematopoietic stem cell transplantation. Therefore, monitoring of the disease on MRI, MRS, and neuropsychological tests from the presymptomatic stage onwards is extremely important. As soon as there is evidence of beginning cerebral disease, hematopoietic stem cell transplantation should be attempted. MRI provides important information for monitoring purposes: the presence of lesions, progression of lesion size, and presence or absence of contrast enhancement. The presence of contrast enhancement is predictive of progressive disease. MRS also provides important information. In an area of active demyelination, not only a decrease in NAA is found, but also an increase in Cho, Cr, mIns, and lactate, related to enhanced membrane turnover, increased cellular density, inflammation, macrophage infiltration, and gliosis. In the inner area of inactive, burnt-out demyelination, NAA is very low, but Cho and lactate are no longer elevated. The spectrum in the burnt-out area has a pattern reflecting gliosis dominated by Cr and mIns. The spectroscopic findings in the area just outside the MRI-visible lesion are highly predictive of disease progression. Elevated levels of Cho, decreased NAA/Cr ratios, and elevated mIns in this area are highly predictive of progressive disease, whereas normal Cho and mIns levels and NAA/Cr ratios are predictive of stable disease. Thus, MRS is more sensitive than MRI in detecting incipient demyelination. It is, however, important to realize that even in normal-appearing white matter remote from the lesion and in the white matter of patients in whom the disease has not yet started, NAA is often below normal in XALD males (Fig. 108.30). In addition, MRS has a predictive value for the outcome of patients treated with a hematopoietic stem cell transplantation. A good outcome is highly correlated with the NAA concentration in the affected white matter, and thus the preservation of neuronal tissue, before the transplantation.

MRS is also a very important tool for purposes of monitoring and prediction of the course of the disease in acute brain injury, including diffuse axonal in-

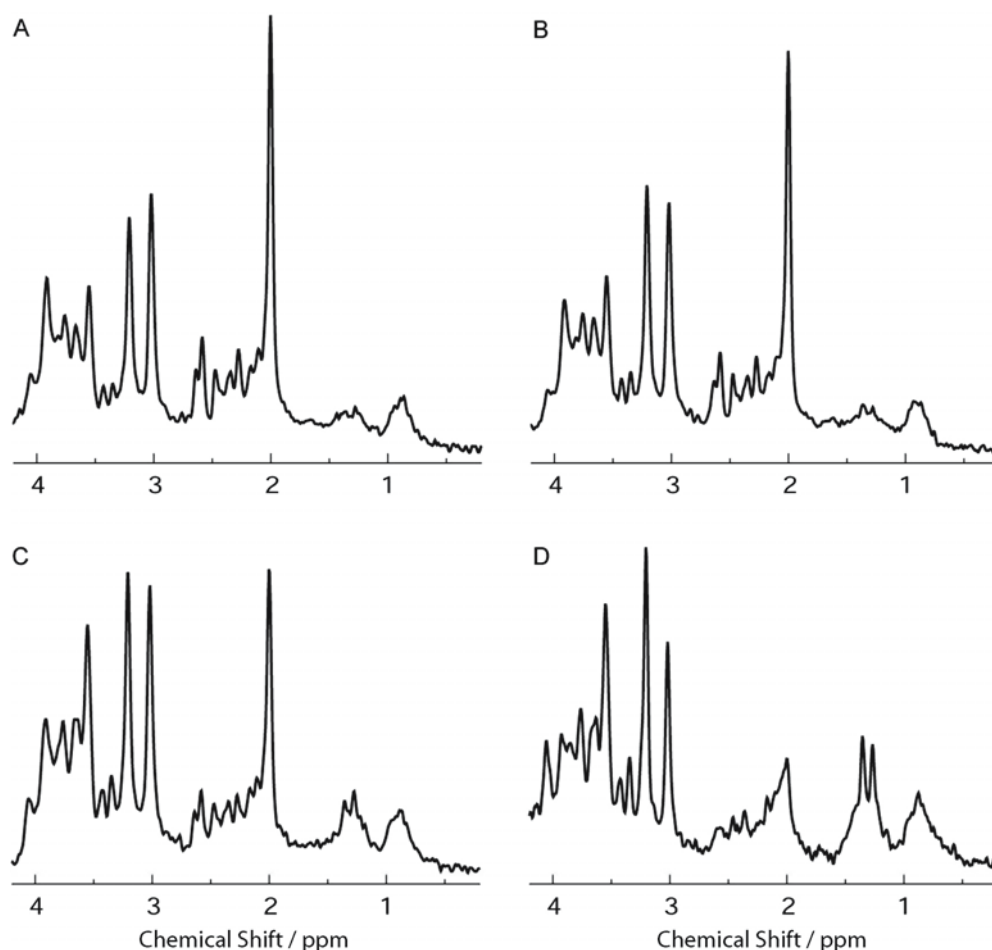


Fig. 108.30. Average ^1H spectra of controls and patients with X-linked adrenoleukodystrophy, obtained with STEAM (TR/TE = 6000/20 ms) at 2.0 T. In comparison to (A) white matter spectra of an age-matched control group ($n = 19$), the spectra of (B) normal-appearing white matter of patients without neurological symptoms ($n = 47$) show on average slightly lower NAA and higher Cho. (C) Spectra of actively demyelinating white

matter in patients without neurological symptoms ($n = 21$) are characterized by decreased NAA and increased concentrations of Cho, Cr, mIns, and on average an increase of lactate. (D) Ongoing demyelination in patients with advanced cerebral X-linked adrenoleukodystrophy ($n = 9$) leads to severe neuronal loss (almost complete absence of NAA and decrease of Cr)

jury after head trauma, near-drowning, and meningoencephalitis. There is a good correlation between early NAA measurements and outcome: the lower the NAA levels, the poorer the outcome. The presence of elevated lactate and lipid peaks adds to the prediction of poor outcome. Elevated Cho may be found, but this finding does not seem to have predictive value. This information can be used in making important decisions in the continuation of treatment of such patients.

Multiple sclerosis (MS) is probably the most important indication for monitoring by MRS. Therapeutic trials require objective and preferably quantitative measures of changes in disease. Spectroscopic imaging with acquisition of data in multiple transverse

slices allows monitoring of spectroscopic changes of large areas of the brain with a spatial resolution that is adequate for the purpose. Single voxel spectroscopy has the advantage of better spectral quality and use of shorter echo times. The spectroscopic abnormalities found depend on the stage of the lesion. Cho is already increased in a prelesional area up to 12 months before the lesion becomes visible on conventional MRI. Acute lesions, as identified by gadolinium enhancement on MRI, show a reduction of NAA, and an increase in Cho, mIns, lipids, and, often, lactate. The earliest spectroscopic changes consist of increased Cho and lactate, whereas a decrease in NAA occurs a few days later. Lactate disappears in a matter of weeks. Enhanced Cho decreases within a couple of

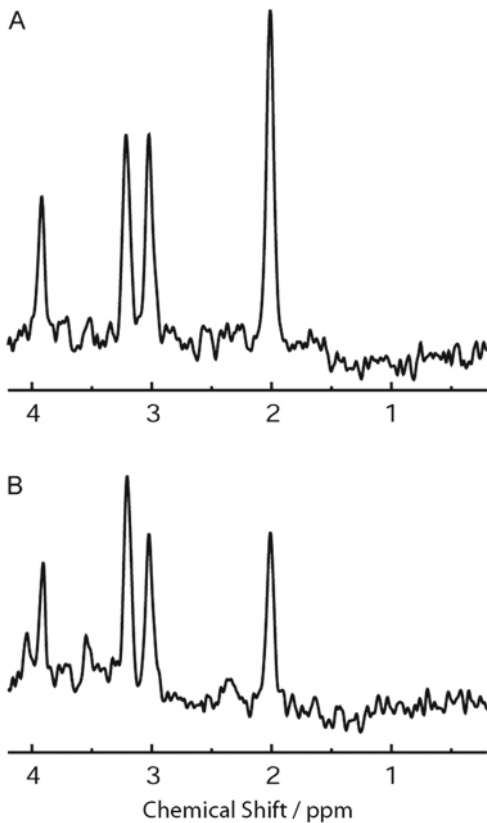


Fig. 108.31. ^1H spectra (8 ml, TR/TE = 2500/135 ms, 1.5 T) of two patients with secondary progressive MS. **A** The normal-appearing white matter of a 45-year-old male with MS is comparable to the white matter of age-matched controls, apart from a slight decrease of NAA, whereas **(B)** a lesion that is hypointense on T_1 -weighted images (a “black hole”) of a 43-year-old male is characterized by a severe decrease of NAA, accompanied by a decrease of Cr

months and eventually returns to normal. A partial recovery of NAA is often seen over a period of months after acute onset of the lesion – probably the result of a combination of actual recovery of axonal integrity and tissue contraction due to disappearance of edema and removal of disintegrated tissue components. The lipid resonances remain elevated for several months. The rise in mIns may be temporary or permanent. ^{31}P -MRS reveals decreased PDE in acute lesions. Spectroscopic findings reflect the changes at the histological level. Correlation with pathological findings in biopsy specimens confirms an association between acute inflammation, hypercellularity due to a mixed macrophage–astrocyte response, and demyelination with increased levels of Cho and lactate. In acute lesions myelin sheaths show signs of disintegration and breakdown accompanied by liberation of polypep-

tides and neutral fat, reflected in elevated protein and lipid signals in MRS. From early on axons are damaged, with decreasing NAA. The decrease in NAA reflects not only axonal transections in acute lesions, but also a significant component of metabolic dysfunction of injured axons. The first component concerns the permanent damage, the second may be transient. Large destructive lesions can additionally show transient decreases in Cr during the hyperacute phase, probably reflecting metabolic dysfunction. The decrease in PDE reflects myelin loss. Chronic and inactive lesions are hypocellular, demyelinated, and gliotic. Inflammation is no longer present. Chronic lesions that are very hypointense on T_1 -weighted images – the so-called “black holes” – have the lowest NAA and Cr, correlating with the profound tissue destruction, axonal loss, and hypocellularity of these lesions (Fig. 108.31). An additional important finding has been that normal-appearing white matter in MRI is not completely normal in MRS (Fig. 109.31). This is true for all MS variants, although observations vary. A decreased or normal NAA, normal or increased Cr, and increased mIns in ^1H -MRS and a decrease in total ^{31}P peak integrals in ^{31}P -MRS are seen, as well as a reduction in the broad component of the ^{31}P spectrum, consistent with a low-grade demyelination, gliosis, and neuronal damage too subtle to be detected by MRI. In the cerebral cortex of MS patients, too, decreased NAA and Cr have been found, ascribed to neuronal metabolic dysfunction, damage, and loss. Several studies have indicated a correlation between the extent of decrease in NAA and disability, which is stronger than the correlation between T_2 lesion load and disability. The total brain content of NAA has been used as an indicator of total neuronal and axonal damage, which is the irreparable part of the pathology in MS.

108.7 Conclusion

Reviewing the information provided by MRS about brain metabolism in normal cerebral maturation, in disturbed maturation, and in disease conditions, shows that MRS has proven itself to be a tool of significant usefulness in clinical medicine and of great potential for research purposes. For clinical applications, the greatest power of MRS is found in monitoring disease processes, in particular with a view to evaluating therapeutic interventions and establishing prognosis. In particular in the early stages of disease processes, MRS often appears to be more sensitive than MRI. For research applications, the greatest potential of MRS may be in contributing to the elucidation of pathophysiological processes in cerebral disorders.

Pattern Recognition in White Matter Disorders

109.1 Introduction

MRI is highly sensitive in the detection of white matter lesions. A close association has been demonstrated between the occurrence of white matter abnormalities observed with MRI and those found at autopsy. It has been generally assumed that the specificity of MRI is much lower than its sensitivity. The specificity of MRI, however, depends not only on the potential and limitations of the method, but also on the capabilities of the person interpreting the MR images (Fig. 109.1). Hence, optimization of the diagnostic specificity of MRI in white matter disorders is achieved by optimizing the quality of both the imaging and its interpretation.

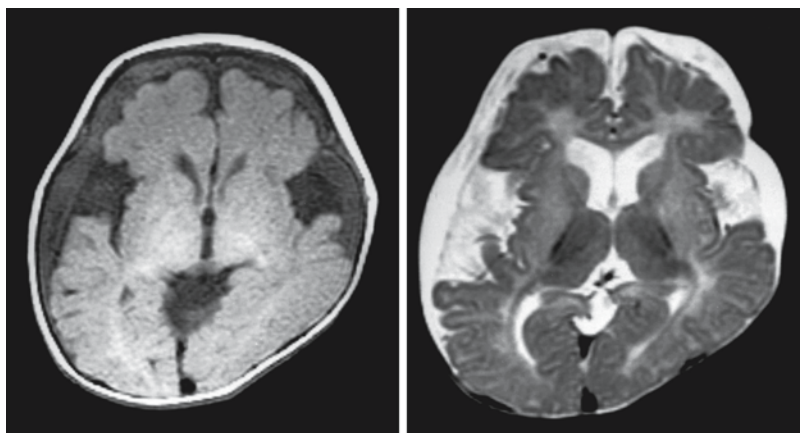
Aids to the perceptual and decision processes can be constructed to support the interpretative process. One such aid is systematic and detailed image analysis. A checklist or score list, which prompts the image reader to assess and record a scale value for each feature, is helpful in this respect. A second aid is a computer program that integrates these scale values into a pattern, compares the pattern obtained with the known patterns in a database, and then reaches a differential diagnosis. The reader of the images can use the computer estimates of the likelihood of various disorders as a guide in the diagnostic process.

It is important to realize that MRI pattern recognition has its limitations. In the first place, MRI patterns have characteristic features only during a certain phase of progressive disorders. This is well illus-

trated in Fig. 109.2. In the early phase of the disease, the MRI pattern is diagnostic. In the end phase almost all cerebral white matter is affected and distinguishing characteristics have been lost. A second problem is illustrated in Fig. 109.3, where the pattern, for reasons unknown, is the inverse of the pattern commonly observed in this disease. The computer program should allow for these exceptions to the rule when they are known to occur. The third problem is illustrated in Fig. 109.4. Sometimes superficial reading of the images strongly suggests a certain diagnosis, whereas on closer examination only some but not all of the main MRI features of a disease are present. And sometimes the resemblance between patterns is so strong that it is difficult or impossible to discriminate disorders on the basis of the MRI pattern recognition program alone.

The benefits of MRI pattern recognition are diverse. First of all, it facilitates the diagnostic process and reduces the list of necessary laboratory tests. Sometimes the activity of only one enzyme has to be assessed or only one gene has to be analyzed after reading the MRI. In this way, MRI pattern recognition reduces the burden for patients and families and is a money-saving strategy. Secondly, the recognition of patterns provides important scientific information. Selective vulnerability of brain structures for different noxious influences underlies the development of different patterns of involvement of brain structures in different disorders. So far, our understanding of the reasons for the selective vulnerability has remained highly limited.

Fig. 109.1. T₁- and T₂-weighted images of a 10-month-old male with glutaric aciduria type I. The images show diffuse bilateral subdural hygromas and frontotemporal hypoplasia. Myelination is severely retarded. Note that the arachnoid and subdural spaces can be clearly distinguished. The presence of bilateral subdural hygromas could be wrongly interpreted as evidence of child battering. Knowledge of the specific features of glutaric aciduria type I with presence of frontotemporal opercular hypoplasia precludes this mistake. Courtesy of Osaka et al. (1993), with permission



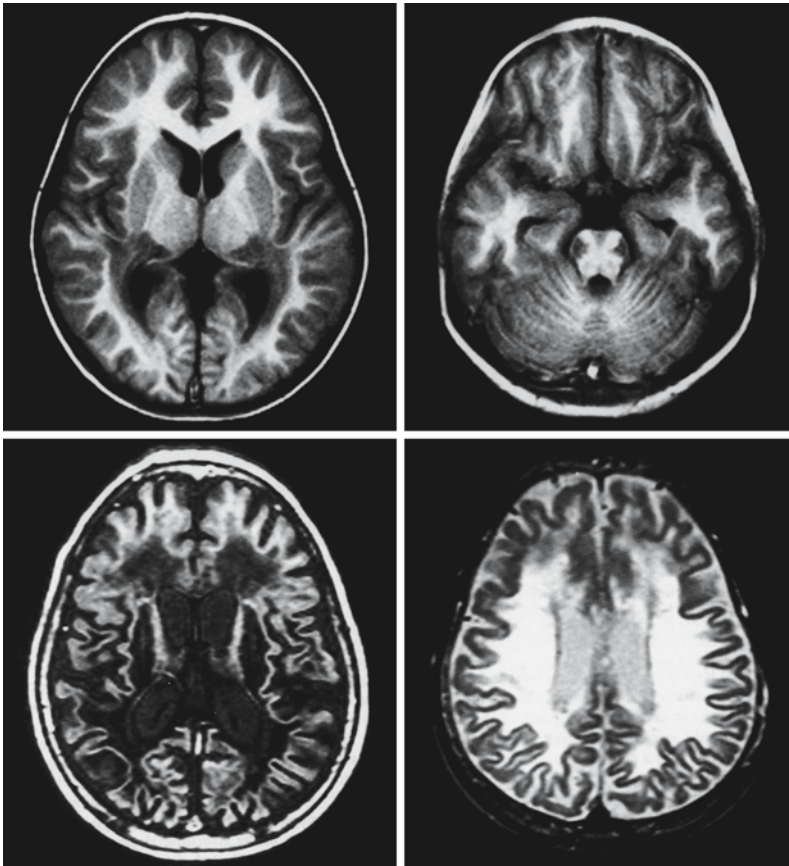


Fig. 109.2. The upper row of T₁-weighted (IR) images in this 3-year-old boy show the pattern that is typical for the childhood cerebral form of X-linked adrenoleukodystrophy: peritrigonal and occipital leukoencephalopathy, sparing the U fibers, involving the geniculate bodies and the splenium of the corpus callosum, with typical involvement of corticospinal tracts in pons and mesencephalon. The lower row of one T₁- and one T₂-weighted image are of the same child, 3 years later. No pattern is recognizable as all white matter structures are involved and all characteristic features of the disease are lost

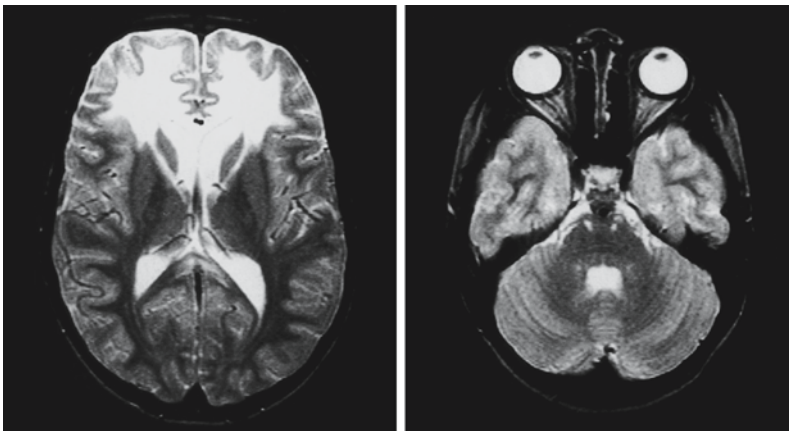


Fig. 109.3. T₂-weighted images in a 6-year-old boy show bilateral, symmetrical involvement of the frontal white matter and the frontospinal tracts in the anterior limb of the internal capsule, which can be followed in the brain stem. The spread of the disease is evidently in a ventrodorsal direction. The diagnosis is X-linked adrenoleukodystrophy with reversed pattern. Courtesy of Dr. P. Hoogland and Dr. W.F.M. Arts, Juliana Children's Hospital, The Hague, The Netherlands

109.2 Noncomputerized Pattern Recognition

Pattern recognition in the daily practice of medical imaging involves three levels of action which are necessary to permit optimal interpretation of the image. These levels can be described as image formation, image analysis, and image interpretation.

The first level is the technological level and has to do with the formation of the image. Although the

reader of the image can regard large parts of an MR system and the imaging process as a "black box," he or she needs to have a more than general knowledge of the imaging process, the parameters involved (repetition time, echo time, inversion time, number of excitations, slice thickness, gradient strength and performance, diffusion sensitivity), the influence of parameter settings on the image, the possible artifacts, and the ways improving quality when special answers are required.

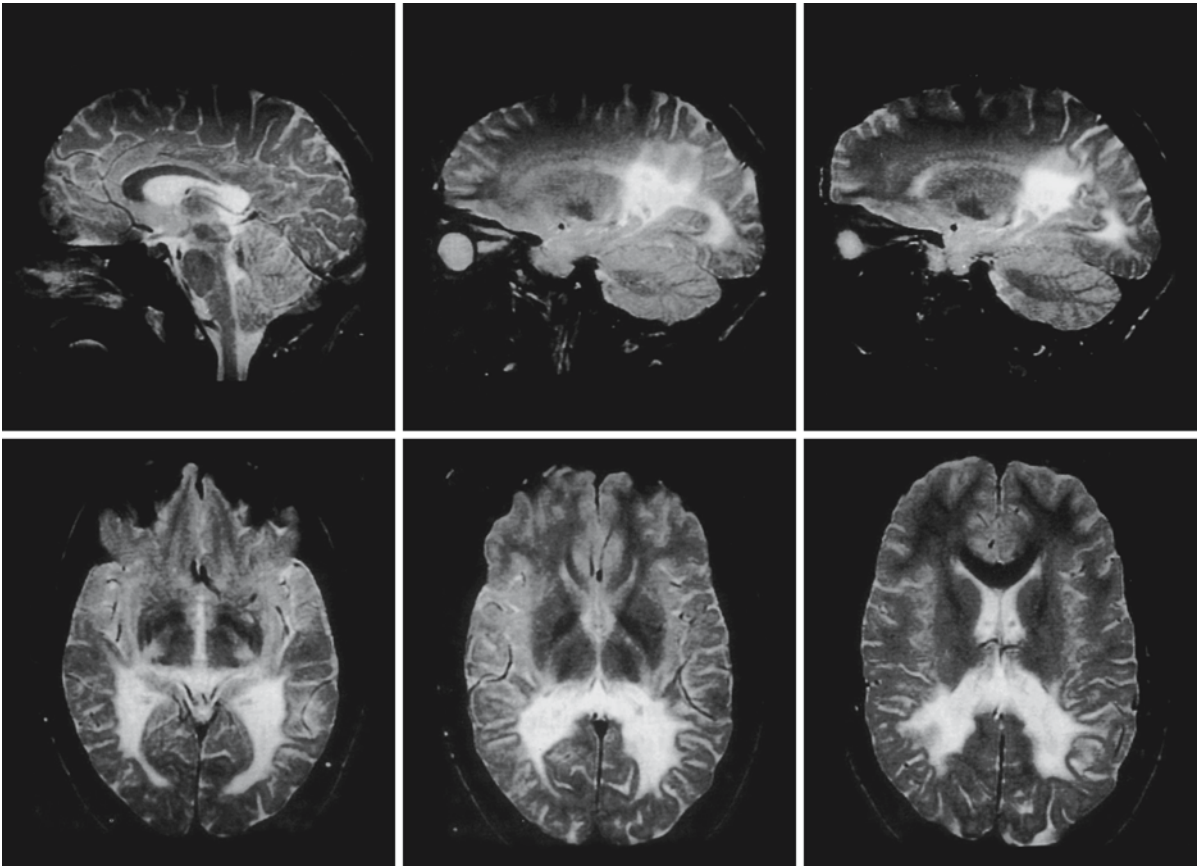


Fig. 109.4. A 23-year-old man had experienced moderate psychomotor retardation from birth onwards and progressive disturbances of gait for the last 2 years. The T_2 -weighted sagittal and transverse images show bilateral peritrigonal and occipital involvement of the white matter; the splenium of the corpus callosum and the posterior limb of the internal capsule are also affected. There is no enhancement after gadolinium injection, which argues against X-linked adrenoleukodystro-

phy. There was no laboratory evidence for a peroxisomal disorder. Although the changes in the peritrigonal area and occipital lobe could be the remnants of periventricular leukomalacia, the involvement of the internal capsule and the involvement of the splenium of the corpus callosum make this diagnosis highly improbable. Despite the highly characteristic image and perfect symmetry this remains an unsolved case, which needs to be followed up

The second level is the level of image analysis, in which the structural elements of the image are analyzed, weighed as to their normality or abnormality, and described as such. This is an important step in the process of teaching and learning, because the analysis of structural elements depends very much on experience, knowledge of anatomy, knowledge of normal brain maturation, and knowledge of pathology.

The first and second levels lay the foundation for the third, the interpretation of the image. In this process the image as such is transcended. Interpreting the image requires a combination of a certain understanding of image formation, analysis of the structural elements, experience, and knowledge of disease entities, histopathology, pathophysiology, biochemistry, and toxicology, and possibly knowledge from

still other sources, in an assessment that aims at answering the clinical question.

The first level, image formation, will not be discussed in this chapter. Some details of special techniques are discussed in Chaps. 106, 107, and 108.

The second level is the analytical level, which includes a systematic analysis and classification of structural elements of the image (see Tables 109.1–109.3). Many separate gray and white matter structures should be scored as normal or abnormal. Which structural elements of an image need to be evaluated has been determined by experience of their discriminating value. For example, if one were not aware from previous experience and histopathological studies that the arcuate fibers are spared in many white matter disorders, but that, for example, L-2-hydroxyglu-

Table 109.1. List of structural elements to be analyzed for MRI pattern recognition

Cerebral cortex	Occipital/frontal/parietal/temporal
Arcuate fibers	Occipital/frontal/parietal/temporal
Lobar (deep) white matter	Occipital/frontal/parietal/temporal
Periventricular white matter	Occipital/frontal/parietal/temporal
Internal capsule	Anterior limb/posterior limb
External capsule + extreme capsule	
Caudate nucleus	
Putamen	
Globus pallidus	
Thalamus	
Corpus callosum	Rostrum/genu/corpus/splenium
Cerebellar cortex	
Cerebellar white matter	
Hilus of dentate nucleus	
Cerebellar pedunculi	
Dentate nucleus	
Midbrain	Central part/peripheral rim/tectum and tegmentum/specific tracts
Pons	Central part/peripheral rim/tegmentum/specific tracts
Medulla	Dorsal part/specific tracts

Scoring: no abnormality/slight to mild abnormality/severe abnormality

Table 109.2. List of general characteristics to be analyzed for MRI pattern recognition

Predominance	Frontal/occipital/parietal/temporal Periventricular/lobar (deep)/ arcuate fibers Supratentorial/posterior fossa
Symmetry	Perfectly symmetrical/slightly asymmetrical/asymmetrical
Extension	Small isolated lesions/large isolated lesions/irregularly confluent lesions/highly confluent lesions/combination of these
Appearance	Swelling/atrophy/rarefaction/cystic degeneration
Signal intensity	Slightly to mildly abnormal/severely abnormal/mixed
Homogeneity	Homogeneous/inhomogeneous/ two zones
Demarcation	Sharp/vague/mixed

Table 109.3. List of extra characteristics to be analyzed for MRI pattern recognition

Calcium deposition	Absent/present
Hemorrhage	Absent/present
Contrast enhancement	Absent/present
Ventricular enlargement	No/slight to mild/severe
Enlargement of pericerebral subarachnoid spaces	No/slight to mild/severe
Cerebellar atrophy	No/slight to mild/severe
Myelination	Normal/ delayed/no or hardly any myelin

taric aciduria starts in the arcuate fibers, it would be senseless to make involvement of the arcuate fibers a point of discrimination in the diagnostic process. The structural elements that need to be scored may also have to be adapted to the diseases under investigation. Some diseases affect very special brain stem structures, as for example in leukoencephalopathy with brain stem and spinal cord abnormalities and elevated lactate (LBSL). In this disease brain stem structures need to be scored in detail, which is not necessary for most other disorders. Then there are so-called “general characteristics” that need to be scored, including symmetry, confluent versus isolated/multifocal involvement of the white matter, predominant localization of the abnormalities, white matter swelling, atrophy, rarefaction, cystic degeneration, and the evolution over time. Finally, analysis of “extra characteristics” is important, including contrast enhancement, calcium deposits, hemorrhages, and the presence of localized cysts.

Structural elements that have been identified by us as having in general the highest discriminating value are: symmetry versus asymmetry, confluent involvement of the white matter versus multifocal isolated lesions, the predominant localization of lesions in the brain, the additional involvement of gray matter structures, contrast enhancement, and the presence of calcium deposits.

In many cases, symmetry is a striking feature of inherited white matter disorders and toxic encephalopathies, although not without exceptions, whereas asymmetry is most often seen in acquired white matter disorders, particularly inflammatory disorders and infections. The appearance of the lesions is important: isolated, or confluent, or both. In most inherited white matter disorders, in toxic encephalopathies, and in diffuse white matter injury af-

ter irradiation and chemotherapy, the lesions are confluent; as a rule no isolated lesions are seen. Multifocal and isolated lesions are more commonly seen in acquired conditions. In multiple sclerosis a mixture of isolated and confluent lesions is the rule. The same is true of Binswanger disease. A global survey of the distribution of the lesion may give an indication of the type of disorder we are dealing with. Sparing of the U fibers is seen in many inherited white matter disorders, in vascular disorders, and in subacute HIV encephalitis. Several organic and amino acidopathies, contrariwise, preferentially involve the U fibers. Extra characteristics such as calcifications occur in Cockayne syndrome, in some patients with X-linked adrenoleukodystrophy, in malignant phenylketonuria, in Aicardi-Goutières syndrome, in some patients with systemic lupus erythematosus, in children with AIDS encephalopathy, in congenital cytomegalovirus infection, in some patients with a mitochondrial leukoencephalopathy, and in some children after cranial irradiation and chemotherapy. In some white matter disorders enhancement with contrast is seen in part of the lesion, often in the active border. This observation can be very helpful in the diagnostic process. In X-linked adrenoleukodystrophy the enhancing border separates the area of complete demyelination from the area with ongoing demyelination. Enhancement is also a prominent feature of multiple sclerosis and Alexander disease.

Perhaps other criteria could also be used in the recognition of patterns of white matter disorders on the images, such as measurements of the absolute signal intensities and measurements of T_1 and T_2 , ADC, fractional anisotropy, and MTR. For instance, in subacute HIV encephalitis, the signal intensity of the white matter lesion, at least in the beginning of the disease, is not as high on T_2 -weighted images as it is in most other white matter disorders. Neuropathological examinations confirm that demyelination in subacute HIV encephalitis is only partial and mild. On the MR images the involved white matter has a coarse, granular texture, which corresponds well with the histological finding of numerous small foci of more complete demyelination.

In our definition, specificity exists in degrees. The pattern emerging from the image can be expressed as being diagnostic (pathognomonic), highly suggestive, suggestive, possible, atypical, and impossible. It is only in the first category that the MRI pattern is pathognomonic for one specific disorder. In the other categories, clinical and laboratory evidence is necessary to complete the diagnosis. The lists given should be considered as examples; they are by no means complete (Table 109.4).

Quite a few white matter disorders can be listed under the categories "diagnostic" or "highly suggestive," implying that MRI makes a firm contribution to

Table 109.4. Specificity of MRI patterns

<i>Diagnostic</i>
Cerebral form of X-linked adrenoleukodystrophy
Zellweger syndrome
Cerebrotendinous xanthomatosis (if fat deposits are present)
Periventricular leukomalacia
Megalencephalic leukoencephalopathy with subcortical cysts
Canavan disease
Maple syrup urine disease
L-2-Hydroxyglutaric aciduria
Alexander disease
Some toxic encephalopathies
Kearns-Sayre syndrome
Multiple sclerosis, when McDonald criteria are met
<i>Highly suggestive</i>
Metachromatic leukodystrophy
Globoid cell leukodystrophy
Mucopolysaccharidoses
Leigh syndrome
MELAS
Cockayne syndrome
Phenylketonuria
Glutaric aciduria type I
Acute disseminated encephalomyelitis
Wilson disease
Central pontine myelinolysis
<i>Suggestive</i>
Lowe syndrome
Pelizaeus-Merzbacher disease
Multiple sclerosis
Subacute HIV encephalitis
Binswanger disease
Wallerian degeneration
Toxic encephalopathies
<i>Possible</i>
Multiple sclerosis, less advanced cases
Extrapontine myelinolysis
<i>Atypical</i>
Unusual appearance with established diagnosis, e.g., asymmetric cerebral involvement in X-linked adrenoleukodystrophy; Alexander disease starting in the cerebellum
<i>Impossible</i>
The pattern excludes the suspected diagnosis

the diagnostic process in these disorders. Very often, by adding clinical information or laboratory data, a higher diagnostic category can be achieved. Additional facts that will help to reach a diagnosis are many and include facts in the clinical history and findings

at physical examination. The latter may include abnormalities of eyes, face, hair, internal organs, skin, skeleton, and peripheral nerves. Examples are facial dysmorphism in Cockayne syndrome and mucopolysaccharidoses, ectopic lenses in hyperhomocysteinuria, and multiple organ involvement in Zellweger syndrome and in mitochondrial disorders.

109.3 Computer-Assisted Pattern Recognition

With the increasing complexity of diagnostic processes and with the increase in number of recognized, rare disorders, the need to implement expert systems is felt. To develop these, it is essential to collect data systematically and quantitatively and to set up large data banks. We created a database that could be used to develop a computer-assisted pattern recognition program in white matter disorders, with the exception of ischemic white matter disease related to arteriosclerosis (van der Knaap et al. 1991). Over a certain period of time, the MR images of all patients under the age of 50 years or, when risk factors for vascular disease were present, under the age of 40 years, with lesions exclusively or predominantly involving the white matter, were scored with the help of a detailed scoring list (see Tables 109.1–109.3). The total study population numbered 1483. The diagnosis in the patients was known. The patients were grouped into diagnostic categories according to the classification we proposed, which stresses etiological and histological similarities between disorders of the same category.

The data obtained were analyzed. The frequency of occurrence of image abnormalities and features per disease category or subcategory were counted and the results presented as histograms (examples in Figs. 109.5–109.8). The outlines of the histograms – the “skylines” – can be considered to be characteristic of the disease or disease category.

In addition, a computer program was developed to estimate post-MRI probabilities of possible diagnoses in new patients with white matter abnormalities. The computer program was based on Bayes’ theorem. Prevalences of the different disease categories and subcategories and frequencies of image abnormalities per disease were estimated from the data of this study. When the imaging findings of a new patient were entered, the computer program would provide a differential diagnosis. For each possible diagnosis the positive predictive value and a two-sided 95% confidence interval could be computed.

Of course, there are several limitations to the practical use of a computer-assisted diagnostic system. The large amounts of data involved make clustering necessary; for example, a two-point scale (yes/no) had to be used instead of a three-point scale (se-

vere/mild/not involved) indicating the severity of involvement of the structures. Also, disease groups had to be clustered to some extent. This would seem to be sensible, because it is practically impossible to differentiate all individual conditions on MR criteria alone. Another limitation of such a computer program is that its quality is highly dependent on the quantity and quality of the data it contains. To improve the quality of the program in this respect a multicenter database with well-defined criteria for inclusion of cases would be extremely helpful in narrowing the confidence intervals in rare disorders.

Of course, such a computer system cannot compete with the flexibility and speed of the human brain in pattern recognition. Computer systems are, therefore, not to be regarded as competing, but as complementary: a support to the experienced and a learning tool for the inexperienced.

109.4 Practical Application of Pattern Recognition

Usually MR images are interpreted without the help of a computer program. However, in daily practice, our approach should also be systematic and we should progress logically through the diagnostic process. We will analyze the logical steps involved in systematic reading of the MR image, well aware that several steps may occur synchronously and that the sequence is variable.

The first step identifies the nature of the cerebral abnormalities. In the global analysis of MR images of the brain, the first consideration relates to the structures involved: gray matter, white matter, or both. Next, the examiner tries to identify the nature of the disorder with which he or she is confronted. If gray matter is involved, are there signs of a congenital anomaly with ectopic gray matter? Is there gray matter atrophy or are there parenchymatous lesions? If there is a white matter disorder, of what nature is it? Is it demyelination, delayed myelination, or hypomyelination? Is there white matter swelling? Is there white matter rarefaction or cystic degeneration? Are there white matter cysts? Is there a loss of white matter volume or gliotic retraction?

The second step considers the symmetry or asymmetry of the abnormalities. Symmetrical white matter involvement occurs in most of the inherited white matter disorders, toxic encephalopathies, and some of the other acquired white matter disorders. Many of the acquired disorders lead to asymmetrical lesions, with some exceptions. A tendency towards symmetry is present in periventricular leukomalacia, subcortical arteriosclerotic encephalopathy, subacute HIV encephalitis, and congenital CMV encephalopathy.

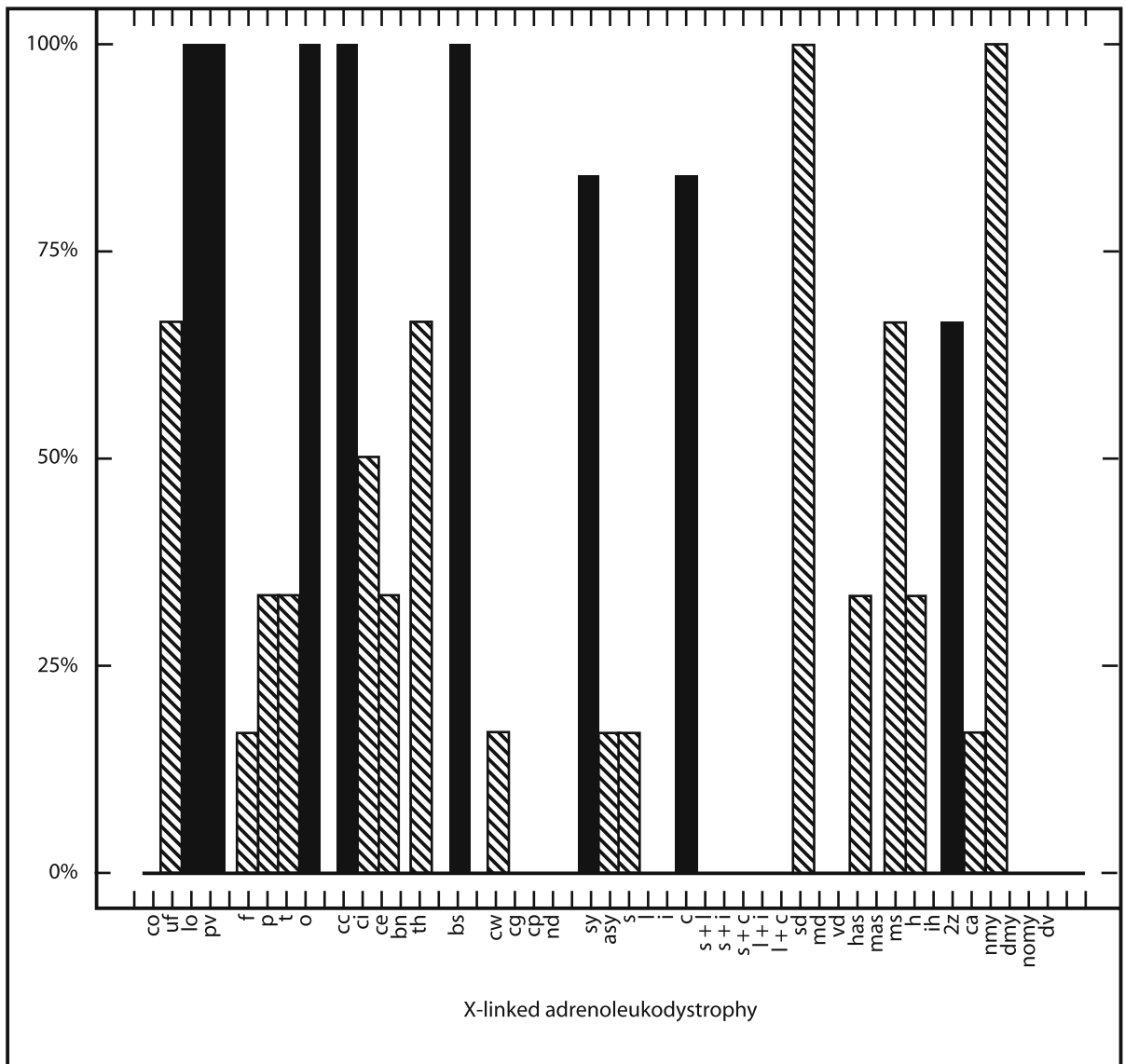


Fig. 109.5. Histogram of the frequency of involvement of the structural elements in the cerebral form of X-linked adrenoleukodystrophy. *co*, cortex; *uf*, arcuate fibers; *lo*, lobar (deep) white matter; *pv*, periventricular white matter; *f*, frontal; *p*, parietal; *t*, temporal; *o*, occipital; *cc*, corpus callosum; *ci*, internal capsule; *ce*, external and extreme capsules; *bn*, basal nuclei (globus pallidus, putamen, caudate nucleus); *th*, thalamus; *bs*, brain stem; *cw*, cerebellar white matter; *cg*, cerebellar cortical gray matter; *cp*, middle cerebellar pedunculi; *nd*, dentate nucleus; *sy*, symmetrical distribution; *asy*, asymmetrical distribu-

tion; *s*, small isolated lesions; *l*, large isolated lesions; *i*, irregularly confluent lesions; *c*, highly confluent lesions; *sd*, sharp demarcation; *md*, mixed demarcation; *vd*, vague demarcation; *has*, highly abnormal signal intensity; *mas*, mildly abnormal signal intensity; *ms*, mixed signal intensity; *h*, homogeneous signal intensity; *ih*, inhomogeneous signal intensity; *2z*, two zones discernible in the lesion; *ca*, calcification; *nmy*, normal myelination; *dmy*, delayed myelination; *nomy*, no or hardly any myelin present; *dv*, deformation of the ventricular system

The third step defines the aspect of the lesions. Are they confluent, isolated, or both; diffuse or multiple? In the inherited white matter disorders lesions are often confluent and diffuse. Multiple sclerosis, of course, is the prototype of a disease with lesions that

are usually asymmetrical, partly confluent, but mainly isolated, and located in rather specific areas of the brain.

The fourth step establishes the predominant location of the lesions. Confluent, symmetrical lesions in

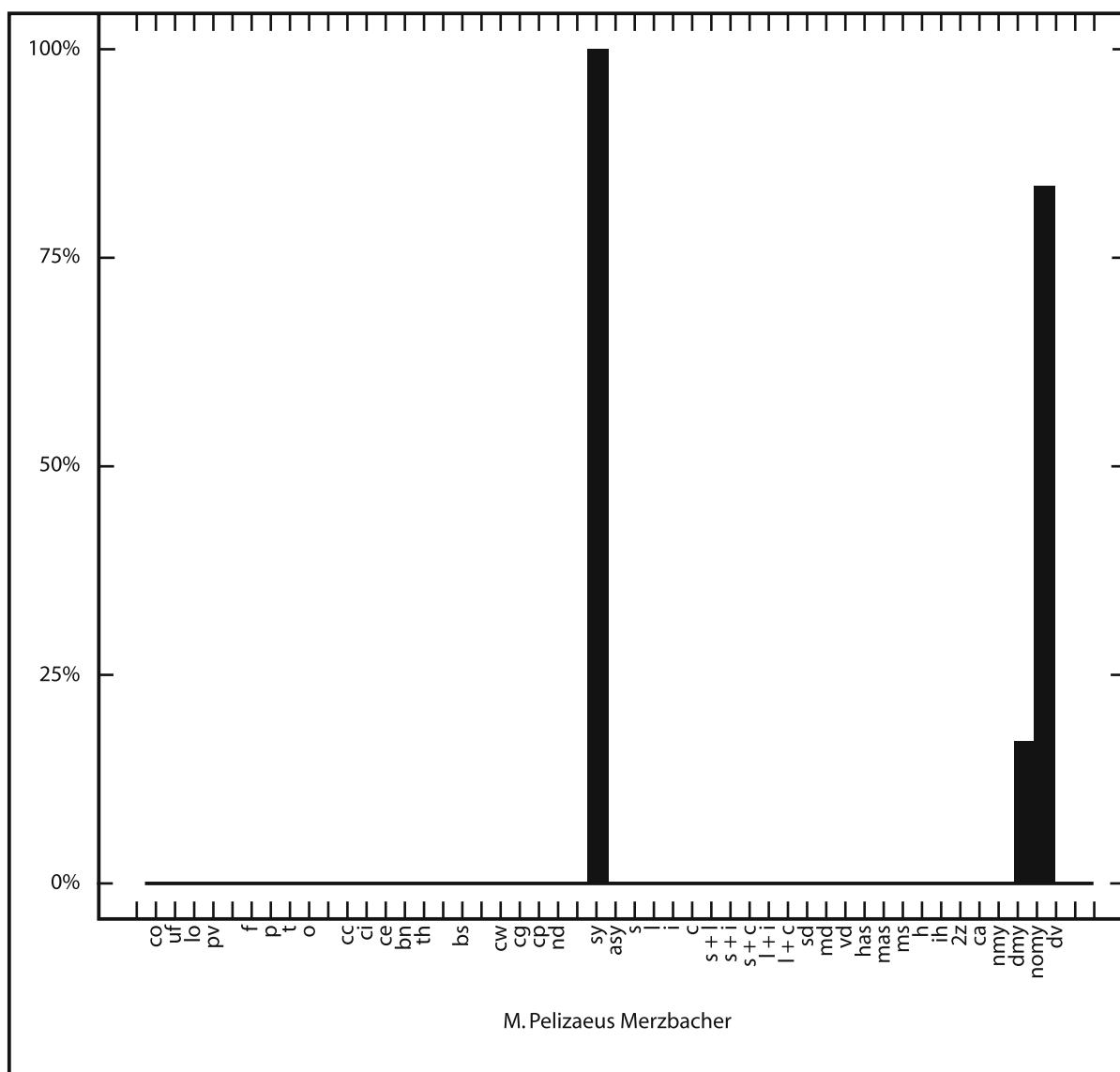


Fig. 109.6. Histogram of the frequency of involvement of the structural elements in Pelizaeus–Merzbacher disease. Abbreviations, see Fig. 109.5

the periventricular area narrow the number of diagnostic possibilities considerably. Sparing of the arcuate fibers is characteristic of the sphingolipidoses, whereas the reverse is true of some of the organic and amino acidopathies, which start in the U fibers. Lesions confined to the cerebellar white matter are rare. Cerebrotendinous xanthomatosis, adrenomyeloneuropathy, Refsum disease, and Langerhans cell histiocytosis can be examples. Multiple sclerosis has a preference for the upper edges of the lateral ventricles and the centrum semiovale. The cerebral form of X-linked adrenoleukodystrophy usually presents in the occipital lobes. Herpes simplex virus infections favor the frontal and temporal lobes.

The fifth step defines the pattern of spread of the disease. Adding the pattern of spread to the analysis further helps to distinguish certain entities. The cerebral form of X-linked adrenoleukodystrophy usually spreads in a dorsoventral direction; the direction of spread of Alexander disease is ventrodorsal, that of Canavan disease centripetal, and that of metachromatic leukodystrophy centrifugal.

The sixth step weighs the contribution of gray matter involvement relative to white matter involvement. Is the gray matter involvement a major or a minor part of the disease? Are cortical or central gray matter structures involved? Deep gray matter is often involved in mitochondrial disorders, in Bin-

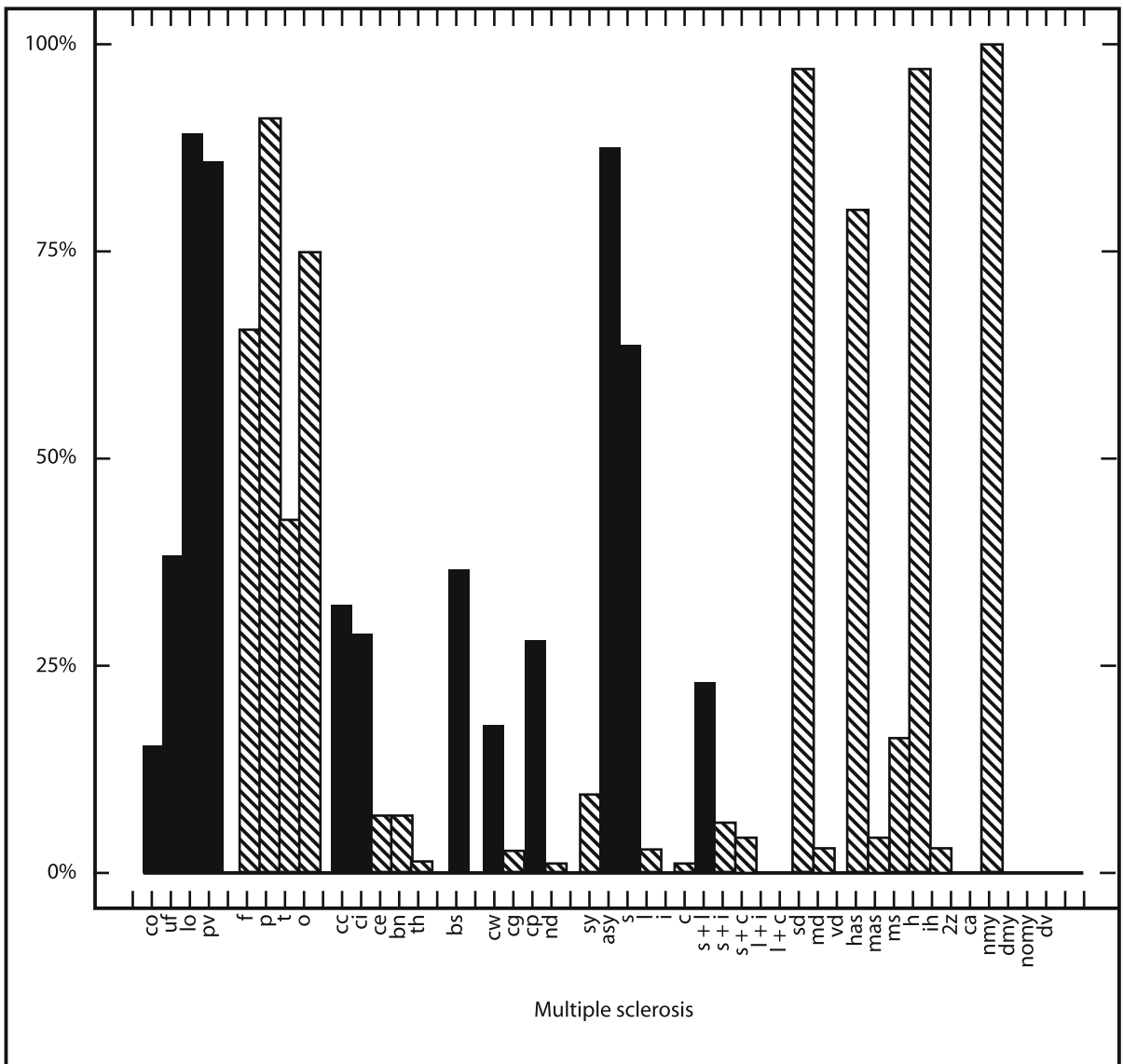


Fig. 109.7. Histogram of the frequency of involvement of the structural elements in multiple sclerosis. Abbreviations, see Fig. 109.5

swanger disease, in vasculitides, in glutaric aciduria type I and many other organic acidurias, in toxic encephalopathies such as carbon monoxide intoxication, cyanide intoxication, amphetamine intoxication, and in post-hypoxic-ischemic conditions. Involvement of the basal ganglia is rare in multiple sclerosis.

The seventh step evaluates whether the lesions enhance after contrast injection. Sometimes enhancement of the lesions leads to a characteristic pattern, as in cerebral X-linked adrenoleukodystrophy and Alexander disease. Active lesions in multiple sclerosis enhance. In acute disseminated encephalomyelitis not all lesions enhance or no lesions enhance at all; in

progressive multifocal leukoencephalitis enhancement occurs occasionally.

109.5 Pattern Recognition in Unclassified Leukoencephalopathies

MRI pattern recognition has not changed the fact that in about 50% of the children with significant white matter abnormalities on MRI, no specific diagnosis can be established despite an extensive laboratory work-up; the disease remains unclassified. The percentage is lower in adults. Pattern recognition works well in patients with a diagnosis that can be con-

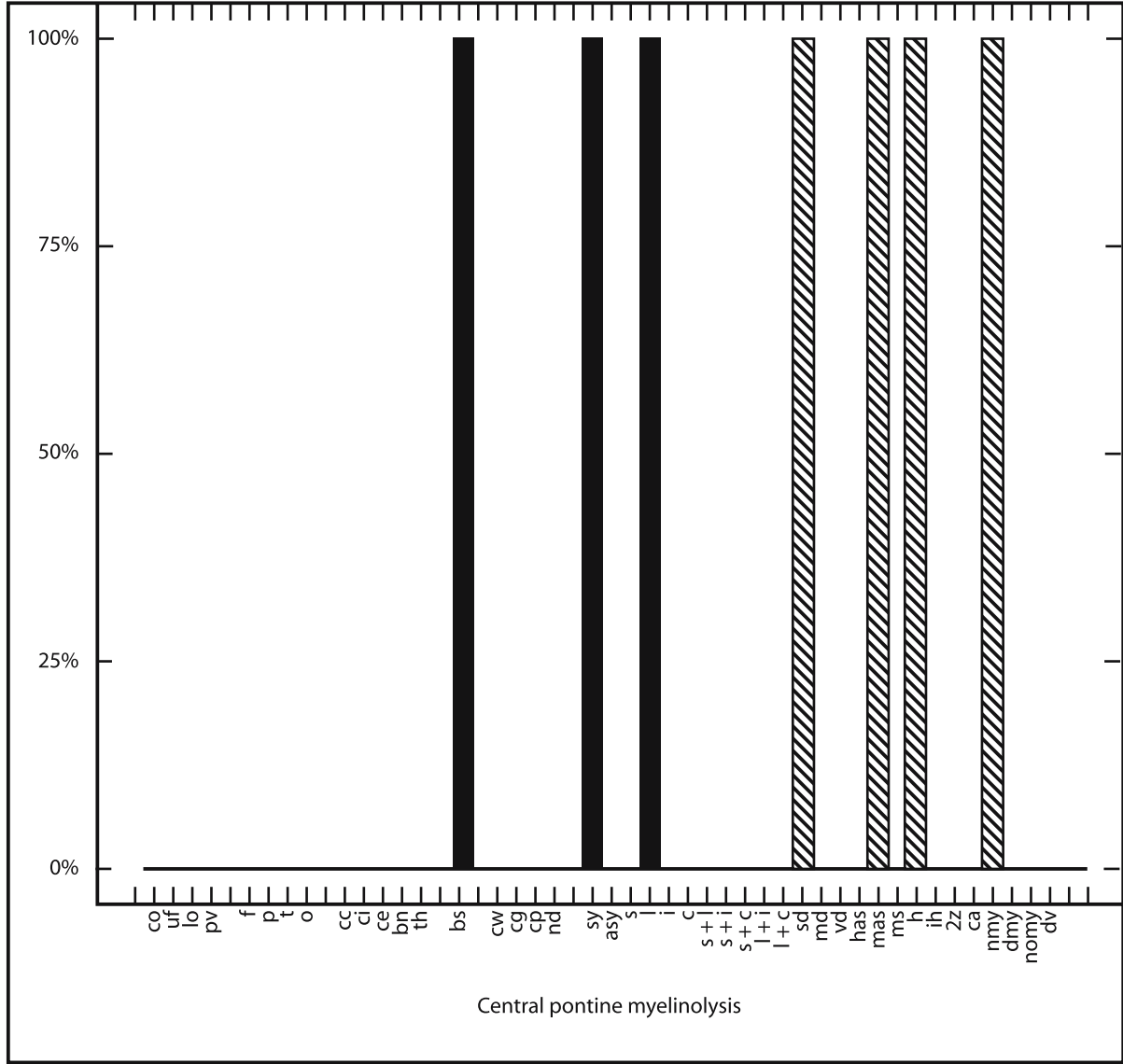


Fig. 109.8. Histogram of the frequency of involvement of the structural elements in central pontine myelinolysis. Abbreviations, see Fig. 109.5

firmed by laboratory tests because patients with the same or a similar disorder have been shown to share the MRI pattern. We decided to apply MRI pattern recognition to the large group of patients with an unclassified leukoencephalopathy, assuming that patients with the same disease entity would again share MRI characteristics. Application of pattern recognition to the MR images of large numbers of patients with an unclassified leukoencephalopathy led to the identification of several distinct patterns seen in multiple patients. MRI pattern recognition has

contributed to the identification of several hitherto unidentified white matter disorders: megalencephalic leukoencephalopathy with subcortical cysts (MLC); vanishing white matter disease (VWM); hypomyelination with atrophy of the basal ganglia and cerebellum (HABC); and leukoencephalopathy with brain stem and spinal cord involvement and elevated white matter lactate (LBSL).
The general MRI-oriented approach to unclassified leukoencephalopathies has been described elsewhere (van der Knaap et al. 1999). Seven major cate-

gories can be identified using simple and robust MRI criteria, mainly based on the predominant location of the white matter abnormalities. Our aim was to divide the unclassified leukoencephalopathies into more workable groups. These categories are distinct, as has been validated statistically.

Group A is characterized by severe hypomyelination. This is the largest single category among the unclassified leukoencephalopathies. In all patients currently known disorders leading to hypomyelination were ruled out, including Pelizaeus–Merzbacher disease, Salla disease, and DNA repair disorders.

Group B is characterized by global involvement of the cerebral white matter. In this group two separate disease entities were identified: *B1*, megalencephalic leukoencephalopathy with subcortical cysts, and *B2*, leukoencephalopathy with vanishing white matter. These diseases, initially identified by their MRI pattern as separate entities, are now also confirmed to be genetic entities.

Group C is characterized by extensive, predominantly frontal white matter abnormalities, relatively sparing of the occipital lobes, with basal ganglia abnormalities and also in many cases brain stem abnormalities. Most of the patients in this category had Alexander disease, a diagnosis that can now also be genetically confirmed.

Group D is characterized by predominantly periventricular white matter abnormalities. This is a heterogeneous group of disorders, often genetic, with a progressive clinical disease course.

Group E is characterized by predominant involvement of the deep (lobar) white matter. Deep or lobar white matter is located in between the periventricular white matter and the U fibers. In most patients the white matter abnormalities consisted of multifocal isolated lesions. In most patients the encephalopathy was static. A considerable proportion of the patients probably had congenital cytomegalovirus infection, a diagnosis that can now be confirmed using PCR for cytomegalovirus DNA on the filter paper containing neonatal blood spots (the Guthrie card).

Group F is characterized by predominant involvement of the U fibers.

Group G is characterized by abnormalities predominantly in the white matter of the posterior fossa.

Subdividing patients with an unclassified leukoencephalopathy using these categories will facilitate future research on homogeneous subgroups of patients and allow pooling of data across multiple centers.

109.6 Typical and Atypical MRI Patterns

The steps leading to the identification of so far unclassified white matter disorders are based upon a strict adherence to MRI criteria. The resulting homogeneous group allows further exploration of the biochemical or genetic background. Once the biochemical or genetic background is established, less typical cases can be analyzed, so that information can be obtained about the phenotypic variations of the disease, including variations in MRI patterns. Important examples can be found in the chapter on Alexander disease (Chap. 57) and the chapter on vanishing white matter (Chap. 65).

109.7 Examples

The following examples serve as illustrations of the described approach.

109.7.1 Example I

A 4-year-old girl presented with bilaterally diminished vision. The initial MRI showed optic neuritis, more severe on the right side. There was one lesion in the cerebral parenchyma on the right side around and under the anterior commissure. She responded favorably to a short course of methylprednisolone, but within a week after discontinuation she returned with severe symptoms of myelopathy in addition to decreased vision. Figure 109.9 shows the MRI findings at that time. The lower row of FLAIR images shows involvement of the caudate nucleus and putamen on the right side and bilateral lesions in the pulvinar. The lesion around the right anterior commissure is conspicuous. The signal intensity of the external/extreme capsules on both sides is too high and there is a distinct lesion in the parietal operculum on the left. There is also involvement of the dorsal part of the pons. At upper left, a sagittal T₂-weighted image of the cervicothoracic spine shows swelling of the cord with central high signal intensity (white arrows). At upper right, a STIR image at the level of the chiasm demonstrates swelling of the right part of the optic chiasm with a central lesion (arrow). Although the combination of optic neuritis followed by myelopathy is reminiscent of Devic neuromyelitis optica, the extent of cerebral lesions in this case argues in favor of the diagnosis acute disseminated encephalomyelitis.

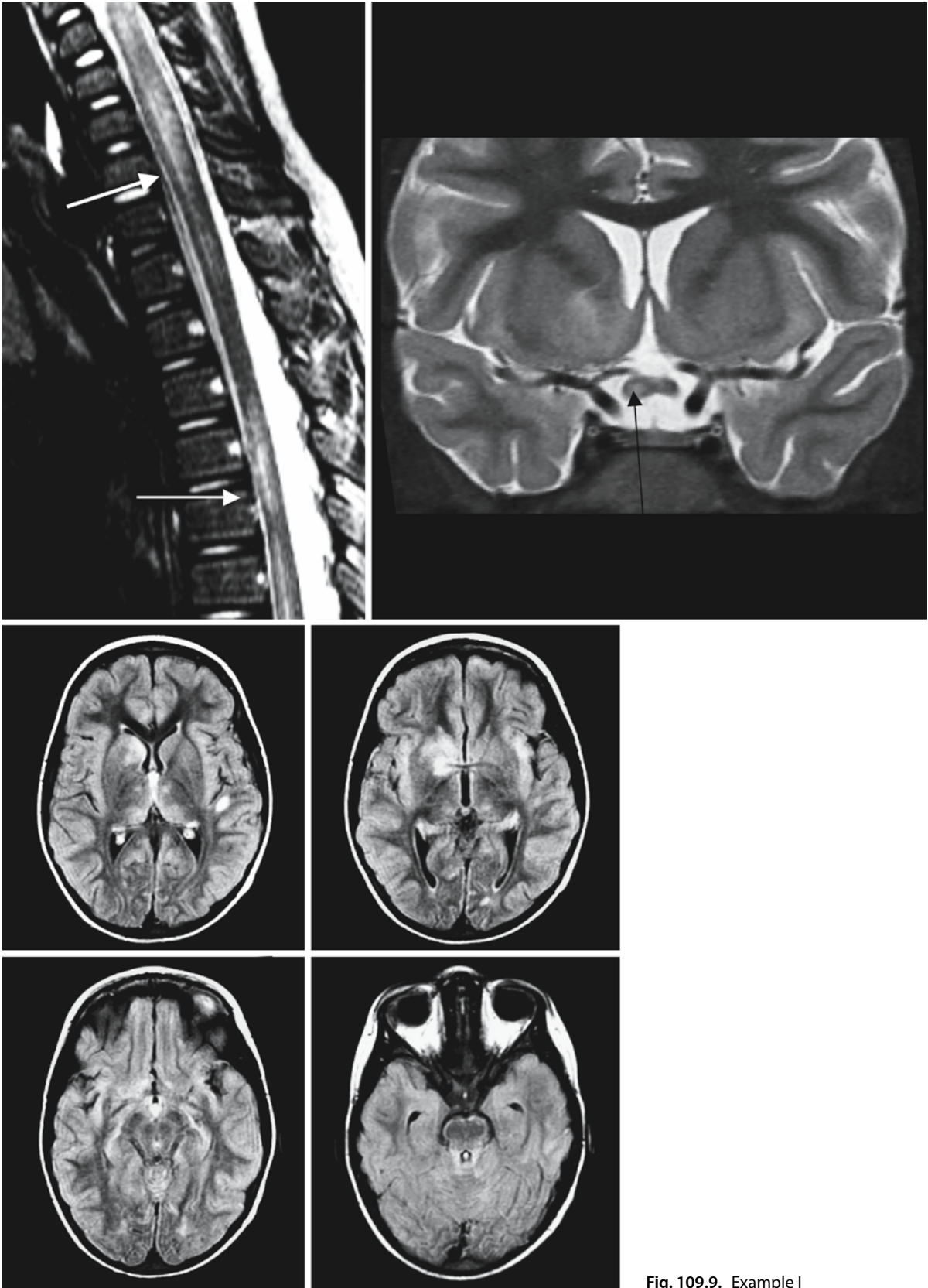


Fig. 109.9. Example I

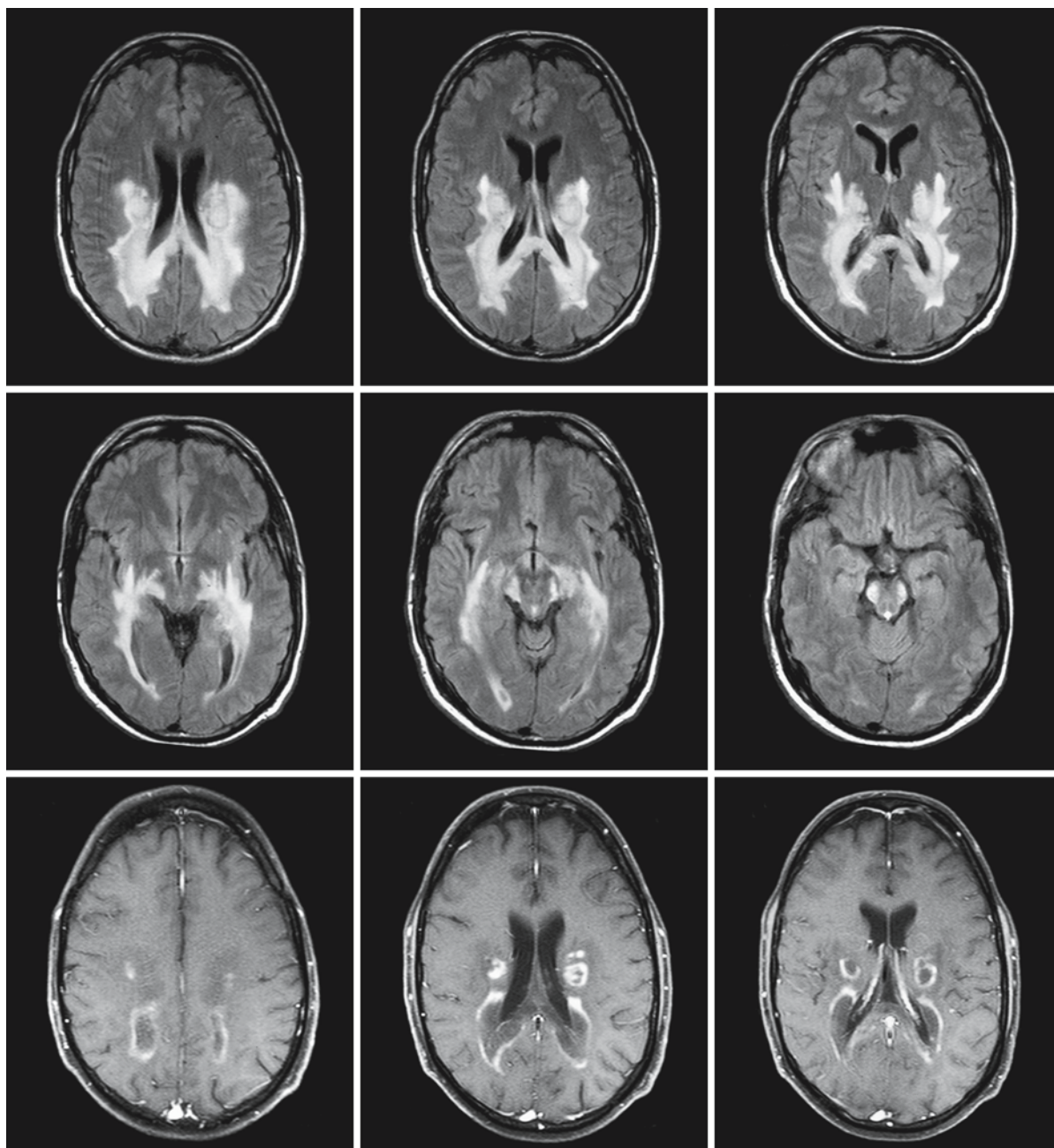


Fig. 109.10. Example II

109.7.2 Example II

The images shown in Fig. 109.10 reveal a diagnostic pattern. They relate to a 32-year-old man with progressive neurological disability. The FLAIR images (first and second rows) show perfectly symmetrical, confluent white matter lesions, mainly involving the

posterior white matter, but also affecting the splenium of the corpus callosum, extending towards the basal ganglia, and including the corticospinal tracts. After contrast (third row), enhancement of a rim within the lesion is seen. Although unusual at this age, the pattern is diagnostic of the cerebral form of X-linked adrenoleukodystrophy.

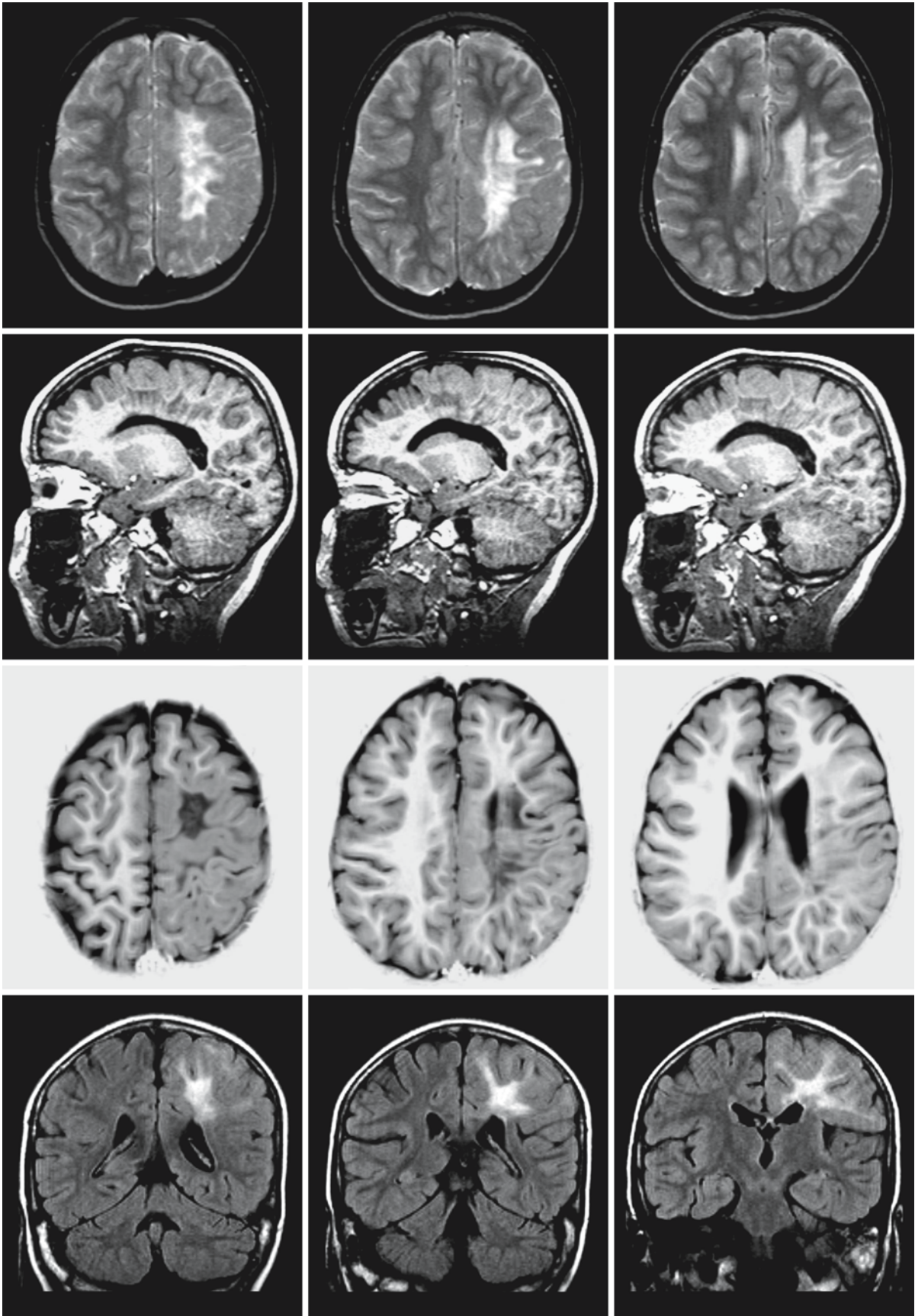


Fig. 109.11. Example III

109.7.3 Example III

A 7-year-old boy presented with intractable seizures on the right. An MRI was obtained, which showed extensive white matter abnormalities for which no metabolic cause could be found (Fig. 109.11). The boy was sent for a second opinion. Clinical history and neurological examination revealed evidence of an old, mild, right-sided hemiparesis. Sequential MRIs taken during the following 2 years showed static white matter abnormalities. The T₂-weighted images (first row) show white matter abnormalities in the up-

per part of the left hemisphere, involving both centrum semiovale and periventricular region. The cortex in contact with this lesion appears too thick. Parasagittal T₁-weighted images of the left hemisphere (second row) show the abnormalities in both the gray and white matter. The IR images (third row) also show the cortical and subcortical abnormalities. The coronal FLAIR images (fourth row) show the triangular shape of the signal abnormalities, tapering as they approach the lateral ventricle. The pattern is that of a balloon-type focal cortical dysplasia (Taylor type), simulating a white matter disease.

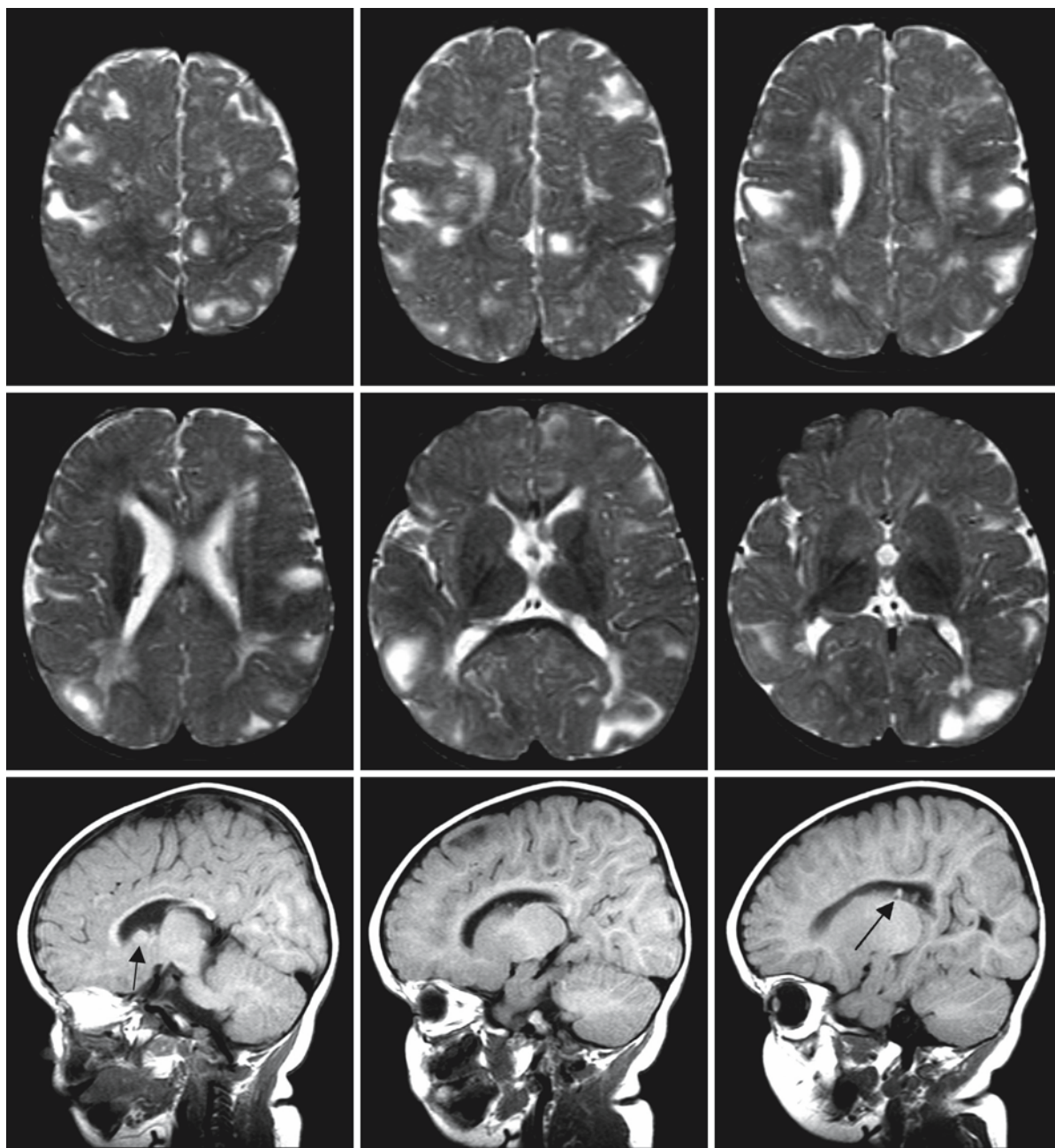


Fig. 109.12. Example IV

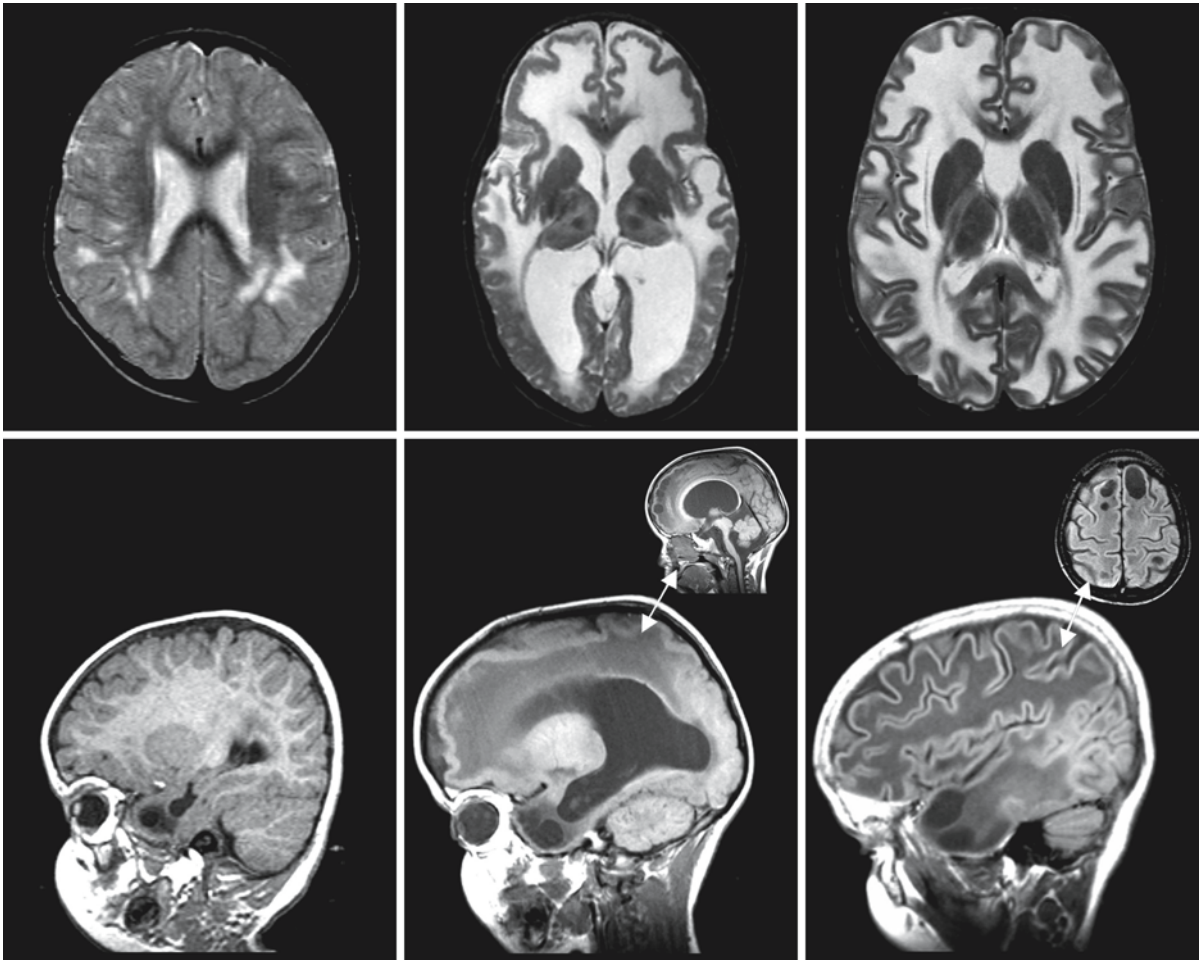


Fig. 109.13. Example V

109.7.4 Example IV

The images of this 1-year-old girl were sent for an opinion because of an unclassified white matter disease (Fig. 109.12). The upper two rows of T₂-weighted images show subcortical white matter lesions with broadening of the overlying cortex. The sagittal T₁-weighted images (third row) show small indentations in the ventricular lining (arrows), representing subependymal nodules. These nodules are dark on the T₂-weighted images, while they are white on T₁-weighted images. The pattern of cortico-subcortical tubers and subependymal nodules is indicative of tuberous sclerosis.

109.7.5 Example V

The T₁-weighted parasagittal images (second row of Fig. 109.13) show abnormalities in the temporal lobe of three different patients: cysts in the temporal pole in all three patients and widened temporal horns in the first two. The diagnosis in each case can be made in conjunction with the axial T₂-weighted images (first row). The images on the left showing multifocal lesions with the largest lesions in the deep parietal white matter, together with the temporal abnormalities, in a microcephalic child are highly suggestive of congenital cytomegalovirus infection. The images in the middle showing diffuse cerebral white matter abnormalities, diffuse cortical dysplasia, and pontine hypoplasia (small sagittal image) demonstrate the

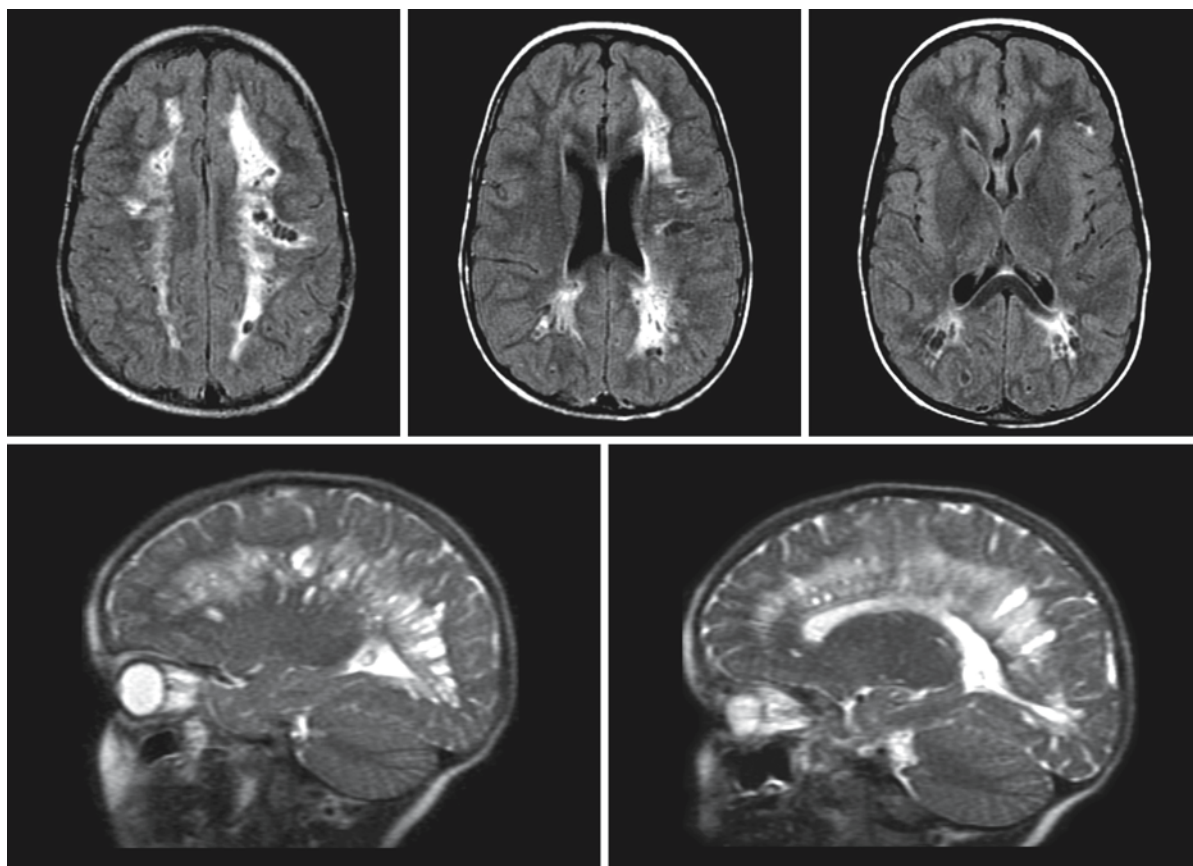


Fig. 109.14. Example VI

pattern of Walker–Warburg congenital muscular dystrophy. The images on the right showing, in addition to the cysts in the anterior temporal lobe, diffuse cerebral white matter abnormalities and frontoparietal subcortical cysts (small image) in a megalencephalic child are diagnostic of megalencephalic leukoencephalopathy with subcortical cysts.

In the next series of examples (VI–X) unusual MR findings are presented: black and white dots and stripes.

109.7.6 Example VI

In this patient with hypomelanosis of Ito (Fig. 109.14), the FLAIR images (first row) show confluent white matter abnormalities in the centrum semiovale and periventricular region. In addition, multiple black dots are seen, some arranged in rows. The sagittal T_2 -weighted images (second row) show that the dots are related to radially arranged widened perivascular spaces.

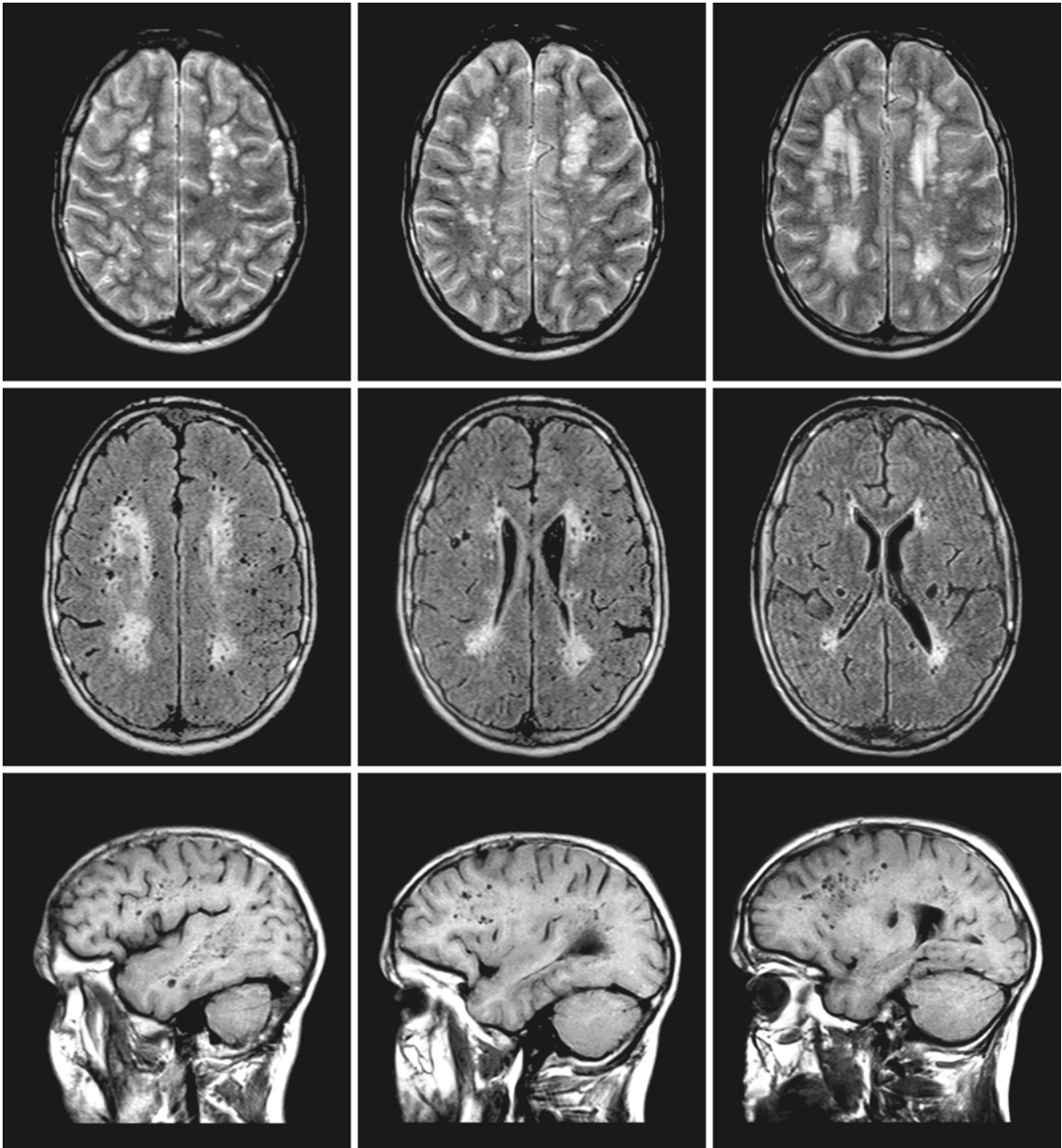


Fig. 109.15. Example VII

109.7.7 Example VII

In this case of Lowe syndrome (Fig. 109.15), the first row of T_2 -weighted images show symmetrical white matter abnormalities in the deep and periventricular white matter. Horizontal stripes in the corpus callosum indicate widened perivascular spaces. The sec-

ond row of FLAIR images shows a multitude of black dots but no stripes. They represent focal cysts, not clearly following the perivascular spaces. The third row of T_1 -weighted sagittal images confirms that the black holes do not or do not only represent widened perivascular spaces.

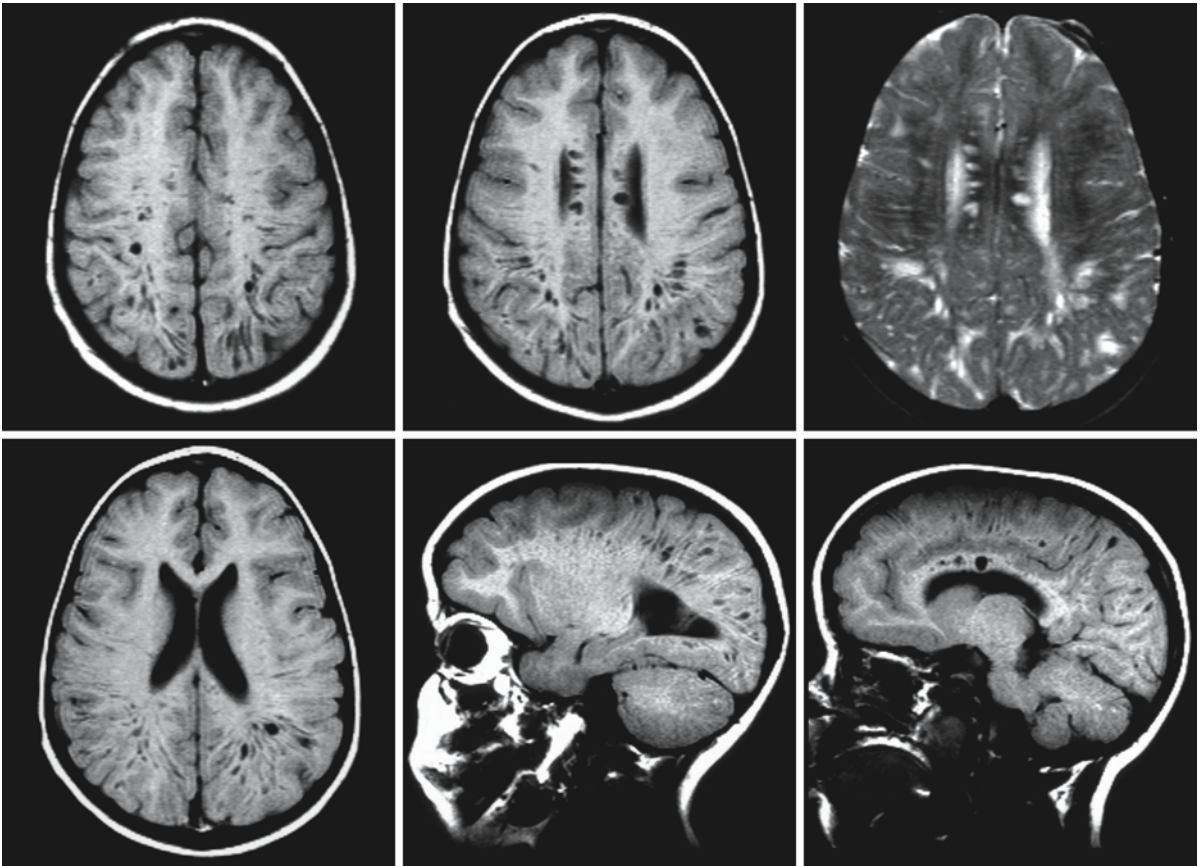


Fig. 109.16. Example VIII

109.7.8 Example VIII

In some subtypes of mucopolysaccharidosis, widened perivascular spaces are the hallmark of the MR pattern. This is demonstrated in the T_1 - and T_2 -weighted transverse images and T_1 -weighted sagittal images (Fig. 109.16) of a patient with Hurler syndrome. Often the corpus callosum is involved.

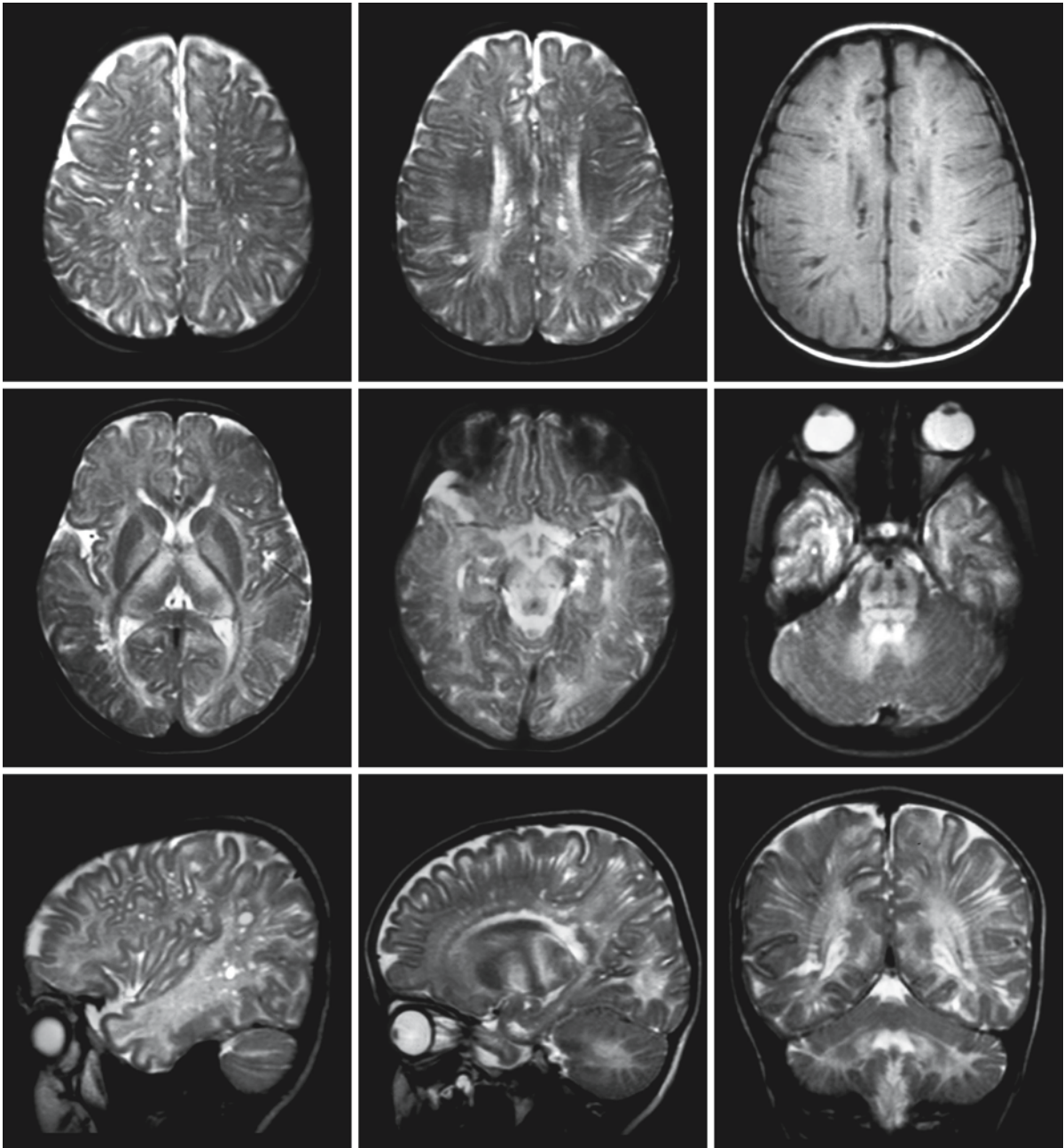


Fig. 109.17. Example IX

109.7.9 Example IX

Figure 109.17 contains the T₂-weighted transverse, sagittal, and coronal images and one T₁-weighted image of a 4-year-old child with a mild variant of maple syrup urine disease. In addition to the abnormalities in the globus pallidus, thalamus, midbrain, pons, and

dentate nucleus, there is a striking widening of the perivascular spaces, especially well depicted in the T₁-weighted image (first row, right) and the sagittal and coronal T₂-weighted images (third row). Myelin deposition also seems to have happened mainly in perivascular areas, leading to dark stripes on T₂-weighted images.

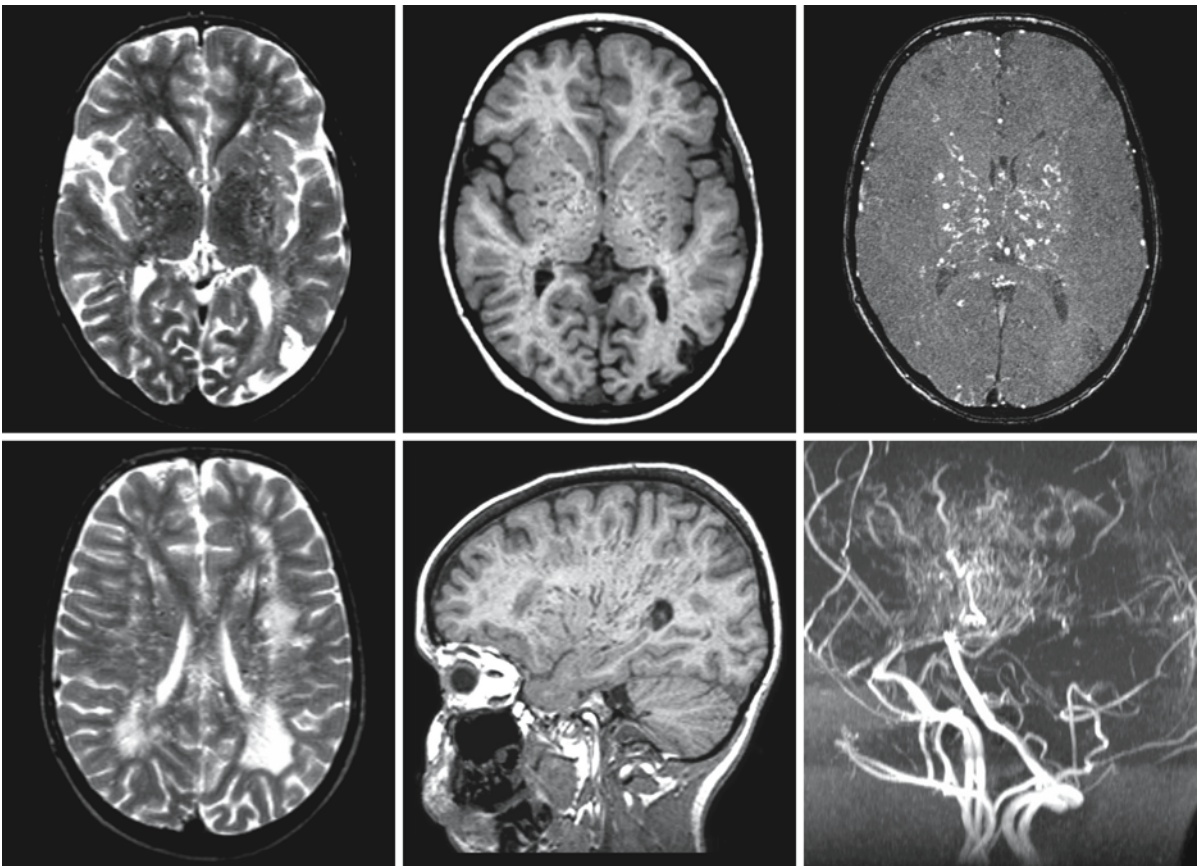


Fig. 109.18. Example X

109.7.10 Example X

A 10-year-old boy presented with multiple transient episodes of neurological dysfunction. In Fig. 109.18, the T_2 -weighted images on the left show a multitude of tiny lesions in the white matter and basal ganglia on a background of more confluent cerebral white matter lesions. The T_1 -weighted images in the middle show a multitude of dark stripes, which were confirmed to be abnormal vessels on the MRA (source image shown upper right), whereas the conventional angiography shows the pattern of moyamoya syndrome.

The next three examples show leukoencephalopathies linked to chromosomal abnormalities.

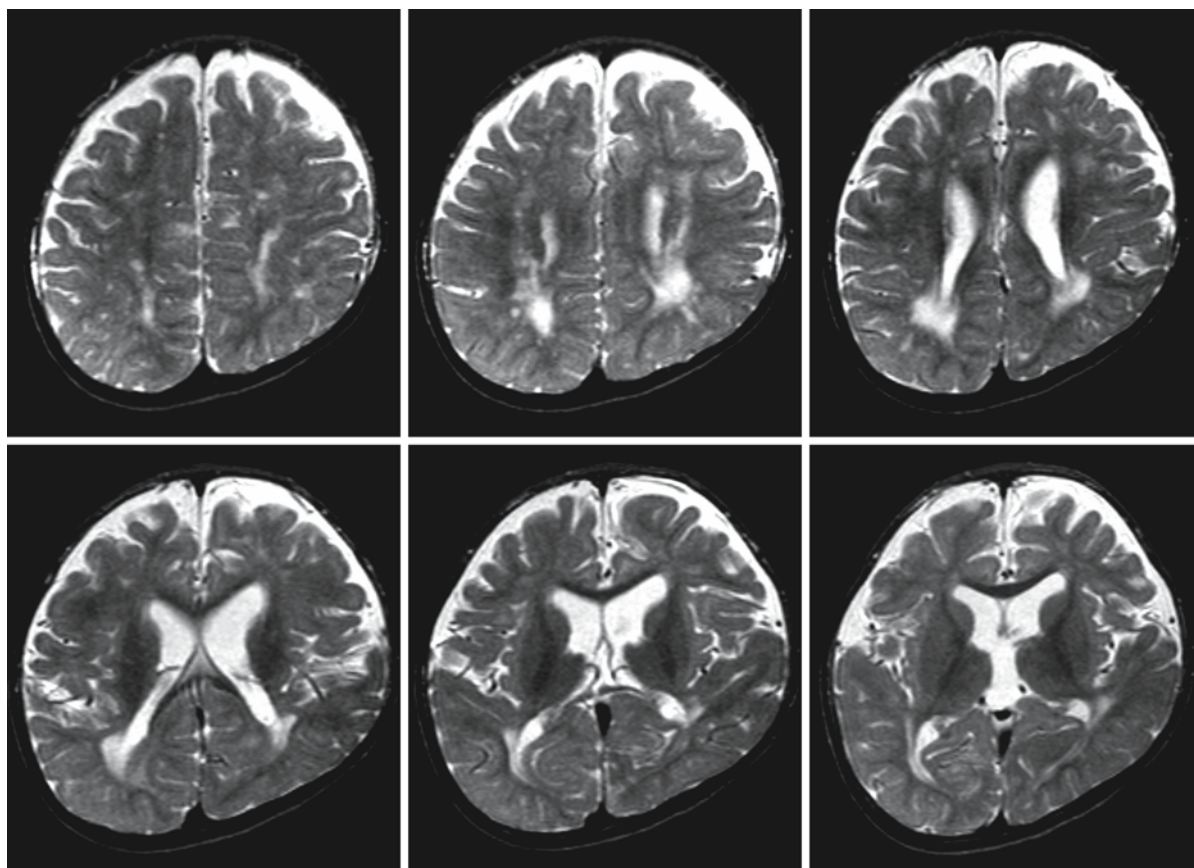


Fig. 109.19. Example XI

109.7.11 Example XI

A 2-year-old boy presented with borderline macrocephaly, retarded development, and dysmorphic features. Chromosomal analysis revealed an inversion-duplication of chromosome 8p. The T_2 -weighted MR images (Fig. 109.19) show dilated CSF spaces and multiple white matter abnormalities. They were found to be stable on follow-up.

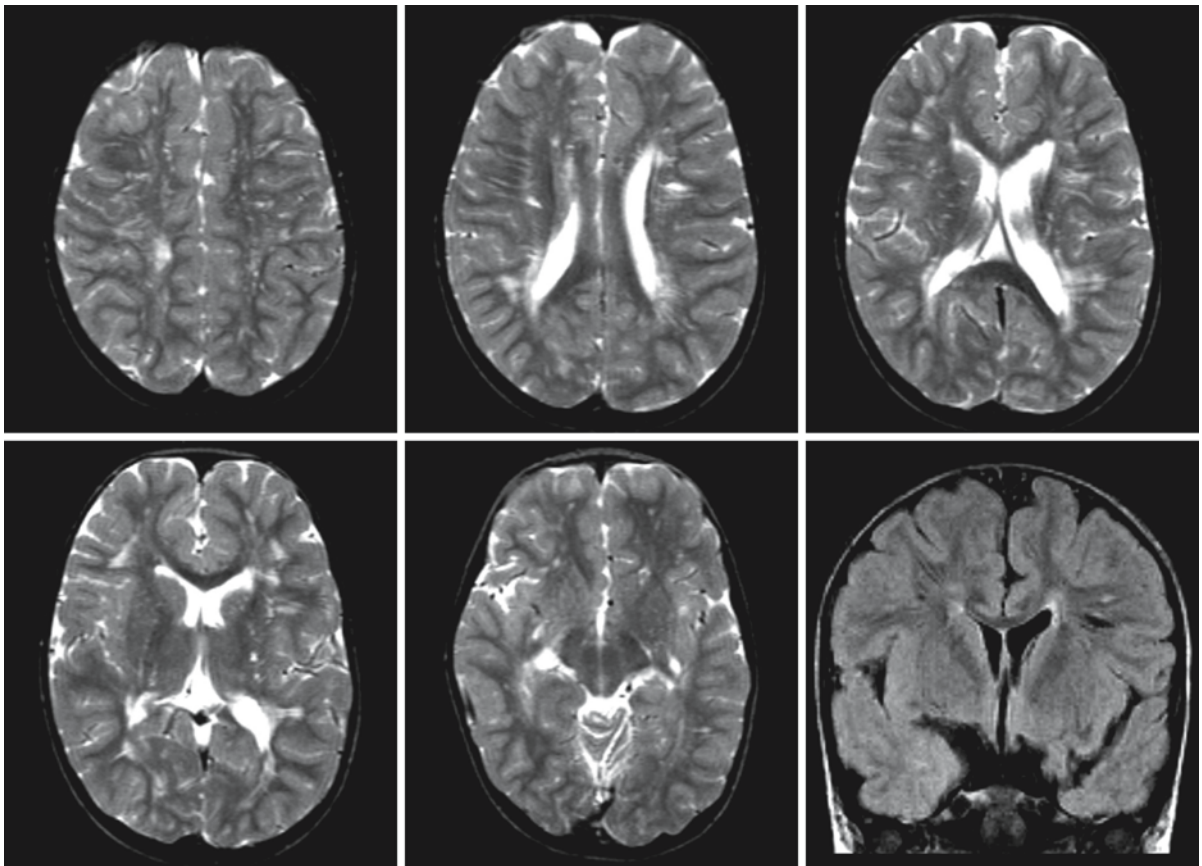


Fig. 109.20. Example XII

109.7.12 Example XII

A 5-year-old girl was known to have psychomotor retardation, dysmorphic features, eye abnormalities, and hearing difficulties. Chromosomal analysis revealed an unbalanced translocation between chromosome 6p25 and chromosome 20q13. The T_2 -weighted images (Fig. 109.20) show spotty white matter abnormalities in the deep and periventricular white matter and several dot-like lesions in the basal ganglia. The coronal FLAIR image (lower right) confirms that some of the abnormalities are related to enlarged perivascular spaces.

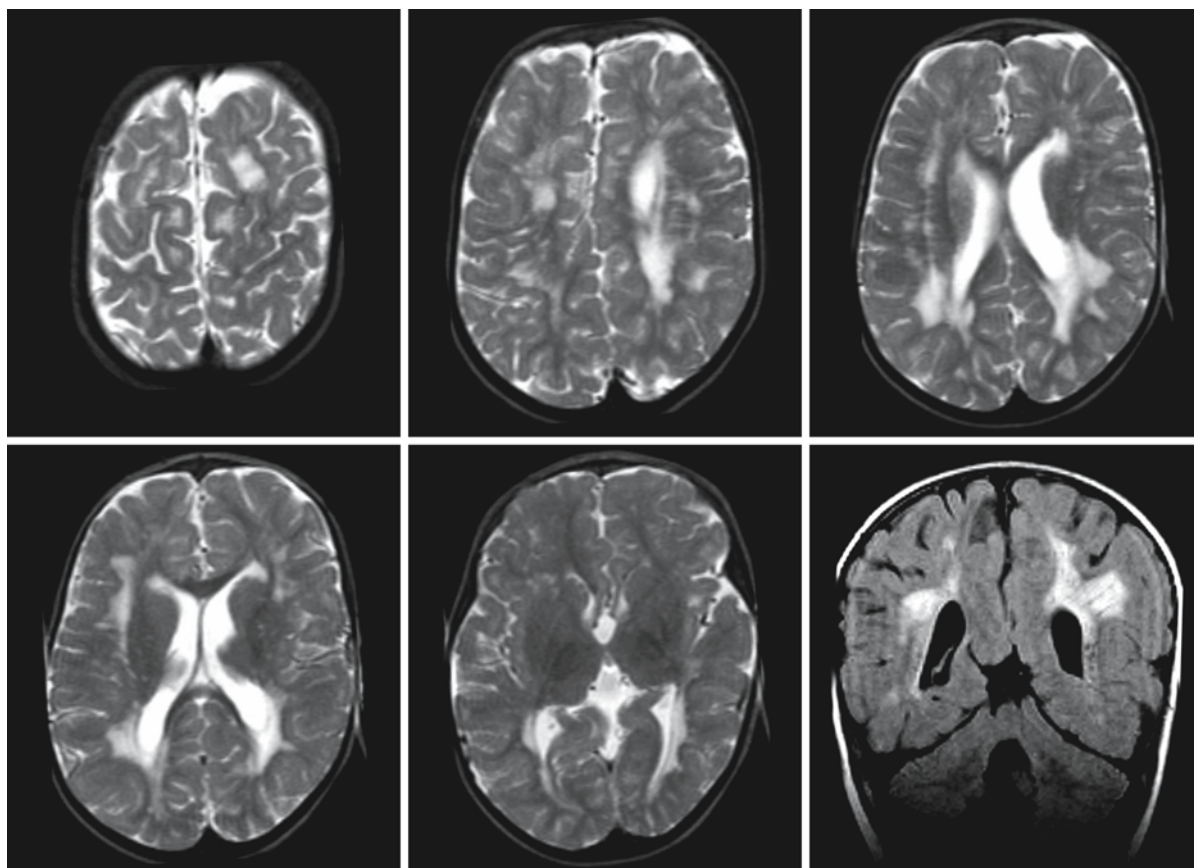


Fig. 109.21. Example XIII

109.7.13 Example XIII

A 2-year-old girl had a similar clinical picture and MRI findings (Fig. 109.21; compare with Fig. 109.20). Chromosomal analysis was normal. Because of the striking clinical and MRI similarities, a submicroscopic deletion of chromosome 6p25 was suspected. FISH analysis confirmed the chromosome 6p25 deletion, illustrating the power of pattern recognition in the reading of MR images.

References and Further Reading

1 Myelin and White Matter

- Asotra K, Macklin WB. Protein kinase C activity modulates myelin gene expression in enriched oligodendrocytes. *J Neurosci Res* 1993; 34: 571–588
- Baumann N, Pham-Dinh D. Biology of oligodendrocyte and myelin in the mammalian central nervous system. *Physiol Rev* 2001; 81: 871–927
- Benjamins JA, Iwata R, Hazlett J. Kinetics of entry of proteins into the myelin membrane. *J Neurochem* 1978; 31: 1077–1085
- Benveniste EN, Merrill JE. Stimulation of oligodendroglial proliferation and maturation by interleukin-2. *Nature* 1986; 321: 610–613
- Berlet HH, Volk B. Studies of human myelin proteins during old age. *Mech Ageing Dev* 1980; 14: 211–222
- Berndt JA, Kim JG, Hudson LD. Identification of cis-regulatory elements in the myelin proteolipid protein (PLP) gene. *J Biol Chem* 1992; 267: 14730–14737
- Boiron F, Spivack WD, Deshmukh DS, Gould RM. Basis for phospholipid incorporation into peripheral nerve myelin. *J Neurochem* 1993; 60: 320–329
- Bologa L. Oligodendrocytes, key cells in myelination and target in demyelinating diseases. *J Neurosci Res* 1985; 14: 1–20
- Bongarzone ER, Howard SG, Schonmann SG, Schonmann V, Campagnoni AT. Identification of the dopamine D3 receptor in oligodendrocyte precursors: potential role in regulation differentiation and myelin formation. *J Neurosci* 1998; 18: 5344–5353
- Brody BA, Kinney HC, Kloman AS, Gilles FH. Sequence of central nervous system myelination in human infancy. I. An autopsy study of myelination. *J Neuropathol Exp Neurol* 1987; 46: 283–301
- Brown MC, Moreno MB, Bongarzone ER, Cohen PD, Soto EF, Pasquini JM. Vesicular transport of myelin proteolipid and cerebroside sulfates to the myelin membrane. *J Neurosci Res* 1993; 35: 402–408
- Burger D, Steck AJ, Bernard CCA, Kerlero de Rosbo N. Human myelin/oligodendrocyte glycoprotein: a new member of the L2/HNK-1 family. *J Neurochem* 1993; 61: 1822–1827
- Butt AM, Berry M. Oligodendrocytes and the control of myelination in vivo: new insights from the rat anterior medullary velum. *J Neurosci Res* 2000; 59: 477–488
- Campagnoni AT. Molecular biology of myelin proteins from the central nervous system. *J Neurochem* 1988; 51: 1–14
- Campagnoni AT, Verdi JM, Verity AN, Amur-Umarjee S. Post-transcriptional events in the expression of myelin protein genes. *Ann NY Acad Sci* 1990; 605: 270–279
- Carson MJ, Behringer RR, Brinster RL, McMorris FA. Insulin-like growth factor I increases brain growth and central nervous system myelination in transgenic mice. *Neuron* 1993; 10: 729–740
- Compston A, Zajicek J, Sussman J, Webb A, Hall G, Muir D, Shaw C, Wood A, Scolding N. Glial lineages and myelination in the central nervous system. *J Anat* 1997; 190: 161–200
- Dambska M, Laure-Kaminowska M. Myelination as a parameter of normal and retarded brain maturation. *Brain Dev* 1990; 12: 214–220
- Davison AN, Dobbing J. Myelination as a vulnerable period in brain development. *Br Med Bull* 1966; 20: 40–44
- Deshmukh DS, Vorbrodt AW, Lee PK, Bear WD, Kuizon S. Studies on the submicrosomal fractions of bovine oligodendroglia: lipid composition and glycolipid biosynthesis. *Neurochem Res* 1988; 13: 571–582
- De Vries GH, Norton WT. The fatty acid composition of sphingolipids from bovine CNS axons and myelin. *J Neurochem* 1974; 22: 251–257
- Dietrich RB, Bradley WG, Zaragoza IV, Otto RJ, Taira RK, Wilson GH, Kangerloo H. MR evaluation of early myelination patterns in normal and developmentally delayed infants. *AJNR Am J Neuroradiol* 1988; 9: 69–76
- Dobbing J. Vulnerable periods in developing brain. In: Davison AN, Dobbing J, eds. *Applied neurochemistry*. Oxford: Blackwell, 1968: 287–316
- Dobbing J, Sands J. Quantitative growth and development of human brain. *Arch Dis Child* 1973; 48: 757–767
- Duhamel-Clerin E, Villarroja H, Mehtali M, Lapie P, Besnard F, Gumpel M, Lachapelle F. Cellular expression of an HMGR promoter-cat fusion gene in transgenic mouse brain: evidence for a developmental regulation in oligodendrocytes. *Glia* 1994; 11: 35–46
- Dziewulska D, Jamrozik Z, Podlecka A, Rafalowska J. Do astrocytes participate in rat spinal cord myelination? *Folia Neuropathol* 1999; 37: 81–86
- Farrer RG, Benjamins JA. Entry of newly synthesized gangliosides into myelin. *J Neurochem* 1992; 58: 1477–1484
- Fishman MA, Agrawal HC, Alexander A, Golterman J, Martenson RE, Mitchell RF. Biochemical maturation of human central nervous system myelin. *J Neurochem* 1975; 24: 689–694
- Flechsig P. Developmental (myelogenetic) localisation of the cerebral cortex in the human subject. *Lancet* 1901; 11: 1027–1029
- Flechsig P. *Anatomie des menschlichen Gehirns und Rückenmarks*. Leipzig: Georg Thieme, 1920, 7–119
- Fors L, Hood L, Saavedra RA. Sequence similarities of myelin basic protein promoters from mouse and shark: implications for the control of gene expression in myelinating cells. *J Neurochem* 1993; 60: 513–521
- Futerman AH, Stieger B, Hubbard AL, Pagano RE. Sphingomyelin synthesis in rat liver occurs predominantly at the cis and medial cisternae of the Golgi apparatus. *J Biol Chem* 1990; 265: 8650–8657
- Gilles FH. Myelination in the neonatal brain. *Hum Pathol* 1976; 7: 244–248
- Gilles FH, Shankle W, Dooling EC. Myelinated tracts: growth patterns. In: Gilles FH, Leviton A, Dooling EC. *The developing human brain*. Boston: Wright, 1983, 117–192
- Goddard DR, Berry M, Butt AM. In vivo actions of fibroblasts growth factor-2 and insuline-like growth factor-I on oligodendrocyte development and myelination in the central nervous system. *J Neurosci Res* 1999; 57: 74–85

- Goodrum JF, Earnhardt T, Goines N, Bouldin TW. Fate of myelin lipids during degeneration and regeneration of peripheral nerve: an autoradiographic study. *J Neurosci* 1994; 14: 357–367
- Gould RM, Spivack W, Cataneo R, Holshek J, Konat G. Lipids and myelination. In: Crescenzi S, ed. *A multidisciplinary approach to myelin diseases*. New York: Plenum, 1987: 87–102
- Gould RM, Freund CM, Palmer F, Feinstein DL. Messenger RNAs located in myelin sheath assembly sites. *J Neurochem* 2000; 75: 1834–1844
- Gupta SK, Pringle J, Poduslo JF, Mezei C. Induction of myelin genes during peripheral nerve remyelination requires a continuous signal from the ingrowing axon. *J Neurosci Res* 1993; 34: 14–23
- Hasegawa M, Houdou S, Mito T, Takashima S, Asanuma K, Ohno T. Development of myelination in the human fetal and infant cerebrum: a myelin basic protein immunohistochemical study. *Brain Dev* 1992; 14: 1–6
- Jacoby CG, Yuh WTC, Afifi AK, Bell WE, Schelper RL, Sato Y. Accelerated myelination in early Sturge-Weber syndrome demonstrated by MR imaging. *J Comput Assist Tomogr* 1987; 11: 226–231
- Jeckel D, Karenbauer A, Birk R, Schmidt RR, Wieland F. Sphingomyelin is synthesized in the cis Golgi. *FEBS Lett* 1990; 261: 155–157
- Kamholz J, Toffenetti, Lazzarini RA. Organization and expression of the human myelin basic protein gene. *J Neurosci Res* 1988; 21: 62–70
- Keene LMF, Hewer EE. Some observations on myelination in the human central nervous system. *J Anat* 1931; 66: 1–13
- Kinney HC, Brody BA, Kloman AS, Gilles FH. Sequence of central nervous system myelination in human infancy. II. Patterns of myelination in autopsied infants. *J Neuropathol Exp Neurol* 1988; 47: 217–234
- Kinney HC, Karthigasan J, Borenshteyn NI, Flax JD, Kirschner DA. Myelination in the developing human brain: biochemical correlates. *Neurochem Res* 1994; 19: 983–996
- Konola JT, Yamamura T, Tyler B, Lees MB. Orientation of the myelin proteolipid protein C-terminus in oligodendroglial membranes. *Glia* 1992; 5: 112–121
- Langworthy OR. Development of behavior patterns and myelination of the nervous system in human fetus and infant. (Contributions to embryology, vol XXIV) Washington DC: Carnegie Institute of Washington, 1933: 1–57
- Lappe-Siefke C, Goebbels S, Gravel M, Nicksch E, Lee J, Braun PE, Griffiths IR, Vane K-A. Disruption of *Cnp1* uncouples oligodendroglial functions in axonal support and myelination. *Nat Genet* 2003; 33: 366–374
- Larocca JN, Rodriguez-Gabin AG. Myelin biogenesis: vesicle transport in oligodendrocytes. *Neurochem Res* 2002; 27: 1313–1329
- Lemke G. Unwrapping the genes of myelin. *Neuron* 1988; 1: 535–543
- Lemke G. The molecular genetics of myelination: an update. *Glia* 1993; 7: 263–271
- Ludwin SK. Remyelination in the central nervous system and the peripheral nervous system. In: Waxman SG, ed. *Advances in neurology: functional recovery in neurological disease*, vol 47, New York: Raven Press, 1988: 215–254
- Martin DW. Membranes. In: Martin DW, Mayes PA, Rochwel VW, Granner DK, eds. *Harper's review of biochemistry*, 20th ed. Los Altos: Lange Medical Publications, 1985, 448–463
- Martin E, Boesch C, Zuerr M, Kikinis R, Molinari L, Kaelin P, Boltshauser E, Duc G. MR imaging of brain maturation in normal and developmentally handicapped children. *J Comput Assist Tomogr* 1990; 14: 685–692
- Matthieu JM. An introduction to the molecular basis of inherited myelin diseases. *J Inher Metab Dis* 1993; 16: 724–732
- Matthieu JM, Comte V, Tosic M, Honegger P. Myelin gene expression during demyelination and remyelination in aggregating brain cell cultures. *J Neuroimmunol* 1992; 40: 231–234
- McLaurin J, Ackerley CA, Moscarello MA. Localization of basic proteins in human myelin. *J Neurosci Res* 1993; 35: 618–628
- Menkes JH. The leukodystrophies. *N Engl J Med* 1990; 322: 54–55
- Meyer-Franke A, Shen S, Barres BA. Astrocytes induce oligodendrocyte processes to align with and adhere to axons. *Mol Cell Neurosci* 1999; 14: 385–397
- Mickel HS, Gilles FH. Changes in glial cells during human telencephalic myelinogenesis. *Brain* 1970; 93: 337–346
- Mikol DD, Rongnoparut P, Allwardt BA, Marton LS, Stefansson K. The oligodendrocyte-myelin glycoprotein of mouse: primary structure and gene structure. *Genomics* 1993; 17: 604–610
- Mitchell LS, Gillespie SC, McAllister F, Fanarraga ML, Kirkham D, Kelly B, Brophy PJ, Grittiths IR, Montague P, Kennedy PGE. Developmental expression of major myelin protein genes in the CNS of X-linked hypomyelinating mutant rumpshaker. *J Neurosci Res* 1992; 33: 205–217
- Morell P, ed. *Myelin*, 2nd ed. New York: Plenum Press, 1984
- Morell P, Wiesmann U. A correlative synopsis of the leukodystrophies. *Neuropediatrics* 1984; 15 (suppl): 62–65
- Morell P, Quarles RH, Norton WT. Formation, structure, and biochemistry of myelin. In: Siegel GJ, Agranoff BW, Albers RW, eds. *Basic neurochemistry: molecular, cellular and medical aspects*, 4th ed. New York: Raven Press, 1989, 109–136
- Norton WT. Recent advances in myelin biochemistry. *Ann NY Acad Sci* 1984; 436: 5–10
- Norton WT, Autilio LA. The lipid composition of purified bovine brain myelin. *J Neurochem* 1966; 13: 213–222
- Norton WT, Cammer W. Isolation and characterization of myelin. In: Morell P, ed. *Myelin*. Plenum, New York, 1984, pp 147–195
- Notterpek LM, Rome LH. Functional evidence for the role of axolemma in CNS myelination. *Neuron* 1994; 13: 473–485
- Pagano RE. The Golgi apparatus: insights from lipid biochemistry. *Biochem Soc Trans* 1990; 18: 361–366
- Patsalos PN, Wiggins RC. Brain maturation following administration of phenobarbital, phenytoin, and sodium valproate to developing rats or to their dams: effects on synthesis of brain myelin and other subcellular membrane proteins. *J Neurochem* 1982; 39: 915–923
- Percy AK, McKhann GM. The biochemistry of myelin and the leukodystrophies. In: Vinken PJ, Bruyn GW, eds. *Handbook of clinical neurology*, vol 10, Amsterdam: North Holland Publishing Company, 1970, 134–149
- Poduslo SE, Jang Y. Myelin development in infant brain. *Neurochem Res* 1984; 9: 1615–1626
- Pope A. Neuroglia: quantitative aspects. In: Schoffeniels E, Franck G, Hertz L, Tower DB, eds. *Dynamic properties of glia cells*. New York: Pergamon Press, 1977, 13–20
- Poser CM. Discussion des rapports sur les maladies démyélinisantes. *Proc Third Intern Congr Neuropathol. Brussels: Editions Acta Medica Belgica*, 1957, 106–111
- Poser CM. Leukodystrophy and the concept of dysmyelination. *Arch Neurol* 1961; 4: 323–332
- Poser CM. Dysmyelination revisited. *Arch Neurol* 1978; 35: 401–407

- Probstmeier R, Fahrigh T, Spiess E, Schachner M. Interactions of the neural cell adhesion molecule and the myelin-associated glycoprotein with collagen type I: involvement in fibrillogenesis. *J Cell Biol* 1992; 116: 1063–1070
- Richardson EP. Myelination in the human central nervous system. In: Haymaker W, Adams RD, eds. *Histology and histopathology of the nervous system*. Springfield: Charles C Thomas, 1982, 146–173
- Rodriguez M. Central nervous system demyelination and remyelination in multiple sclerosis and viral models of disease. *J Neuroimmunol* 1992; 40: 255–264
- Rodriguez M, Prayoonwivat N, Howe C, Sanborn K. Proteolipid protein gene expression in demyelination and remyelination of the central nervous system: a model for multiple sclerosis. *J Neuropathol Exp Neurol* 1994; 53: 136–143
- Rorke LB, Riggs HE, Showers MJC, Cabrera CV, Cohn M. Myelination of the brain in the newborn. Philadelphia: Lippincott, 1969: 1–105
- Royland J, Konat GW, Kanoh M, Wiggins RC. Down regulation of myelin-specific mRNAs in the mechanism of hypomyelination in the undernourished developing brain. *Dev Brain Res* 1992; 65: 223–226
- Royland JE, Konat G, Wiggins RC. Abnormal upregulation of myelin genes underlies the critical period of myelination in undernourished developing rat brain. *Brain Res* 1993; 607: 113–116
- Royland JE, Konat GW, Wiggins RC. Myelin gene activation: a glucose sensitive critical period in development. *J Neurosci Res* 1993; 36: 399–404
- Russell JW, Chen H-L, Golovoy D. Insuline-like growth factor-1 promotes myelination of peripheral sensory axons. *J Neuropathol Exp Neurol* 2000; 59: 575–584
- Saito M, Yu RK. Role of myelin-associated neuraminidase in the ganglioside metabolism of rat brain myelin. *J Neurochem* 1992; 58: 83–87
- Schousboe A, Westergaard N, Waagepetersen HS, Larsson OM, Bakken IJ, Sonnewald U. Trafficking between glia and neurons of TCA cycle intermediates and related metabolites. *Glia* 1997; 21: 99–105
- Seitelberger F. Structural manifestations of leukodystrophies. *Neuropediatrics* 1984; 15 (suppl): 53–61
- Shine HD, Readhead C, Popko B, Hood L, Sidman RL. Morphometric analysis of normal, mutant, and transgenic CNS: correlation of myelin basic protein expression to myelinogenesis. *J Neurochem* 1992; 58: 342–349
- Sinoway MP, Kitagawa K, Timsit S, Hashim GA, Colman DR. Proteolipid protein interactions in transfectants: implications for myelin assembly. *J Neurosci Res* 1994; 37: 551–562
- Skoff RP. Neuroglia: a reevaluation of their origin and development. *Pathol Res Pract* 1980; 168: 279–300
- Smith R. The basic protein of CNS myelin: its structure and ligand binding. *J Neurochem* 1992; 59: 1589–1608
- Stevens B, Porta S, Haak LL, Gallo V, Fields RD. Adenosine: a neuron-glial transmitter promoting myelination in the CNS in response to action potentials. *Neuron* 2002; 36: 855–868
- Stryer L. Introduction to biological membranes. In: Stryer L, ed. *Biochemistry*, 2nd ed. New York: Freeman, 1981, 205–230
- Svennerholm L. Some aspects of the biochemical changes in leukodystrophy. In: Folch PJ, Bauer H, eds. *Brain lipids and lipoproteins and the leukodystrophies*. Amsterdam: Elsevier, 1963, 104–119
- van der Knaap MS, Valk J, Bakker CJ, Schooneveld M, Faber JAJ, Willemse J, Gooskens PHJM. Myelination as expression of the functional maturity of the brain. *Dev Med Child Neurol* 1991; 33: 849–857
- Vinore SA, Herman MM. Phagocytosis of myelin by astrocytes in explants of adult rabbit cerebral white matter maintained on Gelfoam matrix. *J Neuroimmunol* 1993; 43: 169–176
- Vogel US, Thompson RJ. Molecular structure, localization, and possible functions of the myelin-associated enzyme 2',3'-cyclic nucleotide 3'-phosphodiesterase. *J Neurochem* 1988; 50: 1667–1677
- Vogt O. Quelques considérations générales sur la myélo-architecture du lobe frontal. *Rev Neurol* 1910; 20: 405–420
- Vourc'h P, Andres C. Oligodendrocyte myelin glycoprotein (OMgp): evolution, structure and function. *Brain Res Rev* 2004; 45: 115–124
- Waxman SG, Ritchie JM. Molecular dissection of the myelinated axon. *Ann Neurol* 1993; 33: 121–136
- Waxman SG, Sims TJ. Specificity in central myelination: evidence for local regulation of myelin thickness. *Brain Res* 1984; 292: 179–185
- Waxman AG, Black JA, Sontheimer H, Kocsis JD. Glial cells and axo-glial interactions: implications for demyelinating disorders. *Clin Neurosci* 1994; 2: 202–210
- Weimbs T, Stoffel W. Proteolipid protein (PLP) of CNS myelin: positions of free, disulfide-bonded and fatty acid thioester-linked cysteine residues and implications for the membrane topology of PLP. *Biochemistry* 1992; 31: 12289–12296
- Wiggins RC. Myelination: a critical stage in development. *Neurotoxicology* 1986; 7: 103–120
- Williams KA, Deber CM. The structure and function of central nervous system myelin. *Crit Rev Clin Lab Sci* 1993; 30: 29–64
- Wisniewski KE, Schmidt-Sidor B. Postnatal delay of myelin formation in brains from Down syndrome infants and children. *Clin Neuropathol* 1989; 8: 55–62
- Wood PM, Bunge RP. The origin of remyelinating cells in the adult central nervous system: the role of the mature oligodendrocyte. *Glia* 1991; 4: 225–232
- Yakovlev PI, Lecours AR. The myelogenetic cycles of regional maturation of the brain. In: Minkowski A, ed. *Regional development of the brain in early life*. Oxford: Blackwell, 1967: 3–70
- Yamamoto Y, Yoshikawa H, Nagano S, Kondoh G, Sadahiro S, Gotow T, Yanagihara T, Sakoda S. Myelin-associated oligodendrocyte basic protein is essential for normal arrangement of the radial component in central nervous system myelin. *Eur J Neurosci* 1999; 11: 847–855
- Ye P, Carlson J, D'Ercole AJ. Insuline-like growth factor-I influences the initiation of myelination: studies of the anterior commissure of transgenic mice. *Neurosci Lett* 1995; 201: 235–238
- Zurbruggen A, Vandevelde M, Steck A, Angst B. Myelin-associated glycoprotein is produced before myelin basic protein in cultured oligodendrocytes. *J Neuroimmunol* 1984; 6: 41–49

2 Classification of Myelin Disorders

- Adams RD, Kubik CS. The morbid anatomy of the demyelinating diseases. *Am J Med* 1952; 12: 510–546
- Adams RD, Richardson EP. The demyelinating diseases of the human nervous system. In: Folch P, Folch J, eds. *Chemical pathology of the nervous system*. Oxford: Pergamon Press, 1961: 162–194
- Alzheimer A. Beiträge zur Kenntnis der pathologischen Neuroglia und ihrer Beziehungen zu den Abbauvorgängen im Nervengewebe. *Nissl-Alzheimer Arbeiten* 1910; 3: 401–562

- Austin J, McAfee D, Armstrong D, O'Rourke M, Shearer L, Bachhawatt B. Low sulfatase activities in metachromatic leukodystrophy. *Trans Am Neurol Assoc J* 1964;147:150
- Bérard-Badier M, Paillas JE, Gastaut H, Edgar GWF. Essai sur la signification des démyélinisations dans l'idiotie amaurotique infantile. *Psychiatr Neurol* 1958; 132: 50–93
- Bielschowsky M, Henneberg R. Ueber familiäre diffuse Sklerose (leukodystrophie cerebralis progressiva hereditaria) *J Psychol Neurol* 1928; 36: 131–181
- Blackwood W. The histological classification of diffuse demyelinating cerebral sclerosis. In: *Cerebral lipidosis, a symposium*. Oxford: Blackwell Scientific Publications, 1957: 1–10
- Carswell R. Pathological anatomy: illustrations of the elementary forms of disease. London: Longmans, Green, 1938
- Challa VR. White matter lesions in MR imaging of elderly subjects. *Radiology* 1987; 164: 874–875
- Charcot JM. Lectures on the diseases of the nervous system, vol. 3. London: New Sydenham Society, 1868 (Lectures delivered in 1868, English translation published in 1877)
- Cruveilhier J. Anatomie pathologique du corps humain, vol II, fasc XXXII. Paris: Baillière, 1835–1842
- Davison AN, Dobbing J. Myelination as vulnerable period in brain development. *Br Med Bull* 1966; 20: 40–44
- Diezel PB. Histochemische Untersuchungen an den Globoidzellen der familiären infantilen diffusen Sklerose vom Typus Krabbe. *Virchows Arch Pathol Anat* 1955; 327: 206–228
- Edgar GWF. Approche biochimique des lipidoses et des leukodystrophies. *Rev Neurol* 1955; 92: 277–284
- Fardeau M, Lapresle J. Maladie de Tay-Sachs avec atteinte importante de la substance blanche. A propos de deux observations anatomo-cliniques. *Rev Neurol* 1963; 109: 157–175
- Foelling A. Ueber Ausscheidung von Phenylbrenztraubensäure in den Harn als Stoffwechselanomalie in Verbindung mit Imbezilität. *Z Physiol Chem* 1934; 227: 169–176
- George AE, de Leon MJ, Gentes CI, Miller J, London E, Budzilovich GN, Ferris S, Chase N. Leukoencephalopathy in normal and pathologic aging: CT of brain lucencies. *AJNR Am J Neuroradiol* 1986; 7: 561–566
- Gupta SR, Naheedy MH, Young JC, Ghobrial M, Rubino FA, Hinde W. Periventricular white matter changes and dementia. Clinical, neuropsychological, radiological and pathological correlation. *Arch Neurol* 1988; 45: 637–641
- Hallervorden J. Die zentralen Entmarkungskrankheiten. *Dtsch Z Nervenheilk* 1940; 150: 201–239
- Hauw JJ, Delaère P, Seilhean D, Cornu P. Morphology of demyelination in the human central nervous system. *J Neuroimmunol* 1992; 40: 139–152
- Herschkowitz N, Schulte FJ. The lipidoses: from detect to dysfunction. *Neuropediatrics* 1984; 15: 110–111
- Heubner O. Ueber diffuse Hirnsklerose. *Charité-Ann* 1897; 22: 298–310
- Huk WJ, Bydder GM, Curati WL. Degenerative disorders of the brain and white matter diseases. In: Huk WJ, Gademann G, Friedmann G, eds. *Magnetic resonance imaging of central nervous system diseases*. Berlin: Springer, 1990: 197–224
- Jervis GA. Studies on phenylpyruvic oligofrenia: the position of the metabolic error. *J Biol Chem* 1947; 169: 651–656
- Johnson MA, Pennock JM, Bydder GM, Steiner RE, Thomas DJ, Hayward R, Bryant DRT, Payne JA, Levene MI, Whitelaw A, Dubowitz LMS, Dubowitz V. Clinical NMR imaging of the brain in children: normal and neurologic disease. *AJR Am J Roentgenol* 1983; 141: 1005–1018
- Krabbe K. A new familial infantile form of diffuse brain-sclerosis. *Brain* 1916; 39: 74–114
- Lassmann H, Ammerer HP, Kulnig W. Ultrastructural sequence of myelin degradation. Wallerian degeneration in the rat optic nerve. *Acta Neuropathol (Berl)* 1978; 44: 91–102
- Matthieu JM. An introduction to the molecular basis of inherited myelin diseases. *J Inher Metab Dis* 1993; 16: 724–732
- Menkes JH. The leukodystrophies. *N Engl J Med* 1990; 322: 54–55
- Merzbacher L. Eine eigenartige familiär-hereditäre Erkrankungsform (aplasia axialis extracorticalis congenita). *Z Gesamte Neurol Psychiatrie* 1910; 3: 1–138
- Morell P, Wiesmann U. A correlative synopsis of the leukodystrophies. *Neuropediatrics* 1984; 15 (suppl): 62–65
- Neubürger K. Histologisches zur Frage der diffusen Hirnsklerose. *Z Gesamte Neurol Psychiatrie* 1921; 73: 336–352
- Peiffer J. Differentiation of various types of leukodystrophy. *World Neurology* 1962; 3: 580–597
- Pelizaes F. Ueber eine eigenartige familiäre Entwicklungshemmung vornehmlich auf motorischem Gebiet. *Arch Psychiatrie Nervenkr* 1899; 31: 100–104
- Poser CM. Discussion des rapports sur les maladies demyelinisantes. *Proc Third Intern Congr Neuropathol. Brussels. Editions Acta Medica Belgica* 1957, 106–111
- Poser CM. Leukodystrophy and the concept of dysmyelination. *Arch Neurol* 1961; 4: 323–332
- Poser CM. Dysmyelination revisited. *Arch Neurol* 1978; 35: 401–407
- Poser CM. The dysmyelinating diseases. In: Baker AB, Joynt RJ, eds. *Clinical neurology*, vol 3. Philadelphia: Harper & Row, 1987: chap 34
- Raine CS. The neuropathology of myelin diseases. In: Morell P, ed. *Myelin*, 2nd ed. New York: Plenum Press, 1984, 259–310
- Ranvier L-A (1878) *Leçons sur l'histologie du système nerveux* (2 vol.). Weber E. ed. Paris: Savy
- Schilder P. Zur Kenntnis der sogenannten diffusen Sklerose. Ueber Encephalitis periaxialis diffusa. *Z Gesamte Neurol Psychiatrie* 1912; 10, 1–60
- Scholz W. Klinische, pathologisch-anatomische und erbbiologische Untersuchungen bei familiärer, diffuser Hirnsklerose im Kindesalter. *Z Gesamte Neurol Psychiatrie* 1925; 99: 651–717
- Seitelberger F. Structural manifestations of leukodystrophies. *Neuropediatrics* 1984; 15 (suppl): 53–61
- Stam FC, Heslinga JM, Deierkauf FA, Booi HL. Leukodystrophy of the Norman-Greenfield and Krabbe type. *Psychiatry Neurol Neurosurg* 1962; 65: 254–265
- Stam FC. Concept, classification and nosology of the leukodystrophies. In: Vinken PJ, Bruyn GW, eds. *Handbook of clinical neurology*, vol 10. Amsterdam: North Holland Publishing Company, 1970, 1–42
- Suzuki K, Suzuki Y. Globoid cell leukodystrophy (Krabbe's disease): deficiency of galactocerebroside beta-galactosidase. *Proc Natl Acad Sci* 1970; 66: 302–309
- Thieffry S, Bertrand I, Bargeton E, Edgar GWF, Arthuis M. Idiotie amaurotique infantile avec altérations graves de la substance blanche. *Rev Neurol* 1960; 102: 130–152
- Virchow R. Ueber das ausgebreitete Vorkommen einer dem Nervenmark analogen Substanz in den tierischen Geweben. *Virchows Arch Pathol Anat* 1854; 562–572
- Von Hirsch T, Peiffer J. Ueber histologische Methoden in der Differentialdiagnose von Leukodystrophien und Lipidosen. *Arch Psychiatrie Z Neurol* 1955; 194: 88–104
- Von Hirsch T, Peiffer J. A histochemical study of the pre-lipid and metachromatic degenerative products in leukodystrophy. In: *Cerebral lipidoses, a symposium*. Oxford: Blackwell Scientific Publications, 1957, 68–76

3 Selective Vulnerability

- Albin RL. Basal ganglia neurotoxins. *Neurol Clin* 2000; 18: 665–680
- Barboriak DP, Provenzale JM, Boyko OB. MR diagnosis of Creutzfeldt-Jakob disease: significance of high signal intensity of the basal ganglia. *AJR Am J Roentgenol* 1994; 162: 137–140
- Davison AN, Dobbing J. Myelination as a vulnerable period in brain development. *Br Med Bull* 1966; 22: 40–44
- Dubeau F, De Stefano N, Zifkin BG, Arnold DL, Shoubbridge EA. Oxidative phosphorylation defect in the brains of carriers of the tRNA^{Leu}(UUR) A3243G mutation in a MELAS pedigree. *Ann Neurol* 2000; 47: 179–185
- Gosztonyi G, Koprowski H. The concept of neurotropism and selective vulnerability ("pathoclosis") in virus infections of the nervous system- a historical overview. *Curr Top Microbiol Immunol* 2001; 253: 1–13
- Gosztonyi G, Koprowski H. The concept of neuropotism and selective vulnerability ("pathoclosis") in virus infections of the nervous system – a historical overview. *Curr Top Microbiol Immunol* 2001; 253: 1–13
- Govaert P, Lequin M, Swarte R, Robben S, de Coo R, Weisglas-Kuperus N, de Rijke Y, Sinaasappel M, Barkovich J. Changes in globus pallidus with (pre)term kernicterus. *Pediatrics* 2003; 112: 1256–1263
- Guentchev M, Wanschitz J, Voigtlander T, Flicker H, Badka H. Selective neuronal vulnerability in human prion diseases. Fatal familial insomnia differs from other types of prion diseases. *Am J Pathol* 1999; 155: 1453–1457
- Hawker K, Lang AE. Hypoxic-ischemic damage of the basal ganglia. *Mov Disord* 1990; 5: 219–224
- Johnston MV, Goldstein GW. Selective vulnerability of the developing brain to lead. *Curr Opin Neurol* 1998; 11: 689–693
- Johnston MV, Hoon AH. Possible mechanisms in infants for selective basal ganglia damage from asphyxia, kernicterus or mitochondrial encephalopathies. *J Child Neurol* 2000; 15: 588–591
- Kodama T, Numaguchi Y, Gellad FE, Dwyer BA, Kristt DA. Magnetic resonance imaging of limbic encephalitis. *Neuroradiology* 1991; 33: 520–523
- Kölker S, Kohr G, Ahlemeyer B, Okun JG, Pawlak V, Horster F, Mayatepek E, Kriegelstein J, Hoffmann GF. Ca²⁺ and Na⁺ dependence of 3-hydroxyglutarate-induced excitotoxicity in primary neuronal cultures from chick embryo telencephalons. *Pediatr Res* 2002; 52: 199–206
- Kölker S, Mayatepek E, Hoffmann GF. White matter disease in cerebral organic acid disorders: clinical implications and suggested pathomechanisms. *Neuropediatrics* 2002; 33: 225–231
- Lipton SA, Rosenberg PA. Excitatory amino acids as a final common pathway for neurologic disorders. *N Engl J Med* 1994; 330: 613–622
- Ludolph AC, Riepe M, Ullrich K. Excitotoxicity, energy metabolism and neurodegeneration. *J Inher Metab Dis* 1993; 16: 716–723
- McCann UD, Szabo Z, Scheffel U, Dannals RF, Ricaurte GA. Positron emission tomography evidence of toxic effect of MDMA (ecstasy) on brain serotonin neurons in human beings. *Lancet* 1998; 352: 1433–1437
- Meyer A. Section of psychiatry. The selective regional vulnerability of the brain and its relation to psychiatric problems. *Proc R Soc Med* 1936; 29: 1175–1181
- Okun JG, Horster F, Farkas LM, feyh P, Hinz A, Sauer S, Hoffmann GF, Unsicker K, Mayatepek E, Kolker S. Neurodegeneration in methylmalonic aciduria involves inhibition of complex II and the tricarboxylic acid cycle, and synergistically acting excitotoxicity. *J Biol Chem* 2002; 277: 14674–14680
- Pasternak JF, Predey TA, Mikhael MA. Neonatal asphyxia: vulnerability of basal ganglia, thalamus, and brainstem. *Pediatr Neurol* 1991; 7: 147–149
- Pulsinelli WA. Selective neuronal vulnerability: morphological and molecular characteristics. *Prog Brain Res* 1985; 63: 29–37
- Reneman L, Majoie CB, Habraken JB, Den Heeten GJ. Effects of ecstasy (MDMA) on the brain in abstinent users; initial observations with diffusion and perfusion MR imaging. *Radiology* 2001; 220: 611–617
- Reneman L, Majoie CBLM, Flick H, den Heeten GJ. Reduced N-acetyl aspartate levels in the frontal cortex of 3,4-methylenedioxymetamphetamine (ecstasy) users: preliminary results. *AJNR Am J Neuroradiol* 2002; 23: 231–237
- Ricaurte GA, Yuan J, Hatzidimitriou G, Cord BJ, McCann UD. Severe dopaminergic neurotoxicity in primates after a common recreational dose regimen of MDMA ("ecstasy"). *Science* 2002; 297: 2260–2263
- Schmidt R, Offenbacher H, Fazekas F, Payer F, Kleinert R, Porsch G. Magnetic resonance imaging, computed tomography, and autopsy findings after cardiorespiratory arrest. *J Neuroimaging* 1991; 1: 197–199
- Scholz W. Selective neuronal necrosis and its topistic patterns in hypoxemia and oligemia. *J Neuropathol Exp Neurol* 1953; 12: 249–261
- Scholz W. Topistic lesions. In: Schädé JP, McMenemey WH, eds. *Selective vulnerability of the brain in hypoxaemia*. Oxford: Blackwell Scientific Publications, 1963: 257–267
- Sims NR. Energy metabolism and selective neuronal vulnerability following global cerebral ischemia. *Neurochem Res* 1992; 17: 923–931
- Spielmeyer W. Zur Pathogenese örtlicher elektiver Gehirnveränderungen. *Z Neurol Psychiatrie* 1925; 99: 756–777
- Suzuki H, Takanashi J, Saeki N, Kohno Y. Temporal parental nutrition in children causing T1 shortening in the anterior pituitary gland and globus pallidus. *Neuropediatrics* 2003; 34: 200–204
- Tarasów E, Panasiuk A, Siemieńczyk L, Orzechowska-Bobkiewicz A, Lewszuk A, Waleck J, Porkopowicz D. MR and ¹H MR spectroscopy of the brain in patients with liver cirrhosis and early stages of hepatic encephalopathy. *Hepatogastroenterology* 2003; 50: 2149–2153
- Valk J. Selective involvement of CNS structures in pediatric neuroradiology. *Riv Neuroradiol* 1993; 6: 3–10
- Valk J, van der Knaap MS. Selective vulnerability in toxic encephalopathies and metabolic disorders. *Riv Neuroradiol* 1996; 9: 749–760
- Vogt C, Vogt O. Sitz und Wesen der Krankheiten im Licht der topistischen Hirnforschung und des Variierens der Tiere. *J Psychol Neurol* 1937; 47: 237–457
- Yamada M, Inaba A, Yamawaki M, Ishida K, Yokota T, Uchiyama T, Eishi Y, Okeda R. Paraneoplastic encephalo-myelo-ganglionitis: cellular binding sites of the antineuronal antibody. *Acta Neuropathol (Berl)* 1994; 88: 85–92

4 Myelination and Retarded Myelination

- Ajayi-Obe M, Saeed N, Cowan FM, Rutherford MA, Edwards AD. Reduced development of cerebral cortex in extremely preterm infants. *Lancet* 2000; 356: 1162–1163
- Autti T, Raininko R, Vanhanen SL, Kallio M, Santavuori P. MRI of the normal brain from early childhood to middle age. II. Age dependence of signal intensity of T2-weighted images. *Neuroradiology* 1994; 36: 649–651
- Ball WS Jr. Imaging of the brain in children. *Curr Opin Radiol* 1991; 3: 895–905
- Barkovich AJ, Kjos BO, Jackson DE, Norman D. Normal maturation of the neonatal and infant brain: MR imaging at 1.5T¹. *Radiology* 1988; 166: 173–180
- Barkovich AJ, Gressens P, Evrard P. Formation, maturation, and disorders of brain neocortex. *AJNR Am J Neuroradiol* 1992; 13: 423–446
- Barkovich AJ. Concepts of myelin and myelination in neuro-radiology 2000; 21: 1099–1109
- Battin MR, Maalouf EF, Counsell SJ, Herlihy AH, Rutherford MA, Azzopardi D, Edwards AD. Magnetic resonance imaging of brain in very preterm infants: visualization of the germinal matrix, early myelination, and cortical folding. *Pediatrics* 1998; 101: 957–962
- Benes FM, Turtle M, Khan Y, Farol P. Myelination of a key relay zone in the hippocampal formation occurs in the human brain during childhood, adolescence, and adulthood. *Arch Gen Psychiatry* 1994; 51: 477–484
- Blaser S, Harwood-Nash DCF. Radiology of the developing central nervous system. *Curr Opin Neurol Neurosurg* 1992; 5: 843–848
- Breger RK, Yetkin FZ, Fisher ME, Papke RA, Haughton VM, Rimm AA. T₁ and T₂ in the cerebrum: correlation with age, gender, and demographic factors. *Radiology* 1991; 181: 545–547
- Chi JG, Dooling EC, Gilles FH. Gyral development of the human brain. *Ann Neurol* 1977; 1: 86–93
- Childs AM, Remenghi LA, Evans DJ, Ridgeway J, Saysell M, Martinez D, Arthur R, Tanner S, Levene MI. MR features of developing periventricular white matter in preterm infants: evidence of glial cell migration. *AJNR Am J Neuroradiol* 1998; 19: 971–976
- Childs AM, Ramenghi LA, Cornette L, Tanner SF, Arthur RJ, Martinez D, Levene MI. Cerebral maturation in premature infants: quantitative assessment using MR imaging. *AJNR Am J Neuroradiol* 2001; 22: 1577–1582
- Counsell SJ, Maalouf EF, Fletcher AM, Duggan P, Battin M, Lewis HJ, Herlihy AH, Edwards D, Bydder GM, Rutherford MA. MR imaging assessment of myelination in the very preterm brain. *AJNR Am J Neuroradiol* 2002; 23: 872–881
- Counsell SJ, Kennea NL, Herlihy AH, Allsop JM, Harrison MC, Cowan FM, Hajnal JV, Edwards B, Edwards AD, Rutherford MA. T2 relaxation values in the developing preterm brain. *AJNR Am J Neuroradiol* 2003; 24: 1654–1660
- Dietrich RB, Badley WG, Zaragoza EJ IV, Otto RJ, Taira RK, Wilson GH, Kangaroo H. MR evaluation of early myelination patterns in normal and developmentally delayed infants. *AJNR Am J Neuroradiol* 1988; 9: 69–76
- Dooling EC, Chi JG, Gilles FH. Telencephalic development: changing gyral patterns. In: Gilles FH, Leviton A, Dooling EC. *The developing human brain. Growth and epidemiologic neuropathology*. Boston: John Wright, 1983: 94–104
- Duprez T, Ghaniani S, Smith AM, Gadisseux JF, Evrard P. Focal seizure-induced premature myelination: speculation from serial MRI. *Neuroradiology* 1998; 40: 580–582
- Engelbrecht V, Malms J, Kahn T, Grünwald S, Mödder U. Fast spin-echo MR imaging of the pediatric brain. *Pediatr Radiol* 1996; 26: 259–264
- Engelbrecht V, Rassek M, Preiss S, Wald C, Mödder U. Age-dependent changes in magnetization transfer contrast of white matter in the pediatric brain. *AJNR Am J Neuroradiol* 1998; 19: 1923–1929
- Engelbrecht V, Scherer A, Rassek M, Witsack HJ, Mödder U. Diffusion-weighted MR imaging in the brain in children: findings in the normal brain and in the brain with white matter diseases. *Radiology* 2002; 222: 410–418
- Ferrie JC, Barantin L, Saliba E, Akoka S, Tranquart F, Sirinelli D, Pourcelot L. MR assessment of the brain maturation during the perinatal period: quantitative t2 MR study in premature newborns. *Magn Reson Imaging* 1999; 17: 1275–1288
- Finelli DA, Hurst GC, Amantia P Jr, Gullapali RP, Apicella A. Cerebral white matter: technical development and clinical applications of effective magnetization transfer (MT) power concepts for high-power transfer, thin-section, quantitative MT examinations. *Radiology* 1996; 199: 219–226
- Flechsich P. Anatomie des menschlichen Gehirns und Rückenmarks auf myelogenetischer Grundlage. Leipzig: Georg Thieme, 1920
- Forbes KPN, Pipe JG, Bird CR. Changes in brain water diffusion during the 1st year of life. *Radiology* 2002; 222: 405–409
- Garel C, Chantrel E, Brisse H, Elmaleh M, Luton D, Oury JF, Sebarg G, Hassan M. Fetal cerebral cortex: normal gestational landmarks identified using prenatal MR imaging. *AJNR Am J Neuroradiol* 2001; 22: 184–189
- Ge Y, Grossman RI, Babb JS, Rabin ML, Mannon LJ, Kolson DL. Age-related total gray matter and white matter changes in normal adult brain. Part I: volumetric MR imaging analysis. *AJNR Am J Neuroradiol* 2002; 23: 1327–1333
- Ge Y, Grossmann RI, Babb JS, Rabin ML, Mannon LJ, Kolson DL. Age-related total gray matter and white matter changes in normal adult brain. Part II: Quantitative magnetization transfer ratio histogram analysis. *AJNR Am J Neuroradiol* 2002; 23: 1334–1341
- Girard N, Raybaud C, du Lac P. Étude de la myélinisation cérébrale en IRM. MRI study of brain myelination. *J Neuro-radiol* 1991; 18: 291–307
- Hansen PE, Ballesteros MC, Soila K, Garcia L, Howard JM. MR imaging of the developing human brain. Part 1: prenatal development. *Radiographics* 1993; 13: 21–36
- Hittmair K, Wimberger D, Rand T, Prayer L, Bernert G, Kramer J, Imhof H. MR assessment of brain maturation: comparison of sequences. *AJNR Am J Neuroradiol* 1994; 15: 425–433
- Hittmair K, Kramer J, Rand T, Bernert G, Wimberger D. Infratentorial brain maturation: a comparison of MRI at 0.5 and 1.5 T. *Neuroradiology* 1996; 38: 360–366
- Holland BA, Haas DK, Norman D, Brant-Zawadski M, Newton TH. MRI of normal brain maturation. *AJNR Am J Neuroradiol* 1986; 7: 201–208
- Hosoya T, Adachi M, Yamaguchi K, Haku T. MRI anatomy of white matter layers around the trigone of the lateral ventricle. *Neuroradiology* 1998; 40: 477–482
- Huisman TAGM, Wissner J, Martin E, Kubik-Huch R, Marineck B. Fetal magnetic resonance imaging of the central nervous system: a pictorial essay. *Eur Radiol* 2002; 12: 1952–1261
- Hüppi PS, Maier SE, Peled S, Zientara GP, Barnes PD, Jolenz FA, Volpe JJ. Microstructural development of human in assessed in vivo by diffusion tensor magnetic resonance imaging. *Pediatr Res* 1998; 44: 584–590

- Hüppi PS, Warfield S, Kikinis R, Barnes PD, Zientara GP, Jolensz FA, Tsuij MK, Volpe JJ. Quantitative magnetic resonance imaging of brain development in premature and mature newborns. *Ann Neurol* 1998; 43: 224–235
- Johnson MA, Pennock JM, Bydder GM, Steiner RE, Thomas DJ, Hayward R, Bryant DRT, Payne JA, Levene MI, Whitelay A, Dubowitz LMS, Dubowitz V. Clinical NMR imaging of the brain in children: normal and neurologic disease. *AJNR Am J Neuroradiol* 1983; 4: 1013–1025
- Jolensz FA, Polak JF, Adams DF, Ruenzel PW. Myelinated and nonmyelinated nerves: comparison of proton MR properties. *Radiology* 1987; 164: 89–91
- Jones RA, Palasis S, Grattan-Smith JD. The evolution of the apparent diffusion coefficient in the pediatric brain at low and high diffusion weightings. *J Magn Reson Imaging* 2003; 18: 665–674
- Keene MFL, Hewer EE. Some observations on myelination in the human nervous system. *J Anat* 1931; 6: 1–13
- Korogi Y, Takahashi M, Sumi M, Hirai T, Sakamoto Y, Ikushima I, Miyayama H. MR signal intensity of the perirolandic cortex in the neonate and infant. *Neuroradiology* 1996; 38: 578–584
- Krier EL, Truwit CL. The normal and abnormal genu of the corpus callosum: an evolutionary, embryologic, anatomic, and MR analysis. *AJNR Am J Neuroradiol* 1996; 17: 1631–1641
- Lövblad KO, Schneider J, Ruoss K, Steinlin M, Fusch C, Schroth G. Isotropic apparent diffusion coefficient mapping of postnatal cerebral development. *Neuroradiology* 2003; 45: 400–403
- Martin E, Kikinis R, Zuerrer M, Boesch C, Briner J, Krewitz G, Kaelin P. Developmental stages of human brain: an MR study. *J Comput Assist Tomogr* 1988; 12: 917–922
- Martin E, Boesch C, Zuerrer M, Kikinis R, Molinari L, Kealin P, Boltshauser E, Duc G. MR imaging of brain maturation in normal and developmentally handicapped children. *J Comput Assist Tomogr* 1990; 14: 685–692
- Martin E, Krassnitzer S, Kealin P, Boesch Ch. MR imaging of the brainstem: normal postnatal development. *Neuroradiology* 1991; 33: 391–395
- McArdle CB, Richardson CJ, Nicholas DA, Mirfakhraee M, Hayden CK, Amparo EG. Developmental features of the neonatal brain: MR imaging. 1. Gray-white matter differentiation and myelination. *Radiology* 1987; 162: 223–229
- Miller SP, Vigneron DB, Henry RG, Bohland MA, Ceppi-Cozzio C, Hoffman C, Newton N, Partridge JC, Ferriero DM, Barkovich AJ. Serial quantitative diffusion tensor MRI of the premature brain: development in newborns with and without injury. *J Magn Reson Imaging* 2002; 16: 621–632
- Mukherjee P, Miller JH, Lee BCP, Almlí CR, McKinstry RC. Normal brain maturation during childhood: developmental trends characterized with diffusion tensor MR imaging. *Radiology* 2001; 221: 349–358
- Mukherjee P, Miller JH, Shimony JS, Philip JV, Nehra D, Snyder AZ, Conturo TE, Neil JJ, McKinstry RC. Diffusion-tensor MR imaging of gray and white matter development during normal brain maturation. *AJNR Am J Neuroradiol* 2002; 23: 1445–1456
- Murakami JW, Weinberger E, Shaw DWW. Normal myelination of the pediatric brain imaged with fluid-attenuated inversion-recovery (FLAIR) MR imaging. *AJNR Am J Neuroradiol* 1999; 20: 1406–1411
- Naidich TP, Grant JL, Altman N, Zimmerman RA, Birchansky SB, Braffman B, Daniel JL. The developing cerebral surface. Preliminary report on the patterns of sulcal and gyral maturation – anatomy, ultrasound, and magnetic resonance imaging. *Pediatr Neuroradiol* 1994; 4: 201–239
- Naidich TP, Grant JL, Altman N, Zimmerman RA, Birchansky SB, Braffman BM, Daniel JL. The developing cerebral surface. *Neuroimaging Clin N Am* 1994; 4: 201–240
- Neill JJ, Shiran SI, McKinstry RC, Scheffé GL, Snyder AZ, Almlí CR, Akbubak E, Aronovitz JA, Miller JP, Lee BCP, Conturo TE. Normal brain in human newborns: apparent diffusion coefficient and diffusion anisotropy measured by using diffusion tensor MR imaging. *Radiology* 1998; 209: 57–66
- Parazzini C, Baldoli C, Scotti G, Triulzi F. Terminal zones of myelination: MR evaluation of children aged 20–40 months. *AJNR Am J Neuroradiol* 2002; 23: 1669–1673
- Pennock JM, Bydder GM, Dubowitz LMS, Johnson MA. Magnetic resonance imaging of the brain in children. *Magn Reson Imaging* 1986; 4: 1–9
- Rademacher J, Engelbrecht V, Bürgel U, Freund H-J, Zilles K. Measuring in vivo myelination of human white matter fiber tracts with magnetization transfer MR. *Neuroimage* 1999; 9: 393–406
- Robertson RL, Robson CD. Diffusion imaging in neonates. *Neuroimaging Clin N Am* 2002; 12: 55–70
- Ruoss K, Lövblad K, Schroth G, Moessinger AC, Fusch C. Brain development (sulci and gyri) as assessed by early postnatal MR imaging in preterm and term newborn infants. *Neuropediatrics* 2001; 32: 69–74
- Schmithorst VJ, Wilke M, Dardzinski BJ, Holland SK. Correlation of white matter diffusivity and anisotropy with age during childhood and adolescence: a cross-sectional diffusion-tensor MR imaging study. *Radiology* 2002; 222: 212–218
- Schneider JFL, Il'yasov KA, Hennig J, Martin E. Fast quantitative diffusion-tensor imaging of cerebral white matter from the neonatal period to adolescence. *Neuroradiology* 2004; 46: 258–266
- Shaw DWW, Weinberger E, Astley SJ, Tsuruda JS. Quantitative comparison of conventional spin echo and fast spin echo during brain myelination. *J Comput Assist Tomogr* 1997; 21: 867–871
- Sie LT, van der Knaap MS, van Wezel-Meijler G, Valk J. MRI assessment of myelination of motor and sensory pathways in the brain of preterm and term-born infants. *Neuropediatrics* 1997; 28: 97–105
- Sie LT, Barkhof F, Lefeber HN, Valk J, van der Knaap MS. Value of fluid-attenuated inversion recovery sequences in early MRI of the brain in neonates with a perinatal hypoxic-ischemic encephalopathy. *Eur Radiol* 2000; 10: 1594–1601
- Stricker T, Martin E, Boesch C. Development of the human cerebellum observed with high-field-strength MR imaging. *Radiology* 1990; 177: 431–435
- Takeda K, Nomura Y, Sakuma H, Tagami T, Okuda Y, Nakagawa T. MR assessment of normal brain development in neonates and infants: comparative study of T1- and diffusion-weighted images. *J Comput Assist Tomogr* 1997; 21: 1–7
- Tanner SF, Ramenghi LA, Ridgway JP, Berry E, Saysell MA, Martinez D, Arthur RJ, Smith MA, Levene MI. Quantitative comparison of intrabrain diffusion in adults and preterm and term neonates and infants. *AJR A J Roentgenol* 2000; 174: 1643–1649
- Toft PB, Leth H, Peitersen B, Lou HC, Thomson C. The apparent diffusion coefficient of water in gray and white matter of the infant brain. *J Comput Assist Tomogr* 1996; 20: 1006–1011
- Van Buchem MA, Steens SCA, Vrooman HA, Zwinderman AH, McGowan JC, Rassek M, Engelbrecht V. Global estimation of myelination in the developing brain on the basis of magnetization transfer imaging: a preliminary study. *AJNR Am J Neuroradiol* 2001; 22: 762–766

- van der Knaap MS, Valk J. MR imaging of the various stages of normal myelination during the first year of life. *Neuroradiology* 1990; 31: 459–470
- van der Knaap MS, van Wezel-Meijler G, Barth PG, Barkhof F, Ader H, Valk J. Normal gyration and sulcation in preterm and term neonates: appearance on MR images. *Radiology* 1996; 200: 389–396
- Wimberger DM, Roberts TP, Barkovich AJ, Prayer LM, Moseley ME, Kucharczyk J. Identification of 'premyelination' by diffusion-weighted MRI. *J Comput Assist Tomogr* 1995; 19: 28–33
- Yakovlev PI, Lecours AR. The myelogenetic cycles of regional maturation of the brain. In: Minkowski A, ed. *Regional development of the brain in early life*. Oxford: Blackwell, 1967: pp 3–70
- Zhai G, Lin W, Wilber KP, Gerig G, Gilmore JH. Comparison of regional white matter diffusion in healthy neonates and adults performed with a 3.0T head-only MR imaging unit. *Radiology* 2003; 229: 673–681
- Zilles K, Schleicher A, Langemann C, Amunts K, Morosan P, Palomero-Gallagher N, Schormann T, Mohlberg H, Bürgel U, Steinmetz H, Schlaug G, Roland PE. Quantitative analysis of sulci in the human cerebral cortex: development, regional heterogeneity, gender difference, asymmetry, intersubject variability and cortical architecture. *Hum Brain Map* 1997; 5: 218–221

5 Lysosomes and Lysosomal Disorders

- Cavalli V, Corti M, Gruenberg J. Endocytosis and signaling cascades: a close encounter. *Febs Lett* 2001; 498: 190–196
- Dierks T, Schmidt B, Borissenko LV, Peng J, Preusser A, Mariappan M, von Figura K. Multiple sulfatase deficiency is caused by mutations in the gene encoding the human C_{α} -formylglycine generating enzyme. *Cell* 2003; 113: 435–444.
- Gerasimenko JV, Gerasimenko OV, Petersen OH. Membrane repair: Ca^{2+} -elicited lysosomal exocytosis. *Curr Biol* 2001; 11: R971–R974
- Ghosh P, Dahms NM, Kornfeld S. Mannose 6-phosphate receptors: new twists in the tale. *Nat Rev* 2003; 4: 202–212
- Haltia M. The Neuronal Ceroid-Lipofuscinoses. *J Neuropathol Exp Neurol* 2003; 62: 1–13
- Mullins C, Bonifacino JS. The molecular machinery for lysosome biogenesis. *Bioessays* 2001; 23: 333–343
- Scriber CR, Beaudet AL, Sly WS, Valle D (eds). *The metabolic and molecular basis of inherited disease*. Lysosomal disorders. McGraw-Hill, New York, 8th ed., 2001: pp 3371–3896.

6 Metachromatic Leukodystrophy

- Arbour LT, Silver K, Hechtman P, Treacy EP, Coulter-Mackie MB. Variable onset of metachromatic leukodystrophy in a Vietnamese family. *Pediatr Neurol* 2000; 23: 173–176
- Aurebeck G, Osterberg K, Blaw M, Chou S, Nelson E. Electron microscopic observations on metachromatic leukodystrophy. *Arch Neurol* 1964; 11: 273–288
- Austin JH. Metachromatic form of diffuse cerebral sclerosis; diagnosis during life by urine sediment examination. *Neurology* 1957; 7: 415–426
- Barth ML, Fensom A, Harris A. The arylsulphatase A gene and molecular genetics of metachromatic leukodystrophy. *J Med Genet* 1994; 31: 663–666

- Bass NH, Witmer EJ, Dreifuss FE. A pedigree study of metachromatic leukodystrophy. *Neurology* 1970; 20: 52–62
- Baumann N, Masson M, Carreau V, Lefevre M, Herschkowitz N, Turpin JC. Adult forms of metachromatic leukodystrophy: clinical and biochemical approach. *Dev Neurosci* 1991; 13: 211–215
- Baumann N, Turpin JC, Lefevre M, Colsch B. Motor and psychocognitive types in adult metachromatic leukodystrophy: genotype-phenotype relationship? *J Physiol* 2002; 96: 301–306
- Berger J, Löschi B, Bernheimer H, Lugowska A, Tytki-Szymanska A, Gieselmann V, Molzer B. Occurrence, distribution, and phenotype of arylsulphatase A mutations in patients with metachromatic leukodystrophy. *Am J Med Genet* 1997; 69: 335–340
- Berger J, Gmach M, Mayr U, Molzer B, Bernheimer H. Coincidence of two novel arylsulphatase A alleles and mutation 459+1G>A within a family with metachromatic leukodystrophy: molecular basis of phenotypic heterogeneity. *Hum Mutat* 1999; 13: 61–68
- Cengiz N, Özbenli T, Onar M, Yildiz L, Erta OB. Adult metachromatic leukodystrophy: three cases with normal nerve conduction velocities in a family. *Acta Neurol Scand* 2002; 105: 454–457
- Clarke JTR, Skomorowski MA, Chang PL. Marked clinical difference between two sibs affected with juvenile metachromatic leukodystrophy. *Am J Med Genet* 1989; 33: 10–13
- Comabella M, Waye JS, Raguer N, Eng B, Domínguez C, Navarro C, Borrás C, Krivit W, Montalbán X. Late-onset metachromatic leukodystrophy clinically presenting as isolated peripheral neuropathy: compound heterozygosity for the IVS2+1G A mutation and a newly identified missense mutation (Thr408Ile) in a Spanish family. *Ann Neurol* 2001; 50: 108–112
- Consiglio A, Quattrini A, Martino S, Bensadoun JC, Dolcetta D, Trojani A, Benaglia G, Marchesini S, Cestari V, Oliverio A, Bordignon C, Naldini L. In vivo gene therapy of metachromatic leukodystrophy by lentiviral vectors: correction of neuropathology and protection against learning impairments in affected mice. *Nat Med* 2001; 7: 310–316
- Coulter-Mackie MB, Gagnier L. Two novel mutations in the arylsulphatase A gene associated with juvenile (R390Q) and adult onset (H397Y) metachromatic leukodystrophy. *Hum Mutat* 1998; suppl 1: S254–S256
- Dayan AD. Peripheral neuropathy of metachromatic leukodystrophy: observations on segmental demyelination and remyelination and the intracellular distribution of sulphatide. *J Neurol Neurosurg Psychiatry* 1967; 30: 311–318
- Faerber EN, Melvin JJ, Smergel EM. MRI appearances of metachromatic leukodystrophy. *Pediatr Radiol* 1999; 29: 669–672
- Felice KJ, Gomez Lira M, Natowicz M, Grunnet ML, Tsongalis GJ, Sima AAF, Kaplan RF. Adult-onset MLD: a gene mutation with isolated polyneuropathy. *Neurology* 2000; 55: 1036–1039
- Francis GS, Bonni A, Shen N, Hechtman P, Yamut B, Carpenter S, Karpati G, Chang PL. Metachromatic leukodystrophy: multiple nonfunctional and pseudodeficiency alleles in a pedigree: problems with diagnosis and counseling. *Ann Neurol* 1993; 34: 212–218
- Gieselmann V, von Figura K. Advances in the molecular genetics of metachromatic leukodystrophy. *J Inher Metab Dis* 1990; 13: 560–571
- Gieselmann V, Polten A, Kreysing J, von Figura K. Arylsulphatase A pseudodeficiency: loss of a polyadenylation signal and N-glycosylation site. *Proc Natl Acad Sci* 1989; 86: 9436–9440

- Gieselmann V, Fluharty AL, Tonnesen T, von Figura K. Mutations in the arylsulfatase A pseudodeficiency allele causing metachromatic leukodystrophy. *Am J Hum Genet* 1991; 49: 407–413
- Gieselmann V, Zlotogora J, Harris A, Wenger DA, Morris CP. Molecular genetics of metachromatic leukodystrophy. *Hum Mutat* 1994; 4: 233–242
- Gieselmann V, Polten A, Kreysing J, von Figura K. Molecular genetics of metachromatic leukodystrophy. *J Inher Metab Dis* 1994; 17: 500–509
- Gieselmann V, Polten A, Kreysing J, von Figura K. Molecular genetics of metachromatic leukodystrophy. *J Inher Metab Dis* 1994; 17: 500–509
- Gieselmann V, Matzner U, Hess B, Lüllmann-Rauch R, Coenen R, Hartmann D, D'Hooge R, Dedejn P, Nagels G. Metachromatic leukodystrophy: molecular genetics and an animal model. *J Inher Metab Dis* 1998; 21: 564–574
- Gieselmann V. Metachromatic leukodystrophy: recent research developments. *J Child Neurol* 2003; 18: 591–594
- Gieselmann V, Franken S, Klein D, Mansson JE, Sandhoff R, Lüllmann Rauch R, Hartmann D, Saravanan VPM, de Deyn PP, D'Hooge R, van der Linden AM, Schaeren-Wiemers N. Metachromatic leukodystrophy: consequences of sulphatide accumulation. *Acta Paediatr Suppl* 2003; 443: 74–79
- Ginsberg L, Gershfeld NL. Membrane bilayer instability and the pathogenesis of disorders of myelin. *Neurosci Lett* 1991; 130: 133–136.
- Gort L, Coll MJ, Chabàs A. Identification of 12 novel mutations and two new polymorphisms in the arylsulfatase A gene: haplotype and genotype-phenotype correlation studies in Spanish metachromatic leukodystrophy patients. *Hum Mutat* 1999; 14: 240–248
- Grégoire A, Périer O, Dustin P. Metachromatic leukodystrophy, an electron microscopic study. *J Neuropathol Exp Neurol* 1966; 25: 617–636
- Guffon N, Souillet A, Maire I, Dorche C, Mathieu M, Guibaud P. Juvenile metachromatic leukodystrophy: neurological outcome two years after bone marrow transplantation. *J Inher Metab Dis* 1995; 18: 159–161
- Haltia T, Palo J, Haltia M, Icen A. Juvenile metachromatic leukodystrophy: clinical, biochemical, and neuropathologic studies in nine new cases. *Arch Neurol* 1980; 37: 42–46
- Harvey JS, Carey WF, Morris CP. Importance of the glycosylation and polyadenylation variants in metachromatic leukodystrophy pseudodeficiency phenotype. *Hum Mol Genet* 1998; 7: 1215–1219
- Holtschmidt H, Sandhoff K, Kwon HY, Harzer K, Nakano T, Suzuki K. Sulfatide activator protein. *J Biol Chem* 1991; 266: 7556–7560
- Inui K, Furukawa M, Nishimoto J, Okada S, Yabuuchi H. Metabolism of cerebroside sulphate and subcellular distribution of its metabolites in cultured skin fibroblasts derived from controls, metachromatic leukodystrophy, globoid cell leukodystrophy and Farber disease. *J Inher Metab Dis* 1987; 10: 293–296
- Inui K, Furukawa M, Okada S, Yabuuchi H. Metabolism of cerebroside sulfate and subcellular distribution of its metabolites in cultured skin fibroblasts from controls, metachromatic leukodystrophy, and globoid cell leukodystrophy. *J Clin Invest* 1988; 81: 310–317
- Jayakumar PN, Aroor SR, Jha RK, Arya BYT. Computed tomography (CT) in late infantile metachromatic leukodystrophy. *Acta Neurol Scand* 1989; 79: 23–26
- Jervis GA. Infantile metachromatic leukodystrophy. *J Neuropathol Exp Neurol* 1960; 19: 323–340
- Kapaun P, Dittmann RW, Granitzny B, Eickhoff W, Wulbrand H, Neumaier-Probst E, Zander A, Kohlschütter A. Slow progression of juvenile metachromatic leukodystrophy 6 years after bone marrow transplantation. *J Child Neurol* 1999; 222–228
- Kappler J, von Figura K, Gieselmann V. Late-onset metachromatic leukodystrophy: molecular pathology in two siblings. *Ann Neurol* 1992; 31: 256–261
- Kidd D, Nelson J, Jones F, Dusoir H, Wallace I, McKinstry S, Patterson V. Long-term stabilization after bone marrow transplantation in juvenile metachromatic leukodystrophy. *Arch Neurol* 1998; 55: 98–99
- Kim TS, Kim IO, Kim WS, Choi YS, Lee JY, Kim OW, Yeon KM, Kim KJ, Hwang YS. MR of childhood metachromatic leukodystrophy. *AJNR Am J Neuroradiol* 1997; 18: 733–738
- Kreysing J, von Figura K, Gieselmann V. Structure of the arylsulfatase A gene. *Eur J Biochem* 1990; 191: 627–631
- Krivit W, Shapiro E, Kennedy W, Lipton M, Lockman L, Smith S, Gail Summers C, Wenger DA, Tsai MY, Ramsay NKC, Kersey JH, Yao JK, Kaye E. Treatment of late infantile metachromatic leukodystrophy by bone marrow transplantation. *N Engl J Med* 1990; 322: 28–32
- Krivit W, Shapiro E, Hoogerbrugge PM, Moser HW. State of the art review: bone marrow transplantation treatment for storage diseases. *Bone Marrow Transplant* 1992; 10 (suppl 1): 87–96
- Krivit W, Lockman LA, Watkins PA, Hirsch J, Shapiro EG. The future for treatment by bone marrow transplantation for adrenoleukodystrophy, metachromatic leukodystrophy, globoid cell leukodystrophy and Hurler syndrome. *J Inher Metab Dis* 1995; 18: 398–412
- Landrieu P, Blanche S, Vanier MT, Metral S, Husson B, Sandhoff K, Fischer A. Bone marrow transplantation in metachromatic leukodystrophy caused by saposin-B deficiency: a case report with a 3-year follow-up period. *J Pediatr* 1998; 133: 129–132
- Leistner S, Young E, Meaney C, Winchester B. Pseudodeficiency of arylsulphatase A: strategy for clarification of genotype in families of subjects with low ASA activity and neurological symptoms. *J Inher Metab Dis* 1995; 18: 710–716
- McKhann GM. Metachromatic leukodystrophy: clinical and enzymatic parameters. *Neuropediatrics* 1984; 15: 4–10
- Malm G, Ringdén O, Winiarski J, Gröndahl E, Uvebratt P, Eriksson U, Håkansson H, Skjeldal O, Månsson JE. Clinical outcome in four children with metachromatic leukodystrophy treated by bone marrow transplantation. *Bone Marrow Transplant* 1996; 17: 1003–1008
- Matzner U, Hartmann D, Lüllmann-Rauch R, Coenen R, Rothert F, Månsson JE, Fredman P, D'Hooge R, De Deyn PP, Gieselmann V. Bone marrow stem cell-based gene transfer in a mouse model for metachromatic leukodystrophy: effects on visceral and nervous system disease manifestations. *Gene Ther* 2002; 9: 53–63
- Mei Liu H. Ultrastructure of central nervous system lesions in metachromatic leukodystrophy with special reference to morphogenesis. *J Neuropathol Exp Neurol* 1968; 27: 624–644
- Minamikawa-Tachino R, Maeda Y, Fujishiro I, Itoh K, Satake A, Aoki S, Yamada H, Suzuki Y, Sakuraba H. Three-dimensional brain visualization for metachromatic leukodystrophy. *Brain Dev* 1996; 18: 394–399
- Navarro C, Fernández JM, Domínguez C, Fachal C, Albarez M. Late juvenile metachromatic leukodystrophy treated with bone marrow transplantation: a 4-year follow-up study. *Neurology* 1996; 46: 254–256

- Norman RM, Urich H, Tingey AH. Metachromatic leuco-encephalopathy: a form of lipidosis. *Brain* 1960; 83: 369–380
- Penzien JM, Kappler J, Herschkowitz N, Schuknecht B, Keinekugel P, Propping P, Tonnesen T, Lou H, Moser H, Zierz S, Conzelmann E, Gieselmann V. Compound heterozygosity for metachromatic leukodystrophy and arylsulfatase A pseudodeficiency alleles is not associated with progressive neurological disease. *Am J Hum Genet* 1993; 52: 557–564
- Polten A, Fluharty AL, Fluharty CB, Kappler J, von Figura K, Gieselmann V. Molecular basis of different forms of metachromatic leukodystrophy. *N Engl J Med* 1991; 324: 18–22
- Pridjian G, Humbert J, Willis J, Shapira E. Presymptomatic late-infantile metachromatic leukodystrophy treated with bone marrow transplantation. *J Pediatr* 1994; 125: 755–758
- Qu Y, Shapira E, Desnick RJ. Metachromatic leukodystrophy: subtype genotype/phenotype correlations and identification of novel missense mutations (P148L and P191T) causing the juvenile-onset disease. *Mol Genet Metab* 1999; 67: 206–212
- Regis S, Filocamo M, Corsolini F, Caroli F, Keulemans JLM, Diggele van OP, Gatti R. An Asn >Lys substitution in saposin B involving a conserved amino acidic residue and leading to the loss of the single N-glycosylation site in a patient with metachromatic leukodystrophy and normal arylsulphatase A activity. *Eur J Hum Genet* 1999; 7: 125–130
- Regis S, Corsolini F, Stroppiano M, Cusano R, Filocamo M. Contribution of arylsulfatase A mutations located on the same allele to enzyme activity reduction and metachromatic leukodystrophy severity. *Hum Genet* 2002; 110: 351–355
- Reider-Grosswasser I, Bornstein N. CT and MRI in late-onset metachromatic leukodystrophy. *Acta Neurol Scand* 1987; 75: 64–69
- Sangalli A, Taveggia C, Salviati A, Wrabetz L, Bordignon C, Severini GM. Transduced fibroblasts and metachromatic leukodystrophy lymphocytes transfer arylsulfatase A to myelinating Glia and deficient cells in vitro. *Hum Gene Ther* 1998; 9: 2111–2119
- Schlote W, Harzer K, Christomanou H, Paton BC, Kustermann B, Schmid B, Seeger J, Beudt U, Schuster I, Langenbeck U. Sphingolipid activator protein 1 deficiency in metachromatic leukodystrophy with normal arylsulphatase A activity. A clinical, morphological, biochemical, and immunological study. *Eur J Pediatr* 1991; 150: 584–591
- Scholz W. Klinische, pathologisch-anatomische und erbbiologische Untersuchungen. *Z Neurol Psychiatrie* 1925; 99: 651–717
- Shapiro EG, Lockman LA, Knopman D, Krivit W. Characteristics of the dementia in late-onset metachromatic leukodystrophy. *Neurology* 1994; 44: 662–665
- Solders G, Celsing G, Hagenfeldt L, Ljungman P, Isberg B, Ringdén O. Improved peripheral nerve conduction, EEG and verbal IQ after bone marrow transplantation for adult metachromatic leukodystrophy. *Bone Marrow Transplant* 1998; 22: 1119–1122
- Stillman AE, Krivit W, Shapiro E, Lockman L, Latchaw RE. Serial MR after bone marrow transplantation in two patients with metachromatic leukodystrophy. *AJNR Am J Neuroradiol* 1994; 15: 1929–1932
- Tylki-Szymańska A, Czartoryska B, Lugowska A. Practical suggestions in diagnosing metachromatic leukodystrophy in probands and in testing family members. *Eur Neurol* 1998; 40: 67–70
- Van Bogaert L, Dewulf A. Diffuse progressive leukodystrophy in the adult with production of metachromatic degenerative products (Alzheimer-Baroncini). *Arch Neurol Psychiatrie* 1939; 42: 1083–1097
- Von Hirsch T, Pfeiffer J. Über histologische Methoden in der Differentialdiagnose von Leukodystrophien und Lipoidosen. *Arch Psychiatrie Z Neurol* 1955; 194: 88–104
- Wrobe D, Henseler M, Huettler S, Pascual Pascual SI, Chabas A, Sandhoff K. A non-glycosylated and functionally deficient mutant (N215H) of the sphingolipid activator protein B (SAP-B) in a novel case of metachromatic leukodystrophy (MLD). *J Inher Metab Dis* 2000; 23: 63–76
- Zafeiriou DI, Kontopoulos EE, Michelakakis HM, Anastasiou AL, Gombakis NP. Neurophysiology and MRI in late-infantile metachromatic leukodystrophy. *Pediatr Neurol* 1999; 21: 843–846
- Zhang XL, Rafi MA, DeGala G, Wenger DA. Insertion in the mRNA of a metachromatic leukodystrophy patient with sphingolipid activator protein-1 deficiency. *Proc Natl Acad Sci* 1990; 87: 1426–1430

7 Multiple Sulfatase Deficiency

- Al-Moutaery KR, Choudhury AR, Hassanen MO. Cervical cord compression and severe hydrocephalus in a child with Saudi variant of multiple sulfatase deficiency. *Acta Neurol (Wien)* 1994; 131: 160–163
- Aqeel AA, Ozand PT, Brismar J, Gascon GG, Brismar G, Nester M, Sakati N. Saudi variant of multiple sulfatase deficiency. *J Child Neurol* 1992; 7 (suppl): S12–S21
- Austin JH. Studies in metachromatic leukodystrophy. *Arch Neurol* 1973; 28: 258–264
- Basner R, von Figura K, Glössl J, Klein U, Kresse H, Mlekusch W. Multiple deficiency of mucopolysaccharide sulfatases in mucosulfatidosis. *Pediatr Res* 1979; 13: 1316–1318
- Bateman BJ, Philippart M, Isenberg SJ. Ocular features of multiple sulfatase deficiency and a new variant of metachromatic leukodystrophy. *J Pediatr Ophthalmol Strabismus* 1984; 21: 133–139
- Bharucha BA, Nalk G, Savliwala AS, Joshi RM, Kumta NB. Siblings with the Austin variant of metachromatic leukodystrophy multiple sulfatidosis. *Indian J Pediatr* 1984; 51: 477–480
- Burch M, Fesnom AH, Jackson M, Pitts-Tucker T, Congdon PJ. Multiple sulphatase deficiency presenting at birth. *Clin Genet* 1986; 30: 409–415
- Burk RD, Valle D, Thomas GH, Miller C, Moser A, Moser H, Rosenbaum KN. Early manifestations of multiple sulfatase deficiency. *J Pediatr* 1984; 104: 574–578
- Conary JT, Hasilik A, von Figura K. Synthesis and stability of steroid sulfatase in fibroblasts from multiple sulfatase deficiency. *Biol Chem Hoppe-Seyler* 1988; 369: 297–302
- Constantopoulos G. Multiple sulfatase deficiency with a novel biochemical presentation. *Eur J Pediatr* 1988; 147: 634–638
- Cosmo MP, Pepe S, Annuziata I, Newbold RF, Grompe M, Parenti G, Ballabio A. The multiple sulfatase deficiency gene encodes an essential and limiting factor for the activity of sulfatases. *Cell* 2003; 113: 445–456
- Fedde K, Horwitz AL. Complementation of multiple sulfatase deficiency in somatic cell hybrids. *Am J Hum Genet* 1984; 36: 623–633
- Guerra WF, Verity A, Fluharty AL, Nguyen HT, Philippart M. Multiple sulfatase deficiency: clinical, neuropathological, ultrastructural and biochemical studies. *J Neuropathol Exp Neurol* 1990; 49: 406–423
- Harbord M, Buncic JR, Chuang SA, Skomorowski MA, Clarke JTR. Multiple sulfatase deficiency with early severe retinal degeneration. *J Child Neurol* 1991; 6: 229–235

- Horwitz AL, Warshawsky L, King J, Burns G (1986) Rapid degradation of steroid sulfatase in multiple sulfatase deficiency. *Biochem Biophys Res Commun* 1986; 135: 389–396
- Kepes JJ, Berry A, Zacharias DL. Multiple sulfatase deficiency: bridge between neuronal storage diseases and leukodystrophies. *Pathology* 1988; 20: 285–291
- Landgrebe J, Dierks T, Schmidt B, von Figura K. The human *SUMF1* gene, required for posttranslational sulfatase modification, defines a new gene family, which is conserved from pro- to eukaryotes. *Gene* 2003; 316: 47–56
- Loffeld A, Gray RGF, Green SH, Roper HP, Moss C. Mild ichthyosis in a 4-year-old boy with multiple sulphatase deficiency. *Br J Dermatol* 2002; 147: 353–355
- Macaulay RJB, Lowry NJ, Casey RE. Pathologic findings of multiple sulfatase deficiency reflect the pattern of enzyme deficiencies. *Pediatr Neurol* 1998; 19: 372–376
- Mancini GMS, Diggelen van OP, Huijman JG, Stroink H, Coe de RFM. Pitfalls in the diagnosis of multiple sulfatase deficiency. *Neuropediatrics* 2001; 32: 38–40
- Nevsimanova S, Elleder M, Smid F, Zemankova M. Multiple sulphatase deficiency in homozygotic twins. *J Inher Metab Dis* 1984; 7: 38–40
- Perlmutter-Cremer N, Libert J, Vámos E, Spel M, Kiebaers I. Unusual early manifestation of multiple sulfatase deficiency. *Ann Radiol* 1981; 24: 43–48
- Raynaud EJ, Escourolle R, Baumann N, Turpin JC, Dubois G, Malpuech G, Lagarde R. Metachromatic leukodystrophy. *Arch Neurol* 1975; 32: 834–838
- Rommerskirch W, von Figura K. Multiple sulfatase deficiency: catalytically inactive sulfatases are expressed from retrovirally introduced sulfatase cDNAs. *Proc Natl Acad Sci* 1992; 89: 2561–2565
- Schmidt B, Selmer T, Ingendoh A, von Figura K. A novel amino acid modification in sulfatases that is defective in multiple sulfatase deficiency. *Cell* 1995; 82: 271–278
- Soong BW, Casamassima AC, Fink JK, Constantopoulos G, Horwitz AL. Multiple sulfatase deficiency. *Neurology* 1988; 38: 1273–1275
- Tanaka A, Hirabayashi M, Ishii M, Yamaoka S. Complementation studies with clinical and biochemical characterizations of a new variant of multiple sulphatase deficiency. *J Inher Metab Dis* 1987; 10: 103–110
- Vámos E, Lubairs I, Bousard N, Liberti J, Pirimutter N. Multiple sulphatase deficiency with early onset. *J Inher Metab Dis* 1981; 4: 103–104
- Waheed A, Hasilik A, von Figura K. Enhanced breakdown of arylsulfatase A in multiple sulfatase deficiency. *Eur J Biochem* 1982; 123: 317–321
- Austin J, Suzuki K, Armstrong D, Brady R, Bachhawat BK, Schlenker J, Stumpf D. Studies in globoid (Krabbe) leukodystrophy (GLD). *Arch Neurol* 1970; 23: 502–512
- Bajaj NPS, Waldman A, Orrell R, Wood NW, Bhatia KP. Familial adult onset of Krabbe's disease resembling hereditary spastic paraplegia with normal neuroimaging. *J Neurol Neurosurg Psychiatry* 2002; 72: 635–638
- Baker RH, Trautmann JC, Younge BR, Nelson KD, Zimmerman R. Late juvenile-onset Krabbe's disease. *Ophthalmology* 1990; 97: 1176–1180
- Baram TZ, Goldman AM, Percy AK. Krabbe disease: specific MRI and CT findings. *Neurology* 1986; 36: 111–115
- Barone R, Brühl K, Stoeter P, Fiumara A, Pavone L, Beck M. Clinical and neuroradiological findings in classic infantile and late-onset globoid-cell leukodystrophy (Krabbe disease). *Am J Med Genet* 1996; 63: 209–217
- Bernal OG, Lenn N. Multiple cranial nerve enhancement in early infantile Krabbe's disease. *Neurology* 2000; 54: 2348–2349
- Bernardi B, Fonda C, Franzoni E, Marchiani V, Della Guistina E, Zimmerman RA. MRI and CT in Krabbe's disease: case report. *Neuroradiology* 1994; 36: 477–479
- Bernardi GL, Herrera DG, Carson D, DeGasperi R, Gama Sosa MA, Kolodny EH, Trifiletti R. Adult-onset Krabbe's disease in siblings with novel mutations in the galactocerebrosidase gene. *Ann Neurol* 1997; 41: 111–114
- Bischoff A, Ulrich J. Peripheral neuropathy in globoid cell leukodystrophy (Krabbe's disease). Ultrastructural and histochemical findings. *Brain* 1969; 92: 861–870
- Biswas S, Levine SM. Substrate-reduction therapy enhances the benefits of bone marrow transplantation in young mice with globoid cell leukodystrophy. *Pediatr Res* 2002; 51: 40–47
- Cavanagh N, Kendall B. High density on computed tomography in infantile Krabbe's disease: a case report. *Dev Med Child Neurol* 1986; 28: 799–802
- Choi S, Enzmann DR. Infantile Krabbe disease: complementary CT and MR findings. *AJNR Am J Neuroradiol* 1993; 14: 1164–1166
- Demaerel Ph, Wilms G, Verdrup P, Carton H, Baert AL. MR findings in globoid cell leukodystrophy. *Neuroradiology* 1990; 32: 520–522
- De Stefano N, Dotti MT, Mortilla M, Pappagallo E, Luzi P, Rafi MA, Formichi P, Inzitari D, Wenger DA, Federico A. Evidence of diffuse brain pathology and unspecific genetic characterization in a patient with an atypical form of adult-onset Krabbe disease. *J Neurol* 2000; 247: 226–228
- Ellis WG, Schneider EL, McCulloch JR, Suzuki K, Epstein CJ. Fetal globoid cell leukodystrophy (Krabbe disease). Pathological and biochemical examination. *Arch Neurol* 1973; 29: 253–257
- Epstein MA, Zimmerman RA, Rorke LB, Sladky JT. Late-onset globoid cell leukodystrophy mimicking an infiltrating glioma. *Pediatr Radiol* 1991; 21: 131–132
- Eto Y, Suzuki K. Brain sphingolipids in Krabbe's globoid cell leukodystrophy. *J Neurochem* 1971; 18: 503–511
- Eto Y, Suzuki K, Suzuki K. Globoid cell leukodystrophy (Krabbe's disease): isolation of myelin with normal glycolipid composition. *J Lipid Res* 1970; 11: 473–479
- Farina L, Bizzi A, Fiocchiaro G, Pareyson D, Shghirlanzoni A, Bertagnolio B, Savoiardo M, Naidu S, Wenger DA. MR imaging and proton MR spectroscopy in adult Krabbe disease. *AJNR Am J Neuroradiol* 2000; 21: 1478–1482
- Farley TJ, Ketonen LM, Bodensteiner JB, Wang DD. Serial MRI and CT findings in infantile Krabbe disease. *Pediatr Neurol* 1992; 8: 455–458

8 Globoid Cell Leukodystrophy

- Andrews JM, Cancilla PA, Grippo J, Menkes JH. Globoid cell leukodystrophy (Krabbe's disease): morphological and biochemical studies. *Neurology* 1971; 21: 337–352
- Arvidsson J, Hagberg B, Mansson J-E, Svennerholm L. Late onset globoid cell leukodystrophy (Krabbe's disease) – a Swedish case with 15 years of follow-up. *Acta Paediatr* 1995; 84: 218–221
- Austin J. Studies in globoid (Krabbe) leukodystrophy. *Arch Neurol* 1963; 9: 207–231
- Austin J. Studies in globoid (Krabbe) leukodystrophy. *J Neurochem* 1963; 10: 921–930

- Feanny SJ, Chuang SH, Becker LE, Clarke JTR. Intracerebral paraventricular hyperdensities: a new CT sign in Krabbe globoid cell leukodystrophy. *J Inherit Metab Dis* 1987; 10: 24–27
- Finelli DA, Tarr RW, Sawyer RN, Horwitz SJ. Deceptively normal MR in early infantile Krabbe disease. *AJNR Am J Neuroradiol* 1994; 15: 167–171
- Fu L, Inui K, Nishigaki T, Tatsumi N, Tsukamoto H, Kokubu C, Muramatsu T, Okada S. Molecular heterogeneity of Krabbe disease. *J Inherit Metab Dis* 1999; 22: 155–162
- Giri S, Jatana M, Rattan R, Won J-S, Singh I, Sing AK. Galactosylsphingosine (psychosine) –induced expression of cytokine-mediated inducible nitric oxide synthases via AP-1 and C/EBP: implications for Krabbe disease. *FASEB J* 2002; 16: 661–672
- Given CA 2nd, Santos CC, Durden DD. Intracranial and spinal MR imaging findings associated with Krabbe's disease : case report. *AJNR Am J Neuroradiol* 2001; 22: 1782–1785
- Goebel HH, Harzer K, Ernst JP, Bohl J, Klein H. Late-onset globoid cell leukodystrophy: unusual ultrastructural pathology and subtotal β -galactocerebrosidase deficiency. *J Child Neurol* 1990; 5: 299–307
- Goebel HH, Kimura S, Harzer K, Klein H. Ultrastructural pathology of eccrine sweat gland epithelial cells in globoid cell leukodystrophy. *J Child Neurol* 1993; 8: 171–174
- Grewal RP, Petronas N, Barton NW. Late onset globoid cell leukodystrophy. *J Neurol Neurosurg Psychiatry* 1991; 54: 1011–1012
- Hagberg B. Krabbe's disease: clinical presentation of neurological variants. *Neuropediatrics* 1984; 15: 11–15
- Hagberg B, Kollberg H, Sourander P, Akesson HO. Infantile globoid cell leukodystrophy. *Neuropediatrics* 1969; 1: 74–88
- Harzer K, Knoblich R, Rolfs A, Bauer P, Eggers J. Residual galactosylsphingosine (psychosine) β -galactosidase activities and associated *GALC* mutations in late and very late onset Krabbe disease. *Clin Chim Acta* 2002; 317: 77–84
- Henderson RD, MacMillan JC, Bradfield JM. Adult onset Krabbe disease may mimic motor neurone disease. *J Clin Neurosci* 2003; 10: 638–639
- Hittmair K, Wimberger D, Wiesbauer P, Zehetmayer M, Budka H. Early infantile form of Krabbe disease with optic hypertrophy: serial MR examinations and autopsy correlation. *AJNR Am J Neuroradiol* 1994; 15: 1454–1458
- Ida H, Rennert OM, Watabe K, Eto Y, Maekawa K. Pathological and biochemical studies of fetal Krabbe disease. *Brain Dev* 1994; 16: 480–4
- Ishima A, Eda I, Matsui A, Yoshino K, Takashima S, Takeshita K. Computed tomography in Krabbe's disease: comparison with neuropathology. *Neuroradiology* 1983; 25: 323–327
- Igisu H, Nakamura M. Inhibition of cytochrome C oxidase by psychosine (galactosylsphingosine). *Biochem Biophys Res Commun* 1986; 137: 323–327
- Itoh M, Hayashi M, Fujioka Y, Nagashima K, Morimatsu Y, Matsuyama H. Immunohistological study of globoid cell leukodystrophy. *Brain Dev* 2002; 24: 284–290
- Jardim LB, Giugliani R, Fensom AH. Thalamic and basal ganglia hyperdensities – a CT marker for globoid cell leukodystrophy? *Neuropediatrics* 1992; 23: 30–31
- Jardim LB, Giugliani R, Pires RF, Haussen S, Burin MG, Rafi MA, Wenger DA. Protracted course of Krabbe disease in an adult patient bearing a novel mutation. *Arch Neurol* 1999; 56: 1014–1017
- Jatana M, Giri S, Singh AK. Apoptotic positive cells in Krabbe brain and induction of apoptosis in rat C6 glial cells by psychosine. *Neurosci Lett* 2002; 330: 183–187
- Jones BV, Barron TF, Towfighi J. Optic nerve enlargement in Krabbe's disease. *AJNR Am J Neuroradiol* 1999; 20: 1228–1231
- Kapoor R, McDonald WI, Crockard A, Moseley IF. Clinical onset and MRI features of Krabbe's disease in adolescence. *J Neurol Neurosurg Psychiatry* 1992; 55: 331–332
- Kobayashi T, Shinoda H, Goto I, Yamanaka T, Suzuki Y. Globoid cell leukodystrophy is a generalized galactosylsphingosine (psychosine) storage disease. *Biochem Biophys Res Commun* 1987; 144: 41–46
- Kobayashi T, Goto I, Yamanaka T, Suzuki Y, Nakano T, Suzuki K. Infantile and fetal globoid cell leukodystrophy: analysis of galactosylceramide and galactosylsphingosine. *Ann Neurol* 1988; 24: 517–522
- Kolodny EH, Raghavan S, Krivit W. Late-onset Krabbe disease (globoid cell leukodystrophy): clinical and biochemical features of 15 cases. *Dev Neurosci* 1991; 13: 232–239
- Krabbe K. A new familial, infantile form of diffuse brain sclerosis. *Brain* 1916; 39: 74–114
- Krivit W, Lockman LA, Watkins PA, Hirsch J, Shapiro EG. The future for treatment by bone marrow transplantation for adrenoleukodystrophy, metachromatic leukodystrophy, globoid cell leukodystrophy and Hurler syndrome. *J Inherit Metab Dis* 1995; 18: 398–412
- Krivit W, Shapiro EG, Peters C, Wagner JE, Cornu G, Kurtzberg J, Wenger DA, Kolodny EH, Vanier MT, Loes DJ, Dusenbery K, Locman LA. Hematopoietic stem-cell transplantation in globoid-cell leukodystrophy. *N Engl J Med* 1998; 338: 1119–1126
- Krivit W, Peters C, Shapiro EG. Bone marrow transplantation as effective treatment of central nervous system disease in globoid cell leukodystrophy, metachromatic leukodystrophy, adrenoleukodystrophy, mannosidosis, fucosidosis, aspartylglucosaminuria, Hurler, Maroteaux-Lamy, and Sly syndromes, and Gaucher disease type III. *Curr Opin Neurol* 1999; 12: 167–176
- Kurokawa T, Chen YJ, Nagata M. Late infantile Krabbe leukodystrophy: MRI and evoked potentials in a Japanese girl. *Neuropediatrics* 1987; 18: 182–183
- Kwan E, Drace J, Enzmann D. Specific CT findings in Krabbe disease. *AJNR Am J Neuroradiol* 1984; 5: 453–458
- LeVine SM, Pedchenko TV, Bronshteyn IG, Pinson DM. L-cycloserine slows the clinical and pathological course in mice with globoid cell leukodystrophy (twitcher mice). *J Neurosci Res* 2000; 60: 231–236
- Liu HM. Ultrastructure of globoid leukodystrophy (Krabbe's disease) with reference to the origin of globoid cells. *J Neuropathol Exp Neurol* 1970; 29: 441–462
- Loes DJ, Peters C, Krivit W. Globoid cell leukodystrophy: distinguishing early-onset from late-onset disease using a brain MR imaging scoring method. *AJNR Am J Neuroradiol* 1999; 20: 316–323
- Loonen MCB, van Diggelen OP, Janse HC, Kleijer WJ, Arts WFM. Late-onset globoid cell leukodystrophy (Krabbe's disease): clinical and genetic delineation of two forms and their relation to the early-infantile form. *Neuropediatrics* 1985; 16: 137–142
- Lyon G, Hagberg B, Evrard Ph, Allaire C, Pavone L, Vanier M. Symptomatology of late onset Krabbe's leukodystrophy: the European experience. *Dev Neurosci* 1991; 13: 240–244
- Malone MJ, Szöke MC, Looney GL. Globoid leukodystrophy: I. Clinical and enzymatic studies. *Arch Neurol* 1975; 32: 606–612
- Marks HG, Scavina MT, Kolodny EH, Palmieri M, Childs J. Krabbe disease presenting as a peripheral neuropathy. *Muscle Nerve* 1997; 20: 1024–1028

- Matsuda J, Vanier MT, Saito Y, Tohyama J, Suzuki K, Suzuki K. A mutation in the saposin A domain of the sphingolipid activator protein (prosaposin) gene results in a late-onset, chronic form of globoid cell leukodystrophy in the mouse. *Hum Mol Genet* 2001; 10: 1191–1199
- Matsumoto R, Oka N, Nagahama Y, Akiguchi I, Kimura J. Peripheral neuropathy in late-onset Krabbe's disease: histochemical and ultrastructural findings. *Acta Neuropathol (Berl)* 1996; 92: 635–639
- McKelvie P, Vine P, Hopkins I, Poulos A. A case of Krabbe's leukodystrophy without globoid cells. *Pathology* 1990; 22: 235–238
- Menkes JH, Duncan C, Moossy J. Molecular composition of the major glycolipids in globoid cell leukodystrophy. *Neurology* 1966; 16: 381–393
- Mitsuo K, Kobayashi T, Shinnoh N, Goto I. Biosynthesis of galactosylsphingosine (psychosine) in the Twitcher mouse. *Neurochem Res* 1989; 14: 899–903
- Olsson Y, Sourander P, Svennerholm L. Experimental studies on the pathogenesis of leucodystrophies. I. The effect of intracerebrally injected sphingolipids in the rat's brain. *Acta Neuropathol (Berl)* 1966; 6: 153–163
- Percy AK, Odreizin GT, Knowles PD, Rouah E, Armstrong DD. Globoid cell leukodystrophy: comparison of neuropathology with magnetic resonance imaging. *Acta Neuropathol (Berl)* 1994; 88: 26–32
- Phelps M, Aicardi J, Vanier MT. Late onset Krabbe's leukodystrophy: a report of four cases. *J Neurol Neurosurg Psychiatry* 1991; 54: 293–296
- Sabatelli M, Quaranta L, Madia F, Lippi G, Conte A, Lo Monaco M, Di Trapani G, Rafi MA, Wenger DA, Vaccaro AM, Tonali P. Peripheral neuropathy with hypomyelinating features in adult-onset Krabbe's disease. *Neuromusc Disord* 2002; 12: 386–391
- Sasaki M, Sakuragawa N, Takashima S, Hanaoka S, Arima M. MRI and CT findings in Krabbe disease. *Pediatr Neurol* 1991; 7: 283–288
- Satoh J-I, Tokumoto H, Kurohara K, Yukitaka M, Matsui M, Kuroda Y, Yamamoto T, Ruruya H, Shinnoh N, Kobayashi T, Kukita Y, Haysashi K. Adult-onset Krabbe disease with the homozygous T1853C mutation in the galactocerebrosidase gene. *Neurology* 1997; 49: 1392–1399
- Shen JS, Watabe K, Ohashi T, Eto Y. Intraventricular administration of recombinant adenovirus to neonatal twitcher mouse leads to clinicopathological improvements. *Gene Ther* 2001; 8: 1081–1087
- Sourander P, Hansson HA, Olsson Y, Svennerholm L. Experimental studies on the pathogenesis of leucodystrophies. II. The effect of sphingolipids on various cell types in cultures from the nervous system. *Acta Neuropathol (Berl)* 1966; 6: 231–242
- Suzuki K. Twenty five years of the "psychosine" hypothesis: a personal perspective of its history and present status. *Neurochem Res* 1998; 23: 251–259
- Suzuki K. Globoid cell leukodystrophy (Krabbe's disease): update. *J Child Neurol* 2003; 18: 595–603
- Suzuki K, Grover WD. Krabbe's leukodystrophy (globoid cell leukodystrophy). *Arch Neurol* 1970; 22: 385–396
- Suzuki K, Suzuki Y. Globoid cell leucodystrophy (Krabbe's disease): deficiency of galactocerebrosidase β -galactosidase. *Proc Natl Acad Sci* 1970; 66: 302–309
- Suzuki Y, Suzuki K. The twitcher mouse: a model for Krabbe disease and for experimental therapies. *Brain Pathol* 1995; 5: 249–258
- Svennerholm L, Vanier MT, Mansson JE. Krabbe disease: a galactosylsphingosine (psychosine) lipidosis. *J Lipid Res* 1980; 21: 53–64
- Tada K, Taniike M, Tsukamoto H, Inui K, Okada S. Serial magnetic resonance imaging studies in a case of late onset globoid cell leukodystrophy. *Neuropediatrics* 1992; 23: 306–309
- Taniike M, Mohri I, Eguchi N, Irikura D, Urade Y, Okada S, Suzuki K. An opoptotic depletion of oligodendrocytes in the twitcher, a murine model of globoid cell leukodystrophy. *J Neuropathol Exp Neurol* 1999; 58: 644–653
- Tullu MS, Muranjan MN, Kondurkar PP, Bharucha BA. Krabbe disease – clinical profile. *Indian Pediatr* 2000; 37: 939–946
- Turazzini M, Beltramello A, Bassi R, Del Colle R, Silvestri M. Adult onset Krabbe's leukodystrophy: a report of 2 cases. *Acta Neurol Scand* 1997; 96: 413–415
- Vanhanen L-L, Raininko R, Santavuori P. Early differential diagnosis of infantile neuronal ceroid lipofuscinosis, Rett Syndrome, and Krabbe disease by CT and MR. *AJNR Am J Neuroradiol* 1994; 15: 1443–1453
- Vasconcelles E, Smith M. MRI nerve root enhancement in Krabbe disease. *Pediatr Neurol* 1998; 19: 151–152
- Verdrum P, Lammens M, Dom R, Van Elsen A. Globoid cell leukodystrophy: a family with both late-infantile and adult type. *Neurology* 1991; 41: 1382–1384
- Wenger DA, Louie E. Pseudodeficiencies of arylsulfatase A and galactocerebrosidase activities. *Dev Neurosci* 1991; 13: 216–221
- Wenger DA, Rafi MA, Luzi P. Molecular genetics of Krabbe disease (globoid cell leukodystrophy): diagnosis and clinical implications. *Hum Mutat* 1997; 10: 268–279
- Wenger DA, Rafi MA, Luzi P, Datto P, Constantino-Ceccarini E. Krabbe disease: genetic aspects and progress toward therapy. *Mol Genet Metab* 2000; 70: 1–9
- Zafeiriou DI, Michelakaki EM, Anastasiou AL, Gombakis NP, Kontopoulos EE. Serial MRI and neuropsychological studies in late-infantile Krabbe disease. *Pediatr Neurol* 1996; 15: 240–244
- Zafeiriou DI, Anastasiou AL, Michelakaki EM, Augoustidou-Savvopoulou PA, Katzos GS, Kontopoulos EE. Early infantile Krabbe disease: deceptively normal magnetic resonance imaging and serial neurophysiological studies. *Brain Dev* 1997; 19: 488–491
- Zarif MK, Tzika AA, Astrakas LG, Poussaint TY, Anthony DC, Darvas BT. Magnetic resonance spectroscopy and magnetic resonance imaging findings in Krabbe's disease. *J Child Neurol* 2001; 16: 522–526

9 GM₁ Gangliosidosis

- Al-Essa M, Bakheet SM, Patay ZJ, Nounou RM, Ozand TP. Cerebral fluorine-18 labeled 2-fluoro-2-deoxyglucose positron emission tomography (FDG PET), MRI, and clinical observations in a patient with infantile GM₁ gangliosidosis. *Brain Dev* 1999; 21: 559–562
- Beratis NG, Varvarigou-Frimas A, Beratis S, Sklower SL. Angiokeratoma corporis diffusum in GM₁ gangliosidosis, type 1. *Clin Genet* 1989; 36: 59–64
- Cabral A, Portela R, Tasso T, Eusebio F, Moreira A, Marques dos Santos H, Soares J, Moura-Nunes JF. A case of GM₁ gangliosidosis type I. *Ophthalmic Paediatr Genet* 1989; 10: 63–67

- Callahan JW. Molecular basis of GM1 gangliosidosis and Morquio disease, type B. Structure-function studies of lysosomal β -galactosidase and the non-lysosomal β -galactosidase-like protein. *Biochim Biophys Acta* 1999; 1455:85–103
- Chen CY, Zimmerman RA, Lee CC, Chen FH, Yuh YS, Hsiao HS. Neuroimaging findings in late infantile GM1 gangliosidosis. *AJNR Am J Neuroradiol* 1998; 19: 1628–1630
- Folkerth RD, Alroy J, Bhan I, Kaye EM. Infantile GM₁ gangliosidosis: complete morphology and histochemistry of two autopsied cases, with particular reference to delayed central nervous system myelination. *Pediatr Dev Pathol* 2000; 3: 73–86
- Gascon GG, Ozand PT, Erwin RE. GM₁ Gangliosidosis type 2 in two siblings. *J Child Neurol* 1992; 7: S41–S50
- Goebel HH. Morphology of the gangliosidoses. *Neuropediatrics* 1984; 15: 97–106
- Guazzi GC, D'Amore I, van Hoof F, Fruschelli C, Alessandrini C, Palmeri S, Federico A. Type 3 (chronic) GM₁ gangliosidosis presenting as infanto-choreo-athetotic dementia, without epilepsy, in three sisters. *Neurology* 1988; 38: 1124–1127
- Hinek A, Zhang S, Smith AC, Callahan JW. Impaired elastic-fiber assembly by fibroblasts from patients with either Morquio B disease or infantile GM1-gangliosidosis is linked to deficiency in the 67-kD spliced variant of β -galactosidase. *Am J Hum Genet* 2000; 67: 23–36
- Inui K, Namba R, Ihara Y, Nobukuni K, Taniike M, Midorikawa M, Tsukamoto H. A case of chronic GM₁ gangliosidosis presenting as dystonia: clinical and biochemical studies. *J Neurol* 1990; 237: 491–493
- Kasama T, Taketomi T. Abnormalities of cerebral lipids in GM₁-gangliosidoses, infantile, juvenile, and chronic type. *Jpn J Exp Med* 1986; 56: 1–11
- Kaye EM, Alroy J, Raghavan SS, Schwarting GA, Adelman LS, Runge V, Gelblum D, Johann G, Thalhammer DVM, Zuniga G. Dysmyelinogenesis in animal model of GM₁ gangliosidosis. *Pediatr Neurol* 1992; 8: 255–261
- Kobayashi T, Suzuki K. Chronic GM₁ gangliosidosis presenting as dystonia: II. Biochemical studies. *Ann Neurol* 1981; 9: 476–483
- Kobayashi O, Takashima S. Thalamic hyperdensity on CT in the infantile GM1-gangliosidosis. *Brain Dev* 1994; 16: 472–474
- Kohlschütter A. Clinical course of GM₁ gangliosidoses. *Neuropediatrics* 1984; 15: 71–73
- Lin H-C, Tsai F-J, Shen C-H, Peng C-T. Infantile form GM₁ gangliosidosis with dilated cardiomyopathy: a case report. *Acta Paediatr* 2000; 89: 880–883
- Morrone A, Bardelli T, Donati MA, Giorgi M, di Rocco M, Gatti R, Parini R, Ricci R, Tadeucchi G, D'Azzo A, Zammarchi E. β -Galactosidase gene mutations affecting the lysosomal enzyme and the elasin-binding protein in GM₁-gangliosidosis patients with cardiac involvement. *Hum Mutat* 2000; 15: 354–366
- Nardocci N, Bertagnolio B, Rumi V, Combi M, Bardelli P, Angelini L. Chronic GM₁ gangliosidosis presenting as dystonia: clinical and biochemical studies in a new case. *Neuropediatrics* 1993; 24: 164–166
- O'Brien JS, Storb R, Raff RF, Harding J, Appelbaum F, Morimoto S, Kishimoto Y, Graham T, Ahern-Rindell A, O'Brien SL. Bone marrow transplantation in canine GM₁ gangliosidosis. *Clin Genet* 1990; 38: 274–280
- Pampiglione G, Harden A. Neurophysiological investigations in GM₁ and GM₂ gangliosidoses. *Neuropediatrics* 1984; 15: 74–84
- Sandhoff K, Conzelmann E. The biochemical basis of gangliosidoses. *Neuropediatrics* 1984; 15: 85–92
- Shen W-C, Tsai FJ, Tsai C-H. Myelination arrest demonstrated using magnetic resonance imaging in a child with type GM₁ gangliosidosis. *J Formos Med Assoc* 1998; 97: 296–299
- Silva CMD, Severini MH, Sopelsa A, Coelho JC, Zaha A, d'Azzo A, Giugliani R. Six novel β -galactosidase gene mutations in Brazilian patients with GM₁-gangliosidosis. *Hum Mutat* 1999; 13: 401–409
- Suzuki K, Suzuki K, Chen GC. Morphological, histochemical and biochemical studies on a case of systemic late infantile lipidoses (generalized gangliosidosis). *J Neuropathol Exp Neurol* 1968; 27: 15–38
- Suzuki K, Suzuki K, Kamoshita S. Chemical pathology of GM₁ gangliosidosis (generalized gangliosidosis). *J Neuropathol Exp Neurol* 1969; 28: 25–73
- Suzuki Y, Sakuraba H, Oshima A, Yoshida K, Shimmoto M, Takano T, Fukuhara Y. Clinical and molecular heterogeneity in hereditary β -galactosidase deficiency. *Dev Neurosci* 1991; 13: 299–303
- Tanaka R, Momoi T, Yoshida A, Okumura M, Yamakura S, Takasaki Y, Kiyomasu T, Yamanaka C. Type 3 GM₁ gangliosidosis: clinical and neurological findings in an 11-year-old girl. *J Neurol* 1995; 242: 299–303
- Tominaga L, Ogawa Y, Taniguchi M, Ohno K, Matsuda J, Oshima A, Suzuki Y, Nanba E. Galactonojirimycin derivatives restore mutant human β -galactosidase activities expressed in fibroblasts from enzyme-deficient knockout mouse. *Brain Dev* 2001; 23: 284–287
- Urban Z, Boyd CD. Elastic-fiber pathologies: primary defects in assembly – and secondary disorders in transport and delivery. *Am J Hum Genet* 2000; 67: 4–7
- Uyama E, Terasaki T, Watanabe S, Naito M, Owada M, Araki S, Ando M. Type 3 GM₁ gangliosidosis: characteristic MRI findings correlated with dystonia. *Acta Neurol Scand* 1992; 86: 609–615
- van der Voorn JP, Kamphorst W, van der Knaap MS, Powers JM. The leukoencephalopathy of infantile GM₁ gangliosidosis: oligodendrocytic loss and axonal dysfunction. *Acta Neuropathol (Berl)* 2004; 107: 539–545
- Walkley SU, Baker HJ, Rattazzi MC, Haskins ME, Wu JY. Neuroaxonal dystrophy in neuronal storage disorders: evidence for major GABAergic neuron involvement. *J Neurol Sci* 1991; 104: 1–8
- Wood PA, McBride MR, Baker HJ, Christian ST. Fluorescence polarization analysis, lipid composition, and Na⁺, K⁺-ATPase kinetics of synaptosomal membranes in feline GM₁ and GM₂ gangliosidosis. *J Neurochem* 1985; 44: 947–956
- Yoshida K, Oshima A, Sakuraba H, Nakano T, Yanagisawa N, Inui K, Okada S, Uyama E, Namba R, Kondo K, Iwasaki S, Takamiya K, Suzuki Y. GM₁ gangliosidosis in adults: clinical and molecular analysis of 16 Japanese patients. *Ann Neurol* 1992; 31: 328–332

10 GM₂ Gangliosidosis

- Argov Z, Navon R. Clinical and genetic variations in the syndrome of adult GM₂ gangliosidosis resulting from hexosaminidase A deficiency. *Ann Neurol* 1984; 16: 14–20
- Bach G, Tomczak J, Risch N, Ekstein J. Tay-Sachs screening in the Jewish Ashkenazi population: DNA testing is the preferred procedure. *Am J Med Genet* 2001; 99: 70–75
- Barnes D, Misra VP, Young EP, Thomas PK, Harding AE. An adult onset hexosaminidase A deficiency syndrome with sensory neuropathy and internuclear ophthalmoplegia. *J Neurol Neurosurg Psychiatry* 1991; 54: 1112–1113

- Barness LA, Henry K, Kling P, Laxova R, Kaback M, Gilbert-Barness E. A 7-year old white-male boy with progressive neurological deterioration. *Am J Med Genet* 1991; 40: 271–279
- Beck M, Sieber N, Goebel HH. Progressive cerebellar ataxia in juvenile GM₂-gangliosidosis type Sandhoff. *Eur J Pediatr* 1998; 157: 866–867
- Brett EM, Ellis RB, Haas L, Ikonne JU, Lake BD, Patrick AD, Stephens R. Late onset GM₂ gangliosidosis: clinical, pathological, and biochemical studies on 8 patients. *Arch Dis Child* 1973; 48: 775–785
- Brismar J, Brismar G, Coates R, Gascon G, Ozand P. Increased density of the thalamus on CT scans in patients with GM₂ gangliosidosis. *Am J Neurol* 1990; 11: 125–130
- Çaliskan M, Özmen M, Beck M, Apak S. Thalamic hyperdensity – is it a diagnostic marker for Sandhoff disease? *Brain Dev* 1993; 15: 387–388
- Chavany C, Jendoubi M. Biology and potential strategies for the treatment of GM₂ gangliosidosis. *Mol Med Today* 1998; 4: 158–165
- Chen B, Rigat B, Curry C, Mahuran DJ. Structure of the GM2A gene: identification of an exon 2 nonsense mutation and a naturally occurring transcript with an in-frame deletion. *Am J Hum Genet* 1999; 65: 77–87
- Conzelmann E, Kytzia HJ, Navon R, Sandhoff K. Ganglioside GM₂ N-acetyl-β-D-galactosaminidase activity in cultured fibroblasts of late-infantile and adult GM₂ gangliosidosis patients and of healthy probands with low hexosaminidase level. *Am J Hum Genet* 1983; 35: 900–913
- Cordeiro P, Hechtman P, Kaplan F. The GM₂ gangliosidosis databases: allelic variation at the *HEXA*, *HEXB*, and *GM2A*. *Genet Med* 2000; 2: 319–327
- Di Gregorio F, Ferraro G, Marini P, Siliprandi R, Gorio A. The influence of gangliosidosis on neurite growth regeneration. *Neuropediatrics* 1984; 15: 93–96
- D'Souza G, McCann CL, Hedrick J, Fairley C, Nagel HL, Kushner JD, Kessel R. Tay-Sachs disease carrier screening: a 21-year experience. *Genet Test* 2000; 4: 257–263
- Federico A, Palmeri S, Malandrini A, Fabrizi G, Mondelli M, Guazzi GC. The clinical aspects of adult hexosaminidase deficiencies. *Dev Neurosci* 1991; 13: 280–287
- Fukumizu M, Yoshikawa H, Takashima N, Kurokawa T. Tay-Sachs disease: progression of changes on neuroimaging in four cases. *Neuroradiology* 1992; 34: 483–486
- Goebel HH, Stolte G, Kustermann-Kuhn B, Harzer K. B₁ Variant of GM₂ gangliosidosis in a 12-year-old patient. *Pediatr Res* 1989; 25: 89–93
- Gordon BA, Gordon KE, Hinton GG, Cadera W, Feleki V, Bayleran J, Hechtman P. Tay-Sachs disease: B₁ variant. *Pediatr Neurol* 1988; 4: 54–57
- Gray RGF, Green A, Rabb L, Broadhead DM, Besley GTN. A case of the B₁ variant of GM₂-gangliosidosis. *J Inher Metab Dis* 1990; 13: 280–282
- Grosso S, Farnetani MA, Berardi R, Margollicci M, Galluzzi P, Vivarelli R, Morgese G, Balestri P. GM₂ gangliosidosis variant B₁. *Neuroradiologic features*. *J Neurol* 2003; 250: 17–21
- Guidotti JE, Mignon A, Haase G, Caillaud C, McDonnell N, Kahn A, Poenaru L. Adenoviral gene therapy of the Tay-Sachs disease in hexosaminidase A-deficient knock-out mice. *Hum Mol Genet* 1999; 8: 831–838
- Hittmair K, Wimberger D, Bernert G, Mallek R, Schindler EG. MRI in a case of Sandhoff's disease. *Neuroradiology* 1996; 38: S178–S180
- Hund E, Grau A, Fogel W, Fosting M, Cantz M, Kunstermann-Kuhn B, Harzer K, Navon R, Goebel HH, Meinck H-M. Progressive cerebellar ataxia, proximal neurogenic weakness and ocular motor disturbances: hexosaminidase A deficiency with late onset in four siblings. *J Neurol Sci* 1997; 145: 25–31
- Jeyakumar M, Butters TD, Cortina-Borja M, Hunnam V, Proia RL, Pery VH, Dwek RA, Platt FM. Delayed symptom onset and increased life expectancy in Sandhoff disease mice treated with N-butyldeoxynojirimycin. *Proc Natl Acad Sci* 1999; 96: 6388–6393
- Jeyakumar M, Norflus F, Tifft CJ, Cortina-Borja M, Butters TD, Proia RL, Perry VH, Dwek RA, Platt FM. Enhanced survival in Sandhoff disease mice receiving a combination of substrate deprivation therapy and bone marrow transplantation. *Blood* 2001; 97: 327–329
- Johnson WG, Chutorian A, Miranda A. A new juvenile hexosaminidase deficiency disease presenting as cerebellar ataxia: clinical and biochemical studies. *Neurology* 1977; 27: 1012–1018
- Karni A, Navon R, Sadeh M. Hexosaminidase A deficiency manifesting as spinal muscular atrophy of late onset. *Ann Neurol* 1988; 24: 451–453
- Koelfen W, Freund M, Jaschke W, Koenig S, Schultze C. GM₂ gangliosidosis (Sandhoff's disease): two year follow-up by MRI. *Neuroradiology* 1994; 36: 152–154
- Kotagal S, Wenger DA, Alcala H, Gomez C, Horenstein S. AB variant GM₂ gangliosidosis: cerebrospinal fluid and neuropathologic characteristics. *Neurology* 1986; 36: 438–440
- Kroll RA, Pagel MA, Roman-Goldstein S, Barkovich AJ, D'Agostino AN, Neuwelt EA. White matter changes associated with Feline GM₂ gangliosidosis (Sandhoff disease): correlation of MR findings with pathologic and ultrastructural abnormalities. *AJNR Am J Neuroradiol* 1995; 16: 1912–1226
- Lui Y, Wada R, Kawai H, Sango K, Deng C, Tai T, McDonald MP, Araujo K, Crawley JN, Bierfreund U, Sandhoff K, Suzuki K, Proia RL. A genetic model of substrate deprivation therapy for a glycosphingolipid storage disorder. *J Clin Invest* 1999; 103: 497–505
- Meek D, Wolfe LS, Andermann E, Andermann F. Juvenile progressive dystonia: a new phenotype of GM₂ gangliosidosis. *Ann Neurol* 1984; 15: 348–352
- Mugikura S, Takahashi S, Higano S, Kurihara N, Kon K, Sakamoto K. MR findings in Tay-Sachs disease. *J Comput Assist Tomogr* 1996; 20: 551–555
- Nassogne MC, Commare MC, Lellouch-Tubiana A, Emond S, Zerah M, Caillaud C, Hertz-Pannier L, Saudubray JM. Unusual presentation of GM₂ gangliosidosis mimicking a brain stem tumor in a 3-year-old girl. *AJNR Am J Neuroradiol* 2003; 24: 840–842
- Navon R. Molecular and clinical heterogeneity of adult GM₂ gangliosidosis. *Dev Neurosci* 1991; 13: 295–298
- Navon R, Argov Z, Brand N, Sandbank U. Adult GM₂ gangliosidosis in association with Tay-Sachs disease: a new phenotype. *Neurology* 1981; 31: 1397–1401
- Navon R, Argov Z, Frisch A. Hexosaminidase A deficiency in adults. *Am J Med Genet* 1986; 24: 179–196
- Neote K, Mahuran DJ, Gravel RA. Molecular genetics of β-hexosaminidase deficiencies. *Adv Neurol* 1991; 56: 189–207
- Neufeld EF. Natural history and inherited disorders of a lysosomal enzyme α-hexosaminidase. *J Biol Chem* 1989; 264: 10927–10930
- Norflus F, Tifft CJ, McDonald MP, Goldstein G, Crawley JN, Hoffmann A, Sandhoff K, Suzuki K, Proia RL. Bone marrow transplantation prolongs life span and ameliorates neurologic manifestations in Sandhoff disease mice. *J Clin Invest* 1998; 101: 1881–1888

- Oya Y, Proia RL, Norflus F, Tifft CJ, Langaman C, Suzuki K. Distribution of enzyme-bearing cells in GM₂ gangliosidosis mice: regionally specific pattern of cellular infiltration following bone marrow transplantation. *Acta Neuropathol (Berl)* 2000; 99: 161–168
- Paw BH, Moskowitz SM, Uhrhammer N, Wright N, Kaback MM, Neufeld EF. Juvenile GM₂ gangliosidosis caused by substitution of histidine for arginine at position 499 or 504 of the α -subunit of β -hexosaminidase. *J Biol Chem* 1990; 265: 9452–9457
- Platt FM, Butters TD. New therapeutic prospects for the glycosphingolipid lysosomal storage diseases. *Biochem Pharmacol* 1998; 56: 421–430
- Platt FM, Neises GR, Reinkensmeier G, Townsend MJ, Perry VH, Proia RL, Winchester B, Dwek RA, Butters TD. Prevention of lysosomal storage in Tay-Sachs mice treated with *N*-butyldeoxynojirimycin. *Science* 1997; 276: 428–431
- Platt FM, Jeyakumar M, Andersson U, Priestman DA, Dewk RA, Butters TD. Inhibition of substrate synthesis as a strategy for glycolipid lysosomal storage disease therapy. *J Inher Metab Dis* 2001; 24: 275–290
- Pullarkat RK, Reha H, Beratis NG. Accumulation of ganglioside GM₂ in cerebrospinal fluid of a patient with the variant AB of infantile GM₂ gangliosidosis. *Pediatrics* 1981; 68: 106–108
- Rapin I, Suzuki K, Suzuki K, Valsamis MP. Adult (chronic) GM₂ gangliosidosis: atypical spinocerebellar degeneration in a Jewish sibship. *Arch Neurol* 1976; 33: 120–130
- Rattazzi MC, Dobrenis K. Treatment of GM₂ gangliosidosis: past experiences, implications, and future prospects. *Adv Genet* 2001; 44: 317–339
- Rubin M, Karpati G, Wolfe LS, Carpenter S, Klavins MH, Mahuran DJ. Adult onset motor neuropathy in the juvenile type of hexosaminidase A and B deficiency. *J Neurol Sci* 1988; 87: 103–119
- Salaman MS, Clarke JTR, Midroni G, Waxman MB. Peripheral and autonomic nervous system involvement in chronic GM₂-gangliosidosis. *J Inher Metab Dis* 2001; 24: 65–71
- Sandhoff K, Harzer K, Wässle W, Jatzkewitz H. Enzyme alterations and lipid storage in three variants of Tay-Sachs disease. *J Neurochem* 1971; 8: 2469–2489
- Schepers U, Glombitza G, Lemm T, Hoffmann A, Chabas A, Ozand P, Sandhoff K. Molecular analysis of a GM₂-activator deficiency in two patients with GM₂-gangliosidosis AB variant. *Am J Hum Genet* 1996; 59: 1048–105
- Schnorf H, Gitzelmann R, Bosshard NU, Spycher M, Waespe W. Early and severe sensory loss in three adult siblings with hexosaminidase A and B deficiency (Sandhoff disease). *J Neurol Neurosurg Psychiatry* 1995; 59: 520–523
- Specola N, Vanier MT, Goutières F, Mikol J, Aicardi J. The juvenile and chronic forms of GM₂ gangliosidosis: clinical and enzymatic heterogeneity. *Neurology* 1990; 40: 145–150
- Streifler JY, Gornish M, Hadar H, Gadoth N. Brain imaging in late-onset GM₂ gangliosidosis. *Neurology* 1993; 43: 2055–2058
- Suzuki K, Vanier MT. Biochemical and molecular aspects of late-onset GM-2 gangliosidosis: B1 variant as a phenotype. *Dev Neurosci* 1991; 13: 288–294
- Thomas PK, Young E, King RHM. Sandhoff disease mimicking adult-onset bulbospinal neuropathy. *J Neurol Neurosurg Psychiatry* 1989; 52: 1103–1106
- Wada R, Tifft CJ, Proia RL. Microglial activation precedes acute neurodegeneration in Sandhoff disease and is suppressed by bone marrow transplantation. *Proc Nat Acad Sci* 2000; 97: 10954–10959
- Walkley SU, Siegel DA, Dobrenis K. GM₂ Gangliosidosis and pyramidal neuron dendritogenesis. *Neurochem Res* 1995; 20: 1287–1299
- Walkley SU, Siegel DA, Dobrenis K, Zervas M. GM₂ gangliosidosis as a regulator of pyramidal neuron dendritogenesis. *Ann NY Acad Sci* 1998; 845: 188–199
- Walkley SU, Zervas M, Wiseman S. Gangliosidosis as modulators of dendritogenesis in normal and storage disease-affected pyramidal neurons. *Cereb Cortex* 2000; 10: 1028–1037
- Ward CP, Fensom AH, Green PM. Biallelic discrimination assays for the three common Ashkenazi Jewish mutations and a common non-Jewish mutation, in Tay-Sachs disease, using fluorogenic taqman probes. *Genet Test* 2000; 4: 351–358
- Willner JP, Grabowski GA, Gordon RE, Bender AN, Desnick RJ. Chronic GM₂ gangliosidosis masquerading as atypical Friedreich ataxia: clinical, morphologic, and biochemical studies of nine cases. *Neurology* 1981; 31: 787–798
- Yoshikawa H, Yamada K, Sakuragawa N. MRI in the early stage of Tay-Sachs disease. *Neuroradiology* 1992; 34: 394–395
- Yüksel A, Yalçinkaya C, Iolak C, Gündüz E, Seven M. Neuroimaging findings in four patients with Sandhoff disease. *Pediatr Neurol* 1999; 21: 562–565

11 Fabry Disease

- Abe A, Gregory S, Lee L, Killen PD, Brady RO, Kulkarni A, Shayman JA. Reduction of globotriasylceramide in Fabry disease mice by substrate deprivation. *J Clin Invest* 2000; 105: 1563–1571
- Altarescu G, Moore DF, Pursley R, Campia U, Goldstein S, Bryant M, Panza JA, Schiffmann R. Enhanced endothelium-dependent vasodilation in Fabry disease. *Stroke* 2001; 32: 1559–1562
- Asano N, Ishii S, Kizu H, Ikeda H, Ikeda K, Kato A, Martin OR, Fan JQ. In vitro inhibition and intracellular enhancement of lysosomal α -galactosidase A activity in Fabry lymphoblasts by 1-deoxygalactonojirimycin and its derivatives. *Eur J Biochem* 2000 267: 4179–4186
- Ashley GA, Shabbeer J, Yasuda M, Eng CM, Desnick RJ. Fabry disease: twenty novel α -galactosidase A mutations causing the classical phenotype. *J Hum Genet* 2001; 46: 192–196
- Baehner F, Kampmann C, Whybra C, Miebach E, Wiethoff CM, Beck M. Enzyme replacement therapy in heterozygous females with Fabry disease: results of a phase IIIB study. *J Inher Metab Dis* 2003; 26: 617–627
- Brantom MH, Schiffmann R, Sabnis SG, Murray GJ, Quirk JM, Altarescu G, Goldfarb L, Brady RO, Balow JE, Austin HA, Kopp JB. Natural history of Fabry renal disease. *Medicine* 2002; 81: 122–138
- DeVeber GA, Schwarting GA, Kolodny EH, Kowall NW. Fabry disease: immunocytochemical characterization of neuronal involvement. *Ann Neurol* 1992; 31: 409–415
- Dütsch M, Marthol H, Stemper B, Brys M, Haendl T, Hilz MJ. Small fiber dysfunction predominates in Fabry neuropathy. *J Clin Neurophysiol* 2002; 19: 575–586
- Eng CM, Guffon N, Wilcox WR, Germain DP, Lee P, Waldek S, Caplan L, Linthorst GE, Desnick RJ. Safety and efficacy of recombinant human α -galactosidase a replacement therapy in Fabry's disease. *N Engl J Med* 2001; 345: 9–16
- Feldt-Rasmussen U, Rasmussen AK, Mersebach H, Rosenberg KM, Hasholt L, Sorensen S. Fabry disease: a new challenge in endocrinology and metabolism? *Eur J Endocrinol* 2002; 146: 741–742

- Filling-Katz MR, Merrick HF, Fink JK, Miles RB, Sokol J, Barton NW. Carbamazepine in Fabry's disease: effective analgesia with dose-dependent exacerbation of autonomic dysfunction. *Neurology* 1989; 39: 598–600
- Frustazi A, Chimenti C, Ricci R, Natale L, Russo MA, Pieroni M, Eng CM, Desnick RJ. Improvement in cardiac function in the cardiac variant of Fabry's disease with galactose-infusion therapy. *N Engl J Med* 2001; 345: 25–32
- Gahl WA. New therapies for Fabry's disease. *N Engl J Med* 2001; 345: 55–57
- Grewal RP. Stroke in Fabry's disease. *J Neurol* 1994; 241: 153–156
- Grewal RP, McLatchey SK. Cerebrovascular manifestations in a female carrier of Fabry's disease. *Acta Neurol Belg* 1992; 92: 36–40
- Hajioff D, Enever Y, Quiney R, Zuckerman J, Macdermot K, Mehta A. Hearing loss in Fabry patients: the effect of agalsidase alpha replacement therapy. *J Inher Metab Dis* 2002; 26: 787–794
- Kaye EM, Kolodny EH, Logigian EL, Ullman MD. Nervous system involvement in Fabry's disease: clinicopathological and biochemical correlation. *Ann Neurol* 1988; 23: 505–509
- Kleijer WJ, Hussaarts-Odijk LM, Sachs ES, Jahoda MGJ, Niermeijer MF. Prenatal diagnosis of Fabry's disease by direct analysis of chorionic villi. *Prenat Diagn* 1987; 7: 283–287
- Kornreich R, Bishop DF, Desnick RJ. α -galactosidase A gene rearrangements causing Fabry disease. *J Biol Chem* 1990; 265: 9319–9326
- MacDermot KD, Holmes A, Miners AH. Anderson-Fabry disease: clinical manifestations and impact of disease in a cohort of 60 obligate carrier females. *J Med Genet* 2001; 38: 769–775
- MacDermot KD. Anderson-Fabry disease: clinical manifestations and impact of disease in a cohort of 98 hemizygous males. *J Med Genet* 2001; 37: 750–760
- Menzies DG, Campbell IW. Magnetic resonance in Fabry's disease. *J Neurol Neurosurg Psychiatry* 1988; 51: 1240–1241
- Mitsias P, Levine SR. Cerebrovascular complications of Fabry's disease. *Ann Neurol* 1996; 40: 8–17
- Moore DF, Scott LTC, Gladwin MT, Altarescu G, Kaneski C, Suzuki K, Pease-Fye M, Ferri R, Brady RO, Herscovitch P, Schiffmann R. Regional cerebral hyperperfusion and nitric oxide pathway dysregulation in Fabry disease. Reversal by enzyme replacement therapy. *Circulation* 2001; 104: 1506–1512
- Moore DF, Altarescu G, Ling GSF, Jeffries N, Frei KP, Weibel T, Charria-Ortiz G, Ferri R, Arai AE, Brady RO, Schiffmann R. Elevated cerebral blood flow velocities in Fabry disease with reversal after enzyme replacement. *Stroke* 2002; 33: 525–531
- Moore DF, Altarescu G, Barker WC, Patronas NJ, Herscovitch P, Schiffmann R. White matter lesions in Fabry disease occur in 'prior' selectively hypometabolic and hyperperfused brain regions. *Brain Res Bull* 2003; 62: 231–240
- Moore DF, Ye F, Schiffmann R, Butman JA. Increased signal intensity in the pulvinar on T1-weighted images: a pathognomonic MR imaging sign of Fabry disease. *AJNR Am J Neuroradiol* 2003; 24: 1096–1101
- Morgan SH, Rudge P, Smith SJM, Bronstein AM, Kendall BE, Holly E, Young EP, Crawford MA, Bannister R. The neurological complications of Anderson-Fabry disease (α -galactosidase A deficiency): investigation of symptomatic and presymptomatic patients. *QJM [N Ser]* 1990; 75: 491–504
- Moumdjian R, Tampieri D, Melanson D, Ethier R. Anderson-Fabry disease: a case report with MR, CT and cerebral angiography. *AJNR Am J Neuroradiol* 1989; 10: S69–S70
- Nakao S, Takenaka T, Maeda M, Kodama C, Tanaka A, Tahara M, Yoshida A, Kuriyama M, Hayashibe H, Sakuraba H, Tanaka H. An atypical variant of Fabry's disease in men with left ventricular hypertrophy. *N Engl J Med* 1995; 333: 288–293
- Nelis GF, Jacobs GJA. Anorexia, weight loss, and diarrhea as presenting symptoms of angiokeratoma corporis diffusum (Fabry-Anderson's disease). *Dig Dis Sci* 1989; 34: 1798–1800
- Pastores GM, Thadhani R. Enzyme-replacement therapy for Anderson-Fabry disease. *Lancet* 2001; 358: 601–603
- Rahman AN, Lindenberg R. The neuropathology of hereditary dystopic lipidosis. *Arch Neurol* 1963; 9: 373–385
- Schiffmann R, Kopp JB, Austin HA, Sabnis S, Moore DF, Weibel T, Balow J, Brady RO. Enzyme replacement therapy in Fabry disease. A randomized controlled trial. *JAMA* 2001; 285: 2743–2749
- Takanashi J, Barkocich JA, Dillon WP, Sherr EH, Hart KA, Packman S. T1 hyperintensity in the pulvinar: key imaging feature for diagnosis of Fabry disease. *AJNR Am J Neuroradiol* 2003; 24: 916–921
- Takenaka T, Murray GH, Qin G, Quirk JM, Oshima T, Qasba P, Clark K, Kulkarni AB, Brady RO, Medin JA. Long-term enzyme correction and lipid reduction in multiple organs of primary and secondary transplanted Fabry mice receiving transduced bone marrow cells. *Proc Natl Acad Sci USA* 2000; 97: 7515–7520
- Whybra C, Kampmann C, Willers I, Davies J, Winchester B, Kriegsmann J, Brühl K, Gal A, Bunge S, Beck M. Anderson-Fabry disease: clinical manifestations of disease in female heterozygotes. *J Inher Metab Dis* 2001; 24: 715–724
- Wiedemann F, Breuning F, Beer M, Sandstedt J, Turschner O, Voelker W, Ertl G, Knoll A, Wanner C, Strotmann JM. Improvement of cardiac function during enzyme replacement therapy in patients with Fabry disease, a prospective strain rate imaging study. *Circulation* 2003; 108: 1299–1301

12 Fucosidosis

- Darby JK, Willems PJ, Nakashima P, Johnsen J, Ferrell RE, Wijsman EM, Gerhard DS, Dracopoli NC, Housman D, Henke J, Fowler ML, Shows TB, O'Brien JS, Cavalli-Sforza LL. Restriction analysis of the structural α -L-fucosidase gene and its linkage to fucosidosis. *Am J Hum Genet* 1988; 43: 749–755
- Galluzzi P, Rufa A, Balestri P, Cerase A, Federico A. MR brain imaging of fucosidosis type I. *AJNR Am J Neuroradiol* 2001; 22: 777–780
- Gordon BA, Gordon KE, Seo JC, Yang M, DiCioccio RA, O'Brien JS. Fucosidosis with dystonia. *Neuropediatrics* 1995; 26: 325–327
- Inui K, Akagi M, Nishigaki T, Muramatsu T, Tsukamoto H, Okada S. A case of chronic infantile type of fucosidosis: clinical and magnetic resonance imaging. *Brain Dev* 2000; 22: 47–49
- Ismail EAR, Rudwan M, Shafik MK. Fucosidosis: immunological studies and chronological neuroradiological changes. *Acta Paediatr* 1999; 88: 224–227
- Kretz KA, Cripe D, Carson GS, Fukushima H, O'Brien JS. Structure and sequence of the human α -L-fucosidase gene and pseudogene. *Genomics* 1992; 12: 276–280
- Miano M, Lanino E, Gatti R, Morreale G, Fondelli P, Celle ME, Stroppiano M, Crescenzi F, Dini G. Four-year follow-up of a case of fucosidosis treated with unrelated donor bone marrow transplantation. *Bone Marrow Transplant* 2001; 27: 747–751

- Michalski J-C, Klein A. Glycoprotein lysosomal storage disorders: α - and β -mannosidosis, fucosidosis and α -N-acetylgalactosaminidase deficiency. *Biochim Biophys Acta* 1999; 1455: 69–84
- Ng Ying Kin NMK. Composition of the urinary glycoconjugates excreted by patient with type I and type II fucosidosis. *Clin Chem* 1987; 33: 44–47
- Provenzale JM, Barboriak DP, Sims K. Neuroradiologic findings in fucosidosis, a rare lysosomal storage disease. *AJNR Am J Neuroradiol* 1995; 16: 809–813
- Taylor RM, Farrow BRH, Stewart GJ, Healy PJ, Tiver K. Lysosomal enzyme replacement in neural tissue by allogeneic bone marrow transplantation following total lymphoid irradiation in canine fucosidosis. *Transplant Proc* 1987; 9: 2730–2734
- Taylor RM, Farrow BRH, Stewart GJ. Amelioration of clinical disease following bone marrow transplantation in fucosidase-deficient dogs. *Am J Med Genet* 1992; 42: 628–632
- Terespolsky D, Clarke JTR, Blaser SI. Evolution of the neuroimaging changes in fucosidosis type II. *J Inher Metab Dis* 1996; 19: 775–781
- Tiberio G, Filocamo M, Gatti R, Durand P. Mutations in fucosidosis gene: a review. *Acta Genet Med Gemellol* 1995; 44: 223–232
- Vellodi A, Cragg H, Winchester B, Young E, Downie CJC, Hoare RD, Stokes R, Banerjee GK. Allogeneic bone marrow transplantation for fucosidosis. *Bone Marrow Transplant* 1995; 15: 153–158
- Willems PJ, Gatti R, Darby JK, Romeo G, Durand P, Dumon JE, O'Brien JS. Fucosidosis revisited: a review of 77 patients. *Am J Hum Genet* 1991; 38: 111–131
- Willems PJ, Seo H-C, Coucke P, Tonorenzi R, O'Brien JS. Spectrum of mutations in fucosidosis. *Eur J Hum Genet* 1999; 7: 60–67
- Kachur E, del Maestro R. Mucopolysaccharidoses and spinal cord compression: case report and review of the literature with implications of bone marrow transplantation. *Neurosurgery* 2000; 47: 223–229
- Kulkarni MV, Williams JC, Yeakley JW, Andrews JL, McArdle CB, Narayana PA, Howell RR, Jonas AJ. Magnetic resonance imaging in the diagnosis of the cranio-cervical manifestations of the mucopolysaccharidoses. *Magn Reson Imaging* 1987; 5: 317–323
- Lee C, Dineen TE, Brack M, Kirsch JE, Runge VM. The mucopolysaccharidoses: characterization by cranial MR imaging. *AJNR Am J Neuroradiol* 1993; 14: 1285–1292
- Levin TL, Berdon WE, Lachman RS, Anyane-Yeboah K, Ruzal-Shapiro C, Roye DP. Lumbar gibbus in storage diseases and bone dysplasias. *Pediatr Radiol* 1997; 27: 289–294
- Martin JJ, Ceuterick C. The contribution of pathology to the study of storage disorders. *Pathol Res Pract* 1988; 183: 375–385
- Murata R, Nakajima S, Tanaka A, Miyagi N, Matsuoka O, Kogame S, Inoue Y. MR imaging of the brain in patients with mucopolysaccharidosis. *AJNR Am J Neuroradiol* 1989; 10: 1165–1170
- Nelson J, Shields D, Mulholland HC. Cardiovascular studies in the mucopolysaccharidoses. *J Med Genet* 1990; 27: 94–100
- Perretti A, Petrillo A, Pelosi L, Balbi P, Parenti G, Riemma A, Strisciuglio P. Detection of early abnormalities in the mucopolysaccharidoses by the use of visual and brainstem auditory evoked potentials. *Neuropediatrics* 1989; 21: 83–86
- Purpura DP, Suzuki K. Distortion of neuronal geometry and formation of aberrant synapses in neuronal storage disease. *Brain Res* 1976; 116: 1–21
- Schiffmann R, Brady RO. New prospects for the treatment of lysosomal storage diseases. *Drugs* 2002; 62: 733–742
- Scott HS, Bunge S, Gal A, Clarke LA, Morris CP, Hopwood JJ. Mutation update. Molecular genetics of mucopolysaccharidosis type I: diagnostic, clinical, and biological implications. *Hum Mutat* 1995; 6: 288–302
- Seto T, Kono K, Morimoto K, Inoue Y, Shintaku H, Hattori H, Matsuoka O, Yamano T, Tanaka A. Brain magnetic resonance imaging in 23 patients with mucopolysaccharidoses and the effect of bone marrow transplantation. *Ann Neurol* 2001; 50: 79–92
- Shih S-L, Lee Y-J, Lin S-P, Sheu C-Y, Blickman JG. Airway changes in children with mucopolysaccharidoses. CT evaluation. *Acta Radiol* 2002; 43: 40–43
- Sly WS, Vogler C. Brain-directed gene therapy for lysosomal storage disease: going well beyond the blood-brain barrier. *Proc Natl Acad Sci* 2002; 9: 5760–5762
- Stone JE. Urine analysis in the diagnosis of mucopolysaccharide disorders. *Ann Clin Biochem* 1998; 35: 207–225
- Wraith JE. The mucopolysaccharidoses: a clinical review and guide to management. *Arch Dis Child* 1995; 72: 263–267

13 Mucopolysaccharidoses

General

- Albano LMJ, Sugayama SSMM, Bertola DR, Andrade CEF, Utagawa CY, Puppi F, Nader HB, Toma L, Coelho J, Leistner S, Burin M, Giugliani R, Kim CA. Clinical and laboratorial study of 19 cases of mucopolysaccharidoses. *Rev Hosp Clin Fac Med S Paulo* 2000; 55: 213–218
- Barone R, Parano E, Trifiletti RR, Fiumara A, Pavone P. White matter changes mimicking a leukodystrophy in a patient with mucopolysaccharidosis: characterization by MRI. *J Neurol Sci* 2002; 195: 171–175
- Dekaban AS, Constantopoulos G. Mucopolysaccharidosis types I, II, IIIA and V. Pathological and biochemical abnormalities in the neural and mesenchymal elements of the brain. *Acta Neuropathol (Berl)* 1977; 39: 1–7
- Ero Y, Ohashi T. Gene therapy / cell therapy for lysosomal storage disease. *J Inher Metab Dis* 2000; 23: 293–298
- Fensom AH, Benson PF. Recent advances in the prenatal diagnosis of the mucopolysaccharidoses. *Prenat Diagn* 1994; 14: 1–12
- Gieselmann V. Lysosomal storage diseases. *Biochim Biophys Acta* 1995; 1270: 103–136
- Herrick IA, Rhine EJ. The mucopolysaccharidoses and anaesthesia: a report of clinical experience. *Can J Anaesth* 1988; 35: 67–73
- Affi AK, Sato Y, Waziri MH, Bell WE. Computed tomography and magnetic resonance imaging of the brain in Hurler's disease. *J Child Neurol* 1990; 5: 235–241
- Barone R, Parano E, Trifiletti RR, Fiumara A, Pavone P. White matter changes mimicking a leukodystrophy in a patient with mucopolysaccharidosis: characterization by MRI. *J Neurol Sci* 2002; 195: 171–175

Hurler Disease

- Baxter MA, Wynn RF, Deakin JA, Bellantuono I, Edington KG, Cooper A, Besley GTN, Church HJ, Wraith JE, Carr TF, Fairbairn LJ. Retrovirally mediated correction of bone marrow-derived mesenchymal stem cells from patients with mucopolysaccharidosis type I. *Blood* 2002; 99: 1857–1859
- Beesley CE, Meaney CA, Greenland G, Adams V, Vellodi A, Young EP, Winchester BG. Mutational analysis of 85 mucopolysaccharidosis type I families: frequency of known mutations, identification of 17 novel mutations and in vitro expression of missense mutations. *Hum Genet* 2001; 109: 503–511
- Braunlin EA, Rose AG, Hopwood JJ, Candel RD, Krivit W. Coronary artery patency following long-term successful engraftment 14 years after bone marrow transplantation in the Hurler syndrome. *Am J Cardiol* 2001; 88: 1075–1077
- Di Natale P, di Domenico C, Villani GRD, Lombardo A, Follenzi A, Naldini L. *In vitro* gene therapy of mucopolysaccharidosis type I by lentiviral vectors. *Eur J Biochem* 2002; 269: 2764–2771
- Gabrielli O, Salvolini U, Maricotti M. Cerebral MRI in two brothers with mucopolysaccharidosis type I and different clinical phenotypes. *Neuroradiology* 1992; 34: 313–315
- Grewal SS, Krivit W, Defor TE, Shapiro EG, Orchard PJ, Abel SL, Lockman LA, Ziegler RS, Dusenbery KE, Peters C. Hurler syndrome. Outcome of second hematopoietic cell transplantation in Hurler syndrome. *Bone Marrow Transplant* 2002; 29: 491–496
- Hite SH, Peters C, Krivit W. Correction of odontoid dysplasia following bone-marrow transplantation and engraftment (in Hurler syndrome MPS 1H). *Pediatr Radiol* 2000; 30: 464–470
- Johnson MA, Desai S, Hugh-Jones K, Starer F. Magnetic resonance imaging of the brain in Hurler syndrome. *AJNR Am J Neuroradiol* 1984; 5: 816–819
- Kakkis ED, Muenzer J, Tiller GE, Waber L, Belmont J, Passage M, Izykowski B, Phillips J, Doroshow R, Walot I, Hoft R, Neufeld EF. Enzyme-replacement therapy in mucopolysaccharidosis I. *N Engl J Med* 2001; 344: 182–188
- Keeling KM, Brooks DA, Hopwood JJ, Li P, Thompson JN, Bedwell DM. Gentamicin-mediated suppression of Hurler syndrome stop mutations restores a low level of α -L-iduronidase activity and reduces lysosomal glycosaminoglycan accumulation. *Hum Mol Genet* 2001; 10: 291–299
- Krivit W, Lockman LA, Watkins PA, Hirsch J, Shapiro EG. The future for treatment by bone marrow transplantation for adrenoleukodystrophy, metachromatic leukodystrophy, globoid cell leukodystrophy and Hurler syndrome. *J Inherit Metab Dis* 1995; 18: 398–412
- Loeb H, Jonniaux G, Resibois A, Cremer N, Dodion J, Tondeur M, Gregoire PE, Richard J, Cieters P. Biochemical and ultrastructural studies in Hurler's syndrome. *J Pediatr* 1968; 73: 860–874
- Rauch RA, Friloux LA III, Lott IT. MR Imaging of cavitory lesions in the brain with Hurler/Scheie. *AJNR Am J Neuroradiol* 1989; 10: S1–S3
- Schmidt H, Ullrich K, von Lengerke H-J, Kleine M, Brämswig J. Radiological findings in patients with mucopolysaccharidosis I H/S (Hurler-Scheie syndrome). *Pediatr Radiol* 1987; 17: 409–414
- Vellodi A, Young EP, Cooper A, Wraith JE, Winchester B, Meaney C, Ramaswami U, Will A. Bone marrow transplantation for mucopolysaccharidosis type I: experience of two British centres. *Arch Dis Child* 1997; 76: 92–99
- Walkley SU, Haskins ME, Shull RM. Alterations in neuron morphology in mucopolysaccharidosis type I*: a Golgi study. *Acta Neuropathol (Berl)* 1988; 75: 611–620
- Watis RWE, Spellacy E, Adams JH. Neuropathological and clinical correlations in Hurler disease. *J Inherit Metab Dis* 1986; 9: 261–272
- Winters PR, Harrod MJ, Molenich-Heetred SA, Kirkpatrick J, Rosenberg RN. α -L-Iduronidase deficiency and possible Hurler-Scheie genetic compound. Clinical, pathologic and biochemical findings. *Neurology* 1976; 26: 1003–1007
- Wraith JE. Enzyme replacement therapy in mucopolysaccharidosis type I: progress and emerging difficulties. *J Inherit Metab Dis* 2001; 24: 245–250

Hunter Disease

- Adinolfi M. Hunter syndrome: cloning of the gene, mutations and carrier detection. *Dev Med Child Neurol* 1993; 35: 79–85
- Bergstrom SK, Quinn JJ, Greenstein R, Ascensao J. Long-term follow-up of a patient transplanted for Hunter's disease type IIB: a case report and literature review. *Bone Marrow Transplant* 1994; 14: 653–658
- Clarke JTR, Willard HF, Teshima I, Chang PL, Skomorowski MA. Hunter disease (mucopolysaccharidosis type II) in a karyotypically normal girl. *Clin Genet* 1990; 37: 355–362
- Clarke JTR, Greer WL, Strasberg PM, Pearce RD, Skomorowski MA, Ray PN. Hunter disease (mucopolysaccharidosis type II) associated with unbalanced inactivation of the X chromosomes in a karyotypically normal girl. *Am J Hum Genet* 1991; 49: 289–297
- Davitt SM, Hatrick A, Sabharwal T, Pearce A, Gleeson M, Adam A. Tracheobronchial stent insertions in the management of major airway obstruction in a patient with Hunter syndrome (type II mucopolysaccharidosis). *Eur Radiol* 2002; 12: 458–462
- Flomen RH, Green PM, Bentley DR, Giannelli F, Green EP. Detection of point mutations and a gross deletion in six Hunter syndrome patients. *Genomics* 1992; 13: 543–550
- O'Brien DP, Cowie RA, Wraith JE. Cervical decompression in mild mucopolysaccharidosis type II (Hunter syndrome). *Child Nerv Syst* 1997; 13: 87–90
- Parsons VJ, Hughes DG, Wraith JE. Magnetic resonance imaging of the brain, neck and cervical spine in mild Hunter's syndrome (mucopolysaccharidosis type II). *Clin Radiol* 1996; 51: 719–723
- Shimoda-Matsubayashi S, Kuru Y, Sumie H, Ito T, Hattori N, Okuma Y, Mizuno Y. MRI findings in the mild type of mucopolysaccharidosis II (Hunter's syndrome). *Neuroradiology* 1990; 32: 328–330
- Shinomiya N, Nagayama T, Fujioka Y, Aoki T. MRI in the mild type of mucopolysaccharidosis II (Hunter's syndrome). *Neuroradiology* 1996; 38: 483–485
- Vellodi A, Young E, Cooper A, Lidchi V, Winchester B, Wraith JE. Long-term follow-up following bone marrow transplantation for Hunter disease. *J Inherit Metab Dis* 1999; 22: 638–648
- Vinchon M, Cotten A, Clarisse J, Chiki R, Christiaens J-L. Cervical myelopathy secondary to Hunter syndrome in an adult. *AJNR Am J Neuroradiol* 1995; 16: 1402–1403
- Wehnert M, Hopwood JJ, Schröder W, Herrmann FH. Structural gene aberrations in mucopolysaccharidosis II (Hunter). *Hum Genet* 1992; 89: 430–432

- Wilson PJ, Morris CP, Anson DS, Occhiodoro T, Bielicki J, Clements PR, Hopwood JJ. Hunter syndrome: isolation of an iduronate-2-sulfatase cDNA clone and analysis of patient DNA. (mucopolysaccharidosis type II / lysosomal storage disorder / X chromosome-linked mutations / sulfatase sequence homology) *Proc Natl Acad Sci* 1990; 87: 8531–8535
- Young ID, Harper PS, Newcombe RG, Archer IM. A clinical and genetic study of Hunter's syndrome. 2. Differences between the mild and severe forms. *J Med Genet* 1982; 19: 408–411
- Zafeiriou DI, Augoustidou-Savvopoulou PA, Papadopoulou FA, Gombakis NP, Katzos GS, Kontopoulos EE, van Diggelen OP. Magnetic resonance imaging findings in mild mucopolysaccharidosis II (Hunter's syndrome). *Eur J Paediatr Neurol* 1998; 2: 153–156

Sanfilippo Disease

- Andria G, di Natale P, del Giudice E, Strisciuglio P, Murino P. Sanfilippo B syndrome (MPS III B): mild and severe forms within the same sibship. *Clin Genet* 1979; 15: 500–504
- Barone R, Nigro F, Triulzi F, Musumeci S, Fiumara A, Pavone L. Clinical and neuroradiological follow-up in mucopolysaccharidosis type III (Sanfilippo syndrome). *Neuropediatrics* 1999; 30: 270–274
- Fu H, Samulski RJ, McCown TJ, Picornell YJ, Fletcher D, Muenzer J. Neurological correction of lysosomal storage in a mucopolysaccharidosis IIIB mouse model by adeno-associated virus-mediated gene delivery. *Mol Ther* 2002; 5: 42–49
- Gingöör N, Tunçbilek E. Sanfilippo disease type B. A case report and review of the literature on recent advances in bone marrow transplantation. *Turk J Pediatr* 1995; 37: 157–163
- Haust MD, Gordon BA, Hong R, Choi JH, Langer LO, Spranger J, Opitz JM. Clinicopathological conference: an adolescent girl with severe mental impairment and mucopolysacchariduria. *Am J Med Genet* 1985; 22: 1–27
- Jones MZ, Alroy J, Rutledge JC, Taylor JW, Alvord EC Jr, Toone J, Applegarth D, Hopwood JJ, Skutelsky E, Ianelli C, Thorley-Lawson D, Mitchell-Herpolsheimer C, Arias A, Sharp P, Evans W, Sillence D, Cavanagh KT. Human mucopolysaccharidosis IIID: clinical, biochemical, morphological and immunohistochemical characteristics. *J Neuropathol Exp Neurol* 1997; 56: 1158–1167
- Kurihara M, Kumagai K, Yagishita S. Case reports. Sanfilippo syndrome type C: a clinicopathological autopsy study of a long-term survivor. *Pediatr Neurol* 1996; 14: 317–321
- Ozand PT, Thompson JN, Gascon GG, Sarvepalli SB, Rahbeeni Z, Nester MJ, Brismar J. Sanfilippo type D presenting with acquired language disorder but without features of mucopolysaccharidosis. *J Child Neurol* 1994; 9: 408–411
- Petitti N, Holder CA, Williams DW III. Mucopolysaccharidosis III (Sanfilippo syndrome) type B. Cranial imaging in two cases. *J Comput Assist Tomogr* 1997; 21: 897–899
- Vallani GRD, Follenzi A, Vanacore B, di Domenico C, Naldini L, di Natale P. Correction of mucopolysaccharidosis type IIIB fibroblasts by lentiviral vector-mediated gene transfer. *Biochem J* 2002; 364: 747–753
- van de Kamp JJP, Niermeijer MF, von Figura K, Giesberts MAH. Genetic heterogeneity and clinical variability in the Sanfilippo syndrome (types A, B and C). *Clin Genet* 1981; 20: 152–160
- van Schrojenstein-de Valk HMJ, van de Kamp JJP. Follow-up on seven adult patients with mild Sanfilippo B-disease. *Am J Med Genet* 1987; 28: 125–129

- Zafeiriou DI, Savvopoulou-Augoustidou PA, Sewell A, Papadopoulou F, Badouraki M, Vargiami E, Gombakis NP, Katzos GS. Serial magnetic resonance imaging findings in mucopolysaccharidosis IIIB (Sanfilippo's syndrome B). *Brain Dev* 2001; 23: 385–389

Morquio Disease

- Giugliani R, Jackson M, Skinner SJ, Vimal CM, Fensom AH, Fahmy N, Sjövall A, Benson PF. Progressive mental regression in siblings with Morquio disease type B (mucopolysaccharidosis IVB). *Clin Genet* 1987; 32: 313–325
- Hughes DG, Chadderton RD, Cowie RA, Wraith JE, Jenkins JPR. MRI of the brain and craniocervical junction in Morquio's disease. *Neuroradiology* 1997; 39: 381–385
- Mikles M, Stanton RP. A review of Morquio syndrome. *Am J Orthopod* 1997; 26: 533–540
- Nelson J, Grebbell FS. The value of computed tomography in patients with mucopolysaccharidosis. *Neuroradiology* 1987; 29: 544–549
- Nelson J, Kinirons M. Clinical findings in 12 patients with MPS IVA (Morquio's disease). *Clin Genet* 1988; 33: 121–125
- Nelson J, Thomas PS. Clinical findings in 12 patients with MPS IVA (Morquio's disease). Further evidence for heterogeneity. III. Odontoid dysplasia. *Clin Genet* 1988; 33: 126–130
- Nelson J, Broadhead D, Mossman J. Clinical findings in 12 patients with MPS IVA (Morquio's disease). Further evidence for heterogeneity. I. Clinical and biochemical findings. *Clin Genet* 1988; 33: 111–120
- Northover H, Cowie RA, Wraith JE. Mucopolysaccharidosis type IVA (Morquio syndrome): a clinical review. *J Inherit Metab Dis* 1996; 19: 357–365
- Oshima A, Yoshida K, Shimmoto M, Fukuhara Y, Sakuraba H, Suzuki Y. Human β -glycosidase gene mutations in Morquio B disease. *Am J Hum Genet* 1991; 49: 1091–1093
- Rigante D, Antuzzi R, Ricci R, Segni G. Cervical myelopathy in mucopolysaccharidosis type IV. *Clin Neuropathol* 1999; 18: 84–86
- Stevens JM, Kendall BE, Crockard HA, Ransford A. The odontoid process in Morquio-Brailsford's disease; the effects of occipitocervical fusion. *J Bone Joint Surg [Br]* 1991; 73: 851–858

Maroteaux-Lamy Disease

- Herskhovitz E, Young E, Rainer J, Hall CM, Lidchi V, Chong K, Velodi A. Bone marrow transplantation for Maroteaux-Lamy syndrome (MPS VI): long-term follow-up. *J Inherit Metab Dis* 1999; 22: 50–62
- Hite SH, Krivit W, Haines SJ, Whitley CB. Syringomyelia in mucopolysaccharidosis type VI (Maroteaux-Lamy syndrome): imaging findings following bone marrow transplantation. *Pediatr Radiol* 1997; 27: 736–738
- Tamaki N, Kojima N, Tanimoto M, Suyama T, Matsumoto S. Myelopathy due to diffuse thickening of the cervical dura mater in Maroteaux-Lamy syndrome: report of a case. *Neurosurgery* 1987; 21: 416–419
- Uçakhan OO, Brodie SE, Desnick R, Willner J, Asbell PA. Long-term follow-up of corneal graft survival following bone marrow transplantation in the Maroteaux-Lamy syndrome. *CLAO J* 2001; 27: 234–237

- Vestermarck S, Tønnesen T, Schultz Andersen M, Güttler F. Mental retardation in a patient with Maroteaux-Lamy. *Clin Genet* 1987; 31: 114–117
- Vougioukas VI, Berlis A, Kopp MV, Korinthenberg R, Spreer J, van Velthoven V. Neurosurgical interventions in children with Maroteaux-Lamy syndrome. Case report and review of the literature. *Pediatr Neurosurg* 2001; 35: 35–38
- Wicker G, Prill V, Brooks D, Gibson G, Hopwood J, von Figura K, Peters C. Mucopolysaccharidosis VI (Maroteaux-Lamy syndrome). *J Biol Chem* 1991; 266: 21386–21391

Sly Disease

- Bernsen PLJA, Wevers RA, Gabreëls FJM, Lamers KJB, Sonnen AEH, Schuurmans Stekhoven JH. Phenotypic expression in mucopolysaccharidosis VII. *J Neurol Neurosurg Psychiatry* 1987; 50: 699–703
- Fukuda S, Tomatsu S, Sukegawa K, Sasaki T, Yamada Y, Kuwahara T, Okamoto H, Ikeda Y, Yamaguchi S, Orii T. JSSIM Meeting. Molecular analysis of mucopolysaccharidosis type VII. *J Inherit Metab Dis* 1991; 14: 800–804
- Kyle JW, Birkenmeier EH, Gwynn B, Vogler C, Hoppe PC, Hoffmann JW, Sly WS. Correction of murine mucopolysaccharidosis VII by a human β -glucuronidase transgene. *Proc Natl Acad Sci* 1990; 87: 3914–3918
- Ross CJD, Bastedo L, Maier SA, Sands MS, Chang PL. Treatment of a lysosomal storage disease, mucopolysaccharidosis VII, with microencapsulated recombinant cells. *Hum Gene Ther* 2000; 11: 2117–2127
- Sewell AC, Gehler J, Mittermaier G, Meyer E. Mucopolysaccharidosis type VII (β -glucuronidase deficiency): a report of a new case and a survey of those in the literature. *Clin Genet* 1982; 21: 366–373
- Tomatsu S, Fukuda S, Sukegawa K, Ikeda Y, Yamada S, Yamada Y, Sasaki T, Okamoto H, Kuwahara T, Yamaguchi S, Kiman T, Shintaku H, Isshiki G, Orii T. Mucopolysaccharidosis type VII: characterization of mutations and molecular heterogeneity. *Am J Hum Genet* 1991; 48: 89–96

14 Free Sialic Acid Storage Disorder

- Aula N, Salomäki P, Timonen R, Verheijen F, Mancini G, Månsson J-E, Aula P, Peltonen L. The spectrum of SLC17A5 gene mutations resulting in free sialic acid-storage diseases indicates some genotype-phenotype correlation. *Am J Hum Genet* 2000; 67: 832–840
- Autio-Harminen H, Oldfors A, Sourander P, Renlund M, Dammert K, Similä S. Neuropathology of Salla disease. *Acta Neuropathol (Berl)* 1988; 75: 481–490
- Baumkötter J, Cantz M, Mendla K, Baumann W, Friebohn H, Gehler J, Spranger J. N-Acetylneuraminic acid storage disease. *Hum Genet* 1985; 71: 155–159
- Biancheri R, Verbeek E, Rossi A, Gaggero R, Roccatagliata L, Gatti R, van Diggelen OP, Verheijen FW, Mancini GMS. An Italian severe Salla disease variant associated with a SLC17A5 mutation earlier described in infantile sialic acid storage disease. *Clin Genet* 2002; 61: 443–447
- Blom HJ, Andersson HC, Seppala R, Tietze F, Gahl WA. Defective glucuronic acid transport from lysosomes of infantile free sialic acid storage disease fibroblasts. *Biochem J* 1990; 268: 621–625

- Chigorno V, Tettamanti G, Sonnino S. Metabolic processing of gangliosidosis by normal and Salla human fibroblasts in culture. *J Biol Chem* 1996; 36: 21738–21744
- Daneman A, Stringer D, Reilly BJ. Neonatal ascitis due to lysosomal storage disease. *Radiology* 1983; 149: 463–467
- Echenne B, Vidal M, Maire I, Michalski JC, Baldet P, Astruc J. Salla disease in one non-Finnish patient. *Eur J Pediatr* 1986; 145: 320–322
- Fois A, Balestri P, Mancini GMS, Borgogni P, Margollicci MA, Molinelli M, Alessandri C, Gerli R. Free sialic acid storage disease. *Eur J Pediatr* 1987; 146: 195–198
- Gillan JE, Lowden JA, Gaskin K, Cutz E. Congenital ascitis as a presenting sign of lysosomal storage disease. *J Pediatr* 1984; 104: 225
- Grosso S, Berardi R, Farnetani MA, Margollicci M, Mancini GMS, Morgese G, Balestri P. Multiple neuroendocrine disorder in Salla disease. *J Child Neurol* 2001; 16: 775–777
- Haataja L, Parkkola R, Sonninen P, Verhanen S-L, Scheutker J, Äärimala T, Turpeinen U, Renland M, Aula P. Phenotypic variation and magnetic resonance imaging (MRI) in Salla disease, a free sialic acid storage disorder. *Neuropediatrics* 1994; 25: 238–244
- Havelaar AC, Mancini GMS, Beerens CEMT, Souren RMA, Verheijen FW. Purification of the lysosomal sialic acid transporter. Functional characteristics of a monocarboxylate transporter. *J Biol Chem* 1998; 273: 34568–34574
- Havelaar AC, Beerens CEMT, Mancini GMS, Verheijen FW. Transport of organic anions by the lysosomal sialic acid transporter: a functional approach towards the gene for sialic acid storage disease. *FEBS Lett* 1999; 446: 65–68
- Jonas AJ. Studies of lysosomal sialic acid metabolism: retention of sialic acid by Salla disease lysosomes. *Biochem Biophys Res Commun* 1986; 137: 175–181
- Kirchner L, Kircher S, Salzer-Muhar U, Paschke E, Birnbacher R, Stöckler-Ipsiroglu S. Infantile sialic acid storage disease and protein-losing gastroenteropathy. *Pediatr Neurol* 2003; 28: 313–317
- Lemyre E, Russo P, Melançon SB, Gagné R, Potier M, Lambert M. Clinical spectrum of infantile free sialic acid storage disease. *Am J Med Genet* 1999; 82: 385–391
- Linnankivi T, Lönnqvist T, Autti T. A case of Salla disease with involvement of the cerebellar white matter. *Neuroradiology* 2003; 45: 107–109
- Mancini GMS, Verheijen FW, Glaajard H. Free N-acetylneuraminic acid (NANA) storage disorders: evidence for defective NANA transport across the lysosomal membrane. *Hum Genet* 1986; 73: 214–217
- Mancini GMS, Verheijen FW, Beerens CEMT, Renlund M, Aula P. Sialic acid storage disorders: observations on clinical and biochemical variation. *Dev Neurosci* 1991; 13: 327–330
- Mancini GMS, Beerens CEMT, Aula PP, Verheijen FW. Sialic acid storage diseases. A multiple lysosomal transport defect for acidic monosaccharides. *J Clin Invest* 1991; 87: 1329–1335
- Mancini GMS, Hu P, Verheijen FW, van Diggelen OP, Janse HC, Kleijer WJ, Beemer FA, Jennekens FGI. Salla disease variant in a Dutch patient. Potential Value of polymorphonuclear leucocytes for heterozygote detection. *Eur J Pediatr* 1992; 151: 590–595
- Mancini GMS, Havelaar AC, Verheijen FW. Lysosomal transport disorders. *J Inherit Metab Dis* 2000; 23: 278–292
- Nakano C, Hirabayashi Y, Ohno K, Yano K, Yano T, Sakurai M. A Japanese case of infantile sialic acid storage disease. *Brain Dev* 1996; 18: 153–156

- Parazzini C, Arena S, Marchetti L, Menni F, Filocamo M, Verheijen FW, Mancini GMS, Parini R. Infantile sialic acid storage disease: serial ultrasound and magnetic resonance imaging features. *AJNR Am J Neuroradiol* 2003; 24: 398–400
- Paschke E, Höfler G, Roscher A. Infantile sialic acid storage disease: the fate of biosynthetically labelled *N*-acetyl-(^3H)-neuraminic acid in cultured human fibroblasts. *Pediatr Res* 1986; 8: 773–777
- Paschke E, Trinkl G, Erwa W, Pavelka M, Mutz I, Roscher A. Infantile type of sialic acid storage disease with sialuria. *Clin Genet* 1986; 29: 417–424
- Pueschel SM, O'Shea PA, Alroy J, Ambler MW, Dangond F, Daniel PF, Kolodny EH. Infantile sialic acid storage disease associated with renal disease. *Pediatr Neurol* 1988; 4: 207–212
- Renlund M. Clinical and laboratory diagnosis of Salla disease in infancy and childhood. *J Pediatr* 1984; 104: 232–236
- Renlund M, Aula P, Raivio KA, Autio S, Sainio K, Rapola J, Koskela S-L. Salla disease: a new lysosomal storage disorder with disturbed sialic acid metabolism. *Neurology* 1983; 33: 57–66
- Renlund M, Chester MA, Lundblad A, Parkkinen J, Krusius T. Free *N*-acetylneuraminic acid in tissues in Salla disease and the enzymes involved in its metabolism. *Eur J Biochem* 1983; 130: 39–45
- Renlund M, Kovanen PT, Raivio K, Aula P, Gamhberg CG, Ehnholm C. Studies of the defect underlying the lysosomal storage of sialic acid in Salla disease. *J Clin Invest* 1986; 77: 568–574
- Renlund M, Tietze F, Gahl WA. Defective sialic acid egress from isolated fibroblast lysosomes of patients with salla disease. *Science* 1986; 232: 579–763
- Robinson RO, Fenson AH, Lake BD. Salla disease—rare or underdiagnosed? *Dev Med Child Neurol* 1997; 39: 153–157
- Salomäki P, Aula N, Juvonen V, Renlund M, Aula P. Prenatal detection of free sialic acid storage disease: genetic and biochemical studies in nine families. *Prenat Diagn* 2001; 21: 354–358
- Schleutker J, Leppänen P, Månson J-E, Erikson A, Weissenbach J, Peltonen L, Aula P. Lysosomal free sialic acid storage disorders with different phenotypic presentations – infantile-form sialic acid storage disease and Salla disease – represent allelic disorders. *Am J Hum Genet* 1995; 57: 893–901
- Schmid JA, Mach L, Paschke E, Glössl. Accumulation of sialic acid in endocytic compartments interferes with the formation of mature lysosomes. *J Biol Chem* 1999; 274: 19063–19071
- Seppala R, Renlund M, Bernardini I, Tietze F, Gahl WA. Renal handling of free sialic acid in normal humans and patients with Salla disease or renal disease. *Lab Invest* 1990; 63: 197–203
- Sewell AC, Poets CF, Degen I, Stöb, Pontz BF. The spectrum of free neuraminic acid storage disease in childhood: clinical, morphological and biochemical observations in three non-Finnish patients. *Am J Med Genet* 1996; 63: 203–208
- Sewell AC, Murphy HC, Illes R. Proton nuclear magnetic resonance spectroscopic detection of sialic acid storage disease. *Clin Chem* 2002; 48: 357–359
- Sonninen P, Autti T, Varho T, Hämäläinen, Raininko R. Brain involvement in Salla disease. *AJNR Am J Neuroradiol* 1999; 20: 433–443
- Sperl W, Gruber W, Quatacker J, Monnens L, Thoenes W, Fink FM, Paschke E. Nephrosis in two siblings with infantile sialic acid storage disease. *Eur J Pediatr* 1991; 49: 447–482
- Stevenson RE, Lubinsky M, Taylor HA, Wenger DA, Schoer RJ, Olmstead PM. Sialic acid storage disease with sialuria: clinical and biochemical features in the severe infantile type. *Pediatr* 1983; 72: 441–449
- Thomas GH, Scocca J, Libert J, Vámos E, Miller CS, Reynolds LW. Alterations in cultured fibroblasts of sibs with an infantile form of free (unbound) sialic acid storage disorder. *Pediatr Res* 1983; 17: 307–312
- Tietze F, Seppala R, Renlund M, Hopwood JJ, Harper GS, Thomas GH, Gahl WA. Defective lysosomal egress of free sialic acid (*N*-acetylneuraminic acid) in fibroblasts of patients with free sialic acid storage disease. *J Biol Chem* 1989; 264: 15316–15322
- Tondeur M, Libert J, Vámos E, Van Hoof F, Thomas GH, Strecker G. Infantile form of sialic acid storage disorder: clinical, ultrastructural, and biochemical studies in two siblings. *Eur J Pediatr* 1982; 139: 142–147
- Varho T, Komu M, Sonninen P, Holopainen I, Nyman S, Manner T, Sallinpää M, Aula P, Lundbom N. A new metabolite contributing to *N*-acetyl signal in ^1H MRS of the brain in Salla disease. *Neurology* 1999; 52: 1668–1672
- Varho T, Jääskeläinen S, Tolonen U, Sonninen P, Vainionpää L, Aula P, Sillanpää M. Central and peripheral nervous system dysfunction in the clinical variation of Salla disease. *Neurology* 2000; 55: 99–103
- Varho TT, Alajoki LE, Posti KM, Korhonen TT, Renlund GG, Nyman SRG, Sillanpää, Aula PP. Phenotypic spectrum of Salla disease, a free sialic acid storage disorder. *Pediatr Neurol* 2002; 26: 267–273
- Verheijen FW, Verbeel E, Aula N, Beerens CEMT, Havelaar AC, Joosse M, Peltonen L, Aula P, Galjaard H, van der Spek PJ, Mancini GMS. A new gene, encoding an anion transporter, is mutated in sialic acid storage diseases. *Nat Genet* 1999; 23: 462–465
- Wolburg-Buchholz K, Schlote W. Familial lysosomal storage disease with generalized vacuolisation and sialic aciduria. Sporadic Salla disease. *Neuropediatrics* 1985; 16: 67–75

15 Neuronal Ceroid Lipofuscinoses

General

- Autti T, Raininko R, Vanhanen SL, Santavuori P. Magnetic resonance techniques in neuronal ceroid lipofuscinoses and some other lysosomal diseases affecting the brain. *Curr Opin Neurol* 1997; 10: 519–524
- Autti T, Raininko R, Santavuori P, Vanhanen SL, Poutanen VP, Haltia M. MRI of neuronal ceroid lipofuscinosis. II. Post-mortem MRI and histopathological study of the brain in 16 cases of neuronal ceroid lipofuscinosis of juvenile or late infantile type. *Neuroradiology* 1997; 29: 371–377
- Boldrini R, Biselli R, Santorelli FM, Bosman C. Neuronal ceroid lipofuscinosis: an ultrastructural, genetic, and clinical study report. *Ultrastruct Pathol* 2001; 25: 51–58
- Boustany RMN, Kolodny EH. Neurological progress. The neuronal ceroid lipofuscinoses: a review. *Rev Neurol* 1989; 145: 105–110
- Brooks SS. Genetic counseling in the neuronal ceroid lipofuscinoses. *Adv Genet* 2001; 45: 141–158
- Dawson G, Cho S. Batten's disease: clues to neuronal protein metabolism in lysosomes. *J Neurosci Res* 2000; 60: 133–140
- Dunn DW. CT in ceroid lipofuscinosis. *Neurology* 1987; 37: 1025–1026
- Elleder M, Franc K, Kraus J, Nevšimalová S, Sixtová K, Zeman J. Neuronal ceroid lipofuscinosis in the Czech Republic: analysis of 57 cases. Report of the 'Prague NLC group'. *Eur J Paediatr Neurol* 1997; 4: 109–114

- Gardiner RM. The molecular genetic basis of the neuronal ceroid lipofuscinoses. *Neurol Sci* 2000; 21: S15-S19
- Goebel HH. Prenatal ultrastructural diagnosis in the neuronal ceroid lipofuscinoses. *Pathol Res Pract* 1994; 190: 728-733
- Goebel HH. The neuronal ceroid-lipofuscinoses. *J Child Neurol* 1995; 10: 424-437
- Goebel HH. Morphological diagnosis in neuronal ceroid lipofuscinosis. *Neuropediatrics* 1997; 28: 67-69
- Goebel HH. The new nosography of the neuronal ceroid-lipofuscinoses. *Ann Pathol* 2000; 20: 479-491
- Goebel HH. Morphological aspects of the neuronal ceroid lipofuscinoses. *Neurol Sci* 2000; 21: S27-S33
- Goebel HH, Mole SE, Lake BD, eds. The neuronal ceroid lipofuscinoses (Batten disease). Amsterdam: IOS Press, 1999
- Goebel HH, Schochet SS, Jaynes M, Brück W, Kohlschütter A, Hentati F. Progress in neuropathology of the neuronal ceroid lipofuscinoses. *Mol Genet Metab* 1999; 66: 367-372
- Haltia M. The neuronal ceroid-lipofuscinoses. *J Neuropathol Exp Neurol* 2003; 62: 1-13
- Jolly RD, Dalefield RR, Palmer DN. Ceroid, lipofuscin and the ceroid-lipofuscinoses (Batten disease). *J Inher Metab Dis* 1993; 16: 280-283
- Junaid NA, Pullarkat RK. Biochemistry of neuronal ceroid lipofuscinoses. *Adv Genet* 2001; 45: 93-106
- Kida E, Golabek AA, Wisniewski KE. Cellular pathology and pathogenic aspects of neuronal ceroid lipofuscinoses. *Adv Genet* 2001; 45: 35-68
- Kleijer WJ, van Diggelen OP. Prenatal diagnosis of neuronal ceroid lipofuscinoses. *Prenat Diagn* 2000; 20: 819-821
- Machen BC, Williams JP, Lum GB, Dyken P, Joslyn JN, Harpen MD, Dotson P. Magnetic resonance imaging in neuronal ceroid lipofuscinosis. *J Comput Tomogr* 1987; 11: 160-166
- Mitchison GM, Mole SE. Neurodegenerative disease: the neuronal ceroid lipofuscinoses (Batten disease). *Curr Opin Neurol* 2001; 14: 795-803
- Mole SE, Mitchison HM, Munroe PB. Molecular basis of the neuronal ceroid lipofuscinoses: mutations in *CLN1*, *CLN2*, *CLN3* and *CLN5*. *Hum Mutat* 1999; 14: 199-215
- Peltonen L, Savukoski M, Vesa J. Genetics of the neuronal ceroid lipofuscinoses. *Curr Opin Genet Dev* 2000; 10: 299-305
- Raininko R, Santavuori P, Heiskala H, Sainio K, Palo J. CT findings in neuronal ceroid lipofuscinoses. *Neuropediatrics* 1990; 21: 95-101
- Santavuori P. Neuronal ceroid-lipofuscinoses in childhood. *Brain Dev* 1988; 10: 80-83
- Santavuori P, Linnankivi T, Jaeken J, Vanhanen S-L, Telakivi T, Heiskala H. Psychological symptoms and sleep disturbances in neuronal ceroid-lipofuscinoses (NCL). *J Inher Metab Dis* 1993; 16: 245-248
- Santavuori P, Lauronen L, Kirveskari E, Åberg L, Sainio K, Autti T. Neuronal ceroid lipofuscinoses in childhood. *Neurol Sci* 2000; 21: S35-S41
- Santavuori P, Vanhanen S-L, Autti T. Clinical and neuroradiological diagnostic aspects of neuronal ceroid lipofuscinoses disorders. *Eur J Paediatr Neurol* 2001; 5: 157-161
- Wisniewski KE, Kida E, Patxot OF, Connell F. Variability in the clinical and pathological findings in the neuronal ceroid lipofuscinoses: review of data and observations. *Am J Med Genet* 1992; 42: 525-532
- Wisniewski KE, Kida E, Connell F, Zhong N. Neuronal ceroid lipofuscinoses: research update. *Neurol Sci* 2000; 21: S49-S56
- Wisniewski KE, Zhong N, Philippart M. Pheno-/genotypic correlations of neuronal ceroid lipofuscinoses. *Neurology* 2001; 57: 576-581
- Wisniewski KE, Kida E, Golabek AA, Kaczmarek W, Connell F, Zhong N. Neuronal ceroid lipofuscinoses: classification and diagnosis. *Adv Genet* 2001; 45: 1-34
- Zhong N. Neuronal ceroid lipofuscinoses and possible pathogenic mechanism. *Mol Genet Metab* 2000; 71: 195-206
- Zhong N. Molecular genetic testing for neuronal ceroid lipofuscinoses. *Adv Genet* 2001; 45: 141-158

Neuronal Ceroid Lipofuscinosis: CLN1

- Åberg K, Heiskala H, Vanhanen S-L, Himberg JJ, Hosking G, Yuen A, Santavuori P. Lamotrigine therapy in infantile neuronal ceroid lipofuscinosis (INCL). *Neuropediatrics* 1997; 28: 77-79
- Barohn RJ, Dowd DC, Kagen-Hallet KS. Congenital ceroid lipofuscinosis. *Pediatr Neurol* 1992; 8: 54-59
- Bizzozero GA. The mechanisms and functional roles of protein palmitoylation in the nervous system. *Neuropediatrics* 1997; 28: 23-26
- Confort-Gouny S, Chabrol B, Vion-Dury J, Mancini J, Cozzone PJ. MRI and localized proton MRS in early infantile form of neuronal ceroid-lipofuscinosis. *Pediatr Neurol* 1993; 9: 57-60
- Haltia M, Rapola J, Santavuori P, Keränen A. Infantile type of so-called neuronal ceroid-lipofuscinosis. 2. Morphological and biochemical studies. *J Neurol Sci* 1973; 18: 269-285
- Haltia M, Rapola J, Santavuori P. Infantile type of so-called neuronal ceroid-lipofuscinosis. Histological and electron microscopic studies. *Acta Neuropathol (Berl)* 1973; 26: 157-170
- Hofmann SL, Das AD, Lu JY, Wisniewski KE, Gupta P. Infantile neuronal ceroid lipofuscinosis: no longer just a 'Finnish' disease. *Eur J Paediatr Neurol* 2001; 5: 47-51
- Jongen PJH, Gabreëls FJM, Schuurmans Stekhoven JH, Renier WO, Le Coulter R, Begeer JH. Early infantile form of neuronal ceroid lipofuscinosis. *Clin Neurol Neurosurg* 1987; 89: 161-167
- Lake BD, Brett EM, Boyd SG. A form of juvenile Batten disease with granular osmiophilic deposits. *Neuropediatrics* 1996; 27: 265-269
- Lönnqvist T, Vanhanen SL, Vetterranta K, Autti T, Rapola J, Santavuori P, Saarinen-Pihkala UM. Hematopoietic stem cell transplantation in infantile neuronal ceroid lipofuscinosis. *Neurology* 2001; 57: 1411-1416
- Lu J-Y, Verkruyse KA, Hofmann SL. The effects of lysomotrophic agents on normal and INCL cells provide further evidence for the lysosomal nature of palmitoyl-protein thioesterase function. *Biochim Biophys Acta* 2002; 1583: 35-44
- O'Rawe A, Mitchison HM, Williams R, Wheeler R, Andermann F, Andermann E, Hart YM, Martin JJ, Philippart M, Stephanson JBP, Gardiner RM, Mole SE. Genetic linkage analysis of a variant of juvenile onset neuronal ceroid lipofuscinosis with granular osmiophilic deposits. *Neuropediatrics* 1997; 28: 21-22
- Philippart M, Chugani HT, Bateman JB. New Spielmeier-Vogt variant with granular inclusions and early brain atrophy. *Am J Med Genet* 1995; 57: 160-164
- Salonen J, Heinonen-Kopra O, Vesa J, Jalanko A. Neuronal trafficking of palmitoyl protein thioesterase provides an excellent model to study the effects of different mutations, which cause infantile neuronal ceroid lipofuscinosis. *Mol Cell Neurosci* 2001; 18: 131-140
- Santavuori P, Haltia M, Rapola J. Infantile type of so-called neuronal ceroid lipofuscinosis. *Dev Med Child Neurol* 1974; 16: 644-653

- Santavuori P, Raininko R, Vanhanen SL, Launes J, Sainio K. MRI of the brain, EEG sleep spindles and SPECT in the early diagnosis of infantile neuronal ceroid lipofuscinosis. *Dev Med Child Neurol* 1992; 34: 61–79
- Santavuori P, Vanhanen S-L, Sainio K, Nieminen M, Wallden T, Launes J, Raininko R. Infantile neuronal ceroid-lipofuscinosis (INCL): diagnostic criteria. *J Inher Metab Dis* 1993; 16: 227–229
- Svennerholm L, Fredman P, Jungbjer B, Mansson JE, Rynmark BM, Boström K, Hagberg B, Noren L, Santavuori P. Large alterations in ganglioside and neutral glycosphingolipid patterns in brains from cases with infantile neuronal ceroid lipofuscinosis/polyunsaturated fatty acid lipidosis. *J Neurochem* 1987; 49: 1772–1783
- Tyynelä J, Palmer DN, Baumann M, Haltia M. Storage of saposins A and D in infantile neuronal ceroid-lipofuscinosis. *FEBS Lett* 1991; 330: 8–12
- Van Diggelen OP, Thobois S, Tilikete C, Zabet M-T, Keulemans JLM, van Bunderen PA, Taschner PEM, Losekoot M, Voznyi YV. Adult neuronal ceroid lipofuscinosis with palmitoyl-protein thioesterase deficiency: first adult-onset patients of a childhood disease. *Ann Neurol* 2001; 50: 269–272
- Vanhanen S-L, Raininko R, Santavuori P. Early differential diagnosis of infantile neuronal ceroid lipofuscinosis, Rett syndrome, and Krabbe disease by CT and MR. *AJNR Am J Neuroradiol* 1994; 15: 1443–1543
- Vanhanen S-L, Liewendahl K, Raininko R, Nikkinen P, Autti T, Sainio K, Santavuori P. Brain perfusion SPECT in infantile neuronal ceroid-lipofuscinosis (INCL) comparison with clinical manifestations and MRI findings. *Neuropediatrics* 1995; 27: 76–83
- Vanhanen S-L, Raininko R, Santavuori O, Autti T, Haltia M. MRI Evaluation of the brain in infantile neuronal ceroid-lipofuscinosis. 1. Postmortem MRI with histopathological correlation. *J Child Neurol* 1995; 10: 438–443
- Vanhanen S-L, Raininko R, Autti T, Santavuori P. MRI Evaluation of the brain in infantile neuronal ceroid-lipofuscinosis. 2. MRI findings in 21 patients. *J Child Neurol* 1995; 10: 444–450
- Vanhanen S-L, Sainio J, Lappi M, Santavuori P. EEG and evoked potentials in infantile neuronal ceroid-lipofuscinosis. *Dev Med Child Neurol* 1997; 39: 456–463
- Vanhanen SL, Puranen J, Autti T, Raininko R, Liewendahl K, Nikkinen P, Santavuori P, Suominen P, Vuori K, Häkkinen AM. Neuroradiological findings (MRS, MRI, SPECT) in infantile neuronal ceroid-lipofuscinosis (infantile CLN1) at different stages of the disease. *Neuropediatrics* 2004; 35: 27–35
- Vesa J, Hellsten E, Verkruijse LA, Camp LA, Rapola J, Santavuori P, Hofmann SL, Peltonen L. Mutations in the palmitoyl protein thioesterase gene causing infantile neuronal ceroid lipofuscinosis. *Nature* 1995; 376: 584–587
- Ezaki J, Tadeka-Ezaki M, Kominami E. Tripeptidyl peptidase I, the late infantile neuronal ceroid lipofuscinosis gene product, initiates the lysosomal degeneration of subunit c of ATP synthase. *J Biochem* 2000; 128: 506–516
- Fueki N, Linuma K, Kojima A, Yanai K, Haginoya K, Tada K, Ido T, Ito M. Reduced regional cerebral metabolic rate for glucose at the terminal stage in a case of late infantile neuronal ceroid lipofuscinosis. *J Child Neurol* 1990; 5: 98–100
- Kurata K, Hayashi M, Satoh J, Kojima H, Nagata J, Tamagata K, Shinohara T, Morimatsu Y, Kominami E. Pathological study on sibling autopsy cases of the late infantile form of neuronal ceroid lipofuscinosis. *Brain Dev* 1999; 21: 63–67
- Petersen B, Handwerker M, Huppertz H-I. Neurological findings in classical late onset infantile neuronal ceroid-lipofuscinosis. *Pediatr Neurol* 1996; 15: 344–347
- Seitz D, Grodd W, Schwab A, Seeger U, Klose U, Nägele T. MR imaging and localized proton MR spectroscopy in late infantile neuronal ceroid lipofuscinosis. *AJNR Am J Neuroradiol* 1998; 19: 1373–1377
- Sondhi D, Hackett NR, Alpbelt RL, Kaminsky SM, Pergolizzi RG, Crystal RG. Feasibility of gene therapy for late neuronal ceroid lipofuscinosis. *Arch Neurol* 2001; 58: 1793–1798
- Umehara F, Higuchi I, Tanaka HK, Niiyama T, Ezaki J, Kominami E, Osame M. Accumulation of mitochondrial ATP synthase subunit c in muscle in a patient with ceroid lipofuscinosis (late infantile form). *Acta Neuropathol (Berl)* 1997; 93: 628–632
- Warburton MJ, Bernardini F. Tripeptidyl-peptidase I deficiency in classical late-infantile neuronal ceroid lipofuscinosis brain tissue. Evidence for defective peptidase rather than proteinase activity. *J Inher Metab Dis* 2000; 23: 145–154

Neuronal Ceroid Lipofuscinosis: CLN 3

- Autti T, Raininko R, Vanhanen SL, Santavuori P. MRI of neuronal ceroid lipofuscinosis. I. Cranial MRI of 30 patients with juvenile neuronal ceroid lipofuscinosis. *Neuroradiology* 1996; 38: 476–482
- Bennett MJ, Gayton AR, Rittey CDR, Hosking GP. Juvenile neuronal ceroid-lipofuscinosis: developmental progress after supplementation with polyunsaturated fatty acids. *Dev Med Child Neurol* 1994; 36: 630–638
- Boustany RMN, Filipek P. Seizures, depression and dementia in teenagers with Batten disease. *J Inher Metab Dis* 1993; 16: 252–255
- Brod RD, Packer AJ, Van Dyk HJL. Diagnosis of neuronal ceroid lipofuscinosis by ultrastructural examination of peripheral blood lymphocytes. *Arch Ophthalmol* 1987; 105: 1388–1393
- Bruun I, Reske-Nielsen E, Oster S. Juvenile ceroid-lipofuscinosis and calcifications of the CSF. *Acta Neurol Scand* 1991; 83: 1–8
- Hofman IL. Observations in institutionalized neuronal ceroid-lipofuscinosis patients, with special reference to involuntary movements. *J Inher Metab Dis* 1993; 16: 249–251
- Järvelä I, Autti T, Lamminranta S, Aberg L, Raininko R, Santavuori P. Clinical and magnetic resonance imaging findings in Batten disease: analysis of the major mutation (1.02-kb deletion). *Ann Neurol* 1997; 42: 799–802
- Kimura S, Goebel HH. Light and electron microscopic study of juvenile neuronal ceroid-lipofuscinosis lymphocytes. *Pediatr Neurol* 1988; 4: 148–152

- Lauronen L, Munroe PB, Järvelä I, Autti T, Mitchison HM, O'Rawe AM, Gardiner RM, Mole SE, Puranen J, Häkkinen AAM, Kireverski E, Santavuori P. Delayed classical and protracted phenotypes of compound heterozygous juvenile neuronal ceroid lipofuscinosis. *Neurology* 1999; 52: 360–365
- Manca V, Kanitakis J, Zambruno G, Thiovielle J, Gonnaud P. Ultrastructural study of the skin in a case of juvenile ceroid-lipofuscinosis. *Am J Dermatopathol* 1990; 12: 412–416
- Mitchison HM, Taschner PEM, Kremmidiotis G, Callen DF, Doggert NA, Lerner TJ, Janes RB, Wallace BA, Munroe PB, O'Rawe AM, Gardiner RM, Mole SE. Structure of the CLN3 gene and predicted structure, location and function of CLN3 protein. *Neuropediatrics* 1997; 28: 12–14
- Piattella L, Cardinali C, Zamponi N, Papa O. Spielmeyer-Vogt disease: clinical and neurophysiological aspects. *Child Nerv Syst* 1991; 7: 226–230
- Pullarkat RK, Morris GN, Pullerker PS, LaBadie GU, Zawitosky SE. Biochemical studies of the juvenile form of ceroid-lipofuscinosis. *Am J Med Genet* 1992; 42: 575–579
- Wisniewski KE, Zhong N, Kaczmarek W, Kaczmarek A, Sklower-Brooks S, Brown WT. Studies of atypical JNCL suggest overlapping with other NCL forms. *Pediatr Neurol* 1998; 18: 36–40
- Wisniewski KE, Zhong N, Kaczmarek W, Kaczmarek A, Kida E, Brown WT, Schwarz KO, Lazzirini AM, Rubin AJ, Stenroos ES, Johnson WG, Wisniewski TM. Compound heterozygous genotype is associated with protracted neuronal ceroid lipofuscinosis. *Ann Neurol* 1998; 43: 106–110
- Neuronal Ceroid Lipofuscinosis: CLN4**
- Augustine A, Fricchione G, Woznicki R, Broberg D, Holt J. Adult neuronal ceroid lipofuscinosis presenting with psychiatric symptoms (case report). *Int J Psychiatry Med* 1993; 19: 315–322
- Berkovic S, Carpenter S, Andermann F, Andermann E, Wolfe LS. Kufs' disease: a critical reappraisal. *Brain* 1988; 111: 27–62
- Constantinidis J, Wisniewski KE, Wisniewski TM. The adult and a new late adult forms of neuronal ceroid lipofuscinosis. *Acta Neuropathol (Berl)* 1992; 83: 461–468
- Donnet A, Habib M, Pellissier JF, Régis H, Farnarier G, Pelletier J, Gosset A, Roger J, Khalil R. Kufs' disease presenting as progressive dementia with late-onset generalized seizures: a clinicopathological and electrophysiological study. *Epilepsia* 1992; 33: 65–74
- Gelot A, Maurage CA, Rodriguez D, Perrier-Pallissib D, Larmande P, Ruchoux MM. In vivo diagnosis of Kufs' disease by extracerebral biopsies. *Acta Neuropathol (Berl)* 1998; 96: 102–108
- Martin J-J. Adult type of neuronal ceroid-lipofuscinosis. *Dev Neurosci* 1991; 13: 331–338
- Martin J-J. Adult type of neuronal ceroid-lipofuscinosis. *J Inher Metab Dis* 1993; 16: 237–240
- Tobo M, Misuyama Y, Ikari K, Itio K. Familial occurrence of adult-type neuronal ceroid lipofuscinosis. *Arch Neurol* 1984; 41: 1091–1094
- Holmberg V, Lauronen K, Autti T, Santavuori P, Savukoski M, Uvebrand P, Hofman I, Peltonen L, Järvelä I. Phenotype-genotype correlation in eight patients with Finnish variant late infantile NCL (CLN5). *Neurology* 2000; 55: 579–581
- Isosomppi J, Vesa J, Jalanko A, Peltonen L. Lysosomal localization of the neuronal ceroid lipofuscinosis CLN5. *Hum Mol Genet* 2002; 11: 885–891
- Lauronen L, Huttunen J, Kirveskari E, Wikström H, Sainio K, Autti T, Santavuori P. Enlarged Si and SII somatosensory evoked responses in the CLN5 form of neuronal ceroid lipofuscinosis. *Clin Neurophysiol* 2002; 113: 1491–1500
- Rapola J, Lake BD. Lymphocyte inclusions in Finnish-variant late infantile neuronal ceroid lipofuscinosis (CLN5). *Neuropediatrics* 2000; 31: 33–34
- Rapola J, Lähdetie J, Isosomppi J, Helminen P, Penttinen M, Järvelä I. Prenatal diagnosis of variant late infantile neuronal ceroid lipofuscinosis (vLINCL^{finnish} CLN5). *Prenat Diagn* 1999; 19: 685–688
- Santavuori P, Rapola J, Nuutila A, Raininko R, Lappi M, Launes J, Herva R, Sainio K. The spectrum of Jansky-Bielschowsky disease. *Neuropediatrics* 1991; 22: 92–96
- Santavuori P, Rapola J, Raininko R, Autti T, Lappi M, Nuutila A, Launes J, Sainio K. Early juvenile neuronal ceroid-lipofuscinosis or variant Jansky-Bielschowsky disease: diagnostic criteria and nomenclature. *J Inher Metab Dis* 1993; 16: 230–232
- Savukoski M, Klockars T, Holmberg V, Santavuori P, Lander ES, Peltonen L. CLN5, a novel gene encoding a putative transmembrane protein mutated in Finnish variant late infantile neuronal ceroid lipofuscinosis. *Nat Genet* 1998; 19: 286–288
- Tynnelä J, Suopanki J, Santavuori P, Baumann M, Haltia M. Variant late infantile neuronal ceroid-lipofuscinosis: pathology and biochemistry. *J Neuropathol Exp Neurol* 1997; 56: 369–375
- Uvebrand P, Hagberg B. Neuronal ceroid lipofuscinosis in Scandinavia. Epidemiology and clinical pictures. *Neuropediatrics* 1997; 28: 6–8
- Varilo T, Savukoski M, Norio R, Santavuori P, Peltonen L, Järvelä J. The age of human mutation: genealogical and linkage disequilibrium analysis of the CLN5 mutation in the Finnish population. *Am J Hum Genet* 1996; 58: 506–512
- Vesa J, Chin MH, Oelgeschläger K, Isosomppi J, DellAngelica EC, Jalanko A, Peltonen L. Neuronal ceroid lipofuscinoses are connected at molecular level: interaction of CLN5 protein with CLN2 and CLN3. *Mol Biol Cell* 2002; 13: 2410–2420
- Williams R, Santavuori P, Peltonen L, Gardiner RM, Järvelä I. A variant form of late infantile neuronal ceroid lipofuscinosis (CLN5) is not an allelic form of Batten (Spielmeyer-Vogt-Sjögren, CLN3) disease: exclusion of linkage to the CLN3 region of chromosome 16. *Genomics* 1994; 20: 289–290
- Wisniewski KE, Kida E, Connell F, Elleder M, Eviatar L, Konkol RJ. New subform of the late infantile form of neuronal ceroid lipofuscinosis. *Neuropediatrics* 1993; 24: 155–163
- Neuronal Ceroid Lipofuscinosis: CLN 6**
- Auger KJ, Ajene A, Lerner T. Progress toward the cloning of CLN6, the gene underlying a variant LINCL. *Mol Genet Metab* 1999; 66: 332–336
- Gao H, Boustany R-MN, Espanola JA, Cotman SL, Srinidhi L, Antonellis KA, Gillis T, Qin X, Liu S, Donahue LR, Bronson RT, Faust JR, Stout D, Haines JL, Lerner TJ, MacDonald ME. Mutations in a novel CLN6-encoded transmembrane protein cause variant neuronal ceroid lipofuscinosis in man and mouse. *Am J Hum Genet* 2002; 70: 324–335

Neuronal Ceroid Lipofuscinosis: CLN 5

- Autti T, Raininko R, Launes J, Nuutila A, Santavuori P, Jansky-Bielschowsky variant disease: CT, MRI, and SPECT findings. *Pediatr Neurol* 1992; 2: 121–126

- Heine C, Koch B, Storch S, Kohlschütter A, Palmer DN, Braulke T. Defective endoplasmic reticulum-resident membrane protein CLN6 affects lysosomal degradation of endocytosed arylsulfatase A. *J Biol Chem* 2004; 279: 22347–22352
- Pena HA, Cardozo JJ, Montiel CM, Molina OM, Boustany R-M. Serial MRI findings in the Costa Rican variant of neuronal ceroid-lipofuscinosis. *Pediatr Neurol* 2001; 25: 78–80
- Sharp JD, Wheeler RB, Lake BD, Fox M, Gardiner RM, Williams RE. Genetic and physical mapping of the *CLN6* gene on chromosome 15q21–23. *Mol Genet Metab* 1999; 66: 329–331
- Wheeler RB, Sharp JD, Schultz RA, Joslin JM, Williams RE, Mole SE. The gene mutated in variant late-infantile neuronal ceroid lipofuscinosis (*CLN6*) and *nclf* mutant mice encodes a novel predicted transmembrane protein. *Am J Hum Genet* 2002; 70: 537–542

Neuronal Ceroid Lipofuscinosis: CLN 7

- Mitchell WA, Wheeler RB, Sharp JD, Bate SL, Gardiner RM, Ranta US, Lonka L, Williams RE, Lehesjoki AE, Mole SE. Turkish variant late infantile neuronal ceroid lipofuscinosis (CLN7) may be allelic to CLN8. *Eur J Paediatr Neurol* 2001; 5: 21–27
- Topçu M, Tan H, Yalnizoglu D, Usubütün A, Saatçi I, Aynaci M, Anlar B, Topaloglu H, Turanlı G, Köse G, Aysun S. Evaluation of 36 patients from Turkey with neuronal ceroid lipofuscinosis: clinical, neurophysiological, neuroradiological and histopathologic studies. *Turk J Pediatr* 2004; 46: 1–10
- Wheeler RB, Sharp JD, Mitchell WA, Bate SL, Williams WA, Lake BD, Gardiner RM. A new locus for variant late infantile neuronal ceroid lipofuscinosis-CLN7. *Mol Genet Metab* 1999; 66: 337–378

Neuronal Ceroid Lipofuscinosis: CLN8

- Hirvasniemi A, Lang H, Lehesjoki A-E, Leisti KJ. Northern epilepsy syndrome: an inherited childhood-onset epilepsy with associated mental deterioration. *J Med Genet* 1994; 31: 177–182
- Lonka L, Kyttälä A, Ranta S, Jalanko A, Lehesjoki A-E. The neuronal ceroid lipofuscinosis CLN8 membrane protein is a resident of the endoplasmic reticulum. *Hum Mol Genet* 2000; 9: 1691–1697
- Ranta S, Lehesjoki A-E. Northern epilepsy, a new member of the NCL family. *Neurol Sci* 2000; 21: S43–S47
- Ranta S, Lehesjoki A-E, Hirvasniemi A, Weissenbach J, Ross B, Leal SM, de la Chapelle A, Gilliam TC. Genetic and physical mapping of the progressive epilepsy with mental retardation (EPMR) locus on chromosome 8p. *Genome Res* 1996; 6: 351–360
- Ranta S, Zhang Y, Ross B, Lonka L, Takkunen E, Messer A, Sharp J, Wheeler R, Kusumi K, Mole S, Liu W, Soares MB, de Fatima Bonaldo M, Hirvasniemi A, de la Chapelle A, Gilliam TC, Lehesjoki A-E. The neuronal ceroid lipofuscinosis in human EPMR and *mnd* mutant mice are associated with mutations in CLN8. *Nat Genet* 1999; 23: 233–236
- Tahvanainen E, Ranta S, Hirvasniemi A, Karila E, Leisti J, Sistonen P, Weissenbach J, Lehesjoki E-E, de la Chapelle A. The gene for a recessively inherited human childhood progressive epilepsy with mental retardation maps to the distal short arm for chromosome 8. *Proc Natl Acad Sci* 1994; 91: 7267–7270

16 Adult Polyglucosan Body Disease

- Berkhoff M, Weis J, Schroth G, Sturzenegger M. Extensive white-matter changes in case of adult polyglucosan body-disease. *Neuroradiology* 2001; 43: 234–236
- Bigio EH, Weiner MF, Bonte FJ, White CL. Familial dementia due to adult polyglucosan bodydisease. *Clin Neuropathol* 1997; 16: 227–234
- Boulan-Predseil P, Vital A, Brochet B, Darriet D, Henry P, Vital C. Dementia of frontal lobe due to adult polyglucosan body-disease. *J Neurol* 1995; 242: 512–516
- Bruno C, Servidei S, Shanske S, Karpatis G, Carpenter S, McKee D, Barohn RJ, Hirano M, Rifai Z, DiMauro S. Glycogen branching enzyme deficiency in adult polyglucosan bodydisease. *Ann Neurol* 1993; 33: 88–93
- Busard HLSM, Gabreëls-Festen AAWM, Reinier WO, Gabreëls FJM, Joosten EGM, van 't Hof MS, Rensing JBM. Adult polyglucosan bodydisease: the diagnostic value of axilla skin biopsy. *Ann Neurol* 1991; 29: 448–451
- Cafferty MS, Lovelace RE, Hays AP, Servidei S, DiMauro S, Rowland LP. Polyglucosan body disease. *Muscle Nerve* 1991; 14: 102–107
- Cavanagh JB. Corpora-amylacea and the family of polyglucosan diseases. *Brain Res Rev* 1999; 29: 265–295
- Gray F, Gherardi R, Mashall A, Path MRC, Janota I, Poirier J. Adult polyglucosan body disease (APBD) *J Neuropathol Exp Neurol* 1988; 47: 259–474
- Klein CM, Peter Bosch E, Dyck PJ. Probable adult polyglucosan bodydisease. *Mayo Clinic Proc* 2000; 75: 1327–1331
- Lossos A, Baresh V, Soffer D, Argov Z, Gomori M, Ben-Nariah Z, Abramsky O, Steiner I. Hereditary branching enzyme dysfunction in adult polyglucosan bodydisease: a possible metabolic cause in two patients. *Ann Neurol* 1991; 30: 655–662
- McDonald TD, Faust PL, Bruno C, DiMauro S, Goldman JE. Polyglucosan bodydisease simulating amyotrophic lateral sclerosis. *Neurology* 1993; 43: 785–790
- Milde P, Guccion JG, Kelly J, Locatelli E, Jones RV. Adult polyglucosan bodydisease. Diagnosis by sural nerve and skin biopsy. *Arch Pathol Lab Med* 2001; 125: 519–522
- Moses SW, Parvari R. The variable presentations of glycogen storage disease type IV: a review of clinical, enzymatic and molecular studies. *Curr Mol Med* 2002; 2: 177–188
- Negishi C, Sze G. Spinal cord MRI in adult polyglucosan body disease. *J Comput Assist Tomogr* 1992; 16: 824–826
- Okamoto K, Llena JF, Hirano A. A type of adult polyglucosan bodydisease. *Acta Neuropathol (Berl)* 1982; 58: 73–77
- Rifai Z, Klitzke M, Tawil R, Kazee AM, Shanske S, DiMauro S, Griggs RC. Dementia of adult polyglucosan body disease. Evidence of cortical and subcortical dysfunction. *Arch Neurol* 1994; 51: 90–94
- Robertson NP, Wharton S, Anderson J, Scolding NJ. Adult polyglucosan body disease associated with an extrapyramidal syndrome. *J Neurol Neurosurg Psychiatry* 1998; 65: 788–790
- Robitaille Y, Carpenter S, Karpatis G, DiMauro S. A distinct form of adult polyglucosan bodydisease with massive involvement of central and peripheral neuronal processes and astrocytes. A report of four cases and a review of the occurrence of polyglucosan bodies in other conditions such as Lafora's disease and normal ageing. *Brain* 1980; 103: 315–336

- Sindern E, Patzold T, Vorgerd M, Shin YS, Podskarbi T, Schröder JM, Malin JP. Adult polyglucosan body disease. Report of a case with predominant involvement of the central and peripheral nervous system and branching enzyme deficiency in leukocytes. *Nervenarzt* 1999; 70: 745–749
- Sindern E, Ziemssen F, Ziemssen T, Podskarbi T, Shin Y, Brasch F, Müller KM, Schröder JM, Malin JP, Vorgerd M. Adult polyglucosan body disease. A postmortem correlation study. *Neurology* 2003; 61: 263–265
- Vos AJM, Joosten EGM, Gabreëls-Festen AAWM. Adult polyglucosan body disease: clinical and nerve biopsy findings in two cases. *Ann Neurol* 1983; 13: 440–444
- Wierzbicka-Bobrowicz T, Strońska-Kús B. Adult polyglucosan body disease. *Folia Neuropathol* 1994; 32: 37–41
- Ziemssen F, Sindern E, Michael Schröder J, Shin YS, Zange J, Kilimann MW, Malin J-P, Vorgerd M. Novel missense mutations in the glycogen-branching enzyme gene in adult polyglucosan body disease. *Ann Neurol* 2000; 47: 536–540
- ## 17 Peroxisomes and Peroxisomal Disorders
- Aubourg P, Scotto J, Rocchiccioli F, Feldmann-Pautrat D, Robain O. Neonatal adrenoleukodystrophy. *J Neurol Neurosurg Psychiatry* 1986; 49: 77–86
- Barth PG, Gootjes J, Bode H, Vreken P, Majoie CB, Wanders RJA. Late onset white matter disease in peroxisome biogenesis disorder. *Neurology* 2001; 57: 1949–1955
- Barth PG, Majoie CB, Gootjes J, Wanders RJA, Waterham HR, van der Knaap MS, de Klerk JB, Smeitink J, Poll-The BT. Neuroimaging of peroxisome biogenesis disorders (Zellweger spectrum) with prolonged survival. *Neurology* 2004; 62: 439–444
- Braverman N, Chen L, Lin P, Obie C, Steel G, Douglas P, Chakraborty PK, Clarke JT, Boneh A, Moser A, Moser H, Valle D. Mutation analysis of PEX7 in 60 probands with rhizomelic chondrodysplasia punctata and functional correlations of genotype with phenotype. *Hum Mutat* 2002; 20: 284–297
- Corzo D, Gibson W, Johnson K, Mitchell G, LePage G, Cox GF, Casey R, Zeiss C, Tyson H, Cutting GR, Raymond GV, Smith KD, Watkins PA, Moser AB, Moser HW, Steinberg SJ. Contiguous deletion of the X-linked adrenoleukodystrophy gene (ABCD1) and DXS1357E: a novel neonatal phenotype similar to peroxisomal biogenesis disorders. *Am J Hum Genet* 2002; 70: 1520–1531
- Ferdinandusse S, Denis S, Clayton PT, Graham A, Rees JE, Allen JT, Mclean BN, Brown AY, Vreken P, Waterham HR, Wanders RJA. Mutations in the gene encoding peroxisomal alpha-methylacyl-CoA racemase cause adult-onset sensory motor neuropathy. *Nat Genet* 2000; 24: 188–191
- Gould SJ, Valle D. Peroxisome biogenesis disorders: genetics and cell biology. *Trends Genet* 2000; 16: 340–345
- Gould SJ, Raymond GV, Valle D. The peroxisomal biogenesis disorder. In: Scriver CR, Beaudet AL, Sly WS, Valle D, eds. *The metabolic and molecular bases of inherited disease*. New York: McGraw-Hill, 2001, pp 3181–3217
- Kelley RI, Datta NS, Dobyns WB, Hajra AK, Moser AB, Noetzel MJ, Zackai EH, Moser HW. Neonatal adrenoleukodystrophy: new cases, biochemical studies, and differentiation from Zellweger and related peroxisomal polydystrophy syndromes. *Am J Med Genet* 1986; 23: 869–901
- Mannaerts GP, van Veldhoven PP. Functions and organization of peroxisomal beta-oxidation. *Ann NY Acad Sci* 1996; 804: 99–115
- Moser HW, Smith KD, Watkins PA, Powers J, Moser AB. X-Linked Adrenoleukodystrophy. In: Scriver CR, Beaudet AL, Sly WS, Valle D, eds. *The metabolic and molecular bases of inherited disease*. New York: McGraw-Hill, 2001, pp 3257–3301
- Motley AM, Brites P, Gerez L, Hogenhout EM, Haasjes J, Benne R, Tabak HF, Wanders RJA, Waterham HR. Mutational spectrum in the PEX7 gene and functional analysis of mutant alleles in 78 patients with rhizomelic chondrodysplasia punctata type 1. *Am J Hum Genet* 2002; 70: 612–624
- Poll-The BT, Saudubray JM, Ogier HA, Odievre M, Scotto JM, Monnens L, Govaerts LC, Roels F, Cornelis A, Schutgens RBH. Infantile Refsum disease: an inherited peroxisomal disorder. Comparison with Zellweger syndrome and neonatal adrenoleukodystrophy. *Eur J Pediatr* 1987; 146: 477–483
- Setchell KD, Heubi JE, Bove KE, O'Connell NC, Brewsaugh T, Steinberg SJ, Moser A, Squires RH Jr. Liver disease caused by failure to racemize trihydroxycholestanic acid: gene mutation and effect of bile acid therapy. *Gastroenterology* 2003; 124: 217–232
- Shimozawa N, Suzuki Y, Orii T, Moser A, Moser HW, Wanders RJA. Standardization of complementation grouping of peroxisome-deficient disorders and the second Zellweger patient with peroxisomal assembly factor-1 (PAF-1) defect. *Am J Hum Genet* 1993; 52: 843–844
- Van den Brink DM, Brites P, Haasjes J, Wierzbicka AS, Mitchell J, Lambert-Hamill M, de Belleruche J, Jansen GA, Waterham HR, Wanders RJA. Identification of PEX7 as the second gene involved in Refsum disease. *Am J Hum Genet* 2003; 72: 471–477.
- van der Knaap MS, Valk J. The MR spectrum of peroxisomal disorders. *Neuroradiology* 1991; 33: 30–37
- Wanders RJA. Metabolic and molecular basis of peroxisomal disorders: a review. *Am J Med Genet* 2004; 126: 355–375
- Wanders RJA, Heymans HSA, Schutgens RBH, Barth PG, van den Bosch H, Tager JM. Peroxisomal disorders in neurology. *J Neurol Sci* 1988; 88: 1–39
- Wanders RJA, Barth PG, Heymans HSA. Single peroxisomal enzyme deficiencies. In: Scriver CR, Beaudet AL, Sly WS, Valle D, eds. *The metabolic and molecular bases of inherited disease*. New York: McGraw-Hill, 2001, pp 3219–3256.
- Wanders RJA, Jakobs C, Skjeldal OH. Refsum disease. In: Scriver CR, Beaudet AL, Sly WS, Valle D, eds. *The metabolic and molecular bases of inherited disease*. New York: McGraw-Hill, 2001, pp 3303–3321
- Wanders RJA, Vreken P, Ferdinandusse S, Jansen GA, Waterham HR, van Roermund CWT, van Grunsven EG. Peroxisomal fatty acid alpha- and beta-oxidation in humans: enzymology, peroxisomal metabolite transporters and peroxisomal diseases. *Biochem Soc Trans* 2001; 29: 250–267
- ## 18 Peroxisome Biogenesis Defects
- Agamanolis DP, Patre S. Glycogen accumulation in the central nervous system in the cerebro-hepato-renal syndrome. *J Neurol Sci* 1979; 41: 325–334
- Agamanolis DP, Robinson HB, Timmons GD. Cerebro-hepato-renal syndrome. Report of a case with histochemical and ultrastructural observations. *J Neuropathol Exp Neurol* 1976; 35: 226–246
- Aikawa J, Chen WW, Kelley RI, Tada K, Moser HW, Chen GL. Low-density particles (W-particles) containing catalase in Zellweger syndrome and normal fibroblasts. *Proc Natl Acad Sci USA* 1991; 88: 10084–10088

- Aubourg P, Robain O, Rocchiccioli F, Dancea S, Scotto J. The cerebro-hepato-renal (Zellweger) syndrome: lamellar lipid profiles in adrenocortical, hepatic mesenchymal, astrocyte cells and increased levels of very long chain fatty acids and phytanic acid in the plasma. *J Neurol Sci* 1985; 69: 9–25
- Aubourg P, Scotto J, Rocchiccioli R, Feldmann-Pautrat D, Robain O. Neonatal adrenoleukodystrophy. *J Neurol Neurosurg Psychiatry* 1986; 49: 77–86
- Bader PI, Dougherty S, Cangany N, Raymond G, Jackson CE. Infantile Refsum disease in four Amish sibs. *Am J Med Genet* 2000; 90: 110–114
- Barkovich AJ, Peck WW. MR of Zellweger syndrome. *AJNR Am J Neuroradiol* 1997; 18: 1163–1170
- Barth PG, Schutgens RBH, Bakkeren JAJM, Dingemans KP, Heymans HSA, Douwes AC, van der Klei-van Moorsel JM. A milder variant of Zellweger syndrome. *Eur J Pediatr* 1985; 144: 338–342
- Barth PG, Wanders RJA, Schutgens RBH, Bleeker-Wagemakers EM, van Heemstra D. Peroximal β -oxidation defect with detectable peroxisomes: a case with neonatal onset and progressive course. *Eur J Pediatr* 1990; 149: 722–726
- Barth PG, Gootjes J, Bode H, Vreken P, Majoie CBLM, Wanders RJA. Late onset white matter disease in peroxisome biogenesis disorder. *Neurology* 2001; 57: 1949–1955
- Barth PG, Majoie CBLM, Gootjes J, Wanders RJA, Waterham HR, van der Knaap MS, de Klerk JBC, Smeitink J, Poll-The BT. Neuroimaging of peroxisome biogenesis disorders (Zellweger spectrum) with prolonged survival. *Neurology* 2004; 62: 439–444
- Beard ME, Moser AB, Sapirstein V, Holtzman E. Peroxisomes in infantile phytanic acid storage disease: a cytochemical study of skin fibroblasts. *J Inherit Metab Dis* 1986; 9: 321–334
- Benke PJ, Reyes PF, Parker JC Jr. New form of adrenoleukodystrophy. *Hum Genet* 1981; 58: 204–208
- Bizzozero OA, Ziñiga G, Lees MB. Fatty acid composition of human myelin proteolipid protein in peroxisomal disorders. *J Neurochem* 1991; 56: 872–878
- Brosius U, Gärtner J. Cellular and molecular aspects of Zellweger syndrome and other peroxisome biogenesis disorders. *Cell Mol Life Sci* 2002; 59: 1058–1069
- Budden SS, Kennaway NG, Buist NRM, Poulos A, Weleber RG. Dismorphic syndrome with phytanic acid oxidase deficiency, abnormal very long chain fatty acids, and pipelicolic acidemia: studies in four children. *J Pediatr* 1986; 108: 33–39
- Burdette DE, Kremser K, Fink JK, Pahan K, Stanley W, Sing I. Late-onset generalized disorder of peroxisomes. *Neurology* 1996; 46: 829–831
- Chow CW, Poulos A, Fellenberg AJ, Christodoulou J, Danks DM. Autopsy findings in two siblings with infantile Refsum disease. *Acta Neuropathol (Berl)* 1992; 83: 190–195
- De Leon GA, Grover WD, Huff DS, Moringo-Meure G, Punnett HH, Kistenmacher ML. Globoid cells, glial nodules, and peculiar fibrillary changes in the cerebro-hepato-renal syndrome of Zellweger. *Ann Neurol* 1977; 2: 473–484
- Dimmick JE, Applegarth DA. Pathology of peroxisomal disorders. *Perspect Pediatr Pathol* 1993; 17: 45–98
- Dodt G, Braverman N, Wong C, Moser A, Moser HW, Watkins P, Valle D, Gould SJ. Mutations in the PTS1 receptor gene, *PXR1*, define complementation group 2 of the peroxisome biogenesis disorders. *Nat Genet* 1995; 9: 115–125
- Dubois J, Sebag G, Argyropoulou M, Brunelle F. MR findings in infantile Refsum disease: case report of two family members. *AJNR Am J Neuroradiol* 1991; 12: 1159–1160
- Evrard P, Caviness VS, Prats-Vinas J, Lyon G. The mechanism of arrest of neuronal migration in the Zellweger malformation: an hypothesis based upon cytoarchitectonic analysis. *Acta Neuropathol (Berl)* 1978; 41: 109–117
- Ferninandusse S, Denis S, Mooijer PAW, Zhang Z, Reddy JK, Spector AA, Wanders RJA. Identification of the peroxisomal β -oxidation enzymes involved in the biosynthesis of docosahexaenoic acid. *J Lipid Res* 2001; 42: 1987–1995
- Folz SJ, Trobe JD. The peroxisome and the eye. *Surv Ophthalmol* 1991; 35: 353–368
- Ghaedi K, Honsho M, Shimozawa N, Suzuki Y, Kondo N, Fujiki Y. *PEX3* is the casual gene responsible for peroxisome membrane assembly-defective Zellweger syndrome of complementation group G. *Am J Hum Genet* 2000; 67: 976–981
- Goldfischer S, Powers JM, Johnson AB, Axe S, Brown FR, Moser HW. Striated adrenocortical cells in cerebro-hepato-renal (Zellweger) syndrome. *Virchows Arch* 1983; 401: 355–361
- Gould SJ, Valle D. Peroxisome biogenesis disorders. *Genetics and cell biology. Trends Genet* 2000; 16: 340–345
- Govaerts L, Sippell WG, Monnens L. Further analysis of the disturbed adrenocortical function in the cerebro-hepato-renal syndrome of Zellweger. *J Inherit Metab Dis* 1989; 12: 423–428
- Groenendaal F, Bianchi MC, Battini R, Tosetti M, Boldrini A, de Vries LS, Cioni G. Proton magnetic resonance spectroscopy (¹H-MRS) of the cerebrum in two young infants with Zellweger syndrome. *Neuropediatrics* 2001; 32: 23–27
- Heikoop JC, van den Berg M, Strijland A, Weijers PJ, Just WW, Meijer AJ, Tager JM. Turnover of peroxisomal vesicles by autophagic proteolysis in cultured fibroblasts from Zellweger patients. *Eur J Cell Biol* 1992; 59: 165–171
- Heymans HSA, Schutgens RB, Tan R, van den Bosch H, Borst P. Severe plasmalogen deficiency in tissues of infants without peroxisomes (Zellweger syndrome). *Nature* 1983; 306: 69–70
- Holmes RD, Wilson GN, Hajra A. Oral ether lipid therapy in patients with peroxisomal disorders. *J Inherit Metab Dis* 1987; 10: 239–241
- Imamura A, Shimozawa N, Suzuki Y, Zhang Z, Tsukamoto T, Fujiki Y, Osumi T, Wanders RJA, Kondo N. Temperature-sensitive mutations of *PEX6* in peroxisome biogenesis disorders in complementation group C (CG-C): comparative study of *PEX6* and *PEX1*. *Pediatr Res* 2000; 48: 541–545
- Jaffe R, Crumrine P, Hashida Y, Moser HW. Neonatal adrenoleukodystrophy. Clinical, pathologic, and biochemical delineation of a syndrome affecting both males and females. *Am J Pathol* 1982; 108: 100–111
- Janssen A, Baes M, Gressens P, Mannaerts GP, Declercq P, van Veldhoven PP. Docosahexaenoic acid deficit is not a major pathogenic factor in peroxisome-deficient mice. *Lab Invest* 2000; 80: 31–35
- Kelley RI, Datta NA, Dobyns WB, Hajra AK, Moser AB, Noetzel MJ, Zackal EH, Moser HW. Neonatal adrenoleukodystrophy: new cases, biochemical studies, and differentiation from Zellweger and related peroxisomal polydystrophy syndromes. *Am J Med Genet* 1986; 23: 869–901
- Liu HM, Bangaru BS, Kidd J, Boggs J. Neuropathological considerations in cerebro-hepato-renal syndrome (Zellweger's syndrome) *Acta Neuropathol (Berl)* 1976; 34: 115–123
- Manz HJ, Schuelein M, McCullough DC, Kishimoto Y, Eiben RM. New phenotypic variant of adrenoleukodystrophy. Pathologic, ultrastructural, and biochemical study in two brothers. *J Neurol Sci* 1980; 45: 245–260
- Martinez M. Restoring the DHA levels in the brain of Zellweger patients. *J Mol Neurosci* 2001; 16: 309–316

- Martinez M, Vasques E. MRI evidence that docosahexaenoic acid ethyl ester improves myelination in generalized peroxisomal disorders. *Neurology* 1998; 51: 26–32
- Matsumoto N, Tamura S, Moser A, Moser HW, Braverman N, Suzuki Y, Shimozaawa N, Kondo N, Fujiki Y. The peroxin *Pex6p* gene is impaired in peroxisomal biogenesis disorders of complementation group 6. *J Hum Genet* 2001; 46: 273–277
- Matsumoto N, Tamura S, Furuki S, Miyata N, Moser A, Shimozaawa N, Moser HW, Suzuki Y, Kondo N, Fujiki Y. Mutations in novel peroxin gene *PEX26* that causes peroxisome-biogenesis disorders of complementation group 8 provide a genotype-phenotype correlation. *Am J Hum Genet* 2003; 73: 233–246
- Matsumoto N, Tamura S, Fujiki Y. The pathogenic peroxin *Pex26p* recruits the *Pex1p*-*Pex6p* AAA ATPase complexes to peroxisomes. *Nat Cell Biol* 2003; 5: 454–60
- Maxwell MA, Allen T, Solly PB, Svingen T, Paton BC, Crane DL. Novel *PEX1* mutations and genotype-phenotype correlations in Australian peroxisome biogenesis disorder patients. *Hum Mutat* 2002; 20: 342–351
- Mito T, Takada K, Akaboshi S, Takashima S, Takeshita K, Origuchi Y. A pathological study of a peripheral nerve in a case of neonatal adrenoleukodystrophy. *Acta Neuropathol (Berl)* 1989; 77: 437–440
- Muntau AC, Mayerhofer PU, Paton PC, Kammerer S, Roscher AA. Defective peroxisome membrane synthesis due to mutations in human *PEX3* causes Zellweger syndrome, complementation group G. *Am J Hum Genet* 2000; 67: 967–975
- Nakai A, Shigematsu Y, Nishida K, Kikawa Y, Konishi Y. MRI findings of Zellweger syndrome. *Pediatr Neurol* 1995; 13: 346–348
- Okumoto K, Fujiki Y. *PEX12* encodes an integral membrane protein of peroxisomes. *Nat Genet* 1997; 17: 265–266
- Panjan DJ, Megliè NP, Neubauer D. A case of Zellweger syndrome with extensive MRI abnormalities and unusual EEG findings. *Clin Electroencephalogr* 2001; 32: 28–31
- Passarge E, McAdams AJ. Cerebro-hepato-renal syndrome. *J Pediatr* 1967; 71: 691–702
- Poll-The BT, Poulos A, Sharp P, Boue J, Ogier H, Odièvre M, Saudubray JM. Antenatal diagnosis of infantile Refsum's disease. *Clin Genet* 1985; 27: 524–526
- Poll-The BT, Gootjes J, Duran M, de Klerk JBC, Wenniger-Prick LJ, Admiraal RJC, Waterham HR, Wanders JA, Barth PG. Peroxisome biogenesis disorders with prolonged survival: phenotypic expression in a cohort of 31 patients. *Am J Med Genet [A]* 2004; 126: 333–338
- Portsteffen H, Beyer A, Becker E, Epplen C, Pawlak A, Kunau W-H, Dodt G. Human *PEX1* is mutated in complementation group 1 of the peroxisome biogenesis disorders. *Nat Genet* 1997; 17: 449–452
- Poulos A, Sharp P, Johnson D. Plasma polyenoic very-long-chain fatty acids in peroxisomal disease: biochemical discrimination of Zellweger's syndrome from other phenotypes. *Neurology* 1989; 39: 44–47
- Powers JM. The pathology of peroxisomal disorders with pathogenetic considerations. *J Neuropathol Exp Neurol* 1995; 54: 710–719
- Powers JM, Tummons RC, Caviness VS, Moser AB, Moser HW. Structural and chemical alterations in the cerebral maldevelopment of fetal cerebro-hepato-renal (Zellweger) syndrome. *J Neuropathol Exp Neurol* 1989; 48: 270–289
- Powers JM, Moser HG. Peroxisomal disorders: genotype, phenotype, major neuropathologic lesions, and pathogenesis. *Brain Pathol* 1998; 8: 101–120
- Preuss N, Brosius U, Biermanns M, Muntau AC, Conzelmann E, Gärtner J. *PEX1* Mutations in complementation group 1 of Zellweger spectrum patients correlate with severity of disease. *Pediatr Res* 2002; 51: 706–714
- Raafat F, Smith K, Halloran EA, Lacy D. Zellweger syndrome: a histochemical diagnosis of two cases. *Pediatr Pathol* 1991; 11: 413–420
- Raas-Rothschild A, Wanders RJA, Mooijer PAW, Gootjes J, Waterham HR, Gutman A, Suzuki Y, Shimozaawa N, Kondo N, Eshel G, Espeel M, Roels F, Korman SH. A *PEX6*-defective peroxisomal biogenesis disorder with severe phenotype in an infant, versus mild phenotype resembling Usher syndrome in the affected parents. *Am J Hum Genet* 2002; 70: 1062–1068
- Raymond GV. Peroxisomal disorders. *Curr Opin Neurol* 2001; 14: 783–787
- Reuber BE, Germain-Lee E, Collins CS, Morrell JC, Ameritunga R, Moser HW, Valle D, Gould SJ. Mutations in *PEX1* are the most common cause of peroxisome biogenesis disorders. *Nat Genet* 1997; 17: 445–448
- Robertson EF, Poulos A, Sharp P, Manson J, Wise G, Jaunzems A, Carter R. Treatment of infantile phytanic acid storage disease: clinical, biochemical and ultrastructural findings in two children treated for 2 years. *Eur J Pediatr* 1988; 147: 133–142
- Roels F, Espeel M, de Craemer D. Liver pathology and immunocytochemistry in congenital peroxisomal diseases: a review. *J Inher Metab Dis* 1991; 14: 853–875
- Roels F, Espeel M, Poggi F, Mandel H, van Maldergem L, Saudubray JM. Human liver pathology in peroxisomal diseases: a review including novel data. *Biochimie* 1993; 75: 281–292
- Sarnat HB, Trevenen CL, Darwish HZ. Ependymal abnormalities in cerebro-hepato-renal disease of Zellweger. *Brain Dev* 1993; 15: 270–277
- Schutgens RBH, Schrakamp G, Wanders RJA, Heymans HSA, Tager JM, van den Bosch H. Prenatal and perinatal diagnosis of peroxisomal disorders. *J Inher Metab Dis* 1989; 12: 118–134
- Scotto JM, Hadchouel M, Odièvre M, Laudat MH, Saudubray JM, Dulac O, Beucler I, Beaune P. Infantile phytanic acid storage disease, a possible variant of Refsum's disease: three cases, including ultrastructural studies of the liver. *J Inher Metab Dis* 1982; 5: 83–90
- Sharp P, Johnson D, Poulos A. Molecular species of phosphatidylcholine containing very long chain fatty acids in human brain: enrichment in X-linked adrenoleukodystrophy brain and diseases of peroxisome biogenesis brain. *J Neurochem* 1991; 56: 30–37
- Shimozaawa N, Suzuki Y, Zhang Z, Imamura A, Ghaedi K, Fujiki Y, Kondo N. Identification of *PEX3* as the gene mutated in a Zellweger syndrome patient lacking peroxisomal remnant structures. *Hum Mol Genet* 2000; 9: 1995–1999
- Slawekci ML, Dodt G, Steinberg S, Moser AB, Moser HW, Gould SJ. Identification of three distinct peroxisomal protein import defects in patients with peroxisome biogenesis disorders. *J Cell Sci* 1995; 108: 1817–1829
- Torvik A, Torp S, Kase BF, Ek J, Skjeldal O, Stokke O. Infantile Refsum's disease: a generalized peroxisomal disorder. Case report with postmortem examination. *J Neurol Sci* 1988; 85: 39–53
- Ulrich J, Herschkowitz N, Heitz Ph, Sigrist Th, Baerlocher P. Adrenoleukodystrophy. Preliminary report of a connatal case. Light- and electron microscopical immunohistochemical and biochemical findings. *Acta Neuropathol (Berl)* 1978; 43: 77–83

- Vamecq J, Draye JP, van Hoof F, Misson JP, Evrard P, Verellen G, Eyssen HJ, van Eldere J, Schutgens RH, Wanders RJA, Roels F, Goldfischer SL. Multiple peroxisomal enzymatic deficiency disorders. A comparative biochemical and morphologic study of Zellweger cerebrohepatorenal syndrome and neonatal adrenoleukodystrophy. *Am J Pathol* 1986; 125: 524–535
- Van Roermund CWT, Brul S, Tager JM, Schutgens RBH, Wanders RJA. Acyl-CoA oxidase, peroxisomal thiolase and dihydroxyacetone phosphate acyltransferase: aberrant subcellular localization in Zellweger syndrome. *J Inher Metab Dis* 14: 152–164
- Volpe JJ, Adams RD. Cerebro-hepato-renal syndrome of Zellweger: an inherited disorder of neuronal migration. *Acta Neuropathol (Berl)* 1972; 20: 175–198
- Walter C, Gootjes J, Mooijer PA, Portsteffen H, Klein C, Waterham HR, Barth PG, Epplen JT, Kunau W-H, Wanders RJA, Dodt G. Disorders of peroxisome biogenesis due to mutations in *PEX1*: phenotypes and *PEX1* protein levels. *Am J Hum Genet* 2001; 69: 35–48
- Wanders RJA, Boltshauser E, Steinmann B, Spycher MA, Schutgens RBH, Bosch van den H, Tager JM. Infantile phytanic acid storage disease, a disorder of peroxisome biogenesis: a case report. *J Neurol Sci* 1990; 98: 1–11
- Wanders RJA, Schutgens RBH, van den Bosch H, Tager JM, Kleijer WJ. Prenatal diagnosis of inborn errors in peroxisomal β -oxidation. *Prenat Diagn* 1991; 11: 253–261
- Wanders RJA, Schutgens RBH, Barth PG, Tager JM, van den Bosch H. Postnatal diagnosis of peroxisomal disorders: a biochemical approach. *Biochimie* 1993; 75: 269–279
- Warren JS, Morrell JC, Moser HW, Valle D, Gould SJ. Identification of *PEX10*, the gene defective in complementation group 7 of the peroxisome-biogenesis disorders. *Am J Hum Genet* 1998; 63: 347–359
- Warren DS, Wolfe BD, Gould SJ. Phenotype-genotype relationships in *PEX10*-deficient peroxisome biogenesis disorder patients. *Hum Mutat* 2000; 15: 509–521
- Wei H, Kemp S, McGuinness MC, Moser AB, Smith KD. Pharmacological induction of peroxisomes in peroxisome biogenesis disorders. *Ann Neurol* 2000; 47: 286–296
- Wilson GN, Holmes RD, Hajra AK. Peroxisomal disorders: clinical commentary and future prospects. *Am J Med Genet* 1988; 30: 771–792
- Wolff J, Nyhan WL, Powell H, Takahashi D, Hutzler J, Hajra AK, Datta NS, Singh I, Moser HW. Myopathy in an infant with a fatal peroxisomal disorder. *Pediatr Neurol* 1986; 2: 141–146
- Yahruas T, Braverman N, Dodt G, Kalish JE, Morrell JC, Moser HW, Valle D, Gould S. The peroxisome biogenesis disorder group 4 gene, *PXAAA1*, encodes a cytoplasmic ATPase required for stability of the PTS1 receptor. *EMBO J* 1996; 15: 2914–2923
- Clayton PT, Lake BD, Hjelm M, Stephenson JBP, Besley GTN, Wanders RJA, Schram AW, Tager JM, Schutgens RBH, Lawson AM. Bile acid analysis in “pseudo-Zellweger” syndrome; clues to the defect in peroxisomal β -oxidation. *J Inher Metab Dis* 1988; 11: 165–168
- Espeel M, Roels F, van Maldergem L, de Craemer D, Dacremont G, Wanders RJA, Hashimoto T. Peroxisomal localization of the immunoreactive β -oxidation enzymes in a neonate with a β -oxidation defect. *Pathological observations in liver, adrenal cortex and kidney. Virchows Arch [A]* 1991; 419: 301–308
- Ferdinandusse S, van Grunsven EG, Oostheim W, Denis S, Hogenhout EM, Ijlst L, van Roermund CWT, Waterham HR, Goldfischer S, Wanders RJA. Reinvestigation of peroxisomal 3-ketoacyl-CoA thiolase deficiency: identification of the true defect at the level of D-bifunctional protein. *Am J Hum Genet* 2002; 70: 1589–1593
- Goldfischer S, Collins J, Rapin I, Neumann P, Neglia W, Spiro AJ, Ishii T, Roels F, Vamecq J, van Hoof F. Pseudo-Zellweger syndrome: deficiencies in several peroxisomal oxidative activities. *J Pediatr* 1986; 108: 25–32
- Itoh M, Suzuki Y, Akaboshi S, Zhang Z, Miyabara S, Takashima S. Developmental and pathological expression of peroxisomal enzymes: their relationship of D-bifunctional protein deficiency and Zellweger syndrome. *Brain Res* 2000; 858: 40–47
- Kaufman WE, Theda C, Naidu S, Watkins PA, Moser AB, Moser HW. Neuronal migration abnormality in peroxisomal bifunctional enzyme defect. *Ann Neurol* 1996; 39: 268–271
- McGuinness MC, Moser AB, Poll-The BT, Watkins PA. Complementation analysis of patients with intact peroxisomes and impaired peroxisomal β -oxidation. *Biochem Med Metab Biol* 1993; 49: 228–242
- Möller G, van Grunsven EG, Wanders RJA, Adamski J. Molecular basis of D-bifunctional protein deficiency. *Mol Cell Endocrinol* 2001; 171: 61–70
- Naidu S, Hoefler G, Watkins PA, Chen WW, Moser AB, Hoefler S, Rance NE, Powers JM, Beard M, Green WR, Hashimoto T, Moser HW. Neonatal seizures and retardation in a girl with biochemical features of X-linked adrenoleukodystrophy: a possible new peroxisomal disease entity. *Neurology* 1988; 38: 1100–1107
- Nakada Y, Hyakuna N, Suzuki Y, Shimozawa N, Takaesu E, Ikema R, Hirayama K. A case of pseudo-Zellweger syndrome with a possible bifunctional enzyme deficiency but detectable enzyme protein. *Brain Dev* 1993; 15: 453–456
- Nakano K, Zhang Z, Shimozawa N, Kondo N, Ishii N, Funatsuka M, Shirakawa S, Itho M, Takashima S, Une M, Kana-aki RR, Mukai K, Osawa M, Suzuki Y. D-Bifunctional protein deficiency with fetal ascites, polyhydramnios, and contractures of hands and toes. *J Pediatr* 2001; 139: 865–867
- Paton BC, Solly PB, Nelson PV, Pollard AN, Sharp PC, Fietz MJ. Molecular analysis of genomic DNA allows rapid, and accurate, prenatal diagnosis of peroxisomal D-bifunctional protein deficiency. *Prenat Diagn* 2002; 22: 38–41
- Suzuki Y, Shimozawa N, Yajima S, Tomatsu S, Kondo N, Nakada Y, Akaboshi S, Iai M, Tanabe Y, Hashimoto T, Wanders RJA, Schitgens RBH, Moser HW, Orii T. Novel subtype of peroxisomal acyl-CoA oxidase deficiency and bifunctional protein enzyme deficiency with detectable enzyme protein: identification by means of complementation analysis. *Am J Hum Genet* 1994; 54: 35–43

19 Peroxisomal D-Bifunctional Protein Deficiency

- Akaboshi S, Tomita Y, Suzuki Y, Une M, Sohma O, Takashima S, Takeshita K. Peroxisomal bifunctional protein deficiency: serial neurophysiological examinations of a case. *Brain Dev* 1997; 19: 295–299
- Clayton PT. Clinical consequences of defects in peroxisomal β -oxidation. *Biochem Soc Trans* 2001; 29: 298–305

- Suzuki Y, Jiang LL, Soury M, Miyazawa S, Fukuda S, Zhang Z, Une M, Shimozawa N, Kondo N, Orii T, Hashimoto T. D-3-Hydroxy-CoA dehydratase / D-3-hydroxyacyl-CoA dehydrogenase bifunctional protein deficiency: a newly identified peroxisomal disorder. *Am J Hum Genet* 1997; 61: 1153–1162
- Suzuki Y, Zhang Z, Shimozawa N, Muro M, Shono H, Toda S, Miyahara S-I, Hashimoto T, Usuda N, Ito M, Takashima S, Kondo N. Prenatal diagnosis of peroxisomal D-3-hydroxyacyl-CoA dehydratase / D-3-hydroxyacyl-CoA dehydrogenase bifunctional protein deficiency. *J Hum Genet* 1999; 44: 143–147
- Van Grunsven EG, van Roermund CWT, Denis S, Wanders RJA. Complementation analysis of fibroblasts from peroxisomal fatty acid oxidation deficient patients shows high frequency of bifunctional protein enzyme deficiency plus intragenic complementation: unequivocal evidence for differential defects in the same enzyme protein. *Biochem Biophys Res Commun* 1997; 235: 176–179
- Van Grunsven EG, van Berkel E, Ijlst L, Vreken P, De Klerk JBC, Adamski J, Lemonde H, Clayton PT, Cuebas DA, Wanders RJA. Peroxisomal D-hydroxyacyl-CoA dehydrogenase deficiency: resolution of the enzyme defect and its molecular basis in bifunctional protein deficiency. *Proc Natl Acad Sci* 1998; 95: 2128–2133
- Van Grunsven EG, van Berkel E, Lemonde H, Clayton PT, Wanders RJA. Bifunctional protein deficiency: complementation within the same group suggesting differential enzyme defects and clues to the underlying basis. *J Inherit Metab Dis* 1998; 21: 298–301
- Van Grunsven EG, van Berkel E, Mooijer PAW, Watkins PA, Moser HW, Suzuki Y, Jiang LL, Hashimoto T, Hoefler G, Adamski J, Wanders RJA. Peroxisomal bifunctional protein deficiency revisited: resolution of its true enzymatic and molecular basis. *Am J Hum Genet* 1999; 64: 99–107
- Van Grunsven EG, Mooijer PAW, Aubourg P, Wanders RJA. Enoyl-CoA hydratase deficiency: identification of a new type of D-bifunctional protein deficiency. *Hum Mol Genet* 1999; 8: 1509–1516
- Van Maldergem L, Espeel M, Wanders RJA, Roels F, Gerard P, Scalais E, Mannaerts GP, Casteels M, Gillerot Y. Neonatal seizures and severe hypotonia in a male infant suffering from a defect in peroxisomal β -oxidation. *Neuromusc Disord* 1992; 2: 217–234
- Wanders RJA, van Roermund CWT, Schelen A, Schutgens RBH, Tager JM, Stephenson JBP, Clayton PT. A bifunctional protein with deficient enzymatic activity: identification of a new peroxisomal disorder using novel methods to measure the peroxisomal β -oxidation enzyme activities. *J Inherit Metab Dis* 1990; 13: 375–379
- Wanders RJA, van Roermund CWT, Brul S, Schutgens RBH, Tager JM. Bifunctional protein deficiency: identification of a new type of peroxisomal β -oxidation of unknown aetiology by means of complementation analysis. *J Inherit Metab Dis* 1992; 15: 385–388
- Watkins PA, Chen WW, Harris CJ, Hoefler G, Hoefler S, Blake DC Jr, Balfe A, Kelley RI, Moser AB, Beard ME, Moser HW. Peroxisomal bifunctional protein deficiency. *J Clin Invest* 1989; 83: 771–777
- Watkins PA, McGuinness MC, Raymond GV, Hicks BA, Sisk JM, Moser AB, Mower HW. Distinction between peroxisomal bifunctional enzyme and acyl-CoA oxidase deficiencies. *Ann Neurol* 1995; 38: 472–477
- ## 20 Acyl-CoA Oxidase Deficiency
- Clayton PT. Clinical consequences of defects in peroxisomal β -oxidation. *Biochem Soc Trans* 2001; 29: 298–305
- Christensen E, Woldseth B, Hagve T-A, Poll-The BT, Wanders RJA, Sprecher H, Stokke O, Christophersen BO. Peroxisomal β -oxidation of polyunsaturated long chain fatty acids in human fibroblasts. The polyunsaturated and the saturated long chain fatty acids are retroconverted by the same acyl-CoA oxidase. *Scand J Clin Lab Invest* 1993; 53: 61–74
- Kurian MA, Ryan S, Besley GTN, Wanders RJA, King MD. Straight-chain acyl-CoA oxidase deficiency presenting with dysmorphism, neurodevelopmental autistic type regression and a selective pattern of leukodystrophy. *J Inherit Metab Dis* 2004; 27: 105–108
- Mandel H, Berant M, Aizin A, Gershony R, Hemmli S, Schutgens RBH, Wanders RJA. Zellweger-like phenotype in two siblings: a defect in peroxisomal β -oxidation with elevated very long-chain fatty acids but normal bile acids. *J Inherit Metab Dis* 1992; 15: 381–384
- Poll-The BT, Roels F, Ogier H, Scotto J, Vamecq J, Schutgens RBH, Wanders RJA, van Roermund CWT, van Wijland MJA, Schram AW, Tager JM, Saudubray J-M. A new peroxisomal disorder with enlarged peroxisomes and a specific deficiency of acyl-CoA oxidase (pseudo-neonatal adrenoleukodystrophy). *Am J Hum Genet* 1988; 42: 422–434
- Su H-M, Moser AB, Moser HW, Watkins PA. Peroxisomal straight-chain acyl-CoA oxidase and D-bifunctional protein are essential for the retroconversion step in docosahexaenoic acid synthesis. *J Biol Chem* 2001; 276: 38115–38120
- Suzuki Y, Shimozawa N, Yajima S, Tomatsu S, Kondo N, Nakada Y, Akaboshi S, Iai M, Tanabe Y, Hashimoto T, Wanders RJA, Schitgens RBH, Moser HW, Orii T. Novel subtype of peroxisomal acyl-CoA oxidase deficiency and bifunctional protein enzyme deficiency with detectable enzyme protein: identification by means of complementation analysis. *Am J Hum Genet* 1994; 54: 35–43
- Suzuki Y, Iai M, Kamei A, Tanabe Y, Chida S, Yamaguchi S, Zhang Z, Takamoto Y, Shimozawa N, Kondo N. Peroxisomal acyl-CoA oxidase deficiency. *J Pediatr* 2002; 140: 128–130
- Watkins PA, McGuinness MC, Raymond GV, Hicks BA, Sisk JM, Moser AB, Mower HW. Distinction between peroxisomal bifunctional enzyme and acyl-CoA oxidase deficiencies. *Ann Neurol* 1995; 38: 472–477
- ## 21 X-Linked Adrenoleukodystrophy
- Afifi AK, Menezes AH, Reed LA, Bell WE. Atypical presentation of X-linked childhood adrenoleukodystrophy with an unusual magnetic resonance imaging pattern. *J Child Neurol* 1996; 11: 497–499
- Asano J-I, Suzuki Y, Yajima S, Ioué K, Shimozawa N, Kondo N, Murase M, Orii T. Effects of erucic acid therapy on Japanese patients with X-linked adrenoleukodystrophy. *Brain Dev* 1994; 16: 454–458
- Aubourg P, Dubois-Dalcq M. X-linked adrenoleukodystrophy enigma: how does the ALD peroxisomal transporter mutation affect CNS glia? *Glia* 2000; 29: 186–190
- Aubourg P, Blanche S, Jambaqué I, Rocchiccioli F, Kalifa G, Naud-Saudreau C, Rolland MO, Debré M, Chaussain JL, Griscelli C, Fischer A, Bougnères P-F. Reversal of early neurologic and neuroradiologic manifestations of X-linked adrenoleukodystrophy by bone marrow transplantation. *N Engl J Med* 1990; 322: 1860–1866

- Aubourg P, Adamsbaum C, Lavallard-Rousseau M-C, Rocchiccioli F, Cartier N, Jambaqué I, Jakobezak C, Lemaître A, Boureau F, Wolf C, Bougnères P-F. A two-year trial of oleic and erucic acids ("Lorenzo's oil") as treatment for adrenomyeloneuropathy. *N Engl J Med* 1993; 329: 745–752
- Aubourg P, Mandel JL. X-linked adrenoleukodystrophy. *Ann NY Acad Sci* 1996; 804: 461–476
- Barkovich AJ, Ferriero DM, Bass N, Boyer R. Involvement of the pontomedullary corticospinal tracts: a useful finding in the diagnosis of X-linked adrenoleukodystrophy. *AJNR Am J Neuroradiol* 1997; 18: 95–100
- Baumann M, Korenke GC, Widdige-Diedrichs A, Wilichowski E, Hunneman DH, Wilken B, Brockmann K, Klingebiel T, Niethammer D, Kühl J, Ebell W, Hanefeld F. Haematopoietic stem cell transplantation in 12 patients with cerebral X-linked adrenoleukodystrophy. *Eur J Pediatr* 2003; 162: 6–14
- Bekiesińska-Figatowska M, Tyłki-Szymańska A, Walecki J, Stradomska TJ. MRI findings in a asymptomatic boy with X-linked adrenoleukodystrophy and his symptomatic mother. *Neuroradiology* 2001; 43: 951–952
- Bezman L, Moser AB, Raymond GV, Rinaldo P, Watkins PA, Smith KD, Kass NE, Moser HW. Adrenoleukodystrophy: incidence, new mutation rate, and results of extended family screening. *Ann Neurol* 2001; 49: 512–517
- Borker A, Yu LC. Unrelated allogeneic bone marrow transplant in adrenoleukodystrophy using CD34⁺ stem cell selection. *Metab Brain Dis* 2002; 17: 139–142
- Boutin B, Matsuguchi L, Lebon P, Ponsol G, Arthuis C. Immunohistochemical analysis of brain macrophages in adrenoleukodystrophy. *Neuropediatrics* 1989; 20: 202–206
- Brown FR, Chen WW, Kirschner DA, Frayer KL, Powers JM, Moser AB, Moser HW. Myelin membrane from adrenoleukodystrophy brain white matter – biochemical properties. *J Neurochem* 1983; 41: 341–348
- Cartier N, Guidoux S, Rocchiccioli F, Aubourg P. Simvastatin does not normalize very long chain fatty acids in adrenoleukodystrophy mice. *FEBS Lett* 2000; 478: 205–208
- Confort-Gouny S, Vion-Dury J, Chabrol B, Nicoli F, Cozzone PJ. Localised proton magnetic resonance spectroscopy in X-linked adrenoleukodystrophy. *Neuroradiology* 1995; 37: 568–575
- Di Rocco M, Doria-Lamba L, Caruso U. Monozygotic twins with X-linked adrenoleukodystrophy and different phenotypes. *Ann Neurol* 2001; 50: 424
- Dodd A, Rowland SA, Hawkes SLJ, Kennedy MA, Love DR. Mutations in the adrenoleukodystrophy gene. *Hum Mutat* 1997; 9: 500–511
- Domagk J, Linke I, Argyrakos A, Spaar FW, Rahlf G, Schulte FJ. Adrenoleukodystrophy. *Neuropediatrics* 1975; 6: 41–64
- Dubois-Dalcq M, Feigenbaum V, Aubourg P. The neurobiology of X-linked adrenoleukodystrophy, a demyelinating peroxisomal disorder. *Trends Neurosci* 1999; 22: 4–12
- Dumic M, Gubarev n, Sikic N, Roscher A, Plavsic V, Filipovic-Grčić B. Sparse hair and multiple endocrine disorders in two women heterozygous for adrenoleukodystrophy. *Am J Med Genet* 1992; 43: 829–832
- Dunne E, Hyman NM, Huson SM, Németh AH. A novel point mutation in X-linked adrenoleukodystrophy presenting as spinocerebellar degeneration. *Ann Neurol* 1999; 45: 652–655
- Dziewas R, Stögbauer F, Oelerich M, Ritter M, Husstedt IW. A case of adrenomyeloneuropathy with unusual lesion pattern in magnetic resonance imaging. *J Neurol* 2001; 248: 341–342
- Edwin D, Speedie LJ, Kohler W, Naidu S, Kruse B, Moser HW. Cognitive and brain magnetic resonance imaging findings in adrenomyeloneuropathy. *Ann Neurol* 1996; 40: 675–678
- Eichler FS, Barker PB, Cox C, Edwin D, Ulug AM, Moser HW, Raymond GV. Proton MR spectroscopic imaging predicts lesion progression or MRI in X-linked adrenoleukodystrophy. *Neurology* 2002; 58: 901–907
- Eichler FS, Itoh R, Barker PB, Mori S, Garrett ES, van Zijl PCM, Moser HW, Raymond GV, Melhem ER. Proton MR spectroscopic and diffusion tensor brain MR imaging in X-linked adrenoleukodystrophy: initial experience. *Radiology* 2002; 225: 245–252
- Elrington GM, Bateman DE, Jeffrey MJ, Flawton N. Adrenoleukodystrophy: heterogeneity in two brothers. *J Neurol Neurosurg Psychiatry* 1989; 52: 310–313
- Engelbrecht V, Rassek M, Gärtner J, Kahn T, Mödder U. The value of new MRI techniques in adrenoleukodystrophy. *Pediatr Radiol* 1997; 27: 207–215
- Farrell DF, Hamilton SR, Knauss TA, Sanocki E, Deeb SS. X-Linked adrenoleukodystrophy: adult cerebral variant. *Neurology* 1993; 43: 1518–1522
- Fatemi A, Barker PB, Ulug AM, Nagae-Poetcher LM, Beauchamp NJ, Moser AB, Raymond GV, Moser HW, Naidu S. MRI and proton MRSI in women heterozygous for X-linked adrenoleukodystrophy. *Neurology* 2003; 60: 1301–1307
- Feigenbaum V, Gélot A, Casanova P, Daumas-Duport C, Aubourg P, Dubouis-Dalcq M. Apoptosis in the central nervous system of cerebral adrenoleukodystrophy patients. *Neurobiol Dis* 2000; 7: 600–612
- Gärtner J, Braun A, Holzinger A, Roerig P, Lenard H-G, Roscher AA. Clinical and genetic aspects of X-linked adrenoleukodystrophy. *Neuropediatrics* 1998; 29: 3–13
- Garg BP, Markand ON, DeMeyer WE, Warren C Jr. Evoked response studies in patients with adrenoleukodystrophy and heterozygous relatives. *Arch Neurol* 1983; 40: 356–359
- Garside S, Rosebush PI, Levinson AJ, Mazurek MF. Late-onset adrenoleukodystrophy associated with long-standing psychiatric symptoms. *J Clin Psychiatry* 1999; 60: 460–468
- Hershkovitz E, Narkis G, Shorer Z, Moser AB, Watkins PA, Moser HW, Manor E. Cerebral X-linked adrenoleukodystrophy in a girl with Xq27-Ter deletion. *Ann Neurol* 2002; 52: 234–237
- Hitomi T, Mezaki T, Tsujii T, Kinoshita M, Tomimoto H, Ikeda A, Shimohama S, Okazaki T, Uchiyama T, Shibasaki H. Improvement of central motor conduction after bone marrow transplantation in adrenoleukodystrophy. *J Neurol Neurosurg Psychiatry* 2003; 74: 373–375
- Hong-Magno ET, Muraki AS, Huttenlocher PR. Atypical CT scans in adrenoleukodystrophy. *J Comput Assist Tomogr* 1987; 11: 333–336
- Igarashi M, Schaumburg HH, Powers J, Kishimoto Y, Kolodny E, Suzuki K. Fatty acid abnormality in adrenoleukodystrophy. *J Neurochem* 1976; 26: 851–860
- Ito M, Blumberg BM, Mock DJ, Goodman AD, Moser AB, Moser HW, Smith KD, Powers JM. Potential environmental and host participants in the early white matter lesions of adrenoleukodystrophy: morphologic evidence for CD8 cytotoxic T cells, cytolysis of oligodendrocytes, and CD-1 mediated lipid antigen presentation. *J Neuropathol Exp Neurol* 2001; 60: 1004–1019
- Ito R, Melhem ER, Mori S, Eichler FS, Raymond GV, Moser HW. Diffusion tensor brain MR imaging in X-linked cerebral adrenoleukodystrophy. *Neurology* 2001; 56: 544–547
- Jensen ME, Sawyer RW, Braun IF, Rizzo WB. MR imaging appearance of childhood adrenoleukodystrophy with auditory, visual, and motor pathway involvement. *Radiographics* 1990; 10: 53–66

- Izquierdo M, Adamsbaum C, Benosman A, Aubourg P, Bittoun J. MR spectroscopic imaging of normal-appearing white matter in adrenoleukodystrophy. *Pediatr Radiol* 2000; 30: 621–629
- Jorge P, Quelhas D, Oliveira P, Pinto R, Nogueira A. X-Linked adrenoleukodystrophy in patients with idiopathic Addison disease. *Eur J Pediatr* 1994; 153: 594–597
- Kano S, Watanabe M, Kanai M, Koike R, Onodera O, Tsuji S, Okamoto K, Shoji M. A Japanese family with adrenoleukodystrophy with a codon 291 deletion: a clinical, biochemical, pathological, and genetic report. *J Neurol Sci* 1998; 158: 187–192
- Kaplan PW, Tusa RJ, Shankroff J, Heller J, Moser HW. Visual evoked potentials in adrenoleukodystrophy: a trial with glycerol trioleate and Lorenzo oil. *Ann Neurol* 1993; 34: 169–174
- Kemp S, Mooyer PAW, Bolhuis PA, van Geel BM, Mandel JL, Barth PG, Aubourg P, Wanders RJA. ALDP Expression in fibroblasts of patients with X-linked adrenoleukodystrophy. *J Inherit Metab Dis* 1996; 19: 667–674
- Kemp S, Wei H-M, Lu J-F, Braiterman LT, McGuinness MC, Moser AB, Watkins PA, Smith KD. Gene redundancy and pharmacological gene therapy: implications for X-linked adrenoleukodystrophy. *Nat Med* 1998; 4: 1261–1268
- Kemp S, Pujol A, Waterham HR, van Geel BM, Boehm CD, Raymond GV, Cutting GR, Wanders RJA, Moser HW. ABCD1 Mutations and the X-linked adrenoleukodystrophy mutation database: role in diagnosis and clinical correlations. *Hum Mutat* 2001; 18: 499–515
- Koike R, Tsuji S, Ohno T, Suzuki Y, Orii T, Miyatake T. Physiological significance of fatty acid elongation system in adrenoleukodystrophy. *J Neurol Sci* 1991; 103: 188–194
- Kok F, Neumann S, Sarde C-O, Zheng S, Wu K-H, Wei H-M, Bergin J, Watkins PA, Gould S, Sack G, Moser H, Mandel J-L, Smith KD. Mutational analysis of patients with X-linked adrenoleukodystrophy. *Hum Mutat* 1995; 6: 104–115
- Korenke GC, Christen H-J, Kruse B, Hunneman DH, Hanefeld F. Progression of X-linked adrenoleukodystrophy under interferon- β therapy. *J Inherit Metab Dis* 1997; 20: 59–66
- Kukowski B. Magnetic transcranial brain stimulation and multimodality evoked potentials in an adrenoleukodystrophy patient and members of his family. *Electroencephalogr Clin Neurophysiol* 1991; 78: 260–262
- Kumar AJ, Rosenbaum AE, Naidu S, Wener L, Citrin CM, Lindenberg R, Kim WS, Zinreich SJ, Molliver ME, Mayberg HS, Moser HW. Adrenoleukodystrophy: correlating MR imaging with CT. *Radiology* 1987; 165: 497–504
- Kumar AJ, Köhler W, Kruse B, Naidu S, Bergin A, Edwin D, Moser HW. MR findings in adult-onset adrenoleukodystrophy. *AJNR Am J Neuroradiol* 1995; 16: 1227–1237
- Kurihara M, Kumagai K, Yagishita S, Imai M, Watanabe M, Suzuki Y, Orii T. Adrenoleukomyeloneuropathy presenting as cerebellar ataxia in a young child: a probable variant of adrenoleukodystrophy. *Brain Dev* 1993; 15: 377–380
- Kurihara M, Kumagai K, Noda Y, Yagishita S. An autopsy case of atypical adrenoleukomyeloneuropathy in childhood. *Brain Dev* 2000; 22: 394–397
- Kusaka H, Imai T. Ataxic variant of adrenoleukodystrophy: MRI and CT findings. *J Neurol* 1992; 239: 307–310
- Loes DJ, Hite S, Moser H, Stillman AE, Shapiro E, Lockman L, Latchaw RE, Krivit W. Adrenoleukodystrophy: a scoring method for brain MR observations. *AJNR Am J Neuroradiol* 1994; 15: 1761–1766
- Loes DJ, Stillman AE, Hite S, Shapiro E, Lockman L, Latchaw RE, Moser H, Krivit W. Childhood cerebral form of adrenoleukodystrophy: short-term effect of bone marrow transplantation on brain MR observations. *AJNR Am J Neuroradiol* 1994; 15: 1767–1771
- Loes DJ, Fatemi A, Melhem ER, Gupte N, Bezman L, Moser HW, Raymond GV. Analysis of MRI patterns aids prediction of progression in X-linked adrenoleukodystrophy. *Neurology* 2003; 61: 369–374
- Maier EM, Kammerer S, Muntau AC, Wichers M, Braun A, Roscher AA. Symptoms in carriers of adrenoleukodystrophy relate to skewed X inactivation. *Ann Neurol* 2002; 52: 683–688
- Maris T, Androulidakis EJ, Tzagournissakis M, Papavassiliou S, Moser H, Plaitakis A. X-linked adrenoleukodystrophy presenting as neurologically pure familial spastic paraparesis. *Neurology* 1994; 45: 1101–1104
- Marsh WW, Hurst DL. Variable phenotypes in a family kindred with adrenoleukodystrophy. *Pediatr Neurol* 1991; 7: 50–52
- Martin JJ, Ceuterick C, Libert J. Skin and conjunctival nerve biopsies in adrenoleukodystrophy and its variants. *Ann Neurol* 1980; 8: 291–295
- McGuinness MC, Lu J-F, Zhang H-P, Dong G-X, Heinzer AK, Watkins PA, Powers J, Smith KD. Role of ALDP (ABCD1) and mitochondria in X-linked adrenoleukodystrophy. *Mol Cell Biol* 2003; 23: 744–753
- Melhem ER, Breitner SN, Ulug AM, Raymond GV, Moser HW. Improved tissue characterization in adrenoleukodystrophy using magnetization transfer imaging. *AJR Am J Roentgenol* 1996; 166: 689–695
- Melhem ER, Loes DJ, Georgiades CG, Raymond GV, Moser HW. X-linked adrenoleukodystrophy: the role of contrast-enhanced MR imaging in predicting disease progression. *AJNR Am J Neuroradiol* 2000; 21: 839–844
- Melhem ER, Gotwald TF, Itho R, Zinreich SJ, Moser HW. T2 relaxation measurements in X-linked adrenoleukodystrophy performed using dual-echo fast fluid-attenuated inversion recovery MR imaging. *AJNR Am J Neuroradiol* 2001; 22: 733–776
- Mo YH, Chen YF, Liu HM. Adrenomyeloneuropathy, a dynamic disorder: brain magnetic resonance imaging of two cases. *Neuroradiology* 2004; 46: 296–300
- Molzer B, Bernheimer H, Budka H, Pilz P, Toifl K. Accumulation of very long chain fatty acids is common to 3 variants of adrenoleukodystrophy (ALD). *J Neurol Sci* 1981; 51: 301–310
- Moser H, Dubey P, Fatemi A. Progress in X-linked adrenoleukodystrophy. *Curr Opin Neurol* 2004; 17: 263–269
- Moser HW. Adrenoleukodystrophy: natural history treatment and outcome. *J Inherit Metab Dis* 1995; 18: 435–447
- Moser HW. Adrenoleukodystrophy. *Curr Opin Neurol* 1995; 8: 221–226
- Moser HW. Adrenoleukodystrophy: phenotype, genetics, pathogenesis and therapy. *Brain* 1997; 120: 1485–1508
- Moser HW, Moser AB, Frayer KK, Chen W, Schulman JD, O'Neill BP, Kishimoto Y. Adrenoleukodystrophy: increased plasma content of saturated very long chain fatty acids. *Neurology* 1981; 31: 1241–1249
- Moser HW, Moser AB, Naidu S, Bergin A. Clinical aspects of adrenoleukodystrophy and adrenomyeloneuropathy. *Dev Neurosci* 1991; 13: 254–261
- Moser HW, Moser AB, Smith KD, Bergin A, Borel J, Shankroff J, Stine OC, Merette C, Ott J, Krivit W, Shapiro E. Adrenoleukodystrophy: Phenotypic variability and implications for therapy. *J Inherit Metab Dis* 1992; 15: 645–664

- Moser HW, Loes DJ, Melhem ER, Raymond GV, Bezman L, Cox CS, Lu S-e. X-linked adrenoleukodystrophy: overview and prognosis as a function of age and brain magnetic resonance imaging abnormality. A study involving 372 patients. *Neuropediatrics* 2000; 31: 227–239
- Moser HW, Brezman L, Lu SE, Raymond GV. Therapy of X-linked adrenoleukodystrophy: prognosis based upon age and MRI abnormality and plans for placebo-controlled trials. *J Inher Metab Dis* 2000; 23: 273–277
- Moser HW, Raymond GV, Koehler W, Sokolowski P, Hanefeld F, Korenke GC, Green A, Loes DJ, Hunneman DH, Jones RO, Lu SE, Uziel G, Giros ML, Roels F. Evaluation of the preventive effect of glyceryl trioleate-trierythrate ("Lorenzo's oil") therapy in X-linked adrenoleukodystrophy: results of two concurrent trials. *Adv Exp Med Biol* 2003; 544: 369–387
- Mosser J, Douar AM, Sarde CO, Kioschis P, Feil R, Moser H, Poustka AM, Mandel JL, Aubourg P. Putative X-linked adrenoleukodystrophy gene shares unexpected homology with ABC transporters. *Nature* 1993; 361: 726–730
- Nishio H, Kodama S, Tsubota T, Takumi T, Takahashi T, Yokoyama S, Matsuo T. Adrenoleukodystrophy without adrenal insufficiency and its magnetic resonance imaging. *J Neurol* 1985; 232: 265–270
- Nowaczyk MJM, Saunders EF, Tein I, Blaser SI, Clarke JTR. Immunoablation does not delay the neurologic progression of X-linked adrenoleukodystrophy. *J Pediatr* 1997; 131: 453–455
- O'Neill BP, Marmion LC, Feringa ER. The adrenoleukomyeloneuropathy complex: expression in four generations. *Neurology* 1981; 31: 151–156
- O'Neill BP, Moser HW, Saxena KM. Familial X-linked Addison disease as an expression of adrenoleukodystrophy (ALD): elevated C₂₆ fatty acid in cultured skin fibroblasts. *Neurology* 1982; 32: 543–547
- O'Neill GN, Aoki M, Brown RH Jr. ABCD1 translation-initiator mutation demonstrates genotype-phenotype correlation for AMN. *Neurology* 2001; 57: 1956–1962
- Pai GS, Khan M, Barbosa E, Key L, Craver JR, Curé JK, Betros R, Singh I. Lovastatin therapy for X-linked adrenoleukodystrophy: clinical and biochemical observations on 12 patients. *Mol Genet Metab* 2000; 69: 312–322
- Paintlia AS, Gilg AG, Khan M, Singh AK, Barbosa E, Singh I. Correlation of very long chain fatty acid accumulation and inflammatory disease progression in childhood X-ALD: implications for potential therapies. *Neurobiol Dis* 2003; 14: 425–439
- Pasco A, Kalifa G, Sarrazin JL, Adamsbaum C, Aubourg P. Contribution of MRI to the diagnosis of cerebral lesions of adrenoleukodystrophy. *Pediatr Radiol* 1991; 21: 161–163
- Philips JP, Lockman LA, Shapiro EG, Blazar BR, Loes DJ, Moser HW, Krivit W. CSF findings in adrenoleukodystrophy: correlation between measures of cytokines, IgG production, and disease severity. *Pediatr Neurol* 1994; 10: 289–294
- Poulos A, Gibson R, Sharp P, Beckman K, Grattan-Smith P. Very long chain fatty acids in X-linked adrenoleukodystrophy brain after treatment with Lorenzo's oil. *Ann Neurol* 1994; 36: 741–746
- Powell H, Tindall R, Schultz P, Paa D, O'Brien J, Lampert P. Adrenoleukodystrophy. Electron microscopic findings. *Arch Neurol* 1975; 32: 250–260
- Powers JM, Moser HG. Peroxisomal disorders: genotype, phenotype, major neuropathologic lesions, and pathogenesis. *Brain Pathol* 1998; 8: 101–120
- Powers JM, Schaumburg HH. Adreno-leukodystrophy (sex-linked Schilder's disease). A pathogenetic hypothesis based on ultrastructural lesions in adrenal cortex, peripheral nerve and testis. *Am J Pathol* 1974; 76: 481–491
- Powers JM, Liu Y, Moser AB, Moser HW. The inflammatory myelinopathy of adreno-leukodystrophy: cells, effector molecules, and pathogenetic implications. *J Neuropathol Exp Neurol* 1992; 51: 630–643
- Powers JM, DeCiero DP, Ito M, Moser AB, Moser HW. Adrenomyeloneuropathy: a neuropathologic review featuring its noninflammatory myelopathy. *J Neuropathol Exp Neurol* 2000; 59: 89–102
- Powers JM, DeCiero DP, Cox C, Richfield EK, Ito M, Moser AB, Moser HW. The dorsal root ganglia in adrenomyeloneuropathy: neuronal atrophy and abnormal mitochondria. *J Neuropathol Exp Neurol* 2001; 60: 493–501
- Rajanayagam V, Balthazor M, Shapiro EG, Krivit W, Lockman L, Stillman AE. Proton MR spectroscopy and neuropsychological testing in adrenoleukodystrophy. *AJNR Am J Neuroradiol* 1997; 18: 1909–1914
- Ramsey RB, Banik NL, Scott T, Davison AN. Neurochemical findings in adreno-leukodystrophy. *J Neurol Sci* 1976; 29: 277–294
- Ravid S, Diamond AS, Eviatar L. Coma as an acute presentation of adrenoleukodystrophy. *Pediatr Neurol* 2000; 22: 237–239
- Restuccia D, Di Lazzaro V, Valeriani M, Oliviero A, Le Pera D, Colosimo C, Brudi N, Cappa M, Bertini E, Di Biase A, Tonali P. Neurophysiological abnormalities in adrenoleukodystrophy carriers. Evidence of different degrees of central nervous system involvement. *Brain* 1997; 120: 1139–1148
- Rizzo WB, Leshner RT, Odone A, Dammann AL, Craft BS, Jensen ME, Jennings SS, Davis S, Jaitly R, Sgro JA. Dietary erucic acid therapy for X-linked adrenoleukodystrophy. *Neurology* 1989; 39: 1415–1422
- Ronghe MD, Barton J, Jardine PE, Crowne EC, Webster MH, Armitage M, Allen JT, Steward CG. The importance of testing for adrenoleukodystrophy in males with idiopathic Addison's disease. *Arch Dis Child* 2002; 86: 185–189
- Samadja D, Cabre Ph, Kujas M, Vernant J-C, Rivierez M. Intracranial hypertension as an unusual presentation of adrenoleukodystrophy. *Eur J Neurol* 1997; 4: 413–415
- Schaumburg HH, Powers JM, Raine CS, Suzuki K, Richardson EP. Adrenoleukodystrophy: a clinical and pathological study of 17 cases. *Arch Neurol* 1975; 32: 577–591
- Schaumburg HH, Powers JM, Raine CS, Spencer PS, Griffin JW, Prineas JW, Boehme DM. Adrenomyeloneuropathy: a probable variant of adrenoleukodystrophy. General pathologic, neuropathologic, and biochemical aspects. *Neurology* 1977; 27: 1114–1119
- Scholte W, Molzer B, Peiffer J, Poremba M, Schumm F, Harzer K, Schnabel R, Bernheimer H. Adrenoleukodystrophy in an adult female. A clinical, morphological and neurochemical study. *J Neurol* 1987; 235: 1–9
- Schmidt S, Träber F, Block W, Keller E, Pohl C, von Oertzen J, Schild H, Schlegel U, Klockgether T. Phenotype assignment in symptomatic female carriers of X-linked adrenoleukodystrophy. *J Neurol* 2001; 248: 36–44
- Schneider JFL, Il'yasov KA, Boltshauser E, Hennig J, Martin E. Diffusion tensor imaging in cases of adrenoleukodystrophy: preliminary experience as a marker for early demyelination? *AJNR Am J Neuroradiol* 2003; 24: 819–824
- Schöder JM, Mayer M, Weis J. Mitochondrial abnormalities and intrafamilial variability of sural nerve biopsy findings in adrenomyeloneuropathy. *Acta Neuropathol (Berl)* 1996; 92: 64–69

- Shapiro E, Krivit W, Lockman L, Jambaqué, Peters C, Cowan M, Harris R, Blanche S, Bordigoni P, Loes D, Ziegler R, Crittenden M, Ris D, Berg B, Cox C, Moser H, Fisher A, Aubourg P. Long-term effect of bone-marrow transplantation for childhood-onset cerebral X-linked adrenoleukodystrophy. *Lancet* 2000; 356: 713–718
- Singh I, Khan M, Key L, Pai S. Lovastatin for x-linked adrenoleukodystrophy. *N Engl J Med* 1998; 339: 702–703
- Smith KD, Kemp S, Braiterman LT, Lu J-F, Wei H-M, Geraghty M, Stetten G, Bergin JS, Pevsner J, Watkins PA. X-linked adrenoleukodystrophy: genes, mutations, and phenotypes. *Neurochem Res* 1999; 24: 521–535
- Snyder RD, King JN, Keck GM, Orrison WW. MR imaging of the spinal cord in 23 subjects with ALD-AMN complex. *AJNR Am J Neuroradiol* 1991; 12: 1095–1098
- Sobue G, Ueno-Natsukari IU, Okamoto H, Connell TA, Aizawa I, Mizoguchi K, Honma M, Ishakawa G, Mitsuma T, Natsukari N. Phenotypic heterogeneity of an adult form of adrenoleukodystrophy in monozygotic twins. *Ann Neurol* 1994; 36: 912–915
- Steinberg SJ, Kemp S, Braiterman LT, Watkins PA. Role of very-long-chain-acyl-coenzyme A synthetase in X-linked adrenoleukodystrophy. *Ann Neurol* 1999; 46: 409–412
- Stephenson DJ, Bezman L, Raymond GV. Acute presentation of childhood adrenoleukodystrophy. *Neuropediatrics* 2000; 31: 293–297
- Tan E-K, Lim S-H, Chan L-L, Wong M-C, Tan K-P. X-linked adrenoleukodystrophy: spinocerebellar variant. *Clin Neurol Neurosurg* 1999; 101: 137–140
- Tanaka K, Koyama A, Koike R, Ohno T, Atsumi T, Miyatake T. Adrenomyeloneuropathy: report of a family and electron microscopical findings in peripheral nerve. *J Neurol* 1985; 232: 73–78
- Terakawa H, Yanagihara T, Abe K. Unusual lateralization of adrenoleukodystrophy lesions on neuroimaging. *J Neuroimaging* 1997; 7: 121–123
- Theda C, Moser AB, Powers JM, Moser HW. Phospholipids in X-linked adrenoleukodystrophy white matter: fatty acid abnormalities before the onset of demyelination. *J Neurol Sci* 1992; 110: 195–204
- Uchiyama M, Hata Y, Tada S. MR imaging of adrenoleukodystrophy. *Neuroradiology* 1991; 33: 25–29
- Uyama E, Iwagoe H, Maeda J, Nakamura M, Terasaki T, Ando M. Presenile-onset cerebral adrenoleukodystrophy presenting as Balint's syndrome and dementia. *Neurology* 1993; 43: 1249–1251
- Uziel G, Bertini E, Bardelli P, Rimoldi M, Gambetti M. Experience on therapy of adrenoleukodystrophy and adrenomyeloneuropathy. *Dev Neurosci* 1991; 13: 274–279
- van der Knaap MS, Valk J. MR of adrenoleukodystrophy: histopathologic correlations. *AJNR Am J Neuroradiol* 1989; 10: S12–S14
- van Geel BM, Assies J, Weverling GJ, Barth PG. Predominance of the adrenomyeloneuropathy phenotype of X-linked adrenoleukodystrophy in the Netherlands: a survey of 30 kindreds. *Neurology* 1994; 44: 2343–2346
- van Geel BM, Assies J, Wanders RJA, Barth PG. X-linked adrenoleukodystrophy: clinical presentation, diagnosis, and therapy. *J Neurol Neurosurg Psychiatry* 1997; 63: 4–14
- van Geel BM, Assies J, Haverkort EB, Koelman JHTM, Verbeeten B Jr, Wanders RJA, Barth PG. Progression of abnormalities in adrenomyeloneuropathy and neurologically asymptomatic X-linked adrenoleukodystrophy despite treatment with "Lorenzo's oil." *J Neurol Neurosurg Psychiatry* 1999; 67: 290–299
- van Geel BM, Bezman L, Loes DJ, Moser HW, Raymond GV. Evolution of phenotypes in adult male patients with X-linked adrenoleukodystrophy. *Ann Neurol* 2001; 49: 186–194
- Verris A, Willemsen MAA, Rubio-Gozalbo E, de Jong J, Smeitink JAM. Simvastatin and plasma very-long-chain fatty acids in X-linked adrenoleukodystrophy. *Ann Neurol* 2000; 47: 552–553
- Wanders RJA, van Roermund CWT, Lageweg W, Jakobs BS, Schutgens RBH, Nijenhuis AA, Tager JM. X-Linked adrenoleukodystrophy: biochemical diagnosis and enzyme defect. *J Inher Metab Dis* 1992; 15: 634–644
- Wanders RJA, Mooyer PW, Dekker C, Vreken P. X-Linked adrenoleukodystrophy: improved prenatal diagnosis using both biochemical and immunological methods. *J Inher Metab Dis* 1998; 21: 285–287
- Waragai M, Takaya Y, Hayashi M, Shibata N, Kobayashi M. MRI of adrenoleukodystrophy involving predominantly the cerebellum and brain stem. *Neuroradiology* 1996; 38: 788–791
- Watkins PA, Gould JS, Smith MA, Braiterman LT, Wei H-M, Kok F, Moser AB, Moser HW, Smith KD. Altered expression of ALDP in X-linked adrenoleukodystrophy. *Am J Hum Genet* 1995; 57: 292–301
- Weinhofer I, Forss-Petter S, Žigman M, Berger J. Cholesterol regulates *ABCD2* expression: implications for the therapy of X-linked adrenoleukodystrophy. *Hum Mol Genet* 2002; 11: 2701–2708
- Weller M, Liedtke W, Petersen D, Opitz H, Poremba M. Very-late-onset adrenoleukodystrophy: possible precipitation of demyelination by cerebral contusion. *Neurology* 1992; 42: 367–370
- Wilken B, Dechent P, Brockmann K, Finsterbusch J, Baumann M, Ebell W, Korenke GC, Pouwels PJW, Hanefeld FA, Frahm J. Quantitative proton magnetic resonance spectroscopy of children with adrenoleukodystrophy before and after hematopoietic stem cell transplantation. *Neuropediatrics* 2003; 34: 237–246
- Wilson R, Sargent JR. Lipid and fatty acid composition of brain tissue from adrenoleukodystrophy patients. *J Neurochem* 1993; 61: 290–297
- Zammarchi EM, Donati MA, Tucci F, Fonda C, Fanelli F, Pazzaglia R. Acute onset of X-linked adrenoleukodystrophy mimicking encephalitis. *Brain Dev* 1994; 16: 238–240
- Zhang LX, Baski R, Fine E, Moser HW. Clinical and electrophysiological improvement of adrenomyeloneuropathy with steroid treatment. *J Neurol Neurosurg Psychiatry* 2002; 74: 822–823

22 Refsum Disease

- Baumgartner MR, Jansen GA, Verhoeven NM, Mooyer PAW, Jakobs C, Roels F, Espeel M, Fourmaintraux A, Bellet H, Wanders RJA, Saudubray JM. Atypical Refsum disease with pipecolic academia and abnormal catalase distribution. *Ann Neurol* 2000; 47: 109–113
- Cammermeyer J. Neuropathological changes in hereditary neuropathies: manifestation of the syndrome here-dopathia atactica polyneuritiformis in the presence of interstitial hypertrophic polyneuropathy. *J Neuropathol Exp Neurol* 1956; 15: 340–367
- Casteels M, Croes K, van Veldhoven PP, Mannaerts GP. Peroxisomal localization of α -oxidation in human liver. *J Inher Metab Dis* 1997; 20: 665–673

- Chahal A, Khan H, Pai SG, Barbosa E, Singh I. Restoration of phytanic acid oxidation in Refsum disease fibroblasts from patients with mutations in the phytanoyl-CoA hydroxylase gene. *FEBS Lett* 1998; 429: 119–122
- Dick JPR, Gibberd FB, Meeran K, Rose CF. Hypokalaemia in acute Refsum's disease. *J R Soc Med* 1993; 86: 171–172
- Dickson N, Mortimer JG, Faed JM, Pollard AC, Styles M, Peart DA. A child with Refsum's disease: successful treatment with diet and plasma exchange. *Dev Med Child Neurol* 1989; 31: 81–97
- Djupestrand G, Flottorp G, Refsum S. Phytanic acid storage disease: hearing maintained after 15 years of dietary treatment. *Neurology* 1983; 33: 237–240
- Dotti MT, Rossi A, Rizzuto N, Hayek G, Bardelli N, Bardelli AM, Federico A. Atypical phenotype of Refsum's disease: Clinical, biochemical, neurophysiological and pathological study. *Eur Neurol* 1985; 24: 85–93
- Ferdinandusse S, Denis S, Clayton PT, Graham A, Rees JE, Allen JT, McLean BN, Brown AY, Vreken P, Waterham HR, Wanders RJA. Mutations in the gene encoding peroxisomal α -methylacyl-CoA racemase cause adult-onset sensory motor neuropathy. *Nat Genet* 2000; 24: 188–191
- Flament-Durand J, Noel P, Rutsaert J, Toussaint D, Malmendier C, Lyon G. A case of Refsum's disease: clinical, pathological, ultrastructural and biochemical study. *Pathol Eur* 1971; 6: 172–191
- Gibberd FB, Billimoria JD, Goldman JM, Clemens ME, Evans R, Whitelaw MN, Retsas S, Sherratt RM. Heredopathia atactica polyneuritiformis: Refsum's disease. *Acta Neurol Scand* 1985; 72: 1–17
- Gelot A, Vallat JM, Tabaraud F, Rocchiccioli F. Axonal neuropathy and late detection of Refsum's disease. *Muscle Nerve* 1995; 18: 667–670
- Gordon N, Hudson REB. Refsum's syndrome heredopathia atactica polyneuritiformis. A report of three cases, including a study of the cardiac pathology. *Brain* 1959; 82: 41–55
- Harari D, Gibberd FB, Dick JPR, Sidey MC. Plasma exchange in the treatment of Refsum's disease (heredopathia atactica polyneuritiformis). *J Neurol Neurosurg Psychiatry* 1991; 54: 614–617
- Hungerbühler JP, Meier C, Rousselle L, Quadri P, Bogousslavsky J. Refsum's disease: management by diet and plasmapheresis. *Eur Neurol* 1985; 24: 153–159
- Jansen GA, Ofman R, Ferdinandusse S, IJlst L, Muijsers AO, Skjeldal OH, Stokke O, Jakobs C, Besley GTN, Wraith JE, Wanders RJA. Refsum disease is caused by mutations in the phytanoyl-CoA hydroxylase gene. *Nat Genet* 1997; 17: 190–193
- Jansen GA, Hogenhout EM, Ferdinandusse S, Waterham HR, Ofman R, Jakobs C, Skjeldal OH, Wanders RJA. Human phytanoyl-CoA hydroxylase: resolution of the gene structure and the molecular basis of Refsum's disease. *Hum Mol Genet* 2000; 9: 1195–1200
- Kuntzer T, Ochsner F, Schmid F, Regli F. Quantitative EMG analysis and longitudinal nerve conduction studies in a Refsum's disease patient. *Muscle Nerve* 1993; 16: 857–863
- Lemotte PK, Keidel S, Apfel CM. Phytanic acid is a retinoid X receptor ligand. *Eur J Biochem* 1996; 236: 328–333
- Leppert D, Schanz U, Burger J, Gmür J, Blau N, Waespe W. Long-term plasma exchange in a case of Refsum's disease. *Eur Arch Psychiatry Clin Neurosci* 1991; 241: 82–84
- MacBrinn M, O'Brien JS. Lipid composition of the nervous system in Refsum's disease. *J Lipid Res* 1968; 9: 552–561
- Mihalik SJ, Morrell JC, Kim D, Sacksteder KA, Watkins PA, Gould SJ. Identification of *PAHX*, a Refsum disease gene. *Nat Genet* 1997; 17: 185–189
- Millar JHD. Refsum disease – the effect of diet. *Ulster Med J* 1985; 54: 41–45
- Nadal N, Rolland MO, Tranchant C, Reutenauer L, Gyapay G, Warter JM, Mandel JL, Koenig M. Localization of Refsum disease with increased pipecolic acidemia to chromosome 10p by homozygosity mapping and carrier testing in a single nuclear family. *Hum Mol Genet* 1995; 4: 1963–1966
- Oysu C, Aslan I, Basaran B, Baserer N. The site of the hearing loss in Refsum's disease. *Int J Pediatr Otorhinolaryngol* 2001; 61: 129–134
- Plant GR, Hansell DM, Gibberd FB, Sidey MC. Skeletal abnormalities in Refsum's disease (heredopathia atactica polyneuritiformis). *Br J Radiol* 1990; 63: 537–541
- Reese H, Bareta J. Heredopathia atactica polyneuritiformis. *J Neuropathol Exp Neurol* 1950; 9: 385–395
- Singh I, Lazo O, Kalipada P, Singh AK. Phytanic acid α -oxidation in human cultured skin fibroblasts. *Biochim Biophys Acta* 1992; 1180: 221–224
- Singh I, Pahan K, Dhaunsi GS, Lazo O, Ozand P. Phytanic acid α -oxidation. *J Biol Chem* 1993; 268: 9972–9979
- Skjeldal OH, Nyberg-Hansen R, Stokke O. Neurological disorders and phytanic acid metabolism. *Acta Neurol Scand* 1988; 78: 324–328
- Tranchant C, Aubourg P, Mohr M, Rocchiccioli F, Zaenker C, Warter JM. A new peroxisomal disease with impaired phytanic acid and pipecolic acid oxidation. *Neurology* 1993; 43: 2044–2048
- Van den Brink DM, Brites P, Haasjes J, Wierzbicki AS, Mitchell J, Lambert-Hamill M, de Belleruche J, Jansen GA, Waterham HR, Wanders RJA. Identification of *PEX7* as the second gene involved in Refsum disease. *Am J Hum Genet* 2003; 72: 471–477
- Verhoeven NM, Schor DSM, Roe CR, Wanders RJA, Jakobs C. Phytanic acid α -oxidation in peroxisomal disorders: studies in cultured human fibroblasts. *Biochim Biophys Acta* 1997; 1361: 281–286
- Verhoeven NM, Schor DSM, ten Brink HJ, Wanders RJA, Jakobs C. Resolution of the phytanic acid α -oxidation pathway: identification of pristanal as product of the decarboxylation of 2-hydroxyphytanoyl-CoA. *Biochem Biophys Res Commun* 1997; 237: 33–36
- Verhoeven NM, Wanders RJA, Poll-The BT, Saudubray J-M, Jakobs C. The metabolism of phytanic acid and pristanic acid in man: a review. *J Inher Metab Dis* 1998; 21: 697–728
- Wall WJH, Worthington BS. Skeletal changes in Refsum's disease. *Clin Radiol* 1979; 30: 657–659
- Wanders RJA, Heymans HSA, Schutgens RBH, Poll-Thé BT, Saudubray JM, Tager JM, Schrakamp G, van den Bosch H. Peroxisomal functions in classical Refsum's disease: comparison with the infantile form of Refsum's disease. *J Neurol Sci* 1988; 84: 147–155
- Wanders RJA, Jansen GA, Skjeldal OH. Refsum disease, peroxisomes and phytanic acid oxidation: a review. *J Neuropathol Exp Neurol* 2001; 60: 1021–1031
- Weinstein R. Phytanic acid storage disease (Refsum's disease): clinical characteristics, pathophysiology and the role of therapeutic apheresis in its management. *J Clin Apheresis* 1999; 14: 181–184
- Wierzbicki AS, Mitchell J, Lambert-Hamill M, Hancock M, Greenwood J, Sidney MC, de Belleruche J, Gibberd FB. Identification of genetic heterogeneity in Refsum's disease. *Eur J Hum Genet* 2000; 8: 649–651
- Wierzbicki AS, Sankaralingam A, Lumb PJ, Hardman TC, Sidey MC, Gibberd FB. Transport of phytanic acid on lipoproteins in Refsum disease. *J Inher Metab Dis* 1999; 22: 29–36

- Wierzbicki AS, Lloyd MD, Schofield CJ, Feher MD, Gibberd FB. Refsum's disease: a peroxisomal disorder affecting phytanic acid α -oxidation. *J Neurochem* 2002; 80: 727–735
- Wills AJ, Manning NJ, Reilly MM. Refsum's disease. *Q J Med* 2001; 94:403–406
- Young SP, Johnson AW, Muller DPR. Effects of phytanic acid on the vitamin E status, lipid composition and physical properties of retinal cell membranes: implications for adult Refsum disease. *Clin Sci* 2001; 101:697–705

23 Mitochondria and Mitochondrial Disorders

- Andreu AL, Bruno C, Dunne TC, Tanji K, Shanske S, Sue CM, Krishna S, Hadjigeorgiou GM, Shtilbans A, Bonilla E, DiMauro S. A nonsense mutation (G15059A) in the cytochrome b gene in a patient with exercise intolerance and myoglobinuria. *Ann Neurol* 1999; 45: 127–130
- Andreu AL, Tanji K, Bruno C, Hadjigeorgiou GM, Sue CM, Jay C, Ohnishi T, Shanske S, Bonilla E, DiMauro S. Exercise intolerance due to a nonsense mutation in the mtDNA ND4 gene. *Ann Neurol* 1999; 45: 820–823
- Astuti D, Latif F, Dallol A, Dahia PL, Douglas F, George E, Skoldberg F, Husebye ES, Eng C, Maher ER. Gene mutations in the succinate dehydrogenase subunit SDHB cause susceptibility to familial pheochromocytoma and to familial paraganglioma. *Am J Hum Genet* 2001; 69: 49–54
- Benz R. Biophysical properties of porin pores from mitochondrial outer membrane of eukaryotic cells. *Experientia* 1990; 46: 131–137
- Bosbach S, Kornblum C, Schroder R, Wagner M. Executive and visuospatial deficits in patients with chronic progressive external ophthalmoplegia and Kearns-Sayre syndrome. *Brain* 2003; 126: 1231–1240
- Bourgeron T, Rustin P, Chretien D, Birch-Machin M, Bourgeois M, Viegas-Pequignot E, Munnich A, Rotig A. Mutation of a nuclear succinate dehydrogenase gene results in mitochondrial respiratory chain deficiency. *Nat Genet* 1995; 11: 144–149
- Brown MD, Voljavec AS, Lott MT, Torroni A, Yang CC, Wallace DC. Mitochondrial DNA complex I and III mutations associated with Leber's hereditary optic neuropathy. *Genetics* 1992; 130: 163–73
- Bruno C, Martinuzzi A, Tang Y, Andreu AL, Pallotti F, Bonilla E, Shanske S, Fu J, Sue CM, Angelini C, DiMauro S, Manfredi G. A stop-codon mutation in the human mtDNA cytochrome c oxidase I gene disrupts the functional structure of complex IV. *Am J Hum Genet* 1999; 65: 611–620
- Bruno C, Sacco O, Santorelli FM, Assereto S, Tonoli E, Bado M, Rossi GA, Minetti C. Mitochondrial myopathy and respiratory failure associated with a new mutation in the mitochondrial transfer ribonucleic acid glutamic acid gene. *J Child Neurol* 2003; 18: 300–303
- Cheng MY, Hartl FU, Martin J, Pollock RA, Kalousek F, Neupert W, Hallberg EM, Hallberg RL, Horwich AL. Mitochondrial heat-shock protein hsp60 is essential for assembly of proteins imported into yeast mitochondria. *Nature* 1989; 337: 620–625
- Chol M, Lebon S, Benit P, Chretien D, de Lonlay P, Goldenberg A, Odent S, Hertz-Pannier L, Vincent-Delorme C, Cormier-Daire V, Rustin P, Rotig A, Munnich A. The mitochondrial DNA G13513A MELAS mutation in the NADH dehydrogenase 5 gene is a frequent cause of Leigh-like syndrome with isolated complex I deficiency. *J Med Genet* 2003; 40: 188–191
- Coates PM, Tanaka K. Molecular basis of mitochondrial fatty acid oxidation defects. *J Lipid Res* 1992; 33: 1099–1110
- Cuezva JM, Flores AI, Liras A, Santaren JF, Alconada A. Molecular chaperones and the biogenesis of mitochondria and peroxisomes. *Biol Cell* 1993; 77: 47–62
- De Lonlay P, Valnot I, Barrientos A, Gorbatyuk M, Tzagoloff A, Taanman JW, Benayoun E, Chretien D, Kadhom N, Lomès A, de Baulny HO, Niaudet P, Munnich A, Rustin P, Rotig A. A mutant mitochondrial respiratory chain assembly protein causes complex III deficiency in patients with tubulopathy, encephalopathy and liver failure. *Nat Genet* 2001; 29: 57–60
- DeVivo DC. The expanding clinical spectrum of mitochondrial disorders. *Brain Dev* 1993; 15: 1–22
- De Vries DD, Ruitenbeek W, de Wijs IJ, Trijbels JM, van Oost BA. Enzymological versus DNA investigations in mitochondrial (encephalo-myopathies). *J Inher Metab Dis* 1993; 16: 534–536
- DiMauro S, Moraes CT. Mitochondrial encephalomyopathies. *Arch Neurol* 1993; 50: 1197–1208
- DiMauro S, Schon EA. Mitochondrial respiratory-chain diseases. *N Engl J Med* 2003; 348: 2656–2668
- Glick B, Schatz G. Import of proteins into mitochondria. *Annu Rev Genet* 1991; 25: 21–44
- Harding AE, Hammans SR. Deletions of the mitochondrial genome. *J Inher Metab Dis* 1992; 15: 480–486
- Heuvel S, Smeitink JAM. The oxidative phosphorylation (OXPHOS) system: nuclear genes and human genetic diseases. *Bioessays* 2001; 23: 518–525
- Hsieh RH, Li JY, Pang CY, Wei YH. A novel mutation in the mitochondrial 16S rRNA gene in a patient with MELAS syndrome, diabetes mellitus, hyperthyroidism and cardiomyopathy. *J Biomed Sci* 2001; 8: 328–335
- Loeffen JL, Smeitink JAM, Trijbels JM, Janssen AJ, Triepels RH, Sengers RC, van den Heuvel LP. Isolated complex I deficiency in children: clinical, biochemical and genetic aspects. *Hum Mutat* 2000; 15: 123–134
- Poulton J. Duplications of mitochondrial DNA: implications for pathogenesis. *J Inher Metab Dis* 1992; 15: 487–498
- Rahman S, Taanman JW, Cooper JM, Nelson I, Hargreaves I, Meunier B, Hanna MG, Garcia JJ, Capaldi RA, Lake BD, Leonard JV, Schapira AH. A missense mutation of cytochrome oxidase subunit II causes defective assembly and myopathy. *Am J Hum Genet* 1999; 65: 1030–1039
- Rosenberg MJ, Agarwala R, Bouffard G, Davis J, Fiermonte G, Hilliard MS, Koch T, Kalikin LM, Makalowska I, Morton DH, Petty EM, Weber JL, Palmieri F, Kelley RI, Schaffer AA, Biesecker LG. Mutant deoxynucleotide carrier is associated with congenital microcephaly. *Nat Genet* 2002; 32: 175–179
- Saada A, Shaag A, Mandel H, Nevo Y, Eriksson S, Elpeleg O. Mutant mitochondrial thymidine kinase in mitochondrial DNA depletion myopathy. *Nat Genet* 2001; 29: 342–344
- Scholte HR, Busch HF, Luyt-Houwen IE, Vaandrager-Verduin MH, Przyrembel H, Arts WF. Defects in oxidative phosphorylation. Biochemical investigations in skeletal muscle and expression of the lesion in other cells. *J Inher Metab Dis* 1987; 10: 81–97
- Shoubridge EA. Cytochrome c oxidase deficiency. *Am J Med Genet* 2001; 106: 46–52
- Simon DK, Friedman J, Breakefield XO, Jankovic J, Brin MF, Provias J, Bressman SB, Charness ME, Tarsy D, Johns DR, Tarnopolsky MA. A heteroplasmic mitochondrial complex I gene mutation in adult-onset dystonia. *Neurogenetics* 2003; 4: 199–205
- Smeitink JA. Mitochondrial disorders: clinical presentation and diagnostic dilemmas. *J Inher Metab Dis* 2003; 26: 199–207
- Smeitink J, van den Heuvel L, DiMauro S. The genetics and pathology of oxidative phosphorylation. *Nat Rev Genet* 2001; 2: 342–352

- Smeitink JAM, van den Heuvel LWPJ, Koopman WJH, Nijtmans LGJ, Ugalde C, Willems PHGM. Cell biological consequences of NADH: Ubiquinone oxidoreductase Deficiency. *Curr Neurol Res* 2004; 1:29–40
- Stadhouders AM, Sengers RCA. Morphological observations in skeletal muscle from patients with a mitochondrial myopathy. *J Inher Metab Dis* 1987; 10: 62–80
- Suomalainen A, Kaukonen J. Diseases caused by nuclear genes affecting mtDNA stability. *Am J Med Genet* 2001; 106: 53–61
- Taylor RW, Morris AA, Hutchinson M, Turnbull DM. Leigh disease associated with a novel mitochondrial DNA ND5 mutation. *Eur J Hum Genet* 2002; 10: 141–144
- Tiranti V, Corona P, Greco M, Taanman JW, Carrara F, Lamantea E, Nijtmans L, Uziel G, Zeviani M. A novel frameshift mutation of the mtDNA COIII gene leads to impaired assembly of cytochrome c oxidase in a patient affected by Leigh-like syndrome. *Hum Mol Genet* 2000; 9: 2733–2742
- Tulinius MH, Holme E, Kristiansson B, Larsson NG, Oldfors A. Mitochondrial encephalomyopathies in childhood. I. Biochemical and morphologic investigations. *J Pediatr* 1991; 119: 242–250
- Tulinius MH, Holme E, Kristiansson B, Larsson NG, Oldfors A. Mitochondrial encephalomyopathies in childhood. II. Clinical manifestations and syndromes. *J Pediatr* 1991; 119: 251–259
- Tulinius M, Moslemi AR, Darin N, Westerberg B, Wiklund LM, Holme E, Oldfors A. Leigh Syndrome with cytochrome-c oxidase deficiency and a single T insertion nt 5537 in the mitochondrial tRNA^{Trp} gene. *Neuropediatrics* 2003; 34: 87–91
- Visapaa I, Fellman V, Vesa J, Dasvarma A, Hutton JL, Kumar V, Payne GS, Makarow M, Van Coster R, Taylor RW, Turnbull DM, Suomalainen A, Peltonen L. GRACILE syndrome, a lethal metabolic disorder with iron overload, is caused by a point mutation in BCS1L. *Am J Hum Genet* 2002; 71: 863–876
- Vives-Bauza C, Del Toro M, Solano A, Montoya J, Andreu AL, Roig M. Genotype-phenotype correlation in the 5703G>A mutation in the tRNA (ASN) gene of mitochondrial DNA. *J Inher Metab Dis* 2003; 26: 507–508
- Wallace DC. Mitochondrial genetics: a paradigm for aging and degenerative diseases? *Science* 1992; 256: 628–632
- Wallace DC, Lott MT, Shoffner JM, Brown MD. Diseases resulting from mitochondrial DNA point mutations. *J Inher Metab Dis* 1992; 15: 472–479
- Zeviani M, DiDonato S. Neurological disorders due to mutations of the mitochondrial genome. *Neuromusc Disord* 1991; 1: 165–172
- Zeviani M, Spinazzola A, Carelli V. Nuclear genes in mitochondrial disorders. *Curr Opin Genet Dev* 2003; 13: 262–270
- Balestri P, Grosso S. Endocrine disorders in two sisters affected by MELAS syndrome. *J Child Neurol* 2000; 15: 755–758
- Barak Y, Arnon S, Wolach B, Raz Y, Ashkenasi A, Glick B, Shapira Y. MELAS syndrome: peripheral neuropathy and cytochrome c-oxidase deficiency: a case report and review of the literature. *Isr J Med Sci* 1995; 31: 224–229
- Barisic N, Bernert G, Ipsiroglu O, Stromberger C, Muller T, Gruber S, Prayer D, Moser E, Bittner RE, Stöckler-Ipsiroglu S. Effects of oral creatine supplementation in a patient with MELAS phenotype and associated nephropathy. *Neuropediatrics* 2002; 33: 157–161
- Bataillard M, Chatzoglou E, Rumbach L, Sternberg D, Tounade A, Laforêt P, Jardel C, Maisonneuve T, Lombès A. Atypical MELAS syndrome associated with a new mitochondrial tRNA glutamine point mutation. *Neurology* 2001; 56: 405–407
- Brenningstall GN, Lockman LA. Massive focal brain swelling as a feature of MELAS. *Pediatr Neurol* 1988; 4: 366–370
- Campos Y, Garcia-Silva T, Barrionuevo CR, Cabello A, Muley R, Arenas J. Mitochondrial DNA deletion in a patient with mitochondrial myopathy, lactic acidosis, and stroke-like episodes (MELAS) and Fanconi's syndrome. *Pediatr Neurol* 1995; 13: 69–72
- Castillo M, Kwok L, Green C. MELAS syndrome: imaging and proton MR spectroscopic findings. *AJNR Am J Neuroradiol* 1995; 16: 233–239
- Chinnery PF, Howell N, Lightowlers RN, Turnbull DM. Molecular pathology of MELAS and MERRF. The relationship between mutation load and clinical phenotypes. *Brain* 1997; 120: 1713–1721
- Chinnery PF, Howell N, Lightowlers RN, Turnbull DM. MELAS and MERRF. The relationship between maternal mutation load and the frequency of clinically affected offspring. *Brain* 1998; 121: 1889–1894
- Ciafaloni E, Ricci E, Shanske S, Moraes CT, Silvestri G, Hirano M, Simonetti S, Servidei S, Zamarchi E, Bonilla E, DeVivo DC, Rowland LP, Schon EA, DiMauro S. MELAS: clinical features, biochemistry, and molecular genetics. *Ann Neurol* 1992; 31: 391–398
- Clark JM, Marks MP, Adalsteinsson E, Spielman DM, Shuster D, Horoupain D, Albers GW. MELAS: clinical and pathologic correlations with MRI, xenon/CT, and MR spectroscopy. *Neurology* 1996; 46: 223–227
- Corona P, Antozzi C, Carrara F, D'Incerti L, Lamantea E, Tiranti V, Zeviani M. A novel mtDNA mutation in the ND5 subunit of complex I in two MELAS patients. *Ann Neurol* 2001; 49: 106–110
- Damian MS, Hertel A, Seibel P, Reichmann H, Bachmann G, Sachenmayr W, Hoer G, Dorndorf W. Follow-in in carriers of the 'MELAS' mutation without strokes. *Eur Neurol* 1998; 39: 9–15
- De Coo IFM, Sistermans EA, de Wijs IJ, Catsman-Berrevoets C, Busch HFM, Scholte HR, de Klerk JBC, van Oost BA, Smeets HJM. A mitochondrial tRNA^{val} gene mutation (G1642A) in a patient with mitochondrial myopathy, lactic acidosis, and stroke-like episodes. *Neurology* 1998; 50: 293–295
- De Coo IFM, Reinier WO, Ruitenbeek W, Ter Laak HJ, Bakker M, Schägger H, Van Oost BA, Smeets HJM. A 4-base pair deletion in the mitochondrial cytochrome *b* gene associated with Parkinsonism/MELAS overlap syndrome. *Ann Neurol* 1999; 45: 130–133
- Degoul F, Diry M, Pou-Serradell A, Lloreta J. Myo-leukoencephalopathy in twins: study of 3243-myopathy, encephalopathy, lactic acidosis, and stroke-like episodes mitochondrial DNA mutation. *Ann Neurol* 1994; 35: 365–370

24 Mitochondrial myopathy, encephalopathy, lactic acidosis and stroke-like episodes

- Abe K, Fujimura H, Nishikawa Y, Yorifuji S, Mezaki T, Hirono N, Nishitani N, Kameyama M. Marked reduction in CSF lactate and pyruvate levels after CoQ therapy in a patient with mitochondrial myopathy, encephalopathy, lactic acidosis and stroke-like episodes (MELAS). *Acta Neurol Scand* 1991; 83: 356–359
- Allard JC, Tilak S, Carter AP. CT and MR of MELAS syndrome. *AJNR Am J Neuroradiol* 1988; 9: 1234–1238

- Dubeau F, De Stefano N, Zifkin BG, Arnold DL, Shoubridge EA. Oxidative phosphorylation defect in the brains of carriers of the tRNA^{Leu(UUR)} A3243G mutation in a MELAS pedigree. *Ann Neurol* 2000; 47: 179–185
- Fang W, Huang C-C, Lee C-C, Cheng S-Y, Pang C-Y, Wei Y-H. Ophthalmologic manifestations in MELAS syndrome. *Arch Neurol* 1993; 50: 977–980
- Förster Ch, Hübner G, Müller-Höcker J, Pongratz D, Baierl P, Senger R, Ruitenbeek W. Mitochondrial angiopathy in a family with MELAS. *Neuropediatrics* 1992; 23: 165–168
- Fujii T, Okuno T, Ito M, Motoh K, Hamazaki S, Okada S, Kusaka H, Mikawa H. CT, MRI, and autopsy findings in brain of a patient with MELAS. *Pediatr Neurol* 1990; 6: 253–256
- Goto Y-I, Nonaka I, Horai S. A mutation in the tRNA^{Leu(UUR)} gene associated with the MELAS subgroup of mitochondrial encephalomyopathies. *Nature* 1990; 348: 651–653
- Goto Y, Horai S, Matsuoka T, Koga Y, Nihei K, Kobayashi M, Nonaka I. Mitochondrial myopathy, encephalopathy, lactic acidosis, and stroke-like episodes (MELAS): a correlative study of the clinical features and mitochondrial DNA mutation. *Neurology* 1992; 42: 545–550
- Hamazaki S, Okada S, Kusaka H, Fujii T, Okuno T, Kashu I, Midorikawa O. Mitochondrial myopathy, encephalopathy, lactic acidosis, and stroke-like episodes. *Acta Pathol Jpn* 1989; 39: 599–606
- Hamman SR, Sweeney MG, Hanna MG, Brockington M, Morgan-Hughes JA, Marding AE. The mitochondrial DNA transfer RNA^{Leu(UUR)} A→G⁽³²⁴³⁾ mutation. A clinical and genetic study. *Brain* 1995; 118: 721–734
- Hanna MG, Nelson IP, Morgan-Hughes JA, Wood NW. MELAS: a new disease associated mitochondrial DNA mutation and evidence for further genetic heterogeneity. *J Neurol Neurosurg Psychiatry* 1998; 65: 512–517
- Hirano M, Ricci E, Koenigsberger R, Defendini R, Pavlakis ST, DeVivo DC, DiMauro S, Rowland LP. MELAS: an original case and clinical criteria for diagnosis. *Neuromusc Disord* 1992; 2: 125–135
- Hirano M, Pavlakis SG. Mitochondrial myopathy, encephalopathy, lactic acidosis, and stroke-like episodes (MELAS): current concepts. *J Child Neurol* 1994; 9: 4–13
- Ihara Y, Namba R, Kuroda S, Sato T, Shirabe T. Mitochondrial encephalomyopathy (MELAS): pathological study and successful therapy with coenzyme Q₁₀ and idebenone. *J Neurol Sci* 1989; 90: 263–271
- Iizuka T, Sakai F, Suzuki N, Hata T, Tsukahara S, Fukuda M, Takiyama Y. Neuronal hyperexcitability in stroke-like episodes of MELAS syndrome. *Neurology* 2002; 59: 816–824
- Iizuka T, Sakai F, Kan S, Suzuki N. Slowly progressive spread of the stroke-like lesion in MELAS. *Neurology* 2003; 61: 1238–1244
- Inui K, Fukushima H, Tsukamoto H, Taniike M, Midorikawa M, Tanaka J, Nishigaki T, Okada S. Mitochondrial encephalomyopathies with the mutation of the mitochondrial tRNA^{Leu(UUR)} gene. *J Pediatr* 1992; 120: 62–66
- Johns DR, Stein AG, Wityk R. MELAS syndrome masquerading as herpes simplex encephalitis. *Neurology* 1993; 43: 2471–2473
- Joko T, Iwashige K, Hashimoto T, Ono Y, Kobayashi K, Sekiguchi N, Kuroki T, Yanasa R, Takayanagi R, Umeda F, Nawata H. A case of mitochondrial encephalopathy, lactic acidosis and stroke-like episodes associated with Diabetes Mellitus and hypothalamo-pituitary dysfunction. *Endocr J* 1997; 44: 805–809
- Kärppä M, Syrjälä P, Tolonen U, Majamaa K. Peripheral neuropathy in patients with the 3243A>G mutation in mitochondrial DNA. *J Neurol* 2003; 250: 216–221
- Kamada K, Takeuchi F, Houkin K, Kitagawa M, Kuriki S, Ogata A, Tashiro K, Koyanagi I, Mitsumori K, Iwasaki Y. Reversible brain dysfunction in MELAS: MEG and ¹H MRS analysis. *J Neurol Neurosurg Psychiatry* 2001; 70: 675–678
- Kato T, Murashita J, Shiori T, Terada M, Inubushi T, Kato N. Photic stimulation-induced alteration of brain energy metabolism measured by ³¹P-MR spectroscopy in patients with MELAS. *J Neurol Sci* 1998; 155: 182–185
- Kim H-S, Kim D-I, Lee B-I, Lee B-I, Jeong E-K, Choi C, Lee JD, Yoon P-H, Kim E-J, Yoon YK. Diffusion-weighted image and MR spectroscopic analysis of a case of MELAS with repeated attacks. *Yonsei Med J* 2001; 42: 128–133
- Kim I-O, Kim JY, Kim WS, Hwang WS, Yeon KM, Han MC. Mitochondrial myopathy-encephalopathy-lactic acidosis-and stroke-like episodes (MELAS) syndrome: CT and MRI findings in seven children. *AJR Am J Roentgenol* 1996; 166: 641–645
- Kimata KG, Goran L, Ajax ET, Davis PH, Grabowski T. A case of late-onset MELAS. *Arch Neurol* 1998; 55: 722–725
- Kimura M, Hasegawa Y, Yasuda K, Sejima H, Inoue M, Yamaguchi S, Ando Y, Ohno S. Magnetic resonance imaging with fluid-attenuated inversion recovery pulse sequences in MELAS syndrome. *Pediatr Radiol* 1997; 27: 153–154
- Koga Y, Ishibashi M, Ueki I, Yatsuga S, Fukiyama R, Akita Y, Matsui T. Effects of L-arginine on the acute phase of strokes in three patients with MELAS. *Neurology* 2002; 58: 827–828
- Kolb SJ, Costello F, Lee AG, White M, Wong S, Schwartz ED, Messé SR, Ellenbogen J, Kasner SE, Galetta SL. Distinguishing ischemic stroke from the stroke-like lesions of MELAS using apparent diffusion coefficient mapping. *J Neurol Sci* 2003; 216: 11–15
- Koo B, Becker LE, Chuang S, Merante F, Robinson BH, MacGregor D, Tein I, Ho VB, McGreal DA, Wherrett JR, Logan WJ. Mitochondrial encephalomyopathy, lactic acidosis, stroke-like episodes (MELAS): clinical, radiological, pathological, and genetic observations. *Ann Neurol* 1993; 34: 25–32
- Kuriyama M, Umezaki H, Fukuda Y, Osame M, Koike K, Tateishi J, Igata A. Mitochondrial encephalomyopathy with lactate-pyruvate elevation and brain infarctions. *Neurology* 1984; 34: 72–77
- Kaufmann P, Koga Y, Shanske S, Hirano M, DiMauro S, King MP, Shon EA. Mitochondrial DNA and RNA processing in MELAS. *Ann Neurol* 1996; 40: 172–180
- Lee M-L, Chaou W-T, Yang AD, Jong Y-J, Tsai J-L, Pang C-Y, Wei Y-H. Mitochondrial myopathy, encephalopathy, lactic acidosis and stroke-like episodes (MELAS); report of a sporadic case and review of the literature. *Acta Paediatr Sin* 1994; 35: 148–156
- Lertrit P, Noer AS, Jean-Francois MJB, Kapsa R, Dennett X, Thyagarajan D, Lethlean K, Byrne E, Marzuki S. A new disease-related mutation for mitochondrial encephalopathy, lactic acidosis, and stroke-like episodes (MELAS) syndrome affects the ND4 subunit of the respiratory complex I. *Am J Hum Genet* 1992; 51: 457–468
- Lioltis D, Rahman S, Benton S, Carr LJ, Hanna MG. Is the mitochondrial complex I ND5 gene a hot-spot for MELAS causing mutations? *Ann Neurol* 2003; 53: 128–132
- Mariotti C, Saverese N, Soualain A, Rimoldi M, Comi G, Prella A, Antozzi C, Servidei S, Jarre L, DiDonato S, Zeviani M. Genotype to phenotype correlations in mitochondrial encephalomyopathies associated with the A3224G mutation of mitochondrial DNA. *J Neurol* 1995; 242: 304–312

- Matsuzaki M, Izumi T, Shishikura K, Suzuki H, Hirayama Y. Hypothalamic growth hormone deficiency and supplementary GH therapy in two patients with mitochondrial myopathy, encephalopathy, lactic acidosis and stroke-like-episodes. *Neuropediatrics* 2002; 33: 271–273
- Matthews PM, Tampieri D, Berkovic SF, Andermann F, Silver K, Chityat D, Arnold DL. Magnetic resonance imaging shows specific abnormalities in the MELAS syndrome. *Neurology* 1991; 41: 1043–1046
- Miyamoto A, Oki J, Takahashi S, Itoh J, Kusunoki Y, Cho K. Serial imaging in MELAS. *Neuroradiology* 1997; 39: 427–430
- Möller HE, Wiedermann D, Kurlmann G, Hilbich T, Schuierer G. Application of NMR spectroscopy to monitoring MELAS treatment: a case report. *Muscle Nerve* 2002; 25: 593–600
- Mongini T, Doriguzzi C, Chaiaò-Piat L, Silvestri G, Servidei S, Palmucchi L. MERFF/MELAS overlap syndrome in a family with A3243G mtDNA mutation. *Clin Neuropathol* 2002; 21: 72–76
- Mori O, Yamazaki M, Ohaki Y, Arai Y, Oguro T, Shimizu H, Asano G. Mitochondrial encephalomyopathy with lactic acidosis and stroke like episodes (MELAS) with prominent degeneration of the intestinal wall and cactus-like cerebellar atrophy. *Acta Neuropathol (Berl)* 2000; 100: 712–717
- Mosewich RK, Donat JR, DiMauro S, Ciafaloni E, Shanske S, Erasmus M, George D. The syndrome of mitochondrial encephalomyopathy, lactic acidosis, and stroke-like episodes presenting without stroke. *Arch Neurol* 1993; 50: 275–278
- Nariai T, Ohno K, Ohta Y, Hirakawa K, Ishii K, Senda M. Discordance between cerebral oxygen and glucose metabolism, and hemodynamics in a mitochondrial encephalomyopathy, lactic acidosis, and stroke-like episode patient. *J Neuroimaging* 2001; 11: 325–329
- Ohama E, Ohara S, Ikuta F, Tanaka K, Nishizawa M, Miyatake T. Mitochondrial angiopathy in cerebral blood vessels of mitochondrial encephalomyopathy. *Acta Neuropathol (Berl)* 1987; 74: 226–233
- Ohshita T, Oka M, Imon Y, Wanatabe C, Katayama S, Yamaguchi S, Kajima T, Momori Y, Nakamura S. *Neuroradiology* 2000; 42: 651–656
- Ooiwa Y, Uematsu Y, Terada T, Nakai K, Itakura T, Komai N, Moriwaki H. Cerebral blood flow in mitochondrial myopathy, encephalopathy, lactic acidosis, and stroke-like episodes. *Stroke* 1993; 24: 304–309
- Oppenheim C, Galanaud D, Samson Y, Sahel M, Dormont D, Wechsler B, Marsault C. Can diffusion weighted magnetic resonance imaging help differentiate stroke from stroke-like events in MELAS? *J Neurol Neurosurg Psychiatry* 2000; 69: 248–250
- Park H, Davidson E, King MP. The pathogenic A3243G mutation in human mitochondrial tRNA^{Leu(UUR)} decreases the efficiency of aminoacylation. *Biochemistry* 2003; 42: 958–964
- Pavakis SG, Phillips PC, DiMauro S, de Vivo DC, Rowland LP. Mitochondrial myopathy, encephalopathy, lactic acidosis, and stroke-like episodes: a distinctive clinical syndrome. *Ann Neurol* 1984; 16: 481–488
- Penn AMW, Lee JWK, Thuillier P, Wagner M, MacLure KM, Menard MR, Hall LD, Kennaway NG. MELAS syndrome with mitochondrial tRNA^{Leu(UUR)} mutation: correlation of clinical state, nerve conduction, and muscle ³¹P magnetic resonance spectroscopy during treatment with nicotinamide and riboflavin. *Neurology* 1992; 42: 2147–2152
- Pulkes T, Eunson L, Patterson V, Siddiqui A, Wood NW, Nelson IP, Morgan-Hughes JA, Hanna MG. The mitochondrial DNA G13513A transition in ND5 is associated with a LHON/MELAS overlap syndrome and may be a frequent cause of MELAS. *Ann Neurol* 1999; 46: 916–919
- Ravn K, Wibbrand F, Hansen FJ, Horn N, Rosenberg T, Schwartz M. An mtDNA mutation, 1445GA, in the NADH dehydrogenase subunit 6 associated with severe MELAS syndrome. *Eur J Hum Genet* 2001; 9: 805–809
- Rosen L, Philips S, Enzmann D. Magnetic resonance imaging in MELAS syndrome. *Neuroradiology* 1990; 32: 168–171
- Sakuta R, Nonaka I. Vascular involvement in mitochondrial myopathy. *Ann Neurol* 1989; 25: 594–601
- Sakuta R, Honzawa S, Murakami N, Goto Y, Nagai T. Atypical MELAS associated with mitochondrial tRNA^{lys} gene A8296G mutation. *Pediatr Neurol* 2002; 27: 397–400
- Satoh M, Ishikawa N, Yoshizawa T, Takeda T, Akisada M. N-Iso-propyl-p-[¹²³I]-iodoamphetamine SPECT in MELAS syndrome: comparison with CT and MR imaging. *J Comput Assist Tomogr* 1991; 15: 77–82
- Serra G, Piccinu R, Tondi M, Muntoni F, Zeviani M, Mastropalo C. Clinical and EEG findings in eleven patients affected by mitochondrial encephalomyopathy with severe MERFF–MELAS overlap. *Brain Dev* 1996; 18: 185–191
- Seyama K, Suzuki K, Mizuno Y, Yoshida M, Tanaka M, Ozawa T. Mitochondrial encephalomyopathy with lactic acidosis and stroke-like episodes with special reference to the mechanism of cerebral manifestations. *Acta Neurol Scand* 1989; 80: 561–568
- Shoji Y, Sato W, Hayasaka K, Takada G. Tissue distribution of mutant mitochondrial DNA in mitochondrial myopathy, encephalopathy, lactic acidosis and stroke-like episodes (MELAS). *J Inher Metab Dis* 1993; 16: 27–30
- Sparaco M, Simonati A, Cavellaro T, Bartelomei L, Grauso M, Piscicelli F, Morelli L, Rizzuto N. MELAS: clinical phenotype and morphological brain abnormalities. *Acta Neuropathol (Berl)* 2003; 106: 202–212
- Sue CM, Crimmins DS, Soo YS, Pamphlett R, Presgrave CM, Kotsimbos N, Jean-Francois MJB, Morris JGL. Neuroradiological features of six kindreds with MELAS tRNA^{Leu} A3243G point mutation: implications for pathogenesis. *J Neurol Neurosurg Psychiatry* 1988; 65: 233–240
- Suzuki T, Koizumi J, Shiraishi H, Ishikawa N, Ofuku K, Sasaki M, Hori T, Ohkoshi N, Anno I. Mitochondrial encephalomyopathy (MELAS) with mental disorder CT, MRI and SPECT findings. *Neuroradiology* 1990; 32: 74–76
- Takahashi S, Tohgi H, Yonezawa H, Obara S, Nagane Y. Cerebral blood flow and oxygen metabolism before and after stroke-like episode in patient with mitochondrial myopathy, encephalopathy, lactic acidosis and stroke-like episodes (MELAS). *J Neurol Sci* 1998; 158: 58–64
- Tanahashi C, Nakayama A, Yoshida M, Ito M, Mori M, Mori N, Hashizume Y. MELAS with mitochondrial DNA 3243 point mutation: a neuropathological study. *Acta Neuropathol (Berl)* 2000; 99: 31–38
- Tanji K, Gamez J, Cervera C, Mearin F, Ortega A, de la Torre J, Montoya J, Andreu AL, DiMauro S, Bonilla E. The A8344G mutation in mitochondrial DNA associated with stroke-like episodes and gastro-intestinal dysfunction. *Acta Neuropathol (Berl)* 2003; 105: 69–75
- Taylor RW, Chinnery PF, Haldane F, Morris AAM, Bindoff FF, Wilson J, Turnbull DM. MELAS associated with a transfer RNA in the valine transfer RNA gene of mitochondrial DNA. *Ann Neurol* 1996; 40: 459–462
- Terauchi A, Tamagawa K, Morimatsu Y, Kobayashi M, Sano T, Yoda S. An autopsy like case of mitochondrial encephalomyopathy, lactic acidosis and stroke-like episodes (MELAS) with a point mutation of mitochondrial DNA. *Brain Dev* 1996; 18: 224–229

- Tokunaga M, Mita S, Murakami T, Kumamoto T, Uchino M, Nonaka I, Ando M. Single muscle fiber analysis of mitochondrial myopathy, encephalopathy, lactic acidosis, and stroke-like episodes (MELAS). *Ann Neurol* 1994; 35: 413–419
- Tsuchiya K, Miyazaki H, Akebane H, Yamamoto M, Kondo H, Mizusawa H, Ideka K. MELAS with prominent white matter gliosis and atrophy of the cerebellar granular layer: a clinical, genetic, and pathological study. *Acta Neuropathol (Berl)* 1999; 97: 520–524
- Valenne L, Peatau A, Soumalainen A, Ketonen L, Pihko H. Laminar cortical necrosis in MELAS syndrome: MR and neuropathological observations. *Neuropediatrics* 1996; 27: 154–160
- Van Hellenberg Hubar JLM, Gabreëls FJM, Ruitenbeek W, Sengers RCA, Renier WO, Thijssen HOM, ter Laak HJ. MELAS syndrome. Report of two patients, and comparison with data of 24 patients derived from the literature. *Neuropediatrics* 1991; 22: 10–14
- Wang XY, Noguchi K, Takashima S, Hayashi N, Ogawa S, Seto H. Serial diffusion-weighted imaging in a patient with MELAS and presumed cytotoxic oedema. *Neuroradiology* 2003; 45: 640–643
- Yanagihara C, Oyama A, Tanaka M, Nakaji K, Nishimura Y. An autopsy case of mitochondrial encephalomyopathy with lactic acidosis and stroke-like episodes syndrome with chronic renal failure. *Intern Med* 2001; 40: 662–665
- Yoneda M, Maeda M, Kimura H, Fujii A, Katayama K, Kuriyama M. Vasogenic edema on MELAS: a serial study with diffusion-weighted MR imaging. *Neurology* 1999; 53: 2182–2184
- Yonemura K, Hasegawa Y, Kimura K, Minematsu K, Yamaguchi T. Diffusion-weighted MR imaging in a case of mitochondrial myopathy, encephalopathy, lactic acidosis, and stroke-like episodes. *AJNR Am J Neuroradiol* 2001; 22: 269–272
- ## 25 Leber Hereditary Optic Neuropathy
- Barbiroli B, Montagna P, Cortelli P, Lotti S, Lodi R, Barboni P, Monari L, Lugaesi E, Frassinetti C, Zaniol P. Defective brain and muscle energy metabolism shown by in vivo ³¹P magnetic resonance spectroscopy in nonaffected carriers of 11778 mtDNA mutation. *Neurology* 1995; 45: 1364–1369
- Batioğlu F, Atilla H, Eryilmaz T. Chiasmal high signal on magnetic resonance imaging in the atrophic phase of Leber hereditary optic neuropathy. *J Neuroophthalmol* 2003; 23: 28–30
- Bet L, Moggio M, Comi GP, Mariani C, Prella A, Checcarelli N, Bordoni A, Bresolin, Scarpini E, Scarlato G. Multiple sclerosis and mitochondrial myopathy: an unusual combination of diseases. *J Neurol* 1994; 241: 511–516
- Brown MD, Voljavec AS, Lott MT, MacDonald I, Wallace DC. Leber's hereditary optic neuropathy: a model for mitochondrial neurodegenerative diseases. *FASEB J* 1992; 6: 2791–2799
- Brown MD, Allan JC, van Stavern GP, Newman NJ, Wallace DC. Clinical, genetic, and biochemical characterization of a Leber hereditary optic neuropathy family containing both the 11778 and 11484 primary mutations. *Am J Med Genet* 2001; 104: 331–338
- Bruyn GW, Vielvoe GJ, Went LN. Hereditary spastic dystonia: a new mitochondrial encephalopathy? Putaminal necrosis as a diagnostic sign. *J Neurol Sci* 1991; 103: 195–202
- Bu X, Rotter JL. X chromosome-linked and mitochondrial gene control of Leber hereditary optic neuropathy: evidence from segregation analysis for dependence on X chromosome inactivation. *Proc Natl Acad Sci USA* 1991; 88: 8198–8202
- Buhmann C, Ghadamosi J, Heesen C. Visual recovery in a man with the rare combination of mtDNA 11778m LHON mutation and a MS-like disease after mitoxantrone therapy. *Acta Neurol Scand* 2002; 106: 236–239
- Chalmers RM, Harding AE. A case-control study of Leber's hereditary optic neuropathy. *Brain* 1996; 119: 1481–1486
- Cornelissen JC, Wanders RJA, Bolhuis PA, Bleeker-Wagemakers E, Oostra RJ, Wijburg FA. Respiratory chain function in Leber's hereditary optic neuropathy: lack of correlation with clinical disease. *J Inher Metab Dis* 1993; 16: 531–533
- Cortelli P, Montagna P, Avoni P, Sangiorgi S, Bresolin N, Moggio M, Zaniol P, Mantovani V, Barboni P, Barbiroli B, Lugaesi E. Leber's hereditary optic neuropathy: genetic, biochemical, and phosphorus magnetic resonance spectroscopy study in an Italian family. *Neurology* 1991; 41: 1211–1215
- De Vries DD, Went LN, Bruyn GW, Scholte HR, Hofstra RMW, Bolhuis PA, van Oost BA. Genetic and biochemical impairment of mitochondrial complex I activity in a family with Leber hereditary optic neuropathy and hereditary spastic dystonia. *Am J Hum Genet* 1996; 58: 703–711
- Dotti MT, Caputo N, Signorini E, Federico A. Magnetic resonance imaging findings in Leber's hereditary optic neuropathy. *Eur Neurol* 1992; 32: 17–19
- Fausser S, Leo-Kottler B, Besch D, Lubrichs J. Confirmation of the 14568 mutation in the mitochondrial ND6 gene as causative in Leber's hereditary optic neuropathy. *Ophthalmic Genet* 2002; 23: 191–197
- Flanigan KM, Johns DR. Association of the 11778 mitochondrial DNA mutation and demyelinating disease. *Neurology* 1993; 43: 2720–2722
- Funakawa I, Kato H, Terao A, Ichihashi K, Kawashima S, Hayashi T, Mitani K, Miyazaki S. Cerebellar ataxia in patients with Leber's hereditary optic neuropathy. *J Neurol* 1995; 242: 75–77
- Funalot B, Reynier P, Vighetto A, Ranoux D, Bonnefont J-P, Godinot C, Malthiery Y, Mas J-L. Leigh-like encephalopathy complicating Leber's hereditary optic neuropathy. *Ann Neurol* 2002; 52: 374–377
- Guy J, Qi X, Pallotti F, Schon EA, Manfredi G, Carelli V, Martinuzzi A, Hauswirth WW, Lewin AS. Rescue of a mitochondrial deficiency causing Leber hereditary optic neuropathy. *Ann Neurol* 2002; 52: 534–542
- Harding AE, Sweeney MG, Miller DH, Mumford CJ, Kellar-Wood H, Menard D, McDonald WI, Compston DAS. Occurrence of a multiple sclerosis-like illness in women who have a Leber's hereditary optic neuropathy mitochondrial DNA mutation. *Brain* 1992; 115: 979–989
- Horváth R, Abicht A, Shoubbridge EA, Karcagi V, Rózsa C, Komoly S, Lochmüller H. Leber's hereditary optic neuropathy presenting as multiple sclerosis-like disease of the CNS. *J Neurol* 2000; 247: 65–67
- Huoponen K. Leber hereditary optic neuropathy: clinical and molecular genetic findings. *Neurogenetics* 2001; 3: 119–125
- Inglese M, Rovaris M, Bianchi S, La Mantia L, Mancardi GL, Ghezzi A, Montagna P, Salvi F, Filippi M. Magnetic resonance imaging, magnetisation transfer imaging, and diffusion weighted imaging correlates of optic nerve, brain, and cervical cord damage in Leber's hereditary optic neuropathy. *J Neurol Neurosurg Psychiatry* 2001; 70: 444–449

- Jansen PHP, van der Knaap MS, de Coe IFM. Leber's hereditary optic neuropathy with the 11778 mtDNA mutation and white matter disease resembling multiple sclerosis: clinical, MRI and MRS findings. *J Neurol Sci* 1996; 135: 176–180
- Kellar-Wood H, Robertson N, Govan GG, Compston DAS, Harding AE. Leber's hereditary optic neuropathy mitochondrial DNA mutations in multiple sclerosis. *Ann Neurol* 1994; 36: 109–112
- Kermode AG, Moseley IF, Kendall BE, Miller DH, MacManus DG, McDonald WI. Magnetic resonance imaging in Leber's optic neuropathy. *J Neurol Neurosurg Psychiatry* 1989; 52: 671–674
- Kim JY, Hwang J-M, Park SS. Mitochondrial DNA C4171A/ND1 is a novel primary mutation of Leber's hereditary optic neuropathy with a good prognosis. *Ann Neurol* 2002; 51: 630–634
- Larsson NG. Leber hereditary optic neuropathy: a nuclear solution of a mitochondrial problem. *Ann Neurol* 2002; 52: 529–530
- Larsson NG, Andersen O, Holme E, Oldfors A, Wahlström J. Leber's hereditary optic neuropathy and complex I deficiency in muscle. *Ann Neurol* 1991; 30: 701–708
- Leo-Kottler B, Luberichs J, Besch D, Christ-Adler M, Fauser S. Leber's hereditary optic neuropathy: clinical and molecular genetic results in a patient with a point mutation at np T11253C (isoleucine to threonine) in the ND4 gene and spontaneous recovery. *Graefes Arch Clin Exp Ophthalmol* 2002; 240: 758–764
- Leuzzi V, Bertini E, de Negri AM, Gallucci M, Garavaglia B. Bilateral striatal necrosis, dystonia and optic atrophy in two siblings. *J Neurol Neurosurg Psychiatry* 1992; 55: 16–19
- Lev D, Yanoov-Sharav M, Watenberg N, Leshinsky-Silver E, Lerman-Sagie T. White matter abnormalities in Leber's hereditary optic neuropathy due to the 3460 mitochondrial DNA mutation. *Eur J Paediatr Neurol* 2002; 6: 121–123
- Lodi R, Carelli V, Cortelli P, Lotti S, Valentino ML, Barboni P, Pallotti F, Montagna P, Barbiroli B. Phosphorus MR spectroscopy shows a tissue specific in vivo distribution of biochemical expression of the G3460A mutation in Leber's hereditary optic neuropathy. *J Neurol Neurosurg Psychiatry* 2002; 72: 805–807
- Luberichs J, Leo-Kottler B, Besch D, Fauser S. A mutation hot spot in the mitochondrial ND6 gene in patients with Leber's hereditary optic neuropathy. *Graefes Arch Clin Exp Ophthalmol* 2002; 240: 96–100
- Man PYW, Turnbull DM, Chinnery PF. Leber hereditary optic neuropathy. *J Med Genet* 2002; 39: 162–169
- Man PYW, Griffiths PG, Brown DT, Howell N, Turnbull DM, Chinnery PF. The epidemiology of Leber hereditary optic neuropathy in the North East of England. *Am J Hum Genet* 2003; 72: 333–339
- Marsden CD, Lang AE, Quinn NP, McDonald WI, Abdallat A, Nimri S. Familial dystonia and visual failure with striatal CT lucencies. *J Neurol Neurosurg Psychiatry* 1986; 49: 500–509
- Newman NJ. Leber's hereditary optic neuropathy. *Arch Neurol* 1993; 50: 540–548
- Newman NJ, Lott MT, Wallace DC. The clinical characteristics of pedigrees of Leber's hereditary optic neuropathy with the 11778 mutation. *J Ophthalmol* 1991; 111: 750–762
- Newman –Toker DE, Horton JC, Lessell S. Recurrent visual loss in Leber hereditary optic neuropathy. *Arch Ophthalmol* 2003; 121: 288–291
- Nikoskelainen EK, Marttila RJ, Huoponen K, Juvonen V, Lamminen T, Sonninen P. Savontaus M-L. Leber's "plus": neurological abnormalities in patients with Leber's hereditary optic neuropathy. *J Neurol Neurosurg Psychiatry* 1995; 59: 160–164
- Novotny EJ, Sing G, Wallace DC, Dorfman LJ, Louis A, Sogg RL, Steinman L. Leber's disease and dystonia: a mitochondrial disease. *Neurology* 1986; 36: 1053–1060
- Parker WD Jr, Oley CA, Parks JK. A defect in mitochondrial electron-transport activity (NADH-coenzyme Q oxidoreductase) in Leber's hereditary optic neuropathy. *N Engl J Med* 1989; 320: 1331–1333
- Paulus W, Straube A, Bauer W, Harding AE. Central nervous system involvement in Leber's optic neuropathy. *J Neurol* 1993; 240: 251–253
- Riordan-Eva P, Sanders MD, Govan GG, Sweeney MG, da Costa J, Harding AE. The clinical features of Leber's hereditary optic neuropathy defined by the presence of a pathogenic mitochondrial DNA mutation. *Brain* 1995; 118: 319–337
- Sadun AA, Carelli V, Salomao SR, Berezovsky A, Quiros P, Sadun F, de Negri A-M, Andrade R, Schien S, Belfort R. A very large Brazilian pedigree with 11778 Leber's hereditary optic neuropathy. *Trans Am Ophthalmol Soc* 2002; 100: 169–179
- Shoffner JM, Brown MD, Stugard C, Jun AS, Pollock S, Haas RH, Kaufman A, Koontz D, Kim Y, Graham JR, Smith E, Dixon J, Wallace DC. Leber's hereditary optic neuropathy plus dystonia is caused by a mitochondrial DNA point mutation. *Ann Neurol* 1995; 38: 163–169
- Sudoyo H, Suryadi H, Lertrit P, Pramoonjage P, Lyrwati D, Marzuki S. Asian-specific mtDNA backgrounds associated with the primary G11778A mutation of Leber's hereditary optic neuropathy. *J Hum Genet* 2002; 47: 594–604
- Valentino ML, Avoni P, Barboni P, Pallotti F, Rengo Ch, Torroni A, Bellan M, Baruzzi A, Garrelli V. Mitochondrial DNA nucleotide changes C14482G and C14482A in the ND6 gene are pathogenic for Leber's hereditary optic neuropathy. *Ann Neurol* 2002; 51: 774–778
- Vanopdenbosch L, Dubois B, D'Hooge M-B, Meire F, Carton H. Mitochondrial mutations of Leber's hereditary optic neuropathy: a risk factor for multiple sclerosis. *J Neurol* 2002; 247: 535–543
- Wallace DC, Singh G, Lott MT, Hodge JA, Schurr TG, Lezza AMS, Elsas LJ, Nikoskelainen EK. Mitochondrial DNA mutation associated with Leber's hereditary optic neuropathy. *Science* 1988; 242: 1427–1430
- Weiner NC, Newman NJ, Lessell S, Johns DR, Lott MT, Wallace DC. Atypical Leber's hereditary optic neuropathy with molecular confirmation. *Arch Neurol* 1993; 50: 470–473

26 Kearns Sayre syndrome

- Artuch R, Pavia C, Playán A, Vilaseca MA, Colomer J, Valls C, Risch M, González MA, Pou A, Briones P, Montoya J, Pineda M. Multiple endocrine involvement in two pediatric patients with Kearns-Sayre syndrome. *Horm Res* 1998; 50: 99–104
- Ashizawa T, Subramony SH. What is Kearns-Sayre syndrome after all? *Arch Neurol* 2001; 58: 1053–1054
- Barthélémy C, Ogier de Baulny H, Diaz J, Cheval MA, Franchon P, Romero N, Goutières F, Fardeau M, Lombès A. Late-onset mitochondrial DNA depletion: DNA copy number, multiple deletions, and compensation. *Ann Neurol* 2001; 49: 607–617

- Becher MW, Wills ML, Noll WW, Hurko O, Price DL. Kearns-Sayre syndrome with features of Pearson's marrow-pancreas syndrome and a novel 2905-base pair mitochondrial DNA deletion. *Hum Pathol* 1999; 30: 577–581
- Boles RG, Roe T, Sanadheera D, Mahnovski V, Wong LJC. Mitochondrial DNA deletion with Kearns Sayre syndrome. *Eur J Pediatr* 1998; 157: 643–647
- Brockington M, Alsanjari N, Sweeney MG, Morgan-Hughes JA, Scaravilli F, Harding AE. Kearns-Sayre syndrome associated with mitochondrial DNA deletion or duplication: a molecular genetic and pathological study. *J Neurol Sci* 1995; 131: 78–87
- Chu BC, Terae S, Takahasi C, Kikuchi Y, Miyasaka K, Abe S, Minowa K, Sawamura T. MRI of the brain in the Kearns-Sayre syndrome: report of four cases and a review. *Neuroradiology* 1999; 41: 759–764
- Coultier DL, Allen RJ. Abrupt neurological deterioration in children with Kearns-Sayre syndrome. *Arch Neurol* 1981; 38: 247–250
- Curless RG, Flynn J, Bachynski B, Gregorios JB, Benke P, Cullen R. Fatal metabolic acidosis, hyperglycemia, and coma after steroid therapy for Kearns-Sayre syndrome. *Neurology* 1986; 36: 872–873
- Daroff RB, Solitare GB, Pincus JH, Glaser GH. Spongiform encephalopathy with chronic progressive external ophthalmoplegia. *Neurology* 1966; 16: 161–169
- Demange P, Pham Gia H, Kalifa G, Sellier N. MR of Kearns-Sayre syndrome. *AJNR Am J Neuroradiol* 1989; 10: S91
- Flynn JT, Bachynski BR, Rodrigues MM, Curless RG, Joshi B. Hyperglycemic acidotic coma and death in Kearns-Sayre syndrome. *Trans Am Ophthalmol Soc* 1985; 83: 131–161
- Gallastegui J, Hairiman RJ, Handler B, Lev M, Bharati S. Cardiac involvement in the Kearns-Sayre syndrome. *Am J Cardiol* 1987; 60: 385–388
- Herzberg NH, van Schooneveld MJ, Bleeker-Wagemakers EM, Zwart R, Cremers FPM, van der Knaap MS, Bolhuis PA, de Visser M. Kearns-Sayre syndrome with a phenocopy of choroideremia instead of pigmentary retinopathy. *Neurology* 1993; 43: 218–221
- Ishikawa Y, Goto Y-I, Ishikawa Y, Minami R. Progression in a case of Kearns-Sayre syndrome. *J Child Neurol* 2000; 15: 750–755
- Kamata Y, Mashima Y, Yokoyama M, Tanaka K, Goto Y-I, Oguchi Y. Patient with Kearns-Sayre syndrome exhibiting abnormal magnetic resonance image of the brain. *J Neuroophthalmol* 1998; 18: 284–288
- Kleber FX, Park J-W, Hübner G, Johannes A, Pongratz D, König E. Congestive heart failure due to mitochondrial cardiomyopathy in Kearns-Sayre syndrome. *Klin Wochenschr* 1987; 65: 480–486
- Klopstock T, Bishof F, Gerock K, Deuschl G, Seibel P, Ketelson UP, Reichmann H. 3.1-kb Deletion of mitochondrial DNA in a patient with Kearns-Sayre syndrome. *Acta Neuropathol (Berl)* 1995; 90: 26–129
- Larsson NG, Holme E, Kristiansson B, Oldfors A, Tulinius M. Progressive increase of the mutated mitochondrial DNA fraction in Kearns-Sayre syndrome. *Pediatr Res* 1990; 28: 131–136
- Lertrit P, Imsumran A, Karnkirawattana P, Devahasdin V, Sangruchi T, Atchaneeysakul L-o, Mungkornkarn C, Neungton N. A unique 3.5-kb deletion of the mitochondrial genome in Thai patients with Kearns-Sayre syndrome. *Hum Genet* 1999; 105: 127–131
- Leung TF, Hui J, Shoubridge E, Li CK, Chik KW, Shing MMK, Wong GWK, Yeung WL, Yeun PMP. Aplastic anaemia in association with Kearns-Sayre syndrome. *J Inher Metab Dis* 1999; 22: 86–87
- Marin-Garcia J, Goldenthal MJ, Sarnat HB. Kearns-Sayre syndrome with a novel mitochondrial DNA deletion. *J Child Neurol* 2000; 15: 555–558
- Marín-García J, Goldenthal MJ, Flores-Sarnat L, Sarnat HB. Severe mitochondrial cytopathy with complete A-V, PEO, and mtDNA deletions. *Pediatr Neurol* 2002; 27: 213–216
- McShane MA, Hammans SR, Sweeney M, Holt IJ, Beattie TJ, Brett EM, Harding AE. Pearson syndrome and mitochondrial encephalomyopathy in a patient with a deletion of mtDNA. *Am J Hum Genet* 1991; 48: 39–42
- Mohri I, Taniike M, Fujimura H, Matsuoka T, Inui K, Nagai T, Okada S. A case of Kearns-Sayre syndrome showing a constant proportion of deleted mitochondrial DNA in blood cells during 6 years of follow-up. *J Neurol Sci* 1998; 158: 106–109
- Muñoz A, Meteos F, Simón R, García-Silva MT, Cabello S, Arenas J. Mitochondrial diseases in children: neuroradiological and clinical features in 17 patients. *Neuroradiology* 1999; 41: 920–928
- Nakagawa E, Hirano S, Yamanouchi H, Goto Y-I, Nonaka I, Takashima S. Progressive brainstem and white matter lesions in Kearns-Sayre syndrome: a case report. *Brain Dev* 1994; 16: 416–418
- Nakagawa E, Osari S-i, Yamanouchi H, Matsuda H, Goto Y-I, Nonaka I. Long-term therapy with cytochrome c, flavin mononucleotide and thiamine diphosphate for a patient with Kearns-Sayre syndrome. *Brain Dev* 1996; 18: 68–70
- Nakano T, Imanaka K, Uchida H, Isaka N, Takezawa H. Myocardial ultrastructure in Kearns-Sayre syndrome. *Angiology* 1987; 38: 28–35
- Oldfors A, Fyhr I-M, Holme E, Larsson N-G, Tulinius M. Neuropathology in Kearns-Sayre syndrome. *Acta Neuropathol (Berl)* 1990; 80: 541–546
- Poulton J, Morten KJ, Weber K, Brown GK, Bindoff L. Are duplications of mitochondrial DNA characteristic of Kearns-Sayre syndrome? *Hum Mol Genet* 1994; 3: 947–951
- Provenzale JM, VanLandingham K. Cerebral infarction associated with Kearns-Sayre syndrome – related cardiomyopathy. *Neurology* 1996; 46: 826–828
- Robertson Jr WC, Viseskul C, Lee YE, Lloyd RV. Basal ganglia calcification in Kearns-Sayre syndrome. *Arch Neurol* 1979; 36: 711–713
- Rötig A, Bourgeron T, Chretien D, Rustin P, Munnich A. Spectrum of mitochondrial DNA arrangements in the Pearson marrow-pancreas syndrome. *Hum Mol Genet* 1995; 4: 1327–1330
- Schröder R, Vielhaber S, Wiedemann FR, Kornblum C, Pappasotiropoulos A, Broich P, Zierz S, Elger CE, Reichmann H, Seibel P, Klockgether T, Kunz WS. New insights into the metabolic consequences of large-scale mtDNA deletions: a quantitative analysis of biochemical, morphological, and genetic findings in human skeletal muscle. *J Neuropathol Exp Neurol* 2000; 59: 353–360
- Seneca S, Verhelst H, De Meirleir L, Meire F, Ceuterick-De Grootte C, Lissens W, Van Coster R. A new mitochondrial point mutation in the transfer RNA^{leu} gene in a patient with clinical phenotype resembling Kearns-Sayre syndrome. *Arch Neurol* 2001; 58: 1113–1118
- Simaan EM, Mikati MA, Touma EH, Rötig A. Unusual presentation of Kearns-Sayre syndrome in early childhood. *Pediatr Neurol* 1999; 21: 830–831
- Valanne L, Ketonen L, Majander A, Soumalainen A, Pihko H. Neuroradiologic findings in children with mitochondrial disorders. *AJNR Am J Neuroradiol* 1998; 19: 369–377

- Vásquez-Acevedo M, Vázquez-Memije ME, Mutchinick OM, Morales JJ, García-Ramos G, Gonzáles-Halphen D. A case of Kearns-Sayre syndrome with the 4,977-bp common deletion associated with a novel 7,704-bp deletion. *Neurol Sci* 2002; 23: 247–250
- Wilichowski E, Korenke GC, Ruitenbeek W, De Meirleir L, Hagen-dorff A, Janssen AJM, Lissens W, Hanefeld F. Pyruvate dehydrogenase complex deficiency and altered respiratory chain function in a patient with Kearns-Sayre syndrome / MELAS overlap syndrome and A3243G mtDNA mutation. *J Neurol Sci* 1998; 157: 206–213
- Wray SH, Provenzale JM, Johns DR, Thulborn KR. MR of the brain in mitochondrial myopathy. *AJNR Am J Neuroradiol* 1995; 16: 1167–1173
- Yoda S, Terauchi A, Kitahara F, Akabane T. Neurologic deterioration with progressive CT changes in a child with Kearns-Shy syndrome. *Brain Dev* 1984; 6: 322–327
- Zanssen S, Molnar M, Buse G, Schröder JM. Mitochondrial cytochrome b gene deletion in Kearns-Sayre syndrome associated with a subclinical type of peripheral neuropathy. *Clin Neuropathol* 1998; 17: 291–296
- Zeviani M, Moraes CT, DiMauro S, Nakase H, Bonilla E, Schon EA, Rowland LP. Deletions of mitochondrial DNA in Kearns-Sayre syndrome. *Neurology* 1988; 38: 1339–1346
- ## 27 Myo-, Neuro-, Gastrointestinal Encephalopathy
- Bardosi A, Creutzfeldt W, DiMauro S, Felgenhauer K, Friede RL, Goebel HH, Kohlschütter A, Mayer G, Rahlf G, Servidei S, van Lessen G, Wetterling T. Myo-, neuro-, gastrointestinal encephalopathy (MNGIE syndrome) due to partial deficiency of cytochrome-c-oxidase. A new mitochondrial multisystem disorder. *Acta Neuropathol (Berl)* 1987; 74: 248–258
- Carrozzo R, Davidson MM, Walker WF, Hiranio M, Miranda AF. Cellular and molecular studies in the muscle and cultures from patients with multiple mitochondrial DNA deletions. *J Neurol Sci* 1999; 170: 24–31
- Gamez J, Ferriero C, Accarino ML, Guarner L, Tadesse S, Marti RA, Andreu AL, Raguer N, Cervera C, Hirano M. Phenotypic variability in a Spanish family with MNGIE. *Neurology* 2002; 59: 455–457
- Hirano M, Silvestri G, Blake DM, Lombes A, Minetti C, Bonilla E, Hays AP, Lovelace RE, Butler I, Bertorini TE, Threlkeld AB, Mitsumoto H, Salberg LM, Rowland LP, DiMauro S. Mitochondrial neurogastrointestinal encephalomyopathy (MNGIE): clinical, biochemical, and genetic features of an autosomal recessive mitochondrial disorder. *Neurology* 1994; 44: 721–727
- Hirano M, Garcia-de-Yebenes J, Jones AC, Nishino I, DiMauro S, Carlo JR, Bender AN, Hahn AF, Salberg LM, Weeks DE, Nygaard TG. Mitochondrial neurogastrointestinal encephalomyopathy syndrome maps to chromosome 22q13.32-qter. *Am J Hum Genet* 1998; 63: 526–533
- Hirano M, Nishigaki Y, Marti R. Mitochondrial neurogastrointestinal encephalomyopathy (MNGIE): a disease of two genomes. *Neurologist* 2004; 10: 8–17
- Ionasescu V. Oculogastrointestinal muscular dystrophy. *Am J Hum Med Genet* 1983; 15: 103–112
- Kaidar-Person O, Golz A, Netzer A, Goldsher D, Joachims HZ, Goldenberg D. Rapidly progressive bilateral sensory neural hearing loss as a presentation of mitochondrial neurogastrointestinal encephalomyopathy. *Am J Otolaryngol* 2003; 24: 128–130
- Kocaeefe YC, Erdem S, Özgüç M, Tan E. Four novel thymidine phosphorylase gene mutations in mitochondrial neurogastrointestinal encephalomyopathy syndrome (MNGIE) patients. *Eur J Hum Genet* 2003; 11: 102–104
- Labauge P, Durant R, Castelnovo G, Dubois A. MNGIE: diarrhea and leukoencephalopathy. *Neurology* 2002; 25: 58
- Marti R, Spinazzola A, Nishino I, Andreu AL, Naini A, Tadesse S, Oliver JA, Hirano M. Mitochondrial neurogastrointestinal encephalomyopathy and thymidine metabolism: results and hypothesis. *Mitochondrion* 2002; 2: 143–147
- Martí R, Nishigaki Y, Hirano M. Elevated plasma deoxyuridine in patients with thymidine phosphorylase deficiency. *Biochem Biophys Res Commun* 2003; 303: 14–18
- Millar WS, Lignelli A, Hirano M. MRI of five patients with mitochondrial neurogastrointestinal encephalomyopathy. *AJR Am J Roentgenol* 2004; 182: 1537–1541
- Nishino I, Spinazzola A, Hirano M. Thymidine phosphorylase gene mutations in MNGIE, a human mitochondrial disorder. *Science* 1999; 283: 689–692
- Nishino I, Spinazzola A, Papadimitriou A, Hammans S, Steiner I, Hahn CD, Connolly AM, Verloes A, Guimarães J, Maillard I, Hamano H, Donati MA, Semrad CE, Russell JA, Andreu AL, Hadjigeorgiou GM, Vu TH, Tadesse S, Nygaard TG, Nonaka I, Hirano I, Bonilla E, Rowland LP, DiMauro S, Hirano M. Mitochondrial neurogastrointestinal encephalomyopathy: an autosomal recessive disorder due to thymidine phosphorylase mutations. *Ann Neurol* 2000; 47: 792–800
- Nishino I, Spinazzola A, Hirano M. MNGIE: from nuclear DNA to mitochondrial DNA. *Neuromusc Disord* 2001; 11: 7–10
- Papadimitrou A, Comi GP, Hadjigeorgiou GM, Bordonni A, Sciacco M, Napoli L, Prella A, Moggio M, Fagioli G, Bresolin N, Salani S, Anastasopoulos I, Giassakis G, Divari R, Scarlao G. Partial depletion and multiple deletions of muscle mtDNA in familial MNGIE syndrome. *Neurology* 1998; 51: 1086–1092
- Simon LT, Horoupian DS, Dorf LJ, Marks M, Herrick MK, Wasserstein P, Smith ME. Polyneuropathy, ophthalmoplegia, leukoencephalopathy and intestinal pseudo-obstruction: *POLIP* syndrome. *Ann Neurol* 1990; 28: 349–360
- Soykan I, Cetinkaya H, Erdem S, Tan E, Aydin F, Bahar K, Özden A. Mitochondrial neurogastrointestinal encephalomyopathy. Diagnostic features in two patients. *J Clin Gastroenterol* 2002; 34: 446–448
- Spinazzola A, Marti R, Nishino I, Andreu AL, Naini AL, Tadesse S, Pela I, Zammarchi E, Donati MA, Oliver JA, Hirano M. Altered thymidine metabolism due to defects of thymidine phosphorylase. *J Biol Chem* 2002; 277: 4128–4133
- Suomalainen A, Kaukainen J. Diseases caused by nuclear genes affecting mtDNA stability. *Am J Med Genet* 2001; 106: 53–61
- Teitelbaum JE, Berde CB, Nurko S, Buonomo C, Perez-Atayade AR, Vox VL. Diagnosis and management of MNGIE syndrome in children: case report and review of the literature. *J Pediatr Gastroenterol Nutr* 2002; 35: 377–383
- Uncini A, Servidei S, Silvestri G, Manfredi G, Sabatelli M, Di Muzio A, Ricci E, Mirabella M, DiMauro S, Tonali P. Ophthalmoplegia, demyelinating neuropathy, leukoencephalopathy, myopathy, and gastrointestinal dysfunction with multiple deletions of mitochondrial DNA: a mitochondrial multisystem disorder in search of a name. *Muscle Nerve* 1994; 17: 667–674

28 Leigh Syndrome and Mitochondrial Leukoencephalopathies

General

- Absalon MJ, Harding CO, Fain DR, Li L, Mack KJ. Leigh syndrome in an infant resulting from mitochondrial DNA depletion. *Pediatr Neurol* 2001; 24: 60–63
- Anzil AP, Weindl A, Struppler A. Ultrastructure of a cerebral white matter lesion in a 41-year-old man with Leigh's encephalomyelopathy (LEM). *Acta Neuropathol (Berl)* 1981; Suppl VII: 233–238
- Arri J, Tanabe Y. Leigh syndrome: serial MR imaging and clinical follow-up. *AJNR Am J Neuroradiol* 2000; 21: 1502–1509
- Barkovich AJ, Good WV, Koch TK, Berg BO. Mitochondrial disorders: analysis of their clinical and imaging characteristics. *AJNR Am J Neuroradiol* 1993; 14: 1119–1137
- Campos Y, Martin MA, Rubio JC, Solana LG, García-Benayas C, Terradas JL, Arenas J. Leigh syndrome associated with the T9176C mutation in the ATPase 6 gene of mitochondrial DNA. *Neurology* 1997; 49: 595–597
- Coenen MJH, van den Heuvel LP, Smeitink JAM. Mitochondrial oxidative phosphorylation system assembly in man: recent achievements. *Curr Opin Neurol* 2001; 14: 777–781
- Crompton MR. Spongiform subacute necrotising encephalomyelopathy. *Acta Neuropathol (Berl)* 1969; 13: 204–208
- Davis PC, Hoffman JC, Braun IF, Ahmann P, Krawiecki N. MR of Leigh's disease (subacute necrotizing encephalomyelopathy). *AJNR Am J Neuroradiol* 1987; 8: 71–75
- De Lonlay-Debeney P, von Kleist-Retzow J-C, Hertz-Pannier L, Peudener S, Cormier-Daire V, Berquin P, Chrétien D, Rötig A, Saudubray J-M, Baraton J, Brunelle F, Rustin P, van der Knaap M, Munnich A. Cerebral white matter disease in children may be caused by mitochondrial respiratory chain deficiency. *J Pediatr* 2000; 136: 209–214
- Egger J, Wynne-Williams CJE, Erdohazi M. Mitochondrial cytopathy or Leigh's syndrome? Mitochondrial abnormalities in spongiform encephalopathies. *Neuropediatrics* 1982; 13: 219–224
- Egger J, Pincott JR, Wilson J, Erdohazi M. Cortical subacute necrotizing encephalomyelopathy. A study of two patients with mitochondrial dysfunction. *Neuropediatrics* 1984; 15: 150–158
- Feigin I, Kim HS. Subacute necrotizing encephalomyelopathy in a neonatal infant. *J Neuropathol Exp Neurol* 1977; 36: 364–372
- Filiano JJ, Goldenthal MJ, Mamourian AC, Hall CCC, Marin-Garcia J. Mitochondrial DNA depletion in Leigh syndrome. *Pediatr Neurol* 2002; 26: 239–242
- Goebel HH, Bardosi A, Friede RL, Kohlschütter A, Albani M, Siemes H. Sural nerve biopsy studies in Leigh's subacute necrotizing encephalomyelopathy. *Muscle Nerve* 1986; 9: 165–173
- Greenberg SB, Faerber EN, Riviello JJ, de Leon G, Capitanio MA. Subacute necrotizing encephalomyelopathy (Leigh disease): CT and MRI appearances. *Pediatr Radiol* 1990; 21: 5–8
- Howell N, Kubacka I, Smith R, Frerman F, Parks JK, Parker WD Jr. Association of the mitochondrial 8344 MERRF mutation with maternally inherited spinocerebellar degeneration and Leigh disease. *Neurology* 1996; 46: 219–222
- Jiang Y-W, Qin J, Yuan U, Qi Y, Wu X-R. Neuropathologic and clinical features in eight Chinese patients with Leigh disease. *J Child Neurol* 2002; 17: 450–452
- Kang PB, Hunter JV, Melvin JJ, Selak MA, Faerber EN, Kaye EM. Infantile leukoencephalopathy owing to mitochondrial enzyme dysfunction. *J Child Neurol* 2002; 17: 421–428
- Kimura S, Kobayashi T, Amemiya F. Myelin splitting in the spongy lesion in Leigh encephalopathy. *Pediatr Neurol* 1991; 7: 56–58
- Kirby DM, Kahler SG, Freckmann M-L, Reddihough D, Thornburn DR. Leigh disease caused by the mitochondrial DNA G14459A mutation in unrelated family. *Ann Neurol* 2000; 48: 102–104
- Kissel JT, Kolkin S, Chakeres D, Boesel C, Weiss K. Magnetic resonance imaging in a case of autopsy-proved adult subacute necrotizing encephalomyelopathy (Leigh's disease). *Arch Neurol* 1987; 44: 563–566
- Kohlschütter A, Kraus-Ruppert R, Rohrer T, Herschkowitz NN. Myelin studies in a case of subacute necrotizing encephalomyelopathy (SNE). *J Neuropathol Exp Neurol* 1978; 37: 155–164
- Krägeloh-Mann I, Grodd W, Nägele T. Proton spectroscopy in patients with Leigh's disease and mitochondrial enzyme deficiency. *Dev Med Child Neurol* 1994; 36: 839–845
- Majoie CB, Akkerman EM, Blank C, Barth PG, Poll-The BT, den Heeten GJ. Mitochondrial encephalomyopathy: comparison of conventional MR imaging with diffusion-weighted and diffusion tensor imaging: case report. *Am J Neuroradiol* 2002; 23: 813–816
- Malandrini A, Palmeri S, Fabrizi GM, Villanova M, Berti G, Salvadori C, Gardini G, Motti L, Solimé F, Guazzi GC. Juvenile Leigh syndrome with protracted course presenting as chronic sensory motor neuropathy, ataxia, deafness and retinitis pigmentosa: a clinicopathological report. *J Neurol Sci* 1998; 155: 218–221
- Masó E, Ferrer I, Herraiz J, Roquer J, Serrano S. Leigh's syndrome in an adult. *J Neurol* 1984; 231: 253–257
- Medina L, Chi TL, DeVivo DC, Hilal SK. MR findings in patients with subacute necrotizing encephalomyelopathy (Leigh syndrome): correlation with biochemical defect. *AJNR Am J Neuroradiol* 1990; 11: 379–384
- Montpetit VJA, Andermann F, Carpenter S, Fawcett JS, Zborowska-Sluis D, Giberson HR. Subacute necrotizing encephalomyelopathy. A review and a study of two families. *Brain* 1971; 94: 1–30
- Moroni I, Bugiani M, Bizzi A, Castelli G, Lamantea E, Uziel G. Cerebral white matter involvement in children with mitochondrial encephalopathies. *Neuropediatrics* 2002; 33: 79–85
- Morris AAM, Leopard JV. The treatment of congenital lactic acidosis. *J Inher Metab Dis* 1996; 19: 573–580
- Nakagawa M, Kaminishi Y, Isashiki Y, Yamada H, Higuchi I, Uchida Y, Osame M. Familial mitochondrial encephalomyopathy with deaf-mutism, ophthalmoplegia and leukodystrophy. *Acta Neurol Scand* 1995; 92: 102–108
- Niers L, van den Heuvel L, Trijbels F, Sengers R, Smeitink J. Pre-requisites and strategies for prenatal diagnosis of respiratory chain deficiency in chorionoc villi. *J Inher Metab Dis* 2003; 26: 647–658
- Rahman S, Blok RB, Dahl H-HM, Danks DM, Kirby DM, Chow CW, Christodoulou J, Thornburn DR. Leigh syndrome: clinical features and biochemical and DNA abnormalities. *Ann Neurol* 1996; 39: 343–351
- Sandhu FS, Dillon WP. MR demonstration of leukoencephalopathy associated with mitochondrial encephalomyopathy (case report). *AJNR Am J Neuroradiol* 1991; 12: 375–379

- Santorelli FM, Barmada MA, Pons R, Zhang LL, DiMauro S. Leigh-type neuropathology in Pearson syndrome associated with impaired ATP production and a novel mtDNA deletion. *Neurology* 1996; 47: 1320–1323
- Santorelli FM, Tanji K, Shanske S, Krishna S, Schmidt RE, Greenwood RS, DiMauro S, De Vivo DC. The mitochondrial DNA A8344G mutation in Leigh syndrome revealed by analysis in paraffin-embedded sections: revisiting the past. *Ann Neurol* 1998; 44: 962–964
- Seitz RJ, Langes K, Frenzel H, Kluitmann G, Wechsler W. Congenital Leigh's disease: panencephalomyelopathy and peripheral neuropathy. *Acta Neuropathol (Berl)* 1984; 64: 167–171
- Shtilbans A, Shanske S, Goodman S, Sue CM, Bruno C, Johnson TL, Lava NS, Waheed N, DiMauro S. G8363A mutation in the mitochondrial DNA transfer ribonucleic acid^{lys} gene: another case of Leigh syndrome. *J Child Neurol* 2000; 15: 759–761
- Valanne L, Ketonen L, Majander A, Suomalainen A, Pihko H. Neuroradiologic findings in children with mitochondrial disorders. *AJNR Am J Neuroradiol* 1998; 19: 369–377
- van der Knaap MS, Jakobs C, Valk J. Magnetic resonance imaging in lactic acidosis. *J Inherit Metab Dis* 1996; 19: 535–547
- Walter GF, Brucher JM, Martin JJ, Ceuterick C, Pilz P, Freund M. Leigh's disease – several nosological entities with an identical histopathological complex? *Neuropathol Appl Neurobiol* 1986; 12: 95–107
- Weinstock A, Giglio P, Cohen ME, Bakshi R, Januario J, Balos L. Diffuse magnetic resonance imaging white-matter changes in a 15-year-old boy with mitochondrial encephalomyopathy. *J Child Neurol* 2002; 17: 47–49
- ### Pyruvate Dehydrogenase Complex Deficiency
- Aleck KA, Kaplan AM, Sherwood WG, Robinson BH. In utero central nervous system damage in pyruvate dehydrogenase deficiency. *Arch Neurol* 1988; 45: 987–989
- Bindhoff LA, Brich-Machin MA, Farnsworth L, Gardner-Medwin D, Lindsay JG, Turnbull DM. Familial intermittent ataxia due to defect of the E₁ component of pyruvate dehydrogenase deficiency. *J Neurol Sci* 1989; 93: 311–318
- Bonne G, Benelli C, de Meirleir L, Lissens W, Chaussain M, Diry M, Clot J-P, Ponsot G, Geoffroy V, Leroux J-P, Marsac C. E1 pyruvate dehydrogenase deficiency in a child with motor neuropathy. *Pediatr Res* 1993; 33: 284–288
- Brown GK. Pyruvate dehydrogenase E1 α deficiency. *J Inherit Metab Dis* 1992; 15: 625–633
- Brown GK, Otero LJ, LeGris M, Brown RM. Pyruvate dehydrogenase deficiency. *J Med Genet* 1994; 31: 875–879
- Cederbaum SD, Blass JP, Minkoff N, Brown WJ, Cotton ME, Harris SH. Sensitivity to carbohydrate in a patient with familial intermittent lactic acidosis and pyruvate dehydrogenase deficiency. *Pediatr Res* 1976; 10: 713–720
- Chabrol B, Mancini J, Benelli C, Gire C, Munnich A. Leigh syndrome: pyruvate dehydrogenase defect. A case with peripheral neuropathy. *J Child Neurol* 1994; 9: 52–55
- Chow CW, Anderson RMcD, Kenney GCT. Neuropathology in cerebral lactic acidosis. *Acta Neuropathol (Berl)* 1987; 74: 393–396
- Cross JH, Connelly A, Gadian DG, Kendall BE, Brown GK, Leonard JV. Clinical diversity of pyruvate dehydrogenase deficiency. *Pediatr Neurol* 1994; 10: 276–283
- Dahl H-HM, Hansen LL, Brown RM, Danks DM, Rogers JG, Brown GK. X-linked pyruvate dehydrogenase E1 α subunit deficiency in heterozygous females: variable manifestation of the same mutation. *J Inherit Metab Dis* 1992; 15: 835–847
- Dahl J-HM. Pyruvate dehydrogenase E1 α deficiency: males and females differ yet again. *Am J Hum Genet* 1995; 56: 553–557
- De Meirleir L, Lissens W, Denis R, Wayenberg J-L, Michotte A, Brucher J-M, Vamos E, Gerlo E, Liebaers I. Pyruvate dehydrogenase deficiency: clinical and biochemical diagnosis. *Pediatr Neurol* 1993; 9: 216–220
- De Meirleir L, Specola N, Seneca S, Lissens W. Pyruvate dehydrogenase E1 α deficiency in a family: different clinical presentation in two siblings. *J Inherit Metab Dis* 1998; 21: 224–226
- De Meirleir L, Lissens W, Benelli C, Marsac C, de Klerk J, Scholte J, van Diggelen O, Kleijer W, Seneca S, Liebaers I. Pyruvate dehydrogenase complex deficiency and absence of subunit X. *J Inherit Metab Dis* 1998; 21: 9–16
- Dey R, Mine M, Desguerre I, Llama A, van den Berghe L, Brivert M, Aral B, Marsac C. A new case of pyruvate dehydrogenase deficiency due to a novel mutation in the *PDX1* gene. *Ann Neurol* 2003; 53: 273–277
- Fujii T, van Coster RN, Old SE, Medori R, Winter S, Gubits RM, Matthews PM, Brown RM, Brown GK, Dahl H-HM, de Vivo DC. Pyruvate dehydrogenase deficiency: molecular basis for intrafamilial heterogeneity. *Ann Neurol* 1994; 36: 83–89
- Geoffroy V, Fouque F, Benelli C, Poggi F, Saudubray JM, Lissens W, Meirleir LD, Marsac C, Lindsay JG, Sanderson SJ. Defect in the X-lipoyl-containing component of the pyruvate dehydrogenase complex in a patient with a neonatal lactic acidemia. *Pediatrics* 1996; 97: 267–272
- Harada M, Tanouchi M, Arai K, Nishitani H, Miyoshi H, Hashimoto T. Therapeutic efficacy of a case of pyruvate dehydrogenase complex deficiency monitored by localized proton magnetic resonance spectroscopy. *Magn Res Imaging* 1996; 14: 129–133
- Heckmann JM, Eastman R, Handler L, Wright M, Owen P. Leigh disease (subacute necrotizing encephalomyelopathy): MR documentation of the evolution of an acute attack. *AJNR Am J Neuroradiol* 1993; 14: 1157–1159
- Kimura S, Osaka H, Saitou K, Ohtuki N, Kobayashi T, Nezu A. Improvement of lesions shown on MRI and CT scan by administration of dichloroacetate in patients with Leigh syndrome. *J Neurol Sci* 1995; 134: 103–107
- Kimura S, Ohtuki N, Nezu A, Tanaka M, Takeshita S. Clinical and radiologic improvements in mitochondrial encephalomyelopathy following sodium dichloroacetate therapy. *Brain Dev* 1997; 19: 535–540
- Kinosita H, Sakuragawa N, Tada H, Naito E, Kuroda Y, Nonaka I. Recurrent muscle weakness and ataxia in thiamine-responsive pyruvate dehydrogenase complex deficiency. *J Child Neurol* 1997; 12: 141–144
- Kretzschmar HA, DeArmond SJ, Koch TK, Patel MS, Newth CJL, Schmidt KA, Packman S. Pyruvate dehydrogenase complex deficiency as a cause of subacute necrotizing encephalopathy (Leigh disease). *Pediatrics* 1987; 79: 370–373
- Lie SO, Loken AChr, Strömme JH, Aagaens O. Fatal congenital lactic acidosis in two siblings. Clinical and pathological findings. *Acta Paediatr Scand* 1971; 60: 129–137
- Lissens W, de Meirleir L, Seneca S, Liebaers I, Brown GK, Brown RM, Ito M, Naito E, Kuroda Y, Kerr DS, Wexler IS, Patel MS, Robinson BH, Seyda A. Mutations in the X-linked pyruvate dehydrogenase (E1) α subunit gene (*PDHA1*) in patients with a pyruvate dehydrogenase complex deficiency. *Hum Mutat* 2000; 15: 209–219

- Marsac C, Stansbie D, Bonne G, Cousin J, Jehenson P, Benelli C, Leroux J-P, Lindsay G. Defect in the lipoyl-bearing protein X subunit of the pyruvate dehydrogenase complex in two patients with encephalomyelopathy. *J Pediatr* 1993; 123: 915–920
- Matthews PM, Brown RM, Otero L, Marchington D, Leonard JV, Brown GK. Neurodevelopmental abnormalities and lactic acidosis in a girl with a 20-bp deletion in the X-linked pyruvate dehydrogenase E1 α subunit gene. *Neurology* 1993; 43: 2025–2030
- Matthews PM, Brown RM, Otero LJ, Marchington DR, LeGris M, Howes R, Meadows LS, Shevell M, Scriver CR, Brown GK. Pyruvate dehydrogenase deficiency. Clinical presentation and molecular genetic characterization of five new patients. *Brain* 1994; 117: 435–443
- Michotte A, de Meirleir L, Lissens W, Denis R, Wayenberg JL, Liebaers I, Brucher JM. Neuropathological findings of a patient with pyruvate dehydrogenase E1 α deficiency presenting as a cerebral lactic acidosis. *Acta Neuropathol (Berl)* 1993; 85: 674–678
- Morten KJ, Beattie P, Brown GK, Matthews PM. Dichloroacetate stabilizes the mutant E1 α subunit in pyruvate dehydrogenase deficiency. *Neurology* 1999; 53: 612–616
- Naito E, Ito M, Yokota I, Saijo T, Chen S, Maehara M, Kuroda Y. Concomitant administration of sodium dichloroacetate and thiamine in West syndrome caused by thiamine-responsive pyruvate dehydrogenase complex deficiency. *J Neurol Sci* 1999; 171: 56–59
- Otero LJ, Brown GK, Silver K, Arnold SL, Matthews PM. Association of cerebral dysgenesis and lactic acidemia with X-linked PHD E1 α subunit mutations in females. *Pediatr Neurol* 1995; 13: 327–332
- Robinson BH, MacMillan H, Petrova-Benedict R, Sherwood WG. Variable clinical presentation in patients with defective E1 α component of pyruvate dehydrogenase complex. *J Pediatr* 1987; 111: 525–533
- Robinson BH, MacKay N, Petrova-Benedict R, Ozalp I, Coskun T, Stacpoole PW. Defects in the E $_2$ lipoyl containing component of the pyruvate dehydrogenase complex in patient with lactic acidemia. *J Clin Invest* 1990; 85: 1821–1824
- Robinson BH, MacKay N, Chun K, Ling M. Disorders of pyruvate dehydrogenase carboxylase and the pyruvate dehydrogenase complex. *J Inher Metab Dis* 1996; 19: 452–462
- Rubio-Gozalbo ME, Heerschap A, Trijbels JMF, de Meirleir L, Thijssen HOM, Smeitink JAM. Proton MR spectroscopy in a child with pyruvate dehydrogenase complex deficiency. *Magn Res Imaging* 1999; 17: 939–944
- Shany E, Saada A, Landau D, Shaag A, HersHKovitz E, Elpeleg ON. Lipoamide dehydrogenase deficiency due to a novel mutation in the interface domain. *Biochem Biophys Res Commun* 1999; 262: 163–166
- Shevell MI, Matthews PM, Scriver CR, Brown RM, Otero LJ, Legris M, Brown GK, Arnold DL. Cerebral dysgenesis and lactic acidemia: an MRI/MRS phenotype associated with pyruvate dehydrogenase deficiency. *Pediatr Neurol* 1994; 11: 224–229
- Stacpoole PW, Barnes CL, Hurbanis MD, Cannon SL, Kerr DS. Treatment of congenital lactic acidosis with dichloroacetate. *Arch Dis Child* 1997; 77: 535–541
- Takahashi S, Oki J, Tokumitsu A, Obata M, Ogawa K, Tokusashi Y, Saijo H, Okuno A. Autopsy findings in pyruvate dehydrogenase E1 α deficiency: case report. *J Child Neurol* 1997; 12: 519–524
- Wallace SJ. Deficiencies within the pyruvate dehydrogenase complex: clinical and pathological correlates. *Dev Med Child Neurol* 1985; 27: 249–260
- Weber TA, Antognetti MR, Stacpoole PW. Caveats when considering ketogenic diets for the treatment of pyruvate dehydrogenase complex deficiency. *J Pediatr* 2001; 138: 390–395
- Wexler ID, Hemalatha SG, McConnell J, Buist NRM, Dahl H-HM, Berry SA, Cederbaum SD, Patel MS, Derr DS. Outcome of pyruvate dehydrogenase deficiency treated with ketogenic diets. Studies in patients with identical mutations. *Neurology* 1997; 49: 1655–1661
- Wijburg FA, Barth PG, Bindoff LA, Birch-Machin MA, van der Blij JF, Ruitenbeek W, Turnbull DM, Schutgens RBH. Leigh syndrome associated with a deficiency of the pyruvate dehydrogenase complex: results of treatment with a ketogenic diet. *Neuropediatrics* 1992; 23: 147–152
- Zand DJ, Simon EM, Pulitzer SB, Wang DJ, Wang ZJ, Rorke LB, Palmieri M, Berry GT. In vivo pyruvate detected by MR spectroscopy in neonatal dehydrogenase deficiency. *AJNR Am J Neuroradiol* 2003; 24: 1471–1474

Complex I Deficiency

- Andreu AL, Tanji K, Bruno C, Hadjigeorgiou GM, Sue CD, Jay C, Ohnishi T, Shanske S, Bonilla E, diMauro S. Exercise intolerance due to a nonsense mutation in the mtDNA ND4 gene. *Ann Neurol* 1999; 45: 820–823
- Bénit P, Chretien D, Kadhon N, de Lonlay-Debeney P, Cormier-Daire V, Cabral A, Peudenier S, Rustin P, Munnich A, Rötig A. Large-scale deletion and point mutations of the nuclear *NDUFV1* and *NDUFS1* genes in mitochondrial complex I deficiency. *Am J Hum Genet* 2001; 68: 1344–1352
- Bentlage HACM, Wendel U, Schägger H, ter Lak HJ, Janssens AJM, Trijbels JMF. Lethal infantile mitochondrial disease with isolated complex I deficiency in fibroblasts but with combined complex I and IV deficiencies in muscle. *Neurology* 1996; 47: 243–248
- Budde SMS, van den Heuvel LPWJ, Janssen AJ, Smeets RJP, Buskens CAF, deMeirleir L, van Coster R, Baethmann M, Voit T, Trijbels JMF, Smeitink JAM. Combined enzymatic complex I and III deficiency associated with mutations in the nuclear encoded *NDUFS4* gene. *Biochem Biophys Res Commun* 2000; 275: 63–68
- Chol M, Lebon S, Bénit P, Chretien D, de Lonlay P, Goldenberg A, Odent S, Hertz-Pennier L, Vincent-Delorme C, Cormier-Daire V, Rustin P, Rötig A, Munnich A. The mitochondrial DNA G13513A MELAS mutation in the NADH dehydrogenase 5 gene is a frequent cause of Leigh-like syndrome with isolated complex I deficiency. *J Med Genet* 2003; 40: 188–191
- Cooper JM, Mann VM, Krige D, Shapira AHV. Human mitochondrial complex I dysfunction. *Biochim Biophys Acta* 1992; 1101: 198–2003
- Dionisi-Vici C, Ruitenbeek W, Fariello G, Bentlage H, Wanders RJA, Schägger H, Bosman C, Piontadosi C, Sabetta G, Bertini E. New familial mitochondrial encephalopathy with macrocephaly, cardiomyopathy, and complex I deficiency. *Ann Neurol* 1997; 42: 661–665
- Fiellet F, Mousson Y, Grignon Y, Leonard JV, Vidailhet M. Necrotizing encephalopathy with mitochondrial complex I deficiency. *Pediatr Neurol* 1999; 20: 305–308
- Houshmand M, Larsson N-G, Oldfors A, Tulinius M, Holme E. Fatal mitochondrial myopathy, lactic acidosis and complex I deficiency associated with a heteroplasmic AG mutation at position 3251 in the mitochondrial tRNA^{Leu}(UUR) gene. *Hum Genet* 1996; 97: 369–273

- Kirby DM, Crawford M, Cleary MA, Dahl H-HM, Dennett X, Thornburn DR. Respiratory chain complex I deficiency. An underdiagnosed energy generation disorder. *Neurology* 1999; 52: 1255–1264
- Kirby DM, Boneh A, Chow CW, Ohtake A, Ryan MT, Thyagarajan D, Thornburn DR. Low mutant load of mitochondrial DNA G13513A mutation can cause Leigh's disease. *Ann Neurol* 2003; 54: 473–478
- Loeffen J, Smeitink J, Triepels R, Smeets R, Schuelke M, Sengers R, Trijbels F, Hamel B, Mullaart R, van den Heuvel L. The first nuclear-encoded complex I mutation in a patient with Leigh syndrome. *Am J Hum Genet* 1998; 63: 1598–1608
- Loeffen J, Smeets R, Smeitink J, Ruitenbeek W, Janssen A, Mariman E, Sengers R, Trijbels F, van den Heuvel L. The X-chromosomal *NDUFA1* gene of complex I in mitochondrial encephalomyopathies: tissue expression and mutation detection. *J Inher Metab Dis* 1998; 21: 210–215
- Loeffen JLCM, Smeitink JAM, Trijbels JMF, Janssen AJM, Triepels RH, Sengers RCA, van den Heuvel LP. Isolated complex I deficiency in children: clinical, biochemical and genetic aspects. *Hum Mutat* 2000; 15: 123–134
- Loeffen J, Elpeleg O, Smeitink J, Smeets R, Stockler-Ipsiroglu S, Mandel H, Sengers R, Trijbels F, van den Heuvel L. Mutations in the complex I *NCUFS2* gene of patients with cardiomyopathy and encephalomyopathy. *Ann Neurol* 2001; 49: 195–201
- Morris AAM, Leonard JV, Brown GK, Bidouki SK, Bindhoff LA, Woodward CE, Harding AE, Lake BD, Harding BN, Farrell MA, Bell JE, Mirakhur M, Turnbull DM. Deficiency of respiratory chain complex I is a common cause of Leigh disease. *Ann Neurol* 1996; 40: 25–30
- Ogle RF, Christodoulou J, Fagan E, Blok RB, Kirby DM, Seller KL, Dahl H-HM, Thornburn DR. Mitochondrial myopathy with tRNA^{Leu(uur)} mutation and complex I deficiency responsive to riboflavin. *J Pediatr* 1997; 130: 138–145
- Pitkänen S, Feigenbaum A, Laframboise R, Robinson BH. NADH-coenzyme Q reductase (complex I) deficiency: heterogeneity in phenotype and biochemical findings. *J Inher Metab Dis* 1996; 19: 675–686
- Dubio-Gozalbo ME, Ruitenbeek W, Wendel U, Sengers RCA, Trijbels JMF, Smeitink JAM. Systemic infantile complex I deficiency with fatal outcome in two brothers. *Neuropediatrics* 1998; 29: 43–45
- Schuelke M, Smeitink J, Mariman E, Loeffen J, Plecko B, Trijbels F, Stockler-Ipsiroglu S, van den Heuvel L. Mutant *NDUFV1* subunit of mitochondrial complex I causes leukodystrophy and myoclonic epilepsy. *Nat Genet* 1999; 21: 260–261
- Smeitink JAM, Loeffen JLCM, Triepels RH, Smeets RJP, Trijbels JMF, van den Heuvel LP. Nuclear genes of human complex I of the mitochondrial electron transport gene: state of the art. *Hum Mol Genet* 1998; 7: 1573–1579
- Triepels RH, van den Heuvel LP, Loeffen JLCM, Buskens CAF, Smeets RJP, Rubio Gozalbo ME, Budde SMS, Mariman EC, Wijburg FA, Barth PG, Trijbels JMF, Smeitink JAM. Leigh syndrome associated with a mutation in the *NDUFS7* (PSST) nuclear encoded subunit of complex I. *Ann Neurol* 1999; 45: 787–790
- Triepels RH, van den Heuvel LP, Trijbels JM, Smeitink JA. Respiratory chain complex I deficiency. *Am J Med Genet* 2001; 106: 37–45
- Trijbels JMF, Ruitenbeek W, Sengers RCA, Janssen AJM, van Oost BA. Benign mitochondrial encephalomyopathy in a patient with complex I deficiency. *J Inher Metab Dis* 1996; 19: 149–152
- Van den Heuvel L, Ruitenbeek W, Smeets R, Gelman-Kohan Z, Elpeleg O, Loeffen J, Trijbels F, Mariman E, de Bruijn D, Smeitink J. Demonstration of a new pathogenic mutation in the human complex I deficiency: a 5-bp duplication in the nuclear gene encoding the 18-kD (AQDQ) subunit. *Am J Hum Genet* 1998; 62: 262–268
- Vogel R, Nijtmans L, Ugalde C, van den Heuvel L, Smeitink J. Complex I assembly: a puzzling problem. *Curr Opin Neurol* 2004; 17: 179–168
- Wolf NI, Seitz A, Harting I, Smeitink JAM, Trijbels F, van den Heuvel LP, Schlemmer H, Ebinger F, Evert W, Rating D. New pattern of brain MRI lesions in isolated complex I deficiency. *Neuropediatrics* 2003; 34: 156–159

Complex II Deficiency

- Birch-Machin MA, Taylor RW, Cochran B, Ackrell BAC, Turnbull DM. Late-Onset optic atrophy, ataxia, and myopathy associated with a mutation of a complex II gene. *Ann Neurol* 2000; 48: 330–335
- Bourgeois M, Goutieres F, Chretien D, Rustin P, Munnich A, Aicardi J. Deficiency in complex II of the respiratory chain, presenting as a leukodystrophy in two sisters with Leigh syndrome. *Brain Dev* 1992; 14: 404–408
- Bourgeron T, Rustin P, Chretien D, Birch-Machin M, Bourgeois M, Viegas-Péquignot E, Munnich A, Rötig A. Mutation of a nuclear succinate dehydrogenase gene results in mitochondrial respiratory chain deficiency. *Nat Genet* 1995; 11: 144–148
- Brockmann K, Bjornstad A, Dechent P, Korenke CG, Smeitink J, Trijbels JMF, Athanassopoulos S, Villagran R, Sjkeldal AH, Wilichowski E, Frahm J, Hanefeld F. Succinate in dystrophic white matter: a proton magnetic resonance spectroscopy finding characteristic for complex II deficiency. *Ann Neurol* 2002; 52: 38–46
- Taylor RW, Birch-Machin MA, Schaefer J, Taylor L, Shakir R, Ackrell BAC, Cochran B, Bindhoff LA, Jackson MJ, Griffiths P, Turnbull DM. Deficiency of complex II of the mitochondrial respiratory chain in late-onset optic atrophy and ataxia. *Ann Neurol* 1996; 39: 224–232

Complex IV Deficiency

- Antonicka H, Mattman A, Carlson CG, Glerum DM, Hoffbuhr KC, Leary SC, Kennaway NG, Shoubridge EA. Mutations in *COX15* produce a defect in the mitochondrial heme biosynthetic pathway, causing early-onset fatal hypertrophic cardiomyopathy. *Am J Hum Genet* 2003; 72: 104–114
- Antonicka H, Leary SC, Guercin G-H, Agar JN, Horvath R, Kennaway NG, Harding CO, Jaksch M, Shoubridge EA. Mutations in *COX10* result in a defect in mitochondrial heme A biosynthesis and account for multiple, early-onset clinical phenotypes associated with isolated COX deficiency. *Hum Mol Genet* 2003; 12: 2693–2702
- Bakker HD, van den Bogert C, Drewes JG, Barth PG, Scholte HR, Wanders RJA, Ruitenbeek W. Progressive generalized brain atrophy and infantile spasms associated with cytochrome c oxidase deficiency. *J Inher Metab Dis* 1996; 19: 153–156
- Bruno C, Martinuzzi A, Tang Y, Andreu AL, Pallotti F, Bonilla E, Shanske S, Fu J, Sue CM, Angelini C, DiMauro S, Manfredi G. A stop-codon mutation in the human mtDNA cytochrome c oxidase I gene disrupts the functional structure of complex IV. *Am J Hum Genet* 1999; 65: 611–620

- Campos Y, García-Redondo A, Fernández-Moreno MA, Martínez-Pardo M, Goda G, Rubio JC, Martín MA, del Hoyo P, Cabello A, Bornstein B, Garesse R, Arenas J. Early-onset multisystem mitochondrial disorder caused by a nonsense mutation in the mitochondrial DNA cytochrome C oxidase II gene. *Ann Neurol* 2001; 50: 409–413
- Clark KM, Taylor RW, Johnson MA, Chinnery PF, Chrzanowska-Lightowlers ZMA, Andrews RM, Nelson IP, Wood NW, Lamont PJ, Hanna MG, Lightowlers RN, Turnbull DM. An mtDNA mutation in the initiation codon of the cytochrome C oxidase subunit II results in lower levels of the protein and a mitochondrial encephalomyopathy. *Am J Hum Genet* 1999; 64: 1330–1339
- Comi GP, Bordon A, Salani S, Franceschina L, Sciacco M, Prelle A, Fortunato F, Zeviani M, Napoli L, Bresolin N, Moggio M, Ausenda CD, Taanman J-W, Scarlato G. Cytochrome c oxidase subunit I microdeletion in a patient with motor neuron disease. *Ann Neurol* 1998; 43: 110–116
- DiMauro S, Nicholson JF, Hays AP, Eastwood AB, Papadimitriou A, Koenigsberger R, DeVivo DC. Benign infantile mitochondrial myopathy due to reversible cytochrome c oxidase deficiency. *Ann Neurol* 1983; 14: 226–234
- DiMauro S, Servidei S, Zeviani M, DiRocco M, DeVivo DC, DiDonato S, Uziel G, Berry K, Hoganson G, Johnsen SD, Johnson PC. Cytochrome c oxidase deficiency in Leigh syndrome. *Ann Neurol* 1987; 22: 498–506
- Èaèiæ M, Wilichowski E, Mejaški-Bošnjak V. Cytochrome c oxidase partial deficiency-associated with Leigh disease presenting as an extrapyramidal syndrome. *J Child Neurol* 2001; 16: 616–619
- Elia M, Musumeci SA, Ferri R, Colamaria V, Azan G, Greco D, Stefanini MC. Leigh syndrome and partial deficit of cytochrome c oxidase associated with epilepsy partialis continua. *Brain Dev* 1996; 18: 207–211
- Farina L, Chiapparini L, Uziel G, Bugiani M, Zeviani M, Savoiardo M. MR findings in Leigh syndrome with COX deficiency and *SURF-1* mutations. *AJNR Am J Neuroradiol* 2002; 23: 1095–1100
- Goldenberg PC, Steiner RD, Merckens LS, Dunaway T, Egan RA, Zimmerman EA, Nesbit G, Robinson B, Kennaway NG. Remarkable improvement in adult Leigh syndrome with partial cytochrome c oxidase deficiency. *Neurology* 2003; 60: 865–868
- Hanna MG, Nelson IP, Rahman S, Lane RJM, Land J, Heales S, Cooper MJ, Shapira AHV, Morgan-Hughes JA, Wood NW. Cytochrome c oxidase deficiency associated with the first stop-codon point mutation in human mtDNA. *Am J Hum Genet* 1998; 63: 29–36
- Harpey J-P, Heron D, Prudent M, Charpentier C, Rustin P, Ponsot G, Cormier-Daire V. Diffuse leukodystrophy in an infant with cytochrome-c oxidase deficiency. *J Inher Metab Dis* 1998; 21: 4748–752
- Kaido M, Fujimura H, Taniike M, Yoshikawa H, Toyooka K, Yoifuji S, Inui K, Okada S, Sparaco M, Yanagihara T. Focal cytochrome c oxidase deficiency in the brain and dorsal root ganglia in a case with mitochondrial encephalomyopathy (tRNA^{leu} 4269 mutation): histochemical, immunohistochemical, and ultrastructural study. *J Neurol Sci* 1995; 131: 170–176
- Mootha VK, Lepage P, Miller K, Bunkenborg J, Reigh M, Hjerrild M, Delmonte T, Villeneuve A, Sladek R, Xu F, Mitchell GA, Morin C, Mann M, Hudson TJ, Robinson B, Rioux JD, Lander ES. Identification of a gene causing human cytochrome c oxidase deficiency by integrative genomics. *Proc Natl Acad Sci U S A* 2003; 100: 605–610
- Morin C, Dubé J, Robinson BH, Lacroix J, Michaud J, De Braekeleer M, Geoffroy G, Lortie A, Blanchette C, Lambert MA, Mitchell GA. Stroke-like episodes in autosomal recessive cytochrome oxidase deficiency. *Ann Neurol* 1999; 45: 389–392
- Papadopoulou LC, Sue CM, Davidson MM, Tanji K, Nishino I, Sadlock JE, Krishna S, Walker W, Glerum DM, van Coster R, Lyon G, Scalais E, Lebel R, Kaplan P, Shanske S, de Vivo DC, Bonilla E, Hirano M, DiMauro S, Schon EA. Fatal infantile cardioencephalomyopathy with COX deficiency and mutations in *SCO2*, a COX assembly gene. *Nat Genet* 1999; 23: 333–337
- Parfait B, Percheron A, Chretien D, Rustin P, Munnich A, Rötig A. No mitochondrial cytochrome oxidase (COX) gene mutations in 18 cases of COX deficiency. *Hum Genet* 1997; 101: 247–250
- Péquignot MO, Dey R, Zeviani M, Tiranti V, Godinot C, Payau A, Sue C, Di Mauro S, Abitbol M, Marsac C. Mutations in the *SURF1* gene associated with Leigh syndrome and cytochrome c oxidase deficiency. *Hum Mutat* 2001; 17: 374–381
- Rahman S, Taanman J-W, Cooper JM, Nelson I, Hargreaves I, Meunier B, Hanna MG, García JJ, Capaldi RA, Lake BD, Leonard JV, Schapira AHV. A missense mutation of cytochrome oxidase subunit II causes defective assembly and myopathy. *Am J Hum Genet* 1999; 65: 1030–1039
- Rahman S, Brown RM, Chong WK, Wilson CJ, Brown GK. A *SURF1* gene mutation presenting as isolated leukodystrophy. *Ann Neurol* 2001; 49: 797–800
- Robinson BH. Human cytochrome oxidase deficiency. *Pediatr Res* 2000; 48: 581–585
- Rossi A, Biancheri R, Bruno C, Di Rocco M, Calvi A, Pessagno A, Tortori-Donati P. Leigh syndrome with COX deficiency and *SURF1* gene mutations: MR imaging findings. *AJNR Am J Neuroradiol* 2003; 24: 1188–1191
- Sacconi S, Salviati L, Sue CM, Shanske S, Davidson MM, Bonilla E, Niani AB, de Vivo DC, DiMauro S. Mutation screening in patients with isolated cytochrome c oxidase deficiency. *Pediatr Res* 2003; 53: 224–230
- Salviati L, Sacconi S, Rasalan MM, Kronn DF, Braun A, Canoll P, Davidson M, Shanske S, Bonilla E, Hays AP, Schon EA, DiMauro S. Cytochrome c oxidase deficiency due to a novel *SCO2* mutation mimics Werdnig-Hoffmann disease. *Arch Neurol* 2002; 59: 862–865
- Santoro L, Carozzo R, Malandrini A, Piemonte F, Patrono C, Villanova M, Tessa A, Palmeri S, Bertini E, Santorelli FM. A novel *SURF1* mutation results in Leigh syndrome with peripheral neuropathy caused by cytochrome c oxidase deficiency. *Neuromusc Disord* 2000; 10: 450–453
- Savasta S, Comi GP, Perini MP, Lupi A, Strazzer S, Rognoni F, Rossoni R. Leigh disease: clinical, neuroradiologic, and biochemical study of three new cases with cytochrome c oxidase deficiency. *J Child Neurol* 2001; 16: 608–613
- Savoiardo M, Uziel G, Strada L, Visciani A, Grisoli M, Wang G. MRI findings in Leigh's disease with cytochrome-c-oxidase deficiency. *Neuroradiology* 1991; 33: 507–508
- Shoubridge EA. Cytochrome c oxidase deficiency. *Am J Med Genet* 2001; 106: 45–52
- Silvestri G, Mongini T, Odoardi F, Modoni A, de Rosa G, Doriguzzi C, Palmucci L, Tonali P, Servidei S. A new mtDNA mutation associated with a progressive encephalopathy and cytochrome c oxidase deficiency. *Neurology* 2000; 54: 1693–1696

- Sue CM, Karadimas C, Checcarelli N, Tanji K, Papadopoulou LC, Pallotti F, Guo FL, Shanske S, Hirano M, de Vivo DC, van Coster R, Kaplan P, Bonilla E, DiMauro S. Differential features of patients with mutations in two COX assembly genes, *SURF-1* and *SCO2*. *Ann Neurol* 2000; 47: 589–595
- Tiranti V, Hoernagel K, Carrozzo R, Galimberti C, Munaro M, Granatiero M, Zelante L, Gasparini P, Marzella R, Rocchi M, Bayona-Bafaluy MP, Enriquez J-A, Uziel G, Bertini E, Dionisi-Vici C, Franco B, Meitinger T, Zeviani M. Mutations of *SURF-1* in Leigh disease associated with cytochrome c oxidase deficiency. *Am J Hum Genet* 1998; 63: 1609–1621
- Tiranti V, Jaksch M, Hofmann S, Galimberti C, Hoernagel K, Lulli L, Freisinger P, Bindhoff L, Gerbitz KD, Comi G-P, Uziel G, Zeviani M, Meitinger T. Loss-of-function mutations of *SURF-1* are specifically associated with Leigh syndrome with cytochrome c oxidase deficiency. *Ann Neurol* 1999; 46: 161–166
- Topçu M, Saatci I, Apak A, Söylemezoglu F, Akçören Z. Leigh syndrome in a 3-year-old boy with unusual brain MR imaging and pathologic findings. *AJNR Am J Neuroradiol* 2000; 21: 224–227
- Tulinus M, Moslemi AR, Darin N, Westerberg B, Wiklund LM, Holme E, Oldfors A. Leigh syndrome with cytochrome-c oxidase deficiency and a single T insertion nt 5537 in the mitochondrial *tRNA^{trp}* gene. *Neuropediatrics* 2003; 34: 87–91
- Valnot I, Osmond S, Gigarel N, Mehaye B, Amiel J, Cormier-Daire V, Munnich A, Bonnefont J-P, Rustin P, Rötig A. Mutations of the *SCO1* gene in mitochondrial cytochrome c oxidase deficiency with neonatal-onset hepatic failure and encephalopathy. *Am J Hum Genet* 2000; 67: 1104–1109
- Valnot I, von Kleist-Retzow J-C, Barrientos A, Gorbatyuk M, Taanman J-W, Mehanye B, Rustin P, Tzagoloff A, Munnich A, Rötig A. A mutation in the human heme A: farnesyltransferase gene (*COX10*) causes cytochrome c oxidase deficiency. *Hum Mol Genet* 2000; 9: 1245–1249
- Van Coster R, Lombes A, De Vivo DC, Chi TL, Dodson WE, Rothman S, Orrechio EJ, Grover W, Berry GT, Schwartz JF, Habib A, DiMauro S. Cytochrome c oxidase-associated Leigh syndrome: phenotypic features and pathogenetic speculations. *J Neurol Sci* 1991; 104: 97–111
- Varlamov DA, Kudin AP, Vielhaber S, Schröder R, Sassen R, Becker A, Kunz D, Haug K, Rebstock J, Heils A, Elger CE, Kunz WS. Metabolic consequences of a novel missense mutation of the *mtDNA CO 1* gene. *Hum Mol Genet* 2002; 11: 1997–1805
- Von Kleist-Retzow J-C, Yao J, Taanman J-W, Chantrel K, Chretien D, Cormier-Daire V, Rötig A, Munnich A, Rustin P, Shoubridge EA. Mutations in *SURF1* are not specifically associated with Leigh syndrome. *J Med Genet* 2001; 2001: 109–113
- Willis TA, Davidson J, Gray RGF, Poultron K, Ramani P, Whitehouse W. Cytochrome oxidase deficiency presenting as birth asphyxia. *Dev Med Child Neurol* 2000; 42: 414–417
- Zafeiriou DI, Koletzko B, Mueller-Felber W, Paetzke I, Kueffer G, Jensen M. Deficiency in complex IV (cytochrome c oxidase) of the respiratory chain, presenting as a leukodystrophy in two siblings with Leigh syndrome. *Brain Dev* 1995; 17: 117–121
- Zeviani M, Corona P, Nijtmans L, Tiranti V. Nuclear gene defects in mitochondrial disorders. *Ital J Neurol Sci* 1999; 20: 401–408
- Zhu Z, Yao J, Johns T, Fu K, de Bie I, Macmillan C, Cuthbert AP, Newbold RF, Wang J-C, Brown GK, Brown RM, Shoubridge AE. *SURF1*, encoding a factor involved in the biogenesis of cytochrome c oxidase, is mutated in Leigh syndrome. *Nat Genet* 1998; 20: 337–343
- ## ATPase 6 Gene Defect
- Baracca A, Bagori S, Carelli V, Lenaz G, Solaini G. Catalytic activities of mitochondrial ATP synthase in patients with mitochondrial DNA T8993G mutation in the ATPase 6 gene encoding subunit a. *J Biol Chem* 2000; 275: 4177–4182
- Carelli V, Baracca A, Bagogi S, Pallotti F, Valentino ML, Montagna P, Zeviani M, Pini A, Lenaz G, Baruzzi A, Solaini G. Biochemical-clinical correlation in patients with different loads of the mitochondrial DNA T8993G mutation. *Arch Neurol* 2002; 59: 264–270
- Chowers I, Lerman-Sagie T, Elpeleg ON, Shaag A, Merin S. Cone and rod dysfunction in the NARP syndrome. *Br J Ophthalmol* 1999; 83: 190–193
- Degoul F, François D, Diry M, Ponsot G, Desguerre I, Héron B, Marsac C, Moutard ML. A near homoplasmic T8993G mtDNA mutation in a patient with atypical Leigh syndrome not present in the mother's tissues. *J Inher Metab Dis* 1997; 20: 49–53
- De Meirleir L, Seneca S, Lissens W, Schoentjes E, Desprechins B. Bilateral striatal necrosis with a novel point mutation in the mitochondrial ATPase 6 gene. *Pediatr Neurol* 1995; 13: 242–246
- De Vries DD, van Engelen BGM, Gabreëls FJM, Ruitenbeek W, van Oost BA. A second missense mutation in the mitochondrial ATPase 6 gene in Leigh's syndrome. *Ann Neurol* 1993; 34: 410–412
- Dionisi-Vici C, Seneca S, Zeviani M, Fariello G, Rimoldi M, Bertini E, de Meirleir L. Fulminant Leigh syndrome and sudden unexpected death in a family with the T9176C mutation of the mitochondrial ATPase 6 gene. *J Inher Metab Dis* 1998; 21: 2–8
- Ferlin T, Landrieu P, Ramboud C, Fernandez H, Dumoulin R, Rustin R, Mousson B. Segregation of the G8993 mutant mitochondrial DNA through generations and embryonic tissues in a family at risk of Leigh syndrome. *J Pediatr* 1997; 131: 447–449
- Fryer A, Appleton R, Sweeney MG, Rosenbloom L, Harding AE. Mitochondrial DNA 8993 (NARP) mutation presenting with a heterogeneous phenotype including 'cerebral palsy'. *Arch Dis Child* 1994; 71: 419–422
- Fujii T, Hattori H, Higuchi Y, Tsuji M, Mitsuyoshi I. Phenotypic differences between T C and T G mutations at nt 8993 of mitochondrial DNA in Leigh syndrome. *Pediatr Neurol* 1998; 18: 275–277
- García JJ, Ogilvie I, Robinson BH, Capaldi RA. Structure, functioning, and assembly of the ATP synthase in cells from patients with the T8993G mitochondrial DNA mutation. *J Biol Chem* 2000; 275: 11075–11081
- Holt IJ, Harding AE, Petty RKH, Morgan-Hughes JA. A new mitochondrial disease associated with mitochondrial DNA heteroplasmy. *Am J Hum Genet* 1990; 46: 428–433
- Leshinsky-Silver E, Perach M, Basilevsky E, HersHKovitz E, Yanoov-Sharav M, Lerman-Sagie T, Leve D. Prenatal exclusion of Leigh syndrome due to T8993C mutation in the mitochondrial DNA. *Prenat Diagn* 2003; 23: 31–33
- Lodi R, Montagna P, Iotti S, Zaniol P, Barboni P, Puddo P, Barbiroli B. Brain and muscle energy metabolism studied in vivo by ³¹P-magnetic resonance spectroscopy in NARP syndrome. *J Neurol Neurosurg Psychiatry* 1994; 57: 1492–1496
- Mak S-C, Chi C-S, Tsai C-R. Mitochondrial DNA 8993T >C Mutation presenting as juvenile Leigh syndrome with respiratory failure. *J Child Neurol* 1998; 13: 349–351

- Mäkelä-Bengs P, Suomalainen A, Majander A, Rapola J, Kalimo H, Nuutila A, Pihko H. Correlation between the clinical symptoms and the proportion of mitochondrial DNA carrying the 8993 point mutation in the NARP syndrome. *Pediatr Res* 1995; 37: 634–639
- Nagashima T, Mori M, Katayama K, Nunomura M, Nishihara H, Higara H, Tanaka S Goto Y-I, Nagashima K. Adult Leigh syndrome with mitochondrial DNA mutation at 8993. *Acta Neuropathol (Berl)* 1999; 97: 416–422
- Pastores GM, Santorelli FM, Shanske S, Gelb BD, Fyfe B, Wolfe D, Willner JP. Leigh syndrome and hypertrophic cardiomyopathy in an infant with a mitochondrial DNA point mutation (T8993G). *Am J Med Genet* 1994; 50: 265–271
- Porto FBO, Mack G, Sterboul M-J, Lewin P, Flament J, Sahel J, Dofflus H. Isolated late-onset cone-rod dystrophy revealing a familial neurogenic muscle weakness, ataxia, and retinitis pigmentosa syndrome with the T8993G mitochondrial mutation. *Am J Ophthalmol* 2001; 132: 935–937
- Santorelli FM, Shanske S, Macaya A, DeVivo DC, DiMauro S. The mutation at nt 8993 of mitochondrial DNA is a common cause of Leigh's syndrome. *Ann Neurol* 1993; 34: 827–834
- Santorelli FM, Shanske S, Jain KD, Tick D, Schon EA, DiMauro S. A T C mutation at nt 8993 of mitochondrial DNA in a child with Leigh syndrome. *Neurology* 1994; 44: 972–974
- Santorelli FM, Mak S-C, Vazquez-Memije ME, Shanske S, Kranz-Eble P, Jain KD, Bleustone DL, de Vivo DC, DiMauro S. Clinical heterogeneity associated with the mitochondrial DNA T8993C point mutation. *Pediatr Res* 1996; 39: 914–917
- Shoffner JM, Fernhoff PM, Krawiecki NS, Caplan DB, Holt PJ, Koontz DA, Takei Y, Newman NJ, Ortiz RG, Polak M, Ballinger SW, Lott MT, Wallace DC. Subacute necrotizing encephalopathy: oxidative phosphorylation defects and the ATPase 6 point mutation. *Neurology* 1992; 42: 2168–2174
- Suzuki Y, Wada T, Sakai T, Ishikawa Y, Minami R, Tachi N, Saitoh S. Phenotypic variability in a family with a mitochondrial DNA T8993C mutation. *Pediatr Neurol* 1998; 19: 283–286
- Takahashi S, Oki J, Miyamoto A, Okuno A. Proton magnetic resonance spectroscopy to study the metabolic changes in the brain of a patient with Leigh syndrome. *Brain Dev* 1999; 21: 200–204
- Takanashi J-I, Sugita K, Tanabe Y, Maetomo T, Niimi H. Dichloroacetate treatment in Leigh syndrome caused by mitochondrial DNA mutation. *J Neurol Sci* 1997; 145: 83–86
- Tatuch Y, Christodoulou J, Feigenbaum A, Clarke JTR, Wherret J, Smith C, Rudd N, Petrova-Benedict R, Robinson BH. Heteroplasmic mtDNA mutation (T→G) at 8993 can cause Leigh disease when the percentage of abnormal mtDNA is high. *Am J Hum Genet* 1992; 50: 852–858
- Tsao C-Y, Mendell JR, Bartholomew D. High mitochondrial DNA T8993G mutation (>90%) without typical features of Leigh's and NARP syndromes. *J Child Neurol* 2001; 16: 533–535
- Uziel G, Moroni I, Lemantea E, Fratta GM, Ciceri E, Carrara E, Zeviani M. Mitochondrial disease associated with the T8993G mutation of the mitochondrial ATPase 6 gene: a clinical, biochemical, and molecular study in six families. *J Neurol Neurosurg Psychiatry* 1997; 63: 16–22
- Vásquez-Memije ME, Shanske S, Santorelli FM, Franz-Elbe P, DeVivo DC, DiMauro S. Comparative biochemical studies of ATPases in cells from patients with the T8993G or T8993C mitochondrial DNA mutations. *J Inherit Metab Dis* 1998; 21: 829–836
- White SL, Shanske S, Biros I, Warwick L, Dahl HM, Thornburn DR, DiMauro S. Two cases of prenatal analysis for the pathogenic T to G substitution at nucleotide 8993 in mitochondrial DNA. *Prenat Diagn* 1999; 19: 1165–1168
- Wilson CJ, Wood NW, Leonard JV, Surtees R, Rahman S. Mitochondrial DNA point mutation T9176C in Leigh syndrome. *J Child Neurol* 2000; 15: 830–833
- Yamada T, Hayasaka S, Hongo K, Kubota H. Retinal dystrophy in a Japanese boy harboring the mitochondrial DNA T8993G mutation. *Jpn J Ophthalmol* 2002; 46: 460–462

29 Pyruvate Carboxylase Deficiency

- Ahmad A, Kahler SG, Kishnani PS, Artigas-Lopez M, Pappu AS, Steiner R, Millington DS, van Hove JLK. Treatment of pyruvate carboxylase deficiency with high doses of citrate and aspartate. *Am J Med Genet* 1999; 87: 331–338
- Arnold GL, Griebel ML, Porterfield M, Brewster M. Pyruvate carboxylase deficiency. *Clin Pediatr* 2001; 40: 519–521
- Atkin BM, Buist NRM, Utter MF, Leiter AB, Banker BQ. Pyruvate carboxylase deficiency and lactic acidosis in a retarded child without Leigh's disease. *Pediatr Res* 1979; 13: 109–116
- Baal MG, Gabreëls FJM, Renier WO, Hommes FA, Gijsbers THJ, Lamers KJB, Kok JCN. A patient with pyruvate carboxylase deficiency in the liver: treatment with aspartic acid and thiamine. *Dev Med Child Neurol* 1981; 23: 521–530
- Bartlett K, Ghneim HK, Stirk JH, Dale G, Alberti GMM. Pyruvate carboxylase deficiency. *J Inherit Metab Dis* 1984; 7: 74–78
- Brun N, Robitaille Y, Grignon A, Robinson A, Robinson BH, Mitchell GA, Lambert M. Pyruvate carboxylase deficiency: prenatal onset of ischemia-like brain lesions in two sibs with the acute neonatal form. *Am J Med Genet* 1999; 84: 94–101
- Carbone MA, MacKay N, Ling M, Cole DEC, Douglas C, Rigat B, Feigenbaum A, Clarke JTR, Haworth JC, Greenberg CR, Seargant L, Robinson BH. Amerindian pyruvate carboxylase deficiency is associated with two distinct missense mutations. *Am J Hum Genet* 1998; 62: 1312–1319
- Carbone MA, Applegarth DA, Robinson BH. Intron retention and frameshift mutations result in severe pyruvate carboxylase deficiency in two male siblings. *Hum Mutat* 2002; 20: 48–56
- Greter J, Gustafsson J, Holme E. Pyruvate-carboxylase deficiency with urea cycle impairment. *Acta Paediatr Scand* 1985; 74: 982–986
- Hamilton J, Rae MD, Logan RW, Robinson PH. A case of benign pyruvate carboxylase deficiency with normal development. *J Inherit Metab Dis* 1997; 20: 401–403
- Higgins JJ, Glasgow AM, Lusk M, Kerr DS. MRI, clinical, and biochemical features of partial pyruvate carboxylase deficiency. *J Child Neurol* 1994; 9: 436–439
- Higgins JJ, Ide SE, Oghalai JS, Polymeropoulos MH. Lack of mutations in the biotin-binding region of the pyruvate carboxylase (PC) gene in a family with partial PC deficiency. *Clin Biochem* 1997; 30: 79–81
- Murphy JV, Isohashi F, Weinberg MB, Utter MF. Pyruvate carboxylase deficiency: an alleged biochemical cause of Leigh's disease. *Pediatrics* 1981; 368: 401–404
- Oizumi J, Shaw KNF, Giudici TA, Carter M, Donnell GN, Ng WG. Neonatal pyruvate carboxylase deficiency with renal tubular acidosis and cysturia. *J Inherit Metab Dis* 1983; 6: 89–94
- Oizumi J, Donnell GN, Ng WG, Mulivor RA, Greene AE, Coriell LL. Congenital lactic acidosis associated with pyruvate carboxylase deficiency. *Cytogenet Cell Genet* 1984; 38: 81
- Pineda M, Campistol J, Vilaseca MA, Briones P, Ribes A, Temudo T, Pons M, Cusi V, Rolland M-O. An atypical French form of pyruvate carboxylase deficiency. *Brain Dev* 1995; 17: 276–279

- Robinson BH, Oei J, Sherwood WG, Applegarth D, Wong L, Hawthorn J, Goodyer P, Casey R, Zaleski LA. The molecular basis for the two different clinical presentations of classical pyruvate carboxylase deficiency. *Am J Hum Genet* 1984; 36: 283–294
- Robinson BH, Toone JR, Benedict P, Dimmick JE, Oei J, Applegarth DA. Prenatal diagnosis of pyruvate carboxylase deficiency. *Prenat Diagn* 1985; 5: 67–71
- Robinson BH, Oei J, Saudubray JM, Marsac C, Bartlett K, Quan F, Gravel R. The French and North American phenotypes of pyruvate carboxylase deficiency, correlation with biotin containing protein by ^3H -biotin incorporation, ^{35}S -streptavidin labeling, and Northern blotting with a cloned cDNA probe. *Am J Hum Genet* 1987; 40: 50–59
- Robinson BH, MacKay N, Chun K, Ling M. Disorders of pyruvate carboxylase and the pyruvate dehydrogenase complex. *J Inher Metab Dis* 1996; 19: 452–462
- Rutledge SL, Snead OC, Kelly DR, Kerr DS, Swann JW, Spink DL, Martin DL. Pyruvate carboxylase deficiency: acute exacerbation after ACTH treatment of infantile spasms. *Pediatr Neurol* 1989; 5: 249–252
- Sander J, Packman S, Berg BO, Hutchison HT, Caswell N. Pyruvate carboxylase activity in subacute necrotizing encephalopathy (Leigh's disease). *Neurology* 1984; 34: 515–516
- Saudubray JM, Marsac C, Charpentier C, Cathelineau L, Leaud MB, Leroux JP. Neonatal congenital lactic acidosis with pyruvate carboxylase deficiency in two siblings. *Acta Paediatr Scand* 1976; 65: 717–724
- Stern HJ, Nayar R, Depalma L, Fifai N. Prolonged survival in pyruvate carboxylase deficiency: lack of correlation with enzyme activity in cultured fibroblasts. *Clin Biochem* 1995; 28: 85–89
- Tada K, Takada G, Omura K, Itokawa Y. Congenital lactic acidosis due to pyruvate carboxylase deficiency: absence of an inhibitor of TPP-ATP phosphoryltransferase. *Eur J Pediatr* 1978; 127: 141–147
- Tsuchiyama A, Oyanagi K, Hirano S, Tachi N, Sogawa H, Wagatsuma K, Nakao T, Tsugawa S, Kawamura Y. A case of pyruvate carboxylase deficiency with later prenatal diagnosis of an unaffected sibling. *J Inher Metab Dis* 1983; 6: 85–88
- Van Coster RN, Fernhoff PM, De Vivo DC. Pyruvate carboxylase deficiency: a benign variant with normal development. *Pediatr Res* 1991; 30: 1–4
- Van Coster RN, Janssens S, Misson J-P, Verloes A, Leroy JG. Prenatal diagnosis of pyruvate carboxylase deficiency by direct measurement of catalytic activity on chorionic villi samples. *Prenat Diagn* 1998; 18: 1041–1044
- Wallace JC, Jitrapakdee S, Chapman-Smith S. Pyruvate carboxylase. *Biochem Cell Biol* 1998; 30: 1–5
- Wexler ID, Du Y, Lisgaris MV, Mandal SK, Freytag SO, Yang B-S, Liu T-C, Kwon M, Patel MS, Kerr DS. Primary amino acid sequence and structure of human pyruvate carboxylase. *Biochim Biophys Acta* 1994; 1227: 46–52
- Wexler ID, Kerr DS, Du Y, Kaung MM, Stephenson W, Lusk MM, Wappner RS, Higgins JJ. Molecular characterization of pyruvate carboxylase deficiency in two consanguineous families. *Pediatr Res* 1998; 43: 579–584
- Wong LTK, Davidson GF, Applegarth DE, Dimmick JE, Norman MG, Toone JR, Pirie G, Wong J. Biochemical and histologic pathology in an infant with cross-reacting material (negative) pyruvate carboxylase deficiency. *Pediatr Res* 1986; 20: 274–279
- ## 30 Multiple Carboxylase Deficiency
- Bakker HD, Westra M, Overweg-Plandsoen WCG, Wavere van G, Sillevius-Smit JH, Abeling NGGM, Wanders RJA, Schutgens RBH, Gennip van AH. Normalisation of severe cranial CT scan abnormalities after biotin in a case of biotinidase deficiency. *Eur J Pediatr* 1994; 153: 861–866
- Baumgartner ER, Suormala TM, Wick H, Probst A, Blauenstein U, Bachmann C, Vest M. Biotinidase deficiency: a cause of subacute necrotizing encephalomyelopathy (Leigh syndrome). Report of a case with lethal outcome. *Pediatr Res* 1989; 26: 260–266
- Baumgartner ER, Suormala T. Multiple carboxylase deficiency: inherited and acquired disorders of biotin metabolism. *Int J Vitam Nutr Res* 1997; 67: 377–384
- Bay CA, Berry GT, Glauser TA, Hayward JC, Wolf B, Sladky JT, Kaplan P. Reversible metabolic myopathy in biotinidase deficiency: its possible role in causing hypotonia. *J Inher Metab Dis* 1995; 18: 701–704
- Bousounis DP, Camfield PR, Wolf B. Reversal of brain atrophy with biotin treatment in biotinidase deficiency. *Neuropediatrics* 1993; 24: 214–217
- Casado de Frías E, Campos-Castelló J, Careaga Maldonado J, Pérez Cerdá C. Biotinidase deficiency: result of treatment with biotin from age 12 years. *Eur J Paediatr Neurol* 1997; 1: 173–176
- Cornejo Navarro P, Guerra A, Alvarez JG, Ortiz FJ. Cutaneous and neurologic manifestations of biotinidase deficiency. *Int J Dermatol* 2000; 39: 363–382
- Fuchshuber A, Suormala T, Roth B, Duran M, Michalk D, Baumgartner ER. Holocarboxylase synthetase deficiency: early diagnosis and management of a new case. *Eur J Pediatr* 1993; 152: 446–449
- Gibson KM, Bennett MJ, Nyhan WL, Mize CE. Late-onset holocarboxylase synthetase deficiency. *J Inher Metab Dis* 1996; 19: 739–742
- Ginat-Israeli T, Hurvitz H, Klar A, Blinder G, Branski D, Amir N. Deteriorating neurological and neuroradiological course in treated biotinidase deficiency. *Neuropediatrics* 1993; 24: 103–106
- Haagerup A, Brandt Andersen J, Blichfeldt S, Fjord Christensen M. Biotinidase deficiency: two cases of very early presentation. *Dev Med Child Neurol* 1997; 39: 832–835
- Honavar M, Janota I, Neville BGR, Chalmers RA. Neuropathology of biotinidase deficiency. *Acta Neuropathol (Berl)* 1992; 84: 461–464
- Hymes J, Wolf B. Biotinidase and its roles in biotin metabolism. *Clin Chim Acta* 1996; 255: 1–11
- Kalayci Ö, Coskun T, Tokatli A, Demir E, Erdem G, Güngör C, Yükselen A, Özalp I. Infantile spasms as the initial symptom of biotinidase deficiency. *J Pediatr* 1994; 124: 103–104
- Kimura M, Fukui T, Tagami Y, Fujiwaki T, Yokoyama M, Ishioka C, Kumasaka K, Terada N, Yamaguchi S. Normalization of low biotinidase activity in a child with biotin deficiency after biotin supplementation. *J Inher Metab Dis* 2003; 26: 715–719
- Livne M, Gibson M, Amir N, Eshel G, Elpeleg ON. Holocarboxylase synthetase deficiency: a treatable metabolic disorder masquerading as cerebral palsy. *J Child Neurol* 1994; 9: 170–172
- Mardach R, Zemleni J, Wolf B, Cannon MJ, Jennings ML, Cress S, Boylan J, Roth S, Cederbaum S, Mock DM. Biotin dependency due to a defect in biotin transport. *J Clin Invest* 2002; 109: 1617–1623

- Mitchell G, Ogier H, Munnich A, Saudubray JM. Neurological deterioration and lactic acidemia in biotinidase deficiency – a treatable condition mimicking Leigh's disease. *Neuropediatrics* 1986; 17: 129–131
- Möslinger D, Stöckler-Ipsiroglu S, Scheibenreiter S, Tiefenthaler M, Mühl A, Seidl R, Strobl W, Plecko B, Suormala T, Regula Baumgartner ER. Clinical and neuropsychological outcome in 33 patients with biotinidase deficiency ascertained by nationwide newborn screening and family studies in Austria. *Eur J Pediatr* 2001; 160: 277–282
- Pomponio RJ, Hymes J, Reynolds TR, Meyers GA, Fleischhauer K, Buck GA, Wolf B. Mutations in the human biotinidase gene that cause profound biotinidase deficiency in symptomatic children: molecular, biochemical, and clinical analysis. *Pediatr Res* 1997; 42: 840–848
- Rahman S, Standing S, Dalton RN, Pike MG. Late presentation of biotinidase deficiency with acute visual loss and gait disturbance. *Dev Med Child Neurol* 1997; 39: 830–831
- Ramaekers VT, Suormala TM, Brab M, Duran R, Heimann G, Baumgartner ER. A biotinidase K_m variant causing late onset bilateral optic neuropathy. *Arch Dis Child* 1992; 67: 115–119
- Ramaekers VT, Brab M, Rau G, Heimann G. Recovery from neurological deficits following biotin treatment in a biotinidase K_m variant. *Neuropediatrics* 1993; 24: 98–102
- Salbert BA, Astruc J, Wolf B. Ophthalmologic findings in biotinidase deficiency. *Ophthalmologica* 1993; 206: 177–181
- Salbert BA, Pellock JM, Wolf B. Characterization of seizures associated with biotinidase deficiency. *Neurology* 1993; 43: 1351–1355
- Sander JE, Malamud N, Cowan MJ, Packman S, Amman AJ, Wara DW. Intermittent ataxia and immunodeficiency with multiple carboxylase deficiencies: a biotin-responsive disorder. *Ann Neurol* 1980; 8: 544–547
- Schürmann M, Engelbrecht V, Lohmeier K, Lenard HG, Wendel U, Gärtner J. Cerebral metabolic changes in biotinidase deficiency. *J Inherit Metab Dis* 1997; 20: 755–760
- Schultz PE, Weiner SP, Belmont JW, Fishman MA. Basal ganglia calcifications in a case of biotinidase deficiency. *Neurology* 1988; 38: 1326–1328
- Secor McVoy JR, Levy HL, Lawler M, Schmidt MA, Ebers DD, Hart PS, Dove Pettit D, Blitzer MG, Wolf B. Partial biotinidase deficiency: clinical and biochemical features. *J Pediatr* 1990; 116: 78–83
- Suormala TM, Baumgartner ER, Wick H, Scheibenreiter S, Schweitzer S. Comparison of patients with complete and partial biotinidase deficiency: biochemical studies. *J Inherit Metab Dis* 1990; 13: 76–92
- Suormala T, Ramaekers VTh, Schweitzer S, Fowler B, Laub MC, Schwermer C, Bachmann J, Baumgartner ER. Biotinidase K_m -variants: detection and detailed biochemical investigations. *J Inherit Metab Dis* 1995; 18: 689–700
- Suormala T, Fowler B, Jakobs C, Duran M, Lehnert W, Raab K, Wick H, Baumgartner ER. Late-onset holocarboxylase synthetase-deficiency: pre- and post-natal diagnosis and evaluation of effectiveness of antenatal biotin therapy. *Eur J Pediatr* 1998; 157: 570–575
- Sweetman L, Nyhan WL. Inheritable biotin-treatable disorders and associated phenomena. *Annu Rev Nutr* 1986; 6: 317–343
- Tsao CY, Kien CL. Complete biotinidase deficiency presenting as reversible progressive ataxia and sensorineural deafness. *J Child Neurol* 2002; 17: 146
- Wiznitzer M, Bangert BA. Biotinidase deficiency: clinical and MRI findings consistent with myelopathy. *Pediatr Neurol* 2003; 29: 56–58
- Wolf B, Heard GS. Biotinidase deficiency. *Adv Pediatr* 1991; 38: 1–21
- Wolf B, Hsia YE, Sweetman L, Feldman G, Boychuk RB, Bart RD, Crowell DH, Di Mauro RM, Nyhan WL. Multiple carboxylase deficiency: clinical and biochemical improvement following neonatal biotin treatment. *Pediatrics* 1981; 68: 113–118
- Wolf B, Heard GS, Weissbecker KA, Secor McVoy JR, Grier RE, Leshner RT. Biotinidase deficiency: initial clinical features and rapid diagnosis. *Ann Neurol* 1985; 18: 614–617
- Wolf B, Norrgard K, Pomponio RJ, Mock DM, Secor McVoy JR, Fleischhauer K, Shapiro S, Blitzer MG, Hymes J. Profound biotinidase deficiency in two asymptomatic adults. *Am J Med Genet* 1997; 73: 5–9
- Wolf B, Pomponio RJ, Norrgard KJ, Lott IT, Regula Baumgartner E, Suormala T, Ramaekers VTh, Coskun T, Tokatli A, Ozalp I, Hymes J. Delayed-onset profound biotinidase deficiency. *J Pediatr* 1998; 132: 362–365
- Wolf B, Spencer R, Gleason T. Hearing loss is a common feature of symptomatic children with profound biotinidase deficiency. *J Pediatr* 2002; 140: 242–246
- Wolf B, Jensen K, Hüner G, Demirkol M, Baykal T, Divry P, Rolland MO, Perez-Cerdá C, Ugarte M, Straussberg R, Basel-Vanagaite L, Baumgartner ER, Suormala T, Scholl S, Das AM, Schweitzer S, Pronicka E, Sykut-Cegielska J. Seventeen novel mutations that cause profound biotinidase deficiency. *Mol Gen Metab* 2002; 77: 108–111

31 Cerebrotendinous Xanthomatosis

- Argov Z, Soffer D, Eisenberg S, Zimmerman Y. Chronic demyelinating peripheral neuropathy in cerebrotendinous xanthomatosis. *Ann Neurol* 1986; 20: 89–91
- Ballantyne CM, Vega GL, East C, Richards G, Grundy SM. Low-density lipoprotein metabolism in cerebrotendinous xanthomatosis. *Metabolism* 1987; 36: 270–276
- Barkhof F, Verrips A, van der Knaap MS, van Engelen BGM, Gabreëls FJM, Keyser A, Wevers RA, Valk J. Cerebrotendinous xanthomatosis: the spectrum of imaging findings and the correlation with neuropathologic findings. *Radiology* 2000; 217: 869–876
- Bencze KS, van de Polder DR, Prockop LD. Magnetic resonance imaging of the brain and spinal cord in cerebrotendinous xanthomatosis. *J Neurol Neurosurg Psychiatry* 1990; 53: 166–167
- Berginer VM, Berginer J, Salen G, Shefer S, Zimmerman RD. Computed tomography in cerebrotendinous xanthomatosis. *Neurology* 1981; 31: 1463–1465
- Berginer VM, Salen G, Shefer S. Long-term treatment of cerebrotendinous xanthomatosis with chenodeoxycholic acid. *N Engl J Med* 1984; 311: 1649–1652
- Berginer VM, Salen G, Shefer S. Cerebrotendinous xanthomatosis. *Neurol Clin* 1989; 7: 55–74
- Berginer VM, Berginer J, Korczyn AD, Tamor R. Magnetic resonance imaging in cerebrotendinous xanthomatosis: a prospective clinical and neuroradiological study. *J Neurol Sci* 1994; 122: 102–108
- Canelas HM, Quintao ECR, Scaff M, Vasconcelos KS, Brotto MWI. Cerebrotendinous xanthomatosis: clinical and laboratory study of 2 cases. *Acta Neurol Scand* 1983; 67: 305–311
- Chen W, Kubota S, Teramoto T, Ishida S, Ohsawa N, Katayama T, Takeda T, Kuroda K, Yahara O, Kasuhara T, Neshige R, Seyama Y. Genetic analysis enables definite and rapid diagnosis of cerebrotendinous xanthomatosis. *Neurology* 1998; 51: 865–867

- Claydon PT, Verrips A, Sisterman E, Mann A, Mieli-Vergani G, Wevers R. Mutations in the sterol 27-hydrolase gene (*CYP27A*) cause hepatitis of infancy as well as cerebrotendinous xanthomatosis. *J Inher Metab Dis* 2002; 25: 501–513
- De Stefano N, Dotti MT, Mortilla M, Federico A. Magnetic resonance imaging and spectroscopic changes in brains of patients with cerebrotendinous xanthomatosis. *Brain* 2001; 124: 121–131
- Dotti MT, Federico A. Cerebrotendinous xanthomatosis with predominant parkinsonian syndrome: further confirmation of the clinical heterogeneity. *Mov Disord* 2000; 15: 1017–1019
- Dotti MT, Salen G, Federico A. Cerebrotendinous xanthomatosis as a multisystem disease mimicking premature ageing. *Dev Neurosci* 1991; 13: 371–376
- Dotti MT, Federico A, Signorini E, Caputo N, Venturi C, Filisomi G, Guazzi GC. Cerebrotendinous xanthomatosis (van Bogaert-Scherer-Epstein disease): CT and MR findings. *AJNR Am J Neuroradiol* 1994; 15: 1721–1726
- Dotti MT, Mondillo S, Plewnia K, Agricola E, Federico A. Cerebrotendinous xanthomatosis: evidence of lipomatous hypertrophy of the atrium septum. *J Neurol* 1998; 245: 723–726
- Dotti MT, Rufa A, Federico A. Cerebrotendinous xanthomatosis: heterogeneity of clinical phenotype with evidence of previously undescribed ophthalmological findings. *J Inher Metab Dis* 2001; 24: 696–706
- Elleder M, Michalec Ě, Jirásek A, Khun K, Havlová M, Ranný M. Membranocystic lesion in the brain in cerebrotendinous xanthomatosis. Histochemical and ultrastructural study with evidence of its ceroid nature. *Virchows Arch [B]* 1989; 57: 367–374
- Federico A, Dotti MT. Cerebrotendinous xanthomatosis. *Neurology* 2001; 57: 1743
- Federico A, Dotti MT. Cerebrotendinous xanthomatosis: clinical manifestations, diagnostic criteria, pathogenesis and therapy. *J Child Neurol* 2003; 18: 633–638
- Federico A, Dotti MT, Volpi N. Muscle mitochondrial changes in cerebrotendinous xanthomatosis. *Ann Neurol* 1991; 30: 734–735
- Fiorelli M, Di Piero V, Bastianello S, Bozzao L, Federico A. Cerebrotendinous xanthomatosis: clinical and MRI study (case report). *J Neurol Neurosurg Psychiatry* 1990; 53: 76–78
- Hokezu Y, Kuriyama M, Kubota R, Nakagawa M, Fujiyama J, Osame M. Cerebrotendinous xanthomatosis: cranial CT and MRI studies in eight patients. *Neuroradiology* 1992; 34: 308–312
- Javitt NB. Biologic role(s) of the 25(R),26-hydroxycholesterol metabolic pathway. *Biochim Biophys Acta* 2000; 1529: 136–141
- Kawabata M, Kuriyama M, Mori S, Sakashita I, Osame M. Pulmonary manifestations in cerebrotendinous xanthomatosis. *Intern Med* 1998; 37: 922–926
- Kuriyama M, Fujiyama J, Yoshidome H, Takenaga S, Matsumuro K, Kasama T, Fukuda K, Kuramoto T, Hoshita T, Seyama Y, Okatu Y, Osame M. Cerebrotendinous xanthomatosis: clinical and biochemical evaluation of eight patients and review of the literature. *J Neurol Sci* 1991; 102: 225–232
- Lee M-H, Hazard S, Carpten DJ, Yi S, Cohen J, Gerhardt GT, Salen G, Patel SB. Fine-mapping, mutation analysis, and structural mapping of cerebrotendinous xanthomatosis in U.S. pedigrees. *J Lipid Res* 2001; 42: 159–169
- Leitersdorf E, Reshef A, Meiner V, Levitzki R, Pressman Schwartz S, Dann EJ, Berkman N, Cali JJ, Klapholz L, Berginer VM. Frameshift and splice-junction mutations in the sterol 27-hydroxylase gene cause cerebrotendinous xanthomatosis in Jews of Moroccan origin. *J Clin Invest* 1993; 91: 2488–2496
- Lui C-C, Chang W-N. MRI changes in cerebrotendinous xanthomatosis after treatment with chenodeoxycholic acid. *Riv Neuroradiol* 1998; 11: 10–11
- Meiner V, Meiner Z, Reshef A, Björkem I, Leitersdorf E. Cerebrotendinous xanthomatosis: molecular diagnosis enables presymptomatic detection of a treatable disease. *Neurology* 1994; 44: 288–290
- Moghadasian MH, Salen G, Frohlich JJ, Scudamore CH. Cerebrotendinous xanthomatosis. A rare disease with diverse manifestations. *Arch Neurol* 2002; 59: 527–529
- Mondelli M, Rossi A, Scarpini C, Dotti MT, Federico A. Evoked potentials in cerebrotendinous xanthomatosis and effect induced by chenodeoxycholic acid. *Arch Neurol* 1992; 49: 469–475
- Mondelli M, Sicurelli F, Scarpini C, Dotti MT, Federico A. Cerebrotendinous xanthomatosis: 11-year treatment with chenodeoxycholic acid in five patients. An electrophysiological study. *J Neurol Sci* 2001; 190: 29–33
- Ohno T, Kobayashi S, Hayasi M, Suakurai M, Kanazawa I. Diphenylpyraline-responsive parkinsonism in cerebrotendinous xanthomatosis: long-term follow up of three patients. *J Neurol Sci* 2001; 182: 95–97
- Pedley TA, Emerson RG, Warner CL, Rowland LP, Salen G. Treatment of cerebrotendinous xanthomatosis with chenodeoxycholic acid. *Ann Neurol* 1985; 18: 517–518
- Peynet J, Laurent A, de Liege P, Lecoz P, Gambert P, Legrand A, Mikol J, Warnet A. Cerebrotendinous xanthomatosis: treatments with simvastatin, lovastatin, and chenodeoxycholic acid in 3 siblings. *Neurology* 1991; 41: 434–436
- Restuccia D, Di Lazzaro V, Servidei S, Colosimo C, Tonali P. Somatosensory and motor evoked potentials in the assessment of cerebrotendinous xanthomatosis before and after treatment with chenodeoxycholic acid: a preliminary study. *J Neurol Sci* 1992; 112: 139–146
- Salen G, Zaki G, Sabesin S, Boehme D, Sheper S, Mosbach EH. Intraphepatic pigment and crystal forms in patients with cerebrotendinous xanthomatosis (CTX). *Gastroenterology* 1978; 74: 82–89
- Salen G, Shefer S, Berginer V. Biochemical abnormalities in cerebrotendinous xanthomatosis. *Dev Neurosci* 1991; 13: 363–370
- Schimschock JR, Alvord EC, Swanson PD. Cerebrotendinous xanthomatosis. *Arch Neurol* 1968; 18: 688–698
- Siebner HR, Berndt S, Conrad B. Cerebrotendinous xanthomatosis without tendon xanthomas mimicking Marinesco-Sjögren syndrome: a case report. *J Neurol Neurosurg Psychiatry* 1996; 60: 582–585
- Soffer D, Benharroch D, Berginer V. The neuropathology of cerebrotendinous xanthomatosis revisited: a case report and review of the literature. *Acta Neuropathol (Berl)* 1995; 90: 213–220
- Tai KS, Brockwell J, Chan FL, Janus ED, Lam KSL. Magnetic resonance imaging of cerebrotendinous xanthomatosis. *Australas Radiol* 1995; 39: 61–65
- Tokimura Y, Kuriyama M, Arimura K, Fujiyama J, Osame M. Electrophysiological studies in cerebrotendinous xanthomatosis. *J Neurol Neurosurg Psychiatry* 1992; 55: 52–55

- Van Heijst AFJ, Wevers RA, Tangerman A, Cruysberg JRM, Renier WO, Tolboom JJM. Chronic diarrhoea as a dominating symptom in two children with cerebrotendinous xanthomatosis. *Acta Paediatr* 1996; 85: 932–936
- Van Heijst AFJ, Verrips A, Wevers RA, Cruysberg JRM, Renier WO, Tolboom JJM. Treatment and follow-up of children with cerebrotendinous xanthomatosis. *Eur J Pediatr* 1998; 157: 313–316
- Van Rietvelde F, Lemmering M, Mesprenue M, Crevits L, De Reuck J, Kunnen M. MRI of the brain in cerebrotendinous xanthomatosis (van Bogaert-Scherer-Epstein disease). *Eur Radiol* 2000; 10: 576–578
- Verrips A, Lycklama A, Nijeholt, GJ, Barkhof F, van Engelen BGM, Wesseling P, Luyten JAFM, Wevers RA, Stam J, Wokke JHJ, Van den Heuvel LPWJ, Keyser A, Gabreëls FJM. Spinal xanthomatosis: a variant of cerebrotendinous xanthomatosis. *Brain* 1991; 122: 1589–1595
- Verrips A, Wevers RA, van Engelen BGM, Keyser A, Wolthers BG, Barkhof F, Stalenhoef A, De Graaf R, Jansen-Zijlstra F, Van Spreken A, Gabreëls FJM. Effect of Simvastatin in addition to chenoxcholic acid in patients with cerebrotendinous xanthomatosis. *Metabolism* 1999; 48: 233–238
- Verrips A, van Engelen BGM, Ter Laak H, Gabreëls-Festen A, Janssen A, Zwarts M, Wevers RA, Gabreëls FJM. Cerebrotendinous xanthomatosis controversies about nerve and muscle: observations in ten patients. *Neuromusc Disord* 2000; 10: 407–414
- Verrips A, van Engelen BGM, Wevers RA, van Geel BM, Crusberg JRM, van den Heuvel LPWJ, Keyser A, Gabreëls FJM. Presence of diarrhea and absence of tendom xanthomas in patients with cerebrotendinous xanthomatosis. *Arch Neurol* 2000; 57: 520–524
- Verrips A, Hoefsloot LH, Steenbergen GCH, Theelen JP, Wevers RA, Gabreëls JM, van Engelen BGM, Van den Heuvel LPWJ. Clinical and molecular genetic characteristics of patients with cerebrotendinous xanthomatosis. *Brain* 2000; 123: 908–919
- Wakamatsu N, Hayashi M, Kawai H, Kondo H, Gotoda Y, Nishida Y, Kondo S, Matsumoto T. Mutations producing premature termination of translation and an amino acid substitution in the sterol 27-hydroxylase gene cause cerebrotendinous xanthomatosis associated with parkinsonism. *J Neurol Neurosurg Psychiatry* 1999; 67: 195–198
- Wevers RA, Cruysberg JRM, van Heijst AFJ, Janssen-Zijlstra FSM, Renier WO, van Engelen BGM, Tolboom JJM. Paediatric cerebrotendinous xanthomatosis. *J Inher Metab Dis* 1992; 15: 374–376
- Boltshauser E, Yalcinkaya C, Wichmann W, Reutter F, Prader A, Valavanis A. MRI in Cockayne syndrome type I. *Neuroradiology* 1989; 31: 276–277
- Castillo M, Thomas D, Mukherji SK. Facies to remember. *Int J Neuroradiol* 1997; 3: 35–41
- Cirillo Silengo M, Franceschini P, Bianco R, Biagioli M, Pastorin L, Vista N, Baldassar A, Benso L. Distinctive skeletal dysplasia in Cockayne syndrome. *Pediatr Radiol* 1986; 16: 264–266
- Citterio E, Van der Boom V, Schnitzler G, Kanaar R, Bonte E, Kingston RE, Hoeijmakers JHJ, Vermeulen W. ATP-dependent chromatin remodeling by the Cockayne syndrome B DNA repair–transcription-coupling factor. *Mol Cell Biol* 2000; 20: 7643–7653
- Colabucci F, Rossodivita A, Parigi A, Colavita N. A clinical and radiological study of two brothers affected by Cockayne syndrome type II. *Rays* 1987; 12: 57–63
- Dabbagh O, Swaiman KF. Cockayne syndrome: MRI correlates of hypomyelination. *Pediatr Neurol* 1988; 4: 113–116
- Del Bigio MR, Greenberg CR, Rorke LB, Schnur R, McDonald-McGinn DM, Zackai EH. Neuropathological findings in eight children with cerebro-oculo-facio-skeletal (COFS) syndrome. *J Neuropathol Exp Neurol* 1997; 56: 1147–1157
- Demaerel P, Wilms G, Verdrup P, Carton H, Baert AL. MRI in the diagnosis of Cockayne's syndrome. One case. *J Neuroradiol* 1990; 17: 157–160
- Demaerel P, Kendall BE, Kingsley D. Cranial CT and MRI in diseases with DNA repair defects. *Neuroradiology* 1992; 34: 117–121
- Friedberg EC. Cockayne syndrome – a primary defect in DNA repair, transcription, both or neither? *Bioessays* 1996; 18: 731–738
- Graham JM Jr, Anyane-Yeboah K, Raams A, Appeldoorn E, Kleijer WJ, Garritsen VH, Busch D, Edersheim TG, Jaspers NGJ. Cerebro-oculo-facio-skeletal syndrome with a nucleotide excision-repair defect and a mutated *XPD* gene, with prenatal diagnosis in a triplet pregnancy. *Am J Hum Genet* 2001; 69: 291–300
- Grunnet ML, Zimmerman AW, Lewis RA. Ultrastructure and electrodiagnosis of peripheral neuropathy in Cockayne's syndrome. *Neurology* 1983; 33: 1606–1609
- Hanawalt PC. The basis for Cockayne syndrome. *Nature* 2000; 405: 415–416
- Harbord MG, Finn JP, Hall-Craggs MA, Brett EM, Baraitser M. Early onset leukodystrophy with distinct facial features in 2 siblings. *Neuropediatrics* 1989; 20: 154–157
- Hayashi M, Hayakawa K, Suzuki F, Sugita K, Satoh J, Morimatsu Y. A neuropathological study of early onset Cockayne syndrome with chromosomal anomaly 47XXX. *Brain Dev* 1992; 14: 63–67
- Hayashi M, Itoh M, Araki S, Kumada S, Shioda K, Tamagawa K, Mizutani T, Morimatsu Y, Minagawa M, Oda M. Oxidative stress and disturbed glutamate transport in hereditary nucleotide repair disorders. *J Neuropathol Exp Neurol* 2001; 60: 350–356
- Houston CS, Zaleski WA, Rozdilsky B. Identical male twins and brother with Cockayne syndrome. *Am J Med Genet* 1982; 13: 211–223
- Itoh M, Hayashi M, Shioda K, Minagawa M, Isa F, Tamagawa K, Morimatsu Y, Oda M. Neurodegeneration in hereditary nucleotide repair disorders. *Brain Dev* 1999; 21: 326–333
- Kohji T, Hayashi M, Shioda K, Minagawa M, Morimatsu Y, Tamagawa K, Oda M. Cerebellar neurodegeneration in human hereditary DNA repair disorders. *Neurosci Lett* 1998; 243: 133–136

32 Cockayne Syndrome

- Balajee AS, De Santis LP, Brosh Jr RM, Selzer R, Bohr VA. Role of the ATPase domain of the Cockayne syndrome group B protein in UV induced apoptosis. *Oncogene* 2000; 19: 477–489
- Berneberg M, Lowe JE, Nardo T, Araújo S, Foustier MI, Green MHL, Krutmann J, Wood RD, Stefanini M, Lehmann AR. UV damage causes uncontrolled DNA breakage in cells from patients with combined features of XP-D and Cockayne syndrome. *EMBO J* 2000; 19: 1157–1166
- Berneburg M, Lehmann AR. Xeroderma pigmentosum and related disorders: defect in DNA repair and transcription. *Adv Genet* 2000; 43: 71–102
- Bohr VA. Human premature aging syndrome and genomic instability. *Mech Ageing Dev* 2002; 123: 987–993

- Lee S-K, Yu S-L, Prakash L, Prakash S. Requirement of yeast RAD2, a homolog of human *XPG* gene, for efficient RNA polymerase II transcription: implications for Cockayne syndrome. *Cell* 2002; 109: 823–834
- Leech RW, Brumback RA, Miller RH, Otsuka F, Tarone RE, Robbins JH. Cockayne syndrome: clinicopathologic and tissue culture studies of affected siblings. *J Neuropathol Exp Neurol* 1985; 44: 507–519
- Lehmann AR, Thompson AF, Harcourt SA, Stefanini M, Norris PG. Cockayne's syndrome: correlation of clinical features with cellular sensitivity of RNA synthesis to UV irradiation. *J Med Genet* 1993; 30: 679–682
- Licht CL, Stevsner T, Bohr VA. Cockayne syndrome group B cellular and biochemical functions. *Am J Hum Genet* 2003; 73: 1217–1239
- Lindahl T, Karran P, Wood RD. DNA excision repair pathways. *Curr Opin Genet Dev* 1997; 7: 159–169
- Lindenbaum Y, Dickson DW, Rosenbaum PS, Kraemer KH, Robbins JH, Rapin I. Xeroderma pigmentosum / Cockayne syndrome complex: first neuropathological study and review of eight other cases. *Eur J Pediatr Neurol* 2001; 5: 225–242
- Lowry RB. Early onset of Cockayne syndrome. *Am J Med Genet* 1982; 13: 209–210
- Mallery DL, Tanganelli B, Colella S, Steingrimsdottir H, Van Gool AJ, Troelstra C, Stefanini M, Lehmann AR. Molecular analysis of mutations in the CSB (*ERCC6*) gene in patients with Cockayne syndrome. *Am J Hum Genet* 1998; 62: 77–85
- Meira L, Graham Jr JM, Greenberg CR, Busch DB, Doughty ATB, Ziffer DW, Coleman DM, Savre-Train I, Friedberg EC. Mani-tona aboriginal kindred with original cerebro-oculo-facio-skeletal syndrome has a mutation in the Cockayne syndrome group B (*CSB*) gene. *Am J Hum Genet* 2000; 66: 1221–1228
- Moyer DB, Marquis P, Shertzer ME, Burton BK. Cockayne syndrome with early onset of manifestations. *Am J Med Genet* 1982; 13: 225–230
- Nance MA, Berry SA. Cockayne syndrome: review of 140 cases. *Am J Med Genet* 1992; 42: 68–84
- Nishio H, Kodama S, Matsuo T, Ichihashi M, Ito H, Fujiwara Y. Cockayne syndrome: magnetic resonance images of the brain in a severe form with early onset. *J Inher Metab Dis* 1988; 11: 88–102
- Norman RM, Tingey AH. Syndrome of micrencephaly, strio-cerebellar calcifications, and leucodystrophy. *J Neurol Neurosurg Psychiatry* 1966; 29: 157–163
- Ohnishi A, Mitsudome A, Murai Y. Primary segmental demyelination in the sural nerve in Cockayne's syndrome. *Muscle Nerve* 1987; 10: 163–167
- Özdirim E, Topçu M, Özön A, Cila A. Cockayne syndrome: review of 25 cases. *Pediatr Neurol* 1996; 15: 312–316
- Patton MA, Giannelli F, Francis AJ, Baraiser M, Harding B, Williams AJ. Early onset Cockayne's syndrome: case reports with neuropathological and fibroblast studies. *J Med Genet* 1989; 26: 154–159
- Pena SDJ, Shokeir MHK. Autosomal recessive cerebro-oculo-facio-skeletal (COFS) syndrome. *Clin Genet* 1974; 5: 285–293
- Pena SDJ, Evans J, Hunter AGW. COFS syndrome revisited. *Birth Defects* 1978; XIV: 205–213
- Rapin I, Lindenbaum Y, Dickson DW, Kraemer KH, Robbins JH. Cockayne syndrome and xeroderma pigmentosum. DNA repair disorders with overlaps and paradoxes. *Neurology* 2000; 55: 1442–1449
- Roy S, Srivastava RN, Gupta PC, Meyekar G. Ultrastructure of peripheral nerve in Cockayne's syndrome. *Acta Neuropathol (Berl)* 1973; 24: 345–349
- Sakai T, Kikuchi F, Takashima S, Matsuda H, Watanabe N. Neuropathological findings in the cerebro-oculo-facio-skeletal (Pena-Shokeir II) syndrome. *Brain Dev* 1997; 19: 58–62
- Sasaki K, Tachi N, Shinoda M, Satoh N, Minami R, Ohnishi A. Demyelinating peripheral neuropathy in Cockayne syndrome: a histopathologic and morphometric study. *Brain Dev* 1992; 14: 114–117
- Sato H, Saito T, Kurosawa K, Ootaka T, Furuyama T, Yoshinaga K. Renal lesions in Cockayne's syndrome. *Clin Nephrol* 1988; 29: 206–209
- Savary JB, Vasseur F, Deminatti MM. Routine autorediographic analysis of DNA excision-repair. Report of prenatal and postnatal diagnosis in eleven families. *Ann Genet* 1991; 2: 76–81
- Smits MG, Gabreëls FJM, Renier WO, Joosten EMG, Gabreëls-Festen AAWM, ter Laak HJ, Pinckers AJL, Hombergen GCJ, Notermans SLH, Thijssen HOM. Peripheral and central myelinopathy in Cockayne's syndrome. *Neuropediatrics* 1982; 13: 161–167
- Soffer D, Grotsky HW, Rapin I, Suzuki K. Cockayne syndrome: unusual neuropathological findings and review of the literature. *Ann Neurol* 1979; 6: 340–348
- Sugita K, Takanashi J, Ishii M, Niimi H. Comparison of MRI white matter changes with neuropsychologic impairment in Cockayne syndrome. *Pediatr Neurol* 1992; 8: 295–298
- Takada K, Becker LE. Cockayne's syndrome: report of two autopsies cases associated with neurofibrillary tangles. *Clin Neuropathol* 1986; 5: 64–68
- Talwar D, Smith SA. Camfak syndrome: a demyelinating inherited disease similar to Cockayne syndrome. *Am J Med Genet* 1989; 34: 194–198
- Traboulsi EI, de Becker I, Maumenee IH. Ocular findings in Cockayne syndrome. *Am J Ophthalmol* 1992; 114: 579–583
- Van Gool AJ, van der Horst GTJ, Citterio E, Hoeijmakers JHJ. Cockayne syndrome: defective repair of transcription? *EMBO J* 1997; 16: 4155–4162
- Van Hoften A, Kalle WHJ, De Jong-Versteeg A, Lehmann AR, Van Zeeland AA, Mullenders LHF. Cells from XP-D and XP-D-CS patients exhibit equally inefficient of UV-repair damage in transcribed genes but different capacity to recover UV-inhibited transcription. *Nucl Acids Res* 1999; 27: 2898–2904
- Vos A, Gabreëls-Festen A, Joosten E, Gabreëls F, Renier W, Mul-laert R. The neuropathy of Cockayne syndrome. *Acta Neuropathol (Berl)* 1983; 61: 153–156
- Weliky-Conaway J, Conaway RC. Transcription elongation and human disease. *Annu Rev Biochem* 1999; 68: 301–319
- Winter RM, Donna D, d'A Crawford M. Syndromes of microcephaly, microphthalmia, cataracts, and joint contractures. *J Med Genet* 1981; 18: 29–133
- Zafeiriou DI, Thorel F, Andreou A, Kleijer WJ, Raams A, Garritsen VH, Gombakis N, Jaspers NGJ, Clarkson SG. Xeroderma pigmentosum group G with severe neurological involvement and features of Cockayne syndrome in infancy. *Pediatr Res* 2001; 49: 407–412

33 Trichothiodystrophy with Photosensitivity

- Battistella PA, Peserico A. Central nervous system dysmyelination in PIBI(D)S syndrome: a further case. *Childs Nerv Syst* 1996; 12: 110–113
- Bergmann E, Egly J-M. Trichothiodystrophy, a transcription syndrome. *Trends Genet* 2001; 17: 279–286

- Botta E, Nardo T, Broughton BC, Marinoni S, Lehmann AR, Stefanini M. Analysis of mutations in the *XPD* gene in Italian patients with trichothiodystrophy: site of mutation correlates with repair deficiency, but gene dosage appears to determine clinical severity. *Am J Hum Genet* 1998; 63: 1036–1048
- Botta E, Nardo T, Lehmann AR, Egly JM, Pedrini AM, Stefanini M. Reduced level of the repair/transcription factor TFIIH trichothiodystrophy. *Hum Mol Genet* 2002; 11: 2919–2928
- Bracun R, Hemmer W, Wolf-Abolvahab S, Focke M, Botzi C, Kilian W, Götz M, Jarisch R. Diagnosis of trichothiodystrophy in 2 siblings. *Dermatology* 1997; 194: 74–76
- Broughton BC, Steingrimsdottir H, Weber CA, Lehmann AR. Mutations in the xeroderma pigmentosum group D DNA repair/transcription gene in patients with trichothiodystrophy. *Nat Genet* 1994; 7: 189–194
- Broughton BC, Berneburg M, Fawcett H, Taylor EM, Arlett CF, Nardo T, Stefanini M, Menefee E, Price VH, Queilli S, Sarasin A, Bohnert E, Krutmann J, Davidson R, Kreamer KH, Lehmann AR. Two individuals with features of both xeroderma pigmentosum and trichothiodystrophy highlight the complexity of the clinical outcomes of mutations in the *XPD* gene. *Hum Mol Genet* 2001; 10: 2539–2547
- Cancrini C, Romiti ML, di Cesare S, Angelini F, Gigliotti D, Livadiotti S, Bertini E, Rossi R, Racioppi L. Restriction in T-cell receptor repertoire in a patient affected by trichothiodystrophy and CD4⁺ lymphopenia. *Scand J Immunol* 2002; 56: 212–216
- De Boer J, Hoeijmaker JHJ. Nucleotide excision repair and human syndromes. *Carcinogenesis* 2000; 21: 453–460
- Egly JM. TFIIH: from transcription to clinic. *FEBS Lett* 2001; 24884: 124–128
- Friedberg EC. Hot news: temperature-sensitive humans explain hereditary disease. *Bioessays* 2001; 23: 671–673
- Fortina AB, Alaibac M, Piaserico S, Pererico A. PIBI(D)S: clinical and molecular characterization of a new case. *J Eur Acad Dermatol Venereol* 2001; 15: 65–69
- Happle R, Traupe H, Gröbe H, Bonsmann G. The Tay syndrome (congenital ichthyosis with trichothiodystrophy). *Eur J Pediatr* 1984; 141: 147–152
- Itin PH, Sarasin A, Pittelkow MR. Trichothiodystrophy: update on the sulfur-deficient brittle hair syndromes. *J Am Acad Dermatol* 2001; 44: 891–920
- Jackson CE, Weiss L, Watson JHL. “Brittle” hair with short stature, intellectual impairment and decreased fertility: an autosomal recessive syndrome in an Amish kindred. *Pediatrics* 1974; 54: 201–207
- Jaspers NGJ. Multiple involvement of nucleotide excision repair enzymes: clinical manifestations of molecular intricacies. *Cytokines Mol Ther* 1996; 2: 115–119
- Jorizzo JL, Atherton DJ, Crounse RG, Wells RS. Ichthyosis, brittle hair, impaired intelligence, decreased fertility and short stature (IBIDS syndrome). *Br J Dermatol* 1982; 106: 705–710
- King MD, Gummer CL, Stephenson JBP. Trichothiodystrophy-neurotrichocutaneous syndrome of Pollitt: a report of two unrelated cases. *J Med Genet* 1984; 21: 286–289
- Kousseff BG, Esterly NB. Trichothiodystrophy, IBIDS syndrome or Tay syndrome? *Birth Defects Orig Art Ser* 1988; 24: 169–181
- Kousseff BG. Collodion baby, sign of Tay syndrome. *Pediatrics* 1991; 87: 571–574
- Lehmann AR. The xeroderma pigmentosum group D (*XPD*) gene: one gene, two functions, three cases. *Gene Dev* 2001; 15: 15–23
- McGuaig C, Marcoux D, Rasmussen JE, Werner MM, Gentner NE. Trichothiodystrophy associated with photosensitivity, gonadal failure, and striking osteosclerosis. *J Am Acad Dermatol* 1993; 28: 820–826
- Murrin KL, Clarke DJ. Behavioral aspects of Pollitt syndrome: a 32-year follow-up of a case described by R.J. Pollitt and colleagues in 1968. *J Intellect Disabil Res* 2002; 46: 273–278
- Østergaard JR, Christensen T. The central nervous system in Tay syndrome. *Neuropediatrics* 1996; 27: 326–330
- Pescerico A, Battistella PA, Bertoli P. MRI of a very rare hereditary ectodermal dysplasia: PIBI(D)S. *Neuroradiology* 1992; 34: 316–317
- Porto L, Weis R, Schulz C, Reichel P, Lanfermann H, Zanella FE. Tay’s syndrome: MRI. *Neuroradiology* 2000; 42: 849–851
- Queille S, Drougard C, Sarasin A, Daya-Grosjean L. Effects of *XPD* mutations on ultraviolet-induced apoptosis in relation to skin cancer-proneness in repair-deficient syndromes. *J Invest Dermatol* 2001; 117: 1162–1170
- Racioppi L, Cancrini C, Romiti ML, Angelini F, di Cesare S, Bertini E, Livadiotti S, Gambarara MG, Matarese G, Lago Paz F, Stefanini M, Rossi P. Defective dendritic cell maturation in a child with nucleotide excision repair deficiency and CD4 lymphopenia. *Clin Exp Immunol* 2001; 126: 511–518
- Savary JB, Vasseur F, Vinatier D, Manouvrier S, Thomas P, Deminatti MM. Prenatal diagnosis of PIBIDS. *Prenat Diagn* 1991; 11: 859–866
- Stefanini M, Giliani S, Nardo T, Marinoni S, Nazzaro V, Rizzo R, Trevisan G. DNA repair investigations in the nine Italian patients affected by trichothiodystrophy. *Mutat Res DNA Repair* 1992; 273: 119–125
- Takayama K, Salazar EP, Broughton BC, Lehmann AR, Sarasin A, Thompson LH, Weber CA. Defects in the DNA repair and transcription gene *CRCC2(XPD)* in trichothiodystrophy. *Am J Hum Genet* 1996; 58: 263–270
- Taylor EM, Broughton BCM, Botta E, Stefanini M, Sarasin A, Jaspers NGJ, Fawcett H, Harcourt SA, Arlett CF, Lehmann AR. Xeroderma pigmentosum and trichothiodystrophy are associated with different mutations in the *XPD (ERCC2)* repair/transcription gene. *Proc Natl Acad Sci* 1997; 94: 8658–8663
- Vandenbergh K, Casteels I, Vandenbussche E, de Zegher F, de Boeck K. Bilateral cataract and high myopia in a child with trichothiodystrophy: a case report. *Bull Soc Belge Ophthalmol* 2001; 282: 15–18
- Vermeulen W, Bergmann E, Auriol J, Rademakers S, Frit P, Appeldoorn E, Hoeijmakers JHJ, Egly J-M. Sublimiting concentration of TFIIH transcription/DNA repair factor causes TTD-A trichothiodystrophy disorder. *Nat Genet* 2000; 26: 307–313
- Vermeulen W, Rademakers S, Jaspers NGJ, Appeldoorn E, Raams A, Klein B, Kleijer WJ, Hansen LK, Hoeijmakers JHJ. A temperature-sensitive disorder in basal transcription and DNA repair in humans. *Nat Genet* 2001; 27: 299–303
- Viprakasit V, Gibbons RJ, Broughton BC, Tolmie JL, Brown D, Lunt P, Winter RM, Marioni S, Stefanini M, Brueton L, Lehmann AR, Higgs DR. Mutations in the general transcription factor TFIIH result in β -thalassaemia in individuals with trichothiodystrophy. *Hum Mol Genet* 2001; 10: 2797–2802
- Weeda G, Eveno E, Donker I, Vermeulen W, Chevallier-Lagente O, Taieb A, Stary A, Hoeijmakers JHJ, Mezzina M, Sarasin A. A mutation in the *XPB/ERCC2* DNA repair transcription gene, associated with trichothiodystrophy. *Am J Hum Genet* 1997; 60: 320–329

34 Pelizaeus-Merzbacher Disease

- André M, Monin P, Moret C, Braun M, Picard L. Maladie de Pelizaeus-Merzbacher. *J Neuroradiol* 1990; 17: 216–221
- Apkarian P, Koetsveld-Baart JC, Barth PG. Visual evoked potential characteristics and early diagnosis of Pelizaeus-Merzbacher disease. *Arch Neurol* 1993; 50: 981–985
- Battini R, Bianchi MC, Boespflug-Tanguy O, Tosetti M, Bonanni P, Canapicchi R, Cioni G. Unusual clinical and magnetic resonance imaging findings in a family with proteolipid protein gene mutation. *Arch Neurol* 2003; 60: 268–272
- Boltshauser E, Schinzel A, Wichmann W, Haller D, Valavanis A. Pelizaeus-Merzbacher disease: identification of heterozygotes with magnetic resonance imaging? *Hum Genet* 1988; 80: 393–394
- Bonavita S, Schiffmann R, Moore DF, Frei K, Choi B, Patronas N, Virta A, Boespflug-Tanguy O, Tedeschi G. Evidence for neuroaxonal injury in patients with proteolipid protein gene mutations. *Neurology* 2001; 56: 758–788
- Bond C, Si X, Crisp M, Wong P, Paulson GW, Boesel CP, Dlouhy SR, Hodes ME. Family with Pelizaeus-Merzbacher disease / X-linked spastic paraplegia and a nonsense mutation in exon 6 of the proteolipid protein gene. *Am J Med Genet* 1997; 71: 357–360
- Boulloche J, Aicardi J. Pelizaeus-Merzbacher disease: clinical and nosological study. *J Child Neurol* 1986; 1: 233–239
- Bourre JM, Jacque C, Nguyen-Legros J, Bornhofen JH, Araoz CA, Daudu O, Baumann NA. Pelizaeus-Merzbacher disease: biochemical analysis of isolated myelin (electron-microscopy: protein, lipid and unsubstituted fatty acids analysis). *Eur Neurol* 1978; 17: 317–326
- Bridge PJ, MacLeod PM, Lillicrap DP. Carrier detection and prenatal diagnosis of Pelizaeus-Merzbacher disease using a combination of anonymous DNA polymorphisms and the proteolipid protein (PLP) gene cDNA. *Am J Med Genet* 1991; 38: 616–621
- Cailloux F, Gauthier-Barichard F, Mimault C, Isabelle V, Courtois V, Giraud G, Dastugue B, Boespflug-Tanguy O for Clinical European Network on Brain Demyelinating Disease. Genotype-phenotype correlation in inherited brain myelination defects due to proteolipid protein gene mutations. *Eur J Hum Genet* 2000; 8: 837–845
- Cambi F, Tang X-M, Cordray P, Fain PR, Keppen LD, Barker DF. Refined genetic mapping and proteolipid protein mutations analysis in X-linked pure hereditary spastic paraplegia. *Neurology* 1996; 46: 1112–1117
- Cambi F, Tartaglino L, Lublin F, McCarren D. X-linked pure familial spastic paraparesis. Characterization of a large kindred with magnetic resonance imaging studies. *Arch Neurol* 1995; 52: 665–669
- Caro PA, Marks HG. Magnetic resonance imaging and computed tomography in Pelizaeus-Merzbacher disease. *Magn Reson Im* 1990; 8: 791–796
- Cuddon PA, Lipsitz D, Duncan ID. Myelin mosaicism and brain plasticity in heterozygous females of a canine X-linked trait. *Ann Neurol* 1998; 44: 771–779
- Ellis D, Malcom S. Proteolipid protein gene dosage effect in Pelizaeus-Merzbacher disease. *Nat Genet* 1994; 6: 333–334
- Fanarraga ML, Griffiths IR, McCulloch MC, Barrie JA, Cattanaach BM, Brophy PJ, Kennedy PGE. Rumpshaker: an X-linked mutation affecting CNS myelination. A study of the female heterozygote. *Neuropathol Appl Neurobiol* 1991; 17: 323–334
- Fanarraga ML, Griffiths IR, McCulloch MC, Barrie JA, Kennedy PGE, Brophy PJ. Rumpshaker: an X-linked mutation causing hypomyelination and glial cells between the optic nerve and spinal cord. *Glia* 1992; 5: 161–170
- Feldman JI, Kearns DB, Seid AB, Pransky SM, Jones MC. The otolaryngologic manifestations of Pelizaeus-Merzbacher disease. *Arch Otolaryngol Head Neck Surg* 1990; 116: 613–616
- Garbern JY, Cambi F, Lewis R, Shy M, Sima A, Kraft G, Vallat JM, Bosch EP, Hodes ME, Dlouhy S, Raskind W, Bird T, Macklin W, Kamholz J. Peripheral neuropathy caused by proteolipid protein gene mutations. *Ann NY Acad Sci* 1999; 883: 351–365
- Garbern J, Cambi F, Shy M, Kamholz J. The molecular pathogenesis of Pelizaeus-Merzbacher disease. *Arch Neurol* 1999; 56: 1210–1214
- Garbern J, Shy M, Krajewski K, Kamholz J, Hobson G, Cambi F. Evidence of neuroaxonal injury in patients with proteolipid protein gene mutations. *Neurology* 2001; 57: 1938–1939
- Garbern J, Yool DA, Moore GJ, Wilds IB, Faulk MW, Klugmann M, Nave K-A, Siermans EA, van der Knaap MS, Bird TD, Shy ME, Kamholz JA, Griffiths IR. Patients lacking the major myelin protein, proteolipid protein 1, develop length-dependent axonal degeneration in the absence of demyelination and inflammation. *Brain* 2002; 125: 551–561
- Garg BP, Markand ON, DeMyer WE. Usefulness of BAER studies in the early diagnosis of Pelizaeus-Merzbacher disease. *Neurology* 1983; 33: 955–956
- Gencic S, Abuelo D, Ambler M, Hudson LD. Pelizaeus-Merzbacher disease: an X-linked neurologic disorder of myelin metabolism with a novel mutation in the gene encoding proteolipid protein. *Am J Hum Genet* 1989; 45: 435–442
- Gow A, Lazzarini RA. A cellular mechanism governing the severity of Pelizaeus-Merzbacher disease. *Nat Genet* 1996; 13: 422–428
- Griffiths I, Klugmann M, Anderson T, Yool D, Thomson C, Schwab MH, Schneider A, Zimmermann F, McCulloch M, Nadon N, Nave K-A. Axonal swellings and degeneration in mice lacking the major proteolipid of myelin. *Science* 1998; 280: 1610–1613
- Griffiths I, Klugmann M, Anderson T, Thomson C, Vouyiouklis D, Nave K-A. Current concepts of PLP and its role in the nervous system. *Microsc Rev Tech* 1998; 41: 344–358
- Griffiths IR, Montague P, Dickinson P. The proteolipid protein gene. *Neuropathol Appl Neurobiol* 1995; 21: 85–96
- Grinspan JB, Coulalaglou M, Beesley JS, Carpio DF, Scherer SS. Mutation-dependent apoptotic cell death of oligodendrocytes in myelin-deficient rats. *J Neurosci Res* 1998; 54: 623–634
- Gutmann DH, Fischbeck KH, Kamholz J. Complicated hereditary spastic paraparesis with cerebral white matter lesions. *Am J Med Genet* 1990; 36: 251–257
- Hobson GM, Davis AP, Stowell NC, Kolodny EH, Siermans EA, De Co IFM, Funanage VL, Marks HG. Mutations in noncoding regions of the proteolipid protein gene in Pelizaeus-Merzbacher disease. *Neurology* 2000; 55: 1089–1096
- Hodes ME, DeMyer WE, Pratt VM, Edwards MK, Dlouhy SR. Girl with signs of Pelizaeus-Merzbacher disease heterozygous for a mutation in exon 2 of the proteolipid protein gene. *Am J Med Genet* 1995; 55: 397–401
- Hodes ME, Blank CA, Pratt VM, Morales J, Napier J, Dlouhy SR. Nonsense mutation in exon 3 of the proteolipid protein gene (PLP) in a family with an unusual form of Pelizaeus-Merzbacher disease. *Am J Med Genet* 1997; 69: 121–125

- Hodes ME, Zimmermann AW, Aydanian A, Naidu S, Miller NR, Garcia Oller JL, Barker B, Aleck KA, Hurley TD, Dlouhy SR. Different mutations in the same codon of the proteolipid protein gene, *PLP*, may help in correlating genotype with phenotype in Pelizaeus-Merzbacher disease/X-linked spastic paraplegia (PMD/SPG2). *Am J Med Genet* 1999; 82: 132–139
- Hodes ME, Woodward K, Spinner NB, Emanuel BS, Enrico-Simon A, Kamholz J, Stambolian D, Zackai EH, Pratt VM, Thomas IT, Crandall K, Dlouhy SR, Malcolm S. Additional copies of the proteolipid protein gene causing Pelizaeus-Merzbacher disease arise by separate integration into the X chromosome. *Am J Hum Genet* 2000; 67: 14–22
- Hudson LD. Pelizaeus-Merzbacher disease and spastic paraplegia type 2: two faces of myelin loss from mutations in the same gene. *J Child Neurol* 2003; 18: 616–624
- Hudson LD, Puckett C, Berndt J, Chan J, Gencic S. Mutation of the proteolipid protein gene *PLP* in a human X chromosome-linked myelin disorder. *Proc Natl Acad Sci* 1989; 86: 8128–831
- Inoue K, Osaka H, Imaizumi K, Nezu A, Takanashi J-I, Arai J, Murayama K, Ono J, Kikawa Y, Mito T, Shaffer LG, Lupski JR. Proteolipid protein gene duplications causing Pelizaeus-Merzbacher disease: molecular mechanism and phenotypic manifestations. *Ann Neurol* 1999; 45: 624–632
- Inoue K, Tanaka H, Scaglia F, Araki A, Shaffer LG, Lupski JR. Compensating for central nervous system dysmyelination: females with a proteolipid protein gene duplication and sustained clinical improvement. *Ann Neurol* 2001; 50: 747–754
- Journel H, Roussey M, Gandon Y, Allaire C, Carsin M, le Marec B. Magnetic resonance imaging in Pelizaeus-Merzbacher disease. *Neuroradiology* 1987; 29: 403–405
- Jung M, Sommer I, Schachner M, Nave K-A. Monoclonal antibody 010 defines a conformationally sensitive cell-surface epitope of proteolipid protein (PLP): evidence that PLP misfolding underlies dysmyelination in mutant mice. *J Neurosci* 1996; 16: 7920–7929
- Kaga M, Murakami T, Naitoh H, Nihei K. Studies on pediatric patients with absent auditory brainstem response (ABR) later components. *Brain Dev* 1990; 12: 380–384
- Kagawa T, Ikenaka K, Inoue Y, Kuriyama S, Tsujii T, Nakao J, Nakajima K, Aruga J, Okano H, Mikoshiba K. Glial cell degeneration and hypomyelination caused by overexpression of myelin proteolipid protein gene. *Neuron* 1994; 13: 427–442
- Karthigasani J, Evans EL, Vouyiouklis DA, Inouye H, Borenshteyn N, Ramamurthy GV, Kirschner DA. Effects of Rumpshaker mutation on CNS myelin composition and structure. *J Neurochem* 1996; 66: 338–345
- Kaye EM, Doll RF, Natowicz MR, Smith FI. Pelizaeus-Merzbacher disease presenting as spinal muscular atrophy: clinical and molecular studies. *Ann Neurol* 1994; 36: 916–919
- Kobayashi H, Hoffman EP. The rumpshaker mutation in spastic paraplegia. *Nat Genet* 1994; 7: 351–352
- Koeppen AH, Robitaille Y. Pelizaeus-Merzbacher disease. *J Neuropathol Exp Neurol* 2002; 61: 747–759
- Koeppen AH, Ronca NA, Greenfield EA, Hans MB. Defective biosynthesis of proteolipid protein in Pelizaeus-Merzbacher disease. *Ann Neurol* 1987; 21: 159–170
- Komaki H, Sasaki M, Yamamoto T, Iai M, Takashima S. Congenital Pelizaeus-Merzbacher disease associated with the *Jimpy^{msd}* mice mutation. *Pediatr Neurol* 1999; 20: 309–311
- Learish RD, Brüstle O, Zhang S-C, Duncan ID. Intraventricular transplantation of oligodendrocyte progenitors into a fetal myelin mutant results in widespread formation of myelin. *Ann Neurol* 1999; 46: 716–722
- Merzbacher L. Eine eigenartige familiär-hereditäre Erkrankungsform (aplasia axialis extracorticalis congenita). *Z Ges Neurol Psychiatrie* 1910; 3: 1–138
- Mimault C, Giraud G, Courtois V, Cailloux FN, Boire JY, Dastugue B, Boespflug-Tanguy O. The Clinical European Network on Brain Dysmyelination Disease. Proteolipoprotein gene analysis in 82 patients with sporadic Pelizaeus-Merzbacher disease: duplications, the major cause of the disease, originate more frequently in male germ cells, but point mutations do not. *Am J Hum Genet* 1999; 65: 360–369
- Naidu S, Dlouhy SR, Geraghty MT, Hodes ME. A male child with the rumpshaker mutation, X-linked spastic paraplegia/Pelizaeus-Merzbacher disease and lysinuria. *J Inher Metab Dis* 1997; 20: 811–816
- Nance MA, Boyadjiev S, Pratt VM, Taylor S, Hodes ME, Dlouhy SR. Adult-onset neurodegenerative disorder due to proteolipid protein gene mutation in the mother of a man with Pelizaeus-Merzbacher disease. *Neurology* 1996; 47: 1333–1335
- Nezu A, Kimura S, Takeshita S, Osaka H, Kimura K, Inoue K. An MRI and MRS study of Pelizaeus-Merzbacher disease. *Pediatr Neurol* 1998; 18: 334–337
- Pelizaeus F. Ueber eine eigenartige familiäre Entwicklungshemmung vornehmlich auf motorischem Gebiet. *Arch Psychiatr Nervenkr* 1899; 31: 100–104
- Plecko B, Stockler-Ipsiroglu S, Gruber S, Mlynarik V, Moser E, Simbrunner J, Ebner F, Bernert G, Harrer G, Gal A, Prayer D. Degree of hypomyelination and magnetic resonance spectroscopy findings in patients with Pelizaeus Merzbacher phenotype. *Neuropediatrics* 2003; 34: 127–136
- Readhead C, Schneider A, Griffiths I, Nave K-A. Premature arrest of myelin formation in transgenic mice with increased proteolipid protein gene dosage. *Neuron* 1994; 12: 583–595
- Renier WO, Gabreeels FJM, Hustinx TWJ, Jaspar HHJ, Geelen JAG, van Haelst UJG, Lommen EJP, ter Haar BGA. Congenital Pelizaeus-Merzbacher disease with congenital stridor in two maternal cousins. *Acta Neuropathol (Berl)* 1981; 54: 11–17
- Saugier-Verber P, Munnich A, Bonneau D, Rozet J-M, Le Merrer M, Gil R, Boespflug-Tanguy O. X-linked spastic paraplegia and Pelizaeus-Merzbacher disease are allelic disorders at the proteolipid protein locus. *Nat Genet* 1994; 6: 257–262
- Scheffer IE, Baraitser M, Wilson J, Harding B, Kendall B, Brett EM. Pelizaeus-Merzbacher disease: classical or congenital? *Neuropediatrics* 1991; 22: 71–78
- Schneck L, Adachi M, Volk BW. Congenital failure of myelinization: Pelizaeus-Merzbacher disease? *Neurology* 1971; 21: 817–824
- Shy ME, Hobson G, Jain M, Boespflug-Tanguy O, Garbern J, Sperle K, Li W, Gow A, Rodriquez D, Bertini E, Mancias P, Krajewski K, Lewis R, Kamholz J. Schwann cell expression of PLP1 but not DM20 is necessary to prevent neuropathy. *Ann Neurol* 2003; 53: 354–365
- Silverstein AM, Hirsh DK, Trobe JD, Gebarski SS. MR imaging of the brain in five members of a family with Pelizaeus-Merzbacher disease. *AJNR Am J Neuroradiol* 1990; 11: 495–499
- Simons M, Krämer E-M, Macchi P, Rathke-Hartlieb S, Trotter J, Nave K-A, Schulz JB. Overexpression of the myelin proteolipid protein leads to accumulation of cholesterol and proteolipid protein in endosomes/lysosomes: implications for Pelizaeus-Merzbacher disease. *J Cell Biol* 2002; 157: 327–336

- Sisternans EA, De Wijs IJ, De Coe RFM, Smit LME, Menko FH, Van Oost BA. A (G-to-A) mutation in the initiation codon of the proteolipid protein gene causing a relatively mild form of Pelizaeus-Merzbacher disease in a Dutch family. *Hum Genet* 1996; 97: 337–339
- Sisternans EA, De Coe RFM, De Wijs IJ, Van Oost BA. Duplication of the proteolipid protein gene is the major cause of Pelizaeus-Merzbacher disease. *Neurology* 1998; 50: 1749–1754
- Sivakumar K, Sambuughin N, Selenge B, Nagle JW, Baasanjav D, Hudson LD, Goldfarb LG. Novel exon 3B proteolipid protein gene mutation causing late-onset spastic paraplegia type 2 with variable penetrance in female family members. *Ann Neurol* 1999; 45: 680–683
- Southwood CM, Garbern J, Jiang W, Gow A. The unfolded protein response modulates disease severity in Pelizaeus-Merzbacher disease. *Neuron* 2002; 36: 585–596
- Spalice A, Popolizio T, Parisi P, Scarabino T, Iannetti P. Proton MR spectroscopy in connatal Pelizaeus-Merzbacher disease. *Pediatr Radiol* 2000; 30: 171–175
- Spörkel O, Uschkeureit T, Büsow H, Stoffel W. Oligodendrocytes expressing exclusively the DM20 isoform of the proteolipid protein gene: myelination and development. *Glia* 2002; 37: 19–30
- Takanashi J-I, Sugita K, Osaka H, Ishii M, Niimi H. Proton MR spectroscopy in Pelizaeus-Merzbacher disease. *AJNR Am J Neuroradiol* 1997; 18: 533–535
- Takanashi J-I, Sugita K, Tanabe Y, Nagasawa K, Inoue K, Osaka H, Kohno Y. MR-Revealed myelination in the cerebral corticospinal tract as a marker for Pelizaeus-Merzbacher's disease with proteolipid protein gene duplication. *AJNR Am J Neuroradiol* 1999; 20: 1822–1828
- Takanashi J, Inoue K, Tomita M, Kurihara A, Morita F, Ikehira H, Tandana S, Yoshitome E, Kohno Y. Brain *N*-acetylaspartate is elevated in Pelizaeus-Merzbacher disease with *PLP1* duplication. *Neurology* 2002; 58: 237–241
- Thomson CE, Montague P, Jung M, Nave K-A, Griffiths IR. Phenotypic severity of murine *Plp* mutants reflects in vivo and in vitro variations in transport of PLP isoproteins. *Glia* 1997; 20: 322–332
- Ulrich J, Herschkowitz N. Seitelberger's connatal form of Pelizaeus-Merzbacher disease. *Acta Neuropathol (Berl)* 1977; 40: 129–136
- van der Knaap MS, Valk J. The reflection of histology in MR imaging of Pelizaeus-Merzbacher disease. *AJNR Am J Neuroradiol* 1989; 10: 99–103
- Vaurs-Barriere C, Wong K, Weibel TD, Abu-Asab M, Weiss MD, Kaneshi CR, Mixon TH, Bonavita S, Creveaux I, Heiss JD, Tsokos M, Goldin E, Quarles RH, Boespflug-Tanguy O, Schiffmann R. Insertion of mutant proteolipid protein results in missorting of myelin proteins. *Ann Neurol* 2003; 54: 769–780
- Watanabe I, McCaman R, Dyken P, Zeman W. Absence of cerebral myelin sheaths in a case of presumed Pelizaeus-Merzbacher disease. *J Neuropathol Exp Neurol* 1969; 28: 243–256
- Watanabe I, Patel V, Goebel HH, Siakotos AN, Zeman W, Demyer W, Schroder Dyer J. Early lesion of Pelizaeus-Merzbacher disease: electron microscopic and biochemical study. *J Neuropathol Exp Neurol* 1973; 32: 313–333
- Witter B, Debuch H, Klein H. Lipid investigation of central and peripheral nervous system in connatal Pelizaeus-Merzbacher's disease. *J Neurochem* 1980; 34: 957–962
- Woodward K, Kirtland K, Dlouhy S, Raskind W, Bird T, Malcolm S, Abeliovich D. X Inactive phenotype in carriers of Pelizaeus-Merzbacher disease: skewed in carriers of a duplication and random in carriers of point mutations. *Eur J Hum Genet* 2000; 8: 449–454
- Woodward K, Malcolm S. CNS myelination and *PLP* gene dosage. *Pharmacogenomics* 2001; 2: 263–272
- Yool DA, Edgar JM, Montague P, Malcolm S. The proteolipid protein gene and myelin disorders in man and animal models. *Hum Mol Genet* 2000; 9: 987–992
- Yousem DM, Gutmann DH, Milestone BN, Lenkinski RE. Integrated MR imaging and proton nuclear magnetic resonance spectroscopy in a family with an X-linked spastic paraparesis. *AJNR Am J Neuroradiol* 1991; 12: 785–789
- Zeman W, Demyer W, Falls HF. Pelizaeus-Merzbacher disease. *J Neuropathol Exp Neurol* 1964; 23: 334–354

35 18q⁻ Syndrome

- Davis Ghidoni P, Hale DE, Cody JD, Gay CT, Thompson NM, McClure EB, Danny MM, Leach RJ, Kaye CI. Growth hormone deficiency associated in the 18q deletion syndrome. *Am J Med Genet* 1997; 69: 7–12
- Felding I, Kristoffersson U, Sjöström H, Noren O. Contribution to the 18q⁻ syndrome. A patient with del (18) (q22.3qter). *Clin Genet* 1987; 31: 206–210
- Fryns JP, Logghe N, van Eygen M, van den Berghe H. 18q⁻ Syndrome in mother and daughter. *Eur J Pediatr* 1979; 130: 189–192
- Gabrielli O, Coppa GV, Carloni I, Salvolini U. 18q⁻ Syndrome and white matter alterations. *AJNR Am J Neuroradiol* 1998; 39: 398–399
- Gay CT, Hardies LJ, Rauch RA, Lancaster JL, Plaetke R, DuPont BR, Cody JD, Cornell JE, Herndon RC, Ghidoni PD, Schiff JM, Kaye CI, Leach RJ, Fox PT. Magnetic Resonance Imaging demonstrates incomplete myelination in 18q⁻ syndrome: evidence for myelin basic protein haploinsufficiency. *Am J Med Genet* 1997; 74: 422–431
- Jayaraman V, Swan IRC, Patton MA. Hearing impairment in 18q deletion syndrome. *J Laryngol Otol* 2000; 114: 963–966
- Kamholz J, Spielman R, Gogolin K, Modi W, O'Brien S, Lazzarini R. The human myelin-basic-protein gene: chromosomal localization and RFLP analysis. *Am J Hum Genet* 1987; 40: 365–373
- Keppler-Noreuil KM, Carroll AJ, Finley SC, Descartes M, Cody JD, DuPont BR, Gay CT, Leach RJ. Chromosome 18q paracentric inversion in a family with mental retardation and hearing loss. *Am J Med Genet* 1998; 76: 372–378
- Kline AD, White ME, Wapner R, Rojas K, Biesecker LG, Kamholz J, Zackai EH, Muenke M, Scott Jr CI, Overhauser J. Molecular analysis of the 18q⁻ syndrome – and correlation with phenotype. *Am J Hum Genet* 1993; 52: 895–906
- Lemke G. Unwrapping the genes of myelin. *Neuron* 1988; 1: 535–543
- Linnankivi TT, Autti TH, Pikho SH, Somer MS, Tienari PJ, Wirtavuori KO, Valanne LK. 18q⁻ syndrome: brain MRI shows poor differentiation of gray and white matter on T2-weighted images. *J Magn Reson Imag* 2003; 18: 414–419
- Loevner LA, Shapiro RM, Grossmann RI, Overhauser J, Kamholz J. White matter changes associated with deletions of the long arm of chromosome 18 (18q⁻ syndrome): a dysmyelinating disorder? *AJNR Am J Neuroradiol* 1996; 14: 1843–1848

- Mahr RM, Moberg PJ, Overhauser J, Strathdee G, Kamholz J, Lovner LA, Campbell H, Zackai EH, Reber ME, Mozley DP, Brown L, Turetsky BI, Shapiro RM. Neuropsychiatry of 18q⁻ syndrome. *Am J Med Genet* 1996; 67: 172–178
- Miller G, Mowrey PN, Hopper KD, Frankel CA, Ladda RL. Neurologic manifestations in 18q⁻ syndrome. *Am J Med Genet* 1990; 37: 128–132
- Ono J, Harada K, Yamamoto T, Onoe S, Okada S. Delayed myelination in a patient with 18q⁻ syndrome. *Pediatr Neurol* 1994; 11: 64–67
- Rodichok L, Miller G. A study of evoked potentials in the 18q⁻ syndrome which includes the absence of the gene locus for myelin basic protein. *Neuropediatrics* 1992; 23: 218–220
- Stankiewicz P, Brozek I, Hélias-Rodzewicz Z, Wierzbza J, Pilch J, Bocian E, Balcerska A, Woźniak A, Kardac̨e I, Wirth J, Mazurczak T, Limon J. Clinical and molecular–cytogenetic studies in seven patients with ring chromosome 18. *Am J Med Genet* 2001; 101: 226–239
- Strathdee G, Zackai EH, Shapiro R, Kamholz J, Overhauser J. Analysis of clinical variation seen in patients with 18q terminal deletations. *Am J Med Genet* 1995; 59: 476–483
- Strathdee G, Sutherland R, Jonsson JJ, Sataloff R, Kohonen-Corish M, Grady D, Overhauser J. Molecular characterization of patients with 18q23 deletions. *Am J Hum Genet* 1997; 60: 860–868
- Wang Z, Cody JD, Leach RJ, O'Connell P. Gene expression patterns in cell lines from patients with 18q⁻ syndrome. *Hum Genet* 1999; 104: 347–475
- Wertelecki W, Gerald PS. Clinical and chromosomal studies of the 18q⁻ syndrome. *J Pediatr* 1971; 78: 44–52
- Wilson MG, Towner JW, Forsman I, Siris E. Syndromes associated with deletion of the long arm of chromosome 18 [del (18q)]. *Am J Med Genet* 1979; 3: 155–174
- ## 36 Phenylketonuria
- Alvord EC, Stevenson LD, Vogel FS, Engle RL. Neuropathological findings in phenyl-pyruvic oligophrenia (phenylketonuria). *J Neuropathol Exp Neurol* 1950; 9: 298–310
- Anderson PJ, Wood SJ, Francis D, Coleman L, Warwick L, Casanelia S, Anderson VA, Boneh A. Neuropsychological functioning in children with early-treated phenylketonuria: impact of white matter abnormalities. *Dev Med Child Neurol* 2004; 46: 230–238
- Arnold GL, Vladutiu CJ, Kirby RS, Blakely EM, DeLuca JM. Protein insufficiency and linear growth restriction in phenylketonuria. *J Pediatr* 2002; 141: 243–246
- Battistini S, de Stefano N, Parlanti S, Federico A. Unexpected white matter changes in an early treated PKU case and improvement after dietary treatment. *Funct Neurol* 1991; 6: 177–180
- Bick U, Fahrenndorf G, Ludolph AC, Vassallo P, Weglage J, Ullrich K. Disturbed myelination in patients with treated hyperphenylalaninaemia: evaluation with magnetic resonance imaging. *Eur J Pediatr* 1991; 150: 185–189
- Blau N, Branes I, Dhondt JL. International database of tetrahydrobiopterin deficiencies. *J Inherit Metab Dis* 1996; 19: 8–14
- Bonafé L, Blau N, Burlina AP, Romstad A, Gütter F, Burlina AB. Treatable neurotransmitter deficiency in mild phenylketonuria. *Neurology* 2001; 57: 908–911
- Brenton DP, Pietz J. Adult care in phenylketonuria and hyperphenylalaninaemia: the relevance of neurological abnormalities. *Eur J Pediatr* 2000; 159: S114–S120
- Breysem L, Smet M-H, Johannik K, van Hecke P, François B, Wilms B, Bosmans H, Marchal G, Jaeken J, Demaerel P. Brain MR imaging in dietary treatment phenylketonuria. *Eur Radiol* 1994; 4: 329–331
- Brismar J, Aqeel A, Gascon G, Ozand P. Malignant hyperphenylalaninemia: CT and MR of the brain. *AJNR Am J Neuroradiol* 1990; 11: 135–138
- Burgard P. Development of intelligence in early treated phenylketonuria. *Eur J Pediatr* 2000; 159: S74–S79
- Burri R, Steffen CH, Stieger S, Brodbeck U, Colombo JP, Herschkowitz N. Reduced myelinogenesis and recovery in hyperphenylalaninemic rats. *Mol Chem Neuropathol* 1990; 13: 57–69
- Cerone R, Schiaffino MC, Di Stefano S, Veneselli E. Phenylketonuria: diet for life or not? *Acta Paediatr* 1999; 88: 664–666
- Chien Y-H, Peng S-F, Wang T-R, Hwu W-L. Cranial MR spectroscopy of tetrahydrobiopterin deficiency. *AJNR Am J Neuroradiol* 2002; 23: 1055–1058
- Cleary MA, Walter JH. Assessment of adult phenylketonuria. *Ann Clin Biochem* 2001; 38: 450–458
- Cleary MA, Walter JH, Wraith JE, Jenkins JPR, Alani SM, Tyler K, Whittle D. Magnetic resonance imaging of the brain in phenylketonuria. *Lancet* 1994; 334: 87–90
- Cleary MA, Walter JH, Wraith JE, Jenkins JPR. Magnetic resonance imaging in phenylketonuria: reversal of cerebral white matter change. *J Pediatr* 1995; 127: 251–255
- Costa LG, Guizzetti M, Burry M, Oberdoerster J. Developmental neurotoxicity: do similar phenotypes indicate a common mode of action? A comparison of fetal alcohol syndrome, toluene embryopathy and maternal phenylketonuria. *Toxicol Lett* 2002; 127: 197–205
- Dezortová M, Hájek M, Tintra, Hejzmanová L, Syková E. MR in phenylketonuria-related brain lesions. *Acta Radiol* 2001; 42: 459–466
- Dhondt JL, Farriaux JP, Boudha A, Largillière C, Ringel J, Roger MM, Leeming RJ. Neonatal hyperphenylalaninemia presumably caused by guanosine triphosphate-cyclohydrolase deficiency. *J Pediatr* 1985; 106: 954–956
- Erlandsen H, Stevens RC. The structural basis of phenylketonuria. *Mol Genet Metab* 1999; 68: 103–125
- Erlandsen H, Stevens RC. A structural hypothesis for BH₄ responsiveness in patients with mild forms of hyperphenylalaninaemia and phenylketonuria. *J Inherit Metab Dis* 2001; 24: 213–230
- Fisch RO, Burke B, Bass J, Ferrara TB, Mastro A. Maternal phenylketonuria – chronology of the detrimental effects on embryogenesis and fetal development: pathological report, survey, clinical application. *Pediatr Pathol* 1986; 5: 449–461
- Fisch RO, Chang P-N, Weisberg S, Guldborg P, Güttler F, Tsai MY. Phenylketonuric patients decades after diet. *J Inherit Metab Dis* 1995; 18: 347–353
- Gerstl B, Malamud N, Eng LF, Hayman RB. Lipid alterations in human brains in phenylketonuria. *Neurology* 1967; 17: 51–57
- Giovannini M, Biasucci G, Brioschi M, Ghiglieri D, Riva E. Cofactor defects and PKU: diagnosis and treatment. *Int Pediatr* 1991; 6: 26–31
- Gudinchet F, Maeder P, Meuli RA, Deonna T, Mathieu JM. Cranial CT and MRI in malignant phenylketonuria. *Pediatr Radiol* 1992; 22: 223–224
- Güttler F, Guldborg P. Mutation analysis anticipates dietary requirements in phenylketonuria. *Eur J Pediatr* 2000; 159: S150–S153

- Huijbreghts SCJ, de Sonnevle LMJ, Licht R, van Spronsen FJ, Sergeant JA. Short-term dietary interventions in children and adolescents with treated phenylketonuria: effects on neuropsychological outcome of a well-controlled population. *J Inher Metab Dis* 2002; 25: 419–430
- Huttenlocher PR. The neuropathology of phenylketonuria: human and animal studies. *Eur J Pediatr* 2000; 159: S102–S106
- Jones SJ, Turano G, Kriss A, Shawkat F, Kendall B, Thompson AJ. Visual evoked potentials in phenylketonuria: association with brain MRI, dietary state, and IQ. *J Neurol Neurosurg Psychiatry* 1995; 59: 260–265
- Knudsen GM, Hasselbalch S, Toft PB, Christensen E, Paulson OB, Lou H. Blood–brain barrier transport of amino acids in healthy controls and in patients with phenylketonuria. *J Inher Metab Dis* 1995; 18: 653–664
- Koch R, Hanley W, Levy H, Matalon R, Rouse B, Trefz F, Güttler F, Azen C, Friedman E, Platt L, de la Cruz F. Maternal phenylketonuria: an international study. *Mol Genet Metab* 2000; 71: 233–239
- Koch R, Burton B, Hoganson G, Peterson R, Rhead W, Rouse B, Scott R, Wolff J, Stern AM, Güttler F, Nelson M, de la Cruz F, Coldwell J, Erbe R, Geraghty MT, Shear C, Thomas J, Azen C. Phenylketonuria in adulthood: a collaborative study. *J Inher Metab Dis* 2002; 25: 333–346
- Lässker U, Zschocke J, Blau N, Santer R. Tetrahydrobiopterin responsiveness in phenylketonuria. Two new cases and a review of molecular genetic findings. *J Inher Metab Dis* 2002; 25: 65–70
- Leuzzi V, Gualdi GF, Fabbri F, Trasimeni G, DiBiasi C, Antonozzi I. Neuroradiological (MRI) abnormalities in phenylketonuric subjects: clinical and biochemical correlations. *Neuropediatrics* 1993; 24: 302–306
- Leuzzi V, Trasimeni G, Gualdi GF, Antonozzi I. Biochemical, clinical and neuroradiological (MRI) correlations in late-detected PKU patients. *J Inher Metab Dis* 1995; 18: 624–634
- Levy HL, Lobbregt D, Sansaricq C, Snyderman SE. Comparison of phenylketonuric and nonphenylketonuric sibs from untreated pregnancies in a mother with phenylketonuria. *Am J Med Genet* 1992; 44: 439–442
- Longhi R, Valsasina R, Buttè C, Paccanelli S, Riva E, Giovannini M. Cranial computerized tomography in dihydropterine reductase deficiency. *J Inher Metab Dis* 1985; 8: 109–112
- Lou HC, Toft PB, Andressen J, Mikkelsen I, Olsen B, Güttler F, Wieslander S, Henriksen O. An occipito-temporal syndrome in adolescents with optimally controlled hyperphenylalaninaemia. *J Inher Metab Dis* 1992; 15: 687–695
- Magee AC, Ryan K, Moore A, Trimble ER. Follow up of fetal outcome in cases of maternal phenylketonuria in Northern Ireland. *Arch Dis Child* 2002; 87: F141–F143
- Malamud N. Neuropathology of phenylketonuria. *J Neuropathol Exp Neurol* 1966; 25: 254–268
- McCombe PA, McLaughlin DB, Chalk JB, Brown NN, McGill JJ, Pender MP. Spasticity and white matter abnormalities in adult phenylketonuria. *J Neurol Neurosurg Psychiatry* 1992; 55: 359–361
- Menkes JH. The pathogenesis of mental retardation in phenylketonuria and other inborn errors of amino acid metabolism. *Pediatrics* 1967; 39: 297–308
- Milandi N, Larnaout A, Dhondt J-L, Vincent M-F, Kaabachi N, Hentati F. Dihydropteridine reductase deficiency in a large consanguineous Tunisian family: clinical, biochemical, and neuropathologic findings. *J Child Neurol* 1998; 13: 475–480
- Moats RA, Koch R, Moseley K, Guldberg P, Güttler F, Boles RG, Nelson Jr, MD. Brain phenylalanine concentration of adults with phenylketonuria. *J Inher Metab Dis* 2000; 23: 7–14
- Möller HE, Weglage J, Wiedermann D, Ullrich K. Blood-brain barrier phenylalanine transport and individual vulnerability in phenylketonuria. *J Cereb Blood Flow Metab* 1998; 18: 1184–1191
- Möller HE, Ullrich K, Weglage J. In vivo proton magnetic resonance spectroscopy in phenylketonuria. *Eur J Pediatr* 2000; 159: S121–S125
- Naylor EW, Ennis D, Davidson GF, Wong LTK, Applegarth DA, Niederwieser A. Guanosine triphosphate cyclohydrolase I deficiency: early diagnosis by routine urine pteridine screening. *Pediatrics* 1987; 79: 374–378
- Niederwieser A, Blau N, Wang M, Joller P, Atares M, Cardesa-Garcia J. GTP cyclohydrolase I deficiency, a new enzyme defect causing hyperphenylalaninemia with neopterin, biopterin, dopamine, and serotonin deficiencies and muscular hypotonia. *Eur J Pediatr* 1984; 141: 208–214
- Okano Y, Eisensmith RC, Güttler F, Lichter-Konecki U, Konecki DS, Trefz FK, Dasovich M, Wang T, Henriksen K, Lou H, Woo SLC. Molecular basis of phenotypic heterogeneity in phenylketonuria. *N Engl J Med* 1991; 324: 1232–1238
- Pearson KD, Gean-Marton AD, Levy HL, Davis KR. Phenylketonuria: MR imaging of the brain with clinical correlation. *Radiology* 1990; 177: 437–440
- Philips MD, McGraw P, Lowe MJ, Mathews VP, Hainline BE. Diffusion-weighted imaging of white matter abnormalities in patients with phenylketonuria. *AJNR Am J Neuroradiol* 2001; 22: 1583–1586
- Pietz J, Schmidt E, Matthis P, Kobialka B, Kutscha A, de Sonnevle L. EEGs in phenylketonuria. I. Follow up to adulthood. II. Short-term diet-related changes in EEGs and cognitive function. *Dev Med Child Neurol* 1993; 35: 54–64
- Pietz J, Kreis R, Boesch C, Penzien J, Rating D, Herschkowitz N. The dynamics of brain concentrations of phenylalanine and its clinical significance in patients with phenylketonuria determined by in vivo ¹H magnetic resonance spectroscopy. *Pediatr Res* 1995; 38: 657–663
- Pietz J, Kreis R, Schmidt H, Meyding-Lamadé UK, Rupp A, Boesch C. Phenylketonuria: findings at MR imaging and localized in vivo ¹H MR spectroscopy of the brain in patients with early treatment. *Radiology* 1996; 201: 413–420
- Pietz J, Dunkelmann R, Rupp A, Rating D, Meinck H-M, Schmidt H, Bremer HJ. Neurological outcome in adult patients with early-treated phenylketonuria. *Eur J Pediatr* 1998; 157: 824–830
- Pietz J, Kreis R, Rupp A, Myatepek E, Rating D, Boesch C, Bremer HJ. Large neutral amino acids block phenylalanine transport into brain tissue in patients with phenylketonuria. *J Clin Invest* 1999; 103: 1169–1178
- Pietz J, Rupp A, Burgard P, Boesch C, Kreis R. No evidence for individual blood-brain barrier phenylalanine transport to influence clinical outcome in typical phenylketonuria patients. *Ann Neurol* 2002; 52: 382–385
- Poser CM, van Bogaert L. Neuropathologic observations in phenylketonuria. *Brain* 1959; 82: 1–9
- Ris MD, Weber AM, Hunt MM, Berry HK, Williams SE, Leslie N. Adult psychosocial outcome in early-treated phenylketonuria. *J Inher Metab Dis* 1997; 20: 499–508
- Rouse B, Azen C, Koch R, Matalon R, Hanley W, de la Cruz F, Trefz F, Friedman E, Shifrin H. Maternal phenylketonuria collaborative study (MPKUCS) offspring: facial anomalies, malformations, and early neurological sequelae. *Am J Med Genet* 1997; 69: 89–95
- Schmidt H, Ullrich K, Korinthenberg R, Peters PE. Basal ganglion calcification in hyperphenylalaninemia due to deficiency of dihydropteridine reductase. *Pediatr Radiol* 1988; 19: 54–56

- Shaw DWW, Weinberger E, Maravilla KR. Cranial MR in phenylketonuria. *J Comput Assist Tomogr* 1990; 14: 458–460
- Shaw DWW, Maravilla KR, Weinberger E, Garretson J, Trahms CM, Scott CR. MR imaging in phenylketonuria. *AJNR Am J Neuroradiol* 1991; 12: 403–406
- Smith I. Review of neonatal screening programme for phenylketonuria. *BMJ* 1991; 303: 333–335
- Smith I. Treatment of phenylalanine hydroxylase deficiency. *Acta Paediatr Suppl* 1994; 407: 60–65
- Smith I, Knowles J. Behavior in early treated phenylketonuria: a systematic review. *Eur J Pediatr* 2000; 159: S89–S93
- Sugita R, Takahashi S, Ishii K, Matsumoto K, Ishibashi T, Sakamoto K, Narisawa K. Brain CT and MR findings in hyperphenylalaninemia due to dihydropteridine reductase deficiency (variant of phenylketonuria). *J Comput Assist Tomogr* 1990; 14: 699–703
- Surtees R, Blau N. The neurochemistry of phenylketonuria. *Eur J Pediatr* 2000; 159: S109–S113
- Takashima S, Chan F, Becker LE. Cortical dysgenesis in a variant of phenylketonuria (dihydropteridine reductase deficiency). *Pediatr Pathol* 1991; 11: 771–779
- Thompson AJ, Smith I, Brenton D, Youl BD, Rylance G, Davidson DC, Kendall B, Lees AJ. Neurological deterioration in young adults with phenylketonuria. *Lancet* 1990; 336: 602–605
- Thompson AJ, Tillotson S, Smith I, Kendall B, Moore SG, Brenton DP. Brain MRI changes in phenylketonuria. *Brain* 1993; 116: 811–821
- Toft PB, Lou HC, Krägeloh-Mann I, Andresen J, Güttler F, Guldberg P, Henriksen O. Brain magnetic resonance imaging in children with optimally controlled hyperphenylalaninaemia. *J Inherit Metab Dis* 1994; 17: 575–583
- Trefz FK, Cipic-Schmidt S, Koch R. Final intelligence in late treated patients with phenylketonuria. *Eur J Pediatr* 2000; 159: S145–S148
- Ullrich K, Weglage J, Schuierer G, Fünders B, Pietsch M, Koch HG, Hahn-Ullrich H. Cranial MRI in PKU: evaluation of a critical threshold for blood phenylalanine. *Neuropediatrics* 1994; 25: 278–279
- Ullrich K, Möller H, Weglage J, Schuierer G, Bick U, Ludolph A, Hahn-Ullrich H, Fünders B, Koch D-G. White matter abnormalities in phenylketonuria: results of magnetic resonance measurements. *Acta Paediatr Suppl* 1994; 407: 78–82
- Van Spronsen FJ, Smit PGA, Koch R. Phenylketonuria: tyrosine beyond the phenylalanine-restricted diet. *J Inherit Metab Dis* 2001; 24: 1–4
- Waisbren SE, Zaff J. Personality disorder in young woman with treated phenylketonuria. *J Inherit Metab Dis* 1994; 17: 584–592
- Walter JH, Tyfield LA, Holton JB, Johnson C. Biochemical control, genetic analysis and magnetic resonance imaging in patients with phenylketonuria. *Eur J Pediatr* 1993; 152: 822–827
- Walter JH, White F, Wraith JE, Jenkins JP, Wilson BPM. Complete reversal of moderate/severe brain MRI abnormalities in a patient with classical phenylketonuria. *J Inherit Metab Dis* 1997; 20: 367–369
- Weglage J, Bick U, Schuierer G, Pietsch M, Sprinz A, Zass R, Ullrich K. Progression of cerebral white matter abnormalities in early treated patients with phenylketonuria during adolescence. *Neuropediatrics* 1997; 28: 239–240
- Weglage J, Pietsch M, Denecke J, Sprintz A, Fledmann R, Grenzeback M, Ullrich K. Regression of neuropsychological deficits in early-treated phenylketonurics during adolescence. *J Inherit Metab Dis* 1999; 22: 693–705
- Weglage J, Wiedermann D, Denecke J, Feldmann R, Koch H-G, Ullrich K, Harms E, Möller HE. Individual blood-brain barrier phenylalanine transport determines clinical outcome in phenylketonuria. *Ann Neurol* 2001; 50: 463–467
- Weglage J, Wiedermann D, Denecke J, Fledmann R, Koch H-G, Ullrich K, Möller HE. Individual blood-brain barrier phenylalanine transport in siblings with classical phenylketonuria. *J Inherit Metab Dis* 2002; 25: 431–436
- Woody RC, Brewster MA, Glasier C. Progressive intracranial calcification in dihydropteridine reductase deficiency prior to folinic acid therapy. *Neurology* 1989; 39: 683–675

37 Glutaric Aciduria Type I

- Al-Essa M, Bakheet S, Patay Z, Al-Watban J, Powe J, Joshi S, Ozand PT. Fluoro-2-deoxyglucose (¹⁸FDG) PET scan of the brain in glutaric aciduria type I: clinical and MRI correlations. *Brain Dev* 1998; 20: 295–301
- Alkan A, Baysal T, Yakinici C, Sigerici A, Kutlu R. Glutaric aciduria type I diagnosed after poliovirus immunization: magnetic resonance findings. *Pediatr Neurol* 2002; 26: 405–407
- Altman NR, Rovira MJ, Bauer M. Glutaric aciduria type 1: MR findings in two cases. *AJNR Am J Neuroradiol* 1991; 12: 966–968
- Amir N, Peleg OE, Shalev RS, Christensen E. Glutaric aciduria type I: clinical heterogeneity and neuroradiologic features. *Neurology* 1987; 37: 1654–1657
- Amir N, Elpeleg ON, Shalev RS, Christensen E. Glutaric aciduria type I: enzymatic and neuroradiologic investigations of two kindreds. *J Pediatr* 1989; 114: 983–989
- Bähr O, Mader I, Zschoke J, Dichgans J, Schultz JB. Adult onset glutaric aciduria type I presenting with a leukoencephalopathy. *Neurology* 2002; 59: 1802–1804
- Baria I, Zschocke J, Christensen E, Duran M, Goodman SI, Leonard JV, Muller E, Morton DH, Superti-Furga A, Hoffmann GF. Diagnosis and management of glutaric aciduria type I. *J Inherit Metab Dis* 1998; 21: 326–340
- Baric I, Wagner L, Feyh P, Liesert M, Buckel W, Hoffmann GF. Sensitivity and specificity of free and total glutaric acid and 3-hydroxyglutaric acid measurements by stable-isotope dilution assays for the diagnosis of glutaric aciduria type I. *J Inherit Metab Dis* 1999; 22: 867–882
- Bennett MJ, Marlow N, Pollitt RJ, Wales JKH. Glutaric aciduria type I: biochemical investigations and postmortem findings. *Eur J Pediatr* 1986; 145: 403–405
- Bennett MJ, Pollitt RJ, Goodman SI, Hale DE, Vamecq J. Atypical riboflavin-responsive glutaric aciduria, and deficient peroxisomal glutaryl-CoA oxidase activity: a new peroxisomal disorder. *J Inherit Metab Dis* 1991; 14: 165–173
- Bergman I, Finegold D, Gärtner JC, Zitelli BJ, Claassen D, Scarano J, Roe CR, Stanley C, Goodman SI. Acute profound dystonia in infants with glutaric acidemia. *Pediatrics* 1989; 83: 228–234
- Bismar J, Ozand PT. CT and MR of the brain in glutaric aciduria type I: a review of 59 published cases and a report of 5 new patients. *AJNR Am J Neuroradiol* 1995; 16: 675–683
- Busquets C, Coll MR, Christensen E, Campistol J, Clusellas N, Vilaseca MA, Ribes A. Feasibility of molecular prenatal diagnosis of glutaric aciduria type I in chorionic villi. *J Inherit Metab Dis* 1998; 21: 243–246
- Busquets C, Coll MJ, Merinero B, Ugarte M, Ruiz MA, Martinez Bermejo A, Ribes A. Prenatal molecular diagnosis of glutaric aciduria type I by direct mutation analysis. *Prenat Diagn* 2000; 20: 761–764

- Busquets C, Soriano M, Taveres de Almeida I, Garavaglia B, Rimoldi M, Rivera I, Uziel G, Cabral A, Coll MJ, Ribes A. Mutation analysis of the GCDH gene in Italian and Portuguese patients with glutaric aciduria type I. *Mol Genet Metab* 2000; 71: 535–537
- Busquets C, Merinero B, Christensen E, Gelpi JL, Campistol J, Pineda M, Fernández-Alvarez E, Prats JM, Sans A, Arteaga R, Martí M, Campos J, Martínez-Pardo M, Martínez-Bermejo A, Ruiz-Falcó ML, Vaquerizo J, Orozco M, Ugarte M, Coll MJ, Ribes A. Glutaryl-CoA dehydrogenase deficiency in Spain: evidence of two groups of patients, genetically, and biochemically distinct. *Pediatr Res* 2000; 48: 315–322
- Campistol J, Ribes A, Alvarez L, Christensen E, Millington DS. Glutaric aciduria type I: unusual biochemical presentation. *J Pediatr* 1992; 121: 83–86
- Chow CW, Haan EA, Goodman SI, Anderson RM, Evans WA, Kleinschmidt-de Masters BK, Wise G, McGill JJ, Danks DM. Neuropathology in glutaric acidemia type I. *Acta Neuropathol (Berl)* 1988; 76: 590–594
- Desai NK, Runge VM, Crisp DE, Crisp MB, Naul LG. Magnetic resonance imaging of the brain in glutaric acidemia type I: a review of the literature and a report of four new cases with attention to the basal ganglia and imaging technique. *Invest Radiol* 2003; 38: 489–496
- Drigo P, Piovan S, Battistella PA, Della Puppa A, Burlina AB. Macrocephaly, subarachnoid fluid collection, and glutaric aciduria type I. *J Child Neurol* 1996; 11: 414–417
- Francois B, Jaeken J, Gillis P. Vigabatrin in the treatment of glutaric aciduria type I. *J Inher Metab Dis* 1990; 13: 352–354
- Goodman SE, Norenberg MD, Shikes RH, Breslich DJ, Moe PG. Glutaric aciduria: biochemical and morphologic considerations. *J Pediatr* 1990; 90: 746–750
- Hald JK, Nakstad PH, Skjeldal OH, Strømme P. Bilateral arachnoid cysts of the temporal fossa in four children with glutaric aciduria type I. *AJNR Am J Neuroradiol* 1991; 12: 407–409
- Hartley LM, Khwaja OS, Verity CM. Glutamic aciduria type I and nonaccidental head injury. *Pediatrics* 2001; 107: 174–175
- Hauser S, Peters H. Glutaric aciduria type I: an underdiagnosed cause of encephalopathy and dystonia-dyskinesia syndrome in children. *J Paediatr Child Health* 1998; 34: 302–304
- Hauser SEP, Boneh A. Severe clinical course with recurrent hyperpyrexia in a patient with glutaric aciduria type I. *Neuropediatrics* 1999; 30: 51–52
- Haworth JC, Booth FA, Chudley AE, de Groot GW, Dilling LA, Goodman SI, Greenberg CR, Mallory CJ, McClarty BM, Seshia SS, Seargeant LE. Phenotypic variability in glutaric aciduria type I: report of fourteen cases in five Canadian Indian kindreds. *J Pediatr* 1991; 118: 52–58
- Hoffmann GF, Trefz FK, Barth PG, Böhles HJ, Lehnert W, Christensen E, Valk J, Rating D, Bremer HJ. Macrocephaly: an important indication for organic acid analysis. *J Inher Metab Dis* 1991; 14: 329–332
- Hoffmann GF, Trefz FK, Barth PG, Böhles HJ, Biggemann B, Bremer HJ, Christensen E, Frosch M, Hanefeld F, Hunneman DH, Jacobi H, Kurlmann G, Lawrenz-Wolf B, Rating D, Roe CR, Schutgens RBH, Ullrich K, Weisser J, Wendel U, Lehnert W. Glutaryl-coenzyme A dehydrogenase deficiency: a distinct encephalopathy. *Pediatrics* 1991; 88: 1194–1203
- Hoffmann GF, Böhles HJ, Burlina A, Duran M, Herwig J, Lehnert W, Leonard JV, Muntau A, Plecko-Starting FK, Superti-Furga A, Trefz FK, Christensen E. Early signs and cause of disease of glutaryl-CoA dehydrogenase deficiency. *J Inher Metab Dis* 1995; 18: 173–176
- Hoffmann GF, Althanassopoulos S, Burlina AB, Duran M, de Klerk BC, Lehnert W, Leonard JV, Moravari AA, Müller E, Muntau AC, Naughten ER, Plecko-Starting B, Superti-Furga A, Zschocke J, Christensen E. Clinical course, early diagnosis, treatment, and prevention of disease in glutaryl-CoA dehydrogenase deficiency. *Neuropediatrics* 1996; 27: 115–123
- Hoffmann GF, Zschocke J. Glutaric aciduria type I: from clinical, biochemical and molecular diversity to successful therapy. *J Inher Metab Dis* 1999; 22: 381–391
- Iafolla AK, Kahler SG. Megalencephaly in the neonatal period as the initial manifestation of glutaric aciduria type I. *J Pediatr* 1989; 114: 1004–1006
- Jamjoom ZAB, Okamoto E, Jamjoom A-H B, Al Hajery O, Abu-Melha A. Bilateral arachnoid cysts of the sylvian region in female siblings with glutaric aciduria type I. *J Neurosurg* 1995; 82: 1078–1081
- Kafil-Hussain NA, Monvarvi A, Howell R, Thornton P, Naughten E, O'Keefe M. Ocular findings in glutaric aciduria type I. *J Pediatr Ophthalmol Strabismus* 2000; 37: 289–293
- Kölker S, Ahlemeyer B, Kriegelstein J, Hoffmann GF. 3-Hydroxyglutaric and glutaric acids are neurotoxic through NMDA receptors *in vitro*. *J Inher Metab Dis* 1999; 22: 259–2623
- Kölker S, Ahlemeyer B, Kriegelstein J, Hoffmann GF. Evaluation of trigger factors of acute encephalopathy in glutaric aciduria type I: fever and tumour necrosis factor- α . *J Inher Metab Dis* 2000; 23: 359–362
- Kölker S, Ahlemeyer B, Kriegelstein J, Hoffmann GF. Maturation-dependent neurotoxicity of 3-hydroxyglutaric and glutaric acids *in vitro*: a new pathophysiologic approach to glutaryl-CoA dehydrogenase deficiency. *Pediatr Res* 2000; 47: 495–503
- Kölker S, Ramaekers VT, Zschocke J, Hoffmann GF. Acute encephalopathy despite early therapy in a patient with homozygosity for E365 K in the glutaryl-coenzyme A dehydrogenase gene. *J Pediatr* 2001; 138: 277–279
- Kölker S, Hoffmann GF, Schor DS, Feyh P, Wagner L, Jeffrey I, Pourfarzam M, Okun JG, Zschocke J, Baric I, Bain MD, Jakobs C, Chalmers RA. Glutaryl-CoA dehydrogenase deficiency: region-specific analysis of organic acids and acylcarnitines in post mortem brain predicts vulnerability of the putamen. *Neuropediatrics* 2003; 34: 253–260
- Kyllerman M, Skjeldal OH, Lundberg M, Holme I, Jellum E, von Döbeln U, Fossen A, Carlsson G. Dystonia and dyskinesia in glutaric aciduria type I: clinical heterogeneity and therapeutic considerations. *Mov Dis* 1994; 9: 22–30
- Land JM, Goulder P, Johnson A, Hockaday J. Glutaric aciduria type I. An atypical presentation together with some observations upon treatment and the possible cause of cerebral damage. *Neuropediatrics* 1992; 23: 322–326
- Leibel RL, Shih VE, Goodman SI, Bauman ML, McCabe ERB, Zwerdling RG, Bergman I, Costello C. Glutaric acidemia: a metabolic disorder causing progressive choreoathetosis. *Neurology* 1980; 30: 1163–1168
- Lipkin PH, Roe CR, Goodman SI, Batshaw ML. A case of glutaric acidemia type I: effect of riboflavin and carnitine. *J Pediatr* 1988; 112: 62–65
- Lütcherath V, Waaler PE, Jellum E, Wester K. Children with bilateral temporal arachnoid cysts may have glutaric aciduria type I (GATI); operation without knowing that may be harmful. *Acta Neurochir (Wien)* 2000; 142: 1025–1030
- Mandel H, Braun J, El-Peleg O, Christensen E, Berant M. Glutaric aciduria type I. Brain CT features and a diagnostic pitfall. *Neuroradiology* 1991; 33: 75–78

- Martinez-Lage JF, Casas C, Fernandez MA, Puche A, Rodriguez Costa T, Poza M. Macrocephaly, dystonia, and bilateral temporal arachnoid cysts: glutaric aciduria type I. *Childs Nerv Syst* 1994; 10: 198–203
- Martinez-Lage JF. Neurosurgical treatment for hydrocephalus, subdural hematomas, and arachnoid cysts in glutaric aciduria type I. *Neuropediatrics* 1996; 27: 335–336
- Merinero B, Pérez-Cerdá, Font LM, Garcia MJ, Aparicio M, Lorenzo G, Martínez Pardo M, Garzo C, Martínez-Bermejo A, Castroviejo IP, Christensen E, Ugarte M. Variable clinical and biochemical presentation of seven Spanish cases with glutaryl-CoA-dehydrogenase deficiency. *Neuropediatrics* 1995; 26: 238–242
- Monavari AA, Naughten ER. Prevention of cerebral palsy in glutaric aciduria type I by dietary management. *Arch Dis Child* 2000; 82: 67–70
- Morton DH, Bennett MJ, Seargeant LE, Nichter CA, Kelley RL. Glutaric aciduria type I: a common cause of episodic encephalopathy and spastic paralysis in the Amish of Lancaster county, Pennsylvania. *Am J Med Genet* 1991; 4: 89–95
- Nagasawa H, Yamaguchi S, Suzuki Y, Kobayashi M, Wada Y, Shikura K, Shimao S, Okada T, Orii T. Neuroradiological findings in glutaric aciduria type I: report of four Japanese patients. *Acta Paediatr Jpn* 1992; 34: 409–415
- Nyhan WL, Zschocke J, Hoffmann G, Stein DE, Bao L, Goodman S. Glutaryl-CoA dehydrogenase deficiency presenting as 3-hydroxyglutaric aciduria. *Mol Genet Metab* 1999; 66: 199–204
- Osaka H, Kimura S, Nezu A, Yamazaki S, Saitoh K, Yamaguchi S. Chronic subdural hematoma, as an initial manifestation of glutaric aciduria type-I. *Brain Dev* 1993; 15: 125–127
- Pfluger T, Weil S, Muntau A, Willemsen UF, Hahn K. Glutaric aciduria type I: a serious pitfall if diagnosed too late. *Eur Radiol* 1997; 7: 1264–1266
- Pineda M, Ribes A, Busquets C, Vilaseca MA, Aracil A, Christensen E. Glutaric aciduria type I with high residual glutaryl-CoA dehydrogenase activity. *Dev Med Child Neurol* 1998; 40: 840–842
- Prevett MC, Howard RS, Dalton RN, Olpin SE. Glutaric aciduria type I in adulthood. *J Neurol Neurosurg Psychiatry* 1996; 60: 352–353
- Renner C, Razeghi S, Überall MA, Hartmann P, Lehnert W. Clinically asymptomatic glutaric aciduria type I in a 4 5/12-year-old girl with bilateral temporal arachnoid cysts. *J Inher Metab Dis* 1997; 20: 840–840
- Schwartz M, Christensen E, Superti-Furga A, Brandt NJ. The human glutaryl-CoA dehydrogenase gene: report of intronic sequences and of 13 novel mutations causing glutaric aciduria type I. *Hum Genet* 1998; 102: 452–458
- Soffer D, Amir N, Elpeleg ON, Gomori JM, Shalev RS, Gottschalk-Sabag S. Striatal degeneration and spongy myelinopathy in glutaric acidemia. *J Neurol Sci* 1992; 107: 199–204
- Superti-Furga A, Hoffmann GF. Glutaric aciduria type I (glutaryl-CoA-dehydrogenase deficiency): advances and unanswered questions. *Eur J Pediatr* 1997; 156: 821–828
- Twomey EL, Naughten ER, Donoghue VB, Ryan S. Neuroimaging in glutaric aciduria type 1. *Pediatr Radiol* 2003; 33: 823–830
- Ullrich K, Flott-Rahmel B, Schluff P, Musshoff U, Das A, Lucke T, Steinfeld R, Christensen E, Jakobs C, Ludolph A, Neu A, Roper R. Glutaric aciduria type I: pathomechanisms of neurodegeneration. *J Inher Metab Dis* 1999; 22: 293–403
- Vamecq J, van Hoof F. Implication of a peroxisomal enzyme in the catabolism of glutaryl-CoA. *Biochem J* 1984; 221: 203–211
- Vamecq J, de Hoffmann E, van Hoof F. Mitochondrial and peroxisomal metabolism of glutaryl-CoA. *Eur J Biochem* 1985; 146: 663–669
- Woelfle J, Kreft B, Emons D, Haverkamp F. Subdural hemorrhage as an initial sign of glutaric aciduria type I: a diagnostic pitfall. *Pediatr Radiol* 1996; 26: 779–781
- Yager JY, McClarty BM, Seshia SS. CT scan findings in an infant with glutaric aciduria type I. *Dev Med Child Neurol* 1988; 30: 808–820
- Zafeiriou DI, Zschocke J, Augoustidou-Savvopoulou P, Mauro-matis I, Sewell A, Kontopoulos E, Katzos G, Hoffmann GF. Atypical and variable clinical presentation of glutaric aciduria type I. *Neuropediatrics* 2000; 31: 303–306
- Zschocke J, Quak E, Guldberg P, Hoffmann GF. Mutation analysis in glutaric aciduria type I. *J Med Genet* 2000; 37: 177–181

38 Propionic Acidemia

- Bergman AJIW, van der Knaap MS, Smeitink JAM, Duran M, Dorland L, Valk J, Poll-The BT. Magnetic resonance imaging and spectroscopy of the brain in propionic acidemia: clinical and biochemical considerations. *Pediatr Res* 1996; 40: 404–409
- Böhles H, Lehnert W. The effect of intravenous L-carnitine on propionic acid excretion in acute propionic acidemia. *Eur J Pediatr* 1984; 143: 61–63
- Brismar J, Ozand PT. CT and MR of the brain in disorders of the propionate and methylmalonate metabolism. *AJNR Am J Neuroradiol* 1994; 15: 1459–1473
- Burlina AB, Dionisi-Vici C, Piovan S, Saponara I, Bartuli A, Sabetta G, Zacchello F. Acute pancreatitis in propionic acidemia. *J Inher Metab Dis* 1995; 18: 169–172
- Chemelli AP, Schocke M, Sperl W, Trieb T, Aichner F, Felber S. Magnetic resonance spectroscopy (MRS) in five patients with treated propionic acidemia. *J Magn Reson Imaging* 2000; 11: 596–600
- Clavero S, Martínez MaA, Pérez B, Pérez-Cerdá C, Ugarte M, Desviat LR. Functional characterization of PCCA mutations causing propionic acidemia. *Biochim Biophys Acta* 2002; 1588: 119–125
- Gebarski SS, Gabrielsen TO, Knake JE, Latack JT. Cerebral CT findings in methylmalonic and propionic acidemias. *AJNR Am J Neuroradiol* 1983; 4: 955–957
- Gravel RA, Akerman BR, Lamhonwah AM, Loyer M, Léon-del-Rio A, Italiano I. Mutations participating in interallelic complementation in propionic acidemia. *Am J Hum Genet* 1994; 55: 51–58
- Haas RH, Marsden DL, Capistrano-Estrada S, Hamilton R, Grafe MR, Wong W, Nyhand WL. Acute basal ganglia infarction in propionic acidemia. *J Child Neurol* 1995; 10: 18–22
- Hamilton RL, Haas RH, Nyhan WL, Powell HC, Grafe MR. Neuropathology of propionic acidemia: a report of two patients with basal ganglia lesions. *J Child Neurol* 1995; 10: 25–30
- Harding BN, Leonard JV, Erdohazi M. Propionic acidemia: a neuropathological study of two patients presenting in infancy. *Neuropathol Appl Neurobiol* 1991; 17: 133–138
- Hommes FA, Kuipers JRG, Elema JD, Jansen JF, Jonxis JHP. Propionic acidemia, a new inborn error of metabolism. *Pediatr Res* 1968; 2: 519–524
- Inoue Y, Kuhara T. Rapid and sensitive method for prenatal diagnosis of propionic acidemia using stable isotope dilution gas chromatography-mass spectroscopy and urease pretreatment. *J Chromatogr B Biomed Sci Appl* 2002; 776: 71–77

- Kalloghlian A, Gleispach H, Ozand PT. A patient with propionic acidemia managed with continuous insulin infusion and total parenteral nutrition. *J Child Neurol* 1992; 7: S88-S91
- Kurczynski TW, Hoppel CL, Goldblatt PJ, Gunning WT. Metabolic studies of carnitine in a child with propionic acidemia. *Pediatr Res* 1989; 26: 63-66
- Leonard JV. The management and outcome of propionic and methylmalonic acidemia. *J Inherit Metab Dis* 1995; 18: 430-434
- Leonard JV. Stable isotope studies in propionic and methylmalonic acidemia. *Eur J Pediatr* 1997; 156: S67-S69
- Leonard JV, Walter JH, McKiernan PJ. The management of organic acidemias: the role of transplantation. *J Inherit Metab Dis* 2001; 24: 309-311
- Muro S, Pérez B, Desviat R, Rodríguez-Pombo P, Pérez-Cerdá C, Clavero S, Ugarte M. Effect of *PCCB* gene mutations on the heteromeric and homomeric assembly of propionyl-CoA carboxylase. *Mol Genet Metab* 2001; 74: 476-483
- Nyhan WL, Bay C, Webb Beyer E, Mazi M. Neurologic nonmetabolic presentation of propionic acidemia. *Arch Neurol* 1999; 56: 1153-1147
- Ozand PT, Rahed M, Gascon GG, Youssef NG, Harfi H, Rahbeeni Z, Al Garawi S, Aqeel A Al. Unusual presentation of propionic acidemia. *Brain Dev* 1994; 16: 46-57
- Rolland MO, Divry P, Mandon G, Guibaud P, Mathieu M, Sournies G, Thoulon JM. Early prenatal diagnosis of propionic acidemia with simultaneous sampling of chorionic villus and amniotic fluid. *J Inherit Metab Dis* 1990; 13: 345-348
- Schlenzig JS, Poggi-Travert F, Laurent J, Rabier D, Jan D, Wendel U, Sewell AC, Revellion Y, Kamoun P, Saudubray JM. Liver transplantation in two cases of propionic acidemia. *J Inherit Metab Dis* 1995; 18: 448-461
- Sethi KD, Ray R, Roesel RA, Carter AL, Callagher BB, Loring DW, Hommes FA. Adult-onset chorea and dementia with propionic acidemia. *Neurology* 1989; 39: 1343-1345
- Shigematsu Y, Mori I, Nakai A, Kikawa Y, Kuriyama M, Konishi Y, Fuji T, Sudo M. Acute infantile hemiplegia in a patient with propionic acidemia. *Eur J Pediatr* 1990; 149: 659-660
- Steinman L, Clancy RR, Cann H, Urlich H. The neuropathology of propionic acidemia. *Dev Med Child Neurol* 1983; 25: 87-94
- Surtees RAH, Matthews EE, Leonard JV. Neurologic outcome of propionic acidemia. *Pediatr Neurol* 1992; 8: 333-337
- Ugarte M, Pérez-Cerdá C, Rodríguez-Pombo P, Desviat LR, Pérez B, Richard E, Muro S, Campeau E, Ohura T, Gravel RA. Overview of mutations in the *PCCA* and *PCCB* genes causing propionic acidemia. *Hum Mutat* 1999; 14: 275-282
- Wolf B, Hsia YE, Sweetman L, Gravel R, Harris DJ, Nyhan WL. Propionic acidemia: a clinical update. *J Pediatr* 1981; 99: 835-846
- Yorifuji T, Kawai M, Muroi J, Mamada M, Kurokawa K, Shigematsu Y, Hirano S, Sakura N, Yoshida I, Kuhara T, Endo F, Mishubushi H, Nakahata T. Unexpectedly high prevalence of the mild form of propionic acidemia in Japan: presence of a common mutation and possible clinical implications. *Hum Genet* 2002; 111: 161-165
- Agamanolis DP, Potter JL, Lundgren DW. Neonatal glycine encephalopathy: biochemical and neuropathologic findings. *Pediatr Neurol* 1993; 9: 140-143
- Alejo J, Rincón P, Vaquerizo J, Gil C, Plasencia A, Gallardo R. Transient nonketotic hyperglycemia: ultrasound, CT and MRI (case report). *Neuroradiology* 1997; 39: 658-660
- Alemzadeh R, Gammeltoft K, Matteson K. Efficacy of low-dose dextromethorphan in the treatment of nonketotic hyperglycemia. *Pediatrics* 1996; 97: 924-926
- Aliiefendioğlu D, Aslan AT, Çopkun T, Dursun A, Çakmak FN, Kesimer M. Transient nonketotic hyperglycemia: two case reports and literature review. *Pediatr Neurol* 2003; 28: 151-155
- Anderson JM. Spongy degeneration in the white matter of the central nervous system in the newborn: pathological findings in three infants, one with hyperglycemia. *J Neurol Neurosurg Psychiatry* 1969; 32: 328-337
- Ando T, Nyhan WL, Bicknell J, Harris R, Stern J. Non-ketotic hyperglycemia in a family with an unusual phenotype. *J Inherit Metab Dis* 1978; 1: 79-83
- Appelgarth DA, Toone JR, Rolland MO, Black SH, Yim DKC, Bemis G. Non-concordance of CVS and live glycine cleavage enzyme in three families with non-ketotic hyperglycemia (NKH) leading to false negative prenatal diagnosis. *Prenat Diagn* 2000; 20: 367-370
- Arnold GL, Griebel ML, Valentine JL, Koroma DM, Kearns GL. Dextromethorphan in nonketotic hyperglycemia: metabolic variation confounds the dose-response relationship. *J Inherit Metab Dis* 1997; 20: 28-38
- Bank WJ. A familial spinal cord disorder with hyperglycemia. *Arch Neurol* 1972; 27: 136-144
- Bekiesnińska-Figatowska M, Rokicki D, Walecki J. MRI in nonketotic hyperglycemia: case report. *Neuroradiology* 2001; 43: 792-793
- Boneh A, Degani Y, Harari M. Prognostic clues and outcome of early treatment of nonketotic hyperglycemia. *Pediatr Neurol* 1996; 15: 137-141
- Brun A, Börjeson M, Hultberg B, Sjöblad S, Akesson H, Litwin E. Neonatal non-ketotic hyperglycemia: a clinical, biochemical and neuropathological study including electronmicroscopic findings. *Neuropädiatrie* 1979; 10: 195-205
- Choi C-G, Lee HHK, Yoon J-H. Localized proton MR spectroscopic detection of nonketotic hyperglycemia in an infant. *Korean J Radiol* 2001; 2: 239-242
- Christodoulou J, Kure S, Hayasaka K, Clarke JTR. Atypical nonketotic hyperglycemia confirmed by assay of the glycine cleavage system in lymphoblasts. *J Pediatr* 1993; 123: 100-102
- Dalla Bernardina B, Aicardi J, Goutières F, Plouin P. Glycine encephalopathy. *Neuropädiatrie* 1978; 10: 209-225
- Deutsch SI, Rosse RB, Mostropalo J. Current status of NMDA antagonist interventions in the treatment of nonketotic hyperglycemia. *Clin Neuropharmacol* 1998; 21: 71-79
- Dobyns WB. Agenesis of the corpus callosum and gyral malformations are frequent manifestations of nonketotic hyperglycemia. *Neuroradiology* 1989; 39: 817-820
- Eyskens FJM, van Doorn JWD, Mariën P. Clinical and laboratory observations. *Neuroradiologic sequelae in transient nonketotic hyperglycemia of the neonate. J Pediatr* 1992; 121: 620-621
- Flannery DB, Pellock J, Bousounis D, Hunt P, Nance C, Wolf B. Nonketotic hyperglycemia in two retarded adults: a mild form of infantile nonketotic hyperglycemia. *Neurology* 1983; 33: 1064-1066

39 Nonketotic Hyperglycemia

- Fletcher JM, Bye AME, Nayanar V, Wilcken B. Non-ketotic hyperglycinaemia presenting as pachygyria. *J Inherit Metab Dis* 1995; 18: 665–668
- Frazier DM, Summer GK, Chamberlin HR. Hyperglycinuria and hyperglycinemia in two siblings with mild developmental delays. *Am J Dis Child* 1978; 132: 777–781
- Gabis L, Parton P, Roche P, Lenn N, Tudorica A, Huang W. In vivo ¹H magnetic resonance spectroscopic measurement of brain glycine levels in nonketotic hyperglycinemia. *J Neuroim* 2001; 11: 209–211
- Hamosh A, Maher JF, Bellus GA, Rasmussen SA, Johnston MV. Long-term use of high-dose benzoate and dextromethorphan for the treatment of nonketotic hyperglycinemia. *J Pediatr* 1998; 132: 709–713
- Hayasaka K, Tada K, Fueki N, Kakamura Y, Nyhan WL, Schmidt K, Packman S, Seashore MR, Haan E, Danks DM, Schutgens RBH. Nonketotic hyperglycinemia: analysis of glycine cleavage system in typical and atypical cases. *J Pediatr* 1987; 110: 873–877
- Heindel W, Kugel H, Roth B. Noninvasive detection of increased glycine content by proton MR spectroscopy in the brains of two infants with nonketotic hyperglycinemia. *AJNR Am J Neuroradiol* 1993; 14: 629–635
- Holmgren G, Kison Blomquist H. Non-ketotic hyperglycinemia in two sibs with mild psycho-neurological symptoms. *Neuropädiatrie* 1977; 8: 67–72
- Huisman TAGM, Thiel T, Steinmann B, Zeilinger G, Martin E. Proton magnetic resonance spectroscopy of the brain of a neonate with nonketotic hyperglycinemia: in vivo-in vitro (ex vivo) correlation. *Eur Radiol* 2002; 12: 858–861
- Khong PL, Lam PCC, Chung BHY, Wong KY, Ooi GC. Diffusion-weighted MR imaging in neonatal nonketotic hyperglycinemia. *AJNR Am J Neuroradiol* 2003; 24: 1181–1183
- Kish SJ, Dixon LM, Burnham WM, Perry TL, Becker L, Cheng J, Chang LJ, Rebbetoy M. Brain neurotransmitters in glycine encephalopathy. *Ann Neurol* 1988; 24: 458–461
- Korman SH, Gutman S. Pitfalls in the diagnosis of glycine encephalopathy (non-ketotic hyperglycinemia). *Dev Med Child Neurol* 2002; 44: 712–720
- Kure S, Narisawa K, Tada K. Enzymatic diagnosis of nonketotic hyperglycinemia with lymphoblasts. *J Pediatr* 1992; 120: 95–98
- Kure S, Takayanagi M, Narisawa K, Tada K, Leisti J. Identification of a common mutation in Finnish patients with nonketotic hyperglycinemia. *J Clin Invest* 1992; 90: 160–164
- Kure S, Tada K, Narisawa K. Nonketotic hyperglycinemia: biochemical, molecular, and neurological aspects. *Jpn J Hum Genet* 1997; 42: 13–22
- Kure S, Rolland M-O, Leisti J, Mandel H, Sakata Y, Tada K, Matsubara Y, Narisawa K. Prenatal diagnosis of non-ketotic hyperglycinaemia: enzymatic diagnosis in 28 families and DNA diagnosis detecting prevalent Finnish and Israeli-Arab mutations. *Prenat Diagn* 1999; 19: 717–720
- Kure S, Kojima K, Kudo T, Kanno K, Aoki Y, Suzuki Y, Shinka T, Sakata Y, Narisawa K, Matsubara Y. Chromosomal localization, structure, single-nucleotide polymorphisms, and expression of the human H-protein gene of the glycine cleavage system (*GCSH*), a candidate gene for nonketotic hyperglycinemia. *J Hum Genet* 2001; 46: 378–384
- Kure S, Kojima K, Ichinohe A, Maeda T, Kalmachey R, Feteke G, Berg SZ, Filiano J, Aoki Y, Suzuki Y, Izumi T, Matsubara Y. Heterozygous *GLDC* and *GCSH* gene mutations in transient neonatal hyperglycinemia. *Ann Neurol* 2002; 52: 643–646
- Lu FL, Wang P-J, Hwu W-L, Taou Yau K-I, Wang T-R. Neonatal type of nonketotic hyperglycinemia. *Pediatr Neurol* 1999; 20: 295–300
- Luder AS, Davidson A, Goodman SI, Greene CL. Transient nonketotic hyperglycinemia in neonates. *J Pediatr* 1989; 114: 1013–1015
- Matsuo S, Inoue F, Takeuchi Y, Yoshioka H, Kinugasa A, Sawada T. Efficacy of tryptophan for the treatment of nonketotic hyperglycinemia: a new therapeutic approach for modulating the *N*-methyl-D-aspartate receptor. *Pediatrics* 1995; 95: 142–146
- Nanao K, Okamura-Ikeda K, Motokawa Y, Danks DM, Baumgartner ER, Takada G, Hayasaka K. Identification of the mutations in the T-protein gene causing typical and atypical nonketotic hyperglycinemia. *Hum Genet* 1994; 93: 665–658
- Neuberger JM, Schweitzer S, Rolland M-O, Burghard R. Effect of sodium benzoate in the treatment of atypical nonketotic hyperglycinaemia. *J Inherit Metab Dis* 2000; 23: 22–26
- Nightingale S, Barton ME. Intermittent vertical supranuclear ophthalmoplegia and ataxia. *Mov Disord* 1991; 6: 76–78
- Ohya Y, Ochi N, Mizutani N, Hayakawa C, Watanabe K. Nonketotic hyperglycinemia: treatment with NMDA antagonist and consideration of neuropathogenesis. *Pediatr Neurol* 1991; 7: 65–68
- Press GA, Barshop BA, Haas RH, Nyhan WL, Glass RF, Hesselink JR. Abnormalities of the brain in nonketotic hyperglycinemia: MR manifestations. *AJNR Am J Neuroradiol* 1989; 10: 315–321
- Rushton DL. Spongy degeneration of the white matter of the central nervous system associated with hyperglycinuria. *J Clin Pathol* 1968; 21: 246–462
- Schiffmann R, Kaye EM, Willis JK III, Africk D, Ampola M. Transient neonatal hyperglycinemia. *Ann Neurol* 1989; 25: 201–201
- Schmitt B, Steinmann B, Gitzelmann R, Thun-Hohenstein L, Mascher H, Dumermuth G. Nonketotic hyperglycinemia: clinical and electrophysiologic effects of dextromethorphan, an antagonist of the NMDA receptor. *Neurology* 1993; 43: 421–424
- Shuman RM, Leech RW, Scott CR. The neuropathology of the nonketotic and ketotic hyperglycinemias: three cases. *Neurology* 1978; 28: 139–146
- Singer HS, Valle D, Hayasaka K, Tada K. Nonketotic hyperglycinemia: studies in an atypical variant. *Neurology* 1989; 39: 286–288
- Slager UT, Berggren RL, Marubayashi S. Nonketotic hyperglycinemia: report of a case and review of the clinical, chemical, and pathological changes. *Ann Neurol* 1977; 1: 399–402
- Steiner RD, Sweetser DA, Rohrbaugh JR, Dowton B, Toone JR, Applegarth DA. Nonketotic hyperglycinemia: atypical clinical and biochemical manifestations. *J Pediatr* 1996; 128: 243–246
- Steinman GS, Yudkoff M, Berman PH, Blazer-Yost B, Segal S. Late-onset nonketotic hyperglycinemia and spinocerebellar degeneration. *J Pediatr* 1979; 94: 907–911
- Tada K, Hayasaka K. Non-ketotic hyperglycinaemia: clinical and biochemical aspects. *Eur J Pediatr* 1987; 146: 221–227
- Tada K, Kure S. Non-ketotic hyperglycinaemia: molecular lesion, diagnosis and pathophysiology. *J Inherit Metab Dis* 1993; 16: 691–703
- Takayanagi M, Kure S, Sakata Y, Kurihara Y, Ohya Y, Kajita M, Tada K, Matsubara Y, Narisawa K. Human glycine decarboxylase gene (*GLDC*) and its highly conserved processed pseudogene (*øGLDC*): their structure and expression, and the identification of a large deletion in a family with nonketotic hyperglycinemia. *Hum Genet* 2000; 106: 298–305

- Toone JR, Applegarth DA, Coulter-Mackie M, James ER. Identification of the first reported splice site mutation (IVS7-1GA) in the aminomethyltransferase (T-protein) gene (AMT) of the glycine cleavage complex in 3 unrelated families with nonketotic hyperglycinemia. *Hum Mutat* 2000; 17: 76-81
- Tauner DA, Page T, Green C, Sweetman L, Kulovich S, Nyhan WL. Progressive neurodegenerative disorder in a patient with nonketotic hyperglycinemia. *J Pediatr* 1981; 98: 272-275
- Van Hove JLK, Kishnani PS, Damaerel P, Kahler SG, Miller C, Jaeken J, Rutledge SL. Acute hydrocephalus in nonketotic hyperglycinemia. *Neurology* 2000; 54: 754-756
- Wiltshire EJ, Poplawski NK, Harrison JR, Fletcher JM. Treatment of late-onset nonketotic hyperglycinaemia: effectiveness of imipramine and benzoate. *J Inherit Metab Dis* 2000; 23: 15-21
- Wraith JE. Non-ketotic hyperglycinemia: prolonged survival in a patient with a mild variant. *J Inherit Metab Dis* 1996; 19: 695-696
- Zammarchi E, Donati MA, Ciani F, Pasquini E, Pela I, Fiorini P. Failure of early dextromethorphan and sodium benzoate therapy in an infant with nonketotic hyperglycinemia. *Neuropediatrics* 1994; 25: 274-276
- Zammarchi E, Donati MA, Ciani F. Transient neonatal nonketotic hyperglycinemia: a 13-year follow-up. *Neuropediatrics* 1995; 26: 328-330

40 Maple Syrup Urine Disease

- Backhouse O, Leitch RJ, Thompson D, Kriss A, Charris D, Clayton P, Russel-Eggitt I. A case of reversible blindness in maple syrup urine disease. *Br J Ophthalmol* 1999; 83: 250-251
- Berry GT, Heidenreich R, Kaplan P, Levine F, Mazur A, Palmieri MJ, Yudkoff M, Segal S. Branched-chain amino acid-free parenteral nutrition in the treatment of acute metabolic decompensation in patients with maple syrup urine disease. *N Engl J Med* 1991; 324: 175-179
- Biggemann B, Zass R, Wendel U. Postoperative metabolic decompensation in maple syrup urine disease is completely prevented by insulin. *J Inherit Metab Dis* 1993; 16: 912-913
- Brismar J, Aqeel A, Brismar G, Coates R, Gascon G, Ozand P. Maple syrup urine disease: findings on CT and MR scans of the brain in 10 infants. *AJNR Am J Neuroradiol* 1990; 11: 1219-1228
- Cavalleri F, Berardi A, Burlina AB, Ferrari F, Mavilla L. Diffusion-weighted MRI of maple syrup urine disease encephalopathy. *Neuroradiology* 2002; 44: 449-502
- Chuang DT, Davie JR, Max Wynn R, Chuang JL, Koyata H, Cox RP. Molecular basis of maple syrup urine disease and stable correction by retroviral gene transfer. *J Nutr* 1995; 125: 1766S-1772S
- Chuang JL, Chuang DT. Diagnosis and mutational analysis of maple syrup urine disease using cell cultures. *Methods Enzymol* 2000; 324: 413-464
- Delis D, Michelakakis H, Katsarou E, Bartsocas CS. Thiamin-responsive maple syrup urine disease: seizures after 7 years of satisfactory metabolic control. *J Inherit Metab Dis* 2001; 24: 683-684
- Fariello G, Dionisi-Vice C, Orazi C, Malena S, Bartuli A, Schingo P, Carnavale E, Saponara I, Sabetta G. Cranial ultrasonography in maple syrup urine disease. *AJNR Am J Neuroradiol* 1996; 17: 311-315
- Felber SR, Sperl W, Chemelli A, Murr Ch, Wendel U. Maple syrup urine disease: metabolic decompensation monitored by proton magnetic resonance imaging and spectroscopy. *Ann Neurol* 1993; 33: 396-401
- Giacioia GP, Berry GT. Acrodermatitis enteropathica-like syndrome secondary to isoleucine deficiency during treatment of maple syrup urine disease. *Am J Dis Child* 1993; 147: 954-956
- Gouyon JB, Semama D, Prévot A, Desgres J. Removal of branched-chain amino acids and α -ketosocaproate by haemofiltration and haemodiafiltration. *J Inherit Metab Dis* 1996; 19: 610-620
- Ha JS, Kim TK, Eun BL, Lee HS, Lee KY, Seol HY, Cha SH. Maple syrup urine disease encephalopathy: a follow-up study in the acute stage using diffusion-weighted MRI. *Pediatr Radiol* 2004; 34: 163-166
- Hilliges C, Awiszus D, Wendel U. Intellectual performance of children with maple syrup urine disease. *Eur J Pediatr* 1993; 152: 144-147
- Indo Y, Akaboshi I, Nobukuni Y, Endo F, Matsuda I. Maple syrup urine disease: a possible biochemical basis for the clinical heterogeneity. *Hum Genet* 1988; 80: 6-10
- Jan W, Zimmerman RA, Wang ZJ, Berry GT, Kaplan PB, Kaye EM. MR diffusion imaging and MR spectroscopy of maple syrup urine disease during acute metabolic decompensation. *Neuroradiology* 2003; 45: 393-399
- Jouvet P, Poggi F, Rabier D, Michel JL, Hubert P, Sposito M, Saudubray JM, Man NK. Continuous venovenous haemodiafiltration in the acute phase of neonatal maple syrup disease. *J Inherit Metab Dis* 1997; 20: 463-477
- Jouvet P, Rustin P, Taylor DL, Pocock JM, Felderhoff-Mueser U, Mazarakis ND, Sarraf C, Joashi U, Kozma M, Greenwood K, Edwards DA, Mehmet H. Branched chain amino acids induce apoptosis in neural cells without mitochondrial membrane depolarization or cytochrome c release: implications for neurological impairment associated with maple syrup urine disease. *Mol Biol Cell* 2000; 11: 1919-1932
- Jouvet P, Jugie M, Rabier D, Desgrès J, Hubert P, Saudubray JM, Man NK. Combined nutritional support and continuous extracorporeal removal therapy in the severe acute phase of maple syrup urine disease. *Intensive Care Med* 2001; 27: 1798-1806
- Kamei A, Takashima S, Chan F, Becker LE. Abnormal dendritic development in maple syrup urine disease. *Pediatr Neurol* 1992; 8: 145-147
- Kaplan P, Mazur A, Field M, Berlin JA, Berry GT, Heidenreich R, Yudkoff M, Segal S. Intellectual outcome in children with maple syrup urine disease. *J Pediatr* 1991; 119: 46-50
- Kleopa KA, Raizen DM, Friedrich CA, Brown MJ, Bird SJ. Acute axonal neuropathy in maple syrup urine disease. *Muscle Nerve* 2001; 24: 284-287
- Menkes JH, Philippart M, Fiore RE. Cerebral lipids in maple syrup disease. *J Pediatr* 1965; 66: 584-594
- Menkes JH, Solcher H. Maple syrup disease. *Arch Neurol* 1967; 16: 486-491
- Morton DH, Strauss KA, Robinson DL, Puffenberger EG, Kelly RL. Diagnosis and treatment of maple syrup disease: a study of 36 patients. *Pediatrics* 2002; 109: 999-1008
- Müller K, Kahn T, Wendel U. Is demyelination a feature of maple syrup urine disease? *Pediatr Neurol* 1993; 9: 375-382
- Nellis MM, Danner DJ. Gene preference in maple syrup urine disease. *Am J Hum Genet* 2001; 68: 232-237
- Nobukuni Y, Mitsubuchi H, Akaboshi I, Indo Y, Endo F, Matsuda I. Maple syrup urine disease: clinical and biochemical significance of gene analysis. *J Inherit Metab Dis* 1991; 14: 787-792

- Nord A, van Doorninck WJ, Greene C. Developmental profile of patients with maple syrup urine disease. *J Inherit Metab Dis* 1991; 14: 881–889
- Northrup H, Sigman ES, Hebert AA. Exfoliative erythroderma resulting from inadequate intake of branched-chain amino acids in infants with maple syrup urine disease. *Arch Dermatol* 1993; 129: 384–385
- Nyhan WL, Rice-Kelts M, Klein J, Barshop BA. Treatment of the acute crisis in maple syrup urine disease. *Arch Pediatr Adolesc Med* 1998; 152: 593–598
- Ogier de Baulny H, Saudubray JM. Branched-chain organic acidurias. *Semin Neonatol* 2002; 7: 65–74
- Parini R, Sereni LP, Bagozzi DC, Corbetta C, Rabier D, Narcy C, Hubert P, Saudubray JM. Nasogastric drip feeding as the only treatment of neonatal maple syrup urine disease. *Pediatrics* 1993; 92: 280–283
- Parmar H, Sitoh YY, Ho L. Maple syrup urine disease. Diffusion-weighted and diffusion-tensor magnetic resonance imaging findings. *J Comput Assist Tomogr* 2004; 28: 93–97
- Parsons HG, Carter RJ, Unrath M, Snyder FF. Evaluation of branched-chain amino acid intake in children with maple syrup urine disease and methylmalonic aciduria. *J Inherit Metab Dis* 1990; 13: 125–136
- Prensky AL, Moser HW. Brain lipids, proteolipids, and free amino acids in maple syrup urine disease. *J Neurochem* 1966; 13: 863–874
- Puliyanda DP, Harmon WE, Peterschmitt MJ, Irons M, Somers MJG. Utility of hemodialysis in maple syrup urine disease. *Pediatr Nephrol* 2002; 17: 239–242
- Riviello JJ, Rezvani I, DiGeorge AM, Foley CM. Cerebral edema causing death in children with maple syrup urine disease. *J Pediatr* 1991; 119: 42–45
- Schönberger S, Schweiger B, Schwahn B, Schwarz M, Wendel U. Demyelination in the brain of adolescents and young adults with maple syrup urine disease. *Mol Genet Metab* 2004; 82: 69–75
- Scriver CR, Clow CL, Mackenzie S, Delvin E. Thiamine-responsive maple-syrup-urine disease. *Lancet* 1971; i: 310–312
- Scriver CR, Clow CL, George H. So-called thiamine-responsive maple syrup urine disease: 15-year follow-up of the original patient. *J Pediatr* 1985; 107: 763–765
- Sener RN. Diffusion magnetic resonance imaging in intermediate form of maple syrup urine disease. *J Neuroimaging* 2002; 12: 368–390
- Silberberg DH. Maple syrup urine disease metabolites studies in cerebellum cultures. *J Neurochem* 1969; 16: 1141–1146
- Silberman J, Dancis J, Feigin I. Neuropathological observations in maple syrup urine disease. *Arch Neurol* 1961; 5: 351–363
- Taccone A, Schiaffino MC, Cerone R, Fondelli MP, Romano C. Computed tomography in maple syrup urine disease. *Eur J Radiol* 1992; 14: 207–212
- Tharp BR. Unique EEG pattern (comb-like rhythm) in neonatal maple syrup urine disease. *Pediatr Neurol* 1992; 8: 65–68
- Thompson GN, Francis DEM, Halliday D. Acute illness in maple syrup urine disease: dynamics of protein metabolism and implications for management. *J Pediatr* 1991; 119: 35–41
- Tornqvist K, Tornqvist H. Corneal de-epithelialization caused by acute deficiency of isoleucine during treatment of a patient with maple syrup urine disease. *Acta Ophthalmol Scand* 1996; 74: 48–49
- Treacy E, Clow CL, Reade TR, Chitayat D, Mamer OA, Scriver CR. Maple syrup urine disease: interrelations between branched-chain amino, oxo- and hydroxyacids; implications for treatment; associations with CNS demyelination. *J Inherit Metab Dis* 1992; 15: 121–135
- Tsuruta M, Mitsubuchi H, Mardy S, Miura Y, Hayashida Y, Kinugasa A, Ishitsu T, Matsuda I, Indo Y. Molecular basis of intermittent maple syrup urine disease: novel mutations in the E2 gene of the branched-chain (ALPHA)-keto acid dehydrogenase complex. *J Hum Genet* 1998; 43: 91–100
- Uziel G, Savoiardo M, Nardocci N. CT and MRI in maple syrup urine disease. *Neurology* 1988; 38: 486–488
- Verdu A, Lopez-Herce J, Pascual-Castroviejo I, Martinez-Bermejo A, Ugarte M, Garcia MJ. Maple syrup urine disease variant form: presentation with psychomotor retardation and CT scan abnormalities. *Acta Paediatr Scand* 1985; 74: 815–818
- Wanjer M, Coelho DM, Barschak AG, Araújo PR, Pires RF, Lulhier FLG, Vargas CR. Reduction of large neutral amino acid concentrations in plasma and CSF of patients with maple syrup urine disease during crisis. *J Inherit Metab Dis* 2000; 23: 505–512
- Wendel U, Saudubray JM, Bodner A, Schadeewaldt P. Liver transplantation in maple syrup disease. *Eur J Pediatr* 1999; 158: S60–S64
- Wynn RM, Ho R, Chuang JL, Chuang DT. Roles of active site and novel K⁺ ion-binding site residues in human mitochondrial branched chain α -ketoacid decarboxylase/dehydrogenase. *J Biol Chem* 2001; 9: 4168–4174
- Yoshino M, Aoki K, Akeda H, Hashimoto K, Ikeda T, Inoue F, Ito M, Kawamura M, Kohno Y, Koga Y, Kuroda Y, Maesaka H, Murakami-Soda H, Sugiyama N, Suzuki Y, Yano S, Yoshioka A. Management of acute metabolic decompensation in maple syrup urine disease: a multi-center study. *Pediatr Int* 1999; 41: 132–173
- Zneimer SM, Lau KS, Eddy RL, Shows TB, Chuang JL, Chuang DT, Cox RD. Regional assignment of two genes of the human branched-chain (ALPHA)-keto acid dehydrogenase complex: the E1 β gene (BCKDHB) to chromosome 6p21–22 and the E2 gene (DTB) to chromosome 1p31. *Genomics* 1991; 10: 740–747

41 3-Hydroxy-3-Methylglutaryl CoA Lyase Deficiency

- Bakker HD, Wanders RJA, Schutgens RBH, Abeling NGGM, van Gennip AH. 3-Hydroxy-3-methylglutaryl-CoA lyase deficiency: absence of clinical symptoms due to a self-imposed dietary fat and protein restriction. *J Inherit Metab Dis* 1993; 16: 1061–1062
- Ferris JN, Tien RD. Cerebral MRI in 3-hydroxy-3-methylglutaryl-coenzyme A lyase deficiency: case report. *Neuroradiology* 1993; 35: 559–560
- Gibson KM, Breuer J, Kaiser K, Nyhan WL, McCoy EE, Ferreira P, Greene CL, Blitzer MG, Shapira E, Reverte F, Conde C, Bagnell P, Cole DEC. 3-Hydroxy-3-methylglutaryl-coenzyme A lyase deficiency: report of five new patients. *J Inherit Metab Dis* 1988; 11: 76–87
- Gibson KM, Breuer J, Nyhan WL. 3-Hydroxy-3-methylglutaryl-coenzyme A lyase deficiency: review of 18 reported patients. *Eur J Pediatr* 1988; 148: 180–186
- Gibson KM, Cassidy SB, Seaver LH, Wanders RJA, Kennaway NG, Mitchell GA, Sprak RP. Fatal cardiomyopathy associated with 3-hydroxy-3-methylglutaryl-CoA lyase deficiency. *J Inherit Metab Dis* 1994; 17: 291–294
- Gordon K, Riding M, Camfield P, Bawden H, Ludman M, Bagnell P. CT and MR of 3-hydroxy-3-methylglutaryl-coenzyme A lyase deficiency. *AJNR Am J Neuroradiol* 1994; 15: 1474–1476

- Huemer M, Muehl A, Wandl-Vergesslich K, Strobl W, Wanders RJA, Stoeckler-Ipsiroglu S. Stroke-like encephalopathy in an infant with 3-hydroxy-3-methylglutaryl-coenzyme A lyase deficiency. *Eur J Pediatr* 1998; 157: 743–746
- Leupold D, Bojasch M, Jacobs C. 3-Hydroxy-3-methylglutaryl-coenzyme A lyase deficiency in an infant with macrocephaly and mild metabolic acidosis. *Eur J Pediatr* 1982; 138: 73–76
- Lisson G, Leupold D, Bechinger D, Wallesch C. CT findings in a case of deficiency of 3-hydroxy-3-methylglutaryl-CoA lyase. *Neuroradiology* 1981; 22: 99–101
- Mitchell GA, Jakobs C, Gibson KM, Robert M-F, Burlina A, Dionisi-Vici C, Dallaire L. Molecular prenatal diagnosis of 3-hydroxy-3-methylglutaryl-CoA lyase deficiency. *Prenat Diagn* 1995; 15: 725–729
- Ozand PT, Al Aqeel A, Gascon G, Brismar J, Thomas E, Gleispach H. 3-Hydroxy-3-methylglutaryl-coenzyme A (HMG-CoA) lyase deficiency in Saudi Arabia. *J Inherit Metab Dis* 1991; 14: 174–188
- Robinson BH, Oei J, Sherwood G, Slyper AH, Heininger J, Mamer OA. Hydroxymethylglutaryl CoA lyase deficiency: features resembling Reye syndrome. *Neurology* 1980; 30: 714–718
- Thompson GN, Chalmers RA, Halliday D. The contribution of protein catabolism to metabolic decompensation in 3-hydroxy-3-methylglutaric aciduria. *Eur J Pediatr* 1990; 149: 346–350
- van der Knaap MS, Bakker HD, Valk J. MR imaging and proton spectroscopy in 3-hydroxy-3-methylglutaryl-coenzyme A lyase deficiency. *AJNR Am J Neuroradiol* 1998; 19: 378–382
- Walter JH, Clayton PT, Leonard JV. 3-Hydroxy-3-methylglutaryl-coenzyme A lyase deficiency. *J Inherit Metab Dis* 1986; 9: 287–288
- Wang SP, Robert M-F, Gibson KM, Wanders RJA, Mitchell GA. 3-Hydroxy-3-methylglutaryl-CoA lyase (HL): mouse and human HL gene (*HMGCL*) cloning and detection of large gene deletions in two unrelated HL-deficient patients. *Genomics* 1996; 33: 99–104
- Wilson WG, Cass MB, Søvik O, Gibson KM, Sweetman L. A child with acute pancreatitis and recurrent hypoglycemia due to 3-hydroxy-3-methylglutaryl-CoA lyase deficiency. *Eur J Pediatr* 1984; 142: 289–291
- Wysocki SJ, Hähnel R. 3-Hydroxy-3-methylglutaryl-coenzyme A lyase deficiency: a review. *J Inherit Metab Dis* 1986; 9: 225–233
- Yalçinkaya C, Dinçer A, Gündüz E, Fiçicioğlu C, Koçer N, Aydın A. MRI and MRI in HMG-CoA lyase deficiency. *Pediatr Neurol* 1999; 20: 375–380
- Zoghbi HY, Spence JE, Beaudet AL, O'Brien WE, Goodman CJ, Gibson KM. Atypical presentation and neuropathological studies in 3-hydroxy-3-methylglutaryl-CoA lyase deficiency. *Ann Neurol* 1986; 20: 367–369
- Adachi M, Schneck L, Cara J, Volk BW. Spongy degeneration of the central nervous system (Van Bogaert and Bertrand type; Canavan's disease). *Hum Pathol* 1973; 4: 331–347
- Austin SJ, Connelly A, Gadian DG, Benton JS, Brett EM. Localized ¹H NMR spectroscopy in Canavan's disease: a report of two cases. *Magn Reson Med* 1991; 19: 439–445
- Banker BQ, Robertson JT, Victor M. Spongy degeneration of the central nervous system in infancy. *Neurology* 1964; 14: 981–1001
- Barker PB, Bryan RN, Kumar AJ, Naidu S. Proton NMR spectroscopy of Canavan's disease. *Neuropediatrics* 1992; 23: 263–267
- Baslow MH. Molecular water pumps and the aetiology of Canavan's disease: a case of sorcerer's apprentice. *J Inherit Metab Dis* 1999; 22: 99–101
- Baslow MH. Canavan's spongiform leukodystrophy. A clinical anatomy of a genetic metabolic CNS disease. *J Mol Neurosci* 2000; 15: 61–69
- Baslow MH. Evidence supporting a role for *N*-acetyl-L-aspartate as a molecular water pump in myelinated neurons in the central nervous system. An analytical review. *Neurochem Int* 2002; 40: 295–300
- Baslow MH. Brain *N*-acetylaspargate as a molecular water pump and its role in the etiology of Canavan disease. *J Mol Neurosci* 2003; 21: 185–189
- Baslow MH, Resnik TR. Canavan Disease. Analysis of the nature of the metabolic lesions responsible for development of the observed clinical symptoms. *J Mol Neurosci* 1997; 9: 109–125
- Baslow MH, Suckow RF, Sapirstein V, Hungund BL. Expression of aspartoacylase activity in cultured rat macroglial cells is limited to oligodendrocytes. *J Mol Neurosci* 1999; 13: 47–53
- Bennett MJ, Gibson KM, Sherwood WG, Divry P, Rolland MO, Elpeleg ON, Rinaldo P, Jakobs C. Reliable prenatal diagnosis of Canavan disease (aspartoacylase deficiency): comparison of enzymatic and metabolite analysis. *J Inherit Metab Dis* 1993; 16: 831–836
- Besley GTN, Elpeleg ON, Shaag A, Manning NJ, Jakobs C, Walter JH. Prenatal diagnosis of Canavan disease. Problems and dilemmas. *J Inherit Metab Dis* 1999; 22: 263–366
- Brismar J, Brismar G, Gascon G, Ozand P. Canavan disease: CT and MR imaging of the brain. *AJNR Am J Neuroradiol* 1990; 11: 805–810
- Brown LW, Rorke LB, Deray MJ, Smith SB, Altman N. Psychomotor retardation and macrocephaly in an infant. *Pediatr Neurol* 1985–1986; 12: 266–271
- Burlina AP, Ferrari V, Divry P, Gradowska W, Jakobs C, Bennett MJ, Sewell AC, Dionisi-Vici C, Burlina AB. *N*-Acetylaspargyl-glutamate in Canavan disease: an adverse effector? *Eur J Pediatr* 1999; 158: 406–409
- De Coo IFM, Gabreëls FJM, Renier WO, de Pont JJHMM, Hälst UJGM, Veerkamp JH, Trijbels JMF, Jaspar HHJ, Renkawek. Canavan disease: neuromorphological and biochemical analysis of a brain biopsy specimen. *Clin Neuropathol* 1991; 10: 73–78
- Echenne B, Divry P, Vianey-Liaud C. Spongy degeneration of the neuraxis (Canavan-Van Bogaert disease) and *N*-acetylaspargic aciduria. *Neuropediatrics* 1989; 20: 70–81
- Engelbrecht V, Scherer A, Rassek M, Witsack HJ, Mödder U. Diffusion-weighted MR imaging in the brain in children: findings in the normal brain and in the brain with white matter diseases. *Radiology* 2002; 222: 410–418
- Gascon GG, Ozand PT, Mahdi A, Jamil A, Haider A, Brismar J, Al-Nasser M. Infantile CNS spongy degeneration—14 cases: clinical update. *Neurology* 1990; 40: 1876–1882

42 Canavan Disease

- Gordon N. Canavan disease: a review of recent developments. *Eur J Paediatr Neurol* 2000; 5: 65–69
- Grod W, Krägeloh-Mann I, Petersen D, Trefz FK, Harzer K. In vivo assessment of *N*-acetylaspartate in brain in spongy degeneration (Canavan's disease) by proton spectroscopy. *Lancet* 1990; 336: 437–438
- Hagenfeldt L, Bollgren I, Venizelos N. *N*-Acetylaspartic aciduria due to aspartoacylase deficiency – a new aetiology of childhood leucodystrophy. *J Inherit Metab Dis* 1987; 10: 135–141
- Hamaguchi H, Nihei K, Nakamoto N, Ezoe T, Naito H, Hara M, Yokota K, Inoue Y, Matsumoto I. A case of Canavan disease: the first biochemically proven case in a Japanese girl. *Brain Dev* 1993; 15: 367–371
- Janson C, McPhee S, Bilaniuk L, Haselgrove J, Testaiuti M, Freese A, Wang D-J, Shera D, Hurh P, Rupin J, Saslow E, Goldfarb O, Goldberg M, Larijani G, Sharrar W, Liouterman L, Camp A, Kolodny E, Samulski J, Leone P. Gene therapy of Canavan disease: AAV-2 vector for neurosurgical delivery of aspartoacylase gene (ASPA) to the human brain. *Hum Gene Ther* 2002; 13: 1391–1412
- Kamoshita S, Rapin I, Suzuki K, Suzuki K. Spongy degeneration of the brain. *Neurology* 1968; 18: 975–985
- Kaul R, Gao GP, Balamurugan K, Matalon R. Cloning of the human aspartoacylase cDNA and a predominant missense mutation in Canavan disease. *Nat Genet* 1993; 5: 118–123
- Kendall BE. Disorders of lysosomes, peroxisomes, and mitochondria. *AJNR Am J Neuroradiol* 1992; 13: 621–653.
- Kirmani BF, Jacobowitz DM, Kallarakal AT, Namboodiri MAA. Aspartoacylase is restricted primarily to myelin synthesizing cells in the CNS: therapeutic implications for Canavan disease. *Mol Brain Res* 2002; 107: 176–183
- Kvittingen EA, Guldal G, Borsting S, Skälpe IO, Stokke O, Jellum E. *N*-acetylaspartic aciduria in a child with a progressive cerebral atrophy. *Clin Chim Acta* 1986; 158: 217–227
- Leone P, Janson CG, Bilianuk L, Wang Z, Sorgi F, Huang L, Matalon R, Kaul R, Zeng Z, Freese A, McPhee SW, Mee E, During MJ. Aspartoacylase gene transfer to the mammalian central nervous system with therapeutic implications for Canavan disease. *Ann Neurol* 2000; 48: 27–38
- Mahloudji M, Daneshbod K, Karjoo M. Familial spongy degeneration of the brain. *Arch Neurol* 1970; 22: 294–298
- Marks HG, Caro PA, Wang Z, Detre JA, Bogdan AR, Gusnard DA, Zimmerman RA. Use of computed tomography, magnetic resonance imaging, and localized ¹H magnetic resonance spectroscopy in Canavan's disease: a case report. *Ann Neurol* 1991; 30: 106–110
- Matalon R, Michals-Matalon K. Prenatal diagnosis of Canavan disease. *Prenat Diagn* 1999; 19: 669–670
- Matalon R, Michals-Matalon K. Spongy degeneration of the brain, Canavan disease: biochemical and molecular findings. *Pediatr Pathol Mol Med* 2000; 18: 471–481
- Matalon R, Michals K, Sebesta D, Deanching M, Gashkoff P, Casanova J. Aspartoacylase deficiency and *N*-acetylaspartic aciduria in patients with Canavan disease. *Am J Med Genet* 1988; 29: 463–471
- Matalon R, Kaul R, Casanova J, Michals K, Johnson A, Rapin I, Gashkoff P, Deanching M. Aspartoacylase deficiency: the enzyme defect in Canavan disease. *J Inherit Metab Dis* 1989; 12: 329–331
- Matalon R, Kaul R, Michals K. Canavan disease: biochemical and molecular studies. *J Inherit Metab Dis* 1993; 16: 744–752
- Matalon R, Michals K, Kaul R. Canavan disease: from spongy degeneration to molecular analysis. *J Pediatr* 1995; 127: 511–517
- Matalon R, Kaul R, Gao GP, Michals K, Gray RGF, Bennett-Briton S, Norman A, Smith M, Jakobs C. Prenatal diagnosis for canavan disease: the use of DNA markers. *J Inherit Metab Dis* 1995; 18: 215–217
- Matalon R, Rady PL, Platt KA, Skinner HB, Quast MJ, Campbell GA, Matalon K, Ceci JD, Tyring SK, Nehls M, Surendran S, Wei J, Ezell EL, Szucs S. Knock-out mouse for Canavan disease: a model for gene transfer to the central nervous system. *J Gene Med* 2000; 2: 165–175
- Meyding-Lamadé U, Sartor K. Magnetresonanztomographie bei neurodegenerativen Erkrankungen im Kindesalter. *Klin Neuroradiol* 1993; 3: 52–61
- Toft PB, Geiß-Holtorf R, Roland MO, Pryd SO, Mueller-Forell W, Christensen E, Lehnert W, Lou HC, Ott D, Hennig J, Henriksen O. Magnetic resonance imaging in juvenile Canavan disease. *Eur J Pediatr* 1993; 152: 750–753
- Topçu M, Erdem G, Saatçi I, Aktan G, Şimşek A A, Renda Y, Schutgens RBH, Wanders RJA, Jacobs C. Clinical and magnetic resonance imaging features of L-2-hydroxyglutaric academia: report of three cases in comparison with Canavan disease. *J Child Neurol* 1996; 11: 373–377
- Traeger E, Rapin I. The clinical course of Canavan disease. *Pediatr Neurol* 1998; 18: 207–212
- Van Bogaert L, Bertrand I. Les leucodystrophies progressives familiales. *Rev Neurol* 1933; 2: 249–286
- Wittsack HJ, Kugel H, Roth B, Heindel W. Quantitative measurements with localized ¹H MR spectroscopy in children with Canava's disease. *J Magn Reson Imaging* 1996; 6: 889–893
- Zafeiriou D, Kleijer WJ, Maropoulos G, Anastasiou AL, Augoustidou-Savvopoulou P, Papadopoulou F, Kontopoulou EE, Fagan E, Payne S. Protracted course of *N*-acetylaspartic aciduria in two non-Jewish siblings: identical clinical and magnetic resonance imaging findings. *Brain Dev* 1999; 21: 205–208
- Zelnik N, Amir N, Luder AS, Hemli JA, Elpeleg ON, Fatal A, Gross-Tsur V, Harel S. Protracted clinical course for patients with Canavan disease. *Dev Med Child Neurol* 1993; 35: 346–358

43 L-2-Hydroxyglutaric Aciduria

- Aydin K, Ozmen M, Tatli B, Sencer S. Single-voxel MR spectroscopy and diffusion-weighted MRI in two patients with L-2-hydroxyglutaric aciduria. *Pediatr Radiol* 2003; 33: 872–876
- Barbot C, Fineza I, Diogo L, Maia M, Melo J, Guimarães A, Pires MM, Cardoso ML, Vilarinho L. L-2-Hydroxyglutaric aciduria: clinical biochemical and magnetic resonance imaging in six Portuguese pediatric patients. *Brain Dev* 1997; 19: 268–273
- Barth PG, Hoffmann GF, Jaeken J, Lehnert W, Hanefeld F, van Gennip AH, Duran M, Valk J, Schutgens RBH, Trefz FK, Reimann G, Hartung HP. L-2-Hydroxyglutaric acidemia: a novel inherited neurometabolic disease. *Ann Neurol* 1992; 32: 66–71
- Barth PG, Hoffmann GF, Jaeken J, Wanders RJA, Duran M, Jansen GA, Jakobs C, Lehnert W, Hanefeld F, Valk J, Schutgens RBH, Trefz FK, Hartung HP, Chamoles NA, Sfaello Z, Caruso U. L-2-Hydroxyglutaric acidemia: clinical and biochemical findings in 12 patients and preliminary report on L-2-hydroxyacid dehydrogenase. *J Inherit Metab Dis* 1993; 16: 753–761
- Barth PG, Wanders RJA, Scholte HR, Abeling N, Jakobs C, Schutgens RBH, Vreken P. L-2-Hydroxyglutaric aciduria and lactic acidosis. *J Inherit Metab Dis* 1998; 21: 251–254

- Chen E, Nyhan WL, Jakobs C, Greco CM, Barkovich AJ, Cox VA, Packman P. L-2-Hydroxyglutaric aciduria: neuropathological correlations and first report of severe neurodegenerative disease and neonatal death. *J Inherit Metab Dis* 1996; 19: 335–343
- Clerc C, Bataillard M, Richard P, Divry P, Kreaehenbuhl J, Rumbach L. An adult form of L-2-hydroxyglutaric aciduria revealed by tremor. *Eur Neurol* 2000; 43: 119–120
- De Klerk JBC, Huijman JGM, Stroink H, Robben SGF, Jakobs C, Duran M. L-2-Hydroxyglutaric aciduria: clinical heterogeneity versus biochemical homogeneity in a sibship. *Neuropediatrics* 1997; 28: 314–317
- D'Incenti, Farina L, Moroni I, Uziel G, Savoiardo M. L-2-Hydroxyglutaric aciduria: MRI in seven cases. *Neuropathology* 1998; 40: 727–733
- Diogo L, FINEZA I, Canha J, Borges L, Cardoso ML, Vilarinho L. Macrocephaly as the presenting feature of L-2-hydroxyglutaric aciduria in a 5-month-old-boy. *J Inherit Metab Dis* 1996; 19: 369–370
- Divry P, Jakobs C, Vianey-Saban C, Gibson KM, Michelakakis H, Papadimitriou A, Divari R, Chabrol B, Cournelle MA, Livet MO. L-2-Hydroxyglutaric aciduria: two further cases. *J Inherit Metab Dis* 1993; 16: 505–507
- Duran M, Kamerling JP, Bakker HD, van Gennip AH, Wadman SK. L-2-Hydroxyglutaric aciduria: an inborn error of metabolism. *J Inherit Metab Dis* 1980; 3: 109–112
- Fujitake J, Ishikawa Y, Fujii H, Nishimura K, Inoue F, Terada N, Okochi M, Tatsuoka Y. L-2-Hydroxyglutaric aciduria: two Japanese adult cases in one family. *J Neurol* 1999; 246: 378–382
- Hoffmann GF, Jakobs C, Holmes B, Mitchell L, Becker G, Hartung H-P, Nyhan WL. Organic acids in cerebrospinal fluid and plasma of patients with L-2-hydroxyglutaric aciduria. *J Inherit Metab Dis* 1995; 18: 189–193
- Jansen GA, Wanders RJA. L-2-Hydroxyglutarate dehydrogenase: identification of a novel enzyme activity in rat and human liver. Implications for L-2-hydroxyglutaric aciduria. *Biochim Biophys Acta* 1993; 1225: 53–56
- Kaabachi N, Larnaout A, Rabier D, Jakobs C, Belal S, Hentati F, Parvey P, Bardet J, Ben Hamida M, Mebazaa A, Kamoun P. Familial encephalopathy and L-2-hydroxyglutaric aciduria. *J Inherit Metab Dis* 1993; 16: 893
- Kossoff EH, Keswani SC, Raymond GV. L-2-Hydroxyglutaric aciduria presenting as migraine. *Neurology* 2001; 57: 1731–1732
- Larnaout A, Hentati F, Belal S, Ben Hamida C, Kaabachi N, Ben Hamida M. Clinical and pathological study of three Tunisian siblings with L-2-hydroxyglutaric aciduria. *Acta Neuropathol (Berl)* 1994; 88: 367–370
- Moroni I, D'Incerti L, Farina L, Rimoldi M, Uziel G. Clinical, biochemical and neuroradiological findings in L-2-hydroxyglutaric aciduria. *Neurol Sci* 2000; 21: 103–108
- Moroni I, Bugiani M, D'Incerti L, Maccagnano C, Rimoldi M, Bisola L, Pollo B, Finocchiaro G, Uziel G. L-2-Hydroxyglutaric aciduria and brain malignant tumors. A predisposing condition? *Neurology* 2004; 62: 1882–1884
- Rzem R, Veiga-da-Cunha M, Noël G, Goffette S, Nassogne MC, Tabarki B, Schöller C, Marquardt T, Vikkula M, Van Schaftingen E. A gene encoding a putative FAD-dependent L-2-hydroxyglutarate dehydrogenase is mutated in L-2-hydroxyglutaric aciduria. *Proc Natl Acad Sci USA* 2004; 101: 16849–16854
- Sztrihai L, Gururaj A, Vreken P, Nork M, Lestringant GG. L-2-Hydroxyglutaric aciduria in two siblings. *Pediatr Neurol* 2002; 27: 141–144
- Topçu M, Erdem G, Saatçi I, Aktan G, Şimşek A A, Renda Y, Schutgens RBH, Wanders RJA, Jacobs C. Clinical and magnetic resonance imaging features of L-2-hydroxyglutaric aciduria academia: report of three cases in comparison with Canadian disease. *J Child Neurol* 1996; 11: 373–377
- Topçu M, Jobard F, Halliez S, Coskun T, Yalçinkaya C, Gerceker FO, Wanders RJA, Prud'homme JF, Lathrop M, Özguc M, Fischer J. L-2-Hydroxyglutaric aciduria: identification of a mutant gene C14orf160, localized on chromosome 14q22.1. *Hum Mol Genet* 2004; 13: 2803–2811
- Wanders RJA, Vilarinho L, Hartung HP, Hoffmann GF, Mooijer PAW, Jansen GA, Huijman JGM, de Klerk JBC, ten Brink HJ, Jakobs C, Duran M. L-2-Hydroxyglutaric aciduria: normal L-2-hydroxyglutarate dehydrogenase activity in liver from two new patients. *J Inherit Metab Dis* 1997; 20: 725–726
- Wilcken B, Pitt J, Heath F, Walsh P, Wilson G, Bachanan N. L-2-Hydroxyglutaric aciduria: three Australian cases. *J Inherit Metab Dis* 1993; 16: 501–504
- Zafeiriou DI, Sewell A, Savvopoulou-Augoustidou P, Gombakis N, Katzos G. L-2-Hydroxyglutaric aciduria presenting as a status epilepticus. *Brain Dev* 2001; 23: 255–257

44 D-2-Hydroxy Glutaric Aciduria

- Achouri Y, Noël G, Vertommen D, Rider MH, Veiga-Da-Cunha M, Van Schaftingen E. Identification of a dehydrogenase acting on D-2-hydroxyglutarate. *Biochem J* 2004; 381: 35–42
- Amiel J, de Lonay P, Francannet C, Picard A, Bruel H, Rabier D, Le Merrer M, Verhoeven N, Jakobs C, Lyonnet S, Munnich A. Facial anomalies in D-2-hydroxyglutaric aciduria. *Am J Med Genet* 1999; 86: 124–129
- Baker NS, Sarnat HB, Jack RM, Patterson K, Shaw DW, Herndon SP. D-2-hydroxyglutaric aciduria: hypertonemia, cortical blindness, seizures, cardiomyopathy and cylindrical spirals in skeletal muscle. *J Child Neurol* 1997; 12: 31–36
- Chalmers RA, Lawson AM, Watts WE, Tavill AS. D-2-Hydroxyglutaric aciduria: case report and biochemical studies. *J Inherit Metab Dis* 1980; 3: 11–15
- Clarcke NF, Andrews I, Carpenter K, Jakobs C, van der Knaap MS, Kirk EP. D-2-Hydroxyglutaric aciduria: a case with an intermediate phenotype and prenatal diagnosis of two affected fetuses. *Am J Med Genet* 2003; 120A: 523–527
- Craig WJ, Jakobs C, Sekul EA, Levy ML, Gibson KM, Butler IJ, Herman GE. D-2-Hydroxyglutaric aciduria in neonate with seizures and CNS dysfunction. *Pediatr Neurol* 1994; 10: 49–53
- Da Silva CG, Ribeiro CAJ, Leipnitz G, Duntra-Filho CS, Wyse ATS, Wannmacher CMD, Sarkis JF, Jakobs C, Wajner M. Inhibition of cytochrome c oxidase activity in rat cerebral cortex and human skeletal muscle by D-2-hydroxyglutaric acid in vitro. *Biochim Biophys Acta* 2002; 1586: 81–91
- Eeg-Olofsson O, Zhang WW, Olsson Y, Jagell S, Hagenfeldt L. D-2-Hydroxyglutaric aciduria with cerebral, vascular, and muscular abnormalities in a 14-year-old boy. *J Child Neurol* 2000; 15: 488–492
- Geerts Y, Renier WO, Bakkeren J, de Jong J. 2-Hydroxyglutaric aciduria: a case report on an infant with the D-isomeric form with review of the literature. *J Neurol Sci* 1996; 143: 166–169
- Gibson KM, Craig W, Herman GE, Jakobs C. D-2-Hydroxyglutaric aciduria in a newborn with neurological abnormalities: a new neurometabolic disorder? *J Inherit Metab Dis* 1993; 16: 497–500

- Gibson KM, ten Brink HJ, Schor SM, Kok RM, Bootsma AH, Hoffmann GF, Jakobs C. Stable isotope dilution analysis of D- and L-2-hydroxyglutaric acid: application to the detection and prenatal diagnosis of D- and L-2-hydroxyglutaric acidemias. *Pediatr Res* 1993; 34: 277–280
- Kwong KL, Mak T, Fong CM, Poon KH, Wong SN, So KT. D-2-Hydroxyglutaric aciduria and subdural haemorrhage. *Acta Paediatr* 2002; 91: 716–718
- Muntau AC, Röschinger W, Merckenschlager A, van der Knaap MS, Jakobs C, Duran M, Hoffmann GF, Roscher AA. Combined D-2- and L-2-hydroxyglutaric aciduria with neonatal onset encephalopathy: a third biochemical variant of 2-hydroxyglutaric aciduria? *Neuropediatrics* 2000; 31: 137–140
- Nyhan WL, Shelton D, Jakobs C, Holmes B, Bowe C, Curry CJR, Vance C, Duran M, Sweetman L. D-2-Hydroxyglutaric aciduria. *J Child Neurol* 1995; 10: 137–142
- Struys EA, Verhoeven NM, Roos B, Jakobs C. Disease-related metabolites in culture medium of fibroblasts from patients with D-hydroxyglutaric aciduria, L-2-hydroxyglutaric aciduria and combined D-/L-2-hydroxyglutaric aciduria. *Clin Chem* 2003; 49: 1133–1138
- Struys EA, Verhoeven NM, Brunengraber H, Jakobs C. Investigations by mass isotopomer analysis of the formation of D-2-hydroxyglutarate by cultured lymphoblasts from two patients with D-2-hydroxyglutaric aciduria. *FEBS Lett* 2004; 557: 115–120
- Struys EA, Salomons GS, Achouri Y, van Schaftingen E, Grosso S, Craigen WJ, Verhoeven NM, Jakobs C. Mutations in the D-2-hydroxyglutarate dehydrogenase gene cause D-2-hydroxyglutaric aciduria. *Am J Hum Genet* 2005; 76: 358–360
- Sugita K, Kakinuma H, Okajima Y, Ogawa A, Watanabe H, Niimi H. Clinical and MRI findings in a case of D-2-hydroxyglutaric aciduria. *Brain Dev* 1995; 17: 139–141
- van der Knaap MS, Jakobs C, Hoffmann GF, Nyhan WL, Renier WO, Smeitink JAM, Catsman-Berrevoets CE, Hjalmarson O, Vallance H, Sugita K, Bowe CM, Herrin JT, Craigen WJ, Buist NRM, Brookfield DSK, Cahlmers RA. D-2-Hydroxyglutaric aciduria: biochemical marker or clinical disease entity? *Ann Neurol* 1999a; 45: 111–119
- van der Knaap MS, Jakobs C, Hoffmann GF, Duran M, Muntau AC, Schweitzer S, Kelley RI, Parrot-Rouland F, Amiel J, De Lonay P, Rabier D, Eeg-Olofsson O. D-2-Hydroxyglutaric aciduria: further clinical delineation. *J Inherit Metab Dis* 1999b; 22: 404–413
- Wagner L, Hoffmann GF, Jakobs C. D-2-Hydroxyglutaric aciduria: evidence of clinical and biochemical heterogeneity. *J Inherit Metab Dis* 1998; 21: 247–250
- Wajner M, Vargas CR, Funayama C, Fernandez A, Elias MLC, Goodman SI, Jakobs C, van der Knaap MS. D-2-Hydroxyglutaric aciduria in a patient with a severe clinical phenotype and unusual MRI findings. *J Inherit Metab Dis* 2002; 25: 28–34
- Wanders RJA, Mooyer P. D-2-Hydroxyglutaric aciduria: identification of a new enzyme, D-2-hydroxyglutarate dehydrogenase, localized in mitochondria. *J Inherit Metab Dis* 1995; 18: 194–196
- ## 45 Hyperhomocysteinemias
- ### Defects in the Transsulfuration Pathway
- Abeling NGGM, van Gennip AH, Blom H, Wevers RA, Vreken P, van Tinteren HLG, Bakker HD. Rapid diagnosis and methionine administration: basis for a favourable outcome in a patient with methylene tetrahydrofolate reductase deficiency. *J Inherit Metab Dis* 1999; 22: 240–242
- Al-Essa MA, Al Amir A, Rashed M, Al Jishi E, Abutaleb A, Mobairek K, Shin YS, Ozand PT. Clinical, fluorine-18 labeled 2-fluoro-2-deoxyglucose positron emission tomography of the brain, MR spectroscopy, and therapeutic attempts in methylenetetrahydrofolate reductase deficiency. *Brain Dev* 1999; 21: 345–349
- Baethmann M, Wendel U, Hoffmann GF, Göhlich-Ratmann G, Kleinlein B, Seiffert P, Blom H, Voit T. Hydrocephalus internus in two patients with 5,10-methylenetetrahydrofolate reductase deficiency. *Neuropediatrics* 2000; 31: 314–317
- Beckman DR, Hoganson G, Berlow S, Gilbert EF. Pathological findings in 5,10-methylene tetrahydrofolate reductase deficiency. *Birth Defects* 1987; 23: 47–64
- Beradelli A, Thompson PD, Zaccagnini M, Giardini O, D'Eufemia P, Massoud R, Manfredi M. Two sisters with generalized dystonia associated with homocystinuria. *Mov Disord* 1991; 6: 163–165
- Carson NAJ, Dent CE, Field CMB, Gaull GE. Homocystinuria. *J Pediatr* 1965; 66: 565–583
- Chou SM, Waisman HA. Spongy degeneration of the central nervous system. *Arch Pathol Lab Med* 1965; 79: 357–363
- Clayton PT, Smith I, Harding B, Hyland K, Leonard JV, Leeming RJ. Subacute combined degeneration of the cord, dementia and Parkinsonism due to an inborn error of folate metabolism. *J Neurol Neurosurg Psychiatry* 1986; 49: 920–927
- Dunn HG, Perry TL, Dolman CL. Homocystinuria. A recently discovered cause of mental defect and cerebrovascular thrombosis. *Neurology* 1966; 16: 407–420
- Engelbrecht V, Rassek M, Huismann J, Wendel U. MR and proton MR spectroscopy of the brain in hyperhomocysteinemia caused by methylenetetrahydrofolate reductase deficiency. *AJNR Am J Neuroradiol* 1997; 18: 536–539
- Fattal-Valevski A, Bassan H, Korman SH, Lerman-Sagie T, Gutman A, Harel S. Methylenetetrahydrofolate reductase deficiency: importance of early diagnosis. *J Child Neurol* 2000; 15: 539–543
- Fowler B. Disorders of homocysteine metabolism. *J Inherit Metab Dis* 1997; 20: 270–285
- Gerritsen T, Waisman HA. Homocystinuria, an error in the metabolism of methionine. *Pediatrics* 1964; 33: 413–420
- Haworth JC, Dilling LA, Surtees RAH, Seargeant LE, Shing HL, Cooper BA, Rosenblatt DS. Symptomatic and asymptomatic methylenetetrahydrofolate reductase deficiency in two adult brothers. *Am J Med Genet* 1993; 45: 572–576
- Hyland K, Smith I, Bottiglieri T, Perry J, Wendel U, Clayton PT, Leonard JV. Demyelination and decreased S-adenosylmethionine in 5,10-methylenetetrahydrofolate reductase deficiency. *Neurology* 1988; 38: 459–462
- Kelly PJ, Furie KL, Kistler JP, Barron M, Picard EH, Mandell R, Shih VE. Stroke in young patients with hyperhomocysteinemia due to cystathionine beta-synthase deficiency. *Neurology* 2003; 60: 275–279
- Keskin S, Yalcin E. Case report of homocystinuria: clinical, electroencephalographic, and magnetic resonance imaging findings. *J Child Neurol* 1994; 9: 210–211

- Kishi T, Kawamura I, Harada Y, Eguchi T, Sakura N, Ueda K, Nari-sawa K, Rosenblatt DS. Effect of betaine on S-adenosylmethionine levels in the cerebrospinal fluid in a patient with methylenetetrahydrofolate reductase deficiency and peripheral neuropathy. *J Inherit Metab Dis* 1994; 17: 560–565
- Kraus JP. Molecular basis of phenotype expression in homocystinuria. *J Inherit Metab Dis* 1994; 17: 383–390
- Lee C-C, Surtees R, Duchon LW. Distal motor axonopathy and central nervous system myelin vacuolation caused by cycloleucine, an inhibitor of methionine adenosyltransferase. *Brain* 1992; 115: 935–955
- Li SCH, Stewart PM. Homocystinuria and psychiatric disorder: a case report. *Pathology* 1999; 31: 221–224
- Ludolph AC, Ullrich K, Bick U, Fahrendorf G, Pzyrembel H. Functional and morphological deficits in late-treated patients with homocystinuria: a clinical, electrophysiologic and MRI study. *Acta Neurol Scand* 1991; 83: 161–165
- Nishimura M, Yoshino K, Tomita Y, Takashima S, Tanaka J, Nari-sawa K, Kurobane I. Central and peripheral nervous system pathology of homocystinuria due to 5,10-methylenetetrahydrofolate reductase deficiency. *Pediatr Neurol* 1985; 1: 375–378
- Ruano MM, Castillo M, Thompson JE. MR imaging in a patient with homocystinuria. *AJR Am J Roentgenol* 1998; 171: 1147–1149
- Sakura N, Ono H, Nomura S, Ueda H, Fujita N. Betaine dose and treatment intervals in therapy for homocystinuria due to 5,10-methylenetetrahydrofolate reductase deficiency. *J Inherit Metab Dis* 1998; 21: 84–85
- Surtees R, Leonard J, Austin S. Association of demyelination with deficiency of cerebrospinal-fluid-S-adenosylmethionine in inborn errors of methyl-transfer pathway. *Lancet* 1991; 338: 1550–1554
- Surtees R, Heales S, Bowron A. Association of cerebrospinal fluid deficiency of 5-methyltetrahydrofolate, but not S-adenosylmethionine, with reduced concentrations of the acid metabolites of 5-hydroxytryptamine and dopamine. *Clin Sci* 1994; 86: 697–702
- Visy JM, le Coz P, Chadeaux B, Fressinaud C, Woimant F, Marquet J, Zittoun J, Visy J, Vallat JM, Haguénau M. Homocystinuria due to 5,10-methylenetetrahydrofolate reductase deficiency revealed by stroke in adult siblings. *Neurology* 1991; 41: 1313–1315
- Walk D, Kang SS, Horwitz A. Intermittent encephalopathy, reversible nerve conduction slowing, and MRI evidence of cerebral white matter disease in methylenetetrahydrofolate reductase deficiency. *Neurology* 1994; 44: 344–347
- White HH, Rowland LP, Araki S, Thompson HL, Cowen D. Homocystinuria. *Arch Neurol* 1965; 13: 455–470
- Yap S. Classical homocystinuria: vascular risk and its prevention. *J Inherit Metab Dis* 2003; 26: 259–265
- Yap S, Naughten E. Homocystinuria due to cystathionine β -synthase deficiency in Ireland: 25 years' experience of a newborn screened and treated population with reference to clinical outcome and biochemical control. *J Inherit Metab Dis* 1998; 21: 738–747
- Bellamy MF, McDowell IFW. Putative mechanisms for vascular damage by homocysteine. *J Inherit Metab Dis* 1997; 20: 307–315
- Broers GHJ. The case for mild hyperhomocysteinemia as a risk factor. *J Inherit Metab Dis* 1997; 20: 301–306
- Bushnell CD, Goldstein LB. Homocysteine testing in patients with acute ischemic stroke. *Neurology* 2002; 59: 1541–1546
- Cottingham EM, LaMantia C, Stabler SP, Allen RH, Tangerman A, Wagner C, Zeisel SH, Mudd SH. Adverse event associated with methionine loading test. *Vasc Biol* 2002; 22: 1046–1050
- Diaz-Arrastia R. Homocysteine and neurologic disease. *Arch Neurol* 2000; 57: 1422–1428
- Dufouil C, Alperovitch A, Ducros V, Tzourio C. Homocysteine, white matter hyperintensities, and cognition in healthy elder people. *Ann Neurol* 2003; 53: 214–221
- Ganesan V, Prengler M, McShane MA, Wade AM, Kirkham FJ. Investigation of risk factors in children with arterial ischemic stroke. *Ann Neurol* 2003; 53: 167–173
- Hogveen M, Blom HJ, van Amerongen M, Boogmans B, van Beynum IM, van de Bor M. Hyperhomocysteinemia as risk factor for ischemic and hemorrhagic stroke in newborn infants. *J Pediatr* 2002; 141: 429–431
- Kelly PJ, Rosand J, Kistler JP, Shih VE, Silveira S, Plomaritoglu A, Furie KL. Homocysteine, MTHFR 677CT polymorphism, and risk of ischemic stroke. Results of a meta-analysis. *Neurology* 2002; 59: 529–536
- Kim NK, Choi BO, Jung WS, Choi YJ, Choi KG. Hyperhomocysteinemia as an independent risk factor for silent brain infarction. *Neurology* 2003; 61: 1595–1599
- Kohara K, Fujisawa M, Ando F, Tabara Y, Niino N, Miki T, Shimokata H. MTHFR gene polymorphism as a risk factor for silent brain infarcts and white matter lesions in the Japanese general population. The NILS-LSA study. *Stroke* 2003; 34: 1130–1135
- Madonna P, de Stefano V, Coppola A, Cirillo F, Cerbone AM, Orefice G, Di Minno G. Hyperhomocysteinemia and other inherited prothrombotic conditions in young adults with a history of ischemic stroke. *Stroke* 2002; 33: 51–56
- Meiklejohn DJ, Vickers MA, Dijkhuisen R, Greaves M. Plasma homocysteine concentrations in the acute convalescent periods of atherothrombotic stroke. *Stroke* 2001; 32: 57–62
- Pezzini A, del Zotto E, Archetti S, Negrini R, Bani P, Albertini A, Grassi M, Assanelli D, Gasparotti R, Vignolo LA, Magoni M, Padovani A. Plasma homocysteine concentration, C677T MTHFR genotype, and 844ins68 bp CBS genotype in young adults with spontaneous cervical artery dissection and atherothrombotic stroke. *Stroke* 2002; 33: 664–669
- Prins ND, den Heijer T, Hofman A, Koudstaal PJ, Jolles J, Clarke R, Breteler MMB. Homocysteine and cognitive function in the elderly. The Rotterdam scan study. *Neurology* 2002; 59: 1375–1380
- Rosengarten B, Osthaus S, Auch D, Kaps M. Effects of acute hyperhomocysteinemia on the neurovascular coupling mechanism in healthy young adults. *Stroke* 2003; 34: 446–451
- Sarkar PK, Lambert LA. Aetiology and treatment of hyperhomocysteinemia causing ischaemic stroke. *Int J Clin Pract* 2001; 55: 262–268
- Tan NC-K, Venketasubramanian N, Saw S-M, Tjia HT-L. Hyperhomocyst(e)inemia and risk of ischemic stroke among young Asian adults. *Stroke* 2002; 33: 1956–1962
- Van Beynum IM, Smeitink JAM, den Heijer M, te Poele Pothoff MTWB, Blom HJ. Hyperhomocysteinemia. A risk factor for ischaemic stroke in children. *Circulation* 1999; 99: 2070–2072

Mild Hyperhomocysteinemia

- Aronow WS, Ahn C, Gutstein H. Increased plasma homocysteine is an independent predictor of new atherothrombotic brain infarction in older persons. *Am J Cardiol* 2000; 86: 585–586

- Van Diemen-Steenvoorde R, van Nieuwenhuizen O, de Klerk JBC, Duran M. Quasi-Moyamoya disease and heterozygosity for homocystinuria in a five-year-old girl. *Neuropediatrics* 1990; 21: 110–112
- Vermeer SE, van Dijk EJ, Koudstaal PJ, Oudkerk M, Hofman A, Clarke R, Breteler MMB. Homocysteine, silent brain infarcts, and white matter lesions: the Rotterdam scan study. *Ann Neurol* 2002; 51: 285–289
- Vermeulen EGJ, Stehouwer CDA, Valk J, van der Knaap MS, van den Berg M, Twisk JWR, Prevoe W, Rauwerda JA. Effect of homocysteine-lowering treatment with folic acid plus vitamin B₆ on cerebrovascular atherosclerosis and white matter abnormalities as determined by MRA and MRI: a placebo-controlled, randomized trial. *Eur J Clin Invest* 2004; 34: 256–261
- Welch GN, Loscalzo J. Homocysteine and atherothrombosis. *N Engl J Med* 1998; 338: 1042–1050
- Wilcken DEL, Wilcken B. The natural history of vascular disease in homocystinuria and the effects of treatment. *J Inherit Metab Dis* 1997; 20: 295–300
- ### Folate Deficiency
- Giles WH, Kittner SJ, Anda RF, Croft JB, Casper ML. Serum folate and risk factor for ischemic stroke. First national health and nutrition examination survey. Epidemiologic follow-up study. *Stroke* 1995; 26: 1166–1170
- Hoffbrand AV, Weir DG. The history of folic acid. *Br J Haematol* 2001; 113: 579–589
- Lever EG, Elwes RDC, Williams A, Reynolds EH. Subacute combined degeneration of the cord due to folate deficiency: response to methyl folate treatment. *J Neurol Neurosurg Psychiatry* 1986; 49: 1203–1207
- Robertson DM, Dinsdale HB, Campbell RJ, Kingston ChB. Subacute combined degeneration of the spinal cord. No association with vitamin B₁₂ deficiency. *Arch Neurol* 1971; 24: 203–207
- Scott JM, Weir DG. The methyl folate trap. *Lancet* 1981; 2: 337–340
- Selhub J. Folate, vitamin B12 and vitamin B6 and one carbon metabolism. *J Nutr Health Aging* 2002; 6: 39–42
- Van der Weyden MB, Hayman RJ, Rose IS, Brumley J. Folate-deficient human lymphoblasts: changes in deoxynucleotide metabolism and thymidylate cycle activities. *Eur J Haematol* 1991; 47: 109–114
- Weir DG, Scott JM. Brain function in the elderly: role of vitamin B₁₂ and folate. *Br Med Bull* 1999; 55: 669–682
- ### Inborn Errors of Cobalamin Metabolism
- Augoustides-Savvopoulou P, Mylonas I, Sewell AC, Rosenblatt DS. Reversible dementia in an adolescent with *cblC* disease: clinical heterogeneity within the same family. *J Inherit Metab Dis* 1999; 22: 759–758
- Bartholomew DW, Batshaw ML, Allen RH, Roe CR, Rosenblatt D, Valle DL, Francomano CA. Therapeutic approaches to cobalamin-C methylmalonic acidemia and homocystinuria. *J Pediatr* 1988; 112: 32–39
- Bellini C, Cerone R, Bonacci W, Caruso U, Magliano CP, Serra G, Fowler B, Romano C. Biochemical diagnosis and outcome of 2 years' treatment in a patient with combined methylmalonic aciduria and homocystinuria. *Eur J Pediatr* 1992; 151: 818–820
- Biancheri R, Cerone R, Schiaffino MC, Caruso U, Veneselli E, Perone MC, Rossi A, Gatti R. Cobalamin (Cbl) C/D deficiency: clinical, neurophysiological and neuroradiological findings in 14 cases. *Neuropediatrics* 2001; 32: 14–22
- Bibi H, Gelman-Kohan Z, Baumgartner ER, Rosenblatt DS. Transcobalamin II deficiency with methylmalonic aciduria in three sisters. *J Inherit Metab Dis* 1999; 22: 765–772
- Carmel R, Watkins D, Goodman SI, Rosenblatt DS. Hereditary defect of cobalamin metabolism (*cblG* mutation) presenting as a neurologic disorder in adulthood. *N Engl J Med* 1988; 318: 1738–1741
- Dayan AD, Ramsey RB. An inborn error of vitamin B₁₂ metabolism associated with cellular deficiency of coenzyme forms of the vitamin. *J Neurol Sci* 1974; 23: 117–128
- Enns GM, Barkovich AJ, Rosenblatt DS, Fredrick DR, Weisiger K, Ohnstad C, Packman S. Progressive neurological deterioration and MRI changes in *cblC* methylmalonic acidemia treated with hydroxocobalamin. *J Inherit Metab Dis* 1999; 22: 599–607
- Fenton WA, Rosenberg LE. Genetic and biochemical analysis of human cobalamin mutants in cell culture. *Annu Rev Genet* 1978; 12: 223–248
- Linnell JC, Ray Bhatt H. Inherited errors of cobalamin metabolism and their management. *Balliere's Clin Haematol* 1995; 8: 567–601
- Mitchell GA, Watkins D, Melançon SB, Rosenblatt DS, Geoffroy G, Orquin J, Homsy MB, Dallaire L. Clinical heterogeneity in cobalamin C variant of combined homocystinuria and methylmalonic aciduria. *J Pediatr* 1986; 108: 410–415
- Powers JM, Rosenblatt DS, Schmidt RE, Cross AH, Black JT, Moser AB, Moser HW, Morgan DJ. Neurological and neuropathological heterogeneity in two brothers with cobalamin C deficiency. *Ann Neurol* 2001; 49: 396–400
- Rossi A, Biancheri R, Tortori-Donati P. The pathogenesis of hydrocephalus in inborn errors of the single carbon transfer pathway. *Neuropediatrics* 2001^a; 32: 335–336
- Rossi A, Cerone R, Biancheri R, Gatti R, Schiaffino MC, Fonda C, Zammarchi E, Tortori-Donati P. Early-onset combined methylmalonic aciduria and homocystinuria: neuroradiologic findings. *AJNR Am J Neuroradiol* 2001^b; 22: 554–563
- Schuh S, Rosenblatt DS, Cooper BA, Schroeder M-L, Bishop AJ, Seargeant LE, Haworth JC. Homocystinuria and megaloblastic anemia responsive to vitamin B12 therapy. An inborn error of metabolism due to a defect in cobalamin metabolism. *N Engl J Med* 1984; 310: 686–690
- Shinnar S, Singer HS. Cobalamin C mutation (methylmalonic aciduria and homocystinuria) in adolescence. *N Engl J Med* 1984; 311: 451–454
- Steen C, Rosenblatt DS, Scheying H, Brauer JC, Kohlstätter A. Cobalamin E (*cblE*) disease: a severe neurological disorder with megaloblastic anaemia, homocystinuria and slow serum methionine. *J Inherit Metab Dis* 1997; 20: 705–706
- Surtees R. Demyelination and inborn errors of the single carbon transfer pathway. *Eur J Pediatr* 1998; 157: S118–S121
- Thomas PK, Hoffbrand AV. Hereditary transcobalamin II deficiency: a 22 year follow up. *J Neurol Neurosurg Psychiatry* 1997; 62: 197
- Tuchman M, Kelly P, Watkins D, Rosenblatt DS. Vitamin B₁₂-responsive megaloblastic anemia, homocystinuria, and transient methylmalonic aciduria in *cblE* disease. *J Pediatr* 1988; 113: 1052–1055
- Watkins D, Rosenblatt DS. Genetic heterogeneity among patients with methylcobalamin deficiency. Definition of two complementation groups: *cblE* and *cblG*. *J Clin Invest* 1988; 81: 1690–1694

Zavad'ákoa P, Fowler B, Zeman J, Suomala T, Pøistoupilová K, Kozich V. CblE type of homocystinuria due to methionine synthase reductase deficiency: clinical and molecular studies and prenatal diagnosis in two families. *J Inher Metab Dis* 2002; 25: 461–476

Cobalamin Deficiency

Bassi SS, Bulundwe KK, Greeff GP, Labuscagne JH, Gledhill RF. MRI of the spinal cord in myelopathy complicating vitamin B₁₂ deficiency: two additional cases and a review of the literature. *Neuroradiology* 1999; 41: 271–274

Brattström L, Israelsson B, Lindgärde F, Hultberg B. Higher total plasma homocysteine in vitamin B₁₂ deficiency than in heterozygosity for homocystinuria due to cystathionine β-synthase deficiency. *Metabolism* 1988; 37: 175–178

Carmel R. Pernicious anemia. *Arch Intern Med* 1988; 148: 1712–1714

Chatterjee A, Yapundich R, Palmer CA, Marson DC, Mitchell GW. Leukoencephalopathy associated with cobalamin deficiency. *Neurology* 1996; 16: 832–834

Clementz CL, Schade SG. The spectrum of vitamin B₁₂ deficiency. *Am Fam Physician* 1999; 41: 150–162

Duprez TP, Gille M, vande Berg BC, Malghem J, Grandin CB, Michel P, Ghariani S, Maldague BE. MRI of the spine in cobalamin deficiency: the value of examining both spinal cord and bone marrow. *Neuroradiology* 1996; 38: 511–515

Fine EJ, Soria E, Paroski MW, Petryk D, Thomasula L. The neurophysiological profile of vitamin B₁₂ deficiency. *Muscle Nerve* 1990; 13: 158–164

Flippo TS, Holder WD. Neurologic degeneration associated with nitrous oxide anesthesia in patients with vitamin B₁₂ deficiency. *Arch Surg* 1993; 128: 1391–1395

Garewal G, Narang A, Das KC. Infantile tremor syndrome: a vitamin B₁₂ deficiency syndrome in infants. *J Trop Pediatr* 1988; 34: 174–178

Giloiis C, Wierzbicki AS, Hirani N, Norman PM, Jones SJ, Ponsford S, Alani SM, Kriss A. The hematological and electrophysiological effects of cobalamin. Deficiency secondary to vegetarian diets. *Ann NY Acad Sci* 1992; 669: 345–348

Graham SM, Arvela OM, Wise GA. Long-term neurologic consequences of nutritional vitamin B₁₂ deficiency in infants. *J Pediatr* 1992; 121: 710–714

Grattan-Smith PJ, Wilcken B, Procopis PG, Wise GA. The neurological syndrome of infantile cobalamin deficiency: developmental regression and involuntary movements. *Mov Disord* 1997; 12: 39–46

Green R, Kinsella LJ. Current concepts in the diagnosis of cobalamin deficiency. *Neurology* 1995; 45: 1435–1440

Healton EB, Savage DG, Brust JCM, Garrett TJ, Lindenbaum J. Neurologic aspects of cobalamin deficiency. *Medicine* 1991; 70: 229–245

Heckmann JG, Lang CJG, Ganslandt O, Tomandl B, Neundörfer B. Reversible leukoencephalopathy due to vitamin B₁₂ deficiency in an acromegalic patient. *J Neurol* 2003; 250: 366–368

Hector M, Burton JR. What are the psychiatric manifestations of vitamin B₁₂ deficiency? *J Am Geriatr Soc* 1988; 36: 1105–1112

Hemmer B, Glocker FX, Schumacher M, Deuschl G, Lücking CH. Subacute combined deterioration: clinical, electrophysiological, and magnetic resonance imaging findings. *J Neurol Neurosurg Psychiatry* 1998; 65: 822–827

Higginbottom MC, Sweetman L, Nyhan WL. A syndrome of methylmalonic aciduria, homocystinuria, megaloblastic anemia and neurologic abnormalities in a vitamin B₁₂ deficient breast-fed infant of a strict vegetarian. *N Engl J Med* 1978; 299: 317–323

Hoffbrand AV, Jackson BFA. Correction of the DNA synthesis defect in vitamin B₁₂ deficiency by tetrahydrofolate: evidence in favour of the methyl-folate trap hypothesis as the cause of megaloblastic anaemia in vitamin B₁₂ deficiency. *Br J Haematol* 1993; 83: 643–647

Holloway KL, Alberico AM. Postoperative myeloneuropathy: a preventable complication in patients with B₁₂ deficiency. *J Neurosurg* 1990; 72: 732–736

Karnaze DS, Carmel R. Neurologic and evoked potential abnormalities in subtle cobalamin deficiency states, including deficiency without anemia and with normal absorption of free cobalamin. *Arch Neurol* 1990; 47: 1008–1012

Katsaros VK, Glocker FX, Hemmer B, Schumacher M. MRI of spinal cord and brain lesions in subacute combined degeneration. *Neuroradiology* 1998; 40: 716–719

Kealey SM, Provenzale JM. Tensor diffusion imaging in B₁₂ leukoencephalopathy. *J Comput Assist Tomogr* 2002; 26: 952–955

Kühne T, Bubl R, Baumgartner R. Maternal vegan diet causing a serious infantile neurological disorder due to vitamin B₁₂ deficiency. *Eur J Pediatr* 1991; 150: 205–208

Küker W, Hesselmann V, de Simone A. MRI demonstration of reversible impairment of the blood-CNS barrier function in subacute combined degeneration of the spinal cord. *J Neurol Neurosurg Psychiatry* 1997; 62: 298–299

Lindenbaum J, Healton EB, Savage DG, Brust JCM, Garrett TJ, Podell ER, Marcell PD, Stabler SP, Allen RH. Neuropsychiatric disorders caused by cobalamin deficiency in the absence of anemia or macrocytosis. *N Engl J Med* 1988; 318: 1720–1728

Löfblad K-O, Ramelli G, Remonda L, Nirkko AC, Ozdoba C, Schroth G. Retardation of myelination due to dietary vitamin B₁₂ deficiency: cranial MRI findings. *Pediatr Radiol* 1997; 27: 155–158

Morita S, Miwa H, Kihira T, Kondo T. Cerebellar ataxia and leukoencephalopathy associated with cobalamin deficiency. *J Neurol Sci* 2003; 216: 183–184

Murata S, Naritomi H, Sawada T. MRI in subacute combined degeneration. *Neuroradiology* 1994; 36: 408–409

Narayanan MN, Dawson DW, Lewis MJ. Dietary deficiency of vitamin B₁₂ is associated with low serum cobalamin levels in non-vegetarians. *Eur J Haematol* 1991; 47: 115–118

Perry J, Chanarin I, Deacon R, Lumb M. Methylation of DNA in megaloblastic anaemia. *J Clin Pathol* 1990; 43: 211–212

Rasmussen SA, Fernhoff PM, Scanlon KS. Vitamin B₁₂ deficiency in children and adolescents. *J Pediatr* 2001; 138: 10–17

Reynolds EH, Bottiglieri T, Laundry M, Stern J, Payan J, Linnell J, Faludy J. Subacute combined degeneration with high serum vitamin B₁₂ level and abnormal vitamin B₁₂ binding protein. *Arch Neurol* 1993; 50: 739–742

Saracaceanu E, Tramoni AV, Henry JM. An association between subcortical dementia and pernicious anemia. A psychiatric mask. *Compr Psychiatry* 1997; 38: 349–351

Scott JM, Wilson P, Dinn JJ, Weir DG. Pathogenesis of subacute combined degeneration: a result of methyl group deficiency. *Lancet* 1981; 2: 334–337

Shevell MI, Rosenblatt DS. The neurology of cobalamin. *Can J Neurol Sci* 1992; 19: 472–486

- Soria ED, Fine EJ. Somatosensory evoked potentials in the neurological sequelae of treated vitamin B₁₂ deficiency. *Electromyogr Clin Neurophysiol* 1992; 32: 63–71
- Stabler SP, Allen RH, Savage DG, Lindenbaum J. Clinical spectrum and diagnosis of cobalamin deficiency. *Blood* 1990; 76: 871–881
- Steiner I, Kidron D, Soffer D, Wirguin I, Abramsky O. Sensory peripheral neuropathy of vitamin B₁₂ deficiency: a primary demyelinating disease? *J Neurol* 1988; 235: 163–164
- Stojsavlejević N, Lević Z, Drulović J, Dragutinović G. A 44-month clinical-brain MRI follow-up in a patient with B12 deficiency. *Neurology* 1997; 49: 878–881
- Surtees R. Biochemical pathogenesis of subacute combined degeneration of the spinal cord and brain. *J Inherit Metab Dis* 1993; 16: 762–770
- Timms SR, Curé JK, Kurent JE. Subacute combined degeneration of the spinal cord: MR findings. *AJNR Am J Neuroradiol* 1993; 14: 1224–1227
- Ubbink JB. The role of vitamins in the pathogenesis and treatment of hyperhomocyst(e)inaemia. *J Inherit Metab Dis* 1997; 20: 316–325
- Yamada K, Shrier DA, Tanaka H, Numaguchi Y. A case of subacute combined degeneration: MRI findings. *Neuroradiology* 1998; 40: 398–400
- Zegers de Beyl D, Delecluse F, Veranck P, Borestein S, Capel P, Brunko E. Somatosensory conduction in vitamin B12 deficiency. *Electroencephalogr Clin Neurophysiol* 1988; 69: 313–318

46 Urea Cycle Defects

- Aida S, Ogata T, Kamota T, Nakamura N. Primary ornithine transcarbamylase deficiency. *Acta Pathol Jpn* 1989; 39: 451–456
- Albayram S, Murphy KJ, Gailloud P, Moghekar A, Brunberg JA. CT findings in the infantile form of citrullinemia. *AJNR Am J Neuroradiol* 2002; 23: 334–336
- Bachmann C. Ornithine carbamoyl transferase deficiency: findings, models and problems. *J Inherit Metab Dis* 1992; 15: 578–591
- Bajaj SK, Kurlemann G, Schuierer G, Peters PE. CT and MRI findings in a girl with late-onset ornithine transcarbamylase deficiency: case report. *Neuroradiology* 1996; 38: 796–799
- Batshaw ML. Inborn errors of urea synthesis. *Ann Neurol* 1994; 35: 133–141
- Brockstedt M, Smit LME, de Grauw AJC, van der Klei-van Moorsel JM, Jakobs C. A new case of hyperargininaemia: neurological and biochemical findings prior to and during dietary treatment. *Eur J Pediatr* 1990; 149: 341–343
- Brusilow SW. Arginine, an indispensable amino acid for patients with inborn errors of urea synthesis. *J Clin Invest* 1984; 74: 2144–2148
- Bruton CJ, Corsellis JAN, Russell A. Hereditary hyperammonaemia. *Brain* 1970; 93: 423–434
- Cerone R, Caruso U, Barabino A, Gatt R, Jakobs C, Jacquemyn I, Marescau B, De Deyn PP. Hyperargininemia: pre-natal diagnosis and treatment from birth. In: De Deyn PP, Marescau B, Qureshi IA, Mori A, eds. Guanidino compounds. Eastleigh: John Libbey 1997, pp 71–76
- Chen Y-F, Huang Y-C, Liu H-M, Hwu W-L. MRI in a case of adult onset citrullinemia. *Neuroradiology* 2001; 43: 845–847
- Choi C-G, Yoo HW. Localized proton MR spectroscopy in infants with urea cycle defect. *AJNR Am J Neuroradiol* 2001; 22: 834–837
- Christodoulou J, Qureshi IA, McInnes RR, Clarke JTR. Ornithine transcarbamylase deficiency presenting with stroke-like episodes. *J Pediatr* 1993; 122: 423–425
- Connelly A, Cross JH, Gadian DG, Hunter JV, Kirkham FJ, Leonard JV. Magnetic resonance spectroscopy shows increased brain glutamine in ornithine carbamoyl transferase deficiency. *Pediatr Res* 1993; 33: 77–81
- Dolman CL, Clasen RA, Dorovini-Zis K. Severe cerebral damage in ornithine transcarbamylase deficiency. *Clin Neuropathol* 1988; 7: 10–15
- Donn SM, Thoene JG. Prospective prevention of neonatal hyperammonaemia in argininosuccinic aciduria by arginine therapy. *J Inherit Metab Dis* 1985; 8: 18–20
- Finkelstein JE, Hauser ER, Leonard CO, Brusilow SW. Late-onset ornithine transcarbamylase deficiency in male patients. *J Pediatr* 1990; 117: 897–902
- Gallagher JV, Rifai N, Conry J, Soldin SJ. Role of the clinical laboratory in evaluation of argininosuccinate lyase deficiency. *Clin Chem* 1991; 37: 1384–1389
- Gerrits GPJM, Gabreëls FJM, Monnens LAH, De Abreu RA, van Raaij-Selten B, Niezen-Koning KE, Trijbels JMF. Argininosuccinic aciduria: clinical and biochemical findings in three children with the late onset form, with special emphasis on cerebrospinal fluid findings of amino acids and pyrimidines. *Neuropediatrics* 1993; 21: 15–18
- Grody WW, Kern RM, Klein D, Dodson AE, Wissman PB, Barsky SH, Cederbaum SD. Arginase deficiency manifesting delayed clinical sequelae and induction of a kidney arginase isozyme. *Hum Genet* 1993; 91: 1–5
- Grompe M, Caskey CT, Fenwick RG. Improved molecular diagnostics for ornithine transcarbamylase deficiency. *Am J Hum Genet* 1991; 48: 212–222
- Harding BN, Leonard JV, Erdohazi M. Ornithine carbamoyl transferase deficiency: a neuropathological study. *Eur J Pediatr* 1984; 141: 215–220
- Hommes FA, de Groot CJ, Wilmink CW, Jonxis JHP. Carbamylphosphate synthetase deficiency in an infant with severe cerebral damage. *Arch Dis Child* 1969; 44: 688–693
- Honeycutt D, Callahan K, Rutledge L, Evans B. Heterozygote ornithine transcarbamylase deficiency presenting as symptomatic hyperammonemia during initiation of valproate therapy. *Neurology* 1992; 42: 666–668
- Horiuchi M, Imamura Y, Nakamura N, Maruyama I, Saheki T. Carbamylphosphate synthetase deficiency in an adult: deterioration due to administration of valproic acid. *J Inherit Metab Dis* 1993; 16: 39–45
- Kleijer WJ, Garritsen VH, Linnebank M, Mooyer P, Huijman JGM, Mustonen A, Simola KOJ, Arslan-Kirchner M, Battini R, Briones P, Cardo E, Mandel H, Tschiedel E, Wanders RJA, Koch HG. Clinical, enzymatic, and molecular genetic characterization of a biochemical variant type of argininosuccinic aciduria: prenatal and postnatal diagnosis in five unrelated families. *J Inherit Metab Dis* 2002; 25: 399–410
- Kornfeld M, Woodfin BM, Papile L, Davis LE, Bernard LR. Neuropathology of ornithine carbamyl transferase deficiency. *Acta Neuropathol (Berl)* 1985; 65: 261–264
- Kurihara A, Takanashi J-i, Tomita M, Kobayashi K, Ogawa A, Kanazawa M, Yamamoto S, Kohno Y. Magnetic resonance imaging in late-onset ornithine transcarbamylase deficiency. *Brain Dev* 2003; 25: 40–44
- Lee B, Goss J. Long-term correction of urea cycle disorders. *J Pediatr* 2001; 138: S62–S71
- Légras A, Labarthe F, Maillot F, Garrigue M-A, Kouatchet A, Ogié de Baulny H. Late diagnosis of ornithine transcarbamylase defect in three related female patients: polymorphic presentations. *Crit Care Med* 2002; 30: 241–244

- Maestri NE, Hauser ER, Bartholomew D, Brusilow SW. Prospective treatment of urea cycle disorders. *J Pediatr* 1991; 119: 923–928
- Maestri NE, McGowan KD, Brusilow SW. Plasma glutamine concentration: a guide in the management of urea cycle disorders. *J Pediatr* 1992; 121: 259–261
- Maestri NE, Brusilow SW, Clissold DB, Bassett SS. Long-term treatment of girl with ornithine transcarbamylase deficiency. *N Engl J Med* 1996; 335: 855–859
- Mamourian AC, du Plessis A. Urea cycle defect: a case with MR and CT findings resembling infarct. *Pediatr Radiol* 1991; 21: 594–595
- Marescau B, de Deyn PP, Lowenthal A, Qureshi IA, Antonozzi I, Bachmann C, Cederbaum SD, Cerone R, Chamoles N, Colombo JP, Hyland K, Gatti R, Kang SS, Letarte J, Lambert M, Mizutani N, Possemiers I, Rezvani I, Snyderman SE, Terheggen HG, Yoshino M. Guanidino compound analysis as a complementary diagnostic parameter for hyperargininemia: follow-up of guanidino compound levels during therapy. *Pediatr Res* 1990; 27: 297–303
- Martin JJ, Farriaux JP, de Jonghe P. Neuropathology of citrullinaemia. *Acta Neuropathol (Berl)* 1982; 56: 303–306
- Mathias RS, Kostiner D, Packman S. Hyperammonemia in urea cycle disorders: role of the nephrologist. *Am J Kidney Dis* 2001; 37: 1069–1080
- Matsuura I, Nagata N, Matsuura T, Oyanagi K, Tada K, Narisawa K, Kitagawa T, Sakiyama T, Yamashita F, Yoshino M. Retrospective survey of urea cycle disorders. 1. Clinical and laboratory observations of thirty-two Japanese male patients with ornithine transcarbamylase deficiency. *Am J Med Genet* 1991; 38: 85–89
- Matsuura T, Hoshida R, Fukushima M, Sakiyama T, Owada M, Matsuda I. Prenatal monitoring of ornithine transcarbamoylase deficiency in two families by DNA analysis. *J Inher Metab Dis* 1993; 16: 31–38
- Mattson LR, Lindor NM, Goldman DH, Goodwin JT, Groover RV, Vockley J. Central pontine myelinosis as a complication of partial ornithine carbamoyl transferase deficiency. *Am J Med Genet* 1995; 60: 210–213
- McCullough BA, Yudkoff M, Batshaw ML, Wilson JM, Raper SE, Tuchman M. Genotype spectrum of ornithine transcarbamylase deficiency: correlation with the clinical and biochemical phenotype. *Am J Med Genet* 2000; 93: 313–319
- Msall M, Batshaw ML, Suss R, Brusilow SW, Mellits ED. Neurologic outcome in children with inborn errors of urea synthesis. *N Engl J Med* 1984; 310: 1500–1505
- Oechsner M, Steen C, Stürenberg HJ, Kohlschütter A. Hyperammonaemic encephalopathy after initiation of valproate therapy in unrecognized ornithine transcarbamylase deficiency. *J Neurol Neurosurg Psychiatry* 1998; 64: 680–682
- Olier J, Gallego J, Digon E. Computerized tomography in primary hyperammonemia. *Neuroradiology* 1989; 31: 356–357
- Osafune K, Ichikawa K, Yasui Y, Sekikawa A, Takeoka H, Kanatsu K, Kohigashi K, Koshiyama H. An adult-onset case of argininosuccinate synthetase deficiency presenting with atypical citrullinemia. *Intern Med* 1999; 38: 590–596
- Oshiro S, Kochinda T, Tana T, Yamazato M, Kobayashi K, Komine Y, Muratani H, Saheki T, Iseki K, Takishita S. A patient with adult-onset type II citrullinemia on long-term hemodialysis: reversal of clinical symptoms and brain MRI findings. *Am J Kidney Dis* 2002; 39: 189–192
- Pickler JD, Puga AC, Levy HL, Marsden D, Shih VE, DeGirolami U, Ligon KL, Cederbaum SD, Kern RM, Cox GF. Arginase deficiency with lethal neonatal expression: evidence for the glutamine hypothesis of cerebral edema. *J Pediatr* 2003; 142: 349–352
- Potter M, Hammond JW, Sim K-G, Green AK, Wilcken B. Ornithine carbamoyltransferase deficiency: improved sensitivity of testing for protein tolerance in the diagnosis of heterozygotes. *J Inher Metab Dis* 2001; 24: 5–14
- Prasad AN, Breen JC, Ampola MG, Rosman NP. Argininemia: a treatable genetic cause of progressive spastic diplegia simulating cerebral palsy: case reports and literature review. *J Child Neurol* 1997; 12: 301–309
- Pridmore CL, Clarke JTR, Blaser S. Ornithine transcarbamylase deficiency in females: an often overlooked cause of treatable encephalopathy. *J Child Neurol* 1995; 10: 369–374
- Solitare GB, Shih VE, Nelligan DJ, Dolan Jr DJ, Ariginosuccinic aciduria: clinical, biochemical, anatomical and neuropathological observations. *J Ment Defic Res* 1969; 13: 153–170
- Sperl W, Felber S, Skladal D, Wermuth B. Metabolic stroke in carbamyl phosphate synthetase deficiency. *Neuropediatrics* 1997; 28: 229–234
- Takanashi J, Kurihara A, Tomita M, Kanazawa M, Yamamoto S, Morita F, Ikehira H, Tanada H, Tanada S, Kohno Y. Distinctly abnormal brain metabolism in late-onset ornithine transcarbamylase deficiency. *Neurology* 2002; 59: 210–214
- Takanashi J-I, Barkovic AJ, Cheng SF, Weisiger K, Zlatunich CO, Mudge C, Rosenthal P, Tuchman M, Packman S. Brain MR imaging in neonatal hyperammonemic encephalopathy resulting from proximal urea cycle disorders. *AJNR Am J Neuroradiol* 2003; 24: 1184–1187
- Takanashi J-I, Barkovic AJ, Cheng SF, Kostiner D, Baker JC, Packman S. Brain MR imaging in acute hyperammonemic encephalopathy arising from late-onset ornithine transcarbamylase deficiency. *AJNR Am J Neuroradiol* 2003; 24: 390–393
- Takeoka M, Soman TB, Shih VE, Caviness VS, Krishnamoorthy KS. Carbamyl phosphate synthetase 1 deficiency: a destructive encephalopathy. *Pediatr Neurol* 2001; 24: 193–199
- Tomomasa T, Kobayashi K, Kaneko H, Shimura H, Fukusato T, Tabata M, Ioue Y, Ohwada S, Kasahara M, Morishita Y, Kimura M, Saheki T, Morikawa A. Possible clinical and histological manifestations of adult-onset type II citrullinemia in early infancy. *J Pediatr* 2001; 138: 741–743
- Travers H, Reed JS, Kennedy JA. Ultrastructural study of the liver in argininosuccinase deficiency. *Pediatr Pathol* 1986; 5: 307–318
- Tuchman M. The clinical, biochemical, and molecular spectrum of ornithine transcarbamylase deficiency. *J Lab Clin Med* 1992; 120: 836–850
- Tuchman M. Mutations and polymorphisms in the human ornithine transcarbamylase gene. *Hum Mutat* 1993; 2: 174–178
- Tuchman M, Mauer SM, Holzknecht RA, Summar ML, Vnencak-Jones CL. Prospective versus clinical diagnosis and therapy of acute neonatal hyperammonemia in two sisters with carbamyl phosphate synthetase deficiency. *J Inher Metab Dis* 1992; 15: 269–277
- Whittington PF, Alonso EM, Boyle JT, Molleston JP, Rosenthal P, Emond JC, Millis JM. Liver transplantation for the treatment of urea cycle disorders. *J Inher Metab Dis* 1998; 21: 112–118

Widhalm K, Koch S, Scheibenreiter S, Knoll E, Colombo JP, Bachmann C, Thalhammer O (1992) Long-term follow-up of 12 patients with the late-onset variant of argininosuccinic acid lyase deficiency: no impairment of intellectual and psychomotor development during therapy. *Pediatrics* 87: 1182–1184

47 Serine Synthesis Defect

- De Koning TJ. 3-Phosphoglycerate dehydrogenase in disease and development. Thesis, University of Utrecht. Utrecht: Zuidam en Uithof, 2001
- De Koning TJ, Duran M, Dorland M, Dorland L, Gooskens R, van Schaftingen E, Jaeken J, Blau N, Berger R, Poll-The BT. Beneficial effects of L-serine and glycine in the management of seizures in 3-phosphoglycerate dehydrogenase deficiency. *Ann Neurol* 1998; 44: 261–265
- De Koning TJ, Poll-The BT, Jaeken J. Continuing education in neurometabolic disorders – serine deficiency disorders. *Neuropediatrics* 1999; 30: 1–4
- De Koning TJ, Jaeken J, Pineda M, van Maldergem L, Poll-The BT, van der Knaap MS. Hypomyelination and reversible white matter attenuation in 3-phosphoglycerate dehydrogenase deficiency. *Neuropediatrics* 2000; 31: 287–292
- De Koning TJ, Duran M, van Maldergem L, Pineda M, Dorland L, Gooskens R, Jaeken J, Poll-The BT. Congenital microcephaly and seizures due to 3-phosphoglycerate dehydrogenase deficiency: outcome of treatment with amino acids. *J Inher Metab Dis* 2002; 25: 119–125
- De Koning TJ, Snell K, Duran M, Berger R, Poll-The BT, Surtees R. L-Serine in disease and development. *Biochem J* 2003; 371: 653–661
- Häusler MG, Jaeken J, Mönch E, Ramaekers VT. Phenotypic heterogeneity and adverse effects of serine treatment in 3-phosphoglycerate dehydrogenase deficiency: report on two siblings. *Neuropediatrics* 2001; 32: 191–195
- Jaeken J, Detheux M, van Maldegem L, Foulon M, Carchon H, van Schaftingen E. 3-Phosphoglycerate dehydrogenase deficiency: an inborn error of serine biosynthesis. *Arch Dis Child* 1996; 74: 542–545
- Jaeken J, Detheux M, van Maldegem L, Frijns JP, Alliet P, Foulon M, Carchon H, van Schaftingen E. 3-Phosphoglycerate dehydrogenase deficiency and 3-phosphosine phosphatase deficiency: inborn errors of serine biosynthesis. *J Inher Metab Dis* 1996; 19: 223–226
- Klomp LWJ, de Koning TJ, Malingré HEM, van Beurden EACM, Brink M, Opdam FL, Duran M, Jaeken J, Pineda M, van Maldergem L, Poll-The BT, Van den Berg IET, Berger R. Molecular characterization of 3-phosphoglycerate dehydrogenase deficiency – a neurometabolic disorder associated with reduced L-serine biosynthesis. *Am J Hum Genet* 2000; 67: 1389–1399
- Pineda M, Vilaseca MA, Artuch R, Santos S, García González MM, Sua I, Aracil A, van Schaftingen E, Jaeken J. 3-Phosphoglycerate dehydrogenase deficiency in a patient with West syndrome. *Dev Med Child Neurol* 2000; 42: 629–633

48 Molybdenum Cofactor Deficiency and Isolated Sulfite Oxidase Deficiency

- Appignani BA, Kaye EM, Wolpert SM. CT and MR appearance of the brain in two children with molybdenum cofactor deficiency. *AJNR Am J Neuroradiol* 1996; 17: 317–320
- Arslanoglu S, Yalaz M, Gökben, Çoker M, Tütüncüoğlu S, Akisu M, Darcan S, Kultursay N, Çiris M, Demirtaş E. Molybdenum cofactor deficiency associated with Dandy-Walker complex. *Brain Dev* 2001; 23: 815–818
- Barbot C, Martins E, Vilarinho L, Dorche C, Cardoso ML. A mild form of infantile isolated sulphite oxidase deficiency. *Neuropediatrics* 1995; 322: 322–324
- Brown GK, Scholem RD, Croll HB, Wraith JE, McGill JJ. Sulfite oxidase deficiency: clinical, neuroradiologic, and biochemical features in two new patients. *Neurology* 1989; 39: 252–257
- Dublin AB, Hald JK, Wootton-Gorges SL. Isolated sulfite oxidase deficiency: MR images features. *AJNR Am J Neuroradiol* 2002; 23: 484–485
- Duran M, Beemer FA, van der Heijden C, Korteland J, de Bree PK, Brink M, Wadman SK. Combined deficiency of xanthine oxidase and sulphite oxidase: a defect of molybdenum metabolism or transport. *J Inher Metab Dis* 1978; 1: 175–178
- Endres W, Shin YS, Günther R, Ibel H, Duran M, Wadman SK. Report on a new patient with combined deficiencies of sulphite oxidase and xanthine dehydrogenase due to molybdenum cofactor deficiency. *Eur J Pediatr* 1988; 148: 246–249
- Feng G, Tintrup H, Kirsch J, Nichol MC, Kuhse J, Betz H, Sanes JR. Dual requirement for gephyrin in glycine receptor clustering and molybdoenzyme activity. *Science* 1998; 282: 1321–1324
- Hänzelmann P, Schwartz G, Mendel RR. Functionality of alternative splice forms of the first enzymes involved in human molybdenum cofactor biosynthesis. *J Biol Chem* 2002; 277: 18303–18312
- Hughes EF, Fairbanks L, Simmonds HA, O'Robinson R. Molybdenum cofactor deficiency – phenotypic variability in a family with late-onset variant. *Dev Med Child Neurol* 1998; 40: 57–61
- Johnson JL, Coyne E, Rajagopalan KV, van Hove JLK, Mackay M, Pitt J, Boneh A. Molybdopterins synthase mutations in a mild case of molybdenum cofactor deficiency. *Am J Med Genet* 2001; 104: 169–173
- Johnson JL, Coyne KE, Garret RM, Zabot M-T, Dorche C, Kisker C, Rajagopalan KV. Isolated sulfite oxidase deficiency: identification of 12 novel SUOX mutations in 10 patients. *Hum Mutat* 2002; 20: 74–79
- Lee HF, Mak BSC, Chi CS, Tsai CR, Chen CH, Shu SG. A novel mutation in neonatal isolated sulphite oxidase deficiency. *Neuropediatrics* 2002; 33: 174–179
- Mize C, Johnson JL, Rajagopalan KV. Defective molybdopterins biosynthesis: clinical heterogeneity associated with molybdenum cofactor deficiency. *J Inher Metab Dis* 1995; 18: 283–290
- Reiss J. Genetics of molybdenum cofactor deficiency. *Hum Genet* 2000; 106: 157–163
- Reiss J, Johnson LJ. Mutations in the molybdenum cofactor biosynthetic genes *MOCS1*, *MOCS2*, and *GEPH*. *Hum Mutat* 2003; 21: 569–576
- Reiss J, Cohen N, Dorche C, Mandel H, Mendel RR, Stallmeyer B, Zabot MT, Dierks T. Mutations in a polycistronic nuclear gene associated with molybdenum cofactor deficiency. *Nat Genet* 1998; 20: 51–53

- Reiss J, Christensen E, Kurlmann G, Zabot M-T, Dorche C. Genomic structure and mutation spectrum of the bicistronic *MOCS1* gene defective in molybdenum cofactor deficiency type A. *Hum Genet* 1998; 103: 639–644
- Reiss J, Dorche C, Stallmeyer B, Mendel RR, Cohen N, Zabot MT. Human molybdopter synthase gene: genomic structure and mutations in molybdenum cofactor deficiency type B. *Am J Hum Genet* 1999; 64: 706–711
- Reiss J, Gross-Hart S, Christensen E, Schmidt P, Mendel RR, Schwartz G. A mutation in the gene for the neurotransmitter receptor-clustering protein gephyrin causes a novel form of molybdenum cofactor deficiency. *Am J Hum Genet* 2001; 68: 208–213
- Rupar CA, Gillett J, Gordon BA, Ramsay DA, Johnson JL, Garrett RM, Rajagopalan KV, Jung JH, Bacheyie GS, Sellers AR. Isolated sulfite oxidase deficiency. *Neuropediatrics* 1996; 27: 299–304
- Salvan AM, Chambrol B, Lamoureux S, Confort-Gouny S, Cozzone PJ, Vion-Dury J. In vivo brain proton MR spectroscopy in a case of molybdenum cofactor deficiency. *Pediatr Radiol* 1999; 29: 846–848
- Schuieler G, Kurlmann G, Bick U, Stephani U. Molybdenum-cofactor deficiency; CT and MR findings. *Neuropediatrics* 1995; 26: 5–54
- Shalata A, Mandel H, Reiss J, Szargel R, Cohen-Akenine A, Dorche C, Zabot M-T, Van Gennip A, Abeling N, Berant M, Cohen N. Localisation of a gene for molybdenum cofactor deficiency, on the short arm of chromosome 6, by homozygosity mapping. *Am J Hum Genet* 1998; 63: 148–154
- Shih VE, Abroms IF, Johnson JL, Carney M, Mandell R, Robb RM, Cloherty JP, Rajagopalan KV. Sulfite oxidase deficiency. Biochemical and clinical investigations of a hereditary metabolic disorder in sulfur metabolism. *N Engl J Med* 1977; 207: 1022–1028
- Topcu M, Coskun T, Haliloglu G, Saatci I. Molybdenum cofactor deficiency: report of three cases presenting as hypoxic-ischemic encephalopathy. *J Child Neurol* 2001; 16: 264–270
- Touati G, Rusthoven E, Depondt, Dorche C, Duran M, Héron B, Rabier D, Russo M, Saudubray JM. Dietary therapy in two patients with a mild form of sulphite oxidase deficiency. Evidence for clinical and biochemical improvement. *J Inher Metab Dis* 2000; 23: 45–53
- Van der Klei-van Moorsel JM, Smit LM, Brockstedt M, Jacobs C, Dorche C, Duran M. Infantile isolated sulphite oxidase deficiency: report of a case with negative sulphite test and normal sulphate excretion. *Eur J Pediatr* 1991; 150: 196–197
- Bosch AM, Bakker HD, van Gennip AH, van Kempen JV, Wanders RJA, Wijburg FA. Clinical features of galactokinase deficiency: a review of the literature. *J Inher Metab Dis* 2002; 25: 629–634
- Burke JP, O'Keefe M, Bowell R, Naughten ER. Ophthalmic findings in classical galactosemia – a screened population. *J Pediatr Ophthalmol Strabismus* 1989; 26: 165–168
- Cleary MA, Heptinstall LE, Wraith JE, Walter JH. Galactosemia: relationship of IQ to biochemical control and genotype. *J Inher Metab Dis* 1995; 18: 151–152
- Crome L. A case of galactosaemia with the pathological and neuropathological findings. *Arch Dis Child* 1962; 37: 415–429
- Friedman JH, Levy HL, Boustany R-M. Late onset of distinct neurologic syndromes in galactosemic siblings. *Neurology* 1989; 39: 741–742
- Gitzelmann R. Galactose-1-phosphate in the pathophysiology of galactosemia. *Eur J Pediatr* 1995; 154: S45–S49
- Gitzelmann R, Steinmann B, Mitchell B, Haigis E. Uridine diphosphate galactose 4-epimerase deficiency. Report of eight cases in three families. *Helv Paediatr Acta* 1976; 31: 441–452
- Haberland C, Perou M, Brunngraber EG, Hof H. The neuropathology of galactosemia. *J Neuropathol Exp Neurol* 1971; 30: 431–447
- Henderson MJ, Holton JB. Further observations in a case of uridine diphosphate galactose-4-epimerase deficiency with a severe clinical presentation. *J Inher Metab Dis* 1983; 6: 17–20
- Holton JB. Effects of galactosemia in utero. *Eur J Pediatr* 1995; 154: S77–S81
- Holton JB. Galactosemia: pathogenesis and treatment. *J Inher Metab Dis* 1996; 19: 3–7
- Holton JB, Allen JT, Gillett MG. Prenatal diagnosis of disorders of galactose metabolism. *J Inher Metab Dis* 1989; 12 (suppl 1): 202–206
- Keevill NJ, Holton JB, Allen JT. UDP-glucose and UDP-galactose concentrations in cultured skin fibroblasts of patients with classical galactosaemia. *J Inher Metab Dis* 1994; 17: 23–26
- Kliegman RM, Sparks JW. Perinatal galactose metabolism. *J Pediatr* 1985; 107: 831–841
- Koch TK, Schmidt KA, Wagstaff JE, Won G, Packman S. Neurologic complications in galactosemia. *Pediatr Neurol* 1992; 8: 217–220
- Landing BH, Ang SM, Villarreal-Engelhardt G, Donnell GN. Galactosemia: clinical and pathologic features, tissue staining patterns with labeled galactose- and galactosamine-binding lectins, and possible loci of nonenzymatic galactosylation. *Perspect Pediatr Pathol* 1993; 17: 99–124
- Lesgold Belman A, Moshe SL, Zimmerman RD. Computed tomographic demonstration of cerebral edema in a child with galactosemia. *Pediatrics* 1986; 78: 606–609
- Liu G, Hale GE, Hughes CL. Galactose metabolism and ovarian toxicity. *Reprod Toxicol* 2000; 14: 377–384
- Nelson CD, Waggoner DD, Donnell GN, Tuerck JM, Buist NRM. Verbal dyspraxia in treated galactosemia. *Pediatrics* 1991; 88: 346–350
- Nelson MD, Wolff JA, Cross CA, Donnell GN, Kaufman FR. Galactosemia: evaluation with MR imaging. *Radiology* 1992; 184: 255–261
- Olambiwonnu NO, McVie R, Won G, Frasier SD, Donnell GN. Galactokinase deficiency in twins: clinical and biochemical studies. *Pediatrics* 1974; 53: 314–318

49 Galactosemia

- Acosta PH, Gross KC. Hidden sources of galactose in the environment. *Eur J Pediatr* 1995; 154: S87–S92
- Beigi B, O'Keefe M, Bowell R, Naughten E, Badawi N, Lanigan B. Ophthalmic findings in classical galactosaemia – prospective study. *Br J Ophthalmol* 1993; 77: 162–164
- Berry GT. The role of polyols in the pathophysiology of hypergalactosemia. *Eur J Pediatr* 1995; 154: S53–S64
- Berry GT, Palmieri M, Gross KC, Acosta PB, Henstenburg JA, Mazur A, Reynolds R, Segal S. The effect of dietary fruits and vegetables on urinary galactitol excretion in galactose-1-phosphate uridylyltransferase deficiency. *J Inher Metab Dis* 1993; 16: 91–100
- Böhles H, Wenzel D, Shin YS. Progressive cerebellar and extrapyramidal motor disturbances in galactosaemic twins. *Eur J Pediatr* 1986; 145: 413–417

- Ornstein KS, McGuire EJ, Berry GT, Roth S, Segal S. Abnormal galactosylation of complex carbohydrates in cultured fibroblasts from patients with galactose-1-phosphate uridylyltransferase deficiency. *Pediatr Res* 1992; 31: 508–511
- Ratner Kaufman F, McBride-Chang C, Manis FR, Wolff JA, Nelson MD. Cognitive functioning, neurologic status and brain imaging in classical galactosemia. *Eur J Pediatr* 1995; 154: S2–S5
- Ratner Kaufman F, Horton EJ, Gott P, Wolff JA, Neson Jr. MD, Azen C, Manis FR. Abnormal somatosensory evoked potentials in patients with classic galactosemia: correlation with neurologic outcome. *J Child Neurol* 1995; 10: 32–36
- Sardharwalla IB, Wraith JE, Bridge C, Fowler B, Roberts SA. A patient with severe type of epimerase deficiency galactosaemia. *J Inherit Metab Dis* 1988; 11 (suppl 2): 249–251
- Schwarz HP, Schaefer T, Bachmann C. Galactose and galactitol in the urine of children with compound heterozygosity for Duarte variant and classical galactosemia (Gt^D/gt) after an oral galactose load. *Clin Chem* 1985; 31: 420–422
- Schweitzer S, Shin Y, Jakobs C, Brodehl J. Long-term outcome in 134 patients with galactosaemia. *Eur J Pediatr* 1993; 152: 36–43
- Segal S. Galactosemia unsolved. *Eur J Pediatr* 1995; 154: S97–S102
- Segal S, Rutman JY, Frimpr GW. Galactokinase deficiency and mental retardation. *J Pediatr* 1979; 95: 750–753
- Smetana HF, Olen E. Hereditary galactose disease. *Am J Clin Pathol* 1962; 38: 3–25
- Sokol RJ, McCabe ERB, Kotzer AM, Langendoerfer SI. Pitfalls in diagnosing galactosemia: false negative newborn screening following red blood cell transfusion. *J Pediatr Gastroenterol Nutr* 1989; 8: 266–268
- Tyfield LA, Reichardt J, Fridovich-Keil J, Croke Dt, Elas II LJ, Strobl W, Kozak L, Coskun T, Novelli G, Okano Y, Zekanowski C, Shin Y, Dolores Boleda M. Classical galactosemia and mutations at the galactose-1-phosphate uridylyl transferase (*GALT*) gene. *Hum Mutat* 1999; 13: 417–430
- Tyfield LA. Galactosemia and allelic variation at the galactose-1-phosphate uridylyltransferase gene: a complex relationship between genotype and phenotype. *Eur J Pediatr* 2000; 159: S204–S207
- Waggoner DD, Buist NRM. Long-term complications in treated galactosemia. *Int Pediatr* 1993; 8: 97–100
- Waggoner DD, Buist NRM, Donnell GN. Long-term prognosis in galactosaemia: results of a survey of 350 cases. *J Inherit Metab Dis* 1990; 13: 802–818
- 50 Sjögren-Larsson Syndrome**
- Altmok D, Yildiz YT, Seçkin D, Altmok G, Tacal T, Eryilmaz M. MRI of three siblings with Sjögren-Larsson syndrome. *Pediatr Radiol* 1999; 29: 776–769
- Auada MP, Taube MBZ, Collares EF, Tanaka AMU, Cintra ML. Sjögren-Larsson syndrome: biochemical defects and follow up in three cases. *Eur J Dermatol* 2002; 12: 263–266
- De Laurenzi V, Rogers GR, Hamrock DJ, Marekov LN, Steinert SP, Compton JG, Markova N, Rizzo WB. Sjögren-Larsson syndrome is caused by mutations in the fatty aldehyde dehydrogenase gene. *Nat Genet* 1996; 12: 52–57
- Di Rocco M, Filocamo M, Tortori-Donati P, Veneselli E, Borroni C, Rizzo WB. Sjögren-Larsson syndrome: nuclear magnetic resonance imaging of the brain in a 4-year-old boy. *J Inherit Metab Dis* 1994; 17: 112–114
- Gomori JM, Leibovici V, Zlotogorski A, Wirguin I, Haham-Zadeh S. Computed tomography in Sjögren-Larsson syndrome. *Neuroradiology* 1987; 29: 557–559
- Hussain MZ, Aihara M, Oba H, Ohtomo K, Uchiyama G, Hayashibe H, Nakazawa S. MRI of white matter changes in the Sjögren-Larsson syndrome. *Neuroradiology* 1995; 37: 576–577
- Kelson TL, Craft DA, Rizzo WB. Carrier detection for Sjögren-Larsson syndrome. *J Inherit Metab Dis* 1992; 15: 105–111
- Kelson TL, Secor McVoy JR, Rizzo WB. Human liver fatty aldehyde dehydrogenase: microsomal localization, purification, and biochemical characterization. *Biochim Biophys Acta* 1997; 1335: 99–110
- Lake BD, Smith VV, Judge MR, Harper JI, Besley GTN. Hexanol dehydrogenase activity shown by enzyme histochemistry on skin biopsies allows differentiation of Sjögren-Larsson syndrome from other ichthyoses. *J Inherit Metab Dis* 1991; 14: 338–340
- Mano T, Ono J, Taminaga T, Imai K, Sakurai K, Harada K, Nagai T, Rizzo WB, Okada S. Proton MR spectroscopy of Sjögren-Larsson's syndrome. *AJNR Am J Neuroradiol* 1999; 20: 1671–1673
- Miyanomae Y, Ochi M, Yoshioka H, Takaya K, Kizaki Z, Inoue F, Furuya S, Naruse S. Cerebral MRI and spectroscopy in Sjögren-Larsson syndrome: case report. *Neuroradiology* 1995; 37: 225–228
- Mulder LJMM, Oranje AP, Loonen MCB. Cranial CT in the Sjögren-Larsson syndrome. *Neuroradiology* 1987; 29: 560–561
- Rizzo WB. Inherited disorders of fatty alcohol metabolism. *Mol Genet Metab* 1998; 65: 63–73
- Rizzo WB. Sjögren-Larsson syndrome. Explaining the skin-brain connection. *Neurology* 1999; 52: 1307–1308
- Rizzo WB, Craft DA. Sjögren-Larsson syndrome. Deficient activity of the fatty aldehyde dehydrogenase component of fatty alcohol: NAD⁺ oxidoreductase in cultured fibroblasts. *J Clin Invest* 1991; 88: 1643–1648
- Rizzo WB, Craft DA. Sjögren-Larsson syndrome: accumulation of free fatty alcohols in cultured fibroblasts and plasma. *J Lipid Res* 2000; 41: 1077–1081
- Rizzo WB, Carney G, Lin Z. The molecular basis of Sjögren-Larsson syndrome: mutation analysis of the fatty aldehyde dehydrogenase gene. *Am J Hum Genet* 1999; 65: 1547–1560
- Rizzo WB, Heinz E, Simon M, Craft DA. Microsomal fatty aldehyde dehydrogenase catalyzes the oxidation of aliphatic aldehyde derived from ether glycerolipid catabolism: implications for Sjögren-Larsson syndrome. *Biochim Biophys Acta* 2000; 1535: 1–9
- Rizzo WB, Lin Z, Carney G. Fatty aldehyde dehydrogenase: genomic structure, expression and mutation analysis in Sjögren-Larsson syndrome. *Chem Biol Interact* 2001; 130–132: 297–307
- Sillén A, Anton-Lamprecht I, Braun-Quentin C, Kraus CS, Sitki Sayli B, Ayuso C, Jagell S, Küster W, Waledius C. Spectrum of mutations and sequence variants in the *FALDH* gene in patients with Sjögren-Larsson syndrome. *Hum Mutat* 1998; 12: 377–384
- Sylvester PE. Pathological findings in Sjögren-Larsson syndrome. *J Ment Defic Res* 1969; 13: 267–275
- Tabsh K, Rizzo WB, Holbrook K, Theroux N. Sjögren-Larsson syndrome: technique and timing of prenatal diagnosis. *Obstet Gynecol* 1993; 82 (suppl II): 700–703
- Taube B, Billeaud C, Labrèze C, Entressangles B, Fontan D, Taieb A. Sjögren-Larsson syndrome: early diagnosis, dietary management and biochemical studies in two cases. *Dermatol* 1999; 198: 340–345

- Tsukamoto N, Chang C, Yoshida A. Mutations associated with Sjögren-Larsson syndrome. *Ann Hum Genet* 1997; 61: 235–242
- Van Domburg PHMF, Willemsen MAAP, Rotteveel JJ, de Jong JGN, Thijssen HOM, Heerschap A, Cruysberg JRM, Wanders RJA, Gabreëls FJM, Steijlen PM. Sjögren-Larsson syndrome. Clinical and MRI/MRS findings in *FALDH*-deficient patients. *Neurology* 1999; 52: 1345–1352
- Van Mieghem F, van Goethem JWM, Parizel PM, Cras P, van den Hauwe L, de Meirleire J, de Schepper AM. MR of the brain in Sjögren-Larsson syndrome. *AJNR Am J Neuroradiol* 1997; 18: 1561–1563
- Verhoeven NM, Jacobs C, Carney G, Somers MP, Wanders RJA, Rizzo WB. Involvement of microsomal fatty aldehyde dehydrogenase in the α -oxidation of phytanic acid. *FEBS Lett* 1998; 429: 225–228
- Wester P, Bergström U, Brun A, Jagell S, Karlsson B, Eriksson A. Monoaminergic dysfunction in Sjögren-Larsson syndrome. *Mol Chem Neuropathol* 1991; 15: 13–28
- Willemsen MAAP, Rotteveel JJ, Steijlen PM, Heerschap A, Mayatepek E. 5-Lipoxygenase inhibition: a new treatment strategy for Sjögren-Larsson Syndrome. *Neuropediatrics* 1999; 31: 1–3
- Willemsen MAAP, Rotteveel JJ, Domburg v PHMF, Gabreëls FJM, Mayatepek E, Sengers RCA. Preterm birth in Sjögren-Larsson syndrome. *Neuropediatrics* 1999; 30: 325–327
- Willemsen MAAP, de Jong JGN, van Domburg PHMF, Rotteveel JJ, Wanders RJA, Mayatepek E. Defective inactivation of leukotriene B₄ in patients with Sjögren-Larsson syndrome. *J Pediatr* 1999; 136: 258–260
- Willemsen MAAP, Cruysberg RM, Rotteveel JJ, Aandekerk AL, van Domburg PHMF, Deuteman AF. Juvenile Macular dystrophy associated with deficient activity of fatty aldehyde dehydrogenase in Sjögren-Larsson syndrome. *Am J Ophthalmol* 2000; 130: 782–789
- Willemsen MAAP, Lutt MAJ, Steijlen PM, Cruysberg JRM, van der Graaf M, Nijhuis-van der Sanden MWG, Pasman JW, Mayatepek E, Rotteveel JJ. Clinical and biochemical effects of zileuton in patients with the Sjögren-Larsson syndrome. *Eur J Pediatr* 2001; 160: 711–717
- Willemsen MAAP, Rotteveel JJ, de Jong JGN, Wanders RJA, IJlst L, Hoffmann GF, Mayatepek E. Defective metabolism of leukotriene B₄ in the Sjögren-Larsson syndrome. *J Neurol Sci* 2001; 183: 61–67
- Willemsen MAAP, IJlst L, Steijlen PM, Rotteveel JJ, de Jong JGN, van Domburg PHMF, Mayatepek E, Gabreëls FJM, Wanders RJA. Clinical, biochemical and molecular genetic characteristics of 19 patients with the Sjögren-Larsson syndrome. *Brain* 2001; 124: 1426–1437
- Willemsen MAAP, van der Graaf M, van der Knaap MS, Heerschap A, van Domburg PHMF, Gabreëls FJM, Rotteveel JJ. MR imaging and proton MR spectroscopic studies in Sjögren-Larsson syndrome: characterization of the leukoencephalopathy. *AJNR Am J Neuroradiol* 2004; 25: 649–657
- Attree O, Olivos IM, Okabe I, Bailey LC, Nelson DL, Lewis RA, McInnes RR, Nussbaum RL. The Lowe's oculocerebrorenal syndrome gene encodes a protein highly homologous to inositol polyphosphate-5-phosphatase. *Nature* 1992; 358: 239–242
- Carroll WJ, Woodruff WW, Cadman TE. MR findings in oculocerebrorenal syndrome. *AJNR Am J Neuroradiol* 1993; 14: 449–451
- Charnas LR, Gahl WA. The oculocerebrorenal syndrome of Lowe. *Adv Pediatr* 1991; 38: 75–107
- Charnas L, Bernar J, Pezeshkpour GH, Dalakas M, Harper GS, Gahl WA. MRI findings and peripheral neuropathy in Lowe's syndrome. *Neuropediatrics* 1988; 19: 7–9
- Charnas LR, Bernardini I, Rader D, Hoeg JM, Gahl WA. Clinical and laboratory findings in the oculocerebrorenal syndrome of Lowe, with special reference to growth and renal function. *N Engl J Med* 1991; 324: 1318–1325
- Cibis GW, Waeltermann JM, Whitcraft CT, Tripathi RC, Harris DJ. Lenticular opacities in carriers of Lowe's syndrome. *J Ophthalmol* 1986; 93: 1041–1045
- De Camilli P, Emr SD, McPherson PS, Novick P. Phosphoinositides as regulators in membrane traffic. *Science* 1996; 271: 1533–1539
- Demmer LA, Wippold FJ, Dowton SB. Periventricular white matter cystic lesions in Lowe (oculocerebrorenal) syndrome. *Pediatr Radiol* 1992; 22: 76–77
- Dressman MA, Olivos-Glander IM, Nussbaum RL, Suchy SF. Ocr11, a PtdIns(4,5)P₂ 5-phosphatase, is localized to the trans-Golgi network of fibroblasts and epithelial cells. *J Histochem Cytochem* 2000; 48: 179–189
- Fivush BA, Rausen C, Christenson MJ, Olson JL. Acute tubular necrosis associated with Lowe's syndrome: possible role of rhabdomyolysis. *Am J Kidney Dis* 1992; 20: 396–399
- Garzuly F, Jellinger K, Szabo L, Toth K. Morbid changes in Lowe's oculo-cerebro-renal syndrome. *Neuropediatrics* 1973; 4: 304–313
- Giannakopoulos P, Bouras C, Vallet P, Constantinidis J. Lowe syndrome: clinical and neuropathological studies of an adult case. *J Ment Defic Res* 1990; 34: 491–500
- Irvine R. Second messengers and Lowe syndrome. *Nat Genet* 1992; 1: 315–316
- Kenworthy L, Park T, Charnas LR. Cognitive and behavioral profile of the oculocerebrorenal syndrome of Lowe. *Am J Med Genet* 1993; 46: 297–303
- Kohyama J, Niimura F, Kawashima K, Iwakawa Y, Nonaka I. Congenital fiber type disproportion myopathy in Lowe syndrome. *Pediatr Neurol* 1989; 5: 373–376
- Lin T, Orrison BM, Leahey A-M, Suchy SF, Bernard DJ, Lewis RA, Nussbaum RL. Spectrum of mutations in the *OCRL1* gene in the Lowe oculocerebrorenal syndrome. *Am J Hum Genet* 1997; 60: 1384–1388
- Lin T, Orrison BM, Suchy SF, Lewis RA, Nussbaum RL. Mutations are not uniformly distributed throughout the *OCRL1* gene in Lowe syndrome patients. *Mol Genet Metab* 1998; 64: 58–61
- Monnier N, Satre V, Lerouge E, Berthoin F, Lunardi J. *OCRL1* mutation analysis in French Lowe syndrome patients: implications for molecular diagnosis strategy and genetic counseling. *Hum Mutat* 2000; 16: 157–165
- Mueller OT, Hartsfield JK, Gallardo LA, Essig YP, Miller KL, Papenhausen PR, Tedesco TA. Lowe oculocerebrorenal syndrome in a female with a balanced X;20 translocation: mapping of the X chromosome breakpoint. *Am J Hum Genet* 1991; 49: 804–810
- Athreya BH, Schumacher HR, Getz HD, Norman ME, Borden S, Witzleben CL. Arthropathy of Lowe's (oculocerebrorenal) syndrome. *Arthritis Rheum* 1983; 26: 728–735

51 Lowe Syndrome

- Nielsen KF, Steffensen GK. Congenital nephritic syndrome associated with Lowe's syndrome. *Child Nephrol Urol* 1990; 10: 92–95
- Olivos-Glander IM, Jänne PA, Nussbaum RL. The oculocerebrorenal syndrome gene product is a 105-kD protein localized to the Golgi complex. *Am J Hum Genet* 1995; 57: 817–823
- Ono J, Harada K, Mano T, Yamamoto T, Okada S. MR findings and neurologic manifestations in Lowe oculocerebrorenal syndrome. *Pediatr Neurol* 1996; 14: 162–164
- O'Tuama LA, Laster DW. Oculocerebrorenal syndrome: case report with CT and MR correlates. *AJNR Am J Neuroradiol* 1987; 8: 555–557
- Pueschel SM, Brem AS, Nittoli P. Central nervous system and renal investigations in patients with Lowe syndrome. *Childs Nerv Syst* 1992; 8: 45–48
- Satre V, Monnier N, Berthoin F, Ayuso C, Joannard A, Jouk P-S, Lopex-Pajares I, Megabarne A, Philipe HJ, Plauchu H, Torres ML, Lunardi J. Characterization of a germline mosaicism in families with Lowe syndrome, and identification of seven novel mutations in the *OCRL1* gene. *Am J Hum Genet* 1999; 65: 68–76
- Savolaine ER, Bielke DJ. Cranial magnetic resonance imaging in Lowe's syndrome. *Clin Imaging* 1993; 17: 133–136
- Schneider JF, Boltshauser E, Neuhaus TJ, Rauscher C, Martin E. MRI and proton spectroscopy in Lowe syndrome. *Neuropediatrics* 2001; 32: 45–48
- Shields D, Arvan P. Disease models provide insight into post-Golgi protein trafficking, localization and processing. *Curr Opin Cell Biol* 1999; 11: 489–494
- Suchy SF, Nussbaum RL. The deficiency of PIP₂ 5-phosphatase in Lowe syndrome affects actin polymerization. *Am J Hum Genet* 2002; 71: 1420–1427
- Suchy SF, Olivos-Glander IM, Nussbaum RL. Lowe syndrome, a deficiency of a phosphatidylinositol 4,5-bisphosphate 5-phosphatase in the Golgi apparatus. *Hum Mol Genet* 1995; 4: 2245–2250
- Terslev E. Two cases of aminoaciduria, ocular changes and retarded mental and somatic development (Lowe's syndrome). *Acta Paediatr Scand* 1960; 49: 635–644
- Tripathi RC, Cibis GW, Tripathi BJ. Pathogenesis of cataracts in patients with Lowe's syndrome. *J Ophthalmol* 1986; 93: 1046–1051
- Zhang X, Majerus PW. Phosphatidylinositol signaling reactions. *Semin Cell Dev Biol* 1998; 9: 153–160
- Zhang X, Jefferson AB, Auethavekiat V, Majerus PW. The protein deficient in Lowe syndrome is a phosphatidylinositol-4,5-bisphosphate 5-phosphatase. *Proc Natl Acad Sci* 1995; 92: 4853–4856
- Brewer GJ. Recognition, diagnosis, and management of Wilson's disease. *Proc Soc Exp Biol Med* 2000; 233: 39–46
- Brewer GJ, Askari F. Transplant livers in Wilson's disease for hepatic, not neurologic, indications. *Liver Transplant* 2000; 6: 662–664
- Brewer GJ, Yuzbasiyan-Gurkan V. Wilson disease. *Medicine* 1992; 71: 139–164
- Brewer GJ, Fink JK, Hedera P. Diagnosis and treatment of Wilson's disease. *Semin Neurol* 1999; 19: 261–270
- Brewer GJ, Johnson VD, Dick RD, Hedera P, Fink JK, Kluin KJ. Treatment of Wilson's disease with zinc. XVII. Treatment during pregnancy. *Hepatology* 2000; 31: 364–370
- Brewer GJ, Dick RD, Johnson VD, Fink JK, Kluin KJ, Daniels S. Treatment of Wilson's disease with zinc. XVI. Treatment during the pediatric years. *J Lab Clin Med* 2001; 137: 191–198
- Brewer GJ, Hedera P, Kluin KJ, Carlson M, Askari F, Dick RB, Sitterly J, Fink JK. Treatment of Wilson disease with ammonium tetrathiomolybdate. *Arch Neurol* 2003; 60: 379–385
- Bingle CD, Srai SKS, Epstein O. Copper metabolism in hypercupremic human livers. Studies of its subcellular distribution, association with binding proteins and expressions of mRNAs. *J Hepatol* 1992; 15: 94–101
- Brugieres P, Combes C, Ricolfi F, Degos JD, Poirier J, Gaston A. Atypical MR presentation of Wilson disease: a possible consequence of paramagnetic effect of copper? *Neuroradiology* 1992; 34: 222–224
- Bull PC, Thomas GR, Rommens JM, Forbes JR, Wilson Cox D. The Wilson disease gene is a putative copper transporting P-type ATPase similar to the Menkes gene. *Nat Genet* 1993; 5: 327–337
- Castilla-Higuero L, Romero-Gomez M, Suarez E, Castro M. Acute hepatitis after starting zinc therapy in a patient with presymptomatic Wilson's disease. *Hepatology* 2000; 32: 877
- Chelly J, Monaco AP. Cloning the Wilson disease gene. *Nat Genet* 1993; 5: 317–318
- De Haan J, Grossman RI, Civitello L, Hackney DB, Golberg HI, Bilaniuk LT, Zimmerman RA. High-field magnetic resonance imaging of Wilson's disease. *J Comput Assist Tomogr* 1987; 11: 132–135
- Demirkiran M, Jankovic J, Lewis RA, Cox DW. Neurologic presentation of Wilson disease without Kayser-Fleischer rings. *Neurology* 1996; 46: 1040–1043
- Dening TR, Berrios GE, Walshe JM. Wilson's disease and epilepsy. *Brain* 1988; 111: 1139–1155
- Di Donato M, Sarkar B. Copper transport and its alterations in Menkes and Wilson diseases. *Biochim Biophys Acta* 1997; 1360: 3–16
- Emre S, Atillasoy EO, Ozdemir S, Schilsky M, Rathna Varma CVR, Thung SN, Sternlieb I, Guy SR, Sheiner PA, Schwartz ME, Miller CM. Orthotopic liver transplantation for Wilson's disease: a single-center experience. *Transplantation* 2001; 72: 1232–1236
- Engelbrecht V, Schlaug G, Hefter H, Kahn T, Mödder U. MRI of the brain in Wilson disease: T2 signal loss under therapy. *J Comput Assist Tomogr* 1995; 19: 635–638
- Gaffney D, Walker JL, O'Donnell JG, Fell GS, O'Neill KF, Park RHR, Russell RI. DNA-based presymptomatic diagnosis of Wilson disease. *J Inher Metab Dis* 1992; 15: 161–170
- Giagheddu M, Tamburini G, Piga M, Tacconi P, Giagheddu A, Serra A, Siotto P, Satta L, Demilia L, Marrosu F. Comparison of MRI, EEG, EPS and ECD-SPECT in Wilson's disease. *Acta Neurol Scand* 2001; 103: 71–81
- Gow PJ, Smallwood RA, Angus PW, Smith AL, Wall AJ, Sewell RB. Diagnosis of Wilson's disease: an experience over three decades. *Gut* 2000; 46: 415–419

52 Wilson Disease

- Aisen AM, Martel W, Gabrielsen TO, Glazer GM, Brewer G, Young AB, Hill G. Wilson disease of the brain: MR imaging. *Radiology* 1985; 157: 137–141
- Albernaz VS, Castillo M, Mukherji SK, Siatkowski M, Naidich TP. Facies to remember. *Int J Neuroradiol* 1997; 3: 206–217
- Bertrand E, Lewandowska E, Szpak GM, Hoogenraad T, Blaauwgers HG, Czlonkowska A, Dymecki J. Neuropathological analysis of pathological forms of astroglia in Wilson's disease. *Folia Neuropathol* 2001; 39: 73–79
- Brewer GJ. Penicillamine should not be used as initial therapy in Wilson's disease. *Mov Disord* 1999; 14: 551–554

- Grimm G, Madl C, Katzenschlager R, Oder W, Ferenci P, Gangl A. Detailed evaluation of evoked potentials in Wilson's disease. *Electroencephalogr Clin Neurophysiol* 1992; 82: 119–124
- Heckmann JM, Eastman RW. Wilson's disease: neurological and magnetic resonance imaging improvement on zinc treatment. *J Neurol Neurosurg Psychiatry* 1994; 57: 1273–1274
- Hedera P, Brewer GJ, Arbor A, Fink JK. White matter changes in Wilson disease. *Arch Neurol* 2002; 59: 866–867
- Hefter H, Rautenberg W, Kreuzpainter G, Arendt G, Freund H-J, Pichlmayr R, Strohmeyer G. Does orthotopic liver transplantation heal Wilson's disease? Clinical follow-up of two liver-transplanted patients. *Acta Neurol Scand* 1991; 84: 192–196
- Hoogenraad TU, Koevoet R, de Ruyster-Korver EGWM. Oral zinc sulphate as long term treatment in Wilson's disease. *Eur Neurol* 1979; 18: 205–211
- Houwen RHJ, Roberts EA, Thomas GR, Cox DW. DNA markers for the diagnosis of Wilson disease. *J Hepatol* 1993; 17: 269–276
- Huang C-C, Chu N-S. Acute dystonia with thalamic and brain-stem lesions after initial penicillamine treatment in Wilson's disease. *Eur Neurol* 1998; 39: 32–37
- Huang C-C, Chu N-S. Wilson's disease: resolution of MRI lesions following long-term oral zinc therapy. *Acta Neurol Scand* 1996; 93: 215–218
- Imlya M, Ichikawa K, Matsushima H, Kageyama Y, Fujioka A. MR of the base of the pons in Wilson disease. *AJNR Am J Neuroradiol* 1992; 13: 1009–1012
- Ishino H, Mii T, Hayashi Y, Saito A, Otsuki S. A case of Wilson's disease with enormous cavity formation of cerebral white matter. *Neurology* 1972; 22: 905–909
- Keller R, Torta R, Lagget M, Crasto S, Bergamosso B. Psychiatric symptoms as late onset of Wilson's disease: neuroradiological findings, clinical features and treatment. *Ital J Neurol Sci* 1999; 20: 49–54
- Kobayashi S, Ochiai T, Hori S, Suzuki T, Shimizu T, Gunji Y, Shimada H, Yamamoto S, Ogawa A, Kohno Y, Sunaga M, Shimazu M, Takena K. Copper metabolism after living donor liver transplantation for hepatic failure of Wilson's disease from a gene mutated donor. *Hepatogastroenterology* 2001; 48: 1259–1261
- Komatsu H, Fujisawa T, Inui A, Soga T, Sekine I, Kodama H, Uemoto S, Tanaka K. Hepatic copper concentration in children undergoing living related liver transplantation due to Wilsonian fulminant hepatic failure. *Clin Transplant* 2002; 16: 227–232
- Lang CJG, Rabas-Kolominsky P, Engelhart A. Fatal deterioration of Wilson's disease after institution of oral zinc therapy. *Arch Neurol* 1993; 50: 1007–1008
- Longhi R, Riva E, Rottoli A, Valsasina R, Pinelli P, Giovannini M. Nuclear magnetic resonance brain study in a case of Wilson disease. *J Inher Metab Dis* 1989; 12 (suppl) 386–388
- Lui CC, Chen CL, Cheng YF, Lee TY. Recovery of neurological deficits in a case of Wilson's disease after liver transplantation. *Transplant Proc* 1998; 30: 3324–3325
- Magalhaes ACA, Caramelli P, Menezes JR, Lo LS, Bacheschi LA, Barbosa ER, Rosemberg LA. Wilson's disease: MRI with clinical correlation. *Neuroradiology* 1994; 36: 97–100
- Mason AL, Marsh W, Alpers DH. Intractable neurological Wilson's disease treated with orthotopic liver transplantation. *Dig Dis Sci* 1993; 38: 1746–1750
- Matsuura T, Sasaki H, Tashiro K. Atypical MR findings in Wilson's disease: pronounced lesions in the dentate nucleus causing tremor. *J Neurol Neurosurg Psychiatry* 1998; 64: 160
- McQuaid A, Lamand M, Mason J. The interactions of penicillamine with copper in vivo and the effect on hepatic metallothionein levels and copper/zinc distribution: the implications for Wilson's disease and arthritis therapy. *J Lab Clin Med* 1992; 119: 744–750
- Mercer FJB. The molecular basis of copper-transport diseases. *Trends Mol Med* 2001; 7: 64–69
- Mochizuki H, Kamakura K, Masaki T, Okano M, Nagata N, Inui A, Fujisawa T, Kaji T. Atypical MRI features of Wilson's disease: high signal in globus pallidus on T1-weighted images. *Neuroradiology* 1997; 39: 171–174
- Oder W, Grimm G, Kollegger H, Ferenci P, Schneider B, Deecke L. Neurological and neuropsychiatric spectrum of Wilson's disease: a prospective study of 45 cases. *J Neurol* 1991; 238: 281–287
- Oder W, Prayer L, Grimm G, Spatt J, Ferenci P, Kollegger H, Schneider B, Gangl A, Deecke L. Wilson's disease: evidence of subgroups derived from clinical findings and brain lesions. *Neurology* 1993; 43: 120–124
- Porzio S, Iorio R, Vajro P, Pensati P, Vegnente A. Penicillamine-related neurologic syndrome in a child affected by Wilson disease with hepatic presentation. *Arch Neurol* 1997; 54: 1166–1168
- Prayer L, Wimberger D, Kramer J, Grimm G, Oder W, Imhof H. Cranial MRI in Wilson's disease. *Neuroradiology* 1990; 32: 211–214
- Richard VS, Harris VK, Shankar V, Loganathan G, Chandy GM. Clinical manifestations and survival pattern of Wilson's disease. *Natl Med J India* 2000; 13: 301–303
- Riordan SM, Williams R. The Wilson's disease gene and phenotypic diversity. *J Hepatol* 2001; 34: 165–171
- Roh JK, Lee TG, Wie BA, Lee SB, Park SH, Chang KH. Initial and follow-up brain MRI findings and correlation with the clinical course in Wilson's disease. *Neurology* 1994; 44: 1064–1068
- Saatci I, Topcu M, Baltaoglu FF, Köse G, Yalaz K, Renda Y, Besim A. Cranial MR findings in Wilson's disease. *Acta Radiol* 1997; 38: 250–258
- Saha M, Kumar S, Das A, Gupta RK. Similarities and differences of MR findings between Japanese encephalitis and Wilson's disease. *Eur Radiol* 2002; 12: 872–876
- Sarkar B. Copper transport and its defect in Wilson disease: characterization of the copper-binding domain of Wilson disease in ATPase. *J Inorg Biochem* 2000; 79: 187–191
- Schagen van Leeuwen JH, Christiaens GCML, Hoogenraad TU. Recurrent abortion and the diagnosis of Wilson disease. *Obstet Gynecol* 1991; 78: 547–549
- Schilsky ML. Diagnosis and treatment of Wilson's disease. *Pediatr Transplant* 2002; 6: 15–19
- Schlaug G, Hefter H, Engelbrecht V, Kluwert T, Arnold S, Stöcklin G, Seitz RJ. Neurological impairment and recovery in Wilson's disease: evidence from PET and MRI. *J Neurol Sci* 1996; 136: 129–139
- Schulman S, Barbeau A. Wilson's disease: a case with almost total loss of cerebral white matter. *J Neuropathol Exp Neurol* 1963; 22: 105–119
- Schumacher G, Platz KP, Mueller AR, Neuhaus R, Luck W, Langrehr JM, Settmacher U, Steinmüller T, Becker M, Neuhaus P. Liver transplantation in neurologic Wilson's disease. *Transplant Proc* 2001; 33: 1518–1519
- Scully RE, Mark EJ, McNelly WF, Ebeling SH. Presentation of a case. *N Engl J Med* 1997; 336: 118–125
- Selwa LM, Vanderzant CW, Brunberg JA, Brewer GJ, Drury I, Beydoun A. Correlation of evoked potential and MRI findings in Wilson's disease. *Neurology* 1993; 43: 2059–2064

- Selwa LM, Vanderzant CW, Brunberg JA, Brewer GJ, Drury I, Beydoun A. Correlation of evoked potential and MRI findings in Wilson's disease. *Neurology* 1993; 43: 2059–2064
- Sener RN. Wilson's disease: MRI demonstration of cavitations in basal ganglia and thalami. *Pediatr Radiol* 1993; 23: 157
- Sener RN. The claustrum on MRI: normal anatomy, and the bright claustrum as a new sign in Wilson's disease. *Pediatr Radiol* 1993; 23: 594–596
- Shimizu N, Yamaguchi Y, Aoki T. Treatment and management of Wilson's disease. *Pediatr Int* 1999; 41: 419–422
- Siegmund R, Löbner, Günther K, Kühn H-J, Bachmann H. Mode of action of triethylenetetramine dihydrochloride on copper metabolism in Wilson's disease. *Acta Neurol Scand* 1991; 83: 356–359
- Singcharoen T, Chakkaphak K, Udompanich O. Unusual magnetic resonance findings in Wilson's disease. *Br J Radiol* 1991; 64: 752–754
- Song Y-M, Chen M-D. A single determination of liver copper concentration may misdiagnose Wilson's disease. *Clin Biochem* 2000; 33: 589–590
- Starosta-Rubinstein S, Young AB, Kluin K, Hill G, Aisen AM, Gabrielsen T, Brewer GJ. Clinical assessment of 31 patients with Wilson's disease. Correlations with structural changes on magnetic resonance imaging. *Arch Neurol* 1987; 44: 365–370
- Sternlieb I. The outlook for the diagnosis of Wilson's disease. *J Hepatol* 1993; 17: 263–264
- Suzuki M, Gitlin JD. Intracellular localization of the Menkes and Wilson's disease proteins and their role in intracellular copper transport. *Pediatr Int* 1999; 41: 436–442
- Tanzi RE, Petrukhin K, Chernov I, Pellequer JL, Wasco W, Ross B, Romano M, Parano E, Pavone L, Brzustowicz LM, Devoto M, Peppercorn J, Bush AI, Sternlieb I, Pirastu M, Gusella JF, Evgrafov O, Penchaszaeh GK, Honig B, Eelman IS, Soares MB, Scheinberg IH, Gilliam TC. The Wilson disease gene is a copper transporting ATPase with homology to the Menkes disease gene. *Nat Genet* 1993; 5: 344–350
- Thuomas KA, Aquilonius SMA, Bergström K, Westermarck K. Magnetic resonance imaging of the brain in Wilson's disease. *Neuroradiology* 1993; 35: 134–141
- Van Wassenaar-van Hall HN, van den Heuvel AG, Jansen GH, Hoogenraad TU, Mali WPTM. Cranial MR in Wilson disease: abnormal white matter in extrapyramidal and pyramidal tracts. *AJNR Am J Neuroradiol* 1995; 16: 2021–2027
- Van Wassenaar-van Hall HN, van den Heuvel AG, Algra A, Hoogenraad TU, Mali WPTM. Wilson disease: findings at MR imaging and CT of the brain with clinical correlation. *Radiology* 1996; 198: 531–536
- Walker JM, Tsvikovskii R, Lutsenko S. Metallochaperone Atox1 transfers copper to the NH₂-terminal domain of the Wilson's disease protein and regulates its catalytic activity. *J Biol Chem* 2002; 277: 27953–27959
- Walshe JM. Penicillamine: the treatment of first choice for patients with Wilson's disease. *Mov Disord* 1999; 14: 545–550
- Walshe JM, Yealland M. Wilson's disease: the problem of delayed diagnosis. *J Neurol Neurosurg Psychiatry* 1992; 55: 692–696
- Wu J-C, Huang C-C, Jeng L-B, Chu N-S. Correlation of neurological manifestations an MR images in a patient with Wilson's disease after liver transplantation. *Acta Neurol Scand* 2000; 102: 135–139
- Yarze JC, Martin P, Munoz SJ, Friedman LS. Wilson's disease: current status. *Am J Med* 1992; 92: 643–654
- Yoshi F, Takahashi W, Shinohara Y. A Wilson's disease patient with prominent cerebral white matter lesions: five-year follow-up by MRI. *Eur Neurol* 1996; 36: 392–393
- Yüce A, Koçak N, Özen H, Gürakan F. Wilson's disease patients with normal ceruloplasmin levels. *Turk J Pediatr* 1999; 41: 99–102
- Yuzbasiyan-Gurkan V, Grider A, Nostrant T, Cousins RJ, Brewer GJ. Treatment of Wilson's disease with zinc. X. Intestinal metallothionein induction. *J Lab Clin Med* 1992; 120: 380–386

53 Menkes Disease

- Ambrosini L, Mercer JFB. Defective copper-induced trafficking and localization of the Menkes protein in patients with mild and copper treated classical Menkes disease. *Hum Mol Genet* 1999; 8: 1545–1555
- Aynaci FM, Mocan H, Bahadır S, Sari A, Aksoy A. A case of Menkes' syndrome associated with deafness and inferior cerebellar vermian hypoplasia. *Acta Paediatr* 1997; 87: 121–123
- Barnard RO, Best PV, Erdohazi M. Neuropathology of Menkes' disease. *Dev Med Child Neurol* 1978; 20: 586–597
- Blaser SI, Berns DH, Ross JS, Lanska MJ, Weissman BM. Serial MR studies in Menkes disease. *J Comput Assist Tomogr* 1989; 13: 113–115
- Camakaris J, Voskoboinik I, Mercer JF. Molecular mechanisms of copper homeostasis. *Biochem Biophys Res Commun* 1999; 261: 225–232
- Chelly J, Tümer Z, Tønnesen T, Petterson A, Ishikawa-Brush Y, Tommerup N, Horn N, Monaco AP. Isolation of a candidate gene for Menkes disease that encodes a potential heavy metal binding protein. *Nat Genet* 1993; 3: 14–19
- Christodoulou J, Danks DM, Sarkar B, Baerlocher KE, Casey R, Horn N, Tümer Z, Clarke JTR. Early treatment of Menkes disease with parenteral copper-histidine: long-term follow-up of four treated patients. *Am J Med Genet* 1998; 76: 154–164
- Dagenais SL, Adam AN, Innis JW, Glover TW. A novel frameshift mutation in exon 23 of *ATP7A (MNK)* results in occipital horn syndrome and not in Menkes disease. *Am J Hum Genet* 2001; 69: 420–427
- DiDonato M, Sarkar B. Copper transport and its alterations in Menkes and Wilson diseases. *Biochim Biophys Acta* 1997; 1360: 3–16
- Faerber EN, Grover WD, DeFilipp GJ, Capitanio MA, Lui T-H, Swartz JD. Cerebral MR of Menkes kinky-hair disease. *AJNR Am J Neuroradiol* 1989; 10: 190–192
- Gasch AT, Caruso RC, Kaler SG, Kaiser-Kupfer M. Menkes' syndrome. Ophthalmic findings. *Ophthalmology* 2002; 109: 1477–1483
- Geller TJ, Pan Y, Martin DS. Early neuroradiologic evidence of degeneration in Menkes' disease. *Pediatr Neurol* 1997; 17: 255–258
- George DH, Casey RE. Menkes disease after copper histidine replacement therapy: case report. *Pediatr Dev Pathol* 2001; 4: 281–288
- Gu Y-H, Kodoma H, Murata Y, Mochizuki D, Yanagawa Y, Ushijima H, Shiba T, Lee C-C. *ATP7A* Gene mutations in 16 patients with Menkes disease and a patient with occipital horn syndrome. *Am J Med Genet* 2001; 99: 217–222
- Guimarães Santos LM, da Silva Teixeira C, Pereira Vilanova LC, Micheletti C, Curiati Mendes CS, Borri ML, Martins AM. Menkes disease. Case report of an uncommon presentation with white matter lesions. *Arq Neuropsiquiatr* 2001; 59: 125–127

- Harrison MD, Dameron CT. Molecular mechanisms of copper metabolism and the role of Menkes disease protein. *J Biochem Mol Toxicol* 1999; 13: 93–106
- Hsich GE, Robertson RL, Irons M, Soul JS, du Plessis AJ. Cerebral infarction in Menkes' disease. *Pediatr Neurol* 2000; 23: 425–428
- Ichihashi K, Yano S, Kobayashi S, Miyao M, Yanagisawa M. Serial imaging of Menkes disease. *Neuroradiology* 1990; 32: 56–59
- Jacobs DS, Smith AS, Finelli DA, Lanzieri CF, Wiznitzer M. Menkes kinky hair disease: characteristic MR angiographic findings. *AJNR Am J Neuroradiol* 1993; 14: 1160–1163
- Jankov RP, Boerkoel CF, Hellmann J, Sirkin WL, Tümer Z, Horn N, Feigenbaum A. Lethal neonatal Menkes' disease with severe vasculopathy and fractures. *Acta Paediatr* 1998; 87: 1297–1300
- Jayawant S, Halpin S, Wallence S. Menkes kinky hair disease: an unusual case. *Eur J Paediatr Neurol* 2000; 4: 131–134
- Johnson DE, Coleman L, Poe L. MR of progressive neurodegenerative change in treated Menkes' kinky hair disease. *Neuroradiology* 1991; 33: 181–182
- Kaler SG. Menkes disease. *Adv Pediatr* 1994; 41: 263–304
- Kaler SG. Diagnosis and therapy of Menkes syndrome, a genetic form of copper deficiency. *Am J Clin Nutr* 1998; 67: 1029S–1034S.
- Kaler SG. Metabolic and molecular bases of Menkes disease and occipital horn syndrome. *Pediatr Dev Pathol* 1998; 1: 85–98
- Kaler SG, Tümer Z. Prenatal diagnosis of Menkes disease. *Prenat Diagn* 1998; 18: 287–289
- Kaler SG, Goldstein DS, Holmes C, Salerno JA, Gahl WA. Plasma and cerebrospinal fluid neurochemical pattern in Menkes disease. *Ann Neurol* 1993; 33: 171–175
- Kaler SG, Gallo LK, Proud VK, Percy AK, Mark Y, Segal NA, Goldstein DS, Holmes CS, Gahl WA. Occipital horn syndrome and a mild Menkes phenotype associated with splice site mutations at the *MNK* locus. *Nat Genet* 1994; 8: 195–202
- Kaler SG, Buist NRM, Holmes CS, Goldstein DS, Miller RC, Gahl WA. Early copper therapy in classic Menkes disease patients with a novel splicing mutation. *Ann Neurol* 1995; 38: 921–928
- Kaler SG, Das S, Levinson B, Goldstein DS, Holmes CS, Patronas NJ, Packman S, Gahl WA. Successful early copper therapy in Menkes disease associated with a mutant transcript containing a small in-frame deletion. *Biochem Mol Med* 1996; 57: 37–46
- Kanumakala S, Boneh A, Zacharin M. Pamidronate treatment improves bone mineral density in children with Menkes disease. *J Inher Metab Dis* 2002; 25: 391–398
- Kim BE, Smith K, Meagher CK, Petris MJ. A conditional mutation affecting localization of the Menkes disease copper ATPase. Suppression by copper supplementation. *J Biol Chem* 2002; 277: 44079–44084
- Kim OH, Suh JH. Intracranial and extracranial MR angiopathy in Menkes disease. *Pediatr Radiol* 1997; 7: 782–784
- Kodoma H, Murata Y, Kobayashi M. Clinical manifestations and treatment of Menkes disease and its variants. *Pediatr Int* 1999; 41: 423–429
- Kreuder J, Otten A, Fuder H, Tümer Z, Tønnesen, Horn N, Dralle D. Clinical and biochemical consequences of copper-histidine therapy in Menkes disease. *Eur J Paediatr* 1993; 152: 828–832
- Leventer RJ, Kornberg AJ, Phelan EM, Kean MJ. Early magnetic resonance imaging findings in Menkes' disease. *J Child Neurol* 1997; 12: 222–224
- Linder MC, Hazegh-Azam. Copper biochemistry and molecular biology. *Am J Clin Nutr* 1996; 63: 797S–811S
- Llanos RM, Mercer JFB. The molecular basis of copper homeostasis and copper-related disorders. *DNA Cell Biol* 2002; 21: 259–270
- Lou HC, Hølmer GK, Reske-Nielsen E, Vagn-Hansen P. Lipid composition in gray and white matter of the brain in Menkes' disease. *J Neurochem* 1974; 22: 377–381
- Martin JJ, Leroy JG. Thalamic lesions in a patient with Menkes kinky-hair disease. *Clin Neuropathol* 1985; 4: 206–209
- Martin JJ, Flament-Durand J, Farriaux JP, Buysens N, Ketelbant-Balasse P, Jansen C. Menkes kinky-hair disease. A report on its pathology. *Acta Neuropathol (Berl)* 1978; 42: 25–32
- Martins C, Gonçalves C, Moreno A, Poiares Baptista A, Bairos V. Menkes' kinky hair syndrome: ultrastructural cutaneous alterations of the elastic fibers. *Pediatr Dermatol* 1997; 14: 347–350
- Menkes JH. Menkes disease and Wilson disease: two sides of the same copper coin. I. Menkes disease. *Eur J Paediatr Neurol* 1999; 3: 147–158
- Menkes JH. Subdural haematoma, non-accidental head injury or ...? *Eur J Paediatr Neurol* 2001; 5: 175–176
- Mercer JFB. The molecular basis of copper-transport diseases. *Trends Mol Med* 2001; 7: 64–69
- Mercer JFB, Livingston J, Hall B, Paynter JA, Begy C, Chandrasekharappa S, Lockhart P, Grimes A, Bhave M, Siemieniak D, Glover TW. Isolation of a partial candidate gene for Menkes disease by positional cloning. *Nat Genet* 1993; 3: 20–25
- Møller LB, Tümer Z, Lund C, Petersen C, Cole T, Hanusch R, Seidel J, Jensen LR, Horn N. Similar splice-site mutations of the *ATP7A* gene lead to different phenotypes: classical Menkes disease or occipital horn syndrome. *Am J Hum Genet* 2000; 66: 1211–1220
- Morgello S, Peterson HDC, Kahn LJ, Laufer H. Menkes kinky hair disease with 'ragged red' fibers. *Dev Med Child Neurol* 1988; 30: 808–820
- Okeda R, Gei S, Chen I, Okaniwa M, Shinomiya, Matsubara O. Menkes' kinky hair disease: morphological and immunohistochemical comparison of two autopsied patients. *Acta Neuropathol (Berl)* 1991; 81: 450–457
- Oshio T, Hino M, Kirino A, Matsumura C, Fukuda K. Urologic abnormalities in Menkes' kinky hair disease: report of three cases. *J Pediatr Surg* 1997; 32: 782–784
- Ozawa H, Kodama H, Murata Y, Takashima S, Noma S. Transient temporal lobe changes and a novel mutation in a patient with Menkes disease. *Pediatr Int* 2001; 43: 437–440
- Pasquali-Ronchetti I, Baccarani-Contri M, Young RD, Vogel A, Steinmann B, Royce PM. Ultrastructural analysis of skin and aorta from a patient with Menkes disease. *Exp Mol Pathol* 1994; 61: 36–57
- Petris MJ, Mercer JFB, Culvenor JG, Lockhart P, Gleeson PA, Camakaris J. Ligand-regulated transport of the Menkes copper P-type ATPase efflux pump from the Golgi apparatus to the plasma membrane: a novel mechanism of regulated trafficking. *EMBO J* 1996; 15: 6084–6095
- Petris MJ, Strausak D, Mercer JFB. The Menkes copper transporter is required for the activation of tyrosinase. *Hum Mol Genet* 2000; 9: 2845–2851
- Pinto F, Calderazzi A, Canapicchi R, Taddeucci G, Tarantino E. Radiological findings in a case of Menkes' disease. *Childs Nerv Syst* 1995; 11: 112–114
- Proud VK, Mussell HG, Kaler SG, Young DW, Percy AK. Distinctive Menkes disease variant with occipital horns: delineation of natural history and clinical phenotype. *J Med Genet* 1996; 65: 44–51

- Robain O, Aubourg P, Routon MC, Dulac O, Ponsot G. Menkes disease: a Golgi and electron microscopic study of the cerebellar cortex. *Clin Neuropathol* 1988; 7: 47–52
- Rotilio G, Carri MT, Rossi L, Ciriolo MR. Copper-dependent oxidative stress and neurodegeneration. *IUBMB Life* 2000; 50: 309–314
- Sherwood G, Sarkar B, Sass Kortsak A. Copper histidinate therapy in Menkes' disease: prevention of progressive neurodegeneration. *J Inherit Metab Dis* 1989; 12: 393–396
- Sparaco M, Hirano A, Hirano M, DiMauro S, Bonnilla E. Cytochrome C oxidase deficiency and neuronal involvement in Menkes' kinky hair disease: immunohistochemical study. *Brain Pathol* 1993; 3: 349–354
- Sugio Y, Sugio Y, Kuwano A, Miyoshi O, Yamada K, Niikawa N, Tsukahara M. Translocation t(X;21)(q13.3; p11.1) in a girl with Menkes disease. *Am J Med Genet* 1998; 79: 191–194
- Sztriha L, Janáky M, Kiss J, Buga K. Electrophysiological and ^{99m}Tc-HMPAO-SPECT studies in Menkes disease. *Brain Dev* 1994; 16: 224–228
- Takahashi S, Matsumoto K, Higano S, Ishibashi T, Zuguchi M, Maruoka S, Sakamoto K, Kondo Y. Cranial MRI and MR angiography in Menkes' disease. *Neuroradiology* 1993; 35: 556–558
- Tümer Z, Horn N. Menkes disease: recent advances and new aspects. *J Med Genet* 1997; 34: 265–274
- Tümer Z, Horn N. Menkes disease: underlying genetic defect and new diagnostic possibilities. *J Inherit Metab Dis* 1998; 21: 604–612
- Tümer Z, Lund C, Tolshave J, Vural B, Tønnesen T, Horn N. Identification of point mutations in 41 unrelated patients affected with Menkes disease. *Am J Hum Genet* 1997; 60: 63–71
- Vulpe C, Levinson B, Whitney S, Packman S, Gitschier J. Isolation of a candidate gene for Menkes disease and evidence that it encodes a copper-transporting ATPase. *Nat Genet* 1993; 3: 7–13
- Waslen TA, Stuart Houston C, Tchang S. Menkes' kinky-hair disease: radiologic findings in a patient treated with copper histidinate. *Can Assoc Radiol J* 1995; 46: 114–117
- Yamaguchi Y, Heiny ME, Suzuki M, Gitlin JD. Biochemical characterization and intracellular localization of the Menkes disease protein. *Proc Natl Acad Sci* 1996; 93: 14030–14035
- Devys D, Lutz Y, Rouyer N, Bellocq J-P, Mandel JL. The FMR-1 protein is cytoplasmic, most abundant in neurons and appears normal in carriers of a fragile X premutation. *Nat Genet* 1993; 4: 335–340
- Dorn MB, Mazzocco MMM, Hagerman RJ. Behavioral and psychiatric disorders in adult male carriers of fragile X. *J Am Child Adolesc Psychiatry* 1994; 33: 256–264
- Franke P, Maier W, Hautzinger M, Weiffenbach O, Gänsicke M, Iwers B, Poustka F, Schwab SG, Froster U. Fragile-X carrier females: evidence for a distinct psychopathological phenotype? *Am J Med Genet* 1996; 64: 334–339
- Franke P, Leboyer M, Gänsicke M, Weiffenbach O, Biancalana V, Cornillet-Lefebvre P, Croquette MF, Froster U, Schwab SG, Poustka F, Hautzinger M, Maier W. Genotype-phenotype relationship in female carriers of the premutation and full mutation of *FMR-1*. *Psychiatry Res* 1998; 80: 113–127
- Greco CM, Hagerman RJ, Tassone F, Chudley AE, Del Bigio MR, Jacquemont S, Leehey M, Hagerman PJ. Neuronal intranuclear inclusions in a new cerebellar tremor/ataxia syndrome among fragile X carriers. *Brain* 2002; 125: 1760–1771
- Hagerman PJ, Hagerman RJ. The fragile-X premutation: a maturing perspective. *Am J Hum Genet* 2004; 74: 805–816
- Hagerman PJ, Hagerman RJ. Fragile X-associated tremor/ataxia syndrome (FXTAS). *Ment Retard Dev Disabil Res Rev* 2004; 10: 25–30
- Hagerman RJ, Leehey M, Heinrichs W, Tassone F, Wilson R, Hills J, Grigsby J, Gage B, Hagerman PJ. Intention tremor, parkinsonism, and generalized brain atrophy in male carriers of fragile X. *Neurology* 2001; 57: 127–130
- Hagerman RJ, Leavitt BR, Farzin F, Jacquemont S, Greco CM, Brunberg JA, Tassone F, Hessler D, Harris SW, Zhang L, Jardini T, Gane LW, Ferranti J, Ruiz L, Leehey MA, Grigsby J, Hagerman PJ. Fragile-X-associated tremor/ataxia syndrome (FXTAS) in females with the *FMR1* premutation. *Am J Hum Genet* 2004; 74: 1051–1056
- Jacquemont S, Hagerman RJ, Leehey M, Grigsby J, Zhang L, Brunberg JA, Greco C, Des Portes V, Jardini T, Levine R, Berry-Kravis E, Ted Brown W, Schaeffer S, Kissel J, Tassone F, Hagerman PJ. Fragile X premutation tremor/ataxia syndrome: molecular, clinical, and neuroimaging correlates. *Am J Hum Genet* 2003; 72: 869–878
- Jacquemont S, Hagerman RJ, Leehey MA, Hall DA, Levine RA, Brunberg JA, Zhang L, Jardini T, Gane LW, Harris SW, Herman K, Grigsby J, Greco CM, Berry-Kravis E, Tassone F, Hagerman PJ. Penetrance of the fragile X-associated tremor/ataxia syndrome in a premutation carrier population. *JAMA* 2004; 291: 460–469
- Murphy DGM, Mentis MJ, Pietrini P, Grady CL, Moore CJ, Horwithz B, Hinton V, Dobkin CS, Schapiro MB, Rapoport SI. Premutation female carriers of fragile X syndrome: A pilot study on brain anatomy and metabolism. *J Am Acad Child Adolesc Psychiatry* 1999; 38: 1294–1301
- Riddle JE, Cheema A, Sobesky WE, Gardner SC. Phenotypic involvement in females with the FMR1 gene mutation. *Am J Ment Retard* 1998; 102: 590–601
- Tassone F, Hagerman RJ, Taylor AK, Gane LW, Godfrey TE, Hagerman PJ. Elevated levels of *FMR1* mRNA in carrier males: a new mechanism of involvement in the fragile-X syndrome. *Am J Hum Genet* 2000; 66: 6–15
- Tassone F, Hagerman RJ, Hagerman PJ. A majority of fragile X males with methylated, full mutation alleles have significant levels of FMR1 messenger RNA. *J Med Genet* 2001; 38: 453–456

54 Fragile X Premutation

Tassone F, Hagerman RJ, Garcia-Arocena D, Khandjian EW, Greco CM, Hagerman PJ. Intranuclear inclusions in neural cells with premutation alleles in fragile X associated tremor/ataxia syndrome. *J Med Genet* 2004; 41: e43

55 Hypomelanosis of Ito

- Ardinger HH, Bell WE. Hypomelanosis of Ito. Wood's light and magnetic resonance imaging as diagnostic measures. *Arch Neurol* 1986; 43: 848–850
- Auriemma A, Agostinis C, Bianchi P, Bellan C, Salvoni L, Manara O, Colombo A. Hemimegalencephaly in hypomelanosis of Ito: early sonographic pattern and peculiar MR findings in a newborn. *Eur J Ultrasound* 2000; 12: 61–67
- Battistella PA, Peserico A, Bertoli P, Drigo P, Laverda AM, Casara GL. Hypomelanosis of Ito and hemimegalencephaly. *Childs Nerv Syst* 1990; 6: 421–423
- Bermejo F, Dooms G. Cerebral magnetic resonance imaging in a 2-year-old Caucasian girl, with hypomelanosis of Ito. *J Neuroradiol* 1996; 23: 248–250
- Bhushan V, Gupta RR, Weinreb J, Kairam R. Unusual brain MRI findings in a patient with hypomelanosis of Ito. *Pediatr Radiol* 1989; 20: 104–106
- Echenne BP, Leboucq N, Humbertclaude V. Ito hypomelanosis and moyamoya disease. *Pediatr Neurol* 1995; 13: 169–171
- Fryburg JS, Lin KY, Matsumoto J. Abnormal head MRI in a neurologically normal boy with hypomelanosis of Ito. *Am J Med Genet* 1996; 66: 200–203
- Fujino O, Hashimoto K, Fujita T, Enokido H, Komatsuzaki H, Asano G, Sato J, Morimatsu Y. Clinico-neuropathological study of incontinentia pigmenti achromians – an autopsy case. *Brain Dev* 1995; 17: 425–427
- Glover MT, Brett EM, Atherton DJ. Hypomelanosis of Ito: spectrum of the disease. *J Pediatr* 1989; 115: 75–80
- Griebel V, Krägeloh-Mann I, Michaelis R. Hypomelanosis of Ito – report of four cases and survey of the literature. *Neuropediatrics* 1989; 20: 234–237
- Happle R. Mosaicism in human skin. Understanding the patterns and mechanisms. *Arch Dermatol* 1993; 129: 1460–1470
- Happle R. New aspects of cutaneous mosaicism. *J Dermatol* 2002; 29: 681–692
- Kimura M, Yoshino K, Maeoka Y, Suzuki N. Hypomelanosis of Ito: MR findings. *Pediatr Radiol* 1994; 24: 68–69
- Kuwahara RT, Henson T, Tunca Y, Wilroy SW. Hyperpigmentation along the lines of Blaschko with associated chromosome 14 mosaicism. *Pediatr Dermatol* 2001; 18: 360–361
- Malherbe V, Pariente D, Tardieu M, Lacroix C, Venencie PY, Hibon D, Vedrenne J, Landrieu P. Central nervous system lesions in hypomelanosis of Ito: an MRI and pathological study. *J Neurol* 1993; 240: 302–304
- Mendiratta V, Sharma RC, Arya L, Sardana K. Linear and whorled nevoid hypermelanosis. *J Dermatol* 2001; 28: 58–59
- Montagna P, Procaccianti G, Galli G, Ripamonti L, Patrizi A, Baruzzi A. Familial hypomelanosis of Ito. *Eur Neurol* 1991; 31: 345–347
- Pascual-Castroviejo I, López-Rodríguez L, de la Cruz Medina M, Salamanca-Maesso C, Herrero CR. Hypomelanosis of Ito. Neurological complications in 34 cases. *Can J Neurol Sci* 1988; 15: 124–129
- Pascual-Castroviejo I, Roche C, Martínez-Bermejo A, Arcas J, López-Martin V, Tendero A, Esquiroz JH, Pascual-Pascual S-I. Hypomelanosis of Ito. A study 76 infantile cases. *Brain Dev* 1998; 20: 36–43

- Pini G, Faulkner LB. Cerebellar involvement in hypomelanosis of Ito. *Neuropediatrics* 1995; 26: 208–210
- Ross DL, Liwnicz BH, Chun RWM, Gilbert E. Hypomelanosis of Ito (incontinentia pigmenti achromians) – a clinicopathologic study: macrocephaly and gray matter heterotopias. *Neurology* 1982; 32: 1013–1016
- Rott H-D, Lang GE, Huk W, Pfeiffer RA. Hypomelanosis of Ito (incontinentia pigmenti achromians). Ophthalmological evidence for somatic mosaicism. *Ophthalmic Paediatr Genet* 1990; 4: 273–279
- Ruggieri M, Tigano G, Mazzone D, Tine A, Pavone L. Involvement of the white matter in hypomelanosis of Ito (incontinentia pigmenti achromians). *Neurology* 1996; 46: 485–492
- Steiner J, Adamsbaum C, Desguettes I, Lalande G, Raynaud F, Ponsot G, Kalifa G. Hypomelanosis of Ito and brain abnormalities: MRI findings and literature review. *Pediatr Radiol* 1996; 26: 763–768
- Tagawa T, Futagi Y, Arai H, Mushiake S, Nakayama M. Hypomelanosis of Ito associated with hemimegalencephaly: a clinicopathological study. *Pediatr Neurol* 1997; 17: 180–184
- Thomas IT, Frias JL, Cantu ES, Lafer CZ, Flannery DB, Graham JG Jr. Association of pigmentary anomalies with chromosomal and genetic mosaicism and chimerism. *Am J Hum Genet* 1989; 45: 193–205
- Traupe H. Functional X-Chromosomal mosaicism of the skin: Rudolf Happle and the lines of Alfred Blaschko. *Am J Med Genet* 1999; 85: 324–329
- Tunca Y, Wilroy RS, Kadandale JS, Martens PR, Gunther WM, Tharapel AT. Hypomelanosis of Ito and a “mirror image” whole chromosome duplication resulting in trisomy 14 mosaicism. *Ann Genet* 2000; 43: 39–43
- Williams DW, Elster AD. Cranial MR imaging in hypomelanosis of Ito. *J Comput Assist Tomogr* 1990; 14: 981–983
- Zappella M. Autism and hypomelanosis of Ito in twins. *Dev Med Child Neurol* 1993; 35: 826–832

56 Incontinentia Pigmenti

- Aydingöz Ü, Midia N. Central nervous system involvement in incontinentia pigmenti: cranial MRI of two siblings. *Neuroradiology* 1998; 40: 364–366
- Chatkupt S, Gozo AO, Wolansky LJ, Sun S. Characteristic MR findings in a neonate with incontinentia pigmenti. *Am J Radiol* 1993; 160: 372–374
- Cohen BA. Incontinentia pigmenti. *Neurol Clin* 1987; 5: 361–377
- Fiorillo L, Sinclair DB, O'Byrne ML, Krol AL. Bilateral cerebrovascular accidents in incontinentia pigmenti. *Pediatr Neurol* 2003; 29: 66–68
- Goldberg MF. The blinding mechanisms of incontinentia pigmenti. *Ophthalmic Genet* 1994; 2: 69–76
- Goldberg MF, Custis PH. Retinal and other manifestations of incontinentia pigmenti (Bloch-Sulzberger syndrome). *Ophthalmology* 1993; 100: 1645–1654
- Hennel SJ, Ekert PG, Volpe JJ, Inder TE. Insights into the pathogenesis of cerebral lesions in incontinentia pigmenti. *Pediatr Neurol* 2003; 29: 148–150
- Kasai T, Kato Z, Matsui E, Sakai A, Nishida T, Kondo N, Taga T. Cerebral infarction in incontinentia pigmenti: the first report of a case evaluated by single photon emission computed tomography. *Acta Paediatr* 1997; 86: 665–667
- Mangano S, Barbagallo A. Incontinentia pigmenti: clinical and neuroradiologic features. *Brain Dev* 1993; 15: 362–366

- Pascual-Castroviejo I, Roche MC, Fernández VM, Perez-Romero M, Escudero RM, García-Peñas JG, Sanchez M. Incontinentia pigmenti: MR demonstration of brain changes. *AJNR Am J Neuroradiol* 1994; 15: 1521–1527
- Pellegrino RJ, Shah AJ. Vascular occlusion associated with incontinentia pigmenti. *Pediatr Neurol* 1994; 10: 73–74
- Sha SN, Gibbs S, Upton CJ, Pickworth FE, Garioch JJ. Incontinentia pigmenti associated with cerebral palsy and cerebral leukomalacia: a case report and literature review. *Pediatr Dermatol* 2003; 20: 491–494
- Shuper A, Bryan RN, Singer HS. Destructive encephalopathy in incontinentia pigmenti: a primary disorder? *Pediatr Neurol* 1990; 6: 137–140
- Siemes H, Schneider D, Denning D, Hanefeld F. Encephalitis in two members of a family with incontinentia pigmenti (Bloch-Sulzberger syndrome). *Eur J Pediatr* 1978; 129: 102–115
- Tekin N, Uçar B, Saraçoğlu ZN, Koçak AK, Ürer S, Yakut A. Diagnoses and follow up in four cases of incontinentia pigmenti. *Pediatr Int* 2000; 42: 557–560
- Yang J-H, Ma S-Y, Tsai C-H. Destructive encephalopathy in incontinentia pigmenti: a case report. *J Dermatol* 1995; 22: 340–343
- Yoshikawa H, Uehara Y, Abe T, Oda Y. Disappearance of a white matter lesion in incontinentia pigmenti. *Pediatr Neurol* 2000; 23: 364–367
- ## 57 Alexander Disease
- Aoki Y, Haginoya K, Munakata M, Yokoyama H, Nishio T, Tagashi N, Ito T, Suzuki Y, Kure S, Linuma K, Brenner M, Matsubara Y. A novel mutation in glial fibrillary acidic protein gene in a patient with Alexander disease. *Neurosci Lett* 2001; 312: 71–74
- Bobele GB, Garnica A, Schaefer GB, Leonard JC, Wilson D, Marks WA, Leech RW, Brumback RA. Neuroimaging findings in Alexander's disease. *J Child Neurol* 1990; 5: 253–258
- Borrett D, Becker LE. Alexander's disease. A disease of astrocytes. *Brain* 1985; 108: 367–385
- Brenner M, Johnson AB, Boespflug-Tanguy O, Rodriguez D, Goldman JE, Messing A. Mutations in *GFAP*, encoding glial fibrillary acidic protein, are associated with Alexander disease. *Nat Genet* 2001; 27: 117–120
- Brockmann K, Dechent P, Meins M, Haupt M, Sperner J, Stephani U, Frahm J, Hanefeld F. Cerebral proton magnetic resonance spectroscopy in infantile Alexander disease. *J Neurol* 2003; 250: 300–306
- Clifton AG, Kendall BE, Kingsley DPE, Cross JH, Andar U. Computed tomography in Alexander's disease. An atypical case with extensive low density in both frontal lobes. *Neuroradiology* 1991; 33: 438–440
- Cole G, de Villiers F, Proctor NSF, Freiman I, Bill P. Alexander's disease: case report including histopathological and electron microscopic features. *J Neurol Neurosurg Psychiatry* 1979; 42: 619–624
- Crome L. Megalencephaly associated with hyaline pan-neuropathy. *Brain* 1953; 76: 215–228
- Deprez M, D'Hooze M, Misson JP, de Leval L, Ceuterick C, Reznik M, Martin JJ. Infantile and juvenile presentations of Alexander's disease: a report of two cases. *Acta Neurol Scand* 1999; 99: 158–165
- Duckett S, Schwartzman RJ, Osterholm J, Rorke LB, Friedman D, McLellan TL. Biopsy diagnosis of familial Alexander's disease. *Pediatr Neurosurg* 1992; 18: 134–138
- Farrell K, Chuang S, Becker LE. Computed tomography in Alexander's disease. *Ann Neurol* 1984; 15: 605–607
- French TA, Bower BD, Cameron AH. Alexander's disease presenting as astrocytoma. *J Neurol Neurosurg Psychiatry* 1976; 39: 803–809
- Friede RL. Alexander's disease. *Arch Neurol* 1964; 11: 414–422
- Friedman JH, Ambler M. Progressive parkinsonism associated with Rosenthal fibers: senile-onset Alexander's disease? *Neurology* 1992; 42: 1733–1735
- Garcia L, Gascon G, Ozand P, Yaish H. Increased intracranial pressure in Alexander disease: a rare presentation of white-matter disease. *J Child Neurol* 1992; 7: 168–171
- Garret R, Ames RP. Alexander disease. Case report with electron microscopical studies and review of the literature. *Arch Pathol* 1974; 98: 379–385
- Gingold MK, Bodensteiner JB, Schochet SS, Jaynes M. *J Child Neurol* 1999; 14: 325–329
- Goebel HH, Bode G, Ceasar R, Kohlschütter A. Bulbar palsy with Rosenthal fiber formation in the medulla of a 15-year-old girl. Localized form of Alexander's disease? *Neuropediatrics* 1981; 12: 382–391
- Gorespe JR, Naidu S, Johnson AB, Puri V, Raymond GV, Jenkins SD, Pedersen RC, Lewis D, Knowles P, Fernandez R, de Vivo D, van der Knaap MS, Messing A, Brenner M, Hoffman EP. Molecular findings in symptomatic and pre-symptomatic Alexander disease patients. *Neurology* 2002; 58: 1494–1500
- Guthrie SO, Burton EM, Knowles P, Marshall R. Alexander's disease in a neurologically normal child: a case report. *Pediatr Radiol* 2003; 33: 47–49
- Habib M, Hassoun J, Ali-Cherif A, Alonzo B, Toga M, Khalil R. Maladie d'Alexander de l'adulte. *Rev Neurol* 1984; 140: 179–189
- Honnorat J, Flocard F, Ribot C, Saint-Pierre G, Pineau D, Peysson P, Kopp N. Maladie d'Alexander de l'adulte et gliomatose cérébrale diffuse chez deux membres d'une famille. *Rev Neurol* 1993; 149: 781–787
- Imamura A, Orii KE, Mizuno S, Hoshi H, Kondo T. MR imaging and ¹H-MR spectroscopy in a case of juvenile Alexander disease. *Brain Dev* 2002; 24: 723–726
- Jacob J, Robertson NJ, Hilton DA. Short report. The clinicopathological spectrum of Rosenthal fibre encephalopathy and Alexander's disease: a case report and review of the literature. *J Neurol Neurosurg Psychiatry* 2003; 74: 807–810
- Johnson AB. Alexander disease: a review and the gene. *Int J Dev Neurosci* 2002; 20: 391–394
- Johnson AB, Brenner M. Alexander's disease: clinical, pathologic, and genetic features. *J Child Neurol* 2003; 18: 625–632
- Klein EA, Anzil AP. Prominent white matter cavitation in an infant with Alexander's disease. *Clin Neuropathol* 1994; 13: 31–38
- Li R, Messing A, Goldman JE, Brenner M. GFAP mutations in Alexander disease. *Int J Dev Neurosci* 2002; 20: 259–268
- Liedtke W, Edelmann W, Bieri PL, Chiu F-C, Cowan NJ, Kuchelapatti R, Raine CS. GFAP is necessary for the integrity of CNS white matter architecture and long-term maintenance of myelination. *Neuron* 1996; 17: 607–615
- Madsen JR, Partington MD, Hay TC, Tyson RW. A 2-month-old female infant with progressive macrocephaly and irritability. *Pediatr Neurosurg* 1999; 30: 157–163
- Martidis A, Yee RD, Azzarelli B, Biller J. Neuro-ophthalmic, radiographic, and pathologic manifestations of adult-onset Alexander disease. *Arch Ophthalmol* 1999; 117: 265–267
- Mastri AR, Sung JH. Diffuse Rosenthal fiber formation in the adult: a report of four cases. *J Neuropathol Exp Neurol* 1973; 32: 424–436

- Meins M, Brockmann K, Yadav S, Haupt M, Sperner J, Stephani U, Hanefeld F. Infantile Alexander disease: a GFAP mutation in monozygotic twins and novel mutations in two other patients. *Neuropediatrics* 2002; 33: 194–198
- Messing A, Head MW, Galles K, Galbreath EJ, Goldman JE, Brenner M. Fatal encephalopathy with astrocytes inclusions in GFAP transgenic mice. *Am J Pathol* 1998; 152: 391–398
- Messing A, Goldman JE, Johnson AB, Brenner M. Alexander disease: new insights from genetics. *J Neuropathol Exp Neurol* 2001; 60: 563–573
- Mignot C, Boespflug-Tanguy O, Gelot A, Dautigny A, Pham-Dinh D, Rodriguez D. Alexander disease: putative mechanisms of an astrocytic encephalopathy. *Cell Mol Life Sci* 2004; 61: 369–385
- Namekawa M, Takiyama Y, Aoki Y, Takayashiki N, Sakoe K, Shimazaki H, Taguchi T, Tanaka Y, Nishizawa M, Saito K, Matsubara Y, Nakano I. Identification of GFAP gene mutation in hereditary adult-onset Alexander's disease. *Ann Neurol* 2002; 52: 779–785
- Neal JW, Cave EM, Singhrao SK, Cole G, Wallace SJ. Alexander's disease in infancy and childhood: a report of two cases. *Acta Neuropathol (Berl)* 1992; 84: 322–327
- Neumaier Probst E, Hagel C, Weisz V, Nagel S, Wittkugel O, Zeumer H, Kohlschütter A. Atypical focal MRI lesions in a case of juvenile Alexander's disease. *Ann Neurol* 2003; 53: 118–120
- Ni Q, Johns GS, Manepalli A, Martin DS, Geller TJ. Infantile Alexander's disease: serial neuroradiologic findings. *J Child Neurol* 2002; 17: 463–466
- Okamoto Y, Mitsuyama H, Jonosono M, Hirata K, Arimura K, Osame M, Nakagawa M. Autosomal dominant palatal myoclonus and spinal cord atrophy. *J Neurol Sci* 2002; 195: 71–76
- Pridmore CL, Baraitser M, Harding B, Boyd SG, Kendall B, Brett EM. Alexander's disease: clues to diagnosis. *J Child Neurol* 1993; 8: 134–144
- Reichard EAP, Ball WS Jr, Bove KE. Alexander disease: a case report and review of the literature. *Pediatr Pathol Lab Med* 1996; 16: 327–343
- Riggs JE, Schochet SS Jr, Nelson J. Asymptomatic adult Alexander's disease: entity or nosological misconception? *Neurology* 1988; 38: 152–154
- Rodriguez D, Gauthier F, Bertini E, Bugiani M, Brenner M, N'guyen S, Goizet C, Gelot A, Surtees R, Predespan J-M, Hermandorena X, Troncoso M, Uziel G, Messing A, Ponsot G, Pham-Dinh D, Dautigny A, Boespflug-Tanguy O. Infantile Alexander disease: spectrum of GFAP mutations and genotype-phenotype correlation. *Am J Hum Genet* 2001; 69: 1134–1140
- Russo LS Jr, Aron A, Anderson PJ. Alexander's disease: a report and reappraisal. *Neurology* 1976; 26: 607–614
- Sawaishi Y, Yano T, Takaku I, Takada G. Juvenile Alexander disease with a novel mutation in glial fibrillary acidic protein gene. *Neurology* 2002; 58: 1541–1543
- Schochet CSS Jr, Lampert PW, Earle KM. Alexander's disease. A case report with electron microscopic observations. *Neurology* 1968; 18: 543–549
- Schuster V, Horwitz AE, Kreth HW. Alexander's disease: cranial MRI and ultrasound findings. *Pediatr Radiol* 1991; 21: 133–134
- Schwankhaus JD, Parisi JE, Gullledge WR, Chin L, Currier RD. Hereditary adult-onset Alexander's disease with palatal myoclonus, spastic paraparesis, and cerebellar ataxia. *Neurology* 1995; 45: 2266–2271
- Seil FJ, Schochet SS Jr, Earle KM. Alexander's disease in an adult. Report of a case. *Arch Neurol* 1968; 19: 494–502
- Shah M, Ross JS. Infantile Alexander disease: MR appearance of a biopsy-proved case. *AJNR Am J Neuroradiol* 1990; 11: 1105–1106
- Sherwin RM, Berthrong M. Alexander's disease with sudanophilic leukodystrophy. *Arch Pathol* 1970; 89: 321–328
- Shiroma N, Kanazawa N, Izumi M, Sugai K, Fukumizu M, Sasaki M, Hanaoka S, Kaga M, Tsujino S. Diagnosis of Alexander disease in a Japanese patient by molecular genetic analysis. *J Hum Genet* 2001; 46: 579–582
- Soffer D, Horoupian DS. Rosenthal fibers formation in the central nervous system. Its relation to Alexander's disease. *Acta Neuropathol (Berl)* 1979; 47: 81–84
- Spalke G, Mennel HD. Alexander's disease in an adult: clinicopathologic study of a case and review of the literature. *Clin Neuropathol* 1982; 1: 106–112
- Springer S, Erlewein R, Naegel T, Becker I, Auer D, Grodd W, Krägeloh-Mann I. Alexander disease – classification revisited and isolation of a neonatal form. *Neuropediatrics* 2000; 31: 86–92
- Stumpf E, Masson H, Duquette A, Berthelet F, McNabb J, Lortie A, Lesage J, Montplaisir J, Brais B, Cossette P. Adult Alexander disease with autosomal dominant transmission. A distinct entity caused by mutation in the glial fibrillary acid protein gene. *Arch Neurol* 2003; 60: 1307–1312
- Takanashi J-I, Sugita K, Tanabe Y, Niimi H. Adolescent case of Alexander disease: MR imaging and MR spectroscopy. *Pediatr Neurol* 1998; 18: 67–70
- Torreman M, Smit LME, van der Valk P, Valk J, Scheltens Ph. A case of macrocephaly, hydrocephalus, megacerebellum, white matter abnormalities and Rosenthal fibres. *Dev Med Child Neurol* 1993; 35: 732–736
- Towfighi J, Young R, Sassani J, Ramer J, Horoupian DS. Alexander's disease: further light- and electron-microscopic observations. *Acta Neuropathol (Berl)* 1983; 61: 36–42
- van der Knaap MS, Naidu S, Breiter SN, Blaser S, Stroink H, Springer S, Begeer JC, van Coster R, Barth PG, Thomas NH, Valk J, Powers JM. Alexander disease: diagnosis with MR imaging. *AJNR Am J Neuroradiol* 2001; 22: 541–552
- Vogel PS, Hallervorden J. Leukodystrophy with diffuse Rosenthal fiber formation. *Acta Neuropathol (Berl)* 1962; 2: 126–143
- Walls TJ, Jones RA, Cartledge NEF, Saunders M. Alexander's disease with Rosenthal fibre formation in an adult. *J Neurol Neurosurg Psychiatry* 1984; 47: 399–403
- Wohlwill FJ, Bernstein J, Yakovlev PI. Dysmyelinogenic leukodystrophy. *J Neuropathol Exp Neurol* 1959; 18: 359–383

58 Giant Axonal Neuropathy

- Bomont P, Cavalier L, Blondeau F, Ben Hamida C, Belal S, Tazir M, Demir E, Topaloglu H, Koninthenberg R, Tüysüz B, Landrieu P, Hentati F, Koenig M. The gene encoding gigaxonin, a new member of the cytoskeletal BTB / kelch repeat family, is mutated in giant axonal neuropathy. *Nat Genet* 2000; 26: 370–374
- Bomont P, loos C, Yalcinkaya C, Koninthenberg R, Vallat JM, Assami S, Munnich A, Chabrol B, Kurlmann G, Tazir M, Koenig M. Identification of seven novel mutations in the GAN gene. *Hum Mutat* 2003; 21: 446
- Brockmann K, Pouwels PJW, Dechent P, Flanigan KM, Frahm J, Hanefeld F. Cerebral proton magnetic resonance spectroscopy of a patient with giant axonal neuropathy. *Brain Dev* 2003; 25: 45–50

- Bruno C, Bertini E, Federico A, Tonoli E, Lispi ML, Cassandrini D, Pedemonte M, Santorelli FM, Filocamo M, Dotti MT, Schenone A, Malandrini A, Minetti C. Clinical and molecular findings in patients with giant axonal neuropathy (GAN). *Neurology* 2004; 62: 13–16
- Ding J, Liu JJ, Kowal AS, Nardine T, Bhattacharya P, Lee A, Yang Y. Microtubule-associated protein 1B: a neuronal binding partner for gigaxonin. *J Cell Biol* 2002; 158: 427–433
- Donaghy M, Brett EM, Ormerod IEC, King RHM. Giant axonal neuropathy: observations on a further patient. *J Neurol Neurosurg Psychiatry* 1988; 51: 991–994
- Griffiths IR, Duncan ID. The central nervous system in canine giant axonal neuropathy. *Acta Neuropathol (Berl)* 1979; 46: 169–172
- Igisu H, Ohta M, Tabira T, Hosokawa S, Goto I, Kuroiwa Y. Giant axonal neuropathy; a clinical entity affecting the central as well as the peripheral nervous system. *Neurology* 1975; 25: 717–721
- Kretzschmar HA, Berg BO, Davis RL. Giant axonal neuropathy. *Acta Neuropathol (Berl)* 1987; 73: 138–144
- Kuhlenbäumer G, Young P, Oberwittler C, Hünermund G, Schirmacher A, Domschke K, Ringelstein B, Stögbauer F. Giant axonal neuropathy (GAN): case report and two novel mutations in the gigaxonin gene. *Neurology* 2002; 58: 1273–1276
- Kumar K, Barre P, Nigro M, Jones MZ. Giant axonal neuropathy: clinical, electrophysiologic, and neuropathologic features in two siblings. *J Child Neurol* 1990; 5: 229–234
- Lampl Y, Eshel Y, Ben-David E, Gilad R, Sarova-Pinhas I, Sandbank U. Giant axonal neuropathy with predominant central nervous system manifestations. *Dev Med Child Neurol* 1992; 34: 164–181
- Majnemer A, Rosenblatt B, Watters G, Andermann F. Giant axonal neuropathy: central abnormalities demonstrated by evoked potentials. *Ann Neurol* 1986; 19: 394–396
- Malandrini A, Dotti MT, Battisti C, Villanova M, Capocchi G, Federico A. Giant axonal neuropathy with subclinical involvement of the central nervous system (case report). *J Neurol Sci* 1998; 158: 232–235
- Ouvrier RA. Giant axonal neuropathy – a review. *Brain Dev* 1989; 11: 207–214
- Peiffer J, Schlote W, Bischoff A, Boltshauser E, Müller G. Generalized giant axonal neuropathy – a filament-forming disease of neuronal, endothelial, glial, and schwann cells in a patient without kinky hair. *Acta Neuropathol (Berl)* 1977; 40: 213–218
- Richen P, Tandan R. Giant axonal neuropathy: progressive clinical and radiologic CNS involvement. *Neurology* 1992; 42: 2220–2222
- Stollhoff K, Albani M, Goebel HH. Giant axonal neuropathy and leukodystrophy. *Pediatr Neurol* 1991; 7: 69–71
- Thomas C, Love S, Powell HC, Schultz P, Lampert PW. Giant axonal neuropathy: correlation of clinical findings with postmortem neuropathology. *Ann Neurol* 1987; 22: 79–84
- Treiber-Held S, Budjarjo-Welim H, Riemann D, Richter J, Kretzschmar HA, Hanefeld F. Giant axonal neuropathy: a generalized disorder of intermediate filaments with longitudinal grooves in the hair. *Neuropediatrics* 1994; 25: 89–93
- ## 59 Megalencephalic Leukoencephalopathy with Subcortical Cysts
- Aoki K, Uchihara T, Tsuchiya K, Nakamura A, Ikeda K, Wakayama Y. Enhanced expression of aquaporin 4 in human brain with infarction. *Acta Neuropathol (Berl)* 2003; 106: 121–124
- Ben-Zeev B, Gross V, Kushnir T, Shalev R, Hoffman C, Shinar Y, Pras E, Brand N. Vacuolating megalencephalic leukoencephalopathy in 12 Israeli patients. *J Child Neurol* 2001; 16: 93–99
- Ben-Zeev B, Levy-Nissenbaum E, Lahat H, Anikster Y, Shinar Y, Brand N, Gross-Tzur V, MacGregor D, Sidi R, Kleta R, Frydman M, Pras E. Megalencephalic leukoencephalopathy with subcortical cysts; a founder effect in Israeli patients and a higher than expected carrier rate among Libyan Jews. *Hum Genet* 2002; 111: 214–218
- Bešenski N, Bošnjak V, Cop S, Pavic D, Mikulic D, Orolić K. Neuroimaging and clinically distinctive features in van der Knaap megalencephalic leukoencephalopathy. *Int J Neuro-radiol* 1997; 3: 244–249
- Biancheri R, Pisaturo C, Perrone MV, Passagno A, Rossi A, Vene-selli E. Presence of delayed myelination and macrocephaly in the sister of a patient with vacuolating leukoencephalopathy with subcortical cysts. *Neuropediatrics* 2000; 31: 321–324
- Blattner R, von Moers A, Leegwater PAJ, Hanefeld FA, van der Knaap MS, Köhler W. Clinical and genetic heterogeneity in megalencephalic leukoencephalopathy with subcortical cysts (MLC). *Neuropediatrics* 2002; 34: 215–218
- Boor PKI, de Groot K, Waisfisz Q, Kamphorst W, Oudejans CBM, Powers JM, Pronk JC, Scheper GC, van der Knaap MS. MLC1: a novel protein in distal astroglial processes. *J Neuropathol Exp Neurol* 2005 (in press)
- Brockmann K, Finsterbusch J, Terwey B, Frahm J, Hanefeld F. Megalencephalic leukoencephalopathy with subcortical cysts in an adult: quantitative proton MR spectroscopy and diffusion tensor MRI. *Neuroradiology* 2003; 45: 137–142
- Bugiani M, Moroni I, Bizzi A, Nardocci N, Bettecken T, Gärtner J, Uziel G. Consciousness disturbances in megalencephalic leukoencephalopathy with subcortical cysts. *Neuropediatrics* 2003; 34: 211–214
- Chandrasekar HS, Guruprasad AS, Jayakumar PN, Srikanth SG, Taly AB. Megalencephalic leukoencephalopathy with subcortical cysts: MRI and proton spectroscopic features. *Neurol India* 2003; 51: 525–527
- De Stefano N, Balestri P, Dotti MT, Grosso S, Mortilla M, Morgese G, Federico A. Severe metabolic abnormalities in the white matter of patients with vacuolating megalencephalic leukoencephalopathy with subcortical cysts. A proton MR spectroscopic imaging study. *J Neurol* 2001; 248: 403–409
- Gelaf F, Call C, Apaydin M, Erdem G, Van der Knaap's leukoencephalopathy: report of five new cases with emphasis on diffusion-weighted MRI findings. *Neuroradiology* 2002; 4: 625–630
- Gorospe JR, Singhal BS, Kainu T, Wu F, Stephan D, Trent J, Hoffman EP, Naidu S. Indian Agarwal megalencephalic leukodystrophy with cysts is caused by a common MLC1 mutation. *Neurology* 2004; 62: 878–882
- Goutières F, Bouloche J, Bourgeois M, Aicardi J. Leukoencephalopathy, megalencephaly, and mild clinical course. A recently individualized familial leukodystrophy. Report of five new cases. *J Child Neurol* 1996; 11: 439–444
- Gulati S, Kabra M, Gera S, Ghosh M, Menon PSN, Kalra V. Infantile-onset leukoencephalopathy with discrepant mild clinical course. *Indian J Pediatr* 2000; 67: 769–773

- Harbord MG, Harden A, Harding B, Brett EM, Baraitser M. Megalencephaly with dysmyelination, spasticity, ataxia, seizures and distinctive neurophysiological findings in two siblings. *Neuropediatrics* 1990; 21: 164–168
- Higuchi Y, Hattori H, Tsuji M, Asato R, Nakahata T. Partial seizures in leukoencephalopathy with swelling and a discrepantly mild clinical course. *Brain Dev* 2000; 22: 287–389
- Koeda T, Takeshita K. Slowly progressive cystic leukoencephalopathy with megalencephaly in a Japanese boy. *Brain Dev* 1998; 20: 245–249
- Leegwater PAJ, Qiang Yuan B, van der Steen J, Mulders J, Könst AAM, Ilja Boor PK, Mejaski-Bosnjak V, Van der Maarel SM, Frants RR, Oudejans CBM, Schutgens RBH, Pronk JC, van der Knaap MS. Mutations of *MCL1* (*KIAA0027*), encoding a putative membrane protein cause megalencephalic leukoencephalopathy with subcortical cysts. *Am J Hum Genet* 2001; 68: 831–838
- Leegwater PAJ, Boor PKI, Yuan BQ, van der Steen J, Visser A, Könst AAM, CBM Oudejans, Schutgens RBH, Pronk JC, van der Knaap MS. Identifications of novel mutations in *MCL1* responsible for megalencephalic leukoencephalopathy with subcortical cysts. *Hum Genet* 2002; 110: 279–283
- Mejaški-Bošnjak V, Beenski N. Megalencephalic leukoencephalopathy: a further case of a new neurodegenerative white matter disease. *Dev Med Child Neurol* 1997; 39: 561–563
- Mejaški-Bošnjak V, Bešenski N, Brockmann K, Pouwels PJW, Frahm J, Hanefeld FA. Cystic leukoencephalopathy in a megalencephalic child: clinical and magnetic resonance imaging/magnetic resonance spectroscopy findings. *Pediatr Neurol* 1997; 16: 347–350
- Neely JD, Amiry-Moghaddam M, Ottersen OP, Froehner SC, Agre P, Adams ME. Syntrophin-dependent expression and localization of aquaporin-4 water channel protein. *Proc Natl Acad Sci USA* 2001; 98: 14108–14113
- Patrono C, di Giacinto G, Eymard-Pierre E, Santorelli FM, Rodriguez D, de Stefano N, Federico A, Gatti R, Benigo V, Megarbané A, Tabarki B, Boespflug-Tanguy O, Bertini E. Genetic heterogeneity of megalencephalic leukoencephalopathy with subcortical cysts. *Neurology* 2003; 61: 534–537
- Rubie C, Lichtner P, Gärtner J, Siekiera M, Uziel G, Kohlmann B, Kohlschütter A, Meitinger T, Stöber G, Bettecken T. Sequence diversity of *KIAA0027/MCL1*: are megalencephalic leukoencephalopathy and schizophrenia allelic disorders? *Hum Mutat* 2002; 21: 45–53
- Saijo H, Nakayama H, Ezoe T, Araki K, Sone S, Hamaguchi H, Suzuki H, Shiroma N, Kanazawa N, Tsujino S, Hirayama Y, Arima M. A case of megalencephalic leukoencephalopathy with subcortical cysts (van der Knaap disease): molecular genetic study. *Brain Dev* 2003; 25: 362–366
- Schmitt A, Gofferje V, Weber M, Meyer J, Mössner R, Lesch K-P. The brain-specific protein MLC1 implicated in megalencephalic leukoencephalopathy with subcortical cysts is expressed in glial cells in the murine brain. *Glia* 2003; 44: 283–295
- Sener RN. Van der Knaap syndrome: MR imaging findings including FLAIR, diffusion imaging, and proton MR spectroscopy. *Eur Radiol* 2000; 10: 1452–1455
- Shinar Y, Ben-Zeev B, Brand N, Lahat H, Gross-Zur V, MacGregor D, Bahan T, Kastner DL, Pras E. A common ancestral haplotype in carrier chromosomes from different ethnic backgrounds in vacuolating megalencephalic leukoencephalopathy with subcortical cysts. *J Med Genet* 2002; 39: 54–57
- Singhal BS, Gursahani RD, Udami VPK, Biniwale AA. Megalencephalic leukodystrophy in an Asian Indian Ethnic Group. *Pediatr Neurol* 1996; 14: 291–296
- Singhal BS, Gorospe JR, Naidu S. Megalencephalic leukoencephalopathy with subcortical cysts. *J Child Neurol* 2003; 18: 646–652
- Takanashi J-I, Sugita K, Kohno Y. Vacuolating leukoencephalopathy with subcortical cysts with late onset athetotic movements. *J Neurol Sci* 1999; 165: 90–93
- Teijido O, Martinez A, Pusch M, Zorzano A, Soriano E, Del Rio JA, Palacin M, Estevez R. Localization and functional analyses of the MLC1 protein involved in megalencephalic leukoencephalopathy with subcortical cysts. *Hum Mol Genet* 2004; 13: 2581–2594
- Thele T, Balslev T, Christensen T. Van der Knaap's vacuolating leukoencephalopathy: two additional cases. *Eur J Pediatr Neurol* 1999; 3: 83–86
- Topçu M, Saatci I, Topcuoglu MA, Kose G, Kunak B. Megalencephaly and leukodystrophy with mild clinical course: a report on 12 new cases. *Brain Dev* 1998; 20: 142–153
- Topçu M, Gartioux C, Ribierre F, Yalçinkaya C, Tokus E, Öztekin N, Beckmann JS, Ozguc M, Seboun E. Vacuolating megalencephalic leukoencephalopathy with subcortical cysts, mapped to chromosome 22q_{tel}. *Am J Hum Genet* 2000; 66: 733–739
- Tsujino S, Kanazawa N, Yoneyama H, Shimono M, Kawakami A, Hatanaka Y, Shimizu T, Oba H. A common mutation and a novel mutation in Japanese patients with van der Knaap disease. *J Hum Genet* 2003; 48: 605–608
- van der Knaap MS, Barth PG, Stroink H, van Nieuwenhuizen O, Arts WFM, Hoogenraad F, Valk J. Leukoencephalopathy with swelling and a discrepantly mild clinical course in 8 children. *Ann Neurol* 1995; 37: 324–334
- van der Knaap, Valk J, Barth PG, Smit LME, Van Engelen BGM, Tortori Donati P. Leukoencephalopathy with swelling in children and adolescents: MRI pattern and differential diagnosis. *Neuroradiology* 1995; 37: 679–686
- van der Knaap, Barth PG, Vrensens GFJM, Valk J. Histopathology of an infantile-onset spongiform leukoencephalopathy with a discrepantly mild clinical course. *Acta Neuropathol (Berl)* 1996; 92: 206–212
- Yakinci C, Soyulu H, Kutlu NO, Sener RN. Leukoencephalopathy with a mild clinical course: a case report. *Comput Med Imaging Graph* 1999; 23: 169–172
- Yalçinkaya C, Çomu S, Koçer N, Yüksel A, Güzüz E, Dermirbilek V, Öcal A. Siblings with cystic leukoencephalopathy and megalencephaly. *J Child Neurol* 2000; 15: 690–693
- Yalçinkaya C, Yüksel A, Çomu S, Kiliç G, Çokar Ö, Derwent A. Epilepsy in vacuolating megalencephalic leukoencephalopathy with subcortical cysts. *Seizure* 2003; 12: 388–396

60 Congenital Muscular Dystrophies

Walker-Warburg Syndrome

- Asano Y, Minagawa K, Okuda A, Matsui T, Ando K, Kondo-Iida E, Kobayashi O, Toda T, Nonaka I, Tanizawa T. A case of Walker-Warburg syndrome. *Brain Dev* 2000; 22: 454–457
- Barkovic AJ. Neuroimaging manifestations and classification of congenital muscular dystrophies. *AJNR Am J Neuroradiol* 1998; 19: 1389–1396

- Bertrán-Valero de Bernabé D, Currier S, Steinbrecher A, Celli J, van Beusekom E, van der Zwaag B, Kayserili H, Merlini L, Chitayat D, Dobyns WB, Cormand B, Lehesjoki A-E, Cruces J, Voit Th, Walsh CA, van Bokhoven H, Brunner HG. Mutations in the O-mannosyltransferase gene *POMT1* give rise to the severe neuronal migration disorder Walker-Warburg syndrome. *Am J Hum Genet* 2002; 71: 1033–1043
- Di Rocco M, Leveratto L, Cama A, Bado M, Tortori Donati P, Andreussi L, Borroni C. Report on a patient with congenital muscular dystrophy, hydrocephalus, Dandy-Walker malformation and leukodystrophy. *Genet Couns* 1993; 4: 295–298
- Dobyns WB, Kirkpatrick JB, Hittner HM, Roberts RM, Kretzer FL. Syndromes with lissencephaly. II. Walker-Warburg and cerebro-oculo-muscular syndromes and a new syndrome with type II lissencephaly. *Am J Med Genet* 1985; 22: 157–195
- Dobyns WB, Pagon RA, Armstrong D, Curry CJR, Greenberg F, Grix A, Holmes LB, Laxova R, Michels VV, Robinow M, Zimmerman RL. Diagnostic criteria for Walker-Warburg syndrome. *Am J Med Genet* 1989; 32: 195–210
- Heyer R, Ehrich J, Goebel HH, Christen HJ, Hanefeld F. Congenital muscular dystrophy with cerebral and ocular malformations (cerebro-oculo-muscular syndrome). *Brain Dev* 1986; 8: 614–619
- Kanoff RJ, Curlless RG, Petito C, Falcone S, Siatkowski RM, Pegoraro E. Walker-Warburg syndrome: neurologic features and muscle membrane structure. *Pediatr Neurol* 1998; 18: 76–80
- Kim DS, Hayashi YK, Matsumoto H, Ogawa M, Noguchi S, Murakami N, Sakuta R, Michozuki M, Michele DE, Campbell KP, Nonaka I, Nishino I. *POMT1* mutation results in defective glycosylation and loss of laminin-binding activity in α -DG. *Neurology* 2004; 62: 1009–1011
- Kimura S, Sasaki Y, Kobayashi Y, Ohtsuki N, Tanaka Y, Hara M, Miyake S, Yamada M, Iwamoto H, Misugi N. Fukuyama-type congenital muscular dystrophy and the Walker-Warburg syndrome. *Brain Dev* 1993; 15: 182–191
- Kükner S, Güler Y, Saatçi I, Akçören Z, Topaloğlu H. Laminin- α 2 chain (merosin M) is preserved in the Walker-Warburg syndrome. *Neuropediatrics* 1996; 27: 279–280
- Pabuöçü Y, Bulakbaşı N, Koaoğlu M, Uçöz T. Walker-Warburg syndrome variant. *Comput Med Imaging Graph* 2002; 26: 453–458
- Rhodes RE, Hatten HP, Ellington KS. Walker-Warburg syndrome. *AJNR Am J Neuroradiol* 1992; 13: 123–126
- Sabatelli P, Columbaro M, Mura I, Capanni C, Lattanzi G, Maraldi NM, Beltrán-Valero de Barnabé D, van Bokhoven H, Squarzoni S, Merlini L. Extracellular matrix and nuclear abnormalities in skeletal muscle of a patient with Walker-Warburg syndrome caused by *POMT1* mutation. *Biochim Biophys Acta* 2003; 1638: 57–62
- Simma B, Felber S, Maurer H, Gassner I, Krassnitzer S. MR and ultrasound findings in a case of cerebro-oculo-muscular syndrome. *Pediatr Radiol* 1990; 20: 554–555
- Towfighi J, Sassani JW, Suzuki K, Ladda RL. Cerebro-ocular dysplasia – muscular dystrophy (COD-MD) syndrome. *Acta Neuropathol (Berl)* 1984; 65: 110–123
- Vajsar J, Ackerley C, Chitayat D, Becker LE. Basal lamina skeletal muscle of Walker-Warburg syndrome. *Pediatr Neurol* 2000; 22: 139–143
- Villanova M, Sabatelli P, He Y, Malandrini A, Petrini S, Maraldi NM, Merlini L. Immunofluorescence study of a muscle biopsy from a 1-year-old patient with Walker-Warburg syndrome. *Acta Neuropathol (Berl)* 1998; 96: 651–654
- Voit T, Sewry CA, Meyer K, Hermann R, Straub V, Muntoni F, Kahn T, Unsold R, Helliwell TR, Appleton R, Lenard HG. Preserved merosin M-chain (or laminin- α 2) expression in skeletal muscle distinguishes Walker-Warburg syndrome from Fukuyama muscle dystrophy and merosin-deficient congenital muscular dystrophy. *Neuropediatrics* 1995; 26: 148–155
- Williams RS, Swisher CN, Jennings M, Ambler M, Caviness Jr VS. Cerebro-ocular dysgenesis (Walker-Warburg syndrome): neuropathologic and etiologic analysis. *Neurology* 1984; 34: 1531–1541
- Zaleski CG, Abdenour GE. Pediatric case of the day. *Radiographics* 1997; 17: 1319–1323

Fukuyama Type of Congenital Muscular Dystrophy

- Aida N. Fukuyama congenital muscular dystrophy: a neuroradiologic review. *J Magn Reson Imaging* 1998; 8: 317–326
- Aida N, Yagishita A, Takada K, Katsumata Y. Cerebellar MR in Fukuyama congenital muscular dystrophy: polymicrogyria with cystic lesions. *AJNR Am J Neuroradiol* 1994; 15: 1755–1759
- Aida N, Tamagawa K, Takada K, Yagishita A, Kobayashi N, Chikumaru K, Iwamoto H. Brain MR in Fukuyama congenital muscular dystrophy. *AJNR Am J Neuroradiol* 1996; 17: 605–613
- Aihara M, Tanabe Y, Kato K. Serial MRI in Fukuyama type congenital muscular dystrophy. *Neuroradiology* 1992; 34: 396–398
- Aravind L, Koonin EV. The fukutin protein family – predicted enzymes modifying cell-surface molecules. *Curr Biol* 1999; 9: R836–R837
- Beltrán-Valero de Barnabé D, van Bokhoven H, van Beusekom E, van den Akker W, Kant S, Dobyns WB, Cormand B, Currier S, Hamel B, Talim B, Topaloglu H, Brunner HG. A homozygous nonsense mutation in the *Fukutin* gene causes a Walker-Warburg syndrome phenotype. *J Med Genet* 2003; 40: 845–848
- Chijiwa T, Nishimura M, Inomata H, Yamana T, Yamana T, Narazaki O, Kurokawa T. Ocular manifestations of congenital muscular dystrophy (Fukuyama type). *Ann Ophthalmol* 1983; 15: 921–923 and 926–928
- Colombo R, Bignamini AA, Carobene A, Sasaki J, Tachikawa M, Kobayashi K, Toda T. Age and origin of the FCMD 3'-untranslated gene-region retrotranspositional insertion mutation causing Fukuyama-type congenital muscular dystrophy in the Japanese population. *Hum Genet* 2000; 107: 559–567
- Fukuyama Y, Ohsawa M. A genetic study of the Fukuyama type congenital dystrophy. *Brain Dev* 1984; 6: 373–390
- Fukuyama Y, Osawa M, Suzuki H. Congenital progressive muscular dystrophy of the Fukuyama type – clinical, genetic and pathological considerations. *Brain Dev* 1981; 3: 1–29
- Hayashi YK, Engvall E, Arikawa-Hirasawa E, Goto K, Koga R, Nonaka I, Sugita H, Arahata K. Abnormal localization of laminin subunits in muscular dystrophies. *J Neurol Sci* 1993; 119: 53–64
- Hayashi YK, Ogawa W, Tagawa K, Noguchi S, Ishihara T, Nonaka I, Arahata K. Selective deficiency of α -dystroglycan in Fukuyama-type congenital muscular dystrophy. *Neurology* 2001; 57: 115–121
- Ishii H, Hayashi YK, Nonaka I, Arahata K. Electron microscopic examination of basal lamina in Fukuyama congenital muscular dystrophy. *Neuromusc Disord* 1997; 7: 191–197

- Kato T, Funahashi M, Matsui A, Takashima S, Suzuki Y. MRI of disseminated development dysmyelination in Fukuyama type of CMD. *Pediatr Neurol* 2000; 23: 385–388
- Kihira S, Nonaka I. Congenital muscular dystrophy. A histochemical study with morphometric analysis on biopsied muscles. *J Neurol Sci* 1985; 70: 139–149
- Kobayashi K, Nakahori Y, Miyake M, Matsumura K, Kodo-Lida E, Nomura Y, Segawa M, Yoshioka M, Saito K, Osawa M, Hamano K, Sakikahara Y, Nonaka I, Nakagome Y, Kanazawa I, Nakamura Y, Tokunaga K, Toda T. An ancient retrotransposal insertion causes by Fukuyama-type congenital muscular dystrophy. *Nature* 1998; 394: 388–392
- Kumada S, Tsuchiya K, Takahashi M, Takesue M, Shiotsu H, Nomura Y, Segawa M, Ikeda K, Hayashi M. The cerebellar and thalamic degeneration in Fukuyama-type congenital muscular dystrophy. *Acta Neuropathol (Berl)* 2000; 99: 209–213
- Nakano I, Funahashi M, Takada K, Toda T. Are breaches in the glia limitans the primary cause of the micropolygyria in Fukuyama-type congenital muscular dystrophy (FCMD)? – Pathological study of the cerebral cortex of an FCMD fetus. *Acta Neuropathol (Berl)* 1996; 91: 313–321
- Osawa M, Arai Y, Ikenake H, Murasugi H, Sugahara N, Sumida S, Okada N, Shishikura K, Suzuki H, Hirayama Y, Hirasawa K, Fukuyama Y, Tsutsumi A, Ito K, Uchida Y. Fukuyama type congenital progressive muscular dystrophy. *Acta Paediatr Jpn* 1991; 33: 261–269
- Saito K, Osawa M, Wang Z-P, Ikeya K, Fukuyama Y, Kondo-lida E, Toda T, Ohashi H, Kurosawa K, Wakai S, Kanedo K-i. Haplotype-phenotype correlation in Fukuyama congenital muscular dystrophy. *Am J Med Genet* 2000; 92: 184–190
- Saito Y, Murayama S, Kawai M, Nakano I. Breached cerebral glia limitans-basal lamina complex in Fukuyama-type congenital muscular dystrophy. *Acta Neuropathol (Berl)* 1999; 98: 330–336
- Silan F, Yoshioka M, Kobayashi K, Simsek E, Tunc M, Alper M, Cam M, Guven A, Fukuda Y, Kinoshita M, Kocabay K, Toda T. A new mutation of the fukutin gene in a non-Japanese patient. *Ann Neurol* 2003; 53: 392–396
- Takada K. Fukuyama congenital muscular dystrophy as a unique disorder of neuronal migration: a neuropathological review and hypothesis. *Yonago Acta Med* 1988; 31: 1–16
- Takada K, Nakamura H. Cerebellar micropolygyria in Fukuyama congenital muscular dystrophy: observations in fetal and pediatric cases. *Brain Dev* 1990; 12: 774–778
- Takada K, Nakamura H, Tanaka J. Cortical dysplasia in congenital muscular dystrophy with central nervous system involvement (Fukuyama type). *J Neuropathol Exp Neurol* 1984; 43: 395–407
- Takada K, Nakamura H, Suzumori K, Ishikawa T, Sugiyama N. Cortical dysplasia in a 23-week fetus with Fukuyama congenital muscular dystrophy (FCMD). *Acta Neuropathol (Berl)* 1987; 74: 300–306
- Takada K, Nakamura H, Takashima S. Cortical dysplasia in Fukuyama congenital muscular dystrophy (FCMD): a Golgi and angioarchitectonic analysis. *Acta Neuropathol (Berl)* 1988; 76: 170–178
- Takeda S, Kondo M, Sasaki J, Kurahashi H, Kano H, Arai K, Misaki K, Fukui T, Kobayashi K, Tachikawa M, Imamura M, Nakamura Y, Shimizu T, Murakami T, Sunada Y, Fujikado T, Matsumura K, Terashima T, Toda T. Fukutin is required for maintenance of muscle integrity, cortical histogenesis and normal eye development. *Hum Mol Genet* 2003; 12: 1449–1459
- Terasawa K. Muscle regeneration and satellite cells in Fukuyama-type congenital muscular dystrophy. *Muscle Nerve* 1986; 9: 465–470
- Toda T, Segawa M, Nomura Y, Nonaka I, Masuda K, Ishihara T, Suzuki M, Tomita I, Origuchi Y, Ohno K, Misugi N, Sasaki Y, Takada K, Kawai M, Otani K, Murakami T, Saito K, Fukuyama Y, Shimizu T, Kanazawa I, Nakamura Y. Localization of a gene for Fukuyama type congenital muscular dystrophy to chromosome 9q31–33. *Nat Genet* 1993; 5: 283–286
- Toda Y, Watanabe T, Matsumura K, Sunada Y, Yamada H, Nakano I, Mannen T, Kanazawa I, Shimizu T. Three-dimension MR imaging of brain surface anomalies in Fukuyama-type congenital muscular dystrophy. *Muscle Nerve* 1995; 18: 508–517
- Toda T, Kobayashi K, Kondo-lida E, Sasaki J, Nakamura Y. The Fukuyama congenital muscular dystrophy story. *Neuro-musc Disord* 2000; 10: 153–159
- Tsutsumi A, Uchida Y, Osawa M, Fukuyama Y. Ocular findings in Fukuyama type congenital muscular dystrophy. *Brain Dev* 1989; 11: 413–419
- Wang Z-P, Osawa M, Fukuyama Y. Morphometric study of the corpus callosum in Fukuyama type congenital muscular dystrophy by magnetic resonance imaging. *Brain Dev* 1995; 17: 104–110
- Yamamoto T, Toyoda C, Kobayashi M, Kondo E, Saito K, Osawa M. Pial-glial barrier abnormalities in fetuses with Fukuyama congenital muscular dystrophy. *Brain Dev* 1997; 19: 35–42
- Yamamoto T, Armstrong D, Shibata N, Kanazawa M, Kobayashi M. Immature astrocytes in Fukuyama congenital muscular dystrophy: an immunohistochemical study. *Pediatr Neurol* 1999; 20: 31–37
- Yoshioka M, Kuroki S. Clinical spectrum and genetic studies of Fukuyama congenital muscular dystrophy. *Am J Med Genet* 1994; 53: 245–250
- Yoshioka M, Kuroki S, Kondo T. Ocular manifestations in Fukuyama type congenital muscular dystrophy. *Brain Dev* 1990; 12: 423–426
- Yoshioka M, Saiwai S, Kuroki S, Nigami H. MR imaging of the brain in Fukuyama-type congenital muscular dystrophy. *AJNR Am J Neuroradiol* 1991; 12: 63–65
- Yoshioka M, Toda T, Kuroki S, Hamado K. Broader clinical spectrum of Fukuyama congenital muscular dystrophy manifested by haplotype analysis. *J Child Neurol* 1999; 14: 711–715
- Zanoteli E, Rocha JCC, Narumia LK, Fireman MAT, Moura LS, Oliveira ASB, Gabbai AA, Fukuda Y, Kinoshita M, Toda T. Fukuyama-type congenital muscular dystrophy: a case report in the Japanese population living in Brazil. *Acta Neurol Scand* 2002; 106: 117–121

Muscle-Eye-Brain Disease

- Auranen M, Rapola J, Pihki H, Haltia M, Leivo I, Soinila S, Virtanen I, Kalimo H, Anderson LVB, Santavuori P, Somer H. Muscle membrane-skeleton protein changes and histopathological characterization of muscle-eye-brain disease. *Neuromusc Disord* 2000; 10: 16–23
- Chiba A, Matsumura K, Yamada H, Inazu T, Shimizu T, Kusunoki S, Kanazawa I, Kobata A, Endo T. Structures of sialylated O-linked oligosaccharides of bovine peripheral nerve α -dystroglycan. The role of a novel O-mannosyl-type oligosaccharide in the binding of α -dystroglycan with laminin. *J Biol Chem* 1997; 272: 2216–2262
- Cormand B, Avela K, Pihko H, Santavuori P, Talin B, Topalogly H, de la Chapelle A, Lehesjoki A-E. Assignment of the muscle-eye-brain disease gene to 1p32-p34 by linkage analysis and homozygosity mapping. *Am J Hum Genet* 1999; 64: 126–135

- Goebel HH, Fidzianska A, Lenard HG, Osse G, Hori A. A morphological study of non-Japanese congenital muscular dystrophy associated with cerebral lesions. *Brain Dev* 1983; 5: 292–301
- Haltia M, Leivo I, Somer H, Pihko H, Paetau A, Kivelä T, Tarkkanen A, Tomé F, Engvall E, Santavuori P. Muscle-eye-brain disease: a neuropathological study. *Ann Neurol* 1997; 41: 173–180
- Kano H, Kobayashi K, Herrmann R, Tachikawa M, Manya H, Nishino I, Nonaka I, Straub V, Talim B, Voit T, Topaloglu H, Endo T, Yoshikawa H, Toda T. Deficiency of α -dystroglycan in muscle-eye-brain disease. *Biochem Biophys Res Commun* 2002; 291: 1283–1286
- Korinthenberg R, Palm D, Schlake W, Klein J. Congenital muscular dystrophy, brain malformation and ocular problems (muscle, eye and brain disease) in two German families. *Eur J Pediatr* 1984; 142: 64–68
- Manya H, Sakai K, Kobayashi K, Taniguchi K, Kawakita M, Toda T, Endo T. Loss-of-function of an *N*-acetylglucosaminyltransferase, POMGnT1, in muscle-eye-brain disease. *Biochem Biophys Res Commun* 2003; 306: 93–97
- Michele DE, Barresi R, Kanagawa M, Saito F, Cohn RD, Satz JS, Dollar J, Nishino I, Kelley RI, Somer H, Straub V, Mathews KD, Moore SA, Campbell KP. Post-translational disruption of dystroglycan-ligand interactions in congenital muscular dystrophies. *Nature* 2002; 418: 417–422
- Moore SA, Saito F, Chen J, Michele DE, Henry MD, Messing A, Cohn RD, Ross-Barta SE, Westra S, Williamson RA, Hoshi T, Campbell KP. Deletion of brain dystroglycan recapitulates aspects of congenital muscular dystrophy. *Nature* 2002; 418: 422–425
- Muntoni F, Brockington M, Blake DJ, Torelli S, Brown SC. Defective glycosylation in muscular dystrophy. *Lancet* 2002; 360: 1419–1421
- Pihko H, Lappi M, Raitta C, Sainio K, Valanne L, Somer H, Santavuori P. Ocular findings in muscle-eye-brain (MEB) disease: a follow-up study. *Brain Dev* 1995; 17: 57–61
- Ross ME. Full circle to cobbled brain. *Nature* 2002; 418: 376–377
- Santavuori P, Somer H, Sainio K, Rapola J, Kruus S, Nikitin T, Kettonen L, Leisti J. Muscle-eye-brain disease (MEB). *Brain Dev* 1989; 11: 147–153
- Santavuori P, Valanne L, Autti T, Haltia M, Pihko H, Siano K. Muscle-eye-brain disease. Clinical features, visual evoked potentials and brain imaging in 20 patients. *Eur J Pediatr Neurol* 1998; 1: 41–47
- Taniguchi K, Kobayashi K, Saito K, Yamanouchi H, Ohnuma A, Hayashi YK, Manya H, Jin DK, Lee M, Parana E, Falsaperia R, Pavone P, van Coter R, Talim B, Steinbrecher A, Straub V, Nishino I, Topaloglu H, Voit T, Endo T, Toda T. Worldwide distribution and broader clinical spectrum of muscle-eye-brain disease. *Hum Mol Genet* 2003; 12: 527–534
- Valanne L, Pihko H, Katevuo K, Karttunen P, Somer H, Santavuori P. MRI of the brain in muscle-eye-brain (MEB) disease. *Neuroradiology* 1994; 36: 473–476
- van der Knaap MS, Smit LME, Barth PG, Catsman-Berrevoets CE, Brouwer OF, Begeer JH, de Coe IFM, Valk J. Magnetic resonance imaging in classification of congenital muscular dystrophies with brain abnormalities. *Ann Neurol* 1997; 42: 50–59
- Yoshida A, Kobayashi K, Manya H, Taniguchi K, Kano H, Mizuno M, Inazu T, Matsubashi H, Takahashi S, Takeuchi M, Herrmann R, Straub V, Talim B, Voit T, Topaloglu H, Toda T, Endo T. Muscular dystrophy and neuronal migration disorder caused by mutations in a glycosyltransferase, POMGnT1. *Dev Cell* 2001; 1: 717–724
- Zervos A, Hunt KE, Tong G-Q, Avallone J, Morales J, Friedman N, Cohen BH, Clark B, Guo S, Gazda H, Beggs AH, Traboulsi EI. Clinical, genetic and histopathological findings in two siblings with muscle-eye-brain disease. *Eur J Ophthalmol* 2002; 12: 253–261

Merosin-deficient Congenital Muscular Dystrophy

- Brett FM, Costigan D, Farrell MA, Heapy P, Thornton J, King MD. Merosin-deficient congenital muscular dystrophy and cortical dysplasia. *Eur J Pediatr Neurol* 1998; 2: 77–82
- Caro PA, Scavina M, Hoffman E, Pegoraro E, Marks HG. MR imaging findings in children with merosin-deficient congenital muscular dystrophy. *AJNR Am J Neuroradiol* 1999; 20: 324–326
- Cohn RD, Herrmann R, Sorokin L, Wewer UM, Voit T. Laminin α 2 chain-deficient congenital muscular dystrophy. *Neurology* 1998; 51: 94–101
- Coral-Vazquez RM, Rosas-Vargas H, Meza-Espinosa P, Mendoza I, Huicochea JC, Ramon G, Salamanca F. Severe congenital muscular dystrophy in a Mexican family with a new nonsense mutation (R2578X) in the laminin α -2 gene. *J Hum Genet* 2003; 48: 91–95
- Di Blasi C, Mora M, Pareyson D, Farina L, Sghirlanzoni A, Vignier N, Blasevich F, Cornelio F, Guicheney P, Morandi L. Partial laminin α 2 chain deficiency in a patient with myopathy resembling inclusion body myositis. *Ann Neurol* 2000; 47: 811–816
- Di Muzio A, de Angelis MV, di Fulvio P, Ratti A, Pizzuti A, Stuppia L, Gambi D, Unchini A. Dysmyelinating sensory-motor neuropathy in merosin-deficient congenital muscular dystrophy. *Muscle Nerve* 2003; 27: 500–506
- Echenne B, Pages M, Marty-Double C. Congenital muscular dystrophy with cerebral white matter spongiosis. *Brain Dev* 1984; 6: 491–495
- Farina L, Morandi L, Milanese I, Ciceri E, Mora M, Moroni I, Pantaleoni C, Savoardo M. Congenital muscular dystrophy with merosin deficiency: MRI findings in five patients. *Neuroradiology* 1998; 40: 807–811
- Gilhuis HJ, ten Donkelaar HJ, Tanke RB, Vingerhoets DM, Zwarts MJ, Verrips A, Gabreëls FJM. Nonmuscular involvement in merosin-negative congenital muscular dystrophy. *Pediatr Neurol* 2002; 26: 30–36
- Guicheney P, Vignier N, Helbling-Leclerc A, Nissinen M, Zhang X, Cruaud C, Lambert J-C, Richelme C, topaloglu H, Merlini L, Barois A, Schwartz K, Tome FMS, Tryggvason K, Fardeau M. Genetics of laminin α 2 chain (or merosin) deficient congenital muscular dystrophy: from identification of mutations to prenatal diagnosis. *Neuromusc Disord* 1997; 7: 180–186
- Hillaire D, Leclerc A, Fauré S, Topaloglu H, Chiannikulchai N, Guicheney P, Grinas L, Legos P, Philpot J, Evangelista T, Routon M-C, Mayer M, Pellissier J-F, Estournet B, Barois A, Hentati F, Feingold N, Beckmann JS, Dubowitz V, Tomé FMS, Fardeau M. Localization of merosin-negative congenital muscular dystrophy to chromosome 6q2 by homozygosity mapping. *Hum Mol Genet* 1994; 3: 1657–1661
- Jones KJ, Morgan G, Johnston H, Tobias V, Ouvrier RA, Wilkinson I, North KN. The expanding phenotype of laminin α 2 chain (merosin) abnormalities: case series and review. *J Med Genet* 2001; 38: 649–657

- Lamer S, Carlier R-Y, Pinard J-M, Mompoin D, Bagard C, Burdairon E, Estournet B, Barois A, Vallée C. Congenital muscular dystrophy: use of brain MR imaging findings to predict merosin deficiency. *Radiology* 1998; 206: 811–816
- Mackay MT, Kornberg AJ, Shield L, Phelan E, Kean MJ, Coleman LT, Dennett X. Congenital muscular dystrophy, white matter abnormalities, and neuronal migration disorders: the expanding concept. *J Child Neurol* 1998; 13: 481–487
- Marbini A, Bellanova MF, Ferrari A, Lodesani M, Gemignani F. Immunohistochemical study of merosin-negative congenital muscular dystrophy: laminin $\alpha 2$ deficiency in skin biopsy. *Acta Neuropathol (Berl)* 1997; 94: 103–108
- Martinello F, Angelini C, Trevisan CP. Congenital muscular dystrophy with partial merosin deficiency and late onset epilepsy. *Eur Neurol* 1998; 40: 37–45
- Mercuri E, Pennock J, Goodwin F, Sewry C, Cowan F, Dubowitz L, Dubowitz V, Muntoni F. Sequential study of central and peripheral nervous system involvement in an infant with merosin-deficient congenital muscular dystrophy. *Neuromusc Disord* 1996; 6: 425–429
- Mercuri E, Anker S, Philpot J, Sewry C, Dubowitz V, Muntoni F. Visual function in children with merosin-deficient and merosin-positive congenital muscular dystrophy. *Pediatr Neurol* 1998; 18: 339–401
- Mercuri E, Grunter-Andrew J, Philpot J, Sewry C, Counsell S, Henderson S, Jensen A, Naom I, Bydder G, Dubowitz V, Muntoni F. Cognitive abilities in children with congenital muscular dystrophy: correlation with brain MRI and merosin status. *Neuromusc Disord* 1999; 9: 383–387
- Minetti C, Bado M, Morreale G, Pedemonte M, Cordone G. Disruption of muscle basal lamina in congenital muscular dystrophy with merosin deficiency. *Neurology* 1996; 46: 1354–1358
- Miyagoe-Suzuki Y, Nakagawa M, Takeda S. Merosin and congenital muscular dystrophy. *Microsc Res Tech* 2000; 48: 181–191
- Mora M, Moroni I, Uziel G, di Balsi C, Barresi R, Farina L, Morandi L. Mild clinical phenotype in a 12-year-old boy with partial merosin deficiency and central and peripheral nervous system abnormalities. *Neuromusc Disord* 1996; 6: 377–381
- Mrak RE. The pathologic spectrum of merosin deficiency. *J Child Neurol* 1998; 13: 513–515
- Nissinen M, Helbling-Leclerc A, Zhang X, Evangelista T, Topaloglu H, Cruaud C, Weissenbach J, Fardeau M, Tomé FMS, Schwartz K, Tryggvason K, Guicheney P. Substitution of a conserved cysteine-996 in a cysteine-rich motif of the laminin $\alpha 2$ -chain in congenital muscular dystrophy with partial deficiency of the protein. *Am J Hum Genet* 1996; 58: 1177–1184
- North KN, Specht LA, Sethi RK, Shapiro F, Beggs AH. Congenital muscular dystrophy associated with merosin deficiency. *J Child Neurol* 1996; 11: 291–295
- Osari S-i, Kobayashi O, Yamashita Y, Matsuishi T, Goto M, Tanabe Y, Migita T, Nonaka I. Basement membrane abnormality in merosin-negative congenital muscular dystrophy. *Acta Neuropathol (Berl)* 1996; 91: 332–336
- Pegoraro E, Mancias P, Swerdlow SH, Raikow RB, Garcia C, Marks H, Crawford T, Carver V, di Ciano B, Hoffman EP. Congenital muscular dystrophy with primary laminin $\alpha 2$ (merosin) deficiency presenting as inflammatory myopathy. *Ann Neurol* 1996; 40: 782–791
- Pegoraro E, Marks H, Garcia CA, Crawford T, Mancias P, Connolly AM, Fanin M, Martinello F, Trevisan CP, Angelini C, Stella A, Scavina M, Munk RL, Servidei S, Bönnemann CC, Bertorini T, Acsadi G, Thompson CE, Gagnon D, Hoganson G, Carver V, Zimmerman RA, Hoffman EP. Laminin $\alpha 2$ muscular dystrophy genotype/phenotype studies of 22 patients. *Neurology* 1998; 51: 101–110
- Pegoraro E, Fanin M, Trevisan CP, Angelini C, Hoffman EP. A novel laminin $\alpha 2$ isoform in severe laminin $\alpha 2$ deficient congenital muscular dystrophy. *Neurology* 2000; 55: 1128–1134
- Philpot J, Sewry C, Pennock J, Dubowitz V. Clinical phenotype in congenital muscular dystrophy: correlation with expression of merosin in skeletal muscle. *Neuromusc Disord* 1995; 5: 301–305
- Philpot J, Cowan F, Pennock J, Sewry C, Dubowitz V, Bydder G, Muntoni F. Merosin-deficient congenital muscular dystrophy: the spectrum of brain involvement on magnetic resonance imaging. *Neuromusc Disord* 1999; 9: 81–85
- Pini A, Merlini L, Tomé FMS, Chevally M, Gobbi G. Merosin-negative congenital muscular dystrophy, occipital epilepsy with periodic spasms and focal cortical dysplasia. Report of three Italian cases in two families. *Brain Dev* 1996; 18: 316–322
- Reed U, Marie SK, Vainzof M, Salum PB, Levy JA, Zatz M, Diamant A. Congenital muscular dystrophy with cerebral white matter hypodensity. Correlation of clinical features and merosin deficiency. *Brain Dev* 1996; 18: 53–58
- Sanuda Y, Edgar TS, Lotz BP, Rust RS, Campbell KP. Merosin-negative congenital muscular dystrophy associated with extensive brain abnormalities. *Neurology* 1995; 45: 2084–2089
- Schorer Z, Philpot J, Muntoni F, Sewry C, Dubowitz V. Demyelinating peripheral neuropathy in merosin-deficient congenital muscular dystrophy. *J Child Neurol* 1995; 10: 472–475
- Sewrey CA, Philpot J, Mahoney D, Wilson LA, Muntoni F, Dubowitz V. Expression of laminin subunits in congenital muscular dystrophy. *Neuromusc Disord* 1995; 5: 307–316
- Sewrey CA, Philpot J, Sorokin LM, Wilson LA, Naom I, Goodwin F, D'Allesandro M, Muntoni F. Diagnosis of merosin (laminin-2) deficient congenital muscular dystrophy by skin biopsy. *Lancet* 1996; 347: 582–584
- Sewrey CA, Naom I, D'Allesandro M, Sorokin L, Bruno S, Wildon LA, Dubowitz V, Muntoni F. Variable clinical phenotype in merosin-deficient congenital muscular dystrophy associated with differential immunolabelling of two fragments of the laminin $\alpha 2$ chain. *Neuromusc Disord* 1997; 7: 169–175
- Sewrey CA, D'Alessandro M, Wilson LA, Sorokin LM, Naom I, Bruno S, Ferlini A, Dubowitz V, Muntoni F. Expression of laminin chains in skin in merosin-deficient congenital muscular dystrophy. *Neuropediatrics* 1997; 28: 217–222
- Sewrey CA, Naom I, D'Allesandro M, Sorokin L, Bruno S, Wilson LA, Dubowitz V, Muntoni F. Variable clinical phenotype in merosin-deficient congenital muscular dystrophy associated with differential immunolabelling of two fragments of the laminin $\alpha 2$ chain. *Neuromusc Disord* 1997; 7: 169–175
- Tachi N, Kamimura S, Ohya K, Chiba S, Sasaki K. Congenital muscular dystrophy with partial deficiency of merosin. *J Neurol Sci* 1997; 151: 25–27
- Tan E, Topaloglu H, Sewry C, Zorlu Y, Naom I, Erdem S, D'Allesandro M, Muntoni F, Dubowitz V. Late onset muscular dystrophy with cerebral white matter changes due to partial merosin deficiency. *Neuromusc Disord* 1997; 7: 85–89

- Taratuto AL, Lubieniecki F, Díaz D, Schultz M, Ruggieri V, Saccoliti M, Dubrovski A. Merosin-deficient congenital muscular dystrophy associated with abnormal cerebral cortical gyration: an autopsy study. *Neuromusc Disord* 1999; 9: 86–94
- Tezak Z, Prandini P, Boscaro M, Marin A, Devaney J, Marino M, Fanin M, Trevisan CP, Park J, Tyson W, Finkel R, Garcai C, Angelini C, Hoffman EP, Pagoraro E. Clinical and molecular study in congenital muscular dystrophy with partial laminin $\alpha 2$ (LAMA2) deficiency. *Hum Mutat* 2003; 21: 103–111
- Tomé FMS, Evangelista T, Leclerc A, Sunada Y, Manole E, Estournet B, Barois A, Campbell KP, Fardeau M. Congenital muscular dystrophy with merosin deficiency. *Life Sci* 1994; 317: 351–357
- Trevisan CP, Martinello F, Ferruzza E, Angelini C. Divergence of central nervous system involvement in 2 Italian sisters with congenital muscular dystrophy: a clinical and neuroradiological follow-up. *Eur Neurol* 1995; 35: 230–235
- Trevisan CP, Martinello F, Ferruzza E, Fanin M, Chevallay M, Tomé FMS. Brain alterations in the classical form of congenital muscular dystrophy. *Child Nerv Syst* 1996; 12: 604–610
- Tsao CY, Mendell JR, Rusin J, Luquette M. Congenital muscular dystrophy with complete laminin- $\alpha 2$ -deficiency, cortical dysplasia, and cerebral white-matter changes in children. *J Child Neurol* 1998; 13: 253–256
- Van Engelen BGM, Leyten QH, Bernsen PLJA, Gabreëls FJM, Barkhof F, Joosten EMG, Hamel BCJ, ter Laak HJ, Ruijs MBM, Cruysberg JRM, Valk J. Familial adult-onset muscular dystrophy with leukoencephalopathy. *Ann Neurol* 1992; 32: 577–580
- Villanova M, Malandrini A, Toti P, Salvestrone R, Six J, Martin JJ, Guazzi GC. Localization of merosin in the normal human brain: implications for congenital muscular dystrophy with merosin deficiency. *J Submicrosc Cytol Pathol* 1996; 28: 1–4
- Villanova M, Malandrini A, Sabatelli P, Sewry CA, Toti P, Torelli S, Six J, Scarfó G, Palma L, Muntoni F, Squarzoni S, Tosi P, Maraldi NM, Guazzi GC. Localization of laminin $\alpha 2$ chain in normal human central nervous system: an immunofluorescence and ultrastructural study. *Acta Neuropathol (Berl)* 1997; 94: 567–571
- Wewer UM, Engvall E. Merosin/laminin-2 and muscular dystrophy. *Neuromusc Disord* 1996; 6: 409–418
- Yurchenco PD, Cheng Y-S, Campbell K, Li S. Loss of basement membrane, receptor and cytoskeletal lattices in a laminin-deficient muscular dystrophy. *J Cell Sci* 2004; 117: 735–742
- Brown SC, Torelli S, Brockington M, Yuva Y, Jimenez C, Feng L, Anderson L, Ugo I, Kroger S, Bushby K, Voit T, Sewry C, Muntoni F. Abnormalities in α -dystroglycan expression in MDC1C and LGMD2I muscular dystrophies. *Am J Pathol* 2004; 164: 727–737
- De Paula F, Vieira N, Starling A, Uraco Yamamoto L, Lima B, De Cássia Pavanello R, Vainzof M, Nigro V, Zatz M. Asymptomatic carriers for homozygous novel mutations in the FKRP gene: the other end of the spectrum. *Eur J Hum Genet* 2003; 11: 923–930
- Driss A, Noguchi S, Amouri R, Kefi M, Sasaki T, Surgie K, Souilem S, Hayashi YK, Shimizu N, Minoshima S, Kudoh J, Hentati F, Nishino I. Fukutin-related protein gene mutated in the original kindred limb-girdle MD 2I. *Neurology* 2003; 60: 1341–1344
- Harel T, Goldberg Y, Shalev SA, Chervinski I, Ofir R, Birk OS. Limb-girdle muscular dystrophy 2I: phenotypic variability within a large consanguineous Bedouin family associated with a novel FKRP mutation. *Eur J Hum Genet* 2004; 12: 38–43
- Louhichi N, Triki C, Quijano-Roy S, Richard P, Makri S, Méziou M, Estournet B, Mrad S, Romero NB, Ayadi H, Guicheney P, Fakhfakh F. New FKRP mutations causing congenital muscular dystrophy associated with mental retardation and central nervous system abnormalities. Identification of a founder mutation in Tunisian families. *Neurogenetics* 2004; 5: 27–34
- Mercuri E, Sewry CA, Brown SC, Brockington M, Jungbluth H, DeVille C, Counsell S, Muntoni F. Congenital muscular dystrophy with secondary merosin deficiency and normal brain MRI: a novel entity? *Neuropediatrics* 2000; 31: 186–189
- Mercuri E, Brockington M, Straub V, Quijano-Roy S, Yuva Y, Hermann R, Brown SC, Torelli S, Dubowitz V, Blake DJ, Romero NB, Estournet B, Sewry CA, Guicheney P, Voit T, Muntoni F. Phenotype spectrum associated with mutations in the Fukutin-related protein gene. *Ann Neurol* 2003; 53: 537–542
- Topaloglu H, Brockington M, Yuva Y, Talim B, Haliloglu G, Blake D, Torelli S, Brown SC, Muntoni F. FKRP gene mutations cause congenital muscular dystrophy, mental retardation, and cerebellar cysts. *Neurology* 2003; 60: 988–992

MDC1D

MDC1C

- Brockington M, Blake DJ, Prandini P, Brown SC, Torelli S, Benson MA, Ponting CP, Estournet B, Romero NB, Mercuri E, Voit T, Sewry CA, Guicheney P, Muntoni F. Mutations in the Fukutin-related protein gene (*FKRP*) cause a form of congenital muscular dystrophy with secondary laminin $\alpha 2$ deficiency and abnormal glycosylation of α -dystroglycan. *Am J Hum Genet* 2001; 69: 1198–1209
- Brockington M, Yuva Y, Prandini P, Brown SC, Torelli S, Benson MA, Herrmann R, Anderson LVB, Bashir R, Burgunder J-M, Fallet S, Romero N, Fardeau M, Straub V, Storey G, Pollitt C, Richard I, Sewry CA, Bushby K, Voit T, Blake DJ, Muntoni F. Mutations in the Fukutin-related protein gene (*FKRP*) identify limb girdle muscular dystrophy 2I as a milder allelic variant of congenital muscular dystrophy MDC1C. *Hum Mol Genet* 2001; 10: 2851–2859
- Endo T, Toda T. Glycosylation in congenital muscular dystrophies. *Biol Pharm Bull* 2003; 26: 1641–1647
- Grewal PK, Hewitt JE. Glycosylation defects: a new mechanism for muscular dystrophy? *Hum Mol Genet* 2003; 12: R259–R264
- Hewitt JE, Grewal PK. Glycosylation defects in inherited muscle disease. *Cell Mol Life Sci* 2003; 60: 251–258
- Longman C, Brockington M, Torelli S, Jimenez-Mallebrera C, Kennedy C, Khalil N, Feng L, Saran RK, Voit T, Merlini L, Sewry CA, Brown SC, Muntoni F. Mutations in the human *LARGE* gene cause MDC1D, a novel form of congenital muscular dystrophy with severe mental retardation and abnormal glycosylation of α -dystroglycan. *Hum Mol Genet* 2003; 12: 2853–2861
- Martin PT, Freeze HH. Glycobiology of neuromuscular disorders. *Glycobiology* 2003; 13: 67R–75R
- Martin-Rendon E, Blake DJ. Protein glycosylation in disease: new insights into the congenital muscular dystrophies. *Trends Pharmacol Sci* 2003; 24: 178–183

- Muntoni F, Valero de Bernabe B, Bittner R, Blake D, van Bokhoven H, Brockington M, Brown S, Bushby K, Campbell KP, Fiszman M, Gruenewald S, Merlini L, Quijano-Roy S, Romero N, Sabatelli P, Sewry CA, Straub V, Talim B, Topaloglu H, Voit T, Yurchenco PD, Urtizberea JA, Wewer UM, Guicheney P. 114th ENMC International Workshop on Congenital Muscular Dystrophy (CMD) (8th Workshop of the International Consortium on CMD; 3rd Workshop of the Myo-cluster Project GENRE). *Neuromusc Disord* 2003; 13: 579–588
- Muntoni F, Brockington M, Torelli S, Brown SC. Defective glycosylation in congenital muscular dystrophies. *Curr Opin Neurol* 2004; 17: 205–209

Rest

- Arahata K, Brockington M, Bushby K, Cormand B, Dubowitz V, Engvall E, Flanigan K, Guicheney P, Moghadaszadeh B, Morandi L, Muntoni F, Naom I, Pihko H, Sewry C, Soininen R, Straub V, Toda T, Tomé F, Topaloglu H, Urtizberea A, Villanova M, Vilquin J-T, Voit T. 68th ENMC International Workshop (5th International Workshop): on congenital muscular dystrophy. *Neuromusc Disord* 1999; 9: 446–454
- De Stefano N, Dotti MT, Villanova M, Scarano G, Federico A. Merosin positive congenital muscular dystrophy with severe involvement of the central nervous system. *Brain Dev* 1996; 18: 323–326
- Echenne B, Rivier F, Jallali AJ, Azais M, Mornet D, Pons F. Merosin positive congenital muscular dystrophy with mental deficiency, epilepsy and MRI changes in the cerebral white matter. *Neuromusc Disord* 1997; 7: 187–190
- Kobayashi O, Hayashi Y, Arahata K, Ozawa E, Nonaka I. Congenital muscular dystrophy: clinical and pathologic study of 50 patients with the classical (occidental) merosin-positive form. *Neurology* 1996; 46: 815–818
- Topaloglu H, Kale G, Yalnizoglu D, Taodemir AH, Karaduman A, Topcu M, Kutioglu E. Analysis of “pure” congenital muscular dystrophies in thirty-eight cases. How different is the classical type I from the occidental type cerebromuscular dystrophy? *Neuropediatrics* 1994; 25: 94–100
- Triki C, Louhichi N, Méziou M, Choyakh F, Kéchaou MS, Jlidi R, Mhiri C, Fakhfakh F, Ayadi H. Merosin-deficient congenital muscular dystrophy with mental retardation and cerebellar cysts, unlinked to the LAMA2, FCMD, MEB and CMD1B loci, in three Tunisian patients. *Neuromusc Disord* 2003; 13: 4–12
- Voit T, Cohn RD, Sperner J, Leube B, Sorokin L, Toda T, Herrmann R. Merosin-positive congenital muscular dystrophy with transient brain dysmyelination, pontocerebellar hypoplasia and mental retardation. *Neuromusc Disord* 1999; 9: 95–101
- Brunner HG, Jansen G, Nillesen W, Nelen MR, de Die CEM, Höweler CJ, van Oost BA, Wieringa B, Ropers HH, Smeets HJM. Brief report: Reverse mutation in myotonic dystrophy. *N Engl J Med* 1993; 328: 476–480
- Censori B, Provinciali L, Danni M, Chiaramoni I, Maricotti M, Foschi N, Del Pesce M, Salvolini U. Brain involvement in myotonic dystrophy: MRI features and their relationship to clinical and cognitive conditions. *Acta Neurol Scand* 1994; 90: 211–217
- Damian MS, Bachmann G, Herrmann D, Dorndorf W. Magnetic resonance imaging of muscle and brain in myotonic dystrophy. *J Neurol* 1993; 240: 8–12
- Damian MS, Schilling G, Bachman G, Simon C, Stöppler S, Dorndorf W. White matter lesions and cognitive deficits: relevance of lesion pattern? *Acta Neurol Scand* 1994; 90: 430–436
- Di Costanzo A, Di Salle F, Santoro L, Bonavita V, Tedeschi G. T2 relaxometry of brain in myotonic dystrophy. *J Neuroradiol* 2001; 43: 198–204
- Di Costanzo A, Di Salle F, Santoro L, Tessitore A, Bonavita V, Tedeschi G. Pattern and significance of white matter abnormalities in myotonic dystrophy type 1: an MRI study. *J Neurol* 2002; 249: 1175–1182
- Di Costanzo A, Di Salle F, Santoro L, Bonavita V, Tedeschi G. Brain MRI features of congenital and adult-form myotonic dystrophy type 1: case-control study. *Neuromusc Disord* 2002; 12: 476–483
- Fierro B, Daniele O, Aloisio A, Buffa D, La Bua V, Oliveri M, Manfredi L, Brighina F. Neurophysiological and radiological findings in myotonic dystrophy patients. *Eur J Neurol* 1998; 5: 89–94
- Garcia-Alix A, Cabanas F, Morales C, Pellicer A, Echevarria J, Paisan L, Quero J. Cerebral abnormalities in congenital myotonic dystrophy. *Pediatr Neurol* 1991; 7: 28–32
- Glantz RH, Wright RB, Huckman MS, Garron DC, Siegel IM. Central nervous system magnetic resonance imaging findings in myotonic dystrophy. *Arch Neurol* 1998; 45: 36–37
- Groenen P, Wieringa B. Expanding complexity in myotonic dystrophy. *BioEssays* 1998; 20: 901–912
- Hashimoto T, Tayama M, Miyazaki M, Murakawa K, Kawai H, Nishitani H, Kuroda Y. Neuroimaging study of myotonic dystrophy. I. Magnetic resonance imaging of the brain. *Brain Dev* 1995; 17: 24–7
- Hashimoto T, Tayama M, Miyazaki M, Murakawa K, Kawai H, Nishitani H, Kuroda Y. Neuroimaging study of myotonic dystrophy. II. MRI measurements of the brain. *Brain Dev* 1995; 17: 28–32
- Huber SJ, Kissel JT, Shuttleworth EC, Chakeres DW, Clapp LE, Brogan MA. Magnetic resonance imaging and clinical correlates of intellectual impairment in myotonic dystrophy. *Arch Neurol* 1989; 46: 536–540
- Martinello F, Piazza A, Pastorello E, Angelini C, Trevisan CP. Clinical and neuroimaging study of central nervous system in congenital myotonic dystrophy. *J Neurol* 1999; 246: 186–192
- Miaux Y, Chiras J, Eymard B, Lauriot-Prevost MC, Radvanyi H, Martin-Duverneuil N, Delaporte C. Cranial MRI findings in myotonic dystrophy. *J Neuroradiol* 1997; 39: 166–170
- Mitzukami K, Sasaki M, Baba A, Suzuki T, Shiraishi H. An autopsy case of myotonic dystrophy with mental disorders and various neuropathologic features. *J Psychiatry Clin Neurosci* 1999; 53: 51–55
- Moxley R III. Myotonic disorders in childhood: diagnosis and treatment. *J Child Neurol* 1997; 12: 116–129

61 Myotonic Dystrophy Type 1

- Abe K, Fujimura H, Toyooka K, Yorfuji S, Nishikawa Y, Hazama T, Yanagihira T. Involvement of the central nervous system in myotonic dystrophy. *J Neurol Sci* 1991; 127: 179–185
- Abe K, Fujimura H, Soga F. The fluid-attenuated inversion-recovery pulse sequence in assessment of central nervous system involvement in myotonic dystrophy. *J Neuroradiol* 1998; 40: 32–35
- Bachman G, Damian MS, Koch M, Schilling G, Fach B, Stöppler S. The clinical and genetic correlates of MRI findings in myotonic dystrophy. *J Neuroradiol* 1996; 38: 629–635

- Naka H, Imon Y, Ohshita T, Honjo K, Kitamura T, Mimori Y, Nakamura S. Magnetization transfer measurements of cerebral white matter in patients with myotonic dystrophy. *J Neurol Sci* 2002; 193: 111–116
- Ogata A, Terae S, Fujita M, Tashiro K. Anterior temporal white matter lesions in myotonic dystrophy with intellectual impairment: an MRI and neuropathological study. *J Neuroradiol* 1998; 40: 411–415
- Rosman NP, Rebeiz JJ. The cerebral defect and myopathy in myotonic dystrophy. *Neurology* 1967; 17: 1106–1112
- Spranger M, Spranger S, Tischendorf M, Meinck HM, Cremer M. Myotonic dystrophy the role of large triplet repeat length in the development of mental retardation. *Arch Neurol* 1997; 54: 251–254
- Tanabe Y, Iai M, Tamai K, Fujimoto N, Sugita K. Neuroradiological findings in children with congenital myotonic dystrophy. *Acta Paediatr* 1992; 81: 613–617
- Timchenko L. Trinucleotide repeats myotonic dystrophy: the role of RNA CUG triplet repeats. *Am J Hum Genet* 1999; 64: 360–364
- Timchenko L, Caskey CT. Triplet repeat disorders: discussion of molecular mechanisms. *Cell Mol Life Sci* 1999; 55: 1432–1447
- Timchenko L, Monckton DG, Caskey CT. Myotonic dystrophy: an unstable CTG repeat in a protein kinase gene. *Cell Biol* 1995; 6: 13–19
- Uluc K, Murat Arsava E, Erdem S, Tan E. Proximal myopathy and diffuse white matter involvement in myotonic dystrophy type I. *J Neurol* 2002; 249: 629–630
- Meola G, Sansone V. A newly-described myotonic disorder (proximal myotonic myopathy – PROMM): personal experience and review of the literature. *Ital J Neurol Sci* 1996; 17: 347–353
- Meola G, Sansone V, Perani D, Colleluori A, Cappa S, Cotelli M, Fazio F, Thornton CA, Moxley RT. Reduced cerebral blood flow and impaired visual-spatial function in proximal myotonic myopathy. *Neurology* 1999; 53: 1042–1050
- Meola G, Sansone V, Marinou K, Cotelli M, Moxley III RT, Thornton CA, De Ambroggi L. Proximal myotonic myopathy: a syndrome with a favourable prognosis? *J Neurol Sci* 2002; 193: 89–96
- Moxley RT III, Udd B, Ricker K. 54th ENMC International Workshop: PROMM (proximal myotonic myopathies) and other myotonic syndromes. 10–12th October 1997. *Neuromusc Disord* 1998; 8: 508–518
- Moxley RT III, Meola G, Udd B, Ricker K. Report of the 84th ENMC workshop: PROMM (proximal myotonic myopathy) and other myotonic dystrophy-like syndromes: 2nd workshop. 13–15th October, 2000. *Neuromusc Disord* 2002; 12: 306–317
- Nagamitsu S, Ashizawa T. 18 Myotonic dystrophies. *Adv Neurol* 2002; 88: 293–314
- Ricker K, Grimm T, Koch MC, Schneider C, Kress W, Reimers CD, Schulte-Mattler W, Mueller-Myshok B, Toyka KV, Mueller CR. Linkage of proximal myotonic myopathy to chromosome 3q. *Neurology* 1999; 52: 170–171
- Schneider C, Ziegler A, Ricker K, Grimm T, Kress W, Reimers CD, Meinck H-M, Reiners K, Toyka KV. Proximal myotonic myopathy. Evidence for anticipation in families with linkage to chromosome 3q. *Neurology* 2000; 55: 383–388
- Wieser T, Bönsch D, Eger K, Schulte-Mattler W, Zierz S. A family with PROMM not linked to the recently mapped PROMM locus DM 2. *Neuromusc Disord* 2000; 10: 141–143

62 Myotonic Dystrophy Type 2

- Bönsch D, Neumann C, Lang-Roth R, Witte O, Lamprecht-Dinnesen A, Deufel T. PROMM and deafness: excluding of ZNF9 as the disease in DFNA18 suggests a polygenic origin of the PROMM/DM 2 phenotype. *Clin Genet* 2003; 63: 73–75
- Day JW, Ricker K, Jacobsen JF, Rasmussen LJ, Dick KA, Kress W, Schneider C, Koch MC, Beilman GJ, Harrison AR, Dalton JC, Ranum LPW. Myotonic dystrophy type 2. Molecular, diagnostic and clinical spectrum. *Neurology* 2003; 60: 657–664
- Finsterer J. Monotonic dystrophy type 2. *Eur J Neurol* 2002; 9: 441–447
- Hund E, Jansen O, Koch MC, Ricker K, Fogel W, Niedermaier N, Otto M, Kuhn E, Meinck HM. Proximal myotonic myopathy with MRI white matter abnormalities of the brain. *Neurology* 1997; 48: 33–37
- Kress W, Mueller-Myhsok B, Ricker K, Schneider C, Koch MC, Toyka KV, Mueller CR, Grimm T. Proof of genetic heterogeneity in the proximal myotonic myopathy syndrome (PROMM) and its relationship to myotonic dystrophy type 2 (DM). *Neuromusc Disord* 2000; 10: 478–480
- Liquori CL, Ricker K, Moseley ML, Jacobsen JF, Kress W, Naylor SL, Day JW, Ranum LPW. Myotonic dystrophy type 2 caused by a CCTG expansion in Intron 1 of *ZNF9*. *Science* 2001; 293: 864–867
- Mastaglia FL, Harker N, Philips BA, Day TJ, Hankey GJ, Laing NG, Fabian V, Kakulas BA. Dominantly inherited proximal myotonic myopathy and leukoencephalopathy in a family with an incidental *CLCN1* mutation. *J Neurol Neurosurg Psychiatry* 1998; 64: 543–547
- Meola G. Clinical and genetic heterogeneity in myotonic dystrophies. *Muscle Nerve* 2000; 23: 1789–1799
- Meola G. Motonic dystrophies. *Curr Opin Neurol* 2000; 13: 519–525

63 X-linked Charcot-Marie-Tooth Disease

- Abrams CK, Oh S, Ri Y, Bargiello TA. Mutations in connexin 32: the molecular and biophysical bases for the X-linked form of Charcot-Marie-Tooth disease. *Brain Res Rev* 2000; 32: 203–214
- Abrams CK, Freidin MM, Verselis VK, Bennett MVL, Bargiello TA. Functional alterations in gap junction channels formed by mutant forms of connexin 32: evidence for loss of function as a pathogenic mechanism in the X-linked form of Charcot-Marie-Tooth disease. *Brain Res* 2001; 300: 9–25
- Abrams CK, Bennett MVL, Verselis VK, Bargiello TA. Voltage opens unopposed gap junction hemichannels formed by a connexin 32 mutant associated with X-linked Charcot-Marie-Tooth disease. *Proc Natl Acad Sci USA* 2002; 99: 3980–3984
- Bähr M, Andres F, Timmerman V, Nelis ME, Van Broeckhoven C, Dichgans J. Central visual, acoustic, and motor pathway involvement in a Charcot-Marie-Tooth family with an Asn205Ser mutation in the connexin 32 gene. *J Neurol Neurosurg Psychiatry* 1999; 66: 202–206
- Bergoffen J, Scherer SS, Wang S, Oronzi Scott M, Bone LJ, Paul DL, Chen K, Lensch MW, Chance PF, Fischbeck KH. Connexin mutations in X-linked Charcot-Marie-Tooth disease. *Science* 1993; 262: 2039–2042

- Birouk N, LeGuern E, Maissonobe T, Rouger H, Gouider R, Tardieu S, Gugenheim M, Routon MC, Léger JM, Agid Y, Brice A, Bouche P. X-linked Charcot-Marie-Tooth disease with connexin 32 mutations. Clinical and electrophysiologic study. *Neurology* 1998; 50: 1074–1082
- Bondurand N, Girard M, Pingault V, Lemort N, Dubourg O, Goossens M. Human Connexin 32, a gap junction protein altered in the X-linked form of Charcot-Marie-Tooth disease, is directly regulated by transcription factor SOX10. *Hum Mol Genet* 2001; 10: 2783–2795
- Goto H, Matsuo H, Ohnishi A, Fukudome T, Shibuya N. X-linked motor and sensory neuropathy with pyramidal signs and cerebral white matter lesions. *Muscle Nerve* 2003; 28: 623–625
- Hanemann CO, Bergmann C, Senderek J, Zerres K, Sperfeld A-D. Transient, recurrent, white matter lesions in X-linked Charcot-Marie-Tooth disease with novel connexin 32 mutations. *Arch Neurol* 2003; 60: 605–609
- Ionasescu V, Ionasescu R, Searby C. Correlation between 32 gene mutations and clinical phenotype in X-linked dominant Charcot-Marie-Tooth neuropathy. *Am J Med Genet* 1996; 63: 486–491
- Kawakami H, Inoue K, Sakakihara I, Nakamura S. Novel mutation in X-linked Charcot-Marie-Tooth disease associated with CNS impairment. *Neurology* 2002; 59: 923–926
- Kleopa KA, Yum SW, Scherer SS. Cellular mechanisms of connexin32 associated with CNS manifestations. *J Neurosci Res* 2002; 68: 522–534
- Krutovskikh V, Yamasaki H. Connexin gene mutations in human genetic diseases. *Mutat Res* 2000; 462: 197–207
- Lee M-J, Nelson I, Houlden H, Sweeney MG, Hilton-Jones D, Blake J, Wood NW, Reilly MM. Six novel connexin32 (GJB1) mutations in X-linked Charcot-Marie-Tooth disease. *J Neurol Neurosurg Psychiatry* 2002; 73: 304–306
- Marques W Jr, Sweeney MG, Wood NW, Wroe SJ, Marques W. Central nervous system involvement in a novel connexin 32 mutation affecting identical twins. *J Neurol Neurosurg Psychiatry* 1999; 66: 803–804
- Nicholson GA, Yeung L, Corbett A. Efficient neurophysiologic selection of X-linked Charcot-Marie-Tooth families. Ten novel mutations. *Neurology* 1998; 51: 1412–1416
- Panas M, Karadimas C, Avramopoulos D, Vassilopoulos D. Central nervous system involvement in four patients with Charcot-Marie-Tooth disease with connexin 32 extracellular mutations. *J Neurol Neurosurg Psychiatry* 1998; 65: 947–962
- Paulson HL, Garbern JY, Hoban TF, Krajewski KM, Lewis RA, Fischbeck KH, Grossmann RI, Lenkinski R, Kamholz JA, Shy ME. Transient central nervous system white matter abnormality in X-linked Charcot-Marie-Tooth disease. *Ann Neurol* 2002; 52: 429–434
- Ressot C, Gomès D, Dautigny A, Pham-Dinh D, Burzzone R. Connexin32 mutations associated with X-linked Charcot-Marie-Tooth disease show two distinct behaviors: loss of function and altered gating properties. *J Neurosci* 1998; 18: 4063–4075
- Schelhaas HJ, Van Engelen BMG, Gabreëls-Festen AAWM, Hageman G, Vliegen JHR, Van der Knaap MS, Zwarts MJ. Transient cerebral white matter lesions in a patient with connexin 32 missense mutation. *Neurology* 2002; 59: 2007–2008
- Senderek J, Hermanns B, Bergmann C, Boroojerdi B, Bajbouj M, Hungs M, Ramaekers VT, Quasthoff S, Karch D, Micheal Schröder J. X-linked dominant Charcot-Marie-Tooth neuropathy: clinical electrophysiological, and morphological phenotype in four families with different connexin32 mutations. *J Neurologic Sci* 1999; 167: 90–101
- Stojkovic T, Latour P, Vanderberghe A, Hurtevent JF, Vermersch P. Sensorineural deafness in X-linked Charcot-Marie-Tooth disease with connexin 32 mutation (R142Q). *Neurology* 1999; 52: 1010–1014
- Sutor B, Schmolke C, Teubner B, Schirmer C, Willecke K. Myelination defects and neuronal hyperexcitability in the neocortex of connexin 32-deficient mice. *Cerebr Cortex* 2000; 10: 684–697

64 Oculodentodigital Dysplasia

- Ginsberg LE, Jewett T, Grub R, McLean WT. Oculodental digital dysplasia: neuroimaging in a kindred. *Neuroradiology* 1996; 38: 84–86
- Gladwin A, Donnai D, Metcalfe K, Schrandt-Stumpel C, Brue-ton L, Verloes A, Aylsworth A, Torriello H, Winter R, Dixon M. Localization of a gene for oculodentodigital syndrome to human chromosome 6q22-q24. *Hum Mol Genet* 1997; 6: 123–127
- Gutmann DH, Zackai EH, McDonald-McGinn DM, Fischbeck KH, Kamholz J. Oculodentodigital dysplasia syndrome associated with abnormal cerebral white matter. *Am J Med Genet* 1991; 41: 18–20
- Loddenkemper T, Grote K, Evers S, Oelerich M, Stögbauer F. Neurological manifestations of the oculodentodigital dysplasia syndrome. *J Neurol* 2002; 249: 584–595
- Norton KK, Carey JC, Gutmann DH. Oculodentodigital dysplasia with cerebral white matter abnormalities in a two-generation family. *Am J Med Genet* 1995; 57: 458–461
- Patton MA, Laurence KM. Three new cases of oculodentodigital (ODD) syndrome: development of the facial phenotype. *J Med Genet* 1985; 22: 386–389
- Paznekas WA, Boyadjiev SA, Shapiro RE, Daniels O, Wollnik B, Keegan CE, Innis JW, Dinulos MB, Christian C, Hannibal MC, Jabs EW. Connexin 43 (GJA1) mutations cause the pleiotropic phenotype of oculodentodigital dysplasia. *Am J Hum Genet* 2003; 72: 408–418
- Pizzuti A, Flex E, Mingarelli R, Salpietro C, Zelante L, Dallapiccola B. A homozygous GJA1 gene mutation causes a Hallerman-Streiff/ODDD spectrum phenotype. *Hum Mutat* 2004; 23: 286
- Richardson RR, Donnai D, Meire F, Dixon MJ. Expression of Gja1 correlates with the phenotype observed in oculodentodigital syndrome/type III syndactyly. *J Med Genet* 2004; 41: 60–67
- Schrandt-Stumpel CTRM, Franke CL. Central nervous system abnormalities in oculodentodigital dysoplasia. *Genet Couns* 1996; 7: 233–235
- Schrandt-Stumpel CTRM, de Groot-Wijnands JBG, de Die-Smulders C, Fryns JP. Type III syndactyly and odulodentodigital dysplasia: a clinical spectrum. *Genet Couns* 1993; 4: 271–276
- Shapiro RE, Griffin JW, Stine OC. Evidence for genetic anticipation in the oculodentodigital syndrome. *Am J Med Genet* 1997; 71: 36–41

Spaepen A, Schrandt-Stumpel C, Fryns J-P, de Die-Smulders C, Borghgraef M, van den Berghe H, Hallerman-Streiff syndrome: clinical and psychological findings in children. Nosologic overlap with oculodentodigital dysplasia? *Am J Hum Genet* 1991;41:517–520

65 Vanishing White Matter

Abbott CM, Proud CG. Translation factors: in sickness and in health. *Trends Biochem Sci* 2004; 29: 25–31

Alorainy IA, Patenaude YG, O’Gorman AM, Black DN, Meagher-Villemure K. Cree leukoencephalopathy: neuroimaging findings. *Radiology* 1999; 213: 400–406

Anzil AP, Gessaga E. Late-life cavitating dystrophy of the cerebral and cerebellar white matter. *Eur Neurol* 1972; 7: 79–94

Biancheri R, Rossi A, Di Rocco M, Filocamo M, Pronk JC, van der Knaap MS, Tortori-Domati P. Leukoencephalopathy with vanishing white matter: an adult onset case. *Neurology* 2003; 61: 1818–1819

Black DN, Booth F, Watters GV, Andermann E, Dumont C, Halliday WC, Hoogstraten J, Kabay ME, Kaplan P, Meagher-Villemure K, Michaud J, O’Gorman G. Leukoencephalopathy among native Indian infants in northern Quebec and Manitoba. *Ann Neurol* 1988; 24: 490–496

Blüml S, Philippart M, Schiffmann R, Seymour K, Ross BD. Membrane phospholipids and high-energy metabolites in childhood ataxia with CNS hypomyelination. *Neurology* 2003; 61: 648–654

Boesen T, Mohammed SS, Pavitt GD, Andersen GR. Structure of the catalytic fragment of translation initiation factor 2B and identification of a critically important catalytic residue. *J Biol Chem* 2004; 279: 10584–10592

Boltshauser E, Barth PG, Troost D, Martin E, Stallmach T. “Vanishing white matter” and ovarian dysgenesis in an infant with cerebro-oculo-facio-skeletal phenotype. *Neuropediatrics* 2002; 33: 57–62

Brück W, Herms J, Brockmann K, Schulz-Schaeffer W, Hanefeld F. Myelinopathia centralis diffusa (vanishing white matter disease): evidence of apoptotic oligodendrocyte degeneration in early lesion development. *Ann Neurol* 2001; 50: 532–536

Deisenhammer E, Jellinger K. Höhlenbildende Neuralfett-leukodystrophie mit Schubverlauf. *Neuropediatrics* 1976; 7: 111–121

Duncan RF, Hershey JW. Protein synthesis and protein phosphorylation during heat stress, recovery, and adaptation. *J Cell Biol* 1989; 109: 1467–1481

Eicke WJ. Polycystische Umwandlung des Marklagers mit progredientem Verlauf. Atypische diffuse Sklerose? *Arch Psychiatr Nervenkr* 1962; 203: 599–602

Espay AJ, Bodensteiner JB, Patel H. Episodic coma in a new leukodystrophy. *Pediatr Neurol* 2002; 26: 139–142

Fogli A, Dionisi-Vici C, Deodato F, Bartoli A, Boespflug-Tanguy O, Bertini E. A severe variant of childhood ataxia with central hypomyelination / vanishing white matter leukoencephalopathy related to *EIF2B5* mutation. *Neurology* 2002; 59: 1966–1968

Fogli A, Wong K, Eymard-Pierre E, Wenger J, Bouffard JP, Goldin E, Black DN, Boespflug-Tanguy O, Schiffmann R. Cree leukoencephalopathy and CACH/VWM disease are allelic at the *EIF2B5* locus. *Ann Neurol* 2002; 52: 506–510

Fogli A, Rodriguez D, Eymard-Pierre E, Bouhour F, Labauge P, Meaney BF, Zeesman S, Kaneski CR, Schiffmann R, Boespflug-Tanguy O. Ovarian failure related to eukaryotic initiation factor 2B mutations. *Am J Hum Genet* 2003 72: 1544–1550

Fogli A, Schiffmann R, Hugendubler L, Combes P, Bertini E, Rodriguez D, Kimball SR, Boespflug-Tanguy O. Decreased guanine nucleotide exchange factor activity in *EIF2B*-mutated patients. *Eur J Hum Genet* 2004; 12: 561–566

Fogli A, Schiffmann R, Bertini E, Ughetto S, Combes P, Eymard-Pierre E, Kaneski CR, Pineda M, Troncoso M, Uziel G, Surtees R, Pugin D, Chaunu M-P, Rodriguez D, Boespflug-Tanguy O. The effect of genotype on the natural history of *EIF2B*-related leukodystrophies. *Neurology* 2004; 62: 1509–1517

Francalanci P, Eymard-Pierre E, Dionisi-Vici C, Bolderini R, Piemonte F, Virgili R, Fariello G, Bosman C, Santorelli FM, Boespflug-Tanguy O, Bertini E. Fatal infantile leukodystrophy: a severe variant of CACH/VWM syndrome, allelic to chromosome 3q27. *Neurology* 2001; 57: 265–70

Gallo A, Rocca MA, Falini A, Scaglione C, Salvi F, Gambini A, Guerrini L, Mascalchi M, Pronk JC, van der Knaap MS, Filippi M. Multiparametric MRI in a patient with adult-onset leukoencephalopathy with vanishing white matter. *Neurology* 2004; 62: 323–326

Gautier JC, Gray F, Awada A, Escourolle R. Leucodystrophie orthochromatique cavitaire de l’adulte. Prolifération et inclusion oligodendrogiales. *Rev Neurol* 1984; 140: 493–501

Girard PF, Tommassi M, Rochet M, Boucher M. Leuco-encéphalopathie avec cavitations massives, bilatérales et symétriques. Syndrome de décortication post-traumatique. *Presse Med* 1968; 76: 163–166

Gow A, Sharma R. The unfolded protein response in protein aggregating diseases. *Neuromol Med* 2003; 4: 73–94

Graveleau P, Gray F, Plas J, Graveleau J, Brion S. Leucodystrophie orthochromatique cavitaire avec modifications oligodendrogiales. Un cas sporadique adulte. *Rev Neurol* 1985; 141: 713–718

Hanefeld F, Holzbach U, Kruse B, Wilichowski E, Christen HJ, Frahm J. Diffuse white matter disease in three children: an encephalopathy with unique features on magnetic resonance imaging and proton magnetic resonance spectroscopy. *Neuropediatrics* 1993; 24: 244–248

Harding HP, Zhang Y, Ron D. Protein translation and folding are coupled by an endoplasmic-reticulum-resident kinase. *Nature* 1999; 397: 271–274

Harding HP, Novoa I, Zhang Y, Zeng H, Wek R, Schapira M, Ron D. Regulated translation initiation controls stress-induced gene expression in mammalian cells. *Mol Cell* 2000; 6: 1099–1108

Hershey JWB, Merrick WC. The pathway and mechanism of initiation of protein synthesis. In: Sonenberg N, Hershey JWB, Mathews MB, eds. *Translational control of gene expression*. Cold Spring Harbor: Cold Spring Harbor Laboratory Press, 2000, pp 33–88

Hinnebusch AG. Mechanism and regulation of initiator methionyl-tRNA binding to ribosomes. In: Sonenberg N, Hershey JWB, Mathews MB, eds. *Translational control of gene expression*. Cold Spring Harbor: Cold Spring Harbor Laboratory Press, 2000, pp 185–243

Kleijn M, Scheper GC, Voorma HO, Thomas AA. Regulation of translation initiation factors by signal transduction. *Eur J Biochem* 1998; 253: 531–544

- Krishnamoorthy T, Pavitt GD, Zhang F, Dever TE, Hinnebusch AG. Tight binding of the phosphorylated alpha subunit of initiation factor 2 (eIF2alpha) to the regulatory subunits of guanine nucleotide exchange factor eIF2B is required for inhibition of translation initiation. *Mol Cell Biol* 2001; 21: 5018–5030
- Leegwater PA, Konst AA, Kuyt B, Sandkuijl LA, Naidu S, Oudejans CB, Schutgens RB, Pronk JC, van der Knaap MS. The gene for leukoencephalopathy with vanishing white matter is located on chromosome 3q27. *Am J Hum Genet* 1999; 65: 728–734
- Leegwater PA, Vermeulen G, Konst AA, Naidu S, Mulders J, Visser A, Kersbergen P, Mobach D, Fonds D, van Berkel CG, Lemmers RJ, Frants RR, Oudejans CB, Schutgens RB, Pronk JC, van der Knaap MS. Subunits of the translation initiation factor eIF2B are mutant in leukoencephalopathy with vanishing white matter. *Nat Genet* 2001; 29: 383–388
- Leegwater PAJ, Pronk JC, van der Knaap MS. Leukoencephalopathy with vanishing white matter: from magnetic resonance imaging pattern to five genes. *J Child Neurol* 2003; 18: 639–645
- Li W, Wang X, van der Knaap MS, Proud CG. Mutations linked to leukoencephalopathy with vanishing white matter impair the function of the eukaryotic initiation factor 2B complex in diverse ways. *Mol Cell Biol* 2004; 24: 3295–3306
- Matsui M, Mizutani K, Miki Y, Mezaki T, Takahashi Y, Shibasaki H. Adult-onset leukoencephalopathy with vanishing white matter. *Eur J Radiol Extra* 2003; 46: 90–92
- Ohtake H, Shimohata T, Terajima K, Kimura T, Jo R, Kaseda R, Iizuka O, Takano M, Akaiwa Y, Goto H, Kobayashi H, Sugai T, Muratake T, Hosoki T, Shioiri T, Okamoto K, Onodera O, Tanaka K, Someya T, Nakada T, Tsuji S. Adult-onset leukoencephalopathy with vanishing white matter with a missense mutation in *EIF2B5*. *Neurology* 2004; 62: 1601–1603
- Oldfield S, Jones BL, Tanton D, Proud CG. Use of monoclonal antibodies to study the structure and function of eukaryotic protein synthesis initiation factor eIF-2B. *Eur J Biochem* 1994; 221: 399–410
- Prass K, Brück W, Schröder NWJ, Bender A, Prass M, Wolf T, van der Knaap MS, Zschenderlein R. Adult-onset leukoencephalopathy with vanishing white matter presenting with dementia. *Ann Neurol* 2001; 50: 665–668
- Proud CG. Regulation of eukaryotic initiation factor eIF2B. *Prog Mol Subcell Biol* 2001; 26: 95–114
- Proud CG. Regulation of mammalian translation factors by nutrients. *Eur J Biochem* 2002; 269: 5338–5349
- Richardson JP, Mohammad SS, Pavitt GD. Mutations causing childhood ataxia with central nervous system hypomyelination reduce eukaryotic initiation factor 2b complex formation and activity. *Mol Cell Biol* 2004; 24: 2352–2363
- Rodriguez D, Gelot A, della Gaspera B, Robain O, Ponsot G, Sarliève LL, Ghandour S, Pompidou A, Dautigny A, Aubourg P, Pham-Dinh D. Increased density of oligodendrocytes in childhood ataxia with diffuse central hypomyelination (CACH) syndrome: neuropathological and biochemical study of two cases. *Acta Neuropathol (Berl)* 1999; 97: 469–480
- Rosemberg S, Leite C da C, Arita FN, Kliemann SE, Lacerda MT. Leukoencephalopathy with vanishing white matter: report of four cases from three unrelated Brazilian families. *Brain Dev* 2002; 24: 250–256
- Rowlands AG, Montine KS, Henshaw EC, Panniers R. Physiological stresses inhibit guanine-nucleotide-exchange factor in Ehrlich cells. *Eur J Biochem* 1988; 175: 93–99
- Scheper GC, Mulder J, Kleijn M, Voorma HO, Thomas AAM, van Wijk R. Inactivation of eIF2B and phosphorylation of PHAS-I in heat-shocked rat hepatoma cells. *J Biol Chem* 1997; 272: 26850–26856
- Schiffmann R, Moller JR, Trapp BD, Shih HH, Farrer RG, Katz DA, Alger JR, Parker CC, Hauer PE, Kaneski CR, Heiss JD, Kaye EM, Quarles RH, Brady RO, Barton NW. Childhood ataxia with diffuse central nervous system hypomyelination. *Ann Neurol* 1994; 35: 331–340
- Schiffmann R, Tedeschi G, Kinkel P, Trapp BD, Frank JA, Kaneski CR, Brady RO, Barton NW, Nelson L, Yanovski JA. Leucodystrophy in patients with ovarian dysgenesis. *Ann Neurol* 1997; 41: 654–661
- Schneider RJ. Translational control during heat shock. In: Sonenberg N, Hershey JWB, Mathews MB (eds) *Translational Control of Gene Expression*. Cold Spring Harbor Laboratory Press, Cold Spring Harbor, 2000, pp 581–593
- Şenol U, Haspolat S, Karaali K, Lüleci E. MR imaging of vanishing white matter. *AMJ Am J Roentgenol* 2000; 175: 826–828
- Sugiura C, Miyata H, Oka A, Takashima S, Ohama E, Takeshita K. A Japanese girl with leukoencephalopathy with vanishing white matter. *Brain Dev* 2001; 23: 56–61
- Tedeschi G, Schiffmann R, Barton NW, Shin HH-L, Gospe SM, Brady RO, Alger JR, di Chiro G. Proton magnetic resonance spectroscopy imaging in childhood ataxia with diffuse central nervous system hypomyelination. *Neurology* 1995; 45: 1526–1532
- Topçu I, Saatci I, Anil Apak R, Söylemezoglu F. A case of leukoencephalopathy with vanishing white matter. *Neuropadiatr* 2000; 31: 100–103
- van der Knaap MS, Barth PG, Gabreëls FJ, Franzoni E, Begeer JH, Stroink H, Rotteveel JJ, Valk J. A new leukoencephalopathy with vanishing white matter. *Neurology* 1997; 48: 845–855
- van der Knaap MS, Kamphorst W, Barth PG, Kraaijeveld CL, Gut E, Valk J. Phenotypic variation in leukoencephalopathy with vanishing white matter. *Neurology* 1998; 51: 540–547
- van der Knaap MS, Wevers RA, Kure S, Gabreëls FJM, Verhoeven NM, van Raaij-Selten B, Jaeken J. Increased cerebrospinal fluid glycine: a biochemical marker for a leukoencephalopathy with vanishing white matter. *J Child Neurol* 1999; 14: 728–731
- van der Knaap MS, Leegwater PA, Konst AA, Visser A, Naidu S, Oudejans CB, Schutgens RB, Pronk JC. Mutations in each of the five subunits of translation initiation factor eIF2B can cause leukoencephalopathy with vanishing white matter. *Ann Neurol* 2002; 51: 264–270
- van der Knaap MS, van Berkel CGM, Herms J, van Coster R, Baethmann M, Naidu S, Boltshauser E, Willemsen MAAP, Plecko B, Hoffmann GF, Proud CG, Scheper GC, Pronk JC. eIF2B Related Disorders: Antenatal Onset and Involvement of Multiple Organs. *Am J Hum Genet* 2003; 73: 1199–1207
- van der Knaap MS, Leegwater PAJ, van Berkel CGM, Brenner C, Storey E, di Rocco M, Salvi F, Pronk J. Arg113His mutation in eIF2B0 as cause of leukoencephalopathy in adults. *Neurology* 2004; 62: 1598–1600
- Van Haren K, van der Voorn JP, Peterson DR, van der Knaap MS, Powers JM. The life and death of oligodendrocytes in vanishing white matter disease. *J Neuropathol Exp Neurol* 2004; 63: 631–640
- Watanabe I, Muller J. Cavitating “diffuse sclerosis” *J Neuropathol Exp Neurol* 1976; 26: 437–455
- Welch WJ. Mammalian stress response: cell physiology, structure/function of stress proteins, and implications for medicine and disease. *Physiol Rev* 1992; 72: 1063–1081

Wong K, Armstrong RC, Gyure KA, Morrison AL, Rodriguez D, Matalon R, Johnson AB, Wollmann R, Gilbert E, Le TQ, Bradley CA, Crutchfield K, Schiffmann R. Foamy cells with oligodendroglial phenotype in childhood ataxia with diffuse central nervous system hypomyelination syndrome. *Acta Neuropathol (Berl)* 2000; 100: 635–646

66 Aicardi-Goutières Syndrome

Abdel-Salam GMH, Zaki MS, Lebon P, Meguid NA. Aicardi-Goutières syndrome: clinical and neuroradiological findings of 10 new cases. *Acta Paediatr* 2004; 93: 929–936

Aicardi J. Aicardi-Goutières syndrome: special type early-onset encephalopathy. *Eur J Paediatr* 2002; 6: A1–A7

Aicardi J, Goutières F. A progressive familial encephalopathy in infancy with calcifications of the basal ganglia and chronic cerebrospinal fluid lymphocytosis. *Ann Neurol* 1984; 15: 49–54

Aicardi J, Goutières F. Systemic lupus erythematosus or Aicardi-Goutières syndrome? *Neuropediatrics* 2000; 31: 113

Akwa Y, Hassett DE, Eloranta ML, Sandberg K, Masliah E, Powell H, Lindsay Whitton J, Bloom FE, Campbell IL. Transgenic expression of IFN- α the central nervous system of mice protects against lethal neurotropic viral infection but induces inflammation and neurodegeneration. *J Immunol* 1998; 161: 5016–5026

Al-Dabbous R, Sabry MA, Farah S, Al-Awadi SA, Sineonov S, Farag TI. The autosomal recessive congenital intrauterine infection-like syndrome of microcephaly, intracranial calcification, and CNS disease: report of another Bedouin family. *Clin Dysmorphol* 1998; 7: 127–130

Barbitt DP, Tang T, Dobbs J, Berk R. Idiopathic familial cerebrovascular ferocalcinosis (Fahr's disease) and review of differential diagnosis of intracranial calcification in children. *Am J Roentgenol Radiat Ther Nucl Med* 1969; 105: 352–358

Baraitser M, Brett EM, Piesowicz AT. Microcephaly and intracranial calcification in two brothers. *J Med Gen* 1983; 20: 210–212

Barth PG. The neuropathology of Aicardi-Goutières syndrome. *Eur J Paediatr Neurol* 2002; 6: A27–A31

Barth PG, Walter A, van Gelderen I. Aicardi-Goutières syndrome: a genetic microangiopathy? *Acta Neuropathol (Berl)* 1999; 98: 212–216

Billard C, Dulac O, Bouloche J, Echenne B, Lebon P, Motte J, Robain O, Santini JJ. Encephalopathy with calcifications of the basal ganglia in children. A reappraisal of Fahr's syndrome with respect to 14 new cases. *Neuropediatrics* 1989; 20: 12–19

Black DN, Watters GV, Andermann E, Dumont C, Kabay ME, Kaplan P, Meagher-Villemure K, Michaud J, O'Gorman G, Reece E, Tsoukas C, Wainberg MA. Encephalitis among Cree children in Northern Quebec. *Ann Neurol* 1988; 24: 483–489

Blau N, Bonafé L, Krägeloh-Mann I, Thöny B, Kierat L, Häusler M, Ramaekers V. Cerebrospinal fluid pterins and folates in Aicardi-Goutières syndrome. A new phenotype. *Neurology* 2003; 61: 642–647

Boltshauser E, Steinlin M, Boesch C, Martin E, Schubiger G. Magnetic resonance imaging in infantile encephalopathy with cerebral calcification and leukodystrophy. *Neuropediatrics* 1991; 22: 33–35

Bönnemann CG, Meinecke P. Encephalopathy of infancy with intracerebral calcification and chronic spinal fluid lymphocytosis – another case of the Aicardi-Goutières syndrome. *Neuropediatrics* 1992; 23: 157–161

Bönnemann CG, Meinecke P, Reich H. Encephalopathy with intracerebral calcification, white matter lesions, growth hormone deficiency, microcephaly, and retinal degeneration: two sibs confirming a probably distinct entity. *J Med Genet* 1991; 28: 708–711

Burn J, Wickramasinghe HT, Harding B, Baraitser M. A syndrome with intracranial calcification and microcephaly in two sibs, resembling intrauterine infection. *Clin Genet* 1986; 30: 112–116

Campbell IL, Krucker T, Steffensen S, Akwa Y, Powell HC, Lane T, Carr DJ, Gold LH, Henriksen SJ, Siggins GR. Structural and functional neuropathology in transgenic mice with CNS expression of IFN- α . *Brain Research* 1999; 835: 46–61

Crow Y. The genetics of Aicardi-Goutières syndrome. *Eur J Paediatr Neurol* 2002; 6: A33–A35

Crow YJ, Jackson AP, Roberts E, van Beusekom E, Barth P, Corry P, Ferrie CD, Hamel BCJ, Jayatunga R, Karbani G, Kálmánchey R, Kelemen A, King M, Kumar R, Livingstone J, Massey R, McWilliam R, Meager A, Rittey C, Stephenson JBP, Tolmie JL, Verrips A, Voit T, van Bokhoven H, Brunner HG, Woods CG. Aicardi-Goutières syndrome displays genetic heterogeneity with one locus (AGS1) on chromosome 3p21. *Am J Hum Genet* 2000; 67: 213–221

Dale RC, Ping Tang S, Heckmatt JZ, Tatnall FM. Familial systemic lupus erythematosus and congenital infection-like syndrome. *Neuropediatrics* 2000; 31: 155–158

Fauré S, Bordelais I, Marquette C, Rittey C, Campos-Castello J, Goutières F, Ponsot G, Weissenbach J, Lebon P. Aicardi-Goutières syndrome: monogenic recessive disease, genetically heterogeneous disease, or multifactorial disease? *Clin Genet* 1999; 56: 149–153

Goutières F, Aicardi J, Barth PG, Lebon P. Aicardi-Goutières syndrome: an update and results of interferon- α studies. *Ann Neurol* 1998; 44: 900–907

Jervis GA. Microcephaly with extensive calcium deposits and demyelination. *J Neuropathol Exp Neurol* 1954; 13: 318–329

Kato M, Ishii R, Honma A, Ikeda H, Hayasaka K. Brainstem lesion in Aicardi-Goutières syndrome. *Pediatr Neurol* 1998; 19: 145–147

Koul R, Chacko A, Surendranath J, Sankhla D. Aicardi-Goutières syndrome in siblings. *J Child Neurol* 2001; 16: 759–761

Kuijpers TW. Aicardi-Goutières syndrome: immunophenotyping in relation to interferon-alpha. *Eur J Paediatr Neurol* 2002; 6: A59–A64

Kumar D, Rittey C, Cameron AH, Variend S. Recognizable inherited syndrome of progressive central nervous system degeneration and generalized intracranial calcification with overlapping phenotype of the syndrome of Aicardi and Goutières. *Am J Med Genet* 1998; 75: 508–515

Lanzi G, Fazzi E, D'Arrigo S. Aicardi-Goutières syndrome: a description of 21 new cases and a comparison with the literature. *Eur J Paediatr Neurol* 2002; 6: A9–A22

Lebon P, Badoual J, Ponsot G, Goutières F, Hémeury-Cukier F, Aicardi J. Intrathecal synthesis of interferon-alpha in infants with progressive familial encephalopathy. *J Neurol Sci* 1988; 84: 201–208

Lebon P, Meritet JF, Krivine A, Rozenberg F. Interferon and Aicardi-Goutières syndrome. *Eur J Paediatr Neurol* 2002; 6: A47–A53

- McEntagart M, Kamel H, Lebon P, King MD. Aicardi-Goutières syndrome: an expanding phenotype. *Neuropediatrics* 1998; 29: 163–167
- Mehta L, Trounce JQ, Moore JR, Young ID. Familial calcification of the basal ganglia with cerebrospinal fluid pleocytosis. *J Med Genet* 1986; 23: 157–160
- Monastiri K, Salem N, Korbi S, Snoussi N. Microcephaly and intracranial calcification: two new cases. *Clin Genet* 1997; 51: 142–143
- Østergaard JR, Christensen T, Nehen AM. A distinct difference in clinical expression of two siblings with Aicardi-Goutières syndrome. *Neuropediatrics* 1999; 30: 38–41
- Polizzi A, Pavone P, Parana E, Incorpora G, Ruggieri M. Lack of progression of brain atrophy in Aicardi-Goutières syndrome. *Pediatr Neurol* 2001; 24: 300–302
- Razavi-Encha F, Larroche JC, Gaillard D. Infantile familial encephalopathy with cerebral calcifications and leukodystrophy. *Neuropediatrics* 1988; 19: 72–79
- Reardon W, Hockey A, Silberstein P, Kendall B, Farag TI, Swash M, Stevenson R, Baraitser M. Autosomal recessive congenital intrauterine infection-like syndrome of microcephaly, intracranial calcification, and CNS disease. *Am J Med Genet* 1994; 52: 58–65
- Schwarz KB, Ferrie CD, Woods CG. Two siblings with a new Aicardi-Goutières-like syndrome. *Dev Med Child Neurol* 2002; 44: 422–425
- Slee J, Lam G, Walpole I. Syndrome of microcephaly, microphthalmia, cataracts, and intracranial calcification. *Am J Med Genet* 1999; 84: 330–333
- Tolmie JL, Shillito P, Hughes-Benzie R, Stephenson JBP. The Aicardi-Goutières syndrome (familial, early onset encephalopathy with calcifications of the basal ganglia and chronic cerebrospinal fluid lymphocytosis). *J Med Genet* 1995; 32: 881–884
- Troost D, van Rossum A, Veiga Pires J, Willemse J. Cerebral calcifications and cerebellar hypoplasia in two children: clinical, radiologic and neuropathological studies – a separate neurodevelopmental entity. *Neuropediatrics* 1984; 15: 102–109
- Verrips A, Hiel JAP, Gabreëls FJM, Wesseling P, Rotteveel JJ. The Aicardi-Goutières syndrome: variable clinical expression in two siblings. *Pediatr Neurol* 1997; 16: 323–325
- Vivarelli R, Grosso S, Cioni M, Galluzzi P, Monti L, Morgese G, Balestri P. Pseudo-TORCH syndrome or Baraitser-Reardon syndrome: diagnostic criteria. *Brain Dev* 2001; 23: 18–23
- Wieczorek D, Gillissen-Kaesbach G, Passarge E. A nine-month-old boy with microcephaly, cataracts, intracerebral calcifications and dysmorphic signs: an additional observation of an autosomal recessive congenital infection-like syndrome? *Genet Couns* 1995; 6: 297–302
- Gayatri NA, Hughes MI, Lloyd IC, Wynn RF. Association of the congenital bone marrow failure syndromes with retinopathy, intracerebral calcification and progressive neurological impairment. *Eur J Paediatr Neurol* 2002; 6: 125–128
- Goutières F, Dollfus H, Becquet F, Dufier J-L. Extensive brain calcification in two children with bilateral Coats' disease. *Neuropediatrics* 1990; 30: 19–21
- Kajtár P, Méhes K. Bilateral coats retinopathy associated with aplastic anaemia and mild dyskeratotic signs. *Am J Med Genet* 1994; 49: 374–377
- Labrune P, Lacroix C, Goutières F, de Laveaucoupet J, Chevalier P, Zerah M, Husson B, Landrieu P. Extensive brain calcifications, leukodystrophy, and formation of parenchymal cysts: a new progressive disorder due to diffuse cerebral microangiopathy. *Neurology* 1996; 46: 1297–1301
- Nagae-Poetscher LM, Bibat G, Philippart M, Rosemberg S, Fatiemi A, Lacerda MTC, Costa MOR, Kok F, Costa Leite C, Horská A, Barker PB, Naidu S. Leukoencephalopathy, cerebral calcifications, and cysts. New observations. *Neurology* 2004; 62: 1206–1209
- Niedermeyer I, Reiche W, Graf N, Mestres P, Feiden W. Cerebroretinal vasculopathy and leukoencephalopathy mimicking a brain tumor. *Clin Neuropathol* 2000; 19: 285–295
- Revesz T, Fletcher S, Al-Gazali LI, DeBuse P. Bilateral retinopathy, aplastic anaemia, and central nervous system abnormalities: a new syndrome? *J Med Genet* 1992; 29: 673–675
- Sazgar M, Leonard NJ, Renaud DL, Bhargava R, Sinclair DB. Intracranial calcification, retinopathy, and osteopenia: a new syndrome? *Pediatr Neurol* 2002; 26: 324–328
- Tolmie JL, Browne BH, McGettrick PM, Stephenson JBP. A familial syndrome with Coats' reaction retinal angiomas, hair and nail defects and intracranial calcification. *Eye* 1988; 2: 297–303

67 Leukoencephalopathy with Calcifications and Cysts

- Aynaci FM, Celep F, Ahmetoglu A. Encephalopathy with intracranial calcification, dwarfism, leukodystrophy and neuropathy: a new clinical entity? *Brain Dev* 2002; 24: 639–640
- Crow YJ, McMenamin J, Haenggeli CA, Hadley DM, Tirupathi S, Tracy EP, Zuberi SM, Browne BH, Tolmie JL, Stephenson JBP. Coats' plus: a progressive syndrome of bilateral Coats' disease, characteristic cerebral calcification, leukoencephalopathy, slow pre- and post-natal linear growth and defects of bone marrow and integument. *Neuropediatrics* 2004; 35: 10–19

68 Leukoencephalopathy with Brain Stem and Spinal Cord Involvement and Elevated Lactate

- Linnankivi T, Lundbom N, Autti T, Häkkinen AM, Koillinen H, Kuusi T, Lönnqvist T, Saino K, Valanne L, Äärämaa T, Pihko H. Five new cases of a recently described leukoencephalopathy with high brain lactate. *Neurology* 2004; 63: 688–693
- Serkov SV, Pronin IN, Bykova OV, Maslova OI, Arutyunov NV, Muravina TI, Kornienko VN, Fadeeva LM, Marks H, Bönnemann C, Schiffmann R, van der Knaap MS. Five patients with a recently described novel leukoencephalopathy with brainstem and spinal cord involvement and elevated lactate. *Neuropediatrics* 2004; 35: 1–5
- van der Knaap MS, van der Voorn P, Barkhof F, van Coster R, Krägeloh-Mann I, Feigenbaum A, Blaser S, Vles JSH, Rieckmann P, Pouwels PJW. A new leukoencephalopathy with brainstem and spinal cord involvement and high lactate. *Ann Neurol* 2003; 53: 252–258

69 Hypomyelination with Atrophy of the Basal Ganglia and Cerebellum

van der Knaap MS, Naidu S, Pouwels PJW, Bonavita S, van Coster R, Lagae L, Sperner J, Surtees R, Schiffmann R, Valk J. New syndrome characterized by hypomyelination with atrophy of the basal ganglia and cerebellum. *AJNR Am J Neuroradiol* 2002; 23: 1466–1474

70 Hereditary Diffuse Leukoencephalopathy with Neuroaxonal Spheroids

- Axelsson R, Røyttä M, Sourander P, Åkesson HO, Andersen O. Hereditary diffuse leukoencephalopathy with spheroids. *Acta Psychiatr Scand* 1984; 69 (suppl 314): 7–65
- Browne L, Sweeney BJ, Farrell MA. Late-onset neuroaxonal leukoencephalopathy with spheroids and vascular amyloid. *Eur Neurol* 2003; 50: 85–90
- Goodman LA, Dickson DW. Nonhereditary diffuse leukoencephalopathy with spheroids presenting as early-onset rapidly progressive dementia. *J Neuropathol Exp Neurol* 1995; 54: 471
- Hancock N, Poon M, Taylor B, McLean C. Hereditary diffuse leukoencephalopathy with spheroids. *J Neurol Neurosurg Psychiatry* 2003; 74: 1345–1347
- Lampert PW. A comparative electron microscopic study of reactive, degenerating, regenerating, and dystrophic axons. *J Neuropathol Exp Neurol* 1967; 26: 345–368
- Matsuyama H, Watanabe I, Mihm MC, Richardson EP. Dermatoleukodystrophy with neuroaxonal spheroids. *Arch Neurol* 1978; 35: 329–336
- Moro-de-Casillas ML, Cohen ML, Riley DE. Leukoencephalopathy with neuroaxonal spheroids (LENAS) presenting as the cerebellar subtype of multiple system atrophy. *J Neurol Neurosurg Psychiatry* 2004; 75: 1070–1072
- Seitelberger F. Neuropathological conditions related to neuroaxonal dystrophy. *Acta Neuropathol (Berl)* 1971; 21 (suppl V): 17–29
- Torack R, Hughes CP. Neuroaxonal dystrophy in subacute dementia. *Acta Neuropathol (Berl)* 1972; 22: 267–268
- van der Knaap MS, Naidu S, Kleinschmidt-DeMasters BK, Kamphorst W, Weinstein HC. Autosomal dominant diffuse leukoencephalopathy with neuroaxonal spheroids. *Neurology* 2000; 54: 463–468
- Yamashita M, Yamamoto T. Neuroaxonal leukoencephalopathy with axonal spheroids. *Eur Neurol* 2002; 48: 20–25
- Yazawa I, Nakano I, Yamada H, Oda M. Long tract degeneration in familial sudanophilic leukodystrophy with prominent spheroids. *J Neurol Sci* 1997; 147: 185–191

71 Dentatorubropallidoluysian Atrophy

Becher MW, Rubinstein DC, Loggio J, Wagster MV, Stine OC, Ranen NG, Franz ML, Abbott MH, Sherr M, MacMillan JC, Barron L, Porteous M, Harper PS, Ross CA. Dentatorubral-pallidoluysian atrophy (DRPLA). Clinical and neuropathological findings in genetically confirmed North American and European Pedigrees. *Mov Disord* 1997; 12: 519–530

- Burke JR, Wingfield MS, Lewis KE, Roses AD, Lee JE, Hulette C, Pericak-Vance MA, Vance JM. The Haw River syndrome: dentatorubral-pallidoluysian atrophy (DRPLA) in an African-American family. *Nat Genet* 1994; 7: 521–524
- Filla A, Mariotti C, Caruso G, Coppola G, Coccozza S, Castaldo I, Calabrese O, Salvatore E, De Michelle G, Riggio MC, Pareyson D, Gellera C, Di Donato S. Relative frequencies of CAG expansions in spinocerebellar ataxia and dentatorubropallidoluysian atrophy in 116 Italian families. *Eur Neurol* 2000; 44: 31–36
- Imamura A, Ito R, Tanaka S, Fukutomi O, Shimozawa N, Nishimura M, Suzuki Y, Kondo N, Yamada M, Orii T. High-intensity proton and T2-weighted MRI signals in the globus pallidus juvenile-type of dentatorubral and pallidoluysian atrophy. *Neuropediatrics* 1994; 25: 234–237
- Koide R, Onodera O, Ikeuchi T, Kondo R, Tanaka H, Tokiguchi S, Tomoda A, Miike T, Isa F, Beppu H, Shimizu N, Watanabe Y, Horikawa Y, Shimohata T, Hirota K, Ishikawa A, Tsuji S. Atrophy of the cerebellum and brain stem in dentatorubral-pallidoluysian atrophy. Influence of GAG repeat size on MR findings. *Neurology* 1997; 49: 1605–1612
- Lee I-H, Soong B-W, Lu Y-C, Chang Y-C. Dentatorubral-pallidoluysian atrophy in Chinese. *Arch Neurol* 2001; 58: 1905–1908
- Lopez-Cendez I, Teive HGA, Calcagnotto ME, Da Costa JC, Cardoso F, Viana E, Maciel JA, Radvany J, Arruda WO, Trevisol-Bittencourt PC, Neto PR, Silveira I, Steiner CE, Pinto Jr. W, Santos AS, Neto YC, Werneck LC, Araújo AQC, Carakushansky G, Mello LR, Jardim LB, Rouleau GA. Frequency of the different mutations causing spinobellar ataxia (SCA1, SCA2, MJD/SCA3 and DRPLA) in a large group of Brazilian patients. *Arq Neuropsiquiatr* 1997; 55: 519–529
- Melberg A, Dahl N, Hetta J, Valind S, Nennesmo I, Lundberg PO, Raininko R. Neuroimaging study in autosomal dominant cerebellar ataxia, deafness, and narcolepsy. *Neurology* 1999; 53: 2190–2192
- Miyazaki M, Hashimoto T, Yoneda Y, Tayama M, Harada M, Miyoshi H, Kawano N, Murayama N, Kondo I, Kuroda Y. Proton magnetic resonance spectroscopy in childhood-onset dentatorubral-pallidoluysian atrophy (DRPLA). *Brain Dev* 1966; 18: 142–146
- Mizukami K, Sasaki M, Shiraishi H, Koizumi J, Ogata T, Kosaka K. An autopsied case of dentatorubropallidoluysian atrophy with atypical pathological features. *Jpn J Psy Neurol* 1992; 46: 749–754
- Miyazaki M, Kato T, Hashimoto T, Harada M, Kondo I, Kuroda Y. MR of childhood-onset dentatorubral-pallidoluysian atrophy. *AJNR Am J Neuroradiol* 1995; 16: 1834–1836
- Muñoz E, Milà M, Sánchez A, Latorre P, Ariza A, Codina M, Ballesta F, Tolosa E. Dentatorubral-pallidoluysian atrophy in a Spanish family: a clinical, radiological, pathological, and genetic study. *J Neurol Neurosurg Psychiatry* 1999; 67: 811–814
- Nagafuchi S, Yanagisawa H, Sato K, Shirayama T, Ohsaki E, Bundo M, Takeda T, Tadokoro K, Kondo I, Murayama N, Tanaka Y, Kikushima H, Umino K, Kurosawa H, Furukawa T, Nihei K, Inoue T, Sano A, Komue O, Takahashi M, Yoshizawa T, Kanazawa I, Yamada M. Dentatorubral and pallidoluysian atrophy expansion of an unstable CAG trinucleotide on chromosome 12p. *Nat Genet* 1994; 6: 14–18
- Nagaoka U, Suzuki Y, Kawanami T, Kurita K, Shikama Y, Honda K, Abe K, Nakajima T, Kato T. Regional differences in genetic subgroup frequency in hereditary cerebellar ataxia, and a morphometrical study of brain MR images in SCA1, MJD and SCA6. *J Neurol Sci* 1999; 164: 187–194

- Robitaille Y, Lopez-Cendez I, Becher M, Rouleau G, Clark AW. The neuropathology of CAG repeat diseases: review and update of genetic and molecular features. *Brain Pathol* 1997; 7: 901–926
- Silveira I, Miranda C, Guimarães, Moreira M-C, Alonso I, Mendonça P, Ferro A, Pinto-Basto J, Coelho J, Ferreirinha F, Poirier J, Parreira E, Vale J, Januário C, Barbot C, Tuna A, Barros J, Koide R, Tsuji S, Holmes SE, Margolis RL, Jardim L, Pandolfo M, Coutinho P, Sequeiros J. Trinucleotide repeats in 202 families with ataxia. *Arch Neurol* 2002; 59: 623–629
- Smith JK, Gonda VE, Malamud N. Unusual form of cerebellar ataxia: combined dentatorubral and pallidolusian degeneration. *Neurology* 1958; 13: 266–269
- Tsuchiya K, Oyanani S, Arima K, Ikeda K, Akashi T, Ando S. Kurosawa T, Ikeuchi T, Tsuji S. Dentatorubropallidolusian atrophy: clinicopathological study of dementia and involvement of the nucleus basalis of Meynert in seven autopsy cases. *Acta Neuropathol (Berl)* 1998; 96: 502–508
- Uyama E, Kondo I, Uchino M, Fukushima T, Murayama N, Kuwano A, Inokuchi N, Ohtani Y, Ando M. Dentatorubral-pallidolusian atrophy (DRPLA): clinical, genetic and neuro-radiologic studies in a family. *J Neurol Sci* 1995; 130: 146–153
- Violante V, Luongo A, Pepe S, Annunziata S, Gentile V. Transglutaminase-dependent formation of protein aggregates as possible biochemical mechanism for polyglutamine diseases. *Brain Res Bull* 2001; 56: 169–172
- Warner TT, Lennox GC, Janota I, Harding E. Autosomal-dominant dentatorubropallidolusian atrophy in the United Kingdom. *Mov Disord* 1994; 3: 289–296
- Warner TT, Williams LD, Walker RWH, Flinter F, Robb SA, Bunday SE, Honavar M, Harding AE. A clinical and molecular genetic study of dentatorubropallidolusian atrophy in four European families. *Ann Neurol* 1995; 37: 452–459
- Yabe I, Sasaki H, Kikuchi S, Nonaka M, Moriwake F, Tashiro K. Late onset ataxia phenotype in dentatorubro-pallidolusian atrophy (DRPLA). *J Neurol* 2002; 249: 432–436
- Yamada M, Sato T, Tsuji S, Takahashi H. Oligodendrocytic polyglutamine pathology in dentatorubral-pallidolusian atrophy. *Ann Neurol* 2002; 52: 670–674
- Yoshii F, Tomiyasu H, Shinohara Y. Fluid attenuation inversion recovery (FLAIR) images of dentatorubropallidolusian atrophy: case report. *J Neurol Neurosurg Psychiatry* 1998; 65: 396–399
- Zoghbi HY, Orr HT. Glutamine repeats and neurodegeneration. *Ann Rev Neurosci* 2000; 23: 217–247
- Benyamini H, Gunasekaran K, Wolfson H, Nussinov R. Conservation and amyloid formation: a study of the Gelsolin-like family. *Proteins* 2003; 51: 266–282
- Bornebroek M, van Buchem MA, Haan J, Brand R, Lanser JBK, de Bruïne FT, Roos RAC. Hereditary cerebral hemorrhage with amyloidosis-Dutch type: better correlation of cognitive deterioration with advancing age than with number of focal lesions or white matter hyperintensities. *Alzheimer Dis Assoc Disord* 1996; 10: 224–231
- Bornebroek M, Haan J, Maat-Schieman MLC, van Duinen SG, Roos RAC. Hereditary cerebral hemorrhage with amyloidosis-Dutch type (HCHWA-D). 1. A review of clinical, radiologic and genetic aspects. *Brain Pathol* 1996; 6: 111–114
- Bornebroek M, Haan J, Backhovens H, Deutz P, van Buchem MA, van der Broeke M, Bakker E, Roos RAC, van Broeckhoven C. Presenilin-1 polymorphism and hereditary cerebral hemorrhage with amyloidosis, Dutch type. *Ann Neurol* 1997; 42: 108–110
- Bots GTAM. Neuropathological findings in cerebral B-protein amyloidosis. Differences and similarities in those cases presenting as a cerebral hemorrhage and those presenting as a dementia of the Alzheimer type. *Clin Neurol Neurosurg* 1992; 94 (suppl): S52–S53
- Burgermeister P, Calhoun ME, Winkler DT, Jucker M. Mechanisms of cerebrovascular amyloid deposition. Lessons from mouse models. *Ann NY Acad Sci* 2000; 903: 307–316
- Caulo M, Tampieri D, Brassard R, Guiot MC, Malanson D. Cerebral amyloid angiopathy presenting as nonhemorrhagic diffuse encephalopathy: neuropathologic and neuroradiologic manifestations in one case. *AJNR Am J Neuroradiol* 2001; 22: 1072–1076
- Crooks DA. Cerebral amyloid angiopathy. *J Neurol Neurosurg Psychiatry* 1994; 57: 1457
- Cuny E, Loiseau H, Rivel J, Vital C, Castel J-P. Amyloid angiopathy-related cerebellar hemorrhage. *Surg Neurol* 1996; 46: 235–239
- De la Monte S, Sohn Y, Etienne D, Kraft J, Wands JR. Role of aberrant nitric oxide synthase-3 expression in cerebrovascular degeneration and vascular-mediated injury in Alzheimer's disease. *Ann NY Acad Sci* 2000; 903: 61–71
- Fountain NB, Eberhart DA. Primary angiitis of the cerebral nervous system associated with cerebral amyloid angiopathy. *Neurology* 1996; 46: 190–197
- Fountain NB, Lopez MB. Control of primary angiitis of the CNS associated with cerebral amyloid angiopathy by cyclophosphamide alone. *Neurology* 1999; 52: 660–662
- Frangione B, Vidal R, Rostagno A, Ghiso J. Familial cerebral amyloid angiopathies and dementia. *Alzheimer Dis Assoc Disord* 2000; 14 (suppl 1): S25–S29
- Frangione B, Révész T, Vidal R, Holton J, Lashley T, Houlden H, Wood N, Rostagno A, Plant G, Ghiso J. Familial cerebral amyloid angiopathy related to stroke and dementia. *Amyloid* 2004; 8 (suppl 1): 36–42
- Friedland RP, Majocha RE, Reno JM, Lyle LR, Marotta CA. Development of an anti-a β monoclonal antibody for in vivo imaging of amyloid angiopathy in Alzheimer's disease. *Mol Neurobiol* 1994; 9: 107–113
- Gambetti P, Russo C. Human brain amyloidoses. *Nephrol Dial Transplant* 1998; 13: 33–40
- Good CD, NG VWK, Clifton A, Britton JA, Hart Y, Wilkins P. Amyloid angiopathy causing widespread miliary haemorrhages within the brain evident on MRI. *Neuroradiology* 1998; 40: 308–311

72 Cerebral Amyloid Angiopathy

- Abrahamson M, Jonsdottir S, Olafsson I, Jensson O, Grubb A. Hereditary cystin C amyloid angiopathy: identification of the disease-causing mutation and specific diagnosis by polymerase chain reaction based analysis. *Hum Genet* 1992; 89: 377–380
- Atwood CS, Bishop GM, Perry G, Smith MA. Amyloid- β : a vascular sealant that protects against hemorrhage? *J Neurosci Res* 2002; 70: 356
- Baumann MH, Wisniewski T, Levy E, Plant GT, Ghiso J. C-Terminal fragments of α - and β -tubulin form amyloid fibrils in vitro and associate with amyloid deposits of familial cerebral amyloid angiopathy, British type. *Biochem Biophys Res Commun* 1996; 219: 238–242

- Graffagnino C, Herbstreith MH, Schmechel DE, Levy E, Roses AD, Alberts MJ. Cystatin C mutation in an elderly man with sporadic amyloid angiopathy and intracerebral hemorrhage. *Stroke* 1995; 26: 2190–2193
- Gray F, Dubas F, Roullet E, Escourolle R. Leukoencephalopathy in diffuse hemorrhagic cerebral amyloid angiopathy. *Ann Neurol* 1985; 18: 54–59
- Greenberg SM. Cerebral amyloid angiopathy. Prospects for clinical diagnosis and treatment. *Neurology* 1998; 51: 690–694
- Greenberg SM. Cerebral amyloid angiopathy and dementia. Two amyloids are worse than one. *Neurology* 2002; 58: 1587–1588
- Greenberg SM. Cerebral amyloid angiopathy and vessel dysfunction. *Cerebrovasc Dis* 2002; 13 (suppl 2): 42–47
- Greenberg SM, Hyman BT. Cerebral amyloid angiopathy and apolipoprotein E: bad news for the good allele? *Ann Neurol* 1997; 41: 701–702
- Greenberg SM, Vonsattel JPG. Diagnosis of cerebral amyloid angiopathy. Sensitivity and specificity of cortical biopsy. *Stroke* 1997; 28: 1418–1422
- Greenberg SM, Vonsattel JPG, Stakes JW, Gruber M, Finklestein SP. The clinical spectrum of cerebral amyloid angiopathy: presentations without lobar hemorrhage. *Neurology* 1993; 43: 2073–2079
- Greenberg SM, Rebeck W, Vonsattel JPG, Gomez-Isla T, Hyman BT. Apolipoprotein E ϵ 4 and cerebral hemorrhage associated with amyloid angiopathy. *Ann Neurol* 1995; 38: 254–259
- Greenberg SM, Briggs ME, Hyman BT, Kokoris GH, Takis C, Kanter DS, Kase CS, Pessin MS. Apolipoprotein E ϵ 4 is associated with the presence and earlier onset of hemorrhage in cerebral amyloid angiopathy. *Stroke* 1996; 27: 1333–1337
- Haan J, Roos RAC. Comparison between the Icelandic and Dutch forms of hereditary cerebral amyloid angiopathy. *Clin Neurol Neurosurg* 1992; 94 (suppl): S82–S83
- Haan J, Bakker E, Jennekens-Schinkel A, Roos RAC. Progressive dementia, without cerebral hemorrhage, in a patient with hereditary cerebral amyloid angiopathy. *Clin Neurol Neurosurg* 1992; 94: 317–318
- Haan J, Maat-Schieman MLC, van Duinen MLC, Jansson O, Thorsteinsson L, Roos RAC. Co-localization of β /A4 and cystatin C in cortical blood vessels in Dutch, but not in Icelandic hereditary cerebral hemorrhage with amyloidosis. *Acta Neurol Scand* 1994; 89: 367–371
- Haan J, Maat-Schieman MLC, Roos RAC. Clinical aspects of cerebral amyloid angiopathy. *Dementia* 1994; 5: 210–213
- Haan J, Roos RAC, Bakker E. No prospective effect of apolipoprotein E ϵ 2 allele in Dutch hereditary cerebral amyloid angiopathy. *Ann Neurol* 1995; 37: 282
- Hendricks HT, Franke CL, Theunissen PHMH. Cerebral amyloid angiopathy: diagnosis by MRI and brain biopsy. *Neurology* 1991; 40: 1308–1310
- Holton JL, Ghiso J, Lashley T, Rostagno A, Guerin CJ, Gibb G, Houlden H, Ayling H, Martinain L, Anderton BH, Wood NW, Vidal R, Plant G, Frangione B, Revesz T. Regional distribution of amyloid- β deposition and its association with neurofibrillary degeneration in familial British dementia. *Am J Pathol* 2001; 158: 515–526
- Holtzman DM. Role of apoE/A β interactions in the pathogenesis of Alzheimer's disease and cerebral amyloid angiopathy. *J Mol Neurosci* 2001; 17: 147–155
- Hyman BT, Tanzi RE. Amyloid, dementia and Alzheimer's disease. *Curr Opin Neurol Neurosurg* 1992; 5: 88–93
- Imaoka K, Kobayashi S, Fujihara S, Shimode K, Nagasaki M. Leukoencephalopathy with cerebral amyloid angiopathy: a semiquantitative and morphometric study. *J Neurol* 1999; 246: 661–666
- Itoh Y, Yamada M, Hayakawa M, Otomo E, Miyatake T. Cerebral amyloid angiopathy: a significant cause of cerebellar as well as lobar cerebral hemorrhage in the elderly. *J Neurol Sci* 1993; 116: 135–141
- Itoh Y, Yamada M, Suematsu N, Matsushita M, Otomo E. Influence of apolipoprotein E genotype on cerebral amyloid angiopathy in the elderly. *Stroke* 1996; 27: 216–218
- Kim D-E, Bae H-J, Lee S-H, Kim H, Yoon B-W, Roh J-K. Gradient echo magnetic resonance imaging in the prediction of hemorrhagic vs ischemic stroke. A need for the consideration of the extent of leukoaraiosis. *Arch Neurol* 2002; 59: 425–429
- Knudson KA, Rosand J, Karluk D, Greenberg SM. Clinical diagnosis of cerebral amyloid angiopathy: validation of the Boston Criteria. *Neurology* 2001; 56: 537–539
- Levey AI, Heilman CJ, Lah JJ, Nash NR, Rees HD, Wakai M, Mirra SS, Rey DB, Nochlin D, Brid TD, Mufson EJ. Preselin-1 protein expression in familial and sporadic Alzheimer's disease. *Ann Neurol* 1997; 41: 742–753
- Liberski PP, Barcikowska M. Pathology of the vessels in cerebral amyloid angiopathy. *Folia Neuropathol* 1995; 33: 207–214
- Loes DJ, Biller J, Yuh WTC, Hart MN, Godersky JC, Adams Jr HP, Keefauver SP, Tranel D. Leukoencephalopathy in cerebral amyloid angiopathy: MR imaging in four cases. *AJNR Am J Neuroradiol* 1990; 11: 485–488
- Maat-Schieman MLC, Radder CM, van Duinen SG, Roos RAC. Hereditary cerebral hemorrhage with amyloidosis (Dutch): a model for congophilic plaque formation without neurofibrillary pathology. *Acta Neuropathol (Berl)* 1994; 88: 371–378
- Maury CPJ, Liljeström M, Boysen G, Törnroth T, de la Capelle A, Nurmiaho-Lassila E-L. Danish type gelsolin related amyloidosis: 654G-T mutation is associated with a disease pathogenetically and clinically similar to that caused by the 654G-A mutation (familial amyloidosis of the Finnish type). *J Clin Pathol* 2000; 53: 95–99
- McCarron MO, Nicoll JAR. Apolipoprotein E genotype and cerebral amyloid angiopathy-related hemorrhage. *Ann NY Acad Sci* 2000; 903: 176–179
- Mehdorn HM, Gerhard L, Müller SP, Olbirsch HM. Clinical and cerebral blood flow studies in patients with intracranial hemorrhage and amyloid angiopathy typical of Alzheimer's disease. *Neurosurg Rev* 1992; 15: 111–116
- Natté R, Maat-Schieman MLC, Haan J, Bornebroek M, Roos RAC, van Duinen SG. Dementia in hereditary cerebral hemorrhage with amyloidosis-Dutch type is associated with cerebral amyloid angiopathy but is independent of plaques and neurofibrillary tangles. *Ann Neurol* 2001; 50: 765–771
- Nicoll JAR, Burnett C, Love S, Graham DI, Ironside JW, Vinters HV. High frequency of apolipoprotein E ϵ 2 in patients with cerebral hemorrhage due to cerebral amyloid angiopathy. *Ann Neurol* 1996; 39: 682–683
- Nicoll JAR, Burnett C, Love S, Graham DI, Dewar D, Ironside JW, Stewart J, Vinters HV. High frequency of apolipoprotein E ϵ 2 allele in hemorrhage due to cerebral amyloid angiopathy. *Ann Neurol* 1997; 41: 716–721
- Oh U, Gupta R, Krakauer JW, Khandji AG, Chin Ss, Elkind MSV. Reversible leukoencephalopathy associated with cerebral amyloid angiopathy. *Neurology* 2004; 62: 494–497

- Oide T, Takahashi H, Yutani C, Ishihara T, Ikeda S-I. Relationship between lobar intracerebral hemorrhage and leukoencephalopathy associated with cerebral amyloid angiopathy: clinicopathological study of 64 Japanese patients. *J Protein Folding Disord* 2003; 10: 136–143
- Ólafsson Í, Grubb A. Hereditary cystatin C amyloid angiopathy. *Int J Exp Clin Invest* 2000; 7: 70–79
- Olichney JM, Hansen LA, Hofstetter R, Grundman M, Katzman R, Thal LJ. Cerebral infarction in Alzheimer's disease is associated with severe amyloid angiopathy and hypertension. *Arch Neurol* 1995; 52: 702–708
- Olichney JM, Hansen LA, Lee JH, Hofstetter CR, Katzman R, Thal LJ. Relationship between severe amyloid angiopathy, apolipoprotein E genotype and vascular lesions in Alzheimer's disease. *Ann NY Acad Sci* 2000; 903: 138–143
- O'Riordan S, McMonagle P, Janssen JC, Fox NC, Farrell M, Collinge J, Rossor MN, Hutchinson M. Preselin-1 mutation (E280G), spastic paraparesis, and cranial MRI white matter abnormalities. *Neurology* 2002; 59: 1108–1110
- Osumi AK, Tien RD, Felsberg GJ, Rosenbloom M. Cerebral amyloid angiopathy presenting as a brain mass. *AJNR Am J Neuroradiol* 1995; 16: 911–915
- Pfeifer LA, White LR, Ross GW, Petrovitch H, Launer LJ. Cerebral amyloid angiopathy and cognitive function. *Neurology* 2002; 58: 1629–1634
- Prior R, Wihl G, Urmoneit B. Apolipoprotein E, smooth muscle cells and the pathogenesis of cerebral amyloid angiopathy: the potential role of impaired cerebrovascular A β clearance. *Ann NY Acad Sci* 2000; 903: 180–186
- Revasz T, Holton JL, Lashley T, Plant G, Rostagno A, Ghiso J, Frangione B. Sporadic and familial cerebral amyloid angiopathies. *Brain Pathol* 2002; 12: 343–357
- Roob G, Fazekas F. Magnetic resonance imaging of cerebral microbleeds. *Curr Opin Neurol* 2000; 13: 69–73
- Sarazin M, Amarenco P, Mikol J, Dimitri D, Lot G, Bousser MG. Reversible leukoencephalopathy in cerebral amyloid angiopathy presenting as subacute dementia. *Eur J Neurol* 2002; 9: 353–358
- Schubert P, Morino T, Miyazaki H, Ogata T, Nakamura Y, Marchini C, Ferroni S. Cascading glia reactions: a common pathomechanism and its differentiated control by cycling nucleotide signaling. *Ann NY Acad Sci* 2000; 903: 24–33
- Scully RE, Mark EJ, McNeely WF, Ebeling SH, Ellender SM. Presentation of case. *N Engl J Med* 2000; 342: 957–965
- Shimode K, Kobayashi S, Imaoka K, Umegae N, Nagai A. Leukoencephalopathy-related cerebral amyloid angiopathy with cystatin C deposition. *Stroke* 1996; 27: 1417–1419
- Sillus M, Saeger W, Linke RP, Müller D, Voigt C. Cerebral amyloid angiopathy. Frequency, significance and immunohistochemistry. *Zentrabl Pathol* 1993; 139: 2074–215
- Sveinbjörnsdóttir S, Blöndal H, Gudmundsson G, Kjartansson O, Jónsdóttir S, Gudmundsson G. Progressive dementia and leukoencephalopathy as the initial presentation of late onset hereditary cystatin-C amyloidosis. Clinical presentation of two cases. *J Neurol Sci* 1996; 140: 101–108
- Van Duinen SG, Maat-Schieman MLC, Bruijn JA, Haan J, Roos RAC. Cortical tissue of patients with hereditary cerebral hemorrhage with amyloidosis (Dutch) contains various extracellular matrix deposits. *Lab Invest* 1995; 73: 183–189
- Van Nostrand WE, Melchor J, Wagner M, Davis J. Cerebrovascular smooth muscle cell surface fibrillar A β . Alteration of the proteolytic environment in the cerebral vessel wall. *Ann NY Acad Sci* 2000; 903: 89–96
- Vinters HV. Cerebral amyloid angiopathy and Alzheimer's disease: two entities or one? *J Neurol Sci* 1992; 112: 1–3
- Vonsattel JPG, Myers RH, Hedley-Whyte ET, Ropper AH, Bird ED, Richardson EP Jr. Cerebral amyloid angiopathy without and with cerebral hemorrhages: a comparative histological study. *Ann Neurol* 1991; 30: 637–649
- Walker LC. Animal models of cerebral β -amyloid angiopathy. *Brain Res Rev* 1997; 25: 70–84
- Wattendorf AR, Frangione B, Luyendijk W, Bots GTAM. Hereditary cerebral hemorrhage with amyloidosis, Dutch type (HCHWA-D): clinicopathological studies. *J Neurol Neurosurg Psychiatry* 1995; 58: 699–705
- Weller RO, Massey A, Kuo Y-M, Rohrer AE. Cerebral amyloid angiopathy: accumulation of A β in interstitial fluid drainage pathways in Alzheimer's disease. *Ann NY Acad Sci* 2000; 903: 110–117
- Yamada M. Cerebral amyloid angiopathy: an overview. *Neuropathology* 2000; 1: 8–22
- Yoshimura M, Yamanouchi H, Kuzuhara S, Mori H, Sugiura S, Mizutani T, Shimada H, Tomonaga M, Toyokura Y. Dementia in cerebral amyloid angiopathy: a clinicopathological study. *J Neurol* 1992; 239: 441–450

73 Cerebral Autosomal Dominant Arteriopathy with Subcortical Infarcts and Leukoencephalopathy

- Abe K, Murakami T, Matsubara E, Manabe Y, Nagano I, Shoji M. Clinical features of CADASIL. *Ann NY Acad Sci* 2002; 977: 266–272
- Arborelly-Valasquez JF, Lopera F, Lopez E, Frosch MP, Sepulveda-Falla D, Gutierrez JE, Vargas S, Medina M, Martinez de Arrieta C, Lebo RV, Slangenhuys SA, Betensky RA, Villegas A, Arcos-Burgos M, Rivers D, Restrepo JC, Kosik KS. C455R *notch3* mutation in a Colombian CADASIL kindred with early onset of stroke. *Neurology* 2002; 59: 277–279
- Auer DP, Schirmer T, Heidenreich JO, Herzog J, Pütz B, Dichgans M. Altered white and gray matter metabolism in CADASIL. A proton MR spectroscopy and ¹H-MRSI study. *Neurology* 2001; 56: 635–642
- Auer DP, Pütz B, Gössel C, Elbel G-K, Gasser T, Dichgans M. Differential lesion patterns in CADASIL and sporadic subcortical arteriosclerotic encephalopathy: MR imaging study with statistical parametric group comparison. *Radiology* 2001; 218: 443–451
- Bruening R, Dichgans M, Berchtenbreiter C, Yousry T, Seelos KC, Wu RH, Mayer M, Brix G, Reiser M. Cerebral autosomal dominant arteriopathy with subcortical infarcts and leukoencephalopathy: decrease in regional cerebral blood volume in hyperintense subcortical lesions inversely correlates with disability and cognitive performance. *AJNR Am J Neuroradiol* 2001; 22: 1268–1274
- Bulin P, Godfraind C, Leteurtre E, Ruchoux M-M. Morphometric analysis of ultrastructural vascular changes in CADASIL: analysis of 50 skin biopsy specimens and pathogenic implications. *Acta Neuropathol (Berl)* 2002; 104: 241–248
- Ceroni M, Poloni TE, Tonietti S, Fabozzi D, Uggetti C, Frediani F, Simonetti F, Malaspina A, Alimonti D, Celano M, Ferrari M, Carrera P. Migraine with aura and white matter abnormalities: *notch3* mutation. *Neurology* 2000; 54: 1869–1871
- Chabriat H, Mrissa R, Levy C, Vahedi K, Taillia H, Iba-Zizen MT, Joutel A, Tournier-Lasserre E, Bousser MG. Brain stem MRI signal abnormalities in CADASIL. *Stroke* 1999; 30: 457–459

- Chabriat H, Pappata S, Poupon F, Clark CA, Vahedi K, Poupon F, Magin JF, Pachot-Clouard M, Jobert A, le Bihan D, Bousser M-G. Clinical severity in CADASIL related to ultrastructural damage in white matter. In vivo study with diffusion tensor MRI. *Stroke* 1999; 30: 2637–2643
- Chabriat H, Pappata S, Ostergaard L, Clark CA, Pachot-Clouard M, Vahedi K, Jobert A, le Bihan D, Bousser MG. Cerebral hemodynamics in CADASIL before and after acetazolamide challenge assessed with MRI bolus tracking. *Stroke* 2000; 31: 1904–1912
- Chawda SJ, de Lange RPJ, Hourihan MD, Halpin SFS, St Clair D. Diagnosing CADASIL using MRI: evidence from families with known mutations of *Notch 3* gene. *Neuroradiology* 2000; 42: 249–255
- Coulthard A, Blank SC, Bushby K, Kalaria RN, Burn DJ. Distribution of cranial MRI abnormalities in patients with symptomatic and subclinical CADASIL. *Br J Radiol* 2000; 73: 256–265
- Davous P. CADASIL; a review with proposed diagnostic criteria. *Eur J Neurol* 1998; 5: 219–233
- De Lange RPJ, Bolt J, Reid E, da Silva R, Shaw DJ, St Clair DM. Screening British CADASIL families for mutations in the *NOTCH3* gene. *J Med Genet* 2000; 37: 224–225
- Desmond DW, Moroney JT, Lynch T, Chan S, Mohr JP. The natural history of CADASIL. A pooled analysis of previously published cases. *Stroke* 1999; 30: 1230–1233
- Dichans M, Mayer M, Uttner I, Brüning R, Müller-Höcker J, Rungger G, Ebke M, Klockgether T, Gasser T. The phenotypic spectrum of CADASIL: clinical findings in 102 cases. *Ann Neurol* 1998; 44: 731–739
- Dichgans M, Filippi M, Brüning R, Iannucci G, Berchtenbreiter C, Minicucci L, Uttner I, Crispin A, Ludwig H, Gasser T, Yousry TA. Quantitative MRI and CADASIL. Correlation with disability and cognitive performance. *Neurology* 1999; 52: 1361–1367
- Dichgans M, Holtmannspötter M, Herzog M, Herzog J, Peters N, Bergmann M, Yousry TA. Cerebral microbleeds in CADASIL. A gradient-echo magnetic resonance imaging and autopsy study. *Stroke* 2002; 33: 67–71
- Donahue CP, Kosik KS. Distribution pattern of *Notch3* mutations suggests a gain-of-function mechanisms for CADASIL. *Genomics* 2004; 83: 59–65
- Ducros A, Nagy T, Alamowitch S, Nibbio A, Joutel A, Vahedi K, Chabriat H, Iba-Zizen MT, Julien J, Davous P, Goas JY, Lyon-Caen O, Dubois B, Ducrocq X, Salsa F, Ragno M, Burkhard P, Bassetti C, Hutchinson M, Verin M, Viader F, Chapon F, Levasseur M, Mas JL, Delrieu O, Maciazek J, Prieur M, Mohrenweiser H, Bach JF, Bousser MG, Tournier-Lasserre E. Cerebral autosomal dominant arteriopathy with subcortical infarcts and leukoencephalopathy, genetic homogeneity, and mapping of the locus within a 2-cM interval. *Am J Hum Genet* 1996; 58: 171–181
- Engelter ST, Rueegg S, Kirsch EC, Fluri F, Probst A, Steck AJ, Lyrer PA. CADASIL mimicking primary angiitis of the central nervous system. *Arch Neurol* 2002; 59: 1480–1483
- Feuerhake F, Volk B, Ostertag CB, Jungling FD, Kassubek J, Orszagh M, Dichgans M. Reversible coma with raised intracranial pressure: an unusual clinical manifestation of CADASIL. *Acta Neuropathol (Berl)* 2002; 103: 188–192
- Filley CM, Thompon LL, Sze C-I, Simon JA, Paskavitz JF, Kleinschmidt-deMasters BK. White matter dementia in CADASIL. *J Neurol Sci* 1999; 163: 163–167
- Furby A, Vahedi K, Force, Larrouy S, Ruchoux M-M, Joutel A, Tournier-Lasserre E. Differential diagnosis of a vascular leukoencephalopathy within a CADASIL family: use of skin biopsy electron microscopy study and direct genotypic screening. *J Neurol* 1998; 245: 734–740
- Iannucci G, Dichgans M, Rovaris M, Brüning R, Gasser T, Giacomotti L, Yousry TA, Filippi M. Correlations between clinical findings and magnetization transfer imaging metrics of tissue damage in individuals with cerebral autosomal dominant arteriopathy with subcortical infarcts and leukoencephalopathy. *Stroke* 2001; 32: 643–648
- Ito D, Tanahashi N, Murata M, Sato H, Saito I, Wanatabe K, Fukkuchi Y. *Notch3* gene polymorphism and ischaemic cerebrovascular disease. *J Neurol Neurosurg Psychiatry* 2002; 72: 382–384
- Joutel A, Corpechot C, Ducros A, Vahedi K, Chabriat H, Mouton P, Alamowitch S, Domenga V, Cécillon M, Maréchal E, Maciazek J, Vayssière C, Cruaud C, Cabanis E-A, Ruchoux MM, Weissenbach J, Bach JF, Bousser MG, Tournier-Lasserre E. *Notch3* mutations in CADASIL, a hereditary adult-onset condition causing stroke and dementia. *Nature* 1996; 383: 707–710
- Joutel A, Vahedi K, Corpechot C, Troesch A, Chabriat H, Vayssière C, Cruaud C, Maciazek M, Weissenbach J, Bousser M-G, Bach J-F, Tournier-Lasserre E. Strong clustering and stereotyped nature of *Notch3* mutations in CADASIL patients. *Lancet* 1997; 350: 1511–1515
- Joutel A, Andreux F, Gaulis S, Domenga V, Cecillon M, Battail N, Piga N, Chapon F, Godfrain C, Tournier-Lasserre E. The ectodomain of the *Notch3* receptor accumulates within the cerebrovasculature of CADASIL patients. *J Clin Invest* 2000; 105: 597–605
- Joutel A, Dodick DD, Parisi JE, Cecillon M, Tournier-Lasserre E, Bousser MG. De novo mutation in the *notch3* gene causing CADASIL. *Ann Neurol* 2000; 47: 388–391
- Joutel A, Monet M, Domenga V, Riant F, Tournier-Lasserre E. Pathogenic mutations associated with cerebral autosomal dominant arteriopathy with subcortical infarcts and leukoencephalopathy differently affect *jagged1* binding and *Notch3* activity via the RBP/JK signaling pathway. *Am J Hum Genet* 2004; 74: 338–347
- Kalimo H, Viitanen M, Amberlat K, Juvonen V, Marttila R, Pöyhönen M, Rinne JO, Savontaus M-L, Tuisku S, Winblad B. CADASIL: hereditary disease of arteries causing brain infarcts and dementia. *Neuropathol Appl Neurobiol* 1999; 25: 257–265
- Karlström H, Beatus P, Danneus K, Chapman G, Lendahl U, Lundkvist J. A CADASIL-mutated *Notch 3* receptor exhibits impaired intracellular trafficking and maturation but normal ligand-induced signaling. *Proc Natl Acad Sci* 2002; 99: 17119–17124
- LaPoint SF, Patel U, Rubio A. Cerebral autosomal dominant arteriopathy with subcortical infarcts and leukoencephalopathy (CADASIL). *Adv Anat Pathol* 2000; 7: 307–321
- Le Bler I, Carlier L, Derache N, Lalevée C, Ledoze F, Defer GL. Unusual presentation of CADASIL with reversible coma and confusion. *Neurology* 2002; 59: 1115–1116
- Lesnik Oberstein SAJ, van den Boom R, Middelkoop HAM, Ferrari MD, Knaap YM, van Houwelingen HC, Breuning MH, van Buchem MA, Haan J. Incipient CADASIL. *Arch Neurol* 2003; 60: 707–712
- Lesnik Oberstein SAJ, van Duinen SG, van den Boom R, Maat-Schieman MLC, van Buchem MA, van Houwelingen HC, Hegeman-Kleinn IM, Ferrari MD, Breuning MH, Haan J. Evaluation of diagnostic NOTCH3 immunostaining in CADASIL. *Acta Neuropathol (Berl)* 2003; 106: 107–111

- Malandrini A, Carrera P, Palmeri S, Cavellaro T, Fabrizi GM, Villanova M, Fattapposta M, Vismara L, Brancolini V, Tanganelli P, Cali A, Morocutti C, Zeviani M, Ferrari M, Guazzi GC. Clinicopathological and genetic studies of two further Italian families with cerebral dominant arteriopathy. *Acta Neuropathol (Berl)* 1996; 92: 115–122
- Malandrini A, Carrera P, Giacci G, Gonelli Villanova M, Palmeri S, Vismara L, Brancolini V, Signorini E, Ferrari, Guazzi GC. Unusual clinical features and early brain MRI lesions in a family with cerebral autosomal dominant arteriopathy. *Neurology* 1997; 48: 1200–1203
- Malandrini A, Albani F, Palmeri S, Fattapposta F, Gambelli S, Berti G, Bracco A, Tammara A, Calzavara S, Villanova M, Ferrari M, Rossi A, Carrera P. Asymptomatic and paracrystalline mitochondrial inclusions in CADASIL. *Neurology* 2002; 59: 617–620
- Markus HS, Martin RJ, Simpson MA, Dong YB, Ali N, Crosby AH, Powell JF. Diagnostic strategies in CADASIL. *Neurology* 2002; 59: 1134–1138
- Mayer M, Straube A, Bruening R, Uttner I, Pongratz D, Gasser T, Dichgans M, Müller-Höcker J. Muscle and skin biopsies are sensitive diagnostic tool in the diagnosis of CADASIL. *J Neurol* 1999; 246: 526–532
- Molko N, Pappata S, Magnin JF, Poupon C, Vahedi K, Jobert A, LeBihan D, Bousser MG, Chabriat H. Diffusion tensor imaging study of subcortical gray matter in CADASIL. *Stroke* 2001; 32: 2049–2054
- Molko N, Pappata S, Mangin J-F, Poupon F, LeBihan D, Bousser M-G, Chabriat H. Monitoring disease progression in CADASIL with diffusion magnetic resonance imaging. A study with whole brain histogram analysis. *Stroke* 2002; 33: 2902–2908
- Okeda R, Arima K, Kawai M. Arterial changes in cerebral autosomal dominant arteriopathy with subcortical infarcts and leukoencephalopathy (CADASIL) in relation to pathogenesis of diffuse myelin loss of cerebral white matter. Examination of cerebral medullary arteries by reconstruction of serial sections of an autopsy case. *Stroke* 2002; 33: 2565–2569
- O'Sullivan, M Jarosz JM, Martin RJ, Deasy N, Powell JF, Markus HS. MRI hyperintensities of the temporal lobe and external capsule in patients with CADASIL. *Neurology* 2001; 56: 628–634
- O'Sullivan M, Rich PM, Barrick TH, Clark CA, Markus HS. Frequency of subclinical lacunar infarcts in ischemic leukoaraiosis and cerebral autosomal dominant arteriopathy with subcortical infarcts and leukoencephalopathy. *AJNR Am J Neuroradiol* 2003; 24: 1348–1354
- Robinson W, Galetta SL, McCluskey L, Forman MS, Balcer LJ. Retinal findings in cerebral autosomal dominant arteriopathy with subcortical infarcts and leukoencephalopathy (CADASIL). *Surv Ophthalmol* 2001; 45: 445–448
- Rocca MA, Filippi M, Herzog J, Sormani MP, Dichgans M, Yousry TA. A magnetic resonance imaging study of the cervical cord of patients with CADASIL. *Neurology* 2001; 56: 1392–1394
- Rubio A, Rifkin D, Powers JM, Patel U, Stewart J, Faust P, Goldman JE, Mohr JP, Numaguchi Y, Jensen K. Phenotypic variability of CADASIL and novel morphologic findings. *Acta Neuropathol (Berl)* 1997; 94: 247–254
- Ruchoux M-M, Muarage C-A. CADASIL: cerebral autosomal dominant arteriopathy with subcortical infarcts and leukoencephalopathy. *J Neuropathol Exp Neurol* 1997; 56: 947–964
- Santa Y, Uyama E, Chui de H, Arima M, Kotorii S, Takahashi K, Tabira T. Genetic, clinical and pathological studies of CADASIL in Japan: a partial contribution of *Notch3* mutations and implications of smooth muscle cell degeneration for the pathogenesis. *J Neurol Sci* 2003; 212: 79–84
- Schon F, Martin RJ, Prevett M, Clough C, Enevoldson TP, Markus HS. "CADASIL coma": an underdiagnosed acute encephalopathy. *J Neurol Neurosurg Psychiatry* 2003; 74: 249–252
- Schultz A, Santoianni R, Hewan-Lowe D. Vasculopathic changes of CADASIL can be focal in skin biopsies. *Ultrastruct Pathol* 1999; 23: 241–247
- Thomas NJ, Morris CM, Scaravilli F, Johansson J, Rossor M, de Lange R, St Clair D, Nicoll J, Blank C, Coulthard A, Bushby K, Ince PG, Burn D, Kalaria RN. Hereditary vascular dementia linked to *notch 3* mutations. CADASIL in British families. *Ann N Y Acad Sci* 2000; 903: 293–298
- Tournier-Lasserre E, Joutel A, Melki J, Weissenbach J, Lathrop GM, Chabriat H, Mas J-L, Cabanis E-A, Baudrimont M, Maciazek J, Bach M-A, Bousser M-G. Cerebral autosomal dominant arteriopathy with subcortical infarcts and leukoencephalopathy maps to chromosome 19q12. *Nat Genet* 1993; 3: 256–259
- Trojano L, Ragno M, Manca A, Caruso G. A kindred affect by cerebral autosomal dominant arteriopathy with subcortical infarcts and leukoencephalopathy (CADASIL). A 2-year neuropsychological follow-up. *J Neurol* 1998; 245: 217–222
- Tuominen S, Juvonen V, Amberla K, Jolma T, Rinne JO, Tuisku S, Kurki T, Marttila R, Pöyhönen M, Savontaus M-L, Viitanen M, Kalimo H. Phenotype of a homozygous CADASIL patient in comparison to 9 age-matched heterozygous patients with the same R113C *Notch3* mutation. *Stroke* 2001; 32: 1767–1774
- Utatsu Y, Takashima H, Michizono K, Kanda N, Endou K, Mitsuyama Y, Fujimoto T, Nagai M, Umehara F, Higuchi I, Arimura K, Nakagawa M, Osame M. Autosomal dominant early onset dementia and leukoencephalopathy in a Japanese family: clinical, neuroimaging and genetic studies. *J Neurol Sci* 1997; 147: 55–62
- Van den Boom R, Lesnik Oberstein SAJ, van Duinen SG, Bornebroek M, Ferrari MD, Haan J, van Buchem MA. Subcortical lacunar lesions: an MR imaging finding in patients with cerebral autosomal dominant arteriopathy with subcortical infarcts and leukoencephalopathy. *Radiology* 2002; 224: 791–796
- Van den Boom R, Lesnik Oberstein SAJ, Ferrari MD, Haan J, van Buchem MA. Cerebral autosomal dominant arteriopathy with subcortical infarcts and leukoencephalopathy: MR findings at different ages – 3rd–6th decades. *Radiology* 2003; 229: 683–690
- Viitanen M, Kalimo H. CADASIL: hereditary arteriopathy leading to multiple brain infarcts and dementia. *Ann N Y Acad Sci* 2000; 903: 273–284
- Villa N, Walker L, Lindsell CE, Gasson J, Iruela-Arispe ML, Weinmaster G. Vascular expression of Notch pathway receptors and ligands is restricted to arterial vessels. *Mech Dev* 2001; 108: 161–164
- Wang T, Sharma SD, Fox N, Rossor M, Brown MJ, Sharma P. Description of a simple test for CADASIL disease and determination of mutation frequencies in sporadic ischaemic stroke and dementia patients. *J Neurol Neurosurg Psychiatry* 2000; 69: 652–654

- Wieland R, Bornebroek M, Ophoff RA, Winter-Warnars HAO, Scheltens P, Frants RR, Ferrari MD, Haan J. A four-generation Dutch family with cerebral autosomal dominant arteriopathy with subcortical infarcts and leukoencephalopathy (CADASIL), linked to chromosome 19p13. *Clin Neurol Neurosurg* 1995; 97: 307–313
- Yousry TA, Seelos K, Mayer M, Brünig R, Uttner I, Dichgans M, Mammi S, Straube A, Mai N, Filippi M. Characteristic MR lesion pattern and correlation of T1 and T2 lesion volume with neurologic and neuropsychological findings in cerebral autosomal dominant arteriopathy with subcortical infarcts and leukoencephalopathy (CADASIL). *AJNR Am J Neuroradiol* 1996; 20: 91–100

74 Cerebral Autosomal Recessive Arteriopathy with Subcortical Infarcts and Leukoencephalopathy (CARASIL)

- Fukutake T. Young-adult-onset hereditary subcortical vascular dementia: cerebral autosomal recessive arteriosclerosis with subcortical infarcts and leukoencephalopathy (CARASIL). *Clin Neurol* 1999; 39: 50–52
- Fukutake T, Hirayama K. Familial young-adult-onset arteriosclerotic leukoencephalopathy with alopecia and lumbago without arterial hypertension. *Eur Neurol* 1995; 35: 69–79
- Maeda S, Nakayama H, Isaka K, Aihara Y, Nemoto S. Familial unusual encephalopathy of Binswanger's type without hypertension. *Folia Psychiatr Neurol Jap* 1976; 30: 165–177
- Uchino M, Hirano T, Uyama E, Hashimoto Y. Cerebral autosomal dominant arteriopathy with subcortical infarcts and leukoencephalopathy (CARASIL) and CADASIL-like disorders in Japan. *Ann NY Acad Sci* 2002; 977: 273–278
- Yamamura T, Nishimura M, Shirabe T, Fujita M. Subcortical vascular encephalopathy in a normotensive, young adult with premature baldness and spondylitis deformans. A clinicopathological study and review of the literature. *J Neurol Sci* 1987; 78: 175–188
- Yanagawa S, Ito N, Arima K, Ikeda S-I. Cerebral autosomal recessive arteriopathy with subcortical infarcts and leukoencephalopathy. *Neurology* 2002; 58: 817–820
- Yokoi S, Nakayama H. Chronic progressive leukoencephalopathy with systemic arteriosclerosis in young adults. *Clin Neuropathol* 1985; 4: 165–173

75 Polycystic Lipomembranous Osteodysplasia with Sclerosing Leukoencephalopathy (Nasu-Hakola Disease)

- Amano N, Iwabuchi K, Sakai H, Yaghishta S, Itho Y, Eteki E, Yokoi S, Arai N, Kinoshita J. Nasu-Hakola's disease (membranous lipodystrophy). *Acta Neuropathol (Berl)* 1987; 74: 294–299
- Araki T, Ohba H, Monzawa S, Sakuyama K, Hachiya J, Seki T, Takahashi Y, Yamaguchi M. Membranous lipodystrophy: MR imaging appearance of the brain. *Radiology* 1991; 180: 793–797

- Bianchin MM, Capella HM, Chaves DL, Steindel M, Grisard EC, Ganey GG, Péciles da Silva J, Neto ES, Poffo MA, Walz R, Carloti CG, Sakamoto AC. Nasu-Hakola disease (polycystic lipomembranous osteodysplasia with sclerosing leukoencephalopathy – PLOSL): a dementia associated with bone cystic lesions. From clinical to genetic and molecular aspects. *Cell Mol Neurobiol* 2004; 24: 1–24
- Bird TD, Koerker RM, Leaird BJ, Vlcek BW, Thorning DR. Lipomembranous polycystic osteodysplasia (brain, bone, and fat disease): a genetic cause of presenile dementia. *Neurology* 1983; 33: 81–86
- Chaabane M, Larnaout A, Sebai R, Nagi S, Touibi S, Hentati F. Nasu-Hakola disease in two Tunisian siblings: new radiological findings. *Neuroradiology* 2000; 42: 375–378
- Hakola HPA, Järvi OH, Sourander P. Osteodysplasia polycystica hereditaria combined with sclerosing leukoencephalopathy, a new entity of the dementia praesens group. *Acta Neurol Scand* 1970; 46: 79–80
- Hakola HPA. Neuropsychiatric and genetic aspects of a new hereditary disease characterized by progressive dementia and lipomembranous polycystic osteodysplasia. *Acta Psychiatr Scand* 1972; 232: 1–173
- Hakola HPA, Livanainen M. A new hereditary disease with progressive dementia and polycystic osteodysplasia: neuroradiological analysis of seven cases. *Neuroradiology* 1973; 6: 162–168
- Hakola HPA, Partanen VSJ. Neurophysiological findings in the hereditary presenile dementia characterized by polycystic lipomembranous osteodysplasia and sclerosing leukoencephalopathy. *J Neurol Neurosurg Psychiatry* 1983; 46: 515–520
- Hakola HPA, Puranen M. Neuropsychiatric and brain CT findings in polycystic lipomembranous osteodysplasia with sclerosing leukoencephalopathy. *Acta Neurol Scand* 1993; 88: 370–375
- Haruta K, Matsunaga S, Ito H, Hayashi K, Yokouchi M, Onishi T, Komiya S. Membranous lipodystrophy (Nasu-Hakola disease) presenting an unusually benign clinical course. *Oncol Rep* 2003; 10: 1007–1010
- Livanainen M, Hakola P, Erkinjuntti T, Sipponen JT, Ketonen L, Sulkava R, Sepponen RE. Cerebral MR and CT imaging in polycystic lipomembranous osteodysplasia with sclerosing leukoencephalopathy. *J Comput Assist Tomogr* 1984; 8: 940–943
- Kalimo H, Sourander P, Järvi O, Hakola P. Vascular changes and blood-brain barrier damage in the pathogenesis of polycystic lipomembranous osteodysplasia with sclerosing leukoencephalopathy (membranous lipodystrophy). *Acta Neurol Scand* 1994; 89: 353–361
- Kitajima I, Suganuma T, Murata F, Nagamatsu K. Ultrastructural demonstration of *Maclura pomifera* agglutinin bindings sites in the membranocystic lesions of membranous lipodystrophy (Nasu-Hakola disease). *Virchows Arch [A]* 1988; 413: 475–483
- Kitajima I, Kuriyama M, Usuki F, Izumo S, Osame M, Suganuma T, Murata F, Nagamatsu K. Nasu-Hakola disease (membranous lipodystrophy). Clinical, histopathological and biochemical studies of three cases. *J Neurol Sci* 1989; 91: 35–52
- Kobayashi K, Kobayashi E, Miyazu K, Muramori F, Hiramatsu S, Aoki T, Nakamura I, Koshino Y. Hypothalamic haemorrhage and thalamus degeneration in a case of Nasu-Hakola disease with hallucinatory symptoms and central hypothermia. *Neuropathol Appl Neurobiol* 2000; 26: 98–101

- Malandrini A, Scarpini C, Palmeri S, Villanova M, Parrotta E, Tripodi S, Giani S, DeFalco D, Guazzi GC. Palatal myoclonus and unusual MRI findings in a patient with membranous lipodystrophy. *Brain Dev* 1996; 18: 59–63
- Matsushita M, Oyanagi S, Hanawa S, Shiraki H, Kosaka K. Nasu-Hakola's disease (membranous lipodystrophy). A case report. *Acta Neuropathol (Berl)* 1981; 54: 89–93
- Mii Y, Miyauchi Y, Yoshikawa T, Honoki K, Aoki M, Tsutsumi M, Maruyama H, Funauchi M, Konishi Y, Tamai S. Ultrastructural lipid and glycoconjugate cytochemistry of membranous lipodystrophy (Nasu-Hakola disease). *Virchows Archiv [A]* 1991; 419: 137–142
- Minagawa M, Maeshiro H, Kato K, Shioda K. A rare case of leucodystrophy-neuroaxonal leucodystrophy (Seitelberger). *Psychiatry Neurol Jpn* 1980; 82: 488–503
- Minagawa M, Maeshiro H, Shioda K, Hirano A. membranous lipodystrophy (Nasu disease): clinical and neuropathological study of a case. *Clin Neuropathol* 1985; 4: 38–45
- Miyazu K, Kobayashi K, Fukutani Y, Nakamura I, Hasegawa H, Yamaguchi N, Saitoh T. Membranous lipodystrophy (Nasu-Hakola disease) with thalamic degeneration: report of an autopsied case. *Acta Neuropathol (Berl)* 1991; 82: 414–419
- Motohashi N, Shinohara M, Shioe K, Fukuzawa H, Akiyama Y, Kariya T. A case of membranous lipodystrophy (Nasu-Hakola disease) with unique MRI findings. *Neuroradiology* 1995; 37: 549–550
- Nasu T, Tsukahara Y, Terayama K. A lipid metabolic disease – “membranous lipodystrophy” – an autopsied case demonstrating numerous peculiar membrane-structures composed of compound lipid in bone and bone marrow and various adipose tissues. *Acta Pathol Jpn* 1973; 23: 539–558
- Oishi M, Mori N, Takasu T, Osaka S, Yamamoto M, Uchiyama T, Sawada S. Nasu-Hakola disease. A case accompanied by abnormalities in fatty acid composition of serum total lipids and amino acid analysis. *Acta Neurol (Napoli)* 1993; 15: 53–61
- Paloneva J, Kestilä M, Wu J, Salminen A, Böhling T, Ruotsalainen V, Hakola P, Bakker ABH, Phillips JH, Pekkarinen, Lanier LL, Timonen T, Peltonen L. Loss-of-function mutations in *TYROBP (DAP12)* result in a presenile dementia with bone cysts. *Nat Genet* 2000; 25: 357–361
- Paloneva J, Autti T, Raininko R, Partanen J, Salonen O, Puranen M, Hakola P, Haltia M. CNS manifestations of Nasu-Hakola disease. A frontal dementia with bone cysts. *Neurology* 2001; 56: 1552–1558
- Paloneva J, Manninen T, Christman G, Hovanes K, Mandelin J, Adolfsson R, Bianchin M, Bird T, Miranda R, Salmaggi A, Tranebjærg Y, Konttinen Y, Peltonen L. Mutations in two genes encoding different subunits of a receptor signaling complex results in an identical disease phenotype. *Am J Hum Genet* 2002; 71: 656–662
- Pekkarinen P, Hovatta I, Hakola P, Järvi O, Kestilä M, Lenkkeri U, Adolfsson R, Holmgren G, Nylander P-O, Tranebjærg L, Terwilliger JD, Lönnqvist J, Peltonen L. Assignment of the locus for PLO-SL, a frontal lobe dementia with bone cysts, to 19q13. *Am J Hum Genet* 1998; 62: 362–372
- Snow JL, Su WPD, Gibson LE. Lipomembranous (membranocystic) changes associated with morphea: a clinicopathologic review of three cases. *J Am Acad Dermatol* 1994; 31: 246–250
- Tanaka J. Leukoencephalopathic alteration in membranous lipodystrophy. *Acta Neuropathol (Berl)* 1980; 50: 193–197
- Tanaka J. Nasu-Hakola disease: a review of its leukoencephalopathic and membranolipodystrophic features. *Neuropathology* 2000; 20: S25–S29
- Ueki Y, Kohara N, Oga T, Fukuyama H, Akiguchi I, Kimura J, Shibasaki H. Membranous lipodystrophy presenting with palilalia: a PET study of cerebral glucose metabolism. *Acta Neurol Scand* 2000; 102: 60–64
- Verloes A, Maquet P, Sadzot B, Vivario M, Thiry A, Franck G. Nasu-Hakola syndrome: polycystic lipomembranous osteodysplasia with sclerosing leukoencephalopathy and presenile dementia. *J Med Genet* 1997; 34: 753–757
- Yagishita S, Ito Y, Sakai H, Amano N. Membranocystic lesions of the lung in Nasu-Hakola disease. *Virchows Arch [A]* 1985; 408: 211–217

76 Pigmentary Orthochromatic Leukodystrophy

- Belec L, Gray F, Louarn F, Gherardi R, Morelot D, Destée A, Poirier J, Castaigne P. Leucodystrophie orthochromatique pigmentaire. *Rev Neurol* 1988; 144: 347–357
- Constantinidis J, Wisniewski TM. The dominant form of the pigmentary orthochromatic leukodystrophy. *Acta Neuropathol (Berl)* 1991; 82: 483–487
- Dousset V, Tison F, Vital A, Henry P. Leucodystrophie orthochromatique d'évolution rapide chez l'adulte. *Rev Neurol* 1998; 154: 415–418
- Gray F, Destée A, Bourre J-M, Gherardi R, Krivosic I, Warot P, Poirier J. Pigmentary type of orthochromatic leukodystrophy (OLD); a new case with ultrastructural and biochemical study. *J Neuropathol Exp Neurol* 1987; 46: 585–596
- Knopman D, Sung JH, Davis D. Progressive familial leukodystrophy of late onset. *Neurology* 1996; 46: 429–434
- Marotti JD, Tobias S, Fratkin JD, Powers JM, Rhodes CH. Adult onset leukodystrophy with neuroaxonal spheroids and pigmented glia: report of a family, historical perspective, and review of the literature. *Acta Neuropathol (Berl)* 2004; 107: 481–488
- Oaked R, Matsuo T, Kawahara Y, Eishi Y, Tamai Y, Tanaka M, Kamaiki M, Tsubota N, Yamadera H. Adult pigment type (Pfeiffer) of sudanophilic leukodystrophy. Pathological and morphometrical studies on two autopsied cases of siblings. *Acta Neuropathol (Berl)* 1989; 78: 433–542
- Pietrini V, Tagliavini F, Pilleri G, Trabattini CR, Lechi A. Orthochromatic leukodystrophy with pigmented glial cells. An adult case with clinical-anatomical study. *Acta Neurol Scand* 1979; 59: 140–147
- Seiser A, Jellinger K, Brainin. Pigmentary type of orthochromatic leukodystrophy with early onset and protracted course. *Neuropediatrics* 1990; 21: 48–52
- Shannon P, Wherrett JR, Nag S. A rare form of adult onset leukodystrophy: orthochromatic leukodystrophy with pigmented glia. *Can J Neurol Sci* 1997; 24: 146–150
- Verghese J, Weidenheim K, Malik S, Rapin I. Adult onset pigmentary orthochromatic leukodystrophy with ovarian dysgenesis. *Eur J Neurol* 2002; 9: 663–670

77 Adult-onset Autosomal Dominant Leukoencephalopathies

- Abe K, Ikeda M, Watase K, Tanabe H, Fujimura H, Yorifuji S, Ueno S, Mezaki T, Mori T. A kindred of hereditary adult-onset leukodystrophy with sparing of the optic radiations. *Neuroradiology* 1993; 35: 281–283

- Bergui M, Bradac GB, Leombruni S, Vaula G, Quattrocchio G. MRI and CT in autosomal-dominant adult-onset leukodystrophy. *Neuroradiology* 1997; 39: 423–426
- Calandriello L, Matteucci C, Bertini E, Medolago Albani L, Antonelli A, Manfredi M, Pelladini G. Biopsy diagnosis of a case of adult onset orthochromatic leukodystrophy. Clinical and brain biopsy findings. *Ital J Neurol Sci* 1992; 13: 787–792
- Coffeen CM, McKenna C, Koeppe AH, Plaster NM, Maragakis N, Mihalopoulos J, Schwankhaus JD, Flanigan KM, Gregg RG, Ptáček LJ, Fu Y-H. Genetic localization of an autosomal dominant leukodystrophy mimicking chronic progressive multiple sclerosis to chromosome 5q31. *Hum Mol Genet* 2000; 9: 787–793
- Eldridge R, Anayiotos CP, Schlesinger S, Cowen D, Bever C, Patronas N, McFarland H. Hereditary adult-onset leukodystrophy simulating chronic progressive multiple sclerosis. *N Engl J Med* 1984; 311: 948–953
- Fukazawa T, Sasaki H, Kikuchi S, Hamada K, Hamada T, Tashiro K. Dominantly inherited leukodystrophy showing cerebellar deficits and spastic paraparesis: a new entity? *J Neurol* 1997; 244: 446–449
- Letournel F, Etcharry-Bouyx F, Verny C, Barthelaix A, Dubas F. Two clinicopathological cases of a dominantly inherited, adult onset orthochromatic leukodystrophy. *J Neurol Neurosurg Psychiatry* 2003; 74: 671–673
- Quattrocchio G, Leombruni S, Vaula G, Bergui M, Riva A, Bradac GB, Bergamini L. Autosomal dominant late-onset leukoencephalopathy. *Eur Neurol* 1997; 37: 53–61
- Schwankhaus JD, Patronas N, Dorwart R, Eldridge R, Schlesinger S, McFarland H. Computed tomography and magnetic resonance imaging in adult-onset leukodystrophy. *Arch Neurol* 1988; 45: 1004–1008
- Schwankhaus JD, Katz DA, Eldridge R, Schlesinger S, McFarland H. Clinical and pathological features of an autosomal dominant, adult-onset leukodystrophy simulating chronic progressive multiple sclerosis. *Arch Neurol* 1994; 51: 757–766
- Tagawa A, Ono S, Inoue K, Hosoi N, Kaneda K, Suzuki M, Nagao K, Shimizu N. A new familial adult-onset leukodystrophy manifesting as cerebellar ataxia and dementia. *J Neurol Sci* 2001; 183: 47–55
- Delves PJ, Roitt IM. The immune system. Part 1. *N Engl J Med* 2000; 343: 37–49
- Delves PJ, Roitt IM. The immune system. Part 2. *N Engl J Med* 2000; 343: 108–117
- Dopp JM, de Vellis J. Strategies for the therapeutic manipulation of cytokines and their receptors in inflammatory neurodegenerative diseases. *Ment Retard Dev Disabil Res Rev* 1998; 4: 200–211
- Ghirnikar RS, Lee YL, Eng LF. Inflammation in traumatic brain injury: role of cytokines and chemokines. *Neurochem Res* 1998; 23: 329–340
- Gonzalez-Scarano F, Tyler KC. Molecular pathogenesis of neurotropic viral infections. *Ann Neurol* 1987; 22: 565–574
- Gonzalez-Scarano F, Tyler KC. Molecular pathogenesis of neurotropic viral infections. *Ann Neurol* 1987; 22: 565–574
- Hartung H-P, Archelos JJ, Zielasek J, Gold R, Koltzenburg M, Reiners K-H, Toyka KV. Circulating adhesion molecules and inflammatory mediators in demyelination: a review. *Neurology* 1995; 45: S22–S32
- Hartung HP, Jung S, Stoll G, Zielasek J, Schmidt B, Archelos JJ, Toyka KV. Inflammatory mediators in demyelinating disorders of the CNS and PNS. *J Neuroimmunol* 1992; 40: 197–210
- Henson PM, Murphy RC, eds. Mediators of the inflammatory process. *Handbook of inflammation*, vol 6, 3rd ed. Amsterdam: Elsevier, 1989
- Johnson RT. Selective vulnerability of neural cells to viral infections. *Brain* 1980; 103: 447–472
- Johnson RT. The virology of demyelinating diseases. *Ann Neurol* 1994; 36: S54–S60
- Johnson RT, Mims CA. Pathogenesis of viral infections of the nervous system. *N Engl J Med* 1968; 278: 23–30
- Kieseier BC, Storch MK, Archelos JJ, Martino G, Hartung H-P. Effector pathways in immune mediated central nervous system demyelination. *Curr Opin Neurol* 1999; 12: 323–336
- Klein J, Sato A. The HLA system. First of two parts. *N Engl J Med* 2000; 343: 702–709
- Klein J, Sato A. The HLA system. Second of two parts. *N Engl J Med* 2000; 343: 782–786
- Kuroda Y, Shimamoto Y. Human tumor necrosis factor- α arguments experimental allergic encephalomyelitis in rats. *J Neuroimmunol* 1991; 34: 159–165
- Ledeen RW, Chakraborty G. Cytokines, signal transduction, and inflammatory demyelination: review and hypothesis. *Neurochem Res* 1998; 23: 277–289
- Lewis RA, Austen KF, Soberman RJ. Leukotrienes and other products of the 5-lipoxygenase pathway. *N Engl J Med* 1990; 323: 645–655
- Linington C, Morgan BP, Scolding NJ, Wilkins P, Pridleston S, Compston DAS. The role of complement in the pathogenesis of experimental allergic encephalomyelitis. *Brain* 1989; 112: 895–911
- Luster AD. Chemokines – chemotactic cytokines that mediate inflammation. *N Engl J Med* 1998; 388: 436–445
- MacMicking JD, Willenborg DO, Weidemann MJ, Rockett KA, Cowden WB. Elevated secretion of nitrogen and oxygen intermediates by inflammatory leukocytes in hyperacute experimental autoimmune encephalomyelitis: enhancement by the soluble products of encephalitogenic T cells. *J Exp Med* 1992; 176: 303–307
- Maimone D, Gregory S, Arnason BGW, Reder AT. Cytokine levels in the cerebrospinal fluid and serum of patients with multiple sclerosis. *J Neuroimmunol* 1991; 32: 67–74
- Matyszak MK. Inflammation in the CNS: balance between immunological privilege and immune response. *Prog Neurobiol* 1998; 56: 19–35

78 Inflammatory and Infectious Disorders

- Albert LJ, Inman RD. Molecular mimicry and autoimmunity. *N Engl J Med* 1999; 341: 2068–2074
- Beckman JS. The double edged role of nitric oxide in brain function and super-oxide mediated injury. *J Dev Physiol* 1991; 15: 53–59
- Bradl M, Flügel A. The role of T cells in brain pathology. *Prot Pathol Immune Respons CNS* 2002; 265: 141–162
- Coe-Clough N, Roth JA. *Understanding immunology*. London, Mosby, 1997
- Cuzner ML, Loughlin AJ, Mosley K, Woodroffe MN. The role of microglia macrophages in the processes of inflammatory demyelination and remyelination. *Neuropathol Appl Neurobiol* 1994; 20: 200–201
- Dak Canto M, Rabinowitz SG. Experimental models of virus-induced demyelination of the central nervous system. *Ann Neurol* 1982; 11: 109–127
- De Jong R, Brouwer M, Kuiper HM, Hooibrink B, Miedema F, van Lier RAW. Maturation and differentiation dependent responsiveness of human CD4⁺ T helper subsets. *J Immunol* 1992; 149: 2795–2801

- Mayatepek E, Hoffmann GF. Leukotrienes: biosynthesis, metabolism, and pathophysiologic significance. *Pediatr Res* 1995; 37: 1–9
- Merrill JE, Gerner RH, Myers LW, Ellison GW. Regulation of natural killer cell cytotoxicity by prostaglandin E in the peripheral blood and cerebrospinal fluid of patients with multiple sclerosis and other neurological diseases. *J Neuroimmunol* 1983; 4: 223–237
- Merrill JE, Strom SR, Ellison GW, Myers LW. In vitro study of mediators of inflammation in multiple sclerosis. *J Clin Immunol* 1989; 9: 84–96
- Mims CA, Nash A, Stephen J. MIMS pathogenesis of infectious disease, 5th ed. London: Academic Press, 2000
- Powrie F, Coffman RC. Cytokine regulation of T-cell function: potential for therapeutic intervention. *Immunol Today* 1993; 14: 270–276
- Starzl TE, Zinkernagel RM. Antigen localization and migration in immunity and tolerance. *N Engl J Med* 1998; 339: 1905–1913
- Von Andrian UH, Mackay CR. T-Cell function and migration. Two sides of the same coin. *N Engl J Med* 2000; 14: 1020–1034
- Walport MJ. Complement. First of two parts. *N Engl J Med* 2001; 344: 1058–1066
- Walport MJ. Complement. Second of two parts. *N Engl J Med* 2001; 344: 1140–1144
- Weiner LP, Johnson RT, Herndon RM. Viral infections and demyelinating diseases. *N Engl J Med* 1973; 288: 1103–1110
- Whitley RJ. Viral encephalitis. *N Engl J Med* 1990; 323: 242–250
- Wright SA, Unkeless JC. Innate immunity. Fatal attraction: recognition and killing mechanisms of innate immunity. *Curr Opin Immunol* 1993; 5: 57–61
- Barkhof F, Filippi M, van Waesberghe JHTM, Campi A, Miller DH, Adèr HJ. Interobserver agreement for diagnostic MRI criteria in suspected multiple sclerosis. *Neurology* 1999; 41: 347–350
- Barkhof F, Karas GB, van Walderveen MAA. T1 Hypointensities and axonal loss. *Neuroimaging Clin N Am* 2000; 10: 739–752
- Barkhof F, Rocca M, Francis G, van Waesberghe J-HTM, Uitend Haag BMJ, Hommes OR, Hartung H-P, Durelli L, Edan G, Fernández O, Seeldrayer P, Sørensen P, Margrie S, Rovaris M, Comi G, Filippi M. Validation of diagnostic magnetic resonance imaging criteria for multiple sclerosis and response to interferon β 1a. *Ann Neurol* 2003; 53: 718–724
- Barkhof F, van Waesberghe J-HTM, Filippi M, Yousry T, Miller DH, Hahn D, Thompson AJ, Kappos L, Brex P, Pozzilli C, Polman CH. T1 Hypointense lesions in secondary progressive multiple sclerosis: effect of interferon beta-1b treatment. *Brain* 2001; 124: 1396–1402
- Barkhof F, van Walderveen M. Characterization of tissue damage in multiple sclerosis by nuclear magnetic resonance. *Phil Trans R Soc Lond B* 1999; 354: 1675–1686
- Barkhof F. Imaging of remyelination. *Mult Scler* 1997; 3: 129–132
- Barkhof F. The clinico-radiological paradox in multiple sclerosis revisited. *Curr Opin Neurol* 2002; 15: 239–245
- Barnes G, Benjamin S, Bowen JD, Cutter N, de Lateur BJ, Dietrich WD, Dowling MM, Griffin JW, Hummers L, Irani D, Jorens J, Kaplin AI, Kratz JD, Kerr DA, Krishnan C, Lacey CE, Lucchinetti C, Lynn DJ, Manler RN, McArthur JC, McDonald JW III, Morrison L, Pardo-Villamizar C, Pidcock FS, Ransohoff R, Roos KL, Trovato MK, Vollmer TL, Wegener ST, Weinschenker BG, Wingerchuck DM. Proposed diagnostic criteria and nosology of acute transverse myelinitis. *Neurology* 2002; 59: 499–505
- Beer S, Rösler KM, Hess CW. Diagnostic value of paraclinical tests in multiple sclerosis: relative sensitivities and specificities for reclassification according to the Poser committee criteria. *J Neurol Neurosurg Psychiatry* 1995; 59: 152–159
- Belassy C, Bernert G, Wöber-Bingöl C, Csapó B, Kornek B, Széles J, Fleischmann D, Prayer D. Long-term MRI observations of childhood-onset relapsing-remitting multiple sclerosis. *Neuropediatrics* 2001; 32: 28–37
- Berger T, Rubner P, Schautzer F, Egg R, Ulmer H, Mayringer I, Dilitz E, Deisenhammer F, Reindl M. Antimyelin antibodies as a predictor of clinically definite multiple sclerosis after a first demyelinating event. *N Engl J Med* 2003; 349: 139–145
- Bergers E, Bot JCJ, van der Valk P, Castelijns JA, Lycklama A, Nijeholt GJ, Kamphorst W, Polman CH, Blezer EIA, Nicolay K, Ravid R, Barkhof F. Diffuse signal abnormalities in the spinal cord in multiple sclerosis: direct postmortem in situ magnetic resonance imaging correlated with in vitro high resolution magnetic resonance imaging and histopathology. *Ann Neurol* 2002; 41: 652–656
- Bitsch A, Bruhn H, Vougioukas V, Stringaris A, Lassmann H, Frahm J, Brück W. Inflammatory CNS demyelination: histopathologic correlation with in vivo quantitative proton MR spectroscopy. *AJNR Am J Neuroradiol* 1999; 20: 1619–1627
- Bjartmar C, Kidd G, Mörk S, Ruddick R, Trapp BD. Neurological disability correlates with spinal cord axonal loss and reduced N-acetyl aspartate in chronic multiple sclerosis patients. *Ann Neurol* 2000; 48: 893–901
- Bjartmar C, Kinkel RP, Kidd G, Rudick RA, Trapp BD. Axonal loss in normal-appearing white matter in a patient with acute MS. *Neurology* 2001; 57: 1248–1252
- Achiron A, Gabbay U, Gilad R, Hassin-Baer S, Barak Y, Gornish M, Elizur A, Goldhammer Y, Sarova-Pinhas I. Intravenous immunoglobulin treatment in multiple sclerosis. Effect on relapses. *Neurology* 1998; 50: 398–402
- Álvarez-Lafuente R, Martín-Estefanía C, de las Heras V, Castrillo C, Picazo JJ, Varela de Seijas E, González RA. Active human herpesvirus 6 infection in patients with multiple sclerosis. *Arch Neurol* 2002; 59: 929–933
- Arnold DL, Wolinsky JS, Matthews PM, Falini A. The use of magnetic resonance spectroscopy in the evaluation of the natural history of multiple sclerosis. *J Neurol Neurosurg Psychiatry* 1998; 64: S94–S101
- Barcellos LF, Klitz W, Field LL, Tobias R, Bowcock AM, Wilson R, Nelson MP, Nagotomi J, Thomson G. Association mapping of disease loci using a pooled DNA genomic screen. *Am J Hum Genet* 1997; 61: 734–747
- Barkhof F, Brück W, de Groot CJA, Bergers E, Hulshof S, Geurts J, Polman CH, van der Valk P. Remyelinated lesions in multiple sclerosis. Magnetic resonance image appearance. *Arch Neurol* 2003; 60: 1073–1081
- Barkhof F, Brück W, de Groot JA, Bergers E, Hulshof S, Geurts J, Olman CH, van der Valk P. Remyelinated lesions in multiple sclerosis. *Arch Neurol* 2003; 60: 1073–1081
- Barkhof F, Filippi M, Miller DH, Scheltens P, Campi A, Polman CH, Comi G, Adèr HJ, Losseff N, Valk J. Comparison of MRI criteria at first presentation to predict conversion to clinically definite multiple sclerosis. *Brain* 1997; 120: 2059–2069

79 Multiple Sclerosis

- Bjartmar C, Trapp BD. Axonal and neuronal degeneration in multiple sclerosis: mechanisms and functional consequences. *Curr Opin Neurol* 2001; 14: 271–278
- Bjartmar C, Wujek JR, Trapp BD. Axonal loss in the pathology of MS: consequences for understanding the progressive phase of the disease. *J Neurol Sci* 2003; 206:165–171
- Bö L, Vedeler CA, Nyland HI, Trapp BD, Mørk SJ. Subpial demyelination in the cerebral cortex of multiple sclerosis patients. *J Neuropathol Exp Neurol* 2003; 62: 723–732
- Bö L, Geurts JJ, Ravid R, Barkhof F. Magnetic resonance imaging as a tool to examine the neuropathology of multiple sclerosis. *Neuropathol Appl Neurobiol* 2004; 30: 106–117
- Boonetti B, Raine CS. Multiple sclerosis: oligodendrocytes display cell death-related molecules in situ but do not undergo apoptosis. *Ann Neurol* 1997; 42: 74–84
- Bot JC, Barkhof F, Lycklama à Nijeholt G, van Schaardenburg D, Voskuyl AE, Ader HJ, Pijnenburg JA, Polman CH, Uitdehaag BM, Vermeulen EG, Castelijns JA. Differentiation of multiple sclerosis from other inflammatory disorders and cerebrovascular disease: value of spinal MR imaging. *Radiology* 2002; 223: 46–56
- Bot JC, Barkhof F, Lycklama à Nijeholt GJ, Bergers E, Polman CH, Ader HJ, Castelijns JA. Comparison of a conventional cardiac-triggered dual spin-echo and a fast STIR sequence in detection of spinal cord lesions in multiple sclerosis. *Eur Radiol* 2000; 10: 753–758
- Bot JC, Barkhof F, Lycklama à Nijeholt G, van Schaardenburg D, Voskuyl AE, Ader HJ, Pijnenburg JAL, Polman CH, Uitdehaag BMJ, Vermeulen EGJ, Castelijns JA. Differentiation of multiple sclerosis from other inflammatory disorders and cerebrovascular disease: value of spinal MR imaging. *Radiology* 2002; 223: 46–56
- Brex PA, Miszkil KA, O'Riordan JI, Plant GT, Moseley IF, Thompson AJ, Miller DH. Assessing the risk of early multiple sclerosis in patients with clinically isolated syndromes: the role of a follow-up MRI. *J Neurol Neurosurg Psychiatry* 2001; 70: 390–393
- Buljevac D, Flach HZ, Hop WCJ, Hijdra D, Laman JD, Savekoul HFJ, van der Meché FGA, van Doorn PA, Hintzen RQ. Prospective study on the relationship between infections and multiple sclerosis exacerbations. *Brain* 2002; 125: 952–960
- Caramia F, Pantano P, di Legge S, Piattella MC, Lenzi D, Paolillo A, Nucciarelli W, Lenzi GL, Bozzao L, Pozzilli C. A longitudinal study of MR diffusion changes in normal appearing white matter of patients with early multiple sclerosis. *Magn Reson Imaging* 2002; 20: 383–388
- Caracciolo JT, Murtagh RD, Rojiani AM, Murtagh FR. Pathognomonic MR imaging findings in Baló concentric sclerosis. *AJNR Am J Neuroradiol* 2001; 22: 292–293
- Chard DT, Griffin CM, McLean MA, Kapeller P, Kapoor R, Thompson AJ, Miller DH. Brain metabolite changes in cortical gray and normal-appearing white matter in clinically early relapsing-remitting multiple sclerosis. *Brain* 2002; 125: 2342–2352
- Ciccarelli O, Giugni E, Paolilo A, Mainero C, Gasperini C, Bastianello S, Pozzelli. Magnetic resonance outcome of new enhancing lesions in patients with relapsing-remitting multiple sclerosis. *Eur J Neurol* 1999; 6: 455–459
- Comi G, Filippi M, Wolinsky JS. European/Canadian multicenter, double-blind, randomized, placebo-controlled study of the effects of glatiramer acetate on magnetic resonance imaging – measured disease activity and burden in patients with relapsing multiple sclerosis. *Ann Neurol* 2001; 49: 290–297
- Confavreux C, Vukusic S, Moreau T, Adelaine P. Relapses and progression of disability in multiple sclerosis. *N Engl J Med* 2000; 343: 1430–1438
- Cossins JA, Clements JM, Ford J, Miller KM, Pigott R, Vos W, van der Valk P, de Groot CJA. Enhanced expression of MMP-7 and MMP-9 in demyelinating multiple sclerosis lesions. *Acta Neuropathol (Berl)* 1997; 94: 590–598
- Dalton CM, Brax PA, Miszkil KA, Hickman SJ, MacManus DG, Plant GT, Thompson AJ, Miller DH. Application of the new McDonald criteria to patients with clinically isolated syndromes suggestive of multiple sclerosis. *Ann Neurol* 2002; 52: 47–53
- Dalton CM, Brex PA, Mitzkiel KA, Fernando K, MacManus DG, Plant GT, Thompson AJ, Miller DH. New T2 lesions enable an earlier diagnosis of multiple sclerosis in clinically isolated syndromes. *Ann Neurol* 2003; 53: 673–676
- Degaonkar NM, Jayasundar R, Jagannathan NR. Sequential diffusion-weighted magnetic resonance study of lysophosphatidyl choline-induced experimental demyelinating lesion: an animal model of multiple sclerosis. *J Magn Reson Imaging* 2002; 16: 153–159
- De Groot CJA, Bergers E, Kamphorst W, Ravid R, Polman CH, Barkhof F, van der Valk P. Post-mortem MRI-guided sampling of multiple sclerosis brain lesions. Increased yield of active demyelinating and (p)reactive lesions. *Brain* 2001; 124: 1635–1645
- De Seze J, Stojkovic T, Ferriby D, Gauvrit JY, Montagne C, Mounier-Vehier F, Verier A, Pruvo JP, Hache JC, Vermersch P. Devic's neuromyelitis optica: clinically, laboratory, MRI and outcome profile. *J Neurol Sci* 2002; 197: 57–61
- De Stefano N, Narayanan S, Francis GS, Arnaoutelis R, Tartaglial MC, Antel JP, Matthews PM, Arnold DL. Evidence of axonal damage in the early stages of multiple sclerosis and its relevance to disability. *Arch Neurol* 2001; 58: 65–70
- Dhib-Jablit S. Glatiramer acetate (Copaxone) therapy for multiple sclerosis. *Pharmacol Ther* 2003; 98: 245–255
- Dyment DA, Cader MZ, Willer CJ, Risch N, Sadovnick AD, Ebers GC. A multigenerational family with multiple sclerosis. *Brain* 2002; 125: 1474–1482
- Ebers GC. Treatment of multiple sclerosis. *Lancet* 1994; 343: 275–279
- Epplen C, Jäckel S, Santos EJM, D'Souza M, Poehla D, Dortzauer B, Sindern E, Haupts M, Rüde K-P, Weber F, Stöver J, Poser S, Gehler W, Malin J-P, Przuntek H, Epplen JT. Genetic predisposition to multiple sclerosis as revealed by immunoprinting. *Ann Neurol* 1997 41: 341–352
- Filippi M. In-vivo tissue characterization of multiple sclerosis and other white matter diseases using magnetic resonance based techniques. *J Neurol* 2001; 248: 1019–1029
- Filippi M, Rocca MA. Disturbed functional and plasticity in multiple sclerosis as gleaned from functional magnetic resonance imaging. *Curr Opin Neurol* 2003; 16: 275–282
- Filippi M, Dousset V, McFarland HF, Miller DH, Grossman RI. Role of magnetic resonance imaging in the diagnosis and monitoring of multiple sclerosis: consensus report of the white matter study group. *J Magn Reson Imaging* 2002; 15: 499–504
- Filippi M, Bozzali M, Rovaris M, Gonen O, Kesavadas C, Ghezzi A, Martinelli V, Grossman RI, Scotti G, Comi G, Falini A. Evidence for widespread axonal damage at the earliest clinical stage of multiple sclerosis. *Brain* 2003; 126: 433–437
- Finsen B, Antel J, Owens T. TNF α : kill or cure for demyelinating disease? *Mol Psychiatry* 2002; 7: 820–821

- Fisher E, Rudick RA, Simon JH, Cutter G, Baier M, Lee J-C, Miller D, Weinstock-Guttman B, Mass MK, Dougherty DS, Simonian NA. Eight-year follow-up study of brain atrophy in patients with MS. *Neurology* 2002; 59: 1412–1420
- Frederiksen JL. Bilateral acute optic neuritis: prospective clinical, MRI, CSF, neurophysiological and HLA findings. *Neuroophthalmology* 1997; 17: 175–183
- Gasparini C, Pozzilli C, Bastianello S, Koudriavsteva T, Galgani S, Millefiorini E, Paolillo A, Horsfield MA, Bozzao L, Fieschi C. Effect of steroids on Gd-enhancing lesions before and during recombinant beta interferon 1a treatment in relapsing remitting multiple sclerosis. *Neurology* 1998; 50: 403–406
- Ghorpade A, Holter S, Borgmann K, Persidsky R, Wu L. HIV-1 and IL-1 β regulate Fas ligand expression in human astrocytes through the NF-B pathway. *J Neuroimmunol* 2003; 141: 141–149
- Giovannoni G, Lai M, Thorpe J, Kidd D, Chamoun V, Thompson AJ, Miller DH, Feldmann M, Thompson EJ. Longitudinal study of soluble adhesion molecules in multiple sclerosis: correlation with gadolinium enhanced magnetic resonance imaging. *Neurology* 1997; 48: 1557–1565
- Glasier CM, Robbins MB, Davis MB, Davis PC, Ceballos E, Bates SR. Clinical, neurodiagnostic, and MR findings in children with spinal and brain stem multiple sclerosis. *AJNR Am J Neuroradiol* 1995; 16: 87–95
- Gold R, Lington C. Devic's disease: bridging the gap between laboratory and clinic. *Brian* 2002; 125: 1425–1427
- Gonen O, Moriarty DM, Li BSY, Babb JS, He J, Listerud J, Jacobs D, Markowitz CE, Grossman RI. Relapsing-remitting multiple sclerosis and whole-brain N-acetylaspartate measurement: evidence for different clinical cohorts – initial observations. *Radiology* 2002; 255: 261–268
- Goodin DS, Arnason BG, Coyle PK, Frohman EM, Paty DW. The use of mitoxantrone (Novantrone) for the treatment of multiple sclerosis. *Neurology* 2003; 61: 1332–1338
- Goodin DS, Arnason BG, Coyle PK, Frohman EM, Paty DW; Therapeutics and Technology Assessment Subcommittee of the American Academy of Neurology. The use of mitoxantrone (Novantrone) for the treatment of multiple sclerosis: report of the Therapeutics and Technology Assessment Subcommittee of the American Academy of Neurology. *Neurology* 2003; 61: 1332–1338
- Halfpenny C, Benn T, Scolding N. Cell transplantation, myelin repair, and multiple sclerosis. *Lancet [Neurol]* 2002; 1: 31–40
- Hartung H-P. Pathogenesis of inflammatory demyelination: implications for therapy. *Curr Opin Neurol* 1995; 8: 191–199
- He J, Grossman RI, Ge Y, Mannon LJ. Enhancing patterns in multiple sclerosis: evolution and persistence. *AJNR Am J Neuroradiol* 2001; 22: 664–669
- Hermans G, Stinissen P, Hauben L, van den Berg-Loonen E, Raus J, Zhang J. Cytokine profile of myelin basic protein reactive T cells in multiple sclerosis and healthy individuals. *Ann Neurol* 1997; 42: 18–27
- Herrera BM, Ebers GC. Progress in deciphering the genetics of multiple sclerosis. *Curr Opin Neurol* 2003; 16: 253–258
- Horsfield MA, Barker GJ, Barkhof F, Miller DH, Thompson AJ, Filippi M. Guidelines for using quantitative magnetization transfer resonance imaging for monitoring treatment of multiple sclerosis. *J Magn Reson Imaging* 2003; 17: 389–397
- Iannucci G, Rovaris M, Giacomotti L, Comi G, Filippi M. Correlation of multiple sclerosis measures derived from T2-weighted, T1-weighted, magnetization transfer, and diffusion tensor MR imaging. *AJNR Am J Neuroradiol* 2001; 22: 1462–1467
- Ibrahim SM, Mix E, Böttcher T, Koczan D, Gold R, Rolfs A, Thiesen H-J. Gene expression profiling of the nervous system in murine experimental autoimmune encephalitis. *Brain* 2001; 124: 1927–1938
- Jacobs JD, Cookfair DL, Rudick RA, Herndon RM, Richert JR, Salazar AM, Fischer JS, Goodkin DE, Granger CV, Simon JH, Alam JJ, Bartozak DM, Bourdette DN, Brainam J, Brownschidle CM, Coats ME, Cohan SL, Dougherty DS, Kinkel RP, Mass MK, Munschauer FE, Priore RL, Pullicino PM, Scherokman BJ, Weinstock-Guttman B, Whitham RH. Intramuscular interferon beta-1a for disease progression in relapsing multiple sclerosis. *Ann Neurol* 1996; 39: 285–294
- Jacobsen M, Schweer D, Ziegler A, Gaber R, Schock S, Schwitzer R, Wonigeit K, Lindert R-B, Kantarci O, Schaefer-Klein J, Schipper HI, Oertel WH, Heidenreich F, Weinschenker BG, Sommer N, Hemmer B. A point mutation in *PTPRC* is associated with the development of multiple sclerosis. *Nat Genet* 2000; 26: 495–499
- Johnson KP, Brooks BR, Cohen JA, Ford CC, Goldstein J, Lisak RP, Myers LW, Panitch HS, Rose JW, Schiffer RB, Vollmer T, Weiner LP, Wolinsky JS. Copolymer 1 reduces relapse rate and improves disability in relapsing-remitting multiple sclerosis: results of a phase III multicenter, double-blind, placebo-controlled trial. *Neurology* 1995; 45: 1268–1276
- Johnson KP, Brooks BR, Ford CC, Goodman A, Guarnaccia J, Lisak RP, Myers LW, Panitch HS, Pruitt A, Rose JW, Kachuck N, Wolinsky JS. Sustained clinical benefits of glatiramer acetate in relapsing multiple sclerosis patients observed for 6 years. *Mult Scler* 2000; 6: 255–266
- Kalkers NF, Bergers E, Castelijns JA, van Walderveen MAA, Bot JCJ, Adèr HJ, Polman CH, Barkhof F. Optimizing the association between disability and biological markers in MS. *Neurology* 2001; 57: 1253–1258
- Kapeller P, McLean MA, Griffin CM, Chard D, Parker GJM, Barker GJ, Thompson AJ, Miller DH. Preliminary evidence for neuronal damage in cortical grey matter and normal appearing white matter in short duration relapsing-remitting multiple sclerosis: a quantitative MR spectroscopic imaging study. *J Neurol* 2001; 248: 131–138
- Kappos L, Moeri D, Radue EW, Schoetzau A, Schweikert K, Barkhof F, Miller D, Guttman CR, Weiner HL, Gasparini C, Filippi M. Predictive value of gadolinium-enhanced magnetic resonance imaging for relapse rate and changes in disability or impairment in multiple sclerosis: a meta-analysis. *Gadolinium MRI Meta-analysis Group. Lancet* 1999; 353: 964–969
- Karaarslan E, Altintas A, Senol U, Yeni N, Dincer A, Bayindir C, Karaagac N, Siva A. Baló's concentric sclerosis: clinical and radiologic features of five cases. *AJNR Am J Neuroradiol* 2001; 22: 1362–1367
- Killestein J, Kalkers NF, Meilof JF, Barkhof F, van Lier RA, Polman CH. TNF α production by CD4(+) T cells predicts long-term increase in lesion load on MRI in MS. *Neurology* 2001; 57: 1129–1131
- Killestein J, Eikelenboom MJ, Izeboud T, Kalkers NF, Ader HJ, Barkhof F, van Lier RA, Uitdehaag SM, Polman CH. Cytokine producing CD8+ T cells are correlated to MRI features of tissue destruction in MS. *J Neuroimmunol* 2003; 142: 141–148
- Kornek B, Bernert G, Balassy C, Geldner J, Prayer D, Feucht M. Glatiramer acetate treatment in patients with acute childhood and juvenile onset multiple sclerosis. *Neuropediatrics* 2003; 34: 120–126
- Kotil K, Kalayci M, Köseoğlu T, Tuğrul A. Myelinoclastic diffuse sclerosis (Schilder's disease): a report of a case and review of the literature. *Br J Neurosurg* 2002; 16: 516–519
- Lassmann H. Neuropathology in multiple sclerosis: new concepts. *Multiple Sclerosis* 1998; 4: 93–98

- Lassmann H, Bruck W, Lucchinetti C. Heterogeneity of multiple sclerosis pathogenesis: implications for diagnosis and therapy. *Trends Mol Med* 2001; 7: 115–121
- Li BSY, Regal J, Soher BJ, Mannon LJ, Grossman RI, Gonen O. Brian metabolite profiles of T1-hypointense lesions in relapsing-remitting multiple sclerosis. *AJNR Am J Neuroradiol* 2003; 24: 68–74
- Loevner LA, Grossman RI, Cohen JA, Lexa FJ, Kessler D, Kolson DL. Microscopic disease in normal-appearing white matter on conventional MR images in patients with multiple sclerosis: assessment with magnetization-transfer measurements. *Radiology* 1995; 196: 511–515
- Lublin FD, Reingold SC. Defining the clinical course of multiple sclerosis: results of an international study. *Neurology* 1996; 46: 907–911
- Lucchinetti CF, Rodriguez M. The controversy surrounding the pathogenesis of the multiple sclerosis lesion. *Mayo Clin Proc* 1997; 72: 665–678
- Lucchinetti CF, Mandler RN, McGavern D, Bruck W, Gleich G, Ransohoff RM, Trebst C, Weinschenker B, Wingerchuck D, Parisi JE, Lassmann H. A role for humoral mechanisms in the pathogenesis of Devic's neuromyelitis optica. *Brain* 2002; 125: 1450–1461
- Lycklama à Nijeholt GJ, Thompson A, Filippi M, Miller D, Polman C, Fazekas F, Barkhof F. Spinal-cord MRI in multiple sclerosis. *Lancet Neurol* 2003; 2: 555–562
- Lycklama à Nijeholt GJ, Barkhof F, Castelijns JA, Van Waesberghe JHTM, Valk J, Jongen PJH, Hommes OR. Comparison of two MR sequences for the detection of multiple sclerosis lesions in the spinal cord. *AJNR Am J Neuroradiol* 1996; 17: 1533–1538
- Lycklama à Nijeholt GJ, van Walderveen MAA, Castelijns JA, van Waesberghe JHTM, Polman C, Scheltens P, Rosier PFWM, Jongen PJH, Barkhof F. Brain and spinal cord abnormalities in multiple sclerosis. Correlation between MRI parameters, clinical subtypes and symptoms. *Brain* 1998; 121: 687–697
- Lycklama à Nijeholt GJ, Bergers E, Kamphorst W, Bot J, Nicolay K, Castelijns JA, van Waesberghe JHTM, Ravid R, Polman CH, Barkhof F. Post-mortem high-resolution MRI of the spinal cord in multiple sclerosis. A correlative study with conventional MRI, histopathology and clinical phenotype. *Brain* 2001; 124: 154–166
- Mader I, Roser W, Kappos L, Hagberg G, Seelig J, Radue EW, Steinbrich W. Serial proton MR spectroscopy of contrast-enhancing multiple sclerosis plaques: absolute metabolic values over 2 years during a clinical pharmacological study. *AJNR Am J Neuroradiol* 2000; 21: 1220–1227
- Mader I, Seeger U, Weissert R, Klose U, Naegle T, Melms A, Grodd W. Proton MR spectroscopy with metabolite-nulling reveals elevated macromolecules in acute multiple sclerosis. *Brain* 2001; 124: 953–961
- Martino G, Adorini L, Rieckmann P, Hillerts J, Kallmann B, Comi G, Filippi M. Inflammation in multiple sclerosis: the good, the bad and the complex. *Lancet [Neurol]* 2002; 1: 499–509
- Masden JC, Quinto C, Olivera C, Tenner M, Leslie D, Visintainer P. Open-ring imaging sign. *Neurology* 2000; 54: 1427–1433
- Masden JC, Quinto C, Olivera C, Tenner M, Leslie D, Visintainer P. Open-ring imaging sign. Highly specific for atypical brain demyelination. *Neurology* 2000; 54: 1427–1433
- McAdam LC, Blaser SI, Banwell BL. Pediatric tumefactive demyelination: case series and review of the literature. *Pediatr Neurol* 2002; 26: 18–25
- McDonald WI, Ron MA. Multiple sclerosis: the disease and its manifestations. *Phil Trans R Soc Land B* 1999; 354: 1615–1622
- McDonald WI, Compston A, Edan G, Goodkin D, Hartung H-P, Lublin FD, McFarland HF, Paty DW, Polman CH, Reingold SC, Sandberg-Wolheim M, Sibley W, Thompson A, van der Noort S, Weinshenker BY, Wolinsky JS. Recommended diagnostic criteria for multiple sclerosis: guidelines from the International Panel on the diagnosis of multiple sclerosis. *Ann Neurol* 2001; 50: 121–127
- Medena IM, Esiri MM. Axonal damage: a key predictor of outcome in human CNS diseases. *Brain* 2003; 126: 515–530
- Merimsky O, Reider I, Merimsky E, Chaitchik S. Interferon-related leukoencephalopathy in a patient with renal cell carcinoma. *Tumori* 1991; 77: 361–362
- Miller DH, Khan OA, Sheremata WA, Blumhardt LD, Rice GP, Libonati MA, Willmer-Hulme AJ, Dalton CM, Mischke KA, O'Connor PW. A controlled trial of natalizumab for relapsing multiple sclerosis. *N Engl J Med* 2003; 348: 15–23
- Milligan NM, Newcombe R, Compston DAS. A double-blind controlled trial of high dose methylprednisolone in patients with multiple sclerosis: 1. clinical effects. *J Neurol Neurosurg Psychiatry* 1987; 50: 511–516
- Molyneux PD, Tubridy N, Parker GJM, MacManus DG, Tofts PS, Moseley IF, Miller DH. The effect of section thickness on MR lesions detection and quantification in multiple sclerosis. *AJNR Am J Neuroradiol* 1998; 19: 1715–1720
- Muraro PA, Cassiani R, Ingoni RC, Martin R. Hematopoietic stem cell transplantation for multiple sclerosis: current status and future challenges. *Curr Opin Neurol* 2003; 16: 299–305
- Neumann H. Molecular mechanisms of axonal damage in inflammatory central nervous system diseases. *Curr Opin Neurol* 2003; 16: 267–273
- Noseworthy JH, Gold R, Hartung H-P. Treatment of multiple sclerosis: recent trails and future perspectives. *Curr Opin Neurol* 1999; 12: 279–293
- Pathy DW, Arnold DL. The lesions of multiple sclerosis. *N Engl J Med* 2002; 346: 199–200
- Pathy DW, Oger JF, Kastrukoff LF, Hashimoto SA, Hooge JP, Eisen AA, Eisen KA, Purves SJ, Low MD, Brandeys V, Robertson WD, Li DKB. MRI in the diagnosis of MS: a prospective study with comparison of clinical evaluation, evoked potentials, oligoclonal banding, and CT. *Neurology* 1988; 38: 180–185
- Peterson JW, Bo L, Mork S, Chang A, Trapp BD. Transected neurites, apoptotic neurons, and reduced inflammation in cortical multiple sclerosis lesions. *Ann Neurol* 2001; 50: 389–400
- Polman CH, Hartung H-P. The treatment of multiple sclerosis: current and future. *Curr Opin Neurol* 1995; 8: 200–209
- Poppe M, Bruck W, Hahn G, Weissbrich B, Heubner G, Goebel HH, Todt H. Fulminant course in a case of diffuse myelinoclastic encephalitis— a case report. *Neuropediatrics* 2001; 32: 41–44
- Poser CM. The pathogenesis of multiple sclerosis: a commentary. *Clin Neurol Neurosurg* 2000; 102: 191–194
- Poser CM, Brinar VV. Diagnostic criteria for multiple sclerosis. *Clin Neurol Neurosurg* 2001; 103: 1–11
- Pretorius M-L, Looock DB, Ravenscroft A, Schoeman JF. Demyelinating disease of Schilder type in three young South African children: dramatic response to corticosteroids. *J Child Neurol* 1998; 13: 197–201
- Pretorius PM, Quaghebeur G. The role of MRI in the diagnosis of MS. *Clin Radiol* 2003; 58: 434–448
- Rieckman P, Altenhofen B, Riegel A, Baudewig J, Felgenhauer K. Soluble adhesion molecules (sVCAM-1 and sICAM-1) in cerebrospinal fluid and serum correlate with MRI activity in multiple sclerosis. *Ann Neurol* 1997; 41: 326–333

- Rovaris M, Bozzali M, Iannucci G, Ghezzi A, Caputo D, Montanari E, Bertolotto A, Bergamaschi R, Capra R, Mancardi GL, Martinelli V, Comi G, Filippi M. Assessment of normal-appearing white and gray matter in patients with primary progressive multiple sclerosis diffusion – tensor magnetic resonance imaging study. *Arch Neurol* 2002; 59: 1406–1412
- Rudick RA, Goodkin DE, Jacobs LD, Cookfair DL, Herndon RM, Richert JR, Salazar AM, Fisher JS, Granger CV, Simon JH, Alam JJ, Simonian NA, Campion MK, Bartosak DM, Bourdette DN, Braimain J, Brownschidle CM, Coats ME, Cohand SL, Dougherty DS, Kinkel RP, Mass MK, Munschauer RL, Pullicino PM, Scherokman BJ, Weistock-Guttman BJ, Whitham RH. Impact of interferon beta-1a on neurologic disability in relapsing multiple sclerosis. *Neurology* 1997; 49: 358–363
- Sarchielli P, Presciutti O, Pelliccioli GP, Tarducci R, Gobbi G, Chiarini P, Alberti A, Vicinanza F, Gallai V. Absolute quantification of brain metabolites by proton magnetic resonance spectroscopy in normal appearing white matter of multiple sclerosis patients. *Brain* 1999; 122: 513–521
- Sarchielli P, Presciutti O, Tarducci R, Gobbi G, Alberti A, Pelliccioli GP, Chiarini P, Gallai V. Localized ¹H magnetic resonance spectroscopy in mainly cortical gray matter of patients with multiple sclerosis. *J Neurol* 2002; 249: 902–910
- Sawcer S, Compston A. The genetic analysis of multiple sclerosis in Europeans: concepts and design. *J Neuroimmunol* 2003; 143: 13–16
- Scarlsbrick IA, Blaber SI, Luncheon CF, Genain CP, Blaber M, Rodriguez M. Activity of a newly identified serine protease in CNS demyelination. *Brain* 2002; 125: 1283–1296
- Schapiro RT, Langer SL. Symptomatic therapy of multiple sclerosis. *Curr Opin Neurol* 1994; 7: 229–233
- Schönrock LM, Kuhlmann T, Adler S, Bitsch A, Brück W. Identification of glial cell proliferation in early multiple sclerosis lesions. *Neuropathol Appl Neurobiol* 1998; 24: 320–330
- Scully RE, Mark EJ, McNeely WF, Ebeling SH. Case 26–1998. *N Engl J Med* 1998; 339: 542–549
- Shields DC, Banik NL. Pathophysiological role of calpain in experimental demyelination. *J Neurosci Res* 1999; 55: 533–541
- Silver N, Lai M, Symms M, Barker G, McDonald I, Miller D. Serial gadolinium-enhanced and magnetization transfer imaging to investigate the relationship between the duration of blood–brain barrier disruption and extent of demyelination in new multiple sclerosis lesions. *J Neurol* 1999; 246: 728–730
- Šišková D, Hadač J. Multiple sclerosis in children. *Eur J Paediatr Neurol* 1999; 3: A82
- Smith KJ, Hall SM. Factors directly affecting impulse transmission in inflammatory demyelinating disease: recent advances in our understanding. *Curr Opin Neurol* 2001; 14: 2389–2398
- Smith KJ, Lassmann H. The role of nitric oxide in multiple sclerosis. *Lancet [Neurol]* 2002; 1: 232–241
- Söderström M, Ya-Ping J, Hillert J, Link H. Optic Neuritis. Prognosis for multiple sclerosis from MRI, CSF, and HLA findings. *Neurology* 1998; 50: 708–714
- Soramani MP, Bruzzi P, Beckmann K, Wagner K, Miller DH, Kappos L, Filippi M. MRI metrics as surrogate endpoints for EDSS progression in SPMS patients treated with IFN β -1b. *Neurology* 2003; 60: 1462–1466
- Steinman L, Martin R, Bernard C, Conlon P, Oksenberg JR. Multiple sclerosis: deeper understanding of its pathogenesis reveals new targets for therapy. *Annu Rev Neurosci* 2002; 25: 491–505
- Stevenson VL, Leary SM, Losseff NA, Parker GJM, Barker GJ, Human Y, Miller DH, Thompson AJ. Spinal cord atrophy and disability in MS. A longitudinal study. *Neurology* 1998; 51: 234–238
- Stevenson VL, Smith SM, Matthews PM, Miller FH, Thompson AJ. Monitoring disease activity and progression in primary progressive multiple sclerosis using MRI: sub-voxel registration to identify lesion changes and to detect cerebral atrophy. *J Neurol* 2002; 249: 171–177
- Stinissen P, Medaer R, Raus J. Myelin reactive T cells in the autoimmune pathogenesis of multiple sclerosis. *Mult Scler* 1998; 4: 203–211
- Strangel M, Hartung H-P. Remyelinating strategies for the treatment of multiple sclerosis. *Prog Neurobiol* 2002; 68: 361–376
- Tan IL, van Schijndel RA, Pouwels PJ, van Walderveen MA, Reichenbach JR, Manoliu RA, Barkhof F. MR venography of multiple sclerosis. *AJNR Am J Neuroradiol* 2000; 21: 1039–1042
- Tan IL, van Schijndel RA, Pouwels PJW, van Walderveen MAA, Reichenbach JR, Manoliu RA, Barkhof F. MR Venography of multiple sclerosis. *AJNR Am J Neuroradiol* 2000; 21: 1039–1042
- Tan IL, van Schijndel RA, van Walderveen MAA, Quist M, Bos R, Pouwels PJW, Desmedt P, Adèr HJ, Barkhof F. Magnetic resonance image registration in multiple sclerosis: comparison with repositioning error and observer-based variability. *J Magn Reson Imaging* 2002; 15: 505–510
- Tartaglia MC, Narayanan S, de Stefano N, Arnaoutelis R, Antel SB, Francis SJ, Santos AC, Lapierre Y, Arnold DL. Choline is increased in pre-lesional normal appearing white matter in multiple sclerosis. *J Neurol* 2002; 249: 1382–1390
- Tartaglino LM, Friedman DP, Flanders AE, Lublin FD, Knöber RL, Liem M. Multiple sclerosis in the spinal cord: MR appearance and correlation with clinical parameters. *Radiology* 1995; 195: 725–732
- Tas MW, Barkhof F, van Walderveen MAA, Polman CH, Hommes OW, Valk J. The effect of gadolinium on the sensitivity and specificity of MR in the initial diagnosis of multiple sclerosis. *AJNR Am J Neuroradiol* 1995; 16: 259–264
- Thompson AJ, Montalban X, Barkhof F, Brochet B, Filippi M, Miller DH, Polman CH, Stevenson VL, McDonald WI. Diagnostic criteria for primary progressive multiple sclerosis: a position paper. *Ann Neurol* 2000; 47: 831–835
- Thorpe JW, Kidd D, Mosely IF, Kendall BE, Thompson AJ, MacManus DG, McDonald WI, Miller DH. Serial gadolinium-enhanced MRI of the brain and spinal cord in early relapsing-remitting multiple sclerosis. *Neurology* 1996; 46: 373–378
- Tintoré M, Rovira A, Martínez MJ, Río J, Díaz-Valloslada P, Brieval L, Borrás C, Grivé E, Capellades J, Montalban X. Isolated demyelinating syndromes: comparison of different MR imaging criteria to predict conversion to clinically definite multiple sclerosis. *AJNR Am J Neuroradiol* 2000; 21: 702–706
- Tintoré M, Rovira A, Río J, Nos C, Grivé E, Sastre-Garriga J, Pericot I, Sánchez E, Comabella M, Montalban X. New diagnostic criteria for multiple sclerosis. Application in first demyelinating episode. *Neurology* 2003; 60: 27–30
- Tourbah A, Stievenart J-L, Abanou AA, Iba-Zizen M-T, Hamard H, Lyon-Caen O, Cabanis EA. Normal-appearing white matter in optic neuritis and multiple sclerosis: a comparative proton spectroscopy study. *Neuroradiology* 1999; 41: 738–743

- Trojano M, Avolio C, Ruggieri, de Robertis F, Giuliani F, Paolicelli D, Livrea P. Soluble intracellular adhesion molecule-1 (sICAM-1) in serum and cerebrospinal fluid of demyelinating diseases of the central and peripheral nervous system. *Mult Scler* 1998; 4: 39–44
- Ugawa Y, Shirouzu I, Terao Y, Hanajima R, Machii K, Mochizuki H, Furiybayashi T, Kanazawa I. Physiological analysis of a patient with extreme widening of Virchow-Robin spaces. *J Neurol Sci* 1998; 159: 25–27
- Van Buchem MA, Udupa JK, McGowan, Miki Y, Heyning FH, Boncoeur-Martel M-P, Kolson DL, Polansky M, Grossman RI. Global volumetric estimation of disease burden in multiple sclerosis based on magnetization transfer imaging. *AJNR Am J Neuroradiol* 1997; 18: 1287–1290
- Van Waesberghe JH, Kamphorst W, de Groot CJ, van Walderveen MA, Castelijns JA, Ravid R, Lycklama à Nijeholt GJ, van der Valk P, Polman CH, Thompson AJ, Barkhof F. Axonal loss in multiple sclerosis lesions: magnetic resonance imaging insights into substrates of disability. *Ann Neurol* 1999; 46: 747–754
- Van Walderveen MA, Barkhof F, Hommes OR, Polman CH, Tobi H, Frequin STFM, Valk J. Correlating MR imaging and clinical disease activity in multiple sclerosis: relevance of hypointense lesions on short TR/short TE (T1-weighted) spin echo images. *Neurology* 1995; 45: 1684–1690
- Van Walderveen MA, Lycklama à Nijeholt GJ, Ader HJ, Jongen PJ, Polman CH, Castelijns JA, Barkhof F. Hypointense lesions on T1 weighted spin-echo magnetic resonance imaging: relation to clinical characteristics in subgroups of patients with multiple sclerosis. *Arch Neurol* 2001; 58: 76–81
- Van Walderveen MAA, Barkhof F, Hommes OR, Polman CH, Tobi H, Frequin STFM, Valk J. Correlating MRI and clinical disease activity in multiple sclerosis: relevance of hypointense lesions on short-TR/short-TE (T1-weighted) spin-echo images. *Neurology* 1995; 45: 1684–1690
- Van Walderveen MAA, Kamphorst W, Scheltens P, van Waesberghe JHTM, Ravid R, Valk J, Polman CH, Barkhof F. Histopathologic correlate of hypointense lesions on T1-weighted spin-echo MRI in multiple sclerosis. *Neurology* 1998; 50: 1282–1288
- Van Walderveen MAA, van Schijndel RA, Pouwels PJW, Polman CH, Barkhof F. Multislice T₁ relaxation time measurements in the brain using IR-EPI: reproducibility: normal values, and histogram analysis in patients with multiple sclerosis. *J Magn Reson Imag* 2003; 18: 656–664
- Wang CH, Walsh K. Multiple ring-enhancing lesions in a child with relapsing multiple sclerosis. *J Child Neurol* 2002; 17: 69–72
- Wang P-Y, Tseng C-L, Young C, Liu H-M, Chang Y-C, Shen Y-Z, Lee C-Y. Multiple sclerosis in children: clinical, neuroimaging, and neurophysiological correlations. *Acta Paediatr Sin* 1995; 36: 93–100
- Wasman SG. Do 'demyelinating' diseases involve more than myelin? *Nat Am* 2000; 6: 738–739
- Wingerchuck DM, Hogancamp WF, O'Brien PC, Weinschenker BG. The clinical course of neuromyelitis optica (Devic's syndrome). *Neurology* 1999; 53: 1107–1114
- Wood DD, Bilbao JM, O'Connors P, Moscarello MA. Acute multiple sclerosis (Malburg type) is associated with developmentally immature myelin basic protein. *Ann Neurol* 1996; 40: 18–24
- Wuerfel J, Bellmann-Strobl J, Brunecker P, Aktas O, McFarland H, Villringer A, Zipp F. Changes in cerebral perfusion precede plaque formation in multiple sclerosis: a longitudinal perfusion MRI study. *Brain* 2004; 127: 111–119
- Yao S-Y, Stratton CW, Mitchell WM, Sriram S. CSF Oligoclonal bands in MS include antibodies against *Chlamydomophila* antigens. *Neurology* 2001; 56: 1168–1176
- Zivadinov R, Locatelli L, Stival B, Bratina A, Grop A, Nasuelli D, Brnabic-Razmilic O, Zorzon M. Normalized regional brain atrophy measurements in multiple sclerosis. *Neuroradiology* 2003; 45: 793–798

80 Acute Disseminated Encephalomyelitis and Acute Hemorrhagic Encephalomyelitis

- An SF, Groves M, Martinian L, Kuo LT, Scaravilli F. Detection of infectious agents in brain of patients with acute hemorrhagic leukoencephalitis. *J Neurovirol* 2002; 8: 439–446
- Andreula CD, Recchia Luciani ANM, Milella D. Magnetic resonance imaging in the diagnosis of acute disseminated encephalitis (ADEM). *Int J Neuroradiol* 1997; 3: 21–34
- Anlar B, Basaran C, Kose G, Guven A, Haspolat S, Yakut A, Sedaroglu A, Senbil N, Tan H, Karaagaoglu E, Karli Oguz K. Acute disseminated encephalomyelitis in children: outcome and prognosis. *Neuropediatrics* 2003; 34: 194–199
- Atlas SW, Grossman RI, Goldberg HI, Hackney DB, Bilaniuk LT, Zimmerman RA. MR diagnosis of acute disseminated encephalomyelitis. *J Comput Assist Tomogr* 1986; 10: 798–801
- Archer H, Wall R. Acute haemorrhagic leukoencephalopathy: two case reports and review of the literature. *J Infect* 2003; 46: 133–137
- Battistella PA, Laverda AM, Drigo P, Salandin M, Carollo C. Leucoencefalite acuta disseminata: aspetti clinici e neuroradiologici in 9 casi pediatrici. *Riv Neuroradiol* 1996; 9: 649–657
- Baum PA, Barkovich AJ, Koch TK, Berg BO. Deep gray matter involvement in children with acute disseminated encephalomyelitis. *AJNR Am J Neuroradiol* 1994; 15: 1275–1283
- Bernarding J, Braun J, Koennecke HC. Diffusion- and perfusion-weighted MR imaging in a patient with acute demyelinating encephalomyelitis (ADEM). *J Magn Reson Imaging* 2002; 15: 96–100
- Bizzi A, Uluğ AM, Crawford TO, Passe T, Bugiani M, Bryan N, Barker PB. Quantitative proton MR spectroscopic imaging in acute disseminated encephalomyelitis. *AJNR Am J Neuroradiol* 2001; 22: 1125–1130
- Dale RC, Sousa de C, Chong WK, Cox TCS, Harding B, Neville BGR. Acute disseminated encephalomyelitis, multiphasic disseminated encephalomyelitis and multiple sclerosis in children. *Brain* 2000; 123: 2407–2422
- Feydy A, Carlier R, Mompont D, Clair B, Chillet P, Vallee C. Brain and spinal cord MR imaging in a case of acute disseminated encephalomyelitis. *Eur Radiol* 1997; 7: 415–417
- Gupte G, Stonehouse M, Wassmer E, Coad NAG, Whitehouse WP. Acute disseminated encephalitis: a review of 18 cases in childhood. *J Paediatr Child Health* 2003; 39: 336–342
- Haase CG, Faustmann PM, Diener HC. Idiopathic inflammatory demyelinating diseases of the central nervous system: differentiating between acute disseminated encephalomyelitis and malignant multiple sclerosis. *J Clin Neurosci* 1999; 6: 221–226
- Hartung HP, Grossman RI. ADEM. Distinct disease or part of the MS spectrum? *Neurology* 2001; 56: 1257–1260

- Höllinger P, Sturzenegger M, Mathis J, Schroth G, Hess CW. Acute disseminated encephalomyelitis in adults: a reappraisal of clinical, CSF, EEG, and MRI findings. *J Neurol* 2002; 249: 320–329
- Hynson JL, Kornberg AJ, Coleman LT, Shield L, Harvey AS, Kean MJ. Clinical and neuroradiologic features of acute disseminated encephalomyelitis in children. *Neurology* 2001; 56: 1308–1312
- Inglese M, Salvi F, Iannucci G, Mancardi GL, Mascalchi M, Filippi M. Magnetization transfer and diffusion tensor MR imaging of acute disseminated encephalomyelitis. *AJNR Am J Neuroradiol* 2002; 23: 267–272
- Jaing TH, Lin KL, Chiu CH, Lo WC, Wu PL. Acute disseminated encephalomyelitis in autoimmune hemolytic anemia. *Pediatr Neurol* 2001; 24: 303–305
- Johnson RT, Griffin DE, Hirsch RL, Wolinsky JS, Roedenbeck S, Lindo de Soriano I, Vaisberg A. Measles encephalomyelitis—clinical and immunologic studies. *N Engl J Med* 1984; 310: 137–141
- Kepes JJ. Large focal tumor-like demyelinating lesions of the brain: intermediate entity between multiple sclerosis and acute disseminated encephalomyelitis? A study of 31 patients. *Ann Neurol* 1993; 33: 18–27
- Khong PL, Ho HK, Cheng PW, Wong VCN, Goh W, Chan FL. Childhood acute disseminated encephalomyelitis: the role of brain and spinal cord MRI. *Pediatr Radiol* 2002; 32: 59–66
- Kimura S, Nezu A, Ohtsuki N, Kobayashi T, Osaka H, Uehara S. Serial magnetic resonance imaging in children with postinfectious encephalitis. *Brain Dev* 1996; 18: 461–465
- Klein CJ, Wijdicks EFM, Earnest IV F. Full recovery after acute hemorrhagic leukoencephalitis (Hurst's disease). *J Neurol* 2000; 247: 977–979
- Mader I, Wolff M, Niemann G, Küker W. Acute haemorrhagic encephalomyelitis (ADEM): MRI findings. *Neuropediatrics* 2004; 35: 143–146
- Murthy JMK. MRI in acute disseminated encephalomyelitis following Semple antirabies vaccine. *Neuroradiology* 1998; 40: 420–423
- Murthy SNK, Faden HS, Cohen ME, Bakshi R. Acute disseminated encephalomyelitis in children. *Pediatrics* 2002; 110: e21
- Nagai K, Mori T. Acute disseminated encephalomyelitis with probable measles vaccine failure. *Pediatr Neurol* 1999; 20: 399–402
- O'Riordan JI, Gomez-Anson B, Moseley IF, Miller DH. Long term MRI follow-up of patients with post infectious encephalomyelitis: evidence for a monophasic disease. *J Neurol Sci* 1999; 167: 132–136
- Piyasirisilp S, Hemachudha T. Neurological adverse events associated with vaccination. *Curr Opin Neurol* 2002; 15: 333–338
- Reich H, Lin SR, Goldblatt D. Computerized tomography in acute hemorrhagic leukoencephalopathy: a case report. *Neurology* 1979; 29: 255–258
- Schwarz S, Mohr A, Knauth M, Wildemann B, Storch-Hagenlocher B. Acute disseminated encephalomyelitis, a follow-up study of 40 adult patients. *Neurology* 2001; 56: 1313–1318
- Scully RE, Mark EJ, McNeely WF, Ebeling SH. Case records of the Massachusetts General Hospital. *N Engl J Med* 1996; 334: 715–720
- Scully RE, Mark EJ, McNeely WF, Ebeling SH. Case records of the Massachusetts General Hospital. *N Engl J Med* 1999; 340: 127–135
- Shoji H, Kusuhara T, Honda Y, Hino H, Kojima K, Abe T, Watanabe M. Relapsing acute disseminated encephalomyelitis associated with chronic Epstein-Barr virus infection: MRI findings. *Neuroradiology* 1992; 34: 340–342
- Tachi N, Watanabe T, Wakai S, Sato T, Chiba S. Acute disseminated encephalomyelitis following HTLV-I associated myelopathy. *J Neurol Sci* 1992; 110: 234–235
- Tenembaum S, Chamois N, Fejerman N. Acute disseminated encephalomyelitis, a long-term follow-up study of 84 pediatric patients. *Neurology* 2002; 59: 1224–1231
- Yapici Z, Eraksoy M. Bilateral demyelinating tumefactive lesions in three children with hemiparesis. *J Child Neurol* 2002; 17: 655–660.
- Yoshikawa H, Oda Y. Acquired aphasia in acute disseminated encephalomyelitis. *Brain Dev* 1999; 21: 341–344

81 Acquired Immunodeficiency Syndrome

- Abdoulafia DM, Taylor L. Vacuolar myelopathy and vacuolar cerebellar leukoencephalopathy: a late complication of AIDS after highly active antiretroviral therapy-induced immune reconstruction. *AIDS Pat Care* 2002; 16: 579–584
- Albright AV, Soldan SS, Gonzalez-Scarano F. Pathogenesis of human immunodeficiency virus-induced neurological disease. *J Neurovirol* 2003; 9: 222–227
- Anderson E, Zink W, Xiong H, Gendelman HE. HIV-1-associated dementia: a metabolic encephalopathy perpetrated by virus-infected and immune-competent mononuclear phagocytes. *J Acquir Immune Defic Syndr* 2002; 31: S43–S54
- Annunziata P. Blood–brain barrier changes during invasion of the central nervous system by HIV-1. *J Neurol* 2003; 250: 901–906
- Avison MJ, Nath A, Berger JR. Understanding pathogenesis and treatment of HIV dementia: a role for magnetic resonance? *Trends Neurosci* 2002; 25: 468–473
- Barret B, Tardieu M, Rustin P, Lacroix C, Chabrol B, Desguerre I, Dollfus C, Mayaux M-J, Blance S. Persistent mitochondrial dysfunction in HIV-1-exposed but uninfected infants: clinical screening in a large prospective cohort. *AIDS* 2003; 17: 1769–1785
- Belman AL, Ulmann MH, Horoupian D, Novick B, Spiro AJ, Rubinstein A, Kurtzberg D, Cone-Wesson B. Neurological complications in infants and children with acquired immune deficiency syndrome. *Ann Neurol* 1985; 18: 560–566
- Bencherif B, Rottenberg DA. Neuroimaging of the AIDS dementia complex. *AIDS* 1998; 12: 233–244
- Berger JR, Sheremata WA, Resnick L, Atherton S, Fletcher MA, Norenberg M. Multiple sclerosis-like illness occurring with human immunodeficiency virus infection. *Neurology* 1989; 39: 324–329
- Blanche S, Tardieu M, Rustin P, Slama A, Barret B, Firtion G, Ciraru-Vigneron N, Lacroix C, Rouzioux C, Mabdellbrot L, Desguerre I, Rötig A, Mayaux M-J, Delfraissy JF. Persistent mitochondrial dysfunction and perinatal exposure to antiretroviral nucleoside analogues. *Lancet* 1999; 354: 1084–1089
- Camacho DLA, Smith JK, Castillo M. Differentiation of toxoplasmosis and lymphoma in AIDS patients by using apparent diffusion coefficients. *AJNR Am J Neuroradiol* 2003; 24: 633–637
- Cedis Meltzer C, Wells SW, Bechner MW, Flanigan KM, Oyler GA, Lee RR. AIDS-related MR hyperintensity of the basal ganglia. *AJNR Am J Neuroradiol* 1998; 19: 83–89

- Chamberlain MC, Nichols SL, Chase CH. Pediatric AIDS: comparative cranial MRI and CT scans. *Pediatr Neurol* 1991; 7: 357–362
- Chang L. In vivo magnetic resonance spectroscopy in HIV and HIV-related brain diseases. *Rev Neurosci* 1995; 6: 365–378
- Chong J, di Rocco A, Tagliati M, Danisi F, Simpson DM, Atlas SW. MR findings in AIDS-associated myelopathy. *AJNR Am J Neuroradiol* 1999; 20: 1412–1416
- Chrysikopoulos HS, Press GA, Grafe MR, Hesselink JR, Wiley CA. Encephalitis caused by human immunodeficiency virus; CT and MR imaging manifestations with clinical and pathologic correlation. *Radiology* 1990; 175: 185–191
- Church JA. Reversible leukoencephalopathy in a patient with nucleoside analogue-associated mitochondrial depletion and metabolic disease. *AIDS* 2002; 16: 2366–2367
- Cinque P, Bossolasco S, Bestetti A, Sala S, Pierotti C, Lazzarin A. Molecular studies of cerebrospinal fluid in human immunodeficiency virus type 1-associated opportunistic central nervous system diseases – an update. *J Neurovirol* 2002; 8: 122–128
- Corral I, Quereda C, Hellin T, Navas E, García-Villanueva M. Relapsing and remitting leukoencephalopathy associated with chronic HIV infection. *Eur Neurol* 2002; 48: 39–41
- Côté HCF, Brumme ZL, Craib KJP, Alexander CS, Wynhoven B, Ting L, Wong H, Harris M, Harrigan PR, O'Shaughnessy MV, Montaner JSG. Changes in mitochondrial DNA as a marker of nucleoside toxicity in HIV-infected patients. *N Engl J Med* 2002; 346: 811–820
- Curless RG. Congenital AIDS: review of neurologic problems. *Childs Nerv Syst* 1989; 5: 9–11
- Da Chuna A, Mintz M, Eiden LE, Sharer LR. A neuronal and neuroanatomical correlate of HIV-1 encephalopathy relative to HIV-1 in HIV-1-infected children. *J Neuropathol Exp Neurol* 1997; 56: 974–987
- Delisle MB, Bouissou H, Saidi A. What's new in cerebral pathology in acquired immune deficiencies? *Pathol Res Pract* 1986; 181: 85–92
- Diaz-Marchan PJ, Huang ML, Jackson EF, Norton RE, Hayman LA. Triple-dose contrast-enhanced images in neurologically symptomatic HIV-positive patients. *Neuroradiology* 2000; 42: 256–260
- Di Rocco A, Bottiglieri T, Werner P, Geraci A, Simpson D, Godbold J, Morgello S. Abnormal cobalamin-dependent transmethylation in AIDS-associated myelopathy. *Neurology* 2002; 58: 730–735
- Eggers C. HIV-1 associated encephalopathy and myelopathy. *J Neurol* 2002; 249: 1132–1136
- Ellis RJ, Moore DJ, Childers ME, Letendre S, McCutchan JA, Wolfson T, Spector SA, Hsia K, Heaton RK, Grant I. Progression to neuropsychological impairment in human immunodeficiency virus infection predicted by elevated cerebrospinal fluid levels of human immunodeficiency virus RNA. *Arch Neurol* 2002; 59: 923–928
- Filippi CG, Sze G, Farber SJ, Shahmanesh M, Selwyn PA. Regression of HIV encephalopathy and basal ganglia signal intensity abnormality at MR imaging in patients with AIDS after the initiation of protease inhibitor therapy. *Radiology* 1998; 206: 491–498
- Fliss DM, Parikh J, Freeman JL. AIDS-related Kaposi's sarcoma of the sphenoid sinus. *J Otolaryngol* 1992; 21: 235–237
- Flowers CH, Mafee MF, Crowell R, Raofi B, Arnold P, Dobben G, Wycliffe N. Encephalopathy in AIDS patients: evaluation with MR imaging. *AJNR Am J Neuroradiol* 1990; 11: 1235–1245
- Geremia GK, McCluney KW, Adler SS, Charletta DA, Hoile RD, Huckman MS, Ramsey RG. The magnetic resonance hypointense spine of AIDS. *J Comput Assist Tomogr* 1990; 14: 785–789
- Grafe MR, Press GA, Berthoty DP, Hesselink JR, Wiley CA. Abnormalities of the brain in AIDS patients: correlation of post-mortem MR findings with neuropathology. *AJNR Am J Neuroradiol* 1990; 11: 905–911
- Goldstick L, Mandybur TI, Bode R. Spinal cord degeneration in AIDS. *Neurology* 1985; 35: 103–106
- Gray F, Gherardi R, Scaravilli F. The neuropathology of the acquired immune deficiency syndrome (AIDS). A review. *Brain* 1988; 111: 245–266
- Greene WC. Mechanisms of disease. The molecular biology of human immunodeficiency virus type 1 infection. *N Engl J Med* 1991; 324: 308–317
- Hénin D, Smith TW, de Girolami U, Sughayer M, Hauw J-J. Neuropathology of the spinal cord in the acquired immunodeficiency syndrome. *Hum Pathol* 1992; 23: 1106–1114
- Ho DD, Pomarantz RJ, Kaplan JC. Pathogenesis of infection with human immunodeficiency virus. *N Engl J Med* 1987; 317: 278–286
- Holland NR, Power C, Mathews VP, Glass JD, Forman M, McArthur JC. Cytomegalovirus encephalitis in acquired immunodeficiency syndrome (AIDS). *Neurology* 1994; 44: 507–514
- Holliday RA. Manifestations of AIDS in the oromaxillofacial region. The role of imaging. *Radiol Clin N Am* 1993; 31: 45–60
- Ito M, Baker JV, Mock DJ, Goodman AD, Blumberg BM, Shrier DA, Powers JM. Human herpes 6-meningoencephalitis in an HIV patient with progressive multifocal leukoencephalopathy. *Acta Neuropathol (Berl)* 2000; 100: 337–341
- Jones HR Jr, Ho DD, Forgacs P, Adelman LS, Silverman ML, Baker RA, Locuratolo P. Acute fulminating fatal leukoencephalopathy as the only manifestation of human immunodeficiency virus infection. *Ann Neurol* 1988; 3: 519–522
- Kauffman WM, Sivit CJ, Fitz CR, Rakusan TA, Herzog K, Chandra RS. CT and MR evaluation of intracranial involvement in pediatric HIV infection: A clinical-imaging correlation. *AJNR Am J Neuroradiol* 1992; 13: 949–957
- Kirshenbaum KJ, Nadimpalli SR, Friedman M, Kirshenbaum GL, Cavallino RP. Benign lymphoepithelial parotid tumors in AIDS patients: CT and MR findings in nine cases. *AJNR Am J Neuroradiol* 1991; 12: 271–274
- Kovacs A, Schluchter M, Easley K, Demmler G, Shearer W, la Russa P, Pitt J, Cooper E, Goldfarb J, Hodes D, Kattan M, McIntosh K. Cytomegalovirus infection and HIV-1 disease progression in infants born to HIV-1-infected women. *N Engl J Med* 1999; 341: 77–84
- Kupfer MC, Zee CS, Colletti PM, Boswell WD, Rhodes R. MRI evaluation of AIDS-related encephalopathy: toxoplasmosis vs. lymphoma. *Magn Reson Imaging* 1990; 8: 51–57
- Langford TD, Letendre SL, Marcotte TD, Ellis RJ, McCutchan JA, Grant I, Mallory ME, Hansen LA, Archibald S, Jernigan T, Masliah E. Severe, demyelinating leukoencephalopathy in AIDS patients on antiretroviral therapy. *AIDS* 2002; 16: 1019–1029
- Langford TD, Letendre SL, Larrea GJ, Masliah E. Changing patterns in the neuropathogenesis of HIV during the HAART era. *Brain Pathol* 2003; 13: 195–210
- Leger JM, Bouche P, Bolgert F, Chaunu MP, Rosenheim M, Cathala HP, Gentilini M, Hauw JJ, Brunet P. The spectrum of polyneuropathies in patients infected with HIV. *J Neurol Neurosurg Psychiatry* 1989; 52: 1369–1374

- Levy RM, Pons VG, Rosenblum ML. Central nervous system mass lesions in the acquired immunodeficiency syndrome (AIDS). *J Neurosurg* 1984; 61: 9–16
- Lindegren ML, Rhodos P, Gordon L, Fleming P. Lack of mortality related to mitochondrial dysfunction among perinatally HIV-exposed children in pediatric HIV surveillance. *Ann N Y Acad Sci* 2000; 918: 222–235
- Lüer W, Gerhards J, Poser S, Weber T, Felgenhauer K. Acute diffuse leukoencephalitis in HIV-1 infection. *J Neurol Neurosurg Psychiatry* 1994; 57: 105–107
- Mamidi A, DeSimone JA, Pomerantz RJ. Central nervous system infections in individuals with HIV-1 infection. *J Neurovirol* 2002; 8: 158–167
- Morris AA, Carr A. HIV nucleoside analogues: new adverse effects on mitochondria? *Lancet* 1999; 354: 1046–1047
- Navia BA, Cho E-S, Petito CK, Price RW. The AIDS dementia complex. II. Neuropathology. *Ann Neurol* 1986; 19: 525–535
- Nielsen SL, Petito CK, Urmacher CD, Posner JB. Subacute encephalitis in acquired immune deficiency syndrome: a postmortem study. *Am J Clin Pathol* 1984; 82: 678–682
- Portegies P, Enting RH, Gans de J, Algra PR, Derix MMA, Lange JMA, Goudsmit J. Presentation and course of AIDS dementia complex: 10 years of follow-up in Amsterdam, the Netherlands. *AIDS* 1993; 7: 669–675
- Quencer RM. AIDS-associated myelopathy: clinical severity, MR findings, and underlying etiologies. *AJNR Am J Neuroradiol* 1999; 20: 1387–1388
- Sacktor N. The epidemiology of human immunodeficiency virus-associated neurological disease in the era of highly active antiretroviral therapy. *J Neurovirol* 2002; 8 Suppl 2: 115–1121
- Sánchez-Ramón S, Cantó-Nogués C, Muñoz-Fernández MA. Reconstruction of the course of HIV-1-associated progressive encephalopathy in children. *Med Sci Monit* 2002; 8: RA249–RA252
- Shugar JMA, Som PM, Jacobson AL, Ryan JR, Bernard PJ, Dickman SH. Multicentric parotid cysts and cervical adenopathy in AIDS patients. A newly recognized entity: CT and MR manifestations. *Laryngoscope* 1988; 98: 772–775
- Snider WD, Simpson DM, Nielsen S, Gold JWM, Metroka CE, Posner JB. Neurological complications of acquired immune deficiency syndrome: analysis of 50 patients. *Ann Neurol* 1983; 14: 403–418
- Stankoff B, Tourbah A, Suarez S, Turell E, Stievenart JL, Payan C, Coutellier A, Herson S, Baril L, Bricaire F, Calvez V, Cabanis EA, Lacomblez L, Lubetzki C. Clinical and spectroscopic improvement in HIV-associated impairment. *Neurology* 2001; 56: 112–115
- Starr SE, Fletcher CV, Spector SA, Yong FH, Fenton T, Brundage RC, Manion D, Ruiz NM, Gersten M, Becker M, McNamara J, Mofenson LM. Combination therapy with efavirenz, nelfinavir, and nucleoside reverse-transcript inhibitors in children infected with human immunodeficiency type 1. *N Engl J Med* 1999; 341: 1874–1881
- Steinbrook R, Drazen JM. AIDS – will the next 20 years be different? *N Engl J Med* 2001; 344: 1781–1782
- Swindells S, Zheng J, Gendelman HE. HIV-associated dementia: new insights into disease pathogenesis and therapeutic interventions. *AIDS Pat Care* 1999; 13: 153–163
- Talpos D, Tien RD, Hesselink JR. Magnetic resonance imaging of AIDS-related polyradiculopathy. *Neurology* 1991; 41: 1996–1997
- Tardieu M. HIV-1-related central nervous system diseases. *Curr Opin Neurol* 1999; 12: 377–381
- Thurnher MM, Rieger A, Kleibl-Popov C, Settinek U, Henk C, Haberler C, Schindler E. *Neuroradiology* 2001; 43: 29–35
- Thurnher MM, Schindler EG, Thurnher SA, Pernerstorfer-Schön H, Kleibl-Popov C, Rieger A. Highly active antiretroviral therapy for patients with AIDS dementia complex: effect on MR imaging findings and clinical course. *AJNR Am J Neuroradiol* 2000; 21: 670–678
- Thurnher MM, Thurnher SA, Schindler E. CNS involvement in AIDS: spectrum of CT and MR findings. *Eur Radiol* 1997; 7: 1091–1097
- Trenkwalder P, Trenkwalder C, Feiden W, Vogl TJ, Einhäupl KM, Lydtin H. Toxoplasmosis with early intracerebral hemorrhage in a patient with the acquired immunodeficiency syndrome. *Neurology* 1992; 42: 436–438
- Tucker T. Central nervous system AIDS. *J Neurol Sci* 1989; 89: 119–133
- Vago L, Bonetto S, Nebuloni M, Duca P, Carsana L, Zerbi P, D'Arminio-Monforche. Pathological findings in the central nervous system of AIDS patients on assumed antiretroviral therapeutic regimens: retrospective study of 1597 autopsies. *AIDS* 2002; 16: 1925–1928
- Visudtibhan A, Visudhipan P, Chiemchanya S. Stroke and seizures as the presenting signs of pediatric HIV infection. *Pediatr Neurol* 1999; 20: 53–56
- Vittecoq S, Jardel C, Barthélémy C, Escout L, Cheminot N, Chapin S, Sternberg D, Maisonneuve T, Lombès SA. Mitochondrial damage associated with long-term antiretroviral treatment: associated alteration or causal disorder? *J Acquir Immune Defic Syndr* 2002; 31: 299–308
- Walker UA, Setzer B, Venhoff N. Increased long-term mitochondrial toxicity in combinations of nucleoside analogue reverse-transcriptase inhibitors. *AIDS* 2002; 16: 2165–2173
- Wang H, Lemire BD, Cass CE, Weiner JH, Michalak M, Penn AMW, Fliegel L. Zidovudine and dideoxynucleosides deplete wild-type mitochondrial DNA levels and increase deleted mitochondrial DNA levels in cultured Kearns-Sayre syndrome fibroblasts. *Biochim Biophys Acta* 1996; 1316: 51–59
- Wehn SM, Heinz ER, Burger PC, Boyko OB. Dilated Virchow-Robin spaces in cryptococcal meningitis associated with AIDS: CT and MR findings. *J Comput Assist Tomogr* 1989; 13: 756–762
- Zimmer C, Märzheuser S, Patt S, Rolfs A, Gottschalk J, Weigel K, Gosztanyi G. Stereotactic brain biopsy in AIDS. *J Neurol* 1992; 239: 394–400

82 Progressive Multifocal Leukoencephalopathy

- Agostini HT, Ryschkewitsch CF, Baumhefner RW, Tourtelotte WW, Singer EJ, Komoly S, Stoner GL. Influence of JC virus coding region genotype on risk of multiple sclerosis and progressive multifocal leukoencephalopathy. *J Neurovirol* 2000; 6: S101–S108
- Aksamit AJ, Gendelman HE, Orenstein JM, Pezeshkpour GH. AIDS-associated progressive multifocal leukoencephalopathy (PML): comparison to non-AIDS PML with situ hybridization and immunohistochemistry. *Neurology* 1990; 40: 1073–1078
- Arai Y, Tsutsui Y, Nagashima K, Shinmura Y, Kosugi T, Wakai M, Nishikage H, Yamamoto J. Autopsy case of the cerebellar form of progressive multifocal leukoencephalopathy without immunodeficiency. *Neuropathology* 2002; 22: 48–56
- Berger JR, Pall L, Lanska D, Whiteman M. Progressive multifocal leukoencephalopathy in patients with HIV infection. *J Neurovirol* 1998; 4: 59–68

- Berger JR, Major EO. Progressive multifocal leukoencephalopathy. *Semin Neurol* 1999; 19: 193–200
- Bergui M, Bradac GB, Oguz KK, Boghi A, Geda C, Gatti G, Schiffer D. Progressive multifocal leukoencephalopathy: diffusion-weighted imaging and pathological correlations. *Neuroradiology* 2004; 46: 22–25
- Cardenas RL, Cheng KH, Sack K. The effects of cidofovir on progressive multifocal leukoencephalopathy: an MRI case study. *Neuroradiology* 2001; 43: 379–382
- Del Valle L, Gordon J, Assimakopoulou M, Enam S, Geddes JF, Varakis JN, Katsetos CD, Croul S, Khalili K. Detection of JC virus DNA sequences and expression of the viral regulatory protein T-antigen in tumors of the central nervous system. *Cancer Res* 2001; 61: 4287–4293
- Donovan Post MJ, Yiannoutsos C, Simpson D, Booss J, Clifford DB, Cohen B, McArthur JC, Hall CD. Progressive multifocal leukoencephalopathy in AIDS: are there any MR findings useful to patient management and predictive of patient survival? *AJNR Am J Neuroradiol* 1999; 20: 1896–1906
- Dousset V, Armand J-P, Lacoste D, Miège S, Letenneur L, Dartigues J-F, Caillé J-M. Magnetization transfer study of HIV encephalitis and progressive multifocal leukoencephalopathy. *AJNR Am J Neuroradiol* 1997; 18: 895–901
- Du Pasquier RA, Koralnik IJ. Inflammatory reaction in progressive multifocal leukoencephalopathy: harmful or beneficial? *J Neurovirol* 2003; 9 (Suppl 1): 25–31
- Enting RH, Portegies P. Cytarabine and highly active antiretroviral therapy in HIV-related progressive multifocal leukoencephalopathy. *J Neurol* 2000; 247: 134–138
- García de Viedma D, Díaz Infantes M, Miralles P, Berenguer J, Marin M, Muñoz L, Bouza E. JC Virus load in progressive multifocal leukoencephalopathy: analysis of the correlation between the viral burden in cerebrospinal fluid, patient survival, and the volume of neurological lesions. *Clin Infect Dis* 2002; 34: 1568–1575
- Gentile S, Sacerdote L, Roccatello D, Giordana MT. Progressive multifocal leukoencephalopathy during cyclosporine treatment. A case report. *Ital J Neurol Sci* 1996; 17: 363–366
- Gordon J, Gallia GL, del Valle L, Amini S, Khalili K. Human polyomavirus JCV and expression of myelin genes. *J Neurovirol* 2000; 6: S92–S97
- Hou J, Major EO. Progressive multifocal leukoencephalopathy: JC Virus-induced demyelination in the immune compromised host. *J Neurovirol* 2000; 6: S98–S100
- Hal CD, Dafni U, Simpson D, Clifford D, Wetherill PE, Cohen B, McArthur J, Hollander H, Yiannoutsos C, Major E, Millar L, Timpone J. Failure of cytarabine in progressive multifocal leukoencephalopathy associated with human immunodeficiency virus infection. *N Engl J Med* 1998; 338: 1345–1351
- Hansman Whiteman ML, Donovan Post MJ, Berger JR, Tate LG, Bell MD, Limonte LP. Progressive multifocal leukoencephalopathy in 47 HIV-seropositive patients: neuroimaging with clinical and pathologic correlation. *Radiology* 1993; 187: 233–240
- Hawkins CP, McLaughlin JE, Kendall BE, McDonald WI. Pathological findings correlated with MRI in HIV infection. *Neuroradiology* 1993; 35: 264–268
- Henson J, Saffer J, Furneaux H. The transcription factor Sp 1 binds to the JC virus promoter and is selectively expressed in glial cells in human brain. *Ann Neurol* 1992; 32: 72–77
- Ho JL, Poldre PA, McEniry D, Howley PM, Snyderman DR, Rudders RA, Worthington M. Acquired immunodeficiency syndrome with progressive multifocal leukoencephalopathy and monoclonal B-cell proliferation. *Ann Intern Med* 1984; 100: 693–696
- Houff SA, Major EO, Katz DA, Kufta CV, Sever JL, Pittaluga S, Roberts JR, Gitt J, Saini N, Lux W. Involvement of JC virus-infected mononuclear cells from the bone marrow and spleen in the pathogenesis of progressive multifocal leukoencephalopathy. *N Engl J Med* 1988; 318: 301–305
- Iida T, Kitamura T, Guo J, Taguchi F, Aso Y, Nagashima K, Yogo Y. Origin of JC polyomavirus variants associated with progressive multifocal leukoencephalopathy. *Proc Natl Acad Sci* 1993; 90: 5062–5065
- Kasner SE, Gelatta SL, McGowan JC, Grossman RI. Magnetization transfer imaging in progressive multifocal leukoencephalopathy. *Neurology* 1997; 48: 534–536
- Koralnik IJ. Overview of the cellular immunity against JC virus in progressive multifocal leukoencephalopathy. *J Neurovirol* 2002; 2: 59–65
- Kuchelmeister K, Gullotta F, Bergmann M, Angeli G, Masini T. Progressive multifocal leukoencephalopathy (PML) in the acquired immunodeficiency syndrome (AIDS). *Pathol Res Pract* 1993; 189: 163–173
- Mark AS, Atlas SW. Progressive multifocal leukoencephalopathy in patients with AIDS: appearance on MR images. *Radiology* 1989; 173: 517–520
- Marra CM, Rajicic N, Barker DE, Cohen BA, Clifford D, Donovan Post MJ, Ruiz A, Bowen BC, Huang M-L, Queen-Baker J, Andersen J, Kelly S, Shriver S. A pilot study of cidofovir for progressive multifocal leukoencephalopathy in AIDS. *AIDS* 2002; 16: 1791–1797
- Mock DJ, Powers JM, Goodman AD, Blumenthal SR, Ergin N, Baker JV, Mattson DH, Assouline JG, Bergey EJ, Chem N, Epstein LG, Blumberg BM. *J Neurovirol* 1999; 5: 363–373
- Newton HB, Makley M, Slivka AP, Li J. progressive multifocal leukoencephalopathy presenting as multiple enhancing lesions on MRI: case report and literature review. *J Neuroimaging* 1995; 5: 125–125
- Newton P, Aldridge RD, Lessells AM, Best PV. Progressive multifocal leukoencephalopathy complicating systemic lupus erythematosus. *Arthritis Rheum* 1986; 29: 337–343
- Okada Y, Sawa H, Endo S, Orba Y, Umemura T, Nishihara H, Stan AC, Takana S, Takahashi H, Nagashima K. Expression of JC virus agnoprotein in progressive multifocal leukoencephalopathy brain. *Acta Neuropathol (Berl)* 2002; 104: 130–136
- Padgett BL, Walker DL, ZuRhein GM, Hodach AE, Chou SM. JC papovavirus in progressive multifocal leukoencephalopathy. *J Infect Dis* 1976; 133: 686–690
- Peters ACB, Versteeg J, Bots GTAM, Boogerd W, Vielvoye GJ. Progressive multifocal leukoencephalopathy. Immunofluorescent demonstration of simian virus 40 antigen in CSF cells and response to cytarabine therapy. *Arch Neurol* 1980; 37: 497–501
- Port JD, Miseljic S, Lee RR, Ali SZ, Nicol TL, Royal W, Chin BB. Progressive multifocal leukoencephalopathy demonstrating contrast enhancement on MRI and uptake of thallium-201: a case report. *Neuroradiology* 1999; 41: 895–898
- Roberts MTM, Carmichael A, Lever AML. Prolonged survival in AIDS-related progressive multifocal leukoencephalopathy following anti-retroviral therapy and cidofovir. *Int J Antimicrob Agents* 2003; 21: 347–349
- Rockwell D, Ruben FL, Winkelstein A, Mendelow H. Absence of immune deficiencies in a case of progressive multifocal leukoencephalopathy. *Am J Med* 1976; 61: 433–436
- Rubin DI, Norris S, Flint R. Isolated pontine progressive multifocal leukoencephalopathy: unusual magnetic resonance imaging features. *J Neuroimaging* 2002; 12: 63–66

- Sabath BF, Major EO. Traffic of JC virus from sites of initial infection to the brain: the path to progressive multifocal leukoencephalopathy. *J Infect Dis* 2002; 186: S180-S186
- Safdar A, Rubocki J, Horvath JA, Narayan K, Waldron RL. Fatal immune restoration disease in human immunodeficiency virus type 1-infected patients with progressive multifocal leukoencephalopathy: impact of antiretroviral therapy-associated immune reconstruction. *Clin Infect Dis* 2002; 35: 1250-1257
- Seth P, Diaz F, Major EO. Advances in the biology of JC virus and induction of progressive multifocal leukoencephalopathy. *J Neurovirol* 2003; 9: 236-246
- Shapiro RA, Mullane KM, Camras L, Flowers C, Sutton S. Clinical and magnetic resonance imaging regression of progressive multifocal leukoencephalopathy in an AIDS patient after intensive antiretroviral therapy. *J Neuroimaging* 2001; 11: 336-339
- Sima AAF, Finkelstein SD, McLachlan DR. Multiple malignant astrocytomas in a patient with spontaneous progressive multifocal leukoencephalopathy. *Ann Neurol* 1983; 14: 183-188
- Steiger MJ, Tarnesby G, Gabe S, McLaughlin J, Schapira AHV. Successful outcome of progressive multifocal leukoencephalopathy with cytarabine and interferon. *Ann Neurol* 1993; 33: 407-411
- Stohman SA, Hinton DR. Viral induced demyelination. *Brain Pathol* 2001; 11: 92-106
- Sugimoto C, Ito D, Matsuda H, Saito H, Sakai H, Fujihara K, Itoyama Y, Yamada T, Kira J, Matsumoto R, Mori M, Nagashima K, Yogo Y. Amplification of JC virus regulatory DNA sequences from cerebrospinal fluid: diagnostic value for progressive multifocal leukoencephalopathy. *Arch Virol* 1998; 143: 249-262
- Thurnher MM, Donovan Post MJ, Rieger A, Kleibl-Popov C, Loewe C, Schindler E. Initial and follow-up MR imaging findings in AIDS-related progressive multifocal leukoencephalopathy treated with highly active antiretroviral therapy. *AJNR Am J Neuroradiol* 2001; 22: 977-984
- Trotot PM, Vazeux R, Yamashita HK, Sandoz-Tronca C, Mikol J, Vedrenne C, Thiébaud JB, Gray F, Cikurel M, Pialoux G, Levilain R. MRI pattern of progressive multifocal leukoencephalopathy (PML) in AIDS. *J Neuroradiol* 1990; 17: 233-254
- Weber T, Major EO. Progressive multifocal leukoencephalopathy: molecular biology, pathogenesis and clinical impact. *Intervirology* 1997; 40: 98-111
- Zachoval R, Hunstein W, Ho AD. Progressive multifocal leukoencephalopathy in a patient with Hodgkin's disease. *Blut* 1980; 41: 451-454
- Bahemuka M, Rahman Shemena A, Panayiotopoulos CP, Al-Aska AK, Obeid T, Daif AK. Neurological syndromes of brucellosis. *J Neurol Neurosurg Psychiatry* 1988; 51: 1017-1021
- Bahemuka M, Babiker MA, Wright SF, Al Orainey I, Obeid T. The pattern of infections in the nervous system in Riyadh: a review of 121 cases. *Q J Med* 1988; 68: 517-524
- Bashir R, Al-Kawi MZ, Harder EJ, Jenkins J. Nervous system brucellosis: diagnosis and treatment. *Neurology* 1985; 35: 1576-1581
- Belman AL, Coyle PK, Roque C, Cantos E. MR findings in children infected by *Borrelia burgdorferi*. *Pediatr Neurol* 1992; 8: 428-431
- Bussone G, La Manita L, Grazzi L, Lamperti E, Salmaggi A, Strada L. Neurobrucellosis mimicking multiple sclerosis: a case report. *Eur Neurol* 1989; 29: 238-240
- Çiftçi E, Erden İ, Akyar S. Brucellosis of the pituitary region: MRI. *Neuroradiology* 1998; 40: 383-384
- Coskun E, Züzer T, Yalçın N, Tahta K. Spinal extradural compression caused by granuloma of brucellosis. *Scand J Infect Dis* 1998; 30: 311-312
- Galanakis E, Bourantas KL, Levidotou S, Lapatsanis PD. Childhood brucellosis in north-west Greece: a retrospective analysis. *Eur J Pediatr* 1996; 155: 1-6
- Güven MB, Cirak B, Kutluhan A, Ugras S. Pituitary abscess secondary to neurobrucellosis. *J Neurosurg* 1999; 90: 1142
- Güven H, Kocabay K, Okten A, Bektas S. Brucellosis in a child complicated with multiple brain abscesses. *Scand J Infect Dis* 1989; 21: 333-336
- Martínez-Chamorro E, Muñoz A, Esparza J, Muñoz MJ, Giangaspro E. Focal cerebral involvement by neurobrucellosis: pathological and MRI findings. *Eur J Radiol* 2002; 43: 28-30
- McLean DR, Russell N, Khan MY. Neurobrucellosis: clinical and therapeutic features. *Clin Infect Dis* 1992; 15: 582-590
- Oliveri RL, Materna G, Focà A, Zappia M, Aguglia U, Quattrone A. Polyradiculoneuropathy with cerebrospinal fluid albuminocytological dissociation due to neurobrucellosis. *Clin Infect Dis* 1996; 23: 833-834
- Piampiano P, McLeary M, Young LW, Janner D. Brucellosis: unusual presentations in two adolescent boys. *Pediatr Radiol* 2000; 30: 355-357
- Samdani PG, Patil S. Neurobrucellosis. *Indian Pediatr* 2003; 40: 565-568
- Seidel G, Pardo CA, Newman-Toker D, Olivi A, Eberhart CG. Neurobrucellosis presenting as leukoencephalopathy. The role of cytotoxic T lymphocytes. *Arch Pathol Lab Med* 2003; 127: e374-e377
- Shakir RA, Al-Din ASN, Araj GF, Lulu AR, Mousa AR, Saadah MA. Clinical categories of neurobrucellosis. A report on 19 cases. *Brain* 1987; 110: 213-223
- Sharif HS, Clark DC, Aabed MY, Haddad MC, Al Deeb SM, Yaqub B, Al Moutaery KR. Granulomatous spinal infections: MR imaging. *Radiology* 1990; 177: 101-107
- Trifiletti RR, Restivo DA, Pavone P, Giuffrida S, Parano E. Diabetes insipidus in neurobrucellosis. *Clin Neurol Neurosurg* 2000; 102: 163-165
- Young EJ. Utility of the enzyme-linked immunosorbent assay for diagnosing neurobrucellosis. *Clin Infect Dis* 1998; 26: 1481
- Zaidan R, Al Tahan A-R. Central venous thrombosis: a new manifestation of neurobrucellosis. *Clin Infect Dis* 1999; 28: 399-400

83 Brucellosis

- Akdeniz H, Irmak H, Anlar O, Demiroz AP. Central nervous system brucellosis: presentation, diagnosis and treatment. *J Infect* 1998; 36: 297-301
- Al Deeb SM, Yaqub BA, Sharif HS, Phadke JG. Neurobrucellosis: clinical characteristics, diagnosis, and outcome. *Neurology* 1989; 39: 498-501
- Al-Eissa YA. Unusual suppurative complications of brucellosis in children. *Acta Paediatr* 1993; 82: 987-992
- Al-Sous MW, Bohlega S, Al-Kawi MZ, Alwatban J, McLean DR. Neurobrucellosis: clinical and neuroimaging correlation. *AJNR Am J Neuroradiol* 2004; 25: 395-401

84 Subacute Sclerosing Panencephalitis

- Akdal G, Baklan B, Çakmakçı H, Kovanlıkaya A. MRI follow-up of basal ganglia involvement in subacute sclerosing panencephalitis. *Pediatr Neurol* 2001; 24: 393–395
- Alexander M, Singh S, Gnanamuthu C, Chandi S, Korah IP. Subacute sclerosing panencephalitis: CT and MR imaging in a rapidly progressive case. *Neurol India* 1999; 47: 304–307
- Alkan A, Sarac K, Kutlu R, Yakinci C, Sigirci A, Aslan M, Baysal T. Early- and late-state subacute sclerosing panencephalitis; chemical shift imaging and single-voxel MR spectroscopy. *AJNR Am J Neuroradiol* 2003; 24: 501–506
- Allen IV, McQuaid S, McMaron J, Kirk J, McConnell R. The significance of measles virus antigen and genome distribution in the CNS in SSPE for mechanisms of viral spread and demyelination. *J Neuropathol Exp Neurol* 1996; 55: 471–480
- Anlar B, Saatçi I, Köse G, Yalaz K. MRI findings in subacute sclerosing panencephalitis. *Neurology* 1996; 47: 1278–1283
- Anlar B, Yalaz K, Oktem F, Kose G. Long-term follow-up of patients with subacute sclerosing panencephalitis treated with intraventricular α -interferon. *Neurology* 1997; 48: 526–528
- Anlar B, Yalaz K, Köse G, Saygi S. β -Interferon plus inosiplex in the treatment of subacute sclerosing panencephalitis. *J Child Neurol* 1998; 13: 557–559
- Anlar B, Söylemenzoğlu F, Aysun S, Köse G, Belen D, Yalaz K. Tissue inflammatory response in subacute sclerosing panencephalitis (SSPE). *J Child Neurol* 2001; 16: 895–900
- Arora SC, Al-Tahan AR, Al-Zeer A, Al-Tahan F, Ozo CO, ur-Rahman N. Subacute sclerosing panencephalitis presenting as acute disseminated encephalomyelitis: a case report. *J Neurol Sci* 1997; 146: 13–18
- Barthez Carpentier MA, Billard C, Maheut J, Jourdan ML, Degenne D, Ruchoux MM, Goudeau A, Santini JJ. Acute measles encephalitis of the delayed type: neuroradiological and immunological findings. *Eur Neurol* 1992; 32: 235–237
- Bismar J, Gascon GG, Vult von Steyern K, Bohlega S. Subacute sclerosing panencephalitis; evaluation with CT and MR. *AJNR Am J Neuroradiol* 1996; 17: 761–772
- Bohlega S, Al-Kawi MZ. Subacute sclerosing panencephalitis. *J Neuroimaging* 1994; 4: 71–76
- Callebaut DP, Cras P, Martin JJ. Prolonged and atypical course in some cases of subacute sclerosing panencephalitis. *Acta Neurol Belg* 1997; 97: 39–44
- Cathomen T, Naim HY, Cattaneo R. Measles viruses with altered envelope protein cytoplasmic tails gain cell infection competence. *J Virol* 1998; 72: 1224–1234
- Cruzado D, Massery-Spicher V, Roux L, Delavelle J, Picard F, Haenggeli C-A. Early onset and rapidly progressive subacute sclerosing panencephalitis after congenital measles infection. *Eur J Pediatr* 2002; 161: 438–441
- Dimova P, Bojinova V. Subacute sclerosing panencephalitis with atypical onset: clinical, computed tomographic, and magnetic resonance imaging correlations. *J Child Neurol* 2000; 15: 258–260
- Dlugos DJ, Liu GT. Subacute sclerosing panencephalitis in an American-born adult. *Clin Infect Dis* 2001; 32: 173–174
- Dyken PR. Subacute sclerosing panencephalitis. *Neurol Clin* 1985; 3: 179–196
- Dyken PR. Neuropressive disease of post-infectious origin: a review of a resurging subacute sclerosing panencephalitis (SSPE). *Ment Retard Dev Disabil Res Rev* 2001; 7: 217–225
- Dyken PR, Cunningham SC, Charles Ward L. Changing character of subacute sclerosing panencephalitis in the United States. *Pediatr Neurol* 1989; 5: 339–341
- Ehrengruber MU, Ehler E, Billeter MA, Naim HY. Measles virus spreads in rat hippocampal neurons by cell-to-cell contact and in a polarized fashion. *J Virol* 2002; 76: 5720–5728
- Fayad MN, Yamout BI, Mroueh S. Alpha-interferon in the treatment of subacute sclerosing panencephalitis. *J Child Neurol* 1997; 12: 486–488
- Gascon GG. Subacute sclerosing panencephalitis. *Sem Pediatr Neurol* 1996; 3: 260–269
- Gascon GG, International Consortium on Subacute Sclerosing Panencephalitis. Randomized treatment study of inosiplex versus combined inosiplex and intraventricular interferon-alpha in subacute sclerosing panencephalitis (SSPE): international multicenter study. *J Child Neurol* 2003; 18: 819–827
- Geller TJ, Vern BA, Sarwar M. Focal MRI findings in early SSPE. *Pediatr Neurol* 1987; 3: 310–312
- Gokcil Z, Odabasi Z, Demirkaya S, Eroglu E, Vural O. α -Interferon and isoprinosine in adult-onset subacute sclerosing panencephalitis. *J Neurol Sci* 1999; 162: 62–64
- Gürer YKY, Kükner S, Sarica B. Intravenous γ -globulin treatment in a patient with subacute sclerosing panencephalitis. *Pediatr Neurol* 1996; 14: 72–74
- Haspolat S, Anlar B, Köse G, Coskun M, Yegin O. Interleukin-1 β , interleukin-1 receptor antagonist levels in patients with subacute sclerosing panencephalitis and the effects of different treatment protocols. *J Child Neurol* 2001; 16: 417–420
- Hayashi M, Arai N, Satoh J, Suzuki H, Katayama K, Tamagawa K, Morimatsu Y. Neurodegenerative mechanisms in subacute sclerosing panencephalitis. *J Child Neurol* 2002; 17: 725–730
- Inoue T, Kira R, Nakao F, Ihara K, Bassuny WM, Kusuhara K, Nihei K, Takeshita K, Hara T. Contribution of the interleukin 4 gene to susceptibility of subacute sclerosing panencephalitis. *Arch Neurol* 2002; 59: 822–827
- Jin L, Beard S, Hunjan R, Brown DWG, Miller E. Characterization of measles virus strains causing SSPE: a study of 11 cases. *J Neurovirol* 2002; 8: 335–344
- Johnson KP, Byington DP, Gaddis L. Subacute sclerosing panencephalitis. *Adv Neurol* 1974; 6: 77–86
- Kai C, Yamanouchi K, Sakata H, Miyashita N, Takahashi H, Kobune F. Nucleotide sequences of the M gene of prevailing wild measles viruses and a comparison with subacute sclerosing panencephalitis virus. *Virus Genes* 1996; 12: 85–87
- Kato Z, Siato K, Yamada M, Asano T, Kondo N. Proton magnetic resonance spectroscopy in a case of subacute sclerosing panencephalitis. *J Child Neurol* 2002; 17: 788–790
- Koppel BS, Poon TP, Khandji A, Pavlakis SG, Pedley TA. Subacute sclerosing panencephalitis and acquired immunodeficiency syndrome: role of electroencephalography and magnetic resonance imaging. *J Neuroimaging* 1996; 6: 122–125
- Lawrence DMP, Patterson CE, Gales TL, D'Orazio JL, Vuaghn M, Rall GF. Measles virus spread between neurons requires cell contact but not CD46 expression, syncytium formation, or extracellular virus production. *J Virol* 2000; 74: 1908–1918
- Lee WY, Cho WH, Kim SH, Kim HD, Kim IO. Acute encephalitis associated with measles: MRI features. *Neuroradiology* 2003; 45: 100–106
- Lewandowska E, Szpak Gm, Lechowicz W, Pasennik E, Sobczyk W. Ultrastructural changes in neuronal and glial cells in subacute sclerosing panencephalitis: correlation with disease duration. *Folia Neuropathol* 2001; 39: 193–202

- Lewandowska E, Lechowicz W, Szpak GM, Sobczyk W. Quantitative evaluation of intranuclear inclusions in SSPE: correlation with disease duration. *Folia Neuropathol* 2001; 39: 237–241
- Lum GB, Williams JP, Dyken PR, Machen BC, Dotson PM, Harpen MD, McLeod N. Magnetic resonance and CT imaging correlated with clinical status in SSPE. *Pediatr Neurol* 1986; 2: 75–79
- Mawrin C, Lins H, Koenig B, Heinrichs T, Murayama S, Kirches E, Boltze C, Dietzmann K. Spatial and temporal disease progression of adult-onset subacute sclerosing panencephalitis. *Neurology* 2002; 58: 1568–1571
- McCarron MO, McDonnell GV, Gibson JM. Rapid neurological deterioration in a 22-year-old man. *Postgrad Med J* 1997; 73: 344–347
- McQuaid S, Campbell S, Wallace IJC, Kirk J, Cosby SL. Measles virus infection and replication in undifferentiated and differentiated human neuronal cells in culture. *J Virol* 198; 72: 5245–5250
- Miki K, Komase K, Mgone CS, Kawanishi R, Iijima M, Mgone JM, Asuo PG, Alpers MP, Takasu T, Mizutani T. Molecular analysis of measles virus infection genome derived from SSPE and acute measles patients in Papua, New Guinea. *J Med Virol* 2002; 68: 105–112
- Modi G, Campbell H, Bill P. Subacute sclerosing panencephalitis: changes on CT scan during acute relapse. *Neuroradiology* 1989; 31: 433–434
- Norrby E, Kristensson K. Measles virus in the brain. *Brain Res Bull* 1997; 44: 213–220
- Ogura H, Ayata M, Hayashi K, Seto T, Matsuoka O, Hattori H, Tanaka K, Tanaka K, Takano Y, Murata R. Efficient isolation of subacute sclerosing panencephalitis virus from patient brains by reference to magnetic resonance and computed tomographic images. *J Neurovirol* 1997; 3: 304–309
- Ohya T, Martinez AJ, Jabbour JT, Lemmi, Duenas DA. Subacute sclerosing panencephalitis: correlation of clinical, neurophysiologic and neuropathologic findings. *Neurology* 1974; 24: 211–218
- Öztürk A, Gürses C, Baykan B, Gökyiğit A, Eraksoy M. Subacute sclerosing panencephalitis: clinical and magnetic resonance imaging evaluation of 36 patients. *J Child Neurol* 2002; 17: 25–29
- Panagariya A, Sureka RK, Aurora A. Current developments in the management of subacute sclerosing panencephalitis. *J Assoc Physicians India* 1998; 46: 218–222
- Patterson JB, Cornu TI, Redwine J, Dales S, Lewicki H, Holz A, Thomas D, Billeter MA, Oldstone MBA. Evidence that the hypermutated M protein of a subacute sclerosing panencephalitis measles virus actively contributes to the chronic progressive CNS disease. *Virology* 2001; 291: 215–225
- Salvan AM, Confort-Gouny S, Cozzone PJ, Vion-Dury J, Chabrol B, Manchini J. In vivo cerebral proton MRS in a case of subacute sclerosing panencephalitis. *J Neurol Neurosurg Psychiatry* 1999; 66: 547–555
- Santoshkumar B, Radhakrishnan K. Substantial spontaneous long-term remission in subacute sclerosing panencephalitis (SSPE). *J Neurol Sci* 1998; 154: 83–88
- Sawaishi Y, Yano Y, Watanabe Y, Takada G. Migratory basal ganglia lesions in subacute sclerosing panencephalitis (SSPE): clinical implications of axonal spread. *J Neurol Sci* 1999; 168: 137–140
- Sawaishi Y, Abe T, Yano T, Ishikawa K, Takada G. SSPE following neonatal measles infection. *Pediatr Neurol* 1999; 20: 63–65
- Schneider-Schaulies J, Niewiesk S, Schneider-Schaulies S, ter Meulen V. Measles virus in the CNS: the role of viral and host factors for the establishment and maintenance of a persistent infection. *J Neurovirol* 1999; 5: 613–622
- Senol U, Haspolat S, Cevikol C, Saatçi I. Subacute sclerosing panencephalitis: brain stem involvement in a peculiar pattern. *Neuroradiology* 2000; 42: 913–916
- Takayama S, Iwasaki Y, Yamanouchi H, Sugai K, Takashima S, Iwasaki A. Characteristic clinical features in a case of fulminant subacute sclerosing panencephalitis. *Brain Dev* 1994; 16: 132–135
- Tomoda A, Shiraishi S, Hosoya M, Hamada A, Miike T. Combined treatment with interferon-alpha and ribavirin for subacute sclerosing panencephalitis. *Pediatr Neurol* 2001; 24: 54–59
- Tsuchiya K, Yamauchi T, Furui S, Suda Y, Takenaka E. MR imaging vs CT in subacute sclerosing panencephalitis. *AJNR Am J Neuroradiol* 1988; 9: 943–946
- Tuncay R, Akman-Demir G, Gökyiğit A, Eraksoy M, Barlas M, Tolun R, Gürsoy G. MRI in subacute sclerosing panencephalitis. *Neuroradiology* 1996; 38: 636–640
- Voudris KA, Skardoutsou A, Hasiotou M, Theodoropoulos B, Vagiakou EA. Long-term findings on brain magnetic resonance imaging in acute encephalopathy with bilateral striatal necrosis associated with measles. *J Child Neurol* 2002; 17: 776–777
- Winer JB, Pires M, Kermode A, Ginsberg L, Rossor M. Resolving MRI abnormalities with progression of subacute sclerosing panencephalitis. *Neuroradiology* 1991; 33: 178–180
- Woelk CH, Pybus OG, Jin L, Brown DWG, Holmes EC. Increased positive selection pressure in persistent (SSPE) versus acute measles virus infections. *J Gen Virol* 2002; 83: 1419–1430
- Yalaz K, Anlar B, Oktem F, Aysun S, Ustacelebi S, Gurcay O, Gurcay O, Gucuyener K, Renda Y. Intraventricular interferon and oral inosiplex in the treatment of subacute sclerosing panencephalitis. *Neurology* 1992; 42: 488–491
- Zilber N, Kahana E. Environmental risk factors for subacute sclerosing panencephalitis (SSPE). *Acta Neurol Scand* 1998; 98: 49–54

85 Congenital and Perinatal Cytomegalovirus Infection

- Adler SP. Immunoprophylaxis against cytomegalovirus disease. *Scand J Infect Dis Suppl* 1995; 99: 105–109
- Adler SP. Current prospects for immunization against cytomegalovirus disease. *Infect Agents Dis* 1996; 85: 29–35
- Ahlfors K, Ivarsson S-A, Harris S. Report on a long-term study of maternal and congenital cytomegalovirus infection in Sweden. Review of prospective studies available in the literature. *Scand J Infect Dis* 1999; 31: 443–457
- Alford CA, Stagno S, Pass RF, Britt WJ. Congenital and perinatal cytomegalovirus infections. *Rev Infect Dis* 1990; 12: 45–53
- Allen RD, Pellett PE, Stewart JA, Koopmans M. Nonradioactive PCR-enzyme-linked immunosorbent assay method for detection of human cytomegalovirus DNA. *J Clin Microbiol* 1995; 33: 725–728
- Anderson KS, Amos CS, Boppana S, Pass R. Ocular abnormalities in congenital cytomegalovirus infection. *J Am Optom Assoc* 1996; 67: 273–278
- Atkins JT, Demmler GJ, Williamson WD, McDonald JM, Ista AS, Buffone GJ. Polymerase chain reaction to detect cytomegalovirus DNA in the cerebrospinal fluid of neonates with congenital infection. *J Infect Dis* 1994; 169: 1334–1337

- Bale JR Jr, Bray PF, Bell WE. Neuroradiographic abnormalities in congenital cytomegalovirus infection. *Pediatr Neurol* 1985; 1: 42–47
- Bale JR Jr, Sato Y, Eisert D. Progressive postnatal subependymal necrosis in an infant with congenital cytomegalovirus infection. *Pediatr Neurol* 1986; 2: 367–370
- Bale JR Jr, Blackman JA, Sato Y. Outcome in children with symptomatic congenital cytomegalovirus infection. *J Child Neurol* 1989; 4: 131–136
- Bale JR Jr, Zimmerman B, Dawson JD, Souza IE, Petheram SJ, Murph JR. Cytomegalovirus transmission in child care homes. *Arch Pediatr Adolesc Med* 1999; 153: 75–79
- Barbi M, Binda S, Primache V, Caroppo S, Didò P, Guidotti P, Corbetta C, Melotti D. Cytomegalovirus DNA detection in Guthrie cards: a powerful tool for diagnosing congenital infection. *J Clin Virol* 2000; 17: 159–165
- Barkovich AJ, Lindan CE. Congenital cytomegalovirus infection of the brain: imaging analysis and embryologic considerations. *AJNR Am J Neuroradiol* 1994; 15: 703–715
- Boesch C, Issakainen J, Kewitz G, Kikinis R, Martin E, Boltshauser E. Magnetic resonance imaging of the brain in congenital cytomegalovirus infection. *Pediatr Radiol* 1989; 19: 91–93
- Boom R, Sol C, Weel J, Gerrits Y, de Boer M, Ertheim-van Dillen P. A highly sensitive assay for detection and quantitation of human cytomegalovirus DNA in serum and plasma by PCR and electrochemiluminescence. *J Clin Microbiol* 1999; 37: 1489–1497
- Boppana S, Amos C, Britt W, Stagno S, Alford C, Pass R. Late onset and reactivation of chorioretinitis in children with congenital cytomegalovirus infection. *Pediatr Infect Dis J* 1994; 13: 1139–1142
- Boppana SB, Pass RF, Britt WJ, Stagno S, Alford CA. Symptomatic congenital cytomegalovirus infection: neonatal morbidity and mortality. *Pediatr Infect Dis J* 1992; 11: 93–99
- Boppana SB, Fowler KB, Viad Y, Hedlund G, Stagno S, Britt WJ, Pass RF. Neuroradiographic findings in the newborn period and long-term outcome in children with symptomatic congenital cytomegalovirus infection. *Pediatrics* 1997; 99: 409–414
- Boppana SB, Fowler KB, Britt WJ, Stagno S, Pass RF. Symptomatic congenital cytomegalovirus infection in infants born to mothers with preexisting immunity to cytomegalovirus. *Pediatrics* 1999; 104: 55–60
- Boppana SB, Rivera LB, Fowler KB, Mach M, Britt WJ. Intrauterine transmission of congenital cytomegalovirus to infants of women with preconceptional immunity. *N Engl J Med* 2001; 344: 1366–1371
- Brown HL, Abernathy MP. cytomegalovirus infection. *Semin Perinatol* 1998; 22: 260–266
- Bryant P, Morley C, Garland S, Curtis N. Cytomegalovirus transmission for breast milk in premature babies: does it matter? *Arch Dis Child Fetal Neonatal Ed* 2002; 87: F75–F77
- Ceballos R, Ch'ien LT, Whitley RJ, Brans YW. Cerebellar hypoplasia in an infant with congenital cytomegalovirus infection. *Pediatrics* 1976; 57: 155–157
- Cinque P, Marenzi R, Ceresa D. Cytomegalovirus infections of the nervous system. *Intervirology* 1997; 40: 85–97
- Conboy TJ, Pass RF, Stagno S, Alford CA, Myers GJ, Britt WJ, McCollister FP, Summers MN, McFarland CE, Boll TJ. Early clinical manifestations and intellectual outcome in children with symptomatic congenital cytomegalovirus infection. *J Pediatr* 1987; 111: 343–348
- Connolly PK, Jerger S, Williamson WD, Smith RJH, Demmler G. Evaluation of higher-level auditory function in children with asymptomatic congenital cytomegalovirus infection. *Am J Otol* 1992; 13: 185–193
- Damato EG, Winnen CW. Cytomegalovirus infection: prenatal implications. *J Obstet Gynecol Neonatal Nurs* 2002; 31: 86–92
- Daniel Y, Gull I, Reuben Peyser M, Lessing JB. Congenital cytomegalovirus infection. *Eur J Obstet Gynecol Reprod Biol* 1995; 63: 7–16
- Darin N, Bergström T, Fast A, Kyllerman M. Clinical, seriological and PCR evidence of cytomegalovirus infection in the central nervous system in infancy and childhood. *Neuropediatrics* 1994; 25: 316–322
- Das VK. Aetiology of bilateral sensorineural hearing impairment in children: a 10 year study. *Arch Dis Child* 1996; 74: 8–12
- Davis LE, Stewart JA, Rarey KE, McLaren LC. Recovery and probable persistence of cytomegalovirus in human inner ear fluid without cochlear damage. *Ann Otol Laryngol* 1987; 96: 380–383
- Demmler GJ. Infectious diseases society of America and Centers for disease control. Summary of a workshop on surveillance for congenital cytomegalovirus disease. *Rev Infect Dis* 1991; 13: 315–329
- Demmler GJ. Congenital cytomegalovirus infection and disease. *Adv Pediatr Infect Dis* 1996; 11: 135–162
- De Vries LS, Gunardi H, Barth PG, Bok LA, Verboon-Macielek MA, Groenendaal F. The spectrum of cranial ultrasound and magnetic resonance imaging abnormalities in congenital cytomegalovirus infection. *Neuropediatrics* 2004; 35: 113–9
- Eggers M, Metzger C, Enders G. Differentiation between acute primary and recurrent human cytomegalovirus infection in pregnancy, using a microneutralization assay. *J Med Virol* 1998; 56: 351–358
- Fischler B, Rodensjö P, Nemeth A, Forsgren M, Lewensohn-Fuchs I. Cytomegalovirus DNA detection on Guthrie cards in patients with prenatal cholestasis. *Arch Dis Child Fetal Neonat Ed* 1999; 80: F130–F134
- Fowler KB, McCollister FP, Dahle AJ, Boppana S, Britt WJ, Pass RF. Progressive and fluctuating sensorineural hearing loss in children with asymptomatic congenital cytomegalovirus infection. *J Pediatr* 1997; 130: 624–630
- Fowler SL. A light in the darkness: predicting outcomes for congenital cytomegalovirus infections. *J Pediatr* 2000; 137: 4–6
- Fritschy J-M, Brandner S, Aguzzi A, Koedood M, Lüscher B, Mitchell PJ. Brain cell type specification and gliosis-induced activation of the human cytomegalovirus immediate-early promoter in transgenic mice. *J Neurosci* 1996; 16: 2275–2282
- Gaytant MA, Steegers EAP, Semmekrot BA, Merkus HMMW, Galama JMD. Congenital cytomegalovirus infection: review of the epidemiology and outcome. *Obstet Gynecol Surv* 2002; 67: 245–256
- Gomes AL, Vieira JP, Saldanha J. Non-progressive leukoencephalopathy with bilateral temporal cysts. *Eur J Pediatr Neurol* 2001; 5: 121–125
- Grangeot-Keros L, Cointe D. Diagnosis and prognostic markers of HCMV infection. *J Clin Virol* 2001; 21: 213–221
- Grant EG, Williams AL, Schellinger D, Slovis TL. Intracranial calcification in the infant and neonate: evaluation by sonography and CT. *Radiology* 1985; 157: 63–68
- Griffith BP, Booss J. Neurological infections of the fetus and newborn. *Neurol Clin* 1994; 12: 541–564
- Hagay ZJ, Biran G, Ornoy A, Reece EA. Congenital cytomegalovirus infection: a long-standing problem still seeking a solution. *Am J Obstet Gynecol* 1996; 174: 241–245

- Haginoya K, Ohura T, Kon K, Yagi T, Sawaiishi Y, Ishii KK, Funato T, Higano S, Takahashi S, linuma K. Abnormal white matter lesions with sensorineural hearing loss caused by congenital cytomegalovirus infection: retrospective diagnosis by PCR using Guthrie cards. *Brain Dev* 2002; 24: 710–714
- Hayward JC, Titelbaum DS, Clancy RR, Zimmerman RA. Lissencephaly-pachygyria associated with congenital cytomegalovirus infection. *J Child Neurol* 1991; 6: 109–114
- Istas AS, Demmler GJ, Dobbins JG, Stewart JA. Surveillance for congenital cytomegalovirus disease: a report from the National Congenital Cytomegalovirus Disease Registry. *Clin Infect Dis* 1995; 20: 665–670
- Jauniaux E, Jurkovic D, Gulbis B, Liesnard C, Lees C, Campbell S. Materno-fetal immunoglobulin transfer and passive immunity during the first trimester of human pregnancy. *Hum Reprod* 1995; 10: 3297–330
- Johansson PJH, Jönsson M, Ahlfors K, Ivarsson SA, Svanberg L, Guthenberg C. Retrospective diagnostics of congenital cytomegalovirus infection performed by polymerase chain reaction in blood stored on filter paper. *Scand J Infect Dis* 1997; 29: 465–468
- Jones CA, Isaacs D. Predicting the outcome of symptomatic congenital cytomegalovirus infection. *J Paediatr Child Health* 1995; 31: 70–71
- Kimberlin DW, Lin C-Y, Sanches PJ, Demmler GJ, Danker W, Shelton M, Jacobs RF, Vaudry W, Pass RF, Kiell JM, Soong S-J, Whitley RJ. Effect of ganciclovir therapy on hearing in symptomatic congenital cytomegalovirus disease involving the central nervous system: a randomized, controlled trial. *J Pediatr* 2003; 143: 16–25
- Koedood M, Fichtel A, Meier P, Mitchell PJ. Human cytomegalovirus (HCMV) immediate-early enhancer/promoter specificity during embryogenesis defines target tissues of congenital HCMV infection. *J Virol* 1995; 69: 2194–2207
- Kohyama J, Kajiwara M, Shimohira M, Iwakawa Y, Okawa H. Human cytomegalovirus DNA in cerebrospinal fluid. *Arch Dis Child* 1994; 71: 414–418
- Koi H, Zhang J, Parry S. The mechanisms of placental viral infection. *Ann NY Acad Sci* 2001; 943: 148–156
- Koopmans M, Sánchez-Martínez D, Patton J, Stewart J. Evaluation of antigen and antibody detection in urine specimens from children with congenital human cytomegalovirus infection. *J Med Virol* 1995; 46: 321–328
- Lagasse N, Dhooge I, Govaert P. Congenital CMV-infection and hearing loss. *Acta Otolaryngol Belg* 2000; 54: 431–436
- Lamy ME, Mulongo KN, Gadisseux J-F, Lyon G, Gaudy V, van Lierde M. Prenatal diagnosis of fetal cytomegalovirus infection. *Am J Obstet Gynecol* 1992; 166: 91–94
- Lazzarotto T, Guerra B, Spezzacatena P, Varani S, Gabrielli L, Pradelli P, Rumpianesi F, Banzi C, Bovicelli L, Landini MP. Prenatal diagnosis of congenital cytomegalovirus infection. *J Clin Microbiol* 1998; 36: 3540–3544
- Lazzarotto T, Spezzacatena P, Varani S, Gabrielli L, Pradelli P, Guerra B, Landini MP. Anticytomegalovirus (anti-CMV) immunoglobulin G avidity in identification of pregnant woman at risk of transmitting congenital CMV infection. *Clin Diagn Lab Immunol* 1999; 6: 127–129
- Lazzarotto T, Varani S, Gabrielli L, Spezzacatena P, Landini MP. New advances in the diagnosis of congenital cytomegalovirus infection. II. Diagnostics and antiviral therapy. *Intervirology* 1999; 42: 390–397
- Lazzarotto T, Varani S, Guerra B, Nicolosi A, Lanari M, Landini MP. Prenatal indicators of congenital cytomegalovirus infection. *J Pediatr* 2000; 137: 90–95
- Mahlm G, Gröndahl EH, Lewensohn-Fuchs I. Congenital cytomegalovirus infection: a retrospective diagnosis in a child with pachygyria. *Pediatr Neurol* 2000; 22: 407–408
- Malinger G, Lev D, Zahalka N, Aroia ZB, Waternberg N, Kidron D, Sira LB, Lerman-Sagie T. *AJNR Am J Neuroradiol* 2003; 24: 28–32
- Marques Dias MJ, Harmant-van Rijckevorsel G, Landrieu P, Lyon G. Prenatal cytomegalovirus disease and cerebral microgyria: evidence for perfusion failure, not disturbance of histogenesis, as the major cause of fetal cytomegalovirus encephalopathy. *Neuropediatrics* 1984; 15: 18–24
- Martinez A, Castro A, Gil C, Perez C. Recent strategies in the development of new human cytomegalovirus inhibitors. *Med Res Rev* 2001; 3: 227–244
- Michaels MG, Greenberg FP, Sabo DL, Wald ER. Treatment of children with congenital cytomegalovirus infection with ganciclovir. *Pediatr Infect Dis J* 2003; 22: 504–508
- Morris DJ, Sims S, Chiswick M, Das VK, Newton VE. Symptomatic congenital cytomegalovirus infection after maternal recurrent infection. *Pediatr Infect Dis J* 1994; 13: 61–64
- Murph JR, Souza IE, Dawson JD, Benson P, Petheram SJ, Pfab D, Gregg A, O'Neill ME, Zimmerman B, Bale JF Jr. Epidemiology of congenital cytomegalovirus infection: maternal risk factors and molecular analysis of cytomegalovirus strains. *Am J Epidemiol* 1998; 147: 940–947
- Mussi-Pinhata MM, Yamamoto AY, Figueiredo LTM, Cervi MC, Duarte G. Congenital and perinatal cytomegalovirus infection in infants born to mothers infected with human immunodeficiency virus. *J Pediatr* 1998; 132: 285–290
- Negishi H, Yamada H, Hirayama E, Okuyama K, Sagawa T, Matsumoto Y, Fujimoto S. Intraperitoneal administration of cytomegalovirus hyperimmunoglobulin to the cytomegalovirus-infected fetus. *J Perinatol* 1998; 18: 466–469
- Nelson CT, Istas AS, Wilkerson MK, Demmler GJ. PCR detection of cytomegalovirus DNA in serum as a diagnostic test for congenital cytomegalovirus infection. *J Clin Microbiol* 1995; 33: 3317–3318
- Noyola DE, Demmler GJ, Williamson WD, Griesser C, Sellers S, Llorente A, Littman T, Williams S, Jarrett L, Yow MD. Cytomegalovirus urinary excretion and long term outcome in children with congenital cytomegalovirus infection. *Pediatr Infect Dis J* 2000; 19: 505–510
- Noyola DE, Demmler GJ, Nelson CT, Griesser C, Williamson WD, Atkins JT, Rozelle J, Turcich M, Llorente AM, Sellers-Vinson S, Reynolds A, Bale JF Jr, Gerson P, Yow MD. Early predictors of neurodevelopmental outcome in symptomatic congenital cytomegalovirus infection. *J Pediatr* 2001; 138: 325–331
- Numazaki K. Human cytomegalovirus infection of breast milk. *FEMS Immunol Med Microbiol* 1997; 18: 91–98
- Namazaki K, Chiba S. Current aspects of diagnosis and treatment of cytomegalovirus infections in infants. *Clin Diagn Virol* 1997; 8: 169–181
- Namazaki K, Asanuma H, Ikehata M, Chiba S. Detection of cytomegalovirus DNA in serum as test for congenital infection. *Early Hum Dev* 1998; 52: 43–48
- Olivier M, Lenard HG, Aksu F, Gärtner J. A new leukoencephalopathy with bilateral anterior temporal lobe cysts. *Neuropediatrics* 1998; 29: 225–228
- Pass RF. Immunization strategy for prevention of congenital cytomegalovirus infection. *Infect Agents Dis* 1996; 5: 240–244
- Pass RF. Cytomegalovirus infection. *Pediatr Rev* 2002; 23: 163–169
- Peckham C, Tookey P, Logan S, Giaquinto C. Screening options for prevention of congenital cytomegalovirus infection. *J Med Screen* 2001; 8: 119–124

- Peckham CS, Coleman JC, Hurley R, Chin KS, Henderson K, Preece PM. Cytomegalovirus infection in pregnancy: preliminary findings from a prospective study. *Lancet* 1983; *i*: 1352–1355
- Poland SD, Bambrick LL, Dakaban GA, Rice GPA. The extent of human cytomegalovirus replication in primary neurons is dependent on host cell differentiation. *J Infect Dis* 1994; *170*: 1267–1271
- Raine CS, Fields BN. Neurotropic viruses and the developing brain. *NY State Med* 1973; *73*: 1169–1179
- Ramenghi LA, Domizio S, Quartulli L, Sabatino G. Prenatal pseudocysts of the germinal matrix in preterm infants. *J Clin Ultrasound* 1997; *25*: 169–173
- Revello MG, Baldanti F, Furione M, Sarasini A, Percivalle E, Zavattoni M, Gerna G. Polymerase chain reaction for prenatal diagnosis of congenital human cytomegalovirus infection. *J Med Virol* 1995; *47*: 462–466
- Revello MG, Sarasini A, Zavattoni M, Baldanti F, Gerna G. Improved prenatal diagnosis of congenital human cytomegalovirus infection by a modified nested polymerase chain reaction. *J Med Virol* 1998; *56*: 99–103
- Schackelford GD, Fulling KH, Glasier CM Maj. Cysts of the subependymal germinal matrix: sonographic demonstration with pathologic correlation. *Radiology* 1983; *149*: 117–121
- Schendel DE. Infection in pregnancy and cerebral palsy. *J Am Med Womens Assoc* 2001; *56*: 105–108
- Schneeberger PM, Groenendaal F, de Vries LS, van Loon AM, Vroom TM. Variable outcome of a congenital cytomegalovirus infection in a quadruplet after primary infection of the mother during pregnancy. *Acta Paediatr* 1994; *83*: 986–989
- Schopper K, Lauber E, Krech U. Congenital cytomegalovirus infection in newborn infants of mothers infected before pregnancy. *Arch Dis Child* 1978; *53*: 536–539
- Schwebke K, Henry K, Balfour HH Jr, Olson D, Crane RT, Jordan C. Clinical and laboratory observations. Congenital cytomegalovirus infection as a result of nonprimary cytomegalovirus disease in a mother with acquired immunodeficiency syndrome. *J Pediatr* 1995; *126*: 293–295
- Sener RN. Schizencephaly and congenital cytomegalovirus infection. *J Neuroradiol* 1998; *25*: 151–152
- Shaw C-M, Alvord EC Jr. Subependymal germinolysis. *Arch Neurol* 1974; *31*: 374–381
- Soussotte C, Maugey-Laulom B, Charles D, Diard F. Contribution of transvaginal ultrasonography and fetal cerebral MRI in a case of congenital cytomegalovirus infection. *Fetal Diagn Ther* 2000; *15*: 219–223
- Souza IE, Gregg A, Pfab D, Dawson JD, Benson P, O'Neill ME, Murph JR, Petheram SJ, Bale FJ Jr. Cytomegalovirus infection in newborns and their family members: polymerase chain reaction analysis of isolates. *Infection* 1997; *25*: 144–149
- Stamos JK, Rowley AH. Timely diagnosis of congenital infections. *Pediatr Clin North Am* 1994; *41*: 1017–1033
- Steinlin M. Non-progressive congenital ataxias. *Brain Dev* 1998; *20*: 199–208
- Steinlin M, Zürrer M, Marin E, Boesch CH, Largo RH, Boltshauser E. Contribution of magnetic resonance imaging in the evaluation of microcephaly. *Neuropediatrics* 1991; *22*: 184–189
- Steinlin M, Nadal D, Eich GE, Martin E, Boltshauser EJ. Late intrauterine cytomegalovirus infection: Clinical and neuroimaging findings. *Pediatr Neurol* 1996; *15*: 249–253
- Stronati M, Revello MG, Cerbo RM, Furione M, Rondini G, Gerna G. Ganciclovir therapy of congenital human cytomegalovirus hepatitis. *Acta Paediatr* 1995; *84*: 340–341
- Sugita K, Ando M, Makino M, Takanashi J, Fujimoto N, Niimi H. Magnetic resonance imaging of the brain in congenital rubella virus and cytomegalovirus infections. *Neuroradiology* 1991; *33*: 239–242
- Titelbaum DS, Hayward JC, Zimmerman RA. Pachygyriclike changes: topographic appearance at MR imaging ant CT and correlation with neurologic status. *Radiology* 1989; *173*: 663–667
- van der Knaap MS, Vermeulen G, Barkhof F, Hart AAM, Loeber JG, Weel JFL. A pattern of white matter abnormalities on MRI: polymerase chain reaction on Guthrie cards to link the pattern with congenital CMV. *Radiology* 2004; *230*: 529–536
- Weinberg A. The role of immune reconstruction in cytomegalovirus infection. *Biodrugs* 2002; *16*: 89–95
- Williamson WD, Percy AK, Yow MD, Gerson P, Catlin FI, Koppelman ML, Thurber S. Asymptomatic congenital cytomegalovirus infection. Audiologic, Neuroradiologic, and neurodevelopmental abnormalities during the first year. *Am J Dis Child* 1990; *144*: 1365–1368
- Williamson WD, Demmler GJ, Percy AK, Catlin FI. Progressive hearing loss in infants with asymptomatic congenital cytomegalovirus infection. *Pediatrics* 1992; *90*: 862–866
- Yamashita Y, Outani Y, Kawano Y, Horikawa M, Matsuishi T, Hashimoto T. Clinical analysis and short-term progress of neonates with subependymal cysts. *Pediatr Neurol* 1990; *6*: 375–378
- Zaia JA, Lang DJ. Cytomegalovirus infection of the fetus and neonate. *Neurol Clin* 1984; *2*: 387–410

86 Whipple Disease

- Anderson M. Neurology of Whipple's disease. *J Neurol Neurosurg Psychiatry* 2000; *68*: 2–5
- Brändle M, Ammann P, Spinas GA, Dutley F, Galeazzi RL, Schmid C, Altwegg M. Relapsing Whipple's disease presenting with hypopituitarism. *Clin Endocrinol* 1999; *50*: 399–403
- Brown AP, Lane JC, Murayama S, Vollmer DG. Whipple's disease presenting with isolated neurological symptoms. *J Neurosurg* 1990; *73*: 623–627
- Carella F, Valla P, Bernardi G, Parente F, Costa A, Lodrini S. Cerebral Whipple's disease: clinical and cerebrospinal fluid findings. *Ital J Neurol Sci* 1998; *19*: 101–105
- Coene De B, Gilliard C, Indekeu P, Duprez T, Trigaux JP. Whipple's disease confined to the central nervous system. *Neuroradiology* 1996; *38*: 325–327
- Cooper GS, Blades EW, Remler BF, Salata RA, Bennert KW, Jacobs GH. Central nervous system Whipple's disease: relapse during therapy with trimethoprim-sulfamethoxazole and remission with cefixime. *Gastroenterology* 1994; *106*: 782–786
- Davion T, Rosat P, Sevestre H, Desablens B, Debussche C, Delamarre J, Capron JP. MR Imaging of CNS relapse of Whipple disease. *J Comput Assist Tomogr* 1990; *14*: 815–817
- Duprez TPJ, CrandinCBG, Bonnier C, Thauvoy CW, Gadisseux JF, Dutrieux JL, Evrard P. Whipple disease confined to the central nervous system in childhood. *AJNR Am J Neuroradiol* 1996; *17*: 1589–1591
- Erdem E, Carlier R, Delvalle A, Caquet R, Etienne JP, Doyon D. Gadolinium-enhanced MRI in cerebral Wipple's disease. *Neuroradiology* 1993; *35*: 581–583
- Gérard A, Sarrot-Reynauld F, Liozon E, Cathebras P, Besson G, Robin C, Vighetto A, Mosnier JF, Durieu I, Durand DV, Rousset H. Neurologic presentation of Whipple disease. *Medicine* 2002; *81*: 443–457

- Lynch T, Odel J, Fredricks DN, Louis ED, Forman S, Rotterdam H, Fahn S, Redman DA. Polymerase chain reaction-based detection of *Tropheryma whippelii* in central nervous system Whipple's disease. *Ann Neurol* 1997; 42: 120–124
- Manzel K, Tranel D, Cooper G. Cognitive and behavioral abnormalities in a case of central nervous system Whipple disease. *Arch Neurol* 2000; 57: 399–403
- Mendel E, Khoo LT, Go JL, Hinton D, Zee CS, Apuzzo MLJ. Intracerebral Whipple's disease diagnosed by stereotactic biopsy: a case report and review of the literature. *Neurosurgery* 1999; 44: 203–209
- Messori A, Di Bella P, Polonara G, Logullo F, Pauri P, Haghighipour R, Salvolini U. An unusual spinal presentation of Whipple disease. *AJNR Am J Neuroradiol* 2001; 22: 1004–1008
- Peters G, du Plessis DG, Humphrey PR. Cerebral Whipple's disease with a stroke-like presentation and cerebrovascular pathology. *J Neurol Neurosurg Psychiatry* 2002; 73: 336–339
- Raoult D, Birg ML, Scola la B, Fournier PE, Enea M, Lepidi H, Roux V, Piette JC, Vandenesch F, Vital-Durand D, Marrie TJ. Cultivation of the bacillus of Whipple's disease. *N Engl J Med* 2000; 342: 620–625
- Schnider P, Trattinnig S, Kollegger H, Auff E. MR of cerebral Whipple disease. *AJNR Am J Neuroradiol* 1995; 16: 1328–1329
- Scully RE, Mark EJ, McNeely WF, Ebeling SH, Phillips LD. Case records of the Massachusetts General Hospital. *N Engl J Med* 1997; 37: 1612–1620
- Süzer T, Demirkan N, Tahta K, Coskun E, Cetin B. Whipple's disease confined to the central nervous system: case report and review of the literature. *Scand J Infect Dis* 1999; 31: 411–414
- Swartz MN. Whipple's disease – past, present, and future. *N Engl J Med* 2000; 342: 648–650
- Verhagen WIM, Huygen PLM, Dalman JE, Schuurmans MMJ. Whipple's disease and the central nervous system: a case report and a review of the literature. *Clin Neurol Neurosurg* 1996; 98: 299–304
- Wroe SJ, Pires M, Harding B, Youl BD, Shorvon S. Whipple's disease confined to the CNS presenting with multiple intracerebral mass lesions. *J Neurol Neurosurg Psychiatry* 1991; 54: 989–992
- Cohen JA, Fisher RS, Brigell MG, Peyster RG, Sze G. The potential for vigabatrin-induced intramyelinic edema in humans. *Epilepsia* 2000; 41: 148–157
- Crapper McLachlan DR, De Boni U. Aluminium in human brain disease – an overview. *Neurotoxicology* 1980; 1: 3–16
- Davis LE, Kornfeld M, Mooney HS, Fiedler KJ, Haaland KY, Orrison WW, Cernichiari E, Clarkson TW. Methylmercury poisoning: long-term clinical, radiological, toxicological, and pathological studies of an affected family. *Ann Neurol* 1994; 35: 680–688
- Del Amo M, Berenguer J, Pujol T, Mercader JM. MR in trichloroethane poisoning. *AJNR Am J Neuroradiol* 1995; 17: 1180–1182
- Díez-Tejedor E, Frank A, Gutiérrez M, Barreiro P. Encephalopathy and biopsy-proven cerebrovascular inflammatory changes in a cocaine abuser. *Eur J Neurol* 1998; 5: 103–107
- Dobbing J. Vulnerable periods in developing brain. In: Davison AN, Dobbing J, eds. *Applied neurochemistry*. Oxford: Blackwell, 1968, pp 287–316
- Donaldson J. The physiopathologic significance of manganese in brain: its relation to schizophrenia and neurodegenerative disorders. *Neurotoxicology* 1987; 8: 451–462
- Escobar A, Aruffo C. Chronic thinner intoxication: clinicopathologic report of a human case. *J Neurol Neurosurg Psychiatry* 1980; 43: 986–994
- Filley CM. Toxic leukoencephalopathy. *Clin Neuropharmacol* 1999; 22: 249–260
- Filley CM, Heaton RK, Rosenberg NL. White matter dementia in chronic toluene abuse. *Neurology* 1990; 40: 532–534
- Gacouin A, Lavoue S, Signouret T, Person A, Dinard MD, Shpak N, Thomas R. Reversible spongiform leukoencephalopathy after inhalation of heroin. *Intensive Care Med* 2003; 29: 1012–1015
- Galle P, Meyrignac C, Heine P. Presence of high concentrations of aluminium in neurons of a patient dying from a rapidly developing dementia. *C R Acad Sci III* 1984; 299: 535–539
- Gaul HP, Wallace CJ, Auer RN, Fong TC. MR Findings in methanol intoxication. *AJNR Am J Neuroradiol* 1995; 16: 1783–1786
- Greger JL. Nutrition versus toxicology of manganese in humans: evaluation of potential biomarkers. *Neurotoxicology* 1999; 20: 205–212
- Heier LA, Carpanzano CR, Mast J, Brill PW, Winchester P, Deck MDF. Maternal cocaine abuse: the spectrum of radiologic abnormalities in the neonatal CNS. *AJNR Am J Neuroradiol* 1991; 12: 951–956
- Henry JA. Ecstasy and the dance of death. Severe reactions are unpredictable. *BMJ* 1992; 304: 5–6
- Hormes JT, Filley CM, Rosenberg NL. Neurologic sequelae of chronic solvent vapor abuse. *Neurology* 1986; 36: 698–702
- Hsu HH, Chen CY, Chen FH, Lee CC, Chou TY, Zimmerman RA. Optic atrophy and cerebral infarcts caused by methanol intoxication: MRI. *Neuroradiology* 1997; 39: 192–194
- Huang CC, Chu CC, Chen RS, Lin SK, Shih TS. Chronic carbon disulfide encephalopathy. *Eur Neurol* 1996; 36: 364–368
- Huang CC, Chu CC, Chu NS, Wu TN. Carbon disulfide vasculopathy: a small vessel disease. *Cerebrovasc Dis* 2001; 11: 245–250
- Kamran S, Bakshi R. MRI in chronic toluene abuse: low signal in the cerebral cortex on T2-weighted images. *Neuroradiology* 1998; 40: 519–521
- Keogh CF, Andrews GT, Spacey SD, Forkheim KE, Graeb DA. Neuroimaging features of heroin inhalation toxicity: "chasing the dragon". *AJR Am J Roentgenol* 2003; 180: 847–850
- Andreas K, Blaschke M, Bergsträsser E, Fisher H-D, Schmidt J. Neurochemical characterization of hexachlorophene induced brain oedema. *Arch Toxicol* 1991; 14: 30–32
- Ashikaga R, Araki Y, Miura K, Ishida O. Cranial MRI in chronic thinner intoxication. *Neuroradiology* 1995; 37: 443–444
- Aydin K, Sencer S, Demir T, Ogel K, Tunaci A, Minareci O. Cranial MR findings in chronic toluene abuse by inhalation. *AJNR Am J Neuroradiol* 2002; 23: 1173–1179
- Brown GK. Metabolic disorders of embryogenesis. *J Inher Metab Dis* 1994; 17: 448–458
- Brust JCM. Neurologic complications of substance abuse. *J AIDS* 2002; 31: S29–S34
- Burg JR, Gist GL. Health effects of environmental contaminant exposure: an intrafile comparison of the Trichloroethylene Subregistry. *Arch Environ Health* 1999; 54: 231–241
- Cho SK, Kim RH, Yim SH, Tak SW, Lee YK, Son MA. Long-term neuropsychological effects and MRI findings in patients with CS2 poisoning. *Acta Neurol Scand* 2002; 106: 269–275

87 Toxic Encephalopathies

- Kim JH, Chang KH, Song IC, Kim KH, Kwon BJ, Kim HC, Kim JH, Han MH. Delayed encephalopathy of acute carbon monoxide intoxication: diffusivity of cerebral white matter lesions. *AJNR Am J Neuroradiol* 2003; 24: 1592–1597
- Kimbrough RD, Gaines TB. Hexachlorophene effects on the rat brain. Study of high doses by light and electron microscopy. *Arch Environ Health* 1971; 23: 114–118
- Kondo K. Congenital Minamata disease: warnings from Japan's experience. *J Child Neurol* 2000; 15: 458–464
- Kornfeld M, Moser AB, Moser HW, Kleinschmidt-DeMasters BK, Nolte K, Phelps A. Solvent vapor abuse leukoencephalopathy. Comparison to adrenoleukodystrophy. *J Neuropathol Exp Neurol* 1994; 53: 389–398
- Korogi Y, Takahashi M, Shinzato J, Okajima T. MR findings in seven patients with organic mercury poisoning (Minamata disease). *AJNR Am J Neuroradiol* 1994; 15: 1575–1578
- Korogi Y, Takahashi M, Okajima T, Eto K. MR findings in Minamata disease – organic mercury poisoning. *J Magn Reson Imaging* 1998; 3: 308–316
- Kriegstein AR, Shungu DC, Millar WS, Armitage BA, Brust JC, Chhillrud S, Goldman J, Lynch T. Leukoencephalopathy and raised brain lactate from heroin vapor inhalation (“chasing the dragon”) *Neurology* 1999; 53: 1765–1773
- Ku M-C, Huang C-C, Kuo H-C, Yen T-C, Chen C-J, Shih T-S, Chang H-Y. Diffuse white matter lesions in carbon disulfide intoxication: microangiopathy or demyelination. *Eur Neurol* 2003; 50: 220–224
- Kuteifan K, Oesterlé H, Tajahmady T, Gutbub AM, Lapatte G. Necrosis and haemorrhage of the putamen in methanol poisoning shown on MRI. *Neuroradiology* 1998; 40: 158–160
- Lee JC, Bakay L. Ultrastructural changes in the edematous central nervous system. *Arch Neurol* 1965; 13: 48–57
- Long H, Deore K, Hoffman RS, Nelson LS. A fatal case of spongiform leukoencephalopathy linked to “chasing the dragon”. *J Toxicol Clin Toxicol* 2003; 41: 887–891
- Martin-Bouyer G, toga M, Lebreton R, Stolley PD. Outbreak of accidental hexachlorophene poisoning in France. *Lancet* 1982; i: 91–95
- McCreary M, Emerman C, Hanna J, Simon J. Acute myelopathy following intranasal infusion of heroin; a case report. *Neurology* 2000; 55: 316–317
- Maxwell IC, Le Quesne PM. Conduction velocity in hexachlorophane neuropathy. Correlation between electrophysiological and histological neuropathy. *J Neurol Sci* 1979; 43: 95–110
- Nanan R, von Stockhausen HB, Petersen B, Solymosi L, War-muth-Metz M. Usual pattern of leukoencephalopathy after morphine sulphate intoxication. *Neuroradiologie* 2000; 42: 845–848
- Ohnuma A, Kimura I, Saso S. MRI in chronic paint-thinner intoxication. *Neurology* 1995; 37: 445–446
- Pal KP, Samii A, Calne DB. Manganese neurotoxicity: a review of clinical features, imaging and pathology. *Neurotoxicology* 1999; 20: 227–238
- Palmer K, Inskip H, Martyn C, Coggon D. Dementia and occupational exposure to organic solvents. *Occup Environ Med* 1998; 55: 712–715
- Powell H, Swarner O, Gluck L, Lampert P. Hexachlorophene myelinopathy in premature infants. *J Pediatr* 1973; 82: 976–981
- Rosenberg NL, Kleinschmidt-DeMasters BK, Davis KA, Dreisbach JN, Hormes JT, Filley CM. Toluene abuse causes diffuse central nervous system white matter changes. *Ann Neurol* 1988; 23: 611–614
- Sedman AB, Wilkeling GN, Warady BA, Lum GM, Alfrey AC. Encephalopathy in childhood secondary to aluminium toxicity. *J Pediatr* 1984; 105: 836–838
- Tan TP, Algra PG, Valk J, Wolters EC. Toxic leukoencephalopathy after inhalation of poisoned heroin: MR findings. *AJNR Am J Neuroradiol* 1994; 15: 175–178
- Tokuomi H, Okajima T, Kanai J, Tsunoda M, Ichiyasu Y, Misumi H, Shimomura K, Takaba M. Minamata disease – an unusual neurological disorder occurring in Minamata, Japan. *Kumamoto Med J* 1991; 14: 47–64
- Valk J, van der Knaap MS. Toxic encephalopathy. *AJNR Am J Neuroradiol* 1992; 13: 747–760
- Valk J, van der Knaap MS. Selective vulnerability in toxic encephalopathies and metabolic disorders. *Riv Neuro-radiol* 1996; 9: 749–760
- Vella S, Kreis R, Lovblad KO, Steinlin M. Acute leukoencephalopathy after inhalation of a single dose of heroin. *Neuropediatrics* 2003; 34: 100–104
- Wolters EC, Stam FC, Lousberg RJ, van Wijngaarden CK, Rengelink H, Schipper MEI, Verbeten B. Leucoencephalopathy after inhaling “heroin” pyrolysate. *Lancet* 1982; ii, 1233–1237
- Xiong L, Matthes JD, Jenkins JR. MRI imaging of “spray heads”: toluene abuse via aerosol paint inhalation. *AJNR Am J Neuroradiol* 1993; 14: 1195–1199
- Yamanouchi N, Okada S-I, Kodama K, Hirai S, Sekine H, Murakami A, Komatsu N, Sakamoto T, Sato T. White matter changes caused by chronic solvent abuse. *AJNR Am J Neuroradiol* 1995; 16: 1643–1649

88 Iatrogenic Toxic Encephalopathies

- Appignani BA, Bhadelia RA, Blacklow SC, Wang AK, Roland SF, Freeman RB Jr. Neuroimaging findings in patients on immunosuppressive therapy: experience with tacrolimus toxicity. *AJR Am J Roentgenol* 1996; 166: 683–688
- Bargallo N, Burrell M, Berenguer J, Cofan F, Buñesch L, Mercader JM. Cortical laminar necrosis caused by immunosuppressive therapy and chemotherapy. *AJNR Am J Neuroradiol* 2000; 21: 479–484
- Bartynski WS, Grabb BC, Zeigler Z, Lin L, Andrews DF. Watershed imaging features and clinical vascular injury in cyclosporin A neurotoxicity. *J Comput Assist Tomogr* 1997; 21: 872–880
- Bartynski WS, Zeigler Z, Spearman MP, Lin L, Shaddock RK, Lister J. Etiology of cortical and white matter lesions in cyclosporin-A and FK-506 neurotoxicity. *AJNR Am J Neuroradiol* 2001; 22: 1901–1914
- Bova D, Shownkeen H, Goldberg K, Horowitz S, Azar-Kia B. Delayed transient neurologic toxicity due to tacrolimus: CT and MRI. *Neuroradiology* 2000; 42: 666–668
- Bushara KO, Rust RS. Reversible MRI lesions due to pegaspargase treatment of non-Hodgkin's lymphoma. *Pediatr Neurol* 1997; 17: 185–187
- Casanova B, Prieto M, Deya E, Gisbert C, Mir J, Berenguer J, Vilchez JJ. Persistent cortical blindness after cyclosporine leukoencephalopathy. *Liver Transplant Surg* 1997; 3: 638–640
- Coley SC, Porter DA, Calamante F, Chong WK, Connelly A. Quantitative MR diffusion mapping and cyclosporine-induced neurotoxicity. *AJNR Am J Neuroradiol* 1999; 20: 1507–1510
- Franco DA, Greenberg HS. 5-FU multifocal inflammatory leukoencephalopathy and dihydropyrimidine dehydrogenase deficiency. *Neurology* 2001; 56: 110–112

- Furukawa M, Terae S, Chu BC, Kaneko K, Kamada H, Miyasaka K. MRI in seven cases of tacrolimus (FK-506) encephalopathy: utility of FLAIR and diffusion-weighted imaging. *Neuroradiology* 2001; 43: 615–621
- Gleeson JG, duPlessis AJ, Barnes PD, Riviello JJ Jr. Cyclosporin A acute encephalopathy and seizure syndrome in childhood: clinical features and risk of seizure recurrence. *J Child Neurol* 1998; 13: 336–344
- Honkaniemi J, Kähärä V, Dastidar P, Latvala M, Hietaharju A, Salonen T, Keskinen L, Ollikainen J, Vahamäki L, Kellokumpu-Lehtinen P, Frey H. Reversible posterior leukoencephalopathy after combination chemotherapy. *Neuroradiology* 2000; 42: 895–899
- Hook CC, Kimmel DW, Kvols LK, Scheithauer BW, Forsyth PA, Rubin J, Moertel CG, Rodriguez M. Multifocal inflammatory leukoencephalopathy with 5-fluorouracil and levamisole. *Ann Neurol* 1992; 31: 262–267
- Hwang YH, Suh CK, Park SP. Multifocal inflammatory leukoencephalopathy: use of thallium-201 SPECT and proton MRS. *J Korean Med Sci* 2003; 18: 621–624
- Israel ZH, Lossos A, Barak V, Soffer D, Siegal T. Multifocal demyelinating leukoencephalopathy associated with 5-fluorouracil and levamisole. *Acta Oncol* 2000; 39: 117–120
- Ito Y, Arahata Y, Goto Y, Hirayama M, Nagamatsu M, Yasuda T, Yanagi T, Sobue G. Cisplatin neurotoxicity presenting as reversible posterior leukoencephalopathy syndrome. *AJNR Am J Neuroradiol* 1998; 19: 415–417
- Jäger HR, Williams EJ, Savage DG, Rule SAJ, Hajnal JV, Sikora K, Goldman JM, Bydder GM. Assessment of brain changes with registered MR before and after bone marrow transplantation for chronic myeloid leukemia. *AJNR Am J Neuroradiol* 1996; 17: 1275–1282
- Jansen O, Krieger D, Krieger S, Sartor K. Cortical hyperintensity on proton density-weighted images: an MR sign of cyclosporine-related encephalopathy. *AJNR Am J Neuroradiol* 1996; 17: 337–344
- Jarosz JM, Howlett DC, Cox TCS, Bingham JB. Cyclosporine-related reversible posterior leukoencephalopathy: MRI. *Neuroradiology* 1997; 39: 711–715
- Kelly P, Staunton H, Lawler M, Brennan P, Jennings S, Unger ER, Sung JH, Farrell MA. Multifocal remitting-relapsing cerebral demyelination twenty years following allogeneic bone marrow transplantation. *J Neuropathol Exp Neurol* 1996; 55: 992–998
- Kilinc M, Benli SU, Can U, Yilmaz A, Karakayali H, Çolak T, Tarhan C, Özdemir BH. FK 506-induced fulminant leukoencephalopathy after kidney transplantation: case report. *Transplant Proc* 2002; 34: 1182–1184
- Kimmel DW, Wijdicks EFM, Rodriguez M. Multifocal inflammatory leukoencephalopathy associated with levamisole therapy. *Neurology* 1995; 45: 374–376
- Kuzuhara S, Ohkoshi N, Kanemaru K, Hashimoto H, Nakanishi T, Toyokura Y. Original investigations. Subacute leukoencephalopathy induced by carmustine, a 5-fluorouracil derivative. *J Neurol* 1987; 234: 365–370
- Lanzino G, Cloft H, Hemstreet MK, West K, Alston S, Ishitani M. Reversible posterior leukoencephalopathy following organ transplantation. Description of 2 cases. *Clin Neurol Neurosurg* 1997; 99: 222–226
- Lyass O, Lossos A, Hubert A, Gips M, Peretz T. Cisplatin-induced non-convulsive encephalopathy. *Anti-Cancer Drugs* 1998; 9: 100–104
- Matsumoto S, Nishizawa S, Murakami M, Noma S, Sano A, Kuroda Y. Carmustine-induced leukoencephalopathy: MRI. *Neuroradiology* 1995; 37: 649–652
- Obara S, Hayashi R, Hata S, Itoh N, Hanyu N. Leukoencephalopathy induced by chemotherapy with tegafur, a 5-fluorouracil derivative. *Acta Neuropathol (Berl)* 1998; 96: 527–531
- Pace MT, Slovis TL, Kelly JK, Abella SD. Cyclosporin A toxicity: MRI appearance of the brain. *Pediatr Radiol* 1995; 25: 180–183
- Provenzale JM, Graham ML. Reversible leukoencephalopathy associated with graft-versus-host disease: MR findings. *AJNR Am J Neuroradiol* 1996; 17: 1290–1294
- Sánchez-Carpintero R, Narbona J, López de Mesa R, Arbizu J, Sierrasesúmaga L. Transient posterior encephalopathy induced by chemotherapy in children. *Pediatr Neurol* 2001; 24: 145–148
- Savarese DM, Gordon J, Smith TW, Litofsky NS, Licho R, Ragland R, Recht L. Cerebral demyelination syndrome in a patient treated with 5-fluorouracil and levamisole. The use of thallium SPECT imaging to assist in noninvasive diagnosis – a case report. *Cancer* 1996; 77: 387–394
- Schuuring J, Wesseling P, Verrips A. Severe tacrolimus leukoencephalopathy after liver transplantation. *AJNR Am J Neuroradiol* 2003; 24: 2085–2088
- Schwartz RB, Bravo SM, Klufas RA, Hsu L, Barnes PD, Robson CD, Antin JH. Cyclosporine neurotoxicity and its relationship to hypertensive encephalopathy: CT and MR findings in 16 cases. *AJR Am J Roentgenol* 1995; 165: 627–631
- Scully RE, Mark EJ, McNeely WF, Ebeling SH, Phillips LD, Ellender SM. Case 24–1999. *N Engl J Med* 1999; 341: 512–519
- Shah AK. Cyclosporine A neurotoxicity among bone marrow transplant recipients. *Clin Neuropharmacol* 1999; 22: 67–73
- Small SL, Fukui MB, Bramblett GT, Eidelman BH. Immunosuppression-induced leukoencephalopathy from tacrolimus (FK506). *Ann Neurol* 1996; 40: 575–580
- Stemmer SM, Stears JC, Burton BS, Jones RB, Simon JH. White matter changes in patients with breast cancer treated with high-dose chemotherapy and autologous bone marrow support. *AJNR Am J Neuroradiol* 1994; 15: 1267–1273
- Stone JA, Castillo M, Mukherji SK. Leukoencephalopathy complicating an ommaya reservoir and chemotherapy. *Neuroradiology* 1999; 41: 134–136
- Tahsildar HI, Remler BF, Creger RJ, Cooper BW, Snodgrass SM, Tarr RW, Lazarus HM. Delayed, transient encephalopathy after marrow transplantation: case reports and MRI findings in four patients. *J Neurol-Oncol* 1996; 27: 241–250
- Tha KK, Terae S, Sugiura M, Nishioka T, Oka M, Kudoh K, Kaneko K, Miyasaka K. Diffusion-weighted magnetic resonance imaging in early stage of 5-fluorouracil-induced leukoencephalopathy. *Acta Neurol Scand* 2002; 106: 379–386
- Tomura N, Kurowawa R, Kato K, Takahashi S, Watarai J, Takeda O, Watanabe A, Takada G. *J Comput Assist Tomogr* 1998; 22: 505–507
- Trullemans F, Grignard F, van Camp B, Schots R. Clinical findings and magnetic resonance imaging in severe cyclosporine-related neurotoxicity after allogeneic bone marrow transplantation. *Eur J Haematol* 2001; 67: 94–99
- Wilson DA, Nitschke R, Bowman ME, Chaffin MJ, Sexauer CL, Prince JR. Transient white matter changes on MR images in children undergoing chemotherapy for acute lymphocytic leukemia: correlation with neuropsychologic deficiencies. *Radiology* 1991; 180: 205–209

89 Central Pontine and Extrapontine Myelinolysis

- Adams RD, Victor M, Mancall EL. Central pontine myelinolysis. *Arch Neurol Psychiatry* 1959; 81: 154–172
- Adler S, Verbalis JG, Williams D. Effect of rapid correction of hyponatremia on the blood-brain barrier of rats. *Brain Res* 1995; 679: 135–143
- Ağildere AM, Benli S, Erten Y, Copkun M, Boyvat F, Özdemir N. Osmotic demyelination syndrome with a dysequilibrium syndrome: reversible MRI findings. *Neuroradiology* 1998; 40: 228–232
- Ashrafian H, Davey P A review of the causes of central pontine myelinolysis: yet another apoptotic illness? *Eur J Neurol* 2001; 8: 103–109
- Ayus JC, Arieff AI. Brain damage and postoperative hyponatremia: the role of gender. *Neurology* 1996; 46: 323–328
- Ayus JC, Krothapalli RK, Arieff AI. Treatment of symptomatic hyponatremia and its relation to brain damage. *N Engl J Med* 1987; 317: 1190–1195
- Brown WD. Osmotic demyelination disorders: central pontine and extrapontine myelinolysis. *Curr Opin Neurol* 2000; 13: 691–697
- Brunner JE, Redmond JM, Haggard AM, Kruger DF, Elias SB. Central pontine myelinolysis and pontine lesions after rapid correction of hyponatremia: a prospective magnetic resonance imaging study. *Ann Neurol* 1990; 27: 61–66
- Choe WJ, Cho BK, Kim IO, Shin HY, Wang KC. Extrapontine myelinolysis caused by electrolyte imbalance during the management of suprasellar germ cell tumors. *Childs Nerv Syst* 1998; 14: 155–158
- Chu K, Kang DW, Ko SB, Kim M. Diffusion-weighted MR findings of central pontine and extrapontine myelinolysis. *Acta Neurol Scand* 2001; 104: 385–388
- Chua GC, Sitoh YY, Lim CC, Chua HC, Ng PY. MRI findings in osmotic myelinolysis. *Clin Radiol* 2002; 57: 800–806
- Cramer SC, Stegbauer KC, Schneider A, Mukai J, Maravilla KR. Decreased diffusion in central pontine myelinolysis. *AJNR Am J Neuroradiol* 2001; 22: 1476–1479
- DeLuca GC, Nagy Zs, Esiri MM, Davey P. Evidence for a role for apoptosis in central pontine myelinolysis. *Acta Neuropathol (Berl)* 2002; 103: 590–598
- Giannetti AV, Pittella JEH. Ischemic and hemorrhagic necrosis of the pons with anatomical location similar to that of central pontine myelinolysis in a chronic alcoholic patient. *Clin Neuropathol* 1993; 12: 156–159
- Hadfield MG, Kubal WS. Extrapontine myelinolysis of the basal ganglia without central pontine myelinolysis. *Clin Neuropathol* 1996; 15: 96–100
- Karp BI, Laureno R. Pontine and extrapontine myelinolysis: a neurologic disorder following rapid correction of hyponatremia. *Medicine* 1993; 72: 359–373
- Karp BI, Laureno R. Central pontine and extrapontine myelinolysis after correction of hyponatremia. *Neurologist* 2000; 6: 255–266
- Koch KJ, Smith RR. Gd-DTPA enhancement in MR imaging of central pontine myelinolysis. *AJNR Am J Neuroradiol* 1989; 10 (suppl 5): S58
- Koci TM, Chiang F, Chow P, Wang A, Chiu LC, Itabashi H, Mehringer CM. Thalamic extrapontine lesions in central pontine myelinolysis. *AJNR Am J Neuroradiol* 1990; 11: 1229–1233
- Laubenberger J, Schneider B, Ansorge O, Götz F, Häussinger D, Volk B, Langer M. Central pontine myelinolysis: clinical presentation and radiologic findings. *Eur Radiol* 1996; 6: 177–183
- Laureno R, Karp BI. Myelinolysis after correction of hyponatremia. *Ann Intern Med* 1997; 126: 57–62
- Lien YH. Role of organic osmolytes in myelinolysis. *J Clin Invest* 1995; 95: 1579–1586
- Maraganore DM, Folger WN, Swanson JW, Ahlskog JE. Movement disorders as sequelae of central pontine myelinolysis: report of three cases. *Mov Disord* 1992; 7: 142–148
- Murdoch M, Chang M, McVicar J. Central pontine myelinolysis after liver transplantation: a case report. *Transplant Int* 1995; 8: 399–402
- Menakaya JO, Wassmer E, Bradshaw K, Seri S, Whitehouse WP. Idiopathic central pontine myelinolysis in childhood. *Dev Med Child Neurol* 2001; 43: 697–700
- Menger H, Jörg J. Outcome of central pontine and extrapontine myelinolysis (N = 44). *J Neurol* 1999; 246: 700–705
- Moore K, Midha M. Extra pontine myelinolysis in a tetraplegic patient: case report. *Spinal Cord* 1997; 35: 332–334
- Niehaus L, Kulozik A, Lehmann R. Reversible central pontine and extrapontine myelinolysis in a 16-year-old girl. *Childs Nerv Syst* 2001; 17: 294–296
- Okeda R, Kitano M, Sawabe M, Yamada I, Yamada M. Distribution of demyelinating lesions in pontine and extrapontine myelinolysis – three autopsy cases including one case devoid of central pontine myelinolysis. *Acta Neuropathol (Berl)* 1986; 69: 259–266
- Pradhan S, Jha R, Singh MN, Gupta S, Phadke RV, Kher V. Central pontine myelinolysis following “slow” correction of hyponatremia. *Clin Neurol Neurosurg* 1995; 97: 340–343
- Rouanet F, Tison F, Dousset V, Corand V, Orgogozo JM. Early T₂ hypointense signal abnormality preceding clinical manifestations of central pontine myelinolysis. *Neurology* 1995; 44: 979–980
- Salvesen R. Extrapontine myelinolysis after surgical removal of a pituitary tumour. *Acta Neurol Scand* 1998; 98: 213–215
- Susa S, Daimon M, Morita Y, Kitagawa M, Hirata A, Manaka H, Sasaki H, Kato T. Acute intermittent porphyria with central pontine myelinolysis and cortical laminar necrosis. *Neuroradiology* 1999; 41: 835–839
- Tien R, Arieff AI, Kucharczyk W, Wasik A, Kucharczyk J. Hyponatremic encephalopathy: is central pontine myelinolysis a component? *Am J Med* 1992; 92: 513–522
- Udani VP, Dharnidharka VR, Gajendragadkar AR, D’Souza B. Extra and central pontine myelinolysis in a child with adrenal insufficiency. *Pediatr Neurol* 1997; 17: 158–160

90 Hypernatremia

- Al Orainy IA, I’Gorman A, Decell MK. Cerebral bleeding, infarcts, and presumed extrapontine myelinolysis in hypernatraemic dehydration. *Neuroradiology* 1999; 41: 144–146
- Arieff AI, Guisado R. Effects on the cerebral nervous system of hypernatremic and hyponatremic states. *Kidney Int* 1976; 10: 104–116
- Barer J, Leighton L, Hill RM, Martinez WM. Fatal poisoning from salt used as an emetic. *Am J Dis Child* 1973; 125: 889–890
- Baugh JR, Krug EF, Weir MR. Punishment by salt poisoning. *South Med J* 1963; 76: 540–541
- Brown WD, Caruso JM. Extrapontine myelinolysis with involvement of the hippocampus in three children with severe hyponatremia. *J Child Neurol* 1999; 14: 428–433

- Burnett LS, Wentz AC, King TM. Techniques of pregnancy termination. I, II. *Obstet Gynecol Surv* 1974; 29: 6–42
- Calam J, Krasner N, Haqqani M. Extensive gastrointestinal damage following a saline emetic. *Dig Dis Sci* 1982; 27: 936–946
- Calvin ME, Knepper R, Robertson WO. Hazards to health. *N Engl J Med* 1964; 270: 625–626
- Carter RF, Fotheringham BJ. Fatal salt poisoning due to gastric lavage with hypertonic saline. *Med J Aust* 1971; 1: 539–541
- Dine MS, McGovern ME. Intentional poisoning of children – an overlooked category of child abuse: report of seven cases and review of the literature. *Pediatrics* 1982; 70: 32–35
- Dockery WK. Fatal intentional salt poisoning associated with a radiopaque mass. *Pediatrics* 1992; 89: 964–965
- Elton NW, Elton WJ, Nazereno JP. Pathology of acute salt poisoning in infants. *Am J Clin Pathol* 1963; 39: 252–264
- Finberg L. Pathogenesis of lesions in the nervous system in hypernatremic states. Clinical observations of infants. *Pediatrics* 1959; 23: 40–44
- Finberg L. Unforgettable patients. *J Pediatr* 1992; 121: 323–324
- Finberg L, Harrison HE. Hypernatremia in infants. An evaluation of the clinical and biochemical findings accompanying this state. *Pediatrics* 1955; 16: 1–12
- Finberg L, Luttrell C, Redd H. Pathogenesis of lesions in the nervous system in hypernatremic states. Experimental studies of gross anatomic changes and alterations of chemical composition of the tissues. *Pediatrics* 1959; 23: 46–53
- Fried LF, Palevsky PM. Hyponatremia and hypernatremia. *Med Clin North Am* 1997; 81: 585–609
- Fris-Hansen B, Buchthal F. EEG findings in an infant with water intoxication and convulsions incident to hypernatraemia. *Electroencephalogr Clin Neurophysiol* 1965; 19: 387–390
- Golder W, Felgenhauer N, von Einsiedel H, von Clarmann M. Ausgedehnte Kleinhirnblutungen nach Kochsalzvergiftung. *Klin Neuroradiol* 1992; 2: 21–23
- Götze H. Kochsalzvergiftung infolge übergrosser parenteraler Zufuhr. *Arch Toxikol* 1962; 19: 284–292
- Habbick BF, Hill A, Tchang SPK. Computer tomography in an infant with salt poisoning: relationship of hypodense areas in basal ganglia to serum sodium concentration. *Pediatrics* 1984; 74: 1123–1125
- Hartfield SD, Loewy JA, Yager JY. Transient thalamic changes on MRI in a child with hypernatremia. *Pediatr Neurol* 1999; 20: 60–62
- Klein Schwartz W, Finke HB. Saltwater intoxication. *JAMA* 1978; 240: 1338–1339
- Korkmaz A, Yiğit S, Firat M, Oran O. Cranial MRI in neonatal hypernatraemic dehydration. *Pediatr Radiol* 2000; 30: 323–325
- Meadow R. Non-accidental salt poisoning. *Arch Dis Child* 1993; 68: 448–452
- Paut O, André N, fabre P, Sobraquès P, Drouet G, Arditti J, Camboulives J. The management of extreme hypernatraemia secondary to salt poisoning in an infant. *Paediatr Anaesth* 1999; 9: 171–174
- Peer G, Wigler I, Weintraub M, Liron M, Aviram A. Acute psychosis and hypertensive crisis following oral salt replacement. *Lancet* 1983; II: 634–635
- Postuma R. Whole bowel irrigation in pediatric patients. *J Pediatr Surg* 1982; 17: 350–352
- Roberts CJC, Noakes MJ. Fatal outcome from administration of a salt emetic. *Postgrad Med J* 1974; 50: 513–515
- Roberts CJC, Noakes MJ. Danger of emetics in first-aid for poisoning. *BMJ* 1974; III: 683
- Roscelli JD, Yu CE, Southgate WM. Management of salt poisoning in an extremely low birth weight infant. *Pediatr Nephrol* 1994; 8: 172–174
- Samir El-Dahr, Gomez RA, Campbell FG, Chevalier RL. Rapid correction of acute salt poisoning by peritoneal dialysis. *Pediatr Nephrol* 1987; 1: 602–604
- Saunders N, Balfe JW, Laski B. Severe salt poisoning in an infant. *J Pediatr* 1976; 88: 258–261
- Schiffer MA, Pakter J, Clahr J. Mortality associated with hypertonic saline abortion. *Obstet Gynecol* 1973; 42: 759–764
- Soupart A, Penninckx R, Namias B, Seinuit A, Perier O, Decaux G. Brain myelinolysis following hypernatremia in rats. *J Neuropathol Exp Neurol* 1996; 55: 106–113
- Soupart A, Penninckx R, Stenuit A, Perier O, Deaux G. Reinduction of hyponatremia improves survival in rats with myelinolysis-related neurologic symptoms. *J Neuropathol Exp Neurol* 1996; 55: 594–601
- Walter GF, Maresch W. Irrtümliche kochsalzintoxikation bei neugeborenen. Morphologische befunde und pathogenetische discussion. *Klin Padiatr* 1987; 1999: 269–273
- Winter M, Taylor DJE. Danger of saline emetics in first-aid for poisoning. *BMJ* 1974; III: 802

91 Marchiafava-Bignami Syndrome

- Arbelaez A, Pajon A, Castillo M. Acute Marchiafava-Bignami disease: MR findings in two patients. *AJNR Am J Neuroradiol* 2001; 24: 1955–1957
- Berek K, Wagner M, Chemelli AP, Aichner F, Benke T. Hemispheric disconnection in Marchiafava-Bignami disease: clinical, neuropsychological and MRI findings. *J Neurol Sci* 1994; 123: 2–5
- Caparros-Lefebvre D, Pruvo JP, Josien E, Pertuzon B, Clarisse J, Petit H. Marchiafava-Bignami disease: use of contrast media in CT and MRI. *Neuroradiology* 1994; 36: 509–511
- Çelik Y, Kaya M, Şengün S, Utku U. Marchiafava-Bignami disease: cranial MRI and SPECT findings. *Clin Neurol Neurosurg* 2002; 104: 339–341
- Clavier E, Thiebot J, Delangre T, Hannequin D, Samson M, Benozio M. Marchiafava-Bignami disease. A case studied by CT and MRI imaging. *Neuroradiology* 1986; 28: 376
- Ferracci F, Conte F, Gentile M, Candeago R, Foscolo L, Bendini M, Fassetta G. Marchiafava-Bignami disease. Computed tomographic scan, ^{99m}Tc HMPAO-SPECT, and FLAIR MRI findings in a patient with subcortical aphasia, alexia, bilateral agraphia, and left-handed deficit of constructional ability. *Arch Neurol* 1999; 56: 107–110
- Frieze SA, Bitzer M, Freudenstein D, Voigt K, Küker W. Classification of acquired lesions of the corpus callosum with MRI. *Neuroradiology* 2000; 42: 795–802
- Gambini A, Falini A, Moiola L, Comi G, Scotti G. Marchiafava-Bignami disease: longitudinal MR imaging and MR spectroscopy study. *AJNR Am J Neuroradiol* 2003; 24: 249–253
- Gass A, Birtsch C, Oster M, Schwartz A, Hennerici MG. Marchiafava-Bignami disease: reversibility of neuroimaging abnormality. *J Comput Assist Tomogr* 1998; 22: 503–504
- Hayashi T, Tanohata K, Kunitomo M, Inoue K. Marchiafava-Bignami disease with resolving symmetrical putaminal lesion. *J Neurol* 2002; 249: 227–228
- Helenius J, Tatlisumak T, Soine L, Valanne L, Kaste M. Marchiafava-Bignami disease: two cases with favourable outcome. *Eur J Neurol* 2001; 8: 269–272
- Ishii K, Ikejiri Y, Sasaki M, Kitagaki H, Mori E. Regional cerebral glucose metabolism and blood flow in a patient with Marchiafava-Bignami disease. *AJNR Am J Neuroradiol* 1999; 20: 1249–1251

- Izquierdo G, Quesada MA, Chacon J, Martel J. Neuroradiologic abnormalities in Marchiafava-Bignami disease of benign evolution. *Eur J Radiol* 1992; 15: 71–74
- Kohler CG, Ances BM, Coleman AR, Ragland JD, Lazarev M, Gur RC. Marchiafava-Bignami disease: literature review and case report. *Neuropsychiatry Neuropsychol Behav Neurol* 2000; 13: 67–76
- Mayer JW, de Liège P, Netter JM, Danzé F, Reizine D. Computerized tomography and nuclear magnetic resonance imaging in Marchiafava-Bignami disease. *J Neuroradiol* 1987; 14: 152–158
- Ruiz-Martínez J, Perez-Balsa AM, Ruibal M, Urtasun M, Villanua J, Massó JFM. Marchiafava-Bignami disease with widespread extracallosal lesions and favourable course. *Neuroradiology* 1999; 41: 40–43
- Sano M, Ishii K, Suzuki T, Uchigata M, Senda M. Reductions in the bilateral parietal and occipital cerebral blood flow and metabolism in a patient with Marchiafava-Bignami disease. *J Neurol* 1999; 246: 607–607
- Tarnowska-Dziduszko E, Bertrand E, Szpak GM. Morphological changes in the corpus callosum in chronic alcoholism. *Folia Neuropathol* 1995; 33: 25–29
- Yamamoto T, Ashikaga R, Araki Y, Nishimura Y. A case of Marchiafava-Bignami disease: MRI findings on spin-echo and fluid attenuated inversion recovery (FLAIR) images. *Eur J Neurol* 2000; 34: 141–143
- ## 92 Posterior Reversible Encephalopathy Syndrome
- Çelik M, Forta H, Dalkılıç T, Babacan G. MRI reveals reversible lesions resembling posterior reversible encephalopathy in porphyria. *Neuroradiology* 2002; 44: 839–841
- Chakravarty A, Chakrabarti SD. The neurology of eclampsia: some observations. *Neurol India* 2002; 50: 128–135
- Covarrubias DJ, Luetmer PH, Campeau NG. Posterior reversible encephalopathy syndrome: prognostic utility of quantitative diffusion-weighted MR images. *AJNR Am J Neuroradiol* 2002; 23: 1038–1048
- Delanty N, Vaughan C, Frucht S, Stubgen P. Erythropoietin-associated hypertensive posterior leukoencephalopathy. *Neurology* 1997; 49: 686–689
- De Seze J, Mastain B, Stojkovic T, Ferriby D, Pruvo JP, Destée A, Vermersch P. Unusual MR findings of the brain stem in arterial hypertension. *AJNR Am J Neuroradiol* 2000; 21: 391–394
- Digre KB, Varner MW, Osborn AG, Crawford S. Cranial magnetic resonance imaging in severe preeclampsia vs eclampsia. *Arch Neurol* 1993; 50: 399–406
- Eguchi K, Kasahara K, Nagashima A, Mori T, Nii T, Ibaraki K, Kario K, Shimada K. Two cases of malignant hypertension with reversible diffuse leukoencephalopathy exhibiting a reversible nocturnal blood pressure “riser” pattern. *Hypertens Res* 2002; 25: 467–473
- Eichler FS, Wang P, Wityk RJ, Beauchamp NJ Jr, Barker PB. Diffuse metabolic abnormalities in reversible posterior leukoencephalopathy syndrome. *AJNR Am J Neuroradiol* 2002; 23: 833–837
- Hauser RA, Lacey M, Knight MR. Hypertensive encephalopathy: magnetic resonance description of reversible cortical and white matter lesions. *Arch Neurol* 1988; 45: 1078–1083
- Hinchey J, Chaves C, Appignani B, Breen J, Pao L, Wang A, Pessin MS, Lamy C, Mas JL, Caplan LR. A reversible posterior leukoencephalopathy syndrome. *N Engl J Med* 1996; 334: 494–500
- Holdcroft A, Oatridge A, Fusi L, Hajnal JV, Saeed N, Bydder GM. Magnetic resonance imaging in preeclampsia and eclampsia by visual disturbance and other neurological abnormalities. *Int J Obstet Anesth* 2002; 11: 255–259
- Karampekios SK, Contopoulou E, Basta M, Tzagournissakis M, Gourtsoyannis N. Hypertensive encephalopathy with predominant brain stem involvement: MRI findings. *J Hum Hypertens* 2004; 18: 133–134
- Kastrup O, Maschke M, Wanke I, Diener HC. Posterior reversible encephalopathy syndrome due to severe hypercalcemia. *J Neurol* 2002; 249: 1563–1566
- King PH, Bragdon AC. MRI reveals multiple reversible cerebral lesions in an attack of acute intermittent porphyria. *Neurology* 1991; 41: 1300–1302
- Kumai Y, Toyoda K, Fujii K, Ibayashi S. Hypertensive encephalopathy extending into the whole brainstem and deep structures. *Hypertens Res* 2002; 25: 797–800
- Loureiro R, Leite CC, Kahhale S, Freire S, Sousa B, Cardoso EF, Alves EA, Borba P, Cerri GG, Zugaib M. Diffusion imaging may predict reversible brain lesions in severe pre-eclampsia: initial experience. *Am J Obstet Gynecol* 2003; 189: 1350–1355
- Moore KR, Osborn AG, Townsend JJ, Boyer RS, Orrison WW Jr, Ablin DS. The imaging and pathologic spectrum of hemolytic-uremic syndrome-thrombotic thrombocytopenic purpura (HUS-TTP syndrome). *Int J Neuroradiol* 1997; 3: 147–159
- Morello F, Marino A, Cigolini M, Cappellari F. Hypertensive brain stem encephalopathy: clinically silent massive edema of the pons. *Neurol Sci* 2001; 22: 317–320
- Mukherjee P, McKinstry RC. Reversible posterior leukoencephalopathy syndrome: evaluation with diffuse – tensor MR imaging. *Radiology* 2001; 219: 756–765
- Pavlikis SG, Frank Y, Chusid R. Hypertensive encephalopathy, reversible occipitoparietal encephalopathy, or reversible posterior leukoencephalopathy: three names for an old syndrome. *J Child Neurol* 1999; 14: 277–281
- Primavera A, Audenino D, Mavilio N, Cocito L. Reversible posterior leukoencephalopathy syndrome in systemic lupus and vasculitis. *Ann Rheum Dis* 2001; 60: 534–537
- Provenzale JM, Petrella JR, Cruz LCH Jr, Wong JC, Engelter S, Barboriak DP. Quantitative assessment of diffusion abnormalities in posterior reversible encephalopathy syndrome. *AJNR Am J Neuroradiol* 2001; 22: 1455–1461
- Schwartz RB, Mulkern RV, Gudbjartsson H, Jolesz F. Diffusion-weighted MR imaging in hypertensive encephalopathy: clues to pathogenesis. *AJNR Am J Neuroradiol* 1998; 19: 859–862
- Schwartz RB, Feske SK, Polak JF, Degirolami U, Iaia A, Beckner KM, Bravo SM, Klufas RA, Chai RYC, Repke JT. Preeclampsia-eclampsia: clinical and neuroradiographic correlates and insights into the pathogenesis of hypertensive encephalopathy. *Radiology* 2000; 217: 371–376
- Sengar AR, Gupta RK, Dhanuka AK, Das K. MR imaging, MR angiography, and MR spectroscopy of the brain in eclampsia. *AJNR Am J Neuroradiol* 1997; 18: 1485–1490
- Shimono T, Miki Y, Toyoda H, Egawa H, Eumoto S, Tanaka K, Hattori H, Kanagaki M, Itoh K, Konishi J. MR imaging with quantitative diffusion mapping of tricolimus-induced neurotoxicity in organ transplant patients. *Eur Radiol* 2003; 13: 986–993
- Susa S, Daimon M, Morita Y, Kitagawa M, Hirata A, Manaka H, Sasaki H, Kato T. Acute intermittent porphyria with central pontine myelinolysis and cortical laminar necrosis. *Neuroradiology* 1999; 41: 835–839

- Tajima Y, Isonishi K, Kashiwaba T, Tashiro K. Two similar cases of encephalopathy, possibly a reversible posterior leukoencephalopathy syndrome: serial findings of magnetic resonance imaging, SPECT and angiography. *Int Med* 1999; 38: 54–58
- Urushitani M, Seriu N, Udaka F, Kameyama M, Nishinaka K, Kodama M. MRI Demonstration of a reversible lesion in cerebral deep white matter in thrombotic thrombocytopenic purpura. *Neuroradiology* 1996; 38: 137–138
- Taylor MB, Jackson A, Weller JM. Dynamic susceptibility contrast enhanced MRI in reversible posterior leukoencephalopathy syndrome associated with haemolytic uraemic syndrome. *Br J Radiol* 2000; 73: 438–442
- Thomas SV. Neurological aspects of eclampsia. *J Neurol Sci* 1998; 155: 37–43
- Utz N, Kinkel B, Hedde JP, Bewermeyer H. MR imaging of acute intermittent porphyria mimicking reversible posterior leukoencephalopathy syndrome. *Neuroradiology* 2001; 43: 1059–1062
- Wanatabe Y, Mitomo M, Tokuda Y, Yoshida K, Choi S, Hosoki T, Ban C. Eclamptic encephalopathy: MRI, including diffusion-weighted images. *Neuroradiology* 2002; 44: 981–958
- Weidauer S, Gaa J, Sitzer M, Hefner R, Lanfermann H, Zanella FE. Posterior encephalopathy with vasospasm: MRI and angiography. *Neuroradiology* 2003; 45: 869–876
- ### 93 Langerhans Cell Histiocytosis
- Adle-Biasette H, Chetrit J, Bergemer-Fouquet AM, Wechsler J, Mussini JM, Gray F. Pathology of the central nervous system in Chester-Erdheim disease: report of three cases. *J Neuropathol Exp Neurol* 1997; 56: 1207–1216
- Aricò M, Haupt R, Russotto VS, Bossi G, Scappaticci S, Denasino C. Langerhans cell histiocytosis in two generations: a new family and review of the literature. *Med Pediatr Oncol* 2001; 36: 314–316
- Bohlega S, Alwatban J, Tulbah A, Bakheet SM, Powe J. Cerebral manifestation of Erdheim-Chester disease: clinical and radiologic findings. *Neurology* 1997; 49: 1702–1705
- Broadbent V, Gardner H. Current therapy for Langerhans cell histiocytosis. *Hematol Oncol Clin North Am* 1998; 12: 327–338
- Cervera A, García Penas JJ, Díaz MA, Gutiérrez-Solana LG, Benito A, Ruiz-Falcó M-L, Villa M. CNS sequelae in Langerhans cell histiocytosis: progressive spinocerebellar degeneration as a late manifestation of the disease. *Pediatr Hematol Oncol* 1997; 14: 577–584
- Chu T. Langerhans cell histiocytosis. *Aus J Dermatol* 2001; 42: 237–242
- Evidente VGH, Adler CH, Giannini C, Conley CR, Parisi JE, Fletcher GP. Erdheim-Chester disease with extensive intraaxial brain stem lesions presenting as a progressive cerebellar syndrome. *Mov Disord* 1998; 13: 576–581
- Fuzakawa T, Tsukishima E, Sasaki H, Hamada K, Hamada T, Tashiro K. Erdheim-Chester disease and slowly progressive cerebellar dysfunction. *J Neurol Neurosurg Psychiatry* 1995; 58: 238–240
- Gaetani P, Tancioni F, di Rocco M, Rodriguez y Baena R. Isolated cerebellar involvement in Rosai-Dorfman disease: case report. *Neurosurgery* 2000; 46: 479–481
- Goldberg-Stern H, Weitz R, Zaizov R, Gornish M, Gadoth N. Progressive spinocerebellar degeneration “plus” associated with Langerhans cell histiocytosis: a new paraneoplastic syndrome? *J Neurol Neurosurg Psychiatry* 1995; 58: 180–183
- Grois N, Barkovich AJ, Rosenau W, Ablin AR. Central nervous system disease associated with Langerhans’ cell histiocytosis. *Am J Pediatr Hematol Oncol* 1993; 15: 245–254
- Grois NG, Favara BE, Mostbeck GH, Prayer D. Central nervous system disease in Langerhans cell histiocytosis. *Hematol Oncol Clin North Am* 1998; 12: 287305
- Herzog KM, Tubbs RR. Langerhans cell histiocytosis. *Adv Anat Pathol* 1998; 5: 347–358
- Hund E, Steiner H-H, Jansen O, Sieverts H, Sohl G, Essig M. Treatment of cerebral Langerhans cell histiocytosis. *J Neurol Sci* 1999; 171: 145–152
- Iwuagwu FC, Rigby HS, Payne F, Reid CD. Juvenile xanthogranuloma variant: a clinicopathological case report and review of the literature. *Br J Plast Surg* 1999; 52: 591–596
- Kim IT, Lee SM. Choroidal Langerhans’ cell histiocytosis. *Acta Ophthalmol Scand* 2000; 78: 97–100
- Malpas JS. Langerhans cell histiocytosis in adults. *Hematol Oncol Clin North Am* 1998; 12: 259–268
- Miaux Y, Keime F, Martin-Duverneuil N, Cognard C, Savin D, Chiras J. Hyperintense basal ganglia on T1-weighted MR in a patient with Langerhans cell histiocytosis. *AJNR Am J Neuroradiol* 1996; 17: 1193
- Modan-Moses D, Weintraub M, Meyerovitch J, Segal-Lieberman G, Bielora B, Shimon I. Hypopituitarism in Langerhans cell histiocytosis: seven cases and literature review. *J Endocrinol Invest* 2001; 24: 612–617
- Pautas E, Chérin P, Pelletier S, Vidailhet M, Herson S. Cerebral Erdheim-Chester disease: report of two cases with progressive cerebellar syndrome with dentate abnormalities on magnetic resonance imaging. *J Neurol Neurosurg Psychiatry* 1998; 65: 597–599
- Poe LB, Dubowy RL, Hochhauser L, Collins GH, Crosley CJ, Kanzer MD, Oliphant M, Hodge CJ Jr. Demyelinating and gliotic cerebellar lesions in Langerhans cell histiocytosis. *AJNR Am J Neuroradiol* 1994; 15: 1921–1928
- Polizzi A, Coghill S, McShane MA, Squier W. Acute ataxia complicating Langerhans cell histiocytosis. *Arch Dis Child* 2002; 86: 130–131
- Prayer D, Grois N, Prosch H, Gardner H, Barkovich AJ. MR imaging presentation of intracranial disease associated with Langerhans cell histiocytosis. *AJNR Am J Neuroradiol* 2004; 25: 880–891
- Pritchard J. Acute ataxia complicating Langerhans cell histiocytosis. *Arch Dis Child* 2003; 88: 178–179
- Rosenfield NS, Abrahams J, Komp D. Brain MR in patients with Langerhans cell histiocytosis: findings and enhancement with Gd-DTPA. *Pediatr Radiol* 1990; 20: 433–436
- Saatci L, Baskan O, Haliloglu M, Aydingoz U. Cerebellar and basal ganglion involvement in Langerhans cell histiocytosis. *Neuroradiology* 1999; 41: 443–446
- Schmitz L, Favara BE. Nosology and pathology of Langerhans cell histiocytosis. *Hematol Oncol Clin North Am* 1998; 12: 221–246
- Shuper A, Stark B, Yaniv Y, Zaizov R, Carel C, Sadeh M, Steinmetz A. Cerebellar involvement in Langerhans’ cell histiocytosis: a progressive neuropsychiatric disease. *J Child Neurol* 2000; 15: 824–826
- Strottmann JM, Ginsberg LE, Stanton C. Langerhans cell histiocytosis involving the corpus callosum and cerebellum: gadolinium-enhanced MRI. *Neuroradiology* 1995; 37: 289–292
- Thorpy MJ, Crosley CJ. Multifocal eosinophilic granuloma and the cerebellum. *Ann Neurol* 1980; 8: 454
- Varona L, Sagasta A, Bárcena J, Zarranz J-J. Neurological manifestations following treatment of Langerhans cell histiocytosis. *J Neurol* 1997; 244: 58–60

- Vassallo R, Ryu JH, Colby TV, Hartman T, Limper AH. Pulmonary Langerhans'-cell histiocytosis. *N Engl J Med* 2000; 342: 1969-1978
- Weindauer S, von Stuckrad-Barre S, Dettmann E, Zanella FE, Lanfermann H. Cerebral Erdheim-Chester disease: case report and review of the literature. *Neuroradiology* 2003; 45: 241-245
- Whitsett SF, Kneppers K, Coppes MJ, Egeler RM. Neuropsychologic deficits in children with Langerhans cell histiocytosis. *Med Pediatr Oncol* 1999; 33: 486-492
- Wright RA, Hermann RC, Parisi JE. Neurological manifestations of Erdheim-Chester disease. *J Neurol Neurosurg Psychiatry* 1999; 66: 72-75
- ## 94 Posthypoxic-ischemic Damage
- Albin RL, Greenamyre JT. Alternative excitotoxic hypothesis. *Neurology* 1992; 42: 733-738
- Andersen DL, Tannenberg AEG, Burke CJ, Dodd PR. Regional development of glutamate-N-methyl-D-aspartate receptor sites in asphyxiated newborn infants. *J Child Neurol* 1998; 13: 149-157
- Chan PH, Fishman RA. Transient formation of superoxide radicals in polyunsaturated fatty acid-induced brain swelling. *J Neurochem* 1980; 35: 1004-1007
- Chan PH, Yurko M, Fishman RA. Phospholipid degradation and cellular edema induced by free radicals in brain cortical slices. *J Neurochem* 1982; 38: 525-531
- Chan PH, Schmidley JW, Fishman RA, Longar SM. Brain injury, edema, and vascular permeability changes induced by oxygen-derived free radicals. *Neurology* 1984; 34: 315-320
- Chen M, Bullock R, Graham DI, Frey P, Lowe D, McCulloch J. Evaluation of a competitive NMDA antagonist (D-CPPE) in feline focal cerebral ischemia. *Ann Neurol* 1991; 30: 62-70
- Clark GD. Role of excitatory amino acids in brain injury caused by hypoxia-ischemia, status epilepticus, and hypoglycemia. *Clin Perinatol* 1989; 16: 459-474
- Cotman CW, Monaghan DT, Ottersen OP, Storm-Mathisen J. Anatomical organization of excitatory amino acid receptors and their pathways. *Trends Neurosci* 1987; 10: 273-280
- Doble A. Excitatory amino acid receptors and neurodegeneration. *Thérapie* 1995; 50: 319-337
- Foster AC, Donald AE, Willis CL, Tridgett R, Kemp JA, Priestley T. The glycine site on the NMDA receptor: pharmacology and involvement in NMDA receptor-mediated neurodegeneration. In: Ben-Ari Y, ed. *Excitatory Amino Acids and Neuronal Plasticity*. New York: Plenum Press, 1990: 93-100
- Freund TF, Buzsaki G, Leon A, Baimbridge KG, Somogyi P. Relationship of neuronal vulnerability and calcium binding protein immunoreactivity in ischemia. *Exp Brain Res* 1990; 83: 55-66
- Goldberg MP, Choi DW. Intracellular free calcium increases in cultured cortical neurons deprived of oxygen and glucose. *Stroke* 1990; 21 (suppl III): 75-77
- Groenendaal F, Mishra OP, McGowan JE, Hoffman DJ, Delivoria-Papadopoulos M. Function of cell membranes in cerebral cortical tissue of newborn piglets after hypoxia and inhibition of nitric oxide synthase. *Pediatr Res* 1997; 42: 174-179
- Hasegawa K, Yoshioka H, Sawada T, Nishikawa H. Lipid peroxidation in neonatal mouse brain subjected to two different types of hypoxia. *Brain Dev* 1991; 13: 101-103
- Hattori H, Wasterlain CG. Excitatory amino acids in the developing brain: ontogeny, plasticity, and excitotoxicity. *Pediatr Neurol* 1990; 6: 219-228
- Hosler BA, Brown RH Jr. Superoxide dismutase and oxygen radical neurotoxicity. *Curr Opin Neurol* 1996; 9: 486-491
- Ikeda J, Nagashima G, Saito N, Nowak TS, Joo F, Mies G, Lohr JM, Ruetzler CA, Klatzo I. Putative neuroexcitation in cerebral ischemia and brain injury. *Stroke* 1990; 21 (suppl III): 65-70
- Ikeda Y, Long DM. The molecular basis of brain injury and brain edema: the role of oxygen free radicals. *Neurosurgery* 1990; 27: 1-11
- Jarvis MF, Wagner GC. 1-methyl-4-phenyl-1,2,3,6-tetrahydropyridine-induced neurotoxicity in the rat: characterization and age-dependent effects. *Synapse* 1990; 5: 104-112
- Johnston MV. Neurotransmitters and vulnerability of the developing brain. *Brain Dev* 1995; 17: 301-306
- Koroshetz WJ, Freese A, DiFiglia M. The correlation between excitatory amino acid-induced current responses and excitotoxicity in striatal cultures. *Brain Res* 1990; 521: 265-272
- Kucharczyk J, Mintorovitch J, Moseley ME, Asgari HS, Seivick RJ, Derugin N, Norman D. Ischemic brain damage: reduction by sodium-calcium ion channel modulator RS-87476. *RadioLOGY* 1991; 179: 221-227
- Levin SD. Mechanisms of damage in the developing brain. *Curr Opin Neurol Neurosurg* 1991; 4: 371-376
- Lockerbie RO. Neurotrophic factors and development. *Curr Opin Neurol Neurosurg* 1990; 3: 955-958
- Lundgren J, Zhang H, Agardh CD, Smith ML, Evans PJ, Halliwell B, Siesjö BK. Acidosis-induced ischemic brain damage: are free radicals involved? *J Cereb Blood Flow Metab* 1991; 11: 587-596
- Marret S, Gressens P, Gadisseux J-F, Evrard P. Prevention by magnesium of excitotoxic neuronal death in the developing brain: an animal model for clinical intervention studies. *Dev Med Child Neurol* 1995; 37: 473-484
- Mattson MP. Cellular signaling mechanisms common to the development and degeneration of neuroarchitecture. A review. *Mech Ageing Dev* 1989; 50: 103-157
- Mattson MP. Excitatory amino acids, growth factors, and calcium: a teeter-totter model for neural plasticity and degeneration. In: Ben-Ari Y, ed. *Excitatory amino acids and neuronal plasticity*. New York: Plenum Press, 1990: 211-220
- McCord JM. Oxygen-derived free radicals in postischemic tissue injury. *N Engl J Med* 1985; 312: 159-163
- Meldrum BS. Excitatory amino acid receptors and disease. *Curr Opin Neurol Neurosurg* 1992; 5: 508-513
- Mishra OP, Delivoria-Papadopoulos M. Cellular mechanisms of hypoxic injury in the developing brain. *Brain Res Bull* 1999; 48: 233-237
- Mitrovic B, Ignarro LJ, Montestruque S, Smoll A, Merrill JE. Nitric oxide as a potential pathological mechanism in demyelination: its differential effects on primary glial cells in vitro. *Neuroscience* 1994; 61: 575-585
- Nedelcu J, Klein MA, Aguzzi A, Boesiger P, Martin E. Biphasic edema after hypoxic-ischemic brain injury in neonatal rats reflects early neuronal and late glial damage. *Pediatr Res* 1999; 46: 297-304
- Odeh M. The role of reperfusion-induced injury in the pathogenesis of the Crush syndrome. *N Engl J Med* 1991; 324: 1417-1422
- Omar R, Pappolla M. Oxygen free radicals as inducers of heat shock protein synthesis in cultured human neuroblastoma cells: relevance to neurodegenerative disease. *Eur Arch Psychiatry Clin Neurosci* 1993; 242: 262-267
- Riikonen RS, Kero PO, Simell OG. Excitatory amino acids in cerebrospinal fluid in neonatal asphyxia. *Pediatr Neurol* 1992; 8: 37-40

- Rothman S. Synaptic release of excitatory amino acid neurotransmitter mediates anoxic neuronal death. *J Neurosci* 1984; 4: 1884–1891
- Rothman SM. Synaptic activity mediates death of hypoxic neurons. *Science* 1983; 220: 536–537
- Rothman SM, Olney JW. Glutamate and the pathophysiology of hypoxic-ischemic brain damage. *Ann Neurol* 1986; 19: 105–111
- Rothman SM, Olney JW. Excitotoxicity and the NMDA receptor. *Trends Neurosci* 1987; 10: 299–302
- Rothman SM, Thurston JH, Hauhart RE. Delayed neurotoxicity of excitatory amino acids in vitro. *Neurosci* 1987; 22: 471–480
- Sauer D, Allegrini PR, Thedinga KH, Massieu L, Amacker H, Fagg GE. Evaluation of quinolinic acid induced excitotoxic neurodegeneration in rat striatum by quantitative magnetic resonance imaging in vivo. *J Neurosci Methods* 1992; 42: 69–74
- Schwarcz R, Meldrum B. Excitatory amino acid antagonists provide a therapeutic approach to neurological disorders. *Lancet* 1985; II: 140–143
- Shaw PJ. Excitatory amino acid neurotransmission, excitotoxicity and excitotoxins. *Curr Opin Neurol Neurosurg* 1992; 5: 383–390
- Siesjö BK. Cerebral circulation and metabolism. *J Neurosurg* 1984; 60: 883–908
- Siesjö BK. Pathophysiology and treatment of focal cerebral ischemia. Part I: pathophysiology. *J Neurosurg* 1992; 77: 169–184
- Siesjö BK. Pathophysiology and treatment of focal cerebral ischemia. Part II: mechanisms of damage and treatment. *J Neurosurg* 1992; 77: 337–354
- Simon RP, Swan JH, Griffiths T, Meldrum BS. Blockade of N-methyl-D-aspartate receptors may protect against ischemic damage in the brain. *Science* 1984; 226: 850–852
- Sims NR. Energy metabolism and selective neuronal vulnerability following global cerebral ischemia. *Neurochem Res* 1992; 17: 923–931
- Stephenson FA. Neurotransmitter receptors. *Curr Opin Neurol Neurosurg* 1990; 3: 951–954
- Stys PK, Waxman SG, Ransom BR. Na^+ - Ca^{2+} exchanger mediates Ca^{2+} influx during anoxia in mammalian central nervous system white matter. *Ann Neurol* 1991; 30: 375–380
- Turski L, Turski WA. Towards an understanding of the role of glutamate in neurodegenerative disorders: energy metabolism and neuropathology. *Experientia* 1993; 49: 1064–1072
- Wieloch T. Neuronal injury and cerebrovascular disorders. *Curr Opin Neurol Neurosurg* 1990; 3: 944–950
- Yoshida S, Abe K, Busto R, Watson BD, Kogure K, Ginsberg MD. Influence of transient ischemia on lipid-soluble antioxidants, free fatty acids and energy metabolites in rat brain. *Brain Res* 1982; 245: 307–316
- Young RSK, Petroff OAC, Aquila WJ, Yates J. Effects of glutamate, quisqualate, and N-methyl-D-aspartate in neonatal brain. *Exp Neurol* 1991; 111: 362–368
- Amess PN, Wylezinska M, Lorek A, Townsend J, Wyatt JS, Amiel-Tison C, Cady EB, Stewart A. Early brain proton magnetic resonance spectroscopy and neonatal neurology related to neurodevelopmental outcome at 1 year in term infants after presumed hypoxic-ischaemic brain injury. *Dev Med Child Neurol* 1999; 41: 436–445
- Arzoumanian Y, Mirmiran M, Barnes PD, Woolley K, Ariagno RL, Moseley ME, Fleisher BE, Atlas SW. Diffusion tensor brain imaging findings at term-equivalent age may predict neurologic abnormalities in low birth weight preterm infants. *AJNR Am J Neuroradiol* 2003; 24: 1646–1653
- Azzarelli B, Caldemyer KS, Philipps JP, deMyer WE. Hypoxic-ischemic encephalopathy in areas of primary myelination. A neuroimaging and PET study. *Pediatr Neurol* 1996; 14: 108–116
- Back SA, Gan X, Li Y, Rosenberg PA, Volpe JJ. Maturation-dependent vulnerability of oligodendrocytes to oxidative stress-induced death caused by glutathione depletion. *J Neurosci* 1998; 18: 6241–6253
- Back SA, Luo NL, Borenstein NS, Levine JM, Volpe JJ, Kinney HC. Late oligodendrocyte progenitors coincide with the developmental window of vulnerability for human perinatal white matter injury. *J Neurosci* 2001; 21: 1302–1312
- Baenziger O, Martin E, Steinlin M, Good M, Largo R, Burger R, Fanconi S, Duc G, Buchli R, Rumpel H, Boltshauser F. Early pattern recognition in severe perinatal asphyxia: a prospective MRI study. *Neuroradiology* 1993; 35: 437–442
- Barkovich AJ. MR and CT evaluation of profound neonatal and infantile asphyxia. *AJNR Am J Neuroradiol* 1992; 13: 959–972
- Barkovich AJ, Sargent SK. Profound asphyxia in the premature infant: imaging findings. *AJNR Am J Neuroradiol* 1995; 16: 1837–1846
- Barkovich AJ, Truwit CL. Brain damage from perinatal asphyxia: correlation of MR findings with gestational age. *AJNR Am J Neuroradiol* 1990; 11: 1087–1096
- Barkovich AJ, Westmark K, Partridge C, Sola A, Ferriero DM. Perinatal asphyxia: MR findings in the first 10 days. *AJNR Am J Neuroradiol* 1995; 16: 427–438
- Barkovich AJ, Hajnal BL, Vigneron D, Sola A, Partridge JC, Allen F, Ferriero DM. Prediction of neuromotor outcome in perinatal asphyxia: evaluation of MR scoring systems. *AJNR Am J Neuroradiol* 1998; 19: 143–149
- Barth PG. Prenatal clastic encephalopathies. *Clin Neurol Neurosurg* 1984; 86: 65–75
- Barth PG, Valk J, Olislagers-de Slegte R. Central cortico-subcortical pattern on CT in cerebral palsy. Its relevance to asphyxia. *J Neuroradiol* 1984; 111: 65–71
- Bozzao A, Di Paolo A, Mazzoleni C, Fasoli F, Simonetti A, Fantozzi LM, Floris R. Diffusion-weighted MR imaging in the early diagnosis of periventricular leukomalacia. *Eur Radiol* 2003; 13: 1571–1576
- Bydder GM, Rutherford MA, Cowan FM. Diffusion-weighted imaging in neonates. *Childs Nerv Syst* 2001; 17: 190–194
- Christophe C, Clercx A, Blum D, Hasearts D, Segebarth C, Perlmutter N. Early MR deletion of cortical and subcortical hypoxic-ischemic encephalopathy in full-term infants. *Pediatr Radiol* 1994; 24: 581–584
- Counsell SJ, Allsop JM, Harrison MC, Larkman DJ, Kennea NL, Kapellou O, Cowan FM, Hanjal JV, Edwards AD, Rutherford MA. Diffusion-weighted imaging of the brain in preterm infants with focal and diffuse white matter abnormalities. *Pediatrics* 2003; 112: 1–7

95 Posthypoxic-ischemic Encephalopathy of Neonates

- Amato M, Donati F. Update on perinatal hypoxic insult: mechanism, diagnosis and interventions. *Eur J Paediatr Neurol* 2000; 4: 203–209

- Cowan F, Rutherford M, Groenendaal F, Eken P, Mercuri E, Bydder GM, Meiners LC, Dubowitz LM, de Vries LS. Origin and timing of brain lesions in term infants with neonatal encephalopathy. *Lancet* 2003; 361: 736–742
- Cowan FM, Pennock JM, Hanrahan JD, Manji KP, Edwards AD. Early detection of cerebral infarction and hypoxic ischemic encephalopathy in neonates using diffusion-weighted magnet resonance imaging. *Neuropediatrics* 1994; 25: 172–175
- Dammann O, Hagberg H, Leviton A. Is periventricular leukomalacia an axonopathy as well as an oligopathy. *Pediatr Res* 2001; 49: 453–457
- De Reuck J. The human periventricular arterial blood supply and the anatomy of cerebral infarctions. *Eur Neurol* 1971; 5: 321–334
- De Reuck J, Chattha AS, Richardson EP Jr. Pathogenesis and evaluation of periventricular leukomalacia in infancy. *Arch Neurol* 1972; 27: 229–236
- De Reuck JL. Cerebral angioarchitecture and perinatal brain lesions in premature and full-term infants. *Acta Neurol Scand* 1984; 70: 391–395
- De Vries LS, Wigglesworth JS, Regev R, Dubowitz LMS. Evolution of periventricular leukomalacia during the neonatal period and infancy: correlation of imaging and post-mortem findings. *Early Hum Dev* 1988; 17: 205–219
- De Vries LS, Eken P, Groenendaal F, van Haastert IC, Meiners LC. Correlation between the degree of periventricular leukomalacia diagnosed using cranial ultrasound and MRI later in infancy in children with cerebral palsy. *Neuropediatrics* 1993; 24: 263–268
- Du Plessis AJ, Johnston MV. Hypoxic-ischemic brain injury in the newborn. Cellular mechanisms and potential strategies for neuroprotection. *Clin Perinatol* 1997; 24: 627–654
- Felderhoff-Mueser U, Rutherford MA, Squier WV, Cox P, Maalouf EF, Counsell SJ, Bydder GM, Edwards AD. Relationship between MR imaging and histopathologic findings of the brain in extremely sick preterm infants. *AJNR Am J Neuroradiol* 1999; 20: 1349–1357
- Fellman V, Raivio KO. Reperfusion injury as the mechanism of brain damage after perinatal asphyxia. *Pediatr Res* 1997; 41: 599–606
- Filippi CG, Lin DDM, Tsiouris AJ, Watts R, Packard AM, Heier LA, Uluğ AM. Diffusion-tensor MR imaging in children with developmental delay: preliminary findings. *Radiology* 2003; 229: 44–50
- Forbes KPN, Pipe JG, Bird R. Neonatal hypoxic-ischemic encephalopathy: detection with diffusion-weighted MR imaging. *AJNR Am J Neuroradiol* 2000; 21: 1490–1496
- Grow J, Barks JDE. Pathogenesis of hypoxic-ischemic cerebral injury in the term infant: current concepts. *Clin Perinatol* 2002; 29: 585–602
- Gücüyener K, Atalay Y, Aral YZ, Hasanoğlu A, Türkyılmaz C, Biberoğlu G. Excitatory amino acids and taurine levels in cerebrospinal fluid of hypoxic ischemic encephalopathy in newborn. *Clin Neurol Neurosurg* 1999; 101: 171–174
- Guzzetta F, Deodato F, Randò T. Brain ischemic lesions of the newborn. *Childs Nerv Syst* 2000; 16: 633–637
- Haynes RL, Folkert RD, Keefe RJ, Sung I, Swzeda LI, Rosenberg PA, Volpe JJ, Kiney HC. Nitrosative and oxidative injury to premyelinating oligodendrocytes in periventricular leukomalacia. *J Neuropathol Exp Neurol* 2003; 62: 441–450
- Huang C-C, Wang S-T, Chang Y-C, Lin K-P, Wu P-L. Measurement of the urinary lactate: creatinine ratio for the early identification of newborn infants at risk for hypoxic-ischemic encephalopathy. *N Engl J Med* 1999 341: 328–335
- Hüppi PS, Barnes PD. Magnetic resonance techniques in the evaluation of the newborn brain. *Clin Perinatol* 1997; 24: 693–723
- Inage YW, Itoh M, Takashima S. Correlation between cerebrovascular maturity and periventricular leukomalacia. *Pediatr Neurol* 2000; 22: 204–208
- Inder TE, Hüppi PS, Warfield S, Kikinis FR, Zientara GP, Barnes PD, Jolesz F, Volpe JJ. Periventricular white matter injury in the premature infant is followed by reduced cerebral cortical gray matter volume at term. *Ann Neurol* 1999; 46: 755–760
- Inder TE, Mocatta T, Darlow B, Spencer C, Volpe JJ, Winterbourn C. Elevated free radical products in the cerebrospinal fluids of VLBW infants with cerebral white matter injury. *Pediatr Res* 2002; 52: 213–218
- Inder TE, Wells SJ, Mogridge NB, Spencer C, Volpe JJ. Defining the nature of the cerebral abnormalities in the premature infant: a quantitative magnetic resonance imaging study. *J Pediatr* 2003; 143: 171–179
- Johnston MV. Selective vulnerability in the neonatal brain. *Ann Neurol* 1998; 44: 155–156
- Jouvet P, Cowan FM, Cox PH, Lazda E, Rutherford MA, Wigglesworth J, Mehmet H, Edwards AD. Reproducibility and accuracy of MR imaging of the brain after severe birth asphyxia. *Am J Neuroaradiol* 1999; 20: 1343–1348
- Krägeloh-Mann I, Hagberg B, Petersen D, Riethmüller J, Gut E, Michaelis R. Bilateral spastic cerebral palsy – pathogenetic aspects from MRI. *Neuropediatrics* 1991; 23: 46–48
- Krägeloh-Mann I, Petersen D, Hagberg G, Vollmer B, Hagberg B, Michaelis R. Bilateral spastic cerebral palsy – MRI pathology and origin. Analysis from a representative series of 56 cases. *Dev Med Child Neurol* 1995; 37: 379–397
- Kuban K, Sanocka U, Leviton A, Allred EN, Pagano M, Dammann O, Share J, Rosenfeld D, Abiri M, diSalvo D, Doubilet P, Kairam R, Kazam E, Kirpekar M, Schonfeld S. White matter disorders of prematurity: association with intraventricular hemorrhage and ventriculomegaly. *J Pediatr* 1999; 134: 539–546
- Leth H, Toft PB, Pryds O, Peitersen B, Lou HC, Henriksen O. Brain lactate in preterm and growth-retarded neonates. *Acta Paediatr* 1995; 84: 495–499
- Maalouf EF, Duggan PH, Rutherford MA, Counsell SJ, Fletcher AM, Battin M, Cowan F, Edwards AD. Magnetic resonance imaging of the brain in a cohort of extremely preterm infants. *J Pediatr* 1999; 135: 351–357
- Mader I, Schöning M, Klose U, Küker W. Neonatal cerebral infarction diagnosed by diffusion-weighted MRI. Pseudonormalization occurs early. *Stroke* 2002; 33: 1142–1145
- Marín-Padilla M. Developmental neuropathology and impact of perinatal brain damage. II: white matter lesions of the neocortex. *J Neuropathol Exp Neurol* 1997; 56: 219–235
- Martin E, Barkovich AJ. Magnetic resonance imaging in perinatal asphyxia. *Arch Dis Child* 1995; 72: F62-F70
- Mathew OP, Bland H, Boxerman SB, James E. CSF lactate levels in high risk neonates with and without asphyxia. *Pediatrics* 1980; 66: 224–227
- Mayer PL, Kier EL. The controversy of the periventricular white matter circulation: a review of the anatomic literature. *AJNR Am J Neuroradiol* 1991; 12: 223–228
- McArdle CB, Richardson CJ, Hayden CK, Nicholas DA, Crofford MJ, Amparo EG. Abnormalities of the neonatal brain: MR imaging. I. Intracranial hemorrhage. *Radiology* 1987; 163: 387–394
- Mercuri E, Atkinson J, Braddick O, Anker S, Cowan F, Pennock J, Rutherford MA, Dubowitz LMS. The aetiology of delayed visual maturation: short review and personal findings in relation to magnetic resonance imaging. *Eur J Paediatr Neurol* 1997; 1: 31–34

- Mercuri E, Atkinson J, Braddick O, Anker S, Cowan F, Rutherford M, Pennock J, Dubowitz L. Basal ganglia damage and impaired visual function in the newborn infant. *Arch Dis Child* 1997; 77: F111-F114
- Müller AM, Morales C, Briner J, Baenziger O, Duc G, Bucher HU. Loss of CO₂ reactivity of cerebral blood flow is associated with severe brain damage in mechanically ventilated very low birth weight infants. *Eur J Paediatr Neurol* 1997; 5/6: 157-163
- Nakai T, Rhine WD, Enzmann DR, Stevenson DK, Spielman DM. A model for detecting early metabolic changes in neonatal asphyxia by ¹H-MRS. *J Magn Reson Imaging* 1996; 6: 445-452
- Natsume J, Wanatabe K, Kuno K, Hayakawa F, Hashizume Y. Clinical, neuropsychologic, and neuropathological features of an infant with brain damage of total asphyxia type (Myers). *Pediatr Neurol* 1995; 61-64
- Nelson MD, Gonzalez-Gomez I, Gilles FH. The search for human telencephalic ventriculofugal arteries. *AJNR Am J Neuroradiol* 1991 12: 215-222
- Pasternak JF, Predey TA, Mikhael MA. Neonatal asphyxia: vulnerability of basal ganglia, thalamus, and brainstem. *Pediatr Neurol* 1991; 7: 147-149
- Penrice J, Lorek A, Cady EB, Amess PN, Wylezinska M, Cooper CE, d'Souza P, Brown CG, Kirbride V, Edwards AD, Wyatt JS, Reynolds EOR. Proton magnetic resonance spectroscopy of the brain during acute hypoxia-ischemia and delayed cerebral energy failure in the newborn piglet. *Pediatr Res* 1997; 41: 795-802
- Perlman JM. Markers of asphyxia and neonatal brain injury. *N Engl J Med* 1999; 341: 364-365
- Ramakers RP, van der Knaap MS, Verbeeten B Jr, Barth PG, Valk J. Central cortico-subcortical involvement: a distinct pattern of brain damage caused by perinatal and postnatal asphyxia in term infants. *J Comput Assist Tomogr* 1995; 19: 256-263
- Robertson RL, Ben-Sira L, Barnes PD, Mulkern RV, Robson CD, Maier SE, Rivkin MJ, du Plessis AJ. MR line-scan diffusion-weighted imaging of term neonates with perinatal brain ischemia. *AJNR Am J Neuroradiol* 1999; 20: 1658-1670
- Roelants-van Rijn AM, Groenendaal F, Beek FJA, Eken P, van Haastert IC, de Vries LS. Parenchymal brain injury in the preterm infant: comparison of cranial ultrasound, MRI and neurodevelopmental outcome. *Neuropediatrics* 2001; 32: 80-89
- Roland EH, Poskitt K, Rodriguez E, Lupton BA, Hill A. Perinatal hypoxic-ischemic thalamic injury: clinical features and neuroimaging. *Ann Neurol* 1998; 44: 161-166
- Rorke LB, Zimmerman RA. Prematurity, postmaturity, and destructive lesions in utero. *AJNR Am J Neuroradiol* 1992; 13: 517-536
- Rutherford MA, Pennock JM, Schwieso JE, Cowan FM, Dubowitz LMS. Hypoxic ischaemic encephalopathy: early magnetic resonance imaging findings and their evolution. *Neuropediatrics* 1995; 26: 183-191
- Rutherford M, Pennock J, Schwieso J, Cowan F, Dubowitz L. Hypoxic-ischaemic encephalopathy: early and late magnetic resonance imaging findings in relation to outcome. *Arch Dis Child* 1996; 75: F145-F151
- Sarnat HB, Sarnat MS. Neonatal encephalopathy following fetal distress. *Arch Neurol* 1976; 33: 696-705
- Sawada H, Udaka F, Seriu N, Shindou K, Kameyama M, Tsujimura M. MRI demonstration of cortical laminar necrosis and delayed white matter injury in anoxic encephalopathy. *Neuroradiology* 1990; 32: 319-321
- Shevell MI, Majnemer A, Miller SP. Neonatal neurologic prognostication: the asphyxiated term newborn. *Pediatr Neurol* 1999; 21: 776-784
- Sie LTL, van der Knaap MS, Oosting J, de Vries LS, Lafeber HN, Valk J. MR patterns of hypoxic-ischemic brain damage after prenatal, perinatal or postnatal asphyxia. *Neuropediatrics* 2000; 31: 128-136
- Sie LTL, van der Knaap MS, van Wezel-Meijler G, Taets van Amerongen AHM, Lafeber HN, Valk J. Early MR features of hypoxic-ischemic brain injury in neonates with periventricular densities on sonograms. *AJNR Am J Neuroradiol* 2000; 21: 852-861
- Simonati A, Laverda AM, Rizzuto N. Multicystic encephalomalacia associated with symmetrical necrotizing brain stem lesions in an infant: a case report. *Clin Neuropathol* 1986; 5: 139-145
- Skranes SJ, Vik T, Nilsen G, Smevik O, Andersson HW, Brubakk AM. Cerebral magnetic resonance imaging and motor function of a very low birth weight children at six years of age. *Neuropediatrics* 1997; 28: 149-154
- Skullerud K, Westre B. Frequency and prognostic significance of germinal matrix hemorrhage, periventricular leukomalacia, and pontosubicular necrosis in preterm neonates. *Acta Neuropathol (Berl)* 1986; 70: 257-261
- Sohma O, Mito T, Mizuguchi M, Takashima S. The prenatal age critical for the development of the pontosubicular necrosis. *Acta Neuropathol (Berl)* 1995; 90: 7-10
- Takashima S, Tanaka K. Development of cerebrovascular architecture and its relationship to periventricular leukomalacia. *Arch Neurol* 1978; 35: 11-16
- Truwit CL, Barkovich AJ, Koch TK, Ferriero DM. Cerebral palsy: MR findings in 40 patients. *AJNR Am J Neuroradiol* 1992; 13: 67-78
- Volpe JJ. Current concepts of brain injury in the premature infant. *AJR Am J Roentgenol* 1989; 153: 243-251
- Uluğ AM. Monitoring brain development with quantitative diffusion tensor imaging. *Dev Sci* 2002; 5: 286-292
- Valk J, van der Knaap MS, de Grauw T, Taets van Amerongen AHM. The role of imaging modalities in the diagnosis of posthypoxic-ischemic and hemorrhagic conditions of infants (part I of II). *Klin Neuroradiol* 1991; 1: 72-79
- Valk J, van der Knaap MS, de Grauw T, Taets van Amerongen AHM. The role of imaging modalities in the diagnosis of posthypoxic-ischemic and hemorrhagic conditions of infants (part II of II). *Klin Neuroradiol* 1991; 1: 127-138
- Valkama AM, Pääkkö ELE, Vainionpää LK, Lanning FP, Ilkko EA, Koivisto ME. Magnetic resonance imaging at term and neuromotor outcome in preterm infants. *Acta Paediatr* 2000; 89: 348-355
- Vermeulen RJ, Fetter WPF, Hendriks L, van Schie PEM, van der Knaap MS, Barkhof F. Diffusion-weighted MRI in severe neonatal hypoxic ischaemia: the white cerebrum. *Neuropediatrics* 2003; 34: 72-76
- Victory R, Penava D, da Silva O, Natale R, Richardson B. Umbilical cord pH and base excess values in relation to neonatal morbidity for infants delivered preterm. *Am J Obstet Gynecol* 2003; 189: 803-807
- Vintzileos AM, Gaffney SE, Salinger LM, Kontopoulos VG, Campbell WA, Nochimson DJ. The relationships among the fetal biophysical profile, umbilical cord pH, and Apgar scores. *Am J Obstet Gynecol* 1987; 157: 627-631
- Voit T, Lemburg P. Damage of thalamus and basal ganglia in asphyxiated full-term neonates. *Neuropediatrics* 1987; 18: 176-181
- Volpe JJ. Brain injury in the premature infant. *Clin Perinatol* 1997; 24: 567-587

- Volpe JJ. Brain injury in the premature infant – from pathogenesis to prevention. *Brain Dev* 1997; 19: 519–534
- Volpe JJ. Neurobiology of periventricular leukomalacia in the premature infant. *Pediatr Res* 2001; 50: 553–562
- Volpe JJ. Perinatal brain injury: from pathogenesis to neuroprotection. *Mental Retard Dev Disabil Res Rev* 2001; 7: 56–64
- Westmark KD, Barkovich AJ, Sola A, Ferriero D, Partridge JC. Patterns and implications of MR contrast enhancement in perinatal asphyxia: a preliminary report. *AJNR Am J Neuroradiol* 1995; 16: 685–692
- Wood NS, Marlow N, Costeloe K, Gibson AT, Wilkinson AR. Neurologic and developmental disability after extremely preterm birth. *N Engl J Med* 2000; 343: 378–384
- Yoshioka H, Kadomoto Y, Mino M, Morikawa Y, Kasubuchi Y, Kusunoki T. Multicystic encephalomania in liveborn twin with stillborn macerated co-twin. *J Pediatr* 1979; 95: 798–800
- 96 Neonatal Hypoglycemia**
- Abdul-Rahman A, Agartha A, Siesjö BK. Local cerebral blood flow in the rat during severe hypoglycaemia and the recovery period following glucose injection. *Acta Physiol Scand* 1980; 109: 307–314.
- Anderson JM, Milner RDG, Strich SJ. Effects of neonatal hypoglycaemia on the central nervous system: a pathological study. *J Neurol Neurosurg Psychiatry* 1967; 30: 295–310
- Antunes NL, Small TN, George D, Boulad F, Lis E. Posterior leukoencephalopathy syndrome may not be reversible. *Pediatr Neurol* 1999; 20: 241–3
- Anwar M, Vannucci RC. Autoradiographic determination of regional cerebral blood flow during hypoglycaemia in newborn dogs. *Pediatr Res* 1988; 24: 41–45
- Auer RN, Wieloch T, Olsson Y, Siesjö BK. The distribution of hypoglycaemic brain damage. *Acta Neuropathol (Berl)* 1984; 64: 177–191
- Auer RN, Kalimo H, Olsson Y, Siesjö BK. The temporal evolution of hypoglycaemic brain damage. *Acta Neuropathol (Berl)* 1985; 67: 13–24
- Barkovich AJ, Ali FA, Rowley HA, Bass N. Imaging patterns of neonatal hypoglycaemia. *AJNR Am J Neuroradiol* 1998; 19: 523–528
- Chase HP, Marlow RA, Dabiere CS et al. Hypoglycaemia and brain development. *Pediatrics* 1973; 52: 513–520
- Chugani HT, Phelps ME, Mazziotta JC. Positron emission tomography study of the human brain functional development. *Ann Neurol* 1987; 22: 487–497
- Collins JE, Leonard JV. Hyperinsulinism in asphyxiated and small-for dates infants with hypoglycaemia. *Lancet* 1984; 2: 311–313
- Fahnehjelm KT, Jacobson L, Hellstrom A, Lewensohn-Fuchs I, Ygge J. Visually impaired children with posterior ocular malformations: pre- and neonatal data and visual functions. *Acta Ophthalmol Scand* 2003; 81: 361–72.
- Hawdon JM. Hypoglycemia and the neonatal brain. *Eur J Pediatr* 1999; 158: S9–S12
- Ichord RN, Helfaer MA, Kirsch JR, Wilson D, Traystman RJ. Nitric oxide synthetase inhibition attenuates hypoglycaemic hyperemia in piglets. *Am J Physiol* 1994; 266: 1062–1068
- Lucas A, Morley R, Cole TJ. Adverse neurodevelopmental outcome in moderate neonatal hypoglycaemia. *BMJ* 1988; 297: 1304–1308
- Murakami Y, Yamashita Y, Matsuishi T, Utsunomiya H, Okudera T, Hashimoto T. Cranial MRI of neurologically impaired children suffering from neonatal hypoglycaemia. *Pediatr Radiol* 1999; 29: 23–27
- Pildes RS, Cornblath M, Warren I, et al., A prospective controlled study of neonatal hypoglycaemia. *Pediatrics* 1974; 54: 5–14
- Pryds O, Greisen G, Friis-Hansen B. Compensatory increase of CBF in preterm infants during hypoglycaemia. *Acta Paediatr Scand* 1988; 77: 632–637
- Spar JA, Lewine JD, Orrison WW. Neonatal hypoglycaemia: CT and MR findings. *AJNR Am J Neuroradiol* 1994; 15: 1477–1478
- Suhonen-Polvi H, Ruotsalainen U, Kinnala A, Bergman J, Haaparanta MM, Makel AP, Solin O, Wegelius P. FDG-PET in early infancy: simplified quantification methods to measure cerebral glucose utilization. *J Nucl Med* 1995; 13: 1249–1254
- Traill Z, Squier M, Anslow P. Brain imaging in neonatal hypoglycaemia. *Arch Dis Child Fetal Neonatal Ed* 1998; 79: F145–F147
- Van der Knaap MS, Bakker HD, Valk J. MR imaging and proton spectroscopy in 3-hydroxy-3-methylglutaryl coenzyme A lyase deficiency. *AJNR Am J Neuroradiol* 1998; 19: 378–382
- Vannucci SJ. Developmental expression of GLUT1 and GLUT3 glucose transporters. *J Neurochem* 1994; 62: 240–246
- Vannucci SJ, Maher F, Simpson IA. Glucose transporter proteins in brain: delivery of glucose to neurons and glia. *Glia* 1997; 21: 2–21
- Volpe JJ. *Neurology of the newborn*, 4th ed. Philadelphia: WB Saunders Co, 2002
- Zammarchi E, Filippi L, Fonda C, Benedetti PA, Pistone D, Donati MA. Different neurologic outcomes in two patients with neonatal hyperinsulinemic hypoglycaemia. *Childs Nerv Syst* 1996; 12: 413–416
- 97 Delayed Posthypoxic Leukoencephalopathy**
- Chalela JA, Wolf RL, Maldjian JA, Kasner SE. MRI identification of early white matter injury in anoxic-ischemic encephalopathy. *Neurology* 2001; 56: 481–485
- Chang KH, Han MH, Kim HS, Wie BA, Han MC. Delayed encephalopathy after acute carbon monoxide intoxication: MR imaging features and distribution of cerebral white matter lesions. *Radiology* 1992; 184: 117–122
- De Reuck J. Arterial vascularisation and angioarchitecture of the nucleus caudatus in human brain. *Eur Neurol* 1971; 5: 130–136
- De Reuck J, van der Eecken H. Periventricular leukoencephalopathy and meningo-cortical arterio-venous malformation. *Acta Neurol Belg* 1974; 74: 276–283
- Devine SA, Kirkley SM, Palumbo CL, White RF. MRI and neuropsychological correlates of carbon monoxide exposure: a case report. *Environ Health Perspect* 2002; 110: 1051–1055
- Dragonesco ST, Nereantiu FL, Vuia O. Encéphalopathy hypoxique prolongée. *Acta Neuropathol (Berl)* 1964; 3: 387–391
- Elovaara E, Rantanen J. Carbon monoxide-induced brain injury: neurochemical studies after single and repeated exposures. *J Appl Toxicol* 1983; 3: 154–160
- Feigin I, Budzilovich G, Weinberg S, Ogata J. Degeneration of white matter in hypoxia, acidosis and edema. *J Neuropathol Exp Neurol* 1973; 32: 125–143
- Garland H, Pearce J. Neurological complications of carbon monoxide poisoning. *Q J Med* 1967; 36: 445–455

- Ginsberg MD, Myers RE, McDonagh BF. Experimental carbon monoxide. Encephalopathy in the primate. I. Physiologic and metabolic aspects. *Arch Neurol* 1974; 30: 202–208
- Ginsberg MD, Myers RE, McDonagh BF. Experimental carbon monoxide. Encephalopathy in the primate. II. Clinical aspects, neuropathology, and physiologic correlation. *Arch Neurol* 1974; 30: 209–216
- Ginsberg MD, Hedley-Whyte ET, Richardson EP Jr. Hypoxic-ischemic leukoencephalopathy in man. *Arch Neurol* 1976; 33: 5–14
- Gorman D, Huang YL, Williams C. A lignocaine infusion worsens the leukoencephalopathy due to a carbon monoxide exposure in sheep. *Toxicology* 2003; 186: 143–150
- Gottfried JA, Mayer SA, Shungu DC, Chang Y, Duyn JH. Delayed posthypoxic demyelination. Association with arylsulfatase A deficiency and lactic acidosis on MR spectroscopy. *Neurology* 1997; 49: 1400–1404
- Grinker RR. Ueber einen Fall von Luchtgasvergiftung mit doppelseitiger Pallidumweichung und schwerer Degeneration des tiefen Grosshirnmarklagers. *Z Ges Neurol Psychiatr* 1925; 98: 433–456
- Inagaki T, Ishino H, Seno H, Umegae N, Aoyama T. A long-term follow-up study of serial magnetic resonance image in patients with delayed encephalopathy after acute carbon monoxide poisoning. *Psychiatr Clin Neurosci* 1997; 51: 421–423
- Kamada K, Houkin K, Aoki T, Koiwa M, Kashiwaba T, Iwasaki Y, Abe H. Cerebral metabolic changes in delayed carbon monoxide sequelae studied by proton MR spectroscopy. *Neuroradiology* 1994; 36: 104–106
- Kelafant GA. Encephalopathy and peripheral neuropathy following carbon monoxide poisoning from a propane-fueled vehicle. *Am J Ind Med* 1996; 30: 765–768
- Kim JH, Chang KH, Song IC, Kim KH, Kwon BJ, Kim HC, Kim JH, Han MH. Delayed encephalopathy of acute carbon monoxide intoxication: diffusivity of cerebral white matter lesions. *AJNR Am J Neuroradiol* 2003; 24: 1592–1597
- Klawans HL, Stein RW, Tanner CM, Goetz CG. A pure Parkinsonian syndrome following acute carbon monoxide intoxication. *Arch Neurol* 1982; 39: 302–304
- Kono E, Kono R, Shida K. Computerized tomographies of 34 patients at the chronic stage of acute carbon monoxide poisoning. *Arch Psychiatr Nervenkr* 1983; 233: 271–278
- Koehler RC, Jones MD, Traystman RJ. Cerebral circulatory response to carbon monoxide and hypoxic hypoxia in the lamb. *Am J Physiol* 1982; 243: H27–H32
- Ku MC, Huang CC, Kuo HC, Yen TC, Chen CJ, Shih TS, Chang HY. Diffuse white matter lesions in carbon disulfide intoxication: microangiopathy or demyelination. *Eur Neurol* 2003; 50: 220–224
- Lee MS, Marsden CD. Neurological sequelae following carbon monoxide poisoning clinical course and outcome according to the clinical types and brain computed tomography scan findings. *Mov Disord* 1994; 9: 550–558
- Levine S. Anoxic-ischemic encephalopathy in rats. *Am J Pathol* 1960; 36: 1–18
- Levine S, Stypulowski W. Experimental cyanide encephalopathy. *Arch Pathol* 1959; 67: 306–323
- Mascalchi M, Petrucci P, Zampa V. MRI of cerebral white matter damage due to carbon monoxide poisoning: case report. *Neuroradiology* 1996; 38: S73–S74
- Murata T, Itoh S, Koshino Y, Sakamoto K, Nishio M, Maeda M, Yamada H, Ishii Y, Isaki K. Serial cerebral MRI with FLAIR sequences in acute carbon monoxide poisoning. *J Comput Assist Tomogr* 1995; 19: 631–634
- Okeda R, Funata N, Takano T, Miyazaki Y, Higashino F, Yokoyama K, Manabe M. The pathogenesis of carbon monoxide encephalopathy in the acute phase – physiological and morphological correlation. *Acta Neuropathol (Berl)* 1981; 54: 1–10
- Okeda R, Funata N, Song S-J, Higashino F, Takano T, Yokoyama K. Comparative study on pathogenesis of selective cerebral lesions in carbon monoxide poisoning and nitrogen hypoxia in cats. *Acta Neuropathol (Berl)* 1982; 56: 265–272
- Okeda R, Song SY, Funata N, Higashino F. An experimental study of the pathogenesis of Grinker's myelinopathy in carbon monoxide intoxication. *Acta Neuropathol (Berl)* 1983; 59: 200–206
- Parkinson RB, Hopkins RO, Cleavinger HB, Weaver LK, Victoroff J, Foley JF, Bigler ED. White matter hyperintensities and neuropsychological outcome following carbon monoxide poisoning. *Neurology* 2002; 58: 1525–1532
- Plum F, Posner JB, Hain RF. Delayed neurological deterioration after anoxia. *Arch Intern Med* 1962; 110: 18–25
- Prockop LD, Naidu KA. Brain CT and MRI findings after carbon monoxide toxicity. *J Neuroim* 1999; 9: 175–181
- Roohi F, Kula RW, Metha N. Twenty-nine years after carbon monoxide intoxication. *Clin Neurol Neurosurg* 2001; 103: 92–95
- Sawa GM, Watson CPN, Terbrugge K, Chiu M. Delayed encephalopathy following carbon monoxide intoxication. *J Can Sci Neurol* 1981; 8: 77–79
- Sawada Y, Takahashi M, Ohashi N, Fusamoto H, Maemura K, Kobayashi H, Yoshioka T, Sugimoto T. Computerised tomography as an indication of long-term outcome after acute carbon monoxide poisoning. *Lancet* 1980; i: 783–784
- Sawada Y, Sakamoto T, Nishide K, Sadamitsu D, Fusamoto H, Yoshioka T, Sugimoto T, Onishi S. Correlation of pathological findings with computed tomographic findings after acute carbon monoxide poisoning. *N Engl J Med* 1983; 26: 1296
- Sesay M, Bidabe AM, Guyot M, Bedry R, Caille JM, Maurette P. Regional cerebral blood flow measurements with Xenon-CT in the prediction of delayed encephalopathy after carbon monoxide intoxication. *Acta Neurol Scand Suppl* 1996; 166: 22–27
- Silverman CS, Brenner J, Murtagh FR. Hemorrhagic necrosis and vascular injury in carbon monoxide poisoning: MR demonstration. *AJNR Am J Neuroradiol* 1993; 14: 168–170
- Taylor R, Holgate RC. Carbon monoxide poisoning: asymmetric and unilateral changes on CT. *AJNR Am J Neuroradiol* 1988; 9: 975–977
- Teksam M, Casey SO, Michel E, Liu H, Truwit CL. Diffusion-weighted MR images findings in carbon monoxide poisoning. *Neuroradiology* 2002; 44: 109–113
- Uchino A, Hasuo K, Shida K, Matsumoto S, Yasumori K, Masuda K. MRI of the brain in chronic carbon monoxide poisoning. *Neuroradiology* 1994; 36: 399–401
- Valenzuela R, Court J, Godoy J. Delayed cyanide induced dystonia. *J Neurol Neurosurg Psychiatry* 1992; 55: 198–199
- Vieregge P, Klostermann W, Blümm RG, Borgis KJ. Carbon monoxide poisoning: clinical, neurophysiological, and brain imaging observations in acute disease and follow-up. *J Neurol* 1989; 236: 478–481
- Vion-Dury J, Jiddane M, van Bunnin Y, Rumeau C, Lavielle J. Etude IRM des séquelles d'intoxication au monoxyde de carbone: à propos de deux cas. *J Neuroradiol* 1987; 14: 60–65
- Zagami AS, Lethlean AK, Mellick R. Delayed neurological deterioration following carbon monoxide poisoning: MRI findings. *J Neurol* 1993; 240: 113–116

98 White Matter Lesions of the Elderly

- Awad IA, Spetzler RF, Hodak JA, Awad CA, Carey R. Incidental subcortical lesions identified on magnetic resonance imaging. I. Correlation with age and cerebrovascular risk factors. *Stroke* 1986; 17: 1084–1089
- Awad IA, Spetzler RF, Hodak JA, Awad CA, Williams F, Carey R. Incidental lesions noted on magnetic resonance imaging of the brain: prevalence and clinical significance in various age groups. *Neurosurgery* 1987; 20: 222–227
- Barber R, Scheltens P, Gholkar A, Ballard C, McKeith I, Ince P, Perry R, O'Brien J. White matter lesions on magnetic resonance imaging in dementia with Lewy bodies, Alzheimer's disease, vascular dementia, and normal aging. *J Neurol Neurosurg Psychiatry* 1999; 67: 66–72
- Bowen BC, Barker WW, Loewenstein DA, Scheldon J, Duara R. MR signal abnormalities in memory disorder and dementia. *AJNR Am J Neuroradiol* 1990; 11: 283–290
- Bradley WG Jr, Waluch V, Brant-Zawadzki M, Yadley RA, Wycoff RR. Patchy, periventricular white matter lesions in the elderly: a common observation during NMR imaging. *Noninvas Med Imaging* 1984; 1: 5–41
- Braffman BH, Zimmerman RA, Trojanowski JQ, Gonatas NK, Hickey WF, Schlaepfer WW. Brain MR: pathologic correlation with gross and histopathology. 2. Hyperintense white-matter foci in the elderly. *AJNR Am J Neuroradiol* 1988; 9: 629–636
- Brant-Zawadzki M, Fein G, van Dyke C, Kiernan R, Davenport L, de Groot J. MR imaging of the aging brain: patchy white-matter lesions and dementia. *AJNR Am J Neuroradiol* 1985; 6: 675–682
- Brown WR, Moody DM, Thore CR, Challa VR. Apoptosis in leukoaraiosis. *AJNR Am J Neuroradiol* 2000; 21: 79–82
- Charletta D, Gorelick PB, Dollear TJ, Freels S, Harris Y. CT and MRI findings among Africa-Americans with Alzheimer's disease, vascular dementia, and stroke without dementia. *Neurology* 1995; 45: 1456–1461
- Chun T, Filippi CG, Zimmerman RD, Uluğ AM. Diffusion changes in the aging human brain. *AJNR Am J Neuroradiol* 2000; 21: 1078–1083
- Courchesne E, Chisum HJ, Townsend J, Cowles A, Covington J, Egaas B, Harwood M, Hinds S, Press GA. Normal brain development and aging: quantitative analysis at in vivo MR imaging in healthy volunteers. *Radiology* 2000; 216: 672–682
- Damian MS, Schilling G, Bachmann G, Simon C, Stöppler S, Dorndorf W. White matter lesions and cognitive deficits: relevance of lesion pattern. *Acta Neurol Scand* 1994; 90: 430–436
- De Groot JC, de Leeuw F-E, Oudkerk M, van Gijn J, Hofman A, Jolles J, Breteler MMB. Cerebral white matter lesions and cognitive function: the Rotterdam scan study. *Ann Neurol* 2000; 47: 145–151
- De Groot JC, de Leeuw F-E, Oudkerk M, van Gijn J, Hofman A, Jolles J, Breteler MMB. Periventricular cerebral white matter lesions predict rate of cognitive decline. *Ann Neurol* 2002; 52: 335–341
- De Leeuw F-E, de Groot JC, Achten E, Oudkerk M, Ramos LMP, Heijboer R, Hofman A, Jolles J, van Gijn J, Breteler MMB. Prevalence of cerebral white matter lesions in elderly people: a population based magnetic resonance imaging study. The Rotterdam scan study. *J Neurol Neurosurg Psychiatry* 2001; 70: 9–14
- De Reuck J. The human periventricular blood supply and the anatomy of cerebral infarctions. *Eur Neurol* 1971; 5: 321–334
- De Reuck J. Periventricular leukomalacia in adults. Clinico-pathological study of four cases. *Arch Neurol* 1978; 35: 517–521
- Desmond DW. Cognition and white matter lesions. *Cerebrovasc Dis* 2002; 13: 53–57
- Drayer BP. Imaging of the brain. I. Normal findings. *Radiology* 1988; 166: 785–796
- Drayer BP. Imaging of the brain. II. Pathologic conditions. *Radiology* 1988; 166: 797–806
- Dufouil C, de Kersaint-Gilly A, Besançon V, Levy C, Auffray E, Brunnereau L, Alperovitch A, Tzourio C. Longitudinal study of blood pressure and white matter hyperintensities. The EVA MRI cohort. *Neurology* 2001; 56: 921–926
- Engelter ST, Provenzale JM, Petrella JR, DeLong DM, MacFall JR. The effect of aging on the apparent diffusion coefficient of normal-appearing white matter. *AJR Am J Roentgenol* 2000; 175: 425–430
- Fazekas F, Kleinert R, Offenbacher H, Schmidt R, Kleinert G, Payer F, Radner H, Lechner H. Pathological correlates of incidental MRI white matter signal hyperintensities. *Neurology* 1993; 43: 1683–1689
- Fazekas F, Schmidt R, Scheltens P. Pathophysiologic mechanisms in the development of age-related white matter changes of the brain. *Dement Geriatr Cogn Disord* 1998; 9: 2–5
- Freeborough PA, Woods RP, Fox NC. Accurate registration of serial 3D MR brain images and its application to visualizing changes in neurodegenerative disorders. *J Comput Assist Tomogr* 1996; 20: 1012–1022
- Fukuda H, Kitani M. Differences between treated and untreated hypertensive subjects in the extent of periventricular hyperintensities observed on brain MRI. *Stroke* 1995; 26: 1593–1697
- George AE, de Leon MJ, Gentes CY, Miller J, London E, Budzilovich GN, Ferris S, Chase N. Leukoencephalopathy in normal and pathologic aging: 1. CT of brain lucencies. *AJNR Am J Neuroradiol* 1986; 7: 561–566
- Gerard G, Weisberg LA. MRI periventricular lesions in adults. *Neurology* 1986; 36: 998–1001
- Golomb J, Kluger A, Gianutsos J, Ferris SH, de Leon MJ, George AE. Nonspecific leukoencephalopathy associated with aging. *Neuroimaging Clin North Am* 1995; 5: 33–44
- Gunning-Dixon FM, Raz N. The cognitive correlates of white matter abnormalities in normal aging: a quantitative review. *Neuropsychology* 2000; 14: 224–232
- Gupta SR, Neheedy MH, Young JC, Ghobrial M, Rubino FA, Hindo W. Periventricular white matter changes and dementia. Clinical, neuropsychological, radiological, and pathological correlation. *Arch Neurol* 1988; 45: 637–641
- Guttmann CRG, Jolesz FA, Kikinis R, Killiany RJ, Moss MB, Sandor T, Albert MS. White matter changes with normal aging. *Neurology* 1998; 50: 972–978
- Hachinski VC, Potter P, Merskey H. Leuko-araiosis. *Arch Neurol* 1987; 44: 21–23
- Helenius J, Sionne L, Salonen O, Kaste M, Tatlisumak T. Leukoaraiosis, ischemic stroke, and normal white matter on diffusion-weighted MRI. *Stroke* 2002; 33: 45–50
- Hunt AL, Orrison WW, Yeo RA, Haaland KY, Rhyne RL, Garry PJ, Rosenberg GA. Clinical significance of MRI white matter lesions in the elderly. *Neurology* 1989; 39: 1470–1474
- Inzitari D, Diaz F, Fox A, Hachinski VC, Steingart A, Lau C, Donald A, Wade J, Mulic H, Merskey H. Vascular risk factors and leuko-araiosis. *Arch Neurol* 1987; 44: 42–47

- Janota I, Mirsen TR, Hachinski VC, Lee DH, Merskey H. Neuropathologic correlates of leuko-araiosis. *Arch Neurol* 1989; 46: 1124–1128
- Ketonen LM. Neuroimaging of the aging brain. *Neurol Clin North Am* 1998; 16: 581–598
- Kertesz A, Black SE, Tokar G, Benke T, Carr T, Nicholson L. Periventricular and subcortical hyperintensities on magnetic resonance imaging. 'Rims, caps, and unidentified bright objects'. *Arch Neurol* 1988; 45: 404–408
- Kirkpatrick JB, Hayman LA. White-matter lesions in MR imaging of clinically healthy brains of elderly subjects: possible pathologic basis. *Radiology* 1987; 162: 509–511
- Knopman DS, Parisi JE, Salvati A, Floriach-Robert M, Boeve BF, Ivnik RJ, Smith GE, Dickson DW, Johnson KA, Petersen LE, McDonald WC, Braak H, Petersen RC. Neuropathology of cognitively normal elderly. *J Neuropathol Exp Neurol* 2003; 62: 1087–1095
- Kobari M, Stirling Meyer J, Ichijo M. Leuko-araiosis, cerebral atrophy, and cerebral perfusion in normal aging. *Arch Neurol* 1990; 47: 161–165
- Lee D, Fox A, Vinuela F, Pelz D, Lau C, Donald A, Merskey H. Inter-observer variation in computed tomography of the brain. *Arch Neurol* 1987; 44: 30–31
- Leifer D, Buonanno FS, Richardson EP Jr. Clinicopathologic correlations of cranial magnetic resonance imaging of periventricular white matter. *Neurology* 1990; 40: 911–918
- Leys D, Soetaert G, Petit H, Fauquette A, Pruvo J-P, Steinling M. Periventricular and white matter magnetic resonance imaging hyperintensities do not differ between Alzheimer's disease and normal aging. *Arch Neurol* 1990; 47: 525–527
- Longstreth WT Jr, Manolino TA, Arnold A, Burke GL, Bryan N, Jungreis CA, Enright PL, O'Leary D, Fried L. Clinical correlates of white matter findings on cranial magnetic resonance imaging of 3301 elderly people. The cerebrovascular health study. *Stroke* 1996; 27: 1274–1282
- Malone MJ, Szoke MC. Neurochemical changes in white matter. Aged human brain and Alzheimer's disease. *Arch Neurol* 1985; 42: 1063–1066
- Marchall VG, Bradley WG, Marchall CE, Bhoopat T, Rhodes RH. Deep white matter infarction: correlation of MR imaging and histopathological findings. *Radiology* 1988; 167: 517–522
- Mineura K, Sasajima H, Kikuchi K, Kowads M, Tomura N, Monma K, Segawa Y. White matter hyperintensity in neurologically asymptomatic subjects. *Acta Neurol Scand* 1995; 92: 151–156
- Moody DM, Brown WR, Challa VR, Anderson RL. Periventricular venous collagenosis: association with leukoaraiosis. *Radiology* 1995; 194: 469–476
- Murdoch G. Staining for apoptosis: now neuropathologists can "see" leukoaraiosis. *AJNR Am J Neuroradiol* 2000; 2: 42–43
- O'Sullivan M, Lythgoe DJ, Pereira AC, Summers PE, Jarosz JM, Williams SCR, Merkus HS. Patterns of cerebral blood flow reduction in patients with ischemic leukoaraiosis. *Neurology* 2002; 59: 321–326
- Pantoni L, Garcia JH. Pathogenesis of leukoaraiosis. A review. *Stroke* 1997; 28: 652–659
- Pohjasvaara T, Mäntylä R, Salonen O, Aronen HJ, Ylikoski R, Hietanen M, Kaste M, Erkinjuntti T. How complex interactions of ischemic brain infarcts, white matter lesions, and atrophy relate to poststroke dementia. *Arch Neurol* 2000; 57: 1295–1300
- Prencipe M, Marini C. Leuko-araiosis: definition and clinical correlates – an overview. *Eur Neurol* 1989; 29: 27–29
- Pullicino P, Benedict RHB, Capruso DX, Vella N, Withaim-Leith S, Kwen PL. Neuroimaging criteria for vascular dementia. *Arch Neurol* 1996; 53: 723–728
- Qiwen M, Xie J, Wen Z, Weng Q, Shuyun Z. A quantitative MR study of the hippocampal formation, the amygdala, and the temporal horn of the lateral ventricle in healthy subjects 40–90 years of age. *AJNR Am J Neuroradiol* 1999; 20: 207–211
- Salonen O, Autti T, Raininko R, Ylikoski A, Erkinjuntti T. MRI of the brain in neurologically healthy middle-aged and elderly individuals. *Neuroradiology* 1997; 39: 537–545
- Scheltens P, Barkhof F, Leys D, Wolters EC, Ravid R, Kamphorst W. Histopathologic correlates of white matter changes on MRI in Alzheimer's disease and normal aging. *Neurology* 1995; 45: 883–888
- Scheltens P, Erkinjuntti T, Leys D, Wahlund LO, Inzitari D, de Ser T, Pasquier F, Barkhof F, Mantyla R, Bowler J, Wallin A, Ghika J, Fazekas F, Pantoni L. White matter changes on CT and MRI: an overview of visual rating scales. European task force on age-related white matter changes. *Eur Neurol* 1998; 39: 80–89
- Schmidt H, Schmidt R, Fazekas F, Semmler J, Kapeller P, Reinhart B, Kostner GM. Apolipoprotein E e4 allele in the normal elderly; neuropsychologic and brain MRI correlates. *Clin Genet* 1996; 50: 293–299
- Schmidt R, Fazekas F, Kleinert G, Offenbacher H, Grindl K, Payer F, Freidl W, Niederkorn K, Lechner H. Magnetic resonance imaging signal hyperintensities in the deep and subcortical white matter. A comparative study between stroke patients and normal volunteers. *Arch Neurol* 1992; 49: 825–827
- Shintani S, Shiigai T, Arinami T. Subclinical cerebral lesions accumulation on serial magnetic resonance imaging (MRI) in patients with hypertension: risk factors. *Acta Neurol Scand* 1998; 97: 251–256
- Skoog I. A review on blood pressure and ischaemic white matter lesions. *Dement Geriatr Cogn Disord* 1998; 9: 13–19
- Smith CD, Snowdon DA, Wang H, Markesbery WR. White matter volumes and periventricular white matter hyperintensities in aging and dementia. *Neurology* 2000; 54: 538–542
- Steingart A, Hachinski VC, Lau C, Fox AJ, Diaz F, Cape R, Inzitari D, Merskey H. Cognitive and neurology findings in subjects with diffuse white matter lucencies on computed tomographic scan (leuko-araiosis). *Arch Neurol* 1987; 44: 32–35
- Sullivan P, Pary R, Telang F, Rifai AH, Zubenko GS. Risk factors for white matter changes detected by magnetic resonance imaging in elderly. *Stroke* 1990; 21: 1424–1428
- Tarvonen-Schröder S, Röttä M, Riihä I, Kurki T, Rajala T, Sourander L. Clinical features of leuko-araiosis. *J Neurol Neurosurg Psychiatry* 1996; 60: 431–436
- Van Gijn J. Leukoaraiosis and vascular dementia. *Neurology* 1998; 51: S3–S8
- van Straaten EC, Scheltens P, Knol DL, van Buchem MA, van Dijk EJ, Hofman PAM, Karas G, Kjartansson O, de Leeuw FE, Prins ND, Schmidt R, Visser MC, Weinstein HC, Barkhof F. Operational definitions for the NINDS-AIREN criteria for vascular dementia: an interobserver study. *Stroke* 2003; 34: 1907–1912
- Van Zwielen JC, Staal S, Kapelle LJ, Derix MMA, van Gijn J. Are white matter lesions directly associated with cognitive impairment in patients with lacunar infarcts. *J Neurol* 1996; 243: 196–200
- Vinters HV, Ellis WG, Zarow C, Zaias BW, Jagust WJ, Mack WJ, Chui HC. Neuropathologic substrates of ischemic vascular dementia. *J Neuropathol Exp Neurol* 2000; 59: 931–945

- Wahlund L-O, Agartz I, Almqvist O, Basun H, Foressell L, Sääf J, Wetterberg L. The brain in healthy aged individuals: MR imaging. *Radiology* 1990; 174: 675–679
- Wahlund LO, Barkhof F, Fazekas F, Bronge L, Augustin M, Sjörgen M, Wallin A, Ader H, Leys D, Pantoni L, Pasquier F, Erikjuntti T, Scheltens P. A new rating scale for age-related white matter changes applicable to MRI and CT. *Stroke* 2001; 32: 1318–1322
- Wong KT, Grossman RI, Boorstein JM, Lexa FJ, McGowan J. Magnetization transfer imaging of periventricular hyperintense white matter in elderly. *AJNR Am J Neuroradiol* 1995; 16: 252–258
- Yamauchi H, Fukuyama H, Shio H. Corpus callosum atrophy in patients with leukoaraiosis may indicate global cognitive impairment. *Stroke* 2000; 31: 1515–1520
- Ylikoski A, Erkinjuntti T, Raininko R, Sarna S, Sulkava R, Tilvis R. White matter hyperintensities on MRI in the neurologically nondiseased elderly. Analysis of cohorts of consecutive subjects aged 55–85 years living at home. *Stroke* 1995; 26: 1171–1177
- ## 99 Subcortical Arteriosclerotic Encephalopathy
- Aharon-Peretz J, Cummings JL, Hill MA. Vascular dementia and dementia of the Alzheimer type. *Arch Neurol* 1988; 45: 719–721
- Araki Y, Nomura M, Tanaka H, Yamamoto H, Yamamoto T, Tsukaguchi I, Nakamura H. MRI of the brain in diabetes mellitus. *Neuroradiology* 1994; 36: 101–103
- Caplan LR. Binswanger's disease revisited. *Neurology* 1995; 45: 626–633
- Dantoine TF, Debord J, Merle L, Lacroix-Ramiandrisoa H, Bourzeix L, Charnes JP. Paraoxonase 1 activity: a new vascular marker of dementia? *Ann NY Acad Sci* 2002; 977: 96–101
- Del Ser T, Bermejo F, Portera A, Arredondo JM, Bouras C, Constantindis J. Vascular dementia. A clinicopathological study. *J Neurol Sci* 1990; 96: 1–17
- De Reuck J, Schaumburg HH. Periventricular atherosclerotic leukoencephalopathy. *Neurology* 1972; 22: 1094–1097
- De Reuck J, Crevits L, de Coster W, Sieben G, vander Eecken H. Pathogenesis of Binswanger chronic progressive subcortical encephalopathy. *Neurology* 1980; 30: 920–928
- Drayer BP. Imaging of the aging brain. I. Normal findings. *Radiology* 1988; 166: 785–796
- Drayer BP. Imaging of the aging brain. II. Pathologic conditions. *Radiology* 1988; 166: 797–806
- Erkinjuntti T. Treatment options: the latest evidence with galantamine (Reminyl). *J Neurol Sci* 2002; 203–204: 125–130
- Ferrer I, Bella R, Serrano MT, Martí E, Guionnet N. Arteriolosclerotic leukoencephalopathy in the elderly and its relation to white matter lesions in Binswanger's disease, multi-infarct encephalopathy and Alzheimer's disease. *J Neurol Sci* 1990; 98: 37–50
- Fisher CM. Binswanger's encephalopathy: a review. *J Neurol* 1989; 236: 65–79
- Gupta SR, Naheedy MH, Young JC, Ghobrial M, Rubino FA, Hindo W. Periventricular white matter changes and dementia. *Arch Neurol* 1988; 45: 637–641
- Hachinski V. Binswanger's disease: neither Binswanger's nor a disease. *J Neurol Sci* 1991; 103: 1
- Jellinger K, Danielczyk W, Fischer P, Gabriel E. Clinicopathological analysis of dementia disorders in the elderly. *J Neurol Sci* 1990; 95: 239–258
- Kinkel WR, Jacobs L, Polachini I, Bates V, Heffner RR Jr. Subcortical arteriosclerotic encephalopathy (Binswanger's disease). Computed tomographic nuclear magnetic resonance, and clinical correlations. *Arch Neurol* 1985; 42: 951–959
- Knopman DS, Rocca WA, Cha RA, Edland SD, Kokmen E. Survival study of vascular dementia in Rochester, Minnesota. *Arch Neurol* 2003; 60: 85–90
- Kuwabara Y, Ichiya Y, Sasaki M, Yoshida T, Fukumura T, Masuda K, Ibayashi S, Fujishima M. Cerebral blood flow and vascular response to hypercapnia in hypertensive patients with leukoaraiosis. *Ann Nucl Med* 1996; 10: 293–298
- Lee A, Yu YL, Tsoi M, Woo E, Chang CM. Subcortical arteriosclerotic encephalopathy – a controlled psychometric study. *Clin Neurol Neurosurg* 1989; 91: 235–241
- Liao D, Cooper L, Cai J, Toole JF, Bryan NR, Hutchinson RG, Tyroler HA. Presence and severity of cerebral white matter lesions and hypertension, its treatment and its control. The ARIC study. *Stroke* 1996; 27: 2262–2270
- Loeb C, Meyer JS. Vascular dementia: still a debatable entity? *J Neurol Sci* 1996; 143: 31–40
- Loizou LA, Kendall BE, Marshall J. Subcortical arteriosclerotic encephalopathy: a clinical and radiological investigation. *J Neurol Neurosurg Psychiatry* 1981; 44: 294–304
- Lotz PR, Ballinger WE Jr, Quisling RG. Subcortical arteriosclerotic encephalopathy: CT spectrum and pathologic correlation. *AJNR Am J Neuroradiol* 1986; 7: 817–822
- McQuinn BA, O'Leary DH. White matter lucencies on computed tomography, subacute arteriosclerotic encephalopathy (Binswanger's disease), and blood pressure. *Stroke* 1987; 18: 900–905
- Merino JG. Leukoaraiosis. Reifying rarefaction. *Arch Neurol* 2000; 57: 925–926
- Padovani A, di Piero V, Bragioni M, Iacoboni M, Gualdi GF, Lenzi GL. Patterns of neuropsychological impairment in mild dementia: a comparison between Alzheimer's disease and multi-infarct dementia. *Acta Neurol Scand* 1995; 92: 433–442
- Pantoni L, Garcia JH. The significance of cerebral white matter abnormalities 100 years after Binswanger's report. A review. *Stroke* 1995; 26: 1293–1301
- Pantoni L, Garcia JH. Cognitive impairment and cellular/vascular changes in the cerebral white matter. *Ann NY Acad Sci* 1997; 826: 92–102
- Pulicino P, Ostrow P, Miller L, Snyder W, Munschauer F. Pontine ischemic rarefaction. *Ann Neurol* 1995; 37: 460–466
- Román GC. Senile dementia of the Binswanger type. A vascular form of dementia in the elderly. *J Am Med Assoc* 1987; 258: 1782–1788
- Román GC. From UBOs to Binswanger's disease. Impact of magnetic resonance imaging on vascular dementia research. *Stroke* 1996; 27: 1269–1273
- Román GC. New insight into Binswanger's disease. *Arch Neurol* 1999; 56: 1061–1062
- Sacquegna T, Guttmann S, Giuliani S, Agati R, Daidone R, Morreale A, Ambrosetto G, Gallassi R. Binswanger's disease: a review of the literature and a personal contribution. *Eur Neurol* 1989; 29: 20–22
- Sandijk R. Subcortical arteriosclerotic encephalopathy (Binswanger's disease). *S Afr Med J* 1983; 63: 204–205
- Steingart A, Hachinski VC, Lau C, Fox AJ, Fox H, Lee D, Inzitari D, Merskey H. Cognitive and neurologic findings in subjects with diffuse white matter lucencies on computed tomographic scan (leuko-araiosis). *Arch Neurol* 1987; 44: 32–35

- Tanoi Y, Okeda R, Budka H. Binswanger's encephalopathy: serial sections and morphometry of the cerebral arteries. *Acta Neuropathol (Berl)* 2000; 100: 347–355
- Tomimoto H, Akiguchi I, Wakita H, Osaki A, Hayashi M, Yamamoto Y. Coagulation activation in patients with Binswanger disease. *Arch Neurol* 1999; 56: 1104–1108
- Tomonage M, Yamanouchi H, Tohgi H, Kameyama M. Clinico-pathologic study of progressive subcortical vascular encephalopathy (Binswanger type) in the elderly. *J Am Geriatr Soc* 1982; 30: 524–529
- Vermeer SE, Koudstaal PJ, Oudkerk M, Hofman A, Breteler MMB. Prevalence and risk factors of silent brain infarcts in the population-based Rotterdam scan study. *Stroke* 2002; 33: 21–25
- Wisniewska M, Devuyst G, Bogousslavsky J, Ghica J, van Melle G. What is the significance of leukoariosis in patients with acute ischemic stroke? *Arch Neurol* 2000; 57: 967–973
- Zeumer H, Schonsky B, Sturm KW. Predominant white matter involvement in subcortical arteriosclerotic encephalopathy (Binswanger disease). *J Comput Assist Tomogr* 1980; 4: 14–19

100 Vasculitis

Primary and Secondary Vasculitis of the CNS

- Ay H, Sahin G, Saatci I, Söylemezgülu F, Saribas O. Primary angiitis of the central nervous system and silent cortical hemorrhages. *AJNR Am J Neuroradiol* 2002; 23: 1561–1563
- Campi A, Benndorf G, Filippi M, Reganati P, Martinelli V, Terreni MR. Primary angiitis of the central nervous system: serial MRI of brain and spinal cord. *Neuroradiology* 2001; 43: 599–607
- Ehsan T, Hasan S, Powers JM, Heiserman JE. Serial magnetic resonance imaging in isolated angiitis of the central nervous system. *Neurology* 1995; 45: 1462–1465
- Ferro JM. Vasculitis of the central nervous system. *J Neurol* 1998; 245: 766–776
- Finelli PF, Onyike HC, Uphoff DF. Idiopathic granulomatous angiitis of the CNS manifesting as diffuse white matter disease. *Neurology* 1997; 49: 1696–1699
- Greenan TJ, Grossman RI, Goldberg HI. Cerebral vasculitis: MR imaging and angiographic correlation. *Radiology* 1992; 182: 65–72
- Harada S, Mitsunobu F, Kodama F, Hosaki Y, Mifune T, Tsugeno H, Okamoto M, Yamamura M, Makino H, Tanizaki Y. Giant cell arteritis associated with rheumatoid arthritis monitored by magnetic resonance imaging. *Intern Med* 1999; 38: 675–678
- Hoffmann M, Corr P, Robbs J. Cerebrovascular findings in Takayasu disease. *J Neuroimaging* 2000; 10: 84–90
- Jennette CJ, Falk RJ. Small-vessel vasculitis. *N Engl J Med* 1997; 337: 1512–1523
- Joelson E, Ruthrauff B, Ali F, Lindeman N, Sharp FR. Multifocal dural enhancement associated with temporal arteritis. *Arch Neurol* 2000; 57: 119–122
- Komiyama M. Moyamoya disease a progressive occlusive arteriopathy of the primitive internal carotid artery. *Intervent Neuroradiol* 2003; 9: 39–45
- Lanthier S, Lortie A, Michaud J, Laxer R, Jay V, deVeber G. Isolated angiitis of the CNS in children. *Neurology* 2001; 56: 837–842
- Lee AG, Brazis PW. Temporal arteritis: a clinical approach. *J Am Geriatr Soc* 1999; 47: 1364–1370
- Lee S-K, Kim DI, Jeong E-K, Kim S-Y, Kim SH, In YK, Kim D-S, Choi J-U. Postoperative evaluation of Moyamoya disease with perfusion-weighted MR imaging. *AJNR Am J Neuroradiol* 2003; 24: 741–747
- Miller DH, Haas LF, Teague C, Neale TJ. Small vessel vasculitis presenting as neurological disorder. *J Neurol Neurosurg Psychiatry* 1984; 47: 791–794
- Miller DH, Ormerod IEC, Gibson A, du Boulay EPGH, Rudge P, McDonald WI. MR brain scanning in patients with vasculitis: differentiation from multiple sclerosis. *Neuroradiology* 1987; 29: 226–231
- Moore PM. Diagnosis and management of isolated angiitis of the central nervous system. *Neurology* 1989; 39: 167–173
- Moore PM. Neurological manifestations of vasculitis: update on immunopathogenic mechanisms, diagnostic and therapeutic options. *Ann Neurol* 1995; 37: 131–141
- Moore PM. The vasculitides. *Curr Opin Neurol* 1999; 12: 383–388
- Perez C, Olier J, Rivero M, Montes M. MR imaging of acute encephalopathy associated with polyarteritis nodosa. *AJR Am J Roentgenol* 1997; 169: 1995–1996
- Provenzale JM, Allen NB. Neuroradiologic findings in polyarteritis nodosa. *AJNR Am J Neuroradiol* 1996; 17: 1119–1126
- Reichart MD, Bogousslavsky J, Janzer RC. Early lacunar strokes complicating polyarteritis nodosa: thrombotic microangiopathy. *Neurology* 2000; 54: 883–889
- Rosen CL, DePalma L, Morita A. Primary angiitis of the central nervous system as a first presentation in Hodgkin's disease: a case report and review of the literature. *Neurosurgery* 2000; 46: 1504–1508
- Scharre D, Petri M, Engman E, DeArmond S. Large intracranial arteritis with giant cells in systemic lupus erythematosus. *Ann Intern Med* 1986; 104: 661–662
- Scully RE, Mark EJ, McNelly WF, McNelly BU. Case 5–1995. Presentation of case. *N Engl J Med* 1995; 333: 452–459
- Scully RE, Mark EJ, McNelly WF, McNelly BU. Case 33–1995. Presentation of case. *N Engl J Med* 1995; 333: 1135–1143
- Sener RN. Diffusion MRI findings in isolated intracranial angiitis. *Comput Med Imaging Graph* 2002; 26: 265–269
- Sharma BK, Jain S, Radotra BD. An autopsy study of Takayasu arteritis in India. *Int J Cardiol* 1998; 66: 85–90
- Yuh WTC, Ueda T, Maley JE, Quets JP, White M, Hahn PY, Otake S. Diagnosis of microvasculopathy in CNS vasculitis: value of perfusion and diffusion imaging. *J Magn Reson Imaging* 1999; 10: 310–313

Auto-immune Mediated Disorders

- Akman-Demir G, Serdaroglu P, Tasçi B. Clinical patterns of neurological involvement in Behçet's disease; evaluation of 200 patients. *Brain* 1999; 122: 2171–2181
- Akman-Demir G, Bahar S, Coban O, Tasci B, Serdaroglu P. Cranial MRI in Behçet's disease: 134 examinations of 98 patients. *Neuroradiology* 2003; 45: 851–859
- Alexander EL, Malinow K, Lejewski JE, Jerdan MS, Provost TT, Alexander GF. Primary Sjögren's syndrome with central syndrome with central nervous system disease mimicking multiple sclerosis. *Ann Intern Med* 1986; 104: 323–330
- Al-Fahad SA, Al-Araji AH. Neuro-Behçet's disease in Iraq: a study of 40 patients. *J Neurol Sci* 1999; 170: 105–111
- Al-Watban J, Patay Z, Bohlega S, Larsson S. Magnetic resonance imaging of central nervous system involvement in primary Sjögren's syndrome. *Riv Neuroradiol* 1998; 11: 51–54

- Anderson JR. Intracerebral calcification in a case of systemic lupus erythematosus with neurological manifestations. *Neuropathol Appl Neurobiol* 1981; 7: 161–166
- Ando Y, Kai S, Uyama E, Iyonaga K, Hashimoto Y, Uchino M, Ando M. Involvement of the central nervous system in rheumatoid arthritis: its clinical manifestations and analysis by magnetic resonance imaging. *Intern Med* 1995; 34: 188–191
- Baraczka K, Lakos G, Sipka S. Immunoserological changes in the cerebro-spinal fluid and cerebrum in systemic lupus erythematosus patients with demyelinating syndrome and multiple sclerosis. *Acta Neurol Scand* 2002; 105: 378–383
- Baum KA, Hopf U, Nehrig C, Stöver M, Schörner W. Systemic lupus erythematosus: neuropsychiatric signs and symptoms related to cerebral MRI findings. *Clin Neurol Neurosurg* 1993; 95: 29–34
- Bell CL, Partington C, Robbins M, Graziano F, Turski P, Kornguth S. Magnetic resonance imaging of central nervous system lesions in patients with lupus erythematosus. Correlation with clinical remission and antineurofilament and anticardiolipin antibody titers. *Arthritis Rheum* 1991; 34: 432–441
- Berlis A, Petschner F, Bötterfö IC, Spreer J. Wegener granuloma in the fourth ventricle. *AJNR Am J Neuroradiol* 2003; 24: 523–525
- Besana C, Comi G, del Maschio A, Praderio L, Vergani A, Medagliani S, Martinelli V, Triulzi F, Locatelli T. Electrophysiological and MRI evaluation of neurological involvement in Behçet's disease. *J Neurol Neurosurg Psychiatry* 1089; 52: 749–754
- Bianchi DW, Zickwolf GH, Weil GJ, Sylvester S, DeMaria MA. Male fetal progenitor cells persist in maternal blood for as long as 27 years postpartum. *Proc Nat Acad Sci* 1996; 93: 705–708
- Blaszczyk M, Krolicki L, Krasu M, Glinska O, Jablonska S. Progressive facial hemiatrophy: central nervous system involvement and relationship with scleroderma en coup de sabre. *J Rheumatol* 2003; 30: 1997–2004
- Bosma GPT, Rood MJ, Zwinderman AH, Huizinga TWJ, van Buchem MA. Evidence of central nervous system damage in patients with neuropsychiatric systemic lupus erythematosus, demonstrated by magnetic transfer imaging. *Arthritis Rheum* 2000; 43: 48–54
- Bosma GPT, Huizinga TWJ, Mooijart SP, van Buchem MA. Abnormal brain diffusivity in patients with neuropsychiatric systemic lupus erythematosus. *AJNR Am J Neuroradiol* 2003; 24: 850–854
- Brooks WM, Jung RE, Ford CC, Greinel EJ, Sibbitt WL Jr. Relationship between neurometabolite derangement and neurocognitive dysfunction in systemic lupus erythematosus. *J Rheumatol* 1999; 26: 81–85
- Bruyn RPM, van der Veen JPW, Donker AJM, Valk J, Wolters EC. Sneddon's syndrome. Case report and literature review. *J Neurol Sci* 1987; 79: 243–253
- Cauli A, Montaldo C, Peltz MT, Nurchis P, Sanna G, Garau P, Pala R, Passiu G, Mathieu A. Abnormalities of magnetic resonance imaging of the central nervous system in patients with systemic lupus erythematosus correlate with disease severity. *Clin Rheumatol* 1994; 13: 615–618
- Chung MH, Sum J, Morrell MJ, Horoupian DS. Intracerebral involvement in scleroderma en coup de sabre: report of a case with neuropathologic findings. *Ann Neurol* 1995; 37: 679–681
- Çoban O, Bahar S, Akman-Demir G, Serdaroğlu P, Baykan-Kurt B, Tolun R, Yurdakul S, Yazici H. A controlled study of reliability and validity of MRI findings in neuro-Behçet's disease. *Neuroradiology* 1996; 38: 312–316
- Çoban O, Bahar S, Akman-Demir G, Taşçı B, Yurdakul S, Yazici H, Serdaroğlu P. Masked assessment of MRI findings: is it possible to differentiate neuro-Behçet's disease from other central nervous system. *Neuroradiology* 1999; 41: 255–260
- Colamussi P, Giganti M, Cittaniti C, Dovigo L, Trotta F, Tola MR, Tamarozzi R, Lucignani G, Piffanelli A. Brain single-photon emission tomography with ^{99m}Tc-HMPAO in neuropsychiatric systemic lupus erythematosus: relations with EEG and MRI findings and clinical manifestations. *Eur J Nucl Med* 1995; 22: 17–24
- Cox PD, Hales RE. CNS Sjögren's syndrome: an underrecognized and underappreciated neuropsychiatric disorder. *J Neuropsychiatry Clin Neurosci* 1999; 11: 241–247
- Cristophe C, Azzi N, Bouche B, Dan B, Levivier M, Ferster A. Magnetic resonance imaging in cerebral fungal vasculitis. *Neuropediatrics* 1999; 30: 218–220
- Cutolo M, Nobili F, Sulli A, Pizzorni C, Briata M, Faelli F, Viatali P, Mariani G, Copello F, Seriole B, Barone C, Rodriguez G. Evidence of cerebral hypoperfusion in scleroderma patients. *Rheumatology* 2000; 39: 1366–1373
- Dierckx RA, Aichner F, Gerstenbrand F, Fritsch P. Progressive systemic sclerosis and nervous system involvement: A review of 14 cases. *Eur Neurol* 1987; 26: 134–140
- Friedman SD, Stidley CA, Brooks WM, Hart BL, Sibbitt WL Jr. Brain injury and neurometabolic abnormalities in systemic lupus erythematosus. *Radiology* 1998; 209: 79–84
- Fields RA, Sibbitt WL, Toubbeh H, Bankhurst AD. Neuropsychiatric lupus erythematosus, cerebral infarctions, and anticardiolipin antibodies. *Ann Rheum Dis* 1990; 49: 114–117
- Futrell N, Schultz LR, Milikan C. Central nervous system disease in patients with systemic lupus erythematosus. *Neurology* 1992; 42: 1649–1657
- Futrell N. Connective tissue disease and sarcoidosis of the central nervous system. *Curr Opin Neurol* 1994; 7: 201–208
- Gerber S, Biondi A, Dormont D, Wechsler B, Marsault C. Long-term MR follow-up of cerebral lesions in neuro-Behçet's disease. *Neuroradiology* 1996; 38: 761–768
- Gieron MA, Khoromi S, Campos A. MRI changes in the central nervous system in a child with lupus erythematosus. *Pediatr Radiol* 1995; 25: 184–185
- Gobernado JM, Leiva C, Rabano J, Alvarez-Cermenio JC, Fernandez-Molina A. Recovery from rheumatoid cerebral vasculitis. *J Neurol Neurosurg Psychiatry* 1984; 47: 410–413
- Gonzalez-Crespo MR, Blanco FJ, Ramos A, Circuelo E, Mateo I, Lopez Pino MA, Gomez-Reino JJ. Magnetic resonance imaging of the brain in systemic lupus erythematosus. *Br J Rheumatol* 1995; 34: 1055–1060
- Griffey RH, Brown MS, Bankhurst AD, Sibbitt RR, Sibbitt WL Jr. Depletion of high-energy phosphates in the central nervous system of patients with systemic lupus erythematosus, as determined by phosphorus-31 nuclear magnetic resonance spectroscopy. *Arthritis Rheum* 1990; 33: 827–833
- Grosso S, Fioravanti A, Biasi G, Conversano E, Marcolongo R, Morgese G, Balestri P. Linear scleroderma associated with progressive brain atrophy. *Brain Dev* 2003; 25: 57–61
- Hammad A, Tsukada Y, Torre N. Cerebral occlusive vasculopathy in systemic lupus erythematosus and speculation on the part played by complement. *Ann Rheum Dis* 1992; 51: 550–552
- Hietaharju A, Jaaskeleinen S, Hietarinta M, Frey H. Central nervous system involvement and psychiatric manifestations in systemic sclerosis (scleroderma): clinical and neurophysiological evaluation. *Acta Neurol Scand* 1993; 87: 382–387

- Hiraiwa M, Nonaka C, Abe T, Iio M. Positron emission tomography in systemic lupus erythematosus: relation of cerebral vasculitis to PET findings. *AJNR Am J Neuroradiol* 1983; 4: 541–543
- Ishikawa O, Ohnishi K, Miyachi Y, Ishizaka H. Cerebral lesions in systemic lupus erythematosus detected by magnetic resonance imaging. Relationship to anticardiolipin antibody. *J Rheumatol* 1994; 21: 87–90
- Jennings JE, Sundgren PC, Attwood J, McCune J, Maly P. Value of MRI of the brain in patients with systemic lupus erythematosus and neurologic disturbance. *Neuroradiology* 2004; 46: 15–21
- Jung SM, Lee BG, Joh GY, Cha JK, Chung WT, Kim KH. Primary Sjögren's syndrome manifested as multiple sclerosis and cutaneous erythematous lesions: a case report. *J Korean Med Sci* 2000; 15: 115–118
- Keall AT, Shetty M, Lee BCP, Lockshin MD. The diversity of neurologic events in systemic lupus erythematosus. Prospective clinical and computed tomographic classification of 82 events in 71 patients. *Arch Neurol* 1986; 43: 273–276
- Kashihara K, Nakashima S, Kohira I, Shohmori T, Fujiwara Y, Kuroda S. Hyperintense basal ganglia of T1-weighted MR images in a patient with central nervous system lupus and chorea. *AJNR Am J Neuroradiol* 1998; 19: 284–286
- Kashihara K, Fukase S, Kohira I, Abe K. Laminar cortical necrosis in central nervous system lupus: sequential changes in MR changes. *Clin Neurol Neurosurg* 1999; 101: 145–147
- Kidd D, Steuer A, Denman AM, Rudge P. Neurological complications in Behçet's syndrome. *Brain* 1999; 122: 2183–2194
- Koçer N, Islak C, Siva A, Saip S, Akman C, Kantarci O, Hamuryudan V. CNS involvement in neuro-Behçet syndrome: an MR study. *AJNR Am J Neuroradiol* 1999; 20: 1015–1024
- Kozora E, West SG, Kotzin BL, Julian L, Porter S, Bigler E. Magnetic resonance imaging abnormalities and cognitive deficits in systemic lupus erythematosus patients without overt central nervous system disease. *Arthritis Rheum* 1998; 41: 41–47
- Kwon SU, Koh JY, Kim JS. Vertebrobasilar artery territory infarction as an initial manifestation of systemic lupus erythematosus. *Clin Neurol Neurosurg* 1999; 101: 62–67
- Kwong KL, Chu R, Wong SN. Parkinsonism as unusual neurological complication in childhood systemic lupus erythematosus. *Lupus* 2000; 9: 474–477
- Lambert NC, Evans PC, Hashizumi TL, Maloney S, Gooley T, Furst DE, Nelson JL. Cutting edge: persistent fetal microchimerism in T lymphocytes is associated with HLA-DQA1*0501: implications in autoimmunity. *J Immunol* 2000; 164: 5545–5548
- Lim MK, Suh CH, Kim HJ, Cho YK, Choi SH, Kang JH, Park W, Lee JH. Systemic lupus erythematosus: brain MR imaging and single-voxel hydrogen 1 MR spectroscopy. *Radiology* 2000; 217: 43–49
- Mascalchi M, Cosottini M, Cellerini M, Paganini M, Arnetoli G. MRI of spinal cord involvement in Behçet's disease. *Neuroradiology* 1998; 40: 255–257
- Matsumoto R, Shintaku M, Suzuki S, Kato T. Cerebral perivenous calcification in neuropsychiatric lupus erythematosus: a case report. *Neuroradiology* 1998; 40: 583–586
- McAbee GN, Barasch ES. Resolving MRI lesions in lupus erythematosus selectively involving the brainstem. *Pediatr Neurol* 1990; 6: 186–189
- Miller DH, Kendall BE, Barter S, Johnson G, MacManus DG, Logsdail SJ, Ormerod IEC, McDonald WI. Magnetic resonance imaging in central nervous system sarcoidosis. *Neurology* 1988; 38: 378–383
- Miller DH, Buchanan N, Barker G, Morrissey SP, Kendall BE, Rudge P, Khamashta M, Hughes GRV, McDonald WI. Gadolinium-enhanced magnetic resonance imaging of the central nervous system in systemic lupus erythematosus. *J Neurol* 1992; 239: 460–464
- Mills JA. Systemic lupus erythematosus. *N Engl J Med* 1994; 330: 1871–1879
- Nagaoka S, Matsunaga K, Chiba J, Ishigatsubo Y, Tani K. Five cases of systemic lupus erythematosus with intracranial calcification. *Clin Neurol* 1982; 22: 635–643
- Nelson JL. Maternal-fetal immunology and autoimmune disease. *Arthritis Rheum* 1996; 39: 191–194
- Nelson JL, Furst DE, Malony S, Gooley T, Evans P, Smith A, Bean MR, Ober C, Bianchi DW. Microchimerism and HLA-compatible relationships of pregnancy in scleroderma. *Lancet* 1998; 351: 559–562
- Newman LS, Rose CS, Maier LA. Sarcoidosis. *N Engl J Med* 1997; 336: 1224–1234
- Niemelä RK, Hakela M. Primary Sjögren's syndrome with severe central nervous system disease. *Semin Arthritis Rheum* 1999; 29: 4–13
- Nobili F, Cutolo M, Sulli A, Castaldi A, Sardanelli F, Accardo S, Rosadini G, Rodriguez G. Impaired quantitative cerebral blood flow in scleroderma patients. *J Neurol Sci* 1997; 152: 63–71
- Nobili F, Cutolo M, Sulli A, Vitali P, Vignola S, Rodriguez G. Brain functional involvement by perfusion SPECT in systemic sclerosis and Behçet's disease. *Ann N Y Acad Sci* 2002; 966: 409–414
- Nowak DA, Widenka DC. Neurosarcoidosis: a review of its intracranial manifestation. *J Neurol* 2001; 248: 363–372
- Ohtani H, Imai H, Yasuda T, Wakui H, Komatsuda A, Hamia K, Miura AB. A combination of livedo racemosa, occlusion of cerebral blood vessels, and nephropathy: kidney involvement in Sneddon's syndrome. *Am J Kidney Dis* 1995; 26: 511–515
- Padovan CS, Bise K, Hahn J, Sostak P, Holler E, Kolb H-J, Straube A. Angiitis of the central nervous system after allogeneic bone marrow transplantation? *Stroke* 1999; 30: 1651–1656
- Patel DV, Neuman MJ, Hier DB. Reversibility of CT and MR findings in neuro-Behçet disease. *J Comput Assist Tomogr* 1989; 13: 669–673
- Pelz MT, Casciu L, Manconi FM, Sanna G, Schiffrini P, Mathieu A. Distribution of white matter lesions in multiple sclerosis and systemic lupus erythematosus. Differentiation using MRI. *Riv Neuroradiol* 1998; 11: 17–19
- Pickuth D, Spielmann RP, Heywang-Köhrbrunner SH. Role of radiology in the diagnosis of neurosarcoidosis. *Eur Radiol* 2000; 10: 941–944
- Pickuth D, Heywang-Köhrbrunner SH. Neurosarcoidosis: evaluation with MRI. *J Neuroradiol* 2000; 27: 185–188
- Pierot L, Sauve C, Leger JM, Martin N, Koeger AC, Wechsler B, Chiras J. Asymptomatic cerebral involvement in Sjögren's syndrome: MRI findings of 15 cases. *Neuroradiology* 1993; 35: 378–380
- Pomper MG, Miller TJ, Stone JH, Tidmore WC, Hellmann DB. CNS vasculitis in autoimmune disease: MR imaging findings and correlation with angiography. *AJNR Am J Neuroradiol* 1999; 20: 75–85
- Provenzale JM, Heinz ER, Ortel TL, Macik BG, Charles LA, Alberts MJ. Antiphospholipid antibodies in patients without systemic lupus erythematosus: neuroradiologic findings. *Radiology* 1994; 192: 531–537
- Provenzale JM, Allen NB. Wegener granulomatosis: CT and MR findings. *AJNR Am J Neuroradiol* 1996; 17: 785–792

- Provenzale JM, Allen MB. Neuroradiologic findings in polyarteritis nodosa. *AJNR Am J Neuroradiol* 1996; 17: 1119–1126
- Reichart MD, Bogousslavsky J, Janzer RC. Early lacunar strokes complicating polyarteritis nodosa: thrombotic microangiopathy. *Neurology* 2000; 54: 883–889
- Rovaris M, Viti B, Ciboddo G, Gerevini S, Capra R, Ianucci G, Comi G, Filippi M. Brain involvement in systemic mediated diseases: magnetic resonance and magnetization transfer imaging study. *J Neurol Neurosurg Psychiatry* 2000; 68: 170–177
- Rovaris M, Inglesi M, Viti B, Ciboddo G, Gerevini S, Capra R, Filippi M. The contribution of fast-FLAIR MRI for lesion detection in the brain of patients with systemic immune diseases. *J Neurol* 2000; 247: 29–33
- Sailer M, Burchert W, Ehrenheim C, Smid HGOM, Haas J, Wildhagen K, Wurster U, Deicher H. Positron emission tomography and magnetic resonance imaging for cerebral involvement in patients with systemic lupus erythematosus. *J Neurol* 1997; 244: 186–193
- Sanna G, Piga M, Terberry JW, Peltz MT, Giagheddu S, Satta L, Ahmed A, Cauli A, Montaldo C, Passiu G, Peter JB, Shoenfeld Y, Matthieu A. Central nervous system involvement in systemic lupus erythematosus: cerebral imaging and serological profile in patients with and without overt neuropsychiatric manifestations. *Lupus* 2000; 9: 573–583
- Scully RE, Mark EJ, McNelly WF, Ebeling SH. Case 28–1998. Presentation of a case. *N Engl J Med* 1998; 339: 755–763
- Serdaroğlu P. Behçet's disease and the nervous system. *J Neurol* 1998; 245: 197–205
- Serdaroğlu P, Yazici H, Özdemir C, Yurdakul S, Bahar S, Aktin E. Neurologic involvement in Behçet's syndrome. A prospective study. *Arch Neurol* 1989; 46: 265–269
- Sherman JL, Stern BJ. Sarcoidosis of the CNS: comparison of unenhanced and enhanced MR images. *AJNR Am J Neuroradiol* 1990; 11: 915–923
- Shibata M, Kibe T, Fujimoto S, Ishikawa T, Murakami M, Ichi T, Wada Y. Diffuse central nervous system lupus involving white matter, basal ganglia, thalami and brainstem. *Brain Dev* 1999; 21: 337–340
- Shiotani A, Mukobayashi C, Oohata H, Yamanishi T, Hara T, Itoh H, Nishioka S. Wegener's granulomatosis with dural involvement as the initial clinical manifestation. *Intern Med* 1997; 36: 514–518
- Sigal LH. The neurologic presentation of vasculitic and rheumatologic syndromes. A review. *Medicine* 1987; 66: 157–180
- Siva A, Kantarci OH, Saip S, Altintas A, Hamuryudan V, Islak C, Koçer N, Yazici H. Behçet's disease: diagnostic and prognostic aspects of neurological involvement. *J Neurol* 2001; 248: 95–103
- Smith AS, Meisler DM, Weinstein MA, Tomsak RL, Hanson MR, Rudick RA, Farris BK, Ransohoff RM. High-signal periventricular lesions in patients with sarcoidosis: neurosarcoidosis or multiple sclerosis? *AJNR Am J Neuroradiol* 1989; 10: 485–490
- Stern BJ, Krumholz A, Johns C, Scott P, Nissim J. Sarcoidosis and its neurological manifestations. *Arch Neurol* 1985; 42: 909–917
- Sneddon JB. Cerebrovascular lesions and livedo reticularis. *Br J Dermatol* 1965; 77: 180–185
- Szer IS, Miller JH, Rawlings D, Shaham B, Bernstein B. Cerebral perfusion abnormalities in children with central nervous system manifestations of lupus detected by single proton emission computed tomography. *J Rheumatol* 1993; 20: 2143–2148
- Tah ET, Atilla S, Keskin T, Simonson T, I'ik S, Yuh WTC. MRI in neuro-Behçet's disease. *Neuroradiology* 1997; 39: 2–6
- Tanabe J, Weiner MW. MRI-MRS of the brain in systemic lupus erythematosus. How do we use it to understand causes of clinical signs. *Ann N Y Acad Sci* 1997; 823: 169–184
- Tokumaru AM, Obata T, Kohyama S, Kaji T, Okizuka H, Suzuki K, Kusano S. Intracranial meningeal involvement in Churg-Strauss syndrome. *AJNR Am J Neuroradiol* 2002; 23: 221–224
- Trysberg E, Lindgren I, Tarkowski A. Autologous stem cell transplantation in a case of treatment resistant central nervous system lupus. *Ann Rheum Dis* 2000; 59: 236–238
- Van der Kaaden AJ, Kamphuis DJ, Nossent JC, Rico RE. Long-standing isolated cerebral systemic lupus erythematosus in an 8-year-old Black girl. *Clin Neurol Neurosurg* 1993; 95: 241–244
- Wechsler B, Dell'Isola B, Vidaihet M, Dormont D, Piette JC, Bletry O, Godeau P. MRI in 31 patients with Behçet's disease and neurological involvement: prospective study with clinical correlation. *J Neurol Neurosurg Psychiatry* 1993; 56: 793–798
- Welsh KMA. Scleroderma: chimerism, the blind man and the scientist. *Lancet* 1998; 351: 540–541
- Welsh KMA, Nagesh J, Boska M, Moore PM. Detection of cerebral ischemia in systemic lupus erythematosus by magnetic resonance techniques. *Ann N Y Acad Sci* 1997; 823: 120–131
- Yamamoto K, Nogaki H, Takase Y, Morimatsu M. Systemic lupus erythematosus associated with marked intracranial calcification. *AJNR Am J Neuroradiol* 1992; 13: 1340–1342
- Yuh WTC, Ueda T, Maley JE, Quets JP, White M, Hahn PY, Otake S. Diagnosis of microvasculopathy in CNS vasculitis: value of perfusion and diffusion imaging. *J Magn Reson* 1999; 10: 310–313
- Zajicek JP. Neurosarcoidosis. *Curr Opin Neurol* 2000; 13: 323–325
- Zuheir Al Kawi M, Bohlega S, Banna M. MRI findings in neuro-Behçet's disease. *Neurology* 1991; 41: 405–408

Infectious Vasculitis

- Aasley J, Nilsen G. Cerebral atrophy in Lyme disease. *Neuroradiology* 1990; 32: 253–254
- Ahmad NM, Boruchoff SE. Multiple cerebral infarcts due to varicella-zoster virus large-vessel vasculopathy in an immunocompetent adult without skin involvement. *Clin Infect Dis* 2003; 13: e16–18
- Arvin AM. Varicella-Zoster virus: pathogenesis, immunity, and clinical management in hematopoietic cell transplant recipients. *Biol Blood Marrow Transplant* 2000; 6: 219–230
- Belman AL, Coyle PK, Roque C, Cantos E. MRI findings in children infected by *Borrelia burgdorferi*. *Pediatr Neurol* 1992; 8: 428–431
- Bodensteiner JB, Mille MR, Riggs JE. Clinical features of vascular thrombosis following varicella. *Arch Pediatr Adolesc Med* 1992; 146: 100–106
- Cintrón R, Pachner AR. Spirochetal diseases of the central nervous system. *Curr Opin Neurol* 1994; 7: 217–222
- Coyle PK. Neurologic complications of Lyme disease. *Rheum Dis Clin North Am* 1993; 19: 993–1009
- Cristophe C, Azzi N, Bouche B, Dan B, Levivier M, Ferster A. Magnetic resonance imaging in cerebral fungal vasculitis. *Neuropediatrics* 1999; 30: 218–220

- Daniel RT, Henry PT, Rajshekhar V. Unusual MR presentation of cerebral parenchymal tuberculosis. *Neurol India* 2002; 50: 210–211
- Defer G, Levy R, Burgi res P, Postic D, Degos JD. Lyme disease presenting as a stroke in the vertebrobasilar territory: MRI. *Neuroradiology* 1993; 35: 529–531
- Demaerel P, Wilms G, Casteels K, Silberstein J, Baert AL. Childhood neuroborreliosis: clinico-radiological correlation. *Neuroradiology* 1995; 37: 578–581
- Demaerel P, Crevits I, Casteels-Van Daele M, Baert AL. Meningo-radculitis due to borreliosis presenting as low back pain only. *Neuroradiology* 1998; 40: 126–127
- Fernandez RE, Rothberg M, Ferencz G, Wujack D. Lyme disease of the CNS: MR imaging findings in 14 cases. *AJNR Am J Neuroradiol* 1990; 11: 479–481
- Finkel MJ, Halperin JJ. Nervous system Lyme borreliosis – revisited. *Arch Neurol* 1992; 49: 102–107
- Garg RK. Tuberculosis of the central nervous system. *Postgrad Med J* 1999; 75: 133–140
- Gilden DH, Mahalingam R, Cohrs RJ, Kleinschmidt-DeMasters BK, Forghani B. The protean manifestations of varicella-zoster virus vasculopathy. *J Neurovirol* 2002; 8 (Suppl 2): 75–79
- Gilden DH, Kleinschmidt-DeMasters BK, Laguardia JJ, Mahalingam R, Cohrs RJ. Neurologic complications of the reactivation of varicella-zoster virus. *N Engl J Med* 2000; 342: 635–645
- Hausler MG, Ramaekers VT, Reul J, Meilicke R, Heimann G. Early and late onset manifestations of cerebral vasculitis related to varicella zoster. *Neuropediatrics* 1998; 29: 202–207
- Kr ger H, Heim E, Schuknecht B, Scholtz S. Acute and chronic neuroborreliosis with and without CNS involvement; a clinical, MRI, and HLA study of 27 cases. *J Neurol* 1991; 238: 271–280
- Lorenz S, Pfister HW, Padovan C, Yoursy T. MRI abnormalities in tick-borne encephalitis. *Lancet* 1996; 347: 698–699
- Nelson JA, Wolf MD, Yuh WTC, Peeples ME. Cranial nerve involvement with Lyme borreliosis demonstrated by magnetic resonance imaging. *Neurology* 1992; 42: 671–673
- Oksi J, Kalimo H, Marttila RJ, Marjam ki M, Sonninen P, Nikoskelainen J, Viljanen MK. Inflammatory brain changes in Lyme borreliosis. A report on three patients and review of the literature. *Brain* 1996; 119: 2143–2154
- Pfister H-W, Wilske B, Weber K. Lyme borreliosis: basic science and clinical aspects. *Lancet* 1994; 343: 1013–1016
- Rafto SE, Milton WJ, Galetta SL, Grossman RI. Biopsy-confirmed CNS Lyme disease: MR appearance at 1.5 T. *AJNR Am J Neuroradiol* 1990; 11: 482–484
- Sartoretti-Schefer S, Kollias S, Valavanis A. Ramsay Hunt syndrome associated with brain stem enhancement. *AJNR Am J Neuroradiol* 1999; 20: 278–280
- Sencer S, Sencer A, Aydin K, Hepg l K, Payanli A, Minareci O. Imaging in tuberculosis of the skull and skull-base: case report. *Neuroradiology* 2003; 45: 160–163
- Shaw DR, La Brooy JT. Non-viral infections of the nervous system. *Curr Opin Neurol Neurosurg* 1991; 4: 227–231
- Steere AC. Lyme disease. *N Engl J Med* 2001; 345: 115–125
- Ueno M, Oka A, Koeda T, Okamoto R, Takeshita R. Unilateral occlusion of the middle cerebral artery after varicella zoster virus infection. *Brain Dev* 2002; 24: 106–108

Drug-related Vasculitis

- Aggerwal SK, Williams V, Levine SR, Cassin BJ, Garcia JH. Cocaine-associated intracranial hemorrhage: absence of vasculitis in 14 cases. *Neurology* 1996; 46: 1741–1743
- Ashchi M, Wiedermann HP, James KB. Cardiac complication from use of cocaine and phenylephrine in nasal septoplasty. *Arch Otolaryngol* 1995; 121: 681–684
- Barbieri EJ, Ferko AP, DiGregoria GJ, Ruch EK. The presence of cocaine and benzoylecgonine in rat cerebrospinal fluid after the intravenous administration of cocaine. *Life Sci* 1992; 51: 1739–1746
- Bartzokis G, Goldstein IB, Hance DB, Beckson M, Shapiro D, Lu PH, Edwards N, Mintz J, Bridge P. The incidence of T2-weighted MR imaging signal abnormalities in the brain of cocaine-dependent patients is age-related and region-specific. *AJNR Am J Neuroradiol* 1999; 20: 1628–1635
- Benders MJ, Dorrepaal CA, van de Bor M, van Bel F. Acute effects of indometacin on cerebral hemodynamics and oxygenation. *Biol Neonate* 1995; 68: 91–99
- Buttner A, Mall G, Penning R, Weis S. The neuroanatomy of heroin abuse. *Forensic Sci Int* 2000; 113: 435–442
- Cone EJ. Pharmacokinetics and pharmacodynamics of cocaine. *J Anal Toxicol* 1995; 19: 459–478
- Cuellar ML. Drug-induced vasculitis. *Curr Rheumatol Rep* 2002; 4: 55–59
- De Smet PA. A multidisciplinary overview of intoxicating snuff rituals in the western hemisphere. *J Ethnopharmacol* 1985; 13: 3–49
- Fowler JS, Volkow ND, Wang GJ, Gatley SJ, Logan J. Cocaine: PET studies of cocaine pharmacokinetics, dopamine transporter availability and dopamine transporter occupancy. *Nucl Med Biol* 2001; 28: 561–572
- Gradon JD, Wityk R. Diagnosis of probable cocaine-induced cerebral vasculitis by magnetic resonance angiography. *South Med J* 1995; 88: 1264–1266
- He GQ, Zhang A, Altura BT, Altura BM. Cocaine-induced cerebrovasospasm and its possible mechanisms of action. *J Pharmacol Exp Ther* 1994; 268: 1532–1539
- Heesch CM, Wilhelm CR, Ristich J, Adnane J, Bontempo FA, Wagner WR. Cocaine activates platelets and increases the formation of circulating platelet containing microaggregates in humans. *Heart* 2000; 83: 688–695
- Kaye BR, Fainstat M. Cerebral vasculitis associated with cocaine abuse. *JAMA* 1987; 258: 2104–2106
- Lau CE, Iman A, Ma F, Falk JL. Acute effects of cocaine on spontaneous and discriminative motor functions: relation to route of administration and pharmacokinetics. *J Pharmacol Exp Ther* 1991; 257: 444–446
- Margolis MT, Newton TH. Methamphetamine (“speed”) arteritis. *Neuroradiology* 1971; 2: 179–182
- Martin K, Rogers T, Kavanaugh A. Central nervous system angiopathy associated with cocaine abuse. *J Rheumatol* 1995; 22: 780–782
- McEvoy AW, Kitchen ND, Thomas DG. Intracerebral haemorrhage and drug abuse in young adults. *Br J Neurosurg* 2000; 14: 449–454
- Merkel PA, Koroshetz WJ, Irizarry MC, Cudkowicz ME. Cocaine-associated cerebral vasculitis. *Semin Arthritis Rheum* 1995; 25: 172
- Mockel M, Kampf D, Lobeck H, Frei U. Severe panarteritis associated with drug abuse. *Intensive Care Med* 1999; 25: 113–117

- Neiman J, Haapaniemi HM, Hillbom M. Neurological complications of drug abuse: pathophysiological mechanisms. *Eur J Neurol* 2000; 7: 595
- Niehaus L, Meyer BU. Bilateral borderzone brain infarctions in association with heroin abuse. *J Neurol Sci* 1998; 160: 180–182
- Petitti DB, Sidney S, Quesenberry C, Bernstein A. Stroke and cocaine or amphetamine use. *Epidemiology* 1998; 9: 596–600
- Qureshi AI, Suri MF, Guterman LR, Hopkins LN. Cocaine use and the likelihood of nonfatal myocardial infarction and stroke: data from the Third National Health and Nutrition Examination Study. *Circulation* 2001; 103: 502–506
- Samuels N, Shemesh O, Yinnon AM, Fisher D, Abraham AS. Polyarteritis nodosa and drug abuse: is there a connection? *Postgrad Med J* 1996; 72: 684–685
- Disorders Obstructing the Vascular Lumen**
- Glauser TA, Siegel MJ, Lee BCP, DeBaun MR. Accuracy of neurologic examination and history in detecting evidence of MRI-diagnosed cerebral infarctions in children with sickle cell hemoglobinopathy. *J Child Neurol* 1995; 10: 88–92
- Kenéz J, Barsi P, Majtényi K, Molnár B, Kocher I, Stangi E, Kolomy S. Can intravascular lymphomatosis mimic thrombosis? A case report with 8 months' follow-up and fatal outcome. *Neuroradiology* 2000; 42: 436–440
- Martin-Duverneuil N, Mokhtari K, Behin A, Lafitte F, Hoang-Xuan K, Chiras J. Intravascular malignant lymphomatosis. *Neuroradiology* 2002; 44: 749–754
- Miller D, Hochberg F, Harris N, Gruber M, Louis D, Cohen H. Pathology with clinical correlations of primary central nervous system non-Hodgkin lymphoma: the Massachusetts General Hospital experience. *Cancer* 1994; 74: 1338–1397
- Moran CJ, Siegel MJ, DeBaun MR. Sickle cell disease: imaging of cerebrovascular complications. *Radiology* 1998; 206: 311–332
- Moser FG, Miller ST, Bello JA, Pegelow CH, Zimmerman RA, Wang WC, Ohene-Frempong K, Schwartz A, Vichainsky EP, Gallagher D, Kinney TR. The spectrum of brain MR abnormalities in sickle-cell disease: a report from the cooperative study of sickle cell disease. *AJNR Am J Neuroradiol* 1996; 17: 965–972
- Moussouttas M. Intravascular lymphomatosis presenting as posterior leukoencephalopathy. *Arch Neurol* 2002; 59: 640–641
- Otrakji C, Voight W, Amador A, Gregorius J. Malignant angioendotheliomatosis: a true lymphoma. A case of intravascular lymphomatosis studied by Southern blot hybridization analysis. *Hum Pathol* 1988; 19: 475–478
- Perniciaro C, Winkelmann RK, Daoud MS, Su WP. Malignant angioendotheliomatosis is an angiotropic intravascular lymphoma. Immunohistological, ultrastructural and molecular genetic study. *Am J Dermatopathol* 1995; 17: 242–248
- Steen RG, Emudianughe T, Hankins GM, Wynn LW, Wang WC, Xiong X, Helton KJ. Brain imaging findings in pediatric patients with sickle cell disease. *Radiology* 2003; 228: 216–225
- Steen RG, Miles MA, Helton KJ, Strawn S, Wang W, Xiong XZ, Mulherns RK. Cognitive impairment in children with hemoglobin SS sickle cell disease: relationship to MR imaging findings and hematocrit. *AJNR Am J Neuroradiol* 2003; 24: 382–389
- Strickland-Marmol LB, Fessler RG, Rojiani AM. Necrotizing sarcoid granulomatosis mimicking an intracranial neoplasm: clinicopathologic features and review of the literature. *Mod Pathol* 2000; 13: 909–913
- Tateishi U, Terae S, Ogata A, Sawamura Y, Suzuki Y, Abe S, Miyasaka K. MR imaging of the brain in lymphomatoid granulomatosis. *AJNR Am J Neuroradiol* 201; 22: 1283–1290
- Wang WC, Langstem JW, Steen RG, Wynn LW, Mulhern RK, Williams JA, Kim FM, Figueroa RE. Abnormalities of the central nervous system in very young children with sickle cell anemia. *J Pediatr* 1998; 132: 994–998
- 101 Dural Arteriovenous Fistula**
- Awad IA, Little JR, Akarawi WP, Ahl J. Intracranial dural arteriovenous malformations: factors predisposing to an aggressive neurological course. *J Neurosurg* 1990; 72: 839–850
- Borden JA, Wu JK, Shucart WA. A proposed classification for spinal and cranial dural arteriovenous fistulous malformations and implications for treatment. *J Neurosurg* 1995; 82: 166–179
- Brown RD Jr, Wiebers DO, Nichols DA. Intracranial dural arteriovenous fistulae: angiographic predictors of intracranial hemorrhage and clinical outcome in nonsurgical patients. *J Neurosurg* 1994; 81: 531–538
- Cognard C, Gobin YP, Pierot L, Bailly AL, Houdart E, Casasco A, Chiras J, Merland JJ. Cerebral dural arteriovenous fistulas: clinical and angiographic correlation with a revised classification of venous drainage. *Radiology* 1995; 194: 671–680
- Cognard C, Houdart E, Casasco A, Gabrillargues J, Chiras J, Merland JJ. Long-term changes in intracranial dural arteriovenous fistulae leading to worsening in the type of venous drainage. *Neuroradiology* 1997; 39: 59–66
- Collice M, D'Aliberti G, Talamonti G, Branca V, Boccardi E, Scialfa G et al. Surgical interruption of leptomeningeal drainage as treatment for intracranial dural arteriovenous fistulas without dural sinus drainage. *J Neurosurg* 1996; 84: 810–817
- Davies MA, TerBrugge K, Willinsky R, Coyne T, Saleh J, Wallace MC. The validity of classification for the clinical presentation of intracranial dural arteriovenous fistulas. *J Neurosurg* 1996; 85: 830–837
- Davies MA, Saleh J, TerBrugge K, Willinsky R, Wallace MC. The natural history and management of intracranial dural arteriovenous fistulae. Part 1: Benign lesions. *Interventional Neuroradiology* 1997; 3: 295–302
- Davies MA, TerBrugge K, Willinsky R, Wallace MC. The natural history and management of intracranial dural arteriovenous fistulae. Part 2: Aggressive lesions. *Interventional Neuroradiology* 1997; 3: 303–311
- Duffau H, Lopes M, Janosevic V, Sichez JP, Faillot T, Capelle L, Ismail M, Bitar A, Arthuis F, Fohanno D. Early rebleeding from intracranial dural arteriovenous fistulas: report of 20 cases and review of the literature. *J Neurosurg* 1999; 90: 78–84
- Greenough GP, Mamourian A, Harbaugh RE. Venous hypertension associated with a posterior fossa dural arteriovenous fistula: another cause of bithalamic lesions on MR images. *AJNR Am J Neuroradiol* 1999; 20: 145–147
- Houser OW, Campbell JK, Campbell RJ, Sundt TM. Arteriovenous malformation affecting the transverse dural venous sinus—an acquired lesion. *Mayo Clin Proc* 1979; 54: 651–661

- Hurst RW, Bagley LJ, Galetta S, Glosser G, Lieberman AP, Trojanowski J, Sinson G, Stecker M, Zager E, Raps EC, Flamm ES. Dementia resulting from dural arteriovenous fistulas: the pathologic findings of venous hypertensive encephalopathy. *AJNR Am J Neuroradiol* 1998; 19: 1267–1273
- Ito M, Sonokawa T, Mishina H, Sato K. Reversible dural arteriovenous malformation-induced venous ischemia as a cause of dementia: treatment by surgical occlusion of draining dural sinus: case report. *Neurosurgery* 1995; 3: 1187–1191
- Jaillard AS, Peres B, Hommel M. Neuropsychological features of dementia due to dural arteriovenous malformation. *Cerebrovasc Dis* 1999; 9: 91–97
- Lasjaunias P, Chiu M, ter Brugge K, Tolia A, Hurth M, Bernstein M. Neurological manifestations of intracranial dural arteriovenous malformations. *J Neurosurg* 1986; 64: 724–730
- Lawton MT, Jacobowitz R, Spetzler RF. Redefined role of angiogenesis in the pathogenesis of dural arteriovenous malformations. *J Neurosurg* 1997; 8: 267–274
- Malik GM, Pearce JE, Ausman JI, Mehta B. Dural arteriovenous malformations and intracranial hemorrhage. *Neurosurgery* 1984; 15: 332–339
- Matsuda S, Waragai M, Shinotoh H, Takahashi N, Takagi K, Hattori T. Intracranial dural arteriovenous fistula presenting progressive dementia and parkinsonism. *J Neurol Sci* 1999; 165: 43–47
- Mironov A. Selective transvenous embolization of dural fistulas without occlusion of the dural sinus. *AJNR Am J Neuroradiol* 1998; 19: 389–391
- Newton TH, Cronqvist S. Involvement of dural arteries in intracranial arteriovenous malformations. *Radiology* 1969; 93: 1071–1078
- Noguchi K, Melhem ER, Kanazawa T, Kubo M, Kuwayama N, Seto H. Intracranial dural arteriovenous fistulas: Evaluation with combined 3D Time-of-Flight MR angiography and MR digital subtraction angiography. *AJR Am J Roentgenol* 2004; 182: 183–190
- Rothbart D, Awad IA, Lee J, Kim J, Harbaugh R, Criscuolo GR. Expression of angiogenic factors and structural proteins in central nervous system vascular malformations. *Neurosurgery* 1996; 38: 915–924
- Satomi J, Van Dijk JM, TerBrugge KG, Willinsky RA, Wallace MC. Benign cranial dural arteriovenous fistulas: outcome of conservative management based on the natural history of the lesion. *J Neurosurg* 2002; 97: 767–770
- Uranishi R, Nakase H, Sakaki T. Expression of angiogenic growth factors in dural arteriovenous fistula. *J Neurosurg* 1999; 91: 781–786
- Van Dijk JM, Willinsky RA. Venous congestive encephalopathy related to cranial dural arteriovenous fistulas. *Neuroimaging Clin N Am* 2003; 13: 55–72
- Van Dijk JM, TerBrugge KG, Willinsky RA, Wallace MC. Multiplicity of dural arteriovenous fistulas. *J Neurosurg* 2002; 96: 76–78
- Van Dijk JM, TerBrugge KG, Willinsky RA, Wallace MC. Clinical course of cranial dural arteriovenous fistulas with long-term persistent cortical venous reflux. *Stroke* 2002; 33: 1233–1236
- Willinsky R, TerBrugge K, Montanera W, Mikulis D, Wallace MC. Venous congestion: an MR finding in dural arteriovenous malformations with cortical venous drainage. *AJNR Am J Neuroradiol* 1994; 15: 1501–1507
- Willinsky R, Goyal M, TerBrugge K, Montanera W. Tortuous, engorged pial veins in intracranial dural arteriovenous fistulas: correlations with presentation, location, and MR findings in 122 patients. *AJNR Am J Neuroradiol* 1999; 20: 1031–1036

102 Leukoencephalopathy After Chemotherapy and Radiotherapy

- Antunes NL, Souweidane MM, Lis E, Rosenblum MK, Steinherz PG. Methotrexate leukoencephalopathy presenting as Klüver-Bucy syndrome and uncinat seizures. *Pediatr Neurol* 2002; 26: 305–308
- Bleyer WA. Leukoencephalopathy detectable by magnetic resonance imaging: much ado about nothing? *Int J Radiat Oncol Biol Phys* 1995; 32: 1251–1552
- Brown MS, Stemmer SM, Simon JH, Stears JC, Jones RB, Cagnoni PJ, Sheeder JL. White matter disease induced by high-dose chemotherapy: longitudinal study with MR imaging and proton spectroscopy. *AJNR Am J Neuroradiol* 1998; 19: 217–221
- Cain MS, Burton GV, Holcombe RF. Fatal leukoencephalopathy in a patient with non-Hodgkin's lymphoma treated with CHOP chemotherapy and high-dose steroids. *Am J Med Sci* 1998; 315: 202–207
- Cantini R, Giorgetti W, Vollandiani AM, Burchianti M, Amodeo C. Radiation-induced cerebral lesions in childhood. *Childs Nerv Syst* 1989; 5: 135–139
- Chen C-Y, Zimmerman RA, Bilaniuk LT, Chou T-W, Molloy PT. Childhood leukemia: central nervous system abnormalities during and after treatment. *AJNR Am J Neuroradiol* 1996; 17: 295–310
- DeAngelis LM, Delattre J-Y, Posner JB. Radiation-induced dementia in patients cured of brain metastases. *Neurology* 1989; 39: 789–796
- Dietrich U, Wanke I, Mueller T, Wieland R, Moellers M, Forsting M, Stolke D. White matter disease in children treated for malignant brain tumors. *Childs Nerv Syst* 2001; 17: 731–738
- Gowan GM, Herrington JD, Simonetta AB. Methotrexate-induced toxic leukoencephalopathy. *Pharmacotherapy* 2002; 22: 1183–1187
- Hertzberg H, Huk WJ, Ueberall MA, Langer T, Meier W, Dopfer R, Skalej M, Lackner H, Bode U, Janßen G, Zintl F, Beck JD. CNS late effects after all therapy in childhood. Part I: neuroradiological findings in long-term survivors of childhood. ALL – An evaluation of the interferences between morphology and neurophysiological performances. *Med Pediatr Oncol* 1997; 28: 387–400
- Kishi T, Tanaka Y, Ueda K. Evidence for hypomethylation in two children with acute lymphoblastic leukemia and leukoencephalopathy. *Cancer* 2000; 89: 925–931
- Lai R, Abrey LE, Rosenblum MK, DeAngelis LM. Treatment-induced leukoencephalopathy in primary CNS lymphoma: a clinical and autopsy study. *Neurology* 2004; 62: 451–456
- Laitt RD, Chambers EJ, Goddard PR, Wakeley CJ, Duncan AW, Foreman NK. Magnetic resonance imaging and magnetic resonance angiography in long term survivors of acute lymphoblastic leukemia treated with cranial irradiation. *Cancer* 1995; 76: 1846–1852
- Laxmi SN, Takahashi S, Matsumoto K, Higano S, Kurihara N, Imaizumi M, Abe K, Itoyama Y, Sakamoto K. Treatment-related disseminated necrotizing leukoencephalopathy with characteristic contrast enhancement of the white matter. *Radiat Med* 1996; 14: 303–307

- Löfblad K-O, Kelkear P, Ozdoba C, Ramelli C, Remonda L, Schroth G. Pure methotrexate encephalopathy presenting with seizures: CT and MRI features. *Pediatr Radiol* 1998; 28: 86–91
- Matsumoto K, Takahashi S, Sato A, Imaizumi M, Higano S, Sakamoto K, Asakawa H, Tada K. Leukoencephalopathy in childhood hematopoietic neoplasm caused by moderate-dose methotrexate and prophylactic cranial radiotherapy – an MR analysis. *Int J Radiat Oncol Biol Phys* 1995; 32: 913–918
- Ohmoto Y, Kajiwaru K, Kato S, Nisziaki T, Ito H, Tamura S. Atypical MRI findings in treatment-related leukoencephalopathy: case report. *Neuroradiology* 1996; 38: 128–133
- Oka M, Terae S, Kobayashi R, Sawamura Y, Kudoh K, Tha KK, Yoshida M, Kaneda M, Suzuki Y, Miyasaka K. MRI in methotrexate-related leukoencephalopathy: Disseminated necrotising leukoencephalopathy in comparison with mild leukoencephalopathy. *Neuroradiology* 2003; 45: 493–497
- Peterson K, Clark HB, Hall WA, Truwit CL. Multifocal enhancing magnetic resonance imaging lesions following cranial irradiation. *Ann Neurol* 1995; 38: 237–244
- Price RA, Birdwell DA. The central nervous system in childhood leukemia. III. Mineralizing angiopathy and dystrophic calcification. *Cancer* 1978; 42: 717–728
- Seidl H, Nygaard R, Haave I, Moe PJ. Magnetic resonance imaging and neuroradiological evaluation after treatment with high-dose methotrexate for acute lymphocytic leukaemia in young children. *Acta Paediatr* 1996; 85: 450–453
- Shanley DJ. Mineralizing microangiopathy: CT and MRI. *Neuroradiology* 1995; 37: 331–333
- Tahjeb P. Progressive late delayed postirradiation encephalopathy with Klüver-Bucy syndrome. Serial MRI and clinicopathological studies. *Clin Neurol Neurosurg* 1995; 97: 264–268
- Tekkök IH, Carter DA, Robinson MG, Brinker R. Reversals of CNS-prophylaxis-related leukoencephalopathy after CSF shunting: case histories of identical twins. *Childs Nerv Syst* 1996; 12: 309–314
- Valk PE, Dillon WP. Radiation injury of the brain. *AJNR Am J Neuroradiol* 1991; 12: 45–62
- Vasquez E, Lucaya J, Castelotte A, Piguera J, Sainz P, Olive T, Sanchez-Toledo J, Ortega JJ. Neuroimaging in pediatric leukemia and lymphoma: differential diagnosis. *Radiographics* 2002; 22: 1411–1428
- Wong ET. Recurrent cystic radiation necrosis of the brain. *Oncol Rep* 1998; 5: 685–687
- Di Trapani G, Sabatelli M, Carnevale A, Colosimo C, Mignogna T, Tonali P. Gliomatosis cerebri: report of an atypical case. *Clin Neuropathol* 1995; 14: 13–18
- Enterline DS, Davey NC, Tien RD. Case 3: gliomatosis cerebri. *AJRAm J Roentgenol* 1995; 165: 214–215
- Essig M, Schlemmer H-P, Tronnier V, Hawighorst H, Wirtz R, van Kaick G. Fluid-attenuated inversion-recovery MR imaging of gliomatosis cerebri. *Eur Radiol* 2001; 11: 303–308
- Felsberg GJ, Silver SA, Brown MT, Tien RD. Radiologic-pathologic correlation. Gliomatosis cerebri. *AJNR Am J Neuroradiol* 1994; 15: 1745–1753
- Freund M, Hähnel S, Sommer C, Martmann M, Kiessling M, Tronnier V, Sartor K. CT and MRI findings in gliomatosis cerebri: a neuroradiological and neuropathologic review of diffuse infiltrating brain neoplasms. *Eur Radiol* 2001; 11: 309–316
- Galatioto S, Marafioti T, Cavallari V, Batolo D. Gliomatosis cerebri: clinical, neuropathological, immunohistochemical and morphometric studies. *Zentralbl Pathol* 1993; 139: 251–267
- Hara A, Sakai N, Yamada H, Tanaka T, Mori H. Assessment of proliferative potential in gliomatosis cerebri. *J Neurol* 1991; 238: 80–82
- Hayek J, Valavanis A. Computed tomography of gliomatosis cerebri. *Comput Radiol* 1982; 6: 93–98
- Hecht BK, Turc-Carel C, Chatel M, Lonjon M, Roche JL, Gioanni J, Hecht FI, Gaudray P. Chromosomes in gliomatosis cerebri. *Genes Chromosomes Cancer* 1995; 14: 149–153
- Herrlinger U, Felsberg J, Küker W, Bornemann A, Plasswilm L, Knobbe CB, Strik H, Wick W, Meyermann R, Dichgans J, Bamberg M, Feinberger G, Weller M. Gliomatosis cerebri: molecular pathology and clinical course. *Ann Neurol* 2002; 52: 390–399
- Jennings MT, Frenchman M, Shhab T, Johnson MD, Creasy J, LaPorte K, Dettbarn WD. Gliomatosis cerebri presenting as intractable epilepsy during early childhood. *J Child Neurol* 1995; 10: 37–45
- Kandler RH, Smith CML, Broome JC, Davies-Jones GAB. Gliomatosis cerebri: a clinical, radiological and pathological report of four cases. *Br J Neurosurg* 1991; 5: 187–193
- Keene DL, Jimenez C, Hsu E. MRI diagnosis of gliomatosis cerebri. *Pediatr Neurol* 1999; 20: 148–151
- Koslow SA, Claassen D, Hirsch WL, Jungreis CA. Gliomatosis cerebri: a case report with autopsy correlation. *Neuroradiology* 1992; 34: 331–333
- Lev MH. Gliomatosis cerebri has normal relative blood volume: really? Who cares? Should you? *AJNR Am J Neuroradiol* 2002; 23: 345–346
- Levin N, Gomori JM, Siegal T. Chemotherapy as initial treatment in gliomatosis cerebri: results with temozolomide. *Neurology* 2004; 63: 354–356
- Mawrin C, Kirches E, Schneider-Stock R, Scherlach C, Vorwerk C, von Deimling A, van Landeghem F, Meyermann R, Bornemann A, Müller A, Romeike B, Stoltenberg-Diederich G, Wickboldt J, Pilz P, Dietzmann K. Analysis of *TP53* and *PTEN* in gliomatosis cerebri. *Acta Neuropathol (Berl)* 2003; 105: 529–536
- Mohana-Borges AVR, Imbesi SG, Dietrich R, Alksne J, Amjadi DK. Role of proton magnetic resonance spectroscopy in the diagnosis of gliomatosis cerebri. A unique pattern of normal choline but elevated myo-inositol metabolite levels. *J Comput Assist Tomogr* 2004; 28: 103–105
- Nishioka H, Ito H, Miki T. Difficulties in the antemortem diagnosis of gliomatosis cerebri: report of a case with diffuse increase of gemistocyte-like cells, mimicking reactive gliosis. *Br J Neurosurg* 1996; 10: 103–107
- Pyhtinen J. Proton MR spectroscopy in gliomatosis cerebri. *Neuroradiology* 2000; 42: 612–615

103 Gliomatosis Cerebri

- Balko MG, Blisard KS, Samaha FJ. Oligodendroglial gliomatosis cerebri. *Hum Pathol* 1992; 23: 706–707
- Burger PC. Gliomatosis cerebri: molecular pathology and clinical course. *Ann Neurol* 2002; 52: 389
- Bertrand E, Kryst-Widzowska T, Baranska M. Gliomatosis cerebri at the 17-year-old girl correlations of histological, CT and MRI appearance. *Folia Neuropathol* 1994; 32: 245–249
- Del Caprio-O'Donovan, Korah I, Salazar A, Melancon D. Gliomatosis cerebri. *Radiology* 1996; 198: 831–835
- Dexter MA, Parker GD, Besser M, Ell J, Fulham MJ. MR and positron emission tomography with fludeoxyglucose F 18 in gliomatosis cerebri. *AJNR Am J Neuroradiol* 1995; 16: 1507–1510

- Pyhtinen J, Pääkkö E. A difficult diagnosis of gliomatosis cerebri. *Neuroradiology* 1996; 38: 444–448
- Rippe DJ, Boyko OB, Fuller NF, Friedman HS, Oakes WJ, Schold SC. Gadopentetate-dimeglumine – enhanced MR imaging of gliomatosis cerebri: appearance mimicking leptomeningeal tumor dissemination. *AJNR Am J Neuroradiol* 1990; 11: 800–801
- Ross IB, Robitaille Y, Villemure J-G, Tampieri D. Diagnosis and management of gliomatosis cerebri: recent trends. *Surg Neurol* 1991; 36: 431–340
- Sanson M, Cartalat-Carel S, Taillibert S, Napolitano M, Djafari L, Cougnard J, Gervais H, Laigle F, Carpentier A, Mokhtari K, Taillandier L, Chinot O, Duffau H, Honnorat J, Hoang-Xuan K, Delattre JY for the ANOCEF Group. Initial chemotherapy in gliomatosis cerebri. *Neurology* 2004; 63: 270–275
- Saraf-Lavi E, Bowen BC, Pattany PM, Sklar EML, Murdoch JB, Petito CK. Proton MR spectroscopy of gliomatosis cerebri: case report of elevated myoinositol with normal choline levels. *AJNR Am J Neuroradiol* 2003; 24: 946–951
- Schober R, Mai JK, Volk B, Wechsler W. Gliomatosis cerebri; biopsical approach and neuropathological verification. *Acta Neurochir (Wien)* 1991; 113: 131–137
- Shin YM, Chang KH, Han MH, Myung NH, Chi JE, Cha SH, Han MC. Gliomatosis cerebri: comparison of MR and CT features. *AJR Am J Roentgenol* 1993; 161: 859–862
- Spagnoli MV, Grossman RI, Packer RJ, Hackney DB, Goldberg HI, Zimmerman RA, Bilaniuk LT. Magnetic resonance imaging determination of gliomatosis cerebri. *Neuroradiology* 1987; 29: 15–18
- Vates GE. Gliomatosis cerebri: a review of 22 cases. *Neurosurgery* 2003; 53: 261–271
- Yanaka K, Kamezaki T, Kobayashi E, Matsueda K, Yoshii Y, Nose T. MR imaging of diffuse glioma. *AJNR Am J Neuroradiol* 1992; 13: 349–351
- Yang S, Wetzel S, Cha S. Dynamic contrast-enhanced T2*-weighted MR imaging of gliomatosis cerebri. *AJNR Am J Neuroradiol* 2002; 23: 350–355
- Yip M, Fisch C, Lamarche JB. Gliomatosis cerebri affecting the entire neuraxis. *Radiographics* 2003; 23: 247–253

104 Diffuse Axonal Injury

- Bešenski N. Traumatic injuries: imaging of head injuries. *Eur Radiol* 2002; 12: 1237–1252
- Chan JHM, Tsui EYK, Peh WCG, Fong D, Fok KF, Leung KM, Yuen MK, Fung KKL. Diffuse axonal injury: detection of changes in anisotropy of water diffusion by diffusion-weighted imaging. *Neurology* 2003; 45: 34–38
- Graham DI, Raghupathi R, Saatman KE, Meaney D, McIntosh TK. Tissue tears in the white matter after lateral fluid percussion brain injury in the rat: relevance to human brain injury. *Acta Neuropathol (Berl)* 2000; 99: 117–124
- Hammoud DA, Wasserman BA. Diffuse axonal injuries: pathophysiology and imaging. *Neuroimaging Clin N Am* 2002; 12: 205–216
- Huisman TAGM, Sorensen AG, Hergan K, Gonzalez RG, Schaefer PW. Diffusion-Weighted imaging for the evaluation of diffuse axonal injury in closed head injury. *J Comput Assist Tomogr* 2003; 27: 5–11
- LaPlaca MC, Thibault LE. Dynamic mechanical deformation of neurons triggers an acute calcium response and cell injury involving the N-methyl-D-aspartate glutamate receptor. *J Neurosci Res* 1998; 52: 220–229

- Medana IM, Esiri MM. Axonal damage: a key predictor of outcome in human CNS diseases. *Brain* 2003; 126: 515–530
- Meythaler JM, Brunner RC, Johnson A, Novack TA. Amantadine to improve neurorecovery in traumatic brain injury-associated diffuse axonal injury: a pilot double-blind randomized trial. *J Head Trauma Rehabil* 2002; 17: 300–313
- Onaya M. Neuropathological investigation of cerebral white matter lesions caused by closed head injury. *Neuropathology* 2002; 22: 243–251
- Parizel PM, Özsarlak Ö, van Goethem JW, van den Hauwe L, Dillen C, Verlooy J, Cosyns P. Imaging findings in diffuse axonal injury after closed head trauma. *Eur Radiol* 1998; 8: 960–965
- Reichard RR, White CL, Hladik CL, Dolinak D. Beta-amyloid precursor protein staining of nonaccidental central nervous system injury in pediatric autopsies. *J Neurotrauma* 2003; 4: 347–355
- Scheid R, Preul C, Gruber O, Wiggins C, von Cramon Y. Diffuse axonal injury associated with chronic traumatic brain injury: evidence from T2*-weighted gradient-echo imaging at 3 T. *AJNR Am J Neuroradiol* 2003; 24: 1049–1056
- Strich SJ, Oxon DM. Shearing of nerve fibres as a cause of brain damage due to head injury. *Lancet* 1961; II: 443–449
- Takaoka M, Tabuse H, Kamura E, Nakajima S, Tsuzuki T, Nakamura K, Okada A, Sugimoto H. Semiquantitative analysis of corpus callosum injury using magnetic resonance imaging indicates clinical severity in patients with diffuse axonal injury. *J Neurol Neurosurg Psychiatry* 2002; 73: 289–293

105 Wallerian Degeneration and Myelin Loss Secondary to Neuronal and Axonal Degeneration

- Basak M, Erturk M, Oflazoğlu B, Ozel A, Yildiz GB, Forta H. Magnetic resonance imaging in amyotrophic lateral sclerosis. *Acta Neurol Scand* 2002; 105: 395–399
- Becerra JL, Puckett WR, Hiester ED, Quencer RM, Marcillo AE, Donovan Post MJ, Bunge RP. MR-Pathologic comparisons of wallerian degeneration in spinal cord injury. *AJNR Am J Neuroradiol* 1995; 16: 125–133
- Bignami A, Ralston HJ. The cellular reaction to wallerian degeneration in the central nervous system of the cat. *Brain Res* 1969; 13: 444–461
- Bignami A, Eng LF. Biochemical studies of myelin in wallerian degeneration of rat optic nerve. *J Neurochem* 1973; 20: 165–173
- Bozzali M, Falini A, Franceschi M, Cercignani M, Zuffi M, Scotti G, Comi G, Filippi M. White matter damage in Alzheimer's disease assessed in vivo using diffusion tensor magnetic resonance imaging. *J Neurol Neurosurg Psychiatry* 2002; 72: 742–746
- Castillo M, Mukherji SK. Early abnormalities related to postinfarction Wallerian degeneration: evaluation with MR diffusion-weighted imaging. *J Comp Assist Tomogr* 1999; 23: 1004–1007
- Coleman MP, Hugh Perry V. Axon pathology in neurological disease: a neglected therapeutic target. *Trends Neurosci* 2002; 25: 532–537
- Comi G, Rovaris M, Leocani L. Neuroimaging in amyotrophic lateral sclerosis. *Eur J Neurol* 1999; 6: 629–637
- Cook RD, Wisniewski HM. The role of oligodendroglia and astroglia in wallerian degeneration of the optic nerve. *Brain Res* 1973; 61: 191–206

- Fukui K, Iguchi I, Kito A, Watanabe Y, Sugita K. Extent of pontine pyramidal tract wallerian degeneration and outcome after supratentorial hemorrhagic stroke. *Stroke* 1994; 25: 1207–1210
- Griffin JW, George R, Lobato C, Tyor WR, Yan LC, Glass JD. Macrophage responses and myelin clearance during wallerian degeneration: relevance to immune-mediated demyelination. *J Neuroimmunol* 1992; 40: 153–166
- Igarashi H, Katayama Y, Tsuganezawa T, Yamamuro M, Terashi A, Owan C. Three-dimensional anisotropy contrast (3DAC) magnetic resonance imaging of the human brain: application to assess wallerian degeneration. *Int Med* 1998; 37: 662–668
- Inoue Y, Matsumura Y, Fukuda T, Nemoto Y, Shirahata N, Suzuki T, Shakudo M, Yawata S, Tanaka S, Takemoto K, Onoyama Y. MR imaging of wallerian degeneration in the brainstem: temporal relationships. *AJNR Am J Neuroradiol* 1990; 11: 897–903
- Jacob S, Finsterbusch J, Weishaupt JH, Khorram-Sefat D, Frahm J, Ehrenreich H. Diffusion tensor imaging for long-term follow-up of corticospinal tract degeneration in amyotrophic lateral sclerosis. *Neuroradiology* 2003; 45: 598–600
- Kang DW, Chu K, Yoon BW, Song IC, Chang KH, Roh JK. Diffusion-weighted imaging in wallerian degeneration. *J Neurol Sci* 2000; 178: 167–169
- Khurana DS, Strawsburg RH, Robertson RL, Madsen JR, Helmers SL. MRI signal changes in the white matter after corpus callosotomy. *Pediatr Neurol* 1999; 21: 691–695
- Kuhn JM, Johnson KA, Davis KR. Wallerian degeneration: evaluation with MR imaging. *Radiology* 1988; 168: 199–202
- Kuhn MJ, Mikulis DJ, Ayoub DM, Kosofsky BE, Davis KR, Taveras JM. Wallerian degeneration after cerebral infarction: evaluation with sequential MR imaging. *Radiology* 1989; 172: 179–182
- Lassmann H, Ammerer HP, Kulnig W. Ultrastructural sequence of myelin degradation. *Acta Neuropathol (Berl)* 1978; 44: 91–102
- Lassmann H, Ammerer HP, Jurecka W, Kulnig W. Ultrastructural sequence of myelin degradation. *Acta Neuropathol (Berl)* 1978; 44: 103–109
- Lexa FJ, Grossman RI, Rosenquist AC. MR of wallerian degeneration in the feline visual system: characterization by magnetization transfer rate with histopathologic correlation. *AJNR Am J Neuroradiol* 1994; 15: 201–212
- Mazumdar A, Mukherjee P, Miller JH, Malde H, McKinstry RC. Diffusion-weighted imaging of acute corticospinal tract injury preceding Wallerian degeneration in the maturing human brain. *AJNR Am J Neuroradiol* 2003; 24: 1057–1066
- Miyai I, Suzuki T, Kii K, Kang J, Kubota K. Wallerian degeneration of the pyramidal tract does not affect stroke rehabilitation outcome. *Neurology* 1998; 51: 1613–1616
- Orita T, Tsurutani T, Izumihar A, Kajiwaru K. Early, evolving wallerian degeneration of the pyramidal tract in cerebrovascular diseases: MR study. *J Comput Assist Tomogr* 1994; 18: 943–946
- Peretti-Viton P, Azulay JP, Trefouret S, Brunel H, Daniel C, Viton JM, Flori A, Salazard B, Pouget J, Serratrice G, Salamon G. MRI of the intracranial corticospinal tracts in amyotrophic and primary lateral sclerosis. *Neuroradiology* 1999; 41: 744–749
- Pierpaoli C, Barnett A, Pajevic S, Chen R, Penix L, Virta A, Basser P. Water diffusion changes in wallerian degeneration and their dependence on white matter architecture. *Neuroimaging* 2001; 13: 1174–1185
- Reigner J, Matthieu JM, Kraus-Ruppert R, Lassmann H, Poduslo J. Myelin proteins, glycoproteins, and myelin-related enzymes in experimental demyelination of the rabbit optic nerve: sequence of events. *J Neurochem* 1981; 36: 1986–1995
- Savoiardo M, Pareyson D, Grisoli M, Forester M, D'Incerti L, Farina L. The effects of wallerian degeneration of the optic radiations demonstrated by MRI. *Neuroradiology* 1992; 34: 323–325
- Seitz RJ, Reiners K, Himmelmann F, Heininger K, Hartung HP, Toyka KV. The blood–nerve barrier in wallerian degeneration: a sequential long-term study. *Muscle Nerve* 1989; 627–635
- Sonoda S, Tsubahara A, Saito M, Chino N. Extent of pyramidal tract wallerian degeneration in the brain stem on MRI and degree of motor impairment after supratentorial stroke. *Disabil Rehabil* 1992; 14: 89–92
- Tanabe JL, Vermathen M, Miller R, Gelinas D, Weiner MW, Rooney WD. Reduced MTR in the corticospinal tract and normal T₂ in amyotrophic lateral sclerosis. *Magn Reson Imaging* 1998; 16: 1163–1169
- Terae S, Taneichi H, Abumi K. MRI of wallerian degeneration of the injured spinal cord. *J Comput Assist Tomogr* 1993; 17: 700–703
- Türkdoğan-Sözüer D, Özek MM, Sav A, Dinçer A, Pamir MN. Serial MRI and MRS studies with unusual findings in Rasmussen's encephalitis. *Eur Radiol* 2000; 10: 962–966
- Udaka F, Sawada H, Seriu N, Shindou K, Nishitani N, Kameyama M. MRI and SPECT findings in amyotrophic lateral sclerosis. Demonstration of upper motor neurone involvement by clinical neuroimaging. *Neuroradiology* 1992; 34: 389–393
- Uchino A, Imada H, Ohno M. MR imaging of wallerian degeneration in the human brain stem after ictus. *Neuroradiology* 1990; 32: 191–195
- Uchino A, Sawada A, Takase Y, Egashira R, Kudo S. Transient detection of early wallerian degeneration on diffusion-weighted MRI after an acute cerebrovascular accident. *Neuroradiology* 2004; 46: 183–188
- Werring DJ, Toosy AT, Clark CA, Parker GJM, Barker GJ, Miller DH, Thompson AJ. Diffusion tensor imaging can detect and quantify corticospinal tract degeneration after stroke. *J Neurol Neurosurg Psychiatry* 2000; 269–272
- Wiesmann UC, Symms MR, Clark CA, Lemieux L, Franconi F, Parker GJM, Barker GJ, Shorvon SD. Wallerian degeneration in the optic radiation after temporal lobectomy demonstrated in vivo with diffusion tensor imaging. *Epilepsia* 1999; 40: 1155–1158
- Zhang L, Ulug AM, Zimmerman RD, Lin MT, Rubin M, Beal MF. The diagnostic utility of FLAIR imaging in clinically verified amyotrophic lateral sclerosis. *J Magn Reson Imaging* 2003; 17: 521–527

106 Diffusion-weighted Imaging

- Arfanakis K, Houghton VM, Carew JD, Rogers BP, Dempsey RJ, Meyerand ME. Diffusion tensor MR imaging in diffuse axonal injury. *AJNR Am J Neuroradiol* 2002; 23: 794–802
- Assaf BA, Mohamed FB, Abou-Khaled KJ, Williams M, Yazeji MS, Haselgrove J, Faro SH. Diffusion tensor imaging of the hippocampal formation in temporal lobe epilepsy. *AJNR Am J Neuroradiol* 2003; 24: 1857–1862
- Basser PJ, Mattiello J, LeBihan D. Estimation of the effective self-diffusion tensor from the NMR spin echo. *J Magn Reson* 1994; 103: 247–254

- Basser PJ, Mattiello J, LeBihan D. MR diffusion tensor spectroscopy and imaging. *Biophys J* 1994; 66: 259–267
- Basser PJ, Pierpaoli C. A simplified method to measure the diffusion tensor from seven MR images. *Magn Reson Med* 1998; 39: 928–934
- Bozzao A, Di Paolo A, Mazzoleni C, Fasoli F, Simonetti A, Fantozzi LM, Floris R. Diffusion-weighted MR imaging in the early diagnosis of periventricular leukomalacia. *Eur Radiol* 2003; 13: 1571–1576
- Bydder GM, Rutherford MA, Hajnal JV. How to perform diffusion-weighted imaging. *Childs Nerv Syst* 2001; 17: 195–201
- Cavalleri F, Berardi A, Burlina AB, Ferrari F, Mavilla L. Diffusion-weighted MRI of maple syrup urine disease encephalopathy. *Neuroradiology* 2002; 44: 499–502
- Cercignani M, Bozzali M, Iannucci G, Comi G, Filippi M. Magnetization transfer ratio and mean diffusivity of normal appearing white and gray matter from patients with multiple sclerosis. *J Neurol Neurosurg Psychiatry* 2001; 70: 311–317
- Cercignani M, Inglese M, Pagani E, Comi G, Filippi M. Mean diffusivity and fractional anisotropy histograms of patients with multiple sclerosis. *AJNR Am J Neuroradiol* 2001; 22: 952–958
- Cercignani M, Bozzali M, Iannucci G, Comi G, Filippi M. Intravoxel and inter-voxel coherence in patients with multiple sclerosis assessed using diffusion tensor MRI. *J Neurol* 2002; 249: 875–883
- Chan JHM, Tsui EYK, Peh WCG, Fong D, Kok KF, Leung KM, Yeun MK, Fung KKL. Diffuse axonal injury: detection of changes in anisotropy of water diffusion by diffusion-weighted imaging. *Neuroradiology* 2003; 45: 34–38
- Chen C-Y, Lee K-W, Lee C-C, Chin S-C, Chung H-W, Zimmerman RA. Heroin-induced spongiform leukoencephalopathy: value of diffusion MR imaging. *J Comput Assist Tomogr* 2000; 24: 735–737
- Clark CA, Le Bihan D. Water diffusion compartmentation and anisotropy at high b values in the human brain. *Magn Reson Med* 2000; 44: 852–859
- Clark CA, Hedehus M, Moseley ME. In vivo mapping of the fast and slow diffusion tensors in human brain. *Magn Reson Med* 2002; 47: 623–628
- Doran M, Bydder GM. Magnetic resonance: perfusion and diffusion imaging. *Neuroradiology* 1990; 32: 392–398
- Doran M, Hajnal JV, van Bruggen N, King MD, Young IR, Bydder GM. Normal and abnormal white matter tracts shown by MR imaging using directional diffusion weighted sequences. *J Comput Assist Tomogr* 1990; 14: 865–873
- Ducreux D, Oppenheim C, Vandamme X, Dormont D, Samson Y, Rancurel G, Cosnard G, Marsault C. Diffusion-weighted imaging patterns of brain damage associated with cerebral venous thrombosis. *AJNR Am J Neuroradiol* 2001; 22: 261–268
- Eastwood JD, Engelter ST, MacFall JF, DeLong DM, Provenzale JM. Quantitative assessment of the time course of infarct intensity on diffusion-weighted images. *AJNR Am J Neuroradiol* 2003; 24: 680–687
- Engelbrecht V, Scherer A, Rassek M, Witsack HJ, Mödder U. Diffusion-weighted MR imaging in the brain in children: findings in the normal brain and in the brain with white matter diseases. *Radiology* 2002; 222: 410–418
- Engelter ST, Provenzale JM, Petrella JR. Assessment of vasogenic edema in eclampsia using diffusion imaging. *Neuroradiology* 2000; 42: 818–820
- Fiehler J, Foth M, Kucinski T, Knab R, von Bezold M, Weiller C, Zeumer H, Röther J. Severe ADC decreases do not predict irreversible tissue damage in humans. *Stroke* 2002; 33: 79–86
- Filippi M, Iannucci G, Cercignani M, Rocca MA, Pratesi A, Comi G. A quantitative study of water diffusion in multiple sclerosis lesions and normal-appearing white matter using echo-planar imaging. *Arch Neurol* 2000; 57: 1017–1021
- Filippi M, Cercignani M, Inglese M, Horsfield MA, Comi G. Diffusion tensor magnetic resonance imaging in multiple sclerosis. *Neurology* 2001; 56: 304–311
- Fitzek C, Weissmann M, Specter H, Fitzek S, Hopf HC, Schulte E, Stoeter P. Anatomy of brain-stem white-matter tracts shown by diffusion-weighted imaging. *Neuroradiology* 2001; 43: 953–960
- Forbes KPN, Pipe JG, Heiserman JE. Evidence for cytotoxic edema in the pathogenesis of cerebral venous infarction. *AJNR Am J Neuroradiol* 2001; 22: 450–455
- Forbes KPN, Pipe JG, Bird CR. Changes in brain water diffusion during the 1st year of life. *Radiology* 2002; 222: 405–409
- Ford BJ. Brownian movement in Clarkia pollen: a reprise of first observations. *Microscope* 1992; 40: 235–241
- Gelal F, Calli C, Apaydin M, Erdem G. Van der Knaap's leukoencephalopathy: report of five new cases with emphasis on diffusion-weighted MRI findings. *Neuroradiology* 2002; 44: 625–630
- Gray L, MacFall J. Overview of diffusion imaging. *MRI Clin N Am* 1998; 6: 125–138
- Guo A, Jewells VL, Provenzale JM. Analysis of normal-appearing white matter in multiple sclerosis: comparison of diffusion tensor MR imaging and magnetization transfer imaging. *AJNR Am J Neuroradiol* 2001; 22: 1893–1900
- Guo AC, Petrella JR, Kurzberg J, Provenzale JM. Evaluation of white matter anisotropy in Krabbe disease with diffusion tensor MR imaging: initial experience. *Radiology* 2001; 218: 809–815
- Guo AC, MacFall JR, Provenzale JM. Multiple sclerosis: diffusion tensor MR imaging for evaluation of normal-appearing white matter. *Radiology* 2002; 222: 729–736
- Heide AC, Richards TL, Alvord EC Jr, Peterson J, Rose LM. Diffusion imaging of experimental allergic encephalomyelitis. *Magn Reson Med* 1993; 29: 478–484
- Helenius J, Soinne L, Perkiö J, Salonen O, Kamasmäki A, Kaste M, Carano RAD, Aronen HJ, Tatlisamak T. Diffusion-weighted MR imaging in normal human brains in various age groups. *AJNR Am J Neuroradiol* 2002; 23: 194–199
- Horsfield MA. Using diffusion-weighted MRI in multicenter clinical trials for multiple sclerosis. *J Neurol Sci* 2001; 186: S51–S54
- Horsfield MA, Jones DK. Applications of diffusion-weighted and diffusion tensor MRI to white matter diseases. A review. *NMR Biomed* 2002; 15: 570–577
- Horsfield MA, Lai M, Webb SL, Barker GJ, Tofts PS, Turner R, Rudge P, Miller DH. Apparent diffusion coefficients in benign and secondary progressive multiple sclerosis by nuclear magnetic resonance. *Magn Reson Med* 1996; 36: 393–400
- Hüppi PS, Murphy B, Maier SE, Zientara GP, Inder TE, Barnes PD, Kikinis R, Jolensz FA, Volpe JJ. Microstructural brain development after perinatal cerebral white matter injury assessed by diffusion tensor magnetic resonance imaging. *Pediatrics* 2001; 107: 455–460
- Huisman TAGM. Diffusion-weighted imaging: basic concepts and application in cerebral stroke and head trauma. *Eur Radiol* 2003; 13: 2283–2297
- Igarashi H, Katayama Y, Tsuganezawa T, Yamamuro M, Terashi A, Owan C. Three-dimensional anisotropy contract (3DAC) magnetic resonance imaging of the human brain: application to assess wallerian degeneration. *Intern Med* 1998; 37: 662–668

- Iizuka T, Sakai F, Kan S, Suzuki N. Slowly progressive spread of the stroke-like lesions in MELAS. *Neurology* 2003; 61: 1238–1244
- Inder T, Huppi PS, Zientara GP, Maier SE, Jolensz FA, di Salvo D, Robertson R, Barnes PD, Volpe JJ. Early detection of periventricular leukomalacia by diffusion-weighted magnetic resonance imaging techniques. *J Pediatr* 1999; 134: 631–634
- Ito R, Melhem ER, Mori S, Eichler FS, Raymond GV, Moser HW. Diffusion tensor brain MR imaging in X-linked cerebral adrenoleukodystrophy. *Neurology* 2001; 56: 544–547
- Ito R, Mori S, Melhem ER. Diffusion tensor brain imaging and tractography. *Neuroimaging Clin N Am* 2002; 12: 1–19
- Jan W, Zimmerman RA, Wang ZJ, Berry GT, Kaplan PB, Kaye EM. MR diffusion imaging and MR spectroscopy of maple syrup urine disease during acute metabolic decompensation. *Neuroradiology* 2003; 45: 393–399
- Jones DK, Simmons A, Williams SCR, Horsfield MA. Non-invasive assessment of axonal fiber connectivity in the human brain via diffusion tensor MRI. *Magn Reson Med* 1999; 42: 37–41
- Khong P-L, Lam BCC, Chung BHY, Wong CK-Y, Ooi G-C. Diffusion-weighted MR imaging in neonatal nonketotic hyperglycemia. *AJNR Am J Neuroradiol* 2003; 24: 1181–1183
- Kim H-S, Kim D-I, Lee B-I, Jeong E-K, Choi C, Lee JD, Yoon P-H, Kim E-J, Kim S-H, Yoon YK. Diffusion weighted image and MR spectroscopic analysis of a case of MELAS with repeated attacks. *Yonsei Med J* 2001; 42: 128–133
- Le Bihan D. Diffusion, perfusion MR imaging of the brain: from structure to function. *Radiology* 1990; 177: 328–329
- Le Bihan D, Breton E, Lallamand D, Desbleds MT, Aubin ML, Vignaud J, Roger B. Contribution of intravoxel incoherent motion (IVIM) imaging to neuroradiology. *J Neuroradiol* 1987; 14: 295–312
- Le Bihan D, Breton E, Lallemand D, Aubin M-L, Vignaud J, Laval-Jeantet M. Separation of diffusion and perfusion in intravoxel incoherent motion MR imaging. *Radiology* 1988; 168: 497–505
- Le Bihan D, Mangin J-F, Poupon C, Clark CA, Pappata S, Molko N, Chabriat H. Diffusion tensor imaging: concepts and applications. *J Magn Reson Imaging* 2001; 13: 534–546
- Makris N, Worth AJ, Sorensen AG, Papadimitriou GM, Wu O, Reese TG, Wedeen VJ, Davis TL, Stakes JW, Caviness VS, Kaplan E, Rosen BR, Pandya DN, Kennedy DN. Morphometry of in vivo human white matter association pathways with diffusion-weighted magnetic resonance imaging. *Ann Neurol* 1997; 42: 951–962
- Mazumdar A, Mukherjee P, Miller JH, Malde H, McKinstry RC. Diffusion-weighted imaging of acute corticospinal tract injury preceding Wallerian degeneration in the maturing human brain. *AJNR Am J Neuroradiol* 2003; 24: 1057–1066
- McGraw P, Liang L, Provenzale JM. Evaluation of normal age-related changes in anisotropy during infancy and childhood as shown by diffusion tensor imaging. *AJR Am J Roentgenol* 2002; 179: 1515–1522
- Miller DH, Thompson AJ, Filippi M. Magnetic resonance studies of abnormalities in the normal appearing white matter and gray matter in multiple sclerosis. *J Neurol* 2003; 250: 1407–1419
- Miller JH, McKinstry RC, Philip JV, Mukherjee P, Neil JJ. Diffusion-tensor MR imaging of normal brain maturation: a guide to structural development and myelination. *AJR Am J Roentgenol* 2003; 180: 851–859
- Miller SP, Vigneron DB, Henry RG, Bohland MA, Ceppi-Cozzio C, Hoffman C, Newton N, Patridge JC, Ferriero DM, Barkovich AJ. Serial quantitative diffusion tensor MRI of the premature brain: development in newborn with and without injury. *J Magn Reson Imaging* 2002; 16: 621–632
- Mori S, Crain BJ, Chacko VP, van Zijl PCM. Three-dimensional tracking of axonal projections in the brain by magnetic resonance imaging. *Ann Neurol* 1999; 45: 265–269
- Mori S, Itoh R, Zhang J, Kaufmann WE, van Zijl PCM, Solaiyappan M, Yarowsky P. Diffusion tensor imaging of the developing mouse brain. *Magn Reson Med* 2001; 46: 18–23
- Mori S, van Zijl PCM. Fiber tracking: principles and strategies – a technical review. *NMR Biomed* 2002; 15: 468–480
- Moseley ME, Cohen Y, Kucharczyk J, Mintotovich J, Asgari HS, Wendland MF, Tsuruda J, Norman D. Diffusion weighted MR imaging of anisotropic water diffusion in cat central nervous system. *Radiology* 1990; 176: 439–445
- Mukherjee P, Miller JH, Shimony JS, Conturo TE, Lee PCP, Almlí CR, McKinstry RC. Normal brain maturation during childhood: developmental trends characterized with diffusion-tensor MR imaging. *Radiology* 2001; 221: 349–358
- Mukherjee P, Miller JH, Shimony JS, Philip JV, Nehra D, Snyder AZ, Conturo TE, Neil JJ, McKinstry RC. Diffusion-tensor MR imaging of gray and white matter development during normal human brain maturation. *AJNR Am J Neuroradiol* 2002; 23: 1445–1456
- Neil JJ, Shiran SI, McKinstry RC, Scheffé GL, Snyder AZ, Almlí CR, Akbudak E, Aronovitz JA, Miller JP, Lee BCP, Conturo TE. Normal brain in human newborns: apparent diffusion coefficient and diffusion anisotropy measured by using diffusion tensor MR imaging. *Radiology* 1998; 209: 57–66
- Nusbaum AO, Tang CK, Bushbaum MS, Wei TC, Atlas SW. Regional and global changes in cerebral diffusion with normal aging. *AJNR Am J Neuroradiol* 2001; 22: 136–142
- Ohshita T, Oka M, Imon Y, Wanatabe C, Katayama C, Yamaguchi S, Kajima T, Mimori Y, Nakamura S. Serial diffusion-weighted imaging in MELAS. *Neuroradiology* 2000; 42: 651–656
- Ono J, Harada K, Sakurai K, Kodaka R, Shimidzu N, Tanaka J, Nagai T, Okada S. MR diffusion imaging in Pelizaeus-Merzbacher disease. *Brain Dev* 1994; 16: 219–223
- Ono J, Harada K, Mano T, Sakurai K, Okada S. Differentiation of dys- and demyelination using diffusional anisotropy. *Pediatr Neurol* 1997; 16: 63–66
- Oppenheim C, Galanoud D, Samson Y, Sahel M, Dormont D, Wechsler B, Marsault C. Can diffusion weighted magnetic resonance imaging help differentiate stroke from stroke-like events in MELAS? *J Neurol Neurosurg Psychiatry* 2000; 69: 248–250
- Prayer D, Barkovich J, Kirschner DA, Prayer LM, Roberts TPL, Kucharczyk J, Moseley ME. Visualization of nonstructural changes in early white matter development on diffusion-weighted MR images: evidence supporting premyelination anisotropy. *AJNR Am J Neuroradiol* 2001; 22: 1572–1576
- Rovaris M, Bozzali M, Iannucci G, Ghezzi A, Caputo D, Montanari E, Bertolotto A, Bergamaschi R, Capra R, Mancardi GL, Martinelli V, Comi G, Filippi M. Assessment of normal-appearing white and gray matter in patients with primary progressive multiple sclerosis. A diffusion-tensor magnetic resonance imaging study. *Arch Neurol* 2002; 59: 1406–1412
- Roychowdhury S, Maldjian JA, Grossman RI. Multiple sclerosis: comparison of trace apparent diffusion coefficients with MR enhancement patterns of lesions. *AJNR Am J Neuroradiol* 2000; 21: 869–874

- Scanderberg AC, Tomaiuolo F, Sabatini U, Nocentini U, Grasso MG, Caltagirone C. Demyelination plaques in relapsing-remitting and secondary-progressive multiple sclerosis: assessment with diffusion MR imaging. *AJNR Am J Neuroradiol* 2000; 21:862–868
- Schaefer PW, Grant PE, Gonzalez RG. Diffusion-weighted MR imaging of the brain. *Radiology* 2000; 217: 331–345
- Schneider JFL, Il'yasov KA, Boltshauser E, Hennig J, Martin E. Diffusion tensor imaging in cases of adrenoleukodystrophy: preliminary experience as a marker for early demyelination? *AJNR Am J Neuroradiol* 2003; 24: 819–824
- Schneider JFL, Il'yasov KA, Hennig J, Martin E. Fast quantitative diffusion-tensor imaging of cerebral white matter from the neonatal period to adolescence. *Neuroradiology* 2004; 46: 258–266
- Sundgren PC, Evarsson B, Holtås S. Serial investigation of perfusion disturbances and vasogenic oedema in hypertensive encephalopathy by diffusion and perfusion weighted imaging. *Neuroradiology* 2002; 44: 299–304
- Uluğ AM, Moore DF, Bojko AS, Zimmerman RD. Clinical use of diffusion-tensor imaging for diseases causing neuronal and axonal damage. *AJNR Am J Neuroradiol* 1999; 20: 1044–1048
- Virta A, Barnett A, Pierpaoli C. Visualizing and characterizing white matter fiber structure and architecture in the human pyramidal tract using diffusion tensor MRI. *Magn Reson Imaging* 1999; 17: 1121–1133
- Wakana S, Jiang H, Nagae-Poetscher LM, van Zijl PCM, Mori S. Fiber tract-based atlas of human white matter anatomy. *Radiology* 2004; 230: 77–87
- Wang XY, Noguchi K, Takashima S, Hayashi N, Ogawa S, Seto H. Serial diffusion-weighted imaging in a patient with MELAS and presumed cytotoxic oedema. *Neuroradiology* 2003; 45: 640–643
- Westin C-F, Maier SE, Mamata H, Nabavi A, Jolesz FA, Kikinis R. Processing and visualization for diffusion tensor MRI. *Med Imaging Anal* 2002; 6: 93–108
- Wiegel MR, Larsson HBW, Wedeen VJ. Fiber crossing in human brain depicted with diffusion tensor MR imaging. *Radiology* 2000; 217: 897–903
- Wilson M, Morgan PS, Lin X, Turner BP, Blumhardt LD. Quantitative diffusion weighted magnetic resonance imaging, cerebral atrophy, and disability in multiple sclerosis. *J Neurol Neurosurg Psychiatry* 2001; 70: 318–322
- Yoneda M, Maeda M, Kimura H, Fujii A, Katayama K, Kiruyama M. Vasogenic edema on MELAS: a serial study with diffusion-weighted MR imaging. *Neurology* 1999; 53: 2182–2184
- Yonemura K, Hasegawa Y, Kimura K, Minematsu K, Yamaguchi T. Diffusion-weighted MR imaging in a case of mitochondrial myopathy, encephalopathy, lactic acidosis, and stroke-like episodes. *AJNR Am J Neuroradiol* 2001; 22: 269–272
- Zhai G, Lin W, Wilber KP, Gerig G, Gilmore JH. Comparisons of regional white matter diffusion in healthy neonates and adults performed with 3.0-T head-only MR imaging unit. *Radiology* 2003; 229: 673–681
- Berry I, Barker GJ, Barkhof F, Campi A, Dousset V, Franconi J-M, Gass A, Schreiber W, Miller DH, Tofts PS. A multicenter measurement of magnetization transfer ratio in normal white matter. *J Magn Reson Imaging* 1999; 9: 441–446
- Dehmshki J, Silver NC, Leary SM, Tofts PS, Thompson AJ, Miller DH. Magnetization transfer ratio histogram analysis of primary progressive and other multiple sclerosis subgroups. *J Neurol Sci* 2001; 185: 11–17
- Dousset V, Grossman RI, Ramer KN, Schnall MD, Young LH, Gonzalez-Scarano F, Lavi E, Cohen JA. Experimental allergic encephalomyelitis and multiple sclerosis: lesion characterization with magnetization transfer imaging. *Radiology* 1992; 182: 483–491
- Dousset V, Armand J-P, Lacoste D, Miège S, Letenneur L, Dartigues J-F, Caillé J-M. Magnetization transfer study of HIV encephalitis and progressive multifocal leukoencephalopathy. *AJNR Am J Neuroradiol* 1997; 18: 895–901
- Eng J, Ceckler TL, Balaban RS. Quantitative ¹H magnetization transfer imaging in vivo. *Magn Reson Med* 1991; 17: 304–314
- Engelbrecht V, Rassek M, Preiss S, Wald C, Mödder U. Age-dependent changes in magnetization transfer contrast of white matter in the pediatric brain. *AJNR Am J Neuroradiol* 1998; 19: 1923–1929
- Ernst T, Chang L, Witt M, Walot I, Aronow H, Leonido-Yee M, Singer E. Progressive multifocal leukoencephalopathy and human immunodeficiency virus-associated white matter lesions in AIDS: magnetization transfer MR imaging. *Radiology* 1999; 210: 539–543
- Filippi M. Magnetization transfer imaging to monitor the evolution of individual multiple sclerosis lesions. *Neurology* 1999; 53: S18–S22
- Filippi M, Rovaris M. Magnetization transfer imaging in multiple sclerosis. *J Neurovirol* 2000; 6: s115–s120
- Filippi M, Iannucci G, Tortorella C, Minicucci L, Horsfield MA, Colombo B, Sormani MP, Comi G. Comparison of MS clinical phenotypes using conventional and magnetization transfer MRI. *Neurology* 1999; 52: 588–594
- Filippi M, Rocca MA, Minicucci L, Martinelli V, Ghezzi A, Bergamaschi R, Comi G. Magnetization transfer imaging of patients with definite MS and negative conventional MRI. *Neurology* 1999; 52: 845–848
- Finelli DA. Magnetization transfer in neuroimaging. *MRI Clin North Am* 1998; 6: 31–52
- Fralix TA, Ceckler TL, Wolff SD, Simon SA, Balaban RS. Lipid bilayer and water proton magnetization transfer: effect of cholesterol. *Magn Reson Med* 1991; 18: 214–223
- Ge Y, Grossman RI, Udupa JK, Babb JS, Kolson DL, McGowan JC. Magnetization transfer ratio histogram analysis of gray matter in relapsing-remitting multiple sclerosis. *AJNR Am J Neuroradiol* 2001; 22: 470–475
- Graham SJ, Henkelman RM. Understanding pulsed magnetization transfer. *J Magn Reson Imaging* 1997; 7: 903–912
- Grossman RI, McGowan JC. Perspectives on multiple sclerosis. *AJNR Am J Neuroradiol* 1998; 19: 1251–1265
- Hähnel S, Munkel K, Jansen O, Heiland S, Reidel M, Freund M, Aschoff A, Sartor K. Magnetization transfer measurements in normal-appearing cerebral white matter in patients with chronic obstructive hydrocephalus. *J Comput Assist Tomogr* 1999; 23: 516–520
- Henkelman RM, Stanisz GJ, Graham SJ. Magnetization transfer in MRI: a review. *NMR Biomed* 2001; 14: 57–64
- Kaiser JS, Grossman RI, Udupa JK, Miki Y, Galetta SL. Magnetization transfer histogram analysis of monosymptomatic episodes of neurologic dysfunction: preliminary findings. *AJNR Am J Neuroradiol* 2000; 21: 1043–1047

107 Magnetization Transfer

- Balaban RS, Ceckler TL. Magnetization transfer contrast in magnetic resonance imaging. *Magn Res Q* 1992; 8: 116–137

- Kalkers NF, Hintzen RQ, van Waesberghe JHTM, Lazeron RHC, van Schijndel RA, Adèr HJ, Polman CH, Barkhof F. Magnetization transfer histogram parameters reflect all dimensions of MS pathology, including atrophy. *J Neurol Sci* 2001; 184: 155–162
- Kato Y, Matsumura K, Kinoshita Y, Narita Y, Kuzuhara S, Nakagawa T. Detection of pyramidal tract lesions in amyotrophic lateral sclerosis with magnetization-transfer measurements. *AJNR Am J Neuroradiol* 1997; 18: 1541–1547
- Kita M, Goodkin DE, Bacchetti P, Waubant E, Nelson SJ, Majumdar S. Magnetization transfer ratio in new MS lesions before and during therapy with IFN β -1a. *Neurology* 2000; 54: 1741–1745
- Koenig SH. Cholesterol of myelin is the determinant of gray-white contrast in MRI of brain. *Magn Reson Med* 1991; 20: 285–291
- Koenig SH, Brown RD III, Spiller M, Lundbom N. Relaxometry of brain: why white matter appears bright in MRI. *Magn Reson Med* 1990; 14: 482–495
- Kucharczyk W, Macdonald PM, Stanisz GJ, Henkelman RM. Relaxivity and magnetization transfer of white matter lipids at MR imaging: importance of cerebrospines and pH. *Radiology* 1994; 192: 521–529
- Lexa FJ, Grossman RI, Rosenquist AC. MR of wallerian degeneration in the feline visual system: characterization by magnetization transfer rate with histopathologic correlation. *AJNR Am J Neuroradiol* 1994; 15: 201–212
- MacKay A, Whittall K, Adler J, Li D, Paty D, Graeb D. In vivo visualization of myelin water in brain by magnetic resonance. *Magn Reson Med* 1994; 31: 673–677
- McGowan JC. Magnetic resonance imaging and magnetization transfer. *Adv Imaging Electron Phys* 2001; 118: 1–83
- McGowan JC, Filippi M, Campi A, Grossman RI. Magnetization transfer imaging: theory and application to multiple sclerosis. *J Neurol Neurosurg Psychiatry* 1998; 64: s66–s69
- Mehta RC, Pike B, Enzmann DR. Magnetization transfer MR of the normal adult brain. *AJNR Am J Neuroradiol* 1995; 16: 2085–2091
- Melhem ER, Breiter SN, Ulug AM, Raymond GV, Moser HW. Improved tissue characterization in adrenoleukodystrophy using magnetization transfer imaging. *AJR Am J Roentgenol* 1996; 166: 689–695
- Meyer JR, Androux RW, Salamon N, Rabin B, Callahan C, Parrish TB, Prager J, Russell EJ. Contrast-enhanced magnetization transfer MR of the brain: importance of precontrast images. *AJNR Am J Neuroradiol* 1997; 18: 1515–1521
- Ostuni JL, Richert ND, Lewis BK, Frank JA. Characterization of differences between multiple sclerosis and normal brain: a global magnetization transfer application. *AJNR Am J Neuroradiol* 1999; 20: 501–507
- Phillips MD, Grossman RI, Miki Y, Wei L, Kolson DL, van Buchem MA, Polansky M, McGowan JC, Udupa JK. Comparison of T2 lesion volume and magnetization transfer ratio histogram analysis and of atrophy and measures of lesion burden in patients with multiple sclerosis. *AJNR Am J Neuroradiol* 1998; 19: 1055–1060
- Pike GB, de Stephano N, Narayanan S, Worsely KJ, Pelletier D, Francis GS, Antel JP, Arnold DL. Multiple sclerosis: magnetization transfer MR imaging of white matter before lesion appearance on T2-weighted images. *Radiology* 2000; 215: 824–830
- Rademacher J, Engelbrecht V, Bürgel U, Freund H-J, Zilles K. Measuring in vivo myelination of human white matter giber tracts with magnetization transfer MR. *Neuroimage* 1999; 9: 393–406
- Richert ND, Ostuni JL, Bash CN, Duyn JH, McFarland HF, Frank JA. Serial whole-brain magnetization transfer imaging in patients with relapsing-remitting multiple sclerosis at baseline and during treatment with interferon beta-1b. *AJNR Am J Neuroradiol* 1998; 19: 1705–1713
- Ropele S, Strasser-Fuchs S, Augustin M, Stollberger R, Enzinger C, Hartung H-P, Fazekas F. A comparison of magnetization transfer ratio, magnetization transfer rate, and the native relaxation time of water protons related to relapsing-remitting multiple sclerosis. *AJNR Am J Neuroradiol* 2000; 21: 1885–1891
- Rovaris M, Horsfield MA, Filippi M. Correlations between magnetization transfer metrics and other magnetic resonance abnormalities in multiple sclerosis. *Neurology* 1999; 53: S40–S45
- Rovaris M, Iannucci G, Cercignani M, Sormani MP, De Stefano N, Gerevini S, Comi G, Filippi M. Age-related changes in conventional, magnetization transfer, and diffusion-tensor MR imaging findings: study with whole-brain tissue histogram analysis. *Radiology* 2003; 227: 731–738
- Sailer M, O'Riordan JI, Thompson AJ, Kingsley DP, MacManus DG, McDonald WI, Millder DH. Quantitative MRI in patients with clinically isolated syndromes suggestive of demyelination. *Neurology* 1999; 52: 599–606
- Santos AC, Narayanan S, de Stefano N, Tartaglia MC, Francis SJ, Aranoutelis R, Caramanos Z, Antel JP, Pike GB, Arnold DL. Magnetization transfer can predict clinical evolution in patients with multiple sclerosis. *J Neurol* 2002; 249: 662–668
- Silver NC, Barker GJ, Miller DH. Standardization of magnetization transfer imaging for multicenter studies. *Neurology* 1999; 53: S33–S39
- Tomiak MM, Rosenblum JD, Prager JM, Metz CE. Magnetization transfer: a potential method to determine the age of multiple sclerosis lesions. *AJNR Am J Neuroradiol* 1994; 15: 1569–1574
- Van Buchem MA, Udupa JK, McGowan JC, Miki Y, Heyning FH, Boncoeur-Martel M-P, Kolson DL, Polansky M, Grossman RI. Global volumetric estimation of disease burden in multiple sclerosis based on magnetization transfer imaging. *AJNR Am J Neuroradiol* 1997; 18: 1287–1290
- Van Buchem MA, Steens SCA, Vrooman HA, Zwinderman AH, McGowan JC, Rassek M, Engelbrecht V. Global estimation of myelination in the developing brain on the basis of magnetization transfer imaging: a preliminary study. *AJNR Am J Neuroradiol* 2001; 22: 762–766
- Van Waesberghe JHTM, van Walderveen MAA, Castelijns JA, Scheltens P, Lycklama à Nijeholt GJ, Polman CH, Barkhof F. Patterns of lesion development in multiple sclerosis: longitudinal observations with T1-weighted spin-echo and magnetization transfer MR. *AJNR Am J Neuroradiol* 1998; 19: 675–683
- Van Waesberghe JHTM, Kamphorst W, de Groot, CJA, van Walderveen MAA, Castelijns JA, Ravid R, Lycklama à Nijeholt GJ, van der Valk P, Polman CH, Thompson AJ, Barkhof F. Axonal loss in multiple sclerosis lesions: magnetic resonance imaging insights into substrates of disability. *Ann Neurol* 1999; 46: 747–754
- Wolff SD, Balaban RS. Magnetization transfer contrast (MTC) and tissue water relaxation in vivo. *Magn Res Med* 1989; 10: 135–144
- Wong KT, Grossman RI, Boorstein JM, Lexa FJ, McGowan JC. Magnetization transfer imaging of periventricular hyperintense white matter in the elderly. *AJNR Am J Neuroradiol* 1995; 16: 253–258

108 Magnetic Resonance Spectroscopy

General

- Bottomley PA. Human in vivo NMR spectroscopy in diagnostic medicine: clinical tool or research probe? *Radiology* 1989; 170: 1–15
- Brooks WM, Friedman SD, Stidley CA. Reproducibility of ^1H -MRS in vivo. *Magn Reson Med* 1999; 41: 193–197
- Castillo M, Kwok L, Mukherji SK. Clinical applications of proton MR spectroscopy. *AJNR Am J Neuroradiol* 1996; 17: 1–15
- Cox IJ. Development and applications of in vivo clinical magnetic resonance spectroscopy. *Prog Biophys Mol Biol* 1996; 65: 45–81
- Kreis R. Quantitative localized ^1H MR spectroscopy for clinical use. *J Progr Nucl Magn Reson Spectr* 1997; 31: 155–195
- Novotny E, Ashwal S, Shevell M. Proton magnetic resonance spectroscopy: an emerging technology in pediatric neurology research. *Pediatr Res* 1998; 44: 1–10
- Provencher SW. Estimation of metabolite concentrations from localized in vivo proton NMR spectra. *Magn Reson Med* 1993; 30: 672–679
- Ross B, Bluml S. Magnetic resonance spectroscopy of the human brain. *Anat Rec [New Anat]* 2001; 265: 54–84
- Simmons A, Smail M, Moore E, Williams SCR. Serial precision of the metabolic peak area ratios and water referenced metabolite peak areas in proton MR spectroscopy of the human brain. *Magn Reson Imaging* 1998; 16: 319–330
- Tedeschi G, Bertolino A, Campbell G, Barnett AS, Duyn JH, Jacob PK, Moonen CTW, Alger JR, di Chiro G. Reproducibility of proton MR spectroscopy imaging findings. *AJNR Am J Neuroradiol* 1996; 17: 1871–1879
- Van Zijl PCM, Barker PB. Magnetic resonance spectroscopy and spectroscopic imaging for study of brain metabolism. *Ann NY Acad Sci* 1997; 820: 75–96

Normal Age-dependent and Regional Changes

- Azzopardi D, Wyatt JS, Hamilton PA, Cady EB, Delpy DT, Hope PL, Reynolds EOR. Phosphorus metabolites and intracellular pH in the brains of normal and small for gestational age infants investigated by magnetic resonance spectroscopy. *Pediatr Res* 1989; 25: 440–444
- Bluml S, Seymour KJ, Ross BD. Developmental changes in choline- and ethanolamine-containing compounds measured with proton-decoupled ^{31}P MRS in vivo human brain. *Magn Reson Med* 1999; 42: 643–654
- Buchli R, Boesiger MP, Rumpel H. Developmental changes of phosphorus metabolite concentrations in the human brain: a ^{31}P magnetic resonance spectroscopy study in vivo. *Pediatr Res* 1994; 35: 431–435
- Buchli R, Duc CO, Martin E, Boesiger P. Assessment of absolute metabolite concentrations in human tissue by ^{31}P MRS in vivo. 1. Cerebrum, cerebellum, cerebellar gray and white matter. *Magn Reson Med* 1994; 32: 447–452
- Filippi CG, Uluğ AM, Deck MDF, Zimmerman RD, Heier LA. Developmental delay in children: assessment with proton MR spectroscopy. *AJNR Am J Neuroradiol* 2002; 23: 882–888
- Hanaoka S, Takashima S, Morooka K. Study of the maturation of the child's brain using ^{31}P -MRS. *Pediatr Neurol* 1998; 18: 305–310

- Horská A, Kaufmann WE, Brant LJ, Naidu S, Harris JC, Barker PB. In vivo quantitative proton MRSI study of brain development from childhood to adolescence. *J Magn Reson Imaging* 2002; 15: 137–143
- Hüppi PS, Fusch C, Boesch C, Burri R, Bossi E, Amato M, Herschkowitz N. Regional metabolic assessment of human brain during development by proton magnetic resonance spectroscopy in vivo and high-performance liquid chromatography/gas chromatography in autopsy tissue. *Pediatr Res* 1995; 37: 145–150
- Jacobs MA, Horská A, van Zijl PCM, Barker PB. Quantitative proton MR spectroscopy imaging of normal human cerebellum and brain stem. *Magn Reson Med* 2001; 46: 699–705
- Kok RD, van den Berg PP, van den Bergh AJ, Nijland R, Heerschap A. Maturation of the human fetal brain as observed by ^1H MR spectroscopy. *Magn Reson Med* 2002; 48: 611–616
- Kreis R, Ernst T, Ross BD. Development of the human brain: *in vivo* quantification of metabolite and water content with proton magnetic resonance spectroscopy. *Magn Reson Med* 1993; 30: 424–437
- Kreis R, Hofmann L, Kuhlmann B, Boesch C, Bossi E, Hüppi PS. Brain metabolite composition during early human brain development as measured by quantitative in vivo ^1H magnetic resonance spectroscopy. *Magn Reson Med* 2002; 48: 949–958
- Lam WWM, Wang ZJ, Zhao H, Berry GT, Kaplan P, Gibson J, Kaplan BS, Bilaniuk LT, Hunter JV, Haselgrove JC, Zimmermann RA. ^1H MR Spectroscopy of the basal ganglia in childhood: a semiquantitative analysis. *Neuroradiology* 1998; 40: 315–323
- Mader I, Seeger U, Karitzky J, Erb M, Schick F, Klose U. Proton magnetic resonance spectroscopy with metabolite nulling reveals regional differences of macromolecules in normal human brain. *J Magn Reson Imaging* 2002; 16: 538–546
- Mascalchi M, Burgnoli R, Guerrini L, Belli G, Nistri M, Politi LS, Gavazzi C, Lolli F, Argenti G, Villari N. Single-voxel long TE ^1H -MR spectroscopy of the normal brainstem and cerebellum. *J Magn Reson Imaging* 2002; 16: 532–537
- McLean MA, Woermann FG, Barker GJ, Duncan JS. Quantitative analysis of short echo time ^1H -MRSI of cerebellar gray and white matter. *Magn Reson Med* 2000; 44: 401–411
- Nakada T, Kwee IL. ^{31}P localized spectroscopy of fetal brain in utero. *Magn Reson Med* 1993; 29: 122–124
- Pouwels PJW, Frahm J. Regional metabolite concentrations in human brain as determined by quantitative localized proton MRS. *Magn Reson Med* 1998; 39: 53–60
- Pouwels PJW, Brockmann K, Kruse B, Wilken B, Wick M, Hanefeld F, Frahm J. Regional age dependence of human brain metabolites from infancy to adulthood as detected by quantitative localized proton MRS. *Pediatr Res* 1999; 46: 474–485
- Provencher SW. Estimation of metabolite concentrations from localized in vivo proton NMR spectra. *Magn Reson Med* 1993; 30: 672–679
- Tedeschi G, Bertolino A, Righini A, Campbell G, Raman R, Duyn JH, Moonen CTW, Alger JR, di Chiro G. Brain regional distribution pattern of metabolite signal intensities in young adults by proton magnetic resonance spectroscopy imaging. *Neurology* 1995; 45: 1384–1391
- Toft PB, Leth H, Lou HC, Pryds O, Henriksen O. Metabolite concentrations in the developing brain estimated with proton MR spectroscopy. *J Magn Reson Imaging* 1994; 4: 674–680

- van der Knaap MS, van der Grond J, van Rijen PC, Faber JAJ, Valk J, Willemsse K. Age-dependent changes in localized proton and phosphorus MR spectroscopy of the brain. *Radiology* 1990; 176: 509–515
- Vigneron DB, Barkovich AJ, Noworolski SM, von dem Busche M, Henry RG, Lu Y, Partridge JC, Gregory G, Ferriero DM. Three-dimensional proton MR spectroscopic imaging of prematurity and term neonates. *AJNR Am J Neuroradiol* 2001; 22: 1424–1433

Metabolites: General

- Bhakoo KK, Williams IT, Williams SR, Gadian DG, Noble MD. Proton nuclear magnetic resonance spectroscopy of primary cells derived from nervous tissue. *J Neurochem* 1996; 66: 1254–1263
- Govindaraju V, Young K, Mandsley AA. Proton NMR chemical shifts and coupling constants for brain metabolites. *NMR Biomed* 2000; 13: 129–153
- Michaelis T, Merboldt KD, Hänicke W, Gyngell ML, Bruhn H, Frahm J. On the identification of cerebral metabolites in localized ^1H NMR spectra of human brain in vivo. *NMR Biomed* 1991; 4: 90–98
- Urenjak J, Williams SR, Gadian DG, Noble M. Proton nuclear magnetic resonance spectroscopy unambiguously identifies different neural cell types. *J Neurosci* 1993; 13: 981–989

Phosphomonoester / Phosphodiester

- Daly PF, Lyon RC, Faustino PJ, Cohen JS. Phospholipid metabolism in cancer cells monitored by ^{31}P NMR spectroscopy. *J Biol Chem* 1987; 262: 14875–14878
- Dawson RMC. Enzymic pathways of phospholipid metabolism in the nervous system. In: Eichberg J, ed. *Phospholipids in nervous tissues*. New York: Wiley, 1985, pp 45–78
- Gyulai L, Bolinger L, Leigh JS Jr, Barlow C, Chance B. Phosphorylethanolamine – the major constituent of the phosphomonoester peak observed by ^{31}P -NMR on developing dog brain. *FEBS Lett* 1984; 178: 137–142
- Kilby PM, Bolas NM, Radda GK. ^{31}P -NMR study of brain phospholipid structures in vivo. *Biochim Biophys Acta* 1991; 1085: 257–264
- McNamara R, Arias-Mendoza F, Brown TR. Investigation of broad resonances in ^{31}P NMR spectra of the human brain in vivo. *NMR Biomed* 1994; 7: 237–242
- Murphy EJ, Rajagopalan B, Brindle KM, Radda GK. Phospholipid bilayer contribution to ^{31}P NMR spectra in vivo. *Magn Reson Med* 1989; 12: 282–289
- Porcellati G, Arienti G. Metabolism of phosphoglycerides. In: Lajtha A, ed. *Handbook of neurochemistry*, vol 3: Metabolism in the nervous system. New York, Plenum Press: 1983, pp 133–161
- Stanley JA, Pettegrew JW. Postprocessing method to segregate and quantify the broad components underlying the phosphodiester spectral region of in vivo ^{31}P brain spectra. *Magn Reson Med* 2001; 45: 390–396
- Sun GY, Foudin LL. Phospholipid composition and metabolism in the developing and aging nervous system. In: Eichberg J, ed. *Phospholipids in nervous tissues*. New York: Wiley, 1985, pp 79–134
- Van der Grond J, Dijkstra G, Roelofsen B, Mali WPTM. ^{31}P -NMR determination of phosphomonoesters in relation to phospholipid biosynthesis in testis of the rat at different ages. *Biochim Biophys Acta* 1991; 1074: 189–194

pH

- Madden A, Leach MO, Sharp JC, Collins DJ, Easton D. A quantitative analysis of the accuracy of in vivo pH measurements with ^{31}P NMR spectroscopy: assessment of pH measurement methodology. *NMR Biomed* 1991; 4: 1–11
- Moon RB, Richards JH. Determination of intracellular pH by ^{31}P magnetic resonance. *J Biol Chem* 1973; 248: 7276–7278
- Petroff OAC, Prichard JW, Behar KL, Alger JR, den Hollander JA, Shulman RG. Cerebral intracellular pH by ^{31}P nuclear magnetic resonance spectroscopy. *Neurology* 1985; 35: 781–788
- Pettegrew JW, Withers G, Panchalingham K, Post JFM. Considerations for brain pH assessment by ^{31}P NMR. *Magn Reson Imaging* 1988; 6: 135–142

N-Acetylaspartate

- Baslow MH. Functions of *N*-acetyl-L-aspartate and *N*-acetyl-L-aspartylglutamate in the vertebrate brain: role in glial cell-specific signaling. *J Neurochem* 2000; 75: 453–459
- Baslow MH. *N*-Acetylaspartate in the vertebrate brain: metabolism and function. *Neurochem Res* 2003; 28: 941–953
- Bates TE, Strangward M, Keelan J, Davey GP, Munro PMG, Clark JB. Inhibition of *N*-acetylaspartate production: implications for ^1H MRS studies in vivo. *Neuroreport* 1996; 7: 1397–1400
- Bhakoo KK, Pearce D. In vitro expression of *N*-acetyl aspartate by oligodendrocytes: implications for proton magnetic resonance spectroscopy signal in vivo. *J Neurochem* 2000; 74: 254–262
- Birken DL, Oldendorf WH. *N*-acetyl-L-aspartic acid: a literature review of a compound prominent in ^1H -NMR spectroscopic studies of brain. *Neurosci Biobehav Rev* 1989; 13: 23–31
- Bjartmar C, Battistuta J, Terada N, Dupree E, Trapp BD. *N*-Acetylaspartate is an axon-specific marker of mature white matter in vivo: a biochemical and immunohistochemical study on the rat optic nerve. *Ann Neurol* 2002; 51: 51–58
- Block W, Träber, Flacke S, Jessen F, Pohl C, Schild H. In-vivo proton MR-spectroscopy of the human brain: assessment of *N*-acetylaspartate (NAA) reduction as a marker for neurodegeneration. *Amino Acids* 2002; 23: 317–323
- Chakraborty G, Mekala P, Yahya D, Wu G, Ledeen RW. Intraneuronal *N*-acetylaspartate supplies acetyl groups for myelin lipid synthesis: evidence for myelin-associated aspartoacylase. *J Neurochem* 2001; 78: 736–745
- De Stefano N, Matthews PM, Arnold DL. Reversible decreases in *N*-acetylaspartate after acute brain injury. *Magn Reson Med* 1995; 34: 721–727
- Gasparovic C, Arfai N, Smid N, Feeney DM. Decrease and recovery of *N*-acetylaspartate/creatine in rat brain remote from focal injury. *J Neurotrauma* 2001; 18: 241–246
- Patel TB, Clark JB. Synthesis of *N*-acetyl-L-aspartate by rat brain mitochondria and its involvement in mitochondrial/cytosolic carbon transport. *Biochem J* 1979; 184: 539–546
- Pouwels PJW, Frahm J. Differential distribution of NAA and NAAG in human brain as determined by quantitative localized proton MRS. *NMR Biomed* 1997; 10: 73–78
- Tallan HH, Moore S, Stein WH. *N*-Acetyl-L aspartic acid in brain. *J Biol Chem* 1956; 219: 257–264
- Taylor DL, Davies SEC, Obrenovitch TP, Doheny MH, Patsalos PN, Clark JB, Symon L. Investigation into the role of *N*-acetylaspartate in cerebral osmoregulation. *J Neurochem* 1995; 65: 275–281

Urenjak J, Williams SR, Gadian DG, Noble M. Specific expression of *N*-acetylaspartate in neurons, oligodendrocyte-type-2 astrocyte progenitors, and immature oligodendrocytes in vitro. *J Neurochem* 1992; 59: 55–61

Creatine

Chance B, Leigh JS Jr, Clark BJ, Maris J, Kent J, Nioka S, Smith D. Control of oxidative metabolism and oxygen delivery in human skeletal muscle: a steady-state analysis of the work/energy cost transfer function. *Proc Natl Acad Sci* 1985; 82: 8384–8388

Dringen R, Verleysdonk S, Hamprecht B, Willker W, Leibfritz D, Brand A. Metabolism of glycine in primary astroglial cells: synthesis of creatine, serine and glutathione. *J Neurochem* 1998; 70: 835–840

Wyss M, Kaddurah-Daouk R. Creatine and creatinine metabolism. *Physiol Rev* 2000; 80: 1107–1213

Choline

Gupta RK, Cloughesy TF, Sinha U, Garakian J, Lazareff J, Rubino G, Rubino L, Becker DP, Vinters HV, Alger JR. Relationships between choline magnetic resonance spectroscopy, apparent diffusion coefficient and quantitative histopathology in human glioma. *J Neurooncol* 2000; 50: 215–226

Miller BL. A review of chemical issues in ¹H NMR spectroscopy: *N*-acetyl-L-aspartate, creatine and choline. *NMR Biomed* 1991; 4: 47–52

Miller BL, Chang L, Booth R, Ernst T, Conford M, Nikas D, McBride D, Jenden DJ. In vivo ¹H MRS choline: correlation with in vivo chemistry/histology. *Life Sci* 1996; 58: 1929–1935

Myo-inositol

Brand A, Richter-Landsberg C, Leibfritz D. Multinuclear NMR studies on the energy metabolism of glial and neuronal cells. *Dev Neurosci* 1993; 15: 289–298

Glanville NT, Byers DM. Differences in the metabolism of inositol. *Biochim Biophys Acta* 1989; 104: 169–179

Häussinger D, Laubenberger J, vom Dahl S, Ernst T, Bayer S, Langer M, Gerok W, Hennig J. Proton magnetic resonance spectroscopy studies on human brain myo-inositol in hypo-osmolarity and hepatic encephalopathy. *Gastroenterology* 1994; 107: 1475–1480

Lee JH, Arginue E, Ross BD. Brief report: organic osmolytes in the brain of an infant with hyponatremia. *N Engl J Med* 1994; 331: 439–442

Michaelis T, Helms G, Merboldt KD, Hänicke W, Bruhn H, Frahm J. Identification of *scyllo*-inositol in proton NMR spectra of human brain in vivo. *NMR Biomed* 1993; 6: 105–109

Ross BD. Biochemical considerations in ¹H spectroscopy. Glutamate and glutamine; myo-inositol and related metabolites. *NMR Biomed* 1991; 4: 59–63

Rumpel H, Lim WEH, Chang HM, Chan LL, Ho GL, Wong MC, Tan KP. Is myo-inositol a measure of glial swelling after stroke? A magnetic resonance study. *J Magn Reson Imaging* 2003; 17: 11–19

Seaquist ER, Gruetter R. Identification of a high concentration of *scyllo*-inositol in the brain of a healthy human subject using ¹H- and ¹³C-NMR. *Magn Reson Med* 1998; 39: 313–316

Shonk T, Ross BD. Role of increased cerebral myo-inositol in the dementia of Down syndrome. *Magn Reson Med* 1995; 33: 858–861

Videen JS, Michaelis T, Pinto P, Ross BD. Human cerebral osmolytes during chronic hyponatremia. A proton magnetic resonance spectroscopy study. *J Clin Invest* 1995; 95: 788–793

Lactate

López-Villegas D, Lenkinski RE, Wehrli SL, Ho W-Z, Douglas SD. Lactate production by human monocytes / macrophages determined by proton MR spectroscopy. *Magn Reson Med* 1995; 34: 32–38

Petroff OAC, Graham GD, Blamire AM, Al-Rayess M, Rothman DL, Fayad PB, Brass LM, Shulman RG, Prichard JW. Spectroscopic imaging of stroke in humans: histopathology correlates of spectral changes. *Neurology* 1992; 42: 1349–1354

Prichard JW. What the clinician can learn from MRS lactate measurements. *NMR Biomed* 1991; 4: 99–102

Veech RL. The metabolism of lactate. *NMR Biomed* 1991; 4: 53–58

Glucose

Gruetter R, Rothman DL, Novotny EJ, Shulman GI, Prichard JW, Shulman RG. Detection and assignment of the glucose signal in ¹H NMR difference spectra of the human brain. *Magn Reson Med* 1992; 27: 183–188

Gruetter R, Novotny EJ, Boulware SD, Rothman DL, Shulman RG. ¹H NMR Studies of glucose transport in the human brain. *J Cereb Blood Flow Metab* 1996; 16: 427–438

Rothman DL. Studies of metabolic compartmentation and glucose transport using in vivo MRS. *NMR Biomed* 2001; 14: 149–160

Glutamine / Glutamate / GABA

Chamuleau RAFM, Bosman DK, Bové WMMJ, Luyten PR, den Hollander JA. What the clinician can learn from MR glutamine/glutamate assays. *NMR Biomed* 1991; 4: 103–108

Govindaraju V, Basus VJ, Matson GB, Maudsley AA. Measurement of chemical shifts and coupling constants for glutamate and glutamine. *Magn Reson Med* 1998; 39: 1011–1013

Keltner JR, Wald LL, Frederick BB, Renshaw PF. In vivo detection of GABA in human brain using a localized double-quantum filter technique. *Magn Reson Med* 1997; 37: 366–371

Ross BD. Biochemical considerations in ¹H spectroscopy. Glutamate and glutamine; myo-inositol and related metabolites. *NMR Biomed* 1991; 4: 59–63

Rothman DL, Hanstock CC, Petroff OAC, Novotny EJ, Prichard JW, Shulman RG. Localized ¹H NMR spectra of glutamate in the human brain. *Magn Reson Med* 1992; 25: 94–106

Sonnenwald U, Westergaard N, Schousboe A, Svendsen JS, Unsgaard G, Peterson SB. Direct demonstration by [¹³C]NMR spectroscopy that glutamine from astrocytes is a precursor for GABA synthesis in neurons. *Neurochem Int* 1993; 22: 19–29

Sonnenwald U, Westergaard N, Shousboe A. Glutamate transport and metabolites in astrocytes. *Glia* 1997; 21: 56–63

Taurine

- Hardy DL, Norwood TJ. Spectral editing technique for the *in vitro* and *in vivo* detection of taurine. *Nucl Magn Reson* 1998; 133: 70–78
- Trenkner E, Sturman JA. The role of taurine in the survival and function of cerebral cells in cultures of early postnatal cat. *Int J Dev Neurosci* 1991; 9: 77–88

Neuronal Degeneration

- Block W, Karitzky J, Träber F, Pohl C, Keller E, Mundegar R, Lamerichs R, Rink H, Ries F, Schild HH, Jerusalem F. Proton magnetic resonance spectroscopy of the primary motor cortex in patients with motor neuron disease. *Arch Neurol* 1998; 55: 931–936
- Brockmann K, Pouwels PJW, Christen H-J, Frahm J, Hanefeld F. Localized proton magnetic resonance spectroscopy of cerebral metabolic disturbances in children with neuronal ceroid lipofuscinosis. *Neuropediatrics* 1996; 27: 242–248
- Chan S, Shungu DC, Douglas-Akinwande A, Lange DJ, Rowland LP. Motor neuron diseases: comparison of single-voxel proton MR spectroscopy of the motor cortex with MR imaging of the brain. *Radiology* 1999; 212: 763–769
- Ellis CM, Simmons A, Andrews C, Dawson JM, Williams SCR, Leigh PN. A proton magnetic resonance spectroscopy study in ALS. Correlation with clinical findings. *Neurology* 1998; 51: 1104–1109
- Frederico F, Simone IL, Lucivero V, de Mari M, Gianinni P, Illiceto G, Mezzapesa DM, Lamberti P. Proton magnetic resonance spectroscopy in Parkinson's disease and progressive supranuclear palsy. *J Neurol Neurosurg Psychiatry* 1997; 62: 239–242
- Miyazaki M, Hashimoto T, Yonada Y, Tayama M, Harada M, Miyoshi H, Kawano N, Murayama N, Kondo I, Kuroda Y. Proton magnetic resonance spectroscopy on childhood-onset dentatorubral-pallidoluysian atrophy (DRPLA). *Brain Dev* 1996; 18: 142–146
- Rooney WD, Miller RG, Gelinas D, Schuff N, Maudsley AA, Weiner MW. Decreased *N*-acetylaspartate in motor cortex and corticospinal tract in ALS. *Neurology* 1998; 50: 1800–1805
- Tedeschi G, Bertolini A, Massaquoi SG, Campbell G, Patronas NJ, Bonavita S, Barnett AS, Alger JR, Hallett M. Proton magnetic resonance spectroscopic imaging in patients with cerebellar degeneration. *Ann Neurol* 1996; 39: 71–78
- Tedeschi G, Litvan I, Bonavita S, Bertolini A, Lundbom N, Patronas NJ, Hallett M. Proton magnetic resonance spectroscopic imaging in progressive supranuclear palsy, Parkinson's disease and corticobasal degeneration. *Brain* 1997; 120: 1541–1552
- Tedeschi G, Bonavita S, Barton NW, Bertolino A, Frank JA, Patronas NJ, Alger JR, Schiffmann R. Proton magnetic resonance spectroscopic imaging in the clinical evaluation of patients with Niemann-Pick type C disease. *J Neurol Neurosurg Psychiatry* 1998; 65: 72–79

Demyelination

- Brockmann K, Dechent P, Wilken B, Rusch O, Frahm J, Hanefeld F. Proton MRS profile of cerebral metabolic abnormalities in Krabbe disease. *Neurology* 2003; 60: 819–825

- Degaonkar MN, Khubchandihani M, Dhawan JK, Jayasundar R, Jagannathan NR. Sequential proton MRS study of brain metabolite changes monitored during a complete pathological cycle of demyelination and remyelination in a lysophosphatidyl choline (LPC)-induced experimental demyelinating lesion model. *MNR Biomed* 2002; 15: 293–300
- Farina L, Bizzi A, Finocchiaro G, Pareyson D, Sghirlanzoni A, Bertagnolio B, Savairo M, Naidu SB, Singhal BS, Wenger DA. MR imaging and proton MR spectroscopy in adult Krabbe disease. *AJNR Am J Neuroradiol* 2000; 21: 1478–1482
- Kruse B, Hanefeld F, Christen HJ, Bruhn H, Michaelis T, Hänicke W, Frahm J. Alterations of brain metabolites in metachromatic leukodystrophy as detected by localized proton magnetic resonance spectroscopy *in vivo*. *J Neurol* 1993; 241: 68–74
- Silver NC, Barker RA, MacManus DG, Barker GJ, Thom M, Thomas DGT, McDonald WI, Miller DH. Proton magnetic resonance spectroscopy in a pathologically confirmed acute demyelinating lesion. *J Neurol* 1997; 244: 204–207
- van der Knaap MS, van der Grond J, Luyten PR, den Hollander JA, Nauta JJP, Valk J. ¹H and ³¹P magnetic resonance spectroscopy of the brain in degenerative cerebral disorders. *Ann Neurol* 1992; 31: 202–211

Hypomyelination

- Bonavita S, Schiffmann R, Moore DF, Free K, Choi B, Patronas N, Virta A, Boespflug-Tanguy O, Tedeschi G. Evidence for neuroaxonal injury in patients with proteolipid protein gene mutations. *Neurology* 2001; 56: 785–788
- Gebern JY, Yook DA, Moore GJ, Wilds IB, Faulk MW, Klugmann M, Nave K-A, Siermans ES, van der Knaap MS, Bird TD, Shy ME, Kamholz JA, Griffiths IR. Patients lacking the major CNS myelin protein, proteolipid protein 1, develop length-dependent axonal degeneration in the absence of demyelination and inflammation. *Brain* 2002; 125: 551–561
- Pizzini F, Fatemi AS, Barker PB, Nagae-Poetscher LM, Horská A, Zimmerman AW, Moser HW, Bibat G, Naidu S. Proton MR spectroscopic imaging in Pelizaeus-Merzbacher disease. *AJNR Am J Neuroradiol* 2003; 24: 1683–1689
- Plecko B, Stöckler-Ipsiroglu S, Gruber S, Mlynarik V, Moser E, Simbrunner J, Ebner F, Bernert G, Harrer G, Gal A, Prayer D. Degree of hypomyelination and magnetic resonance spectroscopy findings in patient with Pelizaeus Merzbacher phenotype. *Neuropediatrics* 2003; 34: 127–136
- Spalice A, Popolizio T, Parisi P, Scarabino T, Iannetti P. Proton MR spectroscopy in congenital Pelizaeus-Merzbacher disease. *Pediatr Radiol* 2000; 30: 171–175
- Takanashi J, Inoue K, Tomita M, Kurihara A, Morita F, Ikehira H, Tanada S, Yoshitome E, Kohno Y. Brain *N*-acetylaspartate is elevated in Pelizaeus-Merzbacher disease with *PLP1* duplication. *Neurology* 2002; 58: 237–241
- van der Knaap MS, Naidu S, Pouwels PJ, Bonavita S, van Coster R, Lagae L, Sperner J, Surtees R, Schiffmann R, Valk J. New syndrome characterized by hypomyelination with atrophy of the basal ganglia and cerebellum. *AJNR Am J Neuroradiol* 2002; 23: 1466–1474

Cystic White Matter Degeneration

- Hanefeld F, Holzbach U, Kruse B, Wilichowski E, Christen H-J, Frahm J. Diffuse white matter disease in three children: an encephalopathy with unique features on magnetic resonance imaging and proton magnetic resonance spectroscopy. *Neuropediatrics* 1993; 24: 244–248
- Salvan A-M, Chabrol B, Lamoureux S, Confort-Gouny S, Cozzone PJ, Vion-Dury J. In vivo brain proton MR spectroscopy in a case of molybdenum cofactor deficiency. *Pediatr Radiol* 1999; 29: 846–848
- Schiffmann R, Moller JR, Trapp BD, Shih HH-L, Farrer RG, Katz DA, Alger JR, Parker CC, Hauer PE, Kaneski CR, Heiss JD, Kaye EM, Quarles RH, Brady RO, Barton NW. Childhood ataxia with diffuse central nervous system hypomyelination. *Ann Neurol* 1994; 35: 331–340
- Tedeschi G, Schiffmann R, Barton NW, Shih HH-L, Gospe SM Jr, Brady RO, Alger JR, di Chiro G. Proton magnetic resonance spectroscopic imaging in childhood ataxia with diffuse central nervous system hypomyelination. *Neurology* 1995; 45: 1526–1532
- van der Knaap MS, Kamphorst W, Barth PG, Kraaijeveld CL, Gut E, Valk J. Phenotypic variation in leukoencephalopathy with vanishing white matter. *Neurology* 1998; 51: 540–547
- van der Knaap MS, Barth PG, Gabreëls FJM, Franzoni E, Begeer JH, Stroink H, Rottevel JJ, Valk J. A new leukoencephalopathy with vanishing white matter. *Neurology* 1997; 48: 845–855
- ## Hyperammonemia
- Chol C-G, Yoo HW. Localized proton MR spectroscopy in infants with urea cycle defect. *AJNR Am J Neuroradiol* 2001; 22: 834–837
- Connelly A, Cross JH, Gadian DG, Hunter JV, Kirkham FJ, Leonard JV. Magnetic resonance spectroscopy shows increased brain glutamine in ornithine carbamoyl transferase deficiency. *Pediatr Res* 1993; 33: 77–81
- Haseler LJ, Sibbitt WL Jr, Mojtahzadeh HN, Reddy S, Aragwal VP, McCarthy DM. Proton MR spectroscopic measurement of neurometabolites in hepatic encephalopathy during oral lactulose therapy. *AJNR Am J Neuroradiol* 1998; 19: 1681–1686
- Kraft E, Trenkwalder C, Bergh FT, Auer DP. Magnetic resonance proton spectroscopy of the brain in Wilson's disease. *J Neurol* 1999; 246: 693–699
- Kreis R, Farrow N, Ross BD. Localized ^1H NMR spectroscopy in patients with chronic hepatic encephalopathy. Analysis of changes in cerebral glutamine, choline and inositols. *NMR Biomed* 1991; 4: 109–116
- Kreis R, Ross BD, Farrow NA, Ackerman Z. Metabolic disorders of the brain in chronic hepatic encephalopathy detected with H-1 MR spectroscopy. *Radiology* 1992; 182: 19–27
- Laubenberger J, Häussinger D, Bayer S, Gufler H, Hennig J, Langer M. Proton magnetic resonance spectroscopy of the brain in symptomatic and asymptomatic patients with liver cirrhosis. *Gastroenterology* 1997; 112: 1610–1616
- Lien YHH, Michaelis T, Moats RA, Ross BD. Scyllo-inositol depletion in hepatic encephalopathy. *Life Sci* 1994; 54: 1507–1512
- Naegele T, Grodd W, Viebahn R, Seeger U, Klose U, Seitz D, Kaiser S, Mader I, Mayer J, Lauchart W, Gregor M, Voight K. MR imaging and ^1H spectroscopy of brain metabolites in hepatic encephalopathy: time course of renormalization after liver transplantation. *Radiology* 2000; 216: 683–691
- Ross BD, Jacobson S, Villamil F, Korula J, Kreis R, Ernst T, Shonk T, Moats RA. Subclinical hepatic encephalopathy proton MR spectroscopic abnormalities. *Radiology* 1994; 193: 457–463
- Van den Heuvel AG, van der Grond J, van Rooij LG, van Wassenaeer-van Hall HN, Hoogenraad TU, Mali WPTM. Differential between portal-systemic encephalopathy and neurodegenerative disorders in patients in Wilson disease: H-1 MR spectroscopy. *Radiology* 1997; 203: 539–543
- ## Osmolytes
- Davies SEC, Gotoh M, Richards DA, Obrenovitch TP. Hypoosmolarity induces an increase of extracellular N-acetylaspartate concentration in the rat striatum. *Neurochem Res* 1998; 23: 1021–1025
- Heilig CW, Stromski ME, Blumenfeld JD, Lee JP, Gullans SR. Characterization of the major brain osmolytes that accumulate in salt-loaded rats. *Am J Physiol* 1989; 257: F1108–F1116
- Lee JH, Arcinue E, Ross BD. Organic osmolytes in the brain of an infant with hyponatremia. *N Engl J Med* 1994; 331: 439–442
- Lien Y-H H, Shapiro JJ, Chan L. Study of brain electrolytes and organic osmolites during correction of chronic hyponatremia. Implications for the pathogenesis of central pontine myelinolysis. *J Clin Invest* 1991; 88: 303–309
- Strange K, Emma F, Paredes A, Morrison R. Osmoregulatory changes in myo-inositol content and Na^+ / myo-inositol cotransport in rat cortical astrocytes. *Glia* 1994; 12: 35–43
- Videen JS, Michaelis T, Pinto R, Ross BD. Human cerebral osmolytes during chronic hyponatremia. A proton magnetic resonance spectroscopy study. *J Clin Invest* 1995; 95: 788–793
- ## Perinatal Hypoxia-Ischemia
- Azzopardi D, Wyatt JS, Cady EB, Delphy DT, Baudin J, Stewart AL, Hope PL, Hamilton PA, Reynolds EOR. Prognosis of newborn infants with hypoxic-ischemic brain injury assessed by phosphorus magnetic resonance spectroscopy. *Pediatr Res* 1989; 25: 445–451
- Groenendaal F, Veenhoven RH, van der Grond J, Jansen GH, Witkamp TD, de Vries LS. Cerebral lactate and N-acetyl-aspartate/choline ratios in asphyxiated full-term neonates demonstrated in vivo using proton magnetic resonance spectroscopy. *Pediatr Res* 1994; 35: 148–151
- Groenendaal F, van der Grond J, Witkamp TD, de Vries LS. Proton magnetic resonance spectroscopic imaging in neonatal stroke. *Neuropediatrics* 1995; 26: 243–248
- Groenendaal F, van der Grond J, Eken P, van Haastert IC, Rademaker KJ, Toet MC, de Vries LS. Early cerebral proton MRS and neurodevelopmental outcome in infants with cystic leukomalacia. *Dev Med Child Neurol* 1997; 39: 373–379
- Hanrahan JD, Sargentoni J, Azzopardi D, Manji K, Cowan FM, Rutherford MA, Cox IJ, Bell JD, Bryant DJ, Edwards AD. Cerebral metabolism within 18 hours of birth asphyxia: a proton magnetic resonance spectroscopic study. *Pediatr Res* 1996; 39: 584–590

- Hanrahan JD, Cox IJ, Edwards AD, Cowan FM, Sargentoni J, Bell JD, Bryant DJ, Rutherford MA. Persistent increases in cerebral lactate concentration after birth asphyxia. *Pediatr Res* 1998; 44: 304–311
- Hanrahan JD, Cox IJ, Azzopardi D, Cowan FM, Sargentoni J, Bell JD, Bryant DJ, Edwards AD. Relation between proton magnetic resonance spectroscopy within 18 hours of birth asphyxia and neurodevelopment at 1 year of age. *Dev Med Child Neurol* 1999; 41: 76–82
- Lorek A, Takei Y, Cady EB, Wyatt JS, Penrice J, Edwards AD, Peebles D, Wylezinska M, Owen-Reece H, Kirkbridge V, Cooper CE, Aldridge RF, Roth SC, Brown G, Delpy DT, Reynolds EOR. Delayed (“secondary”) cerebral energy failure after acute hypoxia-ischemia in the newborn piglet: continuous 48-hour studies by phosphorus magnetic resonance spectroscopy. *Pediatr Res* 1994; 36: 699–706
- Martin E, Buchli R, Ritter S, Schmid R, Largo RH, Boltshauser E, Fanconi S, Duc G, Rumpel H. Diagnostic and prognostic value of cerebral ^{31}P magnetic resonance spectroscopy in neonates with perinatal asphyxia. *Pediatr Res* 1996; 40: 749–758
- Moorcraft J, Bolas NM, Ives NK, Ouwerkerk R, Smyth J, Rajagopalan B, Hope PL, Radda GK. Global and depth resolved phosphorus magnetic resonance spectroscopy to predict outcome after birth asphyxia. *Arch Dis Child* 1991; 66: 1119–1123
- Moorcraft J, Bolas NM, Ives NK, Sutton P, Blackledge MJ, Rajagopalan B, Hope PL, Radda GK. Spatially localized magnetic resonance spectroscopy of the brains of normal and asphyxiated newborns. *Pediatrics* 1991; 87: 273–282
- Penrice J, Lorek A, Cady EB, Amess PN, Wylezinski M, Cooper CE, D’Souza P, Brown GC, Kirkbride V, Edwards AD, Wyatt JS, Reynolds EOR. Proton magnetic resonance spectroscopy of the brain during acute hypoxia-ischemia and delayed cerebral energy failure in the newborn piglet. *Pediatr Res* 1997; 41: 795–802
- Robertson NJ, Lewis RH, Cowan FM, Allsop JM, Counsell SJ, Edwards AD, Cox IJ. Early increases in brain myo-inositol measured by proton magnetic resonance spectroscopy in term infants with neonatal encephalopathy. *Pediatr Res* 2001; 50: 692–700
- Roth SC, Azzopardi D, Edwards AD, Baudin J, Cady EB, Townsend J, Delpy DT, Stewart AL, Wyatt JS, Osmund E, Reynolds R. Relation between cerebral oxidative metabolism following birth asphyxia, and neurodevelopmental outcome and brain growth at one year. *Dev Med Child Neurol* 1992; 34: 285–295
- Roth SC, Baudin J, Cady E, Johal K, Townsend JP, Wyatt JS, Reynolds EOR, Stewart AL. Relation of deranged neonatal cerebral oxidative metabolism with neurodevelopmental outcome and head circumference at 4 years. *Dev Med Child Neurol* 1997; 39: 708–725
- Capizzano AA, Schuff N, Armend DL, Tanabe JL, Norman D, Maudsley AA, Jagust W, Chui HC, Fein G, Segal MR, Weiner MW. Subcortical ischemic vascular dementia: assessment with quantitative MR imaging and ^1H MR spectroscopy. *AJNR Am J Neuroradiol* 2000; 21: 621–630
- Oppenheimer SM, Bryan RN, Conturo TE, Soher BJ, Preziosi TJ, Barker PB. Proton magnetic resonance spectroscopy and gadolinium-DTPA perfusion imaging of asymptomatic MRI white matter lesions. *Magn Reson Med* 1995; 33: 61–68
- Van der Grond J, Ramos LMP, Eikelboom BC, Mali WPTM. Cerebral metabolic differences between the severe and critical hypoperfused brain. *Neurology* 1996; 47: 399–404
- Barbierioli B, Montagna P, Martinelli P, Lodi R, Lotti S, Cortelli P, Funicello R, Zaniol P. Defective brain energy metabolism shown by in vivo ^{31}P MR spectroscopy in 28 patients with mitochondrial cytopathies. *J Cereb Blood Flow Metab* 1993; 13: 469–474
- Barbierioli B, Montagna P, Cortelli P, Lotti S, Lod R, Barboni P, Monari L, Laguresi E, Frassinetti C, Zaniol P. Defective brain and muscle energy metabolism shown by in vivo ^{31}P magnetic resonance spectroscopy in nonaffected carriers of 11778 mtDNA mutation. *Neurology* 1995; 45: 1364–1369
- Bianchi MC, Tosetti M, Battini R, Manca ML, Mancuso M, Cioni G, Canapicchi R, Siciliano G. Proton MR spectroscopy of mitochondrial diseases: analysis of brain metabolic abnormalities and their possible diagnostic relevance. *AJNR Am J Neuroradiol* 2003; 24: 1958–1966
- Cross JH, Gadian DG, Connelly A, Leonard JV. Proton magnetic resonance spectroscopy studies in lactic acidosis and mitochondrial disorders. *J Inher Metab Dis* 1993; 16: 800–811
- Detre JA, Wang Z, Bogdan AR, Gusnard DA, Bay CA, Bingham PM, Zimmerman RA. Regional variation in brain lactate in Leigh syndrome by localized ^1H magnetic resonance spectroscopy. *Ann Neurol* 1991; 29: 218–221
- Eleff SM, Barker PB, Blackband SJ, Chatham JC, Lutz NW, Johns DR, Bryan RN, Hurko O. Phosphorus magnetic resonance spectroscopy of patients with mitochondrial cytopathies demonstrates decreased levels of brain phosphocreatine. *Ann Neurol* 1990; 27: 626–630
- Herzberg NH, van Schooneveld MJ, Bleeker-Wagemakers E, Zwart R, Cremers FPM, van der Knaap MS, Bolhuis PA, de Visser M. Kearns-Sayre syndrome with a phenocopy of choroideremia instead of pigmentary retinopathy. *Neurology* 1993; 43: 218–221
- Kamada K, Takeuchi F, Houkin K, Kitagawa M, Kuriki S, Ogata A, Tashiro K, Koyanagi I, Mitsumori K, Iwasaki Y. Reversible brain dysfunction in MELAS: MEG and ^1H MRS analysis. *J Neurol Neurosurg Psychiatry* 2001; 70: 675–678
- Krägeloh-Mann I, Grodd W, Niemann G, Haas G, Ruitenbeek W. Assessment and therapy monitoring of Leigh disease by MRI and proton spectroscopy. *Pediatr Neurol* 1992; 8: 60–64
- Krägeloh-Mann I, Grodd W, Schöning M, Marquard K, Nägele T, Ruitenbeek W. Proton spectroscopy in five patients with Leigh’s disease and mitochondrial enzyme deficiency. *Dev Med Child Neurol* 1993; 35: 769–776
- Lin DDM, Crawford TO, Barker PB. Proton MR spectroscopy in the diagnostic evaluation of suspected mitochondrial disease. *AJNR Am J Neuroradiol* 2003; 24: 33–41

Chronic Hypoxia-Ischemia

- Auer DP, Schirmer T, Heidenreich JO, Herzog J, Pütz B, Dichans M. Altered white and gray matter metabolism in CADASIL. A proton MR spectroscopy and ^1H -MRSI study. *Neurology* 2001; 56: 635–642
- Brooks WM, Wesley MH, Kodituwakku PW, Garry PJ, Rosenberg GA. ^1H -MRS Differentiates white matter hyperintensities in subcortical arteriosclerotic encephalopathy from those in normal elderly. *Stroke* 1997; 28: 1940–1943

- Lodi R, Montagna P, Iotti S, Zaniol P, Barboni P, Puddu P, Barbioli B. Brain and muscle energy metabolism studied in vivo by ^{31}P -magnetic resonance spectroscopy in NARP syndrome. *J Neurol Neurosurg Psychiatry* 1994; 57: 1492–1496
- Matthews PM, Andermann F, Silver K, Karpati G, Arnold DL. Proton MR spectroscopic characterization of differences in regional brain metabolic abnormalities in mitochondrial encephalomyopathies. *Neurology* 1993; 43: 2484–2490
- Pavakis SG, Kingsley PB, Kaplan GP, Stacpoole PW, O'Shea M, Lustbader D. Magnetic resonance spectroscopy. Use in monitoring MELAS treatment. *Arch Neurol* 1998; 55: 849–852
- Rubio-Gozalbo ME, Heerschap A, Trijbels JMF, de Meirleir L, Thijssen HOM, Smeitink JAM. Proton MR spectroscopy in a child with pyruvate dehydrogenase complex deficiency. *Magn Reson Imaging* 1999; 17: 939–944
- Shevell MI, Matthews PM, Scriver CR, Brown RM, Otero LJ, Legris ML, Brown GK, Arnold DL. Cerebral dysgenesis and lactate acidemia: an MRI/MRS phenotype associated with pyruvate dehydrogenase deficiency. *Pediatr Neurol* 1994; 11: 224–229
- Takahashi S, Oki J, Miyamoto A, Okuno A. Proton magnetic resonance spectroscopy to study the metabolic changes in the brain of a patient with Leigh syndrome. *Brain Dev* 1999; 21: 200–204
- Wilichowski E, Pouwels PJW, Frahm J, Hanefeld F. Quantitative proton magnetic resonance spectroscopy in patients with MELAS. *Neuropediatrics* 1999; 30: 256–263
- Zand DJ, Simon EM, Pulitzer SB, Wang DJ, Wang ZJ, Rorke LB, Palmieri M, Berry GT. In vivo pyruvate detected by MR spectroscopy in neonatal pyruvate dehydrogenase deficiency. *AJNR Am J Neuroradiol* 2003; 24: 1471–1474

Encephalitis

- Chang L, Ernst T, Tornatore C, Aronow H, Melchor R, Walot I, Singer E, Conford M. Metabolite abnormalities in progressive multifocal leukoencephalopathy by proton magnetic resonance spectroscopy. *Neurology* 1997; 48: 836–845
- Iranzo A, Moreno A, Pujol J, Marti-Fàbregas J, Domingo P, Molet J, Ris J, Cadafalch J. Proton magnetic resonance spectroscopy pattern of progressive multifocal leukoencephalopathy in AIDS. *J Neurol Neurosurg Psychiatry* 1999; 66: 520–523
- Laubenberger J, Häussinger D, Bayer S, Thielemann S, Schneider B, Mundinger A, Hennig J, Langer M. HIV-related metabolic abnormalities in the brain: depiction with short echo times. *Radiology* 1996; 199: 805–810
- Meyerhoff DJ, MacKay S, Bachman L, Poole N, Dillon WP, Weiner MW, Fein G. Reduced brain *N*-acetylaspartate suggests neuronal loss in cognitively impaired neuronal loss in cognitively impaired human immunodeficiency virus-seropositive individuals. In vivo ^1H magnetic resonance spectroscopic imaging. *Neurology* 1993; 43: 509–515
- Sämann PG, Schlegel J, Müller G, Prantl F, Emminger C, Auer DP. Serial proton MR spectroscopy and diffusion imaging findings in HIV-related herpes simplex encephalitis. *AJNR Am J Neuroradiol* 2003; 24: 2015–2019
- Takanashi J-I, Sugita K, Ishii M, Aoyagi M, Niimi H. Longitudinal MR imaging and proton MR spectroscopy in herpes simplex encephalitis. *J Neurol Sci* 1997; 149: 99–102

- Tracey I, Carr CA, Guimareas AR, Worth JL, Navia BA, González RG. Brain choline-containing compounds are elevated in HIV-positive patients before the onset of AIDS dementia complex: a proton magnetic resonance spectroscopic study. *Neurology* 1996; 46: 783–788

Canavan Disease

- Austin SJ, Connelly A, Gadian DG, Benton JS, Brett EM. Localized ^1H NMR spectroscopy in Canavan's disease: a report of two cases. *Magn Reson Med* 1991; 19: 439–445
- Barker PB, Bryan RN, Kumar AJ, Naidu S. Proton NMR spectroscopy of Canavan's disease. *Neuropediatrics* 1992; 23: 263–267
- Marks HG, Caro PA, Wang Z, Detre JA, Bogdan AR, Gusnard DA, Zimmerman RA. Use of computed tomography, magnetic resonance imaging, and localized ^1H magnetic resonance spectroscopy in Canavan's disease: a case report. *Ann Neurol* 1991; 30: 106–110
- Wittsack H-J, Kugel H, Roth B, Heindel W. Quantitative measurements with localized ^1H MR spectroscopy in children with Canavan's disease. *J Magn Reson Imaging* 1996; 6: 889–893

NAA Synthesis Defect

- Barker PB. *N*-Acetyl aspartate – a neuronal marker? *Ann Neurol* 2001; 49: 423–424
- Martin E, Capone A, Schneider J, Hennig J, Thiel T. Absence of *N*-acetylaspartate in the human brain: impact on neurospectroscopy? *Ann Neurol* 2001; 49: 518–521

Creatine Deficiency Syndromes

- Cecil KM, Salomons GS, Ball WS Jr, Wong B, Chuck G, Verhoeven NM, Jakobs C, DeGrauw TJ. Irreversible brain creatine deficiency with elevated serum and urine creatine: a creatine transporter defect. *Ann Neurol* 2001; 49: 401–404
- DeGrauw TJ, Salomons GS, Cecil KM, Chuck G, Newmeyer A, Shapiro MB, Jakobs C. Congenital creatine transporter deficiency. *Neuropediatrics* 2002; 33: 232–238
- Salomons GJ, van Dooren SJM, Verhoeven NM, Cecil KM, Ball WS, DeGrauw TJ, Jakobs C. X-linked creatine-transporter gene (*SLC6A8*) defect: a new creatine-deficiency syndrome. *Am J Hum Genet* 2001; 68: 1497–1500
- Schultze A. Creatine deficiency syndromes. *Mol Cell Biochem* 2003; 244: 143–150
- Stöckler S, Holzbach U, Hanefeld F, Marquart I, Helms G, Requart M, Hänicke W, Frahm J. Creatine deficiency in the brain: a new, treatable inborn error of metabolism. *Pediatr Res* 1994; 36: 409–413
- Stöckler S, Isbrandt D, Hanefeld F, Schmidt B, von Figura. Guanidinoacetate methyltransferase deficiency: the first inborn error of creatine metabolism in man. *Am J Hum Genet* 1996; 58: 914–922
- Stromberger C, Bodamer OA, Stöckler-Ipsiroglu S. Clinical characteristics and diagnostic clues in inborn errors of creatine metabolism. *J Inher Metab Dis* 2003; 26: 299–308
- van der Knaap MS, Verhoeven NM, Maaswinkel-Mooij P, Pouwels PJW, Onkenhout W, Peeters EAJ, Stöckler-Ipsiroglu S, Jakobs C. Mental retardation and behavioral problems as presenting signs of a creatine synthesis defect. *Ann Neurol* 2000; 47: 450–454

Nonketotic Hyperglycinemia

- Gabis L, Parton P, Roche P, Lenn N, Tudorica A, Huang W. In vivo ^1H magnetic resonance spectroscopic measurement of brain glycine levels in nonketotic hyperglycinemia. *J Neuroimaging* 2001; 11: 209–211
- Heindel W, Kugel H, Roth B. Noninvasive detection of increased glycine content by proton MR spectroscopy in the brains of two infants with nonketotic hyperglycinemia. *AJNR Am J Neuroradiol* 1993; 14: 629–635
- Huisman TAGM, Thiel T, Steinman B, Zeislinger G, Martin E. Proton magnetic resonance spectroscopy of the brain of a neonate with nonketotic hyperglycinemia: in vivo-in vitro (ex vivo) correlation. *Eur Radiol* 2002; 12: 858–861
- Viola A, Chabrol B, Nicoli F, Confort-Gouny S, Viout P, Cozzone PJ. Magnetic resonance spectroscopy study of glycine in nonketotic hyperglycinemia. *Pediatr Res* 2002; 52: 292–300

Phenylketonuria

- Kreis R. Comments on in vivo proton magnetic resonance spectroscopy in phenylketonuria. *Eur J Pediatr* 2000; 159: S126–S128
- Kreis R, Pietz J, Penzien J, Herschkowitz N, Boesch C. Identification and quantitation of phenylalanine in the brain of patients with phenylalanine by means of localized in vivo ^1H magnetic-resonance spectroscopy. *J Magn Reson B* 1995; 107: 242–251
- Leuzzi V, Bianchi MC, Tosetti M, Carducci CI, Carducci Ca, Antonozzi I. Clinical significance of brain phenylalanine concentration assessed by in vivo proton magnetic resonance spectroscopy in phenylketonuria. *J Inherit Metab Dis* 2000; 23: 563–570
- Moats RA, Scadeng M, Nelson MD Jr. MR imaging and spectroscopy in PKU. *Ment Retard Dev Disab Res Rev* 1999; 5: 132–135
- Moats RA, Mosely KD, Koch R, Nelson M Jr. Brain phenylalanine concentrations in phenylketonuria: research and treatment of adults. *Pediatrics* 2003; 112: 1575–1579
- Möller HE, Vermathen, Ullrich K, Weglage J, Koch H-G, Peters PE. In-vivo NMR spectroscopy in patients with phenylketonuria: changes of cerebral phenylalanine levels under dietary treatment. *Neuropediatrics* 1995; 26: 199–202
- Möller HE, Ullrich K, Weglage J. In vivo proton magnetic resonance spectroscopy in phenylketonuria. *Eur J Pediatr* 2000; 159: S121–S125
- Möller HE, Weglage J, Bick U, Wiedermann D, Feldmann R, Ullrich K. Brain imaging and proton magnetic resonance spectroscopy in patients with phenylketonuria. *Pediatrics* 2003; 112: 1580–1583
- Novotny EJ Jr, Avison MJ, Herschkowitz N, Petroff OAC, Prichard JW, Seashore MR, Rothman DL. In vivo measurement of phenylalanine in human brain by proton nuclear magnetic resonance spectroscopy. *Pediatr Res* 1995; 37: 244–249
- Pietz J, Lutz T, Zwygart K, Hoffman GF. Phenylalanine can be detected in brain tissue of healthy subjects by ^1H magnetic resonance spectroscopy. *J Inherit Metab Dis* 2003; 26: 683–691

Salla Disease

- Sewell AC, Murphy HC, Iles RA. Proton magnetic resonance spectroscopic detection of sialic acid storage disease. *Clin Chem* 2002; 48: 35–359
- Varho T, Komhu M, Sonninen P, Holopainen I, Nyman S, Manner T, Sillapää M, Aula P, Lundbom N. A new metabolite contributing to *N*-acetyl signal in ^1H MRS of the brain in Salla disease. *Neurology* 1999; 52: 1668–1672

Maple Syrup Urine Disease

- Felber SR, Sperl W, Chemelli A, Murr C, Wendel U. Maple syrup urine disease: metabolic decompensation monitored by proton magnetic resonance imaging and spectroscopy. *Ann Neurol* 1993; 33: 396–401

Sjögren-Larsson Syndrome

- Mano T, Ono J, Kaminaga T, Imai K, Sakura K, Harada K, Nagai T, Rizzo WB, Okada S. Proton MR spectroscopy of Sjögren-Larsson's syndrome. *AJNR Am J Neuroradiol* 1999; 20: 1671–1673
- Van Domburg PHMF, Willemsen MAAP, Rotteveel JJ, de Jong JGN, Thijssen HOM Heerschap A, Cruysberg JRM, Wanders RJA, Gabreëls FJM, Steijlen PM. Sjögren-Larsson syndrome. Clinical and MRI/MRS findings in FALDH-deficient patients. *Neurology* 1999; 52: 1345–1352
- Willemsen MAAP, van der Graaf M, van der Knaap MS, Heerschap A, van Domburg PHMF, Gabreëls FJM, Thijssen HOM, Rotteveel JJ. MR imaging and proton MR spectroscopy studies in Sjögren-Larsson syndrome: characterization of the leukoencephalopathy. *AJNR Am J Neuroradiol* 2004; 25: 649–657

Galactosemia

- Berry GT, Hunter JV, Wang Z, Dreha S, Mazur A, Brooks DG, Ning C, Zimmerman RA, Segal S. In vivo evidence of brain galactitol accumulation in an infant with galactosemia and encephalopathy. *J Pediatr* 2001; 138: 260–262
- Möller HE, Ullrich K, Vermathen P, Schuierer G, Koch H-G. In vivo study of brain metabolism in galactosemia by ^1H and ^{31}P magnetic resonance spectroscopy. *Eur J Pediatr* 1995; 154: S8–S13
- Wang ZJ, Berry GT, Dreha SF, Zhao G, Segal S, Zimmerman RA. Proton magnetic resonance spectroscopy of brain metabolites in galactosemia. *Ann Neurol* 2001; 50: 266–269

Defect in Polyol Metabolism

- Huck JHJ, Verhoeven NM, Struys EA, Salomons GS, Jakobs C, van der Knaap MS. Ribose 5-phosphate isomerase deficiency: new inborn error in the pentose phosphate pathway associated with a slowly progressive leukoencephalopathy. *Am J Hum Genet* 2004; 74: 745–751
- van der Knaap MS, Wevers RA, Struys EA, Verhoeven NM, Pouwels PJW, Engelke UFH, Feikema W, Valk J, Jakobs C. Leukoencephalopathy associated with a disturbance in the metabolism of polyols. *Ann Neurol* 1999; 46: 925–928

Diabetes Mellitus

- Kreis R, Ross BD. Cerebral metabolic disturbance in patients with subacute and chronic diabetes mellitus: detection with proton MR spectroscopy. *Radiology* 1992; 184: 123–130
- Pan JW, Telang FW, Lee JH, de Graaf RA, Rothman DL, Stein DT, Hetherington HP. Measurement of β -hydroxybutyrate in acute hyperketonemia in human brain. *J Neurochem* 2001; 79: 539–544

X-Linked Adrenoleukodystrophy

- Eichler FS, Itoh R, Barker PB, Mori S, Garrett ES, van Zijl PCM, Moser HW, Raymond GV, Melhem ER. Proton MR spectroscopy and diffusion tensor brain MR imaging in X-linked adrenoleukodystrophy: initial experience. *Radiology* 2002; 225: 245–252
- Eichler FS, Barker PB, Cox C, Edwin D, Ulug AM, Moser HW, Raymond GV. Proton MR spectroscopic imaging predicts lesion progression on MRI in X-linked adrenoleukodystrophy. *Neurology* 2002; 58: 901–907
- Korenke GC, Pouwels PJW, Frahm J, Hunneman DH, Stoeckler S, Krasemann E, Jost W, Hanefeld F. Arrested cerebral adrenoleukodystrophy: a clinical and proton magnetic resonance spectroscopy study in three patients. *Pediatr Neurol* 1996; 15: 103–107
- Pouwels PJW, Kruse B, Korenke GC, Mao X, Hanefeld FA, Frahm J. Quantitative proton magnetic resonance spectroscopy of childhood adrenoleukodystrophy. *Neuropediatrics* 1998; 2: 254–264
- Wilken B, Dechent P, Brockmann K, Finsterbusch J, Baumann M, Ebell W, Korenke GC, Pouwels PJW, Hanefeld FA, Frahm J. Quantitative proton magnetic resonance spectroscopy of children with adrenoleukodystrophy before and after hematopoietic stem cell transplantation. *Neuropediatric* 2003; 34: 237–246

Diffuse Axonal Injury

- Auld KL, Ashwal S, Holshouser BA, Tomasi LG, Perkin RM, Ross BD, Hinshaw BD Jr. Proton magnetic resonance spectroscopy in children with acute central nervous system injury. *Pediatr Neurol* 1995; 12: 323–334
- Friedman SD, Brooks WM, Jung RE, Hart BL, Yeo RA. Proton MR spectroscopic findings correspond to neuropsychological function in traumatic brain injury. *AJNR Am J Neuroradiol* 1998; 19: 1879–1885
- Friedman SD, Brooks WM, Jung RE, Chiulli SJ, Sloan JH, Montoya BT, Hart BL, Yeo RA. Quantitative proton MRS predicts outcome after traumatic brain injury. *Neurology* 1999; 52: 1384–1391
- Garnett MR, Blamire AM, Corkill RG, Cadoux-Hudson TAD, Rajagopalan B, Styles P. Early proton magnetic resonance spectroscopy in normal-appearing brain correlates with outcome in patients following traumatic brain injury. *Brain* 2000; 123: 2046–2054
- Haseler LJ, Arcinue E, Danielsen ER, Bluml S, Ross BD. Evidence from proton magnetic resonance spectroscopy for a metabolic cascade of neuronal damage in shaken baby syndrome. *Pediatrics* 1997; 99: 4–14

- Ross BD, Ernst T, Kreis R, Haseler LJ, Bayer S, Danielsen E, Bluml S, Shonk T, Mandigo JC, Caton W, Clark C, Jensen SW, Lehman NL, Arcinue E, Pudenz R, Shelden CH. ^1H MRS in acute traumatic brain injury. *J Magn Reson Imaging* 1998; 8: 829–840

- Signoretti S, Marmarou A, Tavazzi B, Lazzarino G, Beaumont A, Vagnozzi R. *N*-Acetylaspartate reduction as a measure of injury severity and mitochondrial dysfunction following diffuse traumatic brain injury. *J Neurotrauma* 2001; 18: 977–991

Multiple Sclerosis

- Arnold DL, Wolinsky JS, Matthews PM, Falini A. The use of magnetic resonance spectroscopy in the evaluation of the natural history of multiple sclerosis. *J Neurol Neurosurg Psychiatry* 1998; 64: S94–S101
- Bitsch A, Bruhn H, Vougioukas V, Stringaris A, Lassmann H, Frahm J, Brück W. Inflammatory CNS demyelination: histopathologic correlation with in vivo quantitative proton MR spectroscopy. *AJNR Am J Neuroradiol* 1999; 20: 1619–1627
- Bjartmar C, Kidd G, Mörk S, Rudick R, Trapp BD. Neurological disability correlates with spinal cord axonal loss and reduced *N*-acetyl aspartate in chronic multiple sclerosis patients. *Ann Neurol* 2000; 48: 893–901
- Bonneville F, Moriarty DM, Li BSY, Babb JS, Grossmann RI, Gonen O. Whole-brain *N*-acetylaspartate concentration: correlation with T2-weighted lesion volume and expanding disability status scale score in cases of relapsing-remitting multiple sclerosis. *AJNR Am J Neuroradiol* 2002; 23: 371–375
- Chard DT, Griffin CM, McLean MA, Kapeller P, Kapoor R, Thompson AJ, Miller DH. Brain metabolite changes in cortical gray and normal-appearing white matter in clinically early relapsing-remitting multiple sclerosis. *Brain* 2002; 125: 2342–2352
- Davie CA, Barker GJ, Thompson AJ, Tofts PS, McDonald WI, Miller DH. ^1H magnetic resonance spectroscopy of chronic cerebral white matter lesions and normal appearing white matter in multiple sclerosis. *J Neurol Neurosurg Psychiatry* 1997; 63: 736–742
- De Stefano N, Matthews PM, Antel JP, Preul M, Francis G, Arnold DL. Chemical pathology of acute demyelinating lesions and its correlation with disability. *Ann Neurol* 1995; 38: 901–909
- De Stefano N, Matthews PM, Fu L, Narayanan S, Stanley J, Francis GS, Antel JP, Arnold DL. Axonal damage correlates with disability in patients with relapsing-remitting multiple sclerosis. Results of a longitudinal magnetic resonance spectroscopy study. *Brain* 1998; 121: 1469–1477
- De Stefano N, Narayanan S, Francis GS, Arnaoutelis R, Tartaglia MC, Antel JP, Matthews PM, Arnold DL. Evidence of axonal damage in the early stages of multiple sclerosis and its relevance to disability. *Arch Neurol* 2001; 58: 65–70
- Gonen O, Moriarty DM, Li BSY, Babb JS, He J, Listerud J, Jacobs D, Markowitz CE, Grossman RI. Relapsing-remitting multiple sclerosis and whole-brain *N*-acetylaspartate measurement: evidence for different clinical cohorts – initial observations. *Radiology* 2002; 225: 261–268
- Husted CA, Goodin DS, Hugg JW, Maudsley AA, Tsuruda JS, de Bie SH, Fein G, Matson GB, Weiner MW. Biochemical alterations in multiple sclerosis lesions and normal-appearing white matter detected by in vivo ^{31}P and ^1H spectroscopic imaging. *Ann Neurol* 1994; 36: 157–165

- Kapeller P, McLean MA, Griffin CM, Chard D, Parker GJM, Barker GJ, Thompson AJ, Miller DH. Preliminary evidence for neuronal damage in cortical grey matter and normal appearing white matter in short duration relapsing-remitting multiple sclerosis: a quantitative MR spectroscopy imaging study. *J Neurol* 2001; 248: 131–138
- Leary SM, Davie CA, Parker GJM, Stevenson WL, Wang L, Barker GJ, Miller DH, Thompson AJ. ¹H Magnetic resonance spectroscopy of normal appearing white matter in primary progressive multiple sclerosis. *J Neurol* 1999; 246: 1023–1026
- Mader I, Roser W, Kappos L, Hagberg G, Seeling J, Radue EW, Steinbrich W. Serial proton MR spectroscopy of contrast-enhancing multiple sclerosis plaques: absolute metabolic values over 2 years during clinical pharmacological study. *AJNR Am J Neuroradiol* 2000; 21: 1220–1227
- Mader I, Seeger U, Weissert R, Klose U, Naegel T, Melms A, Grodd W. Proton MR spectroscopy with metabolite-nulling reveals elevated macromolecules in acute multiple sclerosis. *Brain* 2001; 124: 953–961
- Narayana PA, Doyle TJ, Lai D, Wolinsky JS. Serial proton magnetic resonance spectroscopic imaging, contrast-enhanced magnetic resonance imaging, and quantitative lesion volumetry in multiple sclerosis. *Ann Neurol* 1998; 43: 56–71
- Sarchielli P, Presciutti O, Pellicoli GP, Tarducci R, Gobbi G, Chiarini P, Alberti A, Vicinanza F, Gallai V. Absolute quantification of brain metabolites by proton magnetic resonance spectroscopy in normal appearing white matter of multiple sclerosis patients. *Brain* 1999; 122: 513–521
- Sarchielli P, Presciutti O, Tarducci R, Gobbi G, Alberti A, Pellicoli GP, Chiarini P, Gallai V. Localized ¹H magnetic resonance spectroscopy in mainly cortical gray matter of patients with multiple sclerosis. *J Neurol* 2002; 249: 902–910
- Suhy J, Rooney WD, Goodkin DE, Capizzano AA, Soher BJ, Maudsley AA, Waubant E, Andersson PB, Weiner MW. ¹H MR-SI Comparison of white matter and lesions in primary progressive and relapsing-remitting MS. *Mult Scler* 2000; 6: 148–155
- Tartaglia MS, Narayanan S, de Stefano N, Arnaoutelis R, Antel SB, Francis SJ, Santos AC, Lapierre Y, Arnold DL. Choline is increased in pre-lesional normal appearing white matter in multiple sclerosis. *J Neurol* 2002; 249: 1382–1390
- Tourbah A, Stievenart JL, Gout O, Fontaine B, Liblau R, Lubetzki C, Cabanis EA, Lyon-Cean O. Localized proton magnetic resonance spectroscopy in relapsing remitting versus secondary progressive multiple sclerosis. *Neurology* 1999; 53: 1091–1097
- Van Walderveen MAA, Barkhof F, Pouwels PJW, van Schijndel RA, Polman CH, Castelijns JA. Neuronal damage in T1-hypointense multiple sclerosis lesions demonstrated in vivo using proton magnetic resonance spectroscopy. *Ann Neurol* 1999; 46: 79–87
- Blaser SI, Clarke JTR, Becker LE. Neuroradiology of lysosomal disorders. *Neuroimaging Clin N Am* 1994; 4: 283–298
- Blois MS. Clinical judgment and computers. *N Engl J Med* 1980; 303: 192–197
- Boltshauser E, Martin E, Wichmann W, Valavanis A. Grenzen der kernspintomographie aus neuropädiatrischer Sicht. *Klin Neuroradiol* 1993; 3: 79–82
- Brismar J. CT and MRI of the brain in inherited metabolic disorders. *J Child Neurol* 1992; 7: S122–S131
- Cassedy KJ, Edwards MK. Metabolic and degenerative diseases of childhood. *Top Magn Reson Imaging* 1993; 5: 73–95
- Cheon JE, Kim IO, Hwang YS, Kim KJ, Wang KC, Cho BK, Chi JG, Kim CJ, Kim WS, Yeon KM. Leukodystrophy in children: a pictorial review of MR imaging features. *Radiographics* 2002; 22: 461–476
- Edwards MK. Imaging of metabolic diseases of the brain. *Curr Opin Radiol* 1991; 3: 25–30
- Ford CC, Ceckler TL, Karp J, Herndon RM. Magnetic resonance imaging of experimental demyelination lesions. *Magn Reson Med* 1990; 14: 461–481
- Forsting M. MR imaging of the brain: metabolic and toxic white matter diseases. *Eur Radiol* 1999; 9: 1061–1065
- Getty DJ, Pickett RM, D'Orsi CJ, Swets JA. Enhanced interpretation of diagnostic images. *Invest Radiol* 1988; 23: 240–252
- Kendall BE. Disorders of lysosomes, peroxisomes and mitochondria. *AJNR Am J Neuroradiol* 1992; 13: 621–653
- Kendall BE. Inborn errors and demyelination: MRI and the diagnosis of white matter disease. *J Inher Metab Dis* 1993; 16: 771–786
- Kristjánsdóttir R, Uvebrant P, Hagberg B, Kyllerman M, Wiklund L-M, Blennow G, Flodmark O, Gustavsson L, Ekholm S, Månsson J-E. Disorders of the cerebral white matter in children. The spectrum of the lesions. *Neuropediatrics* 1996; 27: 295–298
- Miller DH, Robb SA, Ormerod IEC, Pohl KRE, MacManus DG, Kendall BE, Moseley IF, McDonald WI. Magnetic resonance imaging of inflammatory and demyelinating white matter diseases of childhood. *Dev Med Child Neurol* 1990; 32: 97–107
- Sackett DL, Haynes RB, Tugwell P. Clinical epidemiology: a basic science for clinical medicine. Boston: Little, Brown & Co, 1985
- Valk J, van der Knaap MS. Selective vulnerability in toxic encephalopathies and metabolic disorders. *Riv Neuroradiol* 1996; 9: 749–760
- Valk J, van der Knaap MS. Patterns of myelin breakdown. *Eur Radiol* 1999; 9: S3–S14
- van der Knaap MS. Magnetic resonance in childhood white matter disorders. *Dev Med Child Neurol* 2001; 43: 715–712
- van der Knaap MS, Valk J. Non-leukodystrophic white matter changes in inherited disorders. *Int J Neuroradiol* 1995; 1: 56–66
- van der Knaap MS, Valk J, de Neeling N, Nauta JJP. Pattern recognition in magnetic resonance imaging. *Neuroradiology* 1991; 33: 478–493
- van der Knaap MS, Breiter SN, Naidu S, Hart AAM, Valk J. Defining and categorizing leukoencephalopathies of unknown origin: MR imaging approach. *Radiology* 1999; 213: 121–133

109 Pattern Recognition in White Matter Disorders

Barkhof F, van der Knaap MS. Differential diagnosis with leukodystrophies and non-vascular acquired white matter disorders. In: Erkinjuntti T, Gauthier S, eds. *Vascular cognitive impairment*. London: Martin Dunitz, 2002, pp 485–500

Subject Index

A

acquired immunodeficiency syndrome 616–627

- acute HIV-1 encephalopathy 616
- AIDS in infants and children 617
- AIDS-related dementia 616
- cellular immunodeficiency 616
- diagnostic criteria Centers of Disease Control 616
- diagnostic procedures 617
- high risk groups 616
- highly aggressive antiretroviral therapy (HAART) 622
- HIV-1 virions in brain tissue 617
- human immunodeficiency virus type 1 (HIV-1) 616
- lentovirinae subfamily of retroviruses 620
- magnetic resonance imaging 606–627
- major envelope proteins 620
- mode of infection 620
- MS-like encephalopathy 619
- opportunistic infections 616
- pneumocystis carinii pneumonia 616
- spinal cord involvement 619
- subacute HIV-1 encephalopathy 616
- therapeutic options 621–623

activator protein deficiency 74, 98, 104

acute disseminated encephalomyelitis and acute hemorrhagic encephalomyelitis 604–615

- auto-immune reaction 605
- clinical variants 604
- Guillain-Barré syndrome 604
- magnetic resonance imaging 606–615
- postvaccinal encephalopathy 604
- therapeutic options 605
- viral infections 604

acute intermittent porphyria 700

acute profound hypoxic-ischemic insults 718

adult polyglucosan body disease 147–151

- corpora amylacea 148
- cystic lesions 147
- genetic defect 148
- glucose polymers 148
- glycogen branching enzyme 148

- glycogen storage disease type IV 148
- magnetic resonance imaging 149–151
- polyglucosan bodies 147
- – intra-axonal and astrocytic location 147
- sural nerve biopsy 147

adult-onset autosomal dominant leukoencephalopathies 560–561

- clinical variants 560

Aicardi-Goutières syndrome 496–504

- atypical manifestations 496, 497
- calcium deposits 497, 498, 501
- clinical variants 496
- Cree encephalitis 497
- CSF lymphocytosis 497
- interferonopathy 498
- interferon- α 497
- magnetic resonance imaging 498–504
- pseudo-TORCH syndrome 497

Alexander disease 416–435

- α B-crystallin 416
- clinical variants 416
- genetic defect 418
- glial fibrillary astrocyte protein 418
- magnetic resonance imaging 419–435
- megalencephaly 416
- Rosenthal fibers 416, 417, 418

amyloid angiopathy 535–540

angiokeratomas (Fabry disease) 112

anti-phospholipid antibody syndrome 785

apparent diffusion coefficient (ADC) 840

arginase deficiency 360, 362, 367

argininosuccinate

- lyase deficiency 360, 362, 364
- synthase deficiency 360, 362

astrocyte 5

ATP synthase deficiency 224, 225, 227

Ayala syndrome 709

B

Baló concentric sclerosis 567, 600

basal ganglia damage after perinatal asphyxia 718, 738, 739

Batten disease 137

Behçet disease 789, 791, 792

benign primary angiitis 776

big panda sign 397

Binswanger disease 767–772

biotin metabolism, defects 248

biotinidase deficiency 248–251

Bloch-Sulzberger syndrome 412–415

Borrelia burgdorferi 792

brain maturation

- ADC values 847
- DWI-DTI changes 847
- MTR values 42, 857

brucellosis 635–639

- *Brucella* species 635
- clinical variability 635
- coccobacilli 635
- geographic distribution 635
- magnetic resonance imaging 636–639
- therapeutic options 636
- zoonosis 635

C

CADASIL 541–548

Canavan disease 326–333

- aspartoacylase 327
- clinical variants 326
- genetic defect 327
- magnetic resonance imaging 328–333
- N-acetyl aspartate 327
- spongy degeneration 326
- vacuolating myelinopathy 326, 327
- Van Bogaert-Bertrand disease 326

CARASIL 549–551

carbon monoxide intoxication 755

carboxyl phosphate synthetase deficiency 360, 362

cataracts, microcephaly, failure to thrive, kyphoscoliosis syndrome (CAMFAK) 260

central cortical and subcortical pattern 718, 733, 737–740

central pontine and extrapontine myelinolysis 684–689

- alcohol abuse 685
- hyponatremia 685
- iatrogenic factor 685
- magnetic resonance imaging 686–689
- myelinolysis 684–685
- prevention 686
- rapid correction of hyponatremia 685
- therapeutic options 686

- cerebral amyloid angiopathy
 - 535–540
 - amyloid
 - – cascade 537
 - – precursor proteins 536
 - – Bri fragment 537
 - A β protein subunits 536
 - British variant (Worster-Drought syndrome) 535
 - cystatin C 536
 - Dutch variant 535
 - Flemish variant 535
 - genetic defects 536, 537
 - Iceland variant 535
 - lobar hemorrhage 535
 - magnetic resonance imaging 537–540
 - oculoleptomeningeal amyloidosis 535
 - β -sheet content 536
 - sporadic forms 535
 - therapeutic options 537
 - transthyretin 536
 - cerebral autosomal dominant arteriopathy with subcortical infarcts and leukoencephalopathy (CADASIL) 541–548
 - absence of vascular risk factors 541
 - diagnostic criteria 541
 - epidermal growth factor motif 542
 - familial Binswanger disease 541
 - genetic defect 542
 - granular osmiophilic material 541
 - hereditary multi-infarct dementia 541
 - magnetic resonance imaging 542–548
 - migrainous headache 541
 - therapeutic options 542
 - cerebral autosomal recessive arteriopathy with subcortical infarcts and leukoencephalopathy (CARASIL) 549–551
 - alopecia 549
 - clinical variants 549
 - lumbago 549
 - magnetic resonance imaging 549–551
 - cerebro-oculo-facio-skeletal syndrome (COFS) 260
 - cerebrotendinous xanthomatosis 252–259
 - Achilles tendon 252
 - bile acid metabolism 252, 253, 254
 - cholestanol 253
 - clinical variants 252
 - genetic defect 253
 - 27-hydroxylase 253
 - magnetic resonance imaging 253–258
 - xanthomas 253
 - Charcot-Marie-Tooth disease, X-Linked 476–478
 - clinical variants 476
 - connexin 32 476
 - genetic defect 476
 - magnetic resonance imaging 477, 478
 - chemotherapy-related encephalopathy 808–817
 - childhood ataxia with CNS hypomyelination 481–494
 - cholestanol 253
 - choline phosphoglycerides 7
 - Churg-Strauss syndrome 789
 - classification
 - of lysosomal storage disorders 69
 - of mitochondrial disorders 200
 - of mucopolysaccharidoses 123
 - of neuronal ceroid lipofuscinoses (eponyms) 137
 - of peroxisomal disorders 153
 - of toxic encephalopathies 664–678
 - of white matter disorders 20–24
 - cobalamin
 - deficiency 343, 346, 354, 356
 - defects in metabolism 343, 347
 - Cockayne syndrome 259–267
 - cachectic dwarfism 259
 - CAMFAK syndrome 260
 - clinical variants 259
 - COFS syndrome 260
 - complementation groups 261
 - DNA-repair 261–262
 - genetic defects 261
 - magnetic resonance imaging 263–267
 - therapeutic options 262
 - trichothiodystrophy 261
 - UV hypersensitivity 261
 - complex I deficiency 224, 226, 229
 - complex IV deficiency 224, 226, 232
 - conduction velocity 15
 - congenital and perinatal cytomegalovirus infection 645–657
 - ganciclovir 647
 - herpes viridae family 645
 - magnetic resonance imaging 650–657
 - maternal infection 645
 - mental deficiency 646
 - modes of infection 645
 - retrospective diagnosis 646
 - sensorineural hearing loss 646
 - therapeutic options 648, 649
 - TORCH infections 646
 - viral gene products 648
 - congenital muscular dystrophy 451–468
 - α -dystroglycan 453
 - – hypoglycosylation 454, 455
 - dystrophin-associated glycoprotein complex 454
 - Fukuyama congenital muscular dystrophy 451
 - genetic defects 454, 455
 - laminin- α 2 453–455
 - limb girdle muscular dystrophy 21 452
 - magnetic resonance imaging 457–468
 - MDC1C 451
 - MDC1D 451
 - merosin-deficient congenital muscular dystrophy (MDC1A) 451
 - muscle-eye-brain disease 451
 - therapeutic options 457
 - Walker-Warburg syndrome 451
 - cree leukoencephalopathy 481
 - CREST 786
 - Curschmann-Steinert disease 469–472
 - cyanide intoxication 755
 - cystathionine β -synthase deficiency 342, 347
 - cytochrome c oxidase deficiency 225, 227, 238
 - cytomegalovirus infection
 - congenital or perinatal 645–657
 - in AIDS 624
- D**
- D-2-hydroxyglutaric aciduria 338–341
 - clinical variants 338
 - D-2-hydroxyglutarate dehydrogenase 338
 - genetic defect 338
 - magnetic resonance imaging 339–341
 - secondary respiratory chain deficiency 338
 - delayed posthypoxic leukoencephalopathy 755–758
 - carbon monoxide 755
 - cyanide 755
 - magnetic resonance imaging 756–758
 - therapeutic options 756
 - demyelination 15, 17
 - biochemical changes 17
 - loss of function 18
 - dentatorubropallidolulysian atrophy 530–534
 - anticipation 531
 - atrophin-1 530
 - CAG trinucleotide repeat 530
 - clinical variants 530
 - genetic defect 530
 - magnetic resonance imaging 531–534
 - polyglutamine repeat 531

diabetes insipidus 709
 diffuse axonal injury 823–831
 – acceleration-deceleration trauma 823
 – axonal damage 824
 – Genneralli classification 824, 831
 – magnetic resonance imaging 824–831
 – outcome 824
 – therapeutic options 824
 diffusion sensitivity 840
 diffusion weighted imaging 839–855
 – apparent diffusion coefficient 840
 – Brownian movement 839
 – developmental changes 847
 – diffusion sensitivity 840
 – fractional anisotropy 843
 – hypoxia-ischemia in neonates 733, 736, 738, 745, 747, 847, 848
 – intravoxel coherent and incoherent motion 840
 – relative anisotropy 843
 – Stejskal-Tanner sequence 840
 – trace diffusion-weighted images 843
 dihydropteridine reductase deficiency 286, 291, 292, 293
 DNA
 – content of brain 13
 – repair disorders 259–267, 268–272
 drug-induced vasculitis 797
 dysmyelination 15, 17

E

eclampsia 699
 elderly with mild cognitive impairment 759
 eosinophilic granuloma 709
 Erdheim-Chester disease 709, 710, 711, 713
 etat
 – criblé 767
 – lacunaire 767
 ethanolamine phosphoglycerides 6
 extrapontine myelinolysis 684–689

F

Fabry disease 112–118
 – atypical variants 112
 – early and late manifestations 112
 – α -galactosidase 113
 – recombinant 113
 – genetic defect 114
 – glycosphingolipids accumulation 114
 – heterozygous female patients 112
 – magnetic resonance imaging 115–118
 – pain 112
 – therapeutic options 114
 – vascular changes 113

fatty acid β -oxidation, peroxisomal 152
 folate
 – defects in metabolism 347
 – deficiency 343, 344
 fragile X premutation 406–408
 – clinical variants 406
 – genetic defect 406
 – magnetic resonance imaging 406–408
 – mental retardation 406
 – trinucleotide expansion 406
 free sialic acid storage disorder 133–136
 – bone abnormalities 134
 – clinical types 133
 – free sialic acid
 – excretion in urine 133
 – transporter 134
 – genetic defect 134
 – magnetic resonance imaging 135–136
 – Salla disease 133
 – vacuolar inclusions in sural nerve biopsy 134
 fucosidosis 119–122
 – clinical variants 119
 – fucose 119
 – genetic defect 120
 – internal organs enlargement 119
 – α -L-fucosidase 117
 – magnetic resonance imaging 120–122
 – neuronal ballooning 119
 – therapeutic options 117
 Fukuyama congenital muscular dystrophy 451, 454, 459, 461

G

Gagel granuloma 709
 galactosemia 377–382
 – clinical variants 377
 – Duarte variants 378
 – epimerase 379
 – galacticol 378
 – galactokinase 377
 – galactosed-1-phosphate uridyltransferase 377
 – genetic defects 378, 379
 – incidence 377
 – magnetic resonance imaging 380–382
 – therapeutic options 379
 – uridine diphosphate
 – galactose 379
 – galactose-4-epimerase 377
 gangliosides 7, 81, 95, 102, 104
 Genneralli classification 824, 831
 germinal layer related hemorrhage 720

giant axonal neuropathy 436–441
 – aberrant neurofilaments 437
 – genetic defect 437
 – giant axonal swellings 437
 – gigaxonin 437
 – hair abnormalities 436
 – magnetic resonance imaging 437–441
 – Rosenthal fibers 436
 giant cell arteriitis 775
 gliomatosis cerebri 818–822
 – clinical variants 818
 – delayed gadolinium enhancement 821
 – genetic patterns 818
 – magnetic resonance imaging 818–822
 – therapeutic options 820
 globoid cell leukodystrophy (Krabbe disease) 87–95
 – cerebroside 89
 – clinical variants 87
 – galactocerebroside β -galactosidase 88
 – genetic defect 89
 – magnetic resonance imaging 91–95
 – psychosine 89
 – therapeutic options 90
 – white matter involvement 89
 glutaric aciduria type 1 294–300
 – clinical variants 294, 295
 – genetic defect 295
 – glutaryl-CoA-dehydrogenase 295
 – magnetic resonance imaging 296–299
 – myelin splitting 295, 296
 – therapeutic options 295, 296
 glycosaminoglycans in urine 126
 GM1 gangliosidosis 96–102
 – activator protein 97
 – bone deformities 96
 – clinical variants 96
 – β -galactosidase 98
 – gangliosides 97
 – genetic defect 98
 – magnetic resonance imaging 100–102
 – membranous cytoplasmic bodies 97
 GM2 gangliosidosis 103–111
 – bone deformities 104
 – clinical variants 103
 – gangliosides 106
 – genetic defect 106
 – glycolipid biosynthesis 107
 – hexosaminidase A and B 104
 – magnetic resonance imaging 108–111
 – motor neuron disease 104
 granulomatous angiitis 774, 775, 776

gyration 45

- iconography: preterm-term neonates 45–50

H

- Hachinski scale 760
- Hand-Schüller-Christian disease 709
- hemolytic-uremic syndrome 700
- hepatolenticular syndrome 392–399
- hereditary diffuse leukoencephalopathy with neuroaxonal spheroids 526–529
 - axonal spheroids 526
 - clinical variants 526
 - dermatoleukodystrophy with neuroaxonal spheroids 526
 - magnetic resonance imaging 527–529
 - polycystic lipomembranous osteodysplasia with sclerosing leukoencephalopathy (Nasu-Hakola disease) 526, 552–556
- herpes zoster ophthalmica 797
- histiocytosis X 709
- holocarboxylase synthase deficiency 248–251
- Hunter syndrome 83, 124, 130
- Hurler-Scheie syndrome 123, 124, 130
- Hurler syndrome 123, 124
- 3-hydroxy-3-methylglutaryl-CoA lyase deficiency 321–324
 - clinical variants 321
 - genetic defect 321
 - HMG-CoA lyase 321
 - hypoketotic hypoglycemia 322
 - ketone bodies 321
 - magnetic resonance imaging 321–325
 - therapeutic options 322
- hyperhomocysteinemia 342–359
 - clinical variants 343, 344, 345
 - cobalamin metabolism 342
 - cystathione β -synthase 342
 - folate metabolism 342
 - genetic defects 347, 348
 - homocysteine metabolism 342
 - magnetic resonance imaging 348–359
 - methyl-folate trap 345
 - methylmalonic acidemia 343
 - mild form 342
 - pyridoxine (vitamin B6) 348
 - subacute combined degeneration of the cord 345
 - therapeutic options 348
 - transsulfuration pathway 342
- hyponatremia 690–694
 - magnetic resonance imaging 691–694
 - non-accidental intake of sodium 690

- regulation of fluid balance 691
 - toxicity 690
- hypertensive encephalopathy 699
- hypomelanosis of Ito 409–411
- Blaschkó lines 409
 - chromosomal or genetic mosaicism 409
 - clinical phenotypes 409
 - enlarged perivascular spaces 410
 - incontinentia pigmenti achromians 409
 - magnetic resonance imaging 410, 411
- hypomyelination with atrophy of the basal ganglia and cerebellum 519–525
- clinical variants 519
 - magnetic resonance imaging 519–525
- hyponatremia 685
- hypoxia-ischemia in neonates, DWI 733, 736, 738, 745, 747, 847, 848

I

- iatrogenic toxic encephalopathies 679–683
- host-versus-graft disease 679
 - magnetic resonance imaging 680–683
 - multifocal inflammatory leukoencephalopathy 679
 - posterior reversible encephalopathy syndrome 681
- incontinentia pigmenti 412–415
- Bloch-Sulzberger syndrome 412
 - genetic defect 412
 - magnetic resonance imaging 413–415
 - NF- κ -B activation 412
 - proapoptotic signals 412
 - skin lesions 412
 - type II 412–415
- infantile Refsum syndrome 154–166
- inflammatory and infectious disorders 561–565
- acquired adaptive immune system 561
 - acute phase proteins 561
 - B-cell lymphocytes 561
 - complement 561
 - cytokines 563
 - exotoxins 563
 - human leukocyte antigen (HLA) 581
 - immune system 561
 - inflammatory mediators 561
 - inflammatory process 561
 - innate non-adaptive immune system 561
 - interferons 561
 - Langerhans and dendritic cells 563

- major histocompatibility complex (MHC) 561
 - molecular and soluble components 561
 - myelin involvement in inflammatory and infectious disorders 565
 - natural killer cells 562
 - oxygen radicals 562
 - T-cell lymphocytes 561
- intrapetrous line 3
- intravascular lymphomatosis 798

J

- Jansky Bielschowski disease 137

K

- Kearns-Sayre syndrome 215–220
- endocrine dysfunction 215
 - genetic defects 216
 - magnetic resonance imaging 217–220
 - overlapping syndromes 216
 - Pearson syndrome 215
 - red ragged fibers 215
 - therapeutic options 216
- kinky hair disease 400
- Krabbe disease 87–95
- Kufs disease 137

L

- L-2-hydroxyglutaric aciduria 334–337
- clinical variants 334
 - genetic defect 334
 - L-2-hydroxyglutarate dehydrogenase 334
 - magnetic resonance imaging 334–337
- Langerhans cell histiocytosis 709–714
- diabetes insipidus 709
 - eosinophilic granuloma 709
 - Erdheim-Chester disease 709, 710
 - Hand-Schüller-Christian disease 709
 - histiocytosis X 709
 - Letterer-Siwe disease 709
 - magnetic resonance imaging 710–714
- Leber hereditary optic atrophy 212–214
- genetic defects 213
 - magnetic resonance imaging 213–214
 - multiple sclerosis association 212
 - Uhthoff symptom 212
 - visual dysfunction 212
- Leigh syndrome and mitochondrial leukoencephalopathies 224–244
- ATP synthase deficiency 224, 227
 - causes 224, 226
 - clinical variants 224

- complex I deficiency 224, 226
 - cytochrome c oxidase deficiency 224, 227
 - magnetic resonance imaging 228–244
 - mitochondrial leukoencephalopathies 224–244
 - pyruvate dehydrogenase complex deficiency 224, 226
 - therapeutic options 227
 - Letterer Siwe disease 709
 - leukoaraiosis 759
 - leukodystrophy 15
 - leukoencephalopathy 15
 - leukoencephalopathy with brain stem and spinal cord involvement and elevated white matter lactate 510–518
 - clinical variants 510
 - magnetic resonance imaging 510–518
 - leukoencephalopathy with calcifications and cysts 505–509
 - angiomatic changes 505
 - calcifications 505, 507, 509
 - clinical variants 505
 - magnetic resonance imaging 505–509
 - Rosenthal fibers 505
 - leukoencephalopathy and dural arteriovenous fistulas 801–808
 - basic fibroblast growth factor 801
 - classification of cranial AV fistulas 802
 - magnetic resonance imaging 803–807
 - therapeutic options 802
 - vascular endothelial growth factor 801
 - leukoencephalopathy after radiotherapy and chemotherapy 808–817
 - types of damage 808
 - multifocal inflammatory leukoencephalopathy 808
 - posterior reversible encephalopathy syndrome 808
 - Magnetic Resonance Imaging 810–817
 - leukoencephalopathy with vanishing white matter 481–494
 - childhood ataxia with CNS hypomyelination (CACH) 481
 - clinical variants 487–494
 - Cree leukoencephalopathy 481
 - guanosine diphosphate–guanosine triphosphate conversion 482
 - guanosine exchange factor activity 482
 - magnetic resonance imaging 483–494
 - ovarioleukodystrophy 481
 - regulation of protein synthesis 482
 - stress conditions 482
 - subunits of eIF2B 482
 - therapeutic options 482
 - translation-initiation factor eIF2B 482
 - Lhermitte symptom 566
 - lipofuscin 137
 - Loes score 186
 - Lorentzo oil 181
 - Lowe syndrome 387–391
 - genetic defect 388
 - magnetic resonance imaging 388–391
 - oculocerebrorenal syndrome 387
 - phosphoinositides 388
 - skeletal abnormalities 387
 - therapeutic options 388
 - type II phosphatases 388
 - Lyme disease 792, 793, 794
 - lysosomal storage disorders 68–73
 - classification 69
 - defects
 - in activator proteins 71
 - in postsynthetic modification of lysosomal proteins 71
 - in protective protein 72
 - in structural lysosomal proteins 71
 - in transport systems 72
 - lysosomal lipid metabolism 70
 - lysosomes 66
 - biogenesis 66
 - defects in individual hydrolases 68
 - definition 66
 - disorders 66–73
 - functions 66
 - pathochemistry 68
- M**
- magnetic resonance spectroscopy 859–881
 - ATP 861
 - basic principles 859
 - chemical shift imaging (CSI) 859, 861
 - choline 863
 - creatine 863
 - disease-specific abnormalities 865–873
 - editing techniques 860
 - Fourier transformation 860
 - frequency domain signal 860
 - GABA 864
 - glutamate 864
 - ¹H-MRS peak assignment 862
 - inorganic phosphate 861
 - J-coupling 860
 - lactate 863
 - Larmor
 - frequency 859
 - precession 859
 - myo-inositol 864
 - N-acetylaspartate 863
 - normal values 864
 - parts per million (ppm) 860
 - phosphocreatine 861
 - phosphodiesterases 861
 - phosphomonoesters 861
 - ³¹P-MRS
 - peak assignment 861
 - pH estimation 865
 - process-specific abnormalities 873–880
 - time domain signal 860
 - magnetization transfer imaging 854–858
 - developmental changes 42, 857
 - magnetization transfer ratio (MTR) 855
 - histogram analysis 855
 - axonal density 856
 - major dense line 3
 - maple syrup urine disease 311–320
 - branched-chain
 - α-keto acid decarboxylase (E1) 312
 - α-keto acid dehydrogenase complex 312
 - amino acids 311
 - clinical variants 311
 - dihydrolipoyl
 - acyltransferase (E2) 312
 - dehydrogenase (E3) 312
 - genetic defects 312
 - magnetic resonance imaging 312–320
 - therapeutic options 313
 - Marchiafava-Bignami disease 695–699
 - alcohol 695
 - clinical variants 695
 - corpus callosum splitting 696
 - magnetic resonance imaging 697–698
 - toxic factors 695
 - Maroteaux-Lamy syndrome 83, 125, 132
 - measles 640
 - megalencephalic leukoencephalopathy with subcortical cysts 442–450
 - ethnic distribution 442
 - genetic defect 443
 - macrocephaly 442
 - magnetic resonance imaging 443–450
 - MLC1 protein 443
 - phenotypic variation 443
 - vacuolating myelinopathy 443

- Menkes disease 400–405
 - ceruloplasmin levels 401
 - clinical variants 400
 - copper
 - – -dependent enzyme processes 402
 - – -transporting P-type ATPase 402
 - – levels 401
 - cranial exostoses 400
 - genetic defect 402
 - kinky hair disease 400
 - magnetic resonance imaging 403–405
 - occipital horn syndrome 400
 - skeletal abnormalities 400
 - therapeutic options 403
 - tortuosity of cerebral vessels 403
 - trichopoliodystrophy 400
 - type IX Ehlers-Danlos syndrome 400
 - X-linked cutis laxa 400
- merosin-deficient congenital muscular dystrophy 451, 455, 466
- metachromatic leukodystrophy 74–81
 - arylsulfatase A 75
 - clinical variants 74
 - genetic defect 76
 - magnetic resonance imaging 78–81
 - metachromasia 75
 - pseudodeficiency of arylsulfatase A 75
 - sulfatide 75
 - therapeutic options 78
- 5,10-methylenetetrahydrofolate
 - reductase deficiency 342, 347, 351
 - thermolabile variant 342, 347
- microscopic polyarteritis 789
- mitochondria 195–204
 - citric acid cycle 197
 - mitochondrial DNA 198
 - nuclear DNA 198
 - oxidative phosphorylation 197
 - respiratory chain 197
 - structure and function 195
- mitochondrial disorders 195–204
 - classification 200
 - maternal inheritance 199
 - mitochondrial DNA defects 200–201
 - – deletions, large single 201
 - – duplications 201
 - – point mutations 201
 - genetics 198
 - leukoencephalopathies 224–244
 - nuclear DNA defects 201–202
 - – types of genes 201
 - assembly factors 202
 - DNA maintenance 202
- mitochondrial encephalopathy with lactic acidosis and stroke-like episodes (MELAS) 204–211
 - calcium deposits 205
 - clinical variants 204
 - genetic defects 205
 - magnetic resonance imaging 206–211
 - MELAS-MERFF overlap 204
 - red ragged fibers 204
 - therapeutic options 205
- mitochondrial leukoencephalopathies 224–244
- mitochondrial neurogastrointestinal encephalomyopathy 221–223
 - genetic defect 222
 - magnetic resonance imaging 222–223
 - synonyms 221
- molybdenum cofactor deficiency 372–376
 - isolated sulfite oxidase deficiency 372–376
 - clinical variants 372
 - sulphite oxidase 372
 - genetic defects 372, 373
 - molybdenum cofactor synthesis 372
 - therapeutic options 373
 - magnetic resonance imaging 373–376
- Morquio syndrome 83, 125, 132
- Moyamoya syndrome 777, 778, 779, 780
- mucopolysaccharidoses 123–132
 - classification 123
 - degradation of mucopolysaccharides 126
 - enzyme deficiencies (table) 123
 - enzymes involved 123
 - genetic defects 127
 - glycosaminoglycans 127
 - Magnetic Resonance Imaging 129–132
 - mental deficiency 126
 - proteoglycans 127
 - therapeutic options 127
- multicystic encephalopathy 720, 742, 743
- multifocal inflammatory leukoencephalopathy 679, 680, 808
- multiple carboxylase deficiency 248–251
 - biotinidase deficiency 248
 - clinical variants 248
 - genetic defect 249
 - holocarboxylase synthase deficiency 248
 - magnetic resonance imaging 250, 251
 - skin abnormalities 248
 - therapeutic options 250
- multiple sclerosis 566–613
 - Baló concentric sclerosis 567
 - Barkhof criteria 568
 - benign MS 566
 - CD 4⁺ and CD 8⁺ T cell lymphocytes 572
 - Charcot type 566
 - clinical variants 566
 - clinically isolated symptom (CIS) 566
 - cluster of differentiation markers (CD) 569
 - diagnostic criteria 567
 - environmental factors 574
 - experimental allergic encephalomyelitis (EAE) 572
 - FA and ADC 849, 592, 593
 - gadolinium enhancement 569
 - genetic factors 573
 - incidence 566
 - Lhermitte symptom 566
 - magnetic resonance imaging 577–613
 - Marburg type 566
 - McDonald criteria 568
 - neuromyelitis optica 567
 - oligoclonal banding 568
 - perivenular inflammation 569
 - primary progressive MS 566
 - relapsing-remitting MS 566
 - remyelination 570
 - Schilder diffuse sclerosis 567
 - secondary progressive MS 566
 - spinal cord involvement 579, 587–589
 - therapeutic options 575, 576
 - tumefactive MS 566
 - viral factors 573
- multiple sulfatase deficiency 82–86
 - clinical variants 82
 - genetic defect 83
 - magnetic resonance imaging 83–86
 - mucopolysaccharidoses 82
 - peripheral nerve involvement 83
 - sulfatases involved 83
 - zebra bodies 82
- muscle-eye-brain disease 451, 454, 462
- myelin
 - aging 14
 - basic protein 7, 281
 - biochemical composition 6
 - compositional changes during development 13
 - function 14
 - introduction 1
 - glycoproteins 7
 - levels of involvement 16
 - molecular architecture 9

- morphology 1
- disorders
 - – classification 20–24
 - – definitions 15
 - – levels of myelin involvement 16
- turnover 14
- myelination 10, 11, 12
- myelinogenesis 10
- regulation of myelinogenesis 10
- retarded myelination 18
- myelination 3, 4, 10, 11, 12, 37–65
 - arrest 51
 - delayed myelination 51
 - diffusion tensor imaging 41
 - diffusion weighted imaging 41
 - Flechsig 37
 - hypomyelination 51
 - iconography: preterm-adult pattern 51–65
 - irregular myelination 51
 - magnetization transfer imaging 42
 - marker sites 43
 - MRI pulse sequences 39
 - myelination: time tables 42
- myelinogenesis 10
- myoneurogastrointestinal
 - encephalopathy (MNGIE) 221–223
- myotonic dystrophy, type 1 469–472
 - anticipation 469, 470
 - clinical variants 469
 - Curschmann-Steinert disease 469
 - genetic defect 470
 - magnetic resonance imaging 470–472
 - therapeutic options 470
 - unstable CTG repeat 469
- myotonic dystrophy, type 2 473–475
 - clinical variants 473
 - genetic defect 474
 - magnetic resonance imaging 474, 475
 - proximal myotonic dystrophy 473
 - therapeutic options 474
 - unstable CCTG repeat 474

N

- NARP syndrome 227, 244
- Nasu-Hakola disease 552–556
- neonatal adrenoleukodystrophy 154–166
- neonatal hypoglycemia 749–754
 - causes 749
 - glucose transporters 749
 - magnetic resonance imaging 752–754
 - selective vulnerability in hypoglycemia 749, 750
 - therapeutic options 750, 751
- neuromyelitis optica 567, 597

- neuronal ceroid lipofuscinoses 137–146
 - age pigment 141
 - Batten disease 137
 - classification (table) 137
 - genes involved 141
 - incidence 137
 - lysosomal location 140
 - magnetic resonance imaging 143–146
 - myelin reduction 141
 - neuronal lipofuscin storage 140
 - protein defects 141
 - storage material in subtypes (table) 137
- neurosarcoidosis 787, 788
- node of Ranvier 4, 15
- nonketotic hyperglycinemia 306–311
 - clinical variants 306
 - genetic defect 307
 - glycine cleavage system 306
 - magnetic resonance imaging 309, 310
 - P-, T-, H- and L-proteins 307
 - therapeutic options 308
- Northern epilepsy 137

O

- occipital horn syndrome 400
- oculo-cerebro-renal syndrome 387–391
- oculo-dento-digital dysplasia 479–480
 - clinical variants 479
 - connexin 43 479
 - genetic defect 479
 - magnetic resonance imaging 480
- oculogastrointestinal muscular dystrophy (OGIMD) 221–223
- oligodendrocyte 4
 - specific protein 7
- ornithine transcarbamylase deficiency 360, 362, 365
- ovarioleukodystrophy 481

P

- pattern recognition
 - examples 891–904
 - in unclassified white matter disorders 889
 - in white matter disorders 881–904
 - – computer-aided pattern recognition 886
 - – general characteristics 884
 - – non-computerized pattern recognition 882
 - – practical applications 886
 - – sensitivity and specificity 881
 - – special characteristics 884
 - – structural image elements 884

- Pelizaeus-Merzbacher disease and X linked spastic paraplegia type II 272–284
 - clinical variants 272
 - DM20 274
 - genetic defect 275
 - magnetic resonance imaging 276–284
 - proteolipid protein 274
 - X-inactivation 275
- periventricular leukomalacia 719, 720, 722, 726, 727
- peroxisomal acyl-CoA oxidase deficiency 172–175
 - cranio-facial dysmorphism 172
 - fatty acyl-CoA oxidase 172
 - gene defect 172
 - magnetic resonance imaging 174–175
- peroxisomal biochemical functions 151
- peroxisomal D-bifunctional protein deficiency 167–171
 - clinical phenotype 167
 - gene defect 168
 - magnetic resonance imaging 168–171
- peroxisomal single enzyme defects 153
- peroxisome biogenesis 151
 - disorders 153, 154–166
 - – clinical variants 154
 - – Zellweger syndrome 154
 - – neonatal adrenoleukodystrophy 154
 - – infantile Refsum syndrome 154
 - – pathology 155
 - – pathogenesis 157
 - – genetic defects 157, 158
 - – therapy 159
 - – magnetic resonance imaging 160–166
- peroxisomes and peroxisomal disorders 151–153
- phenylalanine metabolism 284
- phenylketonuria 284–293
 - clinical variants 284
 - genetic defect 287
 - magnetic resonance imaging 289–294
 - maternal phenylketonuria 285
 - neonatal screening 285
 - phenylalanine
 - – hydroxylase 284
 - – metabolism 284
 - tetrahydrobiopterin 284
 - – synthesis 285
 - therapeutic options 288
- 3-phosphoglycerate dehydrogenase deficiency 369–371
- PIBIDS 268–272

pigmentary orthochromatic leukodys-
trophy 557–558

- magnetic resonance imaging 558

Pollit syndrome 268–272

polyarteritis nodosa 777,

polycystic lipomembranous osteodys-
plasia with sclerosing leuken-
cephalopathy 526, 552–556

- clinical variants 552
- genetic defects 553
- magnetic resonance imaging 553–556
- Nasu-Hakola disease 552
- skeletal abnormalities 552

polyneuropathy, ophthalmoplegia,
leukoencephalopathy, intestinal
pseudo-obstruction (POLIP)
221–223

posterior reversible encephalopathy
syndrome 679, 680, 699–709, 808

- complication of medical treatment 699
- eclampsia, pre-eclampsia 699
- hypertensive encephalopathy 699
- magnetic resonance imaging 701–709
- related conditions 699
- reversible posterior leukoen-
cephalopathy syndrome 699
- therapeutic options 700
- uremic encephalopathies 700

posthypoxic-ischemic encephalopathy
in neonates 718–749

- basal ganglia damage 718
- central cortical and subcortical dam-
age 718
- germinal layer hemorrhage 720
- magnetic resonance imaging 723–748
- multicystic encephalopathy 720
- periventricular leukomalacia 718,
719
- prognostic factors 719
- Sarnat classification 719
- subcortical leukomalacia 718
- therapeutic options 723
- venous infarction 720

posthypoxic-ischemic damage
714–719

- anti-oxidance capacity 715
- arachidonic acid 715
- calcium-entry blockers 715
- excitatory amino acids 716
- free radicals 714, 715
- – scavengers 714
- glutamate 716
- Haber-Weiss reaction 714
- nitric oxide 715
- N-methyl-D-aspartate (NMDA) 716
- oxygen paradox 714

- patterns of white matter damage in
oxygen deprivation 716, 717
- reperfusion damage 714
- superoxide dismutase 714

progressive multifocal leukoen-
cephalopathy 628–634

- B-cell infection 629
- JC virus infection 628
- magnetic resonance imaging 630–634
- oligodendrocyte infection 629
- Papova-Polyoma virus 628
- simian virus 40 (SV40) 629
- therapeutic options 630
- tumor induction 630

propionic acidemia 300–306

- biotin cofactor 300
- clinical variants 300
- genetic defect 301
- ketotic hyperglycinemia 300
- magnetic resonance imaging 303–305
- propionyl-CoA carboxylase 300
- therapeutic options 301

proteolipid protein 7, 274

psychosine (in Krabbe disease) 89

pyruvate carboxylase deficiency
245–247

- biotin dependent carboxylases 246
- clinical variants 245
- genetic defect 245
- magnetic resonance imaging 246–247
- pyruvate-oxalate conversion 246
- therapeutic options 246

pyruvate dehydrogenase complex defi-
ciency 226, 229, 224

R

Radiotherapy 808–817

- acute postradiotherapy syndrome 809
- early delayed postradiotherapy
syndrome 809
- late postradiotherapy syndrome 809

recombinant α -galactosidase 113

Refsum disease (heredopathia atactica
polyneuritiformis) 91–194

- cardiomyopathy 191
- clinical variants 191
- genetic defect 193
- hereditary sensory and motor neu-
ropathy type 4 191
- ichthyosis 191
- magnetic resonance imaging 194
- phytanic acid levels 191, 192
- phytanoyl-CoA hydroxylase 193
- pipelic acidemia 193
- skeletal deformities 191
- therapeutic options 194

remyelination 18

retarded myelination 18, 51, 42

reversible posterior leukoencephalopa-
thy syndrome 699–709

rheumatoid disease 781

S

Salla disease 133–136

saltatory conduction 15

Sandhoff disease 103–111

Sanfilippo syndrome 83

Santavuori disease 137, 144, 145

Sarnat classification 719

Scheie syndrome 123, 124

Schilder diffuse sclerosis 567, 598, 599

Schmidt-Lantermann cleft 4

Schwann cell 4

selective vulnerability 25–36

- causes of selective involvement 30–35
- topistic areas 25

serine synthesis defect 369–371

- genetic defect 369
- magnetic resonance imaging 370,
371
- 3-phosphoglycerate dehydrogenase 369
- treatment options 369

sialic acid 134

- transporter 134

sickle cell disease 798

Sjögren syndrome 786

Sjögren-Larsson Syndrome 383–386

- clinical triad 383
- fatty alcohol-NAD⁺ oxidoreductase 383
- fatty aldehyde dehydrogenase 384
- genetic defect 383
- leukotriene B₄ 384
- magnetic resonance imaging 384–386
- therapeutic options 384

Sly syndrome 125

Sneddon syndrome 785

Spielmeijer-Vogt disease 137

Stejskal-Tanner sequence 840

subacute combined degeneration
of the cord 350

subacute sclerosing panencephalitis
640–644

- absence of M protein 642
- anti-measles virus antibody 640,
641
- M protein gene mutations 641
- magnetic resonance imaging 642–644
- measles infection 640
- paramyxoviridae family 641
- slow virus infection 640
- stages of disease 640, 641

subcortical arteriosclerotic
encephalopathy 767–772
– Binswanger disease 767–772
– criteria 767
– état
– – criblé 767
– – lacunaire 767
– lacunar infarctions 767
– magnetic resonance imaging
768–772
– therapeutic options 768
– Virchow-Robin spaces 767
subcortical leukomalacia 718
sulfite oxidase deficiency 372–376
18q⁻ syndrome 281–283
– clinical variants 281
– contiguous gene syndrome 281
– magnetic resonance imaging 282,
283
– myelin basic protein 281
syphilitic arteritis 795
systemic lupus erythematosus
781–784

T

Takayasu arteritis 776, 777
Tay syndrome 268–272
Tay-Sachs disease 103–111
temporal arteritis 775
tetrahydrobiopterin deficiency 285
– synthesis 285
thrombotic thrombocytopenic purpura
699
toxic encephalopathies 664–678
– Bonhoeffer reaction types 664
– chemical affinity 665
– classification 667
– drug abuse 670
– endogenous intoxications 667
– exogenous-external intoxications
667
– fetal intoxications 677
– historic examples 664
– iatrogenic intoxications 669
– lipophilic substances 665
– magnetic resonance imaging
(examples) 665–678
– mechanisms of selective vulnera-
bility 665
– organic solvents 670
– topistic areas 664
trichothiodystrophy with photo-
sensitivity 268–272
– basal transcription factor II H 269
– clinical variants 268
– DNA-repair 269
– genetic defects 269
– hair abnormalities 268
– magnetic resonance imaging
270–271

– Pollit syndrome 268
– Tay syndrome 268
– xeroderma pigmentosum 269
tuberculosis 795, 796

U

Uhthoff symptom 212
urea cycle 360
– disorders 360–369
– – arginase deficiency 360
– – argininosuccinate lyase deficiency
360
– – argininosuccinate synthetase
deficiency 360
– – carbamyl phosphate synthetase
deficiency 360
– – female heterozygotes of ornithine
transcarbamylase deficiency 360
– – genetic defects 362
– – hyperargininemia 360
– – magnetic resonance imaging
363–369
– – ornithine transcarbamylase
deficiency 360
– – therapeutic options 362
– – urea cycle defects 360

V

Van Bogaert-Bertrand disease
326–333
vanishing white matter 481–494
varicella-zoster vasculitis 796
vasculitis 773–800
– ANCA test 789
– angiotensin converting enzyme
787
– anti-phospholipid antibody syn-
drome 785
– Behçet disease 789
– benign primary angiitis 776
– Borrelia burgdorferi 792
– Churg-Strauss syndrome 789
– classification 774
– CREST 786
– drug-induced vasculitis 797
– erythema migrans 793
– giant cell arteritis 775
– granulomatous angiitis 774
– herpes zoster ophthalmica 797
– hydroxyurea 799
– hypercoagulable states 798
– intravascular lymphomatosis 798
– Lyme disease 792
– magnetic resonance imaging
799–800
– microscopic polyarteritis 789
– Moyamoya syndrome 777
– neurosarcoidosis 787
– polyarteritis nodosa 777
– rheumatoid disease 781

– sickle cell disease 798
– Sjögren syndrome 786
– Sneddon syndrome 785
– syphilitic arteritis 795
– systemic lupus erythematosus 783
– Takayasu arteritis 776
– temporal arteritis 775
– tuberculosis 795
– varicella-zoster vasculitis 796
– Wegener disease 789
venous infarction 720, 724
vitamin B₁₂ deficiency (see also cobal-
amin deficiency) 343, 346, 354, 356

W

Walker-Warburg syndrome 451, 455,
466
Wallerian degeneration 832–837
– magnetic resonance imaging
834–838
– stages of myelin degradation 832,
833
Wegener disease 789, 790
Whipple disease 658–663
– clinical triad 658
– CNS involvement 658
– lipofuscin granules 658
– magnetic resonance imaging
659–663
– therapeutic options 659
– Tropheryma Whippelii 658
white matter lesions in the elderly
759–766
– age-related changes 759
– cerebral perfusion 760
– leukoaraiosis 759
– magnetic resonance imaging
761–766
– mild cognitive impairment 759
– MR grading of lesions 762
– quantitative MR techniques 759
– risk factors 760
Wilson disease 392–399
– ceruloplasmin 393
– clinical variants 392, 393
– copper
– – concentration 393
– – homeostasis 394
– – toxicity 395
– genetic defect 394
– hepatolenticular degeneration 392
– Kayser-Fleischer rings 392
– magnetic resonance imaging
396–399
– metallothionein 394
– therapeutic options 395

X

Xeroderma pigmentosum 260, 269
X-linked adrenoleukodystrophy
176–190

1084 Subject Index

- ABCD2 gene 182
 - adrenal insufficiency 176
 - clinical variants 176
 - fatty acid chain elongation 180
 - female carriers 177
 - genetic defect 179
 - Loes score 186
 - Lorenzo oil 181
 - magnetic resonance imaging 182–190
 - MTR 187,857,858
 - pathogenesis 180
 - therapeutic options 181
 - unusual forms of X-ALD 177
 - very-long-chain fatty acids (VLCFA) 177
 - VLCFA β -oxidation 179
 - VLCFA-CoA synthase 179
 - X-linked ichthyosis 83
- Z**
- Zellweger syndrome 154–166